

Polymers and Polymeric Composites:
A Reference Series

SPRINGER
REFERENCE

Mohammad Abu Jafar Mazumder
Heather Sheardown
Amir Al-Ahmed *Editors*

Functional Polymers

 Springer

Polymers and Polymeric Composites: A Reference Series

This series provides a comprehensive collection of reference handbooks on all aspects around polymers and polymeric composites. Polymeric materials of all sorts have been emerging as key materials for many applications and for meeting the challenges of the twenty-first century. From commodity applications to engineering and high-tech applications, even including aerospace subsystems, these materials have an important role to play. The study of polymeric and polymeric composite materials is one of the most important and vibrant focus areas in chemical and material scientific research. "Polymers and Polymeric Composites: A Reference Series" compiles the most comprehensive reference handbooks on these materials under one roof. Readers will find all they need to know in well-organized and thoroughly structured reference works covering various topics, such as the structures and properties of polymers, polymeric materials and composites (e.g. structures of amorphous and crystalline polymers, viscoelastic properties, mechanical and thermal properties, and many more); methods and methodology (including polymer characterization, polymerization reaction engineering, polymer processing, and many more); and different compound classes (from polymer additives, polymer blends, and fiber reinforced composites to liquid crystalline polymers, nano-polymers and nano-polymeric composites, and even bio-polymeric materials). While each volume is dedicated to a selected topic, concisely structured and thoroughly edited by experts, with contributions written by leading scientists, the complete collection provides the most comprehensive and most complete overview over the entire field of polymers and polymeric composites. Volumes in this series serve as reference compilation for every scientist working with or on polymers and polymeric materials and composites, whether at universities or in industry, from graduate student level to practitioners and lead scientists alike.

More information about this series at <http://www.springer.com/series/15068>

Mohammad Abu Jafar Mazumder
Heather Sheardown • Amir Al-Ahmed
Editors

Functional Polymers

With 473 Figures and 65 Tables

 Springer

Editors

Mohammad Abu Jafar Mazumder
Chemistry Department
King Fahd University of Petroleum
and Minerals
Dhahran, Saudi Arabia

Heather Sheardown
McMaster University
Hamilton, ON, Canada

Amir Al-Ahmed
Center of Research Excellence in
Renewable Energy
King Fahd University of Petroleum
and Minerals
Dhahran, Saudi Arabia

ISSN 2510-3458

ISBN 978-3-319-95986-3

ISBN 978-3-319-95988-7 (print and electronic bundle)

<https://doi.org/10.1007/978-3-319-95987-0>

ISSN 2510-3466 (electronic)

ISBN 978-3-319-95987-0 (eBook)

© Springer Nature Switzerland AG 2019

This work is subject to copyright. All rights are reserved by the Publisher, whether the whole or part of the material is concerned, specifically the rights of translation, reprinting, reuse of illustrations, recitation, broadcasting, reproduction on microfilms or in any other physical way, and transmission or information storage and retrieval, electronic adaptation, computer software, or by similar or dissimilar methodology now known or hereafter developed.

The use of general descriptive names, registered names, trademarks, service marks, etc. in this publication does not imply, even in the absence of a specific statement, that such names are exempt from the relevant protective laws and regulations and therefore free for general use.

The publisher, the authors, and the editors are safe to assume that the advice and information in this book are believed to be true and accurate at the date of publication. Neither the publisher nor the authors or the editors give a warranty, express or implied, with respect to the material contained herein or for any errors or omissions that may have been made. The publisher remains neutral with regard to jurisdictional claims in published maps and institutional affiliations.

This Springer imprint is published by the registered company Springer Nature Switzerland AG
The registered company address is: Gewerbestrasse 11, 6330 Cham, Switzerland

Preface

Functional polymers contain chemically bound functional groups on their backbone, which make these polymers chemically active for various applications, for example, as reagents, catalysts, protecting groups, and many others. Normally, functional polymers are prepared from monomers containing the desired functional group. The preformed polymer backbone can also be chemically modified with a preferred functional group. The second approach is more suitable for linear polymers, but in most applications, cross-linked polymers are preferred. Suspension polymerization is the most commonly used technique for cross-linked polymers, but several other techniques, such as photo polymerization, electrochemical polymerization, and different controlled radical polymerizations are also attaining their place. The physicochemical properties of these polymers can be modified as required by chemical or physical means. Specific induced properties by functionalization of polymers have great importance in their applications. Advance technologies require improved material performance. Polymers, especially functional polymers can easily be tuned by new or improved design and processing techniques, which can provide better or specific material characteristics. This facilitates their innovative and technically demanding applications.

To edit or compile a book on functional polymers, one should be very careful to keep a fine balance between the built up knowledge developed over the years, based on experience and intuition, and the new scientific endeavors that continue to advance their development. Our approach is to give a rich collection of data on functional polymers. In this regard, this reference book covers some key aspects of functional polymers, such as synthesis, surface modification, composites and nanocomposites, and important applications. All chapters are contributed by experts in

their respective field and contain up-to-date theoretical and experimental information, which will be helpful for students and researchers to create new avenues for functional polymers – in terms of material development and advance applications.

Chemistry Department

King Fahd University of Petroleum
and Minerals, Dhahran, Saudi Arabia

McMaster University, Hamilton, ON, Canada
Center of Research Excellence in Renewable Energy
King Fahd University of Petroleum and Minerals,
Dhahran, Saudi Arabia

Mohammad Abu Jafar Mazumder, Ph.D.

Heather Sheardown, Ph.D.

Amir Al-Ahmed, Ph.D.

The Editors

Acknowledgments

We are thankful to all contributing authors and co-authors for their valued contribution to this book. The project would never have been possible without their sincere supports and contributions. We would also like to express our gratitude to the publisher, authors, and others for granting us the copyright permission to use their illustrations. Although sincere efforts were made to obtain the copyright permissions from the respective owners to include the citation with the reproduced materials, we would like to offer our sincere apologies to any copyright holder if unknowingly their right is being infringed. Among the editors, Dr. Mohammad A. Jafar Mazumder would like to take this opportunity to express his sincere thanks to Drs. Abdulaziz A. Al-Saadi (Dean, College of Sciences, KFUPM) and Khalid R. Alhooshani (Chairman, Chemistry Department, KFUPM) and also to his colleagues at the King Fahd University of Petroleum and Minerals (KFUPM), Saudi Arabia. Dr. Amir Al-Ahmed, would like to take this opportunity to express his sincere thanks to Dr. Fahad Al-Suliman (Director CORE-RE, KFUPM) and also to his colleagues at the King Fahd University of Petroleum and Minerals, Saudi Arabia. Without their continuous encouragement, this book would have not been brought into its final form. We would also like to acknowledge the sincere efforts of Springer team, especially Dr. Sylvia Blago, Dr. Sofia Costa, and Dr. Judith Hinterberg and others who were always so helpful and provided us their assistance in evolving this book into its final shape. We are most grateful to all of them.

Contents

1 Photo-polymerization	1
Prem Prabhakaran and Kwang-Sup Lee	
2 Polymer Functionalization	53
Lindsey A. Bultema, Xia Huang, Daniel D. Brauer, and Patrick Theato	
3 Electrochemical Polymerization	105
Gertrude Fomo, Tesfaye Waryo, Usisipho Feleni, Priscilla Baker, and Emmanuel Iwuoha	
4 Polymer Processing and Rheology	133
Nickolas D. Polychronopoulos and John Vlachopoulos	
5 Porous Coordination Polymers	181
Abdul Malik P. Peedikakkal and N. N. Adarsh	
6 Polyurethane and Its Derivatives	225
Mohammad Mizanur Rahman, Mohammad Mahbub Rabbani, and Joyanta Kumar Saha	
7 Dielectric Polymers	241
Shah Mohammed Reduwan Billah	
8 Dendrimers	289
Balappa B. Munavalli, Satishkumar R. Naik, Anand I. Torvi, and Mahadevappa Y. Kariduraganavar	
9 Surfaces and Interfaces	347
Manfred Stamm	
10 Membrane Surface Modification and Functionalization	391
Syed Mohammed Javaid Zaidi, Kenneth A. Mauritz, and Mohammad K. Hassan	
11 Fiber-Reinforced Composites	417
Ajithkumar Manayan Parambil, Jiji Abraham, Praveen Kosappallyillom Muraleedharan, Deepu Gopakumar, and Sabu Thomas	

12 Composites and Nanocomposites	447
Shah Mohammed Reduwan Billah	
13 Polymer Blends	513
Ibrahim Khan, Muhammad Mansha, and Mohammad Abu Jafar Mazumder	
14 Conducting Polymers and Composites	551
Abd Almonam Baleg, Milua Masikini, Suru Vivian John, Avril Rae Williams, Nazeem Jahed, Priscilla Baker, and Emmanuel Iwuoha	
15 Shape-Memory Polymers	605
Magdalena Mazurek-Budzyńska, Muhammad Yasar Razzaq, Marc Behl, and Andreas Lendlein	
16 Self-Healing Polymers: From Biological Systems to Highly Functional Polymers	665
Stefan Zechel, Martin D. Hager, and Ulrich S. Schubert	
17 Drug Delivery: Polymers in the Development of Controlled Release Systems	719
Scott Campbell and Niels Smeets	
18 Conjugated Organic Polymers for Optoelectronic Devices	749
Shahid Pervez Ansari and Farman Ali	
19 Electrochromic Polymers for Solar Cells	789
Suru Vivian John and Emmanuel Iwuoha	
20 Textile Coatings	825
Shah Mohammed Reduwan Billah	
21 Anticorrosive Coating	883
Mazen K. Nazal and Mohammad Abu Jafar Mazumder	
22 Conducting Polymer Nanocomposites as Gas Sensors	911
Mohammad Omaish Ansari, Sajid Ali Ansari, Moo Hwan Cho, Shahid Pervez Ansari, Mohamed Shaaban Abdel-wahab, and Ahmed Alshahrie	
23 Polymeric Membranes for Natural Gas Processing: Polymer Synthesis and Membrane Gas Transport Properties	941
Jimoh K. Adewole and Abdullah S. Sultan	
24 Proton Conductions	977
N. Awang, Juhana Jaafar, A. F. Ismail, T. Matsuura, M. H. D. Othman, and M. A. Rahman	
25 Desalination	1011
Rasel Das, Syed Mohammed Javaid Zaidi, and Sayonthoni Das Tuhi	

26	Enhanced Oil Recovery	1045
	Muhammad Shahzad Kamal and Abdullah S. Sultan	
27	Drug Delivery: Localized and Systemic Therapeutic Strategies with Polymer Systems	1079
	Scott Campbell and Niels Smeets	
28	Organic-Inorganic Hybrid Materials and Their Applications	1135
	Rizwana Mobin, Tauseef Ahmad Rangreez, Hamida Tun Nisa Chisti, Inamuddin, and Mashallah Rezakazemi	

About the Editors



Dr. Mohammad Abu Jafar Mazumder is an Associate Professor of Chemistry at King Fahd University of Petroleum and Minerals (KFUPM), Saudi Arabia, who has a wide experience in design, synthesis, modification and characterization of various organic compounds, ionic and thermo-responsive polymers using various spectroscopic and chromatographic techniques. Dr. Jafar Mazumder earned his Ph.D. in Chemistry (2009) from McMaster University, Canada followed by 2 years MITACS-postdoctoral fellowship in Chemical and Biomedical engineering at McMaster University, Canada.

In 17 years of academic research, Dr. Jafar Mazumder has had the opportunity to work with several international collaborative research groups and has exposed himself to a broad range of research areas, including chemistry, engineering and material sciences where he developed and engineered synthetic and natural organic and polymeric materials for various applications. Moreover, he has over three years of working experience in pharmaceutical and polymer industry, worked on the development, optimization and characterization of various polymers/chemicals and exposed with a variety of analytical techniques/instruments.

Dr. Jafar Mazumder secured 5 US patents, 2 books edited, 6 invited book chapters, published more than 50 journal articles in synthesis, characterization and applications based peer reviewed journal of Chemistry and material sciences, and had the opportunity to present his research more than 25 international conferences. Dr. Jafar Mazumder has conducted and completed several internally and externally funded research projects from KFUPM, Saudi Aramco, KACST and NSTIP. Currently, he is actively involved in a number of ongoing university, and

client funded research projects in a capacity of principal and co- investigators where he is responsible for synthesis and characterization of various materials including modification of monomers and polymers for their potential use as corrosion inhibitors and for the removal of heavy metal ions and organic contaminants from aqueous samples.



Heather Sheardown is a Professor in the Department of Chemical Engineering with a cross appointment to the Department of Pathology and Molecular Medicine and an adjunct appointment with the School of Optometry at the University of Waterloo. She holds a Tier 1 Canada Research Chair in Ophthalmic Biomaterials and Drug Delivery and has published more than 140 peer reviewed papers on this subject. She is currently the Scientific Director of C20/20, an ORF funded incubator aimed at the commercialization of ophthalmic biotechnologies. Sheardown was previously the Scientific Director of the 20/20 NSERC Ophthalmic Materials Research Network which brought together 12 researchers and more than 10 companies aimed at the early stage development of novel materials based treatments for ophthalmic conditions. Sheardown is the Associate Director of Biomedical Engineering and Advanced Manufacturing (BEAM), a McMaster partnership with the Fraunhofer IZI which partners with companies for incubation and commercialization of cell based therapies, diagnostics and biomaterials. She holds 18 patents or provisional patents and is currently the Chief Scientific Officer of 20/20 OptimEyes, a McMaster based spin out focused on developing and commercializing a micelle based technology developed in her laboratory. She runs a large and vibrant research group with more than 10 post doctoral fellows, and graduate students.



Dr. Amir Al-Ahmed is working as a Research Scientist-II (Associate Professor) in the Center of Research Excellence in Renewable Energy (CoRE-RE), at King Fahd University of Petroleum and Minerals (KFUPM), Saudi Arabia. He graduated in chemistry from the Department of Chemistry, Aligarh Muslim University (AMU), India. Then completed his M.Phil. (2001) and Ph.D. (2003) degree in Applied Chemistry from the Department of Applied Chemistry, AMU, India, followed by three consecutive postdoctoral fellowships in South Africa

and Saudi Arabia. During this period he worked on various multidisciplinary projects in particular, electrochemical sensors, nano-materials, proton exchange membranes, DMFC, electro-catalysis and solar cells. At present, his research activity is fundamentally focused on 3rd generation solar cell devices such as low band gap semiconductor quantum dot structures, perovskite cells and silicon nano-wire base tandem cells. At the same time, he is also having projects on PCM based latent heat energy storage, evaluation of electricity storage devices and dust repellent coating for Harsh Saudi Arabian weather condition. He has worked on different KACST, NSTIP and Saudi Aramco funded projects in the capacity of a co-investigator and principle investigator. Dr. Amir has two US patents, over 60 journal articles, invited book chapters and conferences publications. He has edited nine books with Trans Tech Publication, and Elsevier and several other books are in progress. He is also the Editor-in-Chief of an international journal "*Nano Hybrids and Composites*" along with Professor Y. H. Kim.

Contributors

Mohamed Shaaban Abdel-wahab Center of Nanotechnology, King Abdulaziz University, Jeddah, Saudi Arabia

Materials Science and Nanotechnology Department, Faculty of Postgraduate Studies for Advanced Sciences, Beni-Suef University, Beni-Suef, Egypt

Jiji Abraham International and Inter University Centre for Nanoscience and Nanotechnology, Mahatma Gandhi University, Kottayam, Kerala, India

N. N. Adarsh Solid State and Materials Chemistry, School of Chemical Sciences, Mahatma Gandhi University, Kottayam, Kerala, India

Jimoh K. Adewole Center for Integrative Petroleum Research, College of Petroleum Engineering and Geosciences, King Fahd University of Petroleum and Minerals, Dhahran, Saudi Arabia

Farman Ali Department of Applied Chemistry, Faculty of Engineering and Technology, Aligarh Muslim University, Aligarh, India

Ahmed Alshahrie Center of Nanotechnology, King Abdulaziz University, Jeddah, Saudi Arabia

Department of Physics, Faculty of Science, King Abdulaziz University, Jeddah, Saudi Arabia

Mohammad Omaish Ansari Center of Nanotechnology, King Abdulaziz University, Jeddah, Saudi Arabia

School of Chemical Engineering, Yeungnam University, Gyeongbuk, South Korea

Sajid Ali Ansari Department of Energy and Materials Engineering, Dongguk University, Seoul, Republic of Korea

Shahid Pervez Ansari Department of Applied Chemistry, Faculty of Engineering and Technology, Aligarh Muslim University, Aligarh, India

N. Awang Advanced Membrane Technology Research Centre (AMTEC), Universiti Teknologi Malaysia, Johor Bahru, Malaysia

Faculty of Chemical and Energy Engineering, Universiti Teknologi Malaysia, Johor Bahru, Malaysia

Priscilla Baker SensorLab, Department of Chemistry, University of the Western Cape, Bellville, South Africa

Abd Almonam Baleg Department of Chemistry, University of the Western Cape, Bellville, South Africa

Marc Behl Institute of Biomaterial Science, Helmholtz-Zentrum Geesthacht, Teltow, Germany

Shah Mohammed Reduwan Billah University of East London, Stratford Campus, London, UK

CCIRA UK limited, Galashiels, UK

Department of Chemistry, Durham University, Durham, UK

School of Textiles and Design, Heriot-Watt University, Galashiels, UK

Daniel D. Brauer Institute of Technical and Macromolecular Chemistry, University of Hamburg, Hamburg, Germany

Lindsey A. Bultema Institute of Technical and Macromolecular Chemistry, University of Hamburg, Hamburg, Germany

Scott Campbell Department of Chemical Engineering, McMaster University, Hamilton, ON, Canada

Hamida Tun Nisa Chisti National Institute of Technology, Srinagar, India

Moo Hwan Cho School of Chemical Engineering, Yeungnam University, Gyeongbuk, South Korea

Rasel Das Chemical Department, Leibniz Institute of Surface Engineering, Leipzig, Germany

Usisipho Feleni SensorLab, University of Western Cape, Cape Town, South Africa
Nanotechnology and Water Sustainability Research Unit, University of South Africa, Johannesburg, South Africa

Gertrude Fomo SensorLab, University of Western Cape, Cape Town, South Africa

Deepu Gopakumar International and Inter University Centre for Nanoscience and Nanotechnology, Mahatma Gandhi University, Kottayam, Kerala, India

Martin D. Hager Laboratory of Organic and Macromolecular Chemistry (IOMC), Friedrich Schiller University Jena, Jena, Germany

Jena Center for Soft Matter (JCSM), Friedrich Schiller University Jena, Jena, Germany

Mohammad K. Hassan Center for Advanced Materials, Qatar University, Doha, Qatar

Xia Huang Institut für Technische Chemie und Polymerchemie, Karlsruher Institut für Technologie, Karlsruhe, Germany

Inamuddin Advanced Functional Materials Laboratory, Department of Applied Chemistry, Faculty of Engineering and Technology, Aligarh Muslim University, Aligarh, India

A. F. Ismail Advanced Membrane Technology Research Centre (AMTEC), Universiti Teknologi Malaysia, Johor Bahru, Malaysia
Faculty of Chemical and Energy Engineering, Universiti Teknologi Malaysia, Johor Bahru, Malaysia

Emmanuel Iwuoha SensorLab, Department of Chemistry, University of the Western Cape, Bellville, South Africa

Juhana Jaafar Advanced Membrane Technology Research Centre (AMTEC), Universiti Teknologi Malaysia, Johor Bahru, Malaysia
Faculty of Chemical and Energy Engineering, Universiti Teknologi Malaysia, Johor Bahru, Malaysia

Mohammad Abu Jafar Mazumder Chemistry Department, King Fahd University of Petroleum and Minerals, Dhahran, Saudi Arabia

Nazeem Jahed Department of Chemistry, University of the Western Cape, Bellville, South Africa

Suru Vivian John Department of Chemistry, University of the Western Cape, Bellville, South Africa

Mahadevappa Y. Kariduraganavar Department of Chemistry, Karnatak University, Dharwad, India

Ibrahim Khan Chemistry Department, King Fahd University of Petroleum and Minerals, Dhahran, Saudi Arabia

Praveen Kosappallyillom Muraleedharan International and Inter University Centre for Nanoscience and Nanotechnology, Mahatma Gandhi University, Kottayam, Kerala, India
Department of Mechanical Engineering, Saintgits College of Engineering, Kottayam, Kerala, India

Kwang-Sup Lee Department of Advanced Materials and Chemical Engineering, Hannam University, Daejeon, South Korea

Andreas Lendlein Institute of Biomaterial Science, Helmholtz-Zentrum Geesthacht, Teltow, Germany
Institute of Chemistry, University of Potsdam, Potsdam, Germany

Ajithkumar Manayan Parambil International and Inter University Centre for Nanoscience and Nanotechnology, Mahatma Gandhi University, Kottayam, Kerala, India

Muhammad Mansha Chemistry Department, King Fahd University of Petroleum and Minerals, Dhahran, Saudi Arabia

Milua Masikini Department of Chemistry, University of the Western Cape, Bellville, South Africa

T. Matsuura Advanced Membrane Technology Research Centre (AMTEC), Universiti Teknologi Malaysia, Johor Bahru, Malaysia

Department of Chemical Engineering, University of Ottawa, Ottawa, ON, Canada

Kenneth A. Mauritz School of Polymers and High Performance Materials, The University of Southern Mississippi, Hattiesburg, MI, USA

Magdalena Mazurek-Budzyńska Institute of Biomaterial Science, Helmholtz-Zentrum Geesthacht, Teltow, Germany

Rizwana Mobin Government College for Women, Srinagar, India

Balappa B. Munavalli Department of Chemistry, Karnatak University, Dharwad, India

Satishkumar R. Naik Department of Chemistry, Karnatak University, Dharwad, India

Mazen K. Nazal Centre for Environment and Water (CEW), King Fahd University of Petroleum and Minerals, Dhahran, Saudi Arabia

M. H. D. Othman Advanced Membrane Technology Research Centre (AMTEC), Universiti Teknologi Malaysia, Johor Bahru, Malaysia

Faculty of Chemical and Energy Engineering, Universiti Teknologi Malaysia, Johor Bahru, Malaysia

Abdul Malik P. Peedikakkal Department of Chemistry, King Fahd University of Petroleum and Minerals, Dhahran, Kingdom of Saudi Arabia

Nickolas D. Polychronopoulos Polydynamics Inc., Dundas, ON, Canada

Prem Prabhakaran Department of Advanced Materials and Chemical Engineering, Hannam University, Daejeon, South Korea

Mohammad Mahbub Rabbani Department of Chemistry, American International University-Bangladesh (AIUB), Dhaka, Bangladesh

M. A. Rahman Advanced Membrane Technology Research Centre (AMTEC), Universiti Teknologi Malaysia, Johor Bahru, Malaysia

Faculty of Chemical and Energy Engineering, Universiti Teknologi Malaysia, Johor Bahru, Malaysia

Mohammad Mizanur Rahman Center of Research Excellence in Corrosion, King Fahd University of Petroleum and Minerals, Dhahran, Saudi Arabia

Tauseef Ahmad Rangreez National Institute of Technology, Srinagar, India

Muhammad Yasar Razaq Institute of Biomaterial Science, Helmholtz-Zentrum Geesthacht, Teltow, Germany

Mashallah Rezakazemi Faculty of Chemical and Materials Engineering, Shahrood University of Technology, Shahrood, Iran

Joyanta Kumar Saha Department of Chemistry, Jagannath University, Dhaka, Bangladesh

Ulrich S. Schubert Laboratory of Organic and Macromolecular Chemistry (IOMC), Friedrich Schiller University Jena, Jena, Germany

Jena Center for Soft Matter (JCSM), Friedrich Schiller University Jena, Jena, Germany

Muhammad Shahzad Kamal Center for Integrative Petroleum Research, King Fahd University of Petroleum and Minerals, Dhahran, Saudi Arabia

Department of Petroleum Engineering, King Fahd University of Petroleum and Minerals, Dhahran, Saudi Arabia

Niels Smeets EcoSynthetix, Burlington, ON, Canada

Manfred Stamm Institute of Physical Chemistry and Physics of Polymers, Leibniz-Institut für Polymerforschung Dresden e. V., Dresden, Germany

Abdullah S. Sultan Department of Petroleum Engineering, College of Petroleum Engineering and Geosciences, King Fahd University of Petroleum and Minerals, Dhahran, Saudi Arabia

Center for Integrative Petroleum Research, King Fahd University of Petroleum and Minerals, Dhahran, Saudi Arabia

Patrick Theato Institut für Technische Chemie und Polymerchemie, Karlsruher Institut für Technologie, Karlsruhe, Germany

Sabu Thomas International and Inter University Centre for Nanoscience and Nanotechnology, Mahatma Gandhi University, Kottayam, Kerala, India

Anand I. Torvi Department of Chemistry, Karnatak University, Dharwad, India

Sayonthoni Das Tuhi Department of Microbiology, University of Chittagong, Chittagong, Bangladesh

John Vlachopoulos Department of Chemical Engineering, McMaster University, Hamilton, ON, Canada

Tesfaye Waryo SensorLab, University of Western Cape, Cape Town, South Africa

Avril Rae Williams Department of Biological and Chemical Sciences, The University of the West Indies, Cave Hill, Barbados

Syed Mohammed Javaid Zaidi Center for Advanced materials, Qatar University, Doha, Qatar

Stefan Zechel Laboratory of Organic and Macromolecular Chemistry (IOMC), Friedrich Schiller University Jena, Jena, Germany

Jena Center for Soft Matter (JCSM), Friedrich Schiller University Jena, Jena, Germany



Photo-polymerization

1

Prem Prabhakaran and Kwang-Sup Lee

Contents

1	Introduction	2
1.1	A Physical View of Photoexcitation	4
2	Radical Photopolymerization	9
2.1	Photoinitiators	10
2.2	Monomers/Oligomers	15
2.3	Visible Light-Sensitized Radical Polymerization	17
2.4	Thiol-Ene Photopolymerization	18
3	Cationic Polymerization	23
3.1	Ionic Photoacid Generators	24
3.2	Spectral Broadening	26
3.3	NonIonic Photoacid Generators	29
3.4	Monomers for Cationic Polymerization	29
4	Anionic Polymerization	34
5	Two-Photon Induced Polymerization	38
6	Scope and Outlook	39
	References	42

Abstract

The synthesis of functional polymers by photopolymerization thrives on the rich tradition of industrial photochemistry. Photo-induced polymerization can be broadly divided based on the initiation mechanism as radical, cationic, and anionic photopolymerization. A wide variety of initiators, photosensitizers, and polymerizable materials have been studied for various applications. This chapter is intended to be a primer to major concepts of photopolymerization. In the beginning of the chapter, physical aspects of light matter interactions are

P. Prabhakaran · K.-S. Lee (✉)
Department of Advanced Materials and Chemical Engineering, Hannam University,
Daejeon, South Korea
e-mail: premp@hnu.kr; kslee@hnu.kr; kslee8857@gmail.com

presented followed by photochemical pathways leading to reactions. In the subsequent sections radical polymerization is discussed by introducing different types of initiating systems and polymerizable materials. Within the section on radical polymerization, visible light polymerization and thio-ene photochemistry are also discussed. The section on thiol-ene looks at the fundamentals of thiol-ene reactions, their initiation, reactivity, and advantages over other radical driven polymerizations. Cationic polymerization is covered based on the material science of ionic and nonionic photoacid generators (PAGs). This section also discusses spectral broadening of reactivity in PAGs to visible wavelengths through electron transfer sensitization and free radical promoted cationic polymerization (FRPCP). Unlike radical and cationic polymerization there are little or no reports of commercial application of anionic polymerization. However, due to typical monomers employed in anionic polymerization and the control over the extent of polymerization afforded by this techniques makes it very attractive for functional applications. The section on anionic polymerization summarizes recent developments in this field. Finally in the section about two-photon initiated polymerization, we discuss the scope of nonlinear optical phenomena in photopolymerization.

1 Introduction

Photopolymerization became popular due to the wide-spread application of ultraviolet radiation for cross-linking of photoactive materials in various industries. Any polymeric species capable of undergoing a chemical change when exposed to light can be termed a photopolymer. Photopolymers started out as materials used in packaging and encapsulation of goods and printing technologies. Their early application in the industry was largely driven by the possibility of formulating photoactive materials that reduced the use of solvent while allowing for a remote triggering of chemical phenomena through irradiation. The subsequent growth of microelectronic industry with its demand for progressive miniaturization of components has led to the increased importance of photopolymers. In fact, the progression of microelectronics predicted by Moore's law would be hardly possible without negative photoresists. This was achieved due to the progress in the development, synthesis, and understanding of the chemistry of photopolymers and the resultant rational design. This has been the case with photopolymers applied to many different fields of activity. Need for efficiency and cost effectiveness has driven the development of the field in various directions.

Depending on how they chemically respond to light, photoresponsive polymers or their precursors can be divided into five classes [1]. The first class constitutes multifunctional monomers or oligomers containing functional groups that undergo radical, cationic, or anionic chain growth polymerization in the presence of a suitable photoinitiator (PI) leading to photo-crosslinked polymer networks (see Fig. 1a). When irradiated with a suitable wavelength, the PI initiates the polymerization reaction, leading to the addition of monomer or oligomers to form polymeric

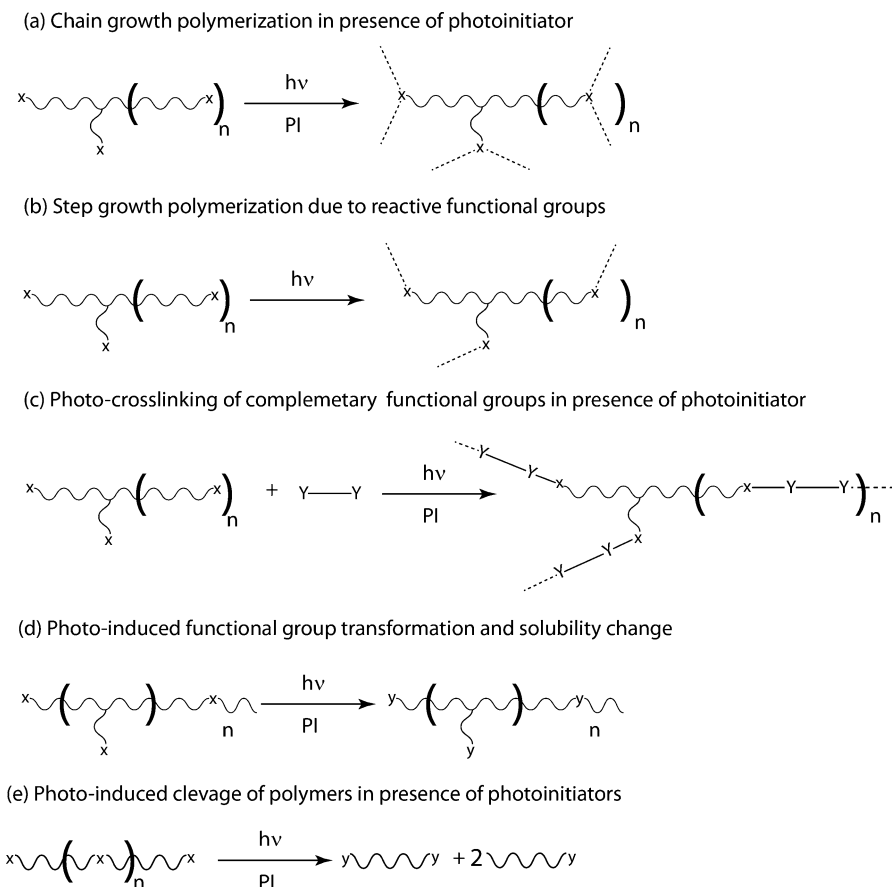


Fig. 1 Five different classes of photopolymers. (Reproduced from Ref. [1])

molecules. The second class of photopolymers consists of oligomers/monomers with integrated photoactive groups capable of initiating polymerization when irradiated with light (see Fig. 1b). In the second class of photopolymeric materials, there is no requirement of a PI. They typically undergo step growth polymerization where polymeric groups are added step by step (e.g., dimer then trimer then tetramer so on). The third class of photopolymer precursors involves component materials with complementary functional groups on them that interact with each other under irradiation in the presence of a suitable PI (see Fig. 1c). The fourth category involves photopolymers with functional groups which, in the presence of a suitable mediator (PI) and light, transform to another functional group with a difference in solubility (see Fig. 1d). The fifth class of photopolymer also undergoes a solubility change due to the photo-induced degradation of polymeric materials (see Fig. 1e).

This chapter deals with photopolymerization and materials for photopolymerization which can be included in categories (a–c) in Fig. 1.

Photopolymerization reactions are normally achieved by combining a number of different materials playing specific roles during polymerization. The combinations are often referred to as photopolymerizable formulations or just formulations. Formulations used for imaging applications are often referred to as photoresists. The most abundant component of a photoresist is a monomer or an oligomer with chemical functionalities capable of undergoing photoinduced chemical change. Different photopolymerization reactions are restricted to certain types of monomers/oligomers. For example, olefins and acrylic monomers/oligomers figure prominently in the materials for radical polymerization, while epoxides and vinyl ethers figure in cationic polymerization. The absorption of light and the initiation of the chemical reaction are mediated by a photoinitiator (PI).

Often another component called photosensitizer (PS) is present in the formulation. The photosensitizer is a molecule that is highly sensitive to light and plays a part in assisting the initiation of the photopolymerization. The PS has a higher sensitivity to a relevant wavelength and would serve to efficiently initiate the reaction in combination with the PI. The photoexcited PS molecule interacts with PI through energy or the electron transfer interaction. Apart from these components, photosensitive systems might contain inhibitor molecules aimed at nullifying the effects of spontaneous degradation of the high-energy bonds in initiators over time during their shelf life. For commercial applications, additional components meant to shape the physical properties of the photopolymerizable medium, such as viscosity, color, wetting, gloss, and matting, are also added to photosensitive systems.

A crucial factor governing the photopolymerization reaction is the choice of the light source. A wide range of optical sources like lamps, lasers, and sun light have been put to use depending on the requirement of the application. Recently, there have been numerous attempts to use sunlight to trigger polymerization, minimizing thus the cost of fabrication. Source like the Xe lamp and sunlight are broad spectrum sources that contain multiple wavelengths. Required wavelength can be filtered out of these sources by using filters. UV producing mercury lamps also converts a high amount of energy it takes up to heat. Mercury lamp emits at specific wavelengths. Doped mercury lamps emit in a range of wavelengths. Microwave lamp, excimer lamp, both continuous and pulsed laser sources are some other examples of the light sources used [2].

In the following chapter, we will discuss photopolymerization based on its modes of initiation. An exhaustive coverage of this broad topic is beyond the scope of the present chapter. Instead, we will focus on initiating the reader to the nuances of the field by providing insights into major developments. In the beginning, we provide a brief physical description of the light-matter interaction; the subsequent sections discuss various types of polymerization from the material perspective.

1.1 A Physical View of Photoexcitation

Photoinitiators and photosensitizers feature polar high-energy bonds between carbon and heteroatoms or metals. Polar bonds have a greater interaction with

electromagnetic radiation due to their strong interactions with the electrical field of light. When the intensity of radiation increases, the materials give rise to new phenomena which can be termed nonlinear optical (NLO) phenomena [3]. In essence, all optical processes are nonlinear, but they become relevant observables only when subjected to an intense radiation. The electric component of the electromagnetic wave is capable of attracting or deflecting the electronic cloud in a molecule, the resultant polarization in the molecule shows a linear behavior at lower intensities. However, in the presence of intense radiations, the polarization of the molecule shows a nonlinear response to light. The polarization (P) or the induced dipole moment (μ_i) of a molecule interacting with radiation can be written as follows (see Eq. 1):

$$P_i = \mu_i = \alpha_{ij}E_j \quad (1)$$

where α_{ij} is the linear polarizability tensor and E_j is the electric field associated with the electromagnetic radiation. The induced dipole moment of a molecule interacting with high intensity radiation can be written as follows (see Eq. 2):

$$\mu_i(E) = \mu_0 + \alpha_{ij}E_j + \frac{\beta_{ijk}}{2}E_jE_k + \frac{\gamma_{ijkl}}{8}E_jE_kE_l \dots \quad (2)$$

where μ_0 is the inherent polarizability of the molecule, α_{ij} is the linear polarizability of the molecule β_{ijk} , and γ_{ijkl} refers to the first and second hyperpolarizabilities. The terms E_i , E_j and E_k describe the electric field components of light. The first two terms explain the single-photon absorption of the molecule, while β_{ijk} and γ_{ijkl} describe the NLO interactions of the molecule with light in the microscopic scale.

For a bulk of molecules, the polarization can be written using Eqs. 3 and 4.

$$P = P_0 + P_i(E) \quad (3)$$

$$P_i(E) = \chi_{ij}^{(1)}E_j + \chi_{ijk}^{(2)}E_jE_k + \chi_{ijkl}^{(3)}E_jE_kE_l \dots \quad (4)$$

In Eq. 3, P_0 is the inherent polarization of a molecule and $P_i(E)$ the induced polarization where $\chi^{(n)}E$ is the nonlinear susceptibility tensor of $(n + 1)^{\text{th}}$ order. The first term in Eq. 4 describes the linear polarizability of the molecule. The terms $\chi_{ijk}^{(2)}$ and $\chi_{ijkl}^{(3)}$ are the bulk analogues of β_{ijk} and γ_{ijkl} , respectively, and are called first and second hyperpolarizability. A number of optical effects arise out of both the first and second hyperpolarizabilities, such as sum and difference-frequency generation, second-harmonic generation, direct four-wave mixing, optical rectification, parametric amplification, self-phase modulation, Kerr lensing, four-wave mixing, two-photon absorption, etc. [4]. In this chapter, we mainly discuss photochemical and photopolymerization triggered by the one-photon absorption (OPA) and two-photon absorption (TPA) excitation of molecules.

The range of wavelengths between 10 nm and 400 nm are defined as ultraviolet (UV) region of the spectrum. Almost all materials including air absorbs UV wavelengths between 10 and 180 nm making it difficult to work with it in the absence of a

vacuum, this range of wavelengths is called far UV region. Wavelengths between 180 and 280 nm constitute the middle-UV region, and those in the range 300–400 nm constitute the near UV region. The range of wavelengths between 200 and 400 nm has been most commonly used in photopolymerization reactions. The energy corresponding to this range of wavelengths can initiate electronic transition in a wide range of materials and cause bond rupture in organic molecules. For a given molecule, the scope of photophysical processes occurring on irradiation is defined by its frontier molecular orbitals, the absorbed wavelength, and the intensity of the light source. All potential photophysical processes during the evolution of a photoexcited molecule are summarized in Fig. 2. Common organic molecules feature σ -bonding molecular orbitals, σ^* antibonding molecular orbitals, π -bonding molecular orbitals, π^* antibonding molecular orbitals, and nonbonding orbitals (n). The transitions between these molecular orbitals (MOs) are subject to conditions of energy difference, symmetry, and occupancy of MOs. The most commonly encountered transitions in organic photoinitiators are $\pi \rightarrow \pi^*$ and $n \rightarrow \pi^*$ transitions. The $\pi \rightarrow \pi^*$ and $n \rightarrow \pi^*$ transitions are localized transitions associated with active bonds in the molecule.

Another set of transitions called charge transfer (CT) transitions are found in the molecules containing extensive conjugation and strong donor and acceptor substitutions. In the CT transitions, the excitation energy is delocalized throughout the molecule. The NLO phenomena are particularly strong in the molecules with strong CT states. The simplest photochemical process in a molecule happens when it absorbs ultraviolet radiation, resulting in the excitation of an electron in its singlet ground state (S_0) to the first singlet excited state (S_1). Photoexcitation is a fast process that occurs at the timescale centering around 10^{-15} s. Alternatively, the absorption of two near IR photons can lead to a singlet excited state. The OPA- and TPA-excited singlet states may or may not be the same, depending on the symmetry of the molecule. They coincide in non-centrosymmetric molecules and differ in symmetric ones. The excited singlet state can follow any of the different paths outlined in Fig. 2, depending on the molecular orbitals and the source of radiation. In the presence of a high intensity laser or non-laser light sources, the excited electron can be further excited to a higher singlet state due to the phenomenon termed excited-state absorption (ESA). The probability of the ESA phenomenon depends on the intensity the light source.

Photoexcitation of a molecule results in the formation of chemically reactive species due to the redistribution of electronic cloud within the molecule. The heavy atoms in the molecule hold their positions (Franck-Condon principle), while the electronic cloud undergoes redistribution. The Franck-Condon principle restricts the inversion of the electronic spin during excitation due to the rules of quantum mechanics. Due to these restrictions, the initial geometry of the excited molecule is not the one that corresponds to an energy minimum (read stable). If an excited state is not immediately quenched after excitation, it undergoes vibrational relaxation to achieve energetically stable geometries, leading to the formation of triplet states [5]. The triplet excited states are more reactive than singlet excited states and lead to

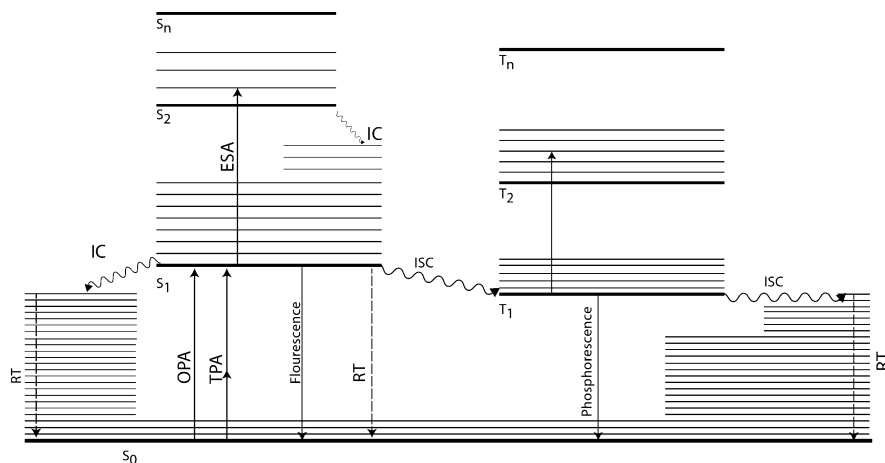


Fig. 2 The fate of the photophysical properties associated with an excited molecule is summarized in the Jablonski's diagram. S_n stands for the n^{th} singlet energy level of the molecules, T_n stands for the n^{th} triplet energy level of the molecule. *OPA* one-photon absorption, *TPA* two-photon absorption, *ESA* excited-state absorption, *ISC* inter system crossing, *IC* internal conversion, *RT* radiationless transfer of electrons

the products that are otherwise inaccessible [6]. Photoexcitation of PI can lead to the following eventualities.

- (i) The excited molecules undergo vibronic relaxation to reach a stable geometry, followed by a release of energy into solvent.
- (ii) The excited electron can undergo intersystem crossing to give a triplet state which further undergoes vibrational relaxation to reach an energy minimum.
- (iii) The emission of energy from the singlet or the triplet excited state, leading to luminescence, fluorescence, or phosphorescence.
- (iv) The excited molecule can undergo excitation quenching through interaction with other molecules; further, the molecule can return to ground state through radiationless thermal or vibrational processes.
- (v) Singlet and triplet excited molecular states can herald photochemical reactions.

Thermally driven reactions go through the singlet excited state. The probability of intersystem crossing and triplet formation in photochemical reactions lead to the formation of the products that are otherwise inaccessible. The use of photoexcitation for driving the reaction also leads to energy-rich excited states. Frequently, such excited states also feature electrons occupying nonbonding molecular orbitals. A photoexcited molecule is susceptible to three different primary photochemical pathways (see Fig. 3a). The first pathway involves the formation of a chemically reactive intermediate (RI) which then leads to the product. The second photochemical pathway leads to the formation of a funnel intermediate by the excited molecule, the funnel intermediate then leads to a product. IUPAC defines a photochemical funnel intermediate as a molecular

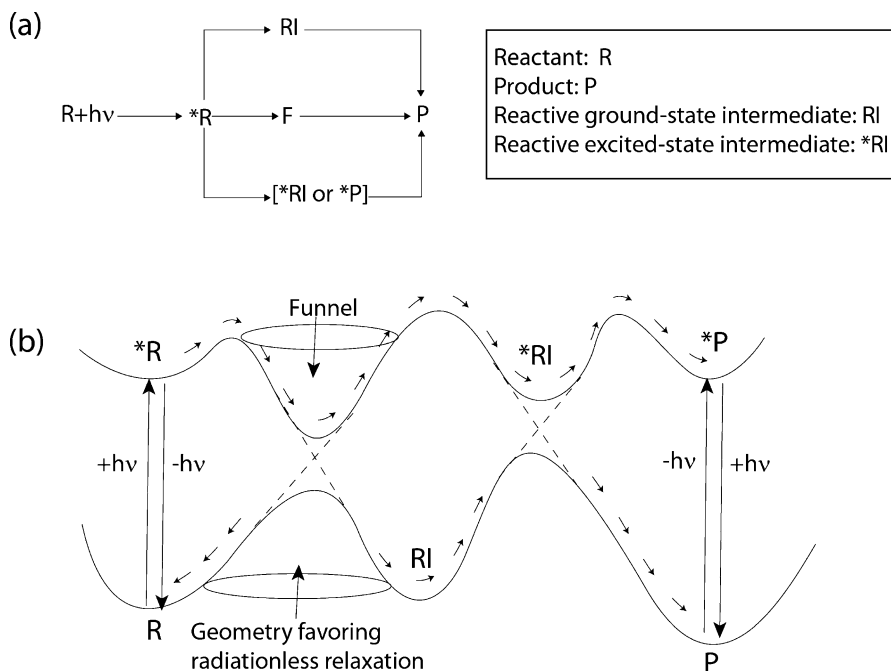


Fig. 3 (a) The photochemical pathways taken by the photoexcited molecule. (b) Potential energy surfaces of a photoreaction from photoexcitation to the formation of the product [8]

structure by means of which the excited-state reactant or intermediate is delivered to the ground state to initiate product formation [7].

The term funnel intermediate itself comes from the local shape of the potential energy surfaces of the ground and excited states (see Fig. 3b) [8]. For many organic reactions, the structure of the funnel can take the form of a conical intersection or a singlet-triplet crossing. The third pathway involves the formation of an excited intermediate state RI^* or an excited state product P^* that eventually gives rise to the product.

Most photoinitiators work through the primary photochemical pathway which progresses through the formation of a reactive intermediate, RI. The RIs formed can include radicals, biradicals, or zwitter ions that then directly or indirectly play a part in the initiation of the polymerization reactions. The role of photosensitizer is primarily that of a mediator in the photoinitiation process. The energy or electron transfer between the photosensitizer and the photoinitiator depends on their frontier molecular orbitals. The LUMO level of the sensitizer should be above the HOMO level of the initiator; when the energy difference is larger, the probability of energy transfer increases. Apart from this, the phase of the polymerizing medium governs the interaction between the photosensitizer and the photoinitiator. In samples permitting flow of materials, diffusion plays a key role in the dynamics and fate of the excited photosensitizer. The transfer of energy between the sensitizer and the initiator could take place through a coulombic interaction or by swapping of a high-energy electron [8].

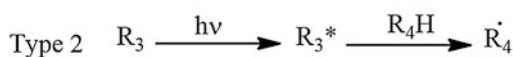
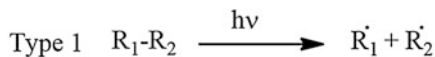
2 Radical Photopolymerization

Radical photopolymerization reactions are initiated by the generation of a free radical (R^\bullet) by a photoexcited photoinitiator (see Fig. 4). The generation of R^\bullet may proceed through the unimolecular process (Type 1) or the bimolecular process (Type 2). The first photochemical pathway outlined in Fig. 3b is responsible for the generation of the free radical. During its course, radical polymerization proceeds through different distinctive steps (see Fig. 4). During the propagation step, the free radical reacts with the monomer/oligomer to give rise to a radical bearing monomer or oligomer (RM^\bullet) called a macroradical. The macroradical then proceeds to grow by addition to more monomers. The reaction proceeds through the propagation step and eventually terminates through coupling or disproportionation reactions.

The presence of inhibitors, such as dissolved oxygen or other added components capable of consuming the radicals in the polymerizing medium, has a detrimental effect on the initiation process. Reactive species formed during initiation react with inhibitors, leading to a period of almost no polymerization reaction at the beginning (see Fig. 5). This phase of the reaction is termed the induction phase. Upon the total consumption of the inhibitors through reactions, the initiating species react with

Fig. 4 Different stages of free radical polymerization

Generation of initiating species



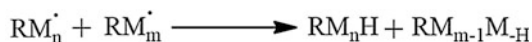
Initiation



Propagation

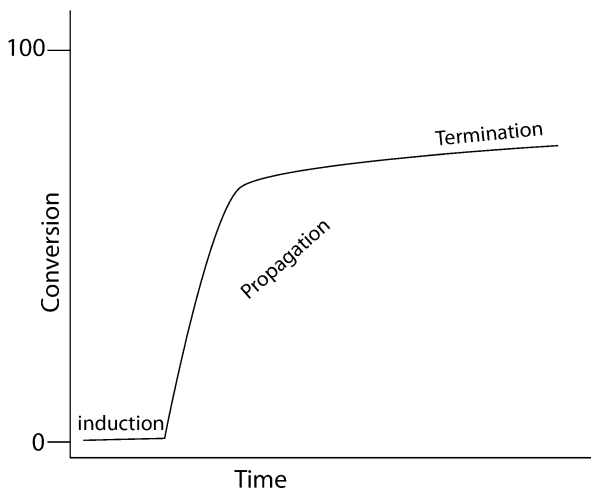


Termination



R^\bullet : Radical
 M : Monomer
 RM^\bullet : Macro Initiator

Fig. 5 Conversion of monomer versus time during photopolymerization



monomer forming a macroradical. The diffusion of the macroradicals throughout the medium leads to a rapid increase in the rate of polymerization until it reaches a maximum.

The development of polymerization is associated with a change in viscosity and refractive index of the polymerizable medium. Viscosity of the polymerizing medium progressively increases to the point where monomers are trapped between growing polymer chains. At this point, the polymerization reaction is terminated by the limited diffusion of the monomer. Due to this, photopolymerization reactions never run to 100% conversion of monomer. A graphical representation of the progression of photopolymerization can be seen in Fig. 5. The induction period is the relatively flat part at the initiation region.

2.1 Photoinitiators

Photoinitiation occurs when the absorption of photon leads to the generation of a free radical. This process is governed by the stability of the photoexcited state, as well as by the energy of the bonds within the excited molecule. As mentioned above, free radical photoinitiators can be classified into two types, based on the number of molecular species involved in the process. Type I photoinitiators constitute a unimolecular process accompanied by a rapid bond cleavage upon the absorption of light. Type II photoinitiators involve more than one molecule. A simple Type II photoinitiator consists of a bimolecular system involving an initiator and a co-initiator. The initiator is first excited into a long-lived triplet state, followed by an electron-transfer or a hydrogen-abstraction reaction with a co-initiator.

Type I photoinitiators are prominently benzoyl compounds; they undergo C–C cleavage at α , β , or γ positions on photoexcitation. The dissociation energy of the C–C bond next to the benzoyl is less than the energy of excitation of the molecule.

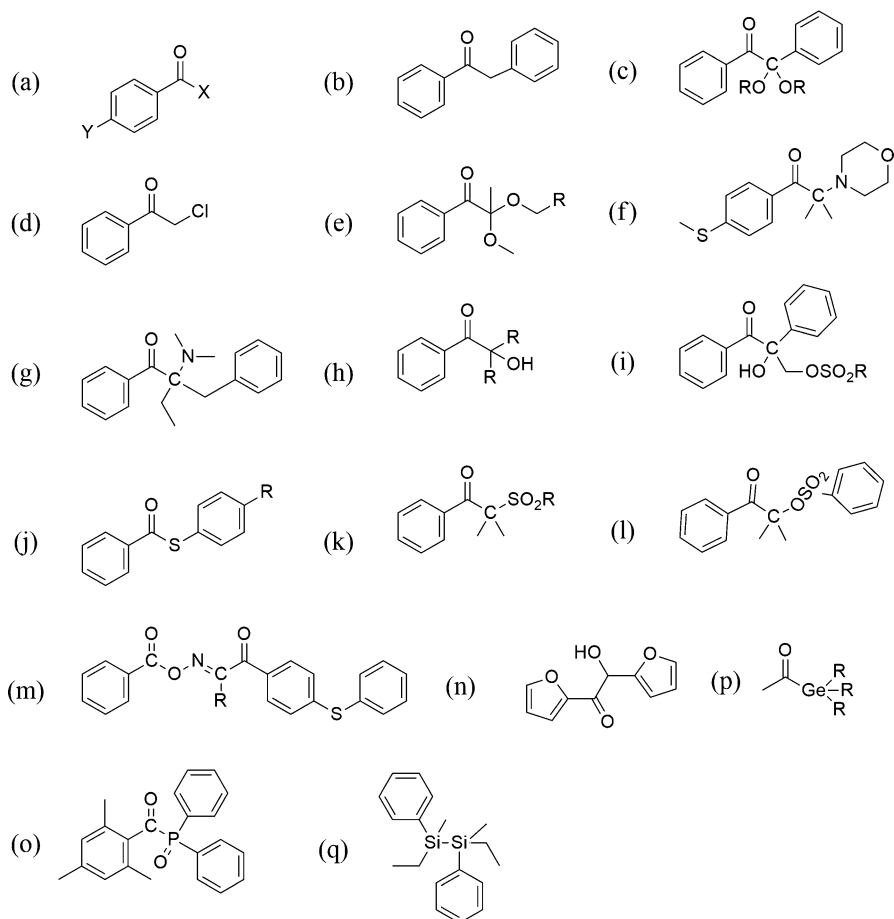
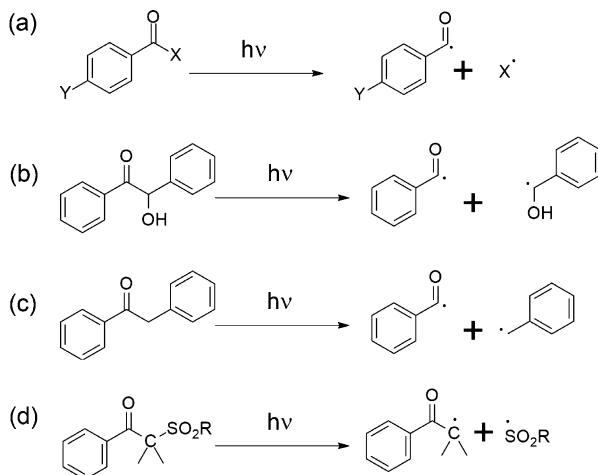


Fig. 6 (a) A model Type I photoinitiator followed by different typical examples; (b) benzoin derivatives; (c) benzoin ether derivatives; (d) halogenated ketones; (e) dialkylacetophenone; (f) morpholinoketone; (g) aminoketone; (h) hydroxyalkylacetophenones; (i) ketone sulfonic ester; (j) thiobenzoate derivatives; (k) sulfonylketone; (l) oxosulfonylketone (m) oximeester; (n) furan hydroxyl alkyl ketone derivative; (o) organometallic ketone; (p) 2,4,6-trimethylbenzoyl diphenylphosphine oxide; (q) organosilanes

The carbonyl chromophore constitute three important molecular orbitals, namely n (nonbonding orbital on oxygen), π (bonding), and π^* (anti-bonding) molecular orbitals on carbonyl double bond. The $\pi \rightarrow \pi^*$ is a high-energy allowed transition and $n \rightarrow \pi^*$ transition is a low-energy forbidden transition. Both these transitions can give rise to singlet and triplet states on excitation. A model Type I radical photoinitiator is shown in Fig. 6a. The substituted groups X and Y influence the optical properties of the benzoyl compounds through electronic interactions, such as electronegativity, +I or -I effects, and delocalization. Some examples of Type I photoinitiators are shown in Fig. 6.

Fig. 7 Photocleavage of type I radical photoinitiator (a) model compound undergoing cleavage at α -carbon; (b–c) benzoin derivatives undergoing photoexcited α -cleavage; (d) sulfonyl ketone derivative undergoing β -cleavage on photoexcitation



The photoinduced cleavage of a model type 1 PI molecule can be seen in Fig. 7a. The rest of Fig. 7 shows the generation of radicals in two benzoin derivatives. The cases in Fig. 7a–c demonstrate cleavage at α -carbon. However, certain type 1 initiators, like sulfonyl ketones, sulfonyloxy ketones, thiosulfonyl ketones, and oxime esters, undergo cleavage at β -carbon upon photoexcitation (see Fig. 7d) [9–11]. The benzoyl radicals in type I photoinitiators are generated by the cleavage of σ bond oriented orthogonally to the π -orbitals of the aromatic group [2]. The substitution on the aromatic ring has little or no effect on the reactivity of the benzoyl radical. Radicals centered on carbon add at a high rate to monomers like acrylate. The nucleophilicity of the radical influences its addition to monomers. In the case of an alkyl radical, the tertiary carbon exhibits the highest nucleophilicity, followed by secondary carbon and primary carbon. Alkyl radicals with -OH substitution are more nucleophilic and would show a greater addition to electron deficient monomers like methacrylates. Carbonyl or nitrile substituted alkyl radical show a greater addition to electron rich monomers. The addition of benzoyl radical to the double bond on a monomer is around two-orders or magnitude (~ 100 -fold) higher as compared a radical centered on an alkyl carbon. Both these species are equally vulnerable to dissolved oxygen in the photopolymerizable medium. Most of the PIs in Fig. 6 feature benzoyl moiety, indicating the prominence of this group in developing useful photoinitiators. There have been several attempts to engineer compounds that do not contain this group in order to address the control over the excitation dynamics or choice of monomers. In compound Fig. 6n, the phenyl ring is substituted with the electron rich five-membered ring furan. Compound in Fig. 6p is organometallic germanium derivative where the germanium atom is attached to a ketone, during photo exposure the Ge–C bond undergoes cleavage to give initiating species. The substituted disilane derivative in Fig. 6q when irradiated undergoes cleavage at the Si–Si to give highly reactive silyl radicals. The advantage of using silyl radical as an initiating species is its ability to overcome oxygen inhibition of polymerization. The ambient oxygen has been shown to play an active part in accelerating the addition of the silyl

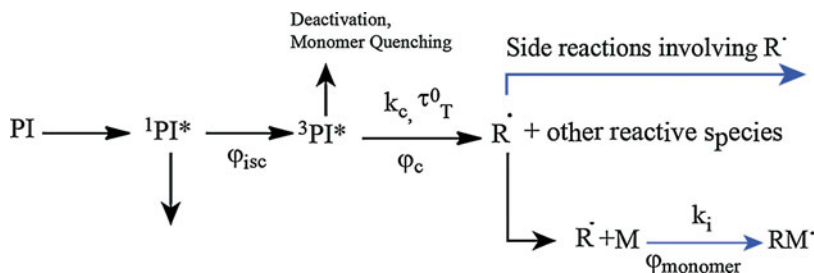


Fig. 8 Reactions governing the excitation and evolution of the photoinitiator

radical to monomers [2, 12, 13]. Another factor governing the effective action of the initiator is the effect of solvent on the stability of the photoexcited transition state. The stabilization of a charged transition state by a polar solvent can lead to an increase in cleavage of the photoinitiator and hence increase the reaction with the monomer.

The mechanism of photopolymerization can be studied through different techniques, such as chemical trapping [14], nuclear magnetic resonance (NMR) [15], time resolved Fourier Transform-Infrared (FT-IR) measurements [16, 17], laser flash photolysis [18], electron spin resonance (ESR) spectroscopy [19–21], chemically induced dynamic nuclear polarization (CIDNP), chemically-induced dynamic electronic polarization [CDEP] [22], femtosecond pump-probe experiments [23, 24], ultrafast fluorescence quenching [25], time-resolved stimulated emission [26], femtosecond-stimulated raman experiments [27], photothermal and photoacoustic methods [28], etc. For further details on the characterization and study of the kinetics of photopolymerization, the readers are referred to previous works [29–33].

Reactions leading to the formation of the macroradical RM^\cdot can be seen in Fig. 8. The rate of polymerization for the early stages of radical polymerization in a deaerated medium can be written as follows (see Eq. 5):

$$R_p = (k_p/k_t^{0.5}) R_i^{0.5} [M] \quad (5)$$

where the rate constants k_p and k_t correspond to propagation and termination steps of polymerization (see Fig. 8), respectively.

$$R_i = I_a \varphi_i \quad (6)$$

Here R_i is the rate of initiation that depends on the amount of absorbed light, I_a , and photoinitiation quantum yield φ_i which defines the efficiency of photoinitiation taking into account all the side processes that could occur during photoexcitation. The initiation quantum yield φ_i describes the number of initiation events associated with the absorption of a photon (or photons, e.g., two-photon-initiated polymerization). It is given by the product of the quantum yield of intersystem crossing φ_{isc} , quantum yield of initiating radical φ_c which is the number of free radical species formed as a result of the absorption of a photon and the quantum yield of the macroinitiator formed by the initial reaction between the initiator radicals and the

monomer ϕ_{monomer} . For a Type I initiator that undergoes cleavage in its triplet state, the initiation quantum yield is given by Eq. 7 [2].

$$\phi_i = \phi_{\text{isc}} \phi_c \phi_{\text{monomer}} \quad (7)$$

The bond cleavage of the photoinitiator is described by the product of ϕ_c and ϕ_{isc} (see Eq. 8) and is called dissociation quantum yield $\phi_{\text{dissociation}}$.

$$\phi_{\text{dissociation}} = \phi_{\text{isc}} \phi_c \quad (8)$$

The quantum yield of formation of radical R^\cdot depends on the rate at which triplets are generated by the photoinitiator k_c and the bimolecular quenching of the triplet by the monomer k_q . It is inversely proportional to the triplet life time τ_T^0 (see Eq. 9).

$$\phi_c = k_c / (1/\tau_T^0 + k_q[M]) \quad (9)$$

The quantum yield of the formation of the macroradical (RM) is denoted by ϕ_{monomer} (see Eq. 10). It depends on k_i , the initiation rate constant that governs the interaction between R^\cdot and monomer M , as well as k_r^0 the pseudo first-order rate constant which is sum of all rate constants leading to the disappearance of R^\cdot (see the processes represented by blue arrows in Fig. 8).

$$\phi_{\text{monomer}} = k_i [M] / (k_r^0 + k_i[M]) \quad (10)$$

Type II PIs form a long-lived triplet state on photoexcitation. Instead of undergoing cleavage, they interact with a co-initiator via a direct hydrogen transfer or an electron transfer reaction (see Fig. 9a). During the direct hydrogen transfer, the excited triplet state of the PI reacts with a co-initiator capable of donating a hydrogen radical to form a new radical species (PI-H $^\cdot$). This radical hydrogen adduct of the PI then initiates polymerization. Alternatively, the donor molecule (RH) forms an electron transfer complex with the photoexcited PI. The degradation of this charge transfer complex leads to PI-H $^\cdot$. Benzophenone initiates polymerization reactions through the formation of the charge transfer complex with amines. A wide range of amines are commonly employed as co-initiators. Other types of molecules, such as mercaptobenzothiazole, substituted silanes, germanes, silylamine derivatives, metal containing amines, boron derivatives, etc., have also been used. Examples of type II PIs and co-initiators can be seen in Figs. 10 and 11, respectively.

The initiation quantum yield for the type II initiators can be written as follows (see Eq. 11):

$$\phi_i = \phi_{\text{isc}} \phi_H \phi_R \phi_{\text{monomer}} \quad (11)$$

where ϕ_{isc} is the intersystem crossing quantum yield, ϕ_H is quantum yield describing the direct transfer of hydrogen, ϕ_R is the quantum yield of initiating radicals, and ϕ_{monomer} is the yield of the macroradical.

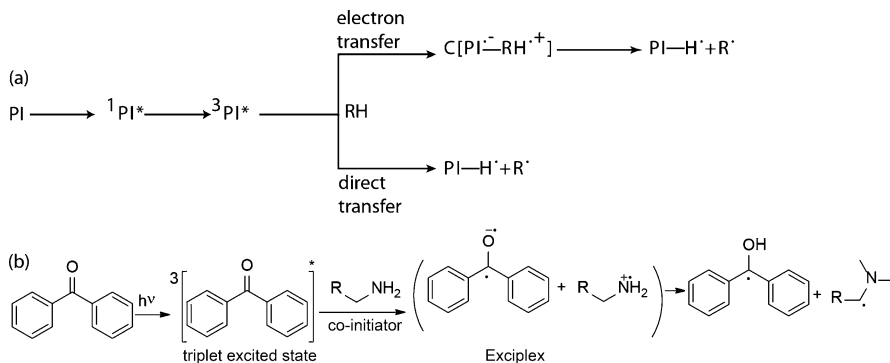


Fig. 9 Mechanism of initiation by type II initiators in the combination with an amine co-initiator

2.2 Monomers/Oligomers

Photopolymerization reactions involving a large variety of monomers/oligomers can be initiated by free radicals. This is because the radical is a neutral species stabilized through interactions with many common groups in monomers, such as halogen, phenyl, and many electron withdrawing groups. Radicals are nonspecific in their reactivity and interact with any available π -bond. Due to different rates of addition of the photogenerated radicals to the monomers, the reactivity of the monomers towards different initiators is variable [34]. Other factors, such as viscosity of the reactive medium, the thickness of the photopolymerizable film, the duration of irradiation, and the dark reaction after the light has been switched off, all govern the end results. Some prominent examples of molecules with chemical groups found in photoresists undergoing radical polymerization are provided in Fig. 12. Multifunctional monomers like epoxyacrylates, polyteracrylate, polytheracrylates, urethane acrylates, etc. are used in commercial formulations for photopolymerization (see Fig. 13).

Depending on the requirement of the application, photopolymerization can be carried out in solutions of monomers in suitable solvents, bulk monomers, or thin films. Due to the relative ease of following reaction and reactive species spectroscopically in solutions, reaction kinetics is often studied in solution. The propagating radical at a low concentration describes a second-order rate constant, while at a high concentrations, it is subject to a pseudo first-order rate constant. The termination reactions in solution phase photopolymerization are diffusion controlled [2, 35].

For many practical applications, polymerization takes place in bulk or thin films. Due to the effects of diffusion, the dynamics of polymerization can be entirely different in solution and in bulk. Owing to its ease of applicability for packaging of materials, photopolymerization has been intensely studied for decades. Despite this, determining the rate constants for addition of the radical produced by the initiator and a monomer is quite difficult. The viscosity of monomer in a bulk sample can be one or two orders of magnitude higher than the monomer solution.

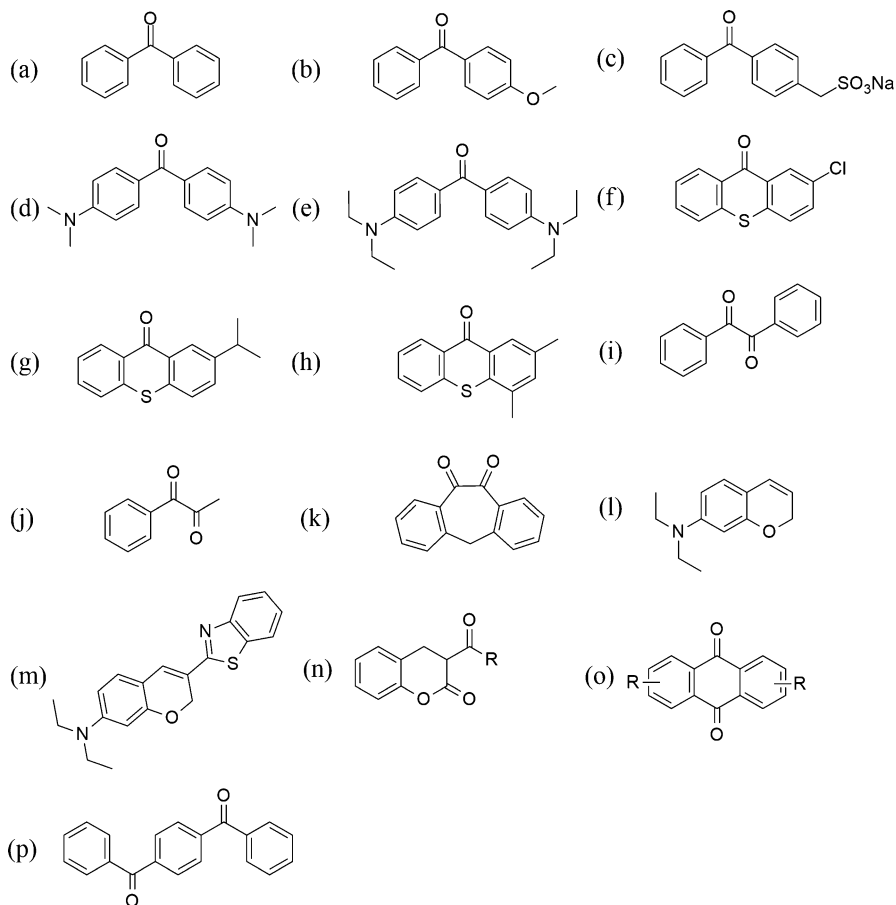


Fig. 10 Examples of type II photoinitiators: (a–e) benzophenone derivatives; (f–h) thioxanthone derivatives; (i–k) diketone (benzil) derivatives; (l–m) coumarin; (n) ketocoumarin; (o) anthraquinone derivatives; (p) terephthalophenone derivatives

The diffusion of the triplet radicals in the medium and its bimolecular quenching in the reactive medium are controlled by the viscosity of the reactive formulation. The rate constant for bimolecular quenching of the triplet radical by monomer (k_q) decreases with viscosity due to the decrease in diffusion, while it increases due to the increased presence of monomers in the bulk material. For a given monomer, the rate of polymerization increases with viscosity and then decreases. Viscosity also governs the cage effects involving the confinement of photogenerated reactive species by solvent molecules. For polymerization to take place, the radical has to escape the cage and react with monomers. In the solution phase, the cage effects are negligible; however, for increased viscosity, it is more difficult for a radical to escape the cage, resulting in a slower reaction [2, 35].

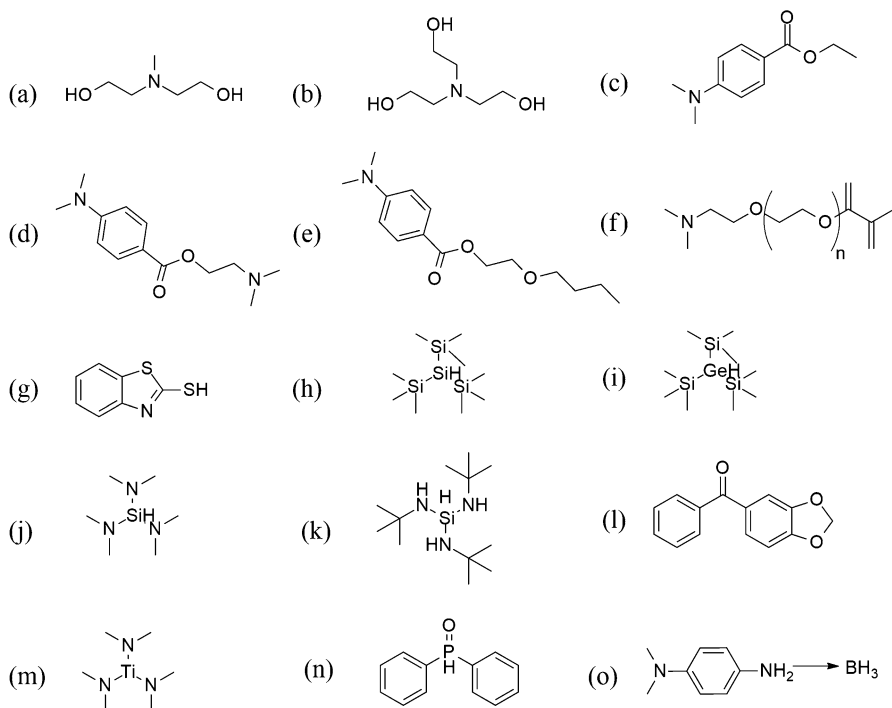
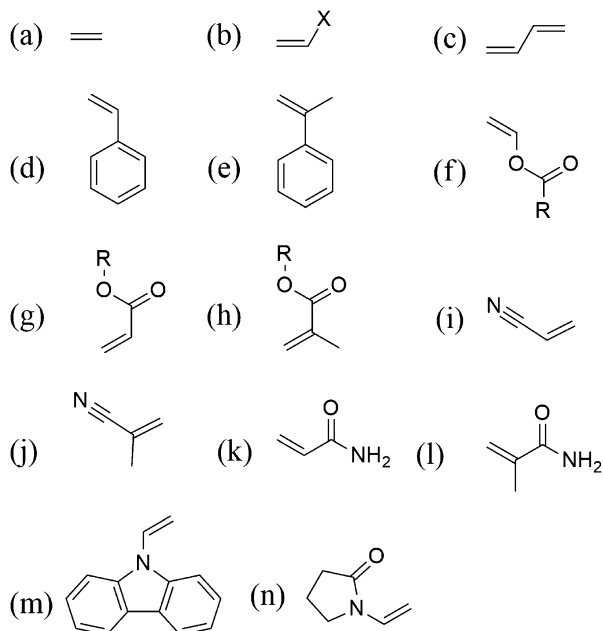


Fig. 11 Co-initiators for type II photoinitiators: **(a)** methyl diethanolamine; **(b)** triethanolamine; **(c)** ethyl 4-(dimethylamino)benzoate; **(d)** 2-(dimethylamino)ethyl 4-(dimethylamino)benzoate; **(e)** 2-butoxyethyl 4-(dimethylamino)benzoate; **(f)** amine containing polyether acrylate; **(g)** mercaptobenzothiazole; **(h)** tris(trimethylsilyl)silane; **(i)** tris(trimethylsilyl)germane; **(j–k)** silylamine derivatives; **(l)** acetal derivatives; **(m)** metal containing amines; **(n)** phosphorus containing co-initiator; **(o)** boron containing co-initiator

2.3 Visible Light–Sensitized Radical Polymerization

A molecule which can absorb visible wavelength and is capable of initiating a polymerization either by itself or in combination with other molecules can be termed a visible light initiator (or initiating systems, in cases when more than one molecule is involved) [36]. They are chosen for their high molar absorptivity at a visible wavelength or wavelengths, their specific interaction with monomers, and their long-lived excited states. Visible light initiating organic molecules can be constructed around UV photoinitiators by incorporating structural changes, such as those shown in Fig. 14a–d which are derivatives of Fig. 10f. The high-energy bonds in UV photoinitiators, when incorporated into molecules with extended conjugation, lead to visible light photoinitiators. The molecules in Fig. 14d are synthesized by incorporating benzophenone, thioxanthone, and pyrene on to a truxene moiety [37, 38]. The planar conjugated truxene moiety forms an efficient bridge for electrons, leading to a red-shifted absorption of the chromophore. The resulting molecules also show very high molar absorptivities, which makes them efficient initiators.

Fig. 12 Some common monomers/oligomers used in radical photopolymerization: (a) ethylene; (b) halogenated alkenes; (c) 1,3-dienes; (d) styrene; (e) *a*-methyl styrene; (f) vinyl ester; (g) acrylate; (h) methacrylate; (i) acrylonitrile; (j) methacrylonitrile; (k) acrylamide; (l) methacrylamide; (m) *N*-vinyl carbazole; (n) *N*-vinyl pyrrolidone



Due to their high interaction with light and stability of the photogenerated species, many organometallic compounds are highly suited for visible light photoinitiation. It should be noted that some organometallic molecules are cytotoxic and care should be taken on their selection in a photoinitiating system. The germane derivatives in Fig. 14i–k initiate radical polymerization in the presence of visible light due to free radicals generated by α -cleavage at the C–Ge bond [39–41]. An increase in the number of germanium atoms in the structure leads to a bathochromic shift in the absorption of the initiator. The photocleavage of germane initiators yield long-lived triplet species that are very efficient radical initiators [42]. Iridium complexes like those in Fig. 14l–m can be combined with suitable co-initiators to be used in free radical polymerization [43, 44]. The introduction of formyl moiety in the latter results in its higher extinction coefficient. Both compounds combine with tris(trimethylsilyl)silane and an iodonium salt to form a photoinitiator system for free radical polymerization. The mechanism of initiation is shown in Fig. 15.

2.4 Thiol-Ene Photopolymerization

Some of the earliest commercially available formulations for photopolymerization were based on photo-induced thiol-ene crosslinking. However, concerns over their shelf life, the odor of the thiols in the formulation, as well as the gradual degradation of the benzophenone photoinitiators used in these formulations causing discoloration led to their failure and disappearance. Many decades of ensuing research rectified the

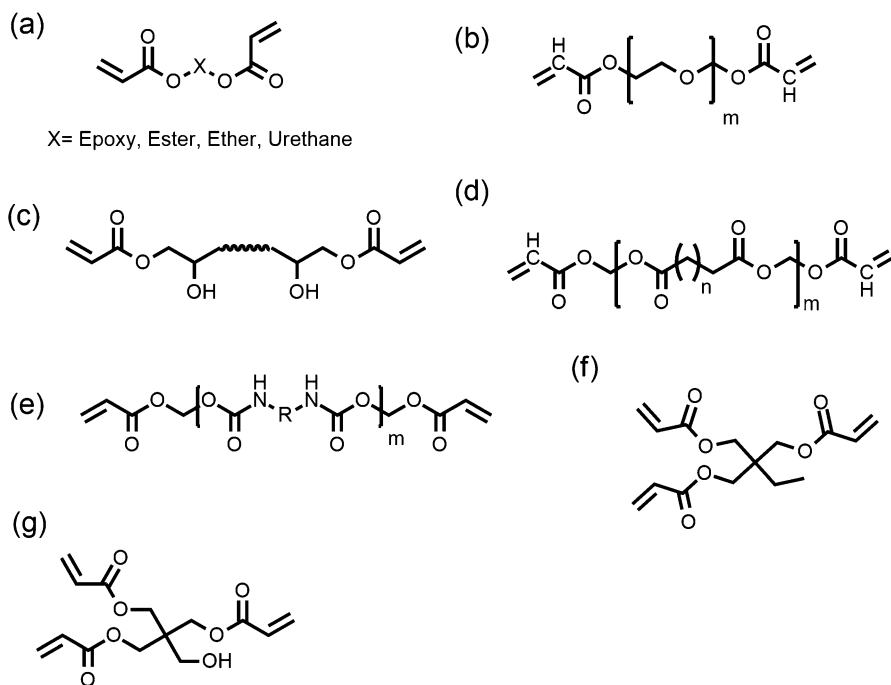


Fig. 13 (a) General structure of multifunctional monomers for free radical polymerization; (b) polyether acrylate; (c) epoxy acrylates; (d) polyester acrylate; (e) polyurethane acrylate; (f) crosslinker monomer trimethylolpropane triacrylate; (g) crosslinker monomer pentaerythritol triacrylate

above problems, leading to the reemergence of this very useful chemistry. The polymer network resulting from thiol-ene polymerization has been suggested as the most ideal from any free-radical polymerization [45, 46]. Since it has been tagged as a “Click reaction,” it has been extensively employed for the synthesis of functional polymers, hybrid materials, and microdevices [47–52]. Thiol-ene reactions are specific and proceed at mostly mild conditions making them attractive for a wide variety of chemical syntheses. Thiol-ene chemistry has been used in the synthesis of various monomers [53–56], polymers, or copolymers [57–65]. Thiol-ene additions are used as a method of direct synthesis or are used for post polymerization modification of polymers [66]. The versatility and mild conditions of thiol-ene reactions are very attractive for chemical modification of monomers, polymers and nanoparticles for biotechnological applications [66–70].

Thiol-ene photopolymerization shows a high curing speed with little or no oxygen and moisture sensitivity to give polymeric films with a very low shrinkage stress and a narrow glass transition temperature [45–47]. The mechanism of thio-ene polymerization shares the characteristics of both addition and condensation polymerization (see Fig. 16a) [46]. Some common enes and thiols that have been employed in thiol-ene polymerization reactions are shown in Fig. 16b.

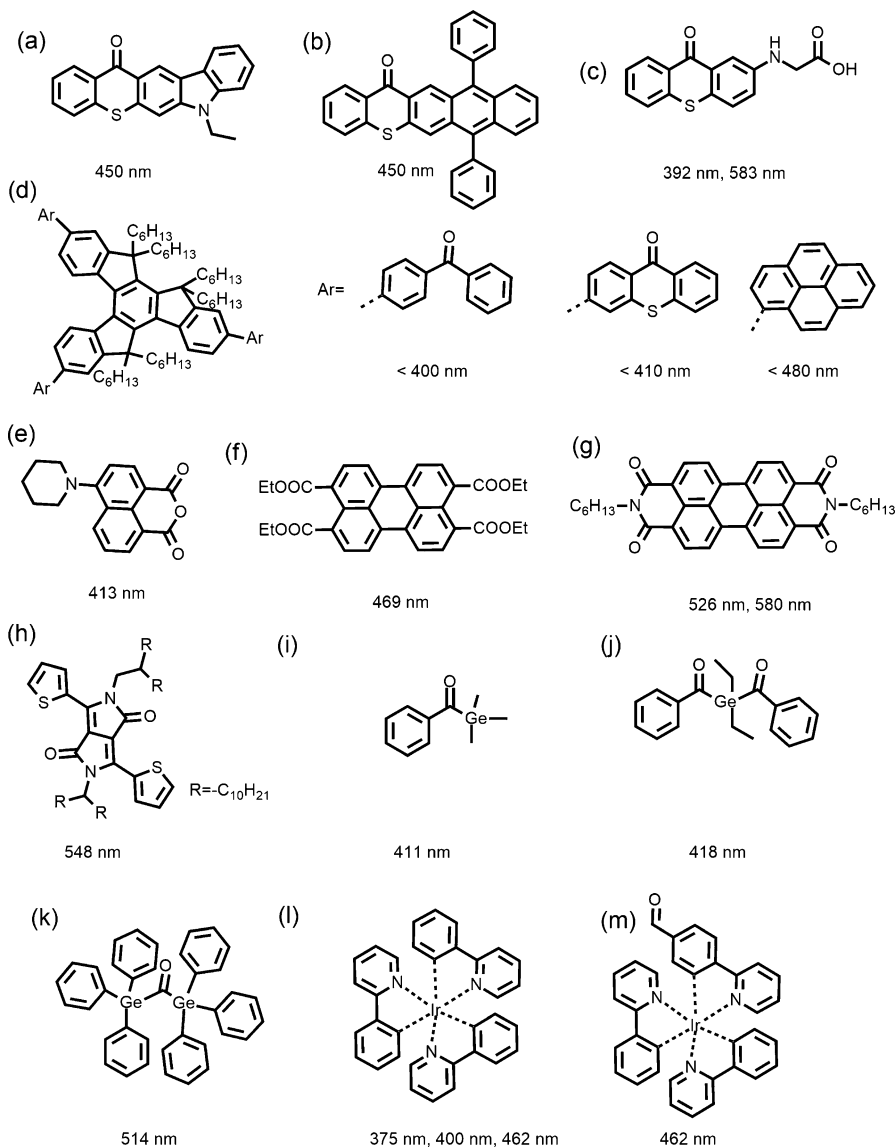


Fig. 14 Some examples of visible light photoinitiators; they are used either by themselves or in combination with other molecules to effect initiation. The absorption maxima or band width of activity are provided underneath each structure

The reaction is easily initiated by a radical photoinitiator and leads to a near quantitative addition of thiol to carbon-carbon double bond. Type I photoinitiators are favored for thiol-ene polymerization due to the improved hydrogen abstraction from thiols [71, 72]. Sterically, unhindered terminal enes show the highest reaction

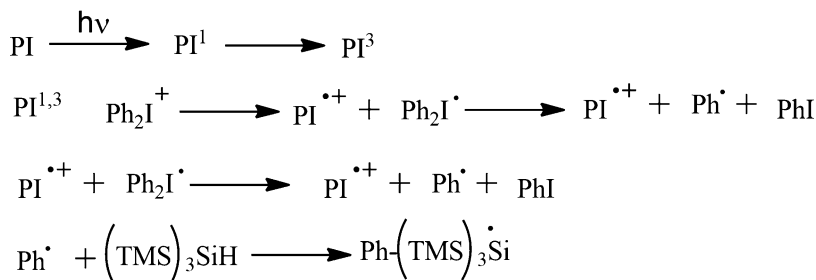


Fig. 15 Initiation of visible light photoinitiating combination; inorganic complexes play the role of the initiator

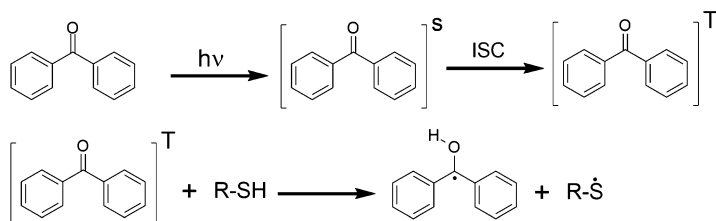
rates during thiol-ene photopolymerization compared to hindered enes [73, 74]. Electron rich or strained enes show higher reaction rates during photopolymerization with a particular thiol. Norbornene seen in Fig. 16b is an example of a strained ene as that undergoes rapid reaction with the thiyl radical leading to an addition product with reduced ring strain at the double bond. Hence, as compared to other enes, the reaction between thiyl and norbornene proceeds quite fast.

Vinyl ethers are examples of electron-rich enes that are highly reactive during thiol-ene polymerization. Conjugated dienes, methacrylates, styrene, and maleimides are examples of low reacting enes (see Fig. 16b) [46, 73]. Alkyl thiols, thiolglycolate esters, and thiol propionate esters have been used in thiol-ene reactions. Esters show a higher reactivity to alkenes, as compared to alkyl thiols. Common multifunctional thiols and enes used in thio-ene photopolymerization are shown in Fig. 17.

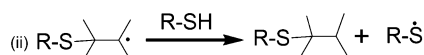
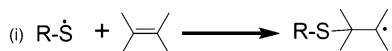
As shown in Fig. 16, the propagation of thiol-ene reaction proceeds in two distinct steps. The first step is called propagation involving the attack of the thiyl radical on the ene. The subsequent step is called the chain transfer step where the thiol-ene adduct radical abstracts hydrogen from a new thiol molecule to regenerate the thiyl radical. The chemical nature of the thiol and ene determines whether the propagation or the chain transfer step forms the rate-determining step during the reaction. Enes that are less reactive cause propagation to be the rate-limiting step. Thiols that structurally limit the abstractability of the hydrogen lead the chain transfer step to be the rate-limiting step. Unlike the conventional free-radical polymerization, a typical thiol-ene polymerization maintains a low cross-linking density characterized by the formation of low molecular weight oligomers for an extended period during the reaction. This, in turn, delays the gel point during polymerization, leading to ease of diffusion of species resulting in the buildup of a uniform network of polymers [75, 76]. In thiol-ene generated polymers, glass transition occurs over a small range of temperature, indicating the uniformity of the formed network. The narrow window of glass transition results in well-defined mechanical properties for the resultant polymers [77].

Thiol-acrylate and thiol-ene-acrylate formulations have been studied to diversify the properties of the thiol-ene crosslinked polymer. In the binary thiol-acrylate systems, multifunctional thiols are combined with traditional acrylate-based monomers. This

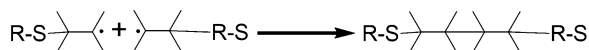
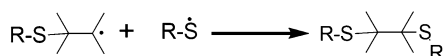
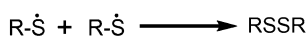
(a) Initiation



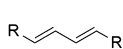
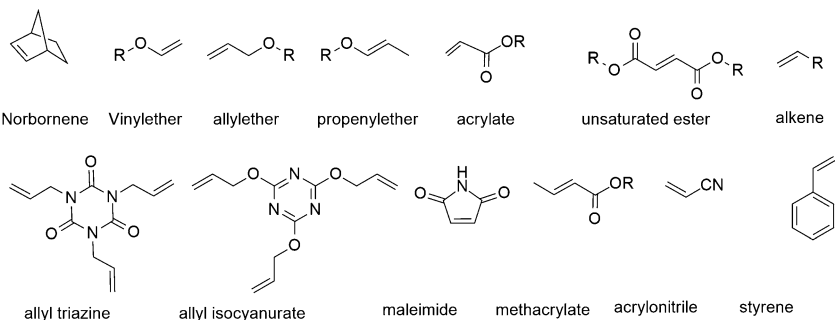
Propagation



Termination



(b) Enes



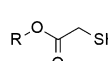
Diene

N-vinyl
amide

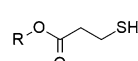
Thiols



alkyl thiol



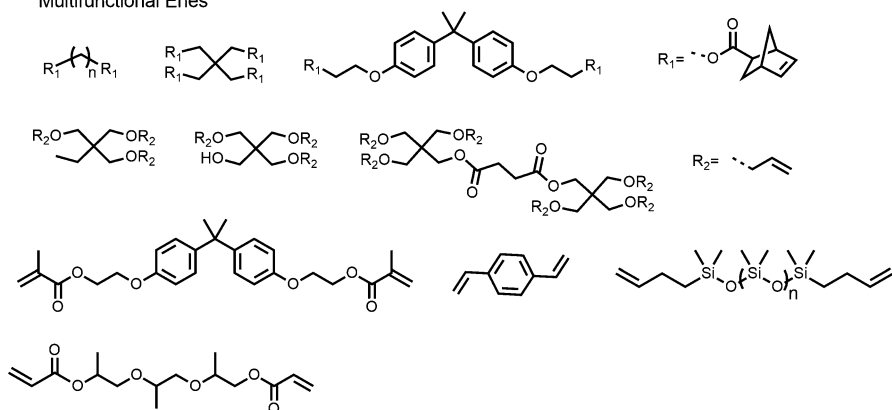
alkyl thioglycolate



alkyl mercaptopropionate

Fig. 16 (a) Thiol-ene polymerization, initiation, propagation, and termination steps and the examples of thiols and enes that could be employed in such reactions. The propagation step can be divided in two steps, namely, propagation (i) where the thiol radical adds to the double bond, and (ii) which involves hydrogen abstraction by the formed monomer radical from thiol is termed chain transfer step (ii). (b) Some enes and thiols that have been used in thiol-ene reaction

Multifunctional Enes



Multifunctional Thiols

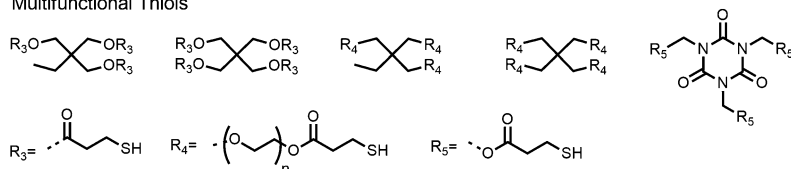


Fig. 17 Common multifunctional ene and thiol monomers employed in thiol-ene photopolymerization

combination leads to polymerization with low oxygen sensitivity, higher conversion, as well as delayed gel point without sizable compromise on the thermo-mechanical properties of the formed polymers, as compared to pure methacrylate polymers. The ternary combination of thiol, ene, and methacrylate is more robust than the binary combinations. Ternary mixtures result in polymers with the high glass transition temperatures similar to those in methacrylate polymers, while imparting the positive traits of thiol-ene polymerization in the system, such as oxygen inhibition and uniform polymerization [78]. With the careful choice of the monomers, there is the possibility of creating polymerization-induced phase separations. Phase separated double polymer networks could be interesting substrates for many applications. Thiol-ene polymerization of some thiol-ene-acrylate formulations results in the formation of two-phases and leads to a reduction in shrinkage stress. The ternary thiol-ene-acrylate formulations are less sensitive to stoichiometry of individual components and hence provide dexterity in designing polymers with desirable properties [78–81].

3 Cationic Polymerization

The oxygen sensitivity of radical polymerization is one of its major drawbacks requiring photocuring to be carried out under inert atmosphere. The high processing costs associated with maintaining inert atmosphere during applications lead to the

exploration of new chemistries capable of delivering effective photopolymerization under ambient conditions [82]. The discovery of photoacid generators enabled the use of chemical amplification reactions to carry out efficient polymerization without inter atmosphere. Chemical amplification refers to a single photochemical event leading to an increasing number of chemical events. Since each photochemical event leads to hundreds of chemical events during chemical amplification reactions, they can be used even with low doses of radiation. Ambient oxygen shows little of no effect on cationic polymerization. In cationic formulations, the photochemical reaction is initiated by a photoacid generator (PAG). A photoacid generator can be an ionic, nonionic, or organometallic compound [1].

3.1 Ionic Photoacid Generators

Photoacid generators (PAGs) are compounds that can generate acidic species on irradiation. Diaryl iodonium and triaryl sulfonium are among the earliest types of PAGs that were investigated for cationic polymerization [83–85]. The light-sensitive organic part of these PAGs features a heteroatom hosting a positive charge; PAGs are also associated with a metal complex anion that acts a counter ion. The counter ion combines with the photogenerated H^+ ion to form Brønsted acids (super acids) capable of catalyzing ring-opening polymerizations. Photoacid generators can be applied to ring-opening reactions of a wide variety of materials, such as multifunctional epoxides, oxetanes, vinyl ethers, cyclic ethers, cyclic acetals, cyclic siloxanes, etc.

Most common onium salt PAGs include iodonium derivatives, sulfonium derivatives, phosphonium derivatives, *N*-alkoxy pyridinium salts, etc. (see Fig. 18a–l). Some organometallic compounds are also used as cationic photo-initiators. Most PAGs absorb radiation in the UV region; however, their activity can be extended to longer wavelength by the use of photosensitizers by the application of free-radical promoted cationic polymerization [86]. Cationic photopolymerization is initiated by either the photogenerated acid or by a stable cation formed due to the photo-scission of the PAG.

Compounds (a–c) in Fig. 18 are examples of iodonium PAGs. The cationic and anionic species in the iodonium salt PAG play specific roles defining its properties. The onium cationic part defines the photochemistry of the PAG. It influences the absorption maximum (λ_{max}), the molar absorption coefficient, quantum yield, photosensitization, and thermal stability of the PAG. The anion determines the acid strength, initiation efficiency (during polymerization), and propagation rate constants (during polymerization). Once the photoacid is generated, the anion determines its role during polymerization. The importance of having non-nucleophilic counteranions was realized during the early investigation of diaryliodonium PAGs. The interaction of the photogenerated cationic species with a nucleophilic anion leads to the suppression of the initiating cationic species and hence the polymerization. In the presence of a suitable anion, the aryl and aryl iodine cationic species formed by photolysis of iodonium PAG can react with monomers, solvents, or impurities to give superacids of the form HMX_n (MX_n^- : BF_4^- , PF_6^- , AsF_6^- ,

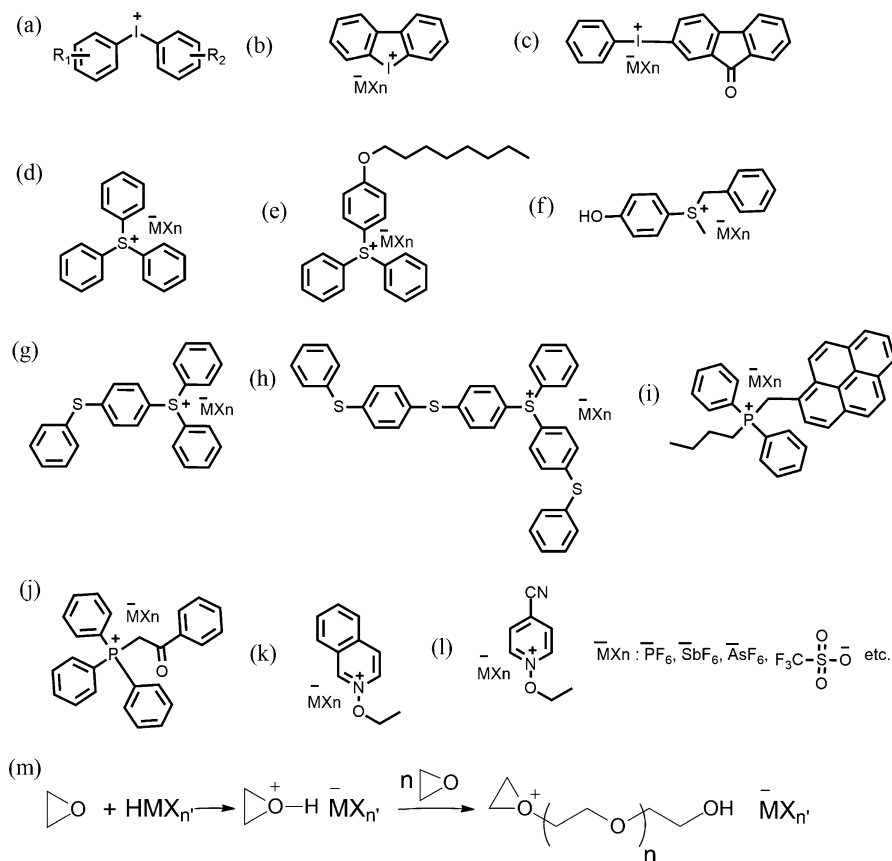


Fig. 18 Onium (ionic) photoacid generators and ring-opening polymerization: (a–c) Iodonium-based PAGs; (d–h) sulfonium-based; (i–j) phosphonium salts; (k–l) *N*-alkoxy pyridinium salts; and (m) ring-opening polymerization of epoxide monomer in the presence of photogenerated acid

SbF_6^- , $(C_6H_5)_4B^-$ etc.). For a series of onium salt with the same cation, the polymerization is dependent on the counterion. The extent of polymerization depends on the nucleophilicity and size of the counterion in the following order, $SbF_6^- > AsF_6^- > PF_6^- > BF_4^-$ [87]. These PAGs undergo photolysis with quantum yields in the range of 0.7–0.9. The λ_{max} and the intensity of absorption of iodonium PAGs can be engineered by substitutions on the aromatic ring. The super acids go on to initiate ring-opening polymerization reactions (see Fig. 18m) [82].

A simplified version of the mechanism of photolysis and photoacid generation in iodonium PAGs is shown in Fig. 19. A diaryliodonium salt undergoes photo-induced scission either through homolytic or through heterolytic cleavage (see Fig. 19). The photoexcited intermediate interacts with water or other protic solvents present during the reaction to give a strong Brønsted acid which can initiate cationic polymerization. In the viscous reaction media, the photogenerated species are subject to cage effects.

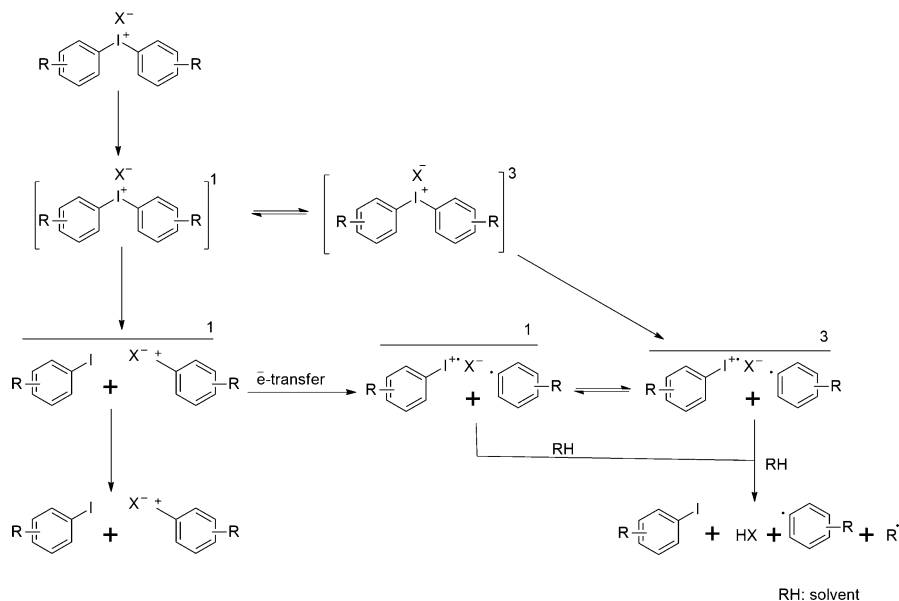


Fig. 19 Mechanism of photoacid generation in an iodonium salt PAG. Here RH is a protic solvent

Sulfonium-based PAGs form another important class of onium salt PAG. Compounds (d–g) in Fig. 18 are examples of sulfonium PAGs. They have a higher reduction potential, than iodonium PAGs, and hence show better thermal stability, allowing them to be used in formulation that is more shelf stable. The higher reduction potential also leads to a lower photosensitivity of the sulfonium-based PAG. The mechanism of photolysis of sulfonium PAGs closely resembles that of iodonium PAGs (see Fig. 20). Homolytic photo-scission pathway is more prominent in sulfonium PAGs, as compared to heterolytic cleavage pathway. Sulfonium PAGs show a longer wavelength absorption band at 305 nm. The substitution of thiophenoxyphenyl groups in compounds (g) and (h) in Fig. 18 increases the molar absorption coefficient of these compounds, as compared to compound (d). This makes them more sensitive photoinitiators. Ferrocenium-based PAGs form a newer class of organometallic initiators that are used mainly with monomers that could complex with iron atom in ferrocenium. They are mainly used for epoxide monomers. Some examples of ferrocenium PAGs and the mechanism of photo-initiation of ferrocenium PAGs are shown in Fig. 21.

3.2 Spectral Broadening

Spectral broadening refers to the technique of increasing the sensitivity of onium salt initiators to visible wavelengths to enable the use of new light sources in the near UV and visible regions of the spectrum. With the use of electron transfer sensitization,

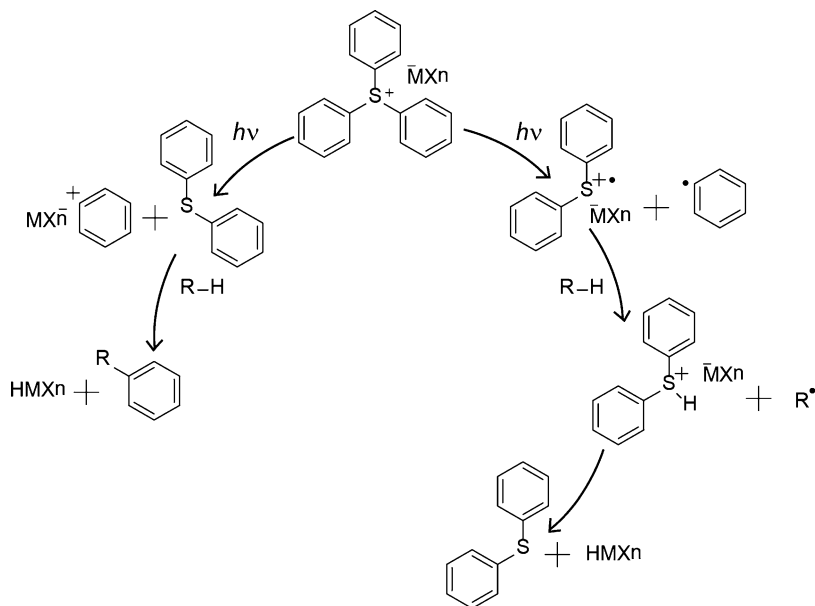
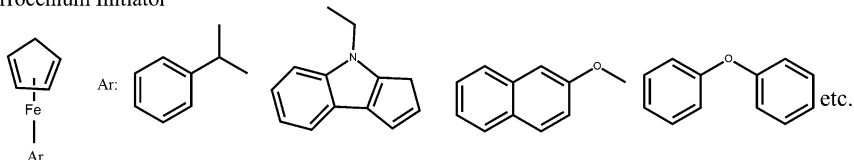


Fig. 20 Mechanism of photoacid generation in sulfonium salt PAG, here RH is a protic solvent

Ferrocenium Initiator



Mechanism of action of Ferrocenium Initiator

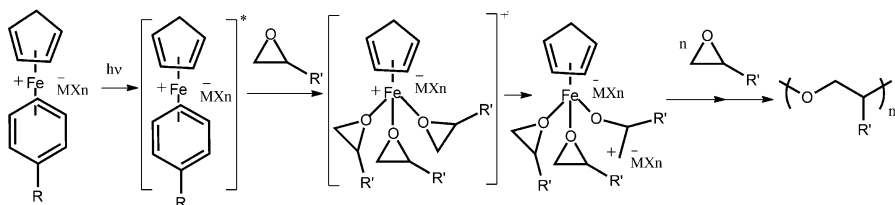
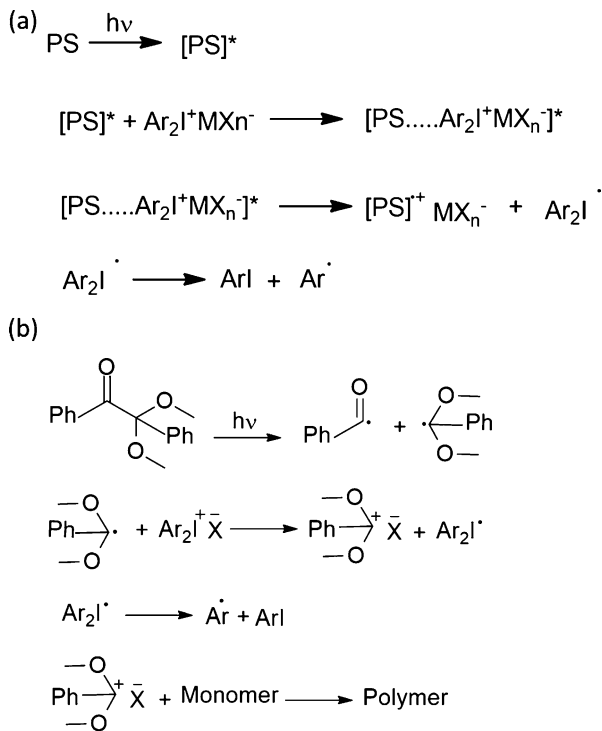


Fig. 21 Examples of ferrocenium photoinitiators and the mechanism of their action as cationic initiators

the absorption of both iodonium and sulfonium PAGs can be shifted to longer wavelengths [88]. Electron-transfer sensitization involves the combination of a photosensitizer (PS) with the PAG to achieve photoinitiation as shown in Fig. 22a. The photoexcitation of PS leads to an electron transfer reaction from PS to the PAG,

Fig. 22 (a) Mechanism of electron transfer sensitization in aryliodonium PAGs; (b) mechanism of free-radical promoted cationic polymerization



leading to the formation of an excited state complex (exciplex) followed by a reduction of the onium cation. This is followed by the irreversible decomposition of the resulting $\text{Ar}_2\text{I}^\bullet$ free radical; this process is very efficient and restricts back electron transfer to the photosensitizer from happening [84, 90]. The positively charged photosensitizer either directly initiates polymerization or generates photoacids through further reactions. Polyaromatic compounds, such as pyrene derivatives, atracene derivatives, carbazole derivatives, etc., are used as electron transfer sensitizers.

Free-radical promoted photosensitization of cationic polymerization (FRPCP) is another method for achieving spectral broadening. In FRPCP a radical initiator is added alongside the PAG. Free radicals formed by the radical initiator interact with onium salt PAG to generate a corresponding cation and $\text{Ar}_2\text{I}^\bullet$. The cation formed from the free radical initiator then goes on to initiate polymerization reactions. The $\text{Ar}_2\text{I}^\bullet$ undergoes a fast and irreversible decay. The mechanism for electron-transfer sensitization is shown in Fig. 22b. Typically, free radicals formed during FRPCP are oxidized to form species containing a positive charge capable of initiating cationic polymerization. A combination of aromatic ketone, disilane, and diaryliodonium salt is a typical example of a FRPCP initiator [89, 90]. Irradiation of the mixture leads to the formation of silyl radical which is then oxidized to give a positively charged initiating species. Acylgermanes like Fig. 14i can be used as a free radical initiator in

FRPCP [91–93]. They give germyl radicals on irradiation; these radicals are then oxidized to germanium ions which can initiate polymerization. Supramolecular complexes of iodonium PAGs-crown ethers and combination of onium salt and zinc halide have also been used for FRPCP [94–97]. Apart from this a combination of an organometallic compound of ruthenium, iridium, selenium or germanium with an organo silane and photoacid generator like those discussed in Sect. 6 can be used for initiating cationic polymerization in the near UV to visible wavelengths [39, 43, 93, 98–103]. These ambivalent initiating systems capable of initiating both radical and cationic polymerization have the potential to be used in complex photo-polymerizable materials.

3.3 Nonionic Photoacid Generators

Nonionic or nonsalt PAGs are another subclass of PAGs extensively studied in recent years. Unlike common onium PAGs, nonionic or nonsalt PAGs exhibit a broad wavelength activity and a good solubility in organic media and polymeric films. On irradiation, nonionic PAGs give rise to various organic acids, such as sulfinic acid, sulfonic acid, carboxylic acid, phosphoric acid, etc. [104, 105]. Some examples of nonionic PAGs are shown in Fig. 23. Under photoirradiation, nonionic PAGs generate organic acids capable of initiating polymerization. Compounds (a–i), except for (h) (see Fig. 23), generate sulfonic acids on irradiation [9]. Compound (f) in Fig. 23 generates a carboxylic acid on irradiation. Sulfone compounds (j) and (k) give rise to sulfinic acid on irradiation. Diphenyl selenide compound (m) in Fig. 23 yields a cationic radical capable of initiating polymerization in the presence of a photosensitizer [106]. The mechanism of photoacid generation in ortho-nitrobenzyl sulfonates, iminosulfonates, and N-hydroxyimide sulfonates is shown in Fig. 24a–c, respectively. Apart from the photoproducts shown in Fig. 24, there are other radical and ionic species that might be formed during the photoacid generation. These side products may or may not intervene in the progress of polymerization depending on the conditions during polymerization. Cage effects in the reaction medium, as well as the interaction of atmospheric oxygen with radical species generated during photoacid generation, can control the dynamics of polymerization. Compound (e) gives an 88% yield of *p*-toluene sulfonic acid in solution and 52–61% of the same compound in polymer films in air [107]. Interestingly, under vacuum conditions, due to the formation of ammonia by hydrolysis of imine, the yield of *p*-toluene sulfonic acid was found to be lower than both cases specified above.

3.4 Monomers for Cationic Polymerization

A wide range of functional groups are compatible to cationic polymerization (see Fig. 25) [82, 86, 109]. They include vinyl derivatives, vinyl ethers, various cyclic ethers, thiranes, cyclic esters, and cyclic siloxane derivatives. Apart from these,

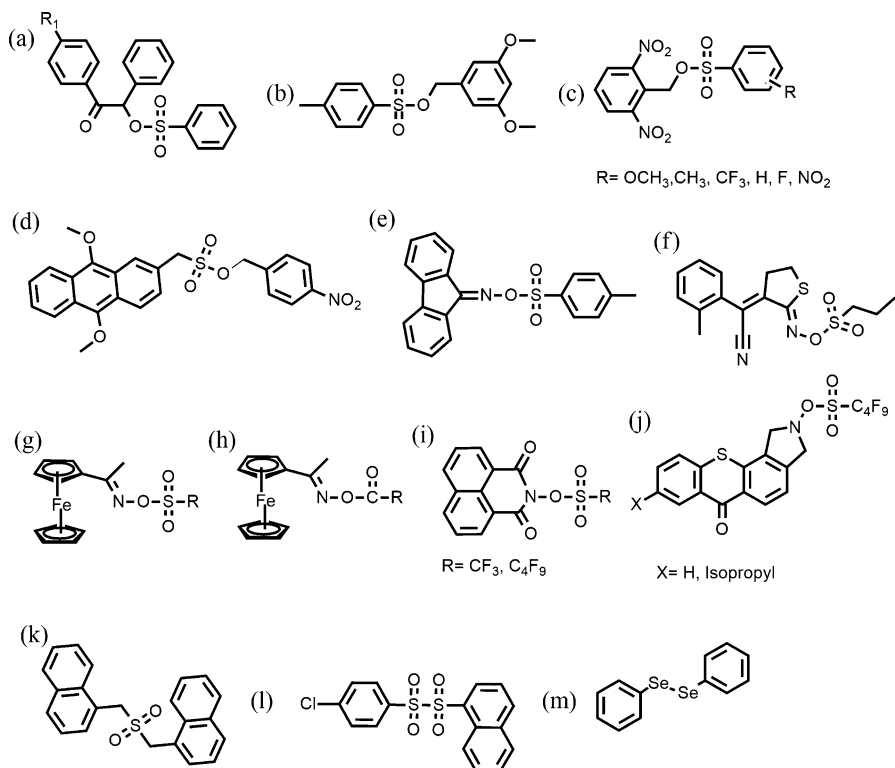


Fig. 23 Some examples of nonionic PAGs: (a–d) based on sulfonates; (e–f) iminosulfonates; (g) acetylferrocene oxime; (h) sulfonylferrocene oxime; (i–j) *N*-hydroxyimide sulfonates; (k–l) sulfones, and (m) selenide-based photoacid generators [106]

many unconventional monomers, such as benzoxazine, epoxy, end functionalized poly caprolactone, thiophene, etc. also undergo cationic polymerization [86, 110].

Practical application demands high reactivity, leading to a high cure speed, lack of oxygen inhibition, low-volume shrinkage, good mechanical properties, little or no toxicity, and good adhesion to various substrates from the monomer. The electron-rich carbon-carbon double bonds in vinyl ethers exhibit a higher curing rate than epoxy functionalized monomers. The high rate of conversion in vinyl ethers is also due to the low glass-transition temperature of the formed polymers [87]. Some examples of multifunctional epoxide monomers that can be polymerized by cationic photoinitiators are shown in Fig. 26a–d. Due to their extensive application in many different fields [1, 87], multifunctional epoxide monomers are the most important class of monomers in cationic polymerization. These monomers polymerize to form three-dimensional networks. The rate of photocuring increases rapidly for multifunctional epoxy groups, reaches a maximum, and then decreases. The presence of the soft counter ion associated with the photoacid minimizes the interaction between polymer chains containing cationic end groups. Cationic polymerization proceeds

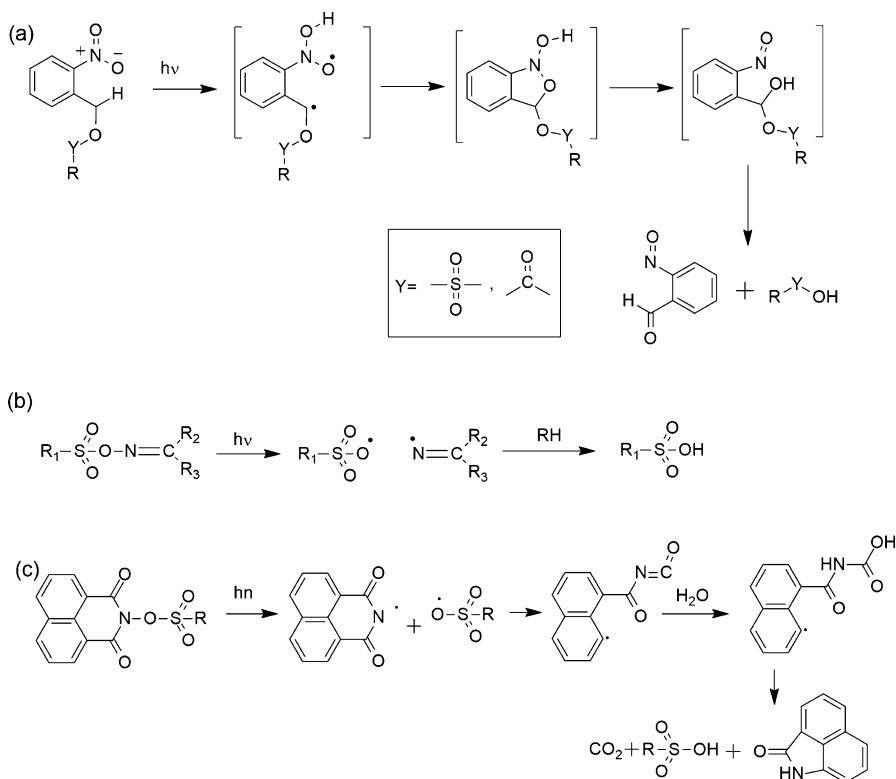


Fig. 24 The mechanism of photoacid generation in nonionic PAGs: (a) Orthonitrobenzyl sulfonates give rise to sulfonic acid and other photoproducts [103]; (b) iminosulfonates give rise to sulfonic acid and other photoproducts [107]; (c) *N*-hydroxyimide sulfonates give rise to sulfonic acid [108]

uninhibited in the dark state; after the light source has been switched off, this process can be accelerated by heating and is called a post-cure step.

The material requirement for applications dictates the design of monomers. The rate of curing of difunctional epoxides monomers was found to be inferior to that of difunctional acrylate monomers. Hence, there have been many attempts to increase the curing speed of the epoxy- based monomers through design. Of the different classes of monomers explored, cycloaliphatic epoxides were found to have the highest curing rates. Rapid polymerization in multifunctional epoxy monomers can lead to gel point, trapping large quantities of residual monomer inside the crosslinked network. This can be circumvented by prolonging the gel point during polymerization by the use of chain transfer agents that attack the cationic end of the polymer while initiating new polymeric chains [111]. Alcohols are among the most efficient chain transfer agents, the oxygen in the alcohol interacts with the cationic end of the growing polymer chain. This results in end-capping of the cationic chain. Further release of an H^+ ion from the alcohol terminated polymer chain initiates free

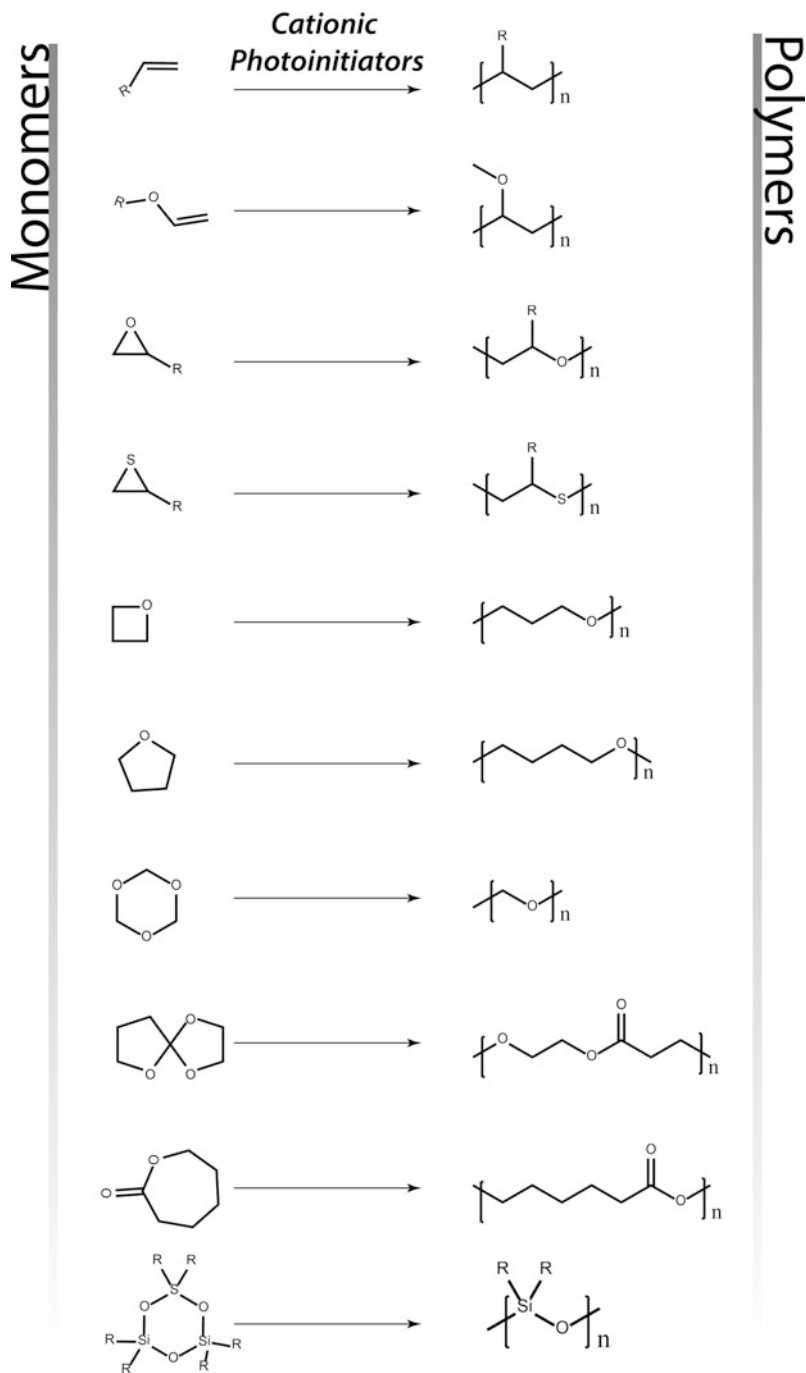


Fig. 25 Various monomers that can be polymerized by cationic polymerization; top to bottom: vinyl, vinyl ether, epoxy, thiirane, oxetane, tetrahydrofuran, 1,3,5-trioxane, 4,6-trioxaspiro[4.4]nonane, 6-caprolactone, hexamethylcyclotrisiloxane [82, 86]

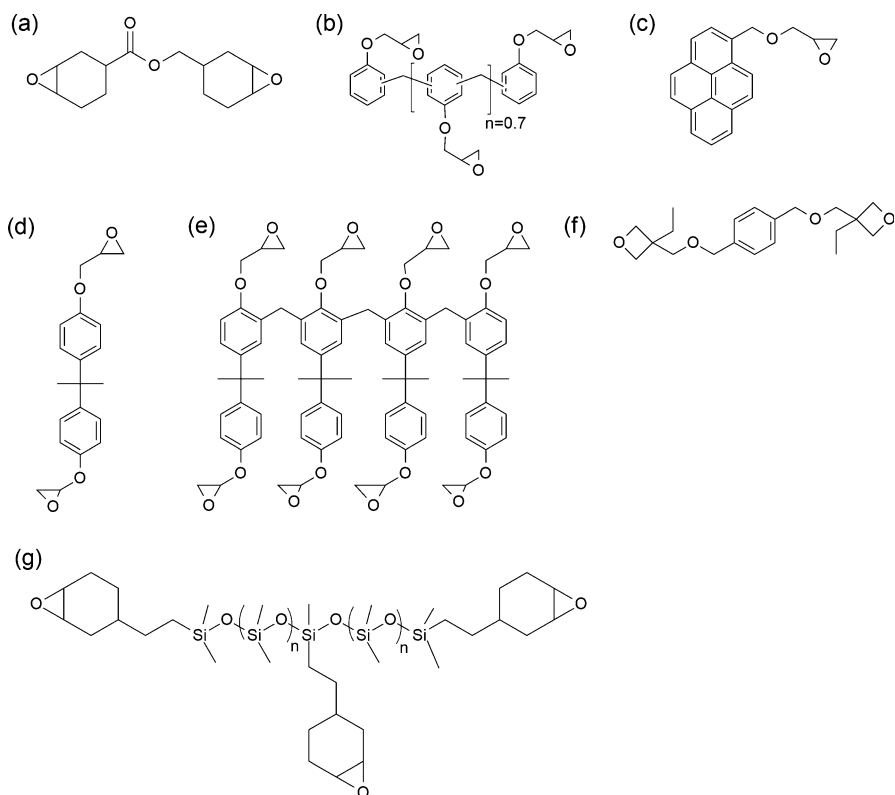


Fig. 26 Ring-opening polymerization in epoxide monomer; examples of multifunctional monomers that can be polymerized by cationic photoinitiators

monomers to progress the reaction. This method of activation of the growing polymer chain is called the activated chain-end mechanism [87, 112]. Apart from this, it has also been proposed that the monomer can be directly activated by alcohol, leading to the activated monomer mechanism [113, 114]. Both these mechanisms check the rapid growth of molecular mass or cross linking and delay the gel point, leading to higher conversions and better mechanical properties.

The high polymerization rates of multifunctional cycloaliphatic monomers make them popular for many commercial applications. Apart from the high curing rates, commercial applications demand high thermo-mechanical properties, chemical stability, abrasion resistance, adhesion, and solvent resistance. The presence of low molecular weight components in the cured polymer after photocuring can adversely affect its thermo-mechanical properties and increase its toxicity. The obvious low molecular weight materials in the cured polymers would be the photosensitizer, the PAG, or its photo-degradation products. Photosensitizers can be functionalized to be incorporated into the polymer; the epoxy functionalized pyrene molecule in Fig. 26c is one such example [115]. Another approach is the development of photosensitizers

attached to a polymer [116]. The photoacid generator can be substituted with long alkyl chains or bound to polymers to increase its molecular weight. The increasing substitution on the photoacid also dictates the diffusion of the photodegradation products from the PAG [117].

Volume shrinkage is one of the major problems faced by radical polymerizable acrylate photopolymers. Simple methyl methacrylate monomer shrinks by about 20–25% of its volume [118]. Multifunctional acrylate monomers show shrinkage lower than the above value (c.a. 10%), but shrinkage is still substantial to hamper application [119–121]. Shrinkage in multifunctional epoxide photopolymers is less than that of acrylate-based photoresists [122]. Some applications, such as dental fixtures, demand minimal shrinkage of the photocured structure. Volume shrinkage can be reduced by designing suitable monomers or a combination of monomers. For example, monomers (f) and (g) in Fig. 26 are used together to make rigid, solvent-resistant films with a low volume shrinkage [123]. Controlled addition of diol derivatives of compound (g) was found to decrease volume shrinkage. Epoxy functionalized hybrid silicone monomers, as the one in Fig. 26h, also undergo rapid polymerization, but yield soft elastomeric and transparent films [124]. Careful selection of monomers and initiators allows the engineering of properties in the final cured film or structure.

4 Anionic Polymerization

The idea of anionic photopolymerization has been around for a long time, but it has been only sporadically advanced over many years [125, 126]. In recent years, the interest in anionic photopolymerization has been renewed, mainly due to the control it provides over the composition and structure of the polymer. Monomers undergoing anionic polymerization should be able to stabilize a negative charge through inductive or resonance effects. Anionic photopolymerization reactions can be initiated by inorganic complexes of chromium, organometallic complexes of chromium, as well as tungsten, metallocenes, triarylmethyl derivatives, Zwitter ions, etc. [127–133]. Ethyl and methyl cyanoacrylates are the most widely studied monomers for anionic photopolymerization. Anionic photopolymerization is initiated by the formation of an anionic species by the photoexcited initiator as shown in see Fig. 27a [127, 129, 134–136]. The photogenerated anion adds to the carbon–carbon double bond in the monomer to generate an anionic adduct setting off the propagation reaction shown in Fig. 27b. Anionic polymerization of ethyl or methyl cyanoacrylates can be carried out in neat samples. Recently, ketoprofen has been used to initiate the polymerization of methoxy acrylate in neat as well as solutions in the presence of a mixture of sodium hydride and sodium hydroxide [137]. Ketoprofen initiated polymerization of methoxy acrylate is shown in Fig. 28.

Sila(I)ferrocenophanes can undergo photoinduced anionic ring-opening polymerization in the presence of a lithium or sodium salt of cyclopentadienyl [138–141]. Though such polymers have been previously prepared by conventional means, the photocontrolled reaction permits the use of ferrocenophanes with

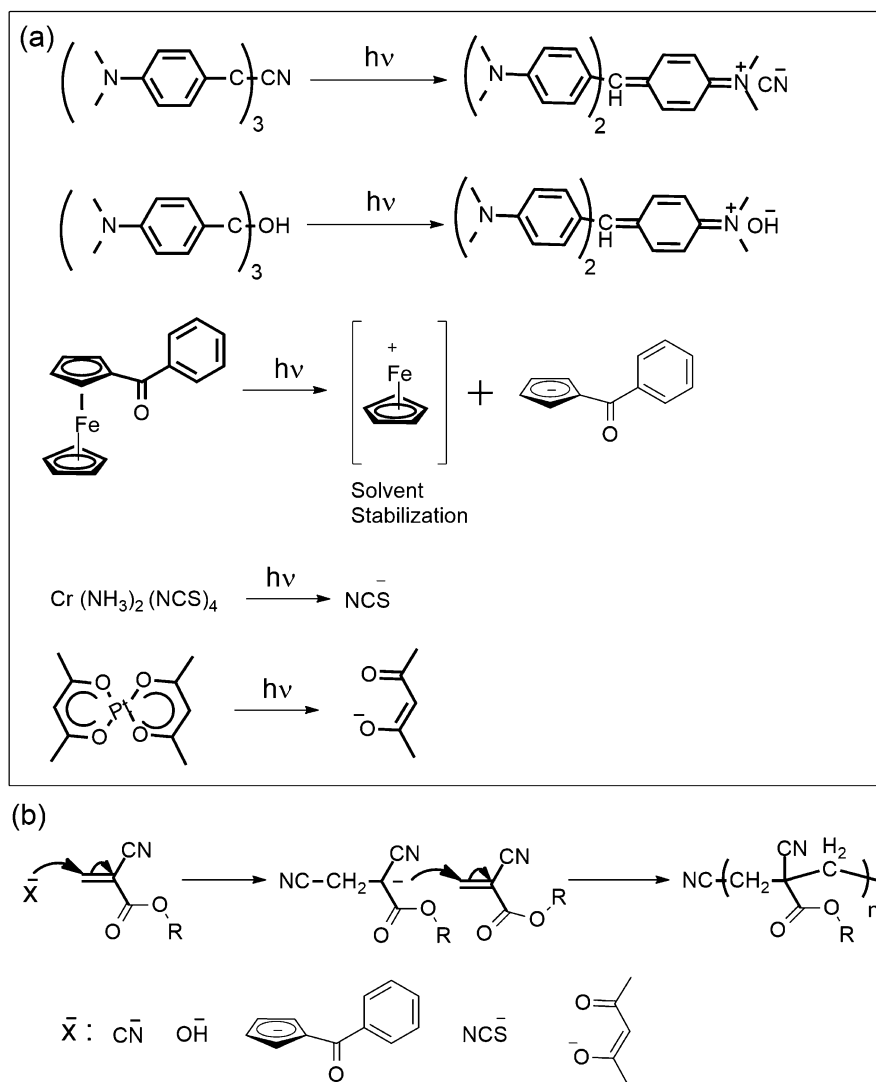


Fig. 27 Anionic photopolymerization of alkyl cyanoacrylate; (a) various photoinitiators; (b) the general scheme for anionic polymerization of alkyl cyanoacrylate [133]

sensitive functional groups as pendants [139, 142, 143]. The scheme in Fig. 29 elaborates the ring-opening polymerization of ferrocenophanes. The mechanism of the photoinduced anionic polymerization is not completely understood, but it is postulated that the strained sila bridge plays a role in weakening the bond between the cyclopentadiene and iron. This bond-weakening effect, alongside with photo-induced ligand to metal charge transfer, increases the electrophilicity of iron.

Fig. 28 Ketoprofen in the presence of NaH and NaOH can polymerize methoxyacrylate with high yields in both liquid and solid state polymerization. The initiation and propagation step of the anionic polymerization of methoxyacrylate can be seen here [137]

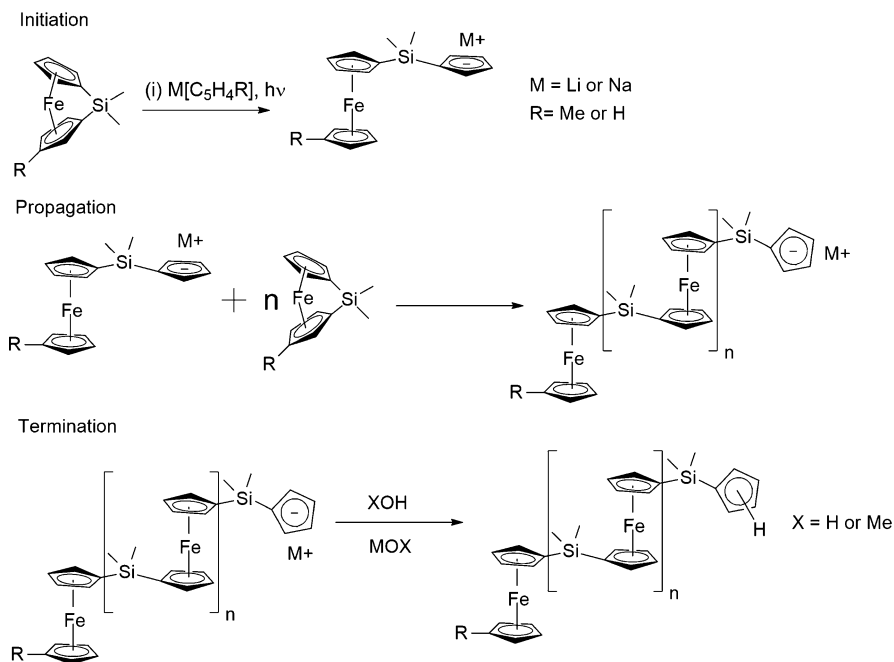
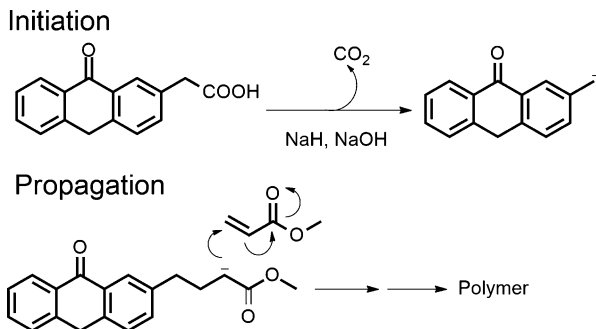


Fig. 29 Ring-opening photopolymerization of ferrocenophanes in the presence of lithium or sodium salt of cyclopentadienyl cation

The nucleophilic metal center then drives the formation of a reactive ring opened species containing cyclopentadienyl anion. This anion is stabilized by a positively charged metal counter ion and leads to the propagation of the ring-opening polymerization by addition of ferrocenophane monomers. The photoreactions are induced using wavelengths greater than 310 nm. This reaction proceeds only in the presence of light, which makes it convenient to add new monomers to make complex polymers [140]. Due to this remarkable control over the addition of monomers, polyferrocenophanes with low polydispersities and a high degree of control

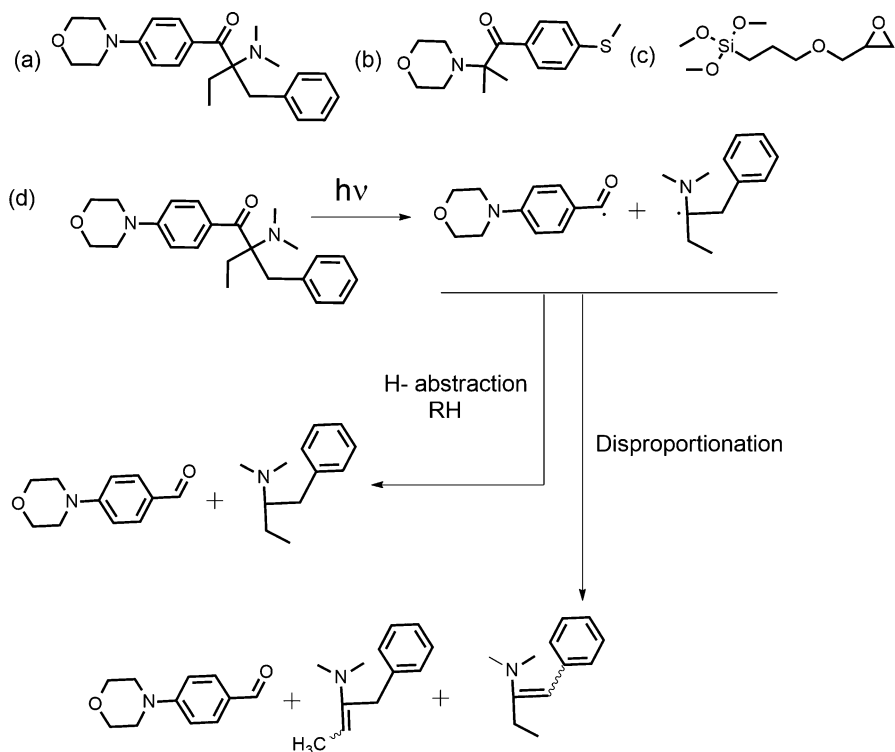


Fig. 30 Photoinitiation of photobase generator that could simultaneously initiate anionic and sol-gel polymerization

over the molecular weights can be obtained. The reaction can be terminated by the addition of a protic solvent which adds hydrogen to the growing negative end of the polymer. Photoinitiated ferrocenophanes have been applied to the synthesis of block copolymers, opening up the possibility of tailoring block copolymers properties suited for different applications [142, 144, 145]. Metal containing polymers and block copolymers synthesized from ferrocenophanes are highly promising functional materials for applications like high refractive index materials, charge transport materials, redox active gels, photoresists for electron beam, plasma etching as well as nanolithography, catalytic materials, etc. [146–156].

Photobases are photolabile compounds capable of releasing a powerful base on irradiation. They have a high reactivity with oxirane type monomers monomer [2, 104, 157]. A recent report featured the simultaneous photoinitiation of anionic and sol-gel polymerization of 3-(glycidyloxypropyl)trimethoxysilane (GPTMS) by an aminoketone based photobase generator [158]. The α -amino acetophenone-based photoinitiators are shown in Fig. 30a–b. They are both well-known type I radical photoinitiators. Upon photoexcitation, the cleavage of the excited photoinitiator yields highly reactive α -amino alkyl and benzoyl radicals.

In the absence of monomers capable of yielding radicals, they undergo H-abstraction and disproportionation, leading to the formation of tertiary amines. The tertiary amino group could initiate both anionic polymerization and sol-gel reaction. The hybrid monomer GPTMS in Fig. 30c undergoes cationic polymerization at the epoxy functional group and sol-gel reaction at the alkoxy silane groups. The aromatic groups around the tertiary amine in the initiator make it stable towards base-sensitive compounds in the patterning media and hence ensure longer shelf stability. After photocleavage, there is a steric release at the amine leaving it highly reactive [11]. The polymerization was carried out in neat monomer with 4 wt% of the photoinitiator. The photoirradiation of the sample was followed by a thermal curing step which was used for the complete drying of the polymerized film. The control over structure and functionality provided by anionic polymerization makes it very desirable for the synthesis of functional materials. A wider application of known techniques and an exploration of new initiating systems and monomers are required to meet this potential.

5 Two-Photon Induced Polymerization

The discussions up to this point have dealt with photopolymerization reactions initiated by the absorption of single photons. Under the condition of a very high-intensity radiation, it is possible for molecules absorbing in UV or visible radiation to simultaneously absorb two lower energy near-IR photons to get excited. This phenomenon is called two-photon absorption. Two near-IR photons of the same or different wavelengths can be absorbed during two-photon absorption. As defined previously, two-photon absorption is a third-order nonlinear optical effect. The energy level to which the electron is excited during a two-photon absorption would be determined by the symmetry of the molecule. In non-centrosymmetric molecules, the lowest two-photon allowed energy level coincides with the lowest one-photon allowed energy level. In a centrosymmetric molecule, the first allowed two-photon energy level is lower than the first one-photon allowed energy level. Two-photon process is an intensity-dependent phenomenon that is confined to the focus of a tightly focused laser beam. Because of this strong confinement, two-photon absorption can be used to initiate spatially confined chemical reactions. Photopolymerization reactions initiated by two-photon absorption are called two-photon polymerization (TPP). Two-photon lithography (TPL) is a lithographic technique based on TPP.

Two-photon absorption has been used to initiate free-radical, cationic, and anionic polymerizations [159]. The efficiency of two-photon absorption by a molecule is described in terms of two-photon absorption cross-section (TPACS) expressed in the GM units ($1 \text{ GM} = 10^{-50} \text{ cm}^4 \text{ s/photon-molecule}$). Due to the low TPACS of common free radical and cationic photoinitiators, early efforts were focused on designing two-photon absorbing molecules with high TPACS. Efficient organic two-photon absorbing (TPA) molecules contain electron-accepting and electron-donating groups bridged by conjugated aromatic constructs of diverse

arrangements. Two-photon absorbers can be dipolar [160–163], quadrupolar [160–172], triagonal [173–177], multibranched [178, 179], dendritic [180–182], oligomeric [170, 183, 184], or polymeric molecules [185–188]. Some typical examples of two-photon sensitizers are shown in Fig. 31.

Two-photon sensitized radical polymerization can be initiated by either a single molecule or a combination of two or more molecules. Single molecules that initiate two-photon polymerization do so from a charge separated excited state. In a two-component initiating system, the excited two-photon absorbing (TPA) molecule interacts with another initiator through electron or energy transfer. Compounds like those shown in Fig. 31 can be combined with previously discussed radical initiators to give efficient initiating systems.

Two-photon absorbing unimolecular initiators for cationic polymerization are rarer than one-component radical initiators [189–191]. Examples of one-component photoinitiating systems used in cationic TPP are shown in Fig. 32. One-component cationic initiators have faced some design challenges due to conflicting electronic criteria for efficient two-photon absorption and photoacid generation [191]. More research is required to reach a molecular understanding of efficient two-photon sensitized photoacid generation from a single molecule. The evidence available so far indicates that PAGs constructed around quadrupolar molecular motifs show a high efficiency as compared to the dipolar ones. Most reports on two-photon initiated cationic polymerization involve two-component initiating system constituting a two-photon absorber and a cationic photoinitiator that interacts with the TPA molecules [192]. Given the availability of the TPA molecule, two-component PI systems can be easily formulated and used. For many applications where high-resolution microstructures are not required, common commercial UV initiators can be used in combination with commercially available PAGs. Two-photon sensitized polymerization is growing in popularity due to the availability of commercial lithographic systems operating with femto-second and picosecond lasers as light sources [193]. TPL has seen a wide adaption in the structuring of biologically relevant microstructures' changes to hardware and light sources are currently driving the maturity of this technique towards commercialization. The recent demonstration of ultra-fast fabrication techniques is a game changer and is poised to revolutionize the applications of TPL in the near future.

6 Scope and Outlook

The application of photopolymers and photopolymerization continues to develop and expand based on the demand of new materials. The demand for sub ten nanometer to few ten nanometer components in electronic circuits has driven the demand for extreme UV (EUV) lithographic systems and materials. The high energy of EUV radiation can cause ionization of materials and excited electrons from inner energy levels. This scenario presents new challenges to the material chemist [194–197]. A new class of photoresists based on nanoparticles is being studied for EUV patterning [198–203]. The emergence and the growth of 3D printing is also a

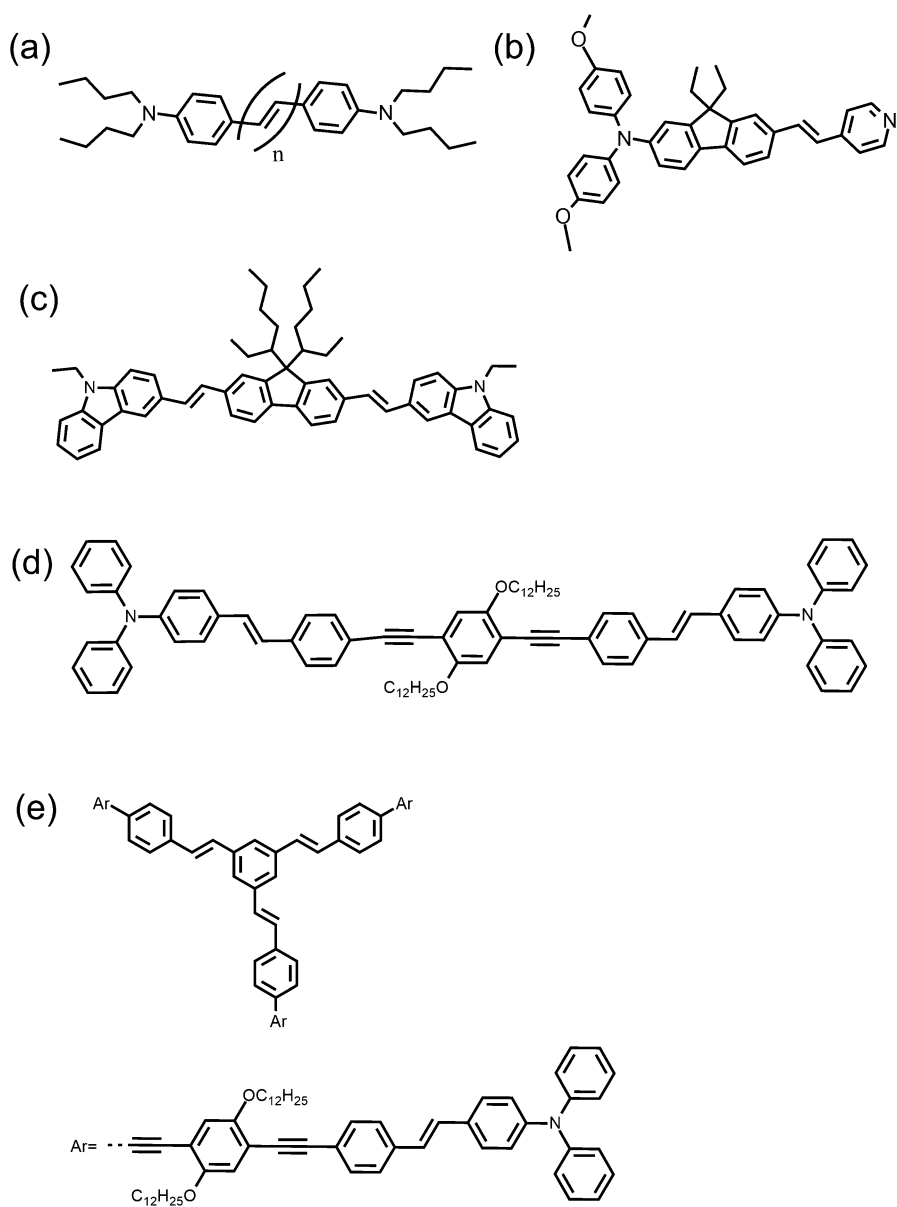
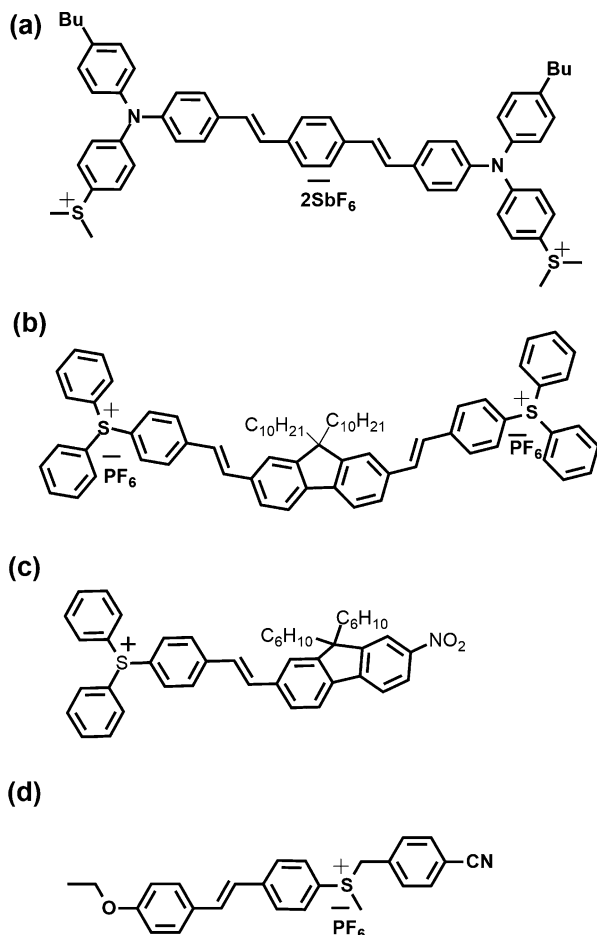


Fig. 31 Examples of two-photon sensitizers; (a) and (b) are examples of dipolar molecules, (c) and (d) are examples of quadrupolar molecules; and (e) is an example of a triangular molecule

Fig. 32 Examples of unimolecular TPA initiators for cationic TPP



major driver behind the growth of novel photopolymerization systems. Recently, De Semione et al. reported ultrafast 3D printing of monolithic 3D structures by engineering the oxygen inhibition of polymerization at the interface between the photopolymer and the cured structure [204]. The development of fast two-photon polymerization and holographic systems demand polymer precursors showing fast response to light and undergoing controlled polymerization [205, 206]. Material demand from medical and industrial applications has led to the development of new photopolymerizable materials [207–210]. The research into medical implants has spurred the growth of many new soft materials which are biocompatible or can be combined with biomaterials to give photo processable materials [211–215]. Human industrial activity and its effect on the environment has been a concern since the turn of the twenty-first century. This concern has contributed to need and awareness of sustainability in the sciences. Many research groups are starting to address the environment in their research for new photopolymers [216–224]. Photopolymers

will continue to play a major role in the future; research into nanomaterial based resists mentioned above may lead to new functional films and microstructures. Large-scale industrial application will continue to be driven by conditions of cost effectiveness. High value applications like microelectronics, biotechnology, health, and space provides a lot of space for growth and development.

References

1. J.V. Crivello, E. Reichmanis, Photopolymer materials and processes for advanced technologies. *Chem. Mater.* **26**, 533–548 (2013)
2. J.-P. Fouassier, J. Lalevée, *Photoinitiators for Polymer Synthesis: Scope, Reactivity, and Efficiency* (Wiley, Weinheim, 2012)
3. G.D. Stucky, S.R. Marder, J.E. Sohn, Linear and Nonlinear Polarizability, S.R. Marder, J.E. Sohn, G.D. Stucky (Eds), *Materials for nonlinear optics chemical perspectives, ACS-Symposium-Series, No. 455907*, 1–30 (Washington, DC, 1991)
4. R.W. Boyd, *Nonlinear Optics* (Academic, San Diego, 2003)
5. J. Jortner, R.S. Berry, Radiationless transitions and molecular quantum beats. *J. Chem. Phys.* **48**, 2757–2766 (1968)
6. B. König, *Organic Photochemistry*. University of Regensburg webpage (<http://www.uni-regensburg.de/>), Germany, 6/12 (2016)
7. A.D. McNaught, A. Wilkinson, *IUPAC. Compendium of Chemical Terminology, (The “Gold Book”)*, 2nd edn. (Blackwell Scientific, Oxford, 1997)
8. N.J. Turro, *Modern Molecular Photochemistry* (University Science Books, Sausalito, 1991)
9. J.P. Fouassier, D. Burr, Triplet state reactivity of α -sulfonyloxy ketones used as polymerization photoinitiators. *Macromolecules* **23**, 3615–3619 (1990)
10. J. Fouassier, D. Lounnot, J. Scaiano, A laser spectroscopy investigation of excited-state processes in α -sulphonyl ketones. *Chem. Phys. Lett.* **160**, 335–341 (1989)
11. K. Dietliker, R. Hüsler, J.-L. Birbaum, S. Ilg, S. Villeneuve, K. Studer, T. Jung, J. Benkhoff, H. Kura, A. Matsumoto, Advancements in photoinitiators – Opening up new applications for radiation curing. *Prog. Org. Coat.* **58**, 146–157 (2007)
12. J. Lalevee, M. El-Roz, F. Morlet-Savary, B. Graff, X. Allonas, J.-P. Fouassier, New highly efficient radical photoinitiators based on si-si bond cleavage. *Macromolecules* **40**, 8527–8530 (2007)
13. C. Chatgililoglu, *Organosilanes in Radical Chemistry* (Wiley, Chichester, 2004)
14. E. Rizzardo, D.H. Solomon, A new method for investigating the mechanism of initiation of radical polymerization. *Polym. Bull.* **1**, 529–534 (1979)
15. D.H. Solomon, G. Moad, Initiation. The reactions of primary radicals. *Macromol. Symp.* **10**, 109–125 (1987)
16. C.S. Colley, D.C. Grills, N.A. Besley, S. Jockusch, P. Matousek, A.W. Parker, M. Towrie, N.J. Turro, P.M. Gill, M.W. George, Probing the reactivity of photoinitiators for free radical polymerization: Time-resolved infrared spectroscopic study of benzoyl radicals. *J. Am. Chem. Soc.* **124**, 14952–14958 (2002)
17. A. Fedorov, E. Danilov, A. Merzlikine, M. Rodgers, D. Neckers, Application of time-resolved step-scan Fourier transform infrared spectroscopy to photochemical mechanistic investigations of alkyl phenylglyoxylates. *J. Phys. Chem. A* **107**, 3208–3214 (2003)
18. W.K. Robbins, R. Eastman, Photodecarbonylation in solution. II. Trapping of intermediates in the photolysis of dibenzyl ketone. *J. Am. Chem. Soc.* **92**, 6077–6079 (1970)
19. M. Kamachi, ESR studies on radical polymerization, in *Polymer Physics*, vol. 82, (Springer, Berlin/Heidelberg, 1987), pp. 207–275
20. K.A. McLauchlan, D. Stevens, Flash photolysis electron spin resonance. *Acc. Chem. Res.* **21**, 54–59 (1988)

21. I. Gatlik, P. Rzadek, G. Gescheidt, G. Rist, B. Hellrung, J. Wirz, K. Dietliker, G. Hug, M. Kunz, J.-P. Wolf, Structure-reactivity relationships in radical reactions: A novel method for the simultaneous determination of absolute rate constants and structural features. *J. Am. Chem. Soc.* **121**, 8332–8336 (1999)
22. P. Hore, C. Joslin, K. McLauchlan, The role of chemically-induced dynamic electron polarization (CIDEP) in chemistry. *Chem. Soc. Rev.* **8**, 29–61 (1979)
23. J.S. Baskin, L. Banares, S. Pedersen, A. Zewail, Femtosecond real-time probing of reactions. 20. Dynamics of twisting, alignment, and IVR in the trans-stilbene isomerization reaction. *J. Phys. Chem.* **100**, 11920–11933 (1996)
24. A.B. Oelkers, L.F. Scatena, D.R. Tyler, Femtosecond pump-probe transient absorption study of the photolysis of $[\text{Cp}^*\text{Mo}(\text{CO})_3]_2$ ($\text{Cp}^* = \eta^5\text{-C}_5\text{H}_4\text{CH}_3$): Role of translational and rotational diffusion in the radical cage effect. *J. Phys. Chem. A* **111**, 5353–5360 (2007)
25. A. Morandeira, A. Fürstenberg, E. Vauthey, Fluorescence quenching in electron-donating solvents. 2. Solvent dependence and product dynamics. *J. Phys. Chem. A* **108**, 8190–8200 (2004)
26. F. Morlet-Savary, C. Ley, P. Jacques, J. Fouassier, Photophysics of a bridged 7-diethylamino-4-methyl-coumarin C102: Studying the hydrogen bonding effect by time resolved stimulated emission. *J. Phys. Chem. A* **105**, 11026–11033 (2001)
27. D.W. McCamant, P. Kukura, R.A. Mathies, Femtosecond stimulated Raman study of excited-state evolution in bacteriorhodopsin. *J. Phys. Chem. B* **109**, 10449–10457 (2005)
28. H. Mohapatra, S. Umaphathy, Influence of solvent on photoinduced electron-transfer reaction: Time-resolved resonance Raman study. *J. Phys. Chem. A* **113**, 6904–6909 (2009)
29. S.E. Braslavsky, G.E. Heibel, Time-resolved photothermal and photoacoustic methods applied to photoinduced processes in solution. *Chem. Rev.* **92**, 1381–1410 (1992)
30. M. Buback, A. M. van Herk (eds.), *Radical Polymerization: Kinetics and Mechanism* (Wiley, Weinheim, 2007)
31. W. Schnabel, J. Fouassier, J. Rabek, *Lasers in Polymer Science and Technology: Applications* (CRC Press, Boca Raton, 1990)
32. J.-P. Fouassier, *Photoinitiation, Photopolymerization, and Photocuring: Fundamentals and Applications* (Hanser, Munich, 1995)
33. X. Allonas, J. Lalevee, J. Fouassier, in *Photoinitiated Polymerization*, ACS Symposium Series, ed. by K.D. Belfield, J.V. Crivello, vol 847 (American Chemical Society, Washington, DC, 2003), p. 140
34. G. Odian, *Principles of Polymerization* (Wiley, Hoboken, 2004)
35. N.S. Allen, *Photochemistry and Photophysics of Polymeric Materials* (Wiley, Weinheim, 2010)
36. P. Xiao, J. Zhang, F. Dumur, M.A. Tehfe, F. Morlet-Savary, B. Graff, D. Gigmes, J.P. Fouassier, J. Lalevée, Visible light sensitive photoinitiating systems: Recent progress in cationic and radical photopolymerization reactions under soft conditions. *Prog. Polym. Sci.* **41**, 32–66 (2015)
37. J. Lalevée, M.-A. Tehfe, F. Dumur, D. Gigmes, B. Graff, F. Morlet-Savary, J.-P. Fouassier, Light-harvesting organic photoinitiators of polymerization. *Macromol. Rapid Commun.* **34**, 239–245 (2013)
38. M.-A. Tehfe, J. Lalevée, S. Telitel, E. Contal, F. Dumur, D. Gigmes, D. Bertin, M. Nechab, B. Graff, F. Morlet-Savary, J.-P. Fouassier, Polyaromatic structures as organo-photoinitiator catalysts for efficient visible light induced dual radical/cationic photopolymerization and interpenetrated polymer networks synthesis. *Macromolecules* **45**, 4454–4460 (2012)
39. B. Ganster, U.K. Fischer, N. Moszner, R. Liska, New photocleavable structures. Diacylgermane-based photoinitiators for visible light curing. *Macromolecules* **41**, 2394–2400 (2008)
40. N. Moszner, U.K. Fischer, B. Ganster, R. Liska, V. Rheinberger, Benzoyl germanium derivatives as novel visible light photoinitiators for dental materials. *Dent. Mater.* **24**, 901–907 (2008)

41. M.-A. Tehfe, N. Blanchard, C. Fries, J. Lalevée, X. Allonas, J.P. Fouassier, Bis(germyl) ketones: Toward a new class of type I photoinitiating systems sensitive above 500 nm? *Macromol. Rapid Commun.* **31**, 473–478 (2010)
42. J. Lalevée, X. Allonas, J.P. Fouassier, Acylgermanes: Excited state processes and reactivity. *Chem. Phys. Lett.* **469**, 298–303 (2009)
43. J. Lalevée, N. Blanchard, M.-A. Tehfe, M. Peter, F. Morlet-Savary, J.P. Fouassier, A novel photopolymerization initiating system based on an iridium complex photocatalyst. *Macromol. Rapid Commun.* **32**, 917–920 (2011)
44. J. Lalevée, M. Peter, F. Dumur, D. Gimes, N. Blanchard, M.-A. Tehfe, F. Morlet-Savary, J.P. Fouassier, Subtle ligand effects in oxidative photocatalysis with iridium complexes: Application to photopolymerization. *Chem. Eur. J.* **17**, 15027–15031 (2011)
45. A.F. Jacobine, Thiol-ene photopolymers, in *Radiation Curing in Polymer Science and Technology*, vol. 3, (Kluwer Academic Publishers Group, Netherlands, 1993), pp. 219–268
46. C.E. Hoyle, T.Y. Lee, T. Roper, Thiol-enes: Chemistry of the past with promise for the future. *J. Polym. Sci. Part A: Polym. Chem.* **42**, 5301–5338 (2004)
47. C.E. Hoyle, C.N. Bowman, Thiol-ene click chemistry. *Angew. Chem. Int. Ed.* **49**, 1540–1573 (2010)
48. A. Dondoni, The emergence of thiol-ene coupling as a click process for materials and bioorganic chemistry. *Angew. Chem. Int. Ed.* **47**, 8995–8997 (2008)
49. A.B. Lowe, Thiol-ene “click” reactions and recent applications in polymer and materials synthesis. *Polym. Chem.* **1**, 17–36 (2010)
50. T.Y. Lee, C.A. Guymon, E.S. Jönsson, C.E. Hoyle, The effect of monomer structure on oxygen inhibition of (meth)acrylates photopolymerization. *Polymer* **45**, 6155–6162 (2004)
51. V.S. Khire, Y. Yi, N.A. Clark, C.N. Bowman, Formation and surface modification of nano-patterned thiol-ene substrates using step and flash imprint lithography. *Adv. Mater.* **20**, 3308–3313 (2008)
52. S.K. Reddy, R.P. Sebra, K.S. Anseth, C.N. Bowman, Living radical photopolymerization induced grafting on thiol-ene based substrates. *J. Polym. Sci. Part A: Polym. Chem.* **43**, 2134–2144 (2005)
53. M. Liu, J. van Hensbergen, R.P. Burford, A.B. Lowe, Thiol-Michael coupling chemistry: Facile access to a library of functional exo-7-oxanorbornenes and their ring-opening metathesis (co)polymerization. *Polym. Chem.* **3**, 1647–1658 (2012)
54. M. Liu, B.H. Tan, R.P. Burford, A.B. Lowe, Nucleophilic thiol-Michael chemistry and hyperbranched (co)polymers: Synthesis and ring-opening metathesis (co)polymerization of novel difunctional exo-7-oxanorbornenes with in situ inimer formation. *Polym. Chem.* **4**, 3300–3311 (2013)
55. S. Ohsawa, K. Morino, A. Sudo, T. Endo, Synthesis of bicyclic bis (γ -butyrolactone) derivatives bearing sulfide moieties and their alternating copolymers with epoxide. *J. Polym. Sci. Part A: Polym. Chem.* **50**, 4666–4673 (2012)
56. M. Firdaus, L. Montero de Espinosa, M.A. Meier, Terpene-based renewable monomers and polymers via thiol-ene additions. *Macromolecules* **44**, 7253–7262 (2011)
57. Y. Li, W.-B. Zhang, J.E. Janoski, X. Li, X. Dong, C. Wesdemiotis, R.P. Quirk, S.Z. Cheng, Anionic synthesis of mono- and heterotelechelic polystyrenes via thiol-ene “click” chemistry and hydrosilylation. *Macromolecules* **44**, 3328–3337 (2011)
58. A.J. Magenau, J.W. Chan, C.E. Hoyle, R.F. Storey, Facile polyisobutylene functionalization via thiol-ene click chemistry. *Polym. Chem.* **1**, 831–833 (2010)
59. J.A. Syrett, M.W. Jones, D.M. Haddleton, A facile route to end-functionalised polymers synthesised by SET-LRP via a one-pot reduction/thiol-ene Michael-type addition. *Chem. Commun.* **46**, 7181–7183 (2010)
60. M. Hong, S.R. Liu, B.X. Li, Y.S. Li, Application of thiol-ene click chemistry to preparation of functional polyethylene with high molecular weight and high polar group content: Influence of thiol structure and vinyl type on reactivity. *J. Polym. Sci. Part A: Polym. Chem.* **50**, 2499–2506 (2012)

61. J. Mazzolini, O. Boyron, V. Monteil, F. D'Agosto, C. Boisson, G.C. Sanders, J.P. Heuts, R. Duchateau, D. Gigmes, D. Bertin, Polyethylene end functionalization using thia-Michael addition chemistry. *Polym. Chem.* **3**, 2383–2392 (2012)
62. H. Durmaz, M. Butun, G. Hizal, U. Tunca, Postfunctionalization of polyoxanorbornene via sequential Michael addition and radical thiol-ene click reactions. *J. Polym. Sci. Part A: Polym. Chem.* **50**, 3116–3125 (2012)
63. H. Mutlu, A.N. Parvulescu, P.C. Bruijninx, B.M. Weckhuysen, M.A. Meier, On the polymerization behavior of telomers: Metathesis versus thiol-ene chemistry. *Macromolecules* **45**, 1866–1878 (2012)
64. J.S. Silverstein, B.J. Casey, M.E. Natoli, B.J. Dair, P. Kofinas, Rapid modular synthesis and processing of thiol-ene functionalized styrene–butadiene block copolymers. *Macromolecules* **45**, 3161–3167 (2012)
65. O. Kreye, T. Tóth, M.A. Meier, Copolymers derived from rapeseed derivatives via ADMET and thiol-ene addition. *Eur. Polym. J.* **47**, 1804–1816 (2011)
66. N.K. Singha, M.I. Gibson, B.P. Koiry, M. Danial, H.-A. Klok, Side-chain peptide-synthetic polymer conjugates via tandem “ester-amide/thiol-ene” post-polymerization modification of poly (pentafluorophenyl methacrylate) obtained using ATRP. *Biomacromolecules* **12**, 2908–2913 (2011)
67. J. Kienberger, N. Noormofidi, I. Mühlbacher, I. Klarholz, C. Harms, C. Slugovc, Antimicrobial equipment of poly (isoprene) applying thiol-ene chemistry. *J. Polym. Sci. Part A: Polym. Chem.* **50**, 2236–2243 (2012)
68. L. Yin, M.C. Dalsin, A. Sizovs, T.M. Reineke, M.A. Hillmyer, Glucose-functionalized, serum-stable polymeric micelles from the combination of anionic and RAFT polymerizations. *Macromolecules* **45**, 4322–4332 (2012)
69. O. Türünc, M.A. Meier, Thiol-ene vs. ADMET: A complementary approach to fatty acid-based biodegradable polymers. *Green Chem.* **13**, 314–320 (2011)
70. J. Mergy, A. Fournier, E. Hachet, R. Auzély-Velty, Modification of polysaccharides via thiol-ene chemistry: A versatile route to functional biomaterials. *J. Polym. Sci. Part A: Polym. Chem.* **50**, 4019–4028 (2012)
71. C.E. Hoyle, A.B. Lowe, C.N. Bowman, Thiol-click chemistry: A multifaceted toolbox for small molecule and polymer synthesis. *Chem. Soc. Rev.* **39**, 1355–1387 (2010)
72. A.F. Senyurt, C.E. Hoyle, Three component ketocoumarin, amine, maleimide photoinitiator II. *Eur. Polym. J.* **42**, 3133–3139 (2006)
73. T.M. Roper, C.A. Guymon, E.S. Jönsson, C.E. Hoyle, Influence of the alkene structure on the mechanism and kinetics of thiol-alkene photopolymerizations with real-time infrared spectroscopy. *J. Polym. Sci. Part A: Polym. Chem.* **42**, 6283–6298 (2004)
74. T.M. Roper, T.Y. Lee, C.A. Guymon, C.E. Hoyle, In situ characterization of photopolymerizable systems using a thin-film calorimeter. *Macromolecules* **38**, 10109–10116 (2005)
75. S.K. Reddy, N.B. Cramer, C.N. Bowman, Thiol-vinyl mechanisms. 2. Kinetic modeling of ternary thiol-vinyl photopolymerizations. *Macromolecules* **39**, 3681–3687 (2006)
76. O. Okay, C.N. Bowman, Kinetic modeling of thiol-ene reactions with both step and chain growth aspects. *Macromol. Theory Simul.* **14**, 267–277 (2005)
77. H. Lu, J.A. Carioscia, J.W. Stansbury, C.N. Bowman, Investigations of step-growth thiol-ene polymerizations for novel dental restoratives. *Dent. Mater.* **21**, 1129–1136 (2005)
78. T.Y. Lee, T.M. Roper, C.A. Guymon, E.S. Jonsson, C.E. Hoyle, *Film Formation*, vol 941 (American Chemical Society, Washington, DC, 2006), pp. 17–28, Chap. 2
79. T.Y. Lee, J. Carioscia, Z. Smith, C.N. Bowman, Thiol-allyl ether-methacrylate ternary systems. Evolution mechanism of polymerization-induced shrinkage stress and mechanical properties. *Macromolecules* **40**, 1473–1479 (2007)
80. T.Y. Lee, Z. Smith, S.K. Reddy, N.B. Cramer, C.N. Bowman, Thiol-allyl ether-methacrylate ternary systems. Polymerization mechanism. *Macromolecules* **40**, 1466–1472 (2007)
81. S.K. Reddy, N.B. Cramer, M. Kalvaitas, T.Y. Lee, C.N. Bowman, Mechanistic modelling and network properties of thiol-vinyl photopolymerizations. *Aust. J. Chem.* **59**, 586–593 (2006)

82. J.V. Crivello, The discovery and development of onium salt cationic photoinitiators. *J. Polym. Sci. A Polym.* **37**, 4241–4254 (1999)
83. J.V. Crivello, J. Lam, Diaryliodonium salts. A new class of photoinitiators for cationic polymerization. *Macromolecules* **10**, 1307–1315 (1977)
84. J.V. Crivello, J. Lam, Photoinitiated cationic polymerization with triarylsulfonium salts. *J. Polym. Sci. Part A: Polym. Chem.* **17**, 977–999 (1979)
85. J. Crivello, *Initiators, Poly-reactions, Optical Activity* (Springer, Heidelberg, 1984), pp. 1–48
86. M.U. Kahveci, A.G. Yilmaz, Y. Yagci, Photoinitiated cationic polymerization reactivity and mechanistic aspects, in *Photochemistry and Photophysics of Polymer Materials*, ed. by N. S. Allen (Wiley, Hoboken, 2010), pp. 421–478
87. M. Sangermano, N. Razza, J.V. Crivello, Cationic UV-curing: Technology and applications. *Macromol. Mater. Eng.* **299**, 775–793 (2014)
88. J.V. Crivello, Diaryliodonium salt photoacid generators, in *Iodine Chemistry and Applications*, ed. by T. Kaiho (Wiley, Weinheim, 2014), p. 459
89. J. Lalevée, A. Dirani, M. El-Roz, X. Allonas, J.P. Fouassier, Germanes as efficient coinitiators in radical and cationic photopolymerizations. *J. Polym. Sci. Part A: Polym. Chem.* **46**, 3042–3047 (2008)
90. J. Lalevée, N. Blanchard, M. El-Roz, B. Graff, X. Allonas, J.P. Fouassier, New photoinitiators based on the silyl radical chemistry: Polymerization ability, ESR spin trapping, and laser flash photolysis investigation. *Macromolecules* **41**, 4180–4186 (2008)
91. N. Moszner, F. Zeuner, I. Lamparth, U.K. Fischer, Benzoylgermanium derivatives as novel visible-light photoinitiators for dental composites. *Macromol. Mater. Eng.* **294**, 877–886 (2009)
92. Y.Y. Durmaz, M. Kukut, N. Moszner, Y. Yagci, Sequential photodecomposition of bisacylgermane type photoinitiator: Synthesis of block copolymers by combination of free radical promoted cationic and free radical polymerization mechanisms. *J. Polym. Sci. Part A: Polym. Chem.* **47**, 4793–4799 (2009)
93. Y.Y. Durmaz, N. Moszner, Y. Yagci, Visible light initiated free radical promoted cationic polymerization using acylgermane based photoinitiator in the presence of onium salts. *Macromolecules* **41**, 6714–6718 (2008)
94. J.V. Crivello, M.F. Aldersley, Supramolecular diaryliodonium salt-crown ether complexes as cationic photoinitiators. *J. Polym. Sci. Part A: Polym. Chem.* **51**, 801–814 (2013)
95. M.U. Kahveci, M.A. Tasdelen, Y. Yagci, Photochemically initiated free radical promoted living cationic polymerization of isobutyl vinyl ether. *Polymer* **48**, 2199–2202 (2007)
96. Y. Yagci, S. Jockusch, N.J. Turro, Photoinitiated polymerization: Advances, challenges, and opportunities. *Macromolecules* **43**, 6245–6260 (2010)
97. M.U. Kahveci, M. Uygun, M.A. Tasdelen, W. Schnabel, W.D. Cook, Y. Yagci, Photoinitiated cationic polymerization of vinyl ethers using substituted vinyl halides. *Macromolecules* **42**, 4443–4448 (2009)
98. J. Lalevée, N. Blanchard, M.-A. Tehfe, F. Morlet-Savary, J.P. Fouassier, Green bulb light source induced epoxy cationic polymerization under air using tris(2,2'-bipyridine)ruthenium (II) and silyl radicals. *Macromolecules* **43**, 10191–10195 (2010)
99. J. Lalevée, N. Blanchard, M.-A. Tehfe, M. Peter, F. Morlet-Savary, D. Gigmes, J.P. Fouassier, Efficient dual radical/cationic photoinitiator under visible light: A new concept. *Polym. Chem.* **2**, 1986–1991 (2011)
100. J. Lalevée, M.-A. Tehfe, F. Dumur, D. Gigmes, N. Blanchard, F. Morlet-Savary, J.P. Fouassier, Iridium photocatalysts in free radical photopolymerization under visible lights. *ACS Macro Lett.* **1**, 286–290 (2012)
101. M.-A. Tehfe, D. Gigmes, F. Dumur, D. Bertin, F. Morlet-Savary, B. Graff, J. Lalevée, J.-P. Fouassier, Cationic photosensitive formulations based on silyl radical chemistry for green and red diode laser exposure. *Polym. Chem.* **3**, 1899–1902 (2012)
102. J. Lalevée, F. Dumur, C.R. Mayer, D. Gigmes, G. Nasr, M.-A. Tehfe, S. Telitel, F. Morlet-Savary, B. Graff, J.P. Fouassier, Photopolymerization of *N*-vinylcarbazole using visible-light harvesting iridium complexes as photoinitiators. *Macromolecules* **45**, 4134–4141 (2012)

103. M.-A. Tehfe, J. Lalevée, S. Telitel, J. Sun, J. Zhao, B. Graff, F. Morlet-Savary, J.-P. Fouassier, Iridium complexes incorporating coumarin moiety as catalyst photoinitiators: Towards household green LED bulb and halogen lamp irradiation. *Polymer* **53**, 2803–2808 (2012)
104. M. Shirai, M. Tsunooka, Photoacid and photobase generators: Chemistry and applications to polymeric materials. *Prog. Polym. Sci.* **21**, 1–45 (1996)
105. H. Yamato, T. Asakura, T. Hintermann, M. Ohwa, *Novel Nonionic Photoacid Generator Releasing Strong Acid for Chemically Amplified Resists*, Proc. SPIE 5376 (SPIE, Bellingham, 2004), pp. 103–114
106. M.K. Gupta, R.P. Singh, Diphenyldiselenide as novel non-salt photoinitiator for photosensitized cationic polymerization of *N*-vinyl carbazole. *Macromol. Symp.* **240**, 186–193 (2006)
107. M. Shirai, H. Okamura, i-Line sensitive photoacid generators for UV curing. *Prog. Org. Coat.* **64**, 175–181 (2009)
108. J.-P. Malval, S. Suzuki, F. Morlet-Savary, X. Allonas, J.-P. Fouassier, S. Takahara, T. Yamaoka, Photochemistry of naphthalimide photoacid generators. *J. Phys. Chem. A* **112**, 3879–3885 (2008)
109. J.-P. Pascault, R. J. Williams (eds.), *Epoxy Polymers* (Wiley, Weinheim, 2009)
110. Y. Yagci, Photoinitiated cationic polymerization of unconventional monomers. *Macromol. Symp.* **240**, 93–101 (2006)
111. J.-P. Fouassier, X. Allonas, *Basics and Applications of Photopolymerization Reactions* (Research Signpost, Trivandrum, 2010)
112. J.V. Crivello, R. Acosta Ortiz, Benzyl alcohols as accelerators in the photoinitiated cationic polymerization of epoxide monomers. *J. Polym. Sci. Part A: Polym. Chem.* **40**, 2298–2309 (2002)
113. S. Penczek, Cationic ring-opening polymerization (CROP) major mechanistic phenomena. *J. Polym. Sci. Part A: Polym. Chem.* **38**, 1919–1933 (2000)
114. P. Kubisa, Hyperbranched polyethers by ring-opening polymerization: Contribution of activated monomer mechanism. *J. Polym. Sci. Part A: Polym. Chem.* **41**, 457–468 (2003)
115. J.V. Crivello, J. Ma, F. Jiang, H. Hua, J. Ahn, R. Acosta Ortiz, Advances in the design of photoinitiators, photo-sensitizers and monomers for photoinitiated cationic polymerization. *Macromol. Symp.* **215**, 165–178 (2004)
116. Y. Hua, J.V. Crivello, Development of polymeric photosensitizers for photoinitiated cationic polymerization. *Macromolecules* **34**, 2488–2494 (2001)
117. J.V. Crivello, J.L. Lee, D.A. Conlon, Developments in the design and applications of novel thermal and photochemical initiators for cationic polymerization. *Macromol. Symp.* **13–14**, 145–160 (1988)
118. R.W. Lenz, in *Polymer Syntheses*, vol 1, ed. by S.R. Sandler, Wolf Karo, Monographs on Organic Chemistry, vol 29-1 (Academic, New York, 1974)
119. K.S. Anseth, L.M. Kline, T.A. Walker, K.J. Anderson, C.N. Bowman, Reaction kinetics and volume relaxation during polymerizations of multiethylene glycol dimethacrylates. *Macromolecules* **28**, 2491–2499 (1995)
120. C.M. Chung, J.G. Kim, M.S. Kim, K.M. Kim, K.N. Kim, Development of a new photocurable composite resin with reduced curing shrinkage. *Dent. Mater.* **18**, 174–178 (2002)
121. M. Atai, D.C. Watts, A new kinetic model for the photopolymerization shrinkage-strain of dental composites and resin-monomers. *Dent. Mater.* **22**, 785–791 (2006)
122. A. del Campo, E. Arzt (eds.), *Generating Micro-and Nanopatterns on Polymeric Materials* (Wiley, Weinheim, 2011)
123. D. Nagai, M. Nishida, T. Nagasawa, B. Ochiai, K. Miyazaki, T. Endo, Non-shrinking networked materials from the cross-linking copolymerization of spiroorthocarbonate with bifunctional oxetane. *Macromol. Rapid Commun.* **27**, 921–925 (2006)
124. S. Putzien, E. Louis, O. Nuyken, J.V. Crivello, F.E. Kühn, UV curing of epoxy functional hybrid silicones. *J. Appl. Polym. Sci.* **126**, 1188–1197 (2012)
125. Y. Fukuchi, T. Takahashi, H. Noguchi, M. Saburi, Y. Uchida, Photoinitiated anionic coordination polymerization of epoxides, a novel polymerization process. *Macromolecules* **20**, 2316–2317 (1987)

126. D.B. Yang, C. Kotal, Radiation curing, in *Inorganic and Organometallic Photoinitiators*, ed. by S. P. Pappas (Springer, Heidelberg, 1992), pp. 21–55
127. C. Kotal, P.A. Grutsch, D.B. Yang, A novel strategy for photoinitiated anionic polymerization. *Macromolecules* **24**, 6872–6873 (1991)
128. Y. Yamaguchi, B.J. Palmer, C. Kotal, T. Wakamatsu, D.B. Yang, Ferrocenes as anionic photoinitiators. *Macromolecules* **31**, 5155–5157 (1998)
129. V.V. Jarikov, D.C. Neckers, Anionic photopolymerization of methyl 2-cyanoacrylate and simultaneous color formation. *Macromolecules* **33**, 7761–7764 (2000)
130. R.B. Paul, J.M. Kelly, D.C. Pepper, C. Long, Photoinduced anionic polymerization of cyanoacrylates using substituted pyridine pentacarbonyl complexes of tungsten or chromium. *Polymer* **38**, 2011–2014 (1997)
131. Y. Yamaguchi, C. Kotal, Benzoyl-substituted ferrocenes: An attractive new class of anionic photoinitiators. *Macromolecules* **33**, 1152–1156 (2000)
132. Y. Watanabe, T. Aida, S. Inoue, First example of photoinduced copolymerizability enhancement: copolymerization of epoxide and episulfide initiated with zinc *N*-substituted porphyrin under visible light irradiation. *Macromolecules* **24**, 3970–3972 (1991)
133. W. Schnabel, *Polymers and Light* (Wiley-VCH, Weinheim, 2007), pp. 273–304
134. C.T. Sanderson, B.J. Palmer, A. Morgan, M. Murphy, R.A. Dluhy, T. Mize, I.J. Amster, C. Kotal, Classical metallocenes as photoinitiators for the anionic polymerization of an alkyl 2-cyanoacrylate. *Macromolecules* **35**, 9648–9652 (2002)
135. B.J. Palmer, C. Kotal, R. Billing, H. Hennig, A new photoinitiator for anionic polymerization. *Macromolecules* **28**, 1328–1329 (1995)
136. R.J. Lavalley, B.J. Palmer, R. Billing, H. Hennig, G. Ferraudi, C. Kotal, Efficient substitutional photochemistry of a third-row transition metal β -diketonate complex. *Inorg. Chem.* **36**, 5552–5558 (1997)
137. Y.-H. Wang, P. Wan, Ketoprofen as a photoinitiator for anionic polymerization. *Photochem. Photobiol.* **14**, 1120–1126 (2015)
138. M. Tanabe, I. Manners, Photolytic living anionic ring-opening polymerization (ROP) of silicon-bridged [1] ferrocenophanes via an iron-cyclopentadienyl bond cleavage mechanism. *J. Am. Chem. Soc.* **126**, 11434–11435 (2004)
139. W.Y. Chan, A.J. Lough, I. Manners, Synthesis, characterization, and photocontrolled ring-opening polymerization of sila[1]ferrocenophanes with multiple alkyne substituents. *Organometallics* **26**, 1217–1225 (2007)
140. R.L.N. Hailes, A.M. Oliver, J. Gwyther, G.R. Whittell, I. Manners, Polyferrocenylsilanes: Synthesis, properties, and applications. *Chem. Soc. Rev.* **45**, 5358–5407 (2016)
141. M. Tanabe, G.W.M. Vandermeulen, W.Y. Chan, P.W. Cyr, L. Vanderark, D.A. Rider, I. Manners, Photocontrolled living polymerizations. *Nat. Mater.* **5**, 467–470 (2006)
142. G.S. Smith, S.K. Patra, L. Vanderark, S. Saithong, J.P. Charment, I. Manners, Photocontrolled living anionic polymerization of silicon-bridged [1] ferrocenophanes with fluorinated substituents: Synthesis and characterization of fluorinated polyferrocenylsilane (PFS) homopolymers and block copolymers. *Macromol. Chem. Phys.* **211**, 303–312 (2010)
143. Z. Wang, G. Masson, F.C. Peiris, G.A. Ozin, I. Manners, Living photolytic ring-opening polymerization of amino-functionalized [1] ferrocenophanes: Synthesis and layer-by-layer self-assembly of well-defined water-soluble polyferrocenylsilane polyelectrolytes. *Chem. Eur. J.* **13**, 9372–9383 (2007)
144. X. Wang, M.A. Winnik, I. Manners, Synthesis, self-assembly, and applications of polyferrocenylsilane block copolymers, in *ACS Symposium Series*, vol 928 (American Chemical Society, Washington, DC, 2006), pp. 274–291
145. F. Wurm, S. Hilf, H. Frey, Electroactive linear–hyperbranched block copolymers based on linear poly(ferrocenylsilane)s and hyperbranched poly(carbosilane)s. *Chem. Eur. J.* **15**, 9068–9077 (2009)
146. I. Hamley, Nanostructure fabrication using block copolymers. *Nanotechnology* **14**, R39 (2003)

147. M.P. Stoykovich, P.F. Nealey, Block copolymers and conventional lithography. *Mater. Today* **9**, 20–29 (2006)
148. J.Y. Cheng, C.A. Ross, H.I. Smith, E.L. Thomas, Templated self-assembly of block copolymers: Top-down helps bottom-up. *Adv. Mater.* **18**, 2505–2521 (2006)
149. J. Bang, U. Jeong, D.Y. Ryu, T.P. Russell, C.J. Hawker, Block copolymer nanolithography: Translation of molecular level control to nanoscale patterns. *Adv. Mater.* **21**, 4769–4792 (2009)
150. C. Hinderling, Y. Keles, T. Stöckli, H.F. Knapp, T. De los Arcos, P. Oelhafen, I. Korczagin, M.A. Hempenius, G.J. Vancso, R. Pugin, Organometallic block copolymers as catalyst precursors for templated carbon nanotube growth. *Adv. Mater.* **16**, 876–879 (2004)
151. C. Acikgoz, B. Vratzov, M.A. Hempenius, G.J. Vancso, J. Huskens, Nanoscale patterning by UV nanoimprint lithography using an organometallic resist. *ACS Appl. Mater. Interfaces* **1**, 2645–2650 (2009)
152. C. Acikgoz, X.Y. Ling, I.Y. Phang, M.A. Hempenius, D.N. Reinhoudt, J. Huskens, G.J. Vancso, Fabrication of free-standing nanoporous polyethersulfone membranes using organometallic polymer resists patterned by nanosphere lithography. *Adv. Mater.* **21**, 2064–2067 (2009)
153. X.Y. Ling, C. Acikgoz, I.Y. Phang, M.A. Hempenius, D.N. Reinhoudt, G.J. Vancso, J. Huskens, 3D ordered nanostructures fabricated by nanosphere lithography using an organometallic etch mask. *Nanoscale* **2**, 1455–1460 (2010)
154. R.G. Lammertink, M.A. Hempenius, V.Z.-H. Chan, E.L. Thomas, G.J. Vancso, Poly (ferrocenyldimethylsilanes) for reactive ion etch barrier applications. *Chem. Mater.* **13**, 429–434 (2001)
155. K.Y. Suh, Y.S. Kim, H.H. Lee, Capillary force lithography. *Adv. Mater.* **13**, 1386–1389 (2001)
156. I. Korczagin, H. Xu, M.A. Hempenius, G.J. Vancso, Pattern transfer fidelity in capillary force lithography with poly (ferrocenylsilane) plasma etch resists. *Eur. Polym. J.* **44**, 2523–2528 (2008)
157. K. Suyama, M. Shirai, Photobase generators: Recent progress and application trend in polymer systems. *Prog. Polym. Sci.* **34**, 194–209 (2009)
158. A. Chemtob, F. Courtecuisse, C. Croutxe-Barghorn, S. Rigolet, Simultaneous sol-gel and anionic photopolymerization of 3-(glycidylxypropyl)trimethoxysilane via photobase catalysis. *New J. Chem.* **35**, 1803–1808 (2011)
159. K.-S. Lee, R.H. Kim, D.-Y. Yang, S.H. Park, Advances in 3D nano/microfabrication using two-photon initiated polymerization. *Prog. Polym. Sci.* **33**, 631–681 (2008)
160. P. Prabhakaran, T.D. Kim, K.S. Lee, in *Polymer Science: A Comprehensive Reference*, ed. by M. Möller (Elsevier, Amsterdam, 2012), pp. 211–260
161. M. Albota, D. Beljonne, J.-L. Brédas, J.E. Ehrlich, J.-Y. Fu, A.A. Heikal, S.E. Hess, T. Kogej, M.D. Levine, S.R. Marder, D. McCord-Maughon, Design of organic molecules with large two-photon absorption cross sections. *Science* **281**, 1653–1656 (1998)
162. H.-K. Yang, M.-S. Kim, S.-W. Kang, K.-S. Kim, K.-S. Lee, S.H. Park, D.-Y. Yang, H.J. Kong, H.-B. Sun, S. Kawata, Recent progress of lithographic microfabrication by the TPA-induced photopolymerization. *J. Photopolym. Sci. Technol.* **17**, 385–392 (2004)
163. O.-K. Kim, K.-S. Lee, H.Y. Woo, K.-S. Kim, G.S. He, J. Swiatkiewicz, P.N. Prasad, New class of two-photon-absorbing chromophores based on dithienothiophene. *Chem. Mater.* **12**, 284–286 (2000)
164. S.J. Pond, O. Tsutsumi, M. Rumi, O. Kwon, E. Zojer, J.-L. Brédas, S.R. Marder, J.W. Perry, Metal-ion sensing fluorophores with large two-photon absorption cross sections: aza-crown ether substituted donor-acceptor-donor distyrylbenzenes. *J. Am. Chem. Soc.* **126**, 9291–9306 (2004)
165. J.-G. Lim, P. Prabhakaran, J.S. Park, Y. Son, T.-D. Kim, D.-Y. Yang, K.-S. Lee, Synthesis and photophysical properties of two-photon absorbing spirofluorene derivatives. *J. Nanosci. Nanotechnol.* **12**, 4403–4408 (2012)
166. N. Cho, P.L. Baldeck, G.S. He, D.-H. Hwang, P.N. Prasad, P. Prabhakaran, T.-D. Kim, K.-S. Lee, Degenerate multi-photon properties of spirofluorene derivatives. *J. Nanosci. Nanotechnol.* **10**, 6958–6961 (2010)

167. N. Cho, G. Zhou, K. Kamada, R.H. Kim, K. Ohta, S.-H. Jin, K. Müllen, K.-S. Lee, The impact of charge defects and resonance enhancement on the two-photon absorption activity of spirofluorene and ladder-type pentaphenylene derivatives. *J. Mater. Chem.* **22**, 185–191 (2012)
168. M. Albota, D. Beljonne, J.L. Breas, J.E. Ehrlich, J.Y. Fu, A.A. Heikal, S.E. Hess, T. Kogej, M.D. Levin, S.R. Marder, Design of organic molecules with large two-photon absorption cross sections. *Science* **281**, 1653 (1998)
169. M. Barzoukas, M. Blanchard-Desce, Molecular engineering of push–pull dipolar and quadrupolar molecules for two-photon absorption: A multivalence-bond states approach. *J. Chem. Phys.* **113**, 3951–3959 (2000)
170. B.H. Cumpston, S.P. Ananthavel, S. Barlow, D.L. Dyer, J.E. Ehrlich, L.L. Erskine, A.A. Heikal, S.M. Kuebler, I.Y.S. Lee, D. McCord-Maughon, J. Qin, H. Rockel, M. Rumi, X.-L. Wu, S.R. Marder, J.W. Perry, Two-photon polymerization initiators for three-dimensional optical data storage and microfabrication. *Nature* **398**, 51–54 (1999)
171. O. Mongin, L. Porrès, L. Moreaux, J. Mertz, M. Blanchard-Desce, Synthesis and photophysical properties of new conjugated fluorophores designed for two-photon-excited fluorescence. *Org. Lett.* **4**, 719–722 (2002)
172. S.L. Oliveira, D.S. Correa, L. Misoguti, C.J.L. Constantino, R.F. Aroca, S.C. Zilio, C.R. Mendonca, Perylene derivatives with large two-photon-absorption cross-sections for application in optical limiting and upconversion lasing. *Adv. Mater.* **17**, 1890–1893 (2005)
173. D. Beljonne, W. Wenseleers, E. Zojer, Z. Shuai, H. Vogel, S.J.K. Pond, J.W. Perry, S.R. Marder, J.L. Bredas, Role of dimensionality on the two-photon absorption response of conjugated molecules: The case of octupolar compounds. *Adv. Funct. Mater.* **12**, 631–641 (2002)
174. A. Bhaskar, G. Ramakrishna, Z. Lu, R. Twieg, J.M. Hales, D.J. Hagan, E. Van Stryland, T. Goodson, Investigation of two-photon absorption properties in branched alkene and alkyne chromophores. *J. Am. Chem. Soc.* **128**, 11840–11849 (2006)
175. B.R. Cho, J.P. Ming, K.H. Son, S.H. Lee, S.J. Yoon, S.-J. Jeon, M. Cho, Nonlinear optical and two-photon absorption properties of 1,3,5-tricyano-2,4,6-tris(styryl)benzene-containing octupolar oligomers. *Chem. Eur. J.* **8**, 3907–3916 (2002)
176. S.J. Chung, K.S. Kim, T.C. Lin, G.S. He, J. Swiatkiewicz, P.N. Prasad, Cooperative enhancement of two-photon absorption in multi-branched structures. *J. Phys. Chem. B* **103**, 10741–10745 (1999)
177. G.S. He, T.C. Lin, J. Dai, P.N. Prasad, R. Kannan, A.G. Dombroskie, R.A. Vaia, L.S. Tan, Degenerate two-photon-absorption spectral studies of highly two-photon active organic chromophores. *J. Chem. Phys.* **120**, 5275 (2004)
178. S.J. Chung, T.C. Lin, K.S. Kim, G.S. He, J. Swiatkiewicz, P.N. Prasad, G.A. Baker, F.V. Bright, Two-photon absorption and excited-state energy-transfer properties of a new multibranched molecule. *Chem. Mater.* **13**, 4071–4076 (2001)
179. F. Meng, B. Li, S. Qian, K. Chen, H. Tian, Enhanced two-photon properties of tri-branched styryl derivatives based on 1,3,5-triazine. *Chem. Lett.* **33**, 470–471 (2004)
180. M. Drobizhev, A. Karotki, Y. Dzenis, A. Rebane, Z. Suo, C.W. Spangler, Strong cooperative enhancement of two-photon absorption in dendrimers. *J. Phys. Chem. B* **107**, 7540–7543 (2003)
181. O. Mongin, J. Brunel, L. Porr, M. Blanchard-Desce, Synthesis and two-photon absorption of triphenylbenzene-cored dendritic chromophores. *Tetrahedron Lett.* **44**, 2813–2816 (2003)
182. Q. Zheng, G.S. He, P.N. Prasad, π -Conjugated dendritic nanosized chromophore with enhanced two-photon absorption. *Chem. Mater.* **17**, 6004–6011 (2005)
183. J.M. Hales, J. Matichak, S. Barlow, S. Ohira, K. Yesudas, J.-L. Bredas, J.W. Perry, S.R. Marder, Design of polymethine dyes with large third-order optical nonlinearities and loss figures of merit. *Science* **327**, 1485–1488 (2010)
184. M.J. Piao, B.R. Cho, K.H. Son, S.H.L. Soo, J.Y. Seung-Joon, J.M. Cho, Nonlinear optical and two-photon absorption properties of 1,3,5-tricyano-2,4,6-tris(styryl)benzene-containing octupolar oligomers. *Chem. Eur. J.* **8**, 3907–3916 (2002)
185. A. Hohenau, C. Cagran, G. Kranzelbinder, U. Scherf, G. Leising, Efficient continuous-wave two-photon absorption in para-phenylene-type polymers. *Adv. Mater.* **13**, 1303 (2001)

186. J. Hua, B. Li, F. Meng, F. Ding, S. Qian, H. Tian, Two-photon absorption properties of hyperbranched conjugated polymers with triphenylamine as the core. *Polymer* **45**, 7143–7149 (2004)
187. S.L. Oliveira, D.S. Correa, L. De Boni, L. Misoguti, S.C. Zilio, C.R. Mendonca, Two-photon absorption cross-section spectrum of a pi-conjugated polymer obtained using the white-light continuum Z-scan technique. *Appl. Phys. Lett.* **88**, 021911–021913 (2006)
188. W.J. Yang, C.H. Kim, M.Y. Jeong, Synthesis and two-photon absorption properties of 9, 10-bis (arylethynyl) anthracene derivatives. *Chem. Mater.* **16**, 2783–2789 (2004)
189. W. Zhou, S.M. Kuebler, K.L. Braun, T. Yu, J.K. Cammack, C.K. Ober, J.W. Perry, S.R. Marder, An efficient two-photon-generated photoacid applied to positive-tone 3D micro-fabrication. *Science* **296**, 1106–1109 (2002)
190. C.O. Yanez, C.D. Andrade, K.D. Belfield, Characterization of novel sulfonium photoacid generators and their microwave-assisted synthesis. *Chem. Commun.* (7), 827–829 (2009)
191. R. Xia, J.-P. Malval, M. Jin, A. Spangenberg, D. Wan, H. Pu, T. Vergote, F. Morlet-Savary, H. Chaumeil, P. Baldeck, O. Poizat, O. Soppera, Enhancement of acid photogeneration through a para-to-meta substitution strategy in a sulfonium-based alkoxystilbene designed for two-photon polymerization. *Chem. Mater.* **24**, 237–244 (2011)
192. P. Prabhakaran, K.-S. Lee, Two-photon sensitized cationic polymerization for 3D nano/micro patterning. *Display Imag.* **1**, 25–45 (2013)
193. C.N. LaFratta, J.T. Fourkas, T. Baldacchini, R.A. Farrer, Multiphoton fabrication. *Angew. Chem. Int. Ed.* **46**, 6238–6258 (2007)
194. I. Toshiro, K. Takahiro, Resist materials and processes for extreme ultraviolet lithography. *Jpn. J. Appl. Phys.* **52**, 010002 (2013)
195. K. Takahiro, O. Hiroaki, I. Toshiro, T. Seiichi, Relationship between chemical gradient and line edge roughness of chemically amplified extreme ultraviolet resist. *Appl. Phys. Exp.* **3**, 036501 (2010)
196. P.D. Ashby, D.L. Olynick, D.F. Ogletree, P.P. Naulleau, Resist materials for extreme ultraviolet lithography: Toward low-cost single-digit-nanometer patterning. *Adv. Mater.* **27**, 5813–5819 (2015)
197. T. Kozawa, H. Oizumi, T. Itani, S. Tagawa, Assessment and extendibility of chemically amplified resists for extreme ultraviolet lithography: consideration of nanolithography beyond 22 nm half-pitch, Japanese J. Appl. Phys. **50**(7R), 076503 (2011)
198. N. Mojarad, M. Hojeij, L. Wang, J. Gobrecht, Y. Ekinici, Single-digit-resolution nano-patterning with extreme ultraviolet light for the 2.5 nm technology node and beyond. *Nanoscale* **7**, 4031–4037 (2015)
199. M. Kryask, M. Trikeriotis, C. Ouyang, S. Chakrabarty, E.P. Giannelis, C.K. Ober, Nanoparticle photoresists: Ligand exchange as a new, sensitive EUV patterning mechanism. *J. Photopolym. Sci. Technol.* **26**, 659–664 (2013)
200. S. Chakrabarty, C. Sarma, L. Li, E.P. Giannelis, C.K. Ober, Increasing sensitivity of oxide nanoparticle photoresists, in *Proc. SPIE*, vol 9048 (SPIE, Bellingham, 2014), pp. 90481C–90485C
201. L. Li, S. Chakrabarty, K. Spyrou, C.K. Ober, E.P. Giannelis, Studying the mechanism of hybrid nanoparticle photoresists: Effect of particle size on photopatterning. *Chem. Mater.* **27**, 5027–5031 (2015)
202. S.K. Sharma, S.P. Pal, P.G. Reddy, P. Kumar, S. Ghosh, K.E. Gonsalves, Design and development of low activation energy based nonchemically amplified resists (n-CARs) for next generation EUV lithography. *Microelectron. Eng.* **164**, 115–122 (2016)
203. L. Li, S. Chakrabarty, J. Jiang, B. Zhang, C. Ober, E.P. Giannelis, Solubility studies of inorganic-organic hybrid nanoparticle photoresists with different surface functional groups. *Nanoscale* **8**, 1338–1343 (2016)
204. J.R. Tumbleston, D. Shirvanyants, N. Ermoshkin, R. Janusziewicz, A.R. Johnson, D. Kelly, K. Chen, R. Pinschmidt, J.P. Rolland, A. Ermoshkin, Continuous liquid interface production of 3D objects. *Science* **347**, 1349–1352 (2015)

205. C.N. Lafratta, L. Li, Making two-photon polymerization faster, in *Three-Dimensional Microfabrication Using Two-Photon Polymerization Fundamentals, Technology and Applications*, ed. by T. Baldacchini (William Andrew, Oxford, 2016), pp. 221–240
206. L. Dhar, M.G. Schnoes, H.E. Katz, A. Hale, M.L. Schilling, A.L. Harris, Photopolymers for digital holographic data storage, in *Holographic Data Storage*, ed. by A. Glass, M. Cardillo, H.J. Coufal, D. Psaltis, G.T. Sincerbox (Springer, Heidelberg, 2012), pp. 199–208
207. F. Karasu, C. Croutxé-Barghorn, X. Allonas, L.G. Ven, Free radical photopolymerization initiated by UV and LED: Towards UV stabilized, tack free coatings. *J. Polym. Sci. Part A: Polym. Chem.* **52**, 3597–3607 (2014)
208. T. Nardi, L.P. Canal, M. Hausmann, F. Dujonc, V. Michaud, J.-A.E. Månson, Y. Leterrier, Stress reduction mechanisms during photopolymerization of functionally graded polymer nanocomposite coatings. *Prog. Org. Coat.* **87**, 204–212 (2015)
209. S. Beke, R. Barenghi, B. Farkas, I. Romano, L. Körösi, S. Scaglione, F. Brandi, Improved cell activity on biodegradable photopolymer scaffolds using titanate nanotube coatings. *Mater. Sci. Eng. C* **44**, 38–43 (2014)
210. K.D. Jandt, R.W. Mills, A brief history of LED photopolymerization. *Dent. Mater.* **29**, 605–617 (2013)
211. R. Gauvin, Y.-C. Chen, J.W. Lee, P. Soman, P. Zorlutuna, J.W. Nichol, H. Bae, S. Chen, A. Khademhosseini, Microfabrication of complex porous tissue engineering scaffolds using 3D projection stereolithography. *Biomaterials* **33**, 3824–3834 (2012)
212. D.L. Elbert, Bottom-up tissue engineering. *Curr. Opin. Biotechnol.* **22**, 674–680 (2011)
213. S. Beke, F. Anjum, H. Tsushima, L. Ceseracciu, E. Chieregatti, A. Diaspro, A. Athanassiou, F. Brandi, Towards excimer-laser-based stereolithography: A rapid process to fabricate rigid biodegradable photopolymer scaffolds. *J. R. Soc. Interface* **9**, 3017 (2012). rsif20120300
214. M. Gonen-Wadmany, L. Oss-Ronen, D. Seliktar, Protein–polymer conjugates for forming photopolymerizable biomimetic hydrogels for tissue engineering. *Biomaterials* **28**, 3876–3886 (2007)
215. S. Suri, L.-H. Han, W. Zhang, A. Singh, S. Chen, C.E. Schmidt, Solid freeform fabrication of designer scaffolds of hyaluronic acid for nerve tissue engineering. *Biomed. Microdevices* **13**, 983–993 (2011)
216. K. Kojima, M. Ito, H. Morishita, N. Hayashi, A novel water-soluble photoinitiator for the acrylic photopolymerization type resist system. *Chem. Mater.* **10**, 3429–3433 (1998)
217. M. Hasegawa, A. Tominaga, Environmentally friendly positive-and negative-tone photopatterning systems of low-K and low-CTE polyimides. *J. Photopolym. Sci. Technol.* **18**, 307–312 (2005)
218. A. Drizo, J. Pegna, Environmental impacts of rapid prototyping: An overview of research to date. *Rapid Prototyping J.* **12**, 64–71 (2006)
219. S.H. Huang, P. Liu, A. Mokasdar, L. Hou, Additive manufacturing and its societal impact: A literature review. *Int. J. Adv. Manuf. Technol.* **67**, 1191–1203 (2013)
220. L. Ionov, S. Diez, Environment-friendly photolithography using poly (*N*-isopropylacrylamide)-based thermoresponsive photoresists. *J. Am. Chem. Soc.* **131**, 13315–13319 (2009)
221. D. Cody, I. Naydenova, E. Mihaylova, New non-toxic holographic photopolymer material. *J. Opt.* **14**, 015601 (2011)
222. S. Chatani, T. Gong, B.A. Earle, M. Podgorski, C.N. Bowman, Visible-light initiated thiol-Michael addition photopolymerization reactions. *ACS Macro Lett.* **3**, 315–318 (2014)
223. G. Bai, S. Ma, R. Qie, Z. Liu, Y. Shi, C. Li, R. Wang, X. Guo, F. Zhou, X. Jia, UV-Triggered surface-initiated polymerization from colorless green tea polyphenol-coated surfaces. *Macromol. Rapid Commun.* **37**, 1256–1261 (2016)
224. E. Sharmin, F. Zafar, D. Akram, M. Alam, S. Ahmad, Recent advances in vegetable oils based environment friendly coatings: A review. *Ind. Crops Prod.* **76**, 215–229 (2015)



Lindsey A. Bultema, Xia Huang, Daniel D. Brauer, and Patrick Theato

Contents

1	General Considerations	54
1.1	Methods for Functional Polymer Synthesis	54
1.2	Classifications	56
2	Short History	57
3	Functional Groups Employed in Chemical Modifications	59
3.1	Activated Esters	59
3.2	Anhydrides, Isocyanates, and Ketenes	62
3.3	Oxazolones and Epoxides	63
3.4	Aldehydes and Ketones	67
3.5	Azides and Alkynes	70
3.6	Dienes and Dienophiles	73
3.7	Tetrazines	76
3.8	Triazolinediones	76
3.9	Halides	79
3.10	Thiols	80
3.11	Future Prospects in Polymer Functionalization	86
3.12	Dibromomaleimide Chemistry	89
3.13	Use of Thiolactone	90
4	Conclusion and Summary	91
	References	91

L. A. Bultema · D. D. Brauer

Institute of Technical and Macromolecular Chemistry, University of Hamburg, Hamburg, Germany
e-mail: lindsey.bultema@chemie.uni-hamburg.de; daniel.d.brauer@gmail.com

X. Huang · P. Theato (✉)

Institut für Technische Chemie und Polymerchemie, Karlsruher Institut für Technologie, Karlsruhe, Germany
e-mail: xia.huang@student.kit.edu; patrick.theato@kit.edu

Abstract

This chapter provides an overview of the many facets of polymer functionalization. To build upon the basic foundation of polymer functionalization, some general considerations are outlined first. This includes various methods to synthesize functional polymers and an overview of reactions frequently employed in postpolymerization modification. Additionally a brief history of polymer functionalization dating back to the vulcanization of rubber in 1840 is discussed. Following the general considerations, the chapter is divided into specific functional groups and modern reactions. The functional groups discussed here include activated esters, anhydrides, isocyanates, and ketenes, oxazolones and epoxides, aldehydes and ketones, azides and alkynes, dienes, and dienophiles, tetrazines, halides, and thiols. To showcase the versatility of the functional groups, side chain modification and end group modification are included within each section. Finally, future prospects in polymer functionalization are briefly mentioned.

1 General Considerations

1.1 Methods for Functional Polymer Synthesis

Functional polymers can be prepared by the direct polymerization of a functional monomer. However, when more than one functional group is required in a polymer, typically a copolymerization of two or more monomers, each featuring one particular functional group, is conducted. These approaches of direct polymerization or copolymerization are only feasible when the functional groups of interest do not interfere with the respective polymerization mechanism.

1.1.1 Copolymerization

Generally in a copolymerization two or more comonomers are reacted to form the respective copolymer. Depending on the nature of the comonomers, a random copolymer, statistical copolymer, or alternating copolymer is formed. If at least one comonomer features reactive characteristics, a postfunctionalization is possible. One of the most classical examples is the alternating copolymerization of maleic anhydride (MA) with styrene (St) resulting in the alternating copolymer poly(St-*alt*-MA). Here MA acts as a reactive anhydride and can react with numerous nucleophiles, such as alcohols or amines [1, 2]. Noteworthy, when copolymerizing other functional monomers, the reactivity ratios of the monomer influence the composition and structure of the obtained copolymer. This may limit the application if the respective distribution of functional groups is not desired. Therefore, the postpolymerization functionalization of a reactive homopolymer with more reactants can be advantageous, as it can lead to a different, often more preferred distribution of functional units in a copolymer.

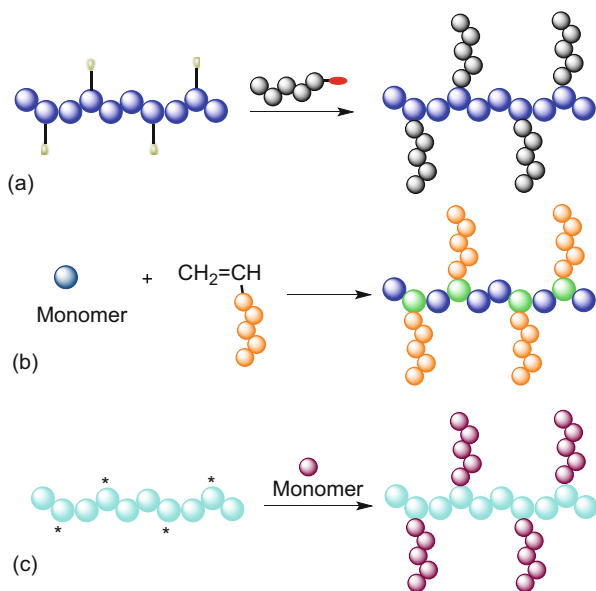
1.1.2 End-Functionalization

End functionalization is possible by the various routes of modifying preexisting polymer chain ends, or halting of the chain growth, followed by end functionalization. These instances are traditionally performed with agents or chemical groups that already contain the desirable functional group [3, 4].

1.1.3 Functionalization-Grafting

Functionalization-grafting briefly consists of the following techniques: (i) use of preexisting polymer chains possessing functional species or chain ends with a chemical affinity to chemical groups on the backbone of another polymer chain. This is considered a “grafting-onto” technique (Fig. 1a) and is frequently used for synthesis of comb polymers. Saldivar-Guerra and coworkers use a grafting from method to functionalize polybutadiene and polyisoprene with different kinds of nitroxide moieties which could further address the controlled growth of poly(maleic anhydride-*co*-styrene) and thus can be used as compatibilizers [5]. (ii) Interchange or reaction of labile atoms on a polymeric backbone by reactive species or functional monomers; use of macromonomers containing highly polymerizable groups, particularly vinyl groups. The addition of a second monomer (comonomer) can lead to various structures, such as brushes, regular grafts, centipede, barbwire, etc., depending on the reactivity ratios and distance between grafts. This is considered “grafting-through” (Fig. 1b). The group of Herrea used the grafting-to method to achieve functionalization of single-walled carbon nanotubes with polystyrene by cycloaddition of polystyrene with N₃-end-groups [6]. (iv) Utilizing a polymer that consists of functional species, reactive groups, or initiator moieties located along the

Fig. 1 (a) grafting-onto, (b) grafting-through, (c) grafting-from methods [7]. (Reprinted with permission of Wiley)



polymer backbone, which in the presence of monomers results in a growth of grafts from the polymer backbone. This is considered a “grafting-from” technique (Fig. 1c) [7]. The group of Wooley reported the usage of grafting through methodology as well as RAFT and ROMP polymerization method for the synthesis of cylindrical molecular brushes with well controlled grafting density and low dispersity [8].

1.2 Classifications

A variety of different organic reactions can be used for the chemical modification (also called functionalization) of polymers. Thus, a brief overview of various reactions will be described in this section to provide a general classification of postpolymerization modifications based on the mechanistic aspects. Subsequently classifications based on functional groups will be provided with modern reactions in greater detail.

1.2.1 Additions

Simplistically speaking an addition reaction involves the reaction of small molecules with functional groups, resulting in a single reaction product containing all atoms of all components. One of the most important addition reactions is the addition of halogens, hydrogen, or oxygen to macromolecules containing carbon-carbon C=C double bonds. Noteworthy, through addition reactions, the solubility and chemical stability of polymers can be altered.

Hydrogenation of polymers is technologically one of the most important modification methods. Hydrogenation of polystyrene has gained interest over the years along with the hydrogenation of polydienes due to the ability to vary the microstructure [9]. Halogenation and hydrohalogenation of unsaturated polymers have also been explored. One example is the bromination of polybutadiene, which results in flame-retardant materials. An alternative method to introduce halogens to polymers is by radiation-induced addition [10]. Finally the epoxidation of double bonds is another useful approach for the functionalization of unsaturated polymers, for example, the epoxidation of polybutadiene [11]. In recent years, the modification of unsaturated polymers with thiols via a thiol-ene reaction has become extremely popular. Details of this are described later in this chapter (Sect. 3.11).

1.2.2 Substitutions

Substitution reactions also belong to a useful class of reactions to produce functional polymers. A practical example would be the chlorination of polyethylene (PE) by free radical substitution. Here chlorination begins in the amorphous areas of the crystalline surface [12]. Esterification and hydrolysis reactions are also numerous utilized. A particularly common reaction is the esterification of poly(methylacrylic acid) utilizing carbodiimides as condensing agents. Often during this reaction, the cyclic anhydride forms first as an intermediate structure, which in turn reacts with the presence of alcohol, to yield an ester. Another common example is the esterification of cellulose, which is still commercially produced [13, 14].

An important example of a hydrolysis reaction is the hydrolysis of poly(vinyl acetate) yielding poly(vinyl alcohol), which is a particularly important reaction because of the inability to directly synthesize the polymer from the respective monomer [10]. Furthermore, varying the degree of hydrolysis can result in polymers with different properties. In particular, increasing the degree of hydrolysis of poly(vinyl alcohol) results in polymers with decreased solubility in water at room temperature due to the high crystallinity of the polymer.

1.2.3 Eliminations

Elimination of water, alcohols, hydrogen halides, or other small molecules are some of the most important polymer modification methods. Following the elimination, unsaturated double or triple bonds or even heterocycles are formed in the macromolecule of the initial polymer. Various polymer elimination reactions are shown in Fig. 2 [15].

1.2.4 Isomerizations

Unlike the previously mentioned reaction classes, isomerizations result in a change in the chemical structure without changing the molecular weight of the macromolecule.

Configurational isomerization is, for example, the *cis-trans* isomerization of polydienes, which can be triggered through UV irradiation in the presence of a radical transfer agent. Additionally, polymers with chromophoric groups have been of interest, in particular azobenzene containing polymers due to *cis-trans* isomerization of azobenzene [10, 16].

Another example that has been developed for protein chemistry is the native chemical ligation. In this reaction, a reversible transthioesterification of a *N*-terminal cysteine residue leads to a thioester intermediate that undergoes a *S,N*-acyl shift isomerization step, resulting in a native amide bond [17].

2 Short History

The transformation of natural rubber into a tough elastic material after treatment with sulfur marks the industrial beginning of the long history of polymer functionalization by postpolymerization modification [18]. This process is called vulcanization and was invented independently by Hancock in England, Ludersdorf in Germany and Charles Goodyear in USA in 1840. Subsequently in 1847, Schönbein introduced cellulose to nitric acid, which resulted in the formation of nitro-cellulose [19]. In 1865, Schützenberger heated cellulose with acetic anhydride which resulted in cellulose acetate. Cellulose acetate subsequently found use in photographic film, membrane material, and artificial silk [20]. Although the use and modification of natural polymers widely occurred during the late nineteenth and early twentieth centuries, there was limited understanding of the mechanism behind the modification reaction of the various materials.

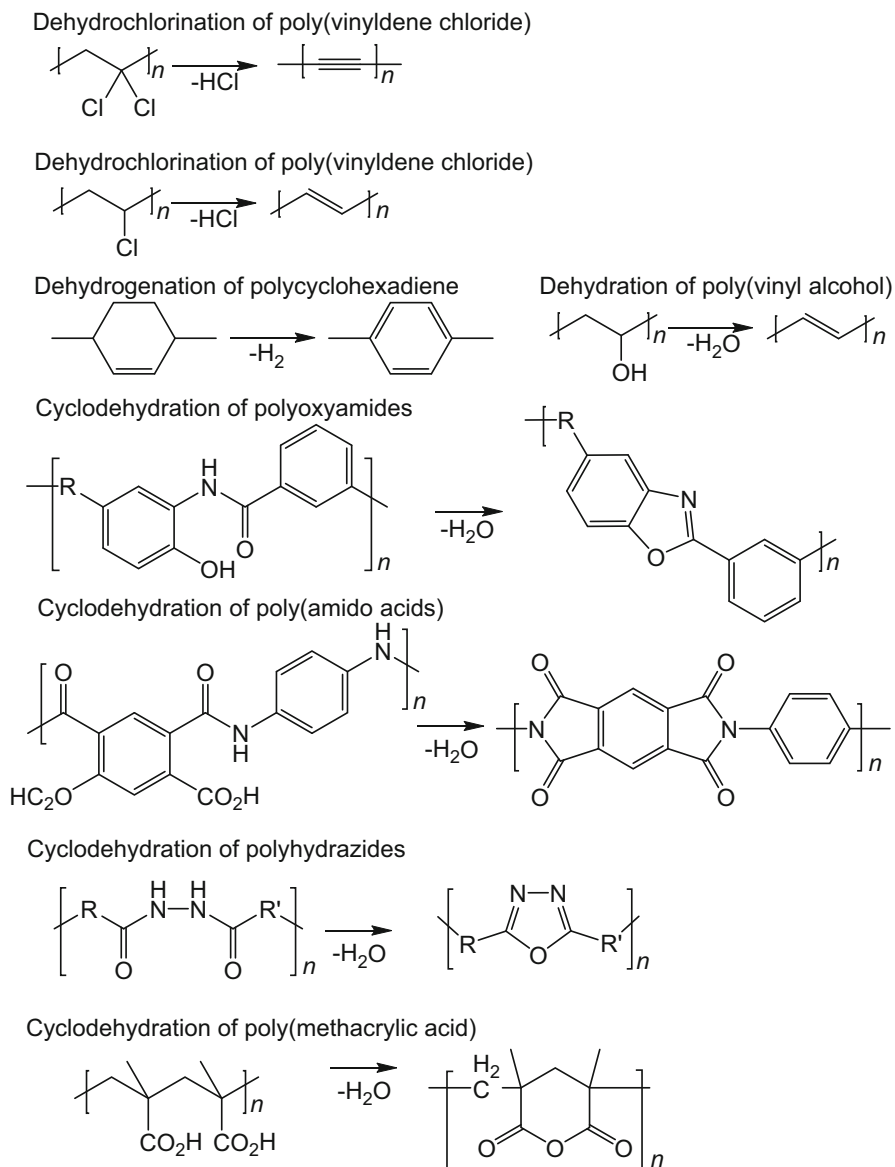


Fig. 2 Various elimination reactions. (Redrawn after [15])

The acceptance and improved understanding of macromolecules came around the time when Staudinger coined the term *polymer analogous reactions*. He defined it as reactions that involve a transformation of a polymer into a derivative of equivalent molecular weight [21]. However, nowadays we refer to reactions that result in derivatives of equivalent degree of polymerization. Following, Sernuik et al. utilized

a thiolene addition to functionalize butadiene polymers with aliphatic thiols [22]. During the early 1950s the use of chlorinated polystyrene-divinylbenzene beads as ion exchange resins rose in popularity [23]. In the late 1950s, Merrifield introduced solid state peptide synthesis [24]. The 1960s brought on the modification of halogenated poly(meth)acrylates and postpolymerization modification of polymers with pendant epoxide groups [25, 26].

The development of living/controlled radical polymerization techniques in the early 1990s allowed for the increase in postpolymerization modification reactions. Note living or controlled radical polymerizations are recommended by IUPAC to be called “reversible deactivation radical polymerizations” and encompass numerous polymerizations of which atom-transfer radical polymerization (ATRP), reversible addition-fragmentation chain transfer (RAFT), and nitroxide mediated polymerization (NMP) are the most popular ones [27–29]. By employing these polymerization techniques under mild conditions, well-defined polymers with a variety of functional groups can be obtained that allow a quantitative and selective modification.

Parallel to the growth of reversible deactivation radical polymerizations, the development of several chemoselective coupling reactions was also taking place. These include, for example, copper-catalyzed azide-alkyne cycloaddition (CuAAC) and thiol-ene addition, often coined as “click chemistry.” All of these developments helped pave the way for the expansion of postpolymerization reactions since the 1990s. A detailed review of click chemistry will not be included in this chapter. Instead click chemistry will be introduced within the respective functional group sections. For a thorough and insightful review on the many facets of click chemistry, the review of Tsdelen et al. is recommended [30]. Thus, the focus of this chapter is solely the development of various classes of postpolymerization modification reactions.

3 Functional Groups Employed in Chemical Modifications

3.1 Activated Esters

First examined by Ferruti and Ringsdorf in the 1970s, postpolymerization modification reactions involving activated ester containing polymers have become one of the most common types of post polymerization modifications [31, 32]. Activated esters are most frequently used for the covalent attachment of functional amines to form amides. This substitution occurs selectively in the presence of weaker nucleophiles like alcohols and without the need for protecting groups or metal catalyst. The production of an amide linkage offers applications in a number of fields, such as peptide chemistry and materials science.

3.1.1 Side-Chain Modification

Polymeric activated esters may be prepared from various monomers using both radical polymerization and metal-catalyzed polymerization. Controlled radical polymerization techniques such as nitroxide-mediated polymerization (NMP), atom-transfer

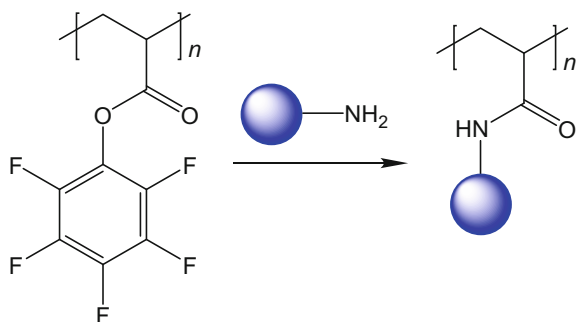
radical polymerization (ATRP), and reversible addition fragmentation chain-transfer (RAFT) polymerization have offered unprecedented precision in the synthesis of polymers containing reactive functional groups like activated esters. Traditionally derivatives of *N*-hydroxysuccinimide (NHS) ester polymers prepared from *N*-acryloxysuccinimide (NAS) or *N*-methacryloxysuccinimide (NMAS) monomers have been used for postmodification because they react with amines under mild conditions and are acceptably resistant to hydrolysis [33, 34]. This polymerization and subsequent postmodification provides access to polyacrylamide and polymethacrylamide derivatives that typically cannot be prepared via direct polymerization of their corresponding acrylamide monomers. Polymerization of the respective activated ester monomers directly offers a number of advantages over the transformation of poly(acrylic acid) with dicyclo-hexylcarbodiimide (DCC) or 1-ethyl-3-[3-dimethyl-aminopropyl]carbodiimide hydrochloride (EDC). The reaction of poly(acrylic acid) with carbodiimides proceeds through cyclic anhydrides and thus limits subsequent conversion. Additionally, urea is formed in the reaction and may be difficult to remove. Further, the change in solubility in the conversion from the starting monomer to polymer causes problems during the synthesis. These NHS ester homopolymers however suffer from poor solubility in solvents other than DMF and DMSO and are susceptible to some side reactions, such as the formation of *N*-substituted glutarimide groups or succinimide ring-opening [35]. These side reactions can be suppressed by the addition of proton scavengers such as DMAP or TEA, or through the use of excess amine [36].

The solubility of activated ester polymers may be improved either by copolymerization or replacement of the NHS ester group with other activating groups [37]. For example, NAS is often copolymerized with *N*-isopropylacrylamide (NIPAM) to produce reactive polyNIPAM. It is possible to adjust the activated ester content of poly(NIPAM-*co*-NAS) by merely altering the comonomer feed ratio. Additionally, the final molecular weight of the copolymer produced from the polymerization in THF/toluene using AIBN as an initiator may be controlled by altering the solvent composition. Higher toluene to THF ratios lead to an increase in molecular weight of poly(NIPAM-*co*-NAS) [38]. PolyNIPAM is normally employed as a thermo-sensitive polymer with a lower critical solution temperature (LCST) in water of 32 °C, which is near body temperature. By varying the amine groups used to postmodify reactive polyNIPAM, one may shift the LCST to higher temperatures via the installation of more hydrophilic units or to lower temperatures with more hydrophobic groups [39].

Thiazolidine-2-thione (TT) bearing activated ester polymers represent a substitute to polyNAS and polyNMAS activated esters which undergo rapid aminolysis in aqueous media and possess good hydrolytic stability [40]. The modification efficiency is influenced by pH, temperature, polymer concentration, and water content. It was found that a pH between 7.4 and 8.0 offers the greatest difference between aminolysis and hydrolysis rates. Unfortunately under identical reaction conditions, TT esters show low selectivity between amines and thiols.

A particularly appealing alternative to NHS-ester monomers is pentafluorophenyl (PFP) ester-based polymers. PFP ester derivatives show higher reactivity than NHS

Fig. 3 Pendant amide formation using polyPFPA activated ester



esters and PFP ester polymers are soluble in a wider range of organic solvents [41]. Both PFP acrylate and methacrylate polymers display good reactivity towards primary and secondary amines, but low conversion rates with aromatic amines and alcohols have been determined. Theato and Nilles examined the reactivity of 4-vinyl benzoic acid-based PFP polymers and found poly(pentafluorophenyl 4-vinyl benzoate) (PolyPFP4VB) to have the highest reactivity among tested polymers [42]. PolyPFP4VB quantitatively reacts with less nucleophilic aromatic or secondary amines. In a subsequent study, they utilized the difference in reactivity between PFP4VB and pentafluorophenyl methacrylate (PFMA) to fabricate bifunctional polymers [43]. Statistic and block copolymers from PFP4VB and PFMA were prepared and sequentially modified with an aromatic and aliphatic amine, respectively.

An exciting new potential for activated ester postpolymerization modification is the trans-esterification of activated esters with alcohols. Theato and coworkers demonstrated for the first time a general methodology for the quantitative conversion of polyPFPA to corresponding polyacrylates [44]. They reported that a DMAP catalyzed transesterification occurs quantitatively and selectively in DMF between PFP groups and primary and secondary alcohols as well as phenols. The reaction strongly prefers primary alcohols and provides an advantage over activated ester postmodification with amines because alcohols tolerate the presence of various functional groups that are reactive towards amines, such as acids, aldehydes, and α , β -unsaturated carbonyl derivatives. Employing this trans-esterification method, fabrication of a number of functional materials was possible, including a pH responsive hydrogel (Fig. 3).

3.1.2 End-Group Modification

Though less commonly employed than side-chain activated ester postmodification, modification via activated ester end groups is a valuable tool for the production of star polymers [45], protein-conjugates [46], and block copolymers [47]. Activated ester groups are installed at the chain end of polymers through the incorporation of activated ester reactive groups in chain-transfer agents or initiators for controlled radical polymerizations. Different derivatives of nitroxide SG1 were studied for use in NMP. The NHS ester of MAMA-SG1 was examined for the polymerization of styrene, *n*-butyl acrylate, and methyl methacrylate. The resultant polymers bearing

NHS ester terminated chains were grafted to amino-coated silica particles. Through this method, grafting densities of 0.1–0.2 chains per nm² were possible. An improved grafting density of 0.9 chains per nm² was achieved using a one-pot grafting approach. In this method, amino-coated silica, NHS ester, and the respective monomer were added to the same reaction flask. Additionally, the NHS ester of MAMA-SG1 could be employed in the synthesis of polystyrene-*block*-poly(*D, L*-lactide) or polystyrene-*block*-poly(propylene oxide) block copolymers [47].

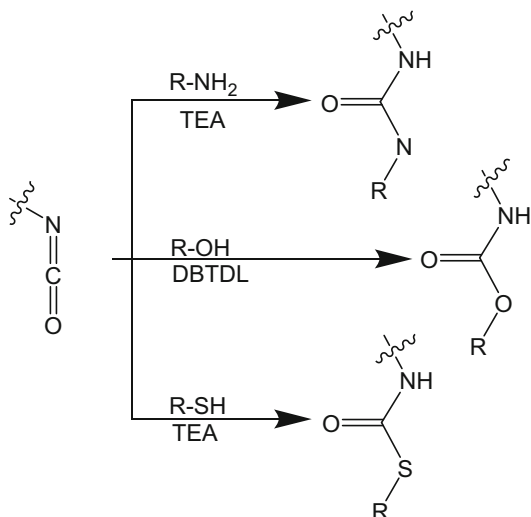
Reactive initiators for ATRP have also been installed with activated ester units successfully, namely, with NHS 2-bromopropionate and NHS 2-bromoisobutyrate. These initiators have mostly been used to prepare protein-polymer conjugates, for example, using glycopolymers functionalized with end group activated esters, bio-compatible poly(2-methacryloxyethyl phosphorylcholine) [48, 49], or poly(oligo(ethylene glycol) methyl ether methacrylate) [50–53]. The conjugation may employ either grafting-to or grafting-from approaches. RAFT polymerizations using activated ester bearing chain-transfer agents have also been explored to prepare end group functionalized polymers. NHS and PFP esters have both been incorporated into chain-transfer agents and used for subsequent preparation of functional polymers and block copolymers. Some notable examples include the preparation of fluorescently labeled thermoresponsive block copolymers from NHS-based dithioesters and the synthesis of poly(*N*-acryloylmorpholine) featuring a biotin or galactose derivative end group [54, 55]. PFP ester-based trithiocarbonates or dithioester also could be used to prepare corresponding PFP ester α -chain terminated polymers [56, 57]. These polymers have been studied for use in conjugation of responsive triblock copolymers to collagen-like peptides [58, 59]. Additionally such polymers could be conjugated to photochromic dyes, leading to thermo- and light-responsive polymers [60].

3.2 Anhydrides, Isocyanates, and Ketenes

Reactive polymer precursors containing anhydrides can easily be synthesized by copolymerization with maleic anhydride. In principle, anhydride and isocyanate containing monomers do not homopolymerize readily but may be copolymerized by radical polymerization techniques with various monomers [61]. Davies has demonstrated the copolymerization of maleic anhydride with various styrene comonomers through RAFT. The obtained series of alternating copolymers of maleic anhydrides have defined structure with a definite and narrow molar mass distribution [62]. Anhydride groups can easily react with alcohols and amines [63]. Functionalization of anhydrides with amines was reported almost quantitatively at ambient temperatures under buffer conditions of dimethyl sulfoxide (DMSO) – 0.5 M NaHCO₃) [63, 64].

Isocyanates, characterized by a N=C=O group, provide reactive carbonyl groups that can react with alcohols, or amines [61]. But reactive isocyanates have also been used in the conjunction of thiol-end-group polymers [65]. The most widely used fabrication method for synthesis of isocyanates is the phosgenation of amines; however, highly toxic phosgenes are used as reagents and involve environmental

Fig. 4 Quantitatively modified of isocyanate functionalized polymers. (Redrawn after [68–70])



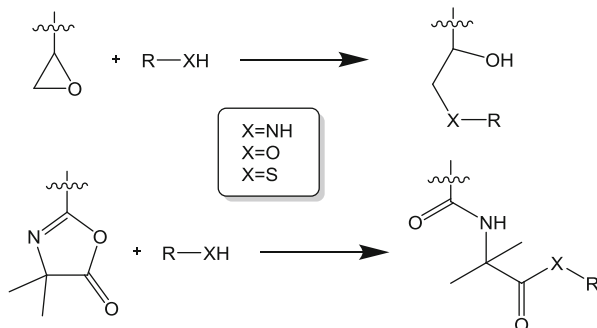
and safety problems. Knolker reported that alkyl- and arylamines can be converted into isocyanates in high yields by reacting activated carbonates (di-*tert*-butyl dicarbonate) in the presence of catalytic amounts of a nucleophilic nitrogen base at room temperature [66]. Modification of isocyanates with amines or thiols proceeds quantitatively, under ambient conditions, and within minutes. Furthermore, this could be facilitated with the addition of TEA or 1,8-diazabicyclo[5.4.0]undec-7-ene (DBU). However, quantitative conversion with alcohols is only possible either in the presence of a catalyst such as dibutyltin dilaurate (DBTDL) or an excess of alcohol (Fig. 4) [67, 68].

Ketenes as an alternative reactive groups in polymer chemistry have the inherent ability to lead to crosslinking by dimerization and can be used as a reactive chemical handle. Both of these features may be used together to provide a simple methodology for preparing a variety of functionalized polymeric materials [71]. Ketenes provide highly reactive carbonyl and alkenyl groups and may undergo various transformations of one or both, which make ketenes versatile organic reactive intermediates [72, 73]. By thermal treatment of 5,5-dialkyl-2,2-dimethyl-1,3-dioxane-4,6-dione (or 5,5-dialkyl Meldrum's acid), ketene derivatives can be prepared. The innovation of Meldrum's acid [74] allowed Hamish's group to prepare ketene intermediates through the pyrolysis of Meldrum's acid (2,2-dimethyl-1,3-dioxane-4,6-dione) derivatives. Further, Leibfarth et al. investigated the preparation of dialkyl ketene precursors based on the modular chemistry of Meldrum's acid by radical and ring-opening metathesis polymerization leading to applications in thin films [75].

3.3 Oxazolones and Epoxides

Oxazolones (or azlactones) and epoxides have long been used in polymer chemistry with monomers bearing these functional moieties. Noteworthy, the functional groups

Fig. 5 General postmodification scheme of oxazolones and epoxides



themselves can be polymerized. Oxazolones and epoxides can both be polymerized via cationic polymerization, while epoxides can also be polymerized by anionic polymerization. Additionally, it has been shown that vinyl monomers featuring these groups can be polymerized by radical polymerization (both conventional and controlled) without affecting the epoxide or oxazolone group. Furthermore, the post-polymerization modification of oxazolone or epoxide containing polymers has primarily allowed access to modification with amine, alcohol, and thiol groups (Fig. 5).

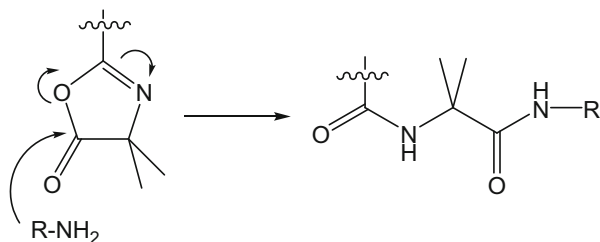
3.3.1 Oxazolones

Taylor and coworkers were the first to produce polymers equipped with oxazolone side chains via the polymerization of 2-vinyl-4,4-dimethyl-5-oxazolone (VDM) [76]. PolyVDM was shown to react quantitatively with amines such as benzylamine at room temperature and produce amide-functional polyacrylamides [77, 78]. This modification can take place rapidly even in aqueous solutions with minimal competitive hydrolysis [79]. The tendency for polyVDM to selectively react with amines in aqueous media was used for the rapid and high-density immobilization of proteins onto polyVDM functionalized beads at pH 7.5 [80]. While less common, oxazolones may also react with alcohols in the presence of either an acid or a base catalyst. The best catalysts for the reaction are trialkylphosphines and cyclic amidines [81].

Postpolymerization modification, where the reactive polymer precursor is directly functionalized, frequently employs some form of click chemistry; however, protection/deprotection chemistries are usually required for “clickable” scaffolds containing the traditional latent functionalities (alkenes and alkynes) when controlled radical polymerizations are used. Thus, to circumvent this alkenyl azlactones such as 2-vinyl-4,4-dimethylazlactone (VDMA) has been used. In particular, Jones et al. used polyVDMA scaffolds as reactive precursors for direct and tandem postpolymerization modifications and subsequent modifications to glycopolymers for antiadhesion therapies against pathogenic toxins [82].

Microphase-separated block copolymers (BCPs) that are separated into periodic domains allow for defined nanoscale structures, interfacial behavior of soft materials, and bulk properties. In particular lamellar or cylindrical morphologies have gained interest with the advancement in lithography to create well defined periodic chemical

Fig. 6 Reaction of azlactone group with primary amine. (Redrawn after [86])



patterns and biological groups on the surface for design of substrates that allow direct growth, deposition, or capture of various molecules. The group of Lynn reported an approach to fabricate reactive microphase-separated azlactone containing BCP thin films that allow for systematic, postfabrication [83].

The azlactone containing block was selected due to the ability of azlactones to react with a wide range of nucleophiles via ring-opening reactions (Fig. 6) [81]. Reactions with primary amines result in amide bonds under mild conditions [81] that maintain phase stability under typical BCP thermal processing conditions [84]. Copolymerization of vinyl azlactones with other vinyl monomers with living/controlled methods results in BCPs with various side chain functionalities [85]. Taking these things into consideration, azlactone-containing BCPs were fabricated that separate into lamellae structures and were subsequently functionalized, through treatment with aqueous solutions containing primary amines [83].

Formation of reactive polyanions was possible via the semi-batch copolymerization of 4,4-dimethyl-2-vinyl-oxazoline-5-one (VDMA) and methacrylic acid (MAA) through free radical and photoinduced radical polymerization. The subsequent 50:50 VDMA:MAA copolymer (PMV50) had up to 40% of the azlactone groups hydrolyzed by water. Further transhydration was possible following the storage in organic solvents. Additionally, solid PMV50 showed a stability for at least 6 months at room temperature. Reduction of transhydration was possible via increasing the VDMA comonomer content, likely due to decreasing the methacrylic acid diads in the backbone. Subsequently the reactive polyanions could bind to poly-*L*-lysine-coated alginate hydrogel beads and crosslink with polyamines. The resulting covalent networks allow the beads to be used for long term therapeutic cell encapsulation [87].

Post-polymerization modification of azlactone functionalized polymers can readily occur through treatment with a variety of nucleophilic species. It has been reported on postpolymerization modification of small molecule diamines for rapid synthesis of amine functionalized polymers. Here tertiary amines did not react with the azlactone ring, but resulted in polymers containing tertiary amine functionalized side chains. Additionally under physiological pH, they exhibited a positive charge and formed electrostatic complexes with DNA in aqueous media.

Furthermore, they reacted PVDMA with hydroxyl-functionalized molecules to result in cationic “charge-shifting” polyelectrolytes (Fig. 7). Here PVDMA was reacted with a molecule containing a hydroxyl and tertiary amine, with DBU

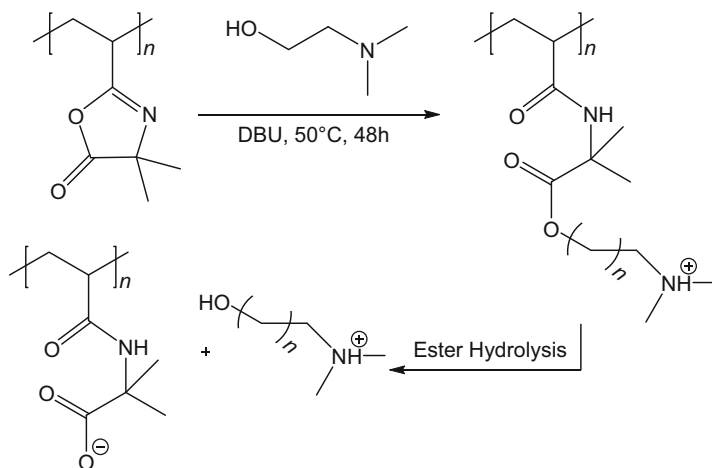


Fig. 7 Synthesis and hydrolysis of "charge-shifting" cationic polymers. ([88]- Reproduced by permission of the Royal Society of Chemistry)

catalyzing the reaction between hydroxyl and azlactone functionality. The resulting polymer consisted of a protonatable tertiary amine side-chain that was attached via an amide/ester functionalized linker. Following hydrolysis of the ester bond, the negatively charged carboxylate group was unmasked, thus resulting in a change or shift in the net charge of the polymer. This concept of charge-shifting materials was utilized to develop multilayered polyelectrolyte thin films for controlled DNA release from surfaces [88].

3.3.2 Epoxides

Epoxide-bearing polymers may be prepared from the radical polymerization of corresponding epoxide functionalized vinyl monomers, such as commercially available glycidyl methacrylate (GMA) and glycidyl acrylate (GA). Epoxide rings are reactive towards a number of functional groups, including amines, alcohols, carboxylic acids, thiols, and anhydrides [89].

The post-polymerization modification of these functional polymers was first explored by Iwakura and coworkers [90–92]. They showed that the post-polymerization modification of polyGA and polyGMA with simple secondary amines (1.0–4.0 equivalents) proceeded with low to moderate yields. Kalal showed in 1974 that postpolymerization modification through epoxide ring opening may be catalyzed with a tertiary amine (TEA) and reported 80 percent conversion of epoxide groups on polyGMA with carboxylic acids [93]. The catalytic ability of TEA for epoxide ring opening modification was furthered by Barbey and Klok, who prepared polyGMA-*co*-polyDMAEMA brushes [94]. The brushes contained pendent TEA groups that could be utilized to accelerate the postpolymerization modification rate of the epoxide groups with amines in aqueous media at room temperature.

The fabrication of fluorescently labeled coreshell nanoparticles was also possible through the use of polyGMA postmodification [95]. Deposition of polyGMA on a silica nanoparticle enabled epoxide-bearing nanoparticles, which subsequently conjugated with Rhodamine B to produce fluorescently modified particles.

Monodisperse poly(glycidyl methacrylate)/polystyrene (PGMA/PS) particles have been fabricated in Janus, raspberry, acorn, and hollow with open mouth shapes. Moreover, the surfaces of these microparticles are high in epoxy groups, which make them applicable for applications in biomolecule immobilization and superhydrophilic/superhydrophobic coatings [96].

Functionally soft interfaces are a great interest for various technologies. Soto-Cantu et al. demonstrated the ability to covalently attach a thin layer of polyGMA to a silica wafer and the versatility of the epoxide groups via a subsequent modification with either propargylamine or 5-hexynoic acid. These modifications resulted in interfacial polymers decorated with alkyne groups that could later undergo various click reactions [97].

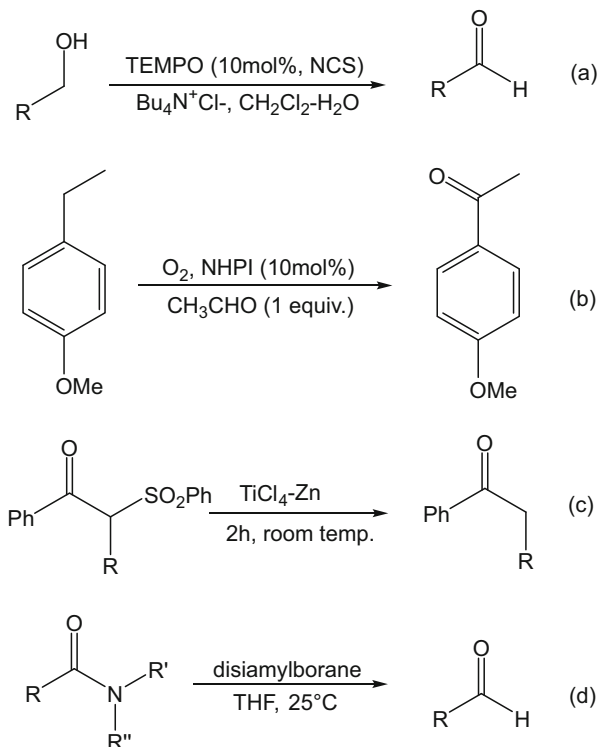
It should be noted that one disadvantage to epoxide-bearing polymers is that their reaction with primary amines can lead to crosslinking [98]. Crosslinking occurs because the reaction between a primary amine and an epoxide produces a secondary amine after the epoxide ring opening, which will subsequently react with an unopened epoxide ring. However, taking into consideration that crosslinking can occur, self-assembled morphologies can be produced. Qin et al. demonstrated this with their bulk self-assembly of diblock copolymer poly(*tert*-butyl acrylate)-*block*-poly(glycidyl methacrylate) (*Pt*BA-*b*-PGMA). Here PGMA bears epoxy groups that act as crosslinkable segments and *Pt*BA as a hydrolyzable segment [99].

3.4 Aldehydes and Ketones

Oxidation of alcohols is a commonly used method for the synthesis of aldehydes and ketones [100]. The group of Einhorn has reported a high yielding and convenient method for the fabrication of aldehydes via oxidation of primary alcohols in biphasic dichloromethane-aqueous buffer systems (Fig. 8a) [101, 102]. The reaction works efficiently under ambient temperature with a high selectivity for the oxidation of primary alcohols into aldehydes. In addition, the inorganic-based supports for chromium and metal-based oxidants such as iron(III)nitrate/montmorillonite K10 are also able to convert less active compounds such as acetals and alkanes into aldehydes and ketones [103]. Hydrocarbons are found oxidized into corresponding ketones in the presence of *N*-hydroxyphthalimide (NHPI), molecular oxygen, and acetaldehyde (Fig. 8b) [104]. Additionally, the α , β -unsaturated aldehydes can be generated from allylic methyl groups by means of microwave activation using selenium dioxide [105].

Also mild reductive methods have been developed for preparing aldehydes and ketones. For instance, under mild conditions β -keto sulfones can result in their corresponding ketones from a reduction by TiCl_4 -Zn (Fig. 8c) [106]. Also,

Fig. 8 Fabrication of aldehydes and ketones functionalized polymer. (Redrawn after [101, 102, 104, 108, 109])



N,N-dialkylamides can react with disiamylborane in THF resulting in aldehydes at room temperature (Fig. 8d) [107].

As previously reported, the acylation reaction is an important method for the synthesis of aromatic ketones. For example, Jia et al. reported the preparation of aromatic ketones by means of palladium-catalyzed regioselective acylations of aromatic C-H bonds. This reaction provided a convenient and atom-economic method for the direct synthesis of aromatic ketones [108].

Aldehydes and ketones are electrophilic groups which can react with alkoxyamines, amines, and hydrazides thus forming oximes, imines and hydrazones, respectively [61]. Besides, aldehydes are also versatile groups which can react with proteins and peptides in aqueous solutions under mild conditions enforcing the biomolecules attaching to surfaces [110]. It was reported that aldehyde functionalized polymers can be polymerized by free radical polymerization as well as ATRP and RAFT conditions from 3,3'-diethoxypropyl polymerization [111–113].

3.4.1 Side Chain Modifications

The polymerization of aldehyde containing monomers dates back to the 1950s. Wiley and Hobson reported the conventional radical polymerization between isophthalaldehyde and malonic acid [114]. Theato's group has synthesized a hybrid

polymer which composed of poly(methylsilsequioxane) and poly(4-vinyl benzaldehyde) and further modified the silica surface in order to achieve zwitterionic thin films containing α -amino phosphonic acid moieties [115]. Another alternative method for the fabrication of aldehyde-functionalized polymers is anionic polymerization. Hirao and Nakahama reported the synthesise of linear poly(4-vinylbenzaldehydes) via anionic living polymerization of 1,3-dimethyl-2-(4-vinylphenyl)imidazolidine; the aldehyde functionality was protected by *N,N'*-dimethylethylenediamine [116]. However, the strict conditions and complex procedures impeded the applicability of this synthetic route [117, 118].

In the past 20 years, RAFT polymerization has found a facile route for homogeneous controlled polymerization of monomers under mild reactive conditions [119]. In order to further simplify the procedures and reaction condition, Wooley and co-workers investigated controlled radical polymerization of aldehyde functionalized monomers. They reported the RAFT polymerization of 4-vinylbenzaldehyde (VBA) for the construction of well-defined aldehyde containing polymers [118]. Afterwards, synthesis of poly(ethylene oxide)-*block*-poly(2-formal-4-vinylphenyl ferrocenecarboxylate) (PEO-*b*-PFVFC) (containing reactive aldehyde groups) was achieved by means of RAFT polymerization; furthermore, the aldehyde group can be covalently modified under simple and mild conditions [120].

Another common synthesis is via the protection of aldehydes as acetals, which is conducted to allow a polymerization of the respective monomers. Maynard's group prepared poly(3,3'-diethoxypropyl methacrylate) (PDEPMA) with acetal functionalized side chains by ATRP, afterwards the acetal protecting group could be hydrolyzed into active aldehyde groups in dilute acids [111]. Polymers with aldehyde side chains are especially useful in the synthesis of polymer drug conjugates. Peptides and antibodies are ubiquitously targeted with amine moieties, which can subsequently react with aldehydes through reductive amination, thus forming a stable bond [109].

Furthermore, ketone containing monomers such as vinylmethylketone (VMK), isopropenyl methyl ketone (IMK), and phenyl vinyl ketone (PVK), can be polymerized via RAFT polymerization as well as free-radical polymerization (FRP). As early as 1938 free-radical polymerization of VMK and its conversion with hydroxylamine was investigated [121]. Cheng and coworkers have studied RAFT polymerization of vinyl ketones and showed that it is a facile way for the synthesis of well-defined ketone containing polymers [122]. These ketone-functionalized polymers can quantitatively be modified with different nucleophiles [123]. Additionally, Yang and Weck reported that via ring-opening metathesis polymerization (ROMP) poly(norbornene)-based copolymers featuring ketone and aldehyde side chain functionalities can be further functionalized and result in hydrazone formation [124, 125].

3.4.2 End-Group Modifications

Aside from functional polymer side groups, aldehyde and ketone functional groups also exist at end groups and could be used for end-group modification. In 1995,

Kataoka and coworkers synthesized a poly(ethylene oxide)-*block*-poly(lactide) (PEO-*b*-PLA) block copolymer which contained an acetal terminal group on the PEO block. As reported, the acetal group could be transformed into an aldehyde group, hence forming an aldehyde end group copolymer which could be further used for conjugation with proteins [126]. With the same method, Kataoka's group also synthesized aldehyde end capped poly(ethylene glycol) (PEG) polymers and PEG-*b*-PLA copolymers, which were utilized for biomedical applications and for the fabrication of supramolecular architectures [127, 128]. Haddleton and Tao synthesized α -aldehyde terminated poly(methoxyPEG) methacrylates by means of ATRP and further conjugated it with lysozymes [129]. In regard to ω -aldehyde-functionalized polymers, Register and Notestein prepared polystyrene and polyisoprene containing an aldehyde at the end of the molecular chain via a prompt and complete termination reaction of a ROMP [130].

In addition to the modification methods which have been mentioned above, utilization of functional initiators or functional chain transfer agents (CTA) has led to polymer end chain functionalization. Fulton and Jackson prepared aldehyde containing trithiocarbonate CTAs in order to fabricate aldehyde end-functionalized polymers via RAFT polymerization methods [131]. It was with ROMP of norbornene (NB) or dicyclopentadiene (DCDP) that Matyjaszewski and Coca reported the preparation of macroinitiators and subsequent chain capping with *p*-(bromomethyl) benzaldehyde for homogeneous ATRP to synthesize styrene block copolymers [132].

3.5 Azides and Alkynes

In 1963, Huisgen was the first to introduce the 1,3-cycloaddition between azides and alkynes, resulting in 1,4- and 1,5-substituted 1,2,3-triazoles (Fig. 9) [133, 134]. Traditionally cycloaddition reactions are an equilibrium process; however, one can push the reaction towards a certain direction with the aid of catalysis, heat, light, and ultrasound [30]. Thus, it was not until 2001 when Meldal and Sharpless promoted the use of copper-catalyzed azide-alkyne cycloaddition (CuAAC) that the

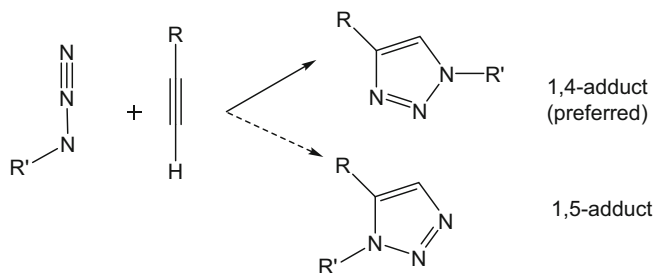


Fig. 9 1,3-Dipolar cycloaddition between azides and alkynes

1,3-cycloaddition gained notoriety. The use of copper as a catalyst not only accelerates the result of a 1,4-adduct but also improves the yield while working under mild conditions in a variety of organic solvents. However, a drawback of the CuAAC is the removal of the copper catalyst, which can be work intensive due to the formation of a complex with a triazole ring, which in turn diminishes the solubility of functionalized polymers [135]. Copper (I) (Cu) species are required for CuAAC reactions; however, the disproportion of Cu(I) to Cu(II) and Cu(0) or the oxidation of Cu(I) to Cu(II) species often is considered catalytic poisoning for the reactions. Luckily reduction of Cu(II) salts is conveniently possible to produce Cu(I). Additionally, Cu(I) can be generated via other reducing agents [136], photochemically [137], electrochemical redox processes [138], and copper containing nanoparticles [139]. Today, Cu(I)-tris((1benzyl-1H-1,2,3-triazolyl)methyl) amine complex and Cu (I)-bathophenanthrolinedisulfonic acid complex are the two most frequently used catalysts for CuAAC reactions [30].

Additionally in 2001, Kolb et al. [140] introduced the concept of click chemistry with “spring loaded” reactions inspired by nature. The following criteria must be met for a reaction to fall under the term “click chemistry”: a modular reaction that is wide in scope, results in high yields, and results in mild byproducts. If purification is required, nonchromatographic methods should be employed. Thus, only reactions that do not employ a copper catalyst will fall under the term click chemistry. A detailed investigation of the mechanism and kinetics will not be discussed here in length. Instead, the use of CuAAC and metal free 1,3-dipolar cycloadditions for modification of polymer side chains and end groups will be the focus. For an in depth overview of the kinetics and mechanistic studies, the review by Binder and Sachsenhofer [141] is recommended.

To ensure the required azide and alkyne functional groups are present, they can either be incorporated during polymerization or directly after polymerization. For example with ATRP, introduction of the azide end group after polymerization frequently occurs due to the simplicity of a nucleophilic substitution of a bromide or chloride substituent. Whereas for the reactive group to be directly incorporated into the polymer side chain, a monomer with the desired functionality is utilized. When the later approach is used, polymerization requirements need to be taken into account. For example when ATRP is used, there is a possibility of alkyne groups (e.g., propargyl methacrylate) interacting with the copper catalyst needed for ATRP [142]. Additionally, the acidic terminal proton of an alkyne group can terminate the propagation of the polymer chain when using anionic polymerization, hence requiring the use of protecting groups for alkynes [143]. Furthermore, terminal alkyne groups can also interfere with radical polymerization, resulting in crosslinking and insolubility in organic solvents in some instances. Although the degree of crosslinking depends partly on the chosen polymerization conditions, i.e., temperature and time. When crosslinking is not warranted, again the use of a protective group is recommended. In contrast azide groups can provide difficulties with cationic ring-opening polymerization (CROP) and decompose at elevated temperatures [144, 145]. Although postpolymerization modifications involving the azide-alkyne cycloaddition are highly efficient, the triazole moiety is often formed which

results in catalytic effects on subsequent cycloaddition reactions and turns the modification into an autocatalytic process [146].

3.5.1 Polymer Side-Chain Modifications

Ring opening polymerization (ROP) has also been employed to synthesize polymers with alkyne side groups. A particular example is the synthesis of poly(α -propargyl- δ -valerolactone) and the copolymerization with ϵ -caprolactone. Subsequent functionalization occurred with azide-terminated PEG monomethylether. Additionally an azide functionalized pentapeptide (GRGDS) was conjugated with the use of copper(II) sulfate and sodium ascorbate in an acetone/water mixture at 80 °C. However, it was found that when less stable polylactides (PLA) are employed nonaqueous conditions should be used, such as copper(I) iodine with triethylamine in THF at 35 °C [147]. Additionally a biocompatible functionalization was possible with an azide functionalized pentapeptide (GRGDS) [148].

Binder and Kluger investigated the preparation of various poly(oxynorbornene)s via ROMP. In particular they found that due to the interaction of the alkyne moiety with the catalyst the polymerization of *exo-N*-prop-2-ynyl-7-oxabicyclo[2.2.1]-hept-5-ene-2,3-dicarboximide resulted in dispersities (\bar{M}_w/\bar{M}_n) over 1.5. To synthesize poly(oxynorbornene)s with alkyne or azide side groups, postpolymerization modification of the reactive polymers has occurred where CuAAC with bromotris(triphenylphosphine) copper(I) was the catalyst and *N,N*-diisopropylethylamine in dimethylformamide (DMF) at 50 °C for 48 h.

RAFT polymerization has also been used to polymerize methacrylate- or styrene-based monomers containing alkyne side groups. One example is the polymerization of propargyl methacrylate with *S*-1-dodecyl-*S'*-(α , α' -dimethyl- α -acetic acid) trithiocarbonate and 2,2'-azobisisobutyronitrile (AIBN) in toluene at 80 °C for 3 h. Subsequently, the resulting poly(propargyl methacrylate) could be grafted with azide-terminated poly(vinyl acetate) in a CuAAC [149].

Postpolymerization modification on azide containing macromolecules has also proven beneficial in the labeling of methionine analogs, found on bacterial cell surface proteins, as azidoalanine with acetylene-functionalized PEG via CuAAC with CuBr [149]. Additionally for biological applications, e.g., drug delivery, sensors, therapeutics, orthogonal multifunctionalization of polymers plays an important role. The orthogonal functionalization of a random copolymer of poly(norbornene) containing azide- and ketone-containing side groups. Here the one-pot strategy proceeded with the copolymer reacting simultaneously with phenylacetylene and benzhydrazide, with copper(II) sulfate and sodium ascorbate for 2 h at 25 °C, wherein the azide and ketone side groups were converted into triazoles and hydrazones, respectively [125].

3.5.2 Polymer End-Group Modifications

Not only can the azide or alkyne end groups be incorporated via post polymerization modification, but also they can be incorporated directly to the initiators used in ATRP, unimers for NMP, or CTAs for RAFT polymerization.

With ATRP, the introduction of an azide at the ω -end group of a polymer is frequently executed through the simple nucleophilic substitution of the resulting halide with sodium azide [149–152]. Subsequently the polymers with azide functionalities could form block copolymers via the conversion with acetylene-terminated polymers [145, 153–155].

Additionally an azide carrying initiator for ATRP has been used for controlled polymerization of methyl methacrylate in combination with *N*-alkyl-2-pyridylmethanimine and copper(I) bromide. The resulting polymer was functionalized via CuAAC at the terminal azide with the same copper catalyst [156].

Chain transfer agents (CTAs) with azide or alkyne groups have been designed for RAFT polymerization. Boyer et al. synthesized heterotelechelic polymers with an azide α -end group and a dithiopyridine ω -end group. Subsequently a heterotelechelic poly(*N*-isopropyl acrylamide) (PNIPAAm) was shown to react with an alkyne-modified biotin using copper(II) sulfate with sodium ascorbate. Under these conditions, the ω -end group was left unmodified, allowing it to be used for further conjugation to thiol containing biomolecules. In this instance, the unmodified end group was conjugated to the protein bovine serum albumin (BSA) [157].

Overall when combining controlled polymerization techniques and this form of click chemistry at polymer end groups, various polymer architectures are possible such as linear architectures of: block copolymers, biohybrids, macromonomers, or heterotelechelic polymers, and other architectures of: cyclic polymers, graft and star copolymers, polymeric networks, dendritic architectures, and nanoparticles [10].

3.5.3 Metal-Free 1,3-Dipolar Cycloaddition

The previously mentioned examples relied mostly on the use of a copper catalyst; however, instances arise in which the toxicology of the catalyst needs to be taken into consideration, in particular for the synthesis of biomedical and pharmaceutical applications. Thus, great efforts have been made to develop copper free click methods. In particular is the use of alkyne species with increased reactivity via a strain-promoted azidealkyne coupling (SPAAC), i.e., cyclooctynes as alkyne components (Fig. 10). First generation cyclooctynes were truly based on ring strain; however, second- and third-generations exhibit one or two fluoro substituents in the α -position, respectively. This leads to accelerated reaction with azides. Additionally 4-dibenzocyclooctynol and benzenes are used as alkynes and result in benzotriazoles following the conversion with azides.

3.6 Dienes and Dienophiles

First described by Diels and Alder in 1928, the cycloaddition reaction between a diene and a dienophile has been widely used for organic synthesis over the years and earned the pioneering scientists a Nobel Prize in Chemistry in 1950 [158]. The reaction specifically involves a molecule containing 1,3 conjugated double bonds (diene) and a molecule that should contain an alkene, alkyne, or double bonds between heteroatoms (dienophile). The resultant product forms via a [4 + 2]

Fig. 10 Chemical structures of various cyclooctynes used in metal-free 1,3-dipolare cycloaddition. (Redrawn after [10])

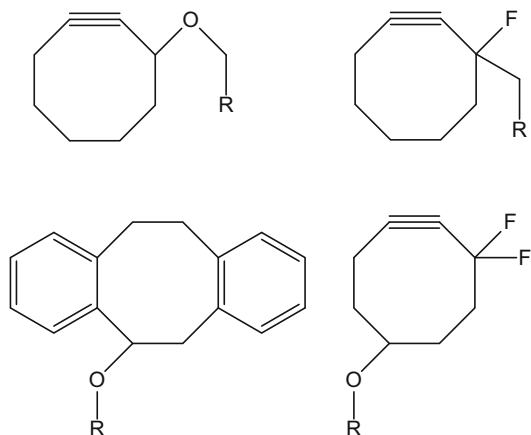
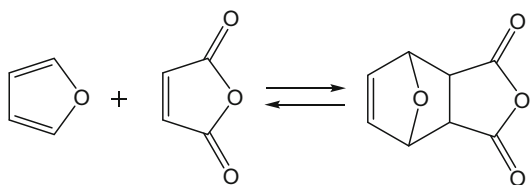


Fig. 11 Diels-Alder reaction between furan and maleimide



cycloaddition in what may be considered “click” chemistry, as the reaction proceeds quantitatively without side reactions, is tolerant to various functional groups and is orthogonal with other chemistries, for example, CuAAC [159]. Notably, these “Diels-Alder” reactions are highly thermally dependent and their cycloadducts may be thermally fragmented via a retro Diels-Alder reaction to obtain new products or recover starting materials from the forward reaction [160]. The stability of the product and thus the ability to reverse the reaction depends upon the compatibility of the chosen diene and dienophile. The energy gap between the highest occupied molecular orbital (HOMO) of the diene and the lowest unoccupied molecular orbital (LUMO) of the dienophile determines their reactivity. As such, electron-rich dienes and dienophiles with electron-deficient double bonds form cycloadducts most readily. Due to this quality, one may tune the reaction temperatures for a number of polymers via adjustment of the diene-dienophile pairs.

The versatile qualities of the Diels-Alder reaction have proved invaluable in multiple areas of chemistry including the preparation of protein-polymer conjugates [161], hydrogels [162–164], dendrimers [165], block copolymers [166], graft, star, telechelic polymers, H-shaped polymers, and dendrimers [167].

One of the most frequently employed pairings for the Diels-Alder reaction in polymer chemistry is the furan-maleimide pair (Fig. 11). The reaction can be adjusted to take place at temperatures up to 80 °C and as low as room temperature with differing reaction kinetics. The temperatures of the reaction are adjusted via the addition of electron-donating or electron-withdrawing substituents to the diene

moiety. One may additionally greatly enhance low temperature reaction rates with the utilization of a Lewis acid catalyst or with high pressure reaction conditions [168]. The coordination of the Lewis acid to the carbonyl oxygen of the dienophile increases the electron withdrawing capacity of the carbonyl group, and in turn its reactivity. Frequently utilized Lewis acids include: trifluoroacetic acid, BF_3 , SnCl_4 , ZnCl_2 , AlCl_3 , and their derivatives [30].

The ability of furan-maleimide cycloadducts to undergo a cycloreversion reaction can be taken advantage of as a protection-deprotection method for diene or dienophile containing polymers [168]. For effective use in this manner, cycloreversion should take place at temperatures below the degradation temperature of the polymer. The cycloreversion of the furan-maleimide cycloadduct occurs around 100 °C and thus presents a viable option for the protection and subsequent unmasking of thiol-reactive maleimide groups.

Another popular diene-dienophile pairing in polymer chemistry is the anthracene-maleimide combination. This reaction takes place at slightly higher temperatures, usually near 110 °C. The corresponding cycloreversion reaction takes place at temperatures above 200 °C and as such is less desirable for alkene functional group masking. Still, the robust and regioselective nature of anthracene as a diene has led to its widespread use in polymer post-modification.

3.6.1 Polymer End-Group Modifications

A useful strategy for harnessing the value of the Diels-Alder reaction in polymer systems is through the synthesis of polymers with either a diene or dienophile at the chain termini. The advances made in living polymerization techniques have produced numerous options for the incorporation of dienes and dienophiles as end groups, such as ATRP, RAFT polymerization, NMP, and ROP. With these living polymerizations, one may design initiators containing the desired functional moiety. Following polymerization, the resultant product will contain the chosen terminal functional group, allowing for subsequent modification through postpolymerization reactions. A benchmark example of producing Diels-Alder accessible end groups to a polymer was reported by Haddleton and coworkers [169]. They presented the first example of the Diels-Alder/retro Diels-Alder reaction for the masking of a dienophile during ATRP. A radical initiator for ATRP in the presence of a Cu(I) catalyst was synthesized bearing a maleimide group. The maleimide was protected by furan, then ATRP took place to produce a poly(ethylene glycol) methacrylate polymer containing furan-maleimide cycloadducts at the chain ends. Finally the maleimide was unmasked quantitatively through reflux in toluene with no polymer degradation. The postmodification of such maleimide end group polymers may even take place in the same step as the deprotection cycloreversion. Reported by Durmaz et al., multiarm polymers and graft copolymers have been prepared via the one-pot cycloreversion of furanmaleimide adducts and subsequent Diels-Alder reaction with anthracene-bearing polymers [170]. PMMA terminated with a furan-protected maleimide was refluxed in toluene with an anthracene terminated poly(styrene) to produce the maleimide-anthracene conjugate without separate removal of the furan. The orthogonality of the [4 + 2] cycloaddition and the copper-catalyzed

Huisgen [3 + 2] cycloaddition between azides and alkynes was demonstrated in the formation of ABC triblock polymer structures [171]. A bifunctional poly(styrene) capable of click reaction via both [4 + 2] and [3 + 2] cycloaddition was prepared by ATRP of an anthracene bearing initiator followed by the substitution of the terminal bromide with azide. The heterotelechelic polymer underwent a one-pot Diels-Alder click reaction and azide-alkyne click reaction with a maleimide terminated PMMA polymer and alkyne terminated poly(ethylene glycol) polymer, respectively.

3.6.2 Polymer Side-Chain Modifications

The application of the Diels-Alder cycloaddition to pendent polymer groups is an additional useful strategy. Shi et al. exploited maleimide side-chains to affix polyenic chromophores to maleimide containing vinyl copolymers. They first synthesized maleimide-functional polymers by the sequential additions of 4-maleimido benzoyl chloride and acetyl chloride under basic conditions to poly[(4-vinylphenol)-*co*-(methyl methacrylate)]. These chemically sensitive anthracene-functional polyenic chromophores could then be attached efficiently via a mild Diels-Alder reaction to produce polymers with pendant novel nonlinear optic functionalities [172].

A diene such as furan may also be installed as a reactive side group for post-polymerization modification. (*p*-vinylphenyl)furfuryl ether was copolymerized with styrene to produce a polymer possessing furan side groups. Subsequently the polymer could be linked to a bismaleimide dienophile [173]. Using a similar concept, a copolymerization of *N*-dimethylacrylamide and furfuryl methacrylate was used to produce hydrogels through bismaleimide crosslinking. Due to the potential for cycloreversion of the Diels-Alder reaction, produced gels were thermally sensitive [174]. The capability of Diels-Alder to readily undergo both the forward and reverse reaction has found application in producing self-healing polymers via side-chain Diels-Alder chemistry [167]. Magana and coworkers were able to produce a furan-maleimide crosslinked poly(ethylene) copolymer film that may be repaired multiple times by adjusting temperature [175].

3.7 Tetrazines

The reaction between tetrazines and strained alkenes or alkynes has been used for bioconjugation reactions. In particular the use of tetrazine-norbornene for post-functionalization of synthetic polymers (Fig. 12) [176].

Additionally the progress of the reaction can be tracked with UV/Vis spectroscopy by the decrease of the absorbance of the tetrazine at roughly 546 nm [177].

3.8 Triazolinediones

Although the Diels-Alder reaction first appeared in the 1920s, due to the problematic synthesis and purification of triazolinedione (TAD) compounds it was not before the 1960s when Cookson et al. obtained the pure crystalline 4-phenyl-TAD (Cookson's reagent) that it was used as a dienophile in the Diels-Alder reaction. Due to the

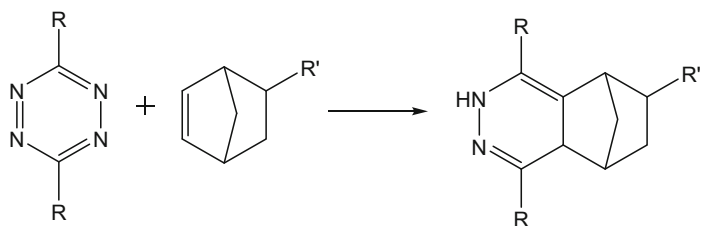


Fig. 12 The tetrazine-norbornene reaction. (Redrawn after [177])

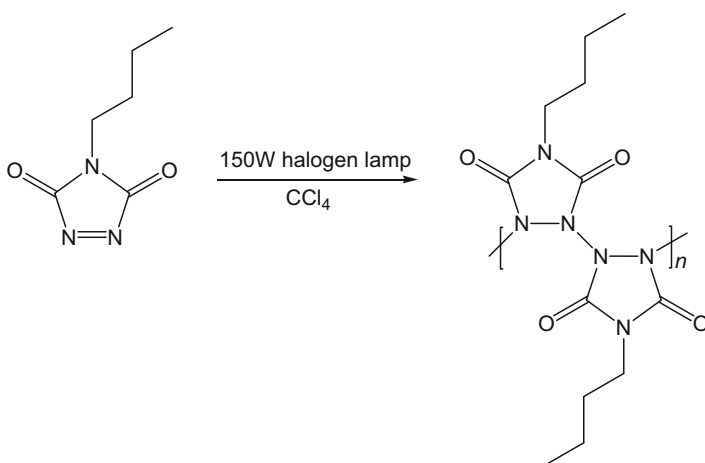


Fig. 13 Homopolymerization of BuTAD

unique reactivity of TADs, the polymer community took an interest during the 1970s with the modification of polydienes. Detailed investigation regarding this early investigation can be found in the review by Butler from the early 1980s [178].

Direct polymerization of TAD-based monomers was first investigated by Pirkle and Stickler in 1970. Here the obtained polymers exhibited an exotic all nitrogen backbone (Fig. 13). However, the obtained polymer had a limited lifetime in the CCl₄ solution (30 min to a few days) and was fully degraded within minutes in the presence of trace amounts of pyridine [178].

It was not until 1985, when Butler et al. investigated the decomposition behavior of TAD molecules that homopolymerization of BuTADs was possible. Here catalytic amounts of pyridine, a solution of a bifunctional TAD molecule in 1,2-dichloroethane was polymerized within 45 minutes and exhibited thermal stability [179] (Fig. 14).

Block copolymers are possible with TAD molecules due to their electron-accepting activity which can react with a variety of electron donating alkenes. Additionally the abundance of research focused on TAD compounds is on their ability to be used as reactive dienophiles or enophiles. However, a major application

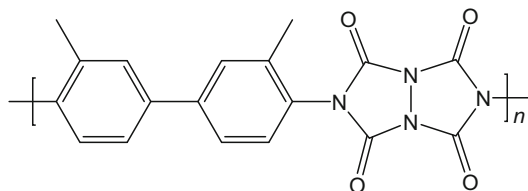


Fig. 14 Resulting structure from the polymerization of 3,3'-dimethyl-4,4'-bis(1,2,4-triazoline-3,5-dione)diphenyl with pyridine. (Redrawn after [179])

of triazolinediones is the low temperature modification of polydienes [180]. Here the alkene-TAD ene reaction results in atom-efficient and site-selective functionalization of substrates [180]. Additionally monofunctional TAD molecules were used in the modification of a variety of polydienes (polybutadiene, polyisoprene, random styrene-butadiene copolymer, and a 1:1 alternating copolymer of furan and maleic anhydride).

Cuttes et al. investigated the use of TAD (mono- and bifunctional) components for surface modification of elastomers. Here the adhesion was improved along with a reduction in peeling of flexible paints. Prior chlorination and halogen donor techniques were used for elastomer modification; thus, this relatively mild and non-corrosive technique became the preferred method [181].

Although hetero-Diels-Alder reactions have been referred to as representations of click chemistry, TAD based chemistry has not widely been discussed in terms of click chemistry, even though TAD compounds have been referred to being the most reactive dienophiles. In particular triazolinediones have been explored as a strategy for tyrosine bioconjugation. Additionally the enetype reaction with tryptophan side chains is not accelerated, thus allowing a way for site selective labeling of tyrosine residues in a natural peptide and protein substrate. The tyrosine-selective click modification was furthered by site-selective and orthogonal protein multifunctionalizations in Barbas' group. Here, orthogonal trifunctionalization of tyrosine, cysteine, and lysine residues on bovine serum albumin (BSA) and human serum albumin (HSA) was conducted. In particular the tyrosine units were reacted with TAD derivatives and cysteine and lysine modified with a maleimide and 11-(dansylamino)-undecanoic acid [182].

An alternative to TAD-based functionalization of peptides was achieved by Madder and coworkers (Fig. 15). Here they incorporated a furan residue into a synthetic peptide with the commercially available furylalanine amino acid. The classical maleimide-furan Diels-Alder conjugation was not very efficient; thus, the more reactive triazolinediones were investigated. However, following investigation it became clear that the expected Diels-Alder adduct was not observed, but a clean furan-TAD electrophilic aromatic substitution. Subsequently this reaction proved useful for quantitative and site selective peptide labeling [178].

The group of Du Prez has recently investigated the control of the TAD-indole reversible click reactions. Here they modified indole reaction parameters to result in easily accessible indole derivatives that result in dynamic TAD-adduct formation at

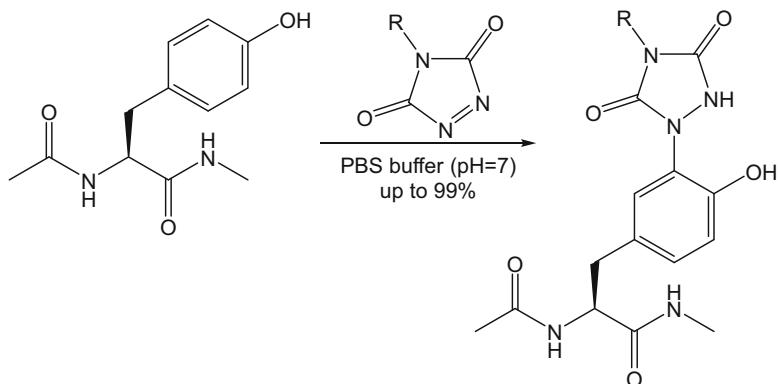


Fig. 15 Model reaction of tyrosine bioconjugation. (Reprinted with permission from [182]. Copyright 2013 American Chemical Society)

lower temperatures [183]. Additionally they demonstrated a simple method to produce TAD endcapped peptides, via different molecular weight, diene end-functionalized poly(ϵ -caprolactone). Here a buildup of *N*-terminal amines of peptides is built up on a resin and functionalized with urazole moieties; following the cleavage from the resin, the TAD is formed from oxidation. Subsequently this reacts with dienes end-capped poly(ϵ -caprolactone) [184].

However, truly expansive development of TAD reagents has been hindered due to the limited availability of reagents required for tailored TAD synthesis. Thus, TAD reagents have found applications that do not require large amounts or cost of synthesis is not an issue [178].

3.9 Halides

3.9.1 Substitution

Aryl halides usually can be activated via reduction and participate in substitution reactions [185]. Among all the transition metal catalysis, palladium is one of the most versatile catalysts that can couple aryl halides to arenes, alkenes, and aryl Grignard reagents as summarized in Fig. 16 [186]. Furthermore, the substitution of aryl halides ($X = \text{Cl}, \text{Br}, \text{F}$) with aryl methyl ethers via organomagnesium reagents catalyzed by manganese chloride (MnCl_2) has been reported [187].

3.9.2 Palladium-Catalyzed Coupling and Cross-coupling Reactions

It is reported that in the presence of copper salts alkyl halides could form C-C bonds, whereas from aryl and alkenyl halides, palladium and nickel complexes are the most used catalysis [188]. C-C cross coupling is one of the most straightforward methods in organic synthesis. It is tolerant to a versatile range of functional groups; thus, alkyl halides containing amide, alcohol, conjugated enone, ester, ether, furan, indole,

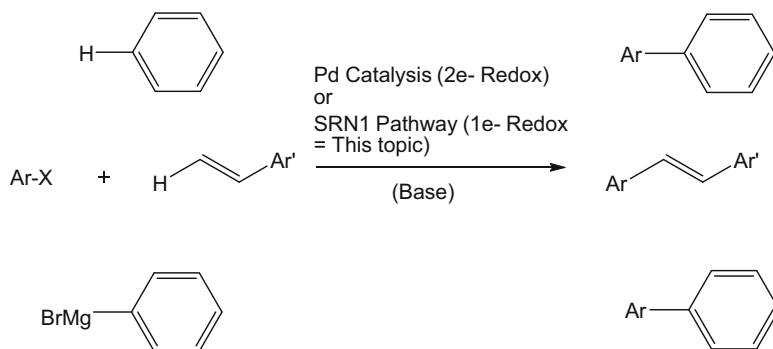


Fig. 16 Palladium catalyzed coupling

nitrile, pyrrole, thioether, and aryl halide moieties were coupled to give high isolated yields of products with functional group stability [189]. Knochel et al. reported that aryl Grignard reagents containing ester or nitrile groups and pyridyl Grignard reagents can be coupled to alkenyl halides, halopyridones, and aryl bromides [190–192]. Additionally, alkyl halides containing heterocyclic groups could be coupled to give furan, indole, and pyrrole derivatives. Vechorkin's group reported that in presence of nickel pincer complex catalysis, Kumada-Corriu-Tamao cross-coupling of nonactivated alkyl halides with aryl and heteroaryl Grignard reagents is possible [192].

3.9.3 Atom Transfer Radical Polymerization

ATRP is one facile polymerization method for the fabrication of a versatile array of materials which could be conveniently modified in post-polymerization modification. End-functionalized polymers can be prepared from initiators containing the desired functional group by means of ATRP [193]. Halide containing initiators such as benzyl halide, *p*-tosyl chloride, 2-bromopropionitrile, and methyl 2-halopropionate could trigger an ATRP reaction [194, 195]. Unprotected functional halides and pseudohalides groups also can serve as an initiation site for radical polymerization techniques [196].

Additionally, alkyl halides can quantitatively form into azides by the reaction with trimethylsilyl azide in the presence of tetrabutylammonium fluoride under mild conditions [197]. The allyl halides can produce radicals by homolytic cleavage of C-X bond in ATRP reaction.

3.10 Thiols

Reactions involving thiols proceed rapidly with high selectivity, result in high yields, and require minimal purification, thus, making thiols a highly versatile functional group that can be employed in a variety of reactions. Additionally due to many biomolecules containing thiols or reducible disulfides, thiol click chemistry is a

useful tool for the preparation of hybrid polymerbiomolecules. Furthermore, thiols can coordinate with metals and enable surface modification via self-assembly [10]. Thiol-ene reactions have also gained notoriety in polymer chemistry due to their similarity to click chemistry. In particular, thiol-ene reactions proceed under two routes: (i) anti-Markovnikov radical addition and (ii) base- or nucleophilic-catalyzed thiol-ene addition reaction. The anti-Markovnikov reaction falls under photochemical conditions and the later with various catalysis (acid/base, nucleophilic) and a solvent promoted process [30].

This section will comprise two main areas of focus: the various click reactions thiols can undergo and a general overview of postpolymerization modifications involving thiols.

3.10.1 Thiol Reactions

Nucleophilic Substitution

Weak bases can be used to deprotonate thiols in aqueous solutions, these resulting thiolates are strong nucleophiles. Nucleophilicity increases on the order of alkyl, propionate, glycolate, and aromatic substituents [198]. Formation of thioethers is possible via ring opening of epoxides with Lewis acid [199].

Nucleophilic Addition

Thiols act as strong nucleophiles, in the presence of a weak base, and can add readily to activated electron poor enes (Fig. 17). Some of the first thiol-ene reactions were reported in 1948 when Serniuk et al. documented the functionalization of butadiene polymers with aliphatic thiols [22]. Reaction of thiols with acrylates, vinylsulfones, or maleimides results in thioethers (Fig. 18). The reaction rate of thiol-Michael addition of esters increases with increasing nucleophilicity of the catalyst. Additionally, increasing electron deficiency of the double bond increases the thiol addition rate [198]. These reactions can occur under physiological conditions and are highly efficient and orthogonal to a variety of functional groups, thus, making them suitable candidates for bioconjugation [10, 198, 200].

However, a drawback to the thiol-ene coupling reaction is the oxidation of the free thiol functionality into disulfide. This can be mitigated by excluding oxygen from the reaction, addition of a reducing agent, or using protected thiol derivatives [198]. If protecting groups are used, they should be quantitatively removed under mild conditions and result in nontoxic byproducts.

Radical Addition

Thiyl radicals can be electrophilic and electrophilicity increases in the order of aromatic, glycolate, propionate, and alkyl substituents and can react with electron-rich enes, and alkynes[10], whereas for cyclic enes increased ring strain increases reaction rates [207]. Generation of radicals is possible via the thermal decomposition of initiators or photo-cleavable initiators. When high temperatures should be avoided, UV light can be used[10]. Photoinitiation has enormous advantages for small molecule synthesis and the modification of surfaces and polymers by allowing

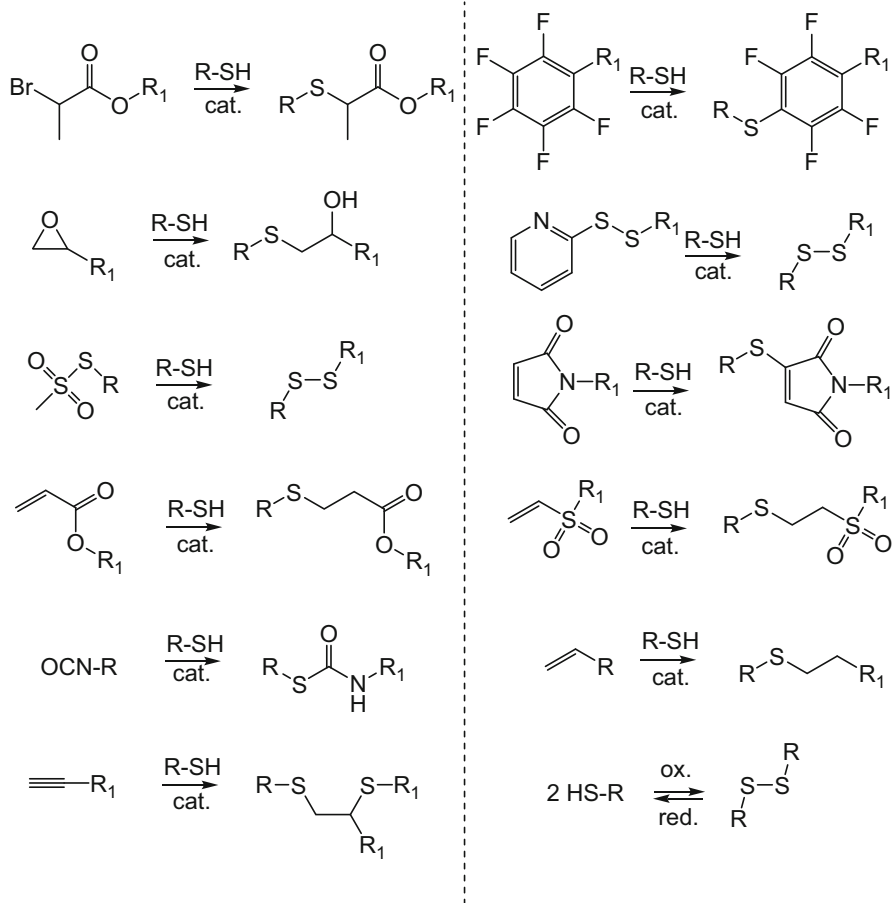


Fig. 17 Overview of reactions of thiols with various substrates. Cat., catalyst; rad., radical; ox., oxidation; red., reduction

the control and manipulation of the reaction rate and extent by simply altering the light intensity, or the duration of the exposure [208].

Generally thiol-ene reactions involve three steps: (i) hydrogen atom abstraction from a thiol by an initiating radical, (ii) the thiyl radical subsequently adding to an alkene or alkyne functionality resulting in a carbon radical, and (iii) the chain transfer of the carbon radical to another thiol, where the resulting thiyl radical propagates a new alkene [30]. The rate of the thiol-ene reaction can be adapted based on the chemical structure of the alkene. A more rapidly occurring reaction would involve electron-rich or strained alkenes as compared to electron-poor alkenes.

Thiyl radicals can be generated from thermal, photo, and redox initiators. Photo-initiation allows control over the whole process through absorption wavelength, light

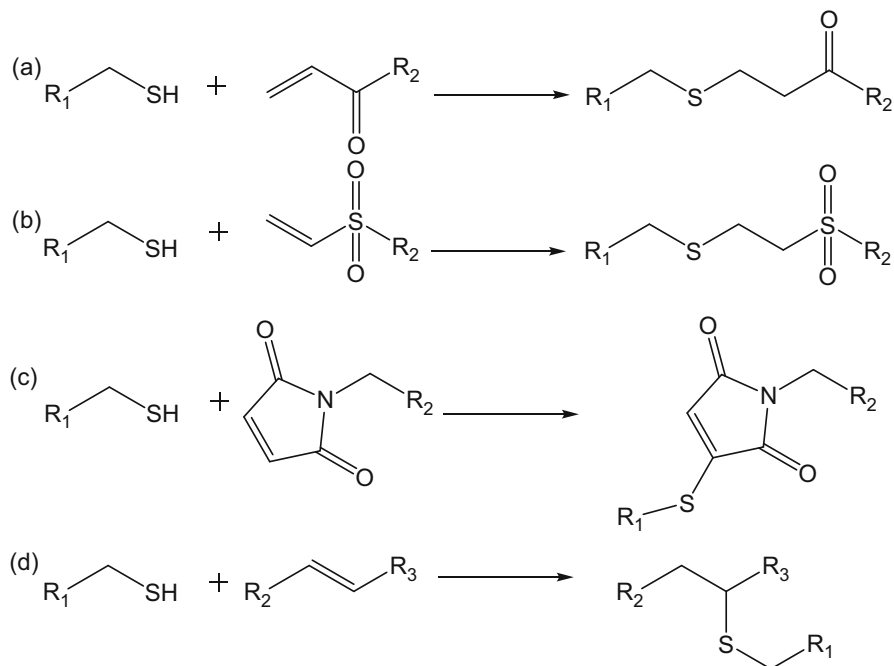


Fig. 18 Thiol-ene reaction variations (a) Michael addition between thiols and acrylates [201], (b) thiols and vinyl sulfones [202, 203], (c) thiols and maleimides [204], (d) thiols and alkenes [205, 206] (R2 and R3 are electron withdrawing groups)

intensity, and length of exposure. Additionally, it can take place under ambient conditions, without metal catalyst, and used with a variety of functional groups. High temperature (over 100°C, irradiation with UV light with UV lamps λ_{max} at 254 or 365 nm), sunlight, or cobalt-60 gamma ray source all can be used for generation of thiyl radicals [30].

Oxidation and Reduction

The half-reaction of $\text{RS-SR} + 2e^- \rightarrow 2\text{RS}^-$ has a reduction potential of -0.25 V. Formation of symmetrical disulfides from thiols is possible with easy-to-handle oxidizing agents, such as oxygen, iodine, hydrogen peroxide, or Fe(III) salts, whereas disulfides can be reduced to thiols with various reducing agents, i.e., dithiothreitol (DTT), *tris*-(carboxyethyl)phosphine (TCEP), or sodium dithionite ($\text{Na}_2\text{S}_2\text{O}_4$) [10].

Jonkheijm et al. demonstrated the bioorthogonality of radical thiol-ene reactions with the immobilization of biomolecules resulting in patterned surfaces. In particular they first treated a silicon oxide surface with aminocaproic acid (acts as a spacer), followed by covalently attaching polyamidoamine dendrimers, and subsequent coupling with previously reduced cystamine to result in a thiol

functionalized surface. Furthermore, the patterned surface was produced via the coating of the surface with ene functional biomolecules, in particular ene-bearing biotin, and directly covering with a photomask and irradiation of the surface. Visualization of the patterned surface was made possible via a Cy5-labeled streptavidin (SAv) [209].

Thiocarbonylthio end groups remaining on polymers synthesized via RAFT polymerization can result in instability of the final polymers [210]. Different methods can be used to remove the RAFT end-group, such as thermolysis, radical transfer, oxidation to give sulfine, and aminolysis [211, 212]. Of these methods, aminolysis (reduction) is frequently used to yield polymers with thiol end-groups that can be further modified. However, a major drawback of aminolysis is the oxidation of the resultant thiol to disulfides, resulting in bimodal populations of polymers containing thiol and disulfide functional polymers [213]. To overcome this problem, Boyer et al. have performed aminolysis of the RAFT containing endgroups with pyridyldisulfide-bearing, ene-bearing, or other thiol reactive compounds. This resulted in a simultaneous protection/functionalization of the thiols, while still controlling the functionality and polymer architecture via thiol-ene reactions [213].

3.10.2 Polymer End-Group Modifications

Various thiol end groups that remain after modification of dithioester, tri-thiocarbonate, or xanthogenate end group moieties from RAFT polymerization subsequently can be modified to obtain terminal thiols via ester/carbon cleavages. In particular, terminal thiols can react with modified maleimides or acrylates as thiol-Michael acceptors in RAFT end group modification. Additionally, star shaped polymers are possible by reacting thiol-terminated polymers with a tri-acrylate core [214].

Terminal-functionalized disulfides are possible via aminolysis of terminal dithioesters on poly(meth)acrylates, poly[(meth)acrylamides] in the presence of functional methane thiosulfonate reagents. Subsequently this approach was employed to various polymers to result in butynyl end groups in CuAAC [214].

Nucleophilic substitution of activated bromides, or thiol-bromo click chemistry, can be employed during aminolysis of RAFT polymers to result in thioether-bound functional groups [214].

Xu et al. demonstrated the efficiency of thiolisocyanate click chemistry on thiol-terminated poly (*N,N*-diethylacrylamide) with isocyanates [215].

Thiol-modified biomolecules can be coupled to RAFT generated polymers by addition of thiolreactive compounds during aminolysis followed by converting trithiocarbonate end group to (i) a stable thiol reactive group that can be used for bio-conjugation or directly (ii) to a bioconjugate (Fig. 19) [216].

ATRP is a good method of choice to produce polymers terminated with halides. Subsequently terminal bromides of poly(methyl acrylate) have been modified with thioglycerol in a thiol-bromo click substitution reaction. In turn, this was used as an effective synthetic pathway for bromoterminated macromolecular dendrimers via

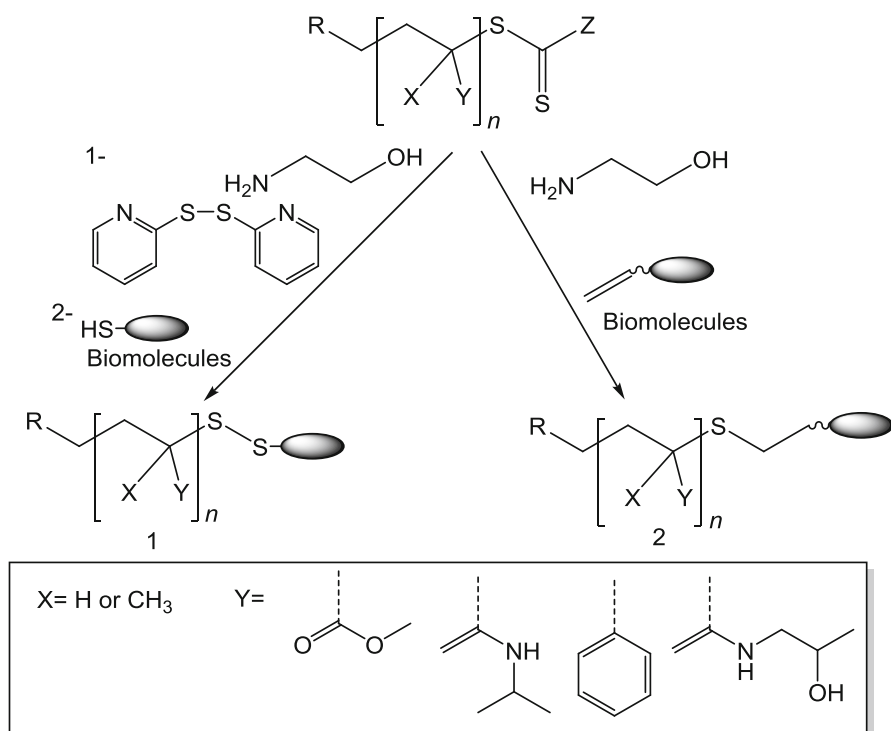


Fig. 19 Atom-efficient (bio)functionalization of a RAFT polymer via simultaneous aminolysis and thiol-specific reactions [216]. Reprinted from permission of JOHN WILEY and SONS

acylation of two terminal hydroxyl groups with 2-bromopropionyl bromide which equipped the end groups with two initiators for ATRP.

3.10.3 Polymer Side-Chain Modifications

Pentafluorostyrene is a readily available monomer that contains a thiol-reactive site that can undergo substitution of the *para*-fluoride with base catalysis after polymerization [217].

Another candidate for side group thiol-ene modification is poly(butadiene), with its pendant vinyl groups. Here the polymer can react with thiolated biomolecules such as amino acids, sugars, or cholesterol. However, the side reaction of cyclization of neighboring side groups can occur due to the closeness of the vinyl groups [218].

Pyridyl disulfide ethyl methacrylate has also been used in thiol conjugation following the polymerization by RAFT and ATRP, resulting in a styrenic derivative carrying two pyridyl disulfide groups that can easily attach to thiolated PEG without endangering the integrity of the acetal bridges within the polymer. Subsequently these bioinspired polymeric carriers became membrane-disruptive and were studied for cellular uptake at different pH [219].

3.11 Future Prospects in Polymer Functionalization

3.11.1 Sulfur Fluoride Exchange

Recently revived by the Sharpless group, the sulfur(VI) fluoride exchange (SuFEx) represents a useful and previously unexplored platform of click chemistry [220]. SuFEx click chemistry is based on the tendency of sulfonyl fluorides to exchange S-F bonds for S-O bonds in the presence of proton or silicon centers. Sulfonyl fluorides exhibit unique properties that make them more suitable for highly efficient reactions than other sulfonyl halides. First, the $\text{SO}_2\text{-F}$ is incredibly resistant to unwanted hydrolysis in harsh reaction conditions. Additionally, the fluoride radical is energetically inaccessible, which allows SuFEx chemistry to avoid radical pathways that hinder other sulfur (VI) halides. Lastly, the $\text{SO}_2\text{-O}$ bonds form rapidly and stably nonprotic conditions with the use of silicon centers, as Si-F forms the strongest single bond found in nature. The Locklin group has successfully employed SuFEx chemistry in the postmodification of polymer brushes [221]. 3-(fluorosulfonyl)propyl methacrylate (FSPMA) monomer was polymerized via UV initiated radical polymerization on an azo-based silane initiator monolayer to form poly(FSPMA) brushes. Subsequently the brushes were exposed to silyl ethers in the presence of a catalyst to encourage the exchange reaction. Sulfonate esters were rapidly formed bearing a number of functional moieties for continued postmodification, notably alkynes, azides, thiols, alkenes, dienes, and dienophiles. The reaction remained dormant until the addition of a catalyst such as triazabicyclodecene and produced an inert silyl fluoride byproduct. Due to its click chemistry features and ability to install other click moieties to for postpolymerization modification, SuFEx functionalization stands as a promising new option for widely expanding the toolbox for polymer tunability.

3.11.2 Nitrile Oxides

The group of Takata has recently reported an attractive new method for 1,3-dipolar cycloaddition to polymers containing unsaturated bonds [222]. Their work incorporates nitrile *N*-oxides as agents for efficient cycloaddition to both alkynes and alkenes. This reaction is advantageous to CuAAC click chemistry because it avoids the use of metal catalysts and solvents, and is safer at higher temperatures than azides [223]. Due to their instability with respect to self-reactions, nitrile *N*-oxides have received relatively little attention in polymer science thus far [224, 225]. However, the Takata group has developed kinetically stabilized nitrile *N*-oxide polymers for subsequent postmodification. Nitrile *N*-oxide terminated polymers were produced via Michael addition of *trans*- β -nitrostyrene to vinyl polymers such as PMMA or PtBMA. The resultant polymers displayed high reactivity towards both pendant and internal olefin-containing polymers at moderate temperatures. With further exploration, nitrile *N*-oxides show promise in accessing 1,3-dipolar cycloadditions in a wider range of systems.

3.11.3 Multicomponent Reactions

Multicomponent reactions (MCR) were first discovered by Strecker in 1850. They refer to reactions that are conducted as one-pot reactions employing at least two starting materials and atoms from starting materials are incorporated in the end product [226]. MCRs have gained attraction over the years and have been utilized in a variety of fields of life sciences, pharmaceuticals, and organic chemistry due to the decrease in chemicals, solvents and their time saving [227]. MCRs also capacitate postpolymerization modifications with a variety of functional groups [228]. Hence, the MCR derived product can be used as a synthetic hub to plenty of novel cyclic or acyclic scaffolds such as branched and star-shaped polymers [229].

As an example of a side chain modification utilizing MCRs, Li's group used poly(*p*-nitrophenyl-methacrylate)-*block*-poly(diethoxypropyl methacrylate) block copolymer as starting materials, afterwards, poly(*p*-nitrophenylmethacrylate) was modified by allylamine and poly(diethoxypropyl methacrylate) was then modified by *O*-benzylhydroxylamine hydrochloride [230].

In order to obtain end-chain modification, Sumerlin's group performed aminolysis of poly(*N*-isopropylacrylamide) into sulfhydryl terminated polymers and further connected with bismaleimide. Thus, they obtained maleimido-terminated macromolecules which allowed near-quantitative coupling with model low molecular weight thiols or dienes [231].

Polymers with tunable properties were synthesized via a Kabachnik-Fields polycondensation reaction in Theato's group. Here the Kabachnik-Fields reaction was chosen to result in α -amino phosphonates in a metal-free reaction that can lead to zwitterionic structures with potential antifouling applications. In particular they investigated the synthesis of various polycondensation polymers with 1,10-bis(4-formylphenyl)-1,4,7,10-tetraoxadecane as a dialdehyde with different diamines and phosphites. It was found that the α -amino phosphonates within the main chain can be deprotected to form zwitterionic species and the glass transition temperature could be varied with different diamines and phosphites [232], thus, allowing for an efficient and diverse synthesis of functional polymers.

Recently Tao's group has developed a strategy for performing MCRs during controlled radical polymerization (CRP) to build one-pot tri-component (enzymatic reaction/click reaction/CRP) and tetracomponent (Biginelli/CRP, Kabachnik-Fields (KF)/CRP) MCR-CRP systems [227]. To build the proper MCR, they utilized components that are efficient and robust under radical conditions and result in excellent yields. Therefore, they investigated the preparation of poly(1,4-dihydropyridine)s through the combination of a Hantzsch reaction and RAFT polymerization (Fig. 20). Hantzsch reactions traditionally consist of four starting materials: an aldehyde, 2 equivalents of β -ketoester, and ammonia to generate 1,4-dihydropyridines (1,4-DHPs). Additionally this reaction can occur under benign conditions, overall efficient, and is atom-economic with the only generated byproduct being water.

Thus, a typical Hantzsch-RAFT system was used to prepare poly(1,4-dihydropyridine), this included: 2-(acetoacetoxy)ethyl methacrylate (AEMA),

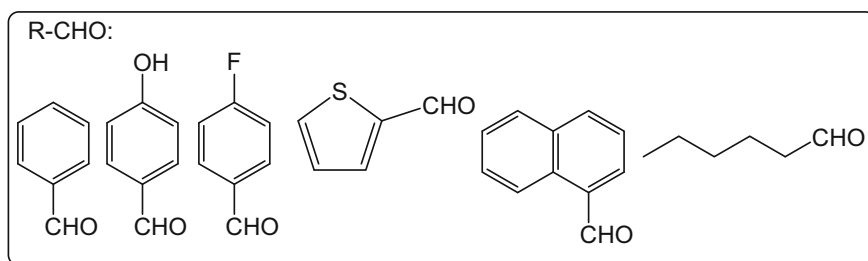
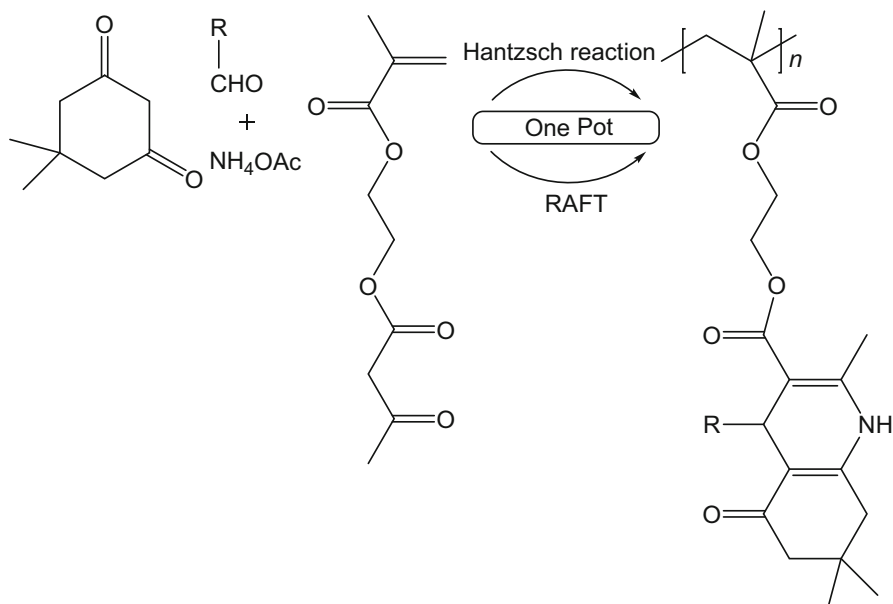


Fig. 20 Hantzsch-RAFT polymerization to one-pot well-defined poly(1,4-DHP)s. (Adapted with permission from [227]. Copyright 2015 American Chemical Society)

benzaldehyde, dimedone, and excess ammonium acetate (1.5 equiv. to AEMA), glycine (10% equiv. to ammonium acetate), azodiisobutyronitrile (AIBN) (initiator for RAFT), and 4-cyano-4-(ethylthio-carbonothioylthio) pentanoic acid (chain transfer agent for RAFT). The reaction proceeded under Schlenk conditions at 70 °C. Under optimal conditions, 1,4-DHP was generated in about 3 h with roughly 90% conversion and RAFT polymerization proceeded with 90% conversion (in relation to vinyl groups) in 12 h. The obtained polymers had controlled molecular weight and narrow dispersities (1.20) [227].

3.11.4 Catalytic Transesterifications

Sawamoto and coworkers demonstrated the use of versatile tandem catalysis in ruthenium-catalyzed living radical polymerization in a one-pot synthesis of multisequence-regulated copolymers (random-gradient and gradient-block

copolymers) and random and block copolymers [233]. The synthesis of gradient polymers takes place by combining the ruthenium-catalyzed living radical polymerization with the in situ transformation of a fed methacrylate (R_1MA) into another (R_2MA) via transesterification with an alcohol (R_2OH) and a metal oxide [$Al(Oi-Pr)_3$, $Ti(i-Br)_4$, etc.] [234].

Here, the metal alkoxide takes on two rolls: first acting as a cocatalyst for promoting propagation and second concurrently catalyzing in situ monomer transformation, which in turn provides a second monomer for copolymerization [233]. Furthermore, efficient transesterification relies on the following factors: (i) it has a higher activity for monomers than the polymers, independent of the monomer concentration (polymerization stage), living radical polymerization is never deactivated or retarded by the cocatalyst, and (iii) the transesterification into the second monomer is kinetically synchronized with the copolymerization [233].

In particular, gradient copolymers based on methyl methacrylate (MMA) and dodecyl methacrylate (DMA) were synthesized with MMA, 1-dodecanol, and titanium isopropoxide. To ensure complete synchronization of the two reactions, molecular sieves were employed to remove methanol from MMA transesterification into DMA. Furthermore, the resulting gradient copolymers exhibited a broad glass transition temperature, making it a potential material for vibration or acoustic dampening [234].

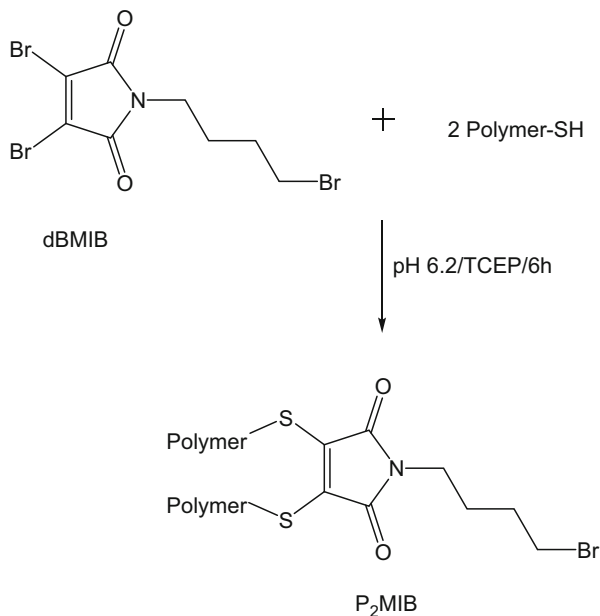
The group of Sawamoto also showed terminal-selective transesterification of chlorine-capped poly (methyl methacrylate)s with alcohols, resulting in telechelic and pinpoint-functionalized polymers that can subsequently be used as a micro-initiator in living radical polymerization due to the chlorine atom at the ω -terminal [235].

The transesterification reactions described by Sawamoto require several purification steps, which limits the development of this creative methodology. To overcome these limitations, enzymatic reactions can be used that exhibit specific catalytic abilities. In particular the use of Lipase B from *Candida antarctica* for the transacylation reaction between esters and nucleophilic compounds (alcohols). Furthermore, to obtain controlled polymerization under mild conditions with external stimuli, light-mediated polymerization has been employed. Tao et al. introduced a photoinduced electron transfer-reversible addition-fragmentation chain transfer (PET-RAFT) polymerization. This technique was used to synthesize (meth)acrylate, (meth)acylamide, vinyl acetate, monomers with great control over the molecular weight and molecular weight distribution. In particular, they prepared functional monomers via transacylation of 1,1,1-trifluoroethylacrylate (TFEA) with different alcohols in the presence of *Candida antarctica*. Following these monomers were polymerized via PET-RAFT to result in high-ordered multiblock copolymers [236].

3.12 Dibromomaleimide Chemistry

Baker et al. reported that bromomaleimides undergo efficient, clean, and selective substitution reactions with the thiol group of cysteines for protein modification and bioconjugation [237]. This rapid and quantitative substitution under mild conditions

Fig. 21 dBMIB as a coupling agent to couple two thiol-terminated polymers into a polymer dimer [238]. (Reprinted with permission from John Wiley and Sons)



showed characteristics of an ideal click reaction and potential use as a polymer-polymer coupling agent for topological polymer engineering [238].

Wang et al. showed that *N*-(4-bromobutyl) dibromomaleimide (dBMIB) can efficiently couple two thiol-terminated polymers that results in double the molecular weight (Fig. 21). Additionally the bromobutylene unit at the chain center may be transferred into an azido unit. This subsequently can be used in a CuAAC reaction for a coupling reaction to a third polymer chain resulting in an A₂B star polymer [238].

3.13 Use of Thiolactone

Although thiols can readily react with alkyl halides, epoxides, isocyanates, and double and triple bonds; the issues of smell, shelf life, and synthetic availability have led to the recent development of thiolactones (cyclic thioesters of mercaptoacids) in synthetic polymer science. Traditionally four-, five-, and six-membered rings are used, β -, γ -, δ -thiolactones, respectively. Here the ring is opened by the functional amine (aminolysis) and the resulting thiol subsequently reacts in an orthogonal manner with a thiol “scavenger” (Fig. 22). This allows for the introduction of two distinct functionalities at the same reactive site. This synthetic approach has two distinct advantages over other chemistries applied in post-polymer modification and polymer synthesis. Thiolactone chemistry results in 100% atom-efficient conjugation reactions and the ability to doubly modify the polymer scaffold [239].

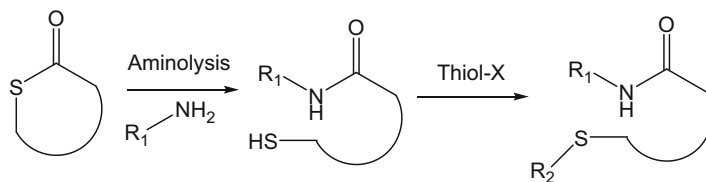


Fig. 22 Thiolactone entity: release of the thiol by nucleophilic ring-opening of the cyclic thioester and a subsequent reaction with a thiol “scavenger.” [239]. (Reprinted with permission from Elsevier)

Additionally, the double modification can occur in a one-pot fashion leading to simplified experimental set-ups [240].

Preparation of saturated γ - and δ -thiolactones occurs by the direct lactonization of the corresponding mercapto-acid. Although several nucleophiles can be used for the ring opening (water, alcohol, etc.) aminolysis requires no additives and can be performed in an aqueous medium, thus, making it an ideal choice for the ring opening [239].

4 Conclusion and Summary

This chapter outlined ways to functionalize polymers by taking a look at specific functional groups and modern reactions. Additionally to showcase the versatility of the functional groups, side chain and end chain modification were included within each section. Polymer functionalization is a versatile tool to tailor a polymer for a specific purpose and in turn develop novel polymer architecture. Additionally through the understanding of various synthetic concepts of organic reactions, the synthesis of well-defined multifunctional polymers is possible. Finally, future prospects in polymer functionalization were briefly mentioned.

Acknowledgments X. Huang kindly acknowledges the financial support of The China Scholarship Council (CSC, Grant 201506240019). D. D. Brauer kindly acknowledges the support of the German American Fulbright Commission through a Fulbright grant.

References

1. M. Hurtgen, A. Debuigne, C.A. Fustin, C. Jérôme, C. Detrembleur, Organometallic-mediated radical polymerization: Unusual route toward (quasi-) diblock graft copolymers starting from a mixture of monomers of opposed reactivity. *Macromolecules* **44**(12), 4623–4631 (2011)
2. J. Bonilla-Cruz, L. Caballero, M. Albores-Velasco, E. Saldívar-Guerra, J. Percino, V. Chapela, Mechanism and kinetics of the induction period in nitroxide mediated thermal auto-polymerizations. Application to the spontaneous copolymerization of styrene and maleic anhydride. *Radic. Polymer. Kinet. Mech.* 132–140 (2007)

3. D.E. Bergbreiter, N. Priyadarshani, Syntheses of terminally functionalized polyisobutylene derivatives using diazonium salts. *J. Polym. Sci. A Polym. Chem.* **49**(8), 1772–1783 (2011)
4. R. Godoy Lopez, C. Boisson, F. D'Agosto, R. Spitz, F. Boisson, P. Tordo, Direct syntheses of macroalkoxyamines based on polyethylene. *Macromolecules* **37**, 3540–3542 (2004)
5. J. Bonilla-Cruz, C. Guerrero-Sánchez, U.S. Schubert, E. Saldivar-Guerra, Controlled grafting-from of poly [styrene-co-maleic anhydride] onto polydienes using nitroxide chemistry. *Eur. Polym. J.* **46**(2), 298–312 (2010)
6. S. Qin, D. Qin, W.T. Ford, D.E. Resasco, J.E. Herrera, Functionalization of single-walled carbon nanotubes with polystyrene via grafting to and grafting from methods. *Macromolecules* **37**(3), 752–757 (2004)
7. J. Bonilla-Cruz, M. Dehonor, E. Saldivar-Guerra, A. Gonzalez-Montiel, in *Handbook of Polymer Synthesis, Characterization, and Processing*. Polymer modification (Wiley, Hoboken, 2013), pp. 205–223
8. Z. Li, K. Zhang, J. Ma, C. Cheng, K.L. Wooley, Facile syntheses of cylindrical molecular brushes by a sequential RAFT and ROMP grafting-through methodology. *J. Polym. Sci. A Polym. Chem.* **47**(20), 5557–5563 (2009)
9. D.A. Hucul, S.F. Hahn, Catalytic hydrogenation of polystyrene. *Adv. Mater.* **12**(23), 1855–1858 (2000)
10. P.J. Roth, K.T. Wiss, P. Theato, *Post-Polymerization Modification*, vol 5 (Elsevier B.V., 2012), Amsterdam, pp. 247–267
11. D. Zuchowska, Polybutadiene modified by epoxidation. 1. Effect of polybutadiene microstructure on the reactivity of double bonds. *Polymer* **21**(5), 514–520 (1980)
12. E.M. Cross, T. J. McCarthy, Radical chlorination of polyethylene film: control of surface selectivity. *Macromolecules*. **25**, 2603–2607 (1992)
13. E. Klesper, D. Strasilla, M.C. Berg, ¹H-NMR of the Esterification of Syndiotacticpoly (methacrylic acid) with Carbodiimides– I Esterification with methanol. *Eur. Polym. J.* **15**, 587–591 (1979)
14. T. Heinze, T. Liebert, Unconventional methods in cellulose functionalization. *Prog. Polym. Sci. (Oxford)* **26**(9), 1689–1762 (2001)
15. V.V. Korshak, The synthesis of polymers by modification methods the synthesis of polymers by modification methods. *Russ. Chem. Rev.* **49**(12), 1135–1980 (1980)
16. A. Ueno, C. Schuerch, Racemization of isotactic poly(isopropyl acrylate). *J. Polym. Sci. Polym. Lett.* **3**, 53–56 (1965)
17. P.E. Dawson, T.W. Muir, I. Clarklewis, S.B.H. Kent, Synthesis of proteins by native chemical ligation. *Science* **266**(5186), 776–779 (1994)
18. W.A. Cunningham, Sulfur. III. *J. Chem. Educ.* **12**(3), 120–124 (1935)
19. R.E. Oesper, Christian Friedrich Schönbein Part II. Experimental labors. *J. Chem. Educ.* **6**(4), 677–685 (1929)
20. P. Rustemeyer, History of CA and evolution of the markets. *Macromol. Symp.* **208**, 1–6 (2004)
21. H. Staudinger, J. Fritschi, Über Isopren und Kautschuk. 5. Mitteilung. Über die Hydrierung des Kautschuks und über seine Konstitution. *Helv. Chim. Acta* **5**(5), 785–806 (1922)
22. G.E. Serniuk, F.W. Banes, M.W. Swaney, Study of the reaction of Buna rubbers with aliphatic mercaptans. *J. Am. Chem. Soc.* **70**(5), 1804–1808 (1948)
23. K. W. Pepper, H. M. Paisley, M. A, Young Properties of ion-exchange resins in relation to their structure. Part VI. Anion-exchange resins derived from styrene-divinyl-benzene copolymers (resumed). *J. Am. Chem. Soc.* **833**, 4097–4105 (1953)
24. R.B. Merrifield, Solid phase peptide synthesis. I. The synthesis of. *J. Am. Chem. Soc.* **85**(14), 2149 (1963)
25. W. Kern, R.C. Schulz, D. Braun, Macro-molecules with groups of high reactivity. *J. Polym. Sci.* **48**, 91–99 (1960)
26. P.E. Blatz, O. Xocony, New polyelectrolytes: Synthesis and preliminary characterization. *J. Polym. Sci.* **58**, 755–768 (1962)

27. C.J. Hawker, A.W. Bosman, E. Harth, New polymer synthesis by nitroxide mediated living radical polymerizations. *Chem. Rev.* **101**(12), 3661–3688 (2001)
28. J.S. Wang, K. Matyjaszewski, Controlled/“living” radical polymerization. Atom transfer radical polymerization in the presence of transition-metal complexes. *J. Am. Chem. Soc.* **117**(6), 5614–5615 (1995)
29. J. Chiefari, Y.K. Bill Chong, F. Ercole, J. Krstina, J. Jeffery, T.P.T. Le, R.T.A. Mayadunne, G.F. Meijs, C.L. Moad, G. Moad, E. Rizzardo, S.H. Thang, Living free-radical polymerization by reversible addition-fragmentation chain transfer: the RAFT process. *Macromolecules* **31**(98), 5559–5562 (1998)
30. M.A. Tasdelen, B. Kiskan, Y. Yagci, Externally stimulated click reactions for macromolecular syntheses dedicated to Prof. Krzysztof Matyjaszewski on the occasion of his 65th birthday. *Prog. Polym. Sci.* **52**, 19–78 (2016)
31. P. Ferruti, A. Bettelli, A. Fer’è, High polymers of acrylic and methacrylic esters of N-hydroxysuccinimide as polyacrylamide and polymethacrylamide precursors. *Polymer* **13**(10), 462–464 (1972)
32. H.-G. Batz, G. Franzmann, H. Ringsdorf, Model reactions for synthesis of pharmacologically active polymers by way of monomeric and polymeric reactive esters. *Angew. Chem. Int. Ed. Engl.* **11**(12), 1103–1104 (1972)
33. G.W. Cline, S.B. Hanna, Kinetics and mechanisms of the aminolysis of N-hydroxysuccinimide esters in aqueous buffers. *J. Org. Chem.* **53**(15), 3583–3586 (1988)
34. D.E. Bergbreiter, R. Hughes, J. Besinaiz, C. Li, P.L. Osburn, Phase-selective solubility of poly (N-alkylacrylamide) s. *J. Am. Chem. Soc.* **125**(c), 8244–8249 (2003)
35. S.R.A. Devenish, J.B. Hill, J.W. Blunt, J.C. Morris, M.H.G. Munro, Dual side-reactions limit the utility of a key polymer therapeutic precursor. *Tetrahedron Lett.* **47**(17), 2875–2878 (2006)
36. S.Y. Wong, D. Putnam, Overcoming limiting side rxns associated w NHS-activated precursor polymethacrylamide-based polymer. *Bioconjug. Chem.* **18**(3), 970–982 (2007)
37. P. Theato, J.-u. Kim, J.-c. Lee, Controlled radical polymerization of active ester monomers: precursor polymers for highly functionalized materials. *Macromolecules* **37**(15), 5475–5478 (2004)
38. S.Y. Wong, N. Sood, D. Putnam, Combinatorial evaluation of cations, pH-sensitive and hydrophobic moieties for polymeric vector design. *Mol. Ther.* **17**(3), 480–490 (2009)
39. C.M. Leon, B.H. Lee, M. Preul, R. McLemore, B.L. Vernon, Synthesis and characterization of radio-opaque thermosensitive poly N-isopropylacrylamide-2,2’-(ethylenedioxy)bis(ethylamine)-2,3,5-triiodobenzamide. *Polym. Int.* **58**(8), 847–850 (2009)
40. V. S`ubr, K. Ulbrich, Synthesis and properties of new N-(2-hydroxypropyl)methacrylamide copolymers containing thiazolidine-2-thione reactive groups. *React. Funct. Polym.* **66**(12), 1525–1538 (2006)
41. M. Eberhardt, R. Mruk, R. Zentel, P. Th’eat, Synthesis of pentafluorophenyl(meth)acrylate polymers: new precursor polymers for the synthesis of multifunctional materials. *Eur. Polym. J.* **41**(7), 1569–1575 (2005)
42. K. Nilles, P. Theato, Synthesis and polymerization of active ester monomers based on 4-vinylbenzoic acid. *Eur. Polym. J.* **43**(7), 2901–2912 (2007)
43. K. Nilles, P. Theato, RAFT polymerization of activated 4-vinylbenzoates. *J. Polym. Sci. A: Polim. Chem.* **47**, 1696–1705 (2009)
44. A. Das, P. Theato, Multifaceted synthetic route to functional polyacrylates by transesterification of poly(pentafluorophenyl acrylates). *Macromolecules* **48**(24), 8695–8707 (2015)
45. J. Parvole, L. Ahrens, H. Blas, J. Vinas, C. Boissiere, C. Sanchez, M. Save, B. Charleux, Grafting polymer chains bearing an N -succinimidyl activated ester endgroup onto primary amine-coated silica particles and application of a simple, one-step approach via nitroxide-mediated controlled/living free-radical polymerization. *J. Polym. Sci. A Polym. Chem.* **48**(1), 173–185 (2010)

46. V. Ladmiral, L. Monaghan, G. Mantovani, D.M. Haddleton, α -Functional glycopolymers: new materials for (poly)peptide conjugation. *Polymer* **46**(19), 8536–8545 (2005)
47. J. Vinas, N. Chagneux, D. Gignes, T. Trimaille, A. Favier, D. Bertin, SG1-based alkoxyamine bearing a N-succinimidyl ester: a versatile tool for advanced polymer synthesis. *Polymer* **49**(17), 3639–3647 (2008)
48. D. Samantha, S. McRae, B. Cooper, Y. Hu, T. Emrick, J. Pratt, S.A. Charles, End-functionalized phosphorylcholine methacrylates and their use in protein conjugation. *Biomacromolecules* **9**(10), 2891–2897 (2008)
49. A. Lewis, Y. Tang, S. Brocchini, J.W. Choi, A. Godwin, Poly(2-methacryloyloxyethyl phosphoryl-choline) for protein conjugation. *Bioconjug. Chem.* **19**(11), 2144–2155 (2008)
50. Z. Zarafshani, T. Obata, J.F. Lutz, Smart PEGylation of trypsin. *Biomacromolecules* **11**(8), 2130–2135 (2010)
51. F. Lecolley, L. Tao, G. Mantovani, I. Durkin, S. Lautru, D.M. Haddleton, A new approach to bioconjugates for proteins and peptides (pegylation) utilising living radical polymerisation. *Chem. Commun.* **23**(18), 2026–2027 (2004)
52. I. Tan, Z. Zarafshani, J.-F. Lutz, M.-M. Titirici, PEGylated chromatography: efficient bioseparation on silica monoliths grafted with smart biocompatible polymers. *ACS Appl. Mater. Interfaces* **1**(9), 1869–1872 (2009)
53. J. Nicolas, E. Khoshdel, D.M. Haddleton, Bioconjugation onto biological surfaces with fluorescently labeled polymers. *Chem. Commun. (Camb.)* **17**, 1722–1724 (2007)
54. T.J.V. Prazeres, M. Beija, M.-T. Charreyre, J.P.S. Farinha, J.M.G. Martinho, RAFT polymerization and self-assembly of thermoresponsive poly(N-decylacrylamide-*b*-N,N-diethylacrylamide) block copolymers bearing a phenanthrene fluorescent α -end group. *Polymer* **51**(2), 355–367 (2010)
55. M. Bathfield, F. D'Agosto, R. Spitz, M.-T. Charreyre, T. Delair, Versatile precursors of functional RAFT agents. Application to the synthesis of bio-related end-functionalized polymers. *J. Am. Chem. Soc.* **128**(8), 2546–2547 (2006)
56. K. Godula, D. Rabuka, K.T. Nam, C.R. Bertozzi, Synthesis and microcontact printing of dual endfunctionalized mucin-like glycopolymers for microarray applications. *Angew. Chem. Int. Ed.* **48**(27), 4973–4976 (2009)
57. K.T. Wiss, P. Theato, Facilitating polymer conjugation via combination of RAFT polymerization and activated ester chemistry. *J. Polym. Sci. A Polym. Chem.* **48**(21), 4758–4767 (2010)
58. K.T. Wiss, O.D. Krishna, P.J. Roth, K.L. Kiick, P. Theato, A versatile grafting-to approach for the bioconjugation of polymers to collagen-like peptides using an activated ester chain transfer agent. *Macromolecules* **42**(12), 3860–3863 (2009)
59. O.D. Krishna, K.T. Wiss, T. Luo, D.J. Pochan, P. Theato, K.L. Kiick, Morphological transformations in a dually thermoresponsive coilrod-coil bioconjugate. *Soft Matter* **8**(14), 3832–3840 (2012)
60. P.J. Roth, K.T. Wiss, R. Zentel, P. Theato, Synthesis of reactive telechelic polymers based on pentafluorophenyl esters. *Macromolecules* **41**(22), 8513–8519 (2008)
61. M.A. Gauthier, M.I. Gibson, H.A. Klok, Synthesis of functional polymers by post-polymerization modification. *Angew. Chem. Int. Ed.* **48**(1), 48–58 (2009)
62. M.C. Davies, J.V. Dawkins, D.J. Hourston, Radical copolymerization of maleic anhydride and substituted styrenes by reversible addition-fragmentation chain transfer (RAFT) polymerization. *Polymer* **46**(6), 1739–1753 (2005)
63. I. Donati, A. Gamini, A. Vetere, C. Campa, S. Paoletti, Synthesis, characterization, and preliminary biological study of glycoconjugates of poly (styrene-co-maleic acid). *Biomacromolecules* **3**(4), 805–812 (2002)
64. S.M. Henry, M.E.H. El-Sayed, C.M. Pirie, A.S. Hoffman, P.S. Stayton, pH-responsive poly (styrene-alt-maleic anhydride) alkylamide copolymers for intracellular drug delivery. *Biomacromolecules* **7**(8), 2407–2414 (2006)

65. H. Willcock, R.K. O'Reilly, End group removal and modification of RAFT polymers. *Polym. Chem.* **1**(2), 149–157 (2010)
66. H.J. Knlker, T. Braxmeier, G. Schlechtingen, A novel method for the synthesis of isocyanates under mild conditions. *Angew. Chem. Int. Ed. Engl.* **34**(22), 2497–2500 (1995)
67. M. Drr, R. Zentel, R. Dietrich, K. Meerholz, C. Bruchle, J. Wichern, S. Zippel, P. Boldt, Reactions on vinyl isocyanate/maleimide copolymers: NLO-functionalized polymers with high glass transitions for nonlinear optical applications. *Macromolecules* **31**(5), 1454–1465 (1998)
68. D. Beyer, W. Paulus, M. Seitz, G. Maxein, H. Ringsdorf, M. Eich, Second harmonic generation in self-assembled alternating multilayers of hemicyanine containing polymers and polyvinylamine. *Thin Solid Films* **271**(1), 73–83 (1995)
69. J.D. Flores, J. Shin, C.E. Hoyle, C.L. McCormick, Direct RAFT polymerization of an unprotected isocyanate-containing monomer and subsequent structopendant functionalization using click-type reactions. *Polym. Chem.* **1**(2), 213–220 (2010)
70. P. Theato, H.A. Klok, *Functional Polymers by Post-Polymerization Modification: Concepts, Guidelines and Applications* (Wiley, Weinheim, 2013)
71. P. Zarras, O. Vogl, Ketenes and bisketenes as polymer intermediates. *Prog. Polym. Sci.* **16**(2), 173–201 (1991)
72. T.T. Tidwell, *Ketenes* (Wiley, Hoboken, 2006)
73. J.A. Hyatt, P.W. Reynolds, Ketene cycloadditions. *Org. React.* **45**, 159 (1994)
74. F.A. Leibfarth, C.J. Hawker, The emerging utility of ketenes in polymer chemistry. *J. Polym. Sci. A Polym. Chem.* **51**(18), 3769–3782 (2013)
75. F.A. Leibfarth, M. Kang, M. Ham, J. Kim, L.M. Campos, N. Gupta, B. Moon, C.J. Hawker, A facile route to ketene-functionalized polymers for general materials applications. *Nat. Chem.* **2**(3), 207–212 (2010)
76. L.D. Taylor, C.K. Chiklis, T.E. Platt, Synthesis and polymerization of 2-vinyl-4,4-dimethyl-5-oxazolone. *J. Polym. Sci. Polym. Lett.* **9**(3), 187–190 (1971)
77. D.C. Tully, M.J. Roberts, B.H. Geierstanger, R.B. Grubbs, Synthesis of reactive poly(vinyl oxazolones) via nitroxide-mediated “living” free radical polymerization. *Macromolecules* **36**(12), 4302–4308 (2003)
78. V. Lapinte, J.C. Brosse, L. Fontaine, Synthesis and ringopening metathesis polymerization (ROMP) reactivity of endo- and exonorbornenylazlactone using ruthenium catalysts. *Macromol. Chem. Phys.* **205**(6), 824–833 (2004)
79. L. Fontaine, T. Lemele, J.C. Brosse, G. Sennyey, J.P. Senet, D. Wattiez, Grafting of 2-vinyl-4,4-dimethylazlactone onto electron-beam activated poly(propylene) films and fabrics. Application to the immobilization of sericin. *Macromol. Chem. Phys.* **203**(10-11), 1377–1384 (2002)
80. P.L. Coleman, M.M. Walker, D.S. Milbrath, D.M. Stauffer, J.K. Rasmussen, L.R. Krepski, S.M. Heilmann, Immobilization of Protein A at high density on azlactone-functional polymeric beads and their use in affinity chromatography. *J. Chromatogr. A* **512**, 345–363 (1990)
81. S.M. Heilmann, J.K. Rasmussen, L.R. Krepski, Chemistry and technology of 2-alkenyl azalactones. *J. Polym. Sci. A Polym. Chem.* **39**, 3655 (2001)
82. M. W. Jones, S. J. Richards, D. M. Haddleton, M. I. Gibson, Poly (azlactone) s: Versatile scaffolds for tandem post-polymerisation modification and glycopolymers synthesis. *Polym. Chem.* **4**(3), 717–723 (2013)
83. F.W. Speetjens, M.C.D. Carter, M. Kim, P. Gopalan, M.K. Mahanthappa, D.M. Lynn, Post-fabrication placement of arbitrary chemical functionality on microphase-separated thin films of amine-reactive block copolymers. *ACS Macro Lett.* **3**(11), 1178–1182 (2014)
84. B.S. Lokitz, J. Wei, J.P. Hinestrota, I. Ivanov, J.F. Browning, J.F. Ankner, S.M. Kilbey, J.M. Messman, Manipulating interfaces through surface confinement of poly(glycidyl methacrylate)-block -poly(vinylidimethylazlactone), a dually reactive block copolymer. *Macromolecules* **45**(16), 6438–6449 (2012)

85. D.C. Tully, M.J. Roberts, B.H. Geierstanger, R.B. Grubbs, Synthesis of reactive poly(vinyl oxazolones) via nitroxidemediated “living” free radical polymerization. *Macromolecules* **36**(12), 4302–4308 (2003)
86. H.T. Ho, M.E. Levere, D. Fournier, V. Montembault, S. Pascual, L. Fontaine, Introducing the azlactone functionality into polymers through controlled radical polymerization: strategies and recent developments. *Aust. J. Chem.* **65**(8), 970–977 (2012)
87. C. Gardner, H. Sto’Iver, Reactive polyanions based on poly(4, 4-dimethyl-2-vinyl-2-oxazoline-5-one-co-methacrylic acid). *Macromolecules* **44**, 7115–7123 (2011)
88. M.E. Buck, D.M. Lynn, Azlactone-functionalized polymers as reactive platforms for the design of advanced materials: Progress in the last ten years. *Polym. Chem.* **3**(1), 66 (2012)
89. D. Navarro-Rodriguez, F.J. Rodriguez-Gonzalez, J. Romero-Garcia, E.J. Jimenez-Regalado, D. Guillon, Chemical modification of glycidyl methacrylate polymers with 4-hydroxy-4-methoxybiphenyl groups. *Eur. Polym. J.* **34**(7), 1039–1045 (1998)
90. Y. Iwakura, K. Toshikazu, Y. Imai, Reaction between amines and epoxy groups of acrylonitrile-glycidyl acrylate copolymers. *Makromol. Chem.* **86**, 73–79 (1965)
91. Y. Iwakura, T. Kurosaki, N. Nakabayashi, Reactive fiber. Part I. Copolymerization and copolymer of acrylonitrile with glycidyl methacrylate and with glycidyl acrylate. *Makromol. Chem.* **44**(1956), 570–590 (1961)
92. Y. Iwakura, T. Kurosaki, N. Ariga, T. Ito, Copolymerization of methyl methacrylat with glycidyl methacrylat and the reaction of the copolymer with amines. *Makromol. Chem.* **97**(2098), 128–138 (1966)
93. J. Kalal, F. S’vec, V. Maroušek, Reactions of epoxide groups of glycidyl methacrylate copolymers. *J. Polym. Sci. Polym. Symp.* **47**(1), 155–166 (1974)
94. R. Barbey, H.A. Klok, Room temperature, aqueous post-polymerization modification of glycidyl methacrylate-containing polymer brushes prepared via surface-initiated atom transfer radical polymerization. *Langmuir* **26**(23), 18219–18230 (2010)
95. V. Tsyalkovsky, V. Klep, K. Ramaratnam, R. Lupitsky, S. Minko, I. Luzinov, Fluorescent reactive core-shell composite nanoparticles with a high surface concentration of epoxy functionalities. *Chem. Mater.* **20**(1), 317–325 (2008)
96. L. Tian, X. Li, P. Zhao, X. Chen, Z. Ali, N. Ali, B. Zhang, H. Zhang, Q. Zhang, Generalized approach for fabricating monodisperse anisotropic microparticles via single-hole swelling PGMA seed particles. *Macromolecules* **48**(20), 7592–7603 (2015)
97. E. Soto-Cantu, B.S. Lokitz, J.P. Hinestrosa, C. Deodhar, J.M. Messman, J.F. Ankner, S.M. Kilbey, Versatility of alkyne-modified poly(glycidyl methacrylate) layers for click reactions. *Langmuir* **27**(10), 5986–5996 (2011)
98. S. Edmondson, W.T.S. Huck, Controlled growth and subsequent chemical modification of poly(glycidyl methacrylate) brushes on silicon wafers. *J. Mater. Chem.* **14**, 730 (2004)
99. J. Qin, X. Jiang, L. Gao, Y. Chen, F. Xi, Functional polymeric nanoobjects by cross-linking bulk self-assemblies of poly(tert-butyl acrylate)-block -poly(glycidyl methacrylate). *Macromolecules* **43**(19), 8094–8100 (2010)
100. A. Marino-gonza, A. Mairata, I.W.C.E. Arends, R.A. Sheldon, Efficient and selective aerobic oxidation of alcohols into aldehydes and ketones using ruthenium / TEMPO as the catalytic system. *J. Am. Chem. Soc.* **123**(23), 6826–6833 (2001)
101. A. De Mico, R. Margarita, L. Parlanti, A. Vescovi, G. Piancatelli, A versatile and highly selective hypervalent iodine (III)/2, 2, 6, 6-tetramethyl-1-piperidinyloxy-mediated oxidation of alcohols to carbonyl compounds. *J. Org. Chem.* **62**(20), 6974–6977 (1997)
102. J. Einhorn, C. Einhorn, F. Ratajczak, J.L. Pierre, Efficient and highly selective oxidation of primary alcohols to aldehydes by N-chlorosuccinimide mediated by oxoammonium salts. *J. Org. Chem.* **61**(9), 7452–7454 (1996)
103. A. Kirschning, H. Monenschein, R. Wittenberg, Functionalized polymersemerging versatile tools for solution-phase chemistry and automated parallel synthesis. *Angew. Chem. Int. Ed.* **40**(4), 650–679 (2001)

104. C. Einhorn, J. Einhorn, C. Marcadal, J.L. Pierre, Oxidation of organic substrates by molecular oxygen mediated by N-hydroxyphthalimide (NHPI) and acetaldehyde. *Chem. Commun.* **5**, 447–448 (1997)
105. J. Singh, M. Sharma, G.L. Kad, B.R. Chhabra, Selective oxidation of allylic methyl groups over a solid support under microwave irradiation. *J. Chem. Res.* **7**, 264–265 (1997)
106. N. Lawrence, Aldehydes and ketones. *J. Chem. Soc. Perkin Trans.* **1**(10), 1739–1750 (1998)
107. G. Godjoian, B. Singaram, Controlled reduction of tertiary amides to the corresponding aldehydes or amines using dialkylboranes. *Tetrahedron Lett.* **38**(10), 1717–1720 (1997)
108. X. Jia, S. Zhang, W. Wang, F. Luo, J. Cheng, Palladium-catalyzed acylation of sp² C-H bond: direct access to ketones from aldehydes. *Org. Lett.* **11**(14), 3120–3123 (2009)
109. G.T. Hermanson, *Bioconjugate Techniques* (Academic Press, Amsterdam, 2013)
110. G.A. Lemieux, C.R. Bertozzi, Chemoselective ligation reactions with proteins, oligosaccharides and cells. *Trends Biotechnol.* **16**(12), 506–513 (1998)
111. R.C. Li, R.M. Broyer, H.D. Maynard, Well-defined polymers with acetal side chains as reactive scaffolds synthesized by atom transfer radical polymerization. *J. Polym. Sci. A Polym. Chem.* **44**(17), 5004–5013 (2006)
112. J. Hwang, R.C. Li, H.D. Maynard, Well-defined polymers with activated ester and protected aldehyde side chains for biofunctionalization. *J. Control. Release* **122**(3), 279–286 (2007)
113. K.L. Christman, H.D. Maynard, Protein micropatterns using a pH-responsive polymer and light. *Langmuir* **21**(18), 8389–8393 (2005)
114. R.H. Wiley, P.H. Hobson, Polymerization of m- and p-formylstyrenes. *J. Polym. Sci.* **5**(4), 483–486 (1950)
115. N. Wagner, P. Zimmermann, P. Heisig, F. Klitsche, W. Maison, P. Theato, Investigation of antifouling properties of surfaces featuring zwitterionic α -aminophosphonic acid moieties. *Macromol. Biosci.* **15**(12), 1673–1678 (2015)
116. A. Hirao, S. Nakahama, Protection and polymerization of functional monomers. 10. Synthesis of well-defined poly(4-vinylbenzaldehyde) by the anionic living polymerization of N-[(4-ethenylphenyl) methylene] cyclohexamine. *Macromolecules* **20**(12), 2968–2972 (1987)
117. T. Ishizone, T. Utaka, Y. Ishino, A. Hirao, S. Nakahama, Anionic polymerization of monomers containing functional groups. 10. Anionic polymerizations of N-Aryl-N-(4-vinylbenzylidene) amines 1. *Macromolecules* **30**(21), 6458–6466 (1997)
118. G. Sun, C. Cheng, K.L. Wooley, Reversible addition fragmentation chain transfer polymerization of 4-vinylbenzaldehyde. *Macromolecules* **40**(4), 793–795 (2007)
119. G. Moad, E. Rizzardo, S.H. Thang, Living radical polymerization by the RAFT process. *Aust. J. Chem.* **58**(6), 379–410 (2005)
120. Z.P. Xiao, Z.H. Cai, H. Liang, J. Lu, Amphiphilic block copolymers with aldehyde and ferrocene-functionalized hydrophobic block and their redox-responsive micelles. *J. Mater. Chem.* **20**(38), 8375–8381 (2010)
121. C.S. Marvel, C.L. Levesque, The structure of vinyl polymers: the polymer from methyl vinyl ketone. *J. Am. Chem. Soc.* **60**(2), 280–284 (1938)
122. C. Cheng, G. Sun, E. Khoshdel, K.L. Wooley, Well-defined vinyl ketone-based polymers by reversible addition-fragmentation chain transfer polymerization. *J. Am. Chem. Soc.* **129**(33), 10086–10087 (2007)
123. A. Mittal, S. Sivaram, D. Baskaran, Unfavorable coordination of copper with methyl vinyl ketone in atom transfer radical polymerization. *Macromolecules* **39**(16), 5555–5558 (2006)
124. S.K. Yang, M. Weck, Covalent and orthogonal multi-functionalization of terpolymers. *Soft Matter* **5**(3), 582–585 (2009)
125. S.K. Yang, M. Weck, Modular covalent multifunctionalization of copolymers. *Macromolecules* **41**(2), 346–351 (2008)
126. C. Scholz, M. Iijima, Y. Nagasaki, K. Kataoka, A novel reactive polymeric micelle with aldehyde groups on its surface. *Macromolecules* **28**(21), 7295–7297 (1995)

127. Y. Nagasaki, T. Okada, C. Scholz, M. Iijima, M. Kato, K. Kataoka, The reactive polymeric micelle based on an aldehyde-ended poly (ethylene glycol)/poly (lactide) block copolymer. *Macromolecules* **31**(5), 1473–1479 (1998)
128. Y. Nagasaki, R. Ogawa, S. Yamamoto, M. Kato, K. Kataoka, Synthesis of heterotelechelic poly (ethylene glycol) macromonomers. Preparation of poly (ethylene glycol) possessing a methacryloyl group at one end and a formyl group at the other end. *Macromolecules* **30**(21), 6489–6493 (1997)
129. L. Tao, G. Mantovani, F. Lecolley, D.M. Haddleton, α -Aldehyde terminally functional methacrylic polymers from living radical polymerization: application in protein conjugation pegylation. *J. Am. Chem. Soc.* **126**(41), 13220–13221 (2004)
130. J.M. Notestein, L.W. Lee, R.A. Register, Well-defined diblock copolymers via termination of living ROMP with anionically polymerized macromolecular aldehydes. *Macromolecules* **35**(6), 1985–1987 (2002)
131. A.W. Jackson, D.A. Fulton, Dynamic covalent diblock copolymers prepared from RAFT generated aldehyde and alkoxyamine end-functionalized polymers. *Macromolecules* **43**(2), 1069–1075 (2009)
132. S. Coca, H. Paik, K. Matyjaszewski, Block copolymers by transformation of living ring-opening metathesis polymerization into controlled/living atom transfer radical polymerization. *Macromolecules* **30**(21), 6513–6516 (1997)
133. R. Huisgen, 1,3-Dipolar cycloadditions. Past and future. *Angew. Chem. Int. Ed. Engl.* **2**(10), 565–598 (1963)
134. R. Huisgen, Kinetics and mechanism of 1,3-dipolar cycloadditions. *Angew. Chem. Int. Ed. Engl.* **2**(11), 633–645 (1963)
135. Y. Li, J. Yang, B.C. Benicewicz, Well-controlled polymerization of 2-azodoethyl methacrylate at near room temperature and click functionalization. *J. Polym. Sci. Part A: Polym. Chem.* **45**, 4300–4306 (2007)
136. M.H.B. Stowell, T.M. McPhillips, D.C. Rees, S.M. Soltis, E. Abresch, G. Feher, Light-induced structural changes in photosynthetic reaction center: implications for mechanism of electron-proton transfer. *Science* **276**, 812–816 (1997)
137. S.C. Ritter, B. König, Signal amplification and transduction by photo-activated catalysis. *Chem. Commun.* **45**, 4694–4696 (2006)
138. V. Hong, A.K. Udit, R.A. Evans, G. Finn, Electrochemically protected copper(I)-catalyzed azide-alkyne cycloaddition. *ChemBioChem* **9**(9), 1481–1486 (2008)
139. G. Molteni, C.L. Bianchi, G. Marinoni, N. Santo, A. Ponti, Cu/Cu-oxide nanoparticles as catalyst in the “click” azide-alkyne cycloaddition. *New J. Chem.* **30**, 1137 (2006)
140. H.C. Kolb, M.G. Finn, K.B. Sharpless, Click chemistry: diverse chemical function from a few good reactions. *Angewandte Chem. Int. Ed.* **40**(11), 2004–2021 (2001)
141. W.H. Binder, R. Sachsenhofer, ‘Click’ chemistry in polymer and materials science. *Macromol. Rapid Commun.* **28**(1), 15–54 (2007)
142. S.S. Brent, V.T. Nicolay, Highly efficient click functionalization of poly(3-azidopropyl methacrylate) prepared by ATRP. *Macromolecules* **38**, 7540–7545 (2005)
143. T. Ishizone, J. Tsuchiya, A. Hirao, S. Nakahama, Anionic polymerization of monomers containing functional groups. 4. Anionic living polymerization of N,N-dialkyl-4-vinylbenzenesulfonamides. *Macromolecules* **25**(19), 4840–4847 (1992)
144. V. Ladmiral, T.M. Legge, Y. Zhao, S. Perrier, “Click” chemistry and radical polymerization: potential loss of orthogonality. *Macromolecules* **41**(18), 6728–6732 (2008)
145. M.Y. Sen, J.E. Puskas, Green polymer chemistry: telechelic poly(ethylene glycol)s via enzymatic catalysis. *Am. Chem. Soc. Polym. Prepr. Div. Polym. Chem.* **49**(1), 487–488 (2008)
146. T.R. Chan, R. Hilgraf, K.B. Sharpless, V.V. Fokin, Polytriazoles as copper (I) -stabilizing ligands in catalysis. *Org. Lett.* **6**(27), 2853–2855 (2004)
147. B. Parrish, R.B. Breitenkamp, T. Emrick, PEG- and peptide-grafted aliphatic polyesters by click chemistry. *J. Am. Chem. Soc.* **127**(20), 7404–7410 (2005)
148. R. Riva, S. Schmeits, F. Stoffelbach, C. Jérôme, R. Jérôme, P. Lecomte, Combination of ring-opening polymerization and “click” chemistry towards functionalization of aliphatic polyesters. *Chem. Commun. (Camb.)* **42**, 5334–5336 (2005)

149. J.A. Link, M.K.S. Vink, D.A. Tirrell, Presentation and detection of azide functionality in bacterial cell surface proteins presentation and detection of azide functionality in bacterial. *J. Am. Chem. Soc.* **2**(126), 10598–10602 (2004)
150. J. Lutz, H.G. Börner, K. Weichenhan, Combining ATRP and “click” chemistry: a promising platform toward functional biocompatible polymers and polymer bioconjugates. *Macromolecules* **39**(19), 6376–6383 (2006)
151. J. Lutz, H.G. Börner, K. Weichenhan, Combining atom transfer radical polymerization and click chemistry: a versatile method for the preparation of end-functional polymers. *Macromol. Rapid Commun.* **26**(7), 514–518 (2005)
152. K. Matyjaszewski, Y. Nakagawa, S.G. Gaynor, Synthesis of well-defined azido and amino end-functionalized polystyrene by atom transfer radical polymerization. *Macromol. Rapid Commun.* **18**(12), 1057–1066 (1997)
153. S.O. Kyeremateng, E. Amado, A. Blume, J. Kressler, Synthesis of ABC and CABAC triphilic block copolymers by ATRP combined with ‘Click’ chemistry. *Macromol. Rapid Commun.* **29**(12-13), 1140–1146 (2008)
154. W. Van Camp, V. Germonpre, L. Mespouille, P. Dubois, E.J. Goethals, F.E. Du Prez, New poly(acrylic acid) containing segmented copolymer structures by combination of “click” chemistry and atom transfer radical polymerization. *React. Funct. Polym.* **67**(11), 1168–1180 (2007)
155. J.A. Opsteen, J.C.M. van Hest, Modular synthesis of block copolymers via cycloaddition of terminal azide and alkyne functionalized polymers. *Chem. Rev.* **109**(11), 5620–5686 (2009)
156. G. Mantovani, V. Ladmiral, L. Tao, D.M. Haddleton, One-pot tandem living radical polymerisation-Huisgens cycloaddition process (“click”) catalysed by N-alkyl-2-pyridylmethanimine/Cu(I)Br complexes. *Chem. Commun. (Camb.)* **16**, 2089–2091 (2005)
157. C. Boyer, J. Liu, V. Bulmus, T.P. Davis, C. Barner-Kowollik, M.H. Stenzel, Direct synthesis of well-defined heterotelechelic polymers for bioconjugations. *Macromolecules* **41**(15), 5641–5650 (2008)
158. A. Otto Diels, Synthesen in der hydroaromatischeii. *Leibigs Ann. Chem* **460**(1906), 98–122 (1928)
159. A. Dag, H. Durmaz, G. Hizal, Umit Tunca: preparation of 3-arm star polymers (A3) via Diels-Alder click reaction. *J. Polym. Sci. A Polym. Chem.* **46**(1), 302–313 (2008)
160. J. Sauer, Diels-Alder reactions. I. New preparative aspects. *Angew. Chem. Int. Ed.* **5**(2), 211–230 (1966)
161. S.M. Ryan, X. Wang, G. Mantovani, C.T. Sayers, D.M. Haddleton, D.J. Brayden, Conjugation of salmon calcitonin to a combed-shaped end functionalized poly(poly(ethylene glycol) methyl ether methacrylate) yields a bioactive stable conjugate. *J. Control. Release* **135**(1), 51–59 (2009)
162. Y. Chujo, K. Sada, T. Saegusa, Reversible gelation of polyoxazoline by means of Diels-Alder reaction. *Macromolecules* **23**, 2636–2641 (1990)
163. J.R. Jones, C.L. Liotta, D.M. Collard, D.A. Schiraldi, Cross-linking and modification of poly(ethylene terephthalate-co-2,6-anthracenedicarboxylate) by Diels-Alder reactions with maleimides. *Macromolecules* **32**(18), 5786–5792 (1999)
164. I. Kosif, E.J. Park, R. Sanyal, A. Sanyal, Fabrication of maleimide containing thiol reactive hydrogels via diels-alder/retro-diels-alder strategy. *Macromolecules* **43**(9), 4140–4148 (2010)
165. M. M. Kose, G. Yesibag, A. Sanyal, Segment block dendrimers via Diels – Alder cycloaddition. *Org. Lett.* **10**(12), 2353–2356 (2008)
166. B. Gacal, H. Durmaz, M.A. Tasdelen, G. Hizal, U. Tunca, Y. Yagci, A.L. Demirel, Anthracene-maleimide-based Diels-Alder “click chemistry” as a novel route to graft copolymers. *Macromolecules* **39**(16), 5330–5336 (2006)
167. M.A. Tasdelen, DielsAlder click reactions: recent applications in polymer and material science. *Polym. Chem.* **2**(10), 2133 (2011)
168. T. Dispinar, R. Sanyal, A. Sanyal, A Diels-Alder/retro Diels-Alder strategy to synthesize polymers bearing maleimide side chains. *J. Polym. Sci. A Polym. Chem.* **45**(20), 4545–4551 (2007)

169. G. Mantovani, F. Lecolley, L. Tao, D.M. Haddleton, J. Clerx, J.J.L.M. Cornelissen, K. Velonia, Design and synthesis of N-maleimido-functionalized hydrophilic polymers via copper-mediated living radical polymerization: a suitable alternative to pegylation chemistry. *J. Am. Chem. Soc.* **127**(9), 2966–2973 (2005)
170. H. Durmaz, A. Dag, C. Onen, O. Gok, A. Sanyal, G. Hizal, U. Tunca, Multiarm star polymers with peripheral dendritic PMMA arms through Diels-Alder click reaction. *J. Polym. Sci. A Polym. Chem.* **48**(21), 4842–4846 (2010)
171. H. Durmaz, A. Dag, O. Altintas, T. Erdogan, G. Hizal, U. Tunca, One-pot synthesis of ABC type triblock copolymers via in situ Click [3 + 2] and Diels-Alder [4 + 2] reactions. *Macromolecules* **40**(2), 191–198 (2007)
172. Z. Shi, J. Luo, S. Huang, Y.J. Cheng, T.D. Kim, B.M. Polishak, X.H. Zhou, Y. Tian, S.H. Jang, D.B. Knorr, R.M. Overney, T.R. Younkin, A.K.Y. Jen, Controlled Diels Alder reactions used to incorporate highly efficient polyenic chromophores into maleimide-containing sidechain polymers for electro-optics. *Macromolecules* **42**(7), 2438–2445 (2009)
173. C. Gouss'e, A. Gandini, P. Hodge, Application of the DielsAlder reaction to polymers bearing furan moieties. 2. DielsAlder and Retro-DielsAlder reactions involving furan rings in some styrene copolymers. *Macromolecules* **31**(97), 314–321 (1998)
174. H.L. Wei, Z. Yang, L.M. Zheng, Y.M. Shen, Thermosensitive hydrogels synthesized by fast Diels-Alder reaction in water. *Polymer* **50**(13), 2836–2840 (2009)
175. S. Magana, A. Zerroukhi, C. Jegat, N. Mignard, Thermally reversible crosslinked polyethylene using Diels-Alder reaction in molten state. *React. Funct. Polym.* **70**(7), 442–448 (2010)
176. A.S. Goldmann, M. Glassner, A.J. Inglis, C. Barner-Kowollik, Post-functionalization of polymers via orthogonal ligation chemistry. *Macromol. Rapid Commun.* **34**(10), 810–849 (2013)
177. C. F. Hansell, P. Espeel, M. M. Stamenovic, I.A. Barker, P. Andrew, F. E. Du Prez, R. K.O. Reilly, Additive-free clicking for polymer functionalization and coupling by tetrazine–norbornene chemistry. *J. Am. Chem. Soc.* **133**(35), 13828–13831 (2011)
178. K. De Bruycker, S. Billiet, H.A. Houck, S. Chattopadhyay, J.M. Winne, F.E. Du Prez, Triazolinediones as highly enabling synthetic tools. *Chem. Rev.* **116**(6), 3919–3974 (2016)
179. Y.-C. Lai, G.B. Butler, Synthesis and polymerization of some new bis-triazolinediones: a stability study of 4-substituted triazolinediones. *J. Macromol. Sci. A Chem.* **22**(10), 1443–1461 (1985)
180. G.B. Butler, Modification of diene polymers and polymer synthesis by reaction of triazolinediones with olefinic bonds. *Polym. Sci. U.S.S.R.* **23**(11), 2587–2622 (1981)
181. R. Lusignan, United States Patent [19], 54–55 (1986)
182. H. Ban, M. Nagano, J. Gavriluyk, W. Hakamata, T. Inokuma, C.F. Barbas, Facile and stable linkages through tyrosine: bioconjugation strategies with the tyrosine-click reaction. *Bioconjug. Chem.* **24**(4), 520–532 (2013)
183. H.A. Houck, K. De Bruycker, S. Billiet, B. Dhanis, H. Goossens, S. Catak, V. Van Speybroeck, J.M. Winne, F.E. Du Prez, Design of a thermally controlled sequence of triazolinedione-based click and transclick reactions. *Chem. Sci.* **8**(4), 3098–3108 (2017)
184. P. Wilke, T. Kunde, S. Chattopadhyay, N. Ten Brummelhuis, F.E. Du Prez, H.G. Börner, Easy access to triazolinedione-endcapped peptides for chemical ligation. *Chem. Commun.* **53**(3), 593–596 (2017)
185. E. Shirakawa, T. Hayashi, Transitionmetal-free coupling reactions of aryl halides. *Chem. Lett.* **41**(2), 130–134 (2012)
186. T. Hosokawa, S.I. Murahashi, in *Handbook of Organopalladium Chemistry for Organic Synthesis*, vol. 2, ed. by E.-i. Negishi (Wiley, New York, 2002), pp. 2141–2159
187. G. Cahiez, F. Lepifre, P. Ramiandrasoa, Manganese-catalyzed substitution of activated aryl halides (X= Cl, Br and F) and aryl ethers by organomagnesium reagents. *Synthesis* **1999**(12), 2138–2144 (1999)
188. A. Suzuki, Organoboron compounds in new synthetic reactions. *Pure Appl. Chem.* **57**(12), 1749–1758 (1985)

189. O. Vechorkin, V. Proust, X. Hu, Functional group tolerant Kumada-Corriu-Tamao coupling of nonactivated alkyl halides with aryl and heteroaryl nucleophiles: catalysis by a nickel pincer complex permits the coupling of functionalized Grignard reagents. *J. Am. Chem. Soc.* **131**(28), 9756–9766 (2009)
190. W. Dohle, D.M. Lindsay, P. Knochel, Copper-mediated cross-coupling of functionalized arylmagnesium reagents with functionalized alkyl and benzylic halides. *Org. Lett.* **3**(18), 2871–2873 (2001)
191. V. Bonnet, F. Mongin, Q. Trcourt, P. Knochel, Syntheses of substituted pyridines, quinolines and diazines via palladium-catalyzed crosscoupling of aryl grignard reagents. *Tetrahedron* **58**(22), 4429–4438 (2002)
192. G. Manolikakes, P. Knochel, Radical catalysis of kumada cross-coupling reactions using functionalized grignard reagents. *Angew. Chem. Int. Ed.* **48**(1), 205–209 (2009)
193. V. Coessens, T. Pintauer, K. Matyjaszewski, Functional polymers by atom transfer radical polymerization. *Prog. Polym. Sci.* **26**(3), 337–377 (2001)
194. J.S. Wang, K. Matyjaszewski, Controlled/“ living” radical polymerization. Halogen atom transfer radical polymerization promoted by a Cu (I)/Cu (II) redox process. *Macromolecules* **28**(23), 7901–7910 (1995)
195. V. Percec, B. Barboiu, A. Neumann, J.C. Ronda, M. Zhao, Metal-catalyzed living radical polymerization of styrene initiated with arenesulfonyl chlorides. From heterogeneous to homogeneous catalysis. *Macromolecules* **29**(10), 3665–3668 (1996)
196. S. Ji, T.R. Hoye, C.W. Macosko, Controlled synthesis of high molecular weight telechelic polybutadienes by ring-opening metathesis polymerization. *Macromolecules* **37**(15), 5485–5489 (2004)
197. M. Ito, K. Koyakumar, T. Ohta, H. Takaya, A simple and convenient synthesis of Alkyl Azides under mild conditions. *Synthesis* **4**, 376–378 (1995)
198. C.E. Hoyle, A.B. Lowe, C.N. Bowman, Thiol-click chemistry: a multifaceted toolbox for small molecule and polymer synthesis. *Chem. Soc. Rev.* **39**(4), 1355–1387 (2010)
199. F. Fringuelli, F. Pizzo, S. Tortoioli, L. Vaccaro, Thiolytic of 1,2-epoxides by thiophenol catalyzed under solvent-free conditions. *Tetrahedron Lett.* **44**(35), 6785–6787 (2003)
200. M. Van Dijk, D.T.S. Rijkers, R.M.J. Liskamp, C.F. Van Nostrum, W.E. Hennink, Synthesis and applications of biomedical and pharmaceutical polymers via click chemistry methodologies. *Bioconjug. Chem.* **20**(11), 2001–2016 (2009)
201. M. Jemal, D.J. Hawthorne, Quantitative determination of BMS186716, a thiol compound, in dog plasma by high-performance liquid chromatography-positive ion electrospray mass spectrometry after formation of the methyl acrylate adduct. *J. Chromatogr. B Biomed. Appl.* **693**(1), 109–116 (1997)
202. M.S. Masri, M. Friedman, Protein reactions with methyl and ethyl vinyl sulfones. *J. Protein Chem.* **7**(1), 49–54 (1988)
203. M. Morpurgo, F.M. Veronese, D. Kachensky, J.M. Harris, S. Farmaceutiche, Preparation and characterization of poly (ethylene glycol) vinyl sulfone. *Bioconjug. Chem.* **7**(96), 363–368 (1996)
204. R.J. Pounder, M.J. Stanford, P. Brooks, S.P. Richards, A.P. Dove, Metal free thiol-maleimide ‘Click’ reaction as a mild functionalisation strategy for degradable polymers. *Chem. Commun. (Camb.)* **41**, 5158–5160 (2008)
205. Y. Geng, D.E. Discher, H. Justynska, J. Schlaad, Grafting short peptides onto polybutadiene-block-poly(ethylene oxide): a platform for self-assembling hybrid amphiphiles. *Angew. Chem. Int. Ed.* **45**(45), 7578–7581 (2006)
206. Z. Hordyjewicz-Baran, L. You, B. Smarsly, R. Sigel, H. Schlaad, Bioinspired polymer vesicles based on hydrophilically modified polybutadienes. *Macromolecules* **40**(11), 3901–3903 (2007)
207. R.P. Sijbesma, Reversible polymers formed from self-complementary monomers using quadruple hydrogen bonding. *Science* **278**(5343), 1601–1604 (1997)
208. C.E. Hoyle, T.Y. Lee, T. Roper, Thiolenes: chemistry of the past with promise for the future. *J. Polym. Sci. A Polym. Chem.* **42**(21), 5301–5338 (2004)

209. P. Jonkheijm, D. Weinrich, M. Koehn, H. Engelkamp, P.C.M. Christianen, J. Kuhlmann, J.C. Maan, D. Nuesse, H. Schroeder, R. Wacker, R. Breinbauer, C.M. Niemeyer, H. Waldmann, Photochemical surface patterning by the thiolene reaction. *Angew. Chem. Int. Ed.* **47**(23), 4421–4424 (2008)
210. P. Vana, L. Albertin, L. Barner, T.P. Davis, C. Barner-Kowollik, Reversible addition-fragmentation chain-transfer polymerization: unambiguous end-group assignment via electro-spray ionization mass spectrometry. *J. Polym. Sci. A Polym. Chem.* **40**(22), 4032–4037 (2002)
211. A. Postma, T.P. Davis, G. Li, G. Moad, M.S. O'Shea, RAFT polymerization with phthalimido-methyl trithiocarbonates or xanthates. On the origin of bimodal molecular weight distributions in living radical polymerization. *Macromolecules* **39**(16), 5307–5318 (2006)
212. A. Postma, T.P. Davis, G. Moad, M.S. O'Shea, Thermolysis of RAFT-synthesized polymers. A convenient method for trithiocarbonate group elimination. *Macromolecules* **38**(13), 5371–5374 (2005)
213. C. Boyer, A. Granville, T.P. Davis, V. Bulmus, Modification of RAFT-polymers via thiol-ene reactions: a general route to functional polymers and new architectures. *J. Polym. Sci. A Polym. Chem.* **47**, 3773–3794 (2009)
214. J.W. Chan, B. Yu, C. Hoyle, A.B. Lowe, Convergent synthesis of 3-arm star polymers from RAFT-prepared poly(N,N-diethylacrylamide) via a thiol-ene click reaction. *Chem. Commun. (Camb.)* **40**, 4959–4961 (2008)
215. J. Xu, L. Tao, C. Boyer, A.B. Lowe, T.P. Davis, Combining thio-bromo click chemistry and raft polymerization: a powerful tool for preparing functionalized multiblock and hyper-branched polymers. *Macromolecules* **43**(1), 20–24 (2010)
216. C. Boyer, V. Bulmus, T.P. Davis, Efficient usage of thiocarbonates for both the production and the biofunctionalization of polymers. *Macromol. Rapid Commun.* **30**(7), 493–497 (2009)
217. A. Bernkop-Schnürch, A. Greimel, Thiomers: the next generation of mucoadhesive polymers. *Am. J. Drug Deliv.* **3**(3), 141–154 (2005)
218. N.T. Brummelhuis, C. Diehl, H. Schlaad, Thiol ene modification of 1, 2-polybutadiene using UV light or sunlight. *Macromolecules* **41**, 9946–9947 (2008)
219. N. Murthy, J. Campbell, N. Fausto, A.S. Hoffman, P.S. Stayton, Bioinspired pH-responsive polymers for the intracellular delivery of biomolecular drugs. *Bioconjug. Chem.* **14**(2), 412–419 (2003)
220. J. Dong, L. Krasnova, M.G. Finn, K. Barry Sharpless, Sulfur(VI) fluoride exchange (SuFEx): another good reaction for click chemistry. *Angew. Chem. Int. Ed.* **53**(36), 9430–9448 (2014)
221. J. Yatvin, K. Brooks, J. Locklin, SuFEx on the surface: a flexible platform for post-polymerization modification of polymer brushes. *Angew. Chem. Int. Ed.* **54**(45), 13370–13373 (2015)
222. C.G. Wang, Y. Koyama, S. Uchida, T. Takata, Synthesis of highly reactive polymer nitrile N-oxides for effective solvent-free grafting. *ACS Macro Lett.* **3**(3), 286–290 (2014)
223. H. Feuer, K. Torrsell, *Nitrile Oxides, Nitrones, and Nitronates in Organic Synthesis*, 2nd edn. (Wiley-Interscience, Hoboken, 2008)
224. I. Singh, Z. Zarafshani, F. Heaney, J.-F. Lutz, Orthogonal modification of polymer chain-ends via sequential nitrile oxidealkyne and azidealkyne Huisgen cycloadditions. *Polym. Chem.* **2**(2), 372 (2011)
225. T. Kanbara, T. Ishii, K. Hasegawa, T. Yamamoto, Preparation of soluble and fluorescent poly(arylene)s by 1, 3-dipolar polycycloaddition and properties. *Polym. Bull.* **679**, 673–679 (1996)
226. I. Ugi, A. Dömling, W. Hörl, Multicomponent reactions in organic chemistry. *Endeavour* **18**(3), 115–122 (1994)
227. Q. Zhang, Y. Zhang, Y. Zhao, B. Yang, C. Fu, Y. Wei, L. Tao, Multicomponent polymerization system combining Hantzsch reaction and reversible addition – fragmentation chain transfer to efficiently synthesize well-defined poly(1,4-dihydropyridine)s. *ACS Macro Lett.* **4**(1), 128–132 (2015)
228. F. Moldenhauer, P. Theato, Sequential reactions for post-polymerization. *Modifications* **269**, 133–162 (2015)

229. A. Domling, W. Wang, K. Wang, Chemistry and biology of multicomponent reactions. *Chem. Rev.* **112**(6), 3083–3135 (2012)
230. R.C. Li, J. Hwang, H.D. Maynard, Reactive block copolymer scaffolds. *Chem. Commun.* **35**, 3631–3633 (2007)
231. M. Li, P. De, S.R. Gondi, B.S. Sumerlin, End group transformations of RAFT-generated polymers with bismaleimides: functional telechelics and modular block copolymers. *J. Polym. Sci. A Polym. Chem.* **46**(15), 5093–5100 (2008)
232. F. Moldenhauer, R. Kakuchi, P. Theato, Synthesis of polymers via kabachnik-fields polycondensation. *ACS Macro Lett.* **5**(1), 10–13 (2016)
233. K. Nakatani, Y. Ogura, Y. Koda, T. Terashima, M. Sawamoto, Sequence-regulated copolymers via tandem catalysis of living radical polymerization and in situ transesterification. *J. Am. Chem. Soc.* **134**(9), 4373–4383 (2012)
234. Y. Ogura, T. Terashima, M. Sawamoto, Synchronized tandem catalysis of living radical polymerization and transesterification: methacrylate gradient copolymers with extremely broad glass transition temperature. *ACS Macro Lett.* **2**(11), 985–989 (2013)
235. Y. Ogura, T. Terashima, M. Sawamoto, Terminal-selective transesterification of chlorine-capped poly (methyl methacrylate)s: a modular approach to telechelic and pinpoint-functionalized polymers poly (methyl methacrylate)s: a modular approach to telechelic and pinpoint-functionalized. *J. Am. Chem. Soc.* **138**(15), 5012–5015 (2016)
236. C. Fu, J. Xu, L. Tao, C. Boyer, Combining enzymatic monomer transformation with photo-induced electron transfer – reversible addition-fragmentation chain transfer for the synthesis of complex multiblock copolymers. *ACS Macro Lett.* **3**(7), 633–638 (2014)
237. M.E.B. Smith, F.F. Schumacher, C.P. Ryan, L.M. Tedaldi, D. Papaioannou, G. Waksman, S. Caddick, J.R. Baker, Protein modification, bioconjugation, and disulfide bridging using bromomaleimides. *J. Am. Chem. Soc.* **132**(6), 1960–1965 (2010)
238. Y. Cui, Y. Yan, Y. Chen, Z. Wang, Dibromomaleimide derivative as an efficient polymer coupling agent for building topological polymers. *Macromol. Chem. Phys.* **214**(4), 470–477 (2013)
239. P. Espeel, F.E. Du Prez, One-pot multi-step reactions based on thiolactone chemistry: a powerful synthetic tool in polymer science. *Eur. Polym. J.* **62**, 247–272 (2015)
240. F. Driessen, S. Martens, B. De Meyer, F.E. Du Prez, P. Espeel, Double Modification of Polymer End Groups through thiolactone chemistry. *Macromol. Rapid Commun.* **37**, 947–951 (2016)



Electrochemical Polymerization

3

Gertrude Fomo, Tesfaye Waryo, Usisipho Feleni, Priscilla Baker, and Emmanuel Iwuoha

Contents

1	History	106
2	Background on Electrochemical Polymerization	107
3	General Principle of Electrochemical Polymerization	107
4	Materials and Equipment Used for Electrochemical Polymerization	110
4.1	Electrodes Materials	110
4.2	Supporting Electrolyte Solution	111
4.3	Solvent	112
5	Reactivity of the Monomer	112
6	Techniques for Electrochemical Polymerization	115
6.1	Galvanostatic Polymerization Technique	115
6.2	Potentiostatic Polymerization Technique	115
6.3	Potentiodynamic Technique	116
7	Factors that Affect Electrochemical Polymerization	118
7.1	Monomer Concentration	118
7.2	pH of Medium	118
7.3	Doping	119
7.4	Mode of Initial Scan	123
8	Advantages and Application of Electrochemical Polymerization	125
8.1	Advantages	125

G. Fomo (✉) · T. Waryo
SensorLab, University of Western Cape, Cape Town, South Africa
e-mail: fomogertrude@gmail.com; twaryo@uwc.ac.za

U. Feleni
SensorLab, University of Western Cape, Cape Town, South Africa

Nanotechnology and Water Sustainability Research Unit, University of South Africa,
Johannesburg, South Africa
e-mail: felenu@unisa.ac.za

P. Baker · E. Iwuoha (✉)
SensorLab, Department of Chemistry, University of the Western Cape, Bellville, South Africa
e-mail: pbaker@uwc.ac.za; eiwuoha@uwc.ac.za

8.2 Applications	125
9 Conclusion	126
References	126

Abstract

Advances in molecular electronic devices such as sensors, organic solar cells, and organic light emitting diodes have increased the interest and research on electro-synthetic conducting polymers. This chapter focuses on electrochemical polymerization (or electropolymerization) as a cost-effective and easy-to-use method for the preparation of electrosynthetic conducting polymer films. Electropolymerized materials, characteristically, possess unique morphological, physical, electronic, and electrochemical properties which make them amenable to various applications. Electropolymerization is initiated by the oxidation of a monomer in an electrochemical cell, followed by the growth of the polymer film on the surface of the working electrode, which may be a carbonaceous, a metallic, or a conducting glass material. As the oxidation of the monomer is voltage- or current-induced, electrochemical polymerization is, therefore, a green chemistry methodology. Being devoid of the use of toxic oxidants, the technique ensures real-time controlled production of very high purity conducting polymer films. The films exhibit excellent electrical, electronic, magnetic, optical, and rheological properties. Polyaniline films in their pristine and doped forms and the films of other conducting polymers are discussed in this chapter.

1 History

Electrochemistry was born as a science especially in chemistry at the end of the eighteenth century by Galvani. Indeed, based on the experiments on the relationship between electricity and muscle contractions by Galvani, Volta (Alessandro Volta, Professor at University of Pavia) announced to the scientific community in 1800, the invention of the electric pile – a “device” which would later revolutionize the concept of energy production [1]. Later, it was found that Galvani’s conclusions were wrong, but his experiments elicited Volta’s interest in this area of study, and today Volta is regarded as the “Father of the Electrochemistry.” For many years, electrochemistry has been an important area of chemistry where technological advances result from the interaction of materials and the electrode in electrochemical cells. The very first effort related to this topic involved the oxidation of aniline in 1835 [2], and the term “aniline black” was given to the resulting polyaniline (PANI). The electrochemical synthesis method came from the notion of conjugated conducting polymers or synthetic metals, where Lethe (a Professor of Chemistry at the College of London Hospital) in 1862 reported the synthesis of a thick layer of dirty bluish-green pigment via the electrochemical polymerization of aniline in aqueous sulfuric acid on a platinum electrode [3]. Within the years 1968–1988, many researchers became interested in the synthesis of polyaniline, using both

chemical and electrochemical techniques with different oxidizing agents and electrolyte solutions [4–9].

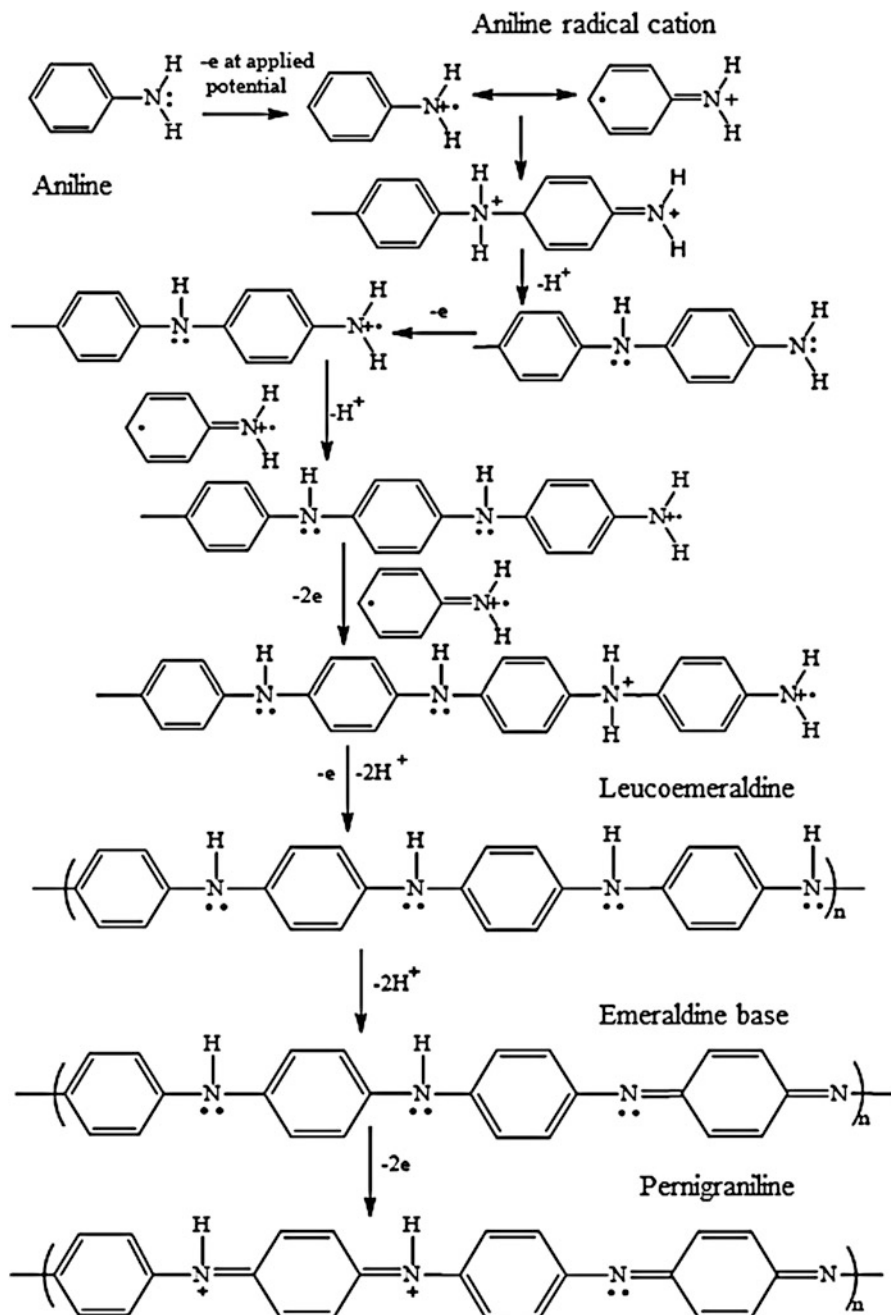
2 Background on Electrochemical Polymerization

Current advancement in electronics and electrochemical technology demands the development of highly sensitive sensors for electrocatalysis and detection, stable photovoltaic cells with high power conversion efficiency, and rechargeable batteries with high specific energy and power. A possible approach for attending to these needs involves the use of electroactive conducting polymer films to fabricate the associated devices [1, 10, 11]. As mentioned earlier, electrochemical polymerization is a typical method that is generally used for the synthesis of electroactive conducting polymers films because of its simplicity and reproducibility [12]. Potentiostatic, galvanostatic, potential step and potential sweep methods are usually used for the electropolymerization of monomers and their derivatives [13–16]. Therefore, factors such as applied potential, doping effect, electrolyte solution, direction of potential sweep, nature of the monomer, pH, solvent effect, temperature, and the voltammetric potential window determine the properties and applications of the polymer films formed [17–19]. Basically, in this method a potential is applied to a working electrode that is immersed in an electrochemical cell containing a monomer, a doping agent (where necessary), and the electrolyte solution. The monomer can, thus, be electrochemically oxidized to form free radicals that initiate the polymerization process and the deposition of the conducting polymer film on the working electrode surface.

3 General Principle of Electrochemical Polymerization

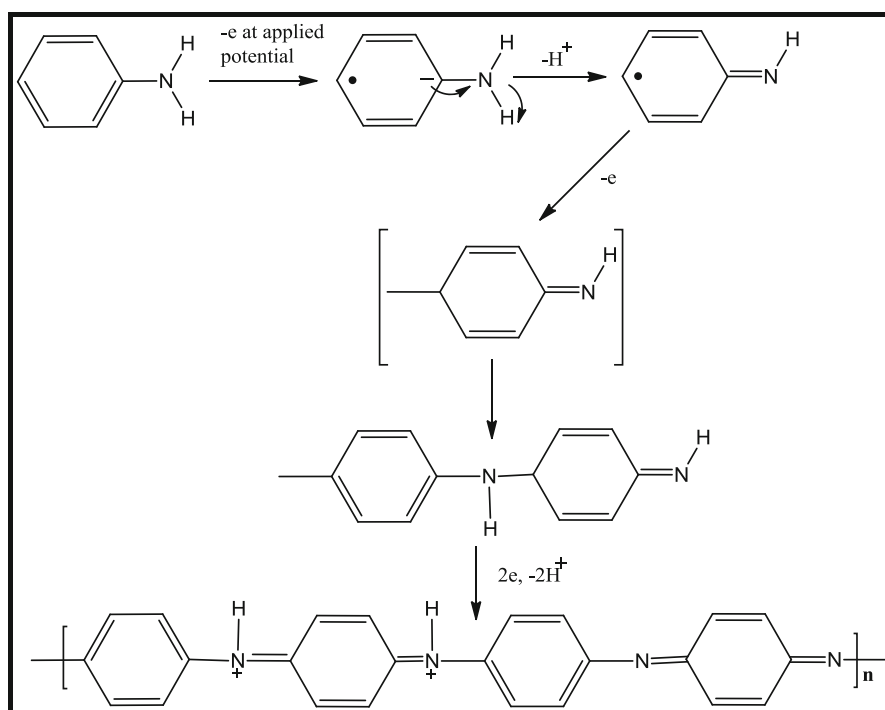
Electrochemical polymerization or electropolymerization is based on the deposition of the polymer onto the surface of a solid electrode material. This occurs through a generally accepted mechanism that involves the formation of cationic radical by the oxidation of the monomer on the solid electrode material. The electrochemical polymerization method can be divided into two important groups, which are anodic and cathodic electrochemical polymerization.

The anodic electrochemical polymerization is the most suitable method of oxidizing monomer species for the preparation of conducting compounds. This process begins with the formation of an oxidative monomer radical cation [20, 21]. The electrochemical stoichiometry of the electro-oxidation process involves $2.07\text{--}2.6 F \text{ mol}^{-1}$ monomer [15]. In most cases, the polymer film formation process requires two electrons per molecule of the monomer, that is, $2 F \text{ mol}^{-1}$. The excess charge is used for the oxidation of the oligomeric compounds that could be observed on the cyclic voltammogram. The mechanism of polymer formation and growth is believed to involve either the coupling between radical cations or the reaction of a radical cation with a neutral monomer. The radical cations can react either with neighboring radical cations or with neutral monomers to produce the polymer.



An example of the mechanism of an electrochemical polymerization involving radical cation-radical cation coupling is illustrated in Scheme 1. It informs that the first step of the electrosynthesis process is the formation of a cation radical via the transfer of an electron from a sp^3 orbital of the atom to the electrode surface when oxidation occurred. During the electropolymerization of aniline, a nonconducting PANI (leucoemeraldine state) is formed, while the most conducting PANI (emeraldine) is formed in the reduced state [22–24].

The cathodic electrochemical polymerization is rarely used for the synthesis of conducting polymers. Indeed, this type of polymerization involves reductive electrosynthetic processes which lead to very low yield of conducting polymers. Only the poly(*p*-phenylenevinylenes) (PPVs) conducting polymers, used as materials for organic light emitting devices [21, 25], have been produced by the cathodic polymerization method. In Sect. 7.4 of this chapter, the synthesis of conducting blue *p*-doped PANI-PSSA thin films by the cathodic polymerization is presented, together with its successful application as biocompatible conducting film for smart DNA aptamer-based biosensor for fish toxin [26]. The mechanism for the cathodic electropolymerization of aniline is as described in Scheme 2 [27].



Scheme 2 Mechanism for the cathodic electrochemical polymerization of aniline

4 Materials and Equipment Used for Electrochemical Polymerization

Electrochemical polymerization experiments are carried out with potentiostatic or galvanostatic electrochemical workstations (see Fig. 1), such as Amel Model 7050 Potentiostat-Galvanostat, Princeton Applied Research (PAR) Potentiostat Model 273, Eco Chemie Metrohm Autolab Potentiostats, Bioanalytical Systems, Incorporated (BASi) 50 and 100 Electrochemical Analyzers, BASi EC Epsilon Potentiostat, Radiometer Analytical VoltaLab 80 Electrochemical Laboratory, and Zhaner IM6e Potentiostat [23, 28–31]. There are also portable, miniaturized, and hand-held electrochemical instruments such as Metrohm Dropsens Potentiostat-Galvanostat, PalmSens Compact Electrochemical Interfaces, and Uniscan/PAR PG580 Potentiostat-Galvanostat that are also used by several laboratories for electrochemical polymerization.

4.1 Electrodes Materials

For electrochemical polymerization, a three-electrode convention in electrochemical cell is used. The working electrode, i.e., the electrode on which the desired reaction takes place, can be an inert metal (e.g., Au, Pt, and Ti) [32–38], a carbon material (e.g., glassy carbon, GC, pyrolytic graphite, PG, and boron-doped diamond (BDD)) [17, 23, 39–45], a conducting glass (e.g., indium tin oxide (ITO)) [46–48], or an alloy. The nature of the working electrode surface [49] influences the ease of the monomer oxidation, the rate of polymerization, and the growth of the polymer films. The use of alloys as working electrodes is limited by the very high potentials

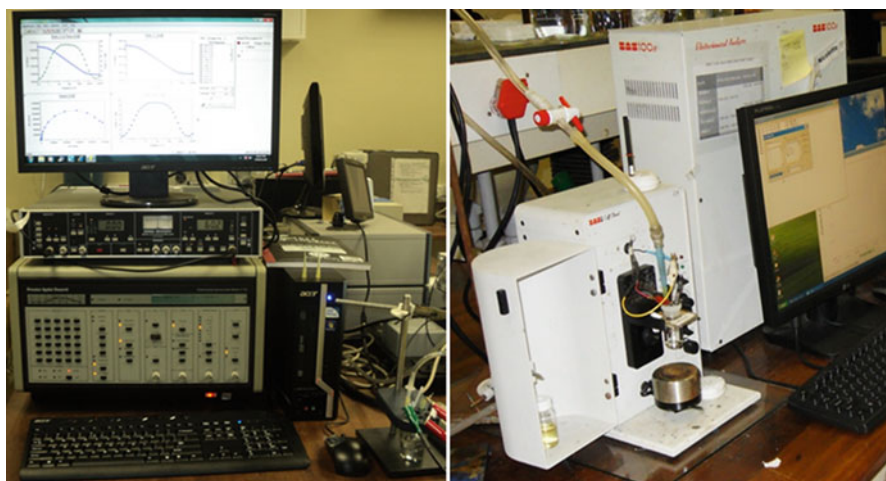


Fig. 1 Examples of instruments used for electrochemical polymerization

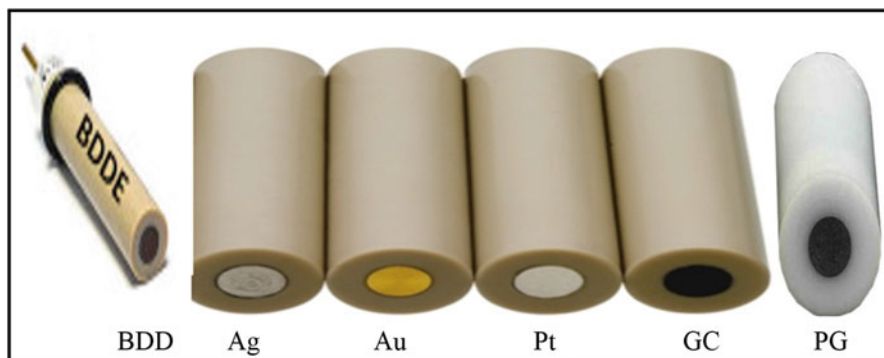


Fig. 2 Examples of working electrodes used for the electropolymerization of conducting polymers

required for the oxidation of monomers. Hence, many researchers use metal, carbon, and ITO glass materials for the electrochemical synthesis of conducting polymer films. The reference electrode in an electropolymerization cell measures the potential at the working electrode surface. It is made of a piece of silver wire immersed in 3 M Ag/AgCl solution, when working with aqueous electrolytes [50]. Silver wire or Ag/AgCl wire is used as pseudoreference electrodes when the medium of the electropolymerization reaction is organic. The auxiliary electrode or counter electrode used for electropolymerization is usually made of an inert material, such as Pt wire [51]. The counter electrode is used to close the current circuit in the electrochemical cell (Fig. 2).

4.2 Supporting Electrolyte Solution

Electrochemical polymerization is known to be a very effective technique for the synthesis of electroactive conductive polymers. The rate of polymer growth, the morphology, and properties of the polymer films deposited on the electrode are strongly influenced by the nature of the supporting electrolyte [19]. Thus, the supporting electrolyte is an important parameter to be taken into account and optimized when designing the electrochemical polymerization protocol. Aqueous and organic solutions have been used as supporting electrolyte, and some examples are listed in Table 1.

In addition to organic and aqueous media used as electrolytes for electrochemical polymerization, new approaches have emerged for the electrochemical polymerization in microemulsion media [15]. Many studies have identified aqueous media as ideal for the electrosynthesis of conducting polymers because of their low pollution and suitability for large-scale applications. However, there are some limitations in the use of aqueous media, including low solubility of many of the organic monomers in water. Microemulsions were introduced as supporting electrolytes for electropolymerization, in order to solve the problem of insolubility of some monomers in aqueous media. This is because a microemulsion is a complex mixture of water, hydrophobic organic material, and surfactant that forms a micellar solution, which is

Table 1 Some supporting electrolytes used for electrochemical polymerization

Medium	Electrolyte	Polymer	References
Aqueous solution	H ₂ SO ₄ , HCl, HNO ₃ , copper (II) nitrate, sodium sulfate, sodium sulfate/sodium perchlorate, lithium perchlorate, sodium benzoate, propylene carbonate/lithium perchlorate, phosphoric acid, and trifluoroacetic acid	PANI	[20, 30, 52, 53]
	Aqueous sulfuric acid and boron trifluoride diethyl etherate	Polyindole	[54–57]
Organic solution	HClO ₄ /acetonitrile, tetramethylammonium trifluoromethane-sulfonate/acetonitrile, periodic acid/tetraethylammonium tetrafluoroborate/acetonitrile, tetrabutylammonium tetrafluoroborate /trifluoroacetic acid, tetrabutylammonium perchlorate/acetonitrile, and perchloric acid/benzenesulfonic acids	PANI	[23, 55, 58, 59]
	Acetonitrile and dichloromethane	Polyindole	[21, 56, 60]
	Acetonitrile, dichloromethane, nitrobenzene, and propylene carbonate	Polypyrrole	[61]
	Ionic liquids	Polypyrrole, PANI, and polypyrrole	[62–64]

stabilized thermodynamically by the amphiphilic surfactant [65]. Microemulsions have been successfully applied in the electrochemical polymerization of aniline derivatives, benzene, pyrrole, and thiophenes, which are usually insoluble in water [18, 66–70].

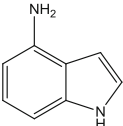
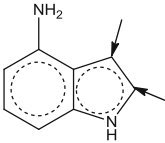
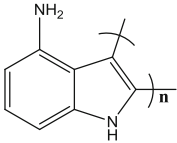
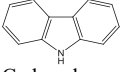
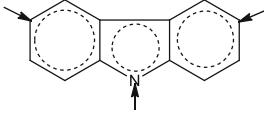
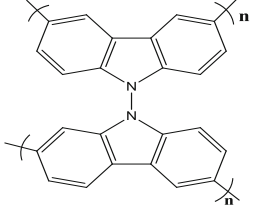
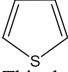
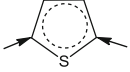
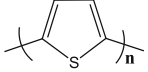
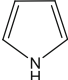
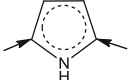
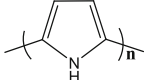
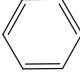

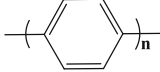
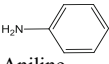
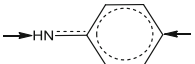
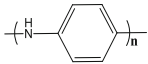
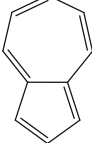
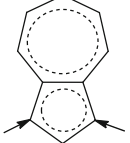
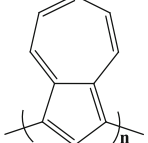
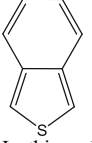
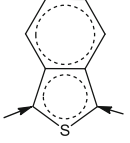
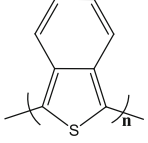
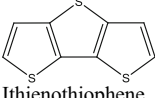
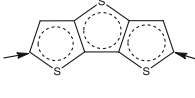
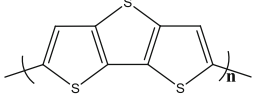
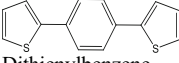
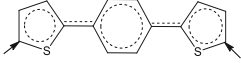
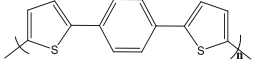
4.3 Solvent

In addition to the supporting electrolyte, the electrochemical cell also contains the solvent in which the monomer is dissolved. Studies have shown that the rate of electrochemical reaction had affected the nature of the solvent in which the monomer was dissolved [71]. The choice of the solvent normally depends on the nucleophilicity and polarity of the solvent [72]. These two properties determine the interaction between the solvent and the aromatic radical cation intermediates formed during the polymerization process. The choice of solvent depends on the solubility of the monomer in the solvent, which should be very pure and oxygen free to avoid the reaction of oxygen with the radical intermediates to form hydroxides on the electrode surface [21].

5 Reactivity of the Monomer

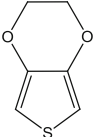
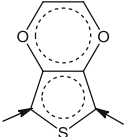
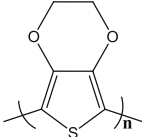
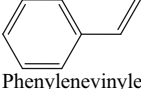
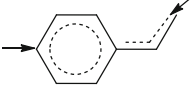
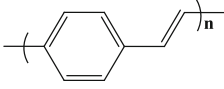
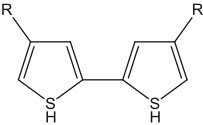
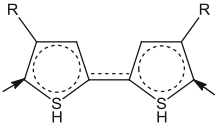
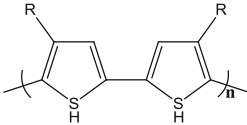
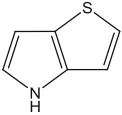
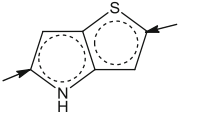
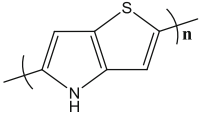
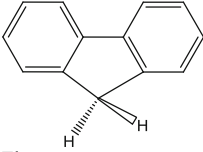
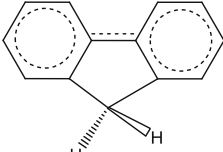
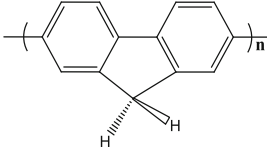
As most of the materials used as monomers for electrochemical polymerization are aromatic compounds (see Table 2), the coupling reaction step is likely to involve electrophilic aromatic substitution. If the nucleophilic character of the solvent

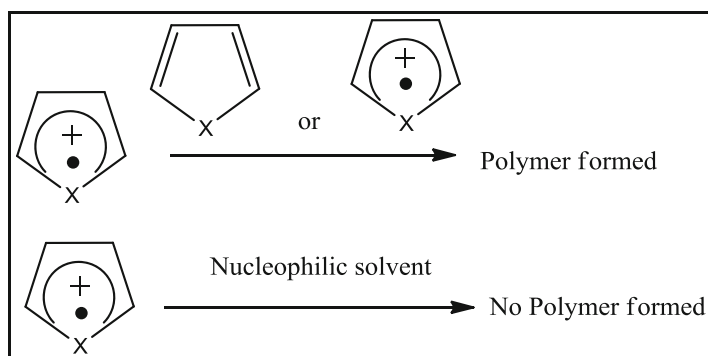
Table 2 The electrophilic reactivity sites of some monomers and their idealized polymer structures obtained on the material surface

Monomer	Electrophilic reactive site(s)	Ideal polymer structure	References
 4-Aminoindole			[34]
 Carbazole			[71]
 Thiophene			[73]
 Pyrrole			[73]
 Benzene			[73]
 Aniline			[73]
 Azulene			[15]
 Isothionaphthalene			[15]
 Ithienothiophene			[15]
 Dithienylbenzene			[15]

(continued)

Table 2 (continued)

Monomer	Electrophilic reactive site(s)	Ideal polymer structure	References
 Ethylenedioxythiophene			[74]
 Phenylevinylene			[15]
 Bithiophene			[75]
 Thieno[3,2-b]pyrrole			[76]
 Fluorene			[75]

**Scheme 3** Reactivity of the monomer depending on the solvent

(in which the monomer is dissolved) is lower than that of the monomer, the solvent can react with the radical cation in the electrolytic solution as shown in Scheme 3. Thus, the monomer's nucleophilicity or reactivity with the radical cation has a limiting effect on polymer film formation. The introduction of an electron donating

substituent into the monomer improves the reactivity of the monomer and favors polymerization in more nucleophilic solvents. If the monomer is very reactive, it could react with other compounds in the electrolyte solution or with the monomers at an undesired position on the aromatic ring that may not lead to polymerization. Another case where there will be no formation of polymer is where the monomer exhibits high stability, which makes it to diffuse away from the anode and thus unavailable for further reaction [20].

6 Techniques for Electrochemical Polymerization

Electrochemical polymerization being the most important method for the synthesis of electroconducting polymer films, the properties of the film formed depend on the choice of technique [22]. Generally, electrochemical polymerization can be achieved by the use of galvanostatic, potentiostatic, or potentiodynamic techniques [39].

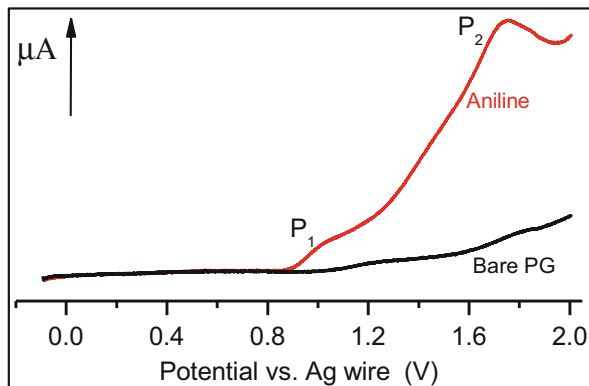
6.1 Galvanostatic Polymerization Technique

Galvanostatic polymerization is performed at a constant current, and it often results in the formation of a doped polymer [77]. This technique is advantageous as it is simple, suitable for practical application, and the thickness of the polymer film can be controlled during the polymerization process by specifying the polymerization time. The current density should be properly chosen to avoid an increase in the resistance at the electrode surface during the growth of the polymer, which might affect the intermediate reactions [78].

6.2 Potentiostatic Polymerization Technique

Potentiostatic technique, on the other hand, involves polymerization reaction carried out at a constant potential. The magnitude of the potential should be such that it will oxidize the monomer, since the polymerization process is initiated by the oxidation of the monomer. Also, the choice of potential should be such that it will avoid overoxidation or secondary reactions [15, 78]. Linear sweep voltammetry (LSV) is first used to oxidize the monomer. This is in order to obtain the potential window within which electro-polymerization can occur without the overoxidation of the monomer – which may impede the polymerization process or cause undesired reactions to take place [15, 78]. Some monomers can easily be oxidized in the presence of oxygen or other oxidizing agents in acid media. Overoxidation of monomers may lead to the formation of polymers with reduced electroactivity and conductivity. In addition, overoxidation may lead to the formation of hydroxyl and oxo derivatives as well as dimer and trimer products rather than the polymer [47]. For example, aniline was oxidized on pyrolytic graphite electrode (PGE) in perchloric acid/acetonitrile ($\text{HClO}_4/\text{CH}_3\text{CN}$) by LSV (Fig. 3). Two oxidation peaks,

Fig. 3 Linear sweep voltammograms of aniline in 0.1 M HClO₄/CH₃CN on PG electrode



P₁ and P₂, were observed at 1.03 and 1.75 V, respectively. The first peak, P₁, refers to the oxidation of aniline, while the second peak, P₂, is characteristic of the oxidation of p-aminodiphenylamine to form the benzidine species diffusing close to the electrode [35]. Moreover, the second peak can be related to the overoxidation of aniline, which results in the deposition of excess of cation on the electrode surface to form dimers. Therefore, the oxidation potential at P₁, which is the potential corresponding to the oxidation of aniline, helps to determine the onset potential (E_{onset}). Indeed, the onset potential is the potential where there is a quick rise of current from a value close to zero and where the oxidation reaction starts taking place. From E_{onset} , the final potential (E_2) used for the electrochemical polymerization can be calculated using the following equation:

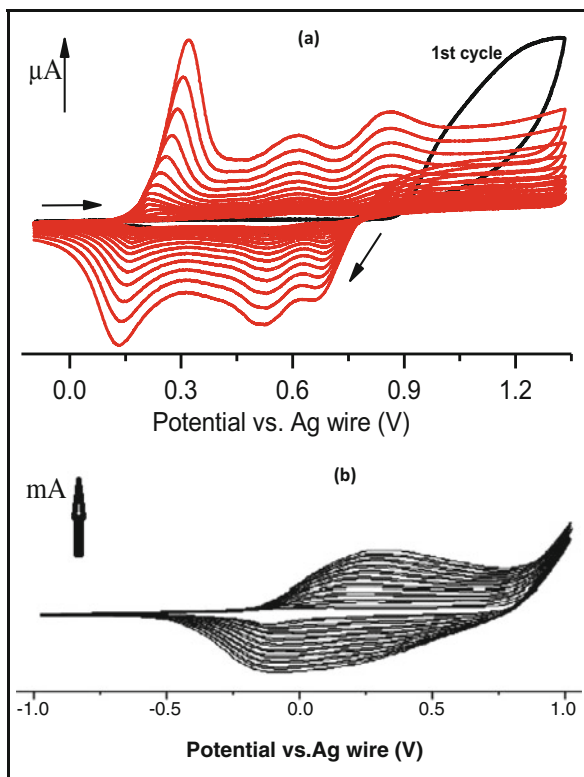
$$E_2 = E_{\text{onset}} + x \quad (1)$$

where x can be $0.1 \leq x \leq 0.5$ V.

6.3 Potentiodynamic Technique

Potentiodynamic technique in electrochemical polymerization involves the use of cyclic voltammetry (CV) technique. During this process, the monomer on the electrode surface is exposed to cyclic (switching between oxidative and reductive scans) regular changes of the applied potential within a potential window. This results in the formation of a conducting polymer film which alternates between the nonconducting (undoped) and the conducting (doped) forms [15], depending on the direction of the cyclic scan. Also, the thickness of the film depends on the number of CV scans performed. Potentiodynamic polymerization results in the formation of cyclic voltammograms (CVs) with several characteristic peaks, depending on the reaction mechanism of the polymerization process. For example, Fig. 4 shows the CVs of PANI film grown on a PG electrode in 0.1 M HClO₄/CH₃CN solution (Fig. 4a) [23] and polypyrrole film grown on Pt electrode in propylene

Fig. 4 Cyclic voltammograms of the formation of (a) 15 cycles of PANI film on PG electrodes in 0.1 M HClO₄/CH₃CN containing 0.05 M aniline at 50 mV s⁻¹; and (b) 10 cycles of polypyrrole film on Pt electrode in PC/TBAPF₆ containing 0.1 M pyrrole at 100 mV s⁻¹



carbonate/tetrabutylammonium hexafluorophosphate (PC/TBAPF₆) solution (Fig. 4b) [79]. The oxidation peak observed for the first cycle in Fig. 4a from 0.9 to 1.4 V is typically the characteristic of the oxidation of aniline, which initiates the polymerization process. This peak is absent in subsequent cycles, indicating that once the cation radicals are activated, the self-catalytic polymerization of aniline controls the film growth in subsequent voltammetry cycles [80]. In the case of polypyrrole and polythiophene [15], as well as polypyrene [81], for example, the first oxidation peak and the entire CV peak currents increase gradually with the number of CV cycles performed, which indicates the growth of conducting film.

For the PANI CV (Fig. 4a), the first redox couple between 0.2 and 0.3 V corresponds to the transformation of the reduced leucoemeraldine state to the partly oxidized emeraldine state. Further increase in potential leads to the appearance of another redox couple between 0.65 and 0.9 V, which is attributed to the transition from the reduced leucoemeraldine state to the fully oxidized pernigraniline state. Intermediate products formed during the polymerization process are trapped in the polymer [82], and the associated redox couple appears between 0.5 and 0.6 V. For polypyrrole, only one redox couple is formed and the properties of the redox peaks depend on the solvent system used in the electro-polymerization reaction [79].

7 Factors that Affect Electrochemical Polymerization

7.1 Monomer Concentration

The concentration of the monomer added into electrolyte solution is one of the important parameters affecting the polymerization reaction and the electrical conductivity properties of the polymer films formed [83]. It has been reported that the current density increases with the increase of concentration of the monomer which is due to the faster dimerization [12], this can also be express by the following equations:

$$i_a = i_0 e^{\frac{(1-\alpha)nF(E-E_{OCV})}{RT}} \quad (2)$$

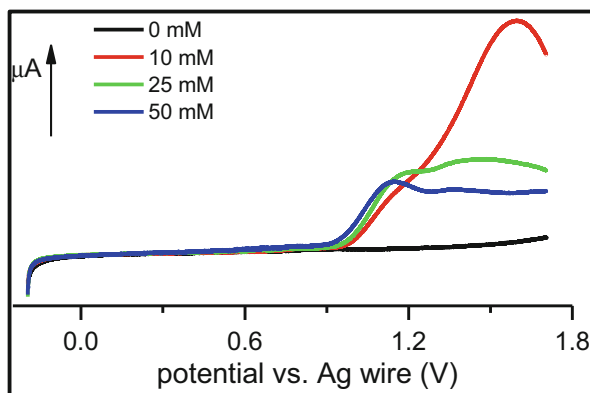
$$i_0 = nFAC_R^{\text{bulk}(1-\alpha)}C_0^{\text{bulk}(\alpha)}k_a \quad (3)$$

where i_a is the oxidation current, i_0 is the exchange current, k_a is the rate of oxidation, R is the ideal gas constant, T is the temperature, C_R and C_0 are concentration of the reduced and oxidized monomer, respectively, F is the Faraday constant, n is the number of electrons exchanged, E is the oxidation potential, and E_{OCV} is the open circuit voltage. However, for some conducting polymers, increase in monomer concentration results in a decrease in the oxidation potential. For example, Fig. 5 contains the oxidation LSVs of different concentration of aniline recorded on PG electrode in 0.1 M HClO₄/CH₃CN at 25 mV s⁻¹. The LSVs show that the aniline oxidation potential decreases as the aniline concentration increases, due to the formation of electro-conductive oligomers on the electrode surface [84] that makes the aniline oxidation process less energetic.

7.2 pH of Medium

In their base form polymers are insulating, regardless of the extent of their oxidation. It means that at pH values greater than 6, no significant protonation of a polymer can

Fig. 5 Linear scan voltammograms of aniline on PG electrode performed in 0.1 M HClO₄/CH₃CN



occur and it will be electrochemically inactive. However, under acidic pH conditions, protonation of the partly oxidized form of the polymer occurs, which makes it conducting. For electrosynthetic polymers, the part that is in contact with the electrode surface can undergo electrochemical redox reactions and serve as a conducting medium for electron transportation to the rest of the polymer chain [85, 86]. Also, some studies have shown that the oxidation and reduction processes of polymers do not occur at $\text{pH} > 4$ [86]. In addition, during polymerization, pH is used to control the critical potential beyond which the degradation of the polymer can occur [17]. Indeed, when polymerization is carried out at low pH, the potential exceeds the critical value for a brief period soon after the start of the polymerization process. The potential subsequently decreases with time to a constant potential value, which is low enough to prevent the degradation of the polymer chain. On the other hand, for polymerization at high pH, the opposite behavior is observed, whereby the increased deposition of insulating polymer species reduces the conductivity of the working electrode. This increases the polymerization potential, resulting in the degradation of the already deposited polymer film, due to the formation of heterojunctions or other unusual chemical bonds [87]. Other parameters, such as the rate of the polymerization reaction and the cathodic charge that determines the mechanisms of polymer growth, strongly depend on the pH of the polymerization medium.

7.3 Doping

With regard to electrochemical polymerization, doping involves the introduction species called dopants or counter ions into a polymer structure. This usually occurs stoichiometrically in order to compensate the positive charge of the polymeric species for it to attain electroneutrality. The insertion of dopants into a polymer is one way of improving its properties, such as morphology, conductivity, electrochemical activity, and the rate of polymerization [17, 88]. The dopant should be both chemically and electrochemically stable within the potential range for the polymerization process [22]. Beside the enhancement of the conductivity and the electroactivity of a polymer, counter ion dopants have significant effect on the polymer growth rate and its redox characteristics. The doping of a conductive polymer is classified as either chemical or electrochemical doping. Chemical doping is more frequently achieved by exposing the polymer to an oxidant (such as iodine or bromine), and less frequently by using a reductant (typically an alkali metal). In electrochemical doping, on the other hand, a polymer film deposited on a working electrode is suspended in an electrolyte solution (in which the polymer is insoluble) along with separate counter and reference electrodes. An electric potential difference is created which charges the polymer and causes appropriate counter ions from the electrolyte to enter the polymer. This charge transfer process creates a localized negative (n-doping) or positive (p-doping) charge on the polymer. This often leads to the distortion of the bonding structure of the polymer backbone and the formation of polarons and bipolarons (i.e., intergap electronic states) which can delocalize along the polymer chain or in an electric field. Electrochemical n-doping is far more common because of the ease of excluding oxygen from a solvent

in a sealed flask. The interaction between the polymer and the p-type dopant usually leads to the partial oxidation of the organic polymer π -backbone – a phenomenon known as oxidative doping. The transfer of electrons from the valence band of the polymer to the acceptor dopant leads to the delocalization of holes within the polymer backbone and the enhancement of the conductivity of the polymer system [89]. The illustration of the concept of n- and p-doping is as shown in Fig. 6.

Many dopants (such as anthracene sulfonic acid, benzene sulfonic acid, chloride ion, dibenzenesulfonic acid, hydrochloric acid, methane sulfonic acid, naphthalene sulfonic acid, perchloric acid, poly(acrylic acid), poly(anilinesulfonic acid), poly(4-styrenesulfonic acid) (PSSA), poly(vinylsulfonic acid), p-toluene sulfonic acid and sulfuric acid) have been used in the electrochemical doping of polymers [90–93]. Figure 7 depicts the electrochemical polymerization of aniline on PG electrodes in the presence and absence of the following dopants: 8-anilino-1-naphthalenesulfonic acid (ANSA), ethylenediaminetetraacetic acid (EDTA), 2-naphthalenesulfonic acid (NSA), and poly(4-styrenesulphonic acid) (PSSA). The CVs obtained during the potentiodynamic polymerization of aniline vary from one dopant to another. It can be observed that the CVs of the undoped PANI have three redox couples, while those of doped PANI have two redox peaks, with the exception of the EDTA-doped PANI that has three redox peaks. On the other hand, Fig. 8 (which contains the CVs of PANI and PANI doped with PSSA in phosphate buffer pH 7) demonstrates the effect of doping on the electroactivity of the PANI films in aqueous medium, at neutral pH. It can be seen that the undoped PANI films formed on the electrode surface loses its electroactivity after the first scan (Fig. 8a). The first cycle shows weak oxidation (E_{pa}) and reduction (E_{pc}) peak potentials at 0.7 and 0.3 V, respectively. The redox peaks disappear on the third scan, indicating that

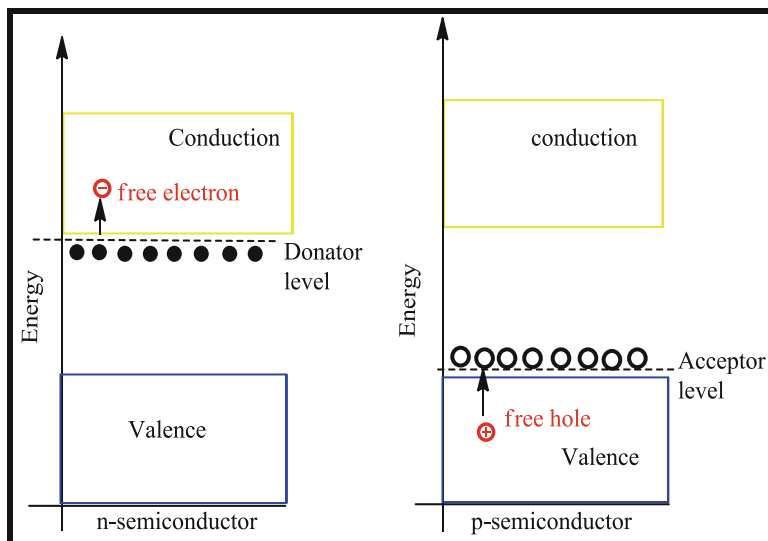


Fig. 6 Schematic representation of the n- and p-doping processes

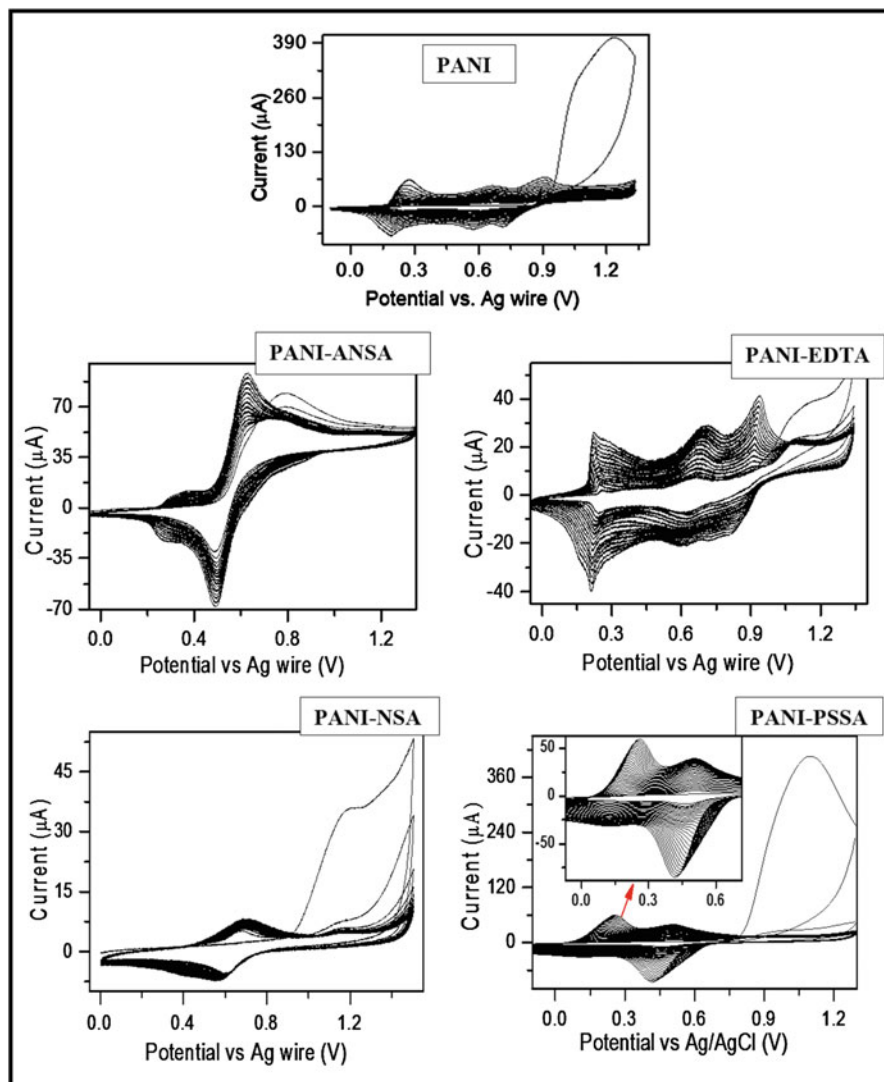


Fig. 7 Cyclic voltammograms (15 cycles) of the polymerization of doped 0.05 M aniline on PG electrode in 0.1 M $\text{HClO}_4/\text{CH}_3\text{CN}$, at 50 mV s^{-1}

the undoped PANI film has decreased electroactivity, which limit its application. Figure 8b shows a voltammogram of PANI-PSSA films which exhibits pronounced E_{pa} and E_{pc} at 0.274 and -0.199 V , respectively, and has a corresponding peak separation ($\Delta E_{\text{p}} = E_{\text{pa}} - E_{\text{pc}}$) value of 0.473 V, which is the characteristic of electroactive polymer films.

Polymers can also be doped with other polymers. For example, Fig. 9 contains the CVs for the doping of poly(3,4-ethylenedioxythiophene) (PEDOT) with poly

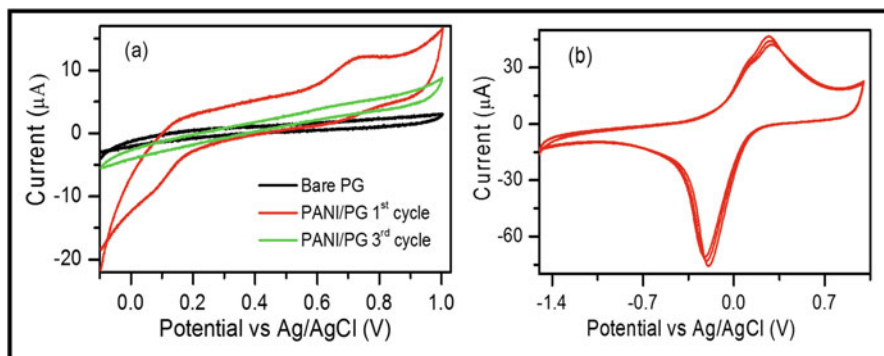


Fig. 8 Cyclic voltammograms of (a) PANI/PG and (b) PANI-PSSA/PG (3 cycles) in phosphate buffer pH 7

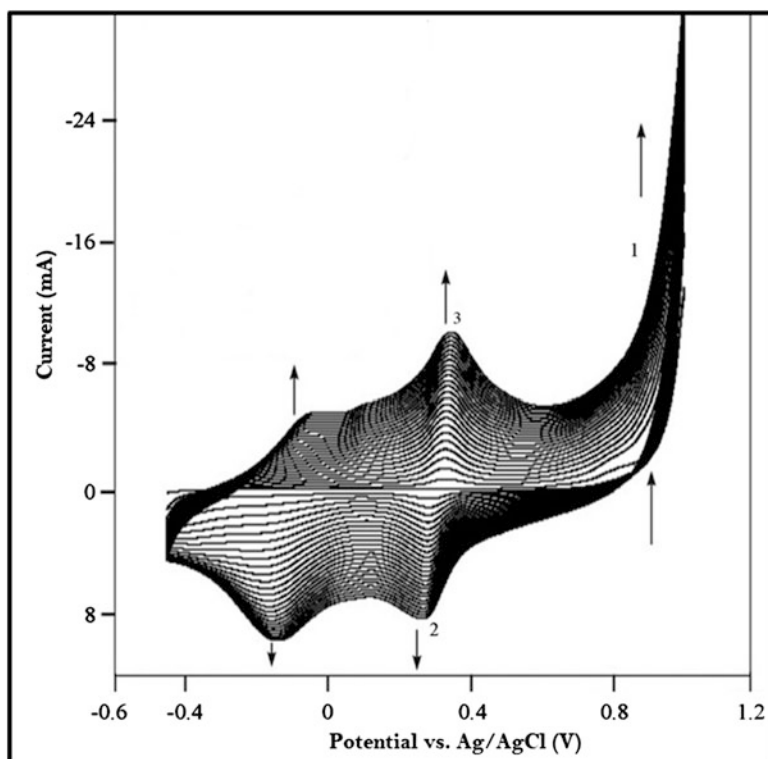


Fig. 9 Cyclic voltammograms of PEDOT-PANS film formation on GCE in 0.2 M HNO_3 solution containing 1.0 mM of ANS and 0.01 M EDOT at 100 mV s^{-1}

(5-amino-2-naphthalenesulfonic acid) (PANS) from a solution containing PEDOT polymer and 5-amino-2-naphthalenesulfonic acid (ANS) monomer. PANS deposits in situ on the PEDOT as it is being electropolymerized from ANS. The PEDOT–PANS polymer films on GCE have been applied in the electrooxidation of dopamine [94].

7.4 Mode of Initial Scan

When the monomer is electrochemically polymerized onto an electrode surface, polymer films of different colors are obtained. The color of the polymeric product obtained depends on the initial scan direction. Indeed, if the scan is carried cathodically, p-doped polymer film is formed, while when the scan is carried out anodically, the polymer formed is neutral. Both form p-doped and neutral polymer vary in solubility, electrochemical properties, and conductivity. For example, PANI–PSSA was electrochemically synthesized in phosphoric acid on Au, GC, PG, and Pt electrodes in order to evaluate the solubility, electrode kinetics, and the influence of the initial scan direction.

Figure 10 shows the CVs of electroactive green neutral and blue p-doped PANI–PSSA thin films recorded during the potentiodynamic polymerization of aniline on four different electrodes in 1 M H_3PO_4 , containing PSSA. The CVs of the neutral PANI–PSSA films exhibit three redox couples between 0.02 to 0.09 V, the actual value of the peak potential depending on the electrode used (Fig. 10a). Compared with the CVs obtained for the electropolymerization of aniline alone (Fig. 4), it is found that the dopant (PSSA) reduced the magnitude of both the E_{pc} and E_{pa} values of the PANI–PSSA films, due to the doping and undoping of PANI film by protons and anions. The redox peaks between 0.1 and 0.4 V (for Au, GC, PG, and Pt electrodes of Fig. 10a) is attributed to leucoemeraldine/emeraldine transformation of PANI–PSSA, while the redox couple that occurs between 0.35 and 0.9 V is due to emeraldine/permanganiline transformation [95]. Pt does not exhibit the redox couple that occurs between 0.3 and 0.6 V, which is attributed to the formation of intermediates products [82].

A major drawback for the application of PANI films is its insolubility in many solvents. To overcome this problem, sulfonated heteronuclear aromatic hydrocarbons (or any dopant) can be incorporated into the PANI backbone and the polymerization mode (anodic or cathodic scan) chosen according to the desired polymer properties and application. Solubility studies showed that the neutral and p-doped PANI–PSSA films exhibited improved solubility in polar organic solvents such as DMSO and DMF compared to PANI. However, it was found that the neutral PANI–PSSA was very dispersed in DMSO, while the p-doped PANI–PSSA was more dispersed in DMF. Similar results have been reported for doped PANI [90, 96, 97] in which the degree of dispersion depended on whether the polymer was neutral or p-doped. The neutral PANI–PSSA films formed on the electrode surface gave a green color in DMSO but not in DMF.

Other factors that influence electrochemical polymerization reactions include temperature and the nature of substituents of the monomer starting materials,

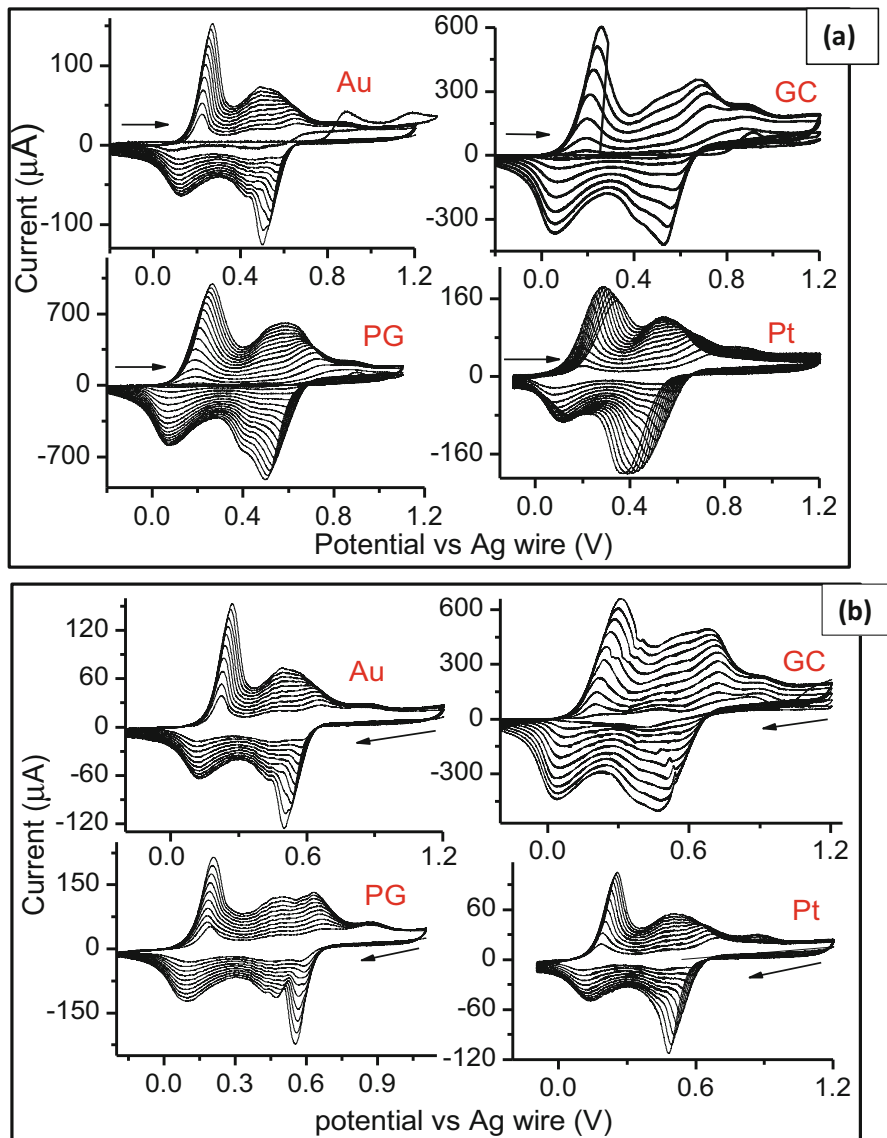


Fig. 10 Cyclic voltammograms (15 cycles) of PANI–PSSA films synthesized (a) anodically and (b) cathodically, at 0.050 V s^{-1} on Au, GC, PG, and Pt electrodes, in $1 \text{ M H}_3\text{PO}_4$ containing 0.05 M aniline and 0.025 M PSSA

particularly in the case of aromatic monomers [39]. Temperature affects the kinetics of the polymerization reaction process and may also determine the extent of the undesired side reactions. For example, since the oxygen species in the reaction medium are sensitive to high temperature, they can easily react with free radicals

formed from anodic processes, thus decreasing the polymerization efficiency [98]. On the other hand, the rate of polymerization increases with temperature due to improved conductivity and electroactivity of the monomer at high temperatures [99].

8 Advantages and Application of Electrochemical Polymerization

8.1 Advantages

The electrochemical synthesis of polymer has the advantage of combining the synthesis and modification steps in one procedure. In this method, the electrochemical oxidation of a monomer gives rise to free radicals that are adsorbed on the electrode surface, which can subsequently undergo a wide variety of reactions, including the primary reaction that produces the desired polymer films. The polymer film formed on the surface of the electrode can be conducting or nonconducting polymer. The difference is that due to the intrinsic conductivity of the conducting polymers, the film thickness can be controlled, and a multilayer film can be also obtained. Electroactive conducting polymer films obtained through electrochemical polymerization can be easily and directly characterized. On the other hand, chemically synthesized polymer may require further purification and characterization in order to confirm the product. Another advantage of electrochemical polymerization is that the polymer formed exhibits physical properties that are inherent to metals or semiconductors, while retaining the mechanical properties of conventional polymers [100].

8.2 Applications

Due to their excellent conductivity and stability, as well as their good magnetic, optical, and electronic properties, conducting polymers are viewed as organic molecular electronic materials. They have thus, found applications as materials for the development of solar cells, light weight batteries, electrochromic devices, sensors, and electronic devices [101–110]. Conducting polymers have been demonstrated to be suitable materials for developing electrochemical capacitors, because of the combination of high charge density and thermal stability with predicted low material cost [111]. Due to their biocompatibility or ease of derivatization, conducting polymers have emerged as promising materials for the development of compact and portable probes and sensors for the detection of biologically significant molecules [112]. Also, heterojunction solar cells have been fabricated by electrochemical polymerization of pyrrole on n-silicon [113]. Moreover, many other conducting polymers, including polyacetylene, polythiophene, polyindole, polypyrrole, and polyaniline, have been used as electrode materials for rechargeable batteries [114–116].

In analytical chemistry, the problem of selectivity, particularly at the low concentrations of analyte and in the presence of interfering substances is extremely

important. Conducting polymers have numerous applications in sensors either as highly selective sensing layers or as suitable materials for sensor development. They have also found applications in biosensors, biotechnology, production of pharmaceuticals, food manufacturing, wastewater treatment, health care products, and organic solar energy production [105].

9 Conclusion

Most conducting polymer films used as transducers in sensors and electrocatalysis are synthesized by chemical and electrochemical polymerization of the monomers, on solid electronic conductor materials with high work function as described in this chapter. However, chemical polymerization has the limitation of requiring more purification and further characterization for their confirmation. Electrochemical polymerization has the disadvantage of low yield and poor solubility of the product, the former making the method unsuitable for large scale production of polymers. However, in electrochemical polymerization, the nature of the product formed can be controlled by doping, redox scan mode, polymerization cycle, and type of electrode material used. Dopant ion-recognition sites can be incorporated into a conducting polymer film as counter ions during electropolymerization, not only to improve the solubility but also to increase the conductivity, electroactivity, and stability of the polymer.

References

1. M.A. De Paoli, W.A. Gazotti, Electrochemistry, polymers and opto-electronic devices: A combination with a future. *J. Braz. Chem. Soc.* **13**, 410–424 (2002)
2. A.A. Syed, M.K. Dinesan, Review: Polyaniline-A novel polymeric material. *Talanta* **38**, 815–837 (1991)
3. P. Monk, R. Mortimer, D. Rosseinsky, Conjugated conducting polymers, in *Electrochromism and Electrochromic Devices* (Cambridge University Press, New York, 2007), p. 312
4. R. de Surville, M. Jozefowicz, L.T. Yu, J. Perichon, R. Buvet, Electrochemical chains using protolytic organic semiconductors. *Electrochim. Acta* **13**, 1451–1458 (1968)
5. A.A. Syed, M.K. Dinesan, E.M. Genies, Basic behavior of chemically synthesized polyanilines. *Bull. Electrochem.* **4**, 737–742 (1988)
6. A.F. Diaz, J.A. Logan, Electroactive polyaniline films. *J. Electroanal. Chem.* **111**, 111–114 (1980)
7. N. Mermillod, J. Tanguy, M. Hoclet, A.A. Syed, Electrochemical characterization of chemically synthesized polyanilines. *Synth. Met.* **18**, 359–364 (1987)
8. A.G. MacDiarmid, J.C. Chiang, M. Halpern, W.S. Huang, S.L. Mu, N.L.D. Somasiri, W. Wu, S.I. Yaniger, Polyaniline: Interconversion of metallic and insulating forms. *Mol. Cryst. Liq. Cryst.* **121**, 173–180 (1985)
9. G. Mengoli, M.T. Munari, C. Folonari, Anodic formation of polynitroanilide films onto copper. *J. Electroanal. Chem.* **124**, 237–246 (1981)
10. S. Cosnier, Biomolecule immobilization on electrode surfaces by entrapment or attachment to electrochemically polymerized films. A review. *Biosens. Bioelectron.* **14**, 443–456 (1999)
11. H.T. Santoso, Electrochemical processing of polythiophene films with enhanced structural order, Thesis, Georgia Institute of Technology, Atlanta, 2011, p. 117

12. S. Yong, W. Kazuya, H. Kazuhito, Hydroxylated and aminated polyaniline nanowire networks for improving anode performance in microbial fuel cells. *J. Biosci. Bioeng.* **112**, 63–66 (2011)
13. R. Gupta, M. Singhal, S.K. Nataraj, D.N. Srivastava, A potentiostatic approach of growing polyaniline nanofibers in fractal morphology by interfacial electropolymerization. *RSC Adv.* **6**, 110416–110421 (2016)
14. M.J. Bleda-Martínez, C. Peng, S. Zhang, G.Z. Chen, E. Morallón, D. Cazorla-Amorós, Electrochemical methods to enhance the capacitance in activated carbon/polyaniline composites. *J. Electrochem. Soc.* **155**, A672–A678 (2008)
15. J. Heinze, B.A. Frontana-Uribe, S. Ludwigs, Electrochemistry of conducting polymers persistent models and new concepts. *Chem. Rev.* **110**, 4724–4771 (2010)
16. W. Schuhmann, C. Kranz, H. Wohlschliiger, J. Strohmeier, Pulse technique for the electrochemical deposition of polymer films on electrode surfaces. *Biosens. Bioelectron.* **12**, 1157–1167 (1997)
17. H. Okamoto, T. Kotaka, Structure and properties of polyaniline films prepared via electrochemical polymerization. I: Effect of pH in electrochemical polymerization media on the primary structure and acid dissociation constant of product polyaniline films. *Polymer* **39**, 4349–4358 (1998)
18. K. Imanishi, M. Satoh, Y. Yasuda, R. Tsushima, S. Aoki, Solvent effect on electrochemical polymerization of aromatic compounds. *J. Electroanal. Chem.* **242**, 203–208 (1988)
19. L.J. Duic, Z. Mandic, F. Kovacecek, The effect of supporting electrolyte on the electrochemical synthesis, morphology, and conductivity of polyaniline. *J. Polym. Sci. Part A* **32**, 105–111 (1994)
20. G. Inzelt, *Conducting Polymers-A New Area in Electrochemistry* (Springer, Berlin, 2008), pp. 123–135
21. G.G. Wallace, P.R. Teasdale, G.M. Spinks, L.A.P. Kane-Maguire, *Conductive Electroactive Polymers*, 3rd edn. (Taylor & Francis Group, Boca Raton, 2009)
22. A.M. Kumar, Z.M. Gasem, In situ electrochemical synthesis of polyaniline/f-MWCNT nanocomposite coatings on mild steel for corrosion protection in 3.5% NaCl solution. *Prog. Org. Coat.* **78**, 387–394 (2015)
23. G. Fomo, T.T. Waryo, P.G. Baker, E.I. Iwuoha, Electrochemical deposition and properties of polyaniline films on carbon and precious metal surfaces in perchloric acid/acetonitrile. *Int. J. Electrochem. Sci.* **11**, 10347–10361 (2016)
24. A.M.P. Hussain, A. Kumar, Electrochemical synthesis and characterization of chloride doped polyaniline. *Bull. Mater. Sci.* **26**, 329–334 (2003)
25. A. Kraft, A.C. Grimsdale, A.B. Holmes, Electroluminescent conjugated polymers—seeing polymers in a new light. *Angew. Chem. Int. Ed.* **37**, 402–428 (1998)
26. G. Fomo, T.T. Waryo, C.E. Sunday, A.A. Baleg, P.G. Baker, E.I. Iwuoha, Aptameric recognition-modulated electroactivity of poly(4-styrenesulfonic acid)-doped polyaniline films for single-shot detection of tetrodotoxin. *Sensors* **15**, 22547–22560 (2015)
27. J.H.P. Utley, J. Gruber, Electrochemical synthesis of poly(p-xylylenes) (PPXs) and poly(p-phenylenevinyls) (PPVs) and the study of xylylene (quinodimethane) intermediates; an underrated approach. *J. Mater. Chem.* **12**, 1613–1624 (2002)
28. B. Sari, M. Talu, F. Yildirim, Electrochemical polymerization of aniline at low supporting-electrolyte concentrations and characterization of obtained films. *Russ. J. Electrochem.* **38**, 707–713 (2002)
29. W.S. Huang, B.D. Humphrey, A.G. MacDiarmid, Polyaniline, a novel conducting polymer morphology and chemistry of its oxidation and reduction in aqueous electrolytes. *J. Chem. Soc. Faraday Trans.* **182**, 2385–2400 (1986)
30. Y. Diamant, E. Furmanovich, A. Landau, J.P. Lellouche, A. Zaban, Electrochemical polymerization and characterization of a functional dicarbazole conducting polymer. *Electrochim. Acta* **48**, 507–512 (2003)
31. <https://www.ch.cam.ac.uk/group/melville/cyclic-voltammetry>
32. B.B. Berkes, G. Inzelt, E. Vass, Electrochemical nanogravimetric study of the adsorption of 4-aminoindole and the surface layer formed by electrooxidation in aqueous acid media. *Electrochim. Acta* **96**, 51–60 (2013)

33. M. Hosseini, M.M. Momeni, M. Faraji, Electrochemical fabrication of polyaniline films containing gold nanoparticles deposited on titanium electrode for electro-oxidation of ascorbic acid. *J. Mater. Sci.* **45**, 2365–2371 (2010)
34. Y. Li, M. Liu, C. Xiang, Q. Xie, S. Yao, Electrochemical quartz crystal microbalance study on growth and property of the polymer deposit at gold electrodes during oxidation of dopamine in aqueous solutions. *Thin Solid Films* **497**, 270–278 (2006)
35. G. Fomo, Ionophoric and aptameric recognition-modulated electroactive polyaniline films for the determination of tetrodotoxin, Thesis, University of the Western Cape, 2015, p. 344
36. B.N. Grgur, A. Žeradžanin, M.M. Gvozdrenović, M.D. Maksimović, T.L. Trišović, B.Z. Jugović, Electrochemical characteristics of rechargeable polyaniline/lead dioxide cell. *J. Power Sources* **217**, 193–198 (2012)
37. D. Bhattacharjya, I. Mukhopadhyay, Controlled growth of polyaniline fractals on HOPG through potentiodynamic electropolymerization. *Langmuir* **28**, 5893–5899 (2012)
38. M.M. Gvozdrenović, B.Z. Jugović, J.S. Stevanović, T.L.J. Trišović, B.N. Grgur, *Electrochemical Polymerization of Aniline, Electropolymerization*, ed. by E. Schab-Balcerzak (InTech, Rijeka, 2011)
39. M.M. Gvozdrenović, B.Z. Jugović, J.S. Stevanović, B.N. Grgur, B.N. Hemijis, Electrochemical synthesis of electroconducting polymers. *Hem. Ind.* **68**, 673–684 (2014)
40. A. Adenier, M.M. Chehimi, I. Gallardo, J. Pinson, N. Vila, Electrochemical oxidation of aliphatic amines and their attachment to carbon and metal surfaces. *Langmuir* **20**, 8243–8253 (2004)
41. R. Zhang, G.D. Jin, D. Chen, X.Y. Hu, Simultaneous electrochemical determination of dopamine, ascorbic acid and uric acid using poly(acid chrome blue K) modified glassy carbon electrode. *Sensors Actuators B Chem.* **138**, 174–181 (2009)
42. X. Huang, Y. Li, Y. Chen, L. Wang, Electrochemical determination of nitrite and iodate by use of gold nanoparticles/poly(3-methylthiophene) composites coated glassy carbon electrode. *Sensors Actuators B Chem.* **234**, 780–786 (2008)
43. J.H. Park, J.M. Ko, O.O. Park, D.W. Kim, Capacitance properties of graphite/polypyrrole composite electrode prepared by chemical polymerization of pyrrole on graphite fiber. *J. Power Sources* **105**, 20–25 (2002)
44. C.C. Hu, C.H. Chu, Electrochemical impedance characterization of polyaniline-coated graphite electrodes for electrochemical capacitors effects of film coverage/thickness and anions. *J. Electroanal. Chem.* **503**, 105–116 (2001)
45. B. Jugović, M. Gvozdrenović, J. Stevanović, T. Trišović, B. Grgur, Characterization of electrochemically synthesized PANI on graphite electrode for potential use in electrochemical power sources. *Mater. Chem. Phys.* **114**, 939–942 (2009)
46. T. Hatano, A.H. Bae, M. Takeuchi, N. Fujita, K. Kaneko, H. Ihara, M. Takafuji, S. Shinkai, Helical superstructure of conductive polymers as created by electrochemical polymerization by using synthetic lipid assemblies as a template. *Angew. Chem.* **116**, 471–475 (2004)
47. L.H. Mascaro, A.N. Berton, L. Micaroni, Electrochemical synthesis of polyaniline/poly-o-aminophenol copolymers in chloride medium. *Int. J. Electrochem.* **2011**, 1–8 (2011)
48. M. Magnuson, J.H. Guo, S.M. Butorin, A. Agui, C. Sâthe, J. Nordgren, A.P. Monkman, The electronic structure of polyaniline and doped phases studied by soft X-ray absorption and emission spectroscopies. *J. Chem. Phys.* **111**, 4756–4761 (1999)
49. http://www.ecochemie.nl/Products/Echem/Accessories/Metal_WE.html
50. <http://www.horiba.com/es/application/material-property-characterization/water-analysis/water-quality-electrochemistry-instrumentation/ph-knowhow/the-basis-of-ph/measuring-ph-using-a-glass-electrode/detector-reference-electrode-temperature-compensation-electrode-combination-ele>
51. <https://orders.gamry.com/platinum-wire-counter-electrode-15-cm.html>
52. A. Eftekhari, Y. Bahareh, Morphological effects of Ni nanostructures on electropolymerization of aniline. *J. Appl. Polym. Sci.* **122**, 1579–1586 (2011)
53. G.L. Zhang, J.H. Xinxì, X. Pang, H. Yang, Y. Wang, K. Ding, Preparation and characterization of polyaniline (PANI) doped-Li₃V₂(PO₄)₃. *Int. J. Electrochem. Sci.* **7**, 830–843 (2012)

54. T.H. Le, T. Ngoc, L.H. Nguyen, H.B. Nguyen, V.A. Nguyen, T.D. Nguyen, Electrosynthesis of polyaniline–multiwalled carbon nanotube nanocomposite films in the presence of sodium dodecyl sulfate for glucose biosensing. *Adv. Nat. Sci. Nanosci. Nanotechnol.* **4**, 025–014 (2013)
55. R. Yue, F. Jiang, Y. Du, J. Xu, P. Yang, Electrosynthesis of a novel polyindole derivative from 5-aminoindole and its use as catalyst support for formic acid electrooxidation. *Electrochim. Acta* **77**, 29–38 (2012)
56. G. Nie, T. Cai, S. Zhang, Q. Bao, J. Xu, Electrodeposition of poly(indole-5-carboxylic acid) in boron trifluoride diethyl etherate containing additional diethyl ether. *Electrochim. Acta* **52**, 7097–7106 (2007)
57. N. Bicak, B. Karagoz, Polymerization of aniline by copper-catalyzed air oxidation. *J. Polym. Sci. A Polym. Chem.* **44**, 6025–6031 (2006)
58. Y. Lee, S. Chen, H. Tu, S. Yau, L.L. Fan, Y. Yang, W.P. Dow, In situ STM revelation of the adsorption and polymerization of aniline on Au (111) electrode in perchloric acid and benzenesulfonic acid. *Langmuir* **26**, 5576–5582 (2010)
59. S. Perc, Electrochemical synthesis of poly(2-iodoaniline) and poly(aniline-co-2-iodoaniline) in acetonitrile. *J. Appl. Polym. Sci.* **89**, 1652–1658 (2003)
60. Y. Sahin, A. Aydin, Y.A. Udum, K. Pekmez, A. Yildiz, Electrochemical synthesis of sulfonated polypyrrole in FSO₃H/acetonitrile solution. *J. Appl. Polym. Sci.* **40**, 526–533 (2004)
61. J.M. Pringle, J. Efthimiadis, P.C. Howlett, J. Efthimiadis, D.R. MacFarlane, A.B. Chaplin, S.B. Hall, D.L. Officer, G.G. Wallace, M. Forsyth, Electrochemical synthesis of polypyrrole in ionic liquids. *Polymer* **45**, 1447–1453 (2004)
62. S. Mu, Pronounced effect of the ionic liquid on the electrochromic property of the polyaniline film: Color changes in the wide wavelength range. *Electrochim. Acta* **52**, 7827–7834 (2007)
63. W. Lu, A.G. Fadeev, B. Qi, E. Smela, B.R. Mattes, J. Ding, G.M. Spinks, J. Mazurkiewicz, D. Zhou, G.G. Wallace, D.R. MacFarlane, S.A. Forsyth, M. Forsyth, Use of ionic liquids for π -conjugated polymer electrochemical devices. *Science* **297**, 983–987 (2002)
64. M.L. Schwuger, K. Stickdorn, R. Schomaecker, Microemulsions in technical processes. *Chem. Rev.* **95**, 849–864 (1995)
65. V. Tsakova, S. Winkels, J.W. Schultze, Anodic polymerization of 3, 4-ethylenedioxythiophene from aqueous microemulsions. *Electrochim. Acta* **46**, 759–768 (2000)
66. C. Lagrost, M. Jouini, J. Tanguy, S. Aeyach, J.C. Lacroix, K.I. Chane-Ching, P.C. Lacaze, Bithiophene electropolymerization in aqueous media: A specific effect of SDS and β -cyclodextrin. *Electrochim. Acta* **46**, 3985–3992 (2001)
67. M. Fall, M.M. Dieng, J.J. Aaron, S. Aeyach, P.C. Lacaze, Role of surfactants in the electrosynthesis and the electrochemical and spectroscopic characteristics of poly(3-methoxythiophene) films in aqueous micellar media. *Synth. Met.* **118**, 149–155 (2001)
68. G.E. Barr, C.N. Sayre, D.M. Connor, D.M. Collard, Polymerization of hydrophobic 3-alkylpyrroles from aqueous solutions of sodium dodecyl sulfate. *Langmuir* **12**, 1395–1398 (1996)
69. A. Mani, K.L.N. Phani, Spherulitic morphology of electrochemically-deposited poly-paraphenylene (PPP) films. *J. Electroanal. Chem.* **513**, 126–132 (2001)
70. M. Kanungo, A. Kumar, A.Q. Contractor, Studies on electropolymerization of aniline in the presence of sodium dodecyl sulfate and its application in sensing urea. *J. Electroanal. Chem.* **528**, 46–56 (2002)
71. K. Matyjaszewski, T. Davys, *Handbook of Radical Polymerization* (Wiley, Hoboken, 2002), pp. 1–177
72. K. Karon, M. Lapkowski, Carbazole electrochemistry: A short review. *J. Solid State Electrochem.* **19**, 2601–2610 (2015)
73. M. Ates, A. Dolapdere, Electrochemical polymerization of thiophene and poly(3-hexyl) thiophene, nanocomposites with TiO₂, and corrosion protection behaviors. *Polym. Plast. Technol. Eng.* **54**, 1780–1786 (2015)
74. P. Novak, K. Muller, K.S.V. Santhana, O. Haas, Electrochemically active polymers for rechargeable batteries. *Chem. Rev.* **97**, 207–281 (1997)

75. J. Bobacka, A. Ivaska, Ion sensors with conducting polymers, as ion-to-electron transducers. *Compr. Anal. Chem.* (Elsevier **49**, 73–86 (2007))
76. R.J. Waltman, J.B. Argon, Electrically conducting polymers: A review of the electropolymerization reaction, of the effects of chemical structure on polymer film properties, and of applications towards technology. *Can. J. Chem.* **64**, 76–95 (1986)
77. R. Lazzaroni, J. Riga, J.J. Verbist, L. Christiaens, M. Renson, Electrochemical synthesis and preliminary characterization of poly(thieno[3,2-b]pyrrole). *J. Chem. Soc. Chem. Commun.*, 999–1000 (1985)
78. V. Gupta, N. Miura, Large-area network of polyaniline nanowires prepared by potentiostatic deposition process. *Electrochem. Commun.* **7**, 995–999 (2005)
79. J.M. Pringle, J. Efthimiadis, P.C. Howlett, J. Efthimiadis, D.R. MacFarlane, A.B. Chaplinc, S.B. Hallc, D.L. Officer, G.G. Wallace, M. Forsyth, Electrochemical synthesis of polypyrrole in ionic liquids. *Polymer* **45**, 1447–1453 (2004)
80. B. Broda, G. Inzelt, Preparation and characterization of poly(5-aminoindole) by using electrochemical quartz crystal nanobalance technique. *Acta Chim. Slov.* **61**, 357–365 (2014)
81. K. Darowicki, J. Kawula, Impedance characterization of the process of polyaniline first redox transformation after aniline electropolymerization. *Electrochim. Acta* **49**, 4829–4839 (2004)
82. X. Li, Y. Li, Electrochemical preparation of polythiophene in acetonitrile solution with boron fluoride-ethyl ether as the electrolyte. *J. Appl. Polym. Sci.* **90**, 940–946 (2003)
83. G. Odian, Y. Atassi, M. Tally, Chapter 3: Radical chain polymerization, in *Principles of Polymerization*, 4th edn., (Wiley, Hoboken, 2004)
84. P. Audebert, J.M. Catel, G.L. Coustumer, V. Duchenet, P. Hapiot, Electrochemistry and polymerization mechanism of thiophene-pyrrole-thiophene oligomers and terthiophenes. Experimental and theoretical modeling studies. *J. Phys. Chem. B* **102**, 8661–8669 (1998)
85. L. Duid, Z. Mandid, Counter-ion and pH effect on the electrochemical synthesis of polyaniline. *Electroanal. Chem.* **335**, 207–221 (1992)
86. W.S. Huang, B.D. Humphrey, A.G. MacDiarmid, Polyaniline, a novel conducting polymer morphology and chemistry of its oxidation and reduction in aqueous electrolytes. *J. Chem. Soc. Faraday Trans. 1*(82), 2385–2400 (1986)
87. D. Seeger, W. Kowalchuk, C. Korzeniewski, Investigation of polymer-dopant interactions in polyaniline-modified electrodes: In situ analysis by FTIR spectroscopy. *Langmuir* **6**, 1527–1534 (1990)
88. H. Okamoto, T. Kotaka, Effect of counter ions in electrochemical polymerization media on the structure and responses of the product polyaniline films III. Structure and properties of polyaniline films prepared via electrochemical polymerization. *Polymer* **40**, 407–417 (1998)
89. M.S. Lee, S.B. Lee, J.Y. Lee, H.S. Kang, H.S. Kang, S. Hyun, J. Joo, A.J. Epstein, All-polymer FET based on simple photolithographic micro-patterning of electrically conducting polymer. *Mol. Cryst. Liq. Cryst.* **405**, 171–178 (2003)
90. M. Immaculate, Synthesis, electrodynamics and biosensor applications of novel sulphonated polyaniline nanocomposites, PhD Thesis, University of the Western Cape, 2007, p. 223
91. W. Yanyan, L. Kalle, Influence of dopant on electroactivity of polyaniline. *Macromol. Symp.* **317**, 240–247 (2012)
92. T. Lindfors, A. Ivaska, Potentiometric and UV–vis characterisation of N-substituted polyanilines. *J. Electroanal. Chem.* **535**, 65–74 (2002)
93. M.H. Pourmaghi-Azar, B. Habibi, Electropolymerization of aniline in acid media on the bare and chemically pre-treated aluminium electrodes: A comparative characterization of the polyaniline deposited electrodes. *Electrochim. Acta* **52**, 4222–4230 (2007)
94. A. Balamurugan, S.M. Chen, Poly(3,4-ethylenedioxythiophene-co-(5-amino-2-naphthalene-sulfonic acid)) (PEDOT-PANS) film modified glassy carbon electrode for selective detection of dopamine in the presence of ascorbic acid and uric acid. *Anal. Chim. Acta* **596**, 92–98 (2007)
95. M.R. Nateghi, M. Zahedi, M.H. Mosslemin, S. Hachemian, S. Behzad, A. Minnai, Auto-acceleration/degradation of electrochemical polymerization of substituted polyanilines. *Polymer* **46**, 11476–11483 (2005)

96. L. Komsijska, T. Tsacheva, V. Tsakova, Electrochemical formation and copper modification of poly-o-methoxyaniline. *Thin Solid Films* **493**, 88–95 (2005)
97. S. Sadki, P. Schottland, N. Brodie, G. Sabouraud, The mechanisms of pyrrole electropolymerization. *Chem. Soc. Rev.* **29**, 283–293 (2000)
98. M. Saraji, A. Bagheri, Electropolymerization of indole and study of electrochemical behavior of the polymer in aqueous solutions. *Synth. Met.* **98**, 57–63 (1998)
99. P. Jennings, A.C. Jones, A.R. Mount, A.D. Thomson, Electrooxidation of 5-substituted indoles. *J. Chem. Soc. Far. Trans.* **93**, 3791–3797 (1997)
100. M.K.L. Coelho, J.D.F. Giarola, A.T.M. Da Silva, C.R.T. Tarley, K.B. Borges, A.C. Pereira, Development and application of electrochemical sensor based on molecularly imprinted polymer and carbon nanotubes for the determination of carvedilol. *Chemosensors* **4**, 1–15 (2016)
101. S. Nambiar, J.T.W. Yeow, Conductive polymer-based sensor for biomedical application. *Biosens. Bioelectron.* **26**, 1825–1832 (2011)
102. P.N. Bartlett, J.M. Cooper, A review of the immobilization of enzyme in electropolymerized films. *J. Electroanal. Chem.* **362**, 1–12 (1993)
103. S. Cosnier, Biosensors based on electropolymerized films: New trends. *Anal. Bioanal. Chem.* **377**, 507–520 (2003)
104. S. Cosnier, Recent advances in biological sensors based on electrogenerated polymers: A review. *Anal. Lett.* **40**, 1260–1279 (2007)
105. M. Gerard, A. Chaubey, B.D. Malhotra, Application of conducting polymers to biosensors. *Biosens. Bioelectron.* **17**, 345–359 (2002)
106. M.A. Rahman, P. Kumar, D.-S. Park, Y.B. Shim, Electrochemical sensor based on organic conjugated polymers. *Sensors* **8**, 118–141 (2008)
107. K.S.V. Santhanam, Conducting polymers for biosensors: Rational based models. *Pure Appl. Chem.* **70**, 1259–1262 (1998)
108. T.D. McQuade, A.E. Pullen, T.M. Swager, Conjugated polymer-based chemical sensors. *Chem. Rev.* **100**, 2537–2574 (2000)
109. U. Lange, N.V. Raznyatovskaya, V.M. Mirsky, Conducting polymers in chemicals sensors and array. *Anal. Chim. Acta* **614**, 1–26 (2008)
110. H. Peng, L. Zhang, C. Soeller, J. Travas-Sejdic, Conducting polymers for electrochemical DNA sensing. *Biomaterials* **30**, 2132–2148 (2009)
111. A. Rudge, I. Raistnck, S. Go-Ite~Fizld, J.P. Ferr, A study of the electrochemical properties of conducting polymers for application in electrochemical capacitors. *Electrochim. Acta* **39**, 273–287 (1994)
112. D. McQuade, A.E.P. Tyler, T.M. Swager, Conjugated polymer-based chemical sensors. *Chem. Rev.* **100**, 2537–2574 (2000)
113. P. Audebert, G. Bidan, Polyhalopyrroles: Electrochemical synthesis and some characteristics. *J. Electroanal. Chem.* **190**, 129–139 (1985)
114. R. Saraswathi, M. Gerard, B.D. Malhotra, Characteristics of aqueous polycarbazole batteries. *J. Appl. Polym. Sci.* **74**, 145–150 (1999)
115. T. Kawai, T. Kuwabara, S. Wang, K. Yoshino, Secondary battery characteristics of poly (3-alkylthiophene). *Jap. J. Appl. Phys.* **29**, 602–605 (1990)
116. K.S.V. Santhanam, N. Gupta, Conducting-polymer electrodes in batteries. *TRIP* **1**, 284–289 (1993)



Nickolas D. Polychronopoulos and John Vlachopoulos

Contents

1	Types of Polymers and Their Flow Behavior	136
2	Rheology of Polymer Melts	138
2.1	Viscosity	138
2.2	Elongational Viscosity	143
2.3	Normal Stresses	145
2.4	Stress Relaxation and Dynamic Measurements	146
2.5	The Role of Shear and Elongation in Mixing	149
2.6	Extrudate Swell	152
2.7	Wall Slip, Sharkskin, Melt Fracture, and Die Lip Buildup	153
2.8	Rheology of Filled Polymers	155
2.9	Rheology of Nanocomposites	157
3	Polymer Melt Processing	161
3.1	Extrusion	161
3.2	Calendering	168
3.3	Injection Molding	170
3.4	Compression Molding	172
3.5	Blow Molding	173
3.6	Thermoforming	173
3.7	Rotational Molding	174
3.8	Melt Spinning	174
3.9	Additive Manufacturing of Polymers	175
4	Considerations in the Polymer Processing Industry	175
	References	177

N. D. Polychronopoulos
Polydynamics Inc., Dundas, ON, Canada
e-mail: polyrheo@polydynamics.com

J. Vlachopoulos (✉)
Department of Chemical Engineering, McMaster University, Hamilton, ON, Canada
e-mail: vlachopj@mcmaster.ca

Abstract

This chapter is devoted to the presentation of the fundamental rheological properties of polymers and their processing technologies. Measurements of the rheological properties offer a fast and reliable way to determine molecular weight distribution and long-chain branching, which, in combination with the processing conditions, have a decisive influence on the end-use product properties. Shear viscosity, elongational viscosity, normal stress differences, stress relaxation, and some other measures and rheological phenomena, of relevance to polymer processing, are discussed. The most widely used polymer processing technologies of extrusion and injection molding are discussed with some details. The discussion includes key features of equipment used and design and operation challenges. Brief descriptions are presented on calendering, compression molding, blow molding, thermoforming, rotational molding, fiber spinning, and additive manufacturing. It is argued that computer-aided flow analysis and rheological measurements are necessary for equipment design, troubleshooting, and optimization in the processing of thermoplastics.

Abbreviations

ABS	Acrylonitrile butadiene styrene
AM	Additive manufacturing
CaBER	Capillary breakup extensional rheometer
EVA	Ethylene-vinyl acetate
FDM	Fused deposition modeling
HDPE	High-density polyethylene
HLMI	High load melt index
LAOS	Large amplitude oscillatory shear
LDPE	Low-density polyethylene
LLDPE	Linear low-density polyethylene
LVE	Linear viscoelasticity
MFI	Melt flow index
MFR	Melt flow rate
MI	Melt index
MWD	Molecular weight distribution
OEMs	Original equipment manufacturers
PA	Polyamide
PC	Polycarbonate
PE	Polyethylene
PET	Polyethylene terephthalate
PP	Polypropylene
PLA	Polylactic acid
PMMA	Polymethyl methacrylate
PS	Polystyrene
PVC	Polyvinyl chloride
RIM	Reaction injection molding

RPM	Revolutions per minute
SAOS	Small amplitude oscillatory shear
SER	Sentmanat extensional rheometer
SLS	Selective laser sintering
SMEs	Small and medium enterprises
SSE	Single screw extruder
TSE	Twin screw extruder
WFC	Wood fiber composite

List of Symbols

α	Fitting parameter in Carreau-Yasuda model
γ	Strain
$\dot{\gamma}$	Shear rate
$\dot{\gamma}_{\text{app}}$	Shear rate (apparent)
$\dot{\gamma}_{\text{true}}$	Shear rate (true)
$\dot{\gamma}_w$	Wall shear rate
ΔP	Pressure drop
ΔP_e	Excess pressure drop
$\dot{\epsilon}$	Elongation rate
η	Viscosity
η_c	Viscosity of the filled system
η_d	Viscosity of the dispersed phase
η_e	Elongational viscosity
η_m	Viscosity of the matrix
η_o	Zero shear viscosity
η^*	Complex viscosity
η_{ref}	Viscosity at a reference temperature
θ	Screw helix angle
λ	Fitting parameter in Carreau-Yasuda, cross models
ρ	Melt density
σ_{11}	Tensile stress
τ	Shear stress
τ_w	Wall shear stress
φ	Volume fraction
φ_{max}	Maximum volume fraction
ω	Frequency
A	Area
A_c	Cross section of a cylindrical fluid element
a	Pressure coefficient
b	Temperature sensitivity coefficient
Ca	Capillary number
d	Extrudate diameter
D	Capillary diameter
D_b	Barrel diameter

E	Activation energy
F	Force
G'	Storage modulus
G''	Loss modulus
h	Gap between plates
H	Channel depth in an extruder
H_o	Minimum distance between two rollers
k	Einstein coefficient frequently denoted as $[\eta]$
K	Consistency index
L	Capillary length
M_w	Weight average molecular weight
N	Rotational speed
N_1	First normal stress difference
N_{1w}	First normal stress difference at the wall
N_2	Second normal stress difference
n	Power law index
n_B	Bagley correction
p	Pressure
P_{\max}	Maximum pressure in calendering
Q	Volume rate of flow
R	Gas constant
R_c	Capillary radius
R_d	Drop radius
R_{rol}	Roller radius
S	Interfacial tension
S_R	Stress ratio
t	Time
T	Temperature
T_{ref}	Reference temperature
U	Velocity/speed

1 Types of Polymers and Their Flow Behavior

Synthetic polymers may be classified into two main categories: thermoplastics and thermosets. Thermoplastics (by far the largest volume with over 300 million tons produced annually) can be melted by heating, shaped by flowing through dies or filling molds, and subsequently solidified into final useful products. In their molten state, they are highly viscous materials, and their viscosity can be more than a million times higher than that of water, under usual processing conditions. This type of polymers can be either amorphous (without regular structure) or semicrystalline (amorphous with embedded regular substructures). Major types are polyethylene (PE), polypropylene (PP), polyvinyl chloride (PVC), polyethylene terephthalate (PET), polycarbonate (PC), polymethyl methacrylate (PMMA), polystyrene (PS), and polyamide (PA, nylon). Thermosets can be hardened by applying

heat or pressure, due to cross-linking, i.e., the creation of permanent three-dimensional networks. They cannot be softened, by heating for reprocessing. Most common types of thermosets are Bakelite, epoxies, melamine, and many polyurethanes. Processing of thermosets is beyond the scope of the present chapter.

Thermoplastics are seldom processed on their own. They are often blended or compounded with other materials to produce pellets, powders, or flakes to be used in subsequent processing operations [1]. The compounds may involve fillers, colorants, other polymers, flame retardants, reinforcements, stabilizers, and various processing aids. The compounded polymers are usually referred to simply as plastics. Polymer processing deals with the conversion of raw polymeric materials into “value-added” finished products, and in addition to compounding and shaping, it may occasionally involve chemical reactions [2]. Several processes are practiced for the processing of thermoplastics, and the most common are extrusion (largest in volume), injection molding (largest in number of people involved), extrusion and injection blow molding, film blowing, film and sheet casting, calendaring, fiber spinning, compression molding, and rotational molding. A common characteristic in these processes is that the polymer is processed in its molten state and it flows. Thus, before describing the various processing methods involving thermoplastics, we present the fundamentals of rheology, which is defined as the science of flow and deformation of materials [3, 4].

Fluids are characterized by a viscosity, which is a quantitative measure of resistance to flow. In Newtonian fluids the viscosity is independent of the shear rate and depends only on temperature and pressure. In polymer melts the viscosity depends also on shear rate. As the shear rate increases, the viscosity decreases due to molecular alignments and disentanglements of the polymer chains. The higher the shear rate, the easier is for the molten polymer to flow through channels of the process equipment. Aside from their viscous behavior, molten polymers and polymer solutions behave as elastic materials, which means that they can exhibit a response resembling that of a rubber-like solid. Due to this dual nature, polymeric liquids are frequently referred to as viscoelastic, and they exhibit some unusual and, perhaps, counterintuitive flow behavior, which can have significant impact on processing and product properties. Such effects are discussed in the rheology section of this chapter and include the rod-climbing effect on a rotating shaft inside a liquid container, the extrudate or die swell phenomenon where the cross-sectional area of the emerging melt from a shaping die is larger than that of the die, and large vortex phenomena in entrance flow from a large reservoir into a smaller diameter tube and various flow instabilities.

For equipment design, optimization, and troubleshooting, both the viscous and elastic nature of polymers must be taken into consideration. Rheology is involved in all aspects of polymer processing from resin characterization to the determination of structure and end-use properties. Such measurements are used for differentiating between different polymer grades. They are more sensitive and easier than many physical or chemical methods for detecting high molecular weight fractions and long-chain branching in polymers. Rheological measurements are necessary as input into computer simulation software, for design of process equipment like extruders, dies, and molds.

2 Rheology of Polymer Melts

2.1 Viscosity

Viscosity represents the resistance to shearing, i.e., forced movement of imaginary fluid slices like a deck of cards. It is the most important polymer processing property. Referring to Fig. 1, we can define viscosity as the ratio of the imposed shear stress (force F applied tangentially, divided by the area A) and the shear rate (velocity U divided by the gap h)

$$\eta = \frac{\text{shear stress}}{\text{shear rate}} = \frac{F/A}{U/h} = \frac{\tau}{\dot{\gamma}} \quad (1)$$

This relation is known as Newton's law of viscosity. The viscosity is measured in Pa·s in SI units (1 Pa·s = 10 poise). When the viscosity is independent of the shear rate, a fluid is called Newtonian. Molten polymers have viscosities dependent on shear rate, exhibit several other unusual flow properties, and are referred to as non-Newtonian. One remarkable property of polymeric liquids (melts and solutions) is their shear-thinning behavior (also known as pseudoplastic behavior). As the shear rate increases, the viscosity decreases, as shown in Fig. 2.

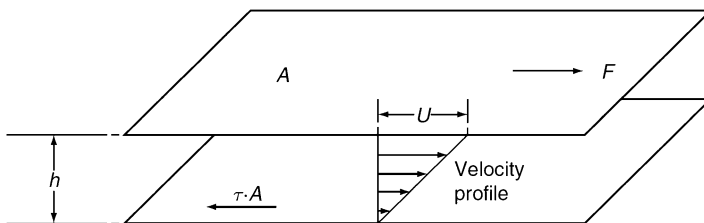
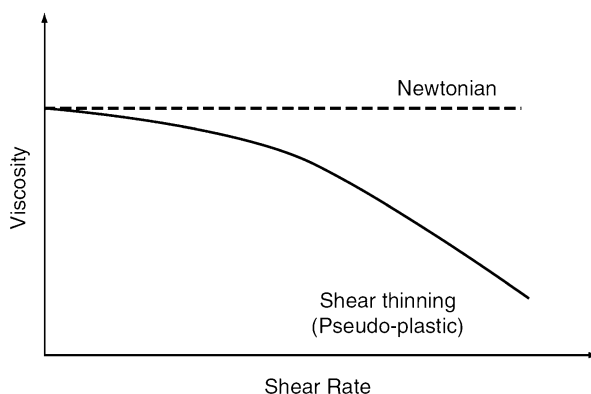


Fig. 1 Shear flow between two plates

Fig. 2 Newtonian and shear-thinning viscosity behavior



This reduction of viscosity is due to molecular alignments and disentanglements of the long polymer chains. The higher the shear rate, the easier it is for polymers to flow through dies and process equipment. The most frequently used model to express the shear-thinning behavior of polymers is the power law:

$$\eta = K\dot{\gamma}^{n-1} \quad (2)$$

This expression is a straight line when plotted on double logarithmic coordinates. This relation does a poor job in fitting low shear rate data (as shear rate approaches zero, the viscosity goes to infinity). The value of the consistency index K is the viscosity at $\dot{\gamma} = 1 \text{ s}^{-1}$. The exponent $(n-1)$ is the slope, because

$$\log \eta = \log K + (n-1) \log \dot{\gamma} \quad (3)$$

For $n = 1$, the power law model reduces to Newton's law (constant viscosity). As n decreases, the polymer becomes more shear thinning. The power law exponent of commercial polymers varies between 0.8 (for some polycarbonate, PC, grades) and 0.2 (for some rubber compounds). For various polyethylene (PE) grades, the range is $0.3 < n < 0.6$ and depends on molecular weight distribution and chain branching and does not change much with temperature. The consistency K varies a lot with temperature, and under usual processing conditions, the consistency index for the most common molten polymers varies between $1,000 \text{ Pa}\cdot\text{s}^n$ (for some polyethylene terephthalate (PET) resins) and $100,000 \text{ Pa}\cdot\text{s}^n$ for highly viscous rigid polyvinyl chloride (PVC). The value depends on chain mobility, molecular weight, and temperature.

During single screw extrusion, shear rates may reach 200 s^{-1} in the screw channel near the barrel wall and much higher between the flight tips and the barrel. At the die lip or exit, the shear rate can be as high as 1000 s^{-1} . During cavity filling in injection molding, shear rates can reach $10,000 \text{ s}^{-1}$, and in some wire coating applications, shear rates may exceed $1,000,000 \text{ s}^{-1}$. However, in the process of rotational molding, shear rates are much less than 1 s^{-1} .

Melt index (MI), melt flow index (MFI), or melt flow rate (MFR) (for polypropylene) refers to the grams per 10 min pushed out of a die of prescribed dimensions according to an ASTM standard [5] under the action of a specified load, as shown in Fig. 3. For PE (ASTM D-1238), the load is 2.16 kg and the die dimensions are $D = 2.095 \text{ mm}$ and $L = 8 \text{ mm}$. The corresponding shear rate at the die wall is approximately $\dot{\gamma}_w = 2.4 \times \text{MFI}$, and the wall shear stress is $\tau_w = 8982 \times 2.16 = 19,401 \text{ Pa}$. The experiment is carried out at $190 \text{ }^\circ\text{C}$. For PP, the same load and die dimensions are used, but the experiment is carried out at $230 \text{ }^\circ\text{C}$. A low melt index means a high molecular weight, highly viscous polymer. A high melt index means a low molecular weight, low-viscosity polymer. When the melt index is less than 1, the material is said to have a fractional melt index. Such materials are used for film extrusion. For some film grades, MI can be less than 0.1. Most extrusion PE grades seldom exceed $\text{MI} = 12$; however, for injection molding, MI is usually in the range of 5–50. The MI (inversely) corresponds to just one point

Fig. 3 Schematic of a melt indexer

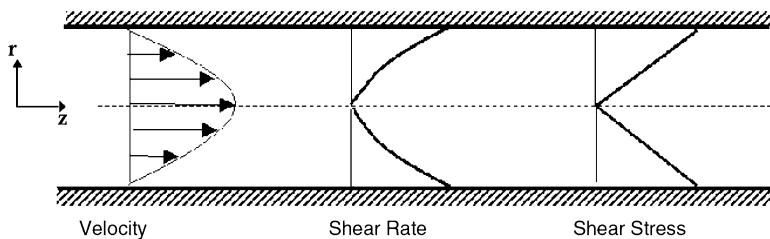
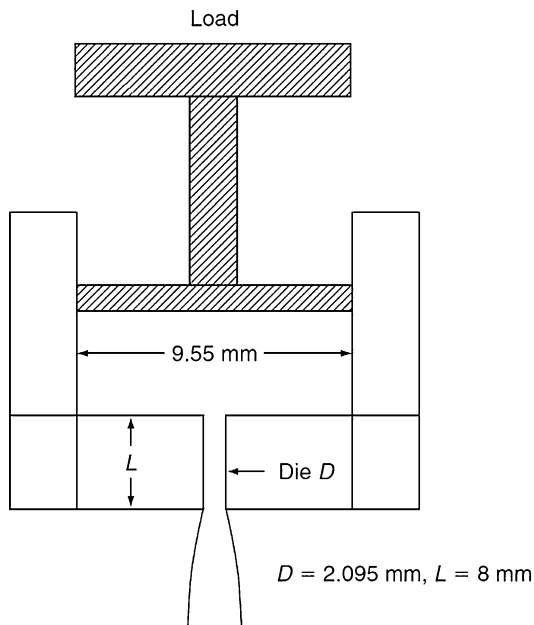


Fig. 4 Velocity, shear rate, and shear stress profiles for pressure-driven flow through a tube of radius R_c

on a viscosity curve (usually at low shear rates). Frequently, the so-called high load melt index (HLMI) is measured, usually with either a 21.6-kg or a 10-kg load on the melt indexer. From two points it is possible to obtain a power law viscosity fit, but such approximations should always be used with extreme caution due to inherent inaccuracies in the melt index measurement method.

For fully developed pressure-driven axial flow (z direction) of a polymeric fluid in a tube (capillary) of radius R_c , the velocity profile is quasi-parabolic, and the shear stress varies linearly with the radius and the shear rate nonlinearly as shown in Fig. 4.

For Newtonian fluids the velocity profile is parabolic, the shear rate varies linearly, and its value at the wall is given by

$$\dot{\gamma}_{\text{app.}} = \frac{4Q}{\pi R_c^3} \quad (4)$$

where Q is the volume rate of flow. This relation is referred to as apparent shear rate when used in non-Newtonian flows. A correction is necessary (Rabinowitsch) for shear-thinning fluids. For the power law model, the true (Rabinowitsch corrected) shear rate becomes

$$\dot{\gamma}_{\text{true}} = \left(\frac{3n+1}{4n} \right) \frac{4Q}{\pi R_c^3} \quad (5)$$

The above equations are used in capillary viscometry for measurement of viscosity from pressure drop ΔP versus volume flow rate Q data. The pressure drop ΔP is measured in the reservoir of the viscometer, and at the entrance to the capillary, there is an excess pressure drop ΔP_e . The easiest way to determine the excess pressure drop ΔP_e is to carry out the experiment using a twin-bore viscometer having two capillaries. One of them has very short length ($L \approx 0$), and the pressure drop recorded is essentially the excess pressure due to the entrance (orifice). This correction is necessary when capillaries are relatively short (L/R_c less than 50) and is known as the Bagley correction. The Bagley correction is usually expressed as

$$n_B = \frac{\Delta P_e}{2\tau_w} \quad (6)$$

The Bagley correction (n_B) may reach perhaps 20 when polymeric materials are extruded at high shear stresses. For a Newtonian fluid, the value for n_B is 0.587. For information on the Bagley correction and entrance and exit pressure drops, the reader is referred to the monographs by Han [6]. Without the Rabinowitsch and Bagley corrections, there can be significant errors in viscosity data obtained from capillary instruments.

In addition to the power law model, two other expressions are frequently used for better fitting of data over the entire range and to include the Newtonian plateau at low shear rates.

The Carreau-Yasuda Model

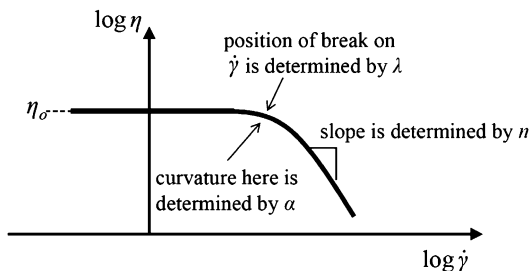
$$\eta = \eta_o [1 + (\lambda\dot{\gamma})^\alpha]^{\frac{n-1}{\alpha}} \quad (7)$$

where η_o is the viscosity at zero shear and λ , α , and n are fitted parameters. The meaning of the fitting parameters is shown in Fig. 5.

The Cross Model

$$\eta = \frac{\eta_o}{1 + (\lambda\dot{\gamma})^{1-n}} \quad (8)$$

Fig. 5 Meaning of Carreau-Yasuda model parameters



where η_o is the viscosity at zero shear and λ and n are fitted parameters. Note that in this model when $\lambda = 1/\dot{\gamma}$, then $\eta = \eta_o/2$.

Regarding viscosity measurements, capillary viscometers are normally used for the shear rate range from 1 s^{-1} to $3,000 \text{ s}^{-1}$. Rotational viscometers (parallel plate or cone and plate) are normally used for the range 10^{-2} – 5 s^{-1} in steady flow. At higher rotational speeds, secondary flows and instabilities may occur which invalidate the simple shear assumption, of imaginary fluid slices motion. For more information about viscosity measurements, the reader is referred to [7].

The viscosity of polymer melts varies with temperature, and it obeys the Arrhenius relation in the form

$$\eta = \eta_{\text{ref}} \exp \left[\frac{E}{R} \left(\frac{1}{T} - \frac{1}{T_{\text{ref}}} \right) \right] \quad (9)$$

where E is the activation energy, R is the gas constant, and T_{ref} is the reference temperature. In polymer processing (especially extrusion), this relation is frequently reduced to a simple exponential which applies over a shorter temperature range

$$\eta = \eta_{\text{ref}} \exp[-b(T - T_{\text{ref}})] \quad (10)$$

The temperature sensitivity coefficient b is usually between 0.01 and $0.1 \text{ }^\circ\text{C}^{-1}$. For HDPE (linear polymer), the value of b is roughly 0.01 , while for LDPE (branched), it may reach 0.03 .

The viscosity increases with pressure in the form

$$\eta(p) = \eta(0) \exp(a \cdot p) \quad (11)$$

The a coefficient is probably of the order $2 \times 10^{-8} \text{ Pa}^{-1}$. Cogswell [8] expresses pressure dependence in terms of an equivalent temperature change. His results suggest that applying 10 MPa is equivalent to decreasing the temperature by about $5 \text{ }^\circ\text{C}$. Usually, pressure dependence of viscosity is not taken into consideration in extrusion, but it is necessary in injection molding calculations and simulations. Pressure drops in die extrusion may reach at most 50 MPa , while in injection molding cavity filling, the pressure may reach 200 MPa .

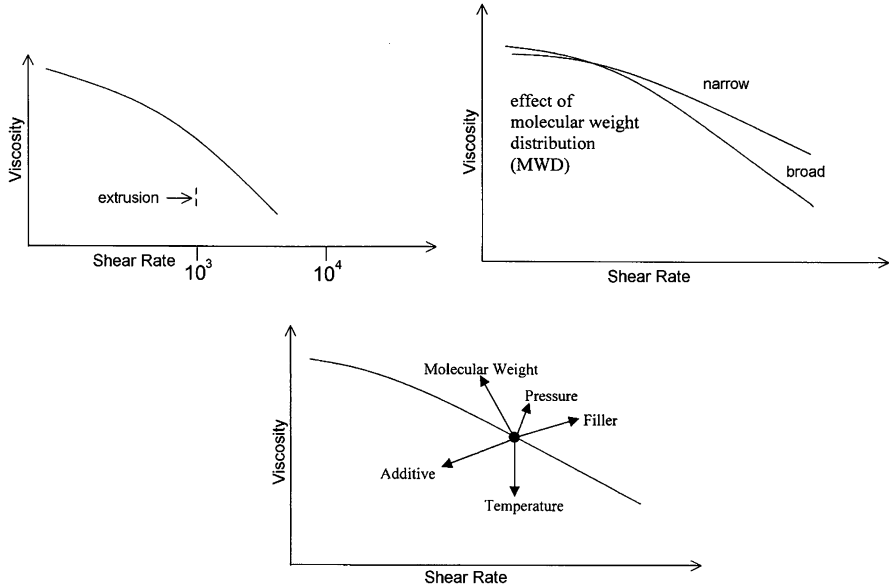


Fig. 6 The influence of various parameters on polymer viscosity

The effects of factors such as shear rate, molecular weight distribution, pressure, filler, temperature, and additives on viscosity are summarized in Fig. 6, as adapted from Cogswell [8]. Linear narrow molecular weight distribution polymers (metallocene catalyzed) are more viscous than their broad distribution counterparts of same average molecular weight. Fillers may increase viscosity (greatly). Various additives are available and are designed to decrease viscosity. The zero shear viscosity increases dramatically with the weight average molecular weight

$$\eta_o = \text{const } M_w^{3.4} \quad (12)$$

For some metallocene-catalyzed PEs with long-chain branching, the exponent might be much higher (perhaps 6.0).

2.2 Elongational Viscosity

Elongational (or extensional) viscosity is the resistance of a fluid to extension [4, 7]. While stretching a low-viscosity fluid like water is difficult to imagine, polymer melts exhibit measurable resistance. The elongational viscosity is defined as

$$\eta_e = \frac{\sigma_{11}}{\dot{\epsilon}} = \frac{F/A_c}{\dot{\epsilon}} \quad (13)$$

where σ_{11} is the tensile stress in the stretching direction, A_c the cross section of a cylindrical fluid element, and $\dot{\epsilon}$ the elongation rate.

Over 100 years ago, Trouton [7] measured the stretching and shearing resistance of some “stiff” (i.e., thick) liquids, including pitch, and found that the extensional-to-shear viscosity ratio is equal to 3

$$\frac{\eta_e}{\eta} = 3 \quad (14)$$

This relation, known as the Trouton ratio, is valid for all Newtonian fluids and has a rigorous theoretical basis that confirms Trouton’s experiments [9]. Note that η_e varies from $\sim 3\eta$ to 100η or more for polymers in molten or semi-molten state, depending upon molecular structure and processing conditions. For the case of polymer solutions, it can reach much higher values. Haward et al. [10] measured $\eta_e \sim 4000\eta$.

Measuring elongational viscosity is considerably more difficult than measuring shear viscosity. One device used involves capillary extrusion and subsequent stretching with a pair of rollers. The maximum force required to break an extruded strand is referred to as melt strength, which is an engineering measure of elongational viscosity for quality control purposes. In industrial practice, the terms elongational (extensional) viscosity and melt strength are sometimes confused. Several processes involve extension, such as film blowing, melt spinning, blow molding, thermoforming, compression molding, and sheet or film drawing.

The excess pressure drop encountered in flow from a large reservoir to a smaller diameter capillary is due to elongational viscosity. In fact, Cogswell [8] has developed a method for measurement of elongational viscosity η_e from excess pressure drop ΔP_e (i.e., the Bagley correction):

$$\eta_e = \frac{9(n+1)^2(\Delta P_e)^2}{32\eta\dot{\gamma}^2} \quad (15)$$

$$\dot{\epsilon} = \frac{4\eta\dot{\gamma}^2}{3(n+1)\Delta P_e} \quad (16)$$

Shear and extensional viscosity measurements reveal that LLDPE (which is linear) is “stiffer” than LDPE (branched) in shear, but “softer” in extension. In extension, the linear LLDPE chains slide by without getting too much entangled. However, the long branches of the LDPE chains result in significantly larger resistance in extension. In the film blowing process, LDPE bubbles exhibit more stability because of their high extensional viscosity. Typical LDPE and LLDPE behavior in shear and extension is shown in Fig. 7. LDPE is often blended with LLDPE to improve the melt strength and consequently bubble stability in film blowing. Most PP grades are known to exhibit very low melt strength. However, recent advances in polymerization catalysts have led to the production of some high melt strength PP grades (with long-chain branching).

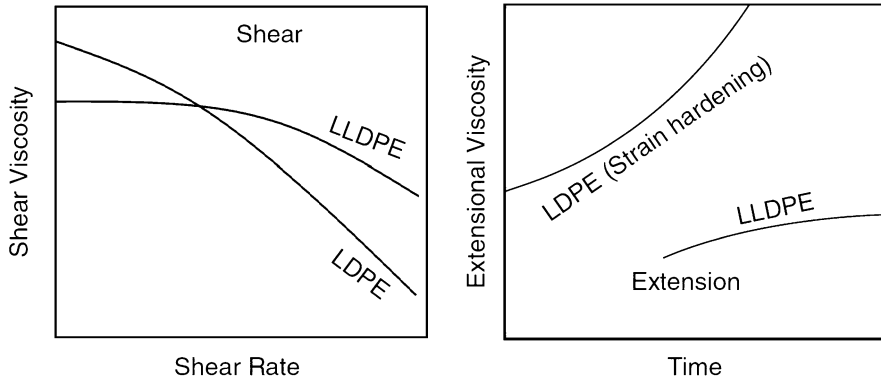


Fig. 7 Schematic representation of LDPE and LLDPE behavior in shear and extension

Measurements of elongational viscosity of polymer melts have been plagued by experimental complexities, lack of repeatability, and considerable inaccuracies over the years. The recently developed SER rheometer [11, 12] seems to have put these problems to rest, and it is expected to play a significant role in the analysis and optimization of polymer processes involving extension in the future. Measuring the elongational viscosity of polymer solutions or, in general, low-viscosity substances (say of the order of 0.1 Pa·s) is even more challenging. Apparently, the capillary breakup extensional rheometer (CaBER) [13] gives satisfactory measurements.

2.3 Normal Stresses

Stress is defined as force divided by the area on which it acts. It has units of N/m^2 (Pascal, Pa) in SI. When a force is acting tangentially on a surface, the corresponding stress is referred to as shear stress. When a force is perpendicular (normal) to a surface, it is termed normal stress. Pressure is a normal stress. When a fluid flows through a conduit, it is acted by the normal (pressure) forces, and it exerts both normal and shear (stress) forces on the conduit walls. For flow through a planar die, the shear stress is zero at the midplane and maximum at the wall, while the corresponding velocity profile is quasi-parabolic. Weissenberg discovered in the 1940s [4, 7] that polymer solutions and melts, when subjected to shearing, tend to develop normal stresses that are unequal in the x (direction of flow), y , and z (normal directions), which are added to or subtracted from the local pressure. They are generated because a polymer's long molecular chains exhibit anisotropic or non-uniform properties when they flow. Any further explanation of the physical origin of normal stresses is likely to be controversial. When an (elastic) polymer solution or melt flows along a pressure gradient, it is less compressed in the direction of flow than in the other two normal directions.

The first normal stress difference N_1 is defined as the total normal stress in the direction of the flow (σ_{xx}) minus the perpendicular (σ_{yy}) stress

$$N_1 = \sigma_{xx} - \sigma_{yy} = (-P + \tau_{xx}) - (-P + \tau_{yy}) = \tau_{xx} - \tau_{yy} \quad (17)$$

The second normal stress difference is

$$N_2 = \sigma_{yy} - \sigma_{zz} = (-P + \tau_{yy}) - (-P + \tau_{zz}) = \tau_{yy} - \tau_{zz} \quad (18)$$

We use normal stress differences rather than just normal stresses to remove the value of the pressure present, so that N_1 and N_2 are fluid properties. Experiments show that N_1 is positive for usual polymers (i.e., extensive, while the compressive pressure forces are negative). For liquid-crystal polymers, N_1 can be negative under certain conditions. N_2 is negative and of the order of 20% of N_1 for most common polymers. N_1 is very sensitive to the high molecular weight tail of a polymer. Broad molecular weight distribution polymers exhibit high N_1 values. The normal stress differences can be very large in high shear rate extrusion through the lips of a die. Some authors suggest a variation for the normal stress difference at the wall in the form

$$N_{1w} = A\tau_w^b \quad (19)$$

The stress ratio

$$S_R = \frac{N_{1w}}{2\tau_w} \quad (20)$$

can reach a value of 10 or more at a flow instability known as melt fracture in extrusion through dies.

The rod-climbing effect observed by Weissenberg when a cylinder rotates in a polymeric liquid is due to some sort of “strangulation” force exerted by the extended polymer chains as shown in Fig. 8a, which results in an upward movement normal to the direction of rotation (normal stress difference). The extrudate swell phenomenon [4, 14] shown in Fig. 8b is due mainly to the contraction of the exiting polymer that is under extension in the die due to N_1 . The uneven extension/compression in the various directions results in a number of unusual flow patterns and instabilities. The secondary flow patterns in square channels observed by Dooley and co-workers [15, 16] are due to the second normal stress difference. Bird et al. [4] state: “A fluid that’s macromolecular is really quite weird, in particular the big normal stresses the fluid possesses give rise to effects quite spectacular.”

2.4 Stress Relaxation and Dynamic Measurements

When flow stops, the stresses become immediately zero for small-molecule Newtonian fluids like water or glycerin. For polymer melts and solutions, the stresses decay

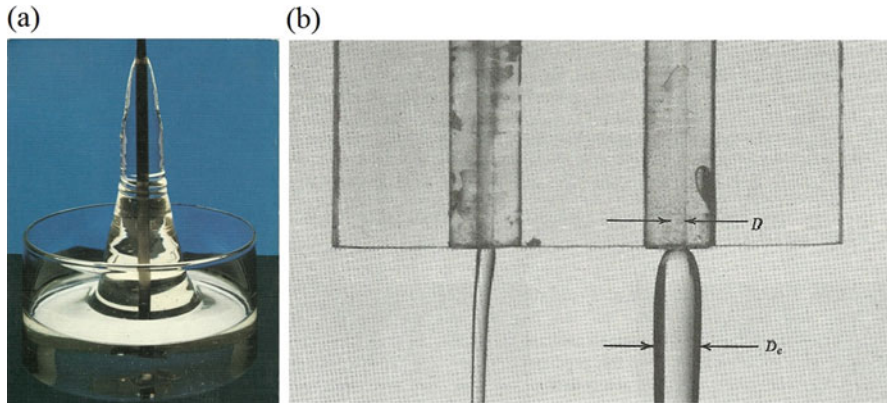


Fig. 8 Phenomena due to normal stresses. (a) Weissenberg (or rod-climbing) effect and (b) extrudate (or die) swell of a Newtonian (left) versus a polymeric (right) liquid. (Adapted from [4])

exponentially after flow stops. Stress relaxation can be measured in a parallel plate or a cone-and-plate rheometer by applying a given shear rate level (rotation speed/gap) and measuring the stress decay after the rotation is brought to an abrupt stop. Such tests, however, are not performed routinely, because of experimental limitations associated with abrupt stopping of rotation and the subsequent measurement of strains and stresses. At start-up of flow, Newtonian fluids reach immediately a stress plateau. The calculated response time for water is of the order of 10^{-12} s. Polymer melts and solutions exhibit a shear and normal stress overshoot and subsequent drop to a plateau. The response times are of the order of 10^{-2} s to a few seconds. Polymer melts that exhibit long relaxation times and large overshoots are likely to produce plastic products having significant amount of frozen-in stresses in case of rapid cooling, which may be released upon reheating. Release of frozen-in stresses results in warpage and other problems.

Dynamic measurements involve the response of a material to an imposed sinusoidal stress or strain on a parallel plate or cone-and-plate instrument. In general, controlled stress rheometers are preferred for polymer solutions and controlled strain rheometers for polymer melts. A perfectly elastic material that behaves like a steel spring, by imposition of extension (strain), would develop stresses that would be in-phase with the strain, because

$$\text{Stress}(\tau) = \text{Modulus}(G) \times \text{Strain}(\gamma) \quad (21)$$

However, for a Newtonian fluid subjected to a sinusoidal strain, the stress and strain will not be in phase because of the time derivative (strain rate) involved

$$\tau = \eta \dot{\gamma} \quad (22)$$

$$\tau = \eta \frac{d\gamma}{d\tau} = \eta \frac{d}{d\tau} (\gamma_o \sin \omega t) = \eta \omega \gamma_o \cos \omega t = \eta \omega \gamma_o \sin (\omega t + 90^\circ) \quad (23)$$

where ω is frequency of oscillation. That is, a Newtonian fluid would exhibit 90° phase difference between stress and strain. Polymeric liquids, which are partly viscous and partly elastic (viscoelastic), will be $0 \leq \varphi \leq 90^\circ$ out of phase.

We can define

$$G'(\omega) = \frac{\text{in - phase stress}}{\text{maximum strain}} \quad \begin{array}{l} \text{storage} \\ \text{modulus} \\ \text{(elastic part)} \end{array} \quad (24)$$

$$G''(\omega) = \frac{\text{out - of - phase stress}}{\text{maximum strain}} \quad \begin{array}{l} \text{loss} \\ \text{modulus} \\ \text{(viscous part)} \end{array} \quad (25)$$

where ω ranges usually from 0.01 to 500 rad/s in most commercially available instruments. Larger G' implies more elasticity. Further, we can define the dynamic viscosity

$$\eta' = \frac{G''(\omega)}{\omega} \quad (26)$$

$$\eta'' = \frac{G'(\omega)}{\omega} \quad (27)$$

and the magnitude of the complex viscosity

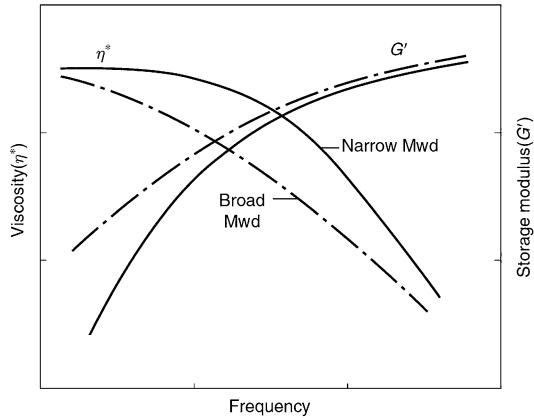
$$|\eta^*| = \left(\eta'^2 + \eta''^2 \right)^{1/2} \quad (28)$$

An empirical relationship called the Cox-Merz rule states that the shear rate dependence of the steady state viscosity η is identical to the frequency dependence of the complex viscosity η^* , that is:

$$\eta(\dot{\gamma}) = |\eta^*(\omega)| \quad (29)$$

The usefulness of this rule, which holds for most conventional polymers, is that while steady measurements of shear viscosity are virtually impossible for shear rates larger than 5/s with rotational instruments, the dynamic measurements can easily be carried out up to 500 rad/s (corresponds to shear rate of 500 s^{-1}) or even higher. Thus, the full range of viscosity needed in extrusion can be covered. Some typical results involving narrow and broad molecular weight distribution samples are shown in Fig. 9. The relative behavior of G' versus ω can be used to identify whether a sample is of narrow or broad molecular weight distribution [17]. In fact, from the crossover point where $G' = G''$ (see also Sect. 2.9), it is possible to get a surprisingly good estimate of the polydispersity M_w/M_n for PP [18]. For such experiments to be meaningful, the imposed strain amplitude must be low, so that the measured G' and G'' values do not vary with the strain, but they are intrinsic properties of the polymer structure. This is the region of the so-called linear viscoelasticity (LVE), and the experiments are frequently referred to as small amplitude oscillatory shear (SAOS) tests. Linearity of the measurements is usually checked by performing strain

Fig. 9 Storage modulus G' and dynamic viscosity η^* behavior of broad and narrow molecular weight distribution polymers



sweeps, i.e., measurements of G' and G'' as a function of strain amplitude at a fixed frequency. After the material's LVE is defined, its structure may be further characterized performing frequency sweeps at a strain amplitude within the LVE region. If the strain amplitude is increased systematically, we enter to the nonlinear viscoelastic regime. In this case the imposed strain amplitude disrupts the polymer network structure, and the test is referred to as large amplitude oscillatory shear (LAOS) test [19]. A review regarding LAOS tests can be found in [20].

Another interesting result is the relation between storage modulus and first normal stress difference at very small deformations ($\omega \rightarrow 0, \dot{\gamma} \rightarrow 0$)

$$2G' = N_1 \quad (30)$$

For higher frequencies an expression developed by Laun [17, 21] is used

$$N_1 = 2 \frac{G'}{\omega^2} \left[1 + \left(\frac{G'}{G''} \right)^2 \right]^{0.7} \quad (31)$$

It is possible to measure N_1 using a cone-and-plate rotational rheometer. The Weissenberg effect results in a separating force between the cone and the plate which can be measured to give N_1 , for very low shear rates (usually less than about 2 s^{-1}), because of secondary flows at higher rates. Instruments capable of measuring N_1 require high-precision construction and very sensitive force gauges. However, measurement of G' and G'' can be carried out more easily and at frequencies corresponding to much higher shear rates.

2.5 The Role of Shear and Elongation in Mixing

Polymers are often compounded (mixed) with pigments, reinforcing agents, fillers, and other polymers for value-added purposes. This is a crucial process operation in the following sense: the minor component must be dispersed (i.e., broken-up,

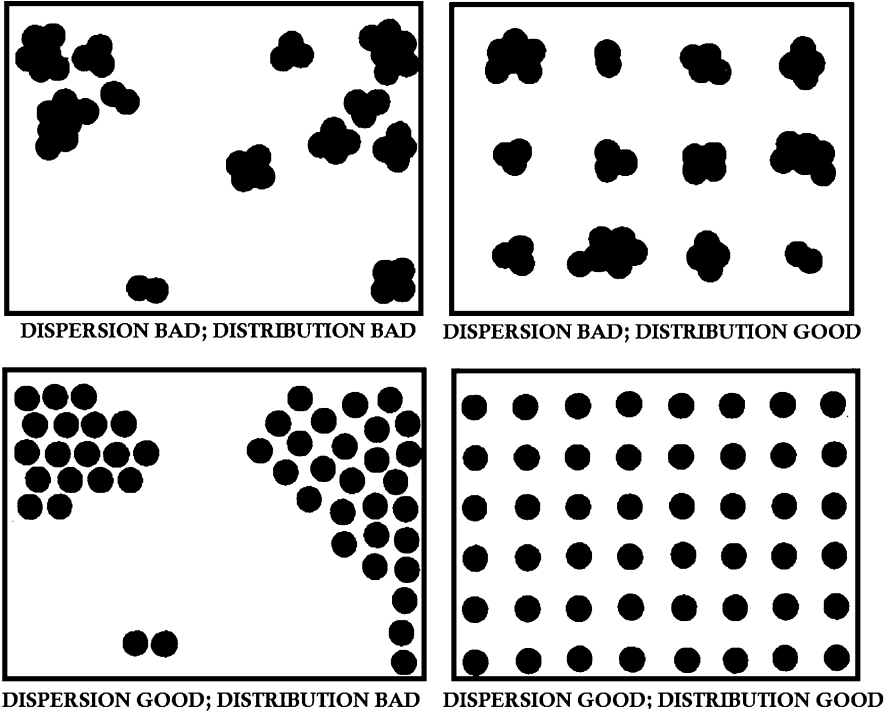


Fig. 10 Effects of dispersive and distributive mixing as adapted from Gale [22]

reduced in size) and distributed (i.e., spread randomly) throughout the polymer matrix as shown schematically in Fig. 10.

Dispersion, in general, is determined by the balance of cohesive forces holding solid agglomerates or liquid drops together and the hydrodynamic disruptive forces. Dispersive mixing is dominated by the stress level within the deforming liquid matrix: a critical stress level must be exceeded to break up whatever cohesive forces hold a solid or liquid particle together. In Newtonian liquids the stresses must exceed the interfacial tension forces.

Taylor [23, 24] studied the breakup of a single Newtonian drop in a simple shear field. The drop size was modeled using the capillary number

$$Ca = \frac{\tau R_d}{S} = \frac{\text{viscous stress} \times \text{drop radius}}{\text{interfacial tension}} \quad (32)$$

and the viscosity ratio

$$\frac{\eta_d}{\eta_m} = \frac{\text{viscosity of dispersed phase}}{\text{viscosity of matrix phase}} \quad (33)$$

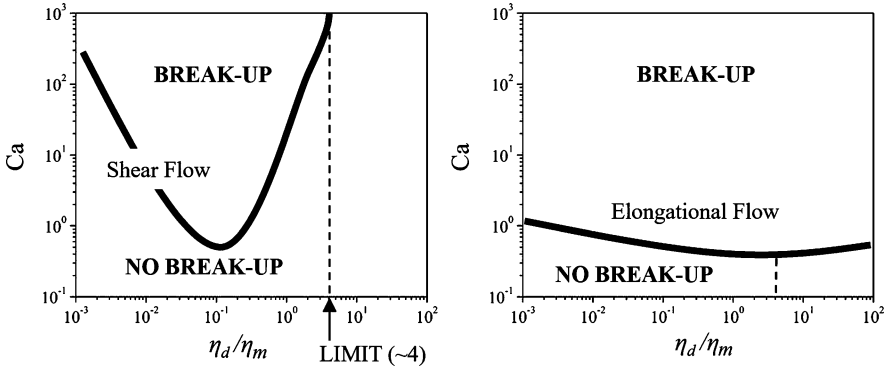


Fig. 11 Grace curves for breakup of droplets in a matrix in shear and elongational flow. (Adapted from [25])

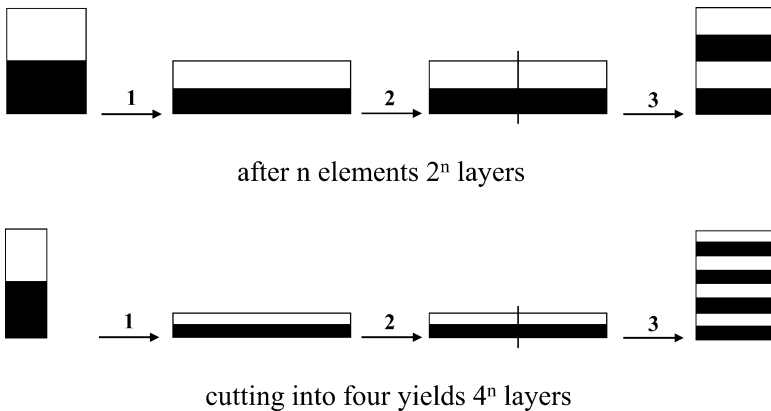


Fig. 12 Schematic representation of baker's transformation. (Adapted from [26])

Grace [25] has performed leading work on breakup of Newtonian drops in both simple shear and elongational flows. The results are summarized in Fig. 11 which are frequently referred to as Grace curves. In shear flow when roughly $\eta_d/\eta_m > 4$, the matrix does not exert sufficient stress to cause rupture, whereas the elongational flow is very effective in causing rupture for virtually all η_d/η_m values. Although Grace curves are for Newtonian fibrils or threads, they correlate qualitatively very well with concentrated blends of polymers. However, it is also possible to have coalescence of small drops. The coalescence process strongly depends on the interface between the drops.

Distributive (or laminar) mixing is quantified by the growth of the interfacial area between two components. This can best be understood by the so-called baker's transformation, since it resembles the way dough is mixed by repeatedly rolling and folding [26] as shown in Fig. 12. For the distributive mixing to be effective, the

layers of the material need to undergo a combination of stretching, folding, and reorientating steps. Devices that do just that can be part of an extruder screw (mixing elements) or attached after the end of an extruder (static mixers).

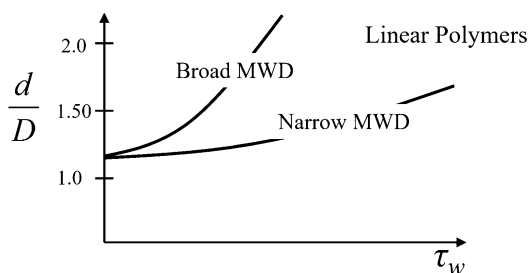
2.6 Extrudate Swell

In extrusion through dies, the extrudate diameter (d) is larger than the die diameter (D). Extrudate swell ratios (d/D) reach values of 400% or more, under certain conditions. This phenomenon (also known as die swell) has been studied by several researchers and is of considerable theoretical and practical importance. While the primary mechanism is the release of normal stresses at the exit, other effects are also important. Extrudate swell is largest for zero-length dies (i.e., orifices). It decreases, for the same throughput, with increasing die length due to fading memory as the residence time in the die increases. Even Newtonian fluids exhibit some swell exiting dies (13% for round extrudates, 19% for planar extrudates). This Newtonian swell is due to streamline rearrangement at the exit. The swell ratio can be influenced by thermal effects due to viscosity differences between the walls and die center. Maximum thermal swell can be obtained when a hot polymer flows through a die with colder walls. Swell ratio of about 5% on top of other mechanisms can be obtained from temperature differences. For linear polymers the swell ratio dramatically increases as the molecular weight distribution broadens as shown in Fig. 13. Several attempts have been made to predict extrudate swell through equations relating the swell ratio d/D (extrudate diameter/die diameter) to the first normal stress difference at the wall N_{1w} . Based on the theory of rubber elasticity, the following equation is obtained [27]

$$N_{1w} = 2\tau_w \left(3 \left[\left(\frac{d}{D} \right)^4 + 2 \left(\frac{d}{D} \right)^{-2} - 3 \right] \right)^{1/2} \quad (34)$$

Based on stress release for a Maxwell fluid [3] exiting from a die, Tanner's equation can be derived [27, 28]

Fig. 13 Schematic of the effect of the molecular weight distribution (MWD) on extrudate swell (d/D) of linear polymers. The horizontal axis corresponds to the wall shear stress



$$N_{1w} = 2\sqrt{2}\tau_w \left[\left(\frac{d}{D} - 0.13 \right)^6 - 1 \right]^{1/2} \quad (35)$$

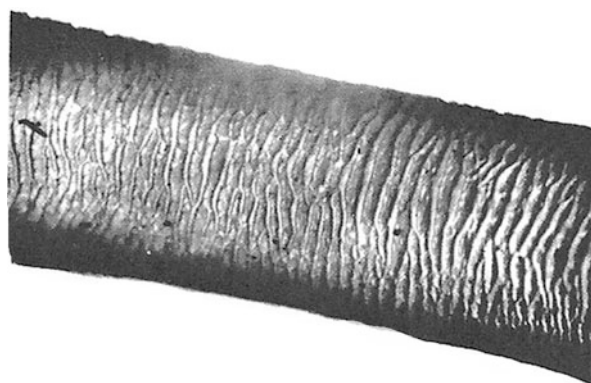
Although this equation has a more rigorous derivation and theoretical basis, the rubber elasticity theory is believed to give better predictions. Unambiguous evaluations are virtually impossible to carry out, because there are no reliable methods for measuring N_{1w} at high shear rates and stresses. At low shear rates (up to perhaps 2 s^{-1}), the first normal stress difference can be determined by measuring the separation force that develops in a cone-and-plate instrument due to the Weissenberg effect. However, in industrial extrusions through dies, wall shear rates at the exit reach or exceed 1000 s^{-1} .

2.7 Wall Slip, Sharkskin, Melt Fracture, and Die Lip Buildup

The no-slip condition at the wall along which a fluid is flowing is a cornerstone of fluid mechanics. The fluid layer adjacent to a wall has the same velocity as the wall itself (zero if not moving). Polymer melts exhibit wall slip when the shear stress level exceeds a certain critical level (about 0.1 MPa for molten HDPE). The existence of wall slip is frequently associated with the onset of polymer flow instabilities or the elimination thereof. The phenomenon of loss of surface gloss on an extrudate is commonly known as sharkskin (also mattness) and occurs at high output rates through dies. The gross flow instability of an extrudate is known as melt fracture occurs at even higher output rates. These phenomena have been studied extensively in the open literature [29, 30]. Die lip buildup, known also as die drool, is not related to sharkskin or melt fracture, and very few studies are available in the open literature.

The sharkskin phenomenon is shown in Fig. 14. It may be described as the appearance of ridges perpendicular to the flow direction, visible to the naked eye.

Fig. 14 Typical sharkskin on an extrudate of about 2 mm, exaggerated due to the enlargement. Note the formation of ridges perpendicular to flow direction



The onset of sharkskin occurs at a critical wall shear stress about $\tau_w \approx 0.14$ MPa, and it is associated with stick-slip phenomena at the die exit.

Ramamurthy [31] suggested that loss of adhesion is responsible for sharkskin, i.e., good adhesion prevents sharkskin. He used dies made of different materials and noticed that the die material has some influence on the loss of extrudate surface gloss. Recent evidence shows that adhesion may diminish sharkskin, but continuous slip is more beneficial. Stick-slip phenomena have always a detrimental effect. With additives, we can postpone sharkskin to higher apparent shear rates (than that corresponding to a critical shear stress of value of 0.14 MPa). For instance, minute amounts of fluorocarbon polymers are used as processing aids in LLDPE [32]. The most recent evidence suggests that sharkskin is the result of tensile failure (rupture) of the emerging extrudate surface [29, 30].

While sharkskin (critical $\tau_w \approx 0.14$ MPa) originates at the die exit, melt fracture as shown in Fig. 15 (with apparent wall shear stress being in the range of $\tau_w = 0.25\text{--}0.5$ MPa) is a gross flow instability and probably the result of more than one mechanism such as (1) entry vortex instability (at high shear rates, the vortex becomes unstable), (2) elastic instability during flow in the extrusion die land when

$$\frac{\text{Normal stress}}{\text{Shear stress}} = \frac{N_1}{2\tau_w} \geq \text{constant} \sim 10 \quad (36)$$

and (3) stick-slip phenomena at the die wall.

It should be noted that the surface tearing phenomenon frequently observed in wood fiber composites (WFC) is not sharkskin nor melt fracture. It appears like some sort of exaggerated sharkskin at very low shear rates as discussed in Sect. 2.8. For very high loadings (over 50%), the tearing disappears due to wall slip. Also at very high shear rates, the surface tearing is reduced [33, 34].

Die lip buildup is the gradual formation of deposit at the extrusion die exit as shown in Fig. 16. Generally, sharp die lips produce more buildup that may be partially relieved using small angle at exit (flaring), e.g., $6^\circ\text{--}12^\circ$. Many additives can cause the severest buildup, and resins with a broad MWD cause more problems.

Fig. 15 Distorted extrudates. Top sample exhibits sharkskin and bottom samples exhibit melt fracture. The defect on the second from the top specimen (HDPE) is due to stick-slip

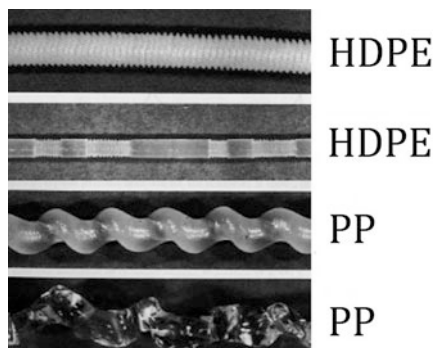
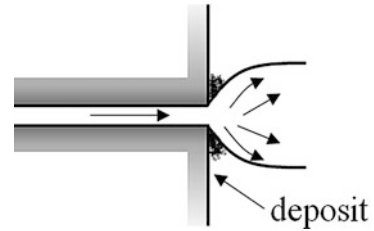


Fig. 16 Schematic representation of the die lip buildup (drool)



Addition of fluorocarbon polymers may sometimes be helpful. According to Gander and Giacomini [35], the main causes of die lip buildup are (1) low molecular weight species, (2) volatiles, (3) fillers, (4) poor dispersion of pigments, (5) drawdown, (6) die swell, (7) low die exit angle, (8) short land length, (9) pressure fluctuations in screw, (10) dissimilar viscosities in blends, (11) dirty die at start-up, (12) high melt temperature, and (13) processing near degradation temperature. An attempt to provide an explanation of die lip buildup has been made by Musil and Zaltoukal [36].

2.8 Rheology of Filled Polymers

Rigid particles are added to polymers either to improve the mechanical properties (reinforcements) or to reduce the cost (fillers) in weight fractions of up to about 70%. Sometimes there might be both improvement of properties and cost reduction. Calcium carbonate is a frequently used filler. Talc is added to increase stiffness and high-temperature creep resistance. Rubber is added to some thermoplastics to increase the impact strength. Carbon black, glass fibers, wood flour, and other natural fibers are also used for a variety of applications.

Einstein solved the problem of resistance to shearing caused by spheres of neutral density, and he showed that the viscosity of the suspensions is related to the viscosity of the matrix η_m as

$$\eta_c = \eta_m(1 + 2.5\varphi) \quad (37)$$

where φ is the volume fraction. This relation is valid for concentrations up to $\varphi = 0.01$. For higher concentrations, the particle-particle interactions are important, and Batchelor's equation is valid up to $\varphi = 0.1$. For strong Brownian motion of spheres,

$$\eta_c = \eta_m(1 + 2.5\varphi + 6.2\varphi^2) \quad (38)$$

and for weak Brownian motion,

$$\eta_c = \eta_m(1 + 2.5\varphi + 7.6\varphi^2) \quad (39)$$

In very dilute solutions, particles will rotate due to the action of the shear field. As the concentration is increased, hydrodynamic interactions between the particles become important. Particles come close to particles on nearby streamlines, and the fluid is disturbed in their vicinity. As the concentration is further increased, colloidal interactions (of attraction or repulsion) involve three, four, or more particles, and the rigorous analyses used in the derivation of the above equations no longer apply [37, 38]. To this end, several semiempirical equations have been proposed by plotting the relative viscosity η_c/η_m as a function of φ/φ_{\max} where φ is the volume fraction and φ_{\max} the limiting concentration called the “maximum packing fraction” of the filler. It is generally difficult to determine the maximum packing fraction φ_{\max} in real situations. For monodisperse spheres packed on a simple cubic lattice, the maximum packing fraction will be $\varphi_{\max} = (4\pi/3)/8 = 0.524$, while for random close packing, $\varphi_{\max} = 0.637$. This value decreases with increasing asymmetry or flocculation due to poorer space filling [38, 39]. The Maron-Pierce equation is used frequently

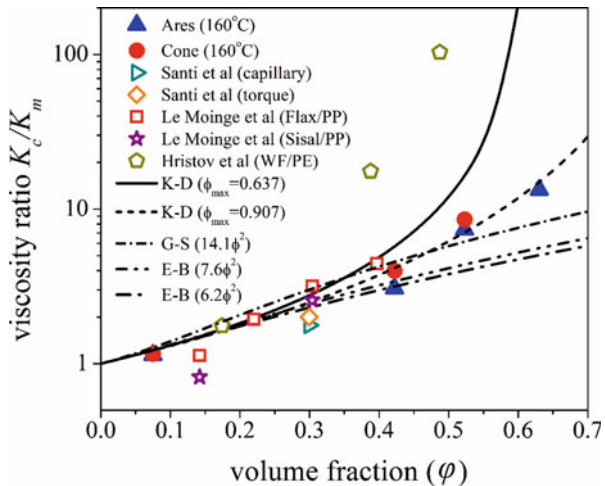
$$\frac{\eta_c}{\eta_m} = \left(1 - \frac{\varphi}{\varphi_{\max}}\right)^{-2} \tag{40}$$

or the Krieger-Dougherty equation

$$\frac{\eta_c}{\eta_m} = \left(1 - \frac{\varphi}{\varphi_{\max}}\right)^{-k\varphi_{\max}} \tag{41}$$

with k being frequently denoted as $[\eta]$ (the intrinsic viscosity) and usually referred to as the Einstein coefficient equal to 2.5 for spheres. High values of k (roughly more than 20), means existence of high aspect ratios. An example of fitting the abovementioned equations to measurements for a relatively wide range of fillers and filler loadings is shown in the semilogarithmic plot of Fig. 17, where the zero

Fig. 17 Relative consistency index as a function of filler volume fraction. K is the consistency index of the power law equation, index c for composite, and m for the matrix. (Adapted from [40])



shear viscosity was replaced by the consistency index K (which is the viscosity at shear rate of 1 s^{-1}).

Measurement of viscosity in filled systems is necessary for extruder and die design purposes and for process optimization. It still remains a challenge, because of significant wall slip as the loading is increased and some problems associated with interference of the relatively large fibers with the walls, in the narrow gaps of rheometrical devices. Another problem is that the Cox-Merz rule (equivalence of steady and dynamic viscosity measurements) is not applicable.

Wood fiber composites have attracted considerable interest in recent years. They are extruded mostly for decking and fencing applications in North America, housing applications in Japan, and injection molded in Europe, for the automotive industry. Fiber loadings usually reach up to 60%. The low cost of the wood fibers and very good end-use properties are strong incentives. Rheologically, they exhibit significant increase in viscosity (Fig. 18a) and storage modulus (Fig. 18b), wall slip phenomena, and a characteristic surface tearing which appears as some sort of exaggerated sharkskin as shown in Fig. 19.

2.9 Rheology of Nanocomposites

Polymeric nanocomposites were first developed and commercialized in the late 1980s by the Toyota research group. They dispersed layered silicate nanofillers in a polymer matrix. Nanosized particles have significant influence on end-use properties of the composites, such as impact strength, flame retardance, liquid and gas permeability reduction, abrasion resistance, and reduced shrinkage, and on electrical and optical properties.

Rheological trends are similar to other filled polymers, with the following differences: (a) loadings are low (less than 10%), (b) the nanosized fillers have very large aspect (length/thickness) ratios, (c) the nanosized fillers have extremely large area-to-volume ratios, and (d) there are interactions at the atomic level [41].

Layered silicate nanocomposites are particle-filled polymers for which at least one dimension of the dispersed phase is in the nanometer range. Three morphologies are possible as shown in Fig. 20: (a) phase-separated, polymer chains do not penetrate into clay; (b) intercalated, polymer chains penetrate deep within the layers of the silicate; and (c) exfoliated, individual layers ($\sim 1 \text{ nm}$) are well dispersed and randomly distributed throughout the polymer matrix (maximum reinforcement due to large surface area of contact).

In steady shear measurements, the viscosity increases with silicate content, and the Newtonian plateau is shifted to lower-and-lower shear rates as shown in Fig. 21a [43]. Similar trends are observed using oscillatory measurements as shown in Fig. 21b for a composite system of montmorillonite and polyethylene using melt compounding. It is evident that " η^* " increased substantially at low frequencies and the Newtonian plateau disappeared as clay content increased above 5 wt%. Increases of such magnitude arise in conventional composites at much higher filler loadings

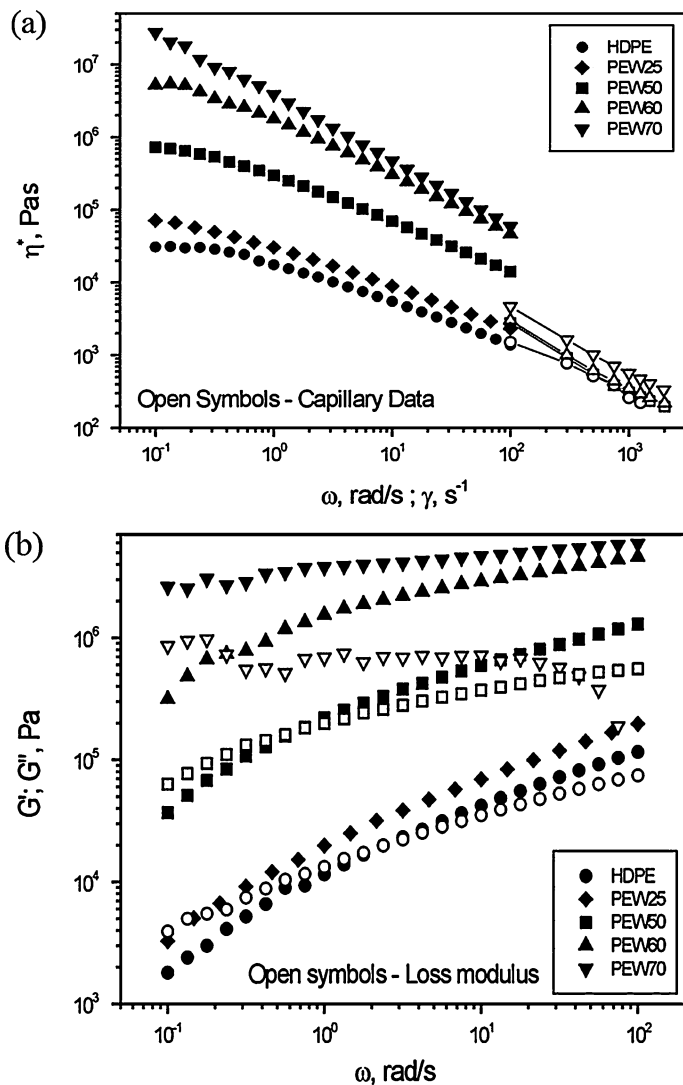


Fig. 18 Effect of wood loading in HDPE on (a) complex viscosity at 180 °C and (b) storage and loss modulus. (Adapted from [33])

(above 20–30 wt%) and may be attributed to weak structure that may remain intact at very low frequencies” [44].

In any dispersion macro-, micro-, or nano-, there will be significant particle-particle interactions at increased concentrations. At some point (threshold), a three-dimensional network is formed. Studies with carbon black show significant changes in electrical properties at the percolation threshold. At the percolation threshold, there are also rheological changes as evidenced by dynamic measurements of storage

Fig. 19 Extrudate surface morphologies under various conditions of wood-filled mPE. In (a) increasing the filler loading for $L/D = 6$, $D = 15$ mm, $\dot{\gamma}_a = 2.5$ s⁻¹ and in (b) increasing the apparent shear rate for 60% filler loading, $L/D = 8$ and $D = 1$ mm. (Adapted from [34])

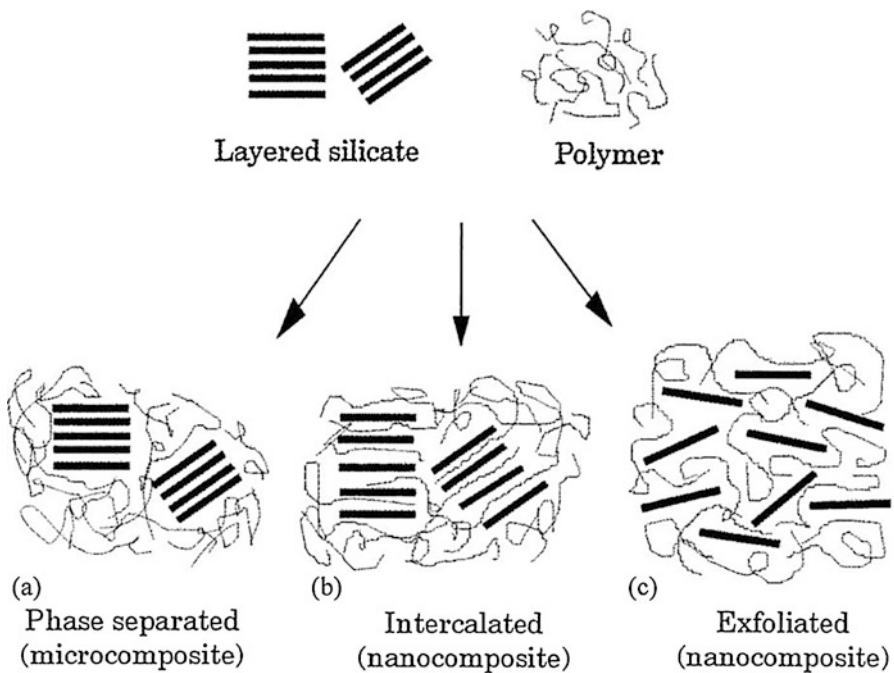
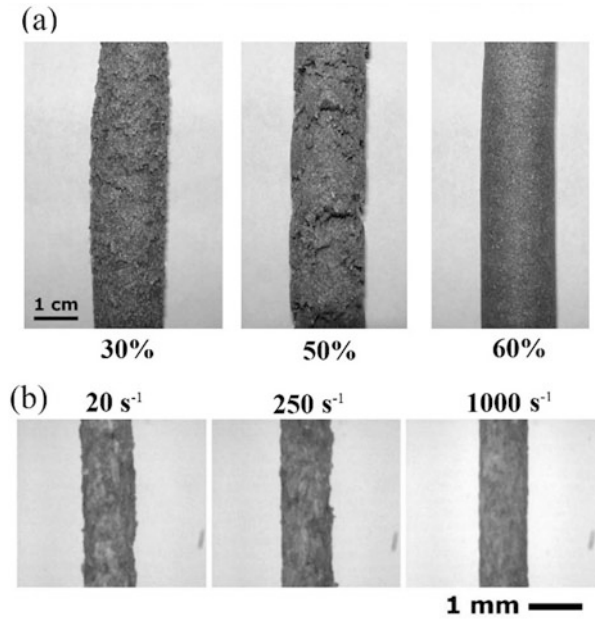


Fig. 20 Morphologies of polymer-layered silicate nanocomposites. (Adapted from [42])

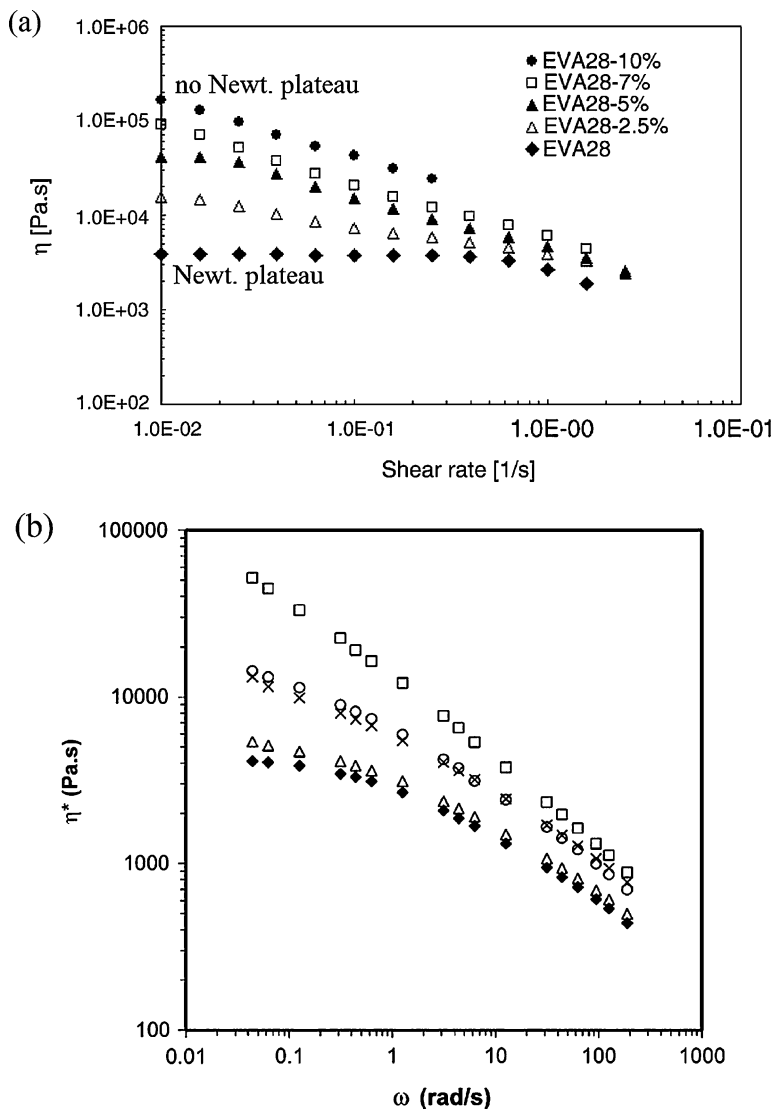
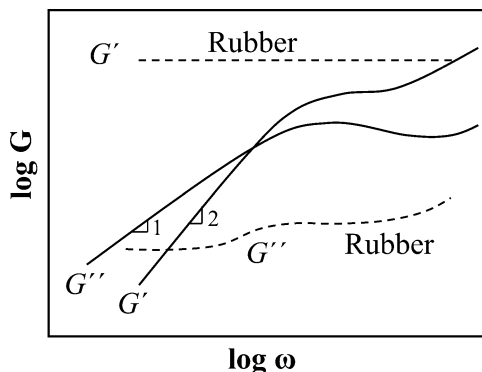


Fig. 21 (a) Steady shear viscosity as a function of shear rate at 130 °C for different bentonite clay loadings in EVA28 adapted from [43] and (b) complex viscosity as a function of frequency at 170 °C for different montmorillonite clay loadings (0-10%) in polyethylene, adapted from [44]

G' and loss modulus G'' . This critical point is dependent upon polymer matrix, filler loading, and temperature. According to a summary of recent publications by Bhattacharya et al. [45], percolation threshold nanocomposite filler loadings range between 0.5% and 6% by weight.

Fig. 22 Typical G' and G'' behavior of a melt or a concentrated solution



When dynamic measurements in the linear viscoelastic regime are performed, the typical G' and G'' behavior of a melt or a concentrated solution is exhibited in Fig. 22 with $G' \sim \omega^2$ and $G'' \sim \omega$ at low frequencies (of less than 0.1 rad/s and preferably less than 0.01 rad/s). If at low frequencies $G'' > G'$, the material exhibits a liquid-like behavior, and if $G'' < G'$, the behavior is more solid-like. An example of such a behavior is shown in Fig. 23a for an EVA28 nanocomposite [46]. At low frequencies the nanocomposite exhibits a liquid-like behavior, and as the filler loading is increased, the behavior tends to be solid-like. It must be noted that the bigger changes in G' and G'' are exhibited in the low frequency range, and therefore G' , in this range, is more sensitive in detecting structural changes. By plotting the slope of $\log G'$ versus $\log \omega$ at low frequencies (< 0.01 rad/s) as a function of the filler loading, the percolation threshold can be determined as shown in Fig. 23b [43].

3 Polymer Melt Processing

3.1 Extrusion

Extrusion is one of the most important polymer processing operations. It involves a sequence of the following steps: (a) heating and melting the polymer, (b) pumping the melted polymer to the shaping unit, (c) forming the melt into the required shape and dimensions via an extrusion die, and (d) cooling and solidification. Steps (a) and (b) above are taking place in an extruder, which consists of a heated hollow cylinder (barrel) into which a screw (single screw extruders – SSE) or a pair of screws rotate (twin screw extruders – TSE). The screw is the heart of the extruder, and it is usually referred to as an Archimedean screw, even though Egyptians were using similar devices before Archimedes. Modern developments, based on understanding of the thermomechanical phenomena, are less than 70 years old [2, 47–49].

Polymer resins in the form of pellets, powders, or flakes flow from a hopper to the gap between the rotating screw and the heated barrel as shown in Fig. 24. The depth

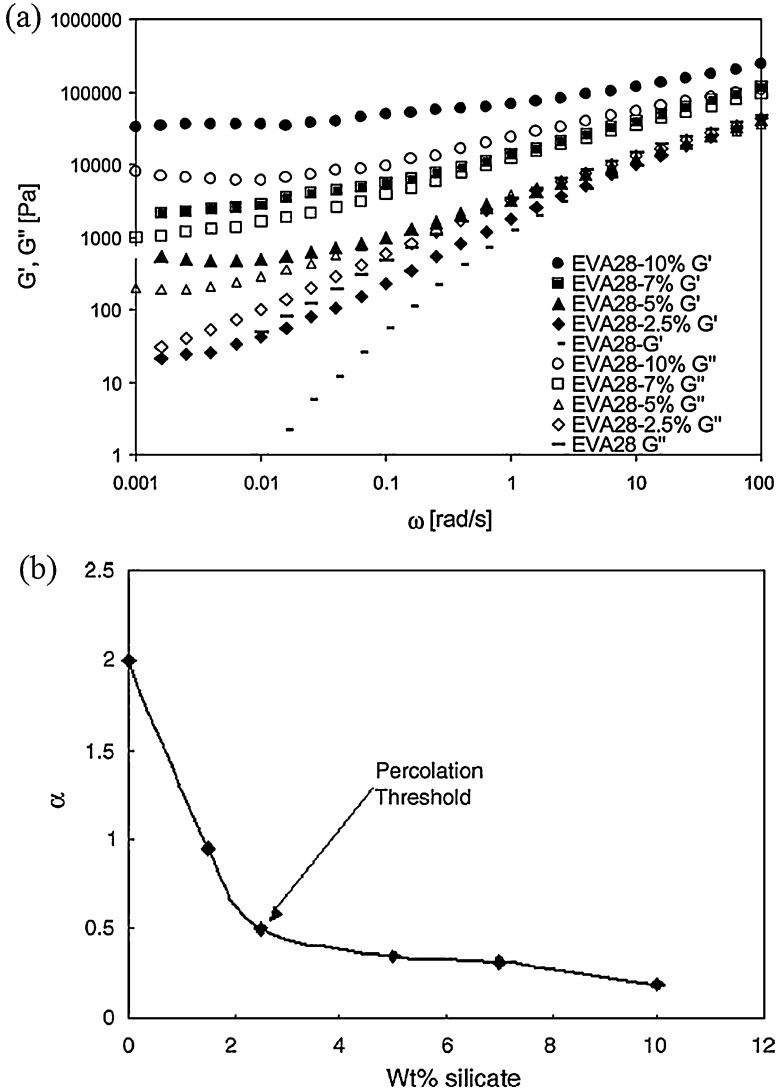


Fig. 23 (a) Storage and loss moduli for EVA28 and EVA28 nanocomposites at 130 °C adapted from [46] and (b) percolation threshold of EVA28 nanocomposites where $\alpha = \log G' / \log \omega$, adapted from [43]

of the conveying channel in the screw is contoured from large to small in the flow direction, to account for the density change from the particulate solid feed to the molten polymer extrudate, and for pressure development. The SSEs normally have diameters between 25 and 250 mm and length/diameter ratios between 20 and 40. Usual rotation speeds range from 20 to 150 RPM. A 60-mm-diameter machine may deliver up to 200 kg/h, while a 150-mm-diameter machine can exceed 1000 kg/h.

Fig. 24 Schematic diagram of a single screw extruder

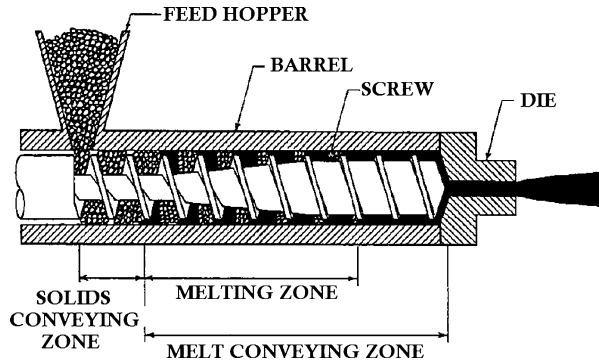
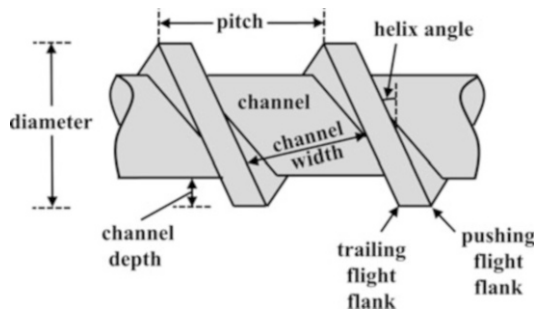


Fig. 25 Typical screw terminology



Recently developed high-speed single screw extruders can produce much higher output rates at rotation speeds exceeding 1000 RPM, usually with small-diameter machines.

In the first region or solids conveying zone of a SSE, the solid polymer particles are compacted together in the screw channel by the rotating action of the screw to form a solid bed of material. At the start of the next extruder section, the plasticating (melting) zone, barrel heaters cause a thin film of molten polymer to form in the gap between the solid bed and the barrel wall. The melt film is subjected to intense shearing in the thin gap, and because of the extremely high viscosities of molten polymers, high rates of viscous dissipation result. The generated heat melts completely the solid packed bed of pellets or powders, usually at 2/3 of the screw length from the feed, in well-designed extruders. In the last zone of the extruder, the metering section, the polymer melt flow is stabilized in the shallow screw channels, and finally the material passes through the die at the end of the machine.

Screw design is very important for achieving high output rates of homogeneous high-quality melt without any solid particles (unmelts). The standard screw has a single flight with 17.66° helix angle (square pitched with the pitch being equal to the diameter as shown in Fig. 25 that represents a typical screw section). Used increasingly in the extrusion industry are barrier screws. Barrier screws have a secondary screw flight in the melting section of the screw, which serves to segregate the solid bed from the molten polymer as shown in Fig. 26. By independently controlling the

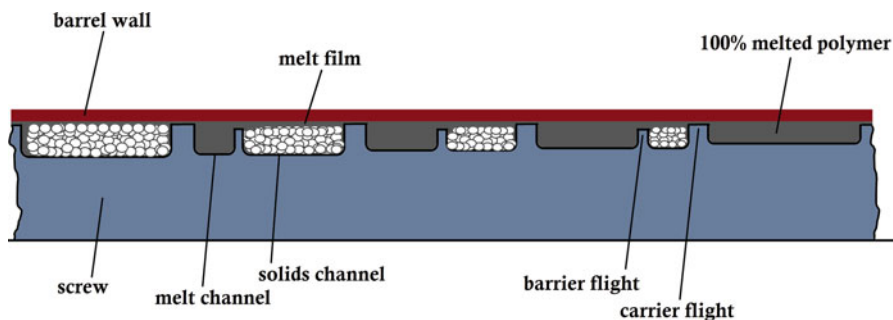


Fig. 26 Schematic diagram of a typical barrier screw

dimensions of the solids and melt channels, the melting process can be accelerated and made more stable, thereby increasing the extruder output and melt quality.

To improve melting and mixing, cutting of the flow field, reorientation, and smearing into thinner sections are necessary. This is achieved by pins or pegs, broken flight sections, reverse flight sections, multiple flighted sections, unflighted torpedo sections, or similar configurations. These devices are normally located at the downstream end of a screw and improve melt quality by reducing temperature non-homogeneities in the polymer stream and improving the dispersion and distribution of additives.

Industrial experience shows that for good functioning extruders, the throughput should not be less than 25% of the drag flow equation

$$\dot{m}_D = \frac{1}{2} \rho \pi^2 D_b^2 H N \sin \theta \cos \theta \quad (42)$$

where ρ is the melt density, D_b barrel diameter, H channel depth in the metering section, N the rotational speed of the screw, and θ the helix angle, as shown in Fig. 25.

Grooved barrel extruders feature axial grooves or slots in the part of the barrel immediately following the feed throat (usually up to $4D_b$). The grooved barrel can significantly enhance the solid transport rate due to high friction on the barrel and increase the pressure buildup significantly, very close to the feed throat. In these extruder types, the compression ratio (i.e., the channel depth in the feed over the depth in metering section) is roughly 1–1.2, while in smooth barrels higher compression ratios are met ranging from 2 to 4. Grooved barrel extruders can deliver double the output rate given by the drag flow equation above. High-speed extruders usually have the entire barrel grooved [50, 51] and even higher outputs.

The power provided by the rotating action of the screw goes to heating the polymer from room temperature to the extrusion temperature, melting the polymer and pumping it through the die [52]. The barrel heaters usually provide less than 25% of the power required to raise the temperature and melt the polymer. Extruders have poor pumping efficiency. The energy required for pumping is about 10% of the total motor power supplied by the rotating screw.

Twin screw extruders (TSEs) are extruders with two screws of the same diameter which turn side by side within the extruder barrel at the same speed [2, 52, 53]. They are used increasingly, in recent years, mainly for mixing, blending, and compounding of thermoplastics with additives, devolatilization, and reactive extrusion. The disadvantage of TSEs compared with SSEs is their significantly higher capital cost. There are twin screw extruders with intermeshing or non-intermeshing screws, depending on whether they engage or not each other's flights. The screws can be corotating or counterrotating. Screws are made up of conveying, kneading blocks and mixing sections. The screw design is frequently modular, which allows for a nearly unlimited number of possible screw configurations. Kneading blocks comprise several disks staggered at an angle to one another. Dispersive mixing takes place in the elongational flow regions formed by thick kneading blocks (shaped like oval disks) wiping the barrel wall. Corotating intermeshing twin screw extruders with thick kneading blocks have excellent mixing capabilities (both distributive and dispersive). Counterrotating intermeshing twin screw extruders operate almost like positive displacement pumps, have limited mixing capabilities, and are used for extruding temperature-sensitive materials (mostly PVC).

Once a polymer has been melted, mixed, and pressurized in an extruder, it is pumped through an extrusion die for continuous forming (after cooling and solidification) into a final product. The most common die types are flat, annular, round, and profile. Products made by extrusion include pipe, tubing, coating of wire, plastic bottles, plastic films and sheets, plastic bags, coating for paper and foil, fibers, filaments, yarns, tapes, and a wide array of profiles (e.g., window frames and sealing systems) [52].

Blown film extrusion is the most important continuous process for the production of thin plastic films from polyethylene. A typical blown film extrusion line is shown in Fig. 27. The molten polymer is extruded through an annular die (normally of spiral mandrel construction as shown in Fig. 28), to form a thin-walled tube which is simultaneously axially drawn and radially expanded. Polymer has the tendency to flow right above the ports of the spiral die, therefore producing tubes of circumferentially thick-thin regions. A good die, in general, should not have thickness variation of more than 5% [54]. This may lead to defects far downstream in the production line. Either way, computer-aided design and knowledge of the polymer's rheology may be used to eliminate or at least suppress in a cost-/time-effective way the above-described thickness variations. In most cases the blown film bubble is formed vertically upward. The maximum bubble diameter is usually 1.2–4 times larger than the die diameter. The hot melt is cooled by annular streams of high-speed air jets from external air rings and occasionally also from internal air distributors. The solidified film passes through a frame which pinches the top of the bubble and is taken up by rollers. Coextruded films with 3–8 layers (sometimes up to 11) are produced by this process, for use in food packaging, having at least 1 polymeric layer with very low permeability to oxygen and moisture. Outputs frequently exceed 1000 kg/h.

Cast film and sheet extrusion is a continuous process and involves extruding a polymer through a flat die, having die lip gap of a couple of mm and width from a

Fig. 27 Schematic representation of a typical film blowing process

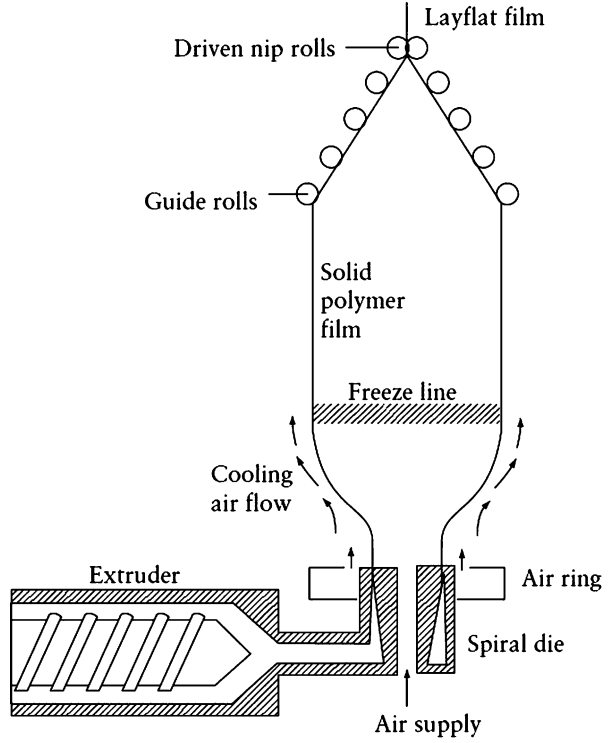
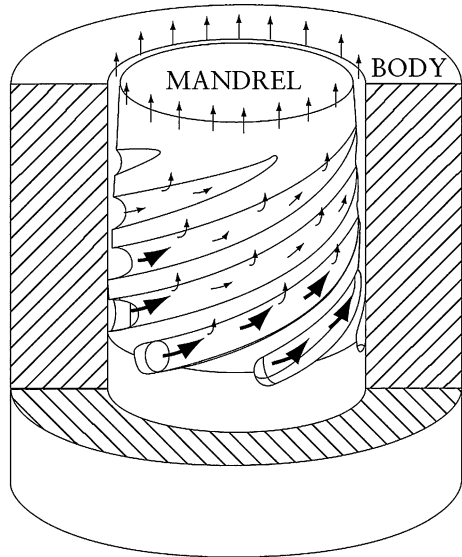


Fig. 28 Schematic of a typical spiral die



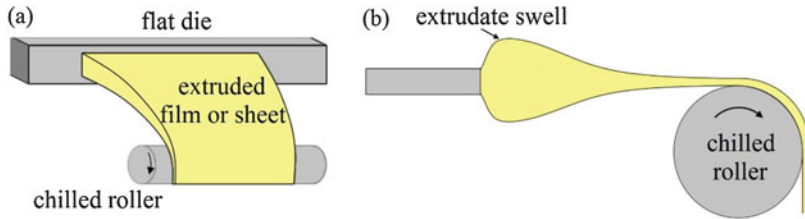
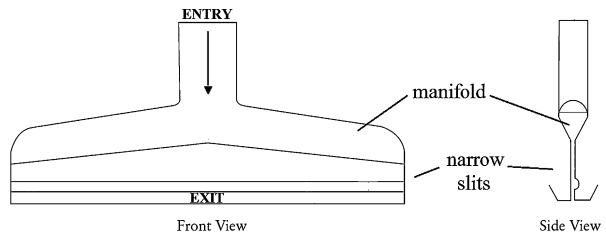


Fig. 29 Schematic representation of cast film extrusion process (a) front and (b) side view. Figure not to scale

Fig. 30 Schematic representation of a typical coat hanger die for film or sheet extrusion



few cm (for tapes) to a few meters. It is subsequently stretched by a chilled steel roller or rollers which quench and solidify the molten material shown in Fig. 29. The final product has reduced width (due to necking) and thickness compared to the corresponding dimensions of the die. The final dimensions are mainly affected by the ratio of the roller speed to the extrusion speed, which is often referred to as draw ratio. Upon emergence from the die, the final product will locally swell. It has been recently shown via numerical methods that this local amount of swell is affected dramatically by the draw ratio [55]. Film is generally defined as a product thinner than 0.25 mm, while sheet is thicker than this. The cast film process is used for very tight tolerances of thin film or for low-viscosity resins. Most flat dies are of T-slot or coat hanger designs, which contain a manifold to spread the flowing polymer across the width of the die, followed downstream by contoured slits to create the desired flow distribution and pressure drop. A typical coat hanger flat die is shown in Fig. 30. Most cast film lines manufactured today are coextrusion lines, combining layers from as many as seven extruders into the product through multi-manifold dies, or single manifold dies with the aid of feedblocks [56].

Pipe extrusion involves dies having lips of annular geometry. Two types of dies are used: either spiral dies (like those used in film blowing but having much wider gaps) or spider leg dies, in which a central mandrel (also called torpedo) is supported by steel supports (rods) around the circumference. Behind the spider legs, weldlines form [57]. Weldlines are lines of weakness in mechanical properties, and their impact must be reduced for avoiding premature pipe failure. PE, PVC, and PP are used extensively in pipe and tube extrusion for a variety of products for water and gas distribution and numerous other applications in housing, automotive, and health industries. Diameters can range from millimeters for medical applications to meters

for sewage and storm water installations. Usually very-high-viscosity materials are used in pipe extrusion (e.g., HDPE having melt index (at 190 °C, 2.16 kg) as low as 0.1 for pressure pipes).

Profile extrusion is a manufacturing process used for products of constant cross section. These can range from simple shapes to very complex profiles with multiple chambers and fingers. Examples range from picture frame moldings and automotive trims to edging for tabletops and window lineals. The extruded materials are classified (roughly) as rigid or flexible. The typical profile extrusion line consists of an extruder pumping a polymer through a profile die, followed by a sizing tank or calibrator, additional cooling troughs, a puller, and a cutoff device. The design of profile dies requires considerable experience and patience. Output limitations in profile extrusion are encountered owing to either sharkskin (for thin products produced from high-viscosity polymers) or the ability to cool thick-walled products.

It should be noted that extrusion die design is a challenging task. Design is much more complex than optimization. In fact, the optimization problem is a standard mathematical one, i.e., to maximize a function subject to constraints. In engineering design, we use inequality specifications of satisfactory performance, rather than maxima and minima, along the lines of Herbert Simon [58] who tried to introduce the term “satisfice” as opposed to “optimize.” In extrusion die design, there are certain considerations that should be taken into account: (a) flow balancing, to produce uniform outflow (i.e., film, profiles of equal thickness), (b) reasonable pressure drop (not too high not too low), (c) no hot spots, (d) no stagnation flow regions, (e) avoidance of die lip buildup, (f) delay onset of sharkskin/melt fracture, (g) avoidance of weldlines or reduction of their influence, and (h) residence time (long enough for homogenized extrudate, but not too long to cause degradation or cross-linking). The nowadays powerful computer systems along with a suitable user-friendly flow analysis software offer a fast way to assess whether a die design can be characterized as satisfactory or not. This is usually carried out by performing a repetitive set of computer simulations before arriving at a satisfactory design. Of course, good viscosity measurements are absolutely necessary for computer simulation of molten polymer flows through dies.

3.2 Calendering

Calendering is a widely used manufacturing continuous process that involves a pair or more of counterrotating heated calenders (rolls) for the production of thin plastic sheets and films. The thermoplastic melt is fed behind the minimum gap of the two calenders, as shown in Fig. 31. The rotational movement forces the material to flow in the machine direction (downstream) and in the lateral direction, with subsequent detachment from the rollers' surface at a specific thickness [59]. Two-roll calendering lines are usually used for rubber processing, whereas four-roll calenders are generally used for the production of double-coated products meeting strict surface quality requirements. The major plastic materials calendered are PVC and ABS.

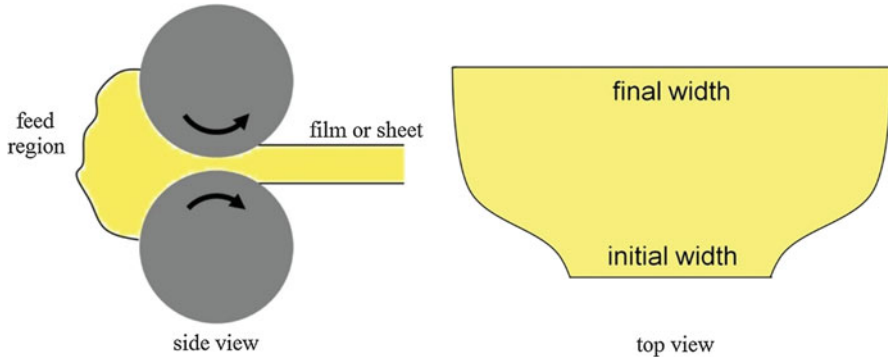


Fig. 31 Schematic representation of a typical calendaring line. Figure not to scale

Products range from wall covering and upholstery fabrics to reservoir linings and agricultural mulching materials. Calendaring is also widely used in the food, paper, and rubber industries.

Calendaring may be characterized as a generally mild process for plastic sheet or film production in terms of the shear rates involved. Typical shear rates are of the order 100 s^{-1} , much lower than in other processes. Assuming the polymer melt viscosity may be expressed by the power law model, the maximum pressure developed P_{max} , between rotating rolls, which can be roughly approximated by

$$P_{\text{max}} = 0.535K \left(\frac{2}{3} \frac{U}{H_o} \right)^{n-1} \left(\frac{U}{H_o} \right) \left(\frac{R_{\text{rol}}}{H_o} \right)^{0.5} \quad (43)$$

where K is the consistency index, n the power law index, U roller speed, H_o the minimum distance between the rollers, and R_{rol} their radius. Two-roll mills are frequently used in the rubber industry, for laboratory mixing trials. It has also been shown that use of a three-roll calendaring-type machine may be an effective process to disperse a nanocomponent in a polymeric matrix such as carbon nanotubes [60] or perhaps graphene [61]. This is mainly due to the strong extensional flow developed in the converging region between the rollers that leads to disaggregation of the agglomerated nanocomposite, resulting in a relatively good dispersion (exfoliation). At the same time, the low shear rates are less likely to cause attrition of the individual nanocomposite particles so that the properties of the added nanocomponent may be exploited to a large degree. For example, it has been recently concluded in the work of Prolongo et al. [62] that the calendaring process is an effective technique for the dispersion of graphene nanofiller, as compared to a high shear mixing process that could induce a reduction of the graphene nanofiller's lateral size by breakage. Determination of the extensional and shear rates in the calendaring gap region, using fully 3D numerical analysis, such as in Polychronopoulos et al. [59], combined with rheological measurements, is of critical importance and may offer new insights in a fast and relatively inexpensive manner.

3.3 Injection Molding

Injection molding is a two-step cyclical process: (a) melt generation by a rotating screw and (b) filling of the mold with molten polymer by the forward ramming of the screw (called a reciprocating screw), followed by a very short packing stage necessary to pack more polymer in the mold to offset the shrinkage after cooling and solidification. The material is held in the mold under high pressure until it has solidified sufficiently to allow ejection.

In polymer injection molding, the melt path into the mold starts with a sprue and splits off into individual melt tubes (called runners) each feeding one of the multiplicities of mold cavities through flow entrances (called gates). Figure 32 shows schematically how these mold components are connected. Molds can contain over 100 cavities, each producing a part per injection cycle. One problem facing mold design is the balancing of runners. Figure 33a shows naturally balanced runners (i.e., it takes the same time for the polymer melt to reach the 16 cavities). Figure 33b

Fig. 32 Schematic representation of injection molding

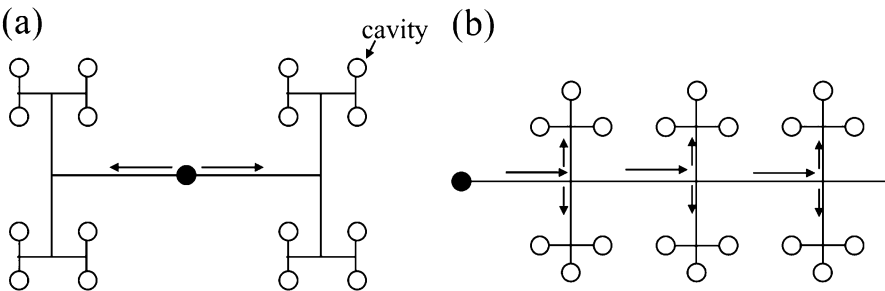
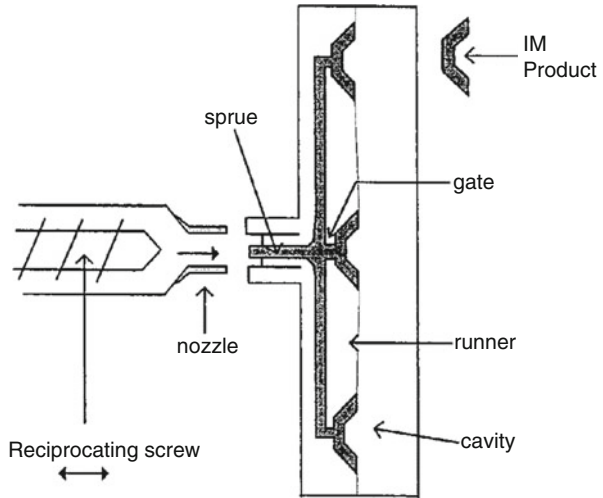


Fig. 33 (a) Naturally balanced and (b) naturally unbalanced runners in injection molding

shows naturally unbalanced runners. To balance a naturally unbalanced system of runners, we must size the runner diameters and lengths so that all cavities fill at the same time. For just a few runners, it is possible to use simple pressure drop versus flow rate equations. For numerous runners, as it is frequently the case, flow simulation software is required.

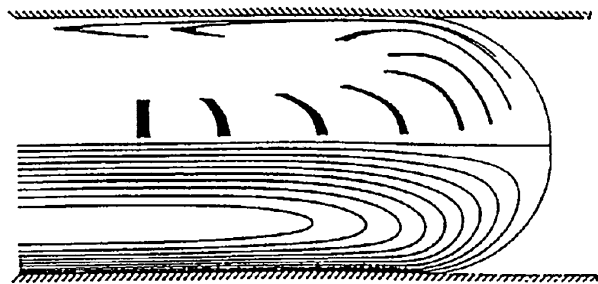
Hydraulic and electric (or hybrid) systems are used, for the purpose of holding the mold closed with sufficient force to resist the injection pressure. The clamping force is determined by multiplying the injection pressure by the projected area, and it is usually reported in tons (1000 kg force). Line pressures can reach up to perhaps 200 MPa. Obviously the larger the projected area, the larger the clamping force required. Commercially available machines range from a few tons to a few thousand tons of clamping capacity.

Cycle times usually range from a few seconds to over a minute. Numerous products ranging from boat hulls, lawn chairs, and appliance housings to radio knobs and bottle caps are injection molded. Very high shear rates arise in injection molding operations (usually up to 10^4 s^{-1}), and to limit temperature increases from viscous heating and to facilitate easy filling, low-viscosity thermoplastic polymer grades are used.

Mold cavity filling is characterized by the fountain effect, in which elements of the molten polymeric fluid undergo complex shear and stretching motions as they catch up to the free flow front and then move outward to the cold walls. This phenomenon can impart considerable orientation to the resulting injection-molded part. While molecular orientation is used in extrusion to improve the mechanical properties, in injection molding, orientation is generally a nuisance [1]. The orientation is further exacerbated during the packing stage. The consequent frozen-in stresses can cause finished parts to become distorted, especially at elevated temperatures. Figure 34 shows streamlines and fluid element deformation in fountain flow [63].

When two flow fronts meet (e.g., when a cavity is filled from two gates from opposite directions), a weldline is formed. Weldlines are also formed behind flow obstructions, just like in the case of spider leg extrusion dies. These are lines of poor bonding and low mechanical strength, due to the relatively large time required for large polymer chains to interdiffuse. Determination of the location of weldlines can be done with the help of suitable flow analysis software. It is advisable to avoid weldlines in load-bearing areas of a molded product.

Fig. 34 Illustration of fountain flow streamlines as seen by an observer moving with the flow front (bottom half) and fluid element orientation (top half)



Simulation of cavity filling is generally carried out on the basis of the Hele-Shaw flow approximation [64, 65] which applies to viscous flow between two closely spaced plates. Recently fully 3D and non-isothermal simulation software packages have also been developed. Computer simulation is used extensively in injection mold design and process/product optimization. Rheological data are absolutely necessary for carrying out reliable simulations of flow of molten polymers through runners and mold cavities.

Among the challenging problems faced in computer simulation is the prediction of shrinkage and warpage. Shrinkage is the difference in dimensions between the mold and the cooled molded part. The main cause is the density increase, which occurs as the melt freezes. Crystalline polymers such as polyamide (PA, nylon), high-density PE, PET, and PP give the worst problems [1] with shrinkages of 1–4%. Amorphous polymers such as PS, PMMA, and PC have fewer problems, shrinking only 0.3–0.7%. Warpage is caused by the density changes mentioned above and orientation imparted to the part during cavity filling and packing, decidedly in a nonuniform manner. In addition to the rheological data, pressure-volume-temperature measurements and knowledge of crystallization behavior are necessary for computer analysis of packing, shrinkage, and warpage phenomena.

Gas-assist injection molding involves the injection of nitrogen with the plastic, which creates a hollow void in the molded part [66]. This allows large parts to be molded with lower clamp tonnage and significant material savings. This innovative process started in the 1980s and its use is growing.

The process of reaction injection molding (RIM) involves the injection of low-viscosity liquids, which become reactive when mixed and polymerize within the mold [67]. The advantage of this process is that the pressures are low owing to the low viscosities. A disadvantage is the requirement to handle highly toxic substances. Although initial projections called for significant growth in RIM, this did not materialize. In fact, some manufacturers of automotive parts by RIM have switched to conventional injection molding of thermoplastics.

3.4 Compression Molding

Compression molding is the oldest technique for the production of polymer products [64] and is mainly used for thermosets. In this process the compound is pressed in the mold by the heated platens of a hydraulic press. This process is to some extent analogous to sheet metal stamping. Injection molding of polymers has replaced compression molding for some polymers, because of the advantages in material handling and automation. However, compression molding has an advantage in the processing of reinforced polymers [68]. Owing to modest levels of deformation and stress involved in compression molding, the reinforcing fibers are not damaged. Very high fiber concentrations and longer fibers can be included in compression-molded products.

3.5 Blow Molding

Blow molding is the process by which articles are formed by inflation of a molten polymer to fill a mold cavity having the desired shape and dimensions. Bottles for soft drinks and other liquids are blow molded. The two most important process variants are extrusion blow molding and injection blow molding [69]. In extrusion blow molding, an extruder pumps the melt through an annular die to form a molten tube or parison with well-defined and controlled dimensions. The parison is clamped between the two mold halves and is inflated by internal air pressure to take the shape of the mold cavity, which is usually cooled. Finally, the formed article solidifies as a result of cooling, and the mold is opened to eject the article without damage. The fuel tanks of cars and trucks are extrusion blow-molded multilayer parisons (usually more than 6 layers with at least 1 layer of a barrier to gasoline vapors).

Injection blow molding is a two-stage process. In the first stage, the plastic is injected into a cavity where the preform is molded. The preform is then transferred to the blow mold for inflation. Injection blow molding offers the advantages of accurate dimensional control, the elimination of scrap, and the molding in of threads before blowing. Extrusion blow molding is preferred for containers with high length/diameter ratios and for products with handles [70].

Polyethylene terephthalate or PET is the polymer most widely used in injection blow molding, for carbonated drinks and water bottles. Stretch blow molding is used to produce PET bottles of enhanced physical properties. In this process, stretching induces the formation of small lamellar crystals. These crystals result in more transparent and tougher products than those produced without stretch blowing, which have spherulitic crystals.

3.6 Thermoforming

Thermoforming techniques involve the softening of thermoplastic sheets by heat, followed by forming by the application of vacuum, pressure, or a moving plug [71]. The sheet may be stretched over a male mold (positive forming) or into a female mold (negative forming). On contact with the mold, heat is lost and the material regains stiffness as it cools. Geometries of thermoformed products are usually simple (boxes, food trays, various containers, refrigerator liners, computer cases). Thermoforming competes with blow molding and injection molding. The main advantages of this process are the relatively low cost of thermoforming machines and the very low cost of the molds and the ease of forming large area, thin section parts. Disadvantages are the limited product shapes possible, difficulties in obtaining the required thickness distribution, difficulty in controlling molecular orientation, and limitations in service temperature which may induce strain recovery or shrinkage. Thermoforming of thermoplastics has certain similarities to sheet metal forming [72]. However, the strain rates involved in polymer sheet forming are much larger than for metals. Figure 35 shows a vacuum thermoforming process. When the

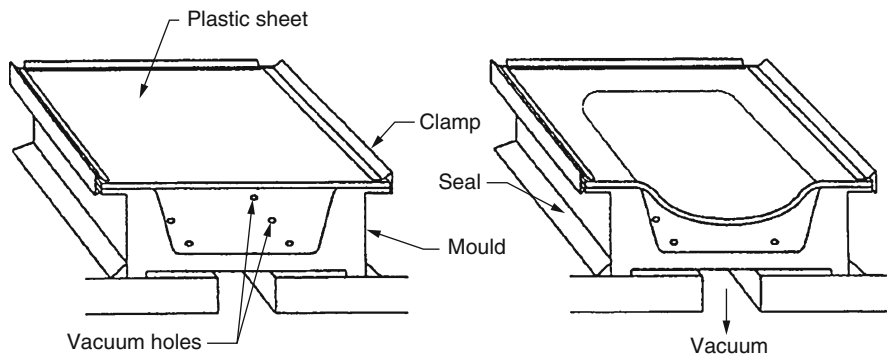


Fig. 35 Thermoforming by application of vacuum

ratio of area of the thermoformed product over the initial area of the sheet (draw ratio) is large, polymers of good melt strength are required.

3.7 Rotational Molding

In rotational molding, a charge of plastic powder is placed in one half of a metal mold. The mold halves are then clamped together and heated, while the mold rotates biaxially. The powder particles melt and coalesce to form a homogeneous layer on the surface of the mold. The mold is then cooled, and the polymer layer densifies and solidifies [73, 74]. Rotational molding competes with blow molding, thermoforming, and injection molding for the production of hollow parts. The main advantages of this process are the simplicity of the molds and the low capital investment requirement. Cycle times are large, ~15–30 min. Rotational molding is mainly used for large tanks (up to 85 m³ reported), toys, and hollow parts that require frequent design modifications. The process of coalescence and subsequent densification [75, 76] is usually referred to as sintering by rotational molding practitioners. In powder metallurgy, however, the term sintering usually refers to compaction of powders below their melting point. Molten particle coalescence is driven by the surface tension and resisted by their viscosity and elasticity [76]. Polymers with melt index of less than 1.5 are not “rotomoldable” due to their high viscosity.

3.8 Melt Spinning

In melt spinning the polymer is melted in an extruder and is delivered under pressure to a die (called spinneret) having numerous small holes, and subsequently the molten filaments (sometimes more than 1000) are heat treated, cooled, and stretched to the desired diameter [14, 77, 78]. Frequently the molten polymer goes through a melt metering pump (for more stable flow) and a filter (to remove impurities and unmelts) upstream of the spinneret holes. The spinneret holes can have circular, square,

pentagonal, octagonal, trilobal, and other cross sections. Structure development occurs as a function of melt spinning conditions involving molecular orientation and morphology of the crystalline structure. Significant enhancement of fiber properties can be achieved, such as in tensile modulus and strength, through proper cooling and drawing conditions. The fibers are, usually, characterized by their linear density expressed in denier or tex. Denier is the weight in grams of 9000 m of synthetic fiber. Tex the weight in grams of 1000 m, and dtex is the weight in grams of 10,000 m. Polyethylene, polypropylene, poly(ethylene terephthalate), and nylon are the most frequently melt-spun polymers.

3.9 Additive Manufacturing of Polymers

Additive manufacturing (AM) is the technology of building 3D objects layer by layer, as opposed to some traditional machining methods like drilling, milling, and grinding which can be classified as subtractive. Frequently, AM is referred to as 3D printing in the mass media, and it is not limited to polymers. AM includes several technologies [79] which offer unique product customization opportunities. From them, selective laser sintering (SLS) and fused deposition modeling (FDM) appear as the most promising methods for the production of plastic parts. In SLS a high-powered laser is used to fuse together small particles. It is similar to the process of particle coalescence (sintering) encountered in rotational molding with the difference that in SLS the heating is localized selectively. At present, polyamide (nylon) 12 is the most frequently used polymer for commercial production, with limited other material options [79]. In FDM a molten polymer is injected from an extrusion nozzle and deposited layer by layer [80, 81]. Modeling the flow in the FDM extrusion nozzle is a relatively straightforward task due to the simplicity of the nozzle geometry (usually of circular cross section). However, modeling the material behavior just after it emerges from the nozzle is a challenging task. Extrudate swell, especially if the material possesses large normal stresses, must be taken into consideration. A lot of research efforts are devoted to SLS and FDM, and it is widely believed that additive manufacturing will spearhead the next industrial revolution [82].

4 Considerations in the Polymer Processing Industry

Commodity polymers (like PE, PP, PVC, PS) and engineering polymers (like PA, PC) are produced by large chemical corporations perhaps numbering less than 100 around the world. However, polymer processing companies number more than 100,000 with their size varying from a handful of employees to several thousand. The vast majority of them can be classified as small or medium enterprises (SMEs). Also, the vast majority of original equipment manufacturers (OEMs) are also SMEs. While polymer (frequently referred to as resin) producers have well-equipped laboratories for physicochemical and rheological characterization, this is

not the case with the SME processing polymers or designing and manufacturing equipment. Traditionally, processors rely heavily on the resin producers and machinery manufacturers for their technology. There is frequent dialogue between processors, OEMs, and polymer suppliers for prevention, reduction, or elimination of problems during processing and defects in the final plastic products.

Extrusion (including extrusion blow molding), calendering, and melt spinning are continuous production methods. Injection molding, compression molding, thermoforming, rotational molding, and additive manufacturing are for production of parts. The decision on which process to use for a particular product is based on several considerations relating product shape and size, quality, quantity, and economics. For example, hollow parts can be produced by injection molding, thermoforming, blow molding, rotational molding, or additive manufacturing. Injection molding requires expensive machines and molds, while for thermoforming and rotational molding the tooling is inexpensive. Injection-molded parts have well-defined surfaces and crisp appearance, and cycle times are very short. Thermoforming is a slow process and rotational molding even slower, but they both have advantages for large parts. Additive manufacturing offers unique advantages for complex designs and customized products. However, it is slow, the raw material selection is limited, and the mechanical properties are likely to be inferior to those of injection molding, due to the poor bonding during the layer-by-layer process in the absence of external pressure.

A typical polymer property data sheet will include solid density and melt index (MI) for the standard load of 2.16 kg. As explained, above, the melt index is inversely proportional to viscosity at one point of a viscosity curve and an indirect measure of the average molecular weight. Frequently the high load melt index (HLMI) for either 10 kg or 21.6 kg is also provided. The ratio HLMI/MI gives an indication of shear thinning; the larger, the more. Melt index is considered as a quality control measure. Detailed rheological characterization can be time-consuming and expensive and might not be always necessary. For problem-solving, it is necessary to have a good understanding of the thermomechanical phenomena and physicochemical interactions that may be involved. Problems may originate from the macromolecular architecture, the processing equipment, or the operating conditions. The rheological measurements must be carefully targeted. The sensitivity of rheological behavior to high molecular weight fractions and long-chain branching is frequently used for differentiating various polymer grades. Rheological measurements and understanding [7, 8, 11, 17, 28, 83] are indispensable in differentiating polymer resin grades and in problem-solving.

Computer flow simulation [2, 52, 54, 56, 65, 84] using suitable non-Newtonian models of viscosity is widely practiced in injection molding for mold design and various other problem-solving purposes. Similarly, computer software is indispensable for extrusion die design and identification of problems originating in dies. In extruder screw design, computer flow analysis is less effective due to the complex aspects of solid transport and melting, before the molten polymer is pumped.

Some problems may be due to other factors, not obviously related to rheology, and not easily amenable to computer flow simulations. For example, inadequate

drying of the raw material may result in surging (fluctuations in output and pressure) in extrusion due to slippage on the barrel wall in the solids conveying zone. Moisture also may result in hydrolysis in processing of PET, nylon, and PLA. Inclusion of even a very small number of tiny air bubbles in the feed of an extruder may result in serious defects in the production of films or fibers. Inclusion of cross-linked gels and other contamination frequently results in deterioration of optical qualities of transparent films. Identification of the root causes of such problems is frequently very difficult. Rheology and computer simulation are sometimes used to exclude other potential causes in the challenging task of fault diagnosis and troubleshooting.

References

1. D.H. Morton-Jones, *Polymer Processing* (Chapman and Hall, London, 1989)
2. Z. Tadmor, C.G. Gogos, *Principles of Polymer Processing* (Wiley, New York, 2006)
3. J. Vlachopoulos, N. Polychronopoulos, Basic concepts in polymer melt rheology and their importance in processing, in *Applied Polymer Rheology: Polymeric Fluids with Industrial Applications*, ed. by M. Kontopoulou (Wiley, Hoboken, 2012), pp. 1–27
4. R.B. Bird, R.C. Armstrong, O. Hassager, *Dynamics of Polymeric Liquids*, vol 1 (Wiley, New York, 1987)
5. A.V. Chenoy, D.R. Saini, *Thermoplastic Melt Rheology and Processing* (Marcel Dekker, New York, 1996)
6. C.D. Han, *Rheology and Processing of Polymeric Materials*, vol 1–2 (Oxford University Press, Oxford, 2007)
7. C.W. Macosko, *Rheology: Principles, Measurements and Applications* (VCH Publishers, New York, 1994)
8. F.N. Cogswell, *Polymer Melt Rheology* (Woodhead Publishing, Cambridge, 1996)
9. J. Vlachopoulos, *Fundamentals of Fluid Mechanics* (Polydynamics Inc., Dundas, 2016)
10. S.J. Haward, J.A. Odell, Z. Li, X.-F. Yuan, The rheology of polymer solution elastic strands in extensional flow. *Rheol. Acta* **49**(7), 781–788 (2010)
11. J.M. Dealy, R.G. Larson, *Structure and Rheology of Molten Polymers* (Hanser, Munich, 2006)
12. M. Sentmanat, B.N. Wang, G.H. McKinley, Measuring the transient extensional rheology of polyethylene melts using the SER universal testing platform. *J. Rheol.* **49**, 585–606 (2005)
13. S.L. Anna, G.H. McKinley, Elasto-capillary thinning and breakup of model elastic liquids. *J. Rheol.* **45**(1), 115–138 (2001)
14. M.M. Denn, *Polymer Melt Processing* (Cambridge University Press, Cambridge, 2008)
15. B. Debbaut, T. Avalose, J. Dooley, K. Hughes, On the development of secondary motions in straight channels induced by the second normal stress difference: experiments and simulations. *J. Non-Newtonian Fluid Mech.* **69**(2–3), 255–271 (1997)
16. J. Dooley, *Viscoelastic Flow Effects in Multilayer Polymer Extrusion*, Doctoral Thesis, University of Eindhoven, Netherlands, 2002
17. J.M. Dealy, K.F. Wissbrun, *Melt Rheology and its Role in Plastics Processing* (Chapman and Hall, London, 1996)
18. S.W. Shang, The precise determination of polydispersity index (PI) in rheological testing of polypropylene. *Adv. Polym. Technol.* **12**(4), 389–401 (1993)
19. R.H. Ewoldt, A.E. Hosoi, G.H. McKinley, New measures for characterizing nonlinear viscoelasticity in large amplitude oscillatory shear. *J. Rheol.* **52**, 1427 (2008)
20. K. Hyun, M. Wilhelm, C.O. Klein, K.S. Cho, J.G. Nam, K.H. Ahn, S.J. Lee, R.H. Ewoldt, G.H. McKinley, A review of nonlinear oscillatory shear tests: Analysis and application of large amplitude oscillatory shear (LAOS). *Prog. Polym. Sci.* **36**(12), 1697–1753 (2001)

21. H.M. Laun, Prediction of elastic strains of polymer melts in shear and elongation. *J. Rheol.* **30**, 459 (1986)
22. M. Gale, Compounding with single-screw extruders. *Adv. Polym. Technol.* **16**(4), 251–262 (1997)
23. G.I. Taylor, The viscosity of a fluid containing small drops of another fluid. *Proc. R. Soc. Lond. A Math. Phys. Sci.* **138**(834), 41–48 (1932)
24. G.I. Taylor, The formation of emulsions in definable fields of flow. *Proc. R. Soc. Lond. A Math. Phys. Sci.* **146**(858), 501–523 (1934)
25. H.P. Grace, Dispersion phenomena in high viscosity immiscible fluid systems and application of static mixers as dispersion devices in such systems. *Chem. Eng. Commun.* **14**, 225–277 (1982)
26. I. Manas-Zloczower, *Mixing and Compounding of Polymers* (Hanser, Munich, 2009)
27. J. Vlachopoulos, Extrudate swell in polymers. *Rev. Deform. Beh. Materials* **3**, 219–248 (1981)
28. R.I. Tanner, *Engineering Rheology* (Oxford Engineering Science, Oxford, 2000)
29. J.-F. Agassant, D.R. Arda, C. Combeaud, A. Merten, H. Münsted, M.R. Mackley, L. Robert, B. Vergnes, Polymer processing extrusion instabilities and methods for their elimination or minimization. *Int. Polym. Process.* **21**(3), 239–255 (2006)
30. B. Vergnes, Extrusion defects and flow instabilities of molten polymers. *Int. Polym. Process.* **30**(1), 3–28 (2015)
31. A.V. Ramamurthy, Extrudate irregularities and the polymer-metal interface connection, in *Proceedings of the Xth International Congress on Rheology* (Sydney, 1988), pp. 85–90
32. E.C. Achilleos, G. Georgiou, S.G. Hatzikiriakos, Role of processing aids in the extrusion of molten polymers. *J. Vinyl Addit. Technol.* **8**(1), 7–24 (2002)
33. V. Hristov, E. Takacs, J. Vlachopoulos, Surface tearing and wall slip phenomena in extrusion of highly filled HDPE/wood flour composites. *Polym. Eng. Sci.* **46**(9), 1204–1214 (2006)
34. V. Hristov, J. Vlachopoulos, A study of viscoelasticity and extrudate distortions of wood polymer composites. *Rheol. Acta* **46**(5), 773–783 (2007)
35. J.D. Gander, A.J. Giacomini, Review of die lip build up in plastics extrusion. *Polym. Eng. Sci.* **37**(7), 1113–1126 (1997)
36. J. Musil, M. Zatloukal, Experimental investigation of flow induced molecular weight fractionation during extrusion of HDPE polymer melts. *Chem. Eng. Sci.* **66**, 4814–4823 (2011)
37. J.W. Goodwin, R.W. Hughes, *Rheology for Chemists an Introduction* (RSC Publishing, Cambridge, 2008)
38. R.K. Gupta, *Polymer and Composites Rheology* (Marcel-Dekker, New York, 2000)
39. L.E. Nielsen, *Polymer Rheology* (Marcel-Dekker, New York, 1977)
40. N.D. Polychronopoulos, Z. Charlton, D. Suwanda, J. Vlachopoulos, Measurements and comparison to predictions of viscosity of heavily filled HDPE with natural fibers. *Adv. Polym. Technol.* **37**(4), 1161–1167 (2018). <https://doi.org/10.1002/adv.21775>
41. L. Theodore, *Nanotechnology* (Wiley, New York, 2006)
42. M. Alexander, P. Dubois, Polymer-layered silicate nanocomposites: preparation, properties and uses of a new class of materials. *Mater. Sci. Eng.* **28**, 1–63 (2000)
43. R.K. Gupta, V. Pasanovic-Zujo, S.N. Bhattacharya, Shear and extensional rheology of EVA/layered silicate-nanocomposites. *J. Non-Newtonian Fluid Mech.* **128**, 116–125 (2005)
44. T.G. Gopakumar, J.A. Lee, M. Kontopoulou, J.S. Parent, Influence of clay exfoliation on the physical properties of montmorillonite/polyethylene composites. *Polymer* **43**(20), 5483–5491 (2002)
45. S.N. Bhattacharya, R.K. Gupta, M.R. Kamal, *Polymeric Nanocomposites* (Hanser, Munich, 2008)
46. V. Pasanovic-Zujo, R.K. Gupta, S.N. Bhattacharya, Effect of vinyl acetate content and silicate loading on EVA nanocomposites under shear and extensional flow. *Rheol. Acta* **43**(2), 99–108 (2004)
47. C.I. Chung, *Extrusion of Polymers* (Hanser, Munich, 2000)
48. G.A. Campbell, M.A. Spalding, *Analyzing and Troubleshooting Single-Screw Extruders* (Hanser, Munich, 2013)

49. C. Rauwendaal, *Polymer Extrusion* (Hanser, Munich, 2014)
50. E. Grünschloß, A powerful universal plasticating system for single-screw-extruders and injection moulding machines. *Int. Polym. Process.* **30**(2), 226–234 (2007)
51. E. Grünschloß, HELIBAR-A powerful Single Screw Plasticating System, SPE-ANTEC Conference, Cincinnati, 2007 pp. 405–410
52. J. Vlachopoulos, J. Wagner Jr. (eds.), *The SPE Guide on Extrusion Technology and Troubleshooting* (Society of Plastics Engineers, Brookfield, 2001)
53. F.G. Martelli, *Twin-Screw Extruders: A Basic Understanding* (Van Nostrand Reinhold, New York, 1983)
54. J. Vlachopoulos, R. Castillo, N. Polychronopoulos, S. Tanifuji, Blown film dies, chapter 5, in *Design of Extrusion Forming Tools*, ed. by O. Carneiro, J.M. Nobrega (Smithers-Rapra, Shawbury 2012), pp. 141–168
55. N.D. Polychronopoulos, T.D. Papathanasiou, A study of the effect of drawing on extrudate swell in film casting. *Appl. Rheol.* **25**, 42425 (2015)
56. J. Vlachopoulos, N. Polychronopoulos, S. Tanifuji, J. Peter Müller, Flat film and sheet dies, chapter 4, in *Design of Extrusion Forming Tools*, ed. by O. Carneiro, J.M. Nobrega (Smithers-Rapra, Shawbury 2012), pp. 113–140,
57. Y. Huang, P. Prentice, Experimental study and computer simulation of the effect of spider shape on the weld-lines in extruded plastic pipe. *Polym. Eng. Sci.* **38**(9), 1506–1532 (1998)
58. H.A. Simon, *The Sciences of the Artificial* (MIT Press, Cambridge, MA, 1996)
59. N.D. Polychronopoulos, I.E. Sarris, T.D. Papathanasiou, 3D features in the calendering of thermoplastics: A computational investigation. *Polym. Eng. Sci.* **54**(7), 1712–1722 (2013)
60. E.T. Thostenson, T.-W. Chou, Processing-structure-multi-functional property relationship in carbon nanotube/epoxy composites. *Carbon* **44**, 3022–3029 (2006)
61. H. Oxfall, J. Rondin, M. Bouquey, R. Muller, M. Rigdahl, R.W. Rychwalski, Elongational flow mixing for manufacturing of graphite nanoplatelet/polysterene composites. *J. Appl. Polym. Sci.* **128**(5), 2679–2686 (2013)
62. S.G. Prolongo, A. Jimenez-Suarez, R. Moriche, A. Ureña, In situ processing of epoxy composites reinforced with graphene nanoplatelets. *Compos. Sci. Technol.* **86**, 185–191 (2013)
63. H. Mavridis, A.N. Hrymak, J. Vlachopoulos, The effect of fountain flow on molecular orientation in injection molding. *J. Rheol.* **32**(6), 639–663 (1988)
64. A. I. Isayev (ed.), *Injection and Compression Molding Fundamentals* (Marcel Dekker, New York, 1987)
65. J.A. Dantzig, C.L. Tucker, *Modeling in Materials Processing* (Cambridge University Press, Cambridge, 2001)
66. J. Avery, *Gas-Assist Injection Molding* (Hanser Gardner, Cincinnati, 2001)
67. C.W. Macosko, *Fundamentals of Reaction Injection Molding* (Hanser, Munich, 1988)
68. P. K. Mallick, S. Newman (eds.), *Composite Materials Technology* (Hanser, Munich, 1990)
69. D.V. Rosato, D.V. Rosato, *Blow Molding Handbook* (Hanser, Munich, 1988)
70. M.R. Kamal, in *Concise Encyclopedia of Polymer Processing and Applications*, ed. by P.J. Corish (Pergamon Press, New York 1992), pp. 71–76
71. J.L. Throne, *Technology of Thermoforming* (Hanser, Munich, 1996)
72. D. Bhattacharya, *Composite Sheet Forming* (Elsevier Science, Amsterdam, 1997)
73. R.J. Crawford, *Rotational Molding of Plastics* (Wiley, New York, 1992)
74. R.J. Crawford, J.L. Throne, *Rotational Molding Technology* (William Andrew Publishing, New York, 2002)
75. M. Narkis, N. Rosenzweig, *Polymer Powder Technology* (Wiley, New York, 1995)
76. M. Kontopoulou, J. Vlachopoulos, Melting and densification of thermoplastic powders. *Polym. Eng. Sci.* **41**(2), 155–169 (2001)
77. A. Ziabicki, *Fundamentals of Fiber Formation: The Science of Fiber Spinning and Drawing* (Wiley, New York, 1976)
78. T. Nakajima (ed.), *Advanced Fiber Spinning Technology* (Woodhead Publishing, Cambridge, 1994)

79. M. Schmid, A. Amado, K. Wegener, Polymer powders for selective laser sintering (SLS). AIP Conf. Proc. **1664**, 160009 (2015)
80. B.N. Turner, R. Strong, S.A. Gold, A review of melt extrusion additive manufacturing processes: I. Process design and modeling. Rapid Prototyp. J. **20**(3), 192–204 (2014)
81. B.N. Turner, S.A. Gold, A review of melt extrusion additive manufacturing processes: II. Materials, dimensional accuracy, and surface roughness. Rapid Prototyp. J. **21**(3), 250–261 (2015)
82. J. Hornick, *3D Printing Will Rock the World* (CreateSpace, North Charleston, 2015)
83. F.A. Morrison, *Understanding Rheology* (Oxford University Press, Oxford, 2001)
84. H. Zhou, *Computer Modeling for Injection Molding: Simulation, Optimization, and Control* (Wiley, New York, 2013)



Abdul Malik P. Peedikakkal and N. N. Adarsh

Contents

1	Coordination Polymers	182
2	Synthesis	186
3	Topology	187
4	Interpenetration	188
5	Surface Area	191
6	Gas Storage	195
6.1	Hydrogen Storage	196
6.2	Methane Storage	200
6.3	Carbon Dioxide Storage	206
7	Conclusion and Future Perspectives	216
	References	218

Abstract

This chapter discusses about porous coordination polymers (PCPs) and/or metal-organic frameworks and mainly emphasizes the historical background, their synthesis, structural properties, and potential applications (mainly gas storage). We organize the gas storage application of PCPs into three sections – H₂, CH₄, and CO₂ storage – in order to highlight the important concerns we must know before designing new functional MOFs. In the case of H₂ storage application of MOFs, we have discussed four important parameters which effect their successful design for H₂ storage application with examples from the literature, such as (1) H₂

A. M. P. Peedikakkal (✉)

Department of Chemistry, King Fahd University of Petroleum and Minerals,
Dhahran, Kingdom of Saudi Arabia
e-mail: abdulmalik@kfupm.edu.sa

N. N. Adarsh

Solid State and Materials Chemistry, School of Chemical Sciences, Mahatma Gandhi University,
Kottayam, Kerala, India
e-mail: adarshnn@gmail.com

adsorption condition (pressure and temperature), (2) inclusion of reducing agents in the MOF, (3) effect of structural defect in MOF, and (4) effect of adsorption sites in the MOF structure (examples: MOF-177, Pt/AC/IRMOF-8, UiO-66(Zr), Yb-BTC). Further, we highlight the investigation results of methane storage application of MOFs, with appropriate examples such as PCN-14, $M_2(\text{dhtp})$ [M: open metal = Mg, Mn, Co, Ni, Zn; dhtp = 2,5-dihydroxyterephthalate], and UTSA-20. And then we discuss more details of various factors which we must take care before the successful design and synthesis of new MOFs for more CO_2 storage such as: (1) the effect of open metal sites in the MOF, (2) the effect of the pore size and surface area of the framework, (3) effect of doping metals, (4) effect of amine functionalization in MOFs, (5) effect of nitrogen-rich MOFs, (6) effect of water molecules, with some important examples such as M-MOF-74 (M = Mg, Co, Fe, Zn, Ni), HKUST-1, etc.

1 Coordination Polymers

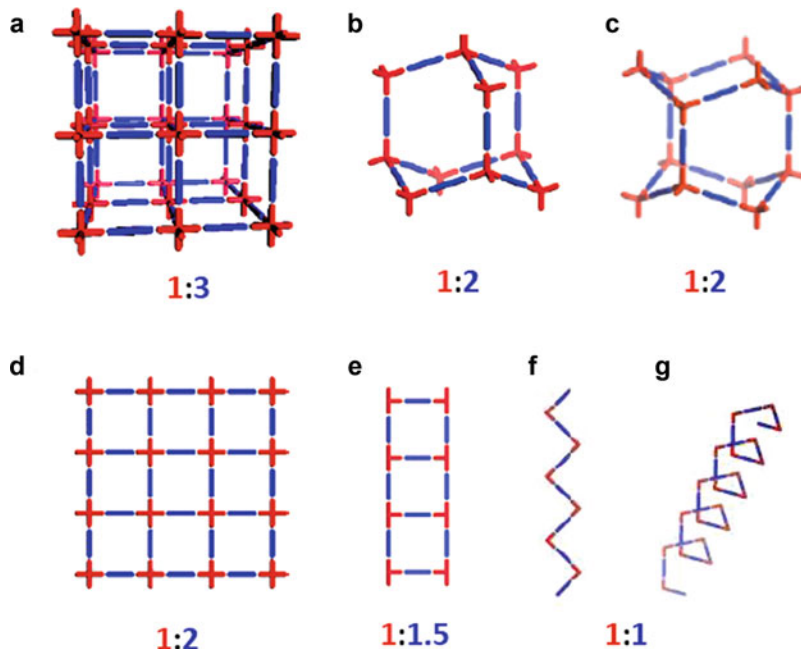
Coordination polymers (CPs) are rapidly emerging inorganic–organic solid state materials which provide boundless opportunity for designing their chemical and physical properties [1]. These highly crystalline materials are constructed from assembling of *metal ion* or *metal cluster* with *organic ligands* through *coordination bonds* to form one-, two-, and three-dimensional structures. CPs are also known as metal-organic frameworks (MOFs) [1], and some of these solid networks exhibit permanent porosity which is termed as porous MOFs or porous coordination polymers (PCPs). These extended solid networks collectively are also termed as metal-organic materials (MOMs) [2]. These materials have drawn ever-increasing scientific and technological interest due to their widespread application such as gas storage/separation, catalysis, ion exchange, drug delivery, and optoelectronics, etc. A collective approach such as design and synthesis, molecular modeling, functional properties towards application from several research groups have significantly helped the growth and development of these materials in the last two decades.

The spectacular growth of these materials attracted researchers from material science, biology, and medicine. In the beginning of 1990, Robson uncovered the remarkable discovery using Wells net-based approach [3] in his laboratory which was the greatest success that helped the rapid expansion and development of the coordination polymers [4]. Robson and co-workers proposed a novel design approach to synthesize these new classes of materials with interesting properties [5]. Supramolecular chemistry and crystal engineering have enhanced the development of the coordination polymers. Lehn defined supramolecular chemistry as the *chemistry beyond the molecules* [6]. A single crystal is the best example of a supermolecule with repetitive arrangement of molecules in three-dimension, according to Dunitz as, “Supermolecule(s) *par excellence*” [7].

In 1970, G.M.J Schmidt coined the term “crystal engineering” to understand the crystal structure of cinnamic acid derivatives and their photochemical reactivity in the solid-state [8]. Schmidt’s investigations provide the information that the physical

and chemical properties of crystalline solids profoundly depend on the distribution of the components inside the lattice. Later, this field has been developed rapidly due to its importance in material science. Desiraju's significant contribution for the past two decades evolves systematic and logical ways to design and understand the properties which led to the development of crystal engineering [9]. Desiraju provided a wider definition for crystal engineering as "*the understanding of intermolecular interaction in the context of crystal packing and in the utilization of such understanding in the design of new solids with desired physical and chemical properties.*" Although crystal engineering was first designed for solid-state reaction in crystals, it has been rediscovered in various fields in designing the solids which have the properties such as porosity, luminescence, nonlinear optical activity, ferroelectricity, and piezoelectricity. The mutual coincidence of supramolecular chemistry and crystal engineering assisted in understanding the self-assembly process and understanding the intermolecular interactions and structure-function relationships in solids. The terminologies such as *synthons* and *tectons* have been used for directing the packing arrangement of molecules in the organic solids in crystal engineering. A similar terminology has been used for designing the infinite network solid of coordination polymers. The organic ligands are linked by metal cation or metal clusters in constructing coordination polymers. Rapid developments in the last 28 years indicate the predictability of the coordination polymers relatively easier since they are more controllable than organic solids (directed via hydrogen bonding). Even though reasonable achievement has been occurred in engineering crystals, the structural predication or Maddox's statement "*One of the continuing scandals in the physical sciences is that it remains in general impossible to predict the structure of even the simplest crystalline solids from a knowledge of their chemical composition*" is still valid today [10]. Even, absolute prediction of the dimensionality and connectivity in coordination polymers is still a challenge when assembling a chosen ligand with a metal center. Depending on the properties of metal cations (various geometry can be used such as linear, tetrahedral, square-planar, square-pyramidal, trigonal-bipyramidal, octahedral, trigonal-prismatic, pentagonal-bipyramidal, and the corresponding distorted forms), binding strength, and directionality of ligands and the reaction conditions, coordination polymers exhibit a wide variety of infinite (1D, 2D, and 3D) networks [1a, 2]. This has been realized through self-organization of various metal cations, and bifunctional ligands (e.g., 4,4'-bipy) can form linear, zig-zag, ladder, honeycomb, square-grid, diamondoid, and octahedral frameworks (Scheme 1) [11].

The diversity of above network structures is very well-known. Zaworotko proposed this diversity of structures as supramolecular isomerism is the *existence of more than one type of network superstructures for the same molecular building blocks* in coordination polymers [12]. It has been categorized to structural, conformational, catenane, and optical supramolecular isomerism. Supramolecular isomerism has its own importance in coordination polymers due to various reasons: (1) it is an opportunity to get better understanding of the factors that influence the crystal nucleation and growth, (2) it represents a significant limitation on the number of the possible superstructures, (3) it provides an opportunity to control the supramolecular

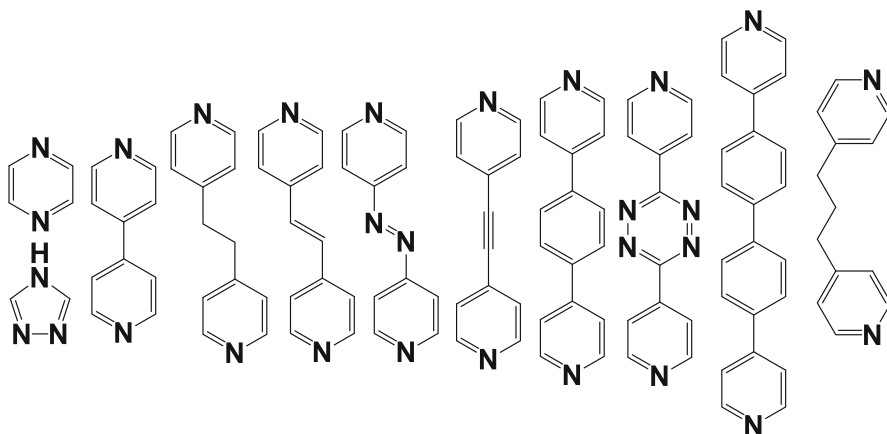


Scheme 1 Schematic representation of some of the simple 1D, 2D, and 3D coordination polymers formed from the metal “nodes”(red) and organic “spacers” (blue): (a) cubic, (b) cubic diamondoid, (c) hexagonal diamondoid, (d) square grid, (e) molecular ladder, (f) zigzag chain, and (g) helix [12]. (This figure is reprinted from Ref. [12] with permission. Copyright 2001, American Chemical Society)

isomers and help to design the desired one, (4) implication of gaining better understanding of polymorphism in crystals, (5) the diversity of these structures profoundly effect on their bulk properties, and (6) it provides the information that the structures can occur from the same building blocks under similar crystallization conditions.

The diversity of networks does not absolutely depend on the geometrical features of metal cations. For example, a zig-zag network can be formed from a linear, square-planar, trigonal-bipyramidal, and octahedral metal cation. In some instances, the assemblies of networks are metal-to-ligand ratio dependent. For example, 4,4'-bipy by coordinating to metals 1:1 metal:ligand ratios can afford molecular polygons or chains (zig-zag, linear, or helical) and 1:1.5 stoichiometry can form 1-D molecular ladder; 1:2 stoichiometry can afford 2-D square grid or 3-D diamondoid topologies; and 1:3 stoichiometry has been shown to produce a 3-D cubic framework (Scheme 1). Different products can be isolated from a reaction that proceeds through kinetically favorable conditions.

Transition metal ions or metal clusters are the most well-known joints (or connectors) in coordination polymers [1]. The main reason is the easiness of designing the coordination polymers from the labile M-L coordination bond and



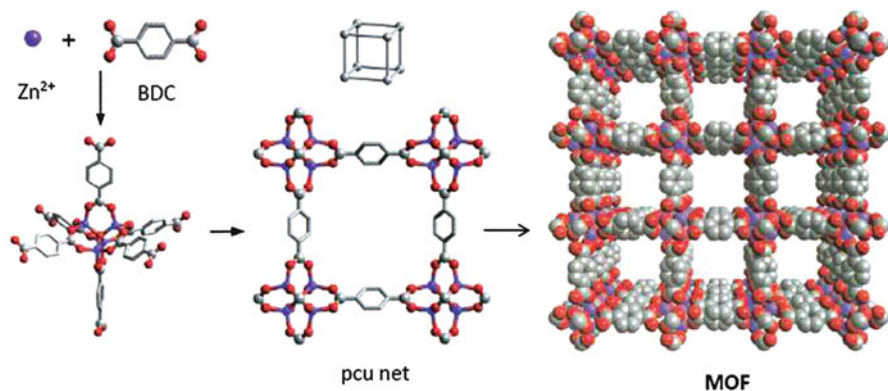
Scheme 2 A few examples of neutral pyridyl donor ligands used in coordination polymers. The ligands exhibit variation in ligand length, rigidity, flexibility, and functionality

the strength of the ordered crystalline network solid formed from the coordination bond with high regularity. The more directional strong coordination bond of metal ions with ligands provides more robust materials.

Ligand design is one of the important factors in getting the desired topological network. Pyridyl donor ligands are one of the most versatile building blocks (or linkers) in the construction of coordination polymers [13]. In these ligands, two-connecting linear bifunctional spacer and three-connecting trifunctional ligands are the most common; four-connecting ligands are far less than two- and three-connecting ligands. Several coordination polymers have been reported using linear and angular spacer ligands (Scheme 2). An anionic source (e.g., ClO_4^- , BF_4^- , NO_3^- , NCS^- , PF_6^- , SiF_6^{2-} , CN^- , and CF_3SO_3^- , etc.) neutralizes the overall charge of the compound.

Later, several modified two-connecting ligands (Scheme 2) are used such as modification in ligand length or flexibility by introducing aliphatic or aromatic group and modification of binding angle via changing position of nitrogen atom in the pyridyl rings. This provides wide variety of structures through ligand design. However, cationic frameworks formed from nitrogen donor ligands can collapse while guest exchange or evacuation. In these two-connecting ligands, 4,4'-bpe (4,4'-bpe: 1,2-bis(4-pyridyl)ethylene) have given particular interest which is the modified form of bpy in terms of ligand length and functionality by introducing C=C bonds [14].

Because of their diverse coordination modes and bridging ability, polycarboxylates have been widely used in the construction of coordination polymers. Carboxylic acid ligands provides wide range of rigid network due to their ability to aggregate metal ions into M-O-C clusters termed as secondary building (SBU) units. Yaghi and co-workers introduced SBU units with large rigid vertices that can be joined by rigid organic links to produce extended frameworks of high structural stability (Scheme 3).



Scheme 3 The formation of MOF is shown from rigid metal carboxylate clusters linked by benzene to form rigid extended frameworks with large void space [1d]

The need for counterions in their cavities is obviating since the frameworks is neutral. In this way, large class of metal-organic frameworks (MOFs) materials has been synthesized and termed as “Reticular Chemistry” which concerns *the linking of molecular building blocks into predetermined structures using strong bonds* [15]. It was one of the major breakthroughs of coordination polymeric materials due to their superior capacity of gas storage properties which can be used for clean energy purpose such as hydrogen and methane storage and CO_2 capture [16].

The stability of coordination polymers is also improved by introducing mixed ligands or mixed functionality in single ligand. For example, ligands containing both pyridyl and carboxylic functional groups have been successfully used for the construction of various coordination polymers [17]. Further, several coordination polymers have been designed and synthesized from more than one bridging ligand [18]. In this case, controlling the reaction may be more challenging since the building blocks can interfere with the reaction which affords various topologies and obviating the desired network. For example, both dicarboxylate ligands and pyridyl ligands can be used to construct pillar-like networks. Similarly, monocarboxylate ligands with pyridyl donors affords ladder like networks [19]. Owing to their bridging ability, acetate and trifluoroacetate are efficiently utilized to orient the $C=C$ double bonds of bpe ligands in ladder coordination polymers for photo-dimerization reaction [20].

2 Synthesis

Normally, coordination polymer is prepared in single step through self-assembly process such as slow evaporation of the solution of the reactants, layering of two solutions, or slow diffusion of the one component to another and other methods have been implemented to get the crystalline products of coordination polymers. The formation of coordination polymers not only depends on the properties of metal

cation, ligand, and metal-to-ligand ratio but also the crystallization conditions such as solvent, temperature, concentration, pH, time, and inorganic counterion. This exemplifies the complexity of predicting the desired connectivity, dimensionality, and topology of the networks. The normal synthetic methods may take weeks and months to get the product which is hampered in some extent in studying of these materials. Hydrothermal/solvothermal techniques have been found to be quite successful by greatly reducing the time for crystallization of coordination polymers to few days [21]. The important parameters such as pH, concentrations, and temperatures can be varied to produce variety of network topologies. There are several other methods being developed for the synthesis of coordination polymers such as electrochemical route [22], microwave synthesis [22, 23], high-throughput synthesis [24], etc. Microwave synthesis has been found very promising since the method provides an efficient way to synthesize in a short period of time. A good understanding of the properties and interactions of the building blocks (noncovalent interactions), the effect of solvent system, and counterion will provide advantage of the stepwise control in constructing the predictable topology.

3 Topology

In 1977, Wells in his famous book described the crystal structures in term of their topology through reducing them to networks (or nets) [3]. Net is formed from series of points (nodes) that are connected to a fixed number of other points. These structures coined with mathematical notations which can be discrete (0D), polyhedra, or infinite (1D, 2D, and 3D) periodic nets. Robson, Hoskins, and co-workers who pioneered the development of coordination polymers applied the net approach to design the coordination polymers by using the metal ion (nodes) and ligands (connection between the nodes) with certain geometries towards targeting a particular topology [4, 5]. For example, diamondoid (**dia**) topology has been known to form from tetrahedral metal ions (Cu(I), Zn(II), and Cd(II)) and linear bridging ligands (cyanide) [5b]. Similarly, **dia** topology also can be formed from tetrahedral bridging ligands and tetrahedral ligands. In this way, 2D and 3D coordination polymers have topologies comparable to minerals. For example, coordination polymers adopt similar structure of PtS (**pts**), SrAl₂ (**sra**), α -Po (**pcu**), NbO (**nbo**), rutile, sodalite, and several analogues of zeolites [1d, g]. Figure 1 represents some of the common inorganic topologies.

Topological description has been found very useful in describing the connectivity of coordination polymers [1d, g]. There are several excellent reviews which are devoted to the topology of coordination polymers [1d, g, 25]. Based on the Wells's description, large number of topological networks has been identified in coordination polymers. Robson and co-workers described the net as the collection of interlinked nodes; each link connects two nodes and each node is linked to three or more other nodes [5]. In each net, a shortest circuit can be formed around the nodes. If net form *uniform net* (same sized circuits), and similar connectivity, the net can be described by the mathematical notation (n, p), where n is the size of shortest

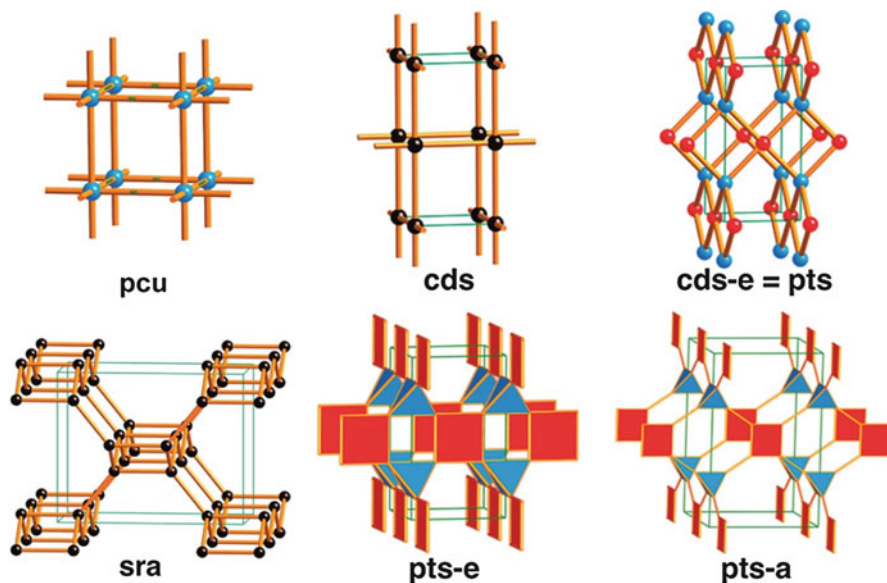


Fig. 1 Common inorganic topologies found in MOFs or coordination polymers. (This figure is reprinted from Ref. [1g] with permission. Copyright 2012, American Chemical Society)

circuit and p is the connectivity of the nodes. Examples of such nets are given in Fig. 2. Specifically, not all the net follow this criterion. For example, the net contains dissimilar shortest circuits or connectivity. In such cases, a modified description is used, called the Schläfli symbol (or point symbol).

Schläfli symbol is also useful in the description of the nets that contain more than one node (e.g., binodal and trinodal net) and interpenetrated nets. A node or link can be formed from a metal cation or metal cluster or ligand. For example, three- and four-connecting ligands can act as three- and four-connecting nodes, respectively. Connectivity and geometry of the node can be different from the geometry of metal cation or metal cluster. For example, octahedral metal can act as three-connecting nodes through bonding in bidentate fashion. A tetrahedral metal can act as square-planar nodes if they are linked by bent ligands. Finally, a topological description *should always simplify the structural description of coordination polymers and not complicate it* [1d].

4 Interpenetration

One of the most exciting features of the coordination polymer is exceptional porous nature of the frameworks due to large voids formed from the net. These voids can accommodate either solvent or guest molecules or multiple interpenetrating networks since “nature abhors a vacuum” in crystals. A crystal can increase its packing efficiency through *intercalation*, *interdigitation*, or *interpenetration* [1d, 26]. A rectangular channel

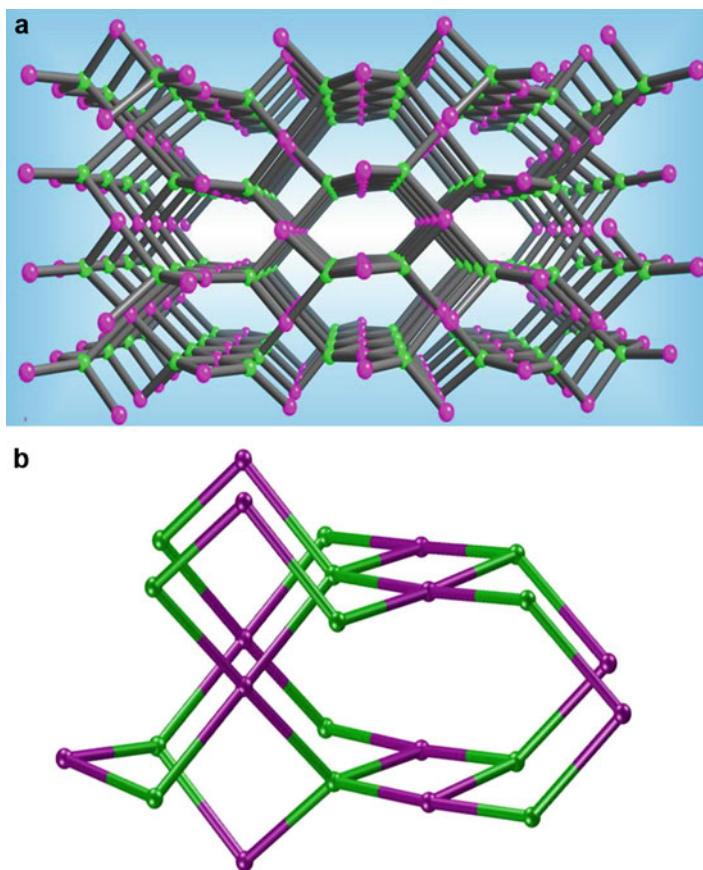


Fig. 2 (a) Topology **ptt** (pts twisted) net with Schläfli symbol for the net is $(4.6^3.8^2)_2-(4^2.6^2.8^2)(6^2.8^4)$. (b) Showing the underlying shortest circuits and connectivity in **ptt** with two tetrahedral and two square planar nodes

of 2D (4,4) sheet can accommodate guest molecules or solvent molecules (*intercalation*), 2D sheets can align themselves like fingers of folded hands (*interdigitation*) as shown in Fig. 3. Batten et al. defined *interpenetration occurs when two or more polymeric networks are not strictly connected but cannot be separated topologically without breaking of bond*. If the network can be separated without breaking the bonds, then it is *interwoven*.

Interpenetration has been thought as a negative factor for long time since it reduces the pore size in coordination polymers. However, recent reports show that interpenetration enhances the stability and selectivity of binding guest molecules [27, 28]. The interpenetrated networks have been shown higher hydrogen uptake compared to the noninterpenetrated counterpart [29]. This may be due to the reduction of pore size, which eventually increases the interaction of dihydrogen molecules and wall of the network. The topology of the interpenetrated networks will be completely different

from the parent structure; hence, the properties also changed. To describe a complete structure of coordination polymeric structure, the topology of the network must be illustrated with network topology. Batten et al. defined a notation, $mD \rightarrow nD$ for the description of entangled networks, where mD represents *the dimensionality of the constituent net*, and nD represent *the overall entanglement* [1d].

Due to their predictable pore size and selective inclusion of guest molecules, square-grid networks with (4,4) topology have gained special attention [30]. Zaworotko et al. have described topologically different modes of interpenetration for (4,4) networks such as parallel/parallel, diagonal/diagonal, and parallel/diagonal inclined interpenetrations (Fig. 4) [30].

The diagonal/diagonal interpenetration contains windows of sheets with the nodes of their interpenetrating partners [25a]. The first diagonal/diagonal networks has been reported by Robson and co-workers in 1990 [4b]. Although diagonal/diagonal interpenetration is commonly encountered in inclined interpenetration, exact diagonal/diagonal inclined sheets with connecting at the midpoint of square-grid sheets are very rare.

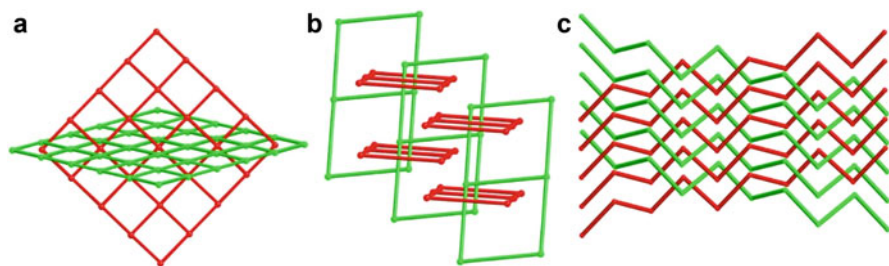


Fig. 3 (a) Interpenetration of 3D nets, (b) interpenetration 2D nets, and (c) interwoven of 1D chains

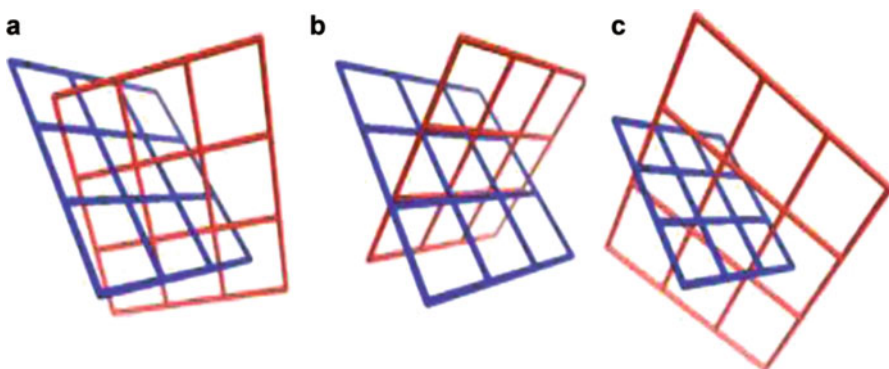


Fig. 4 A schematic representation that demonstrates three modes of inclined interpenetration that have been found in 2D square grid networks: (a) diagonal/diagonal (b) parallel/parallel, (c) parallel/diagonal interpenetration [30]. (This figure is reprinted from Ref. [12] with permission. Copyright 2001, American Chemical Society)

The structural motifs observed with T-shaped connecting nodes are of particular interest in constructing ladders, brick wall, bilayer, and 3D frameworks [31]. Interpenetration of molecular ladders is not very common due to the guest solvent molecules in the cavities [1e]. Long linear spacer ligands favor the formation of square-grid networks or tend to favor higher-folded interpenetrated 3D nets [32]. Despite a few three-fold interpenetrated ladder structures have been reported, molecular ladders formed by bpe spacer ligand with rigid backbone is not fully understood [18].

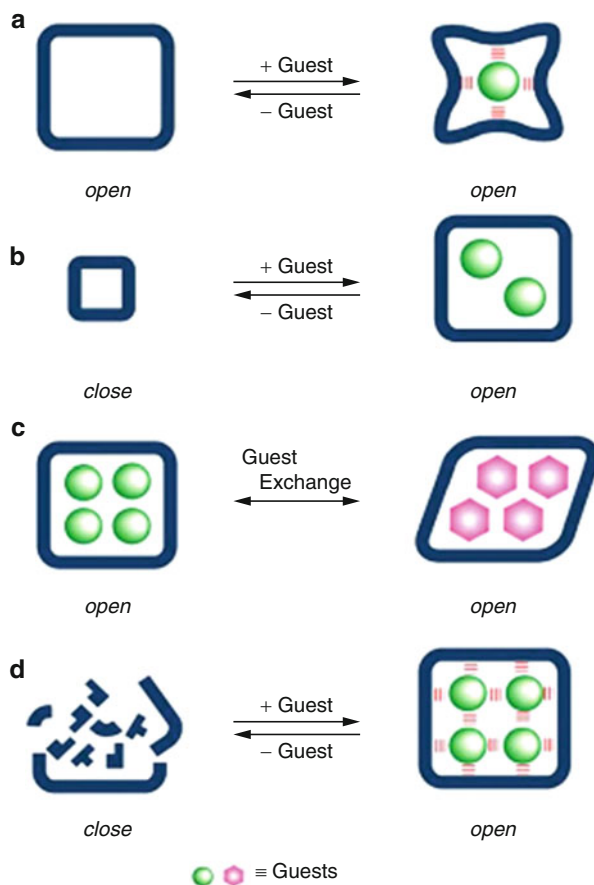
5 Surface Area

The research activities on porous coordination polymers (PCPs) have been intensified in the past three decades because of the obvious flexibility to control their structure and property by tuning the organic ligand and proper choice of metal center [1]. PCPs are usually synthesized under mild conditions by bottom-up approach [33]. The possibilities of generating new materials with intriguing properties based on PCPs were initially demonstrated by Robson, Moore, Yaghi and Fujita. In 1990, Robson et al. reported a PCP that was capable of exchanging anions [4], and later in 1994, Fujita and co-workers demonstrated the catalytic properties of a 2D PCP [34]. In 1995, the adsorption of guest molecules in porous materials was studied by Yaghi et al. [35], and in 1997, gas adsorption at ambient temperature was reported by Kitagawa [36]. Later, contribution by the group of Yaghi on the structure of MOF-5 in late 1999 [37] motivated the interest in the field of PCPs. Surface area is one of the crucial properties which determine the sorption property of PCPs, which depend on their pore size, shape and volume. Depending upon the dynamic nature of the coordination polymer, the deformation of the pore occurs by involving two fundamental operations, namely, shrinking and expansion. Based on these observations, Kitagawa [38] proposed the pore behaviors of PCPs which can be classified into four types based on the correlation between the pores (shape/size) and guest molecules (Fig. 5).

1. Induced-fit type pores: The shrinkage occurs on guest molecule inclusion and gives rise to a pore that is well-suited to the size and shape of the guest molecule, and therefore, short range attractive interactions work effectively.
2. Breathing type pores: The expansion makes a guest molecule fit tightly into the host when the size of the pore is smaller than the guest molecule.
3. Guest-exchange deformation type pores: The pore shape is induced to change responding to guest shape in simultaneous guest exchange.
4. Healing type pores: The collapsed pore in the absence of guest molecules are regenerated with the guest accommodation.

The specific surface area of the porous structure can be determined by Brunauer–Emmett–Teller (BET) method. Due to the high surface area of PCPs,

Fig. 5 Schematic representation of microporous behaviors observed in adsorption/desorption of guest molecules: (a) induced-fit typed pores, (b) breathing pores, (c) guest-exchanging pores with deformation, and (d) healing pores. (This figure is reprinted from Ref. [38] with permission. Copyright 2005, Elsevier)



it tends to have low-density compounds. Some of the early reported PCPs showed excellent surface area in their porous structure having a surface area in the range of $4000\text{--}6260\text{ m}^2\text{ g}^{-1}$ (Fig. 6). One of the first innovations in obtaining MOFs with permanent microporosity was reported by Yaghi et al., who demonstrated the material, namely, $\text{Zn}(\text{BDC})$ (BDC = 1,4-Benzenedicarboxylate), having a Langmuir surface area of $310\text{ m}^2/\text{g}$ [39]. Later, the same group synthesized MOF-5, which shows a BET surface area of $3800\text{ m}^2\text{ g}^{-1}$ [37]. Inspired by the intriguing results of MOF-5, later a series of MOFs, namely, MOF-177 [40] and MOF-200, were also synthesized by the self-assembly of Zn_4O cluster with 1,3,5-benzenetricarboxylate (**btb**) and 4,4',4''-[benzene-1,3,5-triyltris(benzene-4,1-diyl)]tribenzoate (**bbc**), respectively; both MOF-177 [40] and MOF-200 [41] also showed high porosity having a BET surface area of 4746 and $6260\text{ m}^2\text{ g}^{-1}$, respectively.

Interpenetration is one of the intrinsic challenges of PCPs [42], as their pores were blocked by the coordination networks. In order to get rid of from this problem,

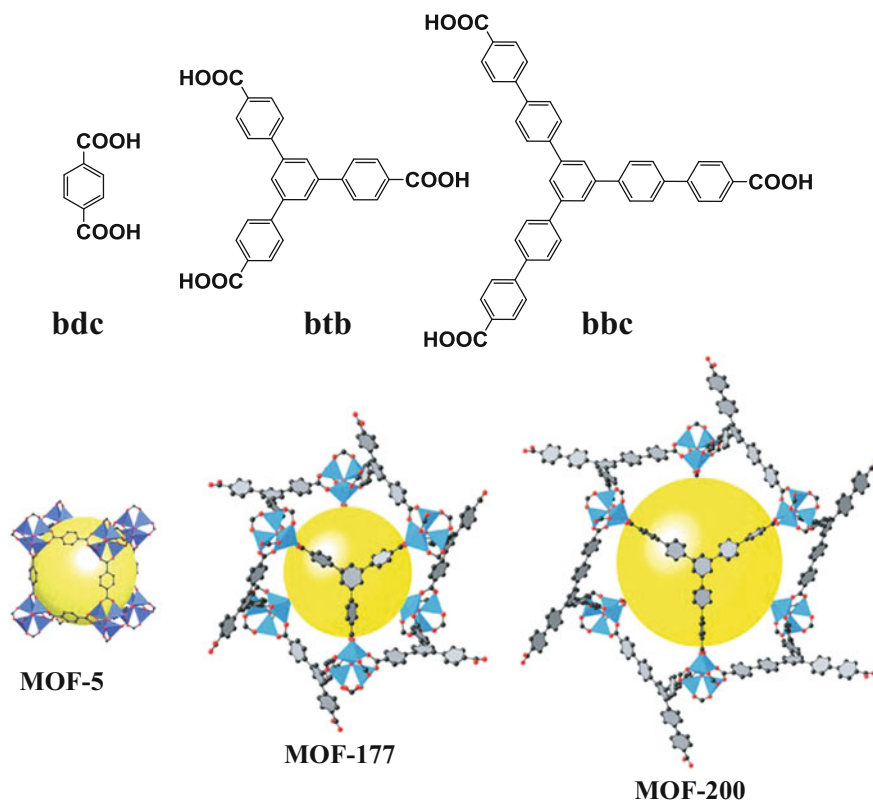
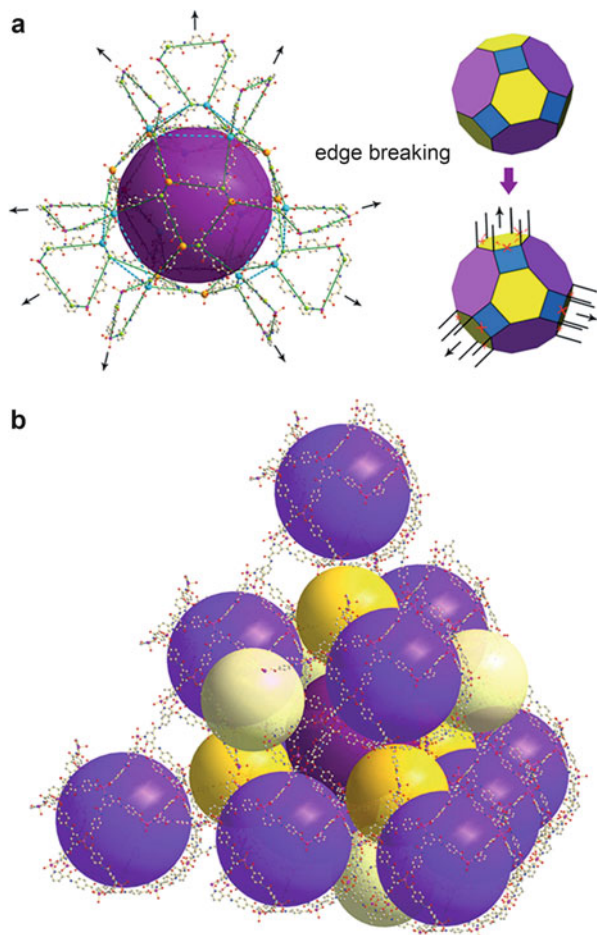


Fig. 6 Crystal structures of MOF-5, MOF-177, and MOF-200. Note the lengthening of the linkers and the increased size of the yellow sphere representing free pore space. (This figure is reprinted from Ref. 37, 39, 40] with permission. Copyright 1999 and 2004, Nature Publishing Group, and 2010, American Association for the Advancement of Science)

judicious choice of ligand and metal ion are important. Bai and co-workers reported a mesoporous MOF, namely, $\{[Zn(\text{BCP})\cdot\text{H}_2\text{O}]\cdot 3.5\text{H}_2\text{O}\cdot\text{DMF}\}_n$ (where BCP = 3,5-bis[4-carboxyanilino-carbonyl]pyridine and DMF = *N,N*-dimethylformamide), also called as NJU-Bai9 [43]. In fact NJU-Bai9 exhibits a three-dimensional (3D) structure having Archimedean-solid-type cages and the structure is highly mesoporous in nature. The mesoporous structure undergoes interpenetration with pbz topology. Interestingly, NJU-Bai9 exhibits unprecedented breaking edges off truncated cuboctahedral cage structure in which the coordination network assembled into a 3D network (Fig. 7).

BET surface area analysis of NJU-Bai9 revealed its uptake of H_2 , CH_4 , and CO_2 with a surface area of $4258\text{ m}^2\text{ g}^{-1}$ which is the highest surface area among the interpenetrated porous MOFs reported to date. Many efforts for even better surface area were carried out by various research groups, despite the daunting task to achieve it due to the tendency of these materials to collapse upon removal

Fig. 7 (a) Edge breaking off in NJU-Bai9; (b) overall packing of NJU-Bai9 displaying the four various types of cages, even after interpenetration. (This figure is reprinted from Ref. [43] with permission. Copyright 2013, Wiley-VCH Verlag)



of lattice occluded solvent molecules [44]. Two MOFs, namely, MOF-210 [45] and NU-100 [46] (NU = Northwestern University; NU-100 is also known as PCN-610 [47]), were reported by Farha et al., which show large cavity structure (surface area $> 6000 \text{ m}^2 \text{ g}^{-1}$) and robustness even after evacuating the guest molecules. Recently, Farha and co-workers reported two MOFs, namely, NU-109 and NU-110, derived from two hexacarboxylic acid ligands (Fig. 8), which showed the highest experimental BET surface areas of any porous materials reported to date ($\sim 7000 \text{ m}^2 \text{ g}^{-1}$). In the same work, they showed computationally that by simply changing phenyl groups with “space efficient” acetylene functionalities as linker expansion units, the hypothetical maximum surface area for a MOF material is substantially greater than previously envisioned ($\sim 14,600 \text{ m}^2 \text{ g}^{-1}$ (or greater) versus $\sim 10,500 \text{ m}^2 \text{ g}^{-1}$).

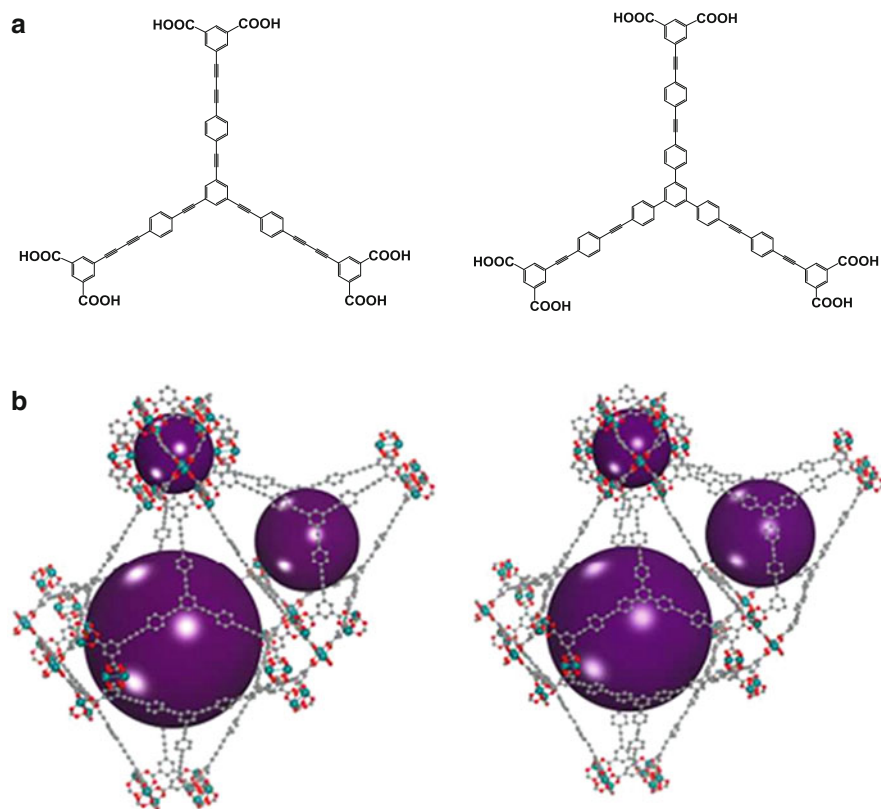


Fig. 8 *Top* – the hexacarboxylic acid ligands; *down* – crystal structure of NU-109 and NU-110, displaying the various cages (shown in purple color). (This figure is reprinted from Ref. [52c] with permission. Copyright 2012, American Chemical Society)

6 Gas Storage

Porous materials were explored by various groups for gas storage application. For example, activated carbon and zeolites have been widely investigated due to easy availability, cheap, and nontoxic nature. Despite of its positive aspects, these porous materials do not exhibit enough gravimetric and volumetric storage capacity due to their relatively weak interactions with adsorbate gas molecules [48a]. In fact the adsorption enthalpies within these materials are significantly less than -15 to -20 kJ/mol, an ideal storage capacity at ambient temperature and 100 bar [48b]. Interestingly, MOFs or PCPs have emerged as smart materials to overcome the aforementioned problems to some extent. Due to the comparable size of gas molecules with the host microporous compounds having a pore size of nanometer scale,

PCPs or MOFs has been developed as an efficient material to entrap or adsorb gas molecules, which plays a crucial roles in modern gas technology [48c].

The gas adsorption application of PCPs was first reported by Kitagawa and co-workers, exploring a three-dimensional framework built from 4,4'-bpy = 4,4'-bipyridine and $M(II) = Co, Ni, Zn$ [36]. Later, owing to their intrinsic property of porosity and tunability (by changing the metal node and organic linker), PCPs/MOFs were already proved as an ideal candidate for gas storage application [20]. A wide variety of isoreticular MOFs were reported by Yaghi, by modifying their structure, pore size, and functional groups of organic linkers [21]. The thermodynamic and kinetic aspects of sorption behavior are very important factors to be considered while designing new PCPs for selective gas adsorption or separation. One of the most crucial factors affecting the gas storage property of PCP is the size of their pore. In fact, once the pore size become equivalent to the molecular size of the gaseous molecules, the adsorption energy potential increases due to the overlapping of energy potentials from the surrounding walls. As a result, the guest gas molecules tend to strongly bind to the framework of PCPs [49]. In the following section, we discuss the H_2 , CH_4 , and CO_2 storage application of PCPs or MOFs.

6.1 Hydrogen Storage

Hydrogen is one of the intriguing fuel gases which is used as an excellent energy source [50]. Among various hydrogen storage materials such as metal hydrides [51a], carbohydrates [51b], clathrates [51c], and nanotubes [51d], PCPs or MOFs have attracted considerable interest because of their diverse structure, extraordinarily high surface areas (experimental value of up to $7140 \text{ m}^2 \text{ g}^{-1}$, against theoretical limit of $14,600 \text{ m}^2 \text{ g}^{-1}$), ultrahigh porosity (up to 90% free volume), tunable pore size, and adaptable internal surface [52]. One of the first MOFs investigated for hydrogen storage was the cubic carboxylate-based framework MOF-5, which showed a hydrogen gas uptake of 4.5 weight % at 78 K and 1.0 weight % at room temperature and pressure of 20 bar [53a]. Secondly, Férey and co-workers reported two MOFs derived from 1,4-benzenedicarboxylic acid and Al^{3+} , Cr^{3+} ; these MOFs showed a hydrogen adsorption capacity of 3.8 and 3.1 wt.%, respectively when the sample loaded at 77 K under 1.6 MPa [53b]. Motivated from these seminal results of MOF-5 by Yaghi et al., and MOFs developed by Férey et al., many research groups gave dedicated efforts for the investigation of H_2 storage in MOFs at low temperature and room temperature [54]. Later, MOF-5 has been explored by many research groups. One of the first studies exhibited an excess gravimetric uptake of 1.3 wt% at 1 bar 66 and 5.1 wt% at 50 bar at 77 K [55]. Interestingly, it was later proved that the method of synthesis and activation of MOF-5 sample is one of the crucial factors for the successful H_2 sorption capability; Langmuir surface areas range between 1010 and $4400 \text{ m}^2 \text{ g}^{-1}$ and H_2 uptake capacity vary accordingly.

In fact, the research of MOFs for hydrogen sorption application emphasizes on various approaches for the design and synthesis of MOFs to increase the hydrogen storage capacity as much as possible, in order to achieve greater gravimetric and

volumetric storage capacity. These approaches depends on various parameters such as (1) H_2 adsorption condition (pressure and temperature), (2) inclusion of reducing agents in the MOF, (3) effect of structural defect in MOF, and (4) effect of adsorption sites in the MOF structure. Hereafter we will discuss the hydrogen storage application of MOFs according to these parameters.

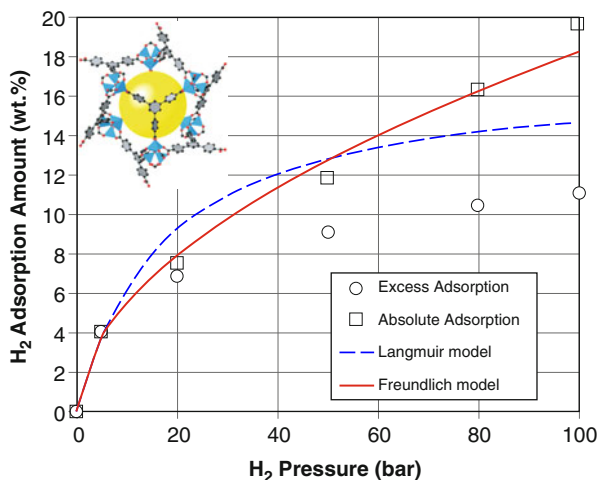
6.1.1 H_2 Adsorption Condition (Pressure and Temperature)

Various research groups have investigated the effect of adsorption condition of a particular MOF on their H_2 storage capacity. For example, MOF-177 exhibits a maximum storage of H_2 at temperature 77 K and pressure 100 atm [40]. Interestingly, Deng et al. synthesized MOF-177 by following a modified method and the resultant material showed a hydrogen saturation uptake of 11.0 wt% at about 100 atm and 77 K. Freundlich isotherm model correlation plot revealed that the absolute amount of hydrogen adsorbed in MOF-177 at these conditions is about 19.67 wt% (Fig. 9). The reason behind the more hydrogen uptake is the high surface area ($5994 \text{ m}^2 \text{ g}^{-1}$) of MOF-177 synthesized by Deng et al. [56].

6.1.2 Inclusion of Reducing Agents in the MOF

Yang and Li reported the synthesis of a modified form of MOF, which showed greater hydrogen binding within their porous framework [57], constructed by introducing the phenomena “hydrogen spillover” [58] by following two methods: (1) by mixing the individual components such as IRMOF-8 and Pt/AC mixture and synthesize a modified MOF, namely, Pt/AC/IRMOF-8, and (2) by bridging the Pt/AC with IRMOF-8, namely, Pt/AC-bridges-IRMOF-8, where AC = activated carbon. Thus by the inclusion of reducing agents Pt/AC, Pt performs as a catalyst and participates in the reduction of H_2 or spillover of H_2 into hydrogen atoms and finally increases the hydrogen storage in MOFs. This study revealed the importance of

Fig. 9 Hydrogen adsorption plot of MOF-177 at high pressure and 77 K, displaying the excess, absolute, Langmuir and Freundlich adsorption. (This figure is reprinted from Ref. [56a] and [56b] with permission. Copyright 2008, Elsevier Ltd., and Copyright 2005, Wiley-VCH Verlag)

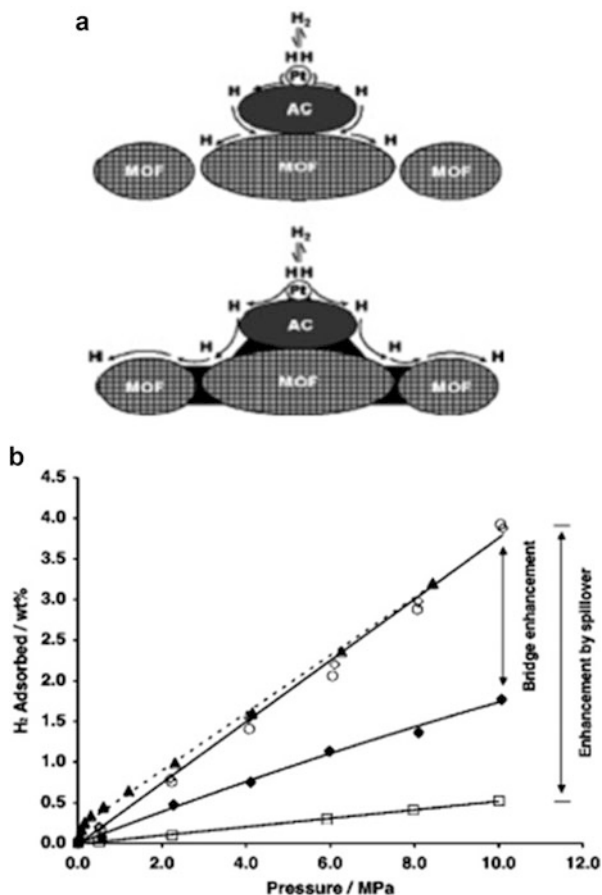


spillover for the hydrogen storage using MOFs. The Pt/AC/IRMOF-8 and Pt/AC-bridges-IRMOF-8 showed a reversible H_2 uptake of 1.8 wt % and 4.0 wt %, respectively at room temperature and 10 atm pressure. Interestingly, the modified forms of IRMOF-8 showed a spillover enhancement factors for hydrogen storage of 3.1 and 6.8 times more than the original form of IRMOF-8 (Fig. 10). These results gave motivation to the materials chemist researchers for the development of other MOFs by spillover and concomitant capacity enhancement of the modified MOFs.

6.1.3 Effect of Structural Defect in MOF

It is well-known that the kinetic diameter of the porous material must be within the range of the kinetic diameter 2.89 \AA , for a successful H_2 adsorption material. This is due to the fact that as the diameter having a pore size of more or equal to 2.89 \AA is essential for the passage of hydrogen molecules through the MOF material [59]. Various research groups investigated to tune the pore size of the MOFs within this range and some groups focused on the effect of defects for the same case, which makes the

Fig. 10 (a) Primary spillover of hydrogen atom supported by Pt and activated carbon (*top*), primary and secondary spillover resulted from carbon (shown in dark color) (*bottom*); (b) hydrogen adsorption and desorption isotherms at 298 K, of pure IRMOF-8, Pt/AC, and IRMOF-8 physical mixture. (This figure is reprinted from Ref. [57b] with permission. Copyright 2006, American Chemical Society)



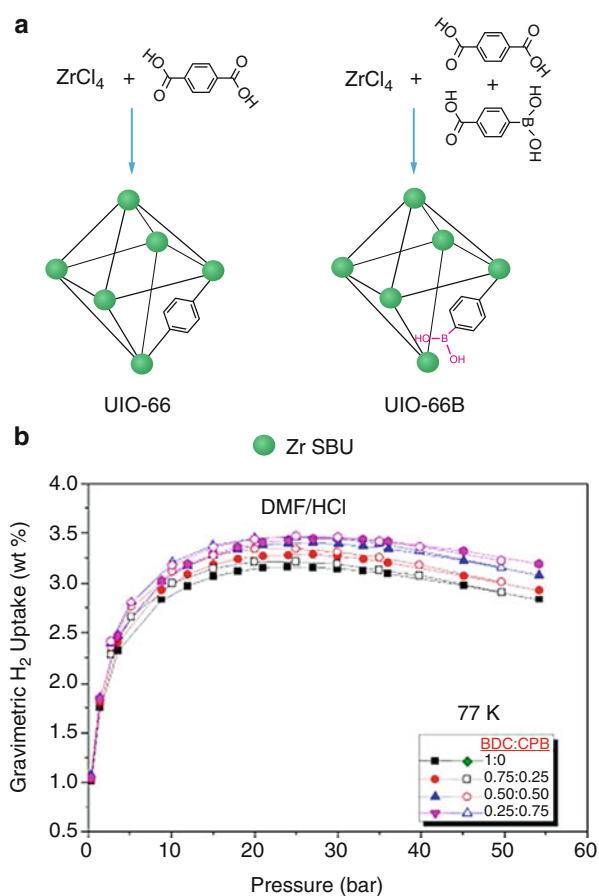
hydrogen molecule to adsorb on the MOF matrix via physisorption at low pressure and ambient temperature [60]. Bai et al. [61] and Feng et al. [62] demonstrated the synthesis of defected MOFs with the incorporation of micro- and mesopores and its capability of improved H₂ adsorption than the nondefected counterpart. Ren et al. studied the structural defects in core-shell MIL-101(Cr)@UiO-66(Zr) by comparing with the parent Zr-based MOF, UiO-66(Zr) [63]. The organic compounds [1,4-benzenedicarboxylic acid (BDC) linker and modulator (HCOOH)], especially the modulator and time of the reaction, played a crucial role for the formation of defects in the parent MOF UiO-66(Zr), which lead to the formation of core-shell MIL-101(Cr)@UiO-66(Zr). Longer synthesis time facilitated to the formation of larger crystals and the presence of the modulator promotes defects in the MOF. Interestingly, the defects created on the MOF structure of UiO-66(Zr) enhanced the diffusion of H₂ and thus store more H₂.

More recently, Erkartal and Sen explored boronic acid functionalities into UiO-66 and thus examine the effect of structural defects on the H₂ adsorption behavior [64]. In order to compare the H₂ sorption behavior of pure parent MOF UiO-66 and defect-induced (with boronic acid) MOF, namely, UiO-66B, both MOFs were synthesized separately via hydrothermal synthesis method. The UiO-66B having various stoichiometric ratios (BDC/CPB ratios from 0.87:0.13 to 0.50:0.50) of the ligands 1,4-benzenedicarboxylic acid (BDC) and 4-carboxyphenylboronic acid (CPB) were synthesized (Fig. 11a) in the presence and absence of HCl and characterized by powder X-ray diffraction (PXRD). The stoichiometric ratios of BDC/CPB present in various samples of UiO-66B were further characterized by proton nuclear magnetic resonance spectroscopy (¹H NMR) and X-ray photoelectron spectroscopy (XPS). The as-synthesized UiO-66Bs having boronic acid functionality showed higher BET surface area (BDC:CPB = 0.25:0.75, BET surface area of 1512 m²/g) and facilitate considerably the hydrogen uptake, 3.44 wt% at 21 bar, 77 K (Fig. 11b) than the pure phase of UiO-66 (BET surface area 1361 m²/g and 2.38 wt% H₂ uptake). Interestingly, UiO-66 exhibits fully reversible isotherm whereas UiO-66B samples showed hysteric adsorption. This unprecedented result is due to the replacement of coordination environment from fully occupied (UiO-66) to partially occupied coordination sites in UiO-66B, which gave more flexibility to the defected MOF (UiO-66B).

6.1.4 Effect of Adsorption Sites in the MOF Structure

In order to understand the mechanism of adsorption in the MOF structure, Yaghi and co-workers studied the inelastic neutron scattering experiment on the H₂ adsorbed MOFs. This study confirmed that both the metal-oxide clusters and the ligand units are responsible for the adsorption sites for hydrogen molecules [53a]. Later, a series of reports were published by various research groups, illustrating the hydrogen storage enhancement by simply replacing the metal ions (for example, Zn²⁺ with other similar metal ions, such as, Mg²⁺, Ni²⁺, or Cu²⁺) or organic linkers [57a]. Zhou et al. demonstrated that the presence of open metal sites in the MOFs have more tendency to attract the hydrogen molecule and facilitate to store H₂, with the support of experimental and computational evidence [65]. Postsynthetic functionalization of MOF, based on conversion of pendant alcohols to metal alkoxides, was explored by Karen and co-workers for better adsorption of H₂ [66].

Fig. 11 (a) Schematic representation for the synthesis of UiO-66 and defect-induced MOF, UiO-66B; (b) hydrogen uptake isotherms of UiO-66-HCl and UiO-66B-HCl at high pressure and 77 K. (This figure is reprinted from Ref. [64] with permission. Copyright 2018, American Chemical Society)

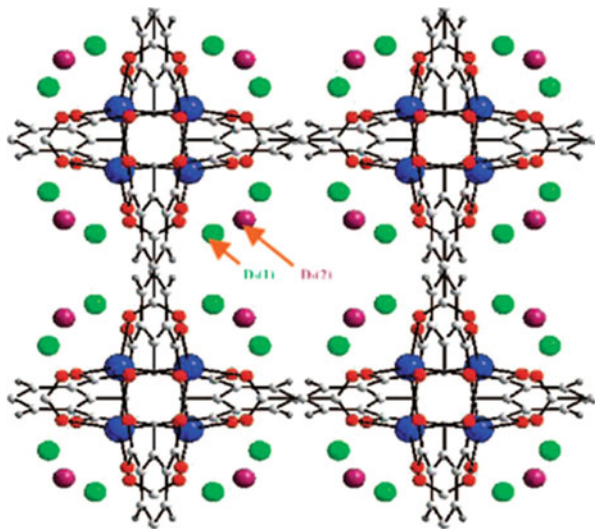


A thermally stable porous MOF derived from Ytterbium and 1,3,5-benzenetricarboxylate (BTC) and its unprecedented H₂ adsorption property was reported [67]. In order to understand the mechanism of interaction of H₂ on the Yb-BTC framework, powder neutron diffraction experiment was carried out. The diffraction data revealed that optimal pore size (6 Å) of the framework reinforces between the H₂ molecule and pore walls, which resulted in the H₂ adsorption. Thus it is confirmed that in this case of MOF, the interaction is between H₂ and the pore walls, not with the open metal sites within the framework. There are four D₂ adsorbing sites found within the framework of Yb-MOF (Fig. 12).

6.2 Methane Storage

Methane is one of the important components of natural gas, and primary concerned fuel due to its potentiality of environment friendliness, compare to other

Fig. 12 Structure of Yb-BTC MOF, displaying the two distinct adsorption sites of H₂ (shown in green and orange ball). (This figure is reprinted from Ref. [67] with permission. Copyright 2008, American Chemical Society)



components. Methane is the first member of saturated hydrocarbon having least number of carbon atoms and more number of hydrogen atoms, and as a result, it exhibits greater octane number. Moreover, combustion of methane yields least amount of CO₂ as the byproduct for each unit of energy released from vehicles. Therefore, it is important to use methane as the fuel gas because of the climate change issue and economy concern. One of the primary and important challenges of the environmental scientists and engineers is to find a best solution to replace petrol with the methane as the fuel for vehicles. In the current scenario, methane is stored as compressed natural gas (>200 atm), in cylinder, which is quite expensive. Therefore, serious efforts were explored by researchers to discover an alternative storage method by using adsorption phenomena on a porous solid compound at low pressure and ambient temperature. In order to attain the practical application of methane storage in vehicles, the U.S. Department of Energy (DOE) has fixed a targeted goal for methane storage at 180 v/v at STP for the adsorbent material [68]. PCPs or MOFs already showed a reasonable uptake of methane at 298 K and lower pressure [69].

Kitagawa et al. reported the first functional coordination polymer CuSiF₆(4,4'-bipyridine)₂, which showed remarkable methane adsorption [70]. In the crystal structure, Cu(II) metal center exhibits distorted octahedral geometry, in which the equatorial and axial positions are occupied with 4,4'-bipyridine and counter anion SiF₆²⁻. Interestingly, the extended coordination of both equatorial and axial ligands resulted in a three-dimensional (3D) porous structure with square shape channels (8 × 8 Å²) and exhibited very good methane adsorption property than zeolite 5 Å, under low pressure (0–36 atm) and room temperature (Fig. 13).

Yaghi and co-workers self-assembled a series of nanoporous isoreticular MOFs (IRMOFs) having an open space of up to 91.1% of the crystal volume and homogeneous square shape channels within the range of 3.8 to 28.8 Å [71]. Interestingly, IRMOF-6 derived from BDC with cyclobutyl functionality showed exceptionally

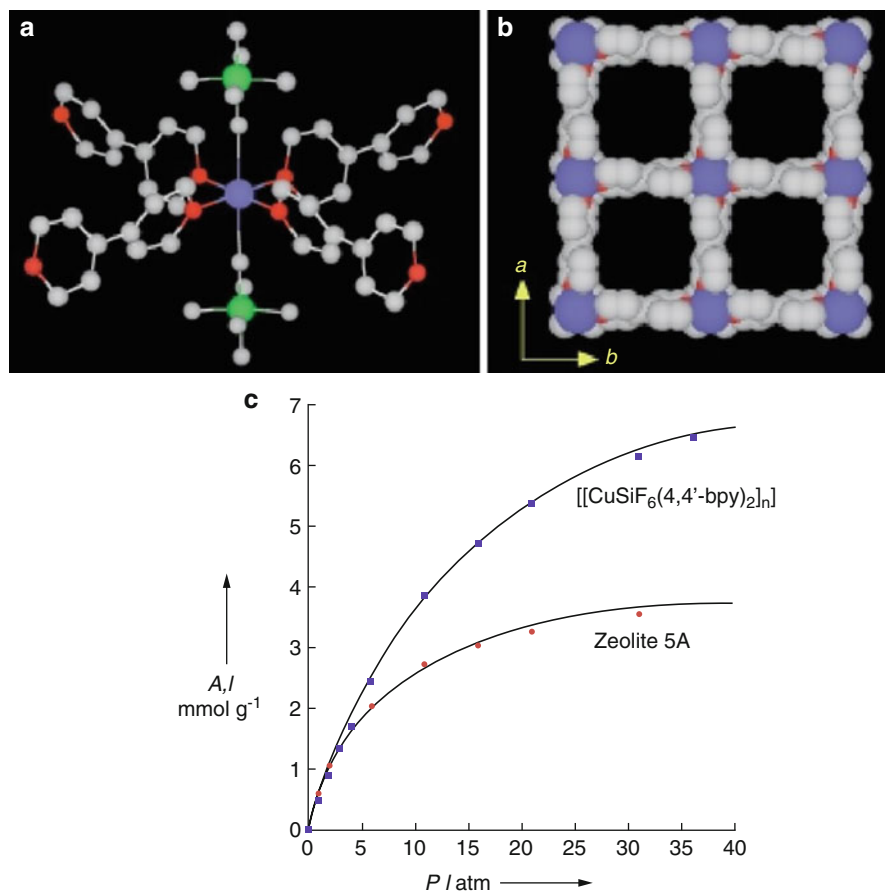


Fig. 13 (a) Coordination geometry of Cu(II) in $\text{CuSiF}_6(4,4'\text{-bipyridine})_2$, displaying the equatorial and axial coordination of 4,4'-bipyridine and SiF_6^{2-} , respectively. (b) 3D porous structure of $\text{CuSiF}_6(4,4'\text{-bipyridine})_2$, along the crystallographic axis "c." (c) Methane adsorption of $\text{CuSiF}_6(4,4'\text{-bipyridine})_2$ and zeolite 5 Å at various pressure. (This figure is reprinted from Ref. [70] with permission. Copyright 2000, Wiley-VCH Verlag GmbH & Co. KGaA, Weinheim)

high methane storage capacity having 240 cm^3 at standard temperature and pressure per gram at 36 atm and ambient temperature. This result is a breakthrough in the research of methane storage application of MOF, because the methane uptake of IRMOF-6 is much more than other well-known crystalline materials like zeolite 5 Å ($87 \text{ cm}^3 \text{ (STP)g}^{-1}$) [72] and other coordination compounds (until $213 \text{ cm}^3 \text{ (STP)g}^{-1}$) [73].

Zhou and co-workers synthesized a MOF, namely, PCN-14, derived from carboxylate ligand having anthracene backbone [74]. The single crystal X-ray structure analysis of PCN-14 confirmed the presence of cuboctahedral nanoscopic cages, in the structure. The crystal structure exhibits a void volume of 1150 Å^3 having capable

for uptake of gas molecules. The BET surface area measurement of PCN-14 further revealed its porous structure having a surface area of $2176 \text{ m}^2/\text{g}$ and pore volume of $0.87 \text{ cm}^3/\text{g}$. Interestingly, PCN-14 displays an absolute methane adsorption capability of 230 v/v [74], which is much greater than (28% more) than the DoE fixed goal (180 v/v) (Fig. 14) [68]. And PCN-14 is the first member of MOFs which come across the target of DoE. This unprecedented methane adsorption behavior of PCN-14 is due to two structural features such as (1) the anthracene backbone present in the ligand presumably participates in the intermolecular interaction with the methane molecules and thus binds strongly with the framework and (2) the size and shape of the nanopores present in the PCN-14 are almost ideal for various interactions between the CH_4 molecules and the host framework.

The observation of coordinatively unsaturated Cu ions present in PCN-14 inspired Wu and co-workers to study the effect of unsaturated metal sites in the MOFs on their methane uptake capacity [75]. The effect of open metal sites on the binding strength of H_2 is already discussed (vide supra) by various research groups [65–67]. Thus Wu et al. selected a series of isostructural $\text{M}_2(\text{dhtp})$ [M: open metal = Mg, Mn, Co, Ni, Zn], dhtp = 2,5-dihydroxyterephthalate] MOFs because of the presence of open metal sites in the crystal structure of these series. Moreover, these isostructural series have significantly higher densities of open metal sites in their crystal structures ($\sim 4.5 \text{ sites}/\text{nm}^3$) than PCN-14 ($\sim 1.6 \text{ sites}/\text{nm}^3$). The single

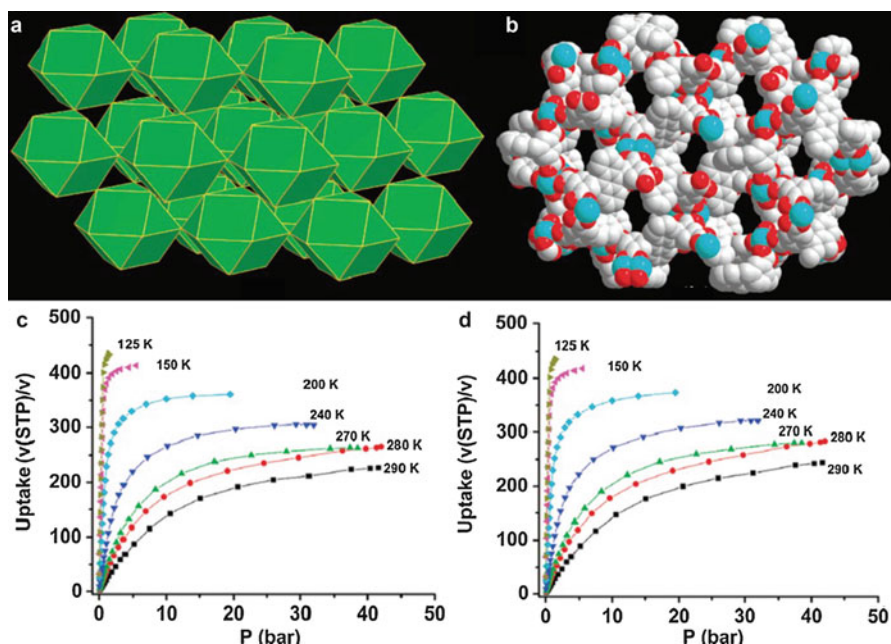
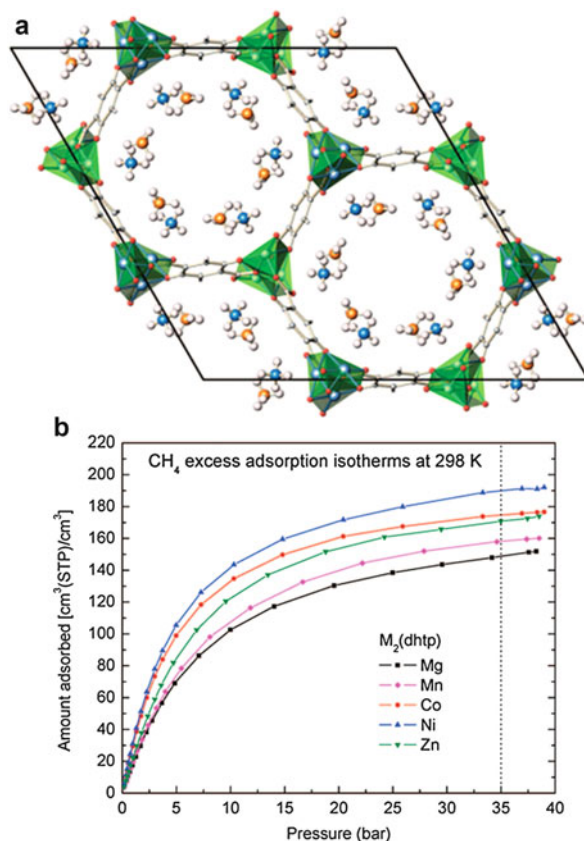


Fig. 14 3D porous structure of PCN-14, displaying (a) cuboctahedral net, (b) space-filling model on the [1 0 3] plane. (This figure is reprinted from Ref. [74] with permission. Copyright 2008, American Chemical Society)

crystal X-ray structure of $M_2(\text{dhtp})$ revealed their porous structure with large one-dimensional (1D) channels having pore diameter of $\sim 13.6 \text{ \AA}$, and such structure can be utilized for methane gas uptake. From the methane adsorption isotherms of the isostructural series, it is revealed that $\text{Ni}_2(\text{dhtp})$ exhibits the highest absolute methane uptake ($\sim 200 \text{ cm}^3(\text{STP})/\text{cm}^3$) and known as the second member of MOFs to potentially exceed the DOE's targeted goal. Neutron diffraction experiment analysis revealed that there are two CH_4 adsorption sites in the crystal structure and the CH_4 molecules interact with the open metal sites via intermolecular interactions. Moreover, initial first-principles calculations of this molecular system displayed that the binding energies associated with the CH_4 on the open metal sites are higher than the MOFs having characteristic adsorption sites reported so far (Fig. 15).

A 3D porous MOF, namely, UTSA-20, was reported by Chen et al. and are synthesized via coordination-driven supramolecular assembly of paddle-wheel $\text{Cu}_2(\text{COO})_4$ SBU and a hexacarboxylate organic linker H_6BHB ($\text{H}_6\text{BHB} = 3,3',3'',5,5',5''$ -benzene-1,3,5-triylhexabenzic acid) [76]. The 3D structure of UTSA-20 was determined by using high resolution PXRD data, which helped to refine the crystal

Fig. 15 (a) Crystal structure of $\text{Mg}_2(\text{dhtp})$, displaying the adsorption of methane at two distinct sites (shown in orange-white and blue-white ball and stick model). (b) The CH_4 adsorption isotherm plots on $M_2(\text{dhtp})$, displaying the highest uptake of CH_4 by Ni derivative of the series. (This figure is reprinted from Ref. [75] with permission. Copyright 2009, American Chemical Society)



structure. The structure analysis revealed that the extended coordination of paddlewheel $\text{Cu}_2(\text{COO})_4$ SBUs with the BHB linkers, resulted in a 3D porous architecture having a novel “zyg” topology involving two kinds of three-coordinated nodes and a four-coordinated paddlewheel $\text{Cu}_2(\text{CO}_2)_4$ cluster (as shown in Fig. 16a). Interestingly, the crystal structure consists of two type of channels having a rectangular ($3.4 \times 4.8 \text{ \AA}$) and a cylindrical (8.5 \AA) shape, along the c' axis with a total accessible free volume of 3471.0 \AA^3 , or 63.0% of the unit volume 5512.9 \AA^3 . Such kind of porous MOF involving open metal (Copper in UTSA-20) sites and enough pore size are crucial factors for the binding of CH_4 molecules in the framework. Nitrogen sorption isotherm at 77 K on the activated sample of UTSA-20 revealed the type I reversible sorption isotherm and moderate porosity, corresponding to a BET surface area of $1156 \text{ m}^2 \text{ g}^{-1}$ (Fig. 16). Despite of the moderate porosity and surface area exhibited by UTSA-20, compared to other well-known MOFs, the presence of open copper sites and optimal pore spaces helped UTSA-20 to achieve a high density methane storage (0.222 g cm^{-3}) and listed to third position in absolute volumetric methane storage, among other MOF materials such as PCN-14, $\text{Ni}_2(\text{dhtp})$, IRMOF-6, etc.

Snurr et al. demonstrated a computational approach to find out the best MOFs (known or unknown) for a particular application, for example, methane storage

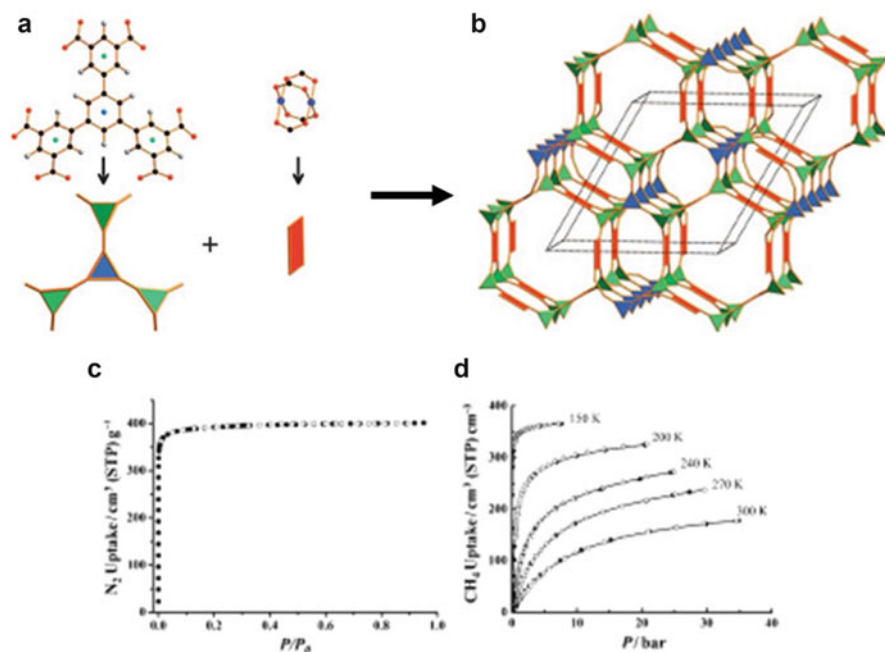


Fig. 16 (a) Crystal structure illustration of UTSA-20, displaying the SBU and 3D porous structure with augmented zyg net topology. (b) N_2 adsorption isotherm of UTSA-20 at 77 K. (c) CH_4 adsorption isotherm of UTSA-20 at variable temperature and high pressure. (This figure is reprinted from Ref. [76] with permission. Copyright 2011, Wiley-VCH Verlag GmbH & Co. KGaA, Weinheim)

capacity of a MOF [77]. They selected a library of 102 building blocks of MOFs, generated 137,953 hypothetical MOFs from these selected building blocks, and finally calculated the pore size, surface area, and methane storage capacity of each MOFs by computational method. Among these MOFs, 300 showed very good methane uptake capacity than the MOFs reported so far. Interestingly, methyl functionalized ligands (building block) showed very good methane adsorption capability.

Zhang et al. engineered a series of mesoporous MOFs UMCM-1, MOF-205, MUF-7a, and the newly synthesized MOFs, termed ST-1, ST-2, ST-3, and ST-4 (ST = ShanghaiTech University), and demonstrated the importance of tuning of mesoporosity for the successful design and synthesis of new MOFs for methane storage application at ultrahigh pressure [78]. All mesoporous MOFs were synthesized from $\text{Zn}_4\text{O}(\text{-COO})_6$ by mixing with tritopic linkers and ditopic linkers (Fig. 17). Interestingly, one of the mesoporous MOFs, namely, ST-2, exhibit excellent capacity of methane uptake ($289 \text{ cm}^3 \text{ STP/cm}^3$ (567 mg/g) at 298 K and 5–200 bar), which is the highest record to date.

6.3 Carbon Dioxide Storage

The emission of CO_2 from industrial waste, mainly from coal-fired power plant, oil, and natural gas, is one of the issues facing by the environmental concern due to climatic change [79]. The coal-fired power plant produces post-combustion flue gases having a concentration of $\sim 15\%$ CO_2 . Moreover, a recent investigation revealed that average concentration of CO_2 emission to earth reached 406.75 parts per million (ppm) in January, 2018 [80]. This is mainly due to the contribution from human activities in the past decades. Thus, various research groups have contributed different approaches to find a good solution to solve the problem of CO_2 such as (1) by cooling and forcing power plant emission and convert CO_2 to CaCO_3 by using lime water and (2) by passing the fumes through aqueous amine solution. These two methods are very expensive and incompetent [81]. Several porous materials were explored to capture and store CO_2 by chemisorption and physisorption [82]. Among these porous materials, MOFs or PCPs show very high CO_2 storage ability even at ambient temperature and pressure, due to their capability for adsorption of gases via physisorption, and tunability of their structure [83].

One of the first results of CO_2 adsorption property of MOFs was reported by Yaghi et al. They explored a series of nanoporous MOFs, such as MOF-2, MOF-505, MOF-74, $\text{Cu}_3(\text{BTC})_2$, IRMOF-11, IRMOF-3, IRMOF-6, IRMOF-1, MOF-177, and systematically study their gravimetric uptake of CO_2 [84]. From the room-temperature CO_2 adsorption isotherms of these MOFs, it is clear that the MOFs having open metal sites in their framework showed type I isotherm with high uptake of CO_2 at low pressure. In contrast to this result, MOFs with $\text{Zn}_4\text{O}(\text{O}_2\text{C})_6$ -type frameworks, such as IRMOFs-1, -3, -6, and, -11, exhibit sigmoidal shape isotherms with high uptake of CO_2 at ambient pressure. The amine functionalized IRMOF-3 is more attracted towards CO_2 uptake, compared to others, due to the nonbonded

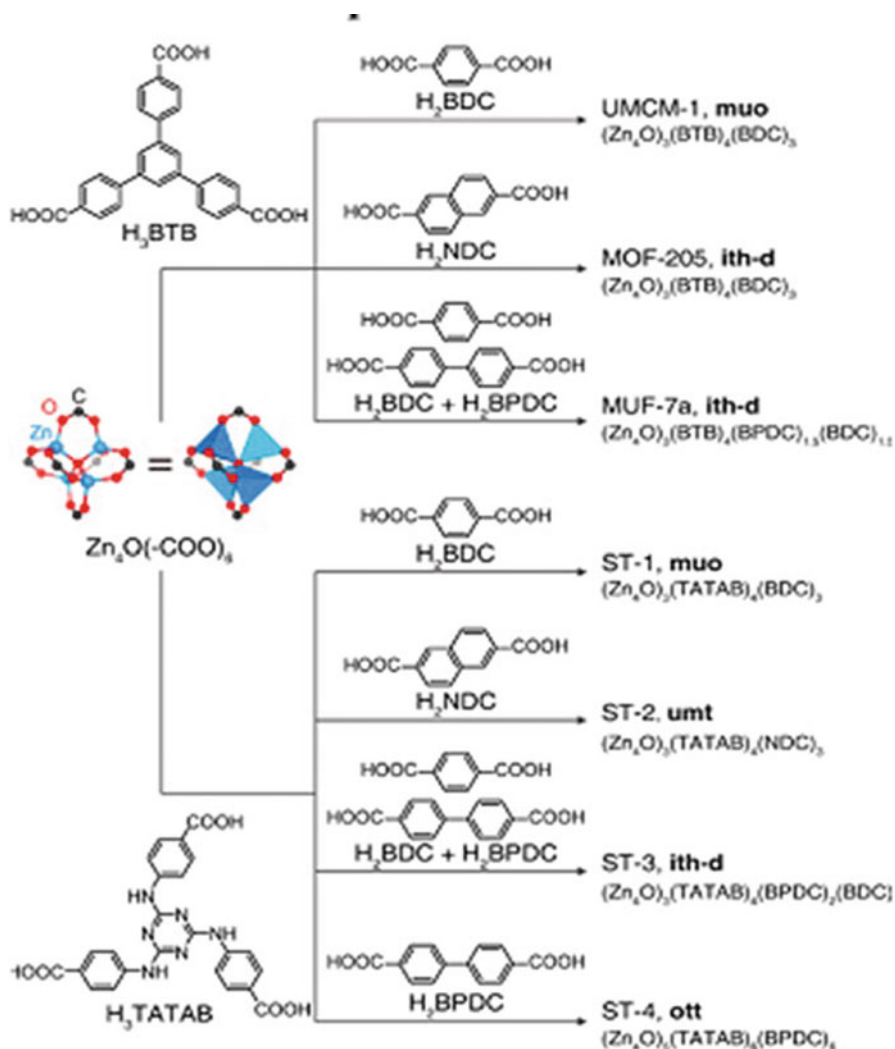


Fig. 17 Schematic representation of the synthesis of MOFs derived from $Zn_4O(-COO)_6$ and tritopic linkers/ditopic linkers. (This figure is reprinted from Ref. [78] with permission. Copyright 2017, American Chemical Society)

interaction of adsorbed CO_2 with the $-NH_2$ group of the framework. Interestingly, the comparison of volumetric CO_2 uptake data of MOF-177 with other well-known CO_2 -capturing materials like zeolite 13X and Maxsorb revealed that MOF-177 can uptake nine times more CO_2 relative to an adsorbent-free container and about two times more than that of zeolite 13X and Maxsorb at 35 atm. These remarkable results of CO_2 storage capacity of MOFs indicate the importance of MOFs to represent a strong candidate for the capturing of CO_2 from coal-fired power plants and exhaust

gases. Later, the same research group explored the possibility of Zeolitic imidazolate frameworks (ZIFs) to mimic Zeolite behavior for adsorption and retention of CO₂ and discovered that the ZIFs showed unprecedented selectivity for CO₂ from a mixture of other gaseous molecules. One liter of ZIF-69 showed a capacity to store and sustain 83 liters of CO₂ at 273 K and ambient pressure [85].

In fact, there are several factors which effect on the successful adsorption capacity of CO₂ on MOFs, which are discussed below.

6.3.1 The Effect of Open Metal Sites in the MOF

The coordination environments in some of the MOFs become unsaturated, once the loosely bound solvent molecules escape from the metal ions, when we activate the MOF crystals by heat or vacuum. For example, M-MOF-74 series derived from the ligand 2,5-dihydroxyterephthalic acid and metal ion (M = Mg, Co, Fe, Zn, Ni) have very high density of open metal sites [86]. Among these series, Mg-MOF-74 showed the best record of CO₂ capture of 228 cm³/g at 273 K, 180 cm³/g at 298 K and 1 atm. The reason behind such unprecedented CO₂ uptake of Mg-MOF-74 than other metal series of MOF-74 is due to the fact that the more ionic behavior of Mg–O bond in Mg-MOF-74 helps the CO₂ molecule to bind to the framework more strongly (Fig. 18).

Thus, the result of Mg-MOF-74 showed the importance of main group elements in designing new high-performance gas sorption materials, than that of the transition metals. Inspired by this thought, Zhai and co-workers developed a series of mixed-metal isostructural MOFs, namely, CPM-200, having a combination of trivalent (In³⁺, Ga³⁺, Fe³⁺, V³⁺, Sc³⁺) and divalent (Mg²⁺, Mn²⁺, Co²⁺, Ni²⁺) metal ions, by using heterometallic cooperative crystallization (Fig. 19a) [87]. The idea behind such an attempt may be due to the fact that the presence of different metal contents (as nodes) lead to defects in the resultant MOFs, and such defects may influence the CO₂ sorption capacity. The crystal structures of these MOF series were determined by single-crystal X-ray diffraction and the phase purity was confirmed by PXRD technique. The stoichiometric ratio between M²⁺ and M³⁺ was determined by site occupancy refinement and further supported by energy dispersive X-ray analysis (EDS) analysis. Interestingly, CPM-200-Fe/Mg showed significant CO₂ uptake (9.27 mmol/g at 273 K and 1 bar) which is the best among the other trimer based and other heterometallic MOFs under the same conditions. Moreover, the CPM-200-V/Mg exhibits the highest isosteric heat of adsorption (−79.6 kJ/mol) for CO₂ binding, compared to other MOFs with Lewis acid sites.

HKUST-1 is another example of MOF having high density of open metal sites, which was synthesized from Cu paddle-wheel SBU and terephthalic acid. The solvent DMF coordinated to the Cu metal center in HKUST-1 can be easily removed by ethanol/NH₄Cl solvent exchange, and the resultant activated (with open metal site) showed excellent CO₂ uptake 7.5 mmol g^{−1} at 1 bar and 298 K [88]. Various research groups further established the importance of open Cu^{II} sites to the enhancement of CO₂ adsorption capacity [89]. Outstanding CO₂ volumetric uptake observed in rare earth (RE) MOFs is due to the localized charge density induced by the presence of high nuclear clusters [90].

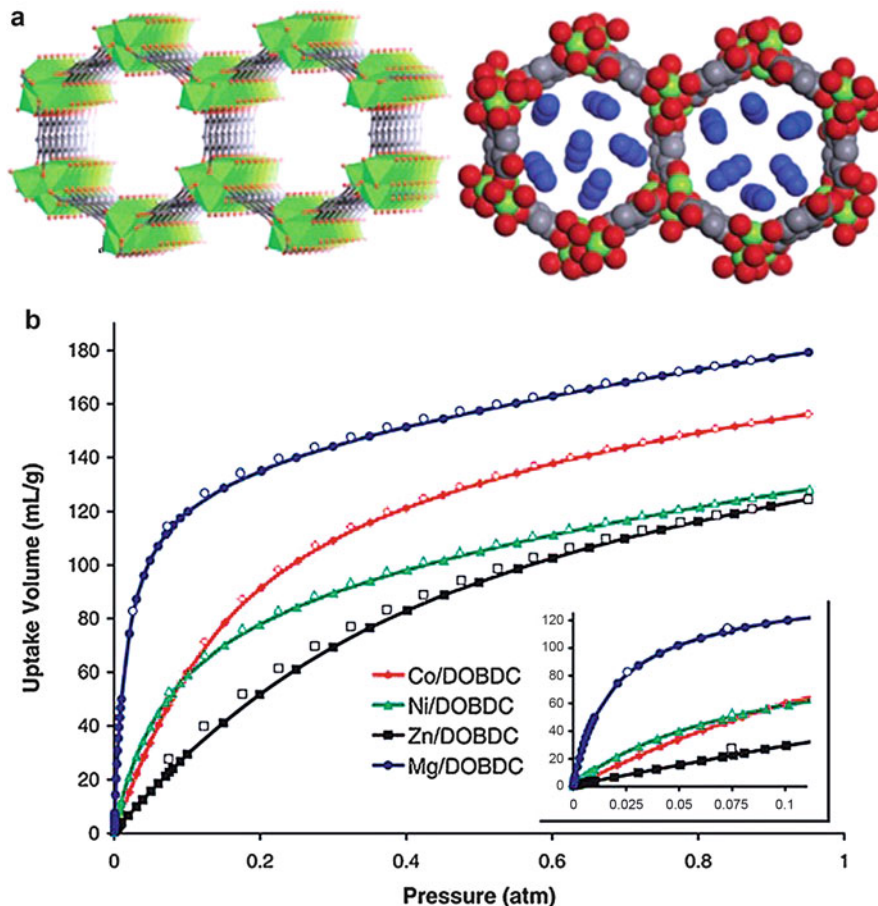
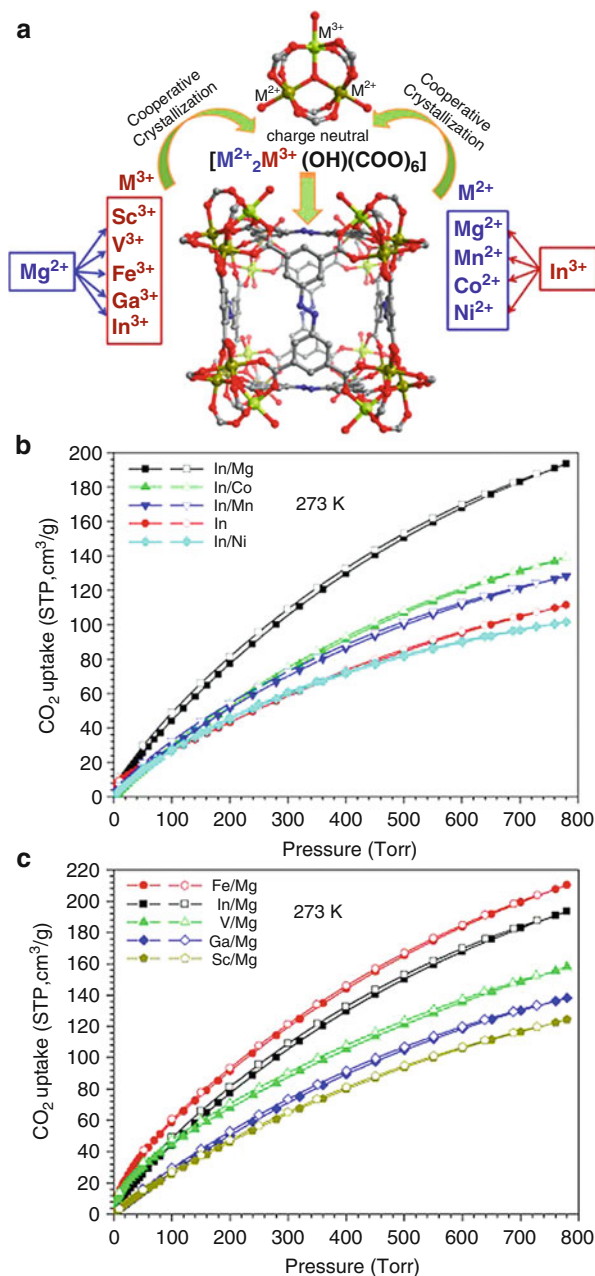


Fig. 18 (a) Crystal structure of M-MOF-74 (where M = Mg, Co, Fe, Zn, Ni), displaying 1D channels (*left*). Porous structure of Mg-MOF-74 (space-filling model), displaying the adsorption of CO₂ molecules (blue color) (*right*). (b) CO₂ adsorption isotherm of M-MOF-74 series at 296 K and various temperatures (0 to 1 atm). Inset – low pressure range (0 to 0.1 atm). Adsorption and desorption plots are shown in filled and open marks, respectively. (This figure is reprinted from Ref. [86] with permission. Copyright 2008, American Chemical Society)

6.3.2 The Effect of the Pore Size and Surface Area of the Framework

The pore size and surface area of the MOFs also play a crucial factor for the CO₂ adsorption capacity, along with the presence of open metal sites. It is worthwhile to mention here that there are examples of MOFs (PCN-61, PCN-66 and PCN-68) [91] with open metal sites which showed very less CO₂ adsorption at low pressures. These MOFs [92] are built from huge dendritic hexacarboxylic acids ligands and showed rht-type topology or (3,24)-connected nets with mesoporous cages in their structure and exhibit very high surface areas. In fact, despite of their mesoporous structure, they did not show any reasonable CO₂ adsorption capacity at low pressure.

Fig. 19 (a) Heterometallic cooperative crystallization of CPM-200 MOF series involving trivalent divalent metal ions and bis-pyridyl ligand. (b) CO₂ adsorption isotherms of In/M MOF (CPM-200) series (M = Mg²⁺, Co²⁺, Mn²⁺, Ni²⁺). (c) CO₂ adsorption isotherms of M/Mg MOF (CPM-200) series (M = Fe³⁺, In³⁺, V³⁺, Ga³⁺, Sc³⁺). (This figure is reprinted from Ref. [87] with permission. Copyright 2016, American Chemical Society)



Thus, with the intention to improve the CO₂ adsorption capacity of these kind of mesoporous MOFs, Zaworotko and co-workers designed a flexible C₃-symmetric hexacarboxylate ligand with acylamide functionality and built the MOF, namely, Cu₃(TPBTM), with open metal sites, which is isostructural with PCN-61 derived

from hexacarboxylate ligand with alkyne groups: TPBTM = N,N',N'' -tris(isophthalyl)-1,3,5-benzenetricarboxamide [93]. The single crystal X-ray structure analysis of $\text{Cu}_3(\text{TPBTM})$ revealed the structure consists of three polyhedra [cuboctahedron (cub-Oh), truncated tetrahedron (T-Td), and truncated octahedron (T-Oh)] packed in a 1:2:1 ratio. The thermal and crystal phase stability of $\text{Cu}_3(\text{TPBTM})$ was confirmed by using PXRD and thermogravimetric analysis (TGA); the material showed stability until 300 °C. The high surface area ($3570 \text{ m}^2 \text{ g}^{-1}$) and large pore volume ($1.268 \text{ cm}^3 \text{ g}^{-1}$) of $\text{Cu}_3(\text{TPBTM})$ MOF prompted the authors to perform CO_2 adsorption experiment. The gas adsorption (CO_2 and N_2) isotherm data at 298 K and various pressure (0 to 20 bar) revealed the unsaturation excess CO_2 uptake of $\text{Cu}_3(\text{TPBTM})$ MOF ($23.53 \text{ mmol g}^{-1}$), which is lower than that of MOF-177 ($\sim 28 \text{ mmol g}^{-1}$) [84] under the same experimental conditions. Moreover, $\text{Cu}_3(\text{TPBTM})$ MOF showed excellent volume of CO_2 adsorbed per volume of sample (330 v/v), which is almost near to MIL-101 (330 v/v at 50 bar and 304 K) [94]. From the ligand structures (TPBTM and BTEI), it is known that the difference between $\text{Cu}_3(\text{TPBTM})$ and PCN-61 is the replacement of the acetylene moiety in PCN-61 with an amide moiety in $\text{Cu}_3(\text{TPBTM})$. In order to get a better understanding of this functionality difference, coverage-dependent isosteric heats of CO_2 adsorption (Qst) for $\text{Cu}_3(\text{TPBTM})$ and PCN-61 was calculated separately. It is observed from this data that the adsorption enthalpy for $\text{Cu}_3(\text{TPBTM})$ is high ($\sim 26.3 \text{ kJ/mol}$) at zero load of CO_2 , indicates strong CO_2 interaction with the framework, and decrease to 23.4 kJ/mol at 15 mmol g^{-1} . On the other hand, the Qst for PCN-61 is much lower than $\text{Cu}_3(\text{TPBTM})$. This difference in the values of Qst of $\text{Cu}_3(\text{TPBTM})$ and PCN-61 may be due to the fact that the amide groups (-CONH) having more dipole moments lead to the dipole-quadrupole interactions between acylamide groups in $\text{Cu}_3(\text{TPBTM})$ and CO_2 , and N-H...O hydrogen bonding involving amide and CO_2 (Fig. 20).

6.3.3 Effect of Doping Metals

The metallic doping on MOFs and its consequential effect on CO_2 adsorption capacity was first demonstrated by Botas et al. by taking MOF-5 as the precursor MOF. The doping of Co on MOF-5 resulted in the doped MOF-5, namely, Co-MOF-5, which showed higher adsorption of CO_2 than that of the parent MOF-5 [95]. Postsynthetic exchange of a metal ion with another is a well-known method in MOF chemistry (for example, exchange of Zr with Ti ions) to build up or enhance any application-related property of MOFs [96]. In fact, the small size of Ti ions assist to decrease the pore size of the framework and bring to ideal size for CO_2 uptake, and further boost the CO_2 uptake of Ti exchanged with Zr in UiO-66. Lau et al. explored this approach in the famous Zr-based MOF, namely, UiO-66, in order to increase their CO_2 adsorption capacity [97]. The Zr(IV) in the parent MOF UiO-66(Zr_{100}) was postsynthetically exchanged with Ti(IV) by soaking it into a DMF solution containing $\text{TiCl}_4(\text{THF})_2$. Thus, a series of Ti-incorporated MOFs derived from the parent Zr-MOF, such as UiO-66(Ti_{32}), UiO-66(Ti_{44}), and UiO-66(Ti_{56}), were synthesized and characterized by various techniques. The BET surface areas of all Ti-doped MOFs are greater than [UiO-66(Ti_{32}) = $1418 \text{ m}^2 \text{ g}^{-1}$, UiO-66

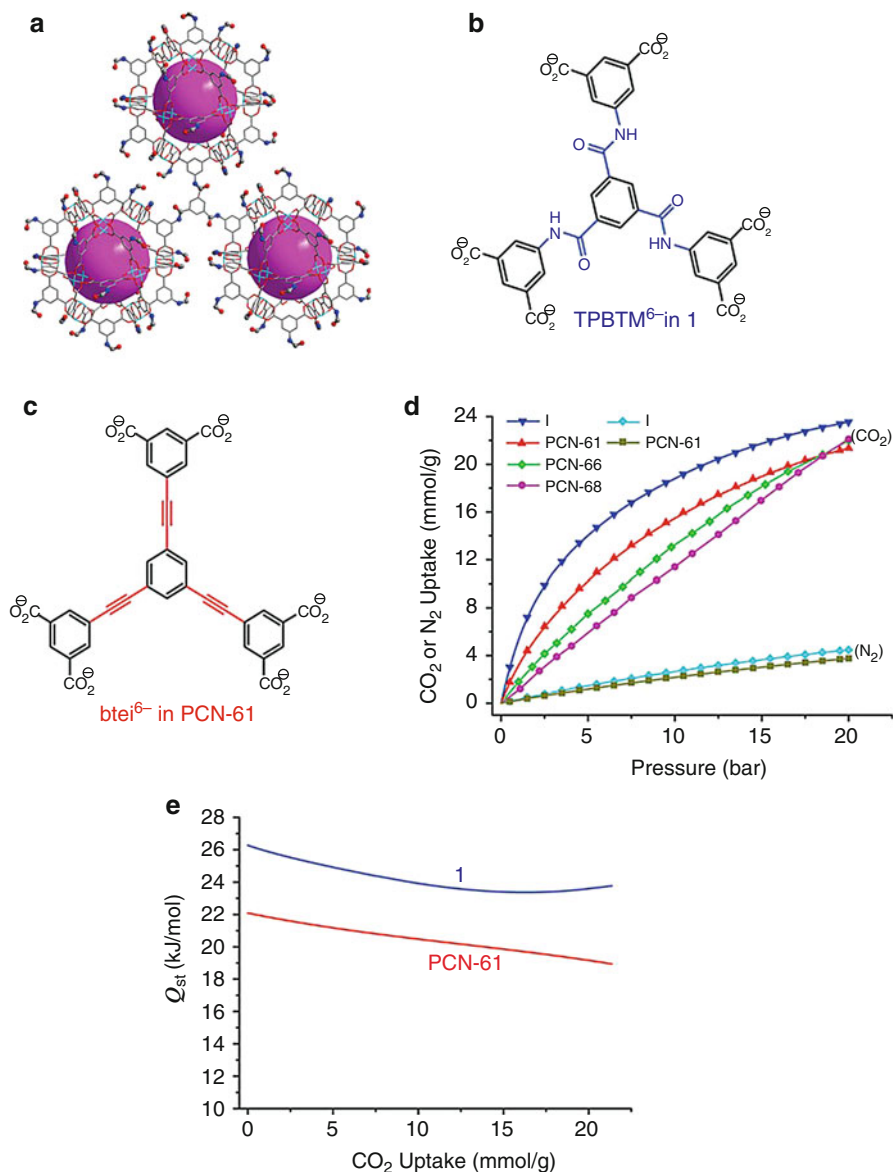


Fig. 20 (a) Crystal structure of $\text{Cu}_3(\text{TPBTM})$ MOF derived from C₃-symmetric hexacarboxylate ligand with acylamide functionality having (3, 24)-connected rht-type topology. Chemical structure of TPBTM (b) and BTEI (c). Gravimetric excess CO_2 and N_2 adsorption isotherms at 298 K and high pressure. (d) and (e) Isothermic heats of CO_2 adsorption comparison plot of $\text{Cu}_3(\text{TPBTM})$ and PCN-61. (This figure is reprinted from Ref. [93] with permission. Copyright 2011, American Chemical Society)

(Ti_{44}) = $1749 \text{ m}^2 \text{ g}^{-1}$, and $\text{UiO-66}(\text{Ti}_{56}) = 1844 \text{ m}^2 \text{ g}^{-1}$] the precursor MOF, $\text{UiO-66}(\text{Zr}_{100})$ [$1390 \text{ m}^2 \text{ g}^{-1}$]. This is due to a well-known fact that the surface area of MOFs increase with the replacement of heavy metals with light metals [98]. Interestingly, the theoretical and experimental CO_2 uptake data of the parent UiO-66 and the Ti-doped MOFs revealed that, with increase in the % of Ti, the amount of CO_2 adsorption increases (Fig. 21).

6.3.4 Effect of Amine Functionalization in MOFs

MOFs derived from amine functionalized ligands [99] attracted many chemists and materials scientists owing to their basic character and its affinity to acidic gas molecules, for example, CO_2 , which helps the MOF to capture CO_2 . Furthermore, such MOFs act as an excellent precursor for postsynthetic modification. In fact, alkylamine have more basicity than aromatic amine, and therefore, MOFs derived from alkylamine functionalized ligands exhibit more active Lewis acid behavior and CO_2 capture capacity. Ferey et al. reported the alkyl-derived MOFs for the first time via postsynthetic functionalization on the open Cr(III) sites of MIL-101(Cr) by using ethylenediamine or diethylenetriamine, and the resultant functionalized MOF showed excellent catalytic activity in Knoevenagel condensation reaction [100]. Later, Long and co-workers reported a MOF, namely, $[\text{Mg}_2(\text{dobpdc})(\text{mmen})_{1.6}(\text{H}_2\text{O})_{0.4}(\text{mmen-Mg}_2(\text{dobpdc}))]$ [where $\text{dobpdc}^{4-} = 4,4'$ -dioxido-3,3'-biphenyldicarboxylate, $\text{mmen} = N,N'$ -dimethylethylenediamine], and the single crystal X-ray structure analysis revealed that the extended coordination of dobpdc^{4-} and Mg^{2+} resulted in a 3D porous structure having honeycomb architecture, with one-dimensional channels of $\sim 18.4 \text{ \AA}$ in width [101]. Interestingly, this Mg-MOF showed unprecedented CO_2 adsorption capacity of 2.0 mmol/g at 0.39 mbar , $25 \text{ }^\circ\text{C}$ and 3.14 mmol/g at 0.15 bar , $40 \text{ }^\circ\text{C}$, ideal condition for CO_2 capture from air and flue gas, respectively (Fig. 22). It is worthwhile to mention here that the structure of this MOF is basically an expanded variant of MOF-74 [102].

6.3.5 Effect of Nitrogen-Rich MOFs

Another important factor for the successful adsorption capacity of CO_2 is the presence of uncoordinated N atoms in the pore walls of the MOFs, which can boost the CO_2 uptake via base-acid and dipole-quadrupole interactions involving CO_2 and N atoms of the uncoordinated ligands. For example, Qin et al. developed a porous MOF, namely, IFMC-1, derived from a bis-tetrazole ligand having 1,2,3-triazole backbone and Zn(II) [103]. Single crystal X-ray structure analysis revealed that the metal ion [Zn(II)] exhibits tetrahedral geometry, and the four coordination sites are occupied by the N atoms of the bridging ligands and its extended coordination lead to the formation of an infinite 3D framework. The structure of IFMC-1 is similar to classical zeolitic SOD topology, which consist of truncated octahedral supercages with eight hexagonal faces and six square faces shared with neighboring cages. The nitrogen adsorption isotherm analysis revealed that the BET and Langmuir surface areas of IFMC-1 were $780 \text{ m}^2 \text{ g}^{-1}$ and $932 \text{ m}^2 \text{ g}^{-1}$, respectively with a

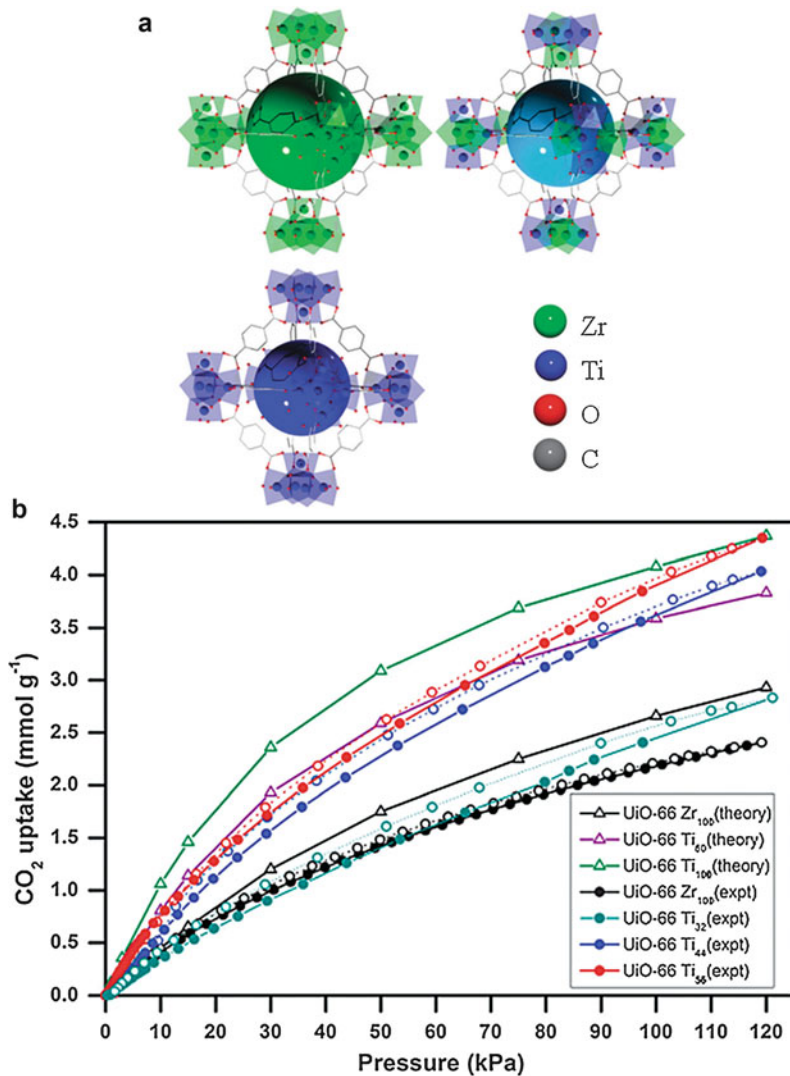


Fig. 21 (a) Crystal structure of MOF UiO-66(Zr100) and its Ti(IV) derivatives, displaying the decrease in the cage size with increase in the % of Ti(IV) than that of Zr(IV). (b) Theoretical and experimental CO₂ adsorption-desorption isotherms of MOF UiO-66(Zr100) and its Ti(IV) derivatives. The empty and solid circles represent desorption and adsorption data, respectively. (This figure is reprinted from Ref. [96] with permission. Copyright 2013, Royal Society of Chemistry)

micropore volume of $0.37 \text{ cm}^3 \text{ g}^{-1}$. The crystals of IFMC-1 were used to explore CO₂ adsorption isotherm experiment at various temperature, which revealed that CO₂ uptake capacity at saturation of $166.9 \text{ cm}^3 \text{ g}^{-1}$ (7.5 mmol g^{-1} , 184.9 L/L), $91.4 \text{ cm}^3 \text{ g}^{-1}$ (4.1 mmol g^{-1} , 101.3 L/L), and $60.3 \text{ cm}^3 \text{ g}^{-1}$ (2.7 mmol g^{-1} , 66.8 L/L),

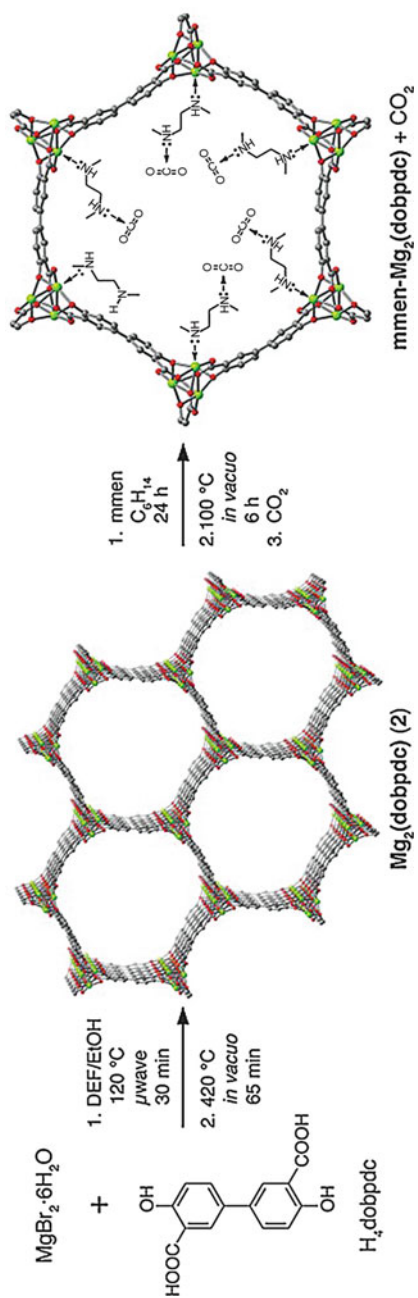


Fig. 22 The schematic representation of the route of synthesis of $\text{mmen-Mg}_2(\text{dobpdc})$. (Reproduced with permission. This figure is reprinted from Ref. [100] with permission. Copyright 2012, American Chemical Society)

respectively at 195 K, 273 K, and 298 K. The CO₂ uptake greater than 60 L/L at 298 K is a remarkable result, owing to the fact that MOFs coming in this category of list of CO₂ uptake at 298 K are very rare [104]. Such unprecedented CO₂ adsorption capability of IFMC-1 is due to the promising nonbonded interactions involving uncoordinated N atoms from N-rich bis-tetrazole ligand and CO₂ molecules (Fig. 23).

6.3.6 Effect of Water Molecules

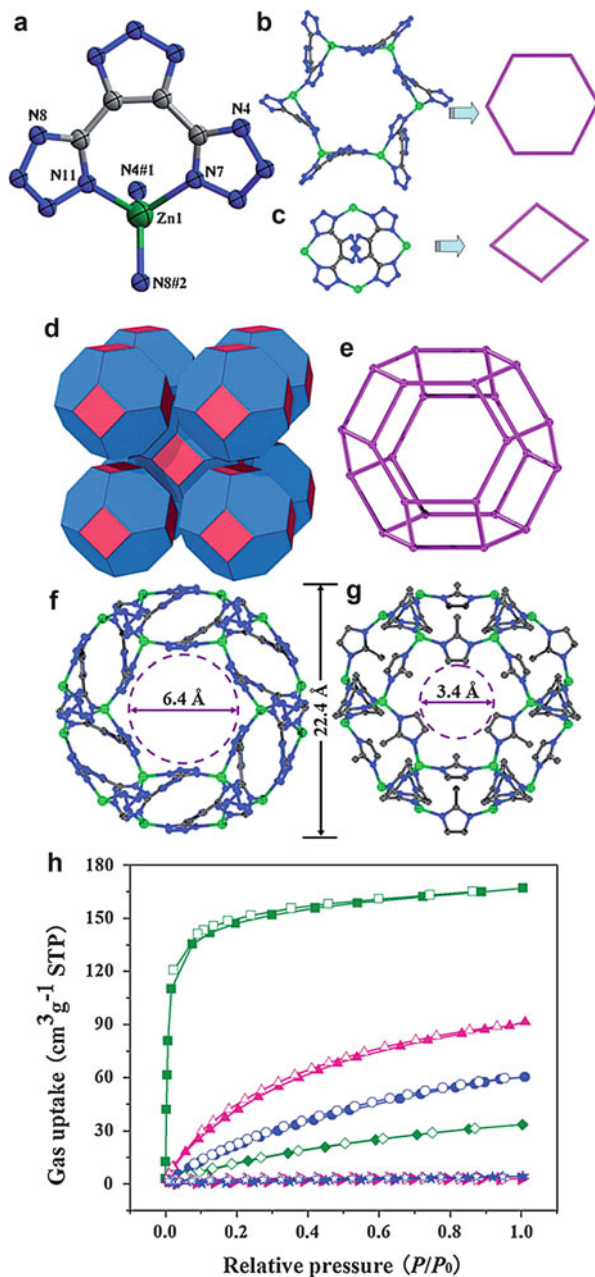
The presence of water molecules within the pore and the open metal sites of MOFs usually decrease their CO₂ adsorption capacity [105]. In contrast to this general concept, there are a few reports in which the MOFs showed good CO₂ uptake in the presence of metal bound or lattice included water molecules. The effect of water molecules in the MOF on their CO₂ adsorption capacity was, experimentally and theoretically (molecular simulations), studied by Yazaydin et al. [106] by taking Cu-BTC MOF as an example. The Cu-BTC MOF having water molecules (coordinated to open-metal sites in the framework) showed enhanced CO₂ uptake and selectivity over N₂ and CH₄. The reason behind such unprecedented CO₂ adsorption was investigated by using simulation and experimental data. The combination of these two data revealed that the nonbonded interaction between the CO₂ and water molecules via quadrupole moment and electric field, respectively is responsible for such great CO₂ uptake.

7 Conclusion and Future Perspectives

A brief introduction of porous coordination polymers (PCPs) and/or metal organic frameworks (MOFs), their synthesis, structure, and gas storage application have been highlighted in this chapter. Several research groups have been contributed well to the development of functional PCPs by following various approaches such as design and synthesis, molecular modeling, structure-property correlation study, etc. We started this chapter with answering several questions: What are CPs? How CPs are formed? What are the factors effecting the final structure of CPs? What are the potential applications of CPs? etc. From the results of various research groups, it is evident that the metal to ligand stoichiometric ratio, reaction condition for the synthesis, the type of counter-anion, nature of the ligand (flexible or rigid), etc. are the important factors, for the design and synthesis of CPs. So we must be seriously concerned of all these factors before we go to synthesize a CP for a particular application. The crystal structures of PCPs are sometime difficult to understand due to their complicated network topology (for example, interpenetrated networks). Thus, a detailed description is very important to understand the topology of CPs, and nowadays, it is easy to analyze the topology of CPs by using TOPOS [107]. Another important issue we need to consider is the phenomena of “*interpenetration*,” owing to the fact that it may lead to blockage of the free space (voids) in the crystal lattice of CPs.

Further, we emphasize the gas storage application of PCPs or MOFs, especially the storage of H₂, CH₄, and CO₂. The intrinsic properties of PCPs or MOFs such as surface area, pore size, pore volume, etc. influence their gas storage application.

Fig. 23 Crystal structure illustration of IFMC-1: (a) coordination environment of Zn(II) in IFMC-1, (b) hexagonal and (c) square windows present in IFMC-1, (d) tiling, and (e) stick diagram, displaying the SOD cage topology. SOD cage topology present in IFMC-1 (f), and ZIF-8 displaying pore size of 6.4 Å and 3.4 Å, respectively. (h) CO₂ and N₂ adsorption isotherm at various temperatures (olive: 195 K, pink: 273 K, blue: 298 K). Filled symbols: adsorption; open symbols: desorption. (This figure is reprinted from Ref. [103] with permission. Copyright 2012, The Royal Society of Chemistry)



The research development of MOFs for gas storage is basically focused on different approaches, which indeed influence to achieve more gravimetric and volumetric gas storage capacity. In fact, the interaction of a gas molecule with the framework of the MOF is basically via van der Waals forces and hydrogen bonding, which is

supported by the pore size/volume of MOFs. Moreover, some specific open metal sites, various functional groups present in the framework, N-rich ligands associated with the framework, etc. further support the MOF–gas molecules interactions.

Acknowledgments A. M. P. Peedikakkal would like to acknowledge the support provided by KACST for funding through NSTIP. Project No. 14-ENE2278-04 for his research.

References

- (a) S. Kitagawa, R. Kitaura, S.I. Noro, Functional porous coordination polymers. *Angew. Chemie Int. Ed.* **43**(18), 2334–2375 (2004). (b) N.L. Rosi, J. Kim, M. Eddaoudi, B. Chen, M. O’Keeffe, O.M. Yaghi, Rod packings and metal–organic frameworks constructed from rod-shaped secondary building units, *J. Am. Chem. Soc.* **127**, 1504–1518 (2005) (c) O.M. Yaghi, M. O’Keeffe, N.W. Ockwig, H.K. Chae, M. Eddaoudi, J. Kim, Reticular synthesis and the design of new materials. *Nature*, **423**, 705–714 (2003) (d) M. Eddaoudi, D.B. Moler, H.L. Li, B.L. Chen, T.M. Reineke, M. O’Keeffe, O.M. Yaghi, Modular chemistry: Secondary building units as a basis for the design of highly porous and robust metal–organic carboxylate frameworks. *Acc. Chem. Res.* **34**, 319–330 (2001) (e) S.R. Batten, R. Robson, Interpenetrating nets: Ordered, periodic entanglement. *Angew. Chem. Int. Ed.* **37**, 1460–1494 (1998) (f) W.L. Leong, J.J. Vittal, One-dimensional coordination polymers: Complexity and diversity in structures, properties, and applications. *Chem. Rev.* **111**(2), 688–764 (2010) (g) S.R. Batten, S.M. Neville, D.R. Turner, *Coordination Polymers: Design, Analysis and Application* (Royal Society of Chemistry, Cambridge, 2009) (h) M. O’Keeffe, O.M. Yaghi, Deconstructing the crystal structures of metal–organic frameworks and related materials into their underlying nets. *Chem. Rev.* **112**, 675–702 (2012)
- (a) C. Janiak, J.K. Vieth, MOFs, MILs and more: Concepts, properties and applications for porous coordination networks (PCNs). *New J. Chem.* **34**, 2366–2388 (2010) (b) K. Biradha, A. Ramanan, J.J. Vittal, Coordination polymers versus metal–organic frameworks. *Cryst. Growth Des.* **9**(7), 2969–2970 (2009)
- A.F. Wells, *Three-Dimensional Nets and Polyhedra* (Wiley, New York, 1977)
- (a) B.F. Hoskins, R. Robson, Infinite polymeric frameworks consisting of three dimensionally linked rod-like segments. *J. Am. Chem. Soc.* **111**(15), 5962–5964 (1989) (b) B.F. Hoskins, R. Robson, Design and construction of a new class of scaffolding-like materials comprising infinite polymeric frameworks of 3D-linked molecular rods. A reappraisal of the zinc cyanide and cadmium cyanide structures and the synthesis and structure of the diamond-related frameworks $[N(CH_3)_4][CuIZnII(CN)_4]$ and $CuI[4,4',4'',4''']$ -tetracyanotetraphenylmethane] $BF_4 \cdot xC_6H_5NO_2$. *J. Am. Chem. Soc.* **112**(4), 1546–1554 (1990)
- R. Robson, A net-based approach to coordination polymers. *J. Chem. Soc. Dalton Trans.*, 3735–3744 (2000)
- J.-M. Lehn, *Supramolecular Chemistry: Concepts and Perspectives* (Wiley-VCH, Weinheim, 1995)
- (a) G.R. Desiraju, *The Crystal as a Supramolecular Entity Perspectives in Supramolecular Chemistry* (Wiley, New Jersey, 1996) (b) D. Dunitz, A. Gavezzotti, Supramolecular synthons: Validation and ranking of intermolecular interaction energies. *Cryst. Growth Des.* **12**, 5873–5877 (2012)
- G.M.J. Schmidt, Photodimerization in the solid-state. *Pure Appl. Chem.* **27**, 647–678 (1971)
- G.R. Desiraju, Crystal engineering: A holistic view. *Angew. Chem. Int. Ed.* **46**, 8342–8356 (2007)
- J. Maddox, Crystals from first principles. *Nature* **335**, 201 (1988)
- K. Biradha, M. Sarkar, L. Rajput, Crystal engineering of coordination polymers using 4,4'-bipyridine as a bond between transition metal atoms. *Chem. Commun.*, 4169–4179 (2006)

12. B. Moulton, M.J. Zaworotko, From molecules to crystal engineering: Supramolecular isomerism and polymorphism in network solids. *Chem. Rev.* **101**(6), 1629–1658 (2001)
13. N.N. Adarsh, P. Dastidar, Coordination polymers: What has been achieved in going from innocent 4, 4'-bipyridine to bis-pyridyl ligands having a non-innocent backbone? *Chem. Soc. Rev.* **41**(8), 3039–3060 (2012)
14. M. Nagarathinam, A.M.P. Peedikakkal, J.J. Vittal, Stacking of double bonds for photochemical [2+2] cycloaddition reactions in the solid state. *Chem. Commun.* (42), 5277–5288 (2008)
15. O.M. Yaghi, Reticular chemistry – Construction, properties, and precision reactions of frameworks. *J. Am. Chem. Soc.* **138**(48), 15507–15509 (2016)
16. M. Witman, S. Ling, A. Gladysiak, K.C. Stylianou, B. Smit, B. Slater, M. Haranczyk, Rational design of a low-cost, high-performance metal–organic framework for hydrogen storage and carbon capture. *J. Phys. Chem. C* **121**(2), 1171–1181 (2017)
17. B.-Q. Ma, K.L. Mulfort, J.T. Hupp, Microporous pillared paddle-wheel frameworks based on mixed-ligand coordination of zinc ions. *Inorg. Chem.* **44**(14), 4912–4914 (2005)
18. A.M.P. Peedikakkal, Y. M, R.-G. Song, S. Xiong, J.J.V. Gao, Influence of the anions on the formation of coordination polymeric structures of Co(II) with *trans*-1,2-bis(4-pyridyl)ethylene. *Eur. J. Inorg. Chem.* **2010**, 3856–3865 (2010)
19. A.M.P. Peedikakkal, J.J. Vittal, Solid-state photochemical behavior of triple-stranded ladder coordination polymer. *Inorg. Chem.* **49**, 10–12 (2010)
20. A.M.P. Peedikakkal, L.L. Koh, J.J. Vittal, Photodimerization of a 1D hydrogen-bonded zwitter-ionic Lead(II) complex and its isomerization in solution. *Chem. Commun.* (4), 441–443 (2008)
21. X.-M. Chen, M.-L. Tonga, Solvothermal in situ metal/ligand reactions: A new bridge between coordination chemistry and organic synthetic chemistry. *Acc. Chem. Res.* **40**, 162–170 (2007)
22. S.S.-Y. Chui, S.M.-F. Los, J.P.H. Charmant, A.G. Open, I.D. Williams, A chemically functionalizable nanoporous material. *Science* **238**, 1148–1150 (1999)
23. D.M.P. Mingos, D.R. Baghurst, Tilden Lecture. Applications of microwave dielectric heating effects to synthetic problems in chemistry. *Chem. Soc. Rev.* **20**, 1–47 (1991)
24. N. Stock, T. Bein, High-throughput synthesis of phosphonate based inorganicorganic hybrid compounds under hydrothermal conditions. *Angew. Chem. Int. Ed.* **43**, 749–752 (2004)
25. (a) S.R. Batten, Topology of interpenetration. *Cryst. Eng. Comm.* **3**, 67–73 (2001) (b) M. O’Keeffe, M. Eddaoudi, H. Li, T. Reineke, O.M. Yaghi, Frameworks for extended solids: Geometrical design principles. *J. Solid State Chem.* **152**, 3–20 (2000) (c) M. O’Keeffe, M.A. Peskov, S.J. Ramsden, O.M. Yaghi, The reticular chemistry structure resource. (RCSR) database of, and symbols for, crystal nets. *Acc. Chem. Res.* **41**, 1782–1789 (2008) (d) I.A. Baburin, V.A. Blatov, L. Carlucci, G. Ciani, D.M. Proserpio, Interpenetrated three-dimensional networks of hydrogen-bonded organic species: A systematic analysis of the Cambridge structural database. *Cryst. Growth Des.* **8**, 519–539 (2008)
26. S.R. Batten, B.F. Hoskins, R. Robson, Interdigitation, interpenetration and intercalation in layered cuprous tricyanomethanide derivatives. *Chem. Eur. J.* **6**, 156–161 (2000)
27. M.J. Manos, M.S. Markoulides, C.D. Malliakas, G.S. Papaefstathiou, N. Chronakis, M.G. Kanatzidis, P.N. Trikalitis, A.J. Tasiopoulos, A highly porous interpenetrated metal–organic framework from the use of a novel nanosized organic linker. *Inorg. Chem.* **50**, 11297–11299 (2011)
28. J.L.C. Rowsell, O.M. Yaghi, Effects of functionalization, catenation, and variation of the metal oxide and organic linking units on the low-pressure hydrogen adsorption properties of metal–organic frameworks. *J. Am. Chem. Soc.* **128**, 1304–1315 (2006)
29. S. Ma, D. Sun, M.W. Ambrogio, J.A. Fillingner, S. Parkin, H.-C. Zhou, Framework-catenation isomerism in metal–organic frameworks and its impact on hydrogen uptake. *J. Am. Chem. Soc.* **129**, 1858–1859 (2007)
30. M.J. Zawortko, Superstructural diversity in two dimensions: Crystal engineering of laminated solids. *Chem. Commun.*, 1–9 (2001)

31. H. Gudbjartson, K. Biradha, K.M. Poirier, M.J. Zaworotko, Novel nanoporous coordination polymer sustained by self-assembly of T-shaped moieties. *J. Am. Chem. Soc.* **121**(11), 2599–2600 (1999)
32. B. Fernández, J.M. Seco, J. Cepeda, A.J. Calahorra, A. Rodríguez-Diéguez, Tuning the porosity through interpenetration of azobenzene-4,4'-dicarboxylate-based metal–organic frameworks. *Cryst Eng Comm* **17**, 7636–7645 (2015)
33. S. Furukawa, J. Reboul, S. Diring, K. Sumida, S. Kitagawa, Structuring of metal–organic frameworks at the mesoscopic/macrosopic scale. *Chem. Soc. Rev.* **43**, 5700–5734 (2014)
34. M. Fujita, Y.J. Kwon, S. Washizu, K. Ogura, Preparation, clathration ability, and catalysis of a two-dimensional square network material composed of cadmium(II) and 4,4'-bipyridine. *J. Am. Chem. Soc.* **116**, 1151–1152 (1994)
35. O.M. Yaghi, G. Li, H. Li, Selective binding and removal of guests in a microporous metal–organic framework. *Nature* **378**, 703–706 (1995)
36. M. Kondo, T. Yoshitomi, K. Seki, H. Matsuzaka, S. Kitagawa, Three-dimensional framework with channeling cavities for small molecules: $\{[M_2(4,4'\text{-bpy})_3(\text{NO}_3)_4]\cdot x\text{H}_2\text{O}\}_n$ (M Co, Ni, Zn) *S. Angew. Chem. Int. Ed. Engl.* **36**, 1725–1727 (1997)
37. H. Li, M. Eddaoudi, M. O’Keeffe, O.M. Yaghi, Design and synthesis of an exceptionally stable and highly porous metal–organic framework. *Nature* **402**, 276–279 (1999)
38. K. Uemura, R. Matsuda, S. Kitagawa, Flexible microporous coordination polymers. *J. Solid State Chem.* **178**, 2420–2429 (2005)
39. H. Li, M. Eddaoudi, T.L. Groy, O.M. Yaghi, Establishing microporosity in open metal–organic frameworks: Gas sorption isotherms for Zn(BDC) (BDC = 1,4-Benzenedicarboxylate). *J. Am. Chem. Soc.* **120**, 8571–8572 (1998)
40. H.K. Chae, D.Y. Siberio-Pérez, J. Kim, Y.B. Go, M. Eddaoudi, A.J. Matzger, M. O’Keeffe, O.M. Yaghi, A route to high surface area, porosity and inclusion of large molecules in crystals. *Nature* **427**, 523–527 (2004)
41. H. Furukawa, N. Ko, Y.B. Go, N. Aratani, S.B. Choi, E. Choi, A.O. Yazaydin, R.Q. Snurr, M. O’Keeffe, J. Kim, O.M. Yaghi, Ultra-high porosity in metal–organic frameworks. *Science* **329**, 424–428 (2010)
42. S.-Y. Zhang, Z. Zhang, M.J. Zaworotko, Topology, chirality and interpenetration in coordination polymers. *Chem. Commun.* **49**, 9700–9703 (2013)
43. R.R. Yun, Z.Y. Lu, Y. Pan, X.Z. You, J.F. Bai, Formation of a metal–organic framework with high surface area and gas uptake by breaking edges off truncated cuboctahedral cages. *Angew. Chem. Int. Ed.* **52**, 11282 (2013)
44. A.P. Nelson, O.K. Farha, K.L. Mulfort, J.T. Hupp, Supercritical processing as a route to high internal surface areas and permanent microporosity in metal–organic framework materials. *J. Am. Chem. Soc.* **131**(2), 458–460 (2008)
45. H. Furukawa, N. Ko, Y.B. Go, N. Aratani, S.B. Choi, E. Choi, A.Ö. Yazaydin, R.Q. Snurr, M. O’Keeffe, J. Kim, O.M. Yaghi, Ultrahigh porosity in metal–organic frameworks. *Science* **329**, 424–428 (2010)
46. O.K. Farha, A.Ö. Yazaydin, I. Eryazici, C.D. Malliakas, B.G. Hauser, M.G. Kanatzidis, S.T. Nguyen, R.Q. Snurr, J.T. Hupp, De novo synthesis of a metal–organic framework material featuring ultrahigh surface area and gas storage capacities. *Nat. Chem.* **2**, 944–948 (2010)
47. D. Yuan, D. Zhao, D. Sun, H.-C. Zhou, An Isoreticular series of metal–organic frameworks with dendritic hexacarboxylate ligands and exceptionally high gas-uptake capacity. *Angew. Chem. Int. Ed.* **49**, 5357–5361 (2010)
48. (a) Z. Yang, Y. Xia, R. Mokaya, Enhanced hydrogen storage capacity of high surface area zeolite-like carbon materials. *J. Am. Chem. Soc.* **129**, 1673–1679 (2007) (b) S.K. Bhatia, A.L. Myers, Optimum conditions for adsorptive storage, *Langmuir*, **22**, 1688–1700 (2006) (c) Y. Ren, G.H. Chia, Z. Gao, Metal–organic frameworks in fuel cell technologies. *Nanotoday* **8**, 577–597 (2013)
49. T.L. Easun, F. Moreau, Y. Yan, S. Yang, M. Schröder, Structural and dynamic studies of substrate binding in porous metal–organic frameworks. *Chem. Soc. Rev.* **46**, 239–274 (2017)

50. M.P. Suh, H.J. Park, T.K. Prasad, D.-W. Lim, Hydrogen storage in metal–organic frameworks. *Chem. Rev.* **112**, 782–835 (2012)
51. (a) B. Sakintuna, F. Lamari-Darkrimb, M. Hirscher, Metal hydride materials for solid hydrogen storage: A review. *Int. J. Hydrogen Energy* **32**, 1121–1140 (2007) (b) Y.-H. P. Zhang, Renewable carbohydrates are a potential high-density hydrogen carrier. *Int. J. Hydrogen Energy* **35**, 10334–10342 (2010) (c) V.V. Struzhkin, B. Militzer, W.L. Mao, H.-K. Mao, R.J. Hemley, Hydrogen storage in molecular clathrates. *Chem. Rev.* **107**, 4133–4151 (2007) (d) H.-M. Cheng, Q.-H. Yang, C. Liu, Hydrogen storage in carbon nanotubes. *Carbon* **39**, 1447–1454 (2001)
52. (a) H.W. Langmi, J. Ren, B. North, M. Mathe, D. Bessarabov, Hydrogen storage in metal–organic frameworks: A review. *Electrochim. Acta* **128** 368–392 (2014) (b) L.J. Murray, M. Dinca, J.R. Long, Hydrogen storage in metal–organic frameworks. *Chem. Soc. Rev.* **38**, 1294–1314 (2009) (c) O.K. Farha, I. Eryazici, N.C. Jeong, B.G. Hauser, C.E. Wilmer, A.A. Sarjeant, Metal–organic framework materials with ultrahigh surface areas: Is the sky the limit? *J. Am. Chem. Soc.* **134**, 15016–15021 (2012)
53. (a) N.L. Rosi, J. Eckert, M. Eddaoudi, D.T. Vodak, J. Kim, M. O’Keeffe, O.M. Yaghi, Hydrogen storage in microporous metal–organic frameworks. *Science*, **300**, 1127–1129 (2003) (b) G. Férey, M. Latroche, C. Serre, F. Millange, T. Loiseau, A. Percheron-Guégan, Hydrogen adsorption in the nanoporous metal–benzenedicarboxylate M(OH) (O₂C–C₆H₄–CO₂) (M = Al³⁺, Cr³⁺), MIL-53. *Chem. Commun.* 2976–2977 (2003)
54. J. Sculley, D. Yuan, H.-C. Zhou, The current status of hydrogen storage in metal–organic frameworks – Updated. *Energy Environ. Sci.* **4**, 2721–2735 (2011)
55. B. Panella, M. Hirscher, H. Putter, U. Muller, Hydrogen adsorption in metal–organic frameworks: Cu-MOFs and Zn-MOFs compared. *Adv. Funct. Mater.* **16**, 520–524 (2006)
56. (a) D. Saha, Z. Wei and S. Deng: Equilibrium, kinetics and enthalpy of hydrogen adsorption in MOF-177. *Int. J. Hydrog. Energy*, **33**, 7479–7488 (2008). (b) J. L. Rowsell and O. M. Yaghi: Strategies for hydrogen storage in metal–organic frameworks, *Angew. Chem. Int. Ed.*, **2005**, **44**, 4670–4679.
57. (a) Y. Li, R.T. Yang, Significantly enhanced hydrogen storage in metal–organic frameworks via spillover. *J. Am. Chem. Soc.* **128**, 726–727 (2006) (b) Y. Li, R.T. Yang, Hydrogen storage in metal–organic frameworks by bridged hydrogen spillover. *J. Am. Chem. Soc.* **128**, 8136–8137 (2006)
58. W.C. Conner, J.L. Falconer, Spillover in heterogeneous catalysis. *Chem. Rev.* **95**, 759–788 (1995)
59. D.W. Breck, *Zeolite Molecular Sieves: Structure, Chemistry and Use* (Wiley, New York, 1974), pp. 593–724
60. J. Ren, M. Ledwaba, N.M. Musyoka, H.W. Langmi, M. Mathe, S. Liao, W. Pang, *Coord. Chem. Rev.* (2017) ASAP
61. A. Xin, J. Bai, Y. Pan, M.J. Zaworotko, Synthesis and enhanced H₂ adsorption properties of a mesoporous nanocrystal of MOF-5: Controlling nano-/mesostructures of MOFs to improve their H₂ heat of adsorption. *Chem. Eur. J.* **16**, 13049–13052 (2010)
62. Y.F. Feng, H. Jiang, M. Chen, Y.R. Wang, Construction of an interpenetrated MOF-5 with high mesoporosity for hydrogen storage at low pressure. *Powder Technol.* **249**, 38–42 (2013)
63. J.W. Ren, H. Langmi, N. Musyoka, M. Mathe, X.D. Kang, Tuning defects to facilitate hydrogen storage in core-shell MIL-101(Cr)@UiO-66(Zr) nanocrystals. *Mater. Today: Proc.* **2**, 3964–3972 (2015)
64. M. Erkartal, U. Sen, Boronic acid moiety as functional defect in UiO-66 and its effect on hydrogen uptake capacity and selective CO₂ adsorption: A comparative study. *ACS Appl. Mater. Interfaces* **10**(1), 787–795 (2018)
65. D. Zhao, D. Yuan, H.-C. Zhou, The current status of hydrogen storage in metal–organic frameworks. *Energy Environ. Sci.* **1**, 222–235 (2008)

66. K.L. Mulfort, O.K. Farha, C.L. Stern, A.A. Sarjeant, J.T. Hupp, Post-synthesis alkoxide formation within metal–organic framework materials: A strategy for incorporating highly coordinatively unsaturated metal ions. *J. Am. Chem. Soc.* **131**(11), 3866–3868 (2009)
67. J. Luo, H. Xu, Y. Liu, Y. Zhao, L.L. Daemen, C. Brown, T.V. Timofeeva, S. Ma, H. Zhou, *J. Am. Chem. Soc.* **130**(30), 9626–9627 (2008)
68. T. Burchell, M. Rogers. SAE Tech. Pap. Ser. 2000, 2000-01-2205
69. Y. He, W. Zhou, G. Qian, B. Chen, Methane storage in metal–organic frameworks. *Chem. Soc. Rev.* **43**, 5657–5678 (2014)
70. S. Noro, S. Kitagawa, M. Kondo, K. Seki, A new, methane adsorbent, porous coordination polymer [$\{\text{CuSiF}_6(4,4'\text{-bipyridine})_2\}_n$]. *Angew. Chem. Int. Ed.* **39**, 2081–2084 (2000)
71. M. Eddaoudi, J. Kim, N. Rosi, D. Vodak, J. Wachter, M. O’Keeffe, O.M. Yaghi, Systematic design of pore size and functionality in isorecticular MOFs and their application in methane storage. *Science* **295**, 469–472 (2002)
72. K. Seki, Design of an adsorbent with an ideal pore structure for methane adsorption using metal complexes. *Chem. Commun.*, 1496–1497 (2001)
73. V.C. Menon, S. Komarneni, Porous adsorbents for vehicular natural gas storage: A review. *J. Porous. Mater.* **5**, 43–58 (1998)
74. S. Ma, D. Sun, J.M. Simmons, C.D. Collier, D. Yuan, H.-C. Zhou, Metal–organic framework from an anthracene derivative containing nanoscopic cages exhibiting high methane uptake. *J. Am. Chem. Soc.* **130**(3), 1012–1016 (2008)
75. H. Wu, W. Zhou, T. Yildirim, High-capacity methane storage in metal–organic frameworks M2 (dhpt): The important role of open metal sites. *J. Am. Chem. Soc.* **131**, 4995–5000 (2009)
76. Z. Guo, H. Wu, G. Srinivas, Y. Zhou, S. Xiang, Z. Chen, Y. Yang, W. Zhou, M. O’Keeffe, B. Chen, A metal–organic framework with optimized open metal sites and pore spaces for high methane storage at room temperature. *Angew. Chem. Int. Ed.* **50**, 3178–3181 (2011)
77. C.E. Wilmer, M. Leaf, C.Y. Lee, O.K. Farha, B.G. Hauser, J.T. Hupp, R.Q. Snurr, Large-scale screening of hypothetical metal–organic frameworks. *Nat. Chem.* **4**, 83–89 (2012)
78. C. Liang, Z. Shi, C. He, J. Tan, H. Zhou, H. Zhou, Y. Lee, Y. Zhang, Engineering of pore geometry for ultrahigh capacity methane storage in mesoporous metal–organic frameworks. *J. Am. Chem. Soc.* **139**, 13300–13303 (2017)
79. C. Figueres, H.J. Schellnhuber, G. Whiteman, J. Rockström, A. Hobley, S. Rahmstorf, Three years to safeguard our climate. *Nature* **546**, 593–595 (2017)
80. <https://www.co2.earth/>
81. J. Johnson, *Chem. Eng. News* **82**, 36 (2004)
82. A. Lu, G. Hao, Porous materials for carbon dioxide capture. *Annu. Rep. Prog. Chem. Sect. A: Inorg. Chem.* **109**, 484–503 (2013)
83. K. Sumida, D.L. Rogow, J.A. Mason, T.M. McDonald, E.D. Bloch, Z.R. Herm, T. Bae, J.R. Long, Carbon dioxide capture in metal–organic frameworks. *Chem. Rev.* **112**, 724–781 (2012)
84. A.R. Millward, O.M. Yaghi, Metal–organic frameworks with exceptionally high capacity for storage of carbon dioxide at room temperature. *J. Am. Chem. Soc.* **127**, 17998–17999 (2005)
85. R. Banerjee, A. Phan, B. Wang, C. Knobler, H. Furukawa, M. O’Keeffe, O.M. Yaghi, High-throughput synthesis of zeolitic imidazolate frameworks and application to CO₂ capture. *Science* **319**, 939–943 (2008)
86. S.R. Caskey, A.G. Wong-Foy, A.J. Matzger, Dramatic tuning of carbon dioxide uptake via metal substitution in a coordination polymer with cylindrical pores. *J. Am. Chem. Soc.* **130**, 10870–10871 (2008)
87. Q.-G. Zhai, X. Bu, C. Mao, X. Zhao, P. Feng, Systematic and dramatic tuning on gas sorption performance in heterometallic metal–organic frameworks. *J. Am. Chem. Soc.* **138**(8), 2524–2527 (2016)
88. X. Yan, S. Komarneni, Z. Zhang, Z. Yan, Extremely enhanced CO₂ uptake by HKUST-1 metal–organic framework via a simple chemical treatment. *Microporous Mesoporous Mater.* **183**, 69–73 (2014)

89. E. Garcia-Perez, J. Gascon, V. Morales-Florez, J.M. Castillo, F. Kapteijn, S. Calero, Identification of adsorption sites in Cu-BTC by experimentation and molecular simulation. *Langmuir* **25**, 1725–1731 (2009)
90. D. Alezi, A.M.P. Peedikakkal, L.J. Weselinski, V. Guillerm, Y. Belmabkhout, A.J. Cairns, Z. Chen, L. Wojtas, M. Eddaoudi, Quest for highly connected metal-organic framework platforms: Rare earth polynuclear clusters versatility meets net topology needs. *J. Am. Chem. Soc.* **137**, 5421–5430 (2015)
91. D.Q. Yuan, D. Zhao, D.F. Sun, H.C. Zhou, An isoreticular series of metal-organic frameworks with dendritic hexacarboxylate ligands and exceptionally high gas-uptake capacity. *Angew. Chem. Int. Edit.* **49**, 5357–5361 (2010)
92. C.E. Wilmer, O.K. Farha, T. Yildirim, I. Eryazici, V. Krungleviciute, A.A. Sarjeant, R.Q. Snurr, J.T. Hupp, Gram-scale, high-yield synthesis of a robust metal-organic framework for storing methane and other gases. *Energy Environ. Sci.* **6**, 1158–1163 (2013)
93. B.S. Zheng, J.F. Bai, J.G. Duan, L. Wojtas, M.J. Zaworotko, Enhanced CO₂ binding affinity of a high-uptake rht-type metal-organic framework decorated with acylamide groups. *J. Am. Chem. Soc.* **133**(4), 748–751 (2011)
94. P.L. Llewellyn, S. Bourrelly, C. Serre, A. Vimont, M. Daturi, L. Hamon, G.D. Weireld, J.-S. Chang, D.-Y. Hong, Y.K. Hwang, S.H. Jung, G. Ferey, High uptakes of CO₂ and CH₄ in mesoporous metal-organic frameworks MIL-100 and MIL-101. *Langmuir* **24**, 7245–7250 (2008)
95. J.A. Botas, G. Calleja, M. Sanchez-Sanchez, M. Gisela Orcajo, Cobalt doping of the MOF-5 framework and its effect on gas-adsorption properties. *Langmuir* **26**, 5300–5303 (2010)
96. M. Kim, J.F. Cahill, H. Fei, K.A. Prather, S.M. Cohen, Postsynthetic ligand and cation exchange in robust metal-organic frameworks. *J. Am. Chem. Soc.* **134**, 18082–18088 (2012)
97. C.H. Lau, R. Babarao, M.R. Hill, A route to drastic increase of CO₂ uptake in Zr metal organic framework UiO-66. *Chem. Commun.* **49**, 3634–3636 (2013)
98. S.S. Kaye, J.R. Long, Hydrogen storage in the dehydrated Prussian blue analogues M₃[co(CN)₆]₂ (M = Mn, Fe, Co, Ni, Cu, Zn). *J. Am. Chem. Soc.* **127**, 6506–6507 (2005)
99. Y. Lin, C. Konga, L. Chen, Amine-functionalized metal-organic frameworks: Structure, synthesis and applications. *RSC Adv.* **6**, 32598–32614 (2016)
100. Y.K. Hwang, D.Y. Hong, J.S. Chang, S.H. Jung, Y.K. Seo, J. Kim, A. Vimont, M. Daturi, C. Serre, G. Ferey, Amine grafting on coordinatively unsaturated metal centers of MOFs: Consequences for catalysis and metal encapsulation. *Angew. Chem. Int. Edit.* **47**, 4144–4148 (2008)
101. T.M. McDonald, W.R. Lee, J.A. Mason, B.M. Wiers, C.S. Hong, J.R. Long, Capture of carbon dioxide from air and flue gas in the alkylamine appended Metal-organic framework mmen-Mg₂(dobpdc). *J. Am. Chem. Soc.* **134**, 7056–7065 (2012)
102. K. Lee, J.D. Howe, L.-C. Lin, B. Smit, J.B. Neaton, Small-molecule adsorption in open-site metal-organic frameworks: A systematic density functional theory study for rational design. *Chem. Mater.* **27**, 668–678 (2015)
103. J.-S. Qin, D.-Y. Du, W.-L. Li, J.-P. Zhang, S.-L. Li, Z.-M. Su, X.-L. Wang, Q. Xu, K.-Z. Shao, Y.-Q. Lan, N-rich zeolite-like metal-organic framework with sodalite topology: High CO₂ uptake, selective gas adsorption and efficient drug delivery. *Chem. Sci.* **3**, 2114–2118 (2012)
104. A. Phan, C.J. Doonan, F.J. Uribe-Romo, C.B. Knobler, M. O’Keefe, O.M. Yaghi, Synthesis, structure, and carbon dioxide capture properties of zeolitic imidazolate frameworks. *Acc. Chem. Res.* **43**, 58–67 (2010)
105. A.C. Kizzie, A.G. Wong-Foy, A.J. Matzger, Effect of humidity on the performance of microporous coordination polymers as adsorbents for CO₂ capture. *Langmuir* **27**, 6368–6373 (2011)
106. A.O. Yazaydin, A.I. Benin, S.A. Faheem, P. Jakubczak, J.J. Low, R.R. Willis, R.Q. Snurr, Enhanced CO₂ adsorption in metal-organic frameworks via occupation of open-metal sites by coordinated water molecules. *Chem. Mater.* **21**, 1425–1430 (2009)
107. V.A. Blatov, D.M. Proserpio, TOPOS 4.0, A program package for multipurpose crystallochemical analysis



Polyurethane and Its Derivatives

6

Mohammad Mizanur Rahman, Mohammad Mahbub Rabbani, and Joyanta Kumar Saha

Contents

1	Introduction	226
2	Chemistry of Polyurethanes	227
3	Synthesis of Polyurethane and Their Derivatives	228
3.1	Polyol	229
3.2	Isocyanate	230
3.3	Catalysts	230
3.4	Chain Extenders	231
3.5	Cross-Linker	232
4	Types of Polyurethanes	232
4.1	Polyurethane Ionomers (PUI)	232
4.2	Polyurethane Foams	232
4.3	Coatings, Adhesives, Sealants, and Elastomers	232
4.4	Binders	233
4.5	Waterborne Polyurethane (WBPU) Dispersions	233
5	Recent Advances in Polyurethane and Their Derivatives	233
5.1	Polyurethane Nanocomposites	233
5.2	Polyurethane Click Coupling Reaction	235
5.3	Heterocyclic Compound-Based Polyurethanes	235
5.4	Polyurethane from Renewable Resources	235
6	Polyurethane Applications	235
6.1	Building Material Application	235
6.2	Automotive Application	236

M. M. Rahman (✉)

Center of Research Excellence in Corrosion, King Fahd University of Petroleum and Minerals,
Dhahran, Saudi Arabia

e-mail: mrahman@kfupm.edu.sa

M. M. Rabbani

Department of Chemistry, American International University-Bangladesh (AIUB),
Dhaka, Bangladesh

J. K. Saha

Department of Chemistry, Jagannath University, Dhaka, Bangladesh

6.3	Marine Applications	236
6.4	Coating and Adhesive Application	236
6.5	Medical Application	236
6.6	Appliances Flooring, and Packaging Application	237
7	Conclusion	237
	References	237

Abstract

Polyurethane (PU) is one of the widely used materials with great potential for multipurpose applications due to their excellent physical, chemical, and mechanical properties. PU materials are widely being used in many applications all over the world. The targeted PU properties for different applications can be achieved by changing the base monomers and their ratios as well as different synthesis process. This chapter highlights the PU application, its chemistry, and its base monomers. The latest modification and new application of PU and its derivatives are also considered.

1 Introduction

Any polymer which contains urethane group is called polyurethane (PU). German Scientist Otto Bayer and his co-workers first introduced PU. Nowadays PU are used in multipurpose applications such as coatings, paints, elastomers, textiles, insulators, elastic fibers, foams, foot wear, etc. At early stage most of the PU was prepared by using toxic solvents and monomers. Later less toxic solvent and water were considered to make PU to make it environmentally friendly. Recently, introducing monomers from natural sources makes PU more attractive in industry due to green nature of PU materials [1–5].

The basic PU structure is shown in Fig. 1. The urethane and urea are the major repeating units in PU. The urethane group is produced from the reaction between isocyanate (NCO) and hydroxyl (–OH) groups, whereas the urea group formed by the reaction between isocyanate (NCO) and amine (–NH₂) groups [2, 6–10]. PU also contains other groups, such as esters, ethers, and some aromatic groups. As there are varieties of monomers in PU preparation and thus given a wide range of specific applications, PU derivatives can be classified into several groups such as flexible, rigid, thermoplastic, waterborne, coating, binders, sealants, adhesives, and elastomers. Every year the use of PU derivatives is being increased in significant level. Counting all different uses, PU foam is one of the leading derivatives, which is being

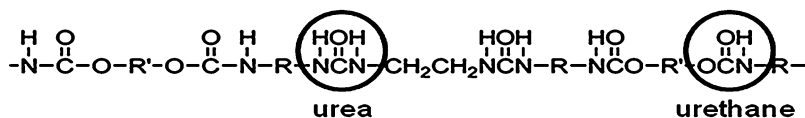


Fig. 1 Urethane/urea group in PU

used globally in significant amounts. Both rigid and flexible foams are being used in different sectors. PU foams can be simply modified to get specific properties by changing blowing agents, isocyanates, fillers, surfactants, and polyols used in their preparation. PU finds a strong level in coatings and adhesives as these materials have excellent mechanical and adhesive strength. Elastomer is another attractive using area of PU, such kind of PU can easily incorporated into different engineered products and extend their properties [1, 11, 12].

PU can be prepared from different monomers of polyols, diisocyanates, and chain extenders; their properties also varied with changing the contents of polyols, diisocyanates, and chain extenders [13, 14]. At early stage of mid-1980s, the major monomers were come from fossil fuel; however, due to environmental concerns, the necessity for more environmentally friendly polyol was shown by many researchers. This has recently drawn enormous commercial and academic attention to renewable resources, such as vegetable oils which mainly consist of triglyceride molecules with different reactive sites, such as carbon–carbon double bonds, hydroxyl, and ester groups. Unfortunately, most of the diisocyanates and chain extenders are toxic and nonnatural sources. To make more environmentally friendly PU, few researchers also made PU without isocyanates [15–19].

To improve the properties of PU and their derivatives, recently nanotechnology has been introduced for these polymers. Different PU nanomaterials have been prepared by using different nanoparticles. The nanomaterial-based PU broadened its applications. PU is being used for 60 years. Plenty of studies have been carried out in academic and industry. In this chapter, a summary of the advances made in the preparation of PU, as well as their application into several products in multisectors, has been highlighted. The basic monomers to prepared PU are also considered [1, 2, 20–23].

2 Chemistry of Polyurethanes

The chemistry of polyurethane is very straightforward. Usually, PU can be prepared by the reaction of polyol and isocyanate. This is commonly used catalyst to fast the reaction between polyol and isocyanate. Isocyanate (termed as hard segment) and polyol (termed as soft segment) may contain single or multiple reactive groups which ultimately determine the properties of final materials. The different ratios between isocyanate and polyol also contribute to achieve the properties. Soft segment maintains elastomeric properties, whereas hard segment controls rigid and tough properties. This is also common to make cross-linkable PU. The cross-linking can be obtained by adding either excess isocyanate or external cross-linker. The cross-linkable PU has better mechanical properties. However, excess cross-linkable PU structure decreased the mechanical properties. A combination of hard segment and soft segment with average cross-linking can produce foam PU. The soft segment, hard segment, and additional cross-linker contribute the molecular weight which finally make small or giant molecule. Besides, the addition of nanofillers and

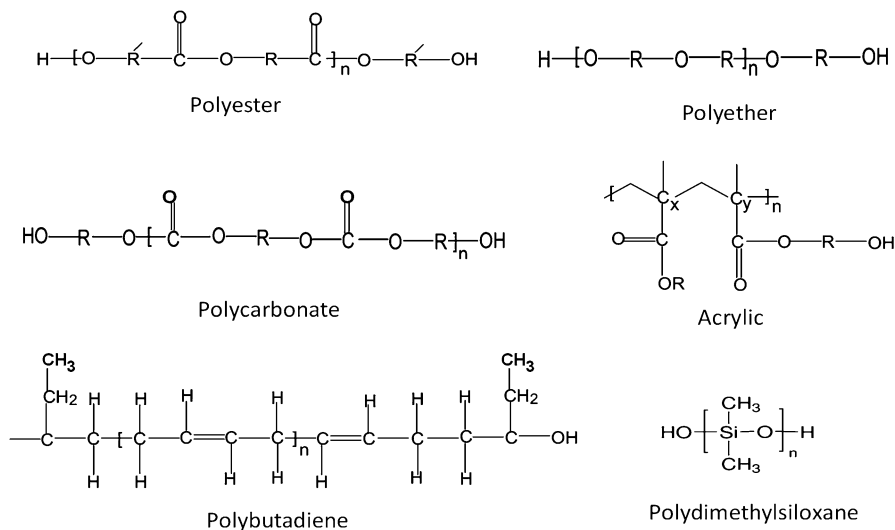


Fig. 2 Structure of different polyols

additives and the processing conditions (temperature, time, addition method, etc.) make PU suitable for different applications [1, 2, 24–28].

One of the important monomers of PU is polyol which can be obtained commercially, as well as it can be synthesized in laboratories by different techniques. Different structures of various polyols are presented in Fig. 2. The widely used polyols are polyether polyol and polyester polyol. It is also common to use mixed polyols with different molecular weights and ratios to obtain specific properties [1].

Phase incompatibility is the vital factor of speed as polyol (polar and less dense) and isocyanates (nonpolar and denser) are opposite in nature. Therefore, a suitable surfactant/catalyst is usually used to make a faster reaction rate between polyol and isocyanate. Isocyanate is very reactive to polyol especially with the presence of catalyst. Aromatic isocyanates are more preferable to aliphatic isocyanates due to high reactivity and low cost. Besides, the final PU products possess high mechanical strength using aromatic isocyanates. Using mixed isocyanates of aliphatic and aromatic is also common in PU materials [2, 29–31].

3 Synthesis of Polyurethane and Their Derivatives

PU and its derivatives are prepared by different processes [1]. Figure 3 illustrates the typical synthesis of a conventional PU. Different cross-linkers, additives, and nanoparticles may also be incorporated during synthesis of PU.

Based on the applications, surfactants, blowing agents, and pigments are also mixed into the PU. Widely used monomers in PU synthesis is summarized in Table 1.

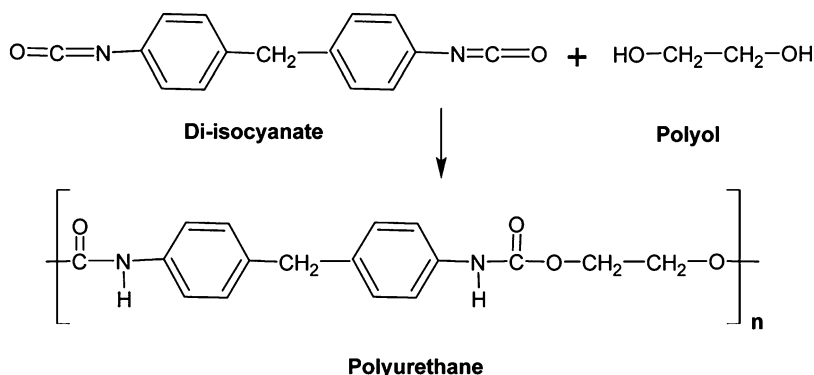


Fig. 3 General way of PU synthesis

Table 1 Polyurethane monomers/additives and their specific reason for using

Monomer/additives	Specific reason for using
Polyol	Maintain elastomeric properties
Isocyanate	Reactivity and curing properties
Chain extender	Control molecular weight
Catalyst	Speed up the reaction between polyol and isocyanate
Cross-linker	Structural modification to improve the mechanical and barrier properties
Filler	Improve thermal, mechanical, and barrier properties
Plasticizer	Reduce material hardness
Hardener	Post crosslinking reaction to improve adhesive strength
Smoke retardant	Reduce smoke
Flame retardant	Reduce flammability
Bowing agent/surfactant	Control the formation of bubble during synthesis
Hydrophilic agent	Make dispersion stable
Pigment	Produce colored materials

3.1 Polyol

One of the major monomers in PU synthesis is polyol, which usually termed as a soft segment. Widely used polyols are either polyester polyols or polyether polyols. The polyether polyol is prepared from epoxy monomers through the ring-opening polymerization, whereas polyester polyol is prepared from polycondensation reaction using carboxylic acid with hydroxyl group. Recently, hydroxy-terminated siloxane is also being used in PU synthesis. It is important to choose the proper polyol as the properties highly depend on polyol and its contents. Different molecular weight of similar generic type of polyols is also available. Low molecular weight polyol controls rigidity, whereas high molecular weight polyol contributes to elastomeric properties. Besides polycaprolactone (PCL), polycarbonate (PC), polysulfide (PS),

and polybutadiene (PB), polyol is also being used in PU materials. Polyether polyol of different molecular weight is also used in PU [2, 32–35].

Poly(tetramethylene ether) glycol (PTMG) is prepared through polymerization of tetrahydrofuran with different molecular weights. PTMG is being widely used in many different PU preparations to broaden their application. Besides, poly(propyleneoxide) glycol (PPG) and poly(ethyleneoxide) glycol (PEG) can be prepared using different weight of ethylene oxide/propylene oxide. By changing the total hydroxyl group and polymer chain, the polyol properties such as reactivity, compatibility, and solubility also can be changed. Usually polyol of propylene oxide is less reactive than those for ethylene oxide. There are available different high molecular weight graft polyols which are prepared by using polyurea, acrylonitrile, or styrene-acrylonitrile, with polyether ketone. Fluoro-based polyol such as fluoroethylene vinyl ether (FEVE) polyols which can be obtained by the copolymerization reaction of tetrafluoroethylene or chlorotrifluoroethylene with vinyl ethers containing hydroxyalkyl vinyl ethers. PU with fluoro-based polyol is useful for antibacterial and antifouling materials [1, 2, 36–45].

Very recently polyols can also be obtained from natural resources. The polyol can be obtained from fatty acid-rich soybean, castor, neem, and cotton seed. Different PU elastomers and foams have been made by using triacylglyceride-based vegetable oils. The presence of such kind of oils used to produce flexible molded foams, elastomers, etc. The advantage of using natural polyols is unmodified synthetic process. Even changing the solvent systems, the PU can be prepared. Nowadays PU is being prepared using renewable resources such as polyol in both solvent- and water-based coating, adhesive, and foam materials without sacrificing their properties [2, 36, 39, 46–53].

3.2 Isocyanate

Isocyanate is one of the important monomers in PU. Mainly diisocyanates (aliphatic/aromatic) are used in PU and their derivatives. Widely used diisocyanates are summarized in Table 2. Aromatic isocyanates are comparatively cheaper. The properties of PU and their derivatives are also influenced by aliphatic or aromatic isocyanates. Aromatic isocyanate-based PU has higher mechanical properties; however, yellowing with time of PU material is one important drawback of using aromatic isocyanates. Recently PU without isocyanates is getting priority due to toxicity of isocyanates. Few researchers have already prepared PU without diisocyanate [1–5, 45].

3.3 Catalysts

Using proper catalyst is also important in PU synthesis because a small amount of catalyst makes a faster reaction between polyol and isocyanates. Popular catalysts for PU synthesis and their derivatives are summarized in Table 3. Both metal complexes and amine compounds are being used as a catalyst for PU synthesis [1, 2].

Table 2 Structure of widely used isocyanates

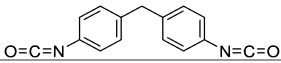

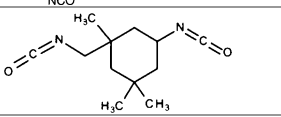
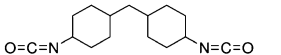
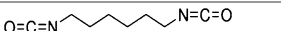
Isocyanate	Structure
4,4'-Methylenebis(phenyl isocyanate), MDI	
Toluene 2,4-diisocyanate, TDI	
Isophorone diisocyanate, IPDI	
4,4'-Methylenebis(cyclohexyl isocyanate), HMDI	
Hexamethylene diisocyanate, HDI	

Table 3 Widely used catalyst in PU synthesis

Name	Nature
Dibutyltin dilaurate	Organometallic catalyst
Dibutyltin dilauryl mercaptide	Organometallic catalyst
Stannous octoate	Organometallic catalyst
Dibutyltin diacetate	Organometallic catalyst
Pentamethyldipropylenetriamine	Amine catalyst
Dimethylethanolamine	Amine catalyst
Dimethylaminoethoxyethanol	Amine catalyst
1,8-Diazabicyclo[5,4,0]undec-7-ene	Amine catalyst

Unfortunately, the metal-based catalysts especially tin, lead, and mercury are reported as very toxic, thus leading to the recent use of very less toxic such as zinc and bismuth as replacements. Scientists are also trying to avoid catalyst by using mixer of aliphatic and aromatic diisocyanates. The selection of catalyst also depends on the solvent systems of PU materials. Tin-based catalysts (such as dibutyltindilaurate) are widely being used in PU synthesis.

3.4 Chain Extenders

Chain extender is usually termed as terminator of the PU reaction. The molecular weight of PU highly depends on the nature of chain extenders and their contents. The chain extenders are usually hydroxyl and amine terminated, with low molecular weights. They are also highly useful for improving the morphology of PU adhesives, coatings, and foams. The mechanical properties also highly depend on chain extender content. Very less amount of chain extender makes PU to have less mechanical strength; with increasing chain extender, the mechanical strength also increased. However, a very higher amount of chain extender makes PU brittle [1, 2, 45].

3.5 Cross-Linker

Polyisocyanate hardener, melamine, and multifunctional polyol are usually used as a cross-linker. The content and addition step of cross-linker also influence the properties. Excess cross-linker has detrimental effect on properties [1, 2].

4 Types of Polyurethanes

4.1 Polyurethane Ionomers (PUI)

Different ionic groups in PU backbone make PU ionomer which have identical properties such as mechanical strength, thermal stability, and dispersion stability in polar solvents. Especially, PUI is very useful in biomedical devices (such as artificial hearts, connector tubing for heart pacemakers) due to shape memory effect. PUI can be prepared by incorporation of ionic groups as a pendant group or using ionic diols during PU synthesis. PUI can be classified as a cationomer or anionomer. Quaternization (for nitrogen) or ternization (for sulfur) makes a cationomer PU [1, 2].

4.2 Polyurethane Foams

Different types (rigid and flexible) of PU foams are being used in different sectors. The major applications of rigid PU foam are insulation and flame retardant. The main applications of flexible PU are packaging, cushion materials, bedding furniture, carpet underlays, biomedicine automotive interior parts, and nano-composites. The main two steps of PU preparation are blowing and gelling. By controlling the monomers and their ratios, the properties of PU foam are usually modified [1, 2].

4.3 Coatings, Adhesives, Sealants, and Elastomers

The most promising fields of PU and its derivatives are adhesives, coatings, liners, and elastomers. This is due to excellent mechanical, thermal, chemical, and physical properties. Different PU adhesives offer excellent bonding properties. PU coating possess sufficient adhesive strength, low temperature flexibility, excellent barrier and UV resistance, adequate corrosion and scratch resistance, and high chemical resistivity. It is easy to apply PU-coating and PU-adhesive materials on different metals, leather, textile, and wood substrates. Another important application of PU and their derivatives is elastomer for shoe soles, ski boots, goggles, and household and car items. These elastomers are attractive as it is easy to make different shapes and colors. The elastomers are light and possess stress-recovering properties. Most

importantly PU and their derivative elastomers withstand several critical environmental factors. Recently the mentioned properties dramatically improved by using different nanomaterials in PU and their derivative elastomers [1, 2].

4.4 Binders

PU binders which act as a glue are usually used to bond materials. This is useful in fiberboards, particle boards, ink-jet printing, flooring surfaces, wood panel, sand casting, and foundry industries. Like other PU materials, the properties such as thermal stability, hydrophobicity, and rubbery state all depend on monomer and their contents. To improve the mentioned properties, other functional groups such as acrylate, siloxane, etc. are also incorporated in PU and their derivatives [1, 2].

4.5 Waterborne Polyurethane (WBPU) Dispersions

PU and their derivatives are prepared by using either organic solvent or water. When water is used as main solvent, the PU and their derivatives are termed as waterborne PU (WBPU). WBPU is an environmentally friendly material as this material is free from toxic solvent. WBPU has advantages such as low viscosity, cheaper, and easy application. WBPU is a two-phase colloidal system, in which the PU particle dispersed in water. A pendant salt in PU parent chain makes the PU dispersible in water. The types and amount of polyol, isocyanate, ionomers, and chain extender used are responsible for different properties of this dispersion [1, 2]. The typical synthesis process of WBPU is summarized in Fig. 4.

5 Recent Advances in Polyurethane and Their Derivatives

5.1 Polyurethane Nanocomposites

Since the last decade, the PU and their derivatives' properties have been improved by using different nanomaterials. There are many different types of nanoparticles, which are being considered as pristine or functionalized nanoparticles. The widely used nanoparticles are different clay, carbon nanotube, graphene, hydroxyapatite, cellulose, and fly ash. The mechanical, thermal, and barrier properties are improved by using nanoparticle in PU and their derivatives. However, it is important to use proper content, because excess nanoparticle can cause detrimental effect on properties. The proper or optimum content depends on nanoparticle nature, PU monomers and their contents, and nanoparticle addition during synthesis [1, 2, 51–53].

5.2 Polyurethane Click Coupling Reaction

Very recently, click coupling reaction attracted in PU and their derivative synthesis. Click chemistry is a copper(I)-catalyzed alkyne-azide cycloaddition reaction which produces a single compound with high yield. The main advantages of click chemistry are highly selective, able to work on both homogeneous and heterogeneous, and fast. Properties such as flame retardant, thermal, mechanical, anti-microbial, and anti-corrosion have improved significantly of PU materials synthesized by click coupling reaction. Different monomers are functionalized by click coupling reaction followed by in situ or atom transfer radical polymerization process to synthesize PU and their derivatives [54–57].

5.3 Heterocyclic Compound-Based Polyurethanes

Heterocyclic compounds have advantages in corrosion protection, anti-flammability, and heat release. Different heterocyclic compounds in PU and their derivatives are used as a monomer. Toxic halogen-based compound is widely used as nonflammable material, but nitrogen-phosphorus-based heterocyclic compound in PU is proved to be a proper replacement for halogen as a flame-retardant material. Imidazole-based compound is used in PU material to improve the corrosion protection [1, 2].

5.4 Polyurethane from Renewable Resources

Most of the monomers of PU are usually based on fossil feedstocks. However, global warming and increasing oil prices push a change from fossil feedstocks to renewable resources. Recently, researchers use vegetable oils and animal fats as a renewable resource for polyol monomer. Different polysaccharides and lignin have been used as filler, chain extender, and cross-linker. The properties of using natural resources are almost the same as the fossil feedstock monomers [1, 2, 45–47].

6 Polyurethane Applications

At early stage, PU application was not very wide. With increasing the choice of monomers, the application of PU material also increased. Besides, with the use of less toxic solvent and green solvent, the application of PU increased rapidly [1, 2].

6.1 Building Material Application

The use of PU in building material is not new. Due to excellent strength, heat insulation capacity, and durability, PU materials are being used in building materials. Every year the use of PU in building material is increasing. Another advantage of PU

in building material is their light weight. The cheap price of PU building materials also makes it attractive to replace the current concrete material. PU material can be used in flooring, roofing, and wall. Besides, PU also can be used in concrete structure [1, 2, 58].

6.2 Automotive Application

PU has a huge application in automotive industry. Different parts such as doors, bumpers, windows, and wheels are made by PU and their derivatives. Due to less weight and proper insulation, the PU materials are attractive in automotive sector. PU adhesive and coating materials are also used in automotive industry. Due to excellent adhesive strength and UV and corrosion resistance, the PU materials are being widely used in this sector. Proper monomer and nanofiller make PU as a suitable material in automotive application [2, 59].

6.3 Marine Applications

Marine area is a new application field for PU and its derivatives. Different PU foams are being used as an insulator for extreme noise and temperature. PU coating for corrosion and fouling protection is another area in marine field. The most successful antifouling coating was tin-based compound which has been banned since 2008. The reason was toxicity of tin-based compound for aquatic environment. PU consists of hard segment and soft segment. The soft segment usually moves to the surface due to its less free surface energies. Using siloxane- and fluorine-based monomer makes PU surface as foul-release coating to protect the surface from fouler attachment. Besides, different biocides can be used in PU coating to protect the surface from fouling [60–62].

6.4 Coating and Adhesive Application

A continuous research is going on PU materials for adhesive and coating application for different purposes. PU possesses different structures such as linear, cross-linkable, and hyperbranched which can be useful in coating and adhesive application by increasing thermal stability, mechanical strength, adhesive strength, and hydrophobicity. Available polyols and diisocyanates give an opportunity to choose a proper combination of PU coating and adhesive material to combat harsh condition. Different biodegradable monomers make PU coating and adhesive material less toxic and replace other toxic coating and adhesive materials [1, 2].

6.5 Medical Application

PU materials are used in different medical applications due to their proper mechanical strength and biocompatibility. It is mainly used in wound dressing, surgical drapes, tubing, hospital bedding, and injection equipment implants. Recently PU

implants attracted due to cost-effectiveness with similar or better protective properties of metals and their alloys and ceramics. Very recently biocompatible and biodegradable PUs were synthesized to apply on biomedical devices [63–65].

6.6 Appliances Flooring, and Packaging Application

Different PU foams are leading in appliance application especially in freezers and refrigerators. The main advantage of using PU foam is its prevention capacity of heat transfer due to close structure. Flooring by PU material is also common as this type of floor is durable, easy to maintain, and good looking. The carpets' life span can be increased by using PU foam as underlays of those carpets. Packaging industry also considered PU as an important material due to excellent barrier properties, super mechanical strength, and antibacterial properties. Using different filler and biodegradable monomers in PU material makes it more attractive as many countries have regulation to avoid the toxic and non-biodegradable packaging products [66, 67].

7 Conclusion

Available monomer, easy synthesis, and variety of applications make PU an important material to the industry. Excellent mechanical strength, long time durability, and low price make PU an alternative to rubber, plastic, and metal in many different products. PU is useful as paint, elastomer, adhesive material, foam, and elastic fiber. At early stage, PU material was made mainly from petroleum sources. The new techniques to use monomers of renewable resources make PU more promising in respect of environmental legislation. Most of the commercially available PU and their derivatives are made using organic solvents. Only few products are made using water as a solvent in PU. Besides, isocyanate which is a very toxic material makes a huge barrier to make PU as a nontoxic material. Very recently few researchers synthesize PU without isocyanate. To broaden PU application, it is necessary to use all nontoxic monomer without sacrificing their properties.

References

1. D. Chattopadhyay, K. Raju, Structural engineering of polyurethane coatings for high performance applications. *Prog. Polym. Sci.* **32**, 352–418 (2007)
2. D. Chattopadhyay, D.C. Webster, Thermal stability and flame retardancy of polyurethanes. *Prog. Polym. Sci.* **34**, 1068–1133 (2009)
3. O. Bayer, Das di-isocyanate-polyadditionsverfahren (polyurethane). *Angew. Chem.* **59**(9), 257–272 (1947)
4. M.R. Islam, M.D.H. Beg, S.S. Jamari, Development of vegetable-oil-based polymers. *J. Appl. Polym. Sci.* **131**(18), 40787–40790 (2014)
5. E. Delebecq, J.-P. Pascault, B. Boutevin, F.O. Ganachaud, On the versatility of urethane/urea bonds: reversibility, blocked isocyanate, and non-isocyanate polyurethane. *Chem. Rev.* **113**, 80–118 (2012)

6. R.B. Seymour, G.B. Kauffman, Polyurethanes: a class of modern versatile materials. *J. Chem. Educ.* **69**, 909 (1992)
7. Z.S. Petrović, J. Ferguson, Polyurethane elastomers. *Prog. Polym. Sci.* **16**, 695–836 (1991)
8. Z. Rafiee, V. Keshavarz, Synthesis and characterization of polyurethane/microcrystalline cellulose bionanocomposites. *Prog. Org. Coat.* **86**, 190–193 (2015)
9. K.M. Zia, S. Anjum, M. Zuber, M. Mujahid, T. Jamil, Synthesis and molecular characterization of chitosan based polyurethane elastomers using aromatic diisocyanate. *Int. J. Biol. Macromol.* **66**, 26–32 (2014)
10. C. Prisacariu, *Polyurethane Elastomers: From Morphology to Mechanical Aspects* (Springer Science & Business Media, 2011), Vienna
11. M. Ionescu, Chemistry and technology of polyols for polyurethanes, Rapra Technology, Shrewsbury, UK. *Polym. Int.* **56**, 820 (2007)
12. S.A. Madbouly, J.U. Otaigbe, Recent advances in synthesis, characterization and rheological properties of polyurethanes and POSS/polyurethane nanocomposites dispersions and films. *Prog. Polym. Sci.* **34**, 1283–1332 (2009)
13. P. Vermette, H.J. Griesser, G. Laroche, R. Guidoin, *Biomedical Applications of Polyurethanes*, vol 6 (Landes Bioscience, Georgetown, 2001)
14. G.T. Howard, Biodegradation of polyurethane: a review. *Int. Biodeterior. Biodegrad.* **49**, 245–252 (2002)
15. T. Romaškevič, S. Budrienė, K. Pielichowski, J. Pielichowski, Application of polyurethane-based materials for immobilization of enzymes and cells: a review. *Chemija* **17**, 74–89 (2006)
16. M. Szycher, *Handbook of Polyurethanes* (CRC Press, Boca Raton, 1999)
17. U. Lochner, H. Chin, Y. Yamaguchi, Polyurethane foams, in *Chemical Economics Handbook, Report No. 580.1600 A* (IHS Group, Englewood, 2012)
18. <http://www.grandviewresearch.com/industry-analysis/bio-based-polyurethane-industry>
19. N. Taheri, S. Sayyahi, Effect of clay loading on the structural and mechanical properties of organoclay/HDI-based thermoplastic polyurethane nanocomposites. *E-Polymers* **16**(1), 65–73 (2016)
20. D. Sridaeng, B. Sukkaneewat, N. Chueasakol, N. Chantarasiri, Copper-amine complex solution as a low-emission catalyst for flexible polyurethane foam preparation. *E-Polymers* **15**(2), 119–126 (2015)
21. E.A. Ismail, A. Motawie, E. Sadek, Synthesis and characterization of polyurethane coatings based on soybean oil–polyester polyols. *Egypt. J. Pet.* **20**, 1–8 (2011)
22. K.M. Zia, M. Zuber, M.J. Saif, M. Jawaid, K. Mahmood, M. Shahid, Chitin based polyurethanes using hydroxyl terminated polybutadiene, part III: surface characteristics. *Int. J. Biol. Macromol.* **62**, 670–676 (2013)
23. K.M. Zia, H.N. Bhatti, I.A. Bhatti, Methods for polyurethane and polyurethane composites, recycling and recovery: a review. *React. Funct. Polym.* **67**, 675–692 (2007)
24. T. Gurunathan, S. Mohanty, S.K. Nayak, Effect of reactive organoclay on physicochemical properties of vegetable oil-based waterborne polyurethane nanocomposites. *RSC Adv.* **5**, 11524–11533 (2015)
25. P. Alagi, Y.J. Choi, S.C. Hong, Preparation of vegetable oil-based polyols with controlled hydroxyl functionalities for thermoplastic polyurethane. *Eur. Polym. J.* **78**, 46–60 (2016)
26. P. Alagi, S.C. Hong, Vegetable oil-based polyols for sustainable polyurethanes. *Macromol. Res.* **23**(12), 1079–1086 (2015)
27. A. Fridrihsone-Girone, U. Stirma, M. Misāne, B. Lazdiņa, L. Deme, Spray-applied 100% volatile organic compounds free two component polyurethane coatings based on rapeseed oil polyols. *Prog. Org. Coat.* **94**, 90–97 (2016)
28. M. Ionescu, D. Radojčić, X. Wan, M.L. Shrestha, Z.S. Petrović, T.A. Upshaw, Highly functional polyols from castor oil for rigid polyurethanes. *Eur. Polym. J.* **88**, 736–749 (2016)
29. A. Guo, Y. Cho, Z.S. Petrović, Structure and properties of halogenated and nonhalogenated soy-based polyols. *J. Polym. Sci. A Polym. Chem.* **38**, 3900–3910 (2000)

30. Z.S. Petrovic, W. Zhang, I. Javni, Structure and properties of polyurethanes prepared from triglyceride polyols by ozonolysis. *Biomacromolecules* **6**, 713–719 (2005)
31. U. Schuchardt, R. Sercheli, R.M. Vargas, Transesterification of vegetable oils: a review. *J. Braz. Chem. Soc.* **9**, 199–210 (2008)
32. A. Guo, D. Demydov, W. Zhang, Z.S. Petrovic, Polyols and polyurethanes from hydroformylation of soybean oil. *J. Polym. Environ.* **10**, 49–52 (2002)
33. Y. Kojima, A. Usuki, M. Kawasumi, V. Okada, Y. Fukushima, T. Kurauchi, Mechanical properties of nylon 6-clay hybrid. *J. Mater. Res.* **8**, 1185–1189 (1993)
34. A. Usuki, Y. Kojima, M. Kawasumi, A. Okada, Y. Fukushima, T. Kurauchi, Synthesis of nylon 6-clay hybrid. *J. Mater. Res.* **8**, 1179–1184 (1993)
35. F. Bergaya, C. Detellier, J.-F. Lambert, G. Lagaly, Introduction to clay–polymer nanocomposites (CPN), in *Handbook of Clay Science*, vol. 5, (Elsevier, Oxford, 2013), pp. 655–677
36. B. Chen, J.R. Evans, H.C. Greenwell, P. Boulet, P.V. Coveney, A.A. Bowden, A critical appraisal of polymer–clay nanocomposites. *Chem. Soc. Rev.* **37**, 568–594 (2008)
37. E.D. Weil, in *Reaction Polymers*, ed. by W.F. Gum, H. Ulrich, W. Riese (Hanser Publishers, Oxford University Press, Munich/New York, 1992), p. 838, Wiley Online Library, 1993
38. H. Ulrich, *Chemistry and Technology of Isocyanates* (Wiley, Chichester, 1996)
39. M. Soto, R.M. Sebastián, J. Marquet, Photochemical activation of extremely weak nucleophiles: highly fluorinated urethanes and polyurethanes from polyfluoro alcohols. *J. Organomet. Chem.* **79**, 5019–5027 (2014)
40. M. Charlon, B. Heinrich, Y. Matter, E. Couzigné, B. Donnio, L. Avérous, Synthesis, structure and properties of fully biobased thermoplastic polyurethanes, obtained from a diisocyanate based on modified dimer fatty acids, and different renewable diols. *Eur. Polym. J.* **61**, 197–205 (2014)
41. N.N.P.N. Pauzi, R.A. Majid, M.H. Dzulkifli, M.Y. Yahya, Development of rigid bio-based polyurethane foam reinforced with nanoclay. *Compos. Part B* **67**, 521–526 (2014)
42. Z.S. Petrović, Polyurethanes from vegetable oils. *Polym. Rev.* **48**, 109–155 (2008)
43. B.F. Richard, B.A.R.D. Edmund, Mechanically Frothed Gel Elastomers and Methods of Making and Using Them, US 20160017084 A1, US 14/730,867, Jan 21, 2016
44. G.P. Rajendran, V. Mahadevan, M. Srinivasan, Synthesis of some low glass transition temperature polytetrahydrofuran polymers. *Eur. Polym. J.* **25**(5), 461–463 (1989)
45. M.F. Sonnenschein, *Polyurethanes. Science, Technology, Markets, and Trends* (The Dow Chemical Company, Midland, 2014)
46. M.R. Anisur, M.A. Kibria, M.H. Mahfuz, R. Saidur, I.H.S.C. Metselaar, Latent heat thermal storage (LHTS) for energy sustainability, in *Energy Sustainability Through Green Energy*, Part of the series *Green Energy and Technology* (2015), Springer, New Delhi, pp. 245–263
47. M. Heinen, A.E. Gerbase, C.L. Petzhold, Vegetable oil-based rigid polyurethanes and phosphorylated flame-retardants derived from epoxydized soybean oil. *Polym. Degrad. Stab.* **108**, 76–86 (2014)
48. M.Z. Arniza, S.S. Hoong, Z. Idris, S.K. Yeong, H.A. Hassan, A.K. Din, Y.M. Choo, Synthesis of transesterified palm olein-based polyol and rigid polyurethanes from this polyol. *J. Am. Oil Chem. Soc.* **92**, 243–255 (2015)
49. V.B. Veronese, R.K. Menger, M.M.C. Forte, C.L. Petzhold, Rigid polyurethane foam based on modified vegetable oil. *J. Appl. Polym. Sci.* **120**, 530–537 (2011)
50. M. Zhang, Z. Luo, J. Zhang, S. Chen, Y. Zhou, Effects of a novel phosphorus–nitrogen flame retardant on rosin-based rigid polyurethane foams. *Polym. Degrad. Stab.* **120**, 427–434 (2015)
51. M. Zhang, J. Zhang, S. Chen, Y. Zhou, Synthesis and fire properties of rigid polyurethane foams made from a polyol derived from melamine and cardanol. *Polym. Degrad. Stab.* **110**, 27–34 (2014)
52. L. Zhang, M. Zhang, L. Hu, Y. Zhou, Synthesis of rigid polyurethane foams with castor oil-based flame retardant polyols. *Ind. Crop. Prod.* **52**, 380–388 (2014)
53. S. Semenzato, A. Lorenzetti, M. Modesti, E. Ugel, D. Hrelja, S. Besco, A novel phosphorus polyurethane FOAM/montmorillonite nanocomposite: preparation, characterization and thermal behaviour. *Appl. Clay Sci.* **44**, 35–42 (2009)

54. A.M. Borreguero, P. Sharma, C. Spiteri, M.M. Velencoso, M.S. Carmona, J.E. Moses, J.F. Rodriguez, A novel click-chemistry approach to flame retardant polyurethanes. *React. Funct. Polym.* **73**, 1207–1212 (2013)
55. D. Fourmier, B.G.D. Geest, F.E.D. Prez, On-demand click functionalization of polyurethane films and foams. *Polymer* **50**, 5362–5367 (2009)
56. G. Chen, X. Guan, R. Xu, J. Tian, M. He, W. Shen, J. Yang, Synthesis and characterization of UV-curable castor oil-based polyfunctional polyurethane acrylate *via* photo-click chemistry and isocyanate polyurethane reaction. *Prog. Org. Coat.* **93**, 11–16 (2016)
57. S. Kantheti, P.S. Sarath, R. Narayan, K.V.S.N. Raju, Synthesis and characterization of triazole rich polyether polyols using click chemistry for highly branched polyurethanes. *React. Funct. Polym.* **73**, 1597–1605 (2013)
58. A. Serrano, A.M. Borreguero, I. Garrido, J.F. Rodríguez, M. Carmona, Reducing heat loss through the building envelope by using polyurethane foams containing thermoregulating microcapsules. *Appl. Therm. Eng.* **103**, 226–232 (2016)
59. J. Njuguna, S. Michałowski, K. Pielichowski, K. Kayvantash, A.C. Walton, Fabrication, characterization and low-velocity impact testing of hybrid sandwich composites with polyurethane/layered silicate foam cores. *Polym. Compos.* **32**, 6–13 (2011)
60. P. Xiao, Y. Dudal, P.F.X. Corvini, U. Pieses, P. Shahgaldian, Cyclodextrin-based polyurethanes act as selective molecular recognition materials of active pharmaceutical ingredients (APIs). *Polym. Chem.* **2**, 1264–1266 (2011)
61. Y.P. Chin, S. Mohamad, M.R.B. Abas, Removal of parabens from aqueous solution using β -cyclodextrin cross-linked polymer. *Int. J. Mol. Sci.* **11**, 3459–3471 (2010)
62. P. Davies, G. Evrard, Accelerated ageing of polyurethanes for marine applications. *Polym. Degrad. Stab.* **92**, 1455–1464 (2007)
63. B. Zhou, Y. Hu, J. Li, B. Li, Chitosan/phosvitin antibacterial films fabricated *via* layer-by-layer deposition. *Int. J. Biol. Macromol.* **64**, 402–408 (2014)
64. X. Zhou, T. Zhang, D. Guo, N. Gu, A facile preparation of poly(ethylene oxide)-modified medical polyurethane to improve hemocompatibility. *Colloids Surf. A Physicochem. Eng. Asp.* **441**, 34–42 (2014)
65. Y. Wang, Q. Hong, Y. Chen, X. Lian, Y. Xiong, Surface properties of polyurethanes modified by bioactive polysaccharide-based polyelectrolyte multilayers. *Colloids Surf. B. Biointerfaces* **100**, 77–83 (2012)
66. M. Garrido, J.R. Correia, T. Keller, Effect of service temperature on the shear creep response of rigid polyurethane foam used in composite sandwich floor panels. *Constr. Build. Mater.* **118**, 235–244 (2016)
67. M.A. Mekewi, A.M. Ramadan, F.M. ElDarse, M.H.A. Rehim, N.A. Mosa, M.A. Ibrahim, Preparation and characterization of polyurethane plasticizer for flexible packaging applications: natural oils affirmed access. *Egypt. J. Pet.* **26**, 9–15 (2017)



Shah Mohammed Reduwan Billah

Contents

1	Dielectric Materials	243
2	Basic Concept of Dielectric Polymers	244
2.1	Dielectric Polymers	246
3	Dielectric Mechanism of Dielectric Polymers	246
4	Useful Terms Usually Used to Analyze Dielectric Materials or Dielectric Polymers	247
4.1	Dielectric Constant	247
4.2	Dielectric Strength	248
4.3	Dielectric Loss	248
4.4	Dissipation Factor	248
5	Basic Characteristic of Dielectric Polymers	249
5.1	Electrical Properties	249
5.2	Physical Properties	249
5.3	Water Absorption, Planarization, and Chemical Resistance	250
6	Different Types of Dielectric Polymers	250
6.1	Low- <i>k</i> Dielectric Materials	250
6.2	Property Requirements of Low- <i>k</i> Dielectric Polymers	251
6.3	High- <i>k</i> Dielectric Materials	252
7	Different Selected Aspects of Dielectric Polymers	255
7.1	Dielectric Fluoropolymers and their Copolymers	255
7.2	Dielectric Polymer Composites	256
7.3	Dielectric Polymer Nanocomposites	260
8	Performance Enhancement of High- <i>k</i> Nanocomposites	264
8.1	Filler Size Effect	264
8.2	Micron-Sized Nanoparticles	265

S. M. R. Billah (✉)

University of East London, Stratford Campus, London, UK

CCIRA UK limited, Galashiels, UK

Department of Chemistry, Durham University, Durham, UK

School of Textiles and Design, Heriot-Watt University, Galashiels, UK

e-mail: reduwan.shah@gmail.com

8.3	Controlled Dispersion	265
8.4	Control of Dielectric Loss for Conductive Filler/Polymer Nanocomposites	265
9	Dielectric Elastomers	266
9.1	Bioinspired Dielectric Elastomers	267
9.2	Different Aspects of Dielectric Elastomers	267
9.3	Large Deformation Capability and Typical Failure Modes of Dielectric Elastomers	268
10	Dielectric Breakdown of Other Polymers	268
10.1	Dielectric Breakdown Behavior of Polymer Composites and Nanocomposites	269
11	Recent Trends in Dielectric Polymer Applications	269
11.1	Microelectronic and Dielectric Polymers	270
12	Challenges for Embedded Capacitor Materials and Dielectric Polymers and Composites and Future Perspectives	271
13	Conclusions	272
	References	273

Abstract

Polymer-based dielectric materials have attractive features making them potentially promising alternatives to usually used inorganic and ceramic-based dielectric materials due to a number of reasons including (a) higher flexibility; (b) easy, cost-effective processing feasibility; and (c) attractive chemical stability along with readily changeable characters. However, one of the main disadvantages of this type of polymer dielectric is their lower thermal stability which limits their wider application potentials. In addition, usually polymer dielectric materials show low dielectric constants compared to inorganic dielectric materials. In addition, dielectric characters can be designed by introducing polarizable groups into polymer chains by increasing free volume by inducing porosity as well as copolymerization. Besides this, the value of dielectric constant can be effectively increased by synthesizing nanocomposites by introducing inorganic fillers into composite structure to acquire high dielectric constants. Dielectric polymers have many applications in electronics. For example, the performance of advanced polymer dielectrics is useful to realize high-power electronic circuits in a miniature form. However, these polymeric materials are required to fulfill different criteria (such as thermal, environmental, and electrical stability, low moisture uptake, high breakdown voltage or low leakage current, low dielectric constant, low loss tangent, high glass transition temperature, and low surface roughness) for their effective applications in different devices including in microelectronics. Many investigations have been reported on the use of polymer dielectrics and evaluated the feasibility of utilizing these materials for various applications. Briefly three types of polymer dielectrics (such as dielectric polymers, organic-inorganic material-based hybrid composites, and coated polymer dielectrics) along with other necessary elements are selectively discussed in this chapter. In addition, behaviors of dielectric elastomers are also briefly covered.

Keywords

Dielectric polymers · Composites · Nanocomposites · Ferroelectric · Dielectric breakdown

1 Dielectric Materials

Dielectricity, a physical model, is commonly used to state how an electric field interacts with atoms or molecules inside a material. For example, when a metal body is exposed to an electric field, the free electrons flow due to the impact of the electric forces against the field until the field in the body vanishes. It gives rise to a charge transport or conduction. The word dielectric is derived from the prefix “dia,” originally from Greek, which usually refers to “through” or “across.” So, the dielectric material can be termed as a material that permits the passage of the electric field or electric flux; however, they are not any type of charge carriers. In addition, in strict consideration, there is no a truly insulating substance which will resist the transport of electric charge through it under all circumstances. Dielectric materials are nonconducting substances, such as insulators. However, the term “dielectric” is usually used to consider the effect of alternating electric fields on the substance, whereas the term “insulator” is often used to express the electrical nature of the material when it is exposed to withstand high electric field. Dielectric materials have different applications where one of the main applications is their use in controlling and storing electrical charges and electrical energies which play key role in modern electronics and electric power systems. For example, a dielectric capacitor is usually made by sandwiching a dielectric material between two metal plates as electrodes where an external electric potential is applied between the metal plates. When the electron distributions around constituent atoms or molecules in dielectric materials are polarized due to charge separation, they can be used as capacitors to store electrical energy in the form of electric field [1–18]. Dielectric materials are frequently applied to electrical energy for charge separation when the electron distributions around constituent atoms or molecules are polarized due to the impact of an external electric field; for this type of system, the complex permittivity (ϵ^*) of a dielectric material can be given as

$$\epsilon^* = \epsilon' - j\epsilon'' \quad (1)$$

For this equation, ϵ' represents real permittivity, while ϵ'' indicates imaginary parts of the complex permittivity, and j is equal to $\sqrt{-1}$. In addition, Kramers-Kronig relation is popularly used to relate the magnitudes of ϵ' and ϵ'' that depend on the frequency ω of the applied electric field; the Kramers-Kronig relation is expressed as:

$$\epsilon'(\omega) = \epsilon_0 + \frac{2}{\pi} \int_0^{\infty} \frac{u\epsilon''(u)}{u^2 - \omega^2} du \quad (2)$$

Additionally, the real part of the permittivity is expressed as:

$$\epsilon' = \epsilon_0 \epsilon_r \quad (3)$$

For the Eq. 3, ϵ_0 indicates the permittivity of vacuum (8.85×10^{-12} F/m) and ϵ_r represents the relative permittivity or dielectric constant of the material and the magnitude of ϵ' (or the dielectric constant ϵ_r) imparts the ability of the material to store energy from the applied electric field [7–17].

2 Basic Concept of Dielectric Polymers

Generally, the term dielectric is used to indicate the energy storing capacity of the material by means of polarization. When exposed to an external electric field, materials show polarization due to a dielectric displacement. Typically, most common polarization mechanisms are (a) electronic polarization, (b) orientational polarization, (c) vibrational polarization, and (d) interfacial polarization, which are shown in Fig. 1. Electronic polarization is effective in every atom or molecule as the center of charge of electrons surrounding the positive atomic cores that are displaced by the action of the electric field in order to create a dipole moment. Orientational polarization or dipolar polarization occurs in materials that contain molecules with permanent dipole moments (such as water) where the dipoles show some type of alignment on exposure to an electric field in order to induce a polar character to the material [1–7].

Orientation of molecular dipoles is a relatively slow process in comparison with electronic transitions or molecular vibrations. In addition, when an orientational polarization is measured immediately after an electric field is applied, the observed

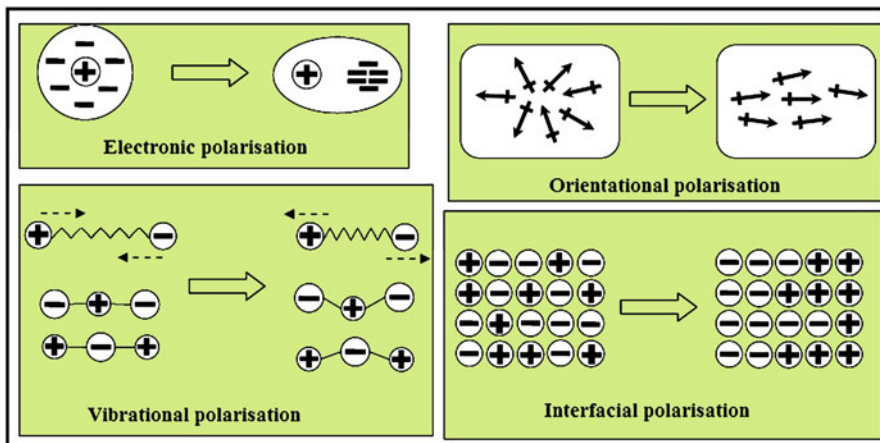


Fig. 1 Schematic representation of (a) electronic, (b) vibrational, (c) orientational, and (d) interfacial polarization mechanisms

instantaneous relative permittivity is usually low due to the fact that no time is allowed for the orientation of the dipoles. In contrast, when a sufficient time is allowed after the application of an electric field, maximum orientational polarization is usually achieved that corresponds to the highest observable relative permittivity (also called the static relative permittivity). Besides this, atomic polarization occurs when an applied electric field distorts the arrangement of atomic nuclei in a molecule or lattice, and it happens at a lower frequency than electronic polarization due to the larger mass of the atom when compared to the electron [1–7].

A dielectric material, a poor conductor of electricity, efficiently supports electrostatic fields. When the flow of current between opposite electric charge poles is kept to a minimum while the electrostatic lines of flux are not impeded or interrupted, an electrostatic field can store energy which is essential for capacitors (particularly at radio frequencies). Dielectric materials are also useful for the construction of radio-frequency transmission lines. Practically, most dielectric materials are solid, for example, porcelain (ceramic), mica, glass, plastics, and the oxides of various metals. In addition, some liquids and gases also show good dielectric properties. For example, dry air shows dielectric character which is usually used in variable capacitors and some specific types of transmission lines. Distilled water also shows a fair dielectric character, and a vacuum also indicates an exceptionally efficient dielectric behavior. An important property of a dielectric polymer or a dielectric material is its ability to support an electrostatic field while dissipating minimal energy in the form of heat. When a material shows a low dielectric loss (the amount of energy lost as heat), it is considered to be a good dielectric material. The dielectric constant is the extent to which a substance concentrates the electrostatic lines of flux. Substances with a low dielectric constant include a perfect vacuum, dry air, and most pure, dry gases (e.g., helium and nitrogen). As for instances, some materials with moderate dielectric constants are – (a) ceramics, (b) distilled water, (c) paper, (d) mica, (e) polyethylene, (f) glass; whereas, typically, metal oxides have high dielectric constants [18–55]. Dielectric materials have a wide range of applications, for example, they are widely used in transistors. In organic thin-film transistors, polymer-based dielectric materials are frequently used. A brief general introduction of the use of dielectric materials in transistors is shown in Fig. 2. Organic thin-film transistors can have different configurations depending on the position of the gate electrode (G) and the sequence of the source (S) and drain (D) electrodes deposited relative to the semiconductor layer. These configurations are stated as (1) top-gate top-contact, (2) top-gate bottom-contact, (3) bottom-gate top-contact, and (4) bottom-gate bottom-contact [8, 56–61].

In principle, the characteristic that best defines organic thin-film transistors is the presence of an electric field which controls and modulates the conductivity of the channel between the source and drain, and this electric field is created by the voltage applied between the source and the gate electrodes (such as gate voltage, V_G). Application of a negative (or positive) gate voltage will induce holes (or electrons) at the dielectric-semiconductor interface where charge transport takes place, and the density of accumulated charge carriers in the channel is modulated by V_G and is dependent on the capacitance C of the dielectric layer [62–69].

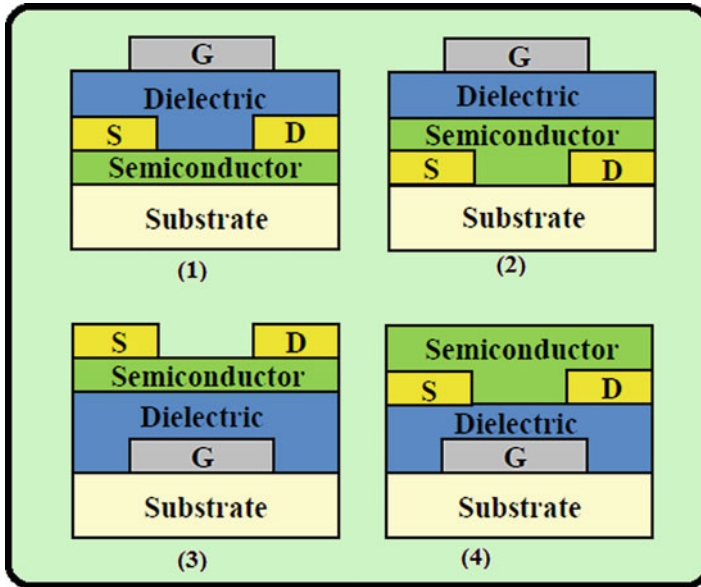


Fig. 2 Schematic representation of (1) top-gate top-contact-, (2) top-gate bottom-contact-, (3) bottom-gate top-contact-, and (4) bottom-gate bottom-contact-based thin-film transistors

2.1 Dielectric Polymers

Polymers (e.g., epoxies, benzocyclobutenes, polyimides) have been applied as dielectrics in microelectronic industry by various coating techniques followed by moderate temperature cure. At first, in 1990, Peng et al. reported the use of polymers as gate dielectrics in OTFTs [70]. They fabricated devices with different types of organic polymer insulators using evaporated R-sexithienyl films to serve as the semiconductor. Polymer-based dielectric materials have some advantage and disadvantages. Most polymers are para-electric capable to provide stable capacitance with regard to temperature and frequency. In addition, they possess good mechanical property, easy processing, low dissipation factor, and high dielectric breakdown strength. Dielectric polymers include (a) polypropylene, (b) cyclic transparent optical fluoropolymer (CYTOP), (c) polypropylene-*co*-1-butene, (d) poly-*p*-xylylene, (e) polyisobutylene, (f) polyvinylphenol, (g) polyvinyl alcohol, (h) PMMA, (i) polyethylene terephthalate, and (j) poly- α -methylstyrene. In contrast, a group of polymers with a polar backbone, so-called ferroelectric polymers, possess higher values of dielectric constant [70–78].

3 Dielectric Mechanism of Dielectric Polymers

The dielectric mechanism of a dielectric polymer is directly related to resonance and relaxation processes (Fig. 3). Resonances process depends on two polarizations, and they are (a) electronic polarization (occurs in a neutral atom when the electric displaces the electronic density relative to the nucleus in its surrounding environment) and

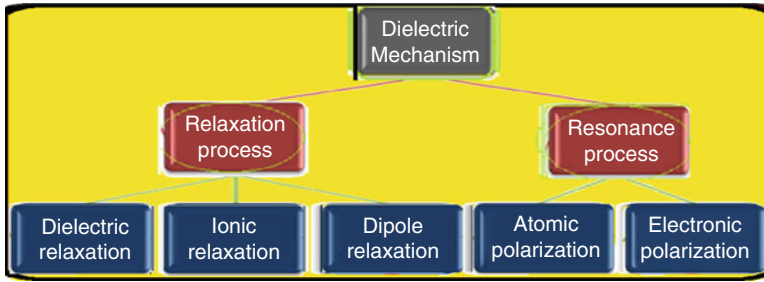


Fig. 3 Dependence of dielectric mechanism

(b) atomic polarization (occurs when the electronic cloud is deformed under the force of the applied field). However, relaxation process relies on three types of relaxation processes, which are (i) dipole relaxation (permanent and induced dipoles aligning to an electric field), (ii) ionic relaxation (comprises ionic conductivity and interfacial and space charge relaxation), and (iii) dielectric relaxation (it is a result of a movement of dipoles due to dipole relaxation and electric charges due to ionic relaxation) [1–7].

4 Useful Terms Usually Used to Analyze Dielectric Materials or Dielectric Polymers

4.1 Dielectric Constant

Dielectric constant (ϵ') is considered to be a critical electrical parameter for a dielectric polymer where the magnitude of ϵ' is a function of the amount of mobile (polarizable) electrical charges and the degree of mobility of these charges in the polymer or material. Charge mobility and ϵ' exhibit temperature dependency. Additionally, since polarization of the material requires a finite amount of time, the frequency of the electric field also influences the measurement of dielectric constant. Besides this, a lower dielectric constant allows for wider signal traces and decrease in the dielectric thickness. It also allows to maintain the same characteristic impedance while lowering the line resistance and crosstalk. A good dielectric polymer usually has different attractive properties including the invariance of the dielectric constant with respect to frequency and temperature. For example, polyimides typically have dielectric constants greater than 3.0, unless they are modified through the inclusion of fluorinated groups. In additions, it has also been shown that low-stress polyimides show highly anisotropic dielectric constants, for example, BCBs and fluoropolymers show dielectric constants which are less than 3.0 [61–78]. The dielectric constant is termed as the permittivity of a material which represents the ability of a material to concentrate electrostatic lines of flux. In other way, it shows the ability of a material to store electrical energy in the presence of an electric field. When placed in an electric field, all materials (including vacuum) store energy and the permittivity of vacuum is defined as the physical constant (ϵ_0 , which is approximately $\epsilon_0 = 8.854 \times 10^{-12}$ farads per meter). This constant appears in many electromagnetism formulas.

4.2 Dielectric Strength

Dielectric strength or breakdown voltage is used to illustrate the voltage at which current begins to flow through the insulating dielectric film and for thin films, for example, avalanche breakdown ultimately defines the breakdown strength of the polymer. In addition, it is possible that a breakdown can also occur due to thermal effects as power dissipated by the insulation, in which an exponential increase in conductivity creates thermal runaway and most polymeric materials show specific values for breakdown voltage. For instance, BCBs have slightly higher values which are suitable for high-voltage power applications. Besides this, an insulator has a limited capability to withstand the voltage before conducting electricity, and all materials have an upper voltage limit which is termed as breakdown voltage. Air is considered as an insulator, however, it can flow current under certain circumstances, for example, during a lightning strike air works as a conductor. During this case, air is ionized (electrons are torn away from the atom's nucleus) when the breakdown field strength is exceeded, and electrons begin moving under the influence of the electric field to produce electrical current [61–78].

4.3 Dielectric Loss

Dielectric loss is a loss of energy during heating of an object made of a dielectric material when a variable voltage is applied to it. However, a dielectric loss is strongly influenced by the changes of material polarization where a tiny electron shifts can be deemed as a tiny alternating current flow. Additionally, at different frequencies, different materials have different losses which must be taken into account for an effective design of dielectric materials with suitable high frequency applications.

4.4 Dissipation Factor

At high frequencies, different electrical parameters such as dissipation factor (ϵ'') and loss tangent (ϵ''/ϵ' or $\tan \delta$) are significantly important. With an increase in the frequency, the inertia of the charged particles has an impact to prohibit the dislocations of the particles from keeping in phase with the field changes that causes a frictional damping mechanism and eventually results in a power loss (due to the work performed in order to overcome these damping forces). Ohmic losses (due to free charge carriers) are also included in the complex permittivity, and the effects of both the damping and the ohmic losses in the imaginary part of the complex permittivity, ϵ^* , are also considered (to deduce Eq. 4) [61–78].

$$\sigma = \omega\epsilon'' \quad (4)$$

5 Basic Characteristic of Dielectric Polymers

Dielectric polymers have many characteristic properties. For example, a dielectric electrical insulator is different from a conductor or a semiconductor and contains a large band gap so that no electric charges can freely flow through this material. The inherent physical characters of polymers are highly important criteria in order to select their suitability as dielectric materials; some of these characters are (a) signal speed, (b) power consumption, (c) thermal stability, (d) interaction with other materials, and (e) wiring density. These polymers should also show particular properties, such as electrical, mechanical, and thermal properties in order to provide easy processing capability [18–43, 79–80].

5.1 Electrical Properties

Dielectric polymers are similar to insulators since they resist electrical conduction to some extent. However, these polymers should have some important electrical characters to be suitable for particular applications. For example, when this type of material is exposed to an electric field, the electric charges of this dielectric material including permanent and induced electric dipoles can be moved to show change in the polarization of the material. Additionally, the equilibrium polarization of this material is constant for a given electrical field (also called the dielectric constant ϵ or also symbolized by k) which is used to characterize the dielectric properties of this dielectric polymer [79–80]. However, for an alternating electrical field, the dielectric constant is a complex quantity (ϵ^*) expressed as the combination of a real component termed as the relative permittivity or dielectric constant (ϵ') and an imaginary component called as the dielectric loss or dissipation factor (ϵ''). In addition, this form is also termed as the complex dielectric permittivity usually defined by the following:

$$\epsilon^* = \epsilon' - j\epsilon'' \quad (5)$$

A key issue is the variation of both ϵ' and ϵ'' with respect to frequency.

5.2 Physical Properties

Different suitable polymers, such as high thermal stability polymers, are very attractive as dielectric polymers for their particular uses in thin-film multilayer interconnections (however, silicon oxide-based products can also provide similar performances). Usually, dielectric polymers are popular for their attractive electrical characters and their easy processing (e.g., deposition and patterning) and their relative stability in the presence of chemical attack and extreme tolerance in temperature and humidity. For example, polyimides (which show stability over 400 °C)

exhibit higher mechanical stability and flexibility and resistance to solvents and chemicals. In addition, a dielectric polymer is expected to planarize the interconnect topology, and it should have a coefficient of thermal expansion closely matched with the substrate and also capable to be applied in thick layers (up to 25 μm) with low stress and no cracks or pinholes [79–80].

5.3 Water Absorption, Planarization, and Chemical Resistance

The electrical properties and the processing capability of dielectric polymers show direct impacts due to water absorption which is usually measured by the maximum amount of water uptake (that depends upon the degree of cure, on temperature, and on relative humidity of the dielectric polymers). The surface roughness of a substrate surface (either due to existing interconnect structures or the polymer deposition process) can directly affect the resolution, and quality of subsequent thin-film layers and the planarity of the multilayer structure are useful for the uniformity of electrical properties across the entire substrate. In addition, one of the main functions of the dielectric layer is to planarize the underlying topography in order to provide a flat focal plane for the next layer. Besides this, dielectric polymers are expected to show chemical resistance when exposed to different chemicals during processing and cleaning. Swelling, cracking, and crazing of the polymer layer are some of the signs of poor chemical resistance. However, thermosetting polymers are usually more chemically resistant compared to thermoplastic materials [18–43, 79–80].

6 Different Types of Dielectric Polymers

Dielectric materials can be grouped into two groups using a simple method of classification, which are (a) low- k dielectric materials and (b) high- k dielectric materials. Both low- k and high- k materials can be used with different suitable polymeric materials to produce composite- or nanocomposite-based dielectric polymers. As a result in this section, both dielectric polymers and other dielectric materials are briefly described.

6.1 Low- k Dielectric Materials

Two primary approaches are usually used to achieve low- k dielectric materials, and they are (a) lowering the electronic contribution by adding fluorine (F) and/or carbon (C), to provide the material with an inherently lower electronic polarizability, and (b) lowering the contribution due to the orientation and or the ionic contribution (by introducing free volume in a material in order to decrease the number of polarizable groups per unit volume and also to lower the atomic or dipolar contributions) [18–43]. Low- k materials can usually be divided into three groups – (a) inorganic, (b) organic, and (c) hybrid (e.g., organo-silicates). Organic dielectric

materials show lower k values than from inorganic materials because of their low polarizability and hydrophobic character. However, inorganic materials retain a SiO_2 -like matrix that assists their easy integration to the existing SiO_2 -like processes, whereas hybrid materials, on the other hand, are usually doped with carbon (C) for taking advantages of both organic and inorganic characters. As a result, in most cases, it is observed that when the base material is selected (organic/inorganic/hybrid), usually the next step is the integration of the material in the sub-100 nm device. Selection of ideal low- k dielectric materials usually depends on their applications and the chip architecture in electronic devices.

Fundamental requirements for a processed dielectric material are quite a few in number, however, for simplicity, some of the desired criteria are selectively mentioned here, they are (in particular for sub-100 nm level electronic devices) (Table 1):

- (a) dielectric constant < 3.0 ;
- (b) sufficient thermal stability at least at the processing temperatures of the device, and low coefficient of thermal expansion;
- (c) strongly adherence to the substrate along with conformity after deposition;
- (d) low thermal shrinkage, ability to resist cracking and compatible with chemical mechanical polishing;
- (e) having isotropic dielectric constant (k);
- (f) high dielectric breakdown, low charge trapping and leakage current;
- (g) low solubility in H_2O and low moisture absorption from the ambient;
- (h) friendly to surrounding environments and safe during handling;
- (i) simple to process and relatively cheap;
- (j) chemically inert;
- (k) having high etch selectivity;
- (l) Strong mechanical characters (such as, the film should have sufficient mechanical strength in order to prevent cohesive failure, and interfaces delamination). [79–124].

6.2 Property Requirements of Low- k Dielectric Polymers

Dielectric polymers have many stringent property requirements in order for their successful integration into the interconnect structures as low- k dielectric materials,

Table 1 Low- k dielectric materials

Materials	Dielectric constant
Silicon dioxide	3.8–3.9
Carbon-doped silicon dioxide	2.2–2.7
Benzocyclobutane	2.49–2.65
Diamond-like carbon	2.7–2.8
Fluorinated diamond-like carbon	2.4–2.8
Aromatic thermosets	2.6–2.8
Polyarelene	2.8

which have required characteristics that show (a) electrical characters, (b) thermal stability, (c) thermomechanical and thermal stress characters, and (d) chemical stability. In that case, desired electrical properties include (i) low dielectric constant, (ii) low dielectric loss and leakage current, and (iii) high breakdown voltage. Many polymeric materials satisfy these electrical criteria; the dimensional stability, thermal and chemical stability, mechanical strength, and thermal conductivity of polymers are inferior to those of silicon dioxide. Low- k dielectric polymers are required to show certain electrical, chemical, mechanical, and thermal properties. These electrical characters are specific range of dielectric constant, anisotropy, low dissipation, low leakage current, low charge trapping, high electric field strength, and high reliability. They should also show particular chemical properties which include certain level of chemical resistance, etch selectivity, low moisture uptake, low solubility in water, low gas permeability, high purity, no corrosion to metal, long storage life, and environmentally safe. They should exhibit particular mechanical properties, some of which are uniform thickness, good adhesion, low stress, high hardness, low shrinkage, crack resistance, and high tensile modulus. They should also show particular thermal properties, some of which include (a) high thermal stability, (b) low coefficient of thermal expansion, (c) low thermal weight loss, and (d) high thermal conductivity [44–60, 80–131]. Table 2 shows dielectric constants of important low- k dielectric materials or polymers with respect to 1 MHz frequency.

6.3 High- k Dielectric Materials

High- k dielectric materials are highly important for a wide range of electronic applications. However, there are many issues with high- k dielectric materials. For example, an important issue that prevents the implementation of high- k gate material is charge trapping in preexisting traps inside the dielectric material, which affects the

Table 2 Important low- k dielectric materials @ 1 MHz

Dielectric materials	Dielectric constant
SiO _x F _y	3.20–3.50
Hydrogen silsesquioxane	3.00
Polysiloxane	2.89
Benzocyclobutane	2.70
Black diamond	2.70
Polyethylene	2.40
Polypropylene	2.30
Fluoropolymer	2.24
Perylene	2.20
Air	1.00
Carbon dioxide	1.00

threshold voltage. In this context, scaling the thickness of the gate dielectric has long been recognized as one of the keys to scaling devices. However, when the oxide is made thinner and the substrate doping is increased, the electric field applied to the oxide/silicon interface results in a significant quantization of the carrier's perpendicular to the interface. In addition, during device fabrication with high- k , etching of Si wafer is usually carried out with hydrofluoric acid followed by an ammonium hydroxide surface treatment. The operation reduces but degrades mobility because of surface nitridation, whereas the chemical oxidation by ozone contributes to increase mobility at the expense of equivalent oxide thickness. But compared to chemical oxide, in situ steam generated interfaces usually observed to show higher overall electrical performances [79–124].

Different metal oxides (and some nitrides) and similar type of compounds are popular high- k dielectric materials, some of which include (a) nitrides and oxynitrides, (b) tantalum oxide (Ta_2O_5), (c) titanium oxide (TiO_2), (d) hafnium oxide (HfO_2), (e) zirconium oxide (ZrO_2), (f) lanthanum aluminate (LaAlO_3), (g) titanate compounds of barium (BaTiO_3), barium strontium (BaSrTiO_3), and lead (PbTiO_3). High- k dielectric materials have recently become important mainly in three areas: (a) memory cell dielectrics, (b) gate dielectrics, and (c) passive components [125–158]. For example, Table 3 exhibits the dielectric constants of some important high- k dielectric materials and their usual applications. These types of dielectric materials can be used with suitable polymers to produce high- k dielectric composites and nanocomposites using different techniques.

High- k gate dielectrics have been investigated as alternative gate dielectrics for certain technology (such as the 65 nm CMOS technology), and it also studied the feasibility to replace conventional SiO_2 or silicon oxynitrides (SiO_xN_y). Most important requirements for high- k dielectric applications include – (a) high dielectric constant and large band gap, (b) high band offset with electrodes, (c) thermally and chemically stable in contact with semiconductor substrate, (d) scalable equivalent oxide thickness (EOT) $<10\text{\AA}$, (e) compatibility with gate electrode material, (f) density of interface states comparable to SiO_2 , (g) low lattice mismatch and similar

Table 3 Important high- k dielectric materials

Dielectric materials	Dielectric constant	Applications
$\text{PbMgNbO}_3 + \text{PbTiO}_3$	22,600	Capacitor dielectrics
PbLaZrTiO_3	1000	Capacitor dielectrics
BaSrTiO_3	300	Capacitor dielectrics
TiO_2	50	Gate dielectrics, Capacitor dielectrics
Ta_2O_5	25	Gate dielectrics, Capacitor dielectrics
CeO_2	20	Gate dielectrics
BaZrTiO_3	17.3	Gate dielectrics for organic transistors on plastic
Al_2O_3	9	Capacitor dielectrics
$\text{CaF}_2, \text{SrF}_2$	7.3	Epitaxial dielectrics

thermal expansion coefficient with Si mobility comparable to SiO₂, (h) negligible capacitance-voltage hysteresis (<20 mV), and (i) good reliability (no charge trapping, high breakdown voltage) [44–60, 125–158]. Table 4 demonstrates the values of dielectric permittivity of generally used ceramics for capacitors.

On the contrary, polymers are easily processed into large-area films, and several polymers have relatively high breakdown field strengths; however, they also have low dielectric constants (Table 5) and thus have low-energy densities. Table 5 indicates a list of dielectric permittivities of commonly used polymers in capacitors.

Table 4 Dielectric permittivity values of generally used ceramics for capacitors

Composition	Dielectric permittivity
La _{1.8} Sr _{0.2} NiO ₄	~100,000
CaCu ₃ Ti ₄ O ₁₂	~60,000
SrTiO ₃	2000
BaTiO ₃	1700
TiO ₂	80
La ₂ O ₃	30
a-LaAlO ₃	30
ZrO ₂	25
HfO ₂	25
Ta ₂ O ₅	22
Y ₂ O ₃	15
HfSiO ₄	11
Al ₂ O ₃	9
SiO ₂	3.9

Table 5 List of dielectric permittivities of commonly used polymers in capacitors

Polymer	Dielectric permittivity
Poly(vinylidene fluoride-co-hexafluoropropylene)	~12
Poly(ether ketone ketone)	~3.5
Nonfluorinated aromatic polyimides	~3.2–3.6
Silsesquioxane	2.8–30
Poly(arylene)	2.9
Fluorinated polyimide	2.6–2.8
Poly(phenyl quinoxaline)	2.8
Fluorinated poly(arylene ether)	2.7
Polystyrene	2.6
Poly(norbornene)	2.4
Perfluorocyclobutane polyether	2.4
Polynaphthalene	2.2
Poly(tetrafluoroethylene)	1.9

7 Different Selected Aspects of Dielectric Polymers

Many polymers are dielectrics or insulators which have poor bulk conductivity and can survive high electric fields as they have no free charge carrier and large band gaps in their electronic structures. Because of their simpler fabrication and lower cost with respect to traditional inorganic materials, polymer dielectrics are extruded into thin films or sheets and are widely used as capacitors, gate dielectrics in transistors, electrical cable wraps, and microelectronic encapsulation. Opposite charges accumulate on both surfaces of the dielectric film after a high electric field is applied on a dielectric polymer film and an electrostatic attraction force builds up between the opposite charges where the like charges on the same electrode repel each other. In stage, the synergistic effect of the two forces presses the polymer film in the direction of the electric field and stretches in the orthogonal directions which cause it to shrink in thickness and expand in the area. The phenomenon has been named after James Clerk Maxwell, as Maxwell stress or Maxwell pressure, with the expression as shown in Eq. 6:

$$P = \varepsilon_0 \varepsilon E^2 \quad (6)$$

where ε_0 is the vacuum permittivity, ε is dielectric constant of the dielectric material, and E is the electric field applied across the material thickness. This equation is only valid on the assumption that ε does not change in its value along with the applied electric field, the stress or strain in the material. Maxwell pressure is a phenomenon to avoid in usual capacitor industries where even slight shape changes will crack the thin-film metal electrodes used in capacitors and prevent the device from functioning. In addition, localized thinning of the dielectric sheet may lead to drastic charge and electric field localization where an ultimate outcome is that the device is most likely to be shorted. The phenomenon has been observed in a number of dielectrics including using polyethylene and polyisobutylene [70–80, 122].

7.1 Dielectric Fluoropolymers and their Copolymers

Fluorinated polymers are very attractive for their interesting properties and have applied for various high-tech applications. In this connection, two families of fluorinated polymers are briefly discussed here. Of these two, the first one corresponds to those where the fluorinated groups are located in the polymer backbone, which are chemically inert, thermally stable, and have low refractive index and low dielectric constant. The polymers or copolymers having crystalline structures with large dipole moments can exhibit high piezoelectricity when their main chain shows an all-trans conformation, for instance, the poly(vinylidene fluoride) (PVDF) particularly β -type conformation, the crystalline copolymers of vinylidene fluoride and trifluoroethylene, and the terpolymers of vinylidene fluoride, trifluoroethylene, and chlorotrifluoroethylene. There are reports on novel ferroelectric polymers based on PVDF and its copolymers with hexafluoropropene which was proposed for high

electric energy storage and low loss performance have been reported. The second family concerns the polymers with a fluorinated dangling group which improves the surface properties and also exhibits low dielectric constant. Several fluoroalkyl acrylate and methacrylate polymers have been developed, and their physical properties have been rigorously studied. Dielectric relaxation studies have been carried on a series of poly(fluoroalkylmethacrylate)s where the α relaxations above T_g and γ relaxations below T_g have been reported and assigned to reorientation of segments and local molecular motion of fluoroalkyl side groups. In advanced electronic devices, the use of high dielectric constant polymers is a crucial component, for example, memory and gate dielectrics for integrated circuits, stationary power generation, and miniature capacitors for telecommunication. Polymers with cyano groups directly attached to the main chain are of potential interest for these developments due to the high dipole moments that can be induced along the macromolecular chain. For instance, vinylidene cyanide (or 1,1-dicyanoethylene, VCN) has often been employed in the preparation of high-polar polymers as a useful starting monomer [79–108, 122].

Other polymers based on commercially available cyano monomer, for example, acrylonitrile, (AN) have been used, and the dielectric behavior of polyacrylonitrile, PAN, in its pristine and cyclized states, has been reported. In addition, a soluble organic PAN material was studied for its potential applications as gate dielectric material. Functional transistors have been reported by using PAN along with poly(3-hexylthiophene) as a semiconductor material. Poly(acrylonitrile-*ter*-methyl methacrylate-*ter*-indene) terpolymers have been synthesized and rigorously studied by isochronal dielectric tests which illustrated their glass-rubber transition values (T_g) are highly dependent on the composition. In addition, there are reports on the measurements of the pyroelectric constants of these copolymers which provided a good approximation for a piezoelectric behavior. Advances in portable electronic devices, stationary power systems, and hybrid electric vehicles create a great need for low-cost, compact, and high-performance electrical energy storage devices. The development of dielectric polymers (capacitor systems) which have high energy density is governed by the dielectric constant of the materials that separate the opposite static charges [79–108, 122].

7.2 Dielectric Polymer Composites

Typically, a composite material is a mixture of two or more component materials behaving like one system with combined characters of multiple constituents. Certain types of polymer composites can be used as dielectric materials, such as ferroelectric ceramics. However, dielectric materials (e.g., ferroelectric ceramics and polymers) have a number of drawbacks that limit their integration as high- k materials in certain applications. For example, high- k ceramics frequently lack stability that allows very low-voltage operation, whereas low- k polymers offer low leakage currents and high stability but require higher operating voltages [109–130]. Different methods are usually employed for preparing ultra-high k materials from conductive filler/polymer

composites which are suitable to be used in embedded capacitors. Ultrahigh- k values have been investigated with conductive filler/polymer composites when the concentration of the conductive filler approaches the percolation threshold that can be explained by the percolation theory for conductor-insulator percolation system. For conductive filler/polymer composites, the effective electrical properties approaching to the percolation threshold are determined by the scaling theory that can be demonstrated in Eq. 7 through Eq. 9.

$$\sigma = \sigma M (f - f_c) t f > f_c \quad (7)$$

$$\sigma = \sigma D (f_c - f) - q f < f_c \quad (8)$$

$$\varepsilon = \varepsilon D / |f - f_c| \quad |q = \varepsilon D (\sigma M / \sigma M) s \quad (9)$$

Here, σM and σD are the electrical conductivity of conductive filler and polymer, respectively; f and f_c are the concentration and the percolation threshold concentration of the conductive filler within the polymer matrix, respectively; εD is the dielectric constant of the polymer matrix; and q , s , and t are scaling constants, related to the material property, microstructure, and connectivity of the phases in the conductive filler/polymer system. In addition, sometimes, the effective dielectric constant of the metal-insulator composite could be three or four orders higher than the dielectric constant of the insulating polymer matrix. This phenomenon can be stated in terms of a “supercapacitor network” with very large area and small thickness. In addition, when the concentration of the metal is close to the percolation threshold, large amount of conducting clusters are in proximity to each other; however, they are insulated by thin layers of dielectric material. Besides this, the percolative approach needs much lower volume concentration of the filler compared to traditional approach of high- k fillers in a polymer matrix. As a result, this material option shows advantageous characteristics over the conventional ceramic/polymer composites, particularly ultrahigh- k with balanced mechanical properties including the adhesion strength. In addition, various metal particles or other conductive fillers, for example, silver (Ag), aluminum (Al), nickel (Ni), and carbon black, have also been used to synthesize the polymer conductive filler composites or three-phase percolative composite systems. High dielectric loss, low dielectric strength, and narrow processing window are technical barriers for this category of materials. In addition, because the highly conductive particles are easy to form, a conductive path in the composite as the filler concentration approaches the percolation threshold. Recently, much work has been engaged with solving these problems of the conductive filler/polymer composites, and much progress has been achieved [109–130].

7.2.1 Ferroelectric Ceramic/Polymer Composites

As a major material candidate for embedded capacitor applications, different studies on ferroelectric ceramic/polymer composites with high- k values have been rigorously investigated. In these studies, the methodologies of different approaches have been used for combining the advantages of the polymers which meet the

requirements for the low-cost organic substrate process. Some of these advantages include (a) low-temperature processibility, (b) mechanical flexibility, and (c) low cost. These materials show easy processing capability since the high temperature steps required to reach high- k from the ferroelectric phase can be executed in advance of application to the organic substrate. Additionally, almost any high- k ferroelectric material can be produced in quantity as submicron powders. These high- k particles can be mixed with a polymer resin at up to 60 to 80% loading by volume which can be screen printed, spun on, or stenciled onto the substrate and the polymer phase that can be cured at temperatures tolerable to organic boards. However, there are still some challenging issues related to these polymer composites for high- k applications, for example, limited dielectric constants and capacitance density and low adhesion strength which results in air gaps and lowers capacitance. The k of the final composite will be much closer to that of the low- k material. This is generally the polymer with a k of about 3 to 5 according to the mixing rules for a two-phase combination of two materials with different k . Similarly, most of the k values of ceramic/polymer composites developed to date are between 10 and 50 at room temperature, and the corresponding film can be made in thickness of around 8 μm pinhole free by screen printing and delivers specific capacitance (up to approximately, 5 nF/cm^2). Polar polymers can increase k of the composites at low frequencies, whereas the presence of polar groups in the polymer matrix also increases dielectric losses especially within the intermediate- and high-frequency ranges. Besides this, the k values of ceramic/polymer composites can be effectively enhanced using polymer matrix with relatively high- k which is mainly due to k values of polymer matrix that shows very strong influence on the k of the final composites. For example, $\text{Pb}(\text{Mg}_{1/3}\text{Nb}_{2/3})\text{O}_3$ - PbTiO_3 /P(VDF-TrFE) composites exhibit k values above 200. Additionally, lead magnesium niobate-lead titanate (PMN-PT) + BaTiO_3 /high- k epoxy system (effective k : 6.4) composite shows k value around 150, in which ceramic filler loading is as high as 85% by volume. Different investigation demonstrated that the k of 0–3 connectivity type composite is dominated by the matrix, and as a result, a relatively large volume fraction of high- k ferroelectric inorganic phase is required. The high filler loading of ceramic powders is still the technical barriers for real application of ceramic/polymer composites in the organic substrate. It shows a poor dispersion of the filler within the organic matrix and shows no adhesion toward other layers in PWB as well because of the low polymer content [131–170].

7.2.2 Dielectric Character of All-organic Polymer Composites

The composites fabricated by dispersing an organic filler material have very high dielectric constant in a polymer matrix which can show high- k as well. Copper-phthalocyanine (CuPc) oligomer based organic semiconductor materials exhibit higher k value (i.e. 105) and when they are dispersed in P(VDF-TrFE) matrix to prepare a composite they show higher k value (such as, 225) and a loss factor of 0.4 at 1 Hz. In this case, the high dielectric loss can be attributed to the long-range intermolecular hopping of electron. In addition, there are reports that chemically modified copper phthalocyanine (CuPc) can be bonded to the backbone of

P(VDF-TrFE) in order to improve the dispersion of CuPc in polymer matrix. However, as a direct impact of chemical modification CuPc/P(VDF-TrFE) composites, there can be a reduction of dielectric loss and weakening of dielectric dispersion (over a particular frequency). A k value above 1000 (@ 1 kHz) has been reported for an all-polymer high- k percolative material-based composite which has been fabricated by a combination of conductive polyaniline (PANI) with a poly(vinylidene fluoride-trifluoroethylene-chlorotrifluoroethylene) [P(VDF-TrFECTFE)] terpolymer matrix ($k > 50$). However, further rigorous studies are a prerequisite in order to realize all-organic based composites with high- k values suitable for their uses in capacitors [171–191].

7.2.3 Dielectric Polymer Composite for Energy Storage

Particular type of polymer composites with required dielectric properties can cater the need for pulse power energy storage systems with high energy density by combining the scope of processibility and breakdown field strength of the polymer(s) along with materials of high dielectric constants (such as ceramic fillers). In typical sense, the fillers are used to enhance the effective dielectric constant of the composite system avoiding the loss of the high inherent breakdown strength of specific polymers. In addition, one of important points is that any improvement in the effective dielectric constant should be realized avoiding any type of higher compromise in dielectric loss (such as energy dissipation). In practical consideration, it is very difficult to achieve various objectives like (a) high dielectric constant, (b) high breakdown field strength, and (c) low dielectric loss; however, a suitable compromise is one of the best solutions. As a result, a lion share of research in this area is mostly focused to boost targeted electrical and other required properties of polymer composite materials using a sound understanding of the physical phenomena that have impact on composite dielectric permittivity and breakdown field strength. The behavior of the polymer-filler interface is directly related to the chemistry and structure of dielectric composites. In this respect, in some recent studies, for enhancing dielectric permittivity of dielectric polymer composites, different types of metal oxides are popularly used; some of these metal oxides include $\text{Pb}(\text{Zr,Ti})\text{O}_3$, $\text{Pb}(\text{Mg}_{0.33}\text{Nb}_{0.77})\text{O}_3$ - PbTiO_3 , and BaTiO_3 . For example, it is highly attractive to boost the dielectric constant of a dielectric polymer composite in the order of hundreds or even thousands by using suitable inorganic fillers in accurate proportions. But there are different challenges to realize these practical expectations, some of which include the following: (a) when the filler with higher level of permittivity in comparison to that of the polymer matrix is incorporated in the system, it causes an increase in the effective dielectric constant comes through an increase in the average field in the polymer matrix that allows relatively little energy storing capacity in the high permittivity phase; (b) there are chances that the large contrast in permittivity between two phases can lead to highly inhomogeneous electric fields; and (c) it is also possible to cause a loss in compatibility between the organophilic polymer matrix and the hydrophilic metal oxide filler that may contribute to poor level of homogenous composite. As a result, the modification of the inorganic filler surface

to achieve suitable compatibility of the inorganic filler with the polymer matrix is one of the main focal points of current research in this area [191–201].

7.3 Dielectric Polymer Nanocomposites

The interfaces between the polymers and the nanoparticles have critical influence in order to control the dielectric properties of polymer nanocomposites. For example, polymer-ceramic nanocomposites are promising dielectric materials for many electronic and power devices that can effectively combine the high dielectric constant of ceramic particles along with the high dielectric breakdown strength of a polymer. In addition, it has been reported that as the size of filler particles decreases to the nanometer scale, the properties of the polymer-filler interface becomes dominant over the bulk properties of the constituents [107]. This concept goes beyond the modification of the filler surface to achieve better dispersion of the dielectric filler particles. In a true nanocomposite dielectric (simply, nano-dielectric), the unique properties of the interface are amplified by the high surface area of the filler [107–111, 202–225].

7.3.1 Current Trends in Dielectric Polymer Nanocomposites

Nanocomposite materials are composed of multiple constituents in particular combinations which have nano-dimensional phases with distinct differences in structure, chemistry, and properties. Generally, nanocomposites contain inorganic components in organic hosts or vice versa. Otherwise, they may also have two or more inorganic/organic phases in some combinatorial forms with the constraint that at least one of the phases or features in the nanosize. Nanocomposites show unique combinations of mechanical, electrical, optical, electrochemical, catalytic, and structural properties compared to those of each individual component to make this composition. In addition, their micron-size filled counterparts have a few advantages such as different structure, composition and properties of their constituents [109–225].

Nanofillers

Nanofillers are fillers with sub-100 nm size in at least one dimension. One of the main objectives for the application of nanoparticle instead of micron-scale traditional fillers is the impact of particle size on their properties. Due to the incorporation of nanofillers into nanocomposite structures, they can achieve some unique and excellent properties, some of which include (a) electrical, (b) magnetic, (c) optical, (d) catalytic, (e) mechanical, and (f) chemical or biological properties. For example, due to the incorporation of carbon nanotube into a nanocomposite structure, it may achieve ultrahigh modulus and conductivity of carbon nanotubes. As a result, nanocomposite materials provide the scope of enhancing functionality in contrast with their single-component counterparts. For instance, nanocomposites with modified electrical or mechanical properties that retain their optical clarity can be obtained due to the fact that very small nanoparticles incorporated into their structure do not scatter light significantly. In addition, nanoparticles are less likely to create

large stress concentrations and thus can avoid the compromise of the material ductility while they contribute to improvement of other mechanical properties. Nanoparticles have a much higher surface area per unit volume than larger particles, and they also possess a much greater interface with their surroundings. As a result when nanoparticles are incorporated into nanocomposite structures as fillers, the small size of the fillers leads to an exceptionally large interfacial area in the nanocomposites. The interface has a significant impact in controlling the degree of interaction between the nanofiller and the polymer matrix which eventually controls the properties of the nanocomposites. The method of preparation sometimes influences the size and characteristics of the nanoparticles. The nanoparticle size depends on the kinetics of nucleation and growth from a supersaturated solution as well as processes, for example, (a) coarsening, (b) oriented attachment, and (c) aggregation. Because of the reduction of lattice constants, the large surface energy and thermodynamic instability resulted from the large ratio of the surface to interior atoms exert great challenges to stabilize nanoparticles. One way to prevent the nanoparticles from growth in size is to reduce the surface energy by insertion (such as adsorption and bonding) of surface active components into the particle surface. Synthesis of nanoparticles in confined geometries and structured reaction media can contribute to yield anisotropic and size-controlled nanoparticles. A basic understanding is very important in order to tailor and optimize properties by controlling the size, shape, volume fraction, interface, and degree of dispersion or aggregation of nanoparticles to guide enhanced development. In addition, the ability to manipulate the size, morphology, and arrangements of nanoparticles in such a fashion that their unique properties (such as, optical, electrical, and magnetic) can be utilized for different applications remains a challenge [109–151].

Processing of Polymer Nanocomposites

One of the main limitations in the commercialization of nanocomposites is their processing which involves with a major difficulty relating to proper dispersion of the nanofillers in the polymer matrix. This is mainly due to the impact of nanoparticles which are aggregated or agglomerated very easily due to the interparticle surface forces (e.g., van der Waals forces, capillary forces, and electrostatic forces) which often leads to undesirable materials properties. The processing of polymer nanocomposites has different type of impacts on the state of the arrangement of nanofiller in the nanocomposites that can be understood from the distribution and dispersion. The quality of nanofiller dispersion in the polymer matrix directly correlates with its effectiveness in the improvement of mechanical, electrical, thermal, impermeability, and other characteristics. In addition, the natures of a composite are also closely related to the aspect ratio and surface-to-volume ratio of the filler. Three general methods generally are involved with dispersing nanofillers in polymers, and they are (a) direct mixing of the nanoparticle and the polymer either as discrete phases or in solution phase, (b) in situ polymerization in the presence of the nanoparticles, and (c) in situ formation of the nanoparticles and in situ polymerization simultaneously. However, hybrid nanocomposites are prepared by the intimate mixing of the two phases ((a) + (b)) [109–225].

Direct Mixing

Direct mixing of the nanoparticle and the polymer can be carried out in different ways, such as in discrete phases or in solution phase. Polymer processing techniques (such as melt mixing or elastomeric mixing through roll mill, twin screw extruder, Brabender high-shear mixer, or thermal spraying) can be applied for direct mixing of the nanofillers and the polymer as discrete phases. For instance, nano silica (SiO_2)/polypropylene, nano alumina/poly(ethylene terephthalate) (PET) or low-density polyethylene (LDPE), and nanoparticle-filled nylon can be prepared using some of these techniques. However, the rapid increase of the viscosity in addition to significant volume fractions of nanofiller limits the viability of the processing technique. Solution-phase mixing is related to dissolving or dispersing the polymer and the nanoparticles in solution, and using solvent evaporation or precipitation technique, the nanoparticle/polymer solution can be cast into a film or can be isolated from solution. This technique allows to modify the particle surface without drying which reduces the chances of particle agglomeration and thereby helps to overcome some of the limitations of direct mixing.

For example, electrically conductive graphene/polymer nanocomposites were synthesized by solution-phase mixing of the exfoliated phenyl isocyanate-treated graphite oxide sheets with polystyrene, followed by their chemical reduction [151–177].

In Situ Polymerization

In situ polymerization refers to the dispersion of the nanofillers in the monomer or monomer solution followed by standard polymerization of the resulting mixture. Some examples include (a) nano SiO_2 /nylon 6, titania (TiO_2)/polymethylmethacrylate (PMMA), and calcium carbonate (CaCO_3)/PMMA. The potential feasibility to graft the polymer onto the particle surface is one of the main advantages of this method. One of the main points of this technique is the appropriate dispersion of the filler in the monomer which often relates to the modification of the nanoparticle surface. It is due to the settling process which is more rapid in a liquid than in a viscous melt although dispersion is easier. [109–121, 178–188].

In Situ Nanoparticle Processing/Formation

In situ nanoparticle processing or formation is another type of technique to produce nanoparticle-filled polymers. Ceramic/polymer composites can be synthesized using an in situ processing of the SiO_2 and TiO_2 in a range of polymer matrices by mixing SiO_2 or TiO_2 precursor with a polymer followed by the sol-gel reaction. There are reports on the processing of metal/polymer nanocomposites via an in situ formation of metal nanoparticles in the polymer matrix from suitable metal precursors where the presence of the protective polymer can prevent the agglomeration and limit the size of the nanoparticles. For example, the parameters which affect the size, stability, and morphology of as-formed nanoparticles have been reviewed. Primary parameters that control the nanoparticle size include the choice of metal precursor and the metal-polymer interaction. The nanoparticle size tends to reduce when the polymer has a stronger interaction with the metal precursor (since the precursors are prevented from phase separation) [129–157, 189–211]. Spherical micelle formation from amphiphilic block copolymers or crosslinked/gelled matrices have some

particular control over nanoparticle size and morphology. In this case, metal precursors either penetrate into the micelles or stabilize in the micelle corona, and thus metal nanoparticles can form either within the micelles or in corona after the addition of reducing agent which contributed to produce various morphological structures. Various conductive, semiconductive, or magnetic nanoparticles (such as gold, silver, palladium, platinum, semiconductors, and metal oxides) can be formed using this method which provides tremendous opportunity to tune the properties of these nanocomposite systems [158–179, 211–231].

Modification of Nanoparticle Interfaces

The interfacial region within the polymer matrix has properties significantly different from those of the bulk polymer. In addition, the local chemistry, degree of cure, chain mobility, chain conformation, and degree of chain ordering or crystallinity can vary continuously from the filler/polymer matrix boundary to some point in the bulk polymer. Nanofillers have many controlling effects on the resultant behaviors of polymer composites. Additionally, a specified size and shape that is controlled by the surface chemistry of nanoparticles is often needed to understand the special advanced functionalities for various studies and uses of polymer composites. The encapsulation of nanoparticles gives them important characters which are not usually present in the uncoated nanoparticles. For example, organic or inorganic coatings on metal or other inorganic particles improve compatibility with organic ingredients, protect particle surfaces from oxidation, and thus improve dispersibility, chemical stability, and so on. As a result, nanofiller interface modification is also essential [180–192, 232–243].

Modification of Nanoparticles by Organic Coatings

In this case, two principal techniques in order to modify the surface of inorganic nanoparticles with organic molecules are either connecting a short chain molecule onto the surface via grafting or strong hydrogen bonding or applying a polymer coating onto the surface via polymerization. Usually these coatings contribute to have the control over the compatibility of the modified nanoparticles with the polymer matrix and the strength of the interaction in between. For example, in the first method, hydroxyl groups on the metal and metal-oxide nanoparticle surface can react with a silane coupling agent, and the large variety of functionalities attached to the silanol modifies the nanoparticle surface with long or short, hydrophilic or hydrophobic, and linear or bulky chains. As a result, the strength of the interaction between the filler and the polymer matrix can be controlled from covalent bonding to repulsion, leading to increases or decreases in glass transition temperature, modulus, or other properties of nanocomposites. Many research activities are engaged with the control of the size and the degree of aggregation of nanoparticles. In addition, the coating layer with reactive sites on the nanoparticles can be used to bond particles together and also to control aggregation of the nanoparticles. Monomer adsorption and subsequent polymerization on the nanoparticle surface have been illustrated on micrometer-scale filler surfaces. In addition, another method involves the grafting on an initiator and then polymerizing a grafted polymer onto the nanoparticle surface. Besides this, a multilayer structure can be achieved on the nanoparticle surface by

self-assembled polymer layers by the use of layer-by-layer (LbL) colloid templating strategy. LbL assembly has the advantages of simplicity, universality, thickness control in nanoscale, low cost, and being environmentally friendly, and uniform multilayers can be formed by this approach on a number of 3D objects because of the conformal nature of the polyelectrolyte adsorption process besides the 2D surfaces. The buildup of polyelectrolyte multilayers on colloidal surfaces ranging in size from several micrometers down to nanometers has been illustrated. A frequently utilized method to create nanoparticle-loaded thin-film coatings on colloidal particles is via layer-by-layer assembly of a polyelectrolyte and preformed nanoparticles of an opposite surface charge, and this approach provides a simple route to create core-shell [109–119].

Inorganic Coatings

Inorganic coatings have also been applied to nanoparticles via precipitation or deposition of the inorganic species onto the particle surfaces by a sol-gel type process; for example, SiO₂, TiO₂, titanium nitride, and zirconia have been coated on nanoparticles, usually metal oxides, in this way [109–119].

Nanodielectrics

Nanodielectrics are a new class of dielectric material which emerges with the increased enthusiasm and activity toward the research on the nanotechnology, and it is also anticipated that nanocomposites are highly promising nanodielectrics. Dielectric polymer nanocomposites based on nanoparticles are a category of nanocomposites that provide a potential solution in order to meet the present and future technological demands, some of which are (a) the good processibility and (b) synergistic properties (such as mechanical properties of polymers combined with the unique electrical, magnetic, or dielectric properties of nanoparticles) of polymer nanocomposites. The heterogeneous inclusions although they are nonpolar sometimes cause heterogeneous dielectric polarization due to the accumulation of a virtual charge at the interface of two media with different permittivities or conductivities. Additionally, nano-sized particles are preferred for high-*k* dielectric composite materials due to the fact that they could help achieve thinner dielectric films leading to a higher specific capacitance. As a result, there is recent progress on the introduction of more nanoparticles of ceramic, metallic, or even organic semiconductor to prepare high-*k* dielectric materials [119–170].

8 Performance Enhancement of High-*k* Nanocomposites

8.1 Filler Size Effect

Several issues of nanoparticle-based dielectric composite materials require to be addressed. In this case, inner particle size is needed in order to obtain a thin dielectric film and also to increase the capacitance density. For example, in the case of ferroelectric ceramics, extremely fine particles may lead to the change of crystal structure from tetragonal that results from the high permittivity which is cubic or pseudo-cubic [109–131].

8.2 Micron-Sized Nanoparticles

BaTiO₃ powders disappear finally when the particle size decreases to approximately 100 nm and 60–70 nm, respectively. For example, there are reports on the synthesis of BaTiO₃/epoxy composite embedded capacitor films (ECFs) with average particle size of 916 nm (P1) and 60 nm (P2); the k values of ECFs made of P1 were higher than those made of P2. As a result, the coarser particle is more useful than the finer particle to obtain high- k of ECFs using unimodal powder in this case. However, by adopting bimodal fillers, fine nanoparticle can effectively improve the k values by maximizing packing density and removing the voids and pores formed in the dielectric films. A dielectric constant of about 90 was obtained at a frequency of 100 kHz by using these two different sizes of BaTiO₃ powders [109, 119–131].

8.3 Controlled Dispersion

Uniform dispersion of nanoparticles in nanocomposite materials is very important since nanoparticles have the capability to agglomerate which may lead to undesirable electrical or materials properties. Thus, the dispersion of nanoparticles is an extremely important contributor in order to achieve improved dielectric properties and reproducibility. Similarly, addition of surfactant or dispersant such as phosphate esters can enhance the dispersion of nanoparticles in polymer matrix in order to improve the overall film quality and dielectric performance of the nanocomposites. Chemical modification of nanoparticles is also a useful method to enhance the dispersion of nanoparticles. For example, surface modification of BaTiO₃ and related perovskite-type metal oxide nanoparticles with phosphonic acid ligands leads to well-dispersed BaTiO₃/polymer nanocomposite films with high dielectric strength. This methodology is straightforward and easily adapted to a wide range of systems by using appropriate ligand functionality [109, 119–135].

8.4 Control of Dielectric Loss for Conductive Filler/Polymer Nanocomposites

Conductive filler/polymer nanocomposites have been identified as a promising method in order to meet the material requirements for embedded capacitors. However, the dielectric loss of this type of materials is very difficult to control since the highly conductive particles are easy to form a conductive path in the composite as the filler concentration approaches the percolation threshold. Recently much work has been devoted to the control of the dielectric loss of this system to solve this drawback. In addition, the direct contact of the conductive metal fillers will lead to high dielectric loss or even conduction for the conductive filler/polymer composites at or above percolation threshold. Thus, core-shell structured fillers have the

potentials to be used as fillers instead of using conductive filler directly. It is due to the fact that the nonconductive shell can serve as electrical barrier between the conductive cores in order to form a continuous interparticle barrier layer network in order to achieve high- k and low loss [111–167, 243–248].

9 Dielectric Elastomers

Elastomers are polymers which show high degree of flexibility and low modulus when crosslinked and exhibit significant reversible deformations under applied mechanical stress. Elastomers are generally dielectrics with dielectric constant ranging from about 2 to 25. Cross-linked elastomers, alone or together with other compounding ingredients, are referred to as rubbers. Rubbers more frequently studied for dielectric elastomer actuator (DEA) applications include silicone (PDMS), polyacrylate, and polyurethane. Moreover, different pieces of research have been conducted on DEAs utilizing acrylonitrile-butadiene rubber (NBR), natural rubber (NR), chloroprene (CR), ethylene-propylene-diene (EPDM), fluorinated rubbers, and polyester-based elastomer [243–257]. Table 6 briefly shows the actuation response and particular features of some selected commonly used dielectric elastomers [257].

Table 6 Different particular features of some commonly used dielectric elastomers [257, 259–265]

Dielectric elastomer	Dielectric constant	Electric field, V/ μm	Coupling efficiency %	Strain, %	Young's modulus, MPa	Pressure, MPa	Elastic energy density, J/cm ³
Silicone nutil CF19–2186	2.8	235	54	32	1.0	1.36	0.22
Silicone DC HS3	2.8	72	64	41	0.125	0.13	0.026
Silicone DC Sylgard 186	2.8	144	54	32	0.7	0.51	0.082
Polyurethane Deerfield PT6100S	7.0	160	21	11	17	1.6	0.087
Fluorosilicone DC 730	6.9	80	48	28	0.5	0.39	0.055
Fluoroelastomer Lauren L143HC	12.7	32	15	8	2.5	0.11	0.0046
Isoprene natural Rubber	2.7	67	21	11	0.85	0.11	0.0059
SEBS161 Copolymer 5–30w% Midblock	1.7–2	133	80	Areal 180	0.007–0.163	–	0.151

9.1 Bioinspired Dielectric Elastomers

Nature provides ideas how to create new functional materials resembling those already existing in the biosphere where the bioinspired and biomimetic materials have recently gained a huge interest in the scientific community. It looks impossible to surpass the creations of Mother Nature; however, many recent pieces of research aim to develop artificial muscles for many potential industrial exploitations. In this context, artificial muscle is synonymous to muscle-like material, and such materials have been developed for non-biomedical applications rather than replacing natural muscles. Some of the possible applications of artificial muscles include (a) refreshable braille displays, (b) robotic arms and other moving parts, (c) loudspeakers, (d) optical zoom lenses, (e) active damping and force-feedback systems, and (f) energy generators. In addition, dielectric elastomers are currently investigated for their uses as smart materials for their potential applications in muscle-like actions. To a good extent, dielectric elastomers have some attractive features suitable to resemble the natural muscles, and some of the important features are (a) strain, (b) actuation pressure, (c) density, (d) efficiency, and (e) response speed. Compared to other electroactive polymers, dielectric elastomers are attractive because of their overall desired features like their high strains and relatively cheaper cost. Thus, rigorous current researches in this area are focused on their cost-effective multipurpose high-tech applications [226–236, 243–257].

9.2 Different Aspects of Dielectric Elastomers

Dielectrics work as insulators which can be polarized when subject to an electric field. Among the dielectric polymers, dielectric elastomers fall in one of the important category of dielectric polymers which are soft electroactive materials that can be developed as electromechanical transducers and convert energy from one form to another. Dielectric elastomers which transduce electrical energy to mechanical energy when they act on actuator mode can also convert mechanical energy to electrical energy in a reverse mode (such as generator mode). Dielectric elastomers are usually crosslinked above the glass transition temperature of polymer materials which have lower shear moduli (a few kilopascal) and more mechanical compliance compared with the stiff or hard dielectrics with moduli of a few gigapascal and achievable strains typically less than 1% (like piezoelectric crystals and ceramics) [226–236]. Dielectric elastomers are capable of undergoing a large voltage-induced deformation and have other characteristic properties, some of which include high energy density, softness, and flexibility. These materials have been used and also explored for many applications including in (a) artificial muscles, (b) programmable haptic surfaces, (c) conformal loudspeakers, (d) energy harvesters, (e) tunable lens, (f) soft robots, (g) sensors of force and pressure, (h) active noise control devices, (i) oscillators, and (j) resonators and adaptive optical elements [226–236, 257–260].

9.3 Large Deformation Capability and Typical Failure Modes of Dielectric Elastomers

Dielectric elastomers (DEs) have many advantages (such as large deformation capability), but this voltage-induced deformation capability of dielectric elastomers is strongly affected by multiple failure modes. The actuation of DEs is also limited by electrical breakdown (EB) failure similar to any other dielectric materials. The material rupture and the electrical breakdown because of the electric field induced by the applied voltage sometimes can exceed the dielectric strength of the material. The determination of the dielectric strength of dielectric elastomers presents many challenges due to the impacts of a number of influencing factors [237–246]. The dielectric strength of dielectric elastomers monotonically increased with the increasing stretch ratio while decreased with the increasing thickness. The dielectric constant of dielectric elastomers is non-monotonic to the temperature. The configuration of the electrodes on the dielectric elastomers and the loading rate of the applied voltage have significant effect on the dielectric strength of dielectric elastomers [247–251]. A constant dielectric strength is commonly assumed in the theoretical analysis on dielectric elastomers, because the mechanisms related to these phenomena are not well understood. The compliant electrodes coated on the dielectric elastomer membrane exert no constraint to both the top and bottom surfaces, when an electric voltage is applied to the electrodes. The induced electric field along the thickness direction forces the unconstrained dielectric elastomer membrane to contract in thickness and stretch in area. The thickness reduction of the dielectric elastomer membrane in turn causes a higher electric field under the same applied voltage which results in a higher attractive electrostatic force to further thin down the dielectric elastomer membrane. This feedback mechanism may lead to excessive thinning of the dielectric elastomer and results in the electromechanical instability (EMI) (or pull-in instability), at a particular level of the applied voltage. This excessive thinning may cause a premature electrical breakdown or result in a desirable large deformation which depends on the dielectric strength of the dielectric elastomer. As the advantages of dielectric elastomers mainly present in their capability of undergoing large deformation, much effort has been devoted in order to tackle the EMI to improve the actuation performance or even to harness the EMI for giant voltage-induced deformation of dielectric elastomers [252–256].

10 Dielectric Breakdown of Other Polymers

Dielectric breakdown is the catastrophic failure of an insulating material under an external applied field resulting in mechanical damage and electrical conduction, depending upon the defect density of a solid material or a dielectric polymer. Electrical breakdown testing of polymers for insulator applications has long been a subject of interest. Table 7 is a selective compilation of the dielectric strengths of some commonly used polymers [257, 259–269].

Table 7 List of dielectric strengths of insulating polymers [257, 259–265]

Polymer	Dielectric strength (V/ μm)
Polyester	300
Polyimide	280
Polycarbonate	252
Polyethylene	200
Polypropylene (biaxially oriented)	200
Polytetrafluoroethylene	88–176
Epoxy resin	25–45

10.1 Dielectric Breakdown Behavior of Polymer Composites and Nanocomposites

Active current research activities are focused on enhancing dielectric properties of composites and nanocomposites based on a wide range of polymers and other materials (such as inorganic fillers and organic-inorganic hybrid systems). For example, in a study, inorganic filler has been added to polymers in order to increase the effective dielectric constant and energy density [269]. Typically used filler particles in conventional composites are very little in size (such as micron-sized or larger). However, the addition of micron-sized fillers has often had a negative impact on breakdown strength which may be due to aggregation of filler particles which may introduce defect centers that distort and enhance the local electric field that results in reduced breakdown strength [269]. This type of field distortion is mainly due to the difference in permittivities of the filler and the polymer matrix under alternating current (AC) conditions and may also be due to differences in conductivities under direct current (DC) conditions. Similar types of results are also observed in related other studies [269–278].

11 Recent Trends in Dielectric Polymer Applications

Dielectric polymers have wide range of applications including in (a) electrical insulation, (b) dielectric capacitors, and (c) electromechanical actuators. Some dielectric polymers show large strain deformations when exposed to electric field (also called dielectric elastomers, as already stated in a previous section) due to their relative low modulus, high elongation at break, and outstanding resilience characters. Dielectric elastomers can be used as actuators which have many advantages over traditional transducers, some of which include – (a) large strains, (b) high energy densities, (c) high coupling efficiency, (d) quiet operation, and (e) light weight. There are many applications of dielectric polymers and a growing interest has recently been shown on fluorinated materials which show the desired characteristics. Advanced pulsed power and power conditioning technologies for power generation/regulation and all electric vehicles/ships need a capacitor material in order to achieve a high discharged electric energy density as well as low loss

performance. Besides this, advanced dielectric applications including power conditioning, electric launch platform, and all electrical or hybrid vehicles require a polar material, because of their large effective dielectric constants and in turn high electrical energy storage [279–289]. For example, PVDF is very popular among commercially available polymer capacitor films, due to its high dielectric constant and high dc breakdown strength. Electrical and electronic applications and future trends of fluoropolymers based on vinylidene fluoride (e.g., jacketing of cables for plenum areas including signaling, communication, and power lines, insulating compounds for jacketing wires and cable assemblies, cathodic protection, industrial power control systems, high temperature wiring, and wire and cable sheathing) are worth to mention here. Fluorinated materials prepared from different polymorphisms and crystallite sizes have been achieved in PVDF and P(VDF-*stat*-HFP) (HPF, hexafluoropropene) films, and the practical applications of ferroelectric polymers for advanced high energy density dielectric film capacitors have been reported [122–132]. A significantly reduced ferroelectric loss and relatively high discharged energy density were investigated due to this antiferroelectric-like behavior even at high poling fields. Most recently, there are reports on multilayer films for high energy density storage. The 65-layer poly(carbonate)/poly(methyl methacrylate)/Poly(VDF-*co*-HFP) (PC/PMMA/ Poly(VDF-*co*-HFP)) system showed a 25% enhanced dielectric breakdown strength, 50% higher energy density, 40% decreased hysteresis loss energy density, and slower ion migration behavior. The improved dielectric properties were attributed to the high interactivity between PMMA layers and both PC and poly(VDF-*co*-HFP) layers. In addition, cyano polymers bearing CN groups are interesting as dielectric materials. Piezoelectricity of the poly(VCN-*alt*-VA) copolymer, stimulated investigations on the copolymerization of cyano-containing monomers with various vinyl and diene comonomers. Electrical characteristics of copolymers based on acrylonitrile have also been reported. Polar polymers containing C–F and C–CN (alternating copolymers of VCN, block copolymers of PVDF, and random copolymers of AN) are a potential candidate as dielectric materials and find many applications in the field above [290–302].

11.1 Microelectronic and Dielectric Polymers

Microelectronic industry uses a variety of polymers, some of which include (a) epoxies, (b) silicones, (c) benzocyclobutenes (BCB), and (d) polyimides (PI), and can be applied different techniques such as by spin on or various coating methods followed by a moderate temperature cure. As a result, these polymer dielectrics are similar to the organic printed wiring board (PWB) manufacture. Usually, polymers have low dielectric constant in the range of 2 to 5 (e.g., approx. 2.5 for polystyrene, approx. 2.65 for BCB, approx. 2.7 for parylene, approx. 2.72 for silicone, and approx. 3.5 for epoxy and polyimide). These modest k values combined with relatively thick layers in 5–50 μm result in specific capacitances which are usually from only 0.07 to 0.3 nF/cm² that make polymer materials useful to embed only the smallest valued capacitors into the board. It is possible to deposit polymer

dielectric layers which are from 2 to 5 μm through coating and curing liquid resins that can contribute for a significant increase of their specific capacitance up to around 1.5 nF/cm^2 . Due to para-electric nature of some polymers, the resultant capacitance is stable with regard to temperature, frequency, and the like. In addition, the dissipation factor of polymers is also very low which is usually much lower than ferroelectric ceramics. Epoxy resins have been of particular interest for embedded capacitor applications due to its compatibility with PWB manufacturing process. In addition, an epoxy system is basically composed of epoxy resin which works as hardener and catalyst as well as the adjusting nature of the dielectric constant of epoxy which can be tailored the components of epoxy system. For instance, the dielectric constant of epoxy system can be enhanced to a significant extent from 3.2 to 5.0 by proper choice of the catalyst (e.g., metal acetylacetonate). Due to polar backbone of ferroelectric polymers compared to conventional polymers, these polymers can have higher k values (which may be above 10). For instance, at 1 kHz and 25°C , pure poly(vinylidene fluoride) (PVDF) polymer shows a k value of about 11. Besides this, poly(vinylidene fluoride-trifluoroethylene) (P(VDF-TrFE)) copolymer is a type of relaxor ferroelectric which can have a relatively high- k around 40 at room temperature after irradiation treatment. For example, a report stated the method of synthesis of polyvinylidene fluoride-trifluoroethylenechlorotrifluoroethylene [P(VDF-TrFE-CTrFE)] terpolymers in order to obtain a similar structure as irradiated P(VDF-TrFE) copolymer by introducing CTrFE block in the polymer (which done to avoid the requires of irradiation process that needs expensive and complicated equipment). It was reported that P(VDF-TrFE-CTrFE) terpolymer with VDF: Tr-Fe:CTrFE molar ratio of 65:35:9 showed a high- k of about 60 (@ 1 kHz) at 33°C , and its dielectric loss tangent was about 0.1. In addition, its dielectric constant can be as high as 320 (@ 10 kHz) at 145°C , whereas the abovementioned high- k polymers have non-conjugated backbones. Besides this, in the case of a conductive polymer with conjugated backbone the k value can be even higher [290–302].

12 Challenges for Embedded Capacitor Materials and Dielectric Polymers and Composites and Future Perspectives

Different states of progress in the field of high- k materials for embedded capacitor applications have been briefly presented in the previous sections. In usual terms, certain types of high- k materials show different properties which make them suitable for a variety of applications. Some of these properties include (a) high dielectric constant, (b) low dissipation factor, (c) high thermal stability, (d) simple processibility, and (e) good dielectric properties over broad frequency range. However, there is no such ideal materials that satisfy all of the abovementioned properties realized till today. In this connection, polymer nanocomposites present the most promising features which have been studied extensively, and efforts to enhance the overall dielectric performance of these nanocomposites have been focused in order to maximize the dielectric constant and also to suppress the dielectric loss. In order

to enhance dielectric property of high- k nanocomposites, new insights into the unique properties of the nanoparticle filler, filler modification, and the dispersion between filler and polymer matrix are anticipated. In specific terms some of the required knowledge and technology which have been used in this direction include (a) optimizing dielectric materials with high filler loading of high- k ceramics for ceramic-polymer nanocomposites and appropriate loading level of conductive fillers in the neighborhood of percolation threshold for conductive filler-polymer nanocomposites; (b) improving microstructure of dielectric materials (which include filler size and distribution, morphology, degree of aggregation, packing, and dispersion in the polymer matrix); (c) enhancing k values of nanocomposites by using high- k polymer matrix; and (d) modifying the filler interface in order to facilitate dispersion in the polymer matrix and also to suppress the dielectric loss of the composite materials.

13 Conclusions

Dielectric polymers work as insulators which implies that no current will flow through the polymer when a voltage is applied to it although certain changes do happen at the atomic scale. For instance, when a voltage is applied across a dielectric polymer, it becomes polarized where the polarization is an effect which slightly shifts electrons toward the positive voltage due to the fact that atoms are made of a positively charged nucleus and negatively charged electrons. These charges do not travel far enough to create a current flow through the dielectric material, because the shift is very tiny, however the effect is very significant particularly when they are used in capacitors. In addition, when the voltage source is removed from the material, it either returns to its original nonpolarized state or stays polarized if the molecular bonds in the material are weak. The distinction between the term dielectric and insulator is very thin, for example, all dielectric materials are insulators; however, a good dielectric is one which is easily polarized. When a certain voltage is applied to an object, it influences the amount of electrical energy and it also causes to generate the amount of polarization which is stored in the electric field, typically it is termed as the dielectric constant of the material. Due to ever-growing requirements of miniaturization, increased functionality, high performance, and low cost for microelectronic products and packaging, new and unique solutions in integrated circuits (IC) and system integrations (e.g., system on chip or SOC, system in package or SiP, system on package or SOP) have been the topics of current active research interests. In addition, embedded passives are one of the key emerging techniques for realizing the system integration. In this case, as an alternative to discrete components, embedded passives offer various advantages some of which include (a) higher component density, (b) increased functionality, (c) improved electrical performance, (d) increased design flexibility, (e) improved reliability, and (f) reduced unit cost. Additionally, novel materials for embedded capacitor applications are in great demand, for which a high dielectric constant (k), low dielectric loss, and process compatibility with printed circuit boards (PCBs) are some of the most important prerequisites. However, to date, it is very difficult to find materials which can

satisfy all desired requirements. In this context, conductive filler/polymer composites are very promising materials which can demonstrate a dramatic increase in their dielectric constant close to the percolation threshold. One of the major challenges for this type of high- k composites is the high dielectric loss inherent in these systems. As a result, there have been many investigations to designed and developed nanocomposites based on nanoparticles with controlled parameters in order to fulfill the balance between sufficiently high- k and low dielectric loss, which satisfied the requirements for embedded capacitor applications. This chapter selectively and briefly stated different features of dielectric polymers (both pristine polymers and composite polymers doped or coated with inorganic dielectric materials) and their applications and related aspects. It also briefly stated different aspects of dielectric elastomers and their applications along with the different applications of dielectric polymers, in general. Detailed explanation and in-depth analysis of various topics related to dielectric polymers and their specific application mechanisms in different devices are beyond the scope of this chapter, so interested readers are advised to consult related books and references, some of which are included in the reference section.

References

1. H. S. Nalwa (ed.), *Ferroelectric Polymers: Chemistry, Physics and Applications* (Marcel Dekker, New York, 1995), pp. 5–75
2. G.S. Neugschwandtner, R. Schwödauer, M. Vieytes, S. Bauer-Gogonea, S. Bauer, J. Hillenbrand, R. Kressmann, G.M. Sessler, M. Paajanen, J. Lekkala, Large and broadband piezoelectricity in smart polymer-foam spacecharge electrets. *Appl. Phys. Lett.* **77**, 3827–3829 (2000)
3. J. Peltonen, M. Paajanen, J. Lekkala, Determination of the actuator sensitivity of electromechanical polypropylene films by atomic force microscopy. *J. App. Phys.* **88**, 4789–4793 (2000)
4. Y. Shi, C. Zhang, H. Zhang, J.H. Bechtel, L.R. Dalton, B.H. Robinson, W.H. Steier, Low (Sub-1-volt) Halfwave voltage polymeric electro-optic modulators achieved by controlling Chromophore shape. *Science* **288**, 119–122 (2000)
5. Q.M. Zhang, V. Bharti, X. Zhao, Giant electrostriction and Relaxor ferroelectric behavior in Electron-irradiated poly(vinylidene fluoridetrifluoroethylene) copolymer. *Science* **280**, 2101–2104 (1998)
6. Q.M. Zhang, H. Li, M. Poh, F. Xia, Z.-Y. Cheng, H. Xu, C. Huang, An all-organic composite actuator material with a high dielectric constant. *Nature* **419**, 284–287 (2002)
7. H. Nalwa, *Handbook of Low and High Dielectric Constant Materials and their Applications* (Academic Press, London, 1999), pp. 2–93
8. T. Osaka, M. Datta, *Energy Storage Systems for Electronics* (Gordon and Breach, Amsterdam, 2001), pp. 3–75
9. C. Brosseau, Modelling and simulation of dielectric heterostructures: A physical survey from an historical perspective. *J. Phys. D. Appl. Phys.* **39**, 1277–1294 (2006)
10. V. Myroshnychenko, C. Brosseau, Finite-element modeling method for the prediction of the complex effective permittivity of two-phase random statistically isotropic heterostructures. *J. Appl. Phys.* **97**, 044101 (2005)
11. Y. Rao, J. Qu, T. Marinis, C.P. Wong, A precise numerical prediction of the effective dielectric constant for polymer-ceramic composite based on effective-medium theory. *IEEE Trans. Comp. Pack. Tech.* **23**, 680–683 (2000)
12. K.L. Ying, T.E. Hsieh, Sintering behaviors and dielectric properties of nanocrystalline barium titanate. *Mater. Sci. Eng. B-Sol. St. Mater. Adv. Technol.* **138**, 241–245 (2007)

13. D.-H. Yoon, J. Zhang, B.I. Lee, Dielectric constant and mixing model of barium titanate composite thick films. *Mater. Res. Bull.* **38**, 765–772 (2003)
14. Y. Rao, C.P. Wong, Material characterization of a high-dielectric constant polymer-ceramic composite for embedded capacitor for RF applications. *J. Appl. Polym. Sci.* **92**, 2228–2231 (2004)
15. M.G. Todd, F.G. Shi, Complex permittivity of composite systems: A comprehensive interphase approach. *IEEE Dielect. El. In.* **12**, 601–611 (2005)
16. H.T. Vo, F.G. Shi, Towards model-based engineering of optoelectronic packaging materials: Dielectric constant modelling. *Microelec.* **33**, 409–415 (2002)
17. P. Murugaraj, D. Mainwaring, N. Mora-Huertas, Dielectric enhancement of polymer-nanoparticle through interphase polarizability. *J. App. Phy.* **98**, 054304 (2005)
18. Z. Yu, C. Ang, L.E. Cross, A. Petchsuk, T.C. Chung, Dielectric and electroactive strain properties of poly(vinylidene fluoride-trifluoroethylene-chlorotrifluoroethylene) terpolymers. *Appl. Phys. Lett.* **84**, 1737–1739 (2004)
19. J. Joo, S.M. Long, J.P. Pouget, E.J. Oh, A.G. MacDiarmid, A.J. Epstein, Charge transport of the mesoscopic metallic state in partially crystalline polyanilines. *Phys. Rev. B* **57**, 9567–9579 (1998)
20. R. Gregorio, M. Cestari, F.E. Bernardino, Dielectric behavior of thin films of beta-PVDF/PZT and beta-PVDF/BaTiO₃ composites. *J. Mat. Sci.* **31**, 2925–2930 (1996)
21. Y. Bai, Z.Y. Cheng, V. Bharti, H.S. Xu, Q.M. Zhang, High-dielectric-constant ceramic-powder polymer composites. *Appl. Phys. Lett.* **76**, 3804–3806 (2000)
22. K. Mazur, Polymer-ferroelectric ceramic composites, in *Ferroelectric Polymers: Chemistry, Physics, and Applications*, ed. by H.S. Nalwa, (Marcel Dekker Inc., New York, 1995)
23. D.K. Dasgupta, K. Doughty, Polymer-ceramic composite materials with high dielectric constants. *Th. Sol. Film.* **158**, 93–105 (1988)
24. S. Liang, S. Chong, E. Giannelis, Barium titanate/epoxy composite dielectric materials for integrated thin film capacitors, Proceedings of 48th Electronic Components and Technology Conference, pp. 171–175, 1998
25. H. Windlass, P.M. Raj, D. Balaraman, S.K. Bhattacharya, R.R. Tummala, Processing of polymer-ceramic nanocomposites for system-on-package applications, Proceedings of the 51st Electronic Components and Technology Conference, pp. 1201–1206, 2001
26. Y. Rao, S. Ogitali, P. Kohl, C.P. Wong, Novel polymer-ceramic nanocomposite based on high dielectric constant epoxy formula for embedded capacitor application. *J. Appl. Polym. Sci.* **83**, 1084–1090 (2002)
27. Z.M. Dang, Y.H. Lin, C.W. Nan, Novel ferroelectric polymer composites with high dielectric constants. *Adv. Mat.* **15**, 1625–1629 (2003)
28. S.D. Cho, J.Y. Lee, J.G. Hyun, K.W. Paik, Study on epoxy/BaTiO₃ composite embedded capacitor films (ECFs) for organic substrate applications. *Mater. Sci. Eng. B* **110**(3), 233–239 (2004)
29. R. Popielarz, C.K. Chiang, R. Nozaki, J. Obrzut, Dielectric properties of polymer/ferroelectric ceramic composites from 100 Hz to 10 GHz. *Macromolecules* **34**, 5910–5915 (2001)
30. M. Arbatti, X.B. Shan, Z.Y. Cheng, Ceramic-polymer composites with high dielectric constant. *Adv. Mater.* **19**, 1369–1372 (2007)
31. P. Kim, S.C. Jones, P.J. Hotchkiss, J.N. Haddock, B. Kippelen, S.R. Marder, J.W. Perry, Phosphonic acid-modified barium titanate polymer nanocomposites with high permittivity and dielectric strength. *Adv. Mater.* **19**, 1001–1005 (2007)
32. Y. Rao, C.P. Wong, J. Xu, Ultra high k polymer metal composite for embedded capacitor application, US Patent 6864306, 2005
33. J. Xu, C.P. Wong, Low loss percolative dielectric composite. *Appl. Phys. Lett.* **87**, 082907 (2005)
34. Z.M. Dang, Y. Shen, C.W. Nan, Dielectric behavior of three-phase percolative Ni-BaTiO₃/Polyvinylidene fluoride composites. *Appl. Phys. Lett.* **81**, 4814–4816 (2002)

35. H.W. Choi, Y.W. Heo, J.H. Lee, J.J. Kim, H.Y. Lee, E.T. Park, Y.K. Chung, Effects of BaTiO₃ on dielectric behavior of BaTiO₃-Ni-polymethylmethacrylate composites. *Appl. Phys. Lett.* **89**, 132910 (2006)
36. P. M. Raj, D. Bahaman, V. Govind, L. Wan, R. Abothu, R. Gerhardt, S. Bhattacharya, M. Swaminathan, R. Tununala, High frequency characteristics of nanocomposite thin film ‘Supercapacitors’ and their suitability for embedded decoupling, Proceedings of the 54th IEEE Electronic Components and Technology Conference, Las Vegas, NV, pp. 154–161, 2004
37. J. Xu, C.P. Wong: Super high dielectric constant carbon black-filled polymer composites as integral capacitor dielectrics, Proceedings of the 54th IEEE Electronic Components and Technology Conference, Las Vegas, NV, pp. 536–541, 2004
38. H. Xu, Z. Dang, M. Jiang, S. Yao, J. Bai, Enhanced dielectric properties and positive temperature coefficient effect in the binary polymer composites with surface modified carbon black. *J. Mat. Chem.* **18**, 229–234 (2008)
39. L. Qi, B.I. Lee, S. Chen, W.D. Samuels, G.J. Exarhos, High-dielectric-constantsilver-epoxy composites as embedded dielectrics. *Adv. Mat.* **17**, 1777–1781 (2005)
40. Y. Shen, Y. Lin, M. Li, C.-W. Nan, High dielectric performance of polymer composite films induced by a percolating interparticle barrier layer. *Adv. Mat.* **19**, 1418–1422 (2007)
41. Q.M. Zhang, H.F. Li, M. Poh, F. Xia, Z.Y. Cheng, H.S. Xu, C. Huang, An allorganic composite actuator material with a high dielectric constant. *Nature* **419**, 284–287 (2002)
42. J. Wang, Q. Shen, C. Yang, Q. Zhang, High dielectric constant composite of P(VDFTrFE) with grafted copper phthalocyanine oligmer. *Macromolecules* **37**, 2294–2298 (2004)
43. C. Huang, Q.M. Zhang, J. Su, High dielectric constant all polymer percolative composites. *Appl. Phys. Lett.* **82**, 3502–3504 (2003)
44. High-k Transistor, Advanced Process Technology. NEC Electronics Corporation, 2005; <https://www.nec.com/en/global/techrep/journal/g06/n05/g0605pa.html>, accessed on 14th July 2018
45. IBM and Intel make high-k gate breakthrough, Compound semiconductor net, 2007, https://compoundsemiconductor.net/article/84384/IBM_and_Intel_make_high-k_gate_breakthrough, accessed on 14th July 2018
46. R.D. Shannon, Dielectric polarizabilities of ions in oxides and fluorides. *J. Appl. Phys.* **73**(1), 348 (1993)
47. G.D. Wilk, R.M. Wallace, J.M. Anthony, Hafnium and zirconium silicates for advanced gate dielectrics. *J. Appl. Phys.* **15**(1), 484 (2000)
48. S. Ezhilvalavan, T. Tseng, Conduction mechanisms in amorphous and crystalline Ta₂O₅ thin films. *J. Appl. Phys.* **83**(9), 4797 (1998)
49. D. Park, Y. King, Q. Lu, T.-J. King, C. Hu, A. Kalnitsky, S.-P. Tay, C.-C. Cheng, Transistor characteristics with Ta₂O₅ gate dielectric, *IEEE Elec. Dev. Lett.* **19**, 441 (1998)
50. J. Robertson, Band offsets of wide-band-gap oxides and implications for future electronic devices. *J. Vac. Sci. Tech. B: Microelec. Nanomet. Struc.* **18**(3), 1785 (2000)
51. M.C. Tarplee, V.P. Madangagly, Q. Zhang, T.S. Surdarshan, Design rules for field pate edge termination in SiC Schottky diodes, *IEEE trans. El. Dev.* **48**, 2659 (2001)
52. D.C. Sheridan, G. Niu, J.N. Merrett, J.D. Cresler, C. Ellis, C.C. Tin, Design and fabrication of planar guard ring termination for high voltage SiC diodes. *Sol. St. Electron.* **44**, 1367 (2000)
53. G. Brezeanu, M. Badila, M. Brezeanu, F. Udrea, C. Boianceanu, I. Enache, F. Draghici, A. Visoreanu, Breakdown performances improvements of SiC diodes using high-k dielectrics, in Proc. of the 28nd International Semiconductor Conference, 2–4 Oct, 2005, Sinaia, Romania, p. 357
54. M. Brezeanu, M. Badila, G. Brezeanu, F. Udrea, C. Boianceanu, G.A.J. Amaratunga, K. Zekentes, An Effective Field Plate Termination for SiC Devices Based on High-k Dielectrics, Proceedings of International Conference on Silicon Carbide and Related Materials-ICSCRM 2005, 18–23 Sept, 2005, Pittsburg, USA, p.21
55. R.D. Shannon, Dielectric polarizabilities of ions in oxides and fluorides. *J. Appl. Phys.* **73**(1), 348 (1993)

56. G.D. Wilk, R.M. Wallace, J.M. Anthony, Hafnium and zirconium silicates for advanced gate dielectrics. *J. Appl. Phys.* **15**(1), 484 (2000)
57. S. Ezhilvalavan, T. Tseng, Conduction mechanisms in amorphous and crystalline Ta₂O₅ thin films. *J. Appl. Phys.* **83**(9), 4797 (1998)
58. D. Park, Y. King, Q. Lu, T. King, C. Hu, A. Kalnitsky, S. Tay, C.C. Cheng, Transistor characteristics with Ta₂O₅ gate dielectric. *IEEE Electron Device Letters* **19**(1), 441
59. J. Robertson, Band offsets of wide-band-gap oxides and implications for future electronic devices. *Journal of Vacuum Science & Technology B: Microelec. Nanomet. Struc* **18**(3), 1785 (2000)
60. M.C. Tarplee, V.P. Madangagly, Q. Zhang, T.S. Surdarshan, Design rules for field pte edge termination in SiC Schottky diodes. *IEEE Trans. El. Dev.* **48**, 2659 (2001)
61. D.C. Sheridan, G. Niu, J.N. Merrett, J.D. Cresler, C. Ellis, C.C. Tin, Design and fabrication of planar guard ring termination for high voltage SiC diodes, *solid St. Electron.* **44**, 1367 (2000)
62. (a) J.H. Lee, S.H. Kim, G.H. Kim, J.I. Lee, Y.S. Yang, H.Y. Chu, J. Oh, L.M. Do, T. Zyung, Organic transistors using polymeric gate dielectrics. *J. Kor. Phys. Soc.* **42**, S614-S617 (2013); (b) G. Brezeanu, M. Badila, M. Brezeanu, F. Udrea, C. Boianceanu, I. Enache, F. Draghici, A. Visoreanu, Breakdown performances improvements of SiC diodes using high-k dielectrics, in *Proc. of the 28nd International Semiconductor Conference*, 2–4 Oct, 2005, Sinaia, Romania, p. 357
63. M. Brezeanu, M. Badila, G. Brezeanu, F. Udrea, C. Boianceanu, G.A.J. Amaratunga, K. Zekentes, An Effective Field Plate Termination for SiC Devices Based on High-k Dielectrics, in *Proc. of International Conference on Silicon Carbide and Related Materials-ICSCRM 2005*, 18–23 Sept, 2005, Pittsburg, USA, p. 21
64. F. Xia, L. Jiang, Bio-inspired, smart, multiscale interfacial materials. *Adv. Mat.* **20**(15), 2842–2858 (2008)
65. Pelrine R, Kornbluh RD, Pei Q, et al., Dielectric elastomer artificial muscle actuators: toward biomimetic motion, *Proceedings of SPIE 4695, Smart Structures and Materials 2002: Electroactive Polymer Actuators and Devices (EAPAD)*, 10 July 2002, pp. 126–137
66. P. Brochu, Q. Pei, Advances in dielectric elastomers for actuators and artificial muscles. *Macromol. Rap. Comm.* **31**(1), 10–36 (2010)
67. C. Löwe, X. Zhang, G. Kovacs, Dielectric elastomers in actuator technology. *Adv. Eng. Mat.* **7** (5), 361–367 (2005)
68. R. Shankar, T.K. Ghosh, R.J. Spontak, Dielectric elastomers as next-generation polymeric actuators. *Sof. Mat.* **3**(9), 1116–1129 (2007)
69. Y. Bar-Cohen, Biomimetics: Nature-based innovation, chapter 6. Electroactive polymer actuators as artificial muscles, in *Electroactive Polymer Actuators as Artificial Muscles*, ed. by B.-C. Yoseph, (CRC Press, 2011), pp. 1–53
70. (a) T.B. Singh, N.S. Sariciftci: Progress in plastic electronics devices. *Annu. Rev. Mater. Res.* **36**, 199–230 (2006); (b) T. Mirfakhrai, J.D.W. Madden, R.H. Baughman, Polymer artificial muscles. *Mat. Tod.* **10**(4): 30–38 (2007)
71. K.J. Kim, S. Tadokoro (eds.), *Electroactive Polymers for Robotic Applications: Artificial Muscles and Sensors* (Springer, 2007), pp. 1–43
72. G. Gallone, F. Galantini, F. Carpi, Perspectives for new dielectric elastomers with improved electromechanical actuation performance: Composites versus blends. *Polym. Int.* **59**(3), 400–406 (2010)
73. L. Chen, C. Liu, K. Liu, C. Meng, C. Hu, J. Wang, S. Fan, High-performance, low-voltage, and easy-operable bending actuator based on aligned carbon nanotube/polymer composites. *ACS Nano* **5**(3), 1588–1593 (2011)
74. H. Stoyanov, M. Kolloosche, S. Risse, D.N. McCarthy, G. Kofod, Elastic block copolymer nanocomposites with controlled interfacial interactions for artificial muscles with direct voltage control. *Sof. Mat.* **7**(1), 194–202 (2011)
75. F. Carpi, D.D. Rossi, R. Kornbluh, R. Pelrine, P. Sommer-Larsen, *Dielectric Elastomers as Electromechanical Transducers: Fundamentals, Materials, Devices, Models and Applications of an Emerging Electroactive Polymer Technology*, 1st edn (Academic Press, 2008), pp. 2–96

76. J. B. Birks (ed.), *Modern Dielectric Materials* (Heywood & Company, London, 1960), pp. 1–23
77. A. Maliakal, Chapter 3.2 Dielectric materials: Selection and design, in *Organic Field-Effect Transistors*, ed. by Z. Bao, J. Locklin (CRC Press, 2007), pp. 229–251
78. D.W. Van Krevelen, K.T. Nijenhuis, Chapter 11 - electrical properties, in *Properties of Polymers*, ed. by D.W.V. Krevelen, K.T. Nijenhuis, 4th edn., (Elsevier, Amsterdam, 2009), pp. 319–354
79. E. Riande, R. Diaz-Calleja, *Electrical Properties of Polymers* (Marcel Dekker, New York, 2004), pp. 632–657
80. (a) L.A. Wall, *Fluoropolymers* (Wiley Interscience, New York, 1972), pp. 1–79; (b) A.E. Feiring, Fluoroplastics, in *Organofluorine Chemistry: Principles and Commercial Applications*, ed. by R.E. Banks, B.E. Smart, J.C. Tatlow (Plenum Press, New York, 1994), pp. 339–372; (c) B. G. Willoughby, R. E. Banks, Fluoropolymers, in *Encyclopedia of Advanced Materials*, ed. by B.G. Bloor, R.J. Brook, M.C. Flemings, S. Mahajan, R.W. Cahn (Pergamon: Oxford, UK, 1994), pp. 887–895
81. R. Seilers, Chapter 25: Polyvinylidene fluoride in the chemical industries, in *Modern Fluoropolymers*, ed. by J. Scheirs (New York, Wiley, 1997), pp. 487–506
82. G. Hougham, P.E. Cassidy, K. Johns, T. Davidson, *Fluoropolymers: Synthesis and Applications*, vol 1–2 (Plenum Press, New York, 1999)
83. B. Ameduri, B. Boutevin, *Well-Architected Fluoropolymers: Synthesis, Properties and Applications* (Elsevier, Amsterdam, 2004), pp. 1–93
84. B. Ameduri, From Vinylidene fluoride (VDF) to the applications of VDF-containing polymers and copolymers: Recent developments and future trends. *Chem. Rev.* **109**(12), 6632–6686 (2009)
85. (a) B. Baradie, M.S. Shoichet, Synthesis of Fluorocarbon–Vinyl Acetate Copolymers in Supercritical Carbon Dioxide: Insight into Bulk Properties, *Macromolecules*: **35**(9), 3569–3575 (2002); (b) F. Boschet, B. Ameduri, *Chem. Rev.* **114**, 927 (2014)
86. (a) Y. Patil, H. Hori, H. Tanaka, T. Sakamoto, B. Ameduri, First radical homopolymerisation of 2-trifluoromethacrylic acid in water and study of the degradation of the resulting homopolymers, *Chem. Commun.* **49**, 6662–6664 (2013); (b) Y. Patil, B. Ameduri, *Prog. Polym. Sci.* **38**, 703 (2013)
87. A.J. Lovinger, G.T. Davis, T. Furukawa, M.G. Broadhurst, Structural and dielectric investigation on the nature of the transition in a copolymer of vinylidene fluoride and trifluoroethylene (52/48 mol %). *Macromolecules* **5**(2), 329–333 (1982)
88. (a) M. Raihane, B. Ameduri, Radical copolymerization of 2,2,2-trifluoroethyl methacrylate with cyano compounds for dielectric materials: Synthesis and characterization. *J. Fluor. Chem.* **127**(3), 391–399 (2006); (b) M. Uchidari, T. Iwamoto, K. Iwata, M. Tamur, *Rep. Prog. Phys. Jpn.* 1979, 22, 345
89. (a) L. Pan, H. Qiu, C. Dou, Y. Li, L. Pu, J. Xu, Y. Shi, Conducting polymer nanostructures: Template synthesis and applications in energy storage. *Int. J. Mol. Sci.* **11**, 2636–2657(2010); (b) F. Guan, J. Wang, L. Yang, J.-K. Tseng, K. Han, Q. Wang, L. Zhu, *Macromolecules* **44**, 2190 (2011)
90. F. Guan, J. Pan, J. Wang, Q. Wang, L. Zhu, Crystal orientation effect on electric energy storage in poly (vinylidene fluoride-co-hexafluoropropylene) copolymers. *Macromolecules* **43**, 384–392 (2010)
91. (a) L. Zhu, Q. Wang, Novel ferroelectric polymers for high energy density and low loss dielectrics. *Macromolecules*, **45**(7), 2937–2954 (2012); (b) F. Guan, J. Wang, J. Pan, Q. Wang, L. Zhu *Macromolecules* 2010, **43**, 6739
92. Y. Liu, L. Cui, F. Guan, Y. Gao, N.E. Hedin, L. Zhu, H. Fong, Crystalline morphology and polymorphic phase transitions in electrospun nylon-6 nanofibers. *Macromolecules* **40**(17), 6283–6290 (2007)
93. (a) G.M. Spinks, V. Mottaghitlab, M. Bahrami-Saniani, P.G. Whitten, G.G. Wallace, Carbon nanotube-reinforced polyaniline fibers for high-strength artificial muscles. *Adv. Mater.* **18**, 637–640 (2006); (b) B. Boutevin, Y. Pietrasanta, *Les Acrylates et Polyacrylates Fluorés* (Erec, Paris, 1989)

94. (a) Y. Wu, G. Alici, G.M. Spinks, G.G. Wallace, Fast trilayer polypyrrole bending actuators for high speed applications. *Synth. Met.* **156**, 1017–1022 (2006); (b) O. Chiantore, M. Lazzari, M. Aglietto, V. Castelvetro, F. Ciardelli, *Polym. Degrad. Stab.* **67**, 461 (2000); (c) G. Alessandrini, M. Aglietto, V. Castelvetro, F. Ciardelli, R. Peruzzi, L. J. Toniolo, *J. Appl. Polym. Sci.* **76**, 962 (2000); (d) M Lazzari, O. Chiantore, V. Castelvetro, *Polym. Int.* **50**, 863 (2001)
95. (a) Y.G. Wang, H.Q. Li, Y.Y. Xia, Ordered whisker like polyaniline grown on the surface of mesoporous carbon and its electrochemical capacitance performance, *Adv. Mater.* **18**, 2619–2623 (2006); (b) S.D. Xiong, X.L. Guo, L. Li, S. Wu, P.K. Chu, Z.J. Xu, *Fluor. Chem.* **131**, 417 (2010)
96. (a) N. Oyama, T. Tatsuma, T. Sato, T. Sotomura, Dimercaptan-polyaniline composite electrodes for lithium batteries with high-energy density. *Nature* **373**, 598–600 (1995); (b) M. Obata, N. Matsuura, K. Mitsuo, H. Nagai, K. Asai, M. Harada, S. Hirohara, M. Tanihara, S.J. Yano, *Polym. Sci. A: Polym. Chem.* **48**, 663 (2010)
97. (a) Y.Z. Long, J.L. Duvail, M.M. Li, C.Z. Gu, Z.W. Liu, S.P. Ringer, Electrical conductivity studies on individual conjugated polymer nanowires: Two-probe and four-probe results. *Nanoscale Res. Lett.* **5**, 237–242 (2010); (b) E. Princi, S. Vicini, E. Pedemonte, V. Arrighi, I.J.J. McEwen, *Appl. Polym. Sci.* **103**, 90 (2007); (c) E. Alyamac, M.D. Soucek, *Prog. Org. Coat.* **71**, 213 (2011)
98. (a) Y.Z. Long, L.J. Zhang, Z.J. Chen, K. Huang, Y.S. Yang, H.M. Xiao, M.X. Wan, A.Z. Jin, C.Z. Gu, Electronic transport in single polyaniline and polypyrrole microtubes. *Phys. Rev. B* **71**, 165412:1–165412:7 (2005); (b) G. He, G. Zhang, J. Hu, J. Sun, S. Hu, Y. Li, F. Liu, D. Xiao, H. Zou, G. J. Liu, *Fluorine Chem.* **132**, 562 (2011); (c) S. Zhang, J. Zhao, G. Chu, L. Zhang, A. Xu, G.J. Liu, *Fluorine Chem.* **132**, 915 (2011)
99. (a) L.J. Pan, L. Pu, Y. Shi, T. Sun, R. Zhang, Y.D. Zheng, Hydrothermal synthesis of polyaniline mesostructures. *Adv. Funct. Mater.* **16**, 1279–1288 (2006); (b) S. Koizumi, K. Tadano, Y. Tanaka, T. Shimidzu, S. Kutsumizu, S. Yano, *Macromolecules* **95**, 6563 (1992)
100. (a) E.S. Forzani, H.Q. Zhang, L.A. Nagahara, I. Amlani, R. Tsui, N.J.A. Tao, A conducting polymer nanojunction sensor for glucose detection. *Nano Lett.* **4**, 1785–1788 (2004); (b) R. Gerhard-Multhaupt, *Ferroelectrics* **75**, 385 (1987); (c) N.R. Chiou, C.M. Lui, J.J. Guan, L.J. Lee, A.J. Epstein, Growth and alignment of polyaniline nanofibres with superhydrophobic, superhydrophilic and other properties. *Nat. Nanotechnol.* **2**, 354–357 (2007); (d) H. Gilbert, F.F. Miller, S.J. Averill, R.F. Schmidt, F.D. Stewart, H.L. Trumbull, *J. Amer. Chem. Soc.* **76**, 1074 (1954)
101. B. Conciatore, L.E. Trapasso, R.W. Stackman, Vinylidene Cyanide Polymers, in *Encyclopedia of Polymer Science and Technology*, vol. 14, 1st edn., (Wiley, New York, 1971), pp. 580–593
102. (a) S. Tasaka, T. Toyama, N. Inagaki, Ferro- and Pyroelectricity in amorphous Polyphenylethynitrile. *Jap. J. Appl. Phys.* **33**(1), No. 10; (b) S. Miyata; M. Yoshikawa, S. Tasaka, M. Ko, *Polym. J.* **12**, 875 (1980)
103. (a) Y. Patil, B. Ameduri, Advances in the (co)polymerization of alkyl 2-trifluoromethacrylates and 2-(trifluoromethyl)acrylic acid, *Prog. Polym. Sci.* **38**(5), 703–739 (2013); (b) S. Tasaka, K. Miyasato, M. Yoshikawa, S. Miyata, M. Ko, *Ferroelectrics* **57**, 267 (1984)
104. J.S. Harrison, Z. Ounaies, Piezoelectric Polymers; NASA/Cr2001–21142. ICASE, 2001; Report No. 43
105. A.F. Thünemann, Dielectric relaxation of polyacrylonitrile in its pristine and cyclized stage. *Macromolecules* **33**, 1790–1795 (2000)
106. (a) H. Kaji, K. Schmidt-Rohr, Conformation and dynamics of Atactic poly(acrylonitrile). 2. Torsion Angle Distributions in Meso Dyads from Two-Dimensional Solid-State Double-Quantum ¹³C NMR, *Macromolecules*, **34**(21), 7368–7381 (2001); (b) H. Kaji, N. Miura, K. Schmidt-Rohr, *Macromolecules* **36**, 6100 (2003)
107. (a) T.J. Lewis, Interfaces are the dominant feature of dielectrics at the nanometric level. *IEEE Dielect.El. In.* **11**, 739–753 (2004); (b) T.J. Lewis, Interfaces: Nanometric dielectrics. *J. Phys. D. Appl. Phys.* **38**, 202–212 (2005); (c) P. Murugaraj, D. Mainwaring, N. Mora-Huertas,

- Dielectric enhancement of polymernanoparticle through interphase polarizability. *J. App. Phy.* **98**, 054304 (2005); (d) H. Hui-Lin, Y. Wei-Chang, L. Ya-Lien, Y. Tri-Rung: *Appl. Phys. Lett.* **91**, 23501 (2007)
108. (a) Y. Sun, Z. Zhang, C.P. Wong, Influence of interphase and moisture on the dielectric spectroscopy of epoxy/silica composites. *Polym.* **46**, 2297–2305 (2005); (b) D.P. Almond, C.R. Bowen, D.A.S. Rees, Composite dielectrics and conductors: Simulation, characterization and design. *J. Phys. D. Appl. Phys.* **39**, 1295–1304 (2006)
109. T. Tanaka, Dielectric nanocomposites with insulating properties. *IEEE Trans. Dielec. Elec. Insul.* **12**, 914–928 (2005)
110. (a) E. Tuncer, A.J. Rondinone, J. Woodward, I. Sauers, D.R. James, A.R. Ellis, Cobalt iron-oxide nanoparticle modified poly(methyl methacrylate) nanodielectrics, *Appl. Phys. A Mater. Sci. Process.* **94**, 843–852 (2009); (b) J.W. Gilman, T. Kashiwagi, J. Lichtenhan, Nanocomposites: A revolutionary new flame retardant approach. *SMMPE J.* **33**(4), 40–46 (1997)
111. T. Tanaka, G.C. Montanari, R. Mulhaupt, Polymer nanocomposites as dielectrics and electrical insulation-perspective for processing technologies, material characterization and future applications. *IEEE Trans. Dielec. Elec. Insul.* **11**, 763–784 (2004)
112. X. Yi, H.L. Duan, Y. Chen, J. Wang, Prediction of complex dielectric constants of polymer-clay nanocomposites. *Phys. Lett. A* **372**, 68–71 (2007)
113. (a) N. Goulbourne, M. Frecker, E. Mockensturm, Electro-elastic modeling of a dielectric elastomer diaphragm for a prosthetic blood pump, smart structures and materials 2004: Electroactive polymer actuators and devices, in Y. Bar-Cohen, ed by, Proceedings of SPIE, San Diego, CA. vol. **5385**, (2004), pp. 122–133; (b) M. Kato, A. Usuki, *Polymer-clay nanocomposites*, ed by T.J. Pinnavaia, G.W. Beall (Wiley, West Sussex, 2000), pp. 1–91
114. R. Bergman, F. Alvarez, A. Alegria, J. Colmenero, The merging of the dielectric α - and β -relaxations in poly-(methyl methacrylate). *J. Chem. Phys.* **109**(17), 7546–7555 (1998)
115. M. Avella, M.E. Errico, E. Martuscelli, Novel PMMA/CaCO₃ nanocomposites abrasion resistant prepared by an in situ polymerization process. *Nano Lett.* **1**, 213–217 (2001)
116. A.B.R. Mayer, Formation of noble metal nanoparticles within a polymeric matrix: Nanoparticle features and overall morphologies. *Mat. Sci. Eng. C. Biomim. Mat., Sens. Syst* **6**, 155–166 (1998)
117. S. Wang, M. Wang, Y. Lei, L. Zhang, Anchor effect in poly(styrene maleic anhydride)/TiO₂ nanocomposites. *J. Mat. Sci. Lett.* **8**, 2009–2012 (1999)
118. L. Nicolais, G. Carotenuto, *Metal-Polymer Nanocomposites* (Wiley, Hoboken, 2005), pp. 1–83
119. M. Roy, J.K. Nelson, R.K. MacCrone, L.S. Schadler, Polymer nanocomposite dielectrics—the role of the interface. *IEEE Trans. Dielec. Elect. Ins.* **125**, 629–642 (2005)
120. E. Tuncer, I. Sauers, D.R. James, A.R. Ellis, M.P. Paranthaman, A. Goyal, K. L. More: Enhancement of dielectric strength in nanocomposites. *Nanotechnol.* **18**, 325704 (2007)
121. J.K. Nelson, J.C. Fothergill, Internal charge behavior of. Nanocomposites. *Nanotechnol.* **15**, 586–595 (2004)
122. J.J. O'Dwyer, *The Theory of Dielectric Breakdown of Solids* (Oxford University Press, 1964), pp. 1–43
123. J.C. Huang, Carbon black filled conducting polymers and polymer blends. *Adv. Polym. Technol.* **21**, 299–313 (2002)
124. M. Moniruzzaman, K.I. Winey, Polymer Nanocomposites containing carbon nanotubes. *Macromolecules* **39**, 5194–5205 (2006)
125. (a) P. Barber, S. Balasubramanian, Y. Anguchamy, S. Gong, A. Wibowo, H. Gao, H. Ploehn, H. Loye, Polymer composites and nanocomposites dielectric materials for pulse power energy storage. *Materials* **2**, 1697 (2009); (b) M. Okamoto, *Polymer/clay Nanocomposites*, Vol. 8 (American Scientific Publishers, Stevenson Ranch, 2004)
126. A.K. Geim, K.S. Novoselov, The rise of graphene. *Nature Mater.* **6**, 183–191 (2007)
127. H. Kim, A.A. Abdala, C.W. Macosko, Graphene/polymer Nanocomposites. *Macromolecules* **43**, 6515–6530 (2010)

128. C. Xu, X. Wang, J. Zhu, Graphene-Metal Particle Nanocomposites. *J. Phys. Chem. C* **112**(50), 19841–19845 (2008)
129. D. David, J. Evanoff, G. Chumanov, Synthesis and optical properties of silver nanoparticles and arrays. *Chem. Phys. Chem.* **6**, 1221–1231 (2005)
130. S. Stankovich, D.A. Dikin, G.H.B. Dommett, K.M. Kohlhaas, E.J. Zimney, E.A. Stach, R.D. Piner, S.T. Nguyen, R.S. Ruoff, Graphene-based composite materials. *Nature* **442**, 282–286 (2006)
131. A. Okada, M. Kawasumi, A. Usuki, Y. Kojima, T. Kurauchi, O. Kamigaito, Synthesis and properties of nylon-6/clay hybrids, in *Polymer Based Molecular Composites. Vol. 171. MRS Symposium Proceedings*, ed. by D.W. Schaefer, J.E. Mark (Materials Research Society, Pittsburgh, 1990), pp. 45–50
132. D.Y. Godovsky, Device applications of polymer-nanocomposites. *Adv. Polym. Sci.* **153**, 163–205 (2000)
133. M. Alexandre, P. Dubois, Polymer-layered silicate nanocomposites: Preparation, properties and uses of a new class of materials. *Mater. Sci. Eng.* **28**, 1–63 (2000)
134. S.S. Ray, M. Okamoto, Polymer/layered silicate nanocomposites: A review from preparation to processing. *Prog. Polym. Sci.* **28**, 1539–1641 (2003)
135. Z. Zhihao, Q. Shi, J. Peng, J. Song, Q. Chen, J. Yang, Y. Gong, R. Ji, X. He, J.H. Lee, Partial delamination of the organo-montmorillonite with surfactant containing hydroxyl groups in maleated poly(propylene carbonate). *Polymer* **47**, 8548–8555 (2006)
136. L. Peng, N.H. Kim, S. Bhadra, J.H. Lee, Electroresponsive property of novel poly(acrylate-acryloyloxyethyl trimethyl ammoniumchloride)/ clay nanocomposite hydrogels. *Adv. Mater. Res.* **79**, 2263–2266 (2009)
137. L. Peng, N.H. Kim, D. Hui, K.Y. Rhee, J.H. Lee, Improved mechanical and swelling behavior of the composite hydrogels prepared by ionic monomer and acid-activated laponite. *Appl. Surf. Sci.* **46**, 414–417 (2009)
138. F. Leroux, J.P. Besse, Polymer intercalated layered double hydroxide: A new emerging class of nanocomposites. *Chem. Mater.* **13**, 3507–3515 (2001)
139. T. Kuila, S.K. Srivastava, A.K. Bhowmick, A.K. Saxena, Thermoplastic polyolefin based polymer-blend-layered double hydroxide nanocomposites. *Compos. Sci. Technol.* **68**, 3234–3139 (2008)
140. E.P. Giannelis, Polymer layered silicate nanocomposites. *Adv. Mater.* **8**, 29–35 (1996)
141. E.P. Giannelis, R. Krishnamoorti, E. Manias, Polymer-silicate nanocomposites: Model systems for confined polymers and polymer brushes. *Adv. Polym. Sci.* **138**, 107–147 (1999)
142. M. Zanetti, G. Camino, P. Reichert, R. Mulhaupt, Thermal behaviour of poly(propylene) layered silicate nanocomposites. *Macromol. Rapid Commun.* **22**, 176–180 (2001)
143. S. Pavlidou, C.D. Papaspyrides, A review on polymer layered silicate nanocomposites. *Prog. Polym. Sci.* **33**, 1119–1198 (2008)
144. H. Acharya, S.K. Srivastava, A.K. Bhowmick, Synthesis of partially exfoliated EPDM/LDH nanocomposites by solution intercalation: Structural characterization and properties. *Compos. Sci. Technol.* **67**, 2807–2816 (2007)
145. F.R. Costa, B.K. Satapathy, U. Wagenknecht, R. Weidisch, G. Heinrich, Morphology and fracture behaviour of polyethylene/mg-Al layered double hydroxide (LDH) nanocomposites. *Eur. Polym. J.* **42**, 2140–2152 (2006)
146. N.J. Garcia, J.C. Bazan, Electrical conductivity of montmorillonite as a function of relative humidity: La-montmorillonite. *Clay Miner.* **44**, 81–88 (2009)
147. F. Uddin, Clays, nanoclays, and montmorillonite minerals. *Metal. Mat Trans* **39**, 2805–2814 (2008)
148. Y.Z. Bao, L.F. Cong, Z.M. Huang, Z.X. Weng, Preparation and proton conductivity of poly(vinylidene fluoride)/layered double hydroxide nanocomposite gel electrolytes. *J. Mater. Sci.* **43**, 390–394 (2008)
149. Q. Li, O.K. Park, J.H. Lee, Positive temperature coefficient behaviour of HDPE/EVA blends filled with carbon black. *Adv. Mater. Res.* **79**, 2267–2270 (2009)

150. T. Jeevananda, Y.K. Jang, J.H. Lee, C. Siddaramaiah, Ranganathaiah: Investigation of multi-walled carbon nanotube reinforced high-density polyethylene/carbon black nanocomposites using electrical DSC and positron lifetime spectroscopy techniques. *Polym. Int.* **58**, 755–780 (2009)
151. Q. Li, N.H. Siddaramaiah, G.H. Kim, J.H.L. Yoo, Positive temperature coefficient characteristic and structure of graphite nanofibers reinforced high-density polyethylene/carbon black nanocomposites. *Compos. Part B* **40**, 218–224 (2009)
152. N.M. Renukappa, S.R.D. Siddaramaiah, J.S. Sudhaker, J.H.L. Rajan, Dielectric properties of carbon black: SBR composites. *J. Mat. Sci. Mat. Elect.* **20**, 648–656 (2009)
153. Q. Li, J.W. Kim, T.H. Shim, Y.K. Jang, J.H. Lee, Positive temperature coefficient behavior of the graphite nanofibre and carbon black filled high-density polyethylene hybrid composites. *Adv. Mater. Res.* **47**, 226–229 (2008)
154. W. Zhang, R.S. Blackburn, A. Dehghani-Sanij, Electrical conductivity of epoxy resin-carbon black-silica nanocomposites: Effect of silica concentration and analysis of polymer curing reaction by FTIR. *Scrip. Mat.* **57**, 949–952 (2007)
155. K. Chrissafis, K.M. Paraskevopoulos, S.Y. Stavrev, A. Docoslis, A. Vassiliou, D.N. Bikiaris, Characterization and thermal degradation mechanism of isotactic polypropylene/carbon black nanocomposites. *Thermoch. Act.* **465**, 6–17 (2007)
156. H. Wang, H. Zhang, W. Zhao, W. Zhang, G. Chen, Preparation of polymer/oriented graphite nanosheet composite by electric field inducement. *Compos. Sci. Technol.* **68**, 238–243 (2008)
157. A. Yu, P. Ramesh, M.E. Itkis, B. Elena, R.C. Haddon, Graphite nanoplatelet-epoxy composite thermal interface materials. *J. Phys. Chem. C* **111**, 7565–7569 (2007)
158. B. Debelak, K. Lafdi, Use of exfoliated graphite filler to enhance polymer physical properties. *Carbon* **45**, 1727–1734 (2007)
159. X. Chen, Y.P. Zheng, F. Kang, W.C. Shen, Preparation and structure analysis of carbon/carbon composite made from phenolic resin impregnation into exfoliated graphite. *J. Phys. Chem. Sol.* **67**, 1141–1144 (2006)
160. S. Mazinani, A. Aji, C. Dubois, Morphology, structure and properties of conductive PS/CNT nanocomposite electrospun mat. *Polym.* **50**, 3329–3342 (2009)
161. Y. Geng, M.Y. Liu, J. Li, X.M. Shi, J.K. Kim, Effects of surfactant treatment on mechanical and electrical properties of CNT/epoxy nanocomposites. *Compos. Part A* **39**, 1876–1883 (2008)
162. S.H. Liao, C.Y. Yen, C.C. Weng, Y.F. Lin, C.C.M. Ma, C.H. Yang, M.C. Tsai, M.Y. Yen, M.C. Hsiao, S.J. Lee, X.F. Xie, Y.H. Hsiao, Preparation and properties of carbon nanotube/polypropylene nanocomposite bipolar plates for polymer electrolyte membrane fuel cells. *J. Pow. Sour.* **185**, 1225–1232 (2008)
163. Z. Spitalsky, D. Tasis, K. Papagelis, C. Galiotis, Carbon nanotube–polymer composites: Chemistry, processing, mechanical and electrical properties. *Prog. Polym. Sci.* **35**, 357–401 (2010)
164. O.K. Park, T. Jeevananda, N.H. Kim, S. Kim, J.H. Lee, Effects of surface modification on the dispersion and electrical conductivity of carbon nanotube/polyaniline composites. *Scrip. Mat.* **60**, 551–554 (2009)
165. T. Jeevananda, N.H. Siddaramaiah, S.B. Kim, J.H.L. Hoe, Synthesis and characterization of polyaniline-multiwalled carbon nanotube nanocomposites in the presence of sodium dodecyl sulfate. *Polym. Adv. Technol.* **19**, 1–9 (2008)
166. T. Jeevananda, T.S. Siddaramaiah, O.M. Lee, R. Samir, J.H.L. Somashekar, Polyaniline-multiwalled carbon nanotubes composites: Characterization by WAXS and TGA. *J. Appl. Polym. Sci.* **108**, 25–34 (2008)
167. C.E. Hong, K. Prashantha, S.G. Advani, J.H. Lee, Effects of oxidative conditions on properties of multi-wall carbon nanotubes of polymer nanocomposites. *Compos. Sci. Technol.* **67**, 1027–1034 (2007)
168. S.K. Kim, N.H. Kim, J.H. Lee, Effects of the addition of multiwalled carbon nanotubes on the positive temperature coefficient characteristics of carbon-black-filled high density polyethylene nanocomposites. *Scrip. Mat.* **55**, 1119–1122 (2006)

169. V. Khanna, B.R. Bakshi, Carbon nanofiber polymer composites: Evaluation of life cycle energy use. *Environ. Sci. Technol.* **43**, 2078–2084 (2009)
170. G.G. Tibbetts, M.L. Lake, K.L. Strong, B.P. Rice, A review of the fabrication and properties of vapor-grown carbon nanofiber/polymer composites. *Compos. Sci. Technol.* **67**, 1709–1718 (2007)
171. M. Chipara, K. Lozano, A. Hernandez, M. Chipara, TGA analysis of polypropylene-carbon nanofibers composites. *Polym. Degrad. Stab.* **93**, 871–876 (2008)
172. S. Ansari, E.P. Giannelis, Functionalized graphene sheetpoly(vinylidene fluoride) conductive nanocomposites. *J. Polym. Sci. Part B Polym. Phys.* **47**, 888–897 (2009)
173. T. Ramanathan, A.A. Abdala, S. Stankovich, D.A. Dikin, M.H. Alonso, R.D. Piner, D.H. Adamson, H.C. Schniepp, X. Chen, R.S. Ruoff, S.T. Nguyen, I.A. Aksay, R.K. Prud'homme, L.C. Brinson, Functionalized graphene sheets for polymer nanocomposites. *Nat. Nanotechnol.* **3**, 327–331 (2008)
174. Y.R. Lee, A.V. Raghunath, H.M. Jeong, B.K. Kim, Properties of waterborne polyurethane/functionalized graphene sheet nanocomposites prepared by an in situ method. *Macromol. Chem. Phys.* **210**, 1247–1254 (2009)
175. Y. Xu, Y. Wang, L. Jiajie, Y. Huang, Y. Ma, X. Wan, Y. Chen, A hybrid material of graphene and poly(3,4-ethyldioxythiophene) with high conductivity, flexibility, and transparency. *Nano Res.* **2**, 343–348 (2009)
176. N. Liu, F. Luo, H. Wu, Y. Liu, C. Zhang, J. Chen, One step ionic-liquid assisted electrochemical synthesis of ionic-liquid-functionalized graphene sheets directly from graphene. *Adv. Funct. Mat.* **18**, 1518–1525 (2008)
177. J.E. Allison, G.S. Cole, Metal-matrix composites in the automotive industry: Opportunities and challenges. *JOM* **45**(1), 19–24 (1993)
178. S. Alwarappan, A. Kumar, *Graphene-Based Materials: Science and Technology* (CRC Press, Taylor & Francis Group, 2014), pp. 2–89
179. B. An, L. Li, H. Li, Electrodeposition in the Ni-plating bath containing multi-walled carbon nanotubes. *Mat. Chem. Phys.* **110**, 481–485 (2008)
180. S. Arai, Ni-deposited multi-walled carbon nanotubes by electrodeposition. *Carbon* **42**, 641–644 (2004)
181. S. Arai, M. Endo, Various carbon nanofiber–copper composite films prepared by electrodeposition. *Electrochem. Commun.* **7**(1), 19–22 (2005)
182. D.J. Blackwood et al., Corrosion behaviour of porous titanium–graphite composites designed for surgical implants. *Corros. Sci.* **42**(3), 481–503 (2000)
183. E. Breval, Synthesis routes to metal matrix composites with specific properties: A review. *Compos. Eng.* **5**(9), 1127–1133 (1995)
184. A.R. Bunsell, J. Renard, *Fundamentals of Fibre Reinforced Composite Materials* (IOP Publishing, 2005)
185. V.V. Ivanov et al., Synergistic effect in nickel-Teflon composite electrolytic coatings. *Rus. J. Appl. Chem.* **81**(12), 2169–2171 (2009)
186. A. Hovestad, L.J.J. Janssen, Electroplating of metal matrix composites by Codeposition of suspended particles, in *Modern Aspects of Electrochemistry No.38*, (Kluwer Academic Publishers, New York, 2005)
187. J. Koráb, P. Štefánek, Š. Kavecký, P. Šebo, G. Korb, Thermal conductivity of unidirectional copper matrix carbon fibre composites. *Composites Part A: Appl. Sci. Manufac.* **33**(4), 577–581 (2002)
188. T. Tanaka, G.C. Montanari, R. Mulhaupt, Polymer nanocomposites as dielectrics and electrical insulation - perspectives for processing technologies, material characterization and future applications. *IEEE Trans. Dielectr. Electr. Insul.* **11**(5), 763–784 (2004)
189. T. Tanaka, Dielectric nanocomposites with insulating properties. *IEEE Transac. Dielec. Elect. Insul.* **12**, 914–928 (2005)
190. G. Banhegyi, Comparison of electrical mixture rules for composites. *Coll. Polym. Sci.* **264**, 1030–1050 (1986)

191. P. Bowen, J.G. Highfield, A. Mocellin, T.A. Ring, Degradation of aluminum nitride powder in aqueous environment. *J. Am. Ceram. Soc.* **73**(3), 724–728 (1990)
192. L. Qiu, R. Xie, P. Ding, B. Qu, Preparation and characterisation of $\text{mg}(\text{OH})_2$ nanoparticles and flame-retardant property of its nanocomposites with eva. *Compos. Struct.* **62**, 391–395 (2003)
193. M. Okoshi, H. Nishizawa, Flame retardancy of nanocomposites. *Fir. Mater.* **28**, 423–429 (2004)
194. L.A. Fredin, Z. Li, M.T. Lanagan, M.A. Ratner, T.J. Marks, Sustainable high capacitance at high frequencies: Metallic aluminum - polypropylene Nanocomposites. *ACS Nano* **7**, 396–407 (2013)
195. D. Pitsa, G. Vardakis, M.G. Danikas, M. Kozako, Electrical treeing Propagation in Nanocomposites and the role of Nanofillers: Simulation with the aid of cellular automata. *J. Electric. Engineer. –Elektrotech. Casop.* **61**, 125–128 (2010)
196. C.A. Grabowski, S.P. Fillery, N.M. Westing, C. Chi, J.S. Meth, M.F. Durstock, R.A. Vaia, Dielectric breakdown in silica-amorphous polymer Nanocomposite films: The role of the polymer matrix. *ACS Appl. Mater. Interfaces* **5**, 5486–5492 (2013)
197. S. Siddabattuni, T.P. Schuman, F. Dogan, Dielectric properties of polymer-particle Nanocomposites influenced by electronic nature of filler surfaces. *ACS Appl. Mater. Interfaces* **5**, 1917–1927 (2013)
198. J. Jancar, J.F. Douglas, F.W. Starr, S.K. Kumar, P. Cassagnau, A.J. Lesser, S.S. Sternstein, M.J. Buehler, Current issues in research on structure-property relationships in polymer Nanocomposites. *Polymer* **51**, 3321–3343 (2010)
199. A. Okada, A. Usuki, Twenty years of polymer-clay Nanocomposites. *Macromol. Mater. Eng.* **291**, 1449–1476 (2006)
200. D.R. Paul, L.M. Robeson, Polymer nanotechnology: Nanocomposites. *Polymer* **49**, 3187–3204 (2008)
201. M.Z. Rong, M.Q. Zhang, W.H. Ruan, Surface modification of Nanoscale fillers for improving properties of polymer Nanocomposites: A review. *Mater. Sci. Technol.* **22**, 787–796 (2006)
202. D.W. Schaefer, R.S. Justice, How nano are nanocomposites? *Macromolecules* **40**, 8501–8517 (2007)
203. S.C. Tjong, Structural and mechanical properties of polymer Nanocomposites. *Mater. Sci. Eng.:R.* **53**, 73–197 (2006)
204. C.L. Wu, M.Q. Zhang, M.Z. Rong, K. Friedrich, Tensile performance improvement of low nanoparticles filled-polypropylene composites. *Compos. Sci. Technol.* **62**, 1327–1340 (2002)
205. S.-W. Kuo, F.-C. Chang, POSS related polymer Nanocomposites. *Prog. Polym. Sci.* **36**, 1649–1696 (2011)
206. E. Ayandele, B. Sarkar, P. Alexandridis, Polyhedral Oligomeric Silsesqui-oxane (POSS)-containing polymer Nanocomposites. *Nano* **2**, 445–475 (2012)
207. B.X. Fu, M.Y. Gelfer, B.S. Hsiao, S. Phillips, B. Viers, R. Blanski, P. Ruth, Physical gelation in ethylene-propylene copolymer melts induced by Polyhedral Oligomeric Silsesquioxane (POSS) molecules. *Polymer* **44**, 1499–1506 (2003)
208. M. Pracella, D. Chionna, A. Fina, D. Tabuani, A. Frache, G.i. Camino, Polypropylene-POSS Nanocomposites: Morphology and crystallization behaviour. *Macromol. Symp.* **234**, 59–67 (2006)
209. F. Baldi, F. Bignotti, A. Fina, D. Tabuani, T. Ricco, Mechanical Characterization of polyhedral Oligomeric Silsesquioxane/polypropylene blends. *J. Appl. Polym. Sci.* **105**, 935–943 (2007)
210. A. Fina, D. Tabuani, A. Frache, G. Camino, Polypropylene-polyhedral Oligomeric Silsesquioxanes (POSS) Nanocomposites. *Polymer* **46**, 7855–7866 (2005)
211. C.Y. Jung, H.S. Kim, H.J. Hah, S.M. Koo, Self-assembly growth process for polyhedral Oligomeric Silsesquioxane cubic crystals. *Chem. Commun. (Cambridge, U. K.)* **10**, 1219–1221 (2009)
212. M. Joshi, B.S. Butola, Isothermal crystallization of HDPE/Octamethyl polyhedral Oligomeric Silsesquioxane Nanocomposites: Role of POSS as a Nano-filler. *J. Appl. Polym. Sci.* **105**, 978–985 (2007)

213. M. Takala, M. Karttunen, P. Salovaara, S. Kortet, K. Kannus, T. Kalliohaka, Dielectric properties of nanostructured polypropylene- polyhedral Oligomeric Silsesquioxane compounds. *IEEE Trans. Dielectr. Electr. Insul.* **15**, 40–51 (2008)
214. J. Horwath, D. Schweickart, G. Garcia, D. Klosterman, M. Galaska: Im-proved performance of Polyhedral Oligomeric Silsesquioxane Epoxies, *Electrical Insulation and Dielectric Phenomena, CEIDP '05. Annual Report Conference on* (2005). pp. 155–157
215. J.I. Weon, K.T. Gam, W.J. Boo, H.J. Sue, C.M. Chan, Impact-toughening mechanisms of calcium carbonate-reinforced polypropylene Nanocomposite. *J. Appl. Polym. Sci.* **99**, 3070–3076 (2006)
216. M.-R. Meng, Q. Dou, Effect of filler treatment on crystallization, Mor-phology and mechanical properties of polypropylene/calcium carbonate composites. *J. Macromol. Sci. B: Phys.* **48**, 213–225 (2009)
217. M.Y.A. Fuad, H. Hanim, R. Zarina, Z.A.M. Ishak, A. Hassan, Polypro-pylene/calcium carbonate Nanocomposites - effects of processing techniques and Maleated polypropylene Compatibiliser. *Expr. Polym. Let.* **4**, 611–620 (2010)
218. H. Huang, B. Han, L. Wang, N. Miao, H. Mo, N.-L. Zhou, Z.-M. Ma, J. Zhang, J. Shen, Crystallization kinetics of polypropylene composites filled with Nano calcium carbonate modified with maleic anhydride. *J. Appl. Polym. Sci.* **119**, 1516–1527 (2011)
219. D. Eiras, L.A. Pessan, Mechanical properties of polypropylene/calcium carbonate Nano-composites. *Mat. Res.* **12**, 517–522 (2009)
220. B. Cioni, A. Lazzeri, The role of interfacial interactions in the toughening of precipitated calcium carbonate-polypropylene Nanocomposites. *Compos. Inter.* **17**, 533–549 (2010)
221. P. Eteläaho, S. Haveri, P. Järvelä, Comparison of the morphology and me-chanical properties of unmodified and surface-modified Nanosized calcium carbonate in a polypropylene matrix. *Polym. Compos.* **32**, 464–471 (2011)
222. Y. Lin, H. Chen, C.-M. Chan, J. Wu, Effects of coating amount and particle concentration on the impact toughness of polypropylene/CaCO₃ Nanocompo-sites. *Eur. Pol. J.* **47**, 294–304 (2011)
223. M. Kamal, C.S. Sharma, P. Upadhyaya, V. Verma, K.N. Pandey, V. Kumar, D.D. Agrawal, Calcium carbonate (CaCO₃) nanoparticle filled polypro-pylene: Effect of particle surface treatment on mechanical, thermal, and Mor-phological performance of composites. *J. Appl. Polym. Sci.* **124**, 2649–2656 (2012)
224. Y. Li, P. Tao, A. Viswanath, B.C. Benicewicz, L.S. Schadler, Bimodal Sur-face ligand engineering: The key to tunable Nanocomposites. *Langmuir* **29**, 1211–1220 (2013)
225. P. Tao, Y. Li, A. Rungta, A. Viswanath, J. Gao, B.C. Benicewicz, R.W. Siegel, L.S. Schadler, TiO₂ Nanocomposites with high refractive index and trans-parency. *J. Mater. Chem.* **21**, 18623–18629 (2011)
226. F. Carpi, C. Salaris, D.D. Rossi, Folded dielectric elastomer actuators. *Smart Mater. Struct.* **16**, S300–S305 (2007)
227. D. Gatti, H. Haus, M. Matysek, B. Frohnapfel, C. Tropea, H.F. Schlaak, The dielectric breakdown limit of silicone dielectric elastomer actuators. *Appl. Phys. Lett.* **104**, 052905 (2014)
228. S.M. Ha, W. Yuan, Q. Pei, R. Pelrine, S. Stanford, Interpenetrating polymer networks for high-performance electroelastomer artificial muscles. *Adv. Mater.* **18**, 887–891 (2006)
229. R. Heydt, R. Kornbluh, J. Eckerle, R. Pelrine, Sound radiation properties of dielectric elastomer electroactive polymer loadspeakers. *Proc. SPIE* **6168**, 61681M (2006)
230. J. Huang, S. Shian, R.M. Diebold, Z. Suo, D.R. Clarke, The thickness and stretch dependence of the electrical breakdown strength of an acrylic dielectric elastomer. *Appl. Phys. Lett.* **101**, 122905 (2012)
231. J. Huang, T. Lu, J. Zhu, D.R. Clarke, Z. Suo, Large, unidirectional actuation in dielectric elastomers achieved by fiber stiffening. *Appl. Phys. Lett.* **100**, 211901 (2012)
232. J. Huang, S. Shian, Z. Suo, D.R. Clarke, Maximizing the energy density of dielectric elastomer generators using equibiaxial loading. *Adv. Funct. Mater.* **23**, 5056–5061 (2013)

233. R. Huang, Z. Suo, Electromechanical phase transition in dielectric elastomers. *Proc. R. Soc. A* **468**, 1014–1040 (2011)
234. R. Karsten, K. Flittner, H. Haus, H.F. Schlaak, Development of an active isolation mat based on dielectric elastomer stack actuators for mechanical vibration cancellation. *Proc. SPIE* **8687**, 86870Y (2013)
235. C. Keplinger, M. Kaltenbrunner, N. Arnold, S. Bauer, Röntgen's electrode free elastomer actuators without electromechanical pull-in instability. *Proc. Natl. Acad. Sci. U. S. A.* **107**, 4505–4510 (2010)
236. C. Keplinger, T. Li, R. Baumgartner, Z. Suo, S. Bauer, Harnessing snap through instability in soft dielectrics to achieve giant voltage-triggered deformation. *Soft Mat* **8**, 285–288 (2012)
237. Y. Hu, R.C. Smith, J.K. Nelson, L.S. Schadler, Some mechanistic understanding of the impulse strength of nanocomposites. *IEEE Conf. Electr. Insul. Dielectr. Phenomena (CEIDP)* (2006) pp. 31–34
238. M. Kozako, S. Yamano, R. Kido, Y. Ohki, M. Kohtoh, S. Okabe, T. Tanaka, Preparation and Preliminary Characteristic Evaluation of Epoxy/Alumina Nanocomposites, *Intern. Sympos. Electr. Insulating Materials (ISEIM)* (2005) 231–234
239. T. McKay, B. O'Brien, E. Calius, I. Anderson, An integrated, self-priming dielectric elastomer generator. *Appl. Phys. Lett.* **97**, 062911 (2010)
240. A. O'Halloran, F. O'Malley, P. McHugh, A review on dielectric elastomer actuators, technology, applications and challenges. *J. Appl. Phys.* **104**, 071101 (2008)
241. R.E. Pelrine, R.D. Kornbluh, J.P. Joseph, Electrostriction of polymer dielectrics with compliant electrodes as a means of actuation. *Sens. Actuators A* **64**, 77–85 (1998)
242. R. Pelrine, R. Kornbluh, Q. Pei, J. Joseph, High-speed electrically actuated elastomers with greater than 100%. *Science* **287**, 836–839 (2000)
243. R. Pelrine, R.D. Kornbluh, Q. Pei, S. Stanford, S. Oh, J. Eckerle, R. Full, M. Rosenthal, K. Meijer, Dielectric elastomer artificial muscle actuators: Toward biomimetic motion. *Proc. SPIE* **4695**, 126–137 (2002)
244. J. Plante, S. Dubowsky, Large-scale failure modes of dielectric elastomer actuators. *Int. J. Solids Struct.* **43**, 7727–7751 (2006)
245. J. Plante, S. Dubowsky, On the performance mechanisms of dielectric elastomer actuators. *Sens. Actuat. A* **137**, 96–109 (2007)
246. Y. Saito, H. Takao, T. Tani, T. Nonoyama, K. Takatori, T. Homma, T. Nagaya, M. Nakamura, Lead-free piezo-ceramics. *Nature* **432**, 84–87 (2004)
247. J. Sheng, H. Chen, B. Li, L. Chang, Temperature dependence of the dielectric constant of acrylic dielectric elastomer. *Appl. Phys. A Mater. Sci. Process.* **110**, 511–515 (2013)
248. A. Trols, A. Kogler, R. Baumgartner, R. Kaltseis, C. Keplinger, R. Schwodiauer, I. Graz, S. Bauer, Stretch dependence of the electrical breakdown strength and dielectric constant of dielectric elastomers. *Smart Mater. Struct.* **22**, 104012 (2013)
249. M. Wissler, E. Mazza, Mechanical behavior of an acrylic elastomer used in dielectric elastomer actuators. *Sens. Actuators A* **134**, 494–504 (2007)
250. X.Q. Zhang, M. Wissler, B. Jaehne, R. Broennimann, G. Kovacs, Effects of crosslinking, prestrain and dielectric filler on the electromechanical response of a new silicone and comparison with acrylic elastomer. *Proc. SPIE* **5385**, 78–86 (2004)
251. X. Zhao, Z. Suo, Theory of dielectric elastomers capable of giant deformation of actuation. *Phys. Rev. Lett.* **104**, 178302 (2010)
252. G. Kofod, P. Sommer-Larsen, R. Kornbluh, R. Pelrine, Actuation response of polyacrylate dielectric elastomers. *J. Intell. Mater. Syst. Struct.* **24**, 1667–1674 (2003)
253. S.J.A. Koh, T. Li, J. Zhou, X. Zhao, W. Hong, J. Zhu, Z. Suo, Mechanisms of large actuation strain in dielectric elastomers. *J. Polym. Sci. B* **49**, 504–515 (2011)
254. M. Kollosche, G. Kofod, Z. Suo, J. Zhu, Temporal evolution and instability in a viscoelastic dielectric elastomer. *J. Mech. Phys. Solids* **76**, 47–64 (2015)
255. M. Kollosche, J. Zhu, Z. Suo, G. Kofod, Complex interplay of nonlinear processes in dielectric elastomers. *Phys. Rev. E* **85**, 051801 (2012)

256. R. Kombluh, R. Pelrine, J. Joseph, R. Heydt, Q. Pei, S. Chiba, High-field electrostriction of elastomeric polymer dielectrics for actuation. *Proc. SPIE* **3669**, 149–161 (1999)
257. (a) R. Shankar, A.K. Krishnan, T. K. Ghosh, R.J. Spontak, Triblock copolymer organogels as high-performance dielectric elastomers. *Macromolecules* **41**, 6100–6109 (2008); (b) G.G. Raju, *Dielectrics in Electric Field* (Marcel Dekker Inc, New York, 2003)
258. A.A. Vorob'ev, Excitation and electrical breakdown of solid insulators. *Russ. Phys. J.* **23**, 382–386 (1980)
259. I. Bunget, M. Popescu, *Physics of Solid Dielectrics*, vol 19 (Elsevier, Amsterdam, 1984)
260. E. Kuffel, W.S. Zaengl, *High Voltage Engineering Fundamental* (Pergamon, New York, 1984)
261. J. Artbauer, Electric strength of polymers. *J. Phys. D. Appl. Phys.* **29**, 446–456 (1996)
262. M.H. Sabuni, J.K. Nelson, The effects of plasticizer on the electric strength of polystyrene. *J. Mater. Sci.* **14**, 2791–2796 (1979)
263. T. Imai, F. Sawa, T. Ozaki, Y. Inoue, T. Shimizu, T. Tanaka, Comparison of insulation breakdown properties of epoxy nanocomposites under homogeneous and divergent electric fields, *IEEE Conf. Electr. Insul. Dielectr. Phenomena (CEIDP)* (2006), pp. 306–309
264. I.L. Hosier, A.S. Vaughan, S.G. Swingler, The effects of measuring techniques and sample preparation on the breakdown strength of polyethylene. *IEEE Dielect. El. In.* **9**, 353–361 (2002)
265. A. Schnewly, P. Groning, L. Schlapbach, C. Irrang, J. Vogt, Breakdown behavior of oilimpregnated polypropylene as dielectric in film capacitors. *IEEE Dielect. El. In.* **5**, 862–868 (1998)
266. A.E. Job, N. Alves, M. Zanin, M.M. Ueki, L.H. Mattoso, M.Y. Teruya, J.A. Giacometti, Increasing the dielectric breakdown strength of poly(ethylene terephthalate) films using a coated polyaniline layer. *J. Phys. D. Appl. Phys.* **36**, 1414–1417 (2003)
267. V.A. Zakrevski, N.T. Sudar, A. Zappo, Y.A. Dubitsky, Mechanism of electrical degradation and breakdown of insulating polymers. *J. Appl. Phys.* **93**, 2135–2139 (2003)
268. M. Ieda, Dielectric breakdown process of polymers. *IEEE Electr. Insul.* **15**, 206–224 (1980)
269. (a) Y. Shen, Y. Lin, M. Li, C.W. Nan, High dielectric performance of polymer composite films induced by a percolating interparticle barrier layer. *Adv. Mater.* **19**, 1418–1422 (2007); (b) E. Tuncer, A.J. Rondinone, J. Woodward, I. Sauers, D.R. James, A.R. Ellis, Cobalt iron-oxide nanoparticle modified poly(methyl methacrylate) nanodielectrics, *Appl. Phys. A Mater. Sci. Process.* **94**, 843–852 (2009)
270. G. Chen, A.E. Davies, The influence of defects on the short-term breakdown characteristics and long-term dc performance of LDPE insulation. *IEEE Dielect. El. In.* **7**, 401–407 (2000)
271. (a) T.J. Lewis, Nanometric dielectrics. *IEEE Dielect. El. In.* **1**, 812–825 (1994); (b) T. Tanaka, M. Kozaka, N. Fuse, Y. Ohki, Proposal of a multi-core model for polymer nanocomposite dielectrics. *IEEE Dielect. El. In.* **12**, 669–681 (2005)
272. T. Tanaka, G.C. Montanari, R. Mulhaupt, Polymer nanocomposites as dielectrics and electrical insulation-perspectives for processing technologies, material characterization, and future applications. *IEEE Dielect. El. In.* **11**, 763–784 (2004)
273. D. Ma, T.A. Hugener, R.W. Siegel, A. Christerson, E. Martensson, C. Onneby, L. Schadler, Influence of nanoparticle surface modification on the electrical behavior of polyethylene nanocomposites. *Nanotechnol.* **16**, 724–731 (2005)
274. G.C. Montanari, D. Fabiani, F. Palmieri, D. Kaempfer, R. Thomann, R. Mulhaupt, Modification of electrical properties and performance of EVA and PP insulation through nanostructure by organophillic silicates. *IEEE Dielect. El. In.* **11**, 754–762 (2004)
275. R.C. Smith, C. Liang, M. Landry, J.K. Nelson, L.S. Schadler, The mechanisms leading to the useful electrical properties of polymer nanodielectrics. *IEEE Dielect. El. In.* **15**, 187–196 (2008)
276. P.J. Kim, C. Simon, P.J. Hotchkiss, N. Joshua, B. Kippelen, S.R. Marder, J.W. Perry, Phosphonic acid-modified barium titanate polymer nanocomposites with high permittivity and dielectric strength. *Adv. Mater.* **19**, 1001–1005 (2007)
277. J. Li, J. Claude, L.E. Norena-Franco, S.I. Seok, Q. Wang, Electrical energy storage in ferroelectric polymer nanocomposites containing surface-functionalized BaTiO₃ nanoparticles. *Chem. Mater.* **20**, 6304–6306 (2008)

278. M. Roy, J.K. Nelson, R.K. MacCrone, L.S. Schadler, Candidate mechanisms controlling the electrical characteristics of silica/XLPE nanodielectrics. *J. Mater. Sci.* **42**, 3789–3799 (2007)
279. F. Guan, J. Wang, L. Yang, J.-K. Tseng, K. Han, Q. Wang, L. Zhu, Confinement-induced high-field Antiferroelectric-like behavior in a poly (vinylidene fluoride-co-trifluoroethylene-co-chlorotrifluoroethylene)-graft-polystyrene graft copolymer. *Macromolecules* **44**, 2190–2199 (2011)
280. F. Guan, J. Pan, J. Wang, Q. Wang, L. Zhu, Crystal orientation effect on electric energy storage in poly (vinylidene fluoride-co-hexafluoropropylene) copolymers. *Macromolecules* **43**, 384–392 (2010)
281. F. Guan, J. Wang, J. Pan, Q. Wang, L. Zhu, Effects of polymorphism and crystallite size on dipole reorientation in poly (vinylidene fluoride) and its random copolymers. *Macromolecules* **43**, 6739–6748 (2010)
282. (a) E. Allahyarov, H. Löwen, L. Zhu, Dipole correlation effects on the local field and the effective dielectric constant in composite dielectrics containing high- k inclusions. *Phys. Chem. Chem. Phys.* (2016) Advance Article; (b) L. Zhu, Q. Wang, *Macromolecules* **45**, 2937 (2012)
283. Y. Zou, L. Han, G. Yuan, B. Liu, X. Zhao, B. Tian, J. Wang, S. Sun, J. Sun, X. Meng, Enhanced ferroelectric and dielectric properties of the P(VDF-TrFE)/Ag nanoparticles composite thin films. *J. Mater. Sci. Mat.* **25**, 3461–3465 (2014)
284. (a) P. Barber, S. Balasubramanian, Y. Anguchamy, S. Gong, A. Wibowo, H. Gao, H.J. Ploehn, H.C.Z. Loye, Polymer composite and nanocomposite dielectric materials for pulse power energy storage. *Materials* **2**, 1697–1733 (2009); (b) O. Chiantore, M. Lazzari, M. Aglietto, V. Castelvetro, F. Ciardelli, *Polym. Degrad. Stab.* **67**, 461 (2000). (c) G. Alessandrini, M. Aglietto, V. Castelvetro, F. Ciardelli, R. Peruzzi, L. Toniolo, *J. Appl. Polym. Sci.* **76**, 962 (2000); (d) M. Lazzari, O. Chiantore, V. Castelvetro *Polym. Int.* **50**, 863 (2001)
285. (a) L. Nyholm, G. Nyström, A. Mihranyan, M. Strømme, Toward flexible polymer and paper-based energy storage devices. *Adv. Mater.* **23**, 3751–3769 (2011); (b) S.D. Xiong, X.L. Guo, L. Li, S. Wu, P.K. Chu, Z. Xu, *J. Fluor. Chem.* **131**, 417 (2010)
286. (a) J. Li, J. Claude, L.E. Norena-Franco, S.I. Seok, Q. Wang, Electrical energy storage in ferroelectric polymer nanocomposites containing surface-functionalized BaTiO₃ nanoparticles, *Chem. Mater.* **20**, 6304–6306 (2008); (b) M. Obata, N. Matsuura, K. Mitsuo, H. Nagai, K. Asai, M. Harada, S. Hirohara, Ma Tanihara, S. Yano, *J. Polym. Sci. A Polym. Chem.* **48**, 663 (2010)
287. (a) X. Hao, J. Zhai, X. Yao: Improved energy storage performance and fatigue endurance of Sr-doped PbZrO₃ antiferroelectric thin films, *J. Am. Ceram. Soc.* **92**, 1133–1135 (2009); (b) E. Princi, S. Vicini, E. Pedemonte, V. Arrighi, I.J. McEwen, *J. Appl. Polym. Sci.* **103**, 90 (2007); (b) E. Alyamac, M.D. Soucek, *Prog. Org. Coat.* **71**, 213 (2011)
288. (a) B. Ma, D.K. Kwon, M. Narayanan, U. Balachandran, Dielectric properties and energy storage capability of antiferroelectric Pb_{0.92}La_{0.08}Zr_{0.95}Ti_{0.05}O₃ film-on-foil capacitors. *J. Mater. Res.* **24**, 2993–2996 (2009); (b) G. He, G. Zhang, J. Hu, J. Sun, S. Hu, Y. Li, F. Liu, D. Xiao, H. Zou, G. Liu, *J. Fluor. Chem.* **132**, 562 (2011); (c) S. Zhang, J. Zhao, G. Chu, L. Zhang, A. Xu, G. Liu, *J. Fluor. Chem.* **132**, 915 (2011)
289. (a) K.J. Choi, M. Biegalski, Y. Li, A. Sharan, J. Schubert, R. Uecker, P. Reiche, Y. Chen, X. Pan, V. Gopalan, Enhancement of ferroelectricity in strained BaTiO₃ thin films. *Science* **306**, 1005–1009 (2004); (b) S. Koizumi, K. Tadano, Y. Tanaka, T. Shimidzu, S. Kutsumizu, S. Yano, *Macromolecules* **95**, 6563 (1992)
290. P. Tsoira, O. Gryshchuk, K. Friedrich, Morphological studies of epoxy/polyaniline blends. *Macromol. Chem. Phys.* **206**, 787–793 (2005)
291. P. Dutta, S. Biswas, S.K. De, Dielectric relaxation in polyaniline-polyvinyl alcohol composites. *Mater. Res. Bul.* **37**, 193–200 (2002)
292. C. Chwang, C. Liu, S. Huang, D. Chao, S. Lee, Synthesis and characterization of high dielectric constant polyaniline/polyurethane blends. *Synth. Met.* **142**, 275–281 (2004)
293. W.C. Chiou, D.Y. Yang, J.L. Han, S.N. Lee, Synthesis and characterization of composites of polyaniline and polyurethane-modified epoxy. *Polym. Intern.* **55**, 1222–1229 (2006)

294. M. Tabellout, K. Fatyeyeva, P.-Y. Baillif, J.-F. Bardeau, A.A. Pud, The influence of the polymer matrix on the dielectric and electrical properties of conductive polymer composites based on polyaniline. *J. Non-Cryst. Sol.* **351**, 2835–2841 (2005)
295. N. Kohut-Svelko, F. Dinant, S. Magana, G. Clisson, J. Francois, C. Dagron-Lartigau, S. Reynaud, Overview of the preparation of pure polyaniline and conductive composites in dispersed media and by thermal processes: From laboratory to semiindustrial scale. *Polym. Intern.* **55**, 1184–1190 (2006)
296. H. Deligoz, B. Tieke, Conducting composites of polyurethane resin and polypyrrole: Solvent-free preparation, electrical, and mechanical properties. *Macromol. Mat. Engin.* **291**, 793–801 (2006)
297. V.X. Moreira, F.G. Garcia, B.G. Soares, Conductive epoxy/amine system containing polyaniline doped with dodecylbenzenesulfonic acid. *J. Appl. Polym. Sci.* **100**, 4059–4065 (2006)
298. X. Yang, T. Zhao, Y. Yu, Y. Wei, Synthesis of conductive polyaniline/epoxy resin composites: Doping of the interpenetrating network. *Synth. Met.* **142**, 57–61 (2004)
299. W. Łuzny, E. Banka, Relations between the structure and electric conductivity of polyaniline protonated with camphorsulfonic acid. *Macromolecules* **33**, 425–429 (2000)
300. M.G. Han, S.S. Im, Morphological study of conductive polyaniline/polyimide blends. I. Determination of compatibility by small-angle X-ray scattering method. *Polym.* **42**, 7449–7454 (2001)
301. J. Jang, J. Bae, K. Lee, Synthesis and characterization of polyaniline nanorods as curing agent and nanofiller for epoxy matrix composite. *Polym.* **46**, 3677–3684 (2005)
302. Q.H. Yang, S.G. Wei, G.X. Cheng, Preparation of conductive polyaniline/epoxy composite. *Polym. Compos.* **27**, 201–204 (2006)



Balappa B. Munavalli, Satishkumar R. Naik, Anand I. Torvi, and Mahadevappa Y. Kariduraganavar

Contents

1	An Overview of Dendrimers	290
2	Classifications of Dendrimers	291
2.1	Simple Dendrimers	292
2.2	Hybrid Dendrimers	292
2.3	Peptide Dendrimers	292
2.4	Multilingual Dendrimers	292
2.5	Amphiphilic Dendrimers	293
2.6	PAMAM Dendrimers	294
2.7	PAMAMOS Dendrimers	295
2.8	Tecto Dendrimers	296
2.9	Chiral Dendrimers	296
2.10	Fréchet-Type Dendrimers	296
2.11	PPI Dendrimers	297
2.12	Metallo Dendrimers	297
2.13	Micellar Dendrimers	298
2.14	Liquid Crystalline Dendrimers	298
3	Synthetic Approaches	298
3.1	Divergent Approach	299
3.2	Convergent Approach	302
4	Properties of Dendrimers	308
4.1	Structure and Shape	308
4.2	Reactivity	309
4.3	Solubility	309
4.4	Viscosity	311
4.5	Ionic Conductivity	313
4.6	Compressibility	313
4.7	Polydispersity	314
4.8	Host–Guest Chemistry	315

B. B. Munavalli · S. R. Naik · A. I. Torvi · M. Y. Kariduraganavar (✉)
Department of Chemistry, Karnatak University, Dharwad, India
e-mail: bbmunavalli712@gmail.com; naikrsatish@gmail.com; anandtorvi49@gmail.com;
mahadevappayk@gmail.com

4.9	Catalytic Properties	317
4.10	Degree of Branching (DB)	318
4.11	Melt Properties	320
4.12	Electrochemical Properties	321
4.13	Biocompatibility and Toxicity	321
5	Applications of Dendrimers	323
5.1	Biomedical Applications	323
5.2	Engineering Applications	328
5.3	Miscellaneous Dendrimer Applications	332
6	Future Prospects and Conclusions	333
	References	334

Abstract

Dendrimers are the new class of materials, characterized by the combination of compact molecular assembly and high number of functional groups, which can make them potential candidates in both medical and engineering applications. Thus, this chapter presents an overview of dendrimers, which includes the classification of dendrimers, different methods employed for the syntheses of dendrimers, and properties and applications of dendrimers. An attempt was also made to discuss the progress made in the variety of dendrimeric materials. A special attention was made in discussing the properties of dendrimers and their structures, which play predominant role in deciding the applications of dendrimers in various fields. During the review, we came to know that dendrimers can also demonstrate as novel carriers for drug delivery across the cell membranes and organ barriers such as blood-brain barrier (BBB) and have a host of applications in treating tumors and cerebral gliomas and delivery of drugs for specific site of a brain. This anticipates that a new era of research on the dendrimers would focus on the development of dendrimers-clusters to form multifunctional therapeutic systems, which could subsequently open a new path for clinical applications. At the end, while concluding, we have also discussed the future prospects of dendrimers for various applications. To compile this chapter and to provide adequate information to the readers, we have explored all the possible ways, such as research articles, reviews, books, book chapters, and Google sites.

1 An Overview of Dendrimers

Dendrimers are highly branched, globular, monodispersed, radially symmetric, and well-defined homogeneous structures [1]. The dense architecture of the dendrimers originates from the monomer compositions and their arrangement. These are highly ordered artificial macromolecules, which are characterized by the combination of compact molecular structure and high number of functional groups [2]. These contain uniform branching segments built around a small molecule or a linear core [3, 4].

The term dendrimers derived from Greek words; “dendros” means “tree” or “branch” and “meros” means “part.” These were first synthesized by Fritz Vogtle

in 1978 and Donald Tomalia and co-workers in 1980s. During the same time, Newkome and his group [5] independently synthesized the similar macromolecules and called as “arborols.” The word “arbor” means a tree in Latin.

A dendrimer is classically symmetric around the core and often adopts a three-dimensional globular structure. In dendritic polymers, generally there are four main subgroups which are closely related to one another: hyperbranched polymers, dendronized polymers, dendrigrafts, and dendrimers. These subgroups have the same concept of synthetic protocols, but the difference lies in the amount of branching units. Hyperbranched and dendronized polymers are statistically ordered polymers with polydispersity index (PDI) ranging from 1.5 to 10. Dendrigrafts are the semi-controlled polymers with PDI values range between 1.1 and 1.5. On the other hand, dendrimers present unprecedented control over the addition reaction with the PDI values occurred between 1.0 and 1.05.

Dendrimers consist of three main architectural components, such as core, interior, and end-groups. The core is positioned at the center, while the branched wedges (dendrons) are attached at the core. The size of dendron depends on the number of monomer layers built and each layer is called as a generation (G). The interior consists of monomers branching that have AB_x functionality, where $x \geq 2$. From the central core, the dendrons are grown through different synthetic protocols [6, 7]. The interior part of the dendrimer is traditionally dormant and not accessible for post modifications. But in some cases, dendrimers are allowed to functionalization by treating with super acids or super bases to generate active sites within the interior.

Macromolecular architectural are traditionally classified as linear, crosslinked, and branched structure to generate polydispersed products of different molecular weights. However, the synthetic dendrimers offer the chances of generating monodispersed and structure-controlled macromolecular architecture. Upon functionalization of the end groups, the physicochemical properties of the dendrimers can be altered [8–13]. The globular shaped, nanoscale sized structures with low intrinsic viscosity could be generally obtained with dendrimers of larger structures. Consequently, branched materials are being attracted both in material research and in industry. Any deviation during the dendrimer synthesis generally creates structural defects, and thereby the purification process becomes tedious or sometimes it is impossible. As a result, the need of good chemistry background is crucial to achieve high efficiency in dendrimer synthesis. In spite of this, dendrimers are still seen as tedious, time consuming and expensive materials to synthesize. Though it is synthetically more challenging, the dendritic molecules can be tailor-made to include the functional domains so as to achieve the desired physical and chemical properties.

2 Classifications of Dendrimers

Generally, dendrimers can be classified based on their shapes, structures, branchings, chirality, etc. They are:

2.1 Simple Dendrimers

These have been made with simple monomer units. The convergent synthesis of monodispersed dendrimers is based on symmetrically substituted benzene tricarboxylic acid ester groups. The resulting dendrimers comprise of 4, 10, 22, and 46 benzene rings linked symmetrically with a molecular diameter of 45 Å [14].

2.2 Hybrid Dendrimers

These dendrimers have been obtained by complete monofunctionalization of the peripheral amines of a “zero-generation” polyethyleneimine dendrimer and thus provide structurally diverse lamellar, cubic, and columnar self-organized lattices that are less readily available from other modified dendritic structures [15]. These dendrimers possess the characteristic properties of both linear and dendritic polymers [16]. Preparation of linear and dendritic polymers can be made in hybrid block or graft copolymer form which makes them suitable to use as surface active agents, compatibilizers, or adhesives, for example, hybrid dendritic linear polymers [14]. The supermolecular hybrid dendrimers (SHDs) exhibit characteristic properties such as well-defined nanostructure, fluorescent signaling, and arginine-rich peptide corona. Bio-inspired supramolecular hybrid dendritic systems stimulate for biomedical applications both in vitro and in vivo as shown in Fig. 1. In addition, bio-inspired supramolecular hybrid strategy largely intensifies the gene transfection efficiency of SHDs around 50,000-fold as compared to single peptide dendrons (PDs) at the same reserves-to-production ratio [17].

2.3 Peptide Dendrimers

Peptide dendrimers are radial or wedge-like branched macromolecules consisting of a peptidyl branching core and/or covalently attached surface functional units. These dendrimers contain amino acid as branching or interior unit as illustrated in Fig. 2 [18]. The multimeric nature, unambiguous composition, and the ease of production make these type of dendrimers well suited for various biotechnological and biochemical applications, generally diagnostic purpose and vaccine delivery [19]. In addition, peptide dendrimers can also be used as contrast agents for magnetic resonance imaging (MRI), magnetic resonance angiography (MRA), fluorogenic imaging, and sero diagnosis.

2.4 Multilingual Dendrimers

Multilingual dendrimers are built with multiple copies of a particular functional group on their surface [16].

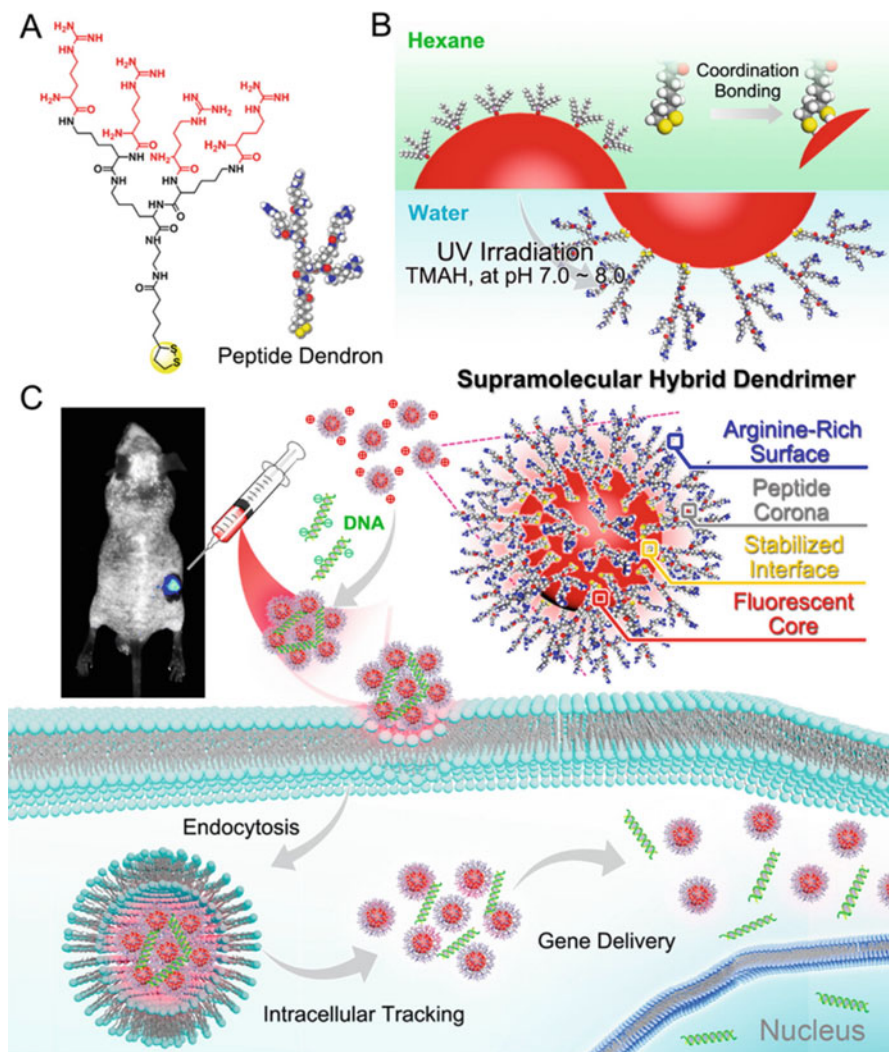


Fig. 1 Schematic illustrations for self-assembly and biomedical applications of SHDs. (a) Chemical structure of the dual functionalized PDs, (b) self-assembly of PDs onto quantum dots through the coordination interactions, (c) SHDs with hierarchical nanostructures for biological tracking and gene delivery in vitro and in vivo. (Adopted with kind permission from Ref. [17] from © ACS)

2.5 Amphiphilic Dendrimers

Amphiphilic dendrimers are the class of globular dendrimers made with two segregated sites of chain end. These have one half that is electron donating site and another half is electron withdrawing site as illustrated in Fig. 3 [20]. These dendrimer structures have asymmetrical but highly controlled division of chain

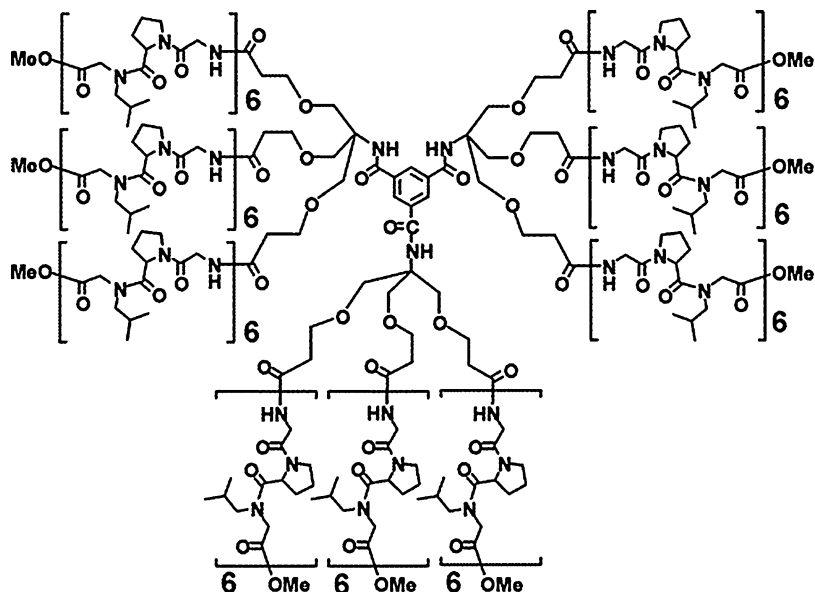


Fig. 2 Synthesis of peptide dendrimer: TMA[β -Ala-TRIS[(Gly-Pro-Nleu) $_6$ -OMe] $_3$] $_3$. Poly(propylene imine) (PPI) dendrimers are available as AstramolTM. (Adopted with kind permission from Ref. [18] from © ACS)

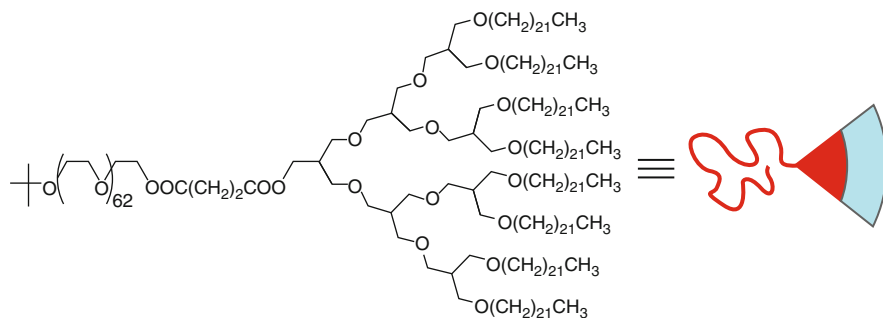


Fig. 3 Molecular architecture of extended amphiphilic dendrimer. (Adopted with kind permission from Ref. [20] from © ACS)

end chemistry. The orientation of these structures at the interface form interfacial liquid membranes for neutralizing aqueous organic emulsion [14].

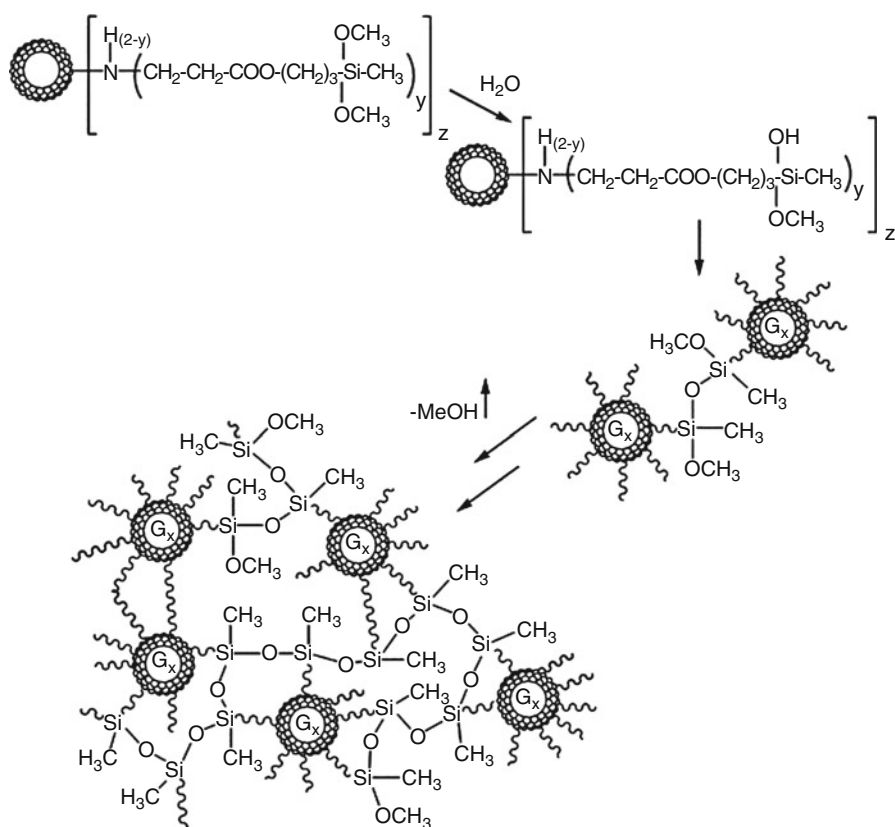
2.6 PAMAM Dendrimers

Poly (amido amine) (PAMAM) dendrimers are ellipsoidal or spheroidal in shape. These are most studied macromolecules and are commercially available [21]. The divergent

method is used for their synthesis using ammonia or ethylenediamine as a starting material. The high solubility and reactivity of these dendrimers is due to the presence of a number of functional end groups and empty internal cavities [22–24]. PAMAM dendrimers contain high amino group density than the conventional macromolecules [21]. They are commercially available as methanol solutions and in generation G0–10 with 5 different core type and 10 functional surface groups [25, 26].

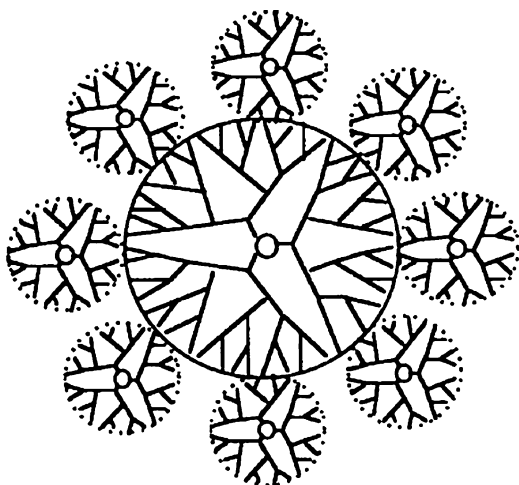
2.7 PAMAMOS Dendrimers

Polyamidoamine organosilicon (PAMAMOS) dendrimers were discovered by Petar Dvornic and his colleagues at Michigan Molecular Institute in 1990. These are inverted unimolecular micelles consist of hydrophilic, nucleophilic polyamidoamine interiors, and hydrophobic organosilicon (OS) exteriors as shown in Scheme 1.



Scheme 1 Formation of honeycomb-like nano-domained PAMAMOS dendrimer networks from alkoxy-silyl functionalized PAMAMOS dendrimers. Circular shapes represent PAMAM dendritic domains of generation G_x . (Adopted with kind permission from Ref. [27] from © ACS)

Fig. 4 Schematic representation of a core-shell tecto-(dendrimer) molecule in solution. (Adopted with kind permission from Ref. [28] from © ACS)



The excellent networks regularity and their ability to complex and encapsulate various guest species offer unprecedented potentials for new applications such as nanolithography, electronics, photonics, chemical catalysis, and useful precursors for the preparation of honeycomb like networks with nanoscopic PAMAM and OS domains [27].

2.8 Tecto Dendrimers

These are made up of core dendrimer which is surrounded by other dendrimers as shown in Fig. 4 [28]. Each dendrimer performs a specific function leading to a smart therapeutic system which can simultaneously diagnose the diseased state and deliver API to the recognized diseased cell [16].

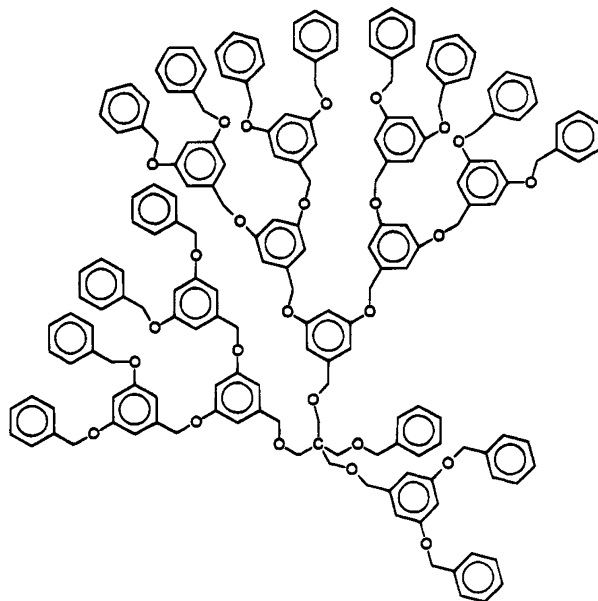
2.9 Chiral Dendrimers

The chirality of the dendrimers is based upon the construction of constitutionally different but chemically similar branches to chiral core [29], for example, chiral dendrimers obtained from pentaerythritol (Fig. 5) [30]. They are potentially used as chiral hosts and chiral catalysts for enantiomeric resolutions and asymmetric synthesis, respectively.

2.10 Fréchet-Type Dendrimers

These are the hydrophobic dendrimer types having carboxylic acid groups as surface groups, serving as a good anchoring point for further surface functionalization as

Fig. 5 Racemic form of the chiral dendrimer (The chirality is based on a pentaerythritol core with four dendrimer substituents of different generation). (Adopted with kind permission from Ref. [30] from © ACS)



shown in Fig. 6. The polar surface groups increase the solubility of these dendrimers in polar solvents or aqueous media [31].

2.11 PPI Dendrimers

The poly(propylene imine) (PPI) dendrimers shown in Fig. 7 made of diamino butane with tertiary-propylene amines as interior and primary amines as the end groups [32]. These are commercially available up to generation G-5 and are chosen as potential molecules in material science and biology.

2.12 Metallo Dendrimers

These dendrimers attached with the metal ion to form the complexation either in the interior or on the peripheral, thus named as metallo dendrimers. Currently, the incorporation of metal centers into macromolecules to develop well-defined molecules with new advantageous properties is one of the most active areas of research in chemistry. The schematic representation of metallo dendrimer is shown in Fig. 8 [33]. The ruthenium bipyridine complex-based dendrimer exhibit both electrochemical and luminescence properties. Thus, the introduction of metals into dendritic structures results in highly ordered materials with attractive magnetic, electronic, and photo-optical properties [34–44].

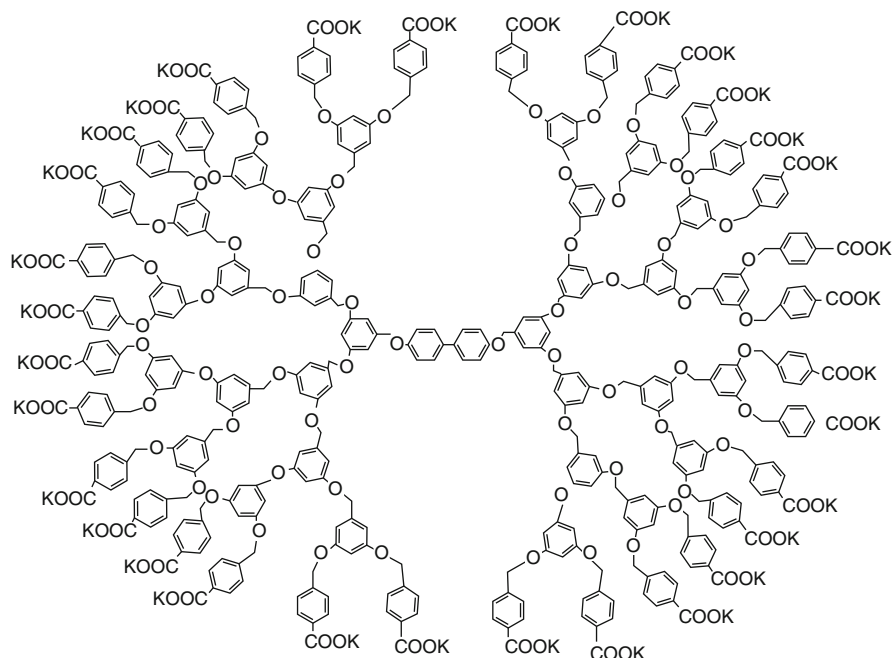


Fig. 6 Structure of G3-Fréchet-type dendrimer. (Adopted with kind permission from Ref. [31] from © RSC)

2.13 Micellar Dendrimers

These are the water-soluble dendrimers with unimolecular micellar arrangement forming a collection of aromatic polymeric chain. Because of micellar structures, these are able to generate an environment for the complex formation with small organic molecules in water [14].

2.14 Liquid Crystalline Dendrimers

These are made of mesogenic monomers. For example, mesogen functionalized carbosilane dendrimer. Functionalization to the end group of carbosilane dendrimers with 36 mesogenic units can be attached through a C-5 spacer and leads to liquid crystalline dendrimers that form broad smectic phase in the temperature range of 17–130 °C [14].

3 Synthetic Approaches

Dendrimers can be developed by two major synthetic approaches, namely, divergent and convergent. In the divergent approach, the synthesis starts from the core of the dendrimer to which the arms are attached by step-wise addition of building blocks.

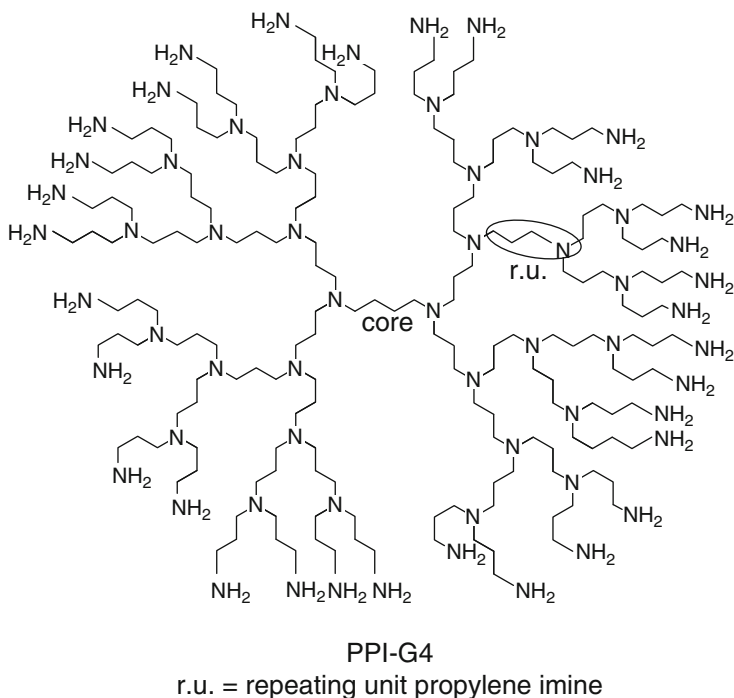


Fig. 7 Poly(propylene imine) PPI-G4 with surfaces of amine groups modified by attaching maltotriose. (Adopted with kind permission from Ref. [32] from © RSC)

However, in the convergent approach, synthesis starts from the exterior, beginning with the molecular structure that finally becomes the outermost arm of the formed dendrimer.

3.1 Divergent Approach

The divergent synthesis of dendrimers is done by Fritz Vögtle in 1978 [45] for the first time and is followed by Denkwalter from Allied Corporation in 1981 [46], Donald Tomalia from Dow Chemicals in 1983 [47], and George Newkome in 1985 [5].

In this approach, monomers are added to a multifunctional core which allows radial growth of dendrimers outwards layer by layer, resulting in approximately doubled molecular weight. Since the partially substituted dendrimers are very similar to the perfect structure both chemically and in size, it is crucial to obtain full substitution of the end-groups. Through the careful monitoring of the reaction using analytical methods, such as matrix assisted laser desorption ionization time of flight (MALDITOF) and nuclear magnetic resonance (NMR), partially substituted dendrimers can be avoided if a large excess of monomer is used in the addition step.

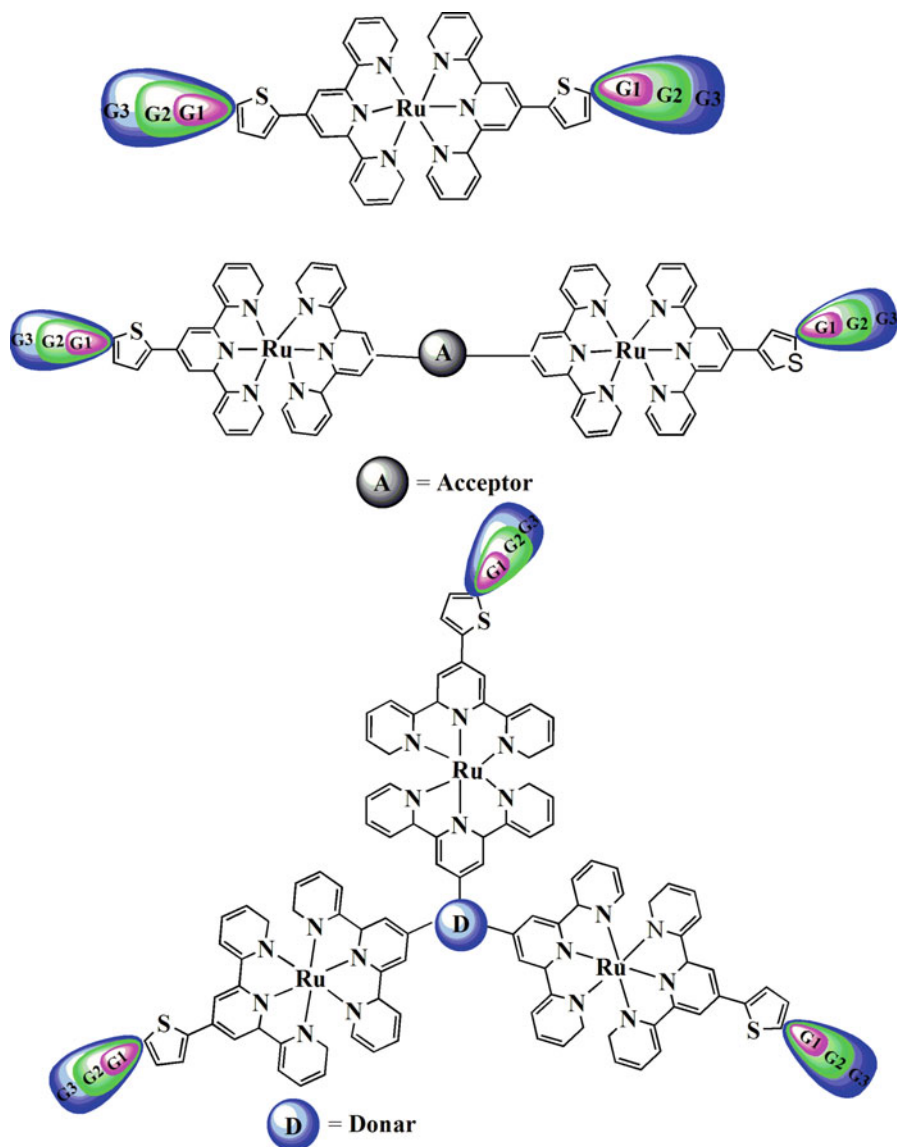
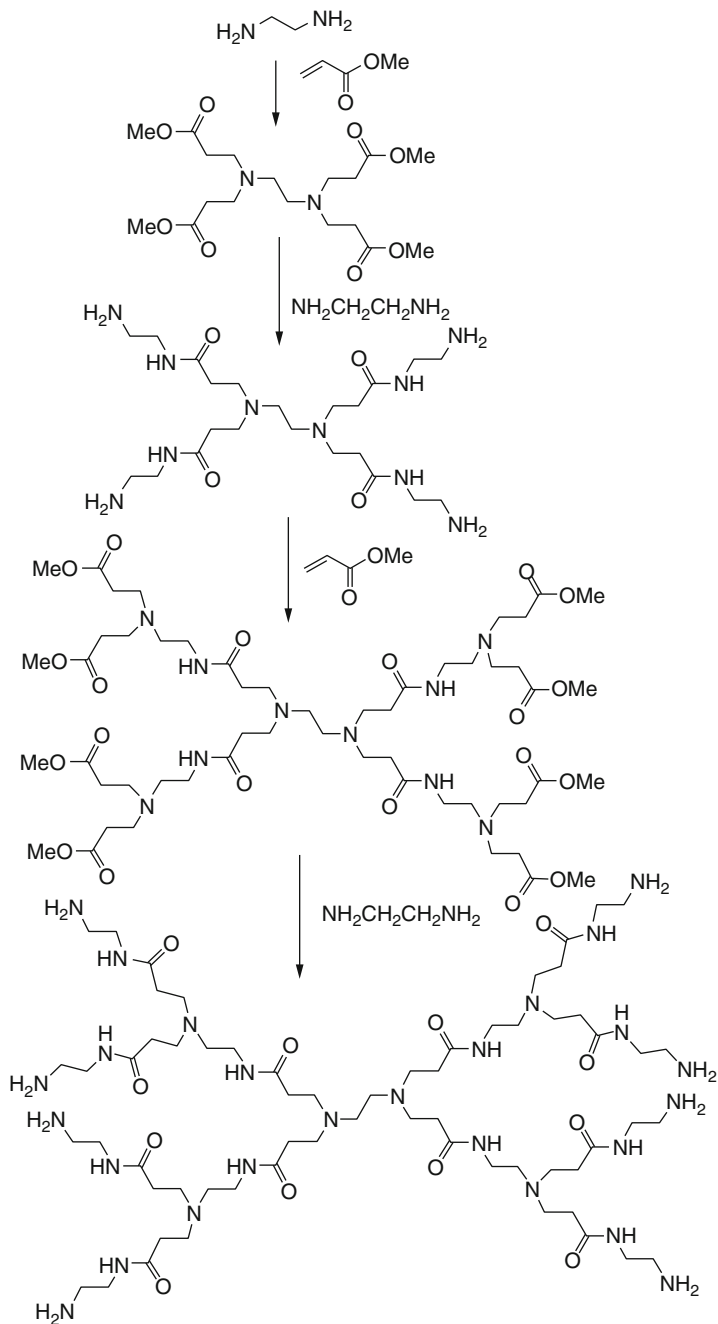


Fig. 8 Schematic representations of the mono-, bis-, and tris-Ru-based systems. (Reproduced with consent from Ref. [33] from © RSC)

Divergent synthesis is generally initiated with a multifunctional core molecule like ethylenediamine (EDA), then four arms are added on nitrogen of EDA with the help of Michael type addition reaction (two arms possible on each nitrogen). In the second step, EDA is again reacted with the resulted four arms through the amidation reaction as shown in Scheme 2 [48].



Scheme 2 Synthesis of dendrimer through the divergent approach. (Reproduced with consent from Ref. [48] from © ACS)

These two steps can be repeated multiple times so as to form different generations of dendrimers. In each generation, the number of arms is doubled than the previous generation. The excess amount of Michael donor (EDA) is used to avoid the structural defects at higher generations. This divergent route is advantageous to get higher yield of dendrimer with lower purity or we can say that the purity is compromised for getting higher yield. Therefore, this approach of synthesis is used worldwide in commercial scale for the production of dendrimers. The purity of the dendrimers is less basically due to one of the reasons: intramolecular and intermolecular cyclization, Retro Michael reaction, or hydrolysis of ester.

Although the divergent approach is conceptually straight forward, there are some synthetic problems. As the size of the dendrimers increases, the number of surface functionalities will also increase. Therefore, to reach the subsequent generation of dendritic molecule, an exponentially increasing number of reactions need to be performed on a single molecule, but it is quite challenging even with highly efficient reactions. The separation of the required product from the by-products is difficult as the mass, size, and properties of bi-products are often very close to the structurally perfect dendrimer. Well-known dendrimers which are synthesized using the divergent approach are: poly(amidoamine) PAMAM, poly(propylene imine) POPAM, and 2,2-bis(methylol) propionic acid (bis-MPA) dendrimers.

3.2 Convergent Approach

The synthesis of dendrimer through the convergent approach was first introduced by Jean Fréchet in 1990 [49]. In this approach, dendrons that end up to terminal groups are synthesized first and these are linked together to a core molecule in the final step for getting complete dendrimer structure.

Convergent approach of dendrimer synthesis overcomes the purity and structural defect issues of divergent synthesis. With this approach, more uniform and symmetric dendrimers can be synthesized but with lower overall yield. In other words, yield is sacrificed for purity. This approach is generally used for laboratory scale dendrimer synthesis. The dendrimer synthesis is initiated from small molecules that end up at the surface of the sphere and the reactions proceed inward building and are finally attached to a core. This method makes it much easier to remove impurities and shorter branches along the way, so that the final dendrimer is more monodisperse. The dendrimers synthesized by this way are not as large as those synthesized by divergent methods, because the convergent approach does not allow the formation of high generations due to the steric hindrance in the reactions of the dendrons and the core molecule.

A variety of convergent syntheses have been developed in the past decade by introducing a wide range of functionalities. The most widely used convergent dendrimer syntheses include: poly(phenylene), poly(alkyl ester), poly(aryl alkyne), poly(aryl alkene) poly(alkyl ether), poly(aryl ether) dendrimers. Some of these syntheses will be described more in detail below.

3.2.1 Poly(aryl ether) Dendrimers

Poly(aryl ether) dendrimers were developed by Hawker and Fréchet in 1989–1990 [50]. The synthesis makes use of 3,5-dihydroxybenzyl alcohol as the monomer **1** and two phenolic groups of this monomer were coupled to the benzylic bromide **2**, in the presence of K_2CO_3 and 18-crown-6, producing the two new ether linkages of the second generation benzylic alcohol **3** as shown in Scheme 3. Through the reaction with carbon tetrabromide and triphenyl phosphine, the focal benzylic alcohol functionality was then activated for the next coupling step affording brominated dendron **4**. The coupling step was then repeated using two equivalent of activated dendron and one equivalent of the monomer, resulting in the third generation benzylic alcohol **5**. The Williamson coupling and bromination steps were repeated subsequently to yield the sixth generation dendron **11**.

The synthesis method utilized Williamson coupling reaction between a highly nucleophilic phenolate and a highly activated benzylic bromide, ensuring exceptional yields during all the generation growth steps. The elimination side reactions were prevented by the benzylic substrates that frequently accompany nucleophilic displacements.

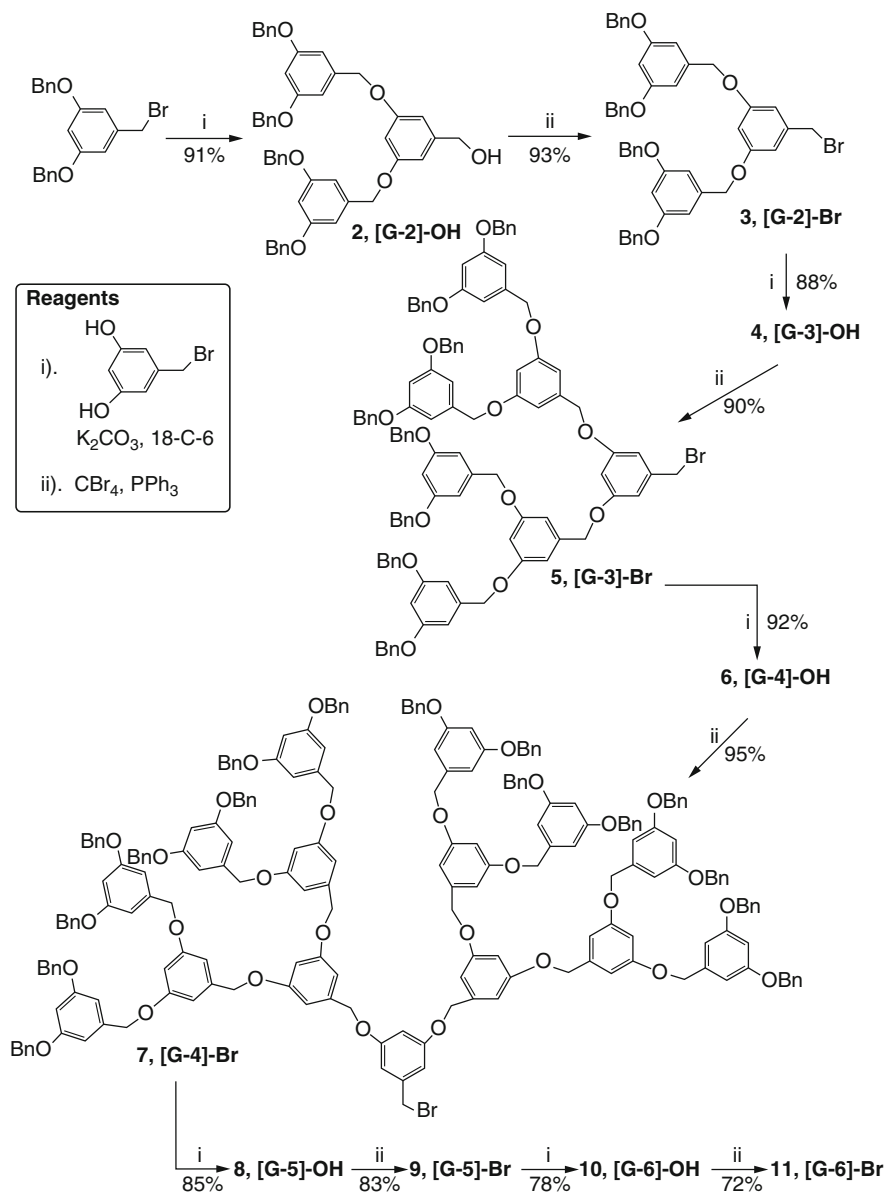
3.2.2 Poly(phenylene) Dendrimers

The convergent approach for the synthesis of a family poly(1,3,5-phenylene) dendrimers [4, 51] was reported by Miller and Neenan soon after the report of the poly(benzyl ether) dendrimer [52].

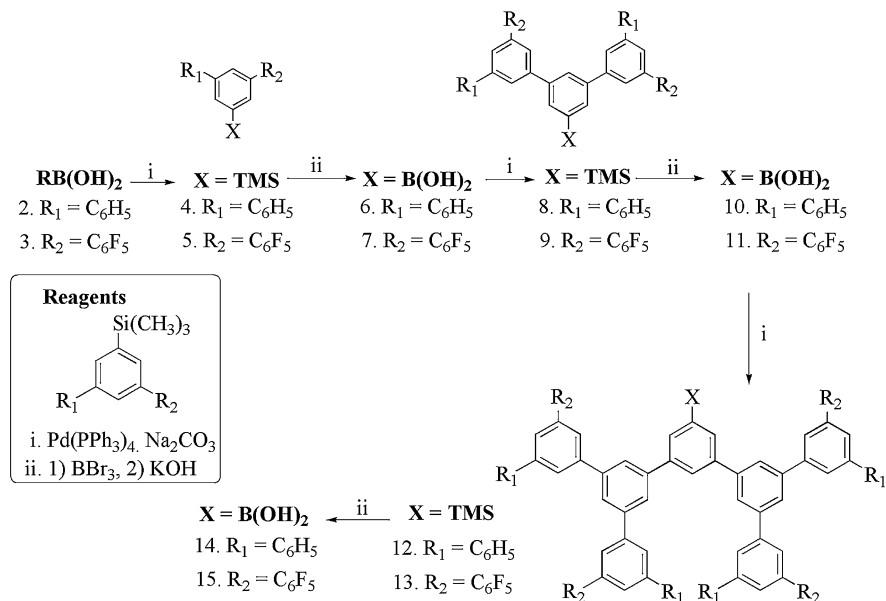
In the preparation of these polyphenylenes and their fluorinated analogs, aryl boronic acids **2** or **3** undergo Suzuki coupling with the monomer **1**, 3,5-dibromo-1-(trimethylsilyl)benzene as shown in Scheme 4. Further coupling to the monomer is initiated owing to the conversion of the trimethylsilyl (TMS) protecting group of products **4** and **5** to the boronic acid functionality in **6** and **5**. This procedure results in the preparation of dendrons up to third generation **13–16**. The rigid repeat units provide well-defined shapes and diameters of these dendritic structures. Recently, Mullen et al. have reported the synthesis of poly(phenylene) dendrimers by the convergent approach [51] similar to the divergent [4 + 2] cycloaddition route reported previously [52] as shown in Scheme 3.

3.2.3 Poly(alkyl ester) Dendrimers

The convergent syntheses of Poly(alkyl ester) dendrimers was reported by Hult and co-workers utilizing a repeat unit based on 2,2-bis-(hydroxymethyl)propanoic acid as shown in Scheme 5 [53]. The two alcohol moieties of the benzyl 2,2-bis-(hydroxymethyl)propanoate monomer **1** undergo coupling with an activated acid chloride end-group **2** followed by the removal of the focal benzyl ester by hydrogenolysis. The carboxylic acid could be transformed to the corresponding acid chloride **4**, in nearly quantitative yields using oxalyl chloride. The repeating coupling deprotection procedure results in the fourth generation dendron **7**. Due to ether or hydrocarbon linkages, these polyesters do not exhibit the chemical stability of other dendritic macromolecules, but as their ester functionalities are shielded from nucleophilic attack by the neighboring quaternary carbon, the dendrons show rather high stability to acidic conditions. The efficient [54] and versatile [55] synthesis of analogous dendrimers is reported recently by Ihre et al.



Scheme 3 Convergent approach for the synthesis of poly(aryl ether) dendrimers. (Reproduced with consent from Ref. [50] from © ACS)



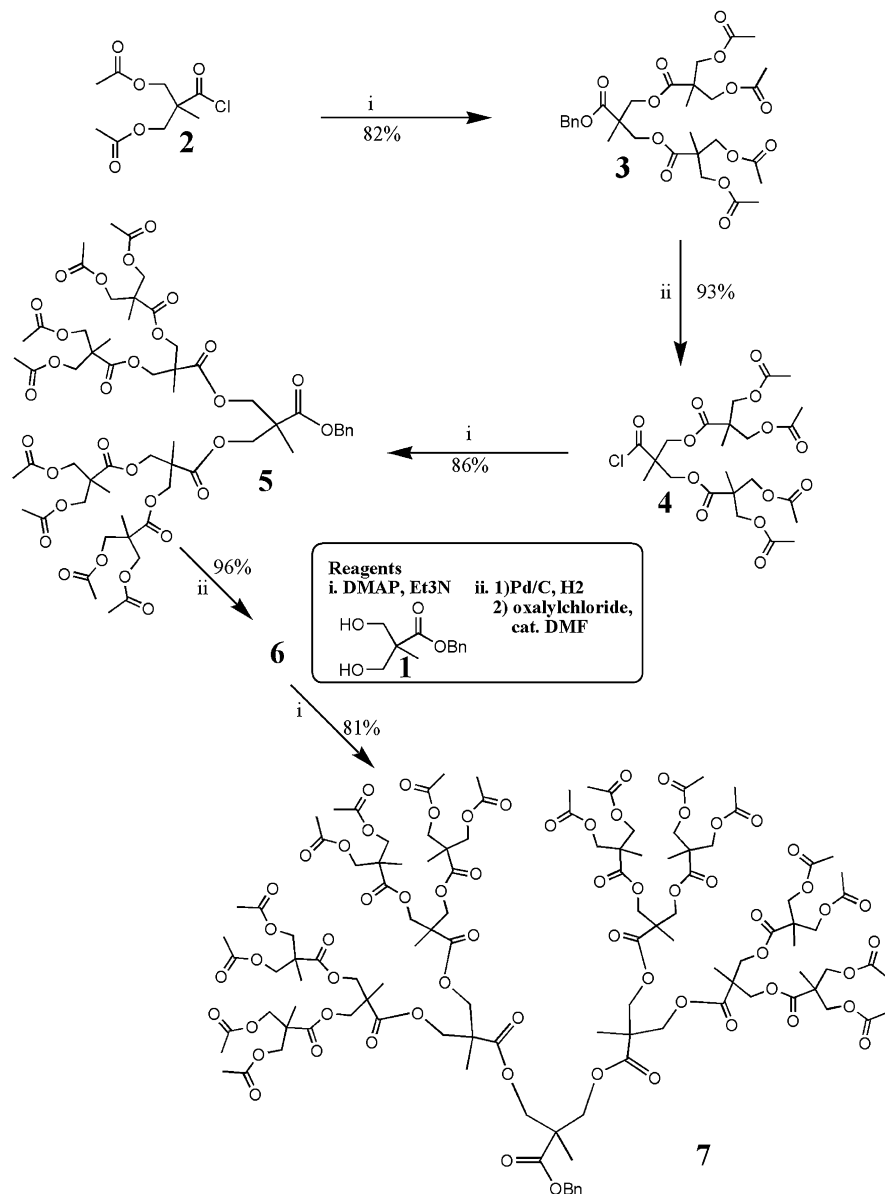
Scheme 4 Convergent approach for the synthesis of poly(phenylene) dendrimers. (Reproduced with consent from Ref. [52] from © ACS)

3.2.4 Poly(alkyl ether) Dendrimers

The convergent approach for the synthesis of an aliphatic analogue of the poly(benzyl ether) dendrimer was recently developed by Fréchet and coworkers as shown in Scheme 6 [56]. The synthesis was initiated by coupling the end groups to the monomer **1**, 3-chloro-2-chloromethyl-propene using the Williamson ether coupling of a bis-protected triol **2** or **3**, with the allylic chloride functionalities of the monomer [57].

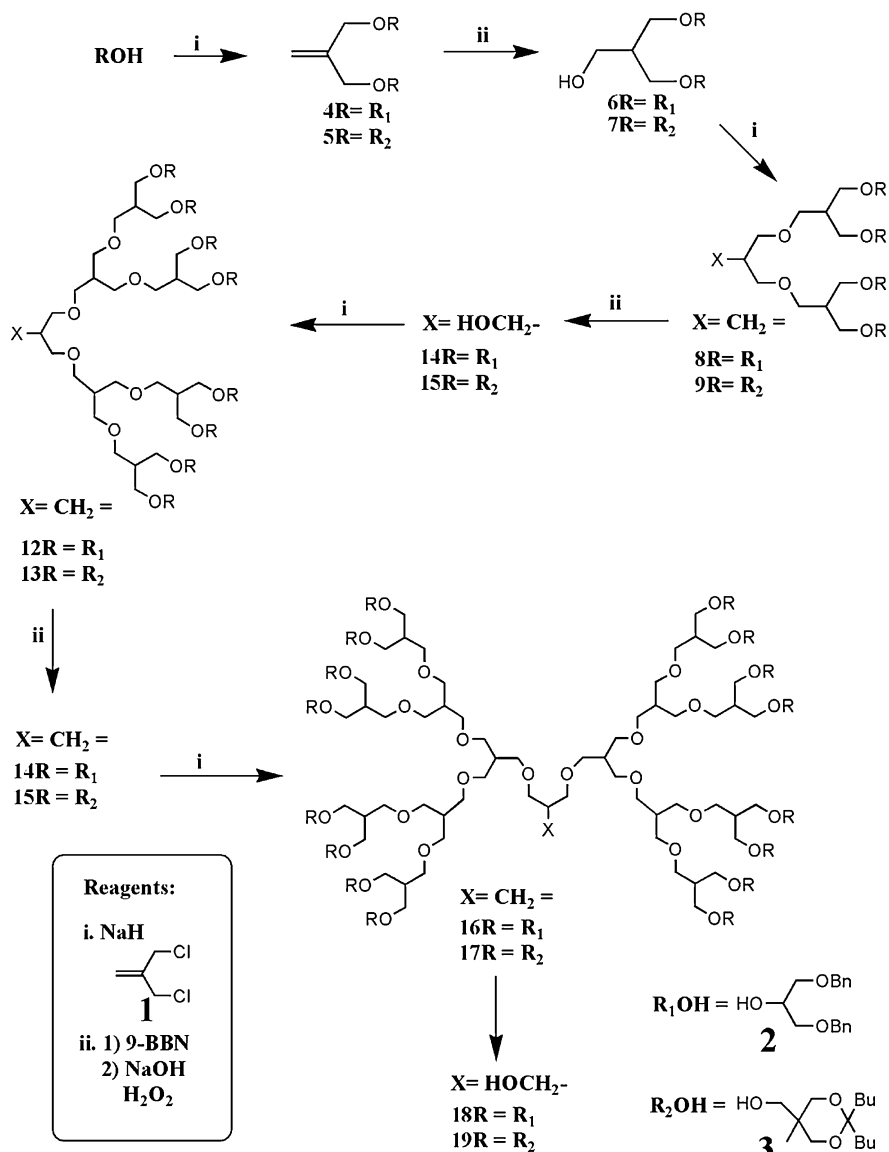
During the synthesis, the double bond of the resulting product **4** or **5** was converted to the corresponding primary alcohol **6** or **7** via hydroboration/oxidation, thereby enabling further coupling and this procedure could be repeated in high yields through fifth generation dendrons **16–19**. Although the more demanding purification of these compounds will likely prevent them from replacing the poly(benzyl ether) family for many applications, they allow a wide range of chemical modification. For example, the peripheral ketal and benzyl ether protecting groups can be quantitatively removed by acid-catalyzed hydrolysis or palladium-catalyzed hydrogenolysis exposing multiple peripheral hydroxyl groups capable of further modification by alkylation or esterification [58].

Since the poly(alkyl ether) dendrons did not interfere with the *N*-bromosuccinimide bromination of the pendant oligothiophene or subsequent Stille couplings,



Scheme 5 Convergent approach for the synthesis of poly(alkyl ester) dendrimers. (Reproduced with consent from Ref. [53] from © ACS)

they were selected as solubilizing scaffolds for otherwise intractable oligothiophenes [59, 60]. Also, the significant polar backbone, similar to poly(ethylene glycol), of these compounds may prove useful in macromolecular catalysts or biomedical applications.



Scheme 6 Convergent approach for the synthesis of poly(alkyl ether) dendrimers. (Reproduced with consent from Ref. [56] from © ACS)

3.2.5 Other Convergent Dendrimer Syntheses

Convergent approach has been developed for the preparation of dendritic poly(amides) [61–68], poly(esters) [69], poly(urethanes) [70, 71], poly(carbonates) [72], poly(arylamines) [73–76], poly(aryl ketones) [77], poly(aryl alkynes) [78],

poly(aryl methanes) [79], poly(arylammonium) salts [80], poly (thioureas) [81], poly- (ether imides) [82], poly(keto ethers) [83–85], poly(amine ethers) [86], poly (amino esters) [87], etc.

4 Properties of Dendrimers

The properties such as well-defined size, shape, molecular weight, monodispersity, and unimolecular micellar nature make the dendrimers a smart choice for drug delivery application and enhance the solubility of poorly soluble drug. Despite several advantages, dendrimers-based drug delivery is still in its infancy even after three decades of discovery [88].

The typical architecture of a dendrimer has consequences for its physical behavior. The research in the past decade revealed the true nature of dendrimers, regarding their appearance and physical characteristics. Since many of the proposed uses of dendrimers rely on the availability of the large amount of functional groups, the localization of the end groups in dendritic systems is the crucial requirement. The properties of dendrimers are deviating as compared to their linear macromolecular counterparts and encompass the transition in physical properties when a sequence of dendrimer generations is considered. This nature results in the unexpected conformational features for dendritic molecules. Thus for the intended use in applications such as drug delivery, biocides, gene transfer, catalyst supports, energy, and processing aids controlling the molecular architecture of dendrimers is crucial [89–91].

4.1 Structure and Shape

Dendrimers are the type of dendritic molecules with two or more dendrons attaching to a multivalent core molecule. A dendron is a highly branched sector with surface groups at the periphery, branching units, and a focal point.

Dendrimers of lower generations (G-0, G-1, and 2) have highly asymmetric shape and possess more open structures as compared to higher generation dendrimers. For example, rotaxanes have a linear dumbbell-shaped component bearing bulky end-groups or stoppers around which one or more macrocycles are trapped [92–95].

As the chains growing from the core, molecule becomes longer and more branched (in 4 and higher generations) and the dendrimers adopt a globular structure [96]. Gradually, the dendrimers become densely packed and they extend out to the periphery, forming a closed membrane-like structure. When a critical branched state is reached, because of a lack of space dendrimers cannot grow further. This is termed as the “starburst effect” [21]. For example, in case of PAMAM dendrimer synthesis, it is observed after the tenth generation. The rate of reaction drops suddenly and further reactions of the end groups will stop. The tenth generation PAMAM contains 6141 monomer units with a diameter of about 124 Å [97]. In addition, the increasing branch density with generation is also believed to have striking effects on the

structure of dendrimers. They are characterized by the presence of internal cavities and large number of reactive end groups.

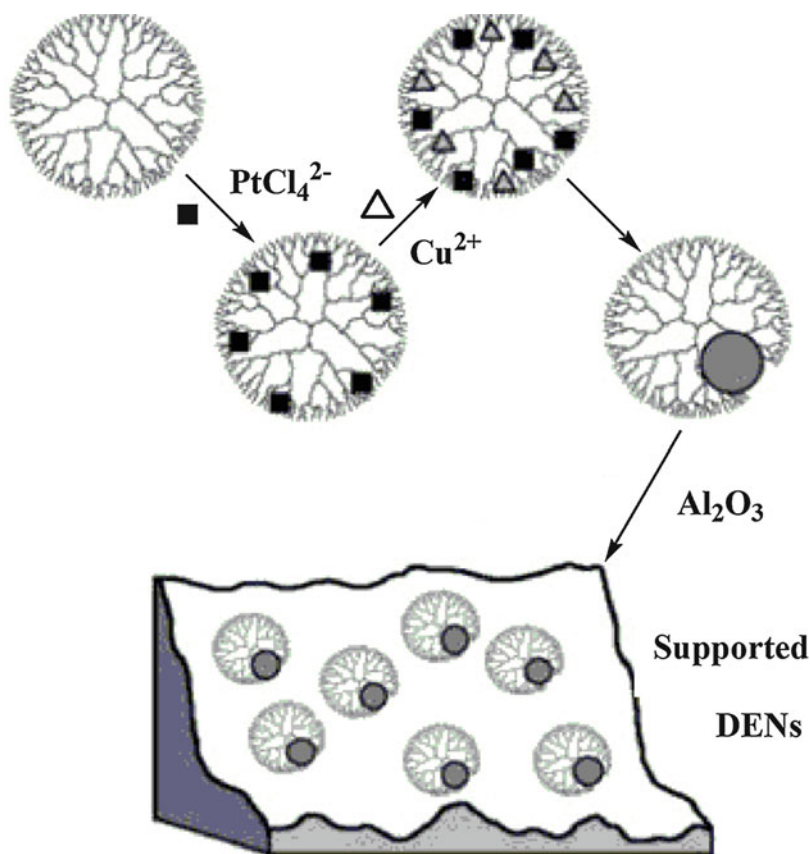
Generally, owing to steric crowding, the structures of dendrimers changed from the extended form to the globular conformation with increasing generations [98–100]. Their properties also vary based on the functionalities attached at surface groups, interiors or cores/focal points, polarities of dendrons/dendrimers, branching multiplicities (AB_2 versus AB_3), etc. [31, 101]. The subsequent dendrimer organizations and assemblies can furnish secondary dendritic structures [102–107]. These characteristics make the use of dendrons/dendrimers feasible in various applications such as nanomedicines [108], catalysis [109–111], light-harvesting [112], and nano-capsules for drug or gene deliveries [113].

4.2 Reactivity

The interaction of dendrimers with their environment depends largely on the functional groups. The design of molecular interactions such as hydrogen bonding and the control of polymer architecture strengthened the interfaces between different polymers or between polymers and other surfaces. To encapsulate reactive sites or provide highly controlled surfaces and interfaces, three dimensional synthetic dendrimers have been fashioned. For example, Hoover et al. [114] demonstrate that PAMAM dendrimers can be used to template bimetallic Pt-Cu nanoparticles with controlled metal stoichiometries in solution as shown in Scheme 7. Active supported bimetallic nanoparticle catalysts can be formed by the deposition of nanoparticles onto a high surface-area oxide support and the thermal dendrimers removal process. The surface dilution of Pt in Cu is indicated by Infrared spectroscopy of adsorbed CO and suggested only weak electronic donation from Cu to Pt. Importantly, the stoichiometry set in the initial solution syntheses of the nanoparticles has a direct influence on the activity of the resulting catalysts. This offers new opportunities for studying particle composition effects for a variety of catalytic reactions.

4.3 Solubility

Due to the hydrophobicity, the solubility of drugs and bioactive compounds in water reduces and significantly diminishes their activity in vivo [115, 116]. Only 60% of drug compounds reach the patients, whereas the remaining 40% of compounds are eliminated during the screening owing to their poor bioavailability, low water solubility, and low permeability through biological membranes [117–120]. Therefore, a thorough understanding of solubility enhancement is the fundamental task of drug delivery. Dendrimers are a novel type of materials with a unique structure and properties which are suitable for drug delivery and solubilization. The solubilization facilitated by dendrimers is based on the ionic interactions, hydrogen bonding, and hydrophobic interactions. Generally, hydrophobic interior core of dendrimers is responsible for the encapsulation of



Scheme 7 Synthesis of dendrimer-templated Pt-Cu nanoparticles. (Adopted with kind permission from Ref. [114] from © ACS)

hydrophobic drugs and the hydrophilic shell of the dendrimers (e.g., carbohydrates) involved in interactions with water and solubilization [118–120].

The presence of many chain-ends offers high solubility, miscibility, and high reactivity to the dendrimers. The nature of surface groups strongly influences the solubility of dendrimers. Dendrimers terminated with hydrophilic groups and hydrophobic groups are soluble in polar and nonpolar solvents, respectively. In tetrahydrofuran (THF), the solubility of dendritic polyester was found remarkably higher than that of analogous linear polyester and also a marked difference was also observed in chemical reactivity. Single-walled carbon nanotube (SWNT) is a nanocarrier of bioactive molecules in aqueous solution. Surface modification of SWNT with a series of dendritic galactopyranosides and mannopyranosides as illustrated in Fig. 9 improves its solubility in water. Generally, sugars with higher branching were more effective in solubilization of SWNT [121].

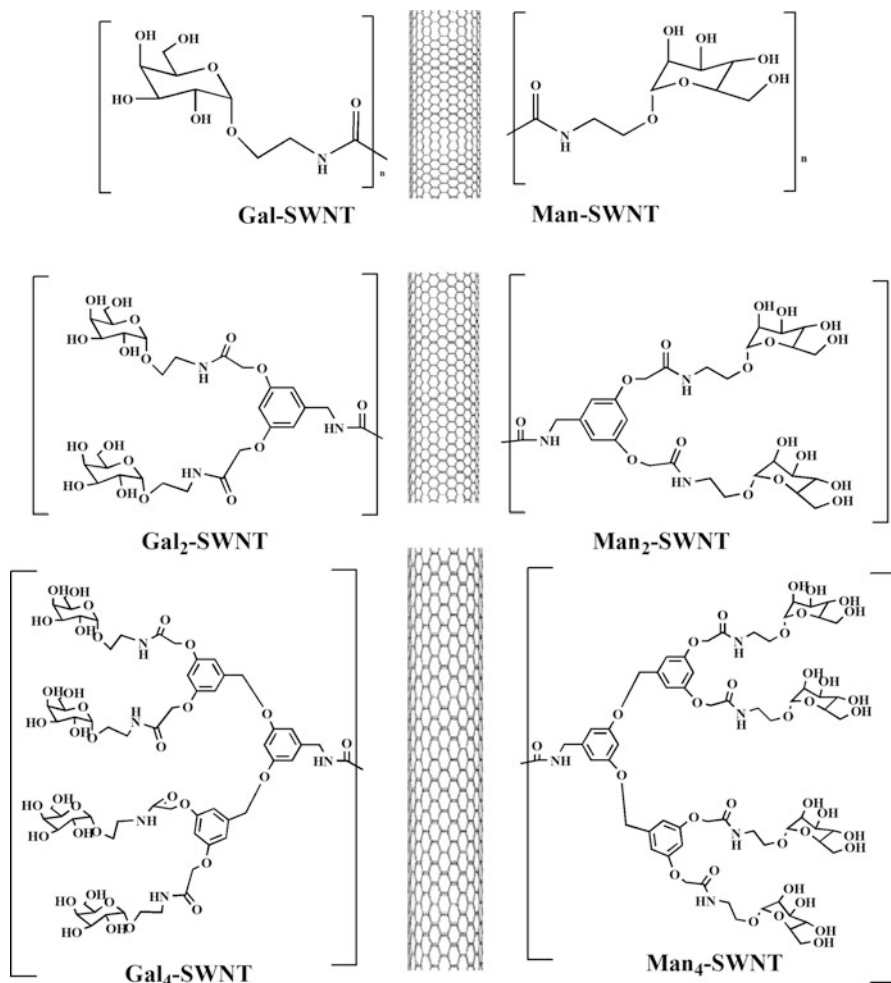


Fig. 9 Carbon nanotubes functionalized with Gal-, Man-, or their dendrons. (Reproduced with consent from Ref. [121] from © ACS)

4.4 Viscosity

Dendrimer solutions are significantly less viscous than the linear polymers. Molecular weight (MW) and degree of branching (DB) strongly influences the viscosity of dendrimers. However, the intrinsic viscosity of dendrimers in solution shows several anomalous behaviors that have hitherto not been explained within the existing theoretical frameworks. Lu et al. [122] proposed a simple two-zone model for a dendrimer based on the radial segmental density profile as illustrated in Fig. 10a, b, which suggests a combined Zimm and Rouse description of the intrinsic viscosity.

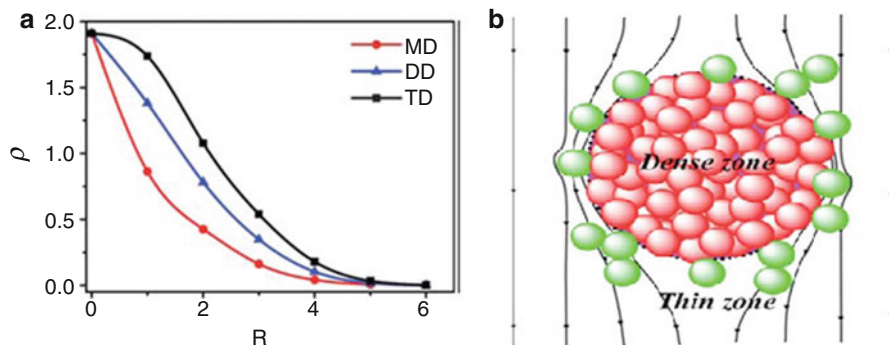


Fig. 10 The two-zone model representing the radial segmental density profiles. (a) The radial segmental density profile of monodendron (MD), didendron (DD), and tridendron (TD). (b) A schematic of the two-zone model: the balls inside and outside the dotted circle belongs to the dense part and thin part, respectively; the distorted lines denote the flow field around the structure. (Adopted with kind permission from Ref. [122] from © RSC)

Based on this simple model, the intrinsic viscosity of the dendrimers can be calculated using Einstein's intrinsic viscosity formula for solid spheres assuming the contributions of dense zone and thin zones the viscosity as additive [97].

$$N_1(G) = \int_{R_c}^{\infty} \rho(R,G) 4\pi R^2 dR \quad (1)$$

The intrinsic viscosity is then,

$$[\eta(G)] = \frac{10\pi [R_c (G)^3 + kN_1(G)\sigma^3]}{3N(G)M_0} \quad (2)$$

where σ is the radius of a monomer, M_0 is the mass of a monomer, k is the ratio between the total effective volume of the segments in the thin zone and their real volume termed as coefficient of correlation, and $N(G)$ is the total number of monomers in the dendrimer calculated from the equation below.

$$\text{where } N(G) = 1 + j(2^{G+1} - 1) \quad (3)$$

where $j = 1, 2, 3, \dots$, for monodendron, didendron, tridendron, etc.

For classical polymers, the intrinsic viscosity increases continuously with molecular mass. In case of polyether dendrimers, it is found that the intrinsic viscosity increases up to fourth generation and then decreases [123, 124]. Such behavior is not found in linear polymers. These properties differ significantly in some of the dendrimers. For example, for polyamidoamine (tridendrons) synthesized by the divergent approach, a maximum intrinsic viscosity as a function of generation has been reported [125]. On the other hand, lysine-based monodendrons have intrinsic viscosities equal to 0.025 dL/g for all generations [126]. A possible reason for this

difference lies on the different density profiles, depending on the length and flexibility of spacers and the interaction between monomer units.

4.5 Ionic Conductivity

The unique properties of dendritic polymers such as the possibility of obtaining tailored made barrier properties, as well as the introduction of crosslinking points and other functional groups to a dendritic polymer by end-group modification, suggest that they have potential as proton exchange membrane fuel cell (PEMFC) components. Several research groups have been investigated the possibility of using dendritic polymers as possible electrolyte materials in lithium-battery applications [127]. Dendritic polymers are highly branched polymers based on AB_x type monomers introducing potential branching points in every repeating unit. The presence of numerous end-groups results in the extensive branching in few entanglements, giving a globular shape and properties. However, there are only a very few publications on dendritic polymers-based proton-conducting membranes in PEFC. Taylor et al. have studied the effect of sulfonated poly(propylene imine) dendrimers in Nafion on morphology and methanol cross-over [128]. Similarly, the development of sulfonated poly(3-ethyl-3-(hydroxymethyl)oxetane) (sPTMPO) by end-capping the hydroxy-groups in the poly-TMPO with 1,4-butane sultone was reported by Gode et al. [128]. Furthermore, the potential use of the dendritic polymer as the acidic component in proton-conducting membranes is explored. Chu et al. [129] developed anhydrous proton-conducting membranes by in situ crosslinking of polymerizable oils containing poly(amido amine) (PAMAM) dendrimer-based macromolecular protic ionic liquids (PILs). Minimal correlation of height observed in AFM images shown in Fig. 11b, d indicates that phase-lag images (Fig. 11a, c) are unlikely to be an artifact of surface roughness. One can observe that the macromolecular PIL droplets with the diameter of ~ 30 nm (dark areas) are dispersed in a continuous polymeric matrix (bright areas) as shown in Fig. 11a. In Fig. 11c, 20–35 nm size of PIL with long and winding channels can be seen. The conductivity of the composite membranes enhances due to the formation of proton transport channel created by homogenous distribution and continuous PIL networks.

4.6 Compressibility

The inverse osmotic compressibility of the poly(propylene imine) dendrimers in deuterated methanol as a function of concentration with small-angle neutron scattering was measured by Rietveld et al. [130]. As increasing the concentration, the scattering intensity of fourth and fifth generations does not increase anymore or increases less than the second and third generations. This effect clearly indicates that the inverse osmotic compressibility was increased as a function of volume fraction as shown in Fig. 12a, b. Zhang et al. [131] for the first time characterized the modification of surface interactions by adsorbed dendrimers of fifth-generation

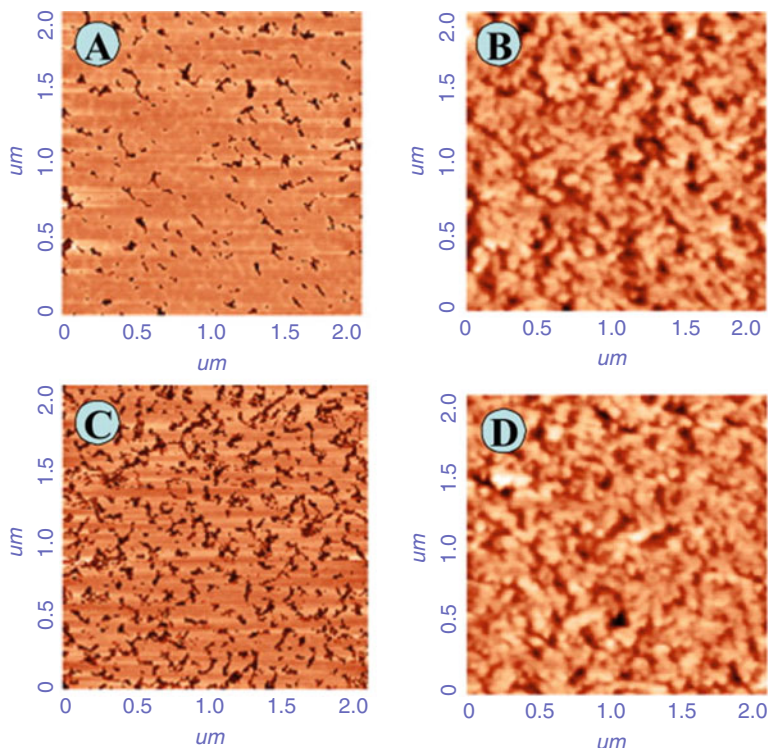


Fig. 11 AFM phase (a, c) and height (b, d) images of the fracture cross-section of polymer composite membranes containing PAMAM dendrimer. (Adopted with kind permission from Ref. [129] from © Elsevier)

poly(propylene imine) by exposing the low energy methyl groups on its outer surface. The experiment results in decrease of compressibility as the dendrimers are progressively compressed.

4.7 Polydispersity

The properties such as low polydispersity index, highly regular branching pattern, and a well-defined number of peripheral groups can be achieved by the stepwise synthesis of dendrimers [5, 132]. In addition, the reproducible pharmacokinetic behavior is resulted due to low polydispersity of dendrimers in contrast to that of some linear polymers containing fractions with vastly different molecular weight within a given sample [133]. The hydrodynamic volume controls the rate of renal filtration. Larger the molecules slower will be the elimination [9]. The synthetic preparation of well-defined high-generation dendrimers is time consuming and the globular architectures of the dendrimers increase the hydrodynamic volume moderately. Figure 13a–c illustrates an alternative approach for the preparation of hybrids

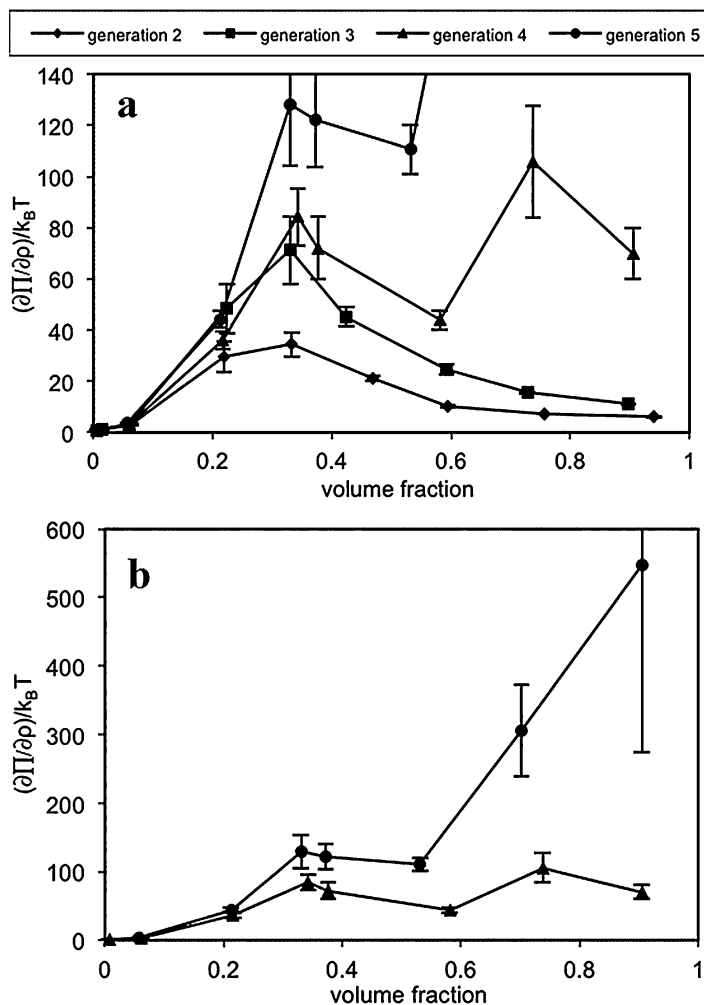


Fig. 12 Inverse osmotic compressibility as a function of volume fraction for generations (a) 2 to 4 and (b) 4 and 5. (Adopted with kind permission from Ref. [131] from © Academic Press)

of polyester dendrimers and PEO star polymers with an increase in molecular weight to 22,000 [9]. PEO was chosen for renal filtration considering its high biocompatibility [134] and low polydispersity of 1.02.

4.8 Host–Guest Chemistry

Several research groups are inspired by host–guest chemistry to prepare dendrimers with specific functionalities at the core. Thus, molecular systems are created in

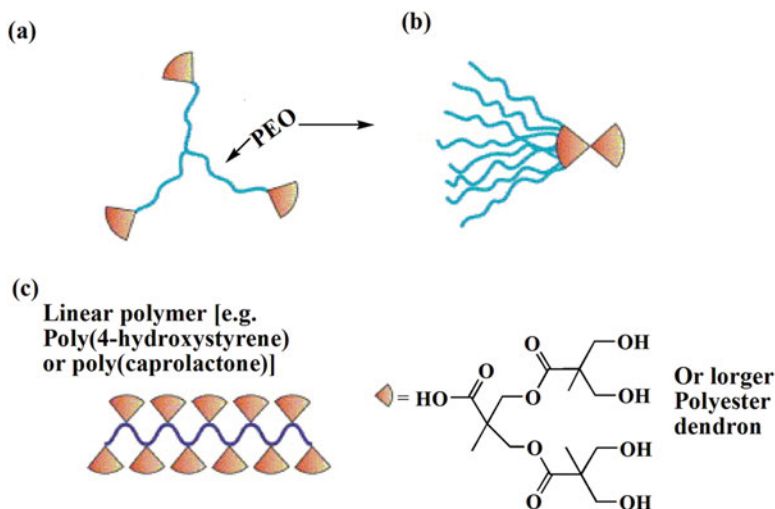


Fig. 13 Polyester dendrimer-linear polymer hybrids. (a) Hybrid of PEO star polymer and polyester dendrons in which the multivalent dendron can carry several copies of drug and the linear PEO provide solubility. (b) “Bow-tie” hybrid of polyester dendrimers and PEO. (c) Polyester dendronized linear polymer. (Adopted with kind permission from Ref. [9] from © Elsevier)

which certain functionality is surrounded by a particular satirically congested structure and the functionality is isolated at a specific site. In dendrimers the ions or neutral molecules can be hosted inside the internal cavities [135]. Such an important property of dendrimers can potentially be exploited for a variety of purposes, such as catalysis, drug delivery, and light harvesting. An advantage shown by such host–guest systems in contrast to dendrimers with a luminescent core is that the wavelength of the sensitized emission can be tuned by changing the guest hosted in the same dendrimer. Dendrimers of the poly(propylene amine) family functionalized with fluorescent dansyl units at the periphery have been chosen as hosts for fluorescent dye molecules [136]. Due to their molecular design, polyphenylene dendrimers create a lot of empty space in their interior, giving rise to unique host–guest interactions, which can be explored in sensor fabrication [41, 137, 138]. Especially porphyrin-based dendrimers have attracted a lot of attention in this research area and they play an essential role as photoactive, redox, guest-binding, and catalytic entities. Diederich et al. have extrapolated the concept of a site-isolated functionality by preparing mimics for cytochrome c, an electron-transferring protein, and have acquired water soluble dendritic iron porphyrins by using peripheral triethyleneglycolmonomethyl ether (PEG-like) moieties (Fig. 14) [41].

Cyclodextrins (CDs), one of the most widely used hosts in the study of host–guest chemistry as well as in the synthesis of rotaxanes are shown in Fig. 15 [139–142].

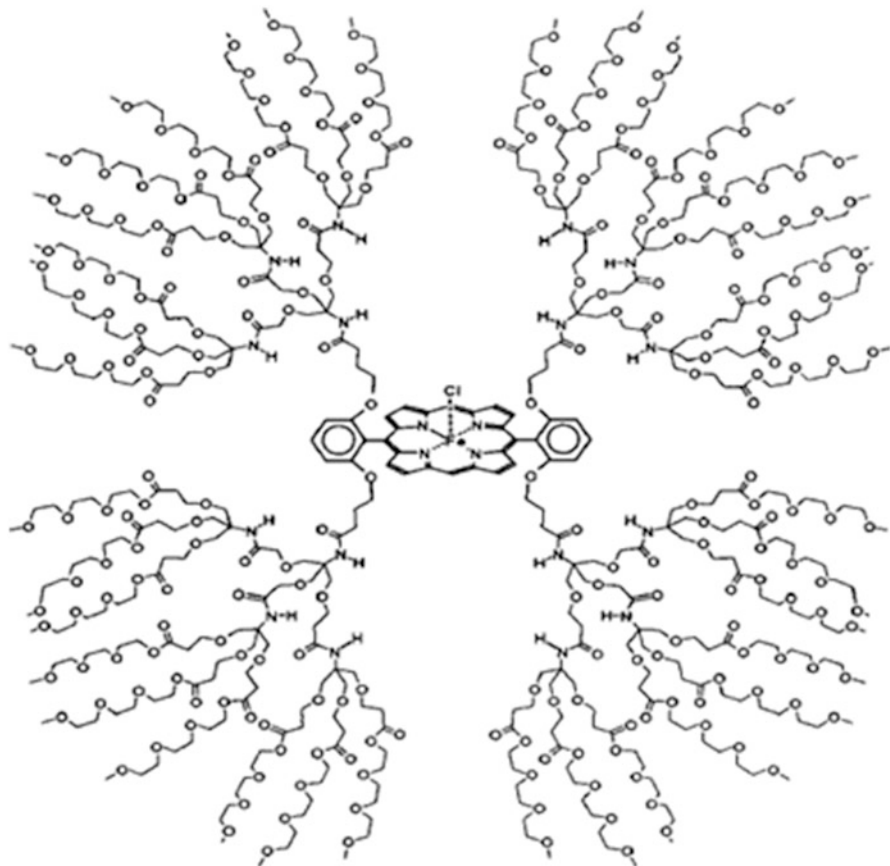


Fig. 14 A dendritic water-soluble heme analog. (Adopted with kind permission from Ref. [41] from © ACS)

4.9 Catalytic Properties

The combined features of dendrimers particularly nanoscopic dimensions and the ability to molecular solvation make them suited to fill the gap between homo- and heterogeneous catalysis. In other words, dendrimers will combine the advantages of homo- and heterogeneous catalysts, if soluble dendrimers with defined catalytic sites are developed that can be removed from homogeneous reaction mixtures by simple separation techniques (i.e., ultrafiltration or dialysis) [143]. In the catalytic dendrimer systems, the active center is located at the core. The exterior functionalities of dendrimers can be used to accommodate many catalytic sites on one molecule, possibly resulting in anomalous and favorable catalytic behavior. Brunner has been one of the first authors to report on branched molecules containing internal catalytic sites. He introduced the word “dendrzymes” for the presented molecules considering the resemblance of the produced structures to prosthetic groups in

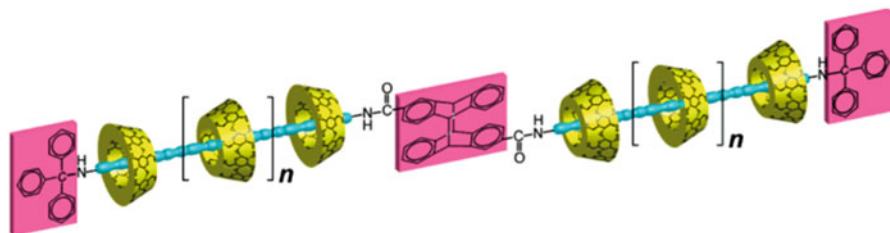


Fig. 15 Schematic diagram of preparation of a β -CD polyrotaxane via photodimerization. (Adopted with kind permission from Ref. [139] from © ACS)

enzymes [144]. The reported first generation dendrzymes are formed in situ by adding Cu(I) triflate to the chiral compounds. Fréchet-type wedges with a chiral pyridyl alcohol at the focal point have been used by Bolm et al. [145] as catalysts in the enantioselective diethylzinc addition to benzaldehyde. Click nonaxylose dendrimers stabilized platinum nanoparticles and were catalytically active in olefin hydrogenation in water at room temperature as shown in Scheme 8 [146].

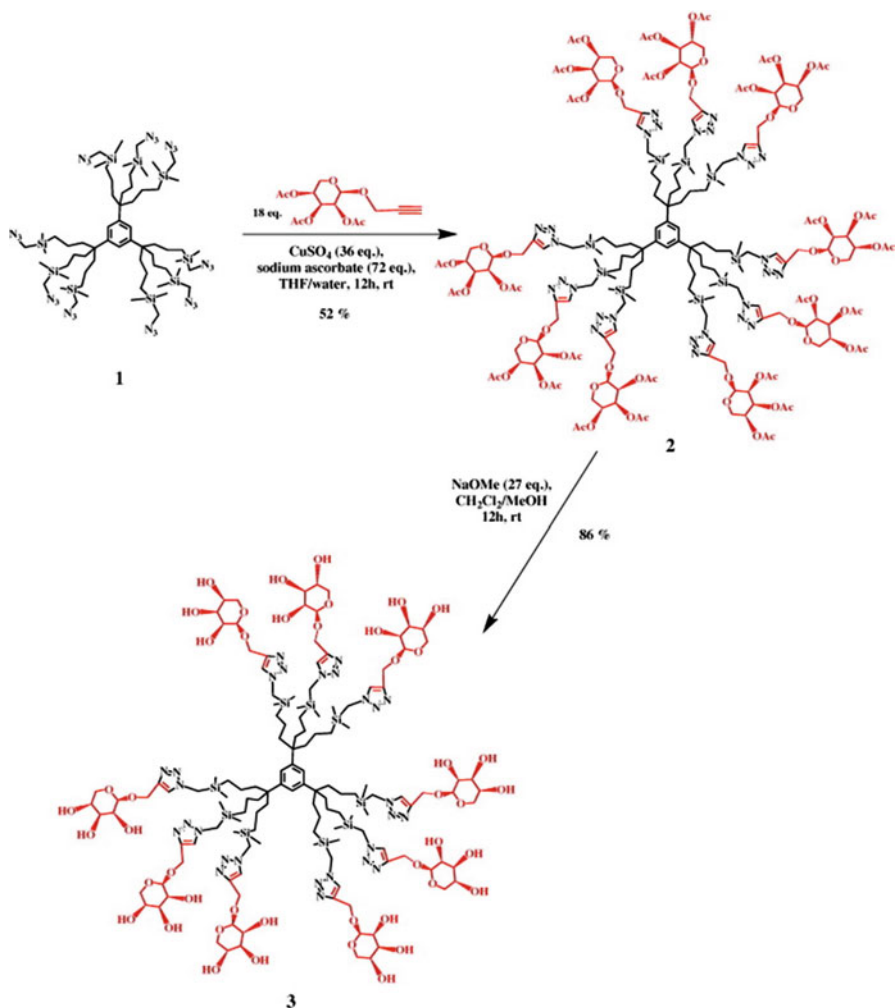
4.10 Degree of Branching (DB)

Degree of branching has been well studied in systems that involve the direct condensation reaction between bifunctional A2 monomers, such as diacids and trifunctional B3 monomers, such as glycerol, in the presence of lipase and chemical catalysts to form hyperbranched polymers [147, 148]. To identify the potential applications, understanding the relationship between percentage of DB and the physical and chemical properties of hyperbranched polymers is necessary. Degree of branching is a structural property that is determined by the concentration of linear (L), terminal (T), and dendritic (D) units within the polymer matrix.

The degree of branching can be regarded as the ratio of branched units in the polymer to those in a perfect dendrimer. Thus, the limiting values are $DB = 0$ for linear polymers and $DB = 1$ for a perfect dendrimer. Various definitions of DB have been given. If we do not take into account the vinyl group or initiator unit (core unit), the DB is defined as

$$DB = \frac{(\text{number of branched units}) + (\text{number of terminal units}) - 1}{(\text{total number of units}) - 1} \quad (4)$$

Here, one unit has been subtracted from the numerator and the denominator to take into account that even a linear polymer has one initiating and one terminal unit. From the topology of branched systems with trifunctional branch points, for any given molecule the number of branched units is equal to the number of terminal unit minus one. Thus, Eq. 4 can be further simplified as:



Scheme 8 Synthesis of the glycodendrimer 3 in two steps from the nona-azide core 1. (Adopted with kind permission from Ref. [146] from © Elsevier)

$$\text{DB} = \frac{2 \times (\text{number of branched units})}{(\text{total number of units}) - 1} \quad (5)$$

Alternatively, the fraction branch points can be defined as

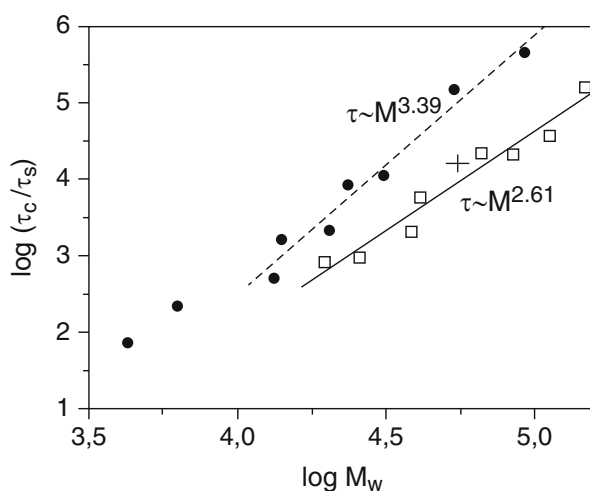
$$\text{FB} = \frac{\text{number of branched units}}{(\text{total number of units}) - (\text{number of monomers})} \quad (6)$$

In the semi-batch system, DB is slightly affected by the presence of polyinitiator and is mostly governed by the comonomer content. The calculations are also applied to polymerizations from surface-bound initiators.

4.11 Melt Properties

The viscoelastic or rheological behavior of polymer melts governed by the size of the macromolecules and their topology is strongly related to their industrial applications. For melts of linear monodisperse chains, the viscoelastic spectra provide information about both segmental and chain relaxation times, which, through known scaling dependences, allow for a determination of the macromolecular sizes of test samples. The situation is more complicated for the macromolecules with nonlinear topologies for which the scaling dependences are different. Systems in which both the sizes and the topologies of molecules are not precisely known and can vary in an undefined way seem to be especially difficult. This seems to be the case for the broad distribution of sizes of highly branched but poorly defined molecular topologies [150, 159]. Both linear and branched molecules can be represented by scaling power laws, but with remarkably different scaling exponents. For the melts of linear chains, the exponent 3.39 is observed, which is closed to the typical value of 3.4. However, the fractions of the branched polymer exhibit considerably lower exponent of 2.61. It is interesting to note that the value of the normalized chain relaxation time for the feed polymer with the broad molecular weight distribution (MWD) fits nicely into the data for the fractions with narrow MWDs. This seems to indicate that conclusions can also be drawn from a series of hyperbranched polymers with broad MWDs as shown in Fig. 16 [149].

Fig. 16 Molecular weight dependences of the normalized chain relaxation time, τ_c/τ_s , for branched fractions (\bullet), linear polymers (\square), and branched feed polymer (+). (Adopted with kind permission from Ref. [149] from © ACS)

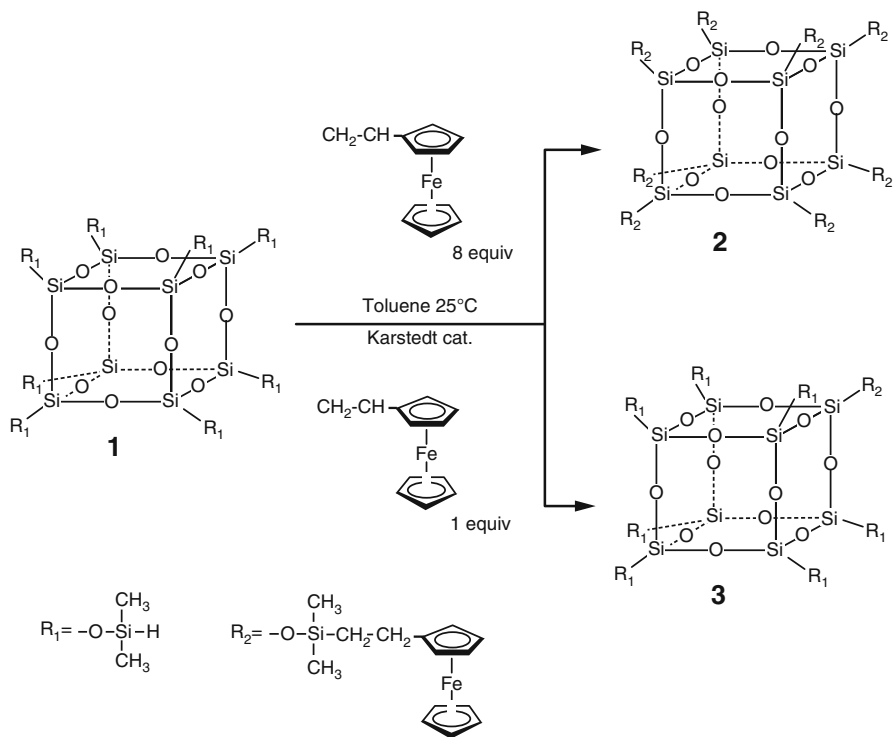


4.12 Electrochemical Properties

Since redox-active organometallic units play a key role as multielectron-transfer mediators in electrocatalytic processes of biological and industrial importance, the incorporation of such molecules at well-defined locations within dendrimeric structures is an important objective. In particular, the ferrocene moiety is an attractive organometallic redox center to integrate into dendritic structures as illustrated in Scheme 9 [151–153]. This system is not only electrochemically well behaved in most common solvents undergoing a reversible one-electron oxidation, but also such electron removal commonly does not involve fragmentation of the original molecular framework. The techniques such as cyclic voltammetry, differential pulse voltammetry, and bulk coulometry have been used to study the redox behavior in solution of the peripherally functionalized ferrocenyl dendritic macromolecules [154–156, 170–173].

4.13 Biocompatibility and Toxicity

In the field of drug delivery, dendrimers have brought the tremendous advances. A great optimism is expected regarding their potential in biomedical field owing to



Scheme 9 Synthesis of ferrocenyl monosubstituted octasilsesquioxane. (Adopted with kind permission from Ref. [151] from © ACS)

their nanometric size lies between 1 and 100 nm. Therefore, they may interact effectively and specifically with the components of cell such as plasma membranes, cell organelles (endosomes, mitochondria, nucleus), and proteins such as enzyme, as all these cellular components are themselves in nanometer in size range [157, 158].

Closely related terms toxicity and biocompatibility of dendrimers are important for biomedical applications. Dendrimers should be devoid of toxicity and immunogenicity. The pharma companies mainly applied the concept of toxicity for the description of adverse effects to cells, organs, or patients. The second concept of biocompatibility belongs to the field of biomedical materials as an extent of their compatibility with the studied system. One can say that biocompatibility and toxicity are inversely proportional, i.e., more is the biocompatible lesser be the toxicity. Therefore, understanding of the precise context of material usage is needed to describe biocompatibility of a material. However, clinical expertise with dendrimers is still in its infancy and thus it is difficult to specify any chemistry insistently biocompatible or toxic [116, 159–161].

The electrostatic interactions between the negative charges of most cell membranes and the amino surface groups of dendrimers significantly influence the stability and permeability of membranes. Also, dendrimer–membrane interactions are responsible for their high cellular uptake by endocytosis. However, G3 and higher generations of amino terminated dendrimers have a destructive interaction with the membrane, which causes cellular lysis and high cytotoxicity. Obviously, negatively charged dendrimers repulse with negatively charged membranes and therefore do not have generation-dependent cytotoxicity. For noncharged dendrimers, their cytotoxicity is influenced by polarity of surface groups. For instance, polar groups like PEG do not induce a toxic behavior. On the contrary, nonpolar groups like lipids could invade the membranes by hydrophobic interactions thus resulting toxicity in dendrimers. Lipids can act as immune stimulators and positively influence the cells. The particle size is a key player for biodistribution, clearance, and toxicity of dendrimers. The clinical applications of PAMAM dendrimer in drug delivery are restricted due to their inherent toxicity, reticuloendothelial system uptake, and hemolysis [162]. Regardless of the extensive pharmaceutical and biomedical applications of dendrimers, toxicity due to terminal-NH₂ groups and multiple cationic charges limits their clinical applications [163–165]. Dendrimers like PPI, PAMAM, and poly-L-lysine (PLL) exert significant *in vitro* cytotoxicity due to their surface cationic groups [166, 167]. Evidence regarding dendrimer safety is conflicting [168]. There are reports of concentration and generation-dependent toxicity of free peripheral amine groups [169]. The cytotoxicity of cationic melamine dendrimers having surface groups like amine, guanidine, carboxylate, sulphonate, or phosphonate was reported by Chen et al. Their study concluded that cationic dendrimers were much more cytotoxic than anionic or PEGylated dendrimers. Not only dendrimers but also cationic macromolecules in general cause destabilization of the cell membrane and thus result in cell lysis [170–172].

5 Applications of Dendrimers

The unique structural characteristics like nanoscopic size, spheroidal surface, high branching, cavernous interior and the exciting properties such as low viscosity, high solubility, high reactivity make dendrimers a good candidate for broad number of prospective applications in various fields. The emerging role of dendritic macromolecules for anticancer therapies, diagnostic imaging, and nanoscale delivery devices is remarkable. These integrated medicinal and diagnosis applications include gene therapy and chemical sensors drug delivery system. In addition, these special classes of materials also have applications for adhesive and coatings, light harvesting material, catalyst, electronic applications, separating agents, and many more. The illustration of various applications of dendrimers is shown in Fig. 17.

5.1 Biomedical Applications

5.1.1 Drug Delivery

Oral Drug Delivery

Among the many drug delivery routes, the oral route is preferred because of its significant advantages such as less fluctuating plasma drug level with the controlled drug delivery systems. This is because the drug released slowly from the dosage

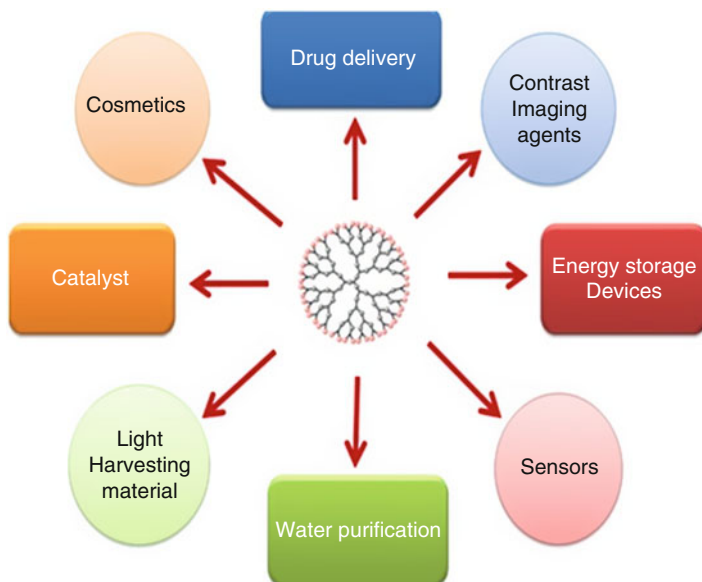


Fig. 17 Various applications of dendrimers

continuously and thus maintains the constant blood level in the body. Because of ease of production, low cost, convenience of ease of administration, and flexibility in designing of dosage, this has received more attention in the pharmaceutical field. Also, it is the most convenient administration route with good patient compliance, especially in the patient opinions. In spite of these benefits, defects of oral delivery route are also obvious. The issues such as less solubility in the aqueous solutions and low penetration across intestinal membranes are common in oral drugs delivery. Currently, to overcome these problems, researchers focus on several strategies in which drugs are loaded into oral drug carriers. The absorption and distribution of drugs in such systems mainly depended on the properties of these macromolecular carriers. Through the modification of these macromolecular structures, minimization of the side effects can be achieved. The ability to protect the drugs from degrading is the main requirement for an ideal macromolecular carrier for orally administered drugs. They might reduce nonspecific interactions with food proteins and enhanced the absorption across the intestinal epithelium. Dendrimers with featured properties may act as potential candidates for orally controlled release systems by conjugating/encapsulating the drug molecules. They can simplify dosing schedules as they maintain the drug concentrations within the therapeutic range at the injured regions. Also, the dendrimers can significantly increase the solubility of these orally administered drugs and even the stability of drugs in biological environments. PAMAM dendrimers are expected to have potential applications in enhancing the solubility for drug delivery systems [110, 173]. The unimolecular micelle nature of dendrimers is because of the presence of hydrophilic exteriors and hydrophilic interiors. Solubilization behavior is due to the formation of covalent and noncovalent complexes with drug molecules and hydrophobes [174]. Studies on Caco-2 monolayers, as models of intestinal epithelial barrier, show that it is possible to minimize toxicity while maximizing transepithelial transport by engineering surface chemistry of PAMAM dendrimers [175]. The effect of dendrimer generation and conjugation on the cytotoxicity, permeation, and transport mechanism of PAMAM dendrimer investigated by D'Emanuele and his research group [176] suggests that, as the concentration and generation increased, cytotoxicity and permeation of dendrimers increased. However, it is observed that conjugation with lauryl chloride resulted in reduction in cytotoxicity.

Ocular Drug Delivery

Drug delivery to the eye has been the most challenging tasks to the pharmaceutical scientists. Drug delivery to the eye can be generally classified into anterior and posterior segments based on ocular application [177]. Conventional drug delivery systems, including eye drops, suspension, and ointments, are not effective enough to meet the requirements in the treatment of ocular diseases [178]. However, more than 90% of the marketed ophthalmic formulations are in the form of eye drops and most of them target the front of the eye termed as anterior segment eye diseases [179]. The precorneal loss factors such as solution drainage, lacrimation, tear dynamics, tear dilution, tear turnover, conjunctival absorption, transient residence time, and low permeability of the corneal epithelial membrane cause poor bioavailability of drugs

from ocular dosage forms and thus act as the major challenges to the drug delivery. A supreme ocular drug delivery system must be nonirritating, biocompatible, sterile, isotonic and biodegradable, improved bioavailability of drugs, increased retention time, reduced side effects, cellular targeting, better patient compliance, and providing extended therapeutic effects [180]. Dendrimers can offer unique solutions to such complex delivery problems like ocular drug delivery.

Vandamme et al. [181] have evaluated several series of (PAMAM) dendrimers for controlled ocular drug delivery. The residence time of pilocarpine nitrate and tropicamide was found to be longer for the anionic dendrimer solutions. Results of a “miotic activity test” on albino rabbits showed that these PAMAM formulations enhance pilocarpine nitrate bioavailability and also prolonged the reduction of intraocular pressure (IOP), indicating increased precorneal residence time. Durairaj et al. [182] studied the dendrimeric polyguanidilylated translocators (DPTs), which are a class of dendrimers with tritolyl branches and surface guanidine groups as potential ophthalmic carriers for gatifloxacin, a “fourth generation fluoro quinolone” approved for conjunctivity treatment. The results have indicated that the DPT forms stable gatifloxacin complexes allowing once a day dosing with enhanced solubility, permeability, antimethicillin resistant *Staphylococcus aureus* (MRSA) activity, and in vivo delivery of gatifloxacin and thus seems like a potential delivery system.

Shaunak et al. [183] synthesized dendrimer-glucosamine (DG) and dendrimer-glucosamine 6-sulfate (DGS) using carboxylated PAMAM dendrimer ($G_{3.5}$) and then these were, respectively, conjugated with immuno-modulatory and anti-angiogenic properties. To increase the long-term success after glaucoma filtration and prevent scar tissue formation, these two conjugates were used together in a validated and clinically relevant rabbit model of wound healing. By subconjunctival injection, DG (60.30 mg/animal) and DGS (30.15 mg/animal) were administered. Bleb survival was evaluated as the primary efficacy end point of treatment. The results showed that the long-term success of the surgery increased from 30% to 80% and inhibited the pro-inflammatory and pro-angiogenic responses for the combination of subconjunctival treatment with DG and DGS. Minimal scar tissue formation was observed for DG and DGS treated rabbits as compared to placebo-treated animals. Furthermore, during the entire experimental period, no clinical, hematological, biochemical toxicity, or microbial infections were observed in all animals. The results thus suggested that ocular administration of DG and DGS might be effective, reasonable, and safe routes in clinical practice.

Transdermal Drug Delivery

Drug delivery through a skin to achieve a systemic effect of a drug is commonly known as transdermal drug delivery. The human skin is a readily accessible surface for drug delivery. Generally, for the patients who cannot tolerate oral dosage forms and who are nauseated or unconscious, transdermal drug delivery system (TDDS) is an alternative route of administration. On the other hand, transdermal delivery of drug has some limitations due to the slow rate of delivery. Thus, the use of transdermal enhancers is the most common method to improve drug penetration through the skin. Various organic solvents act as an effective transdermal enhancers

as they can directly react with the skin and thus cause transient increase in their permeability and induce immune responses in the skin. Also, the polymeric enhancers with hydrophilic and hydrophobic properties have gained tremendous interest. Particularly, PAMAM dendrimers with hydrophilic outer shells and hydrophobic interiors can improve either the water solubility or stability of hydrophobic drugs, which are expected to act as effective penetration enhancers. PAMAM dendrimer complex with nonsteroidal anti-inflammatory drugs such as Ketoprofen and Diflunisal are very effective for the treatment of acute and chronic rheumatoid and osteoarthritis and could improve the drug permeation through the skin as penetration enhancers. The model drugs Ketoprofen and Diflunisal were conjugated with G5 PAMAM dendrimer [184].

The utilization of polyhydroxyalkanoate (PHA) and G3 PAMAM dendrimer was reported by Wang et al. [185] as a novel TDDS. PHA used in this experiment was composed of 3-hydroxyhexanoic acid (8%) and 3-hydroxyoctanoic acid (92%). Both the model drug tamsulosin hydrochloride and PHA were mixed together and laid on the transdermal delivery patches before the *in vitro* permeation experiments performed on snake skins. They pretreated the snake skin with PAMAM dendrimer solution for 24 h to determine the effect of the PAMAM dendrimer on *in vitro* penetration efficiency of tamsulosin hydrochloride. However, permeation amount of the model drug could not enhance significantly. The penetration amount of tamsulosin in the PAMAM dendrimer containing PHA matrix was 24.0 mg/cm²/day, but for the dendrimer-lacking PHA matrix it is 15.7 mg/cm²/day. Note that the required amount of this drug in clinical trials is 20 mg/cm²/day. Thus, PHA-dendrimer matrix reached the clinical aim and could be developed as a useful delivery system for clinical TDDS.

Pulmonary Drug Delivery

Pulmonary drug release is the best alternative to the noninvasive administration for systemic delivery of therapeutic agent (mainly proteins and peptides) due to the fact that lungs could provide a large absorptive surface area up to 100 m² but extremely thin (0.1–0.2 mm) absorptive mucosal membrane and good blood supply. Dendrimers have been reported for pulmonary drug delivery also [186]. The study indicates that the relative bioavailability of pulmonary drug delivery of Enoxaparin was increased by 40% by the positively charged PAMAM dendrimers (G2 and G3 generation). Thus, for Enoxaparin pulmonary delivery, the positively charged dendrimers are the best suitable carriers.

Controlled Drug Delivery

Controlled drug delivery is one which delivers the drug at a predetermined rate, for a specified period of time. In this drug delivery system, therapeutic agents may be released for long periods of time, ranging from days to months from drug-encapsulating devices at controlled rates. Advantages of such systems over traditional methods of drug delivery include tailoring of drug release rates, protection of fragile drugs, and increased patient comfort and compliance. The drug molecule is encapsulated inside the cavity of dendrimers from which the drug released slowly.

Thus, these macromolecules are used to control the release of drug. Encapsulation of Ketoprofen with dendrimer and sustain release of the drug both *in vitro* and *in vivo* was demonstrated by Man et al. [187] that extended pharmacological response. As indicated by the *in vivo* bioavailability evaluation study, PAMAM dendrimers could be considered as a potential drug carrier of Ketoprofen with sustained release behavior under suitable conditions.

Targeted Drug Delivery

Targeted drug delivery is a system that delivers a certain amount of a therapeutic agent to a targeted diseased area within the body for a prolonged period of time. Through this drug delivery system, required plasma and tissue drug levels maintained in the body, and thereby preventing any damage to the healthy tissue via drug. Presence of wide variety of surface functional groups makes dendrimers highly potential for drug delivery applications. If one of these segments is attached with active drug molecule, the other can be highlighted as targeting group. Due to this double functional group, the plasma level of the drugs maintained at desired level for longer period of time with increasing pharmaceutical efficiency [188–190].

Patri et al. [191] synthesized G-5 PAMAM dendrimer conjugates with folic acid and modified surface to give, respectively, a hydrophilic, neutral, hydroxyl surface. Methotrexate inclusion complexes were formed in water and their cytotoxicity was compared with Methotrexate (MTX) covalently conjugated by an ester linkage that mediates release of the active drug through hydrolysis. The study showed that the activity of MTX is proportional to the number of MTX molecules in the inclusion complex, and all the covalently coupled drug–dendrimer conjugates were stable in both water and phosphate buffered saline (PBS) buffer solution. This suggests that drug complex with dendrimer as an inclusion complex improves its aqueous solubility. Thus, a cleavable, covalently linked dendrimer conjugate is suitable for targeted drug delivery as it does not release the drug prematurely in biological conditions.

5.1.2 Diagnostic Applications

The multiplicity of reactive chain ends of dendrimers make them well suited for the medical imaging applications. This allows introduction of large number of contrast agents onto a single molecule in a controlled manner, thereby enhancing the imaging sensitivity. Magnetic resonance imaging (MRI) is a well-developed technique that permits organs, blood vessels, or tissues to be visualized in the human body. Injection of contrast agents containing paramagnetic metal ions could significantly reduce the relaxation time of the water protons in the targeted organ. Some of the dendrimers combining with certain kinds of compounds act as imaging reagents in clinical detection [192, 193]. Recently Raymond's group reported significant enhancement of the relaxivity, solubility, and biocompatibility of MRI contrast agents connecting PAMAM dendrimer with 1,4,7-triazacyclononane TACN-Gd complex. The relaxation times of Gd T_1 and T_2 have increased and the toxicity of PAMAM dendrimer is less than small molecule complexes. Thus, it could provide an effective alternative imaging reagent for early diagnosis of cancer [194].

Dendrimers are under investigation as potential polymeric X-ray contrast agents. Various organometallic complexes such as bismuth and tin are used as potential dendritic X-ray contrast agents to obtain a high resolution X-ray image [195]. Because of their distinct morphology and unique characteristics, dendrimers are fascinating molecules to use as molecular probes. For example, to the generation of an integrated molecular probe, the immobilization of sensor units on the surface of dendrimers is a very efficient way, owing to their large surface area and high density of surface functionalities [196].

5.2 Engineering Applications

5.2.1 Sensors

Development of dendrimer-based sensors has received special attention, in view of their several unique features that could improve optical sensor performance. For dendrimers to be used in sensor applications, they must react with the analyte and the resulting interaction such as absorption, reflectance, luminescence, lifetime, refractive index, scattering, diffraction, and polarization must change quantitatively. Development of electrochemical biosensors using dendrimers for analytical applications has been reported in number of studies [197] for the detection of different types of analyte, such as uric acid, ascorbic acid, dopamine, phenols, glucose, and hydrogen peroxide. Dendrimer-modified sensor surfaces have revealed remarkable stability, even after numerous cycles of regeneration for deoxyribo nucleic acid (DNA) hybridization and antigen-antibody assays. These matrices have been found stable in various types of regeneration system, such as urea stripping [198], glycine-HCl stripping [199], thermal stripping [200], and alkaline stripping. The high stability of the dendrimer film is attributed to the attachment of each bioreceptor molecule by forming multiple bonds with several functional groups on the sensor substrates, as well as the higher holding capacity of the bioaffinity groups. Immobilization of dendrimers on electrode surfaces and bulk materials can be achieved using polyvalent interactions, such as adhesives, surface coatings, or polymer crosslinking [201].

Recently, glucose biosensor preparation based on an Au/AuNP/(FeSH⁺Cyst)/PAMAM/GOD system was described by Karadag et al. [202] as shown in Fig. 18. The biosensor proposed by this group was successfully applied for glucose analysis in beverages.

Dendrimers conjugated with multiple functional molecules are being explored for usages within a wide variety of biomedical applications. The targeted drug delivery system could also serve as a sensor delivering a cytotoxic drug into the desired cells and thereby monitoring the real-time apoptotic effect of the drug. Myc et al. [203] reported the synthesis and in vitro apoptosis-sensing function of a bifunctional G5.0-PAMAM-based dendrimer nanodevice, in which folic acid (FA) was used as the targeting agent as well as the fluorescence resonance energy transfer (FRET) reagent.

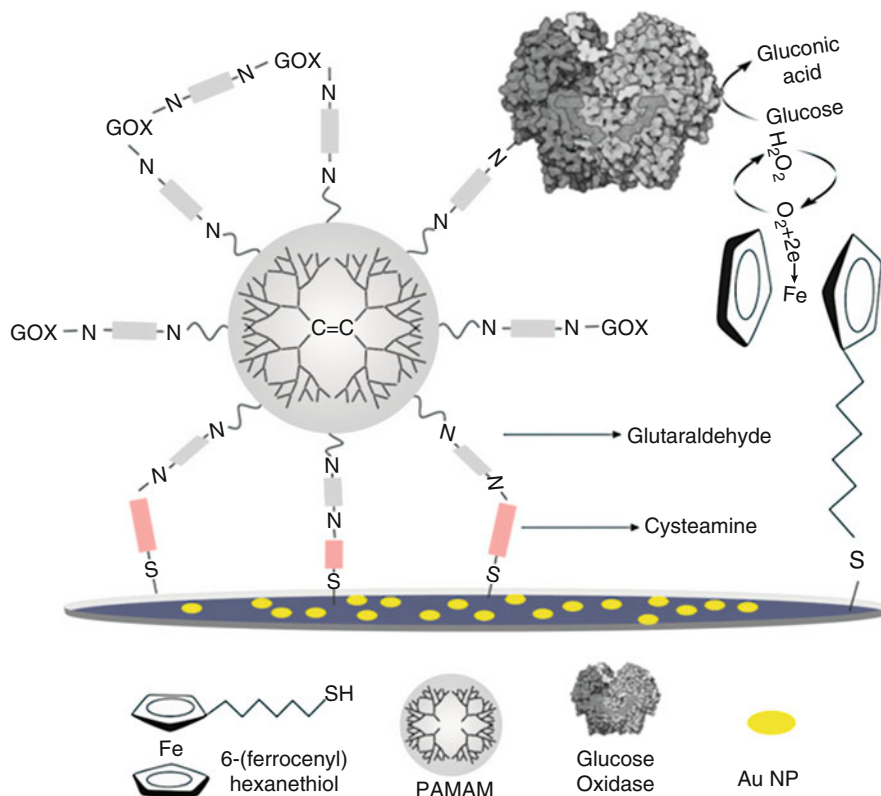


Fig. 18 Preparation of biosensor made of Au/AuNP/(FeSH⁺Cyst)/PAMAM/GOx system. (Adopted with kind permission from Ref. [202] from Elsevier)

5.2.2 Light Harvesting Material

Dendrimers are perfectly branched synthetic macromolecules with numerous chain ends all emanating from core and are used as an interesting scaffolds for light harvesting applications. Light harvesting is the conversion of light energy into photon energy or into chemical energy by trapping energy via peripheral chromophores. The tree-like structure of dendrimers could potentially act as an energy gradient for the funneling process. The periphery of dendrimers can be functionalized with multiple light absorbing chromophore units that gives a high probability to capture light. The relatively short through-space distance from the periphery to the core, due to back folding, allows for high efficiency energy transfer.

The π -conjugated dendrimers based on truxene and thienylethynylene synthesized by Nantalaksakul et al. [204] have shown intrinsic energy gradient from periphery to the core along with broad absorption in the UV-vis range and proficient energy transfer to the lower energy center. They are highly potential as light harvesting materials.

Dendrimer backbones themselves can also be used as the energy donor. The conjugated dendrimers such as phenylacetylene chains were mainly selected for these applications. By controlling over the conjugation length of dendritic branches in these dendrimers, rapid and directional energy transport could be obtained to achieve an efficient energy transfer. The synthesis of phenylacetylene dendrimers by Xu et al. [205] showed an efficient, unidirectional energy transfer to a single core chromophore. The robust, high-yielding synthesis allowed for the preparation of high-generation (G-n) molecules up to G-6. A strong UV absorption features in the range of 250–350 nm observed for these cross-conjugated structures and that is double than the increasing generation. Also, these dendrimers exhibit emission in the range of 350–450 nm. An energy “sink” was introduced into the system by functionalizing the core of these structures with the lower band gap, perylene chromophore. Hence, the phenylacetylene monomer units act as the peripheral energy donors and perylene acts as the central energy acceptor.

5.2.3 Catalyst

Dendrimers are potential candidates in the field of catalysis, as they will retain the benefits of homogeneous catalysts such as high activity, good reproducibility, high selectivity, accessibility of the metal site, and so on. Unlike most other polymeric species, they will be readily recoverable after reaction. In principle, dendrimers are the most promising candidates that can meet the needs for an ideal catalyst: persistent and controllable nanoscale dimensions, chemically reactive surface, favorable configuration in which all the active sites would always be exposed towards the reaction mixture so that they are easily accessible to migrating reactants and soluble but can be easily recovered by filtration. These properties of dendrimers, or some combination of them, make them so useful for their application in catalysis. Till today, many reports have revealed the designing and application of dendrimer-based catalyst for various reactions [81, 99, 108, 206–212]. It is well recognized that the properties such as well-defined structures and small sizes typically $10 \pm 15 \text{ \AA}$ make the homogeneous catalysts more selective and effective catalysts. The controlled molecular size and shape of dendrimers and the disposition of functional groups are highly attractive as scaffold of polymer catalysts.

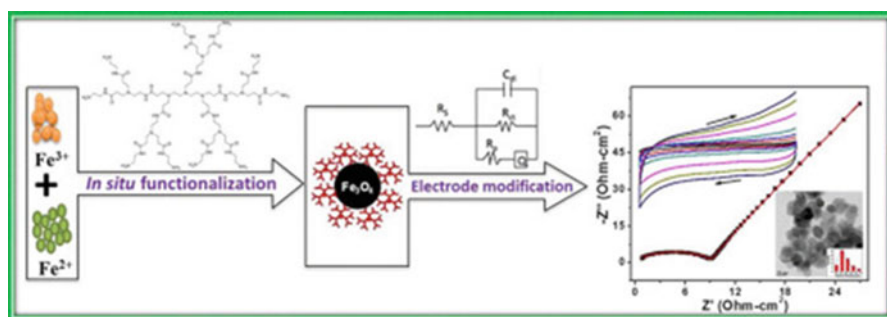
The leaching of metal from the particle can be achieved through the multipoint binding sites on the surface of dendritic polymers. Therefore, it is worth noting that a high catalytic activity can be obtained using dendrimer-templated bimetallic nanoparticle catalysts, which is hardly achievable in the case of monometallic nanoparticles. In view of this, Zhao et al. [213] have synthesized dendrimers encapsulated with Pt and Pd nanoparticles and found an excellent catalytic activity for the electron-deficient alkenes and hydrogenation of simple alkenes. Such catalysts were simply prepared by the incorporation of metal ions into hydroxy-terminated PAMAM dendrimers followed by reduction with BH_2 . The intradendrimer metal nanoparticles are quite monodispersed and stable before, during, and after hydrogenation reactions as observed from high resolution transmission electron microscopy (TEM). It is observed that the fourth generation dendrimer-encapsulated Pd40 nanoparticles showed high catalytic activity for the hydrogenation of allyl alcohol

and *N*-isopropyl acrylamide. Interestingly, the generation has its control over the hydrogenation rates. For higher generation dendrimers, the hydrogenation rates were significantly slow, probably due to their less porous surface.

5.2.4 Energy Storage Devices

Dendrimers are the macromolecules with controlled shape and size connected from branches to a central core. The electron conducting nature resulted from the presence of internal voids and cavities inside the dendrimers offers them energy storage device applications. Till date, only few reports are available for dendrimer-based energy storage devices. The synthesise of a 10-arm NH_2 terminated polyamidoamine dendrimer with a diethylenetriamine core and a redox center reported by Chandra et al. [214] is presented in Scheme 10. This dendrimer is further used to develop dendrimers with functionalized magnetic nanoparticles ($\text{Fe}_3\text{O}_4@D\text{-NH}_2$), which are potential electrode materials for electrochemical supercapacitors. The electron charge transfer mechanism between core and the branched surface of the dendrimers is ideal for energy storage process. The large surface area, diversified composition, unique porous structure, and excellent electronic conductivity resulted from the combined advantages of both dendrimers and iron oxide nanoparticles make porous $\text{Fe}_3\text{O}_4@D\text{-NH}_2$ a potential electrode material for electrochemical supercapacitors.

Dendrimers special structural characters also find application in fuel cells. Dendrimers have also been used to encapsulate the electrocatalysts [215] to modify the proton-conducting membranes [216, 217] and as components in the electro-catalytic ink [218]. It is worthy to mention that in all these cases, polyamidoamine dendrimers have been used due to the presence of amino and amidic groups that can interact with ionic metal precursors, besides amino group allows a subsequent functionalization, which expands its application potential. Recently, Alvarez et al. [219] have synthesized and characterized composite of Nafion and PAMAM (G4OH) dendrimer membrane. Methanol crossover and permeability measurements showed that the dendritic molecule as modifiers of Nafion membranes acts as a barrier hindering the methanol access. This result could be attributed to the affinity with methanol of peripheral groups of PAMAM



Scheme 10 Dendrimer functionalized magnetic nanoparticles ($\text{Fe}_3\text{O}_4@D\text{-NH}_2$). (Adopted with kind permission from Ref. [214] from Elsevier)

(G4-OH) dendrimer. This proves the potential application of dendrimer-based composite membrane to be used in the direct methanol fuel cells (DMFC).

5.3 Miscellaneous Dendrimer Applications

5.3.1 Cosmetics

Dendrimers have wide range of applications in cosmetics such as UV sunscreens, hair treatment, and an oxidant. Due to UV radiation absorbing nature of dendrimers, these are used in sun screen preparations. A variety of hair grooming compositions including permanent shaping composition, hair care compositions, hair bleaching composition, oxidative after-treatment compositions, and hair fixing compositions will be composed of these dendrimeric derivatives [220]. Polyamine macromolecules are used as an antioxidant agents and film forming agents containing disulfide-functionalized polymers and dendrimers in cosmetics.

5.3.2 Water Purification Process

Various critical physicochemical properties of dendrimers offer an excellent separation and reaction media for water purification. Dendritic nanoparticles can be used for the encapsulation of a broad range of solutes in water including anions (e.g., perchlorate, nitrate, and phosphate), cations (e.g., copper, silver, gold, and uranium), and organic compounds (e.g., pharmaceuticals and pesticides). Dendritic nanoparticles also find its applications as nanoscale reactors and catalysts. They can bind and deactivate bacteria and viruses [221]. As compared to linear polymers, it is easier to filter dendrimers because of their globular shape and larger size. Exploring these unique properties, Diallo and coworkers [222, 223] developed enhanced microfiltration (MF) and ultrafiltration (UF) techniques for recovering dissolved cations and anions from aqueous solutions.

5.3.3 Additives, Printing Inks, and Paints

Due to highly ordered and branched structure, dendrimers or hyperbranched polymers offer numerous commercial applications. They have been widely used as additives in ink formulations (0.5–2% level) to enhance adhesion to a variety of substrates. They also provide excellent film color characteristics while maintaining good ink formulation stability and reliable printer operation. The lower “generation” PAMAM dendrimers are particularly effective for such applications. Their Newtonian viscosity characteristics in solution, amorphous, noncrystallizing nature, and their solubility in polar solvents (tailorable) provide them formulation flexibility and reproducible ink application characteristics. In fact, their molecular uniformity and highly functional “Molecular Velcro” surface facilitate their applications even in micro- and nano-lithography. The modification of surface functional groups of PAMAM with polyethyleneoxy-side chains could also improve the ink latency [224]. In addition, dendrimers can also be used for radiation-curable ink formulations in order to achieve good adhesion, water resistance, and humidity resistance [225, 226].

Polyurethane paints made of dendritic polymers are widely used in furniture and automotive industries because of some beneficial characteristics such as surface hardness, chemical resistance, light fastness, scratch resistance, and weathering resistance. Through the use of dendrimer as additives, it is easy to alter the surface characterization of thermoplastic resin after the molding process. For examples, polycarbonates are widely used as an engineering thermoplastic for providing a unique combination of stiffness, toughness, high softening temperature, and processibility.

6 Future Prospects and Conclusions

Dendrimers are highly defined artificial macromolecules, characterized by high number of functional groups and compact molecular assembly, which make them hopeful candidate for various applications. Since last two decades, significant developments are being occurred in dendrimer research for the establishment of synthetic procedures and investigation of various properties of the novel class of macro- and micromolecules.

Today, dendrimer research has created great excitement and immense interest among the scientific community. This has resulted in tremendous progress into a synthesis, fabrication, and in arriving potential applications of dendrimers in a wide variety of technologies. The progress made in the discovery and commercialization of dendrimers are bound to have the impact on the chemical, energy, electronics, and space industries in addition to medicine and health care areas. Particularly, in drug delivery systems, dendrimers research provides an excellent platform for the attachment of drugs and their release to explore the use of dendrimers for various applications in transdermal, ophthalmic, oral, and gene delivery. Dendrimers can be designed to improve the properties of some drugs in topical and transdermal formulations, in delivering the drug to its destination [227–229].

Dendrimers demonstrated as novel carriers of drugs across cell membranes and organ barriers such as blood-brain barrier (BBB) and have a host of applications such as treating tumors, cerebral gliomas, and for brain specific delivery of drugs. A new era of research in dendrimers is the development of dendrimer cluster to form a multifunctional therapeutic system, which will open a new path for clinical applications.

The controlled synthesis and purification process of dendrimers is required to facilitate further research in dendrimer for the specific applications [230]. The low polydispersity of dendrimers is beneficial to predict its pharmacokinetic behavior in biological systems. Due to their nanometric scales and the properties similar to proteins, dendrimers gain attention in studies of their biomimetic properties [231]. The dendrimers architecture can be monitored by molecular engineering, to construct structure resembling to enzymes, antibodies, and globular proteins.

Furthermore, there are different areas of biological chemistry where dendrimer systems found its diverse applications. Some of the significant and fascinating areas of dendrimer research ongoing include highly sensitive analytical devices [232, 233],

magnetic resonance imaging contrast agents [234], prion research [235], burn treatment [236], and electron paramagnetic resonance (EPR) imaging with spin-labeled dendrimers [237–240], etc.

As dendrimer holds great potential adding value in various fields like pharmaceutical, therapeutics, and diagnostics, future development in dendrimer technology must be focused on various aspects, which include:

- (i) Reducing the cost of synthesis so as to achieve extensive use of dendrimers as membranes in various fields.
- (ii) Enlarging application of hyperbranched polymers for membrane applications in the fields of resources and environment.
- (iii) Reducing the cytotoxicity of dendrimers by careful surface engineering.
- (iv) Multistep synthesis still requires great effort.
- (v) Purity aspects of dendrimers and dendrons must be continuously considered and carefully checked.
- (vi) Monitoring the nature of functional groups to control the solubility, related biological properties, enhanced penetration, and retention effect.
- (vii) The applications of dendrimer-based drug delivery systems in cancer treatments are still not acceptable due to difficulty of maintaining clinical grade purity during synthesis.
- (viii) The clinical trial demands detailed investigations of the polymeric carriers including the incorporated drug and linkages.

To conclude, dendrimers offer various advantages including design, type, and mode of reactions. At the same time, some of the issues such as complex synthetic routes, structure-property relationship, biocompatibility, and processability need to be resolved.

Acknowledgments Authors sincerely thank the DST, New Delhi, for providing the financial support under DST-PURSE-Phase-II Program. The authors particularly Balappa Munavalli and Satishkumar Naik thank the UGC, New Delhi, for awarding (RFSMS) fellowship to pursue Ph.D. degree.

References

1. S. Srinivasa, K.J. Yarema, *Dendrimers in Cancer Treatment and Diagnosis* (Wiley, New York, 2007)
2. D.A. Tomalia, J.M.J. Frechet, Discovery of dendrimers and dendritic polymers: a brief historical perspective. *J. Polym. Sci. Part A* **40**, 2719 (2002)
3. D.A. Tomalia, H. Baker, J. Dewald, M. Hall, M. Kallos, S. Martin, J. Roeck, J. Ryder, P. Smith, A new class of polymers: starburst-dendritic macromolecules. *Polym. J.* **17**, 117–132 (1985)
4. C.J. Hawker, J.M.J. Frechet, Preparation of polymers with controlled molecular architecture: a new convergent approach to dendritic macromolecules. *J. Am. Chem. Soc.* **112**, 7638–7647 (1990)
5. G.R. Newkome, Z.Q. Yao, G.R. Baker, V.K. Gupta, Cascade molecules: a new approach to micelles. *J. Org. Chem.* **50**, 2003–2004 (1985)

6. D. Boris, M. Rubinstein, A self-consistent mean field model of a starburst dendrimers: dense core vs. dense shells. *Macromolecules* **29**, 7251–7260 (1996)
7. G. Spataro, F. Malecaze, C.O. Turrin, V. Soler, C. Duhayon, P.P. Elena, Designing dendrimers for ocular drug delivery. *Eur. J. Med. Chem.* **45**, 326–334 (2010)
8. A.W. Bosman, E.W. Meijer, About dendrimers: structure, physical properties and applications. *Chem. Rev.* **99**, 1665–1688 (1999)
9. E.R. Gilles, J.M.J. Fréchet, Dendrimers and dendritic polymers in drug delivery. *Drug Discov. Today* **10**, 35–43 (2005)
10. D.A. Tomalia, H. Baker, J.R. Dewald, M. Hall, G. Kallos, S. Martin, J. Roeck, J. Ryder, P. Smith, Dendritic macromolecules: synthesis of starburst dendrimers. *Macromolecules* **9**, 2466–2468 (1986)
11. Y. Kim, S.C. Zimmerman, Applications of dendrimers in bio-organic chemistry. *Curr. Opin. Chem. Biol.* **2**, 733–742 (1998)
12. D.K. Smith, F. Diederich, Functional dendrimers: unique biological mimics. *Chem. Eur. J.* **4**, 1353–1361 (1998)
13. S.E. Stiriba, H. Frey, R. Haag, Dendritic polymers in biomedical applications: from potential to clinical use in diagnostics and therapy. *Angew. Chem. Int. Ed.* **41**, 1329–1334 (2002)
14. G.V. Shinde, G.S. Bangale, D.K. Umalkar, B.S. Rathinaraj, C.S. Yadav, P. Yadav, Dendrimers. *J. Pharm. Biomed. Sci.* **3**, 1–8 (2010)
15. G. Tarun, S. Onkar, A. Saahil, R.S.R. Murthy, Dendrimer- a novel scaffold for drug delivery. *Int. J. Pharm. Sci. Rev. Res.* **7**(2), 211–220 (2011)
16. S. Pushkar, A. Philip, K. Pathak, D. Pathak, Dendrimers: nanotechnology derived novel polymers in drug delivery. *Indian J. Pharm. Educ.* **40**, 153–158 (2006)
17. X. Xianghui, J. Yeting, L. Yunkun, Z. Xiao, T. Zhaoxu, G. Zhongwei, Bio-inspired supramolecular hybrid dendrimers self-assembled from low-generation peptide dendrons for highly efficient gene delivery and biological tracking. *ACS Nano* **8**, 9255–9264 (2014)
18. A.K. Garth, C. Weibo, G. Murray, Collagen mimetic dendrimers. *J. Am. Chem. Soc.* **124**, 15162–15163 (2002)
19. S. Kristen, P.M. James, Peptide dendrimers: applications and synthesis. *Rev. Mol. Biotechnol.* **90**, 195–229 (2002)
20. K.C. Byoung, J. Anurag, M. Surbhi, O. Hooisweng, S.M. Gruner, U. Wiesner, Nanohybrids from liquid crystalline extended amphiphilic dendrimers. *J. Am. Chem. Soc.* **126**, 4070–4071 (2004)
21. D.A. Tomalia, A.M. Naylor, W.A. Goddard, Starburst dendrimers: molecular-level control of size, shape, surface chemistry, topology and flexibility from atoms to macroscopic matter. *Angew. Chem. Int. Ed. Engl.* **29**, 138–175 (1990)
22. E. Roseita, D.A. Tomalia, Poly (amidoamine) (PAMAM) dendrimers: from biomimicry to drug delivery and biomedical applications. *Drug Deliv. Today* **6**, 427–436 (2001)
23. O. Schiavon, G. Pasut, S. Moro, PEG-Ara-C conjugates for controlled release. *Eur. J. Med. Chem.* **39**, 123–133 (2004)
24. M.F. Brana, G. Dominguez, B. Saez, Synthesis and anti-tumor activity of new dendritic polyamines-(imide-DNA-intercalator) conjugates: potent Lck inhibitors. *Eur. J. Med. Chem.* **37**, 541–551 (2002)
25. D.A. Tomalia, J.R. Dewald, M.R. Hall, S.J. Martin, P.B. Smith, *Reprints 1st SPSJ International Polymer Conference* (Society Polymer Science, Japan, Kyoto, 1984), p. 65
26. C. Hawker, J.M.J. Fréchet, A new convergent approach to monodisperse dendritic macromolecules. *J. Chem. Soc. Chem. Commun.* 1010–1013 (1990)
27. P.R. Dvornic, M.J. Owen, *Poly(amidoamine organosilicon) Dendrimers and Their Derivatives of Higher Degree of Structural Complexity* (American Chemical Society, Washington, DC, 2002)
28. J. Li, D.R. Swanson, D. Qin, H.M. Brothers, L.T. Piehler, D. Tomalia, D.J. Meier, Characterizations of core-shell tecto-(dendrimer) molecules by tapping mode atomic force microscopy. *Langmuir* **15**, 7347–7350 (1999)

29. C. Hawker, K.L. Wooley, J.M.J. Frechet, Unimolecular micelles and globular amphiphiles: dendritic macromolecules as novel recyclable solubilization agents. *J. Chem. Soc. Perkin Trans. 1*, 1287–1289 (1993)
30. J.A. Kremers, E.W. Meijer, Synthesis and characterization of a chiral dendrimer derived from pentaerythritol kremers. *J. Org. Chem.* **59**, 4262–4266 (1994)
31. U. Boas, J.B. Christensen, P.M.H. Heegaard, Dendrimers: design, synthesis and chemical properties. *J. Mater. Chem.* **16**, 3785–3798 (2006)
32. A. Janaszewska, K. Maczynska, G. Matuszko, D. Appelhans, B. Voit, B. Klajnert, M. Bryszewska, Cytotoxicity of PAMAM, PPI and maltose modified PPI dendrimers in Chinese hamster ovary (CHO) and human ovarian carcinoma (SKOV3) cells. *New J. Chem.* **36**, 428–437 (2012)
33. R. Satapathy, M. Ramesh, H. Padhy, I.H. Chiang, C.W. Chu, K.H. Wei, H.C. Lin, Novel metallo-dendrimers containing various Ru core ligands and dendritic thiophene arms for photovoltaic applications. *Polym. Chem.* **5**, 5423–5435 (2014)
34. C. Gorman, Metallo-dendrimers: structural diversity and functional behavior. *Adv. Mater.* **10**, 295–309 (1998)
35. V. Balzani, S. Campagna, G. Denti, A. Juris, S. Serroni, M. Venturi, Designing dendrimers based on transition-metal complexes. Light-harvesting properties and predetermined redox patterns. *Acc. Chem. Res.* **31**, 26–34 (1998)
36. G.R. Newkome, E. He, Nanometric dendritic macromolecules: stepwise assembly by double (2,2':6',2''-terpyridine)ruthenium(I) connectivity. *J. Mater. Chem.* **7**, 1237–1244 (1997)
37. G.R. Newkome, R.G. Guthrie, C.N. Moorefield, F. Cardullo, L. Echegoyen, E.C. Perez, H. Luftmann, Routes to dendritic networks: bis-dendrimers by coupling of cascade macromolecules through metal centers. *Angew. Chem. Int. Ed. Engl.* **34**, 2023–2026 (1995)
38. E.C. Constable, A.J. Edwards, D. Phillips, P.R. Raithby, Self-assembly of a supramolecular oligomer containing three different cobalt(II) environments; the first structurally characterised polymer derived from 2,3,5,6-tetra(2-pyridyl)pyrazine(tppz). *J. Supramol. Chem.* **5**, 93–95 (2006)
39. P. Lange, A. Schier, H. Schmidbaur, Dendrimer-based multinuclear gold(I) complexes. *Inorg. Chem.* **35**, 637–642 (1996)
40. C.B. Gorman, B.L. Parkhurst, W.Y. Su, K.Y. Chen, Encapsulated electroactive molecules based upon an inorganic cluster surrounded by dendron ligands. *J. Am. Chem. Soc.* **119**, 1141–1142 (1997)
41. P.J. Dandliker, F. Diederich, J.P. Gisselbrecht, A. Louati, M. Gross, Water-soluble dendritic iron porphyrins: synthetic models of globular heme proteins. *Angew. Chem. Int. Ed. Engl.* **34**, 2725–2728 (1995)
42. H.F. Chow, I.Y.K. Chan, D.T.W. Chan, R.W.M. Kwok, Dendritic models of redox proteins: X-ray photoelectron spectroscopy and cyclic voltammetry studies of dendritic bis(terpyridine) iron(II) complexes. *Chem. Eur. J.* **2**, 1085–1091 (1996)
43. J. Issberner, F. Vogtle, L.D. Cola, V. Balzani, Dendritic bipyridine ligands and their tris (bipyridine)ruthenium(II) chelates-syntheses, absorption spectra, and photophysical properties. *Chem. Eur. J.* **3**, 706–712 (1997)
44. M. Cuadrado, J. Moran, C.M. Losada, C. Casado, B. Pascual, F. Alonso, F. Lobete, in *Advances in Dendritic Macromolecules*, ed. by G.R. Newkome (JAI, Greenwich, 1996)
45. E. Buhleier, W. Wehner, F. Vögtle, Cascade and nonskid-chain-like syntheses of molecular cavity topologies. *Synthesis-Stuttgart* **2**, 155–158 (1978)
46. R.G. Denkwalter, J.F. Kolc, W.J. Lukasavage, Macromolecular highly branched homogeneous compound, U.S. Patent 4,410,688 (1981)
47. D.A. Tomalia, J.R. Dewald, Dense star polymers having core, core branches, terminal groups, U.S. Patent 4,507,466 (1983)
48. J.M.J. Frechet, Y. Jiang, C.J. Hawker, A. Philippides, *Proceedings of IUPAC International Symposium on Macromolecules* (Seoul, Korea 1989), pp. 19–20
49. T.M. Miller, T.X. Neenan, Convergent synthesis of monodisperse dendrimers based upon 1,3,5-trisubstituted benzenes. *Chem. Mater.* **2**, 346–349 (1990)

50. T.M. Miller, T.X. Neenan, R. Zayas, H.E. Bair, Synthesis and characterization of a series of monodisperse, 1,3,5-phenylene-based hydrocarbon dendrimers including C276H186 and their fluorinated analogs. *J. Am. Chem. Soc.* **114**, 1018–1025 (1992)
51. U.M. Wiesler, K. Mullen, Polyphenylene dendrimers via Diels–Alder reactions: the convergent approach. *Chem. Commun.* **22**, 2293–2294 (1999)
52. F. Morgenroth, E. Reuther, K. Mullen, Polyphenylene dendrimers: from three-dimensional to two-dimensional structures. *Angew. Chem. Int. Ed. Engl.* **36**, 631–634 (1997)
53. H. Ihre, A. Hult, E. Soderlind, Synthesis, characterization, and ¹H NMR self-diffusion studies of dendritic aliphatic polyesters based on 2,2-bis(hydroxymethyl)propionic acid and 1,1,1-tris(hydroxyphenyl)ethane. *J. Am. Chem. Soc.* **118**, 6388–6395 (1996)
54. H. Ihre, D.J.O.L. Padilla, J.M.J. Fréchet, Fast and convenient divergent synthesis of aliphatic ester dendrimers by anhydride coupling. *J. Am. Chem. Soc.* **123**, 5908–5917 (2001)
55. S.M. Grayson, J.M.J. Fréchet, Divergent synthesis of dendronized poly(p-hydroxystyrene). *Macromolecules* **34**, 6542–6544 (2001)
56. M. Jayaraman, J.M.J. Fréchet, A convergent route to novel aliphatic polyether dendrimers. *J. Am. Chem. Soc.* **120**, 12996–12997 (1998)
57. S.M. Grayson, M. Jayaraman, J.M.J. Fréchet, Convergent synthesis and surface functionalization of a dendritic analog of poly(ethylene glycol). *Chem. Commun.* 1329–1330 (1999)
58. S.M. Grayson, J.M.J. Fréchet, Synthesis and surface functionalization of aliphatic polyether dendrons. *J. Am. Chem. Soc.* **122**, 10335–10344 (2000)
59. P.R.L. Malenfant, M. Jayaraman, J.M.J. Fréchet, Dendrimer-supported oligothiophene synthesis: aliphatic ether dendrimers in the preparation of oligothiophenes with minimal substitution. *Chem. Mater.* **11**, 3420–3422 (1999)
60. P.R.L. Malenfant, J.M.J. Fréchet, Dendrimers as solubilizing groups for conducting polymers: preparation and characterization of polythiophene functionalized exclusively with aliphatic ether convergent dendrons. *Macromolecules* **33**, 3634–3640 (2000)
61. A.J. Brouwer, S.J.E. Mulders, R.M.J. Liskamp, Convergent synthesis and diversity of amino acid based dendrimers. *Eur. J. Org. Chem.* 1903–1915 (2001)
62. K.E. Uhrich, J.M.J. Fréchet, Synthesis of dendritic polyamides via a convergent growth approach. *J. Chem. Soc. Perkin Trans. 1*, 1623–1630 (1992)
63. G. Wu, R.F. Barth, W. Yang, M. Chatterjee, W. Tjarks, M.J. Ciesielski, R.A. Fenstermaker, Site-specific conjugation of boron-containing dendrimers to anti-EGF receptor monoclonal antibody cetuximab (IMC-C225) and its evaluation as a potential delivery agent for neutron capture therapy. *Bioconjug. Chem.* **15**, 185–194 (2004)
64. S.J.E. Mulders, A.J. Brouwer, R.M. Liskamp, Molecular diversity of novel amino acid based dendrimers. *J. Tetrahedron Lett.* **38**, 3085–3088 (1997)
65. S.J.E. Mulders, A.J. Brouwer, P.G.J. van der Meer, R.M. Liskamp, Synthesis of a novel amino acid based dendrimer. *J. Tetrahedron Lett.* **38**, 631–634 (1997)
66. S.J.E. Mulders, A.J. Brouwer, P. Kimkes, E.J.R. Sudholter, R.M.J. Liskamp, Sizing of amino acid based dendrimers in Langmuir monolayers. *J. Chem. Soc. Perkin Trans. 2*, 1535–1538 (1998)
67. B.I. Voit, D. Wolf, Perfectly branched polyamide dendrons based on 5-(2-aminoethoxy)-isophthalic acid. *Tetrahedron* **53**, 15535–15551 (1997)
68. T.M. Miller, E.W. Kwock, T.X. Neenan, Synthesis of four generations of monodisperse aryl ester dendrimers based on 1,3,5-benzenetricarboxylic acid. *Macromolecules* **25**, 3143–3148 (1992)
69. E.W. Kwock, T.X. Neenan, T.M. Miller, Convergent synthesis of monodisperse aryl ester dendrimers. *Chem. Mater.* **3**, 775–777 (1991)
70. R.T. Taylor, U. Paupaiboon, Polyurethane dendrimers via curtius reaction. *Tetrahedron Lett.* **39**, 8005–8008 (1998)
71. U. Paupaiboon, R.T. Taylor, Characterization and monitoring reaction of polyurethane dendritic wedges and dendrimers using matrix-assisted laser desorption/ionization time-of-flight mass spectrometry. *Rapid Commun. Mass Spectrom.* **13**, 508–515 (1999)

72. S.P. Rannard, N.J. Davis, A highly selective, one-pot multiple-addition convergent synthesis of polycarbonate dendrimers. *J. Am. Chem. Soc.* **122**, 11729–11730 (2000)
73. K. Kadei, R. Moors, F. Vogtle, Dendrimere und dendrimer-bausteine mit trisubstituiertem benzol und "hexacyclen" als kern. *Chem. Ber.* **127**, 897–903 (1994)
74. J. Louie, J.F. Hartwig, A.J. Fry, Discrete high molecular weight triarylamine dendrimers prepared by palladium-catalyzed amination. *J. Am. Chem. Soc.* **119**, 11695–11696 (1997)
75. J. Lim, E.E. Simanek, Synthesis of water-soluble dendrimers based on melamine bearing 16 paclitaxel groups. *Org. Lett.* **10**, 201–204 (2008)
76. K. Bronk, S. Thayumanavan, Design and synthesis of non-conjugated monodendrons with triarylamine repeating units. *Org. Lett.* **3**, 2057–2060 (2001)
77. K. Matsuda, N. Nakamura, K. Inoue, N. Koga, H. Iwamura, Toward dendritic two-dimensional polycarbenes: syntheses of 'starburst'-type nona- and dodecadiazo compounds and magnetic study of their photoproducts. *Bull. Chem. Soc. Jpn.* **69**, 1483–1494 (1996)
78. Z. Peng, Y. Pan, B. Xu, J. Zhang, Synthesis and optical properties of novel unsymmetrical conjugated dendrimers. *J. Am. Chem. Soc.* **122**, 6619–6623 (2000)
79. A. Rajca, S. Utamapanya, Toward organic synthesis of a magnetic particle: dendritic polyradicals with 15 and 31 centers for unpaired electrons. *J. Am. Chem. Soc.* **115**, 10688–10694 (1993)
80. P.R. Ashton, K. Shibata, A.N. Shipway, J.F. Stoddart, Polycationic dendrimers. *Angew. Chem. Int. Ed. Engl.* **36**, 2781–2783 (1997)
81. I. Baussanne, H. Law, J. Defaye, J.M. Benito, C.O. Mellet, J.M. Garcia Fernandez, Synthesis and comparative lectin-binding affinity of mannosyl-coated β -cyclodextrin-dendrimer constructs. *Chem. Commun.* **16**, 1489–1490 (2000)
82. A. Morikawa, M. Kakimoto, Y. Imai, Convergent synthesis of starburst poly(ether ketone) dendrons. *Macromolecules* **26**, 6324–6329 (1993)
83. A. Morikawa, K. Ono, Preparation of poly(ether ketone) dendrons with graded structures. *Macromolecules* **32**, 1062–1068 (1999)
84. A. Morikawa, K. Ono, Preparation of poly[(ether)-(ether ether ketone)] dendrimers by the convergent method. *Polym. J.* **32**, 255–262 (2000)
85. Y. Pan, W.T. Ford, Dendrimers with alternating amine and ether generations. *J. Org. Chem.* **64**, 8588–8593 (1999)
86. L.J. Twyman, A.E. Beezer, J.C. Mitchell, An approach for the rapid synthesis of moderately sized dendritic macromolecules. *J. Chem. Soc. Perkin Trans.* **1**, 407–411 (1994)
87. A. Malik, S. Chaudhary, G. Garg, A. Tomar, Dendrimers: a tool for drug delivery. *Adv. Biol. Res.* **6**, 165–169 (2012)
88. A.W. Bosman, H.M. Janssen, E.W. Meijer, About dendrimers: structure, physical properties, and applications. *Chem. Rev.* **99**, 1655–1688 (1999)
89. C.J. Hawker, 3-Dimensional dendritic macromolecules. *Curr. Opin. Colloid Interface Sci.* **4**, 117–121 (1999)
90. G.R. Newkome, E. He, C.N. Moorefield, Suprasuper molecules with novel properties: metallodendrimers. *Chem. Rev.* **99**, 1689–1746 (1999)
91. F. Arico, J.D. Badjic, S.J. Cantrill, A.H. Flood, K.C.-F. Leung, Y. Liu, J.F. Stoddart, *Top. Curr. Chem.* **249**, 203–259 (2005)
92. I. Yoon, M. Narita, T. Shimizu, M. Asakawa, *J. Am. Chem. Soc.* **126**, 16740–16741 (2004)
93. C.W. Chiu, C.C. Lai, S.H. Chiu, "Threading-followed-by-swelling": a new protocol for rotaxane synthesis. *J. Am. Chem. Soc.* **129**, 3500–3501 (2007)
94. K. Nørgaard, B.W. Laursen, S. Nygaard, K. Kjaer, H.R. Tseng, A.H. Flood, J.F. Stoddart, T. Bjørnholm, Structural evidence of mechanical shuttling in condensed monolayers of bistable rotaxane molecules. *Angew. Chem. Int. Ed.* **44**, 7035–7039 (2005)
95. G. Caminati, N.J. Turro, D.A. Tomalia, Photophysical investigation of starburst dendrimers and their interactions with anionic and cationic surfactants. *J. Am. Chem. Soc.* **112**, 8515–8522 (1990)
96. M. Fischer, F. Vögtle, Dendrimers: from design to applications – a progress report. *Angew. Chem. Int. Ed.* **38**, 884–905 (1999)

97. T.H. Mourey, S.R. Turner, M. Rubenstein, J.M.J. Frechet, C.J. Hawker, K.L. Wooley, Unique behavior of dendritic macromolecules: intrinsic viscosity of polyether dendrimers. *Macromolecules* **25**, 2401–2406 (1992)
98. C.J. Hawker, Dendritic and hyperbranched macromolecules – precisely controlled macromolecular architectures. *Adv. Polym. Sci.* **147**, 113–160 (1999)
99. S. Hecht, J.M.J. Frechet, Dendritic encapsulation of function: applying nature's site isolation principle from biomimetics to materials science. *Angew. Chem. Int. Ed.* **40**, 74–91 (2001)
100. P. Milosevic, S. Hecht, Design of branched and chiral solvatochromic probes: toward quantifying polarity gradients in dendritic macromolecules. *Org. Lett.* **7**, 5023–5026 (2005)
101. F. Zeng, S.C. Zimmerman, Dendrimers in supramolecular chemistry: from molecular recognition to self-assembly. *Chem. Rev.* **97**, 1681–1712 (1997)
102. S.C. Zimmerman, L.J. Lawless, Supramolecular chemistry of dendrimers. *Top. Curr. Chem.* **217**, 95–120 (2001)
103. D.K. Smith, Dendritic supermolecules – towards controllable nanomaterials. *Chem. Commun.* 34–44 (2006)
104. R. Hirst, B. Escuder, J.F. Miravet, D.K. Smith, High-tech applications of self-assembling supramolecular nanostructured gel-phase materials: from regenerative medicine to electronic devices. *Angew. Chem. Int. Ed.* **47**, 8002–8018 (2008)
105. K.N. Lau, H.F. Chow, M.-C. Chan, K.W. Wong, Dendronized polymer organogels from click chemistry: a remarkable gelation property owing to synergistic functional-group binding and dendritic size effects. *Angew. Chem. Int. Ed.* **47**, 6912–6916 (2008)
106. B.M. Rosen, C.J. Wilson, D.A. Wilson, M. Peterca, M.R. Imam, V. Percec, Dendron-mediated self-assembly, disassembly, and self-organization of complex systems. *Chem. Rev.* **109**, 6275–6540 (2009)
107. N. Nishiyama, W.D. Jang, K. Kataoka, Supramolecular nanocarriers integrated with dendrimers encapsulating photosensitizers for effective photodynamic therapy and photochemical gene delivery. *New J. Chem.* **31**, 1074–1082 (2007)
108. D. Astruc, F. Chardac, Dendritic catalysts and dendrimers in catalysis. *Chem. Rev.* **101**, 2991–3023 (2001)
109. P. Arya, G. Panda, N.V. Rao, H. Alper, S.C. Bourque, L.E. Manzer, Solid-phase catalysis: a biomimetic approach toward ligands on dendritic arms to explore recyclable hydroformylation reactions. *J. Am. Chem. Soc.* **123**, 2889–2890 (2001)
110. T. Muraki, K. Fujita, M. Kujime, Synthesis of novel dendritic 2,2'-bipyridine ligands and their application to Lewis acid-catalyzed Diels–Alder and three-component condensation reactions. *J. Org. Chem.* **72**, 7863–7870 (2007)
111. W.S. Li, T. Aida, Dendrimer porphyrins and phthalocyanines. *Chem. Rev.* **109**, 6047–6076 (2009)
112. S.H. Medina, M.E.H. El-Sayed, Dendrimers as carriers for delivery of chemotherapeutic agents. *Chem. Rev.* **109**, 3141–3157 (2009)
113. A.-M. Caminade, C.-O. Turrin, J.-P. Majoral, Dendrimers and DNA: combinations of two special topologies for nanomaterials and biology. *Chem. Eur. J.* **14**, 7422–7432 (2008)
114. N.N. Hoover, B.J. Auten, B.D. Chandler, Tuning supported catalyst reactivity with dendrimer-templated Pt-Cu nanoparticles. *J. Phys. Chem. B* **110**, 8606–8612 (2006)
115. J. Sebestik, P. Niederhafner, J. Jezek, Peptide and glycopeptide dendrimers and analogous dendrimeric structures and their biomedical applications. *Amino Acids* **40**, 301–370 (2011)
116. D. Astruc, E. Boisselier, C. Ornelas, Dendrimers designed for functions: from physical, photophysical and supramolecular properties to applications in sensing, catalysis, molecular electronics, photonics and nanomedicine. *Chem. Rev.* **110**, 1857–1959 (2010)
117. U. Gupta, H. Agashe, A. Asthana, N. Jain, Dendrimers: novel polymeric nano architectures for solubility enhancement. *Biomacromolecules* **7**, 649–658 (2006)
118. Y. Shi, W. Porter, T. Merdan, L. Li, Recent advances in intravenous delivery of poorly water soluble compounds. *Expert Opin. Drug Deliv.* **6**, 1261–1282 (2009)
119. S. Svenson, Dendrimers as versatile platform in drug delivery applications. *Eur. J. Pharm. Biopharm.* **71**, 445–462 (2009)

120. J.M.J. Fréchet, Functional polymers and dendrimers: reactivity, molecular architecture and interfacial energy. *Science* **263**, 1710–1715 (1994)
121. L. Gu, P.G. Luo, H. Wang, M.J. Mezzani, Y. Lin, L.M. Veca, L. Cao, F. Lu, X. Wang, R.A. Quinn, W. Wang, P. Zhang, S. Lacher, Y.P. Sun, Single-walled carbon nanotube as a unique scaffold for the multivalent display of sugars. *Biomacromolecules* **9**, 2408–2418 (2008)
122. Y. Lu, T. Shi, L. An, L. Jin, Z.-G. Wang, A simple model for the anomalous intrinsic viscosity of dendrimers. *Soft Matter* **6**, 2619–2622 (2010)
123. A. Einstein, Berichtigung zu meiner arbeit: Eine neue bestimmung der molekuldimensionen. *Ann. Phys.* **339**, 591–592 (1911)
124. D.A. Tomalia, D.M. Hedstrand, L.R. Wilson, *Encyclopedia of Polymer Science and Engineering*, 2nd edn. (Wiley, New York, 1990)
125. S.M. Aharoni, C.R. Crosby, E.K. Walsh, Stability of the crosslinked tropomyosin dimer: crosslink effect on the cooperativity of the ordering process and on the maximum in the helix probability profile. *Macromolecules* **15**, 1093 (1982)
126. C.J. Hawker, F.K. Chu, P.J. Pomery, D.J.T. Hill, Hyperbranched poly(ethylene glycol)s: a new class of ion-conducting materials. *Macromolecules* **29**, 3831 (1996)
127. Z.Y. Wen, T. Itoh, M. Ikeda, N. Hirata, M. Kubo, O. Yamamoto, Characterization of composite electrolytes based on a hyperbranched polymer. *J. Power Sources* **90**, 20–26 (2000)
128. P. Gode, A. Hult, P. Jannasch, M. Johansson, L.E. Karlsson, G. Lindbergh, E. Malmström, D. Sandquist, A novel sulfonated dendritic polymer as the acidic component in proton conducting membranes. *Solid State Ionics* **177**, 787–794 (2006)
129. F. Chu, B. Lin, F. Yan, L. Qiu, J. Lu, Macromolecular protic ionic liquid-based proton-conducting membranes for anhydrous proton exchange membrane application. *J. Power Sources* **196**, 7979–7984 (2011)
130. I.B. Rietveld, D. Bedeaux, J.A.M. Smit, Osmotic compressibility of poly(propylene imine) dendrimers in deuterated methanol. *J. Colloid Interface Sci.* **232**, 317–325 (2000)
131. X. Zhang, M. Wilhelm, J. Klein, M. Pfaadt, E.W. Meijer, Modification of surface interactions and friction by adsorbed dendrimers: 1. Low surface-energy fifth-generation amino acid-modified poly(propyleneimine) dendrimers. *Langmuir* **16**, 3884–3892 (2000)
132. R. Duncan, The dawning era of polymer therapeutics. *Nat. Rev. Drug Discov.* **2**, 347–360 (2003)
133. R.S. Greenfield et al., In vitro evaluation of adriamycin immunoconjugates synthesized using an acid-sensitive hydrazine linker. *Cancer Res.* **50**, 6600–6607 (1990)
134. M.W.P.L. Baars, E.W. Meijer, Host-guest chemistry of dendritic molecules. *Top. Curr. Chem.* **210**, 131–182 (2001)
135. V. Balzani, P. Ceroni, S. Gestermann, M. Gorka, C. Kauffmann, M. Maestri, F. Vögtle, Eosin molecules hosted into a dendrimer which carries thirty-two dansyl units in the periphery: a photophysical study. *Chem. Phys. Chem.* **1**, 224–227 (2000)
136. V. Balzani, P. Ceroni, S. Gestermann, M. Gorka, C. Kauffmann, F. Vögtle, Fluorescent guests hosted in fluorescent dendrimers. *Tetrahedron* **58**, 629–637 (2002)
137. T.S. Qin, J.Q. Ding, L.X. Wang, M. Baumgarten, G. Zhou, K. Müllen, A divergent synthesis of very large polyphenylene dendrimers with iridium(III) cores: molecular size effect on the performance of phosphorescent organic light-emitting diodes. *J. Am. Chem. Soc.* **131**, 14329–14336 (2009)
138. P.J. Dandliker, F. Diederich, A. Zingg, J.-P. Gisselbrecht, M. Gross, A. Louati, E. Sanford, Dendrimers with porphyrin cores: synthetic models for globular heme proteins. *Helv. Chim. Acta* **80**, 1773–1801 (1997)
139. G. Wenz, B.H. Han, A. Muller, Cyclodextrin rotaxanes and polyrotaxanes. *Chem. Rev.* **106**, 782–817 (2006)
140. K.A. Connors, The stability of cyclodextrin complexes in solution. *Chem. Rev.* **97**, 1325–1358 (1997)
141. M.V. Rekharsky, Y. Inoue, Complexation thermodynamics of cyclodextrins. *Chem. Rev.* **98**, 1875 (1998)

142. R. Castro, I. Cuadrado, B. Alonso, C.M. Casado, M. Morán, A.E. Kaifer, Multisite inclusion complexation of redox active dendrimer guests. *J. Am. Chem. Soc.* **119**, 5760–5761 (1997)
143. D.A. Tomalia, P.R. Dvornic, What promise for dendrimers? *Nature* **372**, 617–618 (1994)
144. H. Brunner, Dendrzymes: expanded ligands for enantioselective catalysis. *J. Organomet. Chem.* **500**, 39–46 (1995)
145. C. Bolm, N. Derrien, A. Seger, Hyperbranched macromolecules in asymmetric catalysis. *Synlett* **40**, 387–388 (1996)
146. S. Gatard, L. Liang, L. Salmon, J. Ruiz, D. Astruc, S. Bouquillon, Water-soluble glycodendrimers: synthesis and stabilization of catalytically active Pd and Pt nanoparticles. *Tetrahedron Lett.* **52**, 1842–1846 (2011)
147. C.A. Schally, F. Vogtle, H. Mori, H.E.A. Muller (eds.), *Dendrimer V Functional and Hyperbranched Building Blocks Photophysical Properties, Applications in Materials and Life Science* (Springer, Heidelberg, 2003)
148. V.T. Wyatt, G.D. Strahan, Degree of branching in hyperbranched poly(glycerol-co-diacid) synthesized in toluene. *Polymers* **4**, 396–407 (2012)
149. P.F.W. Simon, A.H.E. Muller, T. Pakula, Characterization of highly branched poly(methyl methacrylate) by solution viscosity and viscoelastic spectroscopy. *Macromolecules* **34**, 1677–1684 (2001)
150. M. Antonietti, C. Rosenauer, Properties of fractal divinylbenzene microgel. *Macromolecules* **24**, 3434–3442 (1991)
151. M. Moises, C.M. Casado, I. Cuadrado, Ferrocenyl substituted octa kis(dimethylsiloxy) octa silsesquioxanes: a new class of supramolecular organometallic compounds-synthesis, characterization, and electrochemistry. *Organometallics* **12**, 4327–4333 (1993)
152. D. Felder, H. Nierengarten, J.P. Gisselbrecht, C. Boudon, E. Leize, J.F. Nicoud, M. Gross, A. Van Dorselaer, J.F. Nierengarten, Synthesis, electrochemistry and reduction in the electro-spray source for mass spectrometry analysis. *New J. Chem.* **24**, 687–695 (2000)
153. U. Hahn, K. Hosomizu, H. Imahori, J.F. Nierengarten, Synthesis of dendritic branches with peripheral fullerene subunits. *Eur. J. Org. Chem.* 85–91 (2006)
154. B. Alonso, I. Cuadrado, M. Moran, J. Losada, Organometallic silicon dendrimers. *J. Chem. Soc. Chem. Commun.* 2575–2576 (1994)
155. C.M. Casado, I. Cuadrado, M. Moran, B. Alonso, M. Barranco, J. Losada, Cyclic siloxanes and silsesquioxanes as cores and frameworks for the construction of ferrocenyl dendrimers and polymers. *Appl. Organomet. Chem.* **13**, 245–259 (1999)
156. B. Alonso, M. Moran, C.M. Casado, F. Lobete, J. Losada, I. Cuadrado, Electrodes modified with electroactive films of organometallic dendrimers. *Chem. Mater.* **7**, 1440–1442 (1995)
157. S.H. Lee, S.H. Choi, S.H. Kim, T.G. Park, Thermally sensitive cationic polymer nanocapsules for specific cytosolic delivery and efficient gene silencing of siRNA: swelling induced physical disruption of endosome by cold shock. *J. Control. Release* **125**, 25–32 (2008)
158. S.H. Choi, S.H. Lee, T.G. Park, Temperature-sensitive pluronic/poly(ethylenimine) nanocapsules for thermally triggered disruption of intracellular endosomal compartment. *Biomacromolecules* **7**, 1864–1870 (2006)
159. Y.M. Chabre, R. Roy, Dendrimer-coated carbohydrate residues as drug delivery Trojan horses in glycoscience, in *Dendrimer-Based Drug Delivery Systems: From Theory to Practice*, ed. by Y. Cheng (Wiley, Hoboken, 2012)
160. Y. Cheng, Y. Gao, T. Rao, Y. Li, T. Xu, Dendrimer-based prodrugs: design, synthesis, screening and biological evaluation. *Comb. Chem. High Throughput Screen.* **10**, 336–349 (2007)
161. Y. Cheng, Z. Xu, M. Ma, T. Xu, Dendrimers as drug carriers: applications in different routes of drug administration. *J. Pharm. Sci.* **97**, 123–143 (2008)
162. V. Yellepeddi, A. Kumar, S. Palakurthi, Surface modified poly(amido) amine dendrimers as diverse nanomolecules for biomedical applications. *Expert Opin. Drug Deliv.* **6**, 835–850 (2009)
163. N. Malik, R. Wiwattanapatapee, R. Klopsch, K. Lorenz, H. Frey, J.W. Weener, E.W. Meijer, W. Paulus, R. Duncan, Dendrimers: relationship between structure and biocompatibility

- in vitro and preliminary studies on the biodistribution of 125 I-labelled polyamidoamine dendrimers in vivo. *J. Control. Release* **65**, 133–148 (2000)
164. D. Wilbur, P. Pathare, D. Hamlin, K. Bhular, R. Vessela, Biotin reagents for antibody pretargeting: synthesis, radioiodination and evaluation of biotinylated starburst dendrimers. *Bioconjug. Chem.* **9**, 813–825 (1998)
 165. G.A. Brazeau, S. Attia, S. Poxon, J.A. Hughes, In vitro myotoxicity of selected cationic macromolecules used in non-viral gene delivery. *Pharm. Res.* **15**, 680–684 (1998)
 166. H.B. Agashe, T.D. Dutta, M. Garg, N.K. Jain, Investigations on the toxicological profile of functionalized fifth-generation poly (propylene imine) dendrimer. *J. Pharm. Pharmacol.* **58**, 1491–1498 (2006)
 167. R.B. Kolhatkar, K.M. Kitchens, P.W. Swaan, H. Ghandehari, Surface acetylation of polyamidoamine (PAMAM) dendrimers decreases cytotoxicity while maintaining membrane permeability. *Bioconjug. Chem.* **18**, 2054–2060 (2007)
 168. J.C. Roberts, M.K. Bhalgat, R.T. Zera, Preliminary biological evaluation of polyaminoamine (PAMAM) starburst dendrimers. *J. Biomed. Mater. Res.* **30**, 53–65 (1996)
 169. H.T. Chen, M.F. Neerman, A.R. Parrish, E. Simanek, Cytotoxicity, haemolysis and acute in vivo toxicity of dendrimer based on melamine, candidate vehicles for drug delivery. *J. Am. Chem. Soc.* **32**, 10044–10048 (2004)
 170. K. Rittner, A. Benavente, S. Bompard, F. Heitz, G. Divita, R. Brasseur, E. Jacobs, New basic membrane-destabilizing peptides for plasmid-based gene delivery in vitro and in vivo. *Mol. Ther.* **5**, 104–114 (2002)
 171. S. Hong, J.A. Hessler, M.M.B. Holl, P. Leroueil, A. Mecke, B.G. Orr, Physical interaction of nanoparticles with biological membranes: the observation of nanoscale hole formation. *J. Chem. Health Saf.* **13**, 16–20 (2006)
 172. D. Fischer, Y. Li, B. Ahlemeyer, J. Krieglstein, T. Kissel, In vitro cytotoxicity testing of polycations: influence of polymer structure on cell viability and hemolysis. *Biomaterials* **24**, 1121–1131 (2003)
 173. P.E. Froehling, Dendrimers and dyes – a review. *Dyes Pigments* **48**, 187–195 (2001)
 174. N.K. Jain, U. Gupta, Application of dendrimer-drug complexation in the enhancement of drug solubility and bioavailability. *Expert Opin. Drug Metab. Toxicol.* **8**, 1035–1045 (2008)
 175. R. Jeyprasesphant, J. Penny, D. Attwood, N.B. McKeown, A. D’Emanuele, Engineering of dendrimer surface to enhance transepithelial transport and reduce cytotoxicity. *Pharm. Res.* **20**, 1543–1550 (2003)
 176. S. Sadekar, H. Ghandehari, Transepithelial transport and toxicity of PAMAM dendrimers: implications for oral drug delivery. *Adv. Drug Deliv. Rev.* **64**, 571–588 (2012)
 177. R.C. Nagarwal, S. Kant, P.N. Singh, P. Maiti, J.K. Pandit, Polymeric nano particulate system: a potential approach for ocular drug delivery. *J. Control. Release* **136**, 2–13 (2009)
 178. R. Gaudana, J. Jwala, S.H.S. Boddu, A.K. Mitra, Recent perspectives in ocular drug delivery. *Pharm. Res.* **26**, 1197–1216 (2009)
 179. J.C. Lang, Ocular drug delivery conventional ocular formulations. *Adv. Drug Deliv. Rev.* **16**, 39–43 (1995)
 180. S.K. Sahoo, F. Diinawaz, S. Krishnakumar, Nano technology in ocular drug delivery. *Drug Discov. Today* **13**, 144–151 (2008)
 181. T.F. Vandamme, L. Brobeck, Poly(amidoamine) dendrimers as ophthalmic vehicles for ocular delivery of pilocarpine nitrate and tropicamide. *J. Control. Release* **102**, 23–38 (2005)
 182. C. Durairaj, R.S. Kadam, J.W. Chandler, S.L. Hutcherson, U.B. Kompella, Nano sized dendritic polyguanidilyated translocators for enhanced solubility, permeability and delivery of gatifloxacin. *Invest. Ophthalmol. Vis. Sci.* **51**, 5804–5816 (2010)
 183. S. Shaunak, S. Thomas, E. Gianasieta, Polyvalent dendrimer glucosamine conjugates prevent scar tissue formation. *Nat. Biotechnol.* **22**, 977–984 (2004)
 184. Y. Cheng, N. Man, T. Xu, R. Fu, X. Wang, L. Wen, Transdermal delivery of nonsteroidal anti-inflammatory drugs mediated by polyamidoamine (PAMAM) dendrimers. *J. Pharm. Sci.* **96**, 595–602 (2007)

185. Z.X. Wang, Y. Itoh, Y. Hosaka, I. Kobayashi, Y. Nakano, I. Maeda, F. Umeda, J. Yamakawa, M. Kawase, K. Yag, Novel transdermal drug delivery system with polyhydroxyalkanoate and starburst polyamidoamine dendrimer. *J. Biosci. Bioeng.* **95**, 541–543 (2003)
186. S. Bai, C. Thomas, F. Ahsan, Dendrimers as a carrier for pulmonary delivery of enoxaparin, a low molecular weight heparin. *J. Pharm. Sci.* **96**, 2090–2106 (2007)
187. N. Man, Y.Y. Cheng, T.W. Xu, Y. Ding, Z.W. Li, G.Y. Huang, Y.Y. Shi, L.P. Wen, Dendrimers as potential drug carriers: part II- prolonged delivery of ketoprofen by in vitro and in vivo studies. *Eur. J. Med. Chem.* **41**, 670–674 (2006)
188. R. Langer, Dendrimers II: architecture, nanostructure and supramolecular chemistry. *Chem. Eng. Sci.* **50**, 4109 (1995)
189. R. Duncan, J. Kopecek, Soluble synthetic polymers as potential drug carrier and dendrimers in medicine and biotechnology. *Adv. Polym. Sci.* **57**, 51 (1984)
190. P.A. Brady, E.G. Levy, Inorganic and organometallic macromolecules: design and applications. *Chem. Ind.* 18–21 (1995)
191. A.K. Patri, F. Jolanta, L. Kukowska, R. James, J. Baker, Targeted drug delivery with dendrimers: comparison of the release kinetics of covalently conjugated drug and non-covalent drug inclusion complex-B. *Adv. Drug Deliv. Rev.* **57**, 2203–2214 (2005)
192. C. Peng, X. Shi, Dendrimer-related nanoparticle system for computed tomography imaging, in *Dendrimer Based Drug Delivery Systems: From Theory to Practice*, ed. by Y. Cheng (Wiley, Hoboken, 2012)
193. H. Cai, M. Shen, X. Shi, Dendrimer-based medical nanodevices for magnetic resonance imaging applications, in *Dendrimer-Based Drug Delivery Systems: From Theory to Practice*, ed. by Y. Cheng (Wiley, Hoboken, 2012)
194. P.J. Klemm, W.C. Floyd, D.E. Smiles, J.M. Fréchet, K.N. Raymond, Improving T_1 and T_2 magnetic resonance imaging contrast agents through the conjugation of an esteramide dendrimer to high-water-coordination Gd(III) hydroxypyridinone complexes. *Contrast Media Mol. Imaging* **7**, 95–99 (2012)
195. W. Krause, S.N. Hackmann, F.K. Maier, R. Muller, Dendrimers in diagnostics. *Top. Curr. Chem.* **210**, 261–308 (2000)
196. H. Schumann, B.C. Wassermann, S. Schutte, J. Velder, Y. Aksu, W. Krause, Synthesis and characterization of water-soluble tin-based metallo-dendrimers. *Organometallics* **22**, 2034–2041 (2003)
197. J. Satija, V.V.R. Sai, S. Mukherji, Dendrimers in biosensors: concept and applications. *J. Mater. Chem.* **21**, 14367–14386 (2011)
198. S.S. Mark, N. Sandhyarani, C. Zhu, C. Campagnolo, C.A. Batt, Dendrimer functionalized self-assembled monolayers as a surface plasmon resonance sensor surface. *Langmuir* **20**, 6808–6817 (2004)
199. P. Singh, T. Onodera, Y. Mizuta, K. Matsumoto, N. Miura, K. Toko, Dendrimer modified biochip for detection of 2,4,6 trinitrotoluene on SPR immune sensor fabrication and advantages. *Sensors Actuators B Chem.* **137**, 403–409 (2009)
200. C.M. Yam, M. Deluge, D. Tang, A. Kumar, C. Cai, Preparation, characterization, resistance to protein adsorption, and specific avidin-biotin binding of poly(amidoamine) dendrimers functionalized with oligo(ethylene glycol) on gold. *J. Colloid Interface Sci.* **296**, 118–130 (2006)
201. J. Yan, J. Pei, Chromophore-functionalized dendrimers for sensing applications. *Front. Chem. China* **5**, 134–149 (2010)
202. M. Karadag, C. Geyik, D.O. Demirkol, F.N. Ertas, S. Timur, Modified gold surfaces by 6-(ferrocenyl)hexanethiol dendrimer gold nanoparticles as a platform for the mediated biosensing applications. *Mater. Sci. Eng. C* **33**, 634–640 (2013)
203. A. Myc, I.J. Majoros, T.P. Thomas, J.R. Baker, Dendrimer-based targeted delivery of an apoptotic sensor in cancer cells. *Biomacromolecules* **8**, 13–18 (2007)
204. A. Nantalaksakul, D.R. Reddy, T.S. Ahn, R.A. Kaysi, C.J. Bardeen, S. Thayumanavan, Dendrimer analogues of linear molecules to evaluate energy and charge-transfer properties. *Org. Lett.* **8**, 2981–2984 (2006)

205. Z. Xu, J.S. Moore, Rapid construction of large-size phenylacetylene dendrimers up to 12.5 nanometers in molecular diameter. *Angew. Chem. Int. Ed.* **32**, 1354 (1993)
206. D. Seebach, P.B. Rheiner, G. Greiveldinger, T. Butz, H. Sellner, Chiral dendrimers, in *Dendrimers*, ed. by F. Vögtle (Springer, Berlin/Heidelberg, 1998)
207. G. van Koten, J.T.B.H. Jastrzebski, Periphery-functionalized organometallic dendrimers for homogeneous catalysis. *J. Mol. Catal. A* **146**, 317–323 (1999)
208. G.E. Oosterom, N.J.H. Reek, P.C.J. Kramer, P.W.N.M. van Leeuwen, Transition metal catalysis using functionalized dendrimers. *Angew. Chem. Int. Ed.* **40**, 1828–1849 (2001)
209. R. Kreiter, A.W. Klej, R.J.M.K. Gebbink, G. van Koten, Dendritic catalysts. *Top. Curr. Chem.* **217**, 163–197 (2001)
210. R. van Heebeek, P.C.J. Kamer, P.W.N.M. van Leeuwen, J.N.H. Reek, Dendrimers as support for recoverable catalysts and reagents. *Chem. Rev.* **102**, 3717–3756 (2002)
211. L.J. Twyman, A.S.H. King, I.K. Martin, Catalysis inside dendrimers. *Chem. Soc. Rev.* **31**, 69–82 (2002)
212. S.H. King, L.J. Twyman, Heterogeneous and solid supported dendrimer catalysts. *J. Chem. Soc. Perkin Trans. 1*, 2209–2218 (2002)
213. M. Zhao, R.M. Crooks, Homogeneous hydrogenation catalysis with monodisperse, dendrimer-encapsulated Pd and Pt nanoparticles. *Angew. Chem. Int. Ed.* **38**, 364–366 (1999)
214. S. Chandra, M.D. Patel, H. Lang, D. Bahadur, Dendrimer-functionalized magnetic nanoparticles: a new electrode material for electrochemical energy storage devices. *J. Power Sources* **280**, 217–226 (2015)
215. G.J. Ledesma, G.I.L. Escalante, T.W. Chapman, L.G. Arriaga, V. Baglio, V. Antonucci, Pt dendrimer nanocomposites for oxygen reduction reaction in direct methanol fuel cells. *J. Solid State Electrochem.* **12**, 835–840 (2010)
216. J.H. Lee, H.S. Shin, H.W. Rhee, Y.T. Kim, M.K. Song, M.S. Kim, Composite electrolyte membrane with nanoscopic dendrimers and method of preparing the same, US 2006116479 (2006)
217. A.D. Liyanage, J.P. Ferraris, I.H. Musselman, Y.D. Joo, T.E. Andersson, D.Y. Son, Nafion-sulfonated dendrimer composite membranes for fuel cell applications. *J. Membr. Sci.* **392**, 175–180 (2012)
218. J.H. Lee, J. Won, I.H. Oh, H.Y. Ha, E.A. Cho, Y.S. Kang, Effects of polyamidoamine dendrimers on the catalytic layers of a membrane electrode assembly in fuel cells. *Macromol. Res.* **12**, 101–106 (2006)
219. A. Alvarez, C. Guzman, S. Rivas, L.A. Godinez, A. Sacca, A. Carbone, E. Passalacqua, L.G. Arriaga, J.L. Garcá, Composites membranes based on Nafion and PAMAM dendrimers for PEMFC applications. *Int. J. Hydrog. Energy* **39**, 16686–16693 (2014)
220. J. Maignan, S. Genard, Use of hyperbranched polymer and dendrimers comprising a particular group as film-forming agent, film-forming composition comprising same and use particularly in cosmetics and pharmaceuticals, L'Oreal, U.S. Patent 6432423 (2002)
221. J.M.J. Frechet, D.A. Tomalia (eds.), *Dendrimers and Other Dendritic Polymers* (Wiley, New York, 2001)
222. M.S. Diallo, Water treatment by dendrimer enhanced filtration, U.S. Patent Application, US 1006/0021938 A1 (2006)
223. M.S. Diallo, S. Christie, P. Swaminathan, J.H. Johnson, W.A. Goddard, Dendrimer enhanced ultrafiltration: recovery of Cu(II) from aqueous solutions using Gx-NH₂ PAMAM dendrimers with ethylene diamine core. *Environ. Sci. Technol.* **39**, 1366–1377 (2005)
224. M.P. Breton, Ink compositions with dendrimer grafts; Xerox Corporation, U.S. Patent 5,266,106 (1993)
225. E. Verdonck, L. Vanmaele, Ink compositions for ink jet printing; Agfa-Gevaert, U.S. Patent 6,300,388 B1 (2001)
226. L. Vanmaele, E. Verdonck, Ink compositions for ink jet printing, U.S. Patent 6,310,115 (2001)
227. T.T. Gaurav, C.H. Hannah, The role of dendrimers in topical drug delivery. *Pharm. Technol.* **32**, 88–98 (2008)

228. A. Patidar, D.S. Thakur, Dendrimers-potential carriers for drug delivery. *Int. J. Pharm. Sci. Nanotechnol.* **4**, 1383–1389 (2011)
229. S. Jana, Dendrimers: synthesis, properties, and drug delivery biomedical applications. *Am. J. Res. Pharmtech* **2**, 32–55 (2012)
230. P. Kumar, Dendrimer: a novel polymer for drug delivery. *J. Innov. Trends Pharm. Sci.* **1**, 252–269 (2010)
231. D.A. Tomalia, Dendrimers – an enabling synthetic science to controlled organic nanostructures, in *Handbook of Nanoscience, Engineering and Technology*, ed. by W.A. Goddard III, S.E. Lyshevski (CRC Press LLC, Washington, DC, 2002)
232. H.C. Yoon, D. Lee, H.S. Kim, Reversible affinity interactions of antibody molecules at functionalized dendrimer monolayer: affinity-sensing surface with reusability. *Anal. Chim. Acta* **456**, 209–218 (2002)
233. R. Benters, C.M. Niemeyer, D. Drutschmann, D. Blohm, D. Wöhrle, DNA microarrays with PAMAM dendritic linker systems. *Nucleic Acid Res.* **30**, 1–11 (2002)
234. S.D. Konda, S. Wang, M. Brechbiel, E.C. Wiener, Biodistribution of a 153 Gd folate dendrimer, generation = 4, in mice with folate-receptor positive and negative ovarian tumor xenografts. *Investig. Radiol.* **37**, 199–204 (2002)
235. S. Supattapone, K. Nishina, J.R. Rees, Pharmacological approaches to prion research. *Biochem. Pharmacol.* **63**, 1383–1388 (2002)
236. S.B.A. Halkes, I. Vrasidas, G.R. Rooijer, A.J.J. Van den Berg, R.M.J. Liskamp, R.J. Pieters, Synthesis and biological activity of polygalloyl-dendrimers as stable tannic acid mimics. *Bioorg. Med. Chem. Lett.* **12**, 1567–1570 (2002)
237. A.T. Yordanov, K.I. Yamada, M.C. Krishna, J.B. Mitchell, E. Woller, M. Cloninger, M.W. Brechbiel, Spin-labeled dendrimers in EPR imaging with low molecular weight nitroxides. *Angew. Chem. Int. Ed. Engl.* **40**, 2690–2692 (2001)
238. A. Akbarzadeh, H. Mikaeili, D. Asgari, N. Zarghami, R. Mohammad, S. Davaran, Preparation and in-vitro evaluation of doxorubicin-loaded Fe₃O₄ magnetic nanoparticles modified with biocompatible copolymers. *Int. J. Nanomedicine* **7**, 511–526 (2012)
239. A. Abolfazl, Z. Nosratollah, M. Haleh, A. Davoud, A.G. Mohammad, K.H. Khaksar, D. Soodabeh, Synthesis, characterization and in vitro evaluation of novel polymer-coated magnetic nanoparticles for controlled delivery of doxorubicin. *Int. J. Nanotechnol. Sci. Environ.* **5**, 13–25 (2012)
240. A. Akbarzadeh, M. Samiei, S.W. Joo, M. Anzaby, Y. Hanifepour, H.T. Nasrabadi, Synthesis, characterization and in vitro studies of doxorubicinloaded magnetic nanoparticles grafted to smart copolymers on A549 lung cancer cell line. *J. Nanobiotechnol.* **10**, 46–58 (2012)



Manfred Stamm

Contents

1	Introduction	348
2	Specific Aspects of Polymer Surfaces	352
2.1	Chain Conformation	352
2.2	Surface and Interfacial Tension	357
2.3	Functional Polymer Surfaces	360
3	Interfaces in Blends, Copolymers, and Composites	367
3.1	Interfaces Between Homopolymers	368
4	Characterization Techniques of Polymer Surfaces and Interfaces	375
4.1	Surface and Interfacial Tension	378
4.2	Scanning Force Microscopy (SFM)	378
4.3	Ellipsometry (ELLI) and Surface Plasmon Spectroscopy (SP)	379
4.4	Scanning and Transmission Electron Microscopy (SEM, TEM)	379
4.5	X-Ray Photoelectron Spectroscopy (XPS)	380
4.6	Electrokinetic Methods (Zeta Potential)	381
4.7	Infrared Spectroscopy (ATR-FTIR)	381
4.8	Raman Spectroscopy	381
4.9	X-Ray and Neutron Reflectometry (XR, NR, GISAXS)	382
4.10	Secondary Ion Mass Spectrometry (SIMS)	383
4.11	Ion Techniques	383
4.12	Optical Microscopy Techniques (OM)	384
4.13	Indentation, Adhesion, Mechanical Properties	384
4.14	Inverse Gas Chromatography (IGC)	385
5	Summary and Outlook	386
	References	386

M. Stamm (✉)

Institute of Physical Chemistry and Physics of Polymers, Leibniz-Institut für Polymerforschung
Dresden e. V., Dresden, Germany
e-mail: stamm@ipfdd.de

Abstract

Polymer surfaces and interfaces are present with all polymer materials. They determine many properties like optical appearance, wetting, and adhesion, but with blends and composites also for instance toughness, hardness, modulus, and elongation at break. A short outline of polymer surfaces at molecular scale is given with reference to special aspects of chain conformation and surface dynamics. The surface tension as a fundamental property of a surface is discussed and surface functionalization in particular by grafting of polymer brushes onto surfaces described. In this way, a very versatile surface functionalization and even responsive polymer brush surfaces can be obtained. They may be used to control wetting, adhesion, bio-functionality, catalytic activity, and sensing ability. The interface between polymers can be formulated on the basis of mean-field theory with introduction of an effective interaction parameter, which is related with interface width and fluctuations at the interface. Polymer blends, copolymers as compatibilizers, and composites are discussed as examples, where interfaces play an essential role. Several techniques for surface and interface characterization including scanning force and electron microscopy, photoelectron and IR/Raman spectroscopy, as well as x-ray and neutron reflectometry or scattering techniques are critically reviewed. Guidelines for resolution and typical information obtained are provided. The importance of surface and interface design for future high-tech devices and advanced materials is highlighted.

Keywords

Surfaces · Interfaces · Wetting · Blends · Copolymers · Composites · Functionalization · Brushes · Analysis · Characterization · Surface tension · Contact angle · Electron microscopy · X-ray scattering · Neutron scattering · Reflectometry · Scanning force microscopy · XPS · SIMS · Ion beam techniques

1 Introduction

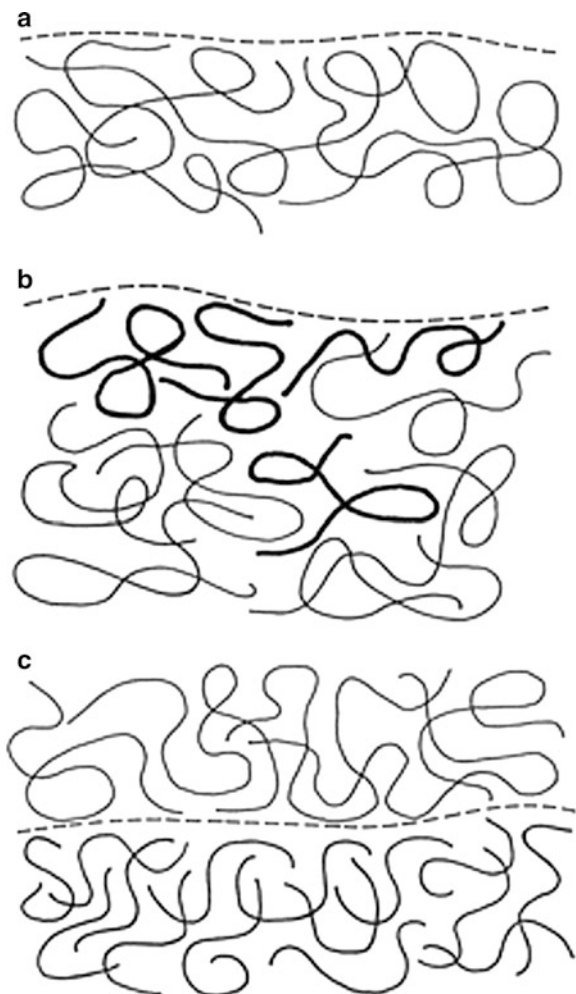
The surfaces and interfaces of polymers are important for many properties of polymeric materials, and their design can introduce interesting functionalities. This is for instance true for polymer blends, where the interface between incompatible polymers strongly influences the mechanical properties, or for the application of lightweight composite materials in cars or airplanes, where adhesion between the reinforcing fibers and the soft polymer matrix plays an essential role. Very special properties can be achieved with polymer nanocomposites, where functional nanoparticles are dispersed in a polymer matrix or with thin smart polymer brush layers as coatings on surfaces, which allow control of wetting and adhesion properties. Looking on everyday polymeric parts in household, cars, or sports, one could ask questions like “how do they feel” or “how do they look,” which in many cases will critically influence the decision for the purchase of a product. The appearance depends on “the surface,” and the optical or mechanical properties but also corrosion or scratch resistance depend largely on surface

composition and structure. A thin functional layer at the surface can influence those properties significantly. This is in particular the case, when even functional or smart surfaces or interfaces are used, which can provide biocompatibility, switching or adaptive properties. The characterization of polymer surfaces and interfaces in many cases requires special or adapted techniques, and often only a combination of different techniques will provide necessary information. A careful characterization is however the prerequisite for the understanding and dedicated design of materials properties [1, 2].

One should be aware of the fact that one may understand quite different aspects when talking about polymer surfaces and interfaces. Depending on the properties under consideration, the surface or interfacial region may extend from subnanometers to micro- or even millimeters, which covers a range of more than 6 orders of magnitude [1–10]. If one is looking at individual polymer chains (Fig. 1), the surface and interfacial region will typically range over one chain, where a measure of the chain size, the radius of gyration, is of the order of 3–30 nm depending on molecular weight. On the other hand, very different microscopic properties or in general a combination of them could be important to achieve a particular surface macroscopic property or appearance. So for instance, for the wetting of a smooth surface by a liquid, the composition of the outermost surface layer will be important for the wetting behavior and one has to consider the composition of the first atomic layer even at subnanometer scale. When on the other hand the optical properties of a surface are important, one is dealing with a surface layer in the range of the wavelength of light, that is typically several hundred nanometers large, while for the adhesion between two sheets of polymeric materials a plastic deformation region in the vicinity of the interface of up to millimeters may be important because a large part of the deformation energy is dissipated in this plastic zone. Thus, different applications require different approaches with respect to desired surface or interface modifications as well as the use of different characterization techniques, and one needs a careful definition of the problem before looking for details of surfaces and interfaces.

A compilation of some common surface and interface analysis techniques is presented in Tables 1 and 2 indicating typical information that can be obtained utilizing a particular technique as well as its typical minimal information depth. With most techniques, the sample preparation and proper adoption of the technique is of particular importance. The parameters indicated will in most cases depend on the mode used, the sample system, the available contrast, the addition of, e.g., fluorescent dyes, and some quantities cannot be obtained completely independent from each other. Thus for instance, there exist several different optical microscopy techniques ranging from simple dark and bright field to differential interference, fluorescent, or phase measurement interference techniques. For those different optical microscopy techniques, the available information is quite different from each other. This is similarly true for scanning force microscopy, electron microscopy, etc., where always techniques are improved, extended, and further developed. So these tables can only be seen as a rough guide for selection of particular techniques and of course are far from being complete.

Fig. 1 Schematics of polymer surfaces and interfaces, (a) homopolymer surface, (b) blend surface with surface enrichment of one component, and (c) interface between polymers with no interdiffusion. (From Ref. [3])



There are plenty of reviews and books available which cover polymer surfaces and interfaces (see [1, 2, 4, 5]) as well as particular aspects and characterization (see [3, 6–11]). In the following, we cover briefly some basic aspects of polymer surfaces and interfaces including some ways for particular functionalization and shortly outline some important analytical techniques from Tables 1 and 2.

We distinguish in Tables 1 and 2 between surface and interface analysis techniques, while this distinction is not rigorously true [3]. So several techniques are applicable for both surface and interface analysis (e.g., x-ray reflectometry, SIMS, optical techniques, etc.), when they are used in different modes of application. Also the optimal sample requirements are different from one technique to the next, and the surface might be facing air, liquid, vacuum, or even a polymer solution. For a particular technique, the choice and the information content will depend of course very much on this environment, and therefore one has to be very careful, to analyze

Table 1 Most common techniques for surface characterization

Technique	Probe in/out	Smallest information depth/width lateraly (nm)	Information	Comments
Surface tension/ contact angle ST	Liquid drop	0.1/–	Surface energy	Easy to use, molecular information difficult
Scanning force microscopy SFM	Cantilever	0.05/1	Surface topography, composition, toughness etc.	Atomic resolution. Many different modes
Ellipsometry ELLI	Polarized light	0.1/300	Thin surface layer	Molecular interpretation difficult
Scanning electron microscopy SEM	Electrons	1/1	Surface topography	Vacuum technique
X-ray photoelectron spectroscopy XPS	X-rays/ electrons	5/2000	Chemical composition, binding state	Quantitative, vacuum technique, lateral imaging possible
Electrokinetic measurements/ zeta potential	Voltage	0.1/–	Surface charge	Measurement in aqueous medium
Infrared attenuated total reflection ATR-FTIR	Infrared light	2000/2000	Surface composition, binding state	Specific ATR-crystal needed
Raman spectroscopy/ microscopy RS (resonance enhanced)	Light	0.5/300	Surface composition, binding state	Resonance enhancement with metal clusters
X-ray reflectometry XR Grazing incidence x-ray small angle scattering GISAX	X-rays	0.5/2000 0.5/0.1	Surface roughness, thin surface layers, lateral structure	Flat surfaces required
Focused ion beam FIB	Ions (electrons)	2/10 (1 with SEM)	Imaging, cutting, deposition	Nanomanipulation possible, often in combination with SEM
Scanning tunneling microscopy STM	Cantilever	0.05/1	Tunneling current	Surface conductivity required
Optical microscopy/ interferometry OM	Light	0.1/300	Surface roughness, structure	Many possibilities, good height resolution with interference techniques
Surface plasmon spectroscopy SP	Light/ plasmons	0.1/300	Thin surface layers	Metallic layer on prism necessary

(continued)

Table 1 (continued)

Technique	Probe in/out	Smallest information depth/width laterally (nm)	Information	Comments
Secondary ion mass spectroscopy SIMS	Ions	0.1/1000	Surface composition, contaminations	“Static” mode, vacuum technique
Micro-indentation MI	Cantilever	100/200	Surface hardness, module	Quantitative interpretation difficult
Neutron reflectometry NR	Neutrons	0.5/2000	Surface roughness, enrichment layer	Deuterated compounds needed
Auger spectroscopy AS High-resolution electron energy loss spectroscopy HREELS	Electrons	0.2/100 1	Electronic excitation, surface composition Vibration spectrum	Surface conductivity needed Vacuum technique
Scanning near field optical microscopy SNOM	Light	1/50	Vibrational modes, fluorescence, orientation	Local optical spectroscopy possible
Inverse gas chromatography IGC	Gas	0.1/–	Gas adsorption, surface functionality, energetics	Measurement on powder

the true materials behavior and not artifacts. On the other hand, one could also just be interested in a thin contamination layer at the surface, which can change surface appearance of materials quite significantly. Also resolution does depend on many parameters and is sensitive in particular on sample conditions and on preparation, so only “typical” values for favorable conditions are given in the tables. With those comments, one should be aware that in this short review not all aspects of polymer surfaces and interfaces can be discussed, and many techniques have elegant ways to focus on particular aspects and can overcome some of their shortages.

2 Specific Aspects of Polymer Surfaces

2.1 Chain Conformation

Polymers are very long molecules with specific properties, which are determined by conformational aspects as well as by chemistry given by the constitution of monomers. The architecture of the molecules, i.e., linear, branched, crosslinked, or even

Table 2 Most common techniques for interface characterization

Technique	Probe in/out	Typical smallest information depth (nm)	Typical information	Comments
Pendent drop	Liquid	0.2	Interface tension	Indirect technique
Transmission electron microscopy TEM	Electrons	0.5	Absorption/reflection of electrons, interface width	Cut perpendicular to interface, staining
Focused ion beam FIB	Ions (electrons)	10 (1 with SEM)	Concentration profile, element distribution, interface width	Cut perpendicular to interface with ions, imaging with SEM
X-ray reflectometry XR	X-rays	0.2	Interference fringes, interface width/roughness	Contrast of heavy elements
Secondary ion mass spectrometry dynamic SIMS	Ions	20	Element distribution, interface width	Dynamic (destructive) technique
Neutron reflectometry NR	Neutrons	0.2	Interference fringes, interface width/roughness	Contrast by deuteration
Scanning force microscopy SFM	Cantilever	0.2	Interface width/roughness/topography	Cut perpendicular to interface/etching, dissolution/hard tapping
Elastic recoil detection ERD Forward recoil spectroscopy FRD	$^4\text{He}/^1\text{H}$, ^2H (H, D)	20	H/D distribution, interface width	Contrast by deuteration
Nuclear reaction analysis NRA	$^{15}\text{N}/\gamma$ (4.4 MeV) $^3\text{He}/^4\text{He}$	12	H/D distribution, interface width	Contrast by deuteration
Rutherford backscattering RBS	$^4\text{He}/^4\text{He}$	30	Backscattering from heavy atoms, interface width	Contrast from heavy atoms
Small angle x-ray scattering SAXS	X-rays	1	Porod analysis, electron density variation, interface width	Bulk sample possible
Nuclear magnetic resonance NMR	Magnetic field	1	Spin diffusion from species, interface width	Bulk sample possible
Fluorescence quenching	Light	0.3	Quenching of donor/acceptor molecules	Fluorescence tagging of molecules necessary

star-like or H-shaped, plays a major role on the properties. At the surface, chain conformations are specific, and various chemical surface modifications are possible. So the surface properties can be largely modified by surface functionalization caused for instance by surface enrichment of components, adsorption, or grafting of chains at the surface or coating of a thin film. In that way, surface properties can be tuned independently from bulk properties, and also switching of surface properties is possible. Those aspects are addressed below, and we first discuss some basic properties of linear homopolymers at surfaces connected with chain conformations, topography, and structure. Because of the wealth of possibilities, we will concentrate on homopolymer surfaces, while many of the polymer surface topics are covered by books and reviews [1–11].

A long, flexible polymer chain possesses a huge number of internal degrees of freedom which is the origin of conformational entropy [10, 12–14]. This property related with the length of polymer chains is the key for the understanding of polymer behavior and distinguishes polymers from small and stiff molecules. It leads to unique properties also at surfaces. The simplest model for a flexible polymer molecule in melt, glassy state and in solution is the Gaussian chain. The chain is artificially subdivided into segments, whose directions are uncorrelated in space. These segments, so-called statistical or Kuhn segments, typically consist of several chemical repeat units of the real chain. The size of the segments corresponds to the persistence length of the chain, i.e., the distance over which orientation correlations between monomers decay. Chemical details of the original chain are mapped into the actual length of the statistical segment and into (effective) interaction parameters between pairs of such segments. For instance, the statistical segment length of polyethylene corresponds to about 5 CH₂ units which is about half a nanometer.

The size of a polymer chain is characterized by the average distance between the chain ends R or the radius of gyration R_g (average distances of segments from the center of mass of the chain). For an ideal chain we have.

$$\langle R^2 \rangle = a^2 N = 6 \langle R_g^2 \rangle \quad (1)$$

Here, a denotes the statistical segment length and N the number of segments (repeat units). The brackets indicate the statistical average. It is obvious that the size of the (statistical) coil formed by a polymer chain is much smaller than its contour length: $R \ll Na$. Typically, the size of synthetic polymer chains is in the range between a few nanometers up to some tens of nanometers. Long stiff biological polymers such as DNA can have a size in the range of several micrometers.

To discuss specific properties of polymer chains in solution at solid surfaces, we have to distinguish the cases, here the surface has attractive (absorbent) or repulsive character with respect to the monomers. Free surfaces, i.e., surfaces formed against air (or vacuum) are considered as a special class of repulsive surfaces where the surface tension of the polymers is the characteristic property. If we consider a chain close to a surface, its conformational degrees of freedom are reduced by the geometrical constraints and so is the chain entropy.

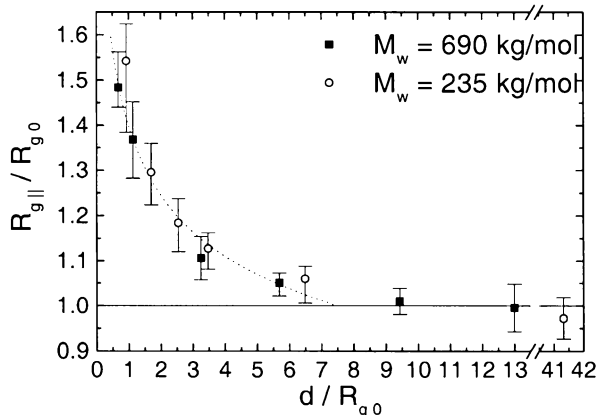
In order to keep a polymer chain in a *dilute solution* close to the surface, an energetic compensation is necessary. This leads to a phase transition scenario for attractive surfaces: Above a critical temperature of adsorption T_c or below a critical adsorption strength of the surface, the polymer chains avoid the surface and form a depletion zone, while below T_c , polymer chains are adsorbed and conformations change into “pancake-like,” quasi two-dimensional shape [15–17]. This is in particular true if individual chains are adsorbed on a flat surface from highly diluted solution. In case of strong adsorption at a flat surface, the chain conformation in the adsorbed state can be directly measured by atomic force microscopy [17]. Under special conditions, it is expected that the adsorbed chain conformations reflect the ones in solution which allows the direct visualization of those chain conformations. In this way, for instance, conformational phase transition in polyelectrolytes can be followed in detail [18].

When the bulk phase is dense (*melt, glassy state*), the layer close to the surface is densely filled independently on substrate interactions. In computer simulations, evidence can be found for changes of chain conformations in the vicinity of the free surface at a scale related to R_g but also deviations on smaller length scales. This includes an enrichment of chain ends at the surface [20] and a flattened chain conformation in direct vicinity at the surface [19]. However, the contribution of chain ends to the free energy and surface tension is rather weak (neglecting chemical effects), typically of the order $1/N$. Despite the problem of free energy and surface tension, a solid surface influences the chain conformations in other subtle ways. This regards the interpenetration or entanglements between the chains close to the surface [22]. As a consequence of neutral boundary conditions, the chain volume is squeezed if chains are located close to the surface. Therefore, the number of other chains penetrating the volume of a chain close to the surface is reduced. Conservation of monomer number (dense melt) leads to a reduction of entanglements by a factor of $1/2$ for long chains close to the surface. Since entanglement properties are essential material properties which determine dynamic properties of polymers, this effect can be important. Experiments give indication for such a reduction of the entanglement density [23]. Generally, it is difficult to observe individual chain conformations close to the surfaces experimentally, but some experiments are available in thin films. From neutron scattering experiments, where the radius of gyration is measured in very thin films, it is concluded that the chain conformation in confined dimensions flattens and R_g changes as much as 50% [19, 24] (Fig. 2).

One has to take into account that neutron scattering averages laterally over a certain region. Taking those effects into account, one can conclude that surface effects on the conformation extend over several R_g . So there is a quite good agreement between experiment and theory. In that range, also entanglement effects are expected (but not directly measured), where entanglements should be reduced in the vicinity of the free surface.

As a trivial effect, there is however also a surface tension connected with capillary waves at polymer melt surfaces. In comparison to low-molecular-weight samples, the capillary waves depend not only on surface tension and temperature but also on viscoelasticity [16] and reflect entanglement effects [25]. With polymers, the surface

Fig. 2 Measurement of the radius of gyration by small-angle neutron scattering SANS in thin films of polystyrene of different molecular weights. When the film thickness d approaches $6R_{g0}$, the flattening of the chains is observed. R_{g0} is the radius of gyration in the bulk film, while $R_{g\parallel}$ denotes the radius of gyration in the plane of the film measured in the experiment. (Data from Ref. [19])



structures are however in many cases not at equilibrium, but frozen-in into the glassy state from preparation. Upon heating, one then can observe formation of surface roughness due to development of capillary waves at larger scales as well as smoothing at small length scales [26, 27].

The presence of an interface or a solid surface influences also dynamical processes. Since reptation requires strong interpenetration of chains, close to a surface reptation dynamics should be accelerated. However, it is rather difficult to measure dynamical effects in the surface region (some nm above the surface only). Computer simulations gave first indications for surface effects on entanglement properties [28]. Polymers below the glass-transition temperature T_g display solid-state mechanical properties. Here, fluctuations are frozen on larger time scales. The temperature T_g is specific for each polymer. With the growing interest in thin polymer films, also measurements of the glass-transition temperature has been carried out for polymers under various geometrical constraints (thin films, pores, with or without substrate). The results obtained are controversial. Based on the previous discussion of dynamics in polymer melts, one might expect a higher mobility of polymer chains close to the surface and thus a decrease of T_g . In fact, such results have been reported experimentally for free-standing polystyrene films where a reduction of T_g of about 70 K has been observed [67]. Other authors found a strong dependence of the substrate/polymer interaction on the change of T_g [29] and reported an increase of T_g close to the surface. Part of the controversy may be due to the fact that different experimental methods and sample preparation techniques are used in different publications. There are recent results that surface effects on dynamics are only minor [30]. Also from neutron reflectivity experiments, one can conclude that chain dynamics is only influenced in a region of the order of R_g [31] (Fig. 3). In this case, the interdiffusion between two films is measured at a temperature close to T_g , where the thickness of one film is varied from $d = 0.3$ to $4.6 R_g$. The interdiffusion is sensitive on the region close to the surface, where a slight increase of dynamics at film thicknesses smaller than R_g is observed. This is reflected by an increased interdiffusion width σ at given interdiffusion time τ_d between two films, where one film has thickness smaller than R_g .

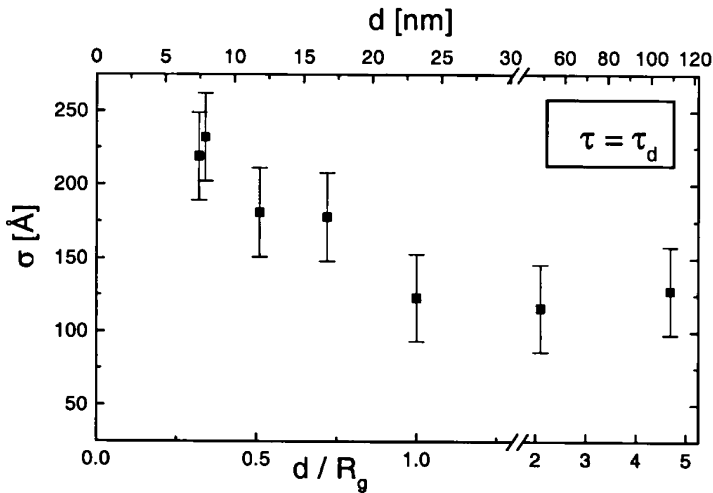


Fig. 3 Determination of chain mobility in thin films of thickness d via neutron reflectometry. The interdiffusion width σ after interdiffusion of time τ equal to disentanglement time τ_d is determined for polystyrene films as function of film thickness d . (From Ref. [31])

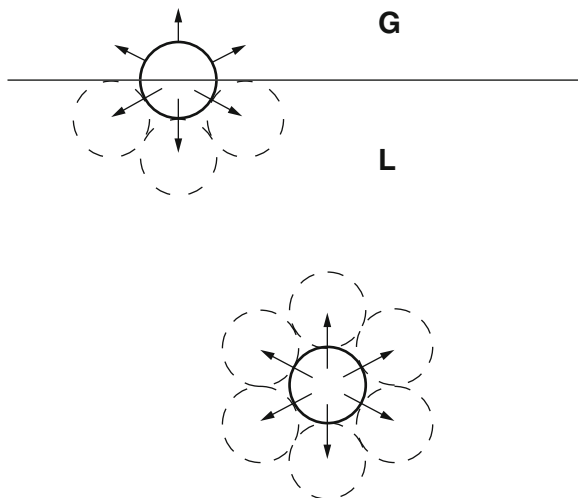
This could be attributed to effects of entanglements, which are expected to be reduced close to the surface, and chain ends, which should be enriched at the surface. One therefore can conclude that surface effects on chain conformation and chain dynamics are restricted to a region of the order of R_g .

2.2 Surface and Interfacial Tension

The most common way to obtain a picture of the surface properties [3, 8, 9, 11, 32, 33] and to measure the surface energetic state is the determination of the *surface tension*. It is determined by the outermost layers of atoms and therefore by a surface region of typically 0.2 nm. It arises from the asymmetric surrounding of atoms at the surface, where an atom at the surface is missing some of its neighboring atoms and consequently experiences a force due to the remaining asymmetric interactions (Fig. 4).

The surface tension turns out to be a very fundamental property of solids and liquids [3, 8], since it reflects directly the strength of the bonding within the bulk material which is schematically shown in Fig. 4. There are very different binding forces, and hard solids (covalent, ionic, metallic) typically reveal “high-energy” surfaces (surface tension ~ 500 to 5000 mJ/m²), which is in contrast to weak molecular solids and liquids (soft matter) with their “low-energy” surfaces (surface tension < 100 mJ/m²). It is clear that most polymers belong to the second class of materials and interactions between the chains are dominated typically by van der Waals forces, and in some cases by hydrogen bonds. Surface tension however also depends on surface roughness and will be influenced by surface segregation of

Fig. 4 Schematics of a molecule in bulk (liquid) and at the surface (interface liquid/gas) showing neighboring molecules and interaction forces [33]



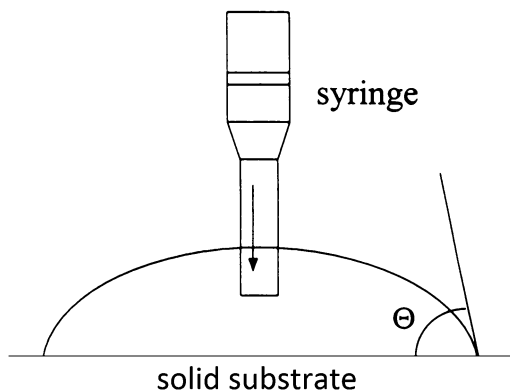
components (surfactants, antioxidants, etc.) and in particular by contaminations (catalyst, solvent, etc.). Therefore, in many practical cases, it may not reflect the properties of bulk material but of a thin surface layer or even end groups which may also segregate to the surface. Using surface tension measurements provides information on surface composition and structure only in a very indirect way, while it is relatively easy to measure in the lab and may provide helpful practical information for application.

In applications, surface and interfacial tensions of polymers are quite important such as in wetting and coating processes, in blending of polymers, in biocompatibility, and in adsorption and corrosion processes. The adhesion, and friction as well as behavior of colloidal dispersions (paints, cosmetics, etc.) are influenced by surface and interface tension. The interrelationships between interfacial aspects and materials properties are despite of their importance still poorly understood. The measurement of surface tensions of polymers is usually performed by determination of the *contact angle*, where a liquid drop is positioned on the sample surface. The equilibrium contact angle Θ for such a drop on a homogeneous smooth surface depends on corresponding interfacial tensions as expressed by the Young equation [8, 32]:

$$\gamma_{LV} \cos \Theta = \gamma_{SV} - \gamma_{SL} \quad (2)$$

γ_{LV} denotes the surface tension of the liquid with its saturated vapor, γ_{SV} the surface tension of the solid with the saturated vapor, and γ_{SL} the interfacial tension between solid and liquid. It is a consequence of the equilibrium of interfacial forces at the three-phase boundary at the edge of the drop. While the contact angle between drop and sample surface is typically measured at the drop edge, also drop profile analysis techniques may be used which enhance the sensitivity. The drop volume can be continuously enlarged (advancing contact angle) or decreased (receding contact angle), and measurements may be performed in a dynamic way. For inhomogeneous

Fig. 5 Scheme of contact angle measurement. A drop is put on a solid substrate via a syringe and the contact angle Θ at the edge of the drop is measured



and rough surfaces, one often observes that the advancing and receding contact angles are significantly different from each other. Dynamic measurements are performed with the goniometer sessile drop technique where the drop is deposited on the surface by a motor-driven syringe, and the volume is increased or decreased at given speed to measure dynamic advancing and receding contact angles (Fig. 5).

With the so-called ADSA technique (axisymmetric drop shape analysis), a silicon wafer with a small hole is used where the polymer to be investigated is deposited as a thin film [3]. From below the wafer, the liquid is put via the hole onto the wafer with a motor-driven syringe at constant speed and the increasing drop is monitored by a video camera. By computer analysis of the drop profile, the advancing contact angle is determined. Then the volume of the drop is decreased at constant speed via the syringe, and the receding contact angle is determined. Those contact angles will in general depend on the speed and possibly reach after some initial time a constant value, but in most cases advancing and receding contact angles are different from each other. For ideal surfaces, they should coincide. One has to be in particular careful to avoid influence of surface contaminations like antioxidants, catalyst, etc., which may be enriched at the surface and where already small amounts can influence the contact angle significantly. Also the liquid used (in most cases water) has to be inert to the surface material. If the surface interacts or swells with the liquid, one can use the captive air bubble technique, where in an inverted setup, the surface is constantly covered with the liquid and the syringe introduces from the top an air bubble via a small hole in the silicon wafer. There are several other techniques used (e.g., Wilhelmy balance technique with a plate or capillary penetration/Washborn technique with a powder) and several types of commercial instruments are available to measure contact angles accurately. If disperse and polar contributions to surface tension are obtained from measurements with several liquids of different polarity, the free surface energy can be calculated [8].

The contact angle of a surface against water is of particular interest. One distinguishes between hydrophobic surfaces, where the contact angle Θ is larger than 90° , and hydrophilic surfaces, where the contact angle Θ is smaller than 90° . Here the polarity of the surface plays a major role. Very interesting is the so-called

ultra-hydrophobic behavior, where the contact angle Θ is even larger than 150° and water is strongly repelled. This is achieved by a combination of surface roughness with a hydrophobic surface [3, 8, 34], where the roughness causes an amplification effect for the contact angle. Ultra-hydrophobic surfaces are observed in many cases in nature (wing of butterfly, Lotus leaf, etc.) and often also show self-cleaning properties, i.e., dirt is easily removed by water.

The *interfacial tension* is measured between different polymers or between a polymer and a substrate. In general, it is much more difficult to determine than the surface tension and therefore it only has been measured for specific examples [3]. The reason is that high viscosities of the polymeric materials, long time scales for the achievement of equilibrium, and sample decomposition make measurements for high-molecular-weight polymer materials quite difficult. The determination of interfacial tension, however, allows determination of interface width and compatibility of polymer materials using model assumptions (mean field theory) [1]. In practical cases, typically the pendant or rotating drop techniques are used.

2.3 Functional Polymer Surfaces

The fascinating aspect of functionalization of surfaces is that a very thin nanoscopic surface layer can completely change appearance and functionality of a material while bulk properties are essentially unchanged. This can include wetting, color, hardness, biocompatibility, conductivity, adhesion, friction, corrosion resistance, and many more properties [1–5, 7, 34–37]. It is even possible to generate switching, adaptive, or smart surfaces, which change their properties according to a stimulus. There are various ways to generate functional polymer surfaces. They have in common that a thin layer of a functional material is put at the surface. This can be achieved by chemical bonding, physical adsorption, or segregation of components from the bulk to the surface. It includes the deposition of a coating to the surface which again can be achieved in different ways. This is a wide field and it is hardly possible to cover here all aspects. Several reviews exist [34–37] and we will focus in the following on the particular way of surface functionalization by polymer brushes which form a stable nanoscopic thin layer that is chemically attached to the surface.

With polymer brush layers, one can nicely tune surface properties of materials [34–43]. They can be tightly attached to most materials by the choice of suitable chemistry. With mixed brush layers, it is possible to achieve switching or adaptive properties of the surface. Similarly, one can introduce multifunctionality at the surface by attachment of different chains, nanoparticles, and by incorporation of chemical functional groups.

For this reason, their use has grown over the last years, and polymer brush layers are adopted in several areas of application. This includes for instance flat substrates, but similarly colloidal particles, fibers, or rough surfaces. A big area of application is related to bio-interfaces, where blood interaction, cell growth, or protein adsorption is investigated [36, 41, 43]. This happens in aqueous environment and in many cases water soluble or polyelectrolyte brushes are utilized [38]. Other areas of application

include coatings, where wetting, adhesion, friction, local sensing, or the reflection and emission of light is controlled. Some examples will be discussed below.

We should first define in more detail, what we mean with polymer brushes. The rigorous definition of Alexander and de Gennes [44–46] assumes that brushes are end-attached polymer chains, which are grafted to the surface at high grafting density where the chains are significantly stretched due to mutual interactions. There are much more than one chain in a volume which an unperturbed chain would adopt at the surface (grafting density $\Sigma \gg 1$). It has been shown theoretically and experimentally that chains are highly stretched chains under those conditions and show properties that are significantly different from unperturbed chains [46]. One example is the autophobicity of a so-called dry brush, where free chains cannot penetrate into the brush layer, which even leads to the dewetting of chains of the same kind on top of the brush layer.

We will however not use this rigorous definition, and call already chains with some stretching a brush layer [43, 46]. So we only assume that there are more than one chain in a volume that an unperturbed chain would adopt at the surface ($\Sigma > 1$). The reason is that already this layer can shield the surface nearly completely and that it can be achieved much easier experimentally. There is still sufficient chain mobility left to allow mixed layers to switch and to rearrange their conformation on response to external stimuli. In the following, we will in particular concentrate on mixed brush layers, which can switch and adapt their properties in response to external stimuli.

If we graft two different polymers onto a solid surface, this surface may adopt the properties of one or the other material or in between which can be tuned by external stimuli ([34, 35, 43] and references therein). It even allows to achieve intermediate or new properties. The scheme of switching is schematically illustrated in Fig. 6. Two polymers are attached by covalent bonds to the surface either by

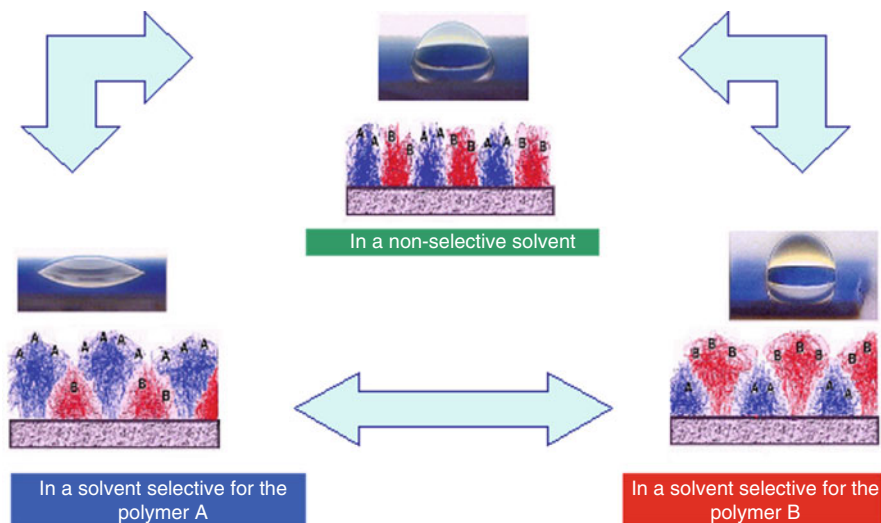


Fig. 6 Scheme of switching of surface properties with polymer brushes with selective solvents [43]. (Reprinted from Ref. [48] with permission from Elsevier)

grafting-to or by grafting-from techniques. One assumes that they are statistically distributed on the surface. The blue polymer could be hydrophilic (e.g., poly(2-vinyl pyridine)) and the red polymer then would be hydrophobic (e.g., polystyrene). In most cases, the two components would be incompatible with each other, but like a copolymer, they only phase segregate at the scale of their molecular dimension. In a solvent selective for the blue polymer (e.g., acidic water), the blue chains are swollen, while the red chains would be collapsed at the surface. There is a complex interplay of lateral and perpendicular phase segregation at molecular level [34], which results in a nanoscopic phase segregation in the surface plane, while the blue polymer might be enriched at the surface. After drying of the film, one might expect hydrophilic behavior, since the wetting is determined by the outermost hydrophilic layer. A water drop on such a surface thus will show a low contact angle.

Exposing this surface to a nonpolar solvent (e.g., toluene), now selective for the red polymer, the situation reverses. The red polymer is typically enriched at the surface, and the dried film might exhibit hydrophobic behavior. The contact angle of water then will be high. This switching is achieved entirely by a conformational change, and therefore is completely reversible. The covalently attached chains cannot perform changes at long range, and they are neither dissolved nor removed, as it could be the case for purely adsorbed molecules. Also intermediate states are possible if one applies less selective solvents.

The situation is however more complex as it might appear at first glance. One definitely needs some chain mobility to achieve switching; chains should be not too short to be able to form a complete upper layer, while they should not be too long to assure reasonable switching times for conformational readjustment. The solvent should partly penetrate the other (upper) component, since otherwise it might not reach the lower layer to cause swelling. Swelling is also difficult, if the grafting density is too high. So there are some limitations and requirements to achieve reasonable switching. Those details of course will largely influence the switching times.

The timescales of switching can vary over a wide range, and have to be adjusted with respect to the application. So switching can be fast (less than seconds), the surface may be called adaptive. A hydrophobic surface then may immediately switch to hydrophobic behavior with exposure to water – and vice versa. For a raincoat, on the other hand, this would not be suitable, and a water repelling brush layer should be stable upon exposure to water and keep the hydrophobic properties. This can be achieved, when the upper brush layer is thick, quite immobile (e.g., in the glassy state), and if this layer is mostly impenetrable to water. The switching times then should be very large (possibly days) and the brush coating is constantly water repelling.

A significant enhancement of the switching effect can be achieved by a combination of surface chemistry and surface topography. The amplification effect causes so-called ultra-hydrophobicity, which is observed at a particular surface roughness. Combining binary brushes with a particular high surface roughness results in a water contact angle that can be switched between virtually 0 and 150 degrees! This is then simply achieved by attaching brushes to a surface with appropriate roughness. In a

model experiment (Fig. 7a), a rough PTFE surface is obtained by etching with plasma. Roughness values can be up to several micrometers. From plasma treatment, one also generates functional groups at the surface, and the mixed polymer brush can be attached by grafting-to technique. After acidic water treatment, the contact angle is close to 0, while exposure to 1,4-dioxane or toluene switches the contact angle to 150 degrees (Fig. 7h). We should note that contact angles of corresponding smooth surfaces switch only between 70 and 90 degrees, and that roughness provides the amplification to smaller and larger contact angles, respectively [43]. In the ultra-hydrophobic state of the brush also the contact angle hysteresis is not observed, which is another criterion for ultra-hydrophobicity.

Using mixed polymer brushes, a wettability gradient can be generated in one or two directions [43, 47]. These brushes are generated by grafting in a temperature gradient which results in a composition gradient. With a linear temperature gradient, the first homopolymers is grafted, and the second polymer is then put into the remaining reactive sites at the substrate. Those gradient brushes can for instance be created with polystyrene PS and the incompatible polyelectrolytes (poly(acrylic acid) PAA, and poly(2-vinyl pyridine) P2VP. The corresponding binary gradient brush shows a gradient of wettability in response to different pH values (Fig. 8). At pH = 2, the wettability gradient proceeds along the P2VP content in the brush. In neutral media, the gradient is essentially “switched off,” whereas it appears again at pH = 9–10 in opposite direction along with increasing PAA fraction. So direction and amplitude of the wettability gradient of a binary polyelectrolyte brush is tuned by pH. These properties may be used for microfluidics or for transport of liquids and particles. Gradient surfaces can similarly be used for separation of binary liquid mixtures. In a lab-on-a-chip [68] device with an integrated FET sensor, the separation of a fluid mixture was achieved.

For many analytical applications, the development of chemical and biological sensors is of interest which includes monitoring of environmental and industrial processes, quality control of nutrition and water, as well as medical and security applications. So the change of fluorescence of organic dyes or the plasmon resonance of inorganic nanoparticles in different environments can be used to detect chemical substances and ions. In this respect, the combination of the responsiveness of polymer brushes and the special properties of nanoparticles turns out to be very interesting for fabrication of thin film sensors (Fig. 9) [43]. As an example, gold nanoparticles may be immobilized via hydrogen bonding on end-functionalized polystyrene brushes (Fig. 9). The presence of the Au nanoparticles on polystyrene brushes was visualized by AFM, XPS, and UV-VIS spectroscopy. By the solvent responsiveness of the polystyrene brushes, the detection of nanoscale optical changes was possible based on localized surface plasmon resonance (LSPR) of the immobilized Au nanoparticles. The change of the proximity of the immobilized Au nanoparticles as a consequence of the solvent-induced reversible swelling-deswelling of polystyrene chains is the basis of the sensing mechanism. The shift in plasmon resonance band caused by variation in the surrounding media is used for sensing, and a chemical nanosensor for the detection of a variety of organic solvents could be demonstrated.

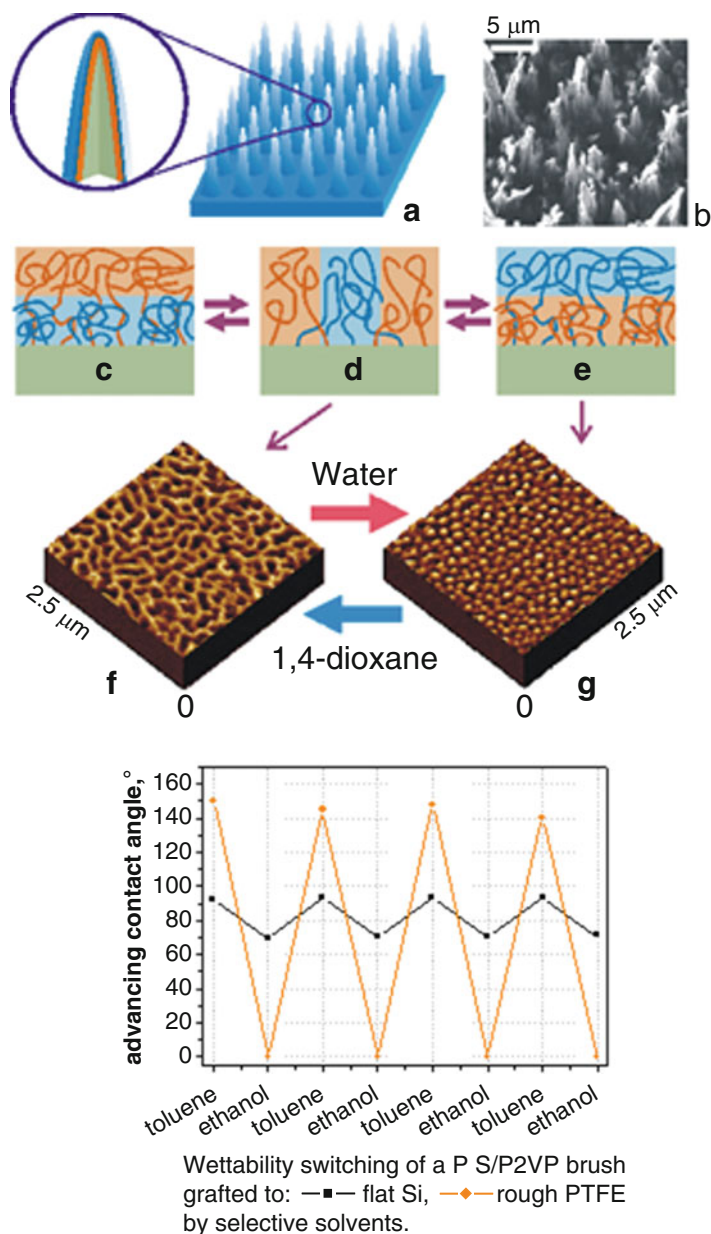


Fig. 7 Two-level structure of a self-adaptive surface: switching of surface properties by a combination of a rough surface morphology and binary brush on a PTFE surface (a–e) where (b) shows the SEM image of the PTFE surface after 600 s of plasma etching. The rough surface is covered by covalently grafted mixed polymer brushes that consist of hydrophobic and hydrophilic chains as shown schematically in (c–e). By the interplay between lateral and vertical phase segregation, the morphology and composition of the surface is switching upon exposure to selective solvents.

Another sensor works with amino-functionalized CdTe quantum dots that are covalently bonded with carboxylic groups of polyacrylic acid brushes via amide bonding. AFM images show a change in surface morphology and roughness before and after the immobilization with NPs. Covalent linkage between the nanoparticles and polymer brushes was investigated with XPS. Photoluminescence spectroscopy and fluorescence microscopy show that the quantum dots retain their optical properties even after the immobilization. The swelling and collapse of the polymer brush layer with nanoparticles attached in different solvents resulted in an intensity modulation of emitted light of the nanoparticles due to interference effects that can be used to detect the swelling of the brush and in this way perform local sensing of solvent quality [49].

Thus, it was demonstrated that the fabrication of straightforward and highly sensitive solvent and pH nano-sensors is possible, based on solvent and pH-induced swelling of polymer brushes coupled with surface plasmon resonance of Au (or Ag) nanoparticles, respectively. The change in plasmon absorption band of immobilized Au/Ag nanoparticles can be detected via UV-VIS absorption spectroscopy where sensitivity is of comparable level as for more complex techniques. Particles have a good adhesion to the polymer support, which minimizes their leakage even after multiple uses and the P2VP-Ag NPs system is quite stable at lower pH. This approach is quite versatile and can be used for the fabrication of nano-sensor devices based on temperature, pH, and ionic strength responsive polymer brushes.

Surfaces with polymer brushes can also be used to control catalytic activity [50]. Catalytically active Pd and Pt NP in P2VP brushes can be synthesized by adsorption of either Pd^{2+} - or PtCl_6^{2-} -ions to the polymer and subsequent reduction to NP by sodium borohydride (NaBH_4). The amount and distribution of nanoparticles on the surface depends strongly on the employed concentrations and length of adsorption and reduction steps. Parameters have to be selected carefully to achieve high surface coverage and ensure the fine dispersion of nanoparticles at the same time. Both Pd and Pt NP show high catalytic activity, which can be switched by use of PNIPAM brushes. The stimuli-responsive catalytic coatings are fabricated by in situ synthesis of metallic nanoparticles in binary PNIPAM–P2VP (poly(N-isopropyl acrylamide)–poly(2-vinyl pyridine)) brushes (Fig. 10). The amount of immobilized nanoparticles is controlled by the polymer ratio, since solely P2VP interacts with the nanoparticles. To investigate the temperature-dependent catalytic activity of the nano-assemblies, the reduction of 4-nitrophenol to 4-aminophenol by NaBH_4 was monitored by UV-VIS spectroscopy as a model reaction. The peak at 400 nm, owing



Fig. 7 (continued) In corresponding solvents, the individual polymers preferentially move to the top of the surface (c and e), while in a common solvent both polymers are present at the surface (d). In f and g, AFM images of the different morphologies after exposure to selective solvents are shown. The amplification effect for contact angle switching for untreated (back) and functionalized (orange) surfaces is shown in (h) [34]. (Reprinted with permission from Ref. [34]. Copyright 2003 American Chemical Society (a–e) and from Ref. [48] with permission from Elsevier (h))

Fig. 8 Scheme of the switching of a wettability gradient obtained from a polyelectrolyte gradient mixed brush (P2VP mixed with PAA) by pH [43]. (Reprinted with permission from Ref. [47]. Copyright 2004 American Chemical Society)

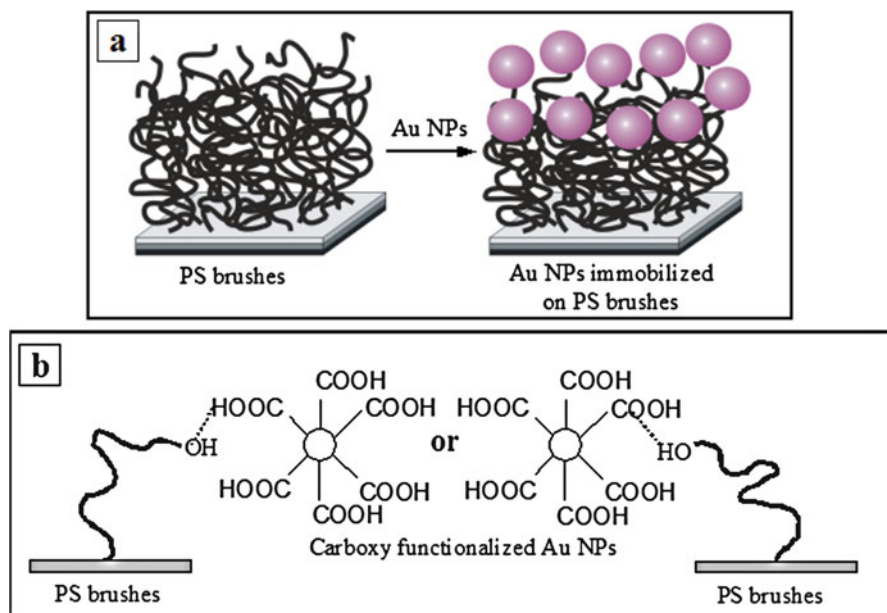
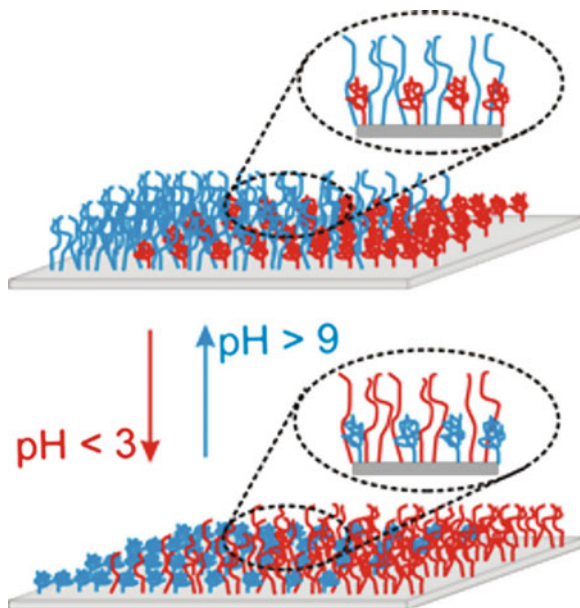


Fig. 9 Sensing by nanoparticles attached to polymer brushes: (a) carboxy-functionalized gold nanoparticles are attached on end-functionalized PS brushes and (b) scheme of hydrogen bonding between carboxy-functionalized Au NPs and hydroxy end groups of PS chain ends [43]

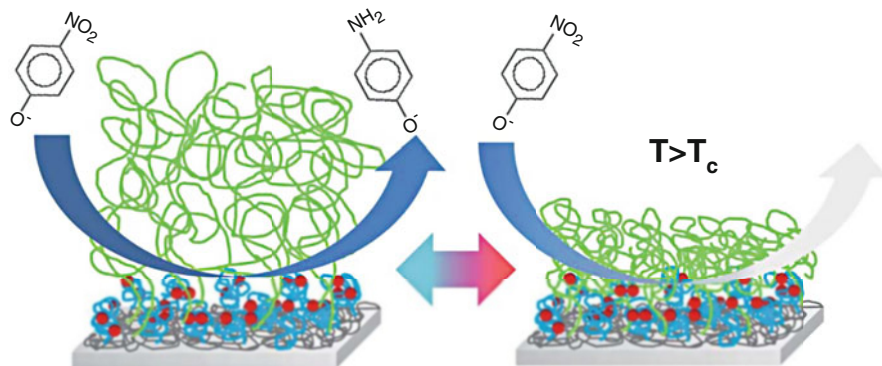


Fig. 10 Scheme of stimuli-responsive catalysis of nanoparticles deposited on binary polymer brushes; the temperature-induced collapse of PNIPAM chains (green) at T_c is proposed to lead to a diffusion barrier blocking the access of reactants to the catalyst (red) [50]

to 4-nitrophenol, decreases and the peak at 300 nm increases with time which indicates the reduction of 4-nitrophenol to 4-aminophenol. Control of the catalytic activity by the temperature-induced deswelling of PNIPAM at T_c is observed, which is explained by the formation of a barrier layer of PNIPAM with increasing temperature. In this way, diffusion of components to catalytic active sites is controlled.

Functional polymer brush layers can be used in various ways to control bio-activity [36, 41]. So adsorption or desorption of proteins as well as cell growth and cell attachment can be performed with polymer brushes. As an example, it was shown that functionalized substrates exhibit cell-guiding properties based on incorporated bioactive signaling cues [41]. The surface was functionalized by polymer brushes made of poly(acrylic acid) PAA, which were functionalized with hepatocyte (HGF) and basic fibroblast growth factor (bFGF) either by physisorption or chemisorption (Fig. 11). The GF release kinetics shows a high initial burst followed by a constant slow release in the case of both physisorbed HGF and bFGF. In contrast, chemisorbed HGF remained bound to the brush surface for over 1 week, whereas 50% of chemisorbed bFGF was released slowly. These GF-functionalized PAA brushes produce a measurable effect on human hepatoma cell lines (HepG2) and mouse embryonic stem cells (mESCs) and can be used as bioactive cell culture substrates to tune cell growth and differentiation.

3 Interfaces in Blends, Copolymers, and Composites

The interfaces between polymers in blends and copolymers as well as between polymers and mostly solid components of composites (typically particles and fibers) determine to a large extent the properties of the materials [1–5]. The interfacial region, which is formed between phases of an immiscible polymer blend, will influence the mechanical behavior of the blend under stress. Similarly the adhesion

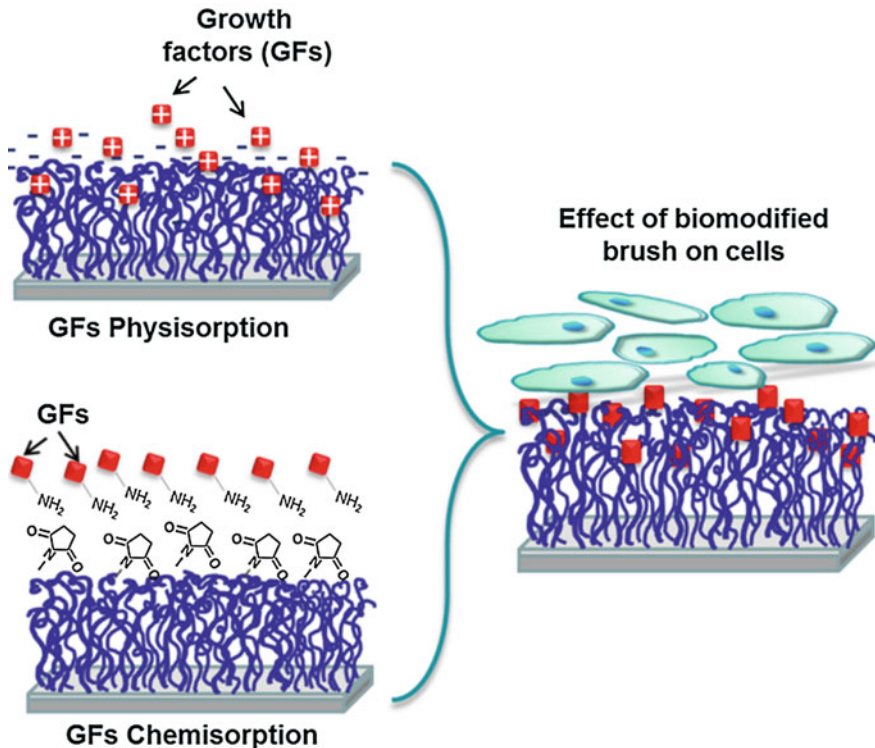


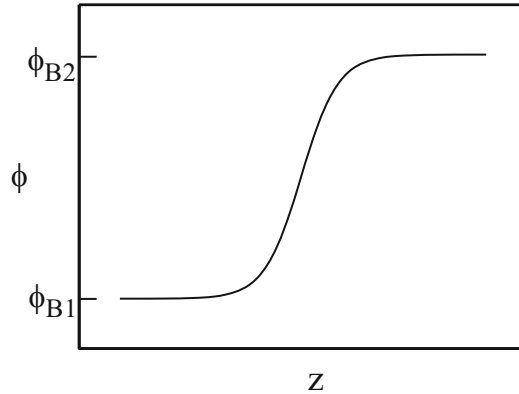
Fig. 11 Grafting of pol(acrylic acid) PAA as brush on solid substrates: Bio-functionalization of PAA brush with growth factor (red squares) through physisorption or chemisorption (left). Interaction of GF-modified PAA brush with HepG2 cells (for HGF-PAA) or mESC cells (for bFGF-PAA) (right) [41]

between particles or fibers and the polymer matrix of a composite will influence the strength of the composite. So we first shortly discuss the theoretical background and then provide some examples. The investigation of interfaces inside of bulk materials turns out to be much more complicated than the investigation of surfaces. We discuss some experimental techniques in Sect. 4.

3.1 Interfaces Between Homopolymers

When two polymer sheets are put together in the melt, an interface is forming. The width of this interface depends on the chain compatibility and determines for instance the adhesion between the sheets [1–5, 8–10, 12, 13]. If the two polymers are compatible, they will interdiffuse with each other and depending on diffusion time and diffusion coefficient at given temperature, an interface will form. This is typically controlled by Ficks law. The situation is however more complicated at short interdiffusion times and if the two polymers are chemically different or possess

Fig. 12 Interface profile between the phases of a blend of two incompatible polymers. The concentrations of the polymers in the blend are Φ_{B1} and Φ_{B2} , respectively, and are determined by the phase diagram. Z is a spatial coordinate across the interface [51]



different mobility (e.g., different molecular weight). Taking chain reptation into account with different diffusion laws at different time scales and the enhancement of chain ends at the surface, a different interdiffusion behavior is expected at small diffusion times. Similarly the situation becomes more complicated, if mobilities of the two polymers are different. The mean position of the interface will move and an asymmetric profile will form. For the development of adhesion, the formation of entanglements during interdiffusion is important. There are plenty of investigations of those effects. At longer diffusion times, the compatible polymers will intermix and at thermodynamic equilibrium form a homogeneous blend.

Most polymers are however incompatible with each other and blends of polymers will be inhomogeneous in nature [10, 12, 13, 51]. Phase segregation between components will occur and only small interfaces between the phases will form. These interfaces between incompatible polymers are typically in the range of 2–50 nm, depending on compatibility. We first will provide a short introduction to mean field theory of interface formation and interfacial tension, and then present some specific examples. Experimental methods employed for the investigation of polymer interfaces are important to gain an understanding and will be discussed in the following Sect. 4 with respect to their accuracy and advantages, with emphasis on neutron- and X-ray reflection, electron microscopy, ellipsometry, interfacial tension, and nuclear reaction analysis techniques.

For most incompatible materials, the interface is not very wide depending on compatibility [3, 10, 12, 13, 51]. A typical interface profile is shown in Fig. 12. When two incompatible polymers are put into contact, segments will move if the materials are heated above the glass transition, and some interpenetration will occur. Therefore the interface width increases with time and reaches an equilibrium value, which is determined by the Flory-Huggins interaction parameters χ according to mean-field theory. The quantity χ expresses polymer compatibility, while it is not completely understood on a molecular basis. In practice, it is often used as an empirical parameter and then allows a thermodynamic description of phase separation for a particular polymer pair within mean-field theory. Besides equilibrium thermodynamic effects, other factors originating from sample preparation and

experimental conditions also influence interface formation. When two films are put together to form an interface, there is the influence of initial surface roughness, surface composition, contaminations, and chain conformation at the surface of the films, which may largely depend on sample history. In specific cases, it is difficult to reach equilibrium, for instance, when segment mobility is slowed down by the glass transition T_g .

When comparing experimentally determined interface widths with calculated ones, e.g., from interfacial tension data, one must be cautious, because there are influences from end-group effects, molecular weight distributions, chain orientation, capillary waves, or initial interface roughness that are not very well understood. We also assume that additives like antioxidants or plasticizers are not present, since those materials might migrate to the surface or interface even if present only in trace amounts.

The description of phase behavior in polymer blends is of fundamental interest in polymer research [10]. A first approach is based on Flory, Huggins, and Staverman (FHS) theory. Using a lattice model, a simple form for the free energy of binary polymer blends including the interaction parameter is derived

$$\frac{F_{FHS}}{kT} = \frac{\phi \ln \phi}{N_1} + \frac{(1 - \phi) \ln(1 - \phi)}{N_2} + \chi \phi (1 - \phi) \quad (3)$$

N_1 and N_2 are the degrees of polymerization and ϕ the volume fraction of one of the polymers. The interaction parameter χ is related to the interactions between segments. It is on the other hand an effective interaction parameter, which takes into account the difference between interactions of the same and different segments of the blend. So it typically is very small quantity although the actual interaction energies are much larger. Many theories have been derived to describe the interaction parameter as a function of temperature to reproduce phase diagrams observed in different experiments. For complicated phase diagrams, it may be necessary to introduce a ϕ -dependence of χ in addition. Equation 3 now contains first the entropic terms, which are small at large N , and second the enthalpic term with χ , which includes the interaction energies and which dominates the free energy. As a consequence, most polymers are immiscible with each other.

In order to discuss the problem of an interface between two polymers [10], Equation 3 has to be extended by the so-called quadratic gradient term $\kappa(\nabla\phi)^2$ introduced by Cahn and Hilliard to take fluctuations into account. This allows the derivation of the equilibrium volume fraction profile. An analytical solution for the volume fraction profile can be calculated for the case of infinite degrees of polymerization ($\chi N \gg 1$), which is equivalent to strong segregation,

$$\phi(z) = \frac{1}{2} \left(1 + \tanh \frac{z}{l} \right) \quad (4)$$

with

$$l = \frac{a}{\sqrt{6\chi}} \quad (5)$$

a is the mean characteristic segment length of the polymers. So even for strong segregation, the two components interpenetrate over some distance. In the same approximation also the interfacial tension γ depends on χ

$$\gamma = \frac{kT}{a^2} \left(\frac{\chi}{6}\right)^2 \quad (6)$$

A simple way to estimate the influence of finite chain length is possible for the case of two polymers with the same degree of polymerization N

$$l = \frac{a}{\sqrt{6\left(\chi - \frac{2}{N}\right)}} \quad (7)$$

As a result, the interface width l and the interfacial tension γ are directly related to the Flory Huggins Stavermann effective interaction parameter χ . For the experimental determination of l , one has to be careful, however, since besides this intrinsic interface width also lateral fluctuations are depending on interfacial tension and consequently on χ . In many cases, it is difficult to distinguish between “intrinsic interface” and capillary wave effects. This is reflected in computer simulations where both effects contribute to the apparent interface width and a correction of the measured interface width with respect to capillary waves is necessary.

As mentioned before, the interface width may be determined by neutron reflectometry [51, 52], if one of the components has been deuterated and a contrast at the interface has been generated. Two highly smooth films are put on top of each other and after annealing in the melt the interface width is determined.

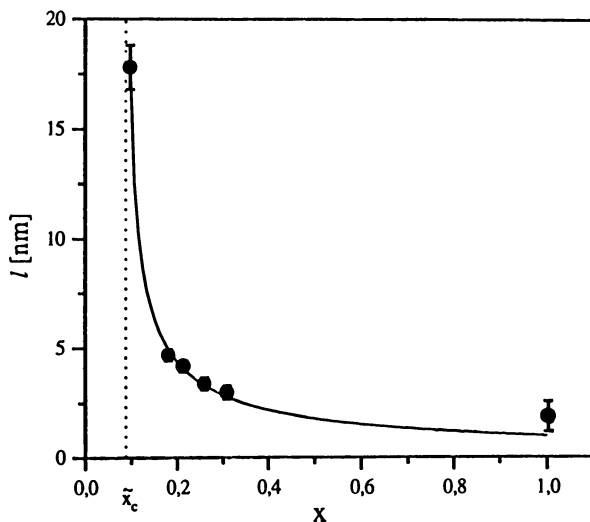
One of the most intensively studied incompatible blend systems is poly(styrene) PS versus poly (methyl methacrylate) PMMA. Values of interface widths l determined with different techniques are of the order of $l = 1.3$ nm [51]. The most accurate value has been obtained with neutron reflectometry from a blend system and has been confirmed from studies of diblock copolymers, where the interface width between lamellae is found to be of the same size. Also, temperature-dependent ellipsometry investigations and TEM yield similar results within error bars. A serious discrepancy, however, arises when the interface width is calculated from interfacial tension data on the basis of meanfield theory. Those interface widths are approximately a factor of two smaller than the measured ones. This might indicate that capillary wave effects might significantly contribute to experimental values, which may contain “intrinsic” and capillary wave effects as discussed above. Of course also other effects could contribute like end-group effects, conformational changes or surface contaminations.

Several other systems have been investigated including interfaces between compatible polymers [51, 52]. Theory predicts at initial stages of interdiffusion a special behavior due to reptation effects. In reptation theory one assumes that initially chains diffuse across the interface mostly via chain ends, which results in a particular time dependence of the growth of the interface width. Other studies deal with partially compatible polymers or blends, where one of the components is in the glassy state.

The blend system of PS and the statistical copolymer poly(styrene-statpara bromo styrene) $\text{PBr}_x\text{S}_{1-x}$ [51] was chosen for systematic investigations of the dependence of interface width on compatibility. Here compatibility between components can be adjusted between completely compatible to highly incompatible by a change in degree of bromination x . Since materials can be obtained by bromination of polystyrene with narrow molecular weight distribution, where the degree of bromination can be high, the contrast between components may be sufficient also for X-ray reflectivity experiments. However, at low degree of bromination, deuterated PS has to be utilized, and NR experiments are performed. The results from all experiments are shown in Fig. 13. At low x , the interface width diverges because the system becomes compatible at x_c . The functional form is fitted empirically by a composition-dependent χ -parameter, which contains the concentration-weighted individual segment-segment interaction parameters of the components. Values at large χ can be compared to other X-ray and neutron reflectivity data. There is good agreement between different data sets and theory, where mean field theory is used to calculate the interface width at different compatibility. Also, the influence of the glass transitions on the interface width has been studied, since the glass transition also increases with degree of bromination. If the sample is annealed between the glass transitions of the components, segment interdiffusion is strongly reduced. In this temperature regime, the interface width depends strongly on temperature until both components become mobile and the glass transition temperature also of the second component is reached. At higher temperatures, dewetting phenomena are observed that are a consequence of the strong incompatibility of the components.

Copolymers are also used for compatibilization of incompatible polymer blends, where a small addition of a diblock copolymer can significantly improve the mechanical properties of the blend [3, 53, 54]. This is due to the fact that the diblock copolymer might be enriched at the interface and provides a mechanical bridge

Fig. 13 Dependence of interface width l on degree of bromination x for the blend system PS versus $\text{PBr}_x\text{S}_{1-x}$. The system becomes strongly incompatible at large x , while it is compatible for $x < x_c$ [51]



between the segregated phases of the two components where interface width and mutual interpenetration otherwise are small. It has been predicted by theory [53] that the diblock copolymer will be enriched at the interface and that the interface is broadened by addition of the copolymer. It is assumed that the two blocks are compatible with the corresponding homopolymers of the blend. With neutron reflectometry or nuclear reaction analysis, those predictions can be tested [54] by utilizing dedicated contrast generation by deuteration: (i) the enrichment of the copolymer at the interface can be visualized if the copolymer has been deuterated with otherwise nondeuterated homopolymers, and (ii) the broadening of the interface is resolved if one of the homopolymers and the corresponding block of the copolymer have been deuterated with otherwise nondeuterated components.

Thin films of copolymers are used in various ways for generation of nanostructures at surfaces [55–57]. The two incompatible blocks phase segregate at the scale of the molecules and form nanoscopic ordered morphologies. The interface to the substrate is important for adhesion but also for alignment of the nanostructured films, while the surface to air determines the wetting behavior and other properties. A particular example are structures formed by a supramolecular approach (SMA) with diblock copolymer thin films of polystyrene, poly(4-vinyl pyridine) PS-*b*-P4VP and 2-(4'-hydroxybenzeneazo) benzoic acid HABA, which is a low molar mass additive associated with one of the blocks by noncovalent interactions [56–58]. This low molar mass additive is removed easily by selective dissolution from the P4VP phase to obtain a nanoporous ordered thin film. SMA with block copolymer self-assembly is a simple and powerful technique for fine tuning of block copolymer morphologies, and has been successfully used in bulk and in thin films. Figure 14 shows the schematic representation of the formation of nanotemplates by this technique. A solution of PS-*b*-P4VP block copolymer and HABA was spin cast on to a silicon wafer as a thin film. A cylindrical morphology was observed either with the cylinder axis parallel or perpendicular to the substrate where orientation

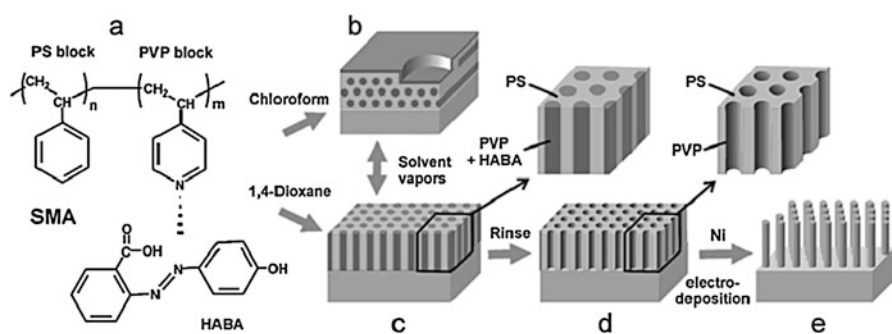


Fig. 14 Generation of ordered nanotemplates with diblock copolymer thin films: the supramolecular assembly SMA of PS-*b*-P4VP block copolymer and HABA (a) is formed by solvent casting. Depending on the solvent, perpendicular (c) or parallel (b) alignment of the structure is achieved. The nanotemplate (d) is prepared by dissolution of HABA. The empty cylinders can be filled by electrodeposition with nickel, and the polymer matrix removed by dissolution in toluene (e) [56]. (Reprinted with permission from Ref. [59]. Copyright 2003 American Chemical Society)

depends on the solvent. By exposure to different solvent vapors, the orientation of the cylindrical microdomains of P4VP(HABA) could also be switched. Annealing in chloroform results in parallel, and annealing in 1,4-dioxane results in perpendicularly oriented cylinders. HABA can be removed from the SMA thin films by immersing in ethanol to transform the block copolymer thin film into a nanotemplate [59]. Due to specific interactions, the P4VP material is enriched both at the surface and at the interface to the silicon wafer. The nanotemplate may be further processed and for instance filled with nickel by electrodeposition. After removal of the polymer matrix the ordered nickel nanorods are left over.

The combination of block copolymers with nanoparticles can add additional functionalities to those coatings. The first commonly used way to prepare hybrid polymer/inorganic nanocomposites is to directly mix presynthesized and suitably functionalized nanoparticles with block copolymers and then allow the whole system to self-assemble [7, 56–61]. Nowadays, nanoparticles of various chemical compositions can be synthesized in solution with precise control over size and shape. The nanoparticles should be stabilized against aggregation and coalescence either electrostatically or sterically by coating with ligands that bind to or adsorb onto the NP surfaces. These ligands might be small molecules, functional (co)polymers, polyelectrolytes, or biomolecules that control interfacial interaction. Such core-shell particles are combined with block copolymers, e.g., by dissolving in common solvent and allowing solvent to evaporate. In particular cases, annealing steps might be required to bring the whole system to an equilibrium state. To achieve domain-selective localization, the particle/polymer interactions are tuned such that particles prefer one block copolymer domain over another. Hydrophobic, electrostatic, or hydrogen bond interactions between monomer units or functional groups can promote domain-selective nanoparticle localization. Various types of inorganic nanoparticles stabilized with small organic molecules can be incorporated in different domains of block copolymers matrices using direct mixing approach. As an example, iron oxide nanoparticles stabilized with oleic acid were selectively segregated into PMMA domains of self-assembled PS-*b*-PMMA matrix [57], but many other examples are reported.

So one can fabricate highly ordered arrays of nanoscopic palladium dots and wires (Fig. 15a) by the direct deposition of presynthesized palladium nanoparticles in aqueous solution [56]. As mentioned before, the cylindrical morphology observed in thin films of PS-*b*-P4VP can be switched from parallel to perpendicular and vice-versa by annealing in vapor of appropriate solvents. By immersion into ethanol, a good solvent for P4VP and a nonsolvent for PS, surface reconstruction of the films was observed with a fine structure. Perpendicular cylinder alignment resulted in a nanomembrane with hexagonal lattice of hollow standing cylinders, and parallel cylinder alignment produced nano-channels. Figure 15b shows AFM height images of nanopores and nano-channels after surface reconstruction. In these templates, the pore or channel walls are formed by functional P4VP chains. A subsequent stabilization of the polymer matrix by UV-irradiation followed by pyrolysis removes the polymer matrix material and produces highly ordered metallic nanostructures. Figure 15c shows AFM height images of palladium nano-dots and nanowires after the removal of the polymer matrix. This method provides a facile approach to fabricate a broad range of

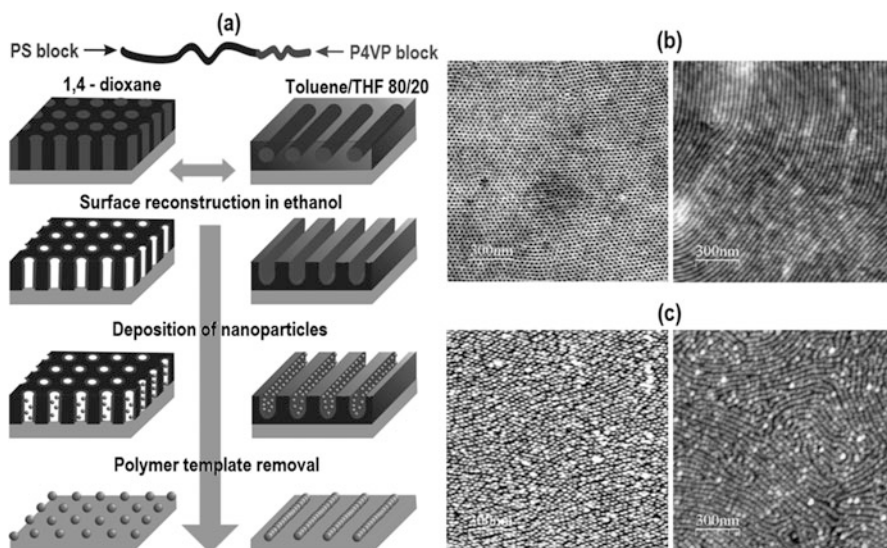


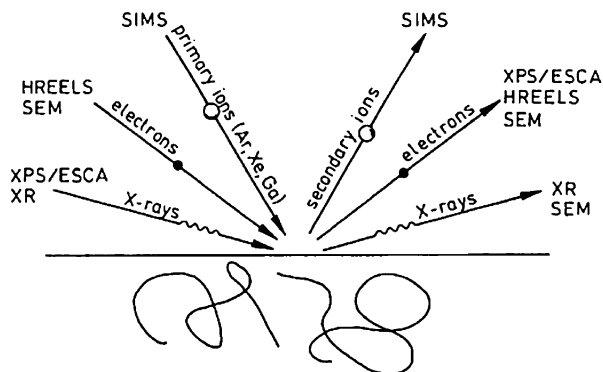
Fig. 15 (a) Schematic diagram of the fabrication process of ordered arrays of nanoscopic palladium dots and assemblies using block copolymer template. (b) AFM height images of PS-b-P4VP nano-templates with perpendicular and parallel arrangement of nanostructures obtained after surface reconstruction in ethanol. (c) AFM height images of palladium nanodots and linear assemblies obtained after the polymer matrix removal [56]. (Reprinted from Ref. [60] with permission of Elsevier)

nano-scaled architectures with tuneable lateral spacing, and can be extended to systems with even smaller dimensions. One can also pattern noble metal nanoparticles such as gold, platinum, and palladium. It is also possible to deposit differently functionalized nanoparticles in or respective on top of the different phases of block copolymer thin films [58]. Also ordered arrays of nanoparticles can be produced inside of the confined space of block copolymer cylindrical phases [60, 61] and nano-objects formed by selective solution [7]. Glass and carbon fibers are widely used for mechanical reinforcement to achieve lightweight materials with good mechanical properties, and oxydic, metallic, or semiconducting nanoparticles are applied for optical, electrical, magnetic, catalytic, or sensing applications. Dispersion and contact of fibers or nano-particles with the surrounding polymer matrix are again highly important, which are determined by the interface between them. The analysis of those interfaces is particularly difficult because properties of the organic and inorganic components are very different.

4 Characterization Techniques of Polymer Surfaces and Interfaces

The characterization of polymer surfaces and interfaces is a difficult task and needs dedicated techniques [1, 3, 11, 20, 32, 51, 52, 62–67]. This is in particular true for the characterization of interfaces, which are hidden inside of the material. To get a

Fig. 16 Schematics of some surface characterization techniques where different types of radiation are used for incident and outgoing beam [3]



reasonable picture, usually a combination of different techniques is necessary. Some of the most common techniques are schematically depicted in Figs. 16 and 17 and listed in Tables 1 and 2, where also typical resolution and information obtained is provided. Those data are however only rough guides and resolution for instance can be much worse or better depending on sample preparation and particular instrumentation used. As an example, for a polymer blend surface, the wetting properties are determined by contact angle measurements, which may provide already a hint on surface composition or segregation of components, the roughness, and lateral nanostructure is determined by scanning force microscopy, the detailed surface composition by x-ray photoelectron spectroscopy, the morphology in the vicinity of the surface by x-ray reflectometry or in more detail by grazing incidence x-ray scattering, and mechanical properties of the surface by nano-indentation. One might of course not need all this information, and characterization techniques have to be carefully chosen for a particular question. Several other and more dedicated techniques are available, which may provide better resolution or additional information, but mostly require more dedicated instrumentation and in many cases also special sample preparation.

From the time dependence of interface formation, one can learn about segment mobility and interdiffusion mechanisms. Techniques are needed that can resolve details of the interface between polymeric components at nanoscopic level. Since the interface width for incompatible polymers is typically much smaller than 50 nm, the resolution of the technique has to be adapted for a determination of such small interface widths. To achieve good resolution, a suitable contrast between components has to be present in order to “see” the interface between the components. Such a contrast can be generated for neutron reflectometry (NR), for example, by deuteration of one of the components [1, 3, 52]. So in multicomponent systems, one particular component and its interfaces with other components can be made visible for neutrons. The application range may be limited by the particular sample geometry needed. Other techniques include ellipsometry, small angle scattering, ion techniques, electron microscopy, and measurements of interface tension.

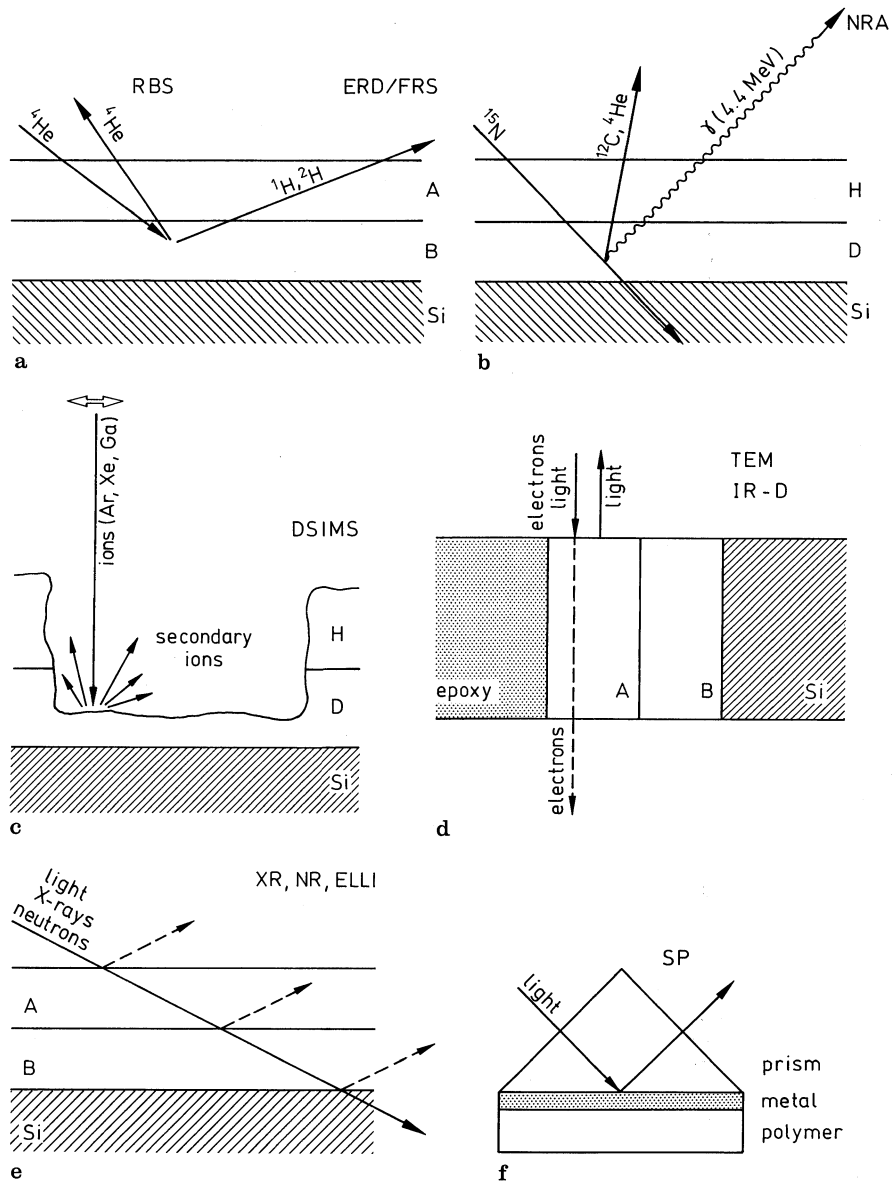


Fig. 17 Schematics of several surface and interface analysis techniques: (a) Rutherford backscattering (RBS), (b) nuclear reaction analysis (NRA), (c) dynamic secondary ion mass spectrometry (DSIMS), (d) transmission electron microscopy (TEM), (e) x-ray (XR) and neutron reflectometry (NR) as well as ellipsometry (ELLI), and (f) surface plasmon spectroscopy (SP) [3]

4.1 Surface and Interfacial Tension

The measurement of surface tension is still one of the easiest and most common techniques for a first surface characterization [3, 8, 32]. Experimental techniques and problems have been discussed in Sect. 2.2. For a detailed surface analysis, other techniques should be used in addition.

The measurement of interfacial tension of polymers is much less straightforward and is determined mostly only in special cases of low-molecular-weight materials.

4.2 Scanning Force Microscopy (SFM)

Scanning force microscopy has been developed as a very versatile technique with many modes for a variety of applications [3, 62, 63]. It provides nanoscopic resolution both in width and height at the surface of a film or substrate, and for instance single polymer molecules adsorbed on a smooth solid substrate have been resolved. Available operation modes include contact, noncontact, hard/soft tapping, materials, adhesion, phase, friction or chemical contrast, indentation, soft or force-distance mode, use of tunneling current, electrostatic, electro-chemical or magnetic interactions, it can be operated in different environments including vacuum, air, liquid or inert/humid atmosphere, and offers various fascinating and versatile possibilities. Nanoscopic resolution of different aspects of a surface can be obtained. So one can measure and visualize the surface with respect to topography, surface hardness, friction, adhesion, conductivity, electrostatic charge, or magnetism. By different operation modes ranging from noncontact to hard tapping, the strength of the interaction of the tip with the substrate can be controlled. To perform depth profiling, the surface can be removed by etching or dissolution techniques, and in this way structures inside the sample and at hidden interfaces may be resolved.

With the tip, individual molecules and atoms at the surface can be manipulated, and for example single atoms may be positioned on a solid surface by the tip. It therefore may not only be used as an analytical but also as a nano-manipulation tool. Its strength comes from the fact that a lateral image can be obtained relatively easily at nanoscopic resolution by different modes, while surface properties at quantitative level are not easy to obtain with this technique. It can be combined with other techniques. Tip-enhanced Raman spectroscopy provides local chemical information, where by plasmon effects at the AFM-tip a local signal enhancement up to a factor of 10^{10} may be achieved, which allows measurement of Raman signals from nanoscopic small spots. An analogous technique is nano-IR, where the local thermal expansion by an IR-beam is detected at nanoscopic level.

A similar technique is scanning tunneling microscopy where the tunneling current between tip and surface is measured and used for tip control. It requires however conductive samples like metals or semiconductors, while nonconducting polymers have to be covered with a conductive layer for measurement. Spectroscopic information is obtained with scanning near-field optical microscopy, SNOM, where a

particular optical fiber is used as a light guiding tip to illuminate the sample. The emitted or absorbed light is then analyzed.

4.3 Ellipsometry (ELLI) and Surface Plasmon Spectroscopy (SP)

Ellipsometry can be used to measure the thickness and index of refraction of a thin layer on a substrate with high precision (the thickness resolution can be better than 1 nm depending on optical contrast) and as a function of time. The change of the polarization state of reflected light from the surface is determined, which provides information on the optical properties of the reflecting medium (Fig. 17) [3, 62]. For very thin films, however, the thickness and index of refraction cannot be measured independently and the so-called optical thickness is determined. For thicker films the technique then reveals thickness and index of refraction of the layer independent from each other (thickness typically larger than 10–20 nm), and may provide information on anisotropy and roughness. By direct ellipsometric imaging (microscopy) or scanning techniques, lateral information on thickness or index of refraction variations at micrometer scale can be resolved too. Problems and limitations may occur from correlations of thickness and index of refraction, low optical contrast in multilayer samples, but also from ambiguities in the evaluation of data in more complex situations, where due to limited experimental data detailed information on the system is difficult to extract. Then spectroscopic or variable angle ellipsometry provides additional information and may help in determination of system parameters. Measurements can be performed under various environmental conditions including for instance the adsorption kinetics of molecules in solution at a solid substrate which may be measured in-situ with a liquid cell. IR ellipsometry can be performed by use of IR radiation from a synchrotron source, which can even provide chemical information in monolayer polymer films or elemental composition.

Surface plasmon spectroscopy (SP) is a very similar technique (Fig. 17) while it uses surface plasmons in a thin metal layer, which are excited by the incident light. The plasmon resonance is influenced by the adjacent polymer layer, which in this way can be analyzed with respect to polymer film thickness and index of refraction. Information content of SP is comparable to ellipsometry, but requires a metallic layer for the excitation of the plasmons.

4.4 Scanning and Transmission Electron Microscopy (SEM, TEM)

Scanning electron microscopy (SEM) [3, 62, 64] is used in scanning and reflection mode for surface investigations. SEM reveals an image of the surface typically at nanometer lateral resolution, and contrast is obtained by electron scattering, absorption, or emission. An image of the element distribution is achieved for instance by electron energy loss (EELS) or x-ray fluorescence spectroscopy (EDX). With organic materials, the sample degradation by the electron beam has to be considered (but also can be used for contrast generation and electron lithography). Contrast and

resolution may be improved, when the surface is covered by a thin conducting film, sputtered at an angle with respect to the surface normal to obtain shading effects. In most cases, quantitative analysis of SEM images is however difficult.

Transmission electron microscopy (TEM), may be used to investigate bulk materials and interfaces where typically a 50 nm thick slice (Fig. 17) is prepared. This slice can be cut with a microtome (using a diamond knife, possibly under cryo-conditions) or with an ion beam (FIB, see below). After staining or other contrasting methods, the interface between materials may be resolved. Limits of resolution arise from intrinsic TEM resolution, but also from preparation, where artefacts and smearing of the interface may occur. Chemical and elemental resolution is obtained using inelastic electron scattering (electron energy loss spectroscopy, EELS) or x-ray emission (EDX). The sample has to withstand ultra-high vacuum during measurement and electron beam damage. For liquid or sensitive samples, cryo-techniques are adapted where the sample slice is shock-frozen and cooled during the experiment. With special setups, experiments at atmospheric conditions or in liquid state are feasible, but require dedicated sample environment with thin windows. TEM however needs in all cases a very special sample preparation, which may be time consuming and difficult to achieve.

4.5 X-Ray Photoelectron Spectroscopy (XPS)

X-ray photoelectron spectroscopy (XPS) can be used to characterize the chemical composition of polymer surfaces. Due to limited electron emission depth, with polymers typically a depth of up to 7 nm is probed [3, 62, 65]. In some cases the acronym *ESCA* for *electron spectroscopy for chemical analysis* is used indicating the possibility of chemical analysis as well as the combination of photoelectron and Auger electron peaks in observed spectra (electron spectroscopy). Electrons from the inner shells or valence bands of the sample are excited and ejected by the incident soft X-rays. The number of photoelectrons which are leaving the sample surface is measured as a function of incident energy. The emission depth of the electrons from the sample is limited, which determines the depth resolution. The measured energy spectrum of the electrons then is characteristic for elemental composition and binding state of atoms of the sample. One can quantitatively determine the surface composition and binding of different species. Measurements are performed under vacuum, and with nonconducting surfaces surface charging has to be avoided.

With conventional scanning XPS instruments, the lateral resolution is typically not better than several micrometers. It may be significantly improved using X-ray photo electron emission microscopy (XPEEM), where an electron microscope is used to image the outgoing electrons. Here the lateral resolution may be of the order of 10–30 nm, when soft x-rays from a synchrotron source are used. Similarly a synchrotron source is needed for transmission x-ray microscopy (TXM), which utilizes the absorption of soft x-rays in a thin film sample for lateral imaging of chemical composition at similarly good resolution.

4.6 Electrokinetic Methods (Zeta Potential)

The preferential adsorption of cations or anions, the dissociation of surface groups, the adsorption of polyelectrolytes, the isomorphic substitution of cations and anions, and the accumulation or depletion of electrons determines the electrokinetic potential on the surface of a solid in contact with a polar medium (usually water) [3]. Usually, one assumes the presence of an electric double layer consisting of two regions of charge distribution at an interface: first a fixed layer and second a diffuse layer. A “surface of shear” or “slipping plane” is located between these two layers. An externally applied electric or mechanic force causes a relative movement between the fixed layer and the diffuse layer. The electrokinetic or zeta (ζ) potential is the potential at this surface. The electrokinetic potential can be measured by applying an external electric field, which results in relative movement of the solid and liquid phases (electrophoresis, electro-osmosis), which generates an electric potential or produces an electric current (called streaming potential/streaming current, sedimentation potential). This can be measured with several experimental techniques, but with planar surfaces often the streaming potential is determined.

4.7 Infrared Spectroscopy (ATR-FTIR)

Infrared spectroscopy provides chemical information and is used for surface and thin film investigations in reflection or attenuated total reflection mode (ATR-FTIR) [3]. Quantitative determination of composition or binding states via vibrational modes is possible. So it is a powerful analytical tool for detection of dynamics at solid/liquid or solid/air interfaces. ATR-FTIR utilizes multiple reflections from a large smooth crystal. The reflecting plane between crystal and surrounding medium is investigated. The IR beam is totally reflected at this interface, but still an evanescent wave penetrates the surrounding medium. Molecules can be distinguished by their IR-spectrum, and deuteration is sometimes used to differentiate between different constituents. The evanescent wave typically penetrates of the order of the wavelength into the other medium, and therefore probes a depth of several micrometers. Utilizing an IR-microscope the lateral resolution similarly can be several micrometers. With an IR array detector, spectroscopic information can be obtained at high speed and spatial resolution. IR synchrotron radiation again enhances time resolution, and allows use of IR ellipsometric imaging techniques for measurement of composition, thickness, orientation, and index of refraction of surfaces and thin films [66].

4.8 Raman Spectroscopy

With Raman spectroscopy also the chemical composition at the surface may be detected [3]. In contrast to IR spectroscopy, those vibrational and rotational states are detected where the polarisation is changing. Since the energy shift of the

scattered light is detected, the observed signal is not so strong and powerful lasers are needed for the investigation of surfaces. With surface enhanced Raman spectroscopy (SERS) the surface signal however can be enhanced by many orders of magnitude. The plasmonic enhancement from metallic nanoparticles (preferentially Ag) is used which are deposited on the surface, and Raman spectroscopy becomes sensitive to the direct environment of those particles [69].

4.9 X-Ray and Neutron Reflectometry (XR, NR, GISAXS)

X-ray and neutron reflectometry techniques (XR, NR) use the fact that x-rays and neutrons are reflected at interfaces (Fig. 17) when a suitable contrast is present [1, 3, 52]. The difference in electron density between materials provides a contrast for x-rays, and x-rays are in particular sensitive for the surface of thin films against air or vacuum. The electron densities between polymers are in most practical cases not very different, and XR cannot easily resolve the interface between two polymer films. The contrast for neutrons on the other hand can be generated by deuteration of one component, i.e., all hydrogens are replaced by deuterium, which chemically is essentially identical to hydrogen, and the interfaces between polymers can then be resolved at nanometer resolution. Both techniques however cannot easily distinguish between lateral fluctuations of the interface (generated by thermal fluctuations, surface roughness, or capillary waves) and the “true” interface (generated by interdiffusion between components). Since both quantities can be in the nanometer range, a quantitative interpretation of reflectometry data in terms of interface width may be difficult (see Sect. 3.1). A separation between interdiffusion and lateral fluctuations may not be necessary however in many cases. Both techniques can on the other hand provide valuable information on film thickness, surface and interface roughness, capillary waves, surface segregation and profile of components in a blend, interdiffusion, interface width and asymmetry etc. The sample should be smooth and flat, and extend laterally typically over several cm. XR and NR can provide information even at sub-nanometer resolution if the quality of the sample (smoothness) is perfect.

For Grazing Incidence Small Angle X-Ray Scattering (GISAXS), two techniques are combined: Grazing Incidence Diffraction (GID), which uses reflection geometry to obtain diffraction from the surface and near surface region, and Small Angle X-ray Scattering (SAXS), which obtains electron density fluctuations and structures at 1–100 nm length scales typically in normal transmission mode. Experiments are carried out close to the critical angle for total external reflection, which results in a considerably enhanced surface sensitivity. The full potential of GISAXS is obtained when it is performed with synchrotron radiation and an area detector. GISAXS is a nondestructive structural probe like other reflectivity and scattering techniques and does not require a conducting surface or special sample preparation. With flat samples GISAXS yields excellent sampling statistics and averages over macroscopic regions while it provides information on lateral nanostructures close to the surface, size distributions, particle geometry, and spatial correlations. Similarly neutrons

can be used at grazing angles (GISANS), but this technique requires high flux neutron sources.

A careful analysis of the decay of the small angle x-ray or neutron scattering (SAXS, SANS) in transmission allows for a determination of the interface width in a two phase system of a bulk sample (Porod law). Because of weak scattering this measurement is only possible with high scattering contrast between components and a strict two component system has to be assumed. An x-ray microbeam (0.05–20 μm in diameter) from a hard x-ray synchrotron source is used for so-called scanning x-ray microscopy where the beam is scanned over the sample to determine at each spot a full x-ray small or wide angle scattering pattern with an area detector. Structural information at micro- to nanometer level is obtained, spatially resolved at different locations of the sample.

4.10 Secondary Ion Mass Spectrometry (SIMS)

Secondary ion mass spectrometry (SIMS) may be used to determine the chemical composition of surfaces and interfaces at high resolution [3, 63, 65]. Secondary ions are generated by bombardment of the sample surface with an ion beam under vacuum. Those generated ions from the sample are analyzed in a mass spectrometer. The organic characteristic fragments are used for identification of the composition (fingerprint technique). In the “static” mode of operation at low ion flux, only a monolayer is removed from the surface (static SIMS). This mode is used for surface investigations and allows for instance very sensitive investigations of surface contaminations.

At high incident ion flux in the “dynamic” mode (Fig. 17), the sample material is continuously sputtered away, and by monitoring the secondary ion flux one generates a depth profile of elements and fragments (dynamic SIMS). At constant sputter rate also interfaces between polymers may be investigated, and depending on sputter rate a depth resolution as small as 12 nm may be achieved.

4.11 Ion Techniques

Several techniques use ions as probes for interface analysis besides SIMS (Figs. 16 and 17) [3]. They require dedicated equipment and are usually applied under ultra-high vacuum. Typically an ion accelerator in the appropriate energy range as well as corresponding ion sources and detectors are needed. Deuteration of one component is again a technique for contrast generation between polymers [54]. While the resolution is reasonably good, ion techniques are quite helpful for interface width determination of polymers. Elastic Recoil Detection/Forward Recoil Detection and Nuclear Reaction Analysis are typical and well-developed techniques. When heavy atoms are present in the sample, Rutherford Backscattering can be used.

A common lab technique uses scanning of a focused ion beam (FIB) for imaging, but in a cross beam set-up is often utilized in combination with a SEM for micro-/

nano-machining of a sample (cutting, milling, etching, ion deposition). The ion beam can etch deep cuts into the sample, which then are investigated by SEM or TEM further. In this way, hidden interfaces may be visualized, and the ion beam is also able to cut soft/hard interfaces, which otherwise may be difficult to achieve. Many possibilities for nano-machining, ion-beam lithography and nano-pattern generation exist, but one should be aware that after FIB treatment there is always a thin surface layer which contains some incident ions and has been modified by the ion beam. By FIB machining, structures may be generated down to the range of 10 nm. The combination of FIB and SEM in commercial instruments offers the possibility of simultaneous imaging of the treated region with the SEM at high resolution, while the ion beam is machining the surface. With added nano-manipulators for instance conductivity measurements can be performed. Various materials like Pt, W, SiO₂, etc. may be locally deposited on a sample surface in the FIB using ion-beam-activated deposition by local decomposition of molecules from a directed gas flow. The FIB in this way can be considered as a nano-lab.

4.12 Optical Microscopy Techniques (OM)

If nanoscopic resolution is not required, optical microscopy techniques provide easy possibilities of lateral imaging of the surface under atmospheric conditions and in some cases also at an interface of the sample. In standard operation, lateral resolution is limited by the wavelength of light, which ranges typically from 300 nm to micrometers. With a tiny waveguide, the lateral resolution can be enhanced to some nanometers (SNOM). Interference techniques improve the sampling depth, and it is enhanced for instance with phase measurement interference microscopy to 0.5 nm. Fluorescence techniques can also reach nanoscopic resolution. Several microscopic techniques are available at different level of sophistication to be used for surface and interface characterization:

Light microscopy in reflection or transmission mode with dark field or differential interference contrast for lateral inhomogeneities, Brewster-angle, ellipsometric, or surface plasmon microscopy for thickness determination, phase measurement interference microscopy for surface topography with subnanometer height resolution, fluorescence microscopy with labeled molecules for distribution and movement of molecules also at nanoscale, IR, or Raman microscopy for lateral distribution and identification of molecules, as well as confocal laser scanning microscopy for lateral and depth sensitivity in sub-micrometer range. The resolution limit of fluorescence microscopy has recently been significantly reduced by specific techniques, which allow for instance measurements of cells and bio-objects at resolution in the nano-range.

4.13 Indentation, Adhesion, Mechanical Properties

A classical mechanical surface characterization is the hardness determination [3]. A hardness measurement is done by indenting a well-defined diamond stylus at a

certain load into the surface measuring the depth of the indent. The test was miniaturized for the investigation of thin layers and anisotropic materials (micro-hardness test). Here a small diamond stylus of well-defined geometry is used, and both indentation depth and indentation load are simultaneously recorded as function of time. From an analysis of the load-displacement data, both the hardness and the Young's modulus can be calculated. Hardness as well as stiffness images of a surface are obtained by scanning the surface. With appropriate tips nano-indentation experiments are performed with a scanning force microscope. The surface can be deformed elastically, and knowing the cantilever stiffness a stiffness image of the surface is obtained. However, quantitative stiffness values are difficult to obtain and the technique is usually used only in a qualitative way to obtain a stiffness contrast between components for lateral imaging.

This is similarly performed for friction and adhesion of the tip at the surface and corresponding images are obtained. Here the adhesion of the cantilever tip to the surface is determined, but also colloidal particles may be attached to the cantilever for example. Tests of adhesion of films deposited on a surface are essentially fracture tests. Adhesion of those films is most commonly measured by peel tests, but may also be determined from blister or double cantilever beam tests. Adhesion tests should be performed in view of the desired application, since values depend in most cases on the measurement technique used. This is similarly true for friction between two solid samples, which can be measured at macroscopic and microscopic level utilizing different techniques and local probes. One should keep in mind that mechanical properties at the surface and interface can be very different from the bulk, and a detailed understanding is still missing.

4.14 Inverse Gas Chromatography (IGC)

From a measurement of the adsorption of test gases (and vapors of liquids) at surface of a material one can get interesting information on surface activity, composition, and phase transitions. While gas chromatography is aiming at the characterization of the adsorbing gas, inverse gas chromatography is aiming at the characterization of the surface of the filler material, which can be a polymer powder or fiber. Specific gases ("probes") of known properties are utilized to determine the interaction behavior, to provide surface characteristics and functionality of the filler material. A commercial gas chromatographic apparatus can be used, and the method is relatively cheap and easy to apply.

As mentioned before, we cannot cover details of the surface and interface characterization techniques because of the wealth of techniques used. In addition, there is fast technical development in many areas and resolution depends largely on experimental conditions and samples, which have to be prepared in a dedicated way to achieve optimal resolution or contrast. The conclusions given above therefore have to be taken with care. One always should keep in mind that the choice of a suitable and optimal technique for a particular problem is of crucial importance and should consider aspects like sample preparation, necessary spatial and depth resolution, contrast generation, as well as environmental conditions needed.

5 Summary and Outlook

Polymer surfaces and interfaces are important for nearly all polymer materials and determine many properties. In this chapter a short outline of polymer surfaces at molecular scale is given with reference to special aspects of chain conformation and surface dynamics. In this respect, the surface tension as a fundamental property of a surface is discussed. Surface functionalization can change appearance of a material very significantly. In particular, the grafting of polymer brushes onto surfaces is described as a very versatile tool, where even responsive polymer brush surfaces can be obtained and wetting, adhesion, bio-functionality, catalytic activity and sensing ability controlled. From the theoretical side, the interface between polymers can be formulated on the basis of mean-field theory with introduction of an effective interaction parameter, which is related with interface width and fluctuations at the interface. Examples are polymer blends, copolymers as compatibilizers and composites, where interfaces play an essential role. Important for surface and interface characterization are dedicated techniques, which include scanning force and electron microscopy, photoelectron and IR/Raman spectroscopy as well as x-ray and neutron reflectometry or scattering techniques. For their efficient use, guidelines for resolution and typical information obtained are provided.

Polymer surfaces and interfaces and the functionalization in their vicinity are becoming more and more important with the development of more complex and nanoscale devices and materials. So requirements for functional coating are getting more and more challenging, and self-cleaning, multifunctional, responsive or adaptive coatings are desired. Similarly nanocomposites with dedicated properties require particular functionalization of the surface of the nanoparticles for good dispersion and interfacial adhesion. In microelectronics industry the design of nanoscopic thin and structured multilayer films provides a challenge to interfacial design concerning adhesion, wetting, roughness, electron transport and optical as well as mechanical properties of polymers used for the design and fabrication of the nano-electronic devices. This becomes even more demanding with the introduction of flexible devices, where typically a flexible polymer film is used as a support. So there are plenty of problems and questions connected with surfaces and interfaces in the design of future advanced devices and materials. They require a good fundamental understanding of surface and interface properties, which is only possible with highly advanced characterization techniques. So this area will also in the future be under constant development.

References

1. I. C. Sanchez (ed.), *Physics of Polymer Surfaces and Interfaces* (Butterworth-Heinemann, Boston, 1992)
2. R.A.L. Jones, *Polymers at Surfaces and Interfaces* (Cambridge University Press, Cambridge, 2008)

3. M. Stamm (ed.), *Polymer Surfaces and Interfaces: Characterization, Modification and Application* (Springer, Berlin/Heidelberg, 2008)
4. G.J. Fleer, *Polymers at Interfaces* (Springer, Berlin, 2013)
5. A. Karim, S. Kumar, *Polymer Surfaces Interfaces and Thin Films* (World Scientific, Singapore, 1999)
6. A.N. Netravali, *Interface/Interphase in Polymer Nanocomposites* (Wiley Academic, New Jersey, 2017)
7. S. Fakirov (ed.), *Nano-size Polymers* (Springer International, Cham, 2016)
8. S. Wu, *Polymer Interface and Adhesion* (Marcel Dekker, New York, 1982)
9. J.N. Israelachvili, *Intermolecular and Surface Forces* (Academic Press, London, 1991)
10. K. Binder, Theories and mechanism of phase transitions, heterophase polymerizations, homopolymerization, addition polymerization. *Adv. Pol. Sci.* **112**, 181 (1994)
11. F. Kremer, W. Richtering (eds.), Characterization of polymer surfaces and thin films. *Progr. Colloid Polym. Sci.* **132**, 1–171 (2006)
12. J.-U. Sommer, M. Stamm, in *Surface and Interface Science*, ed. by K. Wandelt, vol. 1–8 (Wiley, 2019)
13. I.V. Gerasimchuk, J.-U. Sommer, Mean-field treatment of polymer chains trapped between surfaces and penetrable interfaces. *Phys. Rev. E* **76**, 041803, 1–11 (2007)
14. M. Stamm, J.-U. Sommer, Polymer–nanoparticle films: Entropy and enthalpy at play. *Nat. Mater.* **6**, 260–261 (2007)
15. P.G. de Gennes, Polymer solutions near interfaces. 1. Adsorption and depletion layers. *Macromolecules* **14**, 1637 (1981)
16. R. Descas, J.-U. Sommer, A. Blumen, Static and dynamic properties of tethered chains at adsorbing surfaces: A Monte Carlo study. *J. Chem. Phys.* **120**(18), 8831–8840 (2004)
17. G.-L. He, R. Messina, H. Löwen, A. Kiriy, V. Bocharova, M. Stamm, Shear-induced stretching of adsorbed polymer chains. *Soft Matter* **5**, 3014–3017 (2009)
18. S. Minko, A. Kiriy, G. Gorodyska, M. Stamm, Single flexible hydrophobic polyelectrolyte molecules adsorbed on solid substrate: Transition between stretched chain, necklace-like conformation and globule. *J. Am. Chem. Soc.* **124**, 3218–3219 (2002)
19. J. Kraus, P. Müller-Buschbaum, T. Kuhlmann, D.W. Schubert, M. Stamm, Confinement effects on the chain conformation in thin polymer films. *Europhys. Lett.* **49**, 210 (2000). J. Kraus, PhD thesis, Mainz (1999)
20. S.T. Wu, G.H. Fredrickson, J.-P. Carton, A. Ajdari, L. Leibler, Distribution of chain ends at the surface of a polymer melt: Compensation effects and surface tension. *J. Polym. Sci. B* **33**, 2373–2389 (1995)
21. J. Baschnagel, K. Binder, On the influence of hard walls on structural properties in polymer glass simulation. *Macromolecules* **28**, 6808–6818 (1995)
22. A. Galuschko, M. Lang, T. Kreer, J.-U. Sommer, Monte Carlo simulation of thin film polymer melts. *Soft Mater.* **12**, 49–55 (2014)
23. L. Si, M.V. Massa, K. Dalnoki-Veress, H.R. Brown, R.A.L. Jones, Chain entanglement in thin freestanding polymer films. *PRL* **94**, 127801 (2005)
24. R.S. PaiPanandiker, J.R. Dorgan, T. Pakula, Static properties of homopolymer melts in confined geometries determined by Monte Carlo simulation. *Macromolecules* **30**, 6348–6352 (1997)
25. M. Doi, S.F. Edwards, *The Theory of Polymer Dynamics* (Clarendon Press, Oxford, 1986)
26. P. Müller-Buschbaum, M. Stamm, Correlated roughness, long-range correlations and dewetting of thin polymer films. *Macromolecules* **31**, 3686–3692 (1998)
27. N. Rehse, C. Wang, M. Hund, M. Geoghegan, R. Magerle, G. Krausch, Stability of thin polymer films on a corrugated substrate. *Europ. Phys. E* **4**, 69–76 (2001)
28. M. Vlatkov, J.-L. Barrat, Local dynamics and primitive path analysis for a model polymer melt near a surface. *Macromolecules* **40**, 3797–3804 (2007)
29. J.A. Forrest, K. Dalnoki-Veress, J.R. Stevens, J.R. Dutcher, Effect of free surfaces on the glass transition temperature of thin polymer films. *PRL* **77**, 2002 (1996)

30. M. Erber, M. Tress, E.U. Mapesa, A. Serghei, K.-J. Eichhorn, B. Voit, F. Kremer, Glassy dynamics and glass transition in thin polymer layers of PMMA deposited on different substrates. *Macromolecules* **43**, 7729–7733 (2010)
31. T. Kuhlmann, J. Kraus, P. Müller-Buschbaum, D.W. Schubert, M. Stamm, Effects of confined geometry and substrate interaction on the initial stages of interdiffusion in thin polymer films. *J. Non-Cryst. Solids* **235–237**, 457 (1998)
32. A.W. Adamson, A.P. Gast, *Physical Chemistry of Surfaces* (Wiley, New York, 1997)
33. M. Daoud, C.E. Williams, *Soft Matter Physics* (Springer, Berlin, 1999)
34. S. Minko, M. Müller, M. Motornov, M. Nitschke, K. Grundke, M. Stamm, Two-level structured self-adaptive surfaces with reversibly tunable properties. *J. Am. Chem. Soc.* **125**, 3896–3900 (2003)
35. M.A. Cohen Stuart, W.T.S. Huck, J. Genzer, M. Müller, C. Ober, M. Stamm, G.B. Sukhorukov, I. Szleifer, V.V. Tsukruk, M. Urban, F. Winnik, S. Zauscher, I. Luzinov, S. Minko, Emerging applications of stimuli-responsive polymer materials. *Nat. Mater.* **9**, 101–113 (2010)
36. M. Krishnamoorthy, S. Hakobyan, M. Ramstedt, J.E. Gautrot, Surface-initiated polymer brushes in the biomedical field: Applications in membrane science, biosensing, cell culture, regenerative medicine and antibacterial coatings. *Chem. Rev.* **114**, 10976–11026 (2014)
37. L. Wu, J. Baghdachi, *Functional Polymer Coatings: Principles, Methods, and Applications* (Wiley, New York, 2015)
38. J. Rühe, M. Ballauff, M. Biesalski, P. Dzięzok, F. Gröhn, D. Johannsmann, N. Houbenov, N. Hugenberg, R. Konradi, S. Minko, M. Motornov, R.R. Netz, M. Schmidt, C. Seidel, M. Stamm, T. Stephan, D. Usov, H. Zhang, Polyelectrolyte brushes. *Adv. Polym. Sci.: Chem. Mater. Sci.* **165**, 79–150 (2004)
39. P. Mocny, H.A. Klok, Tribology of surface-grafted polymer brushes. *Mol. Syst. Design Eng.* **1**, 141–154 (2016)
40. A. Bousquet, H. Awada, R.C. Hiorns, Conjugated-polymer grafting on inorganic and organic substrates: A new trend in organic electronic material. *Prog. Polym. Sci.* **39**, 1847–1877 (2014)
41. E. Psarra, E. Foster, U. König, J. You, Y. Ueda, K.-J. Eichhorn, M. Müller, M. Stamm, A. Revzin, P. Uhlmann, Growth factor-bearing polymer brushes-versatile bioactive substrates influencing cell response. *Biomacromolecules* **11**, 3530–3542 (2015)
42. R.C. Advincula, W.J. Britain, K.C. Caster, in *Polymer Brushes*, ed. by J. Rühe (Wiley-VCH, Weinheim, 2004)
43. P. Uhlmann, H. Merlitz, J.-U. Sommer, M. Stamm, Polymer brushes for surface tuning. *Macromol. Rapid Commun.* **30**, 732–740 (2009)
44. S. Alexander, Polymer adsorption on small spheres: A scaling approach. *J. Phys. (Paris)* **38**, 977–982 (1977).; P.G. de Gennes, Conformation of polymers attached to an interface. *Macromolecules*, **13**, 1069–1075 (1980)
45. A. Halperin, M. Tirrell, T.P. Lodge, Tethered chains in polymer microstructures. *Adv. Polym. Sci.* **100**, 31–71 (1992)
46. W.J. Brittain, S. Minko, A structural definition of polymer brushes. *J. Polym. Sci., Part A: Polym. Chem.* **45**, 3505–3512 (2007)
47. L. Ionov, N. Houbenov, A. Sidorenko, M. Stamm, Inverse and reversible switching gradient surfaces from mixed polyelectrolyte brushes. *Langmuir* **20**, 9916–9919 (2004)
48. P. Uhlmann, L. Ionov, N. Houbenov, M. Nitschke, K. Grundke, M. Motornov, S. Minko, M. Stamm, Surface functionalization by smart coatings: Stimuli-responsive binary polymer brushes. *Prog. Org. Coat.* **55**, 168–174 (2006)
49. L. Ionov, S. Sapra, A. Synytska, A.L. Rogaci, M. Stamm, S. Diez, Fast and spatially resolved environmental probing using stimuli-responsive polymer layers and fluorescent nanocrystals. *Adv. Mater.* **18**, 1453–1457 (2006)
50. M. König, D. Magerl, M. Philipp, K.-J. Eichhorn, M. Müller, P. Müller-Buschbaum, M. Stamm, P. Uhlmann, Nanocomposit coatings with stimuli-responsive catalytic activity. *RSC Adv.* **4**, 17579–17586 (2014)
51. M. Stamm, D.W. Schubert, Interfaces between incompatible polymers. *Annu. Rev. Mater. Sci.* **25**, 325 (1995)

52. M. Stamm, Polymer surfaces, interfaces and thin films studied by x-ray and neutron reflectometry, in *Scattering in Polymeric and Colloidal Systems*, ed. by W. Brown, K. Mortensen (Gordon and Breach, Amsterdam, 2000), p. 495
53. L. Leibler, Theory of phase equilibria in mixtures of copolymers and homopolymers. *Macromolecules* **15**, 1283–1290 (1982)
54. R. Schnell, M. Stamm, The self-organisation of diblock copolymers at polymer blend interfaces. *Phys. B* **234**, 247 (1997).; R. Schnell, M. Stamm, F. Rauch, Segregation of diblock copolymers to the interface between weakly incompatible polymers. *Macromol. Chem. Phys.* **200**, 1806–1812 (1999)
55. I.W. Hamley, *The Physics of Block Copolymers* (Oxford University Press, Oxford, 1998)
56. E.B. Gowd, M.S. Rama, M. Stamm, Nanostructures based on self-assembly of block copolymers, in *Nanofabrication: Techniques and Principles*, ed. by M. Stepanova, S. Dew (Springer, Berlin, 2012), pp. 191–216
57. B. Nandan, M. Stamm, Self-assembled polymer supramolecules as templates for nanomaterials, in *Supramolecular Chemistry: From Molecules to Nanomaterials*, ed. by J. W. Steed, P. A. Gale, vol. 7 (Wiley, Chichester, 2012), pp. 3563–3586
58. A. Horechyy, B. Nandan, N.E. Zafeiropoulos, P. Formanek, U. Oertel, N.C. Bigall, A. Eychmüller, M. Stamm, A step-wise approach for dual nanoparticle patterning via block copolymer self-assembly. *Adv. Funct. Mater.* **23**, 483–490 (2013)
59. A. Sidorenko, I. Tokarev, S. Minko, M. Stamm, Ordered reactive nanomembranes/nanotemplates from thin films of block copolymer thin films supramolecular assembly. *J. Am. Chem. Soc.* **125**, 12211–12216 (2003)
60. B. Nandan, E.B. Gowd, N.C. Bigall, A. Eychmüller, P. Formanek, P. Simon, M. Stamm, Arrays of inorganic nanodots and nanowires using nanotemplates based on switchable block copolymer supramolecular assemblies. *Adv. Funct. Mater.* **19**, 2805–2811 (2009)
61. S. Sanwaria, A. Horechyy, D. Wolf, C.-Y. Chu, H.-L. Chen, P. Formanek, M. Stamm, R. Srivastava, B. Nandan, Helical packing of nanoparticles confined in cylindrical domains of a self-assembled block copolymer structure. *Angew. Chem. Int. Ed.* **53**(1–5), 9090 (2014)
62. G.J. Vancso, H. Schönherr, *Scanning Force Microscopy of Polymers* (Springer, Berlin, 2016)
63. L. Sabbatini (ed.), *Polymer Surface Characterization* (de Gruyter, Berlin, 2014)
64. G.H. Michler, *Electron Microscopy of Polymers* (Springer, Berlin, 2010)
65. D. Briggs, *Surface Analysis of Polymers by XPS and Static SIMS* (Cambridge University Press, Cambridge, 2009)
66. K. Hinrichs, D. Aulich, L. Ionov, N. Esser, K.-J. Eichhorn, M. Motornov, M. Stamm, S. Minko, Chemical and structural changes in a pH-responsive mixed polyelectrolyte brush studied by infrared Ellipsometry. *Langmuir* **25**, 10987–10991 (2009)
67. D.S. Fryer, P.F. Nealey, J.J. Pablo, Thermal probe measurements of the glass transition temperature for ultrathin polymer films as a function of thickness. *Macromolecules* **33**, 6439–6447 (2000)
68. P. Truman, P. Uhlmann, M. Stamm, Monitoring liquid transport and chemical composition in lab on a chip systems using ion sensitive FET devices. *Lab Chip* **6**, 1220–1228 (2006)
69. S. Gupta, M. Agrawal, M. Conrad, N.A. Hutter, P. Olk, F. Simon, L.M. Eng, M. Stamm, R. Jordan, Poly(2-(dimethylamino)ethyl methacrylate) brushes with incorporated nanoparticles as a SERS active sensing layer. *Adv. Funct. Mater.* **20**, 1756–1761 (2010)



Membrane Surface Modification and Functionalization

10

Syed Mohammed Javid Zaidi, Kenneth A. Mauritz, and
Mohammad K. Hassan

Contents

1	Polyethylene Glycol Grafting Strategy	392
2	Plasma-Induced Surface Treatment	395
3	UV-Induced Surface Treatment	397
4	Zwitterionic Polymer Grafting Strategy	399
5	Layer-by-Layer Technique	402
6	Chemical Vapor Deposition Technique	406
7	Oxidative Stability of Surface Modification and Practical Aspects	407
8	Conclusions and Future Prospective	411
	References	412

Abstract

Surface functionalization of membranes is one of the efficient techniques that can bestow these membranes with novel properties and transform them into valuable finished products. It has been widely applied to polymeric membranes in many fields and has progressed rapidly in recent years. The modified membranes have been widely used in various applications, such as in separation processes for liquid and gaseous mixtures (gas separation, reverse osmosis, pervaporation, nanofiltration, ultrafiltration, microfiltration), biomaterials, catalysis (including fuel cell systems), and “smart” membranes. In this chapter, various approaches to the surface modification and functionalization of polymeric membranes are highlighted and reviewed. Also, the applications of the modified membranes

S. M. J. Zaidi (✉) · M. K. Hassan
Center for Advanced Materials, Qatar University, Doha, Qatar
e-mail: szaidi@qu.edu.qa; mohamed.hassan@qu.edu.qa

K. A. Mauritz
School of Polymers and High Performance Materials, The University of Southern Mississippi,
Hattiesburg, MI, USA
e-mail: Kenneth.Mauritz@usm.edu

will be discussed from the aspect of environmental stimuli-responsive gating membranes, antifouling membranes, adsorption membranes, pervaporation and reverse osmosis membranes, membranes for energy conversion, gas separation membranes, and biomedical membranes. A detailed overview of the usage of polyzwitterions and oxidative stability of surface modifiers to alter membrane surface charge will be outlined. Finally, recent advances and developments in surface modification techniques such as layer-by-layer assembly and chemical vapor deposition will be discussed.

Surface modification of membranes allows better performance and even to implement new functionality. Modifications render better performance in liquid and gaseous mixtures separation (gas separation, reverse osmosis, pervaporation, nanofiltration, ultrafiltration, microfiltration), biomaterials, stimuli-responsive gating, and energy conversion systems.

Membranes for water separation and purification are among the materials that widely use surface treatment due to the fouling phenomena. Fouling in this case originates from microbial growth on membrane surface followed by the production of extracellular polymeric secretions (EPS) containing proteins, glycoproteins, lipoproteins, polysaccharides, and other biomacromolecules [1]. Foulants are typically adsorbed to the membrane surface via hydrophobic interaction, van der Waals attraction, hydrogen bonding, Lewis acid-base interaction, and electrostatic repulsion. Many strategies have been used to exclude or reduce membrane fouling including surface hydrophilicity enhancement, surface roughness reduction, and to alter membrane surface charge [1–6]. Hydrophilic surface modifiers are highly permeable thin-film coating such as crosslinked poly(ethylene glycol) (PEG) [7–10] or grafted chains of PEG brushes [11, 12] or zwitterionic polymers [13, 14].

This chapter presents an overview of the most common strategies and methods used for surface modifications of the membranes in order to eliminate fouling or attain new function and better performance. Also, a detailed overview of the usage of polyzwitterions to alter membrane surface charge will be outlined. Finally, we will cover some of the recent advances in surface coating modification techniques such as layer-by-layer and chemical vapor deposition. Our specific focus on water desalination and cleaning membranes modifications arises from their technological importance as well as abundance in the literature.

1 Polyethylene Glycol Grafting Strategy

Surface grafting and surface segregation are two leading methods for antifouling membrane fabrication. Surface grafting is one of the most commonly used methods to mitigate issues like fouling or to introduce additional functionality to the membrane. Grafting typically happens through one of the two widely used strategies “grafting from” or “grafting to” (Fig. 1) [15]. In the “grafting from” method, active functional groups that exist on the membrane surface are used to initiate

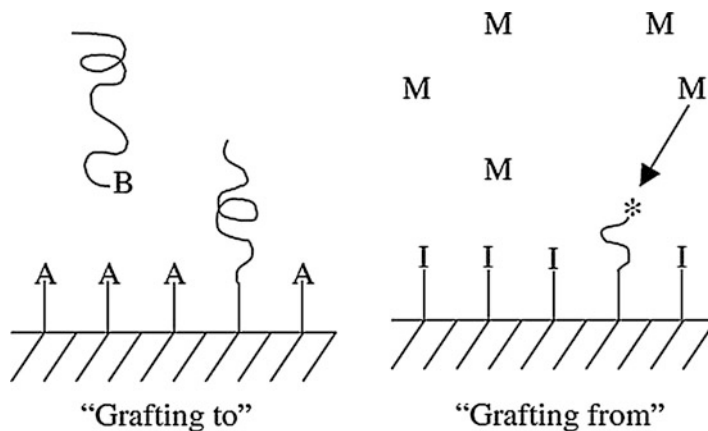


Fig. 1 Surface modification methods using the “grafting from” and “grafting to” approaches. (Figure from [15], with kind permission of Elsevier)

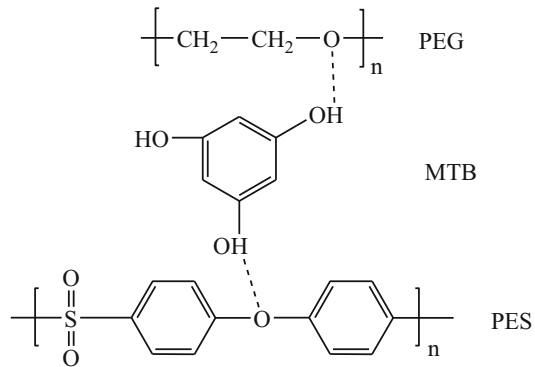
polymerization of monomers from the surface. While in the “grafting to,” polymers carrying reactive groups at their chain ends or on a chain are covalently linked to the membrane surface [16]. Grafting to method became more competent with the recent development of various “click” chemistries. However, the grafting from is proven to be more flexible and useful as a big range of grafting densities and chain lengths can be realized [17]. Overall, grafting has a big advantage over other ways of surface modification as it includes covalent attachment of polymer chains on membrane surface, thus preserving the long-term chemical stability of the modified surface [2].

Polyethylene glycol (PEG) is one of the most widespread modifiers for surface grafting and segregation. Due to its hydrophilicity, neutral charge, and high hydration capacity via hydrogen bonding with water, PEG can help membrane to greatly resist non-specific adhesion of protein and other natural organic materials [1].

Fan et al. used PEG as a surface modifier and pore-forming agent for polyethersulfone (PES) membrane matrix and in the presence of *m*-trihydroxybenzene (MTB) as a hydrogen bond donor [18]. As a common pore-forming agent [19] and during the non-solvent-induced phase separation (NIPS) process, PEG can migrate from the hydrophobic PES membrane matrix to the coagulation bath due to its solubility in water. Therefore, PEG will postpone the solidification of the membrane matrix and promotes fully developed macropores besides its role as hydrophilic surface modifier. Furthermore, MTB mediates the hydrogen bonding interaction between PES and PEG to manipulate the surface segregation behavior of PEG (Fig. 2) [18]. The antifouling performance of PES/PEG-MTB membranes was ominously improved as indicated by the increase in flux recovery ratio from 74.3% to 98.4% and the residence stability of PEG on membrane surface [18].

Furthermore, Liu et al. revealed that using an amphiphilic modifier, consisted of crosslinked hydrophobic melamine formaldehyde (MF) backbone and hydrophilic polyethylene oxide (PEO), helped to reduce the thermodynamic stability of the

Fig. 2 MTB role in forming hydrogen bonding interaction between PES and PEG. (Figure from [18], with kind permission of Elsevier)



casting solution and resulted in PES membranes with high porosity during the NIPS process [20]. Crosslinked hydrophobic MF segments were more compatible with the hydrophobic PES matrix and introduced large diffusion hindrance, due to entanglements with PES chains, which would decrease loss of the amphiphilic modifier during operation. The membranes showed durable antifouling properties after three cycles of ultrafiltration experiment, and the FRR values of the three cycles were bigger than 95% (Fig. 3) [20].

Polydopamine (PDA) represents another attractive strategy for membrane surface hydrophilization and even better when grafted with poly(ethylene glycol) monoamine (PEG-NH₂). It can be easily deposited on almost all types of surfaces from buffered, aqueous dopamine solution under, and it greatly influences hydrophilicity, charge, and surface roughness of the substrate [21–29]. Moreover, simplicity and non-specificity of the PDA deposition process enable improved fouling resistance and enhanced recovery of commercial membrane modules via filling feed side of the module with buffered dopamine solution [30].

Many researchers reported improved fouling performance for different membranes modified with polydopamine, polydopamine-g-poly(ethylene glycol), and polydopamine-g-polyvinyl alcohol. Modified membranes exhibit good mechanical stability, better chemical stability for the grafted layer under acidic and alkaline conditions, and improved antifouling ability [31–34]. In addition, PDA deposition highlighted the importance of applying modifications to membranes with bigger pores than targeted, as surface treatment will effectually reduce the membrane pore size [31]. Figure 4 shows the fouling behavior of modified and unmodified polysulfone ultrafiltration membranes, under constant permeate flux and with a 1500 ppm soybean oil emulsion feed. This operational mode maintains fixed permeate flux while the transmembrane pressure (TMP) increases with time to overcome membrane fouling. It is identical the industrial membrane purification systems which operate at constant permeate flux to guarantee a steady rate of clean water for a particular membrane area [31]. All membranes exhibit similar initial permeances; however, this trend did not last for long as the PDA- and PDA-g-PEG-modified membranes eventually showed lesser TMP comparing to that of the unmodified PS-10 membrane. This result demonstrated the fouling alleviation of the PDA and

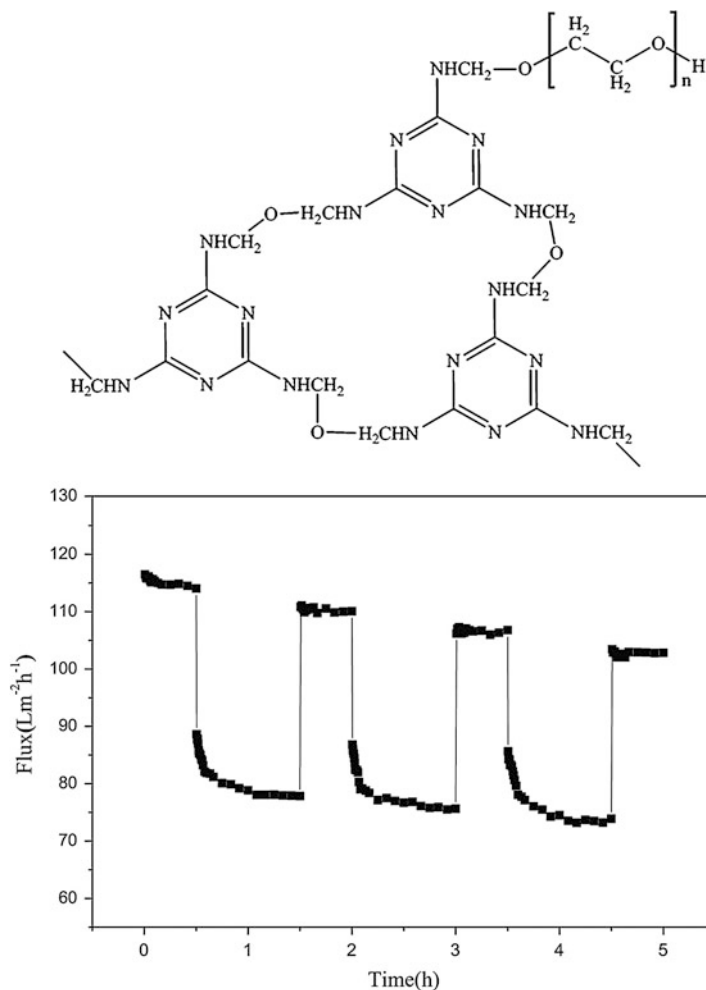


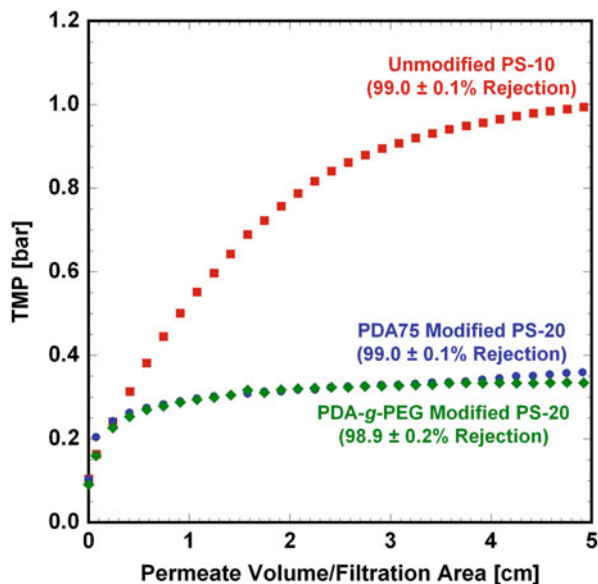
Fig. 3 Chemical structure of the amphiphilic modifier (MF-g-PEG_n) (left) and time-dependent flux of PES/MF-g-PEG2000 (0.36 wt %) in the three cycles of ultrafiltration operation (right). (Figure from [20], with kind permission of Elsevier)

PDA-g-PEG coatings and also the effectiveness of the strategy of using membranes with larger pores to avoid blockage due to surface modifications.

2 Plasma-Induced Surface Treatment

Plasma-induced grafting is a fast, safe, and low cost method that attracted more attention from researchers to modify the membrane surface [35–37]. Ju et al. used low-pressure plasma source, with a radio frequency of 13.56 MHz, to induce surface

Fig. 4 Constant flux fouling of modified and unmodified polysulfone membranes exposed to a 1500 ppm soybean oil emulsion feed. The membranes had a pure water permeance of 570 LMH/bar and fouling performed at 55 LMH. Feed pressure, 2.1 barg, and crossflow velocity, 0.18 m/s. (Figure from [31], with kind permission of Elsevier)



grafting of poly(vinylidene fluoride) (PVDF) membrane with poly(ethylene glycol) diacrylate (PEGDA) [38]. FTIR spectra of the grafted samples revealed the presence of O–C=O absorption from PEGDA and indicate that growth of grafted PEGDA polymer is linked to the increase in the PEGDA monomer concentration. Scanning electron microscopy (SEM) images of samples' cross-section show a uniform microporous structure that consists of spherical particles having roughly the same size. Contact angle of the PEGDA-treated membranes dropped from about 110° to 0° for all the PEGDA monomer concentration used. This instantaneous drop was thought to be due to occupying the PVDF porous rough surface with hydrophilic PEGDA chains, according to the Wenzel model [39]. Moreover, the tensile strength of the PVDF membrane improved after PEGDA modification. The PVDF-g-PEGDA membranes showed high separation efficiency and high fluxes, under ultralow pressure, for different oil-in-water emulsions including colza oil, lubricating oil, and soybean oil (Fig. 5) [38].

Wu et al. also reported grafting of crosslinked collagen on porous PVDF membrane with the aid of low-temperature plasma treatment [40]. Glutaraldehyde was used as a crosslinker for the collagen coated on the membrane surface. This crosslinker has the advantages of high reaction activity with protein, stability of crosslinking points, and the ability to keep the molecular structure of protein chains in space. Glutaraldehyde concentration, crosslinking time, and temperatures were shown to have a great impact on membrane contact angle and pure water flux. Permeability and adsorption capacity of bovine serum albumin as well as cell culture ability of the membrane indicated that they possess good hydrophilicity and biocompatibility [39].

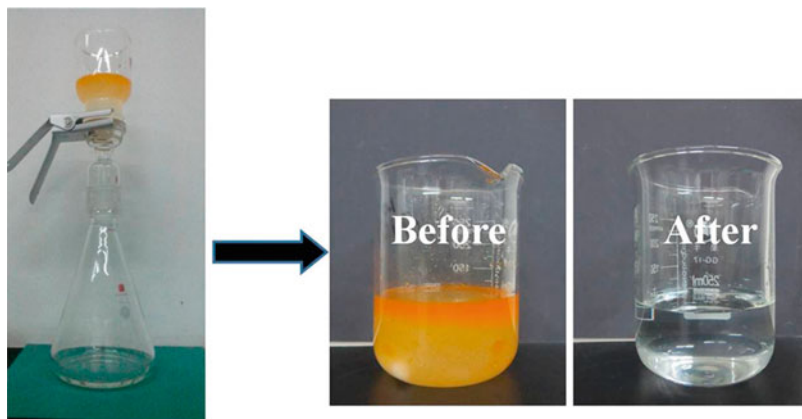


Fig. 5 Images of the lubricating oil-water emulsion (10%, w/w) separation process from PVDF-g-PEGDA-20 membrane. (Figure from [38], with kind permission of Elsevier)

3 UV-Induced Surface Treatment

Graft polymerization induced by UV irradiation is a commonly used surface treatment method due to its high efficiency, low operation cost, simplicity, and distribution of grafted chains near the surface without damaging the bulk polymer [41, 42]. Pan et al. used UV light and benzophenone photoinitiator to graft the hydrophobic polypropylene (PP) surface with acrylic acid [42]. The photoinitiator typically abstracts the active tertiary hydrogen in polypropylene to forming surface radicals which react with the monomer to form acrylic acid chains on the surface. Thin-film composite (TFC) membrane was then formed on the hydrophilic PP surface through interfacial polymerization of piperazine (PIP) and trimesoyl chloride (TMC) monomers [42]. Membranes' separation performance experiments were conducted with methyl orange and fast green (FCF) solutions in the feed. Membrane rejection to both TFC and methyl orange increased, while the flux decreased with increasing the acrylic graft degree (GD). Rejection of FCF solution was higher than that of the methyl orange, while its permeation flux was lower comparing to the methyl orange solution, due to difference in molecular weights of the organic solutes, (Fig. 6a, b). Increasing the GD caused the polyacrylic surface layer to become denser, as indicated by the SEM pictures of Fig. 7, therefore increasing membrane rejection to FCF and methyl orange from the feed solution [41].

Wang et al. highlighted the importance of having membranes with both hydrophilic and antibacterial characteristics in order to reduce biofouling [43]. In their work, UV photo-grafting method proved very effective in introducing both capsaicin derivative (N-(4-hydroxy-3-methoxy-benzyl)-acrylamide, HMBA) and itaconic acid (IA) to the polyethersulfone (PES) membrane surface, in a single reaction step as shown in Fig. 8 [43]. Organic antibacterial compounds, like capsaicin, chitosan, halamine, polycations, and graphene oxide, can be covalently attached to the membrane surface to avoid the drawbacks of the inorganic antibacterial modifiers

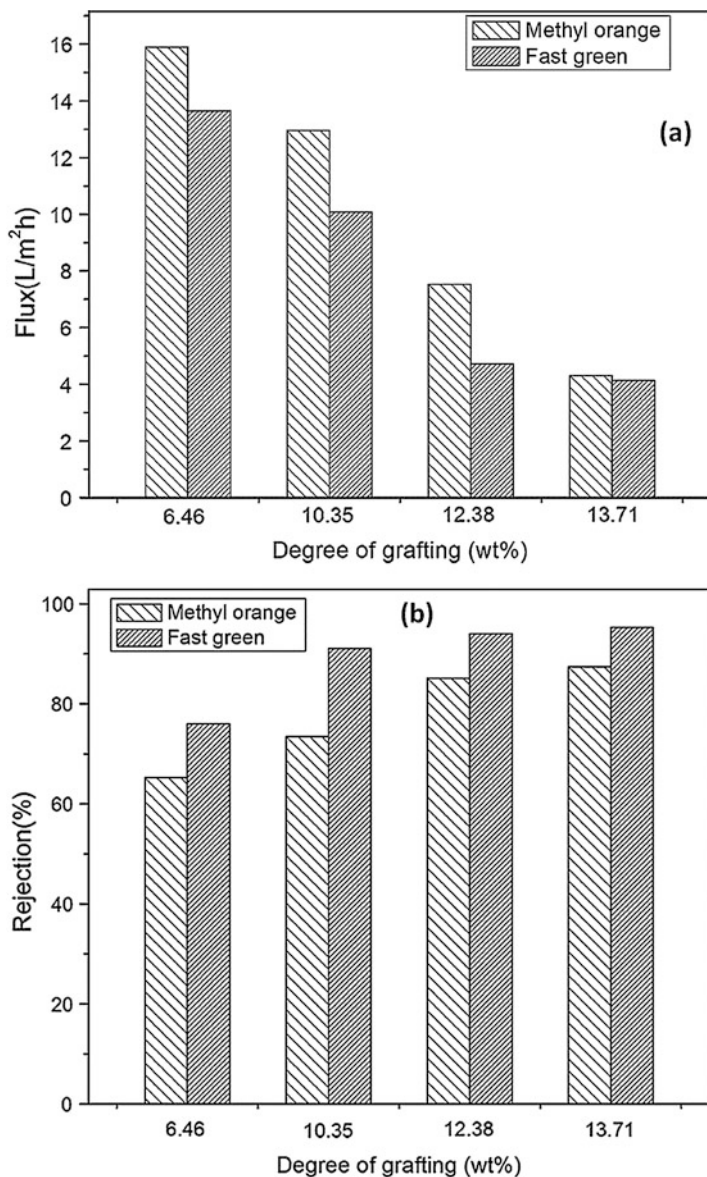


Fig. 6 Separation performance of the TFC membranes with FCF and methyl orange solutions in the feed, showing (a) flux and (b) rejection. (Figure from [42], with kind permission of Springer)

[42, 44, 45]. These drawbacks include inevitable release of inorganic modifier metal ions into feed solution and shorten the lifetime of the antibacterial material [46].

Results showed that grafting of HMBA and IA on PES membrane surface caused significant reduction for the membrane permeability due to the decrease in

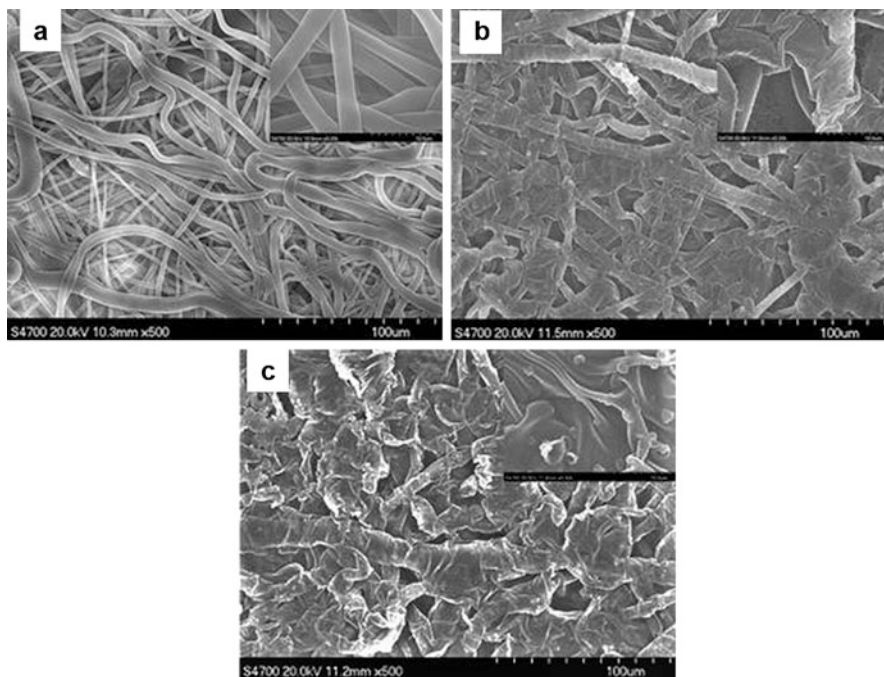


Fig. 7 SEM pictures of neat polypropylene TFC membrane (a) and the membrane after grafting degrees of (b) 6.46 and (c) 13.71 wt%, respectively. (Figure from [42], with kind permission of Springer)

membrane pore size; however, BSA rejection rate increased from 90.1% to 96.4% (Fig. 9a) [43]. Meanwhile, pristine PES showed a massive drop of about 77% for the water flux during 150 min of operation in the presence of significantly high BSA concentration of 1.0 g/L in the feed. Drop of water flux for the modified membranes under the same condition ranged from 7.7% to 42.7% depending on the molar concentration of IA in the grafting solution (Fig. 9b) [43]. Antibacterial activity of the membranes increased considerably with increased UV irradiation time with a slight drop as IA concentration increases. This slight degradation in antibacterial activity was ascribed to dilution of the HMBA density on membrane surface with addition of the IA monomer and thought to be acceptable considering improvements of the antifouling performance of the membranes [43].

4 Zwitterionic Polymer Grafting Strategy

Polyzwitterions (PZs) are antifouling polymer chains, having positively and negatively charged functional groups, which received rising attention due to their great hydration ability and outstanding anti-protein and bacterial adhesion characteristics [47, 48]. Unlike PEG chains, localized charges on PZ chains bind strongly to H₂O

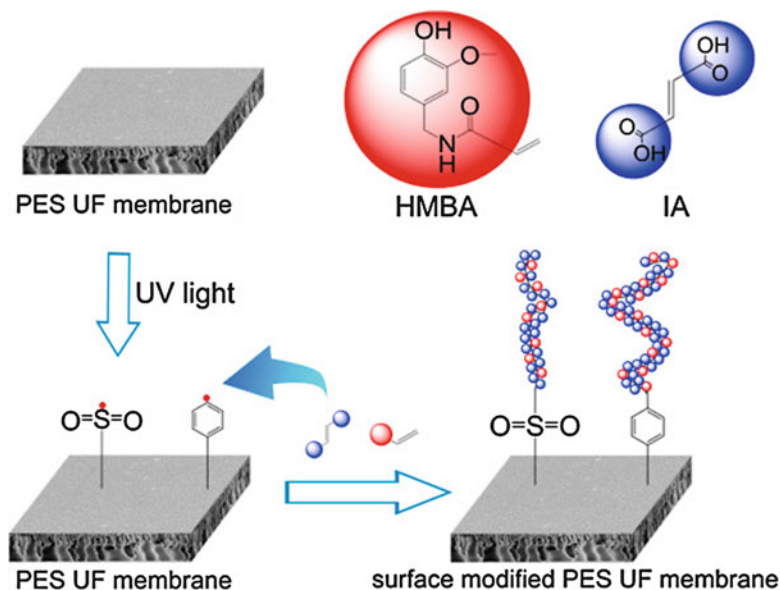


Fig. 8 Schematic diagram of the UV surface modification procedure. (Figure from [43], with kind permission of Elsevier)

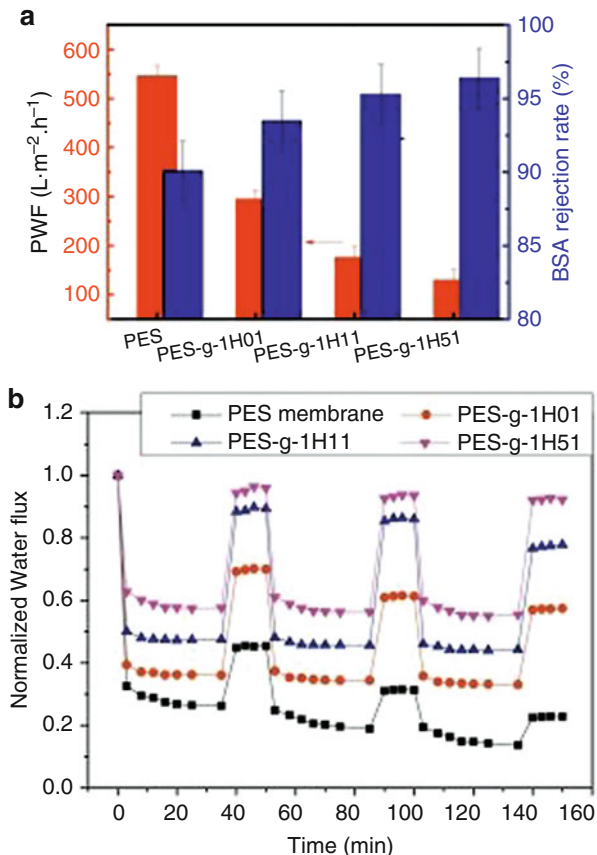
molecules forming electrostatically induced hydration layer, which physically swell the polymer and inhibit protein or bacteria attachment to its surface [49, 50]. Poly (sulfobetaine methacrylate) (polySBMA) is a common PZ, and it was utilized to modify the surfaces of membranes for hemocompatible medical devices and reverse osmosis [51, 52].

The “grafting from” approach was used to grow polysulfobetaine brushes on polyamide membranes coated with polydopamine for reverse osmosis desalination, as shown in Scheme 1 [48]. This approach generated PZ chains of narrow molecular weight distribution at relatively mild polymerization condition and enabled higher polymer densities on membrane surface comparing to the “grafting to” method [47, 53, 54].

The hydrophilic, zwitterionic coating on membrane surface increased water flux by 17% over that of the unmodified polyamide commercial membrane and without significant loss of the salt rejection performance. Meanwhile, the modified membranes displayed considerable suppression of protein and bacterial adhesion of 69% and 88%, respectively, compared to untreated membrane as shown in Fig. 10. Strong repulsive force of polysulfobetaine brushes, to the hydrophobic protein and bacteria, arises from the anionic sulfate and cationic quaternary ammonium groups that form a hydration layer through electrostatic interaction as well as hydrogen bonding [47].

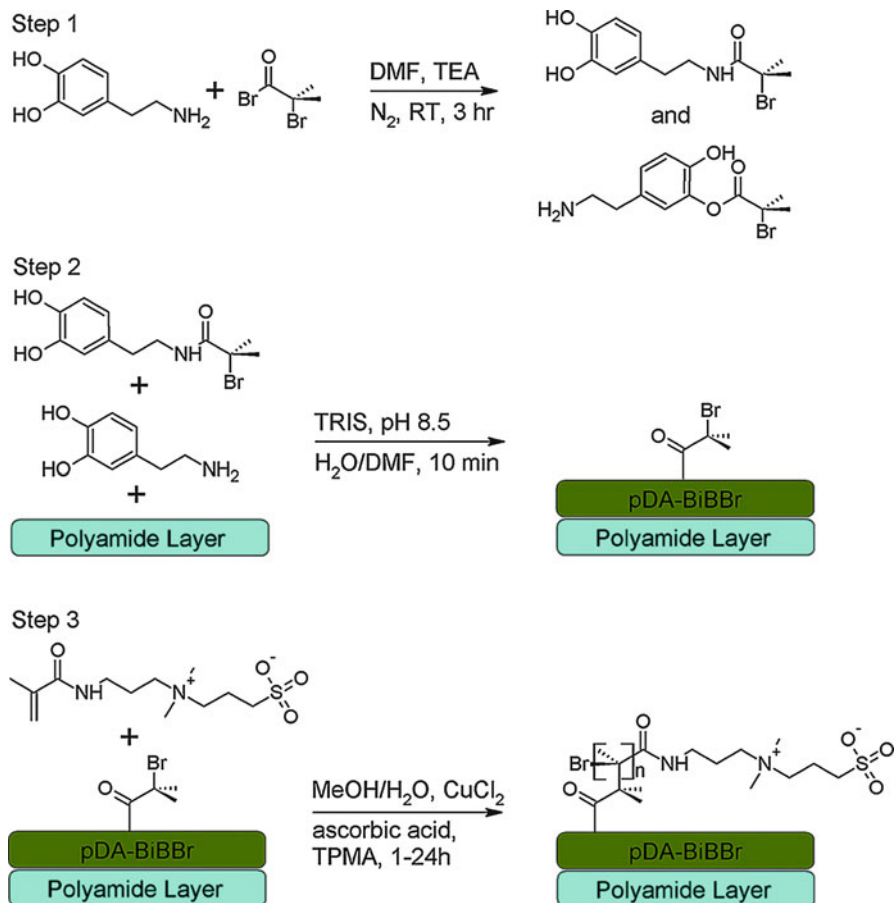
Yu et al. introduced a novel approach to graft alkyne-terminated polyzwitterions onto polyamide (PA) surface using click chemistry in two-step reaction. First, they introduced azide functional group onto polyamide using S_N2 nucleophilic

Fig. 9 (a) Pure water flux and BSA rejection rate for neat and modified membranes under fixed applied pressure of 0.1 MPa, BSA solution concentration of 1.0 g dissolved in 1 L of phosphate buffer (pH = 7.4). (b) Normalized water flux for the same set of samples operated with three cycles of BSA in the feed solution. Samples marked as PES-g-mHnI, where m:n is the molar ratio of HMBA and IA, respectively. (Figure from [43], with kind permission of Elsevier)



substitution on nitrogen atom, a reaction that was facilitated by the adjacent electron-withdrawing C=O and benzene groups. Then, the alkyne groups of PZ were grafted to azide groups of polyamide via an azide-alkyne cycloaddition click reaction as shown in Fig. 11 [55]. In this context, click chemistry offers the benefits of greater site selectivity, almost quantitative conversion under mild conditions, no side reactions or by-products, and stable aromatic triazole ring that makes grafted chains strongly attached to the substrate [56–59].

Forward osmosis mode testing of the membranes indicated that neither the flux nor the NaCl rejection was significantly affected by PZ grafting. Fouling experiments were conducted using humic acid as model foulant. The flux declines significantly for neat polyamide membranes, while the PZ-grafted showed negligible decline after addition of the foulant (Fig. 12a) [55]. To check for fouling reversibility, all membranes were cleaned using 20 mM NaCl cleaning solution after the fouling experiments. After cleaning, water flux of unmodified polyamide showed only $\cong 77\%$ of its original flux, while grafted membranes reserved its original flux before fouling (Fig. 12b) [55]. These excellent antifouling characteristics of surface



Scheme 1 Steps of the “grafting from” approach to grow polysulfobetaine brushes on polyamide membrane surface coated with PDA. (Scheme from [48], with kind permission of the Royal Society of Chemistry)

modified membranes were attributed to combined influences of reduced specific binding, strong hydrophilic repulsion, and steric repulsions of the long flexible PZ chains as illustrated in Fig. 12c [55].

5 Layer-by-Layer Technique

Layer-by-layer (LbL) technique has been used as an effective surface modification method for membranes used in desalination of brackish and seawater, reclamation of wastewater, and membrane bioreactors (MBR) [60–63]. Gao et al. employed a LbL

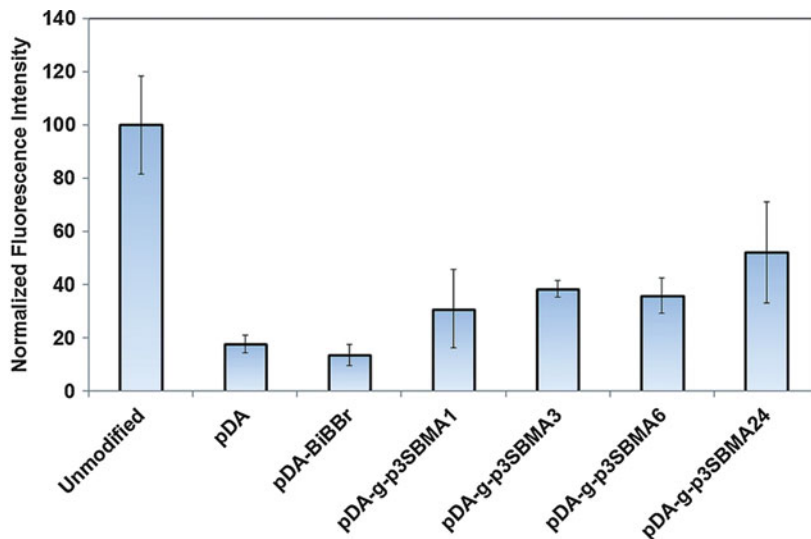


Fig. 10 Normalized fluorescence intensity of surface modified and unmodified polyamide membranes, showing the extent of bovine serum albumin adherence to membrane surface. Values normalized to fluorescence of the untreated PAM, which was given an intensity of 100. Error bars are standard deviation over three replicates. (Figure from [48], with kind permission of the Royal Society of Chemistry)

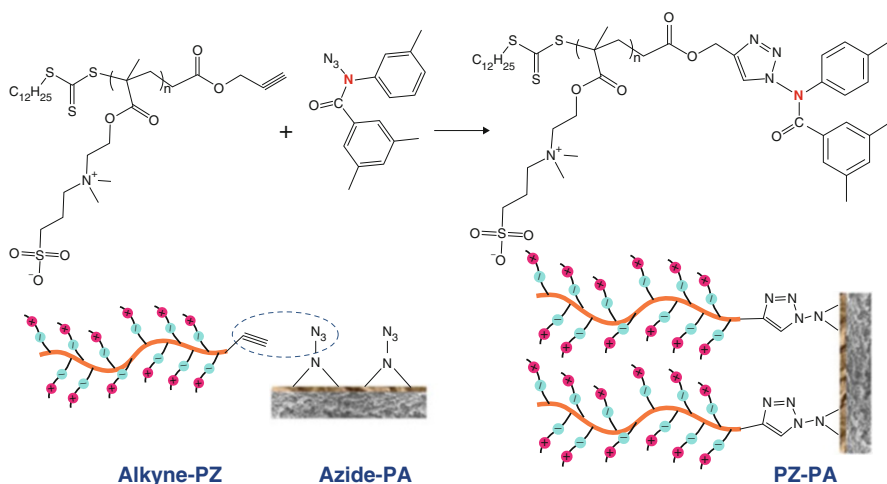


Fig. 11 Cycloaddition click reaction between alkyne-PZ and the azide-polyamide (PA) membrane. (Figure from [55], with kind permission of Elsevier)

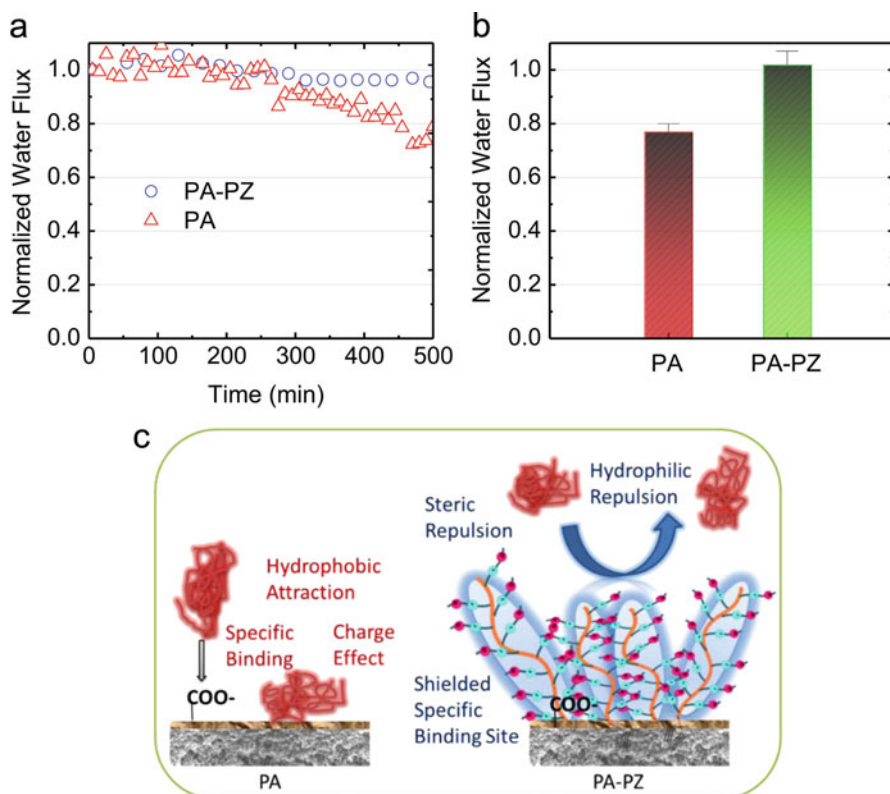


Fig. 12 Performance of grafted PA-PZ comparing to unmodified PA membranes in a forward osmosis system with (a) humic acid fouling experiments and (b) extent of flux recovery after membrane cleaning. The flux data are normalized by the membrane flux prior to the fouling experiments. (c) Schematic diagram of the antifouling characteristics of the PZ-grafted membrane. (Figure from [55], with kind permission of Elsevier)

method to consecutively deposit TiO_2 nanoparticles and GO nanosheets on a commercial porous ultrafiltration polysulfone membrane, followed by partial reduction of GO via ethanol-UV treatment as shown in Fig. 13 [60]. TiO_2 is a very common photocatalyst for decomposing organic pollutants in water to CO_2 and water [64]. Its superior efficacy originates from its high removal efficiency, effective cost, chemical stability, and low toxicity [65]. Combining effective photocatalysts with membrane porosity could ominously improve the separation performance if the catalyst can effectively work in the UV and visible light regions [66]. However, TiO_2 has low photoactivity in visible sunlight due to high band-gap energy (3.2 eV) which requires UV light for the activation of its electron-hole pairs [67]. GO has the ability to expand TiO_2 efficiency to the visible region due to its electron-transferring character and therefore can greatly

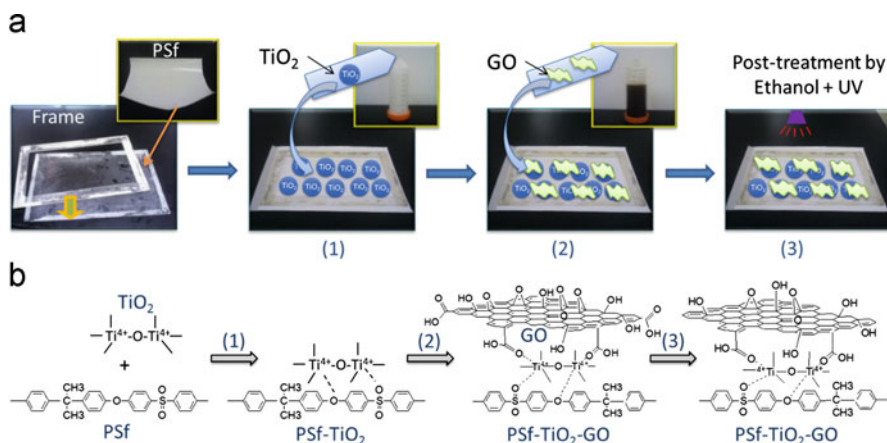


Fig. 13 Illustration (a) and reaction schemes (b) involved in the layer-by-layer method to modify surface of porous polysulfone membrane with the TiO_2 -GO photocatalyst. (Figure from [60], with kind permission of Elsevier)

increase the lifetime of electron-hole pairs [68–72]. In addition, GO's large surface area ($2630 \text{ m}^2/\text{g}$) establishes closer and longer contact between organic pollutant and the photocatalyst [73].

The photocatalytic activity of the membranes in removing methylene blue (MB) is presented in Fig. 14, where C and C_0 are MB concentrations during and at the beginning of the filtration experiment, respectively. Unmodified PSf membrane did not show any photocatalytic activity under dark, UV, or sunlight (Fig. 14a). Coating a single layer of TiO_2 or GO on the PSf membrane did not show more than 10% removal of MB in dark. Under UV light, both TiO_2 and GO are more photocatalytically active than under sunlight as both have a semiconductor character and seem to have similar band-gap energy (Fig. 14b, c). The TiO_2 -GO double layer exhibits highly improved and similar photocatalytic performance in presence of either UV or sunlight irradiation (Fig. 14d). That performance was also much better than a single layer of each photocatalyst under same irradiation. Incorporating TiO_2 with GO decreased the band-gap energy for each semiconductor so that lower energy sunlight irradiation was capable of activating more electrons in the semiconductors and led to improved photocatalytic activities [60]. In addition, ethanol-UV treatment of the TiO_2 -GO membrane further improved the MB degradation kinetics as such treatment partially reduced GO and enhanced the ability of GO to conduct more electrons from TiO_2 nanoparticles. Besides, the TiO_2 -GO-grafted membrane showed enhanced flux increased under UV due to photo-enhanced hydrophilicity and MB degradation. Therefore, surface grafting of TiO_2 -GO provides a very encouraging route to fabricate high-performance photocatalytic PSf membranes for viable water treatment technology [60].

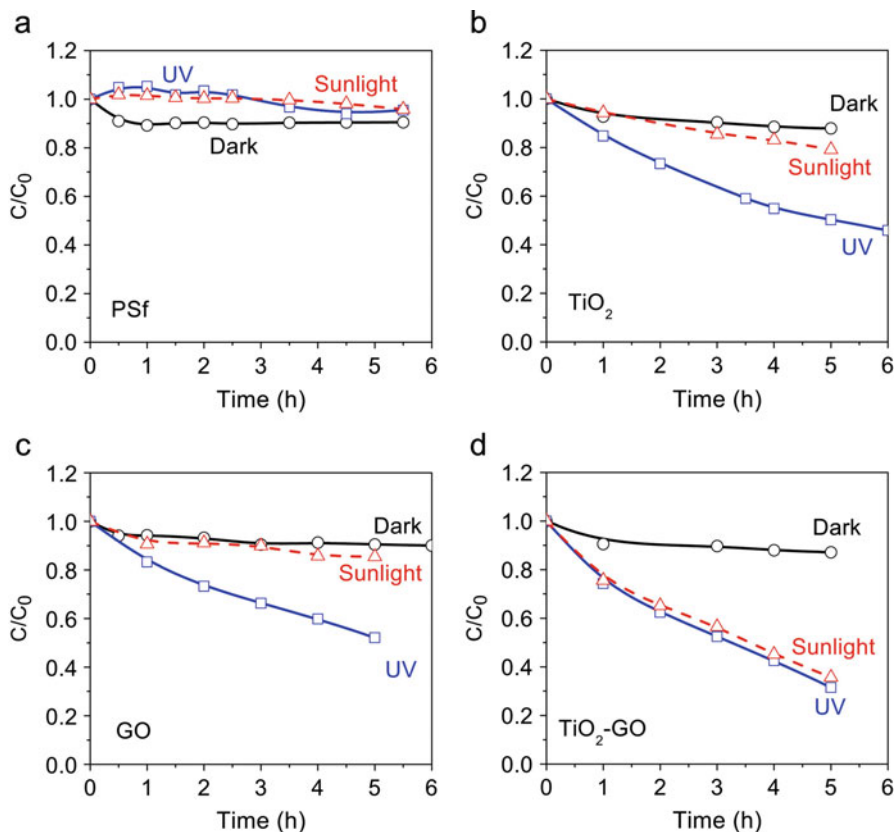


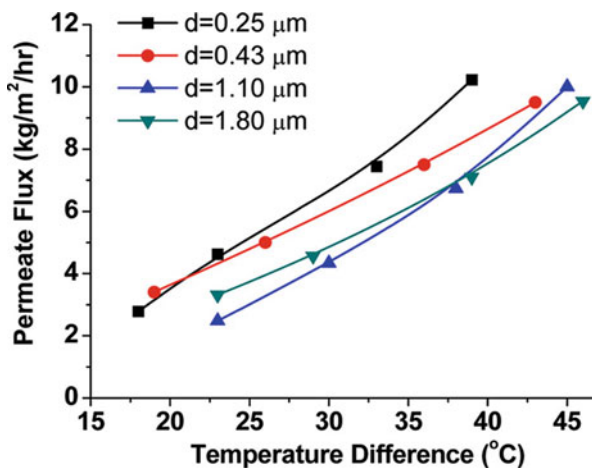
Fig. 14 Methylene blue removal by virgin polysulfone (a) and the membrane after surface modification with (b) TiO_2 , (c) GO, and (d) TiO_2 -GO, respectively. (Figure from [60], with kind permission of Elsevier)

6 Chemical Vapor Deposition Technique

Initiated chemical vapor deposition (iCVD) is a solvent-free method in which thin-film deposition of various polymers occurs on virtually any substrate. Monomers volatilization, their combination to form long chain polymers, and film deposition happen concurrently at modest vacuum and low temperature. Distinctive features of the iCVD technique include long-term stability, conformality, full functional retention, scalability, and ability to control thickness at the nanometer level [74–76].

Electrospun fibrous poly(trimethyl hexamethylene terephthalamide) (PA6(3)T) membrane surface rendered hydrophobic by depositing poly(1H,1H,2H,2H-perfluorodecyl acrylate) (PPFDA) using the iCVD technique [77]. Membrane

Fig. 15 MD performance showing the permeate flux for the PA6(3)T surface-treated fiber membranes with different fiber diameters. (Figure from [77], with kind permission of the American Chemical Society Publications)



distillation (MD) performance revealed that decreasing fiber diameter increased the liquid entry pressure and permeate flux (Fig. 15). This trend was linked to variations in tortuosity rather than difference in membrane thickness or porosity. Porosity typically decreases as fiber diameter decreases and membranes had negligible variation in their thickness. However, this study reported increased curling of the electrospun mats with smaller fiber diameter reflecting high levels of tortuosity. In addition, surface diffusion could also help to enhance flux as smaller diameter for the fiber means high specific surface area [77].

Zaidi et al. copolymerized and deposited hydrophilic hydroxyethyl methacrylate (HEMA) and hydrophobic perfluorodecyl acrylate (PFDA) on commercial RO membranes using the iCVD technique [76, 78]. The iCVD has a unique feature of controlling deposited amphiphilic poly(HEMA-co-PFA) film in a real time, which was then confirmed by SEM as depicted in Fig. 16 [78]. Bacterial adhesion tests showed great reduction in cell attachment on coated membranes comparing to that of the bare membranes (Fig. 17) [76]. The membrane having amphiphilic character (with 40% PFDA) gave the highest resistance to bacterial attachment, which indicates the importance of compositional heterogeneity of amphiphilic chain in rejecting the foulants. Meanwhile, water permeation flux decreased with increasing the PFA content, while the coating chemistry did not affect the NaCl solution salt rejection [78].

7 Oxidative Stability of Surface Modification and Practical Aspects

Oxidative stability of the coat or grafted polymer chains and brushes is crucial for membrane performance over long term. Water treatment and separation environments are very complicated and highly corrosive as it contains harsh

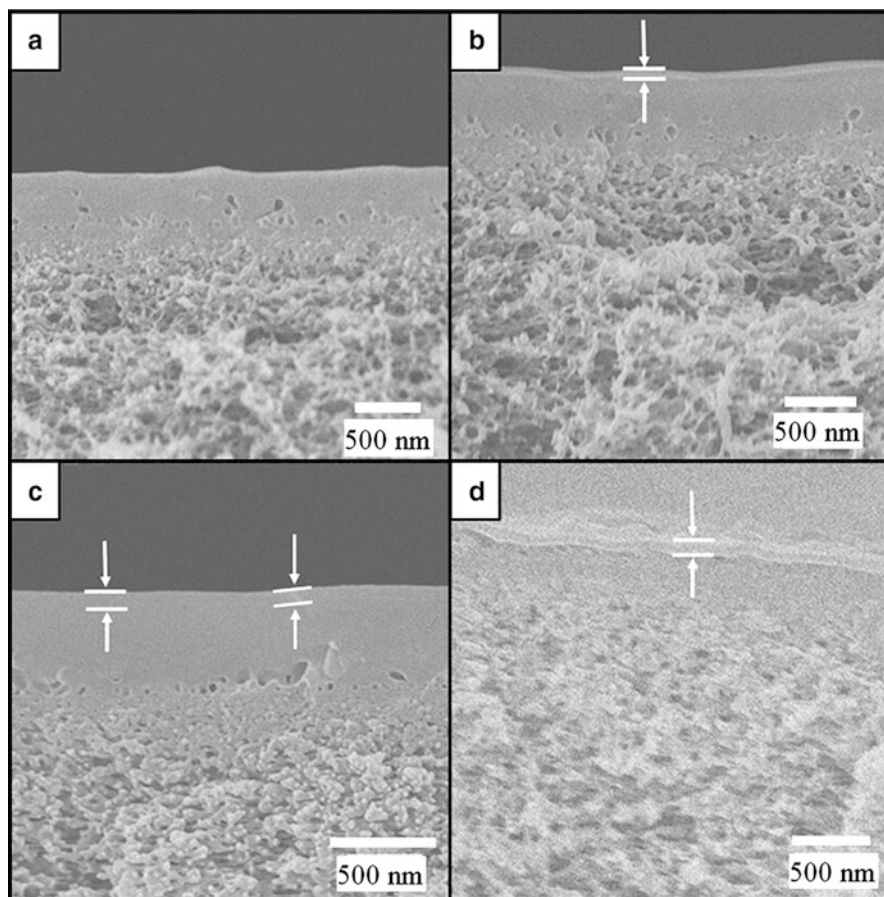
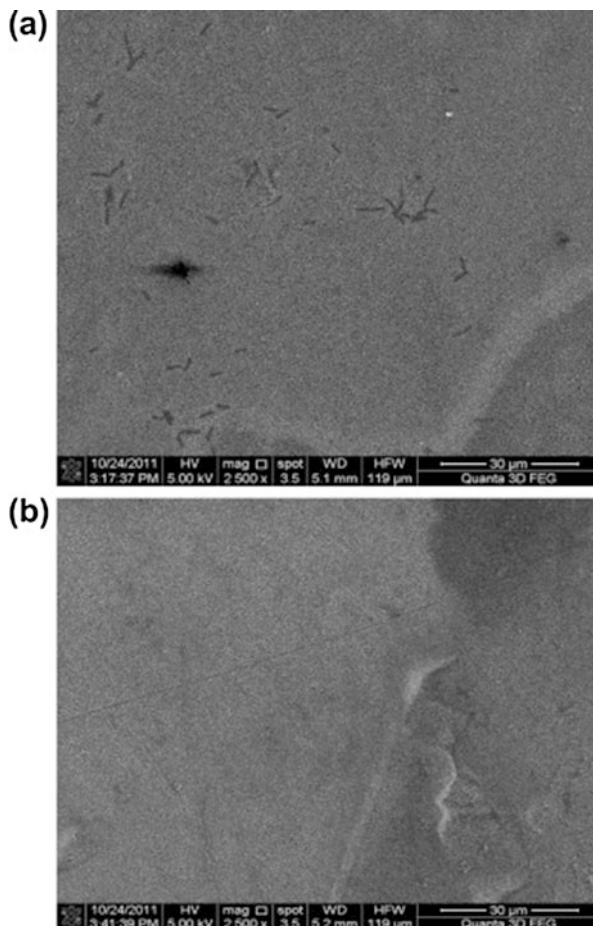


Fig. 16 Cross-section SEM images of unmodified membrane (a) and the membranes after surface treatment with poly(HEMA-co-PFA) films containing 40% of PFA comonomer. Deposited film thickness was measured to be (b) 48 ± 5 , (c) 70 ± 5 , and (d) 96 ± 3 nm, respectively. (Figure from [78], with kind permission of Elsevier)

chemicals like seawater especially at high temperatures. In addition, oxidative solutions like NaClO and $\text{H}_2\text{O}_2/\text{Cu}^{+2}$ are periodically used to clean fouled membranes. Although the chemical and oxidative stabilities are very important aspects for extended membrane lifetime, only few researchers reported such studies [79–82].

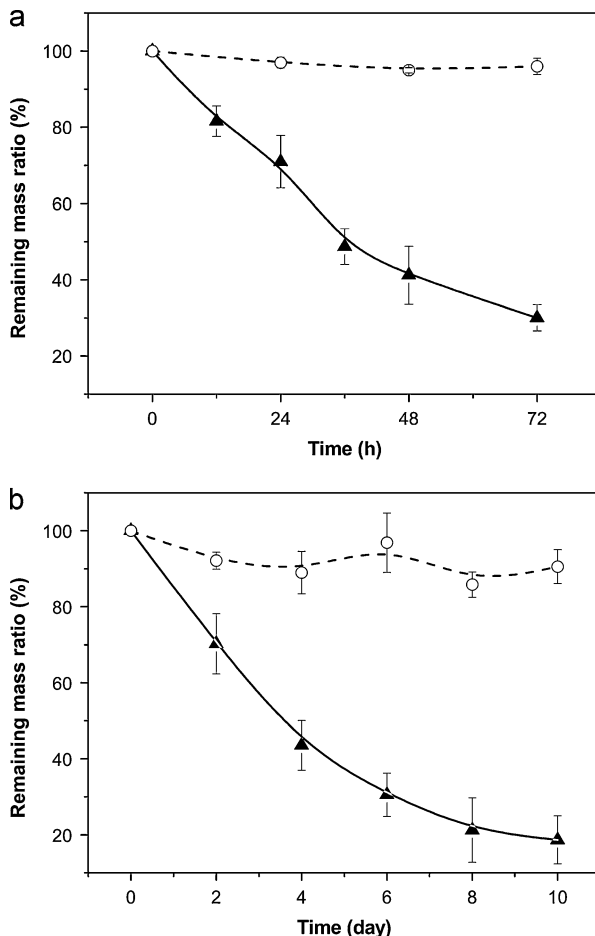
In an effort to understand the oxidative stability of some common surface modifiers, Ren et al. conducted a very interesting study on a UV-induced surface-grafted polypropylene microfiltration membrane (PPMM). They used two typical surface modifiers with good antifouling capability, poly(sulfobetaine

Fig. 17 SEM picture of bacterial colonies on surface of unmodified (a) and the surface after modification with the amphiphilic poly (hydroxyethylmethacrylate-co-perfluorodecylacrylate) (b) using the iCVD technique. (Figure from [76], with kind permission of Elsevier)



methacrylate) (polySBMA) and poly[oligo(ethylene glycol) methyl ether methacrylate] (polyOEGMA) [81]. Modified membranes were immersed in NaClO and $\text{H}_2\text{O}_2/\text{Cu}^{+2}$ oxidants solutions, and their stability was evaluated via monitoring change in remaining mass of graft polymer over extended time periods (Fig. 18). Surprisingly, polySBMA-grafted membranes lost their grafting mass more quickly than the polyOEGMA-grafted ones. PEG chains were in fact reported to be more susceptible to oxidative degradation in the studied solutions. Meanwhile, there was no apparent change in the polySBMA-grafted membrane morphology although it lost about 70% of grafted polymer mass [81]. The authors used the time-of-flight secondary ion mass spectroscopy (TOF-SIMS) to understand the mechanism of the rapid oxidation of the polySBMA chains. Results suggest that hydroperoxide and hydroxyl radicals formed in the Cu^{2+} catalyzed H_2O_2 solution are responsible for the attacks on the polySBMA chains

Fig. 18 Remaining mass ratios of polyOEGMA- (hollow circle) and polySBMA-grafted (solid triangle) PPMs after oxidation in (a) 0.1 mM Cu^{2+} with 0.01 mM H_2O_2 and (b) 6.7 mM NaClO solutions. (Figure from [81], with kind permission of Elsevier)



(Fig. 19). They could cause complete detachment of the grafted chain via ester linkage hydrolysis and also breaking the C-N bonds resulting in elimination of the quaternary amine group [81, 83]. Electrophilic character of the quaternary ammonium group was also thought to accelerate the radical attack and resulted in rapid oxidative loss of polySBMA [81]. Introduction of amide group in the polysulfobetaine chain, instead of the ester bond, made it more stable to NaClO solution [82].

Another aspect of practical importance is to simplify and scalability of the modification processes. Zhou et al. reported a simple one-step co-deposition of dopamine and PSBMA on the surface of microporous polypropylene membranes. Dynamic protein filtration tests confirmed the excellent antifouling property of the modified membranes [84].

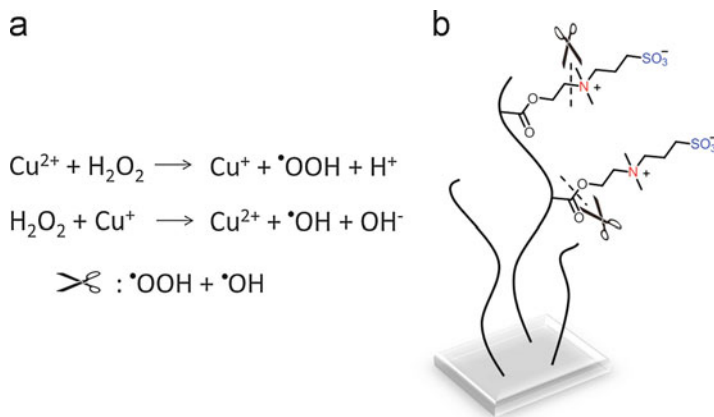


Fig. 19 Hydroxyperoxide and hydroxyl radicals formation in the $\text{Cu}^{2+}/\text{H}_2\text{O}_2$ solution (a) and (b) mechanism of oxidative degradation polySBMA chains on membranes. (Figure from [81], with kind permission of Elsevier)

8 Conclusions and Future Prospective

Surface modification has been used as an effective method to modify the surface of the membranes to tailor it for a specific application. One of the most important surface modification purposes is to protect the membrane from direct exposure to harsh environment such as chlorine or oxidants content in water, foulants, and pH of the water at which the membrane life will be shortened. This technique has been found very effective in reducing the fouling of the membranes in water desalination and treatment, which is a major problem facing the industry today. Among various techniques, such as grafting, plasma treatment, UV treatment, zwitterionic coating on membrane surface, layer-by-layer (LbL) assembly and chemical vapor deposition (CVD), and plasma CVD, are getting more popular as an effective method to fabricate the membranes especially for water treatment and energy applications. They have the better control of the thickness of the surface layer at the nanoscale and are more stable. Moreover, the nanoparticles and various macromolecules can be incorporated into the membrane surfaces. Relatively new technologies, LbL assembly and plasma CVD, offer flexibility and great control over the film properties, which are key to overcome problems, associated with other surface modification techniques. Recently, graphene oxide (GO), a single sheet functionalized graphene with oxygen-rich functional group, has attracted attention from researchers in the field of water treatment. This material provides fast water transport, hydrophilicity, as well as excellent chemical stability.

One of the advantages of these relatively new techniques, LbL assembly and CVD, that has not been thoroughly observed was the flexibility and applicability of

this technique to create ultrathin film from various materials. To the best of our knowledge, most of the works are still focused on polyelectrolyte. Although some people have started introducing nanomaterial such as silver nanoparticles, graphene oxide, and clay, but still there is a gap available to do research in terms of membrane material modification. There were many polymers that have never been investigated because no appropriate technology was applicable to prepare ultrathin film using those polymers; now there is an opportunity to advance the research using these recent techniques. Using LbL assembly, one can create the film either from the polymer itself or from the monomers. One can also combine organic and inorganic material with nano-level control easily to fabricate highly resistant membrane toward chlorine and foulants at the same time giving high flux and high rejection or selectivity, for instance. Tailoring the film properties is one of the strengths and advantages of LbL assembly and CVD that has not been thoroughly investigated yet.

Acknowledgments The authors would like to acknowledge the support of the Center for Advanced Materials (CAM), Qatar University, for this work.

References

1. N. Misdan, A.F. Ismail, N. Hilal, Recent advances in the development of (bio)fouling resistant thin film composite membranes for desalination. *Desalination* **380**, 105–111 (2016)
2. W. Sun, J. Liu, H. Chu, B. Dong, Pretreatment and membrane hydrophilic modification to reduce membrane fouling. *Membranes (Basel, Switzerland)* **3**(3), 226–241 (2013)
3. V. Kochkodan, N. Hilal, A comprehensive review on surface modified polymer membranes for biofouling mitigation. *Desalination* **356**, 187–207 (2015)
4. J. Mueller, Y. Cen, R.H. Davis, Crossflow microfiltration of oily water. *J. Membr. Sci.* **129**(2), 221–235 (1997)
5. D. Rana, T. Matsuura, Surface modifications for antifouling membranes. *Chem. Rev.* **110**(4), 2448–2471 (2010)
6. M. Elimelech, W.A. Phillip, The future of seawater desalination: energy, technology, and the environment. *Science* **333**(6043), 712–717 (2011)
7. H. Ju, B.D. McCloskey, A.C. Sagle, V.A. Kusuma, B.D. Freeman, Preparation and characterization of crosslinked poly(ethylene glycol) diacrylate hydrogels as fouling-resistant membrane coating materials. *J. Membr. Sci.* **330**(1–2), 180–188 (2009)
8. A.C. Sagle, H. Ju, B.D. Freeman, M.M. Sharma, PEG-based hydrogel membrane coatings. *Polymer* **50**(3), 756–766 (2009)
9. H. Ju, B.D. McCloskey, A.C. Sagle, Y.-H. Wu, V.A. Kusuma, B.D. Freeman, Crosslinked poly(ethylene oxide) fouling resistant coating materials for oil/water separation. *J. Membr. Sci.* **307**(2), 260–267 (2008)
10. A.C. Sagle, E.M. Van Wagner, H. Ju, B.D. McCloskey, B.D. Freeman, M.M. Sharma, PEG-coated reverse osmosis membranes: desalination properties and fouling resistance. *J. Membr. Sci.* **340**(1–2), 92–108 (2009)
11. A. Roosjen, H.J. Kaper, H.C. van der Mei, W. Norde, H.J. Busscher, Inhibition of adhesion of yeast sand bacteria by poly(ethylene oxide)-brushes on glass in a parallel plate flow chamber. *Microbiology* **149**(11), 3239–3246 (2003)
12. M. Ulbricht, H. Matuschewski, A. Oechel, H.-G. Hicke, Photo-induced graft polymerization surface modifications for the preparation of hydrophilic and low-protein adsorbing ultrafiltration membranes. *J. Membr. Sci.* **115**(1), 31–47 (1996)

13. Y.-H. Zhao, K.-H. Wee, R. Bai, Highly hydrophilic and low-protein fouling polypropylene membrane prepared by surface modification with sulfobetaine-based zwitterionic polymer through a combined surface polymerization method. *J. Membr. Sci.* **362**(1–2), 326–333 (2010)
14. S. Jiang, Z. Cao, Ultra low-fouling, functionalizable, and hydrolysable zwitterionic materials and their derivatives for biological applications. *Adv. Mater.* **22**(9), 920–932 (2010)
15. B. Zhao, W.J. Brittain, Polymer brushes: surface-immobilized macromolecules. *Prog. Polym. Sci.* **25**, 677–710 (2000)
16. Z.-K. Xu, X.-J. Huang, L.-S. Wan, in *Advanced Topics in Science and Technology in China: Surface Engineering of Polymer Membranes*, Chapter 4 (Springer, Berlin, 2009), pp. 80
17. K. Kato, E. Uchida, E.T. Kang, Y. Uyama, Y. Ikada, Polymer surface with graft chains. *Prog. Polym. Sci.* **28**, 209–259 (2003)
18. X. Fan, Y. Su, X. Zhao, Y. Li, R. Zhang, T. Ma, Y. Liu, Z. Jiang, Manipulating the segregation behavior of polyethylene glycol by hydrogen bonding interaction to endow ultrafiltration membranes with enhanced antifouling performance. *J. Membr. Sci.* **499**, 56–64 (2016)
19. W. Zhao, Y. Su, C. Li, Q. Shi, X. Ning, Z. Jiang, Fabrication of antifouling polyethersulfone ultrafiltration membranes using Pluronic F127 as both surface modifier and pore forming agent. *J. Membr. Sci.* **318**, 405–412 (2008)
20. Y. Liu, Y. Su, X. Zhao, Y. Li, R. Zhang, Z. Jiang, Improved antifouling properties of polyethersulfone membrane by blending the amphiphilic surface modifier with crosslinked hydrophobic segments. *J. Membr. Sci.* **486**, 195–206 (2015)
21. H. Lee, S.M. Dellatore, W.M. Miller, P.B. Messersmith, Mussel-inspired surface chemistry for multifunctional coatings. *Science* **318**(5849), 426–430 (2007)
22. B.D. McCloskey, H.B. Park, H. Ju, B.W. Rowe, D.J. Miller, B.D. Freeman, A bioinspired fouling-resistant surface modification for water purification membranes. *J. Membr. Sci.* **413–414**, 82–90 (2012)
23. J.T. Arena, B. McCloskey, B.D. Freeman, J.R. McCutcheon, Surface modification of thin film composite membrane support layers with polydopamine: enabling use of reverse osmosis membranes in pressure retarded osmosis. *J. Membr. Sci.* **375**(1–2), 55–62 (2011)
24. H. Lee, Y. Lee, A.R. Statz, J. Rho, T.G. Park, P.B. Messersmith, Substrate-independent layer-by-layer assembly by using mussel-adhesive-inspired polymers. *Adv. Mater.* **20**(9), 1619–1623 (2008)
25. G. Han, S. Zhang, X. Li, N. Widjojo, T.-S. Chung, Thin film composite forward osmosis membranes based on polydopamine modified polysulfone substrates with enhancements in both water flux and salt rejection. *Chem. Eng. Sci.* **80**, 219–231 (2012)
26. J.-H. Jiang, L.-P. Zhu, X.-L. Li, Y.-Y. Xu, B.-K. Zhu, Surface modification of PE porous membranes based on the strong adhesion of polydopamine and covalent immobilization of heparin. *J. Membr. Sci.* **364**(1–2), 194–202 (2010)
27. J. Jiang, L. Zhu, L. Zhu, B. Zhu, Y. Xu, Surface characteristics of a self-polymerized dopamine coating deposited on hydrophobic polymer films. *Langmuir* **27**(23), 14180–14187 (2011)
28. Q. Wei, F. Zhang, J. Li, B. Li, C. Zhao, Oxidant-induced dopamine polymerization for multifunctional coatings. *Polym. Chem.* **1**(9), 1430–1433 (2010)
29. Z.-Y. Xi, Y.-Y. Xu, L.-P. Zhu, Y. Wang, B.-K. Zhu, A facile method of surface modification for hydrophobic polymer membranes based on the adhesive behavior of poly(DOPA) and poly(dopamine). *J. Membr. Sci.* **327**(1–2), 244–253 (2009)
30. D.J. Miller, X. Huang, H. Li, S. Kasemset, A. Lee, D. Agnihotri, T. Hayes, D.R. Paul, B.-D. Freeman, Fouling-resistant membranes for the treatment of flowback water from hydraulic shale fracturing: a pilot study. *J. Membr. Sci.* **437**, 265–275 (2013)
31. D.J. Miller, S. Kasemset, L. Wang, D.R. Paul, B.D. Freeman, Constant flux crossflow filtration evaluation of surface-modified fouling-resistant membranes. *J. Membr. Sci.* **452**, 171–183 (2014)
32. F. Li, J. Meng, J. Ye, B. Yang, Q. Tian, C. Deng, Surface modification of PES ultrafiltration membrane by polydopamine coating and poly(ethylene glycol) grafting: morphology, stability, and anti-fouling. *Desalination* **344**, 422–430 (2014)

33. F. Li, C. Deng, C. Du, B. Yang, Q. Tian, Fouling mechanism and cleanability of ultrafiltration membranes modified with polydopamine-graft-PEG. *Water SA* **41**(4), 448–456 (2015)
34. F. Li, J. Ye, L. Yang, C. Deng, Q. Tian, B. Yang, Surface modification of ultrafiltration membranes by grafting glycine-functionalized PVA based on polydopamine coatings. *Appl. Surf. Sci.* **345**, 301–309 (2015)
35. T. Vladkova, P. Atanasova, S. Petrov, P. Dineff, Surface modification of polymeric ultrafiltration membranes: III. Effect of plasma-chemical surface modification onto some characteristics of polyacrylonitrile ultrafiltration membranes. *High Energy Chem.* **47**(6), 346–352 (2013)
36. G. Chen, Z. Wang, L.D. Nghiem, X.-M. Li, M. Xie, B. Zhao, M. Zhang, J. Song, T. He, Treatment of shale gas drilling flow back fluids (SGDFs) by forward osmosis: membrane fouling and mitigation. *Desalination* **366**, 113–120 (2015)
37. G. Zuo, R. Wang, Novel membrane surface modification to enhance anti-oil fouling property for membrane distillation application. *J. Membr. Sci.* **447**, 26–35 (2013)
38. J. Ju, T. Wang, Q. Wang, Superhydrophilic and underwater superoleophobic PVDF membranes via plasma-induced surface PEGDA for effective separation of oil-in-water emulsions. *Colloids Surf. A: Physicochem. Eng. Asp.* **481**, 151–157 (2015)
39. R.N. Wenzel, Resistance of solid surfaces to wetting by water. *Ind. Eng. Chem.* **28**, 988–994 (1936)
40. L. Wu, J. Sun, F. Tong, Surface modification of a PVDF membrane by crosslinked collagen. *RSC Adv.* **4**(109), 63989–63996 (2014)
41. L. Zhi, Z. Wei, W. Xinwei, Surface modification of ultra high molecular weight polyethylene fibers via the sequential photoinduced graft polymerization. *Appl. Surf. Sci.* **257**, 7600–7608 (2011)
42. K. Pan, H. Gu, B. Cao, Interfacially polymerized thin-film composite membrane on UV-induced surface hydrophilic-modified polypropylene support for nanofiltration. *Polymer Bull. (Heidelberg, Germany)* **71**(2), 415–431 (2014)
43. J. Wang, X. Gao, Q. Wang, H. Sun, X. Wang, C. Gao, Enhanced biofouling resistance of polyethersulfone membrane surface modified with capsaicin derivative and itaconic acid. *Appl. Surf. Sci.* **356**, 467–474 (2015)
44. H. Yu, X. Zhang, Y. Zhang, J. Liu, H. Zhang, Development of a hydrophilic PES ultrafiltration membrane containing SiO₂@N-Halamine nanoparticles with both organic antifouling and antibacterial properties. *Desalination* **326**, 69–76 (2013)
45. D. Alves, M. Olivia Pereira, Mini-review: antimicrobial peptides and enzymes as promising candidates to functionalize biomaterial surfaces. *Biofouling* **30**, 1–17 (2014)
46. X. Gao, H. Wang, J. Wang, X. Huang, C. Gao, Surface-modified PSf UF membrane by UV-assisted graft polymerization of capsaicin derivative moiety for fouling and bacterial resistance. *J. Membr. Sci.* **445**, 146–155 (2013)
47. R.E. Holmlin, X. Chen, R.G. Chapman, S. Takayama, G.M. Whitesides, Zwitterionic SAMs that resist nonspecific adsorption of protein from aqueous buffer. *Langmuir* **17**, 2841–2850 (2001)
48. M. Ginic-Markovic, T. Barclay, K.T. Constantopoulos, T. Al-Ghamdi, A. Blok, E. Markovic, A.V. Ellis, A versatile approach to grafting biofouling resistant coatings from polymeric membrane surfaces using an adhesive macroinitiator. *RSC Adv.* **5**(77), 63017–63024 (2015)
49. I. Eshet, V. Freger, R. Kasher, M. Herzberg, J. Lei, M. Ulbricht, Chemical and physical factors in design of antibiofouling polymer coatings. *Biomacromolecules* **12**, 2681–2685 (2011)
50. M.Y. Zhou, H.W. Liu, J.E. Kilduff, R. Langer, D.G. Anderson, G. Belfort, High-throughput membrane surface modification to control NOM fouling. *Environ. Sci. Technol.* **43**, 3865–3871 (2009)
51. M.-C. Sin, S.-H. Chen, Y. Chang, Hemocompatibility of zwitterionic interfaces and membranes, IMP example for biomedical applications, discuss factors below. *Polymer J. (Tokyo, Japan)* **46**(8), 436–443 (2014)
52. R. Bernstein, V. Freger, J.-H. Lee, Y.-G. Kim, J. Lee, M. Herzberg, ‘Should I stay or should I go?’ Bacterial attachment vs biofilm formation on surface-modified membranes “methods to investigate biofouling activity”. *Biofouling* **30**(3), 367–376 (2014)

53. K. Matyjaszewski, H. Dong, W. Jakubowski, J. Pietrasik, Grafting from surfaces for “every-one”: ARGET ATRP in the presence of air. *Langmuir* **23**, 4528–4531 (2007)
54. T. Gillich, E.M. Benetti, E. Rakhmatullina, R. Konradi, W. Li, A. Zhang, A.D. Schlüter, M. Textor, Self-assembly of focal point oligo-catechol ethylene glycol dendrons on titanium oxide surfaces: adsorption kinetics, surface characterization, and nonfouling properties. *J. Am. Chem. Soc.* **133**, 10940–10950 (2011)
55. H.-Y. Yu, Y. Kang, Y. Liu, B. Mi, Grafting polyzwitterions onto polyamide by click chemistry and nucleophilic substitution on nitrogen: a novel approach to enhance membrane fouling resistance. *J. Membr. Sci.* **449**, 50–57 (2014)
56. R. Ranjan, W.J. Brittain, Combination of living radical polymerization and click chemistry for surface modification. *Macromolecules* **40**, 6217–6223 (2007)
57. J.F. Lutz, H.G. Börner, K. Weichenhan, Combining atom transfer radical polymerization and click chemistry: a versatile method for the preparation of end-functional polymers. *Macromol. Rapid Commun.* **26**, 514–518 (2005)
58. D.X. Wu, X.H. Song, T. Tang, H.Y. Zhao, Macromolecular brushes synthesized by grafting from approach based on click chemistry and RAFT polymerization. *J. Polym. Sci. Part A Polym. Chem.* **48**, 443–453 (2010)
59. H.-L. Jiang, D. Feng, T.-F. Liu, J.-R. Li, H.-C. Zhou, Pore surface engineering with controlled loadings of functional groups via click chemistry in highly stable metal-organic frameworks. *J. Am. Chem. Soc.* **134**, 14690–14693 (2012)
60. Y. Gao, M. Hu, B. Mi, Membrane surface modification with TiO₂-graphene oxide for enhanced photocatalytic performance. *J. Membr. Sci.* **455**, 349–356 (2014)
61. P. Kaner, D.J. Johnson, E. Seker, N. Hilal, S.A. Altinkaya, Layer-by-layer surface modification of polyethersulfone membranes using polyelectrolytes and AgCl/TiO₂ xerogels. *J. Membr. Sci.* **493**, 807–819 (2015)
62. W. Ma, M.S. Rahaman, H. Therien-Aubin, Controlling biofouling of reverse osmosis membranes through surface modification via grafting patterned polymer brushes. *J. Water Reuse Desalination* **5**(3), 326–334 (2015)
63. H.M. Hegab, A. ElMekawy, T.G. Barclay, A. Michelmore, L. Zou, C.P. Saint, M. Ginic-Markovic, Fine-tuning the surface of forward osmosis membranes via grafting graphene oxide: performance patterns and biofouling propensity. *ACS Appl. Mater. Interfaces* **7**(32), 18004–18016 (2015)
64. G.L. Liu, C. Han, M. Pelaez, D.W. Zhu, S.J. Liao, V. Likodimos, A.G. Kontos, P. Falaras, D.D. Dionysiou, Enhanced visible light photocatalytic activity of C–N-codoped TiO₂ films for the degradation of microcystin-LR. *J. Mol. Catal. A Chem.* **372**, 58–65 (2013)
65. M.N. Chong, B. Jin, C.W.K. Chow, C. Saint, Recent developments in photocatalytic water treatment technology: a review. *Water Res.* **44**, 2997–3027 (2010)
66. J. Grzechulska-Damszel, M. Tomaszewska, A.W. Morawski, Integration of photocatalysis with membrane processes for purification of water contaminated with organic dyes. *Desalination* **241**, 118–126 (2009)
67. D.C. Hurum, A.G. Agrios, K.A. Gray, T. Rajh, M.C. Thurnauer, Explaining the enhanced photocatalytic activity of Degussa P25 mixed-phase TiO₂ using EPR. *J. Phys. Chem. B* **107**, 4545–4549 (2003)
68. R. Leary, A. Westwood, Carbonaceous nanomaterials for the enhancement of TiO₂ photocatalysis. *Carbon* **49**, 741–772 (2011)
69. Y.H. Zhang, N. Zhang, Z.R. Tang, Y.J. Xu, Improving the photocatalytic performance of graphene–TiO₂ nanocomposites via a combined strategy of decreasing defects of graphene and increasing interfacial contact. *Phys. Chem. Chem. Phys.* **14**, 9167–9175 (2012)
70. D.L. Zhao, G.D. Sheng, C.L. Chen, X.K. Wang, Enhanced photocatalytic degradation of methylene blue under visible irradiation on graphene@TiO₂ dyade structure. *Appl. Catal. B-Environ.* **111**, 303–308 (2012)
71. Y.L. Min, K. Zhang, W. Zhao, F.C. Zheng, Y.C. Chen, Y.G. Zhang, Enhanced chemical interaction between TiO₂ and graphene oxide for photocatalytic decolorization of methylene blue. *Chem. Eng. J.* **193**, 203–210 (2012)

72. G.D. Jiang, Z.F. Lin, C. Chen, L.H. Zhu, Q. Chang, N. Wang, W. Wei, H.Q. Tang, TiO₂ nanoparticles assembled on graphene oxide nanosheets with high photocatalytic activity for removal of pollutants. *Carbon* **49**, 2693–2701 (2011)
73. T.N. Lambert, C.A. Chavez, B. Hernandez-Sanchez, P. Lu, N.S. Bell, A. Ambrosini, T. Friedman, T.J. Boyle, D.R. Wheeler, D.L. Huber, Synthesis and characterization of titania–graphene nanocomposites. *J. Phys. Chem. C* **113**, 19812–19823 (2009)
74. M. Gupta, V. Kapur, N.M. Pinkerton, K.K. Gleason, Initiated chemical vapor deposition (iCVDv) of conformal polymeric nanocoatings for the surface modification of high-aspect-ratio pores. *Chem. Mater.* **20**(4), 1646–1651 (2008)
75. A.M. Coclite, R.M. Howden, D.C. Borrelli, C.D. Petruczuk, R. Yang, J.L. Yague, A. Ugru, N. Chen, S. Lee, W.J. Jo, A. Liu, X. Wang, K.K. Gleason, 25th anniversary article: CVD polymers: a new paradigm for surface modification and device fabrication. *Adv. Mater.* **25**(38), 5392–5423 (2013)
76. A. Matin, Z. Khan, K.K. Gleason, M. Khaled, S.M.J. Zaidi, A. Khalil, P. Moni, R. Yang, Surface-modified reverse osmosis membranes applying a copolymer film to reduce adhesion of bacteria as a strategy for biofouling control. *Sep. Purific. Tech.* **124**, 117–123 (2014)
77. F. Guo, A. Servi, A. Liu, K.K. Gleason, G.C. Rutledge, Desalination by membrane distillation using electrospun polyamide fiber membranes with surface fluorination by chemical vapor deposition. *ACS Appl. Mater. Interfaces* **7**, 8225–8232 (2015)
78. G.O. Ince, A. Matin, Z.U. Khan, S.M.J. Zaidi, K.K. Gleason, Surface modification of reverse osmosis desalination membranes by thin-film coatings deposited by initiated chemical vapor deposition. *Thin Solid Films* **539**, 181–187 (2013)
79. R. Quintana, M. Gosa, D. Jańczewski, E. Kutnyanszky, G.J. Vancso, Enhanced stability of low fouling zwitterionic polymer brushes in seawater with diblock architecture. *Langmuir* **29**, 10859–10867 (2013)
80. S. Rouaix, C. Causserand, P. Aimar, Experimental study of the effects of hypochlorite on polysulfone membrane properties. *J. Membr. Sci.* **277**, 137–147 (2006)
81. P.-F. Ren, Y. Fang, L.-S. Wan, X.-Y. Ye, Z.-K. Xu, Surface modification of polypropylene microfiltration membrane by grafting poly(sulfobetaine methacrylate) and poly(ethylene glycol): oxidative stability and antifouling capability. *J. Membr. Sci.* **492**, 249–256 (2015)
82. Q. Li, H.-H. Lin, X.-L. Wang, Preparation of sulfobetaine-grafted PVDF hollow fiber membranes with a stably anti-protein-fouling performance. *Membranes (Basel, Switzerland)* **4**(2), 181–199 (2014)
83. J. Cardoso, L. Rubio, M. Albores-Velasco, Thermal degradation of poly(sulfobetaines). *J. Appl. Polym. Sci.* **73**, 1409–1414 (1999)
84. R. Zhou, P.-F. Ren, H.-C. Yang, Z.-K. Xu, Fabrication of antifouling membrane surface by poly(sulfobetaine methacrylate)/polydopamine co-deposition. *J. Membr. Sci.* **466**, 18–25 (2014)



Ajithkumar Manayan Parambil, Jiji Abraham,
Praveen Kosappallyillom Muraleedharan, Deepu Gopakumar, and
Sabu Thomas

Contents

1	Macro Fibers	419
1.1	Synthetic Fibers	419
1.2	Natural Fibers	422
1.3	Fiber Size and Length	423
2	Nanofibers	425
2.1	Synthetic Nanofibers	425
2.2	Polymer Nanofibers	425
2.3	Carbon Nano Fibers	426
2.4	Carbon Nanotube Fibers	432
2.5	Metal Oxide Nanofibers	434
3	Nanoscale Bio-Fillers	434
3.1	Nanocelluloses	435
3.2	Nanochitin	437
3.3	Starch Nanocrystals	438
3.4	Bio-Nanofillers as Reinforcement for Polymer Nanocomposites	439
4	Summary	441
	References	441

A. Manayan Parambil · J. Abraham · D. Gopakumar · S. Thomas (✉)
International and Inter University Centre for Nanoscience and Nanotechnology, Mahatma Gandhi
University, Kottayam, Kerala, India
e-mail: ajithkumarp@hotmail.com; jijiabraham02@gmail.com; deepu1789@gmail.com;
sabuthomas@mgu.ac.in; sabupolymer@yahoo.com

P. Kosappallyillom Muraleedharan
International and Inter University Centre for Nanoscience and Nanotechnology, Mahatma Gandhi
University, Kottayam, Kerala, India

Department of Mechanical Engineering, Saintgits College of Engineering, Kottayam, Kerala, India
e-mail: praveenkmiucnn@gmail.com

Abstract

Fiber-reinforced composites (FRC) are widely used in spacecraft, helicopters, aircraft, ships, boats, automobiles, chemical processing equipments, biomedical devices, sports items, buildings, bridges infrastructure, etc. Nowadays, more and more exciting development on advanced forms of FRC materials are happening across the world. Development of high-performance resin systems, incorporating carbon nanotubes and other nanoparticles, are one among them. Polymer fibers have numerous imperative applications apart from using as reinforcement in composite materials. They are widely used in packaging, flooring, rope, textile industries, etc. In this context, the study on fiber-reinforced composites is very much important and the chapter gives an insight on the fiber-reinforced composites from macro to nanoscale.

Composite materials do exist naturally and synthetically. They are synthetically made from two or more constituent materials having considerable difference in chemical and physical properties that will always remain discrete in their structure. Composites are composed of fibers in a matrix and should be strong and stiff with low density. Thermosetting polymers like epoxy and polyester resins are widely used matrices in a composite. This is due to the flexibility in molding after initial fabrication. Similarly, glass and carbon fibers are usually used fibers in composites. The use of metals and ceramics as matrixes for composites are not widely used because of the high manufacturing cost and intricacy in the addition of fibers.

Fiber-reinforced composites are composites having fibers as reinforcement which form the main source of strength and matrix which join and arrange all the fibers together. Matrix transfers the stresses between the reinforcing fibers. Fillers or modifiers are being used to impart special properties and make the process smooth. They are composed of axial particulates embedded in a matrix material. The interfacial bonding is important for fiber-reinforced composites. Aligned, random, and woven fibers are the common geometries for fiber-reinforced composites [1]. Aramid, carbon, glass, boron, alumina, silicon carbide, and natural fibers are the fibers being used in this class of materials.

Fiber-reinforced plastics (FRP) consist of fibers in a polymer matrix, where fibers are the intermittent or disseminated phase and polymer matrix are the continuous phase. They are stout, stiff, have high strength-to-weight ratio and stiffness-to-weight ratio. When compared to unreinforced plastics, they possess ameliorate fatigue resistance, superior toughness, and upper creep resistance. Reinforced plastics are relatively easy to design, fabricate, and repair. Interestingly, they are composed of the combined properties of its constituents. The percentage of fiber by volume ranges from 10% to 60% in reinforced plastics. Similarly, the ratio of fiber integrated in a matrix is constrained by the distance between nearby fibers. It is investigated that higher weight percentage of fibers usually results in poor structural properties. The highest practical fiber content is reported to be 65%.

Generally, hybrids have better properties than single-fiber composites and are more costly. The composites are called a hybrid when more than one type of fibers

are used in reinforced plastics. For higher temperature applications, glass or carbon fiber-reinforced hybrid plastics are developed that ranges about 300 °C. When hybrid fibers are exposed to atmosphere, they showed brittleness, abrasiveness, lack of toughness, and chemical degradation. It is also seen that the fiber properties is significantly influenced when the quality of the material and processing method is varied.

1 Macro Fibers

1.1 Synthetic Fibers

The use of synthetic fibers as reinforcement in plastics is due to well-developed manufacturing base and good mechanical properties. Synthetic fibers used as reinforcement in polymer composites are glass fiber, Kevlar fiber, graphite fiber, boron fiber, and carbon fiber. Table 1 shows the typical properties of synthetic reinforcing fibers. Synthetically designed FRP satisfy the properties required to meet the structure and durability of the materials for numerous application. The different types of synthetic fibers are discussed below.

1.1.1 Glass Fibers

Glass fibers stand as the least expensive fiber and are widely used. The material which is made out of these fibers are called glass-fiber-reinforced plastic (GFRP). These materials contain 30–60% of glass fibers by volume. Glass fibers can also be classified to continuous fibers and discontinuous or staple fibers. Glass is a chemical form of silicon dioxide (SiO_2). Various surface treatments like silane treatment (a silicon hyride) are generally espoused. The different kinds of glass fibers are E, S, and E-CR-type fibers. Calcium aluminoborosilicate glass is the universally employed E-type fiber. Magnesia aluminosilicate is an S-type glass fiber which offers high strength and stiffness. But they are costly. E-CR-type is the one which offer higher resistance to elevated temperatures and are known to be high-performance glass fibers. They are even more resistant toward acid corrosion than E-type glass fibers. The refractive index of S-glass fibers is high to that of resin

Table 1 Properties of synthetic reinforcing fibers [2]

Fibers	Characteristics
Glass	High strength and density, low stiffness, and cheaper, e.g., calcium aluminoborosilicate and magnesia aluminosilicate
Carbon	High modulus/strength, less dense compared glass, used with CNTs in combination and are cheaper
Boron	Higher strength, stiffness, density, contains tungsten filament at its center, and are expensive
Aramids (Kevlar)	Higher strength-to-weight ratio and expensive
Other fibers: Nylon, silicon, silicon carbide, boron nitride, tantalum carbide, steel, tungsten, molybdenum	

matrix and they offers high tensile strength than other glass fibers. In case of resin composites, the flexural properties can be significantly improved by incorporating discontinuous S-glass fibers. Moreover, these fibers will not affect the curing properties of the composites [3].

The main advantage of using glass fibers are the low cost and high strength of the material. These fibers are extensively used in recreational vehicles in order to save weight and for durability [4]. They are extensively used in dentistry as fixed partial dentures, root canal post systems, orthodontic fixed retainers, and periodontal splints [3]. When compared to the organic polymer matrixes, glass fibers have meager wettability. But these properties can be improved by salinizing these fibers with amino propyl tri-methoxy silane [5].

1.1.2 Carbon Fibers

Being more expensive than glass fibers, carbon fiber combines the properties of low density, high strength, and high stiffness. Based on the nature of carbon, these composite material are called as carbon-fiber-reinforced plastic (CFRP) and graphite-fiber-reinforced plastic (GFRP). Carbon and graphite are differentiated based on the purity and processing temperature of the material. Carbon fibers have 90% amorphous carbon while graphite fibers have 99% crystalline carbon. Due to superior mechanical properties, composites containing carbon fibers are used in aeronautical, marine, automobile, sporting equipment, and mechanical engineering applications [6–8]. Carbon fibers show more stiffness, lesser weight, lesser density, lesser coefficient of thermal expansion, lesser abrasion, improved electrical conductivity, vibrating damping, inert to chemicals, elasticity to failure at thermal temperature, higher fracture strength, creep resistance, and biocompatible [9]. Carbon fiber composites are resistant to corrosion and fire and have higher fatigue life [10]. Reduced production cost and shorter composite manufacturing time make carbon-fiber-reinforced epoxy polymer composite a good candidate for automotive application [8]. Carbon fiber-reinforced composites showed optimal biocompatibility and are appropriate for the design of materials for implant sustained full arch dentures [9]. When compared to glass fibers, carbon fibers showed improved stiffness and strength.

The physical interlocking and interfacial adhesion of carbon fiber and polymer matrix can be improved by treating with HNO_3 . This will remove the impurities on the surface and increase the roughness of carbon fiber. Moreover, this may increase the oxygen functional group on the surface, thus improving the properties [7]. The need of the enhancement of electrical and thermal conductivity of reinforced plastic components leads to the development of conductive graphite fibers. The fibers are smeared with metal incessantly by electroplating. The conductive fibers obtained as chopped or continuous form are incorporated directly into injection-molded plastic parts. These type of fibers finds suitable for electromagnetic and radio frequency shielding and lightning strike protection [11].

1.1.3 Ceramic Fibers

Nextels is a ceramic fiber which contains alumina, silica, and boric acid and has oval shape in cross section. These fibers are resistant to chemicals and have very less

elongation and thermal conductivity. They are suitable for high temperature applications. Polyborosilazane fibers (SiBN) can be developed using multistep polymerization and melt spun of hexamethyldisilazane, HSiCl_3 , BCl_3 , and CH_3NH_2 [12]. As the temperature increases, the fiber diameter decreases and the tensile strength improved. Using low-temperature CVD process, boron nitride-coated alumina fibers can be developed [13]. Pyrolysis of cured SiC fibers at different environment resulted in SiC fibers having different electrical resistivity, good mechanical strength, and high temperature performance [14]. SiBNC ceramic fibers were developed using one pot synthesis of polyborosilazane and melt spinning. Similarly, electron beam irradiation of green fibers infusible was also used to develop SiBNC ceramic fibers [15].

1.1.4 Polymer Fibers

Aramid, rayon, and nylon are the source for polymer fibers. Aramids are the most commonly used fibers. In aramid fiber family, Kevlar showed very high specific strength and are toughest among aramid fibers. This is because it undergoes plastic deformation prior to fracture. However, the absorption of moisture and the resulting degradation of properties limit its applications. Similarly, spectra is another polymer fiber which show improved abrasion and flexural fatigue resistance. This fiber belongs to polyethylene polymer fiber which has increased molecular chain orientation and molecular weight. Moreover, their specific strength and stiffness are higher than aramid fibers. This can be attributed due to their lower density. In spite of these benefits, these fibers have meager adhesion and low melting point which can be considered as its major drawbacks.

1.1.5 Boron Fibers

Boron fibers are prepared by depositing boron on tungsten fibers by CVD. They are stronger, stiffer, and resistant to higher temperature. Due to the use of tungsten, these fibers have high density and are very expensive. Boron fibers can also be developed using laser-assisted chemical vapor deposition [16]. By reacting liquid magnesium with boron fibers, superconducting Mg_2B_2 fibers can be developed [17]. Aluminum matrix composites can be reinforced with boron fiber [18]. Low molecular weight and excellently spinnable boron nitride fiber can be fabricated by preceramic method [19].

1.1.6 Other Fibers

Sapphire, steel, tungsten, molybdenum, and tantalum carbide are other fibers used in composites. Whiskers also are used as reinforcing fibers. Whiskers are single crystal with needle-like structure having diameter ranging from 1 to 10 μm and 100 to 15,000 nm aspect ratio. They are free of imperfections, and imperfections do not significantly affect their strength. This is due to their small size. The elastic moduli and tensile strength are observed to vary with material. The tensile strength was observed 15–29 GPa and elastic moduli ranging from 400 to 700 GPa. Multiple shear band formation result in compressive strain to failure and effect in plastic deformation of tungsten fibers/ZrAl-NiCuSi bulk metallic glass composite [20].

Tungsten fiber-reinforced tungsten composites can be used as plasma facing material for future fusion reactors [21]. Further, intercalated graphene/molybdenum disulfide hybrid fiber is developed for capacitive energy storage application [22].

1.1.7 Production of Synthetic Fibers

Polymers are made in to semisolid polymer fibers with continuous filament like arrangement by extruding through spinneret. These fibers are extensively used in plastic reinforcement. The extruder has many holes which allow the polymers to pass through and form fiber. The process starts by converting liquid polymer to rubbery form and later solidifying when the filaments begin to flow through the holes of the spinneret. This process is termed spinning.

The polymer molecules should be oriented in the direction of the fiber. In order to make the direction similar, significant stretching has to be induced. This orientation influences the strength of the fibers and possesses high strength. Thus, this process forms the most important steps during fiber formation. This can be performed soon after extrusion and during pliable stage of the polymer. About 800% strain can be persuaded. Synthetic fiber-reinforced polymer matrix composites have proved their viability in the fabrication of many components in various applications.

1.2 Natural Fibers

As the name points, these fibers are generated from animals, plants, and minerals. The structural performance of the plants is also influenced by these fibers. It also showed significant reinforcement property when it was used in plastic. Further, plant fibers are classified into bast, leaf, seed, fruit, wood, grasses, and reeds. Similarly, animal fibers are classified into animal hair, silk, chicken feather, and avian fibers. In addition, mineral fibers are classified into asbestos, ceramic, and metal fibers.

Natural fibers are complex and three dimensional. Their walls are enclosed with hydroxyl ion-containing polymers like cellulose, hemicellulose, pectin, and lignin. Natural fibers consist of mainly cellulose fibrils (fibers) embedded in lignin matrix (resin). Apart from the polymers, organic with low molecular weight and inorganic matters are also present in lesser ratio in these fibers. The decay resistant, color, and smell are influenced by these extractives. The composition of few natural fibers is given in Table 2 [23]. The use of natural fibers enhances the mechanical properties (strength and stiffness) of plastic or polymer composite. It has to be noted that the density as well as cost is not much influenced by the use of natural fibers. These materials can be effectively employed in automobile industry due to its lighter weight which reduces fuel consumption.

Natural fibers are recyclable, which is their main advantage. There are few technical concerns which have to be addressed for incorporating natural fibers in polymer composites [24]. The fiber properties should be homogenized and the degree of polymerization should be understood before reinforcing natural fibers in polymer composites. Similarly, their crystallization, adhesion property, and flame retardant nature should be known.

Table 2 Composition of natural fibers [23]

Fibers	Cellulose (wt %)	Ligin (wt %)	Hemicellulose (wt %)	Pectin (wt %)	Wax (wt %)	Moisture content (wt %)
Jute	61–71.5	12–13	13.6–20.4	0.4	0.5	12.6
Hemp	70.2–74.4	3.7–5.7	17.9–22.4	0.9	0.8	10
Kenaf	31–39	15–19	21.5	–	1.7	–
Flax	71	2.2	18.6–20.6	2.3	0.3	10
Ramie	68.6	0.6–0.7	13.1–16.7	1.9	0.4	8
Sunn	67.8	3.5	16.6	0.3	2	10
Sisal	67–78	8–11	10.0–14.2	10	–	11
Cotton	82.7	–	5.7	–	–	–
Kapok	64	13	23	23	–	–
Coir	36–43	41–45	10–20	3–4	–	8
Banana	63–67.6	5	19	–	–	8.7
Palf	70–82	5–12	–	–	–	11.8

The structural constitution of natural fiber is shown in Fig. 1. One primary layer and three secondary layers are arranged outside and inside, respectively, for each cell wall. The inner secondary layer has more cellulose content than the outer primary layer. But the primary layer has more lignin content than the secondary layer. Within each layer, microfibrils of cellulose are found to be parallel to each other. Around the longitudinal direction, they are observed to be spiral. The angle between the axis and the fibril of the fiber is called microfibrillar angle/spiral angle. Each layer has different angles of spiraling. The hemicellulose and lignin together holds the cellulose microfibrils in each layer. The properties of fibers are influenced by their chemical components and complex chemical structure [25].

The properties of the fibers can be tailor-made by controlling the structure, microfibrillar angle, cell dimensions, defects, and the chemical composition of fibers. The mechanical properties are summarized in Table 3.

The cellulose content also influences their mechanical properties. Young's modulus and tensile strength was found to increase as the cellulose content increase. Similarly, the structure and morphology are greatly affected by the lignin content of the fiber. The wettability and adhesion of the fibers depend on the waxy substance of the natural rubber. They have more potential to serve as substitute for artificial fiber composite. So the rising global energy crisis and environmental threats can be addressed by carrying out extensive research in this area. Accordingly, extensive studies on the natural fibers with thermoplastic and thermosetting composites were carried out [26].

1.3 Fiber Size and Length

Comparatively, small cross section and orientation of molecules in the longitudinal direction make the fibers robust and stiff in tension. Thus, chance of forming

Fig. 1 Structural constitution of natural fiber

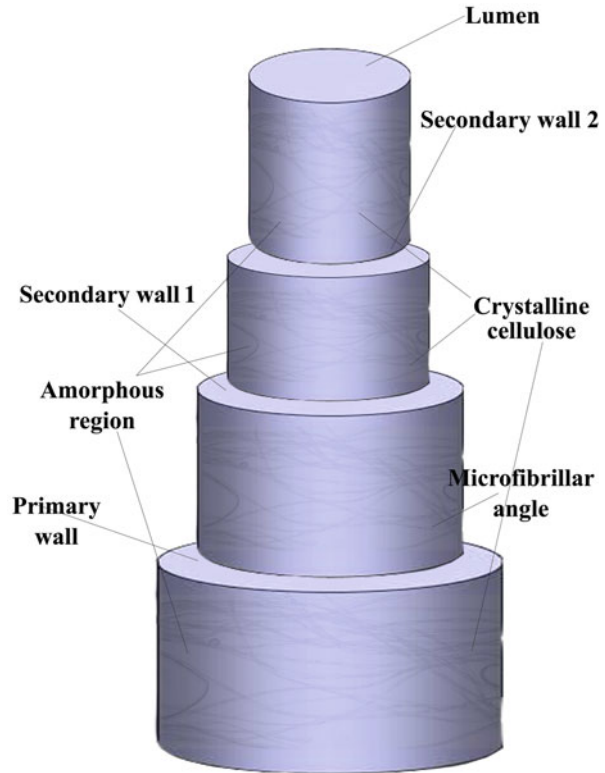


Table 3 Mechanical properties of natural fibers [23]

Fibers	Density (g/cm ³)	Diameter (μm)	Tensile strength (Mpa)	Youngs modulus (GPa)	Elongation at break (%)
Jute	1.3–1.45	25–200	393–773	13–26.5	1.16–1.5
Hemp	–	–	690	–	1.6
Kenaf	–	–	–	–	2.7
Flax	1.5	–	345–1100	27.6	2.7–3.2
Ramie	1	–	400–938	61.4–128	1.2–38
Sunn	–	–	1.17–1.19	–	5.5
Sisal	1.45	50–200	468–640	9.4–22	3–7
Cotton	1.5–1.6	–	287–800	5.5–12.6	7–8
Kapok	–	–	–	–	1.2
Coir	1.15	100–450	131–175	4–6	15–40
Banana	–	–	1.7–7.9	–	1.5–9
Palf	–	20–80	412–1627	34.5–82.5	1.6

significant defects with in the fiber is negligible. The tensile strength of glass fiber is comparatively higher than that of the bulk form up to 4600 MPa. Fibers are usually continuous and discontinuous which are generally long and short, respectively. For short fiber, the average fiber length is increased resulting in their improved mechanical properties. The aspect ratio typically ranges from 20 to 60 for a short fiber and 200 to 500 for long fiber. Reinforcing materials could also exist in the form of shredded fibers, flakes, continuous roving fibers, woven fabric, yarn, and mats of various combinations. Bringing the size of these fibers down from macro to micro level is expected to give several amazing properties to the reinforced polymers.

Composites were fabricated using different polymer processing techniques and fibers with varied length to diameter ratio (L/D). This ratio and size play a crucial role in their strength [27]. Fiber L/D ratio influences the mechanical properties and water absorption characteristics. Low L/D ratio induces stress concentration and may lead to decrease the strength [28]. The use of long fibers increases the mechanical strength of WPC when processed with injection molding technique [29, 30]. Both beneficial and limited or no effects of fiber length on mechanical properties using extrusion were reported [31–33].

2 Nanofibers

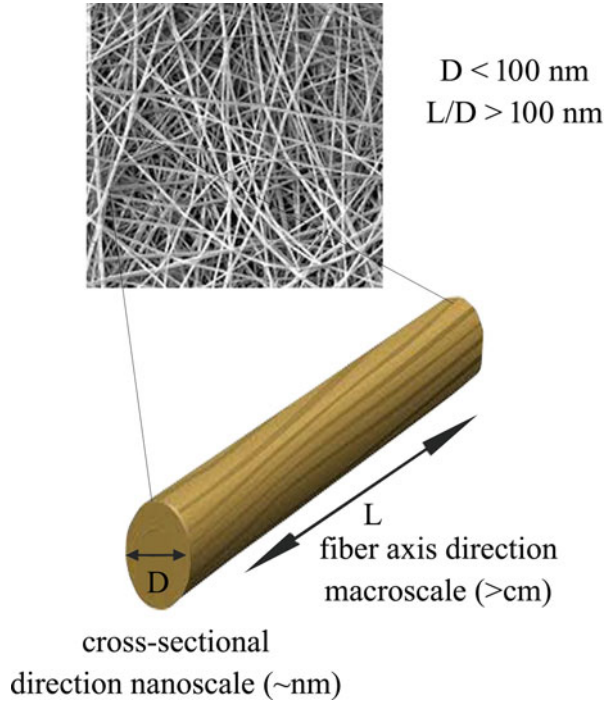
2.1 Synthetic Nanofibers

Nanofibers are defined as fibers with diameters less than 100 nanometers and length about some micrometers. These can be synthesized by melt processing, interfacial polymerization, electrospinning, antisolvent-induced polymer precipitation, and electrostatic spinning [34]. Nanofibers have extreme high aspect ratio which attributes to their special properties when compared to nonwovens. Properties like lower density, huge surface area to mass, tight pore size, and improved pore volume make them ideal candidates for a wide range of filtration applications. The extensive study on one-dimensional structures of nanofibrous compounds and their physical properties points the use of these materials in semiconductors, optical, sensors, electronic, polymer fillers, and nonwoven porous membranes. Basic representation of the nanofibers is given in Fig. 2.

2.2 Polymer Nanofibers

The diameter of polymer nanofibers is in nanometer. The surface area per unit mass is larger and thus the surface can be easily functionalized. This property makes the materials suitable for tissue engineering, clothing, sensors, etc. These fibers can also be employed as reinforcement in composite materials. Electrospinning, phase separation, template synthesis, and self-assembly can be adopted for developing

Fig. 2 Basis representation of nanofibers



polymer nanofibers. A large variety of polymers can be converted to nanofibers by electrospinning technique. Mass production can be achieved through this process [35]. Various applications of polymer nanofibers are depicted in Fig. 3.

2.3 Carbon Nano Fibers

Carbon fibers are developed using anisotropic carbon having carbon content of about 92–100%. Initially, they were prepared by carbonizing bamboo or cotton. Carbon nano fibers are found to be promising candidates in areas such as reinforcement of composites, energy storage, energy conversion, and self-sensing devices. Size is the major difference between conventional carbon fibers (CCF) and carbon nano fibers (CNF). Diameter of CCF is around micrometers and CNF is around 50–200 nm. The typical CCFs were developed from high-strength polyacrylonitrile or meso-phase pitch. Similarly, CNFs were prepared by catalytically vapor deposition growth and electrospinning. The cup-stacked CNF and the platelet CNF can be prepared by catalytically vapor deposition. Polymer fibers were used as precursors for the synthesis of CNF via electrospinning technique, and the final properties of CNF depend on the characteristics of polymer solution and processing parameters [36] (Figs. 4, 5, and 6).

Posttreatment approaches and production procedures highly influence the properties of the CNF [38]. The excellent properties of CNF include impressive creep

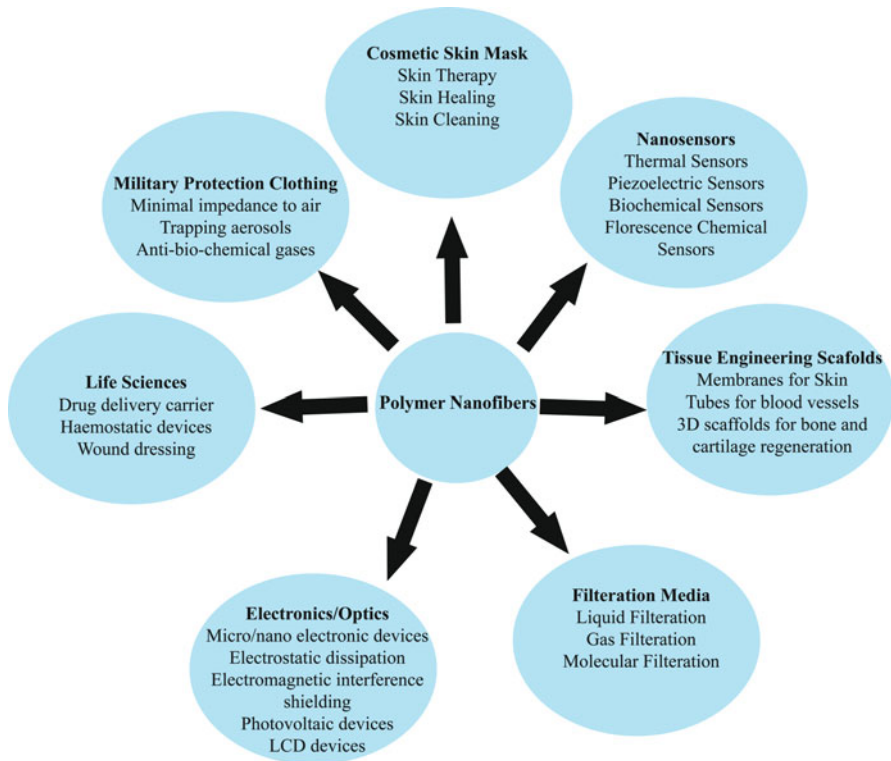
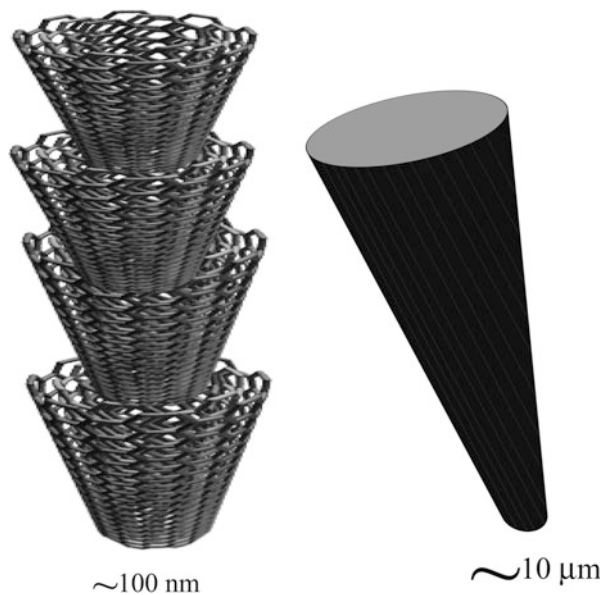


Fig. 3 Various applications of polymer nanofibers

Fig. 4 Difference between CNF and CCF [37]



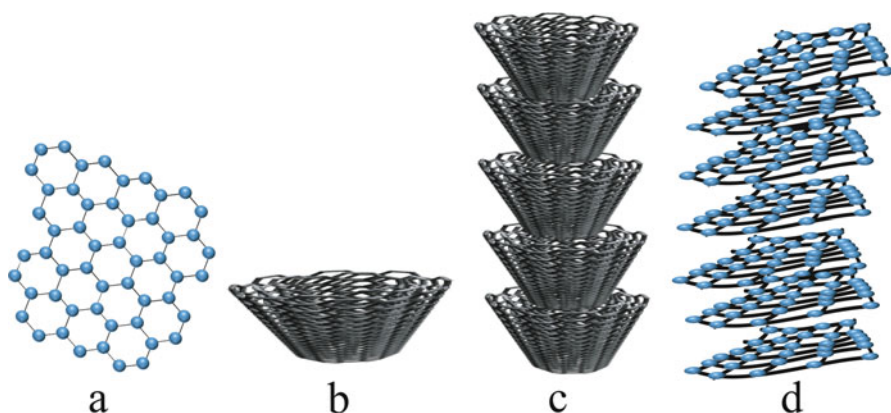


Fig. 5 Cup-stacked CNF structure formation (a–c) and platelet CNF structure (d) [37]

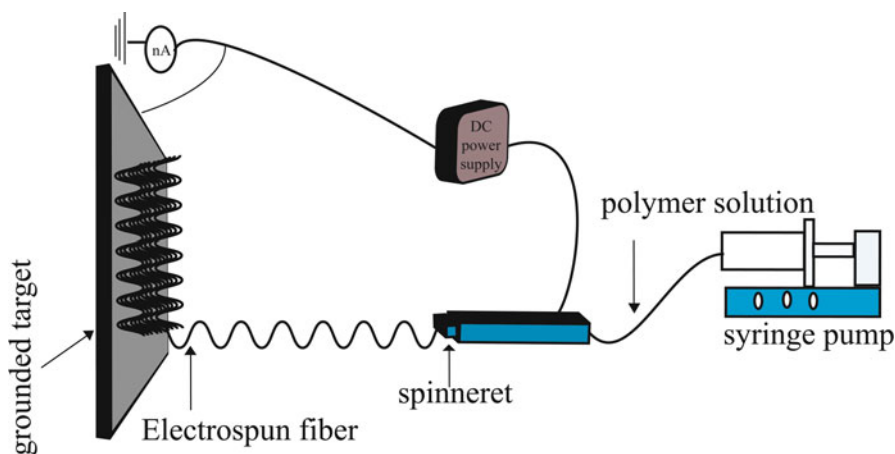


Fig. 6 Electrospinning setup for CNF fabrication [37]

resistance, high tensile strength of ~ 7 GPa, low density of $1.75\text{--}2.00$ g/cm³, improved modulus of <900 GPa, high thermal conductivity (1950 W/mK), and excellent electrical conductivity. The resisting power of these materials against oxidizing agents is very little, but is impervious to other chemicals. Within aluminum or magnesium alloys, metal matrices, CNF showed extraordinary physical properties. Thus, unique composites having astonishing thermal properties are possible to fabricate. The theoretical calculation of the thermal coefficient of expansion and the thermal conductivity reveal the potential of this material. Because of these properties, CNFs can be used as reinforcing agents in polymer matrix, and these novel materials have applications in military, aerospace, construction, medical, and sporting goods [39].

2.3.1 Preparation of CNF Composites

In carbon nano fibers, individual fibers show tendency to form agglomerates due to van der waals force of attraction between them. It will affect the overall performance and final properties of the composites. Proper and uniform dispersion of CNFs is a challenging task to obtain composites with improved properties. So, the dispersion technique has a vital role in fabricating CNF composites. Polymer composites based on CNF can be prepared either by melt mixing process or sonication process in low viscosity solutions. Among these, melt mixing is the widely used method because of its simplicity, less expensiveness, and convenience. Extrusion or roll mill, Haake torque rheometer, and mini-max molder belong to the melt mixing method [40, 41]. All these methods involve shear mixing for getting proper dispersion of CNF. So it is very important to find out low shear mixing technique to preserve the structure of CNF. Surface treatments for CNF are another strategy to get proper dispersion of it in polymer matrix. Here, compatibility between polymer matrix and surface functional groups is the important parameter which predicts the final properties of the composites [42]. This will improve the dispersion and wetting properties of the nanofibers which will also enhance the property of composite materials. This can even be observed even at considerably reduced loads. The conductive filler surface can even be functionalized or grafted. But depending on the thickness and functionalization layer transport properties, the composite transport properties may reduce. So certain parts of conductive layer should be selectively functionalized.

2.3.2 Properties of CNF Composites

Poly(ether ether ketone) nanocomposites incorporated with vapor-grown carbon nanofibers (CNF) were fabricated by typical polymer processing techniques. Investigation of mechanical properties of the composite exposed a steady rise in tensile stiffness and strength with nanofiber filling portions up to 15 wt% without negatively affecting material's ductility [43]. Multiscale fiber-reinforced composites (MFRCS) were fabricated using vacuum-assisted resin infusion molding (VARIM) which contains CNF and epoxy [44]. Similarly, by adopting very low fiber-loaded nanophased matrices, mechanical and thermal properties can be enhanced. During the fabrication, nanoparticles can be trapped within the fiber preform mesh in inter-tow regions which can be considered as its drawback. MRFs are the acceptable method for developing carbon nanofiber/fiber-reinforced polymer composites. The surface functionalization of CNF using amine and carboxylic acid groups improve compressive strength and interlaminar shear strength (ILSS) [44]. Core-shell nanofibers were electrospun for interfacial toughening and self-healing of carbon-fiber/epoxy composites [45]. The ultrathin self-healing fibers were contrived through electrospinning, where a core shell of dicyclopentadiene (DCP)-poly acrylonitrile (PAN) nanofibers is formed in which liquid DCPD was enwrapped into PAN. The interface of the carbon fiber fabrics neighbor to each other was integrated with these core-shell nanofibers. After resin infusion and curing, they form ultrathin self-healing interlayers prior to resin infusion. Interfacial damages in composite laminates are self-repaired using core-shell DCPD/PAN fibers. Vapor-grown carbon nanofibers were found to be interesting additive for polymers in tribological applications since it acts

as a solid lubricant. Several studies have been reported on the effects of various filler concentrations on the tribological and mechanical properties of various polymer composites [46, 47]. Surface treatment of carbon nanofibers on the mechanical behavior of polymer composites were investigated by several researchers. The improved mechanical performance of the composites is due to the enhanced dispersion and interfacial attachment among fibers and the matrix [48, 49]. In addition, decrement in the mechanical properties is also observed in some other cases [50].

Rheological study on polyethylene composites reinforced with vapor-grown carbon nanofiber exposed the impact of temperature, frequency, and concentration of nanofiber (up to 30 wt %) on the rheological properties of the composites [51]. Nanofilled epoxy dispersions structure is highly sensitive to the rheology and is evidenced from the relationship between the morphology and rheology [52]. Studies based on the correlation between electrical and rheological behavior of CNF-filled composites was done by Paleo et al. [53]

Electrical properties, especially percolation threshold of CNF-based polymer nanocomposites, depend on several aspects including CNF aspect ratio, dispersion, distribution, alignment, and conductivity. Similarly, the crystallinity, surface tension of polymer matrix, processing methods, and conditions also influence their electrical properties. Several strategies are developed to diminish the percolation threshold in polymer composites [54]. Table 4 summarizes the percolation threshold concentrations that have been reported so far. It has been shown that posttreatments of CNFs improve the electrical conductivity of composites. These treatments include carbonization, graphitization, etching in air around 400–600 °C, and soaking in nitric acid, sulfuric acid, or sulfuric/nitric acid. Polymer showed improved interaction with nanofibers after surface treatment. Moreover, different dispersion, distribution, wetting, and final aspect ratio of nanofiber after compounding can be observed. The CNF intrinsic conductivity may reduce the percolation threshold. Several other parameters also play major role in improving the conductivity of composites. For determining the conductivity of the composite, CNF surface area and morphology are considerably significant than the intrinsic conductivity [55] Moreover, better EMI shielding capability depends on the surface area of CF for their polymer composites [56].

Compounding or molding instruments available are mini-max molder (MMM), melt mixing in Haake mixer (MM-H), melt mixing in Brabender twin screw kneader (MM-BTS), melt mixing in twin screw extruder (MM-TSE), in situ polymerization (ISP), melt mixing in DACA mixer (MM-DACA), mechanical stirring (MS), mixed in Brabender (MB), melt mixing in a two-roll mill (MM-TRM), heterocoagulation (HT), solution processing (SP), melt mixing in chaotic mixer (MM-CM), and mixing in thinky mixer (M-TM). Similarly, molding methods are injection molding (IM), compression molding (CM), curing (C), and casting (CS).

Polymer nanocomposites containing carbon fibers have been broadly studied in an effort to overcome the deficiencies of metal-based protections to prevent electromagnetic radiations. Carbon nanofibers can be used to raise the permittivity of neat resin so as to attain enhanced radiation absorption in the frequency range 8–12 GHz. Better dielectric properties were obtained at lower filler concentration by using CNF.

Table 4 Percolation threshold of different polymer composites containing CNF [54]

Polymer	Fiber type	Percolation threshold	Compounding/molding
PP	VGCNF	5.6 vol %	MMM/IM
	VGCNF	3 vol %	MMM/IM
	VGCNF	2.47 vol %	MMM/IM
	VGCNF	5.2 vol %	MMM/IM
	VGCNF	4.97 vol %	MMM/IM
	VGCNF	0.5 vol %	MMM/IM
	VGCNF	9–18 wt %	MM-H/CM
	VGCNF	18 wt %	MM-BTS/CM
	VGCNF	7.5 wt %	MM-BTS/CM
	VGCNF	4–5 vol %	MM-TSE/IM
	MWNTs	0.05 vol %	MM-H/CM
	MWNTs	8 wt %	MM-H/CM
	CB	9.5 wt %	MM-H/CM
	CB	3 phr	MM/CM
PC	VGCNF	6.3 wt %	ISP/CM
	VGCNF	7.5	MM-DACA/CM
	MWNT	1–1.5 wt %	MM-DACA/CM
VE		2 wt %	MS/C
		4 wt %	MB/C
PE	VGCNT	2.5 phr	MM-TRM/CM
PA-6	MWNT	4–6 wt %	MM-TSE/IM
P(S-co-BuA)	MWNT	1.5 vol %	HTCS
PS	VGCNF	<1 vol %	HT/CM
	VGCNF	1 wt %	SP/CS
PMMA	VGCNF	8 phr	MM-TRM/CM
		6 wt %	MM-BTS
		2 wt %	MM-CM
Epoxy		0.5 wt %	SP/C
	VGCNF	2.5 wt %	M-TM
	SWNT	0.0052 vol %	SP/C
	SWNT	0.062 wt %	SP/C
	MWNT	0.022–0.04 wt %	SP/C

The investigation of the influence of filler aspect ratio on the electromagnetic properties of epoxy-amine resin reinforce with carbon nanofibers confirmed the role of filler aspect ratio. The study suggest to choose nanofibers with higher value to design conductive lightweight materials with reduced cost, lower filler amounts, and improved electrical properties [57]. Carbon nanofibers-reinforced conductive foam structures are very promising for the use in lightweight EMI shielding materials. Electromagnetic absorbers (EMA) are now attaining ample attention particularly in the field of microwave frequencies applications. CNF/epoxy composites and the effect of carbon nanofibers dispersion on their microwave absorbing properties was investigated by Nanni et al. [58] Two different dispersion techniques are used to

prepare the composites. Different absorbing performance is obtained for different mixing strategies at same filler loading and sample thickness. It was proved that the absorbing performance and the electromagnetic properties are severely influenced by the material microstructure. So, much care should be taken during material preparation. Similarly, repeatability has to be ensured for reliable practical application.

Carbon nanofibers can be used to improve the thermal conductivity of the polymer composites. It was noted that for the thermoplastics, the use of carbon nanofibers increase the working temperature range by 100 °C. Upon the addition of nanofibers, the rate of polymer crystallization get increased with negligible change in the mechanism of nucleation. This was evidenced from the Avrami method [59, 60]. It was found that dispersion of CNF and the formation of percolated network of CNF in polymer matrix have a significant effect on the thermal conductivity of polymer composites [61]. BN/VGCNF/rubbery epoxy hybrid composites can be used for fabricating thermal interface materials (TIMs) having thermal conductivity and electrical insulating property. At thick bond lines, hybrid composites offer improved interfacial thermal transport. This was studied from their thermal contact resistance measurements. Here, thermal conductivity was imparted by CNF. So, as the CNF content is increased, the property is enhanced [62]. Self-assembled multilayered carbon nanofiber nanopaper was used for enhancing electrical actuation of shape memory polyurethane nanocomposite [63]. Bio-based polyester reinforced with vapor-grown carbon nanofiber is employed for electroactive shape memory performance [64]. Life cycle energetic effect concomitant with the production and use of polymer nanocomposites (PNC) reinforced with carbon nanofiber (CNF) is investigated by Vikas et al. [65] The use of PNCs reinforced with CNF and CNF-GF in the automobile body panel exposed the use of lower CNF-loaded PNCs. These composites show potential to save the net life cycle energy when compared to steel. This owes to the enhanced fuel economy benefits.

2.4 Carbon Nanotube Fibers

CNT arrays, films, and fibers can be conveniently utilized than individual CNTs. Individual CNTs provide extraordinary physical and mechanical properties to manufacture these high-performance macrostructures. CNT fibers showed greater specific strength and modulus than polymeric and carbon fibers. This is due to axially aligned and highly packed CNTs along the fibers [66]. Moreover, they require high energy to break and are flexible compared to commercial fibers. Furthermore, they show reasonable thermal and electrical conductivities. Flexible medical devices, transmission lines, biosensors, high-performance composites, and microelectrodes are the expected area of application for CNT fibers [67]. CNT fibers are fabricated through spinning processes. Some are lyotropic liquid crystalline suspension of nanotubes, MWCNTs previously grown on a substrate, aerogel of SWCNTs and MWCNTs. Polymer infiltration and surface modification are very important post-treatment process. Chemical bonding and polymer infiltration can be obtained by introducing abundant amount of functional groups [68]. Figure 7 represents various

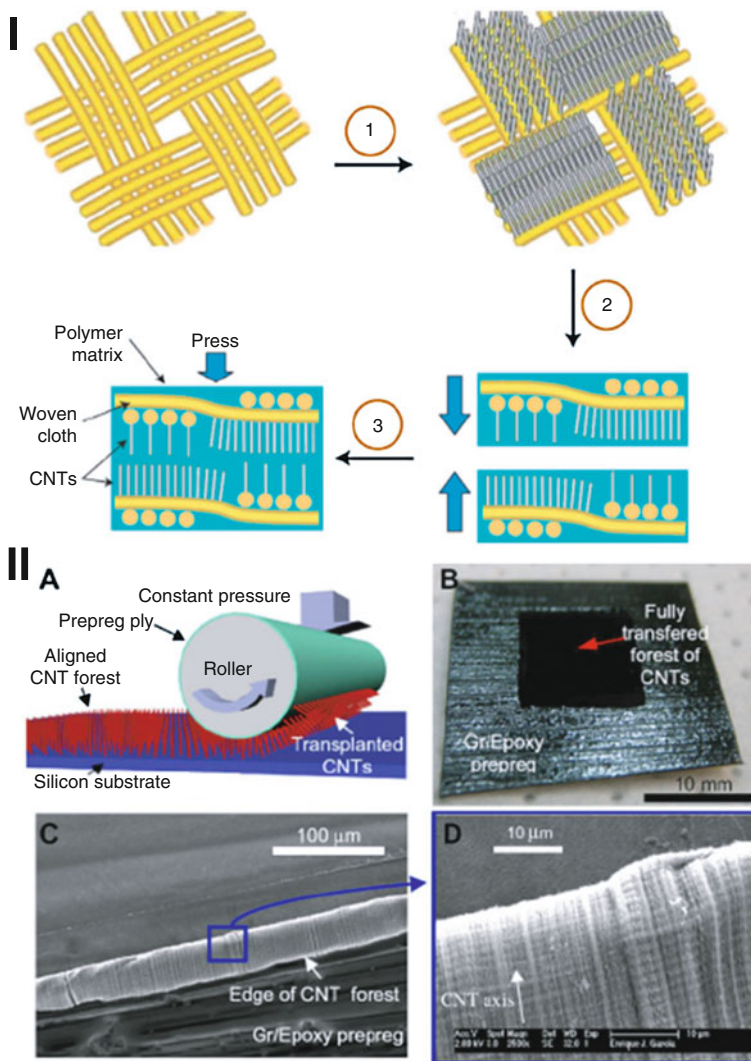


Fig. 7 (I) Representation of laminated composite fabrication: (1) fiber cloth aligned with nanotubes; (2) stacking of fiber cloth grown with matrix-infiltrated CNT; (3) hand lay-up fabrication of nanocomposite laminates. (II) Transfer-printing of vertically-aligned CNTs to prepreg: (A) transfer-printing process demonstration; (B) CNT forest fully transplanted to the surface of a Gr/Ep prepreg ply from its original silicon substrate; (C and D) CNT forest SEM images, indicating the CNT orientation after transplantation

manufacturing routes to produce CNT fiber-reinforced composites to get improved properties [69, 70].

CNT fiber stretchable conductors can be fabricated with modest prestraining – then buckling approach [71]. A thin layer of liquid PDMS is coated on to CNT fibers

before transferring to the prestrained substrate. The fiber-PDMS substrate interfacial bonding can be thus enhanced and facilitate the buckling formation.

2.5 Metal Oxide Nanofibers

Metal oxide nanofibers are produced by the combination of electrospinning and sol gel methods. Metal oxide precursors are first mixed with polymer solution and calcinated at high temperature. During this process, the polymer is removed and metal oxide nanofibers are obtained. Silica is the most common filler used to improve thermomechanical properties of polymers in microelectronic devices. This is because of its electrical insulation properties, low CTE, good mechanical properties and low cost. But micron-sized particles are needed in order to get desirable mechanical properties. This can be achieved by the synthesis of nanosized silica fibers. Enhancements in the thermal conductivity and coefficient of thermal expansion were observed in silica nanofibers-filled epoxy when compared to silica nanoparticle-filled epoxy at low filler loadings. This high aspect ratio-filled epoxy has the potential to be used as a new generation of high-efficiency electronic encapsulation and underfill material [72].

3 Nanoscale Bio-Fillers

Science and technology now focus on producing more sustainable and environmentally-friendly materials due to the problems involved in plastic recycling and scarcity of the petroleum-based materials [73]. Nanoscale bio-fillers have engrossed plentiful attention in practical applications and academic research because of its excellent reinforcing capability to the polymer matrix. Bio-nanofillers, due to its greater aspect ratio, superior surface area, and exceptional properties, show substantial applications in various arenas. The use of nanocomposites with bio-nanofillers offers novel technological and commercial opportunities in automotive, electronics, and biotechnology industries.

We can classify the biomass-based nanofillers into three types:

1. Nanocellulose
2. Nanochitin
3. Starch nanocrystals

The development in the production of bio-fillers like cellulose, chitin, chitosan, and starch at the nanoscale attain abundant potential to diminish most of the sustainability issues. They are biodegradable and renewable. In this perspective, it is essential to generate more knowledge regarding the potential use of these bio-based fillers in various industrial applications. The use of bio-fibers as fillers is a growing trend nowadays and is attracted by many manufactures. The high specific stiffness, low cost, and flexibility during polymerization make them suitable for reinforcing in polymer composites.

3.1 Nanocelluloses

Nowadays, scientists are focused on the isolation and characterization of novel forms of cellulose: various forms are nanocrystals, whiskers, nanofibrils and nanofibers. Nanocelluloses are cellulosic materials having one dimension in nanometer. Chemically, cellulose is composed of D-glucose units linked with unbranched β (1–4) glycosidic bond [74]. Natural fibers consist of lignin matrix embedded with cellulose fibrils and can be considered as natural composites. The crystallinity and cellulose nature influence the reinforcing efficiency of natural fiber. Chemical compositions of some typical cellulose-containing materials are shown in Table 5. Nanocelluloses have drawn much attention due to their unique properties, like high tensile strength, surface area to volume ratio, Young's modulus, and low coefficient of thermal expansion [75, 76]. All of these excellent properties make nanocellulose as a promising and potential material for the reinforcement in polymer nanocomposites [77]. Nanocelluloses can be classified into cellulose nanofibers (CNFs), cellulose nanocrystals (CNCs), and bacterial nanocellulose (BNC). The CNCs have nano-dimensions in both length and diameter wise, whereas the CNFs have diameter at nanoscale and length up to several micrometers. Moreover, CNFs have both amorphous and crystalline region. But CNCs only have crystalline phase as shown in Fig. 8. Normally CNFs and CNCs have been extracted via chem mechanical treatments and strong acid hydrolysis, respectively. In the acid hydrolysis process,

Table 5 Chemical compositions of some typical cellulose-containing materials. (Copyright 2012 [78]. Modified with permission from Elsevier)

Source	Cellulose (%)	Hemicellulose (%)	Lignin (%)
Hard wood	43–47	25–35	16–24
Soft wood	40–44	25–29	25–31
Bagasse	40	30	20
Coir	32–43	10–20	43–49
Corn cobs	45	35	15
Corn stalks	35	25	35
Cotton	95	2	1
EFB	50	30	17
Flax(retted)	71	21	2
Flax (unretted)	63	12	3
Hemp	70	22	6
Henequen	78	4–8	13
Jute	71	14	13
Kenaf	31	26	18
Ramie	76	17	1
Sisal	73	14	11
Sunn	80	10	6
Wheat straw	30	50	15
Banana fibers	63–64	19	5

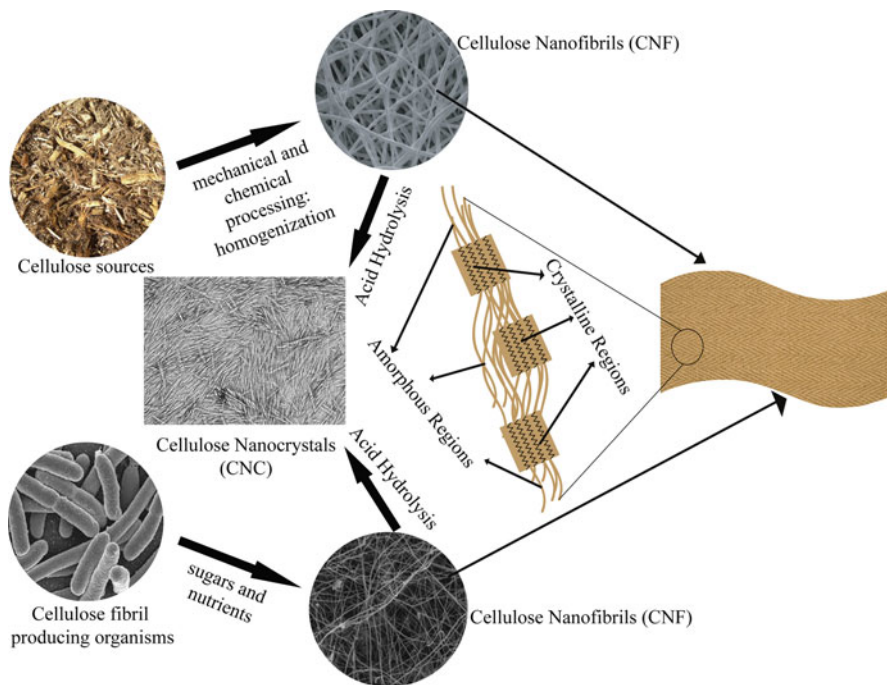


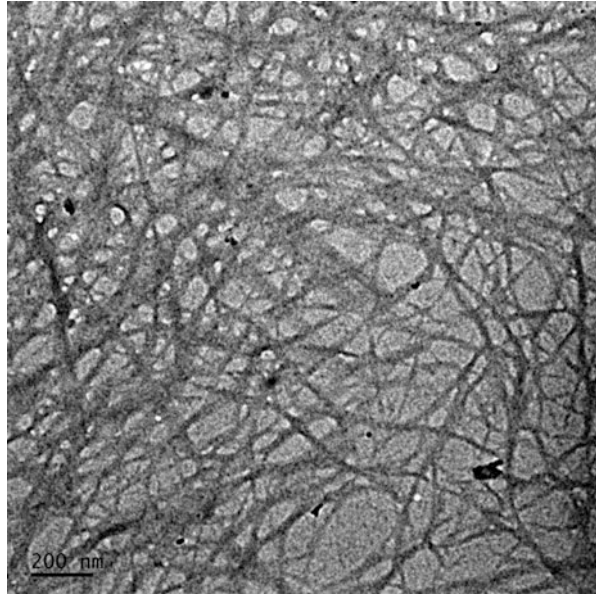
Fig. 8 Representation of fabrication of cellulose nanomaterials from different sources [79]

strong acid like sulfuric acid have been employed for the reaction and it destroys the amorphous portions (disordered region) and lead to the nanocrystal structure.

Many procedures are reported for the extraction of cellulose nanofibers (CNFs). Steam explosion coupled with the mild acid hydrolysis is generally employed as an efficient method to extract cellulose nanofibers. Fortunati et al. [80] reported the extraction of the cellulose nanofibers (shown in Fig. 9) from the sunflower stalks by the steam explosion process in an autoclave. Chirayil et al. [81] employed the steam explosion process for extracting cellulose nanofibers from isora fiber in an autoclave. This techniques involved alkaline treatment, bleaching, acidic steam treatment, and homogenization. The prepared cellulose nanofibers have nanofibrillar network-like structure with high crystallinity and good thermal stability. High-intensity ultrasonic treatment is the technique for the extraction of cellulose nanofibers.

Nanocellulose fibers were prepared by pretreating cellulose in NaOH/urea/thiourea solution. The fibers were then defibrillated by ultrasonication. They achieved high yield of 85.4% [77]. The obtained nanocellulose fibers were about 30 nm in diameter having cellulose II crystal structure. Cryocrushing is an alternative method for producing nanofibers. During the process, the frozen fibers are subjected to high impact forces where the ice crystals exert pressure on the cell wall leading them to rupture and form microfibrils. Nanofibers were isolated from soybean stock using cryocrushing together with a high-pressure fibrillation process. The fibers were having diameters in the range 50–100 nm. Grinding is the process for the extraction of cellulose nanofibers from

Fig. 9 TEM image of the cellulose nanofibers [80]



microcrystalline cellulose [82]. Cellulose nanofibers were obtained with uniform width of 15 nm from wood by the grinding in an undried state [83].

CNCs are typically prepared by acid hydrolysis of the macrocellulose including cotton linters, wood pulp, and microcrystalline cellulose. A strong acid treatment to the amorphous region in the cellulose microfibrils helps to extract the highly crystalline part. The subsequent rod-like crystals after the acid hydrolysis are known as cellulose nanocrystals and their diameter usually ranges from 5 to 20 nm. The size depends on the nature of the cellulosic source and condition of acid hydrolysis.

Danial et al. [84] extracted CNCs from waste paper by acid hydrolysis using 60% (V/V) H_2SO_4 solution at 45 °C with constant stirring. CNCs with length ranged in 100–300 nm, as shown in Fig. 10, were obtained and also observed that newspaper can serve as a precursor for the effective production of CNCs. Similar results were reported by Kargarzadeh et al. [85], using H_2SO_4 acid hydrolysis of kenaf fibers. They extracted the CNCs from kenaf bast fibers by mechanical stirring using 65 wt% of H_2SO_4 at various reaction times.

3.2 Nanochitin

Chitin can be considered as the abundant naturally occurring polymer next to cellulose. They are observed in the cell wall of yeast, fungi, and exoskeleton of arthropods as their structural constituent. Chitin and cellulose are similar type of polysaccharides where cellulose have hydroxyl group and chitin have acetamide group. Chitin has high molecular weight with β (1-4) (*N*-acetyl-D-glucosamine) as shown in Fig. 11. The high crystallinity and mechanical strength of nanochitin make it as a suitable

candidate for reinforcement in polymer nanocomposites. Chitin is natural, nontoxic, nonallergic, antimicrobial, and biodegradable and is insoluble in water.

Several literatures have been reported about the extraction of nanochitin from different sources. Acid hydrolysis is the well-known procedure to extract nanochitin from sea food wastes. Chitin nanowhiskers were successfully extracted from crab shells and squid pens by hydrochloric acid hydrolysis [86].

Similarly, Gopalan et al. [87] prepared protein-free chitin whiskers suspensions via hydrolyzing the purified chitin sample with 3N HCl at the boil for 90 min under stirring. Chitin nanowhiskers had aspect ratio close to 16 which is shown in Fig. 12.

3.3 Starch Nanocrystals

Starch has established substantial attention during the past two decades due to its high strength and biodegradability. Amylose and amylopectin together form starch.

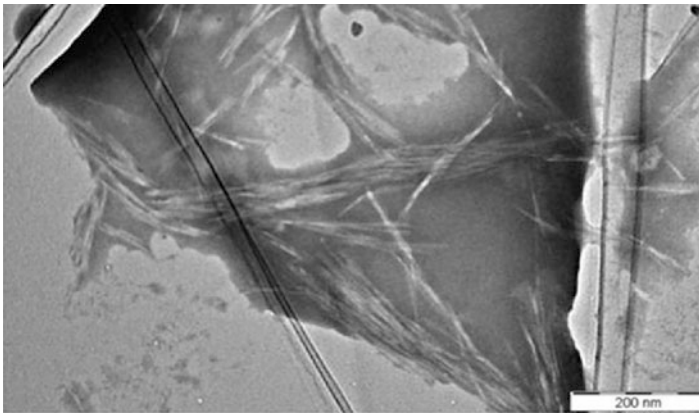
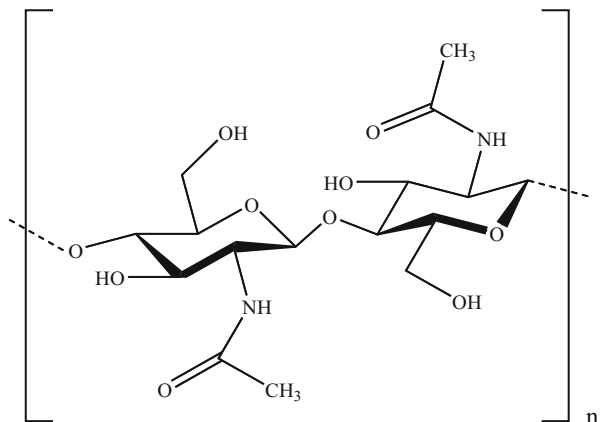


Fig. 10 TEM image of cellulose nanocrystals [84]

Fig. 11 Chitin chemical structure with β -1,4 linkage



Amylose is a linear or slightly branched $(1 \rightarrow 4)\text{-}\alpha\text{-D-glucan}$ and amylopectin is a highly branched $(1 \rightarrow 4)\text{-}\alpha\text{-D-glucan}$ short chains linked through $\alpha\text{-}(1 \rightarrow 6)$ linkages [88]. Figure 13 illustrates the inner structure of the starch granule and chemical structure of amylopectin. Chen et al. [89] extracted starch nanocrystals from potato starch granules having width of 10–20 nm and length of 40–70 nm (Fig. 14). They dispersed 36.725 g of potato starch granules in 250 mL 3.16 M sulfuric acid aqueous solution by stirring for 5 days at 40 °C.

3.4 Bio-Nanofillers as Reinforcement for Polymer Nanocomposites

Abundant reports are there about the reinforcing effect of the bio-nanofillers like cellulose nanocrystals, cellulose nanofibers, chitin nanocrystals, and starch nanocrystals. Cellulose nanocrystals or cellulose nanowhiskers are used as reinforcement

Fig. 12 TEM images of chitin whiskers [87] (inset: typical electron diffractogram of chitin fragments)

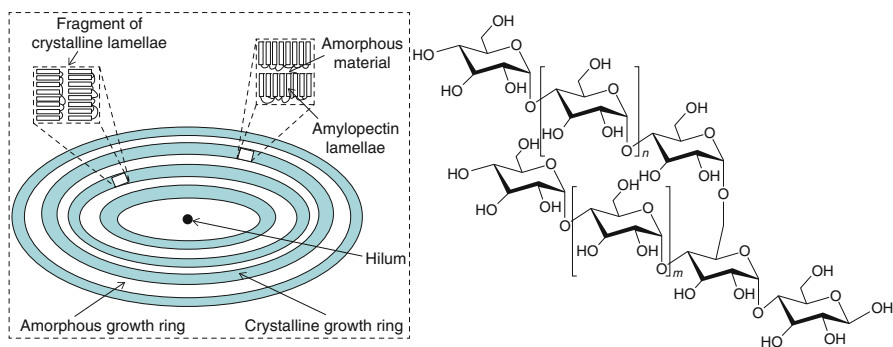
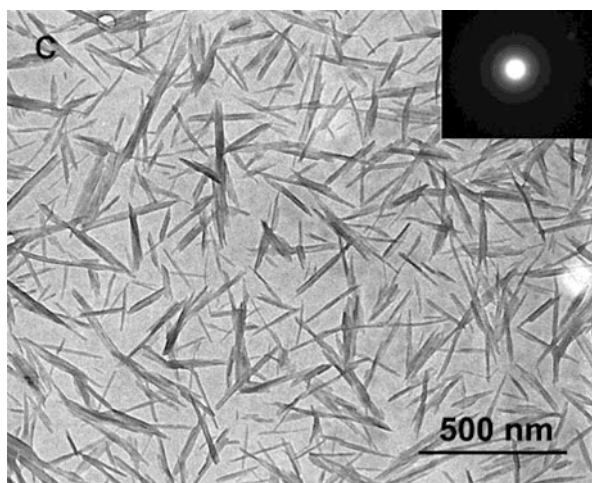
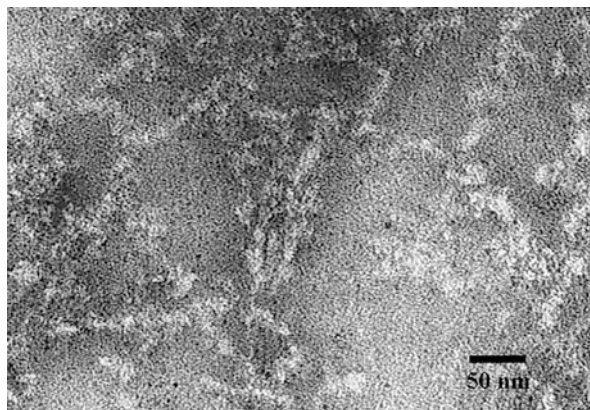


Fig. 13 Representation of starch granule structure and amylopectin molecule [90]

Fig. 14 TEM image of starch nanocrystals from potato starch granules [89]



in plastic and rubber matrices. Nanocellulose are also used as reinforcement for various polymer including poly(propylene), poly(styrene), and high density poly(ethylene) [91]. Similarly, cellulose nanowhiskers showed strong reinforcement capability [92, 93]. Cellulose nanowhiskers are derived from tunicate and reinforced with styrene and butyl acrylate copolymer latex. Even at low cellulose nanowhisker loading, the nanocomposites had significant enhancement in mechanical properties than the neat polymer in its elastomeric effect.

Cellulose nanofibers can be isolated from soybean source via combined mechanical and chemical treatments. The addition of cellulose nanofibers will significantly change the stress-strain behavior of the composites. There will be improvement in the thermal properties of poly(vinyl alcohol) PVA when cellulose nanofibers is added [82]. Cellulose nanofibers-reinforced PLA nanocomposite can be prepared by twin screw extrusion. The tensile modulus and strength were increased for nanocomposites with 5 wt% cellulose nanofibers from 2.9 GPa and 58 MPa to 3.6 GPa and 71 MPa correspondingly [94].

Colloidal suspension of chitin nanowhiskers and latex of both unvulcanized and prevulcanized NR can be used to prepare chitin nanowhisker-reinforced NR nanocomposites. The solid nanocomposite films were developed by casting and evaporating methods. Evaporated samples of chitin whiskers having nano size are observed to form a three-dimensional rigid network. These observations were based on the bound rubber content, diffusion coefficient, and relative weight loss values [87]. On carrageenan polymer matrix, the chitin nanofibers are well dispersed and thus form smooth and flexible composite films. Carrageenan film modulus and tensile strength increase significantly ($p < 0.05$) after reinforcement with chitin nanofibers (up to 5 wt%). Moreover, they were prominent against the growth of Gram-positive foodborne pathogen [95]. The tensile testing of the chitin nanowhisker films prepared by using ionic liquid 1-allyl-3-methylimidazolium bromide (AMIMBr) in polyvinyl alcohol (PVA) matrix indicates mechanical property enhancement with increase in the ratio of PVA to chitin [96]. The mechanical performance were studied for starch-based composite reinforced with novel chitin

nanoparticles prepared by blending glycerol plasticized potato starch (GPS) and chitin nanoparticles (CNP) by casting and evaporation [97]. CNP showed uniform dispersion in the GPS matrix at low loading levels. In GPS/CNP composites, the filler and matrix were having impressive interaction. This results in improving the glass transition temperature, tensile strength, storage modulus, and water vapor barrier properties. But aggregation of CNP occurs at higher loading (greater than 5 wt %) by negatively affecting their properties. The mechanical properties of the cross-linked carboxylated SBR composites reinforced with chitin nanocrystals were water-responsive. The swollen composites exhibited decreased strength and modulus. The significant reinforcement effect of chitin nanocrystals on cross-linked carboxylated SBR was attributed to the unique structure of chitin nanocrystals and their interfacial interactions in the composite [98]. The prominent improvement of mechanical performance of starch nanocrystals developed from potato starch granules is ascribed to persistent stress of rigid starch nanocrystals and stress transferring interceded with robust interaction on the interface between starch nanocrystals nanofiller and waterborne poly urethane matrix [89]. Pullulan film reinforced with starch nanocrystal nanocomposites can be prepared using an amorphous matrix of sorbitol-plasticized pullulan with aqueous suspension of starch nanocrystals as the reinforcing phase. Because of the starch nanocrystals interaction and filler-matrix interaction, there is restriction of the mobility of pullulan chains. These consequences in increasing the amount of nanocrystals and higher temperature shift of glass transition temperature. For the samples conditioned at different environments, the strain at break in the samples are drastically decreased by enhancing the tensile strength and the Young's modulus. This can be attributed to the addition of the nanocrystals [99].

4 Summary

The profuse use of various fiber-reinforced composites in different areas shows the importance of studying and investigation about them. Different types of fibers offer different properties and can be applied in variety of areas. From macro to nanoscale, these materials showed fantabulous changes in their properties. Knowledge on fibers and fillers used in fiber-reinforced composite is very important to tailor-make new materials having superior properties. Development of new composite indeed needs better understanding on fiber-filler interaction. So, studies on these materials show exceptional importance nowadays.

References

1. A.M. Martin, *Introduction of Fiber Reinforced Polymers-Polymer and Composites: Concepts, Properties and Process* (INTECH Open Science, Rijeka, Croatia 2013)
2. S. Kalpakjian, S.R. Schmid, *Manufacturing Engineering and Technology* (Pearson, Upper Saddle River, 2014)

3. H. Qiting, G. Sufyan, L. Zhengmei, J. He, Q. Wei, L. Fang, K.V. Pekka, V.J.L. Lippo, Properties of discontinuous S2-glass fiber-particulate-reinforced resin composites with two different fiber length distributions. *J. Prosthodont. Res.* (2017). <https://doi.org/10.1016/j.jpor.2017.03.002>
4. F.C. Campbell, *Structural Composite Materials* (ASM International, Ohio, 2010)
5. S. Prachi, R. Sonu, R. Sunita, R. K. Diwan, Polypropylene/glass fiber composites for low cost orthotic aid, in *Recent Trends in Materials and Devices* (Springer, Cham, 2017)
6. Z. Zheng, Y. Gangfei, W. Helong, Y. Jie, K. Sritawat, C. Guozhong, Bistable behaviour and microstructure characterization of carbon fiber/epoxy resin anti-symmetric laminated cylindrical shell after thermal exposure. *Compos. Sci. Technol.* (2017). <https://doi.org/10.1016/j.compscitech.2016.11.019>
7. J. Wu, H. Chen, Q. Wu, H. Liu, Z. Luo, Surface modification of carbon fibers and the selective laser sintering of modified carbon fiber/nylon 12 composite powder. *Mater. Des.* (2017). <https://doi.org/10.1016/j.matdes.2016.12.037>
8. T.K. Nicholas, T.D. Lawrence, L. Andre, A. Per, Nanoscale toughening of carbon fiber reinforced/epoxy polymer composites (CFRPs) using a triblock copolymer. *Polymer* (2017). <https://doi.org/10.1016/j.polymer.2017.01.009>
9. M. Maria, P. Paolo, P. Francesco, B. Fabrizio, L. Alberto, B. Ludovica, P. Paolo, Biological and mechanical characterization of carbon fiber frameworks for dental implant applications. *Mater. Sci. Eng. C* **70**, 646–655 (2017)
10. L. Hui, E. Karl, Recycling of carbon fiber-reinforced thermoplastic composite wastes from the aerospace industry. *J. Compos. Mater.* (2017). <https://doi.org/10.1177/0021998316671796>
11. C. Tong, X. Ping, J. Mingyin, The property of polycarbonate/acrylonitrile butadiene styrene-based conductive composites filled by nickel-coated carbon fiber and nickel-graphite powder. *Polym. Compos.* **38**, 157–163 (2017)
12. L. Yong, P. Shuai, C. Yongjie, C. Xuefeng, Z. Chenyu, H. Xianhua, H. Keqing, Y. Muhuo, Fabrication and properties of precursor-derived SiBN ternary ceramic fibers. *Mater. Des.* **128**, 150–156 (2017)
13. N. Sun, W. Chi, J. Liying, Z. Juan, Z. Dahai, Controllable coating of boron nitride on ceramic fibers by CVD at low temperature. *Ceram. Int.* **43**, 1509–1516 (2017)
14. G. Yanzi, W. Hao, J. Ke, S. Changwei, W. Xiaozhou, Preparation and characterization of SiC fibers with diverse electrical resistivity through pyrolysis under reactive atmospheres. *J. Eur. Ceram. Soc.* **37**, 517–522 (2017)
15. J. Xiaoyu, S. Changwei, W. Hao, C. Jun, L. Hao, Curing green fibres infusible by electron beam irradiation for the preparation of SiBNC ceramic fibres. *Ceram. Int.* (2017). <https://doi.org/10.1016/j.ceramint.2017.05.171>
16. T.W. Frederick, Strong, small diameter, boron fibers by LCVD. *Mater. Lett.* **14**, 198–202 (1992)
17. D.D. John, C.D. David, Mechanism and kinetics of MgB₂ synthesis from boron fibers. *Acta Mater.* **56**, 5751–5763 (2008)
18. K.M. Prewo, K.G. Kreider, The transverse tensile properties of boron fiber reinforced aluminum matrix composites. *Metall. Trans.* **3**, 1972–2201 (1972)
19. Y. Kimura, Y. Kubo, N. Hayashi, High-performance boron-nitride fibers from poly (borazine) preceramics. *Compos. Sci. Technol.* **51**, 173–179 (1994)
20. K.Q. Qui, A.M. Wang, H.F. Zhang, B.Z. Ding, Z.Q. Hu, Mechanical properties of tungsten fiber reinforced ZrAlNiCuSi metallic glass matrix composite. *Intermetallics* **10**, 1283–1288 (2002)
21. H. Gietl, J. Riesch, J.W. Coenen, T. Hoschen, C. Linsmeier, R. Neu, Tensile deformation behavior of tungsten fibre-reinforced tungsten composite specimens in as-fabricated state. *Fusion Eng. Des.* (2017). <https://doi.org/10.1016/j.fusengdes.2017.02.054>
22. W. Bingjie, Q. Wu, S. Hao, Z. Jing, R. Jing, L. Yongfeng, W. Min, P. Huisheng, An intercalated graphene(molybdenum disulfide) hybrid fiber for capacitive energy storage. *J. Mater. Chem. A* **5**, 925–930 (2017)
23. R. Malkapuram, V. Kumar, Y.S. Negi, Recent development in natural fiber reinforced polypropylene composites. *J. Reinf. Plast. Compos.* **28**, 1169–1189 (2008)

24. K.M. Praveen, S. Thomas, Y. Grohens, M. Mozetic, I. Junkar, G. Primc, M. Gorjanc, Investigations of plasma induced effects on the surface properties of lignocellulosic natural coir fibers. *Appl. Surf. Sci.* **368**, 146–156 (2016)
25. M.J. John, S. Thomas, Biofibers and biocomposites. *Carbohydr. Polym.* **71**, 343–364 (2008)
26. J. Holbery, D. Houston, Natural-fiber-reinforced polymer composites in automotive applications. *J. Miner. Met. Mater. Soc.* **58**, 80–86 (2006)
27. R.F. Gibson, *Principles of Composites Material Mechanics* (McGraw-Hill, New-York, 1994)
28. E.K. Gamstedt, P. Nygard, M. Lindstrom, Transfer of knowledge from papermaking to manufacture of composite materials, in *Proceedings of the 3rd Wood Fiber Polymer Composites International Symposium*, Bordeaux, 2007
29. N.M. Stark, R.E. Rowlands, Effects of wood fiber characteristics on mechanical properties of wood/polypropylene composites. *Wood Fiber Sci.* **35**, 167–174 (2003)
30. B. Sanschagrín, S.T. Sean, B.V. Kokta, Mechanical properties of cellulose fibers reinforced thermoplastics, in *Proceedings of the 43rd Annual Conference, Composites Institute, February*, The Society of the Plastics Industry, Cincinnati, 1998
31. S. Migneault, A. Koubaa, F. Erchiqui, A. Chaala, K. Englund, C. Krause, Effect of fiber length on processing and properties of extruded wood-fiber/HDPE composites. *J. Appl. Polym. Sci.* **110**, 1085–1092 (2008)
32. M. Le Baillif, K. Oksman, The influence of the extrusion process on bleached pulp fiber and its composites, in *Proceedings of the Progress in Wood and Biofiberplastic Composites Conference*, Toronto, 2006
33. K.L. Yam, B.K. Gogoi, C.C. Lai, S.E. Selke, Composites from compounding wood fibers with recycled high density polyethylene. *Polym. Eng. Sci.* **30**, 693–699 (1990)
34. F.-L. Zhou, R.-H. Gong, Manufacturing technologies of polymeric nanofibers and nanofiber yarns. *Polym. Int.* **57**, 837–845 (2008)
35. K. Jayaraman, M. Kotaki, Y. Zhang, X. Mo, S. Ramakrishna, Recent advances in polymer nanofibers. *J. Nanosci. Nanotechnol.* **4**, 52–65 (2004)
36. E. Frank, F. Hermanutz, R.B. Michael, Carbon fibers: precursors, manufacturing and properties. *Macromol. Mater. Eng.* **297**, 493–501 (2012)
37. L. Feng, N. Xie, J. Zhong, Carbon nanofibers and their composites: a review of synthesizing, properties and applications. *Materials* **7**, 3919–3945 (2014)
38. F.W.J. Van Hattum, P. Serp, J.L. Figueiredo, C.A. Bernardo, The effect of morphology on the properties of vapour-grown carbon fibers. *Carbon* **35**, 860–863 (1997)
39. High Performance Synthetic Fibers for Composites, Commission on Engineering and Technical Systems, National Research Council, *High-Performance Synthetic Fibers for Composites*, vol 23 (National Academy Press, Washington, 1992), pp. 56–64
40. L. Zhang, A. Aboagye, A. Kelkar, C. Lai, H. Fong, A review: carbon nanofibers from electrospun polyacrylonitrile and their applications. *J. Mater. Sci.* **49**, 463–480 (2014)
41. K. Lozano, J. Bonilla-Rios, E.V. Barrera, A study on nanofiber-reinforced thermoplastic composites (II): investigation of the mixing rheology and conduction properties. *J. Appl. Polym. Sci.* **80**, 1162–1172 (2001)
42. J. Li, M.J. Vergne, E.D. Mowles, W.H. Zhong, D.M. Hercules, C.M. Lukehart, Surface functionalization and characterization of graphitic carbon nanofibers. *Carbon* **43**, 2883–2893 (2005)
43. S. Jan, P. Werner, S.P.S. Milo, D. Vitaly, A. Volker, H.W. Alan, Carbon-nanofiber-reinforced poly(ether ether ketone) composites. *Compos. Part A* **33**, 1033–1039 (2002)
44. J.R. Alejandro, M.E. Guzman, L. Chee-Sern, M. Bob, Mechanical properties of carbon nanofiber/fiber-reinforced hierarchical polymer composites manufactured with multiscale-reinforcement fabrics. *Carbon* **49**, 937–948 (2011)
45. X.-F. Wu, R. Arifur, Z. Zhengping, D.P. David, S. Sinha-Ray, C. Bin, P. Scott, A.L. Yarin, Electrospinning core-shell nanofibers for interfacial toughening and self-healing of carbon-fiber/epoxy composites. *J. Appl. Polym. Sci.* **129**, 1383–1393 (2013)

46. Y. Shi, X. Feng, H. Wang, X. Lu, J. Shen, Tribological and mechanical properties of carbon-nanofiber-filled polytetrafluoroethylene composites. *J. Appl. Polym. Sci.* **104**, 2430–2437 (2007)
47. W. Philipp, A. Volker, J. Romy, J. Olaf, J.K.W. Sandler, M.S.P. Shaffere, A.H. Windle, Tribological behaviour of carbon-nanofiber-reinforced poly(ether ether ketone). *Wear* **257**, 1006–1014 (2004)
48. S. Kumara, T. Rath, R.N. Mahaling, C.S. Reddy, C.K. Das, K.N. Pandey, R.B. Srivastava, S.B. Yadaw, Study on mechanical, morphological and electrical properties of carbon nanofiber/polyetherimide composites. *Mater. Sci. Eng. B* **141**, 61–70 (2007)
49. Y. Shi, X. Feng, H. Wang, X. Lu, The effect of surface modification on the friction and wear behavior of carbon nanofiber-filled PTFE composites. *Wear* **264**, 934–939 (2008)
50. P. Cortés, K. Lozano, E.V. Barrera, J. Bonilla-Rios, Effects of nanofiber treatments on the properties of vapor-grown carbon fiber reinforced polymer composites. *J. Appl. Polym. Sci.* **89**, 2527–2534 (2003)
51. L. Karen, Y. Shuying, Z. Qiang, Rheological analysis of vapor-grown carbon nanofiber-reinforced polyethylene composites. *J. Appl. Polym. Sci.* **93**, 155–162 (2004)
52. R.N. Maria, R. Marialuigia, L. Khalid, F. Annalisa, R. Salvatore, G. Liberata, Relationships between nanofiller morphology and viscoelastic properties in CNF/epoxy resins. *Polym. Compos.* **36**, 1152–1160 (2015)
53. J.P. Antonio, J. Silva, F.W.J. Van Hattum, S. Lanceros-Mendez, A.I. Ares, Rheological and electrical analysis in carbon nanofiber reinforced polypropylene composites. *J. Polym. Sci. B Polym. Phys.* **51**, 207–213 (2013)
54. M.H. Al-Saleh, S. Uttandaraman, A review of vapor grown carbon nanofiber/polymer conductive composites. *Carbon* **47**, 2–22 (2009)
55. B.O. Lee, W.J. Woo, M.S. Kim, EMI shielding effectiveness of carbon nanofiber filled poly(vinyl alcohol) coating materials. *Macromol. Mater. Eng.* **286**, 114–118 (2001)
56. J.H. Wu, D.D.L. Chung, Increasing the electromagnetic interference shielding effectiveness of carbon fiber polymer–matrix composite by using activated carbon fibers. *Carbon* **40**, 445–447 (2002)
57. B. De Vivo, P. Lamberti, G. Spinelli, V. Tucci, L. Guadagno, M. Raimondo, The effect of filler aspect ratio on the electromagnetic properties of carbon-nanofibers reinforced composites. *J. Appl. Phys.* **118** (2015). <https://doi.org/10.1063/1.4928317>
58. F. Nanni, P. Travaglia, M. Valentini, Effect of carbon nanofibers dispersion on the microwave absorbing properties of CNF/epoxy composites. *Compos. Sci. Technol.* **69**, 485–490 (2009)
59. K. Lozano, E.V. Barrera, Nanofiber-reinforced thermoplastic composites. I. Thermoanalytical and mechanical analyses. *J. Appl. Polym. Sci.* **79**, 125–133 (2001)
60. A.S. Muhammad, H.E.N. Anwer, Study on the morphological, dynamic mechanical and thermal properties of PLA carbon nanofiber composites. *Compos. Part B Eng.* **91** (2016). <https://doi.org/10.1016/j.compositesb.2016.01.039>
61. A.J. Paleoa, X. Garciaa, L. Arboleda-Clementea, F.W. Van Hattumb, M.J. Abada, A. Aresa, Enhanced thermal conductivity of rheologically percolated carbon nanofiber reinforced polypropylene composites. *Polym. Adv. Technol.* **26**, 369–375 (2015)
62. M.A. Raza, A.V.K. Westwood, C. Stirling, R. Ahmad, Effect of boron nitride addition on properties of vapour grown carbon nanofiber/rubbery epoxy composites for thermal interface applications. *Compos. Sci. Technol.* **120**, 9–16 (2015)
63. H. Lu, F. Liang, Y. Yao, J. Gou, D. Hui, Self-assembled multi-layered carbon nanofiber nanopaper for significantly improving electrical actuation of shape memory polymer nanocomposite. *Compos. Part B* **59**, 191–195 (2014)
64. Z. Tang, D. Sun, D. Yang, B. Guo, L. Zhang, D. Jia, Vapor grown carbon nanofiber reinforced bio-based polyester for electroactive shape memory performance. *Compos. Sci. Technol.* **75**, 15–21 (2013)
65. K. Vikas, R.B. Bhavik, Carbon nanofiber polymer composites: evaluation of life cycle energy use. *Environ. Sci. Technol.* **43**, 2078–2084 (2009)

66. X.F. Zhang, Q.W. Li, T.G. Holesinger, P.N. Arendt, J.Y. Huang, P.D. Kirven, T.G. Clapp, R.F. DePaula, X.Z. Liao, Y.H. Zhao, L.X. Zheng, D.E. Peterson, Y.T. Zhu, Ultrastrong, stiff, and lightweight carbon-nanotube fibers. *Adv. Mater.* **19**, 4198–4201 (2007)
67. W. Lu, M. Zu, J.-H. Byun, B.-S. Kim, T.-W. Chou, State of the art of carbon nanotube fibers: opportunities and challenges. *Adv. Mater.* **24**, 1805–1833 (2012)
68. Y.N. Liu, M. Li, Y. Gu, X. Zhang, J. Zhao, Q. Li, Z. Zhang, The interfacial strength and fracture characteristics of ethanol and polymer modified carbon nanotube fibers in their epoxy composites. *Carbon* **52**, 550–558 (2013)
69. V.P. Veedu, A.Y. Cao, X.S. Li, K.G. Ma, C. Soldano, S. Kar, Multifunctional composites using reinforced laminae with carbon-nanotube forests. *Nat. Mater.* **5**, 457–462 (2006)
70. E.J. Garcia, B.L. Wardle, A.J. Hart, Joining prepreg composite interfaces with aligned carbon nanotubes. *Compos. A: Appl. Sci. Manuf.* **39**, 1065–1070 (2008)
71. M. Zu, Q. Li, G. Wang, J.-H. Byun, T.-W. Chou, Carbon nanotube fiber based stretchable conductor. *Adv. Funct. Mater.* **23**, 789–793 (2013)
72. L. Ren, K. Pashayi, R.F. Hafez, P.K. Shiva, T. Borca-Tasciuc, R. Ozisik, Engineering the coefficient of thermal expansion and thermal conductivity of polymers filled with high aspect ratio silica nanofibers. *Compos. Part B Eng.* **58**, 228–234 (2014)
73. W., P.F. Neto, A.S. Hudson, O.D. Noelio, P. Daniel, Extraction and characterization of cellulose nanocrystals from agro-industrial residue—Soy hulls. *Ind. Crop. Prod.* **42**, 480–488 (2013)
74. J. Kim, Y. Sungryul, O. Zoubaida, Discovery of cellulose as a smart material. *Macromolecules* **39**, 4202–4206 (2006)
75. M.A., S. Azizi Samir, A. Fannie, D. Alain, Review of recent research into cellulosic whiskers, their properties and their application in nanocomposite field. *Biomacromolecules* **6**, 612–626 (2005)
76. T. Nishino, I. Matsuda, K. Hirao, All-cellulose composite. *Macromolecules* **37**, 7683–7687 (2004)
77. M. Li, L.-j. Wang, D. Li, Y.-L. Cheng, B. Adhikari, Preparation and characterization of cellulose nanofibers from de-pectinated sugar beet pulp. *Carbohydr. Polym.* **102**, 136–143 (2014)
78. A.H.P.S. Khalil, A.H. Bhat, A.F.I. Yusra, Green composites from sustainable cellulose nanofibrils: A review. *Carbohydr. Polym.* **87**, 963–979 (2012)
79. A.W. Carpenter, C.F. de Lannoy, M.R. Wiesner, Cellulose nanomaterials in water treatment technologies. *Environ. Sci. Technol.* **49**, 5277–5287 (2015)
80. E. Fortunati, F. Luzi, A. Jimenez, D.A. Gopakumar, D. Puglia, S. Thomas, J.M. Kenny, A. Chiralt, L. Torre, Revalorization of sunflower stalks as novel sources of cellulose nanofibrils and nanocrystals and their effect on wheat gluten bionanocomposite properties. *Carbohydr. Polym.* **149**, 357–368 (2016)
81. J.C. Cintil, J. Jithin, M. Lovely, M. Miran, K. Joachim, T. Sabu, Isolation and characterization of cellulose nanofibrils from *Helicteres isora* plant. *Ind. Crop. Prod.* **59**, 27–34 (2014)
82. B. Wang, S. Mohini, Isolation of nanofibers from soybean source and their reinforcing capability on synthetic polymers. *Compos. Sci. Technol.* **67**, 2521–2527 (2007)
83. K. Abe, I. Shinichiro, Y. Hiroyuki, Obtaining cellulose nanofibers with a uniform width of 15 nm from wood. *Biomacromolecules* **8**, 3276–3278 (2007)
84. W.H. Danial, A.M. Zaiton, N.M.M. Mohd, T. Sugeng, B.B. Mohd, R. Zainab, The reuse of wastepaper for the extraction of cellulose nanocrystals. *Carbohydr. Polym.* **118**, 165–169 (2015)
85. H. Kargarzadeh, A. Ishak, A. Ibrahim, D. Alain, Y.Z. Siti, M.S. Rasha, Effects of hydrolysis conditions on the morphology, crystallinity, and thermal stability of cellulose nanocrystals extracted from kenaf bast fibers. *Cellulose* **19**, 855–866 (2012)
86. M. Paillet, D. Alain, Chitin whisker reinforced thermoplastic nanocomposites. *Macromolecules* **34**, 6527–6530 (2001)
87. K. Gopalan Nair, D. Alain, Crab shell chitin whisker reinforced natural rubber nanocomposites. 1. Processing and swelling behavior. *Biomacromolecules* **4**, 657–665 (2003)

88. M. Paris, H. Bizot, J. Emery, J.Y. Buzare, A. Buleon, Crystallinity and structuring role of water in native and recrystallized starches by ^{13}C CP-MAS NMR spectroscopy: 1: Spectral decomposition. *Carbohydr. Polym.* **39**, 327–339 (1999)
89. G. Chen, M. Wei, J. Chen, J. Huang, D. Alain, P.R. Chang, Simultaneous reinforcing and toughening: new nanocomposites of waterborne polyurethane filled with low loading level of starch nanocrystals. *Polymer* **49**, 1860–1870 (2008)
90. L. Ning, H. Jin, R.C. Peter, P.A. Debbie, Y. Jiahui, Preparation modification and application of starch nanocrystals in nanomaterials: a review. *J. Nanomater.* **2011**, 573687, 13 (2011). <https://doi.org/10.1155/2011/573687>
91. A. Boldizar, C. Klason, J. Kubat, P. Näslund, P. Saha, Prehydrolyzed cellulose as reinforcing filler for thermoplastics. *Int. J. Polym. Mater.* **11**, 229–262 (1987)
92. V. Favier, H. Chanzy, J.Y. Cavaille, Polymer nanocomposites reinforced by cellulose whiskers. *Macromolecules* **28**, 6365–6367 (1995)
93. V. Favier, G.R. Canova, J.Y. Cavaille, H. Chanzy, A. Dufresne, C. Gauthier, Nanocomposite materials from latex and cellulose whiskers. *Polym. Adv. Technol.* **6**, 351–355 (1995)
94. M. Jonoobi, H. Jalaluddin, P.M. Aji, O. Kristiina, Mechanical properties of cellulose nanofiber (CNF) reinforced polylactic acid (PLA) prepared by twin screw extrusion. *Compos. Sci. Technol.* **70**, 1742–1747 (2010)
95. S. Shankar, P.R. Jeevan, R. Jong-Whan, K. Hee-Yun, Preparation, characterization, and antimicrobial activity of chitin nanofibrils reinforced carrageenan nanocomposite films. *Carbohydr. Polym.* **117**, 468–475 (2015)
96. J.-i. Kadokawa, T. Akihiko, M. Shozaburo, P. Kamalesh, Preparation of chitin nanowhiskers using an ionic liquid and their composite materials with poly (vinyl alcohol). *Carbohydr. Polym.* **84**, 1408–1412 (2011)
97. P., R. Chang, R. Jian, J. Yu, X. Ma, Starch-based composites reinforced with novel chitin nanoparticles. *Carbohydr. Polym.* **80**, 420–425 (2010)
98. L. Ma, M. Liu, Q. Peng, Y. Liu, B. Luo, C. Zhou, Crosslinked carboxylated SBR composites reinforced with chitin nanocrystals. *J. Polym. Res.* **23**(7), 1–11 (2016)
99. E. Kristo, G.B. Costas, Physical properties of starch nanocrystal-reinforced pullulan films. *Carbohydr. Polym.* **68**(1), 146–158 (2007)



Shah Mohammed Reduwan Billah

Contents

1	General Aspects of Composites and Nanocomposites	449
2	Composites	450
2.1	Different Types of Microcomposites	452
2.2	Basic Compositions and Selected Features of Composites	454
3	Nanocomposites	456
4	Types of Polymer Nanocomposites	457
4.1	Zero-Dimensional Nanocomposites (Such as Nanoparticles Based Systems)	458
4.2	One-Dimensional Nanocomposites (Such as Nanotubes and Nanowires)	459
4.3	Two-Dimensional Nanocomposites (Nanolayers Based Systems)	459
5	Selected Features of Polymer Nanocomposites	460
5.1	Crack Pinning	460
5.2	Crack Deflection	461
5.3	Immobilized Polymer	461
5.4	Debonding and Plastic Voids Growth	461
6	Discussion on Different Types of Selected Polymer Nanocomposites	461
6.1	Polymer/Carbon Nanotubes Based Nanocomposites	461
6.2	Polymer/Metal Nanocomposites	463
6.3	Polymer/Clay Nanocomposites	464
7	Designing Composites and Nanocomposites	464
8	Processing of Composites and Nanocomposites	467
8.1	Melt Blending	468
8.2	Solution Mixing or Solvent Casting	469
8.3	In Situ Polymerization	469
8.4	Electrospinning	470
8.5	Layer-by-Layer Deposition	471

S. M. R. Billah (✉)

University of East London, Stratford Campus, London, UK

CCIRA UK Limited, Galashiels, UK

Department of Chemistry, Durham University, Durham, UK

School of Textiles and Design, Heriot-Watt University, Galashiels, UK

e-mail: reduwan.shah@gmail.com

9	Environmental Stimuli-Responsive and Functional Polymer Composites and Nanocomposites	472
10	Selected Behaviors of Composites and Nanocomposites	473
	10.1 Reinforcement	473
	10.2 Electrical Conductivity	474
	10.3 Thermal Conductivity	475
	10.4 Thermal Stability	475
	10.5 Glass Transition Temperature	476
	10.6 Barrier Properties	477
	10.7 Antiflammability	478
11	Challenges for Composites and Nanocomposites	478
12	Bio-composites, Green Composites, and Nanocomposites	479
	12.1 Biocomposites	480
	12.2 Cellulose Nanocomposites	480
	12.3 Cellulose Composites	481
	12.4 Stimuli-Responsive Smart Cellulose Composites	482
	12.5 Bio-inspired Stimuli-Responsive Mechanically Dynamic Composites	482
13	Single Polymer Composites	482
14	Future Directions in Composites and Nanocomposites	483
15	Conclusion and Perspectives	486
	References	488

Abstract

In general, a composite is usually made up of two or more materials having two or more phases with heterogeneous characters, where at least one is in a microscopic scale. In addition, a composite can be classified as a nanocomposite when at least one of the reinforcement dimensions is in the nanometer range (from 10 to 200 nm). Both composites and nanocomposites have many promising mechanical, thermal, electrical, optical, and other interesting properties that make them a field of current active research interest both in academia and industry. This chapter selectively covers both fundamental and applied research involved mostly with polymer-based composites and nanocomposites along with a brief discussion on the future research directions for further improvements on high-performance composites and nanocomposites for a variety of conventional and high-tech applications.

A composite is usually made up of two or more materials having two or more phases with heterogeneous characters (where at least one is in a microscopic scale). They can be of different types. For example, a fiber-reinforced composite contains fibers of high strength and modulus, with dimensions on the order of microns, embedded in or bonded to a matrix with distinct interfaces between them. In this system, both fibers and matrix can retain their distinctive physical and chemical characters; however, in the resultant composite system, they produce a combination of properties that cannot be achieved with either of the constituents acting alone. Additionally, a composite can also be classified as a nanocomposite if at least one of the reinforcement dimension is in the nanometer range (10–200 nm). A nanocomposite illustrates many great promises not only in terms of superior mechanical performances, but also in terms of superior thermal, electrical, optical, and other properties. Usually, these properties are

manifested, at relatively low-reinforcement volume fractions. Some of the main reasons for such highly improved properties are (a) the properties of nano-reinforcements are considerably higher than the reinforcing fibers in use; (b) the ratio of their surface area to volume is very high, which provides a greater interfacial interaction with the matrix. Additives used in the production of polymer nanocomposites can be of different types, such as (a) one-dimensional (e.g., nanotubes and fibers), (b) two-dimensional (such as layered minerals like clay), (c) zero-dimensional (e.g., spherical particles). Over the past two decades, both micro- and nanocomposites have been successful to attract active research interests both in academia and industry because of their fantastic properties, such as outstanding mechanical properties (such as improvement in elastic stiffness and strength by adding only a small amount of the nanoadditives). These advantages can be contributed to the large surface area to volume ratio of nanoadditives when compared to the micro- and macroadditives. Some significant and superior characteristics of polymer micro- and nanocomposites include (a) barrier resistance, (b) flame retardancy, (c) scratch/wear resistance, (d) optical, magnetic, and electrical properties. This chapter covers both fundamental and applied research involved mostly with polymer-based micro- and nanocomposites, also presents possible directions for further improvements on high performance micro- and nanocomposites. Additionally, micro- and nanocomposites can also contain a huge variety of materials (such as functional materials, environmental stimuli-responsive materials, materials with specific target applications) with potentials for many conventional and high-tech industrial applications. So, this chapter also briefly covers selective aspects of different types of functional and environmentally responsive micro- and nanocomposites along with their particular current and potential applications.

1 General Aspects of Composites and Nanocomposites

Continuous academic and industrial research and development activities in the field of micro- and nanocomposites and their profound impacts on the designs and applications in materials used in various sectors involved with our everyday life and have an impact in our ever changing life-styles. Traditional materials are being gradually replaced by composite materials for attaining higher technical performances with cost-effectiveness. Composites are practically in use for ages, such as (a) concrete (which is basically a mixture of stones held together by cement) is a familiar material for building; (b) some particular natural composites (which are made of wood and bone) have been known to human civilization for a long time. However, during the last 40 years, the production of synthetic composites has been rapidly increased where one can link the spur of this rapid expansion over the last few decades with the development of carbon fibers (in the UK) and boron fibers (in the USA) in the early 1960s. These new fibers have high elastic characters which provide significant increase in the stiffness of composites (due to high modulus-to-weight and stiffness-to-weight ratio presented by these composites) which are suitable for a variety of applications [1–10]. For example, highly ordered polymer nanocomposites are complex materials which show sound morphological characters

due to their variations in compositions, structures, and properties on a nanometer length scale. Polymer nanocomposites are of different types. Metal-polymer nanocomposites are one of the important class and they are attractive due to their potential applications in low cost, high metal surface areas. A wide range of metals used in polymer nanocomposites are mostly involved with their one of the main application focused on catalytic systems which particularly use specific metals (such as Pt, Ni, Co, and Au, with known catalytic activities). Some of the most frequently utilized techniques usually used to prepare polymer/CNT and/or polymer/clay nanocomposites are (a) melt mixing, (b) solution casting, (c) electrospinning, and (d) solid-state shear pulverization. Variety of high-tech and conventional applications of nanocomposites make them a matter of current active research item and some of the potential applications of polymer/CNT and/or polymer/clay nanocomposites include (i) photovoltaic devices, (ii) optical switches, (iii) electromagnetic interference (EMI) shielding, (iv) aerospace and (v) automotive materials, (vi) packaging, (vii) adhesives, and (viii) coatings [11–32]. This chapter covers a broad range of topics mostly related to polymer based micro- and nanocomposites (such as polymer/carbon nanotubes, polymer/metal nanospheres, polymer/clay nanoplatelets micro- and nanocomposites). This chapter also presents different issues involved with the general overview, synthesis, and applications of micro- and nanocomposites in order to provide a general understanding on the fundamental features of these materials for both conventional and high-tech advanced materials.

2 Composites

Composites are made from two or more constituent materials with significantly different physical or chemical properties which have the capability to provide superior and unique characteristics different from their individual components [1]. Microcomposites are essentially a type of composites and people made and used composite for many centuries, for example, the earliest uses of composites date back to the 1500s B.C. when early Egyptians and Mesopotamian civilizations used a mixture of mud and straw to create strong and durable buildings. Fiber reinforced composites are another type of example which is the most common configuration for composite system. In addition, the modern era of composites begins with the development of synthetic polymers, such as plastics (such as vinyl, polystyrene, phenolic, and polyester) that were developed in early 1900s. These plastics alone could not provide enough strength for structural applications, as a result reinforcement was needed in order to provide the strength and rigidity. In this context, the easy processing character provides the great potential as composite matrix materials for these polymeric materials. As for instance, Owens Corning introduced the first glass fiber in 1935 and later the glass fiber was used to reinforce plastic polymers as the pioneer work of the Fiber Reinforced Polymers (FRP) industry as we know it today. When a reinforced polymer is prepared by the combination of a plastic polymer, it gives an incredibly strong structure and also lightweight materials. Different wars incubated the seeds for many of the greatest advancements in composites. The fiber reinforced polymer industry was brought into

real production from laboratory and developed extremely fast due to the need of lightweight applications in military aircraft during the World Wars. Due to the lightweight and strength of the composites, the engineers used these materials for various diverse range of applications. For instance, it was discovered that fiberglass composites were transparent to radio frequencies, and then the material was applied in sheltering electronic radar equipment. People began to try to fit composite into other markets in order to overcome the lower demand for military products when time elapsed into the peaceful times. As for instance, in the 1970s the composites industry began to mature and better plastic resins and improved reinforcing fibers were developed. A further example include the development of an aramid fiber known as Kevlar by Du Pont and carbon fiber was also developed around this time and these new fibers with improved properties brings more choice for the fiber reinforced composites [1]. At present, the current focus on the composite industry is on various functional applications of composite in different advanced areas, for example, in the areas of renewable energy. In addition, corrosion chemical resistant composites are highly resistant to chemicals and will never rust or corrode and boats made with fiberglass can stay in the highly corrosive salt water without any rusting. Composites with conductive particles dispersed in polymers have the capability to provide tunable conductivity and are widely used in industry as a type of conducting polymers. In most recent scientific studies, composites utilize even better fibers and resins and many of which incorporate nanomaterials to provide nanocomposites [2, 3]. Composites are often carefully designed for specific uses which are unlike many natural and artificial materials that are usually applied by chance only after they have been discovered or invented for particular applications. These composites have now been used for a wide range of products (such as from stealth bombers to smart cars and from bridges to oil rigs) although they were originally developed as light and strong materials for the aerospace industry in the mid-twentieth century [2–5, 8–15, 23–35]. Composites are usually synthesized by the combination of two or more natural or artificial materials in order to maximize their useful properties and minimize their weaknesses. Glass-fiber reinforced plastic (GRP) is one of the oldest and well-known composites which is made by the combination of strong and brittle glass fibers with flexible plastic to provide a composite material that is tough but not brittle. For example, composites have many typical applications in place of metals due to their similar strength but much lighter than metals. Most composites have fibers of one material which are tightly bound into another material that is termed as matrix. Similar to adhesive, the matrix binds the fibers together and makes them more resistant to external damage; however, the fibers make the matrix relatively stronger and stiffer and provide the desired resistance to cracks and fractures in the composite. For fiber-reinforced composites, in usual practice, different types of materials are used as fibers and matrix (although single polymer composites are also developed for various purposes). Typically used materials as fibers include (a) glass, (b) carbon, (c) silicon carbide, (d) asbestos. Examples of generally used materials as matrix include (a) different types of polymers (such as natural and synthetic polymers), (b) metals (e.g., gold, aluminum, silicon, platinum), (c) ceramic materials [36–47]. They are useful for the production of many conventional and high-tech composites widely used in a variety of industrial applications [1, 2, 48–55].

2.1 Different Types of Microcomposites

As already stated above that microcomposites are a type of composites, so the divisions of microcomposites are closely aligned with the types of composites. As a result, for a better explanation, different types of matrix which are used in various applications in order to produce common types of composites are briefly described here.

Polymer matrix composites – GRP (Glass Reinforced Plastic) is a well-known example of this type, where ceramic fibers are commonly used in a combination with a plastic matrix. There are other hundreds of examples of polymer matrix composites where different polymer matrices are used along with different additives.

Metal-matrix composites (MMCs) – this type of composite typically embed silicon carbide fibers in an alloy matrix (made of aluminum and magnesium). However, other matrix materials, for example, titanium, copper, and iron, are also used. There are many applications of MMCs some of main applications include (a) in sports items, (b) in missile guidance systems.

Ceramic-matrix composites (CMCs) – it is another major type composites. For instance, silicon carbide fibers fixed in a matrix made from a borosilicate glass. The ceramic matrix provides them a required suitability for their useful applications in lightweight, high-temperature components, such as parts for airplane jet engines [1–14].

2.1.1 Fiber-Reinforced Composites (FRCs)

A fiber-reinforced composite (FRC) is a mixture of two or more distinct constituents on a microscopic scale with different properties (e.g., the fiber/fabric reinforcement and the matrix) [1]. The reinforcement can be in either in a continuous or discontinuous form. Additionally, fiber-reinforced composites can be classified based on the nature of reinforcement as shown in Table 1.

The orientation of the reinforcement can be designed to give the correct level of mechanical properties where needed. The matrix can be of different types including polymer, ceramic, metals, etc. Polymers are the most common matrix for composite materials [1]. The mechanical properties of different classes of matrix material vary considerably. In addition, the processing techniques of different types of composites also have differences in some aspects which are shown in Table 2.

Another possible classification can be made according to the nature of the additional phase included within the composite structure, so that it is possible to identify two different classes of composite materials.

2.1.2 Nanoreinforced Composites

Nanoreinforced composite systems are based on the embodiment of nanoscaled fillers and nanomodification represents a reliable and solid procedure in order to produce next-generation of composites since small quantities are needed for enhancing their mechanical properties and modifying thermo-electrical behavior. Nanoscaled reinforcing can be in the form of nanoparticles, nanoplatelets, or nanotubes which are usually used by reinforcing both thermoset and thermoplastic polymers. More complex systems can be prepared by applying the nanoreinforced polymers as matrices for preparing multiscaled composites. These systems are characterized by

Table 1 Classification of fiber-reinforced composites

Composites					
Fiber reinforced					
Single layer		Multilayer		Particle reinforced	
Continuous fiber reinforced		Discontinuous fiber reinforced		Structural	
Unidirectional reinforcement	Woven reinforcement	Random orientation	Preferred orientation	Random orientation	Preferred orientation
				Hybrids	Sandwich panels
				Laminates	Laminates

Table 2 A general classification of composite processing. [33–36]

Composite Processings			
Processing of thermoset composites		Processing of thermoplastic composites	
Short-fiber based composites (such as injection, compression and liquid molding, spray-up)	Continuous fiber based composites (e.g., lay-up, filament winding, liquid molding, pultrusion)	Short-fiber based composites (for instance, injection and compression molding)	Continuous fiber based composites (e.g., thermoforming, lay-up, compression molding)

enhanced properties emerged from the superimposition of the nanoeffects provided by the nanofillers and the traditional effects of the traditional microsized long fibers [1, 2, 56–71].

2.1.3 Hybrid Composites

Hybrid composites are prepared including particular engineered phases within the traditional composite structure and by employing specific properties of such components. However, it is possible to enable extra reinforcement mechanisms or activate nonstructural features. For example, components of hybrid composites include metals and nanofluids through thickness reinforcements, optical fibers, and piezoelectric materials [1, 2, 33, 72–88].

2.2 Basic Compositions and Selected Features of Composites

Every major technical and scientific revolution always takes place in accompany of radical transformations in the field of material science which is clearly observed from the study of scientific history. At present microcomposite technology has an important role in modern engineering which is usually used to replace the traditional metallic materials in several industrial applications (e.g., aerospace, automotive, and shipping industry) in order to improve mechanical properties and reduce structural weight. One of the particular advantages of this kind of material include the possibility of using this for tailoring the properties of a specific part for meeting the requirements of different specific applications [89–120]. This opportunity has the capacity for leading to a material specifically designed and manufactured for that application by avoiding the problem of sophisticated designing [121–133]. In principle, a microcomposite is usually prepared by using two or more components that differ in form or composition on a macroscopic scale and are characterized by complementary properties. For example, the main difference with a traditional alloy is that in case of microcomposites each constituent does not dissolve or merge completely into another phase that retains its identity and results in a material characterized by better properties than the ones of the single components considered separately. In addition, a particular role among the large composite materials group is played by fibrous composite materials which are characterized by having a very thin and sharp macroscopic interphase between the different components of which they are made of (e.g., matrix and reinforcement material). It actually acts as another

phase within the material which is characterized by its own properties. Structural composites usually have bi-phasic systems based on the multiple presence of a mainly fibrous reinforcement and a matrix in which the first behaves as the source for key structural properties, while the latter serves as binder to shape the material structural identity. In order to analyze more in depth their unique mechanical properties and fully understand where these properties come from, it is important to focus our attention on the role played by each of these components within the composite structure and how they act both as a single phase and a complex system [134–154].

Materials and structures are two vital elements when a composite has to be defined. However, in this context, it is really difficult to define a material and a structure, although many people try to define a material as a homogeneous thing when it can be seen with bare eyes and a structure is a inhomogeneous material structure that is made up of a fixed geometry or mixing of materials. For example, an alloy is a material even though it contains two or more components; however, a honeycomb core built up of two different components is a structure. Materials are often divided into the six broad classes – (a) metals, (b) ceramics, (c) glasses, (d) elastomers, (e) polymers, and (f) composites [161–181].

Research laboratories around the world are working diligently to find out ways to exploit these materials. One of the limiting factors towards mass customization is that there is little data available on the long-term results of many high-performance materials along with their relatively higher initial cost which retards the potential customers to use this types of materials. As already stated, most of these high performance materials have potentials to use them in the production of high-performance advanced composite materials using many conventional and high-tech methods for a wide range of applications [182–197].

Many challenges are usually observed during the production of high-quality polymer composites, some of which include (a) uniform dispersion of the materials, (b) physical compatibility of different components, (c) ensuring robust technical performances, (d) lightness, (e) cheaper in production cost, (f) inserting required properties (both conventional and functional) [1–3, 198–208]. Manufacturing micro- and nanocomposites with outstanding required technical properties along with strictly maintaining the sustainability by meeting environmental concerns and also ensuring productivity and price compared to the competitor materials are some the very fundamental challenges for micro- and nanocomposite materials. In addition, designing micro- and nanocomposites by incorporating variety of conventional and functional materials suitable for various types of conventional and high-tech industrial exploitations in terms of producing functional intelligent materials and devices with complex structures, high level of integration and miniaturization, recyclability with minimum environmental load are still some way to proceed with in order to utilize the new opportunities and benefits out of these materials. Many pieces of current active research activities are focused in pioneering laboratories around the world in order to address different aspects and issues of advanced micro- and nanocomposites for various applications [1, 2, 33, 50, 209–228].

3 Nanocomposites

Nanocomposites can be defined as a class of materials where one or more phases with nanoscale dimensions (such as zero-, one-, two-dimensions) are embedded in a matrix (such as polymer, metal, ceramic). For example, polymer nanocomposites have at least two-phase systems consisting of polymers and fillers of which at least one dimension is in the nanometer range (1–100 nm) [18–21]. The nanofillers can be one-dimensional nanotubes or nanofibers, two-dimensional clay platelets, or three-dimensional spherical particles. The advantage of nanoparticles is that, because of its high specific surface area, already at low concentrations major effects on the macroscopic properties can be obtained. Over the past years, polymer nanocomposites have attracted considerable interest in both academia and industry, but one of the outstanding problems is to control the state of dispersion of the nanoparticles, which is highly determined by the preparation method. As already stated elsewhere, nanocomposites have many applications where some of which include (a) reinforcement of polymers/structural materials, (b) thermal conductivity, (c) electrical conductivity, (d) light emitting diodes/field effect transistors/actuators, (e) hydrogen storage, (f) absorption of radar waves, (g) dissipation of electric discharge, (h) shielding of electromagnetic radiation [18–31].

Highly ordered polymer nanocomposites exhibit distinct morphological character due to their variations in a number of areas including (a) composition, (b) structure, (c) properties on a nanometer length scale [61–64]. Novel physical characters of soft and bulk polymer nanocomposites are highly influenced by the nature of supramolecular organization of the nanostructures [65]. A typical idea to add a nanoscale second phase is to create a synergy between the various novel constituents with desired properties capable to meet or exceed achievable design expectations. In that case, the properties of nanocomposites depend on a number of variables (more particularly related to the matrix material) with various characters including (a) nanoscale dimensions, (b) loading, (c) degree of dispersion, (d) size, (e) shape, (f) orientation of the nanoscale second phase, (g) interactions between the matrix and the second phase. The presence of the nanoparticle and the interaction of the polymer with the particle, as well as the particle orientation in a dispersed fluid composition may cause to produce a variety of ordered composite materials in the bulk or film [66–68]. When metals are incorporated into polymer matrices, they show unique optical, magnetic, and dielectric properties at the nano- and macroscale in nanocomposites, apparently because of the surface and confinement effects of the nanoparticles [69–75]. The preparation of magnetic nanocomposites which are comprised of polymer shells and magnetic nanoparticles constitutes fascinating approach as the modular nature of polymeric materials facilitates the design of a wide range of hybrid nanocomposites of different compositions [70–73]. Additionally, the inherent dipole moment in ferromagnetic colloids enables the one- and two-dimensional assembly of such materials into novel meso-structures. The development of magnetic assemblies from ferromagnetic and superparamagnetic nanoparticles on supporting surfaces has been reported where some of the structures that have been shown to occur due to the impact of magnetic

assembly which include (i) one dimensional chains [16], (ii) flux closure rings [77], (iii) two dimensional super-lattices of closed packed nanocrystals [78], and (iv) three dimensional labyrinth-like supra-structures [78, 79].

4 Types of Polymer Nanocomposites

From structural consideration, a nanocomposite is a material that contains components which are usually very little (>100 nm in scale) in dimension. In this context, components of a nanocomposite can be divided into three categories – (a) zero-dimensional (nanoparticles, such as metal oxide and ceramic oxide nanoparticles); (b) mono-dimensional (nanotubes and nanowires, such as carbon dot, titanium oxide nanotubes); and (c) bi-dimensional (nanoplatelets, such as layered silicates, nanoclays, and graphene). However, from a design context, nanocomposites can be divided into two classes, such as (a) biphasic nanocomposites (polymer matrix + nanoreinforcement) and (b) triphasic composites (polymer matrix + fibrous reinforcement + nanoreinforcement). Additionally, the specific relationship which relates the structure of the nanoreinforcement with its specific characters is one of the most important morphological features [80–126]. It can be illustrated with the ratio between the surface area and the volume of the little component well within specific nanometer range (Fig. 1).

In specific terms, the variation of the dimensions (or length in case of nanowires and thickness in case of nanoclays) of particle sizes from micrometer scale to nanometer scale, this ratio is usually improved by several orders of magnitude. This type of modification is generally responsible to change the nature of the interphase between reinforcement and matrix that contributes to generate new properties (which control the impressive characteristics of nanocomposites). For a general understanding (within the limited framework of this current chapter), different selected aspects of different types of nanocomposites are included here.

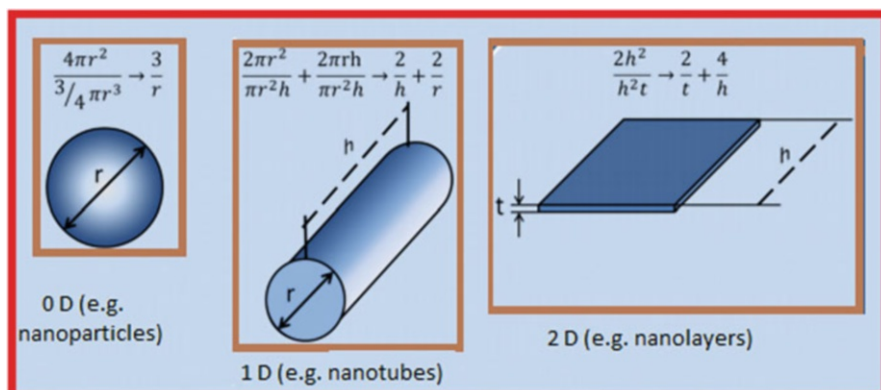


Fig. 1 A schematic representation of surface/volume ratio for various type of nanoreinforcements

4.1 Zero-Dimensional Nanocomposites (Such as Nanoparticles Based Systems)

Nanocomposites reinforced with nanoparticles are one of most widely used materials for various industrial applications. These nanoparticles are generally incorporated into the systems for improving various desired properties of the nanocomposite systems (e.g., enhancing mechanical properties of the matrix, such as elastic modulus, tensile strength and fatigue resistance). For instance, Cho et al. [20] studied the behavior of polymeric composites reinforced with spherical particles made of alumina and glass (of different dimensions from 0.5 μm to 15 nm) and their different impacts on mechanical properties of the nanocomposite systems. Singh et al. [21] analyzed the fracture toughness of polymeric thermoset resins doped with micron- and nanometer-sized aluminum particles and observed that both particles size and volume fraction significantly influenced the composite toughness and fracture behavior and also contributed to enhance the mechanical response of the material when the volume fraction was increased and the particle dimensions were decreased. They also noticed that the incorporation of normal aluminum reduced the strength of the composite system, while after a treatment with organosilicates, fracture toughness was significantly enhanced. Lopez et al. [22] investigated the nature of nanocomposites prepared by embedding alumina nanoparticles in a vinyl ester resin at different percentages and reported similar type of results that established a linear increase of the modulus as the percentage of nanoparticles within the composite structure was raised to higher levels. But these values were relatively lower than the modulus recorded for pure resin which were attributed to the presence of alumina aggregates within the polymer. Zhang et al. [23] studied the effect of nanosilica particles in epoxy based composite and observed their mechanical properties at various selected temperatures and noticed that the presence of a homogeneously dispersed nanometric phase contributed to improve elastic modulus, impact resistance, and fracture toughness when the volume content was increased. Besides this, the analytical models revealed that the nanoparticles induce an improvement of the local deformability around the crack tip. In addition, the effect of nanosilica on the fracture behavior was strongly influenced by the temperatures which contributed in the activation of different mechanisms at various test temperatures. For a better understanding of the mechanisms involved with these improvements, some authors investigated the interactions between polymer chains and nanoparticles using molecular dynamic simulations [24, 25]. They observe that when the polymer-nanoparticles interaction strength is relatively higher compare to that of polymer-polymer one, the elastic modulus is improved with reduction in the dimensions of the nanoparticles. Besides this, a key factor is the density of polymeric chains that surround the nanoparticles this is significantly influenced by the nanoparticles dimensions that create a stiff layer around the reinforcement and contribute to enhance energy absorption rate. Vlasveld et al. studied a multiscaled hybrid system to investigate the mechanical properties of a three phasic system obtained from embedding nanoscaled mica particles in a woven glass fibers reinforced PA6

matrix [26]. They observed that the nanomodification contributed to increase the matrix modulus and enhance matrix-dominated flexural and compressive strength by more than 40%. Another research group also observed similar behavior (a 40% increase of the tensile strength in the transverse direction as a result of an experimental campaign on a three phase composite produced by the modification of a conventional epoxy resin with silica nanoparticles and then using it with E-glass fibers to obtain a multiscaled system) [27]. Nanoparticles are generally used to modify the mechanical character of a composite. However, nanoparticles can also be used to activate particular nonstructural functions. For example, Kagawa reported a unique effect of nanoparticles on nanosilica reinforced epoxy resin and established a relationship of the optical properties of these nanoparticles [28].

4.2 One-Dimensional Nanocomposites (Such as Nanotubes and Nanowires)

Typically, a nanotube is a nanoscaled structure synthesized by a sequence of atoms which are arranged in a long thin cylindrical structure. Several materials such as TiO_2 , silica, silicon carbide, particular type of carbon materials can be used for the synthesis of nanotubes [34–37]. In general terms, a CNT can be defined as a series of carbon atoms arranged in a tube-like shape formed by at least one layer of graphite. Based on the number of layers that form the single CNT structure, it is possible to obtain two different categories of nanotubes, which are: (a) single walled carbon nanotubes (SWCNT), (b) multiwalled carbon nanotubes (MWCNT). Both SWNT and MWNT have been widely used for improving the properties of many composite and nanocomposites for a wide range of applications [80, 99, 108–124].

4.3 Two-Dimensional Nanocomposites (Nanolayers Based Systems)

Nanoplatelets (usually based on phyllosilicates) based nanocomposites have very thin (several nm in thickness) layers embedded within the polymeric matrix [29]. In addition, phyllosilicates mainly composed of alumina and silica which are organized in layered structures where each layer has a sequence of tetrahedral and octahedral type very thin silica sheets that can be dispersed within a polymer in two different ways – (a) tactoids (piled silica/alumina sheets) and (b) intercalated/exfoliated layers (resin-separated layers) [29]. A principal distinction between these two structures is the dispersion of tactoids in a resin that can give rise to classical microcomposite; however, when detached nanoplatelets are used, it is possible to produce nanocomposites. Different structures reinforced with nanoplatelets (typical examples include montmorillonite, saponite, and hectorite) have been rigorously studied and the results indicate significant improvements of tensile strength, tenacity and impact properties [30, 31]. In a separate study, Okada and Usuki observed that the doping of nylon 6 with a small amount of montmorillonite contributed to improve stiffness and

enhance Young's Modulus (structural features) and also to decrease water absorption rate (nonstructural feature) [32]. Tsai and Wu used a multiscaled hybrid system to study and analyze the mechanical behavior of a three phase system obtained by embedding nanoscaled organoclay in glass fibers reinforced epoxy. They noticed that the presence of the nanoscaled phase contributed to improve both tensile strength (+74%) and Young's modulus (+67%) [33]. Besides this, another type of 2D nanocomposites is based on the inclusion of graphene layers within the structure of traditional materials [322–343]. Graphene, a carbon allotrope, made by a single planar sheet of carbon atoms densely packed in a honeycomb crystal lattice, has been rigorously studied and used in producing composites and nanocomposites for a wide range of potential and practical applications [1, 344–360].

5 Selected Features of Polymer Nanocomposites

Many studies have been conducted throughout last couple of decades to produce physically and chemically robust nanocomposites for a wide range of industrial applications. For example, reinforcements are one of them which have many impacts on the overall properties of nanocomposites. When the impact of a reinforcement is reduced, it may lead to an increase of the surface area in contact with the polymeric matrix and generates nanoeffects within the nanocomposite structure. Additionally, the fundamental difference with microscaled reinforcement is that the reinforcement dimensions are of the same magnitude of the radius of gyration of the polymer chains that form the matrix. This relationship may lead to complete new intermolecular interactions which are different from what generally happens in classical micro-reinforced composites that contributes to induce the formation of a polymer inter-phase layer characterized by its own set of properties.

Mechanisms involved with the strengthening of nanocomposites can be divided into two categories, they are (a) in plane mechanisms (such as crack pinning or bowing and crack deflection) and (b) out of plane mechanisms (for instance, immobilized polymer layers and debonding/plastic voids growth).

5.1 Crack Pinning

In 1970 Lange originally postulated this effect where microreinforced composites showed this type of effect even at lower intensity [46–48]. Crack pinning effect is related with dispersion hardening (which usually occurs when the particles act as pinning points during cracks propagation). In this context, the crack is stretched out and forms a secondary nonlinear source, whereas the main one stays pinned at the position where it encounters the particle. A higher energy level is needed to propagate as the dislocation energy is function of its length and this effect could be amplified by reducing the distance between different particles or by using smaller particles since it contributes to the opening of multiple nonlinear cracks in order to dissipate more energy.

5.2 Crack Deflection

Crack deflection takes place when the crack tip arrives in the proximities of a stiffer particle and is deflected after being forced to turn around it. In that situation, the crack shows twisting or tilting from its plane of propagation by increasing its total surface area thus absorbing more energy. Besides this, the crack changes its mode of propagation from normal mode to a superposition that includes contributes from other modes [49].

5.3 Immobilized Polymer

Polymer immobilization relates the creation of a layer of immobilized polymer between the reinforcement particles [50]. This layer can be dislocated throughout the structure in order to create an interphase network that strengthens the composite due to their small size (e.g., several nm). But this substructure alters the chemical natures of the material and changes the glass transition temperature and also can affect other mechanical characters (e.g., storage modulus or damping).

5.4 Debonding and Plastic Voids Growth

The debonding is a toughening effect which is activated by particles embedded within the composite structure that are debonded from the matrix. This process absorbs just a small amount of energy (compared with energies involved in matrix plastic deformation or the other mechanisms); it can reduce the constrains on the crack tip in order to support a subsequent growth of voids that allows larger deformations [51].

6 Discussion on Different Types of Selected Polymer Nanocomposites

6.1 Polymer/Carbon Nanotubes Based Nanocomposites

Recent developments in the fields of nanotechnology, carbon nanotube (CNT) reinforced polymer composites, and related areas have experienced tremendous advancements and they are the most studied polymer nanocomposites due to their potential applications. Carbon nanotubes have the ability to improve the properties of the resultant materials several orders of magnitude relative to the unfilled polymers when these CNTs are finely dispersed within different polymer matrices. In this context, some of the enhanced properties include (a) tensile behavior, (b) strength, (c) toughness, (d) stiffness, (e) electrical and thermal conductivity, and (f) crystallization kinetics. This section briefly provides some information on various selected aspects of polystyrene/CNT and polyethylene/CNT nanocomposites. References have been provided for detail

information on other selective polymer nanocomposites based on carbon nanotubes. Some of these polymers include (i) polystyrene, (ii) poly(ethylene oxide), (iii) poly(ϵ -caprolactone), (iv) polypropylene, (v) various nylons and poly(ethylene terephthalate), and (vi) particular types of elastomers.

6.1.1 Polystyrene/Carbon Nanotubes Composites

A method using electrostatic assembly has been reported to synthesize polystyrene (PS)-carbon nanofibers (CNF) via a bottom-up method [57]. In this method a home-made PS latex has been mixed with an aqueous suspension of oxidized CNF to obtain the nanocomposites through the electrostatic interaction of the cationic PS with the anionic CNF. It shows that the molding temperature has an important effect on the morphology and electrical conductivity of PS-CNF composites, where the optimal temperature and pressure are 185 °C and 25 MPA, respectively. This technique also exhibits a percolation threshold below 2 wt%. This study also shows the thermal analysis in the presence of the CNF that demonstrates an increase in the onset and the thermo-oxidative temperature by 60 °C. The CNF have little impact on the alteration of the glass-transition temperature (T_g) of the polymer. Another research group also reported similar results from their investigation in order to prepare a composite of syndiotactic PS (sPS) filled with carbon nanocapsules (CNC) using a solution-blending method coupled with ultrasonication [58]. They also observed that the addition of filler had no impact on the T_g of the polymer; however, it led to an increase in the melt-crystallization temperature of the β -form sPS. In this case, the presence of the filler triggered a fast crystallization of the sPS that induced either by melt quenching or by slow cooling of the molten state which was attributed to the existence of a profound primary nucleation density. CNCs have been used as high quality nucleating agents in order improve crystallinity and thermal stability of sPS. For example, in a report CNFs have been used as nucleating agents to produce PS microcellular nanocomposite foams with uniform size distributions [129]. It also observed that addition of a small amount of CNFs has the pronounced effect in order to reduce the composite's cell dimensions and increase the cellular density. Additionally, the favorable surface and geometrical characteristics of CNFs have excellent nucleation efficiency when used as fillers. Electrically conductive composites were produced by incorporating single-wall carbon nanotubes (SWCNT) into polystyrene matrices which have good rheological and mechanical properties [130]. In this case, a contiguous SWCNT cellular-structure was synthesized by coating PS pellets with SWCNTs and pressing them afterwards at elevated temperatures [130]. The novel SWCNT cellular-structures showed better electric conductance and lower electrical percolation threshold when compared to nanocomposites with well dispersed SWCNTs. Chang et al. investigated PS composites after dispersing SWCNTs in the polystyrene matrix using a variety of concentrations of SWCNTs and studied morphological, electrical, and mechanical properties of the resultant nanocomposites. They noticed that composites influenced by annealing treatment and annealed composites demonstrated relatively higher electrical conductivities than the raw composites. However, even after annealing, the SWCNT/PS composites showed lower electrical conductivities compared to the

PS/SWCNT cellular-structures. It was also observed that usually it is difficult to disperse SWCNTs in polymers because of the energy of mixing is endothermic up to nanotube diameters of 2.2 nm [132]. Polystyrene and carbon nanotube based composites have a wide range of applications [132–139].

6.1.2 Poly(Ethylene Oxide)/Carbon Nanotubes Composites

There is a range of reports on the synthesis of poly(ethylene oxide) (PEO) nanocomposites containing SWCNTs which have many attractive application potentials [130–140].

Additionally, carbon nanotubes have been extensively used for the synthesis of CNT based composites using different types of polymers such as (a) polystyrene, (b) poly(ethylene oxide), (c) poly(ϵ -caprolactone), (d) polypropylene, (e) nylon, (f) poly(ethylene terephthalate), (g) biopolymers and natural polymers [25, 90–99, 106, 117–128, 192–200, 228–373].

6.2 Polymer/Metal Nanocomposites

Functional materials with special properties and/or combinations of unique properties have been constantly getting evolved since the advanced technologies keep developing by the day. Materials based on nanosized metal particles may assist to meet many of the requirements. This section briefly and selectively presents different pieces of work on the synthesis and characterization of polymer/metal nanocomposites and their applications. Metal containing materials show excellent mechanical properties and/or exceptional electrical or electromagnetic characteristics suitable for a variety of applications. Metal polymer nanocomposites can be synthesized using various types of metals, some of the metals include (a) platinum, (b) cobalt, (c) nickel, (d) silver, (e) palladium, (f) gold, (g) other metals (such as copper, zinc, titanium) [1–2, 10, 13, 17, 20–23, 69–80, 100–107, 210, 217, 226, 294]. Metal-polymer nanocomposites are highly popular for their potential advanced applications with significant industrial scale exploitations which require quite a number of features including low cost, high metal surface areas. For example, catalytic systems are widely investigated along with various metals for the synthesis of polymer nanocomposites. In this context, metals such as Ag, Pt, Ni, Co, and Au are well known for catalytic activities. Metal nanoparticles and conductive polymer matrices are usually embedded for producing electrically active devices for a variety of electronic applications. In addition, metal-polymer nanocomposites are also popular for their uses in optically active devices and magnetically active products. From a muscle like structure to bioactive nanocomposites, these materials provide promising improved characters over the original components that help to expand their usage envelope. In terms of synthetic perspective, currently researchers have developed highly specific pathways in order to produce materials with well-defined tailored properties. Highly cost effective and generally applicable synthesis pathways have been reported by different research groups. Such methods are well suited for a wide range of metals and show the capability to deliver nanoscale metal-polymer composites with significantly enhanced

characters over the starting materials. Some methods of these types sometime use unique chemical bonds and/or treatments that help compatibilize metal surfaces with the organic matrices. Other methods also utilize steric effects similar to mechanical wrapping of the polymers around metal nanospheres to produce metal-polymer nanocomposites. Moreover, compounding techniques to mechanically insert metal particles in polymer substrates are also practiced occasionally to produce metal-polymer nanocomposites [108–125].

6.3 Polymer/Clay Nanocomposites

Polymer and clay nanocomposites are widely investigated for various academic and industrial researches for their potential applications. For example, the exfoliation, intercalation, and aggregation of clays in PEO nanocomposites have been extensively studied in the past. The reality is that the functionality of each component is sometime changed by addition of another, although in complicated multicomponent systems it is difficult to draw conclusions if too many parameters are varied. In addition, all the constituents must be considered at once because of the fact and for a more complete picture of how a system behaves in a real environment. More specifically, in order to examine the polymer-clay interactions a combination of methods is used [108–125].

Different techniques have been extensively used by different researchers some of which include (a) microscopic techniques (such as SEM, TEM, AFM, CLSM), (b) scattering (e.g., WAXS, SAXS) techniques for studying structure and providing a measure of size, shape, and interfacial polymer conformation. Besides this, rheology and mechanical testing are much utilized techniques as they can sufficiently distinguish between properties of chemically versus physically cross-linked polymer-clay materials. In this section only specific selective information on polymer nanocomposites based on laponite and montmorillonite is provided, since these two clays are among the most studied and reported. Laponite and montmorillonite are popular for producing clay composites when they are used in combination with a number of polymers which include (a) poly(urethane urea), (b) poly(methyl methacrylate), (c) polystyrene, (d) poly(ethylene oxide), (e) diblock and triblock copolymers, (f) polyurethane, (g) poly(ϵ -caprolactone), (h) polylactic acid and/or poly(lactic-co-glycolic acid), (i) poly(ethylene oxide), (j) polypropylene [117–128, 199–200, 260–410].

7 Designing Composites and Nanocomposites

Similar to previous sections, information on different aspects of composites has been provided in terms of the information on composite materials. In the context of research conducted on hybrid composites (primarily based on intermingled carbon and glass fiber fabrics) can be traced back to the early 1970s. However, in view of prospective use as lightweight load bearing composite structures, different pieces of work of Bunsell and Harris in the year 1974 or Summerscales and Short in the years 1978 and 1980 are sometimes considered as the first pieces of research work on the

mechanical properties of various material combinations [214–216]. A wide range of combinations emerged since then to prepare fiber reinforced polymer (FRP) composites of viable architectures.

Many reviews primarily focused on polymer-based hybrid composites. For example, in one of the review, Ashby (in the year 2003 and 2011) defines hybrid materials as the combinations of two or more materials assembled in such a way as to have attributes not offered by either components one alone [217, 218]. Additionally, he stated the ingredients to be used in hybrid material design (including the choice of materials to be combined, their configuration, their relative volume fraction, and the scale length of the structural unit). Generally, there are three types of hybridization architectures which are (a) interlayer, (b) intralayer, and (c) intrayarn. In that case, the interlayer hybridization implies reinforcement mixing on the layer level, while the intralayer configurations within each layer. The first architecture is the most general configuration as it is handy to be prepared and the latter is rather difficult to be produced but proved to yield improved mechanical characters [219, 220].

In the light of above, numerous combinations emerged and studied by different investigators from property prediction point of view, cost, and performance, behavior under various loading conditions and application potential based on different features. In 1987, Kretsis at first reviewed hybrid composites and focused particularly on hybrid composites based on epoxy resins reinforced with synthetic fibers, carbon, and glass, especially continuous and unidirectional orientation with effective mechanical characters [221]. Various composites were found to pose challenges in terms of environmental benefits. Thus, natural products were preferred to promote environmental issues [222–224]. One of the primary parameters in the hybrid polymer composites design is the hybrid ratio that has a direct significant control over the overall performance of structure which is intimately related to the hybrid effect. Morom et al. defined the hybrid effect in 1978 and observed that the deviation from linear rule of mixtures can be modified to be used to predict a large spectrum of mechanical properties in addition to the failure strain [225]. Consequently, positive and/or negative hybrid effects obtained from these predictions may be useful to quantify the examined property. This rule is known as the linear rule of hybrid mixtures, but the accuracy of this rule is debated [226]. Many factors have influences on the hybrid effect. For example, high performance composites are expected to show outstanding returns from their individual reinforcement and matrix constituents. Additionally, without limiting the influencing factors, some important ones such as the nature, distribution, amount, layering pattern, and individual features of the composite constituents have strong effective influence on the different properties of the composite. Subsequently, material selection is a significantly important to tackle different issues of the composite made with different constituents since in many cases they share an important part in the composite design. Additionally, other parameters, for example, fiber-matrix interface, interlaminar strength, and fracture toughness, have considerable influences of the hybrid effect of the composite. Theoretical predictions developed in order to address microstructure-property connection have a long and venerable history and have been successful to attract the attention of some of the luminaries of science, including Maxwell, Rayleigh, and

Einstein. Since their very early work on the characters of heterogeneous materials, there has been a huge upsurge of effective contributions in the literature on this subject. For example, one of the outstanding contributors is Torquato [227]. In the most typical sense, the overall characters of heterogeneous materials can be predicted using expressions developed by utilizing various ways including (a) variational principles, (b) local and homogenized solutions to the problems, (c) phase-interchange relations, (c) exact solutions using effective medium approximations, (d) analyzing rigorous bounds and cross-property relations. These significant advances have enabled investigators to overcome the limitations of the models and also allow them to compute property estimations that depend on other requirements imposed real materials. Tailoring composites with unique spectrum of properties depends primarily on the systematic approach to relate the effective characters to the microstructure using accurate expressions. It is possible to relate changes in the microstructure quantitatively due to changes in the macroscopic property.

Major developments in hybrid composites are mainly due to increasingly new industrial demands as well as pressures. Material designers and manufacturers constantly engaged with searching novel combinations to meet desired objectives which allow faster structural optimization based on different things including (a) cost minimization, (b) high performance and lightweight condition, (c) easy manufacturing feasibility. The main development of hybrid polymer composites mostly based on thermosetting resins that range from epoxy to polyester and poly vinyl ester. For example, epoxy resins and derived blends have been rigorously studied due to their versatility in applications with all manufacturing technologies, good compatibility with almost all types of fibers, both synthetic and natural.

Market demand effectively controls the consumption of composites (either thermoplastics or thermosetting). However, the capability to adapt these materials to economic and technical market requirements depends on the innovation in terms of both materials and processes that can be supplemented by adaptability to the environmental constrains (such as circular 3R concept – recycling, reusing, and remanufacturing) [228]. Composites have many application areas, for example, they have some engineering applications. Civil and automotive engineering, marine and aerospace, biomedical and sensing devices have several application domains of modern composite materials [229–233]. In addition, a balance in cost and performance can be sized behind each material design. Particularly, the study of hybrid composites is a multidisciplinary effort that overlaps with various branches of material science, engineering, applied mathematics, and others. The ability to tailor hybrid composites with a unique spectrum of characters depends on microstructure and correlation of experimental retrieved data with theoretical predicted values, bounded by certain processing conditions.

Important material characteristics of a polymer microcomposite depend on a number of things including (a) volume fraction of reinforcements, (b) geometrical parameters (such as length, shape), (c) orientation and layering type, supplemented by interface interactions with the matrix system. The overall characteristic of the resultant composite is defined by each and every components present in the composition [234–236].

A proper control in thermal expansion is highly required for a polymer micro-composite suitable to be used in structural applications. In order to mitigate the effects, different components of the composite should be carefully selected to ensure proper matching with the thermal expansion coefficients at interfaces or at least control the variation within an allowable limit [239–244]. Thermal expansion coefficients of the components used in the composites, particularly particle reinforced composites which are usually used in electronic applications (such as energy harvesting, power electronic, electronic packaging, sensing devices, actuators), need to be controlled adequately in order to ensure high product quality [245–256].

Electrical properties of composites are significantly important criteria for the designs of different types of composites, most particularly composites targeted for electronic applications [257]. In many cases, electrical properties of composites are desired to exhibit required electromagnetic properties along with distinct levels of thermal, and/or mechanical behavior while maintaining structural integrity [258, 259]. As a result, required electronic character along with specific physical and coupling behaviors is also needed to meet certain industrial requirements. For example, electrical properties of particular types of composites can be tailored in order to meet specific industrial applications, such as (a) composites for electronic packaging (e.g., printed circuit boards, thermal interface materials), (b) composites for microelectromechanical systems (MEMS) and BioMEMS where their functions are multifold (both active sensing and housing) [260–270]. In addition, many challenges are usually encountered during the design and development of high-performance composites using different materials, some of which include (a) method of proper combinations and sustaining structural integrity, (b) issues relating to synthesis, (c) characterizing and property modeling or simulation, (d) ensuring higher technical performances at a lower cost [214–238]. In this regard, reflections on the overall behavior, interferences, and synergies with direct consequences on their balanced properties need careful consideration in order to produce high-quality composite structures. Currently, synthetic materials have predominance over natural or 3R materials (such as recycled, reused, recovered), so scientists are focused on producing hybrid composites to ensure many desired industrial needs as well as meeting environmental requirements. In this connection, in order to mitigate the usual challenges in existing and future trends need comprehensive interdisciplinary studies to overcome many issues and produce high-quality composites that can fulfill desired industrial exploitations [259–270].

8 Processing of Composites and Nanocomposites

Designing and processing are critical to produce most sustainable, cost-effective, and environmentally viable micro- and nanocomposites for a wide range of applications. The final characters of micro- and nanocomposites rely on the processing methods and conditions where some of most commonly used method include (a) melt processing, (b) solvent processing, (c) in situ polymerization, (d) electrospinning, and (e) layer by layer (LBL) assembly.

8.1 Melt Blending

Melt blending, a popularly used to prepare composites where the compounding, is usually carried out in a single- or twin-screw extruder by heating the polymer and the nanoparticle mixture in order to form a melt. The mixer provides the required shear and elongational stress to the process for breaking apart the filler agglomerates and dispersing them uniformly in the polymer matrix. This technique is one of the popular techniques to produce composite materials. For example, carbon nanotubes (both Single Wall Nanotube or SWNT and Multi-Wall Nanotube or MWNT) along with different polymers are frequently used to produce conductive polymer composites, where better dispersion is usually achieved with MWNT rather than with SWNT [321]. The extruder, a versatile device, allows to have better control on shear and mixing simply by changing the screw configurations where a higher shear rates generally provides better dispersion and production rates as well as material throughputs in a continuous extrusion process can be high. An important advantage of melt processing is that no organic solvents are needed during processing and the compounded nanoparticle-polymer composite can be processed using various polymer-processing techniques (e.g., injection molding, profile extrusion, blow molding). However, a number of variables (such as temperature, screw-speed, residence time, and shear stress) are directly involved with the mixing process and these parameters should be optimized in order to produce high-quality composite materials because a variation in these parameters usually produce composites with differences in their properties (e.g., agglomerate structure, packing density, length to diameter ratio, dispersion uniformity of the fillers, such as carbon nanotubes in composite polymeric matrix). Besides this, the polymer matrix (particularly, the melt viscosity) also affects the degree of dispersion and the shear forces generated in most mixing equipment are not large enough to break and disperse the fillers in the polymer matrix efficiently. In addition, special mixers where shear rates are an order of magnitude higher than usually obtained from a typical screw-extruder are often used to ensure better dispersion with improved properties, although the high shear has the potential for degrading both the polymer and the filler used in the composite production. A wide range of polymers are popularly used in composite productions using melt blending technique, some of which include low density polyethylene, high density polyethylene, polypropylene, polystyrene, poly methyl methacrylate, polyamide, polyesters, and polycarbonate and a brief details of these can be found in different reviews [293, 306, 313, 322–324].

Melt processing has shown to enhance mechanical properties of composites to some extent [324]. A study reveals that the intensity in the mixing section improves dispersibility over the kneading section and the polymers containing functional groups can react with functional groups on fillers (such as carbon nanotubes) in order to improve dispersions [326]. Another study observes that the extensional flow gives better dispersion of nanotubes compared to that observed from shear flows [327]. For example, several studies on the melt blending of graphene and polymers demonstrate the low thermal stability of most chemically modified graphene and the low bulk density of graphene create difficulties in using melt processing technique.

Additionally, some studies have been carried out where high shear melt mixing technique has been used for the fabrication of graphene based nanocomposite with poly lactic acid [328], polyethylene terephthalate [329], polypropylene [330], nylon 6 [331], polycarbonate [332], polystyrene [333], and elastomers [334] although high shear forces have the tendency to cause buckling, rolling, or shortening of graphene sheets and thus cause a reduction in aspect ratio of a graphene composite.

Melt mixing of clay with polymer has been shown to produce polymer micro- and nanocomposites with improved properties [335–354]. For example, a variety of polymers have been effectively melt compounded using clay to provide various degrees of exfoliation. Additionally, the intercalation during melt processing of clay-polyethylene oxide enhanced further by microwave irradiation [354]. Liu et al. [355] reported an exfoliated composite by compounding organic clay and nylon 6 using a twin-screw extruder. Typically, due to nylon's excellent affinity for the silicate surface, the degree of exfoliation between nylon 6 and clay is quite high [303]. In addition, stresses generated during melt blending can break up the clay aggregates and with an increase in the affinity between the clay and the polymer, the dispersion of the individual platelets in the polymer matrix also increases.

8.2 Solution Mixing or Solvent Casting

Micro- and nanocomposites are also frequently produced by using solution mixing or solvent casting technique which involves the agitation of the filler (such as CNT, nanoparticles) in a polymer that is dissolved in a solvent prior to casting in a mold and then the solvent is removed by evaporation. Both thermoplastic and thermoset polymers have been used to prepare composites using this technique. For example, polymers like PMMA, poly(vinyl alcohol) [358], polyhydroxyaminoether [359], PS [360], PE [361], PEO [362], and epoxy [363–365] with CNTs have been used to prepare composites using solution mixing or solvent casting technique. Polymer solution of lower viscosity (when dissolved in a proper solvent, in contrary to a melt condition) coupled with agitation by mechanical stirrer or ultra-sonication contributes to a better dispersion of nanoparticles in the polymer matrix. Different types of solvents (such as aqueous or organic) are usually used in solution mixing or solvent casting of polymer composites; however, there are environmental implications which are involved with the removal of organic solvents from the casted composites. Solution mixing and solvent casting techniques have been reported to prepare different polymer composites using modified graphene and a range of polymers, some of which include (a) PVA, (b) PMMA, (c) PP, (d) PS, (e) LLDPE, (f) nylon, (g) epoxy, (h) PANI, (i) PU [410–430].

8.3 In Situ Polymerization

It is one of the popular techniques to produce micro- and nanocomposites. For example, different polymer composites (particularly based on carbon nanotube and

polymers) have been synthesized by using in situ polymerization technique. It is possible to use this technique for producing both thermoset and thermoplastic materials. For instance, during the production of CNT based polymer composites, the nanotubes are dispersed in the monomer which is then polymerized and the dispersants may be added to assist in the de-agglomeration of the nanotubes. Besides this, functionalization or polymer adsorption techniques have been reported to assist in the dispersion process where the polymerization is initiated with the increase of temperature and by the addition of a chemical initiator to start the reaction (or by mixing the monomers). Microwaves have been utilized for inducing polymerization reaction as the nanotubes have the capability to absorb microwave that increase temperature which allows the grafting of polymer molecules on to the walls of the nanotubes. The method can be used to make CNT composites with polymers that are insoluble in most common solvents or are thermally unstable which limits the scope of melt processing [102, 362–378, 421–430].

8.4 Electrospinning

Electrospinning, an established and experimentally straight forward technique, has the potential to produce virtually continuous lengths of submicron width fibers, from a wide range of materials that includes many polymers (such as natural polymers like cellulose, synthetic polymers like polystyrene) and their blends. Electrospun fibers have the potential for different types of applications, some of which are (a) production of novel composites, (b) biomedical applications, (c) filtration, (d) textiles, (e) tissue engineering, (f) optical and electronic devices, (g) sensing applications [41–45]. A significant enhancement on the functional properties of electrospun polymer fibers can be achieved by the incorporation of functional materials such as quantum dot, polymer (e.g., to make a blend), metal complexes, nanoparticles, carbon nanotubes, dye molecules, dye loaded zeolite crystals, or proteins. In a typical electrospinning process, a high voltage (kV) is applied to a metallic capillary through which the polymeric solution is fed and the charges induced on the surface of the pendant polymer droplet act in opposition to the surface tension of the fluid. When the repulsive Coulombic interacts above a critical voltage, it overcomes surface tension in order to cause an acceleration of electrified polymer jet from the apex of the droplet towards a grounded collector (such as a metal sheet, e.g., a Cu sheet) which usually kept at certain distance from the metal capillary (Fig. 2). The polymer jet is elongated into a long, thin filament as the solvent evaporates and is deposited onto the collector in the form of fibers and based on the nature of collection, fibers may be collected in random mats or in more ordered assemblies (such as aligned mats). The elongational flow of the polymer exhibits some degree of orientation of the macromolecular chains in the fibers and also shows interesting behaviors of uniaxial properties (such as birefringence). The morphologies and dimensions of electrospun fibers depend on the complex inter-relationship between intrinsic polymeric and solution properties, processing parameters, and also on ambient conditions where electrospinning is carried out. There are

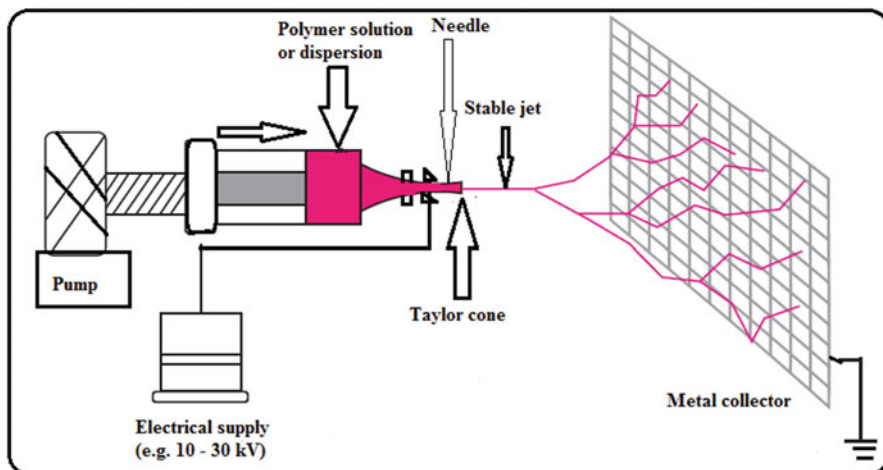


Fig. 2 Schematic diagram of a typical electrospinning rig

reports of using electrospinning technique for producing electrospun nanofibers doped with advanced materials for a variety of applications. For example, one study exhibited the procedure of incorporating cadmium sulfide quantum dots that were co-electrospun with polyethylene oxide for the production of fluorescence nanofiber composite in order to transfer optical properties from quantum dots to polyethylene oxide nanofibers. In addition, the iron oxide nanoparticles were co-electrospun with poly vinylidene fluoride tetrafluoro ethylene to produce electrospun nanocomposite to incorporate strong super paramagnetic properties. Both of these two ways devise a practical method to produce nanostructured which can be extended toward a cellulose-polyethylene oxide-quantum dot nanocomposite by using electrospinning technique. Figure 2 illustrates a schematic diagram of a commonly used typical electrospinning rig for nanofiber production.

Electrospinning technique is also widely used to produce electrospun composites and nanocomposites using a wide range of fillers and polymers for a variety of applications [41–45, 389–407].

8.5 Layer-by-Layer Deposition

Layer-by-layer (LBL) deposition technique is also another popular method for producing micro- and nanocomposites, which involves as immersion process to charge the substrate either negatively or positively using an oppositely charged polyelectrolyte that is adsorbed onto the substrate. In this case, when equilibrium is achieved, the substrate becomes ready to remove for rinsing followed by drying and immersing in a negatively charged polyelectrolyte solution. This process is repeated and continued for achieving required film thickness on the substrate which depends on a number of factors including (a) the concentration of polymer

in the solution, (b) ionic strength, (c) molecular weight of polymer, (d) temperature during assembly, (e) ionic strength, (f) pH. In addition, in case of an irreversible polyelectrolyte absorption, the charge overcompensation can cause charge reversal at the surface. This technique allows to insert different materials between layers as long as they have the opposite charge. For example, when a negatively charged substrate is immersed in the solution of positively charged polyelectrolyte, the latter forms a submonolayer on the surface of the substrate that can switch the surface charge to positive which is then immersed in the dispersion of negatively charged polyelectrolyte or nanoparticles after rinsing with water in order to form a new layer that can switch the surface charge to negative again. This whole cycle is usually repeated for a number of time to achieve the expected result. There are many benefits of LBL assembly, one of which include during this process a high level of dispersion of nanoparticle into a composite that occurs as a result of direct absorption of nanoparticle from a solution to a solid state shows no a phase segregation. Besides this, the typical concept of LBL assembly is a useful versatile method in order to combine various materials (e.g., carbon nanotubes, clays, nanoparticles, polymers, proteins) to produce a wide range of micro- and nanocomposites. This method also allows to control the morphology at nanoscale to provide desired compact and ordered structures relative to other solution-based techniques. LBL assembled thin films have a wide range of applications in various areas, some of which include in (a) producing transparent conducting films, (b) field effect transistors, (c) supercapacitors. However, a slow deposition speeds and cumbersome assembly process are some of the principal limitations of this technique [1, 2, 33, 50].

9 Environmental Stimuli-Responsive and Functional Polymer Composites and Nanocomposites

Materials responsive to surrounding environmental conditions (such as light, pH, temperature, magnetic, and electric fields) are attractive for current intensive fundamental scientific research for their multiple conventional and high-tech applications. In this context, the responsive materials of interest are composite and nanocomposites. A wide range of materials (such as photo-, thermo-, pH-, magnetic, electrical, enzyme-responsive materials or molecular switches) have the potentials to be used with different matrices for producing variety of composites and nanocomposites. Additionally, shape memory polymers or materials, self-healing materials, materials used in different functional applications (such as electromagnetic shielding, electronic applications, energy storage) are widely studied for their applications in particular types of composites and nanocomposite production targeting specific industrial applications [41–51]. Nanocomposites are in the forefront of study due to the fact that when very low load levels (<5%) of the filler are introduced into the nanocomposite structure, they provide a dramatic impact on the final properties of nanocomposite matrices. This is attributed to fact that there is an increase in interfacial interaction of the 1D nanomaterials with the polymeric matrix. Responsive nanocomposites have an impact on a wide ranging areas, including biomedical

applications, energy, security, and military applications. For instance, polymeric materials used in gasket seals have the potential adaptation in order to differ temperatures and humidity in such a way which can maintain an optimal degree of functionality regardless of climate variations [41–51].

The production of responsive nanocomposites is directly involved with a greater understanding on the nature and the interactions of nanomaterials with other polymeric materials or the matrices they are applied in order to realize a specific or multiple objectives. The diverse nature of the effective utilization of responsive nanocomposites multidisciplinary approaches are required in order to investigate the cross-over understanding needed to make the quantum leaps necessary to realize the successful uses in various fields and also on their potential industrial scale applications. Successful applications of nanoparticles and different computational models have been developed by different research groups in order for effective incorporation into responsive nanocomposites. Different research groups have synthesized various metal, semi-conductor, and ceramic nanomaterials and introduced into responsive polymer matrix to produce responsive nanocomposites. Different methods have been investigated for producing responsive nanocomposites some of which include (a) electrospinning, (b) soft templating and photocatalytic nanostructuring, (c) interfacial assembly, (d) inkjet technology, (e) coating, (f) layer by layer deposition. In order to determine the structure of functionalized nanoparticles in solution and also to resolve the interactions between them, different research groups have used large-scale atomistic molecular dynamics simulations for producing responsive nanocomposites. Additionally, simulations have also been used to investigate the effect of nanoparticles on the flow and processibility of polymer nanocomposites for different application purposes. Various methods have been reported for the functionalization of nanocomposites and also to produce responsive nanocomposites for specific as well as multiple application potentials. Some of these methods include (a) electrospinning, (b) templating, (c) layer-by-layer deposition, (d) inkjet technology. Many efforts have also been focused on discovering what effect the existing materials interactions with the polymer matrices have and refining their functionalization strategies for specific or multipurpose applications potentials [41–51].

10 Selected Behaviors of Composites and Nanocomposites

10.1 Reinforcement

When composites and nanocomposites are reinforced with nanofillers, they usually show enhanced mechanical properties. However, excellent properties of nanofillers are yet to be realized (particularly, in the cases of higher volume fractions), when used in composite formulations. In a study, a modulus improvement by a factor of six is predicted at 0.01 filler volume fraction for an aspect ratio of 1000 for 1D nanotubes or 2D platelets using the Halpin-Tsai equation [235]. Additionally, molecular simulations predict similar reinforcing potentials for aspect ratio of approximately 100 as well as relative enhancements in modulus may be much higher than the increase in tensile

strength [236]. There is usually a decrease in strain at break when loaded with nanofillers. For example, when nanotubes are doped or incorporated into micro- and nanocomposites, there is typically an increase in certain properties with an increase with the nanotube content at low volume fractions but there is a decrease at higher fractions due to issues related to dispersions and agglomeration [237–255]. When carbon nanotubes are used as fillers in nanocomposite fabrications, usually modulus of graphene filled nanocomposites shows an increase with an increase in loading fraction which illustrates that the strength of the interface is critical to the improvement of the mechanical properties. An increase in modulus is more pronounced for elastomeric matrices because of their lower intrinsic modulus. Different investigations also confirm that the mechanical reinforcement of graphene is superior over some other fillers (e.g., carbon black, single wall nanotube) [255]. For example, in graphene based epoxy polymer composite, functionalized graphene sheets provide higher fracture toughness, fracture energy stiffness, strength, and fatigue resistance at lower loading fractions as compared to nanotubes [253]. Besides this, normally, there is an increase in tensile strength with increase in graphene content (with some exceptions) [254] and reduction in elongation or remain unchanged. However, for the case of carbon nanotube based composites, the level of mechanical enhancement observed to be relatively lower than the theoretical predictions. Similar trends of mechanical properties of nanoclay are reported for carbon nanotube or graphene based polymer composites which in an addition of this type of fillers increases modulus and tensile strength while decreases elongation at break. However, with clay, the relative reinforcement [256, 292] for a given volume percent of filler in the composite is markedly lower compare to that of graphene based [255] or carbon nanotube based composite [257]. The tensile modulus of a polymeric material shows an increase when nanocomposites are formed with either pristine or organically modified clays, for instance, for nylon 6 based composite shows an increase in tensile strength by 42% and modulus by 90% [257, 258]. In this case, there is an increase in stiffness for an increase in the molecular weight of the matrix at any given loading, even though all the moduli of the neat nylon 6 are almost similar [257–259].

10.2 Electrical Conductivity

Polymer composites and nanocomposites provide an excellent potential to produce electrically conductive materials by incorporating electrically conductive materials (such as carbon nanotubes, graphene, conductive metal oxides) as fillers into their structures or by other suitable means. These types of conductive materials are useful for a wide range of applications including (a) conductive adhesives, (b) antistatic coatings, (c) conductive films, (d) electronics, (e) packaging, (f) electrical appliances. In all these cases, methods of loadings and dispersions of conductive materials have critical importance. For example, in percolation threshold (the critical loading point) when the composite shows a transition from an insulator to a conductor due to the formation of a continuous conducting network, it must be properly controlled to produce desired level of conductive nature. Because, under the percolating threshold, the electrical properties are usually dominated by the dielectric matrix and thus the composite

exhibits nonconductive character, the fillers are unable to form a continuous network in order to ensure flow of electrons. In contrast, beyond the percolation threshold, only a tiny increase in loading with conductive fillers contributes to cause a significant improvement in conductivity, and because of the increase in filler contents, they begin to form a contact with each other. In addition, at percolation threshold, conduction paths are created in the insulating matrix to cause an increase in conduction, although beyond a certain level of filler concentration a plateau in conductivity is reached and some of the main controlling factors which have direct influences on the percolation threshold are (a) aspect ratio, (b) nature of functionalization, (c) method of processing, (d) nature of the polymer matrix, (e) nature of dispersion [292–300].

10.3 Thermal Conductivity

Thermal conductivity of certain types of polymer composites and nanocomposites is sometimes highly desired for their specific applications in particular areas (such as electronic devices, protective applications). Thermal conductivity of polymer composites and nanocomposites depends on a variety of determining factors which include (a) the nature of the polymer matrix and fillers, (b) nature of dispersion of conductive fillers in the polymer matrix. Currently, thermal conductive polymeric composites are being increasingly used in different areas to meet specific application targets. Thermally conductive polymer composites are usually produced by using thermally conductive fillers into composite structures. For example, the polymers filled with the thermally conductive fillers effectively dissipate heat generated from electronic components where the management of heat is directly related to the lifetime of electronic devices. As already mentioned, to improve thermal conductivity of composites, fillers with excellent thermally conductivity (such as metal oxides, CNT, graphene) are popularly employed because they provide several advantages, some of which include (a) easy processibility, (b) low cost, (c) corrosion resistance to certain extend. In this context, carbon-based 1-dimensional nanomaterials (for instance, carbon nanotube, carbon nanofiber) exhibit different useful properties, some of which are (a) high thermal conductivity, (b) corrosion resistance, (c) low thermal expansion coefficient compared to metals. As a result, CNT based polymer composites are highly attractive as thermally conductive materials are suitable for various applications. It has been reported that functionalized nanotubes usually contributed to offer higher thermal conductivity compared to unfunctionalized tubes because of higher dispersion capability [301]. A significant number of studies relating to the thermal conductivity of graphene/polymer composites have been reported [302–303].

10.4 Thermal Stability

Thermal stability of both micro- and composites is an important factor which is mainly designed based on the final use of micro- and nanocomposites. As already stated both micro- and nanocomposites are fascinating materials made from two or more distinct

components with different chemical, physical, and mechanical properties, but when combined, possess better properties than those of each individual components used alone. Composites materials have many advantages, such as (a) high specific strength and modulus, (b) ease of fabrication, (c) high design flexibility, (d) resistance to fatigue and corrosion, (e) desirable thermal expansion characteristics, (f) economic efficiency. Due to these interesting properties, the composites materials are widely used in different industries, some of which include (a) aerospace industry, (b) military industry, (c) automobile industry, (d) construction materials and other engineering applications. At present there is a thrust towards the compaction of electrical power equipment with enhanced insulation electrical stress levels which requires new electrical insulating materials. It is interesting to note that in past few decades, some particular polymeric materials with excellent desired criteria (such as light weight, robust mechanical properties, low cost, and some with unique nonwetting surface characters) have been successful to surpass insulation behaviors of conventional porcelain and glass materials. However, despite these suitable properties, polymeric materials are unable to withstand the high heat from surface arcing that is instigated by the synergism of different factors, such as (a) pollution, (b) moisture, (c) voltage. In addition, surface arcing causes material loss because of different reasons such as (i) heat ablation, (ii) electrical tracking of polymers. In order to overcome these types of problem, inorganic fillers are popularly used along with base polymers for improving various characters which include (a) resistance to surface discharge activities, (b) other technical performances within a cost-effective approach. Usually polymers show higher thermal expansion compared to metals and by adding fillers (such as clay, carbon nanotubes, graphene), this thermal expansion of polymers can be reduced by imposing restriction on the movement of a significant volume of polymer chains due to their interaction with the fillers. However, graphite has a positive thermal expansion coefficient and when incorporated into polymers does not cause a reduction in the expansion of polymers. In contrast, a reduction in thermal expansion was observed when reduced graphene oxide or SWNTs were incorporated into the structure of resins [304]. Fillers with negative thermal expansion coefficients (such as graphene oxide, single walled carbon nanotube) when used in composites fabrication contribute to increase thermal stability by decreasing the thermal expansion coefficient of the composite system. For example, in a study, it was observed that the degradation temperature of PS increased from 400 °C to 450 °C when impregnated with graphene sheets [304–305]. In addition, the thermal stabilities of graphene based PMMA composite system are reported to be higher than that of PMMA. Besides these evidences, there are also reports on clay nanocomposites prepared by using injection molding technique exhibited anisotropy where the expansion coefficient in the flow direction was observed to be relatively lower than in the perpendicular direction which was attributed to the orientation of platelets in the respective direction. Similar types of results were observed when MMT was aligned using magnetic or electric field [304–308].

10.5 Glass Transition Temperature

Methods of preparation and nature of the micro- and nanocomposite structures have pronounced impacts on the glass transition temperature of the composite systems

which are almost all cases different from the individual components of the composite systems. Many factors have direct impact on the T_g of composite system; one of the main reasons include the capability of the fillers to impede the motion of polymer chains due to the interfacial interaction between the polymer and the filler. For example, different investigations have observed that both T_g and the breadth of the transition are usually affected by the presence of fillers in composite structures [304, 309–310]. Other important factors that influence T_g include (a) thickness [304, 311–312], (b) methods of preparation and measurement [313], (c) nanoparticle dimension [309–314], (d) chemical structure of the polymers [315]. Besides this, the interaction of the filler with the surface is significantly important as it can play a role to influence the degree of change of T_g and it is also observed that surfaces that interact strongly with the polymer contribute to improve T_g [304, 316–317]. In contrast, the unadsorbed material may have the same or lower T_g compared to the bulk depending on the nature of the adsorbed layer. Besides this, hydrogen bonds at the polymer-substrate interface may also contribute to enhance T_g relative to bulk values [304, 313, 317]. Graphene platelets with particular characters (such as higher aspect ratio, higher surface roughness) when dispersed uniformly within a composite polymer matrix can improve T_g of the composite. For example, in a study it was noticed that solvent and melt blending processes cause insignificant changes in the T_g of polymer-graphene or polymer-GO composites, while in situ polymerization with unmodified graphene or solvent blending with chemically modified graphene or GO helped to enhance T_g of the composite matrix due to the covalent bonding between the graphene and the polymer. The nature of polymers used in composite structure is also a vital factor to control the glass transition temperature of the composite. For example, nanospherical silica showed an increase in T_g with PVP, decrease in T_g with PMMA, while T_g was unchanged with PS [304, 318]. When a polymer is mixed with a carbon nanotube, the resultant mixture usually shows an increase or a decrease on its glass transition temperature depending on the nature of surface functionalization of nanotubes used in the mixture [304, 319–324].

10.6 Barrier Properties

The structural compositions of micro- and nanocomposites are significantly influenced when they are incorporated with fillers that have large aspect ratios and can show various properties including impeding and changing the diffusion path of penetrating molecules (such as well-dispersed fillers can create a tortuous path for permeants to travel). For example, in a study a decrease in gas permeability (independent of the type of gas) was reported for clay reinforced composites, while in another study a 1% loading of clay in PET showed a two-fold reduction in oxygen gas permeability. Different reports observed a decrease of water vapor permeability of PCL clay nanocomposites over neat PCL. In addition, a decrease in water vapor permeability with an increase in the aspect ratio of the platelets has been reported. Gas molecules find it too difficult to permeate defect-free graphene sheets which provide an opportunity for graphene based polymer composites films to apply as protective elements in electronics and fuel cells (which are sensitive to the

presence of gases, e.g., oxygen and moisture). Additionally, GO conjugated polymer nanocomposite films have the capability to reduce the level of oxygen and carbon dioxide permeation. For example, in different investigations graphene polyimide composite films have been reported to exhibit high moisture barrier characters and some other polymers based composite films also observed similar results [80–99, 108–124, 304, 324–328].

10.7 Antiflammability

Polymers show low fire resistance compared to metals or ceramics. When a polymer is burnt, it decomposes and releases gaseous products. Micro- or nanocomposite matrices having well-dispersed nanoplatelet/nanotube in the structures assist to form continuous networks that contribute to form protective layers on the surfaces and finally exhibit relatively more resistance to fire compared to pristine polymers which are used in this composite matrices. Alternatively, this protective layer that provides heat shielding contributes to prevent the gaseous degradation products from diffusing through it and reacting with the oxygen in the air. A micro- or nanocomposite impregnated with a filler (such as carbon nanotube, graphene, nanoclay, SiO₂) illustrates a significant reduction in the maximum heat release [329] compared to neat polymer although the total heat release remained unchanged. In addition, aspect ratio of dispersed silicate layers and the processing method have a robust influence on the antiflammability characters of composite matrices [304, 330–338].

Besides these selected behaviors, there are many important behaviors (such as physical characters, rheological properties, responsive natures to certain stimuli in the cases of stimuli-responsive composites and nanocomposites, functional properties in case of functional composites) need to be considered properly for realizing desired application potentials from micro- and nanocomposites.

11 Challenges for Composites and Nanocomposites

Different challenges are observed during productions and also dealing with micro- and nanocomposites during practical applications. For example, carbon based nanofillers are relatively at an early stage of development in comparison to nanoclay based nanofillers which are widely used in composites formulations and have met with more relative success. However, several fundamental challenges are required to be addressed in order to achieve full potentials on the uses of nanofillers in polymer composites [304]. Uniform and balanced dispersions of fillers into composite structures are critically important in order to realize the desired full potentials from micro- and nanocomposites. Some of popular techniques used in composite processing are not economically viable, while some other frequently used techniques, such as solvent processing, LBL assembly, and electrospinning although useful for better dispersions of fillers into composite structure but show less cost-effectiveness. In this context, melt processing is one of the most widely used economically viable processing methods which sometimes provides

inadequate dispersion of filler in the composite system to produce poor optimal properties [1–2, 33, 304]. Mechanical reinforcement of melt processed composites exerts many challenges. For example, (a) SWNT shows agglomeration at higher volume fractions, (b) MWNTs require to be disperses at much higher loading. An increase in interfacial area with decrease in easy tube diameter is usually observed. For example, at 0.5 wt% of nanotubes MWNT has 70% of the interfacial area of SWNT, as a result, SWNT lose their intrinsic advantage of higher aspect ratio. Additionally, composites at higher loading do not perform at a similar way when loaded at a lower level; thus, it influences the magnitude of reinforcement. Improvement and ensuring the quality of polymer composites with different fillers (such as CNT, graphene, or clay) depend upon a number of factors, some of which include (a) nature of filler (such as CNTs, MWCNT or SWCNT), (b) layers of graphene or clay, purity, length of CNTs, diameter and length of CNT (aspect ratio), (c) loading of nanofillers, (d) dispersion in the matrix, (e) alignment (tough to align graphene or nanoclay), (f) interaction between the polymer and the nanofiller, (g) nature of the polymer, (h) method of fabrication [304, 333]. In the published pieces of work on composites, in most of the cases, a single type of nanofiller in a polymer matrix has been used, however, simultaneous incorporation of different nanofillers may have some significant impacts on the characters of the composite matrices. The impact of synergy in properties between multiple nanofillers is yet to be investigated. As for instance, 1D fillers may interfere with the stacking of 2D platelets, so the incorporation of CNTs into glass fiber composites inhibits crack formations because of the large density of nucleation sites provided by CNT [1, 304, 334].

Load transfers between nanofillers and polymers are usually obtained by both noncovalent and covalent modifications with functional groups. The introduction of covalently functional bonds disrupts the conjugation of CNTs and graphene which sometimes lead to a negative effect on the electrical properties of the resulting composites. In an investigation, it was observed that a combination of noncovalent and covalently fuctionalization on CNT contributed to enhance compatibilizer-polymer interaction leading to better mechanical and electrical properties [304]. As a result, it is very important to have a better understanding of the interface between the noncovalently functionalized CNT/graphene and the polymeric matrix in order to enable simultaneous improvement of both mechanical and electrical characters of the composites [304, 335–336].

Additionally, selectively some important aspects of biocomposites, green composites and nanocomposites, single polymer composites, stimuli-responsive composites are very briefly covered in the next sections and interested readers are advised to consult relevant references for more detail information [437–458].

12 Bio-composites, Green Composites, and Nanocomposites

Similar to microcomposites and nanocomposites that have been successful to draw active current research interests all over the world due to their wide range of conventional and high-tech industrial applications, biocomposites, green composites, and nanocomposites are widely studied for a huge plethora of potential

industrial applications. Many natural polymers (such as cellulose, chitin, gelatine, collagen) can be used for bio-based composites and nanocomposites which are highly attractive due to the natural abundance that are also renewable in nature. Biopolymers (such as cellulose) have many truly impressive range of diverse properties which can be accessed from the raw resources like cellulose. Cellulosic nanocomposites are usually produced by different techniques commonly applied in nanotechnology where the cellulose component may work as the polymeric matrix or it can also work as a nanoparticle and/or the nanometer-scale constituent (such as cellulose nanocrystals) or can be doped with advanced materials (e.g., quantum dots, functional materials) for functionalization. Since the most abundantly available natural polymers, they can be used to produce environmentally friendly biocompatible renewable material which are focal points for many conventional to high-tech advanced applications [434–455].

12.1 Biocomposites

Environmental concerns along with the development of bio-based composite materials for different industrial applications have been successful to draw active current research interests on biomaterial based composites and nanocomposites (such as cellulose based bio-nanocomposites). For example, many investigations are focused on the use of natural fibers in composites as an alternative to conventional synthetic fillers, which are traditionally used to reinforce thermoplastic matrices. The development of such composite materials using the bio-based and biodegradable reinforcing agent (such as nanofibrillated cellulose) has been thoroughly investigated by different researchers. Additionally, the use of bio-reinforced composites in automotive, construction, packaging, and medical applications also increasingly focused to mitigate specific the requirements for environmental sustainability. So, at present there are quite a lot of interest on green polymer based polymer nanocomposites. Green polymer based nanocomposites have unique characteristic properties for combining the advantages of natural fillers and organic polymers. In this regards, plant fibers are found suitable to reinforce polymers [434–455]. As a result, in this current section cellulose based composites and nanocomposites are briefly described.

12.2 Cellulose Nanocomposites

Cellulose, the most abundant natural biomass possesses very promising properties, some of which include mechanical robustness, hydrophilicity, biocompatibility, and biodegradability. Cellulose based composites have many applications (e.g., in drug delivery systems, hydrogels, electronic active papers, sensors, shape memory materials, and smart membranes) and also offer interesting potential improved properties and new functionalities. Cellulose based stimuli-responsive smart materials have many advantages, some of the most important ones include regulation of stimuli-responsive behaviors during the reactions with the environmental stimuli and wide

application potentials of this smart materials in different fields (e.g., as biomaterials). There are different ways to incorporate different stimuli-responsive materials into the structures of cellulose composites to regulate different properties of the bulk composite structures. Although environmentally stimuli-responsive cellulose composites have many conventional and high-tech applications, there are quite a lot of challenges in order to produce high-quality stimuli-responsive cellulose composites and there are ways how to mitigate these challenges [41–51].

12.3 Cellulose Composites

At present cellulose-fiber-reinforced polymer composites is a very attractive research topic due to their attractive properties, some of which include (a) low density, (b) nonabrasive, (c) combustible, (d) nontoxic, (e) low cost, and (f) biodegradable properties. There are different active current research activities all over the world on the efficient use of cellulose fibers as reinforcing materials for the preparation of various types of composites. However, the use of cellulose-fiber-reinforced composites is relatively less attractive due to a number of reasons, such as (a) relatively less interfacial adhesion, (b) low melting point, and (c) lower hydrophilicity. Different techniques are used to overcome these drawbacks. For example, pretreatments of the cellulose fibers can be used to modify the fiber surface (e.g., influencing moisture adsorption process using chemical functionalization and improving surface roughness techniques). There are different methods of producing cellulose composites; one of the important methods is the use of micro- and nanofibers produced by using electrospinning technique. The production of cellulose based electrospun macro- and nanofibers has been successful to attract increasing interest due to different reasons including (a) high strength and stiffness, (b) biodegradability and renewability, (c) relative ease in the production of high-quality composites using these fibers. The development of electrospun cellulose micro- and nanofibers based composites is relatively a new area of research and these fibers can be used as reinforcement in composite materials due to their contribution in the improvement of mechanical, thermal, and biodegradation properties of composites. Cellulose fibers are hydrophilic in nature and thus important to increase their surface roughness for the development of composites with enhanced properties. There are different methods of the surface modification of cellulose fibers for their applications in the synthesis of high quality nanocellulose and cellulosic composites. For example, a reduction of amorphous parts of fibers obtained from natural plants to cause a break down in the hierarchical structure of the plant into individualized nanofibers of high crystallinity is one of these types of usually used approach. As already mentioned, different advantages of cellulose fibers (e.g., abundantly available, low weight, biodegradable, cheaper, renewable, low abrasive nature, good mechanical properties) have made them attractive reinforcing materials although they have some disadvantages (e.g., moisture absorption, quality variations, low thermal stability, and poor compatibility with the hydrophobic polymer matrix) [41–51, 434–444].

12.4 Stimuli-Responsive Smart Cellulose Composites

Despite specific interesting features of cellulose composites for value additions along with the aim of applying cellulose materials for both conventional and high-tech applications, cellulose composites can be used to fabricate environmental stimuli-responsive smart materials, which will show intelligent behaviors when exposed to specific environmental stimulus. Environmentally stimuli-responsive smart cellulose composites show change in their features (such as morphology, mechanical strength, wettability, color, thermal property, electrical or magnetic property) in a controlled manner in response to the introduction of a predetermined external stimulus. These types of environmentally stimuli-responsive smart cellulose composites are produced by incorporating environmental stimuli-responsive materials into the structure of cellulose composites to make them environmentally responsive. These stimuli-responsive materials are usually used to generate desired controllable changes on the cellulose composite to produce and control a specific alteration on different properties, such as shape, mechanical rigidity/flexibility, opacity, porosity. Environmentally stimuli-responsive smart cellulose composites have great potential in many applications, especially as biomaterials and drug carriers. [41–51, 430–435, 445–455].

12.5 Bio-inspired Stimuli-Responsive Mechanically Dynamic Composites

Polymer nanocomposites which show stimuli responsive changes in their morphology and mechanical behaviors have wide potential applications in the production of smart protective devices or the development of adaptive biomaterials. For example, there are a few reports on the development of bio-inspired stimuli-responsive mechanically dynamic composite materials based on the dermis of sea cucumbers. In this case, a percolating cellulose nanofiber network has been used as reinforcement to a low-modulus matrix polymer. The cellulose nanofibers display strong interactions between themselves which contributed for an even dispersion of percolating nanocomposites to display a high stiffness due to the abundance of surface hydroxyl groups. This study showed that the nanofibers–nanofibers interactions were largely switched off by the introduction of a chemical regulator which allowed a competition in hydrogen bonding and thus caused a significant decrease in the stiffness of the material. They developed nanocomposites which showed three orders of magnitude modulus changes by using a host polymer with a thermal transition with a specific regime [41–51, 446–451].

13 Single Polymer Composites

Environmental regulations relating to safe production and final applications of composites and nanocomposites play provided one of the important impetus to develop single polymer based composites and nanocomposites. As a result, a usual interest to improve

the recyclability of composite and nanocomposite materials has recently emerged and for complying with the environmental regulations and other new requirements, a possible strategy has recently been developed which termed as single polymer composite where both matrix and reinforcement have the same chemical composition. One of the principal advantages of single polymer composites is that, unlike traditional heterogeneous composites (such as glass- or carbon reinforced polymer composites), they can be totally melted down at the end of the product life for recycling. Additionally, life cycle assessment does not produce favorable results for conventional reinforced composites, although high-quality mechanical performances have been achieved to some extent. One of the main reasons behind this is the use of energy-intensive techniques usually used in the production of the reinforced composites and limited recyclability of the corresponding composites. For example, glass fibers are one of the principal component in polymeric matrix composites (PMCs) and this type of reinforcement is severe challenge during both mechanical and thermal recycling. Natural fibers are popularly introduced as reinforcement in order to overcome this problem. Natural fibers are usually renewable in nature which can be thermally recycled, but difficulties arise during recycling because of their low thermal stability. This practical challenge was one of the main impetus to a search for alternative recycling-friendly homocomposites, such as single polymer composites which represent a valuable alternative to the traditional fiber reinforced composites where the matrix and the reinforcement are from the same chemical composition that facilitates an ease in recyclability. Additionally, advantages of single polymer composites include (a) the possibility of manufacturing lightweight parts and structures in comparison with traditional composites because of lower density of polymeric fibers compared with traditional reinforcements (such as glass fiber, carbon fibers, basalt, talc, and silica); (b) better interfacial adhesion fiber-matrix, in comparison with traditional composites, because of a full compatibility with single polymer composites. However, the main challenge on the production single polymer composites is the small difference in melting temperatures of the matrix and reinforcement where both constituents have the same chemical composition. However, there are scopes to expand this processing windows by using polymers with same chemical composition but different chemical structure (e.g., high density polyethylene, low density polyethylene, different types of polylactic acids and their structural homologs) or changing the chemical structure of the polymers. A vast series of single polymer composites has already been reported for a wide range of industrial applications [1–10, 30–79, 456–461].

14 Future Directions in Composites and Nanocomposites

Both micro- and nanocomposites are very wide fields of research where almost everyday there are some notable progresses being made by dedicated research groups from all around the world because micro- and nanocomposites have their applications in a wide range of areas including (a) material sciences, (b) biological sciences, (c) engineering and technologies, (d) electronics, (e) other areas life and physical sciences. As a result, it is almost impossible to cover all areas; however,

very precisely recent trends of current research activities from different selected fields are briefly stated here. Both the micro- and nanocomposites are focused on high-quality, cost-effective, and technically performing environmentally benign products development where one of the main thrust is biocompatibility with cost-effective environmentally friendly product developments [1–10, 33, 304].

The higher strength-to-weight ratios of nanocomposites have made them novel materials to replace metals in applications which requires high material performance (e.g., windmill blades, aircraft components). Nanofiller-reinforced polymer nanocomposites are usually formed by dispersing strong and stiff nanoparticles in various polymeric matrices, and much of the recent work on nanocomposite mechanics only focuses on improving the reinforcement phase (such as the dispersion of nanofillers). However, the design of high-performance nanocomposites requires polymeric matrices with superior mechanical properties and versatile techniques for tailoring these matrices. Additionally, suitable polymeric nanoscale building blocks for advanced composite matrices have been prepared from conventionally strong materials. For instance, a high performance polymer poly-paraphenylene terephthalamide (also known as Kevlar or aramid polymer) has been used as a matrix material in the form of nanoscale building blocks for nanocomposites. Besides this, the synthesis of reactive aramid nanoscale structures has addressed the limitations in the field of synthetic nanocomposites that traditionally relied on a set of polymeric building blocks with low reactivity and of limited variability. Reactive nanoscale aramid structures have been prepared to bond with various moieties to form aramid networks with tailored nanostructures, morphologies, and mechanical properties. Kevlar based metal (such as gold) nanocomposites have been shown to provide a combination of stiffness, strength, and strain to failure due to the reinforcement effect of the metal particles (such as gold nanoparticles) through their bonding with the aramid matrix [1–10, 33, 50–89, 304].

A structure-property relationship has been established by a systematic tailoring and optimizing the mechanical properties of these advanced aramid nanofiber/gold nanoparticle composites. The workers showed the first demonstration of the possibility for aramid nanoscale fibers to form versatile nanosized building blocks that can then be crosslinked or conjugated to fabricate composite structures involving materials that offers a new generation of nanostructured aramid materials. Besides this, the Kevlar/gold nanocomposites synthesized based on aramid nanostructures have a higher strain energy density than that of a commercial plain-woven Kevlar mat tested along its strongest axis which indicates their potential as high performance materials to resist extreme high rate loadings (e.g., blasts). A wide variety of materials have been investigated for producing technically robust high-performance composites and nanocomposites for a huge range of applications. For example, recently, growing prospects of clay (such as layered hydrous aluminosilicates) based nanocomposites have renewed further interest in understanding the fundamental elastic and plastic properties of hydrous aluminosilicates [1–10, 33, 50–89, 304].

In the last two decades, polymer-clay nanocomposites have been successful to attract active research interests due to their significant improvement capability in mechanical and physical properties with minute amount of nanofiller which provide a promise to avoid the typical compromise that exists between properties and

processability of composite materials. However, their success has so far been limited, despite the expectations created by nanoclays in the academic and industrial communities for their huge application potentials. Some of the reasons behind these setbacks include (a) poor dispersion of nanoclays in polymer matrices, (b) weak interfacial interaction with polymers, (c) limited control of nanoclay-orientations. As a result, more pieces of continuous research activities are targeting improve these nanoclay-polymer interactions. These are some examples of current trend of research in a tiny area of composites and nanocomposites. As already mentioned in different earlier sections that both composites and nanocomposites are widely used in a huge range of areas, so the current research and developments in these areas are continuously going on for different reasons, including (a) high-tech and cost effect product developments, (b) incorporating new features on existing products according to customer demands, (c) mitigating environmental concerns, (d) addressing other issues that arise with the change of time, situation, supply, demands, advents of new methods, and scientific tools, (e) incorporating new functionalities [1–10, 33–189, 304–407].

There are increasing trends in using lightweight, high-strength, fiber-reinforced composites for producing different parts of electric cars, aerial vehicles and wind turbines. However, one of the principal limitations is the use of these new materials cause different level of microcracks which can lead to catastrophic failures which are often hard to detect and repair. In this context, a solution to this problem is to use materials with self-healing capability in order to repair themselves in case of any cracks and restore their mechanical properties automatically. It is interesting to note that research on this self-healing capabilities of certain materials has been carried out for over a decade and have been successful to produce self-healing composites capable to recover properties (e.g., interlaminar fracture toughness with over 100% efficiency). As a result, some particular types of current self-healing polymers offer a new route toward safer, longer-lasting, fault-tolerant products and components across a broad cross section of industries (such as coatings, electronics, transportation, energy, security, printing, textiles). Some particular types of composites, such as lightweight ballistic composites, have many applications in defense sectors (e.g., in military and law-enforcement applications). Ballistic composites can be designed in various ways and sometimes they can be designed and produced to give superior properties (in some particular areas) compared to particular type of conventional materials usually used for ballistic purposes. Since they are light weight and have durability against environmental conditions (such as moisture, chemicals, gases, heat) with high performance (e.g., high strength, impact and ballistic resistance, damage tolerance), they have huge range of applications in different areas. For instances, lightweight ballistic composites are widely used in various areas including (a) light weight vehicles, (b) watercraft and aircraft armor giving high performance and light weight protection against bullets and fragments. Additionally, they also show high-quality insulating properties in high temperature environments. There are continuous developments in this area to overcome many existing limitations as well as incorporating more desired properties into the composite structures based on customer demands (mostly from defense and law-enforcement applications).

Composite based textiles are increasingly used in various industrial sectors (e.g., car seats, carpeting). However, the term textile composites is often used to describe a

limited narrow range of materials which are mostly based on three-dimensional reinforcements generally produced by using specialist pieces of equipment. There are intensive research activities on a broad range of polymer composite materials with potentials for textile reinforcements, for example, (a) woven and noncrimp commodity fabrics, (b) high performance 3D textiles.

Increasing environmental regulations along with more customer demands with sustainable and environmentally friendly natures from different products are other important impetus to increase current industrial and academic research interest on green composites. Scientists and engineers are increasingly focused on minimizing the environmental impact on the production of polymer microcomposite and nanocomposites. For example, lifecycle assessment is highly important at every stage of a product's life, such as (a) from initial synthesis through to final disposal, (b) safe handling of materials and environmentally friendly processing methods to ensure a sustainable society. Leading researchers all around the world are actively engaged with research and development activities in this area to produce green composites by using different techniques (including using suitable natural and environmentally benign polymers with environmentally sustainable and safe processing techniques) [1–5, 66–93, 304–407].

In addition, current other trends in main industrial applications of composites and nanocomposites include (a) aerospace industry (for producing wings, fuselage, radomes, antennae, tail-planes, helicopter, blades, landing gears, seats, floors, interior panels, fuel tanks, rocket motors cases, nose cones, launch tubes); (b) automobile industry (for making body panels, cabs, spoilers, consoles, instrument panels, lamp-housings, bumpers, leaf springs, drive shafts, gears, bearings); (c) maritime industry (for the preparation of boats hulls, decks, masts, engine shrouds, interior panels); (d) chemical industry (for producing pipes, tanks, pressure vessels, hoppers, valves, pumps, impellers); (e) domestic applications (such as for making interior and exterior panels, chairs, tables, baths, shower units, ladders); (f) electrical and electronic industries (for producing panels, housings, switchgear, insulators, connectors, packaging); (g) leisure industry (for making motor homes, caravans, trailers, golf clubs, racquets, protective helmets, skis, archery bows, surfboards, fishing rods, canoes, pools, diving boards, playground equipment); (h) health and security; (i) sensoric applications; (j) other branches of material, polymer, and life sciences including engineering and technologies [1–33, 50–96, 236–298, 346–389, 456–466].

15 Conclusion and Perspectives

Composites and nanocomposites are some of the most important topics in modern nanoscience and nanotechnology due to their practical and potential exploitations in industrial and academic studies for ever-growing enormous applications in everyday life. If we look forward to most important focal points of industrial and academic researches for the twenty-first century, both micro- and nanocomposites are some of these fields which will contribute to high level of scientific and technological

developments. Both conventional and functional hybrid composites will play a major role in the development of advanced materials for high-performance materials for advanced high-tech and also cost-efficient applications. Current continuous research in both composite and nanocomposites (including conventional and functional hybrid systems) is being carried by the growing interest of chemists, physicists, biologists, and materials scientists in order to fully realize the potential opportunity to create high-tech cost-effective advanced materials as well as conventional materials with desired criteria. For example, for hybrid composite systems they provide the opportunity to incorporate different components into the structure which can be designed for a simultaneous benefit from the best of the three realms – (a) inorganic, (b) organic, and (c) biological features. In addition, composites also provide the opportunity to use bio-inspired strategies for mimicking the growth processes that occur in biomineralization and design innovative multiscale structured hybrid systems (from nano- to millimetric scale) which are hierarchically organized in terms of structure and functions. Besides these effects, the high versatility in chemical and physical properties and shaping, hybrid nanocomposites offer significant opportunity in order to facilitate integration and miniaturization thus open up to golden door for many promising applications in a variety of areas including (a) optics, (b) electronics, (c) ionics, (d) mechanics, (e) membranes, (f) functional and protective coatings, (g) catalysis, (h) sensors, (i) biology, (j) medicine, (k) biotechnology, (l) security, (m) structural applications. Many conventional and hybrid composite based materials have been continuously appearing in the market either as prototype or commercial products, during the past decades where attempts were made to discuss the applications of some of these composites within this chapter but they only represent a small fraction of the tip of the iceberg.

In addition, currently, molecular approaches of solid state chemistry and nanochemistry have reached a very high level of sophistication where chemists have the tools for taking practical steps to tailor-make any molecular species (e.g., molecules, clusters, nanosized particles, nanolamellar compounds, nanotubes) and also to design new functional hybrid materials with improved technical performances. As a result, at this level of knowledge and understanding in nanoscience and nanotechnology and also following strict rules of environmental issues imposed by the current society, for manufacturing composite based high-tech materials and devices with complex structures, high level of integration and miniaturization is just a question of scientist's imagination and of making industries aware of their opportunities and benefits. In this context, one can bet that advanced composite materials will play a major significant role in oncoming future to shape everyday life.

This chapter covers a broad range of aspects and issues of micro- and nanocomposites and briefly covers different areas of polymer-nanocomposites known to date which include (a) polymer/carbon nanotubes, (b) polymer/metal nanospheres, and (c) polymer/clay nanoplatelets composites. This chapter also presented different issues involved with the general overview, synthesis and applications of micro and nanocomposites in order to provide a general understanding on the fundamental features of these materials for both conventional and high-tech advanced applications. However, besides all these efforts, it is beyond the scope of this current chapter

due to space limitation to cover all important features of micro- and nanocomposites emerging almost everyday because of intensive research in this field. So interested readers are suggested to consult the references provided along with this chapter for more in-depth information and current and future issues of related journals, books, and conference proceedings cited in the reference section to have most update current information on micro- and nanocomposites.

References

1. D. Hull, T.W. Clyne, *An Introduction to Composite Materials* (Cambridge University Press, 1996), pp. 2–92
2. (a) J. Luo, I.M. Danmiel, Characterization and modeling of mechanical behavior of polymer/clay nanocomposites. *Compos. Sci. Technol.* **63**, 1607–1616 (2004); (b) P. Meneghetti, S. Qutubuddin, Synthesis, thermal properties and application of polymer-clay nanocomposites. *Thermoch. Act.* **442**, 74–77 (2006); (c) S.S. Ray, M. Okamoto, Polymer/layered silicate nanocomposites: A review from preparation to processing. *Prog. Polym. Sci.* **28**, 1539–1641 (2003); M. Bhattacharya, Polymer Nanocomposites – A Comparison between Carbon Nanotubes, Graphene, and Clay as Nanofillers by Materials, **9**(4), 262 (2016); <https://doi.org/10.3390/ma9040262>; <http://creativecommons.org/licenses/by/4.0/>
3. P.M. Ajayan, L.S. Schadler, P.V. Braun, *Nanocomposite Science and Technology* (Wiley, New York, 2003), pp. 1–117
4. C. Zeng, L.J. Lee, Poly(methyl methacrylate) and polystyrene/clay nanocomposites prepared by in-situ polymerization. *Macromolecules* **34**, 4098–4103 (2001)
5. R.S. Fertig, M.R. Garnich, Influence of constituent properties and microstructural parameters on the tensile modulus of a polymer/clay nanocomposite. *Compos. Sci. Technol.* **64**, 2577–2258 (2004)
6. W.E. Teo, S. Ramakrishna, Electrospun nanofibers as a platform for multifunctional, hierarchically organized nanocomposite. *Compos. Sci. Technol.* **69**, 1804–1817 (2009)
7. Z.M. Huang, Y.Z. Zhang, M. Kotaki, S. Ramakrishna, A review on polymer nanofibers by electrospinning and their applications in nanocomposites. *Compos. Sci. Technol.* **63**, 2223–2253 (2003)
8. C. Burger, B.S. Hsiao, B. Chu, Nanofibrous materials and their applications. *Annu. Rev. Mater. Res.* **36**, 333–368 (2006)
9. K.M. Sawicka, P. Gouma, Electrospun composite nanofibers for functional applications. *J. Nanopart. Res.* **8**, 769–781 (2006)
10. J.H. He, Y.Q. Wan, J.Y. Yu, Application of vibration technology to polymer electrospinning. *Int. J. Nonlinear Sci. Numer. Simul.* **5**, 253–262 (2004)
11. S. Homaieghar, M. Elbahri, Novel compaction resistant and ductile nanocomposite nanofibrous microfiltration membranes. *J. Colloid Interface Sci.* **372**, 6–15 (2012)
12. P.M. Ajayan, O. Stephan, C. Colliex, D. Trauth, Aligned carbon nanotube arrays formed by cutting a polymer resin – Nanotube composite. *Science* **265**(5176), 1212–1214 (1994)
13. Z.-M. Huang, Y.-Z. Zhang, M. Kotaki, S. Ramakrishna, A review on polymer nanofibers by electrospinning and their applications in nanocomposites. *Compos. Sci. Technol.* **63**(15), 2223–2253 (2003)
14. G. Wei, P.X. Ma, Structure and properties of nano-hydroxyapatite/polymer composite scaffolds for bone tissue engineering. *Biomaterials* **25**(19), 4749–4757 (2004)
15. J.M. Garces, D.J. Moll, J. Bicerano, R. Fibiger, D.G. McLeod, Polymeric Nanocomposites for automotive applications. *Adv. Mater.* **12**(3), 1835 (2000)
16. P. Svoboda, C. Zeng, H. Wang, L. Lee, D. Tomasko, Morphology and mechanical properties of polypropylene/organoclay nanocomposites. *J. Appl. Polym. Sci.* **85**(7), 1562–1570 (2002)

17. P.M. Ajayan, L.S. Schadler, P.V. Braun, *Nanocomposite Science and Technology* (Wiley, New York, 2003), pp. 11–121
18. J. Jordan, K.I. Jacob, R. Tannenbaum, M.A. Sharaf, I. Jasiuk, Experimental trends in polymer nanocomposites – A review. *Mater. Sci. Eng. A* **393**, 1–11 (2005)
19. M. Berta, C. Lindsay, G. Pans, G. Camino, Effect of chemical structure on combustion and thermal behaviour of polyurethane elastomer layered silicate nanocomposites. *Polym. Degrad. Stab.* **91**, 1179–1191 (2006)
20. (a) J. Cho, M. Joshi, C. Sun, Effect of inclusion size on mechanical properties of polymeric composites with micro and nano particles. *Compos. Sci. Technol.* **66**(13), 1941–1952 (2006); (b) C. Sanchez, B. Julián, P. Belleville, M. Popall, Applications of hybrid organic-inorganic nanocomposites. *J. Mater. Chem.* **15**, 3559–3592 (2005)
21. (a) R. Singh, M. Zhang, D. Chan, Toughening of a brittle thermosetting polymer: Effects of reinforcement particle size and volume fraction. *J. Mater. Sci.* **37**(4), 781–788 (2002); (b) P. Hiemenz, R. Rajagopalan, *Principles of Colloid and Surface Chemistry* (Marcel Dekker Inc, New York, 1997), pp. 6–10
22. (a) L. Lopez, B. Song, H. Hahn, The effect of particle size in alumina nanocomposites, in *Proceedings of the 14th International Conference on Composite Materials (ICCM-14)*, July 14–18, (San Diego, 2003); (b) C. Suryanarayana, F.H. Froes, The structure and mechanical properties of metallic nanocrystals. *Metall. Trans. A.* **23**, 1071–1081 (1992)
23. (a) H. Zhang, L.C. Tang, Z. Zhang, K. Friedrich, S. Sprenger, Fracture behaviours of in situ silica nanoparticle-filled epoxy at different temperatures. *Polymer* **49**(17), 3816–3825 (2008); (b) A. Chandra, L.S. Turng, P. Gopalan, R.M. Rowell, S. Gong, Study of utilizing thin polymer surface coating on the nanoparticles for melt compounding of polycarbonate/alumina nanocomposites and their optical properties. *Compos. Sci. Technol.* **68**, 768–776 (2008)
24. (a) C. Cho, C. Sun, A molecular dynamics simulation study of inclusion size effect on polymeric nanocomposites. *Comput. Mater. Sci.* **41**(1), 54–62 (2007); (b) M.A. Osman, J.E.P. Rupp, U.W. Suter, Effect of non-ionic surfactants on the exfoliation and properties of polyethylene-layered silicate nanocomposites. *Polymer* **46**, 8202–8209 (2005)
25. (a) A. Adnan, C. Sun, H. Mahfuz, A molecular dynamics simulation study to investigate the effect of filler size on elastic properties of polymer nanocomposites. *Compos. Sci. Technol.* **67**(3), 348–356 (2007); (b) J.W. Cho, D.R. Paul, Nylon 6 nanocomposites by melt compounding. *Polymer* **42**, 1083–1094 (2001)
26. (a) D.P.N. Vlasveld, H.E.N. Bersee, S.J. Picken, Nanocomposite matrix for increased fibre composite strength. *Polymer* **46**(23), 0269–10278 (2005); (b) J.H. Chang, Y.U. An, D. Cho, E.P. Giannelis, Poly(lactic acid) nanocomposites: Comparison of their properties with montmorillonite and synthetic mica (II). *Polymer* **44**, 3715–3720 (2003)
27. (a) M.F. Uddin, C. Sun, Strength of unidirectional glass/epoxy composite with silica nanoparticle-enhanced matrix. *Compos. Sci. Technol.* **68**(7), 1637–1643 (2008); (b) T. Gupakumar, D. Page, Compounding of Nanocomposites by Thermokinetic mixing. *J. Appl. Polym. Sci.* **96**(5), 1557–1563 (2005)
28. (a) T. Naganuma, Y. Kagawa, Effect of particle size on the optically transparent nano meter-order glass particle-dispersed epoxy matrix composites. *Compos. Sci. Technol.* **62**(9), 1187–1189 (2002); (b) E. Lee, D. Mielewski, R. Baird, Exfoliation and dispersion enhancement in polypropylene Nanocomposites by in-situ melt phase Ultrasonication. *Polym. Eng. Sci* **44**(9), 1773–1782 (2004)
29. (a) S.S. Ray, M. Okamoto, Polymer/layered silicate nanocomposites: A review from preparation to processing. *Prog. Polym. Sci.* **28**(11), 1539–1641 (2003); (b) Y. Wang, F. Chen, K. Wu, Twin-screw extrusion compounding of polypropylene/Organoclay Nanocomposites modified by Maleated polypropylenes. *J. Appl. Polym. Sci.* **93**(1), 100–112 (2004)
30. (a) F. Gao, Clay/polymer composites: The story. *Mater. Today* **7**(11), 50–55 (2004); (b) S.-C. Tjong, Y.Z. Meng, A.S. Hay, Novel preparation and properties of polypropylene-vermiculite Nanocomposites. *Chem. Mater.* **14**(1), 44–51 (2002)
31. (a) M. Alexandre, P. Dubois, Polymer-layered silicate nanocomposites: Preparation, properties and uses of a new class of materials. *Mat. Sci. Eng. R. Rep.* **28**(1), 1–63 (2000); (b) M. Kato,

- M. Matsushita, K. Fukumori, Development of an e-production method for a polypropylene-clay nanocomposite. *Polym. Eng. Sci.* **44**(7), 1205–1211 (2004)
32. (a) A. Okada, A. Usuki, The chemistry of polymer-clay hybrids. *Mat. Sci. Eng. C.* **3**(2), 109–115 (1995); (b) T.D. Fornes, P.J. Yoon, H. Keskkula, D.R. Paul, Nylon 6 nanocomposites: The effect of matrix molecular weight. *Polymer* **42**, 9929 (2001)
33. (a) J.L. Tsai, M.D. Wu, Organoclay effect on mechanical responses of glass/epoxy nanocomposites. *J. Compos. Mater.* **42**(6), 553–568 (2008); (b) E. Manias, A. Touny, L. Wu, K. Strawhecker, B. Lu, T.C. Chung, Polypropylene/Montmorillonite Nanocomposites, review of the synthetic routes and materials properties. *Chem. Mater.* **13**, 3516–3523 (2001)
34. (a) D. Gong, C. Grimes, O. K. Varghese, W. Hu, R. Singh, Z. Chen, et al. Titanium oxide nanotube arrays prepared by anodic oxidation, *J. Mater. Res.* **16**(12):3331–3334 (2001); (b) P. Reichert, H. Nitz, S. Klinke, R. Brandsch, R. Thomann, R. Mulhaupt, Poly(propylene)/Organoclay Nanocomposite formulation: Influence of Compatibilizer functionality and Organoclay modification. *Macromol. Mater. Eng.* **275**, 8–17 (2000)
35. (a) Z. Wang, R.P. Gao, J. Gole, J. Stout, Silica nanotubes and nanofiber arrays. *Adv. Mater.* **12**(24), 1938–1940 (2001); (b) M.T. Ton-That, F. Perrin-Sarazin, K.C. Cole, M.N. Bureau, J. Denault, Polyolefin Nanocomposites: Formulation and development. *Polym. Eng. Sci.* **44**(7), 1212–1219 (2004)
36. T. Taguchi, N. Igawa, H. Yamamoto, S. Jitsukawa, Synthesis of silicon carbide nanotubes. *J. Am. Ceram. Soc.* **88**(2), 459–461 (2005)
37. (a) S. Iijima, Helical microtubules of graphitic carbon. *Nature* **354**(6348), 56–58 (1991); (b) M. Biswas, S.S. Ray, Recent progress in synthesis and evaluation of polymer montmorillonite nanocomposites. *Adv. Polym. Sci.* **155**, 167–221 (2001)
38. (a) H. Rajoria, N. Jalili, Passive vibration damping enhancement using carbon nanotube-epoxy reinforced composites. *Compos. Sci. Technol.* **65**(14), 2079–2093 (2005); (b) M. Alexander, P. Dubois, Polymer-layered silicate nanocomposites: Preparation, properties and uses of a new class of materials. *Mater. Sci. Eng. R. Rep.* **28**, 1–63 (2000)
39. (a) N. Tai, M. Yeh, J. Liu, Enhancement of the mechanical properties of carbon nanotube/phenolic composites using a carbon nanotube network as the Reinforcement. *Carbon* **42**, 2735–2737 (2004); (b) E.P. Giannelis, R. Krishnamoorti, E. Manias, Polymer-silicate nanocomposites: Model systems for confined polymers and polymer brushes. *Adv. Polym. Sci.* **138**, 107–147 (1999)
40. (a) F.H. Gojny, M.H.G. Wichmann, B. Fiedler, K. Schulte, Influence of different carbon nanotubes on the mechanical properties of epoxy matrix composites – A comparative study. *Compos. Sci. Technol.* **65**(15), 2300–2313 (2005); (b) P.C. LeBaron, Z. Wang, T.J. Pinnavaia, Polymer-layered silicate nanocomposites: An overview. *J. Appl. Clay Sci.* **15**, 11–29 (1999)
41. (a) S.M. Reduwan Billah, Synthesis of photochromic dye doped cellulose composite based electrospun Nanofibres for high-tech applications, in *Nanocellulose, Cellulose Nanofibers and Cellulose Nanocomposites: Synthesis and Applications*, ed. by M. I. H. Mondal, (Nova Science Publishers, New York, 2015), pp. 425–442. ISBN: 978-1-63483-885-6; (b) E. Thostenson, W. Li, D. Wang, Z. Ren, T. Chou, Carbon nanotube/carbon fiber hybrid multiscale composites. *J. Appl. Phys.* **91**(9), 6034–6037 (2002); (c) A.K. Mohanty, L.T. Drzal, M. Misra, Nano reinforcement of bio-based polymers-the hope and reality. *Polym. Mater. Sci. Eng.* **88**, 60–61 (2003)
42. (a) S.M. Reduwan Billah, Synthesis of quantum dot doped electrospun cellulose and other polymer based-nanocomposites and their applications, in *Nanocellulose, Cellulose Nanofibers and Cellulose Nanocomposites: Synthesis and Applications*, ed. by M. I. H. Mondal, (Nova Science Publishers, New York, 2015), pp. 387–424. ISBN: 978-1-63483-885-6; (b) R. Sager, P. Klein, D. Lagoudas, Q. Zhang, J. Liu, L. Dai, et al., Effect of carbon nanotubes on the interfacial shear strength of T650 carbon fiber in an epoxy matrix. *Compos. Sci. Technol.* **69**(7), 898–904 (2009); (c) R. Hiroi, S.S. Ray, M. Okamoto, Organically modified layered titanate: A new nanofiller to improve the performance of biodegradable polylactide. *Macromol. Rapid. Commun.* **25**, 1359 (2004)

43. (a) K.H. Hung, W.S. Kuo, T.H. Ko, S.S. Tzeng, C.F. Yan, Processing and tensile characterization of composites composed of carbon nanotube-grown carbon fibers. *Compos. A: Appl. Sci. Manuf.* **40**(8), 1299–1304 (2009); (b) C.A. Mitchell, J.L. Bahr, S. Arepalli, J.M. Tour, R. Krishnamoorti, Dispersion of functionalized carbon nanotubes in polystyrene. *Macromolecules* **35**, 8825–8830 (2002); (c) S.M. Reduwan Billah, Environmental stimuli-responsive electrospun nanofibres and scaffolds for advanced textile applications, in *Conference Proceeding of 2nd NED International Textile Conference*, 17th–18th February, (Karachi, 2016), pp. 1–9
44. (a) S.M. Reduwan Billah, Chapter 8. Environmentally responsive smart cellulose composites, in *Cellulose and Cellulose Derivatives: Synthesis, Modification and Applications*, ed. by M. I. H. Mondal, (Nova Science Publishers, New York, 2015), pp. 211–242, ISBN: 9781634831277 (hardback), 978-1-63483-150-5 (e-book); (b) V.P. Veedu, A. Cao, X. Li, K. Ma, C. Soldano, S. Kar, et al., Multifunctional composites using reinforced laminae with carbon-nanotube forests. *Nat. Mater.* **5**(6), 457–462 (2006); (c) P. PoÈtschke, A. Bhattacharyya, A. Janke, H. Goering, Melt-mixing of polycarbonate/multi-wall carbon nanotube composites. *Compos. Interf.* **10**, 389–404 (2003)
45. (a) E.J. Garcia, B.L. Wardle, A.J. Hart, Joining prepreg composite interfaces with aligned carbon nanotubes. *Compos. A: Appl. Sci. Manuf.* **39**(6), 1065–1070 (2008); (b) R. Andrews, M.C. Wisenberger, Carbon nanotube polymer composites. *Curr. Opinion. Solid State Mater. Sci.* **8**, 31–37 (2004)
46. (a) F. Lange, The interaction of a crack front with a second-phase dispersion. *Phil. Mag.* **22**(179), 983–992 (1970); (b) E. Hackett, E. Manias, E.P. Giannelis, Molecular dynamics simulations of organically modified layered silicates. *J. Chem. Phys.* **108**, 7410–7415 (1998)
47. (a) A. Kinloch, B. Johnsen, R. Mohammed, A. Taylor, S. Sprenger, Toughening mechanisms in novel nano-silica epoxy polymers, in *Proceedings of the 5th Australasian Congress on Applied Mechanics: Engineers*, (Australia), p. 441; (b) E. Hackett, E. Manias, E.P. Giannelis, Computer simulation studies of PEO/layered silicate nanocomposites. *Chem. Mater.* **12**, 2161–2167 (2000)
48. (a) F.F. Lange, K.C. Radford, Fracture energy of an epoxy composite system. *J. Mater. Sci.* **6**(9), 1197–1203 (1971); (b) D.L. Vanderhart, A. Asano, J.W. Gilman, NMR measurements related to clay dispersion quality and organic-modifier stability in nylon 6/clay nanocomposites. *Macromolecules* **34**(12), 3819–3822
49. (a) K.T. Faber, A.G. Evans, Crack deflection processes – I. Theory. *Acta Metall.* **31**(4), 565–576 (1983); (b) P. Kumar, D. Depan, N.S. Tomer, R.P. Singh, Nanoscale particles for polymer degradation and stabilization-trends and future perspectives. *Prog. Polym. Sci.* **34**, 479–515 (2009)
50. (a) H. Zhang, Z. Zhang, K. Friedrich, C. Eger, Property improvements of in situ epoxy nanocomposites with reduced interparticle distance at high nanosilica content. *Acta Mater.* **54**(7), 1833–1842 (2006); (b) P.H.C. Camargo, K.G. Satyanarayana, F. Wypych, Nanocomposites: Synthesis, structure, properties and new application opportunities. *Mater. Res.* **12**(1), 1–39 (2009)
51. (a) B. Johnsen, A. Kinloch, R. Mohammed, A. Taylor, S. Sprenger, Toughening mechanisms of nanoparticle-modified epoxy polymers. *Polymer* **48**(2), 530–541 (2007); (b) G. William, P.V. Kamat, Graphene-semiconductor nanocomposites: Excited-state interactions between ZnO nanoparticles and graphene oxide. *Langmuir* **25**(24), 13869–13873 (2009)
52. M. Zanetti, G. Camino, R. Thomann, R. Mülhaupt, Synthesis and thermal behaviour of layered silicate-EVA nanocomposites. *Polymer* **42**, 4501–4507 (2001)
53. N. Ljungberg, C. Bonini, F. Bortolussi, C. Boisson, L. Heux, J.Y. Cavaille, New nanocomposite materials reinforced with cellulose whiskers in atactic polypropylene: Effect of surface and dispersion characteristics. *Biomacromolecules* **6**, 2732–2739 (2005)
54. S.M. Lai, W.C. Chen, X.S. Zhu, Melt mixed compatibilized polypropylene/clay nanocomposites: Part 1- the effect of compatibilizers on optical transmittance and mechanical properties. *Compos. Part A* **40**, 754–765 (2009)

55. R.N. Choi, C.I. Cheigh, S.Y. Lee, M.S. Chung, Preparation and properties of polypropylene/clay nanocomposites for food packaging. *J. Food Sci.* **76**(8), 62–67 (2011)
56. J.P.G. Villaluenge, M. Khayer, M.A. Lo'pez-Manchado, J.L. Valentin, B. Seoane, J.I. Mengual, Gas transport properties of polypropylene/clay composite membranes. *Eur. Polym. J.* **43**, 1132–1143 (2007)
57. L. Zhu, M. Xanthos, Effects of process conditions and mixing protocols on structure of extruded polypropylene nanocomposites. *J. Appl. Polym. Sci.* **93**, 1891–1899 (2004)
58. Z.-M. Huang, Y.-Z. Zhang, M. Kotaki, S. Ramakrishna, A review on polymer nanofibers by electrospinning and their applications in nanocomposites. *Compos. Sci. Technol.* **63**(15), 2223–2253 (2003)
59. W. Chen, Q. Xu, R.Z. Yuan, Modification of poly(ethylene oxide) with polymethylmethacrylate in polymer-layered silicate nanocomposites. *J. Mater. Sci. Lett.* **18**, 711–713 (1999)
60. H.R. Fischer, L.H. Gielgens, T.P.M. Koster, Nanocomposites from polymers and layered materials. *Acta Polym.* **50**, 122–126 (1999)
61. (a) E.A. Stefanescu, C. Daranga, C. Stefanescu, Insight into the broad field of polymer Nanocomposites: From carbon nanotubes to clay Nanoplatelets, via metal nanoparticles. *Material* **2**, 2095–2153 (2009); (b) E. Loizou, P. Butler, L. Porcar, E. Kesselman, Y. Talmon, A. Dundigalla, G. Schmidt, Large scale structures in nanocomposite hydrogels. *Macromolecules* **38**, 2047–2049 (2005)
62. E. Loizou, P. Butler, L. Porcar, G. Schmidt, Dynamic responses in nanocomposite hydrogels. *Macromolecules* **39**, 1614–1619 (2006)
63. G. Schmidt, A.I. Nakatani, P.D. Butler, A. Karim, C.C. Han, Shear orientation of viscoelastic polymer-clay solutions probed by flow birefringence and SANS. *Macromolecules* **33**, 7219–7222 (2000)
64. G. Schmidt, A.I. Nakatani, C.C. Han, Rheology and flow-birefringence from viscoelastic polymer-clay solutions. *Rheol. Acta* **41**, 45–54 (2002)
65. E.A. Stefanescu, A. Dundigalla, V. Ferreiro, E. Loizou, L. Porcar, I. Negulescu, J. Garno, G. Schmidt, Supramolecular structures in nanocomposite multilayered films. *Phys. Chem. Chem. Phys.* **8**, 1739–1746 (2006)
66. E.A. Stefanescu, W.H. Daly, I.I. Negulescu, Hybrid polymer/clay nanocomposites: Effect of clay size on the structure of multilayered films. *Macromol. Mater. Eng.* **293**, 651–656 (2008)
67. X. Dai, J. Xu, X. Guo, Y. Lu, D. Shen, N. Zhao, X. Luo, X. Zhang, Study on structure and orientation action of polyurethane nanocomposites. *Macromolecules* **37**, 5615–5623 (2004)
68. T. Chatterjee, C.A. Mitchell, V.G. Hadjiev, R. Krishnamoorti, Hierarchical polymer-nanotube composites. *Adv. Mater.* **19**, 3850–3853 (2007)
69. H. Jiang, K. Moon, Y. Li, C.P. Wong, Surface functionalized silver nanoparticles for ultrahigh conductive polymer composites. *Chem. Mater.* **18**, 2969–2973 (2006)
70. P.Y. Keng, I. Shim, B.D. Korth, J.F. Douglas, J. Pyun, Synthesis and self-assembly of polymer-coated ferromagnetic nanoparticles. *ACS Nano* **1**, 279–292 (2007)
71. H.Y. Kwong, Y.W. Wong, K.H. Wong, Temperature dependence of magnetoresistivity of cobalt-polytetrafluoroethylene granular composite films. *J. Appl. Phys.* **102**, 114303 (2007)
72. K. Pirkkalainen, K. Leppänen, U. Vainio, M.A. Webb, T. Elbra, T. Kohout, A. Nykänen, J. Ruokolainen, N. Kotelnikova, R. Serimaa, Nanocomposites of magnetic cobalt nanoparticles and cellulose. *Eur. Phys. J. D.* **49**, 333–342 (2008)
73. G.T. Mohanraj, P.K. Dey, T.K. Chaki, A. Chakraborty, D. Khastgir, Effect of temperature, pressure, and composition on DC resistivity and AC conductivity of conductive styrenebutadiene rubber-particulate metal alloy nanocomposites. *Polym. Compos.* **28**, 696–704 (2007)
74. M. Panda, V. Srinivas, A.K. Thakur, Surface and interfacial effect of filler particle on electrical properties of polyvinylidene fluoride/nickel composites. *Appl. Phys. Lett.* **93**, 242908 (2008)
75. O.P. Valmikanathan, O. Ostroverkhova, I.S. Mulla, K. Vijayamohan, S.V. Atre, The effect of synthesis procedure on the structure and properties of palladium/polycarbonate nanocomposites. *Polymer* **49**, 3413–3418 (2008)

76. Z.Y. Tang, N.A. Kotov, One-dimensional assemblies of nanoparticles: Preparation, properties, and promise. *Adv. Mater.* **17**, 951–962 (2005)
77. S.L. Tripp, R.E. Dunin-Borkowski, A. Wei, Flux closure in self-assembled cobalt nanoparticle rings. *Angew. Chem. Int. Ed.* **42**, 5591–5593 (2003)
78. D. Farrell, Y. Ding, S.A. Majetich, C. Sanchez-Hanke, C.C. Kao, Structural ordering effects in Fe nanoparticle two- and three-dimensional arrays. *J. Appl. Phys.* **95**, 6636–6638 (2004)
79. M. Hilgendorff, B. Tesche, M. Giersig, Creation of 3-D crystals from single cobalt nanoparticles in external magnetic fields. *Aust. J. Chem.* **54**, 497–501 (2001)
80. G. Carotenuto, B. Martorana, P. Perlo, L. Nicolais, A universal method for the synthesis of metal and metal sulfide clusters embedded in polymer matrices. *J. Mater. Chem.* **13**, 2927–2930 (2003)
81. M.V. Jose, B.W. Steinert, V. Thomas, D.R. Dean, M.R. Abdalla, G. Price, G.M. Janowski, Morphology and mechanical properties of Nylon 6/MWNT nanofibers. *Polymer* **48**, 1096–1104 (2007)
82. K. Chrissafis, G. Antoniadis, K.M. Paraskevopoulos, A. Vassiliou, D.N. Bikiaris, Comparative study of the effect of different nanoparticles on the mechanical properties and thermal degradation mechanism of in situ prepared poly(E-caprolactone) nanocomposites. *Compos. Sci. Technol.* **67**, 2165–2174 (2007)
83. J.M. Thomassin, X. Lou, C. Pagnouille, A. Saib, L. Bednarz, I. Huynen, R. Jerome, C. Detrembleur, Multiwalled carbon nanotube/poly(epsilon-caprolactone) nanocomposites with exceptional electromagnetic interference shielding properties. *J. Phys. Chem. C* **111**, 11186–11192 (2007)
84. T.N. Abraham, R. Debdatta, S. Siengchin, J. Karger-Kocsis, Rheological and thermal properties of poly(ethylene oxide)/multiwall carbon nanotube composites. *J. Appl. Polym. Sci.* **110**, 2094–2101 (2008)
85. A.K. Narh, L. Jallo, K.Y. Rhee, The effect of carbon nanotube agglomeration on the thermal and mechanical properties of polyethylene oxide. *Polym. Compos.* **29**, 809–817 (2008)
86. Y.S. Song, Effect of surface treatment for carbon nanotubes on morphological and rheological properties of poly(ethylene oxide) nanocomposites. *Polym. Eng. Sci.* **46**, 1350–1357 (2006)
87. R.D. Averett, M.L. Realff, K.I. Jacob, The effects of fatigue and residual strain on the mechanical behavior of poly(ethylene terephthalate) unreinforced and nanocomposite fibers. *Compos. A: Appl. Sci. Manuf.* **40**, 709–723 (2009)
88. B.W. Steinert, D.R. Dean, Magnetic field alignment and electrical properties of solution cast PET-carbon nanotube composite films. *Polymer* **50**, 898–904 (2009)
89. A.C. Brosse, S. Tence-Girault, P.M. Piccione, L. Leibler, Effect of multi-walled carbon nanotubes on the lamellae morphology of polyamide-6. *Polymer* **49**, 4680–4686 (2008)
90. Y. Li, H. Shimizu, Conductive PVDF/PA6/CNTs nanocomposites fabricated by dual formation of cocontinuous and nanodispersion structures. *Macromolecules* **41**, 5339–5344 (2008)
91. C.A. Mitchell, R. Krishnamoorti, Dispersion of single-walled carbon nanotubes in poly(epsilon-caprolactone). *Macromolecules* **40**, 1538–1545 (2007)
92. T. Chatterjee, R. Krishnamoorti, Steady shear response of carbon nanotube networks dispersed in poly(ethylene oxide). *Macromolecules* **41**, 5333–5338 (2008)
93. T. Chatterjee, K. Yurekli, V.G. Hadjiev, R. Krishnamoorti, Single-walled carbon nanotube dispersions in poly(ethylene oxide). *Adv. Funct. Mater.* **15**, 1832–1838 (2005)
94. H.J. Yoo, Y.C. Jung, J.W. Cho, Effect of interaction between poly(ethylene terephthalate) and carbon nanotubes on the morphology and properties of their nanocomposites. *J. Polym. Sci. B Polym. Phys.* **46**, 900–910 (2008)
95. B.W. Ahn, Y.S. Chi, T.J. Kang, Preparation and characterization of multi-walled carbon nanotube/poly(ethylene terephthalate) nanoweb. *J. Appl. Polym. Sci.* **110**, 4055–4063 (2008)
96. K. Wang, W.W. Li, C. Gao, Poly(epsilon-caprolactone)-functionalized carbon nanofibers by surface-initiated ring-opening polymerization. *J. Appl. Polym. Sci.* **105**, 629–640 (2007)
97. N. Wakamatsu, H. Takamori, T. Fujigaya, N. Nakashima, Self-organized single-walled carbon nanotube conducting thin films with honeycomb structures on flexible plastic films. *Adv. Funct. Mater.* **19**, 311–316 (2009)

98. H. Chen, Z. Liu, P. Cebe, Chain confinement in electrospun nanofibers of PET with carbon nanotubes. *Polymer* **50**, 872–880 (2009)
99. G.J. Hu, X.Y. Feng, S.M. Zhang, M.S. Yang, Crystallization behavior of poly(ethylene terephthalate)/multiwalled carbon nanotubes composites. *J. Appl. Polym. Sci.* **108**, 4080–4089 (2008)
100. A. Nyczzyk, M. Hasik, W. Turek, A. Sniechota, Nanocomposites of polyaniline, its derivatives and platinum prepared using aqueous Pt sol. *Synth. Met.* **159**, 561–567 (2009)
101. G. Zotti, B. Vercelli, A. Berlin, Gold nanoparticle linking to polypyrrole and polythiophene: Monolayers and multilayers. *Chem. Mater.* **20**, 6509–6516 (2008)
102. S.W. Huang, K.G. Neoh, E.T. Kang, H.S. Han, K.L. Tan, Palladium-containing polyaniline and polypyrrole microparticles. *J. Mater. Chem.* **8**, 1743–1748 (1998)
103. J.L. Wilson, P. Poddar, N.A. Frey, H. Srikanth, K. Mohomed, J.P. Harmon, S. Kotha, J. Wachsmuth, Synthesis and magnetic properties of polymer nanocomposites with embedded iron nanoparticles. *J. Appl. Phys.* **95**, 1439 (2004)
104. G. Yurkov, A. Fionov, Y. Koksharov, V. Koleso, S. Gubin, Electrical and magnetic properties of nanomaterials containing iron or cobalt nanoparticles. *Inorg. Mater.* **43**, 834–844 (2007)
105. A. Sarkar, S. Kapoor, G. Yashwant, H.G. Salunke, T. Mukherjee, Preparation and characterization of ultrafine Co and Ni particles in a polymer matrix. *J. Phys. Chem. B* **109**, 7203–7207 (2005)
106. Y. Sun, J. Sun, M. Liu, Q. Chen, Mechanical strength of carbon nanotube-nickel nanocomposites. *Nanotechnology* **18**, 505704–505704 (2007)
107. L. Balan, M. Jin, J.P. Malval, H. Chaumeil, A. Defoin, L. Vidal, Fabrication of silver nanoparticle-embedded polymer promoted by combined photochemical properties of a 2,7-diaminofluorene derivative dye. *Macromolecules* **41**, 9359–9365 (2008)
108. A. Dundigalla, S. Lin Gibson, V. Ferreira, M.M. Malwitz, G. Schmidt, Unusual multi-layered structures in PEO/laponite nanocomposite films. *Macromol. Rapid Commun.* **26**, 143–149 (2005)
109. M.M. Elmahdy, K. Chrissopoulou, A. Afratis, G. Floudas, S.H. Anastasiadis, Effect of confinement on polymer segmental motion and ion mobility in PEO/layered silicate nanocomposites. *Macromolecules* **39**, 5170–5173 (2006)
110. H.I. Inyang, S. Bae, G. Mbamalu, S.-W. Park, Aqueous polymer effects on volumetric swelling of Na-montmorillonite. *J. Mater. Civ. Eng.* **19**:1, 84–90 (2007)
111. A. Loiseau, J.F. Tassin, Model nanocomposites based on laponite and poly(ethylene oxide): Preparation and rheology. *Macromolecules* **39**, 9185–9191 (2006)
112. W. Loyens, F.H.J. Maurer, P. Jannasch, Melt-compounded salt-containing poly(ethylene oxide)/clay nanocomposites for polymer electrolyte membranes. *Polymer* **46**, 7334–7345 (2005)
113. W.L. Qiu, M. Pyda, E. Nowak-Pyda, A. Habenschuss, B. Wunderlich, Reversibility between glass and melting transitions of poly(oxyethylene). *Macromolecules* **38**, 8454–8467 (2005)
114. E.A. Stefanescu, P.J. Schexnailder, A. Dundigalla, I.I. Negulescu, G. Schmidt, Structure and thermal properties of multilayered Laponite/PEO nanocomposite films. *Polymer* **47**, 7339–7348 (2006)
115. E.A. Stefanescu, C. Stefanescu, W.H. Daly, G. Schmidt, I.I. Negulescu, Hybrid polymer-clay nanocomposites: A mechanical study on gels and multilayered films. *Polymer* **49**, 3785–3794 (2008)
116. C.B. Arias, A.A. Zaman, J. Talton, Rheological behavior and wear abrasion resistance of polyethylene oxide/laponite nanocomposites. *J. Dispers. Sci. Technol.* **28**, 247–254 (2007)
117. Y. Xu, B. Higgins, W.J. Brittain, Bottom-up synthesis of PS–CNF nanocomposites. *Polymer* **46**, 799–810 (2005)
118. C. Wang, C.-L. Huang, Y.-C. Chen, G.-L. Hwang, S.-J. Tsai, Carbon nanocapsules-reinforced syndiotactic polystyrene nanocomposites: Crystallization and morphological features. *Polymer* **49**, 5564–5574 (2008)
119. J. Shen, C. Zeng, L.J. Lee, Synthesis of polystyrene–carbon nanofibers nanocomposite foams. *Polymer* **46**, 5218–5224 (2005)

120. M. Mu, A.M. Walker, J.M. Torkelson, K.I. Winey, Cellular structures of carbon nanotubes in a polymer matrix improve properties relative to composites with dispersed nanotubes. *Polymer* **49**, 1332–1337 (2008)
121. A. Chang, A. Kisliuk, S.M. Rhodes, W.J. Brittain, A.P. Sokolov, Conductivity and mechanical properties of well-dispersed single-wall carbon nanotube/polystyrene composite. *Polymer* **47**, 7740–7746 (2006)
122. M.R. Nyden, S.I. Stoliarov, Calculations of the energy of mixing carbon nanotubes with polymers. *Polymer* **49**, 635–641 (2007)
123. L. Xie, F. Xu, F. Qiu, H. Lu, Y. Yang, Single-walled carbon nanotubes functionalized with high bonding density of polymer layers and enhanced mechanical properties of composites. *Macromolecules* **40**, 3296–3305 (2007)
124. K. Putz, R. Krishnamoorti, P.F. Green, The role of interfacial interactions in the dynamic mechanical response of functionalized SWNTePS nanocomposites. *Polymer* **48**, 3540–3545 (2007)
125. B.H. Cipriano, A.K. Kota, A.L. Gershon, C.J. Laskowski, T. Kashiwagi, H.A. Bruck, S.R. Raghavan, Conductivity enhancement of carbon nanotube and nanofiber-based polymer nanocomposites by melt annealing. *Polymer* **49**, 4846–4851 (2008)
126. A.K. Kota, B.H. Cipriano, M.K. Dueterberg, A.L. Gershon, D. Powell, S.R. Raghavan, H.A. Bruck, Electrical and rheological percolation in polystyrene/MWCNT nanocomposites. *Macromolecules* **40**, 7400–7406 (2007)
127. B.H. Cipriano, T. Kashiwagi, S.R. Raghavan, Y. Yang, E.A. Grulke, K. Yamamoto, J.R. Shields, J.F. Douglas, Effects of aspect ratio of MWNT on the flammability properties of polymer nanocomposites. *Polymer* **48**, 6086–6096 (2007)
128. J. Cui, W.P. Wang, Y. You, C. Liu, P. Wang, Functionalization of multiwalled carbon nanotubes by reversible addition fragmentation chain-transfer polymerization. *Polymer* **45**, 8717–8721 (2004)
129. G. Xu, W.-T. Wu, Y. Wang, W. Pang, Q. Zhu, P. Wang, Y. You, Constructing polymer brushes on multiwalled carbon nanotubes by in situ reversible addition fragmentation chain transfer polymerization. *Polymer* **47**, 5909–5918 (2006)
130. X. Jinqi, W.B. Jeremy, A.B.. David, T. Tzu-Chia, E.M. Michael, L.W. Karen, Hierarchical inorganic-organic nanocomposites possessing amphiphilic and morphological complexities: Influence of nanofiller dispersion on mechanical performance. *Adv. Funct. Mater.* **18**, 2733–2744 (2008)
131. A.K. Mohanty, M. Misra, I.T. Drzal, *Natural Fibers, Biopolymers and Biocomposites* (CRC Press, Taylor & Francis, New York, 2005)
132. X. Huang, A.N. Netravali, Characterization of nanoclay reinforced Phytogel- modified soy protein concentrate resin. *Biomacromolecules* **7**, 2783–2789 (2006)
133. P. Iodha, A.N. Netravali, Characterization of Phytogel modified soy protein isolate resin and unidirectional flax yarn reinforced ‘green’ composites. *Polym. Compos.* **26**, 647–659 (2005)
134. D.N. Saheb, J.P. Jog, Natural fiber polymer composites: Review. *Adv. Polym. Technol.* **18**(4), 351–363 (1999)
135. W. Helbert, J.Y. Cavaille, A. Dufresne, Thermoplastic nanocomposites filled with wheat straw cellulose whiskers. Part I: Processing and mechanical behaviour. *Polym. Compos.* **17**(4), 604–611 (1996)
136. T. Nishino, K. Takano, K. Nakamae, Elastic-modulus of the crystalline regions of cellulose polymorphs. *J. Polym. Sci. Polym. Phys.* **33**(11), 1647–1651 (1995)
137. A.N. Nakagaito, H. Yano, Novel high- strength biocomposites based on micro- fibrillated cellulose having nano order unit web-like network structure. *Appl. Phys. A Mater.* **80**(1), 155–159 (2003)
138. I. Turner, C. Karatzas, in *Natural Fibers, Plastics and Composites*, ed. by F. T. Wallenberger, N. Weston, (Kluwer Academic Publishers, Boston, 2004), pp. 2–79
139. D.T. Grubb, I. Jelinski, Fiber morphology of spider silk: The effects of tensile deformation. *Macromolecules* **30**(10), 2860–2867 (1997)

140. S. Salmon, S.M. Hudson, Crystal morphology, biosynthesis and physical assembly of cellulose, chitin and chitosan. *J. Macromol. Sci. C Polym. Rev.* **37**(2), 199–276 (1997)
141. A. Steinbuchel, *Biopolymers – General Aspects and Special Applications*, vol 10 (Wiley-VCH, Weinheim, 2003), pp. 2–342
142. I. Yu, K. Dean, I. Li, Polymer blends & composites from renewable resources. *Prog. Polym. Sci.* **31**(6), 576–602 (2006)
143. A.K. Rana, A. Mandal, B.C. Mitra, R. Jacobson, R. Rowell, A.N. Banerjee, Short jute fiber reinforced polypropylene composites. *J. Appl. Polym. Sci.* **69**(2), 329–338 (1998)
144. A.K. Bledzki, J. Gassan, Composites reinforced with cellulose based fibers. *J. Prog. Polym. Sci.* **24**(2), 221–234 (1999)
145. B.W. Brouwer, Natural fibre composites: Where can flax compete with glass? *J. SAMPE J.* **36**(6), 18–23 (2000)
146. A. Stamboulis, C.A. Baille, T. Pejts, Effects of environmental conditions on mechanical and physical properties of flax fibers. *Compos. A Appl. Sci. Manuf.* **32**(8), 1105–11015 (2001)
147. S. Chabba, A.N. Netravali, ‘Green’ composites Part 1: Characterization of flax fabric and glutaraldehyde modified soy protein concentrate composites. *J. Mater. Sci.* **40**(23), 6263–6273 (2005)
148. S. Chabba, A.N. Netravali, ‘Green’ Composites Part 2: Characterization of flax yarn and glutaraldehyde/poly(vinyl alcohol) modified soy protein concentrate composites. *J. Mater. Sci.* **40**(23), 6275–6282 (2005)
149. N.K. Naik, R. Kuchibhotla, Analytical study of strength and failure behaviour of plain weave fabric composites made of twisted yarns. *Compos. A: Appl. Sci. Manuf.* **33**(5), 697–708 (2002)
150. N.K. Naik, in *Numerical Analysis and Modeling of Composite Materials*, ed. by J. W. Bull, (Blackie, London/New York, 1996), pp. 376–543
151. A.K. Mohanty, A.M. Khan, G. Hinrichsen, Surface modification of jute and its influence on performance of biodegradable jute-fabric/biopol composites. *Compos. Sci. Technol.* **60**(7), 1115–1124 (2000)
152. I.Y. Mwaikambo, E. Martuscelli, M. Avella, Kapok/cotton fabric-polypropylene composites. *Polym. Test.* **19**(8), 905–918 (2000)
153. M. Nardin, I.M. Ward, Influence of surface treatment on adhesion of polyethylene fiber. *Mater. Sci. Technol. Scr.* **3**(10), 814–826 (1987)
154. C.C. Chamis, in *Interfaces in Polymer Matrix Composites*, ed. by E. P. Piuddemann, (Academic Press, New York, 1974), pp. 2–63
155. L. Chen, C. Liu, K. Liu, C. Meng, C. Hu, J. Wang, S. Fan, High-performance, low-voltage, and easy-operable bending actuator based on aligned carbon nanotube/polymer composites. *ACS Nano* **5**(3), 588–1593 (2011)
156. D.K. Seo, T.J. Kang, D.W. Kim, Y.H. Kim, Twistable and bendable actuator: A CNT/polymer sandwich structure driven by thermal gradient. *Nanotechnology* **23**(7), 075501 (2012)
157. S. Ahir, E. Terentjev, Fast relaxation of carbon nanotubes in polymer composite actuators. *Phys. Rev. Lett.* **96**(13), 133902 (2006)
158. S. Lu, B. Panchapakesan, Photomechanical responses of carbon nanotube/polymer actuators. *Nanotechnology* **18**(30), 305502 (2007)
159. H.-C. Jung, J.-H. Moon, D.-H. Baek, J.-H. Lee, Y.-Y. Choi, J.-S. Hong, S.-H. Lee, CNT/PDMS composite flexible dry electrodes for long-term ECG monitoring. *IEEE Trans. Biomed. Eng.* **59**(5), 1472–1479 (2012)
160. P.R. Prajith, R. Ganesan, S. Gobalakrishnan, Design of Electroencephalogram Sensor for long-term bio-signal measurement. *Int. J. Lat. Tren. Eng. Tech.* **2**(3), 198–206 (2013)
161. K.A. Carrado, L.Q. Xu, In-situ synthesis of polymer-clay nanocomposites from silicate gels. *Chem. Mater.* **10**, 1440–1445 (1998)
162. J. Lee, T. Takekoshi, E. Giannelis, Fire retardant polyetherimide nanocomposites. *Mater. Res. Soc. Symp. Proc.* **457**, 513–518 (1997)
163. J.W. Gilman, Flammability and thermal stability studies of polymer layered-silicate (clay) nanocomposites. *Appl. Clay Sci.* **15**, 31–49 (1999)

164. F. Dietsche, R.M. Elhaupt, Thermal properties and flammability of acrylic nanocomposites based upon organophilic layered silicates. *Polym. Bull.* **43**, 395–402 (1999)
165. J.M. Garces, D.J. Moll, J. Bicerano, R. Fibiger, D.G. McLeod, Polymeric Nanocomposites for automotive applications. *Adv. Mater.* **12**(3), 1835–1839 (2000)
166. P. Svoboda, C. Zeng, H. Wang, L. Lee, D. Tomasko, Morphology and mechanical properties of polypropylene/organoclay nanocomposites. *J. Appl. Polym. Sci.* **85**(7), 1562–1570 (2002)
167. J. Jordan, K.I. Jacob, R. Tannenbaum, M.A. Sharaf, I. Jasiuk, Experimental trends in polymer nanocomposites – A review. *Mater. Sci. Eng. A* **393**, 1–11 (2005)
168. M. Berta, C. Lindsay, G. Pans, G. Camino, Effect of chemical structure on combustion and thermal behaviour of polyurethane elastomer layered silicate nanocomposites. *Polym. Degrad. Stab.* **91**, 1179–1191 (2006)
169. C. Sanchez, B. Julián, P. Belleville, M. Popall, Applications of hybrid organic-inorganic nanocomposites. *J. Mater. Chem.* **15**, 3559–3592 (2005)
170. P. Hiemenz, R. Rajagopalan, *Principles of Colloid and Surface Chemistry* (Marcel Dekker Inc., New York, 1997), pp. 6–10
171. C. Suryanarayana, F.H. Froes, The structure and mechanical properties of metallic nanocrystals. *Metall. Trans. A.* **23**, 1071–1081 (1992)
172. A. Chandra, L.S. Turng, P. Gopalan, R.M. Rowell, S. Gong, Study of utilizing thin polymer surface coating on the nanoparticles for melt compounding of polycarbonate/alumina nanocomposites and their optical properties. *Compos. Sci. Technol.* **68**, 768–776 (2008)
173. M.A. Osman, J.E.P. Rupp, U.W. Suter, Effect of non-ionic surfactants on the exfoliation and properties of polyethylene-layered silicate nanocomposites. *Polymer* **46**, 8202–8209 (2005)
174. J.W. Cho, D.R. Paul, Nylon 6 nanocomposites by melt compounding. *Polymer* **42**, 1083–1094 (2001)
175. J.H. Chang, Y.U. An, D. Cho, E.P. Giannelis, Poly(lactic acid) nanocomposites: Comparison of their properties with montmorillonite and synthetic mica (II). *Polymer* **44**, 3715–3720 (2003)
176. T. Gupakumar, D. Page, Compounding of Nanocomposites by Thermokinetic mixing. *J. Appl. Polym. Sci.* **96**(5), 1557–1563 (2005)
177. E. Lee, D. Mielewski, R. Baird, Exfoliation and dispersion enhancement in polypropylene Nanocomposites by in-situ melt phase Ultrasonication. *Polym. Eng. Sci.* **44**(9), 1773–1782 (2004)
178. Y. Wang, F. Chen, K. Wu, Twin-screw extrusion compounding of polypropylene/Organoclay Nanocomposites modified by Maleated polypropylenes. *J. Appl. Polym. Sci.* **93**(1), 100–112 (2004)
179. S.C. Tjong, Y.Z. Meng, A.S. Hay, Novel preparation and properties of polypropylene-vermiculite Nanocomposites. *Chem. Mater* **14**(1), 44–51 (2002)
180. M. Kato, M. Matsushita, K. Fukumori, Development of an e-production method for a polypropylene-clay nanocomposite. *Polym. Eng. Sci.* **44**(7), 1205–1211 (2004)
181. T.D. Fornes, P.J. Yoon, H. Keskkula, D.R. Paul, Nylon 6 nanocomposites: The effect of matrix molecular weight. *Polymer* **42**, 9929 (2001)
182. E. Manias, A. Touny, L. Wu, K. Strawhecker, B. Lu, T.C. Chung, Polypropylene/Montmorillonite Nanocomposites, review of the synthetic routes and materials properties. *Chem. Mater.* **13**, 3516–3523 (2001)
183. P. Reichert, H. Nitz, S. Klinke, R. Brandsch, R. Thomann, R. Mulhaupt, Poly(propylene)/Organoclay Nanocomposite formulation: Influence of Compatibilizer functionality and Organoclay modification. *Macromol. Mater. Eng.* **275**, 8–17 (2000)
184. M.T. Ton-That, F. Perrin-Sarazin, K.C. Cole, M.N. Bureau, J. Denault, Polyolefin Nanocomposites: Formulation and development. *Polym. Eng. Sci.* **44**(7), 1212–1219 (2004)
185. R. Zhang, M. Baxendale, T. Peijs, Universal resistivity-strain dependence of carbon nanotube/polymer composites. *Phys. Rev. B* **76**(19), 195433–195436 (2007)
186. M. Biswas, S.S. Ray, Recent progress in synthesis and evaluation of polymer montmorillonite nanocomposites. *Adv. Polym. Sci.* **155**, 167–221 (2001)

187. M. Alexander, P. Dubois, Polymer-layered silicate nanocomposites: Preparation, properties and uses of a new class of materials. *Mater. Sci. Eng. R. Rep.* **28**, 1–63 (2000)
188. E.P. Giannelis, R. Krishnamoorti, E. Manias, Polymer-silicate nanocomposites: Modelsystems for confined polymers and polymer brushes. *Adv. Polym. Sci.* **138**, 107–147 (1999)
189. P.C. LeBaron, Z. Wang, T.J. Pinnavaia, Polymer-layered silicate nanocomposites: An overview. *J. Appl. Clay Sci.* **15**, 11–29 (1999)
190. (a) S. Sepehri, B.B. Garcia, G. Cao, Tuning dehydrogenation temperature of carbon–ammonia borane nanocomposites. *J. Mater. Chem.* **18**(34), 4034–4037 (2008); (b) A.K. Mohanty, L.T. Drzal, M. Misra, Nano reinforcement of bio-based polymers—the hope and reality. *Polym. Mat. Sci. Eng.* **88**, 60–61 (2003)
191. R. Hiroi, S.S. Ray, M. Okamoto, Organically modified layered titanate: A new nanofiller to improve the performance of biodegradable polylactide. *Macromol. Rap. Com.* **25**, 1359 (2004)
192. C.A. Mitchell, J.L. Bahr, S. Arepalli, J.M. Tour, R. Krishnamoorti, Dispersion of functionalized carbon nanotubes in polystyrene. *Macromolecules* **35**, 8825–8830 (2002)
193. P. PoÈtschke, A. Bhattacharyya, A. Janke, H. Goering, Melt-mixing of polycarbonate/multi-wall carbon nanotube composites. *Compos. Interf.* **10**, 389–404 (2003)
194. R. Andrews, M.C. Wisenberger, Carbon nanotube polymer composites. *Curr. Opin. Sol. Stat. Mat. Sci.* **8**, 31–37 (2004)
195. E. Hackett, E. Manias, E.P. Giannelis, Molecular dynamics simulations of organically modified layered silicates. *J. Chem. Phys.* **108**, 7410–7415 (1998)
196. E. Hackett, E. Manias, E.P. Giannelis, Computer simulation studies of PEO/layered silicate nanocomposites. *Chem. Mater.* **12**, 2161–2167 (2000)
197. D.L. Vanderhart, A. Asano, J.W. Gilman, NMR measurements related to clay dispersion quality and organic-modifier stability in nylon 6/clay nanocomposites. *Macromolecules* **34**(12), 3819–3822 (2001)
198. P. Kumar, D. Depan, N.S. Tomer, R.P. Singh, Nanoscale particles for polymer degradation and stabilization-trends and future perspectives. *Prog. Polym. Sci.* **34**, 479–515 (2009)
199. P.H.C. Camargo, K.G. Satyanarayana, F. Wypych, Nanocomposites: Synthesis, structure, properties and new application opportunities. *Mater. Res.* **12**(1), 1–39 (2009)
200. G. William, P.V. Kamat, Graphene-semiconductor nanocomposites: Excited-state interactions between ZnO nanoparticles and graphene oxide. *Langmuir* **25**(24), 13869–13873 (2009)
201. M. Zanetti, G. Camino, R. Thomann, R. Mülhaupt, Synthesis and thermal behaviour of layered silicate-EVA nanocomposites. *Polymer* **42**, 4501–4507 (2001)
202. N. Ljungberg, C. Bonini, F. Bortolussi, C. Boisson, L. Heux, J.Y. Cavaille, New nanocomposite materials reinforced with cellulose whiskers in atactic polypropylene: Effect of surface and dispersion characteristics. *Biomacromolecules* **6**, 2732–2739 (2005)
203. S.M. Lai, W.C. Chen, X.S. Zhu, Melt mixed compatibilized polypropylene/clay nanocomposites: Part 1- the effect of compatibilizers on optical transmittance and mechanical properties. *Compos. Part A* **40**, 754–765 (2009)
204. R.N. Choi, C.I. Cheigh, S.Y. Lee, M.S. Chung, Preparation and properties of polypropylene/clay nanocomposites for food packaging. *J. Food Sci.* **76**(8), 62–67 (2011)
205. J.P.G. Villaluenge, M. Khayer, M.A. Lo’pez-Manchado, J.L. Valentin, B. Seoane, J.I. Mengual, Gas transport properties of polypropylene/clay composite membranes. *Eur. Polym. J.* **43**, 1132–1143 (2007)
206. L. Zhu, M. Xanthos, Effects of process conditions and mixing protocols on structure of extruded polypropylene nanocomposites. *J. Appl. Polym. Sci.* **93**, 1891–1899 (2004)
207. Z.-M. Huang, Y.-Z. Zhang, M. Kotaki, S. Ramakrishna, A review on polymer nanofibers by electrospinning and their applications in nanocomposites. *Compos. Sci. Technol.* **63**(15), 2223–2253 (2003)
208. W. Chen, Q. Xu, R.Z. Yuan, Modification of poly(ethylene oxide) with polymethylmethacrylate in polymer-layered silicate nanocomposites. *J. Mater. Sci. Lett.* **18**, 711–713 (1999)
209. H.R. Fischer, L.H. Gielgens, T.P.M. Koster, Nanocomposites from polymers and layered materials. *Acta Polym.* **50**, 122–126 (1999)

210. K.A. Carrado, L.Q. Xu, In-situ synthesis of polymer-clay nanocomposites from silicate gels. *Chem. Mater.* **10**, 1440–1445 (1998)
211. J. Lee, T. Takekoshi, E. Giannelis, Fire retardant polyetherimide nanocomposites. *Mater. Res. Soc. Symp. Proc.* **457**, 513–518 (1997)
212. J.W. Gilman, Flammability and thermal stability studies of polymer layered-silicate (clay) nanocomposites. *Appl. Clay Sci.* **15**, 31–49 (1999)
213. F. Dietsche, R.M. Elhaupt, Thermal properties and flammability of acrylic nanocomposites based upon organophilic layered silicates. *Polym. Bull.* **43**, 395–402 (1999)
214. A.R. Bunsell, B. Harris, Hybrid carbon and glass fibre composites. *Composites* **5**(4), 157–164 (1974)
215. J. Summerscales, D. Short, Carbon fibre and glass fibre hybrid reinforced plastics. *Composites* **9**(3), 157–166 (1978)
216. D. Short, J. Summerscales, Hybrids – A review: Part 2. Physical properties. *Composites* **11**(1), 33–38 (1980)
217. M.F. Ashby, Y.J.M. Bréchet, Designing hybrid materials. *Act. Mater.* **51**(19), 5801–5821 (2003)
218. M.F. Ashby, Chapter 11 – Designing hybrid materials, in *Materials Selection in Mechanical Design*, ed. by M. F. Ashby, 4th edn., (Butterworth Heinemann, Oxford, 2011), pp. 299–340
219. A. Pegoretti et al., Intraply and interply hybrid composites based on E-glass and poly(vinyl alcohol) woven fabrics: Tensile and impact properties. *Polym. Int.* **53**(9), 1290–1297 (2004)
220. H. Fukunaga, T.-W. Chou, H. Fukuda, Strength of intermingled hybrid composites. *J. Reinf. Plast. Compos.* **3**(2), 145–160 (1984)
221. G. Kretsis, A review of the tensile, compressive, flexural and shear properties of hybrid fibre-reinforced plastics. *Composites* **18**(1), 13–23 (1987)
222. P. Wambua, J. Ivens, I. Verpoest, Natural fibres: Can they replace glass in fibre reinforced plastics? *Compos. Sci. Technol.* **63**(9), 1259–1264 (2003)
223. O. Faruk et al., Biocomposites reinforced with natural fibers: 2000–2010. *Prog. Polym. Sci.* **37**(11), 1552–1596 (2012)
224. F.P. La Mantia, M. Morreale, Green composites: A brief review. *Compos A: Appl. Sci. Manuf.* **42**(6), 579–588 (2011)
225. G. Marom et al., Hybrid effects in composites: Conditions for positive or negative effects versus rule-of-mixtures behaviour. *J. Mater. Sci.* **13**(7), 1419–1426 (1978)
226. Y. Swolfs, L. Gorbatikh, I. Verpoest, Fibre hybridisation in polymer composites: A review. *Compos. A Appl. Sci. Manuf.* **67**, 181–200 (2014)
227. S. Torquato, *Random Heterogeneous Materials: Microstructure and Macroscopic Properties* (Springer, New York, 2002)
228. M. Biron, 7 – Future prospects for thermosets and composites, in *Thermosets and Composites*, ed. by M. Biron, 2nd edn., (William Andrew Publishing, Oxford, 2014), pp. 475–501
229. F. Ahmad et al., Hybrid composites for engineering application, in *Composite Technologies for 2020*, ed. by L. Ye, Y. W. Mai, Z. Su, (Woodhead Publishing, Cambridge, 2004), pp. 545–550
230. V. Fiore, G. Di Bella, A. Valenza, Glass–basalt/epoxy hybrid composites for marine applications. *Mater. Design* **32**(4), 2091–2099 (2011)
231. D. Lau, Hybrid fiber-reinforced polymer (FRP) composites for structural applications, in *Developments in Fiber-Reinforced Polymer (FRP) Composites for Civil Engineering*, ed. by N. Uddin, (Woodhead Publishing, Cambridge, UK, 2013), pp. 205–225
232. T. Sathishkumar, J. Naveen, S. Satheshkumar, Hybrid fiber reinforced polymer composites – A review. *J. Reinf. Plast. Compos.* **33**(5), 454–471 (2014)
233. D. Lehmhus et al., Taking a downward turn on the weight spiral – Lightweight materials in transport applications. *Mater. Des.* **66**(0), 385–389 (2015)
234. M. Wang, N. Pan, Predictions of effective physical properties of complex multiphase materials. *Mater. Sci. Eng. R. Rep.* **63**(1), 1–30 (2008)
235. (a) J.C. Halpin, J.L. Kardos, The Halpin-Tsai equations: A review. *Polym. Eng. Sci.* **16**, 344–352 (1976); (b) M. Jawaid, H.P.S.A. Khalil, Cellulosic/synthetic fibre reinforced polymer hybrid composites: A review. *Carb. Polym.* **86**(1), 1–18 (2011)

236. (a) M. Terrones, O. Martín, M. González, J. Pozuelo, B. Serrano, J.C. Cabanelas, S.M. Vega-Díaz, J. Baselga, Interphases in graphene polymer-based Nanocomposites: Achievements and challenges. *Adv. Mater.* **23**, 5302–5310 (2011); (b) A. Ashori, S. Sheshmani, Hybrid composites made from recycled materials: Moisture absorption and thickness swelling behaviour. *Bioresour. Technol.* **101**(12), 4717–4720 (2010)
237. (a) M. Cadek, J.N. Coleman, K.P. Ryan, V. Nicolosi, G. Bister, A. Fonseca, J.B. Nagy, K. Szostak, F. Béguin, W.J. Blau, Reinforcement of polymers with carbon nanotubes: The role of nanotube surface area. *Nano Lett.* **4**, 353–356 (2004); (b) A. Kelly, et al., Controlling thermal expansion to obtain negative expansivity using laminated composites. *Compos. Sci. Technol.* **65**(1), 47–59 (2005)
238. (a) R. Haggemueller, H.H. Gommans, A.G. Rinzler, J.E. Fischer, K.I. Winey, Aligned single-wall carbon nanotubes in composites by melt processing methods. *Chem. Phys. Lett.* **330**, 219–225 (2000); (b) A. Kelly, R.J. Stearn, L.N. McCartney, Composite materials of controlled thermal expansion. *Compos. Sci. Technol.* **66**(2), 154–159 (2006)
239. (a) R. Haggemueller, W. Zhou, J.E. Fisher, K.I. Winey, Production and characterization of polymer nanocomposites with highly aligned single-walled carbon nanotubes. *J. Nanosci. Nanotechnol.* **3**, 105–110 (2003); (b) G. Jefferson, T.A. Parthasarathy, R.J. Kerans, Tailorable thermal expansion hybrid structures. *Int. J. Solids Struct.* **46**(11–12), 2372–2387 (2009)
240. (a) X.Q. Chen, T. Saito, H. Yamada, K. Matsushige, Aligning single-wall carbon nanotubes with an alternating-current electric field. *Appl. Phys. Lett.* **78**, 3714–3716 (2001); (b) L.Z. Zhao et al., Thermal expansion of a novel hybrid SiC foam–SiC particles–Al composites. *Compos. Sci. Technol.* **67**(15–16), 3404–3408 (2007)
241. (a) M.S. Kumar, S.H. Lee, T.Y. Kim, T.H. Kim, S.M. Song, J.W. Yang, K.S. Nahm, E.K. Suh, DC electric field assisted alignment of carbon nanotubes on metal electrodes. *Solid State Electron.* **47**, 2075–2080 (2003); (b) H.T. Hatta, T. Takei, M. Taya, Effects of dispersed microvoids on thermal expansion behavior of composite materials. *Mater. Sci. Eng. A* **285** (1–2), 99–110 (2000)
242. (a) M.S. Kumar, T.H. Kim, S.H. Lee, S.M. Song, J.W. Yang, K.S. Nahm, E.K. Suh, Influence of electric field type on the assembly of single walled carbon nanotubes. *Chem. Phys. Lett.* **383**, 235–239 (2004); (b) A.M.D. Pascual, M. Naffakh, M.A. Gómez-Fatou, Mechanical and electrical properties of novel poly(ether ether ketone)/carbon nanotube/inorganic fullerene-like WS₂ hybrid nanocomposites: Experimental measurements and theoretical predictions. *Mater. Chem. Phys.* **130**(1–2), 126–133 (2011)
243. (a) C.A. Martin, J.K.W. Sandler, A.H. Windle, M.K. Schwarz, W.K. Bauhofer, M.S.P. Shaffer, Electric field-induced aligned multi-wall carbon nanotube networks in epoxy composites. *Polymer* **46**, 877–886 (2005); (b) J. Tan, T. Kitano, T. Hatakeyama, Crystallization of carbon fibre reinforced polypropylene. *J. Mater. Sci.* **25**(7), 3380–3384 (1990)
244. C.J. Strobl, C. Schafflein, U. Beierlein, J. Ebbecke, A. Wixforth, Carbon nanotube alignment by surface acoustic waves. *Appl. Phys. Lett.* **85**, 1427–1429 (2004)
245. (a) P.V. Kamat, K.G. Thomas, S. Barazzouk, G. Girishkumar, K. Vinodgopal, D. Meisel, Self-assembled linear bundles of Single Wall carbon nanotubes and their alignment and deposition as a film in a DC field. *J. Am. Chem. Soc.* **126**, 10757–10762 (2004); (b) C. Pradere, C. Sauder, Transverse and longitudinal coefficient of thermal expansion of carbon fibers at high temperatures. *Carbon* **46**(14), 1874–1884 (2008)
246. (a) E. Camponeschi, R. Vance, M.S. Al-Haik, H. Garmestani, R. Tannebaum, Properties of carbon nanotube-polymer composites in a magnetic field. *Carbon* **45**, 2037–2046 (2007); (b) M.H. Gabr et al., Mechanical and thermal properties of carbon fiber/polypropylene composite filled with nano-clay. *Compos. Part B* **69**, 94–100 (2015)
247. (a) H. Garmestani, M.S. Al-Haik, K. Dahmen, R. Tannenbaum, D. Li, S.S. Sablin, M.Y. Hussaini, Polymer-mediated alignment of carbon nanotubes under high magnetic fields. *Adv. Mater.* **15**, 1918–1921 (2003); (b) C. Sauder, J. Lamon, R. Pailler, Thermomechanical properties of carbon fibres at high temperatures (up to 2000°C). *Compos. Sci. Technol.* **62**(4), 499–504 (2002)

248. (a) B.W. Steinart, D.R. Dean, Magnetic field alignment and electrical properties of solution cast PET-carbon nanotube composite films. *Polymer* **50**, 898–904 (2009); (b) R.S. Praveen et al., Hybridization of carbon–glass epoxy composites: An approach to achieve low coefficient of thermal expansion at cryogenic temperatures. *Cryogenics* **51**(2), 95–104 (2011)
249. (a) J. Yang, C. Wang, K. Wang, Q. Zhang, F. Chen, R. Du, Q. Fu, Direct formation of Nanohybrid shish-kebab in the injection molded Bar of polyethylene/multiwalled carbon nanotubes composite. *Macromolecules* **42**, 7016–7023 (2009); (b) M. Esposito et al., Fiber Bragg grating sensors to measure the coefficient of thermal expansion of polymers at cryogenic temperatures. *Sensors Act. A: Phys.* **189**, 195–203 (2013)
250. (a) Y. Bin, M. Kitanaka, D. Zhu, M. Matsuo, Development of highly oriented polyethylene filled with aligned carbon nanotubes by gelation/crystallization from solutions. *Macromolecules* **36**, 6213–6219 (2003); (b) A. Tezvergil, L.V.J. Lassila, P.K. Vallittu, The effect of fiber orientation on the thermal expansion coefficients of fiber-reinforced composites. *Dent. Mater.* **19**(6), 471–477 (2003)
251. (a) W. Chen, X. Tao, Production and characterization of polymer nanocomposite with aligned single wall carbon nanotubes. *Appl. Surf. Sci.* **252**, 3547–3552 (2006); (b) Y.A. Dzenis, Thermal expansion of a composite with a hybrid granular-fibrous filler. *Mech. Compos. Mater.* **25**(2), 173–182 (1989)
252. (a) Q. Wang, J.F. Dai, W. Li, Z.Q. Wei, J.L. Jiang, The effects of CNT alignment on electrical conductivity and mechanical properties of SWNT/epoxy nanocomposites. *Compos. Sci. Technol.* **68**, 1644–1648 (2008); (b) C.W. Camacho et al., Stiffness and thermal expansion predictions for hybrid short fiber composites. *Polym. Compos.* **11**(4), 229–239 (1990)
253. (a) M.A. Rafiee, J. Rafiee, I. Srivastava, Z. Wang, H. Song, Z.Z. Yu, N. Koratkar, Fracture and fatigue in graphene nanocomposites. *Small* **6**, 179–183 (2010); (b) J.S. Jang et al., Experimental and analytical investigation of mechanical damping and CTE of both SiO₂ particle and carbon nanofiber reinforced hybrid epoxy composites. *Compos. A: Appl. Sci. Manuf.* **42**(1), 98–103 (2011)
254. (a) A. Yasmin, J.J. Luo, I.M. Daniel, Processing of expanded graphite reinforced polymer nanocomposites. *Compos. Sci. Technol.* **66**, 1182–1189 (2006); (b) F.-L. Jin, S.-J. Park, Thermal properties of epoxy resin/filler hybrid composites. *Polym. Degrad. Stab.* **97**(11), 2148–2153 (2012)
255. (a) H. Kim, A.A. Abdala, C.W. Macosko, Graphene/polymer Nanocomposites. *Macromolecules* **43**, 6515–6530 (2010); (b) G.C. Papanicolaou, A.S. Bouboulas, N.K. Anifantis, Thermal expansivities in fibrous composites incorporating hybrid interphase regions. *Compos. Struct.* **88**(4), 542–547 (2009)
256. (a) T.D. Fornes, D.R. Paul, Modeling properties of nylon 6/clay nanocomposites using composite theories. *Polymer* **44**, 4993–5013 (2003); (b) C.D. Price et al., Modelling the elastic and thermoelastic properties of short fibre composites with anisotropic phases. *Compos. Sci. Technol.* **66**(1), 69–79 (2006)
257. (a) A. Usuki, N. Hasegawa, M. Kato, Polymer-clay Nanocomposites. *Adv. Polym. Sci.* **179**, 135–195 (2005); (b) H. Tsukamoto, A mean-field micromechanical approach to design of multiphase composite laminates. *Mater. Sci. Eng. A* **528**(7–8), 3232–3242 (2011)
258. (a) A. Usuki, Y. Kojima, M. Kawasumi, A. Okada, Y. Fukushima, T. Kurauchi, O. Kamigaito, Synthesis of nylon 6-clay hybrid. *J. Mater. Res.* **8**, 1179–1184 (1993); (b) S.K. Nayak, S. Mohanty, S.K. Samal, Influence of short bamboo/glass fiber on the thermal, dynamic mechanical and rheological properties of polypropylene hybrid composites. *Mater. Sci. Eng. A* **523**(1–2), 32–38 (2009)
259. (a) E. Manias, Polypropylene/montmorillonite nanocomposites. Review of the synthetic routes and materials properties. *Chem. Mater.* **13**, 3516–3523 (2001); (b) O.L.S. Alsina et al., Thermal properties of hybrid lignocellulosic fabric-reinforced polyester matrix composites. *Polym. Test.* **24**(1), 81–85 (2005)
260. Z. Han, A. Fina, Thermal conductivity of carbon nanotubes and their polymer nanocomposites: A review. *Prog. Polym. Sci.* **36**(7), 914–944 (2011)

261. R.E. Newnham, D.P. Skinner, L.E. Cross, Connectivity and piezoelectric/pyroelectric composites. *Mater. Res. Bull.* **13**(5), 525–536 (1978)
262. M. Taya, *Electronic Composites. Modeling, Characterization, Processing, and MEMS Applications* (Cambridge University Press, Cambridge, 2008)
263. W.J. Kim, M. Taya, M.N. Nguyen, Electrical and thermal conductivities of a silver flake/thermosetting polymer matrix composite. *Mech. Mater.* **41**(10), 1116–1124 (2009)
264. M. El Hasnaoui et al., Modelling of dielectric relaxation processes of epoxy-resin filled with carbon black particles. *Phys. B Condens. Matter* **433**, 62–66 (2014)
265. I. Novák, I. Krupa, I. Janigová, Hybrid electro-conductive composites with improved toughness, filled by carbon black. *Carbon* **43**(4), 841–848 (2005)
266. L. Shen et al., The combined effects of carbon black and carbon fiber on the electrical properties of composites based on polyethylene or polyethylene/polypropylene blend. *Polym. Test.* **30**(4), 442–448 (2011)
267. J. Jin et al., Enhancing the electrical conductivity of polymer composites. *Eur. Polym. J.* **49**(5), 1066–1072 (2013)
268. R.N. Othman, I.A. Kinloch, A.N. Wilkinson, Synthesis and characterisation of silica-carbon nanotube hybrid microparticles and their effect on the electrical properties of poly (vinyl alcohol) composites. *Carbon* **60**, 461–470 (2013)
269. J.A. Puértolas, S.M. Kurtz, Evaluation of carbon nanotubes and graphene as reinforcements for UHMWPE-based composites in arthroplastic applications: A review. *J. Mech. Behav. Biomed. Mater.* **39**, 129–145 (2014)
270. M.H.G. Wichmann et al., Glass-fibre-reinforced composites with enhanced mechanical and electrical properties – Benefits and limitations of a nanoparticle modified matrix. *Eng. Frac. Mech.* **73**(16), 2346–2359 (2006)
271. A. Lonjon et al., Electrical conductivity improvement of aeronautical carbon fiber reinforced polyepoxy composites by insertion of carbon nanotubes. *J. Non Cryst. Solids* **358**(15), 1859–1862 (2012)
272. N. Yamamoto, R.G. de Villoria, B.L. Wardle, Electrical and thermal property enhancement of fiber-reinforced polymer laminate composites through controlled implementation of multi-walled carbon nanotubes. *Compos. Sci. Technol.* **72**(16), 2009–2015 (2012)
273. G. George et al., Dielectric behaviour of PP/jute yarn commingled composites: Effect of fibre content, chemical treatments, temperature and moisture. *Compos. A: Appl. Sci. Manuf.* **47**, 12–21 (2013)
274. C.Q. Yang, Z.S. Wu, H. Huang, Electrical properties of different types of carbon fiber reinforced plastics (CFRPs) and hybrid CFRPs. *Carbon* **45**(15), 3027–3035 (2007)
275. L. Yao et al., Modeling and experimental verification of dielectric constants for three dimensional woven composites. *Compos. Sci. Technol.* **68**(7–8), 1794–1799 (2008)
276. M. Zhan, R.P. Wool, J.Q. Xiao, Electrical properties of chicken feather fiber reinforced epoxy composites. *Compos. A: Appl. Sci. Manuf.* **42**(3), 229–233 (2011)
277. J.-M. Thomassin et al., Polymer/carbon based composites as electromagnetic interference (EMI) shielding materials. *Mater. Sci. Eng. R. Rep.* **74**(7), 211–232 (2013)
278. M.H. Al-Saleh, W.H. Saadeh, Hybrids of conductive polymer nanocomposites. *Mater. Design* **52**, 1071–1076 (2013)
279. G. Zheming et al., Electrical properties and morphology of highly conductive composites based on polypropylene and hybrid fillers. *J. Ind. Eng. Chem.* **16**(1), 10–14 (2010)
280. A.B.. Silva et al., Synergic effect in electrical conductivity using a combination of two fillers in PVDF hybrids composites. *Eur. Polym. J.* **49**(10), 3318–3327 (2013)
281. S.-Y. Yang et al., Synergetic effects of graphene platelets and carbon nanotubes on the mechanical and thermal properties of epoxy composites. *Carbon* **49**(3), 793–803 (2011)
282. C.-R. Yu et al., Electrical and dielectric properties of polypropylene nanocomposites based on carbon nanotubes and barium titanate nanoparticles. *Compos. Sci. Technol.* **71**(15), 1706–1712 (2011)

283. A. Salinier et al., Electrical, rheological and mechanical characterization of multiscale composite materials based on poly(etherimide)/short glass fibers/multiwalled carbon nanotubes. *Compos. Struct.* **102**, 81–89 (2013)
284. A. Motaghi, A. Hrymak, G.H. Motlagh, Electrical conductivity and percolation threshold of hybrid carbon/polymer composites. *J. Appl. Polym. Sci.* (2014)
285. M. Shah, B. Reduwan, Textile Coatings, in *Polymer and Polymer Composites: A Reference Series. Functional Polymers* ed. by M. J. Mazumder, H. Sheardown, A. A. Ahmed, Springer International Publishing AG, Part of Springer Nature, Germany, ISBN: 978-3-319-92067-2. https://doi.org/10.1007/978-3-319-92067-2_30-1, 1–58 (2018)
286. M. Shah, B. Reduwan, Chapter No. 41 Dielectric Polymers, ed. by M. J. Mazumder, H. Sheardown, A. A. Ahmed, Springer, Germany, *Polymer and Polymer Composites: A Reference Series. Functional Polymers*, ISBN: 978-3-319-92067-2. https://doi.org/10.1007/978-3-319-92067-2_8-1, 1–49 (2018)
287. M. Shah, B. Reduwan, Sazzad Hossain, ed. by M. Nahid Pervez, Md Obidul Haque, Chapter on Enzyme Responsive Hydrogels, in the book on Polymer and Polymer Composites: A Reference Series. Cellulose-Based Superabsorbent Hydrogels, I. H. Mondal (Ed), Springer, Germany, ISBN: 978-3-319-76573-0. http://doi.org/10.1007/978-3-319-76573-0_62-1 2–23 (2018)
288. (a) M. Shah, B. Reduwan, I. H. Mondal, Sazzad Hossain, M. Nahid Pervez; Cellulose Based Hydrogels for Industrial Applications, in *Polymer and Polymer Composites: A Reference Series. Cellulose-Based Superabsorbent Hydrogels*, ed. I. H. Mondal, (Springer, Germany, 2018), ISBN: 978-3-319-76573-0, http://doi.org/10.1007/978-3-319-76573-0_63-1, pp. 2–41; (b) M. Shah, B. Reduwan, I. H. Mondal, Sazzad Hossain Somoal, M. Nahid Pervez, Md. Obaidul Haque, Synthesis of external stimuli-responsive hydrogels based CMC and other cellulose derivatives for advanced applications, in *Carboxymethylcellulose. Volume II. Pharmaceutical and Industrial Applications*, ed. by I. H. Mondal, (Nova Science Publishers, New York, USA, 2019), ISBN:978-1-53614-752-0 (eBook), pp. 43–75
289. J. Yan et al., Elastic and electrically conductive carbon nanotubes/chitosan composites with lamellar structure. *Compos. A: Appl. Sci. Manuf.* **67**, 1–7 (2014)
290. J. Yan, Y.G. Jeong, Synergistic effect of hybrid carbon fillers on electric heating behavior of flexible polydimethylsiloxane-based composite films. *Compos. Sci. Technol.* **106**, 134–140 (2015)
291. D.C. Edwards, Polymer-filler interactions in rubber reinforcement. *J. Mater. Sci.* **25**, 4175–4185 (1990)
292. (a) R. Feng, G. Guan, W. Zhou, C. Li, D. Zhang, Y. Xiao, In situ synthesis of poly(ethylene terephthalate)/graphene composites using a catalyst supported on graphite oxide. *J. Mater. Chem.* **21**, 3931–3939 (2011); (b) T.D. Fornes, D.R. Paul, Modeling properties of nylon 6/clay nanocomposites using composite theories. *Polymer* **44**, 4993–5013 (2003)
293. (a) E.J. Garboczi, K.A. Snyder, J.F. Douglas, M.F. Thorpe, Geometrical percolation threshold of overlapping ellipsoids. *Phys. Rev. E* **52**, 819–828 (1996); (b) J.N. Coleman, U. Khan, W.J. Blau, Y.K. Gun'ko, Small but strong: A review of the mechanical properties of carbon nanotube-polymer composites. *Carbon* **44**, 1624–1652 (2006)
294. (a) P. Steurer, R. Wissert, R. Thomann, R. Mülhaupt, Functionalized Graphenes and thermoplastic Nanocomposites based upon expanded graphite oxide. *Macromol. Rapid Commun.* **30**, 316–327 (2009); (b) B. Lin, G.A. Gelves, J.A. Haber, U. Sundararaj, Electrical, rheological, and mechanical properties of polystyrene/copper nanowire Nanocomposites. *Ind. Eng. Chem. Res.* **46**, 2481–2487 (2007)
295. (a) J.B. Bai, A. Allaoui, Effect of the length and the aggregate size of MWNTs on the improvement efficiency of the mechanical and electrical properties of nanocomposites – Experimental investigation. *Compos. A: Appl. Sci. Manuf.* **34**, 689–694 (2003); (b) A. Okada, A. Usuki, Twenty years of polymer-clay Nanocomposites. *Macromol. Mater. Eng.* **291**, 1449–1476 (2006)

296. (a) A. Celzard, E. McRae, C. Deleuze, M. Dufort, G. Furdin, J.F. Marêché, Critical concentration in percolating systems containing a high-aspect-ratio filler. *Phys. Rev. B* **53**, 6209–6214 (1996); (b) A. Fasolino, J.H. Los, M.I. Katsnelson, Intrinsic ripples in graphene. *Nat. Mater.* **6**, 858; E.J. Garboczi, K.A. Snyder, J.F. Douglas, M.F. Thorpe, Geometrical percolation threshold of overlapping ellipsoids. *Phys. Rev. E* **52**, 819–828 (1996)
297. (a) X.Y. Qi, D. Yan, Z. Jiang, Y.K. Cao, Z.Z. Yu, F. Yavari, N. Koratkar, Enhanced electrical conductivity in polystyrene Nanocomposites at ultra-low graphene content. *ACS Appl. Mater. Interfaces* **3**, 3130–3133 (2011); (b) Y. Liu, A. Wang, R. Claus, Molecular self-assembly of TiO₂/polymer Nanocomposite films. *J. Phys. Chem. B* **101**, 1385–1388 (1997)
298. (a) J.K.W. Sandler, J.E. Kirk, I.A. Kinloch, M.S.P. Shaffer, A.H. Windle, Ultra-low electrical percolation threshold in carbon-nanotube-epoxy composites. *Polymer* **44**, 5893–5899 (2003); (b) J. Huang, C. He, Y. Xiao, K.Y. Mya, J. Dai, Y.P. Siow, Polyimide/POSS nanocomposites: Interfacial interaction, thermal properties and mechanical properties. *Polymer* **44**, 4491–4499 (2003)
299. (a) J. Li, M.L. Sham, J.K. Kim, G. Marom, Morphology and properties of UV/ozone treated graphite nanoplatelet/epoxy nanocomposites. *Compos. Sci. Technol.* **67**, 296–305 (2007); (b) E.K. Thostenson, T.W. Chou, Aligned multi-walled carbon nanotube-reinforced composites: Processing and mechanical characterization. *J. Phys. D. Appl. Phys.* **35**, L77–L80 (2002)
300. (a) W. Bauhofer, J.Z. Kovacs, A review and analysis of electrical percolation in carbon nanotube polymer composites. *Compos. Sci. Technol.* **69**, 1486–1498 (2009); (b) E.W. Wong, P.E. Sheehan, C.M. Lieber, Nanobeam mechanics: Elasticity, strength, and toughness of nanorods and nanotubes. *Science* **277**, 1971–1975 (1997)
301. (a) L. Xie, F. Xu, F. Qiu, H. Lu, Y. Yang, Single-walled carbon nanotubes functionalized with high bonding density of polymer layers and enhanced mechanical properties of composites. *Macromolecules* **40**, 3296–3305 (2007); (b) D.A. Brune, J. Bicerano, Micromechanics of nanocomposites: Comparison of tensile and compressive elastic moduli, and prediction of effects of incomplete exfoliation and imperfect alignment on modulus. *Polymer* **43**, 369–387 (2002)
302. (a) R. Verdejo, F. Barroso-Bujans, M.A. Rodriguez-Perez, J.A.D. Saja, M.A. Lopez-Manchado, Functionalized graphene sheet filled silicone foam nanocomposites. *J. Mater. Chem.* **18**, 2221–2226 (2008); (b) K. Hu, D.D. Kulkarni, I. Choi, V.V. Tsukruk, Graphene-polymer nanocomposites for structural and functional applications. *Prog. Polym. Sci.* **39**, 1934–1972 (2014)
303. D.R. Paul, L.M. Robeson, Polymer nanotechnology: Nanocomposites. *Polymer* **49**, 3187–3204 (2008)
304. (a) M. Bhattacharya, Review – Polymer Nanocomposites – A comparison between carbon nanotubes, graphene, and clay as Nanofillers. *Materials* **9**(262), 1–35 (2016); (b) M. Biswas, S.S. Ray, Recent progress in synthesis and evaluation of polymer-montmorillonite nanocomposites. *Adv. Polym. Sci.* **155**, 167–221 (2001)
305. M.A. Rafiee, J. Rafiee, Z. Wang, H. Song, Z.Z. Yu, N. Koratkar, Enhanced mechanical properties of Nanocomposites at low graphene content. *ACS Nano* **3**, 3884–3890 (2009)
306. B.P. Grady, *Carbon Nanotube-Polymer Composites Manufacture, Properties, and Applications* (Wiley, New York, 2011)
307. P. Das, S. Jani-Markus, B.Z. Malho, U. Klemradt, A. Walther, A. Facile access to large-scale, self-assembled, nacre-inspired, high-performance materials with tunable nanoscale periodicities. *ACS Appl. Mater. Interfaces* **5**, 3738–3747 (2013)
308. P. Podsiadlo, Z. Tang, B.S. Shim, N.A. Kotov, Counterintuitive effect of molecular strength and role of molecular rigidity on mechanical properties of layer-by-layer assembled Nanocomposites. *Nano Lett.* **7**, 1224–1231 (2007)
309. N. Bitinis, M. Hernandez, R. Verdejo, J.M. Kenny, M.A. Lopez-Manchado, Recent advances in clay/polymer Nanocomposites. *Adv. Mater.* **23**, 5229–5236 (2011)
310. T. Kashiwagi, F.M. Du, J.F. Douglas, K.I. Winey, R.H. Harris, J.R. Shields, Nanoparticle networks reduce the flammability of polymer nanocomposites. *Nat. Mater.* **4**, 928–933 (2005)

311. D. Qian, E.C. Dickey, R. Andrews, T. Rantell, Load transfer and deformation mechanisms in carbon nanotube-polystyrene composites. *Appl. Phys. Lett.* **76**, 2868–2870 (2000)
312. J.N. Coleman, U. Khan, Y.K. Gun'ko, Mechanical reinforcement of polymers using carbon nanotubes. *Adv. Mater.* **18**, 637–640 (2006)
313. K.H. Liao, S. Aoyama, A.A. Abdala, C.W. Macosko, Does graphene change T_g of Nanocomposites? *Macromolecules* **47**, 8311–8319 (2014)
314. U. Gaur, B. Wunderlich, Study of microphase separation in block copolymers of styrene and -Methylstyrene in the glass transition region using quantitative thermal analysis. *Macromolecules* **13**, 1618–1625 (1980)
315. C.B. Roth, J.R. Dutcher, Glass transition temperature of freely-standing films of atactic poly (methyl methacrylate). *Eur. Phys. J.* **12**, 103–107 (2003)
316. R.S. Tate, D.S. Fryer, S. Pasqualini, M.F. Montague, J.J. de Pablo, P.F. Nealey, Extraordinary elevation of the glass transition temperature of thin polymer films grafted to silicon oxide substrates. *J. Chem. Phys.* **115**, 9982–9990 (2001)
317. J.L. Keddie, R.A.L. Jones, R.A. Cory, Interface and surface effects on the glass-transition temperature in thin polymer films. *Farad. Discuss.* **98**, 219–230 (1994)
318. P. Rittigstein, J.M. Torkelson, Polymer-nanoparticle interfacial interactions in polymer nanocomposites: Confinement effects on glass transition temperature and suppression of physical aging. *J. Polym. Sci. B Polym. Phys.* **44**, 2935–2943 (2006)
319. S.M. Yuen, C.M. Ma, Y.Y. Lin, H.C. Kuan, Preparation, morphology and properties of acid and amine modified multiwalled carbon nanotube/polyimide composite. *Compos. Sci. Technol.* **67**, 2564–2573 (2007)
320. B.P. Grady, Effects of carbon nanotubes on polymer physics. *J. Polym. Sci. B Polym. Phys.* **50**, 591–623 (2012)
321. K.M. Lee, C.D. Han, Effect of hydrogen bonding on the rheology of polycarbonate/organoclay nanocomposites. *Polymer* **44**, 4573–4588 (2003)
322. X. Dai, J. Xu, X. Guo, Y. Lu, D. Shen, N. Zhao, X. Luo, X. Zhang, Study on structure and orientation action of polyurethane Nanocomposites. *Macromolecules* **37**, 5615–5623 (2004)
323. X. Zhang, L.S. Loo, Study of glass transition and reinforcement mechanism in polymer/layered silicate nanocomposites. *Macromolecules* **42**, 5196–5207 (2009)
324. R. Krishnamoorti, R.A. Vaia, E.P. Giannelis, Structure and dynamics of polymer-layered silicate Nanocomposites. *Macromolecules* **8**, 1728–1734 (1996)
325. P.B. Messersmith, E.P. Giannelis, Synthesis and barrier properties of poly(ϵ -caprolactone)-layered silicate nanocomposites. *J. Polym. Sci. A Polym. Chem.* **33**, 1047–1057 (1995)
326. Y.H. Yang, L. Bolling, M.A. Priolo, J.C. Grunlan, Super gas barrier and selectivity of graphene oxide-polymer multilayer thin films. *Adv. Mater.* **45**, 503–508 (2013)
327. H. Liu, T. Kuila, N.H. Kim, B.C. Kud, J.H. Lee, In situ synthesis of the reduced graphene oxide-polyethyleneimine composite and its gas barrier properties. *J. Mater. Chem. A* **1**, 3739–3746 (2013)
328. I.M. Tseng, Y.F. Liao, J.C. Chiang, M.H. Tsai, Transparent polyimide/graphene oxide nanocomposite with improved moisture barrier property. *Mater. Chem. Phys.* **136**, 247–253 (2012)
329. A.B. Morgan, Flame retarded polymer layered silicate nanocomposites: A review of commercial and open literature systems. *Polym. Adv. Technol.* **96**, 206–217 (2006)
330. M.R. Schutz, H. Kalo, T. Lunkenbein, J. Brey, C.A. Wilkie, Intumescent-like behavior of polystyrene synthetic clay nanocomposites. *Polymer* **52**, 3288–3294 (2012)
331. M. Bartholmai, B. Schartel, Layered silicate polymer nanocomposites: New approach or illusion for fire retardancy? Investigations of the potentials and the tasks using a model system. *Polym. Adv. Technol.* **15**, 355–364 (2004)
332. M.C. Costache, M.J. Heidecker, E. Manias, G. Camino, A. Frache, G. Beyer, R.K. Gupta, C.A. Wilkie, The influence of carbon nanotubes, organically modified montmorillonites and layered double hydroxides on the thermal degradation and fire retardancy of polyethylene, ethylene-vinyl acetate copolymer and polystyrene. *Polymer* **48**, 6352–6345 (2007)

333. P. May, U. Khan, A. O'Neill, J.N. Coleman, Approaching the theoretical limit for reinforcing polymers with graphene. *J. Mater. Chem.* **22**, 1278–1282 (2012)
334. C.S. Grimmer, C.K.H. Dharan, High-cycle fatigue of hybrid carbon nanotube/glass fiber/polymer composites. *J. Mater. Sci.* **43**, 4487–4492 (2008)
335. K.T. Kim, W.H. Jo, Non-destructive functionalization of multi-walled carbon nanotubes with naphthalene-containing polymer for high performance Nylon66/multi-walled carbon nanotube composites. *Carbon* **49**, 819–826 (2011)
336. W. Yuan, M.B.C. Park, Covalent cum noncovalent Functionalizations of carbon nanotubes for effective reinforcement of a solution cast composite film. *ACS Appl. Mater. Interf.* **4**, 2065–2073 (2012)
337. S. Aoyama, Y.T. Park, T. Ougizawa, C.W. Macosko, Melt crystallization of poly(ethylene terephthalate): Comparing addition of graphene vs. carbon nanotubes. *Polymer* **55**, 2077–2085 (2014)
338. C.I.W. Calcagno, C.M. Mariani, S.R. Teixeira, R.S. Mauler, The effect of organic modifier of the clay on morphology and crystallization properties of PET nanocomposites. *Polymer* **48**, 966–974 (2007)
339. P.J. Yoon, D.L. Hunter, D.R. Paul, Polycarbonate nanocomposites: Part 2. Degradation and color formation. *Polymer* **44**, 5341–5354 (2003)
340. B. Chen, J.R.G. Evans, Poly(epsilon-caprolactone)-clay Nanocomposites: Structure and mechanical properties. *Macromolecules* **39**, 747–754 (2006)
341. B. Lepoittevin, M. Devalckenaere, N. Pantoustier, M. Alexandre, D. Kubies, C. Calberg, R. Jérôme, P. Dubois, Poly(caprolactone)/clay nanocomposites prepared by melt intercalation: Mechanical, thermal and rheological properties. *Polymer* **43**, 4017–4023 (2002)
342. S.S. Ray, K. Yamada, M. Okamoto, A. Ogami, K. Ueda, New polylactide/layered silicate nanocomposites. 3. High-performance biodegradable materials. *Chem. Mater.* **15**, 1456–1465 (2003)
343. S.S. Ray, P. Maiti, M. Okamoto, K. Yamada, K. Ueda, New Polylactide/layered silicate Nanocomposites. 1. Preparation, characterization, and properties. *Macromolecules* **35**, 3104–3110 (2002)
344. P. Maiti, K. Yamada, M. Okamoto, K. Ueda, K. Okamoto, New polylactide/layered silicate nanocomposites: Role of organoclays. *Chem. Mater.* **14**, 4654–4661 (2002)
345. J.H. Wang, T.H. Young, D.J. Lin, M.K. Sun, H.S. Huang, L.P. Cheng, Preparation of clay/PMMA Nanocomposites with intercalated or exfoliated structure for bone cement synthesis. *Macromol. Mater. Eng.* **291**, 661–669 (2006)
346. Y. Wang, W.C. Chen, Effect of clay modification on the dynamic mechanical and dielectric properties of PMMA nanocomposites via melt blending. *Polymer* **12**, 128–144 (2013)
347. L. Shen, I.Y. Phang, L. Chen, T. Liu, K. Zeng, Nanoindentation and morphological studies on nylon 66 nanocomposites. I. Effect of clay loading. *Polymer* **45**, 3341–3349 (2004)
348. K. Masenelli-Varlot, E. Reynaud, G. Vigier, J. Varlet, Mechanical properties of clay-reinforced polyamide. *J. Polym. Sci. B Polym. Phys.* **40**, 272–283 (2002)
349. J.W. Cho, D.R. Paul, Nylon 6 Nanocomposites by melt compounding. *Polymer* **42**, 1083–1094 (2001)
350. H.A. Stretz, D.R. Paul, P.E. Cassidy, Poly(styrene-co-acrylonitrile)/montmorillonite organoclay mixtures: A model systems for ABS nanocomposites. *Polymer* **46**, 3818–3830 (2005)
351. H. Ma, L. Tong, Z. Xu, Z. Fang, Clay network in ABS-graft-MAH nanocomposites: Rheology and flammability. *Polym. Degrad. Stab.* **92**, 1439–1445 (2007)
352. T.N. Abraham, D. Ratna, S. Siengchin, J. Karger-Kocsis, Structure and properties of polyethylene oxideorgano clay nanocomposite prepared via melt mixing. *Polym. Eng. Sci.* **49**, 379–390 (2009)
353. S. Choudhary, R.J. Sengwa, Dielectric properties and structures of melt-compounded poly(ethylene oxide)-montmorillonite nanocomposites. *J. Appl. Polym. Sci.* **124**, 4847–4853 (2012)

354. P. Aranda, E. Mosqueda, E. Pérez-Cappe, E. Ruiz-Hitzky, Electrical characterization of poly (ethylene oxide)-clay nanocomposites prepared by microwave irradiation. *J. Polym. Sci. B Polym. Phys.* **41**, 3249–3263 (2003)
355. L. Liu, Z. Qi, X. Zhu, Studies on nylon 6/clay Nanocomposites by melt-intercalation process. *J. Appl. Polym. Sci.* **71**, 1133–1138 (1999)
356. M. Kawasumi, N. Hasegawa, M. Kato, A. Usuki, A. Okada, Preparation and mechanical properties of polypropylene-clay hybrids. *Macromolecules* **30**, 6333–6338 (1997)
357. H.R. Dennis, D.L. Hunter, D. Chang, S. Kim, J.L. White, J.W. Cho, D.R. Paul, Effect of melt processing conditions on the extent of the exfoliation in organoclay-based composites. *Polymer* **42**, 9513–9522 (2001)
358. M.S.P. Shaffer, A.H. Windle, Fabrication and characterization of CNT-PVA composites. *Adv. Mater.* **11**, 937–941 (1999)
359. L. Jin, C. Bower, O. Zhou, Alignment of carbon nanotubes in a polymer matrix by mechanical stretching. *Appl. Phys. Lett.* **73**, 1197–1199 (1998)
360. B. Safadi, R. Andrews, E.A. Grulke, Multiwalled carbon nanotube polymer composites: Synthesis and characterization of thin films. *J. Appl. Polym. Sci.* **84**, 2660–2669 (2002)
361. R. Haggemueller, J.E. Fischer, K.I. Winey, Single wall carbon nanotube/polyethylene nanocomposites: Nucleating and templating polyethylene crystallites. *Macromolecules* **39**, 2964–2971 (2006)
362. Y. Xu, W. Hong, H. Bai, C. Li, G. Shi, Strong and ductile poly(vinyl alcohol)/graphene oxide composite films with a layered structure. *Carbon* **47**, 3538–3543 (2009)
363. Y.R. Lee, A.V. Raghun, H.M. Jeong, B.K. Kim, Properties of waterborne polyurethane/functionalized graphene sheet nanocomposites prepared by an in situ method. *Macromol. Chem. Phys.* **210**, 1247–1254 (2009)
364. R. Feng, G. Guan, W. Zhou, C. Li, D. Zhang, Y. Xiao, In situ synthesis of poly(ethylene terephthalate)/graphene composites using a catalyst supported on graphite oxide. *J. Mater. Chem.* **21**, 3931–3939 (2011)
365. E.J. Garboczi, K.A. Snyder, J.F. Douglas, M.F. Thorpe, Geometrical percolation threshold of overlapping ellipsoids. *Phys. Rev. E* **52**, 819–828 (1996)
366. P. Steurer, R. Wissert, R. Thomann, R. Müllhaupt, Functionalized Graphenes and thermoplastic Nanocomposites based upon expanded graphite oxide. *Macromol. Rapid Commun.* **30**, 316–327 (2009)
367. J.B. Bai, A. Allaoui, Effect of the length and the aggregate size of MWNTs on the improvement efficiency of the mechanical and electrical properties of nanocomposites – Experimental investigation. *Compos. A: Appl. Sci. Manuf.* **34**, 689–694 (2003)
368. A. Celzard, E. McRae, C. Deleuze, M. Dufort, G. Furdin, J.F. Maréché, Critical concentration in percolating systems containing a high-aspect-ratio filler. *Phys. Rev. B* **53**, 6209–6214 (1996)
369. X.Y. Qi, D. Yan, Z. Jiang, Y.K. Cao, Z.Z. Yu, F. Yavari, N. Koratkar, Enhanced electrical conductivity in polystyrene Nanocomposites at ultra-low graphene content. *ACS Appl. Mater. Interfaces* **3**, 3130–3133 (2011)
370. J.K.W. Sandler, J.E. Kirk, I.A. Kinloch, M.S.P. Shaffer, A.H. Windle, Ultra-low electrical percolation threshold in carbon-nanotube-epoxy composites. *Polymer* **44**, 5893–5899 (2003)
371. J. Li, M.L. Sham, J.K. Kim, G. Marom, Morphology and properties of UV/ozone treated graphite nanoplatelet/epoxy nanocomposites. *Compos. Sci. Technol.* **67**, 296–305 (2007)
372. W. Bauhofer, J.Z. Kovacs, A review and analysis of electrical percolation in carbon nanotube polymer composites. *Compos. Sci. Technol.* **69**, 1486–1498 (2009)
373. L. Xie, F. Xu, F. Qiu, H. Lu, Y. Yang, Single-walled carbon nanotubes functionalized with high bonding density of polymer layers and enhanced mechanical properties of composites. *Macromolecules* **40**, 3296–3305 (2007)
374. R. Verdejo, F. Barroso-Bujans, M.A. Rodríguez-Perez, J.A.D. Saja, M.A. Lopez-Manchado, Functionalized graphene sheet filled silicone foam nanocomposites. *J. Mater. Chem.* **18**, 2221–2226 (2008)

375. L.M. Veca, M.J. Meziani, W. Wang, X. Wang, F. Lu, P. Zhang, Y. Lin, R. Fee, J.W. Connell, Y.P. Sun, Carbon nanosheets for polymeric nanocomposites with high thermal conductivity. *Adv. Mater.* **21**, 2088–2092 (2009)
376. S. Wang, M. Tambraparni, J. Qiu, J. Tipton, D. Dean, Thermal expansion of graphene composites. *Macromolecules* **42**, 5251–5255 (2009)
377. N. Liu, F. Luo, H. Wu, Y. Liu, C. Zhang, J. Chen, One-step ionic-liquid-assisted electrochemical synthesis of ionic-liquid-functionalized graphene sheets directly from graphite. *Adv. Funct. Mater.* **18**, 1518–1525 (2008)
378. Y. Kayano, H. Keskkula, D.R. Paul, Effect of polycarbonate molecular weight and processing conditions on mechanical behaviour of blends with a core-shell impact modifier. *Polymer* **37**, 4505–4518 (1996)
379. H. Koerner, E. Hampton, D. Dean, Z. Turgut, L. Drummy, P. Mirau, R. Vaia, Generating Triaxial reinforced epoxy/Montmorillonite Nanocomposites with uniaxial magnetic fields. *Chem. Mater.* **17**, 1990–1996 (2005)
380. H. Koerner, J.D. Jacobs, D.W. Tomlin, J.D. Busbee, R.A. Vaia, Tuning polymer Nanocomposite morphology: AC electric field manipulation of epoxy-Montmorillonite (clay) suspensions. *Adv. Mater.* **16**, 297–302 (2004)
381. T. Sasaki, A. Shimizu, T.H. Mourey, C.T. Thurau, M.D. Ediger, Glass transition of small polystyrene spheres in aqueous suspensions. *J. Chem. Phys.* **119**, 8730–8735 (2003)
382. J. Ding, G. Xue, Q. Dai, R. Cheng, Glass transition temperature of polystyrene microparticles. *Polymer* **34**, 3325–3327 (1993)
383. J.A. Forrest, K.D. Veress, J.R. Stevens, J.R. Dutcher, Effect of free surfaces on the glass transition temperature of thin polymer films. *Phys. Rev. Lett.* **77**, 2002–2005 (1996)
384. P. Rittigstein, R.D. Priestley, L.J. Broadbelt, J.M. Torkelson, Model polymer nanocomposites provide an understanding of confinement effects in real nanocomposites. *Nat. Mater.* **6**, 278–282 (2007)
385. K.H. Liao, S. Aoyama, A.A. Abdala, C.W. Macosko, Does graphene change T_g of Nanocomposites? *Macromolecules* **47**, 8311–8319 (2014)
386. W. Yuan, M.B.C. Park, Covalent cum noncovalent Functionalizations of carbon nanotubes for effective reinforcement of a solution cast composite film. *ACS Appl. Mater. Interf.* **4**, 2065–2073 (2012)
387. S. Aoyama, Y.T. Park, T. Ougizawa, C.W. Macosko, Melt crystallization of poly(ethylene terephthalate): Comparing addition of graphene vs. carbon nanotubes. *Polymer* **55**, 2077–2085 (2014)
388. C.I.W. Calcagno, C.M. Mariani, S.R. Teixeira, R.S. Mauler, The effect of organic modifier of the clay on morphology and crystallization properties of PET nanocomposites. *Polymer* **48**, 966–974 (2007)
389. Z. Guo, D. Zhang, S. Wei, Z. Wang, A.B. Karki, Y. Li, P. Bernazzani, D.P. Young, J. Gomes, D. Cocke, T.C. Ho, Effects of iron oxide nanoparticles on polyvinyl alcohol: Interfacial layer and bulk nanocomposites thin film. *J. Nanopart. Res.* **12**, 2415–2426 (2010)
390. W.E. Teo, S.A. Ramakrishna, Review on electrospinning design and nanofibre assemblies. *Nanotechnology* **17**, 89–106 (2006)
391. J. Doshi, D.H. Reneker, Electrospinning process and applications of electrospun fibers. *J. Electrostat.* **35**, 151–160 (1995)
392. S. Ramakrishna, K. Fujihara, W.E. Teo, T. Yong, Z. Ma, R. Ramaseshan, Electrospun nanofibers: Solving global issues. *Mater. Today* **9**, 40–50 (2006)
393. A. Greiner, J.H. Wendorff, Electrospinning: A fascinating method for the preparation of ultrathin fibers. *Angew. Chem. Int. Ed.* **46**, 5670–5703 (2007)
394. W. Zuo, M. Zhu, W. Yang, H. Yu, Y. Chen, Y. Zhang, Experimental study on relationship between jet instability and formation of beaded fibers during electrospinning. *Polym. Eng. Sci.* **45**, 704–709 (2005)
395. J.M. Deitzel, J. Kleinmeyer, D. Harris, T.N.C. Beck, The effect of processing variables on the morphology of electrospun nanofibers and textiles. *Polymer* **42**, 261–272 (2001)

396. T. Lin, H. Wang, X. Wang, M.P. Brenner, The charge effect of cationic surfactants on the elimination of fibre beads in the electrospinning of polystyrene. *Nanotechnology* **15**, 1375–1381 (2004)
397. Z. Yang, S. Chen, W. Hu, N. Yin, W. Zhang, C. Xiang, H. Wang, Flexible luminescent CdSe/bacterial cellulose nanocomposite membranes. *Carbohydr. Polym.* **88**(1), 173–178 (2012)
398. M.M. Hohman, M. Shin, G. Rutledge, M.P. Brenner, Electrospinning and electrically forced jets. I. Stability theory. *Phys. Fluids* **13**, 2201–2220 (2001)
399. M.M. Hohman, M. Shin, G. Rutledge, Electrospinning and electrically forced jets. II. *Appl. Phys. Fluid.* **13**, 2221–2236 (2001)
400. D.H. Reneker, A.L. Yarin, H. Fong, S. Koombhongse, Bending instability of electrically charged liquid jets of polymer solutions in electrospinning. *J. Appl. Phys.* **87**, 4531–4547 (2000)
401. A.L. Yarin, S. Koombhongse, D.H. Reneker, Bending instability in electrospinning of nanofibers. *J. Appl. Phys.* **89**, 3018–3026 (2001)
402. G.M. Kim, R. Lach, G.H. Michler, P. Poetschke, K. Albrecht, Relationships between phase morphology and deformation mechanisms in polymer nanocomposite nanofibres prepared by an electrospinning process. *Nanotechnology* **17**, 963–972 (2006)
403. R. Dersch, M. Steinhart, U. Boudriot, A. Greiner, J.H. Wendorff, Nanoprocessing of polymers: Applications in medicine, sensors, catalysis, photonics. *Polym. Adv. Technol.* **16**, 276–282 (2005)
404. H. Ye, H. Lam, N. Titchenal, Y. Gogotsi, F. Ko, Reinforcement and rupture behavior of carbon nanotubes/polymer nanofibers. *Appl. Phys. Lett.* **85**, 1775–1777 (2004)
405. Y.Q. Wan, J.H. He, J.Y. Yu, Carbon nanotube-reinforced polyacrylonitrile nanofibers by vibration-electrospinning. *Polym. Intern.* **56**, 1367–1370 (2007)
406. C. Pan, L.Q. Ge, Z.Z. Gu, Fabrication of multi-walled carbon nanotube reinforced poly-electrolyte hollow nanofibers by electrospinning. *Compos. Sci. Technol.* **67**, 3271–3277 (2007)
407. H. Lam, N. Titchenal, N. Naguib, H. Ye, Y. Gogotski, F. Ko, Electrospinning of carbon nanotubes reinforced nanocomposite fibrils and yarns. *Mater. Res. Soc. Symp. Proc.* **791**, 353–358 (2004)
408. M.T. Byrne, Y.K. Gun'ko, Recent advances in research on carbon nanotube-polymer composites. *Adv. Mater.* **22**, 1672–1688 (2010)
409. Z. Sun, V. Nicolosi, D. Rickard, S.D. Bergin, D. Aherne, J.N. Coleman, Quantitative evaluation of surfactant-stabilized single-walled carbon nanotubes: Dispersion quality and its correlation with zeta potential. *J. Phys. Chem. C* **112**, 10692–10699 (2008)
410. R.A. Vaia, K.D. Jandt, E.J. Kramer, E.P. Giannelis, Microstructural evolution of melt intercalated polymer-organically modified layered silicates Nanocomposites. *Chem. Mater.* **8**, 2628–2635 (1996)
411. D. Wang, C.A. Wilkie, A stibonium-modified clay and its polystyrene nanocomposite. *Polym. Degrad. Stab.* **82**, 309–315 (2003)
412. J. Zhang, C.A. Wilkie, A carbocation substituted clay and its styrene nanocomposite. *Polym. Degrad. Stab.* **83**, 301–307 (2004)
413. S. Su, D.D. Jiang, C.A. Wilkie, Poly(methyl methacrylate), polypropylene and polyethylene nanocomposite formation by melt blending using novel polymerically-modified clays. *Polym. Degrad. Stab.* **84**, 321–331 (2004)
414. D.H. Kim, P.D. Fasulo, W.R. Rodgers, D.R. Paul, Structure and properties of polypropylene-based nanocomposites: Effect of PP-g-MA to organoclay ratio. *Polymer* **48**, 5308–5323 (2007)
415. E. Manias, Polypropylene/montmorillonite nanocomposites. Review of the synthetic routes and materials properties. *Chem. Mater.* **13**, 3516–3523 (2001)
416. B.P. Grady, *Carbon Nanotube-Polymer Composites Manufacture, Properties, and Applications* (Wiley, New York, 2011), p. 145
417. C. McClory, S.J. Chin, T. McNally, Polymer/carbon nanotube composites. *Aust. J. Chem.* **62**, 762–785 (2009)
418. R. Andrews, M.C. Weisenberger, Carbon nanotube polymer composites. *Curr. Opin. Solid State Mater. Sci.* **8**, 31–37 (2004)

419. J.N. Coleman, M. Cadek, R. Blake, V. Nicolosi, K.P. Ryan, C. Belton, A. Fonseca, J.B. Nagy, Y.K. Gun'ko, W.J. Blau, High performance nanotube-reinforced plastics: Understanding the mechanism of strength increase. *Adv. Funct. Mater.* **14**, 791–798 (2004)
420. T. Villmow, P. Potschke, S. Pegel, L. Haussler, B. Kretzschmar, Influence of twin-screw extrusion conditions on the dispersion of multi-walled carbon nanotubes in poly(lactic acid) matrix. *Polymer* **49**, 3500–3509 (2008)
421. D. Wu, Y. Sun, M. Zhang, Kinetics study on melt compounding of carbon nanotube/polypropylene Nanocomposites. *J. Polym. Sci. B Polym. Phys.* **47**, 608–618 (2009)
422. J.S. Hong, C. Kim, Extension-induced dispersion of multi-walled carbon nanotubes in non-Newtonian fluid. *J. Rheol.* **51**, 833–850 (2007)
423. I.H. Kim, Y.G. Jeong, Polylactide/exfoliated graphite Nanocomposites with enhanced thermal stability, mechanical Modulus, and electrical conductivity. *J. Polym. Sci. B Polym. Phys.* **48**, 850–858 (2010)
424. H.B. Zhang, W.G. Zheng, Q. Yan, Y. Yang, J.W. Wang, Z.H. Lu, G.Y. Ji, Z.Z. Yu, Electrically conductive polyethylene terephthalate/graphene nanocomposites prepared by melt compounding. *Polymer* **51**, 1191–1196 (2010)
425. K. Kalaitzidou, H. Fukushima, L.T. Drzal, Multifunctional polypropylene composites produced by incorporation of exfoliated graphite nanoplatelets. *Carbon* **45**, 1446–1452 (2007)
426. W. Weng, G. Chen, D. Wu, Transport properties of electrically conducting nylon 6/foliated graphite nanocomposites. *Polymer* **46**, 6250–6257 (2005)
427. H. Kim, C.W. Macosko, Processing-property relationship of polycarbonate/graphene composites. *Polymer* **50**, 3797–3809 (2009)
428. G. Chen, C. Wu, W. Weng, D. Wu, W. Yan, Preparation of polystyrene/graphite nanosheet composites. *Polymer* **44**, 1781–1784 (2003)
429. H. Kim, Y. Miura, C.W. Macosko, Graphene/polyurethane Nanocomposites for improved gas barrier and electrical conductivity. *Chem. Mater.* **22**, 3441–3450 (2010)
430. R.A. Vaia, E.P. Giannelis, Polymer melt intercalation in organically-modified layered silicates: Model predictions and experiment. *Macromolecules* **30**, 8000–8009 (1997)
431. R.A. Vaia, H. Ishii, E.P. Giannelis, Synthesis and properties of two-dimensional nanostructures by direct intercalation of polymer melts in layered silicates. *Chem. Mater.* **5**, 1694–1696 (1993)
432. E. Bugnicourt, T. Kehoe, M. Latorre, C. Serrano, S. Philippe, M. Schmid, Recent prospects in the inline monitoring of Nanocomposites and Nanocoatings by optical technologies. *Nano* **6**(150), 1–19 (2016)
433. P.J. Yoon, D.L. Hunter, D.R. Paul, Polycarbonate nanocomposites. Part I. Effect of organoclay structure on morphology and properties. *Polymer* **44**, 5323–5339 (2003)
434. I. Siro, D. Plackett, Microfibrillated cellulose and new nanocomposite materials: A review. *Cellulose* **17**(3), 459–494 (2010)
435. X. Qiu, S. Hu, Smart materials based on cellulose: A review of the preparations, properties, and applications. *Materials* **6**, 738–781 (2013)
436. A.K. Bledzki, S. Reihmane, J. Gassan, Properties and modification methods for vegetable fibers for natural fiber composites. *J. Appl. Polym. Sci.* **59**(8), 1329–1336 (1996)
437. P.R. Hornsby, E. Hinrichsen, K. Tarverdi, Preparation and properties of polypropylene composites reinforced with wheat and flax straw fibres: Part II analysis of composite microstructure and mechanical properties. *J. Mater. Sci.* **32**(4), 1009–1015 (1996)
438. K. Oksman, L. Wallstrom, L.A. Berglund, R.D.T. Filho, Morphology and mechanical properties of unidirectional sisal-epoxy composites. *J. Appl. Polym. Sci.* **84**(13), 2358–2365 (2002)
439. D.N. Saheb, J.P. Jog, Natural fiber polymer composites: A review. *Adv. Polym. Technol.* **18**(4), 351–363 (1999)
440. S.T. Georgopoulos, P.A. Tarantili, E. Avgerinos, A.G. Andreopoulos, E.G. Koukios, Thermoplastic polymers reinforced with fibrous agricultural residues. *Polym. Degrad. Stab.* **90**(2), 303–312 (2005)
441. A. Alemdar, M. Sain, Biocomposites from wheat straw nanofibers: Morphology, thermal and mechanical properties. *Compos. Sci. Technol.* **68**(2), 557–565 (2008)

442. A. Alemdar, M. Sain, Isolation and characterization of nanofibers from agricultural residues – Wheat straw and soy hulls. *Bioresour. Technol.* **99**(6), 1664–1671 (2008)
443. T. Zimmermann, N. Bordeanu, E. Strub, Properties of nanofibrillated cellulose from different raw materials and its reinforcement potential. *Carbohydr. Polym.* **79**(4), 1086–1093 (2010)
444. B. Wang, M. Sain, Dispersion of soybean stock-based nanofiber in a plastic matrix. *Polym. Int.* **56**(4), 538–546 (2007)
445. E. Doelker, Cellulose derivatives. *Adv. Polym. Sci.* **107**, 199–265 (1993)
446. A.K. Bledzki, I.J. Gassan, Composites reinforced with cellulose based fibers. *Prog. Polym. Sci.* **24**, 221–274 (1999)
447. S. Kalia, B.S. Kaith, I. Kaur, Pretreatments of natural fibers and their application as reinforcing material in polymer composites – A review. *Polym. Eng. Sci.* **49**, 1253–1272 (2009)
448. M. Mashkour, M. Tajvidi, T. Kimura, F. Kimura, G. Ebrahimi, Fabricating unidirectional magnetic papers using permanent magnets to align magnetic nanoparticle covers natural cellulose fibers. *BioResources* **6**, 4731–4738 (2011)
449. M.N. Belgacem, A. Gandini, The surface modification of cellulose fibers for use as reinforcing elements in composite materials. *Compos. Interf.* **12**, 41–75 (2005)
450. A.K. Bledzki, J. Gassan, Composites reinforced with cellulose based fibers. *Prog. Polym. Sci.* **24**, 221–274 (1999)
451. M.L. Reid, M.B. Brown, G.P. Moss, S.A. Jones, An investigation into solvent- membrane interactions when assessing drug release from organic vehicles using regenerated cellulose membranes. *J. Pharm. Pharmacol.* **60**, 1139–1147 (2008)
452. K.J. Edgar, C.M. Buchanan, J.S. Debenham, P.A. Rundquist, B.D. Seiler, M.C. Shelton, D. Tindall, Advances in cellulose ester performance and application. *Prog. Polym. Sci.* **26**, 1605–1688 (2001)
453. D. Klemm, B. Heublein, H.P. Fink, A. Bohn, Cellulose: Fascinating biopolymer and sustainable raw material. *Angew. Chem. Int. Ed.* **44**, 3358–3393 (2005)
454. E. Kontturi, T. Tammelin, M. Österberg, Cellulose – Model films and the fundamental approach. *Chem. Soc. Rev.* **35**, 1287–1304 (2006)
455. K.L. Spence, R.A. Venditti, O.J. Rojas, J.J. Pawlak, M.A. Hubbe, Water vapor barrier properties of coated and filled microfibrillated cellulose composite films. *Bioresources* **6**, 4370–4388 (2011)
456. (a) F.L. MAathews, R.D. Rawlings, *Composite Materials: Engineering and Science* (Chapman & Hall, London, 1993); (b) A. Pegoretti, Editorial corner – A personal view. Trends in composite materials: The challenge of single-polymer composites. *Express Polym. Lett.* **1**, 710 (2007)
457. (a) K.P. Matabola, A.R. De Vries, F.S. Moolman, A.S. Luyt, Single polymer composites: A review. *J. Mater. Sci.* **44**, 6213–6222 (2009); (b) A. Kelley, *Concise Encyclopedia of Composites Materials* (Pergamon Press, New York, 1995)
458. R. Seymour, The role of fillers and reinforcements in plastic chemistry, in *Fillers and Reinforcements for Plastic. Advances in Chemistry Series*, ed. by R. D. Deanin, N. R. Schott, vol. 134, (ACS, Washington, DC, 1974), pp. 1–6
459. M.R. Piggot, The effect of the Interface/interphase on Fiber composite properties. *Polym. Compos.* **8**(5), 291–287 (1987)
460. M.R. Piggot, A. Sanadi, P.S. Chua, D. Anderson, Mechanical interactions in the Interphasial region of fibre reinforced thermosets, in *Composite Interfaces*, ed. by H. Ishida, J. L. Koenig, (North-Holland, New York, 1986), pp. 109–121
461. C. Sanchez, B. Julian, P. Belleville, M. Popall, Applications of hybrid organic–inorganic nanocomposites. *J. Mater. Chem.* **15**, 3559–3592 (2005)
462. T.G. Gopakumar, D.J.Y.S. Page, Polypropylene/graphite Nanocomposites by ThermoKinetic mixing. *Polym. Eng. Sci.* **44**(6), 1162–1169 (2004)
463. F. Hussain, M. Hojjati, M. Okamoto, R.E. Gorga, Review article: Polymer-matrix Nanocomposites, processing, manufacturing, and application: An overview. *J. Compos. Mater.* **40**(17), 1511–1575 (2006)

464. X. Jiang, L.T. Drzal, Multifunctional high density polyethylene Nanocomposites produced by incorporation of exfoliated graphite nanoplatelets 1: Morphology and mechanical properties. *Polym. Compos.* **31**, 1091–1098 (2010)
465. K. Kalaitzidou, H. Fukushima, L.T. Drzal, A new compounding method for xfoliated graphite-polypropylene nanocomposites with enhanced flexural properties and lower percolation threshold. *Compos. Sci. Technol.* **67**, 2045–2051 (2007)
466. K. Kalaitzidou, H. Fukushima, L.T. Drzal, Multifunctional polypropylene composites produced by incorporation of exfoliated graphite nanoplatelets. *Carbon* **45**, 1446–1452 (2007)
467. Shah Mohammed, Reduwan Billah, Ibrahim Hossain Mondal, Sazzad Hossain Somoal, M. Nahid Pervez, Md. Obaidul Haque, Synthesis of External Stimuli-Responsive Hydrogels based CMC and Other Cellulose Derivatives for Advanced Applications, in *Carboxymethyl-cellulose. Volume II. Pharmaceutical and Industrial Applications*, ed. by I. H. Mondal, Nova Science Publishers, New York, USA, ISBN: 978-1-53614-752-0 (eBook), 43–75 (2019)



Ibrahim Khan, Muhammad Mansha, and
Mohammad Abu Jafar Mazumder

Contents

1	History of Polymer Blends	516
2	Classification of Polymer Blends	519
2.1	Completely Miscible Polymer Blends	521
2.2	Completely Immiscible Polymer Blends	522
2.3	Partially Miscible Polymer Blends	523
3	Compatibilization Strategy for Good Dispersion	523
4	Methods of Polymer Blending	524
4.1	Melt Blending	524
4.2	Mill Mixing and Fine Powder Mixing Technique	525
4.3	Solution Casting Method	525
4.4	Freeze Drying	526
4.5	Latex Blending	526
4.6	Mechanochemical Blending	526
4.7	Interpenetrating Polymer Network Technology	527
5	Characterization	527
5.1	Spectroscopic Techniques	527
5.2	Energy-Dispersive X-Ray Spectroscopy (EDX)	528
5.3	Scanning Electron Microscopy (SEM)	529
5.4	Transmission Electron Microscopy (TEM)	530
5.5	X-Ray Diffraction (XRD)	530
5.6	Tensile Tester	530
5.7	Differential Scanning Calorimetry (DSC)	531
5.8	Dynamic Mechanical Analysis (DMA)	532
5.9	Thermogravimetric Analysis (TGA)	532
5.10	Rheology	533
5.11	Miscellaneous Characterization Techniques	533

I. Khan · M. Mansha · M. A. Jafar Mazumder (✉)

Chemistry Department, King Fahd University of Petroleum and Minerals, Dhahran, Saudi Arabia
e-mail: ebraheem@kfupm.edu.sa; manshachohan@kfupm.edu.sa; jafar@kfupm.edu.sa

6	Properties of Polymer Blends	534
6.1	Electrical Properties	534
6.2	Mechanical Properties	535
6.3	Thermal Properties	535
6.4	Optical and Glass Properties	536
7	Applications of Polymer Blends	536
7.1	Nanocomposites and Other Nanomaterials	537
7.2	Electronic Device and Batteries	538
7.3	Membrane and Plastic Industry	539
7.4	Supercapacitors	542
7.5	Miscellaneous Applications	543
8	Conclusion	544
	References	545

Abstract

In this chapter, we have presented different aspects of polymer blends, from fundamentals to the synthesis, physical and chemical properties, and applications. Polymer blends are made from the combination of two or more polymer components, having staggering and incredible applications in numerous fields due to their advanced properties. A brief introduction of the polymer blends about its origination and development is presented in the first part of this chapter; then important polymer blend types and synthesis methods are summarized with a brief discussion about their thermodynamic properties. Different characterization techniques were also discussed which can be used to determine the morphological, structural, chemical, and mechanical properties of these materials. The thermal, mechanical, and electrical properties of different polymer blends are discussed considering some recent applications of polymer blends in different industries.

Keywords

Polymer blends · Copolymer · Miscibility · Morphology · Compatibilization · Rheology

Abbreviations

ABS	Acrylonitrile butadiene styrene
ATRP	Atom transfer radical polymerization
BHJ	Bulk heterojunction
BSA	Bovine serum albumin
CAB	Cellulose butyrate
CAGR	Compound annual growth rate
CMCA/CA	Carboxymethyl cellulose acetate/cellulose acetate
CPs	Conjugated polymers
DEC	Diethylene carbonate
DIM	Direct injection molding
DMA	Dynamic mechanical analysis

DMC	Dimethyl carbonate
DSC	Differential scanning calorimetry
EBA	Ethyl butyl acrylate
EC	Ethylene carbonate
EDLC	Electrochemical double-layer capacitor
EDX	Energy-dispersive X-ray spectroscopy
ELSD	Evaporative light scattering detector
EPDM	Ethylene propylene diene
EVA/SAN	Poly(ethylene-co-vinyl acetate)/poly(styrene-co-acrylonitrile)
GO	Graphene oxide
GPC	Gel permeation chromatography
HDPE	High-density polyethylene
HPLC	High-performance liquid chromatography
IPN	Interpenetrating polymer network
LDPE	Low-density polyethylene
LLDPE	Linear low-density polyethylene
MMMs	Mixed matrix membranes
MMT	Montmorillonite
MW	Molecular weight
NC	Nitrocellulose
NMR	Nuclear magnetic resonance spectroscopy
OCP	Open circuit potential
P(VDF-co-HFP)	Poly(vinylidene fluoride-co-hexafluoropropene)
PA	Phosphoric acid
PA 6,6	Polyamide 6,6
PA12	Polyamide-12
PANI-PVC	Polyaniline-polyvinylchloride
PBI	Polybenzimidazole
PBT	Poly(butylene terephthalate)
PCE	Power conversion efficiency
PCL/PLA	Poly ϵ -caprolactone/poly lactic acid
PDA	Photodiode array detector
PDMAEMA	<i>N,N</i> -dimethylamino-2-ethylmethacrylate
PE	Polyethylene
PEDOT	Poly(3, 4-ethylenedioxythiophene)
PEGF	Polyethylene glycol fumarate
PFCE	Partially fluorinated copolyester
PIM-1	Polymer of Intrinsic Microporosity-1
PIPN	Pseudo-interpenetrating polymer networks
PL	Photoluminescence
PLLA	Poly(L-lactide)
PMMA	Poly(methyl methacrylate)
PMMA/EVA	Poly(methyl methacrylate)/ethylene-co-vinyl acetate
PNMPy	Poly(<i>N</i> -methylpyrrole)

PS	Polystyrene
PSCs	Polymer solar cells
PSF	Polysulfone
PSI	Polydispersity index
PV	Pervaporation
PVA	Poly vinyl alcohol
PVB	Polyvinylbutyral
PVC/EVA	Poly(vinyl chloride)/ethylene-co-vinyl acetate
PVC/SAN	Poly(vinyl chloride)/poly(styrene-co-acrylonitrile)
PVdC-AN	Poly(vinylidene chloride-co-acrylonitrile)
PVDF	Polyvinylidene fluoride
PVDF-HFP	Poly(vinylidene fluoride-co-hexafluoro propylene)
PVOH	Poly(vinyl alcohol)
PVPh	Poly (4-vinylphenol)
SBR	Styrene butadiene rubber
SDCDPS	Disodium 3,30-disulfate-4,40-dichlorodiphenyl sulfone
SEM	Scanning electron microscopy
SFPAE	Sulfonated fluorinated poly(arylene ether)
SIPN	Semi-interpenetrating polymer network
SPEEK	Sulfonated poly(etheretherketone)
SPPU	Sulfonated polyphenylene sulphone
SRNF	Solvent resistance nanofiltration
TEM	Transmission electron microscopy
TGA	Thermogravimetric analysis
THF	Tetrahydrofuran
TMPC	Tetramethyl bisphenol-A polycarbonate
UF	Ultrafiltration
UTM	Universal testing machine
VRFB	Vanadium redox flow battery
XLPE	Cross linked polyethylene
XRD	X-ray diffraction
ZIF	Zeolitic imidazolate framework

1 History of Polymer Blends

Since the introduction of nitrocellulose (NC), first synthetic polymer to be used in energetic material formulations, prepared by Braconnot in 1833, has opened a new era in the world of science. No doubt, the polymer industry nowadays is one of the most developing industries in the world and has brought evolutionary changes in everyday life. It is very difficult to consider our daily life without their influence and impacts of these polymeric materials [1]. Considering industrially synthesized available polymers, the scientists started to modify the structure of these materials in different ways to make them suitable for different target applications. One of such modifications of these materials is polymer blending. Polymer blend is a

homogenous or heterogeneous mixture of at least two polymers/copolymers. In some cases, it is also referred as polymer mixture. These polymers can interact chemically or physically depending on their structural properties, and their physical properties obviously differ from their parent components [2].

The history of the polymers is set dates back to 3000 BC, when shellac (natural polymer) was used as varnish in India [3, 4]. When Christopher Columbus discovered the new world in 1495–96, he brought an important product with noticeable elastic properties, called rubber. Gutta percha was introduced in seventeenth century. But the first synthetic polymer available industrially was nitrocellulose (in 1833). In 1850s, Charles Goodyear patented ebonite, which is a hard rubber prepared by the vulcanization of natural rubber or related polymers into more durable materials by the addition of variable amount of sulfur (e.g., 25% to 80%) [3].

In 1846, the first polymer blend patent, prepared from gutta percha and natural rubber, was claimed by an artist Alexander Parkes [3]. That patent was the start of this amazing technology, which has grown so rapidly, and the number of polymer blend patents approached to 3000 within a year. In the recent times, the focus to the polymer blends industries is tremendously increased due to their magnificent applications in every aspect of life [4, 5].

The most important unit of operations in the polymer industry are blending and mixing, which mostly follow the criterion discussed below [3, 5]:

1. Selection of suitable polymers, which can be mixed to a certain extent to form polymer blend. The polymer structure and chemical properties play an imperative role in this case.
2. Selection of a suitable solvent, as a reaction medium for raw polymers. It is pertinent for the polymer components to have some solubility in the solvent for good blending. In certain cases, surfactants can also be used for good mixing.
3. Addition of a copolymer whose one part is soluble in one phase, and other part is soluble in other phase.
4. Addition of a large amount of core-shell (co)polymer.
5. If needed, stabilizers/plasticizers are also added.
6. Provide proper conditions and medium for reaction to occur.

Over the period of time, certain devices have been designed for the purpose of polymer synthesis and its blending. Hancock patented first internal mixer in early 1830s [5], which was improved by Freyburger to a more efficient counter-rotating twin shaft machine in 1876–1877 [6]. Chaffee patented two-roll mills screw extruder in 1836 [7]. In the late nineteenth century, the electric extruders were developed in Britain, while in the early twentieth century, specifically during World War I and II, the world developed Myriad polymer industry to fulfill its need. Following the development of polymer technology, the rapid advancements were observed in the polymer processing devices such as co-extruders, film blowers, crosshead dies, filament extruders, breaker plates, screen packs venting, and two-stage screws in extruders. In the beginning of the 1980s, computer devices came into the picture, which made the polymer blending an ultimate choice for many industrial,

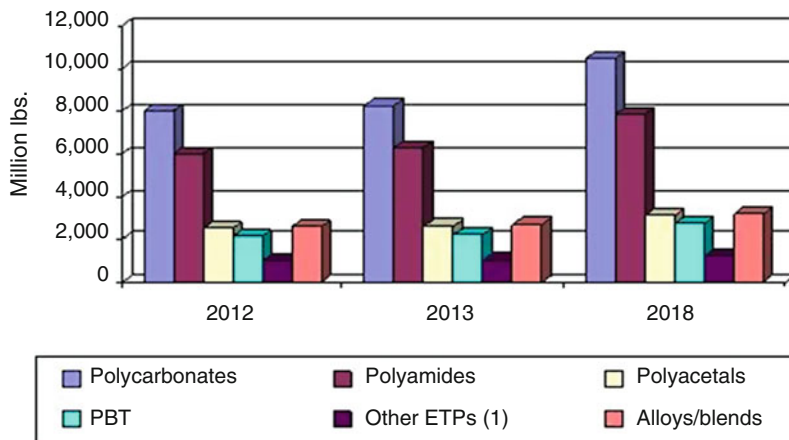
agricultural, medicinal, and domestic applications [8], and turns out as a huge industry. It constitutes approximately 36 wt% of the total polymer consumption, and their applicability continues to increase with industrial development. Nearly 65% of polymer alloys and blends are produced by polymer manufacturers itself, 25% by some related companies, and the remaining 10% by other sources. The expected market growth of polymer blends is tabulated in Table 1, and the diagrammatic representation is shown in Fig. 1. The worldwide market in volume for polymer blends was estimated to be more than 22 billion pounds in 2012, which is expected to increase to 28 billion pounds by 2018 assuming the increasing rate at 4.4% [at a 5-year compound annual growth rate (CAGR)] (Table 1). Asia being the leading polymer market occupied nearly 55% of the total market, followed by Europe and America [9, 10].

The major objective of polymer blending is to achieve cheap, readily available, and commercially viable products with unique properties. Polymer blending is a vast and unlimited subject of interest that requires highest attention theoretically and experimentally. From the literature, it was found that polymer blends have superior properties compared to its component polymers. Blending of different polymers is one of the most important industrial tools to get more efficient and attractive product for various applications. Some characteristics of polymer blending are mentioned below:

1. Provide materials with desired properties at the lowest possible expense, which are within the limit of an ordinary people.
2. It can be used to extend the engineered resin performance that is essential in large-scale applications.
3. Depending on its applications, one can easily design polymer blends of unique properties, e.g., improving specific properties by increasing impact strength or solvent resistance.
4. Polymer blends are suitable for recycling and biodegradation.
5. Blending technology offers striking opportunities for salvage and recycling of polymer wastes, which is impossible in case of their pure component.
6. Polymer blending greatly improved processability, product consistency, and scrap reduction of the primary targeted polymer.

Table 1 Global engineering resin and polymer alloy/blend market by resin type, through 2018 (\$ millions)

Resin	2012	2013	2018	CAGR% 2013–2018
Polycarbonates	8000	8280	10,476	4.8
Polyamides	6000	6279	7883	4.7
Polyacetals	2500	2593	3110	3.7
PBT	2100	2193	2722	4.4
Other ETPs (i.e., PET, PPS, LCPs, polysulfones, etc.)	997	1033	1237	3.7
Alloys/blends	2575	2673	3209	3.7
Total	22,172	23,051	28,637	4.4



(1) Includes PET, PPS, polysulfones, LCPs, polyketones and others

Fig. 1 Expected market growth of polymer blends. (Source: BCC Research Report (2013) global engineering resin and polymer alloy/blend market by resin type, 2012–2018 (\$ millions)

7. Polymer blending is an appropriate method for swift formulation changes, e.g., yearning applications.
8. Considering environmental issues, the polymer blends also increases the life time of the parent polymer.

2 Classification of Polymer Blends

The miscibility of individual polymer is always considered to be a key factor for classifying polymer blends. By definition, miscibility is the capability of a mixture that form a single phase over certain range of temperature, pressure, and compositions. The miscibility term describes the homogeneity of polymer mixtures at a particular temperature. It can be influenced by various factors such as morphology, intermolecular interaction, crystalline phase, and surface tension. The polymer blending miscibility can be judged by various factors such as chemical structure, molecular weight distribution, and molecular architecture of the components that can be confirmed by light scattering, X-ray scattering, and neutron scattering. By using the second law of thermodynamics, one can comment about the miscibility or immiscibility of two polymers considering a factor of entropy involved in it by Eq. 1 [11].

$$\Delta G_M = \Delta H_M - T\Delta S_M \quad (1)$$

where ΔG = change in free energy, ΔH = change in enthalpy, ΔS = change in entropy, T = absolute temperature, and M = mixing.

For a homogeneous miscible blend, the ΔG_M requires a negative value. For high-molecular-weight polymer blends, the gain in entropy (S) is negligible. Hence, ΔG_M

can only be negative if the ΔH_M is negative, which means that the mixing must be exothermic. The system usually requires specific interactions between the blend components. These interactions may range from strongly ionic to nonbonding and/or weak bonding that includes hydrogen bonding, ion–dipole, dipole–dipole, and donor–acceptor interactions. Thus, for complete miscibility of the polymer blends, the following conclusion can be drawn [11, 12]:

Condition 1. Thermodynamically Gibbs free energy of mixing must be negative.

$$\Delta G_{AB} < \Delta G_A + \Delta G_B \quad (2)$$

Or

$$\Delta G_M < 0 \quad (3)$$

Condition 2. The enthalpy of mixing must also be negative.

$$\Delta H_M - T\Delta S_M < 0 \quad (4)$$

As enthalpy depends on pressure, the increasing pressure will increase miscibility as indicated in Eq. 4.

Condition 3. The second derivative of Gibbs free energy of mixing (ΔG_M) with respect to volume fraction (ϕ) must be greater than zero, i.e., positive.

$$[\Delta \partial^2 \Delta G_M / \Delta \phi^2] > 0 \quad (5)$$

The phase diagram, depicted in Fig. 2, can be used to decide the phase behavior of the polymer blends [11–13]. In Fig. 2, the binodal separates miscible and metastable regions from each other, while the spinodal separates two phase regions from metastable.

Considering above discussion, Fig. 2 can also be related with Fig. 3 that explain the miscibility of polymer blends. Figure 3 showed the relationship between Gibbs free energy of mixing (ΔG_M) and composition of the components in terms of volume fraction (ϕ) for binary mixtures [14]. In Fig. 3, miscible mixture, which has positive ΔG_M value between starting point and end point, indicated the component in this blend systems are fully immiscible. The case is reverse for curve immiscible mixture, in which all conditions are applicable and the components are fully miscible. For curve partially miscible mixture, there are two minima, and amorphous phase is observed to its right and left, so partial miscibility can be observed.

Considering the applicable conditions and miscibility of the blend systems, the following three types of blend can be explained:

Fig. 2 Phase diagram for liquid mixtures, showing upper critical (UCST) and lower critical solution temperature (LCST) [12]. (With kind permission from Springer)

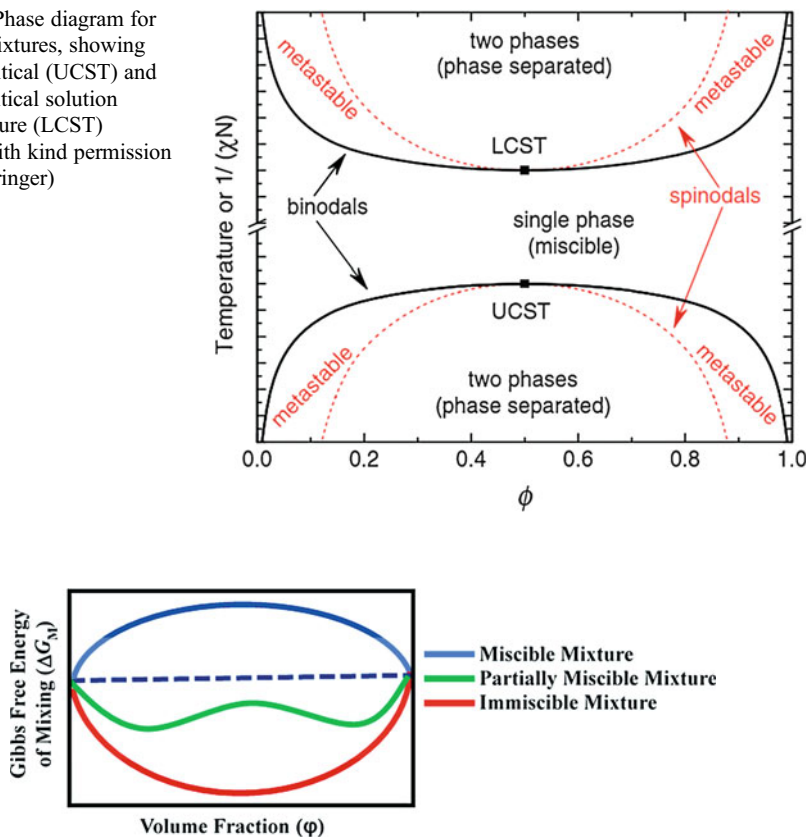


Fig. 3 Gibbs free energy of mixing for binary phases

2.1 Completely Miscible Polymer Blends

As discussed above, the Gibbs free energy and enthalpy of mixing are negative for miscible blends. The homogeneity is achieved at least on a nanometer scale, if not on the molecular scale. The glass transition temperature (T_g) plays an important role in miscible blend. The parent component has their own T_g values that alter and appear with a new value after mixing with other polymers; e.g., polystyrene and poly(phenylene oxide), poly(ethylene terephthalate) with poly(butylene terephthalate), and poly(methylmethacrylate) with poly(vinylidene fluoride) are some important fully miscible polymer blend systems. It is worth to mention that the important chemical and physical compatibilities should be recognized and have an idea before mixing any polymer component to get fully miscible polymer blend products [15, 16]. Table 2 provides some examples of fully miscible polymer blends with their T_g values [17–21].

2.2 Completely Immiscible Polymer Blends

The most distinct features of these blends are their different morphology and inhomogeneous matrix composition. These blends have a sharp interface, coarse morphology, and poor adhesion between the blending component phases. Thus, to make them suitable for different applications, compatibilization is very important, which can be carried out with the help of a specific compatibilizer for a particular system. The compatibilization makes the blending system much stable, and better blended phase morphology is attained by inducing better interactions between two immiscible polymers. One of the important concerns in this kind of blends is the glass transition temperature (T_g). The T_g is not sharp, and usually found more than one values. In binary polymer blends, there are two T_g values, as the components are immiscible so they somewhat retain their own T_g values. Examples of fully immiscible polymer blends systems include polystyrene/polybutadiene, poly(ethylene terephthalate)/poly(vinyl alcohol), and polyvinylidene fluoride/poly(lactic acid) blends [22]. Some typical immiscible polymer blends and their T_g values are listed in Table 3 [23–27]. In these products, one can clearly identify the phases of both components as they are not miscible, though their physical properties are somewhat different from original one. Figure 4 shows the two components of immiscible polymer blend systems in which component A is in small proportion as compared to component B. Therefore, it will be separated as small spheres and the larger component will form a sea (Fig. 4a). After suitable treatment, the component A and B will assume a shape, which can be easily distinguished from each other (Fig. 4b).

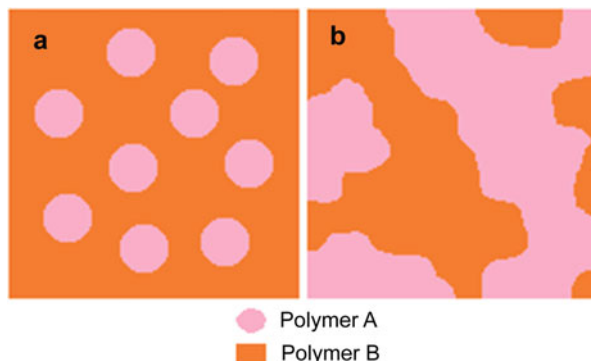
Table 2 Some reported miscible polymer blend system with T_g values

S. no	Components (T_g °C)		Component %	Polymer blend T_g value	References
1.	PB (−100)	SBR (−15)	25:75	−60	17
2.	PBT (40)	PET (81)	25:75	51	18
3.	PVDF (−40)	PMA (16)	25:75	6	19
4.	PS (96)	PPO (216)	20:80	113	20
5.	ABS (105)	PLLA (60)	30:70	73.5	21

Table 3 Some reported fully immiscible polymer blend system with T_g values

S. no	Components (T_g °C)		(Component %)	Polymer blend T_g value (°C)	References
1.	PS (96)	PB (−100)	30:70	103	23
2.	Nylon 6 (54)	Nylon 612 (46)	20:80	49	24
3.	PA-6 (50)	SEBS (95)	50:50	60	25
4.	PET (82)	PC (149)	20:80	123	26
5.	PS (87)	PC (146)	20:80	134	27

Fig. 4 Immiscible polymer blends: (a) before mixing and (b) after mixing



2.3 Partially Miscible Polymer Blends

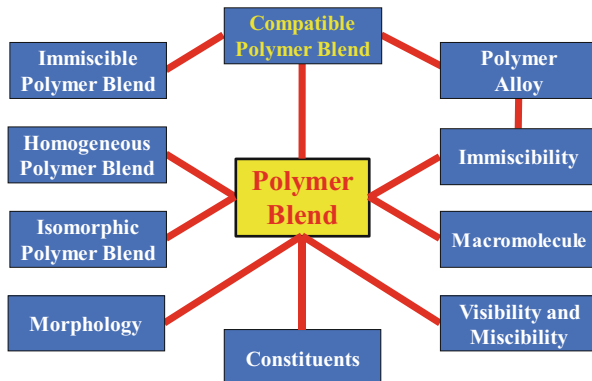
The nature of the partially miscible polymer blends can be depicted from curve **C** in Fig. 3, which represent two regions. These regions specify the existence of some intermediate miscible phase, recognized as partially miscible polymer blend region. The partially miscible blends exhibit properties in between miscible and immiscible polymer blends. In these polymer blends, a small portion of one of the blending components is dissolved in other blending component. These polymer blends are normally compatible and blend phases are homogeneous with their own T_g . But the T_g values are shifted from the neat components to the blend components. Typical example of partially miscible polymer blend is the PC/ABS blends, in which PC and ABS are partially dissolved in one another. The resulted interface is wide and the interfacial adhesion was found to be noble [16, 28–30].

3 Compatibilization Strategy for Good Dispersion

Compatibility is a wide and intriguing arena of research [31–35]. Figure 5 presents some common compatibility strategies for polymer blending [36, 37]. In many cases, particularly in immiscible polymer blends, compatibilization is very useful tool for improving the disparity components in the reaction matrix. It successfully reduces interfacial tension, assist dispersion, and stabilizes the morphology of the combining reactants against offensive stresses and strains (arising out of processing). It enhances adhesion between different phases and improves the overall mechanical properties of the polymer blends. Gravity and interfacial tension are the two important driving forces for the phase segregation of the polymer blend components. The rate of de-mixing greatly depend upon the interfacial tension, density, and viscosity [38, 39].

Various approaches can be used to reduce the interfacial tension in the melted state and improve the adhesion between the immiscible phases in solid states. The selection of the most appropriate blending technique is very important. It could be helpful obtaining continuous or interpenetrating phase morphology that may result in direct load sharing. The addition of a third homopolymer or even block or graft copolymer

Fig. 5 Compatibility strategies of polymer blends



or small molecular active compounds, which is miscible in either of the two phases, called nonreactive compatibilization can also be used. In addition, functionalization can also be successfully used for reactive compatibilization [11]. Noted that in physical compatibilization, the compatibilizing agent is added prior to initiate the reaction. This added agent is capable to reduce the interfacial tension between the blending components which provide emulsification effect and promoting adhesion between the reaction phases [40, 41]. Beside these degradation, coupling and grafting can also be used as an efficient method for achieving compatibility.

4 Methods of Polymer Blending

Several methods can be used to synthesize and/or prepare polymer blends [42]. Each method has their own merits and demerits. Short summary of some feasible polymer blends preparation techniques are presented below.

4.1 Melt Blending

This is one of the most widely used contamination-free techniques for the preparation of polymer blends [42]. Special devices that include different extruders (Fig. 6) and temperature controller devices are used to process and melt individual component. The raw materials are introduced to a special chamber containing extruders to have uniform mixture of all raw materials. Temperature is elevated to a desirable limit and all added materials are consequently melted. Besides the composition of the components, process conditions such as blending duration, operating temperature, and pressure are also important to achieve desirable properties of the blend. This method is usually considered to be a good technique except considering the fact that sometime it appears to be too expensive and the obtained polymer blend might not be uniform (if it is not properly handled) and results mechanically less efficient products [42].

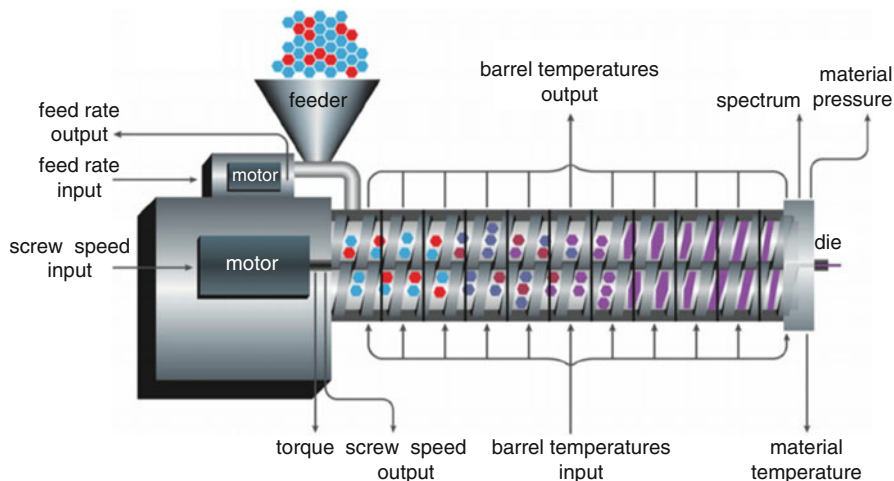


Fig. 6 Twin extruder [42]. (With kind permission from Springer)

4.2 Mill Mixing and Fine Powder Mixing Technique

A simple straightforward method in which the blending components are mixed through milling and grinding. Different kinds of milling devices and grinder are used for this purpose. The raw materials are grinded to achieve the finest powder which are then mixed together to achieve uniform mixing at micro level. The product is then subjected to additional operations to get the desired polymer blend products [43, 44]. Bunbury mixer, which is also known as Master Mixer, is extensively used for mechanical mixing of the polymer ingredients and thus suitable for synthesis of polymer blends [44].

4.3 Solution Casting Method

This is one of the simplest available techniques and very common among the users. In this method, the blend is casted from a common solvent, and this method comprises the following steps:

1. The desired component polymers are selected for blending.
2. The selected polymers are dissolved in a specific solvent. It is noted that the solvent selection is very important and plays an important role in solution casting method.
3. The solution mixture keep stirring for a certain period of time to get the homogenous solution.
4. The binders and compatibilizers are added if required.
5. The resulted product is collected at the end of the process and characterized.

The only limitation of this method is the incompatibility of the component polymer and separation of the solvent from the product, because residual solvent can distress the bulk properties of the blend [45, 46].

4.4 Freeze Drying

Quenching is a well-known method in any chemical laboratory operations, also used in freeze-drying method. In freeze-drying, the component polymers are quenched down to a suitable (normally very low) temperature, and the solution got frozen. The component polymers will have a very least chance to agglomerate and thus all frozen solvent can be collected very easily. The solvent is then removed by the application of sublimation. This method is the best when symmetrical solvents are used in the solution [47–49].

4.5 Latex Blending

A latex is an important word and carry specific meaning in polymer industry. It is used for a stable dispersion (emulsion phase) of polymer particles at micro level in any specific aqueous medium. Thus, the latex blending is a special technique for polymer blending and other polymerization techniques. This method produced rubber-toughened plastic blends. To achieve such blends, the contributing polymers should be in the latex or in the emulsion form, which is followed by mixing. The mixing process is very important since this will provide micro-sized homogenous latex, and distribution of discrete phases [50, 51].

4.6 Mechanochemical Blending

In this method, polymer blends are given by a specific polymeric system in which long-chain monomeric sequences of type one is linked chemically with similar long-chain monomeric sequences of the other kind (Fig. 7). This connection may be axial or in cross



Fig. 7 IPN polymer blend formation

direction. This connection may be axial or in cross direction that produced either block or graft kind of copolymer system. Following this step, crosslinking occurred either by selective or random fashion that leads to inter-crosslinking or graft crosslinking which is termed as mechanochemical polymer blends. This polymer system is appeared as a special network which is interpenetrating in nature. Therefore, it is also called interpenetrating polymer network (IPN). Like other polymer blends, this system also possesses unique mechanical, thermal, and optical properties [52–54].

4.7 Interpenetrating Polymer Network Technology

This is closely related to mechanochemical technique, but uses without external mechanical force in this system. The polymer blend system is highly penetrated into each other, and for separation it requires high energy to break the chemical bonds [2, 54]. In these systems, the components are grown in such a way that they are entangled into each other but not by chemical bond. Thus, special techniques are usually required to produce such polymer systems, as simple mixing will not be enough to get interpenetrating polymer network (IPN). The semi-interpenetrating polymer network (SIPN) is comprising one or more polymer networks that includes linear or nonlinear branch polymer. This system is characterized by embedding at least one network into the polymer at a molecular scale. In this case, the polymer part can be separated from the network without damaging any chemical bond [2]. On the other hand, pseudo-interpenetrating polymer networks (PIPn) are prepared by the partial penetration of polymer into the network system. Thus, the polymer and network parts are distinct, and their properties are retained in greater extent, and their separation is relatively easier than the SIPN [2].

5 Characterization

Characterization of materials provide valuable information about their structure and properties. Variety of characterization techniques can be used to determine the exact nature of the polymer blends [13, 55]. The characterization techniques that usually used to characterize the polymer blends are discussed below.

5.1 Spectroscopic Techniques

The spectroscopic techniques are frequently used for the structural determination of any kind of molecular compounds including polymer blends. Mass spectroscopy provides information about the molecular weight and surface concentration of the polymer blends [56]. In specific operational condition, it also provides information about the propagating chain length at different interval of time. Fourier-transform infrared spectroscopy (FT-IR) has numerous applications in polymer blends, especially in qualitative and quantitative analysis. By comparing the FT-IR spectrum of a

neat component and blends, the chemical information about the functional groups and other properties of the blended polymers can easily be determined. If there is any chemical interaction taking place, some signal would be lost, shifted, or appeared in the polymer blends final spectrum. In addition to chemical information, useful physical information can also be obtained from peak broadening or shifting. FT-IR is also valid for determining hydrogen bonding in polymer blend system. Moreover, FT-IR spectra provide significant information regarding the phase separation of polymer blends [57]. Nuclear magnetic resonance spectroscopy (NMR) can also help deducing the structural properties of polymer blends. In addition to the traditional ^1H and ^{13}C NMR, solid-state NMR technique is also well known for elucidation of certain properties of polymer blends [58].

Typically, the spectroscopic techniques comprise three basic units: (1) The light source, such as neon, xenon, or argon lamps, mercury lamps, etc.; (2) Sample chamber, which is specific for each spectral technique; and (3) The detector, which is also different for different spectroscopies. The data interpreter evaluates the results and transformed them into an individual spectra. Figure 8 shows the schematic representations adopted for various spectroscopies.

5.2 Energy-Dispersive X-Ray Spectroscopy (EDX)

EDX is also called energy-dispersive X-ray analysis (EDXA) or energy-dispersive X-ray microanalysis (EDXMA). This spectroscopic technique primarily relies on an interaction of X-ray excitation and a sample. EDX is helpful in determining the

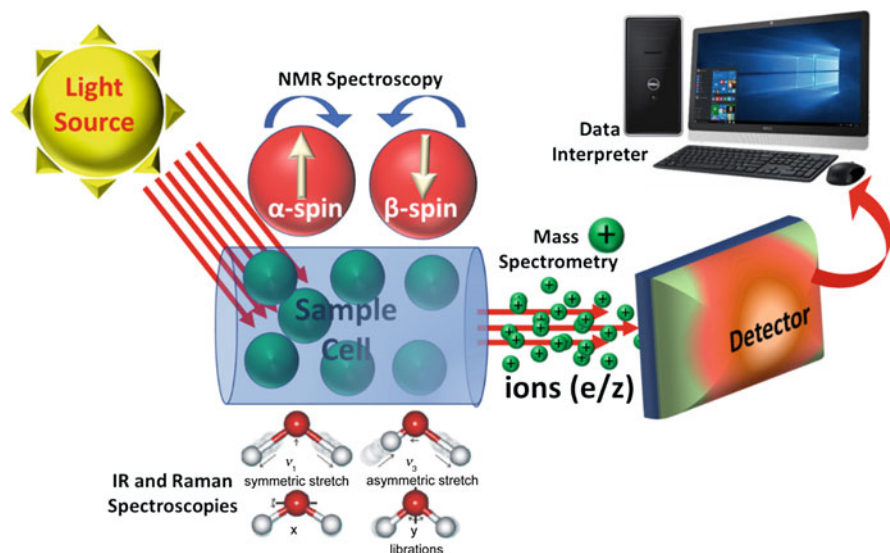


Fig. 8 Schematic representation of basic components used in various spectroscopic techniques

atomic ratio and elemental composition of the components atoms. Moreover, EDX can also be used to determine the contaminants in the mixture of polymer blends. In the recent past, Kindgren investigated the bright spots in different polymer blends consisting of ethyl butyl acrylate (EBA), low-density polyethylene (LDPE), linear low-density polyethylene (LLDPE), high-density polyethylene (HDPE), cross-linked polyethylene (XLPE), poly amide 6 (PA6), and polyamide 6,6 (PA6,6) using EDX. The results showed that the iron and aluminum oxide traces exist in the mixture as contaminants, which came from the processing unit [59].

5.3 Scanning Electron Microscopy (SEM)

Phase morphology of polymer blends is normally characterized by this technique. It is a type of microscopy that generates images of a sample by scanning its surface with a beam of electrons. The electrons interact with the atoms in the sample, producing various signals that is detected and converted into image by computer called micrograph. The micrograph contains valuable information about the sample's surface topography and composition. In the case of polymer blends, this technique assists researcher to predict the distribution of components. Moreover, the homogeneity of phase can also be predicted. In this technique, the samples are cryogenically fractured by immersing the samples in liquid nitrogen. A brittle fracture is obtained avoiding large deformations in the surface to be examined. This technique can be modified depending on the kind of polymer blends. Wang et al. prepared PBT/PFCE polymer blend to study the morphology and structural properties of the polymer components and their distribution [60]. They used different ratios of PFCE polymer to achieve more effective polymer blend having good mechanical and thermal properties. They used SEM images to study the external and internal morphology, properties, and distributions of the PBT/PFCE polymer blend components (Fig. 9). The sample was fractured under nitrogen environment and the brittle portion was used for the analysis. The fractured portion showed homogeneous spherical drop-like distribution of PFCE in PBT matrix (Fig. 9a), which is supported by the backscattered micrograph (Fig. 9b). The uniform

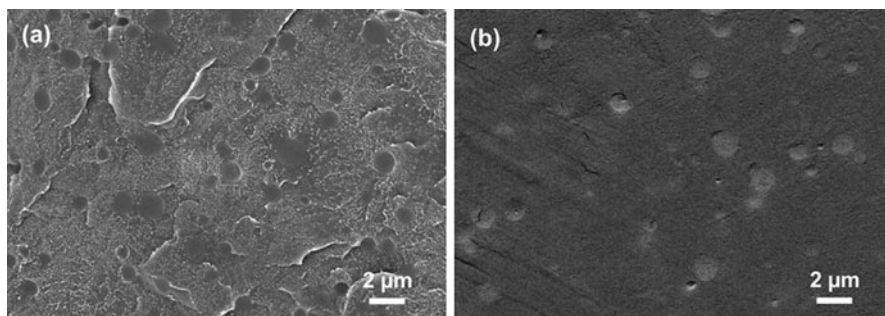


Fig. 9 SEM micrographs of PBT/PFCE polymer blend. (a) Cryofractured portion of the blend system. (b) The backscattered electron micrographs [60]. (With kind permission from ACS)

distribution of mixed phases is very important for better and efficient polymer blend, as it determines the final physiochemical properties of the blend system [59, 60].

5.4 Transmission Electron Microscopy (TEM)

TEM is an optical technique in which a beam of electrons is transmitted through an ultra-thin specimen (sample) and provides a good deal of characteristic information about the sample. To extract the information, the TEM image can be magnified and focused onto an imaging device and the assimilated information regarding polymer blend can easily be achieved. In general, the TEM sample preparation procedure is similar to the SEM. Typically for TEM analysis, some thin portions of the polymer blends were cut with the help of UC6 microtome supported diamond knife. Gold coating is usually applied to most of the polymer blend samples as they are relatively weak conductors. Wang et al. studied the PBT/PFCE polymer blend for the morphology and structural properties of the polymer components by SEM as discussed above [60], and compared the findings obtained by TEM analysis. The results were in good agreement as they obtained in their SEM study, i.e., the polymer matrixes were fully mixed and the phases were uniform.

5.5 X-Ray Diffraction (XRD)

This is one of the most viable characterization techniques for the determination of crystallinity in the polymer blends. In XRD, the ordered atoms cause to deflect the beam of incident X-ray in many specific directions, from which the angles and intensities are obtain in the graph, called crystallograph. This crystallograph provide an excellent information about the crystal lattice and the unit cell. From the electron density, the mean positions of the atoms in the crystal, their chemical bonds, disorder, and various other information can also be determined. In a recent study, Lv and coworkers used XRD technique to study the crystalline properties of the PCL/PLA polymer blend. They determined two extra XRD peaks, which were accountable for PLA along with the characteristic PCL peaks. In addition, they also observed decrease in intensity of PCL X-ray peaks, attributed to the immiscibility of both polymers [61].

5.6 Tensile Tester

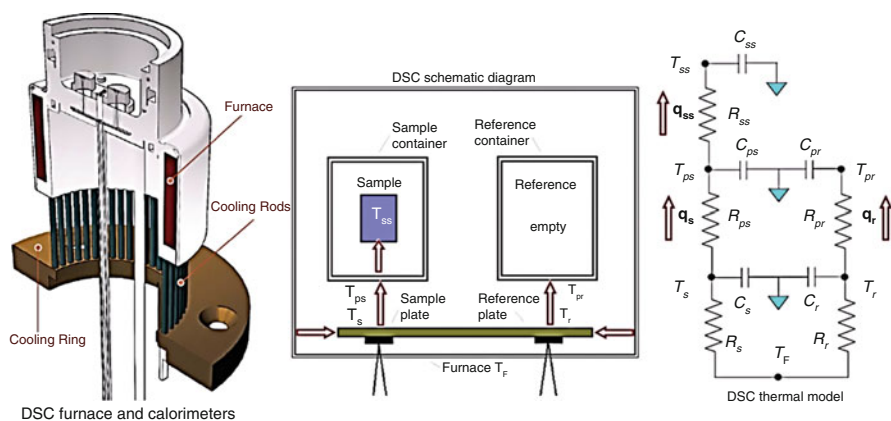
The mechanical properties of polymer blends are the most desirable aspects in blending. These days, research scientists are tapping much efforts to produce mechanically strong products. The mechanical strength of the products can be tested by the tensile tester. A tensile tester, universal testing machine (UTM), generally works on the stress and strain principle, and young modulus can be obtained from thermographs that determine the mechanical strength. The tensile properties of

PLLA was reported in a study [62], in which they found that the block copolymer (5 wt% PEO–PBO)/PLLA blends showed significant increase in mechanical properties after blend formation. Beside this technique, differential scanning calorimetry (DSC), dynamic mechanical analysis (DMA), and rheology can also be used to determine the mechanical properties of polymer blends.

5.7 Differential Scanning Calorimetry (DSC)

DSC is one of the prominent thermo-analytical characterization techniques for polymers and their blends. In this technique, the difference in the amount of heat required to increase the temperature of a sample and/or reference is calculated as a function of temperature. During the experiment, the temperature of the reference and/or sample should linearly increase with time at a specific ramping rate. It is worthwhile to mention that the reference sample should be scanned over the range of temperatures for a well-defined heat capacity. DSC contribute experimental result in the form of a DSC graph as a function of heat flux versus temperature or time. This technique is the best to identify the transition glass temperature (T_g) and enthalpies (H) of the system. Moreover, the depression in the achieved melting point indicated by DSC can be used to determine the miscibility of the blend system. Similarly, the polymer/polymer interaction values can also be judged from the DSC graph [63].

Rady et al. used DSC to investigate the phase-changing behavior of granular composites. They devised simple protocol for DSC (Scheme 1) to obtain accurate results based on the estimation of the thermal resistance between the sample and its enclosure [64].



Scheme 1 Differential scanning calorimetry (DSC) device (left) with schematic representation (right) [64]. (With kind permission of Tech Science)

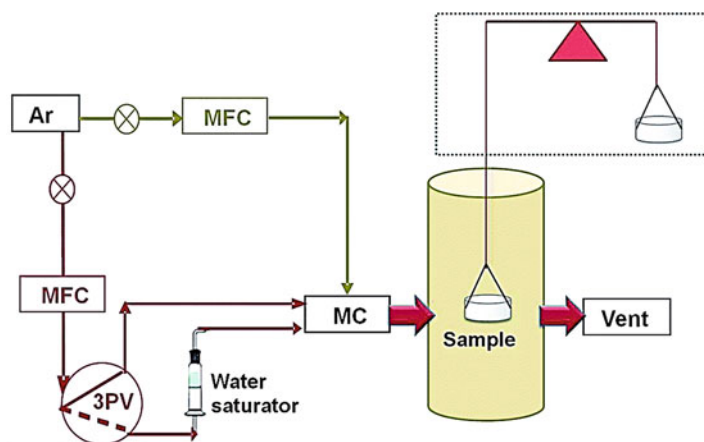
5.8 Dynamic Mechanical Analysis (DMA)

Viscoelastic properties of polymers are of great interest to the researcher, and can be studied by DMA. In DMA, a stress is applied on a polymer blend system in sinusoidal form. Due to the stress, some changes take place in polymer blends from which the strain is calculated, and eventually complex modulus is determined. The DMA can also be used to calculate T_g of the specific material. Beside this, thermo-mechanical analysis (TMA) is also helpful finding transitions analogous to certain molecular motions. Nair et al. prepared polymer blends with different cross-linking density using variable amount of ethylene propylene diene (EPDM) and styrene butadiene rubber (SBR), and studied their crosslinking density by DMA. This study suggested that changing the composition of one of the monomers can lead to difference in T_g and T_c [65].

5.9 Thermogravimetric Analysis (TGA)

Thermal analysis of polymer blends can also be carried out with thermogravimetric analysis (TGA). The thermograph obtained from TGA shows the relationship between physical or chemical changes with temperature. Alongside the temperature, time or mass loss can also be used to get information about the polymer blend [66]. Justin and Guiseppi used TGA to study the thermochemical properties of P (Py-co-PyBA) hydrogel, and found that the inherent and the modified hydrogel-P (Py-co-PyBA) were stable in the range of 25–300 °C. The thermograph indicated intense decomposition at ~400 °C. The comparative T_g result also indicated that the modified hydrogel is more stable than the original one [67].

Thermogravimetric analysis (TGA), shown in Scheme 2, was utilized to study the interface of H_3PO_4 and steam with the polybenzimidazole (PBI) and pyridine-bearing



Scheme 2 Schematic diagram of the TGA experimental set up. *MC* mixing chamber, *MFC* mass flow controllers [68]. (With kind permission from RSC)

aromatic polyether (TPS) systems. It is determined that the evaporation rate is by a factor of two lower than that of the pure phosphoric acid under the same steam partial pressure [68].

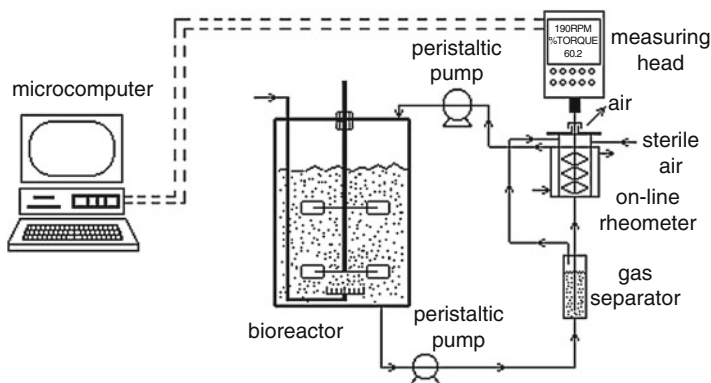
5.10 Rheology

Rheology is the flow of matter in response to an applied force. It can be applied to a variety of materials, especially to macromolecules and polymer blend systems. This technique is entirely dependent on the elasticity and plastic properties of the polymer blend systems. Rheological properties of polymer blends require extensive investigation to understand the basic principles involved in this technique. Yang and Han studied different polymer miscible blend systems constitute of PVPh. They are capable of forming hydrogen bonds due to the presence of active hydrogen and electronegative groups. Various characterizations in addition to rheology indicated that the blend systems are soluble in THF at lower temperature but the solubility decreases at elevated temperature indicating the cross-linking phenomenon takes place in PVPh specimen [69].

Badino et al. [70] indicated that online rheology produced much reasonable data compared to conventional rheological techniques after proper calibration. They further suggested that the impeller is useful for online rheological measurements as in the case of *Aspergillus awamori*. The typical protocol for the online rheology is given in Scheme 3.

5.11 Miscellaneous Characterization Techniques

In recent years, the gradient HPLC techniques, such as gradient polymer elution chromatography (GPEC) are used to find out the compositional drift of copolymers



Scheme 3 Schematic representation of online rheometer apparatus [70]. (With kind permission from Scielo)

or the scrutiny of polymer additives as a form of composition of the polymer blends. With the choice of the selected columns and the gradient conditions, separations are achieved that depend on molecular weight, adsorption mechanism, or kinds of precipitation. The use of a special detector allow researcher to get specific information about the material. For example, an evaporative light scattering detector (ELSD) allows one to perform solvent gradients with a universal mass detector and observe both UV-absorbing and non-UV-absorbing polymer samples without baseline disturbances. The addition of a photodiode array detector (PDA) allows compositional analysis across the molecular weight distribution of many copolymers, can be useful for the identification of components in a polymer blends, and also invaluable for the quantitation of polymer additives and other small molecules in traditional reverse phase separations. The gradient gel permeation chromatography (GPC) is also used to determine the composition and structural information about the polymer blends [71]. Gomez et al. studied the thermodynamics of binary and ternary polymer blend systems by a theoretical approach, and compared the results with experimental calculations obtained from GPC [72]. They theoretically computed the viscosimetric parameters and compared with the experimental data. It was found that their computed values of intrinsic viscosimetric parameters are in good agreement with experimental results.

6 Properties of Polymer Blends

Depending on the structure and compositions, the polymer blends have certain physical and chemical properties. The properties can be controlled by using an appropriate composition of polymer components. Following are some of the most important properties of polymer blends, which needs to be considered for a particular application.

6.1 Electrical Properties

Polymers have distinct electrical and conducting properties that depend on the behavior of the overall structure of the polymer. These properties can be changed with a modification of pure polymer. These modifications can be obtained by adding a filler, i.e., making its nanocomposite or making their blends with other polymer, though many other approaches can also be employed to get the desired product. Therefore, researchers are trying hard to build suitable polymer blends, which can be used as polymer blends in electrical industries. The temperature dependence of direct current (DC) conductivity was studied by S. Ameen et al. [73], in which various film samples were prepared from polyaniline-polyvinylchloride (PANI-PVC) blends. They doped polyaniline by adding different concentrations of sulfamic acid in aqueous tetrahydrofuran (THF) solution. The blended films were prepared by varying the amount of doped PANI, where PVC amount was kept constant. The sample films were used to determine the effect of sulfamic acid (dopant) in the

temperature ranges from 300 to 400 K. In order to evaluate the effect of the dopant on PANI-PVC, the conductivity-derived parameters such as pre-exponential factor (σ^0) and activation energy (ΔE) were calculated first. The structural changes of PANI-PVC blended films were characterized by FTIR spectroscopy from which it was derived that the suitability of the dopant is good in the chemical doping process. They concluded that the conductivity of the blends increased regularly as the percent amount of doped PANI increased in the polymer blend.

6.2 Mechanical Properties

Mechanical strength of polymer blends is the most important aspect in any robust and tangible applications. Normally, polymer blends leads to enhanced mechanical properties. There are certain parameters that includes tensile strength, bulk modulus, young modulus, ductility, hardness, plasticity, and yields strength which are required to calculate determining the overall mechanical strength of the polymer blends. Generally, researcher uses different parameters, and correlate them with the mechanical toughness to evaluate their product [74]. The most recent article published by Aranburu et al. studied the change in the mechanical properties of the constituent's polymer after blending [75]. They synthesized polypropylene/polyamide-12 blends with the help of direct injection molding (DIM), and found that on the gradual cooling crystallization of polypropylene, the nucleating effect of polyamide-12 (PA12) takes place, thus leading to the modification of crystalline morphology. This modification can be attributed to the interaction between the two polymers. Crystallinity of PA12 drops slightly, while that of polypropylene increased to greater extent. This increase in crystallinity is directly proportional to the enhancement in the mechanical properties. Chung and Green reported the synthesis of thin polymer blend film (nanoscale thickness) of miscible polymer blends from polystyrene (PS) and tetramethyl bisphenol-A polycarbonate (TMPC) and determined their elastic moduli and stiffness. They concluded that by varying the composition of the component and the thickness of the nanoscale films, the elastic properties and stiffness behavior alter significantly [76].

6.3 Thermal Properties

Thermal stability of polymer blends is an important marker for thermal industrial applications. For example, thermal aging of certain materials is observed due to their less resistant to solar light and other heat discharging materials. Certain polymeric materials are incapable to resist heat even at very low temperature, deform quickly, and release certain chemical to the object in contact. There are various parameters that can be used to compare the thermal stabilities of different polymer blend systems, i.e., critical temperature, glass transition temperature, heat of fusion, heat of vaporization, flammability, solidus, thermal expansion, thermal conductivity, softness, etc. All these factors are equally important and can be correlated to each other. Lizymol and Thomas investigated the thermal properties of three polymer

blends systems, i.e., PVC/EVA, EVA/SAN, and PVC/SAN, using thermogravimetric methods. It was found that PVC/EVA system was completely miscible, and thermal stability improved significantly [77]. Kim et al. showed that a polymer blend made up of two polymeric components having high miscibility and a suitable linker structure can produce a very homogeneous and dense thermal network, which enhanced mechanical properties of immiscible blend system [23].

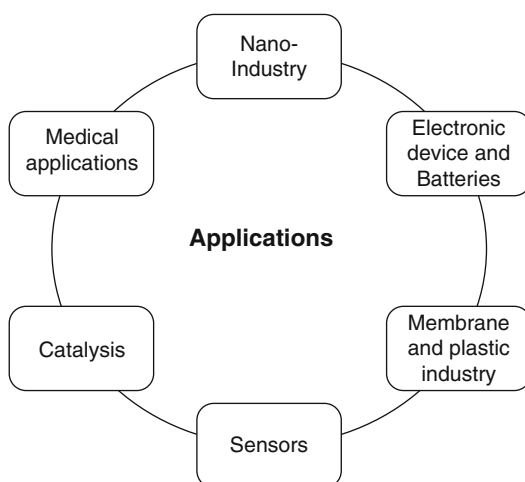
6.4 Optical and Glass Properties

The optical properties of polymer blends are also considered as one of the basic and important properties that helps obtaining variety of information of the blends. Optical property of any substance can be described as the interaction of radiations with the substance mostly in the visible region. In addition to other techniques, UV and photoluminescence (PL) are the two main techniques used to study the interaction of radiations with the substance. Takahashi et al. studied the optical properties of PMMA/EVA polymer blend system [78]. The system showed great transparency (~100%) at room temperature since the refractive index difference for both components were found to be very small at that temperature. They also reported that increasing the temperature significantly decrease the transmittance. Similar observation has been reported in the literature using varieties of other polymer blend systems [79].

7 Applications of Polymer Blends

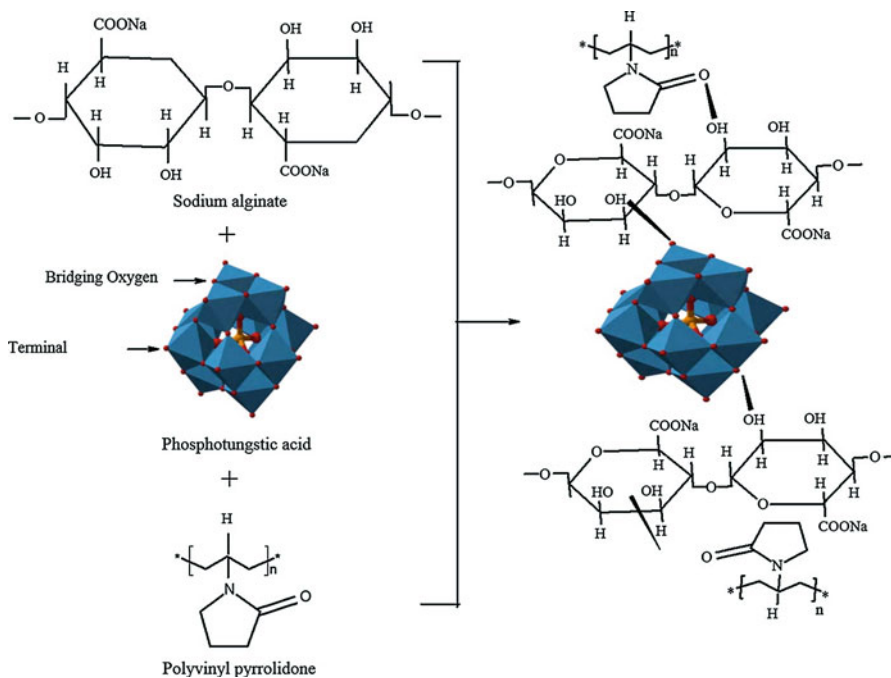
Polymer blends can be used in numerous applications that include synthesis of nanocomposites for improved chemical and mechanical properties, catalysis, medical applications, electronics, and membranes, and are depicted in Fig. 10. Some important applications are discussed below.

Fig. 10 Applications of polymer blends



7.1 Nanocomposites and Other Nanomaterials

The melt extrusion method was used to prepare thermoplastic starch/poly(vinyl alcohol) (PVOH)/clay nanocomposites that exhibited the intercalated and exfoliated structures. These nanocomposites were investigated to realize the effect of clay cation, water, PVOH, and clay contents on clay intercalation and mechanical properties. The taguchi experimental design method was applied on montmorillonite (MMT) having three types of cations or modifiers (Na^+ , alkyl ammonium ion, and citric acid). It was observed that the tensile strength and modulus were increased for nanocomposite samples with 10%, 5%, and 4% (by weight) of water, PVOH, and clay loading, respectively [69]. Sodium alginate/poly(vinyl pyrrolidone) polymers were used to make nanocomposite membranes by varying concentrations of phosphotungstic acid ($\text{H}_3\text{PW}_{12}\text{O}_{40}$) (PWA) using pervaporation (PV) method (Scheme 4). PV performance of the membranes was evaluated in terms of separation factor, and flux was evaluated by considering the effects of filler concentrations, temperature, and feed water surface. It was found that the membrane performance was reduced by increasing the feed water composition due to swelling. Moreover, the membranes showed significantly low Arrhenius activation energies for water than ethanol, suggesting efficient dehydration of ethanol [80].



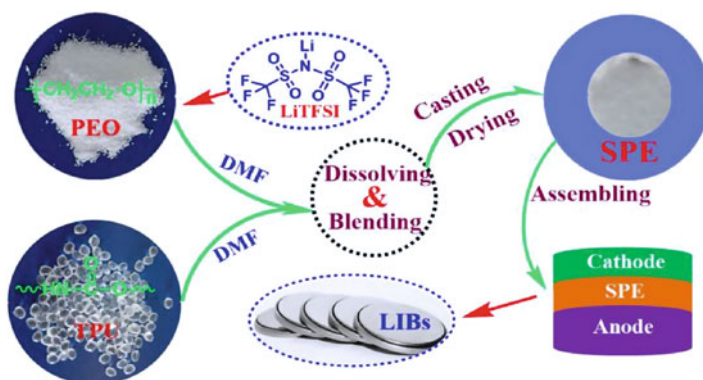
Scheme 4 Polymeric blend nanocomposite membranes for ethanol dehydration – effect of morphology and membrane–solvent interaction [80]. (With kind permission from Elsevier)

7.2 Electronic Device and Batteries

Transport studies were carried out using PVA-chitosan blended polymer on electrolyte system and in proton battery. The electrolyte was prepared by solution casting method. The blend consisting of PVA (36 wt%) and chitosan (24 wt%), doped with NH_4NO_3 (40 wt%), exhibited highest conductivity at the room temperature. Different amount of ethylene carbonate (EC) was used as plasticizer to further enhance the conductivity of the blends. It was found that 70 wt% of EC give the highest conductivity value ($1.60 \times 10^{-3} \text{ Scm}^{-1}$) of the studied sample. The fabricated polymer blends doped with EC is used as electrolyte in the fabrication of $\text{Zn} + \text{ZnSO}_4 \cdot 7\text{H}_2\text{O}/\text{electrolyte}/\text{MnO}_2$ cells. The open circuit potential (OCP) of the polymer blends was found to be in the ranges between 1.6 and 1.7 V [81]. Similarly, polyvinylidene fluoride (PVDF) and cellulose butyrate (CAB) blends supported membrane with polyethylene (PE) were used for gel polymer electrolyte of lithium ion battery. The ratio of PVDF and CAB found more effective in 2:1, which appeared to be the largest ionic conductivity ($2.48 \times 10^{-3} \text{ Scm}^{-1}$), and good compatibility for anode and cathode of lithium ion battery [82].

The electronic properties of thermoplastic polyurethane/poly(ethylene oxide) (TPU)-based polymer blends were found useful in the cathode materials of Li-ion batteries. The results show that the addition of TPU to the blend polymer results in loss of the crystallinity of PEO and improves the dissolution of lithium salts into the solid polymer electrolyte (SPE) matrix. TPU can also improve the mechanical stability and the electrochemical properties. Among the TPU/PEO blend electrolytes, the TPU/PEO = 1:3 based electrolyte presents an ionic conductivity of $5.3 \times 10^{-4} \text{ S cm}^{-1}$ with electrochemical stability above 5 V (vs. Li^+/Li) at 60 °C. The preparation of TPU/PEO blend polymer solid polymer electrolytes (SPEs) is provided in Scheme 5 [83].

Proton-exchange membrane (PEM) was developed by polybenzimidazole (PBI) with poly(vinylidene fluoride-co-hexafluoropropylene) (PVDF-HFP) blend for conducting proton in high temperature fuel cell. The loading of phosphoric acid



Scheme 5 The preparations of TPU/PEO blend SPEs [83]. (With kind permission from Elsevier)

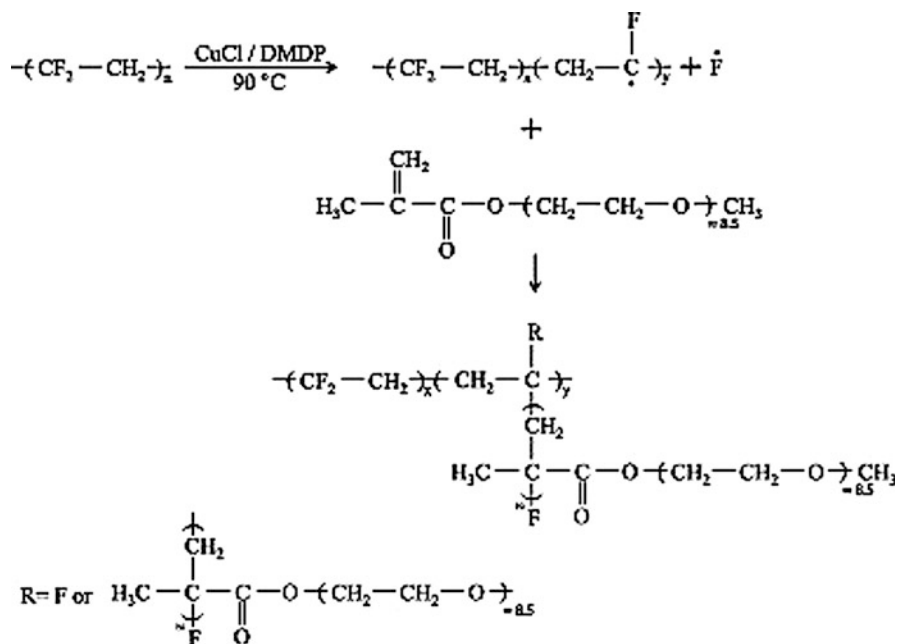
(PA) controlled the hydrophobicity of PVDF-HFP, and supposed to be responsible for low water uptake as compared to pristine PBI. The fluorine atom presence in PVDF-HFP in the blend membranes results higher proton conductivity and also enhances stability. The PA doped blend showed good mechanical stability [84].

Due to high ionic conductivity and leak proof capabilities, the polymer gel electrolytes play potential role in lithium ion batteries. Poly(vinylidene chloride-co-acrylonitrile) (PVdC-AN) and poly(methylmethacrylate) (PMMA) electrolyte blends showed good mechanical properties, less reactivity towards lithium electrode, amorphous in nature, and produces favorable passivation of ions. This polyelectrolyte blend system not only helps in electron pair formation through $C \equiv N$, $C=O$, and $C - O - C$ but also result in the formation of polymer salt complexes with cations of lithium salt, which provide a base for ionic conduction. Solvent casting technique has been used to prepare PVdC-AN based electrolyte. The ionic conductivity of $0.398 \times 10^{-6} \text{ Scm}^{-1}$ was achieved by using EC plasticizer (60 wt%) to PVdC-AN/PMMA blend, and increases the ionic conductivity with increasing the temperature in a linear fashion. It was also found that the plasticizer helps lithium salts remained in the amorphous region of the polymer. FT-IR and thermal analysis also confirmed the presence of complexes and their compositions [85].

The salt leaching method was opted to synthesize microporous polymer membrane of poly(vinylidene fluoride) (PVDF)/sodium hydrogen carbonate (NaHCO_3). The microporous polymer electrode was synthesized by dissolving all the components in a mixture of solvents consisting of dimethyl carbonate (DMC), propylene carbonate (PC), and diethylene carbonate (DEC) in the presence of salt, lithium trifluoromethane sulfonate (LiCF_3SO_3). The lithium salt containing membranes have AC conductivity of $1.34 \times 10^{-5} \text{ Scm}^{-1}$ (GPE100). The stability of the electrolyte was observed at extreme potentials with insignificantly small currents, e.g., $35 \mu\text{A}/\text{cm}^2$ at 4.0 V vs. Li/Li^+ . The potential window in the range of 3.0–4.0 V have shown no peaks [86]. The transport phenomenon has been studied for the polymer blend PVA-chitosan in proton batteries. The preparation of the electrolyte was carried out by solution casting method. It is seen that PVA (36 wt%), chitosan (24 wt%) blend was doped in NH_4NO_3 (40 wt%) showed the highest conductivity at room temperature. The observed conductivity was around $2.07 \times 10^{-5} \text{ Scm}^{-1}$. Further enhancement in conductivity was observed by the addition of plasticizer EC to the 60 wt% of PVA-chitosan and 40 wt% of NH_4NO_3 , and the highest conductivity was found to be $1.60 \times 10^{-3} \text{ Scm}^{-1}$.

7.3 Membrane and Plastic Industry

Moghareh Abed et al. prepared graft copolymers containing poly(vinylidene fluoride) with poly(oxyethylene methacrylate) (PVDF-g-POEM) using atom transfer radical polymerization (ATRP). The hydrophilic blends of PVDF hollow fibers produced by 5 wt% of the copolymer in PVDF spinning dope solution that resulted a pure water flux of approximately $130.5 \text{ Lm}^{-2} \text{ h}^{-1}$ having molecular weight cut-off 200 kDa (Scheme 6). The hydrophilic nature and antifouling characteristics of the



Scheme 6 Synthesis of graft copolymers poly(vinylidene fluoride) with poly(oxyethylene methacrylate) (PVDF-g-POEM) [87]. (With kind permission from Elsevier)

hollow fiber tested by flux recovery method [87]. The sorption and permeation properties were studied for mixed matrix membranes (MMMs) formed by the polymer of PIM-1 and the zeolitic imidazolate framework ZIF-8 (Fig. 11). McBain sorption microbalance and GC gas permeation apparatus was used in self-supported films of ZIF-8, and He, H₂, O₂, N₂, CO₂, and CH₄ gases were used for the permeability coefficients. It was found that increasing the amount of ZIF-8 nanoparticles into PIM-1 results increasing the free volume due to increasing cavities and loosely packed polymer chains [88].

A composite membranes prepared by varying the amount of poly(vinylidene fluoride-co-hexafluoropropene) (P(VDF-co-HFP)) and sulfonated fluorinated poly(arylene ether) (SFPAE), and explored in vanadium redox flow battery (VRFB) application. The SFPAE and P(VDF-co-HFP) showed good compatibility with each other, and P(VDF-co-HFP) enhanced thermal, mechanical, and proton selectivity. The life time of the cell in VRFB increased by 44% with an addition of 10 wt% P(VDF-co-HFP). Thus, the blend made up of SFPAE and P(VDF-co-HFP) is considered as an excellent material for producing low-cost and high-performance VRFB membranes [89].

A three membered ultrafiltration membrane has been formulated by a carboxymethyl cellulose acetate (CMCA)/cellulose acetate (CA) in the presence of 2.5 wt% polyethylene glycol through phase inversion process. The surface roughness of the CA/CMCA blend membranes were analyzed by SEM and AFM, and observed large pore sizes in upper layer and porous structures in cross-sectional area. This novel

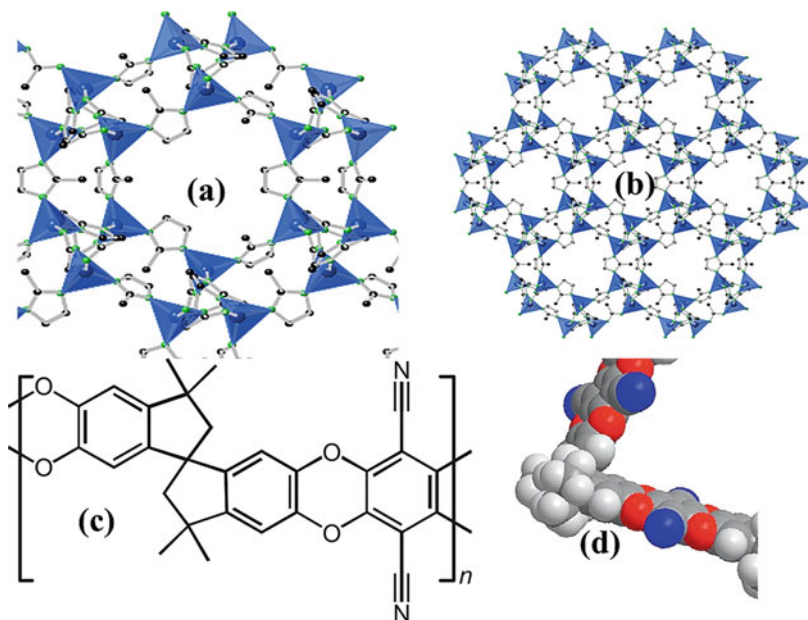
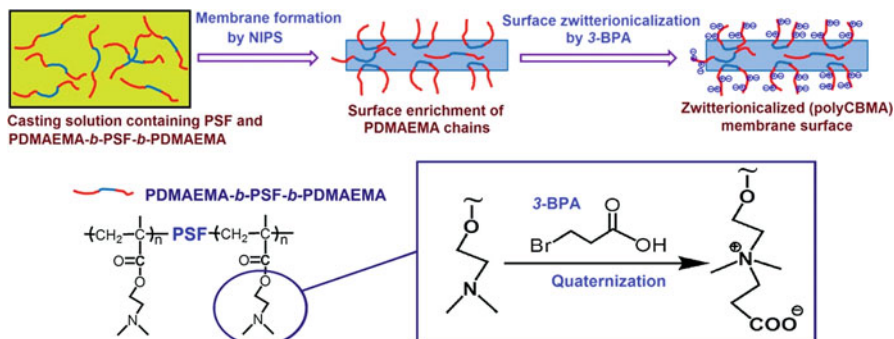


Fig. 11 (a) Magnified and (b) [1 1 1] stacking structure of ZIF-8, with tetrahedral Zn sites in blue, and the N and C atoms in green and black, respectively. (c) Molecular structure and (d) Molecular model of PIM-1

blend membrane appeared with greater ultrafiltration and low contact angle. During the introduction of rejection by blend membrane to bovine serum albumin (BSA), the fouling resistance ability was studied. It was found that this modification has positive influence [90]. A blended film of a copolymer prepared from chitosan/polyethylene glycol fumarate (chitosan/PEGF) was prepared for the evaluation of composition influence on the blending properties as wound dressing material. It is observed that blending chitosan with PEGF removed the brittleness of neat chitosan film, and AFM showed the increase of roughness on the film. Water vapor transportation rates observed in the range of $904\text{--}1447\text{ g}^{-2}\text{ day}^{-1}$ on the wounds. These membranes on wounds show powerful antibacterial activity against *Pseudomonas aeruginosa* and *Staphylococcus aureus* ($> 99.76 \pm 0.16\%$). The film composition comprising 80 wt% chitosan and 20 wt% PEGF is considered to be a suitable candidate for biomedical applications particularly as a wound dressing material [91].

Polysulfone (PSF) ultrafiltration (UF) membranes modified by PSF based block copolymer with an inclusion of additive poly(*N,N*-dimethylamino-2-ethylmethacrylate) (PDMAEMA) blocks were prepared. PDMAEMA-*b*-PSF-*b*-PDMAEMA block polymerization was carried out by condensation and ATRP process. The copolymer and the resin were blended by traditional phase inversion process to synthesize UF membranes as shown in Scheme 7. The modified polymeric chains structured on the membrane surface and pore walls, and the contact angle measurements were carried out. The result showed that the surface hydrophilicity and



Scheme 7 Synthesis of UF membranes by blending copolymer with PSF resin [92]. (With kind permission from Science Direct)

fouling resistance significantly increased. The platelets adhesion experiments results showed that there is a remarkable improvement in hemocompatibility that can lead to the potential applications of blood separation and proteins isolation [92].

7.4 Supercapacitors

Plasticized chitosan and starch blends doped with LiClO_4 have been used as polymer electrolytes for the supercapacitors. Furthermore, the ionic conductivity of non-plasticized blended chitosan/starch was found to be below the T_g of chitosan. The use of plasticizer in the biodegradable polymer increases the amorphous nature and enhances the conductivity of the blend [93]. Electrochemical double-layer capacitor (EDLC) is an inimitable device for the storage of electrical charge. It works on the principle of double-layer capacitance at the electrode/electrolyte interface where electric charges are accumulated on the electrode surfaces and ions of opposite charges are arranged on the electrolyte side. It has the ability to store considerable charge, high power density, lower charging time, long durability as well as environmental friendly features in comparison with the conventional capacitors [94–96]. In 2008, Li et al. reported starch-derived activated carbon electrodes as a promising material for EDLCs [97]. This study not only discussed the effect of temperature on biodegradable blend polymer electrolytes but also discussed the pore size effect of activated carbon for a virtuous carbon based supercapacitor. The blend ratio containing chitosan (60 wt%) showed the conductivity of $3.7 \times 10^{-4} \text{ Scm}^{-1}$. The activation energy measured through the Arrhenius plot was found to be 0.52–0.75 eV. The fabricated supercapacitors have shown reasonably good electrical performance at room temperature like energy density and specific capacitance of 133 Fg^{-1} . It is evident from the galvanostatic studies that the different current density has a significant impact on charge – discharge time. The capacitance of the capacitor is dependent on the affinity of electrolyte towards salt, electrode material under different temperature and ionic conductivity [98].

The multilayer materials were prepared by electrodeposition technique using layer by layer (LbL) deposition of poly (3, 4-ethylenedioxythiophene) (PEDOT) and poly(*N*-methylpyrrole) (PNMPy). This multilayer capacitor showed high ability to store charges and electrochemical behavior in comparison to individual polymeric capacitors. It was seen that the synergistic effect produced by the favorable interactions of PEDOT and PNMPy at the interfaces, and increase in number of layers resulted to enhance charge storage efficiency. It has also been experimentally proven that ml-PEDOT/PNMPy is acting more appropriate capacitor electrodes than the individual PEDOT and PNMPy [99].

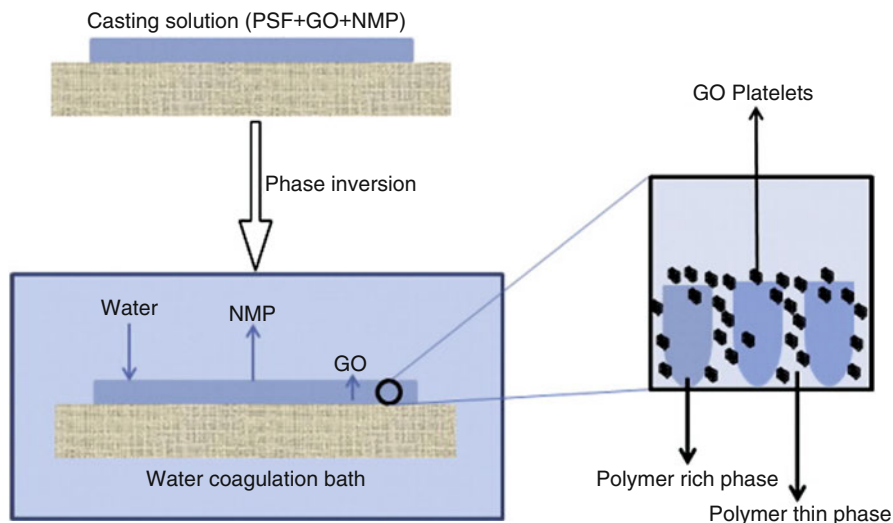
7.5 Miscellaneous Applications

Forward osmosis (FO) membranes supported on thin film composite are formed by the sulfonated polyphenylene sulphone (sPPSU) and 2.5 or 5 mol% of 3,30-disodiumdisulfate-4,40-dichlorodiphenyl sulfone (sDCDPS) monomers. The hydrophilic and sponge-like structures facilitate the membranes with characteristics to transport more water and exhibit anti-fouling properties. This new membrane enhances water flux by 4.4-fold under pressure-retarded osmosis [100].

Mollá et al. prepared sulfonated poly(etheretherketone) (SPEEK) material that has the ability to conduct good proton at higher degrees of sulfonation, and attained glass transition temperature near 200 °C. The higher amount of sulfonation also resulted in excessive swelling and dissolution in water at higher temperature which leads to limit its use in direct methanol fuel cell. Therefore, as a remedy the stable desired membrane was prepared by the addition of sulfonated blend with polyvinyl alcohol (PVA). The inclusion of PVA (more than 25 wt%) in the modified membrane resulted the stability in hot water and increase methanol permeability. While inclusion of hydrophobic polymer, polyvinylbutyral (PVB) (above 30 wt%) the resulted blend appeared to be extremely stable in boiling water but lower the proton conductivity [101].

Graphene oxide (GO) membrane was prepared from polysulfone (PSf) using wet phase inversion method. The hydrophilic properties of the membranes were studied by measuring the surface wettability and swellability. SEM analysis showed that the presences of large spaces while contact angle measurements indicate the membrane is moderate hydrophilic in nature. GO doped (2000 ppm) membranes (Scheme 8) showed improvement in Na₂SO₄ salt rejection up to 72% at 4 bar pressure. It was also found that the salt rejection phenomenon dependent on the pH and rejection efficiency increases with increase in pH [102]. Solvent Resistance nanofiltration (SRNF) membranes were also prepared from the polysulfones (PSf) which obtained from different sources via immersion precipitation. The performance of the synthesized asymmetric membranes was studied considering the effect of purity, polydispersity index (PSI) and molecular weight (MW) [103].

Solar cells based on conjugated polymer bulk heterojunction (BHJ) prepared from conjugate polymer constituted of monomers *N*-9-(heptadec-9-yl)-2,7-bis(4,4,5,5-tetramethyl-1,3,2-dioxaborolan-2-yl)-9*H*-carbazole (CzB), 3,9-bis(4,4,5,5-tetramethyl-1,3,2-dioxaborolan-2-yl)-5,11-di(*N*-heptadec-9-yl)indolo[3,2-*b*]carbazole (ICzB),



Scheme 8 Schematic diagram of GO doped membrane for usage of salt rejection [102]. (With kind permission from Science Direct)

and 2,5-di(4-(5-bromo-4-octylthiophen-2-yl)-2,1,3-benzothiadiazol-7-yl)thiophene (DTBTBr₂), attracted huge attention owing to their flexibility, easy manufacturing, low-cost, and light weight [104]. They are composed of a mixed blend of an electron-donating conjugated polymers and an electron-deficient fullerene derivatives which is a source of renewable and clean energy. In the last decades, the power conversion efficiency (PCE) of polymer solar cells (PSCs) has rapidly improved, which benefited from the design and synthesis of novel conjugated polymers (CPs), the optimization of the device fabrication process and modifying the morphology of the active layer.

Polymer complex was formed by solution casting process using the copolymer of methyl methacrylate (90 wt%) and ethyl methacrylate (10 wt%) with an incorporation of sodium iodide. By addition of sodium iodide, the ionic conductivity ($5.19 \times 10^{-6} \text{ Scm}^{-1}$) and T_g of the polymer complex increases up to 20%. However, the further increase in sodium iodide led to decrease in conductance due to cross-linked effects. LSV analysis showed that copolymer electrolytes were stable electrochemically up to voltage 2.5 V, and the efficiency of this material was found to be only 0.65% [105].

8 Conclusion

A polymer blend is a mixture of two or more polymers that usually blended together by a readily available and cheap polymer blending process to create a new material with different physical properties. In this review chapter, we have provided a comprehensive overview on history, types, miscibility, phase separation, morphology, application, and other fundamental properties of polymer blends, using a wide range

of state-of-the-art techniques. These days' different polymer blend systems received huge importance in industrial and domestic applications due to their unique mechanical, electrical, and optical properties.

Acknowledgments The authors would like to gratefully acknowledge King Fahd University of Petroleum & Minerals (KFUPM) for providing excellent research facilities, and Deanship of Scientific Research, KFUPM, Saudi Arabia for financial assistance to carry out this research through internal grant project No. IN161036.

References

1. P.J. Flory, *Principles of Polymer Chemistry* (Cornell University Press, Ithaca, 1953)
2. A.D. Jenkins, P. Kratochvíl, R.F.T. Stepto, U.W. Suter, Glossary of basic terms in polymer science (IUPAC recommendations, 1996). *Pure Appl. Chem.* **68**, 2287–2311 (1996)
3. L.A. Utracki, History of commercial polymer alloys and blends (from a perspective of the patent literature). *Polym. Eng. Sci.* **35**, 352–417 (1995)
4. T. Kyu, H. Xu, T. Guo, G. Wang, *Encyclopedia of Polymer Blends* (Wiley-VCH, Weinheim, 2010)
5. L.A. Utracki, *Commercial Polymer Blends* (Springer, Boston, 1998)
6. P. Freyburger: Improvement in kneading-eviachines, US Patent, 180568 A (1876)
7. E.M. Chaffee: Making rubber fabrics, US Patent 16 (1836)
8. J.L. White, Development of internal-mixer Technology for the Rubber Industry. *Rubber Chem. Technol.* **65**, 527–579 (1992)
9. BCC Research Report (2013) <https://www.bccresearch.com/market-research/plastics/engineering-resins-polymer-alloys-blends-pls020c.html>. Date retrieved 18 Aug 2015
10. J. Li, G. Ma, J. Sheng, Linear viscoelastic characteristics of in situ compatibilized binary polymer blends with viscoelastic properties of components variable. *J. Polym. Sci. B Polym. Phys.* **48**, 1349–1362 (2010)
11. P.J. Flory, Thermodynamics of high polymer solutions. *J. Chem. Phys.* **10**, 51 (1942)
12. E. Manias, L.A. Utracki, Thermodynamics of polymer blends, in *Polymer Blends Handbook*, (Springer, Dordrecht, 2014), pp. 171–289
13. P.J. Sabu Thomas, Y. Grohens, *Characterization of Polymer Blends: Miscibility, Morphology and Interfaces* (Wiley-VCH, Weinheim, 2014), p. 994
14. I.C. Sanchez, *Polymer Blends*, vol 1 (Academic Press, New York, 1978)
15. J. Yang, L. An, T. Xu, The glass transition temperatures of PS/PPO blends: Couchman volume-based equation and its verification. *Polymer* **42**, 7887–7892 (2001)
16. K.R. Sharma: In: Polym. Blends Copolym. 214th ACS Natl. Meet, ACS, Dallas (1998)
17. P. Shi, R. Schach, E. Munch, H. Montes, F. Lequeux, Glass transition distribution in miscible polymer blends: From calorimetry to rheology. *Macromolecules* **46**, 3611–3620 (2013)
18. Y. Yu, K.J. Choi, Crystallization in blends of poly(ethylene terephthalate) and poly(butylene terephthalate). *Polym. Eng. Sci.* **37**, 91–95 (1997)
19. P. Maiti, A.K. Dikshit, A.K. Nandi, Glass-transition temperature of poly(vinylidene fluoride)-poly(methyl acrylate) blends: Influence of aging and chain structure. *J. Appl. Polym. Sci.* **79**, 1541–1548 (2001)
20. L. Messe, R.E. Prud'homme, Orientation and relaxation study of polystyrene: Polystyrene/poly(phenylene oxide) blends. *J. Polym. Sci. B Polym. Phys.* **38**, 1405–1415 (2000)
21. W. Dong, M. He, H. Wang, F. Ren, J. Zhang, X. Zhao, Y. Li, PLLA/ABS blends compatibilized by reactive comb polymers: Double T_g depression and significantly improved toughness. *ACS Sustain. Chem. Eng.* **3**, 2542–2550 (2015)
22. H. Wang, W. Dong, Y. Li, Compatibilization of immiscible polymer blends using in situ formed janus nanomicelles by reactive blending. *ACS Macro Lett.* **4**, 1398–1403 (2015)

23. W.N. Kim, C.M. Burns, Compatibility studies of polystyrene–polybutadiene blends by thermal analysis. *J. Appl. Polym. Sci.* **32**, 2989–3004 (1986)
24. Y. Shi, Phase behavior of polyamide 6/612 blends. *SPE ANTEC™ Indianapolis* **1**, 76–80 (2016)
25. A.P. Azevedo De Carvalho, A. Da, S. Sirqueira, Effect of compatibilization in situ on PA/SEBS blends. *Polimeros* **26**, 123–128 (2016)
26. A. Al-Jabareen, S. Illescas, M.L. Maspocho, O.O. Santana, Effects of composition and transesterification catalysts on the physico-chemical and dynamic properties of PC/PET blends rich in PC. *J. Mater. Sci.* **45**, 6623–6633 (2010)
27. R.D. Boyd, J.P.S. Badyal, Silent discharge treatment of immiscible polystyrene/polycarbonate polymer blend surfaces. *Macromolecules* **30**, 3658–3663 (1997)
28. D.R. Paul, J.W. Barlow, A binary interaction model for miscibility of copolymers in blends. *Polymer* **25**, 487–494 (1984)
29. K.R. Sharma, Mathematical modeling of partially miscible copolymers in blends. *Polym. Mater. Sci. Eng.* **78**, 193–198 (1998)
30. P.R. Couchman, Compositional variation of glass-transition temperatures. 2. Application of the thermodynamic theory to compatible polymer blends. *Macromolecules* **11**, 1156–1161 (1978)
31. R.V. Sekharan, B.T. Abraham, E.T. Thachil, Utilization of waste expanded polystyrene: Blends with silica-filled natural rubber. *Mater. Des.* **40**, 221–228 (2012)
32. Z. Starý, T. Pemsel, J. Baldrian, H. Münstedt, Influence of a compatibilizer on the morphology development in polymer blends under elongation. *Polymer* **53**, 1881–1889 (2012)
33. B.M. Wood, S.R. Coles, S. Maggs, J. Meredith, K. Kirwan, Use of lignin as a compatibiliser in hemp/epoxy composites. *Compos. Sci. Technol.* **71**, 1804–1810 (2011)
34. A.I. Khalf, D.E.E. Nashar, N.A. Maziad, Effect of grafting cellulose acetate and methyl-methacrylate as compatibilizer onto NBR/SBR blends. *Mater. Des.* **31**, 2592–2598 (2010)
35. B. Kouini, A. Serier, Properties of polypropylene/polyamide nanocomposites prepared by melt processing with a PP-g-MAH compatibilizer. *Mater. Des.* **34**, 313–318 (2012)
36. IUPAC, Definitions of terms relating to the structure and processing of sols, gels, networks, and inorganic-organic hybrid materials. *Pure Appl. Chem.* **79**(1801) (2007)
37. IUPAC, Polymer blend, in *IUPAC Compend. Chem. Terminol.* (IUPAC, Research Triangle Park, 1996)
38. F.W. Billmeyer, *Textbook of Polymer Science*, 2nd edn. (Wiley-Interscience, New York, 1971), p. 598
39. R. Casper, L. Morbitzer, Struktur und eigenschaften von mehrphasenkunststoffen I. Verträglichkeit von polymeren im festen zustand. *Angew. Makromol. Chemie.* **58**, 1–35 (1977)
40. M.L. Huggins, Thermodynamic properties of liquids, including solutions. IX. Thermodynamic properties of polymer solutions. *Polym. J.* **4**, 502–514 (1973)
41. E. Díez, G. Ovejero, M.D. Romero, I. Díaz, Polymer–solvent interaction parameters of SBS rubbers by inverse gas chromatography measurements. *Fluid Phase Equilib.* **308**, 107–113 (2011)
42. H. Patil, R.V. Tiwari, M.A. Repka, Hot-melt extrusion: From theory to application in pharmaceutical formulation. *AAPS Pharm. Sci. Tech.* **17**, 20–42 (2016)
43. J.L. White, S.H. Bumm, Polymer blend compounding and processing, in *Encyclopedia of Polymer Blends*, vol. 2, (Wiley-VCH, Weinheim, 2011), pp. 1–26
44. D.H. Killheffer, *Banbury the Master Mixer*, vol 6 (Palmerton, New York, 1962)
45. U. Siemann, *Solvent Cast Technology – A Versatile Tool for Thin Film Production*, vol 130 (Springer, Berlin/Heidelberg, 2005), pp. 1–14
46. G. Zhu, F. Wang, K. Xu, Q. Gao, Y. Liu, Study on properties of poly(vinyl alcohol)/polyacrylonitrile blend film. *Polímeros Ciência E Tecnol.* **23**, 146–151 (2013)
47. N. Ignjatović, V. Wu, Z. Ajduković, T. Mihajilov-Krsteš, V. Uskoković, D. Uskoković, Chitosan-PLGA polymer blends as coatings for hydroxyapatite nanoparticles and their effect

- on antimicrobial properties, osteoconductivity and regeneration of osseous tissues. *Mater. Sci. Eng. C Mater. Biol. Appl.* **60**, 357–364 (2016)
48. K. Guo, H. Qi, F. Wang, Y. Zhu, Fabrication of boron- and nitrogen-doped carbon nanoparticles by stress from pyrolysis of borazine-containing arylacetylene. *RSC Adv.* **4**, 6330–6336 (2014)
49. R.A.A. Muzzarelli, M. El Mehtedi, M. Mattioli-Belmonte, Emerging biomedical applications of nano-chitins and nano-chitosans obtained via advanced eco-friendly technologies from marine resources. *Mar. Drugs* **12**, 5468–5502 (2014)
50. J.P. Tomba, X. Ye, F. Li, M.A. Winnik, W. Lau, Polymer blend latex films: Miscibility and polymer diffusion studied by energy transfer. *Polymer* **49**, 2055–2064 (2008)
51. J. Feng, M.A. Winnik, R.R. Shivers, B. Clubb, Polymer blend latex films: Morphology and transparency. *Macromolecules* **28**, 7671–7682 (1995)
52. M. Hajian, C. Sadmoghagheh, G. Scott, Polymer blends—IV. *Eur. Polym. J.* **20**, 135–138 (1984)
53. A.L.B. Ramirez, Z.S. Kean, J.A. Orlicki, M. Champhekar, S.M. Elsagr, W.E. Krause, S.L. Craig, Mechanochemical strengthening of a synthetic polymer in response to typically destructive shear forces. *Nat. Chem.* **5**, 757–761 (2013)
54. J.V. Alemán, A.V. Chadwick, J. He, M. Hess, K. Horie, R.G. Jones, P. Kratochvíl, I. Meisel, I. Mita, G. Moad, S. Penczek, R.F.T. Stepto, Definitions of terms relating to the structure and processing of sols, gels, networks, and inorganic-organic hybrid materials (IUPAC recommendations 2007). *Pure Appl. Chem.* **79**, 1801–1829 (2007)
55. L.H. Sperling, *Introduction to Physical Polymer Science*, 2nd edn. (Wiley, New York, 2015)
56. S.F. Wang, X. Li, R.L. Agapov, C. Wesdemiotis, M.D. Foster, Probing surface concentration of cyclic/linear blend films using surface layer MALDI-TOF mass spectrometry. *ACS Macro Lett.* **1**, 1024–1027 (2012)
57. L. Dou, Y. Liu, Z. Hong, G. Li, Y. Yang, Low-bandgap near-IR conjugated polymers/molecules for organic electronics. *Chem. Rev.* **115**, 12633–12665 (2015)
58. J.F. Masson, R.S.J. Manley, Solid-state NMR of some cellulose/synthetic polymer blends. *Macromolecules* **25**, 589–592 (1992)
59. I. Kindgren, *Compounding of Electrically Conductive Two Phase Polymer Blends* (Chalmers University of Technology, Göteborg, 2012), pp. 1–52
60. Z. Wang, C.W. Macosko, F.S. Bates, Fluorine-enriched melt-blown fibers from polymer blends of poly(butylene terephthalate) and a fluorinated multiblock copolyester. *ACS Appl. Mater. Interfaces* **8**, 754–761 (2015)
61. Q. Lv, D. Wu, H. Xie, H. Crystallization of poly(ϵ -caprolactone) in its immiscible blend with polylactide: Insight into the role of annealing histories. *RSC Adv.* **6**, 37721–37730 (2016)
62. T. Li, J. Zhang, D.K. Schneiderman, Toughening glassy poly(lactide) with block copolymer micelles. *ACS Macro Lett.* **5**, 359–364 (2016)
63. C.S. Moran, A. Barthelon, A. Pearsall, Biorenewable blends of polyamide-4,10 and polyamide-6,10. *J. Appl. Polym. Sci.* **43126**, 1–9 (2016)
64. M. Rady, E. Arquis, A comparative study of phase changing characteristics of granular phase change materials using DSC and T-history methods. *FDMP* **6**, 137–152 (2010)
65. T.M. Nair, M.G. Kumaran, G. Unnikrishna, V.B. Pillai, Dynamic mechanical analysis of ethylene-propylene-diene monomer rubber and styrene-butadiene rubber blends. *J. Appl. Polym. Sci.* **112**, 72–81 (2009)
66. A.W. Coats, J.P. Redfern, Thermogravimetric analysis. A review. *Analyst* **88**, 906–924 (1963)
67. G. Justin, A. Guiseppi-Elie, Characterization of electroconductive blends of poly(HEMA-co-PEGMA-co-HMMA-co-SPMA) and poly(Py-co-PyBA). *Biomacromolecules* **10**, 2539–2549 (2009)
68. M.K. Daletou, M. Geormezi, E. Vogli, G.A. Voyiatzis, S.G. Neophytides, The interaction of H₃PO₄ and steam with PBI and TPS polymeric membranes. A TGA and Raman study. *J. Mater. Chem. A* **2**, 1117–1127 (2014)
69. Z. Yang, C.D. Han, Rheology of miscible polymer blends with hydrogen bonding. *Macromolecules* **41**, 2104–2118 (2008)

70. A.C. Badino, M.C.R. Facciotti, W. Schmidell, Construction and operation of an impeller rheometer for on-line rheological characterization of non-Newtonian fermentation broths. *Braz. J. Chem. Eng.* **14** (1997). <https://doi.org/10.1590/S0104-66321997000400010>
71. Y.S. Lipatov, V.F. Shumsky, I.P. Getmanchuk, A.N. Gorbatenko, Rheology of polymer blends. *Rheol. Acta* **21**, 270–279 (1982)
72. C.M. Gómez, J.E. Figueruelo, A. Campos, Thermodynamics of a polymer blend solution system studied by gel permeation chromatography and viscosity. *Macromol. Chem. Phys.* **200**, 246–255 (1999)
73. S. Ameen, V. Ali, M. Zulfeqar, M. Mazharul Haq, M. Husain, Synthesis and characterization of polyaniline-polyvinyl chloride blends doped with sulfamic acid in aqueous tetrahydrofuran. *Open Chem.* **4**, 565–577 (2006)
74. B. Pukánszky, F. Tüdös, Miscibility and mechanical properties of polymer blends, *Makromol. Chemie. Macromol. Symp.* **38**, 221–231 (1990)
75. N. Aranburu, J.I. Eguiazábal, Improved mechanical properties of compatibilized polypropylene/polyamide-12 blends. *Int. J. Polym. Sci.* **2015**, 1–8 (2015)
76. P.C. Chung, P.F. Green, The elastic mechanical response of nanoscale thin films of miscible polymer/polymer blends. *Macromolecules* **48**, 3991–3996 (2015)
77. P.P. Lizymol, S. Thomas, Thermal behaviour of polymer blends: A comparison of the thermal properties of miscible and immiscible systems. *Polym. Degrad. Stab.* **41**, 59–64 (1993)
78. S. Takahashi, H. Okada, S. Nobukawa, M. Yamaguchi, Optical properties of polymer blends composed of poly(methyl methacrylate) and ethylene–vinyl acetate copolymer. *Eur. Polym. J.* **48**, 974–980 (2012)
79. G.H. Kim, D. Lee, A. Shanker, L. Shao, M.S. Kwon, D. Gidley, J. Kim, K.P. Pipe, High thermal conductivity in amorphous polymer blends by engineered interchain interactions. *Nat. Mater.* **14**, 295–300 (2015)
80. V.T. Magalad, G.S. Gokavi, C. Ranganathaiah, M.H. Burshe, C. Han, D.D. Dionysiou, M.N. Nadagouda, T.M. Aminabhavi, Polymeric blend nanocomposite membranes for ethanol dehydration—Effect of morphology and membrane–solvent interactions. *J. Memb. Sci.* **430**, 321–329 (2013)
81. M.F.Z. Kadir, S.R. Majid, A.K. Arof, Plasticized chitosan–PVA blend polymer electrolyte based proton battery. *Electrochim. Acta* **55**, 1475–1482 (2010)
82. J. Liu, W. Li, X. Zuo, S. Liu, Z. Li, Polyethylene-supported polyvinylidene fluoride–cellulose acetate butyrate blended polymer electrolyte for lithium ion battery. *J. Power Sources* **226**, 101–106 (2013)
83. C. Tao, M.H. Gao, B.H. Yin, B. Li, Y.P. Huang, G. Xu, J. J. Bao: A promising TPU/PEO blend polymer electrolyte for all-solid-state lithium ion batteries. *Electrochim. Acta* **257**, 31–39 (2017)
84. M. Hazarika, T. Jana, Novel proton exchange membrane for fuel cell developed from blends of polybenzimidazole with fluorinated polymer. *Eur. Polym. J.* **49**, 1564–1576 (2013)
85. S.M. Mathew, K. Kesavan, S. Rajendran, Structural and electrochemical analysis of PMMA based gel electrolyte membranes. *Int. J. Electrochem.* **2015**, 1–7 (2015)
86. S.Y. Jung, S.Y. Ko, J.O. Park, S. Park, Enhanced ionic polymer metal composite actuator with porous nafion membrane using zinc oxide particulate leaching method. *Smart Mater. Struct.* **24**, 037007 (2015)
87. M.R. Moghareh Abed, S.C. Kumbharkar, A.M. Groth, K. Li, Economical production of PVDF-g-POEM for use as a blend in preparation of PVDF based hydrophilic hollow fiber membranes. *Sep. Purif. Technol.* **106**, 47–55 (2013)
88. A.F. Bushell, M.P. Atfield, C.R. Mason, P.M. Budd, Y. Yampolskii, L. Starannikova, A. Rebrov, F. Bazzarelli, P. Bernardo, J. Carolus Jansen, M. Lanč, K. Friess, V. Shantarovich, V. Gustov, V. Isaeva, Gas permeation parameters of mixed matrix membranes based on the polymer of intrinsic microporosity PIM-1 and the zeolitic imidazolate framework ZIF-8. *J. Memb. Sci.* **427**, 48–62 (2013)

89. D. Chen, S. Kim, V. Sprenkle, M.A. Hickner, Composite blend polymer membranes with increased proton selectivity and lifetime for vanadium redox flow batteries. *J. Power Sources* **231**, 301–306 (2013)
90. B. Han, D. Zhang, Z. Shao, L. Kong, S. Lv, Preparation and characterization of cellulose acetate/carboxymethyl cellulose acetate blend ultrafiltration membranes. *Desalination* **311**, 80–89 (2013)
91. A. Hashemi Doulabi, H. Mirzadeh, M. Imani, N. Samadi, Chitosan/polyethylene glycol fumarate blend film: Physical and antibacterial properties. *Carbohydr. Polym.* **92**, 48–56 (2013)
92. Y.F. Zhao, L.P. Zhu, Z. Yi, B.K. Zhu, Y.Y. Xu, Improving the hydrophilicity and fouling-resistance of polysulfone ultrafiltration membranes via surface zwitterionization mediated by polysulfone-based triblock copolymer additive. *J. Memb. Sci.* **440**, 40–47 (2013)
93. M.Z.A. Yahya, A.K. Arof, Effect of oleic acid plasticizer on chitosan–lithium acetate solid polymer electrolytes. *Eur. Polym. J.* **39**, 897–902 (2003)
94. A. Manuel Stephan, Review on gel polymer electrolytes for lithium batteries. *Eur. Polym. J.* **42**, 21–42 (2006)
95. A. Burke, Ultracapacitors: Why, how, and where is the technology. *J. Power Sources* **91**, 37–50 (2000)
96. M. Winter, R.J. Brodd, What are batteries, fuel cells, and supercapacitors. *Chem. Rev.* **104**, 4245–4270 (2004)
97. Q. Li, H. Wang, Q. Dai, J. Yang, Y. Zhong, Novel activated carbons as electrode materials for electrochemical capacitors from a series of starch. *Solid State Ionics* **179**, 269–273 (2008)
98. Y.N. Sudhakar, M. Selvakumar, Lithium perchlorate doped plasticized chitosan and starch blend as biodegradable polymer electrolyte for supercapacitors. *Electrochim. Acta* **78**, 398–405 (2012)
99. D. Aradilla, F. Estrany, C. Alemán, Symmetric supercapacitors based on multilayers of conducting polymers. *J. Phys. Chem. C* **115**, 8430–8438 (2011)
100. N. Widjojo, T.-S. Chung, M. Weber, C. Maletzko, V. Warzelhan, A sulfonated polyphenylenesulfone (sPPSU) as the supporting substrate in thin film composite (TFC) membranes with enhanced performance for forward osmosis (FO). *Chem. Eng. J.* **220**, 15–23 (2013)
101. S. Mollá, V. Compañ, Polymer blends of SPEEK for DMFC application at intermediate temperatures. *Int. J. Hydrog. Energy* **39**, 5121–5136 (2014)
102. B.M. Ganesh, A.M. Isloor, A.F. Ismail, Enhanced hydrophilicity and salt rejection study of graphene oxide-polysulfone mixed matrix membrane. *Desalination* **313**, 199–207 (2013)
103. A.K. Hořda, M. De Roeck, K. Hendrix, I.F.J. Vankelecom, The influence of polymer purity and molecular weight on the synthesis of integrally skinned polysulfone membranes. *J. Memb. Sci.* **446**, 113–120 (2013)
104. J. Tong, P. Guo, H. Zhang, J. Li, P. Zhang, C. Yang, D. Chen, Y. Xia, Synthesis of modified benzothiadiazole-thiophene-cored acceptor and carbazole/indolocarbazole alternating conjugated polymers and their photovoltaic applications. *Polym. Bull.* **72**, 565–581 (2015)
105. N. Dzulkurnain, A. Ahmad, N. Mohamed, P(MMA-EMA) random copolymer electrolytes incorporating sodium iodide for potential application in a dye-sensitized solar cell. *Polymers (Basel)* **7**, 266–280 (2015)



Abd Almonam Baleg, Milua Masikini, Suru Vivian John,
Avril Rae Williams, Nazeem Jahed, Priscilla Baker, and
Emmanuel Iwuoha

Contents

1	Nature of Conducting Polymer Materials	552
2	Conducting Polymers and Their Properties	552
2.1	Electronic Classification	554
2.2	Band Theory	555
3	Conductivity	559
3.1	The Hopping Process	560
3.2	Solitons, Polarons, and Bipolarons	561
4	Synthesis and Characterization of Conducting Polymers	563
4.1	Polypyrrole	564
4.2	Polythiophene and Its Derivatives	565
5	Principal Conducting Polymers	566
5.1	Polypyrrole (PPy)	566
5.2	Polythiophene (PTh)	568
5.3	Poly(3,4-ethylenedioxythiophene) (PEDOT)	569
5.4	Polyfuran (PFu)	570
5.5	Polyaniline (PANI)	571
6	Conducting Copolymers	573
6.1	Conducting Star Copolymers	574
6.2	Dendrimer Star Copolymers	575
7	Conducting Polymer-Based Composites	581

A. A. Baleg · M. Masikini · S. V. John (✉) · N. Jahed
Department of Chemistry, University of the Western Cape, Bellville, South Africa
e-mail: jv4real44@gmail.com

A. R. Williams
Department of Biological and Chemical Sciences, The University of the West Indies,
Cave Hill, Barbados

P. Baker · E. Iwuoha (✉)
SensorLab, Department of Chemistry, University of the Western Cape, Bellville, South Africa
e-mail: eiwuoha@uwc.ac.za

7.1	Polyaniline–Carbon Nanotubes Composites (CNCs)	581
7.2	Synthesis of the Composites	582
7.3	Interactions Between PANI and CNT	587
8	Conclusions	588
	References	589

Abstract

Conducting polymers (CPs) characteristically form polarons, bipolarons, or solitons and exhibit low band-gap energies. These properties make them to be suitable materials for applications in sensors, semiconductors, anticorrosion coatings, batteries, and display devices, among others. This chapter focuses on the electronics, electrochemistry, and processability of some commonly used CPs in the recent past – namely, polyaniline (PANI), polypyrrole (PPy), polythiophene (PTh), poly(3,4-ethylenedioxythiophene) (PEDOT), and polyfuran (PFu). Also included in the chapter are conducting dendritic star copolymers and polymeric nanocomposites incorporating single-walled and multiwalled carbon nanotubes.

1 Nature of Conducting Polymer Materials

Since the early 1970s, researchers have been focussed on the task of identifying organic solids that exhibit remarkable conducting properties. These organic compounds, with the ability to effectively transfer charge, can be divided into three main groups: radical-ion salt charge-transfer complexes, carbon-based small molecules, and conjugated conducting polymers (CPs). Conducting polymers (more commonly termed *synthetic metals*) are organic polymers that exhibit highly reversible redox behavior and demonstrate the properties of both metals and plastics. CPs gained in popularity owing to their interesting electrical and optical properties, which had previously only been observed in inorganic systems. One of the most remarkable features of CPs is their ability to be nanostructurally tailored for more specialized applications, through innovatively manipulated synthetic transformations. This flexibility has resulted largely in the replacement of traditional inorganic conducting materials with CPs, which, through blending or composite formation, have introduced improved processability, mechanical properties, and stability. These enhancements have allowed CPs to have practical application in various fields, including electromagnetic shielding and microwave absorption [1, 2], static electricity dissipation, heating elements [3], membrane materials [4], paint coatings for anticorrosion protection [5, 6], sensor materials, and molecular devices [7]. This chapter provides an examination of CPs and composites — their properties, synthesis, and applications. In addition, conducting star copolymers, dendritic star copolymers and dendrimers are also explored as they are inextricably connected to their progenitor molecules (the CPs).

2 Conducting Polymers and Their Properties

Conducting polymers (CPs) typically contain a linear backbone of repeating conjugated monomers as the fundamental structural unit, as exemplified by polyacetylene (PAC), polypyrrole (PPy), polyaniline (PANI), and polythiophene (PTh) [8, 9]. Two general

types of conducting polymers exist. The first is a composite material (with dimensions in the nanometre range) that engages a polymer to hold together conductive filler-like metal flakes [10]. Typical examples of conductive components used to prepare this type of CP include conducting solids (carbon black, carbon fibres, aluminium flakes, stainless steel fibers, metal-coated fillers, metal particles, etc.) and conjugated conducting polymers. The latter can be had via polymerization at an electrode (anode) surface coated with a nonconducting polymer film [11]. These conducting nanocomposites (CNCs) can be synthesized from a variety of metals and conjugated polymers as well as oligomers and have attracted considerable interest because of the possibility of using them to create suitable materials for electrocatalysis, microelectronics, and chemical sensors [12]. The second group of CPs consists of a set of polymers whose backbones constitutionally propagate charge, making the polymer itself conductive [13]. The conductivity arises from the chemical bonding which produces an unpaired π -electron per carbon atom in the backbone of the polymer. The carbon atoms are π -bonded in an sp^2p_z hybridized configuration, where the orbitals of successive carbon atoms overlap, providing for delocalization of the electrons along the polymer chain [14]. Consequently, charge mobility is exerted along the polymer backbone, introducing properties such as electrical conductivity, low-energy optical transitions, low ionization potential, and high electron affinity. During doping (addition of known quantities of chemical species) and polymerization of CPs, the π -bonds are highly susceptible to chemical and electrochemical oxidation and/or reduction processes leading to the formation of nonlinear defects, namely, solitons, polarons, and bipolarons, all of which contribute to the electrical conduction in these polymeric materials [15–18].

CPs like PPy, PAC, PTh, and PANI have undergone extensive development over the past 25 years. Thus, organic conducting and semiconducting polymers can now be synthetically bespoke to optimize desirable properties such as melting point, melt viscosity, solubility, electrical and thermal conductivity, etc. Although found in oligomers of 4–10 repeating units, enhanced electrically conductive properties are frequently observed in polymers (e.g., CPs) with hundreds or thousands of repeating units by virtue of the long range ordering of the polymer chains in the solid state [19].

For CPs to be useful in multifarious applications, they need to have excellent electrical and mechanical properties, solution or melt processability, and high environmental stability. Conducting polymer composites (CPCs), resulting from the blending of an insulating polymer matrix with an electrical conductive filler (carbon black, carbon fibers, metal particles), show many interesting features owing to their electrical resistivity variations with temperature [20–22]. For instance, changing the nature of the positive temperature coefficient (PTC) effect, i.e., transition temperature and amplitude, allows for the adjustment of the CPC properties, thereby potentially giving access to a wider range of applications. As such, self-regulated heating can be coerced in a CPC with a sharp positive temperature coefficient effect. Moreover, these materials have the ability to withstand corrosion and can be prepared using common plastics processing techniques such as extrusion or injection. A list of CPs widely in use today are shown in Fig. 1 and include the well-known PAC, poly(3-alkyl-thiophene), PPy, and PANI [23].

Since the early 1990s, CPs have been reported to function as thin films for batteries, capacitors, light-emitting diodes, ion-selective electrodes, and solid-state

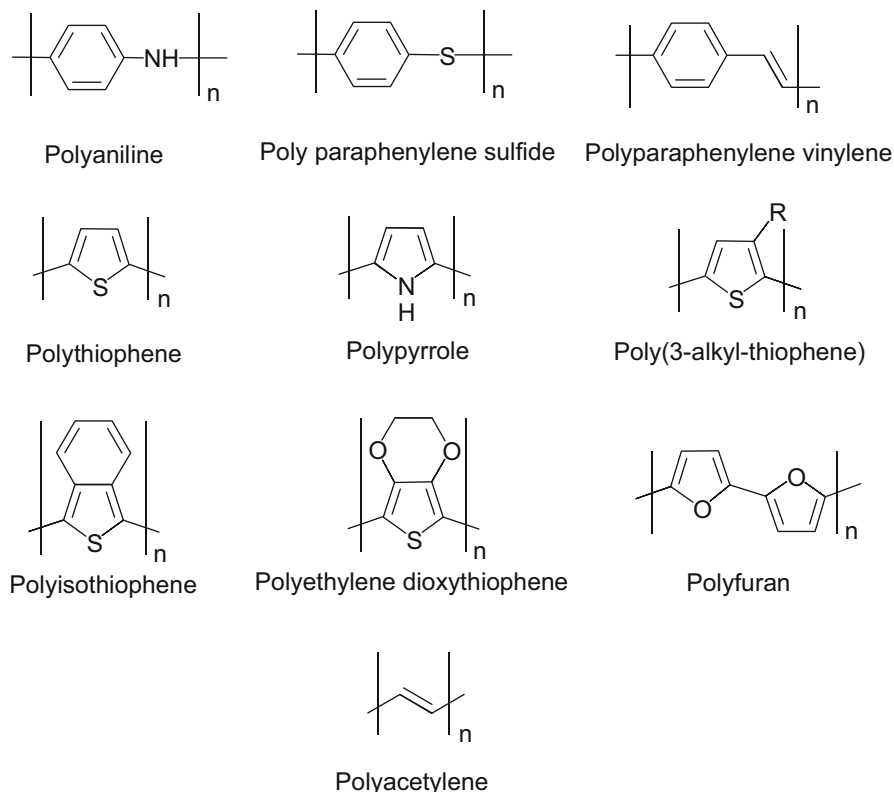


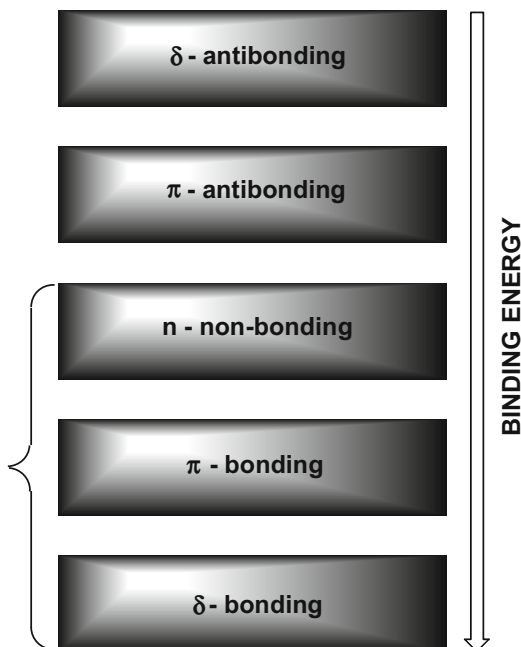
Fig. 1 Chemical structures of common conducting polymers (CPs)

devices [24, 25]. Recently, the application of CPs has extended to include sensors, actuator components in microsurgical tools, controlled drug delivery systems, corrective implantable aids, lifelike prosthetic limbs, actuators, and artificial muscles [26]. It is worth noting that a change in emphasis in the area of materials science and chemistry has opened the doorway to new approaches in analytical sensing, which influences the design of sensors, particularly those that employ electrochemical or spectroscopic transduction methods. Specifically, conducting polymers are frequently used in environmental monitoring and clinical diagnostics to achieve fast detection, high sensitivity, small size and specificity for investigation of a particular analyte through the use of electrochemical sensors [27] and biosensors [28].

2.1 Electronic Classification

Electrons are essential for conductivity and can be loosely categorized into one of four groups. The first type – core electrons – primarily exists close to the nucleus and are rarely removed owing to the relatively large magnitude of the effective nuclear charge felt by these electrons.

Fig. 2 Binding energy levels of σ , π , and n electron states for organic molecules. (Redrawn from Ref. [29])



σ -Electrons constitute the chemical bonds that are responsible for maintaining the structural integrity of the molecule. Nonbonding or n-electrons are usually associated with the lone pairs present on the atoms of some elements and can influence the susceptibility of a bond to reaction. Weaker and less-localized connections than the internuclear bonds of σ -electrons are also present upon the birth of molecules. These entities, known as π -electrons, are likewise involved in bonding but are often thought of as being “free” (delocalized) and hence require the least amount of energy to jump to the next energy state (Fig. 2). This π -electron “cloud” enables conduction and polymers that contain π -electrons, through double bonds, are known as conjugated polymers.

2.2 Band Theory

Band theory is widely used to explain electrical conductivity as it describes the energy states of electrons. When two identical atoms, each having a partially-filled orbital, are brought together, the two atomic orbitals interact to produce two new (molecular) orbitals – one of lower energy and one of higher energy. Two electrons occupy the lower energy orbital. The (now-filled) orbital of lower energy is a bonding orbital and the higher energy (empty) orbital is an antibonding orbital. The magnitude of the energy difference between the highest of the low-energy orbitals (highest occupied molecular orbital – HOMO) and the lowest of the high-energy orbitals (lowest unoccupied molecular orbital – LUMO) is called the energy band gap (E_g).

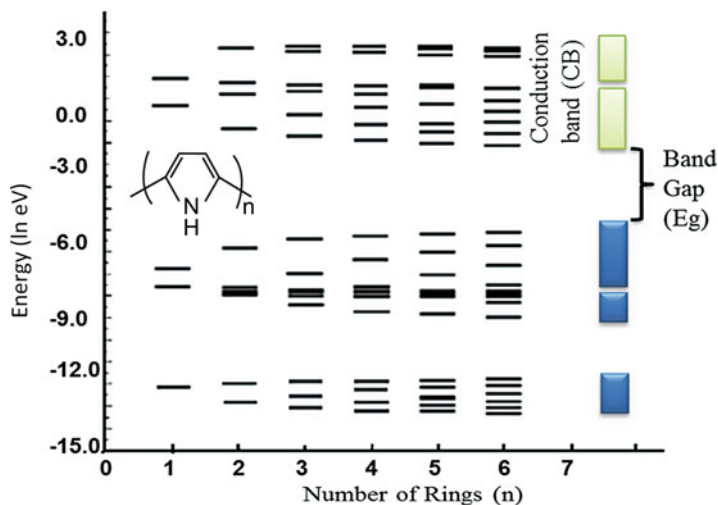


Fig. 3 The origin of band structure in polypyrrole. (Redrawn from Ref. [30])

As shown in Fig. 3, for the PPy system [30], molecular orbital perturbation effects lead to energy states that are comparable. As the length of the polymer chain increases progressively from one to infinity, the occupied valence orbitals form continuous bands called valence bands (VBs), and the empty orbitals coalesce into continuous bands referred to as conduction bands (CBs).

In other words, E_g is the energy difference between the highest energy eigenstate of the valence band (VB) and the lowest energy eigenstate of the conduction band (CB) and represents the minimum energy that is required to excite an electron up into the conduction band where it can participate in the conveyance of charge (Fig. 3). To maintain conductivity, valence electrons must move to the CB through this gain in energy.

In band theory, depending on the size of the energy gap (E_g), the material can be an insulator or a semiconductor (Fig. 4). An insulator has electrons in the valence band that are separated by a large band gap from the conduction band. Hence, these electrons are prevented from participating in conduction. Semiconductors, whose conductivities can range from 10^3 to 10^{-9} S.cm⁻¹, usually have energy gaps ≤ 1 eV. They are mainly inorganic, crystalline solids, and the magnitude of the energy gap is such that electrons may be thermally excited across it into the empty upper band, where they can conduct, leaving holes in the lower band, which can also contribute to conductivity [31].

Contrastingly, a conductive material such as a metal has overlapping of the conduction and valence bands. This means that orbitals are freely available and electrons are “free” to move into the conduction band, increasing the possibility of transference of charge. Metals generally have conductivities of order of magnitude of 10^6 S.cm⁻¹, while insulators are at the other end of the conductivity gamut with magnitudes around 10^{-22} S.cm⁻¹ owing to their very large band gap which renders thermal excitation impossible.

Highly conjugated CPs can display semiconductor properties without the inorganic, crystalline structure. The difference between band energy levels in these materials is such that the bands may be regarded as being continuous, and the electrons can adopt any energy that falls within the upper and lower boundaries of the bands. Both inorganic solids and CPs can be doped using charged chemical species [32, 33] to increase the conductivity (Fig. 5); however, the concentration of dopant is the discerning factor; in the case of semiconductors of the crystalline type, concentrations usually lie in the parts per million (ppm) order of magnitude while the polymer type can have dopant constituents, the concentration levels of which are as high as 50% (relative to the weight of the polymer).

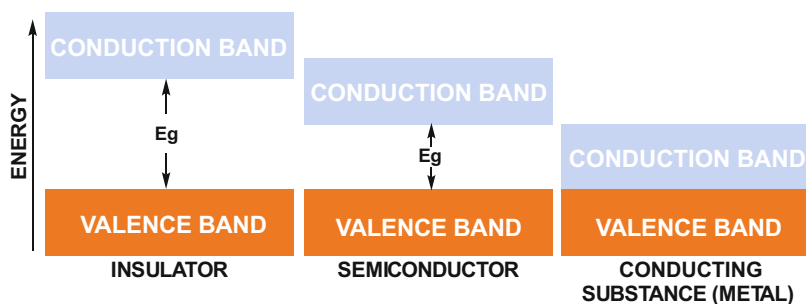
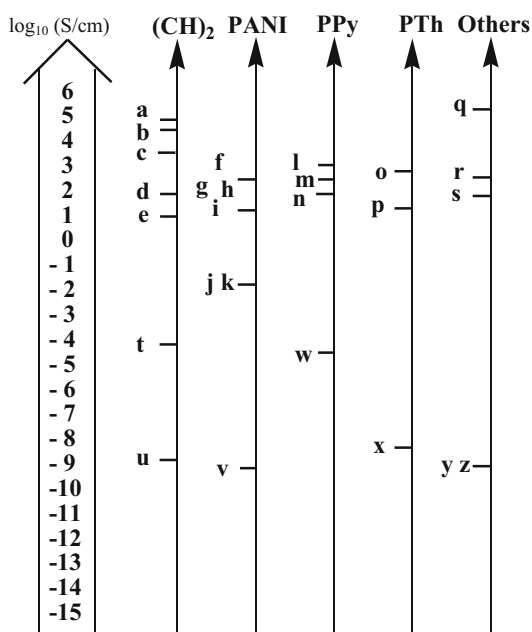


Fig. 4 Energy gap representation of an insulator, a semiconductor, and a metal

Fig. 5 The conductivity of various conducting polymers at 24 °C. (a–e) forms of [CH(I₃)_x], (f–k) forms of PANI, (l, m) PPy doped with PF₆, (n) PPy (TSO), (o, p) forms of PTh, (q) PPV (H₂SO₄), (r) PPP (AsF₅), (s) Kr-implanted poly(phenylenebenzobisazole), (t–z) undoped versions of the respective polymers [32] with kind permission of Cambridge University Press.



2.2.1 Band Theory of Conductive Polymers

While traditional band models have prevailed, for the most part, in explaining the semiconductor physics of inorganic crystalline materials, they have tended to break down when applied to CPs. Although it has been postulated [34] that conducting polymers and conducting inorganic crystalline materials have similar properties, fundamental differences lie in how the electrons move from one location to another. For instance, oxidation or reduction of CPs creates structural deformations along the polymer backbone, where transmission of charge will most likely occur.

When an electron in the valence band of a conducting polymer is exposed to a stimulus that causes it to become excited, a polaron forms. Generally speaking, a polaron is a spin-bearing charge-carrier that is typically linked with radical cations or radical anions. It is thought to consist of two defects – a charged defect (ion) and a neutral defect (radical) (Fig. 6a). Instead of the energized electron leaving a completely empty hole, partial delocalization occurs to offset the new energy level created by the excited electron. This deconfinement of the electrons means that the surrounding monomer units become anatomically distorted – a polaron [35]. Further, conductivity is influenced by the number of polarons (or other quasiparticles such as bipolarons or solitons) generated in the material and their movement across the mass of the material. Doping can, therefore, influence the conductivity of a material as defects in the form of radical cations or anions are introduced.

At low doping levels, charges are stored as polarons and bipolarons (Fig. 6) and so beget an electrically conductive partially filled band. For most conducting polymers such as PPy, bipolarons (pairs of defects) are created when two polarons form on the same polymer chain [38] and since PPy is a highly disordered polymer there are as many as one defect for every three rings [37]. Polarons and bipolarons can also hop to nearby chains to carry the electric current. In single polaron hopping, only one electron moves back and forth between two defect states whereas in bipolaron hopping, two electrons migrate simultaneously between two randomly created defect states. When

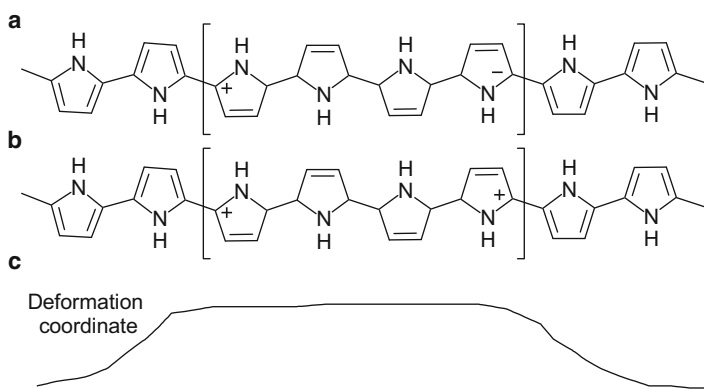


Fig. 6 Schematic of (a) a polaron and (b) a bipolaron on a PPy chain. (c) The bottom schematic represents the deformation of the polymer lattice created from the charge defect. (Redrawn from Refs. [36, 37])

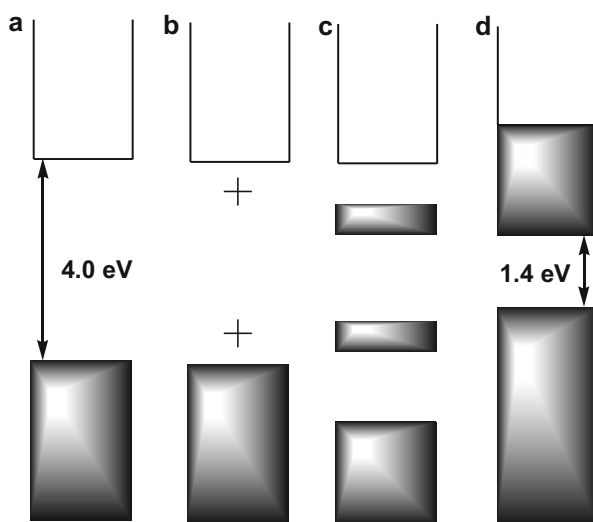
PPy is oxidized and becomes more conductive, it is a polycation with many of these delocalized positive charges (defects) on its backbone, countered by dopant anions.

3 Conductivity

The conductivity of polypyrrole (PPy) can range from nothing tangible ($\sim 10^{-5} \Omega^{-1}\text{cm}^{-1}$) as found in insulators, to $100 \Omega^{-1}\text{cm}^{-1}$ [37]. Electrical conductivity in conducting polymers (CPs) involves movement of positively charged carriers or electrons along polymer chains and hopping of these carriers between chains. It is generally believed that the interchain hopping resistance is much greater than the intrachain transport resistance. PPy is conductive because of the ability of electrons to hop along and across the polymer chains owing to the π -conjugating bonds. In spite of these simple generalizations, conductivity within conducting electroactive polymers is a complex issue. A polymer that can exhibit conductivity across a range of some 15 orders of magnitude, most likely utilizes different mechanisms under different conditions. In addition to the electronic conductivity exhibited by conducting electroactive polymers, ionic conductivity, owing to the solvent/electrolyte incorporated during synthesis, is also a contributing factor [39].

Doping ions help to decrease the band gap (E_g) between the energy levels and hence increase conductivity (Fig. 7). As such, by using small counter anions that are coplanar with the polymer chains, the conductivity can be boosted [40]. Hydrogen peroxide, polyethylene oxide, and dodecylbenzenesulfonate, among others, have all acted as doping ions [41–43]. In addition to the introduction of dopants, conductivity and stability have been reported to result from lower temperatures and plating potentials (as well as degree of roughness of the plating surface), higher concentrations of monomer, electrolyte, and water together with longer deposition times [40, 44, 45].

Fig. 7 Band structure representation of PPy and how E_g is modified with doping: (a) no dopant, (b) intermediate doping level – bipolarons are noninteracting at this point, (c) 33% dopant per monomer, and (d) 100% dopant per monomer. The material has changed from an insulator with a band gap of 4.0 eV to a semiconductor with full doping at 1.4 eV. (Redrawn from Ref. [46])



3.1 The Hopping Process

Conduction via localized electrons implies discrete jumps across an energy barrier from one site to the next. In other words, if two molecules are separated by a potential barrier, a carrier on one side can move to the other side via two mechanisms – either by tunnelling through the barrier or by moving over the barrier via an activated state. The latter process is called hopping. This carrier mobility is the main reason for the transport of the charges in CPs. The mobility of the charge carriers can be restricted as the degree of overlapping decreases at molecular or atomic levels. However, as the electronic states become increasingly localized, transport of the particles escalates through the hopping process. The relative importance of the two mechanisms depends on the shape of the barrier and on the availability of thermal energy, the latter resulting in a thermally activated type of mobility that increases with an increase in temperature and is mainly found in the hopping process. We can learn a lot about the conduction process by determination of the carrier mobility, e.g., its temperature dependence provides a good criterion by which we can distinguish band and hopping types of mechanisms. Though polymers are amorphous materials, a short-range order prevails. Hence, the theory that is used to explain the electronic band structure in a crystalline phase can also be applied to amorphous polymers. If the spatial fluctuations in the interatomic distances are large, the correspondingly large and random fluctuations in the height or depth of the potential wells may lead to the localization of states below a certain critical and well-defined energy. Accordingly, when the carrier mobility is low, and the mean free path is comparable with the interatomic distance, conduction can be expected to take place by a hopping process in the localized states. In order to obtain conduction through hopping, it is necessary to have an insulating or semiconducting material exhibiting a few intrinsic thermal free carriers, at least over a limited energy region, thereby establishing a large density of sites through which charge transfer can take place. There are three principal pathways that ensure carrier mobility – single chain or intermolecular transport (intrachain), interchain transport, and interparticle contact [47]. The intrachain movement depends on the effective conjugation of the polymer, while the interchain hopping is determined by the stacking of the polymer molecules. In a hopping mechanism, only those carriers with an energy kT , where k is the Boltzmann constant and T is the temperature, below the Fermi level have a significant probability of hopping. Mott showed that for strongly localized states, the conductivity at low temperatures must follow a relationship of the form

$$\delta \approx \exp\left(\frac{-B}{T^{1/4}}\right)$$

where δ is the conductivity and B is a constant related to the hopping mechanism. At high temperatures, deviations from $T^{1/4}$ occur, which can be understood in terms of interchain hopping [48]. A carrier trapped in a chain, after detrapping through large energy input, may drift along the same chain or may hop onto an adjacent chain. As such, in amorphous polymers, the conduction occurs due to two distinct processes: a

temperature-dependent trap hopping and a comparatively less temperature-dependent interchain hopping.

3.2 Solitons, Polarons, and Bipolarons

Polymer doping leads to the formation of conjugational defects – solitons, polarons, and bipolarons – in the polymer chain. The presence of localized electronic states of energies less than the band gap, arising from changes in local bond order – including the formation of solitons, polarons, and bipolarons – has led to the possibility of new types of charge conduction [8]. The ground state structure of such polymers is twofold degenerate, thus the charged cations are not bound to each other by a higher energy bonding configuration and so can freely separate along the chain. The effect of this is that the charged defects are independent of one another and can form domain walls that isolate two phases of opposite waveform with identical energy (solitons).

Solitons are subdivided into three categories: a neutral soliton, positive soliton, and negative soliton. An interesting observation is that charged solitons have no spin; however, neutral solitons have spin but no charge. A positively charged soliton occurs when an electron is removed from a localized state of a neutral soliton by oxidation. A negatively charged soliton is produced when an electron is inserted by reduction (Fig. 8). Solitons produced in polyacetylene (PAC) are believed to be delocalized over about 12 CH units, with the maximum charge density existing next to the dopant counterion (A^-). The bonds closer to the defect show decreased bond alternation compared with those further away from the center. Soliton formation results in the creation of new localized electronic states that appear in the middle of the energy gap. At high doping levels, the charged solitons interact with one another to form a soliton band, which can eventually merge with the band (VB and CB) edges (Fig. 8) to create true metallic conductivity [49–51].

A neutral polymer has full VB and empty CB, separated by the band gap. Formation of polarons and bipolarons generates new energy levels located at mid-gap. Bipolarons and polarons are self-localized particle-like defects associated with characteristic distortions of the polymer backbone and with quantum states deep in the energy gap owing to strong electron–lattice coupling. Polarons are obtained through a combination of a neutral and a charged soliton existing on the same polymer chain. Two mechanisms have been put forward to explain the transition from polaron to bipolaron states: polaron recombination into bipolarons [52–54], where the bipolaron is generated when polarons of the same electric charge meet each other; and single-polaron to bipolaron transitions [55–57], where the polaron structure is transformed by the addition of one extra charge. Oxidation causes additional polarons to form and eventually the unpaired electron of the polaron is removed, or two individual polarons combine to form a dication or bipolaron (Fig. 9) [58]. A polaron has a spin $\pm 1/2$ and an electric charge $\pm e$, whereas a bipolaron is spinless with a charge $\pm 2e$ and is of lower energy than the two distinct polarons from which it was created. For example, the bipolarons are located symmetrically with a band gap of 0.75 eV for PPy. With continued doping, continuous bipolaron bands form [59], and the band gap also increases as newly formed bipolarons are made at the expense of

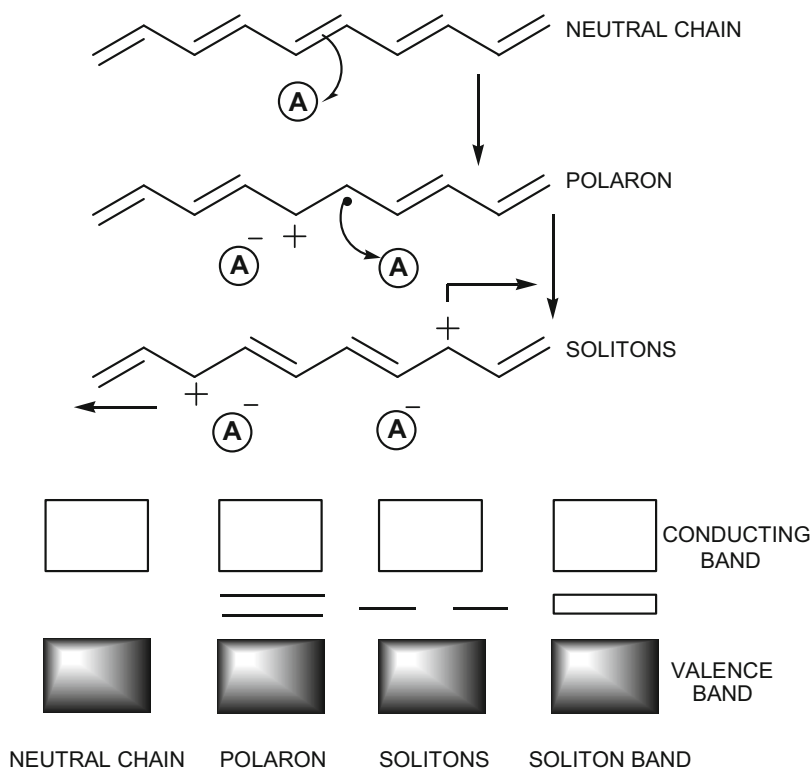


Fig. 8 Soliton structures of polyacetylene

the band edges. For a very heavily doped polymer, it is conceivable that the upper and the lower bipolaron bands will merge with the CBs and the VBs, respectively, to produce partially filled “conducting-like” bands rendering metallic-like conductivity to the polymer, as shown in Fig. 9. Conjugated polymers, e.g., PPy, with a degenerate ground state exhibit a slightly different mechanism. However, in either case, polarons and bipolarons are produced upon oxidation [60]. Indeed, density functional theory calculations showed that the charge carrier in oxidized polypyrrole are bipolarons [61].

The oxidative doping of polypyrrole (PPy) proceeds in the following way. An electron is removed from the π -system of the backbone, producing a free radical and a spinless positive charge. The radical and cation are coupled to each other through local resonance of the charge and the radical, via a sequence of quinoid-like rings, the number of which is limited by the prohibitive amount of energy required for the creation and separation of the defects. For the polaron state of the PPy, it is believed that the lattice distortion extends over four pyrrole rings and can be either a radical cation or radical anion thereby creating a new localized electronic state in the gap, with the lower energy states being occupied by a single unpaired electron. The polaron state of PPy is symmetrically located about 0.5 eV from the band edges [59, 60, 62].

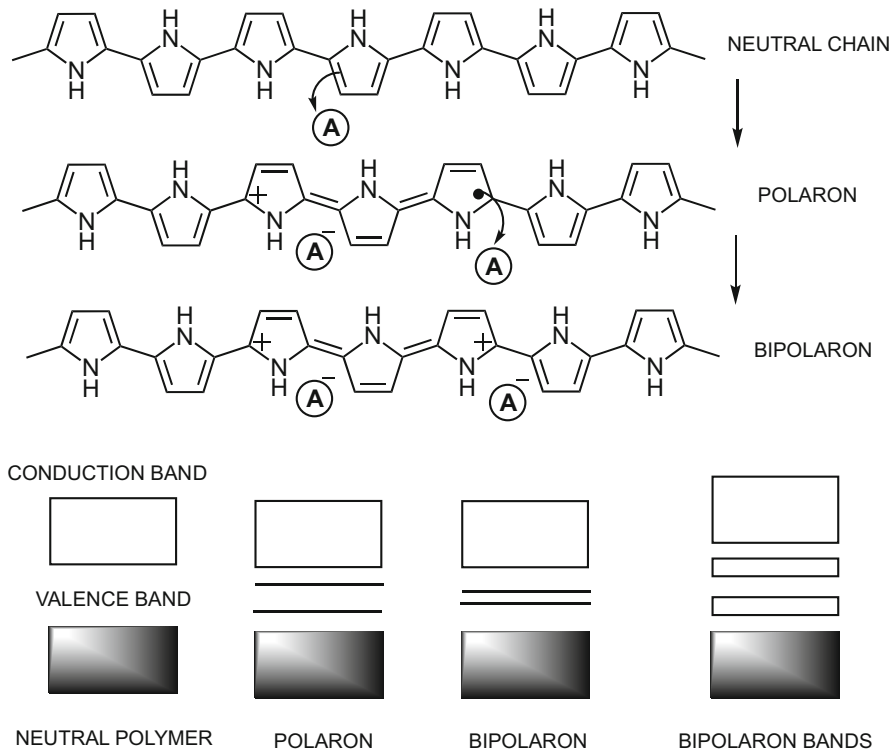


Fig. 9 Formation of polarons and bipolarons for polypyrrole (PPy)

A consistent description of the dynamics of the mechanism of creation, stability, and transition of polarons, and bipolarons constitutes a critical problem in the understanding of these materials. The polaron–bipolaron transition problem was explicitly addressed by Čík et al., in poly(3-dodecyl thiophene) in connection with temperature changes [52]. They found that when the sample was heated and subsequently cooled, there was an amplification of the diamagnetic inter- and intrachain bipolarons. Kaufman et al. studied PPy [53] using optical absorption spectroscopy and electron spin resonance and found that the metastable states possess spin, while the stable states do not. Their data revealed a slow transition, consistent with the diffusion rate limited by the mobility of the dopant.

4 Synthesis and Characterization of Conducting Polymers

It is well known that the conductivity of a polymer is influenced by a number of factors including polaron length, conjugation length, overall chain length, and by charge transfer to adjacent molecules, most of which can be influenced by the method of preparation. Conducting polymers (CPs) are synthesized, either

chemically or electrochemically. Each method has advantages and disadvantages, as summarized in Table 1 [9].

Chemical synthesis includes the usual methods of condensation polymerization (i.e., step growth polymerization) or addition polymerization (i.e., chain growth polymerization). The standard CPs – PPy, PTh, PANI, and poly(3,4-ethylenedioxythiophene) (PEDOT) – can be polymerized both chemically and electrochemically [62]. With chemical synthesis of polymers, it is feasible to synthesize CPs that are currently not possible with electrochemical synthesis. However, because the latter method is relatively straightforward and reproducible [9, 64], it is rapidly becoming the preferred alternative for making CPs and consists of dissolving a monomer in a solvent/electrolyte medium followed by the electrodeposition of a polymer film onto an electrode surface using pulse, galvanostatic, potentiostatic, or sweeping techniques [65]. One advantage associated with the electrochemical polymerization of conducting polymers is that the reactions can be performed at room temperature, either by varying the potential or current for specified periods of time, thereby permitting the thickness of the film to be monitored and controlled. CPs such as PTh, polycarbazole, polyindole polyazulene, and PPy can all be synthesized using this technique [66].

4.1 Polypyrrole

Polypyrrole (PPy), as a model for the CPs, can be obtained chemically or electrochemically. The electrochemical polymerization of pyrrole (Py) has been extensively studied since it is easily obtained in the form of freestanding films and has good environmental stability and conductivity. Electrochemical polymerization is performed using a three-electrode configuration (working, counter, and reference) in a solution of the monomer (Py), appropriate solvent, and electrolyte (dopant) (Fig. 10).

Current is passed through the solution and electrodeposition occurs at the positively charged working electrode or anode. Monomers (Py) at the working electrode surface undergo oxidation to form radical cations that react with other pyrrole monomers or radical cations, forming insoluble polymer chains on the electrode surface

Table 1 Comparison of chemical and electrochemical CP polymerization

Polymerization approach	Advantages	Disadvantages
Chemical polymerization	Larger scale production possible Postcovalent modification of bulk CP possible More options to covalently modify CP backbone	Thin films inaccessible Complicated syntheses
Electrochemical polymerization	Thin film synthesis possible Ease of synthesis Entrapment of molecules in CPs Doping is simultaneous	Difficult to remove film from electrode surface Postcovalent modification of bulk CP is difficult

Fig. 10 Three-electrode setup for electrochemical synthesis of conducting polymers – reference electrode, working electrode, and counter electrode

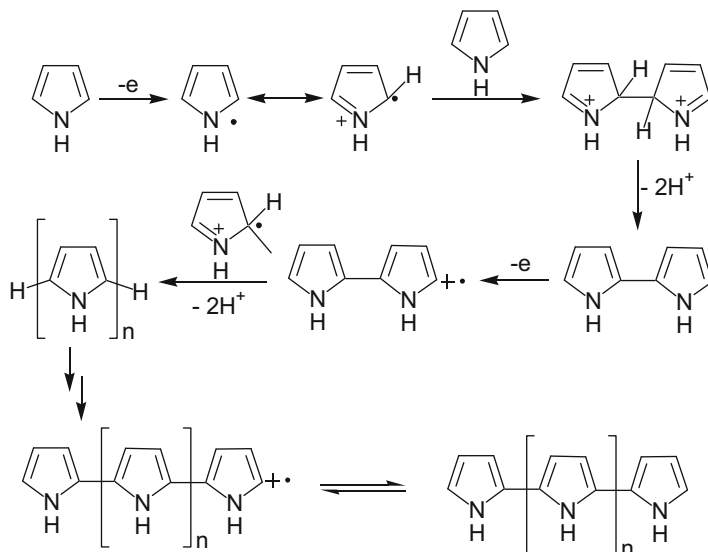


(Scheme 1) [67]. A number of important variables, including deposition time, temperature, solvent system (water content), electrolyte, electrode system, and deposition charge need be considered. Each of these parameters has an effect on film morphology (thickness and topography), mechanics, and conductivity, which are properties that have a direct impact on the utility of the material for specific applications [63].

4.2 Polythiophene and Its Derivatives

In its doped oxidized state, a poly(3,4-ethylenedioxythiophene) (PEDOT) layer/film shows exceptional stability, transparency, and high conductivity ($300 \text{ S}\cdot\text{cm}^{-1}$) [68]. The electrosynthesis of polyalkylenedioxythiophenes was carried out in 1994 by the anodic oxidation of 3,4-ethylenedioxythiophene or 3,4-trimethylenedioxythiophene. This resulted in polymers that were extraordinarily stable during charging and discharging, owing to a narrow band gap [69]. The electropolymerization process may also be executed through *in situ* polymerization of 3,4-ethylenedioxythiophene (EDOT) or via oxidative means [70].

Polymerization of PEDOT is typically carried out in acetonitrile, employing LiClO_4 as electrolyte, which results in a sky-blue doped PEDOT layer containing ClO_4^- as counter ions. Oxidative polymerization, with iron(II) chloride, has been demonstrated to be a satisfactory method of synthesizing neutral, fully undoped



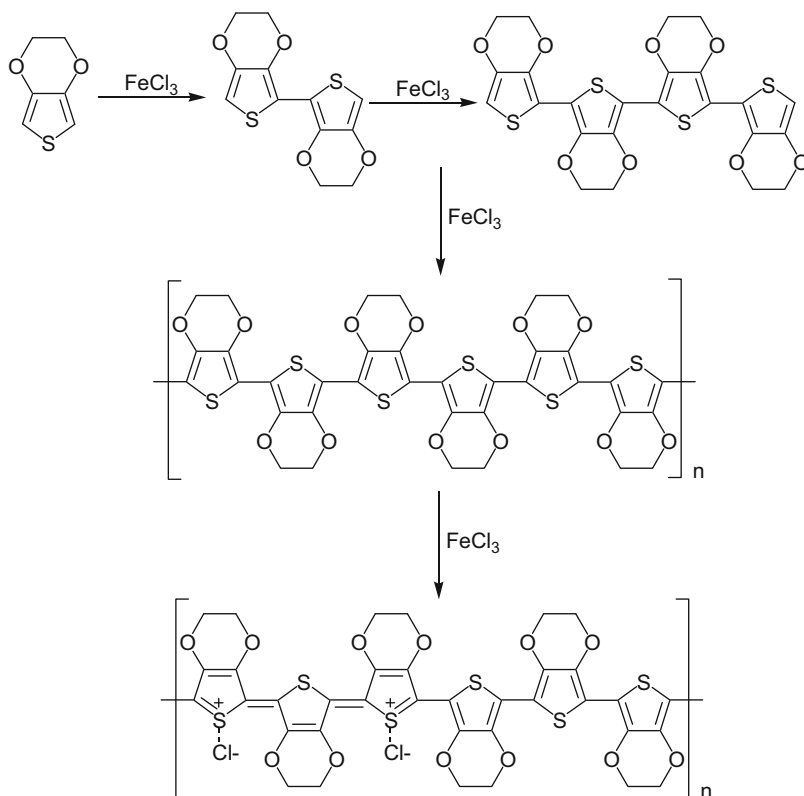
Scheme 1 Mechanism for heterocycle polymerization via electrochemical synthesis. This pathway is initiated by the oxidation of a monomer at the working electrode to give a cation species, which can then react with a neutral monomer species or radical cation oligomeric species to generate the polymer, redrawn from Ref. [67]

molecules with considerable yield [70]. PEDOT (Scheme 2) is an intermediate in the preparation of doped, highly conductive PEDOT and can be isolated through the adjustment of selected reaction conditions.

5 Principal Conducting Polymers

5.1 Polypyrrole (PPy)

Polypyrrole, composed of a number of connected pyrrole rings, has been lauded for its conductivity (resulting from interchain hopping) and high stability. In addition, the ease of oxidation and availability of its monomer, pyrrole, ensured that it would be extensively studied and characterised by thermal analysis and electrochemical techniques that include cyclic voltammetry (CV) and impedance spectroscopy. The chemical synthesis of polypyrrole, through the oxidation of pyrrole, was first accomplished in the early twentieth century. Pyrrole itself is ubiquitous in nature, making appearances in the building blocks of chlorophyll, hemoglobin, bile pigments, and mold metabolites, among others. Much later, the first electrochemical deposition of PPy was accomplished in 1968 [71]. Since then, PPy has been prepared by the electropolymerization of pyrrole onto a variety of conductive substrates, for example, stainless steel, nickel, and platinumized silicon wafers, with promising results [72–76]. The properties – physical, chemical, and electrical – of



Scheme 2 Synthesis of poly(3,4-ethylenedioxythiophene) and doped poly(3,4-ethylenedioxythiophene)

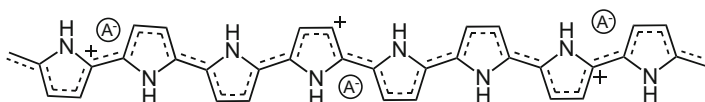


Fig. 11 Polypyrrole (PPy), with counter ions (A^-) to balance charge. (Redrawn from Ref. [81])

electrochemically deposited PPy (Fig. 11) can be reshaped through doping and changeable plating conditions [41, 42, 77–80] thereby increasing its versatility. The easy alteration of these properties, through the judicious choice of dopants, places PPy in a very select group of conducting polymers, increasing its attractiveness for application in biosensor technology, among others.

PPy exhibits good electrical conductivity and high air stability (its conductivity decreases by only 20% per year in an exposed environment) and, by its very nature, has been used in a variety of technological applications in various research areas, namely, secondary batteries [82–85], electrochromic display devices [86, 87], light-emitting diodes [88, 89], capacitors [90–92], sensors, [93–97] membranes [98], and

enzyme electrodes [99–101]. It has been reported that the electrical conductivity is stable even at 200 °C [36, 102]. Consequently, conducting polymeric materials [103, 104], such as PPy, have become an area of increasing research interest as they show great potential for application in solid-state devices [105].

The ability to control polypyrrole's surface properties, such as charge density and wettability, holds promise for effective interaction between biological tissue and the polymer [106–109]. However, polypyrrole itself reveals rather poor properties in terms of electrochromic behavior [110], and often, further enhancement through doping and sensitizing with various dyes is required to obtain good optical properties [109–114]. Additionally, the syntheses of conducting star, graft, and block copolymers are some of the ways to effectively improve electrical and mechanical properties of conducting polymers and polypyrrole is no exception. In order to make conducting polymers processible, several approaches have been developed, one of which is to prepare graft and block copolymers with desired end groups like pyrrole or thiophene [115–118].

5.2 Polythiophene (PTh)

Polythiophenes (PThs) are an important representative class of π -conjugated polymers that exhibit a sought after combination of high environmental/thermal stability, processability, and electrical conductivity. PTh has been used in a variety of applications such as electrical conductors, nonlinear optical devices, light-emitting diodes, transistors, electrochromic or smart windows, photoresists, antistatic coatings, sensors, batteries, electromagnetic shielding materials, artificial noses and muscles, solar cells, microwave absorbing materials, new types of memory devices, nanoswitches, imaging materials, and polymer electronic interconnect batteries [119–121]. PThs have a regular polymeric backbone (Fig. 12) which can be modified by varying the nature of the dopant and through facile ring modifications. Owing to their chemical and electrochemical stability, high conductivity upon doping, and nonlinear optical properties, PThs are among the most widely studied conjugated organic polymers, experimentally and theoretically. However, polythiophene is generally insoluble in common organic solvents and decomposes readily, thereby limiting its use in practical applications. The real interest in this class of CPs was sparked when it was realized that three-carbon substitution of the thiophene ring yielded a wide variety of versatile CPs. The substituted PThs, namely, poly(3-methylthiophene) and poly

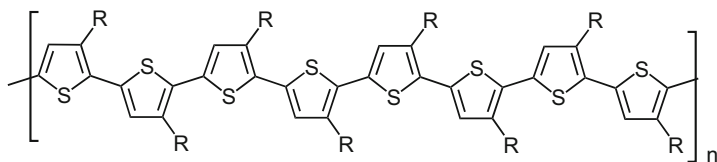


Fig. 12 Structure of polythiophene (PTh) where R = H, poly(3-methylthiophene) where R = CH₃ and poly(3-hexylthiophene) where R = C₆H₁₃

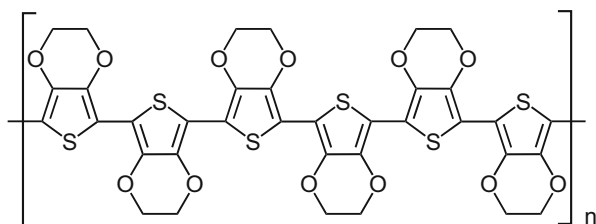
(3-hexylthiophene), etc., all exhibit good solubility in common organic solvents with the latter finding importance as a benchmark hole conductor in organic photovoltaics [122]. The chemical method for the synthesis of PTh is used in bulk production while, electrochemically, very thin and better-ordered films can be prepared. Chemically synthesized PThs are produced in their undoped state and can be doped chemically or electrochemically to increase conductivity [123].

5.3 Poly(3,4-ethylenedioxythiophene) (PEDOT)

The first synthesis of PEDOT was successfully done by scientists at the Bayern A G Laboratories in the late 1980s. The commercial name, Baytron, was given to PEDOT following the chemical polymerization of 3,4-ethylenedioxythiophene [70]. PEDOT [124] has been of interest in numerous studies because of its high transparency, high conductivity, excellent environmental stability, and relatively low band gap [125]. These unique properties make PEDOT an excellent material for utilization in electrochromic devices, antistatic coatings, biocorrosion coatings, light-emitting diodes, sensors, and synthetic textiles [126–129]. PEDOT has also been reported to be excellent for the synthesis of nanostructured materials and devices whose electrical, electronic, magnetic, and optical properties are comparable to those of metals or semiconductors. Compared to other unsubstituted PThs and derivatives, PEDOT exhibits a distinctly low oxidation potential and a small band gap in the oxidized state [130, 131]. It has been revealed that undoped PEDOT has a band gap energy of -1.6 eV and can be electrochemically cycled between its reduced and oxidized states. This superior electrochemical stability may be attributed to the presence of the ethylenedioxy binding group at the α and β position of the thiophene ring in EDOT (Fig. 13), which blocks coupling along the backbone, making the resulting polymer regiochemically defined [130, 132].

Conducting polymers may be employed in their unmodified state or they may be doped to enhance their electrical capability; PEDOT is one of the few examples within the conjugated polymer family which is both p- and n-dopable [133]. It is acknowledged that upon electrochemical p-doping or n-doping, conducting polymers undergo a redox process which involves ion transport into and out of the polymer matrix to balance the electronic charge, resulting not only in an increase in electronic conductivity but also structural transitions which give rise to spectral changes [134–137] which allowed for their exploitation in the field of sensors.

Fig. 13 Structure of poly (3,4-ethylenedioxythiophene) (PEDOT)



Indeed, Nien et al. [138] used PEDOT as the matrix to fabricate an amperometric glucose biosensor; the biosensor showed a detection limit and sensing sensitivity of 0.13 mM and $12.42 \text{ mA cm}^{-2} \text{ M}^{-1}$, respectively. Other incorporations of PEDOT in sensors include a direct detection DNA sensor, that quantifies the targeted single-strand DNA [139], and a self-absorbing piezoelectric sensor consisting of conducting PEDOT [140]. In addition, an amperometric sensor coated with PEDOT for the measurement of chromate ions and an enzyme modified biosensor entrapped by PEDOT for the detection of phenolic compounds, with high catalytic activity have been reported [141]. Moreover, it was found that the increased surface area of the polymer led to a high rate of electron transfer between the electrode and *p*-benzoquinone, when the latter was employed as an electron mediator.

Electrochemical polymerization is widely used to construct conducting polymer films, but the option of using a conducting substrate from which a conducting polymer is formed may limit practical applications [142]. Recently, the incorporation of nanomaterials into a polymer matrix and the study of nanoparticles-matrix interactions have been of interest to material scientists [143]. Polymers are considered a good choice as host matrices for composite materials, because they can easily be designed to yield a variety of bulk physical properties [144, 145]. PEDOT coatings prepared by electrochemical polymerization in aqueous solution allows the direct incorporation of water-soluble anions [146], into its matrix. Xiao et al. developed an adenosine 5'-triphosphate (ATP) doped PEDOT for neural recording devices that displayed great stability and biocompatibility [147]. Balamurugan et al. [124] demonstrated a silver nanograins (AgNGs) incorporated PEDOT modified electrode for electrocatalytic sensing of hydrogen peroxide. The modified electrode exhibited good electrocatalytic activity towards the reduction of hydrogen peroxide without an enzyme or mediator immobilized on the electrode. It showcased a detection limit of 7 μM and a response time of 5 s. Vasantha et al. disclosed the electrochemical synthesis of a poly(3,4-ethylenedioxythiophene)-(PEDOT)|ferricyanide film modified electrode by cyclic voltammetric and chronoamperometric techniques, for the determination of ascorbic acid in aqueous solution with a detection limit of 5×10^{-5} M [148]. Olowu et al., in 2010, constructed an aptasensor for the detection of 17 β -estradiol, an endocrine disrupting chemical, based on a poly(3,4-ethylenedioxythiophene)-gold nanocomposite platform; the detection limit was 0.02 nM [149].

5.4 Polyfuran (PFu)

Furan is one of the five-membered heteroaromatic ring compounds that can be converted into a conducting polymer by both chemical and electrochemical methods in aqueous and organic media. It is lesser known than pyrrole and thiophene because of its high oxidation potential. Polyfuran (Fig. 14), through chemical synthesis, has found application in industry as an insulator and is very sensitive to humidity – its electrical resistivity decreases considerably and reversibly upon contact with moisture.

Ali et al. [150] studied the dispersion of normal modes in polyfuran and this conducting polymer was used in optoelectronic devices, as upon doping the color

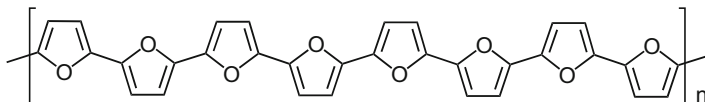
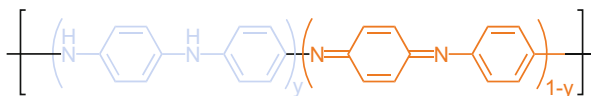


Fig. 14 Chemical structure of polyfuran (PFu)

Fig. 15 General polymeric structure of polyaniline



changes from yellow-brown to black-brown [151, 152]. Meanwhile, Galal et al. developed a promising electrochemical biosensor to determine dopamine, epinephrine and norepinephrine, ascorbic acid, and paracetamol. The sensor was fabricated via electrodeposition of palladium nanoclusters on a polyfuran film modified platinum electrode and saw exceptional improvement in the detection limit. Moreover, diffusion coefficient measurements confirmed the fast electron transfer kinetics of the electrochemical oxidation of the analyte molecules at the sensor/solution interface [153].

5.5 Polyaniline (PANI)

Polyaniline (Fig. 15) has been studied extensively as an important conducting material owing to its promising electronic and optical properties [65, 154]. It has also generated considerable interest because of the many synthetic pathways available to scientists, its chemical stability, good environmental stability, low cost, and ease of redox doping [155]. Although PANI boasts good environmental stability and conductivity, processing of the polymer into useful products has been problematic because of its insolubility in common nontoxic organic solvents and the fact that its ready decomposition before melting. PANI is unique among inherently conducting polymers such as PPys and PThs because its N heteroatom can directly participate in the polymerization process and in the conjugation of the conducting form to a greater extent than the N and S heteroatoms in PPy and PTh.

PANI can be synthesized by either chemical or electrochemical oxidation of aniline under acidic conditions. The most widely used technique is oxidative coupling, involving the oxidation of the monomers, to form radical cations which couple to form dication. Repetition of this propagation step leads to the polymer. Electrochemical synthesis is preferred to chemical synthesis because of the accessibility to thin films and better ordered polymers. The best films are reported to be produced from electrochemical techniques using three electrode systems [156]. The film can be deposited at the working electrode through electropolymerization of monomeric aniline from a suitable medium that limits the dissolution of the substrate. This electropolymerization process is preferably conducted in acidic media at a pH < 1 [157, 158]. PANI-coated electrodes, as components of sensors, presents some

advantages such as acceleration of electron transfer reactions, immobilization of biological compounds, amplification of signal, and elimination of electrode fouling.

5.5.1 Polyaniline Derivatives

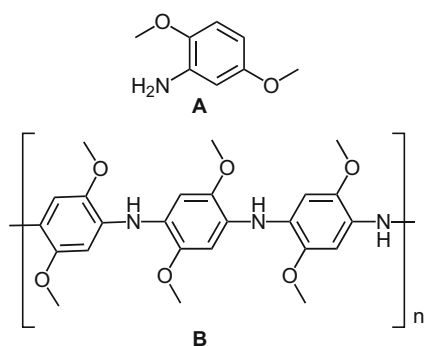
Similar to unsubstituted PANI, polyaniline derivatives are also synthesized by chemical or electrochemical oxidative polymerization of the respective substituted aniline monomers in acidic solution, although some other approaches such as plasma polymerization [159, 160], electroless polymerization [161], solid-state polymerization [162, 163], enzyme-catalyzed polymerization, and photochemically initiated polymerization [164] have also been reported. Conditions related to the formation of PANI and its derivatives, such as the type of supporting electrolyte, monomer concentration, applied potential, the type of solvent, and pH of the electrolyte [158, 164], as well as the influence of anions on the electrodeposition of polyaniline and on polyaniline redox reactions, have also been extensively described in literature [165, 166]. These factors are known to dictate the morphology and properties of the generated polyaniline.

It is well known that the low solubility of PANI, in common organic solvents, ultimately restricts processability. To overcome this challenge, substituted PANI was investigated and polymerization of a typical derivative of aniline resulted in a soluble conducting polymer. The substituent groups present in the units of the polymer chain are thought to contribute to a decrease in the stiffness of the polymer chain resulting in better solubility. Unfortunately, substitution of the phenyl ring or the N-position of polyaniline units has been shown to decrease the conductivity [167]. However, poly(2,5-dimethoxyaniline) (PDMA), bearing anilines substituted with two methoxy groups (2,5-dimethoxyaniline), has been reported to be a soluble polymer (Fig. 16) with a conductivity similar to PANI [168, 169] though the redox transitions occur at lower potentials in comparison with PANI (0.70 V for PANI and 0.27 V for PDMA) [170].

5.5.2 Oxidation States of Polyaniline

Polyaniline has the general formula $[(-B-NH-B-NH)_n (-B-N=Q=N-)]_{1-n}m$, in which B and Q are the rings in the benzenoid and quinonoid forms, respectively.

Fig. 16 Structures of (a) 2,5-dimethoxy aniline and (b) PDMA



PANI can be rapidly converted between the base and salt forms by treatment with acid or base, thus, the general polymeric structure shown in Fig. 15 is now accepted by the scientific community.

PANI can exist in three basic forms depending on the existing oxidation state, which ranges from the fully reduced ($y = 1$) leucoemeraldine state to the half oxidized ($y = 0.5$) emeraldine form to the fully oxidized ($y = 0$) pernigraniline configuration. Reduction of the emeraldine salt to leucoemeraldine and oxidation to pernigraniline both see a decrease in conductivity [171]. In fact, the fully oxidized and fully reduced states of PANI are insulators, although they possess other interesting physical and chemical properties. Beside changes in oxidation levels, different forms of PANI are also characterized by a change in color [172]. For instance, the emeraldine salt obtained by electrochemical polymerization in acidic media is green in color and can be converted into the dark blue form by further oxidation to the fully oxidized pernigraniline salt and even further into the violet pernigraniline through treatment in basic media. It can also be reduced to colorless leucoemeraldine or further converted into the blue nonconducting form of emeraldine in basic media [173] (Scheme 3). Interestingly, the two blue forms of PANI – pernigraniline salt and emeraldine – are of different shades [172].

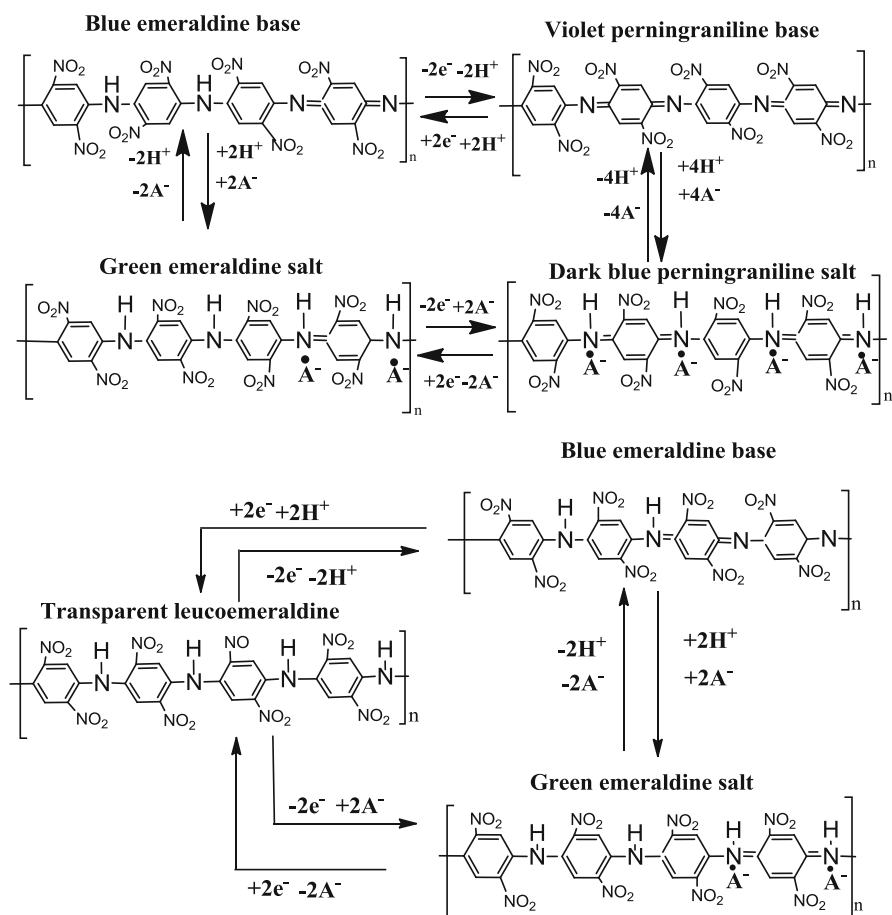
Among the three oxidation states of PANI, the emeraldine salt is the one that displays the highest conductivity, by doping or protonation of the emeraldine base [174] – and is composed of an alternating sequence of three benzenoid units and one quinonoid unit. Further, it consists of amine ($-\text{NH}-$) and imine ($=\text{N}-$) sites in equal proportions [175]. The imine sites are protonated by acids to the bipolaron (dication salt) form. However, further rearrangement occurs to form the delocalized polaron lattice, which is a polysemiquinone radical-cation salt and is responsible for the high conductivity of PANI [164].

6 Conducting Copolymers

Practical use of polypyrrole and other conducting electroactive polymers are limited by their brittle structure, insolubility and poor mechanical and physical properties, all of which restrict their processability [176]. Improvements to the processability of conducting polymers can be had by copolymerizing them with other monomers resulting in star, graft or block copolymers [177, 178]. Copolymerization permits the chemical linking between the insulating matrix (end groups) and the conjugated polymer [179]. Structural modification of conducting polymers via copolymerization has been used to obtain materials with a broad range of electronic, optical, and mechanical properties [180]. Thus, electrochemical syntheses of pyrrole copolymer films with substituted pyrroles, [181], thiophene [182], terthiophene [183], and other combinations of aromatic compounds [184, 185], have been reported. The resulting copolymers have properties different from those of the homopolymers of the constituent monomers.

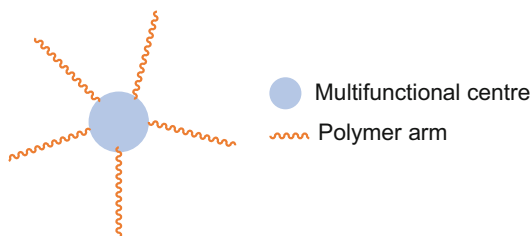
6.1 Conducting Star Copolymers

Star copolymers are a class of branched macromolecules that have a central core to which multiple linear polymer chains are attached – the core consists of a moiety with multiple branching points (Fig. 17). The cores may be formed from



Scheme 3 Different oxidation states of PANI. Redrawn from Ref. [166]

Fig. 17 Representation of a star copolymer



hyperbranched polymers, dendrimers, or other symmetric or semi-symmetric molecules which have multiple attachment sites. The three dimensional (3D) structure, with extended conjugated linear polymer chains, gives star copolymers properties that are different from the typical two-dimensional, linear polymers [19].

Conducting star copolymers are used in their undoped state for applications in which the conductivity requirements are not too high, for example, static dissipation, or where the optical property of the polymer coating is of chief importance as in a pigment or reflective layer. Materials with conductivities in the range of 10^{-6} to 1 S.cm^{-1} are suitable for these purposes. Furthermore, the conducting chains surprisingly can provide sufficient intermolecular overlap to give solid materials with electrical conductivities higher than the corresponding linear, non-star conducting polymers [19, 186–188].

The regular 3D structure of star copolymer gels combines the properties of hardness and flexibility and is being investigated as materials that are hard without being brittle [19]. The combination of star copolymer and conducting polymer structures realises an approach to make materials that possess the favorable properties of both – improved processability and electrical conductivity. The former results from the spheroidal structure of hyperbranched, dendrimeric, and starburst polymers. A conducting star copolymer may be constructed in which two or more different conjugated arms radiate from the central core [86]. Doping of the conducting star copolymers, to increase the electrical conductivity, may be achieved using methods applicable to the conjugated radiating chain moieties. For conjugated chains based on pyrrole, thiophene units or their derivatives, doping may be achieved by treatment with oxidizing agents such as iodine, ferric chloride, ferric tosylate, gold trichloride, and antimony chloride. If the polymer side chains are composed of polyaniline, doping can be brought about by treatment with hydrochloric acid [189]. Doping can also be obtained electrochemically by confining the polymer to an electrode surface and subjecting it to an oxidizing or reducing potential in an electrochemical cell.

6.2 Dendrimer Star Copolymers

Dendritic copolymers (Fig. 18) are a specific group of dendrimers. These exist as two different types of copolymers – segment-block dendrimers built with dendritic segments of different constitution, obtained by attaching different wedges to one polyfunctional core molecule and layer-block dendrimers consisting of concentric layers around the central core. Hawker and Fréchet [190] synthesized a layer-block dendrimer as well as a segment-block dendrimer which consisted of one ether-linked segment and two ester-linked segments. The inner two generations were ester-linked and the outer three ether-linked.

Dendrimer-star copolymers [191] are a novel type of molecular architecture, in which many linear homo- or block copolymer chains are attached to the dendrimer. They have been developed because they combine the properties of star copolymers with those of dendrimers [192–197]. Two general methods have been used to prepare

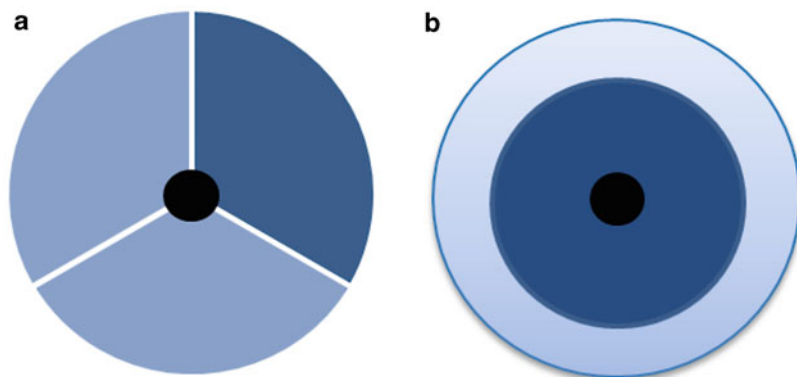


Fig. 18 Copolymers: (a) segment-block dendrimer and (b) layer-block dendrimer

the dendrimer-star copolymers – one is to link monofunctional linear polymers onto the dendrimer surface [192, 196–198] and the other is to grow armed polymer chains from the surface of the dendrimer by “controlled/living” polymerizations, such as anionic polymerization [199], ring-opening polymerization (ROP) [200], and atom transfer radical polymerization (ATRP) [201]. Synthesis of a hybrid dendrimer-star copolymer, through the reversible addition-fragmentation transfer (RAFT) polymerization process, has been reported by Zheng et al. [202]. Wang et al. discussed a conducting star-shaped copolymer, consisting of a regioregular poly(3-hexylthiophene) arm attached to a polyphenylene dendrimer core [203]. Miller and Tomalia announced the conductivities of polyamidoamine (PAMAM) dendrimers modified with cationically substituted naphthalene diimides; the study showed that the conductivity increased with increased humidity, to as high as $18 \text{ S}\cdot\text{cm}^{-1}$ at 90% relative humidity. The conductivity was, in all cases, electrical and isotropic [204].

In 2011, Baleb et al. reported on the synthesis and characterization of a star copolymer based on a PPI dendrimer core (generations 1–4) and polypyrrole [205] (Fig. 19). In the same year, a star copolymer which involved the electro-copolymerization of (3,4-ethylenedioxy thiophene) (EDOT) with G2PPT was developed by Olowu et al. [149, 206].

Poly(propylene imine) (PPI) dendrimers are highly branched macromolecules having terminal amino groups which exhibit a number of interesting characteristics. The dendrimer can be used as a hydrogen donor because of the high density of amino groups; many of the properties of dendrimers are strongly influenced by these terminal groups [207–209].

The use of dendrimer-oligothiophene hybrid macromonomers for the preparation of a soluble, highly conducting PTh, having only dendritic substituents, has been communicated [210]. Roncali et al., in 1999, described electrogenerated poly (dendrimers) containing conjugated poly(thiophene) chains. In his approach, an electroactive conjugated polymer was synthesized by electropolymerization of increasing generations of dendrimer derivatives by a bithiophene group [211]. Deng and others described the synthesis and application of amine-terminated

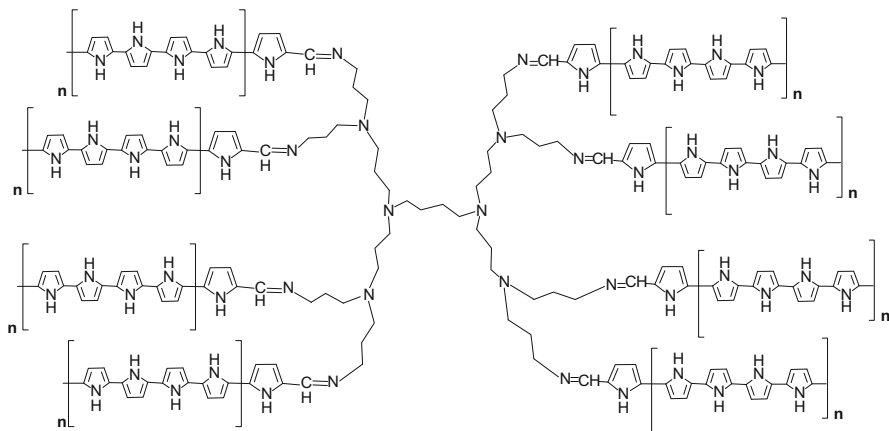


Fig. 19 Poly(propylene imine)-co-polypyrrole

fourth-generation PAMAM dendrimers functionalized with thiophene dendron jackets and their roles in the preparation of dendrimer-encapsulated nanoparticles for energy-transfer and fuel cell application [212]. A series of star-shaped copolymers, using first generation (G1) to the fifth generation (G5) PPIs as the core, were prepared [213, 214] in order to investigate their miscibility properties with linear polystyrene. The unsaturated end groups of polyisobutylene were converted into anhydride termini by Alder-ene reaction with maleic anhydride, and the product was reacted with the PPI dendrimers to generate PPI-polyisobutylene star copolymers [215]. The formation of dendritic stars with conducting polymers such as PANI, PTh, and PPy saw an increase in the conductivity which was attributed to a nanostructural change in the product owing to elongation of the conjugation chains and unhindered π -stacking of the polymer molecule with the dendrimer [205, 212, 216].

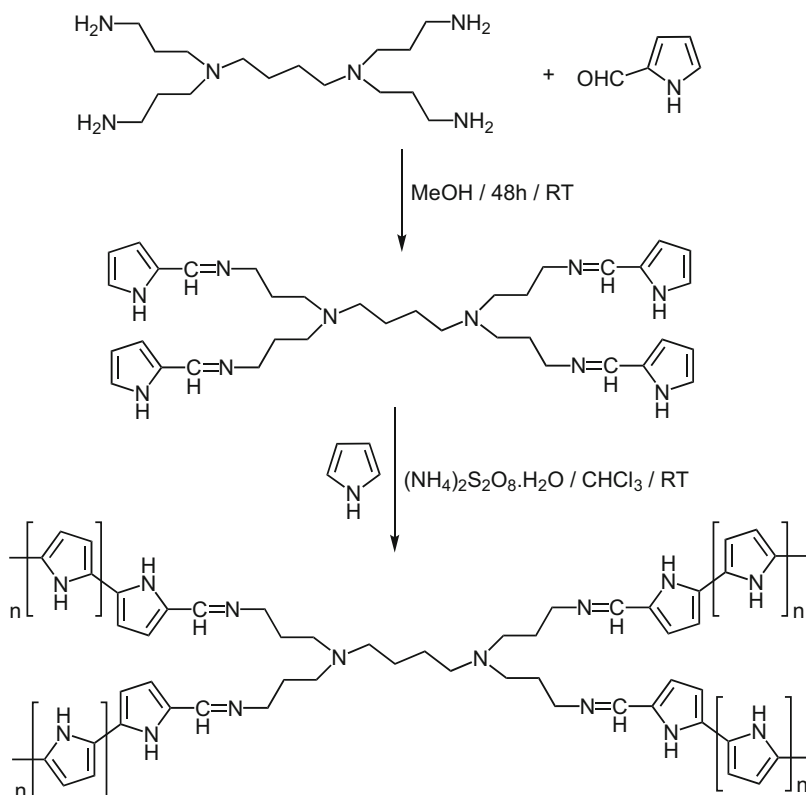
Dendrimer-like star-branched polymers have recently appeared as a new class of hyperbranched polymers and are recognized as nano-ordered globular macromolecules. Based on their architectures which bear many characteristic structural features such as hierarchical hyperbranched structures, generation-based radial architectures, differing branch densities between core (inside) and shell (outside), and many junction points and end-groups [217, 218].

It is also possible to synthesize a variety of dendrimer block copolymers by introducing different polymer segments at each dendrimer branch. Interesting morphologies and nanostructured materials have been reported by several research groups [219–226]. Thus, dendrimer-like star-branched polymers and block copolymers are promising specialty functional materials with many possible applications as drug, vaccine, and gene encapsulated delivery devices, surface modifiers, functional nanosize spheres and micelles, surfactants, molecular recognition systems, and microelectronic materials to name a few. Yoo et al. [227] synthesized a series of dendrimer-like star-branched polystyrenes by developing an iterative

methodology based on the “arm-first” divergent approach. This resulted in high-generation and high-molecular-weight polystyrenes with narrow molecular weight distributions [227].

6.2.1 Poly(propylene imine)-co-polypyrrole Dendritic Star Copolymer

Synthesis of novel star copolymers based on the PPI dendrimer core (generations 1–4) and PPy shell was rendered via a condensation reaction (Scheme 4) between the PPI surface amine moieties and 2-pyrrole aldehyde to give the pyrrole-functionalized PPI dendrimer (PPI-2Py). Subsequently, the pyrrole units on the dendrimer backbone underwent chemical oxidative copolymerization, using ammonium persulfate as an oxidant, providing the conducting star copolymer with polypyrrole side chains in 75% yield. Electrochemical synthesis was achieved via cyclic voltammetric scans of a PPI-2Py drop-coated platinum electrode (Scheme 4). In both cases, the resulting star copolymer, poly(propylene imine)-co-polypyrrole, exhibited higher conductivity than the pristine pyrrole and improved thermal stability over PPI-2Py [205].



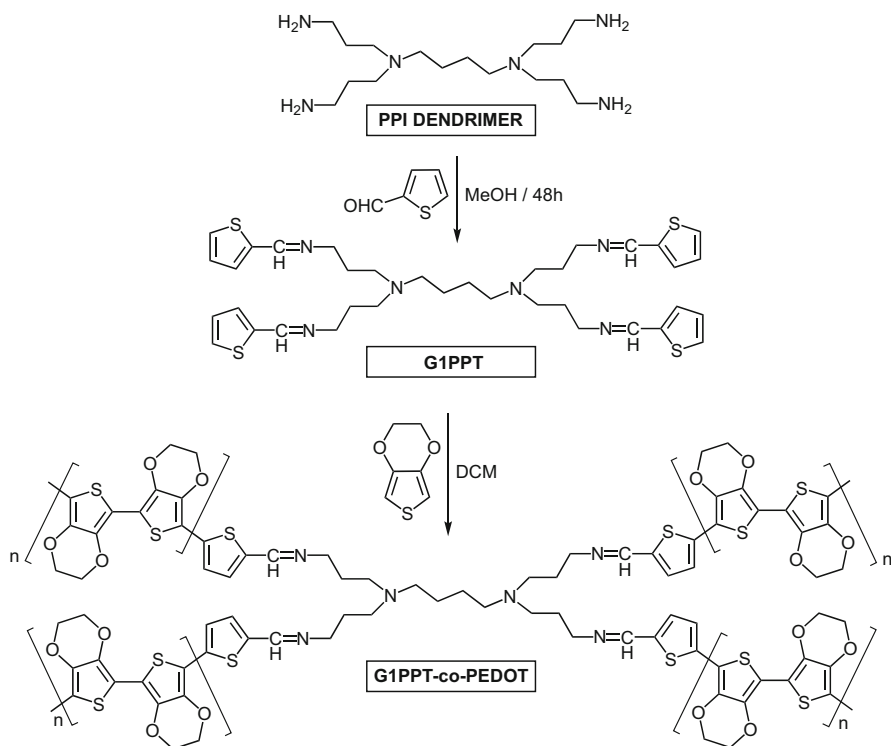
Scheme 4 Chemical synthetic procedure for poly(propylene imine)-co-polypyrrole – a dendritic star copolymer. Redrawn from Ref. [205]

6.2.2 Dendritic Poly(propylene thiophenoimine)-co-poly(3,4-ethylene dioxothiophene) Dendritic Star Copolymer

In another development, Olowu et al., in 2011 [149], also synthesized a star copolymer which involved the electrocopolymerization of 3,4-ethylene dioxothiophene (EDOT) with a G1 poly(propylene thiophenoimine) (G1PPT) modified gold electrode using cyclic voltammetric techniques (Scheme 5) to produce a generation 1 poly(propylene thiophenoimine)-co-poly(3,4-ethylene dioxothiophene) dendritic star copolymer (G1PPT-co-PEDOT) for use in the detection and quantification of the endocrine disrupting compound, 17 β -estradiol. Electrochemical impedance spectroscopy confirmed the more desirable conductive behavior of the star copolymer over PEDOT.

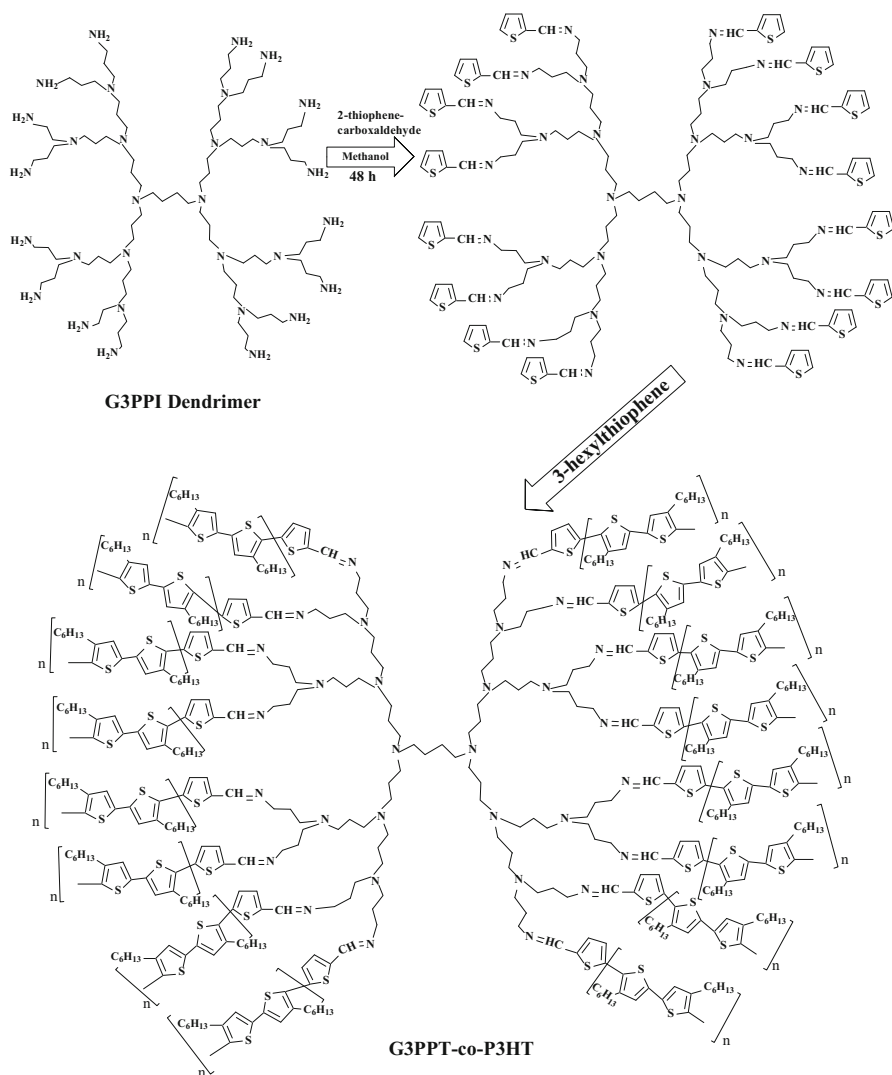
6.2.3 Dendritic Poly(propylene thiophenoimine)-co-poly(-3-hexylthiophene) Dendritic Star Copolymer

Novel star copolymers based on a G3 PPI dendrimer core and a poly(3-hexylthiophene) shell were prepared by Makelane et al. [228]. The synthesis of



Scheme 5 Synthetic pathway to poly(propylene thiophenoimine)-co-poly(3,4-ethylene dioxothiophene) dendritic star copolymer. Redrawn from Ref. [149]

the G3 poly(propylene thiophenoimine) (G3PPT) dendrimer was carried out by condensation of PPI with 2-thiophene carboxaldehyde. The thiophene units on the dendrimer backbone were polymerized electrochemically, in the presence of 3-hexylthiophene on a gold electrode coated with G3PPT using cyclic voltammetry (Scheme 6) resulting in the poly(propylene thiophenoimine)-co-poly(3-hexylthiophene) dendritic star copolymer.



Scheme 6 Synthesis of generation 3 poly(propylene thiophenoimine)-co-poly(3-hexylthiophene) dendritic star copolymer. Redrawn from Ref. [228]

7 Conducting Polymer-Based Composites

Conducting polymers and their composites have been extensively utilized in the fabrication of sensors and other technology that necessarily warrant materials that are responsive in nature. However, as previously mentioned, conducting polymers on their own suffer from low processibility and sensitivity as well as fouling [229]. The expansion of the field of CP-based composites, whose robustness and high detection limits, provided a means of overcoming these challenges associated with neat CPs, expanded.

7.1 Polyaniline–Carbon Nanotubes Composites (CNCs)

The discovery of carbon nanotubes (CNTs) in 1991 [230] led to an explosion of interest in nanoscience and nanotechnology research. Although there were initial high expectations of the potential of the CNTs, it soon became apparent that working with the carbon allotrope in its natural form presented some challenges. One response to facilitate the utilization of CNTs and their extraordinary properties in real-world bulk applications was the development of CNT/polymer nanocomposites (NCs). There now exists ongoing research into new combinations of traditional stock as hybrid materials, blends, and NCs and exploitation of their complementary properties [231, 232]. In this context, the development of conducting polymer–CNT composites, as novel futuristic materials, has attracted the curiosity of investigators because the blending of the two constituents offers the possibility to observe and capitalize on synergistic effects.

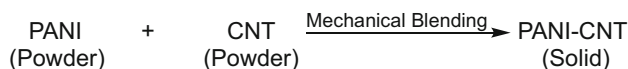
Some studies have emerged in the literature explaining that certain discrete properties of the components of conjugated polymer–CNT composites are enhanced, relative to the individual units, therefore validating their suitability for selected technological applications [233–235]. Incorporating CNT as fillers into conducting polymers results in NCs that possess much higher electrical conductivities than CPs. The CNT has been shown to behave as a transport bridge between the conducting domains of CPs, thus enhancing the electrical conductivity of the CP and by extension, the nanocomposite [236]. Currently, the construction of polymer composites is the biggest area of application for CNTs owing to the nanocomposite's high durability, high strength, light weight, design, and process flexibility. The successful utilization of carbon nanotubes in the assembly of the composite depends heavily on the homogenous dispersion of CNTs individually and uniformly throughout the matrix, without negatively affecting their structural integrity or reducing their aspect ratio [237]. Additionally, the enhanced mechanical properties of the nanocomposites require good interfacial bonding to achieve significant load transfer across the CNT–matrix interface [238]. Therefore, careful processing of the composites is of utmost importance. In the next section, we will discuss the different processing techniques and properties of a polyaniline/carbon nanotube (PANI–CNT) nanocomposite as a benchmark model.

7.2 Synthesis of the Composites

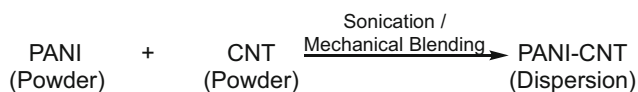
Various methodologies have been developed for chemically and electrochemically [239] preparing PANI–CNT composites, with two of the most common being direct solid-state mixing [240] and dispersal of CNTs in PANI solutions [241, 242] (Scheme 7a, b). However, a cursory scan of the literature reveals that in situ

1. DIRECT MIXING

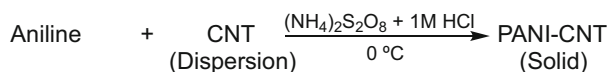
a. Solid-State Mixing



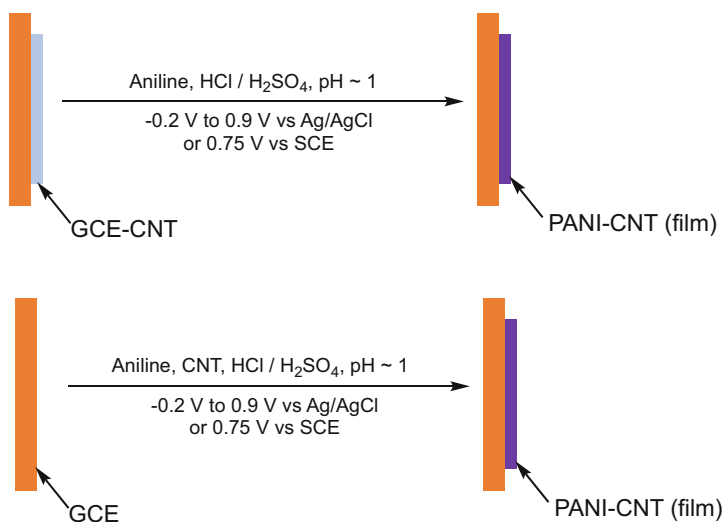
b. Solution Mixing



2. IN SITU CHEMICAL POLYMERIZATION



3. ELECTROCHEMICAL POLYMERIZATION



Scheme 7 General preparative methods of PANI-CNT composites

polymerization (Scheme 7c) is the most favored synthetic method for PANI-CNT NCs as it enables grafting of polymer molecules onto CNT, leading to better dispersion coefficients and augmented interactions between the CNT and the polymer matrix. Arguably, the in situ polymerization of aniline or substituted aniline in an acidic dispersion of multiwalled or single-walled carbon nanotubes, in the presence of an oxidant at low temperatures, is the simplest method reported so far [239, 243, 244]. Nevertheless, several approaches have been successfully adopted to obtain intimate mixing of nanotubes with polymer matrices in general, and polyaniline in particular, including dry powder mixing, solution blending, melt mixing, in situ polymerization, and surfactant-assisted mixing.

7.2.1 Solution Processing of Composites

Solution casting, which involves mixing of carbon nanotubes and the polymer in a suitable solvent, is the most common technique used in the preparation of CNTs/polymer. One benefit is easy deaggregation and dispersion of carbon nanotubes through agitation of the CNTs with the polymer in a solvent. This method consists of three steps:

- (a) Dispersion of carbon nanotubes in either a suitable solvent or polymer solution
- (b) Mixing of carbon nanotubes and the polymer
- (c) Recovery of the nanocomposite by precipitation or casting of a film

The synthesis of nanocomposite CNT/polymer can be done either through an organic or aqueous medium and the choice of solvent is usually dependent on the solubility of the polymer. Lau et al. [245] revealed the influence of solvents on carbon nanotubes dispersion and the thermal and mechanical properties of the composites. Their results demonstrated that, contrary to the general belief that only small traces of CNTs are needed to strengthen the epoxy composites, the choice of solvent used in the dispersion of CNTs cannot be ignored. They concluded that only the acetone-dispersed nanocomposites displayed improvements in flexural strength over the pure epoxy. Ethanol and dimethylformamide (DMF) actually countered the benefits of CNTs in the resulting nanocomposites. Subsequently, thermogravimetric characterization (TGA) proved the existence of remaining solvent in the resulting nanocomposites bringing to the fore the importance of considering the boiling points of solvents in the interest of improving the purity of products. Further study [246] provided evidence of the solvent influence, using Fourier Transform Infrared (FTIR) spectroscopy, on the molecular structure of the final nanocomposite. The presence of remaining solvent altered the reaction mechanism by restricting the nucleophile–electrophile interaction between the hardener and epoxy, thereafter affecting the degree of cross-linking and degrading the transport and mechanical properties of the cured structures.

In general, dispersion of carbon nanotubes can be done by magnetic stirring, shear mixing, reflux or most commonly, ultrasonication. The latter technique can be executed in two ways – mild sonication in a bath or high-powered sonication. Unfortunately, the use of high-powered ultrasonication for long periods of time

can cause shortening of the carbon nanotubes, i.e., reduce the aspect ratio, which is detrimental to the composite [247].

One resolution to this problem has been to disperse higher loadings of nanotubes, through the use of surfactants [246, 248, 249]. As an alternative to the covalent functionalization of CNTs, this approach preserves the integrity of the nanotubes without disrupting the extended π -conjugation [236]. When CNTs are dispersed in aqueous solutions containing surfactants, each individual nanotube (or small bundle) is encased in its own micelle-like envelope with the hydrophobic substituents of the surfactant oriented toward the nanotube and the hydrophilic groups oriented toward the solution. The insertion of aniline in the hydrophobic region within the micelle/CNT hybrid template guides the growth of PANI on the CNT surface. The utilization of surfactants including, anionic sodium dodecylsulfate (SDS) [250], dodecylbenzene sulfonic acid sodium salt [251], dodecylbenzene sulfonic acid (DBSA) [252], cationic cetyltrimethyl ammonium bromide (CTAB) [253], non-ionic poly(ethylene glycol) mono-p-nonyl phenyl ether (O π -10) and polyvinyl alcohol [254, 255], during the micelle/CNT hybrid template directed synthesis of CNT/PANI have produced composites with coaxial nanostructures. In such cases, cationic and nonionic surfactants are not incorporated into the CNT/PANI composites, unlike anionic surfactants that generally are integrated into the composite as a dopant. Zhang et al. [256] reported the template-directed synthesis, characterization, and electrical properties of single-walled carbon nanotube (SWNT)-based coaxial nanowires; that is, core (SWNT)-shell (conducting polypyrrole and polyaniline) nanowires in which an aqueous solution containing the cationic surfactant cetyltrimethylammonium bromide (CTAB) or the nonionic surfactant poly(ethylene glycol) mono-p-nonyl phenyl ether (O π -10) was employed. The results revealed that the micellar molecules could affect the surface morphologies of the resulting coaxial nanowires (SWCNT/polymer composite) but not the molecular structures of the corresponding conducting polymers.

In solvent blending, a slow evaporation step often leads to CNT aggregation. The research groups of Laplaze [257] and Chauvet [258] suggested spin-casting on substrate or drop-casting on a hot substrate CNT/polymer suspension to expedite the evaporation step and hence alleviate the aggregation problem. The solution processing method in the case of PANI/CNT composites generally consists of mixing PANI (Emeraldine Salt or Emeraldine Base) and CNT solutions or dispersions together in an appropriate solvent. Solvents, such as N-methyl-2-pyrrolidone (NMP), dimethylformamide (DMF), or N,N-dimethyl propylene urea (DMPU) are good solvents for the emeraldine base (EB) and are preferred solvents for the preparation of EB-CNT composites [259]. Water processing of emeraldine salt-carbon nanotube (ES-CNT) composites utilize CNT functionalized with hydrophilic moieties, such as carboxylic acid groups [260, 261], and/or hydrophilic PANI (sulfonated [262, 263] or boric acid [264-266]), or self-doped PANI. These modifications are to ensure that the CNTs are properly dispersed in the water. Water processing also refers to the ex-situ processing of ES-CNT composites reported in the literature [242, 260, 262, 267]. The external doping of PANI is important in the

preparation of stable aqueous colloids of ES, which leads to the nanofiber nanoscale structure of PANI [242, 268].

The classic surfactant-free method for the preparation of CNT/PANI composites consists of mixing aniline with an oxidant such as ammonium peroxydisulfate [269], ferric chloride [270], polyphenylene sulfide [271], etc. in an aqueous acidic dispersion [272] of MWCNT or SWCNT in concentrations ranging from 2 to 70 wt% either at low temperatures (0–4 °C) [173, 273] or at room temperature [274]. Among the available surfactant-free preparation methods that have been proposed to facilitate the dispersion of hydrophobic nonfunctionalized CNTs in aqueous media, addition of ethanol to the aqueous reaction medium [274], or refluxing in aniline [275], are generally accepted as being the most efficient. Another approach is to chemically modify the carbon nanotube surface so as to disrupt the rope structure and add reactive species to the nanotubes thereby improving interfacial bonding in CNT/PANI composites. Carboxylic acid [276–278] and amine-functionalized [278–280] CNTs are also frequently used for the same purpose. The oxidation of amino groups, covalently linked to CNT in aminobenzoyl functionalized CNT, generates radical cations that initiate polymerization on the surface [281].

The morphology of CNT/PANI composites depends on the content of CNT [282]. For instance, the morphology of neat PANI is comparable to that of MWCNT/PANI formed as individual nanofibers when MWCNT loading is at 2.7 wt%. However, when the MWCNT loading increases to 10 wt%, granular nanofibers are obtained. Greater than 20 wt% results in a continuous porous matrix formed from the cross-linked smooth-surface nanofibers and increasing the content of PANI to 80 wt% in the composites leads to full encapsulation of the carbon nanotubes by polyaniline [236]. Furthermore, Li and Kim [283] found that the use of a high mass ratio of aniline/MWCNT (4:1) can lead to the formation of nanofibers, with diameters between 10 nm and 15 nm, through in situ polymerization.

7.2.2 Melt Processing of Composites

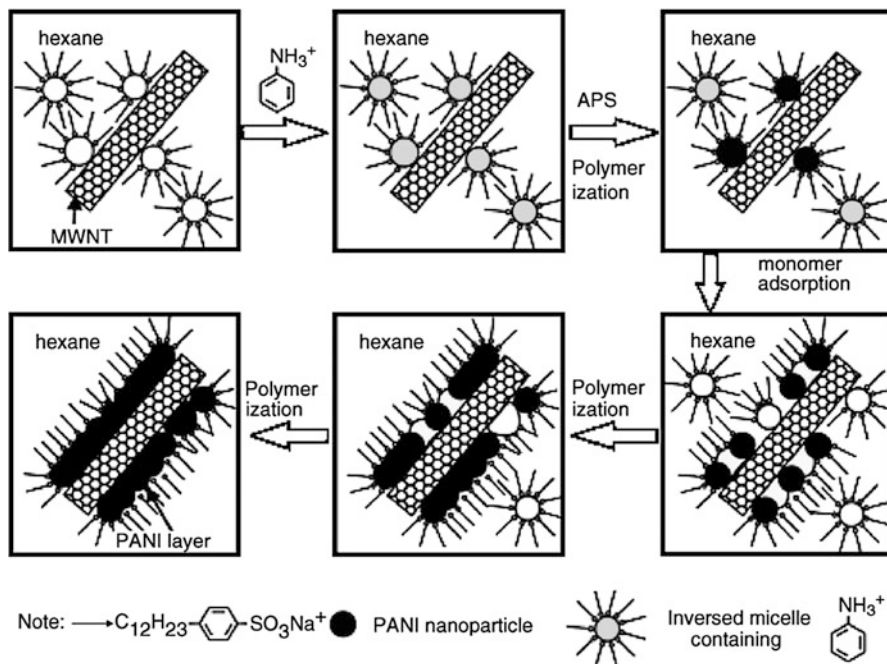
Solution processing is an important technique for both carbon nanotubes dispersion and nanocomposite formation; it is less suitable for industrial scale processes. To facilitate large-scale production for commercial applications, melt processing is the better alternative and the most commonly used method for industrial purposes owing to the low cost and simplicity of process. This technique makes use of the fact that thermoplastic polymers soften when heated. Melt mixing generally requires high temperatures to decrease the viscosity of the substrate and high shear forces to disperse the nanofillers, such as CNTs. Thus, composites of different shapes can be fabricated by techniques such as compression molding, injection molding, or extrusion. While melt blending is presented as a very simple method [284–287], the use of high shear forces and high temperatures can cause deterioration of the nanocomposite structure. To overcome these problems during melt processing, optimization of the processing conditions is required, not only for the different nanotube types but also for the entire range of polymer–nanotube

combinations [288]. For instance, high shear force is required to achieve CNT dispersion but this can lead to CNT fragmentation. Therefore an optimum shear stress is required to achieve the desired dispersion with the least amount of damage to the CNTs. On the other hand, high temperatures enhance CNT dispersion by lowering the viscosity but excessively high temperatures lead to loss of the intrinsic properties of the polymer. Studies have suggested that these challenges can be curtailed through modifications in melt compounding. Haggemueller et al. [289] combined solution and melt blending by subjecting a solvent-cast SWCNT/polymer film to several cycles of melt pressing. Jin et al. [290] introduced polymer-coated MWCNTs (rather than pristine MWCNTs) into the polymer melt to maximize compatibility.

7.2.3 In-situ Polymerization Processing of Composites

In addition to the previously mentioned two methods, which combine nanotubes with high molecular weight polymers, in situ polymerization utilizes CNTs and monomers. In situ polymerization has advantages over other composite fabrication methods, for example a stronger interface results owing to the facile intimate interactions between the polymer and nanotubes during and after the growth stage [291]. The main advantage of this method is that it enables grafting of polymer macromolecules onto the walls of CNTs. In addition, this processing technique allows for the preparation of NCs with high nanotube loading and very good miscibility. It is particularly useful when insoluble and/or thermally unstable polymers are desired, especially when processing by solution or melt processing is not possible. A simple in situ chemical polymerization of aniline, in an acidic dispersion of multiwall carbon nanotubes (MWCNTs) or single-wall carbon nanotubes (SWCNTs), in the presence of an oxidant at low temperature, has been reported by Cochet et al. [243, 244]. Saini et al. [292] described the fabrication process for a highly conducting PANI–MWCNT NC via an in situ polymerization. Carbon nanotube-polyaniline hybrid materials were successfully prepared using in situ emulsion polymerization and an in situ inverse microemulsion route (Scheme 8) [251, 293]. In situ polymerization has also been used for the preparation of composites of substituted PANI in the presence of either SWCNTs or MWCNTs. These include poly(*o*-anisidine) [294], poly(*N*-methylaniline) [295], poly(diphenylamine) [296], and poly(aminobenzoic acid) [297–299].

Another practical approach for the preparation of PANI–CNT composites is electrochemical deposition. Early attempts included the direct electrochemical polymerization of aniline on individual CNT whiskers [299] and an aqueous dispersion containing aniline and CNT [300]. In the latter example, the aniline functionalized CNT was sometimes dispersed in the electrolyte [301], while at other times, substituted PANI was grafted to SWCNT by oxidative coupling during electropolymerization [302, 303]. In 2014, PDMA multiwall carbon nanotubes (PDMA–MWCNTs) nanocomposite films were synthesized by in-situ electrochemical polymerization of a well-dispersed solution of DMA and multiwall carbon nanotubes (MWCNTs) [304].



Scheme 8 In situ synthesis of MWCNT/PANI core-shell nanowires using inverse micro-emulsion [279]

7.3 Interactions Between PANI and CNT

Electrical, thermal, and mechanical properties observed in PANI–CNT composites are intermediate between pure PANI and CNT and is dependent on CNT content and the extent of its integration with PANI. Thus, electrochemical properties of PANI–CNT composites are enhanced compared with the two individual components. For instance, electrochemical growth, redox, and capacitive currents of the composites are several-fold higher than the pure PANI [239, 305]. The same behavior is also observed in composites of CNT with substituted PANI derivatives, but the extent of the current increase depends on the nature of the substituent present on the aniline ring [239]. Such a remarkable current enhancement appears to be unique to PANI–CNT composites and has not been observed for any other conjugated polymer–CNT composite. The augmented properties are a direct result of the intimate interactions between PANI and carbon nanotubes.

There exists various possibilities for interactions between PANI and CNT in the composites. One of the first suggestions was the attachment of aniline radicals, generated during electrochemical oxidative polymerization, onto the CNT lattice especially at defect sites [239]. However, it was also postulated that the carboxylic acid sites on the acid-treated CNTs were the most likely sites of interaction with the

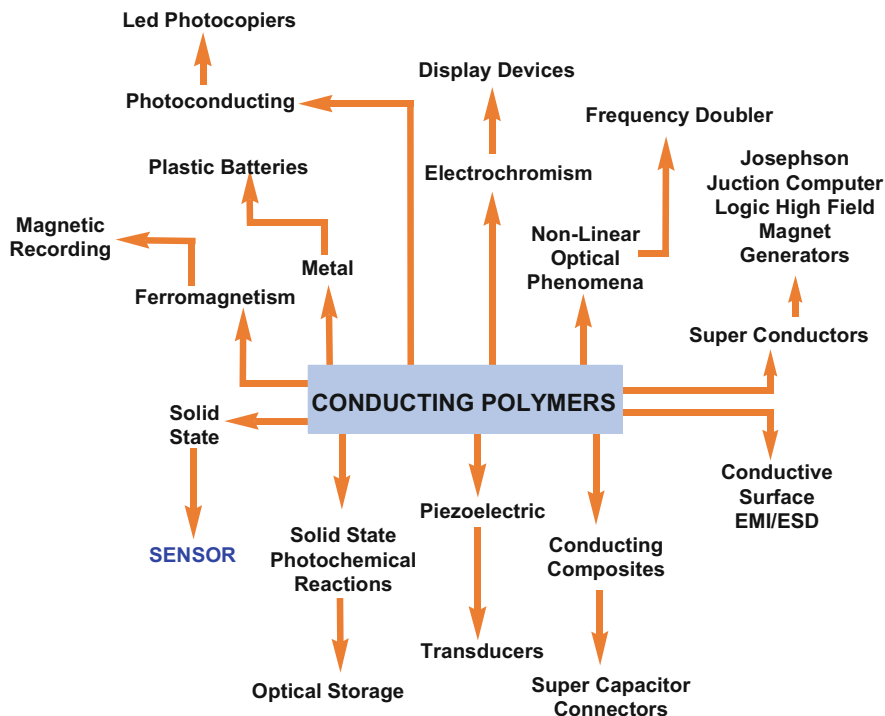


Fig. 20 Applications of conducting polymers

aniline monomer [305]. PANI can interact either with functionalized or with nonfunctionalized CNT.

8 Conclusions

CPs are characterized by a conjugated structure of alternating single and double bonds (extended π -orbital system) through which electrons can move from one end of the polymer to the other. Hence the electrons become delocalized over the whole and are shared by many atoms.

Conducting polymers (CPs) are mainly used in environmental monitoring and clinical diagnostics to achieve fast detection, high sensitivity, small size, and specificity for investigation of a particular analyte through the use of electrochemical sensors and biosensors. Conductivity values for conducting polymers vary from 10^{-10} to 10^6 S.cm⁻¹, covering the range associated with semiconductors and conductive filler composites, at the lower end, to metals at the higher end. Polymers with electrical conductivity and semiconductivity are of interest as lightweight replacements for inorganic metals and semiconductors. CPs have electrical and optical properties similar to those of metals and inorganic semiconductors but also exhibit

the attractive properties associated with conventional polymers such as ease of synthesis and processing.

In addition, conducting polymers have the potential to replace metal coatings and may be applied more economically utilizing nonvacuum processes from solution or from the melt. There are also clear signs that the effectiveness of conducting polymers in transferring electrical charges can be exploited for the preparation of nanocomposites (NCs) in the construction of sensors and in molecular devices. Likewise, organic semiconducting polymers may be synthetically tailored to optimize desirable properties such as melting point, melt viscosity, solubility, electrical and thermal conductivity. Conducting polymer composites (CPCs), resulting from the blending of an insulating polymer matrix with electrical conductive fillers (carbon black, carbon fibres, metal particles), show many interesting features including the variation in their electrical resistivity with thermal solicitations.

The use of pyrrole in the electrochemical synthesis of conducting polymers has proven important in allowing the development of new polymeric materials with worthwhile electrical properties. Recent studies have shown that conducting polymers – namely, PPy, PANI, and PEDOT – all have good biocompatibility and are promising alternatives for use in the development of new biodegradable conduits for restoration function of injured peripheral nerves or in the regeneration of a nerve gap by using in situ electrical stimulation.

Synthesis of conducting star, graft, or block copolymers of the conducting polymer permits chemical linkage between the insulating matrix (end groups) and the conjugated polymer. The new materials formed in this manner possess enhanced processability and chemical stability. Electrochemical copolymerization can produce a variety of conducting materials with different optical, electrical, morphological, and electrochromic properties.

Overall, these unique polymers (CPs) and their derivatives showcase a wide range of specific industrial applications (Fig. 20).

References

1. T. Taka, EMI shielding measurements on poly(3-octyl thiophene) blends. *Synth. Met.* **41**, 1177–1180 (1991)
2. D. Coltevieille, A. Le Méhauté, C. Challioui, P. Mirebeau, J.N. Demay, Industrial applications of polyaniline. *Synth. Met.* **101**, 703–704 (1999)
3. F. Jonas, G. Heywang, Technical applications for conductive polymers. *Electrochim. Acta* **39**, 1345–1347 (1994)
4. V. Misoska, J. Ding, J.M. Davey, W.E. Price, S.F. Ralph, G.G. Wallace, Polypyrrole membranes containing chelating ligands: synthesis, characterisation and transport studies. *Polymer* **42**, 8571–8579 (2001)
5. B. Wessling, J. Posdorfer, Corrosion prevention with an organic metal (polyaniline): corrosion test results. *Electrochim. Acta* **44**, 2139–2147 (1999)
6. C. M. Caldas, L. F. Calheiros, B. G. Soares, Silica-polyaniline hybrid materials prepared by inverse emulsion polymerization for epoxy-based anticorrosive coating, *J. Appl. Polym. Sci.* (2017). <https://doi.org/10.1002/app.45505>

7. Y. Ramanavicius, Z. Oztekin, A. Balevicius, V. Kausaite-Mikstimiene, I. Krikstolaityte, V. Baleviciute, A. Ratautaite, Ramanaviciene: Conducting and electrochemically generated polymers in sensor design. *Procedia Energy* **47**, 825–828 (2012)
8. D. Kumar, R.C. Sharma, *Advances in conductive polymers*. *Eur. Polym. J.* **34**, 1053–1060 (1998)
9. T.A. Skotheim, *Handbook of Conducting Polymers*, vol 2 (Marcel Dekker, New York, 1986)
10. H. Ma, X. Liu, D. Zhang, J. Xiang, Synthesis of polyaniline shell on nickel oxide nanoflake arrays for enhanced lithium ion storage. *Mater. Res. Bull.* **96**, 301–305 (2017)
11. A. Pud, G.S. Shapoval, P.G. Vinogradnyi, Electropolymerization of pyrrole in polymer matrices. *Russ. J. Electrochem.* **36**, 447–447 (2000)
12. M.J. Croissant, T. Napporn, J.M. Leger, C. Lammy, Electrocatalytic oxidation of hydrogen at platinum-modified polyaniline electrode. *Electrochim. Acta* **43**, 2447–2457 (1998)
13. J. Heinze, *Electrochemistry of conducting polymers*. *Synth. Met.* **41–43**, 2805–2823 (1991)
14. P. Bernier, S. Lefrant, G. Bidan, *Advances in synthetic metals. Twenty years of progress in science and technology* (Elsevier, 1999)
15. Y.-C.L. Kuang-Hsuan Yang, Y. Chung-Chin, Temperature effect of electrochemically roughened gold substrates on polymerization electrocatalysts of polypyrrole. *Anal. Chim. Acta* **631**, 40–46 (2009)
16. C. Zhang, X. Yi, H. Yui, S. Asai, M. Sumita, Morphology and electrical properties of short carbon fiber-filled polymer blends: High-density polyethylene/poly(methyl methacrylate). *J. Appl. Polym. Sci.* **69**, 1813–1819 (1998)
17. T. Ahuja, I. Mir, D. Kumar, Rajesh: Biomolecular immobilization on conducting polymers for biosensing applications. *Biomaterials* **28**, 791–805 (2007)
18. B.D. Malhotra, A. Chaudhary, S.P. Singh, Prospects of conducting polymers in biosensors. *Anal. Chim. Acta* **578**, 59–74 (2006)
19. F. Wang, R.D. Rauh, Reflective and conductive star polymers, US Patent 6,025,462 (2000)
20. F. Gubbels, R. Jerome, E. Vanlathem, R. Deltour, S. Blacher, F. Brouers, Kinetic and thermodynamic control of the selective localization of carbon black at the interface of immiscible polymer blends. *Chem. Mater.* **10**, 1227–1235 (1998)
21. C. Lagrève, J.F. Feller, I. Linossier, G. Levesque, Poly(butylene terephthalate)/poly(ethylene-co-alkyl acrylate)/carbon black conductive composites: Influence of composition and morphology on electrical properties. *Polym. Eng. Sci.* **41**, 1124–1132 (2001)
22. F. El-Tantawy, K. Kamada, H. Ohnabe, A novel way of enhancing the electrical and thermal stability of conductive epoxy resin-carbon black composites via the Joule heating effect for heating-element applications. *J. Appl. Polym. Sci.* **87**, 97–109 (2003)
23. V. Saxena, B.D. Malhotra, Prospects of conducting polymers in molecular electronics. *Curr. Appl. Phys.* **3**, 293–305 (2003)
24. L. Huang, T. Wen, A. Gopalan, F. Ren, Structural influence on the electronic properties of methoxy substituted polyaniline/aluminum Schottky barrier diodes. *Mater. Sci. Eng., B* **104**, 88–95 (2003)
25. S. Brahim, A.M. Wilson, D. Narinesingh, E. Iwuoha, A. Guiseppe-Elie, Chemical and biological sensors based on electrochemical detection using conducting electroactive polymers. *Microchim. Acta* **143**, 123–137 (2003)
26. M. Beregoi, A. Evangelidis, E. Matei, I. Enculescu, Polyaniline based microtubes as building blocks for artificial muscle applications. *Sens Actuators B Chem.* **253**, 576–583 (2017)
27. G. Latessa, F. Brunetti, A. Reale, G. Saggio, A. Di Carlo, Piezoresistive behaviour of flexible PEDOT:PSS based sensors. *Sens Actuators B Chem* **139**, 304–309 (2009)
28. K. Arshak, V. Velusamy, O. Korostynska, K. Oliwa-Stasiak, C. Adley, Conducting polymers and their applications to biosensors: Emphasizing on foodborne pathogen detection. *IEEE Sens. J.* **9**, 1942–1951 (2009)
29. W.J. Feast, *Handbook of Conducting Polymers* (Marcel Dekker, New York, 1986)
30. U. Salzner, J.B. Lagowski, P.G. Pickup, R.A. Poirier, Comparison of geometries and electronic structures of polyacetylene, polyborole, polycyclopentadiene, polypyrrole, polyfuran,

- polysilole, polyphosphole, polythiophene, polyselenophene and polytellurophene. *Synth. Met.* **96**, 177–189 (1998)
31. Z.G. Soos, *Handbook of Conductive Polymers* (Marcel Dekker, New York, 1986)
 32. E. Riande, R. Diaz-Calleja, *Electrical Properties of Polymers* (Marcel Dekker, Inc., New York, 2004)
 33. R. Gottan, R. Bhosale, P. Srinivasan, Polyaniline salt containing dual dopants pyrelenediimide tetracarboxylic acid, and sulfuric acid. *J. Appl. Polym. Sci.* (2017). <https://doi.org/10.1002/app.45456>
 34. J. Heeger, Semiconducting and metallic polymers: The fourth generation of polymeric materials. *Synth. Met.* **125**, 23–42 (2001)
 35. H. Masuda, D.K. Asano, Preparation and properties of polypyrrole. *Synth. Met.* **135–136**, 43–44 (2003)
 36. S.W. Kim, Y.H. Bae, T. Okano, Hydrogels: Swelling, drug loading, and release. *Pharm. Res.* **9**, 283–290 (1992)
 37. R. Langer, New methods of drug delivery. *Science* **249**, 1527–1533 (1990)
 38. W. Rehwald, H.G. Kiess, Charge transport in polymers, in *Conjugated Conducting Polymers*, (Springer-Verlag, New York, 1992), pp. 135–173
 39. G. G. Wallace, P.R. Teasdale, G.M. Spinks, L.A.P. Kane-Maguire, Properties of polypyrroles. In: *Conductive Electroactive Polymers: Intelligent Materials Systems*. (CRC Press, 2002)
 40. E.T. Kang, K.G. Neoh, K.L. Tan, Polyaniline: a polymer with many interesting intrinsic redox states. *Prog. Polym. Sci.* **23**, 277–324 (1998)
 41. R.L. Nashat, Temporal characteristics of activation, deactivation, and restimulation of signal transduction following depolarization in the pheochromocytoma cell line PC-12. *Mol. Cell. Biol.* **23**, 4788–4795 (2003)
 42. K. Cysewska, M. Gazda, P. Jasiński, Influence of electropolymerization temperatures on corrosion, morphological and electrical properties of PPy doped with salicylate on iron. *Surf. Coat. Technol.* **328**, 248–255 (2017)
 43. X. Cui, J.F. Hetke, J.A. Wiler, D.J. Anderson, D.C. Martin, Electrochemical deposition and characterization of conducting polymer polypyrrole/PSS on multichannel neural probes. *Sens Actuators A* **93**, 8–18 (2001)
 44. J. Reut, N. Reut, A. Opik, Preparation and characterization of multilayer systems consisting of the soluble and electrochemically synthesized polypyrrole films. *Synth. Met.* **119**, 81–82 (2001)
 45. M.S. Freund, C. Karp, N.S. Lewis, Growth of thin processable films of poly(pyrrole) using phosphomolybdate clusters. *Inorg. Chim. Acta* **240**, 447–451 (1995)
 46. G.B. Street, *Handbook of Conductive Polymers* (Marcel Dekker, New York, 1986)
 47. N.F. Mott, E.A. Davis, *Electronic Processes in Non-crystalline Materials* (Clarendon Press, Oxford, 1979)
 48. N.F. Mott, Electrons in glass. Nobel Lecture (1977)
 49. X. Sun, D. Lu, R. Fu, X.S. Li, D.L. Lin, T.F. George, Gap states of charged solitons in polyacetylene. *Phys. Rev. B* **40**, 12446 (1989)
 50. S. Larsson, L. Rodriguez-Monge, Conductivity in polyacetylene. II. Ab initio and tight-binding calculations of soliton structure and reorganization energy in ordered and disordered structures. *Int. J. Quantum Chem* **58**, 517–532 (1996)
 51. L. Xiaochang, J. Yangsheng, L. Shijin, The syntheses, properties and application of new conducting polymers. *Eur. Polym. J.* **27**, 1345–1351 (1991)
 52. G. Čik, F. Šeršeň, L. Dlhán, Thermally induced transitions of polarons to bipolarons in poly(3-dodecylthiophene). *Synth. Met.* **151**, 124–130 (2005)
 53. J.H. Kaufman, N. Colaneri, J.C. Scott, G.B. Street, Evolution of polaron states into bipolarons in polypyrrole. *Phys. Rev. Lett.* **53**, 1005 (1984)
 54. G.A. Farias, W.B. da Costa, F.M. Peeters, Acoustical polarons and bipolarons in two dimensions. *Phys. Rev. B* **54**, 12835–12840 (1996)

55. S. Irle, H. Lischka, Combined ab initio and density functional study on polaron to bipolaron transitions in oligophenyls and oligothiophenes. *J. Chem. Phys.* **107**, 3021–3032 (1997)
56. M.R. Fernandes, J.R. Garcia, M.S. Schultz, F.C. Nart, Polaron and bipolaron transitions in doped poly(p-phenylene vinylene) films. *Thin Solid Films* **474**, 279–284 (2005)
57. G. Verbist, F.M. Peeters, J.T. Devreese, Large bipolarons in two and three dimensions. *Phys. Rev. B* **43**, 2712–2720 (1991)
58. K. Pichler, D.A. Halliday, D.D.C. Bradley, P.L. Burn, R.H. Friend, A.B. Holmes, Optical spectroscopy of highly ordered poly(p-phenylene vinylene). *J. Phys.: Condens. Matter* **5**, 7155–7172 (1993)
59. J.M. Margolis (ed.), *Conductive Polymers and Plastics*. (Chapman and Hall, 1989). <https://doi.org/10.1002/pi.4990240111>
60. H.K. Chitte, G.N. Shinde, N.V. Bhat, V.E. Walunj, Synthesis of polypyrrole using ferric chloride (FeCl_3) as oxidant together with some dopants for use in gas sensors. *J. Sens Technol.* **1**, 47–56 (2011)
61. J. Chen, X. Zhu, C. Luo, Y. Dai, Electronic and optical properties of pyrrole and thiophene oligomers: A density functional theory study. *Int. J. Quantum Chem.* **117**, (2017) <https://doi.org/10.1002/qua.25453>
62. H. Shirakawa, E.J. Louis, A.G. MacDiarmid, C.K. Chiang, E.J. Louis, A.J. Heeger, Synthesis of electrically conducting organic polymers: Halogen derivatives of polyacetylene, (CH)_x. *J. Chem. Soc. Chem. Commun.*, 578–580 (1977)
63. N.K. Guimard, N. Gomez, C.E. Schmidt, Conducting polymers in biomedical engineering. *Prog. Polym. Sci.* **32**, 876–921 (2002)
64. K. Kanazawa, A.F. Diaz, R.H. Geiss, W.D. Gill, J.F. Kwak, J.A. Logan, J.F. Rabolt, G.B. Street, ‘Organic metals’: polypyrrole, a stable synthetic ‘metallic’ polymer. *J. Chem. Soc. Chem. Commun.*, 854–855 (1979)
65. M. Gerard, A. Chaubey, B.D. Malhotra, Application of conducting polymers to biosensors. *Biosens. Bioelectron.* **17**, 345–359 (2002)
66. R.F. Ngece, *Electrochemical Dynamics of Cytochrome P450 (2D6) Biosensors for Selective Serotonin Re-uptake Inhibitors (SSRIs)* (University of the Western Cape, Cape town, 2007)
67. G. Tourillon, Polythiophene and its derivatives, in *Handbook of Conducting Polymers*, (1986), pp. 293–350
68. L. Groenendaal, G. Zotti, P.H. Aubert, S.M. Waybright, J.R. Reynolds, Electrochemistry of poly(3,4-alkylenedioxythiophene) derivatives. *Adv. Mater.* **15**, 855–879 (2003)
69. M. Dietrich, J. Heinze, G. Heywang, F.J. Jonas, Electrochemical and spectroscopic characterization of polyalkylenedioxythiophenes. *J. Electroanal. Chem.* **369**, 87–92 (1994)
70. E. Andreas, K. Stephan, L. Wilfried, M. Udo, R. Knud, *PEDOT principles and applications of an intrinsically conductive polymer* (Mario En-tech, LLC, Boca Raton, London, New York, 2010)
71. Y. Kudoh, K. Akami, Y. Matsuya, Properties of chemically prepared polypyrrole with an aqueous solution containing $\text{Fe}_2(\text{SO}_4)_3$, a sulfonic surfactant and a phenol derivative. *Synth. Met.* **95**, 191–196 (1998)
72. J. Rodriguez, H.-J. Grande, T.F. Otero, Conductive polymers: Synthesis and electrical properties, in *Handbook of Organic Conductive Molecules and Polymers*, (Wiley Sons, Chichester, 1997)
73. T. Tüken, B. Yazıcı, M. Erbil, The use of polyindole for prevention of copper corrosion. *Surf. Coat. Technol.* **200**, 4802–4809 (2006)
74. M. Bazzzaoui, J.I. Martins, E.A. Bazzzaoui, L. Martins, E. Machnikova, Sweet aqueous solution for electrochemical synthesis of polypyrrole part 1B: On copper and its alloys. *Electrochim. Acta* **52**, 3568–3581 (2007)
75. L. Lehr, S.B. Saidman, Corrosion protection of iron by polypyrrole coatings electro-synthesised from a surfactant solution. *Corros. Sci.* **49**, 2210–2225 (2007)
76. R. Kiefer, S.Y. Chu, P.A. Kilmartin, G. Bowmaker, R.P. Cooney, J. Travas-Sejdic, Mixed-ion linear actuation behaviour of polypyrrole. *Electrochim. Acta* **52**, 2386–2391 (2007)

77. F.W. Scheller, U. Wollenberger, A. Warsinke, F. Lisdat, Research and development in biosensors. *Curr. Opin. Biotechnol.* **12**, 35–40 (2001)
78. G. Sabouraud, S. Sadki, N. Brodie, The mechanisms of pyrrole electropolymerization. *Chem. Soc. Rev.* **29**, 283–293 (2000)
79. N. Zelikin, D. Lynn, J. Farhadi, I. Martin, V. Shastri, R. Langer, Erodible conducting polymers for potential biomedical applications. *Angew. Chem. Int. Ed.* **41**, 141–144 (2002)
80. S. Takeo, O. Akira, I. Tomokazu, H. Kenichi, A novel type of polymer battery using a pyrrole-polyanion composite electrode. *J. Chem. Soc. Chem. Commun.*, 327–328 (1987)
81. P.M. George, *Novel Polypyrrole Derivatives to Enhance Conductive Polymer-Tissue Interactions* (Massachusetts Institute of MIT, 2005)
82. K. Shimizu, M.K. Yamaka, Rechargeable lithium batteries using polypyrrole-poly(styrenesulfonate) composite as the cathode-active material. *Bull. Chem. Soc. Jpn.* **61**, 4401–4406 (1988)
83. R.D. Peres, M.A. De Paoli, S. Panero, B. Scrosati, A new electrode for a poly(pyrrole)-based rechargeable battery. *J. Power Sources* **40**, 299–305 (1992)
84. S. Tarkuc, E. Sahin, L. Toppare, D. Colak, I. Cianga, Y. Yagci, Synthesis, characterization and electrochromic properties of a conducting copolymer of pyrrole functionalized polystyrene with pyrrole. *Polymer* **47**, 2001–2009 (2006)
85. M. Mermillod, J. Tanguy, F. Petiot, A study of chemically synthesized polypyrrole as electrode material for battery applications. *J. Electrochem. Soc.* **133**, 1073–1079 (1986)
86. F. Diaz, J.I. Castillo, J.A. Logan, W.Y. Lee, Electrochemistry of conducting polypyrrole films. *J. Electroanal. Chem.* **129**, 115–132 (1981)
87. G. Sotzing, J.R. Reynolds, P. Steel, Electrochromic conducting polymers via electrochemical polymerization of Bis(2-(3,4-ethylenedioxy)thienyl) Monomers. *Chem. Mater.* **4**, 882–889 (1996)
88. H. Burroughes, D.D.C. Bradley, A.R. Brown, R.N. Marks, K. Mackay, R.H. Friend, P.L. Burns, A.B. Holmes, Light-emitting diodes based on conjugated polymers. *Nature* **347**, 539–541 (1990)
89. D. Braun, A. Heeger, Visible light emission from semiconducting polymer diodes. *Appl. Phys. Lett.* **58**, 1982–1984 (1991)
90. F. Larmat, J.R. Reynolds, Y.J. Qiu, Polypyrrole as a solid electrolyte for tantalum capacitors. *Synth. Met.* **79**, 229–233 (1996)
91. A. Rudge, I. Raistrick, S. Gottesfeld, J. Ferraris, A study of the electrochemical properties of conducting polymers for application in electrochemical capacitors. *Electrochim. Acta* **39**, 273–287 (1994)
92. P. Zhang, Y.X. Zhou, J. Lin, H. Li, Y. Bai, J. Zhu, S. Mao, J. Wang, Gravity assisted synthesis of micro/nano-structured polypyrrole for supercapacitors. *Chem. Eng. J.* **330**, 1060–1067 (2017)
93. F. Selampinar, L. Toppare, U. Akbulut, T. Yalçin, S. Süzer, A conducting composite of polypyrrole II. As a gas sensor. *Synth. Met.* **68**, 109–116 (1995)
94. J.J. Miasik, A. Hooper, B.C. Tofield, Conducting polymer gas sensors. *J. Chem. Soc. Faraday Trans. I* **82**, 1117–1126 (1986)
95. P.N. Bartlett, P.B. Archer, S. Ling-Chung, Conducting polymer gas sensors part I: Fabrication and characterization. *Sens. Actuators* **19**, 125–140 (1989)
96. S. Hwang, J.M. Ko, H.W. Rhee, C.Y. Kim, A polymer humidity sensor. *Synth. Met.* **57**, 3671–3676 (1993)
97. T. Otero, S. Beaumont, Chemical sensors from the cooperative actuation of multistep electrochemical molecular machines of polypyrrole: Voltammetric study. *Sens. Actuators B: Chem* **253**, 958–966 (2017)
98. C.R. Martin, W. Liang, V. Menon, R. Parthasarathy, A. Parthasarathy, Electronically conductive polymers as chemically-selective layers for membrane-based separations. *Synth. Met.* **57**, 3766–3773 (1993)
99. W. Schuhmann, C. Kranz, J. Huber, H. Wohlschläger, Conducting polymer-based amperometric enzyme electrodes. Towards the development of miniaturized reagentless biosensors. *Synth. Met.* **61**, 31–35 (1993)

100. W. Schuhmann, Functionalized polypyrrole. A new material for the construction of biosensors. *Synth. Met.* **41**, 429–432 (1991)
101. F. Selampinar, U. Akbulut, M.Y. Özden, L. Toppare, Immobilization of invertase in conducting polymer matrices. *Biomaterials* **18**, 1163–1168 (1997)
102. X.B. Chen, J. Devaux, J.-P. Issi, D. Billaud, The stability of polypyrrole electrical conductivity. *Eur. Poly. J.* **30**, 809–811 (1994)
103. R. Singh, R.P. Tandon, V.S. Panwar, S. Chandra, Low frequency ac conduction in lightly doped polypyrrole films. *J. Appl. Phys.* **69**, 2504–2508 (1991)
104. S. Kivelson, Electron hopping conduction in the soliton model of polyacetylene. *Phys. Rev. Lett.* **46**, 1344–1348 (1981)
105. M. Ates, T. Karazehir, A.S. Sarac, Conducting polymers and their applications. *Curr. Phys. Chem.* **2**, 224–2410 (2012)
106. Y. Liu, T. Cui, K. Varahramyan, All-polymer capacitor fabricated with inkjet printing technique. *Solid-State Electron.* **47**, 1543–1548 (2003)
107. F.O. Toribio, T.C. Maria, Soft and wet conducting polymers for artificial muscles. *Adv. Mater.* **15**, 279–282 (2003)
108. J. Lee, F. Serna, J. Nickels, C.E. Schmidt, Carboxylic acid-functionalized conductive polypyrrole as a bioactive platform for cell adhesion. *Biomacromolecules* **7**, 1692–1695 (2006)
109. A. Kotwal, C.E. Schmidt, Electrical stimulation alters protein adsorption and nerve cell interactions with electrically conducting biomaterials. *Biomaterials* **22**, 1055–1064 (2001)
110. Y. Furukawa, S. Tazawa, Y. Fujii, I. Harada, Raman spectra of polypyrrole and its 2,5-13C-substituted and C-deuterated analogues in doped and undoped states. *Synth. Met.* **24**, 329–341 (1988)
111. S. Radhakrishnan, P. Somani, Electrochromic response in polypyrrole sensitized by Prussian blue. *Chem. Phys. Lett.* **292**, 218–222 (1998)
112. E.M. Giroto, M.-A. de Paoli, Polypyrrole color modulation and electrochromic contrast enhancement by doping with a dye. *Adv. Mater.* **10**, 790–793 (1998)
113. U. Bulut, F. Yılmaz, Y. Yagci, L. Toppare, Synthesis, characterization and electrochromic properties of conducting copolymers of 3-[(3-thienylcarbonyl)oxy]-2,2-bis{[(3-thienylcarbonyl)oxy]}propyl 3-thiophene carboxylate with thiophene and pyrrole. *React. Funct. Polym.* **61**, 63–70 (2004)
114. J. Xu, G. Nie, S. Zhang, X. Han, J. Hou, S. Pu, Electrochemical copolymerization of indole and 3,4-ethylenedioxythiophene. *J. Mater. Sci.* **40**, 2867–2873 (2005)
115. S. Alkan, L. Toppare, Y. Hepuzer, Y. Yagci, Block copolymers of thiophene-capped poly(methyl methacrylate) with pyrrole. *J. Polym. Sci., Part A: Polym. Chem.* **37**, 4218–4225 (1999)
116. N. Kizilyar, L. Toppare, A. Önen, Y. Yağci, Synthesis of conducting PPy/pTHF copolymers. *J. Appl. Polym. Sci.* **71**, 713–720 (1999)
117. E. Kalaycioglu, L. Toppare, Y. Yagci, V. Harabagiu, M. Pintela, R. Ardelean, B. Simionescu, Synthesis of conducting H-type polysiloxane-polypyrrole block copolymers. *Synth. Met.* **97**, 7–12 (1998)
118. B. Bengü, L. Toppare, E. Kalaycioglu, Synthesis of conducting graft copolymers of 2-(N-pyrrolyl)ethylvinyl ether with pyrrole. *Des. Monomers Polym.* **4**, 53–65 (2001)
119. H. Yamamoto, M. Oshimia, M. Fukuda, I. Isa, K. Yoshino, Characteristics of aluminum solid electrolyte capacitors using a conducting polymer. *J. Power Sources* **60**, 173–177 (1996)
120. Y.-C. Liu, K.-C. Chung, Characteristics of conductivity-improved polypyrrole films via different procedures. *Synth. Met.* **139**, 277–281 (2003)
121. J. Sung, S. Kim, K. Lee, Fabrication of microcapacitors using conducting polymer microelectrodes. *J. Power Sources* **124**, 343–350 (2003)
122. A. Marocchi, D. Lanari, A. Facchetti, L. Vacarro, Poly(3-hexylthiophene): Synthetic methodologies and properties in bulk heterojunction solar cells. *Energy Environ. Sci.* **5**, 8457–8474 (2012)

123. R.L. Elsenbaumer, K.Y. Jen, R. Oboodi, Processible and environmentally stable conducting polymers. *Synth. Met.* **15**, 169–174 (1986)
124. A. Balamurugan, S. Chen, Silver nanograin incorporated PEDOT modified electrode for electrocatalytic sensing of hydrogen peroxide. *Electroanal.* (**12**), 1419–1423 (2009)
125. L. Groenendaal, F. Jonas, D. Freitag, H. Pielartzik, J.R. Reynolds, Poly(3,4-ethylenedioxythiophene) and its derivatives: Past, present, and future. *Adv. Mater.* **12**, 481–494 (2000)
126. G. Sonmez, P. Schottland, J.R. Reynolds, PEDOT/PAMPS: An electrically conductive polymer composite with electrochromic and cation exchange properties. *Synth. Met.* **155**, 130–137 (2005)
127. V.S. Vasantha, R. Thangamuthu, S. Mingchen, Electrochemical polymerization of poly(3,4-ethylene dioxy thiophene) from aqueous solution containing hydroxyl propyl-beta-cyclodextrine and the electrocatalytic behavior of modified electrode towards oxidation of sulphur oxoanion and nitrite. *Electroanal.* **20**, 1754–1759 (2008)
128. M. Zahid, E.L. Papadopoulou, A. Athanassiou, I.S. Bayer, Strain-responsive mercerized conductive cotton fabrics based on PEDIT:PSS/graphene. *Mater. Design* **135**, 213–222 (2017)
129. J. Aguirre, L. Daille, D.A. Fischer, C. Galarce, G. Pizarro, I. Vargas, M. Walczak, R. de la Iglesia, F. Armijo, Study of poly(3,4-ethylenedioxythiophene) as a coating for mitigation of biocorrosion of AISI 304 stainless steel in natural seawater. *Prog. Org. Coat.* **113**, 175–184 (2017)
130. G. Zotti, B. Vercelli, A. Berlin, Gold nanoparticle linking to polypyrrole and polythiophene monolayers and multilayers. *Chem. Mater.* **20**, 6509–6516 (2008)
131. N. Sakmeche, E.A. Bazzaoui, M. Fall, S. Aeiyaeh, M. Jouini, J.C. Lacroix, J.J. Aaron, P.C. Lacaze, Application of sodium dodecyl sulphate (SDS) micellar solution as an organised medium for electropolymerization of thiophene derivatives in water. *Synthetic Met.* **84**, 191–192 (1997)
132. A. Zykwińska, W. Domagala, M. Lapkowski, ESR spectroelectrochemistry of poly(3,4-ethylenedioxythiophene) (PEDOT). *Electrochem. Commun.* **5**, 603–608 (2003)
133. R. Ruffo, A. Celik-Cochet, U. Posset, C.M. Mari, G. Schottner, Mechanistic study of the redox process of an in situ oxidatively polymerised poly(3,4-ethylene-dioxythiophene) film. *Sol. Energy Mater. Sol. Cells* **92**, 140–145 (2008)
134. W.A. Gazotti Jr., G. Casalbore-Miceli, S. Mitzakoff, A. Geri, M.C. Gallazzi, M.A. De Paoli, Conductive polymer blends as electrochromic materials. *Electrochim. Acta* **44**, 1965–1971 (1999)
135. M. Higuchi, Y. Akasaka, T. Ikeda, A. Hayashi, D. Kurth, Electrochromic solid-state devices using organic-metallic hybrid polymers. *J. Inorg. Organomet. Polym. Mater.* **19**, 74–78 (2009)
136. C. Damlin, A.I. Kvarnström, Electrochemical synthesis and in situ spectroelectrochemical characterization of poly(3,4-ethylenedioxythiophene) (PEDOT) in room temperature ionic liquids. *J. Electroanal. Chem.* **570**, 113–122 (2004)
137. C.T. Barry, S. Philippe, Z. Kyukwan, R.R. John, In situ colorimetric analysis of electrochromic polymers and devices. *Chem. Mater.* **12**, 1563–1571 (2000)
138. C. Nien, T.S. Tung, K.C. Ho, Amperometric glucose biosensor based on entrapment of glucose oxidase in a poly(3,4-ethylenedioxythiophene) film. *Electroanal.* **18**, 1408–1415 (2006)
139. W. Chen, G. Güler, E. Kuruvilla, G.B. Schuster, H.C. Chiu, E. Riedo, Development of self-organizing, self-directing molecular nanowires: Synthesis and characterization of conjoined DNA-2,5-Bis(2-thienyl)pyrrole oligomers. *Macromolecules* **43**, 4032–4040 (2010)
140. M. Giannetto, V. Matrià, G. Mori, A. Arduini, A. Secchi, New selective gas sensor based on piezoelectric quartz crystal modified by electropolymerization of a molecular receptor functionalised with 2,2'-bithiophene. *Sens. Actuators B Chem.* **115**, 62–68 (2006)
141. T. Kuwahara, H. Ohta, M. Kondo, M. Shimomura, Immobilization of glucose oxidase on carbon paper electrodes modified with conducting polymer and its application to a glucose fuel cell. *Bioelectrochemistry* **74**, 66–72 (2008)

142. M. Park, H.J. Lee, Recent advances in electrochemical studies of π -conjugated polymers. *Bull. Korean Chem. Soc.* **26**, 697–705 (2005)
143. L.L. Beecroft, K.O. Christopher, Nanocomposite materials for optical applications. *Chem. Mater.* **9**, 1302–1317 (1997)
144. O. Razaq, O. Arotiba, S. Mailu, T. Waryo, P. Baker, E. Iwuoha, Electrochemical aptasensor for endocrine disrupting 17 β -estradiol based on a poly(3,4-ethylenedioxythiophene)-gold nanocomposite platform. *Sensors* **10**, 9872–9890 (2010)
145. P.C. Nien, P.Y. Chen, K.C. Ho, Fabricating an amperometric cholesterol biosensor by a covalent linkage between Poly(3-thiopheneacetic acid) and cholesterol oxidase. *Sensors* **9**, 1794–1806 (2009)
146. L. Pigani, A. Heras, Á. Colina, R. Seeber, J. López-Palacios, Electropolymerisation of 3,4-ethylenedioxythiophene in aqueous solutions. *Electrochem. Commun.* **6**, 1192–1198 (2004)
147. Y.H. Xiao, C.M. Li, M.L. Toh, R. Xue, Adenosine 5' triphosphate incorporated poly(3,4-ethylenedioxythiophene) modified electrode a bioactive platform with electroactivity, stability and biocompatibility. *Chem. Biol. Interact.* **157–158**, 423–426 (2005)
148. V.S. Vasantha, S.-M. Chen, Electrochemical preparation and electrocatalytic properties of PEDOT/ferricyanide film-modified electrodes. *Electrochim. Acta* **51**, 347–355 (2005)
149. P. Olowu, C. Ndangili, N. Ikpo, P. Njomo, E. Baker, Iwuoha: Spectroelectrochemical dynamics of dendritic poly(propyleneimine)-polythiophene star copolymer aptameric 17 β -estradiol biosensor. *Int. J. Electrochem. Sci.* **6**, 1686–1708 (2011)
150. P. Ali, S. Srivastava, I. Ali Khan, V.D. Gupta, S.U.I. Ansari, Phonon dispersion and heat capacity in polyfuran. *Spectrochim. Acta A Mol. Biomol. Spectrosc.* **93**, 149–154 (2012)
151. C.C. Ferrón, M.C.R. Delgado, O. Gidron, S. Sharma, D. Sheberla, Y. Sheynin, M. Bendikov, J.T.L. Navarrete, V. Hernández, α -Oligofurans show a sizeable extent of π -conjugation as probed by Raman spectroscopy. *Chem. Commun.* **48**, 6732–6734 (2012)
152. M. El-Nahas, A.H. Mangood, T.S. El-Shazly, Theoretical investigation of the conducting properties of substituted phosphole oligomers. *Comp. Theor. Chem.* **980**, 68–72 (2012)
153. N.F. Atta, M.F. El-Kady, A. Galal, Palladium nanoclusters-coated polyfuran as a novel sensor for catecholamine neurotransmitters and paracetamol. *Sens. Actuators B-Chem.* **141**, 566–574 (2009)
154. M. Kraljić, Z. Mandić, L. Duić, Inhibition of steel corrosion by polyaniline coatings. *Corros. Sci.* **45**, 181–198 (2003)
155. D. Zhang, Y. Wang, Synthesis and applications of one-dimensional nano-structured polyaniline: An overview. *Mater. Sci. Eng., B* **134**, 9–19 (2006)
156. D. Trivedi, Polyanilines. In: *Handbook of Organic Conductive Molecules and Polymers, Volume 2, Conductive Polymers: Synthesis and Electrical Properties*. (Wiley, 1997) pp. 506–572
157. J.C. Michaelson, A.J. McEvoy, M. Grätzel, Proceedings of the international conference on science and technology of synthetic metals electrochemical behaviour of various polyaniline morphologies in nonaqueous electrolytes. *Synth. Met.* **55**, 1564–1569 (1993)
158. E.I. Iwuoha, D. Saenz de Villaverde, N.P. Garcia, M.R. Smyth, J.M. Pingarron, Reactivities of organic phase biosensors. 2. The amperometric behaviour of horseradish peroxidase immobilised on a platinum electrode modified with an electrosynthetic polyaniline film. *Biosens. Bioelectron.* **12**, 749–761 (1997)
159. L.G. Paterno, S. Manolache, F. Denes, Synthesis of polyaniline-type thin layer structures under low-pressure RF-plasma conditions. *Synth. Met.* **130**, 85–97 (2002)
160. G.J. Cruz, J. Morales, M.M. Castillo-Ortega, R. Olayo, Synthesis of polyaniline films by plasma polymerization. *Synth. Met.* **88**, 213–218 (1997)
161. C. Liao, M. Gu, Electroless deposition of polyaniline film via autocatalytic polymerization of aniline. *Thin Solid Films* **408**, 37–42 (2002)
162. S.-C. Kim, P. Huh, J. Kumar, B. Kim, J.-O. Lee, F.F. Bruno, L.A. Samuelson, Synthesis of polyaniline derivatives via biocatalysis. *Green Chem.* **9**, 44–48 (2007)

163. J. Gong, X.-J. Cui, Z.-W. Xie, S.-G. Wang, L.-Y. Qu, The solid-state synthesis of polyaniline/H4SiW12O40 materials. *Synth. Met.* **129**, 187–192 (2002)
164. G.G. Wallace, M.S. Geoffrey, A.P.K.-M. Leon, *Conductive Electroactive Polymers: Intelligent Materials Systems*, 2nd edn. (CRC Press, Boca Raton, 2003)
165. H. Tang, A. Kitani, M. Shiotani, Effects of anions on electrochemical formation and over-oxidation of polyaniline. *Electrochim. Acta* **41**, 1561–1567 (1996)
166. M. Kalaji, L. Nyholm, L.M. Peter, A microelectrode study of the influence of pH and solution composition on the electrochemical behaviour of polyaniline films. *J. Electroanal. Chem. Interfacial Electrochem.* **313**, 271–289 (1991)
167. S.-S. Chen, T.-C. Wen, A. Gopalan, Electrosynthesis and characterization of a conducting copolymer having S–S links. *Synth. Met.* **132**, 133–143 (2003)
168. G.D. Storrer, S.B. Colbran, D.B. Hibbert, Chemical and electrochemical syntheses, and characterization of poly(2,5-dimethoxyaniline) (PDMA): a novel, soluble, conducting polymer. *Synth. Met.* **62**, 179–186 (1994)
169. B. Palys, A. Kudelski, A. Stankiewicz, K. Jackowska, Influence of anions on formation and electroactivity of poly-2,5-dimethoxyaniline. *Synth. Met.* **108**, 111–119 (2000)
170. T.-C. Wen, L.-M. Huang, A. Gopalan, An in situ spectroelectrochemical investigation of the copolymerization of diaminobenzenesulfonic acid with aniline and its derivatives. *Electrochim. Acta* **46**, 2463–2475 (2001)
171. J. Stejskal, I. Sapurina, M. Trchová, Polyaniline nanostructures and the role of aniline oligomers in their formation. *Prog. Polym. Sci.* **35**, 1420–1481 (2010)
172. J. Stejskal, P. Kratochvíl, A.D. Jenkins, The formation of polyaniline and the nature of its structures. *Polymer* **37**, 367–369 (1996)
173. H. Zengin, W. Zhou, J. Jin, R. Czerw, D.W. Smith, L. Echegoyen, D.L. Carroll, S.H. Foulger, J. Ballato, Carbon nanotube doped polyaniline. *Adv. Mater.* **14**, 1480–1483 (2002)
174. P. Fedorko, M. Trznadel, A. Pron, D. Djurado, J. Planès, J.P. Travers, New analytical approach to the insulator–metal transition in conductive polyaniline. *Synth. Met.* **160**, 1668–1671 (2010)
175. M.G. Milica, Z.J. Branimir, S.S. Jasmina, L.T. Tomislav, B.N. Grgur, *Electrochemical Polymerization of Aniline, Electropolymerization*, (ed.) Dr. Ewa Schab-Balcerzak (InTech, 2011). <https://doi.org/10.5772/28293>. Accessed <http://www.intechopen.com/books/electropolymerization/electrochemical-polymerization-of-aniline2016>
176. R. Qian, J. Qiu, D. Shen, Conducting polypyrrole electrochemically prepared from aqueous solutions. *Synth. Met.* **18**, 13–18 (1987)
177. A. Metin, L. Toppare, Synthesis of star-shaped pyrrole and thiophene functionalized monomers and optoelectrochemical properties of corresponding copolymers. *Mater. Chem. Phys.* **114**, 789–794 (2009)
178. S. Chronakis, A.J. Grapenson, Conductive polypyrrole nanofibers via electrospinning: Electrical and morphological properties. *Polymer* **47**, 1597–1603 (2006)
179. S. Brahim, A. Guiseppi-Elie, Electroconductive hydrogels: Electrical and electrochemical properties of polypyrrole-poly(HEMA) composites. *Electroanal.* **17**, 556–570 (2005)
180. N.S. Sundaresan, S. Basak, M. Pomerantz, J.R. Reynolds, Electroactive copolymers of pyrrole containing covalently bound dopant ions: poly{pyrrole-co-[3-(pyrrol-1-yl)propanesulphonate]}. *J. Chem. Soc. Chem. Comm.* (8), 621–622 (1987)
181. C. Mailhe-Randolph, J. Desilvestro, Morphology of electropolymerized aniline films modified by para-phenylenediamine. *J. Electroanal. Chem. Interfac. Electrochem.* **262**, 289–295 (1989)
182. B.L. Funt, E.M. Peters, J.D. Van Dyke, Preparation of conducting copolymers by oxidative electropolymerization of 2,2'-bithiophene with pyrrole. *J. Polym. Sci. Part A: Polym. Chem.* **24**, 1529–1537 (1986)
183. O. Inganäs, B. Liedberg, W. Chang-Ru, H. Wynberg, A new route to polythiophene and copolymers of thiophene and pyrrole. *Synth. Met.* **11**, 239–249 (1985)
184. H.S.O. Chan, E.T. Kang, K.G. Neoh, K.L. Tan, B.T.G. Tan, Y.K. Lim, XPS studies of copolymers of pyrrole and N-methylpyrrole. *Synth. Met.* **30**, 189–197 (1989)

185. J.P. Ferraris, T.R. Hanlon, Optical, electrical and electrochemical properties of heteroaromatic copolymers. *Polymer* **30**, 1319–1327 (1989)
186. R.D. McCullough, R.D. Lowe, Enhanced electrical conductivity in regioselectively synthesized poly(3-alkylthiophenes). *J. Chem. Soc., Chem. Commun.*, 70–72 (1992)
187. R.D. McCullough, S. Tristram-Nagle, S.P. Williams, R.D. Lowe, M. Jayaraman, Self-orienting head-to-tail poly(3-alkylthiophenes): new insights on structure-property relationships in conducting polymers. *J. Am. Chem. Soc.* **115**, 4910–4911 (1993)
188. A. Chen, X. Wu, R.D. Rieke, Regiocontrolled synthesis of poly(3-alkylthiophenes) mediated by Rieke zinc: Their characterization and solid-state properties. *J. Am. Chem. Soc.* **117**, 233–244 (1995)
189. G. MacDiarmid, A.J. Epstein, Conducting polymers: Past, present and future. *Mater. Res. Soc. Symp. Proc.* **328**, 133–144 (1994)
190. J.M.J. Frechet, Functional polymers and dendrimers: reactivity, molecular architecture, and interfacial energy. *Science* **263**, 1710–1715 (1994)
191. J.L. Hedrick, M. Trollsas, C.J. Hawker, B. Atthoff, H. Claesson, A. Heise, R.D. Miller, D. Mecerreyes, R. Jérôme, P. Dubois, Dendrimer-like star block and amphiphilic copolymers by combination of ring opening and atom transfer radical polymerization. *Macromolecules* **31**, 8691–8705 (1998)
192. J. Roovers, L.L. Zhou, P.M. Toporowski, M. Vanderzwan, H. Iatrou, N. Hadjichristidis, Regular star polymers with 64 and 128 arms. Models for polymeric micelles. *Macromolecules* **26**, 4324–4331 (1993)
193. J. Roovers, B. Comanita, Dendrimers and dendrimer-polymer hybrids, in *Branched Polymers I*, (Springer, Berlin/Heidelberg, 1999), pp. 179–228
194. M. Kimura, M. Kato, T. Muto, K. Hanabusa, H. Shirai, Temperature-sensitive dendritic hosts: synthesis, characterization, and control of catalytic activity. *Macromolecules* **33**, 1117–1119 (2000)
195. A. Cooper, J. Londono, G. Wignall, J. McClain, E. Samulski, J. Lin, A. Dobrynin, M. Rubinstein, A.C. Burke, J. Frechet, J. DeSimone, Extraction of a hydrophilic compound from water into liquid CO₂ using dendritic surfactants. *Nature* **389**, 368–371 (1997)
196. R.C. Hedden, B.J. Bauer, A. Paul Smith, F. Gröhn, E. Amis, Templating of inorganic nanoparticles by PAMAM/PEG dendrimer-star polymers. *Polymer* **43**, 5473–5481 (2002)
197. D. Luo, K. Haverstick, N. Belcheva, E. Han, W.M. Saltzman, Poly(ethylene glycol)-conjugated PAMAM dendrimer for biocompatible, high-efficiency DNA delivery. *Macromolecules* **35**, 3456–3462 (2002)
198. R.C. Hedden, B.J. Bauer, Structure and dimensions of PAMAM/PEG dendrimer–star polymers. *Macromolecules* **36**, 1829–1835 (2003)
199. B. Comanita, B. Noren, J. Roovers, Star poly(ethylene oxide)s from carbosilane dendrimers. *Macromolecules* **32**, 1069–1072 (1999)
200. Y. Zhao, X. Shuai, C. Chen, F. Xi, Synthesis and characterization of star-shaped poly(l-lactide)s initiated with hydroxyl-terminated poly(amidoamine) (PAMAM-OH) dendrimers. *Chem. Mater.* **15**, 2836–2843 (2003)
201. S. Heise, J.L. Diamanti, C.W. Hedrick, R.D.M. Frank, Investigation of the initiation behavior of a dendritic 12-arm initiator in atom transfer radical polymerization. *Macromolecules* **34**, 3798–3801 (2001)
202. Q. Zheng, C.Y. Pan, Preparation and characterization of dendrimer-star PNIPAAm using dithiobenzoate-terminated PPI dendrimer via RAFT polymerization. *Eur. Polym. J.* **42**, 807–814 (2006)
203. F. Wang, M.S. Wilson, R.D. Rauh, Electroactive and conducting star-branched poly(3-hexylthiophene)s with a conjugated core. *Macromolecules* **32**, 4272–4278 (1999)
204. L.L. Miller, R.G. Duan, D.C. Tully, D.A. Tomalia, Electrically conducting dendrimers. *J. Am. Chem. Soc.* **119**, 1005–1010 (1997)
205. N. Baleb, A. Jahed, N. Arotiba, R. Mailu, P. Hendricks, E.I. Baker, Synthesis and characterization of poly(propylene imine) dendrimer – Polypyrrole conducting star copolymer. *J. Electroanal. Chem.* **652**, 18–25 (2011)

206. R.A. Olowu, P.M. Ndagili, C.O. Ikpo, A. Williams, R.F. Ngece, S.N. Mailu, N. Njomo, V. D.V. Wyk, P. Baker, E. Iwuoha, Impedimetry and microscopy of electrosynthetic poly(propylene imine)-co-poly(3,4-ethylene dioxythiophene) dendritic star copolymer. *Int. J. Electrochem. Sci.* **1855–1870** (2011)
207. P.H.J. Schenning, P. Jonkheijm, J. Hofkens, S.D. Feyter, T. Asavei, M. Cotlet, F.C.D. Schryver, E.W. Meijer, Formation and manipulation of supramolecular structures of oligo(p-phenylenevinylene) terminated poly(propylene imine) dendrimers. *Chem. Commun.*, 1264–1265 (2002)
208. P.H.J. Schenning, E. Peeters, E.W. Meijer, Energy transfer in supramolecular assemblies of oligo(p-phenylene vinylene)s terminated poly(propylene imine) dendrimers. *J. Am. Chem. Soc.* **122**, 4489–4495 (2000)
209. K. Miyashita, M. Kamigaito, M. Sawamoto, T. Higashimura, Synthesis of end-functionalized polystyrenes with organosilicon end-capping reagents via living cationic polymerization. *J. Polym. Sci., Part A: Polym. Chem.* **32**, 2531–2542 (1994)
210. P.R.L. Malenfant, J.M.J. Fréchet, Dendrimer solubilizing groups for conducting polymers: Preparation and characterization of polythiophene functionalized exclusively with aliphatic ether convergence dendron. *Macromolecules* **33**, 3634–3640 (2000)
211. J. Roncali, Electrogenerated functional conjugated polymers as advanced electrode materials. *J. Mater. Chem.* **9**, 1875–1893 (1999)
212. S. Deng, J. Locklin, D.B.A. Patton, R.C. Advincula, Thiophene dendron jacketed poly(amidoamine) dendrimers: Nanoparticle synthesis and adsorption on graphite. *J. Am. Chem. Soc.* **127**, 1744–1751 (2005)
213. H.A.M. Van-Aert, M.E.M. Burkard, J.F.G.A. Jansen, M.H.P. Van-Genderen, E.W. Meijer, H. Oevering, G.H.W. Buning, Functional oligomers, telechelics, and graft and star-shaped poly(2,6-dimethyl-1,4-phenylene ether)s prepared by redistribution. *Macromolecules* **28**, 7967–7969 (1995)
214. H.A.M. Van-Aert, M.H.P. Van-Genderen, E.W. Meijer, Star-shaped poly(2,6-dimethyl-1,4-phenylene ether). *Polym. Bull.* **37**, 273–280 (1996)
215. M. Liu, M. Petro, J.M.J. Fréchet, S.A. Haque, H.C. Wang, Preparation of hydrophobic poly(isobutylene) star polymer with hydrophilic poly(propylene imine) dendritic cores. *Polym. Bull.* **43**, 51–58 (1999)
216. E. Sahin, P. Camurlu, L. Toppare, V.M. Mercore, I. Cianga, Y. Yagci, Conducting copolymers of thiophene functionalized polystyrenes with thiophene. *J. Electroanal. Chem.* **579**, 189–197 (2005)
217. A. Hirao, K. Sugiyama, Y. Tsunoda, A. Matsuo, T. Watanabe, Precise synthesis of well-defined dendrimer-like star-branched polymers by iterative methodology based on living anionic polymerization. *J. Polym. Sci., Part A: Polym. Chem.* **44**, 6659–6687 (2006)
218. M. Trollsås, M.A. Kelly, H. Claesson, R. Siemens, J.L. Hedrick, Highly branched block copolymers: Design, synthesis, and morphology. *Macromolecules* **32**, 4917–4924 (1999)
219. R. Francis, D. Taton, J.L. Logan, P. Masse, Y. Gnanou, R.S. Duran, Synthesis and surface properties of amphiphilic star-shaped and dendrimer-like copolymers based on polystyrene core and poly(ethylene oxide) corona. *Macromolecules* **36**, 8253–8259 (2003)
220. M. Trollsås, B. Atthoff, H. Claesson, J.L. Hedrick, Dendritic homopolymers and block copolymers: Tuning the morphology and properties. *J. Polym. Sci. Part A: Polym. Chem.* **42**, 1174–1188 (2004)
221. N. Urbani, D.E. Lonsdale, C.A. Bell, M.R. Whittaker, M.J. Monteiro, Divergent synthesis and self-assembly of amphiphilic polymeric dendrons with selective degradable linkages. *J. Polym. Sci. Part A: Polym. Chem.* **46**, 1533–1547 (2008)
222. M. Stancik, J.A. Pople, M. Trollsås, P. Lindner, J.L. Hedrick, A.P. Gast, Impact of core architecture on solution properties of dendrimer-like star copolymers. *Macromolecules* **36**, 5765–5775 (2003)
223. N. Urbani, C.A. Bell, D.E. Lonsdale, M.R. Whittaker, M.J. Monteiro, Self-assembly of amphiphilic polymeric dendrimers synthesized with selective degradable linkages. *Macromolecules* **41**, 76–86 (2007)

224. R. Matmour, B. Lepoittevin, T.J. Joncheray, R.J. El-khouri, D. Taton, R.S. Duran, Y. Gnanou, Synthesis and investigation of surface properties of dendrimer-like copolymers based on polystyrene and poly(tert-butylacrylate). *Macromolecules* **38**, 5459–5467 (2005)
225. K. Van Ruymbeke, M. Orfanou, H. Kapnistos, M. Iatrou, N. Pitsikalis, D.J. Hadjichristidis, D.V. Lohse, Entangled dendritic polymers and beyond: Rheology of symmetric Cayley-tree polymers and macromolecular self-assemblies. *Macromolecules* **40**, 5941–5952 (2007)
226. L. Yang, W. Wu, Y. Ohki, Y. Feng, S. Li, Enhanced conductivity of polyaniline in the presence of nonionic amphiphilic polymers and their diverse morphologies. *J. Appl. Polym. Sci.* (2017). <https://doi.org/10.1002/app.45547>
227. H. Yoo, T. Watanabe, A. Hirao, Precise Synthesis of dendrimer-like star-branched polystyrenes and block copolymers composed of polystyrene and poly(methyl methacrylate) segments by an iterative methodology using living anionic polymerization. *Macromolecules* **42**, 4558–4570 (2009)
228. H. Makelane, O. Tovide, C. Sunday, T. Waryo, E. Iwuoha, Electrochemical interrogation of G3-poly(propylene thiophenimine) dendritic star polymer in phenanthrene sensing. *Sensors* **15**, 22343 (2015)
229. C. Liu, J. Lee, C. Small, J. Ma, M. Elimelech, Comparison of organic fouling resistance of thin film composite membranes modified by hydrophilic silica nanoparticles and zwitterionic polymer brushes. *J. Membr. Sci.* **544**, 135–142 (2017)
230. S. Iijima, Helical microtubules of graphitic carbon. *Nature* **354**, 56–58 (1991)
231. A. Pud, N. Ogurtsov, A. Korzhenko, G. Shapoval, Some aspects of preparation methods and properties of polyaniline blends and composites with organic polymers. *Prog. Polym. Sci.* **28**, 1701–1753 (2003)
232. J. Anand, S. Palaniappan, D.N. Sathyanarayana, Conducting polyaniline blends and composites. *Prog. Polym. Sci.* **23**, 993–1018 (1998)
233. L. Dai, Electrochemical sensors based on architectural diversity of the π -conjugated structure: Recent advancements from conducting polymers and carbon nanotubes. *Aust. J. Chem.* **60**, 472–483 (2007)
234. M. Baibarac, P. Gómez-Romero, Nanocomposites based on conducting polymers and carbon nanotubes: From fancy materials to functional applications. *J. Nanosci. Nanotechnol.* **6**, 289–302 (2006)
235. A. Bora, K. Mohan, D. Pegu, C.B. Gohain, S.K. Dolui, A room temperature methanol vapor sensor based on highly conducting carboxylated multi-walled carbon nanotube/polyaniline nanotube composite. *Sens. Actuators B: Chem* **253**, 977–986 (2017)
236. C. Oueiny, S. Berlioz, F.-X. Perrin, Carbon nanotube–polyaniline composites. *Prog. Polym. Sci.* **39**, 707–748 (2014)
237. R. Andrews, D. Jacques, M. Minot, T. Rantell, Fabrication of carbon multiwall nanotube/polymer composites by shear mixing. *Macromol. Mater. Eng.* **287**, 395–403 (2002)
238. O. Breuer, U. Sundararaj, Big returns from small fibers: A review of polymer/carbon nanotube composites. *Polym. Compos.* **25**, 630–645 (2004)
239. P. Gajendran, R. Saraswathi, Polyaniline-carbon nanotube composites. *Pure Appl. Chem.* **80**, 2377–2395 (2008)
240. A. Tchmutin, A.T. Ponomarenko, E.P. Krinichnaya, G.I. Kozub, O.N. Efimov, Electrical properties of composites based on conjugated polymers and conductive fillers. *Carbon* **41**, 1391–1395 (2003)
241. M. Baibarac, I. Baltog, S. Lefrant, J.Y. Mevellec, O. Chauvet, Polyaniline and carbon nanotubes based composites containing whole units and fragments of nanotubes. *Chem. Mater.* **15**, 4149–4156 (2003)
242. X.-B. Yan, Z.-J. Han, Y. Yang, B.-K. Tay, Fabrication of carbon nanotube–polyaniline composites via electrostatic adsorption in aqueous colloids. *J. Phys. Chem. C* **111**, 4125–4131 (2007)
243. M. Cochet, W.K. Maser, A.M. Benito, M.A. Callejas, M.T. Martinez, J.-M. Benoit, J. Schreiber, O. Chauvet, Synthesis of a new polyaniline/nanotube composite: “in-situ”

- polymerisation and charge transfer through site-selective interaction. *Chem. Commun.*, 1450–1451 (2001)
244. M.R. Karim, C.J. Lee, Y.-T. Park, M.S. Lee, SWNTs coated by conducting polyaniline: Synthesis and modified properties. *Synth. Met.* **151**, 131–135 (2005)
 245. K.-T. Lau, M. Lu, L. Chun-ki, H.-Y. Cheung, F.-L. Sheng, H.-L. Li, Thermal and mechanical properties of single-walled carbon nanotube bundle-reinforced epoxy nanocomposites: the role of solvent for nanotube dispersion. *Compos. Sci. Tech.* **65**, 719–725 (2005)
 246. M.B. Bryning, D.E. Milkie, M.F. Islam, J.M. Kikkawa, A.G. Yodh, Thermal conductivity and interfacial resistance in single-wall carbon nanotube epoxy composites. *Appl. Phys. Lett.* **87**, 161909 (2005)
 247. S. Badaire, P. Poulin, M. Maugey, C. Zakri, In situ measurements of nanotube dimensions in suspensions by depolarized dynamic light scattering. *Langmuir* **20**, 10367–10370 (2004)
 248. S. Barrau, P. Demont, E. Perez, A. Peigney, C. Laurent, C. Lacabanne, Effect of palmitic acid on the electrical conductivity of carbon nanotubes–epoxy resin composites. *Macromolecules* **36**, 9678–9680 (2003)
 249. M.F. Islam, E. Rojas, D.M. Bergey, A.T. Johnson, A.G. Yodh, High weight fraction surfactant solubilization of single-wall carbon nanotubes in water. *Nano Lett.* **3**, 269–273 (2003)
 250. T. Jeevananda, N.H.K. Siddaramaiah, S.-B. Heo, J.H. Lee, Synthesis and characterization of polyaniline-multiwalled carbon nanotube nanocomposites in the presence of sodium dodecyl sulfate. *Polym. Adv. Tech.* **19**, 1754–1762 (2008)
 251. J. Deng, X. Ding, W. Zhang, Y. Peng, J. Wang, X. Long, P. Li, A.S.C. Chan, Carbon nanotube–polyaniline hybrid materials. *Eur. Polym. J.* **38**, 2497–2501 (2002)
 252. M. Zelikman, A. Narkis, L. Siegmann, J.M.K. Valentini, Polyaniline/multiwalled carbon nanotube systems: Dispersion of CNT and CNT/PANI interaction. *Polym. Eng. Sci.* **48**, 1872–1877 (2008)
 253. M. Zhang, L. Su, L. Mao, Surfactant functionalization of carbon nanotubes (CNTs) for layer-by-layer assembling of CNT multi-layer films and fabrication of gold nanoparticle/CNT nanohybrid. *Carbon* **44**, 276–283 (2006)
 254. A.P. Kane-Maguire, D.L. Officer, S.J. Park, S.Y. Park, M.S. Cho, H.J. Choi, M.S. Jhon, Proceedings of the international conference on science and technology of synthetic metals: Synthesis and electrorheology of multi-walled carbon nanotube/polyaniline nanoparticles. *Synth. Met.* **152**, 337–340 (2005)
 255. C.S. Choi, S.J. Park, H.J. Choi, Carbon nanotube/polyaniline nanocomposites and their electrorheological characteristics under an applied electric field. *Curr. Appl. Phys.* **7**, 352–355 (2007)
 256. X. Zhang, Z. Lü, M. Wen, H. Liang, J. Zhang, Z. Liu, Single-walled carbon nanotube-based coaxial nanowires: Synthesis, characterization, and electrical properties. *J. Phys. Chem. B* **109**, 1101–1107 (2005)
 257. L. de la Chapelle, C. Stéphan, T.P. Nguyen, S. Lefrant, C. Journet, P. Bernier, E. Munoz, A. Benito, W.K. Maser, M.T. Martinez, G.F. de la Fuente, T. Guillard, G. Flamant, L. Alvarez, D. Laplaze, International conference on science and technology of synthetic metals: Raman characterization of singlewalled carbon nanotubes and PMMA-nanotubes composites. *Synth. Met.* **103**, 2510–2512 (1999)
 258. J.M. Benoit, B. Corraze, S. Lefrant, W.J. Blau, P. Bernier, O. Chauvet, Proceedings of the international conference on the science and technology of synthetic metals: Transport properties of PMMA-carbon nanotubes composites. *Synth. Met.* **121**, 1215–1216 (2001)
 259. C. Ramamurthy, W.R. Harrell, R.V. Gregory, B. Sadanadan, A.M. Rao, Mechanical and electrical properties of solution-processed polyaniline/multiwalled carbon nanotube composite films. *J. Electrochem. Soc.* **151**, G502–G506 (2004)
 260. S.I.A. Razak, S.H.S. Zein, A.L. Ahmad, Effect of para-hydroxybenzene sulfonic acid on the properties of ex situ prepared polyaniline/multiwalled carbon nanotubes-MnO₂. *Nano* **05**, 369–373 (2010)

261. J. Shi, Z.-Y. Zhang, Y.-Q. Hu, Y.-X. Hua, Incorporation of 4-aminobenzene functionalized multi-walled carbon nanotubes in polyaniline for application in formic acid electrooxidation. *J. Appl. Polym. Sci.* **118**, 1815–1820 (2010)
262. Y.-W. Lin, T.-M. Wu, Synthesis and characterization of externally doped sulfonated polyaniline/multi-walled carbon nanotube composites. *Compos. Sci. Tech.* **69**, 2559–2565 (2009)
263. Z. Dong-Lin, Z. Xian-Wei, S. Zeng-Min, Synthesis of carbon nanotube/polyaniline composite nanotube and its microwave permittivity. *Acta Phys. Sin.* **54**, 3878–3883 (2005)
264. F. Yakuphanoglu, B.F. Şenkal, Thermoelectrical and optical properties of double wall carbon nanotubes: polyaniline containing boron n-type organic semiconductors. *Polym. Adv. Tech.* **19**, 905–908 (2008)
265. M. Cabuk, B. Gündüz, Controlling the optical properties of polyaniline doped by boric acid particles by changing their doping agent and initiator concentration. *Appl. Surf. Sci.* **424**, 345–351 (2017)
266. M. Cabuk, B. Gündüz, Change of optoelectronic parameters of the boric acid-doped polyaniline conducting polymer with concentration. *Colloids Surf. A: Physiochem. Eng. Asp.* **532**, 263–269 (2017)
267. Y.-W. Lin, H.-H. Chang, Y.-S. Liu, M.-C. Tsai, Y.-C. Tsai, T.-M. Wu, Preparation and electrochemical performance of externally doped sulfonated polyaniline/multiwalled carbon nanotube composites. *J. Electrochem. Soc.* **157**, K15–K20 (2010)
268. F.M. Blighe, D. Diamond, J.N. Coleman, E. Lahiff, Increased response/recovery lifetimes and reinforcement of polyaniline nanofiber films using carbon nanotubes. *Carbon* **50**, 1447–1454 (2012)
269. J. Stejskal, R.G. Gilbert, Polyaniline. Preparation of a conducting polymer (IUPAC technical report). *Pure Appl. Chem.* **74**, 857–868 (2002)
270. G. Khomenko, V.Z. Barsukov, A.S. Katashinskii, The catalytic activity of conducting polymers toward oxygen reduction. *Electrochim. Acta* **50**, 1675–1683 (2005)
271. H. Zhou, Y. Lin, P. Yu, L. Su, L. Mao, Doping polyaniline with pristine carbon nanotubes into electroactive nanocomposite in neutral and alkaline media. *Electrochem. Commun.* **11**, 965–968 (2009)
272. C. Su, G. Wang, F. Huang, Preparation and characterization of composites of polyaniline nanorods and multiwalled carbon nanotubes coated with polyaniline. *J. Appl. Polym. Sci.* **106**, 4241–4247 (2007)
273. E. Zelikman, R.Y. Suckeveriene, G. Mechrez, M. Narkis, Fabrication of composite polyaniline/CNT nanofibers using an ultrasonically assisted dynamic inverse emulsion polymerization technique. *Polym. Adv. Tech.* **21**, 150–152 (2010)
274. J. Xu, P. Yao, L. Liu, Z. Jiang, F. He, M. Li, J. Zou, Synthesis and characterization of an organic soluble and conducting polyaniline-grafted multiwalled carbon nanotube core-shell nanocomposites by emulsion polymerization. *J. Appl. Polym. Sci.* **118**, 2582–2591 (2010)
275. H. Li, B. Wu, J.-E. Huang, J. Zhang, Z.-F. Liu, H.-L. Li, Fabrication and characterization of well-dispersed single-walled carbon nanotube/polyaniline composites. *Carbon* **41**, 1670–1673 (2003)
276. T.-M. Wu, Y.-W. Lin, Doped polyaniline/multi-walled carbon nanotube composites: Preparation, characterization and properties. *Polymer* **47**, 3576–3582 (2006)
277. E. Lafuente, M.A. Callejas, R. Sainz, A.M. Benito, W.K. Maser, M.L. Sanjuán, D. Saurel, J.M. de Teresa, M.T. Martínez, The influence of single-walled carbon nanotube functionalization on the electronic properties of their polyaniline composites. *Carbon* **46**, 1909–1917 (2008)
278. Y.-J. Wu, L. Chao, K.-S. Ho, Y.-J. Huang, Y.-L. Huang, C.-S. Yang, B.-H. Tseng, Characterizations on the amidized multiwalled carbon nanotubes grafted with polyaniline via in situ polymerization. *J. Appl. Polym. Sci.* **124**, 5270–5278 (2012)
279. X. Biju, K.A. Jining, K.V. Jose, Vijay: A new synthetic route to enhance polyaniline assembly on carbon nanotubes in tubular composites. *Smart Mater. Struct.* **13**, 105–107 (2004)

280. N.A. Kumar, Y.T. Jeong, Fabrication of conducting polyaniline–multiwalled carbon nanotube nanocomposites and their use as templates for loading gold nanoparticles. *Polym. Int.* **59**, 1367–1374 (2010)
281. H. Zhang, H.X. Li, H.M. Cheng, Water-soluble multiwalled carbon nanotubes functionalized with sulfonated polyaniline. *J. Phys. Chem. B* **110**, 9095–9099 (2006)
282. L. Cabezas, Z.-B. Zhang, L.-R. Zheng, S.-L. Zhang, Morphological development of nanofibrillar composites of polyaniline and carbon nanotubes. *Synth. Met.* **160**, 664–668 (2010)
283. W. Li, D. Kim, Polyaniline/multiwall carbon nanotube nanocomposite for detecting aromatic hydrocarbon vapors. *J. Mater. Sci.* **46**, 1857–1861 (2011)
284. W.D. Zhang, L. Shen, I.Y. Phang, T. Liu, Carbon nanotubes reinforced nylon-6 composite prepared by simple melt-compounding. *Macromolecules* **37**, 256–259 (2004)
285. A. Soroudi, M. Skrifvars, Melt blending of carbon nanotubes/polyaniline/polypropylene compounds and their melt spinning to conductive fibres. *Synth. Met.* **160**, 1143–1147 (2010)
286. Y. Liao, C. Zhang, Y. Zhang, V. Strong, J. Tang, X.-G. Li, K. Kalantar-zadeh, E.M.V. Hoek, K.L. Wang, R.B. Kaner, Carbon nanotube/polyaniline composite nanofibers: Facile synthesis and chemosensors. *Nano Lett.* **11**, 954–959 (2011)
287. A. Mirmohseni, M.S.S. Dorraji, Effects of dopant, coagulant, and reinforcing nanofiller on mechanical and electrical properties of wet-spun polyaniline nanocomposite fibers. *J. Polym. Res.* **19**, 1–10 (2012)
288. P. Dubois, M. Alexandre, Performant clay/carbon nanotube polymer nanocomposites. *Adv. Engin. Mater.* **8**, 147–154 (2006)
289. R. Haggemueller, H.H. Gommans, A.G. Rinzler, J.E. Fischer, K.I. Winey, Aligned single-wall carbon nanotubes in composites by melt processing methods. *Chem. Phys. Lett.* **330**, 219–225 (2000)
290. K.P. Jin, S.H. Pramoda, G.X. Goh, Poly(vinylidene fluoride)-assisted melt-blending of multi-walled carbon nanotube/poly(methyl methacrylate) composites. *Mater. Res. Bull.* **37**, 271–278 (2002)
291. S. Pande, R.B. Mathur, B.P. Singh, T.L. Dhama, Synthesis and characterization of multiwalled carbon nanotubes-polymethyl methacrylate composites prepared by in situ polymerization method. *Polym. Compos.* **30**, 1312–1317 (2009)
292. P. Saini, V. Choudhary, B.P. Singh, R.B. Mathur, S.K. Dhawan, Polyaniline–MWCNT nanocomposites for microwave absorption and EMI shielding. *Mater. Chem. Phys.* **113**, 919–926 (2009)
293. Y. Yu, B. Che, Z. Si, L. Li, W. Chen, G. Xue, Carbon nanotube/polyaniline core-shell nanowires prepared by in situ inverse microemulsion. *Synth. Met.* **150**, 271–277 (2005)
294. B. Valter, M.K. Ram, C. Nicolini, Synthesis of multiwalled carbon nanotubes and poly(o-anisidine) nanocomposite material: Fabrication and characterization of its Langmuir–Schaefer films. *Langmuir* **18**, 1535–1541 (2002)
295. X. Lu, J. Zheng, D. Chao, J. Chen, W. Zhang, Y. Wei, Poly (N-methylaniline)/multi-walled carbon nanotube composites – Synthesis, characterization, and electrical properties. *J. Appl. Polym. Sci.* **100**, 2356–2361 (2006)
296. X. Lu, D. Chao, J. Zheng, J. Chen, W. Zhang, Y. Wei, Preparation and characterization of polydiphenylamine/multi-walled carbon nanotube composites. *Polym. Int.* **55**, 945–950 (2006)
297. B. Zhao, H. Hu, R.C. Haddon, Synthesis and properties of a water-soluble single-walled carbon nanotube–poly(m-aminobenzene sulfonic acid) graft copolymer. *Adv. Funct. Mater.* **14**, 71–76 (2004)
298. B. Zhao, H. Hu, A. Yu, D. Perea, R.C. Haddon, Synthesis and characterization of water soluble single-walled carbon nanotube graft copolymers. *J. Am. Chem. Soc.* **127**, 8197–8203 (2005)
299. C. Downs, J. Nugent, P.M. Ajayan, D.J. Duquette, K.S.V. Santhanam, Efficient polymerization of aniline at carbon nanotube electrodes. *Adv. Mater.* **11**, 1028–1031 (1999)
300. M. Wu, G.A. Snook, V. Gupta, M. Shaffer, D.J. Fray, G.Z. Chen, Electrochemical fabrication and capacitance of composite films of carbon nanotubes and polyaniline. *J. Mater. Chem.* **15**, 2297–2303 (2005)

301. J.-E. Huang, X.-H. Li, J.-C. Xu, H.-L. Li, Well-dispersed single-walled carbon nanotube/polyaniline composite films. *Carbon* **41**, 2731–2736 (2003)
302. E. Kooi, U. Schlecht, M. Burghard, K. Kern, Electrochemical modification of single carbon nanotubes. *Angew. Chem. Int. Ed.* **41**, 1353–1355 (2002)
303. K. Balasubramanian, M. Friedrich, C. Jiang, Y. Fan, A. Mews, M. Burghard, K. Kern, Electrical transport and confocal Raman studies of electrochemically modified individual carbon nanotubes. *Adv. Mater.* **15**, 1515–1518 (2003)
304. M. Milua, S.N. Mailu, A. Tsegaye, C.O. Ikpo, N.J. Njomo, T.T. Waryo, P.G.L. Baker, E.I. Iwuoha, In-situ electrochemical synthesis, microscopic and spectroscopic characterisations of electroactive poly(2,5-dimethoxyaniline) – Multi-walled carbon nanotubes composite films in neutral media. *Int. J. Electrochem. Sci.* **9**, 7003–7020 (2014)
305. P. Gajendran, R. Saraswathi, Enhanced electrochemical growth and redox characteristics of poly(o-phenylenediamine) on a carbon nanotube modified glassy carbon electrode and its application in the electrocatalytic reduction of oxygen. *J. Phys. Chem. C* **111**, 11320–11328 (2007)



Magdalena Mazurek-Budzyńska , Muhammad Yasar Razzaq,
Marc Behl , and Andreas Lendlein 

Contents

1	Introduction	608
2	Shape-Memory Effect (SME) in Polymers According to Fixation of Temporary Shape	609
2.1	SME Based on Physical Interactions	611
2.2	SME Based on Reversible Covalent Bonds	623
3	Triple/Multiple-Shape Effect (TSE/MSE)	625
4	Temperature-Memory Effect (TME)	633
5	Reversible SME	634
5.1	Reversible Shape-Memory Effect (rSME) Under Constant Stress	635
5.2	Reversible Bidirectional Shape-Memory Effect (rbSME)	636
6	Magnetically Triggered SMPs	642
7	Shape-Memory Hydrogels (SMH)	646
8	Conclusions and Outlook	653
	References	654

Abstract

Shape-memory polymers (SMPs) are stimuli-sensitive materials capable of changing their shape on demand. A shape-memory function is a result of the polymer architecture together with the application of a specific programming procedure. Various possible mechanisms to induce the shape-memory effect (SME) can be realized, which can be based on thermal transitions of switching

M. Mazurek-Budzyńska · M. Y. Razzaq · M. Behl
Institute of Biomaterial Science, Helmholtz-Zentrum Geesthacht, Teltow, Germany
e-mail: magdalena.mazurek-budzynska@hzg.de; muhammad.razzaq@hzg.de; marc.behl@hzg.de

A. Lendlein (✉)
Institute of Biomaterial Science, Helmholtz-Zentrum Geesthacht, Teltow, Germany
Institute of Chemistry, University of Potsdam, Potsdam, Germany
e-mail: andreas.lendlein@uni-potsdam.de

domains or on reversible molecular switches (e.g., supramolecular interactions, reversible covalent bonds). Netpoints, which connect the switching domains and determine the permanent shape, can be either provided by covalent bonds or by physical intermolecular interactions, such as hydrogen bonds or crystallites. This chapter reviews different ways of implementing the phenomenon of programmable changes in the polymer shape, including the one-way shape-memory effect (1-W SME), triple- and multi-shape effects (TSE/MSE), the temperature-memory effect (TME), and reversible shape-memory effects, which can be realized in constant stress conditions (rSME), or in stress-free conditions (reversible bidirectional shape-memory effect (rbSME)). Furthermore, magnetically actuated SMPs and shape-memory hydrogels (SMHs) are described to show the potential of the SMP technology in biomedical applications and multifunctional approaches.

Abbreviations

1-W SME	One-way shape-memory effect
AD	Actuator domains
Alg	Alginate
AMF	Alternating magnetic field
BA	<i>n</i> -Butyl acrylate
BD	1,4-Butanediol
BHECA	<i>N,N</i> -bis(2-Hydroxyethyl) cinnamamide
BM	1,1'-(Methylenedi- <i>p</i> -phenylene)bismaleimide
CA	Cinnamic acid
CAA	Cinnamylidien acetic acid
CD	Cyclodextrine
CIE	Crystallization-induced elongation
CLEG	Copolymer network from PCL with grafted PEG segments
CMF	Cavitation-based mechanical force
cPEVA	Covalently crosslinked poly[ethylene- <i>co</i> -(vinyl acetate)]
CTB	Carboxyl-terminated polybutadiene
DA	Diels-Alder reaction
DETA	Diethylenetriamine
DMPA	Dimethylolpropionic acid
Gly	Glycine
<i>H</i>	Magnetic field strength
H_{def}	Deformation magnetic field strength
HDI	Hexamethylene diisocyanate
HEA-CA	Ethyleneglycol-1-acrylate-2-CA
HEMA	Hydroxyethyl methacrylate
H_{high}	High magnetic field strength
H_{low}	Low magnetic field strength
H-NC	Hybrid nanocomposite
H_{sw}	Switching magnetic field strength
$H_{\sigma, \text{max}}$	Magnetic field strength at maximum stress generated

IPN	Interpenetrating polymer network
IR	Infrared
LU	Low frequency ultrasound
MACL	Copolymer of PCL and poly(cyclohexyl methacrylate)
MDI	4,4'-Diphenylmethane diisocyanate
MIC	Melting-induced contraction
MME	Magnetic-memory effect
MNP	Magnetic nanoparticles
MSE	Multi-shape effect
PBA	Poly(butylene adipate)
PCHMA	Poly(cyclohexyl methacrylate)
PCL	Poly(ϵ -caprolactone)
PDC	Multiblock copolymer from PPDO and PCL
PEG	Poly(ethylene glycol)
PEGDA	Poly(ethylene glycol) diacrylate
PET	Poly(ethylene terephthalate)
PEU	Poly(ester-urethane)
PEVA	Poly[ethylene- <i>co</i> -(vinyl acetate)]
PHEG-Cn	Poly[N ⁵ -(2-hydroxyethyl) L-glutamine] with alkyl side chains -C _n H _{2n+1}
PLA	Poly(lactide)
PLLA	Poly(L-lactide)
PPDL	Poly(ω -pentadecalactone)
PPDL-PCL	Multiblock copolymer from PPDL and PCL
PPDO	Poly(<i>p</i> -dioxanone)
PPGDMA	Poly(propylene glycol) dimethacrylate
PS	Polystyrene
PSVP	Poly[styrene- <i>co</i> -(4-vinylpyridine)]
PTMG	Poly(tetramethylene glycol)
PUR	Polyurethane
PVA	Poly(vinyl alcohol)
Q_{ef}	Deformation fixation efficiency
rbSME	Reversible bidirectional shape-memory effect
r-DA	Retro-Diels-Alder
R_f	Shape fixity ratio
Rh-PCBs	Rhodium-phosphine coordination bonds
r_{mag} -SME	Magnetically controlled rSME
R_r	Shape recovery ratio
rSME	Reversible shape-memory effect
S/V	Surface-to-volume ratio
SAXS	Small-angle X-ray scattering
SGD	Shape shifting geometry domains
SME	Shape-memory effect
SMH	Shape-memory hydrogel
SMP	Shape-memory polymer

sNP	Silica-coated iron oxide nanoparticles
T_{act}	Actuation temperature
T_{d}	Deformation temperature
T_{env}	Environmental temperature
TFX	Polyetherurethane prepared from MDI, BD, and PTMG
T_{g}	Glass transition temperature
THF	Tetrahydrofuran
T_{high}	Highest temperature in the course of shape-memory programming
T_{low}	Lowest temperature in the course of shape-memory programming
T_{m}	Melting transition temperature
TME	Temperature-memory effect
TMPA	Temperature-memory polymer actuator
T_{perm}	Highest thermal transition temperature of a thermoplastic material at which the domains acting as physical crosslinks melt
TSE	Triple-shape effect
TSP	Triple-shape polymer
TSPC	Triple-shape polymeric composites
T_{sw}	Switching temperature
T_{trans}	Thermal transition temperature
T_{u}	Unloading temperature
$T_{\sigma, \text{max}}$	Temperature determined at the maximum of recovery stress
UPy	2-Ureido-4-pyrimidinone
UV	Ultraviolet
ZnCTB	Zinc salt of carboxyl-terminated polybutadiene
ZnOl	Zinc oleate
β -CD	β -Cyclodextrin
ϵ'_{rev}	Reversible elongation
ϵ_{m}	Maximum deformation
ϵ_{p}	Strain of the sample after recovery to the permanent shape
$\epsilon_{\text{u}}(N)$	Free state deformation after cooling
λ	Wave length
σ_{max}	Recovery stress

1 Introduction

Shape-memory polymers (SMPs) are a class of stimuli-responsive polymeric materials in which on demand shape changes can be implemented by tailored programming procedures [1]. The most prominent among the reported shape-memory capabilities of polymers is a one-way, thermally-induced shape-memory effect (1-W SME). A general requirement of polymers capable of 1-W SME is a chemically or physically crosslinked network structure, which could be both, amorphous or semicrystalline in nature. Initially the 1-W SME was realized in γ -radiated polyethylene, which until now is applied in heat-shrinkable tubes for insulating electronic wiring or heat-shrinkable

films for packaging labels. Furthermore, shape-memory polyurethanes have been commercialized for automotive applications as well as for smart textiles and fabrics. Degradable SMPs containing ester moieties are an example of multifunctional polymers and address biomedical applications, such as biodegradable implants and controlled drug release systems [2–5]. SMPs have many advantages compared to metallic shape-memory alloys such as lightweight and capability of much higher deformations. Moreover, according to the broad potential variation of structure architecture, they can be easily tailored for specific applications [6]. Furthermore, by combining the shape-memory capability with other functionalities (hydrolytic degradability, self-healing, drug-release etc.), multifunctional polymers can be obtained [7]. It is important to note that the SME in polymers is a function of a polymer resulting from a combination of the polymer structure and morphology, together with the applied processing and programming [1]. In addition to 1-W SME, the phenomena of programmable changes in shape of polymers can be realized in different manners, including triple- and multiple-shape effect (TSE/MSE), temperature-memory effect (TME), as well as SMEs with reversible shape changes. The latter include the reversible shape-memory effect (rSME) and the reversible bidirectional shape-memory effect (rbSME), in which polymer samples can switch between two shapes under constantly applied stress or under stress-free conditions, respectively. All of them will be discussed in this chapter with the emphasis on the switching mechanisms and examples of polymer systems, in which those concepts are realized.

2 Shape-Memory Effect (SME) in Polymers According to Fixation of Temporary Shape

In this part, general concepts and mechanisms of SMEs will be introduced based on examples of SMPs exhibiting 1-W SME. The phenomena described will be classified according to the types of molecular switching mechanisms. The permanent shape of shape-memory networks is defined by the netpoints, which can be realized by covalent bonds or physical interactions (e.g., crystallites, glassy hard domains, hydrogen bonds, ionic assembly). However, it has to be noted, that netpoints basing on physical interactions are in general not as strong as covalent bonds. Therefore, thermoplastics are more prone to undergo unintended and irreversible changes in a shape-memory cycle, which lead to incomplete shape recovery.

Several polymer architectures have been identified as suitable for exhibiting a SME. The most basic one is a covalently crosslinked polymer network, in which the switching segments create linkages between net points (Fig. 1a). Covalently crosslinked polymer networks can also contain side groups able to form a segregated phase (Fig. 1b) or to cleave covalent bonds reversibly (Fig. 1c). SMPs have been also realized in triblock copolymers able to form multiphase morphologies (Fig. 1d), or copolymers containing liquid-crystalline (Fig. 1e) switching domains [8]. SMP systems, in which the netpoints and the switching domains are not covalently connected to each other, can be realized as interpenetrating polymer networks

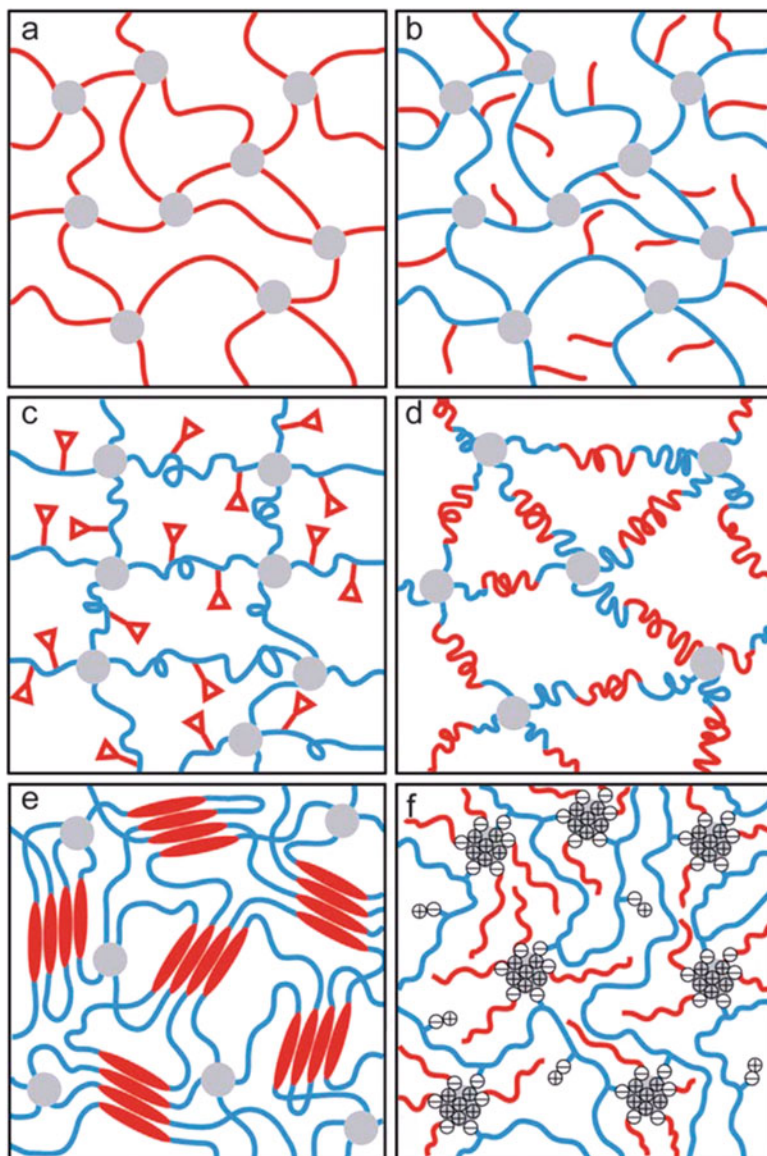


Fig. 1 Examples of polymer network architectures suitable for exhibiting an SME (molecular switches: red; netpoints: gray): (a) switching segments linking netpoints, (b) side chains as switching segments, (c) functional groups as molecular switches capable to reversibly form a covalent bond, (d) ABA triblock segments linking netpoints, (e) liquid-crystalline domains enabling the fixation, (f) ionic switching segments and ionomers containing ion-rich domains as netpoints. ((a–d) taken from Ref. [6] Copyright © 2009, Springer-Verlag Berlin Heidelberg, (e–f) reproduced from Ref. [8] with permission from The Royal Society of Chemistry. <https://doi.org/10.1039/c2sm27077c>)

(IPNs) or polymer blends. Furthermore, netpoints related to physical interaction, such as crystallites, hydrogen bonds, or ion-rich domains (Fig. 1f) can be utilized in SMPs.

Depending on the different architectures of SMPs, various stimuli might be used to induce the shape recovery from the temporary to the permanent shape. Typically, SMPs respond to changes of temperature, ion concentration, pH, IR irradiation, alternating magnetic fields, or ultrasound applied. Examples of various mechanisms of molecular switching based on physical or chemical interactions utilized in SMPs will be described in the following sections.

2.1 SME Based on Physical Interactions

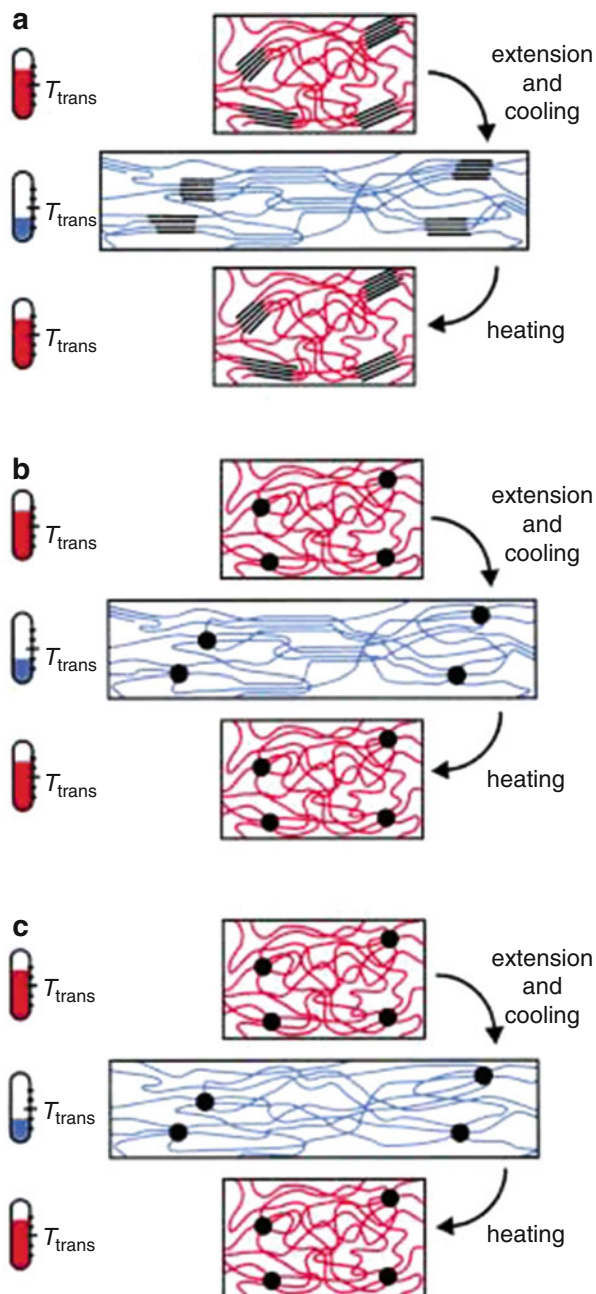
The most commonly utilized switch to induce the shape recovery is a thermal transition temperature (T_{trans}) associated to a melting (T_{m}) or a glass transition temperature (T_{g}) of the switching domains [9]. Furthermore, supramolecular interactions related to hydrogen bond formation, ionic, or metal-ligand interactions enable reversibly crosslinked networks capable of a SME [2, 10].

2.1.1 SME Based on Thermal Transition of Switching Domains

Depending on the polymer architecture and the temperature range of interest for the particular application, a glass transition temperature ($T_{\text{trans}} = T_{\text{g}}$) or a melting transition temperature ($T_{\text{trans}} = T_{\text{m}}$) can be chosen to serve as a T_{trans} . The flexibility of chains below T_{trans} is at least partly limited, whereas upon heating above T_{trans} the mobility of molecular chains increases, resulting in softening of the material. When $T_{\text{trans}} = T_{\text{m}}$, the temporary shape is programmed by stretching the material at $T > T_{\text{trans}}$, followed by cooling, whereby the crystallization of the switching segment is initiated. The crystalline domains formed prevent the polymer chain segments from immediate recoiling, and by this fix the temporary shape. In case of $T_{\text{trans}} = T_{\text{g}}$, the fixation of temporary shape is related to the transition from the rubber-elastic or viscous state to the glassy state, in which the flexibility of the entire segment is limited. The recovery of the original shape is driven by regaining the entropy, which was lost during the orientation of polymer chains [11]. The molecular mechanism of thermally-induced SME, including programming the temporary shape and recovering of the permanent shape, is schematically shown in Fig. 2. Three shape-memory systems are presented: (a) a thermoplastic, linear multiblock copolymer, and covalently crosslinked polymer networks with (b) $T_{\text{trans}} = T_{\text{m}}$ and (c) $T_{\text{trans}} = T_{\text{g}}$, respectively.

The thermally-induced SME is typically quantified by cyclic, thermomechanical investigations [12]. In most of the cases, it is performed with a conventional tensile testing machine equipped with a thermo-chamber, which enables temperature control during mechanical deformation of the specimen according to specific temperature protocols. Besides the cyclic, thermomechanical tests various methods of the characterization of SME have been applied, such as bending tests, compression tests or three-point flexural test [13, 14]. In a schematic representation in Fig. 3, the different

Fig. 2 Schematic representation of the molecular mechanism of the thermally-induced SME for (a) a multiblock copolymer with $T_{\text{trans}} = T_m$, (b) a covalently crosslinked polymer with $T_{\text{trans}} = T_m$, and (c) a polymer network with $T_{\text{trans}} = T_g$. At $T > T_{\text{trans}}$ of the switching segments, these segments are flexible (shown in red) and the polymer can be deformed elastically. The temporary shape is fixed by cooling below $T < T_{\text{trans}}$ (shown in blue). If the temperature is raised again, the permanent shape is recovered. (Reprinted from Ref. [1] with permission, © WILEY-VCH Verlag GmbH, 69,451 Weinheim, Germany, 2002)



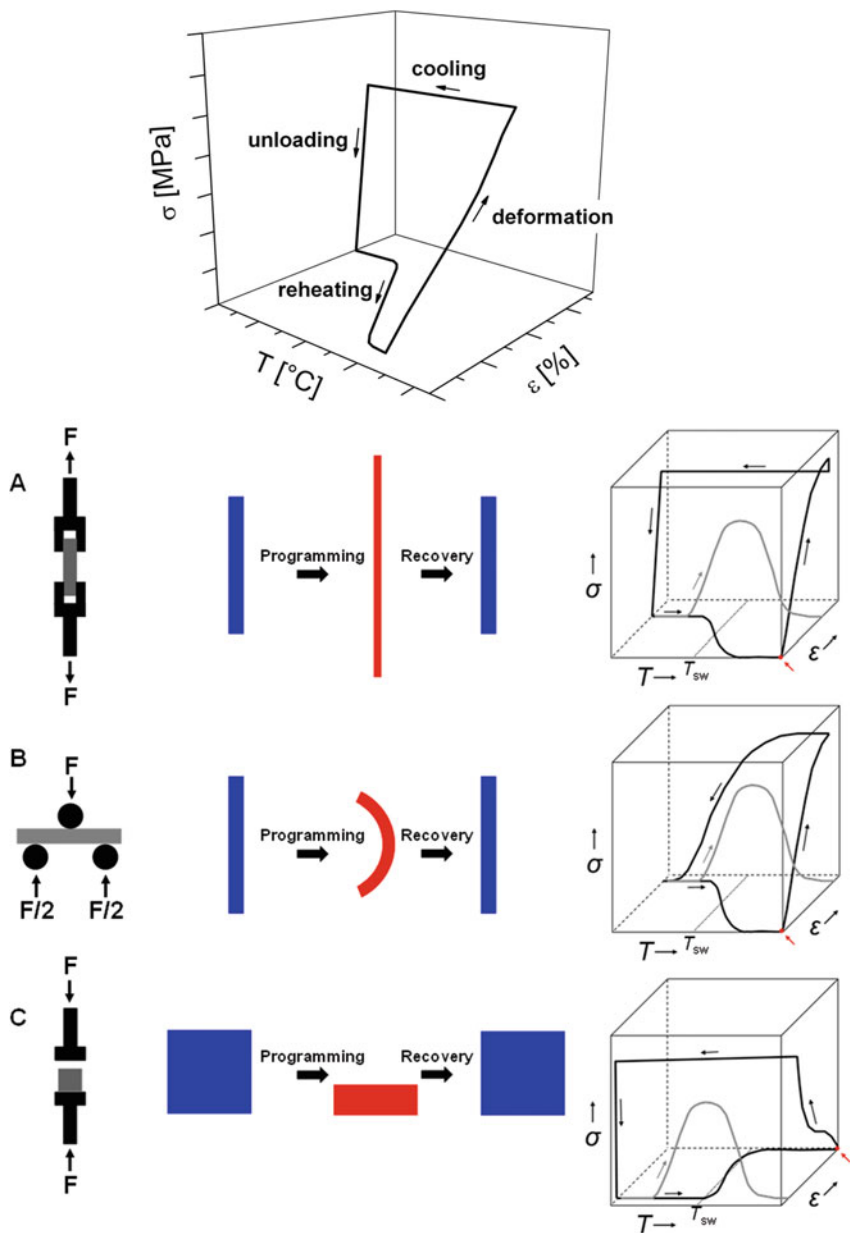


Fig. 3 Three basic methods to quantify the thermally-induced SME by cyclic thermomechanical tests. (A) Tensile test; (B) Bending test; (C) Compression test. The black curve shows a full cycle starting with the programming step at $T_{high} > T_{trans}$ (indicated by the red point and arrow) and the recovery under stress-free conditions. The recovery under constant strain conditions is highlighted by the solid gray curve for thermoplastics (physical netpoints). (Taken from Ref. [13], reprinted with permission (Taylor & Francis Ltd., <http://www.tandfonline.com>))

cyclic testing methods can be overviewed, including the resulting changes in shape during programming and recovery, as well as the related stress-temperature-strain diagrams.

The macroscopic changes of the sample during the cyclic, thermomechanical investigations can be described by two values: the shape fixity ratio (R_f) and the shape recovery ratio (R_r). R_f measures the ability to fix the mechanical deformation applied during the programming process (Eq. 1), whereas R_r quantifies to which extent is the shape recovered in the N_{th} cycle (for $N > 1$) with respect to the recovered shape of the previous $(N-1)_{th}$ cycle (Eq. 2).

$$R_f = \frac{\varepsilon_u(N)}{\varepsilon_m} \cdot 100\% \quad (1)$$

$$R_r = \frac{\varepsilon_m(N) - \varepsilon_p(N)}{\varepsilon_m(N) - \varepsilon_p(N-1)} \cdot 100\% \quad (2)$$

Different test protocols can be applied with various programming procedures. A typical test protocol is as follows: first, the sample is heated up to a temperature $T_{high} > T_{trans}$ and stretched to the certain strain (ε_m), which is typically a maximum of the strain before the break of the sample. In the next step, the sample is cooled to $T_{low} < T_{trans}$, which enables the fixation of the temporary shape (ε_u). This step can be performed in two different ways – in stress-controlled or in stress-free conditions. Afterwards, the sample is heated to T_{high} , whereby it recovers to the permanent shape (ε_p) and the next cycle can begin. The switching temperature (T_{sw}), at which the recovery to original shape is the fastest, is determined at the inflection point of the elongation/temperature curve at the maximum of the absolute value of $\Delta\varepsilon/\Delta T$.

An important group of thermoplastic SMPs are linear block copolymers. The mechanism of SME induction is based on formation of a phase-segregated morphology. The phase with the lower thermal transition provides switching domains and the other phase (with higher thermal transition T_{perm}) provides domains defining the permanent shape. In case of $T_{trans} = T_m$, a relatively sharp thermal transition is observed, whereas the glass transition is always related to a broad temperature range. The most intensively investigated linear block copolymers utilizing $T_m = T_{trans}$ constitute thermoplastic polyurethanes, polyolefins, polyethers, polyesters, copolymers containing poly(ethylene terephthalate) (PET) and poly(ethylene glycol) (PEG), copolymers of polystyrene (PS) and polybutadiene, or triblock copolymers ABA of poly(2-methyl-2-oxazoline) and poly(tetrahydrofuran) [1, 15–17]. Low melting point aliphatic polyesters, mainly poly(ε -caprolactone) (PCL) [18], are the most frequently used building-blocks for the switching segments in the polyurethane, polyamide or polyamide shape-memory systems [19, 20]. Also polymer blends were demonstrated to exhibit a thermally induced SME [21–25].

The second group of thermally-induced shape-memory block copolymers constitutes materials with $T_{trans} = T_g$; however, for this group, the shape change is relatively slow [1, 26, 27]. The most expanded class of these materials are polyurethanes, in which the switching segments are mostly realized by mixed phases, and

are typically based on soft segments from PCL, poly(tetrahydrofuran), PEG or copolymers of lactide and glycolide [1, 28, 29]. Due to their amorphous structure, these shape-memory polyurethanes are more prone to biodegradation.

Thermoplastic elastomers like polyurethanes or polyesters feature excellent processability, however, the lack in chemical crosslinks leads to lower stresses during recovery and lower cyclic recoverable strains [30]. Therefore, covalently crosslinked systems based on linear or branched polymer precursors were designed to be capable of thermally-triggered SME. Netpoints can be created according to two main strategies: during the synthesis step or by post-processing methods (crosslinking by radiation; UV- or γ -radiation, e-beam, neutrons) [1]. The first strategy is realized mainly by the (co)polymerization or (co)polycondensation of monomers, among which at least one is trifunctional or of a higher functionality [31]. An example are poly(tetrahydrofuran)-based polyurethane networks with tailorable switching temperatures synthesized by the precursor method, utilizing 1,1,1-trimethylolpropane as a crosslinking agent [32]. Highly crosslinked networks exhibiting R_r of 96–98% were obtained based on poly(butylene adipate), diphenylene diisocyanate, and hyperbranched polyester Boltorn H30 [33]. Ring-opening polymerization of ϵ -caprolactone initiated by trifunctional glycerol, followed by polyaddition with 4,4'-diphenylmethane diisocyanate (MDI) and 1,6-hexanediol, resulted in shape-memory networks with R_f and R_r of 92% and 99%, respectively [34]. A very important group of crosslinked SMPs constitutes AB networks synthesized by copolymerization of monofunctional telechelic monomers with bifunctional crosslinkers. This type of systems can utilize both, T_m or T_g as T_{trans} . In case of (meth)acrylate-based covalently crosslinked SMPs, most is based on $T_{trans} = T_g$ of the switching segment [10, 35, 36]. One of the examples utilizing $T_{trans} = T_m$ are various crosslinked copolymers of semicrystalline oligo(ϵ -caprolactone)-*co*-glycolide]dimethacrylate with a *n*-butyl acrylate. These SMPs were capable of $R_f > 82\%$ and $R_r > 97\%$, in which T_{trans} could be adjusted in a temperature range between 23 °C and 52 °C [37]. A photopolymerized network containing oligo(ϵ -caprolactone)diacrylate with polyhedral oligosilsesquioxane moieties in the middle of the chains exhibited R_r of 99% when heated to $T_{trans} = 80$ °C [38]. AB polymer networks based on various acrylates containing amorphous poly[(L-lactide)-*ran*-glycolide]dimethacrylate with $T_{trans} = T_g$ in the range of 9–45 °C exhibited SME, with R_f and R_r values above 97% and 98%, respectively [39]. The group of (meth)acrylate-based SMP networks is very important according to potential biomedical applications due to their biodegradability and biocompatibility [10, 35, 36].

2.1.2 SME Based on Reversible Hydrogen Bonds

Two moieties exhibiting hydrogen bonds, pyridine and ureidopyridine units, have been widely studied in SMP systems. Pyridine moieties can be implemented into polymer (typically polyurethane) structure in the form of grafted side chains [40–42]. Reversibility of pyridine-based hydrogen bonds is achieved according to sensitivity to temperature, presence of carboxylic acid, or humidity. In the presence of the latter ones, the hydrogen bonds between the pyridine units in polymer chains

are substituted by the hydrogen bonds between pyridine units and acid or water molecules, resulting in cleavage of crosslinks [43, 44].

Furthermore, 2-ureido-4-pyrimidinone (UPy) units can be incorporated into the main polymer chains. They increase the strength of intermolecular interactions as the UPy units are capable of quadruple-hydrogen bonds formation [45–47]. In the first step, UPy was functionalized with a polymerizable group and afterwards copolymerized with acrylates or bisacrylates [48, 49]. Supramolecular shape-memory elastomers were synthesized from *n*-butyl acrylate, trimethylolpropane trimethacrylate, and the UPy-substituted ethyl methacrylate monomer. Based on the cyclic, thermomechanical analysis, R_r of about 90% and R_r of about 100% were determined [48]. In poly(vinyl alcohol) (PVA) supramolecular networks crosslinked by UPy dimers, thermo- and water-induced shape memory behavior with a R_r of nearly 99% was demonstrated. UPy dimers defined the permanent shape of the samples, whereas the PVA chains provided the switching domains enabling the fixation of a temporary shape [50]. Biodegradable, supramolecular SMPs containing an elastic poly(glycerol sebacate) backbone and multiple hydrogen-bonding UPy grafts (Fig. 4) were designed. The dynamic supramolecular interactions within those multifunctional elastomers enabled also tunable mechanical properties as well as the capability of self-healing [51].

Poly[(methyl acrylate)-*co*-(acrylic acid)] networks were reported to show excellent shape-memory properties ($R_r > 99\%$) due to the combination of hydrogen bonding and controlled crosslinking density [52]. A self-assembling, H-bonding polymeric system containing a polystyrene backbone and polyacrylate amide brushes was designed. The amide formed polyvalent clusters of H-bonds capable of reversible self-assembly and cleavage [53]. A SME based on hydrogen bonding could also be realized in IPN systems [54]. A semi-interpenetrating polymer network based on poly[(methyl methacrylate)-*co*-(*N*-vinyl-2-pyrrolidone)]/poly(ethylene glycol) was capable of SME with R_r of 99%. The PEG-poly(*N*-vinyl-2-pyrrolidone) complexes served as switching domains, whereas covalent netpoints defined the permanent shape [55, 56]. The temporary shape was fixed at pH = 10, whereas the permanent shape was recovered at pH = 1.3. The mechanism of these pH-induced SME is based on the formation of a hydrogen bond interaction between the nitrogen atom of the pyridine ring and the urethane group in neutral or alkaline environment. Under acidic conditions, due to the protonation of the pyridine ring, cleavage of the intermolecular hydrogen bonding takes place resulting in the recovery of permanent shape (Fig. 5). Furthermore, the obtained system could be applied in the drug-delivery field [57].

Poly(carboxylic acid)s can form intermacromolecular complexes with PEG by the hydrogen bonding between the carboxyl groups of poly(carboxylic acid)s and the ether oxygen atoms of PEG. The formation of these hydrogen-bonded complexes is highly sensitive to a change in the temperature. The shape-memory behavior of H-bonded complexes of poly[(acrylic acid)-*co*-(methyl methacrylate)] networks with PEG of varying molecular weight was reported with R_r of 99% [58]. In poly[(acrylic acid)-*co*-acrylonitrile]-based systems, the complexation

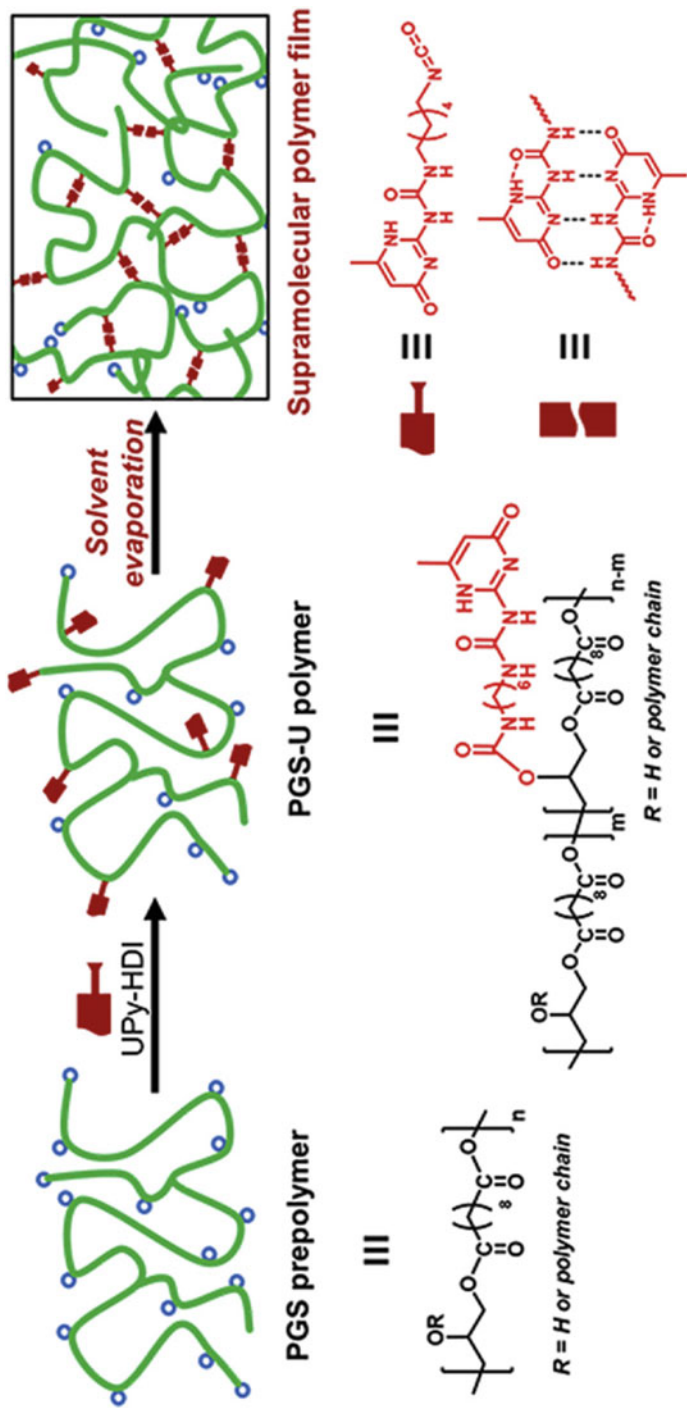


Fig. 4 Schematic presentation of supramolecular SMPs obtained based on poly(glycerol sebacate) backbone and reversible multiple hydrogen-bonding ureidopyrimidinone (UPy) grafts. (Reprinted from Ref. [51], Copyright 2016, with Permission from Elsevier)

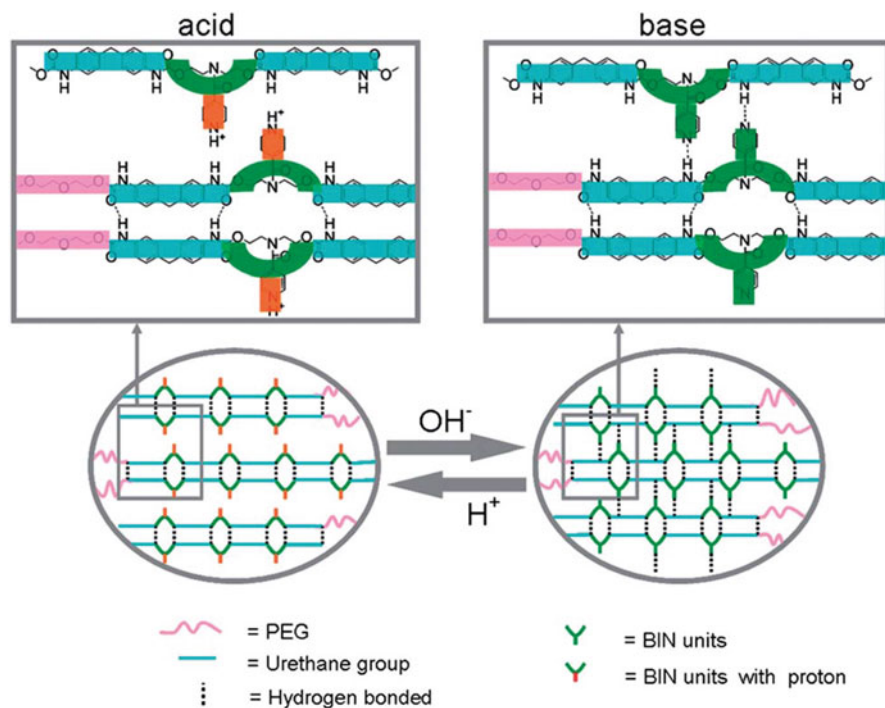


Fig. 5 Schematic representation of the pH-induced SME in PEG-based polyurethane (PUR) containing N,N-bis(2-hydroxyethyl)isonicotinamine (BIN) units. The pyridine rings in PUR are protonated resulting in distortion of the hydrogen bond in acidic condition. Once the pyridine rings are deprotonated under neutral or basic conditions they enable a reversible switching between two shapes. (Reproduced from Ref. [57] with permission of The Royal Society of Chemistry. <https://doi.org/10.1039/c4py00474d>)

occurred through H-bonding of carboxyl group of acrylic acid with ether group of poly(tetramethylene oxide) (PTMO) enabling a SME with $R_f > 93\%$ [59].

2.1.3 SME Based on Ionic Interactions

Usage of ionic interactions as a method to induce an SME was demonstrated by the neutralization of sulfonated polymers with zinc salts [60–62]. SMPs were prepared from mixtures of the zinc salt of a sulfonated poly[ethylene-*co*-propylene-*co*-(5-ethylidene-2-norbornene)] ionomer and zinc oleate (ZnOl). Physical netpoints based on intramolecular ionic interactions provided the permanent network structure. Strong dipolar interactions between the ionomer and a dispersed phase of crystalline ZnOl enabled a fixation of a temporary shape (Fig. 6) [62].

Biodegradable poly[oxyethylene-*b*-(butylene adipate)] ionomers, synthesized by bulk polymerization of adipic acid, bis[poly(oxyethylene)] sulfonated dimethyl fumarate, and 1,4-butanediol, exhibited a SME, with a R_f in the range of 81–95% at 40 °C [63].

Fig. 6 Schematic representation of SMP based on the zinc salt of a sulfonated poly[ethylene-*co*-propylene-*co*-(5-ethylidene-2-norbornene)] ionomer and zinc oleate (ZnOl). (Reprinted with permission from Ref. [62]. Copyright 2011 American Chemical Society)

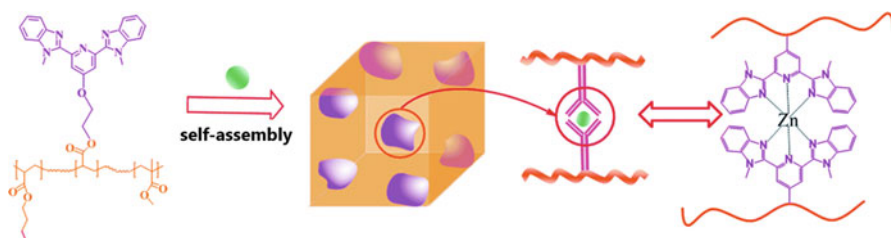
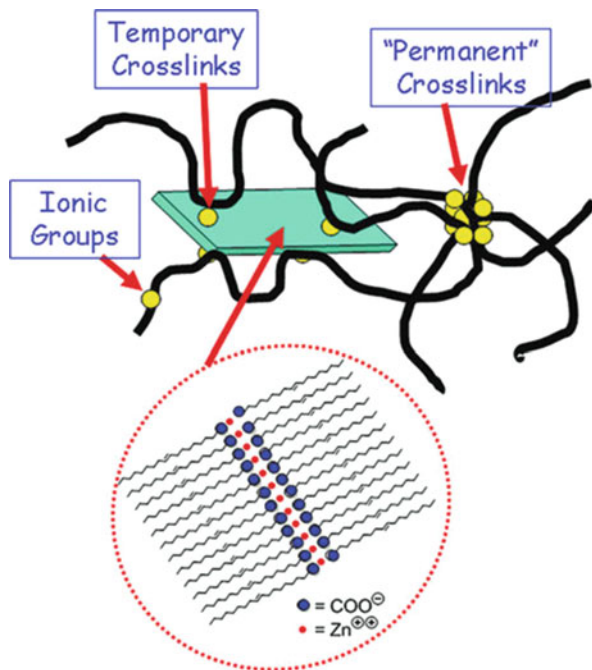


Fig. 7 Schematic diagram of metallosupramolecular interaction exemplarily for poly[(*n*-butyl acrylate)-*co*-(methyl methacrylate)] bearing a side group of the ligand 2,6-bis(10-methylbenzimidazolyl)pyridine. The ligand can be reversibly crosslinked by the zinc trifluoromethanesulfonate upon temperature increase. (Reproduced from Ref. [64] with permission of The Royal Society of Chemistry. <https://doi.org/10.1039/c4ra02843k>)

2.1.4 SME Based on Metal-Ligand Interactions

Another approach to achieve reversible bonds in SMPs is the incorporation of metal-ligand interactions into polymer system. The change of shape is realized by the thermally-triggered association and dissociation of metal-ligand complexes. Structure organization on molecular level is schematically shown in Fig. 7, exemplarily for poly[(*n*-butyl acrylate)-*co*-(methyl methacrylate)] bearing a side group of the ligand 2,6-bis(10-methylbenzimidazolyl)pyridine. The ligand reversibly crosslinks with the zinc trifluoromethanesulfonate when the temperature

is increased, and therefore enables a shape-memory as well as self-healing capability [64].

High-molecular-weight SMPs capable of supramolecular interactions with metal ions were obtained based on europium salts and low molecular weight polybutadiene functionalized with 4-oxy-2,6-bis(N-methylbenzimidazolyl)pyridine ligands. The addition of a tetra-functional thiol and a photoinitiator, followed by photo-crosslinking via the thiolene reaction, resulted in formation of SMP networks. In the solid state the metal ligand complexes formed a separated phase and served as a switching phase enabling the fixation of the temporary shape. The recovery of the permanent shape could be induced under various stimuli such as heat, UV-light or presence of solvents (for example methanol) ($R_r > 80\%$, $R_f > 97\%$) (Fig. 8) [65].

Blends of zinc-neutralized carboxyl-terminated polybutadiene and poly[styrene-co-(4-vinylpyridine)] were tightly bound by the metal coordination interactions between Zn^{2+} ions (Fig. 9). The obtained elastomers were capable of large deformations and exhibited good shape-memory properties with R_r up to 81% in the first and 97% in the following cycles [66].

The phenomenon of ultrasonic cavitation enabled the stimulation of the SME in covalently crosslinked polymer networks containing coordination bonds [67]. In this

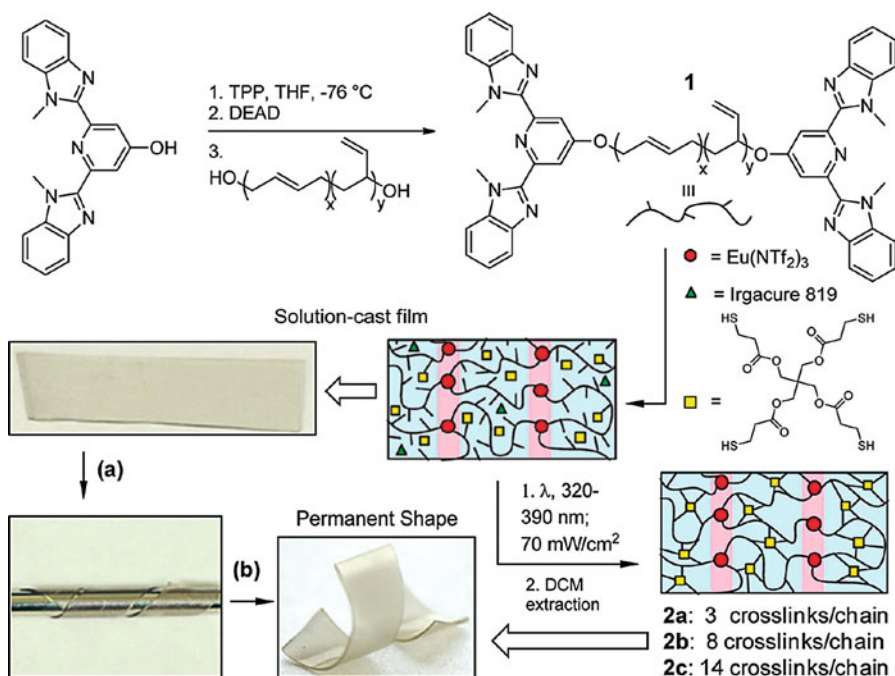


Fig. 8 The solution-cast non-crosslinked films can be fixed into various permanent shapes; (a) a strip of non-crosslinked film is wrapped around a cylinder into a spiral shape; (b) irradiation with low intensity UV-light initiates photo-crosslinking to get the permanent spiral shape. (Reprinted with permission from Ref. [65]. Copyright 2011 American Chemical Society)

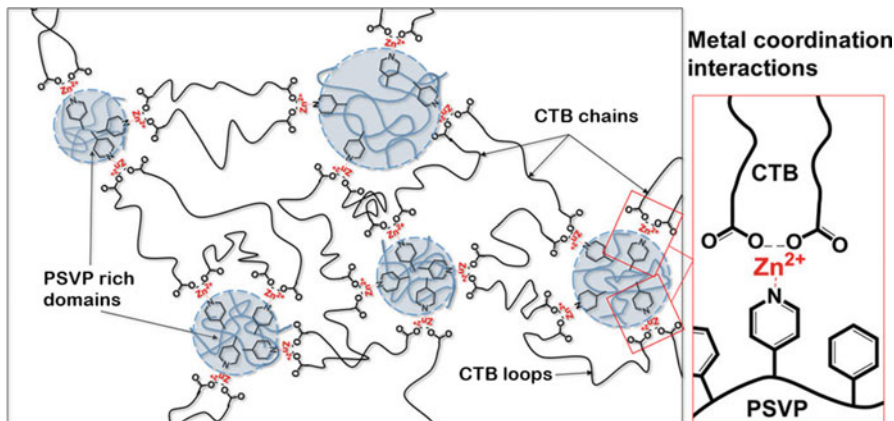


Fig. 9 Scheme of the metal coordination interactions in the blend of zinc salt of carboxyl-terminated polybutadiene (ZnCTB) and poly[styrene-co-(4-vinylpyridine)] (PSVP). The ZnCTB chains crosslink PSVP nanodomains by supramolecular bonds between one zinc ion and two pyridine groups. As indicated in the scheme, some ZnCTB chains may form bonds with the same PSVP nanodomain (CTB loops), resulting in no contribution to growth of the network. (Reprinted with permission from Ref. [66]. Copyright 2016 American Chemical Society)

SME, which is independent of heat, the sonification creates small vacuum bubbles or voids in the liquid medium. When the bubbles attain a volume at which they can no longer absorb energy, a violent collapse takes place resulting in shock waves with a velocity around $100 \text{ m} \cdot \text{s}^{-1}$. These shock waves generate a strong mechanical force near the solid-liquid boundary. For this ultrasound cavitation-induced SME, the key challenge was the design of an appropriate polymer system, which enabled the effective permeation of the mechanical force throughout the bulk polymer sample. Furthermore, selection of suitable mechanoresponsive molecular switches to fix the temporary shape was critical as well. Therefore, interconnected macroporous systems based on poly(*n*-butyl acrylate), diphenylphosphinostyrene, and poly(propylene glycol) dimethacrylate (PPGDMA) (Fig. 10a) were designed. Rhodium-phosphine coordination bonds (Rh-PCBs) served as mechanically sensitive molecular switches, which were able to fix the temporary shape and to control the recovery to permanent shape. The interconnected macroporous structure with thin porous walls provided a large specific surface area and allowed the penetration of the ultrasound waves through the pores. Water captured within the pores acted as an ultrasound transporting medium, whereby the collapse of the cavitation bubbles inside the macropores induced the energy input efficiency from the ultrasound source to the polymer. Rhodium-phosphine complexes formed a separated microphase and provided aggregates, which could be reversibly dissociated under ultrasonic cavitation-based mechanical force (CMF). Furthermore, the CMF accelerate the ligand exchange rate of Rh-PCBs. As a result, once the deformed sample is treated by low frequency ultrasound (LU), the topology of molecular switches is capable to undergo a rapid rearrangement, enabling the deformed polymer chains to

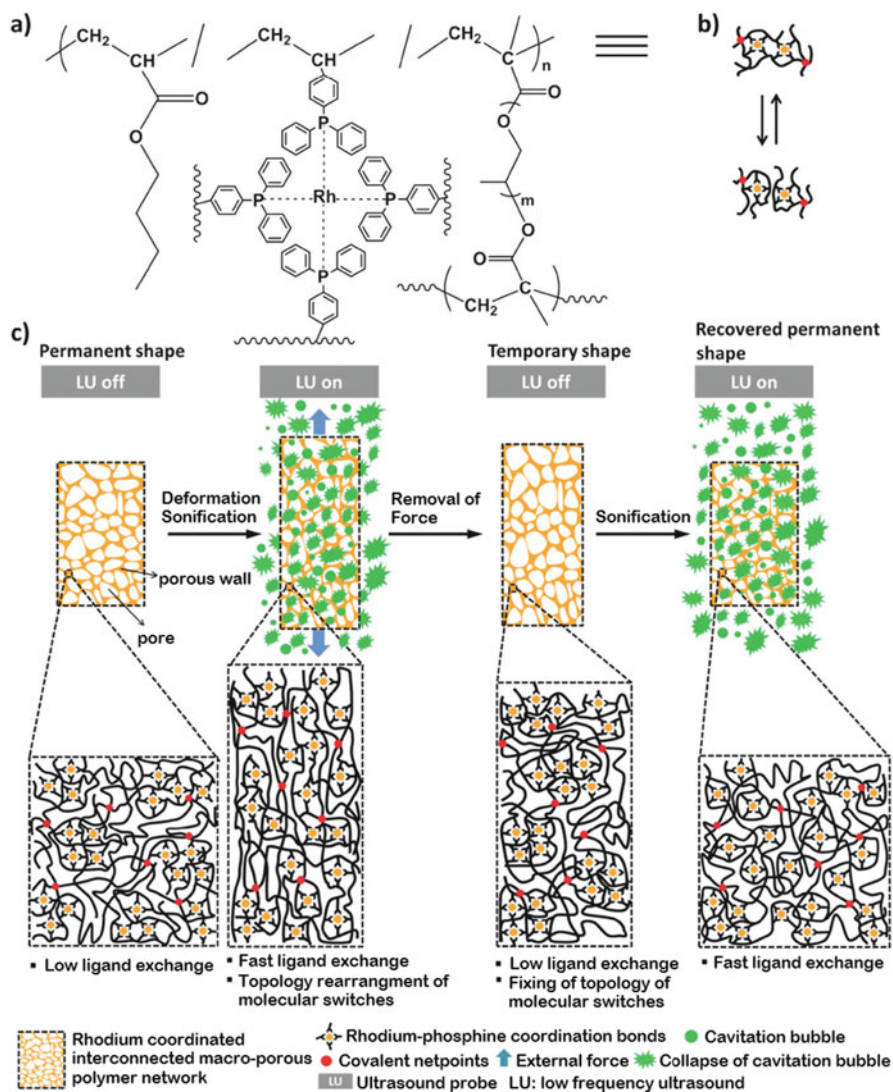


Fig. 10 (a) Chemical structure of rhodium coordinated interconnected macroporous polymer network. (b) Schematic illustration of the ligand-exchange of rhodium-phosphine coordination bonds. (c) Schematic illustration of proposed shape-memory mechanism of the rhodium coordinated interconnected macroporous polymer network. (Reprinted from Ref. [67] with permission, © 2016 WILEY-VCH Verlag GmbH & Co. KGaA, Weinheim)

relax the stress and fix the temporary shape (Fig. 10b). Subsequent LU treatment again causes an increase of the ligand exchange rate of Rh-PCBs and the dissociation of the microphase segregated morphology takes place, resulting in the recovery to the permanent shape (Fig. 10c) [67].

2.2 SME Based on Reversible Covalent Bonds

A fixation of a temporary shape to obtain a SME can also be achieved when reversible crosslinking reactions are used as a switch [68]. The first group of SMPs containing reversible covalent bonds utilizes photodimerization, Diels-Alder reaction, or redox reactions of mercapto groups. The advantage of this concept is the formation of very strong temporary crosslinks, resulting in high R_r . However, optimization of R_r is still a challenge due to the low efficiency of reversibility of these reactions [2].

The most frequently utilized reversible covalent bonds in SMP are based on Diels-Alder (DA) and retro-Diels-Alder (r-DA) reactions. However, it has to be noted that DA reaction is not an on-off switch, but always exists in a dynamic state, in which the temperature change only shifts the equilibrium [69]. In DA-based systems, typically furan derivatives as terminal groups [70–76], pendant groups [77, 78], or as a part of main chains of the polymer [79, 80] are reversibly crosslinked with bismaleimides. For example, PLA and star-shaped PCLs were functionalized with furan moieties. The subsequent crosslinking with bismaleimides resulted in polymer networks exhibiting SME [72–74]. Bio-based polyesters with efficient shape-memory properties were obtained from a furan-diol after polycondensation with succinic acid and crosslinking with bismaleimides [79]. Polyketons functionalized with furan pendant groups and crosslinked with 1,1'-(methylenedi-*p*-phenylene)bismaleimide (BM) resulted in SMP networks with $T_{\text{trans}} = 50\text{ }^\circ\text{C}$ [78].

Besides DA reaction, redox reactions of the mercapto group can also be utilized to create reversible covalent bonds in SMPs [81, 82]. For example, cellulose containing mercaptoic acid terminal groups could be functionalized by dimethylsulfoxide to obtain disulfides capable of gel-sol transition when oxidation/reduction reactions were performed. However, R_r decreased with each redox treatment due to side reactions, which reduced the number of mercaptoacetyl groups [81].

2.2.1 Light-Induced SME

The photodimerization of cinnamic acid (CA) or cinnamyliden acetic acid (CAA) formed the basis for the first light sensitive SMP. These photoresponsive units are able to undergo a reversible [2 + 2] cycloaddition reaction stimulated by light of different wavelength ranges (Fig. 12c). The programming cycle consisted of deformation of the samples to ϵ_m followed by irradiation with UV-light of $\lambda > 260\text{ nm}$. In this way, new covalent bonds between CA molecules were formed and the temporary shape (ϵ_m) could be fixed. When the sample was irradiated with the UV-light of $\lambda < 260\text{ nm}$, the newly formed covalent bonds were cleaved and the permanent shape was recovered (Fig. 11). Two different molecular architectures were explored: a graft-polymer and an interpenetrating polymer network (IPN). The polymer network with the grafted light-sensitive group was realized by a copolymerization of *n*-butyl acrylate (BA), hydroxyethyl methacrylate (HEMA), and ethyleneglycol-1-acrylate-2-CA (HEA-CA). Poly(propylene glycol) dimethacrylate ($M_n = 560\text{ g mol}^{-1}$) was used as a crosslinker. In this system, R_r up to 52% and R_r up to 95% could be realized. The IPN system was obtained by copolymerization of BA

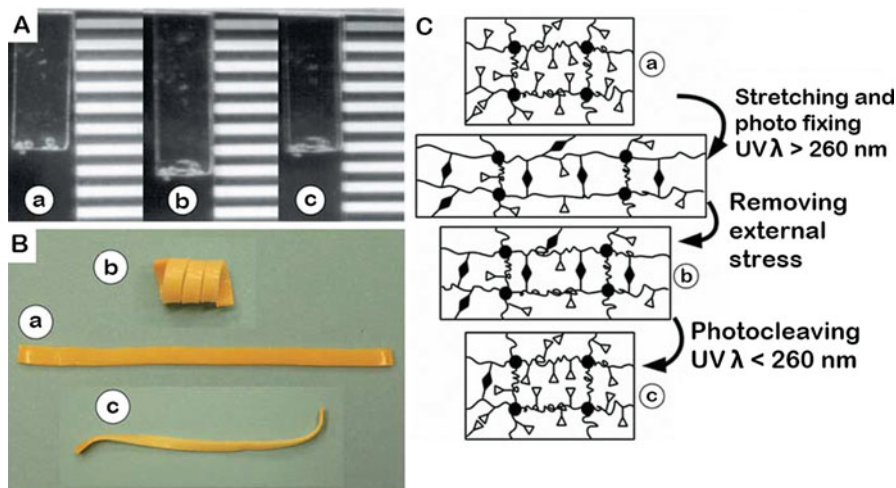


Fig. 11 SME of photoresponsive polymers. (A): a film of grafted polymer; (a) permanent shape; (b) temporary shape; (c) recovered permanent shape. (B): an IPN polymer film. (a) permanent shape; (b) corkscrew spiral temporary shape; (c) recovered shape obtained by irradiation with UV light. (C): Molecular mechanism of SME of the grafted polymer network: the chromophores (Δ) are covalently grafted onto the permanent polymer network (\bullet), forming photoreversible crosslinks (\blacklozenge). (Reproduced from Ref. [83]. © 2005 Nature Publishing Group)

with 3.0 wt% poly(propylene glycol)-dimethacrylate ($M_n = 1,000 \text{ g}\cdot\text{mol}^{-1}$) as a crosslinker, followed by mixing with about 20 wt% star-poly(ethylene glycol) containing CAA terminal groups. The light-induced SME with R_f up to 33% and R_r up to 98% was observed [83]. A light-induced SMP, in which the light-sensitive CA groups were incorporated in the main chain, could be obtained based on α,ω -hydroxyl polyesters (PLA, PCL, PEG). Again based on the [2 + 2] cycloaddition reaction, the reversible gelation of polyesters was achieved by irradiation with UV light [84]. Multiblock biodegradable poly(ester-urethane)s (PEUs) containing pendant cinnamide moieties were synthesized via a two-step polyaddition reaction using N,N-bis(2-hydroxyethyl) cinnamide (BHECA), α,ω -hydroxyl PLLA, and PCL. Hexamethylene diisocyanate (HDI) was used as a coupling agent. The R_f reached 50% at a BHECA content of 20 wt%, whereas the R_r reached >95% at a PLLA content of 50 wt% [85]. Similar PEUs containing pendant photoresponsive moieties (diethyl 2,2'-[cinnamoylazanediy]diacetate and diethyl 3-[cinnamoyloxy]pentanedioate) were reported to show R_f in the range of 70–85%, and R_r in the range of 40–70% [86].

Also coumarin groups are capable to undergo a reversible [2 + 2] cycloaddition, and therefore they can be used in photo-induced SMP [87–89]. PCL with a pendent coumarin group was prepared by solution polycondensation of 7-(3,5-dicarboxyphenyl) carbonylmethoxycoumarin dichloride and α,ω -dihydroxy terminated PCL ($M_n = 1250, 3000, \text{ and } 10,000 \text{ g}\cdot\text{mol}^{-1}$). These photosensitive polymers underwent a rapid, reversible photocrosslinking when exposed to

irradiation with alternating wavelengths (280/254 nm) without an additional photoinitiator. Obtained networks provided the shape-memory properties, in which both R_f and R_r values were between 88% and 100% for tensile strains of 100–500%. The shape-memory ability strongly depended on the degree of the crystallization of PCL segment and the crosslinking density of the polymers [87].

The light-sensitive shape change can also be driven by photoisomerization reactions, typically utilizing azobenzene moieties [10, 90, 91]. Azobenzenes can be switched reversibly from *cis* to *trans* conformations by exposure to light of appropriate wavelength ranges (Fig. 12a). The interconversion between these two photoisomers linked to polymer chains can induce macroscopic changes in the polymeric material. However, this effect was studied more in the context of reversible shape changing of polymeric systems, and not as conventionally understood SME [92–96]. Similarly, changes in the polymer shape were observed in the systems containing triphenylmethane leuco [97, 98] (Fig. 12b) or spiropyran derivatives [99, 100], which dissociate into ion pairs upon exposure to UV light. The recombination reaction of the ion pair occurs thermally in the dark.

3 Triple/Multiple-Shape Effect (TSE/MSE)

Triple-shape polymers (TSPs) are capable to memorize two temporary shapes (A and B) in addition to the original shape (C). TSPs require a polymer system containing at least two phase segregated domains characterized by two transition temperatures $T_{\text{trans,A}}$ and $T_{\text{trans,B}}$ [101–103]. The original shape (C) is defined by covalent netpoints and constitutes a permanent shape. Temporary shapes A and B are created by a two-step programming process. Physical or chemical crosslinks associated to the highest transition temperature ($T_{\text{trans,A}}$) determine shape A, whereas shape B is related to the second highest transition temperature ($T_{\text{trans,B}}$). In the recovery process, upon application of the external stimuli, the TSP switches back from the intermediate shapes (A and B) until the permanent shape C is achieved [8]. Typical chemical structures of TSPs and the processes occurring at the molecular level during the triple-shape change are shown in Fig. 13 [8]. Further increase of the number of phase transitions raises the number of temporary shapes and results in multi-shape effects (MSE). The MSE was realized in thermoplastic polymers providing broad switching transition, covalently crosslinked networks, IPNs, and polymeric multi-material systems [68, 104].

Methods to quantify the efficiency of SME in TSPs are similar to the ones used for 1-W SME. Cyclic, thermomechanical measurements are performed, from which R_f and R_r of each shape can be calculated. Examples of typical cyclic, thermomechanical experiments performed for TSP and the macroscopic changes in the polymer shape are shown in Fig. 14A and B, respectively [108]. The sample is stretched at T_{high} from ε_C (shape C) to ε_B^0 . Cooling under the stress determined at ε_B^0 to T_{mid} results in $\varepsilon_{\text{B,load}}$. Unloading after 30 min leads to ε_B (shape B). The sample is further stretched to ε_A^0 and cooled to T_{low} under the stress determined at ε_A^0 , whereas

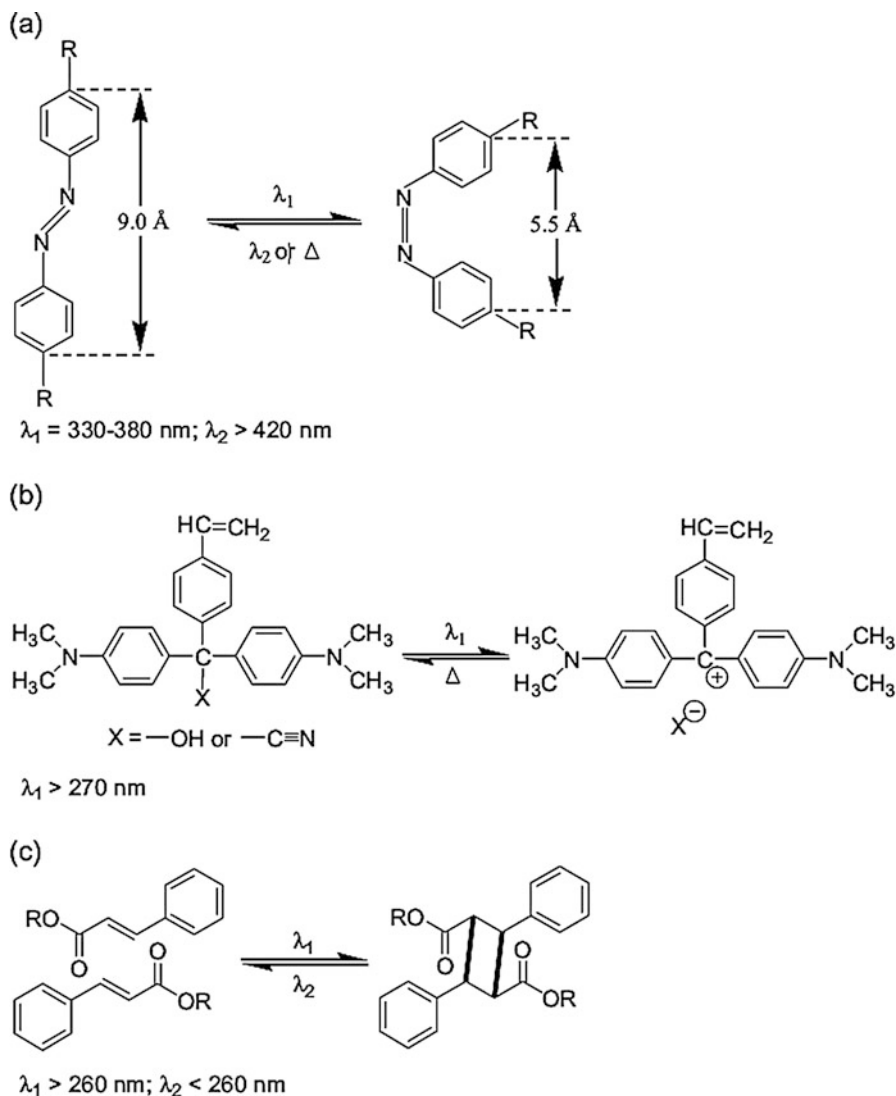


Fig. 12 Schematic illustration of light-induced isomerization and photochemical reactions. (a) Trans–cis photoisomerization of azobenzene groups. (b) Photoinduced ionic dissociation of triphenylmethane leuco derivatives. (c) Photodimerization of the cinnamic acid (CA) group. (Reprinted from Ref. [90] with permission, © 2006 WILEY-VCH Verlag GmbH & Co. KGaA, Weinheim)

the elongation decreases to $\varepsilon_{A,\text{load}}$. Shape A, corresponding to ε_A , is obtained by unloading after 20 min. The recovery process of the sample proceeds during reheating from T_{low} to T_{high} under stress-free conditions. The sample contracts to shape B at $\varepsilon_{B,\text{rec}}$, and further to shape C at $\varepsilon_{C,\text{rec}}$ (Fig. 14A, a). In the second protocol presented in (Fig. 14A, b), the sample is stretched at T_{high} from ε_C (shape C) to ε_B^0 .

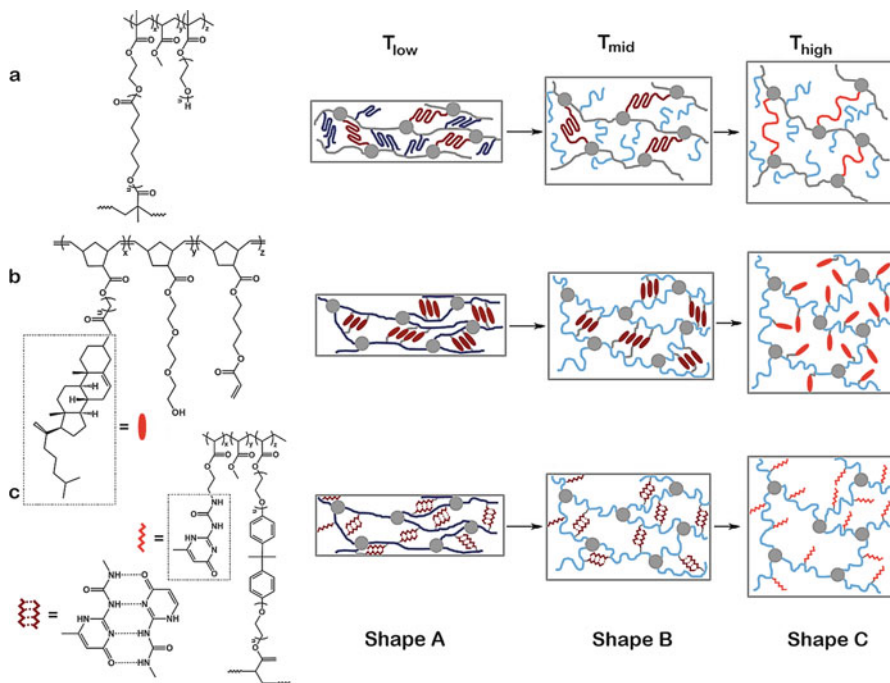


Fig. 13 Chemical structure as well as schematic representation of the changes in the polymer network at the molecular level of selected examples of TSPs. (a) CLEG network [105], (b) side-chain liquid crystalline polymer networks [106], and (c) UPy network [107]. The switching segments related to $T_{\text{trans},B}$ are colored in red. The switching segments related to $T_{\text{trans},A}$ are shown in blue. The segments in light color represent that they are amorphous (flexible), while the segments in dark color represent that they are solidified to form temporary netpoints. The gray dots represent the permanent netpoints, and the gray lines visualize the amorphous polymer chain segments. (Reprinted from Ref. [8] with permission from The Royal Society of Chemistry. <https://doi.org/10.1039/c2sm27077c>)

Cooling to T_{low} under the stress determined at ε_B^0 results in $\varepsilon_{B,\text{load}}$. Subsequently the sample is unloaded for 10 min, heated to T_{mid} and after passing $T_{\text{trans},A}$ with some additional time for equilibration at T_{mid} ε_B (shape B) is reached. The sample is further stretched to ε_A^0 and cooled to T_{low} under the stress determined at ε_A^0 , whereas the elongation $\varepsilon_{A,\text{load}}$ is achieved. Shape A, corresponding to ε_A , is obtained by unloading after 10 min. By reheating from T_{low} to T_{high} under stress-free conditions the recovery process of the sample to shape B at $\varepsilon_{B,\text{rec}}$ and further to shape C at $\varepsilon_{C,\text{rec}}$ is monitored.

The first examples of polymer networks capable of a triple-shape effect (TSE) were realized in two multi-phase polymers. The first one, named MACL, was a copolymer obtained from PCL ($T_m = 50^\circ\text{C}$) and poly(cyclohexyl methacrylate) ($T_g = 140^\circ\text{C}$). The second one, named CLEG (Fig. 13a), was a copolymer obtained from PCL ($T_m = 50^\circ\text{C}$) and grafted PEG segments ($T_m = 34^\circ\text{C}$) introduced as side chains. Both systems were synthesized by photoinduced copolymerization of poly

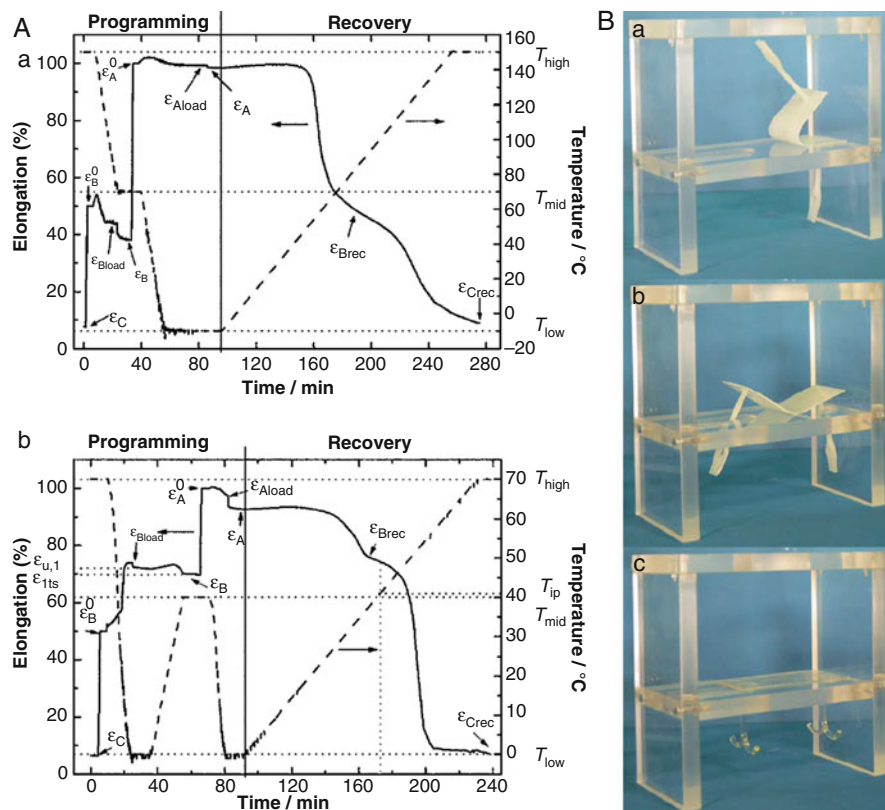


Fig. 14 (A) Example of cyclic, thermomechanical experiment; the strain (solid line) and temperature (dashed line) as a function of time. ((a). Reprinted from Ref. [105], Copyright 2006 National Academy of Sciences. (b) Reprinted from Ref. [109], Copyright 2005, Materials Research Society, Warrendale, PA). (B) Series of photographs illustrating the triple-shape effect. (a) Temporary shape (A) at room-temperature, (b) second temporary shape (B) around T_{mid} , and (c) permanent shape (C) at T_{high} . (Reproduced from Ref. [108] with permission from The Royal Society of Chemistry. <https://doi.org/10.1039/b922992b>)

(PCL)dimethacrylate [105]. Another example describes a maleated-polystyrene-*b*-poly(ethylene-*co*-butylene)-*b*-polystyrene block copolymer with two T_{ms} related to poly(ethylene-*co*-butylene) (EB) (55–65 °C) and polystyrene segments (105–115 °C). EB segments contained maleic anhydride reactive groups, which enabled the grafting of polybutylene succinate to the main polymer backbone. Therefore, the obtained polymer system was capable of TSE based on two melting transitions related to EB and polystyrene segments [110]. Furthermore, a liquid-crystalline polymer network providing two transition temperatures related to a glass transition (80 °C) and an isotropic-nematic transition (150 °C) was realized by an unsaturated, liquid-crystalline polyester, which was further crosslinked with dicumylperoxide [111]. Another crosslinked, glassy network containing

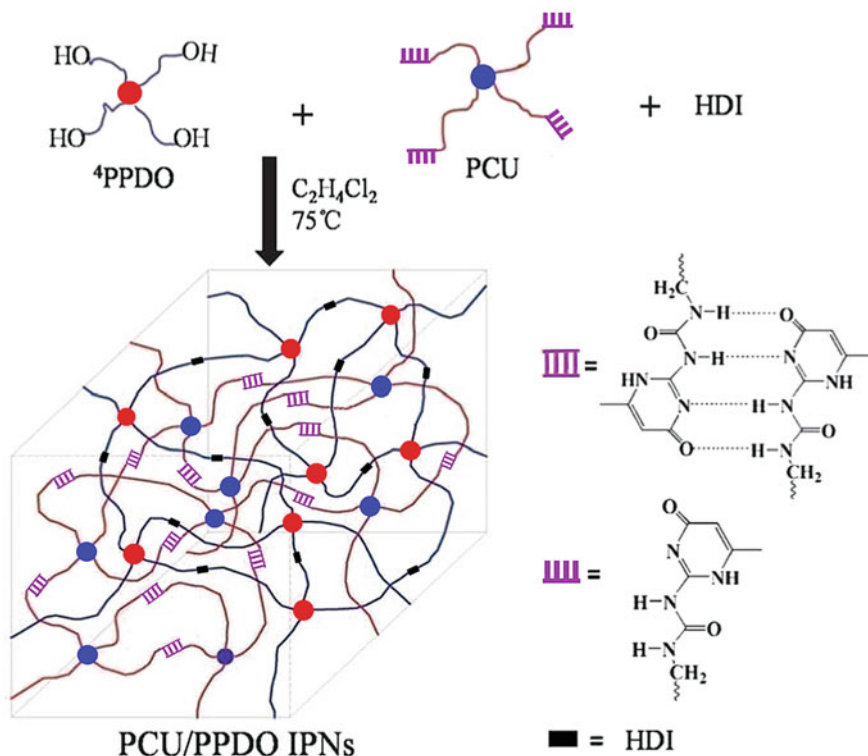


Fig. 15 Schematic representation of PCL-PPDO IPNs capable of TSE. (Reproduced from Ref. [54], with permission of The Royal Society of Chemistry. <https://doi.org/10.1039/c3py01476b>)

liquid-crystalline side chains was synthesized via ring-opening methathesis polymerization followed by radical crosslinking. Two T_{trans} were correlated to the thermal transitions of the domains related to the main network chains and the grafted side chains (Fig. 13b) [106, 112].

Triple-shape poly(ϵ -caprolactone)/poly(*p*-dioxanone) (PCL/PPDO) IPN was synthesized via crosslinking 2-ureido-4-pyrimidinone-functionalized PCL and PPDO. The PPDO network was obtained by coupling a star-shaped PPDO precursor with 1,6-hexamethylene diisocyanate. The PCL network was formed through the quadruple hydrogen bonds between 2-ureido-4-pyrimidinone ligands (Fig. 15). Melting transitions of PCL and PPDO served as T_{trans} of switching domains resulting in TSE with $R_{f,A-B}$ of 99%, $R_{f,B-C}$ of 82%, $R_{r,C-B}$ of 59%, and $R_{r,C-A}$ of 92% [54].

A TSE could also be obtained in systems, in which polymers providing the thermal transitions are macroscopically separated in a bilayer system. For example, two epoxy thermoset layers with two separated T_g s were used to create a macrophase-separated TSP composite with two T_{trans} [113]. Similarly, two-layer shape-memory PUR crosslinked with silica nanoparticles have shown two separated T_g s and exhibited TSE [114]. Non-woven thermoplastic PCL fibers were incorporated into

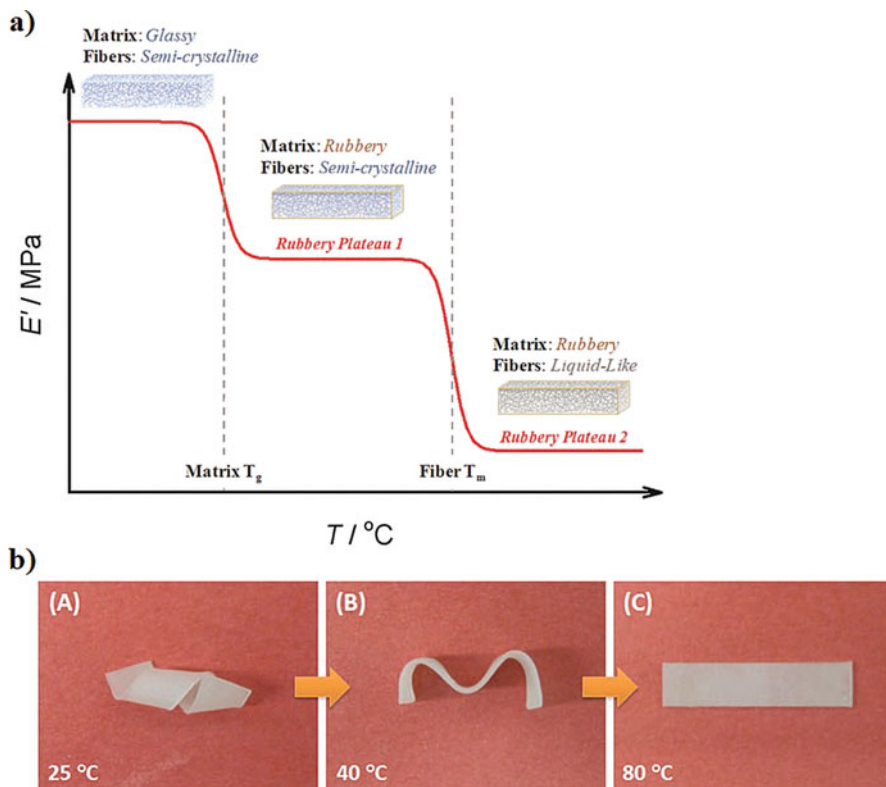


Fig. 16 (a) Schematic illustration of the typical temperature-dependent dynamic mechanical behavior of triple-shape polymeric composites (TSPCs). (b) Photographs showing the sequential recovery of TSPCs from temporary shape A (A), to temporary shape B (B), and to permanent shape C (C). Here the TSCP consists of nonwoven thermoplastic PCL fibers incorporated into a matrix of an epoxy-based SMP. (Reprinted from Ref. [115] with permission, © 2010 WILEY-VCH Verlag GmbH & Co. KGaA, Weinheim)

shape-memory epoxy matrix. Two well-separated thermal transitions ($T_{m,PCL} = 55\text{ °C}$ and $T_{g,epoxy} = 20\text{--}45\text{ °C}$) were utilized to fix two temporary shapes (Fig. 16) [115]. The TSE was also realized in polymeric composites containing small liquid-crystalline molecules (such as cholesteryl isonicotinate or 4-hexadecyloxybenzoic acid), which constituted separated phase and provided additional transition temperature [116, 117].

Instead of multiple discrete thermal transitions, a new approach based on a single broad thermal transition was discovered [118–120]. A thermoplastic copolymer of tetrafluoroethylene and perfluoro-3,6-dioxo-4-methyl-7-octene-sulfonic acid (trade name Nafion[®]) exhibiting a broad T_g (55–130 °C) was capable of a triple- and quadruple-shape effect (Fig. 17) [118, 121]. This broad single thermal transition enabled the programming of two temporary shapes at two deformation temperatures. Furthermore, it was found that Nafion[®] could remember the temperature, at which the deformation was programmed. This effect is referred to the temperature-memory

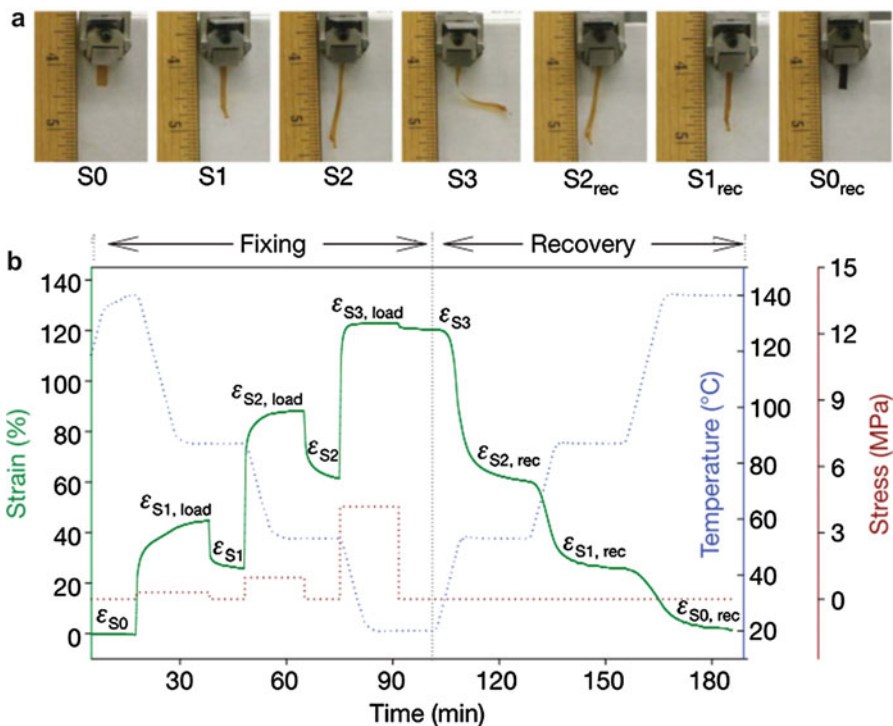


Fig. 17 Quadruple-shape-memory properties of PFSA (Nafion[®]). (a) Macroscopic demonstration of the quadruple memory effect. S0: permanent shape; S1: first temporary shape (T_{d1} : 140 °C); S2: second temporary shape (T_{d2} : 107 °C); S3: third temporary shape (T_{d3} : 68 °C); S2_{rec}: recovered second temporary shape (T_{r1} : 68 °C); S1_{rec}: recovered first temporary shape (T_{r2} : 107 °C); S0_{rec}: recovered permanent shape (T_{r3} : 140 °C). (b) Quantitative thermal mechanical cycle. $R_f(S0 \rightarrow S1)$: 58.7%, $R_f(S1 \rightarrow S2)$: 57.1%, $R_f(S2 \rightarrow S3)$: 96.1%, $R_r(S3 \rightarrow S2)$: 100.0%, $R_r(S2 \rightarrow S1)$: 99.6%, $R_r(S1 \rightarrow S0)$: 93.0%. (Reprinted by permission from Macmillan Publishers Ltd.: Nature Ref. [118] copyright 2010)

effect (TME) (further explained in Sect. 4). Another strategy for preparing tunable SMPs assumes utilization of fillers to adjust polymer behavior. Graphene oxide nanocomposite sheets can act as a physical crosslinker and significantly change the thermomechanical behavior of poly(propylene carbonate), enabling a MSE and TME in the investigated composites [122].

Similarly to 1-W SME, various molecular switching mechanisms based on reversible bonds can be utilized in TSPs. In one of the studies, TSPs were prepared based on amorphous (meth)acrylate copolymers containing grafted UPy capable of reversible hydrogen bonding at T_{trans} around 60 °C [107]. Polyurethanes capable of exhibiting TSE were synthesized through solution polymerization of PEG, dimethylolpropionic acid (DMPA), and MDI. The T_g of PEG chains, together with the association and disassociation of carboxylic dimers, acted as two switches to

control the TSE (Fig. 18). The hydrogen bonding interaction between NH and C=O in urethane groups formed permanent netpoints [123]. Furthermore, a photo-responsive hyperbranched polymer system was obtained based on diester monomer containing 4-hydroxycinnamic acid (coumaric acid) with conjugated double bonds and succinic acid for coupling. Reversible crosslinking was related to photo-dimerization of cinnamic double bonds (Fig. 12c) [124].

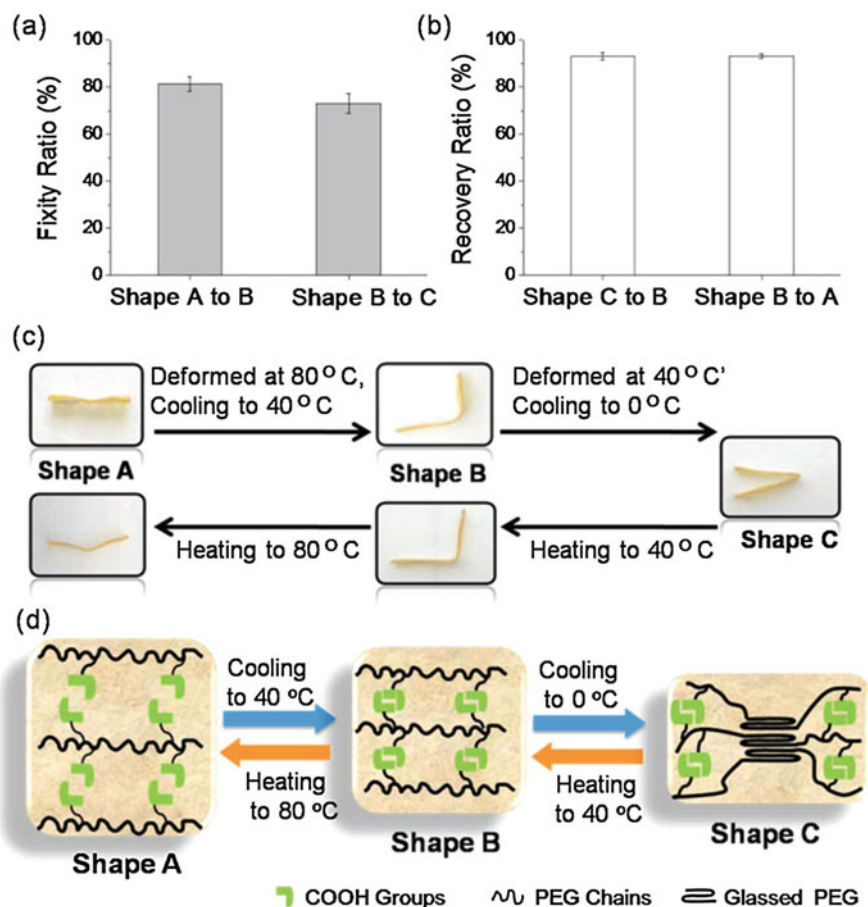


Fig. 18 Shape fixity ratio (a), shape recovery ratio (b), the procedure (c), and the mechanism (d) of TSE. When the sample is heated to 80 °C, the hydrogen bonds between NH and C=O of urethane groups fix the permanent shape. When cooled to 40 °C, the hydrogen bonds between carboxylic dimers fix the temporary shape B. Upon further cooling to 0 °C, PEG segments transform from the rubber state to the glassy state, fixing the temporary shape C. When the sample is reheated to 40 °C and 80 °C, the sample recovers shape B and shape A, respectively. (Reproduced from Ref. [123] with permission of The Royal Society of Chemistry. <https://doi.org/10.1039/c5py02010g>)

4 Temperature-Memory Effect (TME)

Temperature-memory polymers (TMP) are capable of memorizing temperatures, at which they were previously deformed. This temperature-memory effect (TME) provides a flexible approach of adjusting thermosensitivity to certain temperatures without the need of changing their chemical composition [122, 125–128]. TME requires a broad transition temperature ΔT_{trans} , which can be both a T_g or T_m . This broad thermal transition can be considered as an infinite number of thermal transitions $T_{\text{trans}s}$, which can be utilized as separated switching domains. In this way, the temporary shape is fixed only by a fraction of polymer chains associated to certain T_{trans} .

The TME was reported for polymer networks as well as for thermoplastic polymers. Poly(ester-urethane)s with poly(ω -pentadecalactone) as hard segments and PCL segments acting as crystallizable switching units were reported. Response temperatures could be systematically adjusted by variation of the deformation temperature in the range of 32–65 °C [129]. Polymer networks with crystallizable switching domains were formed by blending two poly[ethylene-*co*-(vinyl acetate)]s (PEVA) differing in their comonomer ratio, resulting in very broad melting temperature ranges ($\Delta T_{\text{trans}} = 0\text{--}100$ °C). The recovery under stress-free conditions as well as under constant stress was observed. It was demonstrated that three different parts of the same material piece can be programmed at different T_{prog} , and therefore show the recovery under different T_{trans} of 40 °C, 60 °C, and 80 °C (Fig. 19) [125].

Poly(vinyl alcohol) (PVA)/carbon nanotube (CNT) nanocomposites showed a TME because of their confined structure. In these nanocomposites, the CNTs favor the stabilization of crystalline domains. Therefore, by increasing the stiffness of the polymer, CNTs enable more energy to be absorbed and restored. It has also been shown that significant gradients of T_g can be developed at the interface of nanoparticles. Amorphous polymer shells around the CNTs or around crystalline domains largely overlap and percolate. This results in a distribution of polymer-CNT or amorphous polymer-crystallite distances ranging from molecular contact to several nanometers. This distribution causes a wide broadening of the glass transition [130, 131].

The influence of unloading temperature (T_u) upon the strain and stress recovery was studied in phase-segregated poly(ester-urethane) with crystallizable switching segments of poly(1,4-butylene adipate) (PBA). A novel route of sample programming was explored. An uniaxial stretching and unloading were performed at the same temperature ($T_d = T_u$), followed by specimen cooling below crystallization transition of switching segments (PBA). Independent of the programming route, a maximum tensile strain ε_m of 100% was applied at T_d (Fig. 20a). Almost linear rises of the switching temperatures (T_{sw}) and $T_{\sigma,\text{max}}$ with T_d were observed. Remarkably, the onset temperatures $T_{\text{sw,on}}$ and $T_{\sigma,\text{on}}$, which marked the beginning of strain decrease and stress increase, strongly depended on T_d (Fig. 20b). This illustrates that a temperature-memory onset programming could be achieved over a broad temperature range [132, 133].

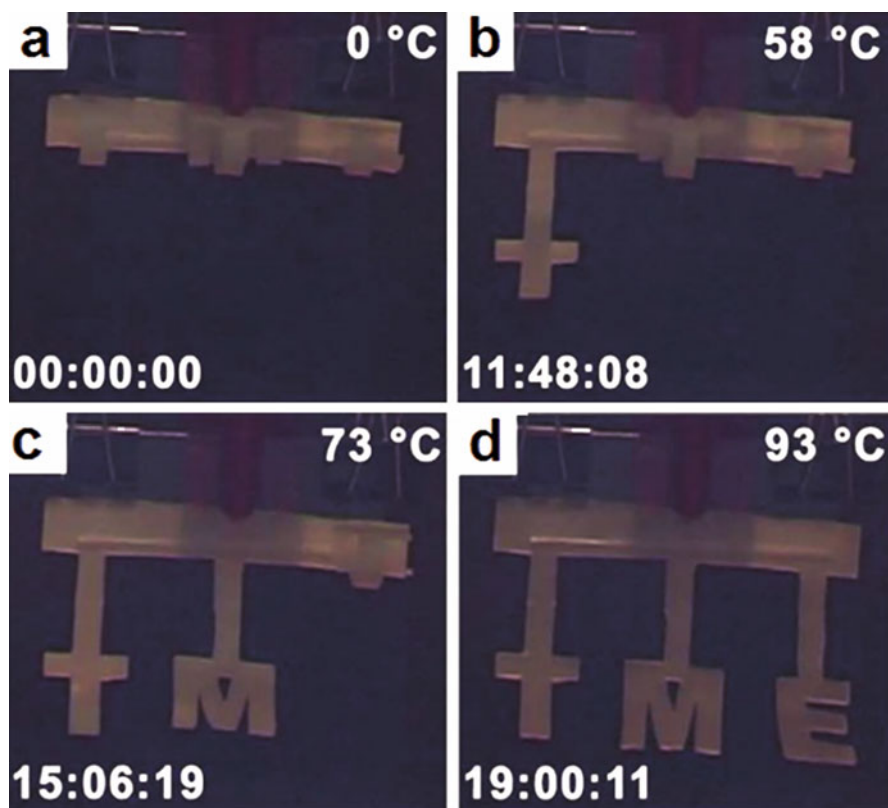
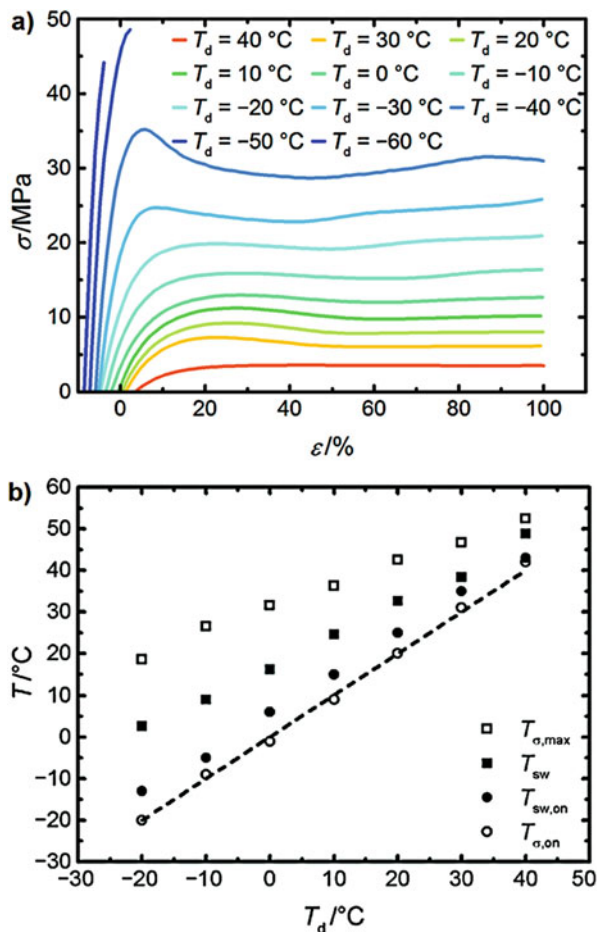


Fig. 19 Photograph series of three different TME demonstration devices prepared from crosslinked PEVA. (a–d) TME shaped temperature-memory demonstrator with three different T_{sw} , here each character was deformed at a different $T_{prog} = 40$ °C (T), $T_{prog} = 60$ °C (M), and $T_{prog} = 80$ °C (E). Heating at 5 K min^{-1} led to three subsequent shape changes. (a) $T = 0$ °C, $t = 00:00$ min; (b) $T = 57.7$ °C, $t = 11:48$ min; (c) $T = 73.4$ °C, $t = 15:06$ min; (d) $T = 93.2$ °C, $t = 19:00$ min. (Reprinted from Ref. [125] with permission, Copyright © 2011 WILEY-VCH Verlag GmbH & Co. KGaA, Weinheim)

5 Reversible SME

Unlike the 1-W SME, in reversible SMEs, polymers can switch between two memorized shapes upon heating and cooling without the requirement of a re-programming step. In reversible shape-memory effect (rSME) [134, 135], an external stress is required to induce the shape shifting of a polymer sample. In contrast to rSME, the reversible bidirectional shape-memory effect (rbSME) enables the polymer sample to change between preprogrammed shapes under stress-free conditions [136, 137]. A development of this revolutionary capability of SMPs enables new and more advanced applications of smart polymeric materials.

Fig. 20 (a) Engineering stress-strain curves of poly (ester-urethane)s at different temperatures (strain rate = $300\% \text{ min}^{-1}$). The corresponding Young's moduli were 1341 MPa (-60°C), 1145 MPa (-50°C), 746 MPa (-40°C), 483 MPa (-30°C), 282 MPa (-20°C), 217 MPa (-10°C), 156 MPa (0°C), 144 MPa (10°C), 116 MPa (20°C), 103 MPa (30°C), and 43 MPa (40°C). (b) Temperature-memory properties: the evolution of T_{sw} , onset temperatures $T_{\text{sw,on}}$, $T_{\sigma,\text{on}}$, and temperature related to maximum recovery stress σ_{max} ($T_{\sigma,\text{max}}$) with T_d . (Reprinted with permission from Ref. [132], Copyright 2014 American Chemical Society)



5.1 Reversible Shape-Memory Effect (rSME) Under Constant Stress

A reversible actuation under constant stress could be observed in semicrystalline polymer networks containing at least one crystalline switching domain. An rSME bases on crystallization-induced elongation (CIE), in which switching segments of polymer chains are oriented by application of constant stress under cooling to $T_{\text{low}} < T_m$, followed by the melting-induced contraction (MIC), which occurs at $T_{\text{high}} > T_m$. Stretching of the sample results in preorientation of polymer chains. During subsequent cooling oriented chain segments serve as raw nuclei in the direction of applied load and induce subsequent epitaxial growth of lamellae of semicrystalline domains. The melting of crystallites while heating to T_{high} under applied stress enables polymer chains to form random coils and contract to original elongation [135, 138]. Similarly to 1-W SME, the cyclic, thermomechanical

measurements are performed to quantitatively analyze the rSME. Firstly, the sample is programmed by elongation at T_{high} , whereby polymer chains become preoriented. The temporary shape A, with the elongation of $\varepsilon_{\text{act,CIE}}$, is achieved as a result of CIE occurring under the direction of load. Reheating to T_{high} under σ_c causes MIC, whereby the shape B ($\varepsilon_{\text{rev,MIC}}$) is obtained. When the temperature is changing between T_{low} and T_{high} , a reversible switching between elongated and contracted shapes under σ_c is observed. Two parameters are quantified based on the cyclic, thermomechanical measurements – the shape change during CIE ($R_{\text{act,CIE}}$) (Eq. 3) and the recovery ratio due to MIC ($R_{r,\text{MIC}}$) (Eq. 4) for each of N cycles.

$$R_{\text{act,CIE}} = \frac{\varepsilon_{\text{act}}(N) - \varepsilon_{\text{rev}}(N - 1)}{\varepsilon_{\text{rev}}(N - 1)} \quad (3)$$

$$R_{r,\text{MIC}} = \frac{\varepsilon_{\text{act}}(N) - \varepsilon_{\text{rev}}(N)}{\varepsilon_{\text{act}}(N - 1) - \varepsilon_{\text{rev}}(N - 1)} \quad (4)$$

One of the first examples of polymeric systems capable of rSME was crosslinked poly(cyclooctene), in which T_{m} s could be adjusted by the crosslinking density [135]. Later on a rSME was also found in the other semicrystalline crosslinked polymers such as PEVA [139], PCL [134, 137, 140] or poly(ω -pentadecalactone) (PPDL) [141, 142]. The approach was even extended to TSE, in which a rSME was shown over two transition temperatures, with a reversible switching under stress between three shapes (A, B and C) (Fig. 21) [138]. The strategy to achieve a reversible TSE under tensile load was to design a multiphase polymer network containing two different semicrystalline segments showing two separated and fully reversible CIE (Fig. 21, cooling from II to III and further IV) and MIC (Fig. 21, heating from IV to III and further to II). Similarly to two-way rSME, the CIE was induced by the crystallization promoted along the uniaxial loading stress.

5.2 Reversible Bidirectional Shape-Memory Effect (rbSME)

For decades, researchers have been trying to enable a stress-free, fully reversible shape shifting of polymer systems to overcome the necessity of a re-programming step and the requirement of external stress application. This challenge could be solved by polymers capable of a rbSME, which possesses a tremendous potential for further application [136]. In such a system, a polymer sample can undergo a reversible change of the shape upon cooling and heating without application of an external force. Polymers exhibiting rbSME contain two crystallizable domains. One is associated to the higher melting transition ($T_{\text{m,SGD}}$) and it determines the shape shifting geometry. The second one is related to the lower melting transition ($T_{\text{m,AD}}$) and is responsible for actuation of the reversible shape shifting (Fig. 22a). The first reported polymer network capable of a rbSME was a poly(ester-urethane)

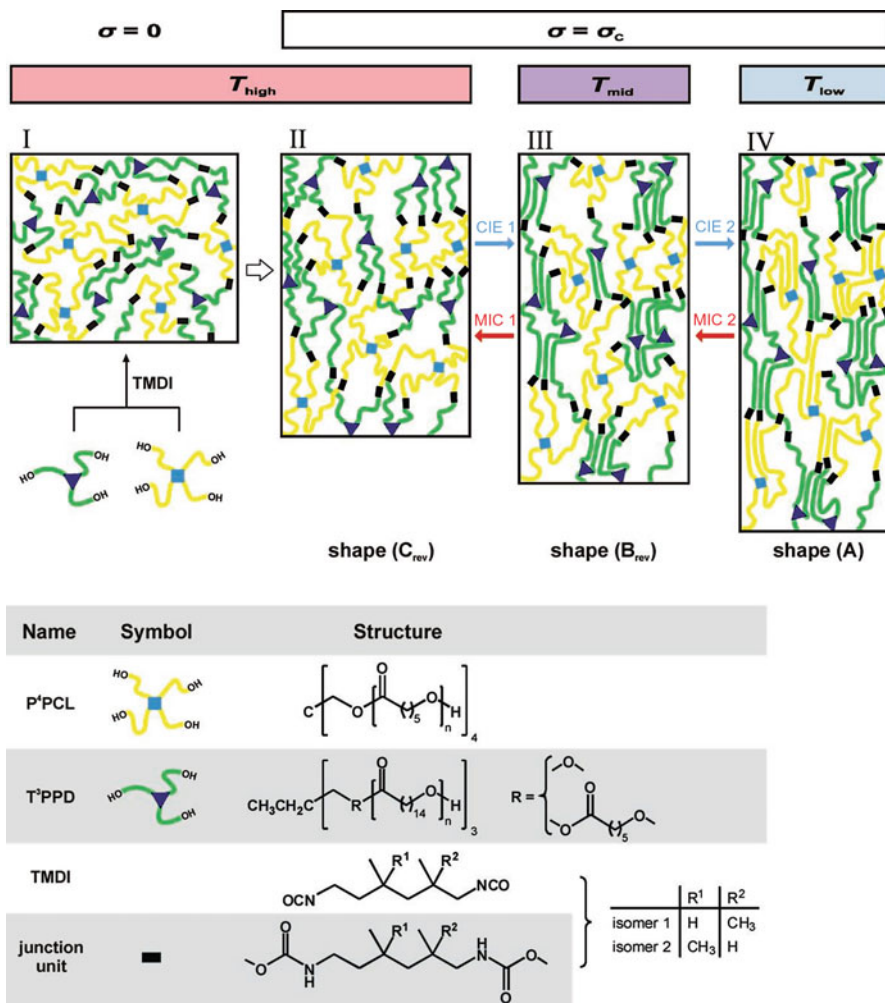


Fig. 21 Polymer network synthesis from star-shaped precursors and the mechanism of reversible TSE under constant stress; I: network synthesis; II: shape (C_{rev}) after application of the constant stress σ_c at T_{high} ; III: shape (B_{rev}) at T_{mid} after PCL-related CIE; IV: shape (A) at T_{low} after PPDL-related CIE. (Reprinted from Ref. [138] with permission, Copyright © 2010 WILEY-VCH Verlag GmbH & Co. KGaA, Weinheim)

containing PPDL and PCL blocks, which provided the shape shifting geometry determining domains and the actuation domains, respectively [136]. The programming step, leading to fixation of the temporary shape B, consists of deformation of the original shape C at $T_{reset} > T_{m,PPDL}$ by applying an external force, then cooling the sample to $T_{low} < T_{m,PCL}$ followed by releasing the stress. Shape A was achieved when the sample was heated to T_{high} ($T_{m,PCL} < T_{high} < T_{m,PPDL}$). Reversible switching between shape A and B was observed under stress free

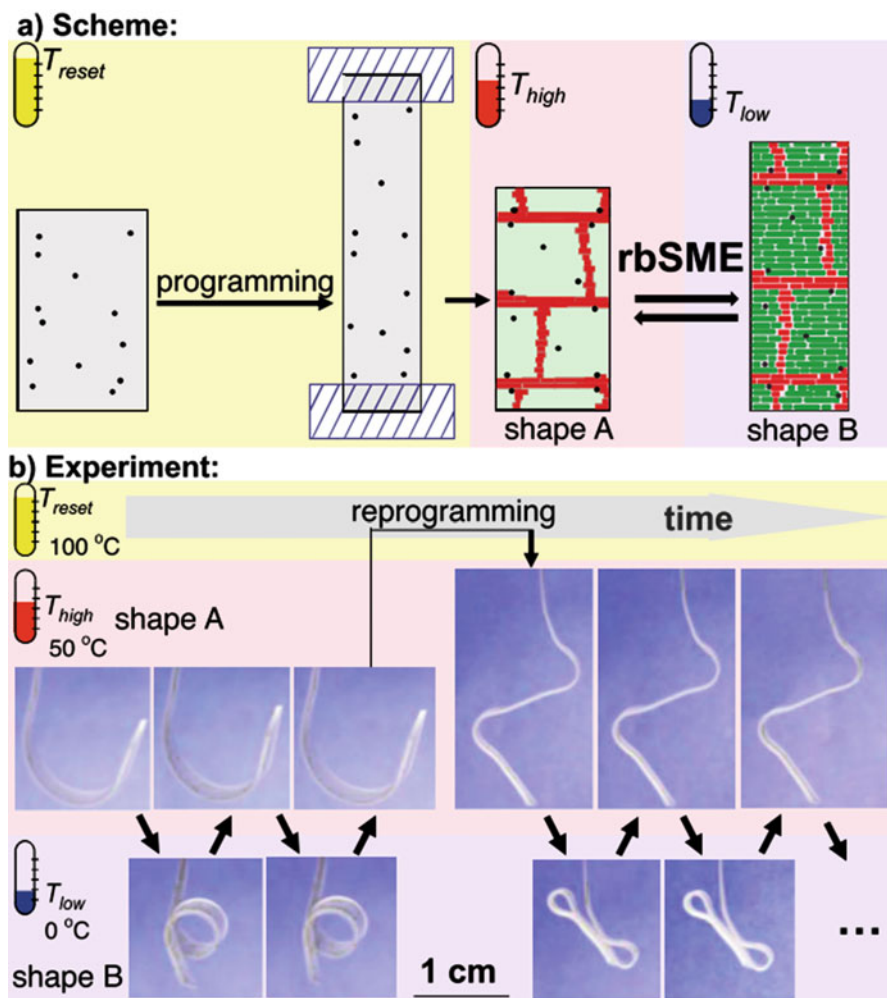


Fig. 22 (a) Scheme of the rbSME for copolymer networks: After deformation at T_{reset} the shifting geometry determining domains (red) are crystallized by cooling (programming). The rbSME is triggered by the reversible crystallization and melting of oriented actuation domains (green). Black dots: crosslinks. (b) Photograph series showing rbSME of a polymer ribbon from PPDL-PCL(75). The sample was reprogrammed by T_{reset} into an open shape (new shape A), which could be shifted reversibly to a folded shape (new shape B). (Reprinted from Ref. [136] with permission, Copyright © 2013 WILEY-VCH Verlag GmbH & Co. KGaA, Weinheim)

condition when the temperature was changed between T_{low} and T_{high} . Reheating to T_{reset} caused recovery of the original shape C (Fig. 22b).

The rbSME is quantified by cyclic, thermomechanical tensile tests, in which two parameters, the reversible elongation $\varepsilon'_{\text{rev}}$, and the deformation fixation efficiency Q_{ef} can be determined according to Eqs. 5 and 6, respectively (Fig. 23).

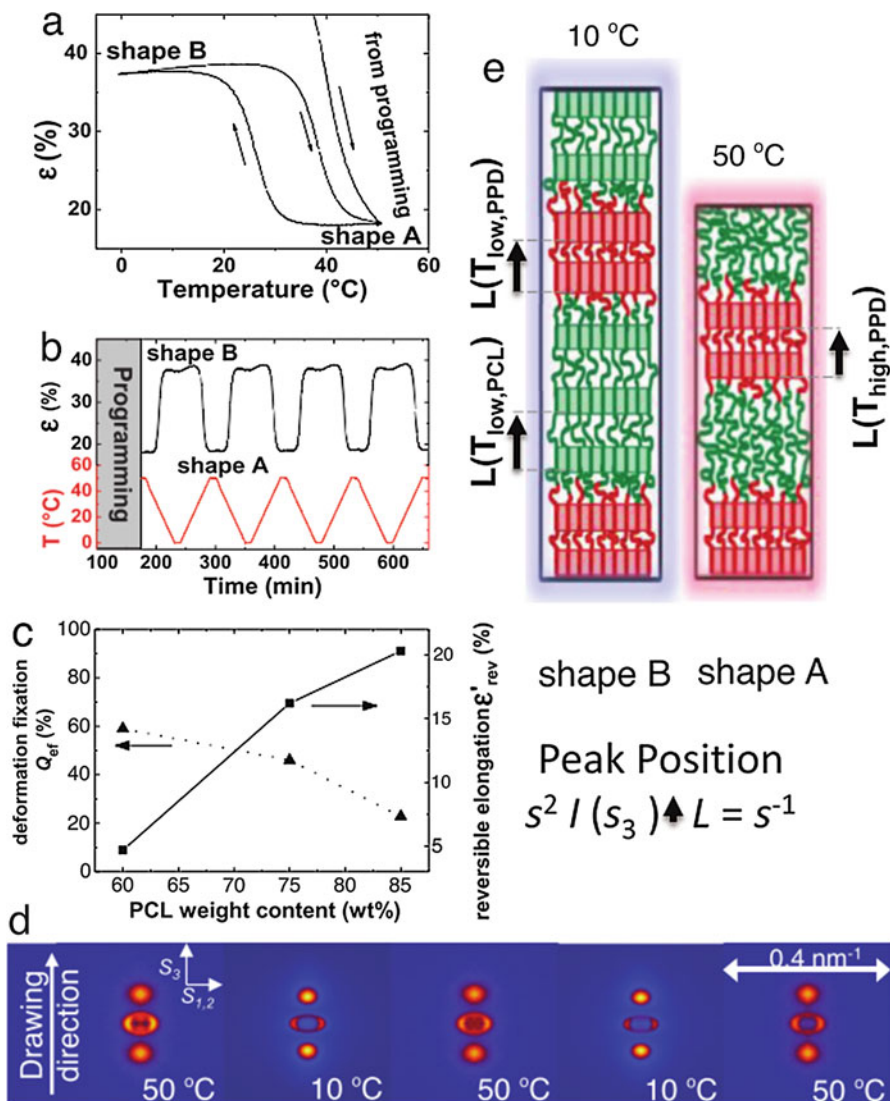


Fig. 23 The rsSME of PPDL-PCL(75) quantified in cyclic, thermomechanical tensile tests. (a) Elongation as function of temperature, reversible shape change between shape A and B. (b) Four reversible cycles, ε (black) and T (red) versus time plot. (c) The deformation fixation efficiency (Q_{eff}) and the reversible elongation ($\varepsilon'_{\text{rev}}$) as a function of the PCL weight content. (d) Structural changes occurring during the rsSME determined by SAXS recorded for shape A and shape B in subsequent reversible cycles. (e) Changes of long periods schematically shown for PPDL-PCL during rsSME. (Reprinted from Ref. [136] with permission, Copyright © 2013 WILEY-VCH Verlag GmbH & Co. KGaA, Weinheim)

$$\varepsilon'_{\text{rev}} = \frac{l_B - l_A}{l_A} \quad (5)$$

$$Q_{ef} = \frac{\varepsilon_A}{\varepsilon_{\text{prog}}} \quad (6)$$

Shape-switchable microparticles based on a crosslinked polymer network, containing well-defined six-arm poly(ethylene glycol)-poly(ε -caprolactone), were elaborated to provide a concept of dynamically shape-switching carriers for drug delivery. These polymer particles have the ability to reversibly change the shape between spherical and elliptical, either extracellularly or intracellularly, when cyclically heated and cooled between 43 °C and 0 °C under stress-free conditions [143].

Recently, a mechanism for rbSME of PCL-based aliphatic polyurethanes (HPL) has been proposed based on molecular flipping and temperature-induced structural changes. PCL domains served as actuating domains, whereas the hard domains, consisting of HDI and 1,4-butanediol, served as shifting geometry determining domains. During heating above T_{trans} , the local reorganization of hard segments in molten soft segment phase is facilitated because the local environment of soft domains became liquid and the interactions of polymer chains within the soft segment are limited. The resulting consolidation of hard segments leads to formation of a more stable pseudohexagonal crystalline phase within the hard domains. During cooling, hard domains in the near of the actuation domains foster the recrystallization by providing the heterogeneous nucleation sites. A “spring model” of the resultant structure was presented, in which two actuation domains acting as springs are chemically attached between two geometry determining domains (Fig. 24b), leading to increase and decrease of the cluster size during the cooling and heating, respectively (Fig. 24c). Therefore, upon the temperature change between 5 °C and 50 °C, the polymer sample was able to exhibit the rbSME by extension and contraction on the macroscopic level, between shape A and B, respectively (Fig. 24a) [144].

5.2.1 Temperature-Memory Polymer Actuators (TMPAs)

In crosslinked copolymer networks exhibiting a broad melting temperature range (ΔT_m), the concept of interchangeable skeleton-forming and actuation domains was realized. These temperature-memory polymer actuators (TMPAs) implemented a temperature-memory with bidirectional actuation. By variation of the parameter called T_{sep} , the actuation temperatures T_{act} of TMPAs can be adjusted. T_{sep} divides ΔT_m into an upper T_m range ($T_{\text{high}} > T_{\text{sep}}$), which constitutes the skeleton-forming domains, and a lower T_m range ($T_{\text{low}} < T_{\text{sep}}$), which provides the actuation domains and enables the temperature-controlled bidirectional actuation by CIE and MIC. Reversible shape changes are realized in the polymer network by crystallization/melting of oriented segments in the actuation domains between T_{low} and T_{sep} (Fig. 25) [127]. In covalently crosslinked poly[ethylene-co-(vinyl acetate)] (cPEVA) containing crystallizable polyethylene (PE) segments, repeating units of vinyl acetate contribute to a broad melting transition of PE crystallites and were used for both, the skeleton-forming and actuation function [127].

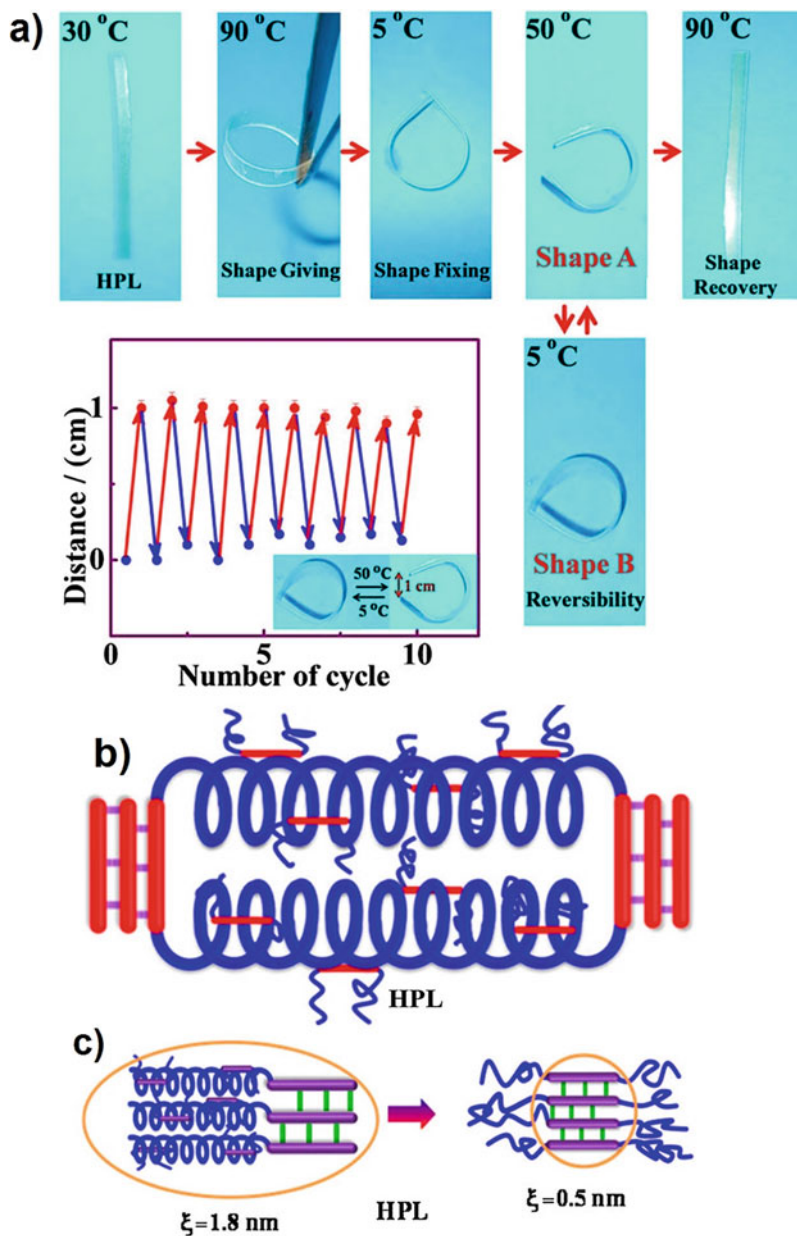
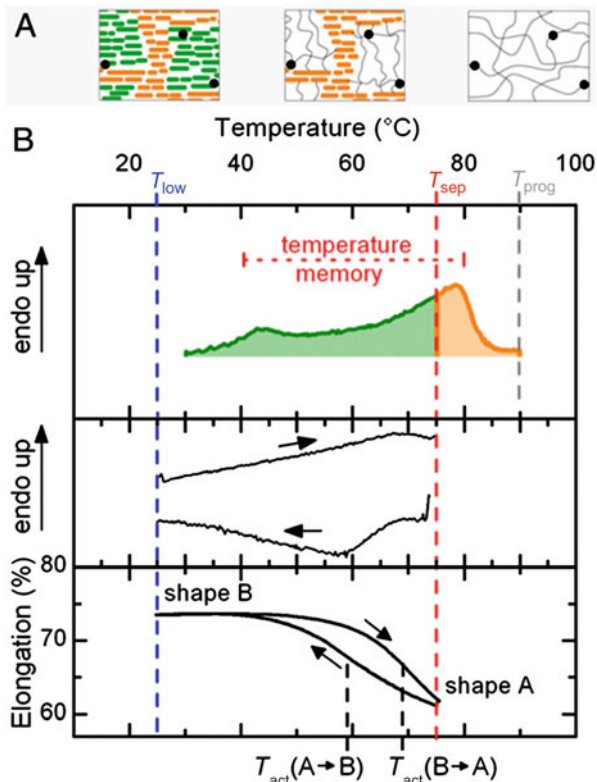


Fig. 24 (a) Photograph series demonstrating rbSME of HPL with a plot showing 10 repeating cycles of rbSME; Opening (shape A) and closing (shape B) of the ring upon heating to 50 °C and cooling to 5 °C. Full recovery to permanent shape at 90 °C. (b) Proposed spring models to demonstrate rbSME in HPL through molecular flipping. (c) Models showing changes in cluster size with the temperature change from 5 °C to 50 °C. (Reprinted with permission from Ref. [144]. Copyright 2016 American Chemical Society)

Fig. 25 Working principle of the programmable temperature-memory polymer actuator. (A) Programming step: amorphous, chemically crosslinked sample is deformed at T_{prog} (● chemical crosslinks) (right). At T_{sep} the crystallization of the internal skeleton-forming domains takes place (marked in orange) (center). Actuation: reversible shape changes of the polymer sample by crystallization/melting of oriented polyethylene segments in the actuation domains (green) between T_{low} and T_{sep} (left). (B) Thermal and thermomechanical investigations of cPEVA. (Reprinted from Ref. [127])



6 Magnetically Triggered SMPs

Thermally-induced SME can also be triggered indirectly, by application of light (IR irradiation), radio frequency, or microwaves [8, 145]. Controlled heating on demand can be realized by introduction of nano- or microfillers sensitive to electrical current or alternating magnetic fields [7, 146]. In case of utilizing an IR irradiation, nanofillers such as carbon nanotubes or gold nanorods were incorporated to enhance the heat transfer [147, 148]. Furthermore, addition of gold nanoparticles results in local control of the shape recovery according to poor thermal conductivity of the filler [149]. Electrical conductivity of polymeric materials can be enhanced by incorporation of carbon black, carbon nanotubes, carbon nanofibers, or metal powders [7, 147, 150–152]. Examples of mechanisms of response to external stimuli in shape-memory composites are presented in Fig. 26.

A remote actuation of the thermally-induced SME without the need of a direct contact has been realized by the incorporation of magnetic nanoparticles (MNP) into

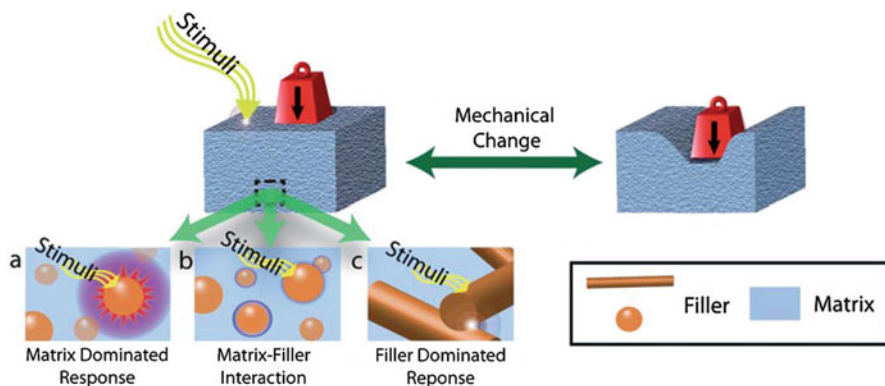


Fig. 26 Examples of mechanisms of response to external stimuli in shape-memory polymeric composites: (a) a matrix dominated response after energy is transferred from the nanofiller to the matrix, (b) a change in the overall matrix–filler interaction, (c) a filler dominated response in which the filler–filler interactions are switched “on” or “off.” (Reproduced from Ref. [151] with permission of The Royal Society of Chemistry. <https://doi.org/10.1039/c0jm02383c>)

the SMP matrix and subsequent triggering of the SME by alternating magnetic fields (AMF) [153]. The MNP dissipate heat in an AMF by hysteresis/or relaxation loss mechanisms. This heat spreads into the polymer matrix and is triggering the shape recovery process. The first example was polymer matrix of an aliphatic poly(ether-urethane) (TFX) obtained from methylene bis(*p*-cyclohexylisocyanate), 1,4-butanediol, and polytetrahydrofuran. Another system was a biodegradable multi-block copolymer (PDC) with poly(*p*-dioxanone) as hard segment and PCL as switching segment containing MNP based on iron(III)oxide core with silica shell (sNP). This silica shell improved the compatibility of the nanoparticles with polymer matrix and helped to gain a homogenous distribution of particles in the polymer matrix. In this composite, the sNP content varied between 0 and 10 wt%. When the sample was placed in the AMF ($f = 258 \text{ kHz}$, $H = 7\text{--}30 \text{ kA} \cdot \text{m}^{-1}$), the bulk temperature of the composite rose by inductive heating of the nanoparticles. Within few minutes the temperature determined at the sample surface reached a constant level (T_{max}), in which the sample was in the thermal equilibrium with the environment. T_{max} increased strongly with increasing sNP concentration and magnetic field strength. When T_{max} exceeded T_{sw} in the bulk of the composite, the shape recovery occurred. A reduction in the frequency and in the magnetic field strength required for triggering the SME was observed when magnetite particles in the range of $9 \mu\text{m}$ were used [146]. Furthermore, when a near single crystal metal alloy comprising of terbium, iron, and dysprosium-d of nominal composition $\text{Tb}_{0.3}\text{Dy}_{0.7}\text{Fe}_{1.92}$ was embedded in an epoxy thermoset, radio frequency could be used to indirectly heat SMP. Here, the radio frequency triggered the magneto-electroelastic effect, which generated the indirect heating [154]. In addition, the indirect magnetic actuation of

thermosets could be achieved by the incorporation of nickel zinc ferrite particles into commercial ester-based thermoset polyurethane [155].

By using a polymer matrix with two switching domains, a magnetically controlled TSE could be realized [156]. In this case, the composite consists of sNP incorporated into a multiphase polymer network named as MACL (see Sect. 3, TSE/MSE). MACL-based composite was prepared by thermally-initiated copolymerization of PCL dimethacrylate and cyclohexyl methacrylate in the presence of sNP. The network composite exhibited two distinct, well separated thermal transitions: a melting transition assigned to the crystalline PCL domains in the range of 41–48 °C, and a glass transition associated to the amorphous PCHMA domains in the range of 131–156 °C. By stepwise increasing the magnetic field strength, a two-step recovery of shapes B and C could be obtained, with the best triple-shape properties achieved for nanocomposites containing 40 wt% of PCL (Fig. 27). In this way, the triple-shape effect could be characterized by two distinct switching magnetic strengths $H_{sw,1}(A \rightarrow B)$ and $H_{sw,2}(B \rightarrow C)$, which correspond to the switching temperatures determined in cyclic, thermomechanical tensile tests. In addition, the magnetically controlled TSE of multiphase polymer networks named CLEG, with two crystallizable switching segments based on PEG side chains and PCL crosslinks, was also demonstrated [156].

Instead of using a multi-phase polymer system with two distinct T_{trans} , a heterogeneous geometry of a polymer composite with one switching domain could also enable a TSE. This geometrically controlled TSE was based on the concept that the composite samples with identical chemical composition but with a higher specific surface area to volume ratio (S/V) required a higher H_{sw} and vice versa. This increase in H_{sw} was attributed to the higher heat transfer to the environment during endogenous heating of the composite by exposure to AMF. In contrast, during exogenous heating (environmental heating), the kinetic of the heating rate could be controlled by the control of the S/V ratio of the sample. Based on these findings, a device having two segments differing in their S/V ratios was fabricated by using a crosslinked PCL + sNP (10 wt%) nanocomposites. Such a composite had shown a dual-shape effect with a shape-recovery exceeding a relatively small temperature interval ($\Delta T_{rec} \approx 10$ °C). After programming by bending and subsequent cooling, the device was exposed to an environmental heating. Here, the segment of the device with the higher S/V ratio was recovered first, while the other segment with lower S/V ratio required a longer time period to recover to the original shape. During magnetically-induced experiments, this sequence of the recovery was reversed. Here, the segment with lower S/V ratio recovered first at lower magnetic field strength (H_{low}), while for the observation of the recovery in the segment with higher S/V ratio, the applied H needed to be increased to H_{high} . This geometrical design enabled a precise control over the shape change process of the two segments. It was speculated that by combining different heat sources (e.g., IR light and T_{env} or microwaves and T_{env}), complex movements from a thermo-sensitive composite can be achieved [157].

Magnetic fields could also be used to generate a magnetic-memory effect (MME) in polymer composites. The MME is defined as the ability of magneto-sensitive

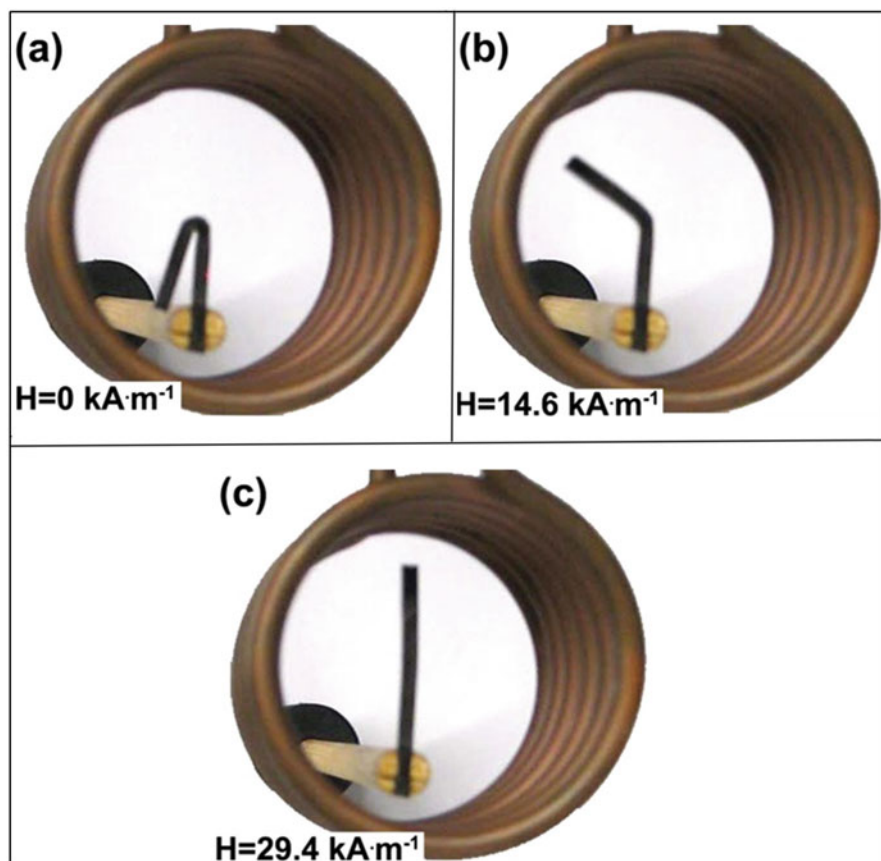


Fig. 27 Images obtained for a triple-shape composite polymer network obtained from cyclohexylmethacrylate, poly(ϵ -caprolactone) dimethacrylate and 12.5 wt% silica coated iron(III)oxide nanoparticles during recovery at a magnetic field strength H of (a) $0 \text{ kA} \cdot \text{m}^{-1}$, (b) $14.6 \text{ kA} \cdot \text{m}^{-1}$, and (c) $29.4 \text{ kA} \cdot \text{m}^{-1}$. (Reproduced from Ref. [156] with permission from The Royal Society of Chemistry. <https://doi.org/10.1039/b923000a>)

materials to remember the magnetic field strength (H_{def}), at which they were deformed recently [158]. To enable MME in polymer composites, MNPs were incorporated into TMP matrices with broad thermal transitions (ΔT_{g} or ΔT_{m}), associated to the switching domains. The MME requires programming (and recovery) of the composite during application of AMF. Therefore, specific magneto-mechanical programming experiments were designed to demonstrate and quantify the MME. A setup consisting of an inductor coil equipped with tensile tester with plastic clamps was used to deform the samples to ϵ_{m} , while being exposed to H_{def} . The recovery of the composites was carried out under stress-free or strain-control conditions by stepwise increasing the applied H . Under stress-free conditions, the composites recovered their initial shape at a switching magnetic field strength H_{sw}

close to H_{def} , while under constant strain conditions they respond by building up stress with a peak maximum at $H_{\sigma, \text{max}}$. While on the one hand the MME required more defined conditions as compared to the TME (such as sample dimension or environmental temperature), on the other hand, the MME enabled a remote actuation with a significantly shorter actuation interval.

Compared to environmental heating, magnetic heating is an endogenous heating process and occurs significantly faster. However, adding MNP adversely affects other material properties, e.g., crystallinity and elasticity of the SMPs. Another important issue in the preparation of such composites is the suppression of nanoparticles aggregation and segregation from the polymer matrix [159]. A potential solution for this challenge is the covalent integration of the MNP into the polymer chain segments, which leads to a cooperative motion of both, the continuous and the dispersed phase. Such a covalent bonding of the MNP in a polymer network has been used to develop hybrid composites, which could enable a magnetically controlled rSME (r_{mag} -SME). The hybrid nanocomposite (H-NC) consisted of oligo(ω -pentadecalactone) (OPDL) matrix crosslinked by OPDL-coated mNP with the usage of diisocyanates. Similar to the magneto-mechanical programming procedure designed for MME exploration, programming of the H-NC in an AMF by stretching was carried out. The H-NC (5 wt% mNP) sample was kept in the center of the inductor coil with the help of plastic clamps, while the deformation $\varepsilon_m = 50\%$ at H_{high} in stress-controlled mode was carried out. Subsequently, the magnetic field was switched “off” to $H_{\text{low}} = 0$ and the cooling to ambient temperature took place. As a result, the sample elongated quite dramatically at the point of crystallization from ε_m to $\varepsilon_{\text{act}} \approx 85\%$ in the direction of applied stress. The effect was reversible, therefore, after applying H_{high} again, the sample contracted back to the original strain ε_{rev} (Fig. 28). The reversible length changes could be explained by a directed crystallization of the crystalline lamellar perpendicular to the load direction when the H-NC cools to ambient temperature. The r_{mag} -SME was quantified by determining the relative increase in strain ($R_{\text{act,CIE}} = 65\%$) between the sample dimensions at H_{low} and at H_{high} [141].

7 Shape-Memory Hydrogels (SMH)

A relatively new group of smart materials, which are capable of combining several functions constitute shape-memory hydrogels (SMH). These highly water-swelling polymer networks have been extensively investigated for drug delivery, cell culture, separation, and sensing applications. SMHs combine stimuli sensitivity with their unique softness, high hydrophilicity, biocompatibility, and ability of rapid diffusion of molecules [68]. Stimuli-sensitive hydrogels are typically crosslinked materials containing hydrophilic and hydrophobic fractions. Hydrophilic components enable swelling in water, whereas a hydrophobic part provides the reversible change of the structure from ordered to disordered under variation of certain external stimuli such as temperature [59, 160–164], pH [165–168], ultrasound [163], or content of ions [169–172].

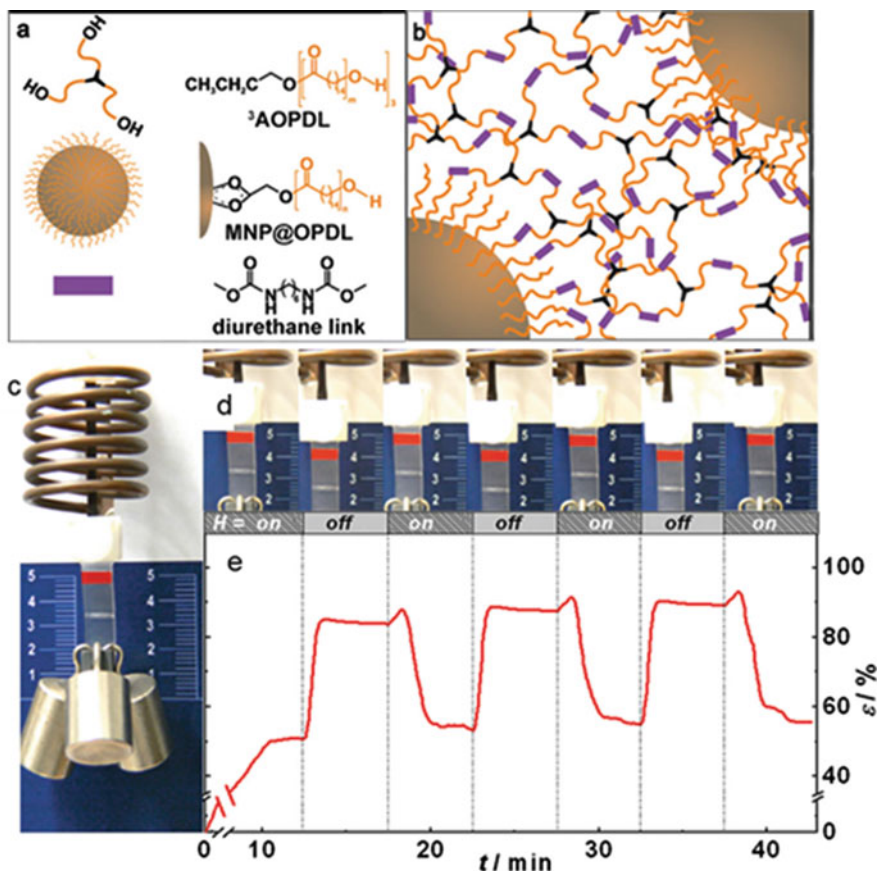


Fig. 28 (a) Formation of the hybrid nanocomposite using iron(III)oxide tetrahydrate nanoparticles with tethered hydroxyl-terminated groups, trifunctional hydroxyl monomers, and 1,6-hexane diisocyanate (HDI) linker. (b) Cartoon depiction of the nanocomposite network. The inclusion of the trifunctional hydroxyl monomer allowed for adjustable elasticity and MNP content in the film. (c, d) Illustration of the setup used to perform magnetic shape-memory cycles under a constant stress provided by a weight (300 g). (e) A plot showing the changes in strain resulting from a pulsed magnetic field. (Reprinted from Ref. [141] with permission, © 2013 WILEY-VCH Verlag GmbH & Co. KGaA, Weinheim)

One of the first hydrogels with programmable, thermally triggered SME was a covalently crosslinked copolymer of acrylic acid, stearyl acrylate, and methylenebisacrylamide used as a crosslinker [173, 174]. The acrylic acid constituted the hydrophilic part, which swells in water, whereas the hydrophobic, crystallizable stearyl side chains of $T_m = T_{sw} = 50$ °C served as switching segments. Heating above T_{sw} was related to significant decrease of the hydrogels' stiffness (from 10 to 0.1 MPa) [175]. In another example, the thermally-triggered SMH was based on

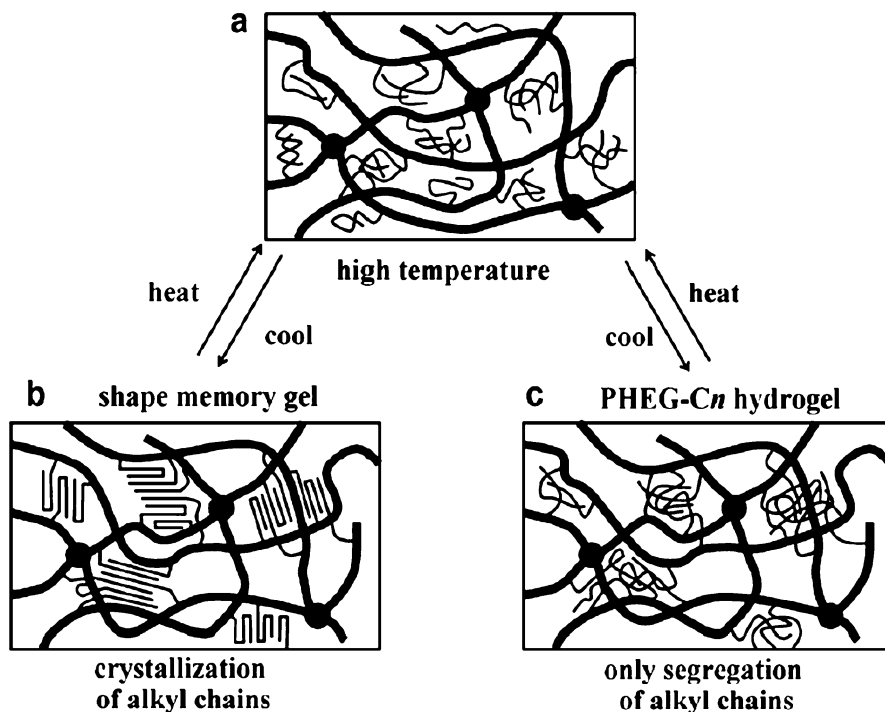


Fig. 29 Schematic representation of the shape-memory mechanism of crystalline shape-memory gel and PHEG-Cn hydrogel. (a) Alkyl chains are in the molten state at high temperature. (b) In the shape-memory gel, alkyl chains are in crystalline state after cooling. (c) In the PHEG-Cn hydrogel, alkyl chains are in non-crystalline state but segregated at low temperature. (Reprinted from Ref. [176], Copyright 2012, with permission of Elsevier)

polypeptides with hydrophobic alkyl side groups. The fixation of the temporary shape was related to segregation of side groups instead of conventional fixation based on a solidification by a phase transition of constituent polymers (Fig. 29) [176, 177]. The segregated hydrophobic alkyl chains fix the temporary shape only partially, and its segregation strength weakened gradually with an increase of the temperature [176]. A similar ability to remember multiple shapes at various recovery temperatures was reported for shape-memory ionomers with broad phase transitions [118].

A double-network hydrogel combining the thermally-induced shape-memory and mechano-responsive shape-changing effects was reported [178]. SMHs based on a crosslinked *N*-vinyl-2-pyrrolidone network containing oligomeric side chains of PPDL acting as switching segments have shown dual-shape memory effect. Independently of the wt% of PPDL, $R_f > 95\%$ and $R_r > 92\%$ were achieved. Furthermore, a degree of swelling of investigated hydrogels was almost independent of the temperature [179]. Similarly, SMHs consisting of the

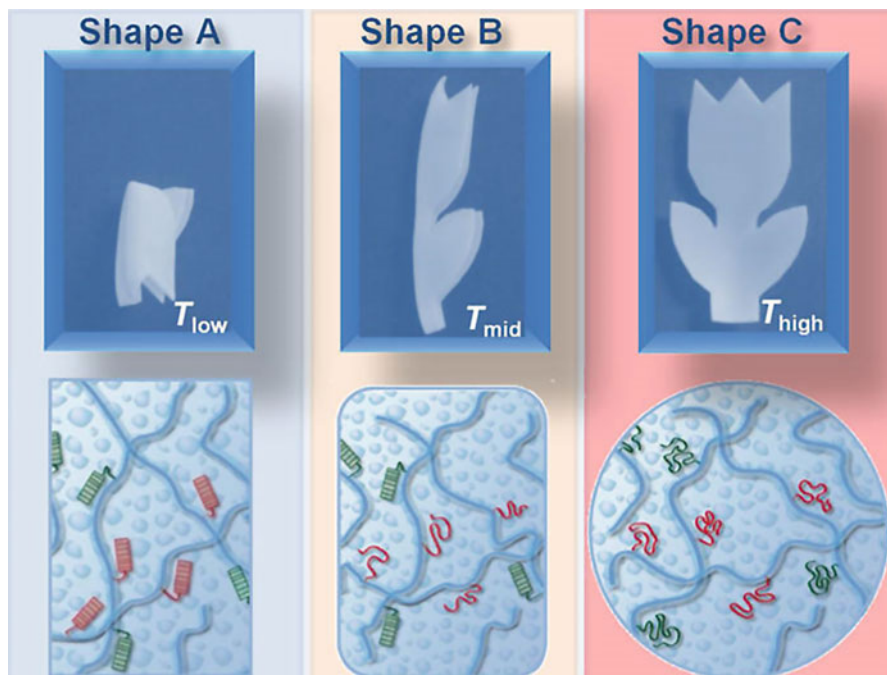


Fig. 30 Recovery process of an OPDL-SA-based triple-shape hydrogel and the molecular mechanism. (Reprinted with permission from Ref. [181]. Copyright 2016 American Chemical Society)

hydrophilic poly(*N*-vinyl-2-pyrrolidone) segment, crosslinked by the oligo(ethylene glycol) dimethacrylate, and grafted crystallizable oligotetrahydrofuran was reported to show SME with T_{trans} around body temperature [180].

Furthermore, a thermally-induced triple-shape-memory hydrogel was obtained by introducing two different hydrophobic crystallizable switching segments (PPDL, THF) in a form of grafted side chains into the hydrophilic poly(*N*-vinyl-2-pyrrolidone) polymer network. In the presented study, a permanent shape C was folded to shape B and further to shape A. Upon heating from T_{low} to T_{high} in the water bath, the subsequent recovery to shape B and then shape C were observed according to sequential melting of semi-crystalline switching segments related to shape A and shape B (Fig. 30) [181].

Considering the limitations of heat as a trigger to recover the original shape, non-covalent interactions such as metal-ligand binding, dynamic covalent bonds and guest-host interactions have been recently investigated as a new way of realizing the SME [65, 68, 169, 182–186]. Furthermore, in comparison with solid SMPs, the presence of water in hydrogels enables new opportunities regarding a shape-memory capability based on molecular switches sensitive to other stimuli than those realized in solid SMPs.

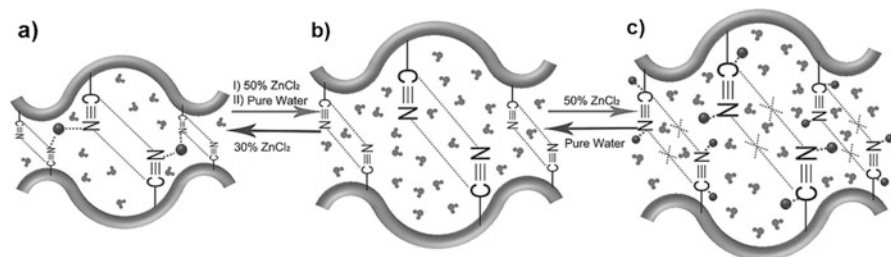


Fig. 31 Schematic presentation of the mechanism of TSE of the hydrogels in response to concentration of zinc ions: (a) In 30% ZnCl₂ solution, formation of CN–CN dipole pairing and Zn–CN linkage, (b) In pure water, only CN–CN dipole-dipole interactions are present, (c) in 50% ZnCl₂ solution, both CN–CN pairs and Zn–CN linkage are dissociated. (Reprinted from Ref. [172] with permission, © 2012 WILEY-VCH Verlag GmbH & Co. KGaA, Weinheim)

Molecular switches based on metal ions–organics complexation can realize a SME in hydrogels by controlling the oxidative state of the metal ions [169–172, 187]. One example of such a system was achieved in a chemically crosslinked copolymer of acrylonitrile and 2-methacryloyloxyethyl phosphoryl choline. The TSE was triggered by the dynamic association and dissociation of dipole–dipole pairs of the cyano groups in response to the presence or absence, as well as concentration of zinc ions (Fig. 31) [172, 187].

Similarly, ion-responsive hydrogels (PVV) strengthened by hydrogen bonding, synthesized by the copolymerization of 2-vinyl-4,6-diamino-1,3,5-triazine (VDT), poly(ethylene glycol) diacrylate (PEGDA), and 1-vinylimidazole (VI) were reported. The introduction of zinc ions further increased the mechanical properties of PVV hydrogels and enabled the fixation of a variety of temporary shapes due to the strong coordination of zinc with imidazole [188, 189]. Also, copper-containing hydrogel materials possess shape-memory functionality. A SMH based on covalently crosslinked PEGDA network with incorporated copper ions was able to change its' shape from A to B under the oxidation process. Figure 32 shows the macroscopic changes of the sample, which can be realized in a solution of sodium metabisulfite or by the exposition to air. The temporary shape is formed by the oxidized Cu²⁺ ions, which serve as a crosslinking agent by coordination with pyridine. The material properties of hydrogels containing Cu²⁺ (blue and rigid) are significantly different from those of hydrogels containing Cu⁺ (yellow and soft) [171].

A supramolecular hydrogel, able to respond to two independent stimuli (ion concentration and change of pH) was reported to show TSE. Initially, the hydrogel sample was deformed and the temporary shape I was fixed by soaking in CaCl₂ solution, whereby Alg–Ca²⁺ complexation occurred. Then the sample was heated to 90 °C, deformed again, and immersed into glycine–NaOH

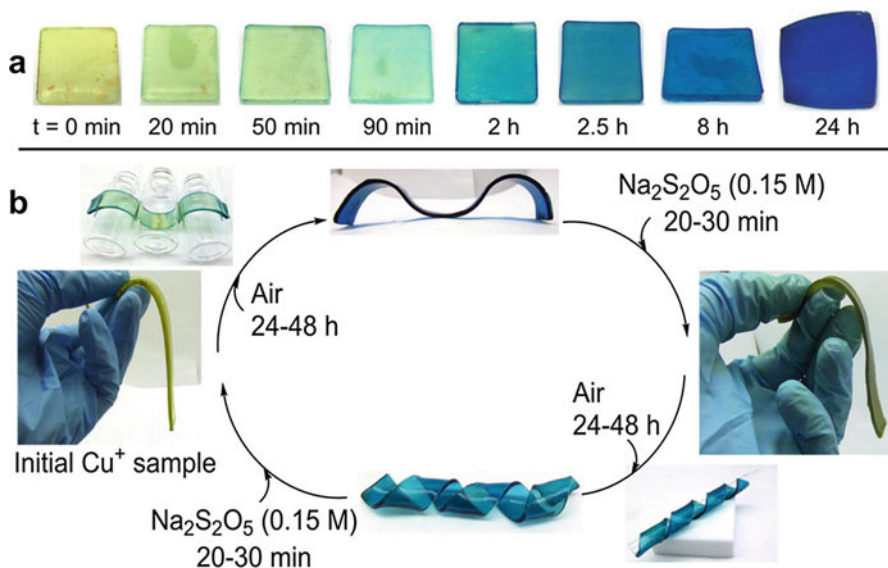


Fig. 32 (a) Conversion of Cu^+ -doped hydrogel to Cu^{2+} in air. (b) Demonstration of shape-memory for copper-crosslinked hydrogels. (Reprinted with permission from Ref. [171]. Copyright 2013 American Chemical Society)

aqueous solution ($\text{pH} = 10.6$), whereby the second temporary shape (II) was fixed. The recovery from shape II to shape I proceeds due to the breakage of PBA-diol ester bonds, whereas the permanent shape would be recovered due to the disassociation of the $\text{Alg}-\text{Ca}^{2+}$ crosslinks upon immersion into K_2CO_3 solution (Fig. 33) [190].

Supramolecular physical crosslinking based on a host-guest complex has been used as molecular switch to enable SME in hydrogels. Cyclodextrins (CDs), which consist of a hydrophilic external surface and a hydrophobic cavity, can be utilized as host compounds. A pH-sensitive, biodegradable and biocompatible SMH was prepared by crosslinking the β -cyclodextrin modified alginate (β -CD-Alg) and diethylenetriamine modified alginate (DETA-Alg). The pH-reversible β -CD-DETA complexes served as a switching phase, whereas the crosslinked alginate chains served as a fixing phase (Fig. 34). A temporary shape was fixed at $\text{pH} = 11.5$ whereas a recovery to the initial shape occurred at $\text{pH} = 7$. The R_r of $95.7 \pm 0.9\%$ and the R_f of $94.8 \pm 1.1\%$ were achieved [167]. Addition of free β -cyclodextrin molecules to poly(*N*-isopropylacrylamide)-based hydrogel network containing β -cyclodextrin-adamantane temporary linkages led to disassociation of temporary netpoints and increase of swelling capacity [191].

A physically crosslinked SMH with two kinds of hydrogen bonds was recently reported. The stronger H-bonding between poly(vinyl alcohol) (PVA) and tannic

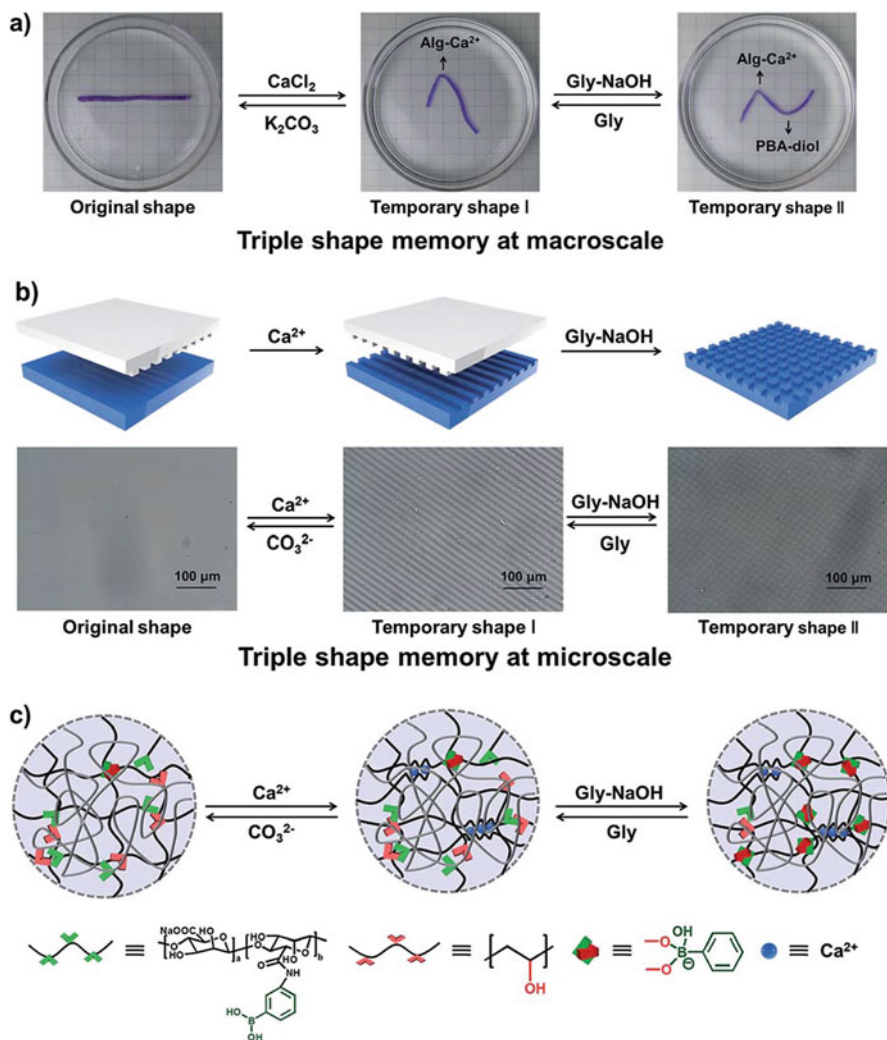
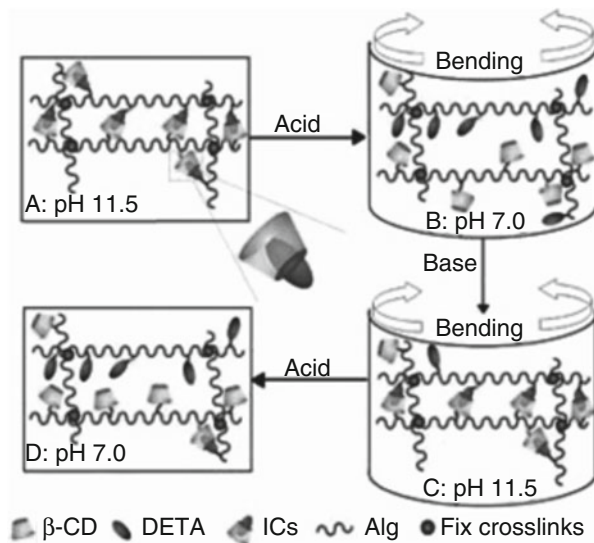


Fig. 33 (a) TSE at the macro-scale. (b) TSE behavior at the micro-scale, microscope images of the original hydrogel and two temporary shapes. (c) The mechanism of the TSE: the original hydrogel can fix its temporary shape I in CaCl_2 solution and memorize temporary shape II in Gly–NaOH solution at $\text{pH} = 10.6$. By immersion in Gly solution ($\text{pH} 6$) the temporary shape I can be recovered, and further by immersion in K_2CO_3 solution, the hydrogel can recover to the original shape. (Reprinted from Ref. [190] – Published by The Royal Society of Chemistry. <https://doi.org/10.1039/c6sc02354a>)

acid (TA) served as the permanent netpoints, whereas the weaker H-bonding between PVA chains were able to reversibly break and act as temporary netpoints. The hydrogel samples were able to recover their original shapes when immersed in water at 60°C , or at 125°C in time periods shorter than 3 min [192].

Fig. 34 Molecular mechanism of the pH-induced SME in β -cyclodextrin modified alginate SMP. (Reprinted from Ref. [167] with permission, © 2012 WILEY-VCH Verlag GmbH & Co. KGaA, Weinheim)



8 Conclusions and Outlook

Different concepts to realize the phenomena of programmed changes in polymer shapes were described. Although conventional SMEs were briefly introduced, the emphasis was placed on new mechanisms as well as new shape-memory concepts. The capability of SME in polymers, enabling a temporary fixation of a new shape, can be realized by physical interactions within the polymer structure utilizing the thermal transition of switching domains, formation of hydrogen bonds, or ionic and metal-ligand interactions. Furthermore, reversible covalent bonds were utilized as molecular switches. In this approach, a photodimerization of cinnamic acid, Diels-Alder reaction, or redox reactions of mercapto groups were capable of fixing a temporary shape. The creation of multiphase polymer systems, polymers with broad phase transitions, and multimaterial systems resulted in the development of novel SMEs such as reversible bidirectional SME or multiple-shape effect, which highly extend the range of potential applications of SMPs [193].

The creation of multifunctional materials based on SMPs is a further focus of recent research. Depending on the molecular design, shape-memory functionality can be combined with other functions such as biodegradability, self-healing, or drug-release capability [182, 188, 194, 195]. Furthermore, shape-memory hydrogels, due to their soft nature, architecture, and capability of gathering the large amounts of water, were found to be promising candidate materials for multifunctional, biomedical approaches. Much attention was paid to magnetically-induced SME, which plays an important role in applications, in which a direct heating by increasing the environmental temperature is not feasible [141, 153].

An important motivation driving the field of shape-memory and actively-moving polymers is the broad application potential for these materials. Thermally-induced SMPs already reached the mass market in the area of textiles and packaging applications [196], however the technology platform of existing materials is moving towards some highly sophisticated applications such as in the field of aerospace or active medical devices. The field of biomedical applications was one of the major driving forces in the past, and due to the tunable properties of SMPs (e.g., soft material, switching around the body temperature, biocompatibility, biodegradability, drug-release capacity, etc.), it will be a strong motivation in the future as well [10]. The most promising areas are self-deployable stents and minimally-invasive surgeries [129, 197]. The first potential applications of SMP-based implants [198] or active prosthesis were already demonstrated [199–201]. The application requirements in the medical field are very complex, therefore, a trend toward the development of multifunctional materials can be seen [7, 202]. With all the progress achieved in the development of new SMPs and corresponding mechanisms within relatively short time periods, we envisage that the progress of SMP research will even intensify in the near future.

Acknowledgments This work was financially supported by the Helmholtz-Association through programme-oriented funding.

References

1. A. Lendlein, S. Kelch, Shape-memory polymers. *Angew. Chem. Int. Ed.* **41**, 2034–2057 (2002)
2. K.K. Julich-Gruner, C. Löwenberg, A.T. Neffe, M. Behl, A. Lendlein, Recent trends in the chemistry of shape-memory polymers. *Macromol. Chem. Phys.* **214**, 527–536 (2013)
3. C. Wischke, A.T. Neffe, A. Lendlein, Controlled drug release from biodegradable shape-memory polymers. *Adv. Polym. Sci.* **226**, 177–205 (2010)
4. C. Wischke, M. Behl, A. Lendlein, Drug-releasing shape-memory polymers – The role of morphology, processing effects, and matrix degradation. *Expert Opin. Drug. Deliv.* **10**, 1193–1205 (2013)
5. A. Lendlein, M. Behl, B. Hiebl, C. Wischke, Shape-memory polymers as a technology platform for biomedical applications. *Expert Rev. Med. Devices* **7**, 357–379 (2010)
6. M. Behl, J. Zotzmann, A. Lendlein, Shape-memory polymers and shape-changing polymers. *Adv. Polym. Sci.* **226**, 1–40 (2010)
7. M. Behl, M.Y. Razzaq, A. Lendlein, Multifunctional shape-memory polymers. *Adv. Mater.* **22**, 3388–3410 (2010)
8. Q. Zhao, M. Behl, A. Lendlein, Shape-memory polymers with multiple transitions: Complex actively moving polymers. *Soft Matter* **9**, 1744–1755 (2013)
9. M. Behl, A. Lendlein, Actively moving polymers. *Soft Matter* **3**, 58–67 (2007)
10. M.D. Hager, S. Bode, C. Weber, U.S. Schubert, Shape memory polymers: Past, present and future developments. *Prog. Polym. Sci.* **49–50**, 3–33 (2015)
11. P.J. Flory, J. Rehner, Statistical mechanics of cross-linked polymer networks II. Swelling. *J. Chem. Phys.* **11**, 521–526 (1943)
12. W. Wagermaier, K. Kratz, M. Heuchel, A. Lendlein, Characterization methods for shape-memory polymers. *Adv. Polym. Sci.* **226**, 97–145 (2010)

13. T. Sauter, M. Heuchel, K. Kratz, A. Lendlein, Quantifying the shape-memory effect of polymers by cyclic thermomechanical tests. *Polym. Rev.* **53**, 6–40 (2013)
14. M. Heuchel, T. Sauter, K. Kratz, A. Lendlein, Thermally induced shape-memory effects in polymers: Quantification and related modeling approaches. *J. Polym. Sci. B Polym. Phys.* **51**, 621–637 (2013)
15. I.S. Kolesov, K. Kratz, A. Lendlein, H.-J. Radusch, Kinetics and dynamics of thermally-induced shape-memory behavior of crosslinked short-chain branched polyethylenes. *Polymer* **50**, 5490–5498 (2009)
16. A. Maksimkin, S. Kaloshkin, M. Zadorozhnyy, V. Tcherdyntsev, Comparison of shape memory effect in UHMWPE for bulk and fiber state. *J. Alloys Compd.* **586**, S214–S217 (2014)
17. J. Zhao, M. Chen, X. Wang, X. Zhao, Z. Wang, Z.-M. Dang, L. Ma, G.-H. Hu, F. Chen, Triple shape memory effects of cross-linked polyethylene/polypropylene blends with cocontinuous architecture. *ACS Appl. Mater. Interfaces* **5**, 5550–5556 (2013)
18. A.L. Sisson, D. Ekinici, A. Lendlein, The contemporary role of ϵ -caprolactone chemistry to create advanced polymer architectures. *Polymer* **54**, 4333–4350 (2013)
19. H.Y. Lee, H.M. Jeong, J.S. Lee, B.K. Kim, Study on the shape memory polyamides. Synthesis and thermomechanical properties of polycaprolactone-polyamide block copolymer. *Polym. J.* **32**, 23–28 (2000)
20. G. Rabani, H. Luftmann, A. Kraft, Synthesis and characterization of two shape-memory polymers containing short aromatic hard segments and poly(ϵ -caprolactone) soft segments. *Polymer* **47**, 4251–4260 (2006)
21. H. Zhang, H. Wang, W. Zhong, Q. Du, A novel type of shape memory polymer blend and the shape memory mechanism. *Polymer* **50**, 1596–1601 (2009)
22. S.H. Ajili, N.G. Ebrahimi, M. Soleimani, Polyurethane/polycaprolactane blend with shape memory effect as a proposed material for cardiovascular implants. *Acta Biomater.* **5**, 1519–1530 (2009)
23. Q. Meng, J. Hu, A review of shape memory polymer composites and blends. *Compos. Part A* **40**, 1661–1672 (2009)
24. X. Jing, H.-Y. Mi, H.-X. Huang, L.-S. Turng, Shape memory thermoplastic polyurethane (TPU)/poly(ϵ -caprolactone) (PCL) blends as self-knotting sutures. *J. Mech. Behav. Biomed. Mater.* **64**, 94–103 (2016)
25. I. Navarro-Baena, V. Sessini, F. Dominici, L. Torre, J.M. Kenny, L. Peponi, Design of biodegradable blends based on PLA and PCL: From morphological, thermal and mechanical studies to shape memory behavior. *Polym. Degrad. Stab.* **132**, 97–108 (2016)
26. M. Behl, A. Lendlein, Shape-memory polymers. *Mater. Today* **10**, 20–28 (2007)
27. J. Hu, Y. Zhu, H. Huang, J. Lu, Recent advances in shape-memory polymers: Structure, mechanism, functionality, modeling and applications. *Prog. Polym. Sci.* **37**, 1720–1763 (2012)
28. J.W. Cho, Y.C. Jung, Y.-C. Chung, B.C. Chun, Improved mechanical properties of shape-memory polyurethane block copolymers through the control of the soft-segment arrangement. *J. Appl. Polym. Sci.* **93**, 2410–2415 (2004)
29. A. Altheld, Y. Feng, S. Kelch, A. Lendlein, Biodegradable, amorphous copolyester-urethane networks having shape-memory properties. *Angew. Chem. Int. Ed.* **44**, 1188–1192 (2005)
30. T. Xie, Recent advances in polymer shape memory. *Polymer* **52**, 4985–5000 (2011)
31. A. Lendlein, J. Zotzmann, Y. Feng, A. Altheld, S. Kelch, Controlling the switching temperature of biodegradable, amorphous, shape-memory poly(rac-lactide)urethane networks by incorporation of different comonomers. *Biomacromolecules* **10**, 975–982 (2009)
32. C.P. Buckley, C. Prisacariu, A. Caraculacu, Novel triol-crosslinked polyurethanes and their thermorheological characterization as shape-memory materials. *Polymer* **48**, 1388–1396 (2007)
33. Q. Cao, P. Liu, Structure and mechanical properties of shape memory polyurethane based on hyperbranched polyesters. *Polym. Bull.* **57**, 889–899 (2006)
34. L. Xue, S. Dai, Z. Li, Synthesis and characterization of three-arm poly(ϵ -caprolactone)-based poly(ester–urethanes) with shape-memory effect at body temperature. *Macromolecules* **42**, 964–972 (2009)

35. N.-Y. Choi, A. Lendlein, Degradable shape-memory polymer networks from oligo[(l-lactide)-ran-glycolide]dimethacrylates. *Soft Matter* **3**, 901–909 (2007)
36. C.M. Yakacki, R. Shandas, D. Safranski, A.M. Ortega, K. Sassaman, K. Gall, Strong, tailored, biocompatible shape-memory polymer networks. *Adv. Funct. Mater.* **18**, 2428–2435 (2008)
37. S. Kelch, S. Steuer, A.M. Schmidt, A. Lendlein, Shape-memory polymer networks from oligo[(ϵ -hydroxycaproate)-co-glycolate]dimethacrylates and butyl acrylate with adjustable hydrolytic degradation rate. *Biomacromolecules* **8**, 1018–1027 (2007)
38. K.M. Lee, P.T. Knight, T. Chung, P.T. Mather, Polycaprolactone–POSS chemical/physical double networks. *Macromolecules* **41**, 4730–4738 (2008)
39. S. Kelch, N.Y. Choi, Z. Wang, A. Lendlein, Amorphous, elastic AB copolymer networks from acrylates and poly[(l-lactide)-ran-glycolide]dimethacrylates. *Adv. Eng. Mater.* **10**, 494–502 (2008)
40. S. Chen, J. Hu, C.-W. Yuen, L. Chan, Fourier transform infrared study of supramolecular polyurethane networks containing pyridine moieties for shape memory materials. *Polym. Int.* **59**, 529–538 (2010)
41. S. Chen, J. Hu, H. Zhuo, S. Chen, Effect of MDI–BDO hard segment on pyridine-containing shape memory polyurethanes. *J. Mater. Sci.* **46**, 5294–5304 (2011)
42. S. Chen, J. Hu, H. Zhuo, C. Yuen, L. Chan, Study on the thermal-induced shape memory effect of pyridine containing supramolecular polyurethane. *Polymer* **51**, 240–248 (2010)
43. S. Chen, J. Hu, C.-w. Yuen, L. Chan, Novel moisture-sensitive shape memory polyurethanes containing pyridine moieties. *Polymer* **50**, 4424–4428 (2009)
44. S. Chen, H. Yuan, S. Chen, H. Yang, Z. Ge, H. Zhuo, J. Liu, Development of supramolecular liquid-crystalline polyurethane complexes exhibiting triple-shape functionality using a one-step programming process. *J. Mater. Chem. A* **2**, 10169–10181 (2014)
45. R.P. Sijbesma, F.H. Beijer, L. Brunsveld, B.J. Folmer, J.H. Hirschberg, R.F. Lange, J.K. Lowe, E.W. Meijer, Reversible polymers formed from self-complementary monomers using quadruple hydrogen bonding. *Science* **278**, 1601–1604 (1997)
46. K.E. Feldman, M.J. Kade, E.W. Meijer, C.J. Hawker, E.J. Kramer, Model transient networks from strongly hydrogen-bonded polymers. *Macromolecules* **42**, 9072–9081 (2009)
47. A. Gooch, N.S. Murphy, N.H. Thomson, A.J. Wilson, Side-chain supramolecular polymers employing conformer independent triple hydrogen bonding arrays. *Macromolecules* **46**, 9634–9641 (2013)
48. J. Li, J.A. Viveros, M.H. Wrue, M. Anthamatten, Shape-memory effects in polymer networks containing reversibly associating side-groups. *Adv. Mater.* **19**, 2851–2855 (2007)
49. J. Li, C.L. Lewis, D.L. Chen, M. Anthamatten, Dynamic mechanical behavior of photo-cross-linked shape-memory elastomers. *Macromolecules* **44**, 5336–5343 (2011)
50. H. Chen, Y. Li, G. Tao, L. Wang, S. Zhou, Thermo- and water-induced shape memory poly(vinyl alcohol) supramolecular networks crosslinked by self-complementary quadruple hydrogen bonding. *Polym. Chem.* **7**, 6637–6644 (2016)
51. Y. Wu, L. Wang, X. Zhao, S. Hou, B. Guo, P.X. Ma, Self-healing supramolecular bioelastomers with shape memory property as a multifunctional platform for biomedical applications via modular assembly. *Biomaterials* **104**, 18–31 (2016)
52. Y. Pan, T. Liu, J. Li, Z. Zheng, X. Ding, Y. Peng, High modulus ratio shape-memory polymers achieved by combining hydrogen bonding with controlled crosslinking. *J. Polym. Sci. B Polym. Phys.* **49**, 1241–1245 (2011)
53. Y. Chen, A.M. Kushner, G.A. Williams, Z. Guan, Multiphase design of autonomic self-healing thermoplastic elastomers. *Nat. Chem.* **4**, 467–472 (2012)
54. L. Xiao, M. Wei, M. Zhan, J. Zhang, H. Xie, X. Deng, K. Yang, Y. Wang, Novel triple-shape PCU/PPDO interpenetrating polymer networks constructed by self-complementary quadruple hydrogen bonding and covalent bonding. *Polym. Chem.* **5**, 2231–2241 (2014)
55. G. Liu, C. Guan, H. Xia, F. Guo, X. Ding, Y. Peng, Novel shape-memory polymer based on hydrogen bonding. *Macromol. Rapid Commun.* **27**, 1100–1104 (2006)

56. G. Liu, W. He, Y. Peng, H. Xia, Shape-memory behavior of poly(methyl methacrylate-co-N-vinyl-2-pyrrolidone)/poly(ethylene glycol) semi-interpenetrating polymer networks based on hydrogen bonding. *J. Polym. Res.* **18**, 2109–2117 (2011)
57. H. Chen, Y. Li, Y. Liu, T. Gong, L. Wang, S. Zhou, Highly pH-sensitive polyurethane exhibiting shape memory and drug release. *Polym. Chem.* **5**, 5168–5174 (2014)
58. G. Liu, X. Ding, Y. Cao, Z. Zheng, Y. Peng, Shape memory of hydrogen-bonded polymer network/poly(ethylene glycol) complexes. *Macromolecules* **37**, 2228–2232 (2004)
59. J.D. Merline, C.P.R. Nair, C. Gouri, T. Shrisudha, K.N. Ninan, Shape memory characterization of polytetra methylene oxide/poly (acrylic acid-co-acrylonitrile) complexed gel. *J. Mater. Sci.* **42**, 5897–5902 (2007)
60. J. Dong, R.A. Weiss, Effect of crosslinking on shape-memory behavior of zinc stearate/ionomer compounds. *Macromol. Chem. Phys.* **214**, 1238–1246 (2013)
61. R.A. Weiss, E. Izzo, S. Mandelbaum, New design of shape memory polymers: Mixtures of an elastomeric ionomer and low molar mass fatty acids and their salts. *Macromolecules* **41**, 2978–2980 (2008)
62. J. Dong, R.A. Weiss, Shape memory behavior of zinc oleate-filled elastomeric ionomers. *Macromolecules* **44**, 8871–8879 (2011)
63. S.-I. Han, B.H. Gu, K.H. Nam, S.J. Im, S.C. Kim, S.S. Im, Novel copolyester-based ionomer for a shape-memory biodegradable material. *Polymer* **48**, 1830–1834 (2007)
64. Z. Wang, W. Fan, R. Tong, X. Lu, H. Xia, Thermal-healable and shape memory metallo-supramolecular poly(n-butyl acrylate-co-methyl methacrylate) materials. *RSC Adv.* **4**, 25486–25493 (2014)
65. J.R. Kumpfer, S.J. Rowan, Thermo-, photo-, and chemo-responsive shape-memory properties from photo-cross-linked metallo-supramolecular polymers. *J. Am. Chem. Soc.* **133**, 12866 (2011)
66. F. Xie, C. Huang, F. Wang, L. Huang, R.A. Weiss, J. Leng, Y. Liu, Carboxyl-terminated polybutadiene–poly(styrene-co-4-vinylpyridine) supramolecular thermoplastic elastomers and their shape memory behavior. *Macromolecules* **49**, 7322–7330 (2016)
67. P. Zhang, M. Behl, X. Peng, M.Y. Razaq, A. Lendlein, Ultrasonic cavitation induced shape-memory effect in porous polymer networks. *Macromol. Rapid Commun.* **37**, 1897–1903 (2016)
68. Q. Zhao, H.J. Qi, T. Xie, Recent progress in shape memory polymer: New behavior, enabling materials, and mechanistic understanding. *Prog. Polym. Sci.* **49–50**, 79–120 (2015)
69. G. Zhang, Q. Zhao, L. Yang, W. Zou, X. Xi, T. Xie, Exploring dynamic equilibrium of Diels–Alder reaction for solid state plasticity in remoldable shape memory polymer network. *ACS Macro Lett.* **5**, 805–808 (2016)
70. M. Yamashiro, K. Inoue, M. Iji, Recyclable shape-memory and mechanical strength of poly(lactic acid) compounds cross-linked by thermo-reversible Diels–Alder reaction. *Polym. J.* **40**, 657–662 (2008)
71. K. Inoue, M. Yamashiro, M. Iji, Recyclable shape-memory polymer: Poly(lactic acid) crosslinked by a thermoreversible Diels–Alder reaction. *J. Appl. Polym. Sci.* **112**, 876–885 (2009)
72. J.-M. Raquez, S. Vanderstappen, F. Meyer, P. Verge, M. Alexandre, J.-M. Thomassin, C. Jérôme, P. Dubois, Design of cross-linked semicrystalline poly(ϵ -caprolactone)-based networks with one-way and two-way shape-memory properties through Diels–Alder reactions. *Chem. Eur. J.* **17**, 10135–10143 (2011)
73. T. Defize, R. Riva, C. Jérôme, M. Alexandre, Multifunctional poly(ϵ -caprolactone)-forming networks by Diels–Alder cycloaddition: Effect of the adduct on the shape-memory properties. *Macromol. Chem. Phys.* **213**, 187–197 (2012)
74. T. Defize, R. Riva, J.M. Raquez, P. Dubois, C. Jerome, M. Alexandre, Thermoreversibly crosslinked poly(epsilon-caprolactone) as recyclable shape-memory polymer network. *Macromol. Rapid Commun.* **32**, 1264–1269 (2011)

75. J. Zhang, Y. Niu, C. Huang, L. Xiao, Z. Chen, K. Yang, Y. Wang, Self-healable and recyclable triple-shape PPDO-PTMEG co-network constructed through thermoreversible Diels-Alder reaction. *Polym. Chem.* **3**, 1390–1393 (2012)
76. T. Defize, R. Riva, J.-M. Thomassin, C. Jérôme, M. Alexandre, Thermo-reversible reactions for the preparation of smart materials: Recyclable covalently-crosslinked shape memory polymers. *Macromol. Symp.* **309–310**, 154–161 (2011)
77. G. Rivero, L.-T.T. Nguyen, X.K.D. Hillewaere, F.E. Du Prez, One-pot thermo-remendable shape memory polyurethanes. *Macromolecules* **47**, 2010–2018 (2014)
78. C. Toncelli, D.C. De Reus, F. Picchioni, A.A. Broekhuis, Properties of reversible Diels–Alder furan/maleimide polymer networks as function of crosslink density. *Macromol. Chem. Phys.* **213**, 157–165 (2012)
79. C. Zeng, H. Seino, J. Ren, K. Hatanaka, N. Yoshie, Bio-based furan polymers with self-healing ability. *Macromolecules* **46**, 1794–1802 (2013)
80. C. Zeng, H. Seino, J. Ren, N. Yoshie, Polymers with multishape memory controlled by local glass transition temperature. *ACS Appl. Mater. Interfaces* **6**, 2753–2758 (2014)
81. D. Aoki, Y. Teramoto, Y. Nishio, SH-containing cellulose acetate derivatives: Preparation and characterization as a shape memory-recovery material. *Biomacromolecules* **8**, 3749–3757 (2007)
82. B.T. Michal, C.A. Jaye, E.J. Spencer, S.J. Rowan, Inherently photohealable and thermal shape-memory polydisulfide networks. *ACS Macro Lett.* **2**, 694–699 (2013)
83. A. Lendlein, H.Y. Jiang, O. Junger, R. Langer, Light-induced shape-memory polymers. *Nature* **434**, 879–882 (2005)
84. M. Nagata, Y. Sato, Synthesis and properties of photocurable biodegradable multiblock copolymers based on poly(ϵ -caprolactone) and poly(L-lactide) segments. *J. Polym. Sci. Part A: Polym. Chem.* **43**, 2426–2439 (2005)
85. L. Wu, C. Jin, X. Sun, Synthesis, properties, and light-induced shape memory effect of multiblock polyesterurethanes containing biodegradable segments and pendant cinnamamide groups. *Biomacromolecules* **12**, 235–241 (2011)
86. J.M. Rochette, V.S. Ashby, Photoresponsive polyesters for tailorable shape memory biomaterials. *Macromolecules* **46**, 2134–2140 (2013)
87. M. Nagata, Y. Yamamoto, Synthesis and characterization of photocrosslinked poly(ϵ -caprolactone)s showing shape-memory properties. *J. Polym. Sci. Part A: Polym. Chem.* **47**, 2422–2433 (2009)
88. M. Nagata, Y. Yamamoto, Photocurable shape-memory copolymers of ϵ -caprolactone and L-lactide. *Macromol. Chem. Phys.* **211**, 1826–1835 (2010)
89. J. He, Y. Zhao, Y. Zhao, Photoinduced bending of a coumarin-containing supramolecular polymer. *Soft Matter* **5**, 308–310 (2009)
90. H. Jiang, S. Kelch, A. Lendlein, Polymers move in response to light. *Adv. Mater.* **18**, 1471–1475 (2006)
91. Y. Li, O. Rios, J.K. Keum, J. Chen, M.R. Kessler, Photoresponsive liquid crystalline epoxy networks with shape memory behavior and dynamic ester bonds. *ACS Appl. Mater. Interfaces* **8**, 15750–15757 (2016)
92. K.M. Lee, H. Koerner, R.A. Vaia, T.J. Bunning, T.J. White, Light-activated shape memory of glassy, azobenzene liquid crystalline polymer networks. *Soft Matter* **7**, 4318–4324 (2011)
93. T. Yoshino, M. Kondo, J.-i. Mamiya, M. Kinoshita, Y. Yu, T. Ikeda, Three-dimensional photomobility of crosslinked azobenzene liquid-crystalline polymer fibers. *Adv. Mater.* **22**, 1361–1363 (2010)
94. M. Yamada, M. Kondo, J.-i. Mamiya, Y. Yu, M. Kinoshita, C.J. Barrett, T. Ikeda, Photomobile polymer materials: Towards light-driven plastic motors. *Angew. Chem. Int. Ed.* **47**, 4986–4988 (2008)
95. Y. Naka, J.-i. Mamiya, A. Shishido, M. Washio, T. Ikeda, Direct fabrication of photomobile polymer materials with an adhesive-free bilayer structure by electron-beam irradiation. *J. Mater. Chem.* **21**, 1681–1683 (2011)

96. O.M. Tanchak, C.J. Barrett, Light-induced reversible volume changes in thin films of azo polymers: The photomechanical effect. *Macromolecules* **38**, 10566–10570 (2005)
97. M. Irie, D. Kungwachakun, Photoresponsive polymers. 8. Reversible photostimulated dilation of polyacrylamide gels having triphenylmethane leuco derivatives. *Macromolecules* **19**, 2476–2480 (1986)
98. A. Mamada, T. Tanaka, D. Kungwachakun, M. Irie, Photoinduced phase transition of gels. *Macromolecules* **23**, 1517–1519 (1990)
99. X. Zhang, Q. Zhou, H. Liu, H. Liu, UV light induced plasticization and light activated shape memory of spiropyran doped ethylene-vinyl acetate copolymers. *Soft Matter* **10**, 3748–3754 (2014)
100. M.-Q. Zhu, L. Zhu, J.J. Han, W. Wu, J.K. Hurst, A.D.Q. Li, Spiropyran-based photochromic polymer nanoparticles with optically switchable luminescence. *J. Am. Chem. Soc.* **128**, 4303–4309 (2006)
101. I. Bellin, S. Kelch, A. Lendlein, Dual-shape properties of triple-shape polymer networks with crystallizable network segments and grafted side chains. *J. Mater. Chem.* **17**, 2885–2891 (2007)
102. M. Behl, I. Bellin, S. Kelch, W. Wagermaier, A. Lendlein, One-step process for creating triple-shape capability of AB polymer networks. *Adv. Funct. Mater.* **19**, 102–108 (2009)
103. S. Chen, J. Hu, C.-W. Yuen, L. Chan, H. Zhuo, Triple shape memory effect in multiple crystalline polyurethanes. *Polym. Adv. Technol.* **21**, 377–380 (2010)
104. A. Lendlein, T. Sauter, Shape-memory effect in polymers. *Macromol. Chem. Phys.* **214**, 1175–1177 (2013)
105. I. Bellin, S. Kelch, R. Langer, A. Lendlein, Polymeric triple-shape materials. *Proc. Natl. Acad. Sci. U. S. A.* **103**, 18043–18047 (2006)
106. S.-K. Ahn, R.M. Kasi, Exploiting microphase-separated morphologies of side-chain liquid crystalline polymer networks for triple shape memory properties. *Adv. Funct. Mater.* **21**, 4543 (2011)
107. T. Ware, K. Hearon, A. Lonneckner, K.L. Wooley, D.J. Maitland, W. Voit, Triple-shape memory polymers based on self-complementary hydrogen bonding. *Macromolecules* **45**, 1062–1069 (2012)
108. M. Behl, A. Lendlein, Triple-shape polymers. *J. Mater. Chem.* **20**, 3335–3345 (2010)
109. M. Behl, I. Bellin, S. Kelch, W. Wagermaier, A. Lendlein, Dual and triple shape capability of AB polymer networks based on poly(ϵ -caprolactone)dimethacrylates. *Mater. Res. Soc. Symp. Proc.* **1140**, 3–8 (2009)
110. K. Suchao-in, S. Chirachanchai, “Grafting to” as a novel and simple approach for triple-shape memory polymers. *ACS Appl. Mater. Interfaces* **5**, 6850–6853 (2013)
111. H. Qin, P.T. Mather, Combined one-way and two-way shape memory in a glass-forming nematic network. *Macromolecules* **42**, 273–280 (2009)
112. S.-K. Ahn, P. Deshmukh, R.M. Kasi, Shape memory behavior of side-chain liquid crystalline polymer networks triggered by dual transition temperatures. *Macromolecules* **43**, 7330–7340 (2010)
113. T. Xie, X. Xiao, Y.-T. Cheng, Revealing triple-shape memory effect by polymer bilayers. *Macromol. Rapid Commun.* **30**, 1823–1827 (2009)
114. C.Y. Bae, J.H. Park, E.Y. Kim, Y.S. Kang, B.K. Kim, Organic-inorganic nanocomposite bilayers with triple shape memory effect. *J. Mater. Chem.* **21**, 11288–11295 (2011)
115. X. Luo, P.T. Mather, Triple-shape polymeric composites (TSPCs). *Adv. Funct. Mater.* **20**, 2649–2656 (2010)
116. H. Chen, Y. Liu, T. Gong, L. Wang, K. Zhao, S. Zhou, Use of intermolecular hydrogen bonding to synthesize triple-shape memory supermolecular composites. *RSC Adv.* **3**, 7048–7056 (2013)
117. S. Chen, H. Yuan, Z. Ge, S. Chen, H. Zhuo, J. Liu, Insights into liquid-crystalline shape-memory polyurethane composites based on an amorphous reversible phase and hexadecyloxybenzoic acid. *J. Mater. Chem. C* **2**, 1041–1049 (2014)

118. T. Xie, Tunable polymer multi-shape memory effect. *Nature* **464**, 267–270 (2010)
119. R. Dolog, R.A. Weiss, Shape memory behavior of a polyethylene-based carboxylate ionomer. *Macromolecules* **46**, 7845–7852 (2013)
120. Q. Zhang, S. Song, J. Feng, P. Wu, A new strategy to prepare polymer composites with versatile shape memory properties. *J. Mater. Chem.* **22**, 24776–24782 (2012)
121. J. Li, T. Xie, Significant impact of thermo-mechanical conditions on polymer triple-shape memory effect. *Macromolecules* **44**, 175–180 (2011)
122. X. Qi, Y. Guo, Y. Wei, P. Dong, Q. Fu, Multishape and temperature memory effects by strong physical confinement in poly(propylene carbonate)/graphene oxide nanocomposites. *J. Phys. Chem. B* **120**, 11064–11073 (2016)
123. Q. Song, H. Chen, S. Zhou, K. Zhao, B. Wang, P. Hu, Thermo- and pH-sensitive shape memory polyurethane containing carboxyl groups. *Polym. Chem.* **7**, 1739–1746 (2016)
124. S.-Q. Wang, D. Kaneko, M. Okajima, K. Yasaki, S. Tateyama, T. Kaneko, Hyperbranched polycoumarates with photofunctional multiple shape memory. *Angew. Chem. Int. Ed.* **52**, 11143–11148 (2013)
125. K. Kratz, S.A. Madbouly, W. Wagermaier, A. Lendlein, Temperature-memory polymer networks with crystallizable controlling units. *Adv. Mater.* **23**, 4058–4062 (2011)
126. K. Yu, H.J. Qi, Temperature memory effect in amorphous shape memory polymers. *Soft Matter* **10**, 9423–9432 (2014)
127. M. Behl, K. Kratz, U. Noechel, T. Sauter, A. Lendlein, Temperature-memory polymer actuators. *Proc. Natl. Acad. Sci. U. S. A.* **110**, 12555–12559 (2013)
128. L. Wang, S. Di, W. Wang, H. Chen, X. Yang, T. Gong, S. Zhou, Tunable temperature memory effect of photo-cross-linked star PCL–PEG networks. *Macromolecules* **47**, 1828–1836 (2014)
129. K. Kratz, U. Voigt, A. Lendlein, Temperature-memory effect of copolyesterurethanes and their application potential in minimally invasive medical technologies. *Adv. Funct. Mater.* **22**, 3057–3065 (2012)
130. L. Viry, C. Mercader, P. Miaudet, C. Zakri, A. Derre, A. Kuhn, M. Maugey, P. Poulin, Nanotube fibers for electromechanical and shape memory actuators. *J. Mater. Chem.* **20**, 3487–3495 (2010)
131. P. Miaudet, A. Derré, M. Maugey, C. Zakri, P.M. Piccione, R. Inoubli, P. Poulin, Shape and temperature memory of nanocomposites with broadened glass transition. *Science* **318**, 1294–1296 (2007)
132. N. Fritzsche, T. Pretsch, Programming of temperature-memory onsets in a semicrystalline polyurethane elastomer. *Macromolecules* **47**, 5952–5959 (2014)
133. N. Mirtschin, T. Pretsch, Designing temperature-memory effects in semicrystalline polyurethane. *RSC Adv.* **5**, 46307–46315 (2015)
134. S. Pandini, F. Baldi, K. Paderni, M. Messori, M. Toselli, F. Pilati, A. Gianoncelli, M. Brisotto, E. Bontempi, T. Riccò, One-way and two-way shape memory behaviour of semi-crystalline networks based on sol–gel cross-linked poly(ϵ -caprolactone). *Polymer* **54**, 4253–4265 (2013)
135. T. Chung, A. Romo-Uribe, P.T. Mather, Two-way reversible shape memory in a semicrystalline network. *Macromolecules* **41**, 184–192 (2008)
136. M. Behl, K. Kratz, J. Zotzmann, U. Nöchel, A. Lendlein, Reversible bidirectional shape-memory polymers. *Adv. Mater.* **25**, 4466–4469 (2013)
137. H. Seok Jin, Y. Woong-Ryeol, Y. Ji Ho, Two-way shape memory behavior of shape memory polyurethanes with a bias load. *Smart Mater. Struct.* **19**, 035022 (2010)
138. J. Zotzmann, M. Behl, D. Hofmann, A. Lendlein, Reversible triple-shape effect of polymer networks containing polypentadecalactone- and poly(ϵ -caprolactone)-segments. *Adv. Mater.* **22**, 3424–3429 (2010)
139. J. Li, W.R. Rodgers, T. Xie, Semi-crystalline two-way shape memory elastomer. *Polymer* **52**, 5320–5325 (2011)
140. S. Pandini, S. Passera, M. Messori, K. Paderni, M. Toselli, A. Gianoncelli, E. Bontempi, T. Riccò, Two-way reversible shape memory behaviour of crosslinked poly(ϵ -caprolactone). *Polymer* **53**, 1915–1924 (2012)

141. M.Y. Razzaq, M. Behl, K. Kratz, A. Lendlein, Multifunctional hybrid nanocomposites with magnetically controlled reversible shape-memory effect. *Adv. Mater.* **25**, 5730–5733 (2013)
142. M. Behl, J. Zotzmann, A. Lendlein, One-way and reversible dual-shape effect of polymer networks based on poly(pentadecalactone) segments. *Int. J. Artif. Organs* **34**, 231–237 (2011)
143. T. Gong, K. Zhao, W. Wang, H. Chen, L. Wang, S. Zhou, Thermally activated reversible shape switch of polymer particles. *J. Mater. Chem. B* **2**, 6855–6866 (2014)
144. A. Biswas, V.K. Aswal, P.U. Sastry, D. Rana, P. Maiti, Reversible bidirectional shape memory effect in polyurethanes through molecular flipping. *Macromolecules* **49**, 4889–4897 (2016)
145. F. Zhang, T. Zhou, Y. Liu, J. Leng, Microwave synthesis and actuation of shape memory polycaprolactone foams with high speed. *Sci. Rep.* **5**, 11152 (2015)
146. M.Y. Razzaq, M. Anhalt, L. Frommann, B. Weidenfeller, Thermal, electrical and magnetic studies of magnetite filled polyurethane shape memory polymers. *Mater. Sci. Eng. A* **444**, 227–235 (2007)
147. H. Koerner, G. Price, N.A. Pearce, M. Alexander, R.A. Vaia, Remotely actuated polymer nanocomposites[mdash]stress-recovery of carbon-nanotube-filled thermoplastic elastomers. *Nat. Mater.* **3**, 115–120 (2004)
148. K.C. Hribar, R.B. Metter, J.L. Ifkovits, T. Troxler, J.A. Burdick, Light-induced temperature transitions in biodegradable polymer and nanorod composites. *Small* **5**, 1830–1834 (2009)
149. H. Zhang, H. Xia, Y. Zhao, Optically triggered and spatially controllable shape-memory polymer-gold nanoparticle composite materials. *J. Mater. Chem.* **22**, 845–849 (2012)
150. Y. Hu, W. Chen, Externally induced thermal actuation of polymer nanocomposites. *Macromol. Chem. Phys.* **212**, 992–998 (2011)
151. L. Hsu, C. Weder, S.J. Rowan, Stimuli-responsive, mechanically-adaptive polymer nanocomposites. *J. Mater. Chem.* **21**, 2812–2822 (2011)
152. S.A. Madbouly, A. Lendlein, Shape-memory polymer composites. *Adv. Polym. Sci.* **226**, 41–95 (2010)
153. M.Y. Razzaq, M. Behl, A. Lendlein, Memory-effects of magnetic nanocomposites. *Nanoscale* **4**, 6181–6195 (2012)
154. C.S. Hazelton, S.C. Arzberger, M.S. Lake, N.A. Munshi, RF actuation of a thermoset shape memory polymer with embedded magneto-electroelastic particles. *J. Adv. Mater. (Covina, CA, US)* **39**, 35–39 (2007)
155. P.R. Buckley, G.H. McKinley, T.S. Wilson, W. Small, W.J. Bennett, J.P. Bearinger, M.W. McElfresh, D.J. Maitland, Inductively heated shape memory polymer for the magnetic actuation of medical devices. *I.E.E.E. Trans. Biomed. Eng.* **53**, 2075–2083 (2006)
156. U.N. Kumar, K. Kratz, W. Wagermaier, M. Behl, A. Lendlein, Non-contact actuation of triple-shape effect in multiphase polymer network nanocomposites in alternating magnetic field. *J. Mater. Chem.* **20**, 3404–3415 (2010)
157. M.Y. Razzaq, M. Behl, K. Kratz, A. Lendlein, Triple-shape effect in polymer-based composites by cleverly matching geometry of active component with heating method. *Adv. Mater.* **25**, 5514–5518 (2013)
158. M.Y. Razzaq, M. Behl, A. Lendlein, Magnetic memory effect of nanocomposites. *Adv. Funct. Mater.* **22**, 184–191 (2012)
159. M.Y. Razzaq, M. Behl, U. Nöchel, A. Lendlein, Magnetically controlled shape-memory effects of hybrid nanocomposites from oligo(omega-pentadecalactone) and covalently integrated magnetite nanoparticles. *Polymer* **55**, 5953–5960 (2014)
160. P.J. Skrzyszewska, L.N. Jong, F.A. de Wolf, M.A. Cohen Stuart, J. van der Gucht, Shape-memory effects in biopolymer networks with collagen-like transient nodes. *Biomacromolecules* **12**, 2285–2292 (2011)
161. J. Hao, R.A. Weiss, Mechanically tough, thermally activated shape memory hydrogels. *ACS Nano. Lett.* **2**, 86–89 (2013)
162. U. Nöchel, C.S. Reddy, N.K. Uttamchand, K. Kratz, M. Behl, A. Lendlein, Shape-memory properties of hydrogels having a poly(ϵ -caprolactone) crosslinker and switching segment in an aqueous environment. *Eur. Polym. J.* **49**, 2457–2466 (2013)

163. G. Li, Q. Yan, H. Xia, Y. Zhao, Therapeutic-ultrasound-triggered shape memory of a melamine-enhanced poly(vinyl alcohol) physical hydrogel. *ACS Appl. Mater. Interfaces* **7**, 12067–12073 (2015)
164. M. Guo, L.M. Pitet, H.M. Wyss, M. Vos, P.Y.W. Dankers, E.W. Meijer, Tough stimuli-responsive supramolecular hydrogels with hydrogen-bonding network junctions. *J. Am. Chem. Soc.* **136**, 6969–6977 (2014)
165. W. Guo, C.-H. Lu, R. Orbach, F. Wang, X.-J. Qi, A. Ceconello, D. Seliktar, I. Willner, pH-stimulated DNA hydrogels exhibiting shape-memory properties. *Adv. Mater.* **27**, 73–78 (2015)
166. V. Kozlovskaya, J. Chen, C. Tedjo, X. Liang, J. Campos-Gomez, J.W. Oh, pH-responsive hydrogel cubes for release of doxorubicin in cancer cells. *J. Mater. Chem. B* **2**, 2494–2507 (2014)
167. X.-J. Han, Z.-Q. Dong, M.-M. Fan, Y. Liu, J.-H. Li, Y.-F. Wang, Q.-J. Yuan, B.-J. Li, S. Zhang, pH-Induced shape-memory polymers. *Macromol. Rapid Commun.* **33**, 1055–1060 (2012)
168. H. Meng, J. Zheng, X. Wen, Z. Cai, J. Zhang, T. Chen, pH- and sugar-induced shape memory hydrogel based on reversible phenylboronic acid–diol ester bonds. *Macromol. Rapid Commun.* **36**, 533–537 (2015)
169. A. Yasin, H. Li, Z. Lu, S.U. Rehman, M. Siddiq, H. Yang, A shape memory hydrogel induced by the interactions between metal ions and phosphate. *Soft Matter* **10**, 972–977 (2014)
170. C.-H. Lu, W. Guo, Y. Hu, X.-J. Qi, I. Willner, Multitrigged shape-memory acrylamide–DNA hydrogels. *J. Am. Chem. Soc.* **137**, 15723–15731 (2015)
171. R.D. Harris, J.T. Auletta, S.A.M. Motlagh, M.J. Lawless, N.M. Perri, S. Saxena, L.M. Weiland, D.H. Waldeck, W.W. Clark, T.Y. Meyer, Chemical and electrochemical manipulation of mechanical properties in stimuli-responsive copper-cross-linked hydrogels. *ACS Macro Lett.* **2**, 1095–1099 (2013)
172. Y. Han, T. Bai, Y. Liu, X. Zhai, W. Liu, Zinc ion uniquely induced triple shape memory effect of dipole-dipole reinforced ultra-high strength hydrogels. *Macromol. Rapid Commun.* **33**, 225–231 (2012)
173. Y. Kagami, J.P. Gong, Y. Osada, Shape memory behaviors of crosslinked copolymers containing stearyl acrylate. *Macromol. Rapid Commun.* **17**, 539–543 (1996)
174. Y. Osada, A. Matsuda, Shape-memory in hydrogels. *Nature* **376**, 219–219 (1995)
175. C. Liu, H. Qin, P.T. Mather, Review of progress in shape-memory polymers. *J. Mater. Chem.* **17**, 1543–1558 (2007)
176. K. Inomata, T. Terahama, R. Sekoguchi, T. Ito, H. Sugimoto, E. Nakanishi, Shape memory properties of polypeptide hydrogels having hydrophobic alkyl side chains. *Polymer* **53**, 3281–3286 (2012)
177. M.H. Kabir, T. Hazama, Y. Watanabe, J. Gong, K. Murase, T. Sunada, H. Furukawa, Smart hydrogel with shape memory for biomedical applications. *J. Taiwan Inst. Chem. Eng.* **45**, 3134–3138 (2014)
178. J.L. Zhang, W.M. Huang, G. Gao, J. Fu, Y. Zhou, A.V. Salvekar, S.S. Venkatraman, Y.S. Wong, K.H. Tay, W.R. Birch, Shape memory/change effect in a double network nanocomposite tough hydrogel. *Eur. Polym. J.* **58**, 41–51 (2014)
179. M. Balk, M. Behl, U. Nöchel, A. Lendlein, Shape-memory hydrogels with switching segments based on oligo(omega-pentadecalactone). *Macromol. Mater. Eng.* **297**, 1184–1192 (2012)
180. M. Balk, M. Behl, U. Nöchel, A. Lendlein, Shape-memory hydrogels with crystallizable oligotetrahydrofuran side chains. *Macromol. Symp.* **345**, 8–13 (2014)
181. U. Nöchel, M. Behl, M. Balk, A. Lendlein, Thermally-induced triple-shape hydrogels: Soft materials enabling complex movements. *ACS Appl. Mater. Interfaces* **8**, 28068–28076 (2016)
182. K. Miyamae, M. Nakahata, Y. Takashima, A. Harada, Self-healing, expansion-contraction, and shape-memory properties of a preorganized supramolecular hydrogel through host–guest interactions. *Angew. Chem. Int. Ed.* **54**, 8984–8987 (2015)
183. G.F. Li, J. Wu, B. Wang, S.F. Yan, K.X. Zhang, J.X. Ding, J.B. Yin, Self-healing supramolecular self-assembled hydrogels based on poly(L-glutamic acid). *Biomacromolecules* **16**, 3508–3518 (2015)

184. N.M. Sangeetha, U. Maitra, Supramolecular gels: Functions and uses. *Chem. Soc. Rev.* **34**, 821–836 (2005)
185. X. Yan, F. Wang, B. Zheng, F. Huang, Stimuli-responsive supramolecular polymeric materials. *Chem. Soc. Rev.* **41**, 6042–6065 (2012)
186. B.Q.Y. Chan, Z.W.K. Low, S.J.W. Heng, S.Y. Chan, C. Owh, X.J. Loh, Recent advances in shape memory soft materials for biomedical applications. *ACS Appl. Mater. Interfaces* **8**, 10070–10087 (2016)
187. T. Bai, Y. Han, P. Zhang, W. Wang, W. Liu, Zinc ion-triggered two-way macro-/microscopic shape changing and memory effects in high strength hydrogels with pre-programmed unilateral patterned surfaces. *Soft Matter* **8**, 6846–6852 (2012)
188. B. Xu, Y. Li, F. Gao, X. Zhai, M. Sun, W. Lu, Z. Cao, W. Liu, High strength multifunctional multiwalled hydrogel tubes: Ion-triggered shape memory, antibacterial, and anti-inflammatory efficacies. *ACS Appl. Mater. Interfaces* **7**, 16865–16872 (2015)
189. W. Nan, W. Wang, H. Gao, W. Liu, Fabrication of a shape memory hydrogel based on imidazole-zinc ion coordination for potential cell-encapsulating tubular scaffold application. *Soft Matter* **9**, 132–137 (2013)
190. X. Le, W. Lu, J. Zheng, D. Tong, N. Zhao, C. Ma, H. Xiao, J. Zhang, Y. Huang, T. Chen, Stretchable supramolecular hydrogels with triple shape memory effect. *Chem. Sci.* **7**, 6715–6720 (2016)
191. O. Peters, H. Ritter, Supramolecular controlled water uptake of macroscopic materials by a cyclodextrin-induced hydrophobic-to-hydrophilic transition. *Angew. Chem. Int. Ed.* **52**, 8961–8963 (2013)
192. Y.-N. Chen, L. Peng, T. Liu, Y. Wang, S. Shi, H. Wang, Poly(vinyl alcohol)-tannic acid hydrogels with excellent mechanical properties and shape memory behaviors. *ACS Appl. Mater. Interfaces* **8**, 27199–27206 (2016)
193. C.L. Lewis, E.M. Dell, A review of shape memory polymers bearing reversible binding groups. *J. Polym. Sci. B Polym. Phys.* **54**, 1340–1364 (2016)
194. L. Qin, F. Xie, P. Duan, M. Liu, A peptide dendron-based shrinkable metallo-hydrogel for charged species separation and stepwise release of drugs. *Chem. Eur. J.* **20**, 15419–15425 (2014)
195. M. Hacker, H. Nawaz, Multi-functional macromers for hydrogel design in biomedical engineering and regenerative medicine. *Int. J. Mol. Sci.* **16**, 26056 (2015)
196. J.L. Hu, J. Lu, Shape memory polymers in textiles. *Adv. Sci. Technol.* **80**, 30–38 (2013)
197. A. Lendlein, R. Langer, Biodegradable, elastic shape-memory polymers for potential biomedical applications. *Science* **296**, 1673 (2002)
198. F. El Feninat, G. Laroche, M. Fiset, D. Mantovani, Shape memory materials for biomedical applications. *Adv. Eng. Mater.* **4**, 91–104 (2002)
199. D.J. Maitland, M.F. Metzger, D. Schumann, A. Lee, T.S. Wilson, Photothermal properties of shape memory polymer micro-actuators for treating stroke. *Lasers Surg. Med.* **30**, 1–11 (2002)
200. W. Small IV, T. Wilson, W. Bennett, J. Loge, D. Maitland, Laser-activated shape memory polymer intravascular thrombectomy device. *Opt. Express* **13**, 8204–8213 (2005)
201. S. Shih-Horn, Mini review of the fully bioabsorbable polymeric stents. *Recent Pat. Eng.* **1**, 244–250 (2007)
202. F. Jung, C. Wischke, A. Lendlein, Degradable, multifunctional cardiovascular implants: Challenges and hurdles. *MRS Bull.* **35**, 607–613 (2010)



Self-Healing Polymers: From Biological Systems to Highly Functional Polymers

16

Stefan Zechel, Martin D. Hager, and Ulrich S. Schubert

Contents

1 From Nature to Synthetic Materials	666
2 General Mechanism and Classification	667
3 Functional Polymeric Materials	692
4 Characterization of Self-Healing Polymers	696
5 Comparison with Other Material Classes	701
6 Commercial Systems	701
7 Conclusion and Outlook	704
References	705

Abstract

The self-healing phenomenon is well-known from nature. Since the last 15 years, several approaches were developed in order to transfer this behavior into synthetic materials and to enable the preparation of multifunctional polymers. The following chapter summarizes the different polymers and their corresponding healing mechanism and provides an overview of the current state of the art. Additionally, the healing of functions as well as the characterization of the self-healing behavior is provided. Furthermore, a short comparison between polymers and other material classes is presented. Finally, the first commercial available systems are summarized showing the way for future developments in this area.

S. Zechel · M. D. Hager (✉) · U. S. Schubert
Laboratory of Organic and Macromolecular Chemistry (IOMC), Friedrich Schiller University Jena,
Jena, Germany

Jena Center for Soft Matter (JCSM), Friedrich Schiller University Jena, Jena, Germany
e-mail: stefan.zechel@uni-jena.de; martin.hager@uni-jena.de; ulrich.schubert@uni-jena.de

© Springer Nature Switzerland AG 2019

M. A. Jafar Mazumder et al. (eds.), *Functional Polymers, Polymers and Polymeric Composites: A Reference Series*, https://doi.org/10.1007/978-3-319-95987-0_19

665

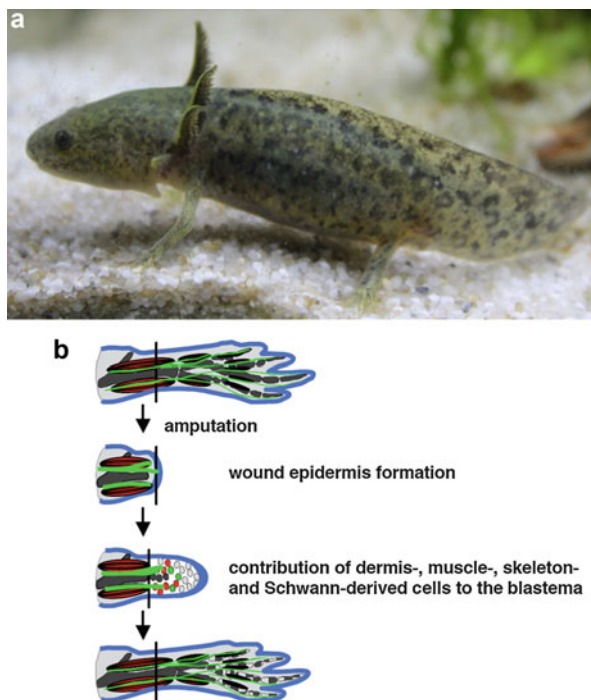
Abbreviations

Cp	Cyclopentadiene
DA	Diels-Alder
DCPD	Dicyclopentadiene
EHM	Eisenberg-Hird-Moore model
ENB	5-Ethylidene-2-norbornene
hDA	Hetero Diels-Alder
IR	Infrared spectroscopy
Mebip	2,6-Bis(methylbenzimidazolyl)pyridine
NMR	Nuclear magnetic resonance spectroscopy
PEG	Poly(ethylene glycol)
PIB	Poly(isobutylene)
PPG	Poly(propylene glycol)
RAFT	Reversible addition-fragmentation chain transfer
ROMP	Ring-opening metathesis polymerization
SAXS	Small angle X-ray scattering
TDCB	Tapered double cantilever beam
TEMPO	2,2,6,6-Tetramethylpiperidiny-1-oxyl

1 From Nature to Synthetic Materials

In the early human history, the usage of materials was limited to natural materials (e.g., stone, wood, fur, etc.). Later on, humans became capable of fabricating synthetic materials resulting in a large variety of different materials utilized nowadays. In recent years, the design of novel materials is increasingly based on natural archetypes. Despite our capability to synthesize and prepare almost every imaginable material, some natural examples are still outstanding and unrivalled, to name just a few examples, gecko feet, which are capable to “stick” to almost every material allowing the reptile to run on the ceiling, [1] spider silk outperforming almost every synthetic fiber [2], as well as natural composites (e.g., nacre) featuring mechanical properties far beyond those properties from the single components [3]. Consequently, a biomimetic material research is ongoing providing a novel blueprint for material design. Important lessons from nature are the hierarchical structuring of materials (e.g., up to seven levels in bone) as well as their ability for repair – some materials are even continuously remodeled (e.g., bone) [4, 5]. In particular, the ability of nature to repair damage and to restore the original properties as well as functions is intriguing. This feature is generally not found in common synthetic materials: Damage will sooner or later lead to the complete failure of the material. In nature, a cut in the finger will be healed; typically 70% of the maximum load and maximum stiffness will be restored within several days [6]. Even a more severe damage/injury can be healed: a broken bone [7]. Depending on the fracture, even full recovery is achieved within a few weeks [8]. Additionally, self-healing is also present at the

Fig. 1 (a) Photograph of an axolotl and (b) schematic representation of the regeneration of a limb. (Reprinted with permission from Ref. [11])



molecular level, for instance, the healing of DNA [9] and the repair cycle of the photosystem II [10]. A masterly performance is the regeneration of whole limbs by the axolotl (*Ambystoma mexicanum*) (see Fig. 1) [11, 12].

These examples provide the basis for the bioinspired design of self-healing materials [13–15]. Important lessons from nature include bleeding (i.e., transport of material to the damage location, mobility for closure of the damage), vascular networks corresponding to our vascular blood system providing transport also after damage, hierarchical structures enabling outstanding material properties, and reversibility (e.g., the constant remodeling of bones or the reversible interaction of molecular building blocks).

2 General Mechanism and Classification

The biological systems described above are very complex, and nature is the expert for the design of materials with self-healing properties. However, the question of what we can learn from nature arises at this point. In general, the strategy of self-healing can partly be adapted from nature [16]. An injury at our finger will subsequently lead to bleeding, which represents the generation of a mobile phase resulting in a filling of the wound. However, the blood would stream out and no real closure, and, thus, self-healing could take place without an immobilization of the mobile

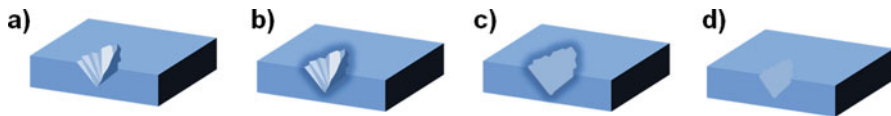


Fig. 2 Schematic representation of the healing of mechanical damage: A scratch occurs and results in a damage of the material (a). The generation of a mobile phase (b) leads to a closure of the crack (c) and to a regeneration of the original mechanical properties (d). (Adapted with permission from Ref. [17])

phase, which is in that case the coagulation. This basic mechanism results in a crack closure and partial restoration of the function. However, nature goes further and substitutes the healing materials (the coagulated blood) with the original material (the skin). This general healing mechanism can also be found in synthetic polymeric materials and consists of the crack propagation, the generation of a mobile phase, and the immobilization (see Fig. 2) [17].

Nevertheless, this general healing mechanism can be achieved in many different ways. Since polymers and polymer composites are easy to functionalize, many different healing strategies were already developed. These approaches can be divided by two different classifications [17]. The first differentiation divides the strategies according to the requirement of an external stimulus. Thus, on the one hand autonomous healing takes place without the utilization of an external trigger like light or heat. Nonautonomous self-healing materials must be activated in order to obtain the mobile phase, which can be obtained in the simplest case by heating to a certain temperature (i.e., the healing temperature). This classification is quite controversially discussed in literature since the final application and the conditions in which the material is used define the final influences [18]. Thus, a material can be an autonomous self-healing material in temperate climate zones, whereas it will be nonautonomous in the Arctic Circle.

A more useful classification divides the self-healing materials into extrinsic and intrinsic [17]. Extrinsic healing requires the presence of an additional self-healing agent. This healing agent is embedded into the polymer matrix (by encapsulation into capsules or the utilization of vascular networks) and is released when the scratch occurs resulting in the formation of the mobile phase [19, 20]. Intrinsic self-healing materials, on the other hand, can heal mechanical damage by itself without any further additives/embedded healing agents. This behavior is realized by the utilization of a specific polymer design and by the incorporation of functional groups, which can provide a certain kind of reversibility in order to later activate the formation of the mobile phase [21]. A general overview of the already used polymeric self-healing materials and the resulting properties as well as the corresponding healing conditions is provided in Table 1. Furthermore, selected examples of intrinsic self-healing polymers are depicted in Fig. 3. Additionally, it can be mentioned that the mechanical properties for extrinsic self-healing systems strongly depend on the matrix. In the case of intrinsic systems, the molecular design and the functional moieties are crucial for the mechanical properties.

Table 1 Summary of selected self-healing polymers and their properties with a comparison to biological systems

Classification	Self-healing mechanism	Chemical compounds	Polymer class	Mechanical data (E-modulus, etc.)	Healing conditions and efficiencies	References
Extrinsic self-healing	The healing is based on the release of healing agent when a crack occurs. The healing agent is encapsulated into capsules or vascular networks	DCPD/ENB ^a	Epoxy	Fracture load up to 200 N	Bulk healing; autonomous healing at RT, 100% efficiency	[22]
			Polystyrene- <i>block</i> -polybutadiene- <i>block</i> -polystyrene	Tensile strength 4 MPa	Bulk healing; healing at RT for 24 h, 80% efficiency	[23]
		Siloxanes ^a	Epoxy	No values provided ^b	Bulk healing; healing at RT for 24 h, 50% efficiency	[24]
			Epoxy-vinyl ester	Fracture load up to 37 N	Bulk healing; autonomous healing at RT, 50% efficiency	[25]
			Poly(dimethyl siloxane)	No values provided ^b	Bulk healing; autonomous healing at RT, 100% efficiency	[26, 27]
		Epoxy ^a	Epoxy	Young's modulus up to 15 GPa	Bulk healing; healing at 130 °C, up to 50% efficiency	[28]
				Failure load 68 N	Bulk healing; healing at 80 °C for 48 h, up to 80% efficiency	[29]
		Amine-epoxy ^a	Epoxy	Critical load 130 N	Bulk healing; healing at 30 °C for 48 h, up to 100% efficiency	[30–32]
		Thiol-epoxy ^a	Epoxy	Young's modulus 3.7 GPa	Bulk healing; healing above 150 °C within minutes; 100% efficiency	[33–36]

(continued)

Table 1 (continued)

Classification	Self-healing mechanism	Chemical compounds	Polymer class	Mechanical data (E-modulus, etc.)	Healing conditions and efficiencies	References
		Thiol-ene ^a	Epoxy	No values provided	Bulk healing; healing at RT for 3 to 5 days, 100% efficiency	[37]
		Thiol-isocyanate ^a	Epoxy	Peak load 84 N	Bulk healing; healing at RT for 1 to 5 days, 100% efficiency	[38]
		Azide-alkyne ^a	Poly(isobutylene)	Storage modulus 2 MPa	Bulk healing; healing at 60 °C for 5 days, 100% efficiency	[39]
		Acylhydrazine/methacrylate ^a	Epoxy	Elastic modulus 1.8 GPa	Bulk healing; autonomous healing at RT; up to 100% efficiency	[40]
		Glycidyl methacrylate ^a	Epoxy	Fracture toughness 0.68 MPa m ^{1/2}	Bulk healing; healing at 25 °C for 72 h, 100% efficiency	[41]
		Maleimide ^a	Epoxy	Flexural strength 3.3 GPa	Bulk healing; healing at RT for 1 to 20 days, up to 80% efficiency	[42–44]
		Isocyanate ^a	Epoxy	Young's modulus 3.3 GPa	Bulk healing; autonomous healing at RT	[45]
			Polyurethane	Fracture toughness 0.02 MPa m ^{1/2}	Bulk healing; healing RT for 24 h, 100% efficiency	[46]

		Cyanoacrylates ^a	Epoxy	Compression strength 180 MPa	Bulk healing; autonomous healing at RT	[47]
			Polyester	Stiffness 0.87 Nm ²	Bulk healing; autonomous healing at RT, 97% efficiency	[48]
		Vinyl ester ^a	Epoxy and vinyl esters	No values provided ^b	Bulk healing; autonomous healing at RT	[49]
		Unsaturated polyester ^a	Epoxy	No values provided ^b	Bulk healing; autonomous healing at RT	[50]
Intrinsic based on covalent bonds	(Retro-) Diels-Alder	Furan-maleimide	Network based on DA-units	Compression modulus: 3.1 GPa	150 °C for 24 h; up to 57% efficiency	[51, 52]
			Epoxy	No values provided	Scratch healing; healing at 140 °C for 30 min	[53]
			Polyurethane	No values provided ^b	Scratch and bulk healing; healing at 120 °C for 5 min, up to 80% efficiency	[54, 55]
			Block copolymer	Indentation modulus 1.8 GPa	Scratch healing; healing at 155 °C for 4 h; up to 100% efficiency	[56]
			Methacrylate	Indentation modulus 1.5 GPa	Scratch healing; healing at 120 °C for 1 h; 100% efficiency	[57–59]
			Anthracene-maleimide	Tensile modulus: 26 MPa	100 °C for several days; up to 55% efficiency	[60]

(continued)

Table 1 (continued)

Classification	Self-healing mechanism	Chemical compounds	Polymer class	Mechanical data (E-modulus, etc.)	Healing conditions and efficiencies	References
		Cyclopentadiene-cyclopentadiene	Network based on Cp-units	Compression modulus: 1560 to 1759 MPa; E-modulus >3 GPa	120 °C for 20 h; up to 110% efficiency	[61]
		Fulvene-cyanoolefine	Network based on DA-units with small PEG spacers	No values provided	10 s at room temperature; no efficiency provided	[62]
	(Retro-) Hetero-Diels-Alder	Dithioesters-cyclopentadiene	Network based on hDA-units	No values provided ^b	Heat press for 10 min. at 120 °C; over 100% efficiency	[63]
	[2 + 2]-Cycloaddition	Coumarin based	Polyurethane	No values provided ^b	Scratch healing; lighting for 1 min. with 254 nm + 90 min. with 350 nm	[64, 65]
		Cinnamate based	Network based on cinnamate groups	Flexural strength: 42 to 50 MPa	Lighting for 10 min. with $\lambda > 280$ nm; ca. 20% efficiency	[66]
	[4 + 4]-Cycloaddition	Anthracene based	Polyglycerol	No values provided	Scratch healing; lighting for 15 min. with 254 nm + 24 h at RT	[67]
	Acylhydrazones	Acylhydrazones crosslinker	Methacrylate	No values provided	Scratch healing; heating for 24 h at 100 °C; 100% scratch closure	[68]
	Imines	Dialdehyde and multivalent imine	Network based on imine units	Tensile strength 4 MPa	Scratch healing; heating at 35 °C	[69]

Disulfides	Disulfide crosslinkers	Epoxy based on PEG and PPG	No values provided ^b	Bulk healing; heating for 1 h at 60 °C; 65% efficiency	[70–72]
		Polyurethane	Tensile strength 0.23 MPa	Bulk healing; heating for 24 h at RT; 90% efficiency	[73]
Polysulfides	Thiuram-disulfide crosslinkers	Polyurethane	Tensile strength 0.81 MPa	Bulk healing; heating for 24 h at RT; 95% efficiency	[74, 75]
		Acrylate	Young's modulus 20 kPa	Scratch healing; applying force using an AFM tip at RT	[76]
		Polyurethane	Young's modulus 12 MPa	Bulk healing; visible light irradiation at RT for 24 h; 100% efficiency	[77]
Urea	Tetrathiol and tetrasulfide as crosslinkers	Organic and inorganic network based on silicone	No values provided ^b	Scratch healing; heating for 10 min at 70 °C; 100% efficiency	[78]
		Poly(urethane-co-urea)	Young's modulus 1.22 MPa	Bulk healing; heating for 24 h at 37 °C; 87% efficiency	[79]
Alkoxyamine	Alkoxyamine crosslinker	Polystyrene	No values provided ^b	Scratch healing; heating for 30 min at 125 °C	[80, 81]
		Polyurethane based on PEG	No values provided ^b	Healing for 150 min at 80 °C; 70% efficiency	[82]
Diarylbibenzofuranone	Diarylbibenzofuranone crosslinker	Poly(propylene glycol)	No values provided ^b	Healing for 24 h at RT; 98% efficiency	[83]
		Epoxy-co-polyesters	Force at break 15 N	Healing for several hours at RT; up to 80% efficiency	[84, 85]
Transesterification	Boronic acids	Network based on boronic esters and thiol-ene adducts	No values provided ^b	Healing for 3 days at RT and 85% humidity; up to 90% efficiency	[86]
		Polycyclooctene	No values provided ^b	Healing for 16 h at 50 °C; up to 90% efficiency	[87]

(continued)

Table 1 (continued)

Classification	Self-healing mechanism	Chemical compounds	Polymer class	Mechanical data (E-modulus, etc.)	Healing conditions and efficiencies	References
Supramolecular intrinsic healing	Hydrogen bonds	Thymine	Poly(isobutylene)	No values provided (for rheology see Ref.)	Bulk healing; healing at 20 °C for 72 h	[88]
		Hamilton wedge	Poly(isobutylene)	No values provided (for rheology see ref.)	Bulk healing; healing at RT for 48 h	[89]
	Amide		Poly(styrene- <i>block</i> -butyl acrylate)	Young's modulus 12 MPa	Bulk healing; healing at 30 °C for 24 h; 95% efficiency	[90]
			Poly(methyl methacrylate) brush polymer	Young's modulus 32 MPa	Bulk healing; healing at RT for 24 h; 80% efficiency	[91]
			Methacrylate	No values provided	Scratch healing; healing at 50 °C for 30 min	[92]
			Polystyrene brush polymer	Young's modulus 35 MPa	Bulk healing; healing at RT for 24 h; 90% efficiency	[93]
	Ureas		Poly (dimethylsiloxane)	No values provided ^b	Bulk healing; healing at RT for few hours	[94]
			Network based on ureas	No values provided ^b	Bulk healing; healing at RT for 3 h	[95, 96]

	Ureidopyrimidone	Poly(butyl acrylate)	No values provided	Bulk healing; healing at RT for 50 h; 100% efficiency of adhesion recovery	[97]
		Poly(lactic acid)- <i>alt</i> -poly(ethylene- <i>co</i> -butylene)	Young's modulus from 4 to 150 MPa	Scratch healing; lighting for 20 min with UV light	[98]
		Poly(styrene- <i>block</i> -butyl acrylate)	Young's modulus up to 40 MPa	Bulk healing; healing at 45 °C for 18 h; 75% efficiency	[99]
		Polysiloxane	No values provided	Scratch healing; heating at 120 °C	[100]
π - π - Interactions	Pyrene-naphthalene diimide	Poly(propylene oxide) and polybutadiene	Tensile modulus 3×10^5 pa	Healing for 240 min at 100 °C; up to 95% efficiency	[101, 102]
		Poly(ethylene- <i>co</i> -methacrylic acid)	No values provided ^b	Healing induced by ballistic impact; healing at different temperatures possible	[103–107]
Ionomers	Surlyn [®]	Acrylates	No values provided	Scratch healing; healing at temperatures between RT and 100 °C for some hours; up to 100% efficiency	[108, 109]
		Copolymers acrylate and acrylic acid	Elastic moduli of 1 MPa	Bulk healing; healing with magnetic-induced heating for 15 min; 100% efficiency	[110]

(continued)

Table 1 (continued)

Classification	Self-healing mechanism	Chemical compounds	Polymer class	Mechanical data (E-modulus, etc.)	Healing conditions and efficiencies	References
	Metallopolymers	Terpyridine ligands	Methacrylates	Indentation modulus of 2 GPa	Scratch healing; heating for several hours at temperatures between 60 °C and 150 °C depending on metal salt	[111–113]
		Mebip ligands	Poly(ethylene-co-butylene)	No values provided ^b	Scratch healing; UV-light irradiation 60 s	[114, 115]
		Histidine ligands	Methacrylates	Indentation modulus of 2 GPa	Scratch healing; heating for several minutes to hours at temperatures between RT and 150 °C depending on metal salt	[116]
		Imidazole ligands	Graft copolymers out of styrene and butyl acrylate	No values provided ^b	Healing for 3 h at RT; 100% efficiency	[117]
		Crown ether based	Acrylate	No values provided ^b	Scratch healing; healing for 3 min at RT	[118, 119]
Host-guest interactions	Cyclodextrin	Methacrylate	Methacrylate	No values provided ^b	Scratch healing; healing for 20 min at RT	[120]
		Methacrylate	Methacrylate	No values provided	Scratch healing; healing for 24 h using 1.5 V at RT	[121]
		Acrylate	Acrylate	Maximum stress at break 73 kPa	Bulk healing; healing for 24 h at RT; 84% efficiency	[122–124]

Selected biological systems

Skin	Wound healing by bleeding		Protein	Elastic modulus 66 MPa	Bulk healing; autonomous healing at 37 °C; healing time depends on wound size; 100% efficiency	[125]
Bone	Transport of new minerals to the broken part	Calcium-phosphate	Mineral	Elastic modulus 20 GPa	Bulk healing; autonomous healing at 37 °C within 4 to 6 weeks; 100% efficiency	[126, 127]
Mussel byssus threads	Interaction between dopamine and iron(III) and zinc(II) and histidine	Zinc(II)-histidine and iron(III)-dopamine	Protein	Young's modulus 500–900 MPa	Bulk healing; healing at 37 °C within 168 h; up to 100% efficiency	[128]

General comment: Efficiencies for the scratch healing tests were not provided only if a 3D analysis of the scratches were performed; furthermore, hydrogel (organogel)-based systems are not listed due to their dependency of the water (or organic solvent) content; the maximum healing efficiency is 100%, and higher values (in particular in the case of extrinsic systems) are normalized to that value.

^aThese mentioned chemistries were adopted from reference [20], and a more detailed overview of the specific chemistry behind the healing is presented in this excellent review article.

^bIn these cases the exact values are not provided; however the graphs of the mechanical testing can be found in the publications.

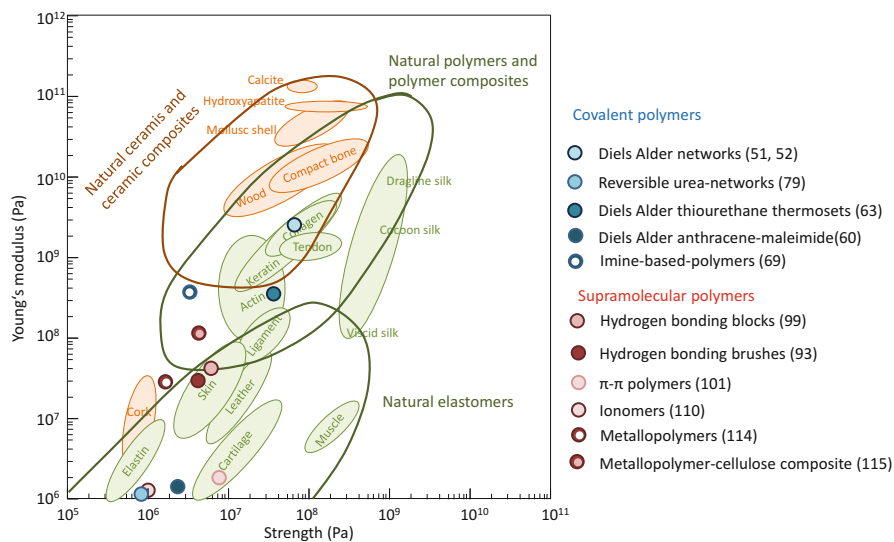


Fig. 3 Schematic representation of the mechanical properties of selected examples of intrinsic self-healing polymers and a comparison to biological materials. (The biological values are adopted from Ref. [3])

In the following paragraph, a more detailed description of each healing mechanism is provided. Firstly, extrinsic self-healing systems will be discussed. Most of the extrinsic self-healing polymers are based on the pioneering work of White and coworkers [22]. The authors incorporated microcapsules filled with dicyclopentadiene into an epoxy resin. When a crack occurs, the capsules are broken and the liquid monomer is released resulting in a filling of the crack. The mobile phase is immobilized by the ring-opening metathesis polymerization (ROMP) of the dicyclopentadiene induced by the contact with the embedded Grubbs catalyst (see Fig. 4).

The basic system could be further improved and different parameters were optimized. Thus, the healing agent, the catalyst (which is not always required), the polymeric matrix, as well as the capsules (composition as well as size) were varied in order to achieve a more robust and better healing system. A summary of the different systems is given in Table 1, and for a detailed overview of the underlying chemistry in capsule-based systems, the interested reader is referred to an excellent review of Du Prez and coworkers [20].

However, the first developed synthetic self-healing systems featured some drawbacks. The most important one is the limited multiple healing behavior at the same position. If the capsules are empty due to a previous healing event, another crack at the same position cannot be healed anymore since no healing agent is present. In order to overcome this problem, several groups focused on the development of vascular networks, which are inspired by the human skin [129, 130]. The blood system in humans is responsible for the delivery of the “healing agent” to the wound. This basic principle was transferred into synthetic materials as depicted in Fig. 5

Fig. 4 Schematic representation of the self-healing principles of capsule-based materials: (a) A crack occurs; (b) the crack leads to the rupture of the capsules resulting in a release of the liquid monomer, which is subsequently polymerized (c) leading to a filling of the crack and the restoration of the original mechanical properties. (Reprinted with permission from Ref. [22])

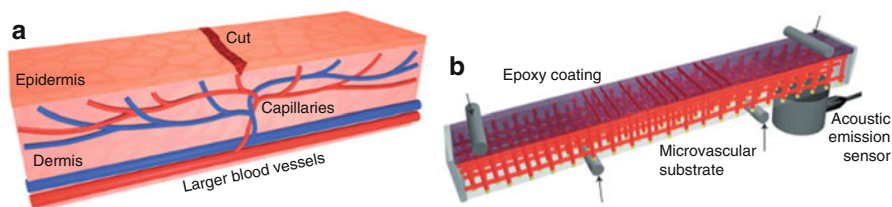
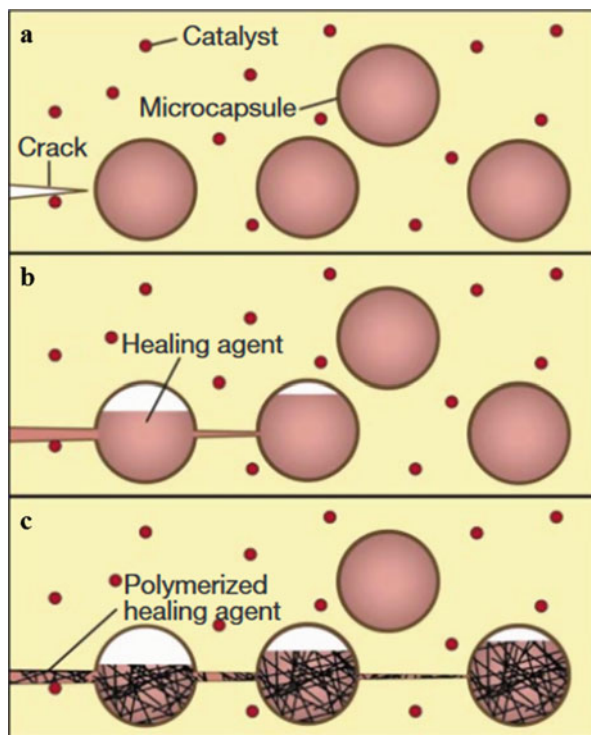


Fig. 5 Schematic presentation of the healing of the human skin (a) and the adopted synthetic material using hollow fibers as transport ways for the healing agent (b). (Reprinted with permission from Ref. [129])

[129]. For this purpose, hollow fibers were incorporated into a polymeric material, and these were utilized for the transport of healing agents [131]. This setup has two advantages compared to the capsule-based system. On the one hand, the transport of the healing agent to the crack is enhanced, and, furthermore, a healing at the same position can be obtained as shown by Toohey et al., who measured a healing efficiency of approximately 50% after seven healing cycles [129]. Furthermore, the microvascular system was further improved by varying the polymeric matrix, the healing agent, the catalyst, as well as the fibers [31, 32, 132–134]. One recent

development in the context of vascular network-based self-healing materials was the possibility to heal large volume damage [40]. For this purpose a two-stage mechanism was required since the healing agent itself is too less viscous and would flow out. Thus, a previous gel formation by the reaction of a *bis*-acylhydrazine and a trialdehyde was required increasing the viscosity of the healing agent. Afterward, the real immobilization by polymerization was obtained resulting in healing of a round crack with a diameter of 35 mm.

The extrinsic self-healing stills lacks in healing over a longer period of time. The vascular networks still lose their mechanical properties during time and a reduced self-healing efficiency after several healing cycles were observed [129]. Thus, further optimization of the flow of the healing agents is required in order to obtain long-term healing and to enable application.

Another concept, which is more promising in terms of healing of a long period of time, is intrinsic self-healing [21]. In this case, the healing is not based on an external healing agent. Instead the material itself has a special design, which offers the possibility to generate a mobile phase. The mussel byssus threads are the most prominent biological examples of such system, [128] which will be discussed in the section about self-healing metallopolymers.

In general, intrinsic self-healing polymers are based on a kind of reversible linkage. This reversible character offers the switching between the solid, non-healing, and the mobile phase. Thus, a smart design of such materials would offer both: high mechanical performance and excellent self-healing properties [21]. However, the realization of the perfect combination is quite difficult, and most intrinsic self-healing materials still lacks in mechanical stability or autonomic self-healing behavior without any external trigger. The reversible character of intrinsic polymeric systems can be generated in many different ways and requires a special molecular process, which can be triggered by an external stimulus and, furthermore, is reversible resulting in the original molecular state. The most useful classification of intrinsic self-healing polymers is the classification into covalent-based [135] and supramolecular-based systems [136].

Firstly, the dynamic covalent system will be discussed in detail. Most of the investigated systems belong to reversible covalent-based self-healing that describes the utilization of cycloadditions [135]. These processes are ring formation reactions, which are, under specific circumstances, reversible. In particular, three different cycloadditions have been utilized for the design of self-healing polymers: Diels-Alder reactions and [2 + 2]- and [4 + 4]-cycloadditions (see Fig. 6). In all three cases, the cycloaddition is reversible and can be switched between the closed state (cycloaddition adduct) and the open state, which is required for the generation of a mobile phase. Whereas the Diels-Alder reaction is thermally reversible, the other two cycloadditions can be switched by light irradiation. However, photo-switchable systems have not often been utilized so far for self-healing polymers, and the [4 + 4] was used, to the best of our knowledge, only once [67]. For the [2 + 2]-cycloaddition, two different structures were incorporated into polymers in order to realize self-healing materials. On the one hand, cinnamate derivatives were utilized [66, 137–139], and the other possibility is the application of coumarin systems [64, 65].

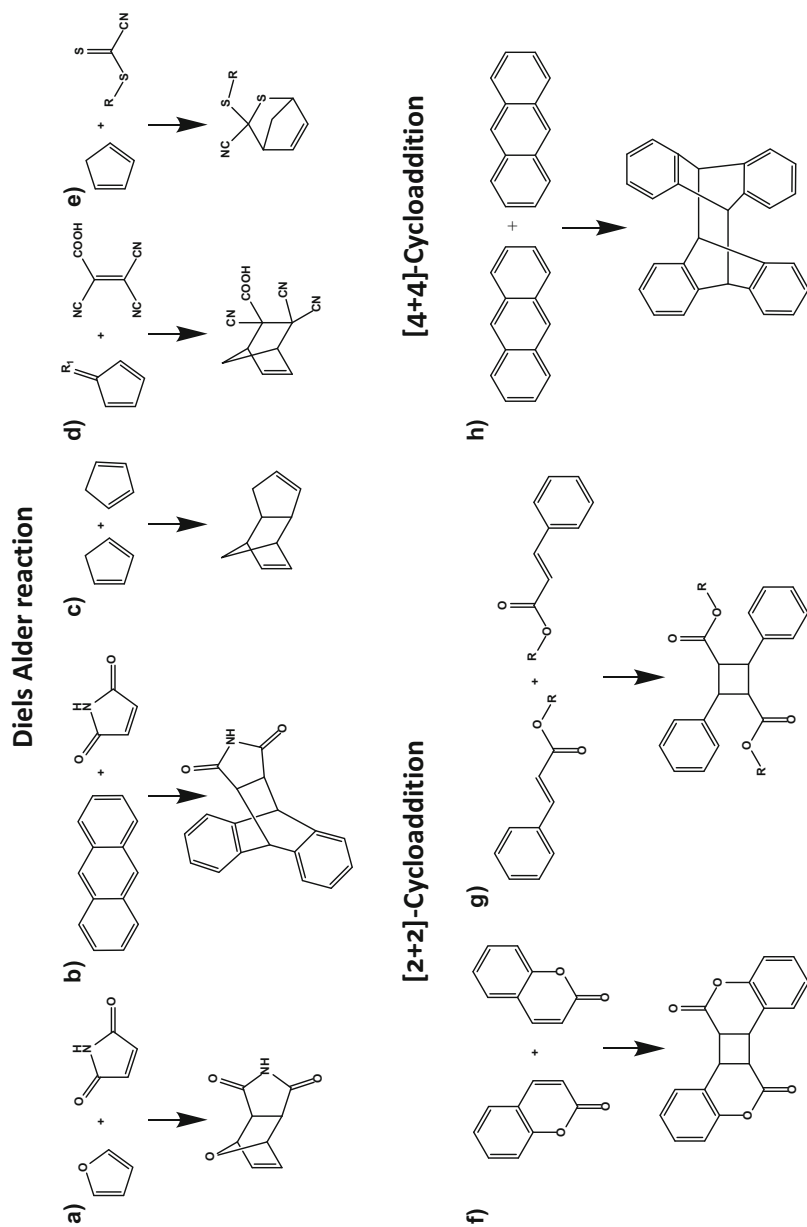


Fig. 6 Schematic representation of the utilized cycloadditions for the design of self-healing polymers: Diels-Alder reaction (**a–e**), [2 + 2]-cycloaddition (**f** and **g**), as well as [4 + 4]-cycloaddition (**h**)

The by far most investigated class of cycloadditions for self-healing polymers is the Diels-Alder reaction. In that case the reversible retro-Diels-Alder reaction proceeds under thermal treatment, and the temperature strongly depends on the chosen dienophile as well as diene and ranges from room temperature up to 200 °C [140]. The diversity of the utilized systems is depicted in Fig. 6. The most promising as well as the most investigated system is the maleimide-furan system. The cycloaddition between these two compounds proceeds even at room temperature, whereas the retro-Diels-Alder temperature happens at temperatures above 100 °C [141]. Furthermore, furan as well as maleimide can easily be functionalized in order to incorporate them into polymeric materials. The pioneering work on this system was performed by the group of Wudl, who were able to design a polymer network consisting of multifunctional furan and maleimide units [51, 52]. During thermal treatment the network opens due to the retro-Diels-Alder reaction enabling the generation of a mobile phase. This process leads to a healing, and during cooling the network is reformed again recovering the excellent mechanical properties (E-modulus of 3.1 GPa). Besides the network based only on furan and maleimide units, also copolymers containing the Diels-Alder units were investigated like epoxy, [142] polyesters [143, 144], or methacrylates [57, 58, 145]. A recent development was the incorporation of this self-healing strategy into block copolymers. Thus, Barthel et al. were able to synthesize a diblock copolymer consisting of poly(ethylene glycol) as well as a furan-glycidyl ether (FGE) [56]. The crosslinking with a low molar mass bismaleimide was performed resulting in a polymer network, which was able to heal scratches within 3 h at 155 °C (see Fig. 7).

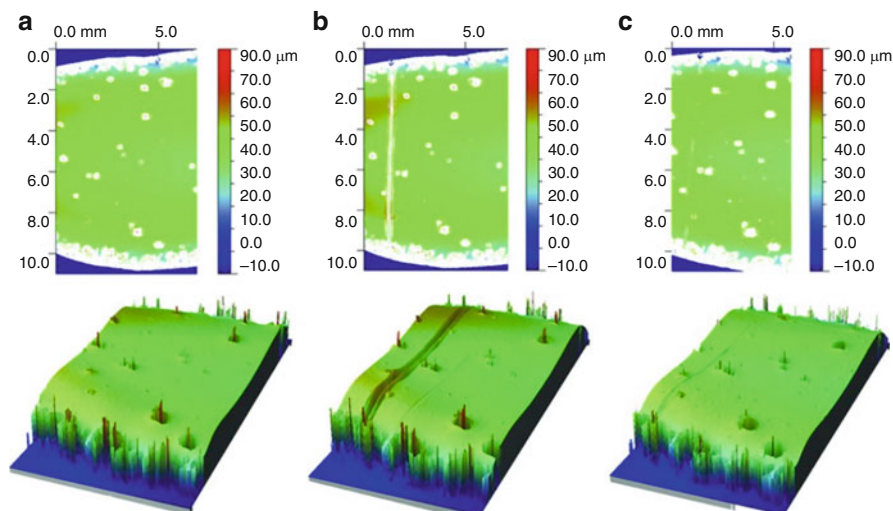


Fig. 7 Schematic representation of the self-healing behavior of a PEG-*b*-PFGE copolymer crosslinked by a low molar mass bismaleimide: (a) Film before scratching, (b) scratch, and (c) self-healing after 3 h at 155 °C. (Reprinted with permission from Ref. [56])

The reversible cycloadditions are not the only utilized reversible covalent interactions, which have been used for the design of self-healing polymers. Di- and polysulfides are other important substance classes in this context. However, the exact molecular mechanism is still not fully understood, and several explanations are provided [135]. Thus, the healing can be based on a reversible metathesis like reaction between two functional groups [70] or the homolytic cleavage of the S-S bond, [146] which can also be promoted by the addition/generation of radicals. Other possibilities are the exchange reaction between a free thiol [71] and the disulfide or the reduction of the S-S bond [147]. All mechanisms are described in literature and can potentially contribute to the overall healing mechanism of disulfide-based materials. Besides disulfides also polysulfides could be utilized for such an approach. For instance, the group of van der Zwaag presented a hybrid material containing inorganic as well as organic compounds [78]. Furthermore, tetrasulfides were incorporated in order to achieve healing. During thermal treatment, the concentration of S-S bonds in the network decreases, resulting in a (partial) decrosslinking and finally healing at 70 °C. This mechanism could be studied using several techniques like IR spectroscopy or rheological measurements.

As already shown with the previous examples, the reversibility or the dynamics of a system is crucial for the self-healing process of intrinsic healable polymers. These dynamic processes were summarized by Lehn and coworkers under the term “dynamers,” which include several substance classes [148]. For instance, imines and acylhydrazones are named in this context since both are able to perform dynamic exchange reactions or cleavage of the covalent bond [149–152]. However, most of the investigations were performed in solution, and the transformation of this knowledge into the solid state is rather difficult. Nevertheless, it was possible to utilize polymers containing these dynamic groups for the preparation of self-healing materials. In particular, the acylhydrazone-based polymers featured self-healing properties, which can either be based on the cleavage of the bonds (at low pH values and in the presence of water) or the dynamic exchange between two functional units. For hydrogels, Deng et al. could report a self-healing process at very low pH values resulting in a depolymerization of the network [153]. However, the healing at high pH values was not possible, but the limitation can be overcome with a double network structure using disulfide bonds as a second reversible element [154]. Changing from hydrogels to solid materials, the healing mechanism changes as reported by Kuhl and coworkers [68]. Therefore, the authors designed a methacrylate-based polymer network crosslinked by acylhydrazone functions and could show the healing ability of these materials. However, a rather low tendency for healing was observed, and higher temperatures were required, which could be explained by the reduced flexibility in the solid state (i.e., bulk polymer) compared to the hydrogels (see Fig. 8). Furthermore, mechanistic investigations were performed using IR and solid-state NMR, revealing that the healing is presumably based on the exchange reaction between two functional groups. Besides the acylhydrazones, also imines were utilized for the design of self-healing polymers, but to a lesser extent [69]. Nevertheless, an impressive example was recently presented by Liu and coworkers [155]. The authors presented the healing of a protein-based hydrogel which was

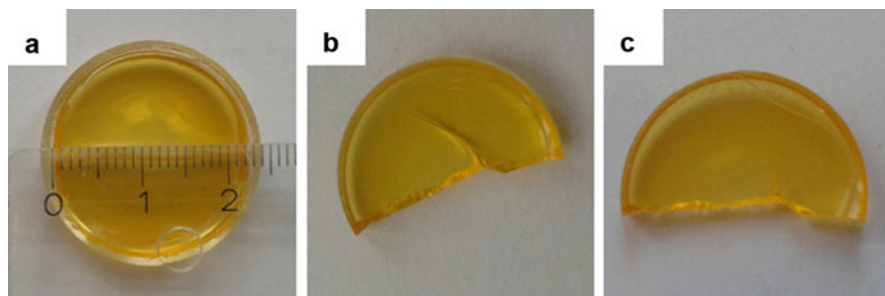


Fig. 8 Representation of the self-healing behavior of a methacrylate-based acylhydrazone network: (a) polymer film, (b) inflicted scratch, and (c) healing after the scratch after 64 h at 100 °C. (Reprinted with permission from Ref. [68])

obtained by the crosslinking of a protein with a dialdehyde. The formation of imine bonds introduced a reversible element, which was further opened by the generation of protons due to an enzymatic process. Thus, healing of the gel at room temperature was observed.

Comparable self-healing phenomena could be obtained for ester crosslinked polymers. Also in these materials a dynamic exchange between functional groups is responsible for the healing mechanism. This so-called transesterification could be found for carboxylic [84] as well as boronic esters [87]. The healing mechanism is based on the exchange between two ester functions, which can be enhanced by the addition of Lewis acids [84].

The last possibility to design self-healing polymers based on reversible interactions is the utilization of stable radicals as well as the corresponding adducts. A typical and well-known stable radical in polymer science is the 2,2,6,6-tetramethylpiperidinyl-1-oxy (TEMPO), which is utilized in the nitroxide-mediated polymerization [156] or organic radical batteries [157]. This concept was also transferred into self-healing polymers. For this purpose, polymer networks crosslinked by a TEMPO unit were prepared, and the self-healing was studied in detail. Firstly, the group of Zhang studied polystyrene-based systems, and these systems revealed a self-healing behavior at 125 °C [80]. Furthermore, the molecular mechanism was studied using various techniques, in particular by ESR [81]. Thus, the authors could demonstrate that the healing is based on a crossover reaction between two functional groups. Additionally the basic principles could also be transferred into polyurethane systems revealing a lower healing temperature of 80 °C due to an increased flexibility of the polymer backbone [82].

Another radical-based concept is the utilization of diarylbibenzofuranon (Fig. 9). In this particular case, the healing is based on the dissociation of the adduct into two stable radicals [83]. The equilibrium between the two species is more dynamic than the TEMPO-based one, and, thus, a healing process at room temperature could be observed.

The class of covalently crosslinked system is investigated in detail, and a wide range of reactions are already applied for this purpose. Furthermore, there are also

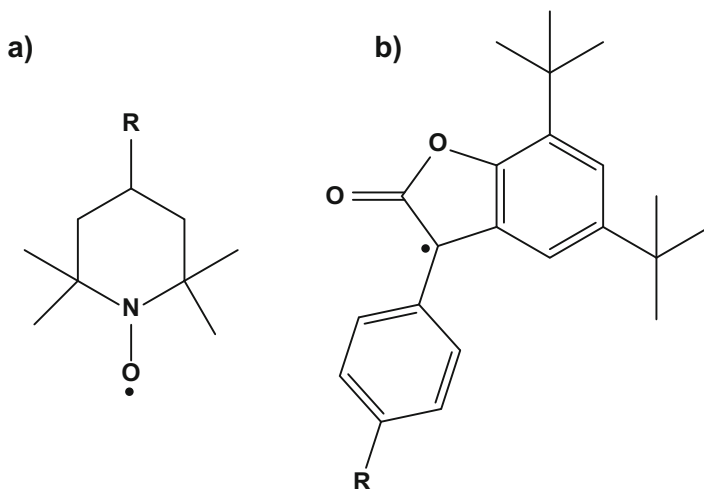


Fig. 9 Schematic representation of the utilized stable radicals for the production of self-healing materials: TEMPO (a) and diarylbibenzofuranon (b)

supramolecular interactions available, which feature also a kind of reversibility. The advantage of these secondary interaction is the simple tunability of the strength and, consequently, of the properties of the material [136]. However, this feature makes it somewhat challenging to design materials offering both self-healing abilities and distinguished mechanical properties [158]. Thus, a high degree of reversibility leads to excellent self-healing properties, but it goes hand in hand with poor mechanical performance. Despite this tightrope walk, it was possible to utilize several supramolecular motifs for the design of self-healing materials, which will be discussed in detail in the following paragraph: hydrogen bonds, ionic interactions, metal-ligand bonds, π - π interactions, as well as host-guest complexes [136].

Hydrogen bonds are by far the most investigated supramolecular interactions in terms of self-healing properties [159]. For this purpose, several structural motifs have been studied, e.g., ureas, ureidopyrimidone or nucleobases. An impressive example of hydrogen-based self-healing polymers was presented by Leibler and his group [95, 96]. The authors synthesized a polymer network containing urea functions, which were responsible for the crosslinking and, additionally, for the self-healing behavior. The authors claimed that the healing of the material is based on the formation of unbound hydrogen bond units at the crack due to the damage event and that these free moieties reform hydrogen bonds if the two parts are placed together. Thus, healing at room temperature could be obtained within minutes. However, if the material parts are kept away from each other and the healing process was started after several hours, an insufficient healing was obtained and the mechanical properties were not restored. This phenomenon was explained by the reassembly of the freshly formed hydrogen bonds, and, thus, no sticking of the polymer was possible anymore.

After the first development of hydrogen bond-based self-healing materials, several other systems were studied in detail. One important moiety is thymine, which is

also a natural building block of the DNA. The utilization of thymine in polymeric materials mostly requires a complementary partner, which can be, e.g., diaminotriazine [160]. However, it is also possible to utilize thymine without any additional partner as shown by Binder and coworkers [88]. In that case, the authors functionalized poly(isobutylene) (PIB) with thymine functions and constructed another network by alkyne-azide click chemistry. The very polar thymine units lead to aggregates within the copolymer, and during a scratch free supramolecular moieties are obtained, which are reformed by the contact of two freshly cut surfaces resulting in a healing. However, the effect of phase separation seems to be more important for the self-healing than the contribution of the reversible hydrogen bonds itself.

One very similar moiety compared to thymine and one of the most frequently investigated molecular units in the context of self-healing materials is barbiturate. Mostly, this system is used with the corresponding Hamilton wedge as shown in Fig. 10 [161]. The rather strong hydrogen bonds as well as the simple functionalization procedure allow a broad range of potential polymer structure. Thus, Herbst et al. were able to end functionalize PIB with either one or two hydrogen bonding motifs [89]. A mixing of the corresponding polymers led to a network formation via clusters since the highly polar functional groups segregated from the unpolar polymer backbone. Furthermore, the healing ability at room temperature was studied, and a healing after 48 h could be obtained. An improvement was reported

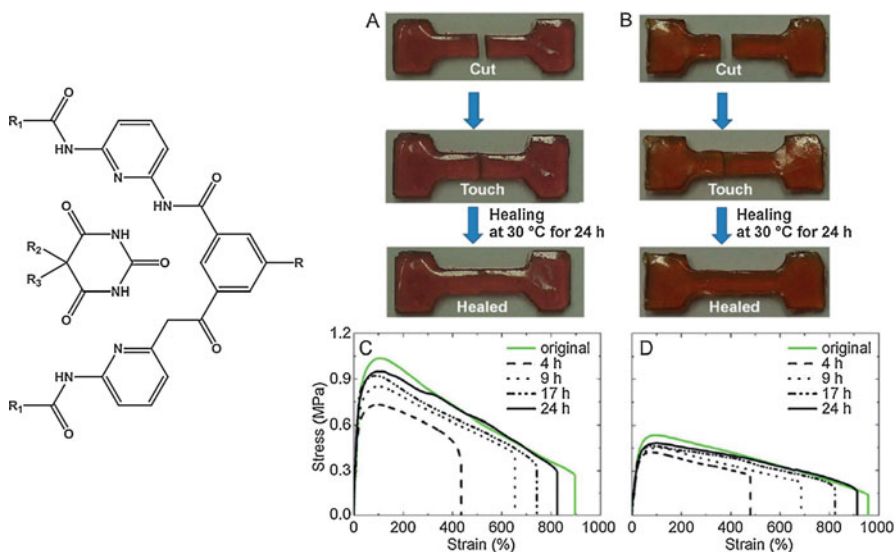


Fig. 10 Schematic representation of the supramolecular pair based on barbiturate and the corresponding Hamilton wedge (left) and the self-healing ability of block copolymers based on these interactions (right). Healing of the block copolymer containing only barbiturate (A and C) and the adduct of the block copolymer containing barbiturate as well as a Hamilton wedge containing polymer (B and C). (Reprinted with permission from Ref. [90])

3 years later by the same group. Therefore, the group prepared block copolymers with the hydrogen bonding (barbiturate) units localized in the hard block (polystyrene) [90]. These materials also featured a healing ability after 24 h at 30 °C as shown in Fig. 10. However, the utilization of α,ω -difunctionalized polyisoprene with two Hamilton wedges and the block copolymer resulted in weaker mechanical properties, but also cracks could be healed at room temperature.

However, the main disadvantage of all the investigated hydrogen bonding-based self-healing polymers is the weak mechanical performance. Thus, only very soft materials were obtained. In order to overcome this problem, Guan and coworkers developed a multiphase phase system offering both mechanical stability and self-healing properties [93]. For this purpose, the authors prepared a polystyrene-based copolymer which featured brushes containing a polyacrylate with an amide function. This function enables hydrogen bonds and, thus, crosslinking. Furthermore, a phase separation was obtained between the hard and the soft block. Although the introduction of non-flexible hard blocks, the copolymer still featured a self-healing ability at room temperature and good mechanical properties (E-modulus of up to 35 MPa).

π - π Interactions represent another important class of supramolecular interactions utilized for self-healing materials. In order to obtain such an interaction, an electron-rich as well as an electron-poor aromatic compound is required [162]. As electron-accepting unit, only naphthalene diimide was utilized, and it was incorporated into polymers as end groups or as repeating units. Furthermore, electron-rich aromatic systems are required, and mostly two different systems were used up to now: perylene [163] and pyrene [100–102, 164]. If both polymers are combined, secondary interaction takes place (see Fig. 11) resulting in crosslinking of the polymer as well as a chain folding. The obtained polymeric materials feature the ability to close cracks during thermal treatment since the thermal activation of the π - π interaction leads to a disassembly and, finally, to mobility, which is required for closing the crack. During cooling, the π - π interactions are reformed, and the original properties of the polymer can be reobtained. Firstly described in 2009, the π - π interaction was already used several times for the preparation of self-healing materials [100]. In the first approach, a polysiloxane containing two pyrene units as end groups were mixed with a naphthalene diimide containing copolymer resulting in the formation of a supramolecular network. This material is able to heal cracks at temperatures above 90 °C. The basic principles could also be transferred into other systems, and, thus, other copolymers for the naphthalene diimide containing part were utilized such as poly(propylene oxide) [101, 102, 164]. Furthermore, polybutadiene was used as building block for the pyrene block [101]. Additionally, the mechanical performance could be enhanced by the utilization of cellulose nanocrystals [165]. Finally, also perylene was incorporated into a polymeric structure resulting in a π - π interaction [163]. In that case, healing after 40 min at 70 °C or after 14 min at 125 °C could be observed.

Ionomers are a very important class of supramolecular healable materials [136]. These copolymers reached already the industrial scale and are sold by DuPont under the trade name Nucrel[®] poly(ethylene-*co*-methacrylic acid) or SulyIn[®]

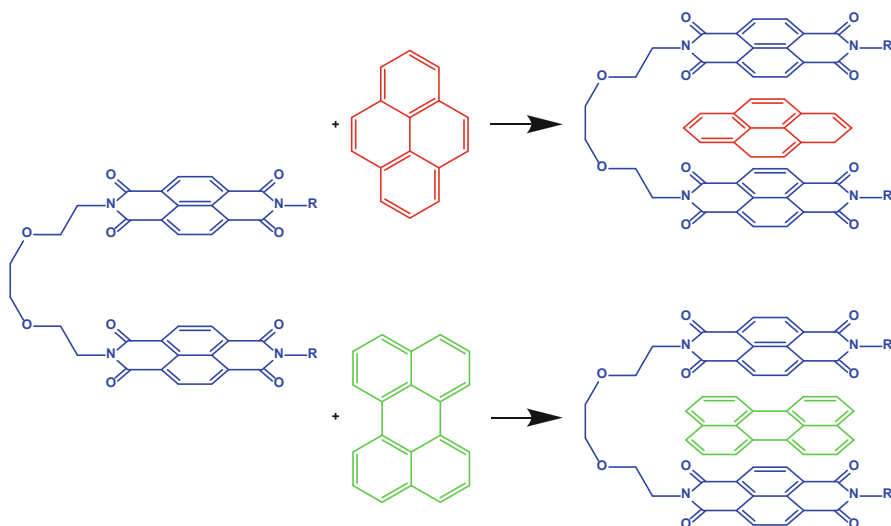


Fig. 11 Schematic representation of the formed complexes by π - π interaction starting from a naphthalene diimide derivatives and pyrene (red) and perylene (green). (Adopted from Ref. [163])

(different salts of poly(ethylene-*co*-methacrylic acid)) [166, 167]. These copolymers feature excellent mechanical properties and are used as packing materials or top layers for, e.g., golf balls [167]. The commercial availability leads to several publications reporting the self-healing ability of Nucrel[®] and Suryln[®]. However, the self-healing effect of those polymers is up to now not used on an industrial scale. Nevertheless, the self-healing phenomenon is studied by several groups and will be described in the following paragraph.

Generally, ionomers are defined as polymers containing a certain amount of ionic groups (1% to 15%), which leads to a special behavior since a phase separation of the ionic groups within the nonpolar backbone is obtained [168]. These so-called multiplets aggregate further to ionic clusters according to the Eisenberg-Hird-Moore model (EHM) [169]. Furthermore, the ionic clusters lead to a crosslinking of the polymer and to a reduced mobility at room temperature. During thermal treatment the order of the ionic clusters itself is destroyed, which can increase the mobility of the polymer chains. In the case of Suryln[®], further thermal treatment would lead to a melting of the polyethylene parts, which are crystalline at room temperature (Fig. 12) [170].

Most investigations on the self-healing behavior of ionomers is focused on the testing of the healing abilities after a ballistic impact [103, 105, 171]. For this purpose, a polymer film was penetrated with a bullet resulting in a hole within the polymer. Furthermore, this kind of damage leads to heating of the polymer, which surrounds the generated hole [171]. Thus, parts of the polymer become sufficiently mobile to close the crack and to heal the damage. Kalista and coworkers investigated this behavior further at different temperatures [104]. The authors could show that the temperature of the film has a crucial influence on the healing abilities. However, the

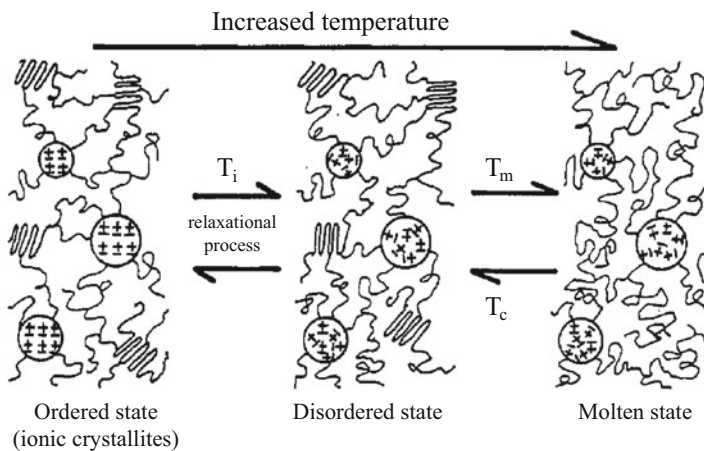


Fig. 12 Schematic representation of the thermal behavior of ionomers (in particular of Suryln[®]): The ordered state at room temperature with crystalline polyethylene as well as ionic cluster undergoes two thermal transitions; disorder of the ionic clusters and melting of the polyethylene. (Reprinted with permission from Ref. [170])

most important parameter is heating of the surrounding polymer, and, consequently, the heating has to be stronger if the polymer film is cooled before the penetration. Additionally, lower temperatures can cause a kind of brittleness of the film resulting in non-healing of the ionomer. This behavior can be in particular observed for low degrees of neutralization of Nucrel[®]. Despite all the ballistic tests, it still requires the access to a shooting place to perform these experiments, and in order to overcome this problem, Varley and van der Zwaag developed a similar method to test the same behavior without a gun [106]. For this purpose, they constructed a hydraulic tensile testing apparatus, which also resulted in hole formation.

The ballistic penetration is not the only method which was reported to test the self-healing capacity of ionomers. Exemplary, Bose et al. studied the scratch healing behavior of ionomers. Furthermore, the utilized copolymers were not based on Suryln or Nucrel. Instead they prepared a copolymer consisting out of *tert*-butyl acrylate and *n*-butyl acrylate [108, 109]. In a second step, the *tert*-butyl ester was cleaved off and the obtained acid was neutralized using different metal salts, i.e., zinc (II) and cobalt(II) acetate as well as sodium hydroxide. Furthermore, the ionic content was varied, and the synthesized materials were investigated using rheology as well as microscopy in order to follow the healing behavior of the scratches. The authors could show that these ionomers are also able to heal scratches, even if they were not generated by high impact damage. Furthermore, a correlation between the mechanical properties and the self-healing abilities was obtained since the crossover frequency of the storage and the elastic modulus obtained by rheology goes hand in hand with the mechanical and self-healing properties. Therefore, the authors could reveal the optimal design principle for having both mechanical stability and self-healing behavior [108, 109].

Metallopolymers are another important class of materials in terms of self-healing and are in some points comparable to the previous mentioned ionomers [172]. Metallopolymers are polymers featuring additionally a metal complex (i.e., a complex consisting of a metal ion and the corresponding ligands). This secondary interaction can influence the properties significantly, and interesting features can be obtained. Thus, metallopolymers were already utilized for special optical, shape memory, or certain biomedical applications [173]. However, the design of metallopolymers is rather challenging since the metal complex as well as the rest of the polymer influences the properties, respectively. The right combination can also lead to self-healing polymers. For this purpose, two basic mechanisms are described in literature: reversible opening of the metal complex or the formation of ionic clusters in analogy to ionomers [172]. The first one is already known in solution but strongly depends on the chosen metal ion-ligand combination. The second possibility requires a phase separation within the formed polymer of the metal complexes, which are mostly charged, from the rest of the polymer. Which contribution is the predominant one depends on the special design (the metal complex, the polymer backbone, the counterion, etc.).

The first self-healing metallopolymer film was described by the groups of Weder and Rowan in 2011 [114]. For this purpose, the authors synthesized a poly(ethylene-*co*-butylene) α,ω -end functionalized with 2,6-*bis*(methylbenzimidazolyl)pyridine (Mebip) ligand. Subsequently, the ligand-containing copolymers were mixed with either zinc(II) or lanthanum(III) bistriflimide resulting in metallopolymers. The healing was studied by inducing a scratch into the polymer film and irradiation with UV light. The lighting leads to a decomplexation resulting in flexibility. However, a secondary effect of the high-power UV light was the heating of the polymer film up to 220 °C, which further enhances the mobility. Thus, a healing was obtained within seconds. The mechanical properties could be enhanced by the utilization of cellulose nanocrystals, and the obtained composite materials featured E-modulus values up to 100 MPa [115]. Another optical healable metallopolymer was reported by Wang and Urban [174]. The authors used a poly(ethylene imine) and incorporated copper(II) complexes. These complexes undergo a geometry change during lighting, resulting in a volume change and, finally, in self-healing properties.

Metallopolymers are multi-stimuli-responsive materials, and, therefore, these polymers can be addressed by several external triggers [173]. The most frequently utilized one in terms of self-healing is temperature. The first thermal-induced self-healing of metallopolymers was reported by the Schubert group in 2013 [112]. The authors synthesized different methacrylate copolymers containing terpyridine moieties in the side chain via RAFT polymerization (see Fig. 13). Crosslinking with iron (II) sulfate resulted in metallopolymers which featured self-healing depending on the chosen copolymers. Whereas copolymers based on methyl methacrylate have a too high glass transition temperature, copolymers with lauryl methacrylate show self-healing abilities at 100 °C. Furthermore, the healing mechanism was investigated using Raman spectroscopy as well as theoretical calculations revealing that the healing process is presumably based on the partial decomplexation [175].

However, the required temperatures were rather high, and a follow-up study of the same group could show that it is possible to reduce the required energy input. For

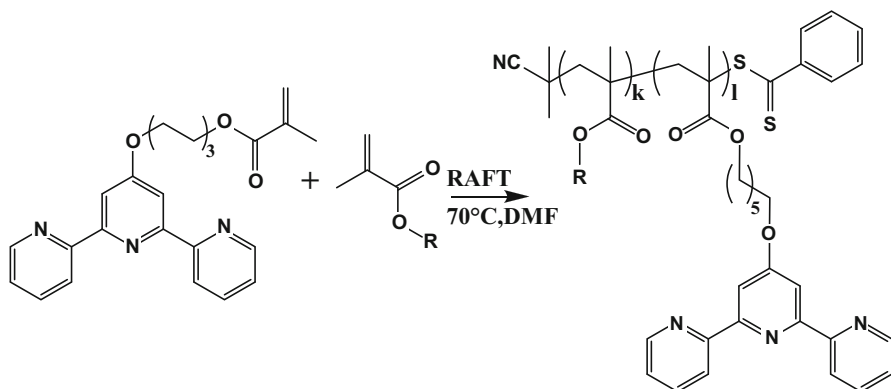


Fig. 13 Schematic representation of the synthesis of a terpyridine-containing copolymer, which can later be utilized for the complexation of different metal ions resulting in metallopolymer networks (Adapted from Ref. [113])

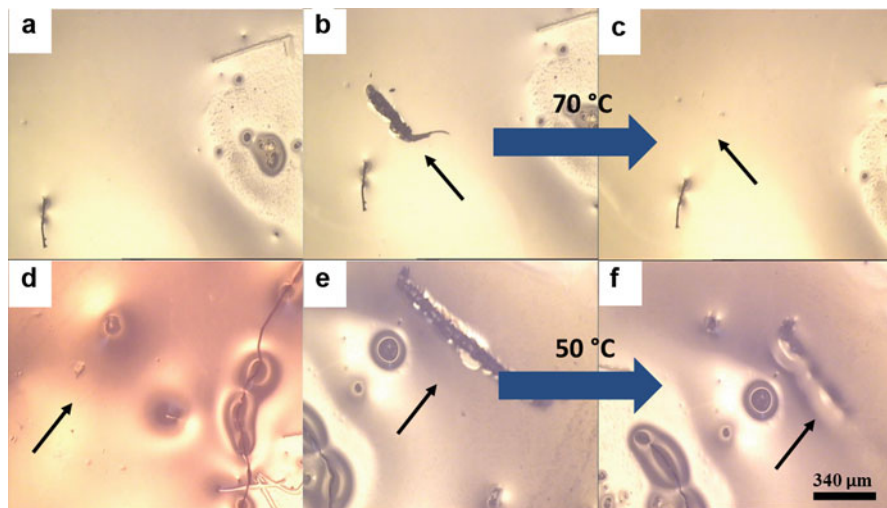


Fig. 14 Self-healing behavior of a metallopolymer network crosslinked by terpyridine-manganese (II) chloride complexes. Self-healing at 70 °C (a–c) and partial healing at 50 °C (d–f). (Reprinted with permission from Ref. [113])

this purpose, cadmium(II) acetate was used resulting in a weaker crosslinking since acetate-bridged complexes were formed [111]. Thus, healing at 70 °C within minutes was possible. Additionally, the required temperature could be further reduced to 60 °C by the utilization of manganese(II) chloride (Fig. 14) [113]. Finally, the Schubert group also presented a general predication of the healing ability of metallopolymer networks showing that rheology can be utilized as a prediction tool. If a crossover of the storage and the elastic modulus at a certain temperature is found, the material

reveals self-healing. However, the film-forming properties are also important for the healing process, and thus, in the case of brittle films, the general correlation is not useful anymore.

The results in the field of synthetic self-healing metallopolymers are promising. However, these are far away from that what nature can do. Mussel byssus threads are also able to heal mechanical damage [176]. This behavior is found under living (harsh) conditions in an ocean at low temperatures [128]. Responsible for that behavior are iron(III)-dopamine as well as zinc(II)-histidine interactions [177, 178]. These interactions lead on one hand to mechanical stiffness and furthermore to the possibility to stick on the surfaces of rocks (mostly the iron(III)-dopamine interaction is responsible for this behavior) [179, 180]. Additionally, the partly opening and the reorganization of the metal complex can lead to a self-healing in mussel byssus threads (Fig. 15) [181]. This impressive behavior was tried to mimic also with synthetic materials. However, no approach comes close to nature so far. Nevertheless, more insights in the behavior of the mussel can be obtained, which can lead to novel materials with outstanding properties in the future.

Thus, iron(III)-dopamine or zinc(II)-histidine units were incorporated into polymeric materials or hydrogels revealing in self-healing abilities [116, 182, 183]. The weak interaction between those moieties led to a healing behavior at room temperature or slightly increased temperature. Furthermore, in the case of iron(III)-dopamine, it was also possible to utilize the pH value as trigger for the self-healing since a lower pH value led to a protonation of the dopamine [183]. Similar to the zinc(II)-histidine interaction, also zinc(II)-imidazole can be utilized for such an effect [117].

Host-guest interactions are the last important class of supramolecular self-healing materials. For the preparation of such polymers, a host (typical for self-healing polymers: cyclodextrin or crown ethers) interacts with a guest, e.g., ferrocene or ammonium salts. The non-covalent interactions are reversible and can be triggered by temperature or, in the case of ferrocene, by oxidation. The reversibility is the crucial aspect for the design of self-healing materials. The pioneering work in this field was performed by Harada and coworkers [122]. The authors could successfully synthesize a cyclodextrin- and ferrocene-containing polyacrylate, which crosslinks due to the host-guest interactions. The oxidation of the obtained gel led to an opening of the interactions resulting in mobility and the ability to self-heal (Fig. 16). Besides the interaction with ferrocene, cyclodextrin can also interact with, e.g., adamantane or azobenzene [123, 184]. Additionally, the host molecule can be changed toward crown ethers, which are more responsible for ammonium salts. This interaction can be triggered by several stimuli like temperature, pH value, or chemicals (e.g., other competing ions) [118]. These special features could already be utilized for the design of self-healing materials, and further development in this area is expected.

3 Functional Polymeric Materials

Most research on self-healing materials was and is still focused on the healing/restoration of mechanical properties. In this context, several mechanisms have been developed, which provide a regeneration of the mechanical properties under specific

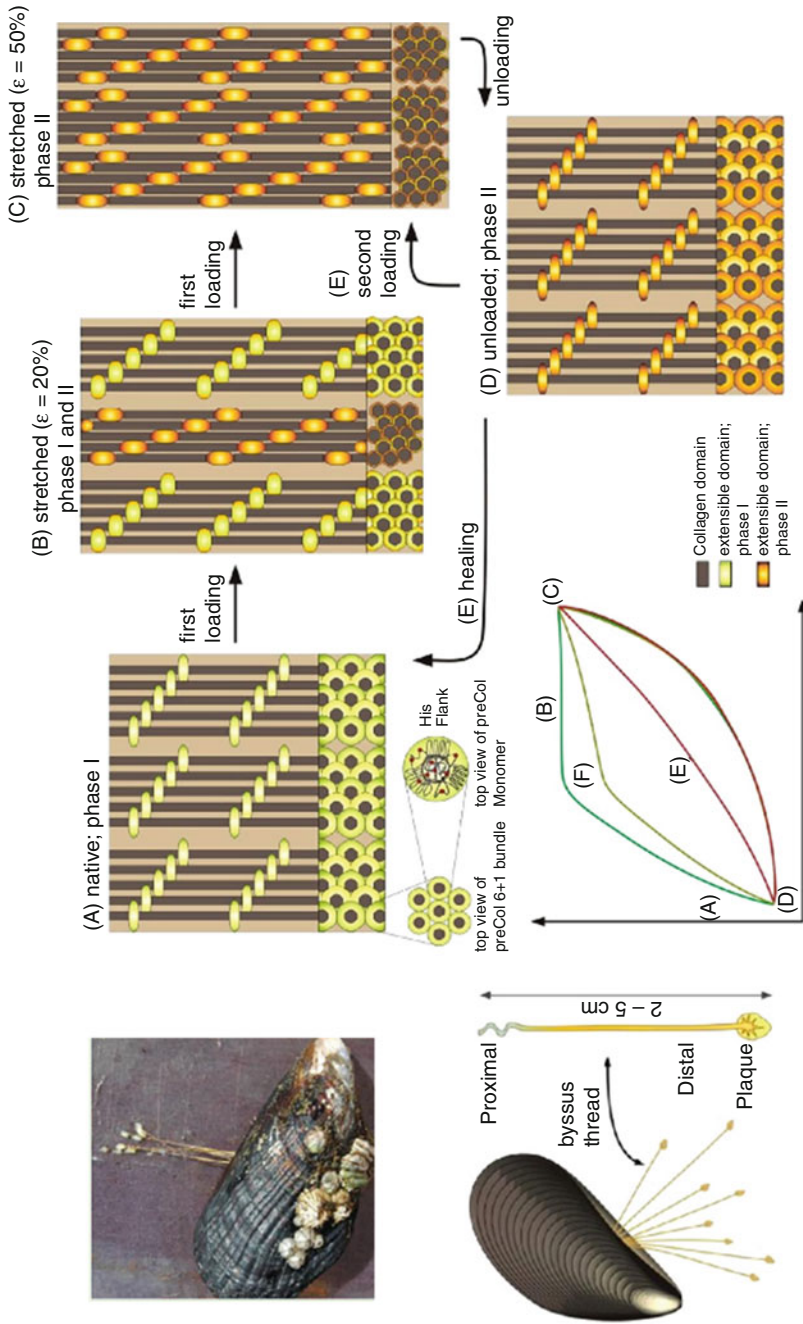


Fig. 15 Schematic representation of the healing mechanism of mussel byssus threads. (Reprinted with permission from Ref. [181])

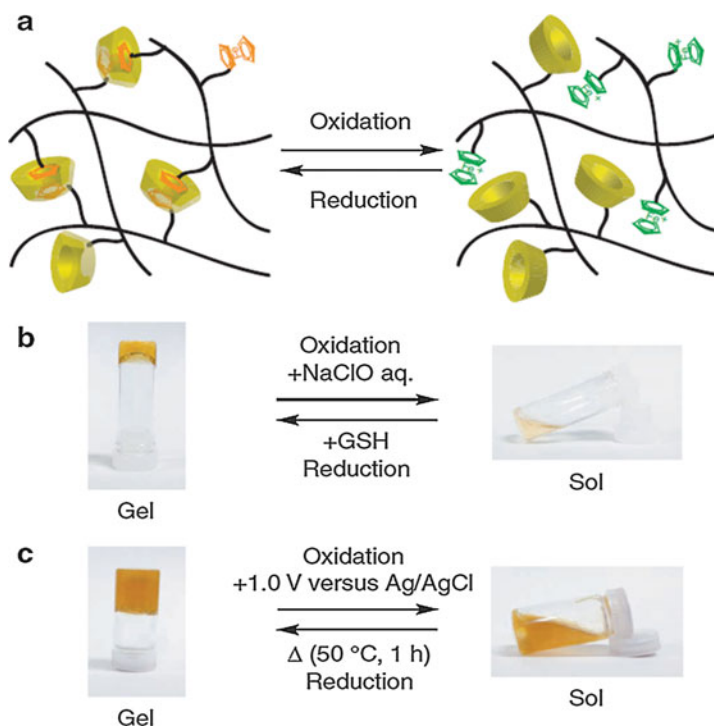


Fig. 16 Schematic representation of the self-healing healing process of polymer networks crosslinked by ferrocene-cyclodextrin interactions and the reversible opening induced by the oxidation of the ferrocene. (Reprinted with permission from Ref. [122])

conditions. Compared to nature, synthetic polymeric materials are still at the beginning of the development to multifunctional materials. Thus, nature can repair the mechanical performance as well as the function. For instance, a scratch in the human skin leads to a loss in both mechanical stability and function (e.g., as barrier against substances from the outside). After the scratch occurs, bleeding starts resulting in a closure of the crack. Up to this point, this behavior can also be found in synthetic materials. However, nature goes further and initiates a second healing step in which new skin is reformed having the same properties as before. Thus, the barrier function or the ability to sweat is reformed. This complex behavior is still influencing the research efforts in developing new materials, which feature both reparation of the mechanical performance and the regeneration of additional functions. The following paragraph will shortly demonstrate which functions can already be healed/restored in functional materials. For a more detailed description, the interested reader is referred to the literature [185].

The two most frequently investigated functions are conductivity as well as optical properties. Furthermore, it is also possible to restore special functions of coatings like superhydrophobicity.

Conductivity can be repaired in different ways, and several strategies have been developed in the past. First of all, it is possible to introduce reversible bonds into a conjugated polymer backbone. In this context, Williams et al. reported a conjugated polymer containing carbene metal complexes, which are able to be reversibly opened at higher temperatures in the presence of DMSO vapor [186]. Furthermore, the polymer featured electric conductivity comparable to silicon. However, the authors only studied the scratch healing behavior, which could be observed at higher temperature, and not the restoration of the conductivity, which has to be improved first.

Another possibility for the generation of self-healing conductors is the embedding of conductive material into a self-healing polymer. Thus, the group of Bao explored several combinations and could show the healing of the function as well as the mechanical stability by utilizing the polymer which was investigated by Leibler [95]. Firstly, the incorporation of nickel microparticles into that polymer matrix led to a material featuring a conductivity of 40 S cm^{-1} , which is a rather high value [187]. After a mechanical damage, 90% of the conductivity could be regenerated within seconds, and the complete recovery of the mechanical properties was obtained after 10 min. However, this basic principle could also be transferred into batteries. In lithium ion batteries, the main challenge is to increase the capacity. One possibility to increase the capacity of the anode is the utilization of silicon anodes. However, these electrodes are mechanically not stable due to a large volume change during charging/discharging, resulting in crack formation (see Fig. 17). However, Bao and coworkers could overcome this problem by the utilization of self-healing polymer, which holds the anode material together and enables the fabrication of a lithium ion battery with a capacity of nearly 3000 mAh g^{-1} over 20 cycles.

The third possibility to enable healing of conductivity is the utilization of the extrinsic healing concept, i.e., the encapsulation a conductive material in capsules. The first approach toward this healing strategy was presented by the

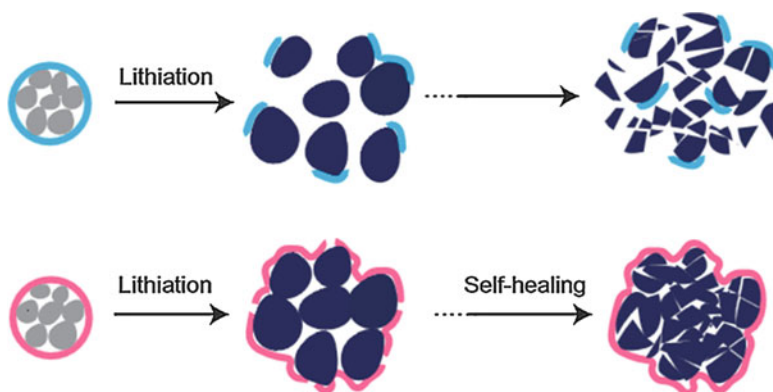


Fig. 17 Schematic representation of the self-healing property of a silicon anode compared to a normal one: Charging of the battery leads to a lithiation and to a volume change of the battery resulting in crack formation and to a total failure of the anode (above) or by the utilization of a self-healing binder (red) to a stable electrode. (Reprinted from Ref. [188])

Moore group in 2009 [189]. The authors were able to encapsulate carbon nanotubes. However, an addition of a nonpolar solvent is required in order to enhance the release. This basic principle could later be used for the reparation of silicon anodes [190]. For this purpose, carbon black as well as *o*-dichlorobenzene was incorporated into microcapsules. However, the addition of a core thickener was required leading to the restoration of the conductivity. Furthermore, it is also possible to utilize liquid metals (alloys) for this process like eutectic gallium indium [191, 192].

The healing of optical properties is still in its infancy, and only very few publications focus on the healing of optical active polymeric systems [185]. However, these properties can range from absorption to emission or in the simplest case to transparency. The latter one is a typical phenomenon known in the daily life. A clear top coating is scratched resulting in worse aesthetics due to the visible scratch. Healing of the scratch requires for certain applications (e.g., as clear top coating in cars) not only the disappearing of the scratch. Furthermore, it is required to obtain afterward again a clear coating, which has the same optical properties as before. One approach toward the solution of that problem was presented in 2011 by Braun and coworkers [193]. The authors tried to overcome scattering phenomena from the encapsulated capsules as well as from the healed polymer. For this purpose, dibutyl phthalate was encapsulated into a PMMA matrix. During crack propagation the capsules are ruptured resulting in a release of the dibutyl phthalate. Thus, a swelling is observed, which leads to healing of the crack and a regeneration of the transparency.

Furthermore, it can be possible to heal also other functions of optical active polymers like absorption or emission, which would be interesting, e.g., for solar cell applications. However, a self-healing polymer featuring this property does not exist so far. Nevertheless, first attempts were created like the utilization of a transport of fluorescent dyes through a polydimethylsiloxane matrix [194].

The last discussed function to be self-healed is the reparation of the surface properties of a polymer coating. One very impressive approach was presented from Esteves and coworkers [195–197]. The authors utilized the so-called self-replenishing of a coating. For this purpose, poly(ϵ -caprolactone) was prepared containing perfluoro-chains as well. These chains phase separate from the rest of the polymers and are moved to the top of the coating, leading to very hydrophobic properties. After the top layer of the coating is removed, the hydrophobicity is lost but is regenerated during time due to a subsequent phase separation process. This effect is schematically shown in Fig. 18.

4 Characterization of Self-Healing Polymers

The characterization of self-healing polymers represents a crucial part of the investigation of such materials. The major task is the investigation of the self-healing phenomenon itself and to quantify or at least to visualize the self-healing effect [198]. Furthermore, the material properties are of significant interest, which allow a

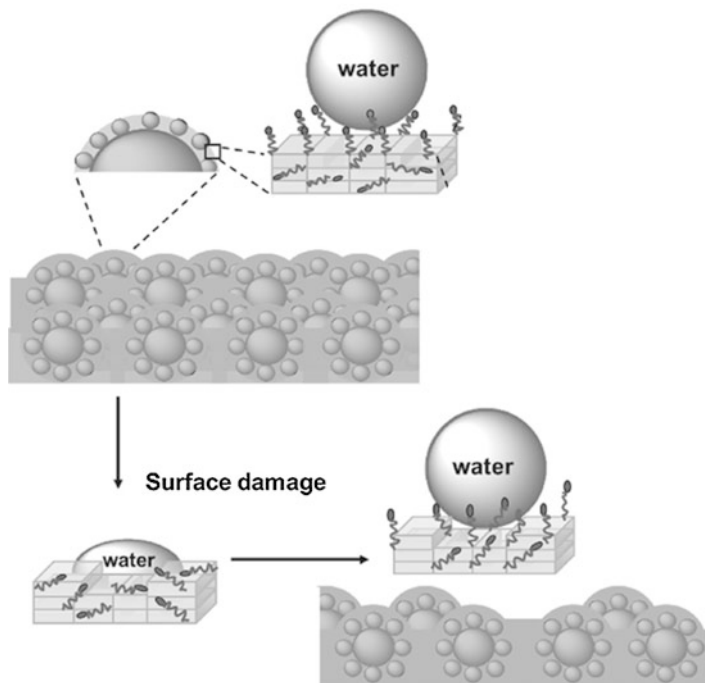


Fig. 18 Schematic representation of the self-replenishing effect of polymer coatings utilizing perfluoro-chains. (Reprinted with permission from Ref. [197])

comparison of the properties to materials without any healing ability. For this purpose, mostly standard mechanical tests are utilized. Additionally, the healing mechanism, in particular for intrinsic systems, should be studied in detail in order to analyze the molecular changes and to understand the basic principles of the self-healing process. Finally, the healing of functional materials, in which specific functions besides the mechanical properties are healed, requires the investigation of the corresponding property like conductivity (see Sect. 3). In the following part, the different methods of the investigation for self-healing processes as well as for the study of the molecular processes will be presented in detail.

The investigation of the self-healing properties can be realized by different tests. Tensile testing, tapered double cantilever beam, and scratch healing are the most common methods to analyze the healing ability. Furthermore, the healing after ballistic impact or the determination of the fracture mechanics was also utilized for this purpose [198]. However, a standardized testing of the self-healing properties is not available at the moment and has still to be developed. The problem behind the standardization of healing quantification is that the testing method strongly depends on the later application. Thus, materials, which will be utilized as coatings, should be studied via scratch healing analysis, whereas bulk material applications require the determination of the mechanical properties before and after the healing event [198].

The tensile test is the one of the most frequently utilized methods in terms of self-healing materials. The method allows the determination of the mechanical properties of the material, like E-modulus, tensile strength, or elongation at break. Furthermore, these properties can also be studied temperature-dependent. Finally, virgin and healed samples can be compared, and the healing efficiency can easily be determined. However, several parameters were utilized in the literature for the calculation of the healing efficiency. Some examples are elongation at break [199], the maximum load at failure [42, 52], or the recovery of the yield point stress [200]. The limitation of this method is the exact determination of the healing efficiency. During the healing event, the surface of the broken tensile specimen has to have contact. However, depending on the hardness of the material, this requirement is difficult to fulfill, and nonoptimal healing events take place resulting in a lower healing efficiency [198, 201]. Nevertheless, the method is widely utilized since it is easy to perform and both the healing process and the mechanical properties of the healed material can be analyzed. The method can also be applied for biological samples since threads can also be investigated by this technique. Thus, Harrington et al. studied the healing of mussel byssus threads using such testing equipment (Fig. 19) [128].

The tapered double cantilever beam (TDCB) represents another possibility to test the mechanical properties as well as the healing efficiency [202]. During the testing a load-displacement curve is generated which can also be utilized for the

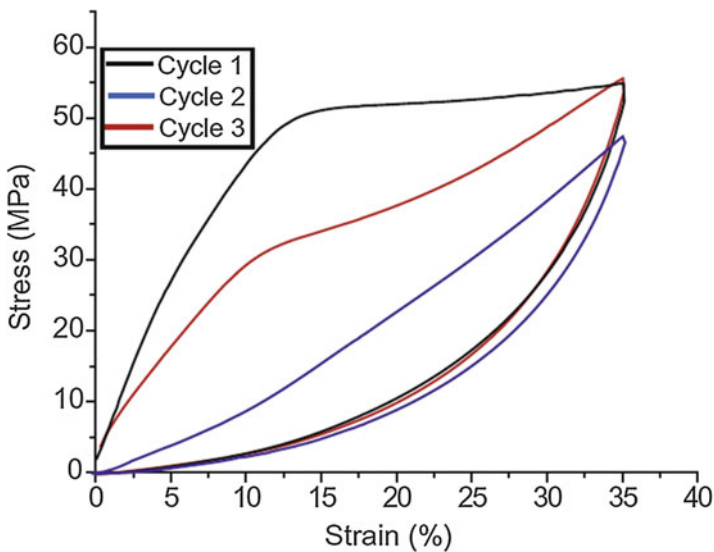


Fig. 19 Schematic representation of the healing within mussel byssus threads within three cycles of tensile testing. Cycle 1 describes the original mechanical properties, and cycle 2 was directly measured after the first cycle with no rest in between. The third cycle represents the healing of the mechanical properties of such a thread after 1 h at ambient conditions. (Reprinted with permission from Ref. [128])

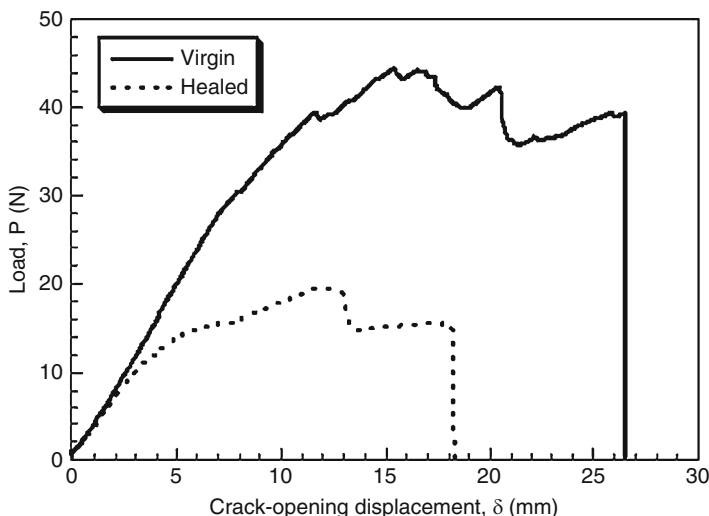


Fig. 20 Schematic representation of the data obtained by a TDCB for capsule-based healing system (dicyclopentadiene encapsulated into capsules in an epoxy resin with a Grubbs catalyst). The original material (solid black line) as well as the healed sample (dotted black line). (Reprinted with permission from Ref. [204])

determination of the healing efficiency. The fraction toughness is a useful parameter for this purpose [203]. The TDCB is mostly utilized for extrinsic self-healing systems. Thus, the capsule-based healing system (dicyclopentadiene encapsulated into capsules in an epoxy resin with a Grubbs catalyst) could be studied using this method, and typical curves revealed from this measurement are depicted in Fig. 20 [204].

A relatively similar approach compared with the TDCB is the testing of the fracture mechanics [198]. Also within this method, the crack propagation is analyzed, and healing efficiency as well as mechanical data can be obtained. However, this kind of testing is not often utilized for the determination of the healing ability of polymers although it seems to be quite promising for the investigation of soft materials [201, 205].

A completely different method for the analysis of the self-healing behavior is the utilization of the scratch healing tests. In this case, no mechanical properties will be analyzed and will also not be utilized for the determination of any kind of efficiency. This testing method focuses more on the ability of the material to close scratches on a surface and is of particular interest for materials utilized later as coating [198]. However, most of the publications simply utilize the optical imaging of the scratch as well as analyze the presence and disappearance of a scratch during healing. This method can just be utilized to show the general healing ability of newly developed system; quantification is not possible. For this purpose, a 3D imaging of the crack is required, which allow the determination of the crack volume, the healing speed, as well as the percentage of healed volume (corresponding to a kind of healing efficiency). Thus,

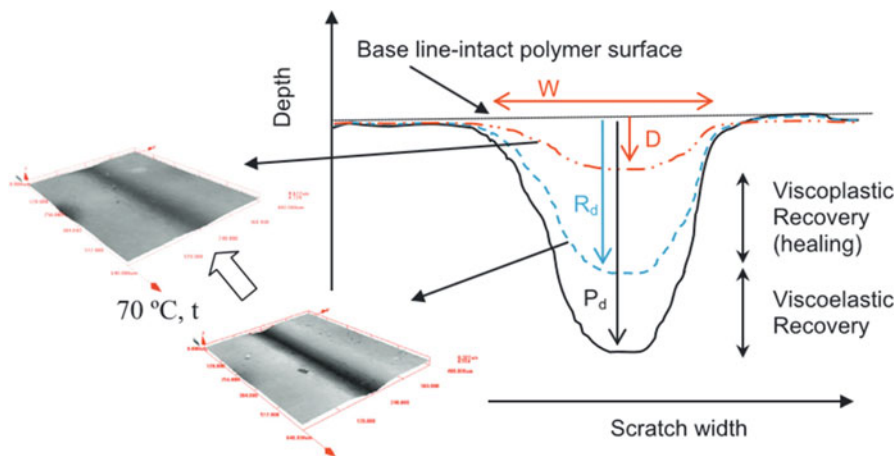


Fig. 21 Schematic representation of the quantification of the scratch healing behavior by the analysis of the residual volume of the scratch. (Reprinted with permission from Ref. [206])

also kinetic studies of the healing process itself would be possible. Such a system was developed by Garcia and coworkers [206]. This procedure requires the utilization of an indenter in order to induce defined cracks, which can later be utilized for the healing studies. Furthermore, the volume is measured using a confocal microscope, and the sample is placed on a heating stage, which enables the simulation of the required healing circumstances (Fig. 21). During the time the scratch is closed as well as the residual volume can be measured and be utilized for the analysis of the healing kinetics and the determination of the healing efficiency. This method was already used for different polymeric systems like ionomer [206], Diels-Alder crosslinked copolymers [57], tetrasulfide [78], or acylhydrazone-based networks [68].

Besides the investigation of the self-healing behavior itself, the characterization of the molecular processes, which enables this phenomenon, is a general important topic [198]. In particular, the behavior in the solid state is of great interest and cannot be simply transferred from solution investigations. Therefore, certain techniques are available which allow the analysis of the materials under healing conditions. The most efficient testing methods seem to be spectroscopic analysis like IR and Raman spectroscopy [198]. Both techniques were already utilized for such investigations, e.g., Raman spectroscopy was used for the analysis of the self-healing mechanism of metallopolymers [175]. The advantage with this kind of analysis is the specific study of molecular fragments which are responsible for the healing process. Thus, Bose et al. were able to follow the Diels-Alder units during thermal treatment and could show the opening of the Diels-Alder adduct at higher temperature [57]. This process is responsible for the generation of a mobile phase and finally for the healing process itself.

Both techniques are the most utilized methods for the understanding of the molecular dynamics. Furthermore, solid-state NMR [111] or scattering techniques

like small angle X-ray scattering (SAXS) can be utilized to determine the behavior in the solid state [112]. Recently, a new method for the investigation of the self-healing phenomenon was presented by Garcia and coworkers [207]. The authors utilized broad dielectric spectroscopy in order to evaluate the flow behavior of the material.

5 Comparison with Other Material Classes

Self-healing materials are by far not limited to polymeric materials. Also other material classes have been investigated within this context. However, polymers are still the by far most studied self-healing material class. This fact can be related to the wide variety of different polymers available as well as the “easier” access to self-healing properties for polymeric materials compared to other systems. Considering the general mechanism, a mobile phase has to be generated. Within a typical polymeric material, the mobility can be provided by (liquid) healing agents as well as by elevated temperatures (ca. 100 °C). Metals as well as ceramics require much higher temperatures (close to 1000 °C) [17]. Particularly the former material class features another intrinsic drawback: The mobile species will be atoms compared to large polymer chains or segments.

Nevertheless, comparable approaches have been investigated for the other material classes. Self-healing metals are still the least studied material class [208]. One approach utilizes the precipitation of hard materials in growing voids (e.g., boron nitride). Similar to metals, most of the approaches for the healing of self-healing ceramics are based on high temperature processes [209]. Comparable to the above described encapsulation of healing agents, also oxidizable compounds (e.g., SiC, TiC) have been encapsulated within ceramics [210, 211]. A crack can be closed by heating resulting in the oxidation of the healing filler material resulting in the formation of an oxide, which closes finally the crack. Moreover, a special ceramic material, MAX phases, has been investigated. These materials can also form oxides upon heating resulting in a healing process [212–214]. Interestingly, concrete materials feature a similarly broad spectrum of different approaches for self-healing properties like polymers. The applied mechanisms range from the encapsulation, the design of damage-tolerant concretes combined with the “natural” ability of concrete for healing, to the encapsulation of bacteria, which can close the crack by precipitation of minerals [215–218].

6 Commercial Systems

The previous illustration of the wide variety of different self-healing polymeric materials sets expectations for further industrial/commercial applications of these materials. The field of smart polymers, particularly self-healing polymers, will strongly grow in the next years resulting in a market volume of 2.7 billion \$ in 2020 [219].

However, not only the offered possibilities as well as the large versatility will determine the success of self-healing polymers, the “real” demands considering the corresponding applications will decide on the success. There are still some challenges to be solved to enable a commercial application of self-healing polymers:

- **Costs** – Many approaches are not based on the common commercial monomers as well as basic chemicals, resulting in higher costs of the resulting polymers. There is still a debate how much more expensive a self-healing material can be compared to the financial benefit which arises from the healing ability. For instance, the double lifetime of a self-healing polymer does not necessarily mean that the double price will be accepted. In fact, in certain application areas, the self-healing ability would be considered as additional asset of the next generation, which should come to the same (or even) lower price. Therefore it is not surprising that the current research on self-healing materials was mainly focused on areas which are not prize sensitive, i.e., aerospace and military.
- **Long-term stability/lifetime** – Many research studies show that the healing is possible multiple times. However, the calendrical lifetime is mostly neglected. Will the material still heal after 5 years?
- **Real-life applications** – The section on the characterization of self-healing polymers illustrated the importance for the selection of the right test/characterization method. Within the scientific community, there is a quest for more standardized test in order to enable a comparison of the performance of different materials. However, real-life applications would require a testing under the specific parameters.
- **Acceptance** – Interestingly, the field of self-healing polymers is easily comprehensible to the general public, e.g., terminology inspired by science fiction: terminator polymers [220]. Nevertheless, the fact that a (totally) new material was developed might hamper the application in more conservative industrial sectors.
- **Material properties** – Admittedly, many of the above described examples do not feature material properties relevant to typical applications. Future developments are required to achieve self-healing polymers with usable properties. Particularly, the supramolecular systems (as well as the highly reversible polymers) might feature an inherent disadvantage. The materials will show creep under load.
- **Need** – In the last years, polymeric materials have developed from *plastics* – sometimes synonymous used for material inferior quality – to high performance materials challenging other material class. For instance, the new generations of airplanes consist of >50% polymer composites as structural parts. Polymers have superseded metals. Considering the possibilities already offered by polymers as well as polymer composites, self-healing might currently be degenerated to a nice add-on instead of being a real asset. However, with a broadened view, self-healing is one aspect of smart materials. Different other properties as well as abilities (e.g., stimuli-responsiveness, shape memory, adaptive materials) will be inherent in the next generation of the materials we use.

Several of the above described general principles have been already utilized in commercial systems – extrinsic as well as intrinsic self-healing polymers have been

utilized. The prime example, i.e., the capsule-based approach, has been commercialized by a company providing solutions for thermosets, coatings, as well as elastomers [221]. Hydrogen bonding self-healing polymers are offered by two companies: Arkema [222] as well as Suprapolix [223]. Another commercial supramolecular polymer is the ionomer Surlyn. The healing capability after ballistic impact is utilized in self-healing targets at shooting grounds [224].

The most common approach for commercial systems is self-healing polyurethane coatings, which are based on a network with a relatively low glass transition temperature. A scratch in the coating can be healed at elevated temperatures (e.g., warming by sunlight) due to the reflow of the material (see Fig. 22). These systems have been commercialized by several companies, including Covestro (formerly Bayer Material Science), Nissan, as well as Rühl. Besides the application as car coating, also the interior of cars (e.g., wooden steering wheel) is covered with this self-healing coating [225].

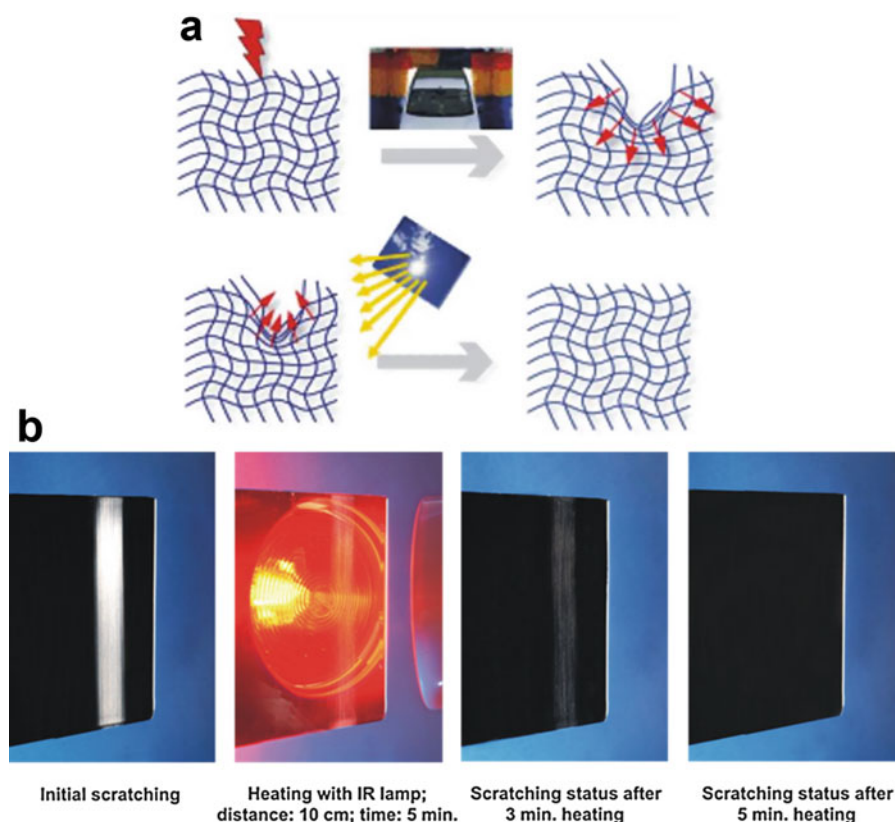


Fig. 22 Schematic representation of self-healing polyurethane coating. (a) Damage of the polymer network leads to deformation and gentle heating the restoration of the network. (b) Initial scratch is vanishing within few minutes. (Reprinted with permission of Covestro)

7 Conclusion and Outlook

Fifteen years ago, self-healing was introduced as a bioinspired research theme. Since this time, researchers aimed for the design of novel materials which feature this outstanding property. However, the comparison between natural and synthetic polymeric materials still is in strong favor for the biological systems; nature had several million years to perfect these materials. Nevertheless several new approaches have been studied in the last decade, and one can expect that the development will continue on a high level.

However, still some important challenges have to be solved. First of all the typical problems of both approaches (extrinsic and intrinsic) are in the main focus. Thus, the extrinsic systems will be developed toward longer stability against cracks enabling more healing cycles. For this purpose, the vascular networks will be of particular interest. However, a continuous flow of the healing agents even after several cracks has to be obtained. On the other hand, the intrinsic systems must be improved toward better mechanical properties. As it can be seen in Table 1, the most intrinsic self-healable materials feature poor mechanical properties with very low E-modulus values. Only the covalent systems based on the Diels-Alder reaction reported by Wudl and coworkers resulted in high moduli [51, 52]. Thus, the intrinsic systems and, in particular, the supramolecular materials have to focus on the combination of high mechanical stability and excellent self-healing properties.

Furthermore, the development toward multifunctional self-healing systems will be a major trend in the next years. Thus, the healing of functions and not only of the mechanical properties will be advanced. Additionally, the combination of both seems to be very promising, and some first results show the high potential of this research topic [185]. Nevertheless, the healing of specific functions is still in its beginning, and new general approaches will be studied in order to go the next steps to self-healing materials.

The development of new materials goes hand in hand with their characterization. However, a standard technique for the investigation of the self-healing phenomenon is still not available, and each material is tested differently [198]. Thus, it is hard to compare different types of polymers in terms of their ability to heal, but also regarding their mechanical properties. Nevertheless, the characterization has to be also suitable for the later application. For instance, the utilization as coating requires scratch healing, whereas bulk healing must be tested by tensile measurements. Therefore, the standardization of the characterization is required and further techniques must be developed.

The next years will provide more self-healing materials, which are based on their natural archetypes. Nature can still provide plenty of inspiration [226].

Acknowledgments The authors thank the Deutsche Forschungsgemeinschaft (DFG, SPP 1568) for financial support.

References

1. K. Liu, J. Du, J. Wu, L. Jiang, Superhydrophobic gecko feet with high adhesive forces towards water and their bio-inspired materials. *Nanoscale* **4**(3), 768–772 (2012). <https://doi.org/10.1039/C1NR11369K>
2. N. Du, X.Y. Liu, J. Narayanan, L. Li, M.L.M. Lim, D. Li, Design of superior spider silk: from nanostructure to mechanical properties. *Biophys. J.* **91**(12), 4528–4535 (2006). <https://doi.org/10.1529/biophysj.106.089144>
3. U.G.K. Wegst, H. Bai, E. Saiz, A.P. Tomsia, R.O. Ritchie, Bioinspired structural materials. *Nat. Mater.* **14**(1), 23–36 (2015). <https://doi.org/10.1038/nmat4089>
4. P. Fratzl, Biomimetic materials research: what can we really learn from nature's structural materials? *J. R. Soc. Interface* **4**(15), 637–642 (2007). <https://doi.org/10.1098/rsif.2007.0218>
5. B. Bhushan, Biomimetics: lessons from nature—an overview. *Philos. Trans. R. Soc. A* **367**(1893), 1445–1486 (2009). <https://doi.org/10.1098/rsta.2009.0011>
6. P.H. Jørgensen, C. Bang, T.T. Andreassen, Mechanical properties of skin graft wounds. *Brit J Plast Surg* **46**(7), 565–569 (1993). [https://doi.org/10.1016/0007-1226\(93\)90106-L](https://doi.org/10.1016/0007-1226(93)90106-L)
7. B. McKibbin, Biology of fracture healing in long bones. *J. Bone Joint Surg. Brit.* **60**, 150–162 (1978)
8. B.A. Uthgenannt, M.H. Kramer, J.A. Hwu, B. Wopenka, M.J. Silva, Skeletal self-repair: stress fracture healing by rapid formation and densification of woven bone. *J. Bone Miner. Res.* **22**(10), 1548–1556 (2007). <https://doi.org/10.1359/jbmr.0070614>
9. Z. Rapti, A. Smerzi, K.Ø. Rasmussen, A.R. Bishop, C.H. Choi, A. Usheva, Healing length and bubble formation in DNA. *Phys. Rev. E* **73**(5), 051902 (2006)
10. J. Komenda, F. Michoux, P.J. Nixon, Keeping the green world alive: the repair cycle, in *Self-Healing at the Nanoscale*, ed. by V. Amendola, M. Meneghetti (Taylor & Francis Group, Boca Raton, 2012), pp. 3–22
11. M. Kragl, D. Knapp, E. Nacu, S. Khattak, M. Maden, H.H. Epperlein, E.M. Tanaka, Cells keep a memory of their tissue origin during axolotl limb regeneration. *Nature* **460**(7251), 60–65 (2009). <https://doi.org/10.1038/nature08152>
12. M.R.J. Carlson, S.V. Bryant, D.M. Gardiner, Expression of Msx-2 during development, regeneration, and wound healing in axolotl limbs. *J. Exp. Zool.* **282**(6), 715–723 (1998). [https://doi.org/10.1002/\(SICI\)1097-010X\(19981215\)282:6<715::AID-JEZ7>3.0.CO;2-F](https://doi.org/10.1002/(SICI)1097-010X(19981215)282:6<715::AID-JEZ7>3.0.CO;2-F)
13. R.S. Trask, H.R. Williams, I.P. Bond, Self-healing polymer composites: mimicking nature to enhance performance. *Bioinspir. Biomim.* **2**(1), P1 (2007)
14. X. Yin, Z. Liu, D. Wang, X. Pei, B. Yu, F. Zhou, Bioinspired self-healing organic materials: chemical mechanisms and fabrications. *J. Bionic. Eng.* **12**(1), 1–16 (2015). [https://doi.org/10.1016/S1672-6529\(14\)60095-0](https://doi.org/10.1016/S1672-6529(14)60095-0)
15. S. van der Zwaag, N.H. van Dijk, H.M. Jonkers, S.D. Mookhoek, W.G. Sloof, Self-healing behaviour in man-made engineering materials: bioinspired but taking into account their intrinsic character. *Philos. Trans. R. Soc. A* **367**(1894), 1689–1704 (2009). <https://doi.org/10.1098/rsta.2009.0020>
16. C.J. Norris, G.J. Meadway, M.J. O'Sullivan, I.P. Bond, R.S. Trask, Self-healing fibre reinforced composites via a bioinspired vasculature. *Adv. Funct. Mater.* **21**(19), 3624–3633 (2011). <https://doi.org/10.1002/adfm.201101100>
17. M.D. Hager, P. Greil, C. Leyens, S. van der Zwaag, U.S. Schubert, Self-healing materials. *Adv. Mater.* **22**(47), 5424–5430 (2010). <https://doi.org/10.1002/adma.201003036>
18. S.J. Garcia, H.R. Fischer, S. van der Zwaag, A critical appraisal of the potential of self healing polymeric coatings. *Prog. Org. Coat.* **72**(3), 211–221 (2011). <https://doi.org/10.1016/j.porgcoat.2011.06.016>
19. S. Billiet, X.K.D. Hillewaere, R.F.A. Teixeira, F.E. Du Prez, Chemistry of crosslinking processes for self-healing polymers. *Macromol. Rapid Commun.* **34**(4), 290–309 (2013). <https://doi.org/10.1002/marc.201200689>

20. X.K.D. Hillewaere, F.E. Du Prez, Fifteen chemistries for autonomous external self-healing polymers and composites. *Prog. Polym. Sci.* **49–50**, 121–153 (2015). <https://doi.org/10.1016/j.progpolymsci.2015.04.004>
21. S.J. Garcia, Effect of polymer architecture on the intrinsic self-healing character of polymers. *Eur. Polym. J.* **53**, 118–125 (2014). <https://doi.org/10.1016/j.eurpolymj.2014.01.026>
22. S.R. White, N.R. Sottos, P.H. Geubelle, J.S. Moore, M.R. Kessler, S.R. Sriram, E.N. Brown, S. Viswanathan, Autonomic healing of polymer composites. *Nature* **409**(6822), 794–797 (2001). <https://doi.org/10.1038/35057232>
23. M.D. Chipara, M. Chipara, E. Shansky, J.M. Zaleski, Self-healing of high elasticity block copolymers. *Polym. Adv. Technol.* **20**(4), 427–431 (2009). <https://doi.org/10.1002/pat.1296>
24. C.L. Mangun, A.C. Mader, N.R. Sottos, S.R. White, Self-healing of a high temperature cured epoxy using poly(dimethylsiloxane) chemistry. *Polymer* **51**(18), 4063–4068 (2010). <https://doi.org/10.1016/j.polymer.2010.06.050>
25. S.H. Cho, H.M. Andersson, S.R. White, N.R. Sottos, P.V. Braun, Polydimethylsiloxane-based self-healing materials. *Adv. Mater.* **18**(8), 997–1000 (2006). <https://doi.org/10.1002/adma.200501814>
26. M.W. Keller, S.R. White, N.R. Sottos, A self-healing poly(dimethyl siloxane) elastomer. *Adv. Funct. Mater.* **17**(14), 2399–2404 (2007). <https://doi.org/10.1002/adfm.200700086>
27. M.W. Keller, S.R. White, N.R. Sottos, Torsion fatigue response of self-healing poly(dimethylsiloxane) elastomers. *Polymer* **49**(13–14), 3136–3145 (2008). <https://doi.org/10.1016/j.polymer.2008.04.041>
28. Y. Tao, Z. Lin, R. Min Zhi, Z. Ming Qiu, Self-healing woven glass fabric/epoxy composites with the healant consisting of micro-encapsulated epoxy and latent curing agent. *Smart Mater. Struct.* **17**(1), 015019 (2008)
29. T.S. Coope, U.F.J. Mayer, D.F. Wass, R.S. Trask, I.P. Bond, Self-healing of an epoxy resin using scandium(III) triflate as a catalytic curing agent. *Adv. Funct. Mater.* **21**(24), 4624–4631 (2011). <https://doi.org/10.1002/adfm.201101660>
30. C.J. Hansen, S.R. White, N.R. Sottos, J.A. Lewis, Accelerated self-healing via ternary interpenetrating microvascular networks. *Adv. Funct. Mater.* **21**(22), 4320–4326 (2011). <https://doi.org/10.1002/adfm.201101553>
31. K.S. Toohey, C.J. Hansen, J.A. Lewis, S.R. White, N.R. Sottos, Delivery of two-part self-healing chemistry via microvascular networks. *Adv. Funct. Mater.* **19**(9), 1399–1405 (2009). <https://doi.org/10.1002/adfm.200801824>
32. C.J. Hansen, W. Wu, K.S. Toohey, N.R. Sottos, S.R. White, J.A. Lewis, Self-healing materials with interpenetrating microvascular networks. *Adv. Mater.* **21**(41), 4143–4147 (2009). <https://doi.org/10.1002/adma.200900588>
33. Y.C. Yuan, X.J. Ye, M.Z. Rong, M.Q. Zhang, G.C. Yang, J.Q. Zhao, Self-healing epoxy composite with heat-resistant healant. *ACS Appl. Mater. Interfaces* **3**(11), 4487–4495 (2011). <https://doi.org/10.1021/am201182j>
34. Y. Yan Chao, Y. Yueping, R. Min Zhi, C. Haibin, W. Jingshen, Z. Ming Qiu, Q. Shi Xiang, Y. Gui Cheng, Self-healing of low-velocity impact damage in glass fabric/epoxy composites using an epoxy–mercaptan healing agent. *Smart Mater. Struct.* **20**(1), 015024 (2011)
35. Y.C. Yuan, M.Z. Rong, M.Q. Zhang, G.C. Yang, Study of factors related to performance improvement of self-healing epoxy based on dual encapsulated healant. *Polymer* **50**(24), 5771–5781 (2009). <https://doi.org/10.1016/j.polymer.2009.10.019>
36. Y.C. Yuan, M.Z. Rong, M.Q. Zhang, J. Chen, G.C. Yang, X.M. Li, Self-healing polymeric materials using epoxy/mercaptan as the healant. *Macromolecules* **41**(14), 5197–5202 (2008). <https://doi.org/10.1021/ma800028d>
37. S. Billiet, W. Van Camp, X.K.D. Hillewaere, H. Rahier, F.E. Du Prez, Development of optimized autonomous self-healing systems for epoxy materials based on maleimide chemistry. *Polymer* **53**(12), 2320–2326 (2012). <https://doi.org/10.1016/j.polymer.2012.03.061>
38. X.K.D. Hillewaere, R.F.A. Teixeira, L.-T.T. Nguyen, J.A. Ramos, H. Rahier, F.E. Du Prez, Autonomous self-healing of epoxy thermosets with thiol-isocyanate chemistry. *Adv. Funct. Mater.* **24**(35), 5575–5583 (2014). <https://doi.org/10.1002/adfm.201400580>

39. M. Gragert, M. Schunack, W.H. Binder, Azide/alkyne-“click”-reactions of encapsulated reagents: toward self-healing materials. *Macromol. Rapid Commun.* **32**(5), 419–425 (2011). <https://doi.org/10.1002/marc.201000687>
40. S.R. White, J.S. Moore, N.R. Sottos, B.P. Krull, W.A. Santa Cruz, R.C.R. Gergely, Restoration of large damage volumes in polymers. *Science* **344**(6184), 620–623 (2014). <https://doi.org/10.1126/science.1251135>
41. L.M. Meng, Y.C. Yuan, M.Z. Rong, M.Q. Zhang, A dual mechanism single-component self-healing strategy for polymers. *J. Mater. Chem.* **20**(29), 6030–6038 (2010). <https://doi.org/10.1039/C0JM00268B>
42. A.M. Peterson, R.E. Jensen, G.R. Palmese, Room-temperature healing of a thermosetting polymer using the Diels–Alder reaction. *ACS Appl. Mater. Interfaces* **2**(4), 1141–1149 (2010). <https://doi.org/10.1021/am9009378>
43. P.A. Pratama, M. Sharifi, A.M. Peterson, G.R. Palmese, Room temperature self-healing thermoset based on the Diels–Alder reaction. *ACS Appl. Mater. Interfaces* **5**(23), 12425–12431 (2013). <https://doi.org/10.1021/am403459e>
44. P.A. Pratama, A.M. Peterson, G.R. Palmese, The role of maleimide structure in the healing of furan-functionalized epoxy-amine thermosets. *Polym. Chem.* **4**(18), 5000–5006 (2013). <https://doi.org/10.1039/C3PY00084B>
45. N.W. Khun, D.W. Sun, M.X. Huang, J.L. Yang, C.Y. Yue, Wear resistant epoxy composites with diisocyanate-based self-healing functionality. *Wear* **313**(1–2), 19–28 (2014). <https://doi.org/10.1016/j.wear.2014.02.011>
46. J.F. Patrick, N.R. Sottos, S.R. White, Microvascular based self-healing polymeric foam. *Polymer* **53**(19), 4231–4240 (2012). <https://doi.org/10.1016/j.polymer.2012.07.021>
47. S.M. Bleay, C.B. Loader, V.J. Hawyes, L. Humberstone, P.T. Curtis, A smart repair system for polymer matrix composites. *Compos. A: Appl. Sci. Manufact.* **32**(12), 1767–1776 (2001). [https://doi.org/10.1016/S1359-835X\(01\)00020-3](https://doi.org/10.1016/S1359-835X(01)00020-3)
48. F. Omosola, R. Kevin, B. Biswajit, Glass fibre polyester composite with in vivo vascular channel for use in self-healing. *Smart Mater. Struct.* **23**(9), 095017 (2014)
49. M. Motuku, U.K. Vaidya, G.M. Janowski, Parametric studies on self-repairing approaches for resin infused composites subjected to low velocity impact. *Smart Mater. Struct.* **8**(5), 623 (1999)
50. S. Zainuddin, T. Arefin, A. Fahim, M.V. Hosur, J.D. Tyson, A. Kumar, J. Trovillion, S. Jeelani, Recovery and improvement in low-velocity impact properties of e-glass/epoxy composites through novel self-healing technique. *Compos. Struct.* **108**, 277–286 (2014). <https://doi.org/10.1016/j.compstruct.2013.09.023>
51. X. Chen, F. Wudl, A.K. Mal, H. Shen, S.R. Nutt, New thermally remendable highly cross-linked polymeric materials. *Macromolecules* **36**(6), 1802–1807 (2003). <https://doi.org/10.1021/ma0210675>
52. X. Chen, M.A. Dam, K. Ono, A. Mal, H. Shen, S.R. Nutt, K. Sheran, F. Wudl, A thermally re-mendable cross-linked polymeric material. *Science* **295**(5560), 1698–1702 (2002). <https://doi.org/10.1126/science.1065879>
53. N. Bai, K. Saito, G.P. Simon, Synthesis of a diamine cross-linker containing Diels–Alder adducts to produce self-healing thermosetting epoxy polymer from a widely used epoxy monomer. *Polym. Chem.* **4**(3), 724–730 (2013). <https://doi.org/10.1039/C2PY20611K>
54. P. Du, M. Wu, X. Liu, Z. Zheng, X. Wang, T. Joncheray, Y. Zhang, Diels–Alder-based crosslinked self-healing polyurethane/urea from polymeric methylene diphenyl diisocyanate. *J. Appl. Polym. Sci.* **131**(9) (2014). <https://doi.org/10.1002/app.40234>
55. P. Du, X. Liu, Z. Zheng, X. Wang, T. Joncheray, Y. Zhang, Synthesis and characterization of linear self-healing polyurethane based on thermally reversible Diels–Alder reaction. *RSC Adv.* **3**(35), 15475–15482 (2013). <https://doi.org/10.1039/C3RA42278J>
56. M.J. Barthel, T. Rudolph, A. Teichler, R.M. Paulus, J. Vitz, S. Hoepfner, M.D. Hager, F.H. Schacher, U.S. Schubert, Self-healing materials via reversible crosslinking of poly(ethylene oxide)-block-poly(furfuryl glycidyl ether) (PEO-b-PFGE) block copolymer films. *Adv. Funct. Mater.* **23**(39), 4921–4932 (2013). <https://doi.org/10.1002/adfm.201300469>

57. R.K. Bose, J. Kötteritzsch, S.J. Garcia, M.D. Hager, U.S. Schubert, S. van der Zwaag, A rheological and spectroscopic study on the kinetics of self-healing in a single-component diels–alder copolymer and its underlying chemical reaction. *J. Polym. Sci. Part A: Polym. Chem.* **52**(12), 1669–1675 (2014). <https://doi.org/10.1002/pola.27164>
58. J. Kötteritzsch, M.D. Hager, U.S. Schubert, Tuning the self-healing behavior of one-component intrinsic polymers. *Polymer* **69**, 321–329 (2015). <https://doi.org/10.1016/j.polymer.2015.03.027>
59. J. Kötteritzsch, S. Stumpf, S. Hoepfener, J. Vitz, M.D. Hager, U.S. Schubert, One-component intrinsic self-healing coatings based on reversible crosslinking by Diels–Alder cycloadditions. *Macromol. Chem. Phys.* **214**(14), 1636–1649 (2013). <https://doi.org/10.1002/macp.201200712>
60. N. Yoshie, S. Saito, N. Oya, A thermally-stable self-mending polymer networked by Diels–Alder cycloaddition. *Polymer* **52**(26), 6074–6079 (2011). <https://doi.org/10.1016/j.polymer.2011.11.007>
61. E.B. Murphy, E. Bolanos, C. Schaffner-Hamann, F. Wudl, S.R. Nutt, M.L. Auad, Synthesis and characterization of a single-component thermally remendable polymer network: staudinger and Stille revisited. *Macromolecules* **41**(14), 5203–5209 (2008). <https://doi.org/10.1021/ma800432g>
62. P. Reutenauer, E. Buhler, P.J. Boul, S.J. Candau, J.M. Lehn, Room temperature dynamic polymers based on Diels–Alder chemistry. *Chem. Eur. J.* **15**(8), 1893–1900 (2009). <https://doi.org/10.1002/chem.200802145>
63. K.K. Oehlenschlaeger, J.O. Mueller, J. Brandt, S. Hilf, A. Lederer, M. Wilhelm, R. Graf, M.L. Coote, F.G. Schmidt, C. Barner-Kowollik, Adaptable hetero Diels–Alder networks for fast self-healing under mild conditions. *Adv. Mater.* **26**(21), 3561–3566 (2014). <https://doi.org/10.1002/adma.201306258>
64. J. Ling, M.Z. Rong, M.Q. Zhang, Coumarin imparts repeated photochemical remendability to polyurethane. *J. Mater. Chem.* **21**(45), 18373–18380 (2011). <https://doi.org/10.1039/C1JM13467A>
65. J. Ling, M.Z. Rong, M.Q. Zhang, Photo-stimulated self-healing polyurethane containing dihydroxyl coumarin derivatives. *Polymer* **53**(13), 2691–2698 (2012). <https://doi.org/10.1016/j.polymer.2012.04.016>
66. C.-M. Chung, Y.-S. Roh, S.-Y. Cho, J.-G. Kim, Crack healing in polymeric materials via photochemical [2+2] cycloaddition. *Chem. Mater.* **16**(21), 3982–3984 (2004). <https://doi.org/10.1021/cm049394+>
67. P. Froimowicz, H. Frey, K. Landfester, Towards the generation of self-healing materials by means of a reversible photo-induced approach. *Macromol. Rapid Commun.* **32**(5), 468–473 (2011). <https://doi.org/10.1002/marc.201000643>
68. N. Kuhl, S. Bode, R.K. Bose, J. Vitz, A. Seifert, S. Hoepfener, S.J. Garcia, S. Spange, S. van der Zwaag, M.D. Hager, U.S. Schubert, Acylhydrazones as reversible covalent crosslinkers for self-healing polymers. *Adv. Funct. Mater.* **25**(22), 3295–3301 (2015). <https://doi.org/10.1002/adfm.201501117>
69. H. Li, J. Bai, Z. Shi, J. Yin, Environmental friendly polymers based on schiff-base reaction with self-healing, remolding and degradable ability. *Polymer* **85**, 106–113 (2016). <https://doi.org/10.1016/j.polymer.2016.01.050>
70. J. Canadell, H. Goossens, B. Klumperman, Self-healing materials based on disulfide links. *Macromolecules* **44**(8), 2536–2541 (2011). <https://doi.org/10.1021/ma2001492>
71. M. Pepels, I. Pilot, B. Klumperman, H. Goossens, Self-healing systems based on disulfide-thiol exchange reactions. *Polym. Chem.* **4**(18), 4955–4965 (2013). <https://doi.org/10.1039/C3PY00087G>
72. U. Lafont, H. van Zeijl, S. van der Zwaag, Influence of cross-linkers on the cohesive and adhesive self-healing ability of polysulfide-based thermosets. *ACS Appl. Mater. Interfaces* **4**(11), 6280–6288 (2012). <https://doi.org/10.1021/am301879z>
73. Z.Q. Lei, H.P. Xiang, Y.J. Yuan, M.Z. Rong, M.Q. Zhang, Room-temperature self-healable and remoldable cross-linked polymer based on the dynamic exchange of disulfide bonds. *Chem. Mater.* **26**(6), 2038–2046 (2014). <https://doi.org/10.1021/cm4040616>

74. R. Martin, A. Rekondo, A. Ruiz de Luzuriaga, G. Cabanero, H.J. Grande, I. Odriozola, The processability of a poly(urea-urethane) elastomer reversibly crosslinked with aromatic disulfide bridges. *J. Mater. Chem. A* **2**(16), 5710–5715 (2014). <https://doi.org/10.1039/C3TA14927G>
75. A. Rekondo, R. Martin, A. Ruiz de Luzuriaga, G. Cabanero, H.J. Grande, I. Odriozola, Catalyst-free room-temperature self-healing elastomers based on aromatic disulfide metathesis. *Mater. Horiz* **1**(2), 237–240 (2014). <https://doi.org/10.1039/C3MH00061C>
76. J.A. Yoon, J. Kamada, K. Koynov, J. Mohin, R. Nicolaÿ, Y. Zhang, A.C. Balazs, T. Kowalewski, K. Matyjaszewski, Self-healing polymer films based on thiol–disulfide exchange reactions and self-healing kinetics measured using atomic force microscopy. *Macromolecules* **45**(1), 142–149 (2012). <https://doi.org/10.1021/ma2015134>
77. Y. Amamoto, H. Otsuka, A. Takahara, K. Matyjaszewski, Self-healing of covalently cross-linked polymers by reshuffling thiuram disulfide moieties in air under visible light. *Adv. Mater.* **24**(29), 3975–3980 (2012). <https://doi.org/10.1002/adma.201201928>
78. A.Z.M. Esteves AC, S. van der Zwaag, S.J. Garcia, Healable dual organic–inorganic crosslinked sol–gel based polymers: crosslinking density and tetrasulfide content effect. *J. Polym. Sci. Part A: Polym. Chem.* **52**(14), 1953–1961 (2014). <https://doi.org/10.1002/pola.27200>
79. H. Ying, Y. Zhang, J. Cheng, Dynamic urea bond for the design of reversible and self-healing polymers. *Nat. Commun.* **5** (2014). <https://doi.org/10.1038/ncomms4218>
80. F. Wang, M.Z. Rong, M.Q. Zhang, Reversibility of solid state radical reactions in thermally remendable polymers with C–ON bonds. *J. Mater. Chem.* **22**(26), 13076–13084 (2012). <https://doi.org/10.1039/C2JM30578J>
81. Y. Ce, M.Z. Rong, M.Q. Zhang, Z.P. Zhang, Y.C. Yuan, Self-healing of polymers via synchronous covalent bond fission/radical recombination. *Chem. Mater.* **23**(22), 5076–5081 (2011). <https://doi.org/10.1021/cm202635w>
82. Y. Ce, M.Z. Rong, M.Q. Zhang, Self-healing polyurethane elastomer with thermally reversible alkoxyamines as crosslinkages. *Polymer* **55**(7), 1782–1791 (2014). <https://doi.org/10.1016/j.polymer.2014.02.033>
83. K. Imato, M. Nishihara, T. Kanehara, Y. Amamoto, A. Takahara, H. Otsuka, Self-healing of chemical gels cross-linked by diarylbibenzofuranone-based trigger-free dynamic covalent bonds at room temperature. *Angew. Chem. Int. Ed.* **51**(5), 1138–1142 (2012). <https://doi.org/10.1002/anie.201104069>
84. M. Capelot, D. Montarnal, F. Tournilhac, L. Leibler, Metal-catalyzed transesterification for healing and assembling of thermosets. *J. Am. Chem. Soc.* **134**(18), 7664–7667 (2012). <https://doi.org/10.1021/ja302894k>
85. D. Montarnal, M. Capelot, F. Tournilhac, L. Leibler, Silica-like malleable materials from permanent organic networks. *Science* **334**(6058), 965–968 (2011). <https://doi.org/10.1126/science.1212648>
86. J.J. Cash, T. Kubo, A.P. Bapat, B.S. Sumerlin, Room-temperature self-healing polymers based on dynamic-covalent boronic esters. *Macromolecules* **48**(7), 2098–2106 (2015). <https://doi.org/10.1021/acs.macromol.5b00210>
87. O.R. Cromwell, J. Chung, Z. Guan, Malleable and self-healing covalent polymer networks through tunable dynamic boronic ester bonds. *J. Am. Chem. Soc.* **137**(20), 6492–6495 (2015). <https://doi.org/10.1021/jacs.5b03551>
88. D. Döhler, H. Peterlik, W.H. Binder, A dual crosslinked self-healing system: supramolecular and covalent network formation of four-arm star polymers. *Polymer* **69**, 264–273 (2015). <https://doi.org/10.1016/j.polymer.2015.01.073>
89. F. Herbst, S. Seiffert, W.H. Binder, Dynamic supramolecular poly(isobutylene)s for self-healing materials. *Polym. Chem.* **3**(11), 3084–3092 (2012). <https://doi.org/10.1039/C2PY20265D>
90. S. Chen, N. Mahmood, M. Beiner, W.H. Binder, Self-healing materials from V- and H-shaped supramolecular architectures. *Angew. Chem. Int. Ed.* **54**(35), 10188–10192 (2015). <https://doi.org/10.1002/anie.201504136>
91. Y. Chen, Z. Guan, Self-healing thermoplastic elastomer brush copolymers having a glassy polymethylmethacrylate backbone and rubbery polyacrylate-amide brushes. *Polymer* **69**, 249–254 (2015). <https://doi.org/10.1016/j.polymer.2015.03.023>

92. M. Yan, J. Tang, H.-L. Xie, B. Ni, H.-L. Zhang, E.-Q. Chen, Self-healing and phase behavior of liquid crystalline elastomer based on a block copolymer constituted of a side-chain liquid crystalline polymer and a hydrogen bonding block. *J. Mater. Chem. C* **3**(33), 8526–8534 (2015). <https://doi.org/10.1039/C5TC01603G>
93. Y. Chen, A.M. Kushner, G.A. Williams, Z. Guan, Multiphase design of autonomic self-healing thermoplastic elastomers. *Nat. Chem.* **4**(6), 467–472 (2012). <https://doi.org/10.1038/nchem.1314>
94. N. Roy, E. Buhler, J.-M. Lehn, The tris-urea motif and its incorporation into polydimethylsiloxane-based supramolecular materials presenting self-healing features. *Chem. Eur. J.* **19**(27), 8814–8820 (2013). <https://doi.org/10.1002/chem.201203518>
95. P. Cordier, F. Tournilhac, C. Soulie-Ziakovic, L. Leibler, Self-healing and thermoreversible rubber from supramolecular assembly. *Nature* **451**(7181), 977–980 (2008). <https://doi.org/10.1038/nature06669>
96. D. Montarnal, P. Cordier, C. Soulié-Ziakovic, F. Tournilhac, L. Leibler, Synthesis of self-healing supramolecular rubbers from fatty acid derivatives, diethylene triamine, and urea. *J. Polym. Sci. Part A: Polym. Chem.* **46**(24), 7925–7936 (2008). <https://doi.org/10.1002/pola.23094>
97. A. Faghihnejad, K.E. Feldman, J. Yu, M.V. Tirrell, J.N. Israelachvili, C.J. Hawker, E.J. Kramer, H. Zeng, Adhesion and surface interactions of a self-healing polymer with multiple hydrogen-bonding groups. *Adv. Funct. Mater.* **24**(16), 2322–2333 (2014). <https://doi.org/10.1002/adfm.201303013>
98. R. Chang, Y. Huang, G. Shan, Y. Bao, X. Yun, T. Dong, P. Pan, Alternating poly(lactic acid)/poly(ethylene-co-butylene) supramolecular multiblock copolymers with tunable shape memory and self-healing properties. *Polym. Chem.* **6**(32), 5899–5910 (2015). <https://doi.org/10.1039/C5PY00742A>
99. J. Hentschel, A.M. Kushner, J. Ziller, Z. Guan, Self-healing supramolecular block copolymers. *Angew. Chem. Int. Ed.* **51**(42), 10561–10565 (2012). <https://doi.org/10.1002/anie.201204840>
100. S. Burattini, H.M. Colquhoun, B.W. Greenland, W. Hayes, A novel self-healing supramolecular polymer system. *Faraday Discuss.* **143**(1), 251–264 (2009). <https://doi.org/10.1039/B900859D>
101. S. Burattini, B.W. Greenland, D.H. Merino, W. Weng, J. Seppala, H.M. Colquhoun, W. Hayes, M.E. Mackay, I.W. Hamley, S.J. Rowan, A healable supramolecular polymer blend based on aromatic π - π stacking and hydrogen-bonding interactions. *J. Am. Chem. Soc.* **132**(34), 12051–12058 (2010). <https://doi.org/10.1021/ja104446r>
102. S. Burattini, B.W. Greenland, W. Hayes, M.E. Mackay, S.J. Rowan, H.M. Colquhoun, A supramolecular polymer based on tweezer-type π - π stacking interactions: molecular design for healability and enhanced toughness. *Chem. Mater.* **23**(1), 6–8 (2011). <https://doi.org/10.1021/cm102963k>
103. S.J. Kalista, T.C. Ward, Thermal characteristics of the self-healing response in poly(ethylene-co-methacrylic acid) copolymers. *J. R. Soc. Interface* **4**(13), 405–411 (2007). <https://doi.org/10.1098/rsif.2006.0169>
104. S.J. Kalista, J.R. Pflug, R.J. Varley, Effect of ionic content on ballistic self-healing in EMAA copolymers and ionomers. *Polym. Chem.* **4**(18), 4910–4926 (2013). <https://doi.org/10.1039/C3PY00095H>
105. S.J. Kalista, T.C. Ward, Z. Oyetunji, Self-healing of poly(ethylene-co-methacrylic acid) copolymers following projectile puncture. *Mech. Adv. Mater. Struct.* **14**(5), 391–397 (2007). <https://doi.org/10.1080/15376490701298819>
106. R.J. Varley, S. van der Zwaag, Development of a quasi-static test method to investigate the origin of self-healing in ionomers under ballistic conditions. *Polym. Test.* **27**(1), 11–19 (2008). <https://doi.org/10.1016/j.polymertesting.2007.07.013>
107. R.J. Varley, S. van der Zwaag, Towards an understanding of thermally activated self-healing of an ionomer system during ballistic penetration. *Acta Mater.* **56**(19), 5737–5750 (2008). <https://doi.org/10.1016/j.actamat.2008.08.008>

108. R.K. Bose, N. Hohlbein, S.J. Garcia, A.M. Schmidt, S. van der Zwaag, Connecting supramolecular bond lifetime and network mobility for scratch healing in poly(butyl acrylate) ionomers containing sodium, zinc and cobalt. *Phys. Chem. Chem. Phys.* **17**(3), 1697–1704 (2015). <https://doi.org/10.1039/C4CP04015E>
109. R.K. Bose, N. Hohlbein, S.J. Garcia, A.M. Schmidt, S. van der Zwaag, Relationship between the network dynamics, supramolecular relaxation time and healing kinetics of cobalt poly (butyl acrylate) ionomers. *Polymer* **69**, 228–232 (2015). <https://doi.org/10.1016/j.polymer.2015.03.049>
110. N. Hohlbein, A. Shaaban, A.M. Schmidt, Remote-controlled activation of self-healing behavior in magneto-responsive ionomeric composites. *Polymer* **69**, 301–309 (2015). <https://doi.org/10.1016/j.polymer.2015.04.024>
111. S. Bode, R.K. Bose, S. Matthes, M. Ehrhardt, A. Seifert, F.H. Schacher, R.M. Paulus, S. Stumpf, B. Sandmann, J. Vitz, A. Winter, S. Hoeppener, S.J. Garcia, S. Spange, S. van der Zwaag, M.D. Hager, U.S. Schubert, Self-healing metallopolymers based on cadmium bis (terpyridine) complex containing polymer networks. *Polym. Chem.* **4**(18), 4966–4973 (2013). <https://doi.org/10.1039/C3PY00288H>
112. S. Bode, L. Zedler, F.H. Schacher, B. Dietzek, M. Schmitt, J. Popp, M.D. Hager, U.S. Schubert, Self-healing polymer coatings based on crosslinked metallosupramolecular copolymers. *Adv. Mater.* **25**(11), 1634–1638 (2013). <https://doi.org/10.1002/adma.201203865>
113. S. Bode, M. Enke, R.K. Bose, F.H. Schacher, S.J. Garcia, S. van der Zwaag, M.D. Hager, U.S. Schubert, Correlation between scratch healing and rheological behavior for terpyridine complex based metallopolymers. *J. Mater. Chem. A* **3**(44), 22145–22153 (2015). <https://doi.org/10.1039/C5TA05545H>
114. M. Burnworth, L. Tang, J.R. Kumpfer, A.J. Duncan, F.L. Beyer, G.L. Fiore, S.J. Rowan, C. Weder, Optically healable supramolecular polymers. *Nature* **472**(7343), 334–337 (2011). <https://doi.org/10.1038/nature09963>
115. S. Coulibaly, A. Roulin, S. Balog, M.V. Biyani, E.J. Foster, S.J. Rowan, G.L. Fiore, C. Weder, Reinforcement of optically healable supramolecular polymers with cellulose nanocrystals. *Macromolecules* **47**(1), 152–160 (2014). <https://doi.org/10.1021/ma402143c>
116. M. Enke, S. Bode, J. Vitz, F.H. Schacher, M.J. Harrington, M.D. Hager, U.S. Schubert, Self-healing response in supramolecular polymers based on reversible zinc–histidine interactions. *Polymer* **69**, 274–282 (2015). <https://doi.org/10.1016/j.polymer.2015.03.068>
117. D. Mozhdehi, S. Ayala, O.R. Cromwell, Z. Guan, Self-healing multiphase polymers via dynamic metal–ligand interactions. *J. Am. Chem. Soc.* **136**(46), 16128–16131 (2014). <https://doi.org/10.1021/ja5097094>
118. F. Zeng, Y. Han, Z.-C. Yan, C.-Y. Liu, C.-F. Chen, Supramolecular polymer gel with multi stimuli responsive, self-healing and erasable properties generated by host–guest interactions. *Polymer* **54**(26), 6929–6935 (2013). <https://doi.org/10.1016/j.polymer.2013.10.048>
119. S. Li, H.-Y. Lu, Y. Shen, C.-F. Chen, A stimulus-response and self-healing supramolecular polymer gel based on host–guest interactions. *Macromol. Chem. Phys.* **214**(14), 1596–1601 (2013). <https://doi.org/10.1002/macp.201300229>
120. M. Zhang, D. Xu, X. Yan, J. Chen, S. Dong, B. Zheng, F. Huang, Self-healing supramolecular gels formed by crown ether based host–guest interactions. *Angew. Chem. Int. Ed.* **51**(28), 7011–7015 (2012). <https://doi.org/10.1002/anie.201203063>
121. T.-W. Chuo, T.-C. Wei, Y.-L. Liu, Electrically driven self-healing polymers based on reversible guest–host complexation of β -cyclodextrin and ferrocene. *J. Polym. Sci. Part A: Polym. Chem.* **51**(16), 3395–3403 (2013). <https://doi.org/10.1002/pola.26736>
122. M. Nakahata, Y. Takashima, H. Yamaguchi, A. Harada, Redox-responsive self-healing materials formed from host–guest polymers. *Nat. Commun.* **2**, 511 (2011). <https://doi.org/10.1038/ncomms1521>
123. T. Kakuta, Y. Takashima, M. Nakahata, M. Otsubo, H. Yamaguchi, A. Harada, Preorganized hydrogel: self-healing properties of supramolecular hydrogels formed by polymerization of

- host–guest-monomers that contain cyclodextrins and hydrophobic guest groups. *Adv. Mater.* **25**(20), 2849–2853 (2013). <https://doi.org/10.1002/adma.201205321>
124. T. Kakuta, Y. Takashima, T. Sano, T. Nakamura, Y. Kobayashi, H. Yamaguchi, A. Harada, Adhesion between semihard polymer materials containing cyclodextrin and adamantane based on host–guest interactions. *Macromolecules* **48**(3), 732–738 (2015). <https://doi.org/10.1021/ma502316d>
125. D.J. Byrne, J. Hardy, R.A.B. Wood, R. McIntosh, A. Cuschieri, Effect of fibrin glues on the mechanical properties of healing wounds. *Br. J. Surg.* **78**(7), 841–843 (1991). <https://doi.org/10.1002/bjs.1800780723>
126. M.B. Schaffler, E.L. Radin, D.B. Burr, Mechanical and morphological effects of strain rate on fatigue of compact bone. *Bone* **10**(3), 207–214 (1989). [https://doi.org/10.1016/8756-3282\(89\)90055-0](https://doi.org/10.1016/8756-3282(89)90055-0)
127. I.H. Kalfas, Principles of bone healing. *Neurosurg. Focus.* **10**(4), 1–4 (2001). <https://doi.org/10.3171/foc.2001.10.4.2>
128. M.J. Harrington, H.S. Gupta, P. Fratzl, J.H. Waite, Collagen insulated from tensile damage by domains that unfold reversibly: in situ X-ray investigation of mechanical yield and damage repair in the mussel byssus. *J. Struct. Biol.* **167**(1), 47–54 (2009). <https://doi.org/10.1016/j.jsb.2009.03.001>
129. K.S. Toohy, N.R. Sottos, J.A. Lewis, J.S. Moore, S.R. White, Self-healing materials with microvascular networks. *Nat. Mater.* **6**(8), 581–585 (2007). <https://doi.org/10.1038/nmat1934>
130. J.W.C. Pang, I.P. Bond, A hollow fibre reinforced polymer composite encompassing self-healing and enhanced damage visibility. *Compos. Sci. Technol.* **65**(11–12), 1791–1799 (2005). <https://doi.org/10.1016/j.compscitech.2005.03.008>
131. I.P. Bond, R.S. Trask, H.R. Williams, Self-healing fiber-reinforced polymer composites. *MRS Bull.* **33**(08), 770–774 (2008). <https://doi.org/10.1557/mrs2008.164>
132. R.S. Trask, C.J. Norris, I.P. Bond, Stimuli triggered self-healing functionality in advanced fibre reinforced composites. *J. Intell. Mater. Syst. Struct.* (2013). <https://doi.org/10.1177/1045389x13505006>
133. T.S. Coope, D.F. Wass, R.S. Trask, I.P. Bond, Metal triflates as catalytic curing agents in self-healing fibre reinforced polymer composite materials. *Macromol. Mater. Eng.* **299**(2), 208–218 (2014). <https://doi.org/10.1002/mame.201300026>
134. A.R. Hamilton, N.R. Sottos, S.R. White, Self-healing of internal damage in synthetic vascular materials. *Adv. Mater.* **22**(45), 5159–5163 (2010). <https://doi.org/10.1002/adma.201002561>
135. N. Kuhl, S. Bode, M.D. Hager, U.S. Schubert, Self-healing polymers based on reversible covalent bonds. *Adv. Polym. Sci.* (2016). https://doi.org/10.1007/12_2015_336
136. M. Enke, D. Döhler, S. Bode, W.H. Binder, M.D. Hager, U.S. Schubert, Intrinsic self-healing polymers based on supramolecular interactions: state of the art and future directions. *Adv. Polym. Sci.* (2016). https://doi.org/10.1007/12_2015_345
137. P. Froimowicz, D. Klinger, K. Landfester, Photoreactive nanoparticles as nanometric building blocks for the generation of self-healing hydrogel thin films. *Chem. Eur. J.* **17**(44), 12465–12475 (2011). <https://doi.org/10.1002/chem.201100685>
138. L. Hu, X. Cheng, A. Zhang, A facile method to prepare UV light-triggered self-healing polyphosphazenes. *J. Mater. Sci.* **50**(5), 2239–2246 (2014). <https://doi.org/10.1007/s10853-014-8786-y>
139. N. Oya, P. Sukarsaatmadja, K. Ishida, N. Yoshie, Photoinduced mendable network polymer from poly(butylene adipate) end-functionalized with cinnamoyl groups. *Polym. J.* **44**(7), 724–729 (2012)
140. Y.-L. Liu, T.-W. Chuo, Self-healing polymers based on thermally reversible Diels–Alder chemistry. *Polym. Chem.* **4**(7), 2194–2205 (2013). <https://doi.org/10.1039/C2PY20957H>
141. A. Gandini, The furan/maleimide Diels–Alder reaction: a versatile click–unlick tool in macromolecular synthesis. *Prog. Polym. Sci.* **38**(1), 1–29 (2013). <https://doi.org/10.1016/j.progpolymsci.2012.04.002>

142. Y.-L. Liu, C.-Y. Hsieh, Crosslinked epoxy materials exhibiting thermal remendability and removability from multifunctional maleimide and furan compounds. *J. Polym. Sci. Part A: Polym. Chem.* **44**(2), 905–913 (2006). <https://doi.org/10.1002/pola.21184>
143. C. Zeng, H. Seino, J. Ren, K. Hatanaka, N. Yoshie, Self-healing bio-based furan polymers cross-linked with various bis-maleimides. *Polymer* **54**(20), 5351–5357 (2013). <https://doi.org/10.1016/j.polymer.2013.07.059>
144. C. Zeng, H. Seino, J. Ren, K. Hatanaka, N. Yoshie, Bio-based furan polymers with self-healing ability. *Macromolecules* **46**(5), 1794–1802 (2013). <https://doi.org/10.1021/ma3023603>
145. J.A. Syrett, G. Mantovani, W.R.S. Barton, D. Price, D.M. Haddleton, Self-healing polymers prepared via living radical polymerisation. *Polym. Chem.* **1**(1), 102–106 (2010). <https://doi.org/10.1039/B9PY00316A>
146. B.D. Fairbanks, S.P. Singh, C.N. Bowman, K.S. Anseth, Photodegradable, photoadaptable hydrogels via radical-mediated disulfide fragmentation reaction. *Macromolecules* **44**(8), 2444–2450 (2011). <https://doi.org/10.1021/ma200202w>
147. A.P. Bapat, J.G. Ray, D.A. Savin, B.S. Sumerlin, Redox-responsive dynamic-covalent assemblies: stars and miktoarm stars. *Macromolecules* **46**(6), 2188–2198 (2013). <https://doi.org/10.1021/ma400169m>
148. N. Roy, B. Bruchmann, J.-M. Lehn, DYNAMERS: dynamic polymers as self-healing materials. *Chem. Soc. Rev.* **44**(11), 3786–3807 (2015). <https://doi.org/10.1039/C5CS00194C>
149. M.E. Belowich, J.F. Stoddart, Dynamic imine chemistry. *Chem. Soc. Rev.* **41**(6), 2003–2024 (2012). <https://doi.org/10.1039/C2CS15305J>
150. M. Ciaccia, S. Di Stefano, Mechanisms of imine exchange reactions in organic solvents. *Org. Biomol. Chem.* **13**(3), 646–654 (2015). <https://doi.org/10.1039/C4OB02110J>
151. G. Schaeffer, E. Buhler, S.J. Candau, J.-M. Lehn, Double dynamic supramolecular polymers of covalent oligo-dynamers. *Macromolecules* **46**(14), 5664–5671 (2013). <https://doi.org/10.1021/ma400449u>
152. A.K.H. Hirsch, E. Buhler, J.-M. Lehn, Biodynamers: self-organization-driven formation of doubly dynamic proteoids. *J. Am. Chem. Soc.* **134**(9), 4177–4183 (2012). <https://doi.org/10.1021/ja2099134>
153. G. Deng, C. Tang, F. Li, H. Jiang, Y. Chen, Covalent cross-linked polymer gels with reversible sol–gel transition and self-healing properties. *Macromolecules* **43**(3), 1191–1194 (2010). <https://doi.org/10.1021/ma9022197>
154. G. Deng, F. Li, H. Yu, F. Liu, C. Liu, W. Sun, H. Jiang, Y. Chen, Dynamic hydrogels with an environmental adaptive self-healing ability and dual responsive sol–gel transitions. *ACS Macro Lett.* **1**(2), 275–279 (2012). <https://doi.org/10.1021/mz200195n>
155. Y. Gao, Q. Luo, S. Qiao, L. Wang, Z. Dong, J. Xu, J. Liu, Enzymatically regulating the self-healing of protein hydrogels with high healing efficiency. *Angew. Chem. Int. Ed.* **53**(35), 9343–9346 (2014). <https://doi.org/10.1002/anie.201404531>
156. J. Nicolas, Y. Guillauneuf, C. Lefay, D. Bertin, D. Gigmes, B. Charleux, Nitroxide-mediated polymerization. *Prog. Polym. Sci.* **38**(1), 63–235 (2013). <https://doi.org/10.1016/j.progpolymsci.2012.06.002>
157. T. Janoschka, A. Teichler, B. Häupler, T. Jähnert, M.D. Hager, U.S. Schubert, Reactive inkjet printing of cathodes for organic radical batteries. *Adv. Energy Mater.* **3**(8), 1025–1028 (2013). <https://doi.org/10.1002/aenm.201300036>
158. R. Hoogenboom, Hard autonomous self-healing supramolecular materials—a contradiction in terms? *Angew. Chem. Int. Ed.* **51**(48), 11942–11944 (2012). <https://doi.org/10.1002/anie.201205226>
159. F. Herbst, D. Döhler, P. Michael, W.H. Binder, Self-healing polymers via supramolecular forces. *Macromol. Rapid Commun.* **34**(3), 203–220 (2013). <https://doi.org/10.1002/marc.201200675>
160. J. Cortese, C. Soulié-Ziakovic, S. Tencé-Girault, L. Leibler, Suppression of mesoscopic order by complementary interactions in supramolecular polymers. *J. Am. Chem. Soc.* **134**(8), 3671–3674 (2012). <https://doi.org/10.1021/ja2119496>

161. A.V. Ambade, S.K. Yang, M. Weck, Supramolecular ABC triblock copolymers. *Angew. Chem. Int. Ed.* **48**(16), 2894–2898 (2009). <https://doi.org/10.1002/anie.200805116>
162. S. Burattini, B.W. Greenland, D. Chappell, H.M. Colquhoun, W. Hayes, Healable polymeric materials: a tutorial review. *Chem. Soc. Rev.* **39**(6), 1973–1985 (2010). <https://doi.org/10.1039/B904502N>
163. L.R. Hart, N.A. Nguyen, J.L. Harries, M.E. Mackay, H.M. Colquhoun, W. Hayes, Perylene as an electron-rich moiety in healable, complementary π - π stacked, supramolecular polymer systems. *Polymer* **69**, 293–300 (2015). <https://doi.org/10.1016/j.polymer.2015.03.028>
164. S. Burattini, H.M. Colquhoun, J.D. Fox, D. Friedmann, B.W. Greenland, P.J.F. Harris, W. Hayes, M.E. Mackay, S.J. Rowan, A self-repairing, supramolecular polymer system: healability as a consequence of donor-acceptor [small pi]-[small pi] stacking interactions. *Chem. Commun.* **44**, 6717–6719 (2009). <https://doi.org/10.1039/B910648K>
165. J. Fox, J.J. Wie, B.W. Greenland, S. Burattini, W. Hayes, H.M. Colquhoun, M.E. Mackay, S.J. Rowan, High-strength, healable, supramolecular polymer nanocomposites. *J. Am. Chem. Soc.* **134**(11), 5362–5368 (2012). <https://doi.org/10.1021/ja300050x>
166. <http://www.dupont.com/products-and-services/plastics-polymers-resins/ethylene-copolymers/brands/nucrel-ethylene-acrylic-acid.html>. (Last accessed: 13 Apr 2016)
167. <http://www.dupont.com/products-and-services/plastics-polymers-resins/ethylene-copolymers/brands/surlyn-ionomer-resin.html>. (Last accessed: 13 Apr 2016)
168. A. Eisenberg, Clustering of ions in organic polymers. A theoretical approach. *Macromolecules* **3**(2), 147–154 (1970). <https://doi.org/10.1021/ma60014a006>
169. A. Eisenberg, B. Hird, R.B. Moore, A new multiplet-cluster model for the morphology of random ionomers. *Macromolecules* **23**(18), 4098–4107 (1990). <https://doi.org/10.1021/ma00220a012>
170. K. Tadano, E. Hirasawa, H. Yamamoto, S. Yano, Order-disorder transition of ionic clusters in ionomers. *Macromolecules* **22**(1), 226–233 (1989). <https://doi.org/10.1021/ma00191a043>
171. T. Haase, I. Rohr, K. Thoma, Dynamic temperature measurements on a thermally activated self-healing ionomer. *J. Intell. Mater. Syst. Struct.* **25**(1), 25–30 (2014). <https://doi.org/10.1177/1045389x12444487>
172. B. Sandmann, S. Bode, M.D. Hager, U.S. Schubert, Metallopolymers as an emerging class of self-healing materials. *Adv. Polym. Sci.* **262**, 239–257 (2013)
173. G.R. Whittell, M.D. Hager, U.S. Schubert, I. Manners, Functional soft materials from metallopolymers and metallosupramolecular polymers. *Nat. Mater.* **10**(3), 176–188 (2011). <https://doi.org/10.1038/nmat2966>
174. Z. Wang, M.W. Urban, Facile UV-healable polyethylenimine-copper (C2H5N-cu) supramolecular polymer networks. *Polym. Chem.* **4**(18), 4897–4901 (2013). <https://doi.org/10.1039/C2PY20844J>
175. S. Kupfer, L. Zedler, J. Guthmuller, S. Bode, M.D. Hager, U.S. Schubert, J. Popp, S. Grafe, B. Dietzek, Self-healing mechanism of metallopolymers investigated by QM/MM simulations and Raman spectroscopy. *Phys. Chem. Chem. Phys.* **16**(24), 12422–12432 (2014). <https://doi.org/10.1039/C4CP00562G>
176. E. Vaccaro, J.H. Waite, Yield and post-yield behavior of mussel byssal thread: a self-healing biomolecular material. *Biomacromolecules* **2**(3), 906–911 (2001). <https://doi.org/10.1021/bm0100514>
177. S. Schmidt, A. Reinecke, F. Wojcik, D. Pussak, L. Hartmann, M.J. Harrington, Metal-mediated molecular self-healing in histidine-rich mussel peptides. *Biomacromolecules* **15**(5), 1644–1652 (2014). <https://doi.org/10.1021/bm500017u>
178. H. Ceylan, M. Urel, T.S. Erkal, A.B. Tekinay, A. Dana, M.O. Guler, Mussel inspired dynamic cross-linking of self-healing peptide nanofiber network. *Adv. Funct. Mater.* **23**(16), 2081–2090 (2013). <https://doi.org/10.1002/adfm.201202291>
179. J.J. Wilker, The iron-fortified adhesive system of marine mussels. *Angew. Chem. Int. Ed.* **49**(44), 8076–8078 (2010). <https://doi.org/10.1002/anie.201003171>

180. M.J. Harrington, A. Masic, N. Holten-Andersen, J.H. Waite, P. Fratzl, Iron-clad fibers: a metal-based biological strategy for hard flexible coatings. *Science* **328**(5975), 216–220 (2010). <https://doi.org/10.1126/science.1181044>
181. S. Krauss, T.H. Metzger, P. Fratzl, M.J. Harrington, Self-repair of a biological fiber guided by an ordered elastic framework. *Biomacromolecules* **14**(5), 1520–1528 (2013). <https://doi.org/10.1021/bm4001712>
182. M. Krogsgaard, M.A. Behrens, J.S. Pedersen, H. Birkedal, Self-healing mussel-inspired multi-pH-responsive hydrogels. *Biomacromolecules* **14**(2), 297–301 (2013). <https://doi.org/10.1021/bm301844u>
183. N. Holten-Andersen, M.J. Harrington, H. Birkedal, B.P. Lee, P.B. Messersmith, K.Y.C. Lee, J.H. Waite, pH-induced metal-ligand cross-links inspired by mussel yield self-healing polymer networks with near-covalent elastic moduli. *Proc. Natl. Acad. Sci.* **108**(7), 2651–2655 (2011). <https://doi.org/10.1073/pnas.1015862108>
184. R. Dong, Y. Liu, Y. Zhou, D. Yan, X. Zhu, Photo-reversible supramolecular hyperbranched polymer based on host-guest interactions. *Polym. Chem.* **2**(12), 2771–2774 (2011). <https://doi.org/10.1039/C1PY00426C>
185. J. Ahner, S. Bode, M. Micheel, B. Dietzek, M.D. Hager, Self-healing functional polymeric materials. *Adv. Polym. Sci.* (2016). https://doi.org/10.1007/12_2015_333
186. K.A. Williams, A.J. Boydston, C.W. Bielawski, Towards electrically conductive, self-healing materials. *J. R. Soc. Interface* **4**(13), 359–362 (2007). <https://doi.org/10.1098/rsif.2006.0202>
187. B.C.K. Tee, C. Wang, R. Allen, Z. Bao, An electrically and mechanically self-healing composite with pressure- and flexion-sensitive properties for electronic skin applications. *Nat. Nanotechnol.* **7**(12), 825–832 (2012). <https://doi.org/10.1038/nnano.2012.192>
188. C. Wang, H. Wu, Z. Chen, M.T. McDowell, Y. Cui, Z. Bao, Self-healing chemistry enables the stable operation of silicon microparticle anodes for high-energy lithium-ion batteries. *Nat. Chem.* **5**(12), 1042–1048 (2013). <https://doi.org/10.1038/nchem.1802>
189. M.M. Caruso, S.R. Schelkopf, A.C. Jackson, A.M. Landry, P.V. Braun, J.S. Moore, Microcapsules containing suspensions of carbon nanotubes. *J. Mater. Chem.* **19**(34), 6093–6096 (2009). <https://doi.org/10.1039/B910673A>
190. S. Kang, A.R. Jones, J.S. Moore, S.R. White, N.R. Sottos, Microencapsulated carbon black suspensions for restoration of electrical conductivity. *Adv. Funct. Mater.* **24**(20), 2947–2956 (2014). <https://doi.org/10.1002/adfm.201303427>
191. E. Palleau, S. Reece, S.C. Desai, M.E. Smith, M.D. Dickey, Self-healing stretchable wires for reconfigurable circuit wiring and 3D microfluidics. *Adv. Mater.* **25**(11), 1589–1592 (2013). <https://doi.org/10.1002/adma.201203921>
192. J.-H. So, J. Thelen, A. Qusba, G.J. Hayes, G. Lazzi, M.D. Dickey, Reversibly deformable and mechanically tunable fluidic antennas. *Adv. Funct. Mater.* **19**(22), 3632–3637 (2009). <https://doi.org/10.1002/adfm.200900604>
193. A.C. Jackson, J.A. Bartelt, P.V. Braun, Transparent self-healing polymers based on encapsulated plasticizers in a thermoplastic matrix. *Adv. Funct. Mater.* **21**(24), 4705–4711 (2011). <https://doi.org/10.1002/adfm.201101574>
194. M. Saito, T. Nishimura, K. Sakiyama, S. Inagaki, Self-healing of optical functions by molecular metabolism in a swollen elastomer. *AIP Adv.* **2**(4), 042118 (2012). <https://doi.org/10.1063/1.4764292>
195. Y. Zhang, C. Rocco, F. Karasu, L.G.J. van der Ven, R.A.T.M. van Benthem, X. Allonas, C. Croutxé-Barghorn, A.C.C. Esteves, G. de With, UV-cured self-replenishing hydrophobic polymer films. *Polymer* **69**, 384–393 (2015). <https://doi.org/10.1016/j.polymer.2015.02.036>
196. T. Dikić, W. Ming, R.A.T.M. van Benthem, A.C.C. Esteves, G. de With, Self-replenishing surfaces. *Adv. Mater.* **24**(27), 3701–3704 (2012). <https://doi.org/10.1002/adma.201200807>
197. A.C.C. Esteves, Y. Luo, M.W.P. van de Put, C.C.M. Carcouët, G. de With, Self-replenishing dual structured superhydrophobic coatings prepared by drop-casting of an all-in-one dispersion. *Adv. Funct. Mater.* **24**(7), 986–992 (2014). <https://doi.org/10.1002/adfm.201301909>

198. S. Bode, M. Enke, M. Hernandez, R.K. Bose, A.M. Grande, S. van der Zwaag, U.S. Schubert, S.J. Garcia, M.D. Hager, Characterization of self-healing polymers: from macroscopic healing tests to the molecular mechanism. *Adv. Polym. Sci.* (2016). https://doi.org/10.1007/12_2015_341
199. D.C. Tuncaboylu, M. Sahin, A. Argun, W. Oppermann, O. Okay, Dynamics and large strain behavior of self-healing hydrogels with and without surfactants. *Macromolecules* **45**(4), 1991–2000 (2012). <https://doi.org/10.1021/ma202672y>
200. E.B. Murphy, The return of photoelastic stress measurements: utilizing birefringence to monitor damage and repair in healable materials. *J. Mater. Chem.* **21**(5), 1438–1446 (2011). <https://doi.org/10.1039/C0JM02308F>
201. A.M. Grande, S.J. Garcia, S. van der Zwaag, On the interfacial healing of a supramolecular elastomer. *Polymer* **56**, 435–442 (2015). <https://doi.org/10.1016/j.polymer.2014.11.052>
202. E. Tsangouri, D. Aggelis, D. Van Hemelrijck, Quantifying thermoset polymers healing efficiency: a systematic review of mechanical testing. *Prog. Polym. Sci.* **49–50**, 154–174 (2015). <https://doi.org/10.1016/j.progpolymsci.2015.06.002>
203. E.N. Brown, Use of the tapered double-cantilever beam geometry for fracture toughness measurements and its application to the quantification of self-healing. *J. Strain Anal. Eng. Des.* **46**(3), 167–186 (2011). <https://doi.org/10.1177/0309324710396018>
204. M.R. Kessler, N.R. Sottos, S.R. White, Self-healing structural composite materials. *Compos. Part A: Appl. Sci. Manufact.* **34**(8), 743–753 (2003). [https://doi.org/10.1016/S1359-835X\(03\)00138-6](https://doi.org/10.1016/S1359-835X(03)00138-6)
205. F. Maes, D. Montarnal, S. Cantournet, F. Tournilhac, L. Corte, L. Leibler, Activation and deactivation of self-healing in supramolecular rubbers. *Soft Matter* **8**(5), 1681–1687 (2012). <https://doi.org/10.1039/C2SM06715C>
206. J.M. Vega, A.M. Grande, S. van der Zwaag, S.J. Garcia, On the role of free carboxylic groups and cluster conformation on the surface scratch healing behaviour of ionomers. *Eur. Polym. J.* **57**, 121–126 (2014). <https://doi.org/10.1016/j.eurpolymj.2014.05.005>
207. M. Hernández, A.M. Grande, S. van der Zwaag, S.J. Garcia, Monitoring network and interfacial healing processes by broadband dielectric spectroscopy: a case study on natural rubber. *ACS Appl. Mater. Interfaces* (2016). <https://doi.org/10.1021/acsami.6b02259>
208. B. Grabowski, C.C. Tasan, Self-healing metals. *Adv. Polym. Sci.* (2016). https://doi.org/10.1007/12_2015_337
209. P. Greil, Generic principles of crack-healing ceramics. *J. Adv. Ceram.* **1**(4), 249–267 (2013). <https://doi.org/10.1007/s40145-012-0020-2>
210. F. Tavangarian, G. Li, Crack healing and strength recovery in SiC/spinel nanocomposite. *Ceram. Int.* **41**(7), 8702–8709 (2015). <https://doi.org/10.1016/j.ceramint.2015.03.088>
211. T. Ouyang, J. Wu, M. Yasir, T. Zhou, X. Fang, Y. Wang, D. Liu, J. Suo, Effect of TiC self-healing coatings on the cyclic oxidation resistance and lifetime of thermal barrier coatings. *J. Alloys Compd.* **656**, 992–1003 (2016). <https://doi.org/10.1016/j.jallcom.2015.07.271>
212. H.J. Yang, Y.T. Pei, J.C. Rao, J.T.M. De Hosson, Self-healing performance of Ti₂AlC ceramic. *J. Mater. Chem.* **22**(17), 8304–8313 (2012). <https://doi.org/10.1039/C2JM16123K>
213. S. Li, G. Song, K. Kwakernaak, S. van der Zwaag, W.G. Sloof, Multiple crack healing of a Ti₂AlC ceramic. *J. Eur. Ceram. Soc.* **32**(8), 1813–1820 (2012). <https://doi.org/10.1016/j.jeurceramsoc.2012.01.017>
214. A.-S. Farle, C. Kwakernaak, S. van der Zwaag, W.G. Sloof, A conceptual study into the potential of Mn+1AX_n-phase ceramics for self-healing of crack damage. *J. Eur. Ceram. Soc.* **35**(1), 37–45 (2015). <https://doi.org/10.1016/j.jeurceramsoc.2014.08.046>
215. K. Van Tittelboom, N. De Belie, Self-healing in cementitious materials—a review. *Materials* **6**(6), 2182 (2013)
216. M. Wu, B. Johansson, M. Geiker, A review: self-healing in cementitious materials and engineered cementitious composite as a self-healing material. *Constr. Build. Mater.* **28**(1), 571–583 (2012). <https://doi.org/10.1016/j.conbuildmat.2011.08.086>
217. D. Snoeck, N. De Belie, From straw in bricks to modern use of microfibers in cementitious composites for improved autogenous healing – A review. *Constr. Build. Mater.* **95**, 774–787 (2015). <https://doi.org/10.1016/j.conbuildmat.2015.07.018>

218. E. Tziviloglou, K. Van Tittelboom, D. Palin, J. Wang, M.G. Sierra-Beltran, Y.C. Ersan, R. Mors, V. Wiktor, H.M. Jonkers, E. Schlangen, N. De Belie, Bio-based self-healing concrete: from research to field application. *Adv. Polym. Sci.* (2016). https://doi.org/10.1007/12_2015_332
219. http://ntechresearch.com/market_reports/markets-for-self-healing-materials-2015-2022. (Last accessed: 02 May 2016)
220. <http://www.rsc.org/chemistryworld/2013/09/polymer-regenerates-elastomer-heals-independently>. (Last accessed: 02 May 2016)
221. <http://www.autonomicmaterials.com/>. (Last accessed: 02 May 2016)
222. <http://www.arkema.com/en/media/news/news-details/Self-healing-elastomer-enters-industrial-production/>. (Last accessed: 02 May 2016)
223. <http://www.suprapolix.com/pages/polymers>. (Last accessed: 21 Feb 2016)
224. <http://www.sportsmansguide.com/product/index/do-all-ground-bouncer-3-pc-self-healing-impact-target-pack?a=1336175>. (Last accessed: 02 May 2016)
225. <http://www.ruehl-ag.de/index.php?id=160>. (Last accessed: 02 May 2016)
226. M.J. Harrington, O. Speck, T. Speck, S. Wagner, R. Weinkamer, Biological archetypes for self-healing materials. *Adv. Polym. Sci.* (2016). https://doi.org/10.1007/12_2015_334



Drug Delivery: Polymers in the Development of Controlled Release Systems

17

Scott Campbell and Niels Smeets

Contents

1	Introduction	720
1.1	Brief Overview of Traditional Delivery Methods	721
1.2	Importance of Concentration and Location	725
1.3	Device Considerations	726
1.4	Drug Considerations	729
2	Polymeric Systems for Controlled Drug Release	731
2.1	Polymeric Implants	732
2.2	Hydrogels	733
2.3	Nanomedicines: Nanoparticles, Microgels, and Micelles	735
3	Conclusions	740
	References	740

Abstract

This chapter comprises an overview of the basic elements that one must take into account when developing a new drug delivery system. It begins with an outline of traditional methods to deliver drugs, relating these to important considerations that must be taken into account when developing a drug delivery system, including the importance of controlling the drug concentration and location, and the properties of the device and the therapeutic. This chapter then continues by describing various types of polymeric delivery systems, including implants, hydrogels, and nanoparticles, microgels, and micelle nanomedicines. This chapter then concludes with a brief perspective on the potential of nanomedicine drug

S. Campbell (✉)

Department of Chemical Engineering, McMaster University, Hamilton, ON, Canada
e-mail: scott.campbell.88@gmail.com

N. Smeets

EcoSynthetix, Burlington, ON, Canada
e-mail: nbmsmeets@gmail.com

© Springer Nature Switzerland AG 2019

M. A. Jafar Mazumder et al. (eds.), *Functional Polymers, Polymers and Polymeric Composites: A Reference Series*, https://doi.org/10.1007/978-3-319-95987-0_20

719

delivery systems; a much more thorough perspective can be found in Chap. 27, “Drug Delivery: Localized and Systemic Therapeutic Strategies with Polymer Systems.”

Abbreviations

BA	Bioavailability
BMA	Butyl methacrylate
CLRP	Controlled-living free radical polymerization
CMC	Carboxymethyl cellulose
DP_A	Hydrophobic block
DP_B	Hydrophilic block
EPR	Enhanced permeability and retention
FDA	US Food and Drug Administration
GI	Gastrointestinal
HA	Hyaluronic acid
IM	Intramuscular
IR	Infrared
IV	Intravenous
MPS	Mononuclear phagocyte system
NIPAM	<i>N</i> -isopropyl acrylamide
PBA	Phenyl boronic acid
PEG	Poly(ethylene glycol)
PGA	Poly(glycolic acid)
PLA	Poly(<i>L</i> -lactic acid)
PLGA	Poly(lactic acid-co-glycolic acid)
PMMA	Poly(methyl methacrylate)
PNIPAM	Poly(<i>N</i> -isopropyl acrylamide)
POEGMA	Poly(oligoethylene glycol methacrylate)
PVA	Polyvinyl alcohol
RGD	Arginine-glycine-aspartic acid
SC	Subcutaneous
SPIONs	Superparamagnetic iron oxide nanoparticles
T_g	Glass transition temperature
Z	Aggregation number

1 Introduction

Achieving better control over drug release is essential to improving the effectiveness of a wide range of therapies targeting specific ailments and diseases throughout the body. The development of drug delivery methods that can deliver controlled, sustained amounts of drug to specific locations while still being tolerable to the body would drastically enhance how healthcare is provided globally. Such a release system could improve the efficacy of the therapeutic, the safety of the treatment, the

duration of the treatment, minimize resistance to medication, patient compliance, decrease the amount of times a treatment is administered, and eventually even be personalized for the treatment to specific individuals [1, 2].

Advancements in the field of polymer synthesis and functionalization have proven essential in the development of better drug delivery technologies. Indeed, the maturation of the field of polymeric drug delivering biomaterials has led to the improved capability in controllably producing polymers with precise molecular weights, structures, and functionalities. This is not to say that it is solely these fields that are linked. In fact, drug delivery as a whole is wildly multidisciplinary; the evolution of improved controlled delivery devices has required advancements in a wide variety of other areas of research to get to where it is today, such as biology, imaging technologies, drug discovery, and gene therapy, to name a few. Once an understanding of the biological response to foreign materials has been acquired, how to maximize the effectiveness of a given drug for a specific therapy (i.e., dosage, duration of treatment, localization, etc.) and the rate at which the drug will be eliminated from the body (the pharmacokinetics) is established, an optimal controlled release system can be designed. This is where the innovations in polymer synthesis technologies come into play. The deft use of polymeric biomaterials can be used to match the ideal release characteristics for a specific drug and therapy, resulting in significant improvements over current conventional clinical methods.

This chapter highlights the use of such polymeric biomaterials as controlled drug delivery systems that are currently commercially available or extensively researched. This chapter first discusses the importance of knowing the characteristics of the therapeutic intended to be released and releasing the correct amount of this therapeutic in the correct location for treatment. We will then delve into the types of polymeric systems that are often used to develop drug releasing materials (polymers in inorganic implants, micro/nanoparticles, micelles, polymeric capsules, and hydrogels).

1.1 Brief Overview of Traditional Delivery Methods

To understand the benefits of controlled release systems, we must first briefly discuss traditional delivery methods. The majority of drugs are intended to ultimately reside in the blood stream, circulating systemically to perform their treatment. This lack of localization of most drug systems is the source of the lengthy list of side effects seen with most therapeutics, with exception to only the safest drugs. Of these systemically delivered drugs, 90–95% are delivered either orally or injected/infused parenterally [3].

Oral dosage forms are incredibly common as they have fairly consistent transit times in the body, are easy to use, and are socially acceptable, leading to good patient compliance [4]. However, oral administration is the least efficient and a highly variable delivery mechanism as the drugs have to transit through myriad of hostile environments on their way to being passed into the systemic blood stream. The majority of drug absorption occurs in the small intestines, so the drugs must first pass

through the low pH and enzyme-containing environment of the stomach. The time the drug spends in the stomach, and consequently drug absorption overall, depends on whether the delivery system is solid or liquid (liquid forms pass through more rapidly), the size of the delivery vehicle, and the amount of food in the stomach [5, 6]. The drug then comes into contact with bile salts in the large intestine that can emulsify fats or lipids to allow them to be absorbed, but ~15–20% of bile salts are ultimately excreted as waste if this is the intended mechanism of drug absorption. The drug then reaches the small intestine and must pass through negatively charged mucus, which readily entraps cationic drugs, to get absorbed by the villi in the small intestine. The absorption is facilitated by the high surface area of the villi and the short distance between the surface of the villi and the blood capillaries that lead to the portal vein. After all of this, the drug still has to pass through the biggest challenge it faces to reach the blood stream, as the liver stands in the way between the portal vein and the systemic blood stream. The liver, the metabolic engine of the body, is able to metabolize a wide range of drugs and severely limits proteins and peptides from being delivered in simple dosage forms [6–8]. The fact that the drugs must pass through the liver before reaching the bloodstream is known as the hepatic “first-pass effect,” which is the primary cause of the inefficiency and low bioavailability (BA), the fraction of the administered dosage that reaches systemic circulation, of oral dosage forms [4, 7].

Intravenous (IV) injections, on the other hand, are the most efficient way to get material into the blood stream. The bioavailability for IV injections is 100%, which allows for any drug to be delivered via this mechanism with a rapid onset of action. There are several disadvantages to these injections: there is a risk of infection; it presents as a shock to the system, where delivering excessive dosages is often not be a recoverable mistake; it requires a professional; they generate medical waste; there is a risk of disease transmission via needle reuse; and the drugs have a short half-life in the blood stream [9]. Intramuscular (IM) and subcutaneous (SC) injections are slightly safer in terms of the degree to which they are a shock to the system, as the drug must diffuse through the tissue and into capillaries to reach systemic circulation. This leads to a lag in the onset of action, as it accumulates in the circulatory system at a slower pace, and bioavailabilities that are <100%. These tissues are more acidic than most tissues, and the diffusion rate is largely dependent on the drug’s size. Larger drugs that are less sensitive to acidic environment can exhibit slower, more sustained release with this method.

Another delivery method that is largely dependent on diffusion is transdermal delivery. If a drug reservoir or a topical solution is applied to the skin, the drug must diffuse through the stratum corneum, which is the hardest layer to pass through and the rate limiting step, the viable epidermis, and the epidermis to partition into circulation [9]. The stratum corneum is particularly thick (10–20 μm) and most drugs are transported on a tortuous lipidic intracellular pathway through this region [10]. A proportion of the absorbed drug is then subject to the first-pass effect, depending on the capillaries that the drug is absorbed into. These factors limit this form of delivery to low molecular weight, potent drugs that can be delivered slowly over prolonged amounts of time, which is particularly beneficial for the treatment of

chronic pain, glaucoma, hypertension, contraception, attention deficit hyperactivity disorder, and smoking cessation, among others [10].

Buccal (inner cheek) and sublingual (under the tongue) are two common delivery methods that take advantage of highly vascularized tissues with a relatively thin epithelial lining [11]. These methods have high bioavailabilities with rapid onset of action that can be comparable to injections, as administered drugs can readily diffuse through the tissue and reach circulation via the jugular vein that avoids the first-pass effect [10]. High bioavailabilities can be achieved via this route for small molecules (15–70%) and, importantly, for peptides as well (<25%). Adhesive tablets, gums, lozenges, and lingual sprays have been commercialized and used to deliver drugs suitable for acute, patient-administered therapies, such as pain management, insomnia, smoking cessation, diabetes, etc. [10]. However, these tissues have low surface areas, the region markedly limits the dosage that can be applied, and the taste can present as a major inconvenience for the patient (particularly if long time scales are required) [11].

Intranasal delivery has similarly high bioavailabilities to buccal and sublingual delivery for many of the same reasons: a thin epithelial lining (even thinner than buccal delivery) that is highly vascularized and relatively leaky in nature in comparison to other mucosae that can allow drugs to bypass the first-pass effect [10, 12]. Nasal tissues also possess high surface area amenable to efficient delivery. The primary inhibiting factor that decreases the BA via this delivery method is the viscous, enzyme-containing mucous that coats this region. This mucous is capable of trapping larger drugs that cannot diffuse rapidly through it. It is also highly anionic and has a pH of 5.5–6.5, which can affect the diffusion and activity of certain drugs. Despite this, the nasal route has proved clinically useful for peptides and small molecules, including lypressin, progesterone, insulin, vitamin B-12, calcitonin, etc., as they have higher viabilities using this route (~10%) than via other strategies ($\leq 1\%$) [10, 12]. Small, lipophilic, nonionic drugs tend to possess greater bioavailabilities via this route.

The pulmonary route also possesses a large available surface area ($>100\text{ m}^2$), combined with an extensive blood supply with only a thin membrane separating the air from the blood and systemic circulation; however, it is difficult to ensure that the drug reaches this site [10]. The particles must be of an optimal size ($\sim 0.5\text{--}5\text{ }\mu\text{m}$) to be delivered to tissues deep within the lung with still highly variable efficiencies between 30 and 60% in the lungs [10, 13]. Some of the drug that does reach the site can also be trapped by the thick mucus layer that is present, which is carried by cilia toward the trachea by what is known as the mucociliary escalator [10]. The fact that low proportions of the drug reach the lungs leads to variable (low) BAs and provided doses. These disadvantages have led to the focus for many pulmonary systems being placed on the treatment of local diseases or conditions, such as congestive obstructive pulmonary disease, asthma, and respiratory infection [10].

The last of the more common delivery routes are rectal, vaginal, or urethral. Of these, rectal is most commonly used, often when the patient is vomiting, immobile, unconscious, or has difficulty swallowing [10]. It is also a highly vascularized region with few layers of epithelial cells with a mucosal layer that can trap materials similar

Table 1 Advantages and limitations of common delivery routes

Route	Pros	Cons
Oral	Convenient Consistent transit time Good compliance Most commercialized dosage route	Lowest BA First-pass effect, gut exposure No protein/peptide delivery
Intravenous (IV) injections	100% BA Rapid onset of action	Inconvenience Infection risk Short half-life Overdosing is a major concern – no time to recover
Intramuscular (IM)/subcutaneous (SC) injections	Good BA Avoids gut exposure Slower, more sustained release compared to IV	Inconvenience Requires a professional Infection risk
Transdermal	Convenience Good compliance Skin resistant to damage	Limited to low molecular weight, potent drugs Toughest barrier
Buccal/sublingual	Good BA Several dosage forms amenable to small molecules/peptides Avoids first-pass effect, gut exposure Easy to access, good compliance	Inconvenience – taste Limited size of drugs, device Clearance by saliva Selective permeability Local toxicity of adhered dose
Intranasal	Good BA Quick onset of action Avoids first-pass effect, gut exposure Convenience, good compliance	Limited size of drugs Mucous limits types of drugs that can penetrate through, can clear drugs Taste and sensory liability
Pulmonary	Convenience Large surface area for absorption Well perfused with blood vessels	Unpredictable BA Limited dose, dose volume, applications Clearance by mucociliary escalator
Rectal	Better BA than oral route Portion avoids first-pass effect	Inconvenient Erratic absorption Sociocultural stigma

to aforementioned mucosal layers. It also has a better BA than oral administration as ~50% of the drug typically bypasses the first-pass effect. Of course, this route is inconvenient, has patient compliance issues, and sociocultural stigma and sensitivities associated with it [10].

All of these typical administration methods are outlined in Table 1 with their primary advantages and disadvantages. Controlled release systems are designed to overcome or alleviate many of the shortcomings listed in this table by mediating the

precise amount of drug being released once they are in the body and/or spatially controlling where the drug is released after it is administered.

1.2 Importance of Concentration and Location

The goal of controlled release is to extend the time frame that the drug is in active use for in a given treatment in comparison to traditional delivery techniques and to improve the efficacy of treatment in the process [3]. For each particular treatment type, there is a minimum drug concentration above which the drug can successfully treat the given malady and below which the concentration is inadequate to effectively treat the condition, termed the minimum effective dose. Simultaneously, there is another concentration above which the amount of drug is toxic to the body known as the toxic limit [14]. The range of concentrations in between the minimum effective dose and the toxic limit is called the therapeutic window, and this is the target region for clinical therapy. A schematic of typical drug concentrations delivered by various different methods after the time of administration is shown in Fig. 1.

Intravenous (IV) injections go directly into the blood stream with the concentration generally above the toxic limit initially. As the drug is rapidly cleared from the blood stream (often renally, however this largely depends on size and hydrophobicity of the drug), it traverses through the therapeutic region until its concentration reaches the minimum effective dose. Extravascular delivery methods, such as oral, pulmonary, and topical treatments take longer to be initially introduced to the blood stream, and their concentration slowly increases until it reaches into the therapeutic window. Once in the blood stream, the drug will be cleared in a similar manner to the IV injections, but the rate of drug supplied to the blood stream should overcome the rate that it is being cleared at for a short time frame before the drug concentration

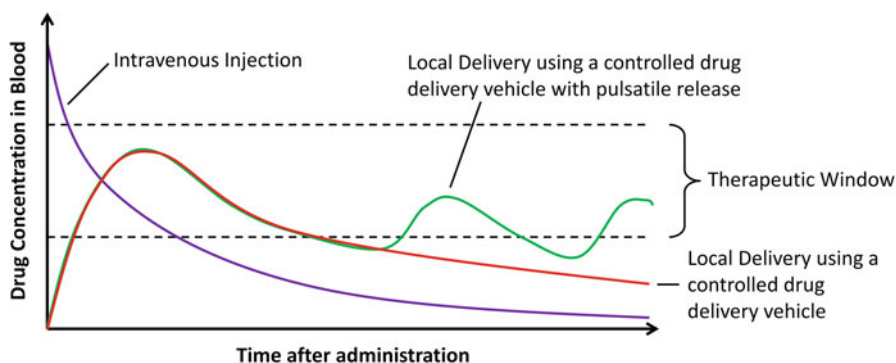


Fig. 1 Representative figure of drug concentration over time for various forms of release. This figure shows the advantage of local delivery over traditional methods: the drug's systemic blood concentration remains below toxic limit (upper dashed line) while persisting above the minimum effective dose for the region (lower dashed line) for a longer period of time

plateaus, ideally still within the therapeutic window, and ultimately falls below the minimum effective dose concentration.

Controlled release systems are often intended to slowly release drugs such that they will slowly head into the therapeutic window, similar to extravascular drug delivery systems, but then persist in this region by continuing to deliver drugs over a much longer time frame while they are therapeutically effective [14, 15]. This is possible because their controlled release capabilities allow them to be loaded with much more drug initially and, if designed correctly, they will slowly deliver their payload without reaching a toxic level of drug concentration. Upon the expulsion of the majority of their payload, their release rate will dip below that of the clearance rate of the drug from the bloodstream until the drug is no longer effective. The pharmacokinetics of controlled release devices could allow for more effective treatment, while lowering the frequency and number of administrations that are required for a given treatment, which could be much more convenient for the patient and, consequently, improve patient compliance.

These benefits could be further enhanced by advances in drug delivery technology which have led to the development of controlled release devices with the ability to deliver drugs in a pulsatile manner [16]. The idea for these is to be capable of a drug release profile similar to controlled release devices initially, but then also have the ability to deliver further pulses of release after it initially leaves the therapeutic window, leaping the drug concentration back into the therapeutic window when desired/required by the patient. This type of mechanism is aiming to mimic how cells, the smartest delivery vehicles, supply growth factors, cytokines, and extracellular matrix materials when necessary based on signals from their surround environment *in vivo* [3]. These more advanced release systems would be particularly relevant as replacements for treatments that require frequent injections (i.e., pain management, diabetes) and could also allow for more personalized clinical treatments where the variations in response that different individuals have to various treatments can be offset by real-time dose management [17, 18].

Note that while Fig. 1 refers to the drugs concentration in the blood, this primarily refers to drugs intended for systemic therapy. An analogous figure could be made for locally focused therapy where the drug concentration in the therapeutic region of interest is the primary consideration (and the label of the y-axis).

1.3 Device Considerations

Much of the initial commercialized controlled release work involved orally delivered systems were improved by using advances in polymer technology to protect the drug as it passes through the gastrointestinal (GI) tract and deliver the drug payload once it reaches the intestines, where the drug can be absorbed into the blood stream [19]. An example of this would be polymer-based capsules that are stable at the low pH of the stomach and then release drug in the higher pH environment of the intestines by the capsule degrading, dissolving, or swelling and bursting [20]. These technologies do not stop a large portion of the drug from being metabolized in the hepatic first-pass

effect but can significantly enhance the bioavailability of the systemic drugs they are delivering.

Greater improvements over current therapies take advantage of one of the clear major benefits of many controlled release systems: the ability to direct delivery at a particular, preordained site in the body. This can be achieved by two major mechanisms: by using a macroscale system that is implanted or injected at the specific site of interest, such as degradable polymers or a polymer as a semi-permeable membrane within a drug-loaded implant, or injectable hydrogel delivery systems; and the use of nanoscale systems that are designed to travel through the circulatory blood stream and accumulate in a specific location via a ligand-targeting mechanism, the enhanced permeability and retention (EPR) effect (the theory that the extra blood supply required by tumorous tissues results in leaky vasculature that promotes the preferential accumulation of certain nanoparticles at these tumorous sites), and/or externally-mediated targeting (i.e., magnetic guidance of metallic nanoparticle-polymeric nanocomposites). If the device can be successfully localized at the desired location, the number of systemic side effects should be limited, the treatment could occur over a longer time frame with any given dosage, and efficacy of treatment can be improved by the fact that the bioavailability of the drug to the target site will be improved [14].

Any foreign material that is placed in the body, particularly foreign materials that are intended to remain located at a specific site for a longer length of time, will be subjected to an immune response from the host. A key parameter in the design of controlled release systems is minimizing this response to negate the removal of the delivery vehicles from the body and/or the formation of a fibrous capsule that can affect the pharmacokinetics of drug release.

For therapeutic delivery using nanoparticles that circulate in the blood stream, the major limitation is the nonspecific uptake of the nanoparticles in healthy organs that prevents the accumulation of enough nanoparticles at the disease site to allow for the concentration of drug to reach therapeutic levels [21]. This is due to the mononuclear phagocyte system (MPS), a system of largely macrophages in the liver, spleen, and lymph nodes, sequestering nanoparticles rapidly postinjection. The cascade begins with what is known as the opsonization of the nanoparticles, where plasma proteins adsorb onto the surface of the nanoparticles, which can also mask targeting ligands on the particles [22]. These proteins promote the attachment of the nanoparticles to specific receptors on phagocytes, which then internalize the particles and transport them to phagosomes which fuse with lysosomes. This process is vital to consider, because if the nanotherapeutic device accumulates in alternative tissues, it can cause undesired release and undesired effects, particularly if the drug or delivery material is toxic in heightened quantities in the tissue it has accumulated in.

Importantly, the initial formation of the protein corona around the nanoparticles is dependent on the nanoparticle's size, surface charge, rheology, hydrophobicity, and surface chemistry, which can all now be engineered fairly well due to advances in materials and polymer science at the nanoscale. To ensure suitable circulation half-lives for nanotherapeutic delivery systems, their size should generally range from ~5 nm to 200 nm, and particles of 50–100 nm are generally long-lasting in circulation and have been shown to accumulate in tumors via the EPR effect [22]. This is

because particles <5 nm are rapidly removed from circulation via renal clearance, and particles >200 nm are larger than the cell slits of the spleen [22]. Larger particles 2–5 μm readily accumulate in the capillaries of the lungs [10]. In terms of surface charge, cationic materials tend to adsorb negatively charged serum proteins, leading to nonspecific accumulation and rapid clearance from circulation. Nanoparticles with neutral and negative surface charges have longer circulation half-lives, as they reduce the adsorption of serum proteins, and negatively charged materials have been shown to experience lower accumulation in the liver and spleen [21].

The rheological properties of the nanoparticles also is important, as softer, more deformable, nanogels have been shown to experience longer circulation half-lives and are less prone to accumulating in the spleen, as they are able to deform and squeeze through the interendothelial slits in the spleen [22]. Highly deformable nanogels that accumulated in the spleen were also shown to migrate back into the circulatory system over time. Similar nanogels have been shown to deform enough to pass through other difficult barriers in the body, such as the blood-brain barrier, which has a cut-off of ~ 400 – 550 Da.

The hydrophobicity of the nanotherapeutic delivery system is also highly important, with proteins attaching to anything that is not hydrophilic enough. The most widely used method to shield nanoparticles from protein adsorption is PEGylation, where the highly hydrophilic poly(ethylene glycol) (PEG) is densely grafted onto the surface of the nanoparticles [22]. The PEG forms strong associations with water molecules, forming a hydrating layer that inhibits protein adsorption. Similar hydrophilic polymers, such as polyvinyl alcohol (PVA) and polysaccharides, can also extend the circulation lifetime of nanoscale vehicles in a similar manner.

Macroscale devices that are injected/implanted into the body will not be rapidly cleared from the body but face some of the same issues as nanoscale circulating systems initially with regards to their biocompatibility. When a foreign material is implanted/injected into the body, it disrupts the anatomic continuity of the tissues, and the wound healing response is triggered [3]. This begins again with proteins adhering to the surface of the biomaterial and platelet cells adhering to these attached proteins and releasing clot-forming proteins, a stage known as hemostasis. This initiates the inflammation stage, where cytokines are released to recruit inflammatory cells (neutrophils, monocyte, lymphocytes, and macrophages) that initiate phagocytosis, the digestion of tissue and biomaterial debris, and release growth factors [3]. The growth factors stimulate the proliferation of cells that can recreate the damaged tissue and may form a tight, fibrous capsule around the biomaterial, a process known as fibrosis, effectively isolating it from the native tissues. The thickness of the fibrous capsule is governed by extent of the foreign body response [3]. Since this fibrous capsule can affect the kinetics of drug release and prevent the integration of the biomaterial with host tissues, which is essential for degradable and/or wound healing systems, limiting the extent of the inflammatory response is often critical for delivery systems.

While one can limit protein adsorption onto these materials, as is done for circulating nanomedicines, it is difficult to stave off protein adsorption entirely for materials that will be present in the body for extended amounts of time. Making the

biomaterial hydrophilic and anionic rather than cationic will limit the extent of the immune response, but the best way to limit this response as much as possible is to mimic the native tissues as much as possible. For example, hydrogels are water-swollen crosslinked networks of water soluble polymers that, with current polymer engineering, are highly tunable such that they can be developed to be mechanically and physiochemically and similar to extracellular matrix of soft tissues [23]. As a result, many hydrogel-based biomaterials have been injected or implanted and are well-tolerated by the body. One must consider the rheology, surface charge, hydrophilicity, and density of the environment of treatment site and compliment these properties as best as possible with the implanted device.

The size and shape of macroscale biomaterials and their components may influence fibrosis and other factors that may be essential to the effectiveness of a biomaterial. For example, surface porosity has been determined to be important parameter influencing angiogenesis in tissue engineering with the strongest angiogenic response occurring with pore sizes of 30–40 μm , much larger than initially believed [24]. While it was not the case for this particular biomaterial, a similar biomaterial could be used to simultaneously release growth factors for tissue engineering or wound healing. A similar finding was seen when observing how the geometry of several materials affected the host recognition and foreign body immune response. It was found that spherical materials, including hydrogels, glass, stainless steel, and latex and natural polymers, were the most biocompatible, but, notably, spheres greater than ≥ 1.5 in diameter markedly mitigated foreign reactions and fibrosis [25]. Both of these results showed that cells seem to prefer surprisingly large, well-contoured smooth surfaces.

Ideally, the material can also slowly degrade into nontoxic components that can be phagocytosed and naturally removed from the body over time [21, 26]. If the material cannot be degraded, it will ultimately be surrounded by a fibrous capsule unless it is surgically removed prior to the formation of the capsule. Biodegradable hydrogels can be used to entrap and hide micro- and nanoscale polymer delivery vehicles, effectively hiding them from the immune response, improving their biocompatibility, while they deliver their payload until they are slowly released as the hydrogel degrades [27]. Degradation might also generally be an important factor of the delivery of the therapeutic if that is how the drug is released. The degradation and subsequent release rate can be controlled by altering the chemistry by which the material degrades in the environment conditions of the desired disease site. Many polymeric release systems utilize enzymatic and hydrolytic degradation to either degrade the polymer by surface erosion to slowly release the therapeutic or to degrade a covalent link between the vehicle and the drug to control release and limit the burst release that is often associated with diffusion-based systems [27].

1.4 Drug Considerations

While considering all of the above factors, it is important to develop the device so that it can be easily delivered to the disease site and to match the properties of the

device with the appropriate drug for treatment to optimize the compatibility between the two. The drug can be associated with the device via charge, hydrophilicity, or even be covalently attached. Generally, the greater the affinity that exists between the drug and the vehicle, the greater the loading efficiency and the cumulative drug loaded is. Improvements in the drug-carrier compatibility can be achieved by altering the carrier, covalently tethering the drug to the carrier, or by drug derivatization, to adjust the drug's hydrophobicity or miscibility with the carrier [28]. The device can also be used to effectively conceal the drug from the body until it is used. However, if the drug is attached such that it is exposed to the external environment, the effects that this may have on protein adsorption and the biocompatibility of the device must be considered [28].

Drug-carrier compatibility is greatly influenced by the hydrophobicity of both components. The better these hydrophobicities match up, the easier it generally is to load drugs into these materials. A wide range of delivery vehicles are designed to slowly deliver hydrophobic drugs, as these are difficult to deliver via traditional methods, particularly with any sort of spatiotemporal control. For example, hydrophobic drugs will preferentially partition into the hydrophobic domains of delivery devices. These hydrophobic domains could consist of a more hydrophobic pocket or region within a hydrogel or capsule to the hydrophobic core of nanoparticles stabilized with a hydrophilic shell. Hydrophilic drugs can also be delivered from delivery vehicles, but they will partition into the generally hydrophilic environment of the body at a more rapid rate.

If ionic interactions are to be used to partner the drug with the delivery vehicle, control of the distribution of charge in the vehicle can also influence where the drug will preferentially be located in the vehicle. For example, distributing the charge such that the majority of charge is located near the center of a nanogel can hide the majority of an oppositely charged drug in the center region of the hydrogel [29]. Anionic drugs could also be loaded into similar zwitterionic nanogels with a cationic core to hold the drug and an anionic surface to repel proteins in circulation. The control of distribution of charge in this manner could be used for a wide variety of systems.

When the drug is intended to diffuse out of the release device, the size of the drug can also be an integral factor. With all other parameters constant, smaller drugs will diffuse out more rapidly than larger drugs. The passive Fickian drug diffusion rate can be altered by adjusting properties of polymeric carriers, such as the porosity, hydrophilicity, average molecular weight, surface charge, and for hydrogel-like material, crosslink density [30–32]. Particularly for hydrophobic systems, the better the drug-carrier affinity, the slower the diffusion rate will be, as the drug will not be as inclined to partition into the relatively hydrophilic environment of the body.

Drugs can be covalently conjugated to their delivery vehicle to slow or mediate their release, either through a degradable linkage that will release the drug over time or by immobilizing the drug on the surface of the vehicle, as is done for numerous nanomedicines. For this latter scenario, the effects of immobilizing a specific drug entity on its biological activity must also be considered [3]. For proteins in particular, the immobilization of certain proteins to the polymeric delivery vehicle could lead to

conformational changes that expose the active portion of the protein and enhance its activity. On the other hand, the opposite could also occur and all biological activity might be lost. Even if the proteins could be released from their associated polymer, their free activity may be adversely affected by the immobilization process. Therefore, choosing the appropriate chemistry for immobilization can be critical.

The stability of the drug-carrier interaction can be critically altered in the *in vivo* environment. This effect has been evident in the use of nanoparticle carriers that carry chemotherapeutics in their hydrophobic cores, either by physical entrapment or covalent attachment. The bioavailability of these systems to the target site is often lower than expected not only due to less than optimal biodistribution but also because the blood components can act as competing drug acceptors [28]. The resulting drug leakage, where a significant amount of the drug being delivered is released prior to the device reaching its target site, can be reduced by drug derivatization to improve the drug-carrier interaction. For these systems, altering the drug's chemistry so that it is more hydrophobic or so that it is more miscible with the core material have been shown to improve the drug-carrier compatibility enough to limit drug leakage [28]. The derivatization of drugs could be used to similarly improve drug-carrier interactions for a wide range of vehicles, provided that the activity of the therapeutic is not negatively affected.

While tuning the characteristics of the drug and delivery vehicle are integral to developing polymeric controlled release systems, a wide range of different types of polymeric systems that were alluded to above, including polymeric capsules, nanoparticles, and hydrogels, can be used for these purposes. Choosing the right polymeric system to suit the therapeutic purpose can be highly important. In order to make this important decision, a deep understanding of the characteristics and synthesis of, and mechanisms of release from these different types of polymeric systems is required.

2 Polymeric Systems for Controlled Drug Release

The diversity of tissues within the human body virtually eliminates the possibility of a “silver bullet” for controlled drug delivery. Consequently, many different polymeric systems have been developed to deliver drugs in a targeted and controlled manner to various tissues. These polymeric systems can be categorized based on their dimensions, ranging from macroscopic (1–10 mm, e.g., polymeric implants and contact lenses) to microscopic (1–100 μm , e.g., hydrogels) and finally nanoscopic (1–100 nm, e.g., polymer nanoparticles, capsules, and micelles) [33]. The design of a polymeric device to deliver a specific therapeutic to a target tissue is governed by the nature of the tissue and the ease and method by which that tissue can be reached. For example, polymeric implants are preferred for delivering therapeutics to the body's exterior organs, such as the skin and eye, or for tissues located directly under the skin that are easily accessible using minor surgical methods. However, for cancerous tissues or delicate internal organs such as the heart and brain, nanoparticles or injectable hydrogels are preferred as these can be administered using minimally

invasive surgical methods such as catheters and injections which reduce patient's level of discomfort and the risk of infection. Irrespective of the type of polymeric drug delivery device selected for the intended application, any device has to be sufficiently stable under physiological conditions, biocompatible, degradable (or at the very least clearable), and should not trigger an adverse immune response from the host. Furthermore, the therapeutic payload should be released at the desired location and, ideally, for a prolonged period of time with a sustained concentration within the therapeutic window. Despite all these requirements, many successful drug delivery devices have been developed and a selected number have found their way into the clinical application [34]. Current developments are now moving towards more sophisticated polymeric devices that can either autonomously respond to queues (e.g., change in the physiological temperature or pH or the presence of specific biomolecules) presented *in vivo* or respond to external stimuli (e.g., magnetic fields or near-infrared (IR) irradiation) to trigger on-demand release of the therapeutic at the desired location.

2.1 Polymeric Implants

The medical community relies heavily on implantable medical devices to treat a variety of diseases such as the vascular stent to preserve blood flow or the acetabular cup that lines acetabulum in a hip replacement. These polymeric devices also hold great potential for the controlled release of therapeutics and have consequently been used, for example, for glaucoma treatment using contact lenses [35] or to treat restenosis using drug eluting stents [36]. There is great diversity in the design, shape, and size of polymeric implantable drug delivery devices, but essentially they consist of a drug reservoir and a polymer matrix that the drug has to diffuse through to become bio-available and deliver its therapeutic effect. The rate at which the drug is released from the polymer matrix is predominantly controlled by the pore size or void space between adjacent polymer chains that make up the matrix.

Implantable polymer drug delivery devices are generally divided into passive and active delivery systems [37]. The principle of passive delivery systems is that release of the therapeutic is predetermined by the choice of the materials, fabrication methods, or drug formulation and cannot be altered once the device is implanted *in vivo*. The simplest example of a passive delivery system are the earliest drug eluting contact lenses, where the contact lens was soaked in a drug containing eye-drop solution followed by diffusional release once applied onto the postlens tear film [38]. More sophisticated designs are based on poly(lactic acid) (PLA), poly(glycolic acid) (PGA), or poly(lactic acid-co-glycolic acid) (PLGA) [39], which are US Food and Drug Administration (FDA) approved, biocompatible, and biodegradable polymers. PLGA-based implants are bioerodible under physiological conditions [40], and the rate at which they erode, and consequently release the therapeutic, can be controlled to great extent. Conversely, active delivery systems provide a means to control release after implantation using external stimuli, requiring an additional level of sophistication in terms of the polymer design. For polymeric devices, this often

results in the use of responsive polymers that exhibit a physiochemical change due to changes in the temperature or pH. Ibuprofen release was triggered externally from an implantable device by heating the poly(methyl methacrylate (MMA)-co-butyl methacrylate (BMA)) matrix above its glass transition temperature (T_g) [41, 42]. Heating was achieved by embedding superparamagnetic iron oxide nanoparticles (SPIONs) that can be selectively heated when placed in an alternating magnetic field. Another example, also utilizing SPIONs, was reported where “on-demand” drug delivery was realized by embedding temperature responsive poly(*N*-isopropyl acrylamide) (PNIPAM) microgels into an ethyl cellulose membrane covering a drug depot. Heating of the SPIONs causes a reversible discontinuous phase transition of the PNIPAAm polymer which results in deswelling of the microgels and, consequently, release of drug from the encapsulated depot [43].

Recent developments in the synthesis of polymeric materials, combined with novel fabrication techniques for polymeric devices (e.g., microfluidics or 3D printing), has resulted more complex and more sophisticated designs [33]. Ultimately, it is the expectation that these complex microfabricated devices can deliver drugs “on-demand,” by coupling sensors to measure local concentrations of bioactive molecules and responding autonomously. Currently, this is only under clinical investigation for implantable devices that can measure blood glucose levels and release appropriate amounts of insulin to treat diabetes [44, 45].

2.2 Hydrogels

Hydrogels are water-swollen polymer networks that are formed as a result of physical or chemical cross-linking of water-soluble polymers [46]. Hydrogels possess high water content, excellent biocompatibility, controllable porosity, and mechanical and (potentially) compositional similarity to native soft tissues [47], and have consequently been of interest for drug delivery applications [23]. However, the hydrophilicity of hydrogels combined with their high water content and high porosity results in low affinity for hydrophobic drugs and fast release kinetics generally ranging from a few hours to a few days [23]. Furthermore, the inherent elasticity of these materials often necessitates surgical implantation. Successful clinical application of hydrogels for drug delivery has yet to reach the market and their biomedical application therefore currently remains limited to contact lenses, hygiene products, and wound dressings [20].

Much of the foundational work on the relationship between the physical hydrogel structure and the drug release kinetics [48] was reported on hydrogels prepared from a “bottom-up” approach, i.e., the polymerization of water-soluble monomers and cross-linker(s). Contact lenses are a good example of “bottom-up” hydrogels [49] and their composition can be easily adjusted by incorporating functional monomers to improve drug affinity and positively affect the release kinetics [38]. A particularly promising approach is the use of functional monomers in combination with imprinting to form high affinity cavities within the hydrogel matrix, as was for example demonstrated by using methacrylic acid in combination with a timolol (cationic drug

used in glaucoma treatment) [50]. Wound dressings are another example where “bottom-up” hydrogels are used to deliver antimicrobials, growth factors, and/or supplements to the wound [51]. A range of hydrophilic monomers have been used to prepare such hydrogels, often including biopolymers such as hyaluronic acid (HA), collagen, or chitosan [51]. Similar to contact lenses, drug release in wound dressing is also governed by molecular diffusion and faces many similar challenges in terms of achieving prolonged drug release. The use hydrogels for *in vivo* drug release often is paired with the use of poly(ethylene glycol)-based polymers and/or macromonomers to improve biocompatibility and mask the hydrogel from the host’s immune system [52].

A major drawback to the use of “bottom-up” hydrogels is that their synthesis conditions often are incompatible with *in vivo* conditions. Hydrogels fabricated from a “top-down” provide a promising route towards clinical *in vivo* application of hydrogels, as these materials are prepared by physical or chemical cross-linking of presynthesized polymer chains [53–55], especially given the extensive range of biorthogonal (click) reactions available for hydrogel synthesis [56]. Furthermore, these hydrogels can be injected into the patient’s body (avoiding invasive surgery) which also enables effective molding of the hydrogel shape *in situ* to fit existing cavities or defects in the native tissue which increases bioavailability of the drug. Our laboratory has reported extensively on injectable poly(oligoethylene glycol methacrylate) (POEGMA) hydrogels for *in vivo* drug delivery applications [57–60]. These hydrogels are prepared by coextruding two oppositely reactive POEGMA polymers (i.e., a hydrazide and aldehyde functionalized polymer, which react in a biorthogonal manner to form a reversible hydrazine bond) [61, 62] using a double barrel syringe with a 25 gauge hypodermic needle. The “top-down” approach provides significant advantages as the hydrogels can be easily injected subcutaneously [58], are fully degradable [60], and can be readily functionalized with hydrophobic moieties to increase affinity for hydrophobic drugs [63]. Another interesting example is the use of oxime cross-linking chemistry [64, 65], which has been used to deliver a PEG hydrogel to the ventricular wall of Sprague Dawley rats by means of a catheter [66]. One major advantage of using the “top-down” approach for hydrogel fabrication is that the resulting hydrogel networks are much more uniform [67, 68], which is a very important physical property that ultimately controls the drug release kinetics [52].

Current research efforts are focusing on the use of extending the use of various biorthogonal cross-link chemistries to achieve even better control over the uniformity of the hydrogel network and associated physiochemical properties such as the mechanical strength, degradation, and release kinetics, as well as to improve the biocompatibility of these materials during and after injection. Furthermore, there is a lot of emphasis on “smart” hydrogels that offer the possibility of a change in drug release kinetics as a response to a change in the environmental conditions [23, 69]. Ultimately, it is expected that hydrogels can reach a level of sophistication that will allow them to mimic natural systems that are able to release drugs on-demand in a self-regulated manner [70]. Some promising first steps are being made in this direction by fabricating hydrogels for self-regulated insulin delivery

[71, 72] and hydrogels that can self-regulate flow in microfluidic channels [73] (which can ultimately be used to control the release rate of therapeutics). Furthermore, many of these hydrogel materials are now being further functionalized with specific cell markers, such as the arginine-glycine-aspartic acid (RGD) peptide [57, 74, 75], to stimulate cell proliferation and tissue regeneration [76].

2.3 Nanomedicines: Nanoparticles, Microgels, and Micelles

Nanomedicine is broadly defined as the use of nanoscale or nanostructured materials in medicine that, due to their structure, have unique medical effects [77]. In light of this chapter, we focus on polymeric colloidal nanoscale materials including nanoparticles, microgels, and micelles. There is a lot of interest, both from academia and industry, for drug delivery applications for these materials, accounting for roughly 75% of the research activity in the nanomedicine market [77]. The increasing interest in these nanomedicine materials can be explained by four paradigm shifting properties [78]: (1) “scaffolds” to build upon: nanomedicines display excellent colloidal stability, even in complex fluids like the blood, and their surface can be easily modified with specific ligands to allow for cell-specific targeting or covalent bonding of drugs [79]; (2) high surface to volume ratio: vitally important property for optimizing drug loading, drug release, and colloidal interactions [78]; (3) shape: many different shapes of nanomedicines have been fabricated (e.g., nanospheres, nanorods, nanoshells, nanocubes, etc.) [80], which has been shown to affect cellular uptake [81–83], where these materials accumulate in the body [84], as well as the cellular responsive in vivo [85]; and (4) unique optical properties. Polymeric nanomedicines, whether they are solid or porous nanoparticles, microgels, or micelles, all display these advantageous properties.

From a biological perspective, there are additional important considerations for nanomedicines. The success of any nanomedicine in vivo is dependent on its blood circulation time [86]. Any foreign nanoscale material is actively removed from the plasma by the reticuloendothelial system (macrophages) and renal filtration (urinary excretion) [87]. Small nanoparticles (< 10 nm) [88, 89] are quickly removed by renal filtration, which is purely size driven and controlled by the endothelial pores in the glomerular capillaries the kidney (~8 nm). Larger particles are eliminated from the plasma by phagocytosis, with increasing efficiency as their size increases [90, 91]. Independent of size, any nanomedicine is first marked by opsonin proteins (opsonization) to trigger an immune response that ultimately results in phagocytosis. Protein adsorption increases with increase size, which in turn results in faster macrophage uptake and elimination from circulation [92]. However, the effects of opsonin adsorption can be reduced by imparting the nanomedicine with the ability to evade the immune system (so-called “stealth” properties), by functionalizing the surface with PEG (known as PEGylation) [93–95], or other hydrophilic polymers such as PVP [96] or dextran [97]. Consequently, nanomedicines of 100 nm and smaller are generally preferred [98], although the size may vary depending on the target tissue. The efficacy of nanomedicines can be further improved by

functionalizing the surface with specific ligands (e.g., small molecules, polypeptides, protein domains, antibodies, and nucleic acid-based aptamers) [99] which possess inherent ability to direct selective binding to cell types or states and, therefore, confer “smartness” to nanoparticles [100]. However, this may not always be necessary as some tissues can be targeted solely by the enhanced permeability and retention (EPR) effect [84]. Finally, the nanomedicine should be biocompatible, nontoxic, and clearable from the body.

2.3.1 Nanoparticles

Nanoparticles have been under investigation as nanomedicines for drug delivery since the 1970s [101, 102], when it was established that dispersions of solids particles could be safely administered intravenously. Polymeric nanoparticles are solid, porous, or hollow particles ranging from 20–500 nm that consist of hydrophobic polymers. These nanoparticles are generally fabricated using a dispersed phase free radical polymerization techniques such as (mini)emulsion polymerization or dispersion polymerization. The fabrication technique used for the synthesis of the nanoparticles governs whether nanospheres (matrix-type nanomedicines) or nanocapsules [103] (reservoir-type nanomedicines) are obtained [101]. Poly(alkyl cyanoacrylate) nanoparticles synthesized via heterogeneous polymerization techniques [104], for example, can be obtained as nanospheres or as nanocapsules and have been investigated as potential nanomedicines for cancer treatment [105]. Alternatively, nanoparticles can be fabricated using a solvent evaporation process, based on the principle that a solid polymer particle forms as the solvent evaporates from a solvent in oil emulsion. PLA and PLGA nanoparticles are typically prepared this way [39] and have been investigated for the controlled release of therapeutics targeting, e.g., cancer, inflammatory diseases, and cardiovascular disease [106].

An early limitation for nanoparticle drug delivery vehicles was that the polymers used were not biocompatible nor biodegradable. Consequently, the majority of nanoparticles are now prepared from biocompatible and/or biodegradable polymers such as poly(alkyl cyanoacrylates) [104], poly(lactic acid-co-glycol acid) [39], or poly(ϵ -caprolactone) [107, 108]. Furthermore, these hydrophobic nanoparticles are prone to opsonization and require modification of their surface with hydrophilic polymers such as dextran [109] and PEG [110]. As a result, PEG-PLGA nanoparticles have become the benchmark polymer nanoparticles for drug delivery applications [39]. Often PEG-PLGA nanoparticles are further modified with specific cell targeting ligands such as lectins [111] or folic acid/folate [112, 113] to increase their targeting efficacy. Another important consideration is the drug loading and drug release kinetics. Drug loading of solid nanoparticles (i.e., matrix-type nanomedicines) is hampered by slow diffusion of the drug into the matrix. One potential strategy circumventing slow diffusion is by preparing the nanoparticles in the presence of drug, a process referred to as molecular imprinting [114]. For example, poly(methyl methacrylate-co-methacrylic acid) nanoparticles were imprinted with paclitaxel, which resulted in a 12 times higher drug affinity and slow controlled release kinetics when compared to conventional nanoparticles [115]. Naturally, it is important that the drug molecule is not altered or degraded by the polymerization

chemistry. Reservoir-type nanoparticles are generally loaded during the solvent evaporation process or interfacial polymerization [116], which alleviates potential chemical modification or degradation of the drug [117]. This was shown by the group of Vauthier [118], who demonstrated that poly(isobutylcyanoacrylate) nanocapsules formed by interfacial polymerization did not affect insulin and the insulin-loaded nanocapsules induced a reduction of the glycemia to normal levels in streptozotocin diabetic rats. Ultimately, the release kinetics is governed by the diffusion of the drug through the polymer particle or capsule wall. However, degradable polymers (such as PLA or PLGA) erode which may have beneficial results for the release kinetics [39].

Although many nanoparticle-based nanomedicines have been investigated for a broad range of illnesses, currently available nanoparticle nanomedicines have not been able to improve the activity of a great number of drugs [101]. Generally, nanoparticles suffer from poor drug loading (usually less than 5% by weight), which results in low effective doses insufficient to reach the pharmacologically active concentration, or substantial amounts of polymer that may cause inflammation or other toxicological effects. Furthermore, the drug release kinetics are generally too fast (i.e., “burst release”), which causes leaching of the drug prior to reaching the target tissue, a small pharmacologically active window, or substantial side effects if the drug concentration exceed the toxic threshold [101].

2.3.2 Microgels

Microgels are water-swollen discrete particles ranging from 20 nm to 50 μm that consist of cross-linked water-soluble polymers [119]. Microgels have been widely recognized for their potential as a nanomedicine for drug delivery, largely due to ease with which responsiveness stimuli can be incorporated into their design [120–122]. Such responsive microgels (also referred to as “smart” microgels) are generally synthesized through free radical precipitation polymerization [123], although many other synthetic routes have been reported (e.g., inverse miniemulsion polymerization [124], polymerization-induced self-assembly [125], or the use of covalent dynamic bonds [126]). Temperature responsive microgels are most commonly used for drug delivery applications as these microgels can undergo a distinct shrinking response, which causes the microgel to deswell and expel water (and other molecules such as drugs) from their interior.

Microgels offer many advantages as a nanomedicine “scaffolds” as these particles can be fabricated over a broad size range and with excellent control over the morphology, internal structure [127, 128], and distribution of functionality [29]. These properties are particularly important as both the swelling/shrinking responses of microgels as well as the drug release kinetics are governed by the homogeneity of the microgel structure [29, 127]. Furthermore, desired functionalities for drug complexation, chemoligation for cell-specific targeting and internalization, or PEGylation can be readily introduced into the microgel structure during synthesis [29]. From a biological perspective, microgels are highly hydrophilic and have low interfacial energy which reduces opsonization and increases bioavailability and biocompatibility. These materials are also highly deformable [129] which may

make these materials excellent candidates for drug delivery that require crossing tight junction barriers such as the blood brain barrier [130]. The potential for drug delivery comes from the high void fraction and the potential to load relatively high amounts of drugs, released under sustained or burst kinetics. The stimuli responsiveness and the ability to release drugs on-demand, as was mentioned earlier, is probably the main reason why microgels have generated the significant amount of academic interest we see today.

However, despite the many advantages that microgels offer as nanomedicines and the maturity of the microgel field from a chemistry point of view, no microgel-based drug delivery therapies are currently in clinical trials [131]. Furthermore, even in academia relatively few microgel drug delivery vehicles are designed and tested specifically for in vivo applications [34, 46]. Clinical application of microgels is in part hampered by the toxicity of the monomers that are used for their synthesis (often *N*-isopropylacrylamide (NIPAM) which is a neurotoxin) and the fact that elaborate chemistry is required to render microgels degradable (obviously this only holds true for synthetic microgels). Furthermore, there is currently no solid understanding how the phase transitions observed in vitro correlate to those in vivo once the microgels are subjected to the inherent complexity blood and both intercellular and intracellular environments [120]. A minor shift of these transitions has the potential to completely alter the predetermined release kinetics. Finally, further improvement over the release kinetics of hydrophobic drugs is required to provide microgels with the ability to offer prolonged drug release capability. The use of covalently bound drugs which are released based on degradation of the microgel or in response to a change in the environmental conditions provides a step in the right direction [16].

2.3.3 Micelles

Amphiphilic block-copolymers consisting of a hydrophilic and a hydrophobic block assemble in water to form micelles ranging from 10 to 100 nm. The advent of controlled-living free radical polymerization (CLRP) [132] in the early 2000s has greatly simplified polymer synthesis and enabled the design of amphiphilic block-copolymers with excellent control over the number-average molecular weight, dispersity, and the relatively length of the respective blocks. The latter is especially important as the ratio of the degree of polymerization of the hydrophobic block (DP_A) and the degree of polymerization of the hydrophilic block (DP_B) governs the aggregation number (Z) as well as the critical micelle concentration (CMC) [133]. The significant interest in micelles for drug delivery applications arises from their particle morphology, consisting of a hydrophobic core that offers loading of hydrophobic drugs surrounded by a water-swollen hydrophilic shell that offers colloidal stability and masks the particle from the host's immune system [134, 135].

The effectiveness of micelles as nanomedicines arises from the extent to which distribution and temporal control can be achieved [136]. The excellent control over the molecular weight and block length ratios result in excellent control over the size and the morphology of the micelle. Furthermore, the low polydispersity of the

block-copolymers translates into micelles with a very narrow size distribution. These size aspects are very important as they control both the blood circulation time and the biodistribution [84], especially when the EPR effect is used as the mode of targeting. The CLRP chemistries used to prepare the block-copolymers offers additional advantage that the functional chain ends can be used to couple cell targeting ligands [137, 138], such as aptamers onto the surface of the micelle [139, 140]. This modification in particular has made micellar nanomedicines a promising tool for intercellular drug delivery [141]. Many of the current research efforts are focused on achieving improved temporal control over drug delivery, exploiting responsive block-copolymers that assemble into micelles able to release their payload once exposed stimuli that are unique to the diseased tissue or the intercellular environment that is targeted [142, 143]. Intercellular drug delivery can be triggered through the presence of increased concentrations of certain biomolecules or existing pH gradients, whereas drug release in cancerous tissue can be triggered through the slightly acidic pH (~6.8) or the abnormal temperature of cancerous tissues [144]. Regardless of the stimuli, the physical (e.g., cloud point transition) or chemical change (e.g., protonation/deprotonation) that occurs affects the solubility of the hydrophilic block, causing the micelle to accumulate, disassemble, and release its payload. Alternative approaches focus on the use of phenyl boronic acid (PBA)-modified micelles that are glucose-responsive for the release of insulin [145, 146] or the disulfide cross-linked micelles that can be disassembled in the presence of glutathione [147–149].

Although micelle-based nanomedicines have, most probably, been established the most promising drug delivery vehicles, due to the great synthetic versatility that can be achieved within their design, clinical application of micelle-based formulations is largely limited to PEG-PLA based systems. This is largely due to the fact that many of the more advanced micellar designs contain block-copolymers that are not yet FDA approved and often require multistep synthesis to be prepared. Furthermore, assembly and long-term stability of these micelles is based on their CMC. Once injected into the bloodstream, the micelles are diluted to the point where the concentration of their components could fall below the CMC, causing the micelles to disassemble and release their payload before the target tissue is reached. Although it should be noted that this can be largely avoided by synthesizing cross-linked micelles [150].

2.3.4 The Overall Potential of Nanomedicines

Nanomedicines offer enormous potential for clinicians to improve the outcome of treatment (e.g., higher therapeutic index due to localization in the diseased tissue) as well as the quality of treatment (e.g., nonsurgical administration, lower doses reduce unwanted side-effects). However, complete understanding of the relationship between the physiochemical properties of nanomedicines (size, shape, surface chemistry, targeting ligands) and their biological properties (circulation time, immune response, biodistribution, penetration of tissues) will be necessary before nanomedicine-based therapies will become commonplace.

3 Conclusions

The development of strategies capable of improved control of drug release could drastically advance patient safety and outcomes, and the healthcare system overall. Prior to the development of novel controlled release strategies, it is important to consider the properties of the drug, the optimal location of release, and the desired release rate of the drug to achieve the intended outcome. This chapter briefly discussed these important considerations, as well as the wide array of potential delivery routes of a drug or drug delivery system and various general methodologies to produce polymeric systems (from macroscale implants to nanomedicines) that can be utilized for drug release. It is of extreme importance to complement a potential controlled delivery device with the drug characteristics, route of delivery, and location of release. In many cases, the best method may be to localize the delivery to a specific local in the body to simplify the process.

► [Chap. 27, “Drug Delivery: Localized and Systemic Therapeutic Strategies with Polymer Systems”](#) will build on the ideas that were introduced in this chapter to concentrate on a variety of strategies for localized delivery to various regions in the body and the systemic delivery of nanomedicines for the treatment of cancer. This chapter will conclude with a perspective on the direction that the drug delivery field could trend towards in the near future and highlights the major challenges that must be overcome to effectively transition more controlled delivery systems from the benchtop to the clinic.

References

1. N. Huebsch, C.J. Kearney, X. Zhao, J. Kim, C.A. Cezar, Z. Suo, D.J. Mooney, Ultrasound-triggered disruption and self-healing of reversibly cross-linked hydrogels for drug delivery and enhanced chemotherapy. *Proc. Natl. Acad. Sci. U. S. A.* **111**, 9762–9767 (2014)
2. D. Maitland, S.B. Campbell, J. Chen, T. Hoare, Controlling the resolution and duration of pulsatile release from injectable magnetic “plum pudding” nanocomposite hydrogels. *RSC Adv.* **6**, 15770–15781 (2016)
3. L.T. Kuhn, *Biomaterials*, ed. By J. Enderle, S. Blanchard, J. Bronzino. Introduction to Biomedical Engineering, 4th edn (Elsevier Academic Press, Burlington, 2005)
4. S.L. Tao, T.A. Desai, Gastrointestinal patch systems for oral drug delivery. *Drug Discov. Today* **10**, 909–915 (2005)
5. D.R. Friend, G. Sri, M. Park, Colon-specific drug delivery. *Adv. Drug Deliv. Rev.* **7**, 149–199 (1991)
6. R. Talukder, R. Fassih, Gastroretentive delivery systems: A mini review. *Drug Dev. Ind. Pharm.* **30**, 1019–1028 (2004)
7. M. Gibaldi, R.N. Boyes, S. Feldman, Influence of first-pass effect on availability of drugs on oral administration. *J. Pharm. Sci.* **60**, 1338–1340 (1971)
8. K. Park, I. Chan, K. Park, Oral protein delivery: Current status and future prospect. *React. Funct. Polym.* **71**, 280–287 (2011)
9. M.R. Prausnitz, R. Langer, Transdermal drug delivery. *Nat. Biotechnol.* **26**, 1261–1268 (2008)
10. N.R. Mathias, M.A. Hussain, Non-invasive systemic drug delivery: Developability considerations for alternate routes of administration. *J. Pharm. Sci.* **99**, 1–20 (2010)
11. M.J. Rathbone, B.K. Drummond, I.G. Tucker, The oral cavity as a site for systemic drug delivery. *Adv. Drug Deliv. Rev.* **13**, 1–22 (1994)

12. L. Illum, Nasal drug delivery – Possibilities, problems and solutions. *J. Control. Release* **87**, 187–198 (2003)
13. J.S. Patton, C.S. Fishburn, J.G. Weers, The lungs as a portal of entry for systemic drug delivery. *Proc. Am. Thorac. Soc.* **1**, 338–344 (2004)
14. J. Kost, R. Langer, Responsive polymeric delivery systems. *Adv. Drug Deliv. Rev.* **46**, 125–148 (2001)
15. S.B. Campbell, M. Patenaude, T. Hoare, Injectable Superparamagnets: Highly elastic and degradable poly(N-isopropylacrylamide)-superparamagnetic iron oxide nanoparticle (SPION) composite hydrogels. *Biomacromolecules* **14**, 644–653 (2013)
16. J. Kost, R. Langer, Responsive polymeric delivery systems. *Adv. Drug Deliv. Rev.* **64**, 327–341 (2012)
17. S. Merino, C. Martin, K. Kostarelos, M. Prato, E. Vázquez, Nanocomposite hydrogels: 3D polymer-nanoparticle synergies for on-demand drug delivery. *ACS Nano* **9**, 4686–4697 (2015)
18. S.B. Campbell, T. Hoare, Externally addressable hydrogel nanocomposites for biomedical applications. *Curr. Opin. Chem. Eng.* **4**, 1–10 (2014)
19. H. Bechgaard, G.H. Nielsen, Controlled-release multiple-units and single-unit doses a literature review. *Drug Dev. Ind. Pharm.* **4**, 53–67 (2008)
20. E. Caló, V.V. Khutoryanskiy, Biomedical applications of hydrogels: A review of patents and commercial products. *Eur. Polym. J.* **65**, 252–267 (2015)
21. M. Elsbahy, K.L. Wooley, Design of polymeric nanoparticles for biomedical delivery applications. *Chem. Soc. Rev.* **41**, 2545–2561 (2012)
22. E. Blanco, H. Shen, M. Ferrari, Principles of nanoparticle design for overcoming biological barriers to drug delivery. *Nat. Biotechnol.* **33**, 941–951 (2015)
23. T.R. Hoare, D.S. Kohane, Hydrogels in drug delivery: Progress and challenges. *Polymer* **49**, 1993–2007 (2008)
24. J.H. Brauker, V.E. Carr-Brendel, L.A. Martinson, J. Crudele, W.D. Johnston, R.C. Johnson, B.H. Corp, B.T. Park, R. Lake, Neovascularization of synthetic membranes directed by membrane microarchitecture. *J. Biomed. Mater. Res.* **29**, 1517–1524 (1995)
25. O. Veisoh, J.C. Dolo, M. Ma, A.J. Vegas, H.H. Tam, A.R. Bader, J. Li, E. Langan, J. Wycko, W.S. Loo, S. Jhunjhunwala, A. Chiu, S. Siebert, K. Tang, J. Hollister-lock, S. Aresta-dasilva, M. Bochenek, J. Mendoza-Elias, Y. Wang, M. Qi, D.M. Lavin, M. Chen, N. Dholakia, R. Thakrar, I. Lacik, G.C. Weir, J. Oberholzer, D.L. Greiner, R. Langer, Size- and shape-dependent foreign body immune response to materials implanted in rodents and non-human primates. *Nat. Mater.* **14**, 643–652 (2015)
26. J. Nicolas, S. Mura, D. Brambilla, N. Mackiewicz, P. Couvreur, Design, functionalization strategies and biomedical applications of targeted biodegradable/biocompatible polymer-based nanocarriers for drug delivery. *Chem. Soc. Rev.* **42**, 1147–1235 (2013)
27. M.K. Nguyen, E. Alsborg, Bioactive factor delivery strategies from engineered polymer hydrogels for therapeutic medicine. *Prog. Polym. Sci.* **39**, 1235–1265 (2014)
28. Y. Zhao, F. Fay, S. Hak, J.M. Perez-aguilar, B.L. Sanchez-Gaytan, C.D.L. Davies, A. Bjørkøy, H. Weinstein, B. Goode, W.J.M. Mulder, Z.A. Fayad, C. Perez-Medina, W.J.M. Mulder, Augmenting drug-carrier compatibility improves tumour nanotherapy efficacy. *Nat. Commun.* **1–11** (2016)
29. T. Hoare, R. Pelton, Impact of microgel morphology on functionalized microgel-drug interactions. *Langmuir* **24**, 1005–1012 (2008)
30. E.A. Appel, R.A. Forster, M.J. Rowland, O.A. Scherman, The control of cargo release from physically crosslinked hydrogels by crosslink dynamics. *Biomaterials* **35**, 9897–9903 (2014)
31. N.A. Peppas, P. Bures, W. Leobandung, H. Ichikawa, Hydrogels in pharmaceutical formulations. *Eur. J. Pharm. Biopharm.* **50**, 27–46 (2000)
32. P.R. Lockman, R.J. Mumper, M.A. Khan, D.D. Allen, Nanoparticle technology for drug delivery across the blood-brain barrier. *Drug Dev. Ind. Pharm.* **28**, 1–13 (2002)
33. D.A. LaVan, T. McGuire, R. Langer, Small-scale systems for in vivo drug delivery. *Nat. Biotechnol.* **21**, 1184–1191 (2003)
34. A.C. Anselmo, S. Mitragotri, An overview of clinical and commercial impact of drug delivery systems. *J. Control. Release* **190**, 15–28 (2014)

35. I.M. Carvalho, C.S. Marques, R.S. Oliveira, P.B. Coelho, P.C. Costa, D.C. Ferreira, Sustained drug release by contact lenses for glaucoma treatment – A review. *J. Control. Release* **202**, 76–82 (2015)
36. G. Acharya, K. Park, Mechanisms of controlled drug release from drug-eluting stents. *Adv. Drug Deliv. Rev.* **58**, 387–401 (2006)
37. M. Staples, K. Daniel, M.J. Cima, R. Langer, Application of micro- and nano-electromechanical devices to drug delivery. *Pharm. Res.* **23**, 847–863 (2006)
38. L.C. Bengani, K.-H. Hsu, S. Gause, A. Chauhan, Contact lenses as a platform for ocular drug delivery. *Expert Opin. Drug Deliv.* **10**, 1483–1496 (2013)
39. H.K. Makadia, S.J. Siegel, Poly lactic-co-glycolic acid (PLGA) as biodegradable controlled drug delivery carrier. *Polymers* **3**, 1377–1397 (2011)
40. B.G. Amsden, Biodegradable elastomers in drug delivery. *Expert Opin. Drug Deliv.* **5**, 175–187 (2008)
41. S.A. Rovers, R. Hoogenboom, M.F. Kemmere, J.T.F. Keurentjes, Repetitive on-demand drug release by magnetic heating of iron oxide containing polymeric implants. *Soft Matter* **8**, 1623–1627 (2012)
42. J.T.F. Keurentjes, M.F. Kemmere, H. Bruinewoud, M.A.M.E. Vertommen, S.A. Rovers, R. Hoogenboom, L.F.S. Stemkens, F.L.A.M.A. Péters, N.J.C. Tielen, D.T.A. van Asseldonk, A.F. Gabriel, E.A. Joosten, M.A.E. Marcus, Externally triggered glass transition switch for localized on-demand drug delivery. *Angew. Chem. Int. Ed.* **48**, 9867–9870 (2009)
43. T. Hoare, J. Santamaria, G.F. Goya, S. Irusta, D. Lin, S. Lau, R. Padera, R. Langer, D.S. Kohane, A magnetically triggered composite membrane for on-demand drug delivery. *Nano Lett.* **9**, 3651–3657 (2009)
44. E. Renard, G. Costalat, J. Bringer, From external to implantable insulin pump, can we close the loop? *Diabetes Metab.* **28**, 2519–2525 (2002)
45. T. Aye, J. Block, B. Buckingham, Toward closing the loop: an update on insulin pumps and continuous glucose monitoring systems. *Endocrinol. Metab. Clin. N. Am.* **39**, 609–624 (2010)
46. S. Van Vlierberghe, P. Dubruel, E. Schacht, Biopolymer-based hydrogels as scaffolds for tissue engineering applications: A review. *Biomacromolecules* **12**, 1387–1408 (2011)
47. M.W. Tibbitt, K.S. Anseth, Hydrogels as extracellular matrix mimics for 3D cell culture. *Biotechnol. Bioeng.* **103**, 655–663 (2009)
48. N.A. Peppas, J.Z. Hilt, A. Khademhosseini, R. Langer, Hydrogels in biology and medicine: From molecular principles to bionanotechnology. *Adv. Mater.* **18**, 1345–1360 (2006)
49. C. Maldonado-Codina, N. Efron, Hydrogel lenses – Materials and manufacture: A review. *Optom. Pract.* **4**, 101–115 (2003)
50. H. Hiratani, C. Alvarez-Lorenzo, Timolol uptake and release by imprinted soft contact lenses made of N,N-diethylacrylamide and methacrylic acid. *J. Control. Release* **83**, 223–230 (2002)
51. J.S. Boateng, K.H. Matthews, H.N.E. Stevens, G.M. Eccleston, Wound healing dressings and drug delivery systems: A review. *J. Pharm. Sci.* **97**, 2892–2923 (2008)
52. C.-C. Lin, K.S. Anseth, PEG hydrogels for the controlled release of biomolecules in regenerative medicine. *Pharm. Res.* **26**, 631–643 (2009)
53. D.J. Overstreet, D. Dutta, S.E. Stabenfeldt, B.L. Vernon, Injectable hydrogels. *J. Polym. Sci. Part B Polym. Phys.* **50**, 881–903 (2012)
54. Y. Li, J. Rodrigues, H. Tomás, Injectable and biodegradable hydrogels: Gelation, biodegradation and biomedical applications. *Chem. Soc. Rev.* **41**, 2193–2221 (2012)
55. M. Patenaude, N.M.B. Smeets, T. Hoare, Designing injectable, covalently cross-linked hydrogels for biomedical applications. *Macromol. Rapid Commun.* **35**, 598–617 (2014)
56. M.A. Azagarsamy, K.S. Anseth, Bioorthogonal click chemistry: An indispensable tool to create multifaceted cell structure scaffolds. *ACS Macro Lett.* **2**, 5–9 (2013)
57. N.M.B. Smeets, E. Bakaic, M. Patenaude, T. Hoare, Injectable and tunable poly(ethylene glycol) analogue hydrogels based on poly(oligoethylene glycol methacrylate). *Chem. Commun.* **50**, 3306–3309 (2014)

58. N.M.B. Smeets, E. Bakaic, M. Patenaude, T. Hoare, Injectable poly(oligoethylene glycol methacrylate)-based hydrogels with tunable phase transition behaviours: Physicochemical and biological responses. *Acta Biomater.* **10**, 4143–4155 (2014)
59. E. Bakaic, N.M.B. Smeets, T. Hoare, Injectable hydrogels based on poly(ethylene glycol) and derivatives as functional biomaterials. *RSC Adv.* **5**, 35469–35486 (2015)
60. E. Bakaic, N.M.B. Smeets, H. Dorrington, T.R. Hoare, “Off-the-shelf” thermoresponsive hydrogel design: Tuning hydrogel properties by mixing precursor polymers with different lower-critical solution temperatures. *RSC Adv.* **5**, 33364–33376 (2015)
61. S.P. Hudson, R. Langer, G.R. Fink, D.S. Kohane, Injectable in situ cross-linking hydrogels for local antifungal therapy. *Biomaterials* **31**, 1444–1452 (2010)
62. A.W. Jackson, D.A. Fulton, Making polymeric nanoparticles stimuli-responsive with dynamic covalent bonds. *Polym. Chem.* **4**, 31–45 (2013)
63. N.M.B. Smeets, M. Patenaude, D. Kinio, F.M. Yavitt, E. Bakaic, F.-C. Yang, M. Rheinstädter, T. Hoare, Injectable hydrogels with in situ-forming hydrophobic domains: oligo(d,l-lactide) modified poly(oligoethylene glycol methacrylate) hydrogels. *Polym. Chem.* **5**, 6811–6823 (2014)
64. D.A. Ossipov, J. Hilborn, Poly(vinyl alcohol)-based hydrogels formed by “click chemistry”. *Macromolecules* **39**, 1709–1718 (2006)
65. G.N. Grover, J. Lam, T.H. Nguyen, T. Segura, H.D. Maynard, Biocompatible hydrogels by oxime click chemistry. *Biomacromolecules* **13**, 3013–3017 (2012)
66. G.N. Grover, R.L. Braden, K.L. Christman, Oxime cross-linked injectable hydrogels for catheter delivery. *Adv. Mater.* **25**, 2937–2942 (2013)
67. H.W. Ooi, K.S. Jack, H. Peng, A.K. Whittaker, “Click” PNIPAAm hydrogels – A comprehensive study of structure and properties. *Polym. Chem.* **4**, 4788–4800 (2013)
68. J.A. Yoon, T. Kowalewski, K. Matyjaszewski, Comparison of thermoresponsive deswelling kinetics of poly(oligo(ethylene oxide) methacrylate)-based thermoresponsive hydrogels prepared by “graft-from” ATRP. *Macromolecules* **44**, 2261–2268 (2011)
69. Y. Qiu, K. Park, Environment-sensitive hydrogels for drug delivery. *Adv. Drug Deliv. Rev.* **64**, 49–60 (2012)
70. S. Cheon, I. Keun, K. Park, Hydrogels for delivery of bioactive agents: A historical perspective. *Adv. Drug Deliv. Rev.* **65**, 17–20 (2013)
71. A. Matsumoto, T. Ishii, J. Nishida, H. Matsumoto, K. Kataoka, Y. Miyahara, A synthetic approach toward a self-regulated insulin delivery system. *Angew. Chem. Int. Ed.* **51**, 2124–2128 (2012)
72. W. Wu, S. Zhou, Responsive materials for self-regulated insulin delivery. *Macromol. Biosci.* **13**, 1464–1477 (2013)
73. D. Beebe, J. Moore, J. Bauer, Q. Yu, R. Liu, C. Devadoss, B. Jo, Functional hydrogel structures for autonomous flow control inside microfluidic channels. *Nature* **404**, 588–590 (2000)
74. D. Guarnieri, A. De Capua, M. Ventre, A. Borzacchiello, C. Pedone, D. Marasco, M. Ruvo, P.A. Netti, Covalently immobilized RGD gradient on PEG hydrogel scaffold influences cell migration parameters. *Acta Biomater.* **6**, 2532–2539 (2010)
75. K.C. Koehler, K.S. Anseth, C.N. Bowman, Diels-Alder mediated controlled release from a poly(ethylene glycol) based hydrogel. *Biomacromolecules* **14**, 538–547 (2013)
76. G.D. Nicodemus, S.J. Bryant, Cell encapsulation in biodegradable hydrogels for tissue engineering applications. *Tissue Eng. Part B Rev.* **14**, 149–165 (2008)
77. V. Wagner, A. Dullaart, A.-K. Bock, A. Zweck, The emerging nanomedicine landscape. *Nat. Biotechnol.* **24**, 1211–1217 (2006)
78. T.L. Doane, C. Burda, The unique role of nanoparticles in nanomedicine: imaging, drug delivery and therapy. *Chem. Soc. Rev.* **41**, 2885–2911 (2012)
79. R. Shenhar, V.M. Rotello, Nanoparticles: Scaffolds and building blocks. *Acc. Chem. Res.* **36**, 549–561 (2003)

80. M.R. Jones, K.D. Osberg, R.J. Macfarlane, M.R. Langille, C.A. Mirkin, Templated techniques for the synthesis and assembly of plasmonic nanostructures. *Chem. Rev.* **111**, 3736–3827 (2011)
81. B.D. Chithrani, W.C.W. Chan, Elucidating the mechanism of cellular uptake and removal of protein-coated gold nanoparticles of different sizes and shapes. *Nano Lett.* **7**, 1542–1550 (2007)
82. B.D. Chithrani, A.A. Ghazani, W.C.W. Chan, Determining the size and shape dependence of gold nanoparticle uptake into mammalian cells. *Nano Lett.* **6**, 662–668 (2006)
83. S.E.A. Gratton, P.A. Ropp, P.D. Pohlhaus, J.C. Luft, V.J. Madden, M.E. Napier, J.M. DeSimone, The effect of particle design on cellular internalization pathways. *Proc. Natl. Acad. Sci. U. S. A.* **105**, 11613–11618 (2008)
84. Y. Matsumura, H. Maeda, A new concept for macromolecular therapeutics in cancer chemotherapy: Mechanism of tumoritropic accumulation of proteins and the antitumor agent Smancs. *Cancer Res.* **46**, 6387–6392 (1986)
85. A. Albanese, E.A. Sykes, W.C.W. Chan, Rough around the edges: The inflammatory response of microglial cells to spiky nanoparticles. *ACS Nano* **4**, 2490–2493 (2010)
86. A.R. Kirtane, Strategies to improve plasma circulation of nanoparticles. *Nirma Univ J Pharm Sci* **1**, 1–18 (2014)
87. M.J. Ernsting, M. Murakami, A. Roy, S.-D. Li, Factors controlling the pharmacokinetics, biodistribution and intratumoral penetration of nanoparticles. *J. Control. Release* **172**, 782–794 (2013)
88. C. Rippe, A. Rippe, O. Torffvit, B. Rippe, Size and charge selectivity of the glomerular filter in early experimental diabetes in rats. *Am. J. Physiol. Renal Physiol.* **293**, F1533–F1538 (2007)
89. D. Asgeirsson, D. Venturoli, B. Rippe, C. Rippe, Increased glomerular permeability to negatively charged Ficoll relative to neutral Ficoll in rats. *Am. J. Physiol. Renal Physiol.* **291**, F1083–F1089 (2006)
90. J. Rejman, V. Oberle, I.S. Zuhom, D. Hoekstra, Size-dependent internalization of particles via the pathways of clathrin- and caveolae-mediated endocytosis. *Biochem. J.* **377**, 159–169 (2004)
91. R. May, L. Machesky, Phagocytosis and the actin cytoskeleton. *J. Cell Sci.* **114**, 1061–1077 (2001)
92. C. Fang, B. Shi, Y.-Y. Pei, M.-H. Hong, J. Wu, H.-Z. Chen, In vivo tumor targeting of tumor necrosis factor- α -loaded stealth nanoparticles: effect of MePEG molecular weight and particle size. *Eur. J. Pharm. Sci.* **27**, 27–36 (2006)
93. S.M. Ryan, G. Mantovani, X. Wang, D.M. Haddleton, D.J. Brayden, Advances in PEGylation of important biotech molecules: delivery aspects. *Expert Opin. Drug Deliv.* **5**, 371–383 (2008)
94. G. Pasut, F.M. Veronese, State of the art in PEGylation: The great versatility achieved after forty years of research. *J. Control. Release* **161**, 461–472 (2012)
95. U. Wattendorf, H.P. Merkle, PEGylation as a tool for the biomedical engineering of surface modified microparticles. *J. Pharm. Sci.* **97**, 4655–4669 (2008)
96. V.P. Torchilin, M.I. Shtilman, V.S. Trubetskoy, K. Whiteman, A.M. Milstein, Amphiphilic vinyl polymers effectively prolong liposome circulation time in vivo. *Biochim. Biophys. Acta Biomembr.* **1195**, 181–184 (1994)
97. A. Moore, E. Marecos, A. Bogdanov, R. Weissleder, Tumoral distribution of long-circulating dextran-coated iron oxide nanoparticles in a rodent model. *Radiology* **214**, 568–574 (2000)
98. V.P. Chauhan, T. Stylianopoulos, J.D. Martin, Z. Popović, O. Chen, W.S. Kamoun, M.G. Bawendi, D. Fukumura, R.K. Jain, Normalization of tumour blood vessels improves the delivery of nanomedicines in a size-dependent manner. *Nat. Nanotechnol.* **7**, 383–388 (2012)
99. R. Liu, B.K. Kay, S. Jiang, S. Chen, Nanoparticle delivery: Targeting and nonspecific binding. *MRS Bull.* **34**, 432–440 (2011)
100. A.D. Friedman, S.E. Claypool, R. Liu, The smart targeting of nanoparticles. *Curr. Pharm. Des.* **19**, 6315–6329 (2013)
101. P. Couvreur, Nanoparticles in drug delivery: Past, present and future. *Adv. Drug Deliv. Rev.* **65**, 21–23 (2013)

102. G. Birrenbach, P.P. Speiser, Polymerized micelles and their use as adjuvants in immunology. *J. Pharm. Sci.* **65**, 1763–1766 (1976)
103. F. Tiarks, K. Landfester, M. Antonietti, Preparation of polymeric nanocapsules by mini-emulsion polymerization. *Langmuir* **17**, 908–918 (2001)
104. J. Nicolas, P. Couvreur, Synthesis of poly(alkyl cyanoacrylate)-based colloidal nanomedicines. *Wiley Interdiscip. Rev. Nanomed. Nanobiotechnol.* **1**, 111–127 (2009)
105. C. Vauthier, C. Dubernet, C. Chauvierre, I. Brigger, P. Couvreur, Drug delivery to resistant tumors: The potential of poly(alkyl cyanoacrylate) nanoparticles. *J. Control. Release* **93**, 151–160 (2003)
106. F. Danhier, E. Ansorena, J.M. Silva, R. Coco, A. Le Breton, V. Préat, PLGA-based nanoparticles: An overview of biomedical applications. *J. Control. Release* **161**, 505–522 (2012)
107. J.S. Chawla, M.M. Amiji, Biodegradable poly(ϵ -caprolactone) nanoparticles for tumor-targeted delivery of tamoxifen. *Int. J. Pharm.* **249**, 127–138 (2002)
108. T.K. Dash, V.B. Konkimalla, Poly- ϵ -caprolactone based formulations for drug delivery and tissue engineering: A review. *J. Control. Release* **158**, 15–33 (2012)
109. C. Chauvierre, D. Labarre, P. Couvreur, C. Vauthier, Novel polysaccharide-decorated poly(isobutyl cyanoacrylate) nanoparticles. *Pharm. Res.* **20**, 1786–1793 (2003)
110. M. Tobío, R. Gref, A. Sánchez, R. Langer, M.J. Alonso, Stealth PLA-PEG nanoparticles as protein carriers for nasal administration. *Pharm. Res.* **15**, 270–275 (1998)
111. J. Piazza, T. Hoare, L. Molinaro, K. Terpstra, J. Bhandari, P.R. Selvaganapathy, B. Gupta, R.K. Mishra, Haloperidol-loaded intranasally administered lectin functionalized poly(ethylene glycol)-block-poly(D,L)-lactic-co-glycolic acid (PEG-PLGA) nanoparticles for the treatment of schizophrenia. *Eur. J. Pharm. Biopharm.* **87**, 30–39 (2014)
112. H.S. Yoo, T.G. Park, Folate receptor targeted biodegradable polymeric doxorubicin micelles. *J. Control. Release* **96**, 273–283 (2004)
113. Z. He, J. Huang, Y. Xu, X. Zhang, Y. Teng, C. Huang, Y. Wu, X. Zhang, H. Zhang, W. Sun, Co-delivery of cisplatin and paclitaxel by folic acid conjugated amphiphilic PEG-PLGA copolymer nanoparticles for the treatment of non-small lung cancer. *Oncotarget* **6**, 42150–42168 (2015)
114. J. Wackerlig, R. Schirhagl, Applications of molecularly imprinted polymer nanoparticles and their advances toward industrial use: A review. *Anal. Chem.* **88**, 250–261 (2015)
115. F.A. Ishkuh, M. Javanbakht, M. Esfandyari-Manesh, R. Dinavand, F. Atyabi, Synthesis and characterization of paclitaxel-imprinted nanoparticles for recognition and controlled release of an anticancer drug. *J. Mater. Sci.* **49**, 6343–6352 (2014)
116. A. Musyanovych, K. Landfester, Polymer micro- and nanocapsules as biological carriers with multifunctional properties. *Macromol. Biosci.* **14**, 458–477 (2014)
117. A.R. Pohlmann, F.N. Fonseca, K. Paese, C.B. Detoni, K. Coradini, R.C. Beck, S.S. Guterres, Poly(ϵ -caprolactone) microcapsules and nanocapsules in drug delivery. *Expert Opin. Drug Deliv.* **10**, 623–638 (2013)
118. M. Aboubakar, F. Puisieux, P. Couvreur, C. Vauthier, Physico-chemical characterization of insulin-loaded poly(isobutyrcyanoacrylate) nanocapsules obtained by interfacial polymerization. *Int. J. Pharm.* **183**, 63–66 (1999)
119. R.H. Pelton, P. Chibante, Preparation of aqueous latices with N-isopropylacrylamide. *Colloids Surf.* **20**, 247–256 (1986)
120. N.M.B. Smeets, T. Hoare, Designing responsive microgels for drug delivery applications. *J. Polym. Sci. Part A: Polym. Chem.* **51**, 3027–3043 (2013)
121. D. Klinger, K. Landfester, Stimuli-responsive microgels for the loading and release of functional compounds: Fundamental concepts and applications. *Polymer* **53**, 5209–5231 (2012)
122. J. Kwon, R. Drumright, D.J. Siegwart, K. Matyjaszewski, The development of microgels/nanogels for drug delivery applications. *Prog. Polym. Sci.* **33**, 448–477 (2008)
123. A. Pich, W. Richtering, Microgels by precipitation polymerization: Synthesis, characterization, and functionalization. *Adv. Polym. Sci.* **234**, 1–37 (2010)

124. K. Landfester, M. Willert, M. Antonietti, Preparation of polymer particles in nonaqueous direct and inverse miniemulsions. *Macromolecules* **33**, 2370–2376 (2000)
125. Z. An, Q. Shi, W. Tang, C. Tsung, C.J. Hawker, G.D. Stucky, Facile RAFT precipitation polymerization for the microwave-assisted synthesis of well-defined, double hydrophilic block copolymers and nanostructured hydrogels. *J. Am. Chem. Soc.* **129**, 14493–14499 (2007)
126. D. Sivakumaran, E. Mueller, T. Hoare, Temperature-induced assembly of monodisperse, covalently cross-linked, and degradable poly(*n*-isopropylacrylamide) microgels based on oligomeric precursors. *Langmuir* **31**, 5767–5778 (2015)
127. T. Hoare, R. Pelton, Charge-switching, amphoteric glucose-responsive microgels with physiological swelling activity. *Biomacromolecules* **9**, 733–740 (2008)
128. T. Hoare, R. Pelton, Functional group distributions in carboxylic acid containing poly(*N*-isopropylacrylamide) microgels. *Langmuir* **20**, 2123–2133 (2004)
129. G.R. Hendrickson, L.A. Lyon, Microgel translocation through pores under confinement. *Angew. Chem. Int. Ed.* **49**, 2193–2197 (2010)
130. K. Gries, K. Bubel, M. Wohlfahrt, S. Agarwal, U. Koert, A. Greiner, Preparation of gold nanoparticle-poly(*L*-menthyl methacrylate) conjugates via ATRP polymerization. *Macromol. Chem. Phys.* **212**, 2551–2557 (2011)
131. H. Kirsebom, I.Y. Galaev, B. Mattiasson, Stimuli-responsive polymers in the 21st century: Elaborated architecture to achieve high sensitivity, fast response, and robust behavior. *J. Polym. Sci. Part B: Polym. Phys.* **49**, 173–178 (2011)
132. K. Matyjaszewski, J. Spanswick, Controlled/living radical polymerization. *Mater. Today* **8**, 26–33 (2005)
133. S. Förster, M. Zisenis, E. Wenz, M. Antonietti, Micellization of strongly segregated block copolymers. *J. Chem. Phys.* **104**, 9956–9970 (1996)
134. M. Yokoyama, Polymeric micelles as a new drug carrier system and their required considerations for clinical trials. *Expert Opin. Drug Deliv.* **7**, 145–158 (2010)
135. K. Kataoka, A. Harada, Y. Nagasaki, Block copolymer micelles for drug delivery: Design, characterization and biological significance. *Adv. Drug Deliv. Rev.* **64**, 37–48 (2012)
136. K.E. Uhrich, S.M. Cannizzaro, R.S. Langer, K.M. Shakesheff, Polymeric systems for controlled drug release. *Chem. Rev.* **99**, 3181–3198 (1999)
137. A.W. York, S.E. Kirkland, C.L. McCormick, Advances in the synthesis of amphiphilic block copolymers via RAFT polymerization: Stimuli-responsive drug and gene delivery. *Adv. Drug Deliv. Rev.* **60**, 1018–1036 (2008)
138. D.J. Siegwart, J.K. Oh, K. Matyjaszewski, ATRP in the design of functional materials for biomedical applications. *Prog. Polym. Sci.* **37**, 18–37 (2012)
139. Y. Wu, K. Sefah, H. Liu, R. Wang, W. Tan, DNA aptamer-micelle as an efficient detection/delivery vehicle toward cancer cells. *Proc. Natl. Acad. Sci. U. S. A.* **107**, 5–10 (2010)
140. S. Dhar, F.X. Gu, R. Langer, O.C. Farokhzad, S.J. Lippard, Targeted delivery of cisplatin to prostate cancer cells by aptamer functionalized Pt(IV) prodrug-PLGA-PEG nanoparticles. *Proc. Natl. Acad. Sci. U. S. A.* **105**, 17356–17361 (2008)
141. D. Sutton, N. Nasongkla, E. Blanco, J. Gao, Functionalized micellar systems for cancer targeted drug delivery. *Pharm. Res.* **24**, 1029–1046 (2007)
142. N. Rapoport, Physical stimuli-responsive polymeric micelles for anti-cancer drug delivery. *Prog. Polym. Sci.* **32**, 962–990 (2007)
143. S. Ganta, H. Devalapally, A. Shahiwala, M. Amiji, A review of stimuli-responsive nanocarriers for drug and gene delivery. *J. Control. Release* **126**, 187–204 (2008)
144. Z. Ge, S. Liu, Functional block copolymer assemblies responsive to tumor and intracellular microenvironments for site-specific drug delivery and enhanced imaging performance. *Chem. Soc. Rev.* **42**, 7289–7325 (2013)
145. O. Veisoh, B.C. Tang, K.A. Whitehead, D.G. Anderson, R. Langer, Managing diabetes with nanomedicine: Challenges and opportunities. *Nat. Rev. Drug Discov.* **14**, 45–57 (2014)

146. G. Liu, R. Ma, J. Ren, Z. Li, H. Zhang, Z. Zhang, Y. An, L. Shi, A glucose-responsive complex polymeric micelle enabling repeated on-off release and insulin protection. *Soft Matter* **9**, 1636–1644 (2013)
147. Q. Zhang, N.R. Ko, J.K. Oh, Recent advances in stimuli-responsive degradable block copolymer micelles: Synthesis and controlled drug delivery applications. *Chem. Commun.* **48**, 7542–7552 (2012)
148. B. Khorsand, G. Lapointe, C. Brett, J.K. Oh, Intracellular drug delivery nanocarriers of glutathione-responsive degradable block copolymers having pendant disulfide linkages. *Biomacromolecules* **14**, 2103–2111 (2013)
149. L. Zhang, W. Liu, L. Lin, D. Chen, M.H. Stenzel, Degradable disulfide core-cross-linked micelles as a drug delivery system prepared from vinyl functionalized nucleosides via the RAFT process. *Biomacromolecules* **9**, 3321–3331 (2008)
150. C.F. van Nostrum, Covalently cross-linked amphiphilic block copolymer micelles. *Soft Matter* **7**, 3246–3259 (2011)



Conjugated Organic Polymers for Optoelectronic Devices

18

Shahid Pervez Ansari and Farman Ali

Contents

1	Organic Molecules in Optoelectronic Devices	750
2	Benefits of OLEDs	751
3	Electronic Structure of Conjugated Organic Molecules and Luminescence	752
4	Energy Transfer in Guest-Host Systems	753
5	Working of an OLED	754
6	Materials for OLEDs	756
6.1	Anode Materials	756
6.2	Hole Injection Materials (HIM)	757
6.3	Hole Transport Layer (HTL)	757
6.4	Electron Transport Layer (ETL)	758
6.5	Cathode Interfacial Materials (CIM)	758
6.6	Cathode Materials	759
6.7	Light-Emitting Materials	759
7	Performance Parameters of OLEDs	760
8	Conjugated Polymers in LED	760
9	Chemical Synthesis of Optoelectronic Polymers	761
9.1	Soluble Precursor Route	761
9.2	Dehydrohalogenation Reactions	762
9.3	Transition Metal-Catalyzed Coupling Polymerizations	763
9.4	Condensation Polymerizations	767
10	Blue, Green, Red, and White Light-Emitting Polymers	769
10.1	Blue-Emitting Polymers	769
10.2	Green-Emitting Polymers	773
10.3	Red-Emitting Polymers	776
10.4	White Light-Emitting Polymers	778
11	Conclusion	782
	References	782

S. P. Ansari · F. Ali (✉)

Department of Applied Chemistry, Faculty of Engineering and Technology, Aligarh Muslim University, Aligarh, India

e-mail: shahidzahir@gmail.com; farmanali.ac@amu.ac.in; farmanfrequent@gmail.com

© Springer Nature Switzerland AG 2019

M. A. Jafar Mazumder et al. (eds.), *Functional Polymers, Polymers and Polymeric Composites: A Reference Series*, https://doi.org/10.1007/978-3-319-95987-0_21

749

Abstract

Organic Light-Emitting Devices (OLEDs) have received much attention in the past two decades. The possibility of cost effective production of large area devices is the main attraction for doing research in this area. There has been a considerable progress in the development of materials and the device engineering for improving the efficiency of OLEDs. These significant developments have resulted in their commercialization. In this chapter we describe OLEDs. We discuss their working principles and the measurements that are normally made in these devices. We also discuss the different types of conjugated polymers which are used for specific purposes in these devices.

Keywords

Electroluminescence · Conjugated polymers · OLEDs · PLEDs

1 Organic Molecules in Optoelectronic Devices

Optoelectronic devices have been the focus of investigation in physics and chemistry for more than 50 years. The electroluminescence (EL) was first observed by Bernanose in 1950s, where he applied a high-voltage alternating current (ac) field to the crystalline thin films of acridine orange and quinacrine [1, 2]. Pope and his co-workers demonstrated the direct current (dc) driven EL using a single crystal of anthracene [3]. In the initial stages of development organic EL devices, the driving voltage was as high as 100 V in order to obtain significant light output [4–6]. A significant decrease in the operating voltage (~30 V) was observed with thermally evaporated film of anthracene [7]. Optoelectronic properties were studied mainly in the academic institutions due to low efficiency of these devices. The breakthrough in EL efficiency was first observed by C. W. Tang and Vanslyke at Eastman Kodak Research Laboratories (USA) by making a bilayer device [8]. This demonstration highlighted the potential of using organic thin films for a new generation of optoelectronic devices.

The motivation for doing research in organic-based optoelectronic devices comes from the possible cost-effective production of large area devices. Also the physical and chemical properties of organic molecules can be tailored according to the requirement of application by modifying the molecular structure. For example, color of emission of organic molecules can be adjusted by increasing or decreasing the pi electron conjugation. The synthesis of a large number of new organic molecules with the desired colors was reported, which emit different colors with good quantum yield. They are promising materials for multicolor displays and flexible devices.

Organic thin films have found to be useful in a number of applications, which are now getting commercialized [9, 10]. Organic light-emitting device (OLED) is the most successful application. Significant progresses have also been made in the thin film transistors and the organic solar cells. Organic light-emitting transistors and

Table 1 History of major developments in OLEDs

S. No.	Discoveries and developments	Year	References
1.	Blue light emission from LED on Li complex	1953	A.B. Bermose, M. Comte, P. Vouaux, Blue emission from LED based on lithium complex, <i>J. Chem. Phys.</i> 50 (1953) 64–69 (in French)
2.	EL reported in anthracene crystals	1963	M. Pope, H. Knllmann, P. Magnante, Electroluminescence in organic crystals, <i>J. Chem. Phys.</i> 38 (1963) 2042–2043
3.	EL reported in tetracene	1976	J. Kalinowski, J. God lewski, R. Singnerski, Electroluminescence in tetracene crystals, <i>Mol. Cryst. Liq. Cryst.</i> 33 (1976) 247–259
4.	EL reported in PVK polymer	1983	R.H Partridge, Electroluminescence from polyvinylcarbazole films, <i>Polymer.</i> 24 (1983) 733–762
5.	Double layered OLED	1987	Tang, Van Slyke, U.S. Patent (1979) 4,164,431. U.S. Patent (1982) 4,356,429. Van Slyke, Organic electroluminescent diodes. 51 (1987) 913–915
6.	Single layered PLED	1990	R.H. Friends, J.H. Burroughes, D. Bardleywo, U.S. Patent 90/13148(1990)
7.	Double layered PLED	1993	N.C. Greenham, R.H. Friend, in <i>Solid state physics</i> (Academic, New York/London 1995), pp. 2–150
8.	Flexible OLED technology	2007	M. Hack, R. Hewitt, K. Urbanik, A. Chwang, J.J. Brown, Full colour top emission AMOLED displays on flexible metal foil, in <i>Proceedings of IMID/IDMC'06, Gigest conference</i> (Daegu, 2006), pp. 305–307

photodetectors have also attracted attention [11, 12]. We may also see organic materials in many more applications such as lasers, super capacitors, and memories in future [13].

This brief overview of organic electronics is not a comprehensive review of the entire field. Rather, it is intended to justify the current enthusiasm in exploring organic materials for various applications. In the latter sections of this chapter, we will describe concepts which will be useful to understand conjugated organic polymers for various applications. We will review the development of new conjugated polymers for OLEDs. A glance of discoveries in OLEDs are given in Table 1.

2 Benefits of OLEDs

The energy policies of present encourage maximum energy saving technologies. OLEDs are very competent in the light of these policies. OLEDs possess many advantages compared to both LCDs and LEDs, some of these are listed below [14]

- OLEDs are highly economical.
- OLEDs offer flexibility of processing.

- OLEDs provide a greater range of colors and brightness.
- OLEDs also offer color tuning.
- OLEDs possess high energy saving potential.
- OLEDs are Mercury-free.
- OLEDs possess high luminous efficiency.

3 Electronic Structure of Conjugated Organic Molecules and Luminescence

The conjugated organic molecules are used in organic electronics. These organic molecules have π -bonds in an alternate fashion. The overlap of atomic pz orbital leads to the formation of π -bond. The π -electrons in conjugated organic molecules are delocalized throughout the molecular backbone. Figure 1 shows a schematic of π -conjugated molecules.

A π -bond is formed after the σ -bond. The electrons in the π -molecular orbitals have higher energy than the electrons in σ -orbitals. Therefore the highest occupied molecular orbital (HOMO) is a π -molecular orbital in conjugated molecules. The ground state of molecules is a singlet as the number of π -electrons in the HOMO is even. It is these π -electrons in HOMO which participate in electronic transitions. The various photophysical processes, absorption, and emission of light in a conjugated organic molecule can be explained with the help of Jablonski diagram (Fig. 2). The HOMO of the molecule has two electrons with paired spin in the ground state and this state is shown as S_0 . When an electron is promoted from HOMO to the lowest unoccupied molecular orbital (LUMO), it becomes the excited state of the molecule. In the excited state, the electron in the LUMO can have its spin paired or unpaired with the spin of the electron in the HOMO. Thus the excited state of the molecule can be singlet (S_1) or triplet (T_1). The radiative electronic transitions from S_1 to S_0 and T_1 to S_0 are known as fluorescence and phosphorescence, respectively. The non-radiative transition between the states of same spin multiplicity like S_1 to S_0 is known as internal conversion (IC). Intersystem crossing (ISC) is a non-radiative transition between the states of different multiplicity. Figure 2 also shows the typical time scale for these

Fig. 1 π -conjugated molecules; formation of π -bond occurs due to the overlap of atomic pz orbitals

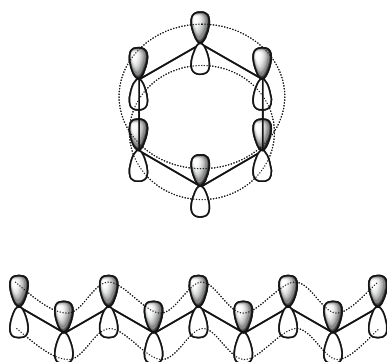
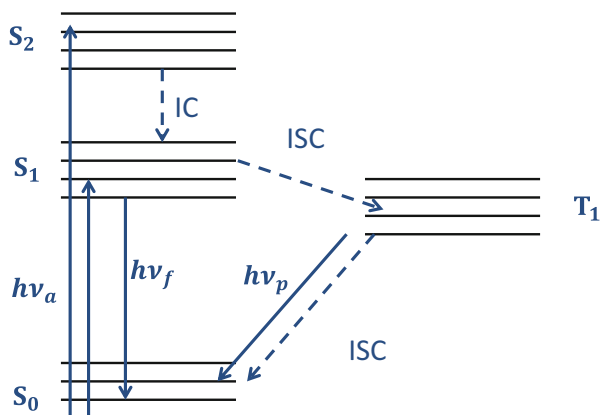


Fig. 2 Jablonski diagram of energy levels in π -conjugated organic molecule



processes. The intensity of molecular fluorescence or phosphorescence is a consequence of interplay between different processes. The band gap in organic molecules depends upon the extent of π -electrons delocalization. The band gap may vary between 1 and 4 eV. Thus, depending upon the band gap the organic molecules may absorb and emit photons anywhere from near-infrared to near-UV region.

For emission to occur, the molecule needs to be in electronically excited state. One way of getting the excited state of a molecule is by absorption of light. The excited state can also be formed by a simple electron transfer reaction between anion and cation radical pair. This principle is used to obtain the chemiluminescence [15] and electrochemiluminescence [16] in solutions. The physical movement of cation and anion radicals in a solvent medium is important to form the excited state of molecules. Light emitting electrochemical cells using gels and polymers [17] are gaining attention but cells using liquids are less attractive for practical applications. A solid state analogue of this process is OLED. In OLEDs, the electrons and holes are pumped in to the LUMO and HOMO levels, respectively, to form the excited state. These electrons and holes then recombine to give electroluminescence.

4 Energy Transfer in Guest-Host Systems

Energy transfer from host donors to guest acceptors via Forster/Dexter mechanism is utilized to tune the color of emission and improve efficiency in OLEDs. Forster energy transfer is a long-range mechanism (up to ~ 10 nm) due to dipole-dipole coupling between donor and acceptor [18]. Dexter energy transfer is a short-range mechanism (typically ~ 1 nm) and it involves intermolecular electron exchange process [18]. Energy transfer from singlet to singlet can either be Forster or Dexter or involve both mechanisms. The triplet-triplet energy transfer is always through Dexter mechanism only. Figure 3 shows the schematic of light emission processes and energy transfer in guest-host systems of phosphorescent emitting layer in OLEDs.

Fig. 3 Schematic of energy transfer and light-emission processes in host-guest systems in phosphorescent OLEDs

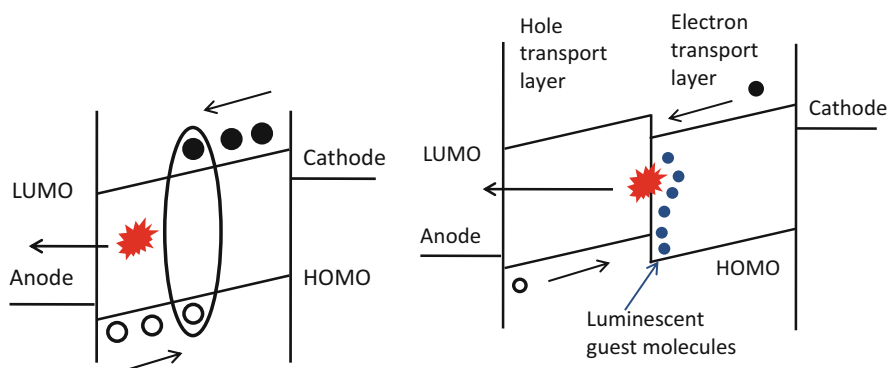
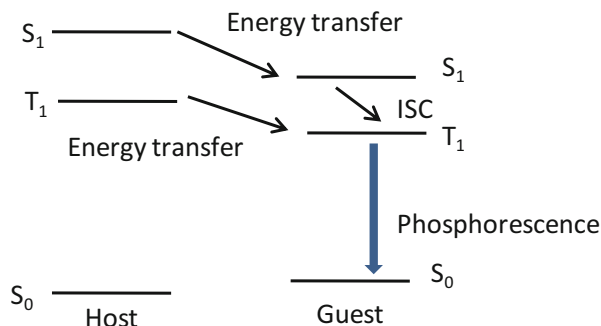


Fig. 4 (a) Schematic diagram of a single layer OLED, and (b) bilayer OLED. Hole transporting layer is a diamine and electron transporting layer is Alq3

5 Working of an OLED

The electrical energy is converted into light energy in an OLED. Figure 4a shows the schematic energy level diagram of the single layer OLED. Cathode and anode injects electrons and holes into the LUMO and HOMO of organic thin film, respectively. These injected electrons and holes move towards each other under the influence of applied electric field and when they meet on to the same organic molecule, that is, hole in the HOMO and electron in LUMO, it becomes the excited state of organic molecule. The excited state may diffuse to other molecules if it is long lived (e.g., triplet), and its properties are conserved during the diffusion. In other words, the excitation of organic molecule behaves like a quasi-particle and this is termed as an exciton. The exciton binding energy in organic molecules is of the order of 0.5–1.0 eV [19]. The electron and hole in the excited molecule may recombine radiatively by emitting a photon. The emission so obtained is called electroluminescence (EL). The energy of the emitted photon depends on the band gap energy of the excited organic molecule.

The recombination of injected electrons and holes gives high electroluminescence efficiency in OLED. In case the injected carriers do not meet each other than the EL efficiency of OLED is less or even zero. In organic molecules, the mobility values of electron and hole are very different. As a result, one of the injected carriers (e.g., hole) moves faster than the other carrier (e.g., electron) and reaches the opposite electrode without recombination. This is normally the case in single-layer device. An efficient strategy to prevent the leakage of injected carriers was first demonstrated by Tang and Vanslyke in 1987 [8]. They fabricated a bilayer device with hole transport layer (HTL) and electron transport layer (ETL). Figure 4b shows the schematic energy level diagram of a bilayer device. In this device, diamine functions as HTL and tris(8-hydroxyquinolino) Al(III) (Alq₃) as a ETL. The injected carriers move towards the diamine/Alq₃ interface and are not able to cross over the interface because of high energy barrier. They pile up at the interface and form the molecular excitons which emit light. The interface may also be doped with other low band gap guest molecules for harvesting the excitons [20]. The other advantage of this bilayer structure is that excitons are formed away from the conductive contacts which are known to quench the excitons. This particular demonstration has highlighted the importance of using multilayer architectures in order to improve the EL efficiency of the OLEDs. Nowadays, functionally distinct organic layers such as hole inducing (HIL), hole transporting (HTL), hole blocking (HBL), electron transporting (ETL), electron blocking (EBL), emissive layers, etc. are used in OLEDs to improve the overall EL efficiency [21]. Table 2 shows the different components of a multilayer OLED. Figure 5 shows the schematic of a multilayer OLED. It also shows the

Table 2 The different components of a multilayer OLED, their function and representative examples

S. No	Component	Functions/properties	Materials
1.	Substrate	Provides support for PLED	Glass/plastic foil
2.	Anode	A transparent anode with good electrical conductivity, high work function suitable for hole injection in HOMO of organic layer	Indium tin oxide
3.	Hole Transport Layer (HTL)	Smooth surface over ITO, supports efficient hole injection by reducing energy barriers in case of red-green emitting polymers	PEDOT:PSS, PVK, cross-linked conjugated polymers
4.	Emissive Layer (EML)	Light emitting polymers	PPV, MEH-PPV, CN-PPV, Derivatives of Polythiophene, Polyfluorenes, poly (1,4-phenylenes) etc.
5.	Electron Transport Layer (ETL)	Provides balanced injection of charge carriers	1,3,4 Oxadiazole
6.	Cathode	Facilitates electron injection in polymeric materials	Li, Ba, Ca, Al etc

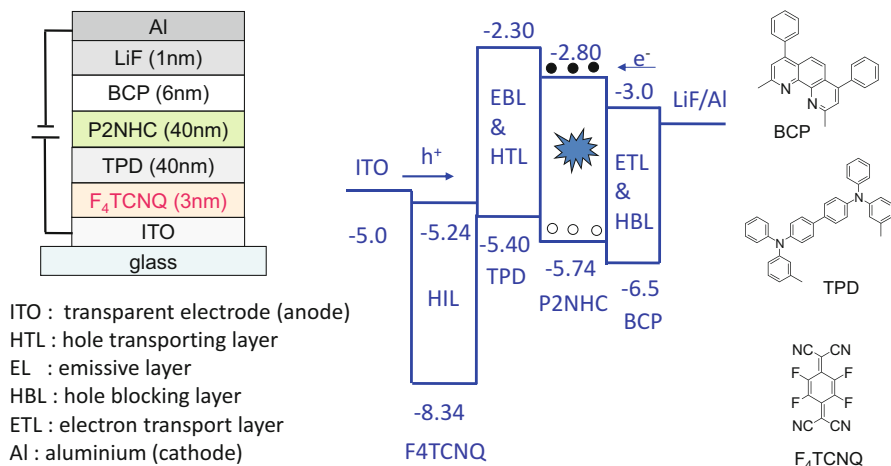


Fig. 5 The schematic of an high efficiency multilayer structure OLED, its corresponding schematic energy level diagram, and the molecular structure of the molecules used

schematic energy level diagram and the molecular structure of the organic molecules performing different functions.

The multilayer OLED is complete in all functional aspects. It has 2,3,5,6-Tetrafluoro-7,7,8,8-tetracyanoquinodimethane (F_4TCNQ)/N,N'-diphenyl-N,N'-bis(3-methylphenyl)-1,1'-biphenyl-4,4'-diamine (TPD) at the anode which efficiently injects and transports holes and 4,7-diphenyl-1,10-phenanthroline (BCP)/LiF/Al as a composite cathode which injects and transports electrons to the P2NHC (emissive layer). TPD and BCP layers also separate the emissive layer from the anode and cathode, respectively, as a result of which the electroluminescence of 3,6-dipyrenyl-N-hexylcarbazole (P2NHC) does not get quenched due to electrodes. TPD and BCP layers also confine the injected electrons and holes in the P2NHC layer. The device exhibit high electroluminescence efficiency at low turn-on field due to efficient hole and electron injection accompanied by exciton formation and radiative recombination.

In the later sections we discuss functionally distinct organic layers which are used in the high efficiency OLED.

6 Materials for OLEDs

6.1 Anode Materials

The function of anode is to inject holes into the HOMO level of organic molecules and therefore high work function materials are desirable for efficient injection of holes into the HOMO level. Indium Tin Oxide (ITO) coated on glass is the most popular anode material because it has the following advantages: (a) transparent in

the visible region, (b) can make “contact” with the organic molecules, and (c) high work function for efficient hole injection. The work function of ITO is typically 4.5 eV, which can be increased up to 5.1 eV by UV ozone treatment [9]. The other materials which can be used for the anode, besides ITO, are Poly (3,4-ethylene dioxy-2,4-thiophen)-polystyrene sulfonate (PEDOT:PSS) [22], noble metals like gold and platinum [23]. PEDOT:PSS is a conducting polymer and its thin films are transparent to the visible spectrum. Thin films (<1 nm) of gold and platinum are also transparent to the visible spectrum. The work function of gold and platinum are 5.1 eV and 5.6 eV, respectively [9].

6.2 Hole Injection Materials (HIM)

An efficient OLED requires a multilayer device architecture, therefore the interfacial structure at the organic-metal and organic-organic interfaces play an important role in devices. A thin film (~1–2 nm) of HIL acts as an interface connection layer between the anode and the HTL. It improves the film forming property and facilitates efficient hole injection from anode to the HTL [24]. As a result, the operational voltage decreases and less amount of heat is generated inside the device. The frequently used HILs are PEDOT:PSS, copper phthalocyanine (CuPc), or various inorganic buffer layers like TiO₂ [25]. CuPc layer on ITO has proved to be an effective HIL [23]. PSS-rich PEDOT:PSS was also used as HIL [23]. The exact mechanism of “modification” by PEDOT:PSS is still unclear but the most accepted one is the creation of interfacial dipoles on surface of PEDOT:PSS that helps the injection of holes to the HTL [26]. The surface of bare ITO is undesirably rough and spikes on bare ITO normally shunt the device. Coating of ITO with PEDOT:PSS layer helps to avoid these problems. However, the commercially available PEDOT:PSS solutions have unpredictable short shelf-life (nearly 6 month). An electron acceptor molecule (F₄TCNQ) is also used as HIL on ITO anode [23]. More recently, inorganic compounds like ZnO have also been used as thin buffer layer between ITO and HTL [27].

6.3 Hole Transport Layer (HTL)

The use of HTL with thickness (40–100 nm) on top of ITO with or without HIL serves the following functions: (a) gives an interface with the emissive layer (b) provides energy barrier for electron and confines them to the emissive layer, and (c) transport holes to the emissive layer for the exciton formation.

The general requirements for organic molecules to be used in as HTL are: (a) high hole mobility, (b) their HOMO level in the thin film should be close to the work function of the anode in order to facilitate easier hole injection, (c) high glass transition temperature, (d) high stability of its cation radical, and (e) large optical band gap in order to avoid the absorption of visible light as emitted by the emissive layer.

The frequently used small molecules in HTL are N,N'-diphenyl-N,N'-bis(3-methylphenyl)-1,1'-biphenyl-4,4'-diamine (TPD), N,N'-diphenyl-N,N'-bis

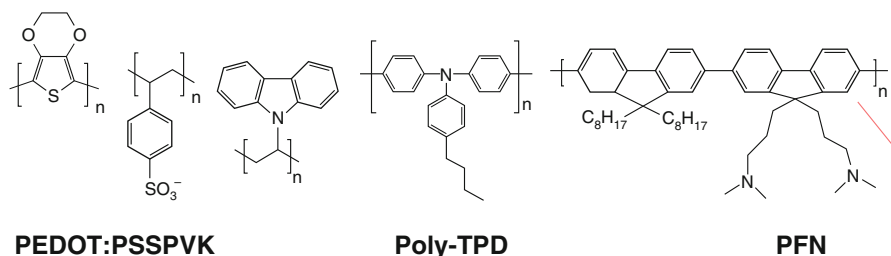


Fig. 6 Molecular structure of polymers used at the interfaces in OLEDs

(1-naphthylphenyl)-1,1'-biphenyl-4,4'-diamine (NPD), and copper phthalocyanine (CuPc). The polymers used as HTL are PEDOT:PSS, poly-N-vinylcarbazole (PVK), poly(4-butyl-phenyl-diphenyl-amine) (poly-TPD), etc. [23, 28] (Fig. 6). The mobility values for holes in small molecules TPD and NPD are 2×10^{-3} and $3 \times 10^{-4} \text{ cm}^2 \text{ V}^{-1} \text{ s}^{-1}$, respectively [9]. The mobility values for holes in polymers PVK and poly-TPD are 2.5×10^{-6} and $1 \times 10^{-4} \text{ cm}^2 \text{ V}^{-1} \text{ s}^{-1}$, respectively. These molecules have low electron affinity (2–2.5 eV), and hence they also function as electron blocking layer.

6.4 Electron Transport Layer (ETL)

The use of ETL with thickness (~6–10 nm) between the emissive layer and cathode facilitates electron injection during the device operation. The ETL also helps to confine holes within the emissive layer due to its large work function. The general requirements for organic molecules to be used as an electron transporting layer are: (a) the energy of LUMO level is close to the work function of cathode for easier electron injection, (b) high mobility values for electrons for efficient transport into the emissive layer, (c) high glass transition temperature, (d) high stability of anion radical, and (e) large optical band.

The frequently used small molecules in ETL are tris(8-hydroxyquinolino) Al (III) (Alq₃), 4,7-diphenyl-1,10-phenanthroline (BCP), 2,9-dimethyl-4,7-diphenyl-1,10-phenanthroline (Bphen), 1,3,5-tris(N-phenylbenzimidazol-2-yl)benzene (TPBI), and Oxidazole derivatives [9]. The mobility value of electron in Alq₃ is $1.4 \times 10^{-6} \text{ cm}^2 \text{ V}^{-1} \text{ cm}^{-1}$ [9] and hole is $2 \times 10^{-8} \text{ cm}^2 \text{ V}^{-1} \text{ s}^{-1}$ [9]. The value electron mobility of BCP and Bphen is in the order of $10^{-5} \text{ cm}^2 \text{ V}^{-1} \text{ s}^{-1}$ [29].

6.5 Cathode Interfacial Materials (CIM)

The electron injection from the cathode can be improved by decreasing the work function of cathode. The use of a thin layer (~1 nm) of a CIM in contact with the cathode decreases the work function of the cathode (e.g., Al) and facilitates electron injection. The popular materials used in CIM are LiF, CsF, and Li₂O [23]. The barrier to electron injection has been shown to decrease by 0.4 eV in the case of Alq₃/LiF/Al

than Alq₃/Al [30]. The mechanism of lowering in work function using CIM is debated. It was speculated that free Li atoms are formed at the Alq₃/LiF/Al interface, which in turn forms Alq₃ anion [31]. However, the use of CIM along with Al (4.2 eV) is equivalent to using low work function cathodes like Ca (2.87 eV) and Mg (3.66 eV) [9]. Water/alcohol soluble conjugated polymers poly [(9,9-bis(3'-(N,N-dimethylamino)propyl)-2,7-fluorene)-alt-2,7-(9,9-dioctylfluorene)] (PFN) have also been used as a cathode interfacial layer in organic devices [32].

6.6 Cathode Materials

The function of cathode is to supply electrons into the LUMO. The requirements for cathode materials are as follows: (a) low work function to facilitate efficient electron injection into the LUMO, (b) wetting properties to ensure good contact with adjacent organic layers, (c) stable to ensure long lifetime of device, and (d) transparent when used in “top-emitting” OLEDs.

The most popular cathode material is Al (4.2 eV). The other materials which are commonly used for cathode are LiF/Al (3.6–3.8 eV), Ca/Al, Mg/Ag (2.9 eV), and Ba/Al (2.6 eV) [21, 23]. Very low work function materials such as Cs, Ca, etc. need to be capped with another stable metal film such as Al, Ag to avoid oxidation.

6.7 Light-Emitting Materials

The material that gets the most value in OLED is the one used in emissive layer. The organic molecules to be used in the emissive layer must have high photoluminescence quantum yield in the thin solid film. The other requirements of a light emitting materials are as follows: (a) compatible HOMO and LUMO for efficient carrier injection from electrodes or adjacent organic layers, (b) good film forming property, (c) large stokes shift, (d) high glass transition temperature, (e) good solubility in suitable solvents is essential for polymers as they can only be deposited via spin coating, and (f) efficient energy transfer from the host, if used as a guest (dopant).

The emitting layer may also be doped with another highly luminescent guest molecule. Energy transfer from the host (primary exciton) to guest (secondary exciton) makes possible to change the color of emission. This strategy is widely used in harvesting triplets excitons in phosphorescent OLEDs [23].

The color of emission of an OLED is decided by the band gap of the polymer used in the emissive layer. If a blue-emitting polymer is used in the emissive layer then electroluminescence spectrum of the device will also be blue. To make a display like television, we require white light emission. For an organic molecule, it is difficult to emit such a broad spectra. The way white light easily generated is by mixing blue, green, and red emitters in suitable ratio in the active layer. The synthesis of white light-emitting polymers is little difficult but has been done. In the later section, we review the polymers synthesized and used in fabricating blue, green, red, and white light-emitting OLEDs.

7 Performance Parameters of OLEDs

The performance of an OLED is measured in terms of various parameters. They are current efficiency (cd/A), brightness (cd/m²), power efficiency (W/W), lifetime, and internal and external quantum efficiency. The internal quantum efficiency (η_{int}) is the number of photons generated in the device per injected carrier, and it can have a maximum value of 100%. External quantum efficiency (η_{ext}) is the number of photons emitted out of the device per injected carrier in the forward or viewing direction. The light out-coupling efficiency (ξ) of device is limited by absorption losses and guiding of electroluminescence within the device and its substrate. For a refractive index of the emissive medium n , ξ for a flat interface is given by: $\xi \approx 1/(2n^2)$ [9].

Internal quantum efficiency is determined by various factors. Charge balance factor (γ) accounts for the ratio of electrons and holes injected (ideally 1) into the device and the probability of their recombination (ideally 1). Spin statistics predicts the formation of triplet and singlet state in the ratio of 3:1 from the uncorrelated electron and hole recombination. The emission from these states depends upon the quantum yields of fluorescence (ϕ_F) and phosphorescence (ϕ_P). In ground state, most organic molecules have a total spin of $S = 0$, and during the course of electronic transition, the spin remains conserved. The fluorescence quantum yields close to 1 have been reported for many organic molecules [23]. The electronic transitions involving a change in spin multiplicity are spin forbidden. Therefore the phosphorescence from the $S = 1$ (triplet) state to the singlet state is generally inefficient and almost all energy is lost to the non-radiative processes. Transition from the triplet state is partially allowed in certain heavy metal complexes, such as Iridium (Ir), due to mixing of metal orbitals. Heavy metal complexes of iridium and platinum have high phosphorescent quantum yield and they are used to harvest the triplet excitons formed in the emitting layer [10].

Taking into all the above factors, external quantum efficiency (η_{ext}) can be written as

$$\eta_{\text{ext}} = \xi \gamma (r_s \phi_F + r_t \phi_P) \dots \quad (1)$$

where r_s and r_t are singlet and triplet state formation efficiencies. Figure 7 shows the various processes that follow electron-hole recombination in OLEDs. Internal quantum efficiency of nearly 100% and external quantum efficiency of $19.0 \pm 0.5\%$ have been demonstrated using a heavy metal (Ir) complex [33].

8 Conjugated Polymers in LED

The EL in conjugated organic polymers based on poly(N-vinyl carbazole) (PVK) and doped with luminescent dyes was first reported by Partridge [34]. Friend and co-workers described an EL device based on conjugated poly(p-phenylenevinylene)

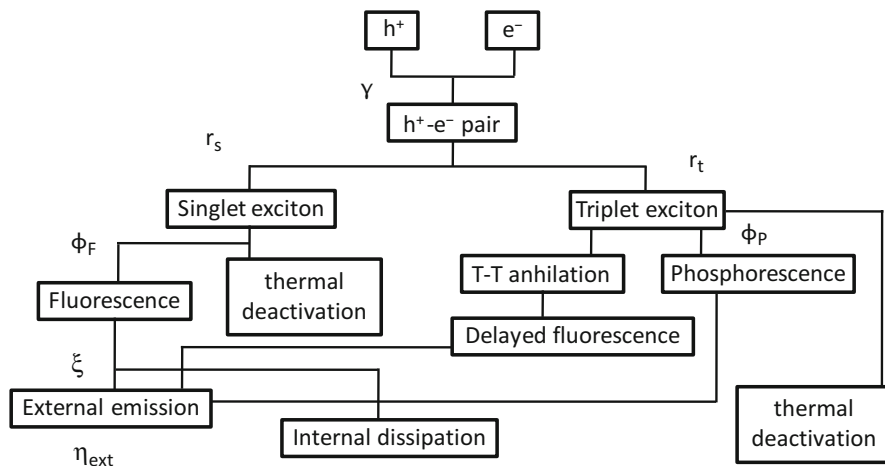


Fig. 7 Schematic of the external quantum efficiency

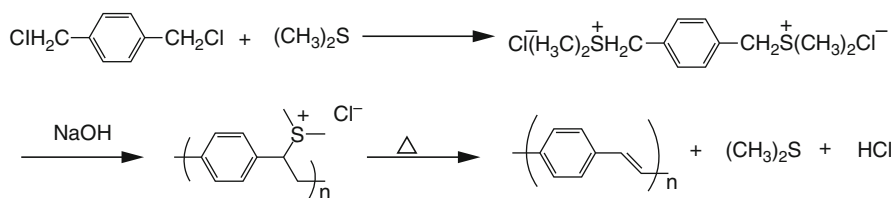
(PPV) [1]. The EL efficiency and low turn-on voltage of this device projected conjugated polymers as promising candidates for commercial application. Since then a number of polymers with different emission color have been synthesized and tested. In the following sections we first describe the popular chemical reactions adopted to synthesize conjugated polymers and then we review the development of most promising polymers for blue, green, red, and white light emission.

9 Chemical Synthesis of Optoelectronic Polymers

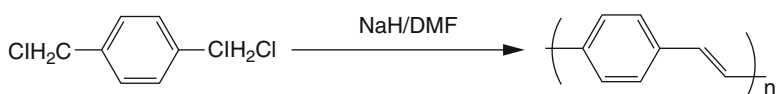
There are many polymerization techniques to prepare light emitting polymers. The synthesis of different light emitting polymers as reported in literature exploited mainly four important C–C bond forming techniques. These include soluble precursor polymer route, dehydrohalogenation reactions, transition metal-catalyzed coupling polymerizations, and condensation polymerizations. In this section, we present representative examples of all the above mentioned reactions.

9.1 Soluble Precursor Route

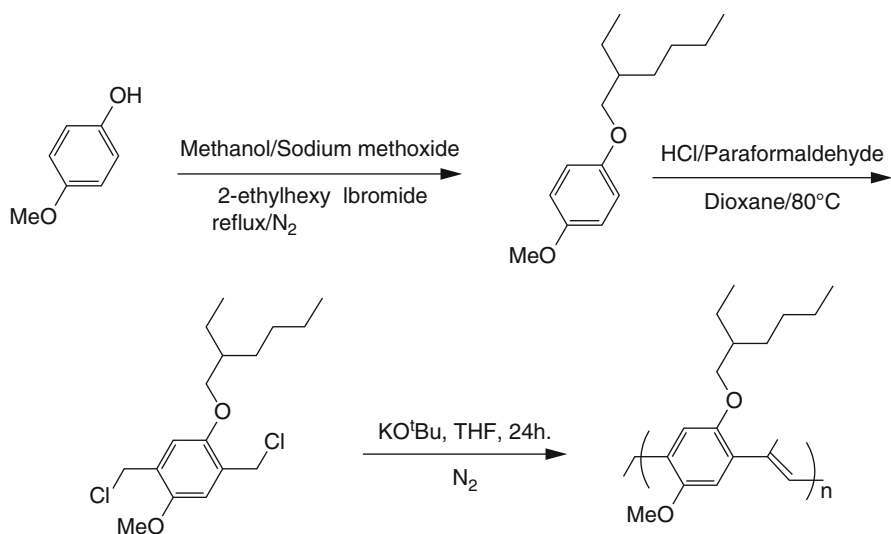
This is the most extensively used strategy for the synthesis of PPV and its derivatives. The polymer produced by this method possess very high molecular weight, and their films are highly oriented by stretching during conversion of the precursor polymer to its conjugated form (Scheme 1) [35]. The conversion temperature can be reduced to 100 °C by using bromide derivatives instead of chlorides, thus enabling the fabrication of flexible devices [36].



Scheme 1 The Wessling-Zimmerman precursor route to PPV



Scheme 2 Synthesis of PPV using dehydrohalogenation reaction

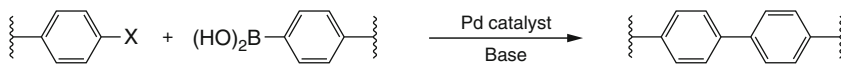


Scheme 3 Gluch polymerization of MEH-PPV

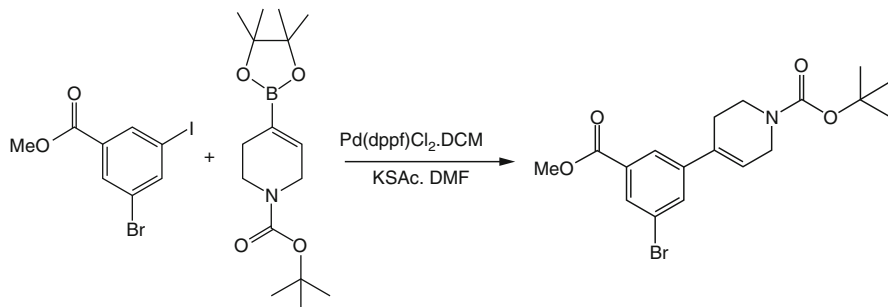
9.2 Dehydrohalogenation Reactions

These reactions are employed to synthesize different PPV derivatives. Unsubstituted PPV is synthesized by the dehydrohalogenation of dichloroethylene in the presence of sodium hydride and DMF solvent [37] (Scheme 2).

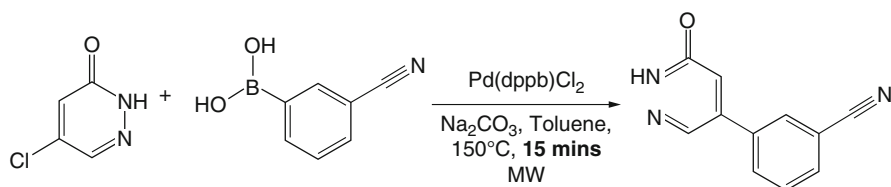
Gluch polymerization is most widely used for the synthesis of PPV derivatives. Mainly alkyl or alkoxy substituted PPV derivatives are synthesized using this method [38, 39] (Scheme 3).



X = Br, I, Cl, sulfonyl



Scheme 4 Representative examples of Suzuki-Miyura Coupling reaction



Scheme 5 Representative example of microwave assisted Suzuki-Miyura Coupling reaction

9.3 Transition Metal-Catalyzed Coupling Polymerizations

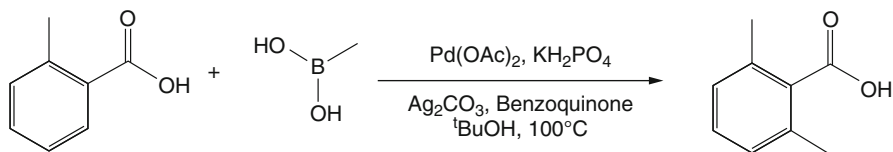
9.3.1 The Suzuki-Miyaura Coupling

The Suzuki coupling reactions are mainly for the cross-coupling reaction of organoborons with organohalides. The organoboron are present in the form of a boronic acid or ester. These reactions offer very high tolerance toward various functional groups and by-products containing boron can easily be removed. These reactions are most commonly used to form aryl-aryl bonds and are very effective for the synthesis of highly substituted conjugated aromatic products. Suzuki coupling has found extensive use for the preparation of alternating copolymers [40, 41] (Scheme 4).

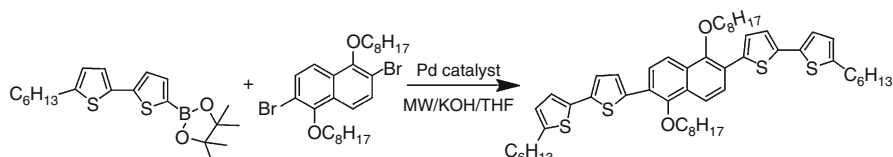
In presence of microwaves, Suzuki reactions get accelerated (Scheme 5).

This reaction can also be used to obtain aromatic alkylations. C-H insertion negates the necessity to begin with an aryl halide, improving the atom efficiency of the process (Scheme 6).

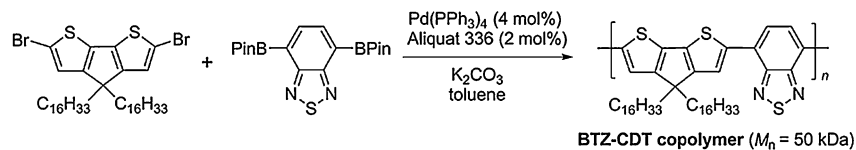
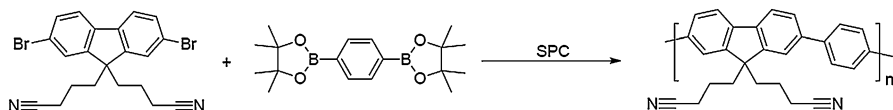
Nehls et al. synthesized thiophene-naphthalene oligomer via microwave-assisted Suzuki coupling of the appropriate bromo and boronic acid derivative [42] (Scheme 7).



Scheme 6 Representative example of Suzuki-Miyura Coupling reaction



Scheme 7 Synthesis of thiophene-naphthalene oligomer via microwave assisted Suzuki-Miyura Coupling reaction



Scheme 8 Synthesis of benzothiadiazole-cyclopentadithiophene (BTZ-CDT) copolymers via Suzuki polycondensation

9.3.2 Suzuki Polycondensation

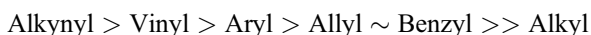
Suzuki polycondensation reaction was discovered in 1987. Since then, it has been utilized for the synthesis of polyarylenes as a powerful tool. A typical procedure for Suzuki polycondensation [43, 44] (Scheme 8).

Advantages of Suzuki Reactions:

- Mild reaction conditions.
- Availability of common boronic acids.
- Inorganic by-products are easily removed from reaction mixture.
- Stereoselective.
- Less toxic than other competitive methods (i.e., Boronic acids are environmentally safer and less toxic than organostannanes.).
- Reaction will take place in the presence of other functional groups.
- Protecting groups are not always necessary.
- Relatively cheap reagents, easy to prepare, and GREEN.

9.3.3 The Stille Coupling

This is a very versatile reaction and an excellent alternative to the Suzuki reaction. In this reaction, organostannanes are used instead of organoboron. The tin atom bears four functional groups; therefore, it is very important to have very good understanding of the rates of transmetallation reaction of each group. Relative rate of transmetallation:



The main attraction and advantage of the Stille coupling reaction is the use of organostannanes which are easily prepared, purified, and stored. An important benefit of these reactions is their tolerance (better than Suzuki Coupling) to many functional groups and can also be carried out in neutral conditions. Compounds like aromatic ketones, biaryl derivatives, and styrenes can be synthesized using this reaction [45, 46] (Scheme 9).

Carsten et al. polymerized thiophene containing monomers with stannyl groups via microwave-assisted Stille coupling reaction [47]. Stille reactions are very versatile and are widely used to synthesize functional/multifunctional light emitting polymers.

9.3.4 Heck Coupling

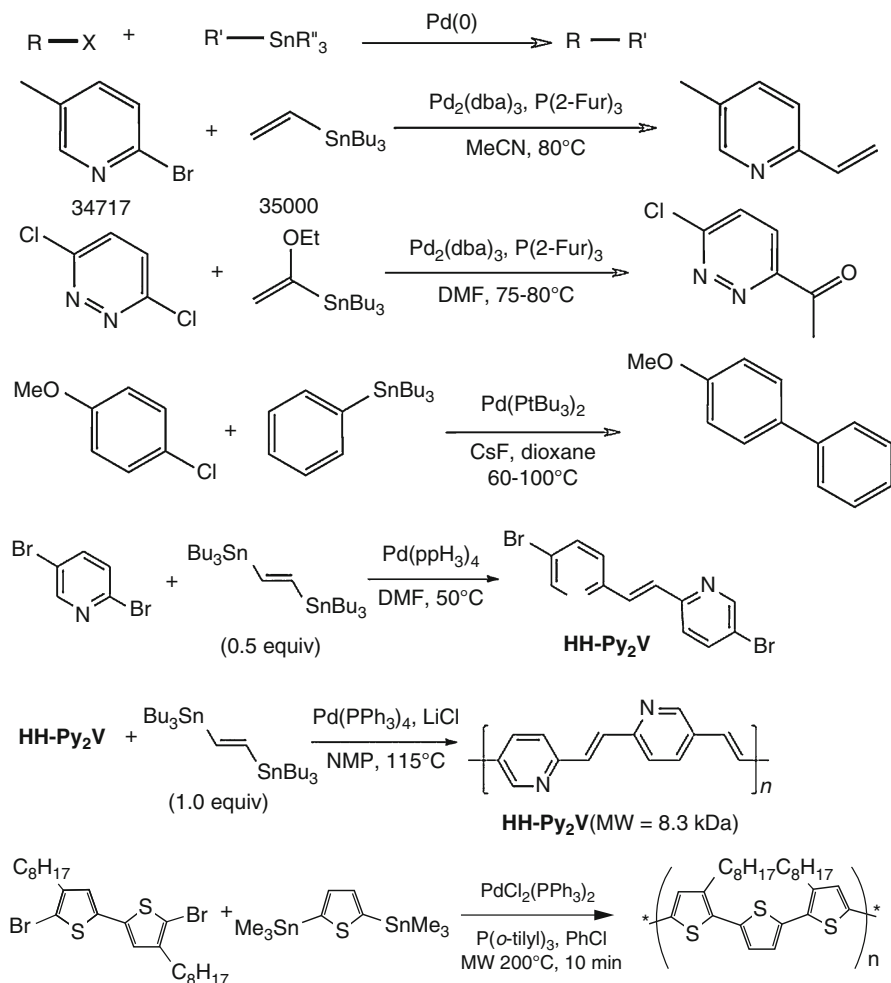
The Heck reaction is a cross-coupling reaction of an organohalide with an alkene to make a substituted alkene using palladium as a catalyst and a base. Heck coupling reaction can be described as a palladium-catalyzed C–C formation between aryl/vinyl halides and activated alkenes in presence of a base. The reaction starts with the oxidative addition of aryl halide to the palladium atom, which is followed by coordination and migratory insertion of the olefin to the palladium. Bond rotation then places the two groups *trans* to each other to relieve the steric strain and subsequent β -hydride elimination results in a *trans* final product. Base-mediated reductive elimination regenerates the palladium(0) catalyst. The Heck reaction is of great importance, as it allows substitution reactions on planar sp^2 -hybridized carbon atoms. Another advantage of this reaction is its excellent *trans* selectivity [48, 49].

Heck method is not suitable for the preparation of PPV homopolymers, but this method is more useful for the preparation of PPV-related block copolymers (Scheme 10). Heck reaction yields the same regular copolymer regiochemistry and double-bond configuration with a much higher yield, better purity, and also high luminescence efficiency.

9.3.5 Yamamoto Coupling

In Yamamoto coupling, C–C bonds of aryl halogenides are formed by mediation from a transition metal as catalyst, like bis(cyclooctadiene)nickel(0), $\text{Ni}(\text{cod})_2$. In Yamamoto coupling, only a single halogen functionalized monomer is required, offering diversity in monomers and simple reaction procedure.

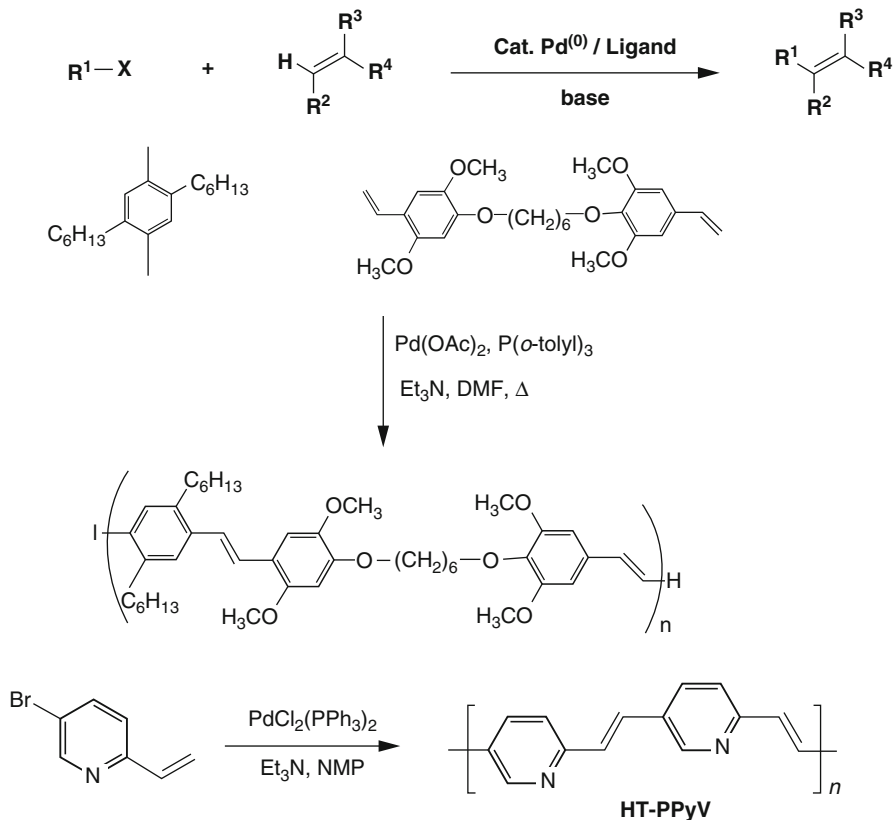
Yamamoto polymerization of a dihaloaromatic compound (AA-type monomer) gives a polymer. The main advantage of Yamamoto polymerization is that AA-type



Scheme 9 Representative examples of Stille coupling reaction

monomers are straightforward to work with. For example, poly(9,9-bis(2-ethylhexyl)fluorene) was prepared by Yamamoto-type polycondensation of a 2,7-dibromofluorene with bis(COD)nickel and bipyridine [50, 51]. However, this method usually requires stoichiometric amounts of catalyst. Investigations on Ni-catalyzed reductive polymerization of 2,7-dibromofluorenes with excess zinc dust as a reductant led to the synthesis of highly conjugated and processable PFs (Scheme 11).

Lee and Hsu synthesized green-emitting polymers using Yamamoto coupling reaction by end capping N-aryl-1,8-naphthalimide and 1,8-naphthoilenearylimidazole derivatives into polyfluorene [52].



Scheme 10 Representative examples of Palladium catalyzed Heck coupling reaction

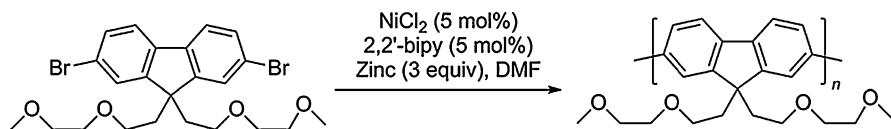
9.4 Condensation Polymerizations

9.4.1 Wittig Reaction

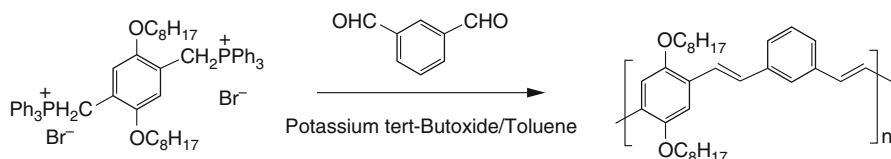
Wittig reaction is one of the most versatile methods for the synthesis of alkenes in which electrophilic carbonyl compounds such as aldehyde and ketone are attacked by a phosphorus ylide. Phosponiumylides are readily formed by the addition of a suitable base to the corresponding phosphonium salt. Wittig polycondensation route was used for the preparation of well-defined alternating copolymers. Here we present one of the example related to PPV, Blau et al. synthesized poly(*m*phenylenevinylene-co-2,5-dioctyloxy-*p*-phenylenevinylene) by Wittig reaction [53] (Scheme 12).

9.4.2 Horner-Emmons Condensation

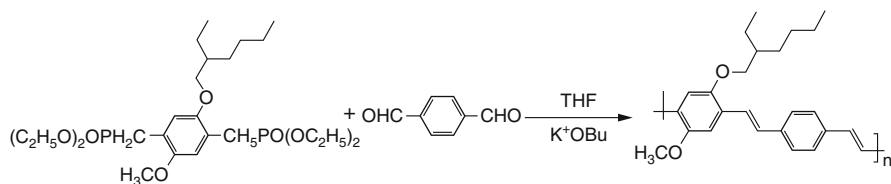
Horner-Emmons condensation is a practical modification of Wittig reaction that is used for the synthesis of PPV related alternating copolymer [54]. Wittig polymers have high molecular weight and it contain certain amount of *cis*-vinylene double bonds. Horner-Emmons condensation has some advantages over Wittig reaction



Scheme 11 Nickel catalyzed Yamamoto coupling



Scheme 12 Synthesis of PPV derivative by Wittig reaction

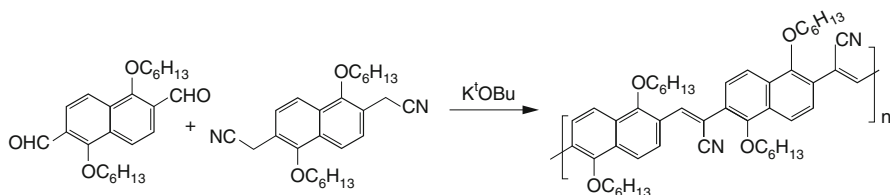


Scheme 13 Synthesis of Poly(MEHPV-alt-PV) by Horner-Emmons condensation

such as, newly formed double bonds are purely *trans* in nature, it shows good regioselectivity, high degree of conversion, and finally good yield [55]. Kim et al. prepared poly (MEHPV-alt-PV) by using Horner-Emmons condensation is displayed in Scheme 13. The reaction consist of substituted phosphonate ester reacted with terephthalaldehyde under the presence of potassium *tert*-butoxide to produce alternating copolymer [55].

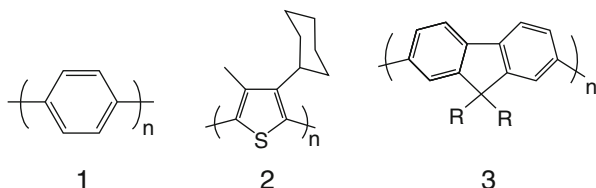
9.4.3 Knoevenagel Coupling Route

Emissive polymers containing vinylene linkages are also prepared by using Knoevenagel coupling reaction, in which carbon-carbon double bonds are formed between respective monomers. Knoevenagel condensation based on the reaction between aldehyde groups with active methylene species requires strong electron withdrawing substituent groups (CN, for example) [55]. Employing Knoevenagel condensation numerous PPV-related homo and copolymers with CN containing vinylene units have been synthesized. Hanack et al. prepared cyano substituted poly(2,6-naphthylenevinylene) (CN-2,6-PNV) by using Knoevenagel condensation reaction between two monomers, namely, 1,5-bis(hexyloxy)-2,6-naphthalenediacetonitrile and 1,5-bis(hexyloxy)-2,6-naphthalenedicarbaldehyde in the presence of a strong base is shown in Scheme 14.



Scheme 14 Synthesis of poly(2,6-naphthylenevinylene) by Knoevenagel condensation

Fig. 8 Molecular structures of different families of blue-emitting polymers



10 Blue, Green, Red, and White Light-Emitting Polymers

10.1 Blue-Emitting Polymers

The fluorophores that are responsible for blue light emission typically contain phenyl, or fluorene, or heterocycles such as thiophene, etc. in their chemical structure. Figure 8 shows the molecular structures of different families of blue-emitting polymers. These fluorophores may be present in the main chain of polymer or as its side chain. The presence of side chain play an important role and its function is to increase interaction, decrease planarity for color shift in the emission spectrum, and to enhance solubility of polymers [56].

Poly(p-phenylenes) (PPPs) is an important class of blue-emitting polymers. Figure 9 shows the molecular structures of different PPPs derivatives. PPPs can make neat thin films which emit at ~460 nm. Electrochemically polymerized Poly(p-phenylene) (PPP) was also observed to exhibit light-emitting properties [56, 57]. It was found that the reaction condition for polymerization affect the light-emitting properties. The polymers obtained electro-reductively with charges of 50 and 100 mC/cm² show EL maxima in the region between 450 and 550 nm while that with a charge of 1 mC/cm² falls at about 600 nm [58, 59]. PPPs have poor solubility and low quantum efficiency (QE) which made them less attractive for blue OLED. The issue of poor solubility was addressed by attaching the alkyl chains in the polymer backbone. Many PPPs derivatives were synthesized. Monoalkoxy substituted PPPs, poly[2-(6'-cyano-6'-methylheptyloxy)-1,4-phenylene] (CN-PPP) (6), poly(2-decyloxy-1,4-phenylene) (DO-PPP) (5), and poly[2-(2'-ethylhexyloxy)-1,4-phenylene] (EHO-PPP) (4) are soluble in organic solvents [60, 61]. The three polymers show nearly identical PL spectra, with PL and EL maxima at 420 nm. A PL quantum yield for the polymers in a 1% solution is 85% and the yields in films

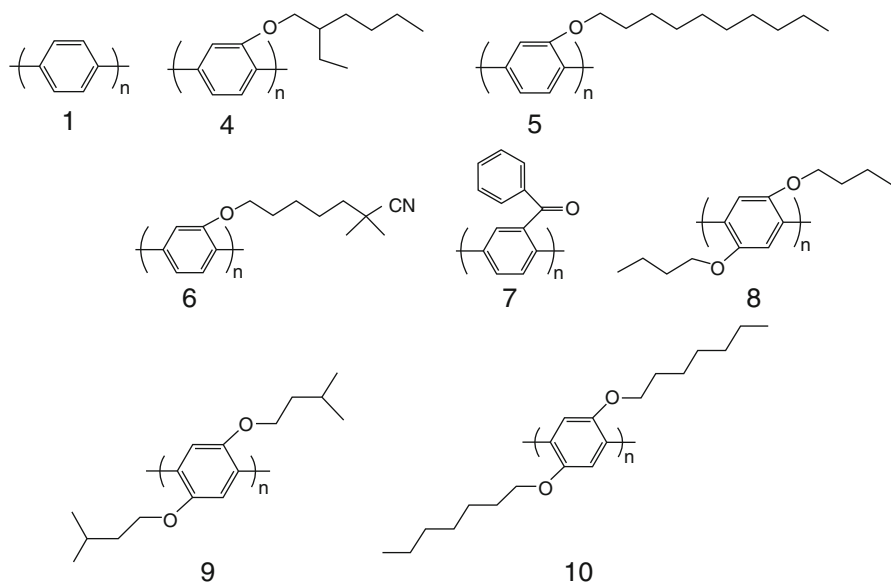


Fig. 9 Molecular structures of PPV polymers

ranges from 35% to 46%. The best external QE for LEDs with a structure of ITO/PVK/PPPs/Ca are 3.0, 2.0, and 1.4% for **4**, **5**, and **6**, respectively, where PVK is poly(N-vinylcarbazole).

Poly(2-benzoyl-1,4-phenylene) (PBP) (**7**) is soluble in common organic solvents and thermally stable up to 400 °C [62]. The polymer film having thickness of 15 nm, when photo excited at 390 nm exhibit PL maximum at 433 nm, slightly less than that of PPPs but higher than that of alkoxy substituted PPPs. Quantum yield of PBP in chloroform was measured to be 15%. A LED having a structure of ITO/PVK-PBP (3:1) blend/PBD-PMMA (3:1) blend/Ca/Al exhibits an EL maximum at 446 nm with an EQE of 0.17%, where PBD and PMMA are 2-(4-biphenyl)-5-(4-tert-butylphenyl)-1,3,4-oxadiazole and poly(methyl methacrylate), respectively.

Photophysical properties of dialkoxy substituted PPVs (**8**, **9**, and **10**) have also been studied [62]. The absorption spectra are reported to be similar and unaffected by the length of the alkyl chain or isomeric structures. The peak absorption wavelength is at about 336 nm. Degree of polymerization, length of alkoxy substituent, and preparation methods affects the absorption maxima of the resultant molecules. The intensity of absorption changes with the length of the alkoxy groups. Poly(2,5-dibutyloxy-1,4-phenylene) (**8**) in methylene chloride shows an extinction coefficient $6.4 \times 10^6 \text{ cm}^2/\text{mol}$ whereas poly[2,5-bis(3'-methylbutyloxy-1,4-phenylene)] (**9**) shows an extinction coefficient $3.8 \times 10^6 \text{ cm}^2/\text{mol}$. The PL maxima of **8**, **9**, and **10** in chloroform appear at 410 nm. Poly(2,5-diheptyloxy-1,4-phenylene) (**10**) when synthesized by oxidative coupling using anhydrous FeCl_3 as a catalyst has a band gap of 3.5 eV and a PL maximum for a film at 400 nm with a strong secondary peak

at 500 nm [63]. The result suggests that during the preparation of the polymer some defects would have been produced which leads to the secondary emission.

Thiophene-based polymers can also give blue emission. The band gap of polythiophenes can be controlled by steric hindrance via bulky side chain substituents on the thiophene unit [64]. Poly(3-cyclohexyl-4-methylthiophene) (PCHMT) (**2**) (Fig. 8) possesses large band gap. The PL maximum of **2** in chloroform was observed at 460 nm. The bilayer device of **2** with PBD as an electron transporting layer sandwiched between ITO and Ca gives an EQE of 0.6% and an EL maximum at 460 nm. It is also reported that single-layer device of polythiophene with crown ether unit attached to positions 3 and 4 (**11**) gives an EL maximum at 470 nm [65]. Poly(dioctylthiophene) (**12**) in toluene shows a PL maximum at 470 nm [66]. A LED with a structure of ITO/**12**/In also shows EL maximum at 470 nm. The stereo interactions between the alkyl chains is likely responsible for short chain length and blue color in polythiophenes. However, the QE values of all LEDs prepared with this material are not promising (Fig. 10).

The fluorine-based polymers is other important family of blue-emitting polymers. Figure 11 show the molecular structures of typical fluorene derivatives such as polyfluorenes (PFs, **3**), 5,6-polyindeno-fluorenes (PIFs, **13**), 7,8 and ladder-type polyphenylenes (LPPPs, **14**). In solution, they emit blue to blue-green which gets

Fig. 10 Molecular structures of polythiophenes

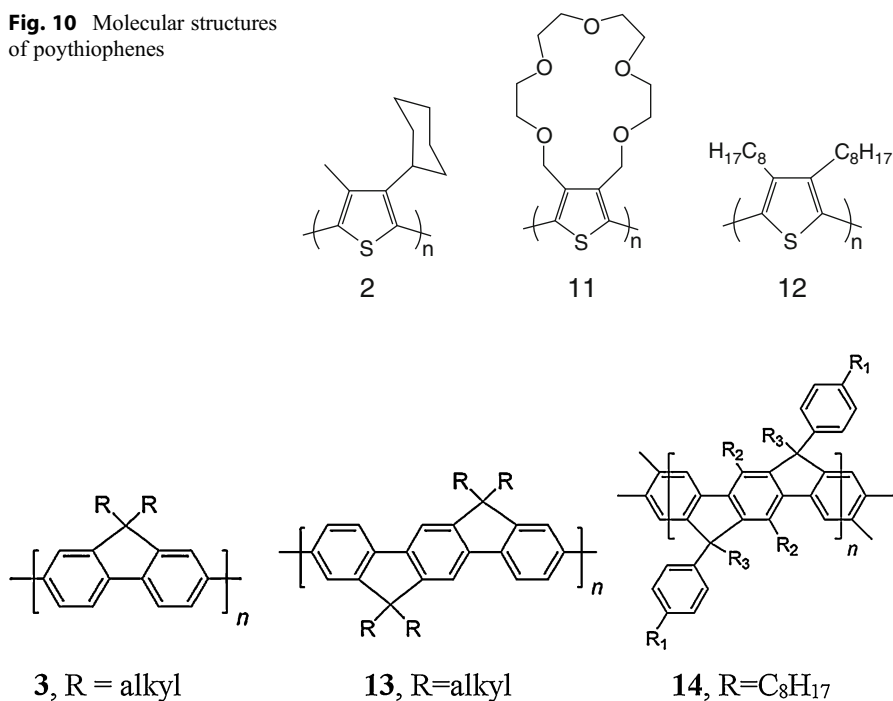


Fig. 11 Typical fluorine based blue-emitting conjugated polymers

red-shifted with increasing rigidity of the polymer chain with emission maxima of 420 nm for **3**, 430 nm for **13**, and 450 nm for **14**. The first PLED for blue color emission was made in 1991 [67]. A layer of poly(9,9'-di-n-hexylfluorene)(PDHF) (**3**) was formed by spin-coating its solution in chloroform onto ITO glass and a layer of magnesium-indium alloy on the polymeric layer was vacuum-deposited. The EL spectrum of PDHF exhibited the emission maximum at 470 nm with a shoulder at 420 nm and a FWHM of ~200 nm. In the solid state broad emission bands at longer wavelengths ~530 nm also appears [68–71]. The cause of long-emission band for **3**, **13**, and **14** has been correlated to the emission from the ketonic defects which get incorporated in the polymer backbone as 9-fluorenone units [72–77].

Craig et al. purified the monomers used in the synthesis of polyfluorenes to ensure reduced levels of fluorenone defects in the corresponding polyfluorenes. The synthesized polymer demonstrated pure blue and more stable electroluminescence when exposed to high temperatures [78]. Green EL was suppressed by incorporating a novel buffer layer of tetrakis(4-(5-(α,α,α -trifluoromethylphenyl))-2-oxidiazolyl)phenyl)methane (CF3OXD) between emissive layer and the Ca/Ag or Ba/Ag cathode [73]. The problem of ketonic defects in fluorene-based polymer was also addressed by replacing the alkyl groups in the methine bridges with the aryl substituents (Fig. 12). The greater stability of blue emission in molecule **15**, **16**, and **17** arises due to high resistance to oxidation and a reduction in excimer diffusion to a ketone defect sites. Efficient, stable blue-emitting LEDs have been fabricated using the polymers **15**, **16**, and **17** [79, 80].

The other important strategy adopted to avoid long-wavelength emission in polyfluorenes was replacing the vulnerable C-9 carbon in polyfluorene by a heteroatom, such as silicon. Many new polymers were synthesized. The optical properties of polymer poly(9,9-dihexyl-2,7-dibenzosilole) (**18**) were similar to that of poly

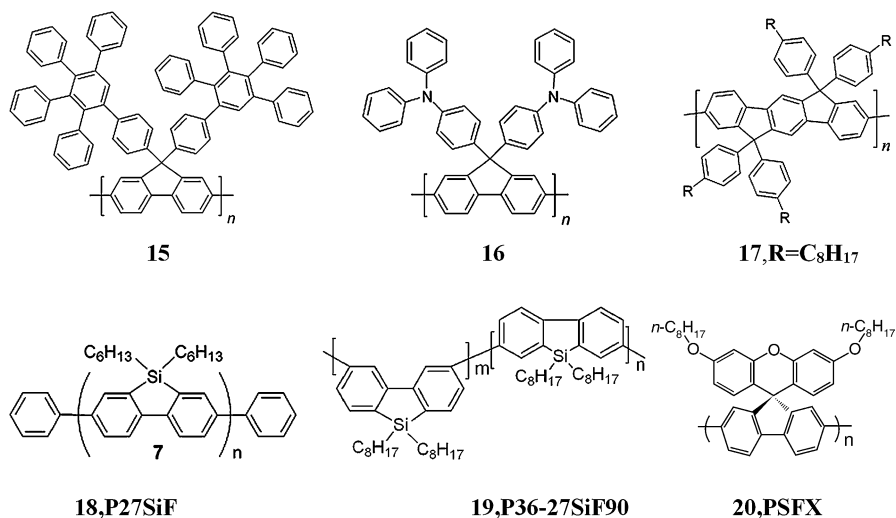


Fig. 12 Stable blue-emitting polyfluorenes

(9,9-dioctyl-2,7-fluorene) (PFO) [81]. Thin film of P27SiF show photoluminescence (PL) emission maxima at 425 nm and has two vibronic sidebands at 449 and 482 nm. The PL efficiencies of **18** and PFO were also similar ~60%. Of the two polymers, **18** was found to be more thermally stable and maintained its color purity even after annealing at 250 °C for 16 h whereas films of PFO degraded as indicated by the appearance of a broad green band centered at 535 nm. The electroluminescence emission spectrum measured on a single layer device in the configuration ITO/PEDOT/**18**/Ba/Al showed emission maxima at 431 and 451 nm and efficiency slightly superior to that of the corresponding device fabricated with a single layer of PFO. The copolymerization of 3,6-silafluorene unit into the 2,7-silafluorene gave P36-27SiF90(**19**) [82]. The copolymer did not show undesirable long wavelength emission and it was thermally stable. The device of the copolymer with a configuration of ITO/PEDOT:PSS/PVK/**19**/Ba/Al exhibited an external quantum efficiency of 1.95%, a luminous efficiency of 1.69 cd/A, and a maximum brightness of 6000 cd/m². Homopolymers and copolymers of spirofluorene were also found to give stable blue emission [83]. Fluorene-9,9'-(2',7'-di-*n*-octyloxyxanthene)](PSFX) (**20**) have high quantum efficiency of close to 1 in solution and 0.92 in thin film. Its optical properties were found similar to PFO. An OLED fabricated using PSFX as the emitting layer ITO/PEDOT/**20**/TPBI/Mg:Ag/Ag exhibits an efficient, stable blue emission and a maximum external quantum efficiency of 1.74%. The EL spectrum remains unchanged even at high brightness (10³cd/m²). High PL quantum efficiencies of fluorene-based polymers and their good performance in devices make them promising candidates for OLEDs.

10.2 Green-Emitting Polymers

In the photoluminescence (PL) spectrum, poly[2-methoxy-5-(2-ethylhexyloxy)-1,4-phenylenevinylene] MEH-PPV as a solid thin film emits yellowish-red light with λ_{\max} at 593 nm and shoulder peaks at 640 nm and 707 nm. Nguyen et al. have blue shifted this emission of MEH-PPV by blending MEH-PPV with poly[9-vinylcarbazole] (PVK) and TiO₂ nanoparticles [84]. The single layer devices based on the blended polymer films were fabricated in the configuration ITO/(PVK: MEH-PPV) + TiO₂/Al have shown green electroluminescence. The optical properties of PPVs were also found to depend on the substitution pattern of the alkoxy groups in the polymer backbone. 2,3-dialkoxy substituted PPVs as synthesized by Holmes and co-workers have shown significant blue-shift in the emission maximum and they were also having high PL and EL efficiency in the solid state [85–87]. The di-butoxy-PPV shows green emission with λ_{\max} at 530 nm and a PL efficiency of 40%. Bigger alkyl groups increases the steric constraints as in (**23**) leads to a further blue-shift in the emission with λ_{\max} at 513 nm and a drop in PL efficiency to 28%. The PL efficiency of MEH-PPV was only in the range of 15%–20% [88–89].

Benzothiadiazole is an electron deficient monomer unit which was used in copolymerization with fluorene to red-shift the blue emission of polyfluorenes (PFs) to green region [90]. The polymer Poly(9,9-dioctylfluorene-alt-benzothiadiazole)

(F8BT, **24**) synthesized shows PL emission peaks at 545 nm and has a shoulder peak at 576 nm and a long wavelengths tail that extends up to 750 nm [91]. Single-layer device with the configuration ITO/ZnO/Cs₂CO₃/F8BT/MoO₃/Au containing thick layer of F8BT as the emissive layer shows excellent current efficiency of more than 20 cd/A at a brightness of ~1000 cd/m² [92]. The peak external quantum efficiency (EQE) of the device was close to 7% (Fig. 13).

Yong Cao and coworkers synthesized green-emitting poly[2,7-silafluorene-co-benzothiadiazole]PSiF-BT10 (**25**) by incorporating 2,1,3-benzothiadiazole (BT) into the backbone of blue-emitting poly(2,7-silafluorene) (PSiF) [93]. The peak emission wavelength and PL quantum efficiency of PSiF-BT10 as a solid thin film were measured to be 530 nm and 0.52, respectively. This λ_{\max} is very close to that of a similar fluorene derivative (PFO-BT10) for which λ_{\max} is 533 nm. The PL quantum efficiency of PFO-BT10 was 0.68, a little higher than PSiF-BT10. The polymer LED with the configuration of ITO/PEDOT:PSS/PVK/PSiF-BT10/Ba/Al showed the maximum EQE of 3.81% and current efficiency of 10.6 cd/A.

Yu et al. (2013) synthesized green-emitting PPF-SO-BT (**26**) polymers containing 9,9-bis(4-(2-ethylhexyloxy) phenyl)fluorene (PPF), dibenzothiophene-*S,S*-dioxide (SO), and benzothiadiazole (BT) units with varying ratios [94]. Of these polymers, PPF-SO15-BT1 exhibited highest fluorescence quantum yield (~0.67) and good thermal stability. Light-emitting diodes (LEDs) using PPF-SO15-BT1 as the emissive layer in the device configuration ITO/PEDOT:PSS/PVK/PPF-SO15-BT1/CsF/Al have shown green electroluminescence. The maximum brightness and the maximum current efficiency measured in this device are 30,314 cd/m² and 17.6 cd/A, respectively.

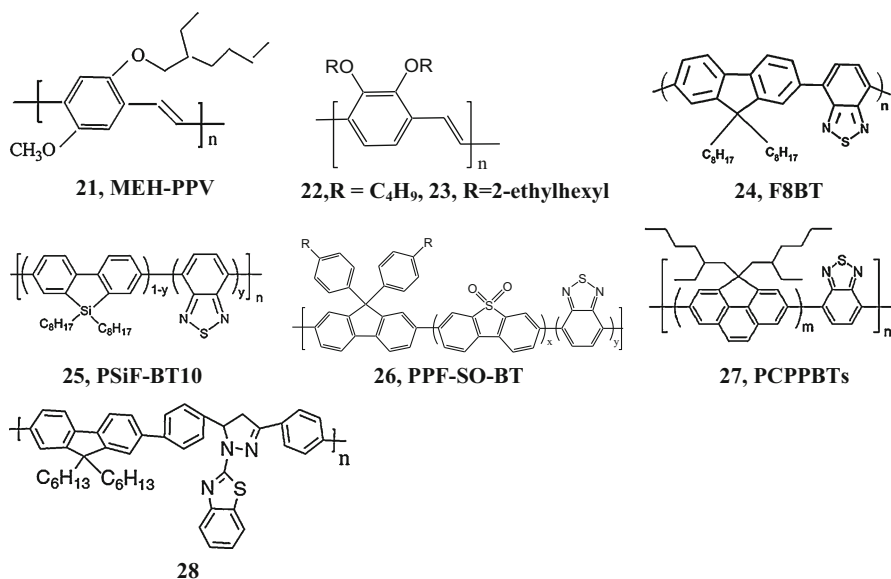


Fig. 13 Molecular structures of different green-emitting polymers

The BT units were also copolymerized with cyclopenta[*def*]phenanthrene derivatives to give poly(4,4-bis(2-ethylhexyl)-4*H*-cyclopenta[*def*]phenanthrene)-*co*-poly(2,1,3-benzothiadiazole) (PCPPBTs, **27**) [95]. The introduction of BT unit resulted red-shifted emission. The color of emission was found to be varying with the amount of BTs. The PL spectra were having two emission peaks at around 410 and 530 nm in thin films. The polymer LEDs of combination (ITO/PEDOT/polymer/Ca:Al) of PCPPBTs exhibited emissions λ_{max} at 508–528 nm. Among all the devices fabricated, the best device was the one with PCPPBT10, which showed the highest luminous efficiency of 1.25 cd/A and the highest brightness of 1170 cd/m². This study established that PL efficiency can be improved by randomly copolymerizing the BT into the PCPP.

Fluorene and benzothiazolopyrazoline units were copolymerized to give Poly(9,9-dihexylfluorene-*alt*-benzothiazolopyrazoline, **28**) [96]. This polymer possessed good thermal stability. As a solid thin film, the polymer emits green light (λ_{max} at 501 nm) with high (PL) quantum yield of 47%. Polymer light-emitting diode (PLED) fabricated with the configuration of ITO/PEDOT/PVK/polymer/Ba(4 nm)/Al(160 nm) emit green light with λ_{max} at 501 nm. The maximum brightness and the maximum EQE achieved were 1726 cd/m² and 1.59%, respectively.

Lee et al. synthesized a series of polyfluorenes (P1–P5) which were end-capped by *N*-aryl-1,8-naphthalimide and 1,8-naphthoilenarylimidazole derivatives in an attempt to red-shift the blue emission of (PFs) into the greenish region [96]. The color of emission was tuned by controlling the content of **29–33**. The electroluminescence (EL) spectra of polymers (**34–38**) exhibit greenish-blue, bluish-green, pure green, and yellowish-green emission with the corresponding peak emission (λ_{max}) at 465 nm (for **35**), 490 nm (for **34** and **36**), 500 nm (for **37**), and 545 nm (for **38**). Of these polymers, **37** could give pure green emission in the device. The maximum brightness achieved for this polymer was ~6500 cd/m² with a current efficiency of 0.56 cd/A (Fig. 14).

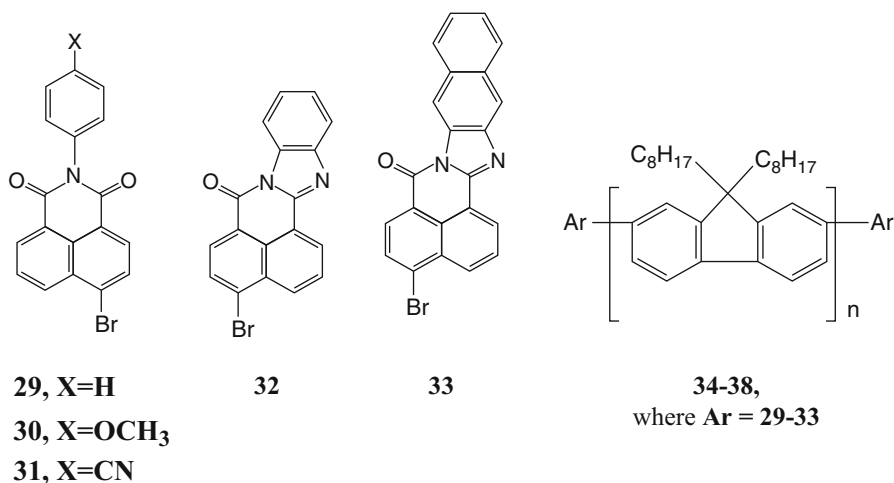


Fig. 14 Molecular structures of green-emitting polymers

10.3 Red-Emitting Polymers

Gurge and co-workers studied the asymmetrically substituted, “push-pull” family of PPVs, i.e., poly(2[5-chloro-5[2]-(*n*-hexyloxy)-1,4-phenylenevinylene) and poly(2[5-bromo-5[2]-(*n*-hexyloxy)-1,4-phenylenevinylene), **39** and **40**, respectively (Fig. 15) [97]. These polymers gave strong EL emission in the ~620 nm (orange-red to red) spectral region even without fine-tuning of emission characteristics. Single-layer LED of configuration ITO/**39**/Ca exhibited an output brightness of ~20 cd/m² at 30 V pulsed input voltage using 1 mA of current [97].

Lo and Burn synthesized polymer (**41**) (Fig. 15) by incorporating a red-emitting porphyrin as a side chain to the PPV unit by a rigid phenylacetylene linker [98]. Red emission with λ_{max} at 604, 653 nm were observed in PL studies which suggest that the red emission originated from the porphyrin chromophore. But the EL device performance was rather poor.

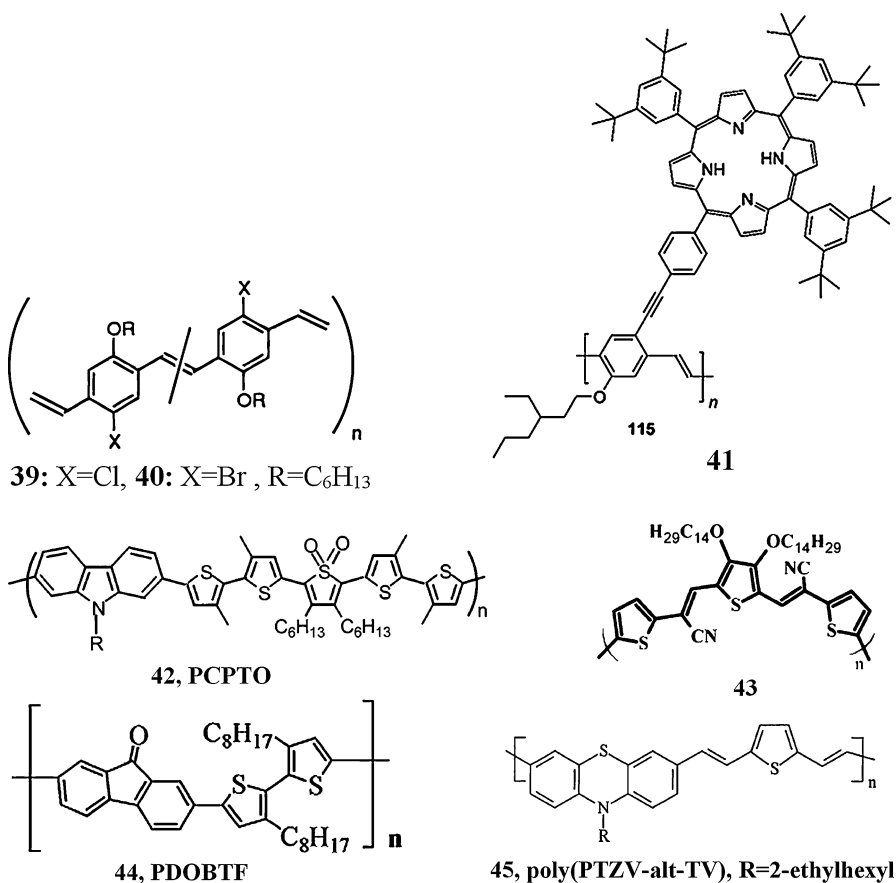


Fig. 15 Molecular structures of red-emitting polymers

Morin and Leclerc synthesized 2,7-carbazole-based light-emitting homopolymers and copolymers [99]. Wherein, poly(*N*-(2-ethylhexyl)-2,7-carbazole-*alt*-3,3',4''',3''''-tetramethyl-3'',4''-dihexyl-2,2':5',2'':5'', 2''':5''',2''''-quinquethiophene-1'', 1''-dioxide) (PCPTO) (**42**) (Fig. 15) emits red light with λ_{max} at 638 and 671 nm. The fluorescence quantum yield in chloroform solution was measured to be 25% for PCPTO.

Manjunatha and co-workers synthesized narrow band gaped donor-acceptor type polymer from cyanovinylenepoly{3,30-(3,4-ditetradecyloxythiophene-2,5-diyl) bis[2-(thiophen-2-yl)prop-2-enenitrile]} (**43**) (Fig. 15) [100]. The polymer exhibited red-fluorescence in solution as well as in solid state. The peak emission wavelength of polymer in solid thin film was measured to be 647 nm. The PL efficiency of the polymer was determined to be 43%.

Fluorenone and dialkylbithiophene were copolymerized to give regioregular, alternate copolymer poly[(5,5'-(3,3'-di-*n*-octyl-2,2'-bithiophene))-*alt*-(2,7-fluoren-9-one)] (PDOBTF) (**44**) (Fig. 15) by different preparation methods [101]. The photoluminescence studies showed that PDOBTF emits red light with λ_{max} at 643 nm in the solid state.

Kim and co-workers synthesized an alternating copolymer poly(PTZV-*alt*-TV) (**45**) (Fig. 15) using Wittig polycondensation between 10-(2-ethylhexyl)-phenothiazine-3,7-dicarbaldehyde and thiophene bis(phosphonium) salt [102]. The PL emission of poly(PTZV-*alt*-TV) as a thin film was having λ_{max} at 584 nm. Electroluminescent device was fabricated in an ITO/PEDOT/poly(PTZV-*alt*-TV)/Ca/Al configuration which showed maximum brightness of 140 cd/m² and a luminous efficiency of 1.3×10^{-2} cd/A. However, at different voltages emission at 650 nm was also observed. The EL emission spectrum of the device showed a broad emission range (500–800 nm).

Cho and co-workers were able to tune the color of emission of polyfuorenes by copolymerization of fluorene with different comonomers. They were able to synthesize pure red-emitting poly{9,9-dioctylfluorene-2,7-diyl-*alt*-2,5-bis(2-thienyl-2-cyanovinyl)-1-(2'-ethylhexyloxy)-4-methoxybenzene-5'',5''-diyl} (PFR4-S) (**46**) by doing Suzuki coupling of 2,7-bis(4,4,5,5-tetramethyl-1,3,2-dioxabororan-2-yl)-9',9'-dioctylfluorene and 2,5-Bis{2-(4'-bromothieryl)-2-cyanovinyl}-2-(2'-ethylhexyloxy)-5-methoxybenzene [103]. The PL and EL emission peaks of PFR4-S as a solid thin film were at 674 nm. Single-layer LED devices fabricated from this polymer emitted pure red light. The CIE coordinate values $x = 0.66$, $y = 0.33$ of the device was almost identical to the standard red ($x = 0.66$, $y = 0.34$) as demanded by the National Television System Committee.

Peng and co-workers synthesized a series of red-light-emitting copolymers (**47–49**) using fluorene and 2-pyran-4-ylidenemalononitrile (PM) [104]. The PL emission of these polymers in thin films emit red color with λ_{max} around 641–662 nm and additional peaks in the range 704–712 nm. The absolute PL quantum yields of the polymer as solid thin films were measured to be about 4–7%. The PLEDs fabricated with the configuration of ITO/PEDOT/polymer/Ba/Al emit red light with EQE of 0.21–0.38%.

Ying and co-workers copolymerized 3,6-dibromo-*N*-alkylcarbazole having red-emitting Iridium complex in the alkyl chain with fluorene to give poly

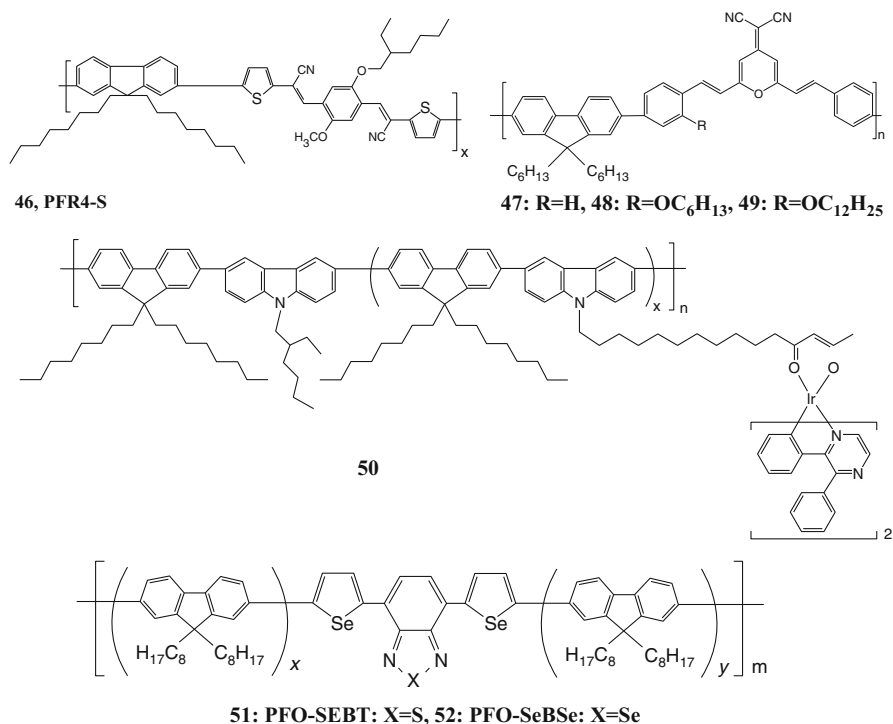


Fig. 16 Molecular structures of red-emitting copolymers of fluorene

(fluorene-alt-carbazole) (**50**, Fig. 16) based copolymers [105]. Iridium complex in the ratio of 1 mol% to that of host polymer was sufficient to completely quench the emission of host polymer. The polymer PFCzIrBpz-1 in the device configuration ITO/PEDOT:PSS/polymer+PBD/Ba/Al gave an orange-red emission. The phosphorescent polymer light-emitting diodes (PhPLEDs) showed a maximum luminous efficiency (LE) of 5.58 cd/A and a maximal luminance of 8625 cd/m².

Yang and co-workers synthesized a series of copolymers, using alkyl-substituted fluorene and 4,7-diselenophen-2'-yl-2,1,3-benzothiadiazole (SeBT), or 4,7-diselenophen-2'-yl-2,1,3-benzoselenadiazole (SeBSe) as the comonomers (**51**, **52**, Fig. 16) [106]. The PL emission peaks as solid thin films were found to depend upon the content of comonomer. The PL and EL is dominated by narrow-band-gap species and peaked at 670–790 nm. The double layer devices made from these two types of copolymers in the configuration ITO/PVK/polymer/Ba/Al reached an EQE of 1.1% and 0.3%, respectively.

10.4 White Light-Emitting Polymers

Single polymer which can emit white light can be synthesized by incorporating two chromophores (blue and orange) or three chromophores (blue, green, and red) into a

polymeric chain. It is very difficult to synthesize the latter; however, it offers better color quality while synthesis of the former type of white light-emitting polymer is easy. Tu and co-workers developed two component polymers for white light emission. They incorporated 1,8-naphthalimide (orange emissive) unit as dopant into polyfluorene (blue-emitting polymer) with varying dopant ratio [107]. A novel single-component polymer system (**53**) with 0.05 mol% of dopant showed white light emission. A white polymeric light-emitting diode (WPLED) fabricated with the configuration ITO/PEDOT:PSS/**53**/Ca/Al showed a current efficiency of 5.3 cd/A and a power efficiency of 2.8 lm/W at 6 V [107].

Sun and co-workers synthesized a series of copolymers by incorporating orange-emitting 2,3-dimethyl-5,8-dithien-2-ylquinoxaline (DDQ) unit in the backbone of PFO with varying mole ratio [108]. White emission could be obtained by carefully controlling the DDQ unit (~0.02 mol%) in the PFO backbone. The two distinguished emission peaks (blue and orange red) leading to white light emission were observed in the polymer PFO-DDQ002 (**54**) due to incomplete energy transfer from the PFO to DDQ. A WPLED fabricated with the configuration ITO/PEDOT/PVK/PFO-DDQ/**54**/Ba/Al showed high EQE and current efficiency of 2.64 and 4.1 cd/A, respectively. The CIE coordinates remained stable for different voltages.

Lee et al. synthesized a series of copolymers by incorporating 2-(2,6-bis-{2-[1-(9,9-dihexyl-9H-fluoren-2-yl)-1,2,3,4-tetrahydro-quinolin-6-yl]-vinyl}-pyran-4-ylidene)-malononitrile as the orange unit into a polyfluorene main chain as the blue host [109]. The polymer (F6DCM005) having 0.05 mol% of orange-emitting comonomer (DCMF) was found to emit white light with peak emission at 423/450 nm (blue) and at 580 nm (orange). The PLED fabricated in the configuration ITO/PEDOT:PSS/**55**/Ca/Al showed white light emission with CIE coordinates (0.33, 0.32). The maximum brightness and current efficiency achieved in the device were 1180 cd/m² and 0.60 cd/A, respectively [109].

Hsieh and co-workers synthesized copolymers (**56**, Fig. 17) by incorporating orange emitting chromophore 2,5-dihexyloxy-1,4-bis(2-thienyl-2-cyanovinyl) benzene in the mole ratio (0.1 and 0.025 mol%) into the polyfluorenes for getting white electroluminescence [110]. The PL peaks of copolymer films ~428 and 570 nm were due to fluorene unit and the orange chromophore unit respectively. The PLEDs of the copolymers PFR1 and PFR2 showed white light emission with CIE coordinates (0.36, 0.35) and (0.32, 0.30), respectively, which are close to white light emission (0.33, 0.33). The maximum EL brightness achieved with PFR1 and PFR2 were 5419 and 3011 cd/m², respectively [110].

Lee and co-workers copolymerized 2-{2-(2-[4-{bis(4-bromophenyl)amino}phenyl]-vinyl)-6-tertbutylpyran-4-ylidene}malonitrile (TPDCM) (red emitter), {4-(2-[2,5-dibromo-4-{2-(4-phenylaminophenyl)vinyl}phenyl]-vinyl)phenyl}-diphenylamine (DTPA) (green emitter), and a 2,7-dibromo-9,9-dihexylfluorene (DHF)(blue emitter) in suitable ratios to get white light-emitting polymer [111]. White emission was observed in the polymer PG3R2 (**57**, Fig. 18) having the comonomers composition as 3 mol% of DTPA and 2 mol% of TPDCM. The WPLED device fabricated in the configuration ITO/PEDOT:PSS/polymer/Ca/Al showed white light emission with CIE coordinated of (0.33, 0.35). The peak luminance and current efficiency achieved were 820 cd/m² and 0.1 cd/A, respectively [111].

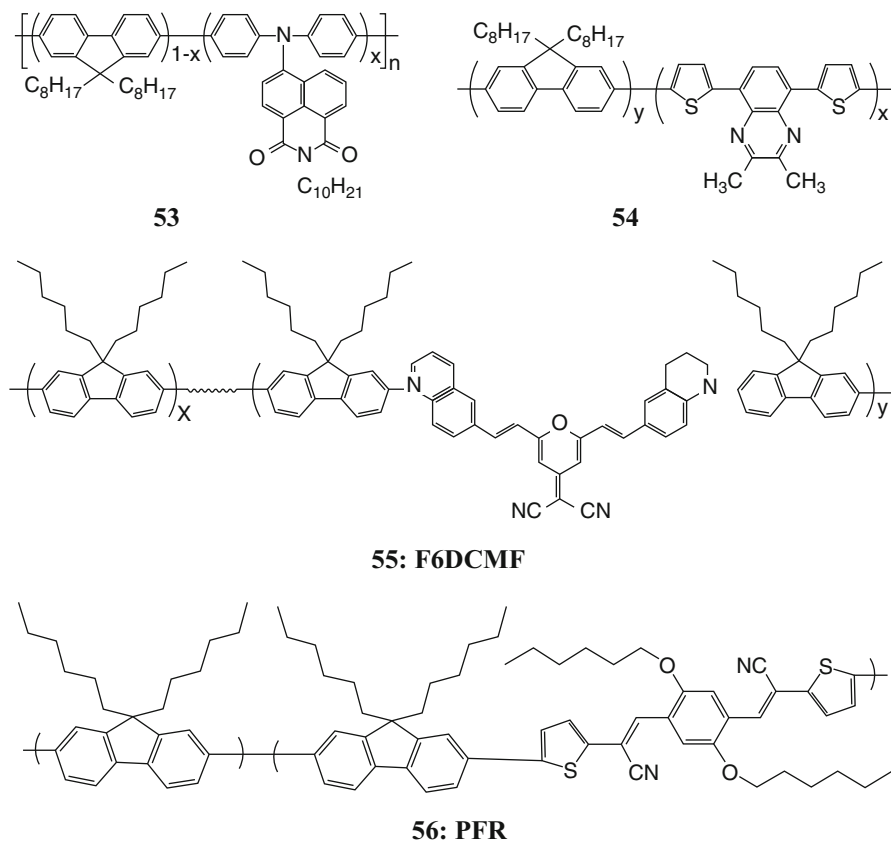


Fig. 17 Molecular structures of white-emitting copolymers

Tokito and co-workers were able to get white light emission by blending red phosphorescent polymer (RPP) (**58**) and blue phosphorescent polymers (BPP) (**59**) [112]. The RPP and BPP when mixed with the ratio of 10:1 in a PLED having the configuration ITO/PEDOT:PSS/**58** + **59**/Ca/Al showed white EL with CIE coordinates of (0.34, 0.36). The EQE of white emission was measured as 4.5%.

Xiong et al. fabricated polymer white light-emitting diodes based on the blend of poly[9,9-di-(2-ethylhexyl)-fluorenyl-2,7-diyl]-end capped with polysilsesquioxane (PFO) and poly[(9,9-bis(3'-(N,N-dimethylamino)propyl)-2,7-fluorene-alt-2,7-(9,9-dioctylfluorene))-co-[2,7-(9,9-dioctylfluorene)-alt-5,5-bis(2-(4-methyl-1-naphthalene) pyridine-C2,N) iridium (III) acetylacetonate]] (PFN-NaIr05) (**60**) [113]. The PLED of the configuration ITO/PEDOT/PVK/PFO: PFN-NaIr05/Al with 5% PFN-NaIr in the blend showed white light emission having CIE coordinates of the (0.34, 0.35).

Xu et al. demonstrated white light emission by doping a blue-emitting oligomeric silsesquioxane-terminated poly(9,9-dioctylfluorene) (PFO-poss) (**61**) with green

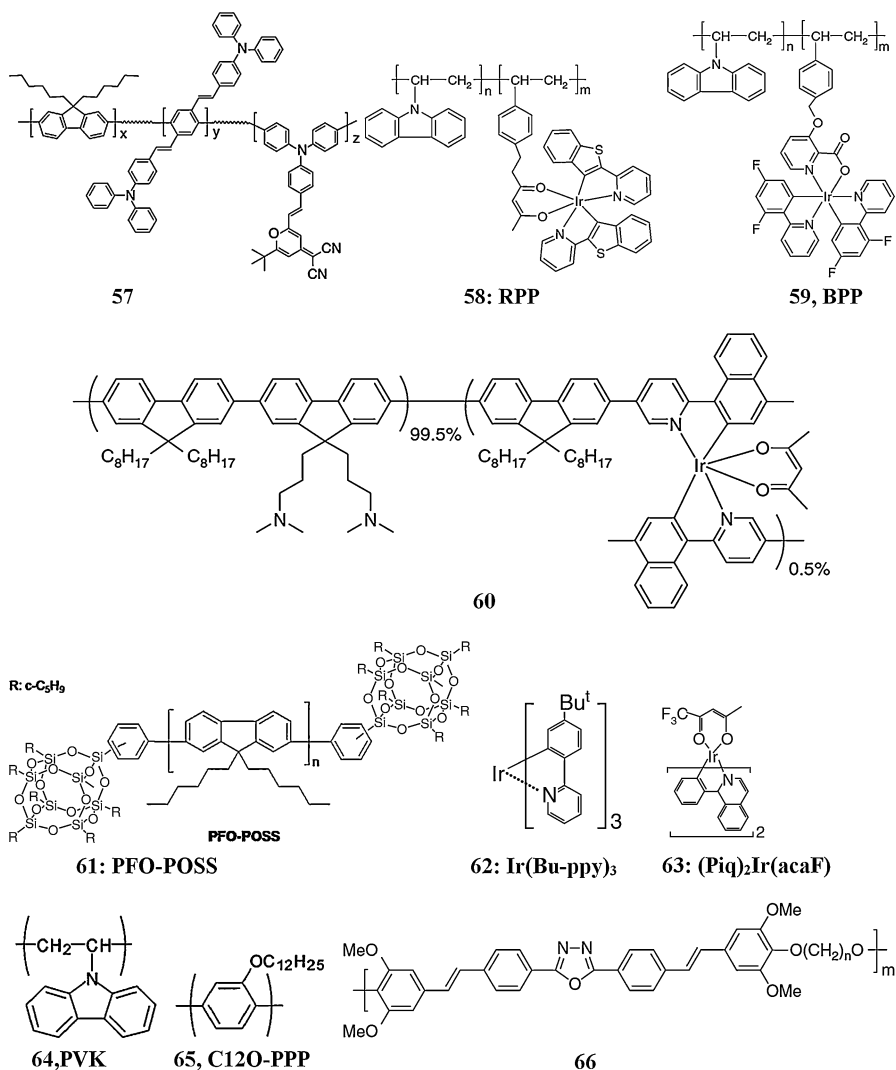


Fig. 18 Molecular structures of some other white-emitting copolymers

emitting fac-tris[2-(4'-ter-butyl)phenylpyridine]Iridium (III) [Ir(Bu-ppy)₃] and red-emitting bis-(1-phenylisoquinolyl)Iridium(III)(1-trifluoro)acetylacetonate [(Piq)₂Ir(acaF)] [114]. The electroluminescence spectrum was found changing with the concentration of the guests. The WPLED with the configuration ITO/PEDOT:PSS/PVK/PFO-poss+**62**+**63**/Ba/Al and with the doping concentrations of 0.14 wt% for **62** and **63**. TheCIE coordinates of WPLED was around (0.33, 0.33). The maximum brightness achieved in the device was ~10,200 cd/m².

White light emission has also been reported by utilizing excimer or exciplex formation. Chao and co-workers reported WPLED which utilized the exciplex formation between poly(N-vinyl carbazole) PVK (**64**) and poly(2-dodecyl-p-phenylene) (C12O-PPP) (**65**) [115]. A broad EL spectrum having emission from 400 to 700 nm was observed. The exciplex emission was arising from the recombination of the electron in the lowest unoccupied molecular orbital (LUMO) of C12O-PPP and the hole in the highest occupied molecular orbital (HOMO) of carbazole groups in PVK.

Lee and co-workers reported white light emission from a single-layered system based on oxadiazole and phenylenevinylene copolymer having ether linkage [116]. The emission spectrum of the above was found to be composed of red and blue-green components from different species, i.e., red component originated from the new excited dimer while blue-green component from an individual lumophore and excimer. The excited dimer generated in the above system was reported to be different from excimers/exciplex, typically observed in electro- and photoluminescence and could not be produced during these processes and could be seen only in the system under high electric field.

11 Conclusion

Herein, the various components of making an efficient OLED are discussed. We first described the electronic transitions and energy transfer processes involved in conjugated polymers. The working of different types of device architectures, their efficiencies, and the measurement that are normally made in OLEDs are also presented. The various types of materials and their functional requirements as needed in the making of multilayer OLEDs are discussed. Several categories of blue, green, red, and white light-emitting polymers have been highlighted. Conjugated polymers have established their importance for optoelectronic device applications. They give high electroluminescence efficiency in OLEDs. The improved efficiencies of these devices are facilitating the commercialization of these devices.

References

1. A. Bernanose, The mechanism of organic electroluminescence. *J. Chim. Phys. Phys.-Chim. Biol.* **52**, 396–400 (1955)
2. A. Bernanose, M. Comte, P. Vouaux, Sur un nouveau mode demission lumineuse chez certains composes organiques. *J. Chim. Phys. Phys.-Chim. Biol.* **50**(1), 64–68 (1953)
3. M. Pope, P. Magnante, H.P. Kallmann, Electroluminescence in organic crystals. *J. Chem. Phys.* **38**(8), 2042 (1963)
4. J. Dresner, Double injection electroluminescence in anthracene. *RCA Rev* **30**(2), 322 (1969)
5. W. Helfrich, W.G. Schneide, Recombination radiation in anthracene crystals. *Phys. Rev. Lett.* **14**(7), 229 (1965)
6. D.F. Williams, M. Schadt, DC and pulsed electroluminescence in anthracene and doped anthracene crystals. *J. Chem. Phys.* **53**(9), 3480 (1970)

7. P.S. Vincett, W.A. Barlow, R.A. Hann, G.G. Roberts, Electrical-conduction and low-voltage blue electro-luminescence in vacuum-deposited organic films. *Thin Solid Films* **94**(2), 171–183 (1982)
8. C.W. Tang, S.A. Vanslyke, Organic electroluminescent diodes. *Appl. Phys. Lett.* **51**(12), 913–915 (1987)
9. J. Shinar, *Organic light-emitting devices* (Springer, New York, 2004)
10. H. Yersin, *Highly efficient OLEDs with phosphorescent materials* (Wiley-VCH, Weinheim, 2008)
11. H. Sirringhaus, N. Tessler, R.H. Friend, Integrated optoelectronic devices based on conjugated polymers. *Science* **280**(5370), 1741–1744 (1998)
12. S.S. Sun, N.S. Sariciftci, *Organic photovoltaics: Mechanisms, materials, and devices* (Taylor & Francis, Singapore, 2005)
13. A.J. Heeger, N.S. Sariciftci, E.B. Namdas, *Semiconducting and metallic polymers* (Oxford University Press, New York, 2010)
14. M.S. AlSalhi, J. Alam, L.A. Dass, M. Raja, Recent advances in conjugated polymers for light emitting devices. *Int. J. Mol. Sci.* **12**(3), 2036–2054 (2011)
15. M. Gordon, W.R. Ware, *The exciplex* (Academic, New York, 1975)
16. A.J. Bard, *Electrogenerated chemiluminescence* (Marcel Dekker, New York, 2004)
17. S.C. Chang, Y. Yang, Polymer gel light-emitting devices. *Appl. Phys. Lett.* **75**(18), 2713–2715 (1999)
18. J.R. Lakowicz, *Principles of fluorescence spectroscopy*, 3rd edn. (Springer, New York, 2006)
19. S. Barth, H. Bassler, Intrinsic photoconduction in PPV-type conjugated polymers. *Phys. Rev. Lett.* **79**(22), 4445–4448 (1997)
20. V. Bulovic, A. Shoustikov, M.A. Baldo, E. Bose, V.G. Kozlov, M.E. Thompson, S.R. Forrest, Bright, saturated, red-to-yellow organic light-emitting devices based on polarization-induced spectral shifts. *Chem. Phys. Lett.* **287**(3–4), 455–460 (1998)
21. F. Ali, N. Periasamy, M.P. Patankar, K.L. Narasimhan, Integrated organic blue LED and visible-blind UV photodetector. *J. Phys. Chem. C* **115**(5), 2462–2469 (2011)
22. J.W. Huh, Y.M. Kim, Y.W. Park, J.H. Choi, J.W. Lee, J.W. Lee, J.W. Yang, S.H. Ju, K.K. Paek, B.K. Ju, Characteristics of organic light-emitting diodes with conducting polymer anodes on plastic substrates. *J. Appl. Phys.* **103**(4), 044502 (2008)
23. Z. Li, H. Meng, *Organic light-emitting materials and devices* (Taylor & Francis, New York, 2007)
24. W.R. Salaneck, S. Seki, A. Kahn, J. Pireaux, *Conjugated polymer and molecular interfaces*, 1st edn. (Marcel Dekker, New York, 2001)
25. Z.F. Zhang, Z.B. Deng, C.J. Liang, M.X. Zhang, D.H. Xu, Organic light-emitting diodes with a nanostructured TiO₂ layer at the interface between ITO and NPB layers. *Displays* **24**(4–5), 231–234 (2003)
26. J. Hwang, F. Amy, A. Kahn, Spectroscopic study on sputtered PEDOT center dot PSS: Role of surface PSS layer. *Org. Electron.* **7**(5), 387–396 (2006)
27. M.H. Song, D. Kabra, B. Wenger, R.H. Friend, H.J. Snaith, Optically-pumped lasing in hybrid organic-inorganic light-emitting diodes. *Adv. Funct. Mater.* **19**(13), 2130–2136 (2009)
28. M.D. Ho, D. Kim, N. Kim, S.M. Cho, H. Chae, Polymer and small molecule mixture for organic hole transport layers in quantum dot light-emitting diodes. *ACS Appl. Mater. Interfaces* **5**(23), 12369–12374 (2013)
29. H.Z. Gao, C.S. Qin, H.Y. Zhang, S.X. Wu, Z.M. Su, Y. Wang, Theoretical characterization of a typical hole/exciton-blocking material bathocuproine and its analogues. *J. Phys. Chem. A* **112**(38), 9097–9103 (2008)
30. A. Mishra, P.K. Nayak, D. Ray, M.P. Patankar, K.L. Narasimhan, N. Periasamy, Synthesis and characterization of spin-coatable tert-amine molecules for hole-transport in organic light-emitting diodes. *Tetrahedron Lett.* **47**(27), 4715–4719 (2006)
31. L.S. Hung, R.Q. Zhang, P. He, G. Mason, Contact formation of LiF/Al cathodes in Alq-based organic light-emitting diodes. *J. Phys. D Appl. Phys.* **35**(2), 103–107 (2002)

32. S. Zhong, R. Wang, H. Ying Mao, Z. He, H. Wu, W. Chen, Y. Cao, Interface investigation of the alcohol-/water-soluble conjugated polymer PFN as cathode interfacial layer in organic solar cells. *J. Appl. Phys.* **114**(11), 113709 (2013)
33. C. Adachi, M.A. Baldo, M.E. Thompson, S.R. Forrest, Nearly 100% internal phosphorescence efficiency in an organic light-emitting device. *J. Appl. Phys.* **90**(10), 5048–5051 (2001)
34. R.H. Partridge, Electroluminescence from polyvinylcarbazole films: 2. Polyvinylcarbazole films containing antimony pentachloride. *Polymer (Guildf)* **24**(6), 739–747 (1983)
35. R.A. Wessling, R.G. Zimmerman, Polyelectrolytes from bis sulfonium salts. U.S. Patent no. 3401152 (1968)
36. R.O. Garay, U. Baier, C. Bubeck, K. Müllen, Low-temperature synthesis of poly(p-phenylenevinylene) by the sulfonium salt route. *Adv. Mater.* **5**(7–8), 561–564 (1993)
37. D.F. Hoeg, D.I. Lusk, E.P. Goldberg, Poly-p-xylylidene. *J. Polym. Sci. Part B Polym. Lett.* **2**(7), 697–701 (1964)
38. F. Wudl, S. Barbara, G. Srdanov, U.S. Patent no. 5189136 (1993)
39. C.J. Neef, J.P. Ferraris, MEH-PPV: Improved synthetic procedure and molecular weight control. *Macromolecules* **33**(7), 2311–2314 (2000)
40. N. Miyaura, K. Yamada, A. Suzuki, A new stereospecific cross-coupling by the palladium-catalyzed reaction of 1-alkenylboranes with 1-alkenyl or 1-alkynyl halides. *Tetrahedron Lett.* **20**(36), 3437–3440 (1979)
41. N. Miyaura, A. Suzuki, Palladium-catalyzed cross-coupling reactions of organoboron compounds. *Chem. Rev.* **95**(7), 2457–2483 (1995)
42. B.S. Nehls, S. Földner, E. Preis, T. Farrell, U. Scherf, Microwave-assisted synthesis of 1,5- and 2,6-linked naphthylene-based ladder polymers. *Macromolecules* **38**(3), 687–694 (2005)
43. H.N. Tsao, D. Cho, J.W. Andreasen, A. Rouhanipour, D.W. Breiby, W. Pisula, K. Müllen, The influence of morphology on high-performance polymer field-effect transistors. *Adv. Mater.* **21**(2), 209–212 (2009)
44. C. Shi, Y. Yao, Yang, Q. Pei, Regioregular copolymers of 3-Alkoxythiophene and their photovoltaic application. *J. Am. Chem. Soc.* **128**(27), 8980–8986 (2006)
45. D. Milstein, J.K. Stille, Mechanism of reductive elimination. Reaction of alkylpalladium (II) complexes with tetraorganotin, organolithium, and Grignard reagents. Evidence for palladium(IV) intermediacy. *J. Am. Chem. Soc.* **101**(17), 4981–4991 (1979)
46. D. Milstein, J.K. Stille, Palladium-catalyzed coupling of tetraorganotin compounds with aryl and benzyl halides. Synthetic utility and mechanism. *J. Am. Chem. Soc.* **101**(17), 4992–4998 (1979)
47. B. Carsten, F. He, H.J. Son, T. Xu, L. Yu, Stille Polycondensation for synthesis of functional materials. *Chem. Rev.* **111**(3), 1493–1528 (2011)
48. R.F. Heck, Palladium-catalyzed vinylation of organic halides, in *Organic reactions* (Wiley, New York, 2004)
49. R.F. Heck, J.P. Nolley, Palladium-catalyzed vinylic hydrogen substitution reactions with aryl, benzyl, and styryl halides. *J. Org. Chem.* **37**(14), 2320–2322 (1972)
50. M. Grell, W. Knoll, D. Lupo, A. Meisel, T. Miteva, D. Neher, H.-G. Nothofer, U. Scherf, A. Yasuda, Blue polarized electroluminescence from a liquid crystalline polyfluorene. *Adv. Mater.* **11**(8), 671–675 (1999)
51. T. Yamamoto, Electrically conducting and thermally stable π -conjugated poly(arylene)s prepared by organometallic processes. *Prog. Polym. Sci.* **17**(6), 1153–1205 (1992)
52. J.-F. Lee, S.L.-C. Hsu, Green polymer-light-emitting-diodes based on polyfluorenes containing N-aryl-1,8-naphthalimide and 1,8-naphthoiline-arylimidazole derivatives as color tuner. *Polymer (Guildf)* **50**(24), 5668–5674 (2009)
53. A. Drury, S. Maier, M. Ruther, W.J. Blau, Investigation of different synthetic routes to and structure-property relationships of poly(m-phenylenevinylene-co-2,5-dioctyloxy-p-phenylenevinylene). *J. Mater. Chem.* **13**(3), 485–490 (2003)
54. S. Pfeiffer, H.-H. Hörhold, Synthesis of soluble MEH-PPV and MEH-PPB by horner condensation polymerization. *Synth. Met.* **101**(1), 109–110 (1999)

55. S. Pfeiffer, H. Hörhold, Investigation of poly(arylene vinylene)s, 41 – Synthesis of soluble dialkoxy-substituted poly(phenylene alkenylidene)s by applying the Horner-reaction for condensation polymerization. *Macromol. Chem. Phys.* **200**(8), 1870 (1999)
56. D.Y. Kim, H.N. Cho, C.Y. Kim, Blue light emitting polymers. *Prog. Polym. Sci.* **25**(8), 1089–1139 (2000)
57. S. Komaba, A. Amano, T. Osaka, Electroluminescence properties of electropolymerized poly (Para-phenylene) films by means of electrochemical oxidation and reduction. *J. Electroanal. Chem.* **430**(1), 97–102 (1997)
58. G. Grem, G. Leising, Electroluminescence of ‘wide-bandgap’ chemically tunable cyclic conjugated polymers. *Synth. Met.* **57**(1), 4105–4110 (1993)
59. G. Grem, G. Leditzky, B. Ullrich, G. Leising, Blue electroluminescent device based on a conjugated polymer. *Synth. Met.* **51**(1), 383–389 (1992)
60. Y. Yang, Q. Pei, A.J. Heeger, Efficient blue polymer light-emitting diodes from a series of soluble poly(paraphenylenes). *J. Appl. Phys.* **79**(2), 934–939 (1996)
61. Y. Yang, Q. Pei, A.J. Heeger, Efficient blue light-emitting diodes from a soluble poly (Paraphenylene) internal field emission measurement of the energy gap in semiconducting polymers. *Synth. Met.* **78**(3), 263–267 (1996)
62. A. Edwards, S. Blumstengel, I. Sokolik, R. Dorsinville, H. Yun, T.K. Kwei, Y. Okamoto, Blue photo- and electroluminescence from poly(benzoyl-1,4-phenylene). *Appl. Phys. Lett.* **70**(3), 298–300 (1997)
63. M. Hamaguchi, K. Yoshino, Blue electroluminescence from poly(2,5-diheptyloxy-1,4-phenylene). *Jpn. J. Appl. Phys.* **34**, L587–L589 (1995)
64. M.R. Andersson, M. Berggren, G. Gustafsson, T. Hjertberg, O. Inganäs, O. Wennerström, Synthesis of poly(alkylthiophenes) for light-emitting diodes. *Synth. Met.* **71**(1), 2183–2184 (1995)
65. Y. Miyazaki, T. Yamamoto, Poly(thiophene-2,5-diyl) having crown ethereal subunit. Preparation, stable n-doped state, and light emitting diode. *Chem. Lett.* **23**(1), 41–44 (1994)
66. R.E. Gill, G.G. Malliaras, J. Wildeman, G. Hadziioannou, Tuning of photo- and electroluminescence in alkylated polythiophenes with well-defined regioregularity. *Adv. Mater.* **6**(2), 132–135 (1994)
67. Y. Ohmori, M. Uchida, K. Muro, K. Yoshino, Blue electroluminescent diodes utilizing poly (alkylfluorene). *Jpn. J. Appl. Phys.* **30**(12B), L1941–L1943 (1991)
68. S. Setayesh, D. Marsitzky, K. Müllen, Bridging the gap between polyfluorene and ladder-poly-p-phenylene: Synthesis and characterization of Poly-2,8-indenofluorene. *Macromolecules* **33** (6), 2016–2020 (2000)
69. D. Neher, Polyfluorene homopolymers: Conjugated liquid-crystalline polymers for bright blue emission and polarized electroluminescence. *Macromol. Rapid Commun.* **22**(17), 1365–1385 (2001)
70. A.C. Grimsdale, P. Leclère, R. Lazzaroni, J.D. MacKenzie, C. Murphy, S. Setayesh, C. Silva, R.H. Friend, K. Müllen, Correlation between molecular structure, microscopic morphology, and optical properties of poly(tetraalkylindenofluorene)s. *Adv. Funct. Mater.* **12**(10), 729–733 (2002)
71. U. Scherf, Ladder-type materials. *J. Mater. Chem.* **9**(9), 1853–1864 (1999)
72. J. Jacob, J. Zhang, A.C. Grimsdale, K. Müllen, M. Gaal, E.J.W. List, Poly(tetraaryllindenofluorene)s: New stable blue-emitting polymers. *Macromolecules* **36**(22), 8240–8245 (2003)
73. B.X. Gong, P.K. Iyer, D. Moses, G.C. Bazan, A.J. Heeger, S.S. Xiao, Stabilized blue emission from polyfluorene-based light-emitting diodes: elimination of fluorenone defects. *Adv. Funct. Mater.* **13**(4), 325–330 (2003)
74. E.J.W. List, R. Guentner, P. Scanducci de Freitas, U. Scherf, The effect of keto defect sites on the emission properties of polyfluorene-type materials. *Adv. Mater.* **14**(5), 374–378 (2002)

75. E. Zojer, A. Pogantsch, E. Hennebicq, D. Beljonne, J.L. Brédas, P. Scandiucci De Freitas, U. Scherf, E.J.W. List, Green emission from poly(flourene)s: The role of oxidation. *J. Chem. Phys.* **117**(14), 6794–6802 (2002)
76. M. Gaal, E.J.W. List, U. Scherf, Excimers or emissive on-chain defects? *Macromolecules* **36** (11), 4236–4237 (2003)
77. P.S. De Freitas, U. Scherf, M. Collon, E.J.W. List, (9,9-Dialkylflourene-co-flourenone) copolymers containing low flourenone fractions as model systems for degradation-induced changes in polyflourene-type semiconducting materials. *E-Polymers* **2**(1), 1–7 (2002)
78. M.R. Craig, M.M. de Kok, J.W. Hofstraat, A.P.H.J. Schenning, E.W. Meijer, Improving color purity and stability in a blue emitting polyflourene by monomer purification. *J. Mater. Chem.* **13**(12), 2861–2862 (2003)
79. A. Pogantsch, F.P. Wenzl, E.J.W. List, G. Leising, A.C. Grimsdale, K. Müllen, Polyflourenes with dendron side chains as the active materials for polymer light-emitting devices. *Adv. Mater.* **14**(15), 1061–1064 (2002)
80. S. Setayesh, A.C. Grimsdale, T. Weil, V. Enkelmann, K. Müllen, F. Meghdadi, E.J.W. List, G. Leising, Polyflourenes with polyphenylene dendron side chains: Toward non-aggregating, light-emitting polymers. *J. Am. Chem. Soc.* **123**(5), 946–953 (2001)
81. K.L. Chan, M.J. McKiernan, C.R. Towns, A.B.. Holmes, Poly(2,7-dibenzosilole): A blue light emitting polymer. *J. Am. Chem. Soc.* **127**(21), 7662–7663 (2005)
82. E. Wang, C. Li, J. Peng, Y. Cao, High-efficiency blue light-emitting polymers based on 3,6-silaflourene and 2,7-silaflourene. *J. Polym. Sci. Part A Polym. Chem.* **45**(21), 4941–4949 (2007)
83. Y.-H. Tseng, P.-I. Shih, C.-H. Chien, A.K. Dixit, C.-F. Shu, Y.-H. Liu, G.-H. Lee, Stable organic blue-light-emitting devices prepared from poly[spiro(flourene-9,9'-xanthene)]. *Macromolecules* **38**(24), 10055–10060 (2005)
84. P.H.N. Nguyen, N.D. Nguyen, Green light-emitting diodes based on a hybrid TiO₂ nanoparticle-conducting polymer blend. *Adv. Nat. Sci. Nanosci. Nanotechnol.* **2**(3), 35012 (2011)
85. R.E. Martin, F. Geneste, B.S. Chuah, C. Fischmeister, Y. Ma, A.B.. Holmes, R. Riehn, F. Cacialli, R.H. Friend, Versatile synthesis of various conjugated aromatic homo- and copolymers. *Synth. Met.* **122**(1), 1–5 (2001)
86. R.E. Martin, F. Geneste, R. Riehn, B.S. Chuah, F. Cacialli, R.H. Friend, A.B.. Holmes, Efficient blue-green light emitting poly(1,4-phenylene vinylene) copolymers. *Chem. Commun.* (4), 291–292 (2000)
87. R.E. Martin, F. Geneste, A.B.. Holmes, Synthesis of conjugated polymers for application in light-emitting diodes (PLEDs). *C. R. Acad. Sci. Ser. IV Phys.* **1**(4), 447–470 (2000)
88. N.C. Greenham, I.D.W. Samuel, G.R. Hayes, R.T. Phillips, Y.A.R.R. Kessener, S.C. Moratti, A.B.. Holmes, R.H. Friend, Measurement of absolute photoluminescence quantum efficiencies in conjugated polymers. *Chem. Phys. Lett.* **241**(1), 89–96 (1995)
89. D. Braun, A.J. Heeger, Erratum: Visible light emission from semiconducting polymer diodes [*Appl. Phys. Lett.* **58**, 1982 (1991)]. *Appl. Phys. Lett.* **59**(7), 878 (1991)
90. E.P. Woo, W.R. Shiang, M. Inbasekaran, G.R. Roof, M.T. Bernius, W. Wu, Flourene-containing polymers and compounds useful in the preparation thereof. US Patent 6,169,163 (1997)
91. R. Xia, G. Heliotis, D.D.C. Bradley, Flourene-based polymer gain media for solid-state laser emission across the full visible spectrum. *Appl. Phys. Lett.* **82**(21), 3599–3601 (2003)
92. D. Kabra, L.P. Lu, M.H. Song, H.J. Snaith, R.H. Friend, Efficient single-layer polymer light-emitting diodes. *Adv. Mater.* **22**(29), 3194–3198 (2010)
93. E. Wang, C. Li, W. Zhuang, J. Peng, Y. Cao, High-efficiency red and green light-emitting polymers based on a novel wide bandgap poly(2,7-silaflourene). *J. Mater. Chem.* **18**(7), 797–801 (2008)

94. L. Yu, J. Liu, S. Hu, R. He, W. Yang, H. Wu, J. Peng, R. Xia, D.D.C. Bradley, Red, green, and blue light-emitting polyfluorenes containing a dibenzothiophene-S,S-dioxide unit and efficient high-color-rendering-index white-light-emitting diodes made therefrom. *Adv. Funct. Mater.* **23**(35), 4366–4376 (2013)
95. Y. Jin, Y. Kim, S.H. Kim, S. Song, H.Y. Woo, K. Lee, H. Suh, Novel green-light-emitting polymers based on Cyclopenta[def]phenanthrene. *Macromolecules* **41**(15), 5548–5554 (2008)
96. H. Zhang, Y. Li, Q. Jiang, M. Xie, J. Peng, Y. Cao, Novel green-emitting polymer containing fluorene and 1-(2-benzothiazolyl)-3,5-diphenylpyrazoline. *J. Mater. Sci.* **42**(12), 4476–4479 (2007)
97. R.M. Gurge, A. Sarker, P.M. Lahti, B. Hu, F.E. Karasz, Red light emitting ‘push-pull’ Disubstituted poly(1,4-phenylenevinylenes). *Macromolecules* **29**, 4287–4292 (1996)
98. S.-C. Lo, P.L. Burn, Synthesis of a porphyrin/conjugated polymer hybrid. *Synth. Met.* **102**, 1089–1090 (1999)
99. J.-F. Morin, M. Leclerc, 2,7-Carbazole-based conjugated polymers for blue, green, and red light emission. *Macromolecules* **35**(22), 8413–8417 (2002)
100. M.G. Manjunatha, A.V. Adhikari, P.K. Hegde, A novel narrow band gap red light-emitting cyanovinylene polymer derived from 3,4-dialkoxy thiophene for optoelectronic applications. *J. Mater. Sci. Mater. Electron.* **21**(8), 751–757 (2010)
101. R. Demadrille, P. Rannou, J. Oddou, A. Pron, Regiochemically well-defined Fluorenone – Alkylthiophene copolymers: Synthesis, spectroscopic characterization, and their Post-functionalization with Oligoaniline. *Macromolecules* **36**, 7045–7054 (2003)
102. S.K. Kim, J.H. Lee, D.H. Hwang, EL properties of an alternating copolymer composed of phenothiazine and thiophene heterocycles. *Synth. Met.* **152**(1–3), 201–204 (2005)
103. N.S. Cho, D.H. Hwang, B.J. Jung, E. Lim, J. Lee, H.K. Shim, Synthesis, characterization, and electroluminescence of new conjugated polyfluorene derivatives containing various dyes as comonomers. *Macromolecules* **37**(14), 5265–5273 (2004)
104. Q. Peng, Z.Y. Lu, Y. Huang, M.G. Xie, S.H. Han, J.B. Peng, Y. Cao, Synthesis and characterization of new red-emitting polyfluorene derivatives containing electron-deficient 2-pyran-4-ylidene- malononitrile moieties. *Macromolecules* **37**(2), 260–266 (2004)
105. L. Ying, J. Zou, A. Zhang, B. Chen, W. Yang, Y. Cao, Novel orange-red light-emitting polymers with cyclometalated iridium complex grafted in alkyl chain. *J. Organomet. Chem.* **694**(17), 2727–2734 (2009)
106. R. Yang, R. Tian, J. Yan, Y. Zhang, J. Yang, Q. Hou, W. Yang, C. Zhang, Y. Cao, Deep-red electroluminescent polymers: Synthesis and characterization of new low-band-gap conjugated copolymers for light-emitting diodes and photovoltaic devices. *Macromolecules* **38**(2), 244–253 (2005)
107. G. Tu, Q. Zhou, Y. Cheng, L. Wang, D. Ma, X. Jing, F. Wang, White electroluminescence from polyfluorene chemically doped with 1,8-naphthalimide moieties. *Appl. Phys. Lett.* **85**(12), 2172–2174 (2004)
108. M. Sun, Q. Niu, B. Du, J. Peng, W. Yang, Y. Cao, Fluorene-based single-chain copolymers for color-stable white light-emitting diodes. *Macromol. Chem. Phys.* **208**(9), 988–993 (2007)
109. S.K. Lee, B.-J. Jung, T. Ahn, Y.K. Jung, J.-I. Lee, I.-N. Kang, J. Lee, J.-H. Park, H.K. Shim, White electroluminescence from a single Polyfluorene containing Bis-DCM units. *J. Polym. Sci. A Polym. Chem.* **45**, 3380–3390 (2007)
110. B.-Y. Hsieh, Y.L. Chen, Polyfluorenes minimally doped with 1,4-Bis(2-thienyl-2-cyanovinyl) benzene chromophore: Their synthesis, characterization, and application to white-light-emitting materials. *J. Polym. Sci. A Polym. Chem.* **46**, 3703–3713 (2008)
111. S.K. Lee, D.H. Hwang, B.J. Jung, N.S. Cho, J. Lee, J.D. Lee, H.K. Shim, The fabrication and characterization of single-component polymeric white-light-emitting diodes. *Adv. Funct. Mater.* **15**(10), 1647–1655 (2005)

112. S. Tokito, M. Suzuki, F. Sato, M. Kamachi, K. Shirane, High-efficiency phosphorescent polymer light-emitting devices. *Org. Electron. Phys. Mater. Appl.* **4**(2–3), 105–111 (2003)
113. Y. Xiong, Y. Zhang, J.L. Zhou, J.B. Peng, W.B. Huang, Y. Cao, Polymer white-light-emitting diodes with high work function cathode based on a novel phosphorescent chelating copolymer. *Chin. Phys. Lett.* **24**(12), 3547–3550 (2007)
114. Y. Xu, J. Peng, J. Jiang, W. Xu, W. Yang, Y. Cao, Efficient white-light-emitting diodes based on polymer codoped with two phosphorescent dyes. *Appl. Phys. Lett.* **87**(19), 1–3 (2005)
115. C. Chao, S. Chen, C. Chao, S. Chen, White light emission from exciplex in a bilayer device with two blue light-emitting polymers White light emission from exciplex in a bilayer device with two blue light- emitting polymers. *Appl. Phys. Lett.* **426**(1998), 72–75 (2011)
116. Y.Z. Lee, X. Chen, M.C. Chen, S.A. Chen, J.H. Hsu, W. Fann, White-light electroluminescence from soluble oxadiazole-containing phenylene vinylene ether-linkage copolymer. *Appl. Phys. Lett.* **79**(3), 308–310 (2001)



Suru Vivian John and Emmanuel Iwuoha

Contents

1	Introduction to Electrochromism	790
1.1	Classes of Electrochromic Materials	791
1.2	Operating Principle of an Electrochromic Device	791
2	Conducting Polymers	793
2.1	Conjugated Polymers as Semiconductors	793
3	Charge Carriers in Conducting Polymers	802
4	Electronics of Conjugated Polymers	804
5	Electrochromism in Conducting Polymers	807
5.1	Electrochromism in Poly(aniline)	807
5.2	Electrochromism in Poly(thiophene) and Its Derivatives	808
5.3	Electrochromism in Triphenylamine Containing Polymers	811
6	Electrochromic Devices with Optically Transparent Polymer Layer	812
7	Electrochromism and Solar Cells	813
8	Conclusion	817
	References	817

Abstract

Electrochromic materials have attracted a lot of research interest for their fascinating spectro-electrochemical properties and commercial applications. A large number of inorganic and organic electrochromic materials ranging from transition metal oxides, metal coordination complexes, viologen systems, and conducting polymers are available. Electrochromic conducting polymers are exciting new

S. V. John (✉)

Department of Chemistry, University of the Western Cape, Bellville, South Africa
e-mail: jv4real44@gmail.com

E. Iwuoha

SensorLab, Department of Chemistry, University of the Western Cape, Bellville, South Africa
e-mail: eiwuoha@uwc.ac.za

class of electronic materials with a huge potential in the rapidly growing area of plastic electronics due to their electronic and optical properties, ease of processing, low-power consumption, flexibility, and low processing cost. They consist of vibrant colors and can be processed under simple ambient temperature. In this chapter, the general field of electrochromism is introduced, with coverage of the classes, operating principle, the experimental methods used in their study, and applications of electrochromic materials. Some of the most important examples of the major classes of electrochromic conducting polymers are highlighted. It surveyed electrochromic conducting polymers with a focus on their chemistry, electrochemistry, stability, and ability to enhance the performance of solar cell device.

Abbreviations

DEG	Diethylene glycol
ECD	Electrochromic device
Eg	Band gap
EPR	Electron paramagnetic resonance spectroscopy
FTIR	Fourier transform infra red spectroscopy
HOMO	Highest occupied molecular orbital
ITO	Indium tin oxide
LUMO	Lowest unoccupied molecular orbital
MVRH	Mott variable range hopping
NIR	Near infra red spectroscopy
NMP	<i>N</i> -methylpyrrolidone
PB	Prussian blue
PDMA	Poly (2,5-dimethoxyaniline)
PEDOT	Poly(3,4-(ethylenedioxy)thiophene)
PET	poly(ethylene terephthalate)
UV-Visible	Ultra violet visible spectroscopy
VTECWs	Variable transmission electrochromic windows
WO ₃	Tungsten oxide

1 Introduction to Electrochromism

Chromism is a general term for reversible color change in material due to response to external stimuli. This change is generally named based on the type of external stimuli. The color change can be as a result of exposure of the material to light (photochromic), vapor (vapochromic), solvent (solvatochromic), heat (thermochromic), or oxidation/reduction of the chemical specie (electrochromic). The reversible change of absorption with distinct electronic (UV-Visible) absorption spectra following an electrochemical (oxidation/reduction) reaction is termed **electrochromism**. It is the switching between redox states which results in the generation of various visible to near infra red (NIR) electronic absorption [1, 2].

It results in the reversible and visible change in the transmittance and/or reflectance of a material due to electrochemical oxidation or reduction. Usually, a color change between a transparent or bleached state and a colored state or between two colored states is observed. On the other hand, cases exist where more than two redox states are electrochemically available. In such cases, the electrochromic material may likely display more than two colors. This is termed *polyelectrochromism*.

Electrochromic materials, therefore, are chemical species that can be electrochemically switched between different colors. They exhibit reversible and highly stable changes of their optical properties upon oxidation or reduction by the passage of an electrical current which takes place as a result of an applied voltage [3, 4]. They have the ability to reversibly change the optical properties (refractive index n , extinction coefficient k) upon insertion and extraction of small charges by application of voltage. Basically, materials are considered to be electrochromic when noticeable visible color changes are observed under illumination. Nevertheless, chemical species have shown possibility for modulation of radiation in the near infrared (NIR), thermal infrared, and microwave regions [5–7]. In this case, “color” can mean response of detectors to these electromagnetic regions, not just the color noticed by the human eye [8].

1.1 Classes of Electrochromic Materials

Synthetic chemistry has produced a number of materials for electrochromic applications. Chemical species such as transition metal oxides, metal coordination complexes, viologen systems, and conducting polymers show electrochromic properties [1, 3, 5, 9–14]. They can be classified as either inorganic, organic, or hybrid. Inorganic electrochromic materials are in the form of transition metal oxides such as tungsten trioxide, oxides of molybdenum and vanadium [15, 16], and transition metal complexes like Prussian blue systems [17, 18]. Viologen derivatives [19, 20] and conducting polymers, e.g., poly(aniline), poly(thiophene), are examples of organic electrochromic materials while hybrid systems are formed by the complexation of metal ions with organic ligands or polymers bearing coordination sites.

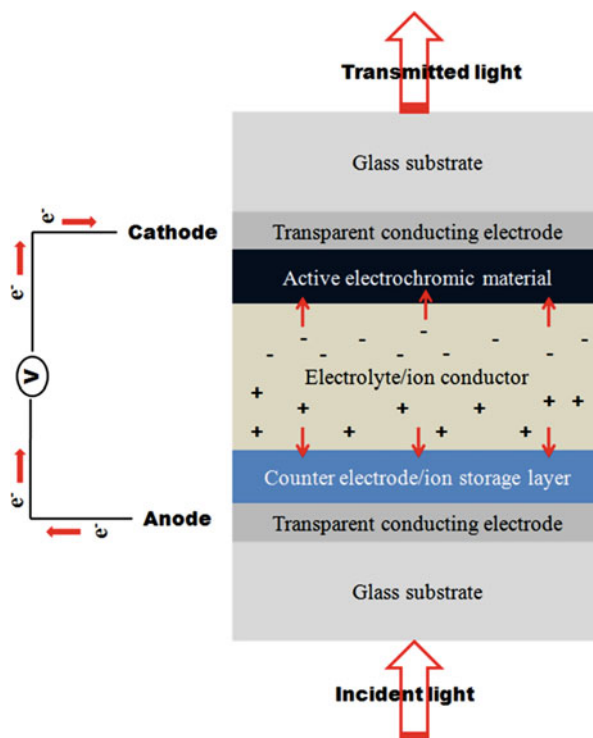
1.2 Operating Principle of an Electrochromic Device

The operating system for the study of electrochromic materials with very few exceptions is a two-terminal electrochemical cell configuration and all employ at least one optically transparent electrode. Materials to be applied for electrochromic device are first studied either as an electro-active solute or surface film under potentiostatic or galvanostatic control and an absorption measurement medium [1]. Conventional electrochemical techniques such as cyclic voltammetry (CV), coulometry, or chronoamperometry [21] are employed. The potentiostat or galvanostat is usually connected to a spectrophotometer and in situ spectroscopic measurement is carried out during the passage of current [22, 23]. Three-electrode circuitry can be employed for testing of materials to investigate their electrochromic parameters [1], while a simple

two-electrode system comprising of the working electrode and the counter electrode can be employed for practical electrochemical device investigations. Basically, the two electrode system involves a working electrode (the primary/electrochromic electrode) and a counter electrode (the secondary electrode) in a sandwiched configuration (Fig. 1). The working or electrochromic electrode is typically made of glass or flexible plastic (mainly poly(ethylene terephthalate) (PET))sheet, coated with an optically transparent electrically conducting film, e.g., tin doped indium oxide (ITO) on which the electrochromic material is deposited. A solid (often polymeric), gel, or liquid electrolyte is sandwiched between the primary electrode and the charge-balancing secondary electrode in the electrochemical cell to separate both electrodes. Upon application of an appropriate electrical potential, the electrochemical cell becomes charged/discharged and the device undergoes color switch which takes place at the working electrode. After the decay of the resulting current pulse and color change effected, the new redox state persists, with little or no power input. During this time, the optical response is monitored and recorded by in situ spectroscopic measurement.

The active electrochromic material can be WO_3 , MoO_3 , V_2O_5 , Prussian blue [PB, iron(III) hexacyanoferrate(II)], viologen systems, e.g., 1,1'-disubstituted-4,4'-bipyridylum salts, conducting polymers or a complexation of organic and inorganic material. This chapter focuses on conducting polymers and their application as the active electrochrome in electrochromic device.

Fig. 1 Schematic representation of the operating principle and testing of an electrochromic material



2 Conducting Polymers

Conducting polymers are conjugated polymers that conduct electricity. They are organic macromolecules which consist of at least one backbone chain of alternating double- and single-bonds. This is due to the conjugation which occurs as a result of the overlap of a p-orbital with another across an intervening σ – bond. The system usually comprises of a region of overlapping p-orbitals bridging the adjacent single bonds and allows delocalization of π -electrons across all p-orbitals aligned adjacently [24]. The π electrons do not belong to a single bond or atom, but rather to a group of atoms. A conjugated compound may be cyclic, acyclic, linear, or mixed. Systems with the largest form of conjugation are graphite, carbon nanotubes, grapheme, and conductive polymers. They have a unique characteristic which is the conjugated molecular structure of the polymer main chain where the π -electrons delocalize over the whole polymer chain and can result in interesting and useful optical and electronic properties. Generally, conducting polymers can either be ionically or electronically conducting. Polymer electrolytes are classified as the ionically conducting polymers while conjugated conducting polymers and the insulating polymers blended with conducting materials are classified as electronically conducting polymers. In this chapter, the conducting polymers are limited to conjugated conducting polymers.

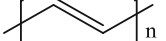
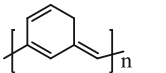
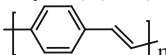
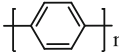
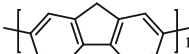
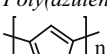
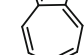
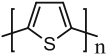
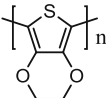
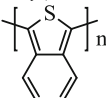
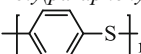
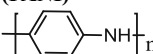
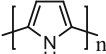
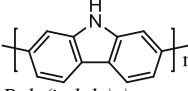
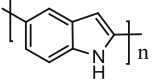
Although known for many years, conjugated polymers did not attract significant research interest until the mid-1970s due to their intractable nature. Research papers based on conjugated polymers were rare and the research was usually not done according to a fixed plan or system as the chemical nature and mechanism of their conductivity was not known. For decades, after the demonstration of polymers by Hermann Staudinger in 1920 as long chain molecules which led to his Nobel Prize in Chemistry in 1953, the general perception about polymers is that they were insulators, until the conductivity of polyacetylene was reported by Shirakawa, McDiarmid, and Heeger in 1977. This report brought about a change in the research in this field of polymers. They showed that poly (acetylene) can be made conductive by reaction with halogen vapors [25]. The reaction was proven to occur by the modification of neutral polymer chains to polycarbocation and concurrently inserting the corresponding halogen anion between the polymer chains in order to neutralize the positive charge on the polymer chain which was induced by doping [26]. They also showed that after doping polyacetylene with electron-withdrawing AsF_5 the conductivity increased, reaching the order of 10^3 S/cm [25, 27]. Extensive research into the chemistry and physics of this field including well-defined methodology both for the doped and undoped forms began after this discovery. Table 1 presents major organic conducting polymers according to their composition. **The well-explored classes are written in bold** and *the less well explored in italics*.

2.1 Conjugated Polymers as Semiconductors

2.1.1 Basic Characteristics

Poly(acetylene), the simplest conjugated polymer, and the prototype of other conjugated polymers exist in two isomeric forms. The structures can either be *trans*- or

Table 1 Major organic conducting polymers according to their composition

Components of the main chain	No hetero-atom present	Heteroatom present	
		Sulfur-containing Polymers	Nitrogen-containing Polymers
Double bonds	Poly(acetylene)s (PAC)  <i>Poly(heptadiyne)s</i> 		
Double bonds coupled with aromatic cycles	Poly(p-phenylene vinylene) (PPV) 		
Aromatic cycles only	<i>Poly(phenylene)</i>  <i>Poly(fluorine)s</i>  <i>Poly(azulene)s</i>  	Poly(thiophene)s  Poly(3,4-ethylenedioxythiophene) (PEDOT)  <i>Poly(isothianaphthene)</i>  <i>Poly(paraphenylene sulfide)</i> 	Poly(aniline)s (PANI)  Poly(pyrrole)s (PPY)  <i>Poly(carbazole)s</i>  <i>Poly(indole)s</i> 

cis- based on the locations of the hydrogen atoms on the double bond carbons. *Trans*-poly(acetylene) has the two hydrogen atoms located on the opposite sides of the double bond carbons, while *cis*-poly(acetylene) has the hydrogen atoms located on the same side of the double bond carbons (Fig. 2a, b). Each carbon atom of poly(acetylene) is sp^2 hybridized and can therefore be handled as a one-dimensional analogue of graphite. Nevertheless, the C-C bond in poly(acetylene) are not equal (Fig. 2d). This is known as the Peierls distortion or Peierls effect. The Peierls effect has an important effect on the electronics of poly(acetylene) and by extension, other conjugated polymers. It modifies the properties of a polymer by opening a gap between the highest occupied molecular orbital (HOMO) and the lowest unoccupied molecular orbital (LUMO) [28, 29]. This occurs when the p_z-orbitals of the polymer align perpendicular to the polymer backbone creating an enabling environment for electronic interaction between the double bonds, an interaction that results in delocalization, improving the conductivity of the conjugated system [30]. A periodic

bond alternation and variation in charge density occurs within the chains due to variation in the delocalization of the double bonds (Fig. 2c).

The π -conjugated system of poly(acetylene) and most polymers is formed by the overlap of carbon p_z orbitals. However, in some systems like that of poly(aniline), the p_z orbitals of nitrogen also take part. The main chain structure of poly(aniline) is in a way complicated compared to other conjugated polymers. The presence of basic centers of amine and imine nitrogens in the conjugated backbone of poly(aniline) makes it show a different chemistry compared to other poly-conjugated systems. Generally, poly(aniline) exists in three main structural forms, namely, *leucoemeraldine*, *emeraldine base*, and *pernigraniline* depending on the level of reduction or oxidation. The neutral or most reduced form of poly(aniline) is *leucoemeraldine*. It consists of rings of phenylene joined together by amine nitrogens. The completely oxidized form of poly(aniline) is *pernigraniline*. It consist of benzenoid and quinoid type of bonds and rings in the ratio 1:1 with imine nitrogens in between the ring, while the partially oxidized form – *emeraldine base* – consists of equal numbers of imine and amine nitrogens with benzenoid and quinoid rings in the ratio 3:1 (Fig. 3).

Fig. 2 Structure of various forms of poly(acetylene)

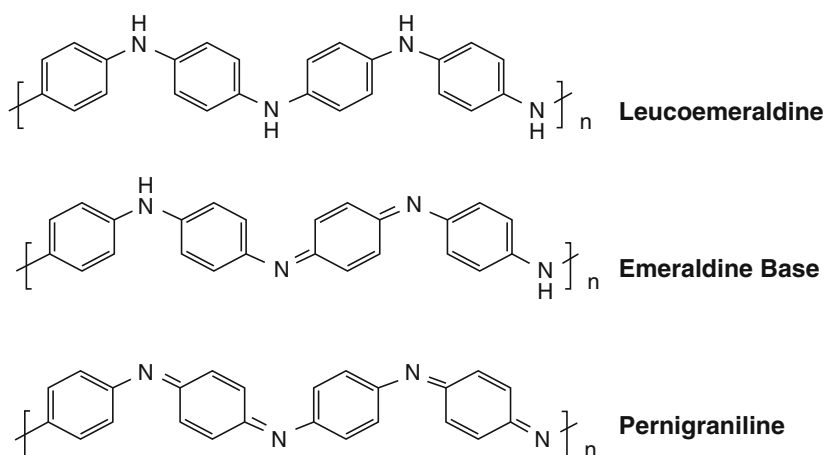
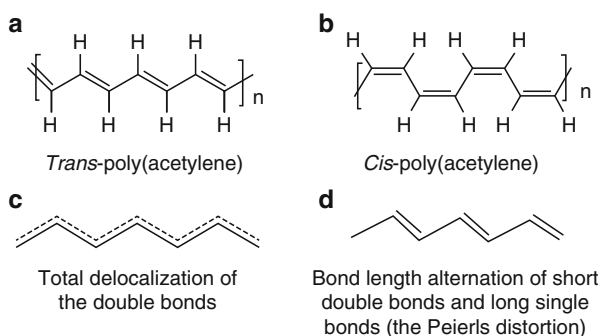


Fig. 3 Structure of tetrameric repeat units of the three forms of poly(aniline)

The conductive ability of a polymer largely depends on the band gap (E_g). The band gap is defined as the energy difference between the highest occupied molecular orbital (HOMO) or valence band and the lowest unoccupied molecular orbital (LUMO) or conduction band [31]. According to the energy difference, materials are classified into three groups as shown in Fig. 4: conductors, semiconductors, and insulators. For conductors, band gap does not exist as the highest energy level of the HOMO combines with the lowest energy level of the LUMO (no energy gap between the HOMO and LUMO). As a result, the electrons easily migrate to the LUMO from the HOMO. Some examples of good conductors are Fe, Cu, Al, Au, Ag, etc.

Semiconductors and insulators on the other hand have defined band gaps. For an insulator, the difference in energy between the HOMO and the LUMO energy level is large; thus, the promotion of electrons from the HOMO to the LUMO in principle is not possible. Due to the large band gap between the HOMO and LUMO of insulators, they do not conduct electricity. Examples of insulators are mainly saturated polymers, Bakelite, rubber, and wood. The band gap for saturated insulated polymers is higher than 10 eV [32]. This hinders the promotion of electrons from the HOMO to the LUMO and therefore prevents conductivity. For conjugated semiconducting polymers, the energy of delocalized HOMO is increased, while that of the LUMO is decreased due to delocalization through the polymer chain. Their conductivity falls in between those of metals and insulators with moderate band gaps. The gap between insulators is usually larger than that of semiconductors as can be seen in Fig. 4. They absorb light with an energy that is equal to or higher than the gap between their HOMO and LUMO. Examples of semiconductors are GaAs, ZnO, conjugated polymers, etc.

When light of certain energy (equal to or higher than the band gap) is absorbed by a semiconductor, electrons are transferred from π to a π^* excited state. This phenomenon is known as excitation and it is represented in Fig. 5 [33].

Conductivity of polymeric materials can be intrinsic or induced (doped). The conductivity of intrinsic conducting polymers ranges from 10^{-11} to 10^{-5} S/cm, while the conductivity of doped conjugated polymers generally ranges from 10^{-3} to 10^3 . Conjugated undoped polymers conduct electricity only in the lower

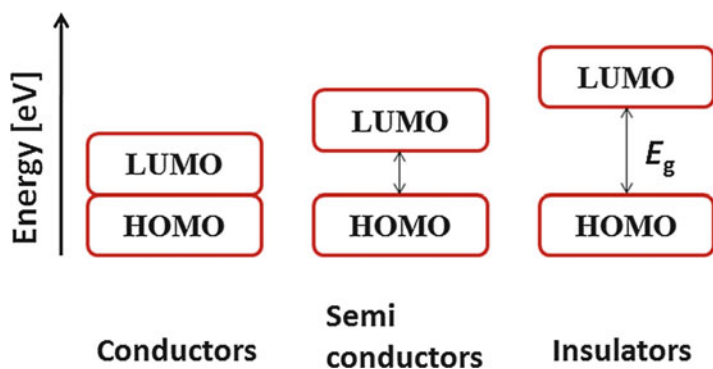


Fig. 4 Representative energy level diagram of energy gap in conductor, semi-conductor, and insulators

semiconducting region. For conjugated polymers to be applied as electrochemically active materials, improving the conductivity is vital. This can be achieved by doping of the polymer materials. Doping lowers the band gap and increases the polymer conductivity up to a range of 10^{-5} – 10^5 S/cm (Fig. 6) [34].

2.1.2 Doping in Conjugated Polymers

Doping in inorganic semiconductors is generally due to the incorporation of holes in the valence band or addition of electron in the conduction band. Doping in

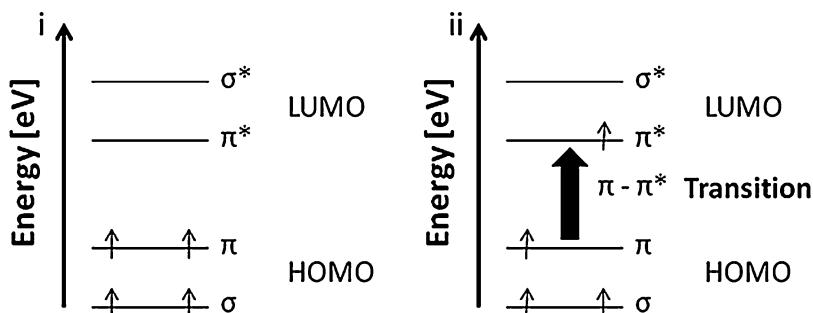


Fig. 5 Orbital diagram of an unsaturated material. (i) Ground state. (ii) Energy is absorbed and an electron is excited from the π orbital to the π^* orbital (excited state)

Conductivity increases with increased doping

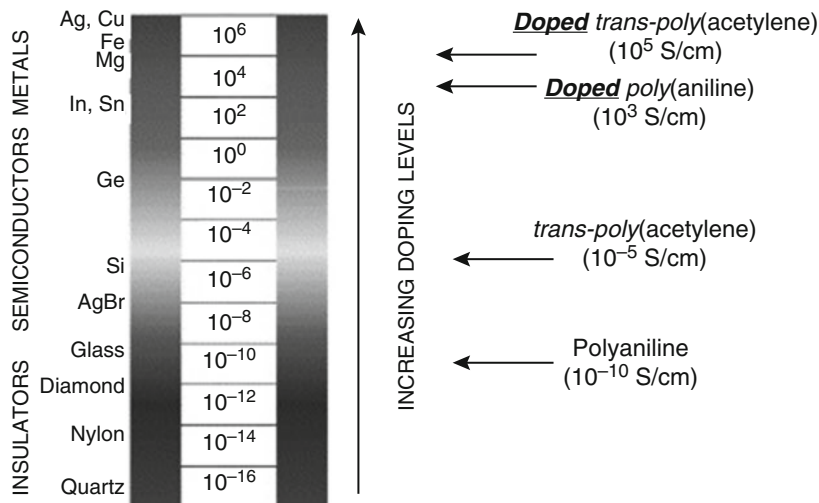


Fig. 6 Conductivity of electronic polymers. (Reprinted from Curr. Appl. Phys., 1, Alan G. MacDiarmid, "Synthetic metals," a novel role for organic polymers (Nobel Prize 2000 Lecture), 269–279, Copyright (2001), with permission from Elsevier.)

conjugated polymers is however different. The mechanism in this case, in addition to electron acceptance or release, involves the simultaneous insertion of counter ions into the polymer matrix. The doped polymers are considered as polymeric organic salts and the oxidizing or reducing agents used for the doping are known as dopants or doping agents. Doping of conjugated polymers can be achieved in two ways. They are:

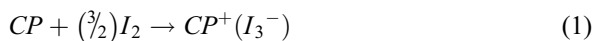
- Redox type doping
- Acid-base doping

Redox Type Doping

Redox type doping is the doping of conjugated polymers by an applied voltage. Conducting polymers can either be p-type doped or n-type doped. In p-type doped polymer, the main chain of the polymer is oxidized by counter-anions leaving holes in the chain. For n-type doping, the polymer main chain is reduced by counter-cations leaving electrons on the main chain.

p-Type Doping

Oxidative or p-type doping can be defined as the loss of electrons by the valence band, i.e., from HOMO of conjugated polymer to the oxidizing agent. The oxidizing agent accepts the electrons and becomes reduced. It leaves the polymer main chain with positive charges. It involves the oxidation of the polymer chains to polycarbonium cations and concurrently inserting a suitable amount of anions between the polymer chains to neutralize the polycarbonium cations charge. The oxidizing agent is termed the p-type dopant. Examples of oxidative or p-type dopants are Br_2 , I_2 , AsF_5 , H_2SO_4 , SO_3 , FeCl_3 , PF_3 , SF_6 , CH_3F , NO_2F , NO_2 , $\text{NO}^+\text{SbCl}_6^-$, HClO_4 , BCl_3 , etc. In oxidative doping, the oxidants gain electrons from the polymer and become the counter-anion according to the reaction represented by Eq. 1



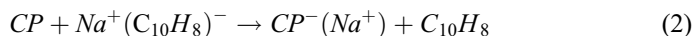
where CP denotes conducting polymers.

The p-type doping can be carried out both chemically and electrochemically on a variety of conjugated polymers like poly(acetylene), poly(aniline), poly(pyrrole), poly(p-phenylene), poly(thiophene), etc.

n-Type Doping

The n-type doping on the other hand is the transfer of an electron from a reducing agent to the empty conduction band, i.e., to the LUMO of conjugated polymer. In n-type doping, the conjugated polymer accepts electrons from the dopant (the reducing agent), an ionic complex is formed having negatively charged conjugated polymer chain and counter cations, and the polymer becomes reduced. The reducing agent in this case is termed the n-type dopant. The n-type dopants are

electron-donating substances. Due to the electron rich nature of conjugated polymers as a result of their π -system, strong reducing agents such as alkali metal are required for n-type doping. The process leaves the polymer main chain with negative charge carriers, and the dopant loses electrons and become the counter-cation. The reaction is represented by Eq. 2



As a result of the electron rich nature of conducting polymers and the strength of the reducing agent required for their n-type doping, there are relatively a small number of reports available on the n-type doped conjugated polymers.

Acid-Based Doping

Conjugated polymers possessing strong basic centers in their backbone can be doped by acid-base doping methods in addition to redox doping method. The *emeraldine* base form of poly(aniline), for example, undergoes protonation in an adequate amount of strong protonic acid to give the corresponding *emeraldine* salt. The protonation involves the imine nitrogens and they are preferentially protonated in a two-step transition from isolated, doubly charged, spinless bipolaron to a polaronic metal (Fig. 7). The first step of the protonation gives the product with the charge stored as *bipolarons* (Fig. 7ii); then due to instability on the polymer chain, redistribution of charge (internal redox process) occurs and transforms the *bipolarons* into *polarons* (Fig. 7iii). The *polarons* then undergoes a second step by separating to form a *polaron lattice* (Fig. 7iv).

Generally, the doping process involves charge transfer to or from the π -system of conjugated polymers, while the σ -system is kept unbroken. Although the structural identity of the individual chains of doped polymers is maintained, the electronic, vibrational, supramolecular structure and other properties of the polymer are altered. The doping process increases the polymer conductivity by several orders of magnitude and in some cases reach the conductivity of metals [35–39].

2.1.3 Doping Methods

There are two main doping methods employed for the doping of conjugated polymers.

- Electrochemical doping
- Chemical doping

Electrochemical Doping

Oxidative or reductive doping can be achieved by electrochemical oxidation or reduction of conducting polymers on an electrode surface. In the electrochemical oxidation or *p*-doping process, the main chain of the polymer loses an electron and becomes oxidized according to Eq. 3 below

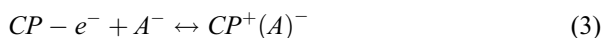
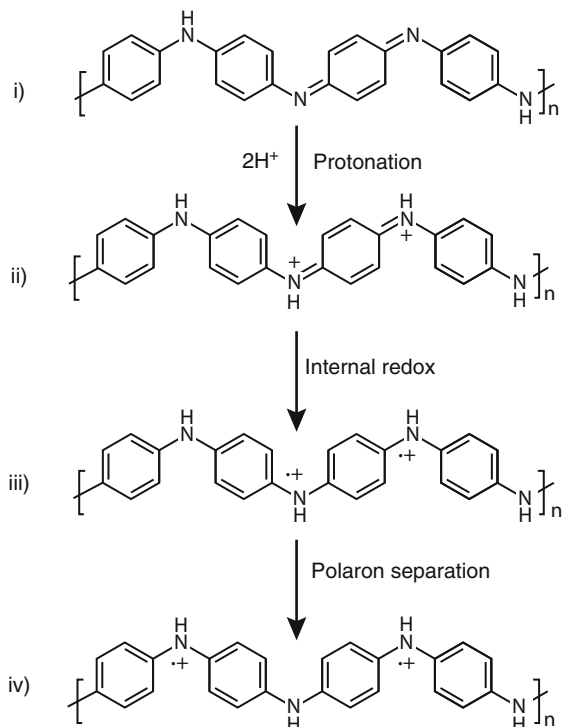
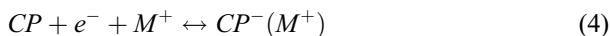


Fig. 7 Preferential protonation of emeraldine base form of poly(aniline).
i) Before protonation, *(ii–iv)* after protonation, *(ii)* formation of *bipolarons*, *(iii)* formation of *polarons*, and *(iv)* formation of *polaron lattice*



where A^- represents the anions in the solution, $CP^+(A^-)$ represents the oxidized conducting polymer and doped counter-anion. In the reduced systems, the main chain of the polymer accepts electrons and becomes reduced according to Eq. 4 below

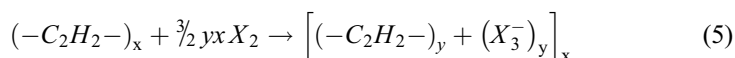


Generally, electrochemical doping is conducted in a nonaqueous electrolyte solution having quaternary amine salts of mono-valent anions either at constant current or constant potential. In most cases, the monomer is used and it undergoes both polymerization and doping simultaneously. The supporting electrolyte supplies the ions and dopes the conjugated polymer by coupling ionically with the monomer. The dopant anions generated from the electrolyte are inserted into the polymer matrix and oxidation takes place concurrently. A variety of supporting electrolytes are available for electrochemical doping and poor nucleophilic aprotic solvents (e.g., acetonitrile, benzonitrile) are employed. Other aprotic solvents such as dimethyl formamide, dimethyl sulfoxide, hexamethyl phosphoramide, and hydroxylic, with nucleophilic character can also be used. The nucleophilicity of this second class of aprotic solvent is reduced by the addition of a suitable protic acid for their application as solvent for electrochemical doping. Quaternary ammonium salts of the form R_4NX (where R = Alkyl, Aryl group and X = Cl^- , Br^- , I^- , PF_6^- , $CF_3SO_3^-$, ClO_4^- , BF_4^- , $CH_3C_6H_4SO_3^-$) are commonly used supporting electrolytes that are soluble in aprotic solvent [40].

Electrochemical doping of conjugated polymers has been extensively employed. In electrochemical doping, polymers are obtained from the monomers by electropolymerization and this results in a doped polymer; they therefore do not require additional doping [41]. Nevertheless, if a different dopant is needed, the polymer can be electrochemically reduced to its neutral form before re-doping with the anion of interests either chemically or electrochemically. The polymer can be deposited from a polymer solution on an electrode surface by spin coating or drop coating. In most cases, electrochemical doping is carried out using cyclic voltammetric electrochemical method and the accompanying spectroscopic changes can be monitored. This is usually made possible by the use of spectro-electrochemical methods where a spectroscopic instrument is coupled with an electrochemical instrument, e.g., UV-Vis/CV [42–44], EPR/CV [45–48], FTIR/CV [49–52], Raman/CV [53, 54].

Chemical Doping

The first report on doping of conjugated polymers was on the use of halogens (Br_2 and I_2) and arsenic pentafluoride (AsF_5) as doping agents for poly(acetylene) [25, 27]. Equation 5 shows the chemical reaction describing the doping of poly(acetylene) with halogen



The doping process involves the conversion of the doping agents into linear polyhalogen anions (I^- , Br^-) which are then inserted into the polymer matrix. The mechanism for the doping of poly(acetylene) with Br_2 is slightly delicate. In the case of Br_2 oxidative doping, the reaction involves the addition of bromine to the double bond and this breaks the conjugation and converts parts of the poly(acetylene) into insulating poly(dibromovinylidene). To avoid this, doping with Br_2 is conducted in very mild conditions. Arsenic pentafluoride can be used to achieve both redox and acid-base types of doping. Transition metals with oxidizing properties, e.g., FeCl_3 [55, 56], strongly or mildly oxidizing acids such as HClO_4 and H_2SO_4 [57] arsenates or antimonates ($\text{NO}_2^+\text{XF}_6^-$, where $\text{X} = \text{P}, \text{As}, \text{Bi}$), nitrosonium salts (NO^+XF_6^- , where $\text{X} = \text{P}, \text{As}, \text{Bi}$), and nitronium salts of hexafluorophosphates can be used for the doping of a good number of conjugated polymers. Chemical doping of conjugated polymers is a useful method of doping of conjugated polymers. However, in this technique, control over the doping level is somewhat poor and complete doping to the optimum concentrations often results in inhomogeneous doping.

Doping brings about a six- and ninefold increase in the conductivity of conjugated polymers. Conducting polymers shows temperature dependence conductivity similar to that of semiconductors. It obeys the Mott variable range hopping (MVRH) model. MVRH is a model that describes low-temperature conduction in strongly disordered systems with localized charge-carrier states [58]. The MVRH has a characteristic temperature dependence represented by

$$\sigma = \sigma_0 e^{-(T_0/T)^{1/4}} \quad (6)$$

For n - space dimension of the material, MVRH is given as

$$\sigma = \sigma_0 e^{-(T_0/T)^{1/(n+1)}} \quad (7)$$

where σ is the prefactor, n is the space dimension number of the material. The prefactor is independent or weakly dependent on temperature.

The degree of ordering and doping of conjugated polymers plays a huge role in their conductivity.

3 Charge Carriers in Conducting Polymers

The charge carriers in conjugated polymers are solitons, polarons, or bipolarons. Solitons are interesting type of excited states which have kinks in the bond alternation. They can exist in the neutral or redox state. The neutral soliton can lose an electron and be oxidized to form a positive soliton or gain an electron and be reduced to form a negative soliton. Neutral soliton S^0 has a spin of $1/2$ while charged soliton is spinless. *Polarons*, on the other hand, are radical ion associated with a lattice distortion. The positively charged and negatively charged *polarons* formed from oxidation and reduction of the polymer main chain are denoted as P^+ and P^- , respectively, and they possess a spin of $1/2$. The coupling of two positively charged *polarons* or two negatively charged *polarons* on the main chain of a conjugated polymer results in *bipolaron*. It is a pair of like charges (dication) associated with strong local lattice distortion. It is formed when the concentration of the *polaron* is high on the polymer main chain. It is thermodynamically more stable than two polarons and it is spinless.

The major charge carriers in conducting polymers, however, are *polarons*. For n -type doping of poly(acetylene), neutral chains of the polymer are either chemically or electrochemically reduced to polycarbonium anions and cations are inserted into the polymer chain simultaneously. In such instance, negatively charged spinless *solitons* are the charge carriers. Figure 8 shows the schematic representation of the p - and n -type doping process of poly(acetylene). The p -type process starts by the removal of an electron from the π -system of the polymer resulting in the formation of a radical cation (*polaron*). It is followed by the removal of a second electron resulting in a second radical cation which recombines or couples with the first to give spinless dication (*bipolaron*). The spinless dication can further be oxidized to solitons [59].

For polyheterocyclic systems, the removal of an electron from the π -system results in the emergence of a radical cation called *polaron*. The presence of the *polaron* creates a domain of quinone-type bond sequence within the aromatic bond

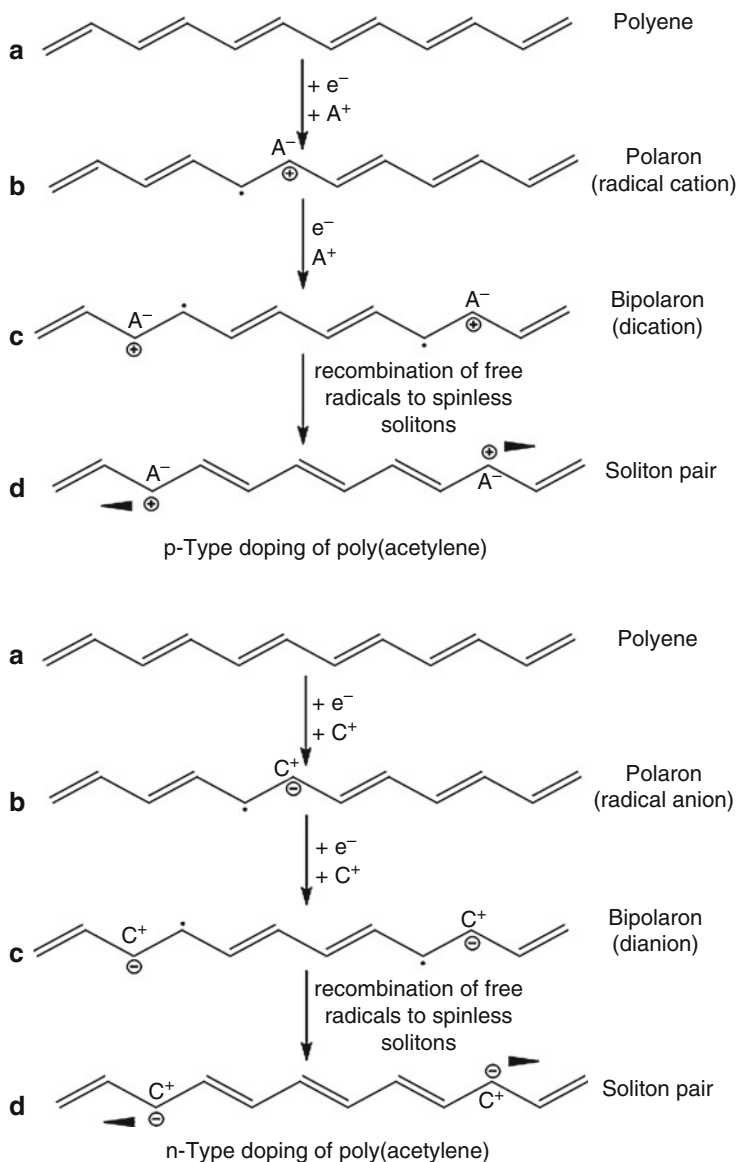


Fig. 8 Schematic representation of p- and n-type doping of poly(acetylene). A^- = anion, C^+ = cation

sequence of the polymer chain. Removal of a second electron may either lead to the formation of another *polaron* or a spinless *bipolaron* [60]. The *bipolaron* in this case is a dication separating the quinone bond domain from the aromatic bond domain in the polymer chain (Fig. 9).

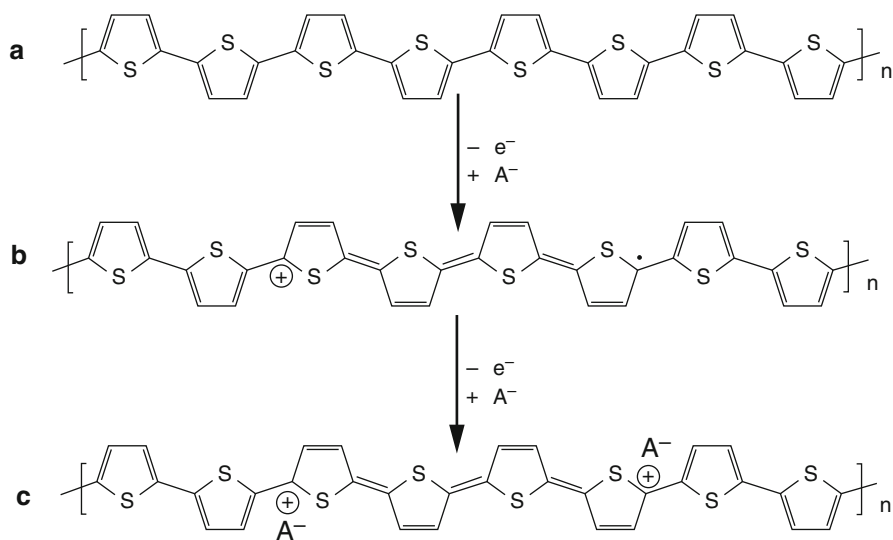


Fig. 9 Schematic representation of p-type doping of poly(thiophene)

4 Electronics of Conjugated Polymers

The absorption spectra of conjugated polymers can be used to distinguish between intrinsic conducting and doped conducting polymers. For doped conducting polymers, strong absorption maximum peak in the visible to near-infrared (NIR) region of the electromagnetic spectrum is generally observed. This is brought about by the presence of polarons and bipolaron in the main chain of the conjugated polymers.

Figure 10 [61], for example, shows the absorption spectra of poly(2,5-dimethoxyaniline) (PDMA) in different doping states at different applied potentials (0.3 V, 1.0 V, and 0.5 V) in 0.001 M HCl as supporting electrolyte. The spectra show three absorption bands at 370, 470, and 690 nm. The peak at 370 nm corresponds to the fully reduced *leucoemeraldine* state of PDMA (yellow). Upon partial oxidation, the peak disappears and a peak at 470 nm is observed. The peak at 470 nm is the intermediate or partially oxidized form of polyaniline (*emeraldine*) which is green in color. The peak disappears upon full or complete oxidation and another peak which corresponds to the completely oxidized form of polyaniline (*pernigraniline*) which is blue-violet to purple in color appears at about 690 nm. The doped poly(aniline) can be reduced to its intrinsic conducting form by dedoping of the polymer. In such case, the absorption band which corresponds to the oxidized form of polyaniline is weakened and finally disappears.

The band gap values are estimated from spectroscopic and electrochemical measurements. For spectroscopic measurements, the onset absorption is estimated from the tangential position where the absorption begins to level to a straight line as shown in Fig. 11.

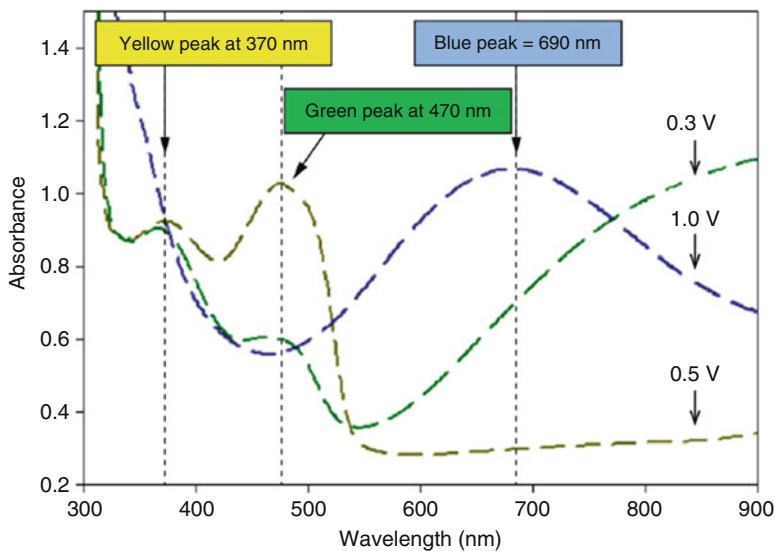
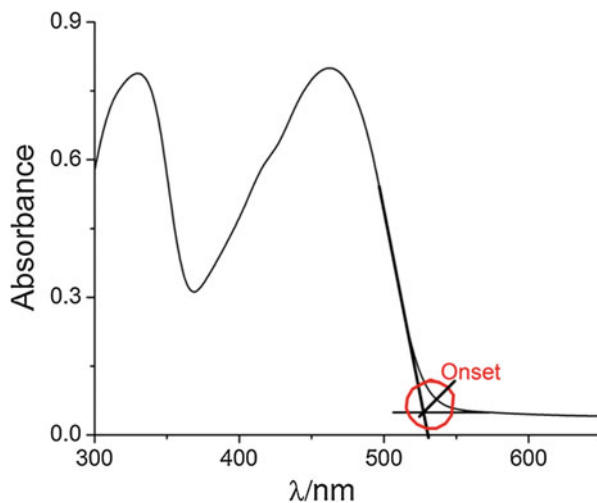


Fig. 10 UV-VIS spectra of the PDMA film recorded at different applied potentials to distinguish doping levels. (Adapted with permission from Ref. [61])

Fig. 11 Representation of onset absorption



From the onset of the absorption, the band gap is calculated using Eq. 8

$$E_g^{\text{op}} = \frac{1240}{\lambda_{\text{onset}}} \text{ (eV)} \quad (8)$$

where E_g^{op} is the optical band gap and λ_{onset} is the onset absorption in nm.

For the electrochemical measurements, the HOMO and LUMO energy levels of the polymers are estimated from the cyclic voltammetric onset oxidation and onset reduction potentials of the polymer or material, respectively. The electrochemical band gap of conjugated polymers can be calculated using the linear correlation between the ionization and oxidation potential with the electron affinity and reduction potential derived by Bredas and co-workers [62] on the basis of a comprehensive comparison between the valence effective Hamiltonian (VEH) theoretical results and experimental electrochemical data (Eqs. 9, 10, and 11)

$$I_p = -(E_{\text{onset}}^{\text{ox}} + 4.4) \text{ eV} \quad (9)$$

$$E_a = -(E_{\text{onset}}^{\text{red}} + 4.4) \text{ eV} \quad (10)$$

$$\text{And } E_g^{\text{cl}} = I_p - E_a \quad (11)$$

where $E_{\text{onset}}^{\text{ox}}$ and $E_{\text{onset}}^{\text{red}}$ are onset oxidation and reduction potentials (determined at the position where the current starts to differ from the baseline) Fig. 12.

Conducting polymers are intrinsic semi-conductors with band gaps which depend on the chemical composition of the conjugated backbone as well as the substituent on the main chain. Their optical and electronic properties can therefore be varied resulting in the fabrication of various types of electronic devices. The conductivity of conducting polymers increases by several folds due to doping. They not only show high conductivity but also impart interesting optical and mechanical properties. They have fascinating properties like good scalability, mechanical strength, flexibility,

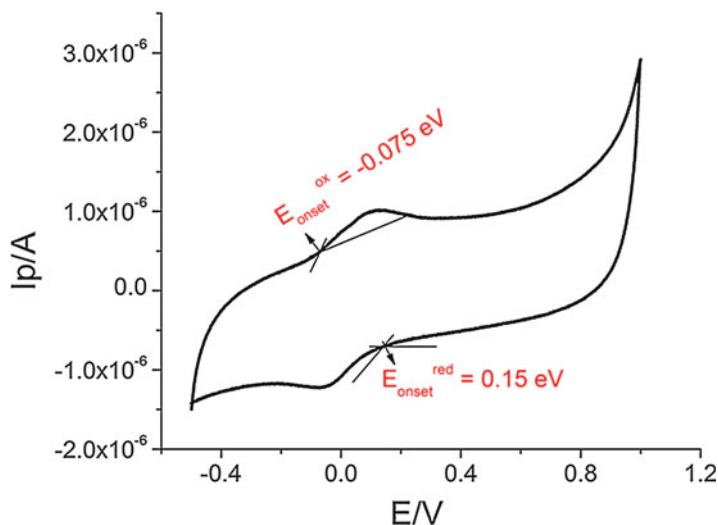


Fig. 12 Representation of electrochemical onset oxidation and reduction

unique optical properties, ease of processing, long shelf life, and low cost for device integration [63, 64]. They therefore find applications as semiconducting materials, in electronics, optoelectronic, and other semiconducting materials. Interestingly, these π -conjugated polymers also possess electrochromic properties like diverse colors, high optical contrast, fast switching speed, and good processability for electrochromic device applications, such as smart windows, mirrors, and displays [64–71]. Also, in addition to having the electronic and optical properties of metals and inorganic semiconductors, conducting polymers have intriguing electrochemical redox properties. They can exhibit more redox states and generate multiple colors unlike their inorganic counterparts [1].

5 Electrochromism in Conducting Polymers

Electrochromism occurs in conjugated polymers when the polymer is induced by redox processes. This results in the modification of the electronic properties of the polymer, giving rise to changes in the color. Upon oxidation or reduction (doping), the gap between the highest occupied molecular orbital (HOMO) and lowest unoccupied molecular orbital (LUMO) potentials (band gap) is modified and color changes. The color changes lead to the ability of such electrochromic materials to exhibit various colors. The energy band between the HOMO and the LUMO determine the intrinsic optical properties of conducting polymers. They are doped with counter anions when oxidized (p-doping) and contain delocalized π -electron. Reduction removes the dopant to give the undoped (neutral) electrically insulating form. The color can be controlled by structural modification of the main-chain of the polymer structure, nature of the monomer substituent, side chains, the pendant group, or the length of the polymer chain. All conducting polymers therefore are potentially electrochromic in nature due to redox switching which give rise to new optical absorption bands and colors together with transfer of electrons/counter ions [72].

5.1 Electrochromism in Poly(aniline)

Poly(aniline) has received considerable attention due to its broad range of tunable properties derived from its structure flexibility. It exists in three distinct oxidation states and can be switched between oxidation states by chemical or electrochemical means through the conversion of some of the amine nitrogen(s) to imine nitrogen(s). The reduced form of poly(aniline), *leucoemeraldine*, is yellow. By chemical or electrochemical doping, poly(aniline) shows reversible transitions to its intermediate oxidized form of blue *emeraldine base form*(EB), while further oxidation to *pernigraniline* state renders the material purple [73, 74]. The *emeraldine base form* can be protonated to its green conducting *emeraldine salt*.

Generally, poly(aniline) is known for insolubility resulting in intractability. With the recent breakthroughs in the synthesis of conducting polymers with

nano-dimensional control, the challenge of poor processability of poly(aniline) has been overcome. The nanosphere mixture of poly(aniline) with poly(sodium 4-styrenesulfonate) (PSS) is highly dispersed in aqueous solution as the emeraldine salt and the electrostatic interaction between poly(aniline) and the surfactant makes this nano-dispersion stable [75, 76]. Figure 13 shows the chemical oxidation of polyaniline with the blue *emeraldine base* and green *emeraldine salt* form [75]. Due to high conductivity and rapid redox switching, nano-sized poly(aniline) has potential advantages in electrochromic application.

5.2 Electrochromism in Poly(thiophene) and Its Derivatives

Poly(thiophene), a polyheterocyclic system, has received wide research interest for applications in organic electronics (organic photovoltaic cells, organic light emitting diodes, organic field effect transistors) and other applications. A good number of publications on organic electronics are based on thiophenes. The success of this group of polymers in organic electronics, particularly in organic photovoltaics, is huge. Its unique properties prompted the research for its possible application as the active material in electrochromic device. The potential of poly(thiophenes) for electrochromic applications was first reported in 1983 [77, 78]. Unsubstituted poly(thiophene) was electrochemically polymerized, and its redox properties were investigated and reportedly revealed a red to blue switch on p-type doping. This corresponds to the bleaching of its $\pi-\pi^*$ transition in the visible region with simultaneous emergence of infrared charge-carrier optical transitions. Electrochemical n-type doping of the unsubstituted poly(thiophene) resulted in a color change of red to black-green [79].

The thin films of polythiophenes are blue in their doped state with a maximum wavelength of 730 nm (oxidized state) and 470 nm in their undoped (reduced) state

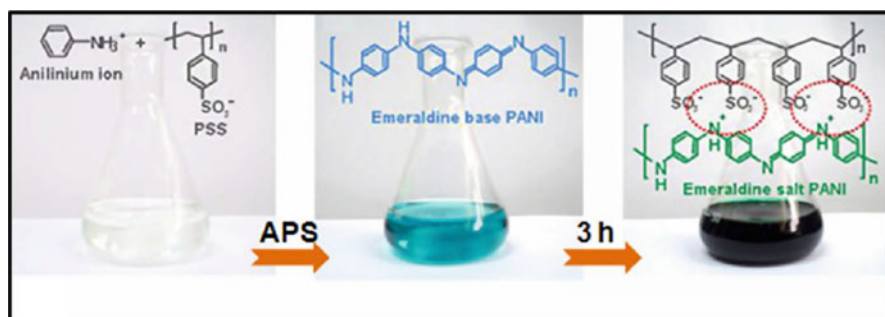


Fig. 13 Schematic diagram and photograph of preparation of PANI/PSS-NPs. (Reprinted from *Electrochemistry Communications*, 12, Sung Jong Yoo, JoonHyuk Cho, Ju Wan Lim, Sun Ha Park, Jyongsik Jang, Yung-Eun Sung, High contrast ratio and fast switching polymeric electrochromic films based on water-dispersible polyaniline-poly(4-styrenesulfonate) nanoparticles, 164–167, Copyright (2010), with permission from Elsevier.)

[80]. Monomer modification can significantly alter optical response. For example, the positions of methyl groups or alkoxy substituents on the polymer backbone of polymer films prepared from 3-methyl-thiophene-based oligomers strongly determined the color [81]. The colors varied from pale blue, blue to violet in the oxidized form and purple, yellow, red to orange in the reduced form. This variation in color is ascribed to changes in the effective conjugation length of the polymer chain. Reynolds' group reported a series of alternating conjugated donor-acceptor polymeric hybrids containing 3,4-dioxythiophenes, 2,1,3-benzothiadiazole, and unsaturated spacers (ethynylene or *trans*-ethylene). The presence of *trans*-ethylene spacers induced narrowing of the energy gaps affording various tones of greens, a color not common to achieve in the field of π -conjugated polymers [82]. The polymer showed excellent optical and redox stabilities to repeated switching of over 3000 cycles, demonstrating the potential of this polymer for electrochromic device applications.

Poly(3,4-(ethylenedioxy)thiophene)s an analogue of poly(thiophene) is a unique electron-rich polymeric material possessing high oxygen content. It was designed in the late 1980s at the Bayer AG research laboratories in Germany to address the lack of processability exhibited by the more conventional unsubstituted poly(thiophenes). Compared to its unsubstituted poly(thiophenes) parent, neutral deep blue PEDOT shows a relatively stable and highly transmissive sky blue oxidized state. In Fig. 14, the onset of the optical absorption of neutral PEDOT lies in the near-IR region of the electromagnetic spectrum. This excellent transmissivity of PEDOT has attracted significant research attention and has been the focus of a considerable number of publications [81, 83].

Havinga and Reynolds et al. [67, 85] introduced solubilizing alkyl side chains to the alkylenedioxy bridge of PEDOT, to produce the first neutral-state solution processable PEDOT derivatives (Fig. 15a). They investigated the electrochemical performance of these materials and compared the response to that of the unsubstituted PEDOT. In addition to the direct effect of this structural modification on the energy gap of the subsequent analogues, which depends on the length and bulkiness of the substituted pendant group (1.75–1.8 eV), the substitution was found to enhance the switching properties of PEDOT and a more effective depletion of the neutral-state optical absorption was observed on full oxidation. Hydrophobic analogue exhibiting particularly high contrast ratios, rapid switching times along with the same dark blue to transmissive sky blue switch on electrochemical oxidation and narrow band gap of 1.65 eV, has been reported for the perfluoroalkyl ester-functionalized derivative PEDOT-F (Fig. 15b) [86].

The electrochromic properties of PEDOT and its derivatives have revealed contrast ranging from 45 to 62% and a fast response time of ~ 10 s in their maximum wavelength of absorption [87–91]. Considering the ease of functionalization and structure controlled optical properties of poly(thiophene) and its analogues, they have attracted research attention as conducting polymer active electrochromes. Various possibilities of fine tuning the colored neutral state taking full advantage of the different substitution-induced backbone conformations have been proposed.

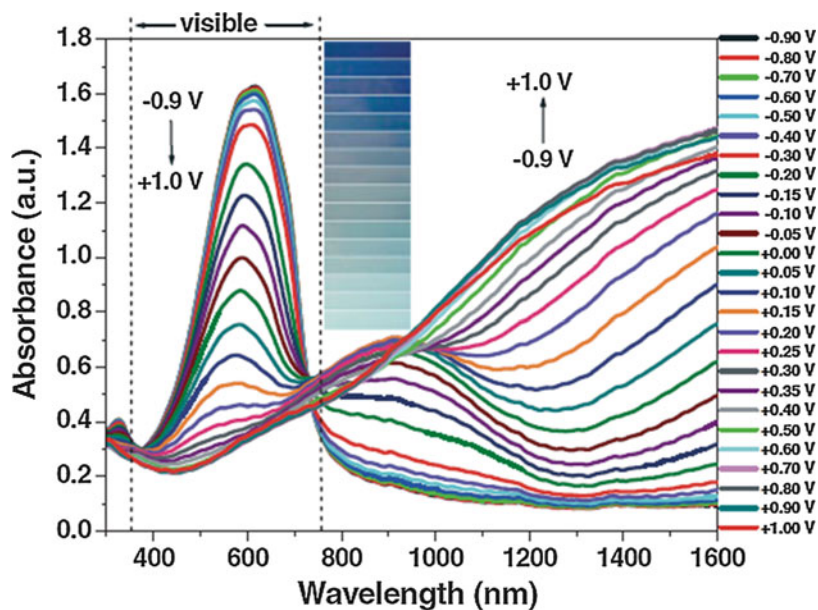


Fig. 14 Spectroelectrochemistry of a thin film of PEDOT at different oxidation states with inset pictures of variation in the blue color on application of different biases. (Reprinted (adapted) with permission from Ref. [84], Copyright (2004) John Wiley and Sons)

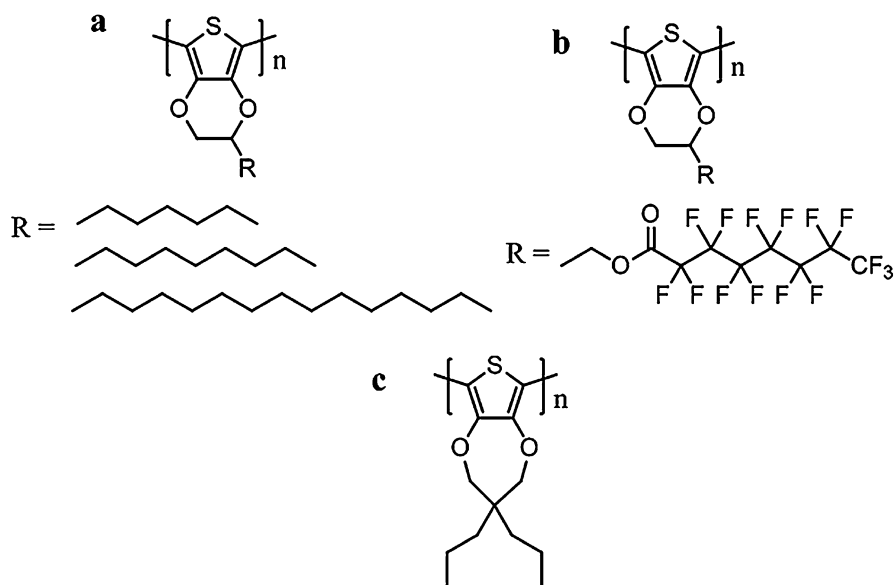


Fig. 15 Structure of PEDOT derivatives

5.3 Electrochromism in Triphenylamine Containing Polymers

Triphenylamine containing polymers are readily soluble aromatic polyamides. They show interesting redox properties that are useful for electrochromic application. The preparation and characterization of a series of novel electrochromic aromatic polyamides have been reported. The electrochromic properties of a series of polyamides with pendent triphenylamine units based on *N,N*-bis(4-aminophenyl)-*N'*, *N'*-diphenyl-1,4-phenylenediamine exhibited two reversible oxidation redox couples at different applied potential ranging from 0 to 0.85 V. They revealed color change from pale yellow to green and then blue at 0.85 and 1.25 V, respectively [92]. Liou reported several triphenylamine containing electrochromic polymers with interesting color transitions that showed good electrochromic reversibility in the visible region and near infrared range [93–96]. However, despite the interesting properties, majority of the polymers only reveal less than two stages of electrochromism due to challenge of increasing electroactive nitrogen atoms within triarylamine-containing structures. In a recent work, the Liou group designed and synthesized a series of novel near infrared electrochromic starburst triarylamine-based materials with the incorporation of electron-donating substituents at the para-position of phenyl groups [97]. This is believed to be able to prevent the coupling reactions by affording stable cationic radicals and lowering the oxidation potentials [98–104]. In the neutral form (when no voltage was applied), the film of one of the reported polymers exhibited strong triarylamine absorption around 346 nm with almost transparent response in the visible region. At an applied voltage of 0.55 V, the intensity of the absorption peak at 346 nm decreased while a new peak at 447 nm and broad intervalence charge transfer absorption around 1170 nm was observed. The broad absorption at 1170 nm was due to the intervalence charge transfer absorption excitation between states in which the positive charge is centered at different nitrogen atoms. The applied voltage was varied between 0.55 V and 1.45 V and the response showed different spectro-electrochemical behavior and colors as shown in Fig. 16.

The electron-donating substituents reportedly stabilized the radical cations and lead to good solubility and film forming property of the polyamide in addition to good thermal stability. The report by Beaupre' et al. of electrochromic polymers containing a 4-butyltriphenylamine (BuTPA) unit on the main chain shows the color transition of these polymers as shown in Fig. 17 [105]. The copolymers show promising optical and electrochemical properties for military camouflage needs with color transition from pale yellow to green, transparent to khaki, or pale green to reddish-brown. The copolymers PC(BuTPA) and PCC(BuTPA) are colorless in their neutral states and show reversible color transition from colorless to khaki fits either desert or forest background for military camouflage. Relatively good electrochromic characteristics such as high contrast ratio both in the visible range and near infrared region, low switching times, high coloration efficiency, and highly electrochromic/electroactive reversibility are reported for these novel polymers. This suggests a good potential for practical applications in both visible and near infrared region.

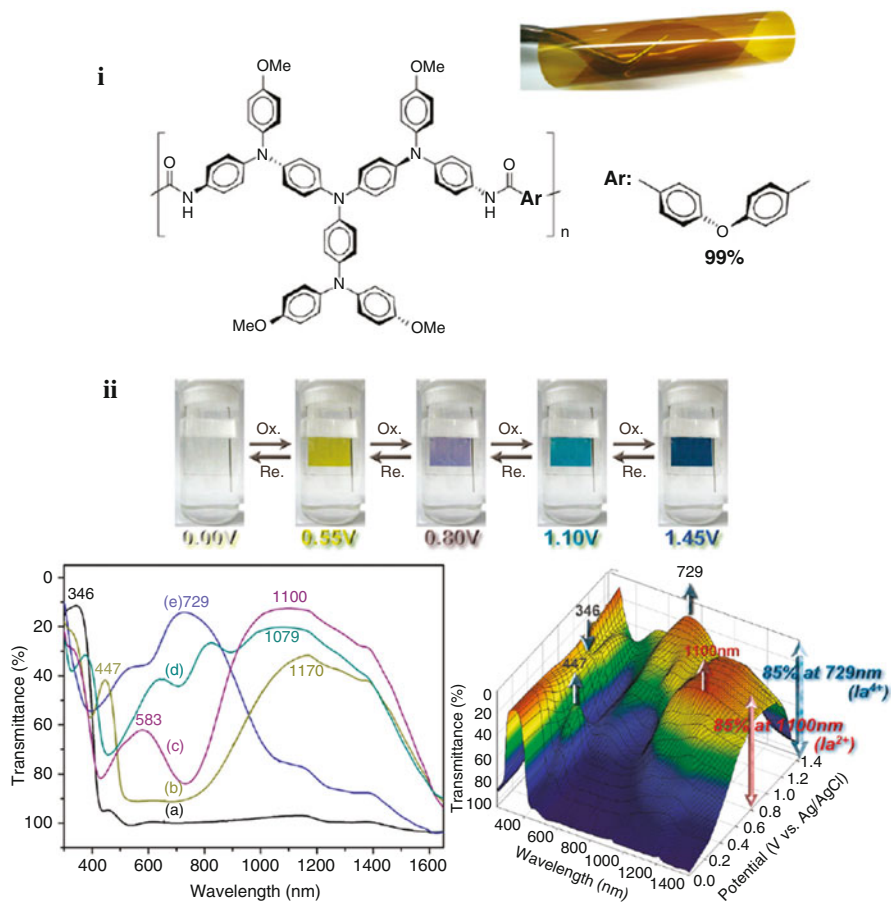


Fig. 16 *i*) Structure of the aromatic polyamide and the appearance of the flexible film; *ii*) Electrochromic behavior (left) at applied potentials of (a) 0.00, (b) 0.55, (c) 0.80, (d) 1.10, (e) 1.45 (V vs. Ag/AgCl), and 3D spectroelectrochemical behavior (right) from 0.00 to 1.45 (V vs. Ag/AgCl) of polyamide thin film (~120 nm in thickness) on ITO-coated glass substrate in 0.1 M TBAP/CH₃CN. (Reprinted (adapted) with permission from (Ref. [97]), Copyright (2011) American Chemical Society)

6 Electrochromic Devices with Optically Transparent Polymer Layer

The replacement of ITO (an optically transparent electrically conducting material) by a polymer in an electrochromic device setup is referred to as an “all-polymer” electrochromic device. PEDOT-PSS in otherwise all-plastic designed device architecture has resulted in a strictly “all-polymer” electrochromic device [106]. In this case, a film of poly(3,4-(ethylenedioxy) thiophene)–poly(styrene sulfonate) (PEDOT–PSS) served as

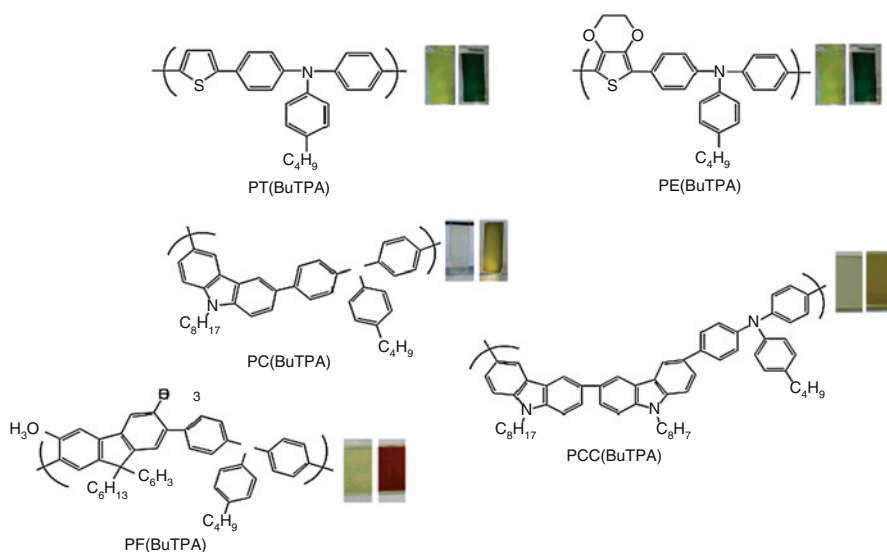


Fig. 17 Chemical structure and color transition of some triarylamine-containing copolymers. (Reprinted (adapted) with permission from (Ref. [105]), Copyright (2006) American Chemical Society)

the electrically conducting material film and was spin-coated on commercial transparent plastic. The prototypes were made from PEDOT-PSS and mixed with *N*-methylpyrrolidone (NMP) or diethylene glycol (DEG) additive by incorporation into the aqueous casting solutions of PEDOT-PSS [106]. Devices which exhibited excellent relative luminance change values as high as 51% with contrast nearly as high as that obtained when using ITO-coated glass electrodes (56%) have been reported [70]. About 51% transmittance change at 540 nm upon switching and high stability with only a few percent contrast loss over more than 30,000 switches was demonstrated by Argun et al. [106].

7 Electrochromism and Solar Cells

It is a well-known fact that the most abundant source of renewable energy is solar radiation. Researchers in the field of renewable energy are working tirelessly and making frantic efforts to make photovoltaic technology an alternative source of energy. As promising and interesting as this may sound, solar radiation is also one of the main causes of energy consumption in buildings (both residential and commercial) through increased cooling demands when the heat generated is high. Increases in the energy consumption of buildings can be mainly attributed to the desire to be comfortable and free from thermal discomfort arising from too high or too low perceived temperatures, while in the building by occupants.

The energy consumed by buildings for heating, cooling, lighting, and ventilation accounts for about 30–40% of the global primary energy [107]. The energy lost through inefficient window stock accounts for ~30% of the heating and cooling in buildings in the USA [108]. It is estimated that 41% of the energy consumed in the USA in 2009 was in the commercial and residential buildings, a 48% increase in the 1980 estimate [109]; 19% of this value is attributed to cooling and lighting and 37% attributed to space heating and the remainder to water heating and consumer electronics/appliances [109]. There is a considerable high energy demand for cooling systems in Europe with electrically driven air conditioning dominating the peak power during summer in parts of Europe as well as in the USA. Therefore, in more extreme climates, the electrical power may be entirely dominated by air conditioning.

A potential technology for reduction in both lighting and cooling energy use through modulation of transmitted light and solar heat is variable transmission electrochromic windows (VTECWs) [110, 111], popularly known as “smart windows.” Smart windows are used in the control of the incident daylight and glare in buildings and automotive applications [112–114]. This technology can modulate the solar energy entering a building as well as other see-through devices by application of an applied voltage. They can be switched from 62% visible transmittance, 0.47 solar heat gain coefficient to a fully tinted state with $\leq 2\%$ visible transmittance and 0.09 solar heat gain efficiency [110]. Their ability to modulate solar energy transmittance keeps the heat from the sun out and provides substantial total energy savings. They offer tunable shading which allows light energy use savings of up to 48–67%, while bringing down annual peak cooling loads to as low as 19–26% when compared to efficient low-e windows [115]. As a result, shade or blinds are not necessary for reduction of glare in buildings and the comfort of building occupants can be significantly enhanced with comfortable working or living environment and a clear view and link to the outdoors.

VTECWs combine electrochromism and light-harvesting ability for power generation. They require an external power source offsetting some of the energy savings. They can be self-powered switchable devices only or can be used as power sources for different applications. This can be achieved by the integration of an electrochromic device with a photovoltaic device. The integration results in so-called self-powered or photo-electrochromic device [116–120]. The photovoltaic component or device is externally incorporated to the periphery of the electrochromic windows [117–120] as part of the device stack. The device is typically based on low band-gap *a*-Si or dye-sensitized solar cells as the power-generating component and transition metal oxides, metal coordination complexes, viologen systems, or conducting polymers as the active electrochrome. The combination of solar cell and electrochromic device results in improved efficiency while saving energy. VTECWs are now preferred over the low e-windows as a result of the awareness of reductions in glare, reflections on the computer monitor, and window luminance. Sbar et al. [110] modeled the performance of commercial office buildings in three US climate zones and demonstrated that electrochromic windows can notably reduce building energy consumption compared to current static glazing systems. Lee et al. summarized the findings from a 15-month monitored pilot demonstration of WO₃ large-area

electrochromic windows with automated controls in a west-facing conference room in Washington DC [121]. The electrochromic windows were automatically controlled in an on-off, fully clear, or fully tinted mode with a dimmable lighting system installed as shown in Fig. 18.



Fig. 18 (a) Interior view of the conference room with upper and lower control zones and (b) Signage instructing occupants on how to switch the windows. (Reprinted from Energy and Buildings, 47, E.S. Lee, E.S. Claybaugh, M. LaFrance, End user impacts of automated electrochromic windows in a pilot retrofit application, 267–284, Copyright (2012), with permission from Elsevier)

Electrochromic materials find applications for transmittance modulation of sunlight control window glazings used in cars and buildings (smart windows), protective eyewear for the military, optical displays, antiglare car rear-view mirrors, controllable aircraft canopies, and storage devices [3, 65, 69, 122]. Materials for electrochromic device applications must possess characteristics such as long-term stability, rapid redox switching, multiple colors within the same material, high coloration efficiency (CE), and high optical transmittance change ($\Delta\%T$). These characteristics play a huge role in electrochromic device performance and it is therefore crucial to obtain a good combination of these characteristics. Usually, the photogenerated current triggers the color of the electrochromic layer [123, 124]. Photo-electrochromic devices using the dye-sensitized solar cell (DSSC) approach have been fabricated based on metal complexes (e.g., Prussian blue) or metal oxide (e.g., WO_3) [116, 125]. The DSSC acts as the solar power generating material while the electrochromic material acts as the active electrochrome in the device. Inorganic materials like WO_3 are the major players in the design of electrochromic devices. They have been extensively studied and found commercial application.

Organic electrochromic devices in which the active electrochromes are polymers have also been reported. Xu et al. reported in a patent, the synthesis, and application of poly(3,4-propylenedioxythiophene) as the active electrochrome in electrochromic devices [126]. Wudl and co-workers reported EDOT derivative which exhibited high coloration efficiency and stability after 5000 switching cycles but only with a contrast ratio of 57% [127, 128]. Ho et al. described the first photo-electrochromic device based on electrochromic polymer PEDOT. The device consists of dual ECD/DSSC all-in-one device. In this device, WO_3 (the conventional metal oxide active electrochrome) was replaced by a film of PEDOT (Fig. 19) [129]. The device reportedly possessed much larger coloration efficiency values than those of other materials like WO_3 . The same group recently reported on alkyl substituted analogue of the parent PEDOT (PProDOT-Et2 (Fig. 15c))-based photo-electrochromic device with enhanced contrasts ($\sim 34\%$ transmittance attenuation) [130].

Despite the fact that inorganic materials have been extensively studied for electrochromic devices and have found commercial application in this field, conducting polymers have become a recent focus of researchers in this field. This is basically due to the fact that all electroactive and conducting polymers are potentially electrochromic materials, more processable than inorganic electrochromic materials, and offer the advantage of a high degree of color tailorability [131]. They have several advantages such as processability, high coloration efficiency, fast switching ability, and multiple colors within the same material over inorganic materials. Inorganic materials offer limited color variation and their use involves complicated processing. The improved advantage of conducting polymers over the inorganic materials for electrochromic device is achieved through the modification of various polymer systems via monomer functionalization and copolymerization [132–135] which result in significant improvement or change in the spectral property and electrochromic response.

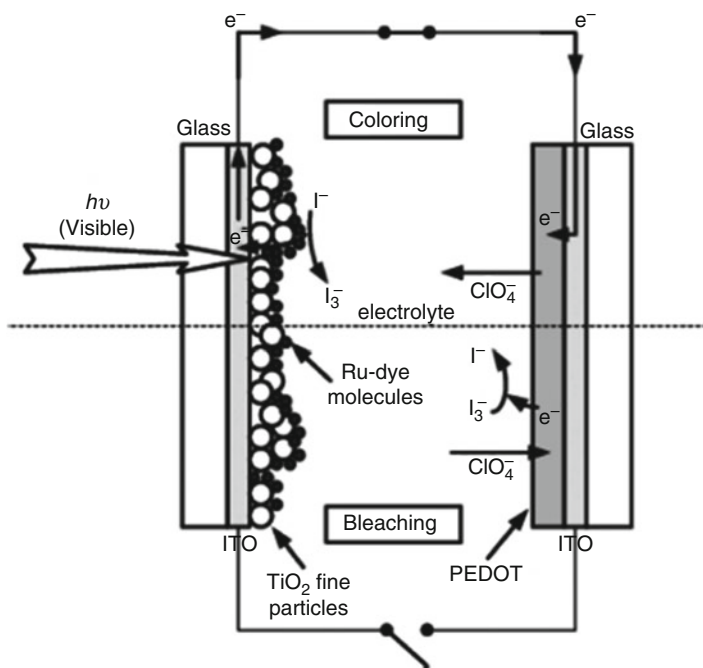


Fig. 19 Photo-electrochemical cell described by Ho et al. (Adapted with permission from Ref. [129])

8 Conclusion

Considering the extent of recent progress in the design of conjugated conducting polymer electrochromes, the current interest of these materials for electrochromics and organic electronics is not unexpected. They have witnessed a surge of interest for their applications in electrochromic devices in the past decade due to their ever-improving physical properties. Given the ability to manipulate the polymer band gap by modifying the molecular structure of its repeat unit and the opportunity to simultaneously tune the colors, ambient-stable materials operating over tens to hundreds of thousands of switching cycles can be achieved. Due to their processability, environmental stability, wide range of colors and spectral properties, electrochromic conducting polymers are on the path to commercialization.

References

1. P.M.S. Monk, R.J. Mortimer, D.R. Rosseinsky, *Electrochromism: Fundamentals and Application* (VCH, Weinheim, 1995)
2. M.M. Verghese, M.K. Ram, H. Vardhan, B.D. Malhotra, S.M. Ashraf, Electrochromic properties of polycarbazole films. *Polymer* **38**, 1625–1629 (1997)

3. C.G. Granqvist, *Handbook of Inorganic Electrochromic Materials* (Elsevier, Amsterdam, 1995)
4. M. Green, The promise of electrochromic systems. *Chem. Ind.* (17), 641–644 (1996)
5. R. J. Mortimer, N. M. Rowley, J. A. McCleverty, T. J. Meyer, M. D. Ward (eds.), *Metal Complexes as Dyes for Optical Data Storage and Electrochromic Materials in: Comprehensive Coordination Chemistry – II: From Biology to Nanotechnology* (Elsevier, Oxford, 2004)
6. M.D. Ward, J.A. McCleverty, Non-innocent behaviour in mononuclear and polynuclear complexes: Consequences for redox and electronic spectroscopic properties. *J. Chem. Soc. Dalton Trans.*, 275–288 (2002)
7. Z.C. Wu, Z.H. Chen, X. Du, J.M. Logan, J. Sippel, M. Nikolou, K. Kamaras, J.R. Reynolds, D.B. Tanner, A.F. Hebard, A.G. Rinzler, Transparent, conductive carbon nanotube films. *Science* **305**, 1273–1276 (2004)
8. R.D. Rauh, Electrochromic windows: an overview. *Electrochim. Acta* **44**, 3165–3176 (1999)
9. P.M.S. Monk, *The Viologens: Physicochemical Properties, Synthesis and Applications of the Salts of 4,40-Bipyridine* (Wiley, Chichester, 1998)
10. T. A. Skotheim, R. L. Elsenbaumer, J. R. Reynolds (eds.), *Handbook of Conducting Polymers* (Marcel Dekker, New York, 1998)
11. J. Heinze, Electronically conducting polymers. *Top. Curr. Chem.* **152**, 1–47 (1990)
12. S.J. Higgins, Conjugated polymers incorporating pendant functional groups – synthesis and characterisation. *Chem. Soc. Rev.* **26**, 247–257 (1997)
13. M. Mastragostino, B. Scrosati (eds.), *Electrochromic Devices in Applications of Electroactive Polymers* (Chapman and Hall, London, 1993)
14. B. Scrosati, B. Scrosati (eds.), *Laminated Electrochromic Displays and Windows in Applications of Electroactive Polymers* (Chapman and Hall, London, 1993)
15. N. Miyata, S. Akiyoshi, Preparation and electrochromic properties of rf-sputtered molybdenum oxide films. *J. Appl. Phys.* **58**, 1651–1655 (1985)
16. L. Guerfi, H. Dao, Electrochromic molybdenum oxide thin films prepared by electrodeposition. *J. Electrochem. Soc.* **136**, 2435–2436 (1989)
17. K. Itaya, K. Shibayama, H. Akahoshi, S. Toshima, Prussian-blue-modified electrodes: an application for a stable electrochromic display device. *J. Appl. Phys.* **53**, 804–805 (1982)
18. D.M. DeLongchamp, P.T. Hammond, High-contrast electrochromism and controllable dissolution of assembled Prussian blue/polymer nanocomposites. *Adv. Funct. Mater.* **14**, 224–232 (2004)
19. D.C. Bookbinder, M.S. Wrighton, Electrochromic polymers covalently anchored to electrode surfaces. Optical and electrochemical properties of a viologen-based polymer. *J. Electrochem. Soc.* **130**, 1080–1087 (1983)
20. R.J. Mortimer, Organic electrochromic materials. *Electrochim. Acta* **44**, 2971–2981 (1999)
21. J. Bard, L.R. Faulkner, *Electrochemical Methods: Fundamentals and Applications* (Wiley, New York, 2001)
22. R.J. Mortimer, J.C. Lindon, G.E. Tranter, J.L. Holmes (eds.), Electronic spectroscopy: spectroelectrochemistry applications, in *Encyclopedia of Spectroscopy and Spectrometry*, vol. 3 (Academic Press, London 1999)
23. R.J. Mortimer, J.C. Lindon, G.E. Tranter, J.L. Holmes (eds.), Electronic spectroscopy: spectroelectrochemistry methods and instrumentation, in *Encyclopedia of Spectroscopy and Spectrometry* (Academic Press, London 1999)
24. M. Jerry, *Advanced Organic Chemistry Reactions, Mechanisms and Structure*, 3rd edn. (Wiley, New York, 1985)
25. H. Shirakawa, E.J. Louis, A.G. MacDiarmid, C.K. Chiang, A.J. Heeger, Synthesis of electrically conducting organic polymers: halogen derivatives of poly(acetylene), $(\text{CH})_x$. *J. Chem. Soc. Chem. Commun.* **16**, 578–579 (1977)
26. S. Lefrant, L.S. Lichtman, M. Temkin, D.C. Fitchten, D.C. Miller, G.E. Whitwell, J.M. Burlich, Raman scattering in $(\text{CH})_x$ and $(\text{CH})_x$ treated with bromine and iodine. *Solid State Commun.* **29**, 191–196 (1979)
27. C.K. Chiang, C.B. Fincher Jr, Y.W. Park, A.J. Heeger, H. Shirakawa, E.J. Louis, S.C. Gau, A.G. MacDiarmid, Electrical conductivity in doped polyacetylene. *Phys. Rev. Lett.* **39**, 1098–1101 (1977)

28. H.A.M. van Mullekom, J.A.J.M. Vekemans, E.E. Havinga, E.W. Meijer, Developments in the chemistry and band gap engineering of donor-acceptor substituted conjugated polymers. *Mater. Sci. Eng.* **32**, 1–40 (1991)
29. A. Pron, P. Rannou, Processible conjugated polymers: from organic semiconductors to organic metals and superconductors. *Prog. Polym. Sci.* **27**, 135–190 (2002)
30. C. Lungenschmied, G. Dennler, G. Czeremuzskin, M. Latrèche, H. Neugebauer, N.S. Sariciftci, Flexible encapsulation for organic solar cells, *Proc. SPIE* 6197, Photonics for Solar Energy Systems 619712 (2006). <https://doi.org/10.1117/1112.662829>
31. J. Heeger, T. A. Skotheim (eds.), *Handbook of Conducting Polymers* (Marcel Dekker, New York, 1986)
32. P. Kar, *Doping in Conjugated Polymers* (Wiley, Hoboken, 2013)
33. N.S. Sariciftci, L. Smilowitz, A.J. Heeger, F. Wudl, Photoinduced electron transfer from a conducting polymer to buckminsterfullerene. *Science* **258**, 1474–1476 (1992)
34. G. MacDiarmid, “Synthetic metals,”: a novel role for organic polymers (Nobel prize 2000 lecture). *Curr. Appl. Phys.* **1**, 269–279 (2001)
35. P. Rannou, A. Gawlicka, D. Berner, A. Pron, M. Nechtschein, D. Djurado, Spectroscopic, structural and transport properties of conducting polyaniline processed from fluorinated alcohols. *Macromolecules* **31**, 3007–3015 (1998)
36. M. Reghu, Y. Cao, D. Moses, A.J. Heeger, Counterion-induced processibility of polyaniline: transport at the metal-insulator boundary. *Phys. Rev. B* **47**, 1758–1764 (1993)
37. H. Naarmann, N. Theophilou, New process for the production of metal-like, stable polyacetylene. *Synth. Met.* **22**, 1–8 (1987)
38. T. Hagiwara, M. Hirasaka, K. Sato, M. Yamamura, Enhancement of the electrical conductivity of polypyrrole film by stretching: influence of the polymerization conditions. *Synth. Met.* **36**, 241–252 (1990)
39. O. Yoon, M. Reghu, D. Moses, A.J. Heeger, Transport near the metal-insulator transition: polypyrrole doped with PF₆. *Phys. Rev. B* **49**, 10851–10863 (1994)
40. K. Gurunathan, A.V. Murugan, R. Marimuthu, U.P. Mulik, D.P. Amalnerkar, Electrochemically synthesised conducting polymeric materials for applications towards technology in electronics, optoelectronics and energy storage devices. *Mater. Chem. Phys.* **61**, 173–191 (1999)
41. G. Zotti, H.S. Nalwa (eds.), Electrochemical synthesis of polyheterocycles and their applications. in *Handbook of Organic Conductive Molecules and Polymers* (Wiley, Chichester, 1997)
42. E.M. Genies, M. Lapkowski, Spectroelectrochemical study of polyaniline versus potential in the equilibrium state. *J. Electroanal. Chem.* **220**, 67–82 (1987)
43. E. Stilwell, S.-M. Park, Electrochemistry of conducting polymers. V. In situ spectroelectrochemical studies of polyaniline films. *J. Electrochem. Soc.* **136**, 427–433 (1989)
44. G. Tourillon, D. Gourier, F. Garnier, D. Vivien, Electron spin resonance study of electrochemically generated polythiophene and derivatives. *J. Phys. Chem.* **88**, 1049–1051 (1984)
45. S.H. Glarum, J.H. Marshall, Electron delocalization in poly(aniline). *J. Phys. Chem.* **92**, 4210–4217 (1988)
46. M. Genies, M. Lapkowski, Electrochemical in situ EPR evidence of two polaron-dipolaron states in polyaniline. *J. Electroanal. Chem.* **236**, 199–208 (1987)
47. J.F. Oudard, R.D. Allendoerfer, R.A. Osteryoung, EPR simultaneous electrochemical measurements on polypyrrole in ambient temperature ionic liquids. *J. Electroanal. Chem.* **241**, 231–240 (1988)
48. F. Genoud, J. Kruszka, M. Nechtschein, M. Zagorska, I. Kulszewicz-Bajer, A. Pron, Electrochemical doping of poly(butylthiophene) and poly(dibutylbithiophene)-in situ EPR and conductivity studies. *J. Chim. Phys.* **87**, 57–66 (1990)
49. N.S. Sariciftci, H. Kuzmany, H. Neugebauer, A. Neckel, Structural and electronic transitions in polyaniline: a Fourier transform infrared spectroscopic study. *J. Chem. Phys.* **92**, 4530–4539 (1990)
50. H. Neugebauer, C. Kvanrmtom, C. Brabec, N.S. Sariciftci, R. Kiebooms, F. Wudl, S. Luzzati, Infrared spectroelectrochemical investigations on the doping of soluble poly(isothianaphthene methine) (pim). *J. Chem. Phys.* **110**, 12108–12115 (1999)

51. S. Srinivasan, H. Neugebauer, N.S. Sariciftci, Electrochemically induced IR/V modes of BeCHA-PPV studied in situ FTIR-ATR spectroscopy. *Synth. Met.* **84**, 635–636 (1997)
52. T. Yohannes, H. Neugebauer, S. Luzzati, M. Catellani, S.A. Jenekhe, N.S. Sariciftci, Multiple electrochemical doping induced insulator to conductor transitions observed in the conjugated ladder polymer polybenzimidazobenzophenanthroline. *J. Phys. Chem.* **104**, 9430–9437 (2000)
53. M. Lapkowski, K. Berrada, S. Quillard, G. Louarn, S. Lefrant, A. Pron, Electrochemical oxidation of polyaniline in nonaqueous electrolytes: in situ Raman spectroscopic studies. *Macromolecules* **28**, 1233–1238 (1995)
54. M. Zagorska, I. Kulszewicz-Bajer, A. Pron, J. Sukiennik, P. Raimond, F. Kajzar, A.-J. Attias, M. Lapkowski, Preparation and spectroelectrochemical characterization of copolymers of 3-alkylthiophenes and thiophenes functionalized with an azo chromophore. *Macromolecules* **31**, 9146–9153 (1998)
55. A. Pron, I. Kulszewicz, D. Billaud, J. Przulski, Reaction of FeCl₃ with polyacetylene, (CH)_x, and poly(p-phenylene), (p-C₆H₄)_x. *J. Chem. Soc. Chem. Commun.* **15**, 783–784 (1981)
56. A. Pron, M. Zagorska, Z. Kucharski, M. Lukasiak, J. Suwalski, Mossbauer spectroscopy studies of polyacetylene doped with iron chloride complexes. *Mater. Res. Bull.* **17**, 1505–1510 (1982)
57. S.C. Gau, J. Milliken, A. Pron, A.G. MacDiarmid, A.J. Heeger, Organic metals. New class of p-type dopants converting polyacetylene, (CH)_x into the metallic state. *J. Chem. Soc. Chem. Commun.* **15**, 662–663 (1979)
58. N.F. Mot, Conduction in non-crystalline materials. *Philos. Mag.* **19**, 835–852 (1969)
59. W.P. Su, J.R. Schrieffer, A.J. Heeger, Solitons in polyacetylene. *Phys. Rev. Lett.* **42**, 1698–1701 (1979)
60. M. Nechtschein, F. Devreux, F. Genoud, E. Vieil, J.M. Pernaut, E. Genies: Polarons, bipolarons and charge interactions in polypyrrole: physical and electrochemical approaches. *Synth. Met.* **15**, 59–78 (1986)
61. P. Mungkalodom, N. Paradee, A. Sirivat, P. Hornnirun, Synthesis of poly(2,5-dimethoxyaniline) and electrochromic properties. *Mater. Res.* **18**, 669–676 (2015)
62. J.L. Bredas, R. Silbey, D.S. Boudreaux, R.R. Chance, Chain-length dependence of electronic and electrochemical properties of conjugated systems: polyacetylene, polyphenylene, polythiophene, and polypyrrole. *J. Am. Chem. Soc.* **105**, 6555–6559 (1983)
63. R.J. Mortimer, A.L. Dyer, J.R. Reynolds, Electrochromic organic and polymeric materials for display applications. *Displays* **27**, 2–18 (2006)
64. A. Argun, P.-H. Aubert, B.C. Thompson, I. Schwendeman, C.L. Gaupp, J. Hwang, N.J. Pinto, D.B. Tanner, A.G. MacDiarmid, J.R. Reynolds, Multicolored electrochromism in polymers: structures and devices. *Chem. Mater.* **16**, 4401–4412 (2004)
65. J.C. Lacroix, K.K. Kanazawa, A. Diaz, Polyaniline: a very fast electrochromic material. *J. Electrochem. Soc.* **136**, 1308–1313 (1989)
66. J.C. Gustafsson, B. Liedberg, O. Inganäs, In situ spectroscopic investigations of electrochromism and ion transport in a poly(3,4-ethylenedioxythiophene) electrode in a solid state electrochemical cell author links open the overlay panel. *Solid State Ionics* **69**, 145–152 (1994)
67. D. Kumar, M. Welsh, M.C. Morvant, F. Piroux, K.A. Abboud, J.R. Reynolds, Conducting poly(3,4-alkylenedioxythiophene) derivatives as fast electrochromics with high-contrast ratios. *Chem. Mater.* **10**, 896–902 (1998)
68. M.-A. De Paoli, G. Casalbore-Miceli, E.M. Giroto, W.A. Gazotti, All polymeric solid state electrochromic devices. *Electrochim. Acta* **44**, 2983–2991 (1999)
69. C. Thompson, P. Schottland, K. Zong, J.R. Reynolds, In situ colorimetric analysis of electrochromic polymers and devices. *Chem. Mater.* **12**, 1563–1571 (2000)
70. I. Schwendeman, R. Hickman, G. Sönmez, P. Schottland, K. Zong, D.M. Welsh, J.R. Reynolds, Enhanced contrast dual polymer electrochromic devices. *Chem. Mater.* **14**, 3118–3122 (2002)
71. W. Lu, A.G. Fadeev, B.H. Qi, E. Smela, B.R. Mattes, J. Ding, G.M. Spinks, J. Mazurkiewicz, D.Z. Zhou, G.G. Wallace, D.R. MacFarlane, S.A. Forsyth, M. Forsyth, Use of ionic liquids for pi-conjugated polymer electrochemical devices. *Science* **297**, 983–987 (2002)

72. R.J. Mortimer, *Electrochromic materials*. *Chem. Soc. Rev.* **26**, 147–156 (1997)
73. A. Nekrasov, V.F. Ivanov, A.V. Vannikov, Analysis of the structure of polyaniline absorption spectra based on spectroelectrochemical data. *J. Electroanal. Chem.* **482**, 1711–1727 (2000)
74. T.-H. Lin, K.-C. Ho, A complementary electrochromic device based on polyaniline and poly(3,4-ethylenedioxythiophene). *Sol. Energy Mater. Sol. Cells* **90**, 506–520 (2006)
75. S.J. Yoo, J. Cho, J.W. Lim, S.H. Park, J. Jang, Y.-E. Sung, High contrast ratio and fast switching polymeric electrochromic films based on water-dispersible polyaniline-poly(4-styrenesulfonate) nanoparticles. *Electrochem. Commun.* **12**, 164–167 (2010)
76. J. Jang, J. Ha, J. Cho, Fabrication of water-dispersible polyaniline-poly(4-styrenesulfonate) nanoparticles for inkjet-printed chemical-sensor applications. *Adv. Mater.* **19**, 1772–1775 (2007)
77. M. Gazard, J.C. Dubois, M. Champagne, F. Garnier, G. Tourillon, Electrooptical properties of thin films of polyheterocycles. *J. Phys. Colloq.* **44**, C3-537-C533-542 (1983)
78. M.A. Druy, R.J. Seymour, Poly(2,2' - Bithiophene): An electrochromic conducting polymer. *J. Phys. Colloq.* **44**, C3-595-C593-598 (1983)
79. M. Aizawa, S. Watanabe, H. Shinohara, H. Shirakawa, Electrochemical cation doping of a polythietylene film. *J. Chem. Soc. Chem. Commun.* (5), 264–265 (1985)
80. J. Zmija, M.J. Malachowski, New organic electrochromic materials and their applications. *J. Achiev. Mater. Manuf. Eng.* **48**, 14–23 (2011)
81. M. Dietrich, J. Heinze, G. Heywang, F. Jonas, Electrochemical and spectroscopic characterization of polyalkylenedioxythiophenes. *J. Electroanal. Chem.* **369**, 87–92 (1994)
82. P.M. Beaujuge, S.V. Vasilyeva, S. Ellinger, T.D. McCarley, J.R. Reynolds, Unsaturated linkages in dioxothiophene-benzothiadiazole donor-acceptor electrochromic polymers: the key role of conformational freedom. *Macromolecules* **42**, 3694–3706 (2009)
83. G. Heywang, F. Jonas, Poly(alkylenedioxythiophene)s – new, very stable conducting polymers. *Adv. Mater.* **4**, 116–118 (1992)
84. H. Sonmez, B. Sonmez, C.K.F. Shen, F. Wudl, Red, green, and blue colors in polymeric electrochromics. *Adv. Mater.* **16**, 1905–1908 (2004)
85. J. Sankaran, R. Reynolds, High-contrast electrochromic polymers from alkyl-derivatized poly(3,4-ethylenedioxythiophenes). *Macromolecules* **30**, 2582–2588 (1997)
86. C. Schwendeman, L. Gaupp, J.M. Hancock, L.B. Groenendaal, J.R. Reynolds, Perfluoralkanoate-substituted PEDOT for electrochromic device applications. *Adv. Funct. Mater.* **13**, 541–547 (2003)
87. P. Lock, S.G. Im, K.K. Gleason, Oxidative chemical vapor deposition of electrically conducting poly 3,4 ethylenedioxythiophene (PEDOT) films. *Macromolecules* **39**, 5326–5329 (2006)
88. S.I. Cho, R. Xiao, S.B. Lee, Electrochemical synthesis of poly(3,4-ethylenedioxythiophene) nanotubes towards fast window-type electrochromic devices. *Nanotechnology* **18**, 405705 (2007)
89. P. Manisankar, C. Vedhi, G. Selvanathan, H. Gurumalles Prabu, Influence of surfactants on the electrochromic behavior of poly(3,4-ethylenedioxythiophene). *J. Appl. Polym. Sci.* **104**, 3285–3291 (2007)
90. M. Deepa, S. Bhandari, M. Arora, R. Kant, Electrochromic response of nanostructured poly(3,4-ethylenedioxythiophene) films grown in an aqueous micellar solution. *Macromol. Chem. Phys.* **209**, 137–149 (2008)
91. S.I. Cho, S.B. Lee, Fast electrochemistry of conductive polymer nanotubes: synthesis, mechanism, and application. *Acc. Chem. Res.* **41**, 699–707 (2008)
92. T.-H. Su, S.-H. Hsiao, G.-S. Liou, Novel family of triphenylamine-containing, hole-transporting, amorphous, aromatic polyamides with stable electrochromic properties. *J. Polym. Sci. Part A Polym. Chem.* **43**, 2085–2098 (2005)
93. G.-S. Liou, S.-H. Hsiao, T.-H. Su, Synthesis, luminescence and electrochromism of aromatic poly(amine–amide)s with pendent triphenylamine moieties. *J. Mater. Chem.* **15**, 1812–1820 (2005)

94. G.-S. Liou, Y.-L. Yang, Y.O. Su, Synthesis and evaluation of photoluminescent and electrochemical properties of new aromatic polyamides and polyimides with a kink 1,2-phenylenediamine moiety. *J. Polym. Sci. Part A Polym. Chem.* **44**, 2587–2603 (2006)
95. G.-S. Liou, H.-W. Chen, H.-J. Yen, Poly(amine-amide-imide)s bearing pendent N-carbazolyphenyl moieties: synthesis and electrochromic properties. *Macromol. Chem. Phys.* **207**, 1589–1598 (2006)
96. G.-S. Liou, S.-H. Hsiao, W.-C. Chen, H.-J. Yen, A new class of high T_g and organosoluble aromatic poly(amine-1,3,4-oxadiazole)s containing donor and acceptor moieties for blue-light-emitting materials. *Macromolecules* **39**, 6036–6045 (2006)
97. H.-J. Yen, H.-Y. Lin, G.-S. Liou, Novel starburst triarylamine-containing electroactive aramids with highly stable electrochromism in near-infrared and visible light regions. *Chem. Mater.* **23**, 1874–1882 (2011)
98. C.-W. Chang, G.-S. Liou, S.-H. Hsiao, Highly stable anodic green electrochromic aromatic polyamides: synthesis and electrochromic properties. *J. Mater. Chem.* **17**, 1007–1015 (2007)
99. G.-S. Liou, C.-W. Chang, Highly stable anodic electrochromic aromatic polyamides containing *N,N,N',N'*-tetraphenyl-*p*-phenylenediamine moieties: synthesis, electrochemical, and electrochromic properties. *Macromolecules* **41**, 1667–1674 (2008)
100. S.-H. Hsiao, G.-S. Liou, Y.-C. Kung, H.-J. Yen, High contrast ratio and rapid switching electrochromic polymeric films based on 4-(dimethylamino)triphenylamine-functionalized aromatic polyamides. *Macromolecules* **41**, 2800–2808 (2008)
101. C.-W. Chang, G.-S. Liou, Novel anodic electrochromic aromatic polyamides with multi-stage oxidative coloring based on *N,N,N',N'*-tetraphenyl-*p*-phenylenediamine derivatives. *J. Mater. Chem.* **18**, 5638–5646 (2008)
102. C.-W. Chang, H.-J. Yen, K.-Y. Huang, J.-M. Yeh, G.-S. Liou, Novel organosoluble aromatic polyimides bearing pendant methoxy-substituted triphenylamine moieties: synthesis, electrochromic, and gas separation properties. *J. Polym. Sci. Part A Polym. Chem.* **46**, 7937–7949 (2008)
103. H.-J. Yen, G.-S. Liou, Solution-processable novel near-infrared electrochromic aromatic polyamides based on electroactive tetraphenyl-*p*-phenylenediamine moieties. *Chem. Mater.* **21**, 4062–4070 (2009)
104. H.-J. Yen, G.-S. Liou, Novel blue and red electrochromic poly (azomethine ether)s based on electroactive triphenylamine moieties. *Org. Electron.* **11**, 299–310 (2010)
105. S. Beaupré, J. Dumas, M. Leclerc, Toward the development of new textile/plastic electrochromic cells using triphenylamine-based copolymers. *Chem. Mater.* **18**, 4011–4018 (2006)
106. A. Argun, A. Cirpan, J.R. Reynolds, The first truly all-polymer electrochromic devices. *Adv. Mater.* **15**, 1338–1341 (2003)
107. World business council for sustainable development, 2009. Energy performance in buildings: transforming the market **IS 2009–65**, (2009)
108. D. Arasteh, S. Selkowitz, J. Apte, M. LaFrance, Zero energy windows, in *Proceedings of the 2006 ACEEE Summer study on energy efficiency in buildings*, Pacific Grove, 2006
109. U.S. Department of Energy, Energy Efficiency and Renewable Energy, 2011 Buildings energy data book, prepared by D&R international, Ltd., March 2012
110. N.L. Sbar, L. Podbelski, H.M. Yang, B. Pease, Electrochromic dynamic windows for office buildings. *Int. J. Sustain. Built Environ.* **1**, 125–139 (2012)
111. C.G. Granqvist, *Switchable Glazing Technology: Electrochromic Fenestration for Energy-Efficient Buildings, in Nearly Zero Energy Building Refurbishment* (Springer, London, 2013)
112. C. M. Lampert, C. G. Granqvist (eds.), *Large-Area Chromogenics: Materials and Devices for Transmittance Control* (SPIE Optical Engineering Press, Bellingham, 1990)
113. C.M. Lampert, Large-area smart glass and integrated photovoltaics. *Sol. Energy Mater. Sol. Cells* **76**, 489–499 (2003)
114. G.P. Smestad, C.M. Lampert, Event report – solar power 2006, San José, CA. *Sol. Energy Mater. Sol. Cells* **91**, 440–444 (2007)

115. S. Lee, S.E. Selkowitz, R.D. Clear, D.L. DiBartolomeo, J.H. Klems, L.L. Fernandes, G.J. Ward, V. Inkarojrit, M. Yazdaniyan, *Advancement of Electrochromic Windows, California Energy Commission*. PIER, 2006 Publication number CEC-500-2006-052
116. C. Bechinger, S. Ferrere, A. Zaban, J. Sprague, B.A. Gregg, Photoelectrochromic windows and displays. *Nature* **383**, 608–610 (1996)
117. S.K. Deb, S.-H. Lee, C.E. Tracy, J.R. Pitts, B.A. Gregg, H.M. Branz, Stand-alone photovoltaic-powered electrochromic smart window. *Electrochim. Acta* **46**, 2125–2130 (2001)
118. A. Hauch, A. Georg, S. Baumgärtner, U.O. Krašovec, B. Orel, New photoelectrochromic device. *Electrochim. Acta* **46**, 2131–2136 (2001)
119. K.-S. Ahn, S.J. Yoo, M.-S. Kang, J.-W. Lee, Y.-E. Sung, Tandem dye-sensitized solar cell-powered electrochromic devices for the photovoltaic-powered smart window. *J. Power Sources* **168**, 533–536 (2007)
120. H. Jensen, F. Dam, J.R. Reynolds, A.L. Dyer, F.C. Krebs, Manufacture and demonstration of organic photovoltaic-powered electrochromic displays using roll coating methods and printable electrolytes. *J. Polym. Sci. Part B Polym. Phys.* **50**, 536–545 (2012)
121. S. Lee, E.S. Claybaugh, M. LaFrance, End user impacts of automated electrochromic windows in a pilot retrofit application. *Energ. Buildings* **47**, 267–284 (2012)
122. D.R. Rosseinsky, R.J. Mortimer, Electrochromic systems and the prospects for devices. *Adv. Mater.* **13**, 783–793 (2001)
123. S. Kuwabata, N. Takahashi, S. Hirao, H. Yoneyama, Light image formations on deprotonated polyaniline films containing titania particles. *Chem. Mater.* **5**, 437–441 (1993)
124. S. Nishizawa, H. Kuwabata, Yoneyama: photoimage formation in a TiO₂ particle-incorporated prussian blue film. *J. Electrochem. Soc.* **143**, 3462–3465 (1996)
125. A. Hauch, A. Georg, U. Opar Krašovec, B. Orel, Comparison of photoelectrochromic devices with different layer configurations. *J. Electrochem. Soc.* **149**, H159–H163 (2002)
126. C. Xu, M. Taya, Electrochromic organic, polymer synthesis and devices utilizing electrochromic organic polymers, US Patent 7,038,828 B2, 2006
127. G. Sonmez, H. Meng, Q. Zhang, F. Wudl, A highly stable, new electrochromic polymer: Poly(1,4-bis(2-(3'-4'-ethylenedioxy)thienyl)-2-methoxy-5-2''-ethylhexyloxybenzene). *Adv. Funct. Mater.* **13**, 726–731 (2003)
128. G. Sonmez, H. Meng, F. Wudl, Organic polymeric electrochromic devices: polychromism with very high coloration efficiency. *Chem. Mater.* **16**, 574–580 (2004)
129. J.-Y. Liao, K.-C. Ho, A Photoelectrochromic device using a pedot thin film. *J. New Mater. Electrochem. Syst.* **8**, 37–47 (2005)
130. C.-Y. Hsu, K.-M. Lee, J.-H. Huang, K.R. Justin Thomas, J.T. Lin, K.-C. Ho, A novel photoelectrochromic device with dual application based on poly(3,4-alkylenedioxythiophene) thin film and an organic dye. *J. Power Sources* **185**, 1505–1508 (2008)
131. D. Brotherson, D.S.K. Mudigonda, J.M. Osborn, J. Belk, J. Chen, D.C. Loveday, J.L. Boehme, J.P. Ferraris, D.L. Meeker, Tailoring the electrochromic properties of devices via polymer blends, copolymers, laminates and patterns. *Electrochim. Acta* **44**, 2993 (1999)
132. S.A. Sapp, G.A. Sotzing, J.L. Reddinger, J.R. Reynolds, Rapid switching solid state electrochromic devices based on complementary conducting polymer films. *Adv. Mater.* **8**, 808–811 (1996)
133. J. Roncali, Synthetic principles for bandgap control in linear π -conjugated systems. *Chem. Rev.* **97**, 173–206 (1997)
134. S.A. Sapp, G.A. Sotzing, J.R. Reynolds, High contrast ratio and fast-switching dual polymer electrochromic devices. *Chem. Mater.* **10**, 2101–2108 (1998)
135. D.S.K. Mudigonda, D.L. Meeker, D.C. Loveday, J.M. Osborn, J.P. Ferraris, Compositional control of electrochromic properties in copolymers of N-vinylcarbazole and N-phenyl-2-(5'-vinyl-2'-thienyl)-5-(2''-thienyl)-pyrrole. *Polymer* **40**, 3407–3412 (1999)



Shah Mohammed Reduwan Billah

Contents

1	General Aspects of Textile Coating	827
1.1	Advanced Functional Coated Textiles	828
1.2	Coated Textiles for Conventional and High-Tech Applications	829
2	Textile Fabrics	830
3	Different Types of Coatings and Application Methods	831
3.1	Knife Coating	831
3.2	Pad Coating	832
3.3	Screen Printing/Coating	833
3.4	Digital Coating Using Inkjet Technology	833
3.5	Other Coating Techniques Usually Used in Textile Coatings	835
3.6	Recent Technological Advancements and Their Impacts on Textile Coatings	837
4	Film Formation	843
5	Polymers and Additives for Typical Textile Coatings	844
5.1	Selected Characters of Commonly Used Polymers in Textile Coatings	845
5.2	Thermoplastic Polymers	846
5.3	Thermosetting Polymers	847
5.4	Rubbers and Their Uses in Textile Coatings	847
6	Textile Coating Formulations	848
7	Functional Coatings on Textiles	848
8	High Thermal-Resistant Coatings	849
9	Fire Retardant Coatings	849
9.1	Application of Flame Retardant Finishes by Coating	850
10	Silicones in Textile Fabric Coatings	850
10.1	Surface Active Agents and Chemical Softeners	851
11	Scratch- and Abrasion-Resistant Coatings	852

S. M. R. Billah (✉)

University of East London, Stratford Campus, London, UK

CCIRA UK Limited, Galashiels, UK

Department of Chemistry, Durham University, Durham, UK

School of Textiles and Design, Heriot-Watt University, Galashiels, UK

e-mail: reduwan.shah@gmail.com

12	Self-Healing Coatings	853
13	Antibacterial Coatings	854
14	Antifouling Coatings	854
15	Enzymatic Biocoatings	855
16	Antimicrobial Coating	855
17	Microencapsulation in Coating and Finishing of Textiles	856
18	Conductive Coatings	856
19	Self-Assembled Nanophase Coatings	857
20	Coated Breathable Fabrics	857
21	High-Tech Superhydrophobic-Coated Textiles	859
21.1	Design, Development, and Evaluation of Superhydrophobic Coatings	860
22	Powder Coating Technology and Coated Textiles	862
22.1	Epoxy Powder Coatings	863
22.2	Hybrid Powder Coatings	863
22.3	Polyester Powder Coatings	864
22.4	Acrylic Powder Coatings	864
22.5	UV-Curable Powder Coatings	864
23	Photonic Coatings on Textiles	865
24	Textile Finishing and Textile Coatings in Future	865
24.1	Main Influencing Factors for Future Developments in Textile Coating and Finishing	867
25	Conclusion and Perspectives	868
	References	868

Abstract

Textile coatings usually provide material layers which adhere to the textile structures. A typical textile coating formulation generally contains polymeric binder(s) along with other additives (such as colorants, adhesion promoter, biocide, plasticizers, etc.) which are applied in the form of a solution or a dispersion or a paste or a similar fashion using a spreading technique onto a textile fabric. Different types of techniques are commonly used for textile coatings, for examples, spray coating techniques, the application of nanoscale technologies, biotechnology, and plasma technology. Certain coating technologies including digital coating technology have many industrial potentials in order to produce higher performance coated textiles with a variety of conventional and functional properties. Textiles with multifunctionalities are increasingly demanded as a part of advanced and future marketing strategies, for instance, garments and technical textiles for outdoor environments can have novelty and durable self-cleaning properties at the same time. Various ways are usually used to impart novelty and functionality into coated textiles. For example, sol-gel chemistry is one of many techniques which can be used to produce superhydrophobic coated textiles suitable for many high-tech and general application purposes. This chapter provides selective pieces of information on different types of popular textile coatings and related specific features which have pronounced impacts on the behaviors of coated textiles. It also briefly provides some selective pieces of information on different advancements in textile coatings in

consideration to the applications of new advanced techniques as well as frequently used general coating techniques (such as spraying, padding, etc.) to produce high-performance coated textiles for conventional and high-tech applications.

1 General Aspects of Textile Coating

Textile coating is one of very highly important topics for aesthetic as well as functional modification of the textile surface in order to produce high-quality textiles and their products suitable for various applications. Additionally, the development of conventional and functional coated textiles with multiple properties have potential applications in different areas including – (a) protective and casual clothing, (b) security, (c) mobility, (d) lightweight construction, (e) geotechnology, (f) environmental technology, (g) health, (h) communication and emotion, (i) fashion and designs, (j) automobile, and (k) filtration. Besides these, coated textiles have diverse range of other applications as well. For example, a military tent can be made of a material that combines nylon fabric with a neoprene coat, whereas a urethane-coated polyester cloth can be used to make the inflatable chutes installed at the emergency exits from the aircrafts. For textile coatings, different types of coating formulations are used. For example, typical textile coating formulations usually contain polymeric binder(s) along with other additives (such as colorants, adhesion promoter, biocide, plasticizers, etc.). Generally, a coating formulation is applied onto the textile surface in the form of a solution or a dispersion or a paste or a similar fashion using a suitable spreading technique [1–3]. In addition, during different textile coating formulations, a wide range of polymers are practically in use for a variety of purposes. For a typical textile coating based on a polymeric system, two or more layers are usually applied on textiles where at least one of the layer is a textile fabric and the other is the thin continuous polymeric layer along with other additives. The nature of each layer and their combined characters determine the overall properties of the coated system. In this context, the textile substrate provides the required strength (such as tear and tensile strengths), elongational, and dimensional properties of the system. The polymer coat provides different desired properties, some of which include – (a) the required resistance to penetration and impermeability (to liquids, gases, and dust particles), (b) improving fabric abrasion, (c) providing other required character on the coated textile surfaces, (d) increasing conductivity, (e) providing shielding from electromagnetic interference/radiofrequency interference (EMI/RFI), (f) introducing antimicrobial properties, (g) modifying the appearance for decorative purposes [2–5]. The layers within the coated textiles are bonded to each other in situ by the adhesive properties of the layers in order to produce “coated fabrics,” or additional adhesives which are sometimes also used to produce “laminated fabric.” Besides this, coating on textiles can be carried out in a variety of ways. For example, in order to produce a typically coated textile, different steps can be used successively,

which include – (a) direct spreading of the thick liquid layer of coating formulation or paste of polymer in liquid form over the textile surface, (b) evaporating the thick liquid layer or liquid in the polymer paste to leave the polymer on the fabric (for solvent-based system), or (c) allowing the transformation into a coat in the case of plastisol- or dispersion-based system (both of these processes are usually carried out in special dryer or ovens). In addition, required level of crosslinking of the polymer coat is achieved during this drying step (also called curing) which helps to enhance durability to abrasion and resistance to solvents (and water). Advantages of this processing type include the production of coats without mechanical or thermal stresses. However, removing large amounts of solvent or dispersion medium involve time and energy which are often very expensive and not environmentally friendly [5–14].

1.1 Advanced Functional Coated Textiles

Textiles are a ubiquitous part of human life which can be incorporated with a number of functional materials in order to provide new useful functional and high-tech application properties. In order to produce advanced functional coated textile, a wide range of functional materials and polymers can be used for textile coatings. Some of these functional materials include – (a) environmentally responsive materials (such as photoresponsive, thermally responsive, electrically responsive, magnetically responsive, biologically responsive materials), (b) chromic sensoric materials (such as photochromic, thermochromic, ionochromic, electrochromic, piezochromic, mechanochromic materials), and (c) other sensoric materials or polymers. For example, photonic materials are widely used in advanced textiles for many high-tech applications [1, 2]. Photonic coatings have the capability to provide some important functional features on photonic-coated textiles useful for various applications, such as in electronic textile applications. The combination of textiles with electronics for producing electronic textile systems provides many potentials in new emerging application fields. The development of photonic polymer coatings can change their volume or surface topology in a reversible, dynamic fashion when exposed to an external stimulus. For instance, topographic response can be established by using hydrogels or liquid crystal polymer networks by the change of the surface corrugation in response to light (by which, various functional coating characters can be modulated, for example, wettability and/or mechanical friction). Similarly, volume changes in photonic coatings can be produced by different stimuli that can lead to a change in light reflection [1–4, 8–20].

Polymer coatings as well as textile coatings have a significant importance in our everyday life which protect everyday objects from environmental influences. In addition, coatings are also widely used for aesthetic purposes which include – (a) adhesion-promotion/reduction and (b) antireflection or antifouling. These functional characters are often determined by the surface topography. Currently, extensive research interests are focused on the improvement in the design or formulation of stimulus-responsive polymer-based coating systems which are

mostly dynamic in nature rather than on their static properties. In this type of coating systems, the changes in characteristic properties in response to an external stimulus (where the functional properties can be adjusted autonomously) depend on user needs or on environmental changes. These types of smart coatings have important potentials in meeting social challenges in many areas including – (a) sustainable energy, (b) health, (c) food safety, (d) sensors, (e) electronics, (f) communication. For instance, the photo-induced dimensional or structural change has many attractive appealing features since it can be done locally without contact and without changing the immediate chemical environment of the polymer coatings or the integration of electrodes. Photoexposure has the potential in order to lead to the structural modification of a polymeric network to generate a change in the surface topography. Additionally, photo-induced changes in the surface roughness or the hydrophilicity of materials are highly attractive because they can alter their wettability and/or also can controllably change in their nature of adhesion. Photoresponsive coatings are sensitive to sunlight, and they have the potential to develop sun-tracking materials or materials with self-cleaning properties involving structural changes [1, 2, 5, 18–35].

1.2 Coated Textiles for Conventional and High-Tech Applications

Coated textiles have huge application potentials. Polymer coating on textiles can be on one or both side(s). Textile coatings are very important on different types of applications of textile substrates, some of which include – (a) specific textile products usually used in aerospace, automotive (e.g., airbags), (b) chemical processing, (c) E-textiles, (d) geotextiles, (e) military textiles, (f) filtration and heating, venting and air conditioning applications, (g) textile products used in carpeting, (h) protective clothing, (i) fuel cells, (j) home furnishing applications, (k) inflatable boats, (l) folding kayaks, (m) gloves, (n) snowshoes, (o) tents, and (p) fuel tanks. Overall properties of a polymer-coated textiles dependent on a number of things including on the nature of textiles, polymers used in coatings along with the nature of additives and application techniques used. The nature of textiles plays a very vital role on the performance of polymer-coated textiles. Some of the usually used textiles for coating with polymers include (a) natural textiles (such as cotton, wool, silk, hemp, jute, linen); (b) synthetic polymer-based textiles (for examples, polyester, nylon, viscose, acetate/triacetate, acrylic/modacrylic, aramid); and (c) other polymeric substrates, such as elastomeric, fluoropolymer, polyamide, olefin, polyolefin, polyester, polyethylene, Rayon, styrene acrylonitrile, and polyvinyl chloride. Certain type of fiber glass-based substrates (such as fibers of glass, fiberglass, E-glass, S-glass, rock wool, slag wool, ceramic, boron, carbon, graphite, silica, metallic fibers, and zirconia-based fibers) can also be coated with particular types of polymer-coating systems. In all of these cases, polymers play a dominating part for textile coatings [27, 36–66].

As a result, a solid background and knowledge of polymer science and technology in addition to knowledge of textile technology and the principles of chemical engineering is very important for producing highly viable and robust textile coating

formulations suitable for different industrial scale exploitations. However, a detail discussion on all of these areas is beyond the scope of this current chapter; it only provides selected brief information on the components of the textile coating systems as well as short discussions on different types of textile coatings, chemistry and technology involved with these methods, along with their applications in textile coatings.

2 Textile Fabrics

The nature of a textile fabric where the textile coating is applied is one of the main determinant on the characters of coating system. A variety of coating techniques are practically in use for textile coatings, for example, conventional, continuous coating methods use substantial tension on textile fabrics, more specifically woven textiles need more applied tension as they show relatively more dimensional stability. Fabrics made from staple fibers, especially cotton, are the most commonly used textile substrate for coating for a long time [4, 43, 60]. However, at present fabrics made from synthetic filaments are most predominant for their use in textile coatings mainly due to their strength and easy processing. Figure 1 illustrates three basic types of textile constructions which are – (a) a woven, (b) a weft-knitted, and (c) a warp-knitted textile fabric. In a plain-woven fabric construction, each weft yarn goes between every warp yarn, where every other weft insertion takes the opposite sides of the warp yarns. This is also the most dimensionally stable woven construction as this system locks every yarn in place. The density of the fabric depends on the thickness (such as dtex) of the yarns and how tightly the yarns are packed, and it also has a control on the rigidity of the fabric. Weft-knitted fabrics can be produced by using flat- and circular-knitting techniques. In principal, a single yarn bobbin can be used as it is made to form loops (held by needles) into which new loops of the same yarn can be formed and the yarn is led from side to side in flat-knitting and circularly

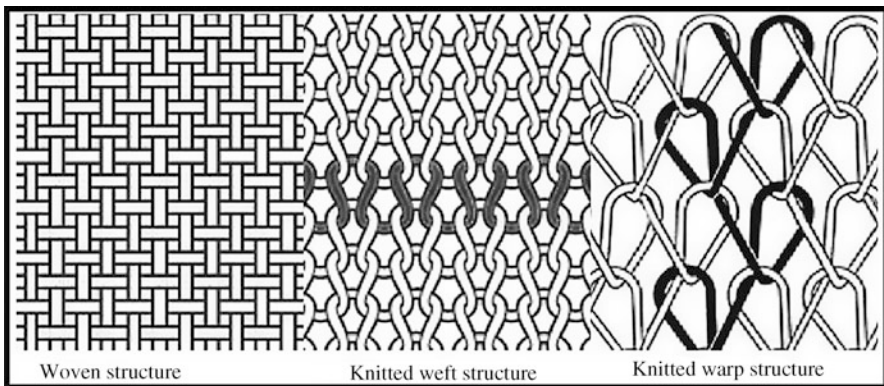


Fig. 1 Illustration of plain textile constructions: (a) woven structure, (b) knitted weft structure, (c) knitted warp structure

upwards in circular knitting. Particularly, knitted fabrics and plain weft-knits have tendency to show deformation which makes the fabrics easy to fit onto a human body; however, this property may be a drawback when stability and rigidity is required. Warp knitting is an intermediate between weaving and weft knitting, but it is probably the most versatile construction technique of textile fabrics where the fabrics can be anything from the finest lace to the most robust automotive interior. In this case, yarns are vertically placed side-by-side, similar to the warp yarns in weaving and placed in guiders in order to allow them to be interlocked with each other horizontally. Additionally, the fabrics often mechanically outshine woven- and weft-knitted fabrics. Synthetic filaments are mainly required for this type of construction for avoiding entanglements. Many noble characters can also be incorporated with this system according to end uses. This makes them ideal for many high-tech applications, some of which include – (a) sports items, (b) products for automotive interior, personal protective equipment, and (c) geo and greenhouse fabrics [4].

3 Different Types of Coatings and Application Methods

Coatings are protective and/or decorative compositions that dry to a cohesive, adherent, tack-free film when applied to a substrate (such as textile substrates). Textile coatings contain polymeric binders along with other additives (such as colorants, adhesion promoter, biocide, plasticizers, etc.). Based on the nature of components used in the coating formulations and also on the objectives of the coated surfaces where they are applied, textile coatings can be of different types. For examples, hydrophobic and hydrophilic coatings; organic and inorganic coatings; aesthetic and functional coatings; conventional and technical coatings; and metallic and nonmetallic coatings. Coating mechanisms also depend on the nature of coating formulations and also on the nature of the substrates [4, 57]. Various types of coating techniques are usually used in textile coatings where main types include – (a) pad coating, (b) direct coating or knife coating, (c) inkjet coating technology, (d) atomic layer deposition, (e) chemical and physical vapor deposition, (f) UV coating, (g) plasma coating, (h) magnetron sputtering, (i) screen printing, (j) sol-gel coating, (k) coating by using evaporation techniques, (l) coating by layer-by-layer deposition, and (m) coating by using general or specific spraying technique [4, 56–59].

3.1 Knife Coating

Knife coating, or direct coating, is one of the most widely used technique for textile coatings. In principle, a blade is used to smear out a thickened polymeric formulation across a moving textile substrate. When the substrate rests on a roll beneath the blade the technique is called knife-over-roll (Fig. 2). Other setups include – knife-over-air (or floating knife) and knife-over-blanket. Different setups mainly deal with the penetration of the coating into the textile substrate where the knife-over-roll yields

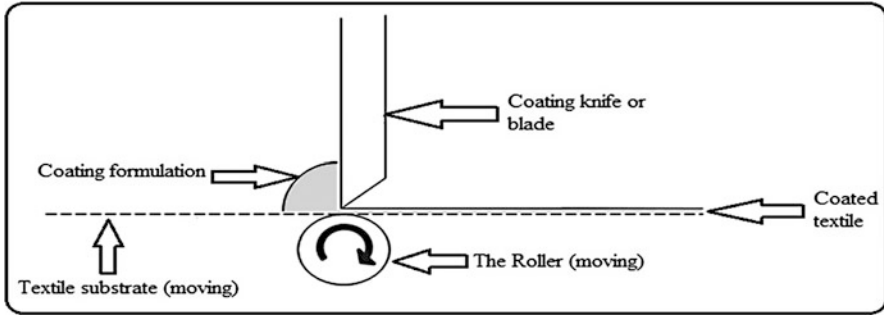


Fig. 2 Schematic illustration of knife-over-roll coating

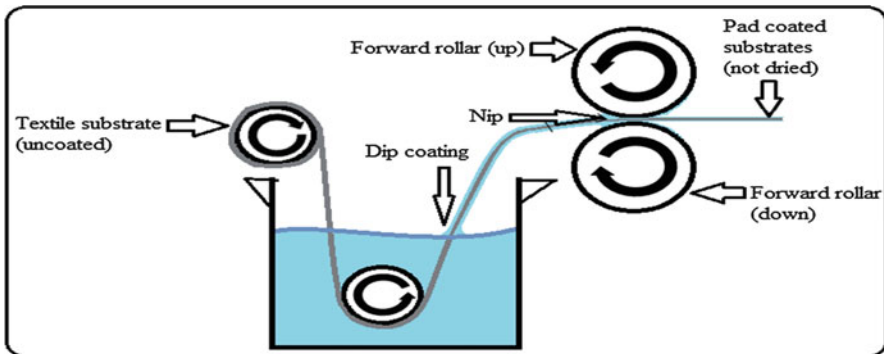


Fig. 3 Schematic illustration of pad (or pad-mangle) coating

the highest degree of penetration and floating knife causes the lowest. In this case, blade angle, gap height, coating speed, and the shear viscosity of the formulation are also important for the degree of penetration which, in turn, affect the adhesion of the coating to the substrate. These parameters are affected by other forces related to textile coatings some of which include – (a) tension, (b) air flow, (c) pressure, (d) temperatures, (e) time, and (f) relative humidity [4, 57].

3.2 Pad Coating

Pad coating (also known as impregnation) is a dipping procedure where excess formulation is squeezed out by the rollers from the textile fabrics. A typical pad coating arrangement is demonstrated in Fig. 3. The method allows coating to penetrate into the interstices in the textile fabric and between the fibers in the yarn. In this case, the coating is on the entire fabric, whereas in most other cases, coating methods lead to a more one-sided coating. The amount of applied material to the fabric depends on coating viscosity as well as the speed by which the fabric moves through

the coating liquid and the time the fabric is in the liquid is referred to as dwell time. From a fluid-mechanical consideration, the pad-mangle coating process is viewed as a combination of dip coating and a forward two-roll coating process (Fig. 3). Main governing factors in the dip coating process include – (a) nature of the textile substrate, (b) substrate speed, (c) surface tension and viscosity of the formulation (with water as solvent, the effect of drying during the process is negligible), (d) nip pressure of the roll coater, (e) roller speed, and (f) rheological properties (such as viscosity, surface tension, flow behavior). Sometimes, it is difficult to control the shear forces applicable during the entire process because of the great number of process parameters [4, 57].

3.3 Screen Printing/Coating

Rotary screen printing is considered as one of the most common printing techniques in the textile industry since it provides many advantages over other techniques, some of which include – (a) efficiency and (b) fast and versatile in character, especially when compared to older methods (such as engraved roller printing and flat-bed screen printing). The basic principle behind both rotary and flat-bed screen printing is that the printing formulation is pressed through a screen onto the textile substrate. Usually, the screen is printed with the inverse of the desired pattern with an UV-curable ink, then with an open screen mesh. Rotary screen printing usually contains a cylindrical screen often made of perforated nickel, whereas the screen is flat in flat-bed screen printing and often made out of polyester mesh. During industrial rotary screen printing, the fabric rests on a rubber mat that moves the fabric forward under the rotating screen. As the friction between the fabric and screen is low, the method is suitable even for delicate, stretchable, lightweight textile substrates with uneven surfaces. A magnetic table is used beneath the substrate and a squeegee or a metal rod is placed over the screen on the top of this table which is used to squeeze out the print through the cylinder. Rotary screen printing allows continuous printing operation without having to move the screen exactly into a new place which is essentially required during flat-bed screen printing process. However, the flat-bed technique still has industrial applications in printing of individual textile products (such as t-shirts and table cloths), and it is also popular for laboratory-scale textile coating using screen coating technique [4, 54–62].

3.4 Digital Coating Using Inkjet Technology

Inkjet technology have many wide range of applications including in digital dyeing, printing, and coating of textile substrates. Inkjet printing, a noncontact printing technology, allows deposition of ink droplets on various substrates, such as textiles, paper, leather, ceramic, glass, and also on many other substrates for different purposes. It is capable to meet the market demand for producing samples and product within a very short time compared to screen printing technology. This technique is

also suitable for mass customization along with the scope of adaptation to unlimited design possibilities with respect to repeat size and color range. Inkjet printing techniques can also be used for the digital dyeing of textiles using a very innovative technique where the colorants and related additives can be applied on the substrates in the form of a jettable ink disposing through the inkjet printhead which is commonly used for inkjet printing technology. Inkjet printing techniques are increasingly gaining the momentum to produce very high-quality printed substrates using a wide variety of materials, including, conventional dyes, functional dyes, pigments to meet the demand for a wide variety of colored substrates for their different applications. All inkjet technologies are basically precise microdisposal techniques which digitally control the fluid droplet (e.g., the ink) ejection from the printhead onto a substrate. Various techniques can be used for a digital control on the fluid droplet ejection from the printhead to the substrates which are sometimes used as a basis for the classification of inkjet printheads. For example, continuous inkjet printing technique or drop-on-demand inkjet printing technique are two mostly used terms for a broader classification of industrial inkjet printing technology (although there are variants within each class). Recently, inkjet technology has been rigorously explored for digital coating of textiles for both conventional and high-tech coated textiles with immense industrial application potentials. There are many advantages of using inkjet technology for digital coating of textiles. For example, using inkjet technology, fluid deposition can be precisely controlled and placed in an exact location. It is particularly beneficial for applications that require multiple coatings on a single substrate (such as coated textile for outdoor work wear). Inkjet technology can also be used for functional coatings on textiles using different types of inkjet printheads. These techniques can also be used for high-throughput productions on both rigid and flexible substrates. In addition, inkjet coating can be used for functional finishing of textiles which may provide different benefits including – (a) fast turnaround time, (b) maximum customization, (c) reduced wastage, and (d) improved energy savings. Table 1 provides a comparison on the benefit of using digital inkjet coating technique along with other usually used coating technique [1, 2].

Table 1 A comparison of digital inkjet coating with other selective coating techniques

Name of coating technologies	Film quality	Nature of productivity	Applicability	Scalability	Type of process	Nature of material waste
Spray-coating or doctor blade	Low	High	Polymer/small molecule	High	Subtractive	High
Screen printing/padding	Low	Very high	Inorganic/polymer/small molecule	Medium	Subtractive	Medium
Inkjet coating technology	Medium	High	Inorganic/polymer/small molecule	High	Additive	Low
Evaporation	High	Low (batch)	Inorganic/small molecule	Low	Subtractive	Medium

3.5 Other Coating Techniques Usually Used in Textile Coatings

A range of other techniques are also popularly used during textile coatings. During particular types of textile coatings, many nanomaterials are applied on textiles using different advanced coating techniques, such as (a) chemical vapor deposition, (b) physical vapor deposition, (c) atomic layer deposition, (d) electrodeposition, (e) spray coating (both plasma and thermal), (f) self-assembling monolayers, (g) plasma coating, (h) sol–gel coating, and (i) nanotechnology. Sometime it is very difficult to separate one technique from another due to the fact that very often a total coating package come with a combination of more than one technology. For example, nanotechnology is widely used to engineer and modify the characters of different ingredients used in textile coating formulations, and sometimes these ingredients are used by other coating techniques. Additionally, there are many versatile and widely used processes for the applications of nanoparticles. Nanotechnology is usually used to provide the tools to control three prominent parameters which are essential to ensure the performances of thin films. These three main parameter are – (a) chemical composition (and crystalline structure at nanosized domains), (b) thickness, (c) topography (including nanoscale patterning of the surfaces of the thin films). These techniques can be used to produce coated textiles with a diverse range of properties [4, 8, 28, 29, 67–150] and some of which have been mentioned in different parts of this chapter (both previous and successive sections).

3.5.1 Chemical Vapor Deposition and Physical Vapor Deposition

These techniques involve heating the material in order to convert the material into the gas phase and also deposit it onto the textile surface by using chemical reactants for triggering the deposition process. For depositing the thin film material, several techniques are widely used, some of which include – (a) thermal evaporation, (b) magnetron sputtering, and (c) pulsed laser deposition [4, 57–62].

3.5.2 Electrodeposition

It is a coating process that uses the electric current in order to produce metallic coatings on textile substrates, and there are different ways to apply this technique. For example, in one method, the deposition is achieved by negatively charging the substrate to be coated and by immersing it into a solution containing a salt of the metal to be deposited [4, 60–64].

3.5.3 Spray Coating

Primarily two methods such as (a) plasma spray coating and (b) thermal spray coating are frequently used in spray coating along with other spray coatings for advanced textiles. During plasma spray coating (also termed as – plasma arc plating, plasma arc spraying, and plasma coating), powders are introduced in a cavity that contains the gas stream of a plasma gun, and after being melted, the powders are projected onto the surface of the substrate (under coating operation, such as textile surface). Thermal spraying coating system contains a feed stock material (powder or wire) for heating and accelerating it to high velocity using a gas stream. Then the particles strike the

surface of the textile substrate and the particles deform and freeze onto the substrate, and the collision speed is an essential element that have direct control on different coating properties [4, 57, 60, 65–68].

3.5.4 Plasma Coating

Originally, plasma coating was developed for coating on the clothing mainly used by the military or for protective applications for saving the wearer from chemical agents. However, at present, it is generally used for producing very high hydrophobic nature on coated substrates (such as bioinspired or lotus effect type hydrophobic nature on coated substrates). In addition, continuous research on this type of technique has been successful to find ways to reduce the amount of functional additive required for the production of nonwovens for the hygiene industry. Plasma, a fourth state of matter, is usually used for modifying textile surfaces during textile coating using plasma treatments. Two main groups of plasma treatments are – (a) degradative surface treatments (such as cleaning, etching, sterilization) and (b) addition treatments, (for examples, activating by temporarily increasing the surface energy, functionalizing by permanently introducing chemical groups, and deposition or coating). Plasma treatments have many advantages where one of which is that it is a dry alternative method of textile processing. Plasma treatments under low pressure (~ 0.01 kPa) or subatmospheric pressures (~ 1 kPa) can be used to provide uniformity of treatment combined with flexibility, but this type of batch treatments use expensive plasma equipment. In addition, the in-line, high-speed continuous plasma processing systems at atmospheric pressure (~ 100 kPa) are less flexible and are influenced by the environment. To produce different desired characteristic properties on textiles, the effective use of plasma technologies in order to functionalize fiber surface is an important step. Plasma treatments are usually carried out on textile for a number of reasons, some of which include – (a) imparting hydrophilicity to polypropylene and polyester; (b) increasing adhesion of coatings; (c) pre-treatment for water, oil- and stain-repellent finishes; (d) pre-treatment for ultra-hydrophobicity/self-cleaning finishes; (e) pre-treatment for printing wool; (f) pre-treatment for inkjet printing; (g) enhancing fiber dyeability; (h) modifying electrical conductivity or antistatic finishes; and (i) application of antimicrobial and flame retardant finishes. Another important area for developing textile finishing is the introduction of plasma-polymerization processes, some of which are – (a) plasma-induced polymerization processes directly on the fiber surface; (b) surface grafting of polymers; (c) functionalization of the fiber surface to accept the deposition of polymers and reaction with the fiber surface; (d) cold plasma discharge synthesis of new polymeric structures to impart novel effects on the fibers surfaces. Besides this, the use of plasma technologies for the production of higher easy-care performance through the production of ultra-hydrophobic finishes in order to produce self-cleaning fabrics with water-, oil-, and stain-repellent characters [4, 57, 58].

3.5.5 Self-Assembling Monolayers

Self-assembling monolayers are one-molecule thick thin layers spontaneously formed by a substance that have many potential applications including scratch-resistant coatings and also producing coated self-cleaning textile surfaces. Crucial

dimension in self-assembling monolayers is the thickness perpendicular to the plane of the monolayer where this dimension and the composition along this axis can be influenced (simply at the scale of 0.1 nm) by controlling the structures of the molecules which are used to make up the monolayer. As for instance, self-assembling monolayers can also be used to provide tailor-made functions by changing the structures of the organic molecules in simple ways where interfacial free energies can be controlled [4, 57, 67, 68].

3.5.6 Atomic Layer Deposition

Atomic layer deposition technique has many uses including producing ultrathin and conformal thin film structures for many semiconductor and thin film device applications. This technique is also used for sequential self-limiting surface reactions in order to control film growth in the monolayer or submonolayer thickness regime. It has many potential applications in advanced electronic devices. In addition, it has many advanced applications, for example, this can be used to control the film structure in the nanometer or subnanometer scale which is useful for coating textile substrates with complex surface topographies [4, 57, 68].

3.6 Recent Technological Advancements and Their Impacts on Textile Coatings

Ongoing progresses in different areas of science and technology have been continuously influencing the nature of textile coatings. However, due to limitation of space, only a few selective scientific achievements on nanotechnology and its impacts of textile coatings are briefly and selectively covered here in this chapter and sol-gel technology is also discussed separately.

3.6.1 Nanotechnology in Textile Coatings

Nanofinishing technique is also used for nanocoating of textiles. Nanotechnology is sometimes used to impart novel qualities on fabric which can repel water and oil without any loss of natural breathability and comfort of the fabric. Nanotechnology has been popularly used to improve molecular organization in order to give fibers and fabrics advanced performance characteristics without losing the original softness, durability, and breathability. Basic principles of designing a breathable fabric involve proper selection of different important things, some of which include – (a) film and coating, (b) fabric substrate, (c) lining material, (d) garment designing, and (e) nature of additional finish.

In addition, nanotechnology has been successful to open up new horizons in the production of high-quality coated textiles along with other multiple application in textile products. For example, nanoscale emulsions are popularly used for chemical finishing of textiles to achieve uniformity and precision onto the textile surface if this technique is used during textile coating. During the use of this method, finishes are usually emulsified into nanomicelles, made into nanosols or wrapped in nanocapsules in order to attach them to textile substrates for uniform coating in particular cases. Many high-quality coated textiles for various applications can be used using

this technique. Many nanomaterials are widely used in textile coating formulations. Generally, the term nanoscale refers to the size range from 100 nm down to 1 nm (ISO 2010). Nanomaterials have a much larger surface area per unit mass and hence they become more reactive at the nanoscale. As the nanomaterials decrease in size towards the molecular and the atomic scale (such as approximately 0.2 nm), the optical, electrical, and magnetic properties become increasingly dependent upon quantum effects, as a result characteristic changes in properties can be observed. Nanoscale technologies encompass a number of enabling technologies (incorporating materials, manufacturing, measurement, and integration techniques) which result in products normally embedded into a larger scale component or system rather than products in their own right. In this case, first generation nanoscale technologies refer to passive technologies (for example, antimicrobial coatings, nanocomposites) and second generation refer to active nanoscale technologies (for instance, controlled release drugs, multifunctional sensors) whereas the third generation refer to active systems of nanoscale technologies (such as where more than one active nanoscale technology is present within a system). In particular types of textile coatings, nanosized particles are applied by coating onto the textile for providing specific specialist performance properties. In this context, textile coating techniques incorporate nanotechnology and the coated textiles produced by using these techniques are useful for variety of advanced applications including in medical textiles (such as antimicrobial or antiviral textiles which usually meet biocidal requirements).

Nanotechnology is widely used to produce inkjet inks which can be delivered on textile surfaces by different techniques including inkjet coating technique. Inkjet coating on textiles involves the application of chemical coatings onto a textile substrate by using the similar method which is usually used for digital inkjet printing technique. Both conventional and advanced functional or technical coated textiles can be produced by using this inkjet coating technique. For examples, specific developments in inkjet-coated fabrics include – (a) textiles with dirt repellency and self-cleaning attributes, (b) stimuli-responsive color changing textiles, (c) rubber-like fabrics which are impermeable to toxic chemicals, (d) stain-resistant fabrics, and (e) waterproof fabrics. In addition, during chemical finishing, it is possible to incorporate different types of nanoscale materials, which are – (a) with one dimension in the nanoscale (for example, thin film coatings or nanocoatings), (b) with two dimensions in the nanoscale (such as nanotubes), and (c) with three dimensions in the nanoscale (for instance, nanoparticles, nanocapsules). There are different types of nanoscale materials which include – (a) nanoparticles, (b) nanowires, (c) nanocomposites, (d) carbon nanotubes (single wall, multiwalled), (e) nanocapsules, (f) quantum dots, (g) nanoporous materials, (h) coatings and surfaces, (i) nanofibers, (j) graphene, (k) fullerenes, and (l) nanostructured materials. Nanofibers and nanotechnology in textiles covers a wide range of materials including textile finishing. In order to impart different functionalities on textiles using different techniques including coating, nanocomposites can be used to utilize different nanoparticles for incorporation into a polymeric matrix. Nanocomposites have many potentials for a wide range of textile applications and also to functionalize the textile substrates for particular set of applications, some of which include (a) UV protection,

(b) biocompatibility, (c) superhydrophobic, self-cleaning finishes, (d) electrical conductivity, (e) water-, oil-, and soil-repellency, (f) flame retardancy, (g) antimicrobial activity, (h) antistatic properties, (i) biocatalysts, (j) abrasion resistance, (k) moisture management, and (l) hydrophilic finishes. In addition, nanocapsules can be used to encapsulate different products, for examples, fragrances, enzymes, catalysts, oils, adhesives, polymers, nanoparticles, biological cells, vitamins, and provitamins. Besides this, nanocoatings can be carried out using a variety of other techniques, where some prominent techniques include – (a) physical vapor deposition, (b) chemical vapor deposition, (c) sol–gel treatments, (d) spin coating, and (e) inkjet technology [4, 57, 58, 69–82]. Nanomaterials are also used for a number of reasons including – (a) producing self-cleaning fabrics, (b) imparting water-, oil-, and soil-repellency, (c) providing antibacterial and antifungal finishes, (d) photocatalytic coatings for detoxifying or color removal, and (e) applying abrasion resistant finishes. In addition, sometimes plasma technologies are used for surface functionalization prior to nanocoating or before the incorporation of chemical finishes. Moreover, the exploration of nanoscale technologies for application of nanofinishes can be used to introduce novel finishes for smart textiles and also to extend the end uses of other type of textiles. However, there are also some potential risks associated with the use of nanoscale materials (for examples, nanoparticles, carbon nanotubes) which may limit the full utilization of nanomaterials and more extensive research is needed to address all these issues [58, 83–99].

3.6.2 Sol–Gel Technology in Textile Coating

Sol–gel technology is popular for particular types of textile coatings. In typical sol–gel coating formulation, the precursor used in the sol–gel process is usually dissolved in a solvent in order to form a sol or gel which depends on the reactor conditions and also to cause precipitation because of chemical reactions. Four basic steps in the sol–gel process are – (a) hydrolysis, (b) condensation and polymerization of particles, (c) growth of particles and agglomeration, and (d) formation of networks. Practically, sol–gel technology has been popularly used for a long time where inorganic materials are used along with other components in the coating formulations. Inorganic components of sol–gel coating compositions are usually used to enhance different desired properties including strength and wear resistance to obtain important effects on thin coated layers. This technique is widely used in many industrial applications including in textile coating. However, there are some issues which limit the wider applications of this technique in textile coatings and some of which include – (a) the use of highly acidic solutions and predominance of organic solvents and (b) high process temperatures and long process sequences. Inorganic sol can be synthesized from various nanopowders of metal oxides (for instances, TiO_2 , ZnO , Fe_3O_4 , Al_2O_3 , and SiO_2). Coated textiles with hydrophilic or hydrophobic surfaces have been reported by using sol–gel techniques [28, 92, 99–122].

Sol–Gel Coatings for the Functionalization of Textiles

Sol–gel technology is popular for the functionalization of textile in order to achieve better physical maintenance and improvement of particular properties with potentials

of various industrial exploitations. During sol–gel coating, textiles are chemically or physically modified with used sols (with particle diameters <50 nm or nanosols) in the coating formulation and change the physico-mechanical, optical, electrical, and biological properties of the coated textiles. In addition, sol–gel coating protects coated textiles from destruction and creates new desired functionalities on coated textiles, some of which include – (a) water, oil and soil repellency, (b) antimicrobial resistance, and (c) improvements on different technical performances (such as abrasion resistance, washfastness, lightfastness). This chapter briefly provides some basic information on the core development on the recent functionalization methods for producing multifunctionalized textiles by coatings and similar other techniques which use modified silica nanosols.

Multifunctional textiles have significant potentials to meet future challenges and also benefit from future changes in overall textile and apparel industries. Functional textiles have vivid application potentials which are sometimes designed to meet consumer demands in terms of comfort, easy care, health, and hygiene and also to protect against mechanical, thermal, chemical, and biological attacks. Besides these, functional textile coatings have significant contributions in order to develop performance and durability for technical textiles (such as in automotive, railroad and aviation engineering, in construction and for home textiles). Coated functional textiles demonstrate particular characteristic properties, some of which are – (a) enhanced stability against mechanical, chemical, photochemical or thermal destruction, (b) strong water-, oil-, and soil-repellence characters, (c) shifting light absorption and emission properties from the UV up to the IR region, in particular cases, (d) enhanced electric conductivity (such as for antistatic and electromagnetic protective effects), (e) immobilization and controlled-release of active species (for instances, with biocidal, therapeutic, and well-being effects). Simultaneously, important textile properties (for example, appearance, feel and durability to laundering) should be maintained as additional feature to newly incorporated functionalities on the coated textiles to make them suitable for their uses as high-tech or smart textiles. In usual terms, the textiles can be functionalized not only by using new production technologies (for example, 3D structures) but also by improving fiber materials or modifying the fiber surface. Principles related to selected methods of textile functionalization using different modification techniques include:

- (a) Incorporating functional additives (such as organic or biological compounds, inorganic particles, polymers) into the polymer melt or polymer solution before spinning. High permanence is a clear advantage, although low flexibility is a drawback whereas the high nontextile portion, and also the procedure is not practically suitable for natural fibers.
- (b) Direct chemical grafting of additives on the textile fiber surface or by using linkers on textile surfaces. In addition, this method produces excellent permanent effects; however, it is restricted to reactive fibers and additive structures.
- (c) Post-treatment of textiles using functional coatings. This technique is flexible with regard to coating technology and shows productive capacity which is

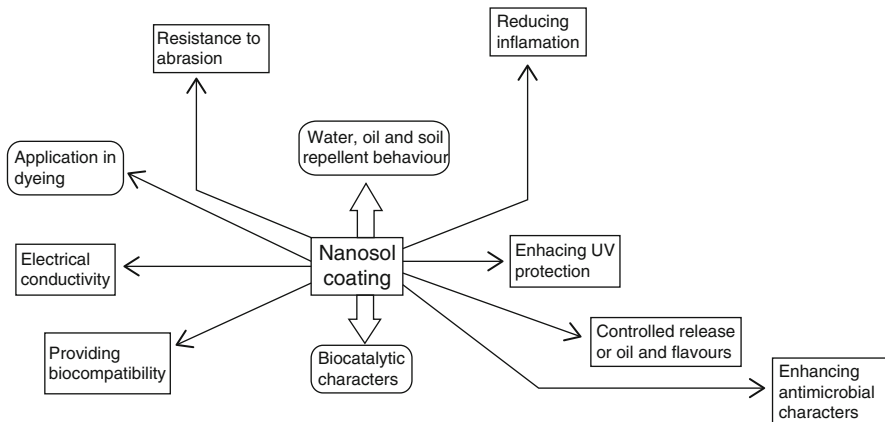


Fig. 4 Various uses of nanosol coatings and their applications on textiles

largely independent from fabric type that requires low quantities of additive and enables the combination of different functionalities in a simple way.

Besides this, textile functionalization by using coating techniques is widely involved with the applications of inorganic sols which are usually produced from modified silica and other metal oxides. Many reasons are usually considered behind the use of inorganic sol coatings for the functionalization of textile surfaces some of which include – (a) sols based on modified silica and other metal oxides (particle size <50 nm) usually form transparent oxide layers on textiles which show good adhesion property; these metal oxide layers also exhibit stability against light, heat, chemical, and microbial attacks; (b) these layers also contribute to enhance the mechanical behaviors of the textiles (for examples, high mechanical strength, wear, and abrasion resistance while offering possible methods of varying the surface characteristics); (c) the oxide coatings can act as carrier for embedded functional additives, such as organic or biological compounds, inorganic particles, and polymers since it is easy to control layer porosity and the degree of immobilization of the embedded compounds; (d) this technique also allows the coating formulations at room temperature and normal pressure using conventional coating devices usually applied for textile finishing (for example, padding, exhaust processing techniques, dip-coating, spraying) [4, 28, 57, 92, 99–122]. Figure 4 illustrates different uses of nanosol coatings and their applications on textiles.

Improved Stability Against Mechanical or Thermal Destruction

Many reports are focused on the modification of textile materials using silica particles in a sol–gel process to produce ceramic-like composites with higher density and enhanced mechanical characters. Treating textiles using inorganic nanosols can be applied in order to enhance abrasive resistance since the inorganic coating improves solidity. As for instance, the coating of polyester sieves used for paper

production with alkyl modified silica nanosols has the potential for enhancing their abrasion characters. Moreover, enhancement in abrasive resistance and tensile strength after nanosol treatments have been reported for other textile substrates (for examples, cotton, polyamide, and glass fibers). For example, when cotton is treated with pure silica sols modified by adding epoxysilanes (such as glycidylpropyloxy-trimethoxysilane or GPTMS), it exhibits a significant improvement in, adhesion property of nanosol coating to the fiber which eventually contributes to enhance the mechanical stability of the coated textile substrates. In addition, this enhanced adhesion property of the nanosol coating on textile is attributed to the chemical bonding which generates from the opening of the epoxy ring of GPTMS and the reaction of the hydroxy groups on the cotton surface. There are many applications for antiabrasion coated textiles, some of which include – the applications of polyester sieves in paper production and for home textiles (such as furniture or carpets), knife- and bullet-proof protective clothing. In addition, nanosol coatings are also popularly used to improve the fire and heat resistance of wooden materials, which usually use silica nanosols modified with phosphorus compounds (for example, diethylphosphite or phenylphosphonic dichloride). On the contrary, only a few reports deal with the improvement of fire resistance of textiles by using nanosols (though for instance, the use of simple silica sol coatings modified with fluorinated silane compounds has been reported to improve the flame resistance of nylon-based carpets). Additionally, the use of $\text{SiO}_2\text{-TiO}_2$ or $\text{SiO}_2\text{-Al}_2\text{O}_3$ nanosols to textile filters can contribute to improve heat resistance up to a particular temperature (such as $300\text{ }^\circ\text{C}$). Besides this, the flame retardant characters of wool can be enhanced by using hydrolyzed $\text{TiCl}_4\text{-NH}_4\text{HF}_2$ -dicarboxylic acid solutions. Enhanced heat and flame resistances have been reported where phosphorus-containing flame-retardants have been embedded into the nanosol coatings on textile fibers [8, 28, 29, 123–132].

Improved Water, Oil and Soil Repellency

Textiles with repellent characters are significantly important because of a broad range of prospective uses (for examples, water-repellent textiles as rainclothes and tents, or easy-to-clean oil-repellent fabrics). Coating with modified nanosols helps to cover the full range between hydrophilic and hydrophobic textile characters. Coating textiles with silica nanosols based on perfluoroalkyl compounds contributes to enhance the hydrophobicity, oleophobicity, and soil repellence of fibers. Additionally, when alkylsilane compounds without fluorine substituents are used in nanosol-based coating formulations, they also help to improve water-repellent characters of the coated textiles [91, 133–135].

Advances in Sol–Gel Coatings for Smart Textiles

In order to meet the increasing demands for comfortable, aesthetic, durable, functional, and safe textile products with advanced characteristic properties, the development of new techniques for processing and designing textiles are highly required. As a result, nanotechnology has been successful to attract its application on various features of textiles in recent years. Nanoscale manipulation and composition are usually used to improve desired properties and to include new functionalities for all kinds of textiles (for examples, self-cleaning, sensing, healing,

decorating, actuating, and communication). The inorganic sol–gel matrix produced by using coating with nanoparticle sols can be combined with organic systems to obtain required characters onto textiles (for instances, good mechanical, thermal, and photochemical stability). These coatings also demonstrate improved adhesion properties to different types of substrates (for examples, paper, textile, and polymer sheets), and the matrices are toxicologically and biologically inert, and their porosity can be controlled. As a result, compounds can be embedded in these matrices and released in a controlled way into the adjacent gaseous or liquid phase. In addition, sols and derived coatings can be synthesized based on ambient conditions using conventional coating processes for textile finishing. In different ongoing research activities, textiles have been functionalized with new functional materials. For example, in different reports biosensors integrated within textiles have been developed using various techniques (for example, incorporating functionalized optical fibers into fabric structures). Sol–gel coatings have been designed for the encapsulation of reactive biological entities to deposit on the optical fiber core and specific interactions with target analytes in order to induce changes in the color of embedded dyes for detection purposes by using light-guided optical fibers. These materials are suitable for various applications including – (a) professional clothing, (b) biomedical textiles, (c) high-tech sportswear, and (d) technical textiles. Additionally, sol–gel technology provides some promising application potentials for tailoring surface characters on the coated substrates and also to combine different functionalities in a single material. For example, the nanoparticulate sols can be applied using commonly used techniques in textile industry for fabrication and functionalization of the textile fibers. Moreover, new functional fibers can be generated by using extrusion and electrospinning techniques from hybrid organic–inorganic sols. The combination of innovative sol–gel materials, specific functionalization, and casting and deposition techniques provides the scope for new perspectives in smart textiles with protection, healing, and comfort by drug delivery mechanisms, wetting, decorative, and sensing properties [20, 135–193].

4 Film Formation

When a coating formulation is applied on a textile substrate, usually the film is formed over the surface after the drying and annealing of the coating formulation. For simplicity, this film formation may be divided into four stages:

- (a) Firstly, the particles are randomly distributed in the medium.
- (b) Secondly, water or solvent evaporates from the formulation and the polymer particles are packed together.
- (c) Thirdly, the polymer particles deform for a more thermodynamically favored structure.
- (d) Fourthly, the inter-diffusion of polymers across particle boundaries (and sometimes they are chemically crosslinked).

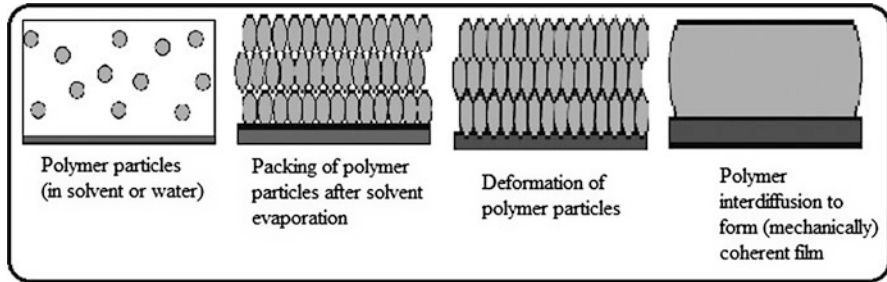


Fig. 5 Schematic diagram for the illustration of different stages of film formation

Since stages two and three are often referred to as drying in an industrial context, the last stage may thus be called curing or annealing, although these terms are highly dependent on the place and main objectives of their uses. Drying is normally performed at a lower temperature for ensuring the solvent evaporation which should not cause irregularities in the coating. However, the annealing operation is performed in higher temperatures for enhancing the inter-diffusion or, when possible, because it is used to catalyze the chemical reaction necessary for crosslinking. For waterborne coatings, the film formation process is often the most energy demanding step in the production [4, 57, 158, 180, 183]. Figure 5 demonstrates the schematic diagram of different stages of film formation process.

5 Polymers and Additives for Typical Textile Coatings

A wide range of polymers are generally used in textile coatings and they perform various activities and also have significant control on the final characteristics of coated textiles. Based on the nature of polymer and other additives used in the textile coating formulations many final characters of the coated textiles can be effectively controlled. These characters could be related to the aesthetic or technical or any other types. For examples, there are different functional characters, where one or more than one final characters may be desired from a functional coated textiles. Some of these functional characters include – (a) chemical resistance, (b) solvent resistance, (c) acid resistance, (d) alkali resistance, (e) flame resistance, (f) water repellancy or resistance, (g) oil resistance, (h) increased rigidity, (i) abrasion resistance, (j) tear resistance, (k) good ability to stretch, (l) high or low friction, and (m) specific response to particular surrounding environment. Using proper selection of polymers, additives, and textile substrates, many of these desired characters can be realized on coated textiles. A wide range of additives are used along with polymers to control many of these desired characters. Some of which have been selectively and briefly discussed in different sections of this chapter.

Compatibility of the nature of the polymer with a particular type of textile is an important issue to select a specific polymer for a particular type of textile coating

formulation. In this case, textile surfaces may denote any material intended for textile use, some of which include – (a) loose staple fibers, (b) filaments, (c) yarns, (d) braids, and (e) nonwoven, woven, and knitted fabrics of both organic and inorganic origins. Textile coatings can also add or change the functionality of textile (a character of a textile that does not form covalent bonds or adhere to the fabric on its own). Polymeric binders usually used in textile coatings are sometimes designed to form enough secondary bonds for adhesion with the textile surface. Additionally, polymers used in textile coatings may also exhibit functional characters (such as hydrophobicity or increased rigidity). Sometimes the polymeric binders generally used in waterborne coating come in the form of waterborne dispersions, into which functional materials and auxiliaries are added. The coating binders can be any types of polymers which have enough adhesion property; however, compatibility with the coating method and the end-use purpose is an essential requirement. Usually used, polymeric binders include – (a) rubbers, (b) polyvinyl chloride, (c) silicones, (d) acrylates, and (e) polyurethanes [4, 20, 57, 166–184].

Textiles coated with polymers can work as flexible composites, and they contain polymer coatings and the textile substrates which adhere together through specific coating processes and provide additional properties for the coated substrates. Mostly high molecular weights polymers are usually used in polymer coatings of textiles. Both natural (such as gelatine, casein, biopolymers), and synthetic polymers can be used in textile coatings. Synthetic polymers can be mainly categorized in three types based on their thermal responses, such as – (a) thermoplastic polymers, (b) thermoset polymers, and (c) rubbers. Thermoplastic polymers are mostly reprocessible with long chain which can be softened with temperature. Thermosets polymers have strong three-dimensional networks where individual long chain molecules are interconnected to each other by strong covalent bonds (or chemically crosslinked). Thermosets are hard and glassy at room temperature, and they cannot be softened by heat and they are not reprocessible. Rubbers have highly flexible networks, and they are soft and elastic at room temperature. Physical entanglements in rubber act as physical crosslinks between the chains. Both thermoplastics and rubbers are widely used as coating materials [20, 57, 178–183].

5.1 Selected Characters of Commonly Used Polymers in Textile Coatings

Several types of thermoplastics (for examples, polyvinylidene chloride, polyvinyl acetate, polyurethanes, acrylics) and most of the natural and synthetic rubbers are commonly used for textile coatings. Different properties of thermoplastic polymers are suitable for textile coating due to their hot-melting and thermally induced welding characters. Selection of polymers for textile coatings depend on the particular natures of the polymers (such as melting points, glass transition temperature, molecular weight, mechanical and chemical properties). Table 2 illustrates selected behaviors of some commonly used polymers in textile coatings. Most frequently used thermoplastic polymers in textiles coatings include – (a) polyvinylchloride,

Table 2 Selected behaviors of some commonly used polymers in textile coatings

Type of polymer	Glass transition temperature (°C)	Melting temperature (°C)
Low density polyethylene	−120	115
Polypropylene	−20	165
Polyvinylchloride	85	220 ^a
Polyvinylidenechloride	−17	185–200
Polyvinylacetate	29	–
Polystyrene (amorphous/atactic)	100	
High density polyethylene	−135	130
Polyethylene terephthalate	69	265
Polyamide	50	215
Polycarbonate	145	295 ^a
Polymethylmethacrylate (amorphous)	105	
Polyacrylonitrile	90	
Polytetrafluoroethylene	20	327 ^a
Polyetheretherketone	145	335
Thermoplastic polyurethane	230	
Polyisoprene (natural rubber)	−73	
Polybutadiene	<−90	
Styrene-butadiene-rubbers	25–75	−55
Polyisobutylene (butyl rubber)	−70	0
Polydimethylsiloxane (silicone rubber)	−125	−55

^aDecomposing

(b) polyvinylidene chloride, (c) polyvinylacetate and acetate copolymers, (d) acrylics, (e) polyurethanes, and (f) different types of rubbers and particular types of thermosetting polymers [4, 20, 57, 177–192].

5.2 Thermoplastic Polymers

Four main types of thermoplastic polymers include – (a) polyethylene, (b) polypropylene, (c) polyvinyl chloride, and (d) polystyrene. Sometimes, these polymers are also termed as commodity thermoplastics. Engineering thermoplastics have better mechanical properties compared to commodity thermoplastics. Some of these engineered thermoplastics include – (a) polyethylene terephthalate, (b) polybutylene terephthalate, (c) polyamides (or nylons), (d) polycarbonate, (e) polymethyl methacrylate, and (f) polyetheretherketone. These polymers show high strengths, with high stability performances in continuous use at temperatures >100 °C. In addition, engineering thermoplastics are produced and used on a small scale and have prices higher than those for commodity thermoplastics. Specialty plastics are also popularly used thermoplastics in textile coatings which have specific

properties some of which include – (a) high heat-resistance and (b) exceptional mechanical properties. These polymers are relatively more expensive. Poly-tetrafluoroethylene is considered to be a specialty plastic with unique low-friction properties. Microstructure-based thermoplastics usually show amorphous glassy or semicrystalline solid behavior and amorphous thermoplastics are glassy up to a specific temperature (the glass transition temperature) above which they transform into a more rubbery structure without a distinct melting point. In addition, semicrystalline thermoplastics are two-phase materials comprising an amorphous phase with the certain glass transition temperature and a crystalline phase with a specific melting temperature [4, 20, 57–60, 178–183].

5.3 Thermosetting Polymers

Most of the thermoset polymers are hard, rigid, and brittle, with high temperature- and chemical-resistances, and they are popularly used as matrices for reinforced composites. These type of thermoset polymers are usually used to provide good adhesion when used along with other additives during textile coatings. Some thermosets (for examples, epoxy, phenolics, and polyester resins) are mainly used as the matrices for fiber-reinforced composites, whereas amino resins are mainly used for bonding chipboard. If the number of branch points in a polymer system is progressively increased, long branched molecules with infinite “tree molecules” are initially formed and ultimately a 3D network system is obtained. In addition, a single-tree molecule (also called as the “gel point”) forms, when most of the polymer becomes nonsoluble, and a swollen gel forms if a solvent is added to the system [4, 57, 185–192].

5.4 Rubbers and Their Uses in Textile Coatings

Rubbers are crosslinked amorphous polymers and their glass transition temperatures are characteristically below 25 °C. In these systems, no rigid groups (for instance, phenyl rings) present in the chain or as side groups, and no polar groups are available that can increase intermolecular forces. Rubbers are dominated by commodity types (for example, natural rubber and styrene-butadiene copolymer rubber) which are mostly used for tire production. For this and many other applications (such as conveyor belts, pressure hoses), rubber systems reinforced by fibers are used. The rubber matrix allows flexibility in bending, whereas the fabric reinforcement limits the in-plane stretching of the product. Raw rubber shows plastic-like deformation which behaves like an elastomer (for examples, a material that can undergo large elastic deformations which are reversible) only after crosslinking by vulcanization. There are also specialty rubbers which have certain properties. For example, butyl rubbers have low air permeability, nitrile rubbers have good oil resistance, and silicone rubbers have low temperature-resistance. Some of these rubbers are also used in textile coatings [4, 57, 185–192].

6 Textile Coating Formulations

Textile coating compositions are of different types which can be very simple to enormously complex in nature based on a number of factors relating to the main objectives of the coating formulations. In general, a typical coating formulation contains three main components which are – (a) colorants, (b) vehicle, and (c) additives. Colorants (such as dyes or pigments) provide the required shade or carry out other functions, while the vehicles (sometimes also termed as binders) act as the adhesive to stick colorant particles to substrate or to each other. Additives are auxiliary chemicals which are used to modify the properties of the coating in fluid or solid state. The chemical and physical properties of organic coatings are directly controlled by a number of main factors some of which include – (a) the nature of main ingredients used in the organic coating formulations, (b) the nature of the substrate where they are used, (c) mode of application of the coatings on the substrates, (d) surrounding environments, (e) drying system used, and (f) nature of pre-treatments on the substrates or post-treatments on the coated substrates. Technological advances on the coating techniques along with recent developments of nanomaterials and their applications on organic coatings for a wide variety of application areas are in the way to achieve many high performance organic coating systems for different technical performances in various coated substrates [4, 8, 28, 29, 57, 95, 108–150, 184]. Generally, textile coatings are applied as multilayered systems which have different coating layers, such as – (a) primer and (b) topcoat. However, in some cases (such as automotive coatings), there can be a number of coating layers depending on the nature of final uses of the coated products. In this case, each coating layer is applied to perform certain specific functions, though its activities are influenced by the other layers in the system. In addition, the interactions among different layers and the interfacial phenomenon play a significant role in the overall performance of the multicoat systems and particular characters of coatings are usually associated with specific parts of a coating system [4, 57, 185–195].

Different types of coatings are usually used for producing functional advanced coated textiles for specific applications some of which are briefly and selectively discussed in the successive sections along with a number of other particular items with specific textile coating applications.

7 Functional Coatings on Textiles

Generally, coatings are applied on surfaces to provide decorative, protective, or functional characters or a combination of these properties. Functional coatings provide additional functionality besides the usual characters of a coating formulation and depending on the actual application of a coated substrate, additional functionality may have diverse features. Some particular examples of functional coatings include – (a) self-cleaning, (b) easy-to-clean (anti-graffiti), (c) antifouling, (d) soft feel, (e) antibacterial, (f) flame retardancy, and (g) antimicrobial. In addition, functional coatings are sometimes designed to provide certain specific characters, some

of which include – (a) durability, (b) reproducibility, (c) easy application and cost effectiveness, (d) tailored surface morphology, and (e) environmental friendliness. Based on functional characteristics of functional coating formulations, this coating system can be of different types. Functional coatings provide the functional character using different means, such as – (a) physical means, (b) chemical means, (c) mechanical means, and (d) thermal means. For example, chemically active functional coatings perform their activities either at film–substrate interfaces (such as anticorrosive coatings), in the bulk of the film (for example, fire-retardant or intumescent coatings), or at air–film interfaces (e.g., antibacterial, self-cleaning) [20, 57, 142–181, 195–247]. Selectively, some specific types of functional coatings along with their certain applications on textile coatings are briefly discussed here.

8 High Thermal-Resistant Coatings

High thermal-resistant coatings are required for a wide variety of thermally resistant textiles for both conventional and high-tech specific applications. Some of these coated textiles include (a) certain types of technical textiles; (b) textiles for fire fighters, coats for extreme environments; and (c) textiles for certain types of automotive applications. Thermal- and fire-resistant coating formulations usually contains fluorine- or silicon-based products to produce a high thermal-resistance for the coated textile products. However, all fluorinated coatings are not suitable for high-temperature applications as they degrade above ~ 300 °C and produce toxic by-products. Although currently silicon containing coatings dominate the textile coatings, there are also other binders (for examples, phenolic or epoxy resins) which are also popularly used to formulate high thermal-resistant textile coatings. Silicon-containing polymers provide better thermal resistance as it takes very high level of energy in order to cleave silicon bonds compared to carbon bonds in analogous molecules. For example, recently developed silicon-based coatings which exhibit thermal resistance up to a very high temperature (such as 1000 °C). Silicon derivatives (for example, silicone resins like siloxanes or inorganic silicates) are commonly used for high-temperature resistance textile coating applications. Silicon containing materials are usually expensive, but copolymers or blends of silicones with acrylate, epoxy or urethanes are very often used to reduce costs. Many investigations have been reported innovative ways to design thermal-resistant coatings; for instance, titanium esters in combination with aluminum flakes have been incorporated into binders which can show resistance to high temperatures [20, 176–179, 181–183].

9 Fire Retardant Coatings

Fire retardant coatings are highly important for producing particular types of clothing, tents, automotive textiles, or similar other types of materials based on coated textiles. Different types of materials used in fire retardant coating formulations.

For example, when phosphorus containing compounds are used in fire coating formulations, these materials form a protective layer as a glassy surface barrier coating. However, halogen- and antimony-based fire retardants are toxic in nature and not eco-friendly. Additionally, intumescent coatings form an expanded carbonaceous layer which acts as a protective barrier against heat transfer and hinders the diffusion of combustible gases and melted polymer to the site of combustion. Fire retardant textile coatings usually composed of three main components which are – (a) an inorganic acid (dehydrating agent), (b) a carbonaceous char-forming material, and (c) a blowing agent. Coating performances of the intumescent system depend on the choice of the ingredients and their appropriate combination. Expandable graphites are popular as fire retardant agents since they contain different compounds including acids which are entrapped with different carbon layers. When exfoliation of the graphite takes place, it provides an insulating layer to the substrate during exposure at higher temperatures. Polyurethanes and phosphates are widely used in the fire-retardant intumescent system whereas the nature of solubility of phosphates in water sometimes causes migration problem. Using proper techniques (such as microencapsulation of phosphates like diammonium hydrogen phosphate within a polyurethane shell) can limit this problem to certain extent. Currently, silicon or inorganic hydroxide-based fire-retardant coatings are very popular for variety of industrial applications including textile coatings. Additionally, polymer clay (layered silicates) nanocomposites have been successful to attract current active research due to their potential use as fire retardants in industrial applications including in textiles [20, 176–179, 181–184].

9.1 Application of Flame Retardant Finishes by Coating

Flame retardant finishes are applied on textiles by using a variety of techniques including spray coating, padding, impregnation, and inkjet coating technology. There are different ways to realize flame retarding character of textiles where some of which include – (a) removal of heat, (b) enhancement of fiber decomposition temperatures, (c) decreased formation of flammable volatiles and increase in char, (d) decreased access to oxygen or flame dilution, and (e) interference with flame chemistry and/or increase in fuel ignition in fuel ignition temperature.

10 Silicones in Textile Fabric Coatings

Silicones are widely used in different steps of textile and other types of fiber processing which range from wet processing to finishing. They are also widely used in textile coatings for a diverse application range comprising fashion wear (for example, women's stockings) to technically demanding air bags applications in the car. These applications are based on cross-linked silicone polymers or elastomers that are usually used to formulate crystal-clear coatings that produce either soft and flexible film or hard and rigid film. All such coatings may have nearly similar

compositions and share common raw materials for up to 70% of their formulation technique. These formulations can exhibit better thermal stability (over a wide range of temperatures) than organics. For example, liquid silicone rubbers (LSR) are popularly used material for such fabric coatings due to their ease of use and rapid cure when exposed to elevated temperatures (there is an exception to this statement relating to one-part Room Temperature Vulcanisable or RTV elastomers used in women's stockings). Addition of SiH functional polymers to SiVi functional polymers using a platinum catalyst cross-linking is usually used to prepare these elastomers. These liquid silicone rubbers similar to other silicone elastomers contain fume silica in these structures because these fillers can dramatically improve mechanical properties. Silicone polymers are used in textile coatings for a variety of purposes where one of the prime applications is to provide some form of protection from exposure to high temperatures (as in conveyor belts), low temperatures (as with many outdoor goods), or exposure to stress over long periods of time (as in air bags or compensator bellows) since silicones are more stable than other elastomers. Typical applications and key properties of silicon elastomer based textile fabric coatings can be divided into two categories which are – (a) soft coatings and (b) hard coatings. Main application areas for silicone elastomer-based soft coatings (whose key properties are given in the bracket) include – hold-up stockings (where key properties are – ease to process, crystal clear, soft, nonslip/high elongation):

- (i) Outdoor clothing and tents (where key properties are – adhesion, flexible, thermal stability, colorless, and hydrophobicity)
- (ii) Air bags (where key properties are – strength, adhesion, slip, and stability at elevated temperature)

Similarly, main application areas for silicone elastomer based hard coatings (whose key properties are given in the bracket) include:

- (i) Conveyor belt coating (where key properties are – adhesion, nonslip/abrasion resistance, thermal stability, and food grade)
- (ii) Compensator bellow (where key properties are – adhesion, flexible, chemical/thermal stability, and abrasion resistance)
- (iii) Medical protective wear (where key properties are – hydrophobic, autoclavable, adhesion) [8, 28, 29, 121–177, 197–219]

10.1 Surface Active Agents and Chemical Softeners

Generally, a soft luxurious handle significantly improves the aesthetic appeal of a cloth, particularly, at the point of sale; however, it equally contributes to the thermopsychological comfort of a garment during wear. In this context, the performance requirements for chemical softeners which function as fiber lubricants have impacts on the decreasing nature of fiber/fiber and fiber/metal frictions which may vary according to the end-use. Additionally, this performance requirements may vary

in a number of specific cases, some of which include – (a) soft, luxurious handle, (b) high durability to machine washing (and dry cleaning), (c) antistatic (protection against garment cling), (d) minimum effects upon color/color fastness, (e) non-yellowing in the presence of heat, sunlight (UV radiation), and atmospheric pollutants (for examples, oxides of Nitrogen, NO_x), and (f) compatible in co-application with other finishes. Different types of chemical softeners are available based upon anionic, nonionic, cationic, pseudo-cationic and amphoteric compounds. Some of the most important softening agents are the cationic aminosilicone derivatives, particularly, aminoethylaminopropyl polysiloxanes. These softeners can be modified in various ways in order to enhance their hydrophilic characters which are important in modern moisture management control systems used in many forms of clothing (such as sportswear, activewear, outdoor performance wear). Epoxy-functional and carboxy-functional silicone softeners can provide yellowing resistance, hydrophilic properties, and soil-release characters. However, softer handling fabrics can be achieved using terpolymers with amine and polyether functionality, while epoxy- and glycol-functional siloxanes can be regarded as durable hydrophilic softeners. Aminosiloxane softeners have been widely used for the preparation of microemulsions but nanoemulsion-based softeners are now being produced with particle sizes down to 10 nm, creating a more luxurious softness. In this case, for multifunctional finishing softeners are usually chemically designed for co-application with other finishes as well as not impairing the overall performance of the finished fabric.

11 Scratch- and Abrasion-Resistant Coatings

Some particular types of textile coatings are designed to show scratch and abrasion resistance.

The consumer prefers to retain the aesthetic appearance of coated textile substrates, so clear coats used on particular coated textile substrates (such as coated textile for automobile applications) are expected to show good scratch and abrasion resistance. Scratches have the tendency to cause damage to the underlying substrate which is an additional problem. There are ongoing research projects around the world to mitigate the challenge of producing scratch resistance coating with little or no adverse impact on other desired properties. Generally, scratch resistance can be obtained by incorporating a greater number of cross links in the binders used for coating formulations although it is a known fact that highly cross linked binders often produce hard films which have poor impact resistance because of less flexibility. However, a less-cross linked binder usually produces soft film and shows better performance with regard to other properties (such as antifingerprint and impact resistance) but shows less scratch and abrasion resistances. As a result, a proper combination of hardness and flexibility is a prerequisite in order to ensure optimal scratch resistance. Clearly, organic-inorganic hybrid films are relatively popular for developing scratch-resistant coatings in this context, and recent progresses in nanotechnology also have significant role in developing scratch-resistant coatings.

For example, the use of siloxane encapsulated SiO₂ nanoparticles has been reported to develop scratch- and abrasion-resistant coatings. In similar type of studies in industrial scale, coating industries have developed scratch-resistant coatings using different techniques including – (a) by incorporating SiO₂ nanoparticles into an organic matrix that can migrate to the surface and (b) by enhancing the enrichment of nanoparticles near the coating surface. In different studies, coatings with good abrasion- and scratch-resistant properties have also been reported [52, 81–87, 91, 137, 167–175].

12 Self-Healing Coatings

Self-healing coatings try to replicate the lesson from the mother nature which often termed as biomimicry. It is a coating technique which deals with special type of polymers along with other additives to produce self-healing effect on the coated film. Self-cleaning coatings provide a special functional property which also frequently termed as “lotus effects” or self-cleaning effects. In this type of coating on textiles or a textile product, manual cleaning is not required because a shower of rain is sufficient to carry out the cleaning process, these surfaces can be soiled though. There are reports that the self-cleaning property of lotus leaves could be attributed to their specialized surface morphology and hydrophobic character. Since the high hydrophobic character of lotus leaves provides pronounced water-repellence to produce special type of surface morphology for these leaves which eventually deny the dirt or the soiling materials any chance to form an intimate contact with the surface; as a consequence, when the water droplets roll onto the leaf surface, they carry along the contaminants or dirt or soiling materials. Different research groups have attempted to mimic lotus effect by developing self-cleaning using different techniques including coating techniques (and detailed discussions on self-cleaning coating surfaces can be found elsewhere, which is beyond the scope of this current chapter). Recent interests to mimic nature using different advanced techniques have produced a huge amount of successful results in various areas of science and technology. For example, in this context, during the past few years, self-cleaning coatings using photocatalytic titanium dioxide (TiO₂; particularly the anatase crystalline form) have attracted significant research interests in academic and industrial sectors. In addition, when photocatalytic TiO₂ particles are irradiated with an ultraviolet light source (for example, sunlight), electrons are seen to be promoted from the valence band to the conduction band of the particle which generates a region of positive charge (h⁺), holes, in the valence band and a free electron in the conduction band. These charge carriers can either recombine or migrate to the surface where the holes can react with the hydroxyl or adsorbed water molecules on the surface and produce different radicals (for examples, hydroxyl radicals and hydroperoxy radicals). On the contrary, the electrons combine with the oxygen and produce superoxide radicals. Photoproduced radicals of this kind usually show strong oxidizing capability in order to cause the deterioration of organic contaminants or microbial pieces on the particle surface. Besides this, TiO₂ can also be used

to produce superhydrophilic behavior (such as, so called, water sheathing effect) which allows contaminants to be washed away relatively easily with water or rainfall if the coatings are applied onto external surfaces. The underlying mechanisms photocatalysis and hydrophilicity are completely different in nature although they occur simultaneously [57–60, 114, 150].

13 Antibacterial Coatings

Antibacterial coatings on textiles and other flexible matrices have been successful to attract active current research interests due to their wide range of application potentials in different areas of science and technology. Antibacterial coated textiles have been reported to contribute in the protection from microbial attacks. Microorganisms (for example, bacteria, fungi, or viruses) exert potential threats and there are limitation of producing antibacterial-coated textile substrates including – (a) problems of aesthetics (discoloration of the coating), (b) risks to health and hygiene, (c) bed smells, and (d) biofilm development or microbial corrosion in the case of metallic substrates. Different types of coating formulations are usually used in textile coatings, and they show different level of antimicrobial resistance when formulated using antibacterial or antifungal chemicals (e.g., biocide and fungicide) into the coating formulations. For example, organic coatings are susceptible to microbial attack and the nature of the coating composition also have direct impact on this. When biocides or fungicides are used in the textile coating formulations, they have different level of control on the growth of microbial organism on the coated substrates. Two typical types of phenomena are usually observed, they are – (a) inhibition of the growth of microorganism and (b) killing the microorganism. Developing biorepulsive (without killing) antibacterial coatings are quite popular nowadays due to new legislations and pressures from environmental agencies [4, 57, 114, 150, 200–203].

14 Antifouling Coatings

The accumulation of unwanted materials on the surface of a material is sometime termed as antifouling. Fouling materials could be of different types – (a) living organisms (biofouling) and (b) nonliving substances (such as inorganic or organic materials). Fouling is usually due to the adhesion of proteins, polysaccharides, and bacteria on a surface (such as textiles), and biofouling is a problem associated with the maritime industry (for instances, ships, cables, aquaculture nets, maritime textiles). Both outdoor and indoor textile substrates are subject to organic and inorganic material depositions which reduce the utility and durability of the fabrics. Different techniques are usually used to protect from fouling where coating is one of them. For examples, both biocidal and nonbiocidal coatings are used to prevent foulings. In this case, biocide-based antifouling coatings reduce leaching of the incorporated biocides into the coating. Biocides are toxic, and there are strong legislation in order to restrict the

use of biocides; for instance, tributyl tin is a highly efficient marine biocide, but it is no longer in use biofouling coatings due to its toxicity [4, 57, 58, 60, 92].

15 Enzymatic Biocoatings

Biological coatings have a wide range of potentials for industrial exploitations, including in coating of medical textiles or similar biomedical applications of the textiles which are required to show biodegradability for specific applications. The range of enzymes available for textile applications is growing by the day. It is possible that many of these enzyme can be used for different treatment on textiles (such as pre-treatment, post-treatment, modification of certain properties) using different techniques including in – coating techniques, padding, and inkjet coating technology. Continuous research and development on smart materials and biomaterials containing enzymes or enzyme substrates and enzyme immobilization on fabrics have been successful to produce novel sophisticated functionalities which are useful for textiles usually used in medical, protective, and defense applications. For examples, textiles incorporated with wound healing, self-cleaning or self-detoxifying properties, or various antimicrobial effects sometimes use oxidoreductases and hydrolases where enzyme immobilization in polymers are usually achieved by using entrapment, covalent attachment, and adsorption bonding. In addition, smart materials can respond to triggers (such as enzymes) in order to allow a controlled release of active agents (for example, drugs, perfumes, antibiotics, and antimicrobial substances) for high-tech textiles for high added-value products [57, 189].

16 Antimicrobial Coating

Microbial growth on textiles or usually used clothing (such as casualwear, sportswear, and activewear) when exposed to certain environmental conditions such as prolong exposure to moisture or damp conditions or perspirations exerts a real problem on health and safety to the users due to a number of reasons including bacterial growth and body odors. Additionally, prolong uses of technical textiles in outdoor environments where bacteria, fungi, and algae may grow on the textile materials may cause a number of problems, such as (a) physical deterioration, (b) rotting, and (c) the growth of unsightly stains. To avoid this type of problem, antimicrobial finishes can be applied in order protect the textile substrates from these microbial attacks and also to make the clothes to smell fresh and increase their life strength. Antimicrobial finishes can be applied by using different techniques where coating is one of them. Antimicrobial finishes of various kinds have been developed which work in various ways some of which include – (a) controlled release of the antimicrobial agent or provide a barrier/blocking action using inert films/coatings to physically block bacteria, (b) provide films/coatings with direct surface activity against bacterial growth, and (c) regenerate active antimicrobial agents, which are regenerated by bleaching during laundering or using ultraviolet radiation.

In addition, there could be a number of other ways to incorporate antimicrobial agents or similar types of materials on textiles or their products. For example, durability to washing treatments can be increased by a number of approaches, some of which include – (i) insolubilization of the antimicrobial agent either in or on the fiber; (ii) fiber treatment with resins, condensates, or fiber cross-linking agents; (iii) microencapsulation of the antimicrobial agent and durable bonding of microcapsules to the fiber surface; (iv) coating of the fiber surface; (v) chemical modification of the fiber by covalent bond formation; (vi) use of graft polymers, homopolymers, and/or copolymerization on the fiber. Textiles usually used in healthcare or biomedical application require protection against microorganisms where different types of antimicrobial agents are used, some of the most commonly used ones are – (a) metals and metal salts (such as silver, copper based salts), (b) quaternary ammonium compounds (for example, 3-trimethoxysilylpropyl-dimethyloctadecyl ammonium chloride), (c) polyhexamethylene biguanide, (d) triclosan (or 2,4,4'-trichloro-2' hydroxyphenol ether), (e) chitosan ($\beta(1,4)$ -2-amino-2-deoxy-D-glycopyranose), and (f) *N*-halamine and peroxyacid. Additionally, some metal-complex dyes also show antimicrobial activity; however, metal-free dyestuffs are now more preferred due to environmental pollution caused by metal-complex dyes [4, 57, 114, 150, 200–203].

17 Microencapsulation in Coating and Finishing of Textiles

Microencapsulation is a type of micropackaging where different types of materials (such as cyclodextrins, urea, preformed synthetic polymers, biopolymers) can be used to work as a container or a cage in order to encapsulate the materials used in the core. The containers or the cages usually worked as a shell for the materials used in the core. For example, for thermoregulation, phase-change materials have been quite widely used in performance clothing.

Macroencapsulation are also popular in a number other areas of textile finishing, some of which are – (a) aromatherapy or controlled fragrance release, (b) antimicrobial finishes or deodorizing finishes, (c) insect-repellent or insect-resist treatments, (d) skin moisturizing or skin cooling finishes, (e) controlled release of vitamins or provitamins, (f) chemical protection, (g) application of UV-absorbers, (h) enzymetic actions, and (i) microclimate control in clothing, especially for thermoregulation of garments [4, 30, 57, 189–191]. Some of these microcapsules can also be used during textile coating formulations in order to realize specific application properties from particular types textiles coated with these microcapsules along with other additives present in the coating formulations.

18 Conductive Coatings

Conducting polymers are widely used for nanocoating on textiles for their various application potentials including their attractive electrochemical properties and their applications in advanced and conventional applications. Nanocoatings are usually

used in host matrices in various composite films. In addition, organic or inorganic particles can be mixed with or incorporated to conductive polymers to modify their behaviors, such as – (a) morphology, (b) conductivity, and (c) different physical and chemical properties, which depend on their target applications [15, 64].

19 Self-Assembled Nanophase Coatings

Conventional sol–gel method includes hydrolysis condensation processes which proceed through condensation polymerization upon film application on the substrate. In this case, the evaporation process results in voids and channels throughout the solid gel and cannot provide adequate corrosion protection because of high crack-forming tendency. Sol–gel technology is limited by the fact that the maximum attainable coating thickness using this technique is typically lower than 2 mm. However, different studies establish that incorporation of nanoparticles to the sol can make it possible to increase the coating thickness, without increasing the sintering temperature [5, 31–42, 68, 87–97].

20 Coated Breathable Fabrics

Coated breathable fabrics are mostly engineered composite materials which can be produced by a combination of a textile fabric and a polymer coating onto the fabric surface. Polymer materials (such as resins or polymer pastes) can be used for coating textiles during the coating process. The polymer coating provides new properties on the coated fabric. Polymers can also be applied to a fabric in terms of polymer membranes or they can be laminated to the fabric afterward in a separate process. Different processes and classes of adhesive and machinery are used during laminating process. Producing a strong bond using lamination technique is relatively simple; however, there are practical challenges when original properties of the fabric are to be preserved. But using flexible lamination technique some of the desired objectives such as appearance, handle, and durability can be preserved to some extent [4, 16–29, 57, 108]. Breathable fabric can be divided into various groups based on fundamental principles and design of the nature of waterproof character and breathability of fabrics. Some of these include – (a) closely woven fabrics, (b) microporous membranes and coating, (c) hydrophilic membranes and coating, (d) combination of microporous and hydrophilic membranes and coating, (e) retroreflective microbeads, (f) smart breathable fabrics, and (g) biomimetics. Differences in underlying mechanisms have significant influences on the vapor regulation of these fabrics which varies widely. In addition, some of the high-performance products mentioned are more expensive than normal waterproof fabrics. For a variety of applications, the technology is continuously evolving in the areas of a cost-effective manufacturing process to produce cost-effective breathable textiles. This technique uses quite a lot of methods to reduce the price, some of which are – (a) improving material formulation to enhance the properties of film and coating material, (b) controlling pore sizes and their distributions, (c) improving characteristics of hydrophilic solid

membrane, and (d) developing new technology combining new required methods (such as biomimetics, smart breathable fabrics) [4, 16–29, 57, 108].

Methods of Incorporation of Membranes and Their Applications in Textile Coatings When microporous fragile films are applied on fabrics, it causes to lose cloth-like feels. So, the incorporation of this type of films onto textile should be done in such a way that can maximize the high-tech function without adversely affecting the classical textile properties, such as handle, drape, and visual impression. Four major techniques are usually used to incorporate membranes onto textiles, they are – (a) laminating membrane and outer fabric, (b) liner or insert processing, (c) laminating membrane and lining fabric, and (d) laminating outer fabric, membrane and lining. Development of an improved and cheaper method (Reifenhauser) for producing breathable waterproof film/nonwoven laminates by a combined film extrusion and lamination process have been reported in different research studies. There are ways of incorporating coating by an electrostatic process rather than by using mechanical pressure. So, a careful selection of lamination process is vital to ensure the breathability of the laminate to maintain at a high level. The membrane has to be laminated with at least one substratum in order to serve varied applications of breathable fabrics. The nature of lamination of particular substrates depends on the final applications, some of which include – (a) woven for garments and wound dressing, (b) nonwovens for wound dressing, inserts/lining, roofing membranes and (c) foams for upholstery. For a number of reasons, nonwovens are usually more cost effective than traditional fabrics. MediSoft (Polymer Group Inc., the Netherlands) is a blend of spunmelt and spunlace which provides enhanced softness and breathability. DuPont Acturel (a product of DuPont) is made of three layers which are – (a) a polyester based nonwoven inner layer, (b) Dupont Hytrel as a breathable membrane layer, and (c) spun-bonded polypropylene as an outer layer. In this case, the first two layers are formed by an extrusion coating process, and the final outer layer is attached to the layer of Hytrel by an adhesive lamination process. Similarly, different type of nonwoven fabrics are made into breathable fabrics. In usual term, most of coated fabrics are treated with coating materials on the outer face sides. The conventional method of applying coating onto the fabric is by the direct application of the knife-over-roller technique. Sometimes textile coatings consist of several layers. Thinner coatings are applied on flexible fabrics (such as coating onto warp knitted, nonwoven, open weave, and elastic fabric) are sometimes achieved by using transfer coating technique. Transfer coating process applies a film by using casting technique on a release paper, which subsequently adhered to the fabric to make laminates. Some commercial products produced by using this transfer coating process include – (a) Cyclone (Carrington), (b) Entrant (Toray), and (c) Keelatex. Transfer coated and laminated fabrics are more permeable compared to direct-coated fabrics of the same fiber type for a particular polymer coating weight due to the blocking of the interstices by coating material in the latter case [4, 16–29, 57].

21 High-Tech Superhydrophobic-Coated Textiles

Durable non-wetting fabrics and their preparation and liquid transport function for high-tech applications. Recently, intensive research interests are focused on superhydrophobic textiles for a variety of application potentials. For example, air-permeable, super-liquid-repellent fabrics exhibit strong resistance to various liquid fluids and have self-cleaning, anti-sticking, and anticontaminating characteristics which have huge industrial application potentials for high-tech textile and textile products. However, most of the liquid-repellent fabrics are not strong enough and sometimes limit the application potentials. In this context, different related current research activities are focused on developing durable super-liquid-repellent fabrics and exploring novel property of liquid-repellent fabrics [8, 20, 125–128, 137–166, 169–185, 200–228].

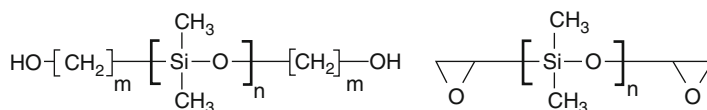
Typical elastomeric nanocomposites are used for the coating of superhydrophobic textile fabrics. For examples, polydimethylsiloxane filled with functionalized silica nanoparticles and fluorinated alkyl silane is popular for producing a superhydrophobic coating on fabrics (such as polyester, cotton, wool). In certain cases, the coated fabrics showed water contact angles higher than 170° and sliding angles lower than 5° . In addition, some coated textiles exhibited remarkable durability against strong acid, strong alkali, repeated machine washes, boiling water, and severe abrasion damages while retaining its superhydrophobic character. Besides this, durable, self-healing superamphiphobic fabrics can be prepared by elastomeric fluoropolymer containing nanoparticle and fluorinated alkyl silane. Many research groups have reported durable, self-healed coated fabrics which can show significant hydrophobic character. For example, a new coating system has been reported which can be used to produce fabrics with a durable self-healed superamphiphobic surface using elastomeric fluoropolymer containing nanoparticle and fluorinated alkyl silane with a two-step wet-chemistry coating technique. In that technique, the coating consists of a commonly used, commercially available fluoro-containing polymer, poly(vinylidene-fluoride-hexafluoropropylene), a fluorinated alkyl silane, and a surface modified silica nanoparticle. Besides this, different studies demonstrated that the treated fabrics showed remarkable liquid repellency (with water contact angle as high as 170° , and a contact angle above 150° to many oil fluids, such as soybean oil and hexadecane). When self-healing polymers are used in the coating formulations, they can show self-healing ability during any chemical damage and can restore their super liquid-repellent properties simply by a short-time heating treatment or room temperature ageing. Superhydrophobic-coated textile substrates have significant uses in various areas. For examples, wetting and non-wetting of fabrics have been involved with various applications. Superhydrophobic textiles (a textile surface with a contact angle larger than 150° to water) using coating techniques or other useful techniques have many applications in self-cleaning and anti-sticking abilities and potential uses in a variety of decontaminations. Significant progress has been reported to improve superhydrophobic fabrics

although most of the superhydrophobic fabrics show low durability to wash and poor abrasion fastness. Superoleophobic surfaces exhibit contact angle more than 150° with organic liquids having very low surface tensions and low contact angle hysteresis. They have huge application potentials in antifouling, anticrawling, decontamination, and microfluidics areas. Superoleophobic surfaces naturally show superhydrophobic characters when liquid repellency is based on a low surface energy (LSE) surface [169, 202–228].

21.1 Design, Development, and Evaluation of Superhydrophobic Coatings

Nanosol coatings are popular for producing hydrophobic-coated textiles where inorganic sols prepared from ordinary metal oxides, such as SiO_2 , TiO_2 . These metal oxides are chemically or physically modified with suitable hydrophobic additives during coating formulations. Some of the usually used hydrophobic additives are – (a) monomeric alkylsilane compounds, (b) polysiloxanes with hydrophobic groups (the chemical structures are shown in Scheme 1), and (c) fluorinated compounds (such as perfluorooctyltriethoxysilane).

However, for the preparation of water-repellent textiles, fluorinated compounds exert some practical limitations due to their high cost and potential risks to human health. Long-chained monomeric alkylsilane compounds can be used in the place of fluorinated compounds to produce hydrophobic nanosols for textile coatings. Additionally, with the increase of chain lengths of alkylsilane additives, the hydrophobicity of coated textiles shows a considerable increase. In addition, sol–gel coatings on textiles have been frequently used for functionalizing and refining the desired characters of coated textiles. Coating solutions can be applied onto the textile substrates using high speed spraying or other conventional coating methods. Very tiny (such as diameter less than 50 nm) size of the sol particles when used in the coating formulations along with other required additives contributes to improve adhesion properties and other mechanical as well as chemical properties of the coated textiles. The application of specially made nanosol solutions on coated textiles also enhance other properties some of which include – (a) abrasion resistance, (b) hydrophobic characters, (c) soil-repellent behaviors, and (d) modification of optical and biological properties. Additionally, it also provides the opportunity for the preparation of multifunctional coatings, for examples – multifunctional and bioactive coatings. A detail discussion on these multiple application methods and their synthetic techniques are beyond the scope of this current chapter. Special type



Scheme 1 Polysiloxanes for hydrophobic modification of nanosols

of sol-gel coated superhydrophobic coated textile have many applications, some of which include – (a) antiadhesive wound dressing, (b) leaching behavior of embedded dyes, (c) photobleaching behavior, (d) UV protection, (e) improved electric conductivity of textiles, (f) immobilization and controlled release of bioactive species, oils, and flavors, (g) antimicrobially finished textiles, (h) photoactive nanosol coatings, (i) nanosol coatings containing nondiffusible antimicrobial additives, (j) nanosol coatings with controlled-release embedded biocides, and (k) oil and flavor released coatings of textiles [5, 8, 18–29, 31–47, 104–141, 151–170]. Besides this, superhydrophobic surfaces are topics of active current research interest both in academic and industrial arena for their many practical applications including – (a) contamination prevention, (b) self-cleaning, (c) antifouling surface designs, (d) anti-icing coatings, (e) corrosion resistance of metals and their alloys, and (f) biomedical and biological applications. By controlling the topographic features and surface energies, coated hydrophobic surfaces can be fabricated. In addition, a surface's water repellency is an important phenomenon in natural and technological processes and a superhydrophobic surface is termed by a water contact angle (WCA) greater than 150° and a sliding angle (SA) lower than 5° . Examples of superhydrophobic surfaces prevail in nature which include – (a) lotus leaves, (b) butterfly wings, (c) duck feathers, etc. Based on bioinspiration from nature, superhydrophobic surfaces can be derived by using two kinds of approaches which are – (a) firstly, the solid surface that is chemically modified with a low-surface-energy material and (b) secondly, nano- and microscale structures which are created on the substrate to prevent water from completely being in contact with the surface. In this method, the water droplets sit mostly on the air and the water droplets on superhydrophobic surfaces can be nearly spherical and therefore have a tiny liquid–solid contact area that leads to easy roll off. Cassie's law states how simply roughing up a substrate can increase the apparent contact angle of a surface to form appropriate surface patterns on hydrophobic surfaces in order to lead to a general change in their wettability for increasing the contact angle substantially. On this theme, an extensive research has been carried out in order to understand the formation of superhydrophobicity on various substrates. For example, organic/inorganic hybrid coatings have been extensively studied based on the sol-gel technique to produce a simple and cost-effective method in order to functionalize different surfaces. The presence of aliphatic hydrocarbon or perfluoro chains in the sol-gel precursors can substantially decrease the surface energy of the derived coatings. In addition, the mechanical properties of the films and adhesion strength to the substrate can be improved by crosslinking the silanol groups in the matrix and introducing chemical bonding between the coating and the substrate [219–268].

21.1.1 Self-Cleaning Fabrics: Superhydrophobic Finishes for Water-, Oil-, and Stain-Repellency

The revolution in this area involves the use of biomimetics to mimic the microstructure and nanostructure of the surface of the lotus leaf (also called “lotus effect”) which essentially provides the lotus leaf with self-cleaning characters where the

contact angle of water on a lotus leaf can reach up to 170° due to the nature of the surface roughness generated by the wax layer. In addition, the water droplets rest on the outermost points of the minute wax mounds with air underneath the droplets so that the surface area contact is as low as 7%. By mimicking this similar idea, researches use nanotechnology approach in order to replicate the “lotus effect” on coated textile surfaces by engineering the micro- and nanoscale surface features of fibers and fabrics using nanomaterials or other suitable materials or techniques. Similarly, fluorochemical-based finishes have been developed that can provide superhydrophobic performance with extremely high water contact angles ($>150^\circ$) which allow water droplets to roll off at slight inclination. In addition, a novel water shedding angle method has been developed in order to evaluate the water-repellent characters of superhydrophobic surfaces [173–177].

21.1.2 Application of Polymer Nanocomposites for Producing Superhydrophobic, Self-Cleaning Textiles

Different types of technique (for examples, sol–gel methods, self-assembly of polymer layers, plasma treatments, and laser etching) are popularly used for incorporating nanoparticles to create a nanoscale surface roughness to meet different required specifications for particular products (such as highly water proof or soil-resistant textiles). Using specific types of polymers and nanoparticles, now it is practically possible to produce multifunctional properties on coated textiles (such as self-cleaned coated textiles), where such fabrics can exhibit higher levels of easy care, but the durability of the effect (particularly oil-repellent character) should preferably persist throughout the wear life of the textile product. Besides this, this area of research in chemical finishing and coating has been successful to emerge as a new vistas in textile finishing. The higher fabric performance along with desired functionality may open up new consumer markets and outdoor technical textile markets in near future. For example, the incorporation of nanoparticles (such as anatase type titanium dioxide) during textile coatings or other suitable operations may contribute to photocatalytically decompose fabric stains (such as certain type of stains) due to the action of ultraviolet radiation from sunlight [20, 176–179, 181–184].

22 Powder Coating Technology and Coated Textiles

Mostly for composite textiles, powder coating technology has some appealing application potentials. In addition, powder coatings have many attractive features which also make them popular day by day. In principle, coatings from solid components are melt mixed during the application of powder coatings on suitable substrates where the insoluble components (such as pigments are dispersed in the matrix of the binder components). In addition, the formulation is pulverized on a substrate and finely fused to become a continuous film; binders for thermosetting powder coatings consist of a mixture of the primary resin and a cross-linker [67–74]. For example, semicrystalline urethane groups containing polymers without

Table 3 Different types of thermosetting powder coatings

Coating types	Usually used binders	Popular cross-linkers
Epoxy coating	Bisphenol A epoxy Novolac epoxy	Polyamines Anhydrides or phenolics
Hybrid coatings	Polyesters with COOH end groups Polyesters with OH end groups	Triglycidylisocyanurate Block isocyanates
Acrylic coatings	Epoxy functional acrylics Hydroxy functional acrylics	Dicarboxylic acids Blocked isocyanates
UV-curable coatings	Acrylate functional resins Epoxy functional resins	Free radical Cationic

using isocyanates or phosgene can be used for powder coating resins. The new development in polyurethane chemistry is generally promoted by the use of non-isocyanate and phosgene free routes [67–75]. Powder coatings are of different types some of which are selectively described in Table 3.

22.1 Epoxy Powder Coatings

Epoxy resins are popularly used in powder coatings which is the largest in proportions in terms of use from the class of thermosetting powder coatings. Additionally, in an epoxy coating, a bisphenol A or a novolac epoxy resin is cross-linked with polyamines or anhydrides. Bisphenol A (BPA) epoxies are usually prepared by reacting BPA with epichlorohydrin to incorporate glycidyl ether end groups. Epoxy resins are prepared from the reaction of *o*- or *p*-cresol-formaldehyde novolacs with epichlorohydrin and the resulting novolac epoxy resins are useful in applications where more than two epoxy groups per molecule are expected. Epoxy powder coatings exhibit attractive sound mechanical properties (such as adhesion, and corrosion protection), and they have many potential uses, some of which include – decorative applications in institutional furniture, shelving, and tools. In addition, protective epoxy coatings include various applications for pipes, electrical equipment, primers, and automotive underbody parts [67–73].

22.2 Hybrid Powder Coatings

Polyesters with carboxylic acid end groups are cross-linked by an epoxy cross-linker during their use in hybrid coatings, and these type of coatings are intermediate between epoxy and polyester coatings. Usually, polyester resins are derived from neopentyl glycol and terephthalic acid with a small amount of other monomers in order to adjust the glass transition temperature and also to introduce branching which increases the functionality above two. This type of coating exhibit color retention and UV resistance than epoxy powder coatings and also used in many applications (such as water heaters, fire extinguishers, radiators, and transformer covers). In

addition, powder coatings containing carboxylic acid terminated polyesters have poorer flow behaviors compared to hydroxy terminated polyesters [67–73].

22.3 Polyester Powder Coatings

Triglycidylisocyanurate (TGIC) is a popular cross-linker for carboxylic acid-terminated polyesters with basic catalysts (with a solid trifunctional epoxy cross-linker) where the presence of three functional groups results in higher cross-link density than obtained with BPA epoxy resins. Typically used binders generally contain 4–10 wt% TGIC and 90–96 wt% of carboxylic acid-terminated polyesters. Additionally, the generally used polyesters are less branched compared to those used in hybrid coatings due to their higher functionality of TGIC than BPA oxides. TGIC-based powder coatings have good exterior stability and mechanical characters which are useful for different applications including in – (a) outdoor furniture, (b) farm equipment, (c) fence poles, and (d) air conditioning units. However, TGIC is considered to be toxic in nature. Tetra(2-hydroxyalkyl)bisamides were introduced as cross-linking agents for carboxylic acid-terminated polyesters in exterior durable coatings, and these coatings also have good mechanical character and flow behaviors. Usually, blocked isocyanates are also used as cross-linkers with polyesters containing hydroxy end groups, and this type of isocyanate-polyester powder coatings typically exhibit better flow compared to most powder coatings due to the unreacted cross-linkers or blocking agents released upon unblocking are good plasticizers. They are usually used for coating different items, some of which include – (a) automobile wheels, (b) lighting fixtures, (c) garden tractors, (d) fence fittings, and (e) playground equipment. In this context, derivatives of isophorone diisocyanate, bis(4-isocyanatocyclohexyl) methane, and tetramethylxylidene diisocyanate are selective examples of blocked isocyanates which show solid physical characters [67–73].

22.4 Acrylic Powder Coatings

The epoxy or hydroxy functional acrylic binder is cross-linked with dicarboxylic acids (such as dodecanedioic acid $(\text{HOOC}(\text{CH}_2)_{10}\text{COOH})_{14}$, or blocked isocyanates) during in acrylic coatings. Usually, acrylic powder coatings exhibit superior detergent resistance and are useful for applications in different types of coatings (such as coating washing machines) [67–73].

22.5 UV-Curable Powder Coatings

Polymers with acrylic functional groups or epoxy functional groups (which are cross-linked within the polymer network through free radical or cationic mechanism) are widely used in UV-curable coatings. Radiation curable coatings are cross-linked through reactions initiated with radiation rather than heat, and they exhibit relative

stability during the storage in the absence of radiation where the crosslinking takes place at ambient temperature when exposed to radiation. In powder coatings, it is very important to control the balance of binder glass transition temperature, molecular weight, and reactivity. When the glass transition temperature of a binder used in the coating formulation is high enough, it provides an option to avoid the sintering operation. However, low glass transition temperature contributes to promote coalescence and levelling at the lowest possible temperature. But the short baking times at low temperatures are possible when the resins are highly reactive and the baking temperature is well above the glass transition temperature of the final cross-linked film. This type of compositions may exhibit crosslinking during extrusion and a rapid increase in viscosity as the particles fuse in the oven limits the ability of the coating to coalesce and level. Different factors have controlling effect on glass transition temperature which include – (a) chemical composition and (b) molecular weight. In addition, it has been reported to use higher molecular weight to ensure more flexibility within the resin systems since these may have adequate package stability and also flow more easily during baking than a low molecular weight resin of similar glass transition temperature that has more rigid chains. Moreover, differential scanning calorimetry is one of the powerful tools to determine glass transition temperature and curing and cure response, and this technique is also often used to study powder coatings [67–73].

All these types of powder coatings have many potentials in different particular types of textiles for specific applications.

23 Photonic Coatings on Textiles

In this type of coatings, usually photonic materials (such as photonic metal oxides, a photoresponsive material or similar other type of materials) are incorporated in the coating formulations for producing certain types of functional coated textile substrates. For example, when a photochromic dye is used as a photonic material in the coating formulation, the textile substrate coated with this formulation shows photoresponsive behavior when exposed to UV light or sunlight. In this case, the dye isomerizes into a different form when exposed to actinic radiation (such as sunlight, UV light). For producing photoresponsive-coated textiles, different types of photochromic dyes are most commonly used, some of which include – (a) azobenzene derivatives (which undergo cis–trans isomerization), (b) hydrophobic spiropyran derivatives (which isomerize into the hydrophilic merocyanine form), (c) spirooxazines, (d) fulgides, and (e) diarylethenes. Isomerization of the photochromic dye can change the functional characters of the coated textile substrates to cause change in topological behaviors [1, 2, 79, 80, 188–192, 204–209, 218].

24 Textile Finishing and Textile Coatings in Future

Textile finishing processes including textile coatings are changing with time and also with the evolution of new environmentally friendly materials (such as polymers, dyes, pigments, additives) and techniques (such as nanocoating technologies, plasma

coating, inkjet coating, and other advanced coating techniques). Different ground breaking noble achievements have recognizable significant impacts on textile sectors that have been realized almost in every decades since 1920 to current age. To keep pace with this evolutions in different areas, there are relative changes in order to adopt these new methods and techniques during the production of finished textile products including the coated textile substrates. Different external factors have significant influences on this textile finishing as well as textile coating sectors. For example, changes in global macroeconomics, politics, global resources (such as sustainable uses and availability of different resources including fibers, energy, water), possible climate change and initiatives towards more environmentally and cost-effective production targets, as well as the growth of domestic developing economies have immense impact on different processing techniques and methods usually used for the production of textile and allied products in the future. The textile finishing (including textile coating) sector is a type of service sector, and it requires to be responsive to the changing market demands where incremental changes are usually apparent. In addition, in almost every decade, some technical developments have been reported which very often bring about quantum changes in textile finishing as well as in textile coatings. For example, textile finishing as well as textile coating sectors have encompassed three main revolutions (which are – mechanical, chemical, and electronic revolutions) which are on the verge of fourth revolution due to their necessary competence with on-coming technological revolution with the advent of the state of art new technologies (some of which include – nanotechnology, biotechnology, plasma technology, other advanced coating technologies, and inkjet technology). Current developments in these areas of textile finishing (including textile coatings) and also in the areas of easy care, durable press, and wrinkle-free finishes and antimicrobial and flame-retardant finishes; softening techniques are worth to mention here. In addition, developments in microencapsulation and also in self-cleaning fabrics with superhydrophobic finishes for water-, oil-, and stain-repellency have significant achievement in these areas to produce high-quality textile products for specific targeted applications. In this context, novel application technologies for chemical finishing which significantly decrease water and energy consumption have also made some very striking notable progresses which have the potentials to shape these industries.

Coating technique is one of many techniques which can also be used for applying easy care, durable press, and wrinkle-free finishes onto the textiles. Significant progresses have been made in the field of textile finishing to produce easy care, durable press, and wrinkle-free textiles using different techniques. Additionally, notable improvements have been realized by giving chemical cross-linking treatments on cotton and other cellulosic fibers and their blends with synthetic fibers. For example, for textile finishing, mainly self-cross-linking resins (such as urea-formaldehyde) have been replaced with *NN*1,3-dimethylol-4,5-dihydroxyethylene urea (DMDHEU) and other derivatives, where the release of formaldehyde is significantly reduced by the use of methylated or glycolated DMDHEU derivatives which show improved stability compared to DMDHEU. The use of such products in along with a formaldehyde acceptor (such as urea or diethylene glycol) can be

applied to minimize formaldehyde generation from the resin finished fabric. Besides this, zero formaldehyde resins (such as DHDMI, or DMeDHEU, or 1,3-dimethyl-4,5-dihydroxyethylene urea) have also been developed; however, a less uniform cross-linked distribution with a reduced easy-care performance is one of the limiting effects of this type of resins. In addition, a higher amount of this type of resin is usually required in order to produce a satisfactory performance, and the curing temperature and cure times are comparatively higher than for DMDHEU. Polycarboxylic acids based other formaldehyde-free resin finishes, for examples, citric acid, malic acid, 1, 2, 3, 4-butanetetracarboxylic acid or polymaleic acid derivatives have been reported for their usefulness in wrinkle-free finishing, but their durable press performance is relatively inferior to that of DMDHEU. In addition, ultra-low formaldehyde resins are very popular in this regard for meeting targets set by the legislation on residual formaldehyde levels in finished fabric. Continuous research activities are going on for a chemical breakthrough to produce new cross-linking agents which are formaldehyde-free and also to prepare new catalysts that can ensure cross-linking of cellulosic and cellulosic blend fabrics cured in considerably short period of time and also at low temperatures [238–288].

24.1 Main Influencing Factors for Future Developments in Textile Coating and Finishing

Textile finishing (as well as textile coatings) in future depends on a number of things where the currently available techniques and methods as well as the future developments in this area needs to satisfy different competing criteria including the consumer demands, innovation, change in process due to environmental causes and sustainability, as well as new product functionalities. In this context, the main drivers of change in textile finishing (including textile coatings) are required to concentrate on a number of areas including in – (a) fashion (such as aesthetics, appearance, image, or prestige), (b) consumer demands (for examples, comfort, changing demands, or lifestyles), (c) environmental causes (such as legal, ecological, care, REACH, BPD), (d) safety requirements (for instance, legal, health, or protection), (e) technical specifications (for instance, innovation, new applications, smart textiles, wearable technologies), (f) meeting sustainability (such as supply chain sustainability, maximizing performance with minimum use of fibers and all utilities like energy, water, chemicals and also incorporating recycling possibilities), and (g) other demand (such as aftercare). Here, REACH stands for registration, evaluation, authorization, and restriction of chemicals, whereas BPD stands for biocidal products directive.

The global market for chemical finishes is increasingly becoming very discerning and is demanding comparatively more technical input from both chemical suppliers and textile wet processors in order for providing more innovations and developments. In addition, there are incremental demands from both the retailers and also from consumers on novel finishes, greater added value, enhanced comfort, protection, and performance from the finished textiles or coated textiles and their products

which they purchase. The continual expansion of technical textile sector with a range of textile applications and end uses involves continuous research in the areas on chemical finishes for self-cleaning textiles and abrasion-resistant textiles, among many other performance-driven criteria which are creating challenges for chemical manufacturers and textile finishing companies as well as industries which are mainly focused on textile coatings.

25 Conclusion and Perspectives

Coated textile fabrics have a wide variety of applications, for examples, their uses in protective clothing to architectural materials. Typically used textile coating technologies use a wide variety of materials (such as elastomers and silicones, polyurethane, polytetrafluoroethylene) for the applications of coating formulations using different techniques which include – direct coating, transfer coating, digital or inkjet coating, and extrusion coating. Recent advances on coating textiles using advanced techniques are enormous, some of which include – (a) plasma coating, (b) nanocoating, (c) inkjet coating with the aim to improve functionality, reduce the costs, and also improve environmentally sustainable manufacturing operations. The chapter has briefly discussed different important topics and items usually used for conventional and advanced textile coatings. For example, it has briefly described the methods and approaches in order to design hydrophobic or superhydrophobic coatings based on sol–gel chemistry by incorporating hydrophobic moieties and controlling surface morphology. It has also provided a brief account of various types of coatings and methods which are usually used in textile coatings. At the end, it has briefly discussed the recent trends in textile coatings and the nature of advanced technologies which are focused in most current progresses and trends in future developments. It is beyond the scope of this current chapter to provide a detail explanation of all the methods and coating systems stated in this chapter, so readers are advised to consult the references for more detailed information.

References

1. S.M.R. Billah, Chapter 4. Inkjet printed photo-responsive textiles for conventional and high-tech applications, in *Textiles: History, Properties & Performance and Applications*, ed. by M.I.H. Mondal (Nova Science Publishers, New York, 2014), pp. 81–122
2. S.M.R. Billah, Chapter 7. Smart textiles and the effective uses of photochromic, thermochromic, ionochromic and electrochromic molecular switches, in *Textiles: History, Properties & Performance and Applications*, ed. by M.I.H. Mondal (Nova Science Publishers, New York, 2014), pp. 187–238
3. (a) E. Amerio, P. Fabbri, G. Malucelli, M. Messori, M. Sangermano, R. Taurino, Scratch resistance of nano-silica reinforced acrylic coatings. *Prog. Org. Coat.* **62**, 129 (2008). (b) J. Baghdachi, Chapter 1. Smart coatings, in *Smart Coatings II*, ACS Symposium Series, vol. 1002 (2009), pp. 3–24
4. (a) A.K. Sen, *Coated Textiles – Principles and Applications*, 2nd edn. (CRC Press, Boca Raton, 2008), pp. 1–225. (b) A.A. Tracton (ed.), *Coating Technology – Fundamentals, Testing,*

- and Processing Techniques, 2nd edn., pp. 1–250. (c) A.A. Tracton (ed.), *Coating Technology Fundamentals, Testing, and Processing Techniques*, 3rd edn. (CRC Press, 2006), pp. 1–320. (d) B. Zorn, *J. Coat. Fabrics* **13**, 166 (1984)
5. M.N. Sathyanarayana, M. Yaseen, Role of promoters in improving adhesion of organic coatings to a substrate. *Prog. Org. Coat.* **26**, 275–313 (1995)
 6. J. Kettle, T. Lamminmaki, P. Gane, A review of modified surfaces for high speed inkjet coating. *Surf. Coat. Technol.* **204**, 2103–2109 (2010)
 7. Y. Ner, C. Asemota, J.R. Olson, G.A. Sotzing, Nanofiber alignment on a flexible substrate: hierarchical order from macro to nano. *Appl. Mater. Interfaces* **1**, 2093–2097 (2009)
 8. S. Sundarajan, A.R. Chandrasekaran, S. Ramakrishna, An update on nanomaterials-based textiles for protection and decontamination. *J. Am. Ceram. Soc.* **93**(12), 3955–3975 (2010)
 9. A. El Shafei, S. Shaarawy, A. Hebeish, Application of reactive cyclodextrin poly butyl acrylate preformed polymers containing nano-ZnO to cotton fabrics and their impact on fabric performance. *Carbohydr. Polym.* **79**, 852–857 (2010)
 10. Y. Li, D.X. Wu, J.Y. Hu, S.X. Wang, Novel infrared radiation properties of cotton fabric coated with nano Zn/ZnO particles. *Colloids Surf. A Physicochem. Eng. Asp.* **300**, 140–144 (2007)
 11. M.H. El-Rafie, A.A. Mohamed, T.I. Shaheen, A. Hebeish, Antimicrobial effect of silver nanoparticles produced by fungal process on cotton fabrics. *Carbohydr. Polym.* **80**, 779–782 (2010)
 12. C. Su, J. Li, The friction property of super-hydrophobic cotton textiles. *Appl. Surf. Sci.* **256**, 4220–4225 (2010)
 13. H. Lu, L. Song, Y. Hu, A review on flame retardant technology in China. Part II: flame retardant polymeric nanocomposites and coatings. *Polym. Adv. Technol.* **22**, 379–394 (2011)
 14. K.H. Ki, J.H. Kim, S.C. Kwon, S.H. Jeong, A study on multifunctional wool textiles treated with nano-sized silver. *J. Mater. Sci., Germany*, **42**, 8020–8024 (2007)
 15. L. Hu, M. Pasta, F.L. Mantia, L.F. Cui, S. Jeong, H.D. Deshazer, J.W. Choi, S.M. Han, Y. Cui, Stretchable, porous, and conductive energy textiles. *Nano Lett.* **10**(2), 708–714 (2010)
 16. B. Leng, Z. Shao, G. With, W. Ming, Superoleophobic cotton textiles. *Langmuir* **25**, 2456–2460 (2009)
 17. G.K. Hyde, K.J. Park, S.M. Stewart, J.P. Hinestroza, G.N. Parsons, Atomic layer deposition of conformal inorganic nanoscale coatings on three-dimensional natural fiber systems: effect of surface topology on film growth characteristics. *Langmuir* **23**, 9844–9849 (2007)
 18. (a) I.P. Parkin, R.G. Palgrave, Self-cleaning coatings. *J. Mater. Chem.* **15**, 1689–1695 (2005). (b) B. Mahltig, T. Textor, *Nanosols and Textiles* (World Scientific Publishing, 2008)
 19. S. Sakka, *Handbook of Sol-Gel Science and Technology* (Springer, 2004), pp. 23–353
 20. J. Alongi, M. Ciobanu, G. Malucelli, Thermal stability, flame retardancy and mechanical properties of cotton fabrics treated with inorganic coatings synthesized through sol–gel processes. *Carbohydr. Polym.* **87**(3), 2093–2099 (2012)
 21. B. Tomšič, B. Simoncic, B. Orel, M. Zerjav, H. Schroers, A. Simoncic, Z. Samardžija, Antimicrobial activity of AgCl embedded in a silica matrix on cotton fabric. *Carbohydr. Polym.* **75**, 618–626 (2009)
 22. K. Qi, J.H. Xin, Room-temperature synthesis of single-phase anatase TiO₂ by aging and its self-cleaning properties. *Appl. Mater. Interfaces* **2**, 3479–3485 (2010)
 23. A. Vilnik, I. Jerman, A. SurcaVuk, M. Kozelj, B. Orel, B. Tomsic, B. Simoncic, J. Kovac, Structural properties and antibacterial effects of hydrophobic and oleophobic sol-gel coatings for cotton fabrics. *Langmuir* **25**(10), 5869–5880 (2009)
 24. T. Textor, B. Mahltig, A sol–gel based surface treatment for preparation of water repellent antistatic textiles. *Appl. Surf. Sci.* **256**, 1668–1674 (2010)
 25. C. Zheng, G. Chen, Z. Qi, Ultraviolet resistant/antiwrinkle finishing of cotton fabrics by sol-gel method. *J. Appl. Polym. Sci.* **122**, 2090–2098 (2011)
 26. M. Messaoud, E. Chadeau, C. Brunon, T. Ballet, L. Rappenne, F. Roussel, D. Leonard, N. Oulahal, M. Langlet, Photocatalytic generation of silver nanoparticles and application to the antibacterial functionalization of textile fabrics. *J. Photochem. Photobiol. A Chem.* **215**, 147–156 (2010)

27. G.Y. Bae, B.G. Min, Y.G. Jeong, S.C. Lee, J.H. Jang, G.H. Koo, Superhydrophobicity of cotton fabrics treated with silica nanoparticles and water-repellent agent. *J. Colloid Interface Sci.* **337**(1), 170–175 (2009)
28. M. Yu, G. Gu, W.D. Meng, F.L. Qing, Superhydrophobic cotton fabric coating based on a complex layer of silica nanoparticles and perfluorooctylated quaternary ammonium silane coupling agent. *Appl. Surf. Sci.* **253**(7), 3669–3673 (2007)
29. C.H. Xue, S.T. Jia, H.Z. Chen, M. Wang, Superhydrophobic cotton fabrics prepared by sol-gel coating of TiO₂ and surface hydrophobization. *Sci. Technol. Adv. Mater.* **9**(3), 035001–035006 (2008)
30. O.A. Hakeim, A.A. Arafa, M.K. Zahran, L.A.W. Abdou, UV-curable encapsulation of surface – modified organic pigments for inkjet printing of textiles. *Colloids Surf. A* **447**, 172–182 (2014)
31. (a) A.S.H. Makhoulf, I. Tiginyanu, *Nanocoatings and Ultra-Thin Films Technologies and Applications* (Woodhead Publishing Limited, Cambridge, 2011), pp. 1–345.
(b) E.P. Plueddemann, *Silane Coupling Agents*, 2nd edn. (Plenum Press, New York, 1991), pp. 1–22
32. E.K. Drown, H.A. Moussawi, L. Drzal, Glass fiber sizings and their role in fiber-matrix adhesion, in *Silanes and Other Coupling Agents*, ed. by K.L. Mittal (VSP, Utrecht, 1992), pp. 513–529
33. M.A. Ansarifar, L.K. Chong, J. Zhang, A. Bell, R.J. Ellis, Effect of bifunctional organosilane on the joint strength of some natural rubber compounds to nylon 6,6. *Int. J. Adhes. Adhes.* **23**(3), 177–188 (2003)
34. A.C. Miller, J.C. Berg, Predicting adhesion between a crystalline polymer and silane-treated glass surfaces in filled composites. *J. Adhes. Sci. Technol.* **16**(14), 1949–1956 (2002)
35. G.L. Witucki, A silane primer: chemistry and applications of alkoxy silanes. *J. Coat. Technol.* **65**(822), 57–60 (1993)
36. M. Guichenuy, M.L. Abel, M. Audenaert, A. Vineer, J.F. Watts, Mechanism of delamination of a thick coating on untreated steel, in *Proceedings of the 27th Annual Meeting of the Adhesion Society, Inc.* (2004), pp. 200–201
37. F.J. Boerio, P. Shah, Adhesion of injection molded PVC to steel substrates. *J. Adhes.* **81**(6), 645–675 (2005)
38. H. Scott, J. Humphries, Novel crosslinking method for polyethylene. *Mod. Plast.* **50**(3), 82 (1973)
39. M.S. Hearn, J.D. Baird, L.P. Nethsinghe, M. Gilbert, Silane crosslinking of plasticized polyvinyl chloride. *Polym. Commun.* **31**(5), 194–197 (1990)
40. F.D. Buyl, Silicone sealants and structural adhesives. *Int. J. Adhes. Adhes.* **21**(5), 411–422 (2001)
41. T.P. Chou, C. Chandrasekaran, S. Limmer, C. Nguyen, G.Z. Cao, Organic-inorganic sol-gel coating for corrosion protection of stainless steel. *J. Mater. Sci. Lett.* **21**, 251–255 (2002)
42. B. Arkles, J.R. Steinmetz, J. Zazyczny, P. Metha, Factors contributing to the stability of alkoxy silanes in aqueous solution, in *Silanes and Other Coupling Agents*, ed. by K.L. Mittal (VSP, Utrecht, 1992), pp. 91–104
43. N. Abidi, H. Eric, L. Cabrales, Functionalization of a cotton fabric surface with titania nanosols: applications for self-cleaning and UV-protection properties. *ACS Appl. Mater. Interfaces* **1**, 2141–2146 (2009)
44. R. Higgins, *Powder Coatings* (Campden Publishing Ltd., New York, USA, 1998), pp. 2–77
45. W.A. Daoud, J.H. Xin, Y.H. Zhang, K. Qi, Surface characterization of thin titania films prepared at low temperatures. *J. Non-Cryst. Solids* **351**(16), 1486–1490 (2005)
46. R. Dastjerdi, M. Montazer, A review on the application of inorganic nano-structure materials in the modification of textiles: focus on anti-microbial properties. *Colloids Surf. B Biointerfaces* **79**, 5–18 (2010)
47. (a) Z. Shi, I. Wymana, G. Liua, H. Hua, H. Zoub, J. Hub, Preparation of water-repellent cotton fabrics from fluorinated diblock copolymers and evaluation of their durability. *Polymer* **54**,

- 6406–6414 (2013). (b) R. Rahal, T. Pigot, D. Foix, S. Lacombe, Photocatalytic efficiency and self-cleaning properties under visible light of cotton fabrics coated with sensitized TiO₂. *Appl. Catal. B Environ.* **104** (2011)
48. D. Wu, M. Long, J. Zhou, W. Cai, X. Zhu, C. Chen, Y. Wu, Synthesis and characterization of self-cleaning cotton fabrics modified by TiO₂ through facile approach. *Surf. Coat. Technol.* **203**, 3728–3733 (2009)
49. M. Hasem, P. Hauser, B. Smith, Wrinkle recovery for cellulosic fabric by means of ionic crosslinking. *Text. Res. J.* **3**(9), 762–766 (2003)
50. M. Hasem, P. Hauser, B. Smith, Reaction efficiency for cellulose cationization using 3-chloro-2-hydroxypropyl trimethyl ammonium chloride. *Text. Res. J.* **73**(11), 1017–1023 (2003)
51. M.M. Kamel, E.A. El Kharadly, B.M. Youssef, Dyeing of chemically modified cellulose with methylolated acrylamide derivatives. *Cellul. Chem. Technol.* **18**(5), 459–468 (1984)
52. R. Butnaru, A. Muresanu, S. Mitu, Influence of crease resist finish treatments upon the comfort indices in cotton-type textiles. *Cellul. Chem. Technol.* **20**(3), 349–355 (1986)
53. P. Bajaj, S. Chakrapani, N.K. Jha, Flame retardant durable-press finishes for cotton and polyester/cellulose blends. *Text. Res. J.* **54**(9), 619–630 (1984)
54. Y. Shin, N.R.S. Hollies, K. Yeh, Polymerization crosslinking of cotton fabric for superior performance properties. I. A preliminary study. *Text. Res. J.* **59**(11), 635–642 (1989)
55. I. Holme, Water repellency and waterproofing, in *Textile Finishing*, ed. by D. Heywood (Society of Dyers and Colourists, West Yorkshire, 2003), pp. 137–213
56. E. Kissa, *Handbook of Fiber Science and Technology*, vol. II Chemical Processing of Fibers and Fabrics Part B, ed. by M. Lewin, S. Sello (Marcel Dekker, New York, 1984), pp. 2–65
57. W. Schindler, P. Hauser, *Chemical Finishing of Textiles* (Woodhead Publishing Limited, Cambridge, 2004), pp. 2–78
58. K. Singha, A review on coating & lamination in textiles: processes and applications. *Am. J. Polym. Sci.* **2**(3), 39–49 (2012)
59. I. Holme, *Coating and Lamination Enhance Textile Performance*, 3rd edn. (Technical Textiles International, Woodhead Publishing Limited, Cambridge, England, 2003)
60. S. Mondal, Phase change materials for smart textiles – an overview. *Appl. Therm. Eng.* **28**(11–12), 1536–1550 (2008)
61. G. Stephen, B. Serge, R. Meryline, V. Isabelle, T. Lan, D. Rene, P. Frank, Flame retarded polyurea with microencapsulated ammonium phosphate. *Polym. Degrad. Stab.* **88**, 106–113 (2005)
62. Y.L. Weijun, M. Fai, X. John, T. Leung, L.D. Kam, L. Pei, Novel core-shell particles with poly (*n*-butyl acrylate) cores & chitosan shells as an antibacterial coating for textiles. *Polymer* **46**, 10538–10543 (2005)
63. S.V. Kangwansupamonkon, Antibacterial effect of apatite-coated titanium dioxide for textiles application. *Nanomed. Nanotechnol. Biol. Med.* **5**, 240–249 (2009)
64. (a) T. Matejmicusik, M. Igor, F. Katarina, M. Chehimi, Conductive polymer coated textiles: the role of fabric treatment by pyrrole-functionalised triethoxysilane. *Synth. Met.* **157**, 914–923 (2007). (b) T. Lin, L. Wang, X. Wang, A. Kaynak, Polymerising pyrrole on polyester textiles and controlling the conductivity through coating thickness. *Thin Solid Films* **489**, 77–82 (2005)
65. S.M. Bidoki, R. Wittlinger, Environmental and economical acceptance of polyvinyl chloride (PVC) coating agents. *J. Clean. Prod.* **18**(3), 219–225 (2010)
66. F.C. Krebs, Fabrication and processing of polymer solar cells: a review of printing and coating techniques. *Sol. Energy Mater. Sol. Cells* **93**(4), 394–412 (2010)
67. (a) I. Bombard, P. Laurent, J. Lieto, G. Jeandel, A model of the infrared cure of powder coatings based on surface absorptivities in-situ measurements. *J. Coat. Technol. Res.* **5**(3), 353–363 (2008). (b) F.C. Krebs, Fabrication and processing of polymer solar cells: a review of printing and coating techniques. *Sol. Energy Mater. Sol. Cells* **93**(4), 394–412 (2009)
68. M.E. Gross, P.M. Martin, Chapter 11: Vacuum polymer deposition, in *Handbook of Deposition Technologies for Films and Coatings*, P.M. Martin, Editor. 2010, Elsevier. pp. 532–553

69. (a) T.F. Degnan, Temperature gradients in electron beam cured coatings. *Radiat. Phys. Chem.* **19**(5), 393–401(1982); (b) Natural wood effect with UV curable powder coatings. *Focus Powder Coat* **2008**(11), 2–5 (2008)
70. H. Zhou, H. Wang, H. Niu, T. Lin, Superphobicity/philicity Janus fabrics with switchable, spontaneous, directional transport ability to water and oil fluids. *Sci. Rep.* **3**, 2964 (2013)
71. H. Zhou, H. Wang, H. Niu, A. Gestos, T. Lin, Robust, self-healing superamphiphobic fabrics prepared by two-step coating of fluoro-containing polymer, fluoroalkyl silane and modified silica nanoparticles. *Adv. Funct. Mater.* **23**, 1664 (2013)
72. H. Zhou, H. Wang, H. Niu, A. Gestos, X. Wang, T. Lin, Fluoroalkyl silane modified silicone rubber/nanoparticle composite: a super durable, robust superhydrophobic fabric coating. *Adv. Mater.* **24**, 2409–2412 (2012)
73. H. Wang, H. Zhou, A. Gestos, J. Fang, H. Niu, J. Ding, T. Lin, Robust, electro-conductive, self-healing superamphiphobic fabric prepared by one-step vapour-phase polymerisation of poly(3,4-ethylenedioxythiophene) in the presence of fluorinated decyl polyhedral oligomeric silsesquioxane and fluorinated alkyl silane. *Soft Matter* **9**, 277 (2013)
74. H. Wang, H. Zhou, A. Gestos, J. Fang, T. Lin, Robust, superamphiphobic fabric with multiple self-healing ability against both physical and chemical damages. *ACS Appl. Mater. Interfaces* **5**, 10221–10226 (2013)
75. (a) Y. Okamoto, Y. Hasegawa, F. Yoshino, Urethane/acrylic composite polymer emulsions. *Prog. Org. Coat.* **29**(1–4), 175–182 (1996). (b) H. Wang, H. Zhou, T. Lin, *Adv. Sci. Technol.* **80**, 152–155 (2013)
76. Z. Yoshimitsu, A. Nakajima, T. Watanabe, L. Hashimoto, Effects of surface structure on the hydrophobicity and sliding behavior of water droplets. *Langmuir* **18**(15), 5818–5822 (2002)
77. R.V. Lakshmi, T. Bharathidasan, B.J. Basu, Superhydrophobic sol–gel nanocomposite coatings with enhanced hardness. *Appl. Surf. Sci.* **257**(24), 10421–10426 (2011)
78. S.S. Lathe, H. Imai, V. Ganesan, A.V. Rao, Superhydrophobic silica films by sol–gel co-precursor method. *Appl. Surf. Sci.* **256**(1), 217–222 (2009)
79. S.M.R. Billah, R.M. Christie, R. Shamey, Direct coloration of textiles with photochromic dyes. Part 3: dyeing of wool with photochromic acid dyes. *Color. Technol.* **128**(6), 488–492 (2012)
80. S.M.R. Billah, R.M. Christie, R.H. Wardman, Inkjet printed textile based molecular switches, in *Conference Proceeding of Textile Institute World Conference*, Manchester, 3–4 Nov 2010 (2010), pp. 1–10
81. A.S. Aly, A.B.E. Mostafa, M.A. Ramadan, A. Hebeish, Innovative dual antimicrobial & antirease finishing of cotton fabric. *Polym. Plast. Technol. Eng.* **46**, 703–707 (2007)
82. (a) R. Schwalm, *UV Coatings: Basics, Recent Developments and New Applications* (Elsevier, San Diego, 2006), (b) I. Holme, Adhesion to textile fibres and fabrics. *Int. J. Adhes. Adhes.* **19**(6), 455–463 (1999)
83. C.M. Carr, I.H. Leaver, A.E. Hughes, X-ray photoelectron spectroscopic study of the wool fiber surface. *Text. Res. J.* **56**(7), 457–461 (1986)
84. R.J. Ward, H.A. Willis, G.A. George, G.B. Guise, R.J. Denning, D.J. Evans, R.D. Short, Surface analysis of wool by X-ray photoelectron spectroscopy and static secondary ion mass spectrometry. *Text. Res. J.* **63**(6), 362–368 (1993)
85. J.D. Leeder, J.H. Bradbury, Effects of shrink proofing and other chemical treatments on the epicuticle of wool. *Text. Res. J.* **41**(3), 215–281 (1971)
86. (a) W.A. Daoud, J.H. Xin, Y. Zhang, Surface functionalization of cellulose fibers with titanium dioxide nanoparticles and their combined bactericidal activities. *Surf. Sci.* **599**(1–3), 69–75 (2005). (b) C.J. Brinker, G.W. Scherer, *Sol-Gel Science: The Physics and Chemistry of Sol-Gel Processing* (Academic, San Diego, 1990)
87. L. Xu, W. Zhuang, B. Xu, Z. Cai, Fabrication of superhydrophobic cotton fabrics by silica hydrosol and hydrophobization. *J. Appl. Polym. Sci.* **257**(13), 5491–5498 (2011)
88. C. Sanchez, F. Ribot, Chemical Design of hybrid organic-inorganic materials synthesized via sol-gel chemistry. *New J. Chem.* **18**, 1007–1047 (1994)

89. S.Y. Chang, T.A. Ring, Map of gel times for three phase region tetraethoxysilane, ethanol and water. *J. Non-Cryst. Solids* **147–148**, 56–61 (1992)
90. D. Knittel, E. Schollmeyer, Technologies for a new century. Surface modification of fibres. *J. Text. Inst.* **91**(3), 151–165 (2000)
91. B. Mahltig, H. Böttcher, Refining of textiles by nanosol coating. *Melliand Textilber.* **83**(4), 251–253, E50–E51 (2002)
92. M. Joshi, A. Bhattacharyya, Nanotechnology – a new route to high performance functional textiles. *Text. Prog.* **43**(3), 155–233 (2011)
93. B. Mahltig, H. Haufe, H. Böttcher, Functionalisation of textiles by inorganic sol-gel coatings. *J. Mater. Chem.* **15**(41), 4385–4398 (2005)
94. I. Holme, Performance under adverse conditions. *Int. Dyer* **187**(7), 11–12 (2002)
95. S. Amberg-Schwab, U. Weber, Functional coatings using nanotechnology. *Int. Text. Bull.* **50**(1), 14–19 (2004)
96. M. Montazer, E. Pakdel, Functionality of nano titanium dioxide on textiles with future aspects: focus on wool. *J. Photochem. Photobiol. C Photochem. Rev.* **12**(4), 293–303 (2011)
97. C. Günesoglu, Performing the electrospraying process for the application of textile nano finishing particles. *Text. Res. J.* **80**(2), 106–115 (2009)
98. (a) T. Textor, T. Bahners, E. Schollmeyer, Organically modified ceramics for coating textile materials. *Prog. Colloid Polym. Sci.* **117**, 76–79 (2001). (b) J.S. Jur, G.N. Parsons, Nanoscale ceramic surface modification of textiles by atomic layer deposition. *Am. Ceram. Soc. Bull.* **91**(6), 24–27 (2012)
99. P. Colomban, E. Bruneton, J.L. Lagrange, E. Mouchon, Sol-gel mullite matrix-SiC and -mullite 2D woven fabric composites with or without zirconia containing interphase: elaboration and properties. *J. Eur. Ceram. Soc.* **16**(2), 301–314 (1996)
100. B. Sun, T. Fan, J. Xu, D. Zhang, Biomorphic synthesis of SnO₂ microtubules on cotton fibers. *Mater. Lett.* **59**(18), 2325–2328 (2005)
101. M. Nacken, S. Heidenreich, M. Hackel, G. Schaub, Catalytic activation of ceramic filter elements for combined particle separation, NO_x removal and VOC total oxidation. *Appl. Catal. B Environ.* **70**(1–4), 370–376 (2007)
102. N.I. Baklanova, T.M. Zima, A.T. Titov, N.V. Isaeva, D.V. Grashchenkov, S.S. Solntsev, Protective coatings for carbon fibers. *Inorg. Mater.* **42**(7), 744–749 (2006)
103. B. Boutevin, Y. Pietrasanta, The synthesis and applications of fluorinated silicones, notably in high-performance coatings. *Prog. Org. Coat.* **13**(5), 297–331 (1985)
104. B. Mahltig, H. Böttcher, Modified silica sol coatings for water-repellent textiles. *J. Sol-Gel Sci. Technol.* **27**, 43–52 (2003)
105. W.A. Daoud, J.H. Xin, X. Tao, Superhydrophobic silica nanocomposite coating by a low-temperature process. *J. Am. Ceram. Soc.* **87**(9), 1782–1784 (2004)
106. T. Textor, T. Bahners, E. Schollmeyer, Surface modification of textile fabrics by coatings based on the sol-gel process. *Melliand Textilber.* **80**(10), 847–848, E229 (1999)
107. J. Trepte, H. Böttcher, Improvement in the leaching behaviour of dye doped modified silica layers coated onto paper or textiles. *J. Sol-Gel Sci. Technol.* **19**(1–3), 691–694 (2000)
108. Q.B. Meng, S. Lee, C. Nah, Y. Lee, Preparation of waterborne polyurethanes using an amphiphilic diol for breathable waterproof textile coatings. *Prog. Org. Coat.* **66**(4), 382–386 (2009)
109. B. Mahltig, F. Audenaert, H. Böttcher, Hydrophobic silica sol coatings on textiles the influence of solvent and sol concentration. *J. Sol-Gel Sci. Technol.* **34**(2), 103–109 (2005)
110. B. Mahltig, Hydrophobic sol-gel based coating agent for textiles: improvement by solvothermal treatment. *J. Text. Inst.* **102**(5), 455–459 (2011)
111. S. Leelajariyakul, H. Noguchi, S. Kiatkamjornwong, Surface-modified and micro-encapsulated pigmented inks for ink jet printing on textile fabrics. *Prog. Org. Coat.* **62**(2), 145–161 (2008)
112. J. Vince, B. Orel, A. Vilčnik, M. Fir, A.S. Vuk, V. Jovanovski, B. Simončič, Structural and water-repellent properties of a urea/poly(dimethylsiloxane) sol-gel hybrid and its bonding to cotton fabric. *Langmuir* **22**(15), 6489–6497 (2006)

113. M. Fir, J. Vince, A.S. Vuk, A. Vilčnik, V. Jovanovski, G. Mali, B. Orel, B. Simončič, Functionalisation of cotton with hydrophobic urea/poly(dimethylsiloxane) sol-gel hybrid. *Acta Chim. Slov.* **54**(1), 144–148 (2007)
114. B. Mahltig, A. Fischer, Inorganic/organic polymer coatings for textiles to realize water repellent and antimicrobial properties – a study with respect to textile comfort. *J. Polym. Sci. B Polym. Phys.* **48**(14), 1562–1568 (2010)
115. T. Bahners, T. Textor, K. Opwis, E. Schollmeyer, Recent approaches to highly hydrophobic textile surfaces. *J. Adhes. Sci. Technol.* **22**(3–4), 285–309 (2008)
116. M. Messaoud, M. Houmard, S. Briche, F. Roussel, M. Langlet, Hydrophobic functionalization of cotton-based textile fabrics through a non-fluorinated sol-gel route. *J. Sol-Gel Sci. Technol.* **55**(2), 243–254 (2010)
117. T. Pipatchanchai, K. Srikulkit, Hydrophobicity modification of woven cotton fabric by hydrophobic fumed silica coating. *J. Sol-Gel Sci. Technol.* **44**(2), 119–123 (2007)
118. A. Khoddami, O. Avinc, F. Ghahremanzadeh, Improvement in poly(lactic acid) fabric performance via hydrophilic coating. *Prog. Org. Coat.* **72**(3), 299–304 (2011)
119. H. Zhang, R.N. Lamb, Superhydrophobic treatment for textiles via engineering nanotextured silica/polysiloxane hybrid material onto fibres. *Surf. Eng.* **25**(1), 21–24 (2009)
120. D. Chen, L. Tan, H. Liu, J. Hu, Y. Li, F. Tang, Fabricating superhydrophilic wool fabrics. *Langmuir* **26**(7), 4675–4679 (2010)
121. L. Xu, W. Zhuang, B. Xu, Z. Cai, Superhydrophobic cotton fabrics prepared by one-step water-based sol-gel coating. *J. Text. Inst.* **103**(3), 311–319 (2012)
122. Z. Li, Y. Xing, J. Dai, Superhydrophobic surfaces prepared from water glass and non-fluorinated alkylsilane on cotton substrates. *Appl. Surf. Sci.* **254**(7), 2131–2135 (2008)
123. W. Huang, Y. Xing, Y. Yu, S. Shang, J. Dai, Enhanced washing durability of hydrophobic coating on cellulose fabric using polycarboxylic acids. *Appl. Surf. Sci.* **257**(9), 4443–4448 (2011)
124. C. Wang, J. He, Citric acid as crosslinking agent for grafting β -cyclodextrin onto wool fabric, in *Proceedings of the 12th International Wool Research Conference*, Shanghai, vol. I (2010), pp. 399–402
125. M. Montazer, E. Pakdel, Self-cleaning and color reduction in wool fabric by nano titanium dioxide. *J. Text. Inst.* **102**(4), 343–352 (2011)
126. K. Satoh, H. Nakazumi, Novel fluorinated inorganic-organic finishing materials for nylon carpeting. *Text. Res. J.* **74**(12), 1079–1084 (2004)
127. W.A. Daoud, J.H. Xin, Nucleation and growth of anatase crystallites on cotton fabrics at low temperatures. *J. Am. Ceram. Soc.* **87**(5), 953–955 (2004)
128. A. Bozzi, T. Yuranova, J. Kiwi, Self-cleaning of wool-polyamide and polyester textiles by TiO₂-rutile modification under daylight irradiation at ambient temperature. *J. Photochem. Photobiol. A Chem.* **172**(1), 27–34 (2005)
129. A. Bozzi, T. Yuranova, I. Guasaquillo, D. Laub, J. Kiwi, Self-cleaning of modified cotton textiles by TiO₂ at low temperatures under daylight irradiation. *J. Photochem. Photobiol. A Chem.* **174**(2), 156–164 (2005)
130. K.T. Meilert, D. Laub, J. Kiwi, Photocatalytic Self-cleaning of modified cotton textiles by TiO₂ clusters attached by chemical spacers. *J. Mol. Catal. A Chem.* **237**(1–2), 101–108 (2005)
131. T. Yuranova, R. Mosteo, J. Bandara, D. Laub, J. Kiwi, Self-cleaning cotton textiles surfaces modified by photoactive SiO₂/TiO₂ coating. *J. Mol. Catal. A Chem.* **244**(1–2), 160–167 (2006)
132. Y.A. Matsuda, Y. Kotani, T. Kogure, M. Tatsumisago, T. Minami, Transparent anatase nanocomposite films by the sol-gel process at low temperatures. *J. Am. Ceram. Soc.* **83**(1), 229–231 (2000)
133. M. Langlet, A. Kim, M. Audier, J.M. Herrmann, Sol-gel preparation of photocatalytic TiO₂ films on polymer substrates. *J. Sol-Gel Sci. Technol.* **25**(3), 223–234 (2002)
134. H. Imai, H. Morimoto, A. Tominaga, H. Hirashima, Structural changes in sol-gel derived SiO₂ and TiO₂ films by exposure to water vapor. *J. Sol-Gel Sci. Technol.* **10**(1), 45–54 (1997)

135. H. Imai, H. Hirashima, Preparation of porous anatase coating from sol-gel-derived titanium dioxide and titanium dioxide-silica by water-vapor exposure. *J. Am. Ceram. Soc.* **82**(9), 2301–2304 (1999)
136. W.A. Daoud, J.H. Xin, Low temperature sol-gel processed photocatalytic titania coating. *J. Sol-Gel Sci. Technol.* **29**(1), 25–29 (2004)
137. K. Qi, W.A. Daoud, J.H. Xin, C.L. Mak, W. Tang, W.P. Cheung, Self-cleaning cotton. *J. Mater. Chem.* **16**(47), 4567–4574 (2006)
138. W.A. Daoud, J.H. Xin, Y.-H. Zhang, Surface functionalization of cellulose fibers with titanium dioxide nanoparticles and their combined bactericidal activities. *Surf. Sci.* **599**(1–3), 69–75 (2005)
139. H.F. Moafi, A.F. Shojaie, M.A. Zanjanchi, The comparison of photocatalytic activity of synthesized TiO₂ and ZrO₂ nanosize onto wool fibers. *Appl. Surf. Sci.* **256**(13), 4310–4316 (2010)
140. W.S. Tung, W.A. Daoud, Effect of wettability and silicone surface modification on the self-cleaning functionalization of wool. *J. Appl. Polym. Sci.* **112**(1), 235–243 (2009)
141. B. Liu, Z. Wang, J. He, SiO₂/TiO₂ multilayer films grown on cotton fibers surface at low temperature by a novel two-step process. *Mater. Lett.* **67**(1), 8–10 (2012)
142. M. Montazer, E. Pakdel, M.B. Moghadam, The role of nano colloid of TiO₂ and butane tetra carboxylic acid on the alkali solubility and hydrophilicity of proteinous fibers. *Colloids Surf. A Physicochem. Eng. Asp.* **375**(1–3), 1–11 (2011)
143. K. Qi, B. Fei, J.H. Xin, Visible light-active iron-doped anatase nanocrystallites and their self-cleaning property. *Thin Solid Films* **519**(8), 2438–2444 (2011)
144. M.J. Uddin, F. Cesano, S. Bertarione, F. Bonino, S. Bordiga, D. Scarano, A. Zecchina, Tailoring the activity of Ti-based photocatalysts by playing with surface morphology and silver doping. *J. Photochem. Photobiol. A Chem.* **196**(2–3), 165–173 (2008)
145. M.J. Uddin, F. Cesano, D. Scarano, F. Bonino, G. Agostini, G. Spoto, S. Bordiga, A. Zecchina, Cotton textile fibres coated by Au/TiO₂ films: synthesis, characterization and self cleaning properties. *J. Photochem. Photobiol. A Chem.* **199**(1), 64–72 (2008)
146. A. Farouk, T. Textor, E. Schollmeyer, A. Tarbuk, A.M. Grancacic, Sol-gel derived inorganic-organic hybrid polymers filled with ZnO nanoparticles as ultraviolet protection finish for textiles. *Autex Res. J.* **9**(4), 114–120 (2009)
147. W.S. Simpson, Chemical processes for enhanced appearance and performance, in *Wool: Science and Technology*, ed. by W.S. Simpson, G.H. Crawshaw (Woodhead Publishing, Abington, 2002), pp. 215–236
148. J.H. Xin, W.A. Daoud, Y.Y. Kong, A new approach to UV-blocking treatment for cotton fabrics. *Text. Res. J.* **74**(2), 97–100 (2004)
149. P. Xu, W. Wang, S.-L. Chen, UV blocking treatment of cotton fabrics by titanium hydrosol. *AATCC Rev.* **5**(6), 28–31 (2005)
150. P. Xu, X. Liu, W. Wang, S. Chen, Improving the antibacterial and UV resistant properties of cotton by the titanium hydrosol treatment. *J. Appl. Polym. Sci.* **102**(2), 1478–1482 (2006)
151. N. Abidi, E. Hequet, S. Tarimala, L.L. Dai, Cotton fabric surface modification for improved UV radiation protection using sol-gel process. *J. Appl. Polym. Sci.* **104**(1), 111–117 (2007)
152. Y. Xing, X. Ding, UV photo-stabilization of tetrabutyl titanate for aramid fibers via sol-gel surface modification. *J. Appl. Polym. Sci.* **103**(5), 3113–3119 (2007)
153. T. Textor, T. Bahners, E. Schollmeyer, Inorganic-organic hybrid polymers improve the stab resistance of ballistic fabrics. *Tech. Text.* **47**(2), 85–87, E72–E74 (2004)
154. H. Kan, L. Zhang, H. Xu, Z. Mao, H. Cao, Optimization of conditions for nanocrystal ZnO in-situ growing on SiO₂-coated cotton fabric. *Text. Res. J.* **80**(7), 660–670 (2010)
155. P.G. Parejo, M. Zayat, D. Levy, Photostability and retention of UV absorber molecules in sol-gel hybrid UV-protective coatings. *J. Sol-Gel Sci. Technol.* **53**(2), 280–286 (2010)
156. M.A. Tshabalala, R. Libert, C.M. Schaller, Photostability and moisture uptake properties of wood veneers coated with a combination of thin sol-gel films and light stabilizers. *Holzforschung* **65**(2), 215–220 (2011)

157. B. Mahltig, H. Böttcher, K. Rauch, U. Dieckmann, R. Nitsche, T. Fritz, Optimized UV protecting coatings by combination of organic and inorganic UV absorbers. *Thin Solid Films* **485**(1–2), 108–114 (2005)
158. B. Mahltig, D. Knittel, E. Schollmeyer, H. Böttcher, Incorporation of triarylmethane dyes into sol-gel matrices deposited on textiles. *J. Sol-Gel Sci. Technol.* **31**(1–3), 293–297 (2004)
159. B. Mahltig, H. Böttcher, D. Knittel, E. Schollmeyer, Light fading and wash fastness of dyed nanosol-coated textiles. *Text. Res. J.* **74**(6), 521–527 (2004)
160. A.C. Aksit, N.A. Onar, Leaching and fastness behavior of cotton fabrics dyed with different type of dyes using sol-gel process. *J. Appl. Polym. Sci.* **109**(1), 97–105 (2008)
161. C. Schramm, B. Rinderer, Dyeing and DP treatment of sol-gel pre-treated cotton fabrics. *Fibers Polym.* **12**(2), 226–232 (2011)
162. L. Min, Z. Xiaoli, C. Shuilin, Enhancing the wash fastness of dyeings by a sol-gel process. Part 1: direct dyes on cotton. *Color. Technol.* **119**(5), 297–300 (2003)
163. D. Juan, Z. Li, C. Shuilin, Wash fastness of dyed fabric treated by the sol-gel process. *Color. Technol.* **121**(1), 29–36 (2005)
164. B. Mahltig, T. Textor, Combination of silica sol and dyes on textiles. *J. Sol-Gel Sci. Technol.* **39**(2), 111–118 (2006)
165. Y. Yin, C. Wang, Sol-gel synthesis and characterizations of organically modified silica coatings on knitted cellulose for fixation applications. *Prog. Org. Coat.* **73**(1), 14–18 (2012)
166. D. Hegemann, M.M. Hossain, D.J. Balazs, Nanostructured plasma coatings to obtain multi-functional textile surfaces. *Prog. Org. Coat.* **58**(2–3), 237–240 (2007)
167. H. Yi, K.-L. Yan, Polyurethane modified with 3-aminopropyltriethoxysilane as wool antifelting agent. *J. Appl. Polym. Sci.* **109**(4), 2169–2175 (2008)
168. Y. Hu, J. Liu, C. Xu, Antifelting-coating for wool from PPD-[Si(OH)₃]₂ agent via a sol-gel process. *Adv. Mater. Res.* **233–235**, 151–154 (2011)
169. C. Schramm, W.H. Binder, R. Tessadri, Durable press finishing of cotton fabric with 1,2,3,4-butanetetracarboxylic acid and TEOS/GLYMO. *J. Sol-Gel Sci. Technol.* **29**(3), 155–165 (2004)
170. C. Schramm, B. Rinderer, W.H. Binder, R. Tessadri, H. Duelli, Treatment of 1,3-dimethylol-4,5-dihydroxyimidazolidine-2-one finished cellulosic material with tetraethoxysilane or glycidylxypropyltrimethoxysilane solutions. *J. Mater. Sci.* **40**(8), 1883–1891 (2005)
171. K.S. Huang, Y.H. Nien, K.C. Hsiao, Y.S. Chang, Application of DMEU/SiO₂ gel solution in the antiwrinkle finishing of cotton fabrics. *J. Appl. Polym. Sci.* **102**(5), 4136–4143 (2006)
172. K.-S. Huang, K.-L. Yang, S.-J. Lin, W.-T. Lian, Antiwrinkle treatment of cotton fabric with a mixed sol of TEOS-TTD/DMDHEU. *J. Appl. Polym. Sci.* **106**(4), 2559–2564 (2007)
173. K.-S. Huang, M.-C. Hwang, J.-S. Chen, S.-J. Lin, S.-P. Wang, Application of mixed gel solution in the anti-wrinkle finishing of cotton fabrics. *J. Text. Inst.* **98**(2), 169–176 (2007)
174. C. Wang, L. Chen, Surface treatment of anti-crease finished cotton fabric based on sol-gel technology. *Surf. Rev. Lett.* **16**(5), 715–721 (2009)
175. S. Hribernik, M.S. Smole, K.S. Kleinschek, M. Bele, J. Jamnik, M. Gaberscek, Flame retardant activity of SiO₂-coated regenerated cellulose fibers. *Polym. Degrad. Stab.* **92**(11), 1957–1965 (2007)
176. A. Cireli, N. Onar, M.F. Ebeoglugil, I. Kayatekin, B. Kutlu, O. Culha, E. Celik, Development of flame retardancy properties of new halogen-free phosphorous doped silica thin films on fabrics. *J. Appl. Polym. Sci.* **105**(6), 3747–3756 (2007)
177. S.A. Chapple, E. Ferg, The influence of precursor ratios on the properties of cotton coated with a sol-gel flame retardant. *AATCC Rev.* **6**(11), 36–40 (2006)
178. B.C. Kim, P.C. Innis, G.G. Wallace, C.T.J. Low, F.C. Walsh, W.J. Cho, K.H. Yu, Electrically conductive coatings of nickel and polypyrrole/poly(2-methoxyaniline-5-sulfonic acid) on nylon Lycra[®] textiles. *Prog. Org. Coat.* **76**(10), 1296–1301 (2013)
179. J. Alongi, M. Ciobanu, G. Malucelli, Novel flame retardant finishing systems for cotton fabrics based on phosphorus-containing compounds and silica derived from sol-gel processes. *Carbohydr. Polym.* **85**(3), 599–608 (2011)
180. S. Hu, Y. Hu, L. Song, H. Lu, Effect of modified organic-inorganic hybrid materials on thermal properties of cotton fabrics. *J. Therm. Anal. Calorim.* **103**(2), 423–427 (2011)

181. J. Alongi, M. Ciobanu, G. Malucelli, Sol-gel treatments on cotton fabrics for improving thermal and flame stability: effect of the structure of the alkoxysilane precursor. *Carbohydr. Polym.* **87**(1), 627–635 (2012)
182. J. Alongi, M. Ciobanu, G. Malucelli, Sol-gel treatments for enhancing flame retardancy and thermal stability of cotton fabrics: optimisation of the process and evaluation of the durability. *Cellulose* **18**(1), 167–177 (2011)
183. J. Alongi, M. Ciobanu, J. Tata, F. Carosio, G. Malucelli, Thermal stability and flame retardancy of polyester, cotton, and relative blend textile fabrics subjected to sol-gel treatments. *J. Appl. Polym. Sci.* **119**(4), 1961–1969 (2011)
184. J. Alongi, M. Ciobanu, G. Malucelli, Cotton fabrics treated with hybrid organic-inorganic coatings obtained through dual-cure processes. *Cellulose* **18**(5), 1335–1348 (2011)
185. P. Xu, W. Wang, S.-L. Chen, Application of nanosol on the antistatic property of polyester. *Melliand Int.* **11**(1), 56–59 (2005)
186. (a) L. Andreozzi et al., Free radical generation upon plasma treatment of cotton fibers and their initiation efficiency in surface-graft polymerization. *J. Colloid Interface Sci.* **289**, 455–465 (2005). (b) G.B. Chu, F.N. Jones, Low-temperature curing higher-solids polyester coatings with melamine-formaldehyde resin cross-linkers. *J. Coat. Technol.* **65**(819), 43–48 (1993). (c) P.K.T. Oldring, SITA Technology Limited, *Resins for Surface Coatings*, 2nd edn. (Wiley, Chichester/New York, 2000)
187. (a) N. Abidi, E. Hequet, Cotton fabric graft copolymerization using microwave plasma. II. Physical properties. *J. Appl. Polym. Sci.* **98**, 896–902 (2005). (b) J.W. Gilman, A.B. Morgan, R.H. Harris, P.C. Trulove, H.C. DeLong, T.E. Sutto, Polymer layered silicate nanocomposites: thermal stability of organic cationic treatments. *Polym. Mater. Sci. Eng.* **83**, 59–60 (2000)
188. (a) J.L.G. Kamlangkla, Multifunctional silk fabrics by means of the plasma induced graft polymerization (PIGP) process. *Surf. Coat. Technol.* **205**, 3755–3762 (2011). (b) W. Caseri, Nanocomposites of polymers and metals or semiconductors: historical background and optical properties. *Macromol. Rapid Commun.* **21**, 705–722 (2000). (c) C. Sanchez, B. Julian, P. Belleville, M. Popall, Applications of hybrid organic/inorganic nanocomposites. *J. Mater. Chem.* **15**, 3559–3592 (2005). (d) H.H. Huang, B. Orlor, G.L. Wilkes, Structure-property behavior of new hybrid materials incorporating oligomeric species into sol-gel glasses. 3. Effect of acid content, tetraethoxysilane content, and molecular weight of poly(dimethylsiloxane). *Macromolecules* **20**, 1322–1330 (1987)
189. (a) A. Cavaco-Paulo, G.M. Gübitz, *Textile Processing with Enzymes* (Woodhead Publishing Ltd., Cambridge, 2003), pp. 1–234. (b) A.J. Barrett, N.D. Rawlings, J.F. Woessner, *The Handbook of Proteolytic Enzymes*, 2nd edn. (Academic, Oxford, 2003)
190. (a) M.J. Tsafack, J. Levalois-Grützmacher, Flame retardancy of cotton textiles by plasma-induced graft-polymerization (PIGP). *Surf. Coat. Technol.* **201**, 2599–2610 (2006). (b) A. Lendlein, R. Langer, Biodegradable, elastic shape-memory polymers for potential biomedical applications. *Science* **296**, 1673–1676 (2002)
191. (a) A. Lendlein, S. Kelch, Shape-memory polymers. *Angew. Chem. Int. Ed.* **41**, 2034–2057 (2002). (b) A. Lendlein, S. Kelch, Shape-memory polymers as stimuli-sensitive implant materials. *Clin. Hemorheol. Microcirc.* **32**, 105–116 (2005)
192. (a) C. Liu, P.T. Mather, Thermomechanical characterization of a tailored series of shape memory polymers. *J. Appl. Med. Polym.* **6**, 47–52 (2002). (b) W. Sokolowsky, A. Metcalfe, S. Hayashi, L. Yahia, J. Raymond, Medical applications of shape memory polymers. *Biomed. Mater.* **2**, 23–27 (2007). (c) Z.W. Wicks, *Organic Coatings: Science and Technology*, 3rd edn. (Wiley-Interscience, Hoboken, 2007). (d) O. Coulembier, P. Degee, J.L. Hedrick, P. Dubois, From controlled ringopening polymerization to biodegradable aliphatic polyester: especially poly(betaamalic acid) derivatives. *Progr. Polym. Sci.* **31**(8), 723–747 (2006)
193. B. Mahltig, D. Fiedler, H. Böttcher, Antimicrobial sol-gel coatings. *J. Sol-Gel Sci. Technol.* **32**(1–3), 219–222 (2004)
194. B. Tomšič, B. Simončič, B. Orel, L. Černe, P.F. Tavčer, M. Zorko, I. Jerman, A. Vilčnik, J. Kovač, Sol-gel coating of cellulose fibres with antimicrobial and repellent properties. *J. Sol-Gel Sci. Technol.* **47**(1), 44–57 (2008)

195. B. Simončič, B. Tomšič, L. Černe, B. Orel, I. Jerman, J. Kovač, M. Žerjav, A. Simončič, Multifunctional water and oil repellent and antimicrobial properties of finished cotton: influence of sol-gel finishing procedure. *J. Sol-Gel Sci. Technol.* **61**(2), 340–354 (2012)
196. X. Liu, T. Lin, B. Peng, X. Wang, Antibacterial activity of capsaicin coated wool fabric. *Text. Res. J.* **82**(6), 584–590 (2012)
197. H. Haufe, K. Muschter, J. Siegert, H. Böttcher, Bioactive textiles by sol-gel immobilised natural active agents. *J. Sol-Gel Sci. Technol.* **45**(1), 97–101 (2008)
198. S. Tarimala, N. Kothari, N. Abidi, E. Hequet, J. Fralick, L.L. Dai, New approach to antibacterial treatment of cotton fabric with silver nanoparticle-doped silica using sol-gel process. *J. Appl. Polym. Sci.* **101**(5), 2938–2943 (2006)
199. B. Mahltig, E. Gutmann, M. Reibold, D.C. Meyer, H. Böttcher, Synthesis of Ag and Ag/SiO₂ Sols by solvothermal method and their bactericidal activity. *J. Sol-Gel Sci. Technol.* **51**(2), 204–214 (2009)
200. Y. Xing, X. Yang, J. Dai, Antimicrobial finishing of cotton textile based on water glass by sol-gel method. *J. Sol-Gel Sci. Technol.* **43**(2), 187–192 (2007)
201. X. Wang, C. Wang, The antibacterial finish of cotton via sols containing quaternary ammonium salts. *J. Sol-Gel Sci. Technol.* **50**(1), 15–21 (2009)
202. L. Song, R.H. Baney, Antibacterial evaluation of cotton textile treated by trialkoxysilane compounds with antimicrobial moiety. *Text. Res. J.* **81**(5), 504–511 (2011)
203. B. Mahltig, D. Fiedler, A. Fischer, P. Simon, Antimicrobial coatings on textiles: modification of sol-gel layers with organic and inorganic biocides. *J. Sol-Gel Sci. Technol.* **55**(3), 269–277 (2010)
204. A.S. Chan, J.D. Valle, K. Lao, C. Malapit, M. Chua, R.C. So, Evaluation of silica sol-gel microcapsule for the controlled release of insect repellent, *N, N*-diethyl-2-methoxybenzamide, on cotton. *Philipp. J. Sci.* **138**(1), 13–21 (2009)
205. A.F. Little, R.M. Christie, Textile applications of photochromic dyes. Part 3: factors affecting the technical performance of textiles screen printed with commercial photochromic dyes. *Color Technol.* **127**(5), 275–281 (2011)
206. R. Pardo, M. Zayat, D. Levy, Photochromic organic-inorganic hybrid materials. *Chem. Soc. Rev.* **40**(2), 672–687 (2011)
207. T. Cheng, T. Lin, R. Brady, X. Wang, Fast response photochromic textiles from hybrid silica surface coating. *Fibers Polym.* **9**(3), 301–306 (2008)
208. R. Zimehl, T. Textor, T. Bahners, E. Schollmeyer, Smart textiles when colloid chemistry bears a challenge. *Progr. Colloid Polym. Sci.* **125**, 49–53 (2004)
209. L.V. Schueren, K.D. Clerck, G. Brancatelli, G. Rosace, E. Van Damme, W.D. Vos, Novel cellulose and polyamide halochromic textile sensors based on the encapsulation of Methyl Red into a sol-gel matrix. *Sens. Actuators B Chem.* **162**(1), 27–34 (2012)
210. R.B. Bhatia, C.J. Brinker, C.S. Ashley, T.M. Harris, *Synthesis of Sol-Gel Matrices for Encapsulation of Enzymes Using an Aqueous Route*, Report SAN098-2610c (Sandia Corporation, Albuquerque, 1998)
211. F.-Y. Li, Y.-J. Xing, X. Ding, Immobilization of papain on cotton fabric by sol-gel method. *Enzyme Microb. Technol.* **40**(7), 1692–1697 (2007)
212. A. Pannier, D. Fiedler, U. Soltmann, S. Matys, H. Böttcher, Cellulose producing Biocer coatings. *Ver. Dtsch. Ing. Ber.* **2027**, 129–132 (2008)
213. C. Schramm, W.H. Binder, R. Tessadri, H. Duelli, Modification of cotton fabrics by means of hydrolyzed TEOS-, GLYMO- and Ti(OiPr)₃(acac)- solutions. *Cellul. Chem. Technol.* **39**(3–4), 303–314 (2005)
214. B. Tomšič, P.K. Lavrič, B. Simončič, B. Orel, D. Jocić, Sol-gel technology for functional finishing of PES fabric by stimuli-responsive microgel. *J. Sol-Gel Sci. Technol.* **61**(3), 463–476 (2012)
215. X. Xiao, F. Chen, Q. Wei, N. Wu, Surface modification of polyester nonwoven fabrics by Al₂O₃ sol-gel coating. *J. Coat. Technol. Res.* **6**(4), 537–541 (2009)

216. B. Orel, A. Surca, U.O. Krasovec, Recent progress in sol-gel derived electrochromic devices. *Acta Chim. Slov.* **45**(4), 487–506 (1998)
217. E.H. Lan, B.C. Dave, J.M. Fukuto, B. Dunn, J.I. Zink, J.S. Valentine, Synthesis of sol-gel encapsulated heme proteins with chemical sensing properties. *J. Mater. Chem.* **9**(1), 45–53 (1999)
218. L.M. Fortes, M.C. Goncalves, R.M. Almeida, Flexible photonic crystals for strain sensing. *Opt. Mater.* **33**(3), 408–412 (2011)
219. S. Mann, S.L. Burkett, S.A. Davis, C.E. Fowler, N.H. Mendelson, S.D. Simms, D. Walsh, N.T. Whilton, Sol-gel synthesis of organized matter. *Chem. Mater.* **9**(11), 2300–2310 (1997)
220. M. Sumper, N. Kröger, Silica formation in diatoms: the function of long-chain polyamines and silaffins. *J. Mater. Chem.* **14**(14), 2059–2065 (2004)
221. S.C. Nunes, N.J.O. Silva, J. Hümmer, R.A.S. Ferreira, P. Almeida, L.D. Carlos, V.Z. Bermudez, Water-mediated structural tunability of an alkyl/siloxane hybrid: from amorphous material to lamellar structure or bilamellar superstructure. *RSC Adv.* **2**(5), 2087–2099 (2012)
222. F.C. Meldrum, H. Cölfen, Controlling mineral morphologies and structures in biological and synthetic systems. *Chem. Rev.* **108**(11), 4332–4432 (2008)
223. Y. Chen, D.W. Lloyd, S.C. Harlock, Mechanical characteristics of coated fabrics. *J. Text. Inst.* **86**(4), 690–700 (1995)
224. F. Rombaldoni, R. Demichelis, G. Mazzuchetti, Prediction of human psychophysical perception of fabric crispness and coolness hand from rapidly measurable low-stress mechanical and thermal parameters. *J. Sens. Stud.* **25**(6), 899–916 (2010)
225. H.T. Amine, S. Msahli, F. Sakli, A new index for evaluating the mechanical comfort of linen fabric. *J. Nat. Fibers* **7**(4), 251–266 (2010)
226. Y. Gao, X. Yu, A.P. Pierlot, R.J. Denning, R. Cranston, A simultaneous antimicrobial and shrink resistance treatment of wool woven fabrics using the polymeric biocide poly-hexamethylene biguanide. *J. Mater. Sci.* **46**(9), 3020–3026 (2011)
227. M. Parvinezadeha, I. Ebrahimib, Atmospheric air-plasma treatment of polyester fiber to improve the performance of nanoemulsion silicone. *Appl. Surf. Sci.* **257**(9), 4062–4068 (2011)
228. K. Wongcharee, M. Brungs, R. Chaplin, Y.J. Hong, E. Sizgek, Influence of surfactant and humidity on sol-gel macroporous organosilicate coatings. *J. Sol-Gel Sci. Technol.* **29**(2), 115–124 (2004)
229. C.D. Volpe, S. Dire, E. Pagani, A comparative analysis of surface structure and surface tension of hybrid silica films. *J. Non-Cryst. Solids* **209**(1–2), 51–60 (1997)
230. G. Dubois, W. Volksen, T. Magbitang, M. Sherwood, R.D. Miller, D.M. Gage, R.H. Dauskardt, Superior mechanical properties of dense and porous organic-inorganic hybrid thin films. *J. Sol-Gel Sci. Technol.* **48**(1–2), 187–193 (2008)
231. D. Aslanidou, I. Karapanagiotis, C. Panayiotou, Superhydrophobic, superoleophobic coatings for the protection of silk textiles. *Prog. Org. Coat.* **97**, 44–52 (2016)
232. D. Avnir, V.R. Kaufman, R. Reisfeld, Organic fluorescent dyes trapped in silica and silicitania thin films by the sol-gel method. Photophysical, film and cage properties. *J. Non-Cryst. Solids* **74**(2–3), 395–406 (1985)
233. G.B. Guise, G.C. Smith, The chemistry of a polyamide-epichlorohydrin resin (Hercosett 125) used to shrink-resist wool. *J. Appl. Polym. Sci.* **30**(10), 4099–4111 (1985)
234. C.H. Giles, G. Baxter, S.M.K. Rahman, Studies of high fastness to light in coloring matters in hydrophilic substrates. *Text. Res. J.* **31**(10), 831–844 (1961)
235. C. Rottman, G.S. Grader, Y. De Hazan, D. Avnir, Sol-gel entrapment of ET(30) in ormosils. Interfacial polarity-fractality correlation. *Langmuir* **12**(23), 5505–5508 (1996)
236. A. Datyner, M.T. Pailthorpe, A study of dyestuff aggregation, Part III. The effect of levelling agents on the aggregation of some anionic dyes. *Dyes Pigments* **8**, 253–263 (1987)
237. H.H. Sumner, T. Vickerstaff, E. Waters, The effects of the soaping after treatment on vat dyeings. *J. Soc. Dye. Colour.* **69**(6), 181–194 (1953)

238. Y. Chen, L. Jin, Y. Xie, Sol-gel processing of organic-inorganic nanocomposite protective coatings. *J. Sol-Gel Sci. Technol.* **13**(1–3), 735–738 (1998)
239. S. Amberg-Schwab, E. Arpac, W. Glaubitt, K. Rose, G. Schottner, U. Schubert, Protective coatings for organic polymers by sol-gel techniques, in *High Performance Ceramic Films and Coatings*, ed. by P. Vincenzini (Elsevier Science, New York City, 1991), pp. 203–310
240. S. Luo, W.J.V. Oij, Surface modification of textile fibres for the improvement of adhesion to polymeric matrices: a review. *J. Adhes. Sci. Technol.* **16**(13), 1715–1735 (2002)
241. R. Krüger, M.J. Bockmeyer, A. Dutschke, P.C. Löberman, Continuous sol-gel coating of ceramic multifilaments: evaluation of fiber bridging by three point bending test. *J. Am. Ceram. Soc.* **89**(7), 2080–2088 (2006)
242. J.G. Dominguez, P. Erra, A. Maza, M.R. Julia, T. Shaw, The use of surfactants to improve the regularity of deposition of resins on wool. *Text. Inst. Ind.* **15**(6), 214–216 (1977)
243. A.-C. Hellgren, P. Weissenborn, K. Holmberg, Surfactants in water-borne paints. *Prog. Org. Coat.* **35**(1–4), 79–87 (1999)
244. N. Brack, R. Lamb, D. Pham, P. Turner, Nonionic surfactants and the wool fibre surface. *Colloids Surf. A Phys. Eng. Asp.* **146**, 405–415 (1999)
245. H.D. Feldtman, J.R. McPhee, The spreading and adhesion of polymers on wool. *Text. Res. J.* **34**(7), 634–642 (1964)
246. R.L. McConnell, M.F. Meyer, F.D. Petke, W.A. Haile, Polyester adhesives in nonwovens and other textile applications. *J. Coat. Fabrics* **16**(1), 199–208 (1987)
247. R.R. Costa, C.A. Custódio, F.J. Arias, J.C. Rodríguez-Cabello, J.F. Mano, Layer-by-layer assembly of chitosan and recombinant biopolymers into biomimetic coatings with multiple stimuli-responsive properties. *Small* **7**, 2640–2649 (2011)
248. G. Decher, Fuzzy nanoassemblies: toward layered polymeric multi-composites. *Science* **277**, 1232–1237 (1997)
249. P.T. Hammond, Engineering materials layer-by-layer: challenges and opportunities in multi-layer assembly. *AIChE J.* **57**, 2928–2940 (2011)
250. Z. Tang, Y. Wang, P. Podsiadlo, N.A. Kotov, Biomedical applications of layer-by-layer assembly: from biomimetics to tissue engineering. *Adv. Mater.* **18**, 3203–3224 (2006)
251. K.V. Rijswijk, H. Bersee, Reactive processing of textile fiber-reinforced thermoplastic composites – an overview. *Compos. A Appl. Sci. Manuf.* **38**, 666–681 (2007)
252. J.M. Yeh, C.P. Chin, Structure and properties of poly(omethoxyaniline)-clay nano-composite materials. *J. Appl. Polym. Sci.* **88**, 1072–1078 (2003)
253. M. Kendig, M. Hon, L. Warren, Smart corrosion inhibiting coating. *Prog. Org. Coat.* **47**, 183–189 (2003)
254. Y. Castro, B. Ferrari, R. Moreno, A. Duran, Coatings produced by electrophoretic deposition from nano-particulate silica sol–gel suspensions. *Surf. Coat. Technol.* **182**, 199–203 (2004)
255. L. Fogelstrom, P. Antoni, E. Malmstrom, A. Hult, UV-curable hyperbranched nanocomposite coatings. *Prog. Org. Coat.* **55**, 284–290 (2006)
256. C. Chen, M. Khoibaib, D. Curliss, Epoxy layered-silicate nanocomposites. *Prog. Org. Coat.* **47**(3–4), 376–383 (2003)
257. L.H. Yang, F.C. Liu, E.H. Han, Effects of P/B on the properties of anticorrosive coatings with different particle size. *Prog. Org. Coat.* **53**, 91–98 (2005)
258. T. Xu, C.S. Xie, Tetrapod-like nano-particle ZnO/acrylic resin composite and its multi-function property. *Prog. Org. Coat.* **46**, 297–301 (2003)
259. A.S. Hamdy, A clean low cost anti-corrosion molybdate based nano-particles coating for aluminum alloys. *Prog. Org. Coat.* **56**, 146–150 (2006)
260. F. Masson, C. Decker, S. Andre, X. Andrieu, UV-curable formulations for UV-transparent optical fiber coatings. I. Acrylic resins. *Prog. Org. Coat.* **49**, 1–12 (2004)
261. J. Kaetsu, M. Yoshida, New coating materials and their preparation by radiation polymerization -antifogging coating composition. *J. Appl. Polym. Sci.* **24**(1), 235 (1979)

262. J. Manara, M. Reidinger, M. Rydzek, M. Arduini-Schuster, Polymer-based pigmented coatings on flexible substrates with spectrally selective characteristics to improve the thermal properties. *Prog. Org. Coat.* **70**(4), 199–204 (2011)
263. W. Fung, M. Hardcastle, *Textiles Automotive Engineering* (The Textile Institute, Woodhead Publishing Limited, Cambridge, 2001)
264. M. Skoko, Investigations of properties and multiaxial strength and deformations of coated textile fabrics. *Tekstil* **47**(7), 339–344 (1998)
265. P. Durst, PU transfer coating of fabrics for leather like fashion products. *J. Coat. Fabrics* **14**, 227–241 (1985)
266. S. Park, J. Kim, C.H. Park, Superhydrophobic textiles: review of theoretical definitions, fabrication and functional evaluation. *J. Eng. Fibers Fabr.* **10**(4), 1–18 (2015)
267. T. Makowski, D. Kowalczyk, W. Fortuniak, D. Jeziorska, S. Brzezinski, A. Tracz, Superhydrophobic properties of cotton woven fabrics with conducting 3D networks of multiwall carbon nanotubes, MWCNTs. *Cellulose* **21**, 4659–4670 (2014)
268. J. Hu, H. Meng, G. Li, S.I. Ibekwe, A review of stimuli-responsive polymers for smart textile applications. *Smart Mater. Struct.* **21**, 1–22 (2012)
269. S. Paul, *Surface Coatings, Science and Technology* (Wiley, Chichester, 1996)
270. Z.W. Wicks, F.N. Jones, S.P. Pappas, *Organic Coatings: Science and Technology* (Wiley-Interscience, Chichester, 1992), pp. 3–89
271. T.A. Misev, *Powder Coatings, Chemistry and Technology* (Wiley, Chichester, 1991), pp. 1–68
272. D.S. Richart, in *Coating Processes (Powder Technology)*, vol. 6 ed. by M. Howe-Grant (Wiley, New York, 1993), pp. 635–661
273. J.D. Pont, Further advances in low temperature cure polyurethane powder coatings, in *Proceedings of the International Waterborne, High Solids and Powder Coatings Symposium*, New Orleans (1999), pp. 232–245
274. M. Sohoni, P. Figlioti, Developments in low temperature cure: urethane powder curing agents, in *Proceedings of the International Waterborne, High Solids and Powder Coatings Symposium*, New Orleans (1998), pp. 267–280
275. R. Subramanian, C.J. Sullivan, Unsaturated polyesters in low temperature cure powder coatings, in *Proceedings of the International Waterborne, High Solids and Powder Coatings Symposium*, New Orleans (2001), pp. 381–389
276. S. Joneydi, A. Khoddami, A. Zadhoush, Novel superhydrophobic top coating on surface modified PVC-coated fabric. *Prog. Org. Coat.* **76**, 821 (2013)
277. G.R.J. Artus, S. Jung, J. Zimmermann, H.P. Gautschi, K. Marquardt, S. Seeger, Silicone nanofilaments and their application as superhydrophobic coatings. *Adv. Mater.* **18**(20), 2758–2762 (2006)
278. J. Zimmermann, F.A. Reifler, G. Fortunato, L.-C. Gerhardt, S. Seeger, A simple, one-step approach to durable and robust superhydrophobic textiles. *Adv. Funct. Mater.* **18**(22), 3662–3669 (2008)
279. S.S. Latthe, A.B. Gurav, C.S. Maruti, R.S. Vhatkar, Recent progress in preparation of superhydrophobic surfaces: a review. *J. Surf. Eng. Mater. Adv. Technol.* **2**, 76–94 (2012)
280. A. Mukhopadhyay, V.K. Midha, Fundamental principles and designing aspects of breathable fabrics: a review on designing the waterproof breathable fabrics. Part I. *J. Ind. Text.* **37**, 225–262 (2008)
281. M. Jassal, A. Khungar, P. Bajaj, T.J.M. Sinha, Waterproof breathable polymeric coatings based on polyurethanes. *J. Ind. Text.* **33**(4), 269–280 (2004)
282. V.M. Desai, V.D. Athawale, Water resistant breathable hydrophilic polyurethane coatings. *J. Coat. Fabrics* **25**(1), 39–46 (1995)
283. G.R. Lomax, Hydrophilic polyurethane coatings. *J. Coat. Fabrics* **20**(2), 88–107 (1990)
284. J. Feng, Z. Ge, C. Chai, S. Wang, D. Yu, G. Wu, Y. Luo, Flame retardant modification of waterborne polyurethane fabric coating agent with high hydrostatic pressure resistance. *Prog. Org. Coat.* **97**, 91–98 (2016)

285. N. Onar, M.F. Ebeoglulil, I. Kayatekin, E. Celik, Low-temperature, sol-gel-synthesized, silver-doped titanium oxide coatings to improve ultraviolet-blocking properties for cotton fabrics. *J. Appl. Polym. Sci.* **106**(1), 514–525 (2007)
286. T. Suratwala, Z. Gardlund, K. Davidson, D.R. Uhlmann, S. Bonilla, N. Peyghambarian, Photostability of silylated coumarin dyes in polyceram hosts. *J. Sol-Gel Sci. Technol.* **8**(1–3), 973–978 (1997)
287. T. Textor, B. Mahltig, A sol-gel, based surface treatment for preparation of water repellent antistatic textiles. *Appl. Surf. Sci.* **256**(6), 1668–1674 (2010)
288. C. Molaison, G. Merfeld, E. Acar, R. Koeniger, S. Mordhorst, J. Suriano, Acid/epoxy catalyst screening for low temperature cure (120 °C) powder coatings, in *Annual Partners in Environmental Technology Technical Symposium and Workshop*, 2–5 Dec 2003, p. 237



Mazen K. Nazal and Mohammad Abu Jafar Mazumder

Contents

1	Basis of Corrosion Protection	884
2	Corrosion Control	886
3	Materials for Anticorrosive Coating	887
3.1	Metallic Coating Materials	888
3.2	Inorganic Coating Materials	889
3.3	Organic Coating Materials	889
4	Mechanism of Anticorrosion Protective Coating	892
5	Performance Testing and Evaluation of Anticorrosion Coating Materials	899
6	Conclusions	905
	References	906

Abstract

Protection of construction tools such as bridges, rails, ships, cars, engines, cargo, and storage containers against corrosion is significant. The scale-up of corrosion in a system can be prevented or at least minimized by altering the environment, changing the material properties, and/or protective coating. The main objective of this book chapter is to present and describe the different types of corrosion control methods in addition to the materials (organic, metallic, and inorganic) used as

M. K. Nazal

Centre for Environment and Water (CEW), King Fahd University of Petroleum and Minerals,
Dhahran, Saudi Arabia

e-mail: mazennazal@kfupm.edu.sa

M. A. Jafar Mazumder (✉)

Chemistry Department, King Fahd University of Petroleum and Minerals, Dhahran, Saudi Arabia

e-mail: jafar@kfupm.edu.sa

anticorrosive coatings and discuss the mechanism of different classes of anti-corrosion protective coating (i.e., barrier, sacrificial, and inhibitive coating). Furthermore, some anticorrosive coating evaluation methods using outdoor exposure and laboratory tests have been discussed.

Keywords

Anticorrosion · Coating · Pigments · Inhibitors · Controlling corrosion

Abbreviations

ACAT	Amine-capped aniline trimer
aq	Aqueous
Cd	Capacitance of double layers
CPE	Constant phase element
DMDDES	Dimethyldiethoxysilane
EMF	Electromotive force
FGNP-TPP	Functionalized graphite nanoplatelets modified with tripolyphosphate anion
FHWA	Federal Highway Agencies
GPTMS	Glycidoxypropyltrimethoxysilane
HEE	Hydrophobic electroactive epoxy
l	Liquid
MAPTS	Methacryloxypropyltrimethoxysilane
MTES	Methyltriethoxysilane
n	Power of the diffusion impedance
PAAMPS	Poly-acetamide-acetoxyl methyl-propylsiloxane
PANI shell with AuNPs	Polyaniline-modified gold nanoparticles
PANI-MWCNT	Multiwall carbon nanotube-polyaniline
RGO	Reduced graphene oxide
R _p	Polarization resistance
R _s	Electrolyte solution resistance
s	Solid
SEPI	Superhydrophobic electroactive polyimide
TEOS	Tetraethoxysilane
W	Warburg impedance
Y ₀	Admittance constant
χ^2	Chi square
ω	Frequency

1 Basis of Corrosion Protection

Corrosion is the phenomenon of destruction and consumption of materials chemically, electrochemically, and/or biologically with the environment [1]. The corrosive environment includes but not limited to air, humidity, and different types of water (i.e., marine, salt, fresh, and distilled), natural atmosphere, ammonia, hydrogen sulfide,

acids, and fuel gases. Based on the exposure, these environments are divided into three different types: (a) atmospheric (i.e. industrials, rural, and marine), (b) splash zone, and (c) immersion (i.e., in soil, seawater, and freshwater). Consequences of corrosion are loss of industrial efficiency, insulation of heat exchanger pipelines, loss of products, and contamination and shutdown of plants, which imply inconvenient increase of cost, destroy the economy, and deplete the resources. Table 1 shows the annual cost of corrosion studies at some countries. In addition, a study conducted by Federal Highway Agencies (FHWA), USA [2], C. C. Technologies Inc., USA [3], and National Association of Corrosion Engineers [4] found that the corrosion is covered by around 3.1% of the national gross domestic product with an approximate cost of \$276 billion. In the United States, the corrosion cost of gas and liquid transportation's pipelines exceeds \$7 billion and is expected to be very high in the future due to the highly corrosive environment in gulf countries. Also, the United States spends around 10% of the maintenance of aircraft on corrosion remediation [4].

Corrosion science and corrosion engineering cannot be separated; virtually they go hand-in-hand. The corrosion science describes classification of different forms of corrosion in addition to the mechanism and rate. On the other hand, the rules and principles established from corrosion science are used in the corrosion engineering.

Corrosion engineering concerns on designing of materials and coating of structures to prevent corrosion. Basic science such as chemistry, physics, and biology and different disciplines of engineering such as mechanical, civil, metallurgical, and electrical engineering contribute to the theme of corrosion and anticorrosion. The following functions affect corrosion and deserve to be considered in corrosion science and engineering: (a) impermeability, (b) mechanical strength, (c) dimensional integrity, (d) physical properties, (e) contaminations, and (f) damage to equipment. Consider the following points and abovementioned direct and indirect hindrance that intrigue and motivate us to study anticorrosion:

- (i) The importance of materials such as iron, aluminum, copper, manganese, and titanium as resources to life.
- (ii) Corrosion may contaminate stored products such as food and water.

Table 1 Overview of cost of corrosion studies at some countries in selected year

Country name	Annual cost	Year
United States	\$ 5.5 billion	1949
United States	\$ 70 billion	1975
United States	\$ 276 billion	2002
Japan	\$ 9.2 billion	1974
West Germany	\$ 6 billion	1967
United Kingdom	£ 1.365 billion	1970
Australia	\$ 2 billion	1982
Kuwait	\$ 1 billion	1987
India	\$ 320 million	1960
Finland	\$ 54 million	1965

- (iii) Fully understand the engineering corrosion to provide better design and construction knowledge for industrial process and transportation medium.
- (iv) Prevent the disaster caused by corrosion, such as crushing civil and military constructions and explosion of oil pipelines and oil tanks.
- (v) Complete understanding of corrosion science is required for designing an efficient artificial tool that can be implemented in the human body.

Corrosion resistance and developing anticorrosion materials depend on many factors such as effect of oxygen, effect of oxidizing materials and conditions, temperature, corrosive concentration, metallurgical factors, velocity of corrosion, and galvanic coupling [5]. A powerful solution that dealt with corrosion and preventing failure occurring in industries and constructions is the main motivating force in the development of anticorrosive coating materials such as alloy, composites, metals, polymers, and ceramics with advanced chemical, physical, and mechanical properties better than the surfaces to be covered. In the last decades, many anticorrosion materials (i.e., metallic, inorganic, and organic materials) were developed and investigated based on corrosion type and their mechanisms in protecting different types of environment such as industrial atmosphere and immersed marine seawater. In recent years, a number of anticorrosive coating materials which showed significant improvements in the resistivity of materials' surface against corrosion have been explored for protection against corrosion, and many of them have appeared with significant advancement. These advanced materials offer better resistant, cheap, more efficient operation, reduction in contamination of products, and highly pure and eco-friendly environment. However, despite very promising and encouraging outcome from anticorrosion research, unraveling of the complex mechanism and/or nature of corrosion has become the impediment in designing new anticorrosive coating materials and methods.

2 Corrosion Control

The pricey damage caused by corrosion could have been reduced by the application of corrosion control. A wide range of methods have been used to protect materials from corrosion. Some of the most common methods are listed below:

1. Alteration of environment: In this method, the corrosion can be reduced by reducing aeration, eliminating moisture, pumping an inert gas, reducing the flow of turbulence, and/or decreasing the surrounding temperature.
2. Introducing inhibitors: The inhibitors are generally added less than 0.1% by weight to the respective system. Consequently, the inhibitors protect the metals by adsorbing on to the metal surface and forming a protective film or eradicating the corrosion agent from the surface.
3. Cathodic protection: It is based on galvanic action, where the metal surface is protected by making it a cathode of an electrochemical cell. The metal protection

can be achieved by sacrificial metal to act as the anode or impressed electromotive force (emf) methods.

4. Anodic protection: It is relatively new compared to the cathodic protection. The corrosion is controlled by keeping an active-passive metal or alloy in the passive region by an externally applied anodic current. It has many advantageous properties over the cathodic protection, namely, (i) it requires low current, (ii) it reduces the corrosion rate largely, and (iii) it is applicable to some strong acids and other highly corrosive media. However, this type of corrosion control possesses some limitations which are as follows:
 - (a) The coating metals must have passivity such as stainless steel, nickels, and chromium and their alloys.
 - (b) This type of protection cannot be used if the media contains chloride ions, because the formed film can be attacked by those ions and be destroyed.
5. Selection of proper materials and design for equipment: The corrosion can be minimized in this method by designing a system with a complete drainage of liquid, eliminating cracks, avoiding direct contact between two different metals specially if there is a large gap in their electrochemical activity, and making the equipment easy to be cleaned, inspected, and maintained.
6. Lining and coating: There are many methods that can be used to apply the coat or line on top of the surface or inside the pipelines such as electroplating, cladding, and organic coating.

As a whole, the chance for corrosion of a certain type can primarily be prevented by a careful choice of suitable materials and the building or machine design. Typically, the scale-up of corrosion in a system can be prevented or at least minimized by altering the environment, changing the material properties, and/or protective coating. This protective coating is particularly important because it includes all the corrosion prevention methods such as barrier effect (inhibition), materials selection (conducting polymers), and cathodic/anodic protection.

3 Materials for Anticorrosive Coating

Protection of the surface of metallic materials or steel is achieved by one or multilayered system using anticorrosive coating materials. These materials can be classified in three major groups [6]: (i) metallic, (ii) inorganic, and (iii) organic coating materials. Many types of materials or elements can be used in each class, as illustrated in Fig. 1.

Corrosion inhibitors, whether inorganic or organic, retard the corrosion rate by affecting the anodic reaction or cathodic reactions or both. For inhibition of anodic reaction, the reaction rate of anodic dissolution turns out to be slow, and/or a thin film over the anode is formed by the produced reaction products. However, in cathodic reaction inhibition, the flow of electrons from the anode to the cathode is disrupted and/or the produced reaction products adsorbed selectively at the cathode sites.

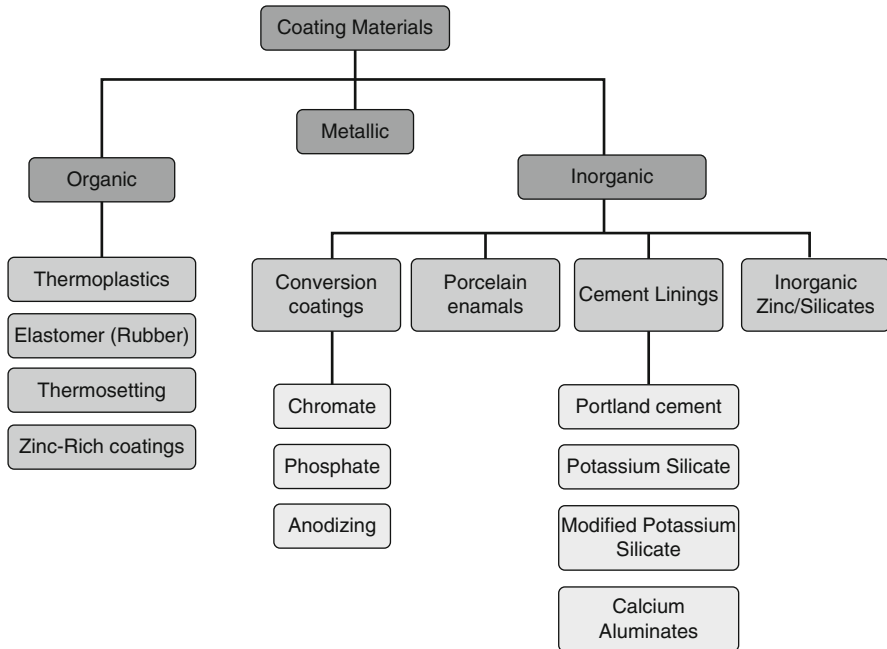


Fig. 1 Classification of materials and methods used in coating

The corrosion inhibitors work on one or more of the following factors:

- Increasing the anodic or cathodic polarization behavior
- Increasing the electrical resistance of the metallic surface
- Adsorbing themselves on the metallic surface and forming a film
- Reducing the movement or diffusion of ions to the metallic surface
- Interacting with the metallic surface or the environment near it

3.1 Metallic Coating Materials

Many metals (such as nickel, alumina, lead, zinc, copper, etc.) and their alloy composites are used as coating materials [7]. These metals are less noble than stainless steel; therefore, the main role of such coating is to form a barrier to protect the active metal (stainless steel) surface. Other factors should also be considered in the selection of metallic coating: (i) the metals should resist direct attack of the environment, (ii) they should be hard, and (iii) they should be nonporous. There are number of methods used to coat the metal surface by anticorrosive coating materials such as hot dipping (galvanizing), electroplating, thermal spray (metal in powder form), cladding stainless steel and weld overlaying are used to coat the stainless steel metal surface. The quality of coating is affected by many factors, such as (1) thickness uniformity, (2) porosity and continuity of coating, (3) its adherence, and (4) the average thickness of coating.

3.2 Inorganic Coating Materials

Chromate, potassium silicate, phosphate, modified potassium silicate, calcium aluminate, and zinc/silicate compounds are used as an inorganic coating (Fig. 1). Inorganic coating is achieved or formed by chemical conversion, spraying, or diffusion [6]. It is worthwhile to mention that the metallic and inorganic coating materials should form a barrier without defects (brittleness and very low porosity). Otherwise these defects can accelerate localized corrosion of the coated metals instead of coating due to galvanic effect.

3.3 Organic Coating Materials

Better coating can be formed by organic coating materials. These organic materials coat the active metal surface by formation of thin film of paint, varnish, and lacquer. Most organic material coatings adhere to the metal surface by two mechanisms: the first one is the mechanical adhesion which is common in porous materials, where a large surface area of metal is used and the organic coat is anchored on the surface physically. The second mechanism is the chemical adhesion. In this mechanism, the organic coat is bound to the surface through a covalent, ionic, hydrogen bonding, dipole-dipole, and/or van der Waals interactions [8]. To obtain good organic coatings, the following three steps should be considered: (i) suitable surface preparation, (ii) selection of proper priming coat, and (iii) top coat. It is noted that without proper surface preparation, the priming coat does not have a good adherence. As a result, the top coat will not be firmed and may peel off any time.

The first and most important step in assuring good coat performance is surface preparation. If there is oil or grease contamination in the surfaces, the oil and grease should be removed first by the solvent or vapor degreasing, for example, a chlorinated hydrocarbon, by alkali or emulsion cleaning, and so forth. The degreased surface can then be sandblasted or pickled.

Painting is one of the long-established methods of corrosion control. Paint consists resin or plasticizer as binder materials, in addition to organic materials as a coloring and protective coat [9]. If the environment can be effectively excluded, paint can do its proposed job. It takes good user technique to be sure a paint works properly otherwise it can be a wastage of money. The main target of painting is to furnish a barrier coating that will exclude the environment and prevent its premature adverse reaction with the substrate. All paint systems fail eventually, but avoidance of premature failure is needed to minimize the cost.

Paint failure normally involves a combination of oxidation and ultraviolet light. Due to the oxidation and/or ultraviolet light, there may be a change in appearance, such as loss of gloss, or reduction in the film thickness. Premature failure is usually characterized by a loss of adhesion, either with the substrate or between successive paint layers. Loss of adhesion to the substrate also can be a secondary process resulting from corrosion. To avoid these problems, adequate cleaning must be done to remove greasy oils of various kinds, poorly adherent prior coatings,

corrosion product salts, and solid corrosion products, such as mill scale. Primers that are to be top coated must be completely cured; manufacturers are tempted to underestimate the time required for this coat. Topcoats on primers or other existing coatings must be compatible. As a general rule, two paint coats will be compatible if the plots of their solubility parameters versus their hydrogen bonding index are appropriately close.

The correlation between solubility parameter and hydrogen bonding, which can be used to judge on the suitability of polymeric paints and the compatibility between resin and solvent system or between an existing polymeric coating and a paint. In general, the existing coating should be swelled somewhat by the solvent system of the topcoat and should not be completely soluble [10].

Two classes of painting should be recognized. The first class is cosmetic painting for noncorrosive indoor applications, whereas a solvent wipe may be the only justified pretreatment, and the coating thickness is not important, for example, painting on fire mains for identification purposes. The second class is intended to protect from corrosion; here the pretreatment is necessarily expensive and extensive. Thickness is also important for optimum performance and should be thin (3–12 mils) for air-dried coatings, depending on type of coating used and the intended service [10].

Three steps should be followed for obtaining the best performance of protective coatings using paints. Firstly, the applied coat of paint at the steel surface produce high quality finishing surface. Secondly, the applied coat helps prompting weldable priming usually by pigmented iron oxide. The resultant prime should be hard enough to withstand handling on the way to the assembly site with minimal damage. Lastly, a hard thin top coat can be applied prior to protect a softer primer. When old paint is recoated, it is necessary to remove the loose and nonadherent layers on the surface. Note that pickled or sandblasted steel usually rusts rapidly. Therefore, a superficial oxide is replaced with a phosphate which acts as a good paint base. Alternatively, a combination paint called Etch primer from phosphoric acid and specialized primer can be used [10].

Protective coating using organic materials are applied to a surface in liquid form and dried to give a prolonging solid film. Drying process usually involves chemical reactions and polymerization or merely consists of solvent evaporation [11]. Polyaniline conducting polymer is commonly used as common materials for organic protective coating, which can easily be prepared as a cheap product, and it has a good tunable properties and thermal stability [12, 13]. It is not like traditional polymeric coating materials which require multilayer coating to protect a metal's surface against corrosion. The main advantage of this material is that it can be used as single-layer coat [14]. The polyaniline nanostructure composites (i.e., nanospheres, granules, nanotubes, and nanofibers) demonstrated an improvement in their application as anticorrosive coating materials [15–18]. Different kinds of polyaniline nanostructure composites are depicted in Fig. 2. Moreover, there are different methods utilized for preparation of polyaniline such as self-assembling, electrochemical polymerizations, and heterophase interfaces which could easily provide different kinds of structures with tunable properties. Table 2

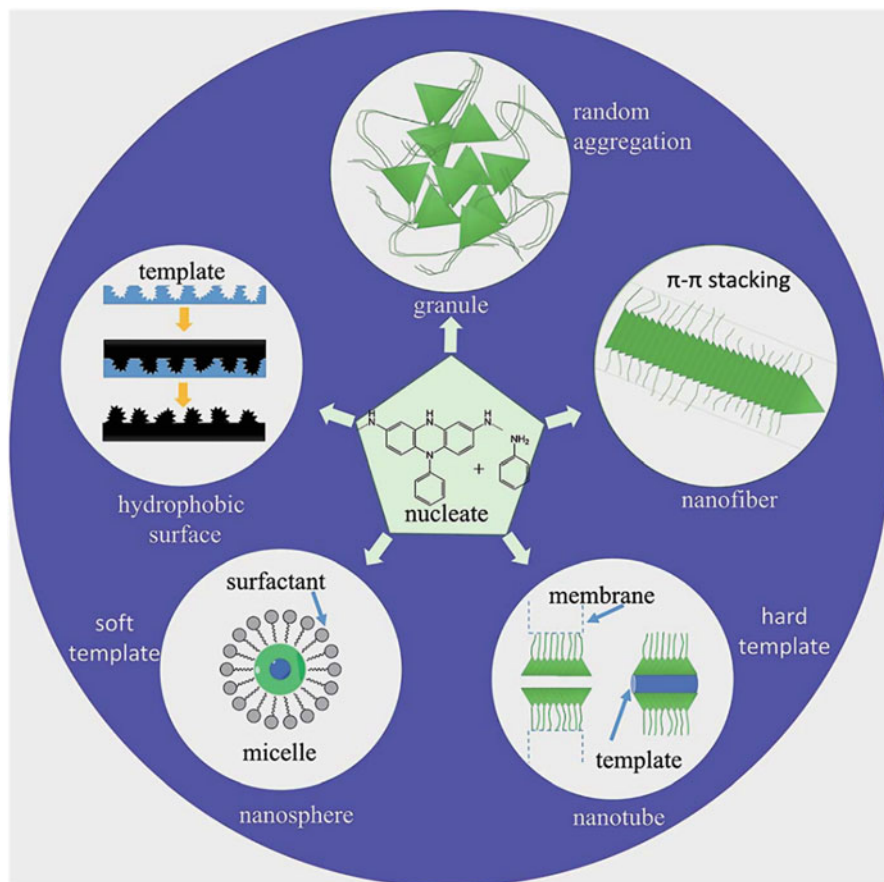


Fig. 2 Schematic illustration of nucleates and monomer of aniline to produce different types of PANI nanostructures [18]. (With kind permission from RSC)

shows different polyaniline nanostructure composites classified based on their structures' morphologies.

One of the important classes of corrosion inhibitors is organic adsorption inhibitors (e.g., primary amine, amide, imidazoline, and polyethoxylated amines). The organic adsorption inhibitors adsorb and form thin film onto the metal surface. The effectiveness of adsorption inhibitors depends on the electrical potential of metals, chemical structure, size, and shape of inhibitor molecules. On the other hand, the inorganic adsorption inhibitors are classified into (i) cathodic inhibitors, such as carbonate, sulfate, and hydrazine, and (ii) anodic inhibitors such as silicate, bicarbonate, phosphate, chromate, or nitrite compounds. These inhibitors are usually added in small amount ($\approx 0.1\%$) to the corrosive media and are able to stop or slow down electrochemical corrosion reaction on the metal surface.

Table 2 Examples on different PANI nanostructure composites

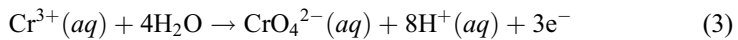
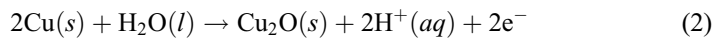
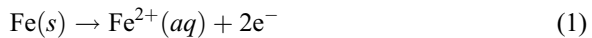
#	Structure	Composition of PANI-based corrosion inhibitor	Methods of composition preparation	Substrate	Corrosion medium	Ref.
1	Nanospheres	PANI shell with AuNPs	In situ polymerization and dispersion mixing	Zinc	1 M KCl	[19]
2	Granules	ND-PANI	In situ polymerization	Steel and aluminum	HCl	[20]
		PANI-CN	Ultrasonic oxidative polymerization	Carbon steel	3.5% NaCl	[21]
3	Nanotubes	PANI-MWCNT	In situ polymerization	Mild steel	3.5% NaCl	[22]
		PANI	Emulsion polymerization	Mild steel	3.5% NaCl	[23]
4	Nanofibers	ZnO-PANI	In situ polymerization	Carbon steel	3.5% NaCl	[24]
		PANI	Direct mixed reaction	Aluminum alloy	0.6 M NaCl	[17]
		PANI	Three different types of reactions	Mild steel	3.5% NaCl	[25]
5	Other nanocomposites	HEE and SEPI synthesized from ACAT	Nanocasting technique	Cold-rolled steel	3.5% NaCl	[26]
		Urchin-like PANI	Emulsion polymerization and in situ polymerization	–	–	[27]

4 Mechanism of Anticorrosion Protective Coating

Corrosion of metals causes a significant shortage in the function of the technical system as a result of the destruction of the metals. The metals are destroyed by converting them to oxides or other form of corrosion products. Consequently, understanding the mechanism and thermodynamic of corrosion is significant for controlling corrosion. Mechanism of corrosion is classified to three main types: (i) physical, (ii) chemical, and (iii) electrochemical corrosion. Chemical corrosion involves chemical reaction and takes place in dry conditions on homogeneous or heterogeneous surface by direct contact with chemical compounds. While physical corrosion occurs by a combination between a corrosive environment and tensile loading cracks resulting in multiple branching cracks such as the corrosion that happens in stainless steel pressure vessels. In electrochemical corrosion, exposing

two different surface structure or composition in different operational environments causes of evolving an electrical potential. This system of corrosion consists of three elements as shown in Fig. 3. The corrosion site (anode), the corrosion media (electrolyte), and the metals, which are active in the system but do not corrode (cathode), are the main components in the electrochemical process. The process usually occurs through a coupled electrochemical half-cell of anodic and cathodic reaction.

In this process, the metals lose an electron in the anodic reaction thus increasing their oxidation number. For example, as shown in Eqs. 1, 2, and 3, Fe, Cu and Cr lost 2, 2, and 3 electrons, respectively, whereas the first two reactions are considered as a corrosion reaction but the third one is not.



where s , aq , and l represent the state of solid, aqueous, and liquid, respectively.

In the third reaction, there is a loss of electrons from Cr^{+3} and a charge transfer in the solution without a phase change. Therefore, the corrosion reaction should have a mass transfer in addition to the electron loss from metals.

In cathodic reaction, the electrons are consumed, whereas the metals gain electrons, and their oxidation number is decreased. For example, in acidic media, the predominant cathodic reaction is the reduction of two hydrogen ions at a metal surface and formation of hydrogen gas, as shown in Eq. 4:

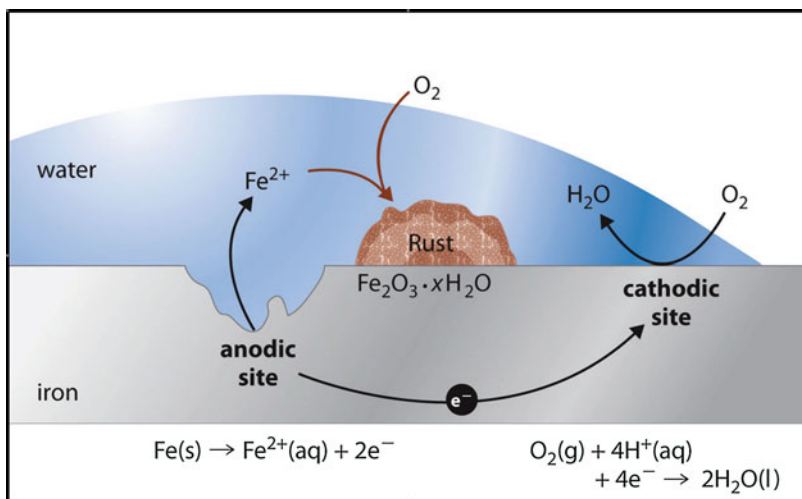
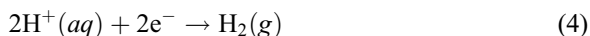


Fig. 3 Corrosion process of steel that leads to the creation of small holes in metal [28]. (Permission for unrestricted use under creative commons attribution license)



In case of availability of the metal surface in a neutral or basic media, the cathodic reaction includes reduction of the dissolved oxygen molecules to hydroxyl ions as shown in Eq. 5:



Coupling of both electrochemical reactions (cathodic and anodic) at the same metal surface occurs at different sites because of the heterogeneity of metal surface or metals containing impurities. For example, in the acidic environment, the iron atoms at metal surface act as anodic half-cell, released two electrons and appear as Fe^{+2} . These released electrons from iron (Eq. 1) is consumed by two hydrogen ions, and got reduced at another sites as cathodic half-cell on the same metal surface.

For the electrochemical corrosion, the protection types can be classified based on their protective mechanism to three main classes, galvanic effect (coating sacrificial), barrier effect, and inhibitive effect. The anticorrosion mechanism by barrier coating is achieved through its role as a barrier to oxygen and water from the environment by forming an ionic impermeability interface with high electrical resistance [29–31]. This leads to very low conductivity which in turn minimizes transferring the corrosion current between the anodic and cathodic side at the substrate [32]. Table 3 shows some of those materials used in protective coating. Because of heat and chemical resistance of SiO_2 , it improves the acidic corrosion and oxidation resistance of metal

Table 3 Various protective coating materials

Substrate	Coating composition	Coating method	Thickness (um)	Reference
Carbon steel	SiO_2	Dip-coating	0.15	[34]
Mild steel	ZrO_2	Dip-coating	0.3–0.6	[36]
Aluminum	SiO_2	Dip-coating	N/A	[38]
Aluminum	Epoxy silane-epoxy	Spraying	30–50	[39]
Aluminum	TEOS-GPTMS-PDMS	Spin-coating	N/A	[40]
Carbon steel	TEOS-MAPTS	Brushing	N/A	[41]
Galvanized steel	TEOS-MTES	Dip-coating	4.0	[42]
Stainless steel	$\text{CaO-P}_2\text{O}_5$	Spin-coating	1.0	[43]
Aluminum	ZrO_2 -TEOS-MAPTS	Spin-coating	1.9–7.5	[44]
Carbon steel	PAAMPS polymer containing a cerium (Ce)	Dip-coating	2.1–2.5	[45]
Stainless steel	Cerium-TEOS-MTES	Spin-coating	1.9–2.0	[46]
Aluminum	MTES	Electrodeposition	0.16–0.18	[47]
AISI 304 stainless steel	MTES and DMDDES	Deposition	0.58–0.76	[48]
Metal substrate of zinc 5% aluminium	Strontium aluminium polyphosphate	Roll bar coater	5	[49]

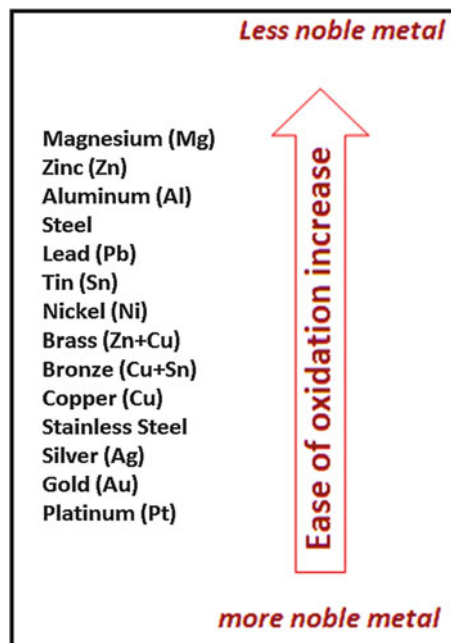
substrate at different temperatures; as a result it has been used efficiently as a protective coat for stainless steel [33, 34]. Zirconium oxide ZrO_2 has a good chemical stability as well as it can minimize the cracking of metal substrate due to its high expansion coefficient that is close to the variety of bulk metal substrates [35, 36].

Recently, the reduced graphene oxide (RGO) has been developed as a protective coating material. A monolayer defect-free RGO with high-barrier properties was synthesized to prevent water and oxygen gas molecules and even strong acids such as hydrofluoric acid (HF) to reach the surface of substrate and cause corrosion [37]. The main challenge for defect-free RGO barrier coating is its synthesis with a large surface area.

The second type of protective coating mechanism is called sacrificial or galvanic coating. In this type, the metallic substrate is protected by another electrochemically more active metal or alloy. In another words, the sacrificial metal or alloy dissolves favorably to protect the substrate metals. This type of coating is unlike the first type of protection mechanism. Since its protection mechanism depends on the electrical conductivity, the coat must be in direct contact with the metal substrate; therefore, it is only applied as a primer. As shown in the electrochemical activity series in Fig. 4, there are some metals that might be used as sacrificial coat such as zinc, aluminum, and chromium on metal substrate. For example, zinc (Zn) is used as primer to protect the metal substrate by forming an anodic site active coat [50]. The cathode protection mechanism using Zn sacrificial coat is illustrated in Fig. 5.

For further improvement of the performance of zinc-rich sacrificial coat, many composites of zinc with other nanoparticles such as aluminum oxide [51], silicon

Fig. 4 Galvanic series



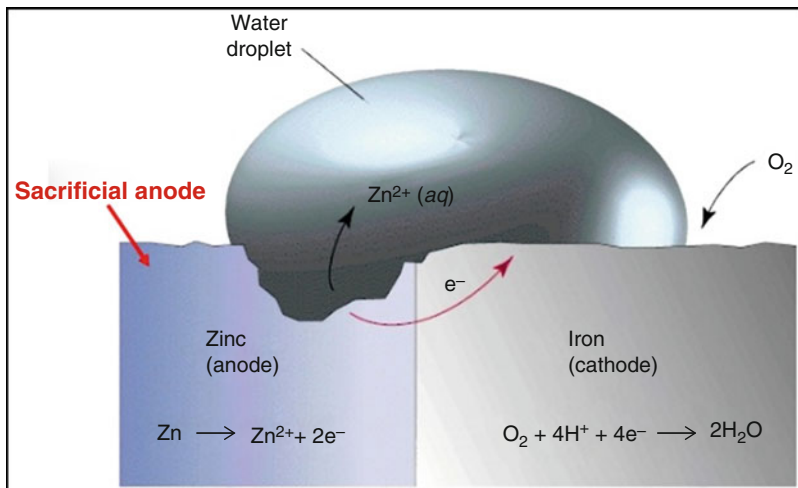


Fig. 5 Scheme illustrates the mechanism of sacrificial coat for cathodic protection

dioxide [52], and titanium dioxide [53, 54] were investigated. In 2011, Khan et al. [55] prepared a zinc-silica nanocomposites coat with different functionalized silicas. They found the functionalized silica with thiol group can interact strongly with zinc metal and form an efficient coating on the surface of metal substrate. To improve the incorporation of sacrificial coat furthermore with surface of metal substrate, recently, Camargo et al. [56] enhanced the electrodeposition of zinc-titanium dioxide coat on steel substrate using ultrasonication method. They reported that using high-speed electrodeposition under ultrasound sonication reduces the titanium dioxide particle agglomeration and forms smaller particle size in addition to its better distribution in zinc sacrificial matrix. Consequently, as a result of enhancement of the hardness of sacrificial coat, it improve the corrosion resistivity. The main challenge for sacrificial coating is to keep its conductivity as high as possible without compromising the hardness as well as the adhesion and cohesion properties on the metal substrate.

Figure 6 shows the setup of anodic protection, where it is used as an example for protection of a steel storage tank for acidic solution. To achieve successful anodic protection, it requires a controlled potential current and formed insoluble film in aggressive solution. In the anodic protection, many factors influence the protective potential such as the chloride ion concentration as well as the temperature. As shown in Fig. 7, the protective potential is inversely proportional to the current, whereas the metallic coating resistance decreases due to the effect of chloride concentration and temperature [57]. The low current density for anodic corrosion rate is due to the limited ionic mobility in the formed insoluble film at the protected surface.

The third protection type based on the anticorrosion mechanism is inhibitive coating. The corrosion inhibitor materials used in this type initially diffuse from bulk solution to the surface of metal, and then their molecules start condensation at the

Fig. 6 Schematic illustration for anodic protection [57]. (With kind permission from Springer)

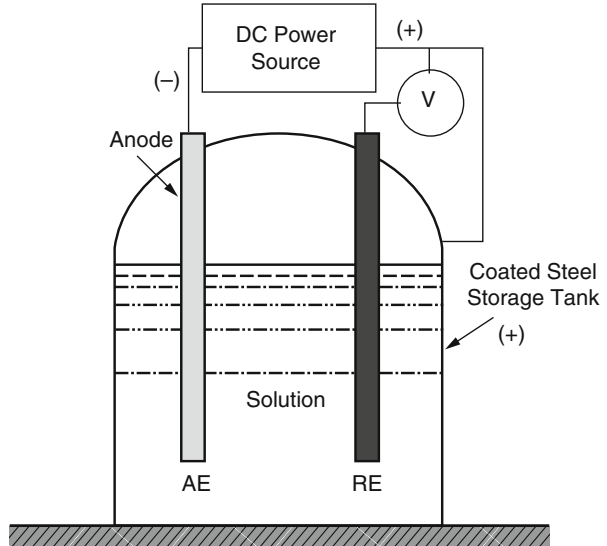
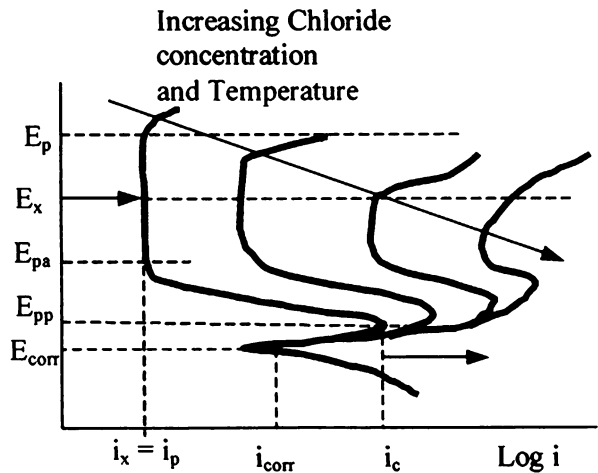


Fig. 7 Polarization curves for the effects of chloride concentration and temperature on the passive region [57]. (With kind permission from Springer)



surface followed by the adsorption to form monolayer or multilayer protective coating on the metal surface [58]. The schematic representation of adsorption of inhibitor molecules on metal surface is shown in Fig. 8.

The inhibitor material adsorbs on the surface of metal and forms monolayer or multilayers mainly through one of the following interaction mechanisms:

1. Electrostatic interaction between the charged molecules and the surface.
2. Interaction of the nonbonding or the π -electrons with the empty orbitals available in the surface chemical structure.
3. A mixed mechanism includes both of the above.

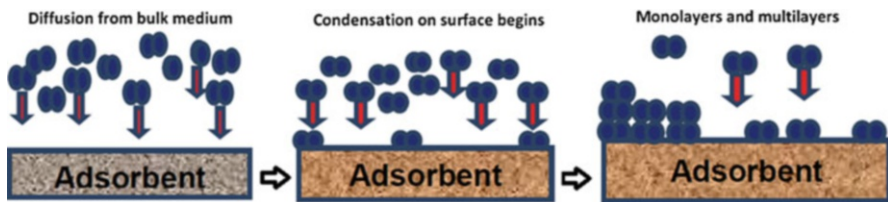


Fig. 8 Schematic representation of adsorption of inhibitor molecules on metal surface from bulk solution [58]. (Permission for unrestricted use under creative commons attribution license)

The main advantages of this type of protection are that (i) it is cheaper than sacrificial zinc-pigmented coatings and (ii) it works in most environments. However, the inhibitive coating is not applicable for coating the immersed structure and must have low water permeability to work effectively. The inhibition coat composition must contain soluble constituent which can react with metal surface. Therefore, it is mainly applied as a primer for substrates exposed to the atmospheric environments such as industrial environment [59]. In inhibitive coating, the substrate passivates the materials' coat that consists mainly of insoluble metallic compounds to protect the surface of the substrate from the aggressive species. The inhibitive coat contains low percentage of slightly water-soluble inorganic salts such as phosphate [60], silicates [61], chromates, and molybdates [62]. These inorganic salts dissolve partially once they are permeated with water, and then the dissolved components are moved to the surface of the metal substrate which reacts with it and form protective products that passivate the metal substrate. Therefore, the inhibitive coat should consist of enough soluble inorganic salt pigments to insure sufficient leaching from the coat to passivate the surface of substrate but not too high to prevent occurrence of blistering [63]. This indicates a balance has to be obtained between compounds which work as a barrier and those as inhibitive inorganic salts.

Generally, molybdates, silicates, and chromate salts are used as an inhibitive pigment in the inhibitive organic coats. However, in Europe, phosphate salts are mainly used [59]. In regard to phosphate salt-based pigments, they can be classified into four generations, namely, (i) pigments which contain only zinc phosphate salt, which has weak inhibitive properties due to its low water solubility [64]; (ii) modified zinc phosphate salts with aluminum, iron, molybdenum, potassium, or sodium [65]; (iii) zinc polyphosphates and zinc tripolyphosphate; and (iv) zinc phosphate which contains organic compounds [66].

Recently, Mohammadi et al. [67] synthesized functionalized graphite nanoplatelets modified with tripolyphosphates anion (FGNP-TPP) to improve the anti-corrosion coating performance of epoxy by dispersing the nanoparticles on it. Their results indicate high coated steel substrate resistivity for corrosion. The proposed mechanism is illustrated in Fig. 9. Tripolyphosphate anions close to the surface of metal substrate are released from the epoxy coating after its exposure to moisture from the environment. Polyphosphate anions compared to chloride anions have high competitive and binding strength to ferric and ferrous oxide at the surface of the

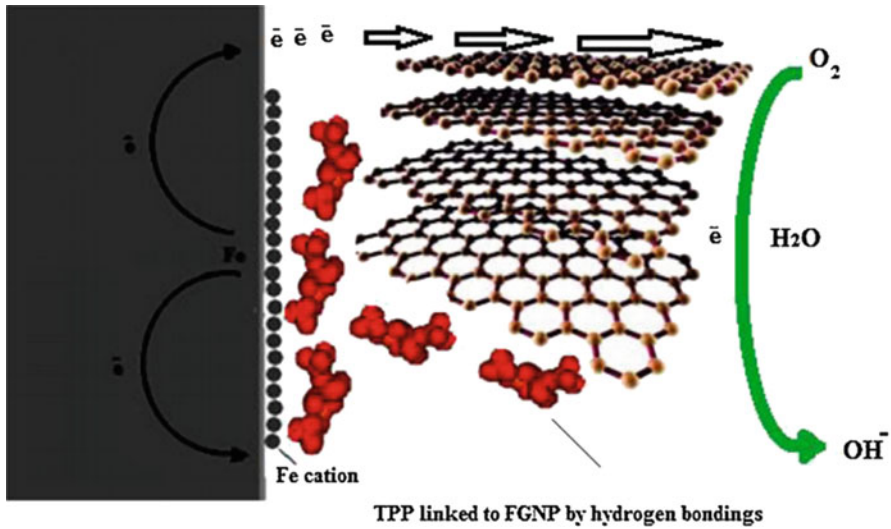


Fig. 9 Illustration for inhibition mechanism using FGNP-TPP epoxy coating composite [67]. (With kind permission from Elsevier)

substrate. Therefore, a stable and dense protective ferric and ferrous phosphate layer is formed.

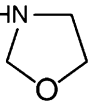
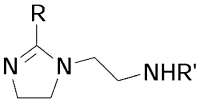
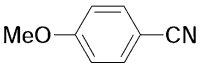
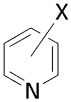
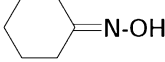
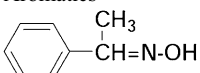
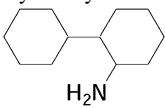
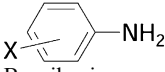
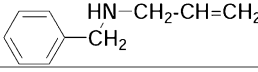
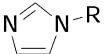
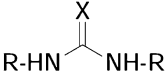
The organic inhibitors have the ability to form an efficient protective film on the surface of metals which might be exposed to media with high hydrocarbon contents. Therefore, the most widely used inhibitors in the oil and gas industry are the organic inhibitors [68]. There are many organic inhibitors that have showed excellent performance as corrosion inhibitors. As shown in Table 4, they have been used as corrosion inhibitors for different metal surfaces immersed in basic or acidic media. They belong to different organic families, such as isoxazolidines [69], pyridines [70–72], fatty amides [73, 74], imidazolines [75–79], and polymers [80].

As a summary, the chart in Fig. 10 shows the main three types of anticorrosion protection, where they are applied, and their advantages and disadvantages.

5 Performance Testing and Evaluation of Anticorrosion Coating Materials

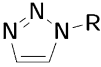
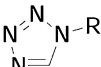
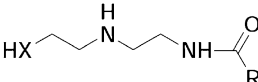
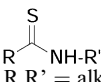
Characterization of anticorrosive coating materials is very important. To characterize a coating material, sample development process, point of interest and evaluation criteria of the coating materials should be taken into consideration. There are many outdoor and laboratory tests which have been used to evaluate the performance of coating materials. The outdoor exposure method is the most reliable way to test the suitability of certain coating materials for certain substrate in specific environment. In this approach, the coated substrate is exposed to real environmental conditions in

Table 4 Chemical family groups of organic inhibitors for anticorrosive coatings

Organic inhibitors (Chemical family)	Structure	Surface	Media
Isoxazolidines		Carbon steel	Acidic
Imidazolines	 R, R' = alkyl, aryl; X = NH ₂ , NHR, OH	Carbon steel	Acidic
Nitriles	Alkyl nitriles C ₁₇ H ₃₅ - CN Aromatics 	Carbon steel	Acidic
Pyridines	 X = CH ₃ , Br, OR	Carbon steel	Acidic
Oximes	Alkyl oximes  Aromatics 	Carbon steel	Acidic
Primary and secondary amines	Cycloalkylic  Aromatic (X = H, NO ₂ , CH ₃ , Cl, COOH)  Benzilamines 	Carbon steel	Acidic
Imidazoles	 R = alkyl, aryl	Copper alloy and carbon steel	Basic
Ureasy Thioureas	 R = O, S, R = alkyl, aryl	Copper alloy and carbon steel	Acidic

(continued)

Table 4 (continued)

Organic inhibitors (Chemical family)	Structure	Surface	Media
Triazoles	 $R = \text{alkyl, aryl}$	Copper alloys	Basic
Tetrazoles	 $R = \text{alkyl, aryl}$	Copper alloys	Basic
Amides and thioamides	<p>Amides</p>  <p>Thioamides</p>  $R, R' = \text{alkyl}$	Carbon steel	Acidic
Polyvinyls	$R - (\text{CH}=\underset{\text{R}}{\text{C}}\text{H})_n$ $R, R' = \text{alkyl, aryl heterocyclic}$	Carbon steel	Acidic
Polyesters	$R - (\text{OCH}_2\text{CH}_2)_n$ $R = \text{alkyl, aryl}$	Carbon steel	Acidic

a long-term study where it will be finally used [81]. Therefore, the outdoor exposure test provides a good representation results for the degradation of the anticorrosive coating materials in specific environment, which consider the main advantage of this test method. However, it has many disadvantages, for example, degradation of coating materials in real environment takes a very long time (>10 years). In addition, the variability of environmental conditions makes obtaining consistence corrosion rate and mode not possible, which affects the accuracy of concluding result [82].

On the other hand, the second approach, where tests are done in the laboratory, can provide reproducible results on the performance of coating materials in a shorter time at different environmental conditions. This approach includes accelerated tests such as salt spray tests, cyclic testing, and advanced cycling testing. The coated surface is evaluated later by visual methods exposing them to outdoor or laboratories corrosion environmental conditions. It is based on translation visual signs of corrosion on the surface that lead to useful conclusion, which depends heavily on the operators' capability and experience. Therefore, combining the previous visual method to an electronic method is very beneficial to understand the mechanism of corrosion and the quality of coating materials.

Since corrosion is mainly an electrochemical process, using electrochemical techniques is considered the best strategy for characterization and evaluation of the anticorrosive coating materials' performance. Particularly, the electrochemical impedance spectroscopy (EIS), which is relatively fast, accurate, and reproducible,

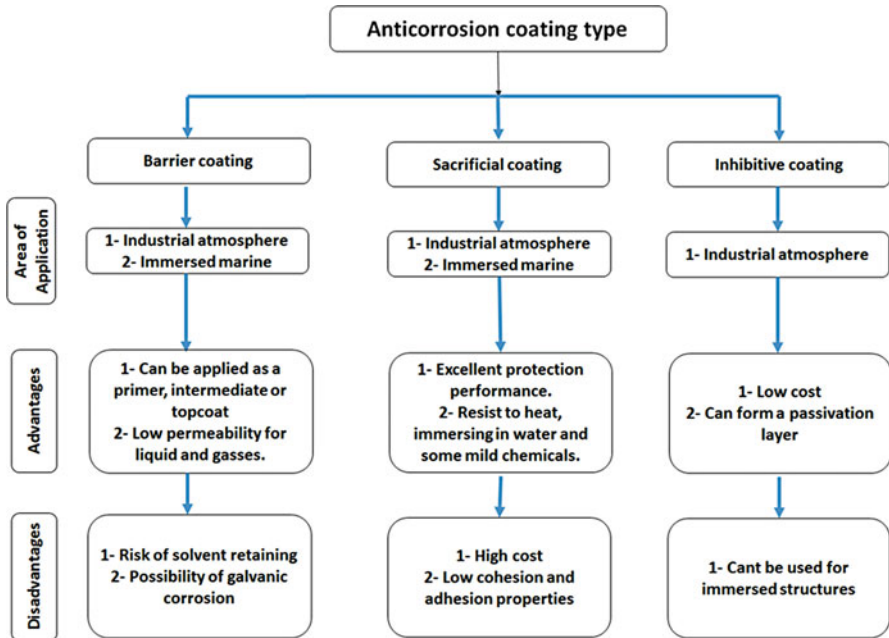


Fig. 10 Types of anticorrosion protection coating with their advantages, disadvantages, and area of applications

has been widely used in studying the performance of coating materials to understand the mechanism of corrosion reaction at the coated surface-solution interface. In addition, the EIS is a well-established and powerful technique for the characterization of coating materials. However, the EIS has some practical limitations, and it requires skilled persons and experts to personally perform data analysis.

Figure 11 shows the illustration for the simplest electrical characteristic of electrode surface-electrolyte solution interface which can also be called Randle electrochemical circuit. This interface mainly consists of (i) a thin film capacitor (double layer capacitance (C_d)) which is divided into two planes, inner and outer Helmholtz planes, (ii) resistivity of charge transfer which is expressed by polarization resistance (R_p), and (iii) another resistor electrical component which expresses the resistivity of electrolyte solution (R_s). In some cases, another electrochemical component appears which is called Warburg impedance (W) due to the impact of neutral and charged species diffusion from and to the surface. The inductive effect is not usually appearing in the electrochemical equivalent circuit, therefore, the more common electrical component is presented in the electrochemical circuit [83].

Generally, the EIS results can be interpreted by one of two approaches: fundamental approach and phenomenological approach. For the fundamental approach, a physico-electrochemical model accounting the processes which take place in the measurement system is required to formulate a mathematical representation including all the parameters and express the relationship between the input and the output

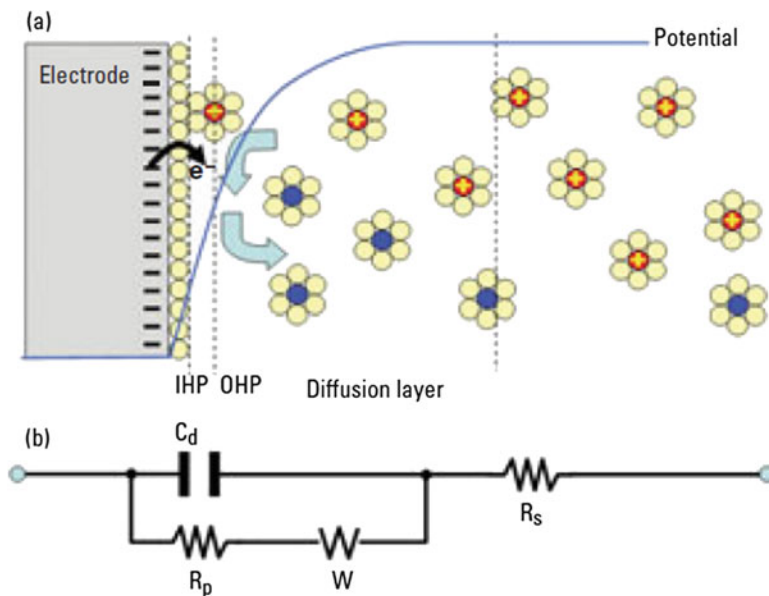






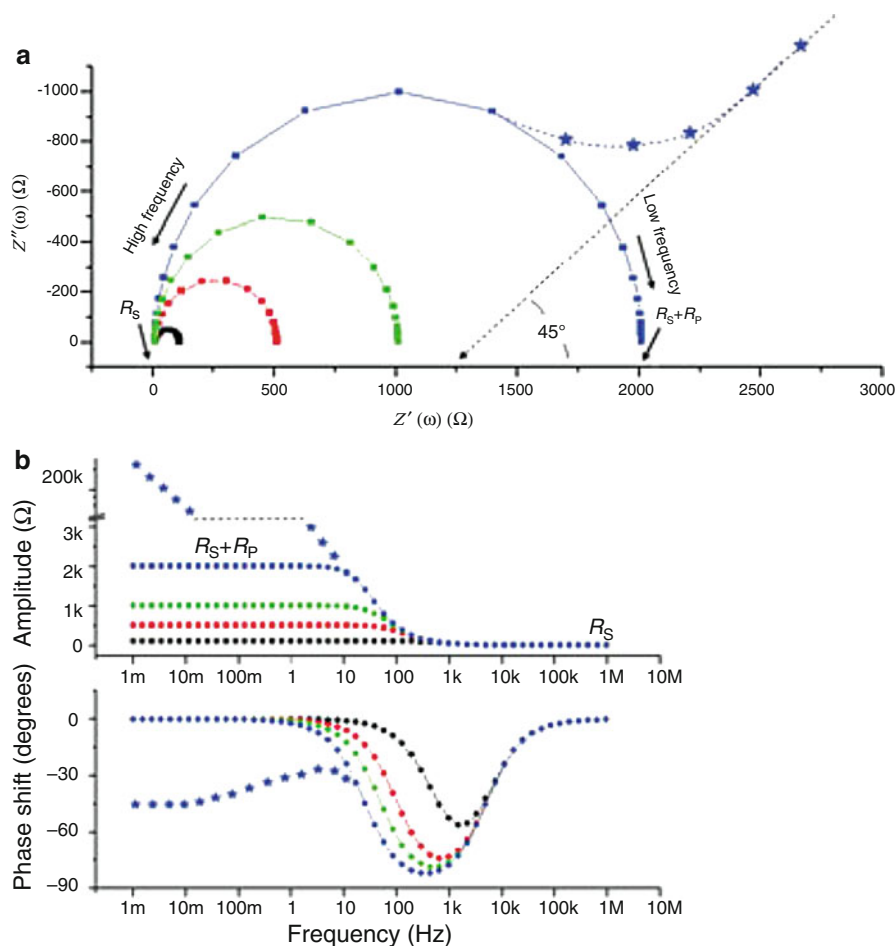
Fig. 11 A simple electrified interface, in which the vertical dotted lines in (a) are represented by the electronic components in (b) [83]. (With kind permission from ACS)

of the tested system to fit the measurement data and then get an information about the reaction mechanism. The main drawback of this approach is that it requires a fully understood reaction mechanism to formulate the model since the electro-chemical system sometimes appear as complex to get a useful model. Therefore, the second approach is often used to analyze the EIS data by using a well-defined electrical equivalent circuit as a physical model that contains electrical parameters, such as resistors and capacitances, and simulates the EIS measured data. The starting model of the most probable equivalent circuit can be constructed based on the following points:

1. It is usually derived based on other research results.
2. Starting with a simple electrical circuit includes resistors, capacitors and constant phase elements, Warburg, and inductor (their symbols and impedance expression are represented in Table 5) extracted from analysis. The graphical information in the Nyquist and Bode plots (typical examples) are shown in Fig. 12.
3. The number of electrical elements should be as low as possible in the proposed equivalent circuit. Any additional element added to the circuit has to decrease the chi square (χ^2) value and enhance the goodness of fit.
4. The ordered electrical elements in the equivalent circuit should be selected with a theoretical meaningful model.
5. The EIS data should be validated using Kramers-Kronig (KK) transforms.
6. When logical changes happen in the tested system, a systematical change should be shown with time for the calculated values of electrical elements in the circuit.

Table 5 Some of the impedance elements' symbols and expression

#	Electrical element	Symbol	Graphical symbol	Impedance expression	Unit
1	Resistor	R		$Z = R$	$[\Omega \cdot \text{cm}^{-2}]$
2	Capacitor	C		$Z = 1/j\omega C$	$[\text{F or s}/\Omega]$
3	Constant phase element (CPE)	Q		$Z = 1/(j\omega)^\alpha Y_o$	$[\text{S}^\alpha \Omega^{-1} \cdot \text{cm}^{-2}]$
4	Warburg	W		$Z = 1 / (j\omega)^{0.5} Y_o$	$\Omega \text{ s}^{-1/2}$

**Fig. 12** A typical EIS result. (a) Nyquist and (b) Bode magnitude and phase shift [83]. (With kind permission from ACS)

6 Conclusions

Regardless of the detailed discussions in the aforementioned sections of this chapter, there are a number of coating technologies and/or methods and materials which are available for protecting metal surface from corrosion; however, so far, to date, no single coating technology has been developed to adequately protect the metallic surface from corrosion in harsh environment. The current coating schemes are complex, multilayer systems that incorporate many different technologies and must be conducted very carefully in order to achieve optimum results. There are a number of factors to be considered when developing a coating process for an industrial application. Significantly some of them are listed below:

1. Development of new inhibitors as a green chemical to replace the existent toxic organic and inorganic inhibitors
2. Development of a new surface treatment for better coating and new corrosion inhibitors to substitute some of the non-environmentally friendly inorganic inhibitors
3. Replacement of toxic chemicals such as chromium and other toxic metals in a new composition of stainless steel
4. Environmental concerns with the use of solvent-borne organic coatings but the development of water-borne and powder coating technologies
5. Employing the fundamental knowledge and understanding of corrosion mechanism to develop alloys with better surface corrosion resistance
6. Development of smart organic inhibitors and coatings that may detect and rebuild automatically a breakdown in the coated stainless steel surface
7. Development of the concern over waste disposal, capital investment, ease of manufacturing, coating performance, and environmental issues
8. Combining two or more inhibitors to make their solubility lower or higher to get long-term or short-term protection, respectively, via sustained release or passivation
9. Adding other components such as pigments, organic inhibitors, or additives to increase the efficiency of anticorrosive coating and reinforce their impermeability with extenders as well as keep the corrosive ions out

Above all, a great deal of research is still required to be done to develop better, simpler, and cheaper coating technologies so that we can take advantage of the economically feasible, environmentally friendly, and excellent mechanical properties of this material.

Acknowledgments The authors would like to gratefully acknowledge King Fahd University of Petroleum and Minerals (KFUPM) for providing excellent research facilities and Deanship of Scientific Research, KFUPM, Saudi Arabia, for financial assistance to carry out this research through internal grant project No. IN131047.

References

1. H.H. Uhlig, The cost of corrosion in the United States. *Chem. Eng. News* **97**, 2764 (1949)
2. G.H. Koch, M.P.H. Brongers, N.G. Thompson, Y.P. Virmani, J.H. Payer, *Corrosion Cost and Preventive Strategies in the United States* (Federal Highway Administration, FHWA-RD-01-156, U.S. Department of Transportation, Washington, DC, 2001)
3. C.C. Technologies Laboratories, Inc, *Cost of Corrosion and Prevention Strategies in the United States*, Ohio: Dublin, USA (2001)
4. National Association of Corrosion Engineers (NACE), C. C. Technologies and Federal Highway Administration (FHWA), *Materials Performance*, Special Issue, Houston (2002)
5. J.M. West, *Basic Corrosion and Oxidation*, 2nd edn. (Ellis Horwood, Chichester, 1986), pp. 312–337
6. C.R. Hegedus, A holistic perspective of coating technology. *JCT Res.* **1**(1), 5–19 (2004)
7. 4MS Common Approach, Acceptance of metallic materials used for products in contact with drinking water, 6th Revision. (2016) http://www.umweltbundesamt.de/sites/default/files/medien/374/dokumente/6th_revision_4ms_scheme_for_metallic_materials_part_b.pdf
8. P.R. Sere, A.R. Armas, C.I. Elsner, A.R. Di Sarli, The surface condition effect on adhesion and corrosion resistance of carbon steel chlorinated rubber artificial sea water systems. *Corros. Sci.* **38**, 853–866 (1996)
9. J. Boxall, J.A. von Fraunhofer, *Paint Formulation: Principles and Practice* (George Godwin Limited, London, UK, 1980)
10. F. Rodriguez, *Principles of Polymer Systems*, 2nd edn. (Hemisphere, New York, 1982)
11. V.D. Atkinson, *Corrosion and its Control*, 2nd edn. (ANACE international, Houston, 1995)
12. S. Bhadra, N.K. Singha, J.H. Lee, D. Khastgir, Progress in preparation, processing and applications of polyaniline. *Prog. Polym. Sci.* **34**, 783–810 (2009)
13. S. Bhadra, N.K. Singha, D. Khastgir, Polyaniline based anticorrosive and anti-molding coating. *J. Chem. Eng. Mater. Sci.* **2**(1), 1–11 (2011)
14. B. Wessling, Scientific engineering of anti-corrosion coating systems based on organic metals (Polyaniline). *J. Corros. Sci. Eng.* **15**(1), 1–13 (1999)
15. T. Wang, Y. Tan, Understanding electrodeposition of polyaniline coatings for corrosion prevention applications using the wire beam electrode method. *Corros. Sci.* **48**, 2274–2290 (2006)
16. A.A. Hermas, M. Abdel Salam, S.S. Al-Juaid, In situ electrochemical preparation of multi-walled carbon nanotubes/polyaniline composite on the stainless steel. *Prog. Org. Coat.* **76**, 1810–1813 (2013)
17. G. Gupta, N. Birbilis, A.B. Cook, A.S. Khanna, Polyaniline-lignosulfonate/epoxy coating for corrosion protection of AA2024-T3. *Corros. Sci.* **67**, 256–267 (2013)
18. Z. Tian, H. Yu, L. Wang, M. Saleem, F. Ren, P. Ren, Y. Chen, R. Sun, Y. Sun, L. Huang, Recent progress in the preparation of polyaniline nanostructures and their applications in anticorrosive coatings. *RSC Adv.* **4**, 28195–28208 (2014)
19. A. Vimalanandan, L. Lv, T.H. Tran, K. Landfester, D. Crespy, M. Rohwerder, Redox-responsive self-healing for corrosion protection. *Adv. Mater.* **25**, 6980–6984 (2013)
20. H. Gomez, M.K. Ram, F. Alvi, E. Stefanakos, A. Kumar, Novel synthesis, characterization, and corrosion inhibition properties of nanodiamond–polyaniline films. *J. Phys. Chem. C* **114**, 18797–18804 (2010)
21. E. Akbarinezhad, M. Ebrahimi, F. Sharif, M.M. Attar, H.R. Faridi, Synthesis and evaluating corrosion protection effects of emeraldine base PAni/clay nanocomposite as a barrier pigment in zinc-rich ethyl silicate primer. *Prog. Org. Coat.* **70**, 39–44 (2011)
22. J. Xu, P. Yao, Z. Jiang, H. Liu, X. Li, L. Liu, M. Li, Y. Zheng, Preparation, morphology, and properties of conducting polyaniline-grafted multiwalled carbon nanotubes/epoxy composites. *J. Appl. Polym. Sci.* **125**, E334–E341 (2012)
23. M.R. Mahmoudian, Y. Alias, W.J. Basirun, Effect of narrow diameter polyaniline nanotubes and nanofibers in polyvinyl butyral coating on corrosion protective performance of mild steel. *Prog. Org. Coat.* **75**, 301–308 (2012)

24. A. Mostafaei, F. Nasirpouri, Epoxy/polyaniline–ZnO nanorods hybrid protection performance of conducting paints. *Prog. Org. Coat.* **77**, 146–159 (2014)
25. X. Yang, B. Li, H. Wang, B. Hou, Anticorrosion performance of polyaniline nanostructures on mild steel. *Prog. Org. Coat.* **69**, 267–271 (2010)
26. C. Weng, C. Chang, C. Peng, S. Chen, J. Yeh, C. Hsu, Y. Wei, Advanced anticorrosive coatings prepared from the Mimicked Xanthosoma Sagittifolium-leaf-like electroactive epoxy with synergistic effects of super hydrophobicity and redox catalytic capability. *Chem. Mater.* **23**, 2075–2083 (2011)
27. A. Prasannan, T.L.B. Truong, P. Hong, N. Somanathan, I. Shown, T. Imae, Synthesis and characterization of “hairy urchin”-like polyaniline by using β -cyclodextrin as a template. *Langmuir* **27**, 766–773 (2010)
28. B. Averill, P. Eldredge, *General Chemistry: Principles, Patterns, and Applications* (Saylor Foundation, Arlington, 2011)
29. R.A. Dickie, A.G. Smith, How paint arrests rust. *Chem. Tech.* **10**, 31 (1980)
30. C.R. Bacon, J.J. Smith, F.G. Rugg, Electrolytic resistance in evaluating protective merit of coatings on metals. *Ind. Eng. Chem.* **40**, 161–167 (1948)
31. W.W. Kittelberger, A.C. Elm, Diffusion of chloride through various paint systems. *Ind. Eng. Chem. Res.* **44**, 326–329 (1952)
32. C. Hare, Barrier coatings. *J. Protect. Coat. Linings* **6**, 59 (1989)
33. P. Galliano, J.J.D. Damborenea, M.J. Pascual, A. Duran, Sol-gel coatings on 316L steel for clinical applications. *J. Sol-Gel Sci. Technol.* **13**, 723–727 (1998)
34. D.C.L. Vasconcelos, J.A.N. Carvalho, M. Mantel, W.L. Vasconcelos, Corrosion resistance of stainless steel coated with sol-gel silica. *J. Non-Cryst. Solids* **273**, 135–139 (2000)
35. M. Atik, P. Neto, L.A. Avaca, M.A. Aegerter, Sol-gel thin films for corrosion protection. *Ceram. Int.* **21**, 403–406 (1995)
36. L. Fedrizzi, F.J. Rodriguez, S. Rossi, F. Deflorian, R.D. Maggio, The use of electrochemical techniques to study the corrosion behaviour of organic coatings on steel pretreated with sol-gel zirconia films. *Electrochim. Acta* **46**, 3715–3724 (2001)
37. Y. Su, V.G. Kravets, S.L. Wong, J. Waters, A.K. Geim, R.R. Nair, Impermeable barrier films and protective coatings based on reduced graphene oxide. *Nat. Commun.* **5**, 4843–4842 (2014)
38. G.P. Thim, M.A.S. Oliveria, E.D.A. Oliveria, F.C.L. Melo, Sol-gel silica film preparation from aqueous solutions for corrosion protection. *J. Non-Cryst. Solids* **273**, 124–128 (2000)
39. Y. Joshua Du, M. Damron, G. Tang, H. Zheng, C.J. Chu, J.H. Osborne, Inorganic/organic hybrid coatings for aircraft aluminum alloy substrates. *Prog. Org. Coat.* **41**, 226–232 (2001)
40. K.H. Wu, C.M. Chao, T.F. Yeh, T.C. Chang, Thermal stability and corrosion resistance of polysiloxane coatings on 2024-T3 and 6061-T6 aluminum alloy. *Surf. Coat. Technol.* **201**, 5782–5788 (2007)
41. L. Jianguo, G. Gaoping, Y. Chuanwei, Enhancement of the erosion–corrosion resistance of Dacromet with hybrid SiO₂ sol-gel. *Surf. Coat. Technol.* **200**, 4967–4975 (2006)
42. A. Conde, J.D. Damborenea, A. Duran, M. Menning, Protective properties of a sol-gel coating on zinc coated steel. *J. Sol-Gel Sci. Technol.* **37**, 79–85 (2006)
43. U. Vijayalakshmi, S. Rajeswari, Synthesis and characterization of sol-gel derived glass-ceramic and its corrosion protection on 316L SS. *J. Sol-Gel Sci. Technol.* **43**, 251–258 (2007)
44. W. Datchary, A. Mehner, H.W. Zoch, D.A. Lucca, M.J. Klopstein, R. Ghisleni, D. Grimme, E. Brinksmeier, High precision diamond machining of hybrid sol-gel coatings. *J. Sol-Gel Sci. Technol.* **35**, 245–251 (2005)
45. T. Sugama, Cerium acetate-modified aminopropylsilane triol: A precursor of corrosion-preventing coating for aluminum-finned condensers. *J. Coat. Technol. Res.* **2**, 649–659 (2005)
46. A. Pepe, M. Aparicio, A. Duran, S. Cere, Cerium hybrid silica coatings on stainless steel AISI 304 substrate. *J. Sol-Gel Sci. Technol.* **39**, 131–132 (2006)
47. M. Sheffer, A. Groysman, D. Mandler, Electrodeposition of sol-gel films on Al for corrosion protection. *Corros. Sci.* **45**, 2893–2904 (2003)

48. M. Aparicio, A. Jitianu, G. Rodriguez, A. Degnah, K. Al-Marzoki, J. Mosa, L.C. Klein, Corrosion protection of AISI 304 stainless steel with melting gel coatings. *Electrochim. Acta* **202**, 325–332 (2016)
49. Y. Liu, X. Zhou, S.B. Lyon, R. Emad, T. Hashimoto, A. Gholinia, G.E. Thompson, D. Graham, S.R. Gibbon, D. Francis, An organic coating pigmented with strontium aluminium polyphosphate for corrosion protection of zinc alloy coated steel. *Prog. Org. Coat.* **102**, 29–36 (2017)
50. C. Hare, M. Steele, S.P. Collins, Zinc loadings, cathodic protection, and post-cathodic protective mechanisms in organic zinc-rich metal primers. *J. Protect. Coat. Linings* **18**, 54–72 (2001)
51. O. Satoshi, N. Hiroaki, K. Shigeo, A. Tetsuya, F. Hisaaki, O. Kazuo, J. Surf. Finish. Soc. Jpn. **53**, 920 (2002)
52. C.T.J. Low, R.G.A. Wills, F.C. Walsh, Electrodeposition of composite coatings containing nanoparticles in a metal deposit. *Surf. Coat. Technol.* **201**, 371–383 (2006)
53. B.M. Praveen, T.V. Venkatesha, Electrodeposition and properties of Zn-nanosized TiO₂ composite coatings. *Appl. Surf. Sci.* **254**, 2418–2424 (2008)
54. A. Vlasa, S. Varvara, A. Pop, C. Bulea, L.M. Muresan, Electrodeposited Zn-TiO₂ nanocomposite coatings and their corrosion behavior. *J. Appl. Electrochem.* **40**, 1519–1527 (2010)
55. T.R. Khan, A. Erbe, M. Auinger, F. Marlow, M. Rohwerder, Electrodeposition of zinc–silica composite coatings: Challenges in incorporating functionalized silica particles into a zinc matrix. *Sci. Technol. Adv. Mater.* **12**, 1–9 (2011)
56. M.K. Camargo, I. Tudela, U. Schmidt, A.J. Cobley, A. Bund, Ultrasound assisted electrodeposition of Zn and Zn-TiO₂ coatings. *Electrochim. Acta* **198**, 287–295 (2016)
57. N. Perez, *Electrochemistry and Corrosion Science* (Kluwer, Boston, 2004)
58. E. Ituen, O. Akaranta, A. James, Evaluation of performance of corrosion inhibitors using adsorption isotherm models: An overview. *Chem. Sci. Int. J.* **18**(1), 1–34 (2017)
59. P.A. Sørensen, S. Kiil, K. Dam-Johansen, Anticorrosive coatings: A review. *J. Coat. Technol. Res.* **6**(2), 135–176 (2009)
60. R. Romagnoli, V.F. Vetere, Heterogeneous reaction between steel and zinc phosphate. *Corrosion* **51**(2), 116–123 (1995)
61. J. Sinko, Challenges of chromate inhibitor pigments replacement in organic coatings. *Prog. Org. Coat.* **42**, 267–282 (2001)
62. Q. Meng, T. Ramgopal, G.S. Frankel, The influence of inhibitor ions on dissolution kinetics of Al and Mg using the artificial crevice technique. *Electrochem. Solid-State Lett.* **5**(2), B1–B4 (2002)
63. T. Prosek, D. Thierry, A model for the release of chromate from organic coatings. *Prog. Org. Coat.* **49**(3), 209–217 (2004)
64. M. Beiro, A. Collazo, M. Izquierdo, X. Novoa, C. Perez, Characterisation of barrier properties of organic paints: The zinc phosphate effectiveness. *Prog. Org. Coat.* **46**(2), 97–106 (2003)
65. S. Mousavifard, P.M. Nouri, M. Attar, B. Ramezanzadeh, The effects of zinc aluminum phosphate (ZPA) and zinc aluminum polyphosphate (ZAPP) mixtures on corrosion inhibition performance of epoxy/polyamide coating. *J. Ind. Eng. Chem.* **19**(3), 1031–1039 (2013)
66. F. Askari, E. Ghasemi, B. Ramezanzadeh, M. Mahdavian, Synthesis and characterization of the fourth generation of zinc phosphate pigment in the presence of benzotriazole. *Dyes Pigments* **124**, 18–26 (2016)
67. S. Mohammadi, H. Shariatpanahi, F.A. Taromi, J. Neshati, Electrochemical and anticorrosion behaviors of hybrid functionalized graphite nano-platelets/tripolyphosphate in epoxy-coated carbon steel. *Mater. Res. Bull.* **80**, 7–22 (2016)
68. R.M. Palou, O. Olivares-Xomelt, N.V. Likhanova, *Environmentally Friendly Corrosion Inhibitors, Developments in Corrosion Protection* (InTech, London, UK, 2014)
69. S.A. Ali, M.T. Saeed, S.U. Rahman, The isoxazolidines: A new class of corrosion inhibitors of mild steel in acidic medium. *Corros. Sci.* **45**(2), 253–266 (2003)
70. S.A. Abd El-Maksoud, A.S. Fouda, Some pyridine derivatives as corrosion inhibitors for carbon steel in acidic medium. *Mater. Chem. Phys.* **93**, 84–90 (2005)

71. Ü. Ergun, D. Yüzer, K.C. Emregül, The inhibitory effect of bis-2,6-(3,5-dimethylpyrazolyl) pyridine on the corrosion behaviour of mild steel in HCl solution. *Mater. Chem. Phys.* **109**, 492–499 (2008)
72. E.A. Noor, Evaluation of inhibitive action of some quaternary *N*-heterocyclic compounds on the corrosion of Al–Cu alloy in hydrochloric acid. *Mater. Chem. Phys.* **114**, 533–541 (2009)
73. O. Olivares-Xometl, N.V. Likhanova, B. Gómez, J. Navarrete, M.E. Llanos-Serrano, E. Arce, J.M. Hallen, Electrochemical and XPS studies of decylamides of alpha-amino acids adsorption on carbon steel in acidic environment. *Appl. Surf. Sci.* **252**(6), 2894–2909 (2006)
74. O. Olivares-Xometl, N.V. Likhanova, M.A. Domínguez-Aguilar, E. Arce, H. Dorante, P. Arellanes-Lozada, Synthesis and corrosion inhibition of alpha-amino acids alkylamides for mild steel in acidic environment. *Mater. Chem. Phys.* **110**(2–3), 344–351 (2008)
75. M.A.J. Mazumder, M.K. Nazal, M. Faiz, S.A. Ali, Imidazolines containing single-, twin- and triple-tailed hydrophobes and hydrophilic pendants $(\text{CH}_2\text{CH}_2\text{NH})_n\text{H}$ as inhibitors of mild steel corrosion in CO_2 – 0.5 M NaCl. *RSC Adv.* **6**(15), 12348–12362 (2016)
76. J. Cruz, R. Martínez-Palou, J. Genesca, E. García-Ochoa, Experimental and theoretical study of 1-(2-ethylamino)-2-methylimidazoline as an inhibitor of carbon steel corrosion in acid media. *J. Electroanal. Chem.* **566**(1), 111–121 (2004)
77. R. Martínez-Palou, J. Rivera, L.G. Zepeda, A.N. Rodríguez, M.A. Hernandez, J. Marín-Cruz, A. Estrada, Evaluation of corrosion inhibitors synthesized from fatty acids and fatty alcohols isolated from sugar cane wax. *Corros. Sci.* **60**(5), 465–470 (2004)
78. O. Olivares-Xometl, N.V. Likhanova, R. Martínez-Palou, M.A. Domínguez-Aguilar, Electrochemistry and XPS study of an imidazoline as corrosion inhibitor of mild steel in an acidic environment. *Mater. Corros.* **60**(1), 14–21 (2009)
79. F.G. Liu, M. Du, J. Zhang, M. Qiu, Electrochemical behavior of Q235 steel in saltwater saturated with carbon dioxide based on new imidazoline derivative inhibitor. *Corros. Sci.* **51**(1), 102–109 (2009)
80. D.E. Tallman, G. Spinks, A. Dominis, G.G. Wallace, Electroactive conducting polymers for corrosion control. Part 1. General introduction and a review of non-ferrous metals. *J. Solid States Electrochem.* **6**(2), 73–84 (2002)
81. M. Morcillo, J. Simanacas, J.M. Bastidas, S. Feliu, C. Blanco, F. Camón, Comparison of laboratory tests and outdoor tests of paint coatings for atmospheric exposure, in *Polymeric Materials for Corrosion Control*, ed. by R.A. Dickie, F.L. Floyd (American Chemical Society, Washington, DC, 1986), pp. 86–100
82. B.R. Appleman, Survey of accelerated test methods for anti-corrosive coating performance. *J. Coatings Technol.* **67**, 57–67 (1990)
83. S.M. Park, J.S. Yoo, Peer reviewed: Electrochemical impedance spectroscopy for better electrochemical measurements. *Anal. Chem.* **75**(21), 455–461 (2003)



Conducting Polymer Nanocomposites as Gas Sensors

22

Mohammad Omaish Ansari, Sajid Ali Ansari, Moo Hwan Cho, Shahid Pervez Ansari, Mohamed Shaaban Abdel-wahab, and Ahmed Alshahrie

Contents

1	General Overview	912
2	Commonly Used Conducting Polymers	914
3	Factors Affecting the Gas Sensing Response in Conducting Polymer Nanocomposites	914
3.1	Electrical Conduction	915

M. O. Ansari (✉)

Center of Nanotechnology, King Abdulaziz University, Jeddah, Saudi Arabia

School of Chemical Engineering, Yeungnam University, Gyeongbuk, South Korea

e-mail: omaishchem@gmail.com

S. A. Ansari

Department of Energy and Materials Engineering, Dongguk University, Seoul, Republic of Korea

e-mail: sajidansari@dongguk.edu

M. H. Cho

School of Chemical Engineering, Yeungnam University, Gyeongbuk, South Korea

e-mail: mhcho@ynu.ac.kr

S. P. Ansari

Department of Applied Chemistry, Faculty of Engineering and Technology, Aligarh Muslim University, Aligarh, India

e-mail: shahidzahir@gmail.com

M. S. Abdel-wahab

Center of Nanotechnology, King Abdulaziz University, Jeddah, Saudi Arabia

Materials Science and Nanotechnology Department, Faculty of Postgraduate Studies for Advanced Sciences, Beni-Suef University, Beni-Suef, Egypt

e-mail: msahassan@kau.edu.sa

A. Alshahrie

Center of Nanotechnology, King Abdulaziz University, Jeddah, Saudi Arabia

Department of Physics, Faculty of Science, King Abdulaziz University, Jeddah, Saudi Arabia

e-mail: aalshahri@kau.edu.sa

3.2	Doping Process	915
3.3	Undoping Process	916
3.4	Surface Area Aspects	917
3.5	Role of Environmental Conditions	918
4	Polyaniline and Its Nanocomposites as Gas Sensing Materials	919
4.1	Effect of Nanoparticles in the Sensing Properties of Pani Nanocomposites	921
4.2	Effect of Dopant in Sensing Properties of Pani Nanocomposites	921
4.3	General Sensing Mechanism for Pani-Based Nanocomposites	922
5	Polypyrrole and Polythiophene Nanocomposite as Gas Sensors	925
6	Polythiophene-Based Optical Gas Sensors	927
7	Functionalized Conducting Polymers in Gas Sensing	930
8	Conclusion and Future Challenges	933
	References	934

Abstract

The great concerns regarding environmental and living beings protection together with the widespread requirements for highly accurate process monitoring have highlighted the need for the development of new and sensitive sensors. Conducting polymers and their nanocomposites have been used widely as sensing materials owing to their special redox chemistry. The electrical properties can be controlled easily by doping and undoping processes resulting into the generation of conducting and nonconducting states, respectively. The electrical conductivity also depends on the type and amount of filler (nanosize filler in some cases) used which produces the positive or negative carriers responsible for the conduction. Any type of interaction of these polymers that affects the number and movement of charge carriers affects the conductivity and is the main principle behind the gas sensing characteristics. Advances in nanotechnology allows for the fabrication of various conducting polymer nanocomposites using different techniques. Conducting polymer nanocomposites have high surface area, small dimension, and show enhanced properties, making them suitable for various sensor devices. This chapter presents the different types of gas sensors based on the conducting polymer (polyaniline, polypyrrole, and polythiophene)-based nanocomposites, their progress, and future scope of ongoing research in this research area. The factors that affect the performance of the gas sensors and the chemistry of the sensing process are also addressed.

1 General Overview

With the publication of the paper entitled “Synthesis of Electrically Conducting Organic Polymers: Halogen Derivatives of Polyacetylene, $(CH)_x$ ” in “Chemical Communications” in 1977, a new field of chemistry, “Electrically Conducting Polymers,” was born [1]. The new concept that the plastics or polymers can conduct electricity became an exciting area of research and the work in this field has made significant advances. Later, many other conjugated polymeric materials and their

derivatives were found to possess electrical conductivity [2–9]. Of these polymers, polyaniline (Pani), polypyrrole (PPy), and polythiophene (PTh) have attracted the highest attention of researchers owing to their wide range of electrical conductivity from insulating to metallic, unique redox properties, good stability, low cost, ease of synthesis, and promising applications in various fields such as corrosion protection, energy storage, supercapacitors, gas sensors, etc. [4–15]. The use of conducting polymers to form conducting nanocomposites has been achieved successfully and has been an area of interest over the past few years. A nanocomposite is generally defined as a two-phase system, in which the dimensions of at least one of the phases are in the order of nanometers. One of the most promising nanocomposite systems is the hybrids based on organic Pani, PPy, or PTh, nanoparticles such as metal oxides (ZnO, TiO₂, etc.) and carbonaceous materials (CNT, graphene (GN), etc.) [16–18]. These nanostructured particles combined with conducting polymers can give rise to the polymer nanocomposites with interesting properties to be the potential materials for newer and novel applications. The resulting nanocomposites can be produced in the form of nanofibers, nanorods, thin films, etc. [19–21].

Pani, PPy, and PTh are used widely as the sensing materials due to their redox nature [22–26]. The electrical conduction can be controlled easily by a doping or undoping process resulting into the generation of conducting and nonconducting states, respectively. The electrical conductivity of these polymers depends on the type and amount of dopant used which produces the charge carriers responsible for electrical conduction. Any interaction with the polymer that affects the number and movement of charge carriers along the chain or by the hopping of charge carriers between chains will affect the conductivity of the doped polymer. This is the main and basic chemical principle that enables them to be used as the chemical-vapor sensing materials. In comparison, conducting polymer-based sensors have high sensitivity and short response times and these features are mostly observed at ambient temperatures [27–29].

The main problems associated with the conducting polymers are their poor stability, low surface area, low sensitivity at room temperatures, and comparatively low conductivity in comparison to metallic conductors. In this regard, the nanocomposite of conducting polymers with metal oxides (TiO₂, ZnO, SnO₂), metals (Ag, Au, Zn), carbonaceous materials (CNT, GN), etc., is expected to effectively promote gas sensing and make sensor operational at low temperature [30]. In the first place, the interaction of polymers with n-type semiconducting particles such as TiO₂, SnO₂ will lead to the formation of p-n heterojunctions at polymer-metal oxide nanoparticle interfaces. Thus, depletion regions may appear at polymer-metal oxide nanoparticle interfaces and when the composite is treated with deprotonating gas (e.g., amines), the width of depletion regions increases, which accounts for the sensing response [31–33]. Apart from this, the nanoparticles also affect the surface area of the polymers composites, which is directly related to the sensing response. The generation of mesoporous structures or coating of polymers on nanoparticles effectively increases the overall surface area of the polymer nanocomposite thereby resulting in better sensitivity [34–36].

As a result of the large number of publications on the research and development of conducting polymer nanocomposites within a short span of time, the main purpose of the present chapter is to outline the status of the applications of these nanocomposites in different fields. The work selected here is far from complete and fully exhaustive of the numerous works published over the last few years but it is meant to highlight some specific important features and furnish a representative scenario of the advances and progress in this field. For convenience, the discussion is divided into a few categories depending on the field of their applications.

2 Commonly Used Conducting Polymers

Polymers that is plastics, we know behave somehow the opposite of metals. They are used as insulators as they do not conduct electricity. Electric wires are coated with polymers to protect us from short circuits.

This view of polymers was changed with the discovery of polyacetylene which can be made conductive almost like a metal by Alan J. Heeger, Alan G. MacDiarmid, and Hideki Shirakawa [1]. For this discovery, the Royal Swedish Academy of Science awarded the Nobel Prize in Chemistry for the year 2000 to these three scientists who have revolutionized the development efforts in the field of electrically conducting polymers.

Conducting polymers have extended π -systems and are quite susceptible to chemical or electrochemical oxidation or reduction. Therefore, the electrical and optical properties of these polymers could be altered precisely by carefully controlling the process of oxidation and reduction. Because these reactions are often reversible, it is possible to control the electrical and optical properties systematically and a great deal of precision switching from a highly conducting state through semiconducting to an insulating state and vice versa [37]. Therefore, conducting polymers can be perceived as macromolecules with a fully conjugated sequence of bonds along the backbone which acquires positive or negative charges by the oxidation or reduction process, respectively. With the advent of many more discoveries in the field of conducting polymers, there is a wide variety of polymers that exhibit electrical conductivity. Figure 1 presents the structures of some of the conducting polymers.

3 Factors Affecting the Gas Sensing Response in Conducting Polymer Nanocomposites

To develop the basic concept of gas sensing by conducting polymer nanocomposites, it is important to understand the phenomenon of doping, undoping, and the effect of the addition of nanoparticles on the surface area and electrical properties of the polymer and its nanocomposites.

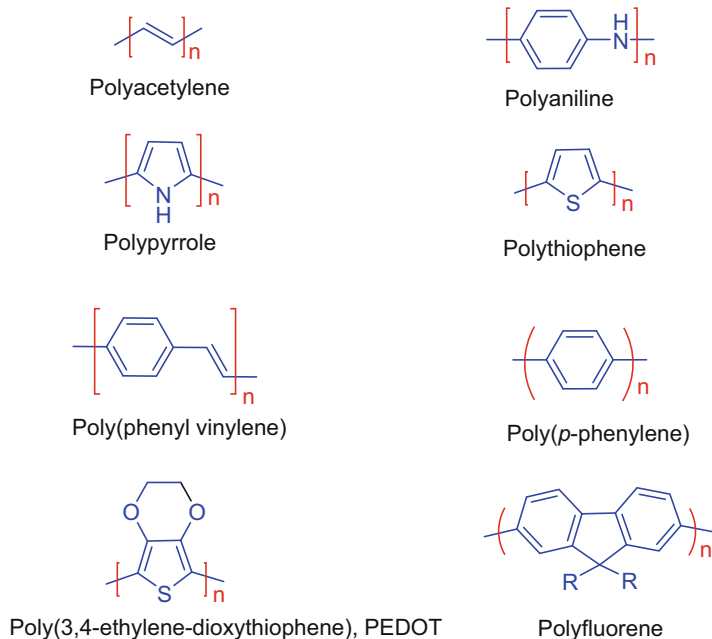


Fig. 1 Common conducting polymers

3.1 Electrical Conduction

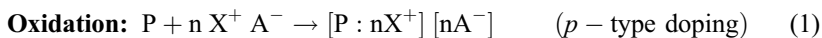
Conjugated polymers can be oxidized or reduced more easily than conventional polymers. Because of the presence of the π -conjugated structure, the electrical conduction is obtained through “doping” leading to the generation of charge-carriers in the form of free electrons or holes. The charge carriers are usually delocalized over the conjugated polymer chain [38].

To conduct, a polymer must have a conjugated backbone for the easy movement of charge carriers. On the other hand, when conjugated polymers do not contain any intrinsic charge-carriers, charge-carriers need to be provided extrinsically, typically by a charge transfer process, generally known as “doping” as a very poor analogy to silicon technology. Polymers have the electronic profiles of either insulators or semiconductors. Therefore, the band gap in a fully saturated chain such as polyethylene is ~ 5 eV and decreases to approximately ~ 1.5 eV in the fully conjugated system of polyacetylene. The respective intrinsic conductivities are $\sim 10^{-17}$ Scm^{-1} and $\sim 10^{-8}$ Scm^{-1} which is very low in both the cases [39].

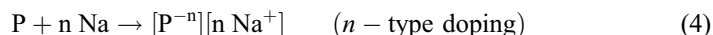
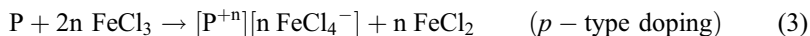
3.2 Doping Process

The role of the dopant is to either remove or to add electrons to the polymers. These dopants acts as charge transfer agents. The electrical conductivity can be increased

by “doping” i.e., *p*-type doping (oxidation) or *n*-type doping (reduction) increase the electrical conductivity by many orders of magnitude. The doping reaction can be represented in the generalized form as:

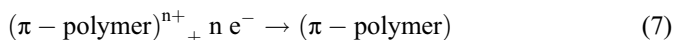
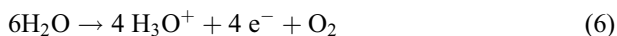
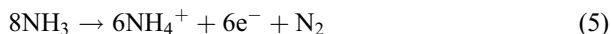


where P is the part of the polymer chain. The soliton or a polaron (cation or anion) formation is the first step which may be followed by second electron transfer leading to the formation of dication or dianion also called as bipolaron. Thus this charged segment can interact with neutral polymer segments to give polymer segments of variable lengths. The general principles can be illustrated best by examining specific examples, particularly polyacetylene, which has been studied intensively. The reactions between conjugated polymers and oxidants (*p*-type doping by an acceptor) or reductants (*n*-type doping by a donor) have been observed to cause a dramatic increase in electrical conductivity. The commonly used oxidants (*p*-type dopant) include HClO₄, FeCl₃, AsF₅, I₂, NH₄BF₄, SO₃CF₃, HCl, HNO₃, H₂SO₄, and H₃PO₄ whereas the reductants (*n*-type dopants) include Li, K, and Na. A general equation for doping of a conjugated polymer may be expressed as [40, 41]:



3.3 Undoping Process

Another important aspect of doping is its reversal, called undoping or dedoping or compensation or electrical neutralization of a doped polymer in which, for example, a *p*-type doped polymer reacts with some reducing agent and regains its insulating state. The undoping agent diffuses into the polymer matrix and neutralizes the charges of the system via a charge-transfer reaction. The process may involve chemical reactions between the undoping agent and carbonium ion or/and dopant leading to neutralization by charge-transfer. The undoping agents generally used for *p*-type doped conjugated polymers include ammonia, water, hydrazine, etc., and the chemistry of the process may be given by the following equations.



Undoping may also be affected by thermal treatments as observed in the case of PTh. The kinetics of undoping may be studied by several methods such as electrical conductivity measurements, x-ray diffraction, optical spectroscopy, etc.

3.4 Surface Area Aspects

The functional groups on the surface of the polymers are generally responsible for the sensing signal. The intercoiled or compressed polymeric structure will give a poor response due to the fewer unexposed functional sites, while porous or mesoporous structures will have large number of exposed functional groups and hence show stronger response. The inclusion of nanomaterials in the polymeric system greatly affects the surface area of the overall polymeric nanocomposite. The electrochemical deposition of conducting polymers may introduce porosity and increase the surface area while solution-cast films of conducting polymers typically exhibit low porosity [42, 43]. The in situ polymerization technique for the formation of the polymer nanocomposites under optimal conditions generally leads to the wrapping of nanomaterials by the polymer thereby increasing the surface area (Fig. 2).

The simultaneous in situ formation of nanocomposites alongside the polymer chain results into the formation of mesoporous structures which can have great applications in gas sensing due to the large surface area. Nazish et al. [11, 44] reported the formation of the nanocomposite of Pani with TiO_2 where Pani chain formation and formation of TiO_2 from the respective precursor occurred simultaneously. The TiO_2 precursor trapped inside the weak growing Pani network upon hydrolysis subsequently broke the Pani chain and made it porous resulting into the generation of mesoporous structures. Figure 3 presents a schematic of this synthesis process.

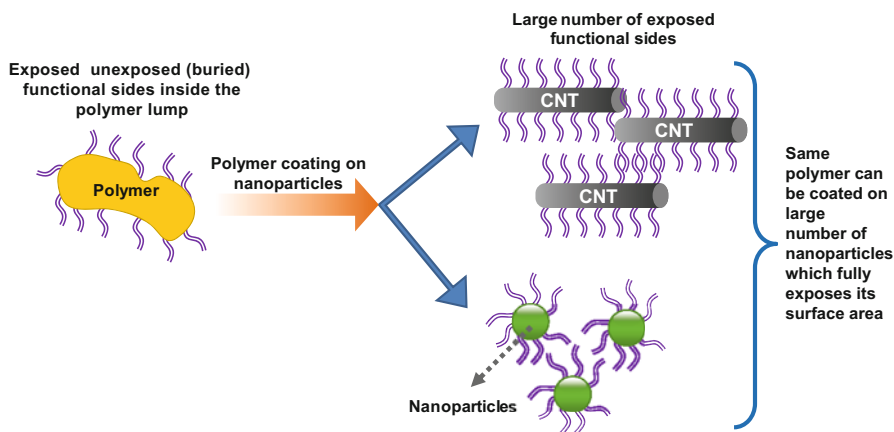


Fig. 2 Effect of nanomaterials on the surface area of polymer nanocomposite

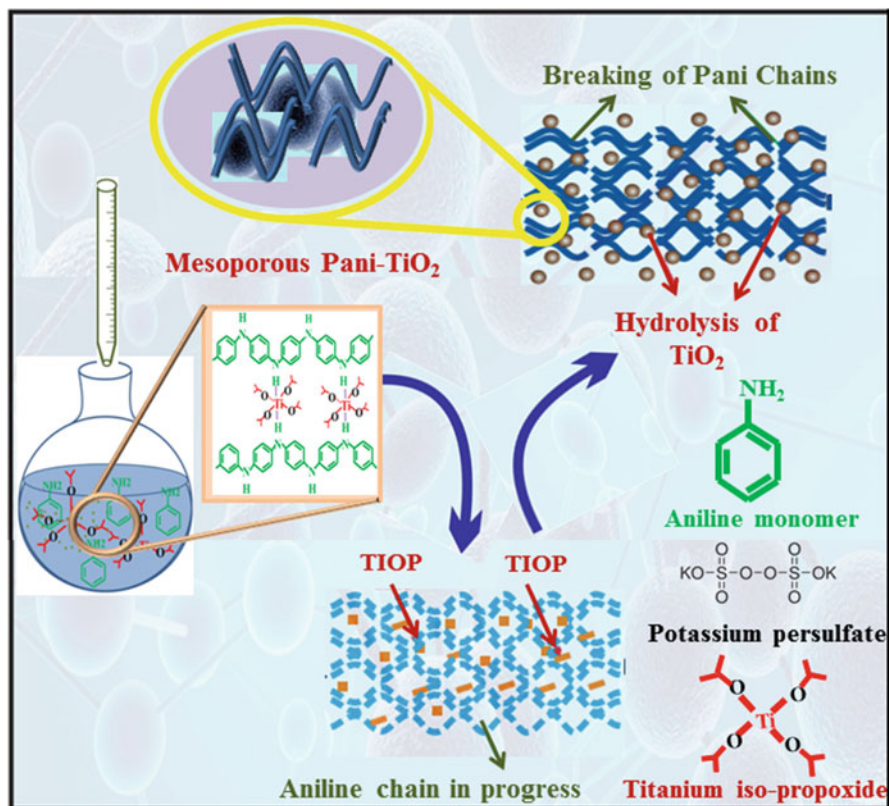


Fig. 3 Schematic diagram of the polymerization mechanism leading to the formation of mesoporous Pani@TiO₂ nanocomposite. (Reprinted with permission from Ref. [44]. Copyright (2015) American Chemical Society)

Hard template-assisted synthesis of Pani and thereafter final removal of the template has also shown to give Pani and its composites with highly ruptured surface morphology which eventually increases the surface area.

3.5 Role of Environmental Conditions

The temperature and humidity are also important factors that play very crucial role in sensing property of conducting polymer-based sensors [45]. Increase in the conductance of the conducting polymers occurs with the rise in temperature and humidity. As most of the sensors are based on chemiresistors, therefore, any change in the temperature or humidity will also affect its conductance [46, 47].

The process of sensing involves two main steps: adsorption of analyte molecules on sensing surface of the film followed by reaction between them. The temperature is able to influence both steps. As adsorption prefers low temperature, any temperature

increase will shift the equilibrium and analyte desorption will become favorable. As the adsorption/desorption are the important steps, sensitivity will decrease with increase in temperature [48, 49]. While the sensitivity of the sensors based on redox reactions increase with the increase of temperature because of the increased reaction rate [50].

As a matter of fact, there are many sensors which are quite sensitive to humidity itself, and here the water vapor becomes analyte. Therefore, the data of sensing property may be misleading in the presence of humidity which may be due to the similar response of the sensing material towards the analyte gas and humidity [51]. When humidity is present while sensing an analyte molecule, the adsorption becomes competitive between water and the analyte molecule. Consequently, water molecules will occupy some active sites, therefore, the sensitivity sensor for the analyte decreases with increase in humidity [48]. However, few cases of cooperative effect analyte and humidity have also been found in sensing film [52]. Sometimes, pressure also affects the sensing property, for eg. with change in pressure, phase transition may occur in PPy, causing alternation of conductivity and thereby its sensing of analyte [53].

4 Polyaniline and Its Nanocomposites as Gas Sensing Materials

Considerable work involving Pani doped with different organic and inorganic acids has been done in the field of chemical vapor sensors. Koul et al. [54], Ayad et al. [55], Pinto et al. [56] used Pani as chemical vapor sensor for sensing alcohols, ammonia, and some derivatives of ammonia and reported Pani to be a good material for their sensing. Redox reactions of PPy and PTh also occurs with volatile organic compounds (VOCs), also making them suitable for gas sensing applications [57, 58]. Nanocomposites of these polymers are expected to give an enhanced sensing response due to the higher surface area, as discussed above.

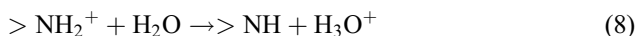
Several studies found that the reaction of Pani nanocomposites with VOCs is reversible. Tai et al. [59] examined the sensing behavior of Pani:TiO₂ composite films towards NH₃ and CO and reported that Pani@TiO₂ films were more sensitive to NH₃ than CO. The good reproducibility towards NH₃ was explained based on NH₄⁺ being formed upon exposure to ammonia which decomposes to gaseous ammonia and a proton added to Pani when exposed to ambient air and results in the restoration of the initial level of doping. The thickness of the films and polymerization temperature also affects the sensing behavior. Thin films show better response due to the better adsorption and desorption during sensing and the films prepared at the optimal temperature are superior to those prepared at other temperatures in terms of the response properties [60].

Ma et al. [61] showed that Pani does not have any specific character to distinguish between different gases and the sensing response, either strong or weak, will be recorded for most chemicals. On the other hand, some gas sensor arrays can be used to identify different gases with aid of an artificial neural network system.

They reported gas-sensitivity of Pani and TiO₂ composite film towards trimethylamine, triethylamine, ethanol, formaldehyde, acetone, and toluene vapors. The results showed different sensitivity and recovery time for different gases. The sensitivity and the response time of triethylamine were much lower than that of trimethylamine, and hence the composite film can be used to distinguish between trimethylamine and triethylamine. In addition, the composite film showed little response to ethanol, formaldehyde, acetone, and toluene.

Therefore, it can be concluded that Pani-based nanocomposites are the excellent sensor for organic bases such as ammonia or ammonia derivatives or other base-based chemical compounds due to the change in electrical conductivity upon interaction with bases and the response and recovery time can be an important parameter for distinguishing between different types of gases. Many other reports on different sensors such as humidity, carbon monoxide, nitrogen oxides, carbon dioxide, etc., also work on the same principle [62, 63]. In general, the sensitivity is lower in these cases due to the smaller change in electrical conductivity upon exposure to these compounds compared to ammonia and ammonia derivatives. The sensing of ammonia-based derivatives can be done at much lower concentrations such as below ~0.5 ppm while for H₂, ethanol, methanol, and acetone, etc., a much higher concentration is required [64]. A comparative study of the sensing response towards CO, methane, and liquefied petroleum gas (LPG) at room temperature by a Pani/Co₃O₄ nanocomposite showed high selectivity towards CO at a very low ppm concentration while in the case of methane and LPG, a very small or no response was recorded even at 100 ppm [65]. This suggests that both methane and LPG consisting of hydrocarbons cannot affect the conductivity of Pani/Co₃O₄ significantly. Therefore, a very small response was recorded in their case while a sharp increase in conductivity was observed in the case of CO gas suggesting an increase in charge carriers in Pani. The resonance structure of CO withdraws a lone pair of electrons from the amine nitrogen in Pani resulting in the transfer of a positive charge from the carbon of CO to the amine nitrogen of Pani which results in an increase in the number of holes and consequently an increase in its conductivity. In contrast to the above findings, the Pani@CdSe and Pani@γ-Fe₂O₃ sensing response was attributed to the sensor's modified depletion layer and the detection of LPG is due to an increase in the depletion depth caused by the adsorption of gas molecules at the depletion region of the *p-n* heterojunction [66, 67].

The electrical properties of Pani and Pani-based nanocomposites in the doped states are sensitive to water which provides a basis for their potential applications as humidity sensors. Humidity affects the resistivity for two reasons; the adsorbed water molecules dissociate at the imine nitrogen centers and the positive charge migrates through the Pani or Pani-based nanocomposites [68]. Jain et al. [69] and other workers [70] reported that the increase in conductivity of Pani films in humid conditions is due to proton exchange between the polymer and the water adsorbed on the surface of Pani. NMR spectroscopy showed that proton transfer takes place in Pani in the presence of water. This transfer can be described by the following redox reaction:



4.1 Effect of Nanoparticles in the Sensing Properties of Pani Nanocomposites

Different types of nanoparticles in Pani nanocomposites respond differently to different gases which may be due to a synergistic effect. The Pani@TiO₂ nanocomposite shows superior NH₃ gas-sensing characteristics in comparison to Pani@SnO₂ and Pani@In₂O₃ films. Pani being a *p*-type polymer and the metal oxide being *n*-type interact to form a *p-n* junction resulting into the formation of a positively charged depletion layer on the surface of the inorganic nanoparticles which results in a lowering of the activation energy and enthalpy of physisorption for NH₃ gas. This leads to a higher gas sensing response compared to that of Pani. The lowest unoccupied molecular orbital (LUMO) of Pani and the conducting band of TiO₂ compared to SnO₂ and In₂O₃ matches well, leading to better sensing characteristics of Pani@TiO₂ [71].

Gong et al. [72] showed that the *p-n* heterojunctions between TiO₂ and Pani nanoparticles acts as an electric on-off current switch when NH₃ gas is absorbed by Pani. The change in bulk resistance of Pani and the combination of the *p-n* depletion layer functions as a current switch which turns on the current circuit by absorbing H⁺ and turns off the current circuit by adsorbing NH₃ gas. Dhawale et al. [73] proposed a similar sensing mechanism where the heterojunctions showed the maximum response of 63% upon exposure to 0.1 vol% LPG at room temperature. Figure 4 shows a schematic diagram of a nanosized *p-n* heterojunction as a switch to control the electric current flow.

Nanoparticles have also been observed to act as catalyst for the redox reactions of Pani. Methanol detection by the Pani@Pd nanocomposite revealed a very strong response in the order of $\sim 10^4$ magnitudes. The Pd acts as a catalyst for the reduction of imine nitrogen in Pani by methanol [74]. Choudhury et al. [33] reported a similar catalytic influence of Ag nanoparticles in ethanol detection by the Pani@Ag nanocomposite. A faster protonation-deprotonation of Pani was observed upon exposure to ethanol in the presence of Ag nanoparticles.

4.2 Effect of Dopant in Sensing Properties of Pani Nanocomposites

Pani or its nanocomposites doped with different types of dopants generally respond differently to various VOCs. Song et al. [75] showed that in the case of Pani doped with HCl, HNO₃, H₂SO₄, and organic protonic acids (e.g., sulfosalicylic acid), the resistance increased upon exposure to ammonia irrespective of the acid used. The noticeable difference is that the recovery and response time of Pani doped with H₂SO₄ was longest while the shortest response and recovery times were recorded for a sulfosalicylic acid-doped Pani. In another study, it was proven that HCl-doped Pani showed superior gas sensing characteristics to *p*-toluenesulfonic acid (*p*TSA)-doped Pani because HCl effectively

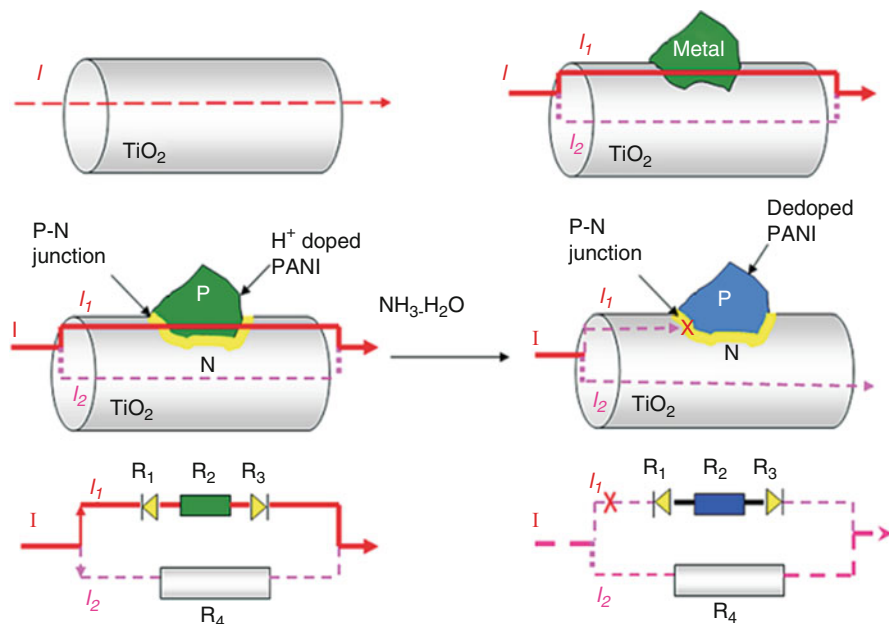


Fig. 4 Schematic diagram of the nanosized *p-n* heterojunction as a switch to control the electric current flow in TiO_2 microfibers. (Reprinted with permission from Ref. [72]. Copyright (2015) American Chemical Society)

improved the conductive properties of Pani in a wide range of concentrations and *p*TSA in a narrow range of concentrations [76].

The optimal dopant concentration for high gas sensitivity is generally required with a bulky dopant such as camphor sulfonic acid (CSA). For high concentrations of CSA, the number of Pani-H^+ reacting with NH_3 would not make up a high proportion of all Pani-H^+ within certain limits and steric hindrance would reduce the chance of NH_3 being absorbed by Pani (Fig. 5). As a result, their ammonia sensing performance was degraded although the high concentration CSA-doped Pani composite showed better conductivity [77].

4.3 General Sensing Mechanism for Pani-Based Nanocomposites

The gas sensing response can be summarized as a combination of the absorption-desorption phenomenon as well as electrical compensation, as a side reaction. The main reasons for the gas-sensitivity should be attributed to the interaction between Pani and the adsorbed gas through strong interactions such as chemical bonding and weak interactions, such as hydrogen bonding, van der Waals forces, etc. Recovery is very difficult in the case of strong interactions while it is much easier for weak interaction systems [61]. This might be due to the formation of weak complex of

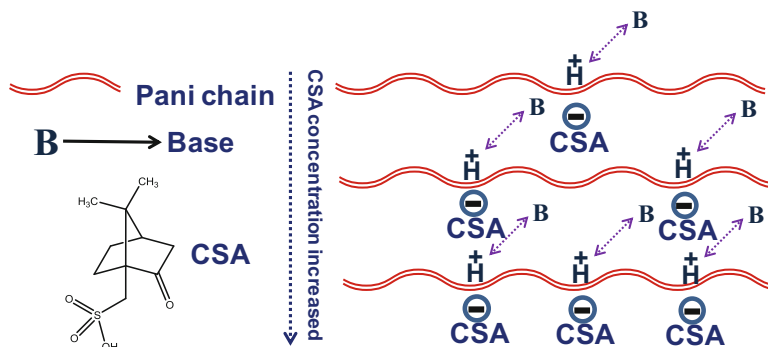


Fig. 5 Effect of the CSA concentration on the sensing of NH_3 by CSA-doped Pani composite

$\text{C}_7\text{H}_7\text{SO}_3 - \text{NH}_4^+$ and after desorption, resistivity slightly higher than the original value is observed [78]. Many workers suggested that the deprotonation reaction causes the conductivity of the Pani to decrease for low concentrations of base [79–82].

In these reports, at low concentrations, the reversible interaction occurs, whereas at high concentrations, the irreversible interaction occurs for short exposure to ammonia vapors [83]. For *p*TSA doped Pani@TiO₂, the interaction of ammonia is similar to the acid/base interaction and at higher concentration of ammonia, the neutralization of the dopant acid occurs rapidly leading to the formation of nonconducting emeraldine base. However, at low concentrations of ammonia, the chemisorption of ammonia molecules occurs on the positively charged nitrogen atoms as proposed in the mechanism. This process is largely reversible but neutralization reaction is also partially involved as discussed above leading to the undoping of Pani. During the chemisorptions, the ammonia molecules interacts by its lone pair with positively charged nitrogen atoms of Pani, thereby decreasing the hole mobility which results in a decrease in electrical conductivity. By this interaction, the nitrogen slightly acquires pentavalent configuration and becomes unstable (nitrogen does not show pentavalency because of the absence of *d* orbitals). Thus favorable desorption of ammonia occurs upon exposure to an ambient atmosphere. Figure 6 presents a schematic representation of the sensing mechanism.

Therefore, Pani and the Pani-based nanocomposites can serve as excellent sensor for a variety of gases such as ammonia or their derivatives, water vapor, carbon monoxide, or carbon dioxides. The sensing generally involves redox reaction in all the cases with a combination of chemisorption and desorption. The more undoping of Pani or its nanocomposites takes place, the lower the cyclic stability while high desorption under ambient conditions or inert atmosphere will provide better sensors.

In addition, a higher operating temperature ($\sim 90^\circ\text{C}$) is unsuitable for the gas sensitivity because it may damage the linear structure of the polymer and hinder the migration of charge carriers [84]. Figure 7 shows a typical resistivity based sensor of Pani and its nanocomposites [85].

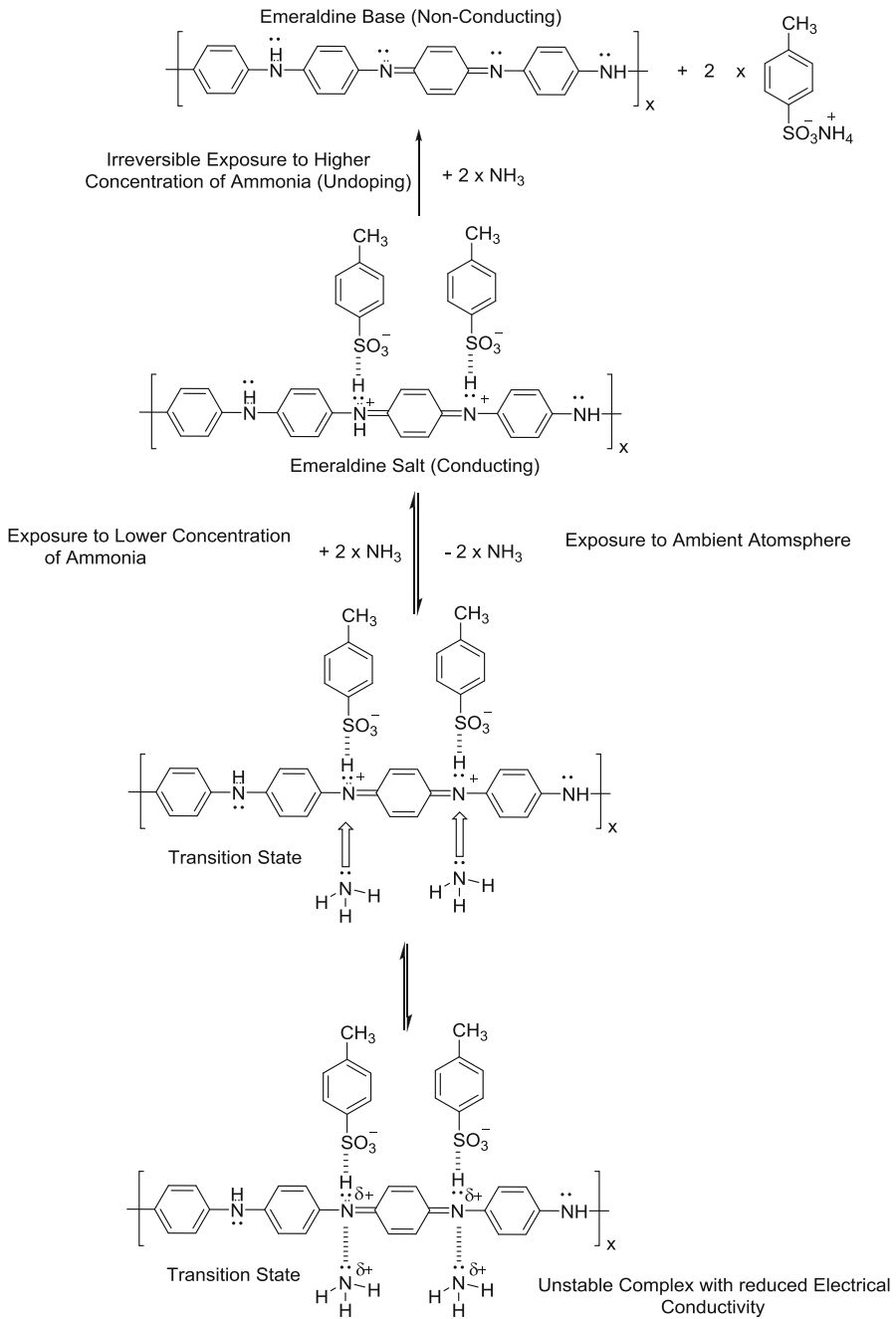


Fig. 6 Schematic sensing mechanism of Pani involving the chemisorption-desorption phenomenon and electrical compensation. (Adapted from Ref. [83] with permission from Elsevier)

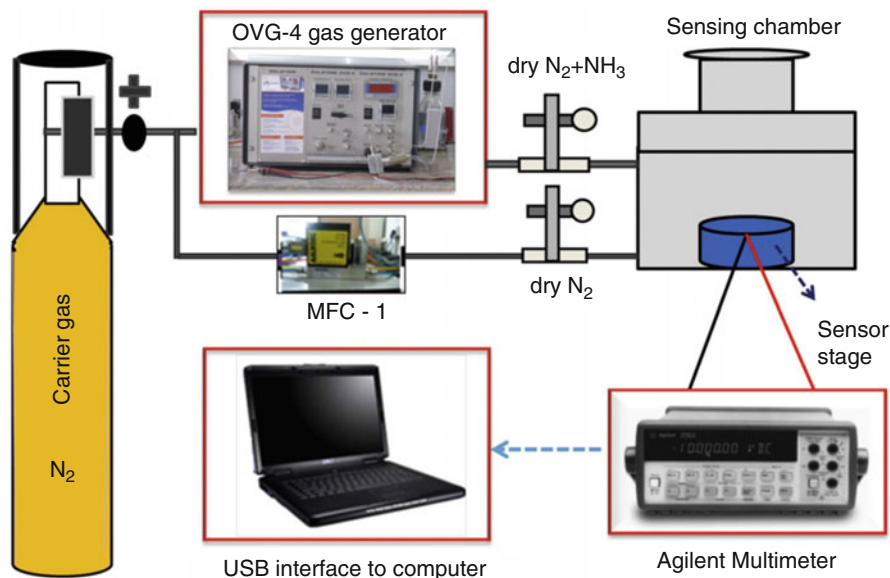


Fig. 7 Schematic illustration of the experimental setup used for gas sensing evaluation. (Adapted from Ref. [85] with permission from Elsevier)

5 Polypyrrole and Polythiophene Nanocomposite as Gas Sensors

Like Pani, PPy and PTh also show similar gas sensing characteristics due to the similar conjugated structures. The derivatives of PTh such as poly (3-hexylthiophene) (P3hT) have been used widely because of its better stability and processability. PPy and P3hT in the doped state behave like *p*-type semiconductor and can interact readily with different gases. Owing to the basic structural similarity of PPy and P3hT with Pani, the sensing reaction also takes place similarly while the response and recovery times can vary widely.

Undoped PPy does not show any gas sensitivity but shows high sensitivity in doped PPy depending on the dopant anion [43]. The gas sensing response of PPy@WO₃ reported by Geng et al. [86] was observed to be different when exposed to 1000 ppm NH₃, H₂S, and NO_x at room temperature. The response time for NH₃, H₂S, and NO_x was 54 s, 135 s and 124 s, respectively. The recovery time of PPy to NH₃ and H₂S was very long and PPy showed irreversibility when exposed to NO_x gases. PPy is a *p*-type semiconductor whose carrier is a hole while WO₃ is *p*-type semiconductor whose carrier is an electron. The irreversibility towards NO_x may be due to the blocking of PPy interaction sites by NO_x. The sensing mechanism of PPy@WO₃ towards H₂S can be explained by the co-effects of the proton doping process and the effects of the *n*-type semiconductor. Similar to ammonia sensors,

PPy being *p*-type reacts with reducing gases such as NH_3 leading to a decrease in charge carrier density and the conductivity decreases once the mobility of the charge carrier decreases as observed in the case of the Pani-based nanocomposites [28]. PTh also responds in a similar manner to redox reactions and upon doping the PTh film with halogens such as iodine, the electrons are removed from the rings of PTh (protonation reaction) thereby increasing the hole density leading to an enhancement of the electrical conductivity. Upon exposure to ammonia, the molecules are physisorbed and undoping takes place. Higher concentrations of ammonia lead to a higher carrier density and consequently a better sensor response. The process of the change in electrical resistance is partially reversible under ambient or inert atmospheres as observed in the case of Pani and PPy-based nanocomposites [87].

Alcohols such as methanol and ethanol upon exposure to PPy nanocomposites increase the conductivity which is in contrast to the reducing gases such as H_2S and NH_3 or their derivatives. The conductivity of PPy changes with the change in the doping level and PPy is a *p*-type semiconductor. Therefore, exposure to electron-donating gases such as alcohol will cause an increase in resistance [88–90]. Chang et al. [91] reported that PTh responds to alcohol with high reversibility. This is in contrast to the inorganic sensors which are poisoned by alcohol. Another interesting report by Goncalves et al. [92] revealed the swelling behavior of P3hT films which affects the interchain spacing thereby affecting charge transport and hence the conductivity. The highest response for tetrahydrofuran (THF) in their case was its polar nature, which imparts high levels of swelling to the P3hT films and enlarges the spacing between the polymeric chains resulting in lower conductivity. The poor response to methanol which is not a solvent for P3hT is due to the absence of its swelling effect.

Li et al. [93] reported that PPy shows high sensitivity towards humid conditions and plenty of works have been done on the low temperature humidity sensing on PPy-based composites [94]. Sun et al. [95] reported that the sensing phenomenon involves an ionic conduction mechanism. Under humid conditions, a layer of water molecules begins to form at the polymer surface and polymers containing hydrophilic groups such as $-\text{COOH}$, $-\text{SO}_3\text{H}$, $-\text{NH}_2$, etc., ionize and produce conductive ions i.e., charge carriers. The concentration of conductive ions increases with increase in relative humidity and the resistance of the sensing materials decreases. The PTh humidity sensor also works in a similar manner, the presence of surface water affects the PTh conduction that occurs through the overlap of adjacent π -bonds and surface water enhances the overlap of π -bonds [96]. Hoshina et al. [97] explained the generation of holes in the film in the vicinity of adsorbed H_2O due to its large dipole. H_2O is expected to adsorb only at the surface and grain boundaries and so the holes induced by H_2O provide conduction paths.

Akbarinejad et al. [98] prepared a 3D PPy film with very high porosity and coated it over copper interdigital electrode by electrospinning of soluble PPy nanoparticles. The coated system was studied for its sensing properties as gas sensor proved to be an excellent material for aliphatic amines with high sensing response, low detection limit, and good repeatability at operating temperature upto 150°C . In addition, it also showed extremely high sensitivity and selectivity to *n*-butylamine. The sensitivity

toward n-butylamine was observed to be approximately three orders of magnitude higher than that of other aliphatic amines. The detection limit was 0.42 ppm and linear range for determination of n-butylamine was 10.54–21.08 ppm.

Kamble et al. [99] synthesized nanofibrous PTh on glass substrate through a simple chemical bath deposition method. The film was tested for its sensing properties toward different gases. Out of these different gases like CO, H₂S, LPG, NH₃, NO₂, and SO₂, the highest selectivity of the PTh film for NO₂ was seen. The morphology, concentration of monomer, and thickness of the deposited film plays significant role in the sensing properties of the film. The film deposited at 0.5 M monomer concentration showed the highest NO₂ gas response of 47.58% at room temperature. These results also showed that initial concentration of monomer plays an important role as the deposition parameters to control the morphological and gas sensing properties of the chemical bath deposited PTh film.

Liao et al. [58] on studying the mechanism of gas sensing on derivatives of PTh films proposed that change in the thickness of films occurs on exposure to vapors which large defines the sensitivity. The X-ray reflectivity, analytical technique can be used to study the structure of films is extremely accurate in measuring film thickness with Angstrom resolution and the swelling and de-swelling of PTh films on exposure to vapors can be easily measured by X-ray reflectivity. The change in the thickness can be characterized to estimate the different amounts of vapor as well as for exposures in a saturated chamber of amines, alcohols, etc. In order to establish the change in thickness as related to vapor exposure, the deswelling of films was also observed in situ. The advantage of X-ray reflectivity measurement is that the insitu characterization of the physical interaction between the PTh and vapors can be easily studied. The thickness change and its relation to the uptake of analyte by the PTh films can be easily studied. Figure 8 shows the reflectivity changes of polybutylthiophene films on interaction with analyte, and a definite swelling of films is observed. Further examining the desorption process, the thickness of polybutylthiophene films was monitored after desorption of acetone from the film. The scans in Fig. 8 show the fringes shifting to the right, as a result of the decrease in film thickness. Thus the X-ray reflectivity measurements confirms the physical interaction between the analyte species and the PTh films and the analytes diffuse to the interface and interacts with the charge carriers, effecting reducing the drain current at a given voltage. It can also be concluded that the physical interaction between the analyte and PTh film results in a few Angstroms increase in the film thickness. This effect must be accounted for any mechanistic model proposed for the sensing response.

6 Polythiophene-Based Optical Gas Sensors

PTh has also been studied as an optical sensor and several studies have utilized the absorbance, reflectance, fluorescence, and refractive index properties, both intensity and wavelength of absorbance and fluorescence are used as a measure of the gas sensing response [100]. Solis et al. [101] examined the absorption and refractive

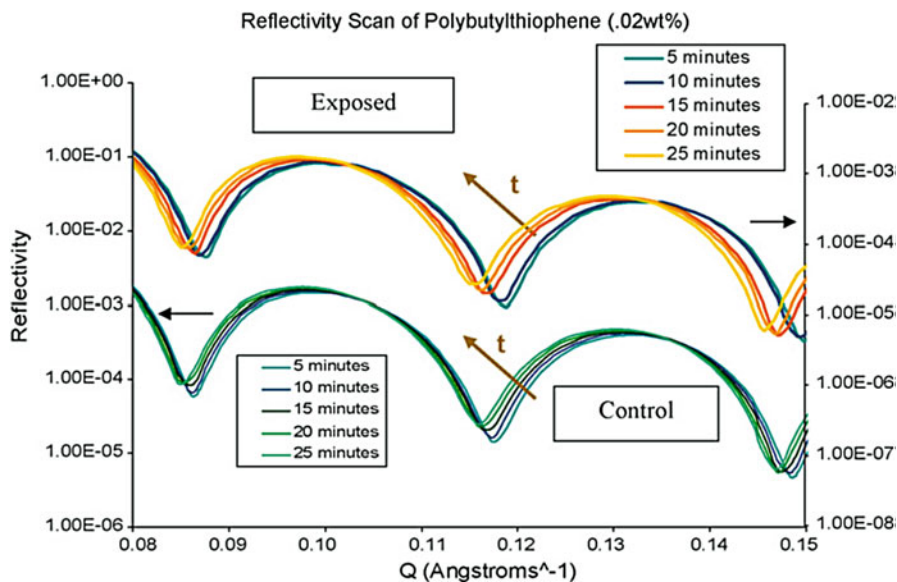


Fig. 8 X-ray reflectivity scan depicting the baseline drift (control) and the clear shift due to analyte exposure (exposed). (Adapted from Ref. [58] with permission from Elsevier)

index change for the detection and high sensitivity and a rapid response time was observed. A small change in the side chain of PTh also induces significant changes in the responses of the optical sensors and the sensors responded differentially towards P3Th and poly(3-dodecylthiophene) suggesting that using PTh with different side chains is a good method for obtaining sensors with better selectivity. The sensing behavior can be due to the physical interactions between the gas and PTh causing swelling of the polymeric films. The redox reaction can also occur but oxidation–reduction reactions are not possible in the case of a neutral gas [102]. The swelling behavior increases the pore volume, accelerates the dilution of chromophores (polymer chains), and results into the decrease in the absorbance which can also affect the aggregation state of the polymer chains changing their conformation and interchain interactions. The change in absorbance affects all the optical parameters and can be a good measure of the sensor performance. Goncalves et al. [103] reported that different types of PTh as an active layer can be used in optical sensors for the detection of *n*-hexane, toluene, tetrahydrofuran, chloroform, dichloromethane, methanol, and water vapor in concentration range of 500–30,000 ppm. On the other hand, the major drawbacks are the poor signal response and either the sensitivity to VOCs needs to be improved or amplifying systems will be needed for future commercial applications [104].

The typical simplest fabrication of sensor involves coating of PTh-based composite on substrate which works as electrode for the sensing purpose. The coated substrate such as silicon wafer/glass coated PTh-based composite results in high

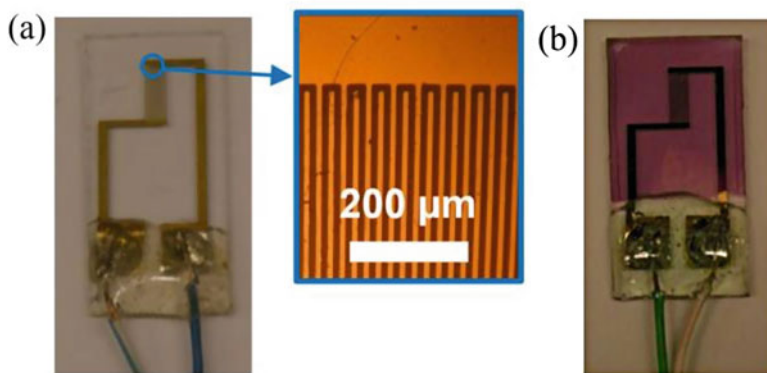


Fig. 9 (a) Bare sensor and (b) poly(3-hexylthiophene) (P3hT) film-based sensor. (Taken from Ref. [105])

effective charge carrier mobility and is directly related to the sensing characteristics. Figure 9 shows the bare sensor and P3hT film-based sensor [105].

In summary, there are various factors which affect the sensing response, i.e., the thickness of polymer films, side chains attached to the polymer unit, and band gap of polymer. The transition from the conducting state to the insulating state changes the optical properties of the PTh derivate. The nonconducting undoped state of poly(3-octylthiophene) which is dark red in color becomes light blue on doping; similarly the neutral state of poly(N-methylpyrrole) is transparent which becomes brown on oxidation and blue to colorless change on oxidation occurs for poly(ethylenedioxythiophene). In insulating state, the materials possess a characteristic $\pi-\pi^*$ transition in the visible region and the extent of which is governed by the band gap and length of conjugation [106]. The exposure of these polymers and their composite to gases results in the change in the structure due to weak interactions, doping-undoping, compensation as observed in their optical spectra, and this is also accompanied by a change in conductivity [107].

Besides their sensing toward the metallic ions, these polymers also exhibit good sensitive to acidic vapor. The changes observed in these cases are reversible and thus offer very promising prospects and application in various fields of application. Deep colored solutions (from violet to yellow) are formed by the reaction of poly(thiophene-3-propionic acid) or poly(thiophene-3-octanic acid) with 1 equivalent alkali metal hydroxide or tetraalkylammonium hydroxide per carboxylic acid group depending on the size of the counter ion. It could be explained on the basis of varying size of counter ions in the carboxylate polymer which affect the stereochemistry of the polymer. Smaller cations favor planar (*p*-stacked purple phase) while larger cations prevent planarity and self assembly (isolated yellow phase) (Fig. 10). When exposed to HCl vapor, the polymer films quickly changed from red, orange, or yellow (depending on the cation) to purple. It is attributed to the protonation of the carboxylate groups in the polymer, which allows the polymer

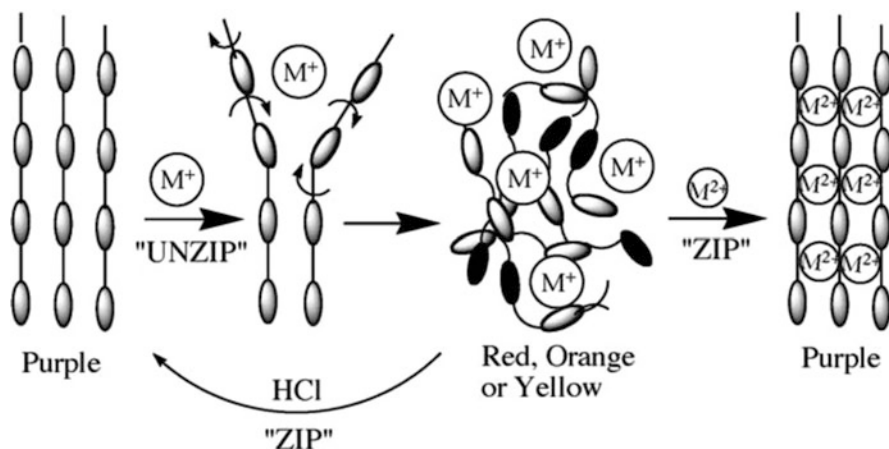


Fig. 10 PTh zipper sensors: analyte driven disassembly and self-assembly. (Adapted from Ref. [108] with permission from Elsevier)

chains to attain a relaxed conformation from a twisted to a violet *p*-stacked conformation with H-bonding, therefore, zipped phase of polymer is an ordered phase. However, when the polymers are left in air, they reverted back to their original color. Thus, a promising future of these polymer and their special stereo structures could be anticipated [108].

7 Functionalized Conducting Polymers in Gas Sensing

Apart from the main stream conducting polymers, functionalized or derivatives of main conducting polymers are also utilized for the sensing purposes. The aim to develop sensors based on the functionalized conducting polymer is solely to remove the specific drawback concerned with the particular conducting polymer. For example, Poly(*N*-alkylanilines) are soluble in common organic solvents while main conducting polymers are insoluble in these solvents. The introduction of bulk alkyl groups into the polymer backbone can be used to dissolve it in common solvents which makes their processing easy [109]. There are numerous reports of gas sensing properties of substituted or functionalized conducting polymer. Patil et al. [110] reported excellent sensing properties of poly(*o*-anisidine)/tin oxide nanocomposites towards the LPG. These nanocomposites possess better sensing properties toward LPG detection than pure poly(*o*-anisidine). The nanocomposite behaves as *p*-type semiconductor and its resistance increases on exposure to LPG, and this feature is employed for the measure of the sensing characteristics. Ratole and Khadayate [111] reported gas sensing properties of poly(*o*-anisidine)/TiO₂ and found higher response than the pure poly(*o*-anisidine). These films of poly(*o*-anisidine)/TiO₂ nanocomposites when exposed to NH₃ not only showed better response than that of poly(*o*-anisidine) but also possessed faster gas desorption from

the surface as compared to poly(*o*-anisidine) itself. Valentini et al. [112] prepared and studied CNT/poly(*o*-anisidine) nanocomposites. The poly(*o*-anisidine) deposition onto the CNTs imparted higher sensitivity to the sensor based on these nanocomposites. On exposure to HCl, CNT/poly(*o*-anisidine) nanocomposites showed higher sensitivity than CNT alone. The increased sensing capability for inorganic vapors is attributed to direct charge transfer with electron hopping effects on intertube conductivity through physically adsorbed poly(*o*-anisidine) between CNT. Casalbore-Miceli et al. [113] electropolymerized 4-(Ferrocenylmethylidene)-4H-cyclopenta[2,1-b:3,4-b]-dithiophene for its humidity sensing properties. Tanaka et al. [114] studied electrical and optical characteristics of poly(3-octyloxythiophene). Because of higher energy of valance band originated from electron donating alkoxy group, poly(3-octyloxythiophene) exhibits more stable doped state and strong interaction with electron accepting molecules and offers its nature to be utilized for gas sensing application. There were reversible changes in its electrical properties on exposure/absence of organic gases. It also exhibited linearity against gas concentration. Other derivatives of Pani, poly(*o*-toluidine), poly(*N*-methylaniline), poly(*N*-ethylaniline), poly(2,3 dimethylaniline), poly(2,5 dimethylaniline) were found to be good sensor for alcohol vapors [115].

Surwade et al. [116] studied poly-*o*-toluidine as gas sensor, herein this study they suggested good and reversible sensing properties of poly-*o*-toluidine toward NO₂ gas in the concentration range 10–100 ppm using UV irradiation at room temperature. They also found that solvent used for casting the film with dipolar aprotic solvents yields the conducting polymer films showing a strong response. The choice of solvents also affects the morphology of the polymer film which is attributed to the chain conformation in the solutions that is preserved in the solid state, i.e., polymer film and it opens a new line to control the sensing and selectivity response of the polymer. Aussawasathien et al. [109] used electrospinning technique to prepare poly(*o*-toluidine) (POT)–polystyrene composite fibers doped with CSA in the form of nonwoven mat on Au substrate as chemical vapor sensor. Owing to the different nature of different sensing gases, the response of the electrospun fiber was also varied. The composite fiber sensor responded to volatile chemicals in different ways, depending on the polarity of sensing chemicals. The change in electrical response with chemical vapor was noticeable even at low amount of fibers. This can be attributed to large specific surface area, high fiber aspect ratio, and high interconnecting network of composite fibers. It was also observed that the surface morphology of the electrospun fibers was unaffected after gas sensing.

As far as substituted pyrrole is concerned, its derivatives have also been utilized as sensor. Poly(*N*-methylpyrrole) was found to be sensitive toward various organic vapors [117, 118]. Costello et al. [119] developed chiral poly(3-substituted-pyrrole) sensor to detect chiral molecules in vapor phase. The polymers were fabricated into chiral sensors by coating the chiral monomer onto poly(vinylidene) difluoride membrane and polymerizing within the membrane structure using ferric chloride oxidant. The sensors exhibited significant chiral discrimination properties, exhibited differential changes in electrical resistance and mass when exposed to different enantiomers in the vapor phase (e.g., (R)- and (S)-menthol, 2-butanol, limonene,

and carvone). Preliminary results obtained in their work proved that chiral conducting polymers have opened up a new approach for detection of gaseous analytes. Paul et al. [120] developed a rapid carbon monoxide detection system by electrochemically functionalizing PPy with ferrocenylmethyl trimethylammonium iodide as a co-dopant which exhibited very high sensitivity to ppm levels of carbon monoxide gas and fast recovery under normal dry room temperature conditions. Iron-based complexes are expected to provide sensitivity for carbon monoxide detection due to the preferential interaction with iron moiety [121]. However, such complexes would have to be modified to suit electrochemical polymerization of conducting polymers. Paul et al. [120] synthesized a new dopant derived from ferrocene attached with tetramethylammonium iodide group so that it can be used during electrochemical polymerization and also dope PPy with the same. These have been then tested for sensitivity and found to be rapidly responsive to ppm levels of carbon monoxide. They functionalized PPy with 5,10,15,20-tetraphenyl-21H,23H-porphyrin iron(III) chloride to detect presence of carbon monoxide gas in ppm level. Controlled functionalization of PPy was done by incorporation of various concentrations of porphyrin. The redox properties of the PPy matrix can be altered strongly by the linkage of electroactive species, especially with coordination compounds. Thus, pyrrole-based polymers containing redox sites of adequately designed transition metal complexes like porphyrin, phthalocyanine, etc., have been prepared by chemical as well as electrochemical methods. The polymerization of these pyrrole substituted complexes has produced interesting polymers aimed at catalyzing redox and organic reactions but not mainly for gas sensor applications. In another research, Paul and Joseph [122] reported NO₂ sensing capacity of PPy functionalized with iron(III)phthalocyanine-4,4,4-tetrasulfonic acid monosodium salt. The increase in conductivity of the functionalized PPy was found on exposure to NO₂ at room temperature. This material exhibited excellent stability, reversibility, and reproducibility. Thuwachaowsoan et al. [123] synthesized perchloric acid doped Poly (3-thiopheneacetic acid), P3TAA, by oxidative polymerization methodology, and later prepared its composite with zeolites (zeolite L, zeolite modenite, zeolite beta) by random dry mixing. The type of zeolites affected the sensitivity and zeolite beta (composite with 20% (v/v) of zeolite beta) showed the highest electrical conductivity and sensitivity due to the lowest amount of Al which leads to large number of available active sites of positive charges on the polymer chain. These positive charges (polaron or the bipolaron) can easily interact with H₂ hence giving the sensing response.

Krondak et al. [124] reported the chemoresistivity of 4,4'-dibutoxy-2,2'-bipyrrole and 4,4'-dimethoxy-2,2'-bipyrrole for electrical and sensing characteristics. These polymers were synthesized by cyclic voltametry and showed high sensitivity for HCl in the ppm range. These polymers also sensed the presence of NH₃, NO, and oxygen, however, less sensitivity than towards HCl. The electrical conductivity of the polymers was observed to be pH dependent; in comparison to 4,4-dibutoxy-2,2-bipyrrole, the conductivity of the methoxy-2,2-bipyrrole shifted to acidic range. This behavior also offers their utilization in the advancement of enzymatic biosensors with pH transducing.

Lange et al. supported that presence of ozone changes the oxidation and protonation states of Pani and *m*-chloro-Pani which could be seen as change in optical absorbance between 500 and 800 nm. The higher sensitivity of Pani and *m*-chloro-Pani in comparison to *N*-methyl-Pani is probably caused by their ability to be oxidized to pernigraniline [125].

Torsi et al. [126] studied alkoxy and alkyl substituted regiochemically defined polyterthiophenes as active layers in sensing organic thin films transistors. The active layers possess polycrystalline morphology and the substituent chains on it bear different associated dipole moments. VOCs carrying moieties that are chemically homologous to the selected polymers' side chains are used as analytes. Both electrical and quartz crystal microbalance sensor responses are evaluated and a rationale for the sensing mechanisms involving weak polar/polar-type interactions is proposed. In another report, Torsi et al. [127], utilized dipentoxy-substituted PTh thin film in configuring an organic thin film transistor. Sensing response of the film was found to be very fast for 1-hexanol and ethanol and sensitive as low as 0.7 ng/ppm.

Xu et al. [128] synthesized SnO₂ hollow spheres and further its composite with PTh, the resulting PTh hybrid composite showed good synergistic interaction between SnO₂ and PTh. The hybrid possessed higher thermal stability than pure PTh. Gas sensing properties (sensor response and selectivity) of these hybrids were found to be good toward NO₂ at temperature below 100 °C. The increased sensing performance of the hybrids is attributed to the large surface area of the hybrids and the *p*-*n* heterojunction formed between *p*-type PTh and *n*-type SnO₂ hollow spheres.

Pirsa and Alizadeh [129] studies gas sensors based on sulfonate ion doped PPy and found rapid response and lowest detection limit for DMSO among different VOCs. These sensors were fast, reversible, and reproducible. Therefore, these hybrids can be utilized for detection of DMSO and other VOCs in the atmosphere or at work place.

Organic field effect transistors based on P3hT and Cu^{II} tetraphenylporphyrin composite were studied for sensing behavior toward nitro-based explosive compounds. For example, 1,3,5-trinitro-1,3,5-triazacyclohexane (RDX), 2,4,6-trinitrotoluene (TNT) and dinitrobenzene. Sufficient changes, suitable for sensing were observed in transistor on current and conductance on exposure [130].

8 Conclusion and Future Challenges

Overall, nanocomposites of Pani, PPy, and PTh offer the safe detection of a wide variety of gases at room temperature. Room temperature sensing gives high stability and prevents structural changes such as polymer deformation. Conducting polymer-based gas sensors have potential applications in different contexts such as industries, household emission, vehicle emission control, environmental monitoring, and biosensors. Sensors are inexpensive, easy to fabricate, and operate at room temperature with very little power consumption. Future works may include the introduction of different chemical moieties and chemically modifying the polymer structure to

customize the properties and enhance the selectivity for different gases. Finally, new strategies will be needed to fully understand the underlying mechanism involved in analyte sensing by conducting polymers and its nanocomposites which will assist in the fabrication and commercialization of highly selective sensors for specific agents.

Pani, PPy, and PTh nanocomposites have high potential in the field of gas sensing and can be used in wide variety of applications. On the other hand, major drawbacks limit their commercialization due to the following demerits:

1. Alan MacDiarmid, one of the pioneers in conducting polymer research, stated that “there are as many different types of polyaniline(s) as there are people who make it!” [72]. Therefore, different reaction setups even with a slight change in the reaction parameters may yield a polymer product with a completely different set of properties. In the case of Pani, PPy, and PTh, optimized conditions are needed to obtain a controlled nanostructure because pH, time of synthesis, and temperature affect the final polymer product considerably.
2. The dopant also plays an important role, and the quantification of dopant by chemical synthesis is a tedious job. Different amounts of dopant may remain in the final product due to the different amount of losses of dopant during filtration which depends on many factors such as suction pressure, filtration time, washing, etc.
3. The shelf life of doped Pani, PPy, and PTh is relatively short due to the undoping reaction which might take place upon exposure to reducing conditions.
4. Such sensors in contrast to metal oxide sensors do not work at high temperatures because polymer degradation is often the competing reaction.
5. The sensor response towards a large number of nanocomposites is influenced by humidity which may cause the false response. Therefore, the development of Pani, PPy, and PTh nanocomposites impervious to humidity will be one of the great challenges of the future.

References

1. H. Shirakawa, E.J. Louis, A.G. MacDiarmid, C.K. Chiang, A.J. Heeger, Synthesis of electrically conducting organic polymers: Halogen derivatives of polyacetylene, (CH)_x. *J. Chem. Soc. Chem. Commun.* (16), 578–580 (1977)
2. T. Yamamoto, Molecular assembly and properties of polythiophenes. *NPG Asia Mater.* **2**, 54–60 (2010)
3. H.C. Kang, K.E. Geckeler, Enhanced electrical conductivity of polypyrrole prepared by chemical oxidative polymerization: Effect of the preparation technique and polymer additive. *Polymer* **41**, 6931–6934 (2000)
4. A.L. Aldaba, Á. González-Vila, M. Debliquy, M.L. Amo, C. Caucheteur, D. Lahem, Polyaniline-coated tilted fiber Bragg gratings for pH sensing. *Sensors Actuators B Chem.* **254**, 1087–1093 (2018)
5. X. Li, Z.-Y. Sui, Y.-N. Sun, P.-W. Xiao, X.-Y. Wang, B.-H. Han, Polyaniline-derived hierarchically porous nitrogen-doped carbons as gas adsorbents for carbon dioxide uptake. *Microporous Mesoporous Mater.* **257**, 85–91 (2018)
6. S. Hong, F.S. Cannon, P. Hou, T. Byrne, C. Nieto-Delgado, Adsorptive removal of sulfate from acid mine drainage by polypyrrole modified activated carbons: Effects of polypyrrole deposition protocols and activated carbon source. *Chemosphere* **184**, 429–437 (2017)

7. A. Ramaprasad, D. Latha, V. Rao, Synthesis and characterization of polypyrrole grafted chitin. *J. Phys. Chem. Solids* **104**, 169–174 (2017)
8. M. Khan, G. Brunklaus, S. Ahmad, Probing the molecular orientation of chemically polymerized polythiophene-polyrotaxane via solid state NMR. *Arab. J. Chem.* **10**, 708–714 (2017)
9. M.R. Chandra, P.S.P. Reddy, T.S. Rao, S. Pammi, K.S. Kumar, K.V. Babu, C.K. Kumar, K. Hemalatha, Enhanced visible-light photocatalysis and gas sensor properties of polythiophene supported tin doped titanium nanocomposite. *J. Phys. Chem. Solids* **105**, 99–105 (2017)
10. N. Parveen, N. Mahato, M.O. Ansari, M.H. Cho, Enhanced electrochemical behavior and hydrophobicity of crystalline polyaniline@graphene nanocomposite synthesized at elevated temperature. *Compos. Part B Eng.* **87**, 281–290 (2016)
11. N. Parveen, M.O. Ansari, M.H. Cho, Simple and rapid synthesis of ternary polyaniline/titanium oxide/graphene by simultaneous TiO₂ generation and aniline oxidation as hybrid materials for supercapacitor applications. *J. Solid State Electrochem.* **21**, 57 (2016). <https://doi.org/10.1007/s10008-016-3310-8>
12. X. Wu, M. Lian, Highly flexible solid-state supercapacitor based on graphene/polypyrrole hydrogel. *J. Power Sources* **362**, 184–191 (2017)
13. C. Kumar, G. Rawat, H. Kumar, Y. Kumar, R. Prakash, S. Jit, Flexible poly(3, 3'-dialkylquaterthiophene) based interdigitated metal-semiconductor-metal ammonia gas sensor. *Sensors Actuators B Chem.* **255**, 203–209 (2018)
14. L. Ai, Y. Liu, X. Zhang, X. Ouyang, Z. Ge, A facile and template-free method for preparation of polythiophene microspheres and their dispersion for waterborne corrosion protection coatings. *Synth. Met.* **191**, 41–46 (2014)
15. Q. Meng, K. Cai, Y. Chen, L. Chen, Research progress on conducting polymer based supercapacitor electrode materials. *Nano Energy* **36**, 268–285 (2017)
16. M.O. Ansari, F. Mohammad, Thermal stability of HCl-doped-polyaniline and TiO₂ nanoparticles-based nanocomposites. *J. Appl. Polym. Sci.* **124**, 4433–4442 (2012)
17. T. Anwer, M.O. Ansari, F. Mohammad, Morphology and thermal stability of electrically conducting nanocomposites prepared by sulfosalicylic acid micelles assisted polymerization of aniline in presence of ZrO₂ nanoparticles. *Polym.-Plast. Technol. Eng.* **52**, 472–477 (2013)
18. R. Kumar, M.O. Ansari, M.A. Barakat, DBSA doped polyaniline/multi-walled carbon nanotubes composite for high efficiency removal of Cr(VI) from aqueous solution. *Chem. Eng. J.* **228**, 748–755 (2013)
19. F.H. Lu, M.G. Mohamed, T.F. Liu, C.G. Chao, L. Daic, S.W. Kuo, A quenching method for the preparation of metal oxide–polythiophene composites having fiber structures. *RSC Adv.* **4**, 64525–64534 (2014)
20. Y. Wang, X. Qing, Q. Zhou, Y. Zhang, Q. Liu, K. Liu, W. Wang, M. Li, Z. Lu, Y. Chen, The woven fiber organic electrochemical transistors based on polypyrrole nanowires/reduced graphene oxide composites for glucose sensing. *Biosens. Bioelectron.* **95**, 138–145 (2017)
21. S.-X. Zhou, X.-Y. Tao, J. Ma, C.-H. Qu, Y. Zhou, L.-T. Guo, P.-Z. Feng, Y.-B. Zhu, X.-Y. Wei, Facile synthesis of self-assembled polyaniline nanorods doped with sulphuric acid for high-performance supercapacitors. *Vacuum* **143**, 63–70 (2017)
22. E.I. Santiago, E.C. Pereira, L.O.S. Bulhões, Characterization of the redox processes in polyaniline using capacitance-potential curves. *Synth. Met.* **98**, 87–93 (1998)
23. V. Tabard-Cossa, M. Godin, P. Grütter, Redox-induced surface stress of polypyrrole-based actuators. *J. Phys. Chem. B* **109**, 17531–17537 (2005)
24. S. Haraguchi, Y. Tsuchiya, T. Shiraki, K. Sada, S. Shinkai, Control of polythiophene redox potentials based on supramolecular complexation with helical schizophyllan. *Chem. Commun.* (40), 6086–6088 (2009)
25. L. Yang, X. Huang, A. Gogoll, M. Strømme, M. Sjödin, Conducting redox polymer based anode materials for high power electrical energy storage. *Electrochim. Acta* **204**, 270–275 (2016)
26. A. Nautiyal, M. Qiao, J.E. Cook, X. Zhang, T.-S. Huang, High performance polypyrrole coating for corrosion protection and biocidal applications. *Appl. Surf. Sci.* **427**, 922–930 (2017)

27. L. Kumar, I. Rawal, A. Kaur, S. Annapoorni, Flexible room temperature ammonia sensor based on polyaniline. *Sensors Actuators B Chem.* **240**, 408–416 (2017)
28. A. Joshi, S.A. Gangal, S.K. Gupta, Ammonia sensing properties of polypyrrole thin films at room temperature. *Sensors Actuators B Chem.* **156**, 938–942 (2011)
29. S.T. Navale, A.T. Mane, G.D. Khuspe, M.A. Chougule, V.B. Patil, Room temperature NO₂ sensing properties of polythiophene films. *Synth. Met.* **195**, 228–233 (2014)
30. S. Pandey, Highly sensitive and selective chemiresistor gas/vapor sensors based on polyaniline nanocomposite: A comprehensive review. *J. Sci. Adv. Mater. Dev.* **1**, 431–453 (2016)
31. C.T.P. da Silva, V.L. Kupfer, G.R. da Silva, M. Pereira, A.W. Rinaldi, One-step electrochemical synthesis of polyaniline/metallic oxide nanoparticle (γ -Fe₂O₃) thin film. *Int. J. Electrochem. Sci.* **11**, 5380–5394 (2016)
32. A.A. Athawale, S. Bhagwat, P.P. Katre, Nanocomposite of Pd–polyaniline as a selective methanol sensor. *Sensors Actuators B Chem.* **114**, 263–267 (2006)
33. A. Choudhury, Polyaniline/silver nanocomposites: Dielectric properties and ethanol vapour sensitivity. *Sensors Actuators B Chem.* **138**, 318–325 (2009)
34. Z.-F. Li, H. Zhang, Q. Liu, L. Sun, L. Stanciu, J. Xie, Fabrication of high-surface-area graphene/polyaniline nanocomposites and their application in supercapacitors. *ACS Appl. Mater. Interfaces* **5**, 2685–2691 (2013)
35. S. Maeda, S. Armes, Polypyrrole-tin (IV) oxide colloidal nanocomposites. *Synth. Met.* **69**, 499–500 (1995)
36. R.A. Naikoo, S.U. Bhat, M.A. Mir, R. Tomar, Composites of various cation exchanged forms of mesoporous zeolite A with polypyrrole-thermal, spectroscopic and gas sensing studies. *Microporous Mesoporous Mater.* **243**, 229–238 (2017)
37. B.-K. Kim, Y.H. Kim, K. Won, H. Chang, Y. Choi, K. Kong, B.W. Rhyu, J. Kim, J.-O. Lee, Electrical properties of polyaniline nanofibre synthesized with biocatalyst. *Nanotechnology* **16**, 1177–1181 (2005)
38. K.M. Molapo, P.M. Ndingili, R.F. Ajayi, G. Mbambisa, S.M. Mailu, N. Njomo, M. Masikini, P. Baker, E.I. Iwuoha, Electronics of conjugated polymers (I): polyaniline. *Int. J. Electrochem. Sci.* **7**, 11859–11875 (2012)
39. S. Etemad, A.J. Heeger, Polyacetylene, (CH)_x: The prototype conducting polymer. *Annu. Rev. Phys. Chem.* **33**, 443–469 (1982)
40. J.M.G. Cowie, *Chemistry and Physics of Modern Materials*, II edn. (Blackie/Chapman and Hall, New York, 1973)
41. R. Kiebooms, R. Menon, K. Lee, in *Handbook of Advance Electronic and Photonic Materials and Devices*, ed. by H.S. Nalwa (Academic, San Diego, 2001)
42. W.-C. Chen, T.-C. Wen, Electrochemical and capacitive properties of polyaniline-implanted porous carbon electrode for supercapacitors. *J. Power Sources* **117**, 273–282 (2003)
43. S. Košina, V. Skákalová, D. Jančula, Electrochemical preparation of thick porous polypyrrole layers. *Synth. Met.* **53**, 227–235 (1993)
44. N. Parveen, M.O. Ansari, M.H. Cho, Route to high surface area, mesoporosity of polyaniline-titanium dioxide nanocomposites via one pot synthesis for energy storage applications. *Ind. Eng. Chem. Res.* **55**, 116–124 (2016)
45. H. Bai, G. Shi, Gas sensors based on conducting polymers. *Sensors* **7**, 267–307 (2007)
46. N. Kemp, G. Fianagan, A. Kaiser, H. Trodahl, B. Chapman, A. Partridge, R. Buckley, Temperature-dependent conductivity of conducting polymers exposed to gases. *Synth. Met.* **101**, 434–435 (1999)
47. S. Krutovtsev, O. Ivanova, S. Sorokin, Sensing properties of polyaniline films doped with Dawson heteropoly compounds. *J. Anal. Chem.* **56**, 1057–1060 (2001)
48. J.-H. Cho, J.-B. Yu, J.-S. Kim, S.-O. Sohn, D.-D. Lee, J.-S. Huh, Sensing behaviors of polypyrrole sensor under humidity condition. *Sensors Actuators B Chem.* **108**, 389–392 (2005)
49. N. Kemp, A. Kaiser, H. Trodahl, B. Chapman, R. Buckley, A. Partridge, P. Foot, Effect of ammonia on the temperature-dependent conductivity and thermopower of polypyrrole. *J. Polym. Sci. B Polym. Phys.* **44**, 1331–1338 (2006)

50. D. Liu, J. Aguilar-Hernandez, K. Potje-Kamloth, H. Liess, A new carbon monoxide sensor using a polypyrrole film grown on an interdigital-capacitor substrate. *Sensors Actuators B Chem.* **41**, 203–206 (1997)
51. S. Christie, E. Scorsone, K. Persaud, F. Kvasnik, Remote detection of gaseous ammonia using the near infrared transmission properties of polyaniline. *Sensors Actuators B Chem.* **90**, 163–169 (2003)
52. K. Hosono, I. Matsubara, N. Murayama, W. Shin, N. Izu, The sensitivity of 4-ethylbenzenesulfonic acid-doped plasma polymerized polypyrrole films to volatile organic compounds. *Thin Solid Films* **484**, 396–399 (2005)
53. P. Fedorko, V. Skakalova, Low pressure effect in the electrical conductivity of doped polypyrrole. *Synth. Met.* **94**, 279–283 (1998)
54. S. Koul, R. Chandra, S.K. Dhawan, Conducting polyaniline composite: A reusable sensor material for aqueous ammonia. *Sensors Actuators B Chem.* **75**, 151–159 (2001)
55. M.M. Ayad, G. El-Hefnawy, N.L. Torad, A sensor of alcohol vapours based on thin polyaniline base film and quartz crystal microbalance. *J. Hazard. Mater.* **168**, 85–88 (2009)
56. N.J. Pinto, I. Ramos, R. Rojas, P.-C. Wang, A.T. Johnson Jr., Electric response of isolated electrospun polyaniline nanofibers to vapors of aliphatic alcohols. *Sensors Actuators B Chem.* **129**, 621–627 (2008)
57. H.-K. Jun, Y.-S. Hoh, B.-S. Lee, S.-T. Lee, J.-O. Lim, D.-D. Lee, J.-S. Huh, Electrical properties of polypyrrole gas sensors fabricated under various pretreatment conditions. *Sensors Actuators B Chem.* **96**, 576–581 (2003)
58. F. Liao, M.F. Toney, V. Subramanian, Thickness changes in polythiophene gas sensors exposed to vapor. *Sensors Actuators B Chem.* **148**, 74–80 (2010)
59. H. Tai, Y. Jiang, G. Xie, J. Yu, X. Chen, Fabrication and gas sensitivity of polyaniline-titanium dioxide nanocomposite thin film. *Sensors Actuators B Chem.* **125**, 644–650 (2007)
60. H. Tai, Y. Jiang, G. Xie, J. Yu, X. Chen, Z. Ying, Influence of polymerization temperature on NH₃ response of PANI/TiO₂ thin film gas sensor. *Sensors Actuators B Chem.* **129**, 319–326 (2008)
61. X. Ma, M. Wang, G. Li, H. Chen, R. Bai, Preparation of polyaniline-TiO₂ composite film with in situ polymerization approach and its gas-sensitivity at room temperature. *Mater. Chem. Phys.* **98**, 241–247 (2006)
62. A.T. Mane, S.T. Navale, S. Sen, D.K. Aswal, S.K. Gupta, V.B. Patil, Nitrogen dioxide (NO₂) sensing performance of p-polypyrrole/n-tungsten oxide hybrid nanocomposites at room temperature. *Org. Electron.* **16**, 195–204 (2015)
63. T. Sen, S. Mishra, N.G. Shimpi, Synthesis and sensing applications of polyaniline nanocomposites: A review. *RSC Adv.* **6**, 42196–42222 (2016)
64. P. Lobotka, P. Kunzo, E. Kovacova, I. Vavra, Z. Krizanova, V. Smatko, J. Stejskal, E.N. Konyushenko, M. Omastova, Z. Spitalsky, M. Micusik, I. Krupa, Thin polyaniline and polyaniline/carbon nanocomposite films for gas sensing. *Thin Solid Films* **519**, 4123–4127 (2011)
65. T. Sen, N.G. Shimpi, S. Mishra, Room temperature CO sensing by polyaniline/Co₃O₄ nanocomposite. *J. Appl. Polym. Sci.* (2016). <https://doi.org/10.1002/APP.44115>
66. S.S. Joshi, C.D. Lokhande, S.-H. Han, A room temperature liquefied petroleum gas sensor based on all-electrodeposited n-CdSe/p-polyaniline junction. *Sensors Actuators B Chem.* **123**, 240–245 (2007)
67. T. Sen, N.G. Shimpi, S. Mishra, R. Sharma, Polyaniline/ γ -Fe₂O₃ nanocomposite for room temperature LPG sensing. *Sensors Actuators B Chem.* **190**, 120–126 (2014)
68. M.V. Fuke, A. Vijayan, M. Kulkarni, R. Hawaldar, R.C. Aiyyer, Evaluation of Co-polyaniline nanocomposite thin films as humidity sensor. *Talanta* **76**, 1035–1040 (2008)
69. S. Jain, S. Chakane, A.B. Samui, V.N. Krishnamurthy, S.V. Bhoraskar, Humidity sensing with weak acid-doped polyaniline and its composites. *Sensors Actuators B Chem.* **96**, 124–129 (2003)

70. S.K. Shukla, V. Minakshi, A. Bharadavaja, A. Shekhar, A. Tiwari, Fabrication of electrochemical humidity sensor based on zinc oxide/polyaniline nanocomposite. *Adv. Mater. Lett.* **3**, 421–425 (2012)
71. H. Tai, Y. Jiang, G. Xie, J. Yu, Preparation, characterization and comparative NH₃-sensing characteristic studies of PANI/inorganic oxides nanocomposite thin films. *J. Mater. Sci. Technol.* **26**, 605–613 (2010)
72. J. Gong, Y. Li, Z. Hu, Z. Zhou, Y. Deng, Ultrasensitive NH₃ Gas sensor from polyaniline nanograin enched TiO₂ fibers. *J. Phys. Chem. C* **114**, 9970–9974 (2010)
73. D.S. Dhawale, R.R. Salunkhe, U.M. Patil, K.V. Gurav, A.M. More, C.D. Lokhande, Room temperature liquefied petroleum gas (LPG) sensor based on p-polyaniline/n-TiO₂ heterojunction. *Sensors Actuators B Chem.* **134**, 988–992 (2008)
74. A.A. Athawale, S.V. Bhagwat, P.P. Katre, Nanocomposite of Pd–polyaniline as a selective methanol sensor. *Sensors Actuators B Chem.* **114**, 263–267 (2006)
75. M. Song, F. Liu, X. Ma, Study of PANI Preparation and Properties in Gas Sensing, CA '14 Proceedings of the 2014 7th International Conference on Control and Automation, IEEE Computer Society Washington, DC, USA ©2014, pp. 37–44. ISBN: 978-1-4799-8206-6
76. L. Yang, C.S. Zhang, Effect of dopants on microstructure and properties of polyaniline and polypyrrole. *Adv. Mater. Res.* **328–330**, 1576–1579 (2011)
77. Z. Pang, J. Fu, P. Lv, F. Huang, Q. Wei, Effect of CSA concentration on the ammonia sensing properties of CSA-Doped PA6/PANI composite nanofibers. *Sensors* **14**, 21453–21465 (2014)
78. S. Koul, R. Chandra, Mixed dopant conducting polyaniline reusable blend for the detection of aqueous ammonia. *Sensors Actuators B Chem.* **104**, 57–67 (2005)
79. A.A. Khan, M. Khalid, Synthesis of nano-sized ZnO and polyaniline-zinc oxide composite: Characterization, stability in terms of DC electrical conductivity retention and application in ammonia vapor detection. *J. Appl. Polym. Sci.* **3**, 1601–1607 (2010)
80. V.V. Chabukswar, S. Pethkar, A.A. Athawale, Acrylic acid doped polyaniline as an ammonia sensor. *Sensors Actuators B Chem.* **77**, 657–663 (2011)
81. P.P. Sengupta, P. Kar, B. Adhikari, Influence of dopant in the synthesis, characteristics and ammonia sensing behavior of processable polyaniline. *Thin Solid Films* **517**, 3770–3775 (2009)
82. A.L. Kukla, Y.M. Shirshov, S.A. Piletsky, Ammonia sensors based on sensitive polyaniline films. *Sensors Actuators B Chem.* **37**, 135–140 (1996)
83. M.O. Ansari, F. Mohammad, Thermal stability, electrical conductivity and ammonia sensing studies on p-toluenesulfonic acid doped polyaniline:titanium dioxide (pTSA/Pani:TiO₂) nanocomposites. *Sensors Actuators B Chem.* **157**, 122–129 (2011)
84. L. Geng, Y. Zhao, X. Huang, S. Wang, S. Zhang, W. Huang, S. Wu, The preparation and gas sensitivity study of polypyrrole/zinc oxide. *Synth. Met.* **156**, 1078–1082 (2006)
85. S. Abdulla, T.L. Mathew, B. Pullithadathil, Highly sensitive, room temperature gas sensor based on polyaniline-multiwalled carbon nanotubes (PANI/MWCNTs) nanocomposite for trace-level ammonia detection. *Sensors Actuators B Chem.* **221**, 1523–1534 (2015)
86. L. Geng, Gas sensitivity study of polypyrrole/WO₃ hybrid materials to H₂S. *Synth. Met.* **160**, 1708–1711 (2010)
87. H. Malkeshi, M. Moghaddam, Ammonia gas-sensing based on polythiophene film prepared through electrophoretic deposition method. *J. Polym. Res.* **23**, 108 (2016)
88. J.J. Miasik, A. Hooper, B.C. Tofield, Conducting polymer gas sensors. *J. Chem. Soc. Faraday Trans.* **1**(82), 1117–1126 (1986)
89. P. Topart, M. Josowicz, Transient effects in the interaction between polypyrrole and methanol vapor. *J. Phys. Chem.* **96**, 8662–8666 (1992)
90. D. Das, P. Choudhury, L.J. Borthakur, I.R. Kamrupi, U. Gogoi, S.K. Dolui, Methanol vapor sensor based on poly(styrene-co-butylacrylate)/polypyrrole-EG core-shell nanocomposites. *Sensors Actuators B Chem.* **199**, 320–329 (2014)
91. J.B. Chang, V. Liu, V. Subramanian, K. Sivula, C. Luscombe, A. Murphy, J. Liu, J.M.J. Fréchet, Printable polythiophene gas sensor array for low-cost electronic noses. *J. Appl. Phys.* **100**, 014506 (2006)

92. V.C. Gonçalves, B.M. Nunes, D.T. Balogh, C.A. Olivati, Detection of volatile organic compounds using a polythiophene derivative. *Phys. Status Solidi A* **207**, 1756–1759 (2010)
93. Y. Li, L. Hong, M. Yang, Crosslinked and quaternized poly(4-vinylpyridine)/polypyrrole composite as a potential candidate for the detection of low humidity. *Talanta* **75**, 412–417 (2008)
94. P.-G. Su, Y.-P. Chang, Low-humidity sensor based on a quartz-crystal microbalance coated with polypyrrole/Ag/TiO₂ nanoparticles composite thin films. *Sensors Actuators B Chem.* **129**, 915–920 (2008)
95. A. Sun, Z. Li, T. Wei, Y. Li, P. Cui, Highly sensitive humidity sensor at low humidity based on the quaternized polypyrrole composite film. *Sensors Actuators B Chem.* **142**, 197–203 (2009)
96. W.M. Sears, The effect of humidity on the electrical conductivity of mesoporous polythiophene. *Sensors Actuators B Chem.* **130**, 661–667 (2008)
97. S. Hoshino, M. Yoshida, S. Uemura, T. Kodzasa, N. Takada, T. Kamata, K. Yase, Influence of moisture on device characteristics of polythiophene-based field-effect transistors. *J. Appl. Phys.* **95**, 5088 (2004)
98. A. Akbarinejad, A. Ghoorchian, M. Kamalabadi, N. Alizadeh, Electrospun soluble conductive polypyrrole nanoparticles for fabrication of highly selective *n*-butylamine gas sensor. *Sensors Actuators B Chem.* **236**, 99–108 (2016)
99. D.B. Kamble, A.K. Sharma, J.B. Yadav, V.B. Patil, R.S. Devan, A.A. Jatratkar, M.A. Yewale, V.V. Ganbavle, S.D. Pawar, Facile chemical bath deposition method for interconnected nanofibrous polythiophene thin films and their use for highly efficient room temperature NO₂ sensor application. *Sensors Actuators B Chem.* **244**, 522–530 (2017)
100. V.C. Gonçalves, D.T. Balogh, Optical VOCs detection using poly(3-alkylthiophenes) with different side-chain lengths. *Sensors Actuators B Chem.* **142**, 55–60 (2009)
101. J. Cerón Solís, E. De la Rosa, E. Peña Cabrera, Absorption and refractive index changes of poly(3-octylthiophene) under NO₂ gas exposure. *Opt. Mater.* **29**, 167–172 (2006)
102. J. Janata, M. Josowicz, Conducting polymers in electronic chemical sensors. *Nat. Mater.* **2**, 19–24 (2003)
103. V.C. Gonçalves, D.T. Balogh, Optical chemical sensors using polythiophene derivatives as active layer for detection of volatile organic compounds. *Sensors Actuators B Chem.* **162**, 307–312 (2012)
104. H. Yoon, Current trends in sensors based on conducting polymer nanomaterials. *Nanomaterials* **3**, 524–549 (2013)
105. M.R. Cavallari, J.E. Izquierdo, G.S. Braga, E.A. Dirani, M.A. Pereira-da-Silva, E.F. Rodríguez, F.J. Fonseca, Enhanced sensitivity of gas sensor based on poly(3-hexylthiophene) thin-film transistors for disease diagnosis and environment monitoring. *Sensors* **15**, 9592–9609 (2015)
106. T.A. Skotheim, *Handbook of Conducting Polymers* (CRC Press, Boca Raton, 1997)
107. K.C. Persaud, Polymers for chemical sensing. *Mater. Today* **8**, 38–44 (2005)
108. P.C. Ewbank, R.S. Loewe, L. Zhai, J. Reddinger, G. Sauvé, R.D. McCullough, Regioregular poly(thiophene-3-alkanoic acid)s: Water soluble conducting polymers suitable for chromatic chemosensing in solution and solid state. *Tetrahedron* **60**, 11269–11275 (2004)
109. D. Aussawasathien, S. Sahasithiwat, L. Menbangpung, Electrospun camphorsulphonic acid doped poly(*o*-toluidine)-polystyrene composite fibers: Chemical vapour sensing. *Synth. Met.* **158**, 259–263 (2008)
110. D. Patil, K. Kolhe, H.S. Potdar, P. Patil, Investigation of poly(*o*-anisidine)-SnO₂ nanocomposites for fabrication of low temperature operative liquefied petroleum gas sensor. *J. Appl. Phys.* **110**, 124501 (2011). <https://doi.org/10.1063/1.3667107>
111. P.M. Raotole, R.S. Khadayate, Deposition and characterization of poly(*O*-anisidine)/TiO₂ nanocomposite for gas sensing application. *Int. J. Polym. Sci. Eng.* **1**, 1–7 (2105)
112. L. Valentini, V. Bavastrello, E. Stura, I. Armentano, C. Nicolini, J.M. Kenny, Sensors for inorganic vapor detection based on carbon nanotubes and poly(*o*-anisidine) nanocomposite material. *Chem. Phys. Lett.* **383**, 617–622 (2004)

113. G. Casalbore-Miceli, A. Zanelli, A.W. Rinaldi, N. Camaioni, M.J. Yang, Y. Li, E.M. Girotto, Electric properties of polyelectrolyte films in moist solvents. *Sensors Actuators B Chem.* **125**, 120–125 (2007)
114. F. Tanaka, T. Kawai, S. Kojima, K. Yoshino, Electrical and optical properties of poly(3-alkoxythiophene) and their application for gas sensor. *Synth. Met.* **102**, 1358–1359 (1999)
115. A.A. Athawale, M.V. Kulkarni, Polyaniline and its substituted derivatives as sensors for aliphatic alcohol. *Sensors Actuators B Chem.* **67**, 173–177 (2000)
116. S.P. Surwade, S.R. Agnihotra, V. Dua, S.K. Manohar, Nitrogen dioxide vapor detection using poly-*o*-toluidine. *Sensors Actuators B Chem.* **143**, 454–457 (2009)
117. X. Li, Y. Wang, X. Yang, J. Chen, H. Fu, T. Cheng, Y. Wang, Conducting polymers in environmental analysis. *Trends Anal. Chem.* **39**, 163–179 (2012)
118. P.N. Barret, S.K. Ling-Chung, Conducting polymers gas sensors part III: Results for four different polymers and five different vapours. *Sensors Actuators* **20**, 287–292 (1989)
119. B.P.J.D.L. Castelo, N.M. Ratcliff, P.S. Sivanand, The synthesis of novel 3-substitutedpyrrole monomers processing chiral side groups: A study of their chiral discrimination properties. *Synth. Met.* **139**, 43–55 (2003)
120. S. Paul, N.N. Chavan, S. Radhakrishnan, Polypyrrole functionalized with ferrocenyl derivative as a rapid carbon monoxide sensor. *Synth. Met.* **159**, 415–418 (2009)
121. K.H. Lee, M.L. Kennedy, M. Buchalova, D.R. Benson, Thermodynamics of carbon monoxide binding by helical hemoprotein models: The effect of a competing intermolecular ligand. *Tetrahedron* **56**, 9725–9731 (2000)
122. S. Paul, M. Joseph, Polypyrrole functionalized with FePcTSA for NO₂ sensor application. *Sensors Actuators B Chem.* **140**, 439–444 (2009)
123. K. Thuwachaowsoan, D. Chotpattananont, A. Sirivat, R. Rujiravanit, J.W. Schwank, Electrical conductivity responses and interactions of poly(3-thiopheneacetic acid)/zeolites L, mordenite, beta and H₂. *Mater. Sci. Eng. B* **140**, 23–30 (2007)
124. M. Krondak, G. Broncová, S. Anikin, A. Merz, V.M. Mirsky, Chemosensitive properties of poly-4, 4'-dialkoxy-2, 2'-bipyrroles. *J. Solid State Electrochem.* **10**, 185–191 (2006)
125. U. Lange, N.V. Roznyatovskaya, V.M. Mirsky, Conducting polymers in chemical sensors and arrays. *Anal. Chim. Acta* **614**, 1–26 (2008)
126. L. Torsi, A. Tafuri, N. Cioffi, M. Gallazzi, A. Sassella, L. Sabbatini, P. Zambonin, Regioregular polythiophene field-effect transistors employed as chemical sensors. *Sensors Actuators B Chem.* **93**, 257–262 (2003)
127. L. Torsi, M.C. Tanese, N. Cioffi, M.C. Gallazzi, L. Sabbatini, P.G. Zambonin, Alkoxy-substituted polyterthiophene thin-film-transistors as alcohol sensors. *Sensors Actuators B Chem.* **98**, 204–207 (2004)
128. M. Xu, J. Zhang, S. Wang, X. Guo, H. Xia, Y. Wang, S. Zhang, W. Huang, S. Wu, Gas sensing properties of SnO₂ hollow spheres/polythiophene inorganic–organic hybrids. *Sensors Actuators B Chem.* **146**, 8–13 (2010)
129. S. Pirsá, N. Alizadeh, A selective DMSO gas sensor based on nanostructured conducting polypyrrole doped with sulfonate anion. *Sensors Actuators B Chem.* **168**, 303–309 (2012)
130. R.S. Dudhe, S. Tiwari, H.N. Raval, M.A. Khaderbad, R. Singh, J. Sinha, M. Yedukondalu, M. Ravikanth, A. Kumar, V.R. Rao, Explosive vapor sensor using poly(3-hexylthiophene) and Cu II tetraphenylporphyrin composite based organic field effect transistors. *Appl. Phys. Lett.* **93**, 263306 (2008)



Polymeric Membranes for Natural Gas Processing: Polymer Synthesis and Membrane Gas Transport Properties

23

Jimoh K. Adewole and Abdullah S. Sultan

Contents

1	Natural Gas	943
2	Natural Gas Processing Using Membrane Separation Technology	943
3	Functional Polymeric Membranes for Natural Gas Processing	945
4	Classification of Membrane Materials	948
5	Theoretical Background of Gas Separation in Polymeric Membranes	950
6	Synthesis, Preparation, and Transport Properties of Functional Polymeric Membrane for Natural Gas Processing	955
6.1	Thermal Rearrangement and Cross-Linking	955
6.2	Grafting of Polymer Backbone	966
6.3	Template Polymerization Technique and Use of Porogens	966
6.4	Sulfonation Method	967
6.5	Technique for Preparing Polymers of Intrinsic Microporosity (PIM)	969
6.6	Membrane Preparation Using 3D Printing Technologies	970
7	Conclusion	970
	References	971

Abstract

Polymers are macromolecules made up of repetition of some simpler units called monomers. To the general public, polymers are used as consumer products in the

J. K. Adewole

Center for Integrative Petroleum Research, College of Petroleum Engineering and Geosciences, King Fahd University of Petroleum and Minerals, Dhahran, Saudi Arabia
e-mail: adekayojih@kfupm.edu.sa

A. S. Sultan (✉)

Department of Petroleum Engineering, College of Petroleum Engineering and Geosciences, King Fahd University of Petroleum and Minerals, Dhahran, Saudi Arabia

Center for Integrative Petroleum Research, King Fahd University of Petroleum and Minerals, Dhahran, Saudi Arabia
e-mail: sultanas@kfupm.edu.sa

forms of plastics, fibers, rubber, adhesive, paints, and coatings. Today, new areas of applications of polymers have emerged due to the continuous growth of new classes of polymers. Varieties of functional polymers have been developed for various applications including organic catalysis, separation, biotechnology, medicines, optoelectronics, photographic, building, and fuel. Natural gas separation using functional polymers is a new area of application where not much information is available. This work seeks to present an overview of the synthesis, preparation, and separation performance of functional polymers in natural gas separation.

Abbreviations

6FDA	2,2'-bis(3,4-Dicarboxyphenyl) hexafluoropropane dianhydride
APTMSD	bis(3-Aminopropyl)-tetramethyldisiloxane)
BAS	bis(Aminopropyl) polydimethylsiloxane
CD	Cyclodextrin
CH ₄	Methane
CMS	Carbon molecular sieve
CO ₂	Carbon dioxide
DADE	Diamino diphenyl ether
EDA	Ethylene diamine
GPU	Gas permeation unit
HPAAc	Hydroxyl poly (amic acid)
HPI	Hydroxyl polyimide
MDI	4,4-Metylenediphenyl diisocyanate
NG	Natural gas
PBO	Polybenzoxazoles
PBT	Polybenzothiazoles (PBT)
PDMC	Propane-diol monoesterified cross-linkable polyimide
PEG	Polyethylene glycol
PEO	Polyethylene oxide
PHA	Polyhydroxyamide
PIM	Polymers of intrinsic microporosity
PIOFG	Ortho-positioned functional groups
PPG	Poly(propylene glycol)
PTMS	Poly[1-(trimethylsilyl)-1-propyne]
S-PEEK	Poly(ether ether ketone)
TCDA	2,3,5-Tricarboxy cyclopentyl acetic dianhydride
THF	Tetrahydrofuran
TR	Thermal rearrangement/thermally rearranged
TR-PBI	Thermally rearranged microporous polybenzimidazole
XLPEGDA	Cross-linked poly(ethylene glycol diacrylate)

List of Symbols

D_D	Gas diffusion coefficient by Henry modes of sorption
E_D	Activation energy of diffusion (kJ/mol)
E_P	Activation energy of permeation

D_H	Gas diffusion coefficient by Langmuir modes of sorption
ΔH_S	Enthalpy of the gas
k_D	Henry's law constant
b	Langmuir affinity constant
C'_H	Langmuir capacity constant
L	Membrane thickness (dense-selective layer thickness)
P	Permeability
α_{AB}	Permselectivity or selectivity or separation factor of component A from B
D_{A0}	Pre-exponential factor
S_{A0}	Pre-exponential factor
P_{A0}	Pre-exponential factor
A or B	Gas components (or permeated and rejected component, respectively)
D	Diffusivity coefficient
R	Universal gas constant, 8.31 J/mol
S	Solubility coefficient
T	Temperature, K

1 Natural Gas

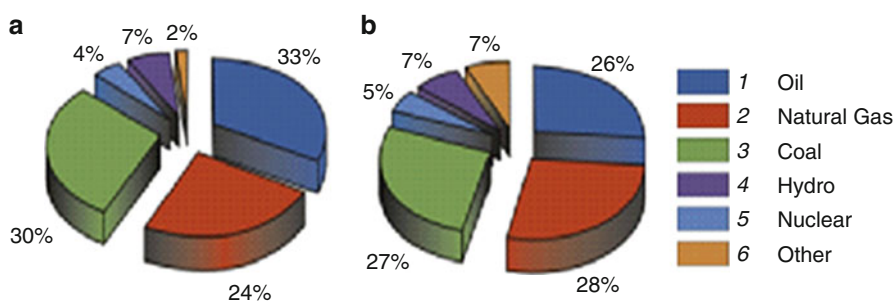
Currently, the world cleanest, safest, and most efficient energy source is natural gas [1–3]. The carbon dioxide emission factor of commercial natural gas is 26% lower than that of oil and 41% lower than the emission from coal during combustion [4]. Natural gas is often found in crude oil or gas reservoirs, condensate wells, and coal beds [2] with methane (CH₄) as its primary constituent [5]. In addition, natural gas contains some heavier hydrocarbons, water (in the form of vapor), mercury, nitrogen, helium, and acid gases [6]. Table 1 contains a detailed composition of a typical raw natural gas. It is important to note that natural gas composition varies from place to place [7]. The composition shown in Table 1 is the range obtained for Eleme (Nigeria), Alberta (Canada), Western Colorado (USA), Miskar (Tunisia), Southwest Kansas (USA), Rio Arriba County (New Mexico), and Bach Ho (Vietnam). In the present global economy, natural gas is indeed one of the fastest growing primary sources of energy [2, 8–10]. In 2012, it constitutes about 24% of the global energy mix and it is expected to rise to 28 by 2040 (Fig. 1). The natural gas world market is estimated as US\$22 billion per annum [11]. Clearly, for natural gas to maintain its position as one of the world's most sought after energy sources, alternative cheaper and energy efficient means of processing technique (such as the membrane) is needed.

2 Natural Gas Processing Using Membrane Separation Technology

Today, membrane gas separation technology is a commercially available process for gas separation and purification. This include separation of nitrogen from air (oxygen enrichment), recovery of hydrogen from process streams, dehydration of gas

Table 1 Natural gas compositions [8, 12–14]

Component	Composition range (mol%)
Helium (He)	0.0–1.8
Nitrogen (N ₂)	0.21–26.10
Carbon dioxide (CO ₂)	0.06–50.00
Hydrogen sulfide (H ₂ S)	0.0–3.3
Methane (CH ₄)	29.98–90.12
Ethane (C ₂ H ₆)	0.55–14.22
Propane (C ₃ H ₈)	0.23–12.54
Butanes (C ₄ H ₁₀)	0.14–8.12
Pentanes and heavier (C ₅ H ₁₂ +)	0.037–3.0

**Fig. 1** Forecast of changes in the global energy mix. (a) 2012. (b) 2040. (Copied from Kontorovich et al. [15] with permission from Elsevier)

streams, recovery of vapors from gases, and natural-gas processing [16–18]. The composition of crude natural gas displayed in Table 1 clearly reveals that the raw natural gas needs further treatment in order to meet a specified quality standard. The standard that is specified by pipeline transmission and distribution companies is shown in Table 2. Membrane separation is one of the major separation techniques that are used in natural gas purification [1, 9, 19]. In membrane natural gas processing, research attention has been focused more on the removal of CO₂ due to its abundance in the raw gas than H₂S. The removal of CO₂ will enhance the calorific value (energy content) of the natural gas, significantly reduce the volume of gas to be transported through pipeline and cylinders, prevent atmospheric pollution, and reduce the susceptibility of the pipeline to corrosion [11, 20]. Presently, commercially available CO₂ separation techniques include adsorption, cryogenic distillation, and membrane [21].

For many reasons, membrane separation has witnessed a much more rate of growth than other separation techniques [17]. This is particularly due to some of the special features of membrane separation technique which distinguishes it from others. Advantages of membrane gas separation include higher separation efficiency, faster separation, simplicity, and high space economy [7, 23–26]. The use of an efficient gas processing technology for producing a cleaner source of energy will

Table 2 Natural gas specifications for various applications [8, 13, 14, 22]

Major components	Mol% range
Methane	≥ 75
Ethane	≤ 10.0
Propane	≤ 5.0
Butanes	≤ 2.0
Pentanes and heavier	≤ 0.5
Nitrogen and other inerts	≤ 3.0
Carbon dioxide	2.0–5.0
Total diluents gases	4.0–5.0

constitute an excellent approach in addressing environmental issues that are associated with greenhouse gas emission at relatively lower cost.

3 Functional Polymeric Membranes for Natural Gas Processing

Review of available literature on membrane gas separation techniques revealed that current research efforts in improving the competitiveness of membrane gas separation with other gas separation processes can be classified into two: namely [27], engineering, which deals with the design and optimization of membrane modules, and materials, which involves the design and development of novel membrane materials.

In materials development, research efforts are twofolds:

- (i) Synthesis of new novel polymers for preparation of new membranes.
- (ii) Modification of existing commercial polymers to improve their gas separation properties.

In both cases, the synthesis of functional polymers and functionalization of existing polymers have dominated research endeavors. Functional polymers are macromolecules which contain specified chemical groups or polymer that has certain specific physical, chemical, and biological properties. The selection of such polymers for certain application depends on the presence of the functional groups it contains. Usually, the properties of such polymers are determined by the presence of functional groups which are different from those of the backbone chains [28]. The polymers can be based on simple linear backbones, three-dimensional (such as stars, hyperbranched polymers) or dendrimers (tree-like structures polymers). All these polymers have been used in the preparation of membrane materials for gas separation. For example, CO_2 has an affinity to amine, polar ether oxygen linkages, and other functional groups. Thus, polymers which bear any of these functional groups are often preferred for preparing membrane materials for CO_2 removal from natural gas. Table 3 showed commercial membranes that are presently being used in industrial gas plants. Also, the performance of other commercially available

membranes in CO₂ removal from CH₄ is shown in Fig. 2. These membranes are made from polymers that contain one or more functional groups.

The presence of these functional groups in a polymer will enhance the solubility and solubility selectivity of such polymers with respect to CO₂. In addition, the presence of the functional groups could also enhance the diffusivity of the natural gas component in membrane especially when they are positioned as branches within the polymer matrixes. The presence contributes seriously to intrasegmental rotational mobility and intersegmental chain packing of polymers [32]. For instance, Table 4 shows two membrane samples, one with ether functional group and the other without. It can be observed that the one with ether has higher solubility as compared to the other one. Also, the second without ether has higher diffusivity which is a result of the gap created by the presence of H₂ branching that is not available in the first one.

The unit of P is Barrer; S is $10^8 \left(\frac{\text{cm}^3}{\text{s}} \right)$, D is $\left(\frac{\text{cm}^3(\text{STP})}{\text{cm}^3(\text{polymer})\text{-atm}} \right)$.

The effect of substitution of the bulkier functional groups (such as trifluoromethyl) in place of the methyl groups has also been investigated for isopropylidene moiety of the diamine. The results shown in Table 5 revealed once

Table 3 Commercial membranes used for CO₂ removal from natural [7, 16, 29–31]

Membrane	Selectivity CO ₂ /CH ₄
Cellulose acetate	10.0–28.0
Polysulfone	22.0
Polyimide	32.5

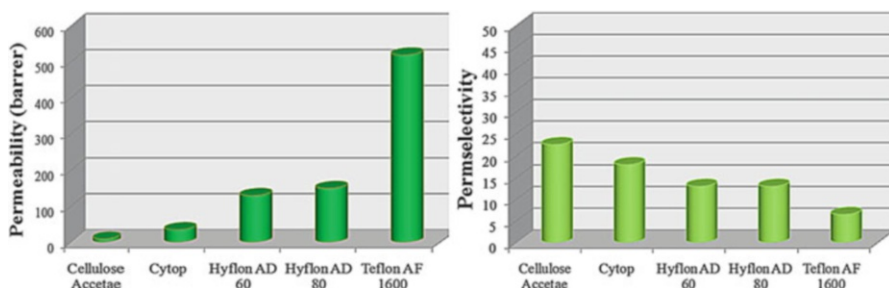


Fig. 2 Gas separation (CO₂/CH₄) performance of some commercial polymeric membranes. (Copied from Adewole et al. [4] with permission from Elsevier)

Table 4 Comparison of effect of functional groups on gas transport and separation properties of polymers [3]

Name	Structure	P	S	D	Permeability
4,4-Oxydianiline (4,4-ODA)	<chem>Nc1ccc(Oc2ccc(N)cc2)cc1</chem>	23	4.89	3.58	60.5
Methylenedianiline (MDA)	<chem>Nc1ccc(Cc2ccc(N)cc2)cc1</chem>	19.3	3.96	3.70	44.9

Table 5 Comparison of effect of bulkier functional groups on gas transport and separation properties of polymers at 10 atm and 35 °C [32]

Name	Structure	Solubility	Diffusivity
6FDA-ODA		4.89	3.58
6FDA-MDA		3.96	3.70
6FDA-6FpDA		4.72	10.3

again that the polymer with ether oxygen linkage has the highest CO₂ solubility than other polymers. This is majorly due to the interaction between the ether linkage and CO₂. Moreover, polymers with bulkier functional groups (placed as branches) have higher diffusivity. For instance, the diffusivity of 6FDA-MDA with H branch is about 64% lower than 6FDA-6FpDA which contains bulkier functional group units as branches. This is because the substitution of the bulkier central moiety for less bulky ones leads to simultaneous disruption in intermolecular packing and suppression of intrarotational flexibility in the diamine segment of polyimides [32].

Permeability unit (Barrer); solubility unit $10^8 \left(\frac{\text{cm}^2}{\text{s}} \right), \left(\frac{\text{cm}^3(\text{STP})}{\text{cm}^3(\text{polymer})\text{-atm}} \right)$.

The main aim of this work is to provide an overview of the method of synthesis and transport properties of polymers that are presently being used for natural gas processing. Particularly, the writing will be limited to functional polymers for separation of major components of natural gas which include helium, nitrogen, carbon dioxide, hydrogen sulfide, methane, ethane, propane, Butanes, pentanes, and heavier hydrocarbon. In addition, functional polymeric membrane gas transport properties in terms of permeability, solubility, diffusivity, and selectivity will be considered. Polymeric membrane materials are often subdivided into two classes, namely, rubbery and glassy polymers. Rubbery polymers are those that are above the glass-transition temperature while glassy polymers are those below the glass-transition temperature [1]. The glassy polymers often possess high selectivity but their permeability are low [33]. Moreover, the permeability may deteriorate over time as a result of polymer aging. In the contrary, the rubbery polymers are known to be highly permeable but their selectivity and plasticization resistance properties are low. Herein, attention has been given to both classes of polymers.

4 Classification of Membrane Materials

Polymeric membranes have been applied in a verity of areas such as filtration (microfiltration, nanofiltration, and ultrafiltration), reverse osmosis, pervaporation, desalination, membrane distillation, membrane crystallization, dialysis, gas and vapor separation, and so on. The classification of membrane materials is carried out based on many factors. Membrane materials can be either synthetic or natural. Natural membrane materials are those polymers that are often found in animals and plants. Examples include polysaccharides and rubbers [34]. Synthetic membranes can be further classified into organic (polymers), inorganic (such as ceramic, metals, zeolites, and carbon [35]), or mixed-matrix (containing both organic and inorganic materials). Figure 3 depicts a pictorial representation of membrane material classification. Moreover, both the synthetic and natural polymers can be used in gas separation in the form of solid or liquid membranes.

In terms of morphology, membrane materials can be classified into porous and nonporous membranes. The scanning electron microscope (SEM) surface images of porous and nonporous membranes are shown in Fig. 4. According to the cross-sectional structure, membranes can be isotropic (symmetric membranes)

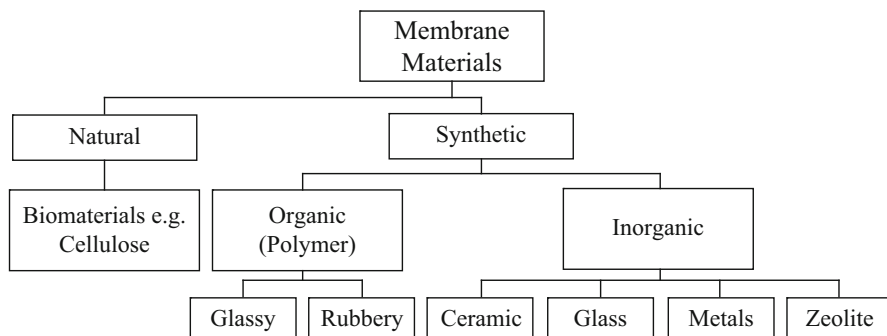


Fig. 3 Membrane material classification for gas separation

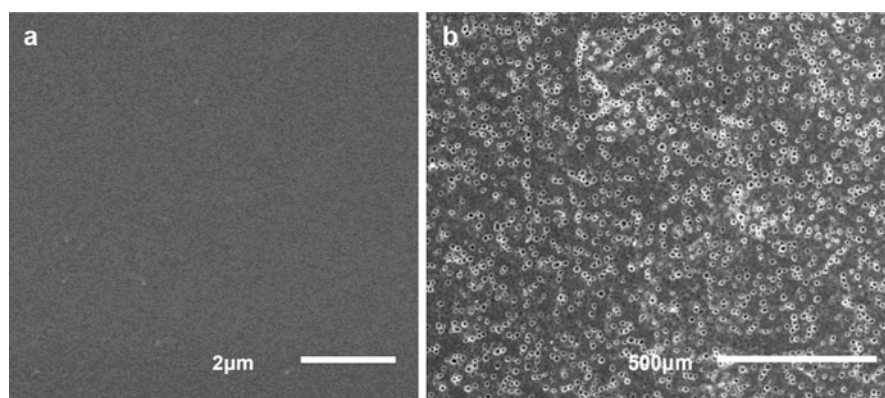


Fig. 4 Surface images of porous and nonporous membranes. (a) Nonporous membrane. (b) Porous membrane

or anisotropic (asymmetric membrane with a thin porous or nonporous selective layer that is supported by a much thicker porous substructure) [34]. Asymmetric membranes are commonly prepared in such a way that they are integrally anisotropic. Dual-layer (or composite) membrane is an example of asymmetric membrane (Fig. 5). The dual-layer technique provides the opportunity to separately optimize the performance of the selective layer and the porous support. The top selective layer could be a barrier with pores in the nanometer range or a nonporous polymer. The porous sublayer provides the mechanical support that is needed during operation.

During operation, all the membrane materials are often packed within a certain housing called modules. There are two major types of membrane modules: the hollow fiber module (containing hollow fiber membranes) and the spiral wound module (housing flat sheet membranes). The two types of module are shown in Figs. 6 and 7, respectively. Majority of the large-scale membrane gas separation plants are operated based on these two modules. A photograph of membrane CO_2 separation plant is shown in Fig. 8.

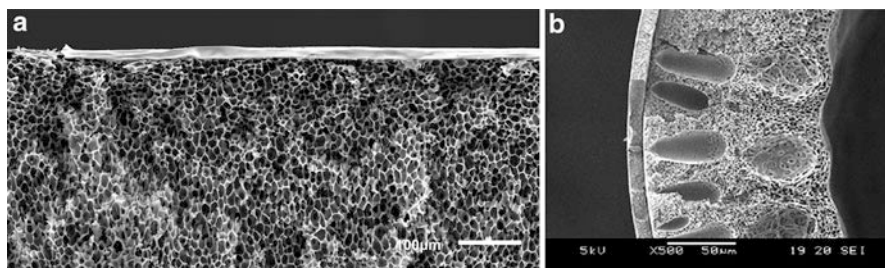


Fig. 5 Cross-sectional images of dual-layer polymeric membranes. (a) Flat sheet dual-layer. (b) Hollow fiber dual-layer. (Reprinted from [36] by permission from Elsevier)

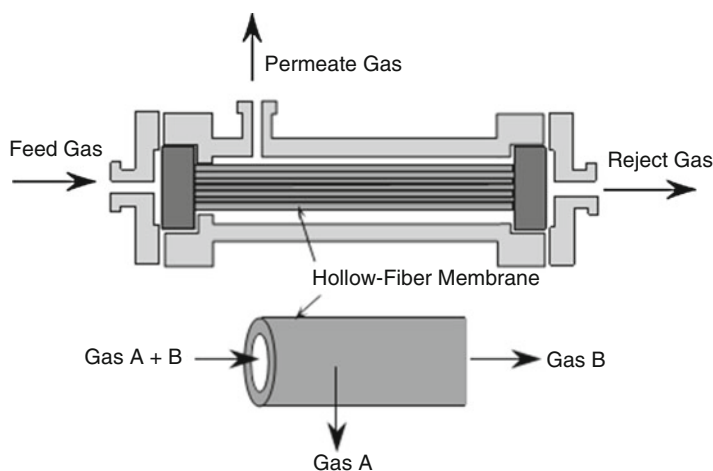


Fig. 6 Hollow fiber membrane module. (Reprinted from [37])

5 Theoretical Background of Gas Separation in Polymeric Membranes

Theoretically, the permeation of gas through nonporous dense polymeric membranes is commonly described using the Solution-diffusion mechanism. Based on this mechanism, gas molecules are first sorbed by the membranes at the upstream (high-pressure) interface, the sorbed gas then diffuses through the membrane, and it is later desorbed at the downstream (low pressure) chamber [39–41]. A schematic illustration of a gas permeation setup is shown in Fig. 9. Gas molecules movement through polymeric membranes is controlled by diffusivity coefficient (D) and solubility coefficient (S). The solubility coefficient is thermodynamic in nature and is determined by the following factors:

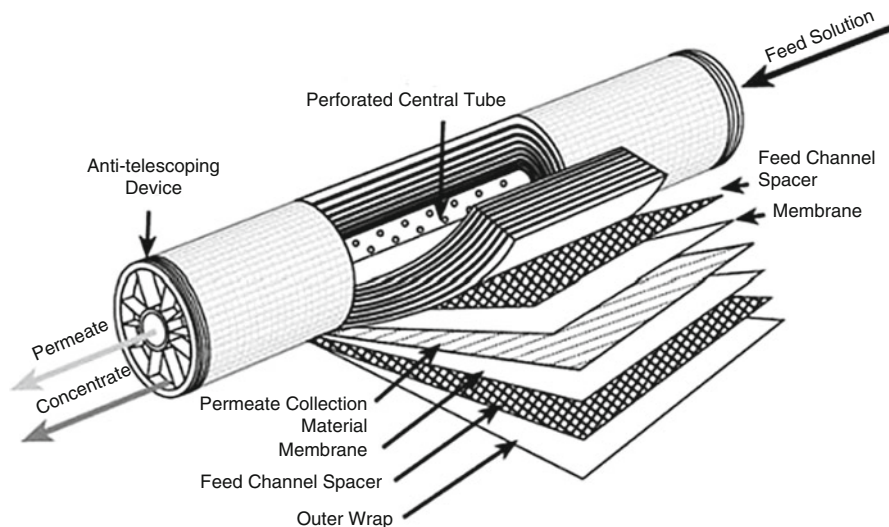


Fig. 7 Schematic representation of spiral wound membrane module. (Copied from [38])



Fig. 8 Photograph of a CO₂ separation plant. (Reprinted from [7] with permission from Elsevier)

- (i) The inherent condensability of the penetrant
- (ii) Polymer–penetrant interactions
- (iii) The amount of excess volume existing in the glassy polymer

Diffusivity coefficient, D , is a kinetic parameter which determines the mobility of individual molecules through the polymer chains [42]. It is determined by packing and motion of the polymer segments and by the size of the penetrant molecule.

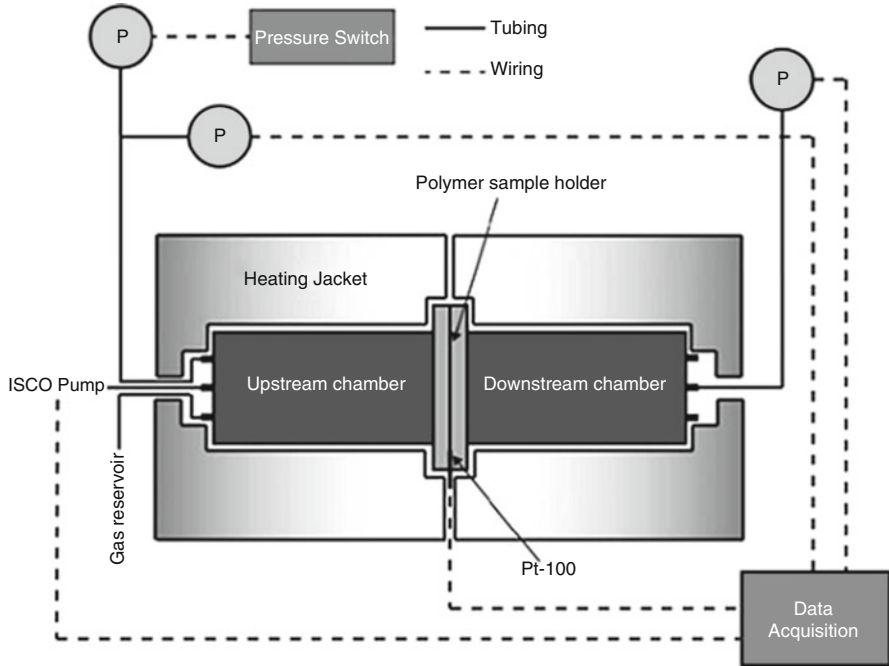


Fig. 9 Schematic diagram of a permeation setup for measuring gas permeability. (Copied from Adewole et al. [43] with permission from Springer)

Increasing the diffusivity or the solubility or both for a particular gas by structural modification of the polymer allows one to raise the gas permeability. Moreover, such modification could also lead to improvement of the permselectivity of a desired gas over an undesired one [4].

The permeability (P), which provides information about the ability of the molecules to pass through a membrane, is therefore defined as the product of diffusivity coefficient and solubility coefficient:

$$P = DS \tag{1}$$

The commonly used unit of permeability in membrane gas separation is the barrer. Conversion from barrer to other unit can be done using the given expression: $1 \text{ barrer} = 1 \times 10^{-10} \text{ cm}^3(\text{STP})\text{cm}/(\text{cm}^2\text{scmHg}) = 7.5005 \times 10^{-18} \text{ m}^2\text{s}^{-1}\text{Pa}^{-1}$ [44].

The ability of a membrane to separate a gas A from a mixture of gases (A and B) referred to as the selectivity (α_{AB}).

$$\alpha_{AB} = \frac{P_A}{P_B} \tag{2}$$

The Eq. (2) above is used for calculating selectivity involving single (pure) gas permeation through a membrane. For the permeation of mixed gases, the selectivity

(which is referred to as mixed gas selectivity or the separation factor) is calculated using the following equation [20, 45, 46]:

$$\text{Separation factor} = \frac{\left(\frac{\text{Composition of A Downstream}}{\text{Composition of B Downstream}} \right)}{\left(\frac{\text{Composition of A Upstream}}{\text{Composition of B Upstream}} \right)} = \frac{\left(\frac{y_A}{y_B} \right)}{\left(\frac{x_A}{x_B} \right)} \quad (3)$$

where A is the gaseous component which permeated through the membrane. B is the gaseous component which was retained or rejected from permeating through the membrane. The x is the mole fraction of the gaseous component which is present in the feed while y is the mole fraction of the gaseous component in the permeate. It is important to note that the type of the permeation experiment (either pure or mixed gas permeation) needs to be mentioned while reporting the selectivity. By combining Eqs. (1) and (2), it is possible to express the selectivity as:

$$\alpha_{AB} = \frac{D_A}{D_B} \times \frac{S_A}{S_B} \quad (4)$$

The $\frac{D_A}{D_B}$ is often referred to as the mobility selectivity or diffusivity selectivity. Also, the $\frac{S_A}{S_B}$ is referred to as the sorption selectivity or solubility selectivity [40].

A parameter that is used for expressing membrane performance depends on the type of membrane module. For hollow fiber membranes, the separation performance is commonly expressed in term of permeance. The permeance of a hollow fiber membrane to gas A is the permeability of the membrane (P_A) divided by the membrane thickness (L). Mathematically,

$$\text{Permeance} = \frac{P_A}{L} \quad (5)$$

For dual-layer hollow fiber, L is the dense-selective layer thickness and can be determined as follows [47]:

$$L = \frac{P_{A(\text{dense_film})}}{(P/L)_A(\text{dual_layer_hollow_fiber_membrane})} \quad (6)$$

Accordingly, the selectivity is expressed as:

$$\alpha_{AB} = \frac{(P/L)_A}{(P/L)_B} \quad (7)$$

The permeance is commonly expressed using the gas permeation unit (GPU) (1GPU is equivalent to $1 \times 10^{-6} \text{cm}^3(\text{STP})/(\text{cm}^2 \text{scmHg})$ or $7.5005 \times 10^{-12} \text{ms}^{-1} \text{Pa}^{-1}$) [47, 48]. It is a common practice to use Eq. 7 for asymmetric membranes especially when the thickness of the active layer is not known.

The relationship between the operating temperature and the gas diffusion coefficient in polymeric membrane can be represented by the Arrhenius equation [40]:

$$D_A = D_{A0} \exp \left[\frac{-E_D}{RT} \right] \quad (8)$$

where D_A represents the diffusion coefficient (cm^2/s) of gas A. D_{A0} , E_D , T , and R are the pre-exponential factor, the activation energy of diffusion (in kJ/mol), the temperature (in K), and the universal gas constant, respectively. Here, the value of the R is 8.31 J/mol .

Similarly, the solubility as a function of temperature can be expressed by the van't Hoff equation:

$$S_A = S_{A0} \exp \left[\frac{-\Delta H_S}{RT} \right] \quad (9)$$

S_{A0} and ΔH_S are the pre-exponential factor and the enthalpy of solution of the gas A, respectively.

The gas permeability can therefore be expressed as a function of temperature by combining Eqs. 8 and 9 substituting them into Eq. 1 as follows:

$$P_A = P_{A0} \exp \left[\frac{-E_P}{RT} \right] \quad (10)$$

$$E_P = E_D + \Delta H_S \quad (11)$$

P_{A0} and E_P are the pre-exponential factor, and the activation energy of permeation, respectively.

Gas transport through polymeric membrane is also affected by the upstream (feed) pressure as well as downstream (permeate) pressure of membrane module. The effect of pressure on gas transport properties of the two major classes of polymeric membrane is very much distinguishable. For example, in rubbery polymers, the well-known solution-diffusion model is used to describe gas transport behavior as a function of feed pressure. On the other hand, gas transport behavior in glassy polymers is more complicated and other equations are needed. Changes in gas permeability as a function of pressure is often explained using the dual-mode model and partial/total immobilization models [40]. In this model, solubility is expressed as:

$$S = k_D + \frac{FC'_H b}{1 + bp} \quad (12)$$

where k_D , C'_H , and b are constants referred to as Henry's law constant, the Langmuir capacity constant, and the Langmuir affinity constant, respectively. In the case for total immobilization model, F is set to 1.

Using a modified form of Eq. 12 allows the permeability of gases to be expressed using the dual-sorption model as follows [16]:

$$P = k_D D_D + \frac{C'_H b D_H}{1 + b p_2} \quad (13)$$

where D_D is the diffusion coefficient for gas molecules absorbed by Henry sorption mode and D_H the coefficient for gas molecules absorbed Langmuir mode of sorption.

Equation (1) provides a better measure of the gas transport properties and separation performance of polymer because all the parameters included in these equations are experimentally measurable. Therefore, all these parameters will be used as indices of the degree of natural gas purification capability of the functional polymers in this discussion.

6 Synthesis, Preparation, and Transport Properties of Functional Polymeric Membrane for Natural Gas Processing

6.1 Thermal Rearrangement and Cross-Linking

High thermal property and chemical resistance are some of the properties that are needed for polymers to be used for separation NG components. Aromatic polymers such as polybenzoxazoles (PBO) and polybenzothiazoles (PBT) are two excellent types of polymers with these properties. However, the high chemical resistance (to common solvents) makes it difficult for them to be used in membrane preparation. This challenge was overcome by using thermal rearrangement method which involves a postfabrication polymer – modifying reaction. The process is carried out by thermally rearranging the aromatic polyimides containing functional groups (PIOFG) such as –OH and –SH in order to obtain a dense PBO and PBT membrane [49]. The whole procedure is a two-stage procedure:

- (i) Synthesis of hydroxyl-containing polyimides: Polyimides containing ortho-positions functional groups (PIOFGs) were prepared via a two-step process. First, formation of hydroxyl-containing poly(amic acids). Then thermal imidization.
- (ii) Synthesis of thermally rearranged membrane: Thermal treatment was done at varying temperature (300 to 450 °C) and time 1 to 3 hours under argon gas in a quartz tube furnace.

A schematic of the proposed scheme for thermal rearrangement is shown in Fig. 10.

The transport properties of TR membranes were evaluated with respect to permeability, solubility, and diffusivity. Results of these properties showed that gas transport properties depend on the final heat treatment temperature and the method of imidization used for preparing the polyimide. Previous reports [50] showed that thermal rearrangement of polyimide was triggered at around 350 °C and at 450 °C, full conversion of polyimide to thermally rearranged polymer occurred. At the

temperature between 350 °C and 450 °C, TR membranes were believed to contain both unchanged segments and thermally rearranged segments. Usually, polyimide shows higher H₂ permeability than CO₂ permeability. This is in consistent with the order or increasing kinetic diameters of penetrant molecules. This means that the diffusion selectivity plays a major role. On the other hand, TR polymer treated at 450 °C has permeability in the order: CO₂ > H₂ > He > O₂ > N₂ > CH₄ with high gas permeability values. By increasing the treatment temperature, the gap between the permeabilities of CO₂ and H₂ reduces and at 450 °C the order of the permeability values for these two gases are completely reversed. The change in behavior suggests that CO₂ solubility is higher in TR polymer than H₂ solubility and this contribute to the higher value of CO₂ permeability as compared to that of H₂. Table 6 shows the comparison of gas transport properties of polyimides made from two imidization methods. The gas selectivity decreases with increase in treatment temperature; however, TR polymer still looks promising because it has higher CO₂ permeability with corresponding high CO₂/CH₄ selectivity than other conventional polymers such as cellulose acetate and polyimides.

The huge success recorded on the use of thermal rearrangement method for the synthesis of TR-PBO membranes encouraged researchers to further dig into investigating the thermally rearranged polymers. Importantly, a detailed fundamental understanding of the behavior of the TR polymers is needed in order to develop a better procedure for the design and synthesis of these polymers.

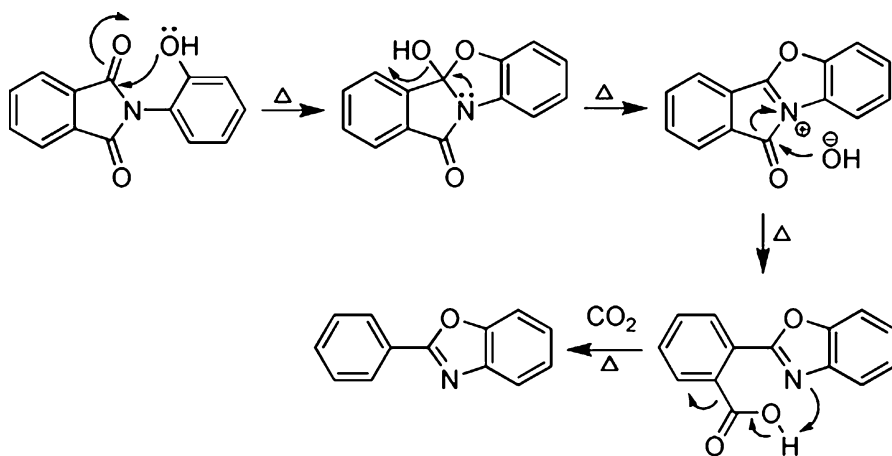


Fig. 10 Proposed thermal rearrangement mechanism from hydroxyl-containing polyimide to polybenzoxazole. (Taken from Park et al. [49] with permission from Elsevier)

Table 6 Gas transport properties of polyimide obtained by various imidization methods [49, 51]

Method of imidization	CO ₂ permeability (Barrer)	CO ₂ /CH ₄ selectivity
Chemical imidization	17	62
Thermal imidization	6	43

Wang and Chang [52] carried out a systematic investigation on the evaluation of the physicochemical and gas transport properties of a representative thermally rearranged polymer (polyhydroxyamide (PHA)) with respect to temperature. The study was aimed at providing solid evidence that will help to elucidate the fundamentals of thermal cyclization and provide molecular illumination of the temperature-induced chain rearrangement. Therefore, the effect of thermal cyclization temperature on the thermal rearrangement process was investigated. The effect of the temperature on the chemical structure transformation, thermal stability, physical properties, gas separation performance, and gas sorption properties of the resulting membranes were evaluated. Results revealed that the thermal cyclization temperature is a factor that affects the degree of thermal conversion, influences the thermal history of polymers, and causes thermal cross-linking.

Table 7 shows the effect the temperature has on gas separation performance of the resulting membrane. Membranes that are cyclized at higher temperature exhibit better performance. According to the authors, the superior performance recorded for these membranes is due to the fact that a higher thermal cyclization temperature caused the suppression of polymer chain segmental rotation, resulted in lower chain packing density, and enhanced the formation of microvoids.

The work carried out by Wang and Chang [52] on TR polymers involved the use of PHA as processors owing to its high rate of conversion at relatively lower temperature. Wang et al. [53] used another similar polymers but with a higher number of functional groups. The authors employed poly(hydroxyl amic acid) (PHAA) as a precursor to synthesize PBO. PHAA comprises of hydroxyl and carboxyl functional group giving room for the exploration of different stages of thermal cyclization of PHAA in a stepwise manner. The first step involved the transformation of PHAA to poly(imide benzoxazole) (PIBO) at temperature up to 300 °C. During the second step, PIBO was finally transformed to polybenzoxazole (PBO) at 400 °C. This was followed by a systematic investigation of the resulting evolution of the structure and gas separation performance of the ensuing membrane. The results of the physicochemical and gas transport properties are shown in Table 8. It was concluded that gas separation efficiency of polymer membrane can be tailored by the use of appropriate thermally induced structure transformation and polymer chain rearrangement.

Table 7 Effects of cyclization temperature on gas transport properties

Membrane	Cyclization temperature	FFY	Permeability			Ideal selectivity	
			CO ₂	CH ₄	N ₂	CO ₂ /CH ₄	CO ₂ /N ₂
PHA	–	0.134	5.76	0.13	0.24	43.0	24.2
PBO 1	300	0.195	44.7	1.56	2.28	28.6	19.6
PBO 2	350	0.198	84.2	3.48	4.42	24.0	18.9
PBO 3	425	0.202	183	8.53	10.10	21.4	18.1
PBO 4	450	0.220	532	28.9	30.30	18.4	17.6

Table 8 Gas transport properties of poly(benzoxazole) membranes prepared from poly(hydroxyamide amic acid) via stepwise thermal cyclization

Membrane	Temperature	d-Spacing	Permeability			Ideal selectivity	
			CO ₂	CH ₄	N ₂	CO ₂ /N ₂	CO ₂ /CH ₄
PHAA	130	5.28	2.12	0.05	0.10	21.1	40.2
PIBO	200	5.39	5.06	0.10	0.24	21.1	49.4
PIBO	220	5.48	9.65	0.20	0.46	21.0	48.5
PIBO	300	5.63	30.2	0.69	1.53	19.8	43.6
PBO	350	5.77	113	3.43	5.73	19.7	33.0
PBO	400	6.16	456	17.4	23.8	19.2	26.2

It is worth mentioning that the authors observed a bimodal distribution for temperatures 350 °C and 400 °C. A detailed explanation of these results can be found in the original article [53].

Various research articles have been published on alternative approaches to molecularly design advanced membrane materials using thermal rearrangement. The conversion of hydroxyl-containing imides to PBO was reported by Tullos et al. [54]. This method was used by many researchers to synthesize membranes for gas separation purposes [49, 55]. Another approach for producing highly permeable polymeric membrane is by controlling the free volume cavities via the synthesis of poly(benzoxazole-co-imide) [56] and the incorporation of heterocyclic compound (such as pyrrolone or ether) during copolymerization [57]. Thus thermally rearranged poly(benzoxazole-co-pyrrolone) was reported by Choi et al. [57] while thermally rearranged poly(ether-benzoxazole) membrane was reported by Calle et al. [58].

Similarly, the change in the intrinsic properties of TR-PBO as a result of the incorporation of a cardo moiety was investigated by Yeong et al. [59]. The work resulted into the synthesis of sets of new copolyimide with different composition of cardo-copolybenzoxazole membranes with enhanced gas transport properties. Sanders et al. [60] employed polycondensation method to prepare thermally rearranged polyimide membranes. The authors used HAB and 6FDA as precursors. A new synthesis route which involves alkaline hydrolysis of carbonyl-group of poly-pyrrolone and thermal treatment was investigated by Han et al. [61]. Highly permeable thermally rearranged microporous polybenzimidazole (TR-PBI) membrane was produced using this method. A new copolyimide was prepared by Lu et al. [62]. This polymer was subsequently thermally treated in air and N₂ atmosphere to attain thermal oxidative and thermally rearranged membranes, respectively. Table 9 contains the summary of the gas transport properties of these polymers.

The thermal rearrangement method has not been limited to flat sheet membrane. Some articles have been published on thermally rearranged hollow fiber membrane as well. The first TR hollow fiber membrane was reported by Kim et al. [63]. The membrane was fabricated by spinning hydroxyl poly(amic acid) (a soluble precursor polymer) via a phase separation process. A hollow fiber membrane (with a high permeability) was produced by thermal imidization and subsequent thermal

Table 9 Gas transport properties of polyimides prepared by thermal oxidative and thermal rearrangement procedure

	Permeability			Selectivity	
	CO ₂	CH ₄	N ₂	CO ₂ /N ₂	CO ₂ /CH ₄
TO	31.22–653.93	3.83–13.42	3.04–15.15	43.16–94.74	48.73–75.20
TR	24.54–5087.49	16.62–245.45	20.44–212.78	15.37–34.65	20.73–42.62

TO thermal treatment in Air, TR thermal treatment in nitrogen

rearrangement of hydroxyl polyimide. The effect of thermal treatment parameter (time from 10 to 60 mins and temperature from 450 °C to 500 °C) on gas separation performance of the membrane was also investigated. An optimum treatment parameter of 500 °C and 10 mins was found to produce a membrane with the highest selectivity of CO₂/CH₄ of 22. The membrane has a permeance of 2326 and 105 GPU for CO₂ and CH₄, respectively. Various other reports and description of thermal rearrangement procedure for polymers have also been published on the use of thermal rearrangement [64–68].

A cross-link is a formation of intermolecular connections through chemical bonds. It is used to develop materials with superior resistance to swelling and plasticization. The possibility of swelling and plasticization phenomenon is very high when using a polymeric membrane to separate natural gas with a high concentration of CO₂ or separation at high feed pressure. Cross-linking methods that have been reported in the literature for developing plasticization resistant membranes include chemical, thermal, and photochemical cross-linking [3, 69, 70].

The mechanism of cross-linking shown in Fig. 11 has been employed in a variety of ways to produce membranes with better gas separation performance. For example, esterification, cross-linking, mono-esterification, transesterification reaction, imide ring opening reactions, thermal cross-linking by decarboxylation, and chemical cross-linking using diamino compounds are some of the methods that have been used successfully prepare membranes with better plasticization resistance properties [71–73].

Cross-linking often results in a reduction in chain mobility and increase in T_g . It has been successfully employed for producing membranes with superior performance at high pressure. When a polymeric membrane is cross-linked, its plasticization pressure increases, consequently, the cross-linking processes helps in stabilizing the membrane at a higher partial pressure of CO₂ [74]. Membranes with higher packing density, smaller free volume, better resistance to CO₂-induced plasticization phenomenon, and higher T_g has been produced using thermal annealing.

Staudt-Bickel and Koros [75] carried out cross-linking in order to determine its effect on the reduction of swelling and plasticization. The work was focused on simultaneous inhibition of chain mobility and intrasegmental packing by changing the backbone structure of the polymer. Polyimides with strong polar associating functional groups were synthesized. In addition, cross-linking polyimides and copolyimide were also synthesized in the study. Gas permeability and permselectivity of CO₂/CH₄ were investigated. It was observed that the presence of

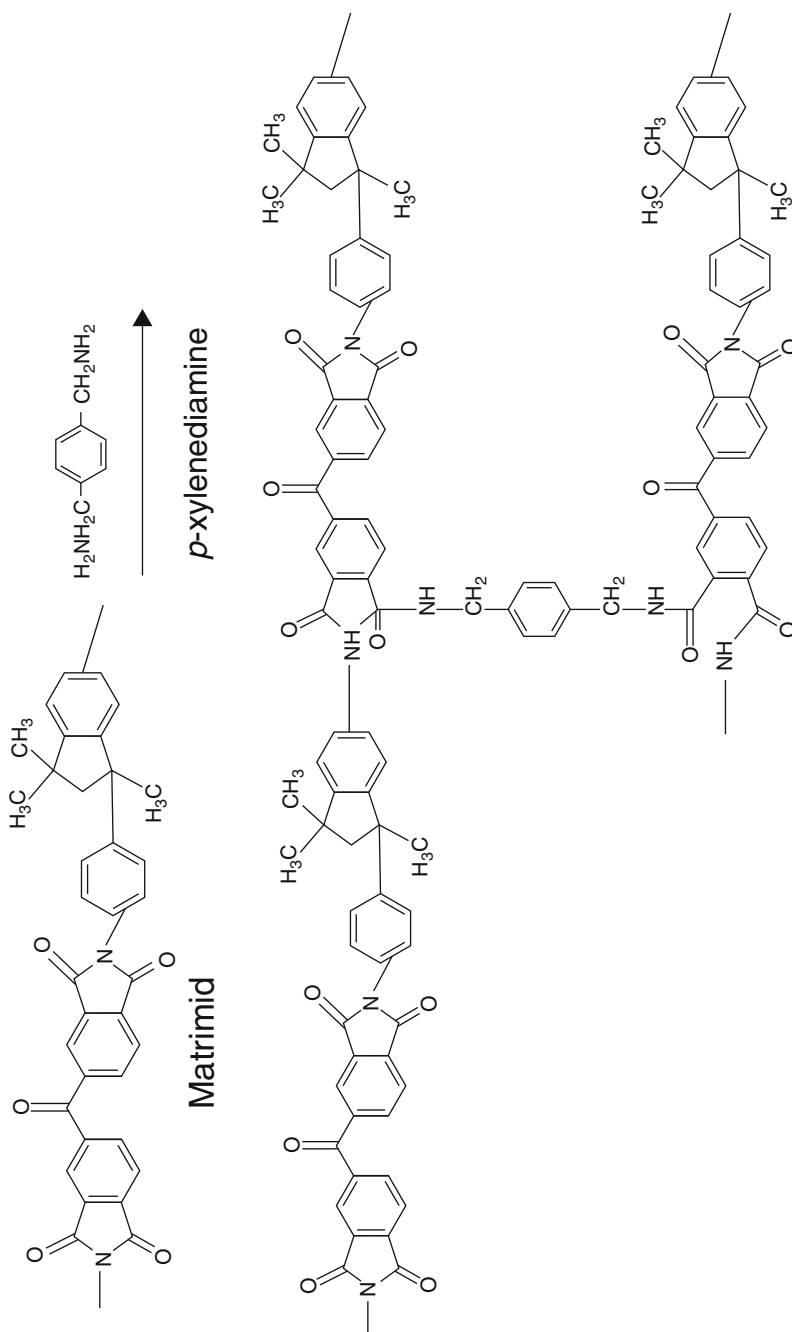


Fig. 11 Mechanisms of chemical cross-linking modification of Matrimid with *p*-xylenediamine. (Taken from Tin et al. [70] with permission from Elsevier)

-C(CF₃)- linkage and polar carboxylic group enhanced the CO₂/CH₄ permselectivity of the polyimides. The effects of cross-linking degree were evaluated using chemical and thermal cross-linking approach. Plasticization and swelling properties were investigated up to 41 atm feed stream pressure using pure CO₂ as feed gas. The authors concluded that cross-linking of polyimide can enhance the plasticization resistance properties of the cross-linked membrane. However, such enhancement is often accompanied with reduced gas permeability.

Copolymer membranes were synthesized and evaluated for natural gas processing by Wind et al. [5]. The authors used cross-linked polyimides copolymers (6FDA-DAM,DABA and 6FpDA,DABA). Transport properties of natural gas components (used as 50/50 CO₂/CH₄ mixtures and multicomponent mixtures) were investigated at 35 °C and an upstream pressure up to 55 atm. The cross-linking procedure was performed at a range of temperature (220 °C to 295 °C) and 1,4-butylene glycol and 1,4-cyclohexanedimethanol were used as cross-linking agents. Posttreatment annealing was done at temperatures between 130 °C and 295 °C. In order to ensure a clearer interpretation of the results, the effect of various treatments (such as thermal treatment and chemical cross-linking) were decoupled with respect to separation performance of the membrane. The composition of the multicomponent gas mixtures is CO₂ (30.01–30.02), CH₄ (61.0–62.95), C₂H₆ (3.99–4.0), C₃H₈ (2.99–3.0), C₄H₁₀ (2.01), and toluene (0.0299) (in mol%) while the mixed gas is 50 mol% each of CO₂ and CH₄. The results obtained on the performance analysis of the membrane were compared with membranes made of commercially available polymers (such as Matrimid and cellulose acetate). It was observed that the resulting membranes from these studies have better transport and penetrant-induced plasticization properties than the commercially available polymers. The summary of the results of transport and plasticization resistance properties are shown in Table 10. It can be observed from the table that by covalently cross-

Table 10 Gas separation and plasticization resistance properties of cross-linked copolyimides membrane [4]

Polymer membrane	Method	T (°C)	P (CO ₂) (Barrer)	α CO ₂ /CH ₄	Plasticization pressure (atm)
6FDA-DAM: DABA 2:1	Annealing	130	135	28	20–25
		220	115	33	>22.5
		295	95	30	35
	Cross-linked with butylenes glycol monoester	220	40	26	>55
		295	150	30	>30
	Cross-linked with benzenedimethanol monoester	295	43	37	33
6FDA-6FpDA: DABA 1:2	Cross-linked with ethylene glycol monoester	220	24	47	27
6FDA-DAM: DABA 2:1	Annealing	220	47	23–28	>40
			50–55	23–27	>10

linking, its plasticization resistance property can be improved. The table also revealed that thermal annealing can serve as an effective tool for suppressing CO₂-induced plasticization challenges.

In a similar study by Omole et al. [76], separation capability of an asymmetric hollow fiber membranes made from propane-diol monoesterified cross-linkable polyimide (PDMC) was investigated. The ability of PDMC to effectively separate CO₂ from gas mixture was studied under aggressive operating conditions. The cross-linked membranes showed a good separation performance for CO₂ and CH₄. A selectivity value of about 49, CO₂ permeability of 161 barrer, were obtained under the operating condition of 65 psia, 35 °C, and 10% CO₂. The membranes also showed good resistance to CO₂-induced plasticization at a CO₂ partial pressure up to 400 psia. Thus, plasticization was effectively suppressed. The improved plasticization resistance was however accompanied by a decline in membrane permeability. The accompanied deterioration of the permeability was as a result of densification of the selective top layer during the annealing process.

High temperature cross-linking is a common procedure for modifying polyimide. There is, therefore, a need to develop a low-temperature protocol in order to reduce the cost of membrane preparation. Liu et al. [77] developed a simple low-temperature (room temperature) chemical cross-linking technology for membrane preparation. The authors tested this technology using 6FDA-durene cross-linked with a *p*-xylenediamine methanol solution. Gas (such as N₂ and CO₂) permeation properties of the cross-linked polyimides were investigated at 35 °C and 10 atm. Low-temperature chemical cross-linking was also applied by Tin et al. [70] for the modification of a commercially available polyimide (Matrimid[®] 5218). Pure and mixed gas permeation properties of the membranes were performed using CH₄ and CO₂ gases. Moreover, the authors also studied the effect of cross-linking on plasticization resistance properties of the membrane. The outcome of the studies showed that plasticization resistance increased significantly. The plasticization pressure was found to increase from 15 atm to 32 atm following a 7-day polymer cross-linking. This is more than 100% increment. Unfortunately, the increase in plasticization resistance property was accompanied by 45% decrease in permeability. There was no significant change in the ideal selectivity.

A critical observation on the side effect of cross-linking revealed that cross-linking is often accompanied by a reduction in permeability. To solve this problem, rapid quenching was introduced into membrane cross-linking procedure. The use of rapid quenching was used for solving the challenge of permeability reduction with no compromise to the plasticization resistance properties of the membranes. In some cases, improved plasticization resistance property was recorded. For instance, decarboxylation-induced cross-linking was utilized by [74] to improve the plasticization resistance of 6FDA-DAM:DABA (2:1) copolyimides. Two sets of membrane samples were employed for the studies. One set of membrane samples was annealed while the other set was rapidly quenched from above its T_g . Gas permeability and solvent dissolution tests were performed on both samples. The sample that was subjected to rapid quenching was observed to exhibit better plasticization resistance

property. The plasticization pressure was observed to increase from 28 atm to more than 49 atm. The results of these plasticization resistance properties are shown in Table 11. In addition, the normalized CO₂ permeability was found to be stable up to 49 atm. Also, the samples did not dissolve in solvents such as cyclohexanone, THF, and NMP which were well-known solvents for dissolving polyimides. In fact, the quenched membranes did not dissolve after boiling in NMP for 18 hr. It was concluded that both responses that were observed are due to cross-linking which occurred in the polyimide.

The outcomes of many investigations on the use of chemical cross-linking indicate that the technology is promising in developing plasticization-resistant membrane. However, the use of chemical cross-linking has its own challenges. Some of these challenges include the formation of ester linkages when diol is used as cross-linking agents. It is highly possible for the linkages so formed to be hydrolyzed when a membrane is used in the presence of aggressive acid gas feed streams. The hydrolysis is known to be capable of reversing the effects of the cross-linking, reduce the membrane separation efficiency, and make it (the membrane) to be more susceptible to penetrant-induced plasticization [74]. For this reason, a new method of cross-linking which does not cause formation ester linkages was developed. The new cross-linking approach involves the use of a high-temperature decarboxylation process. The decarboxylation of the acid pendant (at high temperature) will create free radical sites that are capable of initiating the cross-linking process in the absence of a diol cross-linking agent.

Clearly, the use of decarboxylation approach has a variety of advantages and disadvantages. One of the major concerns of the high-temperature decarboxylation as a cross-linking technique is the possibility of causing the collapse of the transition layers as well as the substructure of asymmetric hollow fiber membrane that was developed using decarboxylated materials. In order to address this challenge, an attempt was made to investigate the possibility of carrying out thermal cross-linking

Table 11 Plasticization properties of polyimide membrane prepared using thermal treatment and chemical cross-linking [4]

Treatment temperature	Cross-linking agents/method	Polymer	P (CO ₂) (barrer)	Plasticization pressure (atm)
	Noncross-linked	6FDA-mPD	9	5–7
35 °C	Ethylene glycol in DMAc	6FDA-DABA	7.5	24
	Noncross-linked	6FDA-mPD / DABA (9:1)	7	15
35 °C	Ethylene glycol in DMAc	6FDA-mPD / DABA (9:1)	11	36
220 °C, 23 h	Decarboxylation	6FDA-DAM: DABA (2:1)	0.65 ^a	25-32
220 °C, 23 h + Quenching	Rapid quenching from above T_g	6FDA-DAM: DABA (2:1)	0.64 ^a	>49

^aThe normalized permeability which was calculated as a ratio of the measured permeability to the initial permeability that was measured at 2 atm

at a temperature below the glass transition temperature. Consequently, a new thermal cross-linking method was reported by Qiu et al. [72]. Using this method, a glassy polymer can be easily cross-linked at a temperature that is lower than the glass transition temperature of such a polymer. The sub- T_g method of cross-linking is a promising method that could facilitate a large-scale method of fabricating asymmetric membranes. The sub- T_g method was used to develop a polyimide (6FDA-DAM: DABA (3:2)) membrane for application in CO₂ separation. The properties of the resulting membranes were evaluated using solubility, thermal, and permeation tests. The gas transport properties and gas separation performance tests were performed using aggressive gas mixtures as feed streams at high feed (upstream) pressure. The feed streams consist of both the pure and mixed gases of CO₂ and CH₄. The results of the permeation tests revealed that there was significant improvement in the plasticization resistance properties of the membranes. Tested membrane samples showed no sign of plasticization at feed pressure as high as 48 bar and 69 bar for pure and mixed gas permeation tests, respectively. The results of the solubility test were used to corroborate the increment in the plasticization resistance properties. It was observed that some membranes did not dissolve in hot solvents such as NMP at 100 °C when soaked in the hot NMP for 1 week. The authors also carried out further studies to discover the range of temperatures at which cross-linking occurred. It was observed that there was no cross-linking at a temperature below 300 °C [72].

Diamino-organosilicone (bis(3-aminopropyl)-tetramethyldisiloxane), APTMDS) is another cross-linking agent that was investigated by Chen et al. [78]. The authors employed two different routes to accomplish the cross-linking and the preparation of two different cross-linked polyimide membranes. In addition, both routes were implemented at ambient temperature. The results of gas separation performance of the resulting membranes are shown in Tables 12 and 13. From these tables, it can be observed that both methods produced membranes with enhanced gas separation properties.

Research focus on CO₂ separation has targeted polymeric materials with relatively higher CO₂ selectivity. Interestingly, the rubbery polymers constitute the most promising materials in this respect [16]. Outstanding rubbery polymers such as those

Table 12 Gas separation performance of cross-linked polyimide membranes [78]

Polymer	Cross-linking method	P (CO ₂) (barrer)	Ideal selectivity	Separation factor
6FDA-ODA	Original sample	19	53	49
	Immersion in APTMDS/methanol	12–17	66–90	39–62
	Direct mixing of APTMDS in polyimide solution	12–14	71–82	55–64
6FDA-ODA TemMPD (50/50%)	Original sample	57	15	14
	Immersion in APTMDS/methanol	18–54	15–41	14–40
	Direct mixing of APTMDS in the polyimide solution	24–33	19–24	15–24

Table 13 Gas transport and plasticization resistance properties of cross-linked polyimide membranes [78]

Polymer	CO ₂ permeability (barrer)	Plasticization pressure (atm)
6FDA-ODA	15	20–24
Cross-linked 6FDA-ODA	8	>41
6FDA-ODA(50%)-TemMPD (50%)	48	14
Cross-linked 6FDA-ODA (50%) -TemMPD (50%) (direct mixing)	12	>41

containing polyethylene oxide (PEO) segments have better solubility selectivities due to their molecular interaction with the CO₂ quadrupole. On the other hand, PEO is crystalline. Therefore, to achieve useful gas separation performance from polymers in which PEO has been incorporated, the PEO crystallization must be suppressed. This will give room to achieving high fluxes and retard swelling. Some of the means by which this could be accomplished include cross-linking, polymer blending, or block-copolymerization [16]. A comprehensive description of polyethylene glycol can be found in Adewole et al. [4]. Within the polyether family, PEO is as an outstanding membrane forming material particularly suitable for processing and purification of gas mixtures containing polar gases (such as CO₂ and H₂S) and nonpolar ones (such as H₂, N₂, and CH₄) [79, 80]. This is due to its polarity and CO₂ affinity [81]. PEO contains an ether oxygen functional group which favorably interacts with CO₂ at the molecular level which then result in increase in selectivity toward the gas [82].

One of the strategies that can be used to improve the gas separation capability of PEO-based membrane is to destroy the crystalline nature of PEO and make it to become more amorphous. A family of cross-linked poly(ethylene glycol diacrylate) (XLPEGDA) was prepared by Lin and Freeman [80]. The effect of cross-linking on the crystallinity and gas permeability of XLPEGDA was investigated. The results revealed that the cross-linking have successfully disrupted the crystallinity. No significant effect was observed with respect to the permeability and diffusivity. Expectedly, it was observed that the solubility selectivity for the CO₂/CH₄ gas pair increased due to the interaction of PEO functional group with CO₂. Lin and Freeman [83] also measured the permeabilities of CO₂ and CH₄ through XLPEGDA membrane as a function of temperature and feed fugacity. The authors observed that permeability of CH₄ is independent of feed fugacity while that of CO₂ increased with increasing fugacity. Therefore, it can be inferred that the cross-linking have no significant effect on the plasticization resistance behavior of the polymer. During the permeation test, the significant quantity of CO₂ sorbed into the polymer caused an increase in polymer chain flexibility as well as an increase in fractional free volume.

Li et al. [84] prepare a series of poly(urethane-urea)s polymers using 4,4-methylene diphenyl diisocyanate (MDI), various types of polyether diols, and ethylene diamine (EDA). Membrane produced using the prepared copolymers were

subjected to pure gas permeation tests using CO₂ and CH₄. The data obtained from the permeability measurements revealed that the CO₂ permeability increased instantaneously with increase in feed pressure for all the samples. Such type of transport phenomenon is commonly associated with rubbery polymers. Usually, rubbery polymers always exhibit a high tendency for CO₂ sorption. Mixed as well as pure gas permeation tests results of highly permeable poly(ethylene) oxide [85], cross-linked poly(ethylene) oxide [86], and blend of polyimide-*b*-ethylene oxide/polyethylene glycol [87] membranes did not show any promising performance with respect to plasticization resistance. Therefore, it can be concluded that polyether-based polymers are not suitable for high-pressure removal of CO₂ gas from CH₄. Studies on how the plasticization pressure of these class of highly permeable polymers can be improved are recommended for further research. Other new membranes and thermal treatment methods have been reported. Details of these can be found in the literature [54, 88–95].

6.2 Grafting of Polymer Backbone

The performance properties of polymeric membranes can be improved by the incorporation or the substitution of small functional groups onto the rotating unit of the polymers. This simple method has been applied by some researchers to enhance the permeability and selectivity of membranes. Pixton and Paul [96] studied the gas transport properties of 2,2-(4-hydroxy-phenyl) adamantane polysulfone and 1,3-(4-hydroxyphenyl)adamantane polysulfone membranes and compared the results with that of bisphenol A-based polysulfone. The results of the pressure-dependent permeability tests that was carried out on the membranes (with a thickness in the range of 50–75 μm) revealed that both polymers can resist CO₂-induced plasticization up to a pressure of 20 atm. It is worth mentioning that 20 atm is the maximum pressure of the experiment. Therefore, there is every possibility for the plasticization pressure to be more than 20 atm. The recorded improvement in the plasticization suppression properties is, however, dependent on the thickness of the membrane. This became evident from the studies that were later carried on ultra-thin film polysulfone membranes where the plasticization pressure was found to be lower [19]. To date, varieties of new and more advanced grafting techniques have been reported for modifying polymers that are used for applications in gas separation. Some of these techniques can be found in the open literature [97–99].

6.3 Template Polymerization Technique and Use of Porogens

Template polymerization is a concept that was derived from natural polymerization processes. The process mimics the polymerization techniques that are found in nature. Examples include DNA replication and biosynthesis of proteins [100]. Template polymerization the technique provides scientists with the opportunity to control and tune polymer properties during polymerization [101]. It is a versatile process

that can be employed in synthesizing ultrathin polymeric membranes. It can be made to proceed in various ways such as template polycondensation, ring opening polymerization, polyaddition, and ionic or radical polymerization [100, 101]. The process is a convenient way of producing poly complexes, poly complex composites, and polymer blends.

The term “porogen” is an acronym for “pore generator” [102]. The mechanisms of porogen-induced pore formation have been investigated by a number of authors. Traditionally, this method is used for the preparation of porous materials for applications in dielectric industries [103, 104]. The porogenesis process can be performed via a sacrificial thermal decomposition of the porogens in the range of 350 °C and 400 °C [103–105]. Marti et al. [106] provided a detailed description of another new approach for using porogens for membrane preparation. Recently, this approach has been found to be very useful in developing membranes with better resistance to plasticization phenomenon. The techniques of template polymerization and use of porogens can be traced back to the preparation of carbon molecular sieve (CMS). A comprehensive explanation of CMS and its preparation are presented in Mohamed [107], Kita [108], and Williams and Koros [109].

Aromatic polyimides have been used as polymer precursors for the preparation of CMS membranes due to their excellent balance of productivity and separation factor or ideal selectivity [110]. CMS membranes are fabricated by heating up the polyimides to a temperature range of 700–900 °C. The high-temperature heating process often results in polyimides degradation [110]. Relatively low-temperature pyrolysis was therefore proposed. Islam et al. [111] and Weiliang et al. [112] employed low-temperature pyrolysis for preparing flexible pyrolytic membranes. Sulfonated polyimides were pyrolyzed at a temperature range of 370 °C and 450 °C to produce dense flat sheet membranes. The membrane contains a large number of microvoids which were caused by “template-like effect” of SO₃H groups. Gas (CO₂) permeability of the membranes was found to have increased by 378 barrer in comparison with the polymer precursor.

Similar approach has been used by other authors such as Xiao and Chung [113] (using beta-cyclodextrin thermal labile molecule with large dimensions) and Chua et al. [114] (using thermal labile saccharide units with different molecular weights and structures: glucose (180 g/mol), sucrose (342 g/mol), and raffinose (504 g/mol)). Based on the permeability of CO₂, membrane prepared using cyclodextrin, porogens was found to be the best membrane (Table 14). A further investigation into the plasticization behaviour of polyimide containing cyclodextrin porogens was performed by Askari et al. [69, 115]. A summary of the plasticization properties of the membrane developed using the copolyimide is displayed in Table 15.

6.4 Sulfonation Method

Sulfonation involves the replacement of a hydrogen atom of an organic compound with a sulfonic acid (-SO₃H) functional group. It is often accomplished reaction of the organic compound (such as a polymer) with sulfuric acid at high temperatures.

Table 14 Gas transport properties of partially pyrolyzed polyimide membranes using various porogens [4]

Porogens	Temperature ^a (°C)	P (CO ₂)	α CO ₂ /CH ₄
Sulfonic group	370–450	145–380	–
Carboxylic acid	425–475	39.1–94.8	60–47
Cyclodextrin	300–450	56–8000	31–17
Saccharides	200–425	533–1389	24.9–26.9

^aThis is the temperature of partial pyrolysis

Table 15 Penetrant-induced plasticization properties of 6FDA-Durene/DABA co-polyimides with α , β , and γ -cyclodextrin [69]

Polymer	Treatment temperature (°C)	Plasticization pressure (atm)
Original polyimide	200	5–10
	300	10–15
	425	15–20
Polyimide grafted with- α -CD	200	7–10
	300	10–15
	425	25
Polyimide grafted with β -CD	200	7–10
	300	10
	425	>30
Polyimide grafted with γ -CD	200	10
	300	10
	425	>30

Sulfonation is one of the new methods that have been proposed for modification of gas transport properties of polymers. Sulfonated polymeric membranes usually exhibit enhanced separation performance than the original ones. Studies on structure–properties relationship of sulfonated polymers was conducted by Piroux et al. [116] for a large series of sulfonated copolyimides. The copolyimides were synthesized with a naphthalenic dianhydride, a sulfonated diamine, and various nonsulfonated diamines. It was observed that the contribution of the dispersed sulfonated phase to the gas transport greatly depends on the structure of the non-sulfonated diamine.

Previously, polymer structures are commonly modified by postsulfonation. Unfortunately, the practice of postsulfonation lead to lower thermal and mechanical stabilities of the polymers compared with the original polymer. In addition, it very difficult to achieve a high degree of sulfonation using postsulfonation process. To overcome this problem, sulfonation of monomers prior to polymerization was proposed. Khan et al. [117] prepared a series of sulfonated poly(ether ether ketone) (S-PEEK) membranes by the sulfonation of its monomers. Commercial-scale application of the membranes (that were prepared from the S-PEEK) for CO₂ separation

Table 16 Transport and plasticization properties of S-PEEK with sodium ions [117]

Polymer	Degree of sulfonation	CO ₂ permeability (barrer)	Plasticization pressure (bar)
S-PEEK-Na-1	0.44	8	11
S-PEEK-Na-2	0.76	10.5	32
S-PEEK-Na-3	1.10	14.5	>40

from gas mixtures was investigated. The authors also investigated the effects of various degree of sulfonation and the presence of different types of ions (H, Na, Li, Mg, Ba, and Al) on the gas separation performance of the membranes were investigated. Results obtained for the plasticization pressure and CO₂ permeability are displayed in Table 16.

6.5 Technique for Preparing Polymers of Intrinsic Microporosity (PIM)

Percentage crystallinity is one of the major morphological properties which determine the transport properties of polymers that are used for making membrane. Less crystalline (amorphous) are commonly recommended candidate for membrane applications. A successful synthesis of nanoporous polymers was reported by Budd et al. [118]. The new set of polymers were prepared from certain microporous networks of functional units including phthalocyanine, porphyrin, and hexaazatrinaphthylene. Due to the microporous nature of the starting materials, the resulting polymer from this synthesis protocol is often called polymers of intrinsic microporosity (PIMs) [119].

PIMs are nanoporous (0.4–0.8 nm), soluble, solution processable, and thermally stable (initial decomposition at around 460 °C) polymers. They have very high surface areas (of ~800 m²/g) and free volume [119, 120]. A detailed description of the concept of PIMs can be found in Budd et al. [118]. Following the pioneering article that was published on PIMs synthesis, the polymers have been further investigated for a variety of applications [120]. In gas separation application, PIMs have high permeability as well as high selectivity that are above the Robeson's upper bound for a number of gas pairs. Table 17 shows the separation performance results of PIMs in separating CO₂ from CH₄. Phthalazinone-based copolymers with intrinsic microporosity (PHPIMs) was reported by [121]. A high temperature aromatic double nucleophilic subcondensation polymerization method was used to synthesize the polymer. Gas separation performance of membrane prepared from the polymers was investigated. The effect of the stiffness of the phthalazinone unit was investigated in order to explore the possibility of using this property to design a new high-performance membrane for gas separation. The results of the investigation showed that the introduction of phthalazinone moiety resulted into amorphous glassy copolymers which exhibit excellent thermal stability and gas separation properties.

Table 17 Gas transport properties of PIMs [4]

Membrane	Experimental parameters		Permeability (Barrer)	
	Feed pressure	Temperature (°C)	CO ₂	CH ₄
PIM-1 ^a	0.2 bar	30	23,000	125
PIM-7 ^b	0.2 bar	30	1100	62
Polybenzodioxane- PIM-1	1 atm	25	4390	310
Thioamide-PIM	1 bar	25	1120	56
Carboxylated PIMs	50 psig	25	620–6715	–
Cross-linked PIMs	3.4 atm	30	1291–2345	52.6–192
PIMs (Trifluoromethyl and Phenylsulfone groups)	50 psig	25	731–3616	–

^aPrepared using 5,5,6,6-tetrahydroxy-3,3,3,3 tetramethyl-1,1-spirobisindane and tetrafluoroterephthalonitrile

^bPrepared using 5,5,6,6-tetrahydroxy-3,3,3,3 tetramethyl-1,1-spirobisindane and 7,7,8,8-tetrachloro-phenazyl-3,3,3,3-tetramethyl-1,1-spirobisindane

6.6 Membrane Preparation Using 3D Printing Technologies

Three-dimensional (3D) printing is a new technology whose applications have been extended into almost all aspects of research and development. The technology is also referred to as additive manufacturing or rapid prototyping. It involves a layer-by-layer building of materials to create materials of various geometries from 3D image data [122, 123]. The 3D technology has been recently applied for membrane materials fabrication. It is a technology that is expected to revolutionize membrane materials and modules fabrication. In membrane technology, the applicable additive manufacturing techniques can be grouped into four: namely, photopolymerization, powder, material extrusion, and lamination [124, 125]. The most promising among these is the photopolymerization. It is the curing of photoreactive polymers (photopolymers) with a laser, UV, or light [124].

Presently, the majority of the polymeric membranes produced by 3D printing technology have been evaluated for liquid. Thus, very few publications can be found on gas separation. Polymers that have been investigated for membrane fabrication include polydimethylsiloxane membrane for use as gas-liquid contactor [126–128], *m*-phenylene diamine [129, 130], polyamide-12 using selective laser sintering [131] and photocurable formulation of diurethane dimethacrylate (DUDA), poly(ethylene glycol) diacrylate (PEGDA), dipentaerythritol penta-/hexaacrylate, and 4-vinylbenzyl chloride [125].

7 Conclusion

Advances in the method of synthesis and gas transport properties of functional polymeric membrane materials were reviewed. The transport properties of both rubbery and glassy polymeric membranes that were prepared by these methods of

synthesis were described in terms of permeability, solubility, diffusivity, and selectivity. It was generally observed that the presence of functional groups such as polar ether oxygen linkages, hydroxyl, and amine enhances the separation efficiency of polymeric membranes. The intermolecular interaction of these functional groups with CO₂ enhances its solubility within the membrane matrix and hence the solubility selectivity of the membrane is improved. The size of such functional groups contributes in the enhancement of CO₂ diffusivity and hence diffusivity-selectivity of the membranes. It was also revealed that porogens such as sulfonic, carboxylic acid, cyclodextrin, and saccharides could be excellent candidates for improving the separation properties of polymeric membranes. Therefore, the introduction of any of these functional groups or similar ones into the polymer backbone is one of the promising methods for producing membranes with superior natural gas separation performance.

References

1. C.A. Scholes, K.H. Smith, S.E. Kentish, G.W. Stevens, CO₂ capture from pre-combustion processes—Strategies for membrane gas separation. *Int. J. Greenh. Gas Control* **4**, 739–755 (2010)
2. J.G. Speight, *Natural gas: A basic handbook* (Gulf Publishing Company, Houston, 2007)
3. Y. Xiao et al., The strategies of molecular architecture and modification of polyimide-based membranes for CO₂ removal from natural gas – A review. *Prog. Polym. Sci.* **34**, 561–580 (2009)
4. J.K. Adewole et al., Current challenges in membrane separation of CO₂ from natural gas: A review. *Int. J. Greenh. Gas Control* **17**, 46–65 (2013)
5. J.D. Wind, D.R. Paul, W.J. Koros, Natural gas permeation in polyimide membranes. *J. Membr. Sci.* **228**, 227–236 (2004)
6. Yergin, D., *Natural gas, in Energy for a sustainable world: From the oil age to a sun-powered future*, N. Armaroli and V. Balzani, 2011, Wiley-VCH Verlag GmbH & Co. KGaA Weinheim 69–84
7. R.W. Baker, K. Lokhandwala, Natural gas processing with membranes: An overview. *Ind. Eng. Chem. Res.* **47**, 2109–2121 (2008)
8. A.J. Kidnay, W.R. Parrish, D.G. McCartney, *Fundamentals of natural gas processing*, 2nd edn. (Taylor & Francis, Boca Raton, 2011)
9. S. Mokhatab, W.A. Poe, J.G. Speight, *Handbook of natural gas transmission and processing* (Gulf Professional Publishing, Oxford, 2006)
10. H. Kumazawa et al., Permeation behavior for mixed gases in poly(4-methyl-1-pentene) membrane near the glass transition temperature. *J. Membr. Sci.* **97**, 7–12 (1994)
11. J. Ren et al., Development of asymmetric 6FDA-2,6DAT hollow fiber membranes for CO₂/CH₄ separation I. The Influence of dope composition and rheology on membrane morphology and separation performance. *J. Membr. Sci.* **207**, 227–240 (2002)
12. E.J. Dung, L.S. Bombom, T.D. Agusomu, The effects of gas flaring on crops in the Niger Delta, Nigeria. *GeoJournal* **73**, 297–305 (2008)
13. P.J. Hickey, F.P. Juricic, C.S. Slater, Effect of process parameters on the pervaporation of alcohols through organophilic membranes. *Sep. Sci. Technol.* **27**(7), 843–861 (1992)
14. M. Safari, A. Ghanizadeh, M.M. Montazer-Rahmati, Optimization of membrane-based CO₂-removal from natural gas using simple models considering both pressure and temperature effects. *Int. J. Greenh. Gas Control* **3**, 3–10 (2009)
15. A.E. Kontorovich, M.I. Epov, L.V. Eder, Long-term and medium-term scenarios and factors in world energy perspectives for the 21st century. *Russ. Geol. Geophys.* **55**(5), 534–543 (2014)

16. Murphy, T.M., G.T. Offord, and D.R. Paul, Fundamentals of membrane gas separation, in *Innovative separations and transformations*, ed. by E. Drioli, L. Giomo (WILEY-VCH Verlag GmbH & Co. KGaA, Weinheim, 2009), pp. 63–82
17. R.W. Baker, Future directions of membrane gas separation technology. *Ind. Eng. Chem. Res.* **41**, 1393–1411 (2002)
18. R.W. Baker, Membrane gas-separation: Applications, in *Membrane operations*, (Wiley-VCH Verlag GmbH & Co. KGaA, Weinheim, 2009), pp. 167–194
19. C.A. Scholes et al., Plasticization of ultra-thin polysulfone membranes by carbon dioxide. *J. Membr. Sci.* **346**(1), 208–214 (2010)
20. T.-L. Chew, A.L. Ahmad, S. Bhatia, Ordered mesoporous silica (OMS) as an adsorbent and membrane for separation of carbon dioxide (CO₂). *Adv. Colloid Interf. Sci.* **153**, 43–57 (2010)
21. G.W. Meindersma, M. Kuczynski, Implementing membrane technology in the process industry: Problems and opportunities. *J. Membr. Sci.* **113**, 285–292 (1996)
22. J.K. Adewole et al., Model-based analysis of polymeric membranes performance in high pressure CO₂ removal from natural gas. *J. Polym. Res.* **22**(3), 1–10 (2015)
23. C. Cao et al., Formation of high-performance 6FDA-2,6-DAT asymmetric composite hollow fiber membranes for CO₂/CH₄ Separation. *J. Membr. Sci.* **209**, 309–319 (2002)
24. Ng, B.C., et al., Formation of asymmetric polysulfone flat sheet membrane for gas separation: Rheological assessment. *Jurnal Teknologi*, 41(F) Keluaran Khas. Dis. **41**, 73–88 (2004)
25. S.R. Reijerkerk et al., On the effects of plasticization in CO₂/light gas separation using polymeric solubility selective membranes. *J. Membr. Sci.* **367**(1–2), 33–44 (2011)
26. J. Zhao et al., Influence of heat-treatment on CO₂ separation performance of novel fixed carrier composite membranes prepared by interfacial polymerization. *J. Membr. Sci.* **283**, 346–356 (2006)
27. G. Clarizia, Polymer-based membranes applied to gas separation: material and engineering aspects. *Desalination* **245**, 763–768 (2009)
28. D.N. Schulz, A.O. Patil, Functional polymers: An overview, in *Functional polymers*, (American Chemical Society, Washington, DC, 1998), pp. 1–14
29. N.R. Horn, D.R. Paul, Carbon dioxide plasticization of thin glassy polymer films. *Polymer* **52**(24), 5587–5594 (2011)
30. P. Bernardo, E. Drioli, G. Golemme, Membrane gas separation: A review/state of the art. *Ind. Eng. Chem. Res.* **48**(10), 4638–4663 (2009)
31. A.L. Ahmad et al., Preparation and gas transport properties of dual-layer polysulfone membranes for high pressure CO₂ removal from natural gas. *J. Appl. Polym. Sci.* **131**(20), 1–10 (2014)
32. M.R. Coleman, W.J. Koros, Isomeric polyimides based on fluorinated dianhydrides and diamines for gas separation applications. *J. Membr. Sci.* **50**(3), 285–297 (1990)
33. Hofmann, D. and E. Tocci, Molecular Modeling, A tool for the knowledge-based design of polymer-based membrane materials, in *Membrane operations innovative separations and transformations*, ed. by E. Drioli, L. Giomo (Wiley-VCH Verlag GmbH & Co. KGaA, Weinheim, 2009), pp. 3–17
34. H. Susanto, M. Ulbricht, Polymeric membranes for molecular separations, in *Membrane operations*, (Wiley-VCH Verlag GmbH & Co. KGaA, Weinheim, 2009), pp. 19–43
35. X.Y. Chen et al., Membrane gas separation technologies for biogas upgrading. *RSC Adv.* **5**(31), 24399–24448 (2015)
36. L. Jiang, Fabrication of Matrimid/polyethersulfone dual-layer hollow fiber membranes for gas separation. *J. Membr. Sci.* **240**(1–2), 91–103 (2004)
37. Y. Kase, Gas separation by polyimide membranes, in *Advanced membrane technology and applications*, (Wiley, New York, 2008), pp. 581–598
38. M.D. Kennedy et al., Water treatment by microfiltration and ultrafiltration, in *Advanced membrane technology and applications*, (Wiley, New York, 2008), pp. 131–170
39. M. Mulder, *Basic principles of membrane technology* (Kluwer Academic Publishers, Dordrecht, 1996)
40. Park, H.B. and Y.M. Lee, Polymeric membrane materials and potential use in gas separation, in *Advanced membrane technology and applications*, N.N. Li, et al., 2008, Wiley: Hoboken. p. 633–664

41. J.K. Adewole et al., Comparative studies on the effects of casting solvent on physico-chemical and gas transport properties of dense polysulfone membrane used for CO₂/CH₄ separation. *J. Appl. Polym. Sci.* **132**(27), 1–10 (2015)
42. Hagg, M.-B., Membrane for gas separation, in *Handbook of membrane separations: Chemical, pharmaceutical, food, and biotechnological applications*, ed. by A. K. Pabby, S. S. H. Rivzi, A. M. Sastre (CRC Press, Boca Raton, 2009), pp. 65–105
43. J.K. Adewole et al., Transport properties of natural gas through polyethylene nanocomposites. *J. Polym. Res.* **19**(2), 1–11 (2012)
44. Y. Li, T.S. Chung, Highly selective sulfonated polyethersulfone (SPES)-based membranes with transition metal counterions for hydrogen recovery and natural gas separation. *J. Membr. Sci.* **308**(1–2), 128–135 (2008)
45. A.M.W. Hillock, S.J. Miller, W.J. Koros, Crosslinked mixed matrix membranes for the purification of natural gas: Effects of sieve surface modification. *J. Membr. Sci.* **314**(1–2), 193–199 (2008)
46. Koros, W.K., et al., Energy and Environmental Issues and Impacts of Membranes in Industry, in *Membrane Operations Innovative Separations and Transformations*, E. Drioli and L. Giorno. 2009, Wiley-VCH Verlag GmbH & Co. KGaA: Weinheim. p. 139–165
47. Y. Li, T.S. Chung, Silver ionic modification in dual-layer hollow fiber membranes with significant enhancement in CO₂/CH₄ and O₂/N₂ separation. *J. Membr. Sci.* **350**(1–2), 226–231 (2010)
48. M.A. Aroon et al., Morphology and permeation properties of polysulfone membranes for gas separation: Effects of non-solvent additives and co-solvent. *Sep. Purif. Technol.* **72**(2), 194–202 (2010)
49. H.B. Park et al., Thermally rearranged (TR) polymer membranes for CO₂ separation. *J. Membr. Sci.* **359**, 11–24 (2010)
50. H.B. Park et al., Polymers with cavities tuned for fast selective transport of small molecules and ions. *Science* **318**, 254–258 (2007)
51. K. Matsumoto, P. Xu, Gas permeation properties of hexafluoro aromatic polyimides. *J. Appl. Polym. Sci.* **47**(11), 1961–1972 (1993)
52. H. Wang, T.-S. Chung, The evolution of physicochemical and gas transport properties of thermally rearranged polyhydroxyamide (PHA). *J. Membr. Sci.* **385–386**, 86–95 (2011)
53. H. Wang et al., The evolution of poly(hydroxyamide amic acid) to poly(benzoxazole) via stepwise thermal cyclization: Structural changes and gas transport properties. *Polymer* **52**(22), 5127–5138 (2011)
54. G.L. Tullos et al., Thermal conversion of hydroxycontaining imides to benzoxazoles: polymer and model compound study. *Macromolecules* **32**, 3598–3612 (1999)
55. S.H. Han et al., Thermally rearranged (TR) polybenzoxazole: Effects of diverse imidization routes on physical properties and gas transport behaviors. *Macromolecules* **43**(18), 7657–7667 (2010)
56. C.H. Jung et al., Highly permeable and selective poly(benzoxazole-co-imide) membranes for gas separation. *J. Membr. Sci.* **350**(1–2), 301–309 (2010)
57. J.I. Choi et al., Thermally rearranged (TR) poly(benzoxazole-co-pyrrolone) membranes tuned for high gas permeability and selectivity. *J. Membr. Sci.* **349**, 358–368 (2010)
58. M. Calle, Y.M. Lee, Thermally rearranged (TR) poly(ether-benzoxazole) membranes for gas separation. *Macromolecules* **44**(5), 1156–1165 (2011)
59. Y.F. Yeong et al., Thermal induced structural rearrangement of cardo-copolybenzoxazole membranes for enhanced gas transport properties. *J. Membr. Sci.* **397–398**, 51–65 (2012)
60. D.F. Sanders et al., Gas permeability, diffusivity, and free volume of thermally rearranged polymers based on 3,3'-dihydroxy-4,4'-diamino-biphenyl (HAB) and 2,2'-bis-(3,4-dicarboxyphenyl) hexafluoropropane dianhydride (6FDA). *J. Membr. Sci.* **409–410**, 232–241 (2012)
61. S.H. Han et al., Highly gas permeable and microporous polybenzimidazole membrane by thermal rearrangement. *J. Membr. Sci.* **357**, 143–151 (2010)
62. Y. Lu et al., Preparation and gas transport properties of thermally induced rigid membranes of copolyimide containing cardo moieties. *React. Funct. Polym.* **119**, 134–144 (2017)
63. S. Kim, S.H. Han, Y.M. Lee, Thermally rearranged (TR) polybenzoxazole hollow fiber membranes for CO₂ capture. *J. Membr. Sci.* **403–404**, 169–178 (2012)

64. H.J. Jo et al., Thermally rearranged poly(benzoxazole-co-imide) membranes with superior mechanical strength for gas separation obtained by tuning chain rigidity. *Macromolecules* **48**(7), 2194–2202 (2015)
65. B. Comesana-Gandara et al., Gas separation membranes made through thermal rearrangement of ortho-methoxy polyimides. *RSC Adv.* **5**(124), 102261–102276 (2015)
66. J.H. Lee et al., Wet CO₂/N₂ permeation through a crosslinked thermally rearranged poly(benzoxazole-co-imide) (XTR-PBOI) hollow fiber membrane module for CO₂ capture. *J. Membr. Sci.* **539**, 412–420 (2017)
67. S. Lee et al., Membrane separation process for CO₂ capture from mixed gases using TR and XTR hollow fiber membranes: Process modeling and experiments. *J. Membr. Sci.* **541**, 224–234 (2017)
68. C.A. Scholes et al., Permeation and separation of SO₂, H₂S and CO₂ through thermally rearranged (TR) polymeric membranes. *Sep. Purif. Technol.* **179**, 449–454 (2017)
69. M. Askari et al., Natural gas purification and olefin/paraffin separation using cross-linkable 6FDA-Durene/DABA co-polyimides grafted with α , β and γ cyclodextrin. *J. Membr. Sci.* **390–391**, 141–151 (2012)
70. P.S. Tin et al., Effects of cross-linking modification on gas separation performance of Matrimid membranes. *J. Membr. Sci.* **225**(1–2), 77–90 (2003)
71. Kanehashi, S., S. Sato, and K. Nagai, Synthesis and gas permeability of hyperbranched and cross-linked polyimide membranes, in *Membrane gas separation*, ed. by Y. Yampol'skii, B. Freeman (Wiley, New York, 2010), pp. 3–27
72. W. Qiu et al., Sub-Tg cross-linking of a polyimide membrane for enhanced CO₂ plasticization resistance for natural gas separation. *Macromolecules* **44**(15), 6046–6056 (2011)
73. M.O. González-Díaz et al., Novel copolyaramides with bulky flexible groups for pure and mixed-gas separation. *Sep. Purif. Technol.* **189**, 366–374 (2017)
74. A.M. Kratochvil, W.J. Koros, Decarboxylation-induced cross-linking of a polyimide for enhanced CO₂ plasticization resistance. *Macromolecules* **41**, 7920–7927 (2008)
75. C. Staudt-Bickel, W.J. Koros, Improvement of CO₂/CH₄ separation characteristics of polyimides by chemical crosslinking. *J. Membr. Sci.* **155**(1), 145–154 (1999)
76. I.C. Omole et al., Effects of CO₂ on a high performance hollow-fiber membrane for natural gas purification. *Ind. Eng. Chem. Res.* **49**(10), 4887–4896 (2010)
77. Y. Liu, R. Wang, T.S. Chung, Chemically cross-linking modification of polyimide membranes for gas separation. *J. Membr. Sci.* **189**, 231 (2001)
78. X. Chen, D. Rodrigue, S. Kaliaguine, Diamino-organosilicone APTMDS: A new cross-linking agent for polyimides membranes. *Sep. Purif. Technol.* **86**, 221–233 (2012)
79. B.D. Freeman et al., Plasticization enhanced hydrogen purification using polymeric membranes. *Science* **311**(5761), 639–642 (2006)
80. H. Lin, B.D. Freeman, Gas and vapor solubility in cross-linked poly(ethylene glycol diacrylate). *Macromolecules* **38**(20), 8394–8407 (2005)
81. C. Charmette et al., Gas transport properties of poly(ethylene oxide-coepichlorohydrin) membranes. *J. Membr. Sci.* **230**, 161–169 (2004)
82. V.A. Kusuma et al., Structure/property characteristics of polar rubbery membranes for carbon dioxide removal, in *Advanced membrane technology and applications*, (Wiley, New York, 2008), pp. 929–953
83. H. Lin, D.B. Freeman, Gas permeation and diffusion in cross-linked poly(ethylene glycol diacrylate). *Macromolecules* **39**, 3568–3580 (2006)
84. H. Li, B.D. Freeman, O.M. Ekiner, Gas permeation properties of poly(urethane-urea)s containing different polyethers. *J. Membr. Sci.* **369**, 49–58 (2011)
85. S.R. Reijerkerk et al., Highly hydrophilic, rubbery membranes for CO₂ capture and dehydration of flue gas. *Int. J. Greenh. Gas Control* **5**, 26–36 (2011)
86. C.P. Ribeiro Jr., B.D. Freeman, D.R. Paul, Pure- and mixed-gas carbon dioxide/ethane permeability and diffusivity in a cross-linked poly(ethylene oxide) copolymer. *J. Membr. Sci.* **377**, 110–123 (2011)

87. W. Yave et al., Gas permeability and free volume in poly(amide-b-ethylene oxide)/polyethylene glycol blend membranes. *J. Membr. Sci.* **339**(1–2), 177–183 (2009)
88. K.-I. Okamoto et al., Gas permeability and permselectivity of fluorinated polybenzoxazoles. *J. Polym. Sci. B Polym. Phys.* **30**(11), 1215–1221 (1992)
89. D.G. Lucero, D. Likhatchev, Imide-to-benzoxazole rearrangement in ortho substituted poly(4,4-diphenylene pyromellitimides)s. *Polym. Bull.* **48**, 261–269 (2002)
90. D.R. Pesiri, B. Jorgensen, R.C. Dye, Thermal optimization of polybenzimidazole meniscus membranes for the separation of hydrogen, methane, and carbon dioxide. *J. Membr. Sci.* **218**(1–2), 11–18 (2003)
91. Barsema, J.N., et al., Intermediate polymer to carbon gas separation membranes based on Matrimid PI. *J. Membr. Sci.*, 2004. 238(1–2): p. 93–102
92. X. Yang et al., Significantly enhanced CH₄ permeability base on poly(styrene-b-butadiene-b-styrene)-poly(dimethylsiloxane-co-methylhydrosiloxane) crosslinked membranes. *React. Funct. Polym.* **124**, 48–54 (2018)
93. C. Zhang, B. Cao, P. Li, Thermal oxidative crosslinking of phenolphthalein-based cardo polyimides with enhanced gas permeability and selectivity. *J. Membr. Sci.* **546**, 90–99 (2018)
94. H. An et al., Bromination/debromination-induced thermal crosslinking of 6FDA-Durene for aggressive gas separations. *J. Membr. Sci.* **545**, 358–366 (2018)
95. K.T. Woo et al., Thermally rearranged poly(benzoxazole-co-imide) hollow fiber membranes for CO₂ capture. *J. Membr. Sci.* **498**, 125–134 (2016)
96. M.R. Pixton, D.R. Paul, Gas transport properties of adamantane- based polysulfones. *Polymer* **36**(16), 3165 (1995)
97. A. Bhattacharya, Grafting: a versatile means to modify polymers techniques, factors and applications. *Prog. Polym. Sci.* **29**(8), 767–814 (2004)
98. J. Luo et al., Improved permeability by incorporating polysiloxane in SBS block copolymers for CH₄/N₂ gas separation. *Polymer* **127**, 52–65 (2017)
99. J.H. Lee et al., Dual-phase all-polymeric membranes with graft copolymer filler for CO₂ capture. *Chem. Eng. J.* **334**, 939–947 (2018)
100. Polowinski, S., Template polymerization, in *Encyclopedia of polymer science and technology*, ed. by H. F. Mark (Wiley-Interscience, Hoboken, 2003), pp. 130–142
101. C.R. South, M. Weck, Template-enhanced ring-opening metathesis polymerization. *Macromolecules* **40**, 1386–1394 (2007)
102. H. Li et al., The effect of porogen loading on the stiffness and fracture energy of brittle organosilicates. *J. Mater. Res.* **24**(1), 107–116 (2009)
103. B. Lee, W. Oh, Y. Hwang, Y.-H. Park, J. Yoon, K.S. Jin, K. Heo, J. Kim, K.-W. Kim, M. Ree, Imprinting well-controlled nanopores in organosilicate dielectric films: Triethoxysilyl-modified six armed poly(ϵ -caprolactone) and its chemical hybridization with an organosilicate precursor. *Chem. Mater.* (6), 1845–1852 (2005, **17**)
104. B. Lee et al., Ultralow-k nanoporous organosilicate dielectric films imprinted with dendritic spheres. *Nat. Mater.* **4**, 147 (2005)
105. B. Cruden et al., Thermal Decomposition of Low Dielectric Constant Pulsed Plasma Fluoro-carbon Films: II. Effect of Postdeposition Annealing and Ambients. *J. Electrochem. Soc.* **146**(12), 4597–4604 (1999)
106. N. Marti et al., Production of polymeric materials with controlled pore structure: the “reactive gelation” process. *Macromol. Mater. Eng.* **290**, 221–229 (2005)
107. A.R. Mohamed, M. Mohammadi, G.N. Darzi, Preparation of carbon molecular sieve from lignocellulosic biomass: A review. *Renew. Sust. Energ. Rev.* **14**(6), 1591–1599 (2010)
108. Kita, H., Gas and vapor separation membranes based on carbon membranes, in *Materials science of membranes for gas and vapor separation*, ed. by Y. Yampolkii, I. Pinnau, B. D. Freeman (Wiley, West Sussex, 2006), pp. 337–354
109. P.J. Williams, W.J. Koros, Gas separation by carbon membranes, in *Advanced membrane technology and applications*, (Wiley, New York, 2008), pp. 599–631

110. E.M. Maya et al., Partially pyrolyzed membranes (PPMs) derived from copolyimides having carboxylic acid groups. Preparation and gas transport properties. *J. Membr. Sci.* **349**(1–2), 385–392 (2010)
111. M.N. Islam et al., Preparation and gas separation performance of flexible pyrolytic membranes by low-temperature pyrolysis of sulfonated polyimides. *J. Membr. Sci.* **261**(1–2), 17–26 (2005)
112. Z. Weiliang et al., Gas permeation properties of flexible pyrolytic membranes from sulfonated polyimides. *Chem. Lett.* **31**(5), 534–535 (2002)
113. Y. Xiao, T.-S. Chung, Grafting thermally labile molecules on cross-linkable polyimide to design membrane materials for natural gas purification and CO₂ capture. *Energy Environ. Sci.* **4**(1), 201–208 (2011)
114. M.L. Chua, Y.C. Xiao, T.-S. Chung, Effects of thermally labile saccharide units on the gas separation performance of highly permeable polyimide membranes. *J. Membr. Sci.* **415–416**, 375–382 (2012)
115. M. Askari, T. Yang, T.-S. Chung, Natural gas purification and olefin/paraffin separation using cross-linkable dual-layer hollow fiber membranes comprising β -Cyclodextrin. *J. Membr. Sci.* **423–424**, 392–403 (2012)
116. F. Piroux et al., Gas transport mechanism in sulfonated polyimides: Consequences on gas selectivity. *J. Membr. Sci.* **209**(1), 241–253 (2002)
117. A.L. Khan, X. Li, I.F.J. Vankelecom, Mixed-gas CO₂/CH₄ and CO₂/N₂ separation with sulfonated PEEK membranes. *J. Membr. Sci.* **372**, 87–96 (2011)
118. P.M. Budd et al., Polymers of intrinsic microporosity (PIMs): robust, solution-processable, organic nanoporous materials. *Chem. Commun.* **2**, 230–231 (2004)
119. Budd, P.M., et al., Gas permeation parameters and other physicochemical properties of a polymer of intrinsic microporosity (PIM-1), in *Membrane gas separation*, ed. by Y. Yampolskii, B. Freeman (Wiley, West Sussex, 2010), pp. 29–42
120. P.M. Budd et al., Gas permeation parameters and other physicochemical properties of a polymer of intrinsic microporosity: Polybenzodioxane PIM-1. *J. Membr. Sci.* **325**(2), 851–860 (2008)
121. K. Yuan et al., Phthalazinone-based copolymers with intrinsic microporosity (PHPIMs) and their separation performance. *J. Membr. Sci.* **541**, 403–412 (2017)
122. J.-Y. Lee et al., The potential to enhance membrane module design with 3D printing technology. *J. Membr. Sci.* **499**(Supplement C), 480–490 (2016)
123. A. Siddiqui et al., Development and characterization of 3D-printed feed spacers for spiral wound membrane systems. *Water Research* **91**(Supplement C), 55–67 (2016)
124. Z.-X. Low et al., Perspective on 3D printing of separation membranes and comparison to related unconventional fabrication techniques. *J. Membr. Sci.* **523**(Supplement C), 596–613 (2017)
125. J. Seo, D.I. Kushner, M.A. Hickner, 3D Printing of Micropatterned Anion Exchange Membranes. *ACS Appl. Mater. Interfaces* **8**(26), 16656–16663 (2016)
126. T. Femmer et al., Print your membrane: Rapid prototyping of complex 3D-PDMS membranes via a sacrificial resist. *Journal of Membrane Science* **478**(Supplement C), 12–18 (2015)
127. T. Femmer, A.J.C. Kuehne, M. Wessling, Print your own membrane: direct rapid prototyping of polydimethylsiloxane. *Lab Chip* **14**(15), 2610–2613 (2014)
128. T. Femmer, A.J.C. Kuehne, M. Wessling, Estimation of the structure dependent performance of 3-D rapid prototyped membranes. *Chem. Eng. J.* **273**(Supplement C), 438–445 (2015)
129. S. Badalov, C.J. Arnusch, Ink-jet printing assisted fabrication of thin film composite membranes. *J. Membr. Sci.* **515**(Supplement C), 79–85 (2016)
130. S. Badalov, Y. Oren, C.J. Arnusch, Ink-jet printing assisted fabrication of patterned thin film composite membranes. *J. Membr. Sci.* **493**(Supplement C), 508–514 (2015)
131. S. Yuan et al., Production of polyamide-12 membranes for microfiltration through selective laser sintering. *J. Membr. Sci.* **525**(Supplement C), 157–162 (2017)



N. Awang, Juhana Jaafar, A. F. Ismail, T. Matsuura,
M. H. D. Othman, and M. A. Rahman

Contents

1	Introduction	978
2	Proton Transport in Cation Exchange Membrane	980
3	Types of Proton Conductive Membrane Materials for Fuel Cell Applications	981
3.1	Perfluorinated Ionomers	983
3.2	Partially Fluorinated Polymers	983
3.3	Nonfluorinated Aliphatic Hydrocarbons	985
3.4	Nonfluorinated Membranes with Aromatic Backbones	986
3.5	Acid–Base Complexes	991
4	Enhancing Proton Conductivity by Electrospinning Technique	994
5	Electrospun Polymer-Based Nanofiber Membranes	996
6	Current Studies and Future Directions	1000
7	Conclusions	1000
	References	1001

N. Awang · J. Jaafar (✉) · A. F. Ismail (✉) · M. H. D. Othman · M. A. Rahman
Advanced Membrane Technology Research Centre (AMTEC), Universiti Teknologi Malaysia,
Johor Bahru, Malaysia

Faculty of Chemical and Energy Engineering, Universiti Teknologi Malaysia,
Johor Bahru, Malaysia

e-mail: nuhaawang@yahoo.com; juhana@petroleum.utm.my; juhana@utm.my; afauzi@utm.my;
dzarfan@utm.my; r-mukhlis@utm.my

T. Matsuura

Advanced Membrane Technology Research Centre (AMTEC), Universiti Teknologi Malaysia,
Johor Bahru, Malaysia

Department of Chemical Engineering, University of Ottawa, Ottawa, ON, Canada

e-mail: matsuura@eng.uottawa.ca

Abstract

The importance of proton conductivity is enormous for biological systems and in devices such as electrochemical sensors, electrochemical reactors, electrochromic devices, and fuel cells. In the book chapter, the phenomenon of proton conductivity in materials was discussed with a special emphasis on five different types of conductive materials, namely, perfluorinated ionomers, partially fluorinated, aromatic polymers, acid-base complexes, non-fluorinated ionomers, and hydrocarbon. In a fuel cell, the proton exchange membranes (PEMs) have a profound influence on its performance. Many researchers have investigated the functionalization methods to solve the methanol crossover problem and to obtain low electronic conductivity, low electroosmotic drag coefficient, good mechanical properties, good chemical stability, good thermal stability, and high proton conductivity. The way forward of developing high-performance proton-conductive polymeric membrane via electrospinning for as fuel cells was also addressed.

1 Introduction

Proton conductivity plays an important role in many processes; for example, the production of electricity in a hydrogen fuel cell and the photosynthesis in green plants. Proton is the main ion which has no electron shell. In this way, it strongly interacts with the electron density of its surroundings, which then takes some of the H (1s) characters [1, 2].

However, in nonmetallic compounds, proton strongly interacts with the valence electron density of only one or two nearest neighbors. If this is a single oxygen, being well separated from other electronegative species resulted in the formation of O-H bond which is less than 100 pm in length compared to ~ 140 pm for the ionic “radius” of the oxide ion. The proton finds its equilibrium position deeply embedded in the valence electron density of the oxygen (Fig. 1a). For medium distances between oxygen and another oxygen (~ 250 – 280 pm), the proton may be involved in two bonds: a short, strong bond with the so-called proton donor and a longer, weak

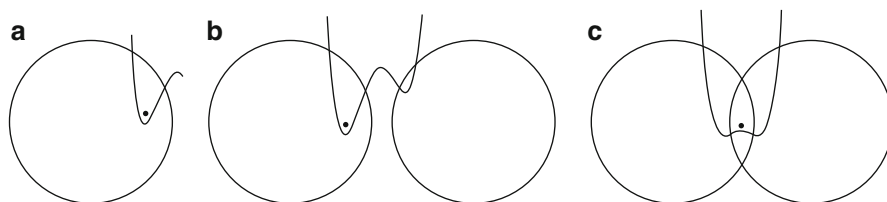


Fig. 1 A schematic representation for different cases of proton binding in a nonmetallic environment where the proton is coordinated to one or two preferentially basic species. Note that the given potential surfaces correspond to the electronic structure of the indicated proton positions [1]

bond with a proton acceptor. This is the case for an asymmetrical hydrogen bond ($\text{O-H}\cdots\text{O}$) which is directional in character (Fig. 1b). For extremely short oxygen separations (~ 240 pm), a symmetrical hydrogen bond may be formed, i.e., the proton is involved in two equivalent bonds (Fig. 1c) [3, 4].

Hydrogen bond is a type of interaction which involves proton conduction process. The stronger the covalent or ionic bonds, the hydrogen bonds have the tendency to fluctuate less [3]. For proton conduction process, distance between proton acceptor and proton donor is important in defining strong hydrogen bond and proton conductivity. It is clear that the compounds with the highest proton diffusivity are hydrogen-bonded liquids (for instance, dilute aqueous solutions of acids) or solids in which weak or medium hydrogen-bond interactions are not or just marginally confined by the vicinity of other sorts of bonds. An essential feature of hydrogen bond is to give a path to proton transfer from a proton donor to a proton acceptor and the part as proton conductor is played by materials which can be a proton conductor especially for ion exchange membrane [4].

Ion exchange membranes are thin films or sheets of ion exchange materials which can be used to allow the transportation of anions or cations and separate the ions [5]. In the 1950s, ion selective membranes in sheet form with high selectivity, low electrical resistance, good chemical stability, and high mechanical strength were observed [6]. In the 1970s, DuPont has invented a cation exchange membrane from sulfonated polytetrafluoroethylene which is chemically stable, known as Nafion[®]. The Nafion[®] is used for the application of energy storage system in the chlor-alkali production industry and energy conversion (fuel cell) [7].

Owing to high electrochemical property as well as chemical resistance, Nafion[®] still widely applied as the fundamental membrane for fuel cell [8]. The polytetrafluoroethylene backbone in Nafion[®] has been made with perfluorinated vinyl ethers pendant side chains which are terminated by a sulfonate ionic group [9, 10]. Since a nanophase separation occurs between hydrophobic matrix and hydrophilic ionic domains in the hydrated Nafion[®] due to the amphiphilic composition (water-soluble group attached to a water-insoluble nonpolar hydrocarbon chain), the membrane has to be fully hydrated for good proton conductivity in order to operate at temperatures below 80 °C. Other than that, the operating temperature must be increased above 100 °C for transportation and to limit the poisoning of anode catalysts by traces of CO, and thus enable high-energy-consumption applications [11].

Nafion[®] membranes, however, show drawbacks and dramatic alteration which are caused by water evaporation. So, at these temperatures, Nafion[®] has weak conductivity performance and the effect can be related to the dehydration of initial ionic domains. Therefore, commercially available Nafion[®] membranes nowadays do not fulfill the specification of a fuel cell that can be applied above 100 °C and hydrated swollen membranes are desirable at elevated temperatures for the purpose of maintaining mechanical properties and proton conductivity [12].

There are two principal mechanisms that portray proton diffusion in a manner that the proton stays shielded by some electron density along the whole diffusion path. One of the well-known principal mechanism is the principal situation where

“vehicles” show to claim local dynamics yet dwell on their destinations, the protons being exchanged inside of the hydrogen bonds from one “vehicle” to another. Extra redesign of proton environment involves reorientation of individual species or significantly more expanded gatherings, then resulted in the formation of continuous trajectory for proton migration. This mechanism is often termed as Grotthuss mechanism.

2 Proton Transport in Cation Exchange Membrane

The transport of proton in cation exchange membrane is greatly affected by the presence of water molecules. Water molecules provide a probe for the local environment, and the hydrogen bond network dynamics of water is confined in the hydrophilic region of cation exchange membrane materials. Therefore, water provides a better medium for protons to freely move than other common ions environment. This is the result of the fact that proton in water does not take place through normal diffusion, but via a process where the hydrogen bonds between water molecules are converted into covalent bonds and vice versa [13].

The movement of proton in hydrated state occurs in two processes which are free solution-diffusion process (Fig. 2a) and proton hopping process (Fig. 2b). Proton diffuses into water phase explained the first process while the movements of protons in sequential steps involving the formation and breakage of hydrogen bonding of a series of water molecules explained the proton hopping mechanism. In Grotthuss mechanism, the original proton that enters the membrane is not the proton that comes out of the membrane. This is because, it is not the proton itself that is transported; only the charge of the proton is transported, and not its mass. The charge is basically passed on from one water molecule to another water molecule [14].

Proton transport through a hydrated ion exchange membrane can, in principle, occur via the two processes mentioned above. The approach to explain the transport in ion exchange membrane is that the water in an ion exchange material can be understood as bound (or “nonfreezable,” “associated”) water and free (“freezable,” “bulk-like”) water. The free water resembles bulk water with hydrogen bonds as the major interactions.

Bound water molecules are in the vicinity of the materials while the free water is further away. The strength of bonding between the bound water molecule and the materials is more prominent than that of hydrogen bonding in free water. The free water is bulk-like but the bound water is thought to be a part of the materials. The free solution diffusion of a proton through a hydrated membrane can, in principle, include both free and bound water. On the other hand, the free diffusion is much slower in bound water. Then again, the proton hopping or the Grotthuss mechanism can happen in both free and bound water. This transport phenomenon in ion exchange membrane clarifies the ion transport in polyelectrolyte membranes [15]. Figure 3 illustrates the domain distribution of proton, water, and methanol transport in polyelectrolyte membranes.

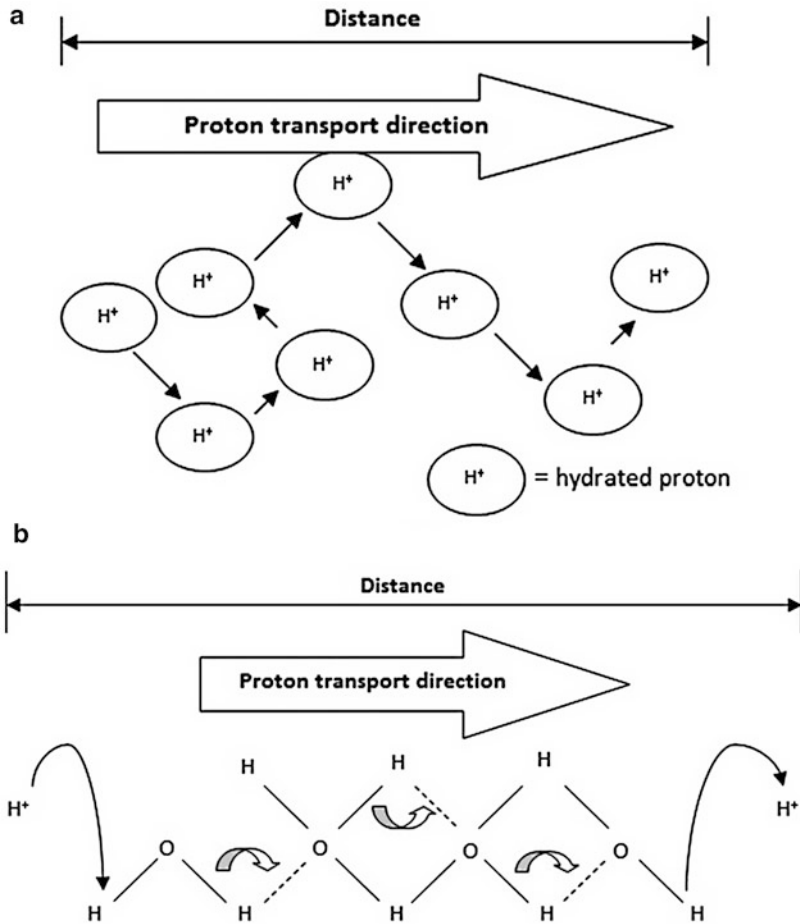


Fig. 2 Proton transport via (a) free solution diffusion and (b) proton hop mechanism (Grotthuss mechanism) [15]

3 Types of Proton Conductive Membrane Materials for Fuel Cell Applications

The materials which represent the majority of all-known fast proton conductors applied in the synthesis of polymer membranes can be generally classified into five different groups: perfluorinated ionomers, partially fluorinated polymers, non-fluorinated hydrocarbons, nonfluorinated membranes with acid-base complexes, and aromatic backbones [16]. Figure 4 shows the categories of membranes based on the materials applied [17].

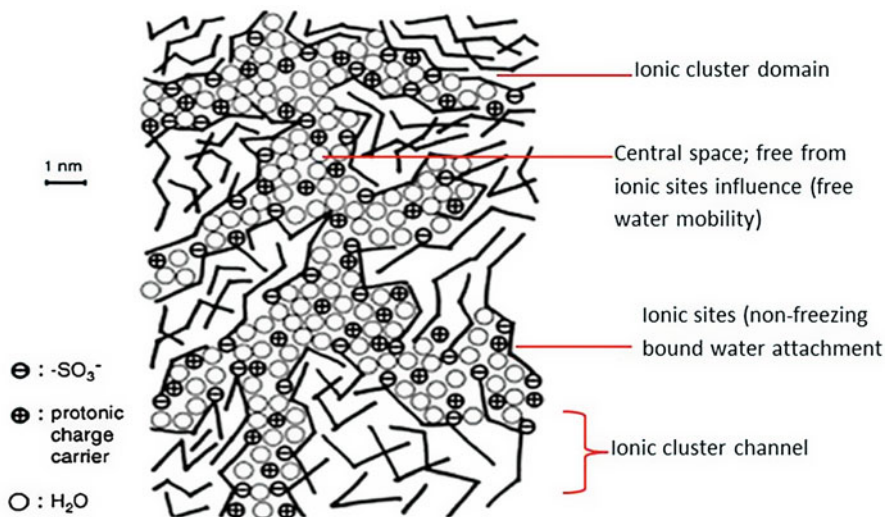


Fig. 3 An illustration of domain distribution in sulfonated polymer electrolyte membranes [16]

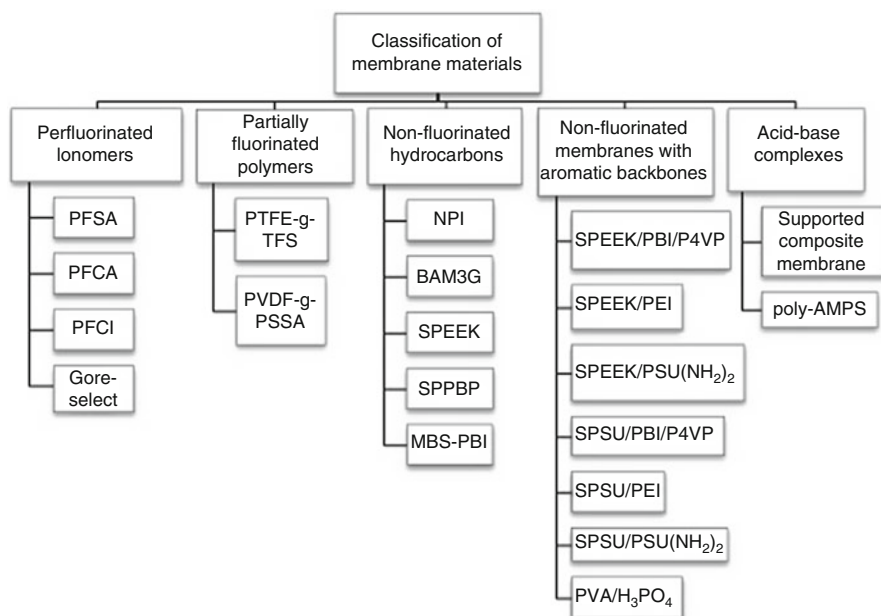


Fig. 4 The categories of membranes based on materials [17]

The most highest proton conductivity happens at 100% relative humidity. Other than the disadvantages of the membrane, proton conductivity which depends on the humidity of Nafion[®] constrains the utilization of Nafion[®] as a membrane in a fuel cell. Other than this, since the fuel that is utilized as a part of the fuel cell framework, for example, alcohol-based fuels and hydrogen are dissolvable in water over a wide range of compositions, this raises an issue based on the fact that not just water diffuses through the polyelectrolyte membrane (PEM) but the fuel as well. Henceforth, the reaction focuses on the cathode which alludes to mixed potential. Apparently, decreasing the water uptake can promptly diminish the methanol crossover issue. Lamentably, decreasing the fuel crossover all this while yields proton conductivity [189].

Based on these disadvantages, analysts have attempted to imagine a low fuel permeability and high conductivity membrane from hydrocarbon polymer and partially perfluorinated ionomer that can dismiss the current inadequacies as of now, and the membranes are utilized in low- and high-temperature operation.

3.1 Perfluorinated Ionomers

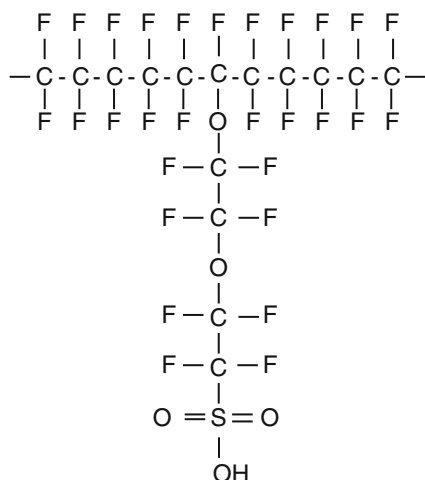
Nowadays, perfluorinated polymers have been intensively studied due to special characteristics which are high electronegativity of fluorine atom with C–F bond, small in size, and low polarization capacity [18]. The membranes usually apply the incorporation of a moiety of a molecule more than sulfonic group ($-\text{CF}_2\text{SO}_3\text{H}$) that can be further treated into the membranes either anionic or cationic way [19]. Owing to good chemical and thermal stability, this type of polymers is also used as part of a chlor-alkali process in producing proton exchange membranes for fuel cell application.

Perfluorinated polymers have been commercially manufactured by three major companies which are DuPont (Nafion[®]), Asahi Glass (Flemion[®]), and Asahi Chemical (Aciplex-S[®]). Nafion[®] was widely applied compared to others commercialized membranes due to high proton conductivity, high mechanical strength, and good synthetic stability [20]. The Nafion[®] chemical structure is shown in Fig. 5.

3.2 Partially Fluorinated Polymers

Over the past 20 years, there are several studies that have been attempted to produce novel proton exchange membranes by utilizing partially fluorinated polymers as the main materials [21]. Few approaches were discovered for instance grafting porous PTFE with partially fluorinated sulfonated poly(arylene ether ketone), sulfonating poly(arylene ether sulfone)s containing fluorophenyl pendant group, and blending polybenzimidazole with a fluorinated polymer [21, 22]. The results have shown several improvements not only mechanically but also

Fig. 5 Chemical structure of Nafion[®]



chemically. This significant improvement in membrane properties can be related to C–F bond strength (460 kJ/mol) which is greater than that of C–H bond (410 kJ/mol) [23].

Further modification of better PEM was done by Kerres' group by arranging the of fractional oxidation of sulfonated polysulfone (PSU) and consequent cross-linking of the remaining sulfonate groups with α,ω -diiodoalkanes by utilizing sodium hypochlorite (NaOCl) [24–27]. The advantages of the process are: (1) no side reaction occurs during oxidation process, (2) the partially oxidized polymer is stable at ambience environment, and (3) the desired oxidation degree is easily balanced. The study found that the application of swelling ratio and water uptake weaken the membrane mechanical and is the using of different types of cross-linker chain length and the difference of oxidation degree in sulfonated polymer. Eventhough the method successfully improve the desired properties, desired proton conductivity still cannot be achieved due to the cross-link interaction that brings down the quantity of free $-\text{SO}_3\text{H}$ groups in the cross-linked membranes [25]. Another characteristic which is marked as failure in this study is the compatibility issue between Nafion[®] bonded anode and cross-linked hydrocarbon membrane.

To date, a research on reinforced partially fluorinated membranes proved to have superior properties than fluorinated hydrocarbon membranes. The membranes demonstrated high water uptake, low interfacial resistance, and high mechanical strength [28–30]. Besides, reinforced composite membranes from partially fluorinated membranes also showed better dimensional stability and low cost [31–35]. In any case, the execution of PTFE composite membrane is profoundly reliant on the combination of state polymer and porous PTFE substrate [36].

The combination of α , β , and β -trifluorostyrene monomer was then discovered to improve the fuel cell properties [37, 38]. Figure 6 shows the chemical structure of

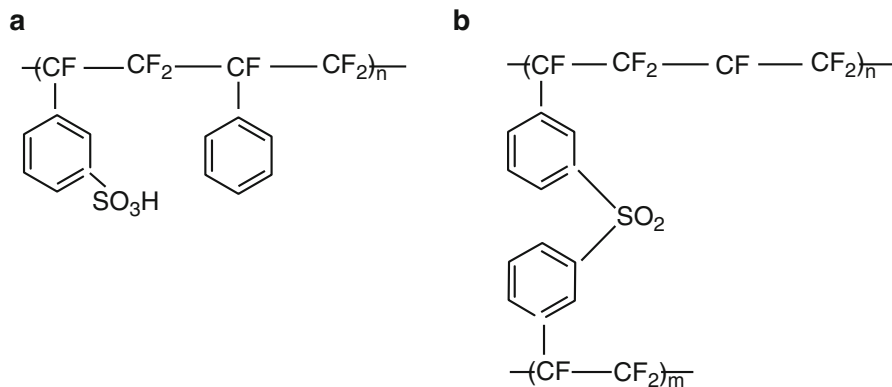


Fig. 6 (a) Linear poly(trifluorostyrene) and (b) cross-linked poly(trifluorostyrene)

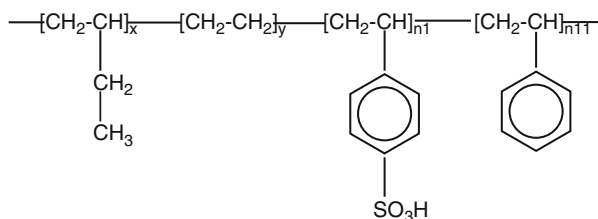
the polymer. The observation was done using the optimization of reaction of ion exchange capacity with multiple equivalent weights from both cross-linked and linear α , β , β -trifluorostyrene. The outcomes showed that the beta coordinating impacted the perfluorinated polyalkyl group attached to the aromatic ring and caused a great problem in the sulfonation of poly- α , β , β -trifluorostyrene. The problem in the sulfonation procedure was due to the meta-coordinating impact of the perfluorinated polyalkyl group attached to the aromatic ring as shown in Fig. 6

3.3 Nonfluorinated Aliphatic Hydrocarbons

Nonfluorinated aliphatic hydrocarbons are one type of membranes that is used to synthesize proton exchange membranes [39, 40]. The polymer materials can be aromatic or aliphatic in bulk pendant groups or in a polymeric backbone of a membrane. Nowadays, the best technique to deliver a high proton conductor electrolyte membrane is by utilizing hydrocarbon polymers as the polymer backbones [41].

Hydrocarbon membranes offer few advantages over PFSA membranes such as less cost, economically accessible, and their structure permits the introduction of pendant groups from the polar site. Hydrocarbon polymers comprise of polar groups which restrict the absorption of water to polar groups of polymer chain and have high water uptake over a large range of temperature. A certain degree of appropriate molecular design can be disintegrated due to the decomposition of hydrocarbon polymers. Likewise, hydrocarbon polymers are effectively reused by ordinary strategies. The chemical structure of the hydrocarbon is shown in Fig. 7.

Table 1 shows the summary of previous studies regarding the synthesis of nonfluorinated aliphatic hydrocarbon materials. Figure 8 shows the prominent structure under this category.

Fig. 7 Poly(butadiene styrene) block copolymer**Table 1** Modification of aromatic polymers

No.	Types of membrane (category)	Design methodology
1	Sulfonated poly(4-phenoxybenzoyl-1,4-phenylene) (SPPBP)	Formulated from poly(<i>p</i> -phenylene) and particle course of action fundamentally like poly ether ether ketone (PEEK). Direct sulfonation created a highly proton conductive polymer [42]
2	Cross-linked/non-cross-linked (SPEEK)	Direct sulfonation of PEEK in corrosive sulfuric acid resulted in high thermal stability alongside proton conductivity [42]
3	BAM3G membrane (Ballard advanced material of third generation membrane)	Polymerization of α , β , β -trifluorostyrene incorporated the monomer screened from a group of substitution α , β , β -trifluorostyrene [43]
4	Membrane of base-doped with S-polybenzimidazoles (PBI)	Presentation of natural inorganic Bronsted bases to sulfonated PBI [44]
5	Methylbenzenesulfonate PBI/methylbenzenesulfonate poly(<i>p</i> -phenylene terephthalamide) membranes	These alkylsulfonated aromatic polymer electrolytes have extremely brilliant proton conductivity and thermal stability when compared to PFSA membranes, even above 80 °C [21]
6	Imidazole-doped sulfonated polyetherketone (SPEK) Methylbenzenesulfonate PBI/ methylbenzenesulfonate poly(<i>p</i> -phenylene terephthalamide) membranes	Complexation with imidazoles to accomplish high proton conductivity [4]. These alkylsulfonated aromatic polymer electrolytes have extremely brilliant proton conductivity and thermal stability when compared to PFSA membranes, even above 80 °C [21]
7	Imidazole-doped sulfonated polyetherketone (SPEK)	Complexation with imidazoles to accomplish high proton conductivity [4]
8	Imidazole-doped sulfonated polyetherketone (SPEK)	Complexation with imidazoles to accomplish high proton conductivity [4]

3.4 Nonfluorinated Membranes with Aromatic Backbones

Thermal stability of a proton exchange membrane can be improved by applying these two major approaches: (a) modification of polymers with bulky groups in the backbone of the aromatic polymer to give them relevant protons conduction and (b) incorporation of aromatic hydrocarbon specifically into the hydrocarbon polymer

Table 2 Findings of electrospun fiber polymer-based membrane for fuel cell application [48]

No.	Membrane type	Proton conductivity (mS cm ⁻¹)	Ion exchange capacity (meq/g)	Modification information
1	Sulfonated polysulfone	–	2.16	Synthesized by utilizing intricate sulfur trioxide-triethyl phosphate as the sulfonating operators. Excellent mechanical properties and generally high IEC were obtained [49].
2	Sulfonated polyethersulfone (SPES)	–	2.22	SPES was covalently cross-linked and integrated by utilizing substituted diamine-sulfone to bring high proton conductivity and mechanical quality for operations above 100 °C [50].
3	Styrenic system of styrene divinyl benzene (SDVB) poly(arylene)	–	3.65	Sulfonated naphthalene type polyimides were combined to accomplish low water/methanol permeability, high proton conductivity, and coefficients different from PFSA [51].
4	Styrenic system of styrene divinyl benzene (SDVB)	–	2.15	SDVB and poly (fluoroethylene-co-hexafluoropropylene) (FEP) were combined, trailed by sulfonation by achieving membranes extremely indistinguishable to PFSA [52].
5	Sulfonated polyether ether ketone (SPEEK) and sulfonated poly (4-phenoxy benzoyl-1,4-phenylene)	10.00	–	PPBP and PEEK were sulfonated by utilizing concentrated sulfuric acid. Thermal stability up to at least 200 °C was obtained. A conductance of around 10 ⁻² S/cm at 65 mol% of sulfonation in the event of SPPBP was observed while SPEEK showed a lower conductance for the same mol% of sulfonation [53].
6	Sulfonated poly [bis (3-methyl phenoxy) phoszene]	9.20	1.40	The base polymer and sulfur trioxide were sulfonated by yielding higher proton conductivity, cross-linking, lower water, and methanol diffusion synthetic mechanical stability when contrasted to Nafion [®] [54]

(continued)

Table 2 (continued)

No.	Membrane type	Proton conductivity (mS cm ⁻¹)	Ion exchange capacity (meq/g)	Modification information
7	Sulfonated polyimide (PI)	29.00	–	PI was sulfonated by utilizing sulfur trioxide to obtain properties proportionate to Nafion 117 [55].
8	Hydrogenated poly (butadiene-styrene) (HPBS) sulfonated polystyrene	54.00	1.43	Polystyrene was sulfonated by utilizing acetyl sulfate as the sulfonating specialists. To expand the sulfonation, ionic conductivity was equipotential to Nafion [®] (10 ⁻³ to 10 ⁻² S/cm). In any case, discontinuity in the properties at 15% sulfonation was noted [56]
9	Hydrogenated poly (butadiene-styrene) (HPBS)	–	1.00	Incorporated by heterogeneous sulfonation of poly (butadiene-styrene). Mixed with polypropylene as an improvement in both proton conductivity and thermal properties [57]
10	Poly [aryloxyphosphazene] polymers	58.00	0.99	Aryloxyphosphazenes bearing bromo-phenoxy side groups were treated with t-butyllithium, continued with diphenylchlorophosphonate by converting to phenyl phosphonic acid groups [58]
11	Sulfonated polyaryls	23.00	–	Polyetherketones were recustomized by mixing it with polymers including immobilized heterocycles; for instance pyrazole, imidazole, or benzimidazole as the proton solvating species to accomplish high proton conductivity. Water crossover was definitely reduced while proton conductivity was kept high [59]
12	Impregnating fleeces on polyte-trafluoro ethylene (PTFE) matrix	0.07	–	Polysulfone, micro glass fiber, and a composite grid constituting both fleeces were impregnated on a PTFE matrix. Different from the two impregnated fleeces, the composite membranes did not show similar or lower resistance than Nafion 117 [60]

(continued)

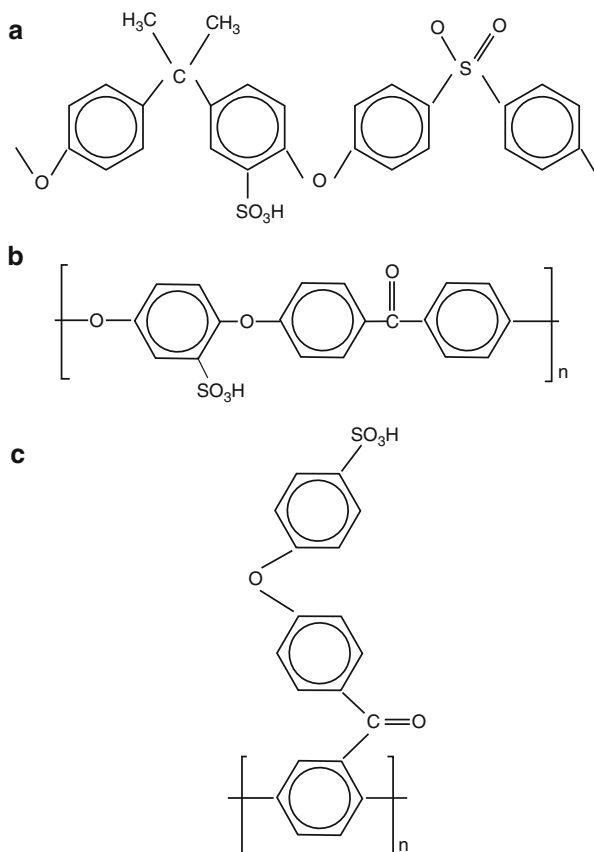
Table 2 (continued)

No.	Membrane type	Proton conductivity (mS cm ⁻¹)	Ion exchange capacity (meq/g)	Modification information
13	Sulfonimide compound	60.00	0.99	Cross-linking sulfonimide was integrated by applying the macromolecular substitution method to deal with the phosphazene bearing pendant sulfonimide gatherings produced to obtain high proton conductivity [58]
14	Polystyrene graft polymerSulfonimide compound	11.00	1.07	Cross-linking sulfonimide was integrated by applying the macromolecular substitution method to deal with the phosphazene bearing pendant sulfonimide gatherings produced to get high proton conductivity [56]
15	Polystyrene graft polymer	–	3.40	Cross-linking styrene/acrylonitrile was acquired from <i>N</i> -vinylpyrrolidone/2-acrylamide-2-methyl-1-propane sulfonic acid graft polymer by applying divinylbenzene and kept it in order to acquire a better stability in an oxidative domain [61]

conductivity up to 10⁻⁵ Scm⁻¹ at 120 °C [58]. The structures of nonfluorinated membranes with aromatic backbones classification are shown in Fig. 9.

Poly(2,6-dimethyl-1,4-phenylene oxide) (PPO) is a hydrophobic polymer with a high glass transition temperature ($T_g = 210$ °C), excellent hydrolytic stability, and high mechanical strength. Eventhough PPO chemical structure is simple compared to other aromatic polymers, it permits many modifications on both benzyl and aryl positions, characteristics of PPO meet most of the requirement for PEMFCs application. The PPO chemical structure also favored for fuel cell application due to their stability in acidic medium and thermally stable: (1) nucleophilic substitution of bromomethylated PPO, (2) electrophilic substitution on benzene ring, (3) coupling and capping of terminal hydroxyl groups in PPO chains, (4) metalation of PPO with organometallic compounds, and (5) radical substitution of hydrogen from methyl groups [42].

Fig. 9 Structures of (a) SPSU, (b) SPEEK, and (c) SPPBP



3.5 Acid–Base Complexes

Acid–base complexes are well known as low-cost and practical substitution for proton exchange membranes. The materials are proved to maintain highly proton conductive in elevated temperatures. The acid–base complexes normally involve the process of incorporating acid component into alkaline polymer base to activate proton conduction [16]. The chemical structures of acid–base complexes polymers are shown in Fig. 10.

Currently, the most outstanding system for high-temperature PEMFC under ambient pressure is phosphoric acid-doped polybenzimidazole ($\text{PBI}/\text{H}_3\text{PO}_4$) membrane. Different studies have used polybenzimidazole ($\text{PBI}/\text{H}_3\text{PO}_4$) for various applications, for example, fuel cell technologies, physicochemical characterizations, and membrane casting. Many researchers have focused on acid-doped PBI membranes. High-temperature PEMFC effectively appears at temperatures of up to 200°C under ambient pressure, and related fuel cell technologies have been created.

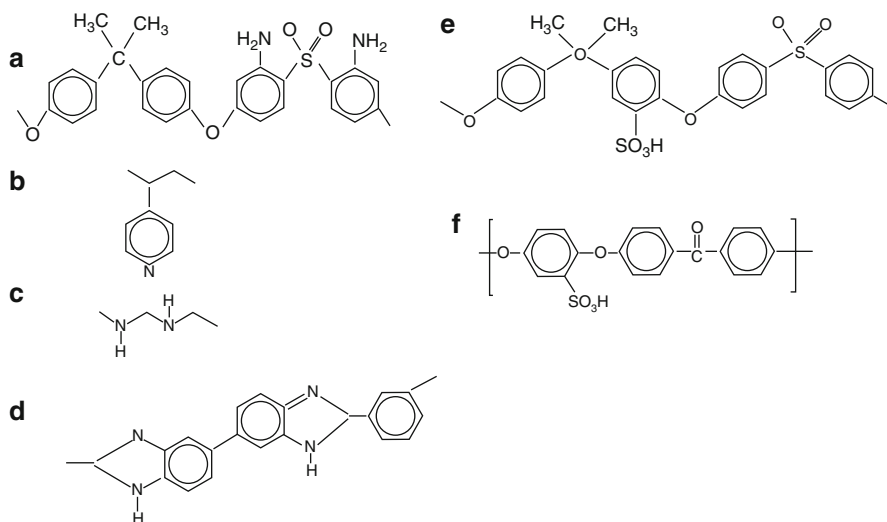


Fig. 10 Structure of basic polymers (a–d) and acidic polymers (e and f)

The upside of the membrane is mandatory for gas humidification which allows the elimination of complicated humidification system in contrast and Nafion[®] cells. Other exceptional working elements of PBI are simple control of cell temperature and air flow [66].

The acid-base membranes comprise of basic polyetherimide (PEI) and sulfonated polymers (aPBEEK, sPPENK, and sPPESK). All the membranes mentioned have been studied and have shown thermostability, oxidative resistance with highly proton conductivity, hydrolysis resistance, and excellent resistance to swelling. From the observation of every attribute, they are anticipated as high potential proton exchange membrane materials later on [67].

As of late, the improvement of membranes selection with sensible cost and great performance, fuel cells have been broadly concentrated on. Acid-base polymer blends are said to be highly potential materials because of the interactions in the middle of polymers and acid, for instance, hydrogen bonding bridges and ionic cross-linking (electrostatic forces) increase the membrane swelling control without reducing the flexibility. Thus, these membranes have high mechanical flexibility and strength, high proton conductivity, low water uptake, great thermal stability, and decrease crossover [46, 68–74].

The mixture of acid-base polymer membranes were prepared by blending sulfonated poly (2, 6-dimethyl-1, 4-phenylene oxide) (sPPO) with (3-aminopropyl) triethoxysilane (A1100) by utilizing a sol-gel process for fuel cell application. Analyses have shown that acid-base interaction enhances membrane homogeneity and thermal stability as well as flexibility and mechanical strength [57, 75, 76].

Poly (2, 21-(*m*-phenylene)- 5, 51-benzimidazole)/phosphoric acid (PBI/H₃PO₄) complex is both promising and captivating. It has demonstrated high potential for

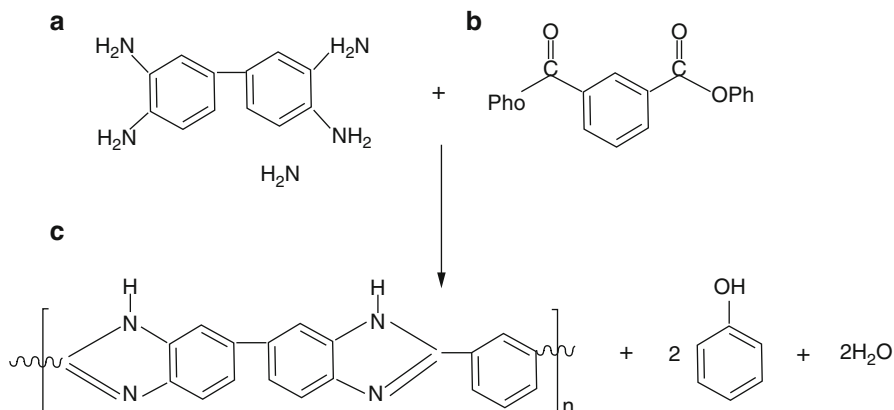


Fig. 11 Structure of (a) tetraaminobiphenyl, (b) diphenyl isophthalate, and (c) poly [2,2'-(*m*-phenylene)-5,5' bibenzimidazole]

fuel cell applications at medium temperature and subsequently numerous investigations have been made to optimize and understand this specific system. A broad observation on the PBI complexes has been completed at Case Western Reserve University. The structure of the reactants and the PBI item are shown in Fig. 11.

A research conducted on blending of sulfonated polysulfones and doped H_3PO_4 – PBI [77, 78]. PBI acid-base membranes are known for their excellent attributes in fuel cell applications (with improvement in conductivities above 10^{-2} S/cm 160°C at 80% relative humidity which is higher than acid-doped PBI membranes under the same condition). However, their long-term stability of doped PBI membranes has yet to be found and proven.

Acid-base complex membranes ($\text{PBI}/\text{H}_3\text{PO}_4$) do not depend on humidity. The materials are highly sensitive to the doping level of complex. As the doping level increases, the proton conduction of the materials increases. A research proved that the conductivity of PBI membrane was about 4.6×10^{-2} S/cm at a temperature of 165°C at 450% doping. It has been shown that conductivity could reach 0.13 S/cm at extremely high doping level around 1600%. The situations occur when the doping constantly increases, the anion moieties support the proton hopping between imidazole sites and the distance between the clusters of acid sites decreases. The significant effects of applying high-temperature specialty polymers are not only for thermal stability purpose but also to promote stability in oxidative, reducing, and acidic environments [28, 79–84].

A study has supported proton hopping mechanism which is called Grotthuss mechanism for PBI membrane doped with phosphoric acid as acid-base complex ($\text{PBI}/\text{H}_3\text{PO}_4$) [85]. The research has been carried on a doped $\text{PBI}/\text{H}_3\text{PO}_4$ membrane at 190°C under atmospheric pressure and produced a current density of $1.2 \text{ A}/\text{cm}^2$ and a power density of $0.55 \text{ W}/\text{cm}^2$. Conductivity data of doped PBI at temperatures below glass transition temperature and the relatively high change in entropy (which

could be related to the molecular rearrangements that is essential for Grotthus mechanism) showed that Grotthus mechanism is possible. At such elevated temperatures, the poison tolerance of the electrode catalysts was significantly improved compared to that at lower temperatures [86].

There are several polymers from the acid-group complex type that have been tested for fuel cell performance [87]. The research on poly(4-vinylimidazole)-H₃PO₄ complexes has shown that the complexes of amorphous polyamide with H₃PO₄ have high conductivity but low mechanical strength and lack chemical stability at temperatures above 90 °C [88]. Another research that synthesized synthesized a new protonic conductor gel (PVAL/H₃PO₂/H₂O) using prime chemicals which were H₃PO₂ (hypophosphorous acid) and PVAL (polyvinyl alcohol) showed improvement in mechanical property. The study reached the highest electrical conductivity at ambient and sub-ambient temperatures in this type of material reported up to now in the literature (in the order of 10⁻¹ Scm⁻¹). In addition, the variation of electrical conductivity with temperature and acid concentration was studied. The highest open fuel cell voltage measured at 23 °C was 435 mV. The performance of the fuel cell improved when it was fed with humidified hydrogen [89].

SPEEK/PBI membranes which comprised of poly(benzimidazole) PBI as the basic compound and sulfonated poly(etheretherketone) SPEEK as the acidic compound have been reviewed by Kerres et al. [90]. The membranes exhibited high thermal stability (decomposition temperatures more than 270 °C), excellent proton conductivity at ion-exchange capacities IEC of 1, and showed good performance when tested in H₂ membrane fuel cell.

Despite these selected polymers have been studied as membrane and have achieved high proton conductivity, some studies regarding the fabrication of polymer are still rare. Hence, the technique needs to be further investigated in order to improve the mass transfer and solve the methanol crossover problem. One of the suggested fabrication methods is electrospinning. The method is believed able to improve the pathway and provide better characteristics for DMFC membranes.

4 Enhancing Proton Conductivity by Electrospinning Technique

Electrospinning is one of the most straightforward, adaptable, and advanced processing technique in delivering nanofibers [91]. The process is grouped into a couple of strategies, for instance, magneto-electrospinning vibration-electrospinning, bubble electrospinning, and siro-electrospinning. The principal patent of electrospinning has been issued by Formhals in October 1934 [92]. In spite of the fact that the procedure has been generally connected for just about 70 years, the utilization of electrospun nanofibers as a part of delivering membrane for fuel cells is still new. In this manner, the situation leads electrospinning process to end a subject of interest for several years [91].

Actually, the electrospinning process became widely known in the sixteenth century prior when William Gilbert recorded the first electrostatic attraction of

a liquid. In 1846, highly nitrate cellulose was delivered by Christian Friedrich Schonbein. In 1900, the first electrospinning patent was filled by John Francis Cooley. John Zenely has distributed the work on fluid droplets qualities towards the end of metal capillaries in 1914. His exertion started the endeavor to simulate a model that conduct fluid mathematically under electrostatic forces [92].

In addition, the majority of work presented by Formhals and Zenely were specifically connected to the polymer. Compared to conventional techniques, for example, melt spinning, wet spinning, and dry spinning, electrospinning can create smaller pore size and larger specific surface area with the diameter of fiber ranging 10~1000 nm, while the conventional system can only deliver fiber with a diameter in the range of 5~500 μm [91].

In the electrospinning method of polymers, high-voltage electrostatic field is connected to the charged surface of the polymer solution bead and subsequently will prompt the ejection of a liquid jet through a spinneret. Due to the current circumstances, the electrostatic force conquers the surface tension of the bead and the formation of Taylor cone occurs when the solution is leaving the tip of the spinneret and thus prompting the charged jet in the long run [20, 93–103]. The formation of Taylor cone is proportional to the connected voltage, the voltage continues to expand until the equilibrium condition is obtained between the surface tension and the electrostatic force (Fig. 12). The electric field controls the course of charge jet and the solidified spun fiber is gathered on the turning or stationary conductive collector [20, 93–102, 104, 105]. A setup for electrospinning is shown as in Fig. 13.

Other than electrospinning process, template synthesis, drawing, phase separation, and self-assembly are the other methods that can be used in developing nanofibers [98, 99]. However, due to the versatility possessed by electrospinning process, it becomes more favorable to be used in developing highly porous, patterned, and nanofibrous polymeric materials nanofibers [100].

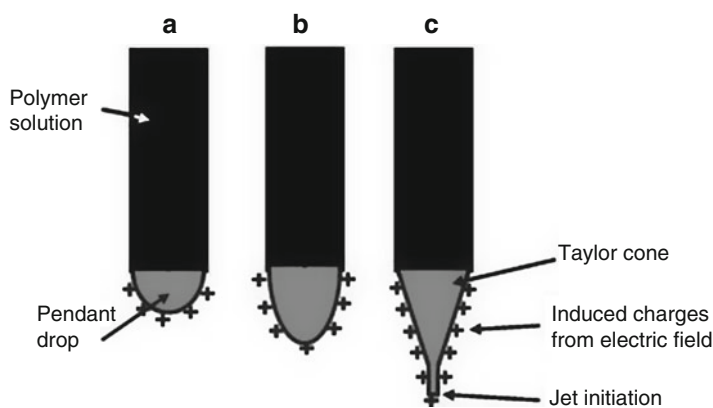


Fig. 12 Formation of Taylor cone. Voltage is increased until the equilibrium between surface tension and electrostatic force is achieved as in Fig. 11c [97]

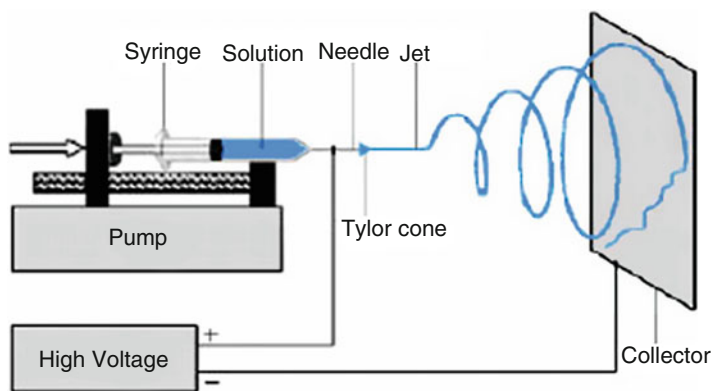


Fig. 13 Electrospinning setup

5 Electrospun Polymer-Based Nanofiber Membranes

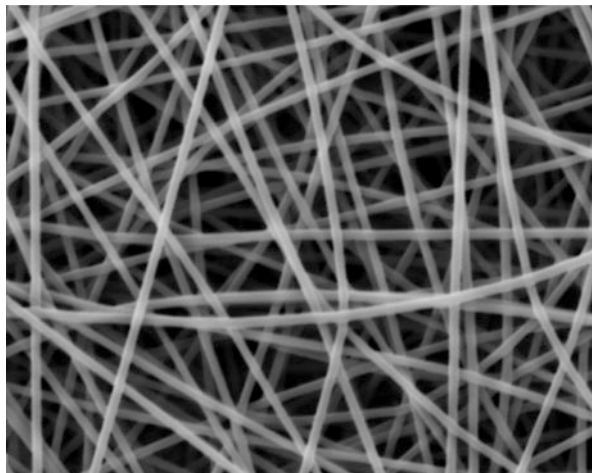
As aforementioned, the work presented by Formhals and Zenely were only connected to the polymer and this turns the initial move towards expanding the improvement of electrospun nanofibers from different kinds of polymers. Nanofibers have been created from hundreds kinds of polymers [48] and just a few concentrates on the impact of polymer-based membrane electrospun fibers in fuel cell application. The following are a few polymer-based membranes that have been mainly utilized lately to make nanofibers for fuel cell application.

Nafion[®] has been economically utilized as a polymer electrolyte membrane and it has demonstrated high performance in proton conductivity [92] which is essential for fuel cell. Another direction for Nafion has been induced being developed of Nafion nanofibers by Dong et al. [102]. A total of 0.1% of high molecular weight carrier polymer, poly (ethylene oxide) PEO ($M_w = 8000 \text{ kg/mol}$), was utilized as a part of their study. They effectively acquired higher purity for Nafion[®], Nafion nanofiber and higher proton conductivity with a magnitude of 1.5 Scm^{-1} compared to bulk Nafion[®], Nafion film. The reduction in diameter of the fiber from 500 nm to 400 nm was found to enhance the proton conductivity of the fuel cell.

The ionic morphology of polymer-based membrane (the morphology of a polymer is based on the impact of proton conductivity) is another essential trademark for improving proton conductivity. The orientation of ionic domains along the fiber pivot direction can be obtained due to the application of shear force during electrospinning process. Figure 14 shows the image of 400 nm wide Nafion nanofiber. The picture portrays the request of magnitude (aligned structure) higher than that of bulk business nafion the aligned electrospun fibers bring higher conductivity and this orientation can be extended if the utilized of shear forces increment as a part of parallel with diminishing the fiber diameter [106].

Tamura and Kawakami [103] have synthesized membrane electrolytes containing sulfonated polyimide nanofibers and sulfonated polyimide for proton exchange

Fig. 14 SEM image of 99.9 wt% Nafion nanofiber



membrane fuel cell. They found that the polyimides inside the nanofiber were fundamentally oriented when electrospun. This membrane demonstrated a change in stability by expanding the measure of aligned nanofiber while the gas crossover permeability diminished when contrasted with membrane without nanofibers because of the total structure inside the nanofibers. Moreover, the proton conductivity of the membrane in parallel direction demonstrated a higher value when contrasted with membrane in perpendicular direction and sulfonated polyimide membrane without nanofibers that was prepared through solvent casting technique.

Pan et al. [104] in their study has concentrated on adding nanowire-based superior in the application of smaller scale fuel cells. Nafion/poly (vinyl pyrrolidone) (PVP) nanowires (NPNWs) were blended by electrospinning. 1.27 g of Nafion (E.I.DuPont Company, identical weight (EW) = 1100), 0.26 g of PVP (Sigma, MW~1300 000), and 2.1 mg tetramethylammonium chloride (Sigma) in 0.7 g ethanol were prepared as the antecedent polymer for electrospinning. Plastic syringes with stainless-steel needle used and the 10 cm separation between the needle tip and the collector was connected. The voltage connected was 16 kV. The use of PVP as a part of this study was devoted to the high subatomic weight of PVP. It was kept in mind that the end goal was to effectively electrospin the Nafion with no commitment on proton conductivity [120–125].

Electrospun Nafion itself is difficult to create alone because it is not soluble in most normal solvents and thus will inevitably lead to the arrangement of micelles which diminish the chain entrapment [105]. Pan et al. [104] have utilized the authority which is made of two conductive substrates (silicon) isolated by a void gap. The study found that the transportation of protons to reach the cathode in NPNWs turned out to be more effective, hence the proton conductivity of NPNWs was found to be bigger corresponding to the diminishing measurement because of the increment in the level of the “texture” coming about because of special orientation [126–139]. They uncovered that the proton conductivity can be upgraded by adjusting the distance across the NPNWs below 2.3 μm . The other findings on the

Table 3 Findings on electrospun fiber polymer-based membrane for fuel cell application [48]

Based polymer	Filler/carrier polymer	Proton conductivity (mS cm ⁻¹)
Poly(vinyl alcohol)	Nafion [®]	22
Polyvinylidene fluoride	Nafion [®]	2
Sulfonated polyethersulfone	Nafion [®]	~85
Sulfonated random copolyimide	Sulfonated polyimide	Up to 370
Bromomethylated sulfonated polyphenylene oxide (BPPO)	Sulfonated poly(2,6-dimethyl-1,4-phenylene oxide) (SPPO)	30–80
3 M perfluorosulfonic acid polymer	PEO	55
Nafion [®]	5 wt% PVA or PEO	8.7–16
3 M perfluorosulfonic acid polymer	PAA	498
Polymerized ionic liquid	Poly(MEBIm-BF ₄), PAA	7.1 × 10 ⁻⁴
Sulfonated poly(ether ether ketone ketone)	None	37 (solvent DMF) 41 (solvent DMAc)
Sulfonated poly(arylene ether sulfone)	None sulfonated polyhedral oligomeric silsesquioxane (sPOSS)	86 94
Sulfonated copolyimide		~100
Polyvinylidene	Phosphotungstic acid (PWA, up to 12.8 wt%)	~0.4
Aquivion TM	PEO (Mw 1x106)	66
Sulfonated Zro2	PVP, poly(2-acrylamido-2-methylpropanesulfonic acid) (pAMPS)	240

electrospun fiber polymer-based membrane for fuel cell application are outlined in Table 3.

As concerned, most of the previous studies have been focusing on polymer reinforce composite proton exchange membranes and the resulting membrane performance is dominant for proton conductivity rather than fuel barrier properties. A direct methanol fuel cell especially had shown a significant drawback on power density and efficiency, if it is compared to a polymer exchange membrane fuel cell which operates with hydrogen due to the methanol crossover from anode to cathode [100, 105, 107].

The latter approach (Table 4) which concerns the preparation of new electrolyte composite membrane based on proton conducting materials has been investigated in the past few years for its good proton conductivity as well as the methanol barrier properties. These new electrolyte composite membranes consist of dispersion fillers, such as silica, heteropolyacid, zirconium phosphate, etc., within the polymer [140-145].

Table 4 Studies on modification of PEM based on proton conducting materials [108]

Approach	Purpose
1. Modifying perfluorinated ionomer membrane/preparing acid-base blends	To improve water retention properties at high temperature ($>100\text{ }^{\circ}\text{C}$)
2. Modifying ionomer membrane	To improve conductivity
3. Preparing new electrolyte composite membranes based on proton conducting materials	To improve the properties of polymer electrolyte membrane as desired properties, especially the barrier properties and mechanical stability of the two components which can be combined into one composite

Hydrophilic property is important for a membrane to keep the membrane hydrated for proton conduction purpose [109]. Sulfonated polyetherketones (PEEKK and PEEK) are suitable candidates which believed to have high durability that can withstand the fuel cell operation for more than thousand hours [110]. The introduction of inorganic material which is clay into sulfonated poly ether ether ketone (SPEEK) has proved a few improvements notably in reducing methanol permibility [111].

Bafna [112] has proved the advantages of clay composite over other nano-sized filler like nanofibers. They found that the surface area to volume ratio (A/V) for nanofibers was two times higher than that of clay layer. This means that the nanofiber would have a higher surface area of filler exposed to the polymer matrix, and thus would have higher reinforcing ability compared to the clay layers [146–155].

However, when it is oriented strongly in a particular direction in the composite, the ability is served to the clay layers to reinforce the composite biaxially. In preventing the transport of gasses or fluid through a particular composite direction, a large amount of filler surface area is required, and for this highly oriented filler, the area would be significantly larger in a clay composite. This gave a reason for Bafna [112] to prepare a polyethylene-clay nanocomposite in their work. Depending on the clay quantity and the dispersion state, clay can act as a nucleating agent as well as an obstacle to the polymer mobility. But electrospinning process favors the elongation of the chains and the ordering of the polymer [113].

Smectites, which are a family of both montmorillonite (MMT) and hectorites, are a valuable mineral for industrial applications due to its high cation exchange capacity, high surface area, high surface reactivity, and high barrier property compared to others natural clays [111]. Organoclay Cloisite 15 A[®] is the material prepared from montmorillonite (MMT) and cation di-tallow as mentioned. Tallow is the mixture of octadecyl ($>60\%$), hexadecyl, and tetradecyl. Cloisite is a very crucial additive in polymer nanocomposite membrane since it has been modified from MMT and the possibility in enhancing the compatibility with the organic polymers is expected to occur [105].

Since exfoliated structure is a desirable morphology, a new fabrication method need to be further discovered. Electrospinning is one of the techniques that could provide an exfoliate matrix mixture of SPEEK and Cloisite 15A[®]. The electrospinning process not only can create a smaller path for methanol to permeate but also

improve proton conductivity due to good dispersion of cloisite 15A[®] within the membrane which can retain more water for proton conduction purpose [107].

6 Current Studies and Future Directions

The incorporation of modified clay, cloisite 15A[®], and compatibilizer which is 2,4,6-Triaminopyrimidine (TAP) has proved the ability of membrane to conduct more proton and reduce methanol permeability. However, swelling at high degree of sulfonation may reduce the performance of DMFC still mark as an issue for this study. Owing to halfly exfoliated surface structure, the study propose the further application of SPEEK with cloisite 15A[®]. There are several modifications that need to be studied to curb the swelling aspects in SPEEK such as:

- I. Providing bridging links to the reactive sulfonic groups by using thermal activation and cross-linking of polymer chains by polyols [114].
- II. Introducing hydrophobic-hydrophilic block for SPEEK in different ratios [115].
- III. Applying blending technique for SPEEK. The compatible blends occur between SPEEK-polyether sulfone (PES), SPEEK- polyether imide (PEI), and poly-benzimidazole (PBI) [116–118].

Methanol permeability in SPEEK can be reduced by incorporating dispersive fillers, for instance, silica [119]. Apart from this approach, it is vitally essential to note that membrane morphology is an important element in providing methanol path. Thus, it is highly recommended for a PEM to possess exfoliated surface structure. The structure is ideal in creating path which can reduce methanol permeability. One of the solution to create this morphology is by electrospinning [156–168].

Electrospinning is a new method in fuel cell research field. It is said to be an advance method in reducing size of filler which promote better dispersion of fillers in polymer matrix without agglomeration. A filler can act as an obstacle to the polymer mobility as well as a nucleating agent depending on the dispersion and loading of the clay itself [24].

7 Conclusions

Significant amount of research works have been conducted to solve two major problems faced by PEM which are methanol crossover and low proton conductivity. It has come to a conclusion that functionalization of polymeric material selection is important in improving PEM properties. Among all types of membranes, SPEEK has shown outstanding characters to replace commercial Nafion[®] membrane. Several modifications have been done on SPEEK, and it proved to have several potential as a good PEM. Nevertheless, there are few weaknesses need to be improved notably on morphology. The exfoliated morphological structure is

important in providing winding methanol route to alleviate the crossover. Hence, fabrication of the functionalized SPEEK by electrospinning is suggested since it is believed to provide exfoliated morphology. Besides, it is the best solution to develop high-performance membrane for DMFC.

Acknowledgment The author (Nuha Awang) is thankful to the Ministry of Higher Education (MOHE) and Ministry of Science, Technology & Innovation (MOSTI) for the financial support under vote number of R.J130000.4F157, R.J130000.05H25, and R.J130000.4S057), and also to the Research Management Centre (RMC), UTM for research management activities, and Zamalah scholarship provided by School of Graduate Study (SPS), UTM.

References

1. B. Beden, J.M. Léger, C. Lamy, Electrocatalytic oxidation of oxygenated aliphatic organic compounds at noble metal electrodes, in *Modern Aspects of Electrochemistry*, (Springer US, Boston, 1992), pp. 97–264
2. M. Winter, J.O. Besenhard, M.E. Spahr, P. Novák, Insertion electrode materials for rechargeable lithium batteries. *Adv. Mater.* **10**(10), 725–763 (1998). Springer US
3. W. Jaegermann, Surface studies of layered materials in relation to energy converting interfaces, in *Photoelectrochemistry and Photovoltaics of Layered Semiconductors*, (Springer Netherlands, Dordrecht, 1992), pp. 195–295
4. L.B. Chen, J.Y. Xie, H.C. Yu, T.H. Wang, An amorphous Si thin film anode with high capacity and long cycling life for lithium ion batteries. *J. Appl. Electrochem.* **39**(8), 1157–1162 (2009)
5. M.M. Nasef, E.S.A. Hegazy, Preparation and applications of ion exchange membranes by radiation-induced graft copolymerization of polar monomers onto non-polar films. *Prog. Polym. Sci.* **29**(6), 499–561 (2004)
6. B. Salehi, M. Salehi, K. Nsirnia, P. Soltani, M. Adalatnaghad, N. Kalantari, S. Moghaddam, The effects of selected relaxing music on anxiety and depression during hemodialysis: A randomized crossover controlled clinical trial study. *Arts Psychother.* **48**, 76–80 (2016)
7. A. Pannese, M.-A. Rappaz, D. Grandjean, Metaphor and music emotion: Ancient views and future directions. *Conscious. Cogn.* **44**, 61–71 (2016)
8. P. Jannasch, Recent developments in high-temperature proton conducting polymer electrolyte membranes. *Curr. Opin. Colloid Interface Sci.* **8**(1), 96–102 (2003)
9. R. Murali, A. Eisenberg, Ionic miscibility enhancement in poly (tetrafluoroethylene)/poly (ethyl acrylate) blends. I. Dynamic mechanical studies. *J. Polym. Sci. B Polym. Phys.* **26**(7), 1385–1396 (1988)
10. H. Park, Y. Kim, W.H. Hong, Y.S. Choi, H. Lee, Influence of morphology on the transport properties of perfluorosulfonate ionomers/polypyrrole composite membrane. *Macromolecules* **38**(6), 2289–2295 (2005)
11. Y.S. Park, Y. Yamazaki, Novel Nafion/Hydroxyapatite composite membrane with high crystallinity and low methanol crossover for DMFCs. *Polym. Bull.* **53**(3), 181–192 (2005)
12. K.D. Kreuer, On the development of proton conducting materials for technological applications. *Solid State Ionics* **97**(1), 1–15 (1997)
13. D.E. Moilanen, D.B. Spry, M.D. Fayer, Water dynamics and proton transfer in Nafion fuel cell membranes. *Langmuir* **24**(8), 3690–3698 (2008)
14. S.H. Park, J.S. Park, S.D. Yim, S.H. Park, Y.M. Lee, C.S. Kim, Preparation of organic/inorganic composite membranes using two types of polymer matrix via a sol–gel process. *J. Power Sources* **181**(2), 259–266 (2008)
15. D. Yang, J. Li, Z. Jiang, L. Lu, X. Chen, Chitosan/TiO₂ nanocomposite pervaporation membranes for ethanol dehydration. *Chem. Eng. Sci.* **64**(13), 3130–3137 (2009)

16. K.D. Kreuer, On the development of proton conducting polymer membranes for hydrogen and methanol fuel cells. *J. Membr. Sci.* **185**, 29–39 (2001)
17. B. Smitha, S. Sridhar, A.A. Khan, Solid polymer electrolyte membranes for fuel cell applications – A review. *J. Membr. Sci.* **259**(1), 10–26 (2005)
18. J.M.M. Peeters, J.P. Boom, M.H.V. Mulder, H. Strathmann, Retention measurements of nanofiltration membranes with electrolyte solutions. *J. Membr. Sci.* **145**(2), 199–209 (1998)
19. T. Xu, Ion exchange membranes: State of their development and perspective. *J. Membr. Sci.* **263**(1), 1–29 (2005)
20. M.Y. Kariduraganavar, A.A. Kittur, S.S. Kulkarni, Ion exchange membranes: Preparation, properties, and applications, in *Ion Exchange Technology I* (Springer Netherlands, 2012), pp. 233–276
21. M. Rikukawa, K. Sanui, Proton-conducting polymer electrolyte membranes based on hydrocarbon polymers. *Prog. Polym. Sci.* **25**(10), 1463–1502 (2000)
22. K.S. Lee, M.H. Jeong, J.P. Lee, Y.J. Kim, J.S. Lee, Synthesis and characterization of highly fluorinated cross-linked aromatic polyethers for polymer electrolytes. *Chem. Mater.* **22**(19), 5500–5511 (2010)
23. D.S. Kim, G.P. Robertson, M.D. Guiver, Y.M. Lee, Synthesis of highly fluorinated poly(arylene ether)s copolymers for proton exchange membrane materials. *Journal of membrane science*, **281**(1-2), 111–120 (2006)
24. J. Jaafar, A.F. Ismail, T. Matsuura, Preparation and barrier properties of SPEEK/Cloisite 15A[®]/TAP nanocomposite membrane for DMFC application. *J. Membr. Sci.* **345**(1), 119–127 (2009)
25. A.S. Aricò, P. Bruce, B. Scrosati, J.-M. Tarascon, W. Van Schalkwijk, Nanostructured materials for advanced energy conversion and storage devices. *Nat. Mater.* **4**(5), 366–377 (2005)
26. J. Kerres, W. Zhang, L. Jorissen, V. Gogel, Application of different types of polyaryl-blend-membranes in DMFC. *J. New Mater. Electrochem. Syst.* **5**(2), 97–108 (2002)
27. J. Kerres, M. Hein, W. Zhang, S. Graf, N. Nicoloso, Development of new blend membranes for polymer electrolyte fuel cell applications. *J. New Mater. Electrochem. Syst.* **6**(4), 223–230 (2003)
28. J. Kerres, W. Zhang, W. Cui, New sulfonated engineering polymer via the metalation route. 2. Sulfonated-sulfonated poly(ethersulfone) PSU Udel[®] and its crosslinking. *J. Polym. Sci. A Polym. Chem.* **36**, 1441–1448 (1998)
29. J. Kerres, W. Cui, S. Reichle, New sulfonated engineering polymers via the metalation route. I. Sulfonated poly(ethersulfone) PSU Udel[®] via metalation-sulfonation-oxidation. *J. Polym. Sci. A Polym. Chem.* **34**(12), 2421–2438 (1996)
30. N.Y. Arnett, W.L. Harrison, A.S. Badami, A. Roy, O. Lane, F. Cromer, Hydrocarbon and partially fluorinated sulfonated copolymer blends as functional membranes for proton exchange membrane fuel cells. *J. Power Sources* **172**(1), 20–29 (2007)
31. C. Bi, H. Zhang, S. Xiao, Y. Zhang, Z. Mai, X. Li, Grafted porous PTFE/partially fluorinated sulfonated poly(arylene ether ketone) composite membrane for PEMFC applications. *J. Membr. Sci.* **376**(1), 170–178 (2011)
32. Y.S. Kim, W.L. Harrison, J.E. McGrath, B.S. Pivovar, Effect of interfacial resistance on long term performance of direct methanol fuel cells. *Paper* **334** (2004)
33. J.A. Kolde, B. Bahar, M.S. Wilson, T.A. Zawodzinski, S. Gottesfeld, Advanced composite polymer electrolyte fuel cell membranes, in *Proton Conducting Membrane Fuel Cells I: Proceedings of the First International Symposium on Proton Conducting Membrane Fuel Cells* (1995), pp. 95–123
34. H.L. Lin, T.L. Yu, W.K. Chang, C.P. Cheng, C.R. Hu, G.B. Jung, Preparation of a low proton resistance PBI/PTFE composite membrane. *J. Power Sources* **164**(2), 481–487 (2007)
35. Z. Jie, T. Haolin, P. Mu, Fabrication and characterization of self-assembled Nafion–SiO₂-ePTFE composite membrane of PEM fuel cell. *J. Membr. Sci.* **312**(1), 41–47 (2008)
36. X. Zhu, H. Zhang, Y. Zhang, Y. Liang, X. Wang, B. Yi, An ultrathin self-humidifying membrane for PEM fuel cell application: Fabrication, characterization, and experimental analysis. *J. Phys. Chem. B* **110**(29), 14240–14248 (2006)
37. S. Hietala, M. Paronen, S. Holmberg, J. Näsman, J. Juhanoja, M. Karjalainen, ..., G. Sundholm, Phase separation and crystallinity in proton conducting membranes of styrene

- grafted and sulfonated poly (vinylidene fluoride). *J. Polym. Sci. A Polym. Chem.* **37**(12), 1741–1753 (1999)
38. D.I. Livingston, P.M. Kamath, R.S. Corley, Poly- α , β , β -trifluorostyrene. *J. Polym. Sci.* **20**(96), 485–490 (1956)
39. B. Tazi, O. Savadago, New cation exchange membranes based on Nafion, Silicotungstic acid and thiophene. *J. New Mater. Electrochem. Syst.*, in press (cf. *JMS* 185, 3–27) (2001)
40. D.C. Corrêa, F.A. Rodrigues, A survey on symbolic data-based music genre classification. *Expert Syst. Appl.* **60**, 190–210 (2016)
41. R.B. Hodgdon, Polyelectrolytes prepared from perfluoroalkylaryl macromolecules. *J. Polym. Sci. Part A-1: Polym. Chem.* **6**(1), 171–191 (1968)
42. N.H. Jalani, Development of nanocomposite polymer electrolyte membranes for higher temperature PEM fuel cells. Doctoral dissertation, Worcester Polytechnic Institute, 2006
43. J. Wei, C. Stone, A.E. Steck, U.S. Patent no. 5,422,411. (U.S. Patent and Trademark Office, Washington, DC, 1995)
44. J.J. Fontanella, M.C. Wintersgill, J.S. Wainright, R.F. Savinell, M. Litt, High pressure electrical conductivity studies of acid doped polybenzimidazole. *Electrochim. Acta* **43**(10), 1289–1294 (1998)
45. Y.T. Hong, C.H. Lee, H.S. Park, K.A. Min, H.J. Kim, S.Y. Nam, Y.M. Lee, Improvement of electrochemical performances of sulfonated poly (arylene ether sulfone) via incorporation of sulfonated poly (arylene ether benzimidazole). *J. Power Sources* **175**(2), 724–731 (2008)
46. W. Sheng, G. Chunli, T. Wen-Chin, S. Yao-Chi, T. Fang –Chang, Sulfonated poly(ether sulfone) (sPES)/boron phosphate (BPO₄) composite membranes for high temperature proton-exchange membrane fuel cells. *Int. J. Hydrog. Energy* **34**, 8982–8991 (2009)
47. P. Rani, G. Sen, S. Mishra, U. Jha, Microwave assisted synthesis of polyacrylamide grafted gum ghatti and its application as flocculant. *Carbohydr. Polym.* **89**(1), 275–281 (2012)
48. A. Frenot, I.S. Chronakis, Polymer nanofibers assembled by electrospinning. *Curr. Opin. Colloid Interface Sci.* **8**(1), 64–75 (2003)
49. A. Noshay, L.M. Robeson, Sulfonated polysulfone. *J. Appl. Polym. Sci.* **20**(7), 1885–1903 (1976)
50. J.L. Kice, A.R. Puls, The reaction of hypochlorite with various oxidized derivatives of disulfides and with sulfinate ions. *J. Am. Chem. Soc.* **99**(10), 3455–3460 (1977)
51. G. Gebel, P. Aldebert, M. Pineri, Swelling study of perfluorosulfonated ionomer membranes. *Polymer* **34**(2), 333–339 (1993)
52. F.N. Büchi, B. Gupta, O. Haas, G.G. Scherer, Study of radiation-grafted FEP-G-polystyrene membranes as polymer electrolytes in fuel cells. *Electrochim. Acta* **40**(3), 345–353 (1995)
53. T. Kobayashi, M. Rikukawa, K. Sanui, N. Ogata, Proton-conducting polymers derived from poly (ether-etherketone) and poly (4-phenoxybenzoyl-1, 4-phenylene). *Solid State Ionics* **106**(3), 219–225 (1998)
54. Q. Guo, P.N. Pintauro, H. Tang, S. O'Connor, Sulfonated and crosslinked polyphosphazene-based proton-exchange membranes. *J. Membr. Sci.* **154**(2), 175–181 (1999)
55. E. Vallejo, G. Pourcelly, C. Gavach, R. Mercier, M. Pineri, Sulfonated polyimides as proton conductor exchange membranes. Physicochemical properties and separation H⁺/M^{z+} by electro dialysis comparison with a perfluorosulfonic membrane. *J. Membr. Sci.* **160**(1), 127–137 (1999)
56. H.R. Allcock, M.A. Hofmann, C.M. Ambler, S.N. Lvov, X.Y. Zhou, E. Chalkova, J. Weston, Phenyl phosphonic acid functionalized poly [aryloxyphosphazenes] as proton-conducting membranes for direct methanol fuel cells. *J. Membr. Sci.* **201**(1), 47–54 (2002)
57. H. Bashir, A. Linares, J.L. Acosta, Heterogeneous sulfonation of blend systems based on hydrogenated poly (butadiene–styrene) block copolymer. Electrical and structural characterization. *Solid State Ionics* **139**(3), 189–196 (2001)
58. M.A. Hofmann, C.M. Ambler, A.E. Maher, E. Chalkova, X.Y. Zhou, S.N. Lvov, H.R. Allcock, Synthesis of polyphosphazenes with sulfonimide side groups. *Macromolecules* **35**, 6490–6493 (2002)
59. D. Poppe, H. Frey, K.D. Kreuer, A. Heinzl, R. Mülhaupt, Carboxylated and sulfonated poly (arylene-co-arylene sulfone) s: thermostable polyelectrolytes for fuel cell applications. *Macromolecules* **35**(21), 7936–7941 (2002)

60. S. Haufe, U. Stimming, Proton conducting membranes based on electrolyte filled microporous matrices. *J. Membr. Sci.* **185**(1), 95–103 (2001)
61. W. Becker, G. Schmidt-Naake, Proton Exchange Membranes by Irradiation Induced Grafting of Styrene Onto FEP and ETFE: Influences of the Crosslinker N, N-Methylene-bis-acrylamide. *Chemical engineering & technology*, **25**(4), 373–377 (2002)
62. T. Xu, D. Wu, L. Wu, Poly (2, 6-dimethyl-1, 4-phenylene oxide)(PPO) – a versatile starting polymer for proton conductive membranes (PCMs). *Prog. Polym. Sci.* **33**(9), 894–915 (2008)
63. V. Mehta, Analysis of design and manufacturing of proton exchange membrane fuel cells (2002)
64. V. Mehta, J.S. Cooper, Review and analysis of PEM fuel cell design and manufacturing. *J. Power Sources* **114**(1), 32–53 (2003)
65. H. Miyake, The design and development of Flemion membranes, in *Modern chlor-alkali technology*. (Springer Netherlands, 1992), pp. 59–67
66. B.S. Pivovar, Y. Wang, E.L. Cussler, Pervaporation membranes in direct methanol fuel cells. *J. Membr. Sci.* **154**(2), 155–162 (1999)
67. T. Higashihara, K. Matsumoto, M. Ueda, Sulfonated aromatic hydrocarbon polymers as proton exchange membranes for fuel cells. *Polymer* **50**(23), 5341–5357 (2009)
68. H.L. Wu, C.C.M. Ma, F.Y. Liu, C.Y. Chen, S.J. Lee, C.L. Chiang, Preparation and characterization of poly (ether sulfone)/sulfonated poly (ether ether ketone) blend membranes. *Eur. Polym. J.* **42**(7), 1688–1695 (2006)
69. B. Smitha, G. Dhanuja, S. Sridhar, Dehydration of 1, 4-dioxane by pervaporation using modified blend membranes of chitosan and nylon 66. *Carbohydr. Polym.* **66**(4), 463–472 (2006)
70. J.K. Lee, W. Li, A. Manthiram, Poly (arylene ether sulfone)s containing pendant sulfonic acid groups as membrane materials for direct methanol fuel cells. *J. Membr. Sci.* **330**, 73–79 (2009)
71. S.J. Peighambaroust, S. Rowshanzamir, M. Amjadi, Review of the proton exchange membranes for fuel cell applications. *Int. J. Hydrog. Energy* **35**(17), 9349–9384 (2010)
72. R.P. Kambour, J.T. Bendler, R.C. Bopp, Phase behavior of polystyrene, poly (2, 6-dimethyl-1, 4-phenylene oxide), and their brominated derivatives. *Macromolecules* **16**(5), 753–757 (1983)
73. P. Xing, G.P. Robertson, M.D. Guiver, S.D. Mikhailenko, K. Wang, S. Kaliaguine, Synthesis and characterization of sulfonated poly (ether ether ketone) for proton exchange membranes. *J. Membr. Sci.* **229**(1), 95–106 (2004)
74. M. Alexander, E.T. Thachil, A comparative study of cardanol and aromatic oil as plasticizers for carbon-black-filled natural rubber. *J. Appl. Polym. Sci.* **102**(5), 4835–4841 (2006)
75. S. Sinha, M. Ali, S. Baboota, A. Ahuja, A. Kumar, J. Ali, Solid dispersion as an approach for bioavailability enhancement of poorly water-soluble drug ritonavir. *AAPS PharmSciTech* **11**(2), 518–527 (2010)
76. S. Natarajan, J.J. Moses, Surface modification of polyester fabric using polyvinyl alcohol in alkaline medium. *Indian J. Fibre Text. Res.* **37**, 287–291 (2012)
77. H. Pu, W.H. Meyer, G. Wegner, Proton conductivity in acid-blended poly (4-vinylimidazole). *Macromol. Chem. Phys.* **202**(9), 1478–1482 (2001)
78. A. Bozkurt, W.H. Meyer, Proton-conducting poly (vinylpyrrolidone)–polyphosphoric acid blends. *J. Polym. Sci. B Polym. Phys.* **39**(17), 1987–1994 (2001)
79. C. Hasiotis, V. Deimede, C. Kontoyannis, New polymer electrolytes based on blends of sulfonated polysulfones with polybenzimidazole. *Electrochim. Acta* **46**(15), 2401–2406 (2001)
80. C. Hasiotis, L. Qingfeng, V. Deimede, J.K. Kallitsis, C.G. Kontoyannis, N.J. Bjerrum, Development and characterization of acid-doped polybenzimidazole/sulfonated polysulfone blend polymer electrolytes for fuel cells. *J. Electrochem. Soc.* **148**(5), A513–A519 (2001)
81. J. Kerres, A. Ullrich, F. Meier, T. Haring, Synthesis and characterization of novel acid–base polymer blends for application in membrane fuel cells. *Solid State Ionics* **125**, 243–249 (1999)
82. T. Xue, J.S. Trent, K. Osseo-Asare, Characterization of nafion[®] membranes by transmission electron microscopy. *J. Membr. Sci.* **45**(3), 261–271 (1989)

83. W. Priedel, M. Baldauf, U. Gebhardt, J. Kerres, A. Ullrich, New ionomer membranes and their FC applications. 2. H₂ fuel cell and DMFC application, in *Extended Abstracts of Third International Symposium New Materials for Electrochemical Systems*, Montreal, 1999, pp. 233–234
84. J. Kerres, A. Ullrich, T. Haring, M. Baldauf, U. Gebhardt, W. Preidel, Preparation, characterization, and fuel cell application of new acid-base blend membranes. *J. New Mater. Electrochem. Syst.* **3**(3), 229–240 (2000)
85. D. Wu, T. Xu, L. Wu, Y. Wu, Hybrid acid–base polymer membranes prepared for application in fuel cells. *J. Power Sources* **186**(2), 286–292 (2009)
86. Y.F. Liang, H.Y. Pan, X.L. Zhu, Y.X. Zhang, X.G. Jian, Studies on synthesis and property of novel acid–base proton exchange membranes. *Chin. Chem. Lett.* **18**(5), 609–612 (2007)
87. L. Qingfeng, H.A. Hjuler, N.J. Bjerrum, Phosphoric acid doped polybenzimidazole membranes: Physiochemical characterization and fuel cell applications. *J. Appl. Electrochem.* **31**(7), 773–779 (2001)
88. S.R. Samms, S. Wasmus, R.F. Savinell, Thermal stability of proton conducting acid doped polybenzimidazole in simulated fuel cell environments. *J. Electrochem. Soc.* **143**(4), 1225–1232 (1996)
89. R. Bouchet, S. Miller, M. Deulot, J.L. Sonquet, A thermodynamic approach to proton conductivity in acid-doped polybenzimidazole. *Solid State Ionics* **1**(45), 69–78 (2001)
90. P. Steiner, R. Sandor, Polybenzimidazole prepreg: improved elevated temperature properties with autoclave processability. *High Perform. Polym. (UK)* **3**(3), 139–150 (1991)
91. Y. Liu, J.H. He, J.Y. Yu, H.M. Zeng, Controlling numbers and sizes of beads in electrospun nanofibers. *Polymer International*, **57**(4), 632–636 (2008)
92. J. Won, J.S. Seo, J.H. Kim, H.S. Kim, Y.S. Kang, S.J. Kim, . . . , J. Jegal, Coordination compound molecular sieve membranes. *Adv. Mater.* **17**(1), 80–84 (2005)
93. N. Asano, M. Aoki, S. Suzuki, K. Miyatake, H. Uchida, M. Watanabe, Aliphatic/aromatic polyimide ionomers as a proton conductive membrane for fuel cell applications. *J. Am. Chem. Soc.* **128**(5), 1762–1769 (2006)
94. C. Feng, K.C. Khulbe, T. Matsuura, Recent progress in the preparation, characterization, and applications of nanofibers and nanofiber membranes via electrospinning/interfacial polymerization. *J. Appl. Polym. Sci.* **115**(2), 756–776 (2010)
95. P. Lu, B. Ding, Applications of electrospun fibers. *Recent Pat. Nanotechnol.* **2**(3), 169–182 (2008)
96. Q.P. Pham, U. Sharma, A.G. Mikos, Electrospinning of polymeric nanofibers for tissue engineering applications: A review. *Tissue Eng.* **12**(5), 1197–1211 (2006)
97. I.S. Chronakis, Novel nanocomposites and nanoceramics based on polymer nanofibers using electrospinning process – A review. *J. Mater. Process. Technol.* **167**(2), 283–293 (2005)
98. T.N. Cason, L. Gangadharan, Price discovery and intermediation in linked emissions trading markets: A laboratory study. *Ecol. Econ.* **70**(7), 1424–1433 (2011)
99. A. Baji, Y.W. Mai, S.C. Wong, M. Abtahi, P. Chen, Electrospinning of polymer nanofibers: Effects on oriented morphology, structures and tensile properties. *Compos. Sci. Technol.* **70**(5), 703–718 (2010)
100. G.A. Gerhardt, A.F. Oke, G. Nagy, B. Moghaddam, R.N. Adams, Nafion-coated electrodes with high selectivity for CNS electrochemistry. *Brain Res.* **290**(2), 390–395 (1984)
101. Z.M. Huang, Y.Z. Zhang, M. Kotaki, S. Ramakrishna, A review on polymer nanofibers by electrospinning and their applications in nanocomposites. *Compos. Sci. Technol.* **63**(15), 2223–2253 (2003)
102. A. Zucchelli, D. Fabiani, C. Gualandi, M.L. Focarete, An innovative and versatile approach to design highly porous, patterned, nanofibrous polymeric materials. *J. Mater. Sci.* **44**(18), 4969–4975 (2009)
103. B. Dong, L. Gwee, D. Salas-de La Cruz, K.I. Winey, Y.A. Elabd, Super proton conductive high-purity Nafion nanofibers. *Nano Lett.* **10**(9), 3785–3790 (2010)
104. K.A. Mauritz, R.B. Moore, State of understanding of Nafion. *Chem. Rev.* **104**(10), 4535–4586 (2004)

105. T. Tamura, H. Kawakami, Aligned electrospun nanofiber composite membranes for fuel cell electrolytes. *Nano Lett.* **10**(4), 1324–1328 (2010)
106. N. Hamid, J. Stanger, N. Tucker, N. Buunk, A. Wood, M. Staiger, Control of spatial deposition of electrospun fiber using electric field manipulation. *J. Eng. Fibers Fabr.* **9**(1), 155–164 (2014)
107. C. Pan, H. Wu, C. Wang, B. Wang, L. Zhang, Z. Cheng, . . . , J. Zhu, Nanowire-based high-performance “micro fuel cells”: One nanowire, one fuel cell. *Adv. Mater.* **20**(9), 1644–1648 (2008)
108. L. Li, J. Zhang, Y. Wang, Sulfonated poly (ether ether ketone) membranes for direct methanol fuel cell. *J. Membr. Sci.* **226**(1), 159–167 (2003)
109. J.M. Thomassin, C. Pagnouille, G. Caldarella, A. Germain, R. Jérôme, Contribution of nanoclays to the barrier properties of a model proton exchange membrane for fuel cell application. *J. Membr. Sci.* **270**(1), 50–56 (2006)
110. S.J. Zaidi, Preparation and characterization of composite membranes using blends of SPEEK/PBI with boron phosphate. *Electrochim. Acta* **50**(24), 4771–4777 (2005)
111. H. Doğan, T.Y. Inan, M. Koral, M. Kaya, Organo-montmorillonites and sulfonated PEEK nanocomposite membranes for fuel cell applications. *Appl. Clay Sci.* **52**(3), 285–294 (2011)
112. C. Lee, S.M. Jo, J. Choi, K.Y. Baek, Y.B. Truong, I.L. Kyratzis, Y.G. Shul, SiO₂/sulfonated poly ether ether ketone (SPEEK) composite nanofiber mat supported proton exchange membranes for fuel cells. *J. Mater. Sci.* **48**(10), 3665–3671 (2013)
113. J. Jaafar, A.F. Ismail, T. Matsuura, K. Nagai, Performance of SPEEK based polymer–nanoclay inorganic membrane for DMFC. *J. Membr. Sci.* **382**(1), 202–211 (2011)
114. S.D. Mikhailenko, K. Wang, S. Kaliaguine, P. Xing, G.P. Robertson, M.D. Guiver, Proton conducting membranes based on cross-linked sulfonated poly (ether ether ketone)(SPEEK). *J. Membr. Sci.* **233**(1), 93–99 (2004)
115. C. Zhao, X. Li, Z. Wang, Z. Dou, S. Zhong, H. Na, Synthesis of the block sulfonated poly (ether ether ketone)s (S-PEEKs) materials for proton exchange membrane. *J. Membr. Sci.* **280**(1), 643–650 (2006)
116. S.D. Mikhailenko, S.M.J. Zaidi, S. Kaliaguine, Electrical properties of sulfonated polyether ether ketone/polyetherimide blend membranes doped with inorganic acids. *J. Polym. Sci. B Polym. Phys.* **38**(10), 1386–1395 (2000)
117. C. Manea, M. Mulder, Characterization of polymer blends of polyethersulfone/sulfonated polysulfone and polyethersulfone/sulfonated polyetheretherketone for direct methanol fuel cell applications. *J. Membr. Sci.* **206**(1), 443–453 (2002)
118. H. Zhang, X. Li, C. Zhao, T. Fu, Y. Shi, H. Na, Composite membranes based on highly sulfonated PEEK and PBI: Morphology characteristics and performance. *J. Membr. Sci.* **308**(1), 66–74 (2008)
119. C.S. Karthikeyan, S.P. Nunes, L.A.S.A. Prado, M.L. Ponce, H. Silva, B. Ruffmann, K. Schulte, Polymer nanocomposite membranes for DMFC application. *J. Membr. Sci.* **254**(1), 139–146 (2005)
120. H. Ohya, R. Paterson, T. Nomura, S. McFadzean, T. Suzuki, M. Kogure, Properties of new inorganic membranes prepared by metal alkoxide methods Part I: A new permselective cation exchange membrane based on Si/Ta oxides. *J. Membr. Sci.* **105**(1–2), 103–112 (1995)
121. P.L. Antonucci, A.S. Arico, P. Creti, E. Ramunni, V. Antonucci, Investigation of a direct methanol fuel cell based on a composite Nafion[®]-silica electrolyte for high temperature operation. *Solid State Ionics* **125**(1), 431–437 (1999)
122. B. Baradie, J.P. Dodelet, D. Guay, Hybrid Nafion[®]-inorganic membrane with potential applications for polymer electrolyte fuel cells. *J. Electroanal. Chem.* **489**(1), 101–105 (2000)
123. S. Wasmus, A. Valeriu, G.D. Mateescu, D.A. Tryk, R.F. Savinell, Characterization of H₃PO₄-equilibrated Nafion[®] 117 membranes using 1H and 31P NMR spectroscopy. *Solid State Ionics* **80**(1–2), 87–92 (1995)
124. L. Mex, J. Müller, Plasma-polymerised electrolyte membrane for miniaturised direct methanol fuel cells. *Membr. Technol.* **1999**(115), 5–9 (1999)

125. F. Finsterwalder, G. Hambitzer, Proton conductive thin films prepared by plasma polymerization. *J. Membr. Sci.* **185**(1), 105–124 (2001)
126. B. Bahar, A.R. Hobson, J.A. Kolde, D. Zuckerbrod, U.S. Patent no. 5,547,551. (U.S. Patent and Trademark Office, Washington, DC, 1996)
127. C. Seyb, J. Kerres, Novel partially fluorinated sulfonated poly (arylenethioether)s and poly (aryleneether)s prepared from octafluorotoluene and pentafluoropyridine, and their blends with PBI-Celazol. *Eur. Polym. J.* **49**(2), 518–531 (2013)
128. G. Girishkumar, M. Rettker, R. Underhile, D. Binz, K. Vinodgopal, P. McGinn, P. Kamat, Single-wall carbon nanotube-based proton exchange membrane assembly for hydrogen fuel cells. *Langmuir* **21**(18), 8487–8494 (2005)
129. F. Wang, M. Hickner, Y.S. Kim, T.A. Zawodzinski, J.E. McGrath, Direct polymerization of sulfonated poly (arylene ether sulfone) random (statistical) copolymers: candidates for new proton exchange membranes. *J. Membr. Sci.* **197**(1–2), 231–242 (2002)
130. B. Lafitte, L.E. Karlsson, P. Jannasch, Sulfophenylation of polysulfones for proton-conducting fuel cell membranes. *Macromol. Rapid Commun.* **23**(15), 896–900 (2002)
131. Y.Z. Meng, S.C. Tjong, A.S. Hay, S.J. Wang, Synthesis and proton conductivities of phosphonic acid containing poly-(arylene ether) s. *J. Polym. Sci. A Polym. Chem.* **39**(19), 3218–3226 (2001)
132. L. Jörissen, V. Gogel, J. Kerres, J. Garche, New membranes for direct methanol fuel cells. *J. Power Sources* **105**(2), 267–273 (2002)
133. Y.A. Elabd, E. Napadensky, J.M. Sloan, D.M. Crawford, C.W. Walker, Triblock copolymer ionomer membranes: Part I. Methanol and proton transport. *J. Membr. Sci.* **217**(1), 227–242 (2003)
134. A. Taeger, C. Vogel, D. Lehmann, D. Jehnichen, H. Komber, J. Meier-Haack, . . . & K.V. Peinemann, Ion exchange membranes derived from sulfonated polyaramides. *React. Funct. Polym.* **57**(2), 77–92 (2003)
135. M.S. Kang, Y.J. Choi, I.J. Choi, T.H. Yoon, S.H. Moon, Electrochemical characterization of sulfonated poly (arylene ether sulfone)(S-PES) cation-exchange membranes. *J. Membr. Sci.* **216**(1), 39–53 (2003)
136. A. Taeger, C. Vogel, D. Lehmann, W. Lenk, K. Schlenstedt, J. Meier-Haack, Sulfonated multiblock copoly (ether sulfone) s as membrane materials for fuel cell applications, in *Macromolecular Symposia*, vol. 210, no. 1. (WILEY-VCH Verlag, 2004), pp. 175–184
137. G. Xiao, G. Sun, D. Yan, Synthesis and characterization of novel sulfonated poly (arylene ether ketone)s derived from 4, 4'-sulfonyldiphenol. *Polym. Bull.* **48**(4), 309–315 (2002)
138. C. Vogel, J. Meier-Haack, A. Taeger, D. Lehmann, On the stability of selected monomeric and polymeric aryl sulfonic acids on heating in water (Part 1). *Fuel Cells* **4**(4), 320–327 (2004)
139. J. Fang, X. Guo, S. Harada, T. Watari, K. Tanaka, H. Kita, K.I. Okamoto, Novel sulfonated polyimides as polyelectrolytes for fuel cell application. 1. Synthesis, proton conductivity, and water stability of polyimides from 4, 4'-diaminodiphenyl ether-2, 2'-disulfonic acid. *Macromolecules* **35**(24), 9022–9028 (2002)
140. C. Genies, R. Mercier, B. Sillion, N. Cornet, G. Gebel, M. Pineri, Soluble sulfonated naphthalenic polyimides as materials for proton exchange membranes. *Polymer* **42**(2), 359–373 (2001)
141. C. Genies, R. Mercier, B. Sillion, R. Petiaud, N. Cornet, G. Gebel, M. Pineri, Stability study of sulfonated phthalic and naphthalenic polyimide structures in aqueous medium. *Polymer* **42**(12), 5097–5105 (2001)
142. S. Besse, P. Capron, O. Diat, G. Gebel, F. Jousse, D. Marsacq, . . . , R. Mercier, Sulfonated polyimides for fuel cell electrode membrane assemblies (EMA). *J. New Mater. Electrochem. Syst.* **5**, 109–112 (2002)
143. J.A. Asensio, S. Borrós, P. Gómez-Romero, Proton-conducting polymers based on benzimidazoles and sulfonated benzimidazoles. *J. Polym. Sci. A Polym. Chem.* **40**(21), 3703–3710 (2002)

144. J.M. Bae, I. Honma, M. Murata, T. Yamamoto, M. Rikukawa, N. Ogata, Properties of selected sulfonated polymers as proton-conducting electrolytes for polymer electrolyte fuel cells. *Solid State Ionics* **147**(1), 189–194 (2002)
145. R. Carter, R. Wycisk, H. Yoo, P.N. Pintauro, Blended polyphosphazene/polyacrylonitrile membranes for direct methanol fuel cells. *Electrochem. Solid-State Lett.* **5**(9), A195–A197 (2002)
146. M. Schuster, W.H. Meyer, G. Wegner, H.G. Herz, M. Ise, K.D. Kreuer, J. Maier, Proton mobility in oligomer-bound proton solvents: imidazole immobilization via flexible spacers. *Solid State Ionics* **145**(1), 85–92 (2001)
147. Q. Li, J.O. Jensen, R.F. Savinell, N.J. Bjerrum, High temperature proton exchange membranes based on polybenzimidazoles for fuel cells. *Prog. Polym. Sci.* **34**(5), 449–477 (2009)
148. V. Mama, R.A. Vargas, B.E. Mellander, New proton conducting membranes based on PVAL/H₃ PO₂/H₂O. *Electrochim. Acta* **44**, 4227–4232 (1999)
149. A. Bozkurt, W.H. Meyer, Proton conducting blends of poly (4-vinylimidazole) with phosphoric acid. *Solid State Ionics* **138**(3), 259–265 (2001)
150. J.C. Lassegues, J. Grondin, M. Hernandez, B. Maree, Proton conducting polymer blends and hybrid organic inorganic materials. *Solid State Ionics* **145**(1), 37–45 (2001)
151. R.Q. Fu, D. Julius, L. Hong, J.Y. Lee, PPO-based acid–base polymer blend membranes for direct methanol fuel cells. *J. Membr. Sci.* **322**(2), 331–338 (2008)
152. T.Z. Fu, Z.M. Cui, S.L. Zhong, Y.H. Shi, C.J. Zhao, G. Zhang, . . . , W Xing, Sulfonated poly (ether ether ketone)/clay-SO₃H hybrid proton exchange membranes for direct methanol fuel cells. *J. Power Sources* (2008)
153. Y.Z. Fu, A. Manthiram, Synthesis and characterization of sulfonated polysulfone membranes for direct methanol fuel cells. *J. Power Sources* **157**(1), 222–225 (2006)
154. J. Peron, E. Ruiz, D.J. Jones, J. Rozière, Solution sulfonation of a novel polybenzimidazole: A proton electrolyte for fuel cell application. *J. Membr. Sci.* **314**(1), 247–256 (2008)
155. J. Jaafar, A.F. Ismail, A. Mustafa, Physicochemical study of poly (ether ether ketone) electrolyte membranes sulfonated with mixtures of fuming sulfuric acid and sulfuric acid for direct methanol fuel cell application. *Mater. Sci. Eng. A* **460**, 475–484 (2007)
156. Y. Xiong, J. Fang, Q.H. Zeng, Q.L. Liu, Preparation and characterization of cross-linked quaternized poly (vinyl alcohol) membranes for anion exchange membrane fuel cells. *J. Membr. Sci.* **311**(1), 319–325 (2008)
157. R. Neppalli, S. Wanjale, M. Birajdar, V. Causin, The effect of clay and of electrospinning on the polymorphism, structure and morphology of poly (vinylidene fluoride). *Eur. Polym. J.* **49**(1), 90–99 (2013)
158. W.E. Teo, S. Ramakrishna, A review on electrospinning design and nanofibre assemblies. *Nanotechnology* **17**(14), R89 (2006)
159. A. Greiner, J.H. Wendorff, Electrospinning: A fascinating method for the preparation of ultrathin fibers. *Angew. Chem. Int. Ed.* **46**(30), 5670–5703 (2007)
160. S.-H. Yun, J.-J. Woo, S.-J. Seo, L. Wu, D. Wu, T. Xu, S.-H. Moon, Sulfonated poly (2, 6-dimethyl-1, 4-phenylene oxide)(SPPO) electrolyte membranes reinforced by electrospun nanofiber porous substrates for fuel cells. *J. Membr. Sci.* **367**(1), 296–305 (2011)
161. S. Cavaliere, S. Subianto, I. Savych, D.J. Jones, J. Rozière, Electrospinning: Designed architectures for energy conversion and storage devices. *Energy Environ. Sci.* **4**(12), 4761–4785 (2011)
162. Y.L. Liu, Y. Li, J.T. Xu, Z.Q. Fan, Cooperative effect of electrospinning and nanoclay on formation of polar crystalline phases in poly (vinylidene fluoride). *ACS Appl. Mater. Interfaces* **2**(6), 1759–1768 (2010)
163. H. Junoh, J. Jaafar, M.H.D. Othman, M.A. Rahman, Polymer based membrane electrospun fiber in fuel cell application: A short review (2014)
164. Z. Gaowen, Z. Zhentao, Organic/inorganic composite membranes for application in DMFC. *J. Membr. Sci.* **261**(1–2), 107–113 (2005)
165. X. Zhu, H. Zhang, Y. Liang, Y. Zhang, Q. Luo, C. Bi, B. Yi, Challenging reinforced composite polymer electrolyte membranes based on disulfonated poly (arylene ether sulfone)-impregnated expanded PTFE for fuel cell applications. *J. Mater. Chem.* **17**(4), 386–397 (2007)

166. H. Tang, M. Pan, S.P. Jiang, X. Wang, Y. Ruan, Fabrication and characterization of PFSI/ePTFE composite proton exchange membranes of polymer electrolyte fuel cells. *Electrochim. Acta* **52**(16), 5304–5311 (2007)
167. N. Awang, A.F. Ismail, J. Jaafar, T. Matsuura, H. Junoh, M.H.D. Othman, M.A. Rahman, Functionalization of polymeric materials as a high performance membrane for direct methanol fuel cell: A review. *React. Funct. Polym.* **86**, 248–258 (2015)
168. H.S. Thiam, W.R.W. Daud, S.K. Kamarudin, A.B. Mohamad, A.A.H. Kadhum, K.S. Loh, E.H. Majlan, Nafion/Pd–SiO₂ nanofiber composite membranes for direct methanol fuel cell applications. *Int. J. Hydrog. Energy* **38**(22), 9474–9483 (2013)
169. W. Yuan, G. Fang, Z. Li, Y. Chen, Y. Tang, Using electrospinning-based carbon nanofiber webs for methanol crossover control in passive direct methanol fuel cells. *Materials* **11**(1), 71 (2018)
170. M. Salahuddin, M.N. Uddin, G. Hwang, R. Asmatulu, Superhydrophobic PAN nanofibers for gas diffusion layers of proton exchange membrane fuel cells for cathodic water management. *Int. J. Hydrog. Energy* **43**(25), 11530–11538 (2018)
171. N. Abdullhah, S.K. Kamarudin, L.K. Shyuan, Novel anodic catalyst support for direct methanol fuel cell: characterizations and single-cell performances. *Nanoscale Res. Lett.* **13**(1), 90 (2018)
172. B. Munavalli, A. Torvi, M. Kariduranavar, A facile route for the preparation of proton exchange membranes using sulfonated side chain graphite oxides and crosslinked sodium alginate for fuel cell. *Polymer* **142**, 293–309 (2018)
173. A.S. Aricó, V. Baglio, V. Antonucci, *Electrocatalysis of Direct Methanol Fuel Cells* (Verlag GmbH & Co., Weinheim, 2009)
174. S. Jang, Y.G. Yoon, Y.S. Lee, Y.W. Choi, One-step fabrication and characterization of reinforced microcomposite membranes for polymer electrolyte membrane fuel cells. *J. Membr. Sci.* **563**, 896–902 (2018)
175. S. Chan, J. Jankovic, D. Susac, M.S. Saha, M. Tam, H. Yang, F. Ko, Electrospun carbon nanofiber catalyst layers for polymer electrolyte membrane fuel cells: structure and performance. *J. Power Sources* **392**, 239–250 (2018)
176. N. Awang, J. Jaafar, A.F. Ismail, Thermal stability and water content study of void-free electrospun SPEEK/Cloisite membrane for direct methanol fuel cell application. *Polymers* **10**(2), 194 (2018)
177. F. Helmer-Metzman, F. Osan, A. Schneller, H. Ritter, K. Ledjeff, R. Nolte, R. Thorwirth, Polymer electrolyte membrane, and process for the production thereof, US Patent 5,438,082 (1995)
178. H. Junoh, J. Jaafar, N.A.M. Nor, N. Awang, M.N.A.M. Norddin, A.F. Ismail, ... & W. N. W. Salleh, *J. Membr. Sci. Res.* (2018)
179. N. Awang, J. Jaafar, A.F. Ismail, M.H.D. Othman, M.A. Rahman, N. Yusof, et al., Development of dense void-free electrospun SPEEK-Cloisite15A membrane for direct methanol fuel cell application: Optimization using response surface methodology. *Int. J. Hydrog. Energy* **42**(42), 26496–26510 (2017)
180. J. Jaafar, Development and characterization of sulfonated poly (ether ether ketone) membrane for direct methanol fuel cell. Universiti Teknologi Malaysia. M.Sc. Thesis, 2006
181. N. Awang, J. Jaafar, A.F. Ismail, M.H.D. Othman, M.A. Rahman, Effects of SPEEK/Cloisite concentration as electrospinning parameter on proton exchange membrane for direct methanol fuel cell application. *Mater. Sci. Forum* **890**, 278 (2017). Trans Tech Publications Ltd
182. N. Awang, J. Jaafar, A.F. Ismail, T. Matsuura, M.H.D. Othman, M.A. Rahman, Electrospun nanocomposite materials for polymer electrolyte membrane methanol fuel cells, in *Organic-Inorganic Composite Polymer Electrolyte Membranes*, (Springer, Cham, 2017), pp. 165–191
183. M.A. Mohamed, M.A. Mutalib, Z.A.M. Hir, M.F.M. Zain, A.B. Mohamad, L.J. Minggu, et al., An overview on cellulose-based material in tailoring bio-hybrid nanostructured photocatalysts for water treatment and renewable energy applications. *Int. J. Biol. Macromol.* **103**, 1232–1256 (2017)
184. M.A. Mohamed, W.N.W. Salleh, J. Jaafar, A.F. Ismail, M.A. Mutalib, A.B. Mohamad, et al., Physicochemical characterization of cellulose nanocrystal and nanoporous self-assembled CNC membrane derived from Ceiba pentandra. *Carbohydr. Polym.* **157**, 1892–1902 (2017)

185. J.P. Luongo, Infrared study of oxygenated groups formed in polyethylene during oxidation. *J. Polym. Sci.* **42**(139), 139–150 (1960)
186. M.A. Abdelkareem, Y. Al Haj, M. Alajami, H. Alawadhi, N.A. Barakat, Ni-Cd carbon nanofibers as an effective catalyst for urea fuel cell. *J. Environ. Chem. Eng.* **6**(1), 332–337 (2018)
187. A.R. Ashraf, J.J. Ryan, M.M. Satkowski, S.D. Smith, R.J. Spontak, Effect of systematic hydrogenation on the phase behavior and nanostructural dimensions of block copolymers. *ACS Appl. Mater. Interfaces* **10**(4), 3186–3190 (2018)
188. Li, J. Zhang, Y. Wang, sulfonated poly (ether ether ketone) mem-branes for direct methanol fuel cell, *J. Membr. Sci.* **226**, 159 (2003)
189. T. Sancho, J. Lemus, M. Urbiztondo, J. Soler, M.P. Pina, Zeolites and zeotype materials as efficient barriers for methanol cross-over in DMFCs. *Microporous and Mesoporous Materials*, **115**(1-2), 206–213 (2008)



Rasel Das, Syed Mohammed Javaid Zaidi, and
Sayonthoni Das Tuhi

Contents

1	Introduction	1013
2	Polymers for Membrane Fabrications	1017
2.1	Synthetic Polymers	1018
2.2	Biopolymers	1027
2.3	Nanomaterial for Mixed-Matrix Polymeric Membrane	1033
3	Conclusion and Future Perspectives	1036
	References	1037

Abstract

Polymeric membranes are currently extensively investigated for water purification. Strong motivations behind this are due to their unique structural characteristics such as high mechanical, thermal, and chemical stabilities. They are also flexible in nature in such a way that one can easily fold them into hollow fiber or flat sheet. Based on such features, an excellent pollutant selectivity and permeability of water have been observed; thereby a remarkable separation capacity is expected. This chapter covers a comprehensive discussion on the fabrication of both synthetic and biopolymeric membranes for water desalination. Fundamental knowledge on structures, types, functionalizations, and optimizations of different advanced polymer-based membranes, especially microfiltration

R. Das (✉)

Chemical Department, Leibniz Institute of Surface Engineering, Leipzig, Germany
e-mail: raselgeneticist@gmail.com; raseldas@daad-alumni.de

S. M. J. Zaidi

Center for Advanced materials, Qatar University, Doha, Qatar
e-mail: szaidi@qu.edu.qa

S. D. Tuhi

Department of Microbiology, University of Chittagong, Chittagong, Bangladesh
e-mail: sayonthonidastuhi@gmail.com

(MF), ultrafiltration (UF), nanofiltration (NF), and reverse osmosis (RO), were discussed in details with their synthesis procedures. MF and UF membranes are suitable to retain larger organic and inorganic molecules, whereas NF and RO are popularly used to purify salty water. MF is usually prepared by cellulose acetate, polysulfone, poly(ether sulfone), and poly(vinylidene fluoride). Secondly, UF membrane is made by polysulfone, poly(ether sulfone), poly(vinylidene fluoride), poly(acrylonitrile), and poly(etherimide). Thirdly, polysulfone, polyamide poly(vinylidene fluoride), chitosan, and aquaporin are the major building blocks for NF membranes. Finally, cellulose acetate, polysulfone, and aromatic polyamides are the major constituents of RO membranes. Carbon nanotube is highlighted as a part of polymers' composites membrane with respect to improved or novel performance, and the potential implications of those developments for future membrane technology are discussed. Finally, some of the research gaps and future prospects of polymeric membrane technologies are also highlighted.

Keywords

Polymers · Structures · Functionalization · Water purification · Desalination

Abbreviations

°C	Degree Celsius
ABA	Triblock copolymer with a hydrophobic B segment flanked by two identical hydrophilic A segments
AQP0	Mammalian aquaporin 0 isoform
AQP1	Mammalian aquaporin 1 isoform
AQP3	Mammalian aquaglyceroporin 3 isoform
AQP4	Mammalian aquaporin 4 isoform
AqpZ	Bacterial (<i>E. coli</i>) aquaporin Z isoform
CA	Cellulose acetate
cm ³ /cm ² /s	Cubic centimeter per centimeter square per second
CNT	Carbon nanotube
CNT	Carbon nanotube
COD	Chemical oxygen demand
CTA	Cellulose triacetate
DOPC	1,2-Dioleoyl- <i>sn</i> -glycero-3-phosphocholine
DOTAP	2-Dioleoyl-3-trimethylammonium-propane (chloride salt)
g/mol	Gram per mol
GFD	Gallons per square foot per day
GO	Graphene oxide
GS	Gas separation
kDA	Kilo Dalton
kg h ⁻¹ m ⁻²	Kilogram per hour per meter square
kg/m ³ ·s	Kilogram per cubic meter second
L m ⁻² h	Liter per meter square hour
L m ⁻² h ⁻¹ bar ⁻¹	Liter per meter square per hour per bar
L m ⁻² h ⁻¹	Liter per meter square per hour

L/h·m ²	Liter per hour meter square
L/m ² h	Liter per meter square per hour
L/min	Liter per minute
m/s	Meter per second
m ² s ⁻¹	Meter square per second
m ³ m ⁻² day ⁻¹	Cubic meter per meter square per day
MF	Microfiltration
mL/cm ² s	Mililitre per centemeter square per second
mm	Millimeter
MM	Mixed matrix
MMCNT	Mixed matrix carbon nanotube
MPa	Megapascal
mPa ⁻¹ s ⁻¹	Meter per pascal per second
MW	Molecular weight
MWCNT	Multiwalled carbon nanotubes
NF	Nanofiltration
NIPS	Nonsolvent-induced phase separation
nm	Nanometer
ppm	Parts per million
PVDF	Polyvinylidene di(fluoride)
RO	Reverse osmosis
SPES	Sulfonated polyethersulfones
SWCNT	Single-walled carbon nanotubes
TFC	Thin film composite
TIPS	Thermally induced phase separation
UF	Ultrafiltration
VA	Vertically aligned
VACNT	Vertical aligned carbon nanotube
VIPS	Vapor-induced phase separation
WP	Water permeation
μm	Micrometer

1 Introduction

Global warming causes severe climate changes that increase ice-melting and sea level. It submerges the available fresh water resources and makes them saltier. Therefore, future water shortage is a must, and the lack of cost-effective sea and brackish water desalination technology has further aggravated the crisis for the rapidly growing population. This paves the way for a big threat to human development, health, sustainability, and social and economic progresses.

In order to secure pure water availability, many water treatment technologies under the category of primary (screening, filtration, centrifugation, separation, sedimentation, coagulation, and flocculation), secondary (aerobic and anaerobic treatments), and tertiary (distillation, crystallization, evaporation, solvent extraction,

oxidation, precipitation, ion exchange, membrane filtration technologies) have been proposed [1]. Among them, membrane technologies such as microfiltration (MF), ultrafiltration (UF), nanofiltration (NF), and reverse osmosis (RO) [2] are commonly used for water purification. Membrane can be simply defined as a thin barrier which allows a very selective mass transport. Although both the organic (e.g., polymers) and inorganic (zeolites, ceramic, etc.) materials have been used, organic polymers are popularly examined for commercial membrane fabrications. Table 1 shows some important commercial organic polymers corresponding to their membrane processes. The major advantage of membrane technologies are high throughput, high pollutants rejection ability, high selectivity, high mechanical strength, and spent media regeneration [2]. In order to make an effective membrane, one needs to ensure these advantages for high water flux and pollutants rejections with low biofouling (long life-span) effects. For manufacturing purpose, membrane needs to be reproducible, low capital costs for packaging.

Membranes are usually classified based on few factors such as nature of the polymers, morphology, geometry, preparation method, separation regime, and

Table 1 Polymers used for industrially established separation membranes [5]

Polymer	Morphology			Membrane process
	barrier type	Cross section	Barrier thickness (mm)	
Cellulose acetates	Nonporous	Anisotropic	~0.1	RO
	Mesoporous	Anisotropic	~0.1	UF
	Macroporous	Isotropic	50–300	MF
Cellulose nitrate	Macroporous	Isotropic	100–300	MF
Cellulose	Mesoporous	Anisotropic	~0.1	UF
Polyacrylonitrile	Mesoporous	Anisotropic	~0.1	UF
Polyetherimides	Mesoporous	Anisotropic	~0.1	UF
Polyethersulfones	Mesoporous	Anisotropic	~0.1	UF
	Macroporous	Isotropic	50–300	MF
Polyethylene terephthalate	Macroporous	Isotropic track-etched	6–35	MF
Polyamide (aliphatic)	Macroporous	Isotropic	100–500	MF
Polyamide (aromatic)	Mesoporous	Anisotropic	~0.1	UF
Polyamide (aromatic)	Nonporous	Anisotropic/composite	~0.05	RO,NF
Polyether (aliphatic)	Nonporous	Anisotropic/composite	~0.05	RO,NF
Polyethylene	Macroporous	Isotropic	50–500	MF
Polyimides	Nonporous	Anisotropic	~0.1	GS,NF
Polypropylene	Macroporous	Isotropic	50–500	MF
Polysiloxanes	Nonporous	Anisotropic/composite	~0.1 < 1–10	NF
Polyvinylidene fluoride	Mesoporous	Anisotropic	~0.1	UF
	Macroporous	Isotropic	50–300	MF

processes [3]. Figure 1 shows the permeability of solutes through several polymeric membranes, such as NF, UF, MF, and RO. Among them, RO has been extensively used for desalination and around 19% of the world’s desalination plants have successfully installed the RO membrane [4].

Classification of membrane depends on several factors as shown in Fig. 2 [6]. It reveals two forms of membrane (a) flat sheet and (b) hollow fiber based on its geometry. Based on structural variations, two types of membranes are classified (a) symmetric or isotropic and (b) asymmetric or anisotropic, as shown in Fig. 3. It shows symmetric membranes are uniform in structure (homogenous) throughout the whole membrane body which controls overall separation performances. On the other hand, the gradient structure in asymmetric membrane is controlled by densest part of the membrane.

Symmetric membranes are synthesized by vapor precipitation and phase inversion processes [7, 8]. Porosity of the membrane is controlled by using the concentration of polymers and the phase compositions. At low polymer with high humidity concentrations, it is possible to synthesize highly porous membrane and vice versa as shown in Fig. 4. Thermally-induced phase inversion process has also found effective to get symmetric porous membrane structure. On the other hand, different types of

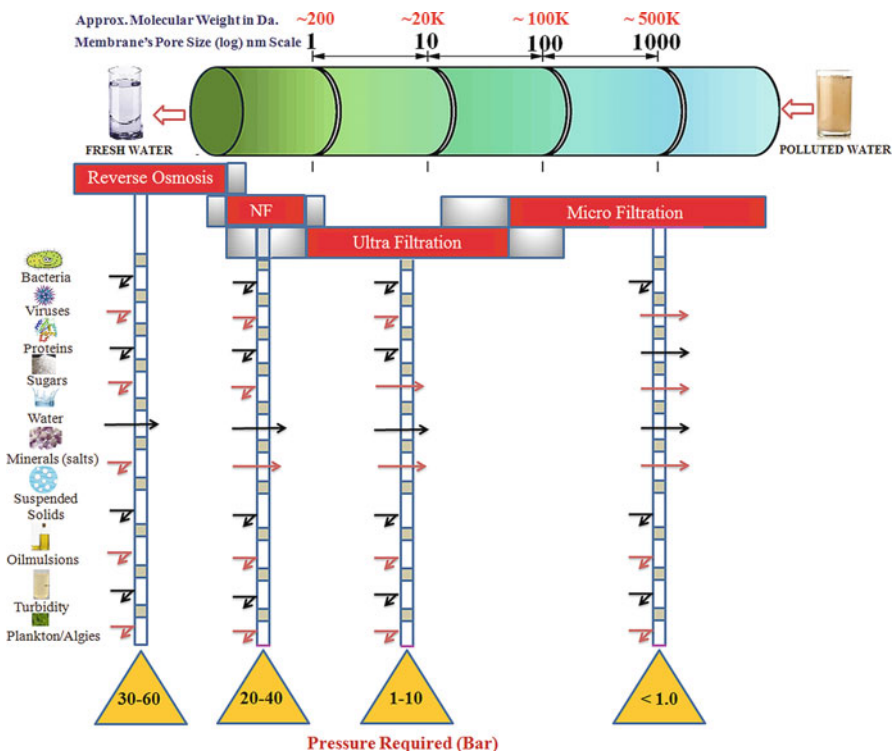


Fig. 1 Major polymeric membranes for water purification

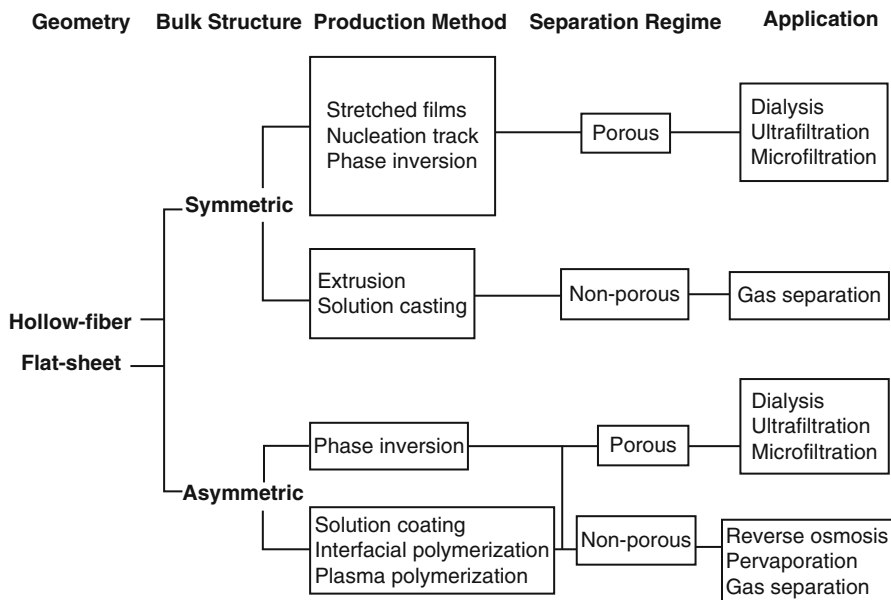


Fig. 2 Classification of synthetic membranes. (Adapted with permission from American Chemical Society [6])

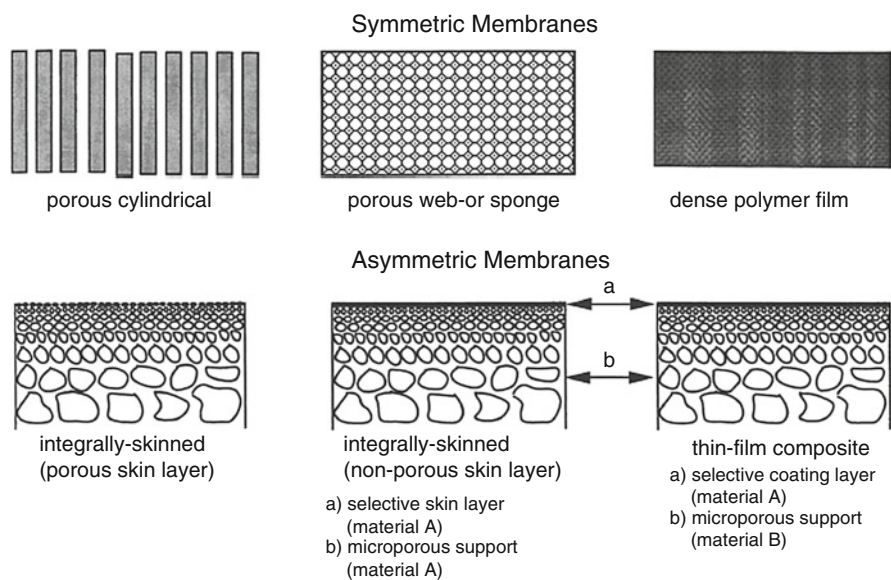


Fig. 3 Structural representation of symmetric and asymmetric membrane structures. (Adapted with permission from American Chemical Society [6])

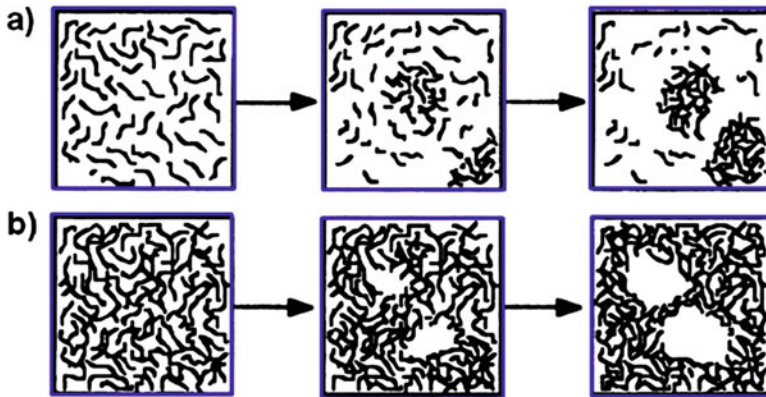


Fig. 4 Effects of polymer concentrations on membrane morphology: (a) membrane resulting from polymer-rich and (b) polymer-poor phases. (Adapted with permission from American Chemical Society [6])

asymmetric membranes are synthesized by different production methods. For example, phase inversion method is suitable for porous integral membrane. The membrane has directly been used for UF and MF processes. However, dense integral membrane is more suitable for RO and gas separations.

2 Polymers for Membrane Fabrications

Ideal polymers are the major building blocks for a membrane which should have high mechanical, thermal, and chemical stabilities. In addition, it should also be flexible in such a way that one can easily fold them into hollow fiber or flat sheet. In general, synthetic organic polymers such as cellulose, cellulose acetates, cellulose acetate butyrate, cellulosic ester, cellulose nitrates, polycarbonate esters, ethyl celluloses, polyacetylenes, polyacrylonitrile, polyamides, polyamide esters, polyamide-hydrazide, polyamideimides, polyaryletherketone, polyetherketones, polycarbonates, poly(phenylene oxide) polyesters, polyestercarbonate, polyethers, polyetherimides, polyetherketones, polyethersulfones, polyethylenes, polyhydrazides, polyimides, polyphenylene oxides, polyphenylene sulfide, poly(phthalazine ether sulfone ketone), sulfonated poly(phthalazine ether sulfone ketone), polypropylene, polysiloxanes, polysulfones, sulfonated polysulfones, polytetrafluoroethylene, poly(trialkylsilylacetylenes), poly(trimethylsilylpropyne), polyureas, polyurethanes, polyvinylalcohol, polyvinylchloride, polyvinylidene fluorides, and so on have been used to fabricate different membrane processes [9]. But all polymers are not commonly practiced industrially. Here we will only highlight those polymers which are commonly used for membrane fabrications. Firstly, both the MF and UF membranes are usually made by poly(vinylidene fluoride), polysulfone, poly(acrylonitrile), and poly(acrylonitrile)-poly(vinyl chloride) copolymers. MF membranes also utilized

the cellulose acetate and cellulose nitrate blends, nylons and poly(tetrafluoroethylene) [10, 11]. Secondly, poly(ether sulfone) is a major building block for UF membranes. Thirdly, NF membranes are made by polyether, polyimide, polyamide, and polyester. Finally, RO membranes are usually prepared by cellulose acetate or polysulfone coated with aromatic polyamides. Although same polymers could be used to fabricate multiple membranes, there are huge physicochemical differences along with their performances for water purification as we summarized in Table 2.

2.1 Synthetic Polymers

Man-made polymers have been synthesized by taking in to account their commercial utility in various sectors and are commonly classified as thermoplastics, thermosets, elastomers, and synthetic fibers. Although most of the synthetic polymers have long-chain structures, they are different in either main or side chain variations. Most of the membranes made by synthetic polymers have been commercialized for industrial or domestic uses. The synthetic polymers for membrane fabrications such as cellulose acetate, polysulfone, polyethersulfone, polyacrylonitrile, polyvinylidene fluoride, polyetherimide, polyamide, and polyimide are widely studied due to their mechanical strength, flexibility, and chemical stability. Here we discussed these polymers in detail including their structure, types, and modification strategies in the subsections below, and also highlighted their applications for water purification in Table 3.

2.1.1 Cellulose and Cellulose Acetate

Cellulose is a naturally abundant polymer and its ester form is the so-called cellulose acetate as shown in Fig. 5a. Cellulose acetate can be obtained from the cellulose acetylation. The degree of acetylation determines the replacement rates of cellulose's OH groups with CH_3COO groups. This substitution is important for controlling membrane properties. Scaling from 0 to 3, where 0 represents unreacted cellulose and 3 depicts completely substituted cellulose, which is called cellulose triacetate (CTA) [27]. Higher degree of acetylation brings high salt retention, but low water permeability. Loeb and Sourirajan [28] used heat treatment to fabricate the RO membrane using cellulose acetate in 1960. The membrane was so effective for water desalination than the other existing membranes at that time, which allow its rapid commercialization in the market. Later, the same fabrication processes were used to form MF. The degree of acetylation for commercial cellulose acetate-mediated RO membrane is about 2.7, which postulates a good balance between salt rejections and permeate flux. Some membranes are prepared by the blending of cellulose acetate and CTA. It increases the membrane's mechanical stability and resistance to hydrolysis, but decreases water permeability. A commercial cellulose acetate-blended membrane exhibits a flux of 22 GFD at 425 psi (Δp), and an average NaCl rejection of 97.5% [29]. The membranes are relatively easy to make and are typically resistant to chlorine attack. It can tolerate up to 5 ppm of free chlorine which is much higher than the aromatic polyamide-based membranes. However, cellulose acetate membrane has some disadvantages such as the low

Table 2 Major differences among some major polymeric membranes

Feature	RO	NF	UF	MF	Refs.
Definition	A process that applies transmembrane pressure to cause selective movement of solvent against the osmotic pressure difference	A separation process in which particles and dissolved macromolecules smaller than 2 nm are rejected	A process whereby a solution containing a solute of >1–100 nm in diameter is removed from the solvent	A separation process in which particles and dissolved macromolecules larger than 100 nm are rejected	[12]
Specific application	Desalination, water reuse, and ultrapure water production	Hardness, heavy metals, and dissolved organic matter removal	Virus and colloid removal	Suspended solids, protozoa, and bacteria removal	[2, 5, 13]
Materials	Organic polymers such as, polyamide, polysulfone, and polyether sulfone	Organic polymers like polyamide, polyester, and other porous polymers	Polysulfone, acrylic, cellulose, and others	Polypropylene, polysulfone, polyurethane, and so on	[14–18]
Pore types and sizes (nm)	Micropores (0.3–0.6)	Micropores (<2)	Mesopores (2–50)	Macropores (>50–500)	[5, 19]
Thickness (μm)	~0.1–0.2	~0.05	150–300	50–100	[20, 21]
Water permeability ($\text{mPa}^{-1} \text{s}^{-1}$)	~ 3×10^{-12}	~ 40×10^{-12}	~ 0.5×10^{-10}	–	[2, 20]
Solute rejection ability	Good	Good	Moderate	Poor	[2, 20]
Self-cleaning capability	Only with functionalization	Only with functionalization especially at ceramic-reactive membranes	Only with functionalization especially at ceramic-reactive membranes	Only with functionalization especially at ceramic-reactive membrane	[2, 22–25]
Tunable selectivity	<i>Mixed matrix only</i>	<i>Mixed matrix only</i>	Mixed matrix with ceramic reactivity	Mixed matrix with ceramic reactivity	[2]
Membrane fouling	Yes	Yes	Yes	Yes	[2]
Pressure uses (bar)	30–60	20–40	1–10	<1.0	[26]

water flux, weak chemical resistance, and high biodegradability. The membrane typically tends to hydrolyze over time which decreases their selectivity and sensitivity toward salt molecules. Water pH determines the stability of the membrane (stable pH: 4–6). Salt rejection of cellulose acetate membranes decreases as temperature increases. Influent water temperature usually should not exceed 35 °C [30]. Therefore, several modifications of the polymer using styrene, poly-(4-vinylpyridine), phenyl isocyanate, propylene oxide, acrylamide, *O*-(carboxy-

Table 3 Major observations of synthetic polymeric membranes for water purification

Type	Synthetic polymers	Key features	Refs.
MF	Polyvinyl alcohol/ polypropylene	Water permeability (WP): 32,346 L/m ² h at 0.24 bar Smaller avg. pore size than nonwoven membranes	[52]
	Poly(vinylidene fluoride) / hydroxyethylmethacrylate	Enhanced hydrophilicity and improved flux	[53]
UF	Cellulose acetate nanofiber	10× higher flux than commercial membranes (WP: 3540 L/m ² h)	[54]
	Polyimide/polyethersulfone	WP: 3565–1780 L/m ² h Enhanced thermal resistance and mechanical strength	[55]
	Polyethylene terephthalate	WP: 0.1–0.21 mL/cm ² s Reversible pH-responsive permeation	[56]
	Polysulfone/poly[2,2'-(<i>m</i> -phenylene)-5,5'-dibenzimidazole]	WP: 355 L/m ² h Enhanced porosity, hydrophilicity, and thermal stability	[57]
	Polyvinyl chloride and polyvinyl formal	WP: 52–323 L/m ² h at 0.1 MPa Enhanced antifouling property	[58]
	Cellulose acetate/polyethylene glycol	WP: Max 360 L/m ² h at 0.05 MPa Antibacterial and antifouling Concurrent separation	[59]
	Polyurethane/polyvinylidene fluoride	WP: 130 L/m ² h Six times higher fluxes than the pure PVDF membranes	[60]
	Cellulose acetate and its derivatives	WP: 316–406 L/m ² h Hollow fiber, and hydrophilicities cellulose acetate > cellulose acetate butyrate > cellulose acetate propionate Cellulose acetate with the highest antifouling properties for humic acid and bovine serum albumin	[61]
	Polysulfone	WP: 227.8 L/m ² h Mixed with polyethylene glycol methyl ether (PEGME) as an additive Decreases contact angle from 71° to 47°	[62]
Nano-chitin whisker/poly(vinylidene fluoride)	WP: 392 L/m ² h Improved mechanical properties Antifouling membrane	[63]	
NF	Polysulfone	WP: 7.5–8.9 L/m ² h Gravity-driven membrane filtration Improved permeate quality in the presence of biofilm on membrane surface	[64]
	Poly(acrylic acid-co-polyethylene glycol methyl ether methacrylate)	WP: 0.794 L/m ² h Hydrophilic surface pH responsive 90% flux recovery ratio after bovine serum albumin separation	[65]

(continued)

Table 3 (continued)

Type	Synthetic polymers	Key features	Refs.
	Cellulose acetate	WP: 3540 L/m ² h (10 times greater than that of most commercial membranes) 71% porous structure	[66]
	Poly(ethylene glycol) diglycidyl ether/polyamide	WP: 50–92 L/m ² h 99.1 to 99.9% NaCl rejection with >95% organic rejection Improved fouling resistance	[67]
	Polysulfone	WP: Max 70 L/m ² h Cadmium removal 98%	[66]
	Cellulose acetate	WP: 5.09 × 10–6 m/s 81.7% NaCl rejection	[68]
	Polyamide	WP: 5.67 × 10–6 m/s 98.3% NaCl rejection	[68]
RO	Sulfonated polyfuran	WP: 0.8 m ³ m ⁻² day ⁻¹ 99.8% NaCl rejection	[69]
	Polyether-polyfuran	WP: 0.5 m ³ m ⁻² day ⁻¹ 99.9% NaCl rejection	[69]
	Sulfonated polysulfone	WP: 0.06 m ³ m ⁻² day ⁻¹ 98% NaCl rejection	[69]
	Polyamide (aliphatic-aromatic)	WP: 0.7 m ³ m ⁻² day ⁻¹ 99% NaCl rejection	[69]
	Polypiperazine-amide	WP: 0.3 m ³ m ⁻² day ⁻¹ 68% NaCl rejection	[69]
	Poly(vinyl) alcohol via network cellulose	1.2 L/h·m ² 98.9% NaCl rejection	[70]
	Cellulose acetate/polyethylene glycol-600	WP: 0.35 L/h·m ² 81.50% NaCl rejection Increased hydrophilicity	[71]
	Polypropylene	WP: 0.9 L/m ² 77.9% NaCl rejection	[72]
	Polysulfone	WP: 1.1 L/m ² h 96.4% NaCl rejection	[72]
	Polysulfone	WP: 6.5–32.8 L/m ² h 83–94% NaCl rejection	[73]
	Polysulfone	WP: 0.15–0.24 L/m ² h 79–95% NaCl rejection	[46]
	Poly(pathalazinone ether sulfone ketone)	WP: 22.9 L m ⁻² h 99.2% NaCl rejection	[74]
	Poly(pathalazinone ether amide)	WP: 270 L/m ² h >18.2% NaCl rejection >99% dyes rejection	[75]
	Polyvinylidene fluoride	WP: 0.55–0.25 L/m ² h 2–99% NaCl rejection	[46]

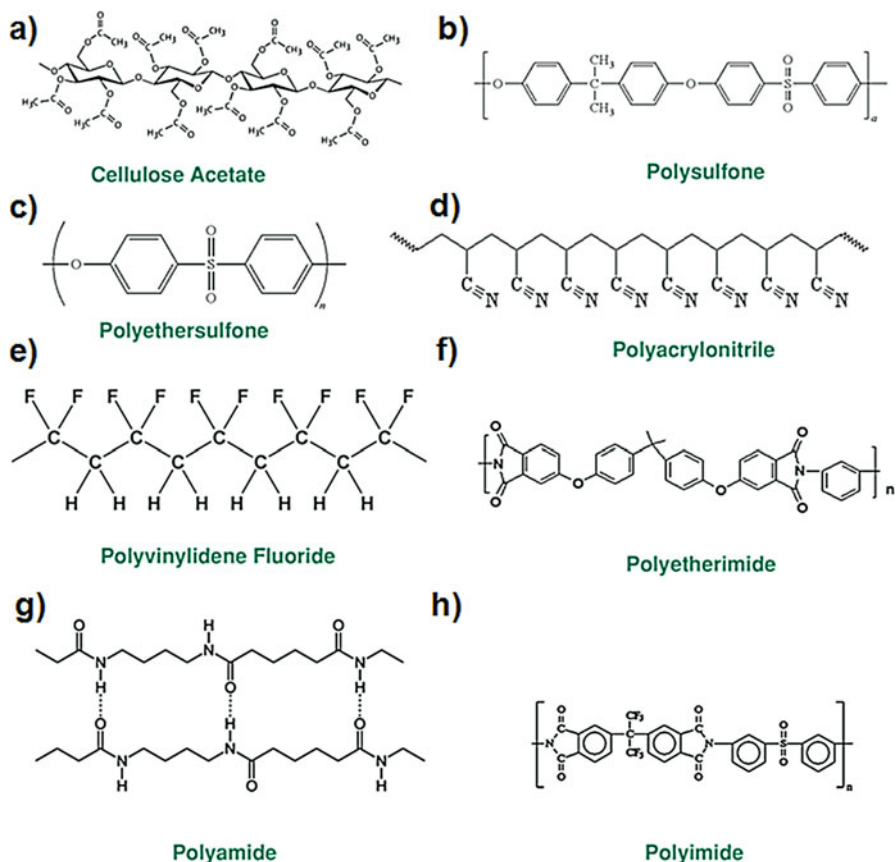
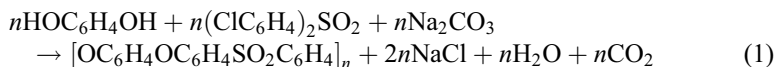


Fig. 5 Chemical structures of some commonly used synthetic polymeric membrane materials

methyl), *O*-nitro, and *O*-(cyanoethyl) groups, and so on have been observed in fabricating the RO membrane for improving its mechanical strength, salt selectivity, and water flux [31, 32].

2.1.2 Polysulfone

Compared to cellulose acetate, polysulfone is more thermostable and is so called thermoplastic polymers and was introduced by Union Carbide in 1965. The polymer is expensive because of its high costs of raw materials. Figure 5b shows a typical repeating unit of polysulfone having aryl-SO₂-aryl subunit. The formation of polysulfone requires the active reaction between the diphenol (bisphenol-A or 1,4-dihydroxybenzene) and bis(4-chlorophenyl)sulfone, forming a polyether by removing of NaCl as shown in Eq. 1. Based on its purity of reactant monomer, one can achieve to get a high-molecular-weight long polymer.



Polysulfone is rigid in structure, but transparent. It can hold its physicochemical properties in temperature between -100 and 150 °C. Polysulfone is highly stable in a wide range of pH (2–13), so that the membranes prepared by them (UF and MF) can be easily washable using both acidic and basic solutions to reuse [33]. Autoclave and steam sterilization of the membrane can also be possible to thwart the microbes clogging into the membrane pores. But special attention should be paid to see whether the integrity and pore structure of the membrane should not be changed. The polymer is popular to use pressure-driven water and gas filtration membranes because of its high compaction resistance and can withstand at high pressure without compromising its strength. Polysulfone allows easy membrane fabrications with the controlled properties (pore sizes and volumes). Yuan et al. [34] synthesized polysulfone-based NF membrane and achieved high Na_2SO_4 (>80%), but low rejection of NaCl (15%). Besides desalination, polysulfone-based membranes also have huge applications in hemodialysis and gas separation. The membranes are popular to build the filter cartridges because of ensuring high flow rates at very low pressures as compared with nylon and polypropylene. Polysulfone can also be used as a copolymer with others, e.g., sulfonated polyethersulfones (SPES), for highly durable proton-exchange membranes in fuel cell [35]. Modification of polysulfone membrane using nanoparticle [36], polyethylene glycol [37], poly(vinyl alcohol), carboxymethyl cellulose [38], and so on has been well documented to improve NF membrane's permeability, selectivity and sensitivity, thermal and solvent resistance, and also mechanical properties.

2.1.3 Polyethersulfone

Polyethersulfone is an important polymer for separation sciences because of its high chemical (oxidative and hydrolytic) and thermal stabilities. Compared to polysulfone, polyethersulfone consists of phenyl rings separated by alternate ether and sulfone linkages as shown in Fig. 5c. Direct sulfonation reactions lead to sulfonation at the ortho position of the ether bond. Since polyethersulfone has sensitivity to aromatic hydrocarbons or ketones, they are widely used in UF, MF, and dialysis membranes. Polyethersulfone-based membrane commonly prepared by phase inversion method and is asymmetric in structure. The two most common used polyethersulfones are Ultrason E6020P (58) and Radel A-100 (15 kDa). Besides desalination, the polyethersulfone membrane has also been used for blood purification. Rastegarpanah and Mortaheb [39] reported that the permeate flux for polyethersulfone is 1.02×10^{-3} as comparable with commercial polytetrafluoroethylene membrane 1.07×10^{-3} kg/m³·s. It helps polyethersulfone to achieve the overall separation factors >99%. However, the hydrophobic character of polyethersulfone-based membranes brings difficulty for membrane fouling as

compared to polysulfone. So, the membrane has short life span and sensitivity. Therefore, anchoring of hydrophilic functional groups such as the sulfonated, pegylated, and carboxylated groups into the polyethersulfone membrane are important to increase the surface free energy, thereby reduced fouling effect. Some polymers such as polyvinylpyrrolidone, polyethylene glycol, cellulose acetate phthalate, Poly(1-vinylpyrrolidone-co-styrene), acrylic acid, and so on have been reported to increase polyethersulfone-based membrane porosity and polarity. Sometimes nanoparticles such as TiO₂, ZnO, SiO₂, ZrO₂, and so on have been used to fabricate organic–inorganic hybrid membrane for controlling the asymmetric structure and membrane porosity [39]. Alternatively, those membranes which are hydrophilic (having tendency to swell in water) could be strengthened by using hydrophobic polyethersulfone. Such compromised membrane between the hydrophilic and hydrophobic junction especially at pores would give high flux and decrease fouling effects.

2.1.4 Polyacrylonitrile

Polyacrylonitrile is a semicrystalline organic polymer resin, which is also known as Creslan 61. Acrylonitrile is a major part of this polymer with a linear formula (C₃H₃N)_n as shown in Fig. 5d. Polyacrylonitrile is synthesized by either the free radical or anionic polymerizations of acrylonitrile monomer. Besides, vinyl could be used as comonomer (1–10%), but it depends on special field applications. Polyacrylonitrile is popular because of its thermostability (<300 °C) and resistance to organic solvents, bacteria, photoirradiation, and membrane-forming ability. Polyacrylonitrile often shows superior performance than polysulfone-based membrane. Polyacrylonitrile is mainly used to prepare UF and RO membranes and porous supports of composite membranes using phase inversion process due to its superior resistance to hydrolysis and oxidation. In spite of having polar group in the backbone of the polymer, polyacrylonitrile is hydrophobic in its pure state. Hence, during preparation, it is typically copolymerized with more hydrophilic monomers to improve its hydrophilicity and processability to make it less brittle [40]. Similar to other membrane, polyacrylonitrile is also susceptible to foul that decreases its reusability. Therefore, modification of polyacrylonitrile with various polymers (amphiphilic) and nanomaterials such as carbon nanotube (CNT), SiO₂, TiO₂, Al₂O₃, and so on is important. Such composite membrane has shown enhanced water permeability (increased porosity), salt retention, and antifouling property and stability in real applications. For instance, polyacrylonitrile-based membrane has shown water flux of about 250, which is further increased to almost 1150 L m⁻² h⁻¹ upon SiO₂ modification [41]. Similarly, graphene oxide (GO)-doped polyacrylonitrile composite membrane shows a high water flux (65.1 L m⁻² h⁻¹) and salt rejection rate of about 99.8% [42].

2.1.5 Polyvinylidene Fluoride

Polyvinylidene di(fluoride) also known as PVDF is a semicrystalline polymer having a repeating unit of -(CH₂CF₂)_n- (Fig. 5e). As like other membranes polymer, polyvinylidene fluoride has high chemical, mechanical, and thermal stabilities. One important beauty of this membrane is its longevity (aging resistance), which is one of

the most important features for a commercial membrane. Because of its smoothness, it can easily be packed as flat sheet or tubular or hollow membrane. Classical nonsolvent-induced phase separation (NIPS) and thermally induced phase separation (TIPS) methods are popularly used to fabricate porous polyvinylidene fluoride membrane. TIPS method has some advantages as compared with NIPS. Polyvinylidene fluoride synthesized by TIPS typically shows high mechanical strength and lower antifouling property. But it needs high energy to pump water through it. So far, MF and UF membranes are commonly prepared by polyvinylidene fluoride polymer. The polymer is also used in gas separation, distillation pump, ion exchange technology, and so on. Many company including Asahi Kasei Chemicals, Merck Millipore, Koch Membrane Systems, Hyflux, and so on are now marketing the polyvinylidene fluoride-based membrane commercially. TIPS is also used for MF, whereas NIPS is useful for UF membrane. But vapor-induced phase separation (VIPS), solution casting and electrospinning can also be used to fabricate both membrane types. Xiao et al. [43] fabricated MF using polyvinylidene fluoride for municipal effluent treatment. The membrane was so stable and decreases chemical oxygen demand (COD) and develops appropriate water quality prior to RO treatment. Zhao et al. [44] synthesized UF membranes by crosslinking chitosan which shows high flux and rejection efficiency and less fouling effects.

Polyvinylidene fluoride has also been used as a support to develop composite membranes such as thin film composite (TFC)-based RO and NF membranes. Although polysulfone was popular at primary level, polyvinylidene fluoride is now getting popularity because of its high mechanical strength and resistance to chemicals. Figure 6 shows the polyvinylidene fluoride-based TFC membrane preparation [46]. The composite membrane shows high water flux and salt rejection abilities as compared with polysulfone as the support. Liang et al. [47] used plasma treatment for surface functionalizations of polyvinylidene fluoride which would be acted as anchoring site for coating of inorganic silica nanoparticles in UF membrane (Fig. 7). This allows improving the hydrophilicity and antifouling properties of polyvinylidene fluoride membranes.

2.1.6 Polyetherimide

Polyetherimide is an amorphous dense polymer having a repeating molecular unit ($C_{37}H_{24}O_6N_2$) (Fig. 5f) with MW of about 592 g/mol. It has been commonly used for UF membrane because of its good thermal and chemical stabilities, excellent film-forming ability, and low cost polymer. Compared to other polymers, polyetherimide is a hydrophobic one and is inadequate to use in membrane fabrication. Bowen et al. [48] modified polyetherimide using charged polymer called sulfonated poly(ether ether ketone) and showed that it increases the overall hydrophilicity of the membrane and enhances water permeability and NaCl rejection. Other modifiers such as Al_2O_3 , Fe_2O_3 , ZrO_2 , ZnO , and TiO_2 have been used to achieve more hydrophilic surface, higher specific surface area, and bactericidal and self-cleaning properties [49].

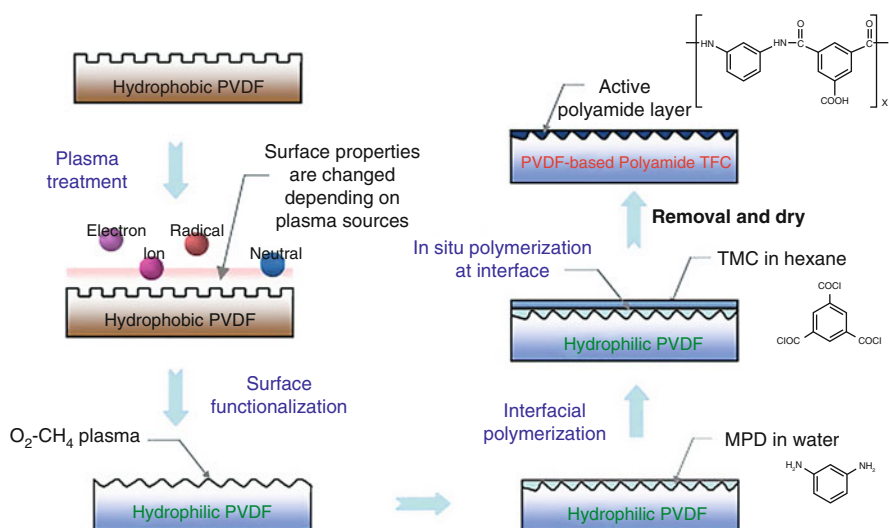


Fig. 6 Preparation of polyamide TFC membrane based on polyvinylidene fluoride. (Adopted with permission from Elsevier [45, 46])

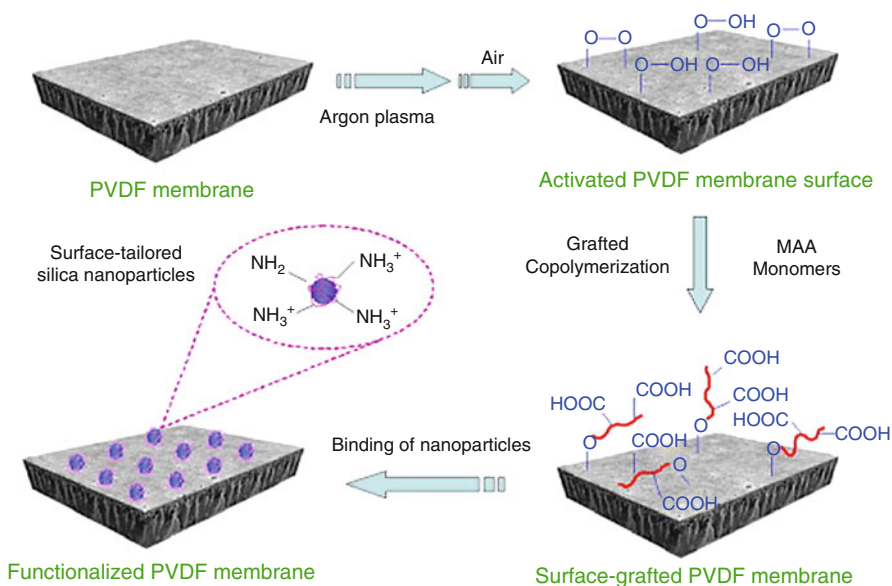


Fig. 7 Illustration of preparation of argon plasma treatment of polyvinylidene fluoride membrane followed by its graft copolymerization and nanoparticle binding. (Adopted with permission from Elsevier [45, 47])

2.1.7 Polyamide

Polyamide is a naturally occurring macromolecular polymer such as proteins, wool, silk, etc., where the repeating units are held together by amide bonds (Fig. 5g). It can also be synthesized artificially to achieve higher durability and strength. Such polyamides are nylons, sodium poly(aspartate), aramids, and so on, which have been commonly used in textiles, automotive applications, carpets, and so on. More than 35% of polyamides are commonly utilized in industry. However, most of the currently available polyamide-based membranes are RO and NF prepared by interfacial polymerization of acyl chlorides and various water-soluble reactants [50]. The method is popular nowadays, because it is possible to optimize individual feature or characteristics of a membrane chain. So, one can even optimize the polymeric structure at the surface which has direct regulatory effects in the water permeability and solute rejection. Chlorine is a common antifouling agent which has been used in wastewater treatment processes. But it can attack polyamide chains and damage its physical structure. In order to increase polyamide's chlorine stability and antifouling property, several modification techniques have been observed for polyamides using polyvinyl alcohol, 3-allyl-5,5-dimethylhydantoin, methylene-bis-acrylamide, and so on [51].

2.1.8 Polyimide

Polyimide is a polymer of imide monomers (Fig. 5h). Polyimide had been in mass production since 1955 because of their strong heat resistance properties. It was first synthesized by reacting naphthalene-1,4,5,8-tetracarboxylic dianhydride or 4,49-oxydiphthalic anhydride with 4,49-diaminobiphenyl-2,29-disulfonic acid and nonsulfonated diamine monomers such as 4,49-oxydianiline. The soluble poly(amic acid) is first formed by polycondensation of aromatic dianhydrides with aromatic diamines. Then, poly(amic acid) is shaped into the polyimide product by dehydration step. Based on the main polymeric chain composition, polyimide could be classified into aliphatic, aromatic, and semiaromatic. In addition, based on inter-main-chain interactions; polyimide can be categorized into thermoplastic and thermosetting. Thermosetting polyimide has good thermal and mechanical properties (very low creep and high tensile strength). Polyimide can hold these morphological properties up to 452 °C. In addition, polyimide is chemically stable in various solvents ethers, alcohol, esters, hydrocarbons, and so on. Although polyimide is relatively stable in weak acid, there is a least evidence to use the polymer in higher alkaline solution.

2.2 Biopolymers

The popularity of synthetic polymers has been decreased because of its stringent environmental regulations. Therefore, researchers are now replacing the synthetic polymers by natural biopolymers because of their sustainability and renewability [76]. Special physicochemical properties of biopolymeric membranes would help

to achieve high water permeation and separation, toxic metal capture, toxic organic dechlorination, and biocatalysts [77]. Most of the biopolymers are typically polysaccharides and a few are protein. The following subsections covered some popular biopolymers that have been used to fabricate current membrane technologies, and some major evidences of biopolymeric membrane performances for water purification are summarized in Table 4.

2.2.1 Chitin and Chitosan

Chitin is an important polysaccharide known as poly(β -(1–4)-*N*-acetyl-D-glucosamine) and was first identified in 1884. Because of structural similarity with chitosan, chitin is often considered as cellulose derivative, but it has acetamide groups at C-2 positions [78]. Aquatic flora and fauna such as fungi, diatoms, nematodes, arthropods, shrimps, crabs, lobsters, krill, and squid are the major natural sources of chitin. Similarly, chitosan is a linear polysaccharide composed of randomly distributed (1–4)-linked glucosamine and *N*-acetyl-D-glucosamine [79]. Generally, the physical characteristics of chitin and chitosan are white, hard, inelastic nitrogenous polysaccharides. Chitosan can be isolated directly from the cell wall of certain fungi. Moreover, it can be obtained from chitin by a chemical method or an enzymatic production method [80]. Chitosan is produced commercially by deacetylation of chitin, which is the structural element in the exoskeleton of the crustaceans crab and shrimp, and the cell walls of fungi (Fig. 8) [81, 82]. When the degree of deacetylation of chitin reaches about 50% (depending on the origin of polymer), it becomes soluble in aqueous acidic media and is called chitosan [83]. Chitosan membranes have been explored in many uses, such as in water–ethanol pervaporation, enzyme immobilization and cationic specimen transportation, protein separation and concentration, controlled ingredient release, and environmental applications [26]. Chitosan is applied in RO membrane preparation, where the degree of acetylation is about 0.3–0.8. Treatment with an organic acid or an acid anhydride, chitosan is converted to the acetylated form which is stable and useful as an RO membrane. Moreover, chitosan membrane has excellent thermal and chemical stabilities and exhibits mechanical strength sufficient for the pressure difference in the operating condition [84].

2.2.2 Carrageenans and Pullulan

Carrageenan is an anionic polysaccharide extracted from marine red algae, large and highly flexible molecules that curl forming helical structures (Fig. 9). Chemically, it is a linear polymer, sulfated galactan, composed of alternating disaccharide repeating units of 3-linked β -D-galactopyranose (G units) and 4-linked α -D-galactopyranose (D units) or 4-linked 3,6-anhydro- α -D-galactopyranose (DA units) [85]. Based on the number and position of sulfate groups, the isomers of carrageenan are known as kappa, iota, and lambda-carrageenan. Carrageenan is biocompatible, biodegradable, nontoxic, cheap, gel forming, and its oligosaccharides possess antibacterial activities against *Escherichia coli*, *Staphylococcus aureus*, *Saccharomyces cerevisiae*, *Pseudomonas citronellolis*, and *Mucor* species [81, 82, 86, 87]. However, these carrageenan films are observed to be very brittle and for this their potential applications also be hindered.

Table 4 Biopolymer-based composite membranes

Type	Membrane materials	Performance/key feature	Refs.
UF/NF	Chitosan/polyacrylonitrile	Water permeability (WP): 1.1 L/m ² h >99.95% organic waste rejection	[109]
Pervaporation	Chitosan and γ -(glycidyloxypropyl) trimethoxysilane	WP: 1730 g/m ² Increased membrane stability	[110]
RO	Chitosan/poly- <i>N</i> -acetyl glucosamine	WP: 1.67 \pm 10 ⁻³ cm ³ /cm ² /s 78.8% NaCl rejection	[111]
NF	<i>N,O</i> carboxymethyl chitosan/ cellulose acetate	WP: 16 L/min 83.40% chromium rejection 72.60% copper rejection	[112]
NF	2-Hydroxypropyltrimethyl ammonium chloride chitosan/ poly(acrylonitrile)	WP: 2.57 kg h ⁻¹ m ⁻² Order of salts rejection: MgCl ₂ > CaCl ₂ > NaCl, KCl > MgSO ₄ > Na ₂ SO ₄ > K ₂ SO ₄	[113]
NF	<i>N,O</i> carboxymethyl chitosan/ polyether sulfone	Nickel sulfate-water (rejection 74–80%) Nickel chloride-water (rejection 57–62%)	[114]
NF	Trimethylallyl ammonium chloride onto chitosan/poly (acrylonitrile)	WP: 6.3 L/h m ² Rejections trend: MgCl ₂ > CaCl ₂ > MgSO ₄ > NaCl > KCl > Na ₂ SO ₄ > K ₂ SO ₄	[115]
Biopolymeric	κ -Carrageenan-pullulan	WP: 0.13 g m ² s ⁻¹ Increase temperature brings increased permeate flux Good dye rejection	[116]
NF	Aquaporin Z/cellulose acetate	WP: 34 L/m ² h >30% NaCl rejection High throughput with lesser energy consumption	[117]
–	D-block copolymer (poly (2-vinylpyridine- <i>b</i> - methacrylicacid)	60–80% NaCl rejection Maximum flux rates at pH 5.5–6.0	[118]
RO	ESPA/PEBAX 1657 (polyether–polyamide block copolymer)	WP: 19.9 \pm 2.6 L/m ² h 99.0 \pm 0.06% NaCl rejection	[119]
UF	Poly(isoprene- <i>b</i> -styrene- <i>b</i> -4- vinylpyridine) triblock terpolymers	WP: 24–850 L m ⁻² h ⁻¹ bar ⁻¹ Membrane pore densities: 4.53 \times 10 ¹⁴ –1.48 \times 10 ¹⁵ pores/m ²	[120]
NF	Aquaporin (AqpZ-DOPC)	WP: 3.6 L m ⁻² h ⁻¹ bar ⁻¹ 20% NaCl rejection	[121]
NF	AqpZ-ABA	WP: 34.2 L m ⁻² h ⁻¹ bar ⁻¹ 32.9% NaCl rejection	[122]
NF	AqpZ-ABA	WP: 8.2 L m ⁻² h ⁻¹ bar ⁻¹ 45.1% NaCl rejection	[123]
NF	AqpZ-DOPC/DOTAP	WP: 5.5 L m ⁻² h ⁻¹ bar ⁻¹ 75% NaCl rejection	[124]
RO	AqpZ-DOPC	WP: 4 L m ⁻² h ⁻¹ bar ⁻¹ 96% NaCl rejection	[125]

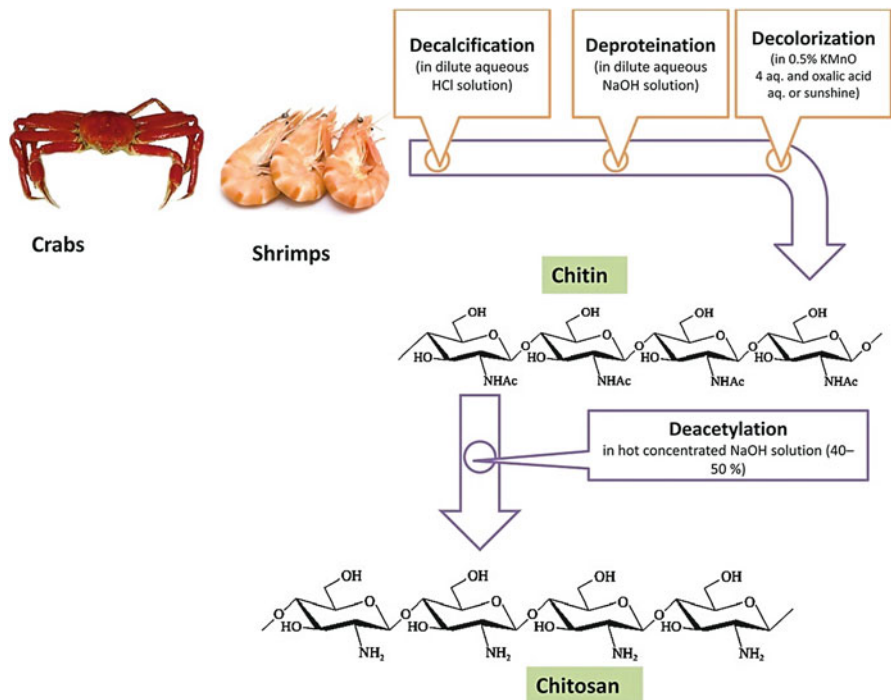


Fig. 8 Production method for chitin and chitosan

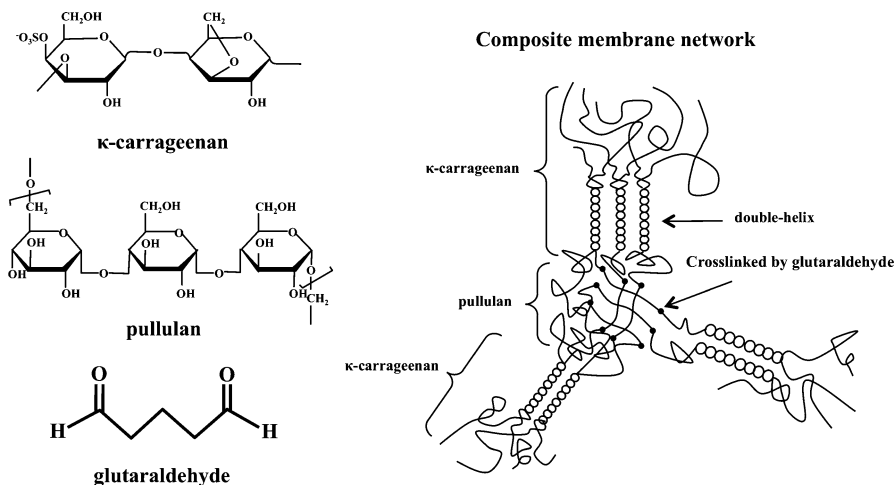


Fig. 9 Composite membrane made by cross-linking of κ-carrageenan-pullulan. (Adapted with permission from Elsevier [92])

Pullulan is another linear glucan polysaccharide consisting of repeating units of maltotriose joined by α -D-(1 \rightarrow 6) linkages (Fig. 9) [88]. It is an extracellular glucan intricate by a fungus of the genus *Aureobasidium*, which is commonly called black yeast. Due to its capacity to form strong, resilient films and fibers, pullulan gains the major interest in its own or combined with other thickeners or gelling agents [89]. Pullulan have a disadvantage for some applications, though this can be improved by mixing a small amount of another polysaccharide such as carrageenan or xanthan gum [90, 91]. Combination of κ -carrageenan and pullulan composite membrane (Fig. 9) shows sufficient mechanical strength for practical use and excellent mass transfer characteristics, especially for molecular-size screening. The fraction of κ -carrageenan (FC) typically determines the membrane characteristics such as mechanical stability and mass transfer effect. Because of its cross-linked hydrophilic structure, it exhibited high selectivity and high water flux [92].

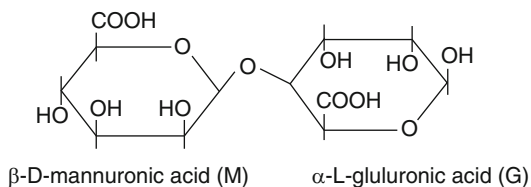
2.2.3 Alginate

Alginate is a biocompatible, nontoxic, nonimmunogenic, and biodegradable biopolymer. It is composed of guluronic acid (G) and mannuronic acid in its chain structure (Fig. 10), and typically extracted from brown algae (Phaeophyceae) including *Laminaria hyperborea*, *Laminaria digitata*, *Laminaria japonica*, *Ascophyllum nodosum*, and *Macrocystis prrifere* by treatment with aqueous alkali solution, e.g., NaOH [93]. Alginates have been traditionally applied in the food industry as thickeners, suspending agents, emulsion stabilizers, gelling, and film-forming agents. The physical properties (e.g., viscosity and mean molecular weight) of sodium alginate are very susceptible to physicochemical factors (e.g., pH and total ionic strength) [93]. For example, at near-neutral pH, the carboxylic functional groups of sodium alginates deprotonated and induce repulsive inter- and intramolecular electrostatic forces and have shown high negative charges [94]. In recent years, alginate membranes have been investigated in diverse ways (e.g., pervaporation, immobilized cell reactor, and UF), and can be prepared by low concentration cross-linker needed support matrix (e.g., glass fiber filter) to maintain flat membrane [94].

2.2.4 Aquaporins

Aquaporins are a class of membrane-spanning proteins, responsible for the water transport across the cell membrane [95]. The first human aquaporin, which was first demonstrated by Agre and coworkers, was named AQP1. The first aquaporins are described by their water channel activity, and since then 12 other human/mammalian

Fig. 10 β -D-mannuronic acid and α -L-guluronic acid monomers of alginate



aquaporins have been discovered (named AQP0 through AQP12) with critical physiological functions [96]. Moreover, aquaporins have been found in plants, yeast, and in the domains of Bacteria and Archaea. Though most of the aquaporins have water transport functions, solute transport [96] and formation of intercellular junctions (AQP0, AQP4) have been reported for selective aquaporins [97]. As an example, the aquaporin obtained from mammalian eye lens, AQP0, is selective for water, nonetheless, does not show high permeability, while in case of AQP2, which is present in kidney tissues and involved in concentrating urine, shows high selectivity and high permeability. The *E. coli* aquaporin AQPZ has high water permeability and no known transport of solutes [98]. The transport of water in aquaporins is more rapidly than existing RO and forward osmosis (FO) membranes, since there is a fundamental difference in transport mechanism. In contrast to the “jump diffusion” mechanism of existing membranes, water transport in aquaporins occurred through narrow hydrophobic nanochannels (diameter < 200 nm) by frictionless movement. Briefly, the pore openings around 3 Å of aquaporins are lined with mostly hydrophobic amino acids as shown in Fig. 11 [99]. Here, the large solutes are rejected through size exclusion, as the narrowest part of the channel is 2.3 Å. A positively charged arginine residue is located at this narrow part and helps to reject positively charged solutes through electrostatic repulsion [100]. And, lastly, molecular reorientation of water molecules occurs by hydrogen bonding with a residue near the pore. This molecular reorientation (water dipole reorientation) breaks the extensive hydrogen bonding that normally allows rapid H⁺ transfer in bulk water and in doing so prevents passage of H⁺ ions. It is that single aquaporins transfer water molecules at rates of 2–8 × 10⁹ molecules per second [100, 101]. However, nowadays, aquaporin-based membranes are not commercially available due to the difficulties of attaining large quantities of proteins and producing large areas of membrane material.

2.2.5 Block Copolymers

Block polymers are macromolecules composed of multiple block polymeric species which have the ability to self-assemble into highly ordered structures (Fig. 12), when it is placed in a selective solvent [103]. Because of having self-assembly properties, block copolymer possesses narrow pore size distributions and high porosities. The property is useful for membrane protein insertion [104]. Block polymers may appear in different forms due to the self-assembly by varying the concentrations and conditions, including densely packed cylindrical pores ideal for water separation membranes [105]. Phase inversion, shear aligning, and controlled substrate–polymer interactions are the common methods for large-scale production of block polymers. Theoretically, aligned cylinders can be formed through nanostructuring of block copolymers, which could enable a fully polymeric analog to aquaporin or align CNT membranes that may give a chance to take advantage of nanopore performance, while maintaining ease and economy of large-scale polymeric membrane fabrication [106]. These block polymers, which are sometimes called amphiphilic block copolymers, can be designed to have hydrophobic and hydrophilic blocks. The amphiphilic block copolymers are mostly used in biomimetic membranes preparation because of having some advantages like high mechanical and chemical stability, customizable properties, and ability to perform end group functionalization

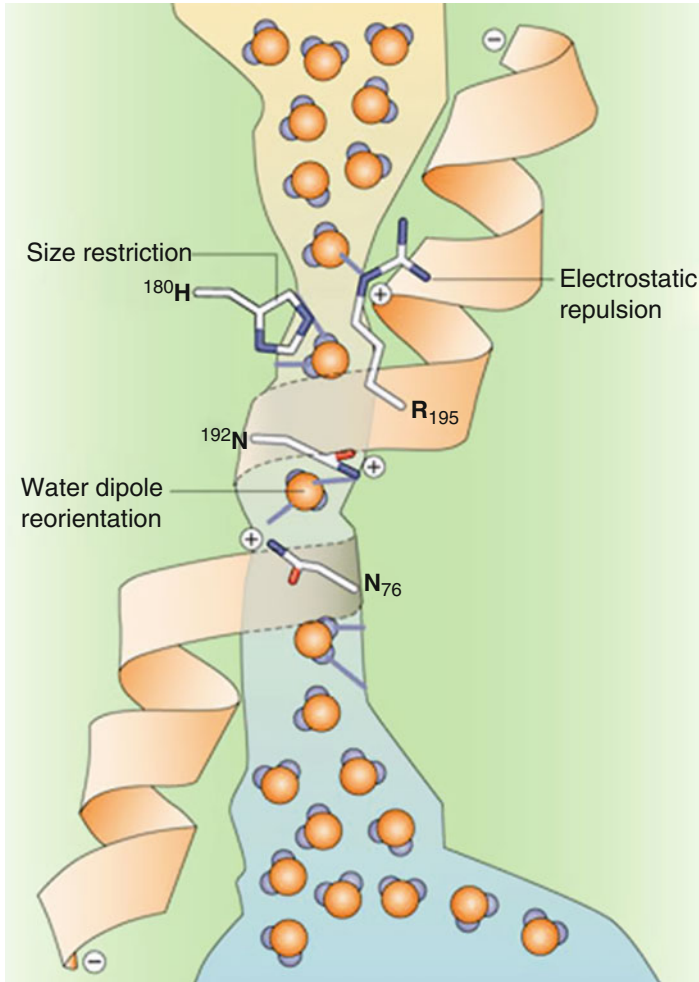


Fig. 11 Longitudinal section of AQP-1 water channel. The aqueous pore (blue color) which has a pre-diameter of 2.8 Å corresponds to the size of water molecules. (Adapted with permission from Nature [102])

[107]. Block copolymers are typically expensive, so using the polymers with other membranes as small percentage could provide large cost savings and improved performances for separation science.

2.3 Nanomaterial for Mixed-Matrix Polymeric Membrane

CNTs are composed of graphite sheets (allotropic form of carbon) rolled up in a tube-like structure with appearance of latticework fence (Fig. 13). Multiwalled carbon

Fig. 12 Assembly of block copolymer. (Adapted with permission from Nature [108])

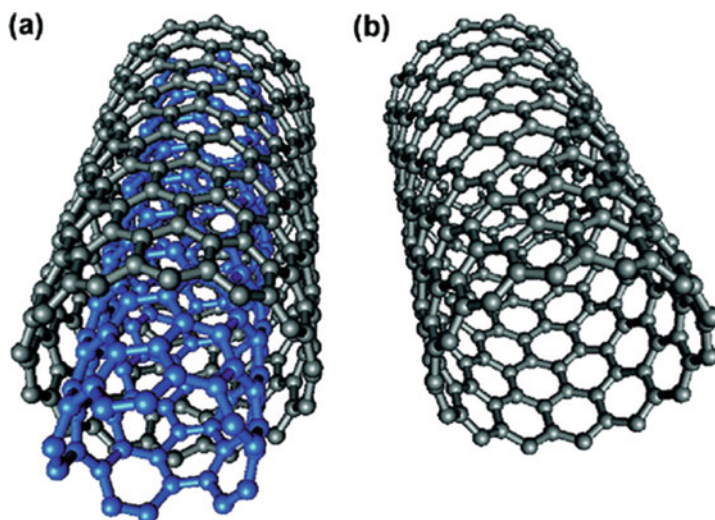
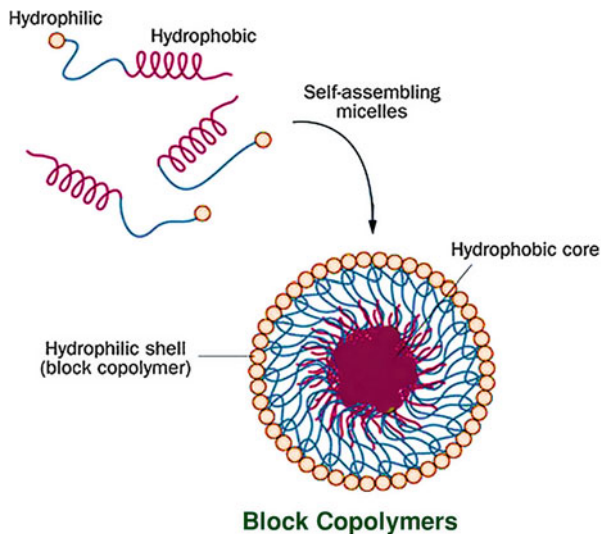


Fig. 13 (Super) structure representations of (a) an MWCNT and (b) an SWCNT. (Adapted with permission from American Chemical Society [128])

nanotubes (MWCNTs) are composed of multiple layers of graphene sheets (Fig. 13a), whereas single-walled carbon nanotubes (SWCNTs) have cylindrical shape consisting of a single graphene shell (Fig. 13b) [126, 127].

CNTs membrane works with low energy consumption because of its frictionless water transport capability through nanotubes hydrophobic hollow cavity (Table 5). The membrane is highly sensitive toward multiple pollutants and salts, antifouling,

Table 5 Potentiality of vertically aligned (VA) and mixed matrix (MM) CNT membranes

Membrane types	Substrate/filler	Major observations	Refs.
MM	Polysulfonate	Increased hydrophilicity Increased water permeability, up to 2 wt% Decreased solute rejection, up to 2 wt% Decreased permeability and increased rejection at 4 wt%	[131]
MM	Polysulfonate	Increased surface roughness Altered surface hydrophilicity Increased mechanical stability	[132]
MM	Poly(vinylidene fluoride)	Eliminated <i>E. coli</i> cells (~2 μm) through size exclusion Inactivated 80% of the bacteria within 20 min contact time Removed viruses with great extent	[133]
MM	Polyamide-polysulfone	Increased water permeability Enhanced bacterial cytotoxicity (60%/h) Decreased biofouling during operation	[134]
MM	Polyethersulfone	Increased water refluxing capacity Greater antifouling activity against whey proteins	[135]
MM	Poly(methyl methacrylate)	Increased water flux (62%) with improved selectivity and sensitivity Retained Na_2SO_4 (99%)	[136]
MM	Polyvinyl- <i>N</i> -carbazole	Cytotoxic for Gram-positive and Gram-negative bacteria (~80–90%) Removed virus (~2.5 logs) Cost-effective method	[137]
MM	Polysulfone	Increased fouling resistance	[138]
MM	Polysulfone	Increased water flux (60–100%) Retained solutes and resistant to protein fouling	[139]
MM	Polysulfone	Enhanced thermal stability Increased heavy metals rejection	[140]
MM	Polyethersulfone	Increased water fluxing without aggressive chemical cleaning Excellent antifouling properties rendered membranes suitable for recycling use	[24]
MM	Polysulfone	Increased water flux (160%)	[141]
MM	Polyvinylidene fluoride	Reduced fouling tendency Improved self-cleaning ability Retained salts ($R(\text{Na}_2\text{SO}_4) > R(\text{MgSO}_4) > R(\text{NaCl})$)	[23]

self-clean, reusable, and good water permeable. CNTs can be doped into existing engineered membranes or membranes themselves by aligning them together. On the basis of current fabrication systems, there are two types of nanotube membranes (i) vertically aligned (VA) CNT membranes and (ii) mixed matrix (MM) CNT membranes [129]. Figure 14 postulates both membrane prototypes along with their distinguishable properties. VACNT membranes can be synthesized by aligning

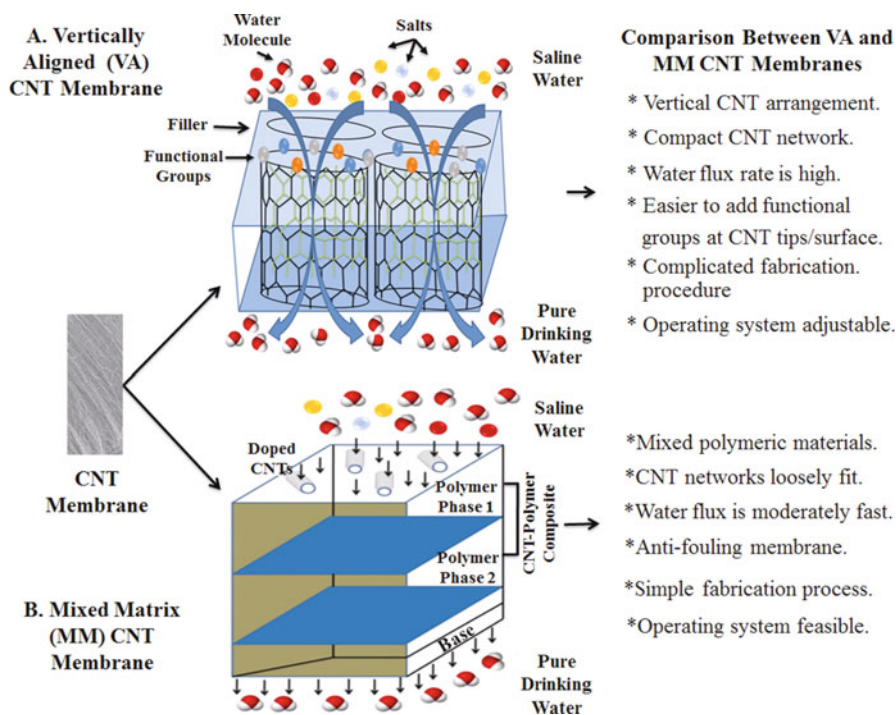


Fig. 14 Schematic illustration of the two types of CNT membranes. (a) vertically aligned and (b) mixed matrix CNT membranes

perpendicular CNTs with supportive filler contents (epoxy, silicon nitride, etc.) between the tubes (Fig. 14a) [130]. On the other hand, MMCNTs membrane consists of several layers of polymers or other composite materials (Fig. 14b).

3 Conclusion and Future Perspectives

Polymeric membranes outperform classical water treatment technologies because of their special physicochemical properties. Different polymer chemistry helps to fabricate membrane with desired properties which contributes significantly to yield potable water. Simple operating procedures of membrane-based water treatment plants at different capacity according to the desired requirements in the given area make membranes technologies more popular commercially. One important conclusion from the activities highlighted in this chapter is that the synthetic polymers that have been produced in such a way that packing of these polymeric membranes into different configurations will not affect membrane's performances. But most of the biopolymers depend on their natural macromolecular configurations for water flux and pollutants retention. Altering their architecture might not be feasible to develop new biopolymer-based membrane technology. However, among all membrane

technologies, RO is a popular one to desalinate both brackish and sea water. About 19% of the world's desalination plants have successfully installed the RO membrane. But energy requirements and fouling problem of the membrane have remained a big issue to think. The theoretical minimum energy that required for sea water desalination is 0.81, 0.97, and 1.29 kWhm⁻³ for a water recovery of 25, 50, and 75%, respectively, suggesting research gaps for further improvement of the technologies. On the other hand, fouling has remained a major problem for recrudescence and reusability of the membrane. Most of the polymers described here are hydrophobic in nature which attracts foulant molecules to adsorb onto the membrane surface. As a corollary, most of the membrane pores become saturated which ultimately decrease water flux and pollutant-rejection ability of the membrane. In order to overcome these, current polymeric membranes have been decorated with guest compounds and nanomaterials, so that the functionalized membrane would have high water permeability, high pollutants selectivity, and antifouling properties for feasible uses. But, there is no evidence to transform these advanced functionalized membranes commercially which is associated to their scaling-up into designed products that can be economically mass produced. Therefore, cross-fertilization between academic research works and industrial research and development activities is important to bring a technology from a lab-bench to field level.

References

1. V.K. Gupta, I. Ali, T.A. Saleh, A. Nayak, S. Agarwal, Chemical treatment technologies for waste-water recycling—An overview. *RSC Adv.* **2**(16), 6380–6388 (2012)
2. M.M. Pendergast, E.M. Hoek, A review of water treatment membrane nanotechnologies. *Energy Environ. Sci.* **4**(6), 1946–1971 (2011)
3. W. Koros, G. Fleming, Membrane-based gas separation. *J. Memb. Sci.* **83**(1), 1–80 (1993)
4. K. Wangnick, IDA Worldwide Desalting Plants Inventory. Report No. 18. Prepared and published by Wangnick Consulting. Wangnick Consulting GmbH Kuhstedtermoor, 19A, D-27442 Gnarrenburg, Germany, 2004
5. M. Ulbricht, Advanced functional polymer membranes. *Polymer* **47**(7), 2217–2262 (2006)
6. I. Pinnau, B. Freeman, Formation and modification of polymeric membranes: Overview, in *Membrane Formation and Modification*, vol. 744 (American Chemical Society, Washington, DC, 2000), pp. 1–22
7. M. C. Porter, Handbook of industrial membrane technology. United States: N. p., (1989). Web
8. I. Pinnau, W.J. Koros, A qualitative skin layer formation mechanism for membranes made by dry/wet phase inversion. *J. Polym. Sci. B Polym. Phys.* **31**(4), 419–427 (1993)
9. J. Ren, R. Wang, Preparation of polymeric membranes, in *Membrane and Desalination Technologies* (Springer, New York, 2011), pp. 47–100
10. I. Pinnau, B.D. Freeman, *Advanced materials for membrane separations* (American Chemical Society, Washington, DC, 2004)
11. S. Nunes, K. V. Peinemann, Membrane Market, in *Membrane Technology: in the Chemical Industry* (Wiley, Weinheim, 2001), pp. 4–5
12. A. Wilkinson, A. McNaught, *IUPAC Compendium of Chemical Terminology, (the "Gold Book")* (Blackwell Scientific Publications, Oxford, 1997)
13. P. Bernardo, E. Drioli, G. Golemme, Membrane gas separation: A review/state of the art. *Ind. Eng. Chem. Res.* **48**(10), 4638–4663 (2009)

14. M. Hirose, H. Ito, M. Maeda, K. Tanaka, Highly permeable composite reverse osmosis membrane, method of producing the same, and method of using the same. Google Patents (1997)
15. M. Paul, H.B. Park, B.D. Freeman, A. Roy, J.E. McGrath, J. Riffle, Synthesis and crosslinking of partially disulfonated poly (arylene ether sulfone) random copolymers as candidates for chlorine resistant reverse osmosis membranes. *Polymer* **49**(9), 2243–2252 (2008)
16. P. Singh, P. Ray, P. Kallem, S. Maurya, G. Trivedi, Structure and performance of nanofiltration membrane prepared in a large-scale at CSIR-CSMCRI using indigenous coating unit. *Desalination* **288**, 8–15 (2012)
17. J.-M. Laine, J.P. Hagstrom, M.M. Clark, J. Mallevalle, Effects of ultrafiltration membrane composition. *J. Am. Water Works Assoc.* **81**, 61–67 (1989)
18. Y. Wang, J.-H. Kim, K.-H. Choo, Y.-S. Lee, C.-H. Lee, Hydrophilic modification of polypropylene microfiltration membranes by ozone-induced graft polymerization. *J. Memb. Sci.* **169**(2), 269–276 (2000)
19. R. Kesting, The four tiers of structure in integrally skinned phase inversion membranes and their relevance to the various separation regimes. *J. Appl. Polym. Sci.* **41**(11–12), 2739–2752 (1990)
20. G. Guillen, E.M. Hoek, Modeling the impacts of feed spacer geometry on reverse osmosis and nanofiltration processes. *Chem. Eng. J.* **149**(1), 221–231 (2009)
21. M. Mondor, C. Moresoli, Experimental verification of the shear-induced hydrodynamic diffusion model of crossflow microfiltration, with consideration of the transmembrane pressure axial variation. *J. Memb. Sci.* **175**(1), 119–137 (2000)
22. S. Madaeni, N. Ghaemi, Characterization of self-cleaning RO membranes coated with TiO₂ particles under UV irradiation. *J. Memb. Sci.* **303**(1), 221–233 (2007)
23. S. Madaeni, S. Zinadini, V. Vatanpour, Preparation of superhydrophobic nanofiltration membrane by embedding multiwalled carbon nanotube and polydimethylsiloxane in pores of microfiltration membrane. *Sep. Purif. Technol.* **111**, 98–107 (2013)
24. L. Liu, M. Son, S. Chakraborty, C. Bhattacharjee, H. Choi, Fabrication of ultra-thin polyelectrolyte/carbon nanotube membrane by spray-assisted layer-by-layer technique: Characterization and its anti-protein fouling properties for water treatment. *Desalin. Water Treat.* **51**(31–33), 6194–6200 (2013)
25. G. Song, A. Sengupta, X. Qian, S.R. Wickramasinghe, Investigation on suppression of fouling by magnetically responsive nanofiltration membranes. *Separation and Purification Technology.* **205**, 94–104 (2018)
26. P. Wu, M. Imai, Novel biopolymer composite membrane involved with selective mass transfer and excellent water permeability, in *Advancing Desalination* (INTECH Open Access Publisher, Rijeka, 2012)
27. R.W. Baker, *Membrane technology* (Wiley Online Library, 2000)
28. S. Loeb, S. Sourirajan, High-flow semipermeable membranes for separation of water from saline solutions. *Adv. Chem. Ser.* **38**, 117 (1961)
29. R. Kesting, S. Sourirajan, in *Reverse Osmosis and Synthetic Membranes: Theory-Technology-Engineering*, ed. by S. Sourirajan (National Research Council Canada, Ottawa, 1977) pp. 89–110
30. A. Sagle, B. Freeman, Fundamentals of membranes for water treatment, in *The future of desalination in Texas*, vol. 2 (Texas Water Development Board, Texas, 2004), pp. 137–154
31. Y. Wen-E, Y. Pu-Chen, W. Yi-Kuan, Modified cellulose acetate flat membranes for desalination. *J. Polym. Sci. A: Polym. Chem.* **26**(10), 2683–2694 (1988)
32. M.A. El-Taraboulsi, M.A. Mandil, H.E.-S.M. Ali, Reverse osmosis studies on desalination membranes formed from chemically modified cellulose acetate. *Carbohydr. Res.* **13**(1), 83–88 (1970)
33. D. Parker, J. Bussink, H. T. Grampel, G. W. Wheatley, E. U. Dorf, E. Ostlinning, K. Reinking, F. Schubert, O. Jünger, R. Wagener, Polymers, High-Temperature, in *Ullmann's Encyclopedia of Industrial Chemistry* (Verlag Chemie, Weinheim, 2002)
34. H.-G. Yuan, T.-Y. Liu, Y.-Y. Liu, X.-L. Wang, A homogeneous polysulfone nanofiltration membrane with excellent chlorine resistance for removal of Na₂SO₄ from brine in chloralkali process. *Desalination* **379**, 16–23 (2016)

35. M.A. Hickner, H. Ghassemi, Y.S. Kim, B.R. Einsla, J.E. McGrath, Alternative polymer systems for proton exchange membranes (PEMs). *Chem. Rev.* **104**(10), 4587–4612 (2004)
36. F. Fayyazi, E.A. Feijani, H. Mahdavi, Chemically modified polysulfone membrane containing palladium nanoparticles: Preparation, characterization and application as an efficient catalytic membrane for Suzuki reaction. *Chem. Eng. Sci.* **134**, 549–554 (2015)
37. W. Wang, X. Huang, H. Yin, W. Fan, T. Zhang, L. Li, C. Mao, Polyethylene glycol acrylate-grafted polysulphone membrane for artificial lungs: Plasma modification and haemocompatibility improvement. *Biomed. Mater.* **10**(6), 065022 (2015)
38. Y. Zhang, C. Yu, Z. Lü, S. Yu, Modification of polysulfone ultrafiltration membrane by sequential deposition of cross-linked poly (vinyl alcohol)(PVA) and sodium carboxymethyl cellulose (CMCNa) for nanofiltration. *Desalin. Water Treat.* **57**(38), 1–12 (2015)
39. A. Ahmad, A. Abdulkarim, B. Ooi, S. Ismail, Recent development in additives modifications of polyethersulfone membrane for flux enhancement. *Chem. Eng. J.* **223**, 246–267 (2013)
40. M.S.A. Rahaman, A.F. Ismail, A. Mustafa, A review of heat treatment on polyacrylonitrile fiber. *Polym. Degrad. Stab.* **92**(8), 1421–1432 (2007)
41. B.P. Tripathi, N.C. Dubey, R. Subair, S. Choudhury, M. Stamm, Enhanced hydrophilic and antifouling polyacrylonitrile membrane with polydopamine modified silica nanoparticles. *RSC Adv.* **6**(6), 4448–4457 (2016)
42. B. Liang, W. Zhan, G. Qi, S. Lin, Q. Nan, Y. Liu, B. Cao, K. Pan, High performance graphene oxide/polyacrylonitrile composite pervaporation membranes for desalination applications. *J. Mater. Chem. A* **3**(9), 5140–5147 (2015)
43. Y. Xiao, X. Liu, D. Wang, Y. Lin, Y. Han, X. Wang, Feasibility of using an innovative PVDF MF membrane prior to RO for reuse of a secondary municipal effluent. *Desalination* **311**, 16–23 (2013)
44. Z. Zhao, J. Zheng, M. Wang, H. Zhang, C.C. Han, High performance ultrafiltration membrane based on modified chitosan coating and electrospun nanofibrous PVDF scaffolds. *J. Memb. Sci.* **394**, 209–217 (2012)
45. G.-d. Kang, Y.-m. Cao, Application and modification of poly (vinylidene fluoride)(PVDF) membranes—a review. *J. Memb. Sci.* **463**, 145–165 (2014)
46. E.-S. Kim, Y.J. Kim, Q. Yu, B. Deng, Preparation and characterization of polyamide thin-film composite (TFC) membranes on plasma-modified polyvinylidene fluoride (PVDF). *J. Memb. Sci.* **344**(1), 71–81 (2009)
47. S. Liang, Y. Kang, A. Tiraferri, E.P. Giannelis, X. Huang, M. Elimelech, Highly hydrophilic polyvinylidene fluoride (PVDF) ultrafiltration membranes via postfabrication grafting of surface-tailored silica nanoparticles. *ACS Appl. Mater. Interfaces* **5**(14), 6694–6703 (2013)
48. W.R. Bowen, S.Y. Cheng, T.A. Doneva, D.L. Oatley, Manufacture and characterisation of polyetherimide/sulfonated poly (ether ether ketone) blend membranes. *J. Memb. Sci.* **250**(1), 1–10 (2005)
49. Y.L. Thuyavan, N. Anantharaman, G. Arthanareeswaran, A. Ismail, R. Mangalaraja, Preparation and characterization of TiO₂-sulfonated polymer embedded polyetherimide membranes for effective desalination application. *Desalination* **365**, 355–364 (2015)
50. Y.-F. Mi, Q. Zhao, Y.-L. Ji, Q.-F. An, C.-J. Gao, A novel route for surface zwitterionic functionalization of polyamide nanofiltration membranes with improved performance. *J. Memb. Sci.* **490**, 311–320 (2015)
51. Y. Hu, K. Lu, F. Yan, Y. Shi, P. Yu, S. Yu, S. Li, C. Gao, Enhancing the performance of aromatic polyamide reverse osmosis membrane by surface modification via covalent attachment of polyvinyl alcohol (PVA). *J. Memb. Sci.* **501**, 209–219 (2016)
52. X. Li, W. Yang, H. Li, Y. Wang, M.M. Bubakir, Y. Ding, Y. Zhang, Water filtration properties of novel composite membranes combining solution electrospinning and needleless melt electrospinning methods. *J. Appl. Polym. Sci.* **132**(10), 1–8 (2015)
53. S.A.A.N. Nasreen, S. Sundarajan, S.A.S. Nizar, R. Balamurugan, S. Ramakrishna, Advancement in electrospun nanofibrous membranes modification and their application in water treatment. *Membranes* **3**(4), 266–284 (2013)

54. F. Soyekwo, Q.G. Zhang, C. Deng, Y. Gong, A.M. Zhu, Q.L. Liu, Highly permeable cellulose acetate nanofibrous composite membranes by freeze-extraction. *J. Memb. Sci.* **454**, 339–345 (2014)
55. T. Sheng, H. Chen, S. Xiong, X. Chen, Y. Wang, Atomic layer deposition of polyimide on microporous polyethersulfone membranes for enhanced and tunable performances. *AIChE J.* **60**(10), 3614–3622 (2014)
56. K. Pan, R. Ren, B. Liang, L. Li, H. Li, B. Cao, Synthesis of pH-responsive polyethylene terephthalate track-etched membranes by grafting hydroxyethyl-methacrylate using atom-transfer radical polymerization method. *J. Appl. Polym. Sci.* **131**(20), 40912 (2014)
57. E. Eren, A. Sarihan, B. Eren, H. Gumus, F.O. Kocak, Preparation, characterization and performance enhancement of polysulfone ultrafiltration membrane using PBI as hydrophilic modifier. *J. Memb. Sci.* **475**, 1–8 (2015)
58. X. Fan, Y. Su, X. Zhao, Y. Li, R. Zhang, J. Zhao, Z. Jiang, J. Zhu, Y. Ma, Y. Liu, Fabrication of polyvinyl chloride ultrafiltration membranes with stable antifouling property by exploring the pore formation and surface modification capabilities of polyvinyl formal. *J. Memb. Sci.* **464**, 100–109 (2014)
59. T. Mohammadi, E. Saljoughi, Effect of production conditions on morphology and permeability of asymmetric cellulose acetate membranes. *Desalination* **243**(1), 1–7 (2009)
60. N. Pezeshk, D. Rana, R. Narbaitz, T. Matsuura, Novel modified PVDF ultrafiltration flat-sheet membranes. *J. Memb. Sci.* **389**, 280–286 (2012)
61. T. Shibutani, T. Kitaura, Y. Ohmukai, T. Maruyama, S. Nakatsuka, T. Watabe, H. Matsuyama, Membrane fouling properties of hollow fiber membranes prepared from cellulose acetate derivatives. *J. Memb. Sci.* **376**(1), 102–109 (2011)
62. M. Sinha, M. Purkait, Increase in hydrophilicity of polysulfone membrane using polyethylene glycol methyl ether. *J. Memb. Sci.* **437**, 7–16 (2013)
63. A. Qin, X. Li, X. Zhao, D. Liu, C. He, Preparation and characterization of nano-chitin whisker reinforced PVDF membrane with excellent antifouling property. *J. Memb. Sci.* **480**, 1–10 (2015)
64. N. Derlon, J. Mimoso, T. Klein, S. Koetzsch, E. Morgenroth, Presence of biofilms on ultrafiltration membrane surfaces increases the quality of permeate produced during ultra-low pressure gravity-driven membrane filtration. *Water Res.* **60**, 164–173 (2014)
65. M. Sinha, M. Purkait, Preparation and characterization of novel pegylated hydrophilic pH responsive polysulfone ultrafiltration membrane. *J. Memb. Sci.* **464**, 20–32 (2014)
66. E. Saljoughi, S.M. Mousavi, Preparation and characterization of novel polysulfone nano-filtration membranes for removal of cadmium from contaminated water. *Sep. Purif. Technol.* **90**, 22–30 (2012)
67. E.M. Van Wagner, A.C. Sagle, M.M. Sharma, Y.-H. La, B.D. Freeman, Surface modification of commercial polyamide desalination membranes using poly (ethylene glycol) diglycidyl ether to enhance membrane fouling resistance. *J. Memb. Sci.* **367**(1), 273–287 (2011)
68. J.O. Abitoye, P. Mukherjee, K. Jones, Ion implantation: Effect on flux and rejection properties of NF membranes. *Environ. Sci. Technol.* **39**(17), 6487–6493 (2005)
69. A. Ghosh, R. Bindal, S. Prabhakar, P. Tewari, Composite polyamide reverse osmosis (RO) membranes—recent developments and future directions. *BARC Newslett.* **321**, 43–51 (2011)
70. S.F. Anis, B.S. Lalia, R. Hashaikeh, Controlling swelling behavior of poly (vinyl) alcohol via networked cellulose and its application as a reverse osmosis membrane. *Desalination* **336**, 138–145 (2014)
71. G. Sabad e, S. Waheed, A. Ahmad, S.M. Khan, M. Hussain, T. Jamil, M. Zuber, Synthesis, characterization and permeation performance of cellulose acetate/polyethylene glycol-600 membranes loaded with silver particles for ultra low pressure reverse osmosis. *J. Taiwan Inst. Chem. Eng.* **57**, 129–138 (2015)
72. H.I. Kim, S.S. Kim, Plasma treatment of polypropylene and polysulfone supports for thin film composite reverse osmosis membrane. *J. Memb. Sci.* **286**(1), 193–201 (2006)

73. A.K. Ghosh, E.M. Hoek, Impacts of support membrane structure and chemistry on polyamide-polysulfone interfacial composite membranes. *J. Memb. Sci.* **336**(1), 140–148 (2009)
74. J. Wei, X. Jian, C. Wu, S. Zhang, C. Yan, Influence of polymer structure on thermal stability of composite membranes. *J. Memb. Sci.* **256**(1), 116–121 (2005)
75. C. Wu, S. Zhang, D. Yang, X. Jian, Preparation, characterization and application of a novel thermal stable composite nanofiltration membrane. *J. Memb. Sci.* **326**(2), 429–434 (2009)
76. A. Sorrentino, G. Gorrasi, V. Vittoria, Potential perspectives of bio-nanocomposites for food packaging applications. *Trends Food Sci. Technol.* **18**(2), 84–95 (2007)
77. J. Bajpai, R. Shrivastava, A. Bajpai, Dynamic and equilibrium studies on adsorption of Cr (VI) ions onto binary bio-polymeric beads of cross linked alginate and gelatin. *Colloids Surf., A: Physicochem. Eng. Asp.* **236**(1), 81–90 (2004)
78. M.N.R. Kumar, A review of chitin and chitosan applications. *React. Funct. Polym.* **46**(1), 1–27 (2000)
79. P.K. Dutta, J. Dutta, V. Tripathi, Chitin and chitosan: Chemistry, properties and applications. *J. Sci. Ind. Res.* **63**(1), 20–31 (2004)
80. M. Rinaudo, Chitin and chitosan: Properties and applications. *Prog. Polym. Sci.* **31**(7), 603–632 (2006)
81. H.-M. Cauchie, Chitin production by arthropods in the hydrosphere. *Hydrobiologia* **470**(1–3), 63–95 (2002)
82. C. Jeuniaux, M.F. Voss-Foucart, Chitin biomass and production in the marine environment. *Biochem. Syst. Ecol.* **19**(5), 347–356 (1991)
83. M.S. Rao, W.F. Stevens, Fermentation of shrimp biowaste under different salt concentrations with amylolytic and non-amylolytic lactobacillus strains for chitin production. *Food Technol. Biotechnol.* **44**(1), 83–87 (2006)
84. S. Arai, F. Akiya, Desalination reverse osmotic membranes and their preparation. Google Patents (1978)
85. E. Brychcy, M. Malik, P. Drożdżewski, Ż. Król, A. Jarmoluk, Physicochemical and antibacterial properties of carrageenan and Gelatine hydrosols and hydrogels incorporated with acidic electrolyzed water. *Polymers* **7**(12), 2638–2649 (2015)
86. A.V. Briones, T. Sato, U.G. Bigol, Antibacterial activity of polyethylenimine/carrageenan multilayer against pathogenic bacteria. *Adv. Chem. Eng. Sci.* **4**(2), 233–241 (2014)
87. L.A. Cira, S. Huerta, G.M. Hall, K. Shirai, Pilot scale lactic acid fermentation of shrimp wastes for chitin recovery. *Process Biochem.* **37**(12), 1359–1366 (2002)
88. T.D. Leathers, Biotechnological production and applications of pullulan. *Appl. Microbiol. Biotechnol.* **62**(5–6), 468–473 (2003)
89. S. Yuen, Pullulan and its applications. *Process Biochem.* **22**, 7–9 (1974)
90. S. Kasapis, I.M. Al-Marhoobi, Bridging the divide between the high-and low-solid analyses in the gelatin/κ-carrageenan mixture. *Biomacromolecules* **6**(1), 14–23 (2005)
91. C. Viebke, P. Williams, Determination of molecular mass distribution of κ-carrageenan and xanthan using asymmetrical flow field-flow fractionation. *Food Hydrocoll.* **14**(3), 265–270 (2000)
92. P. Wu, M. Imai, Outstanding molecular size recognition and regulation of water permeability on K-carrageenan-pullulan membrane involved in synergistic Design of Composite Polysaccharides–Structure. *Procedia Eng.* **42**, 1313–1325 (2012)
93. K.Y. Lee, D.J. Mooney, Alginate: Properties and biomedical applications. *Prog. Polym. Sci.* **37**(1), 106–126 (2012)
94. J.-S. Yang, Y.-J. Xie, W. He, Research progress on chemical modification of alginate: A review. *Carbohydr. Polym.* **84**(1), 33–39 (2011)
95. G.M. Preston, T.P. Carroll, W.B. Guggino, P. Agre, Appearance of water channels in *Xenopus* oocytes expressing red cell CHIP28 protein. *Science* **256**(5055), 385–387 (1992)
96. K. Ishibashi, S. Hara, S. Kondo, Aquaporin water channels in mammals. *Clin. Exp. Nephrol.* **13**(2), 107–117 (2009)

97. A. Engel, Y. Fujiyoshi, T. Gonen, T. Walz, Junction-forming aquaporins. *Curr. Opin. Struct. Biol.* **18**(2), 229–235 (2008)
98. M.J. Borgnia, D. Kozono, G. Calamita, P.C. Maloney, P. Agre, Functional reconstitution and characterization of AqpZ, the *E. coli* water channel protein. *J. Mol. Biol.* **291**(5), 1169–1179 (1999)
99. D. Kozono, M. Yasui, L.S. King, P. Agre, Aquaporin water channels: Atomic structure molecular dynamics meet clinical medicine. *J. Clin. Invest.* **109**(11), 1395–1399 (2002)
100. B.L. de Groot, H. Grubmüller, Water permeation across biological membranes: Mechanism and dynamics of aquaporin-1 and GlpF. *Science* **294**(5550), 2353–2357 (2001)
101. K. Murata, K. Mitsuoka, T. Hirai, T. Walz, P. Agre, J.B. Heymann, A. Engel, Y. Fujiyoshi, Structural determinants of water permeation through aquaporin-1. *Nature* **407**(6804), 599–605 (2000)
102. M. Amiry-Moghaddam, O.P. Ottersen, The molecular basis of water transport in the brain. *Nat. Rev. Neurosci.* **4**(12), 991–1001 (2003)
103. H. Yabu, Y. Hirai, M. Shimomura, Electroless plating of honeycomb and pincushion polymer films prepared by self-organization. *Langmuir* **22**(23), 9760–9764 (2006)
104. G.M. Whitesides, B. Grzybowski, Self-assembly at all scales. *Science* **295**(5564), 2418–2421 (2002)
105. D. Fierro, K. Buhr, C. Abetz, A. Boschetti-de-Fierro, V. Abetz, New insights into the control of self-assembly of block copolymer membranes. *Aust. J. Chem.* **62**(8), 885–890 (2009)
106. T. Smart, H. Lomas, M. Massignani, M.V. Flores-Merino, L.R. Perez, G. Battaglia, Block copolymer nanostructures. *Nano Today* **3**(3), 38–46 (2008)
107. M. Kumar, M.M. Payne, S.K. Poust, J.L. Zilles, Polymer-based biomimetic membranes for desalination, in *Biomimetic Membranes for Sensor and Separation Applications*, (Springer, Dordrecht, 2012), pp. 43–62
108. H. Shimizu, T. Fujita, New short interfering RNA-based therapies for glomerulonephritis. *Nat. Rev. Nephrol.* **7**(7), 407–415 (2011)
109. K. Yoon, K. Kim, X. Wang, D. Fang, B.S. Hsiao, B. Chu, High flux ultrafiltration membranes based on electrospun nanofibrous PAN scaffolds and chitosan coating. *Polymer* **47**(7), 2434–2441 (2006)
110. Y.-L. Liu, Y.-H. Su, K.-R. Lee, J.-Y. Lai, Crosslinked organic–inorganic hybrid chitosan membranes for pervaporation dehydration of isopropanol–water mixtures with a long-term stability. *J. Memb. Sci.* **251**(1–2), 233–238 (2005)
111. T. Yang, R. Zall, Chitosan membranes for reverse osmosis application. *J. Food Sci.* **49**(1), 91–93 (1984)
112. A.G. Boricha, Z.V.P. Murthy, Preparation of N,O-carboxymethyl chitosan/cellulose acetate blend nanofiltration membrane and testing its performance in treating industrial wastewater. *Chem. Eng. J.* **157**(2–3), 393–400 (2010)
113. R. Huang, G. Chen, M. Sun, Y. Hu, C. Gao, Studies on nanofiltration membrane formed by diisocyanate cross-linking of quaternized chitosan on poly (acrylonitrile)(PAN) support. *J. Memb. Sci.* **286**(1), 237–244 (2006)
114. A.G. Boricha, Z. Murthy, Preparation and performance of N, O-carboxymethyl chitosan-polyether sulfone composite nanofiltration membrane in the separation of nickel ions from aqueous solutions. *J. Appl. Polym. Sci.* **110**(6), 3596–3605 (2008)
115. R. Huang, G. Chen, M. Sun, C. Gao, A novel composite nanofiltration (NF) membrane prepared from graft copolymer of trimethylallyl ammonium chloride onto chitosan (GCTACC)/poly (acrylonitrile)(PAN) by epichlorohydrin cross-linking. *Carbohydr. Res.* **341**(17), 2777–2784 (2006)
116. P. Wu, M. Imai, Excellent dyes removal and remarkable molecular size rejection of novel biopolymer composite membrane. *Desalin. Water Treat.* **51**(25–27), 5237–5247 (2013)
117. P.S. Zhong, T.-S. Chung, K. Jeyaseelan, A. Armugam, Aquaporin-embedded biomimetic membranes for nanofiltration. *J. Memb. Sci.* **407–408**, 27–33 (2012)

118. M. Kamachi, M. Kurihara, J. Stille, Synthesis of block polymers for desalination membranes. Preparation of block copolymers of 2-vinylpyridine and methacrylic acid or acrylic acid. *Macromolecules* **5**(2), 161–167 (1972)
119. J.S. Louie, I. Pinnau, I. Ciobanu, K.P. Ishida, A. Ng, M. Reinhard, Effects of poly-ether–polyamide block copolymer coating on performance and fouling of reverse osmosis membranes. *J. Memb. Sci.* **280**(1), 762–770 (2006)
120. R.M. Dorin, W.A. Phillip, H. Sai, J. Werner, M. Elimelech, U. Wiesner, Designing block copolymer architectures for targeted membrane performance. *Polymer* **55**(1), 347–353 (2014)
121. X. Li, R. Wang, C. Tang, A. Vararattanavech, Y. Zhao, J. Torres, T. Fane, Preparation of supported lipid membranes for aquaporin Z incorporation. *Colloids Surf. B. Biointerfaces* **94**, 333–340 (2012)
122. P.S. Zhong, T.-S. Chung, K. Jeyaseelan, A. Armugam, Aquaporin-embedded biomimetic membranes for nanofiltration. *J. Memb. Sci.* **407**, 27–33 (2012)
123. P.H. Duong, T.-S. Chung, K. Jeyaseelan, A. Armugam, Z. Chen, J. Yang, M. Hong, Planar biomimetic aquaporin-incorporated triblock copolymer membranes on porous alumina supports for nanofiltration. *J. Memb. Sci.* **409**, 34–43 (2012)
124. M. Wang, Z. Wang, X. Wang, S. Wang, W. Ding, C. Gao, Layer-by-layer assembly of aquaporin Z-incorporated biomimetic membranes for water purification. *Environ. Sci. Technol.* **49**(6), 3761–3768 (2015)
125. Y. Zhao, C. Qiu, X. Li, A. Vararattanavech, W. Shen, J. Torres, C. Hélix-Nielsen, R. Wang, X. Hu, A.G. Fane, C.Y. Tang, Synthesis of robust and high-performance aquaporin-based biomimetic membranes by interfacial polymerization-membrane preparation and RO performance characterization. *J. Memb. Sci.* **423–424**, 422–428 (2012)
126. S. Iijima, Helical microtubules of graphitic carbon. *Nature* **354**(6348), 56–58 (1991)
127. S. Iijima, T. Ichihashi, Single-shell carbon nanotubes of 1-nm diameter. *Nature* **363**(6430), 603–605 (1993)
128. Y.L. Zhao, J.F. Stoddart, Noncovalent functionalization of single-walled carbon nanotubes. *Acc. Chem. Res.* **42**(8), 1161–1171 (2009)
129. C.H. Ahn, Y. Baek, C. Lee, S.O. Kim, S. Kim, S. Lee, S.-H. Kim, S.S. Bae, J. Park, J. Yoon, Carbon nanotube-based membranes: Fabrication and application to desalination. *J. Ind. Eng. Chem.* **18**(5), 1551–1559 (2012)
130. B.J. Hinds, N. Chopra, T. Rantell, R. Andrews, V. Gavalas, L.G. Bachas, Aligned multiwalled carbon nanotube membranes. *Science* **303**(5654), 62–65 (2004)
131. J.-H. Choi, J. Jegal, W.-N. Kim, Fabrication and characterization of multi-walled carbon nanotubes/polymer blend membranes. *J. Memb. Sci.* **284**(1), 406–415 (2006)
132. L. Brunet, D. Lyon, K. Zodrow, J.-C. Rouch, B. Caussat, P. Serp, J.-C. Remigy, M. Wiesner, P. Alvarez, Properties of membranes containing semi-dispersed carbon nanotubes. *Environ. Eng. Sci.* **25**(4), 565–576 (2008)
133. A.S. Brady-Estévez, S. Kang, M. Elimelech, A single-walled-carbon-nanotube filter for removal of viral and bacterial pathogens. *Small* **4**(4), 481–484 (2008)
134. A. Tiraferri, C.D. Vecitis, M. Elimelech, Covalent binding of single-walled carbon nanotubes to polyamide membranes for antimicrobial surface properties. *ACS Appl. Mater. Interfaces* **3**(8), 2869–2877 (2011)
135. P. Daraei, S.S. Madaeni, N. Ghaemi, M.A. Khadivi, B. Astinchap, R. Moradian, Enhancing antifouling capability of PES membrane via mixing with various types of polymer modified multi-walled carbon nanotube. *J. Memb. Sci.* **444**, 184–191 (2013)
136. J. nan Shen, C. chao Yu, H. min Ruan, C. jie Gao, B. Van der Bruggen, Preparation and characterization of thin-film nanocomposite membranes embedded with poly (methyl methacrylate) hydrophobic modified multiwalled carbon nanotubes by interfacial polymerization. *J. Memb. Sci.* **442**, 18–26 (2013)

137. F. Ahmed, C.M. Santos, J. Mangadlao, R. Advincula, D.F. Rodrigues, Antimicrobial PVK: SWNT nanocomposite coated membrane for water purification: Performance and toxicity testing. *Water Res.* **47**(12), 3966–3975 (2013)
138. S. Kar, M. Subramanian, A. Pal, A. Ghosh, R. Bindal, S. Prabhakar, J. Nuwad, C. Pillai, S. Chattopadhyay, P. Tewari, Preparation, characterisation and performance evaluation of anti-biofouling property of carbon nanotube-polysulfone nanocomposite membranes, in *CARBON MATERIALS 2012 (CCM12): Carbon Materials for Energy Harvesting, Environment, Nanoscience and Technology*, vol. 1 (AIP Publishing, New York, 2013), pp. 181–185
139. J. Yin, G. Zhu, B. Deng, Multi-walled carbon nanotubes (MWNTs)/polysulfone (PSU) mixed matrix hollow fiber membranes for enhanced water treatment. *J. Memb. Sci.* **437**, 237–248 (2013)
140. P. Shah, C. Murthy, Studies on the porosity control of MWCNT/polysulfone composite membrane and its effect on metal removal. *J. Memb. Sci.* **437**, 90–98 (2013)
141. M. Amini, M. Jahanshahi, A. Rahimpour, Synthesis of novel thin film nanocomposite (TFN) forward osmosis membranes using functionalized multi-walled carbon nanotubes. *J. Memb. Sci.* **435**, 233–241 (2013)



Muhammad Shahzad Kamal and Abdullah S. Sultan

Contents

1	Enhanced Oil Recovery	1047
1.1	Evaluation and Screening Techniques for EOR	1049
1.2	Polymer Systems for Enhanced Oil Recovery	1050
2	Drilling Fluids	1055
2.1	Classification of Drilling Fluids	1056
2.2	Evaluation and Screening Techniques	1058
2.3	Polymer Systems for Drilling Fluids	1059
3	Hydrate Inhibition	1060
3.1	Evaluation and Screening Techniques	1061
3.2	Polymer Systems for Kinetic Hydrate Inhibition	1067
4	Conclusion	1068
	References	1069

Abstract

Worldwide energy demand has been increased in last few decades, and it is expected that it will increase up to 50% by the end of next decade. Oil and gas were major sources of energy in past, and it is expected that it will remain the

M. Shahzad Kamal

Center for Integrative Petroleum Research, King Fahd University of Petroleum and Minerals, Dhahran, Saudi Arabia

Department of Petroleum Engineering, King Fahd University of Petroleum and Minerals, Dhahran, Saudi Arabia

e-mail: shahzadmalik@kfupm.edu.sa

A. S. Sultan (✉)

Department of Petroleum Engineering, College of Petroleum Engineering and Geosciences, King Fahd University of Petroleum and Minerals, Dhahran, Saudi Arabia

Center for Integrative Petroleum Research, King Fahd University of Petroleum and Minerals, Dhahran, Saudi Arabia

e-mail: sultanas@kfupm.edu.sa

primary source of energy in next few decades. Therefore, efforts are being made to upgrade drilling, completion, workover, and production operations to maximize the oil recovery at a lower cost. In last few decades, water-soluble polymers have been extensively used in different gas and oilfield applications. In the present chapter, we discuss the various types of polymeric systems that have been applied in various oilfield applications. These applications are mainly enhanced oil recovery, drilling fluids, and kinetic gas hydrate inhibition. Properties required for each application are also discussed and related to the chemical structure of the polymer.

Keywords

Polymer · Enhanced oil recovery · Drilling fluid · Kinetic hydrate inhibitors · Viscosity

Abbreviations

AAs	Antiagglomerates
AM	Acrylamide
AMPS	2-Acrylamido-2-Methylpropane Sulfonic Acid
API	American Petroleum Institute
ASP	Alkali-surfactant-polymer
CEC	Cation exchange capacity
CMC	Carboxymethylcellulose
EOR	Enhanced Oil Recovery
HAPAM	Hydrophobically modified polyacrylamide
HEC	Hydroxyethylcellulose
HPAM	Partially hydrolyzed polyacrylamide
HP- μ DSC	High-pressure microdifferential scanning calorimetry
HTHS	High-temperature high-salinity
IEP	Isoelectric point
k	Permeability
KHIs	Kinetic hydrate inhibitors (), and
k_o	Permeability of oil
k_w	Permeability of water
MD	Molecular dynamic
PAM	Polyacrylamide
PEO	Polyethylene oxide
PVCap	Poly(vinyl caprolactam)
PVIMA	Poly (N-methyl,N-vinylacetamide)
PVP	Poly(vinyl pyrrolidone)
sI	Structure I
sII	Structure II
sIII	Structure III
SP	Surfactant-polymer
sT	Structure T
t_a	Hydrate plug formation time
THIs	Thermodynamic hydrate inhibitors

t_i	Induction time
VIMA	N-methyl,N-vinylacetamide
VP	Vinylpyrrolidone
μ	Viscosity
μ_o	Viscosity of oil
μ_w	Viscosity of water

1 Enhanced Oil Recovery

Oil is the most important source of energy and it is expected that it will remain a primary source of energy in meeting future energy demands [1]. Therefore, it is extremely important to discover new oil fields and/or enhance the production from existing oil reservoir. Oil from reservoirs is recovered in three different stages, namely, primary, secondary, and tertiary stages. In the primary stage, oil is recovered due to natural drive energy available in the reservoir. In secondary recovery, water and/or gas are used to increase the oil recovery. Only 15–20% oil is recovered using primary and secondary oil recovery process. About 7,000 billion barrels of conventional and heavy oil could not be recovered using conventional oil recovery methods [2]. To recover the remaining oil, tertiary oil recovery also called as enhanced oil recovery (EOR) methods are used. A typical classification of EOR method is given in Fig. 1. Thermal EOR, gas EOR, and chemical EOR are three main tertiary oil recovery methods. The worldwide share of each EOR method is given in Fig. 2 [3]. Data show that most of the previous EOR projects were carried out using thermal injection followed by the gas injection. The share of chemical EOR was not significant due to low oil prices, unavailability of suitable chemicals, high chemical cost, and poor understanding of the mechanism. However, chemical EOR could be a preferable choice in future due to bulk production of EOR chemicals that resulted in low oil prices. The oil reservoirs are mainly characterized as sandstone and carbonate reservoirs. The data presented in Fig. 3 show that majority of the EOR projects were carried out in sandstone reservoirs. A major fraction of the residual oil is present in

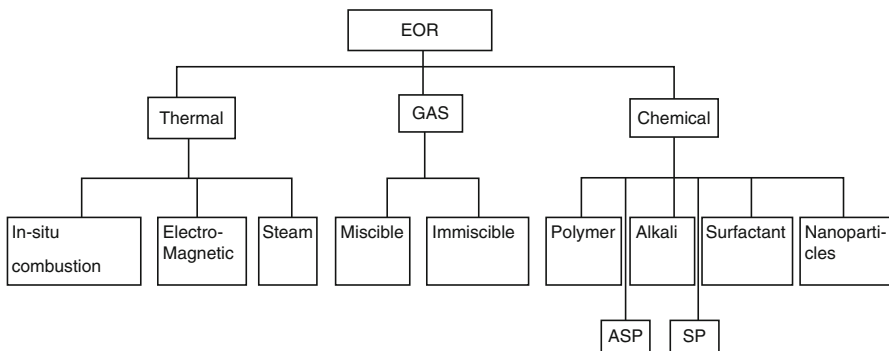


Fig. 1 Classification of EOR processes

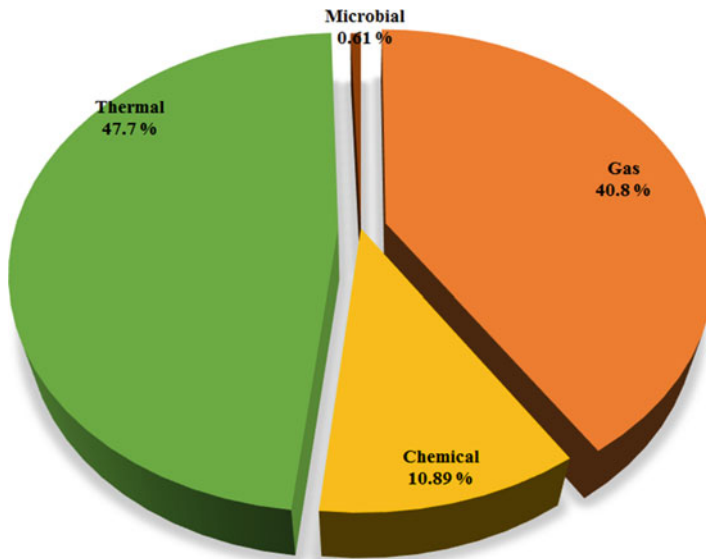


Fig. 2 EOR projects categories [3]. (© Elsevier, published with the kind permission of Elsevier.)

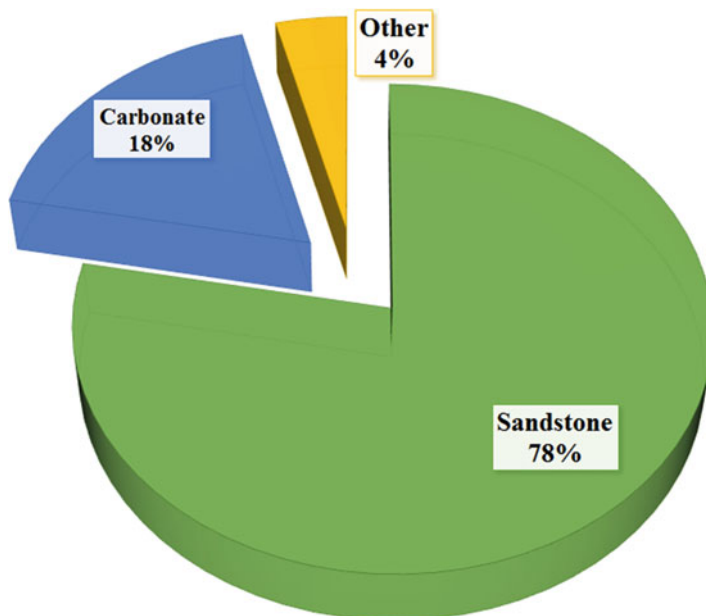


Fig. 3 EOR field projects in different reservoirs [4]. (© Society of Petroleum Engineers, published with the kind permission of Society of Petroleum Engineers.)

carbonate reservoirs. Therefore, it is expected that most of the future EOR projects would be in carbonate reservoirs. Carbonate reservoirs are more challenging compared to sandstone reservoirs due to high temperature high salinity (HTHS) conditions and heterogeneity of carbonate reservoirs.

In chemical EOR, surfactants, polymers, and/or alkalis are used to increase the displacement efficiency and the volumetric sweep efficiency [5–12]. The ultimate objective is to increase the capillary number, which is defined as the ratio of viscous forces to interfacial forces [13–16]. Surfactants are used to lower the interfacial tension between water and oil. An ultra-low value in the range of 10^{-3} mN/m is required to achieve a capillary number higher enough for effective displacement [17]. In addition to IFT reduction, surfactants also improve the oil recovery via microemulsification of trapped residual oil, wettability alteration, and improving the interfacial rheological properties [18–24]. Polymers are used to improve the mobility ratio by enhancing the viscosity of the displacing phase fluid. Mobility ratio is the ratio of mobilities of the water to oil ($k_w\mu_o/k_o\mu_w$). Here k is effective permeability and μ is viscosity. Subscript w represents oil while o denotes water phase. The eventual target in any EOR project using polymer is to achieve a mobility ratio of less than 1 [25]. Higher mobility ratio results in viscous fingering due to high mobility of water. Such a lower mobility ratio is achieved using water-soluble polymers. Surfactant-polymer (SP) and alkaline-surfactant-polymer (ASP) injections are also common to have relative advantage of each component.

1.1 Evaluation and Screening Techniques for EOR

The polymers for EOR are screened by comparing their rheological properties, thermal stability, adsorption, compatibility, chemical stability, injectivity, coreflooding data, and cost. Ideally, a polymer should have good thermal stability for longer time at reservoir conditions (few weeks to few months), high resistance to mechanical degradation (up to $1000 \text{ m}^3/\text{m}^2/\text{d}$ flux during entering into porous rock), low adsorption on reservoir rock ($<1 \text{ mg/g-rock}$), good compatibility with reservoir brine and other chemicals, good tolerance to injection and formation brine, high injectivity, high viscosity, and low cost [26].

As the main purpose of injecting polymer is to achieve and maintain high viscosity, therefore, it is extremely important that polymer should tolerate harsh conditions. At high temperature, the polymer can degrade and precipitate by interaction with the injection of formation brine. The usual expectation from a good polymer is that it should maintain 50% of its original viscosity for at least 6 months [27]. Polymer adsorption on reservoir rock is a serious issue, and it should be considered during screening process due to economic reasons. A high retention on reservoir rock can lower the viscosity of the flood and affect mobility ratio. Polymer retention is measured using static adsorption test or dynamic adsorption core flooding test. Static adsorption tests are performed in sealed aging tubes using a fixed amount of crushed rock and polymer solutions. The solutions are stirred for a particular time (usually 1 day of stirring and another 1 day for equilibrium) at given conditions of

temperatures. Similarly, dynamic adsorption is determined using analysis of core samples and polymer solutions before and after flooding. Adsorption density can be determined by the difference of polymer concentration before and after flooding. An acceptable polymer for EOR must have adsorption lower than 1 mg/g-rock [27]. Adsorption of a polymer depends on several factors such as nature and type of reservoir rock, salinity, and temperature. Adsorption of polymer on the reservoir is related to the isoelectric point (IEP). At a pH lower than IEP, the surface charge is positive and vice versa. The IEP of kaolinite and limestone is 4.7 and 8.2, respectively [28, 29]. It means if $\text{pH} > 4.7$, adsorption of the anionic polymer would be lower compared to cationic polymer due to electrostatic interactions in sandstone reservoirs. If $\text{pH} < 8.2$, the adsorption of the anionic polymer would be higher compared to cationic polymer in limestone reservoirs. Polymers for EOR are supplied in dry powder form; however, the equipment required to dissolve these polymers are bulky, which may not find space on offshore platforms. Polymer solutions experience a very high shear rate that may cause shear degradation in the polymer. A very high initial viscosity of polymer makes it more difficult to inject into the reservoir. If the polymer solution is not prepared properly, debris can plug the pore space around the well-bore [30].

1.2 Polymer Systems for Enhanced Oil Recovery

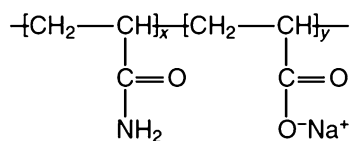
To achieve a favorable mobility ratio, high molecular weight (9–25 million Dalton) polymers are utilized. High viscosity can be achieved using a low concentration of high molecular weight polymers. Other factors that affect the viscosity of polymer solutions are polymer molecular weight, temperature, salinity, and concentration of divalent ions. Subsequent sections will discuss various types of synthetic and biopolymers for EOR applications.

1.2.1 Synthetic polymers

A number of polymers have been investigated in both laboratory and field in last few decades. The most important polymers used in EOR are acrylamide-based copolymer and terpolymer. Polyacrylamide was among the first polymers that were used as mobility control agents in EOR. Many attempts were made to modify the polyacrylamide by copolymerizing acrylamide with different suitable monomers that are more tolerant to temperature and salinity.

Partially hydrolyzed polyacrylamide (HPAM) is widely used in EOR applications [31–36]. The structure of the HPAM is shown in Fig. 4. The aqueous solution of the HPAM is negatively charged and highly viscous. The presence of negative charges on the backbone causes a stretching of polymer chain due to electrostatic repulsion. This stretching results in a high viscosity of the polymer. The fraction of acrylate group (the

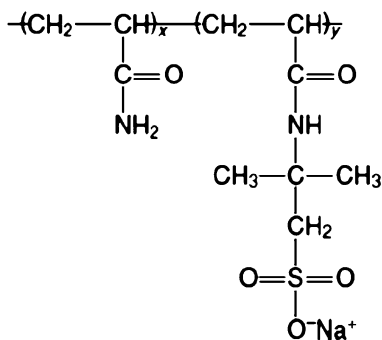
Fig. 4 Structure of HPAM



degree of hydrolysis) usually ranges between 25– and 35% [37]. A higher degree of hydrolysis causes the distortion of flexible chains that can result in viscosity reduction and flocculation in hard brine. The properties of HPAM can be tuned by changing the acrylate contents in the copolymer. The negative charges induced due to hydrolysis increase the viscosity of the polymer; however, the higher percentage of acrylate group in the HPAM can weaken the tolerance to salinity and hardness [38]. Hydrolysis of HPAM strongly depends on the pH and temperature [39]. The rate is speedy at high temperatures compared to low temperatures [40]. Based on the available data, HPAM is stable up to 70 °C in presence of divalent cations; however, without divalent ions, HPAM found to be stable at 100 °C [41, 42]. Therefore, HPAM is recommended only in the reservoir having the temperature up to 75 °C if the divalent concentration is high in the formation brine. However, if the divalent concentration is less than 200 ppm, its application can be extended up to 100 °C. HPAM exhibit excellent rheological properties that depend on polymer concentration, temperature, salinity, pH, shear rate, and the presence of other chemicals such as surfactants and alkalis. Salts cause a dramatic reduction in the viscosity of the HPAM due to charge screening effect [43]. Salts bring the cations in aqueous solution, which interact with the anions present on the polymer backbone. These interactions result in lowering the viscosity of the polymer. In general, the application of HPAM is limited to the reservoir with low temperature and low salinity. For HTHS reservoirs, different copolymers have been developed by incorporating more salt and temperature tolerant monomer. In last four decades, a number of attempts were made to design the water-soluble polymers for HTHS reservoirs. These efforts were focused mainly on the development of acrylamide-based copolymer by incorporating a suitable monomer, hydrophobically modified polyacrylamide, and thermos-thickening polymers [44–50].

The first category consists of those polymers where acrylamide monomer is copolymerized with more temperature and salt tolerant polymers. The two most widely reported polymers include a copolymer of acrylamide (AM) and 2-acrylamido-2-methylpropane sulfonic acid (AMPS) and acrylamide-vinylpyrrolidone (AM/VP) copolymer. Sulfonate makes it resistance to divalent and salinity in general. A typical structure of AM/AMPS copolymer is given in Fig. 5. The AM/AMPS copolymer showed good thermal stability up to 110 °C and no viscosity changes were observed after 16 days. However, at 120 °C, the polymer lost 50% of its original viscosity

Fig. 5 A typical structure of AM/AMPS copolymer



after 10 days of aging [51]. Other monomers that can polymerize with acrylamide include: N-phenylmaleimide [52], allylbenzamide [53], sodium vinyl sulfonate [54], 2-(acrylamido)-2-methylpropyl trimethylammonium chloride [55], sodium 3-acrylamido-3-methylbutanoate [56], carboxymethylcellulose [57], ether carboxylate [58], and sodium (acrylamido) methanesulfonate [53]. Although some of these copolymers have high thermal stability at harsh conditions compared to HPAM, their cost is higher compared to HPAM.

The second category of the polymers includes hydrophobic associating polymers, which contain hydrophobic monomer in the main hydrophilic chain. In aqueous solution, the association among different hydrophobic groups results in the formation of hydrophobic microdomains [59]. At higher concentrations, the formation of network structure takes place due to intermolecular associations. The hydrophobic monomer can be incorporated by grafting on the backbone or by copolymerizing [60]. The viscosity of HPAM changes gradually by increasing polymer concentration; however, the viscosity change of hydrophobically modified polymers with concentration is abrupt as a result of the aggregation of hydrophobic groups [45]. Similarly, the adsorption behavior of associating polymers is different from the adsorption behavior of the unmodified counterpart. The adsorption isotherms of associating polymers have different shapes compared to their unmodified counterpart without any plateau due to multilayer adsorption as shown in Fig. 6. Multilayer adsorption of associating polymers causes high adsorption density of associating polymers that result in an abrupt decrease in the viscosity of the aqueous solution. Although in last few years, the number of publications on associating polymers has been increased tremendously, their field applications are limited. One pilot test was performed using associating polymer in China [61].

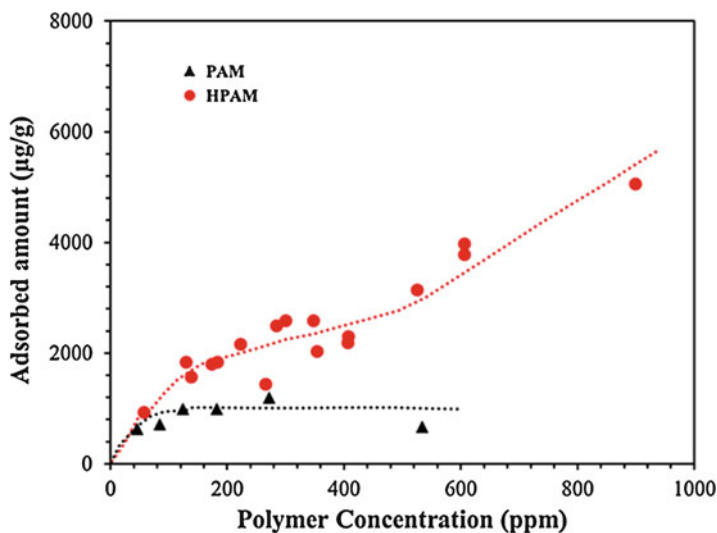


Fig. 6 Adsorption behavior of polyacrylamide (PAM) and hydrophobically modified polyacrylamide (HAPAM) [60]. (© Elsevier, published with the kind permission of Elsevier.)

The third category of modified polymers consists of thermo-thickening polymers that contain thermo-sensitive hydrophobic monomers as pendant chains on the hydrophilic backbone. These thermo-sensitive monomers are soluble in water at low temperatures but show a lower critical solution temperature. By increasing temperature, the hydrophobic chains become insoluble in water and associate to form a microdomain [62]. The viscosity of thermo-thickening polymers increases with temperature after a critical point. Poly (acrylamide-co-2-acrylamido-2-methylpropane sulfonic acid)-g-poly acrylamide-co-N-(1,1-dimethyl-3-oxobutyl) acrylamide is typical example of thermo-thickening polymer [63]. A comparison of viscosity behavior of different polymers is shown in Fig. 7. This unique behavior of thermo-thickening polymers helps in easy injection due to the low viscosity at low temperatures. On the other hand, the high temperature inside the reservoir causes an increase in the viscosity that is a primary requirement for EOR. Thermo-thickening polymers achieve high viscosity only after critical concentration. Therefore, use of high concentration makes the process costly.

1.2.2 Biopolymers

Biopolymers have also been used in EOR applications due to their good water solubility and tolerance to salts. Xanthan gum, guar gum, carboxymethylcellulose, hydroxyethylcellulose, welan gum are some typical examples of biopolymers [64].

Xanthan gum is an extracellular polymer which is obtained mainly by the bacterium *Xanthomonas* [65]. A typical representation of xanthan repeating unit is given in Fig. 8. Xanthan gum mainly consists of glucose units, mannose units, and glucuronic units. In addition, side chains of xanthan gum also consist of charged

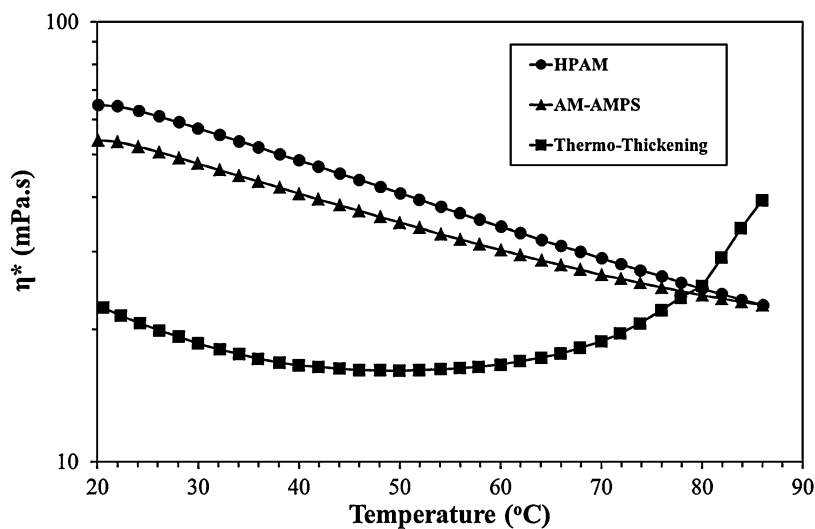
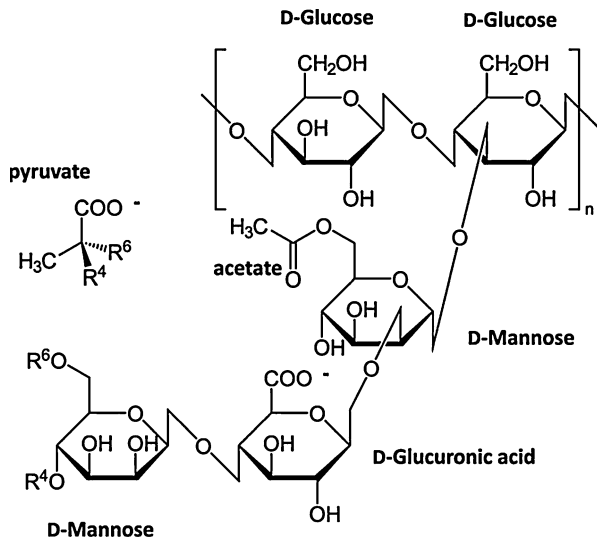


Fig. 7 Comparison of viscosity of different polymers at different temperatures [44]. (© John Wiley and Sons, published with the kind permission of John Wiley and Sons.)

Fig. 8 Representation of chemicals structure of xanthan repeating unit [65]. (© John Wiley and Sons, published with the kind permission of John Wiley and Sons.)



moieties (acetate and pyruvate). The chain length of xanthan gum is similar to that of acetate; therefore, it is also being used in different applications such as viscosifier in food ingredients, in cosmetics, and in pharmaceutical [66–68]. The average molecular weight of typical xanthan gum used for EOR application is between one million Dalton and 15 million Dalton. Its thermal stability depends on the brine salinity. At a particular temperature, xanthan gum is thermally stable if it achieves an ordered structure by addition of salts. However, if it attains a disordered structure by adding salts, it is not thermally stable at that temperature and salinity. For example, a xanthan solution was thermally unstable at 90 °C when its salinity was 1 g/L (disordered structure). But a solution with a salinity of 50 g/L was stable at this temperature (ordered structure) [69]. In summary, the rheological behavior is favorable in high salinity conditions; however, it is not thermally stable at high temperatures (>90 °C) and the addition of a high amount of salts causes the conformational transition [70, 71]. The adsorption of xanthan gum on different rock surface depends on rock type, pH, temperature, and salinity. The other issues associated with xanthan gum are its high cost, biodegradation, biochemical reactions, and difficulties associated with injectivity [72, 73]. The issue of biodegradation is usually overcome by adding a suitable biocide such as formaldehyde [74].

Hydroxyethylcellulose (HEC) is a nonionic hydrophilic polysaccharide and considered as environmental friendly polymer owing to its properties. HEC have better injectivity compared to xanthan gum [75]. It can be hydrophobically modified to improve its viscosity and thermal stability at low concentrations. A typical structure of hydrophobically modified HEC is given in Fig. 9. Addition of sulfonate also improves the thermal stability of the polymer. Another neutral polysaccharide schizophyllan (Fig. 10) was reported for EOR applications [76]. At high salinity, schizophyllan can maintain viscosity for a long time. A field test conducted using schizophyllan showed improved oil production after injection.

Fig. 9 Schematic representation of modified HEC [77]. (© Elsevier, published with the kind permission of Elsevier.)

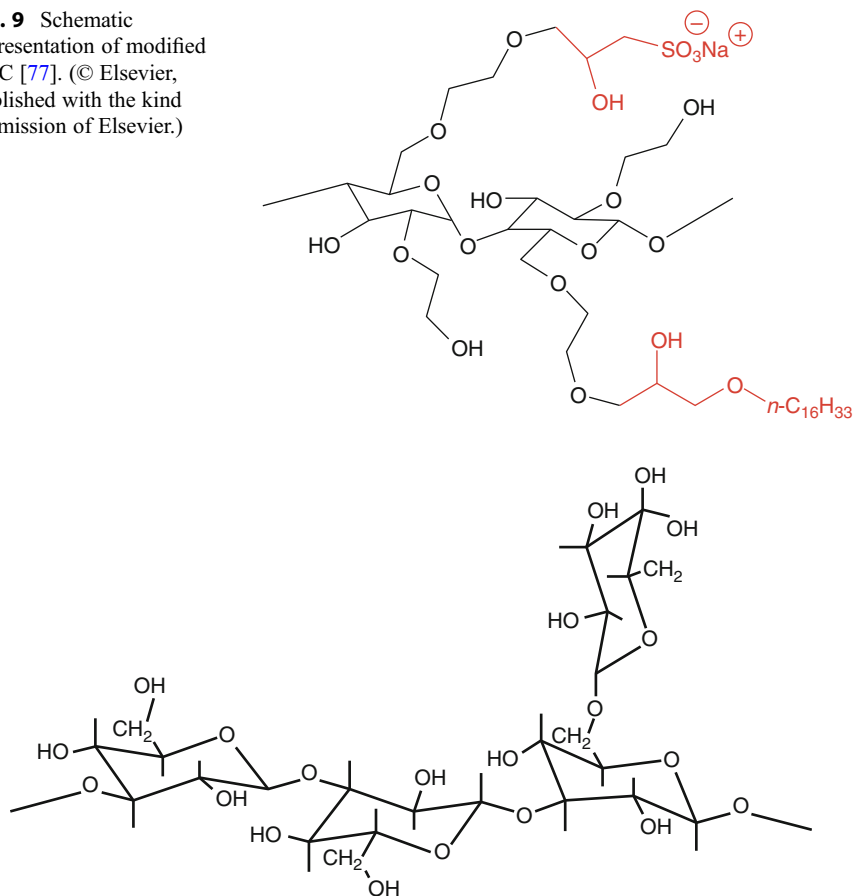


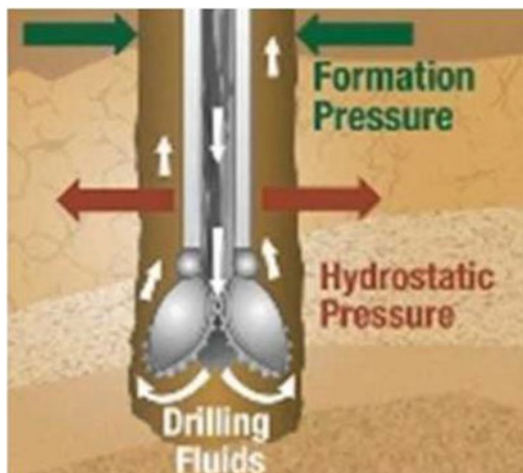
Fig. 10 Molecular structure of schizophyllan [76]. (© Gao (author), (<https://link.springer.com/article/10.1007/s13202-015-0213-7#aboutcontent>), according terms of Creative Commons Attribution 4.0 International License (<http://creativecommons.org/licenses/by/4.0/>)).

In summary, various biopolymers have been evaluated for EOR applications. Despite the fact that biopolymers have good tolerance to temperature and salinity, their poor biodegradation limits their field applications.

2 Drilling Fluids

Drilling of the well bore is the first step in the exploration and recovery of oil (Fig. 11). Drilling fluids are mainly composed of liquids, solids, and chemical additives [78]. Drilling fluids are primarily used in the drilling operations to perform different functions such as removing the formation cutting from the downhole, stabilizing the downhole formation, preventing loss of fluid, and lubricating the bit

Fig. 11 Schematic diagram of drilling process [80]. (© The authors, (<http://www.mdpi.com/1996-1073/10/4/540>), according terms of Creative Commons Attribution 4.0 International License (<http://creativecommons.org/licenses/by/4.0/>).



and drill string [79]. In any drilling operation, drilling fluids are injected down through a drill string that returned to the surface in the annulus formed by borehole wall and bring back the formation cuttings. Before injecting again, the chemical and physical properties of the fluid are tailored again by adding one or more additives. The formulation of drilling fluid is very important to preserve the rock integrity and permeability of the formations during the process. Therefore, the final selection of drilling fluid additives decided after studying the reservoir rock characteristics. The performance of drilling through high permeability zones or through shales rocks (soft rocks) usually results in formation damage. The formation damage occurs because of the invasion of drilling fluids into the formation. The invasion of drilling fluids also results in shale swelling.

2.1 Classification of Drilling Fluids

Drilling fluids are classified into various categories based on the phase of fluid, alkalinity, dispersion ability, and several types of additives used for specific formulations such as pH control agents, weight control agents, viscosity control agents, fluid loss control agent, and shale inhibition. The careful selection of drilling fluid additives is very influential on the performance of drilling fluids. The general selection of drilling fluid is carried out based on petrophysical data, geology, and previously available drilling field data. Drilling fluids are classified into various categories (Fig. 12).

Gas-based drilling fluids are employed to transfer rock cuttings from bottom hole to the surface with high speed along with a minimum fluid loss in the formations. It was observed that problems occurred with extreme complex formation reservoirs where the lifting of drilled cutting could not be completely addressed. Shale

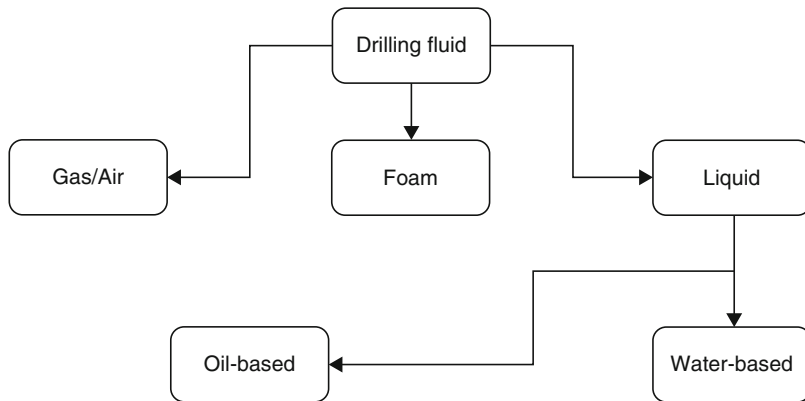


Fig. 12 Classifications of drilling fluids

reservoirs showed enhanced drilling speed with the gas drilling fluid system. It is difficult to maintain the balance between formation pressure and column pressure [81, 82].

Foam-based drilling fluids are formed by embedding gas/air bubbles into liquids and stabilized by surfactants. Foam-based drilling fluids are mainly used to prevent lost circulation during the drilling process. Foam-based fluids showed enhanced drilling performance in terms of quick recovery of drilled cutting towards the surface. However, the stability of foam-based drilling fluids is complicated towards the performance of drilling fluids compared to the conventionally used liquid based drilling fluids [83, 84].

Oil-based drilling fluids are most efficient compared to the all other gas-, foam-, or water-based drilling fluids. Oil-based fluids show better rheological properties, thermal properties, and inhibitive properties for water-sensitive shale reservoirs. However, oil-based drilling fluids are more expensive and toxic compared to other drilling fluids. Disposal to open surface and environmental concerns on oil base fluids are restricting their application. Therefore, water-based drilling fluids are widely recommended for drilling operations [85–88].

Water-based fluids are economical, environmentally friendly, and easily prepared for required drilling formation. The main components of water-based drilling fluid formulations are usually water (continuous phase), viscosity builder (clays or polymers), and other organic agents to control the various properties such as rheology and filtration properties. The water used may be of very high salinity; therefore, alkalis such as potassium hydroxide are used to maintain the pH at which polymers and clays work effectively. Some high specific gravity materials such as barite or hematite are used to attain the required density of drilling fluids. The presence of additives in water-based drilling fluids enhances the rheological properties (viscosity, gel strength, yield stress), reduces the coefficient of friction, and enhances the density of drilling fluid which is used to maintain the balance between column and formation pressure. However, water-based fluids show poor fluid loss properties and

sensitive to shale formations. To avoid fluid loss and inhibit the shale swelling, the high molecular weight polymers are employed [89–92].

Water-soluble polymers are used in drilling fluids as a viscosity enhancer, flocculants, de-flocculants, filtration control agents, and shale stabilizer [79]. Due to interactions of drilling fluid with clay-bearing shale, borehole instability may occur. Borehole stability is one of the many functions that a drilling fluid must fulfill. The water of the drilling fluid formulations can interact with shale and alter the properties of the exposed subsurface. The shale can swell or become mechanically from soft to hard which affect the drilling efficiency. Nature of the water is an important and decisive factor that how it will interact. Freshwater has more effect compared to saline water. Therefore, some salts like sodium chloride and potassium chloride are added to reduce the swelling of shale. Polymers can be used as shale stabilizer as an added electrolyte may not perform effectively. Polymers can be used alone or with electrolytes. The main selection criterion of the polymer is its compatibility with other drilling fluids chemical in addition to its performance as shale stabilizer.

2.2 Evaluation and Screening Techniques

Drilling fluids are characterized based on three different classifications: rheology, fluid loss, and reactivity.

Rheology is a valuable tool for characterization of drilling fluids. Both dynamic and steady shear analyses of drilling fluids are performed to simulate the behavior in real field conditions. Steady shear rheological analysis of drilling fluids is carried out at different shear rates as the polymer may experience a range of shear rates during circulation. The shear rates experienced by the polymer in drill pipe, in the annulus, and at bit nozzle are usually 10^3 s^{-1} , 10^2 s^{-1} and 10^5 s^{-1} , respectively [93]. On the other hand, dynamic tests are used to investigate different material properties such as gel strength, gel formation, and low shear viscosity. The creep-recovery test, the relaxation test, amplitude sweep test, and the frequency sweep test are few examples of rheological analysis important for drilling fluid evaluation. The creep-recovery test is important to understand the material response under constant stress. Linear viscoelasticity is characterized by amplitude sweep test while the frequency sweep test is used to determine the zero shear viscosity and structural strength [93].

Fluid loss is measured using a set of different techniques such as API filtrate, leak off, high-pressure high-temperature filtrate, and dynamic filtrate. Filtration test is performed to evaluate the drilling fluids at different temperature and pressures using multiple filter press stages [94]. Static filtration test simulates the condition of filtration process in drilling operations when drill string at rest and no drilling is carried out, while dynamic filtration test simulates the true filtration process when the drill bit is rotating at high shear rates [95]. Cation exchange capacity (CEC) is an important technique to determine the reactivity of drilling fluids and mainly depends on the pH and types of exchangeable cations in the bentonite used in drilling fluid. According to API standards, 2 ml of drilling fluid is mixed with sulfuric acid, hydrogen peroxide, and methylene blue solution with well stirring. The reactive



Fig. 13 FESEM of: (a) CMC, (b) PAM, (c) CMC-g-PAM [104]. (© The authors, (<https://www.sciencedirect.com/science/article/pii/S1110062114200109#!>), according terms of Creative Commons Attribution 4.0 International License (<http://creativecommons.org/licenses/by/4.0/>))

contents of drilling fluid could be determined by putting a drop of mixture on filter paper. A green or blue halo was formed around the droplet indicates the end point of the test. The CEC of drilling fluids is reported in milliequivalents per ml of drilling fluid [96, 97]. Density measurement of drilling fluid is also important to simulate the commune pressure in drilling well using density meter. The carefully designed density of drilling fluid is used to maintain the balance between formation pressure and column pressure [98].

Bentonite inhibition tests are also used in the characterization of drilling fluids [99]. This test is used to determine the inhibition capacity of drilling fluid for reactive shale formations and maintaining low rheological properties. For this test, the weighted amount of reactive drilled cuttings is dispersed in drilling fluid for 16 h according to API standards in the hot rolling oven. After 16 h, the remaining weight of drilled cuttings was measured and percentage recovery of cuttings are reported [100, 101]. Drilling fluids are characterized to measure chemical contents, solid contents, pH, and lubricity. Particle size measurement can provide an indication of flocculation or deflocculation [99].

Zeta potential of drilling fluids is measured using zeta potential analyzer to determine the stability of drilling fluids and dispersion of drilling fluid additives. Zeta potential was measured as a function of drilling fluid additives such as pH and electrolyte concentration. Zeta potential values are reported in positive and negative magnitude. The lower values of zeta potential represent the low stability of drilling fluids, while higher values indicate the better stability of drilling fluids [102, 103]. Field emission electron microscope images (Fig. 13) are used to determine the morphology of polymer and grafted polymers used as drilling fluid additives [104].

2.3 Polymer Systems for Drilling Fluids

Several polymers have been investigated in drilling fluids such as xanthan gum, guar gum, flaxseed, hydroxyethyl cellulose, carboxymethyl cellulose, and acrylamide-acrylate copolymers [105]. A polymer with narrow molecular weight range and low molecular weight acts as fluid loss reducer, while a polymer with high molecular weight and broader range functions as flocculants and viscosifier [106].

Among synthetic polymers, acrylamide-acrylic acid copolymers with various ratios are most commonly used polymers for drilling fluid applications. Anionic partially hydrolyzed polyacrylamide is most reported polymer for drilling fluid applications. Partially hydrolyzed polyacrylamide is mainly used as flocculants and shale stabilizers due to its high molecular weight. Acrylamide can be copolymerized with various other monomers to have improved properties such as thermal stability. The cationic polymers obtained by copolymerization of positively charged monomer with acrylates or acrylamide are also used in drilling fluids as flocculants. Polymer nanocomposites containing different nanoparticles such as TiO_2 , ZnO , SiO_2 , and CuO are also investigated in drilling fluids [89, 107, 108].

Natural and modified natural polymers are also common in the industry. Polysaccharides such as xanthan gum, guar gum, and scleroglucan gum are used as a rheology modifier in drilling fluids. Polysaccharides are complex structures with high molecular weight and have a high tolerance to salinity. Several grades of natural polymers are available in the market to be used in drilling fluid formulations. Another important natural polymer is starch, which is obtained from either corn or potatoes. It is widely used in drilling fluid formulations as fluid loss control. Among modified natural polymers, anionic carboxymethylcellulose (CMC) is most common. CMC is a linear polysaccharide modified with carboxylic acid groups and is anionic in nature. Depending on molecular weight and degree of the substitution, it can be used as fluid loss control and rheology modifier in drilling fluid formulations. Hydroxyethylcellulose (HEC) is nonionic in nature and mainly used as viscosifier. Carboxymethyl starch is a modified form of starch and has higher thermal stability compared to starch. It is used in drilling fluid formulations as fluid loss reducer.

3 Hydrate Inhibition

Another interesting application of water-soluble polymers is as kinetic hydrate inhibitors in gas transmission lines. Gas Hydrates are solid crystalline ice-like compounds in which gas molecules are trapped in a water cavities at moderate pressures and low temperatures [109–112]. The gas molecules can be propane, ethane, isobutene, methane, and CO_2 . Gas hydrates can be classified as structure I (sI), structure II (sII), structure III (sIII), and structure T (sT) [113–115]. Formation of gas hydrate in gas transmission lines is a serious problem and can result in blockage of pipelines and the explosion of pipelines. The gas hydrates result in severe economic losses in addition to putting hazard to human safety [116–120].

Different methods are being used in industry to avoid hydrate formation. These methods include insulation of pipelines, lowering the water level from a gas stream, changing the operational parameter to keep conditions unfavorable for hydrate formation, and utilizing chemicals [121–123]. Insulation and removal of water are not common due to economic issues as they involve huge cost. Injection of chemicals to delay or prevent hydrate formation is common in the industry. These chemicals are termed as gas hydrate inhibitors and can be classified as thermodynamic hydrate inhibitors (THIs), kinetic hydrate inhibitors (KHIs), and

anti-agglomerates (AAs). THIs change the thermodynamic conditions to that values where hydrate formation is not favored [124–129]. Various organic compounds that are used as THIs include methanol, monoethylene glycols, and an electrolyte such as NaCl. The major drawback associated with using THIs is the cost of the process as high concentrations (10–50%) of the chemicals are required [130, 131]. Storage of bulk amount of chemicals in the offshore environment is not recommended and practical. Anti-agglomerates prevent the agglomeration of hydrates but could not stop the hydrate formation. In presence of AAs, the formation of hydrate takes place in form of finely suspended slush and gas lines can be cleaned easily [132–134]. KHIs are usually water-soluble polymers and prevent/delay nucleation and crystal growth. This way hydrate formation can be avoided due to lesser residence time the pipelines compared to hydrate formation time. Several explanations were proposed to explain the hydrate inhibition using water-soluble polymers. One explanation is that KHIs adsorb on the surface while perturbation of water structure can also inhibit the hydrate formation [135–137]. Another mechanism suggests that polymer chain interact and interfere with the nucleation and/or crystal growth. In this way, guest molecules could not enter into the crystal lattice [138, 139]. The major advantage of using KHIs is that they are used at a very low concentration (0.1–1 wt%), which results in lower cost and easy handling and storage of the chemicals.

3.1 Evaluation and Screening Techniques

Potential water-soluble polymers are assessed with the high-pressure autoclave, the high-pressure microdifferential scanning calorimetry (HP- μ DSC), Raman spectroscopy, nuclear magnetic resonance spectroscopy, the flow loop, the rocking cell, X-ray diffraction, conductivity measurements, and molecular simulation [116, 140–143]. Most of the techniques are used to measure either hydrate nucleation temperature or induction time. Types of the test may be either isothermal (to measure the hydrate induction time) or temperature ramp (to measure the hydrate nucleation temperature). Details of test methods are provided in subsequent sections.

3.1.1 Autoclave System

Hydrate induction time and temperature can be determined using an autoclave. In autoclave systems, hydrate formation is inferred when a sudden pressure drop occurs due to gas uptake into hydrate cages [144–147]. Constant cooling or isothermal methods can be implemented using an autoclave (Fig. 14). In the constant cooling method, the cell is cooled at a low cooling rate at a constant stirring speed. A typical constant cooling plot is shown in Fig. 15. During cooling, pressure drops at a constant rate due to the decreasing temperature before hydrate nucleation. Due to the slow cooling rate, hydrate formation is detected as the point of deviation from a linear decrease in pressure due to gas being used in hydrate formation. Torque data also indicate hydrate formation with an increase of torque signaling hydrate formation. Gas consumption data can also give information about hydrate formation as gas

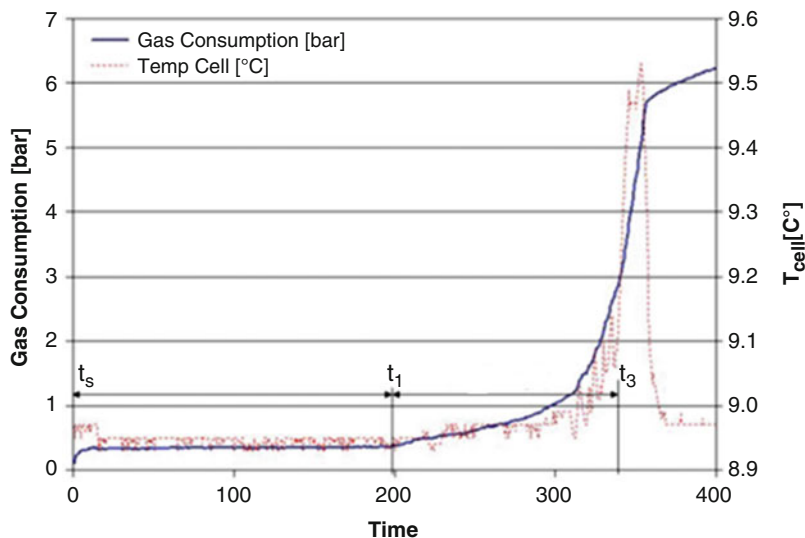


Fig. 16 Results of a typical isothermal test using an autoclave [148]. ©American Chemical Society, published with the kind permission of American Chemical Society

consumption increases suddenly due to hydrate formation. In the isothermal method, fluids in the cell are subjected to a constant temperature at a constant stirring speed. A typical isothermal plot is shown in Fig. 16. The time where the first pressure drop is observed is called the induction time (t_i). The total time taken for the formation of the hydrate plug (t_a) can also be measured. The period between t_a and t_i is known as the slow growth period.

3.1.2 High-Pressure Microcalorimeter

The high-pressure microcalorimeter consists of multiple high-pressure cells. HP- μ DSC can operate in the temperature ramping or isothermal modes. In the temperature ramping mode, a constant cooling is applied, and as the crystal formation is an exothermic process, hydrate nucleation temperature is determined from the first exothermic peak. A typical temperature ramp plot obtained using an HP- μ DSC is shown in Fig. 17, where the first exothermic peak is observed at -12.5 °C. During the heating cycle, hydrate decomposition can be detected using endothermic peaks. In Fig. 17, the two endothermic peaks are due to the melting of ice (0 °C) and the melting of hydrates (13 °C). A typical isothermal plot obtained using an HP- μ DSC is shown in Fig. 18. Hydrate nucleation time is the time taken to observe the exothermic peak. Hydrate conversion can also be obtained by integrating the heat output with respect to time [149]. The advantage of HP- μ DSC is that it requires very small amount of inhibitor and the test takes shorter time compared to other techniques.

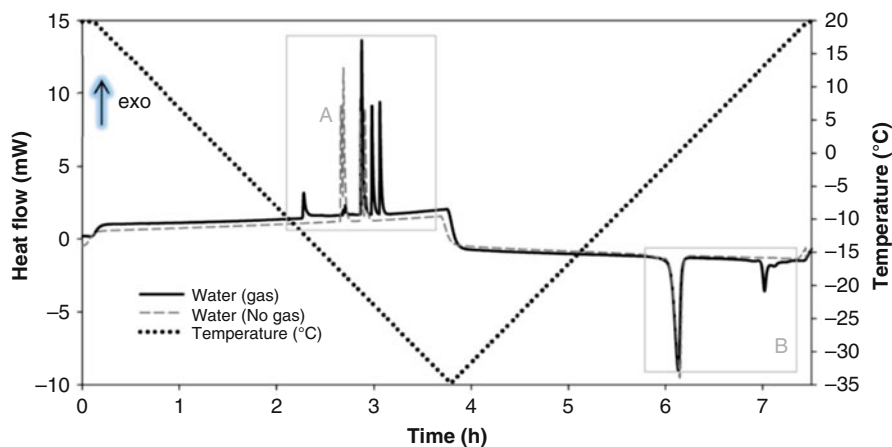


Fig. 17 A typical temperature ramp plot obtained using an HP- μ DSC [150]. (© American Chemical Society, published with the kind permission of American Chemical Society.)

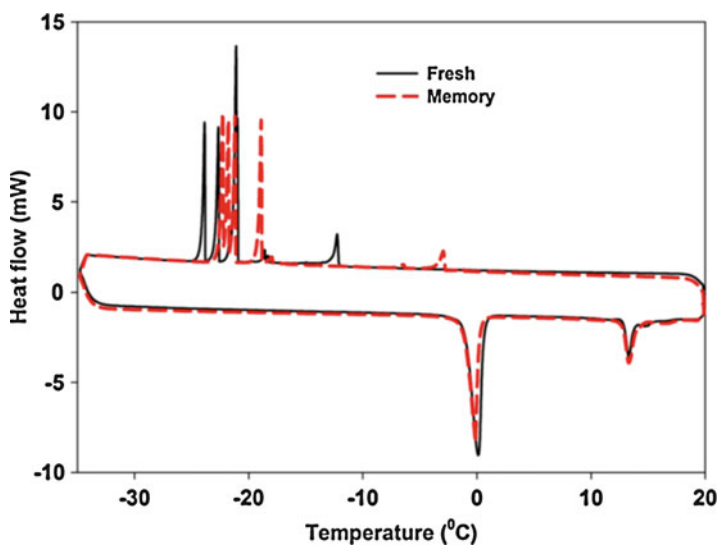


Fig. 18 A typical temperature ramp plot obtained using an HP- μ DSC for fresh and memory solutions [150]. (© American Chemical Society, published with the kind permission of American Chemical Society.)

3.1.3 Rocking Cell

The rocking cell equipment has several cells and can be used to test the effect of inhibitors on gas hydrate nucleation, growth, and decomposition. The stainless steel cells can withstand high pressures. A steel ball is placed inside the cell which rolls back and forth along the length of the cell to agitate the solution inside. Once the

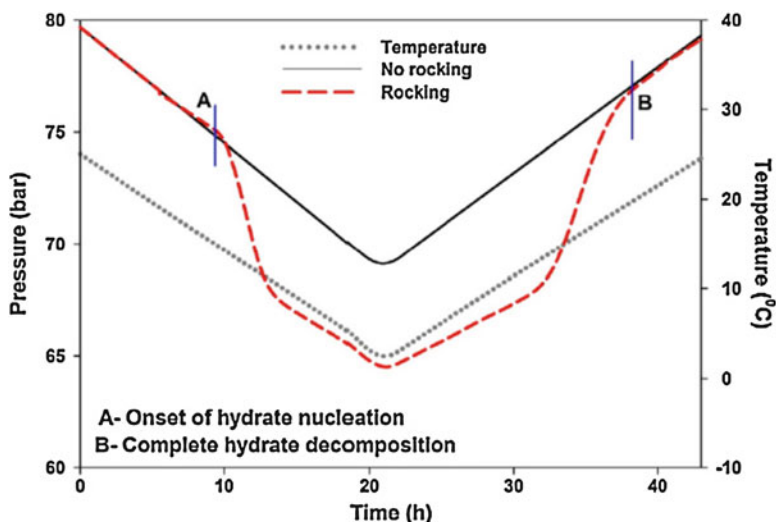


Fig. 19 Results of a typical temperature ramp test conducted using a rocking cell [151]. (© Elsevier, published with the kind permission of Elsevier)

cells are loaded with the desired solution, they are placed in a cooling bath controlled by an external refrigerator. The temperature and pressure of the cells are observed by the data acquisition system. The cells are continuously rocked and the hydrate formation is signaled when the steel ball can no longer move freely inside the cell. Just as with HP- μ DSC, both constant temperature and ramping experiments can be performed. The advantage of the latest model of the rocking cell equipment is that several experiments can be performed at the same time, giving good statistical data with fewer runs. In the temperature ramping mode, the performance of the inhibitor is evaluated in terms of the hydrate nucleation temperature. Results of a temperature ramping test are shown in Fig. 19 and the black solid line is the reference obtained without rocking. Pressure decreases linearly during cooling and increases linearly during heating due to thermal contraction and expansion, respectively. In the temperature ramping experiment with rocking (red dashed line), pressure decreases linearly during cooling due to thermal contraction up to point A. Pressure drops faster at the onset of nucleation of the hydrate due to high gas consumption during hydrate formation. Hydrate decomposition can also be studied using the temperature ramping mode. A linear increase of pressure (point B) with temperature indicates complete hydrate decomposition [151]. The strength of an inhibitor can be evaluated using the time taken for hydrate nucleation at a constant temperature.

3.1.4 Flow Loop Apparatus

The flow loop apparatus has been extensively used in the evaluation and characterization of hydrates under a wide range of conditions [152–158]. The laboratory flow loop apparatus is typically made of stainless steel and essentially composed of a pipe and a pump with a sight glass and a camera used for visual observation and

recording. Water injection and the flow regime is controlled using pumps. The temperature is normally controlled using pump-fed water and cooling is achieved by circulating a coolant such as ethylene glycol. Pressure and temperature inside the pump, which are used to monitor hydrate formation, is monitored using temperature and pressure sensors [159]. The flow loop apparatus is typically used by oil companies to simulate field conditions in the final stages of evaluation. It is relatively expensive than the high pressure autoclave and the rocking cell equipment. However, the flow loop apparatus can give much more realistic values and assessment of the behavior as the tests will be conducted under real field conditions.

3.1.5 Advanced Evaluation Techniques

With the advancement in technology, several novel techniques and methods have been developed to evaluate the performance of KHIs. Ohno et al. used solid state ^{13}C NMR to analyze hydrate formation with and without kinetic inhibitors [160]. Lee et al. also used solid state ^{13}C NMR to analyze hydrate formation behavior of methane and natural gas in the presence and absence of monoethylene glycol [161]. Daraboina et al. investigated the formation kinetics of methane/ethane/propane hydrates using the ^1H nuclear magnetic resonance imaging technique in the presence of biological and commercial inhibitors [162]. The technique is a useful tool particularly for biological inhibitors, which are available in limited quantities. Yang and Tohidi used the ultrasonic test technique for the evaluation of KHIs [163]. Karamoddin and Varaminian investigated the tetrahydrofuran hydrate formation behavior in the presence of different inhibitors using conductivity measurements [164].

3.1.6 Molecular Simulations

Molecular simulation technique has been utilized in hydrate studies by several researchers [165–176]. Baez and Clancy [169] used molecular dynamic (MD) simulations to study crystal growth. A spherical hydrate crystal was implanted in the melt to monitor the kinetics of growth and dissolution of a hydrate crystal and they reported slow crystal growth. In another study, Ota and Qi [177] used MD simulations to investigate the nucleation process of methane hydrates. MD simulations of mixtures of methane and water molecules placed in a cubic cell were used to determine that the nucleation process has three stages. In the first stage, gas molecules undergo a dispersive process followed by water molecules making hydrate cavities in the second stage and finally the hydrate structure becoming steady in the third stage. Other research groups have also studied crystal growth of gas hydrates using MD simulations [178, 179].

Anderson et al. [180] projected the hydrate inhibition efficiency of polyethylene oxide (PEO), PVP, poly(vinyl caprolactam) (PVCap), and poly (N-methyl,N-vinylacetamide) (PVIMA). They found a correlation between the degree of inhibition and the free energy of binding between the inhibitor and the hydrate crystal surface. Experimental data support this conclusion with the most effective inhibitor (PVIMA) having the highest negative binding energy (-45.8) and the least effective inhibitor (PEO) having the lowest negative binding energy (-0.2). Moon et al. [181] found a correlation between the inhibition mechanism of PVP and the surface energy using simulations. They showed that PVP increases the time taken to form the

critical nucleus when the surface energy of the interfacial region is increased. Storr et al. [182] successfully designed and evaluated quaternary ammonium zwitterions based on inhibitors using MD simulations. Zheng [183] used MD simulations to investigate the effects of the molecular weight of hyper branched polyesteramides and showed that low molecular weight inhibitors inhibit crystal growth but do not prevent crystal growth. On the other hand, high molecular weight inhibitors destabilize the crystals and prevent further crystal growth.

3.2 Polymer Systems for Kinetic Hydrate Inhibition

Polymer-based KHIs are primarily vinyl lactam polymers, amide polymers, and natural polymers. Typical examples of vinyl lactam polymers are PVP, PVCap, poly (N-vinyl piperidone), and vinyl pyrrolidone/vinyl caprolactam copolymers. Amide polymers are mainly acrylamide-based polymers and vinyl amide polymers. Natural polymer KHIs are mainly starch, chitosan, and amino acids.

Poly (vinyl pyrrolidone) is most reported KHI in the scientific literature due to its several advantages such as low cost and availability of literature. The structure of PVP is given in Fig. 20. Currently, PVP serve as a benchmark to compare the performance of modern polymeric KHIs. Typical molecular weights of commercial PVP range from 10,000 to 350,000. Surface adsorption is the main mechanism of hydrate inhibition using PVP. PVP shows good performance at low subcooling conditions and it is not an efficient KHI at high subcooling conditions [184]. PVCap is another important kinetic inhibitor, which has been used in industry and compared with PVP for its inhibition performance. Under different conditions, the performance of PVP and PVCap differ and there is no well-defined rule to predict which inhibitor will be more effective at given conditions. Additional experimental work is required to understand the inhibition performance at various given conditions. Poly (N-vinyl piperidone) is another less common investigated polymer for hydrate inhibition applications. Its inhibition performance was found to be intermediate between PVP and PVCap [185]. To utilize the relative advantages of different polymers, several copolymers and terpolymers such as vinyl pyrrolidone/vinyl caprolactam copolymer and vinyl pyrrolidone/vinyl caprolactam/dimethylaminoethyl

Fig. 20 Structure of PVP (a) and PVCap (b)

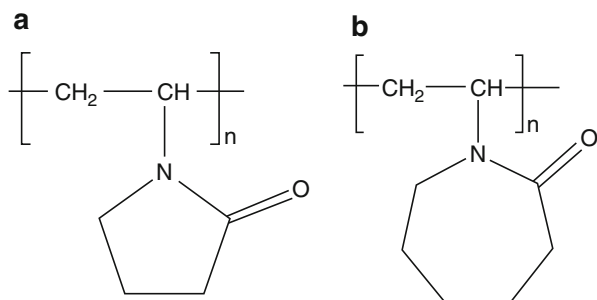
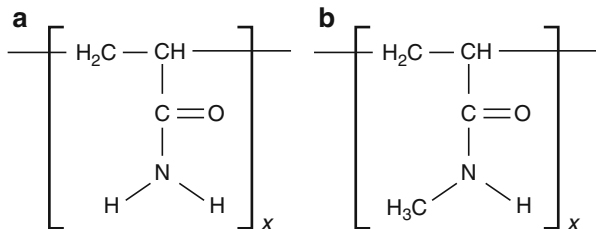


Fig. 21 Structure of polyacrylamide (a) and poly (N-methylacrylamide) (b)



methacrylate terpolymer with different ratios have been evaluated for inhibition performance.

Amine-based polymers include acrylamide, vinyl amide, and allyl amide polymers. Polyacrylamide and poly (N-methylacrylamide) have been investigated and showed similar mechanism as of vinyl lactam polymers [186]. The structure of these polymers is given in Fig. 21. N-methyl,N-vinylacetamide (VIMA) is the most monomer from this class. The copolymer made from VIMA and another suitable monomer from acrylamides, maleimides, and carboxylate have shown good inhibition performance in various investigations. VIMA/VCap copolymer has shown higher subcooling compared to poly (N-methyl, N-vinylacetamide) and PVCap [187].

Besides these classical polymers, research has moved to investigate other classes of polymers. Three dimensional highly branched dendrimeric compounds are also being utilized in hydrate inhibition [188]. Commercially available “HYBRANES” are hyperbranched polyesteramide with a number average molecular weight of 1200 [189]. Fluorinated polymers have also been investigated for hydrate inhibition, despite the fact they showed low inhibition performance compared to nonfluorinated polymers [190]. Due to the poor biodegradability of the KHIs, the research has moved towards the development of natural and biodegradable inhibitors. Starch is a naturally occurring polysaccharide and importantly is biodegradable and environmentally friendly [191]. Another polysaccharide reported for hydrate inhibition is chitosan that is produced by deacetylation of chitin. Despite the fact that starch and chitosan have shown good performance as hydrate inhibitors, their field applications are limited due to high cost and less availability.

4 Conclusion

Water-soluble polymers have been utilized in several gas and oil field applications. HPAM is most commonly used polymer in enhanced oil recovery and drilling fluids due to low cost, high viscosity, and commercial availability. However, its performance is limited to only low-temperature and low-salinity conditions. For HTHS applications, acrylamide copolymers such AM-AMPS with better thermal stability have been developed. Hydrophobically associating polymers and thermo-viscosifying polymers have been specially designed for HTHS.

The use of polymeric kinetic hydrate inhibitors has gained attention in last few years due to their effectiveness at low concentration that makes them economic and

environmentally friendly. Poly (vinyl pyrrolidone) and poly (vinyl caprolactam) are two most commonly reported kinetic inhibitors in literature. To overcome the limitations of classical polymers, research has shifted towards development of cheap, high performance, and environmentally friendly green kinetic inhibitors. The major drawback associated with green kinetic inhibitors is their unavailability in bulk and high cost. Despite the fact that laboratory research has moved towards the development of green kinetic inhibitors, their field application is limited.

References

1. I. Lakatos, Role of chemical IOR/EOR methods in the 21st century, in *18th World Petroleum Congress, 25–29 September*, Johannesburg. 2005. World Petroleum Congress, WPC-18-0883
2. M.S. Kamal et al., Evaluation of rheological and thermal properties of a new fluorocarbon surfactant-polymer system for EOR applications in high-temperature and high-salinity oil reservoirs. *J. Surfactant Deterg.* **17**(5), 985–993 (2014)
3. A. Al Adasani, B. Bai, Analysis of EOR projects and updated screening criteria. *J. Pet. Sci. Eng.* **79**(1), 10–24 (2011)
4. E.J. Manrique et al., *EOR: Current Status and Opportunities*. SPE Improved Oil Recovery Symposium, 24–28 April, (Society of Petroleum Engineers, Tulsa, Oklahoma, USA. 2010)
5. M.S. Kamal, A.S. Sultan, I.A. Hussein, Screening of amphoteric and anionic surfactants for cEOR applications using a novel approach. *Colloids Surf. A Physicochem. Eng. Asp.* **476**, 17–23 (2015)
6. Y. Wang et al., *Optimized Surfactant IFT and Polymer Viscosity for Surfactant- Polymer Flooding in Heterogeneous Formations*. SPE Improved Oil Recovery Symposium, 24–28 April, (Society of Petroleum Engineers, Tulsa, Oklahoma, USA 2010)
7. A. Bera et al., Adsorption of surfactants on sand surface in enhanced oil recovery: Isotherms, kinetics and thermodynamic studies. *Appl. Surf. Sci.* **284**, 87–99 (2013)
8. A. Bera et al., Screening of microemulsion properties for application in enhanced oil recovery. *Fuel* **121**, 198–207 (2014)
9. A. Samanta et al., Effects of alkali, salts, and surfactant on rheological behavior of partially hydrolyzed polyacrylamide solutions. *J. Chem. Eng. Data* **55**(10), 4315–4322 (2010)
10. A. Samanta et al., Comparative studies on enhanced oil recovery by alkali–surfactant and polymer flooding. *J. Pet. Explor. Prod. Technol.* **2**(2), 67–74 (2012)
11. Y. Wang et al., A novel thermoviscosifying water-soluble polymer: Synthesis and aqueous solution properties. *J. Appl. Polym. Sci.* **116**(6), 3516–3524 (2010)
12. D. Zhu et al., Aqueous hybrids of silica nanoparticles and hydrophobically associating hydrolyzed polyacrylamide used for EOR in high-temperature and high-salinity reservoirs. *Energies* **7**(6), 3858–3871 (2014)
13. J.J. Taber, Dynamic and static forces required to remove a discontinuous oil phase from porous media containing both oil and water. *Soc. Pet. Eng. J.* **9**(1), 3 (1969)
14. W.R. Foster, A low-tension waterflooding process. *J. Pet. Technol.* **25**(02), 205–210 (1973)
15. M.A. Ahmadi et al., Preliminary evaluation of mulberry leaf-derived surfactant on interfacial tension in an oil-aqueous system: EOR application. *Fuel* **117**, 749–755 (2014)
16. P. Fernandes et al., Biosurfactant, solvents and polymer production by *Bacillus subtilis* RI4914 and their application for enhanced oil recovery. *Fuel* **180**, 551–557 (2016)
17. M.S. Kamal, A review of gemini surfactants: Potential application in enhanced oil recovery. *J. Surfactant Deterg.* **19**(2), 1–14 (2016)
18. M.A. Ahmadi, S.R. Shadizadeh, Implementation of a high-performance surfactant for enhanced oil recovery from carbonate reservoirs. *J. Pet. Sci. Eng.* **110**, 66–73 (2013)
19. M.A. Ahmadi, M. Galedarzadeh, S.R. Shadizadeh, Wettability alteration in carbonate rocks by implementing new derived natural surfactant: Enhanced oil recovery applications. *Transp. Porous Media* **106**(3), 645–667 (2015)

20. M. Mohammed, T. Babadagli, Wettability alteration: A comprehensive review of materials/methods and testing the selected ones on heavy-oil containing oil-wet systems. *Adv. Colloid Interf. Sci.* **220**, 54–77 (2015)
21. M.A. Ahmadi, S.R. Shadizadeh, Experimental investigation of adsorption of a new nonionic surfactant on carbonate minerals. *Fuel* **104**, 462–467 (2013)
22. M.A. Ahmadi, S. Shadizadeh, Experimental and theoretical study of a new plant derived surfactant adsorption on quartz surface: Kinetic and isotherm methods. *J. Dispers. Sci. Technol.* **36**(3), 441–452 (2015)
23. M.A. Ahmadi, S.R. Shadizadeh, Induced effect of adding nano silica on adsorption of a natural surfactant onto sandstone rock: Experimental and theoretical study. *J. Pet. Sci. Eng.* **112**, 239–247 (2013)
24. L. Fu et al., Study on organic alkali-surfactant-polymer flooding for enhanced ordinary heavy oil recovery. *Colloids Surf. A Physicochem. Eng. Asp.* **508**, 230–239 (2016)
25. M.S. Kamal et al., Review on polymer flooding: Rheology, adsorption, stability, and field applications of various polymer systems. *Polym. Rev.* **55**(3), 491–530 (2015)
26. A.Z. Abidin, T. Puspasari, W.A. Nugroho, Polymers for enhanced oil recovery technology. *Procedia Chem.* **4**, 11–16 (2012)
27. M. Han et al., Laboratory study on polymers for chemical flooding in carbonate reservoirs. SPE EOR Conference at Oil and Gas West Asia, 31 March–2 April, (Society of Petroleum Engineers, Muscat, Oman 2014)
28. G. Atesok, P. Somasundaran, L.J. Morgan, Charge effects in the adsorption of polyacrylamides on sodium kaolinite and its flocculation. *Powder Technol.* **54**(2), 77–83 (1988)
29. M. Celik, S. Ahmad, H. Al-Hashim, Adsorption/desorption of polymers from Saudi Arabian limestone. *J. Pet. Sci. Eng.* **6**(3), 213–223 (1991)
30. A. Muggeridge et al., Recovery rates, enhanced oil recovery and technological limits. *Phil. Trans. R. Soc. A* **372**(2006), 20120320 (2014)
31. H.R. Li et al., Effect of organic alkalis on interfacial tensions of surfactant/polymer solutions against hydrocarbons. *Energy Fuel* **29**(2), 459–466 (2015)
32. A.A. Olajire, Review of ASP EOR (alkaline surfactant polymer enhanced oil recovery) technology in the petroleum industry: Prospects and challenges. *Energy* **77**, 963–982 (2014)
33. X.M. Zhang et al., Adaptability of a hydrophobically associating polyacrylamide/mixed-surfactant combination flooding system to the Shengli Chengdao oilfield. *J. Appl. Polym. Sci.* **131**(12), 40390 (1–9) (2014)
34. F.W. Smith, The behavior of partially hydrolyzed polyacrylamide solutions in porous media. *J. Pet. Technol.* **22**(02), 148–156 (2013)
35. M.S. Kamal et al., Rheological study on ATBS-AM copolymer-surfactant system in high-temperature and high-salinity environment. *J. Chem.* **2013**, 801570 (2013)
36. C. Zhou et al., Synthesis and solution properties of novel comb-shaped acrylamide copolymers. *Polym. Bull.* **66**(3), 407–417 (2011)
37. A. Borthakur et al., Partially hydrolyzed polyacrylamide for enhanced oil-recovery. *Res. Ind.* **40**(2), 90–94 (1995)
38. R.D. Shupe, Chemical stability of polyacrylamide polymers. *J. Pet. Technol.* **33**(08), 1513–1529 (1981)
39. H. Lu et al., Retention behaviors of hydrophobically associating polyacrylamide prepared via inverse microemulsion polymerization through porous media. *J. Macromol. Sci., Part A: Pure Appl. Chem.* **47**(6), 602–607 (2010)
40. R.G. Ryles, Chemical stability limits of water-soluble polymers used in oil recovery processes. *SPE Reserv. Eng.* **3**(01), 23–34 (1988)
41. A. Moradi-Araghi, D.H. Cleveland, I.J. Westerman, *Development and Evaluation of EOR Polymers Suitable for Hostile Environments: II-Copolymers of Acrylamide and Sodium AMPS*. 1987
42. R.S. Seright et al., Stability of partially hydrolyzed polyacrylamides at elevated temperatures in the absence of divalent cations. *SPE J.* **15**(02), 341–348 (2010)

43. H. Nasr-El-Din., B. Hawkins, K. Green, Viscosity behavior of alkaline, surfactant, polyacrylamide solutions used for enhanced oil recovery, in *SPE International Symposium on Oilfield Chemistry*, 20–22 February, (Society of Petroleum Engineers, Anaheim, California 1991)
44. M.S. Kamal et al., Rheological properties of thermoviscosifying polymers in high-temperature and high-salinity environments. *Can. J. Chem. Eng.* **93**(7), 1194–1200 (2015)
45. Y. Niu et al., *Research on hydrophobically associating water-soluble polymer used for EOR*. SPE International Symposium on Oilfield Chemistry, 13–16 February, (Society of Petroleum Engineers, Houston, Texas 2001)
46. M. Buchgraber et al., *The displacement of viscous oil by associative polymer solutions*. SPE Annual Technical Conference and Exhibition, 4–7 October, (Society of Petroleum Engineers, New Orleans, Louisiana 2009)
47. D. Lijian, W. Biao, *Hydrophobically associating terpolymer and its complex with a stabilizer in brine for enhanced oil recovery*. SPE International Symposium on Oilfield Chemistry, 14–17 February, (Society of Petroleum Engineers, San Antonio, Texas 1995)
48. Z. Ye et al., Hydrophobically associating acrylamide-based copolymer for chemically enhanced oil recovery. *J. Appl. Polym. Sci.* **130**(4), 2901–2911 (2013)
49. Y. Wang et al., A novel thermoviscosifying water-soluble polymer for enhancing oil recovery from high-temperature and high-salinity oil reservoirs. *Adv. Mater. Res.* **307**, 654–657 (2011)
50. P. Maroy, et al., *Thermoviscosifying polymers, their synthesis and their uses in particular in the oil industry*. EP Patent 0,583,814. 1998
51. J. Sheng, *Modern Chemical Enhanced Oil Recovery: Theory and Practice* (Gulf Professional Publishing, 2010)
52. X.J. Liu et al., Synthesis and evaluation of a water-soluble acrylamide binary sulfonates copolymer on MMT crystalline interspace and EOR. *J. Appl. Polym. Sci.* **125**(2), 1252–1260 (2012)
53. Z. Ye et al., Synthesis and characterization of a water-soluble sulfonates copolymer of acrylamide and N-allylbenzamide as enhanced oil recovery chemical. *J. Appl. Polym. Sci.* **128**(3), 2003–2011 (2013)
54. Y. Xu et al., Synthesis and aqueous solution properties of a novel nonionic, amphiphilic comb-type polyacrylamide. *J. Macromol. Sci., Part B* **50**(9), 1691–1704 (2011)
55. C.L. McCormick, L.C. Salazar, Water-soluble copolymers. 43. Ampholytic copolymers of sodium 2-(acrylamido)-2-methylpropanesulfonate with [2-(acrylamido)-2-methylpropyl] trimethylammonium chloride. *Macromolecules* **25**(7), 1896–1900 (1992)
56. C.L. McCormick, J.C. Middleton, D.F. Cummins, Water-soluble copolymers. 37. Synthesis and characterization of responsive hydrophobically modified polyelectrolytes. *Macromolecules* **25**(4), 1201–1206 (1992)
57. F. Yang et al., Synthesis, characterization, and applied properties of carboxymethyl cellulose and polyacrylamide graft copolymer. *Carbohydr. Polym.* **78**(1), 95–99 (2009)
58. L. Bai et al., Synthesis and solution properties of comb-like acrylamide copolymers. *J. Wuhan Univ. Technol.-Mater. Sci. Ed.* **27**(6), 1105–1109 (2012)
59. J.F. Berret et al., Fluorocarbon associative polymers. *Curr. Opin. Colloid Interface Sci.* **8**(3), 296–306 (2003)
60. J.F. Argillier et al., Solution and adsorption properties of hydrophobically associating water-soluble polyacrylamides. *Colloids Surf. A Physicochem. Eng. Asp.* **113**(3), 247–257 (1996)
61. W. Zhou et al., *Application of hydrophobically associating water-soluble polymer for polymer flooding in China offshore heavy oilfield*. International Petroleum Technology Conference, 4–6 December, (Dubai, U.A.E. 2007)
62. L. Petit et al., Synthesis of graft polyacrylamide with responsive self-assembling properties in aqueous media. *Polymer* **48**(24), 7098–7112 (2007)
63. X. Liu et al., Effect of inorganic salts on viscosifying behavior of a thermoassociative water-soluble terpolymer based on 2-acrylamido-methylpropane sulfonic acid. *J. Appl. Polym. Sci.* **125**(5), 4041–4048 (2012)

64. M.J. Zohuriaan, F. Shokrolahi, Thermal studies on natural and modified gums. *Polym. Test.* **23**(5), 575–579 (2004)
65. D.F. Petri, Xanthan gum: A versatile biopolymer for biomedical and technological applications. *J. Appl. Polym. Sci.* **132**(23), 42035 (1–13)
66. A. Palaniraj, V. Jayaraman, Production, recovery and applications of xanthan gum by *Xanthomonas campestris*. *J. Food Eng.* **106**(1), 1–12 (2011)
67. C. Kim et al., Drag reduction characteristics of polysaccharide xanthan gum. *Macromol. Rapid Commun.* **19**(8), 419–422 (1998)
68. H.Y. Jang et al., Enhanced oil recovery performance and viscosity characteristics of polysaccharide xanthan gum solution. *J. Ind. Eng. Chem.* **21**, 741–745 (2015)
69. T. Lund, J. Lecourtier, G. Müller, Properties of xanthan solutions after long-term heat treatment at 90°C. *Polym. Degrad. Stab.* **27**(2), 211–225 (1990)
70. I. Norton et al., Mechanism and dynamics of conformational ordering in xanthan polysaccharide. *J. Mol. Biol.* **175**(3), 371–394 (1984)
71. E. Morris et al., Order-disorder transition for a bacterial polysaccharide in solution. A role for polysaccharide conformation in recognition between *Xanthomonas* pathogen and its plant host. *J. Mol. Biol.* **110**(1), 1–16 (1977)
72. S.L. Wellington, Biopolymer solution viscosity stabilization-polymer degradation and antioxidant use. *Soc. Pet. Eng. J.* **23**(06), 901–912 (1983)
73. M. Rashidi, A.M. Blokhuis, A. Skauge, Viscosity study of salt tolerant polymers. *J. Appl. Polym. Sci.* **117**(3), 1551–1557 (2010)
74. C.T. Hou, N. Barnabe, K. Greaney, Biodegradation of xanthan by salt-tolerant aerobic microorganisms. *J. Ind. Microbiol.* **1**(1), 31–37 (1986)
75. S. Abbas, J. Donovan, A. Sanders, Applicability of hydroxyethylcellulose polymers for chemical EOR, in *2013 SPE Enhanced Oil Recovery Conference*, 2–4 July, (Kuala Lumpur, Malaysia 2013)
76. C. Gao, Application of a novel biopolymer to enhance oil recovery. *J. Pet. Explor. Prod. Technol.*, **6**(4) 749–753 (2016)
77. A.-L. Kjøniksen et al., Modified polysaccharides for use in enhanced oil recovery applications. *Eur. Polym. J.* **44**(4), 959–967 (2008)
78. C. Gatlin, *Petroleum engineering, drilling and well completions* (Prentice-hall Inc, Englewood Cliffs, 1960). 341 p
79. R. K. Clark, *Applications of water-soluble polymers as shale stabilizers in drilling fluids*. Advances in Chemistry Series 213, 171–181 (1986)
80. Z. Vryzas, V.C. Kelessidis, Nano-based drilling fluids: A review. *Energies* **10**(4), 540 (2017)
81. C. Moore, V. Lafave, Air and gas drilling. *J. Pet. Technol.* **8**(02), 15–16 (1956)
82. C. Maranuk et al., Unique system for underbalanced drilling using air in the Marcellus Shale, in *SPE Eastern Regional Meeting*, 21–23 October, (Society of Petroleum Engineers, Charleston, WV, USA 2014)
83. S. Saintpere et al., Hole cleaning capabilities of drilling foams compared to conventional fluids, in *SPE Annual Technical Conference and Exhibition*, 1–4 October, (Society of Petroleum Engineers, Dallas, Texas 2000)
84. A. Paknejad, J.J. Schubert, M. Amani, Key parameters in foam drilling operations, in *IADC/SPE Managed Pressure Drilling and Underbalanced Operations Conference & Exhibition*, 12–13 February, (Society of Petroleum Engineers, San Antonio, Texas 2009)
85. J. Davies et al., Environmental effects of the use of oil-based drilling muds in the North Sea. *Mar. Pollut. Bull.* **15**(10), 363–370 (1984)
86. R. Caenn, H.C. Darley, G.R. Gray, *Composition and properties of drilling and completion fluids* (Gulf professional publishing, 2011)
87. J. Shafer, et al., Core and log NMR measurements indicate reservoir rock is altered by OBM filtrate, in *SPWLA 45th Annual Logging Symposium*, 6–9 June, (Society of Petrophysicists and Well-Log Analysts, Noordwijk, Netherlands 2004)

88. R. Minton, B. Secoy, Annular re-injection of drilling wastes. *J. Pet. Technol.* **45**(11), 1081–1085 (1993)
89. M. Sadeghalvaad, S. Sabbaghi, The effect of the TiO₂/polyacrylamide nanocomposite on water-based drilling fluid properties. *Powder Technol.* **272**, 113–119 (2015)
90. S. Elkhatny, H. Nasr-El-Din, M. Al-Bagoury, Properties of ilmenite water-based drilling fluids for HPHT applications, in *IPTC 2013: International Petroleum Technology Conference*, 26–28 March, Beijing, China 2013
91. A. Kamel, A. Hosny, A novel mud formulation for drilling operations in the permafrost, in *SPE Western Regional & AAPG Pacific Section Meeting 2013 Joint Technical Conference*, 19–25 April, (Society of Petroleum Engineers, Monterey, California, USA 2013)
92. F. Huadi et al., Successful KCl free highly inhibitive and cost effective WBM applications, Offshore East Kalimantan, Indonesia, in *IADC/SPE Asia Pacific Drilling Technology Conference and Exhibition*, 1–3 November, (Society of Petroleum Engineers, Ho Chi Minh City, Vietnam 2010)
93. B. Bui, A. Tutuncu, Creep-recovery test: A critical tool for rheological characterization of drilling fluids, in *Unconventional Resources Technology Conference*, 12–14 August, (Society of Petroleum Engineers, Denver, Colorado, USA 2013)
94. R. Caenn, G.V. Chillingar, Drilling fluids: State of the art. *J. Pet. Sci. Eng.* **14**(3), 221–230 (1996)
95. J.P. Simpson, Drilling fluid filtration under stimulated downhole conditions, in *SPE Symposium on Formation Damage Control*, 30 January–2 February, (Society of Petroleum Engineers, New Orleans, Louisiana 1974)
96. C.I.R. de Oliveira et al., Characterization of bentonite clays from Cubati, Paraíba (northeast of Brazil). *Cerâmica* **62**(363), 272–277 (2016)
97. G. Xie et al., Investigation of the inhibition mechanism of the number of primary amine groups of alkylamines on the swelling of bentonite. *Appl. Clay Sci.* **136**, 43–50 (2017)
98. H. Yarranton, Development of Viscosity Model for Petroleum Industry Applications, Doctoral dissertation. University of Calgary, 2013
99. K.S. Hafshejani, A. Moslemzadeh, K. Shahbazi, A novel bio-based deflocculant for bentonite drilling mud. *Appl. Clay Sci.* **127**, 23–34 (2016)
100. H. Zhong et al., Shale inhibitive properties of polyether diamine in water-based drilling fluid. *J. Pet. Sci. Eng.* **78**(2), 510–515 (2011)
101. H. Zhong et al., Inhibitive properties comparison of different polyetheramines in water-based drilling fluid. *J. Nat. Gas Sci. Eng.* **26**, 99–107 (2015)
102. A. Benchabane, K. Bekkour, Effects of anionic additives on the rheological behavior of aqueous calcium montmorillonite suspensions. *Rheol. Acta* **45**(4), 425–434 (2006)
103. K.Y. Choo, K. Bai, Effects of bentonite concentration and solution pH on the rheological properties and long-term stabilities of bentonite suspensions. *Appl. Clay Sci.* **108**, 182–190 (2015)
104. R. Jain et al., Study the effect of synthesized graft copolymer on the inhibitive water based drilling fluid system. *Egypt. J. Pet.* **26**(4), 875–883 (2017)
105. V.C. Kelessidis, M. Zografou, V. Chatzistamou, Optimization of drilling fluid rheological and fluid loss properties utilizing PHPA polymer, in *SPE Middle East Oil and Gas Show and Conference*, 10–13 March, (Society of Petroleum Engineers, Manama, Bahrain 2013)
106. J.C. Estes, Role of water-soluble polymers in oil well drilling muds, in *Water-soluble polymers: Beauty with performance*, vol. 213, (ACS Publications, USA 1986), p. 155
107. J.K.M. William et al., Effect of CuO and ZnO nanofluids in xanthan gum on thermal, electrical and high pressure rheology of water-based drilling fluids. *J. Pet. Sci. Eng.* **117**, 15–27 (2014)
108. A.S. Ragab, A. Noah, Reduction of formation damage and fluid loss using nano-sized silica drilling fluids. *Pet. Technol. Dev. J.* **2**, 75–88 (2014)
109. C.M. Perfeldt et al., Inhibition of gas hydrate nucleation and growth: Efficacy of an antifreeze protein from the longhorn beetle *rhagium mordax*. *Energy Fuel* **28**(6), 3666–3672 (2014)

110. E.D. Sloan, Fundamental principles and applications of natural gas hydrates. *Nature* **426**(6964), 353–363 (2003)
111. N. Daraboina, S. Pachitsas, N. von Solms, Experimental validation of kinetic inhibitor strength on natural gas hydrate nucleation. *Fuel* **139**, 554–560 (2015)
112. V. Mohebbi, R.M. Behbahani, Experimental study on gas hydrate formation from natural gas mixture. *J. Nat. Gas Sci. Eng.* **18**, 47–52 (2014)
113. P. Englezos et al., Kinetics of formation of methane and ethane gas hydrates. *Chem. Eng. Sci.* **42**(11), 2647–2658 (1987)
114. Y.C. Song et al., The status of natural gas hydrate research in China: A review. *Renew. Sust. Energ. Rev.* **31**(0), 778–791 (2014)
115. P. Bishnoi, P. Dholabhai, Experimental study on propane hydrate equilibrium conditions in aqueous electrolyte solutions. *Fluid Phase Equilib.* **83**, 455–462 (1993)
116. M.S. Kamal et al., Application of various water soluble polymers in gas hydrate inhibition. *Renew. Sust. Energ. Rev.* **60**, 206–225 (2016)
117. E.G. Hammerschmidt, Formation of gas hydrates in natural gas transmission lines. *Ind. Eng. Chem. Res.* **26**(8), 851–855 (1934)
118. M.A. Kelland, History of the development of low dosage hydrate inhibitors. *Energy Fuel* **20**(3), 825–847 (2006)
119. X. Zhao, Z. Qiu, W. Huang, Characterization of kinetics of hydrate formation in the presence of kinetic hydrate inhibitors during Deepwater drilling. *J. Nat. Gas Sci. Eng.* **22**, 270–278 (2015)
120. M.A. Kelland, J.E. Iversen, Kinetic hydrate inhibition at pressures up to 760 bar in deep water drilling fluids. *Energy Fuel* **24**(5), 3003–3013 (2010)
121. M. Illbeigi, A. Fazlali, A.H. Mohammadi, Thermodynamic model for the prediction of equilibrium conditions of clathrate hydrates of methane+ water-soluble or-insoluble hydrate former. *Ind. Eng. Chem. Res.* **50**(15), 9437–9450 (2011)
122. A. Eslamimanesh et al., Phase equilibrium modeling of structure H clathrate hydrates of methane plus water “insoluble” hydrocarbon promoter using QSPR molecular approach. *J. Chem. Eng. Data* **56**(10), 3775–3793 (2011)
123. A. Eslamimanesh et al., Application of gas hydrate formation in separation processes: A review of experimental studies. *J. Chem. Thermodyn.* **46**, 62–71 (2012)
124. J. Chen et al., Insights into the formation mechanism of hydrate plugging in pipelines. *Chem. Eng. Sci.* **122**, 284–290 (2015)
125. M. Arjmandi et al., Is subcooling the right driving force for testing low-dosage hydrate inhibitors? *Chem. Eng. Sci.* **60**(5), 1313–1321 (2005)
126. H. Tavasoli et al., Prediction of gas hydrate formation condition in the presence of thermodynamic inhibitors with the Elliott–Suresh–Donohue Equation of State. *J. Pet. Sci. Eng.* **77**(1), 93–103 (2011)
127. Z. Long et al., Phase equilibria of ethane hydrate in MgCl₂ aqueous solutions. *J. Chem. Eng. Data* **55**(8), 2938–2941 (2010)
128. A.H. Mohammadi, D. Richon, Gas hydrate phase equilibrium in the presence of ethylene glycol or methanol aqueous solution. *Ind. Eng. Chem. Res.* **49**(18), 8865–8869 (2010)
129. M. Sun, A. Firoozabadi, New surfactant for hydrate anti-agglomeration in hydrocarbon flowlines and seabed oil capture. *J. Colloid Interface Sci.* **402**, 312–319 (2013)
130. M.A. Kelland et al., Studies on some alkylamide surfactant gas hydrate anti-agglomerants. *Chem. Eng. Sci.* **61**(13), 4290–4298 (2006)
131. E.D. Sloan, A changing hydrate paradigm – From apprehension to avoidance to risk management. *Fluid Phase Equilib.* **228**, 67–74 (2005)
132. Z. Huo et al., Hydrate plug prevention by anti-agglomeration. *Chem. Eng. Sci.* **56**(17), 4979–4991 (2001)
133. J.W. Lachance, E.D. Sloan, C.A. Koh, Determining gas hydrate kinetic inhibitor effectiveness using emulsions. *Chem. Eng. Sci.* **64**(1), 180–184 (2009)

134. P. Naeiji, A. Arjomandi, F. Varaminian, Amino acids as kinetic inhibitors for tetrahydrofuran hydrate formation: Experimental study and kinetic modeling. *J. Nat. Gas Sci. Eng.* **21**, 64–70 (2014)
135. H. Zeng et al., Differences in nucleator adsorption may explain distinct inhibition activities of two gas hydrate kinetic inhibitors. *Chem. Eng. Sci.* **63**(15), 4026–4029 (2008)
136. L. Del Villano, M.A. Kelland, Tetrahydrofuran hydrate crystal growth inhibition by hyperbranched poly (ester amide)s. *Chem. Eng. Sci.* **64**(13), 3197–3200 (2009)
137. R.W. Hawtin, P.M. Rodger, Polydispersity in oligomeric low dosage gas hydrate inhibitors. *J. Mater. Chem.* **16**(20), 1934–1934 (2006)
138. T.Y. Makogon, E.D. Sloan, *Mechanism of kinetic hydrate inhibitors*
139. H. Zeng, V.K. Walker, J.A. Ripmeester, Approaches to the design of better low-dosage gas hydrate inhibitors. *Angew. Chem. – Int. Ed.* **46**(28), 5402–5404 (2007)
140. Z.R. Chong et al., Review of natural gas hydrates as an energy resource: Prospects and challenges. *Appl. Energy* **162**, 1633–1652 (2016)
141. H. Sharifi, J. Ripmeester, P. Englezos, Recalcitrance of gas hydrate crystals formed in the presence of kinetic hydrate inhibitors. *J. Nat. Gas Sci. Eng.* **35**, 1573 (2016)
142. M. Tariq et al., Experimental and DFT approach on the determination of natural gas hydrate equilibrium with the use of excess N₂ and choline chloride ionic liquid as an inhibitor. *Energy Fuel* **30**(4), 2821–2832 (2016)
143. M.F. Qureshi et al., Gas hydrate prevention and flow assurance by using mixtures of ionic liquids and Synergist compounds: Combined kinetics and thermodynamic approach. *Energy Fuel* **30**(4), 3541–3548 (2016)
144. E.F. May et al., Quantitative kinetic inhibitor comparisons and memory effect measurements from hydrate formation probability distributions. *Chem. Eng. Sci.* **107**, 1–12 (2014)
145. N. Daraboina et al., Natural gas hydrate formation and decomposition in the presence of kinetic inhibitors. 2. Stirred reactor experiments. *Energy Fuel* **25**(10), 4384–4391 (2011)
146. T. Svartaas, M. Kelland, L. Dybvik, Experiments related to the performance of gas hydrate kinetic inhibitors. *Ann. N. Y. Acad. Sci.* **912**(1), 744–752 (2000)
147. P.C. Chua, M.A. Kelland, Tetra (iso-hexyl) ammonium bromide – the most powerful quaternary ammonium-based tetrahydrofuran crystal growth inhibitor and synergist with polyvinylcaprolactam kinetic gas hydrate inhibitor. *Energy Fuel* **26**(2), 1160–1168 (2012)
148. P.C. Chua et al., Kinetic hydrate inhibition of poly (N-isopropylmethacrylamide) s with different tacticities. *Energy Fuel* **26**(6), 3577–3585 (2012)
149. K. McNamee, Evaluation of hydrate nucleation trends and kinetic hydrate inhibitor performance by high-pressure differential scanning calorimetry, in *Proceedings of the 7th International Conference on Gas Hydrates (ICGH 2011)* (Edinburgh, 2011)
150. N. Daraboina, C. Malmos, N. von Solms, Investigation of kinetic hydrate inhibition using a high pressure micro differential scanning calorimeter. *Energy Fuel* **27**(10), 5779–5786 (2013)
151. N. Daraboina, C. Malmos, N. Von Solms, Synergistic kinetic inhibition of natural gas hydrate formation. *Fuel* **108**, 749–757 (2013)
152. J. Peytavy, J. Monfort, C. Gaillard, Investigation of methane hydrate formation in a recirculating flow loop: Modeling of the kinetics and tests of efficiency of chemical additives on hydrate inhibition. *Oil Gas Sci. Technol.* **54**(3), 365–374 (1999)
153. M.R. Talaghat, Effect of various types of equations of state for prediction of simple gas hydrate formation with or without the presence of kinetic inhibitors in a flow mini-loop apparatus. *Fluid Phase Equilib.* **286**(1), 33–42 (2009)
154. P. Notz, et al., The application of kinetic inhibitors to gas hydrate problems, in *Offshore Technology Conference*, 1–4 May, Houston, Texas 1995
155. K.-L. Yan et al., Flow characteristics and rheological properties of natural gas hydrate slurry in the presence of anti-agglomerant in a flow loop apparatus. *Chem. Eng. Sci.* **106**, 99–108 (2014)
156. J.-L. Peytavy, P. Glénat, P. Bourg, *Qualification of low dose hydrate inhibitors (LDHIs): Field cases studies demonstrate the good reproducibility of the results obtained from flow loops.*

- Proceedings of the 6th International Conference on Gas hydrates, Vancouver, Canada. Vol. 5499. 2008.
157. S. Jerbi et al., Characterization of CO₂ hydrate formation and dissociation kinetics in a flow loop. *Int. J. Refrig.* **33**(8), 1625–1631 (2010)
 158. L. Frostman, Anti-agglomerant hydrate inhibitors for prevention of hydrate plugs in deepwater systems, in *SPE Annual Technical Conference and Exhibition*, 1–4 October, (Society of Petroleum Engineers, Dallas, Texas 2000)
 159. M.R. Talaghat, F. Esmailzadeh, J. Fathikaljahi, Experimental and theoretical investigation of double gas hydrate formation in the presence or absence of kinetic inhibitors in a flow mini-loop apparatus. *Chem. Eng. Technol.* **32**(5), 805–819 (2009)
 160. H. Ohno et al., Raman studies of methane–ethane hydrate metastability. *Chem. Eur. J.* **113**(9), 1711–1716 (2009)
 161. J.-W. Lee, J. Lee, S.-P. Kang, ¹³C NMR spectroscopies and formation kinetics of gas hydrates in the presence of monoethylene glycol as an inhibitor. *Chem. Eng. Sci.* **104**, 755–759 (2013)
 162. N. Daraboina et al., Assessing the performance of commercial and biological gas hydrate inhibitors using nuclear magnetic resonance microscopy and a stirred autoclave. *Fuel* **105**, 630–635 (2013)
 163. J. Yang, B. Tohidi, Characterization of inhibition mechanisms of kinetic hydrate inhibitors using ultrasonic test technique. *Chem. Eng. Sci.* **66**(3), 278–283 (2011)
 164. M. Karamoddin, F. Varaminian, Performance of hydrate inhibitors in tetrahydrofuran hydrate formation by using measurement of electrical conductivity. *J. Ind. Eng. Chem.* **20**(5), 3815–3820 (2014)
 165. J. Tse et al., The low frequency vibrations in clathrate hydrates. *J. Chem. Phys.* **107**(21), 9271–9274 (1997)
 166. R.E. Westacott, P.M. Rodger, A local harmonic study of clusters of water and methane. *J. Chem. Soc. Faraday Trans.* **94**(23), 3421–3426 (1998)
 167. H. Tanaka, Y. Tamai, K. Koga, Large thermal expansivity of clathrate hydrates. *J. Phys. Chem. B* **101**(33), 6560–6565 (1997)
 168. B. Kvamme, Molecular dynamics simulations as a tool for the selection of candidates for kinetic hydrate inhibitors, in *The Eleventh International Offshore and Polar Engineering Conference*, 17–22 June, Stavanger, Norway 2001
 169. L.A. Baez, P. Clancy, Computer simulation of the crystal growth and dissolution of natural gas hydrates. *Ann. N. Y. Acad. Sci.* **715**(1), 177–186 (1994)
 170. B. Kvamme, T. Kuznetsova, K. Aasoldsen, Molecular simulations as a tool for selection of kinetic hydrate inhibitors. *Mol. Simul.* **31**(14–15), 1083–1094 (2005)
 171. B. Kvamme, T. Kuznetsova, K. Aasoldsen, Molecular dynamics simulations for selection of kinetic hydrate inhibitors. *J. Mol. Graph. Model.* **23**(6), 524–536 (2005)
 172. M.R. Talaghat, Evaluation of various types equations of state on prediction of rate of hydrate formation for binary gas mixtures in the presence or absence of kinetic hydrate inhibitors in a flow mini-loop apparatus. *Fluid Phase Equilib.* **347**, 45–53 (2013)
 173. B.B. KVAMME, G. Huseby, O.K. Forrisdahl, Molecular dynamics simulations of PVP kinetic inhibitor in liquid water and hydrate/liquid water systems. *Mol. Phys.* **90**(6), 979–992 (1997)
 174. E. Sloan, F. Fleyfel, A molecular mechanism for gas hydrate nucleation from ice. *AICHE J.* **37**(9), 1281–1292 (1991)
 175. H. Jiang, K.D. Jordan, C. Taylor, Molecular dynamics simulations of methane hydrate using polarizable force fields. *J. Phys. Chem. B* **111**(23), 6486–6492 (2007)
 176. L.C. Jacobson, W. Hujo, V. Molinero, Amorphous precursors in the nucleation of clathrate hydrates. *J. Am. Chem. Soc.* **132**(33), 11806–11811 (2010)
 177. M. Ota, Y. Qi, Numerical simulation of nucleation process of clathrate hydrates. *JSME Int. J. Ser. B, Fluids Therm. Eng.* **43**(4), 719–726 (2000)
 178. J. Vatamanu, P.G. Kusalik, Molecular insights into the heterogeneous crystal growth of methane hydrate. *J. Phys. Chem. B* **110**(32), 15896–15904 (2006)

179. C. Moon, P.C. Taylor, P.M. Rodger, Molecular dynamics study of gas hydrate formation. *J. Am. Chem. Soc.* **125**(16), 4706–4707 (2003)
180. B.J. Anderson et al., Properties of inhibitors of methane hydrate formation via molecular dynamics simulations. *J. Am. Chem. Soc.* **127**(50), 17852–17862 (2005)
181. C. Moon, R. Hawtin, P.M. Rodger, Nucleation and control of clathrate hydrates: Insights from simulation. *Faraday Discuss.* **136**, 367–382 (2007)
182. M.T. Storr et al., Kinetic inhibitor of hydrate crystallization. *J. Am. Chem. Soc.* **126**(5), 1569–1576 (2004)
183. Z. Zheng, *Molecular dynamics simulations on the inhibition of methane hydrates*. (2010). Graduate Theses and Dissertations. Iowa State University 11911. <https://lib.dr.iastate.edu/etd/11911>
184. S.-P. Kang et al., Experimental measurement of the induction time of natural gas hydrate and its prediction with polymeric kinetic inhibitor. *Chem. Eng. Sci.* **116**, 817–823 (2014)
185. R. O'Reilly et al., Crystal growth inhibition of tetrahydrofuran hydrate with poly (N-vinyl piperidone) and other poly (N-vinyl lactam) homopolymers. *Chem. Eng. Sci.* **66**(24), 6555–6560 (2011)
186. M.A. Kelland et al., A new class of kinetic hydrate inhibitor. *Ann. N. Y. Acad. Sci.* **912**(1), 281–293 (2000)
187. K.S. Colle, R.H. Oelfke, M.A. Kelland, *Method for inhibiting hydrate formation*, Google Patents. 1999
188. U. Klomp, *Method for inhibiting the pluggings of conduits by gas hydrates*, Google Patents. 2003
189. P. Froehling, Development of DSM's Hybrane[®] hyperbranched polyesteramides. *J. Polym. Sci. A Polym. Chem.* **42**(13), 3110–3115 (2004)
190. M.F. Mady et al., The first kinetic hydrate inhibition investigation on fluorinated polymers: Poly (fluoroalkylacrylamide)s. *Chem. Eng. Sci.* **119**, 230–235 (2014)
191. M.R. Talaghat, Enhancement of the performance of modified starch as a kinetic hydrate inhibitor in the presence of polyoxides for simple gas hydrate formation in a flow mini-loop apparatus. *J. Nat. Gas Sci. Eng.* **18**, 7–12 (2014)



Drug Delivery: Localized and Systemic Therapeutic Strategies with Polymer Systems

27

Scott Campbell and Niels Smeets

Contents

1	Introduction	1081
2	Strategies for Drug Delivery: Organs and Systemic Diseases	1082
2.1	The Gastrointestinal Tract: Oral Delivery	1082
2.2	Skin: Topical Treatments and Wound Healing	1086
2.3	The Lungs: Pulmonary Delivery	1092
2.4	The Brain: Traversing the Blood-Brain Barrier	1096
2.5	The Eye: Ocular Delivery	1098
2.6	Other Common Regions	1105
3	Systemic Controlled Release Case Study: Cancer Therapy	1107
3.1	What Is Cancer?	1108
3.2	Passive Targeting	1109
3.3	Active Targeting	1112
3.4	Alternative Cancer Therapies	1118
4	Current Understanding/Trends and Future Prospective	1121
	References	1125

Abstract

This chapter expands upon some of the basic concepts regarding drug delivery and takes a tour through various regions of the body that are commonly treated locally with controlled release systems, investigating current research and commercial strategies involving the use of polymeric systems within each region after briefly describing the biology and the typical biological targets of each region. This section includes drug delivery throughout the gastrointestinal tract and to the

S. Campbell (✉)

Department of Chemical Engineering, McMaster University, Hamilton, ON, Canada
e-mail: scott.campbell.88@gmail.com

N. Smeets

EcoSynthetix, Burlington, ON, Canada
e-mail: nbmsmeets@gmail.com

© Springer Nature Switzerland AG 2019

M. A. Jafar Mazumder et al. (eds.), *Functional Polymers, Polymers and Polymeric Composites: A Reference Series*, https://doi.org/10.1007/978-3-319-95987-0_32

1079

skin, lungs, brain, and eye, along with several others. The use of polymeric materials for systemic controlled release is then briefly described and thoroughly investigated in a case study on the most common target of systemically delivered nanomedicines: cancer. The chapter concludes with a perspective on where the field of drug delivery is headed in the future.

Abbreviations

AMD	Age-related macular degeneration
AMF	Alternating magnetic field
AMT	Adsorptive-mediated transcytosis
APC	Antigen-presenting cells
BA	Bioavailability
BBB	Blood-brain barrier
BCNU	1,3-bis(2-Chloroethyl)-1-nitrosourea
BRB	Blood-retinal barrier
CNS	Central nervous system
COPD	Chronic obstructive pulmonary disease
CPT	Camptothecin
DNA	Deoxyribonucleic acid
Dox	Doxorubicin
DSPE	Distearoylphosphatidylethanolamine
EGF	Epidermal growth factor
EPR	Enhanced permeability and retention
EVA	Ethylene vinyl acetate
F(ab') ₂	Dimers of Fabs
Fab	Antigen-binding fragments
FDA	U.S. Food and Drug Administration
FGF	Fibroblast growth factor
GI	Gastrointestinal
GM-CSF	Granulocyte-macrophage colony-stimulating factor
HA	Hyaluronic acid
HGH	Human growth hormone
HIV	Human immunodeficiency virus
HPV	Human papillomavirus
IGF-1	Insulin-like growth factor
IgG	Immunoglobulin G
IR	Infrared
LbL	Layer-by-layer
LCST	Lower critical solution temperature
LRP	Low-density lipoprotein receptor-related protein
MPEG	Methyl ether poly(ethylene glycol)
MPS	Mononuclear phagocyte system
MRI	Magnetic resonance imaging
NCS	Nanotoxicological classification system
NIPAM	<i>N</i> -Isopropyl acrylamide

PAMAM	Polyamidoamine
PBA	Phenyl boronic acid
PBAE	Poly(β -amino ester)
PCL	Polycaprolactone
PDGF	Platelet-derived growth factor
PDMS	Polydimethylsiloxane
PEG	Poly(ethylene glycol)
PEI	Poly(ethylene imine)
PEM	Polyelectrolyte multilayers
PEO	Poly(ethylene oxide)
HEMA	Poly(2-hydroxyethyl methacrylate)
PLGA	Poly(lactic acid-co-glycolic acid)
PMMA	poly(methyl methacrylate)
PNIPAM	Poly(<i>N</i> -isopropyl acrylamide)
POEGMA	Poly(oligoethylene glycol methacrylate)
PPO	Poly(propylene oxide)
Ptx	Paclitaxel
PVA	Polyvinyl alcohol
RGD	Arginine-glycine-aspartic acid
RNA	Ribonucleic acid
SC	Subcutaneous
scFv	Single-chain fragment variables
siRNA	Small-interfering RNA
SPIONs	Superparamagnetic iron oxide nanoparticles
T_g	Glass transition temperature
TGF- β 1	Transforming growth factor
UV	Ultraviolet
VPPT	Volume phase transition temperature

1 Introduction

Some of the basic concepts regarding drug delivery are discussed in ► [Chap. 17, “Drug Delivery: Polymers in the Development of Controlled Release Systems.”](#) These include traditional delivery methods, the importance of drug location and concentration for release, the necessity to complement the properties of the drug with that of the delivery system, and various techniques to produce polymeric drug delivery devices, including polymeric implants, hydrogels, and nanomedicines.

This chapter develops on those ideas and concepts to discuss various strategies for both localized and systemic controlled drug delivery. For localized treatments, a tour is taken through various regions of the body, including the gastrointestinal (GI) tract, the skin, the lungs, the brain, the eye, etc., where there is a brief description of the important biological aspects of the region, followed by an examination of current and upcoming controlled release strategies using polymeric

systems. Only a handful of controlled delivery devices have been commercialized to date; so much of this discussion involves the current state of research for each given section. The systemic portion is a case study on various strategies that are being studied for the treatment of cancer, mostly via the use of polymeric nanomedicines. The chapter then concludes with a brief discussion on the current trends and a future perspective on the drug delivery field. This includes some of the primary challenges that must be overcome to commercialize new controlled release systems that could benefit people around the world by enhancing the effectiveness, duration, patient compliance, and the safety of a given treatment, while decreasing the frequency at which a given treatment is administered [1, 2].

2 Strategies for Drug Delivery: Organs and Systemic Diseases

Any therapeutic that is intended to be delivered systemically, via oral administration or parenteral injection, is subjected to modification by the liver and/or clearance by the kidney. Orally administered drugs additionally have to traverse the varying harsh pH environment of gastrointestinal (GI) tract and the first-pass metabolism of the liver. Despite this, the vast majority of drugs are still delivered by these methods. As the relatively young field of targeted and controlled drug delivery advances, these traditional methods of administration will be replaced by smarter technologies with more consistent pharmacokinetics, less side effects, with high levels of patient compliance.

This section takes a tour throughout various organs in the body and discuss strategies to deliver drugs to treat diseases associated with these organs. The importance of targeting polymeric materials to the desired site of action and the significant differences in treatment strategies that are present depending on the location are emphasized in this section. For each location, there will be a description of the biology of the region of the body, highlighting the principle obstacles that must be overcome to deliver drugs to the location, examples of specific current or emerging research strategies using polymer-based therapeutics being developed to improve how medicine can be delivered to these regions, and commercialized treatments and/or the barriers to broad commercialization to treat diseases in the specific organ/region of interest.

2.1 The Gastrointestinal Tract: Oral Delivery

Oral delivery of small molecules is the most common and widely accepted delivery method. Oral administration systems are generally easy to ingest, pain-free, versatile in terms of the variety of drugs that can be administered this way, and have high patient compliance [3]. However, as mentioned previously, there are a wide range of obstacles that limit the bioavailability (BA) of orally administered drugs. Both the acidic gastric environment of the stomach and the constant secretion and recycling of

the protective mucus lining of the GI tract must be overcome before even reaching the epithelial lining of the intestine, which is the most vital barrier that must be overcome to achieve efficient oral drug delivery [4, 5]. Furthermore, the fraction of the initial drug dose that successfully traverses past this epithelial layer and into the bloodstream must first come in contact with the portal system, where they are subjected to the hepatic first-pass effect. As a result, even though the majority of tablet-based drugs that we take are via oral administration, their bioavailability is very low with low proportions of drug actually reaching systemic circulation. These obstacles, along with the plentiful number of proteases, nucleases, and lipases throughout this journey also means that protein therapeutics are particularly difficult to administer orally, as GI proteases digest 94–98% of orally taken proteins [5].

Early sustained release approaches focused on taking advantage of the differing pHs throughout the alimentary canal, developing drug-loaded systems that were stable at low pH (1–5) to bypass the stomach, but dissolve at neutral to higher pHs (>7.4) to preferentially release the drug in the small intestines [6]. Acrylic-based polymers that exhibit pH-dependent swelling have been a major focus in the development of particles that can prevent the release of therapeutics until they reach specific locations in the GI tract. For example, poly(methacrylic acid) can be blended with polymers like polyethylacrylate and polymethacrylate to fabricate particles that are in a collapsed state at low pHs and swell or dissolve at specific higher pHs that are associated with certain portions of the intestines [4]. These materials can be used to coat drug pellets or be used as individual microparticles or nanoparticles that have spatially controlled delivery based on their pH responsiveness. A promising orally-delivered system involving pH-responsive chitosan-co-poly- γ -glutamic acid nanoparticles that were loaded with fast-acting insulin was shown to result in comparable blood glucose responses in reaction to a glucose challenge to standard subcutaneous (SC) doses in diabetic rat models [7]. This is particularly surprising, as even if the insulin is delivered locally in the intestines, it still has several barriers to overcome, including the hepatic first-pass system. This nanoparticle system thus represents an impressive potential non-invasive alternative to current insulin, and possibly many other therapeutic, delivery strategies. Despite research like this, no pH-responsive particle systems have completed human trials. Pellets coated with pH-responsive materials may also prove ineffective as a treatment for all populations, as variations in pH between individuals and within an individual's GI tract could severely limit solely pH responsive therapies [4].

Particles that shield drugs and are also able to infiltrate the mucous layers could improve the retention time of the drug-carrying vehicles in the intestines, hopefully leading to longer-term release from orally-administered materials. In order to design particles for this, more information on the mucous layer must be known. Mucous, a complex, shear-thinning hydrogel, has evolved to efficiently trap and rapidly clear pathogens and foreign particulates. This mucous is constantly secreted and turned over to remove undesired compounds and lubricate the GI tract. There are two different layers of mucous throughout the alimentary canal: a firmly adherent mucous layer that neighbors the intestinal epithelium and a thicker loosely adherent mucous layer. The firmly adherent layer contains cell bound mucins that allow them

to adhere to the epithelial layer, while the loosely adherent mucous is less bound to the surface and experiences a much more rapid turnover than the adherent layer.

Knowing these properties about mucous, several strategies have been employed in the engineering of polymeric systems that attempt to improve the retention time of drugs within these mucous layers or to traverse through the mucous to reach the underlying epithelial cells. Polymers such as poly(acrylic acid), PLA, PLGA, and poly(sebacic acid) can adhere to mucous via hydrogen bonding, hydrophobic interactions, polymer entanglements with mucins, or a combination thereof [4]. Particles can also be designed to have a positively charged surface to obtain mucoadhesive properties, as electrostatic interactions between these particles and the negatively charged sugar moieties present on mucins can be quite strong [4]. As a result, PLGA particles have been coated with chitosan and assessed for their mucoadhesive enhancement as a result of this coating. Small molecule therapeutics, proteins, and peptides can be encapsulated and shielded from the harsh gastroenvironment by mucoadhesive polymeric microsphere and nanoparticles. However, passively-targeted mucoadhesive systems tend to be rather limited in terms of oral administration, as nonspecific mucoadhesion to undesired surfaces can readily occur. It is thought that this nonspecific adsorption would result in a wide range of these mucoadhesive systems adhering to portions of the loosely connected mucous layer and rapidly cleared along with it, effectively eliminating the drug carriers just as efficiently as foreign pathogens would be.

Alternatively, particles can be designed to be hydrophobic and negatively charged. These particles are designed to reach specific lymphoid tissues in the intestine, called Peyer's patches, that are covered with M cells. M cells provide antigen sampling for immune surveillance and, as a result, these cells have a particularly high transcytotic capacity [4]. These areas have much thinner and less dense overlying mucin layers, as they also do not secrete mucous [5]. Polystyrene particles as large as 1 μm in size (larger is generally better) [5] have been shown to be transcytosed by these M cells [4]. Targeting ligands, including bacterial adhesins, lectins, and IgA antibodies, can also be attached to the polymer surface to enhance their chances of transcytosis past these M cells [5]. However, the efficiency of these processes are questionable, as Peyer's patches make up less than 1% of the surface area of the intestines [4], and studies using glucan nanoparticles have indicated that a majority of the nanoparticles are taken up by dendritic cells before reaching the bloodstream [5]. The fact that these particles are endocytosed by dendritic cells in such large proportions could initiate an immune response, which could be advantageous for the orally administered vaccines but would generally be undesired.

Nanoparticles can be designed to penetrate the outer mucous layer to reach the firmly adherent mucous layer to have longer residence times and deliver the drugs closer to the epithelium. For alternative systems where the nanoparticles are designed to be delivered into circulation themselves to later release their contents, the penetration of the mucous barrier is necessary first step to reach the underlying absorptive epithelial cells in the GI tract. Viruses have evolved to penetrate mucous by being small enough to not be sterically hindered by the mucin mesh of mucous and possessing a highly hydrophilic surface that lacks any mucoadhesive hydrophobic

areas [4]. There are several strategies that have been employed in attempt to develop mucous-penetrating polymeric systems, to varying degree of successes. While there has not been *in vitro* or *in vivo* proof of successful mucous penetration in the GI tract [4], coating the surface of the drug carrier with a high density of low molecular weight poly(ethylene glycol) (PEG) appears to be a promising technique. This coats the entire surface with highly hydrophilic PEG groups, and the high density ensures that hydrophobic areas are avoided. While this technique hasn't been observed in the GI tract *in vivo*, it has been in vaginal mucous, which could afford similar results for intestinal applications [8]. If particles like this could shield therapeutics from the harsh environments prior to the intestines, as well as the degradative enzymes within the intestines, and subsequently penetrate the mucous lining to the more adherent mucous layer, they could be retained longer and slowly release and deliver the therapeutic for prolonged lengths of time. However, one area of concern is that penetrating nanoparticles may, in some cases, compromise the integrity the mucous barrier that is essential for our health, and the effect of these systems on the mucous that they penetrate through must be studied further [4, 5].

To reach the blood stream drugs have to pass through the epithelial layer of the intestines. The epithelium is composed of villi that dramatically increase the total absorptive surface area of the GI tract to be 300–400 m² [4]. The absorptive nature of these tissues allows for many small molecule drugs to be taken into the blood stream by passing in between the epithelial cells via the paracellular pathway. However larger therapeutics, including cancer drug and biologics like antibodies, enzymes, growth factors, hormones, nucleic acids, and vaccines, must rely on the transcytosis pathway, where receptors actively bind and guide these materials through the cell in endosomes while avoiding the degradation pathway [5, 9]. There are several ways that small nanoparticle systems (<500 nm) loaded with larger therapeutics could be transported across the epithelium via the transcytosis pathway, rather than just the drugs themselves, to enhance the amount of drug that enters the bloodstream by shielding and protecting them all the way there [9]. This is achieved by actively targeting specific receptors that are commonly present on intestinal epithelial cells that allow for efficient transport via the transcytosis pathways. Notably, polymeric nanoparticles can be tagged with vitamin B12 and the neonatal Fc receptor (FcRn) to enhance the transport of nanoparticles across the epithelium of GI tract to reach circulation and areas like the kidneys, liver, lungs, and spleen to release their drug [5]. Both of these tags have been used to deliver orally-administered insulin more effectively, with one study using the FcRn receptor being capable of producing a 15-h hypoglycemic response with a much lower [10], clinically-relevant initial dose than what has been used for many studies involving orally delivered insulin (1.1 U/kg rather than 10–100 U/kg) [11].

Many of these polymeric systems, particularly those involving the delivery of large molecules and biologics, have yet to be developed in a form that is suitable for human clinical trials. There are still several hurdles to overcome in terms of improving orally administered therapeutics, such as further improving the bioavailability of these systems, better understanding the differences between *in vivo* animal models and human systems, accounting for patient-to-patient variations, and even

variations within the patient depending on their lifestyle [5]. Despite this, many of these methodologies are improving at a rapid rate to the point that they are nearing commercialization within the next few decades. There will always be an appeal for advances in oral delivery, particularly if it can be utilized effectively for a wider array of therapeutics, due to the convenience, compliance, and flexibility of this treatment method that has the potential to treat more people while lowering hospital visits and overall healthcare costs.

2.2 Skin: Topical Treatments and Wound Healing

The skin is the largest organ in the human body, and, as such, it is highly important in providing immunity, and maintaining homeostasis and sensory feedback [12]. As a large, easy-to-access organ, its convenience alone presents as an attractive alternative to oral delivery and hypodermic injection if an efficient method of delivery can be achieved through the skin. Delivering materials transdermally (across the skin boundary) could be a non-invasive, self-administered method to get drugs into the body while evading the first-pass effect. Drugs delivered via this method can also be delivered at a constant rate over long durations, and can be halted on demand by simply removing the system [13]. The first transdermal system that took advantage of these benefits was a 3-day patch to treat motion sickness. Since then there are approximately 20 transdermal systems, including nicotine patches, which have greatly improved the public acceptance of patches [14]. These patches often utilize hydrogels in the drug-containing reservoir to keep in moisture and maintain drug activity, and polymeric membranes to control release.

However, as the first line of defense in preventing foreign compounds from entering the body, the skin is designed to be impermeable to a wide variety of materials. Consequently, transdermal delivery has been limited to drugs with molecular masses up to only a couple hundred Daltons. In particular, it has proven difficult to use the transdermal route to deliver hydrophilic drugs, particularly vaccines, and macromolecules and peptides, including small-interfering RNA (siRNA) and DNA [15]. Thus, delivering polymeric nanoparticle carriers transdermally also cannot be done by traditional means, which do not attempt to increase the permeability of the skin.

For transdermal delivery, drugs must traverse first through the outermost layer, the stratum corneum (10–20 μm thick) [12]. The stratum corneum barrier is a brick-like structure, where the bricks are nonliving corneocyte cells bourne in the epidermis surrounded by a mixture of lipids that are mostly arranged in bilayers. This is the most difficult layer for even small drugs to pass through, as hydrophobic and hydrophilic molecules must travel through a tortuous path around the corneocyte cells though the lipid tails or head, respectively [16]. This is the rate limiting step for any drug to be delivered transdermally and the skin structure that primarily limits the number of drugs that can be delivered via the transdermal route. The drugs must then traverse the avascular viable epidermis (50–1,000 μm thick) to reach the dermis [12]. The dermis is 1–2-mm thick and possesses a rich capillary bed just below the dermal-epidermal junction where the drugs can be absorbed into systemic

circulation. Drugs applied topically can also use hair shaft to reach the dermis with less resistance, and many topical drug delivery utilize this route to one degree or another (whether it is designed for or not).

2.2.1 Polymeric Microneedles

Since it was established that penetrating through the stratum corneum is the trickiest step in transdermal drug delivery, a variety of different strategies have been developed to improve transdermal delivery that focus on the targeted permeabilization of this outermost layer of the skin [15]. The emergence of technologies that can locally disrupt the stratum corneum to facilitate transdermal release with improved safety and efficacy, including chemical enhancers, electroporation, cavitation ultrasound, thermal ablation, microdermabrasion, and microneedles, are now medically acceptable. While many of these techniques do not make use of polymers and are thus outside the scope of this chapter (they are discussed in much greater detail in an excellent review article [15]), microneedles are one of the most promising techniques for transporting larger therapeutics across the skin. Microneedle systems are often comprised of polymers to serve their purpose, mainly due to their low cost and ease of manufacture over metallic microneedles.

Microneedles present as a simple but elegant solution to getting drugs across the stratum corneum in a minimally invasive manner. By piercing through the stratum corneum (and often into the epidermis and/or the superficial dermis) microneedles can: generate micron-scale pathways into the skin to increase its permeability; actively transport drugs into the skin via a variety of mechanisms; target the effects only to the stratum corneum; and do all of this in a manner that is considered painless and well-tolerated that can also be achieved without any specific training [15]. This is highly advantageous, as needle phobia and inconvenience (due to the fact that vaccine injections must be performed by a professional) are significant barriers that limit vaccination coverage [17]. The costs associated with administration and patient time are also significant factors that microneedles could significantly influence by being an inexpensive, self-administered technique.

There are several ways in which microneedles can be used to enhance the transdermal delivery of therapeutics. Solid microneedles can be used to first pierce the skin to improve the permeability of a variety of therapeutics from extended-release patches. Drugs can also be coated on the exterior of microneedles or encapsulated within microneedles to deliver drugs across the stratum corneum. Hollow microneedles can also be used to infuse drug into the skin through the needle, however, these are generally made from inorganic components [14]. These strategies can be used to deliver a wide range of small molecules, proteins, DNA, vaccines, and virus particles transdermally in clinically relevant quantities [15].

Over the last couple decades, advances in microneedle design have transitioned from expensive, clean room-based development of silicon-based needles to low-cost methods of fabricating metal and polymeric microneedles. Polymeric needles that are water soluble and degrade over time (generally in a matter of minutes) have been used to encapsulate drugs within the polymeric matrix that are released as the needles degrade, leaving no sharp medical waste after use [15]. The different types of microneedles are depicted in Fig. 1.

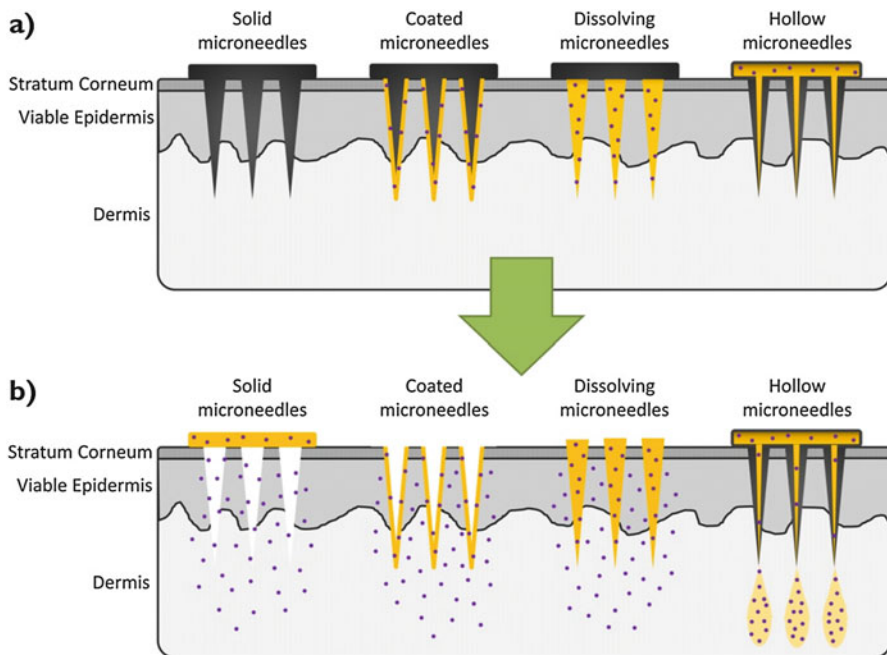


Fig. 1 Drug delivery using microneedles. The various microneedles are: (a) applied to the skin and then (b) are allowed to release drug over a predetermined amount of time via various mechanisms. Solid microneedles are applied and removed, and then hydrogel-based drug releasing systems are often applied to efficiently release the drug to the dermis through the void space afforded by the microneedle. The bioresorbable polymer coating of coated microneedles rapidly disbands from the microneedle and is left there to release drug upon removal of the system. Dissolving microneedles contain biodegradable polymer that remains in place to release their encapsulated therapeutics over time. Hollow microneedles are left in place to continuously inject drug directly into the dermis over extended periods of time. (Original drawing adapted with permission from Ref. [14])

Polymeric microneedles can be made in several ways but the most common, cheap, and commercially viable method involves first creating molds to form the microneedles in. These molds are typically made via photolithography with optically curable polymers, such as the ultraviolet (UV)-curable SU-8. After this, inverse molds are generally made with silicone polymers, such as polydimethylsiloxane (PDMS), by pouring them on the master mold and curing them. Aluminum, polyvinyl alcohol (PVA), and silicon have also been used to make molds, but PDMS is the most prevalent and cheapest. These molds are then filled with softened or molten thermoplastics, such as polycarbonate or poly(methyl methacrylate) (PMMA) at elevated temperatures that resulting in non-degradable microneedles upon cooling [14]. Biodegradable and water soluble polymers, such as PVP, PVA, and PLGA, with encapsulated drugs can also be fabricated with molds in an analogous manner.

Polymeric microneedles can be coated with drugs to facilitate their delivery by dipping or spraying the microneedles with a drug solution and letting the material dry on the surface of the microneedles. A wide range of materials, from very

small molecules to macromolecules, vaccines, DNA, and micron-scale particles can be coated onto the surface in this manner. The microneedles can also be fabricated/coated with ionically charged polymers, which can be used to coat drugs on the exterior of polymeric microneedles via layer-by-layer (LbL) techniques. These technique involves repeatedly dipping the microneedles in two oppositely-charged solutions, such as positively charged polymer and negatively charged protein, to build up polyelectrolyte multilayers (PEMs) coating the surface of the microneedles, that, when applied, will slowly dissolve and release the drug of interest. A variety of materials can be released this way, including negatively charged DNA or protein [18], and even larger poly(lactic-co-glycolic acid) (PLGA) nanoparticles and cationic polypeptides [19]. These drugs will then dissolve in the environment of the dermis to allow for a more facile pathway to systemic circulation. In an interesting example of this, PLGA microneedles were coated with twenty PEM bilayers of positively and negatively charged polymers to create an even coating, followed by 24 bilayers of a hydrolytically degradable cationic polymer poly(β -amino ester) (PBAE) and plasmid DNA or 4 bilayers of PBAE and PLGA nanoparticles [19]. These microneedles were shown to deliver these materials to the viable epidermis successfully *in vivo*, demonstrating that PEMs on the coating of microneedles can be used to potentially deliver materials for gene therapy or co-deliver multiple therapeutics within PEM layers on microneedles. The plasmid DNA delivered from these materials was found to be successfully transfected into dendritic cells *in vivo*, showing that microneedles could potentially be used for gene therapy and DNA vaccine delivery [19].

Another area in which polymer microneedles provide additional benefits over their inorganic counterparts is their capacity to be used to generate degradable or dissolving microneedles. Numerous polymers that have been traditionally developed to dissolve or degrade over time to release therapeutics can be used as microneedles as well. These polymers are typically biocompatible, safe, and are water soluble in nature, and include carboxymethyl cellulose, dextran, PVP, PVA, PLGA, etc. [14]. These dissolving microneedles can be used simply to improve the permeability through the skin, but regularly encapsulate controlled amounts drug molecules to release them as they degrade.

The most common method of producing these microneedles, which was described above, involves by making a solution of drug and the polymer melt and allowing the solution to solidify in a prefabricated PDMS mold. It is imperative to ensure that heat-sensitive therapeutic (i.e., antigens and proteins) should be incorporated in conditions such that they will not forfeit their activity in the development process. One of the primary benefits of this technique is that controlled release can be achieved for extended time frames (up to months), which means that the biodegradable polymeric microneedles need to remain in the skin for long amounts of time as well. This can be inconvenient for the patient. One neat solution to solve this issue involved encapsulating nanogels into the microneedle base that swell when the microneedles are applied and the microneedles rapidly lose their mechanical strength and break away to remain in embedded in the skin to degrade on their own [20].

There have been numerous promising studies that have involved the delivery of multiple small molecules, lidocaine, peptides, protein, DNA, RNA, insulin and

vaccines [17]. Polymeric microneedles are particularly amenable to vaccine delivery. Their low cost, thermostability, ability to dispense consistent doses, and the potential for them to be self-administered effectively, which has been demonstrated with metallic microneedles, could allow for a wide range of vaccines, including live, attenuated, and subunit vaccines, to be administered in a facile manner [17]. This could ultimately greatly improve vaccination coverage as a result. There is currently only one vaccine that can be self-administered, which is Vivotif Berna[®], an orally-delivered typhoid vaccine that has been used at a rate of three million vaccinations per year [17, 21]. Microneedles, and particularly polymeric microneedles, could present as a highly beneficial disruptive technology in this market.

Despite the promising release studies involving polymeric microneedles, the fact that this is still quite a new field combined with the lengthy U.S. Food and Drug Administration (FDA) approval process associated with the delivery of therapeutics means that the number of fully commercialized polymeric microneedles is currently rather limited. There are several metallic microneedles that have been commercialized over the years, mainly for cosmetic purposes, including the Dermaroller[®] that is used for home use to improve skin texture; Soluvia[®], which uses hollow microneedles to deliver influenza vaccine; and MicronJet[®], which consists of four hollow silicon microneedles that have a luer lock adapter to allow it to be attached to standard syringes [14]. The sole polymeric microneedle is the MicroHyla[®], which is a patch of dissolving microneedles that contain hyaluronic acid (HA) to treat wrinkles that is sold in Japan [14]. The relative cost of polymeric microneedles in comparison to metallic counterparts, combined with the numerous benefits of microneedles, should afford for its use in many more commercial products over the next decade.

2.2.2 Wound Healing

A wound to the skin compromises its primary function, increasing the risk of dehydration and infection, particularly for burns. Wound dressings intended to aid the process of healing have been used throughout human history, ranging from primitive applications of plant herbs, animal fat, and honey to tissue engineered scaffold from polymeric sources [22]. The goal with modern wound dressings has been to establish and maintain a moist environment around the wound to assist in wound healing while preventing infection.

Both natural and synthetic polymers play a distinct role in wound dressings, with the majority of wound dressings making use of natural polymers. The most widely used wound dressings are hydrocolloid dressings, which are generally colloidal polymeric materials (often made from natural polymer such as carboxymethyl cellulose and gelatin) that adhere to both moist and dry sites and form a gel upon contact with the wound [22]. These dressings become increasingly more permeable to water and air as the gel forms, but these systems often have an outer cover that prevent water vapor exchange between the wound and its surroundings, which is not ideal for wounds that require oxygen to rapidly heal.

Alginate is natural polysaccharide that is commonly used in wound dressings. Alginates rapidly form hydrogels upon contact with moderate to heavily exuding

wounds, with calcium ions in the exudate forming the crosslinks between the alginic acid polymer components [22]. These materials rapidly absorb the components that the wound secretes and form a protective film that sustains moisture content and healing temperature while minimizing bacterial contamination. Alginates also can be removed with less pain than conventional dressings.

There are several other common natural hydrogels that are useful for wound healing purposes, including collagen, hyaluronic acid, and chitosan. For example, collagen matrices are a natural component of connective tissues that are widely known to play a prominent role in the induction of clotting and minimizing the appearance of scars [22]. Collagen hydrogels also stimulate the formation of fibroblasts and enhance the migration of endothelial cells to the wound site. Hyaluronic acid (HA) is another extracellular matrix component that can be the main component of naturally biocompatible, safe, and effective dressings that deter immune responses. Naturally-derived chitosan hydrogels also are effective wound healing materials, promoting the infiltration of inflammatory cells and tissue granulation and organization in the early stages of the wound healing process [23].

Synthetic hydrogels can be applied either as an amorphous gel, which need a secondary cover to remain in place, or as elastic sheets. Hydrogels are ideal wound healing materials in terms of their capacity to promote moist healing, be non-adherent to allow for facile removal, be non-irritating, be permeable to metabolites, improve reepithelization, to cool the surface of the wound, and to rehydrate and remove dead tissues to improve healing [22]. Hydrogels are also highly malleable, able to heal while reducing the compressive forces on the wound to make the healing process more comfortable. However, they contain large amounts of water, which limits the amount of wound exudate that they can absorb, leading to their use in primarily light to moderately exuding wounds.

Many of these natural components, and several synthetically-designed hydrogels, are also biodegradable, and will be removed as they promote wound healing and new tissue formation. More complex, "smart" hydrogels that take advantage of the advances in the fabrication of biomaterials are an essential part of the development of a new generation of synthetic hydrogel-based skin substitutes that better mimic the tissue and normal physiologic responses of the tissue during wound healing and then ultimately degrade over time. Tissue engineered skin substitutes are often comprised of these more complex hydrogel materials (either natural or synthetic) and can be seeded with naturally-derived cells prior to application.

Importantly, these engineered matrices also contain and release molecules that can inhibit infections and promote and increase the efficacy of wound healing. While there have only been a few clinical studies performed to date, many modern dressings could easily be used to deliver drugs to improve wound healing, especially considering that a large amount of these are polymeric hydrogel or hydrogel-like materials [22]. Consequently, a wide range of the aforementioned wound dressings have also been studied for their capacity to release antimicrobials, growth factors, and genetic material as they protect and encourage the wound healing process. The drug is initially released from these materials as the fluids that exude from wounds further hydrate and swell the polymer matrix, enhancing the diffusional

release in the process. Solely Fickian release will occur in materials that do not degrade. However, most materials are designed to degrade so that any drug remaining in the dressings will be released. This degradation is thought to be the overriding mechanism in the latter part of most release profiles.

The delivery antibiotics or antibacterial component is intended to resist infections, particularly for wounds from surgery, accidents, and for diabetic foot ulcers. Localizing the antibiotics, such as dialkylcarbamoylechloride, minocycline, tetracycline, and silver, along with the wound dressings rather than systemically allows for lower antibiotic doses, lower antibiotic resistance, better tissue compatibility, and reduced interference with the healing process [22]. One of the earlier examples of antimicrobial-releasing materials was a silicone hydrogel that released ofloxacin used to prevent infections in human patients with superficial and deep dermal-depth burn wounds that prevented infection while reducing pain and enhancing the epithelialization process in comparison to more traditional ointment-laden gauze [24].

More recent polymeric wound healing systems tend to deliver growth factors, or, in similar situations described above where infection is a clear risk, releasing growth factors and antimicrobials simultaneously. Growth factors play an active physiological role in various necessary parts of the healing process, including enzyme production, protein expression, and cell division, migration, and differentiation [22]. Growth factors are involved in every stage of wound healing by stimulating angiogenesis and cellular proliferation, which is involved in producing the extracellular matrix, inflammation, and fibroblast activity. Common growth factors that have been researched to improve healing are epidermal growth factor (EGF), fibroblast growth factor (FGF), granulocyte-macrophage colony stimulating factor (GM-CSF), human growth hormone (HGH), insulin-like growth factor (IGF-1), platelet-derived growth factor (PDGF), and transforming growth factor (TGF- β 1) [22]. These all play a distinct role in the healing process. For example, GM-CSF is highly important for rapid wound healing and ensuring the formation of suitable scar tissues [22].

The combination of delivering growth factors alongside has proven to be highly beneficial in certain situations. EGF has been found to reverse the negative effects of the antibiotic silver sulphadiazine when delivered from a hydrogel dressing [25]. Another collagen-hydrogel matrix with the antibiotic tobramycin, FGF, and PDGF exhibited markedly enhanced wound healing compared to the hydrogel matrix with only the antibiotic [26]. DNA can also be delivered from similar polymeric dressing to regenerate tissues as well [27]. A wide variety of materials can be released from polymeric wound dressing biomaterials that are designed to mimic tissues and encourage release to restore skin structure and function after injury.

2.3 The Lungs: Pulmonary Delivery

The pulmonary delivery route has been a well-established route for the local treatment of respiratory diseases. Asthma stands out as a particularly identifiable and commonly used example, with inhaler treatments having been in use since the 1950s [28]. Other disorders that are commonly treated with pulmonary drug

administration are pulmonary hypertension, respiratory inflammation, cystic fibrosis, chronic obstructive pulmonary disease (COPD), and tuberculosis [29–31]. This is a common administration route because a high local concentration of drug can be achieved for the treatment of respiratory diseases and it is a viable option to non-invasively deliver biologics like peptide and proteins [31–33]. It has also been developed for use in delivering insulin to the blood stream non-invasively as this administration method avoids the first pass effect, unlike many alternative approaches. The downside to this method is that the rapid decay of inhaled drugs (without an accompanying delivery vehicle) means that multiple daily inhalations may be required for a given therapy, which is inconvenient for the patient and leads to low compliance [32]. The effectiveness of inhaled administration can be improved with the use of polymeric micro- and nanoparticles, once the underlying nature of the tissues associated with the lung are understood.

The lung consists of two primary sections: the conducting airways and the respiratory region. The upper airway, consisting of the mouth/nasal cavity, pharynx, larynx, trachea, bronchi, and bronchioles, is lined with mucous that is propelled upwards away from the lung, has low regional blood flow, and possesses a small surface area with thick tissues ($>10\ \mu\text{m}$) compared to the lower lung, resulting in many barriers to drug delivery in this region of the lung [32]. However the lower region of the deep lung consists of the respiratory bronchioles and the alveoli, which accounts for around 95% of the lung total surface area. These alveoli have a large surface area ($70\text{--}150\ \text{m}^2$) [29], limited quantities of proteolytic enzymes, and a thin tissue lining ($<0.3\text{--}1\ \mu\text{m}$) [32] leading to an extensive blood supply [6, 16]. This results in the deep lung being particularly suitable as a site for long term systemic delivery of molecules.

Inhaled drug systems disperse throughout the lungs via three mechanisms: Brownian diffusion, impaction, and gravitational sedimentation. While these are dependent upon numerous particle properties, such as charge, surface characteristics, hygroscopicity, temperature, breathing pattern, and the relationship between the timing of the aerosol pulse injection with that of the breathing cycle, the principle factor is generally seen as particle size [31]. Small particles diffuse, based on Brownian motion, throughout the lungs, while larger particles tend to deposit in the lower lungs via gravitational sedimentation and inertial impaction [29]. Currently, most commercial inhalers deliver drug powders into the lungs. These small lone drug particles ($<0.5\ \mu\text{m}$) are so small that much of it fails reach the lower respiratory region and $>90\%$ of the drug is immediately exhaled or rapidly eliminated by mucous clearance in the upper airway [29, 32]. Larger particles that are $>5\ \mu\text{m}$ tend to be delivered via impaction, as when they are administered they travel at such a high velocity that they collide with the respiratory wall and are deposited in the oropharynx regions [34]. Local delivery to tissues deep within the lung can be most efficiently achieved with particles that are of an optimal size ($\sim 0.5\text{--}5\ \mu\text{m}$) for gravitational sedimentation to occur [16, 35]. However, prolonged retention in the deep lung tissues may be difficult in some cases, as many particles that reach deep lung tissues are generally cleared when they are taken up by an army of alveolar macrophages, which is highly efficient for particles from 1 to 3 μm in diameter [30, 32].

There are several methods that have been used to engineer materials that could be delivered to the deep lung while avoiding the lung's natural clearance mechanisms. A very significant study found that the aforementioned particle diameter values that determine which mechanism a given particle will likely be dispersed were not simply the diameters of the particles, but aerodynamic diameters (d_{ac}) [30]. This means that larger, porous particles could be deposited in the deep lung and be too large to be rapidly cleared by the alveolar macrophages. This study involved 8.5 μm PLGA particles with a density of 0.1 g/cm^3 that were loaded with insulin, and these porous particles were ten times more likely to reach deep lung tissues than solid particles with similar a d_{ac} and were shown to deliver insulin for 96 h in diabetic rats, offering nearly as effective insulin bioavailabilities to subcutaneous (SC) injections (87.5%) [30]. These porous particles also showed lesser aggregation between particles (owed to their lower surface area) produced a reduced inflammatory response in comparison to solid microparticles with a similar d_{ac} . The porous PLGA particles were also shown to release significant quantities of testosterone for a prolonged 24-h period from quite large 20.4 μm porous particles, exhibiting that it is truly the d_{ac} that must be considered to deliver particles to the desired region of the lungs [30]. Similar PLGA particles are now being pursued in clinical trials by Pulmatrix for the treatment of chronic obstructive pulmonary disease and similar particles have been developed for a wide range of drugs, including heparin, deslorelin, anthocyanin, and more [33]. Porous PLGA particles have also been shown to deliver rifampicin, an anti-tuberculosis antibiotic, for 8 h in guinea pigs in vivo [36]. While porous nanoparticles have distinct advantages, they have more rapid release than from solid nanoparticles. A study showed that the release of isoniazid, an antibiotic for tuberculosis, was released over 3 days, 6 days, and 7 weeks for porous, non-porous, and hardened PLGA microparticles respectively [37]. Regardless of particle type, all were shown to be more effective at clearing bacteria with a single dose in vivo in a murine model than the daily administration of free drug [38].

Another method to evade macrophage uptake is to use dry polymeric microparticles that swell once they become hydrated. Chitosan-functionalized PEG microparticles were investigated for this purpose. The particles were initially $\sim 10 \mu\text{m}$ and somewhat porous ($\rho \approx 0.7 \text{ g}/\text{cm}^3$) and ballooned to 70 μm upon hydration [39]. These particles were capable of delivering a hydrophilic model drug, sodium fluorescein, and were very effective at avoiding macrophage uptake in vitro, so they could potentially be applicable for pulmonary drug release [39]. Nanoparticle-containing microparticles could also be utilized that take advantage of the ability of microparticles to reach alveolar tissues and the benefits of nanoparticles to avoid clearance to deliver therapeutics to the blood stream or to internalize into cells for the delivery of genes and other biologics. Nanoparticles $< 100 \text{ nm}$ in size are taken up to a larger extent by the alveolar epithelial cells than macrophages, so this "Trojan horse" strategy could be an effective method of delivering small nanoparticles to the deep lung for genetic therapies.

The pulmonary administration of nucleic acids has been investigated treat genetic and chronic lung disorders. To suit this purpose, PLGA has been modified with

polymeric gene delivery vectors like poly(ethylene imine) (PEI). PEI can encapsulate negatively-charged DNA and siRNA into nanoscale complexes and protect their degradation by nucleases and is often grafted with PEG to reduce its toxicity [32]. In order to penetrate cells, additional functionalities are required to efficiently deliver genes. For example, TAT, a cell-penetrating peptide, was coupled to PEG-PEI to form small 90 nm polyplexes that showed significantly enhanced gene delivery efficiency in mice *in vivo* than with PEI alone [40]. Other targeting moieties, including lactose, lactoferrin, galactose, etc., can also be used to target specific receptors of cells to promote internalization [32]. These could be coupled with promising polymeric delivery systems, such as PLGA-based particles, diethyleneaminopropylamine-co-PVA-co-PLGA particles that have shown efficient siRNA delivery [41], and chitosan nanoparticles that have shown effective *in vivo* siRNA delivery in mice [42] and rats [43].

PLGA nanoparticles have also been surface modified with chitosan to deliver the peptide elcatonin more effectively than unmodified nanoparticles [44]. Polyelectrolyte nanoparticles that self-assemble from siRNA and chitosan to form polyplexes that were used to deliver this siRNA to human lung carcinoma cells *in vitro*. These materials have shown successful *in vivo* RNA interference in mice, allowing potential for *in vivo* lung cancer treatment via pulmonary administration.

Living radical polymerization has been used to develop micelles of PEG and the hydrophobic distearoylphosphatidylethanolamine (DSPE) for the pulmonary delivery of paclitaxel (Ptx) to cancerous lung tissues [45]. The localized delivery of this system would be particularly beneficial for cancer treatments to negate the amount of systemic side effects associated with lung cancer treatments. The accumulation of Ptx in the lungs was 45 times higher than intravenously administered Ptx and 3 times higher than a conventional chemotherapeutic delivered intratracheally [45]. The Ptx concentration in other tissues was also much lower in the case of the micelles and the normal lung tissues did not appear to be injured [45]. These micelle-based systems appear to have great efficacy and could lead to more micelle-based strategies for treatment of lung disorders or to other polymeric systems delivering chemotherapeutic agents for lung cancer treatments.

Although vast amounts of research have been performed on polymeric systems for pulmonary administration, there are few examples of systems that have successfully made it to clinical trials. One of the main issues is that the fate of nano- and micro-materials and their long term effects on the functionality of lung tissues is still unknown and difficult to determine. While these particles are supposed to limit the number of required administrations and many of these are biodegradable over time, the effects of the accumulation of particles in the lung and particularly on the lining fluid of the lung are unknown [32]. A deeper knowledge of these effects and an understanding of how best to examine the safety of these materials after *in vivo* use must be established before many of these materials lead to commercially used products. However, the current porous PLGA systems under clinical trials may pave the way for the rest of the field of pulmonary administered micro- and nano-systems.

2.4 The Brain: Traversing the Blood-Brain Barrier

There are many treatments where the brain is the principal target region for therapeutics, including Alzheimer's disease; Parkinson's disease; Huntington's disease; amyotrophic lateral sclerosis (ALS); schizophrenia; learning impairment; HIV infection of the brain; protecting tissues after cerebral ischemia, a condition that occurs when there is an insufficient amount of blood flow to the brain; and brain cancers [46]. Due to the obvious inherent risks of trying to deliver therapeutics directly to the brain, the majority of work that focusses neural drug delivery involves transporting nanotherapeutic carriers from the blood to the brain, through the blood-brain barrier (BBB). The BBB is one of the strictest barriers in therapeutic delivery. It is a contiguous layer of the endothelial cells of the cerebral capillaries connected by tight junctions, <12 nm, that can be 100 times tighter than the junctions of other capillary endothelium [47, 48]. The barrier is analogous to cell membranes, where, in general, it allows for the facile transport of lipophilic molecules across the membrane while restricting the exchange of hydrophilic compounds, small proteins, and charged molecules between the plasma and the central nervous system (CNS). Even small therapeutic molecules have difficulty crossing this barrier.

The approaches for delivering therapeutics to the brain can be invasive or non-invasive. Invasive treatments not only include direct intracerebral/intraventricular injection or intracerebral implantation of the drug/delivery device, but also by techniques that can temporarily increase the permeability of the BBB, which include osmotic disruption and focused ultrasound [49]. These techniques, simply due to their invasive nature, pose the risk of complications, including intracranial infections and brain edema, and are expensive, complex procedures [46]. Noninvasive techniques to deliver drugs to the brain have thus been the focus of the majority of the research in this area, often by conjugating specific functionalities on the surface of nanoscale delivery vehicles.

A wide variety of ligands can be functionalized to the surface of nanosized polymeric carriers to improve their transport across the BBB. These take advantage of transporters native to the endothelial cells that deliver essential hydrophilic and large compounds across the BBB, such as choline, amino acids, and lipoproteins [47]. Transferrin was one the first ligands discovered for this purpose, as the transferrin receptor is overexpressed in the endothelial cells that comprise the BBB [50]. Numerous other ligands have been used to allow nanocarriers to pass through the BBB, including a wide range of peptides; apolipoproteins that are recognized by low-density lipoprotein receptors on the surface of the BBB's endothelial cells; and even insulin, which targets the insulin receptor and can transport carriers across the BBB ten times more efficiently [46]. Receptor-mediated endocytosis in this manner is used to transport many carriers that would otherwise be too large to cross the BBB into the brain.

To target specific neural diseases, nanocarriers can be designed with functionalities that can be used to allow the carrier to travel through the bloodstream and traverse the BBB and target the disease of interest. This is of particular interest for the treatment of brain tumors. Cancers of the brain are particularly difficult to treat,

with patients often having to undergo invasive neurosurgeries to excise the tumorous tissues. However, many cancers often have overexpressed receptors that may be utilized for targeting, similar to the BBB.

In fact, some of the overexpressed receptors on glioma cells correspond with the BBB receptors, including lactoferrin and transferrin proteins [46]. Lactoferrin-functionalized polycaprolactone (PCL)-*b*-PEG polymersomes encapsulating doxorubicin (Dox) and tetradrine, a multidrug resistance inhibitor, exhibited a greater accumulation in brain tumors within an *in vivo* glioma model in rats relative to non-lactoferrin-functionalized controls [51]. This particular study highlighted that the effectiveness of the targeted application of Dox is significantly enhanced by the combined delivery of a multidrug resistance inhibitor, decreasing the tumor growth rate and extending long-term survival compared to controls. Dox alone has been shown to exhibit promising results, including an increase in mice survival time and a reduction in tumor volume, when targeted *in vivo* to glioma cells in mice with similar PCL-*b*-PEG polymersomes using transferrin as the targeting moiety [52]. Another common receptor at the BBB and on human glioma cells is the low-density lipoprotein receptor-related protein (LRP). Similar polymersomes functionalized with Angiopep-2, a small, LRP-binding peptide, were shown to penetrate into the brain by receptor-mediated endocytosis and preferentially accumulate in the gliomal bed and in infiltrating gliomal cells to deliver paclitaxel (Ptx), another common cancer drug.

Alternatively, multiple ligands could be used to treat brain cancers and other ailments. PCL-*b*-PEG nanoparticles with covalently conjugated Pep-TGN peptides and the AS1411 DNA aptamer on their surface was used to selectively target gliomas cells in the brain. The dense Pep-TGN coating could afford the passage of the nanoparticles into the brain and, once there, the aptamers decorated on the surface of the nanoparticles could then bind with the highly expressed nucleolin protein on gliomas cells, which the aptamers have a very high affinity for [53]. *In vivo* imaging confirmed that both particles were needed to best accumulate at the cancerous target, and this nanomedicine with both Pep-TGN peptides and the AS1411 DNA aptamer showed improved survival times when loaded with docetaxel (Dtx), another common chemotherapeutic, in comparison to singly-functionalized nanoparticle controls.

All of the above studies utilized IV administration to rapidly get the carriers into the systemic blood in order to traverse the BBB into the brain utilizing receptor-mediated endocytosis. There are, however, alternative mechanisms. For example, polycationic molecules can be efficiently internalized by the negatively charged membrane of the cerebral endothelial cells in the BBB, in a process known as adsorptive-mediated transcytosis (AMT) [54]. An IV injection of biodegradable PLGA-trimethylated chitosan nanoparticles loaded with coenzyme Q10 was used to treat an Alzheimer's disease animal model using this route, resulting in an increase in learning ability and a reduction in the escape latency from a water maze compared to controls.

Another alternative mechanism to internalize carriers in the brain is to use intranasal administration to allow for the transport of specific functionalized vehicles

to the brain from the nasal cavity via the system of nerves that exists between the two (olfactory and trigeminal nerves) [55]. Lectin-functionalized nanoparticles are able to bind to the glycosylated nasal mucosa to initiate this transport, and a range of biodegradable nanoparticles functionalized with various lectins have been shown to utilize this pathway to accumulate in therapeutically significant quantities in the brain after 2 h [50]. For example, *Solanum tuberosum* lectin-functionalized PEG-*b*-PLGA nanogels loaded with the antipsychotic drug haloperidol were able to use this pathway, with most of the nanocarriers likely traversing to the brain directly via the olfactory receptor cells. The lectin-functionalized nanogels accumulated in the brain tissues 1.5–3-fold more effectively than controls. The haloperidol-loaded nanogel formulations were shown to effectively induce catalepsy, effectively calming the mice down in the way that this antipsychotic drug for the schizophrenia treatment should, when delivered intranasally [56]. The downside of this and other alternative routes of delivery to the brain is that they generally have low bioavailabilities (<0.1%) [46, 55].

Despite the extensive research interest in developing nanotherapeutic delivery vehicles for traversing across the BBB, it is still in its early stages and there are no clinically available treatments currently. This is due to the difficulty in obtaining high bioavailabilities to the cerebral site of interest (significant proportions do not make it past the BBB), the biocompatibility concerns of nanoparticles, and the long FDA process that it difficult to get through. Therefore, invasive delivery methods, namely injections and infusions are frequently used for treating only the most severe ailments. However, there are polymeric brain implants capable of controlled release the is currently used to treat malignant gliomas [57]. The first one was approved by the FDA in 1995 and is a wafer composed of a biodegradable polymer, poly (carboxyphenoxypropane-co-sebacic acid), with the entrapped chemotherapeutic drug 1,3-bis(2-chloroethyl)-1-nitrosourea (BCNU) that is implanted after a malignant tumor is removed and releases its payload as it degrades over 3 weeks in this localized treatment regime [57, 58]. The result was a statistically significant improvement in the survival of the patients. Several other similar bioresorbable implants were developed and placed in clinical trials since [59], notably resorbable microchips made from PLA that significantly reduced tumor sizes in an in vivo rat model via the controlled, localized release of BCNU [60].

2.5 The Eye: Ocular Delivery

The eye is a particularly interesting target tissue for drug delivery as its unique nature presents numerous anatomical and physiological barriers that makes therapeutic delivery through traditional means extraordinarily difficult [61]. Drug delivery to the eye is generally characterized in terms of which of two regions the delivery is intended for: either the anterior or posterior segment of the eye. These segments and the overall anatomy of the eye are depicted in Fig. 2. The anterior segment of the eye is responsible for collecting and focusing light, while the posterior segment is responsible for detecting this light and transferring this information to the optic nerve

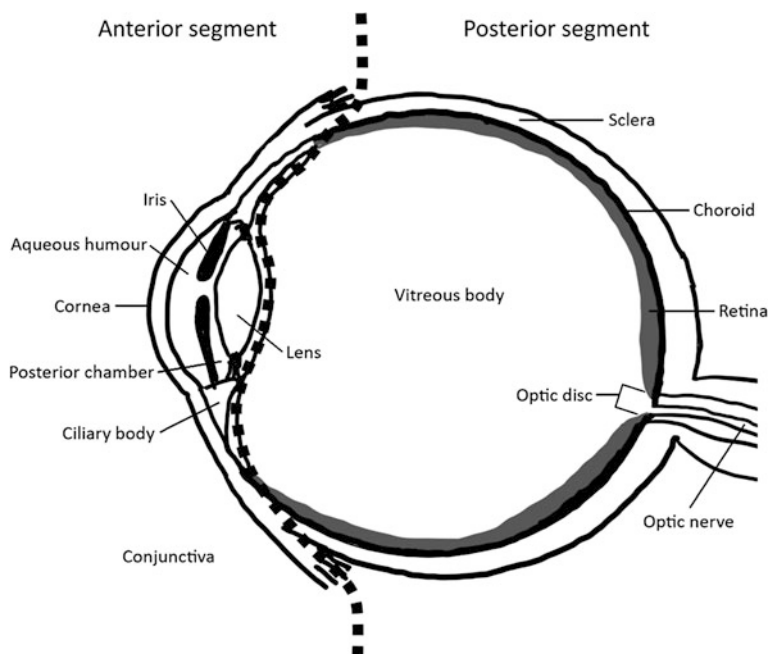


Fig. 2 The anatomy of the eye: a transverse cross-section of the eye. The different components of the anterior and posterior segments are separated by the dotted line. (Original drawing adapted with permission from Ref. [62])

that leads to the brain. The outermost layer of the anterior section is a transparent collagenous layer called the cornea. The anterior chamber, filled with aqueous humor, separates the cornea from the iris, the pigmented portion of the eye that regulates the amount of light that enters the lens, and the lens. This chamber is enclosed on either side by the ciliary body, which secretes aqueous humor that provides nutrients to these avascular tissues and maintains the intraocular pressure. The structure of the lens-iris barrier is what separates the anterior and posterior portions of the eye [62]. The collagenous outer layer in the posterior segment is an opaque white color and called the sclera. Between this structure and the retina is a middle layer called the choroid, which is a network of capillaries that supplies the inner layer, the retina, with nutrients. The retina detects and transduces the light signal, and transfers the neurosensory information to the brain via the optic nerve. The vitreous is the largest part of the posterior segment of the eye, encompassing the space between the lens and the retina [63]. This region is filled with a hydrated gel like extracellular matrix called vitreous humor.

2.5.1 Anterior Segment Treatments

Anterior segment diseases, including dry eye, microbial keratitis, giant papillary conjunctivitis, and vernal keratoconjunctivitis, are treated topically with eye

drops/ointments, systemically, or periocularly via subconjunctival injections or implants [62]. Drugs delivered systemically can reach the aqueous humor, which provides nutrients to the anterior segment of the eye and is secreted from the ciliary body, after it passes through the blood-aqueous barrier [64]. However, only small portions of the drug will partition into the aqueous humor. Thus large amounts of potent drugs are required to deliver therapeutically relevant concentrations of the drug to the desired anterior eye site, which can result in numerous undesired side effects [62].

Of these methods, topical administration is the most common, with numerous small, moderately-charged drugs being known to penetrate the cornea, conjunctiva, and sclera to enter the eye. Topical administration via eye drops is only really useful for anterior segment diseases, particularly for those that can be treated with small therapeutics [64]. The pharmacokinetics of release in this case are very complex, as they are impacted by the flow of tears (lacrimation), blood flow, aqueous production, as well as the physical barriers of the tissues they are trying to penetrate [62]. The correct administration of eye drops involves proper placement of the eye drop, the correct number of administrations per day, and the correct time intervals between multiple dosings or therapeutics [65]. The difficulty in maintaining this procedure leads to low patient adherence, which is an issue that only increases with age. Additionally, the majority of each eye drop will be washed away within minutes. This is the crux of the issue of using eye drops: only a small amount, typically <1–3%, of small drug compounds reach the aqueous humor site with 75% of drug lost rapidly via lacrimation and absorbed systemically by the conjunctiva [64–66]. The degree of permeability steeply drops for larger compounds, meaning the larger the drug is the lower its bioavailability will be. Thus, for any drug within eye drops, in order to be effective high concentrations of drug are required, as most of it will be lost in the process.

There are several strategies that will slightly improve the bioavailability of eye drops involving polymeric particles. Mucoadhesive nanoparticles, microgels, and dendrimers that enhance the retention of drug delivering molecules to the surface of the eye include PEG, poly(acrylic acid), and positively-charged polymers such as polyamidoamine (PAMAM) [61]. These particles can also be uptaken by the corneal epithelial cells for treatment and/or prolonged release to other anterior segments. Viscosity enhancers can also prolong the residence time of an eye drop. For example, in situ gelling hydrogels have been incorporated into eye drops specifically for the purpose of increasing the residence time of a given droplet by delaying its removal via lacrimation.

Injections into the subconjunctival space around the eye have been used to store a drug depot close to the surface of the sclera. This space can be used to store up to 0.5 mL of a drug containing solution and proteins as large as 145 kDa have been shown to penetrate the sclera from this region (via the periocular route), affording an option for both anterior and posterior segment treatments [64]. Most drugs injected into this space are cleared by the systemic circulation, particularly rapidly with small drugs, but this still provides as a simple option for the delivery of larger molecules in particular. An interesting hydrogel-based biomaterial composed of tri

(ethyleneglycol)dimethacrylate and poly(ethyleneglycol)dimethacrylate containing three different small molecular weight model drugs with a controlled release cover made from the same polymers and was implanted in the subconjunctival space [67]. The device was capable of delivering multiple drugs that traverse the sclera at different controlled rates, depending on the composition of the hydrogel and/or hydrogel cover (by altering the ratio of the comprising copolymers) [67]. Microspheres composed of polyester have been injected subconjunctivally and studied for the release of timolol to treat glaucoma, and, promisingly, were shown to be capable of delivering timolol for more than 3 months *in vitro* [65]. Another option that is used for large molecular weight drugs is to inject small reservoirs of drugs into the densely-packed stromal cells of the cornea. The macromolecules immunoglobulin G (IgG) were shown to have an exceptionally high half-life of 26 days when injected intrastromally [68].

Much of the biomaterial strategies that are currently being developed for the anterior region center around the use of contact lenses as the delivery vehicle, as these systems are minimally-invasive and should have relatively good compliance. Contact lens-based delivery systems have great potential for anterior eye segment treatments, as they provide as a potential drug reservoir that is placed against the cornea for long time frames and is currently used by a significant portion of the population in the developed world [69]. Through the advent and consistent improvement of silicone hydrogel-based biomaterials, it is now clinically possible to produce contact lenses that can be worn for 30 days and could be soaked in a drug of interest prior to their use [69]. However, more controlled, sustained release is generally required, resulting in numerous research groups attempting to better control release from drug-containing hydrogel contact lenses. In the development of novel means to deliver therapeutics from hydrogel contact lenses, drug have been immobilized on surface-modified poly(2-hydroxyethyl methacrylate) (PHEMA) hydrogels, incorporated in a colloidal structure dispersed in the lens, electrostatically bound to polymeric hydrogels containing ionic functionalities, and molecularly imprinted in the hydrogel network of contact lens [66]. While none of these materials are commercialized as of yet, contact lenses have the potential to provide as a better solution to eye drops for a wide range of therapies.

2.5.2 Posterior Segment Treatments

Delivery to the posterior segment of the eye is remarkably difficult due to a variety of anatomic and physiologic limitations, as all of the barriers to release for the anterior segment are also present here, but with a much longer required diffusional distance [62, 69]. Additionally, this region is particularly unique in the body in that it is largely acellular in nature. However, the development of improved methods of delivery to the posterior segment of the eye is important as diseases associated with this region, including age-related macular degeneration (AMD), posterior uveitis, diabetic retinopathy, and retinitis due to glaucoma, are the primary causes of vision loss in developed nations [62, 69, 70]. A further complicating factor with these diseases is that they often need to undergo treatment over the course of years

[61]. As a result, alternative strategies are frequently used to deliver drugs to the vitreous, choroid, and retina.

Notably, systemic delivery is particularly difficult for delivery to the eye, as the inner and outer blood-retinal barriers (BRBs), which separate the neurosensory retina from circulation, are known to be similarly exclusive as the BBB [64]. While functionalized nanoparticles delivered intravenously with transferrin or arginine-glycine-aspartic acid (RGD)-peptide have been shown to result in polymeric nanoparticles capable of reaching and treating the eye in a significantly improved manner over non-functionalized particles, this improvement was rather small considering that the bulk of the nanoparticles would have not been capable of crossing the exclusive BRB [61]. As a result, more direct methods of delivery are typically desired to avoid side effects associated with systemic delivery.

Intravitreal injections are the most common method of conventional treatment and, from a therapeutic perspective, have been rather successful, particularly for AMD treatments [64, 69]. These injections are useful for posterior treatments because the vitreous is central to the tissues of the posterior region and high drug loads can be applied [61]. However, many treatments require frequent injections, which greatly increases the risk of complications over time, such as cataracts, vitreal hemorrhage, endophthalmitis, intraocular hemorrhage, retinal detachment, and increase intraocular pressure [63, 69, 71]. Many of these complications could result in permanent vision loss. The injections are also demanding of an ophthalmologist's time, and are inconvenient for the patient (leading to low patient compliance). Frequent intraocular injections are thus only really suitable for treating older patients with advanced forms of posterior segment diseases, leaving younger patients without safe and effective treatment options [69]. Drugs that are injected into the intravitreal space are cleared (with a limited retention half-life of <3 days) via an anterior route through the aqueous humor or via a posterior route that involves the drug crossing retinal space and the BRB [64, 72]. Large molecular weight drugs (>500 Da in this case) have long half-lives in the vitreous from days to weeks and small drugs have been PEGylated to increase their molecular weight to enhance their retention time in the posterior segment [73]. Polymeric nano- and micro-particles, micelles, liposomes, hydrogels, and implants can also be used for the controlled release of drugs over longer time frames in the vitreous.

The main issue is the maintenance of therapeutically-relevant concentration levels of the therapeutic throughout lengthy treatments, which is difficult to achieve long-term [65, 69]. Despite this challenge, several commercial devices have been developed for the delivery of therapeutics to the back of the eye. These FDA-approved devices are all implants. These implants, along with alternative implants currently in FDA trials, utilize polymers such as PLGA, polycaprolactone (PCL), and poly(orthoester) if they are to be biodegradable, and silicone, PVA, and ethylene vinyl acetate (EVA) if they are not degradable in nature [72]. For example, Retisert[®] is a nondegradable device that is surgically implanted in the sclera that can continuously deliver small amounts of drug to treat posterior uveitis over 2.5 years [63, 72]. After this time, the device must also be surgically removed. Iluvien[®] is a new commercially available injectable implant (injected in a similar manner to

typical intraocular injections) capable of long-term delivery of corticosteroids to treat diabetic macular edema [63]. However, once this material is injected it is not erodible or degradable, so it remains in the vitreous. Ozurdex[®] is an implant that is capable of sustained release over 1–3 months for treating either posterior uveitis or diabetic macular edema, but because this implant is composed of PLGA it has biodegradable properties and is approved by the FDA [61, 63]. There are several other implantable systems, both degradable and non-degradable, in development that are currently in the clinical trial process [63].

Commercialized systems that could be facily injected to the back of the eye, deliver therapeutically-relevant drug dosages for posterior eye segment ailments over months, and ultimately degrade would be ideal, but this type of technology is not currently available and presents as a great market opportunity in the future. However, as biomedical sciences and biomaterials research advance, new opportunities to improve therapies are emerging for the treatment of posterior segment diseases.

Iontophoresis has been used to non-invasively drive the permeation of ionized drugs across the sclera, periorcularly, via the application of weak electric currents [62]. This method can be used to deliver high concentrations of drugs to the choroid and tissue, and often use hydrogels as the component that is actually in contact with the sclera due to their soft nature. Transcleral delivery using electrophoresis from HEMA-co-EGDMA hydrogels has shown to be effective with a two minute application and this is a promising method for the delivery of hydrophilic macromolecules, like DNA, siRNA, etc., across the sclera [62, 72].

Microneedles for use on the eye have been adapted from previous work on the use of microneedles to deliver drugs across the skin. These systems have primarily been explored as an option to deliver drugs through the sclera. Microneedles would provide as a simple, less intrusive alternative to the surgical implant strategies for extended release that are currently available on the market. A hollow microneedle system has been developed that partially penetrates the sclera and would allow for the slow release of therapeutics (up to 35 μL) into vitreous in a manner that could be facily administered in a clinical setting [74]. Microneedles can also be designed to a specific length such that they can deliver drugs to the suprachoroidal space for diseases like chorioretinitis, choroidal neovascularization, AMD, and glaucoma [61]. Hollow microneedles were shown to be capable of injecting polymeric nanoparticles from 20 nm to 10 μm in size into the suprachoroidal space and these particles remained for over 2 months [75].

Polymeric nano- and micro-particles have been studied for delivering therapeutics topically, periorcularly, suprachoroidally, and via intravitreal injections [64]. The use of biodegradable polymeric particles is particularly important for the eye, as the degradation of these particles will allow them to be eventually cleared from the eye in their smaller fragments. The biodegradation of polymers like PLGA can also be used to mediate drug release in the eye [64]. The difficulty in designing a system that is stable, can control the release rate, and is made of safe polymeric materials whose degradation products are also safe has hindered the progress of polymeric particle formulations being used for ophthalmic drug delivery in the market. Polymeric

nanoparticles also could not be injected into the vitreous humor, as they diffract light and would cloud one's vision [64]. Larger microparticles would not have this issue, as they would sink to the bottom of this region of the posterior segment. PLGA microspheres have been developed that are large enough to sink after vitreal injection and deliver a growth factor that improves the recovery from ischemic retinal injuries (brain-derived neurotrophic factor) [65], and anti-transforming growth factors to limit fibrosis after glaucoma surgeries [76]. These larger particles also have longer residence times in the subconjunctival space for long term periocular delivery of therapeutics through the sclera [61]. One of the biggest issues related to the use of polymeric nanoparticles is that, due to their size, larger surface-to-volume ratio, and the associated diffusion lengths, they are generally not capable of the long term delivery of weeks to months that would particularly benefit the treatment of eye-related disorders (where it is particularly undesirable to have frequent administrations), even though they may be present for over 4–6 months [72]. This is the major advantage that the previously mentioned commercial implants have over polymeric particles. Larger implants can load more drug and deliver the drug slowly due to their smaller surface-to-volume ratio that allow for prolong release of up to several months. Larger microparticles have this analogous advantage over nanoparticles, but to a lesser extent to typical macro-scale implants [61].

Injectable in situ gelling systems are another potential solution that is being studied, as they can afford long-term release while being capable of being administered with a simple injection as opposed to the invasive surgeries required for implants [64]. These are hydrogels that form upon injection by an increase in temperature, via thermogelation, as the polymer exceeds its lower critical solution temperature (LCST) and interacts with itself to form a physically-crosslinked hydrogels in the vitreous that can later be used to deliver drugs or cells that were in the pre-gelation solutions [70]. Thermogelling hydrogels present as a safe alternative to intravitreal injections and are capable of prolonged therapeutic delivery [61]. Verisome, a thermogelling drug delivery system involving an in situ-forming biodegradable hydrogel containing lipid forms a spherule upon injection into the vitreous, and was able to release therapeutic levels of a drug for macular edema, triamcinolone, for 12 months in early clinical trials [63]. Hydrogels that form via the in situ crosslinking of two reactive functionalized polymers could also be realized, as recent developments in injection devices have allowed for the injection of these types of polymeric systems into the vitreous [77]. These covalently-crosslinked hydrogels can be similarly biodegradable have tunable crosslink densities that could further slow the release of drugs contained within them in a controlled fashion, leading to longer term release from injectable materials [78]. Injectable hydrogels can also be injected into the subconjunctival space to deliver drugs over longer time frames via the periocular route to deliver drugs to the posterior segment through the sclera [61].

Several responsive systems whose release rates can be altered have been investigated as well [63]. These advances generally attempt to take advantage of the fact that light can be easily transmitted to materials within the eye due to the necessary transparent nature of the cornea and the lens. Light-responsive systems can be made from incorporating light sensitive materials that respond to specific wavelengths

or convert light into heat within polymeric micelles or hydrogels. In the case of micelles, a chromophore can be attached to the hydrophobic part of the polymer. When a specific wavelength of light (typically in the visible or near-infrared (IR) range) is applied the chromophore, it is cleaved and this disrupts the micelle, causing it to release its drug-loaded contents. This is usually an irreversible process and a way to deliver bursts of drug using micelles [63]. Verteporfin is a systemically administered liposome that experiences photodynamic disruption of the lipid bilayer, releasing its drug contents, and is currently clinically used for the treatment of subfoveal choroidal neovascularization [61]. Gold nanoparticles (2–3 nm) can also be embedded in the inner and outer layers of liposomes and near-IR light can be used to heat these materials and cause them to irreversibly release their contents in a similar fashion [72]. Hydrogels with reversible photodynamically labile crosslinks can also be used to regulate drug release, where exposure to a certain wavelength of light will cause the crosslink to form while another wavelength may be used to eliminate that same crosslink, affording external control over the crosslink density and tortuosity of the hydrogel, which can regulate drug release. Near-IR induced heating of thermosensitive hydrogels incorporated with gold nanoparticles, or other nanoparticles that transduce near-IR light to produce heat, can also be used to remotely alter the hydrogel's swelling characteristics and, consequently, regulate the associated drug release from the hydrogel networks [72]. Many eye conditions would benefit from a drug release profile that is in tune with the patient's needs associated the state of the condition being treated, all while inhibiting the prevalence of side effects [63]. Thus, if implemented successfully, such advanced systems would serve as a new generation of ophthalmic drug delivery strategies that are capable of altering their drug release kinetics on demand in real time.

2.6 Other Common Regions

There are several other administration methods that can be used to deliver medications, however these methods are generally utilized to a lesser extent than the aforementioned methods and/or they have not been explored in drug delivery research using polymeric particles nearly as readily for a variety of reasons. The nasal route can be used to rapidly and noninvasively deliver drugs for, for example, sinus issues or into circulation, as, similar to the lungs, the tissues are fairly facily penetrated by therapeutics and this region is highly vascularized. However, significantly more small particles are lost via the nasal route than in the lungs and it is difficult to design polymeric particles that will remain in this region for prolonged lengths of time without being cleared by the mucosal turnover [29]. As highlighted in the section on delivery to the brain, the nasal route can be used to deliver materials to the brain [56], but localized delivery by controlled release vehicles has not been extensively studied in order to pursue simpler and likely more efficacious routes of delivery to the brain.

Another region of the body that is widely used for traditional drug delivery is delivery to the anal cavity via suppositories. This region also has tissues that are

easily penetrated to deliver drugs rapidly to the bloodstream (with ~50% of the drugs bypassing the first-pass effect), leading to its widespread use in patients that have difficulty in taking drugs themselves via alternative means. However, the socio-cultural stigma, inconvenience, and low patient compliance associated with this method has led to limited research in the development of controlled release methods via this route [16]. The anal administration method is generally used for acute rather than chronic treatments, also leading to little motivation to engineer devices capable of prolonged release.

Alternatively, localized treatments to the bladder with polymeric devices have been studied, as delivery to the region is so difficult and inconvenient that prolonged release is desired to limit the number of administrations. An example of this is the use of hydrogels for the treatment of bladder cancer. A floating hydrogel made of the thermosensitive polymer poloxamer 407 was developed that could float in the bladder to avoid urinary obstruction and irritation while delivering the anti-cancer drug Dox *in vivo* [79]. While mucoadhesive hydrogels have also been used in the bladder [79], another strategy utilized nanocomposite hydrogels with magnetic nanoparticles to magnetically target the hydrogel to the specific region of the bladder that has cancer to more effectively treat the diseased region [80]. While there are several research groups looking into treating the bladder with polymeric release systems, they are limited to looking into serious ailments of the regions, like bladder cancer, as the difficulty in delivering materials to this region means localized delivery will only be performed under dire circumstances.

The vagina is a principle site of infection for many sexually transmitted infections (STIs). As a result, intravaginal rings composed of extruded polymers, such as elastomeric polyurethane [81], silicone [82], and PEG [83], have been developed for their use in the delivery of therapeutics to prevent and treat sexually transmitted infections and as contraception [6]. These polymeric devices can be used for over 6 months and are periodically removed for 1 week intervals. These systems are also capable of locally deliver antibodies, microbiocides, and siRNA to protect against both pregnancy, human papillomavirus (HPV) infection, human immunodeficiency virus (HIV) infection and many more [6, 84]. Many intravaginal systems have also been commercialized, including a few intravaginal rings [82, 84]. This can also be used as a site of administration for systemic acting therapeutics, as the released materials bypass the hepatic first pass effect and controlled release can take place for over 30 days in some cases [84].

Drug eluting stents have been used for many years to enhance healing and limit the inflammatory response after surgeries where stents are utilized to maintain the structure of the arteries/veins that underwent surgery [85]. These systems often have crystalline drug coated to the surface of the stent and their drug is generally released at a fairly rapid rate. A wide range of drugs have been used for this purpose, including antibiotics, proteins, genes, cardiovascular agents, hormones, and steroids [86]. The use of bioresorbable polymeric coatings, like PLGA, PLA and PCL, can offer long term release and improve the long term biocompatibility of stents after their administration by reducing inflammation [85, 86]. As a very specialized platform, many of these stents have been commercialized and seen great success

in treating local issues [86]. These systems are solely suited for localized treatment, as they are invasive to insert, and, as such, their potential applications are also quite limited. These limitations have, in a way, simplified the applications and requirements of the delivery system to such an extent that they have been successfully commercialized to a great degree to date (which has yet to be achieved for the majority of controlled release systems), although there is still room for improvement in these devices as well.

3 Systemic Controlled Release Case Study: Cancer Therapy

Many biologics, including antibodies, enzymes, growth factors, hormones, peptides, nucleic acids, and vaccines, are clinically limited to parenteral delivery into blood circulation [5]. Many of the diseases that are treated by these materials are chronic in nature [5], meaning short-lived injection treatments must be frequently performed for long periods of time for treatment. The pain and inconvenience of these treatments leads to reduced treatment efficacies and poor patient compliance. Improving the release of these drugs that are introduced systemically could drastically improve healthcare. However, when a disease is not confined to a specific organ in the body, the best method of treatment can be much more complicated to determine.

As we have seen earlier in this and the previous chapter, many ailments that can affect the body systemically can be treated by polymer-based delivery vehicles, which, in turn, may be administered in a wide variety of methods. For example, insulin-releasing systems can be administered systemically or via the oral, nasal, transdermal, pulmonary, etc. routes. Glucose-sensitive hydrogels and microgels, normally composed from phenylboronic acid (PBA) or its derivatives, can also be used to deliver insulin as it is required [6]. Mannan-functionalized PLGA can be used to aid the delivery of vaccines, as mannan is a natural polysaccharide that binds with mannose receptors on antigen-presenting cells and this can be used to enhance the uptake of antigen to elicit improved antigen-specific T-cell responses [50, 87].

Nanoparticles can also be used to access the intracellular environment via the endocytosis process, and, as such, they are currently being investigated as a safe substitute to viral gene-delivery [61]. The plasma membranes of cellular barriers are very restrictive to admission of macromolecules (which are normally hydrophilic) and hydrophilic small molecules into the cell. It is well established that the transferrin receptor of cells regularly undergoes internalization and recycling, and, as such, can be utilized to transport transferrin-functionalized polymeric nanoparticles into cells [61]. Functionalizing these polymeric nanoparticles with ligands such as transferrin, deslorelin, and RGD peptide are known to enhance the cell entry of nanoparticles and consequently also improving the desired therapeutic effect [61]. Polymeric nanocarriers can enhance both gene transfection and its duration by protecting nucleic acids, such as siRNA and miRNA, from degradation by the numerous nucleases in the body, reduce the number of off-target interactions of nucleic acids with cell receptors, enhance the entry of nucleic acids into the target cells, and sustain this intracellular delivery [61]. Although there have been no

clinical success in gene delivery to date [88], approaches that are able to maintain the stability of sensitive molecules, like proteins, hormones, and nucleic acids, are integral for new drug releasing systems and are currently a significant focus of drug delivery research [6]. Similar strategies with functionalized nanomedicines are being researched for a wide range of drugs and, from blood thinners to painkillers to allergy medications, and each with its own set of pros and cons, particularly when considering the drug and disease of interest.

This section in particular will focus on what is one of the most challenging hurdles that modern medicine is currently grappling with: the treatment of cancer. The best means of treatment is not a trivial choice in the case of cancer. There are a wide range of potential directions that could result in a viable treatment option for a variety of cancers, but selecting the optimal direction to proceed in is far from obvious at this point in time. It may simply be the case that each form of cancer may be so different and malleable that individual treatment methods must be applied to any given cancerous tumor. This section aims to briefly examine the state of polymer-focused research and medical treatments that are currently being employed and look at the direction that research in this area may head toward.

3.1 What Is Cancer?

Cancer has provided a persistent challenge to medicine and biomedical research over the last several decades and its devastating effects are still felt today, as it remains one of the leading causes of death in the world. Over 8.2 million deaths were reportedly attributed to cancer in 2012 [88]. The mortality rate of cancer has only recently started to slightly decline, owing to a deeper understanding of the disease and extraordinary advancements in the diagnosis and treatment methods. However, this mortality rate remains high at ~20.2% [88], so there is clearly much that remains to be discovered. The majority of the research involving the delivery of chemotherapeutics to tumorous sites has yet to be commercialized, which means that, while there is still a lot of work that must be done to drastically improve mortality rates from the disease, there is certainly a reason to be optimistic about the treatment of cancer in the future.

Cancer represents a large array of diseases that involve abnormal cell growth due to genetic defects in the regulatory circuits of cells that dictate cell proliferation and homeostasis [89]. These abnormal cells also have the potential to spread to other locations in the body. Cancer cells undergo unregulated, malignant growth may take shape in the form of a mass or lump, but they could also be distributed throughout the body. This malignant growth can be characterized by six distinct alterations in cell physiology: (1) the cells independently grow and divide regardless of the growth signals; (2) their growth is insensitive to growth-inhibitory (antigrowth) signals; (3) they are able to avoid programmed cell death (apoptosis); (4) they possess an unlimited number of potential replications; (5) they continually promote angiogenesis, the formation of blood vasculature; and (6) they are capable of invading healthy tissues and metastasizing to spread to other organs [89].

Cancer is currently treated by surgical intervention, radiation, and chemotherapeutic drugs, often utilizing several different chemotherapeutics to have a better chance of eradicating the cancerous tissues [90]. The drugs themselves are generally deadly to cells that quickly replicate and are delivered intravenously, and these drugs, along with the radiation, often kill healthy tissues and cause toxic side effects to the patient [90]. This is the primary issue associated with cancer treatment: the mortality rate of cancer remains high due to the fact that there is currently no means to which chemotherapeutic drugs can be delivered to tumor sites without also provoking severe, sometimes lethal, side effects to healthy organs and tissues [88]. Developing methods to effectively target and deliver chemotherapeutics to cancerous tissues could minimize the dangerous side effects associated with chemotherapy and reduce the mortality rate of cancer as a whole [90–92]. Thus, investigating systems that could potentially target cancers in a more effective manner has been an important focus of drug delivery research in recent decades.

An idealized treatment system would be a nanocarrier that is capable of overcoming the body's natural biological barriers, parsing through and distinguishing between cancerous and healthy cells, selectively targeting these malignant tissues, and recognizing and responding to the heterogeneity and complexity of the tumor microenvironment in order to deliver an optimal dosage of the therapeutic on-demand [88]. These can be simplified into four steps: retain, evade, target, and release [93]. These are certainly lofty goals for an engineered drug-releasing vehicle, and these systems have consequently been traditionally termed as “magic bullets” [94]. While delivery science is nowhere close to developing a “magic bullet” currently, science is taking small steps towards this ultimate goal. The focus in the last few decades has been to develop systems that can more effectively overcome biological barriers and target cancerous regions in the body to more effectively deliver drug to the region of interest (the tumor) while limiting the side effects of the chemotherapeutic as much as possible. These systems are often polymeric nanoparticles, which have the beneficial characteristics of preventing premature degradation of the drug, protecting the bulk of the drug from interacting with the biological environment before it reaches its target, improving the delivery of poorly soluble drugs (the majority of chemotherapeutics are hydrophobic), possessing the ability to load multiple drugs/diagnostic agents, being capable of possessing controllable pharmacokinetic release profiles, and improving the intracellular transport of the drug [88, 90]. There are two general strategies for systemically delivered drug delivery nanoparticle systems to target cancers: passive targeting and active targeting.

3.2 Passive Targeting

Passive targeting exploits the anatomical and physiological irregularities of solid tumors to target nanoparticles to their location [95]. The rapid growth associated with solid cancerous tumors with high cell densities relies on these tumors receiving increasing quantities of nutrients and oxygen to afford their accelerated growth rate

[95–97]. As a result, they promote substantial angiogenesis, to the point where they often promote the formation of leaky vasculature, or gaps between the endothelial cells of blood vessels that are regularly connected via tight junctions [88]. These gaps in the tumor vasculature are typically balloon from their normal range of 5–10 nm to 100–800 nm [92, 97]. The defective nature of the vasculature around tumors results in substantial leakage of blood plasma components into the tumor tissues. Tumor tissues also tend to have dysfunctional lymphatic drainage which leads to much of the material introduced to the tumorous region also being retained in these tissues [95]. Collectively, these phenomena associated with solid tumors are termed the enhanced permeability and retention (EPR) effect.

Polymeric nanoparticles can exploit the EPR effect to improve their accumulation at the site of the tumor and if they are effectively retained in the tissue they could release their payloads in the vicinity of the tumor cells. This passive strategy, which has been used since the mid-1980s, theoretically should be fairly simple to utilize. Improving the effectiveness of passive targeting should relate to prolonging the length of time that the drug-loaded nanoparticles can be retained in the circulatory system [98]. Polymeric nanoparticles can be engineered to remain stable within the circulatory system and avoid protein adsorption and eventual clearance by the mononuclear phagocyte system (MPS) system and be within the optimal size range for taking advantage of the EPR effect. The accumulation of polymer nanoparticles that can occur around solid tumors due to the EPR effect is depicted in Fig. 3.

As mentioned previously in the chapter, a proven method to improve the circulation half-life of a nanoparticle (and the most commonplace one) is to functionalize the target vehicle with PEG. In fact, several of the early nanocarrier-based drugs that were initially developed to utilize the EPR effect and are currently on the market are PEGylated drug conjugates or PEG-coated liposomes [90, 99]. It is widely regarded that brush-like PEG configurations that form a hydrated shell are shown to better evade protein adsorption and phagocytosis [92]. “Stealth” PEG-functionalized particles should thus allow for the passive accumulation of these particles at the tumor site, where they could release their drug outside of the cluster of malignant cells or enter the cells and release their payload.

Particle size and shape is an important consideration when designing nanoparticle carriers to target tumors. Particles from 30 to 200 nm in size are generally regarded as the optimal size range for passive targeting [100]. The large gaps in the vessel structure around some solid tumors allows large nanoparticles to extravasate into the tumorous regions (depending on the size and the stage of the tumor), so sizes up to the cut off size for the spleen (~200 nm) can be utilized [88]. These sizes also relate to the degree to which the nanoparticles can spread throughout these solid tumors. This is a diffusion-based process, so smaller nanoparticles have a better chance of spreading throughout the tissue. However, nanoparticles smaller than 30 nm tend not be retained at well, as they can diffuse back out into the vasculature network, and may not accumulate at the target site [88].

If they reach and are retained in the target tissues, nanoparticles generally have a high intracellular uptake, and anisotropic structures may provide a better configuration for binding with the target cells. Spherical nanoparticles have been shown to

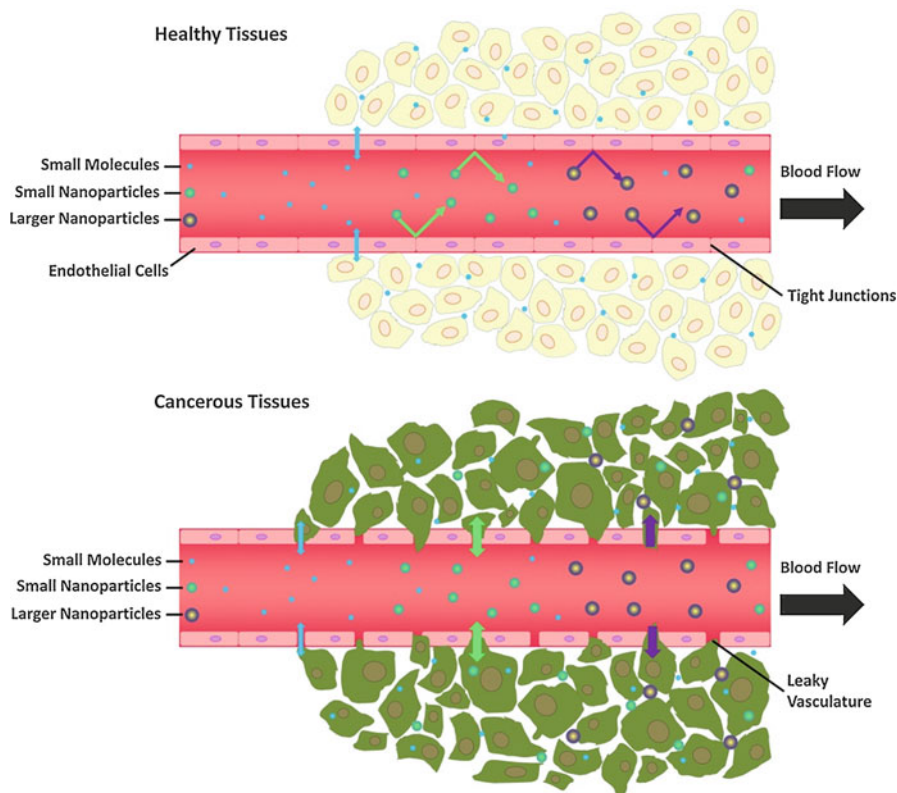


Fig. 3 The delivery of polymeric nanoparticles, small (20–40 nm) and large (40–200 nm), to solid tumors via the enhanced permeation and retention (EPR) effect. The angiogenesis that is promoted by fast-growing tumors enhances the gaps between endothelial cells of blood vessels from 5–10 nm to 100–800 nm to allow for nanoparticles to extravasate and be retained in the tumorous tissues. These particles would otherwise remain in the blood stream in vasculature surrounded by healthy tissues. Small nanoparticles may not be retained as well as large nanoparticles, as they are small enough to escape from the tumor microenvironment, which is much less likely for large nanoparticles

follow a laminar flow pattern, so only the nanoparticles near vessel walls will extravasate via the EPR effect, whereas anisotropic particles have less regular flow patterns and could possibly accumulate in greater quantities if they could avoid the clearance via the MPS [101, 102]. However, these anisotropic structures also generally have a higher degree of opsonization and phagocytotic uptake [88]. Overall, spherical particles are the more popular option for nanocarriers as they are better at avoiding the body's natural barriers and they can be facily and cost-effectively fabricated in a variety of forms. This is especially true of polymeric nanocarriers, from nanoparticles to dendrimers to micelles.

The simplicity of passive targeting has led to it forming the basis of many current clinical therapies [97]. However, relying on the EPR effect alone has not provided a

therapeutic option that is anywhere near a “magic bullet”-like treatment option for cancer. An issue associated with this strategy is the fact that all tumors, even tumors that are of the same type and at the same stage, are different, with varying degrees of density, heterogeneity, angiogenesis (and associated vessel leakage, permeability, and retention capability), etc. In fact, some solid tumors do not exhibit the EPR effect at all and it is difficult to determine the extent to which a given tumor does exhibit this effect [90]. Notably, as Bae and Park importantly revealed in 2012, while the EPR effect may affect the distribution of intravenously injected nanoparticles, in all studies relying on the EPR effect less than 5% of the desired drug from the nanoparticles ultimately reaches the tumor site [93]. In this work, they questioned that if the bulk (>95%) of nanoparticles accumulate in other locations, particularly in the liver, lungs, and spleen, then is passive targeting really targeting at all? [93]. This is the primary issue currently facing nanoparticles that are designed to target specific tissues: they primarily accumulate in undesired locations. Thus, a great deal of recent focus in the area of improving cancer therapy with polymeric nanoparticles has not only relied on the EPR effect, but also active targeting strategies.

3.3 Active Targeting

Active targeting involves the binding of the nanocarriers to specific, targeted cells after they leave the blood stream. This is achieved by functionalizing the nanocarriers with specific ligands that can recognize and bind to particular receptors on the surface of the target cells via a range of conjugation chemistries [103], and these targeting techniques have been attempted since the early 1980s [104]. These functionalization chemistries are highly dependent on the functional groups present on the ligand of interest (that can be conjugated without affecting its targeting efficiency) and the functional groups present on the polymersome, micelle, dendrimer, or polymer nanoparticle. For example, particles functionalized with PEG brushes to promote a longer circulatory half live could also be functionalized with an active targeting ligand via conjugating the ligand with the distal end of the PEG chains. In this case, if the terminal end of the PEG is functionalized with a p-nitrophenylcarbonyl group, amino containing ligands, such as antibodies, could then be readily attached to PEGylated polymer nanocarriers via a carbamate (urethane) bond [103]. Examples such as this exhibit why polymer nanocarriers have a distinct advantage over many other forms of nanocarriers, as they can be designed to possess specific chemistries to enable them to be functionalized with active targeting moieties.

To actively target cancer cells in an effective manner the targeting ligand must bind with a high selectivity to surface markers (antigens or receptors) that are uniquely expressed on the target cells [90]. If this occurs, nanocarriers could bind to these cells and these carriers could be internalized (often via receptor-mediated endocytosis) to release their payload inside the cell [88]. Generally, most surface markers that are present on cancerous cells are present on some other native cells in the body, so exclusively targeting tumors is difficult. However, selective targeting is

possible if the surface marker is sufficiently overexpressed on the target cell relative to healthy native cells [90]. For example, to improve the therapeutic efficacy of delivering liposomes with the anti-CD19 monoclonal antibody to B-cell receptors [105] and the delivery of doxorubicin-containing liposomes to a breast cancer model with ErbB2 receptors [106], 10^4 – 10^6 and 10^5 receptors per cell were required, respectively. Different receptors are also classified as internalizing (such as the anti-CD19 receptor) or non-internalizing (the anti-CD20 receptor), and these could be targeted for different purposes [90]. Internalizing receptors could kill malignant cells individually, whereas noninternalizing receptors could be used to kill cells via the bystander effect, where the nanocarrier is attached to a cell within a solid tumor and releases its contents within range of a wide array of malignant cells [90].

The use of multiple targeting ligands on a single nanocarrier could also improve targeting capacity, as the collective interactions between a carrier with numerous ligands with several receptors on a target cell result in much stronger bonding [90]. For example, many cancers are characterized by a marked overexpression of folate receptors (100–300 times that of healthy tissues), leading extensive amounts of research to focus on using folic acid as a targeting ligand for a wide range of cancers [50]. Dendrimers with multiple folate groups on their periphery (which is very simple to design with dendrimers) target these cancerous cells to a much greater extent than free folate (2,500–17,000-fold) [107]. However, there are downsides to targeting with extremely high binding affinities, as carriers that extravasate into a tumor region may interact with only the first cancerous cells that they come in contact with, anchoring them to tumor cells in close proximity to the leaky vasculature and limiting their degree of penetration into solid tumors [90]. Thus, if active targeting is to be effective, a fine balance must be achieved between binding affinity and other factors that affect the tumor penetration depth of the polymeric nanocarriers (i.e., size, surface chemistry, etc.).

Active targeting moieties that are often employed include proteins (including antibodies and antibody fragments), nucleic acids, peptides, vitamins, and carbohydrates [90]. These moieties have been studied for targeting since 1981 [104] and the first ligand-drug conjugate was commercialized in 2000 [90]. The first attempts at targeting focused on the use antibodies as targeting ligands. Antibodies can be used to treat cancer alone or can be conjugated to nanocarriers and whole, native antibodies with two binding sites per molecule or antibody fragments can be used for targeting. Whole monoclonal antibodies can be used alone to treat cancers, as they have high binding affinities to the surface of cancer cells and immune cells can bind to the exposed Fc portion of the antibody and subsequently initiate a signaling cascade to kill the malignant cell [90]. This process may not be sufficiently selective, as the Fc portion can bind to normal cells and lead to increased immunogenicity and uptake of the nanocarrier in the liver and spleen. Monoclonal antibodies, due to this constant Fc region, are also bulky molecules (~150 kDa) that will dramatically increase the size of the majority of nanocarriers that they are attached to.

Antibody fragments, such as antigen-binding fragments (Fab), dimers of Fabs (F(ab')₂), single-chain fragment variables (scFv), and diabodies (dimers of scFvs), contain the binding components of monoclonal antibodies and a lesser number of

redundant amino acids [90]. The resulting fragments are smaller in size, have lower immunogenicity, and target in a more selective manner [88]. Fusion proteins that consist of two or more genes can also be engineered to bind to target cells with a high affinity. These proteins, and small proteins known as affibodies, could be designed to interact with specific conformations of cell receptors to improve their targeting specificity. This has been examined in a study that aimed to deliver siRNA to activated lymphocytes. These white blood cells possess an integrin LFA-1 receptor whose conformation shifts from a low affinity, non-adhesive form on nonactivated leukocytes to an adhesive, high affinity form upon activation by the immune system [108]. Complexes of siRNA and a fusion protein containing a scFv were shown to selectively deliver the siRNA to activated lymphocytes 10,000-fold more than nonactivated cells [108]. Taking advantage of the conformation of receptors on cancerous cells could be exploited in a similar manner to attempt to target cancer more effectively with antibody fragments.

Aptamers are synthetic, short, single-stranded oligonucleotides that are selected *in vitro* from large arrays of random sequences ($\sim 10^{14}$ – 10^{15}) to bind to specific targets. These nucleic acid oligomers can form complex 3D structures that can specifically bind to cancer cell receptors and can be tethered to polymeric nanoparticles. For example, Farokhzad et al., developed biodegradable PLGA-b-PEG nanoparticles encapsulating docetaxel that were surface functionalized with RNA aptamers to treat prostate cancer [109]. These aptamers recognize and coordinate with prostate-specific membrane antigens, which are situated on the surface of prostate cancer cells. A murine *in vivo* treatment with these nanoparticles resulted in markedly lower toxicity and significantly better treatment outcomes than the drug alone, which was attributed to the selective targeting capacity of the aptamer-polymer nanoparticle system [109]. Screening techniques, including newer forms of high throughput screening, have been employed to attempt to optimize the targeting efficiency and selectivity of various antibodies and their fragments to various varieties of cancer, leading to a vast expansion in the library of potential targeting antibodies and aptamers [99].

Peptides represent another potential targeting ligand. Peptides have a low molecular weight, are easy to produce, lack immunogenicity, and can be facilely (and densely) fastened to the surface of nanoparticles [88]. Peptides regularly have lower binding affinities than most other targeting ligands, but they can also be attached in greater densities than most alternatives to compensate for this relative disadvantage. A range of differing peptides can interact with receptors on cancer cells and have been explored as potential targeting moieties on delivery vehicles. The RGD peptide is one of the peptides that is often used for targeting, as it has an affinity for integrin, which are often overexpressed by the endothelium during tumor angiogenesis [88]. However, small binding peptides can also nonspecifically bind to healthy cells, as RGD is known to do with other integrins on normal cells, negating the intent to selectively target malignant regions [88].

Many of these active targeting strategies still rely on the EPR effect to get within range of tumor before they can make use of their functionality to target cancerous cells. Thus, many nanomedicines must be designed to navigate the circulatory

system for as long as possible while avoiding opsonization and rapid clearance, and are also functionalized with PEG as a result. However, PEG-functionalization can also inhibit interactions between the nanoparticle with the target cells, leading to lower efficacy, especially when active targeting strategies are also being employed [88]. As a response, strategies exploring the use of biomimetic coatings and or particles where the PEG structure is removed upon entering the tumor, often using stimuli-responsive chemistries that interact with the unique qualities of the tumor environment (i.e., higher temperature, lower pH, etc.), have undergone extensive development in recent years [88].

Stimuli-responsive polymeric nanoparticles have the potential to provide better spatial, temporal, and dosage control via on-demand delivery. These nanocarriers would undergo certain protonations or molecular or supramolecular conformational changes in response to a change in its local environment (temperature [110–112], pH [113–115], or solute concentrations [116, 117]), which could be provoked by an external stimulus [118, 119]. Thermosensitive “smart” polymers like poly(*N*-isopropyl acrylamide) (PNIPAM), poly(oligoethylene glycol methacrylate) (POEGMA), and, less famously, poly(γ -2(2-(2-methoxyethoxy)-ethoxy) ethoxy- ϵ -caprolactone)-*b*-poly(γ -octyloxy- ϵ -caprolactone) all have a lower critical solution temperature (LCST). Thermosensitive polymers become less water soluble as their local temperature increases above their LCST, causing the polymers to recoil and take up less hydrodynamic volume. This is a reversible process, such that when the temperature is subsequently lowered below the LCST, the polymers become more soluble and return to their original state. Cross-linked networks of these polymers reversibly deswell (or shrink in size) when their temperature is increased above their volume phase transition temperature (VPTT, which is normally slightly, ~ 1 °C, above the LCST of their comprising polymers) [112, 118]. These particles could be utilized in combination with locally-induced hyperthermia treatments, which is a clinical treatment that involves the targeted short-term exposure of cancerous tissues to elevated temperatures (39–43 °C) that will preferentially eliminate the more temperature-sensitive cancer tissues while being safe for normal tissues [120].

Using microgel nanocarriers composed of these thermosensitive polymers in conjunction with hyperthermia treatments could be used to alter the local temperature of these “smart” microgels at the tumour site, and could allow for the drug-loaded nanocarriers to become insoluble, aggregate, and accumulate as a coacervate at this site (as they become less hydrophilic and less dispersible in aqueous solutions when they deswell), and release drug as they deswell and accumulate in tumorous regions [110, 121]. While this has not been shown for microgels *in vivo*, thermosensitive liposomes have been engineered to release all of their contained drug at hyperthermic temperatures, and have undergone clinical trials in a combined hyperthermia/chemotherapy treatment for both breast cancer, colorectal liver metastasis, hepatocellular carcinoma [118, 122].

Hyperthermia can also be induced by the nanocarriers themselves by adding inorganic nanoparticles to “smart” systems that can produce heat in response to external triggers. For example, PLGA nanoparticles were designed to have a glass

transition temperature (T_g) of 45 °C and were half-coated with a gold layer that could produce enough heat in response to near-IR irradiation to induce hyperthermia, releasing drug to show antitumor activity in breast cancer models in the process [123].

Magnetic nanoparticles have also been coated with PEG to stabilize the nanoparticles for hyperthermia treatments, and have become one of the clinical standards for hyperthermia treatments (and magnetic resonance imaging (MRI)) [124, 125]. When alternating magnetic fields (AMFs) are applied to magnetic nanoparticles like superparamagnetic iron oxide nanoparticles (SPIONs), the SPIONs generate heat that can be used for hyperthermia treatments. Combining hyperthermia with chemotherapy synergistically improves on the cytotoxic effects on cancerous cells of either therapy alone [124, 126, 127], so achieving drug release concurrent to localized hyperthermic heating with these particles could prove quite advantageous. Consequently, numerous core-shell nanoparticles with a magnetic SPION core and polymer coatings loaded with drug have been developed [128, 129]. The polymer coating could also be thermosensitive to improve the diffusion of drug upon hyperthermia heating as well. An example of this is in nanocapsules containing both SPIONs and poly(styrene allyl alcohol) (PS₁₆PAA₁₀) that were capable of releasing hydrophilic fluorescently-labeled DNA plasmids and hydrophobic quantum dots on-demand upon heating induced via short AMF applications [130]. Polymer-coated SPIONs like these can have additional functionalities rather than a drug delivery with hyperthermia alone, but could also be used to generating contrast in MRI, and could be magnetically targeted to the site of interest [131, 132]. The complexity of the magnetic guidance of sufficient quantities of magnetic nanocomposite particles and concurrently using hyperthermia treatments have slowed its clinical application [118], but magnetic nanoparticles are being used for clinical treatments at present [127], so these intriguing advances might be surprisingly close to being realized clinically.

There is also a slight difference in pH that exists between the extracellular environment of solid tumors (6.5–7.2) and healthy tissues (~7.4) that can be exploited for spatially controlled drug release [118]. This disparity is attributed to the abnormal increase in angiogenesis associated with rapidly growing tumors, which leads to a deficit in oxygen and nutrients and a glycolytic metabolism that produces acidic metabolites [118]. This opens the door for the use of pH-responsive polymeric nanomedicines for cancer treatment, provided that their response is sensitive enough to experience a transition due to a subtle change in pH. Chitosan is a pH-sensitive polymer that swells upon the protonation of its amino group ($pK_a \sim 6.3$) and hollow chitosan nanospheres were shown to successfully deliver tumor necrosis factor α (TNF- α) to breast cancer cells upon reaching their slightly acidic environment to suppress their growth of in a murine model [133]. Polymeric micelles have also been designed to possess sharp pH-dependent micellation/demicellation transitions around tumoral pH values (6.4) by using a block copolymer of methyl ether poly(ethylene glycol) (MPEG) and poly(β -amino ester) (PBAE) [134]. These micelles were shown to deliver the chemotherapeutic, camptothecin (CPT), to the target breast cancer site in murine models and burst

due to the low pH of these areas to release an effective quantity of the CPT while lowering the side effects to other tissues over delivery of the free drug alone [134]. Similar micelles of piperidine- and imidazole-modified PEG-PBAE have since been used to treat cerebral ischemia, which is when there is insufficient blood flow to the brain, resulting in a lower pH that can be used to target the therapeutic [135].

These pH-responsive systems can also be combined with inorganic nanoparticles to provide additional functionality. An excellent example of this are the hollow superparamagnetic microgels fabricated via supramolecular assembly by Chiang et al. [132]. These are hollow particles with a pH-sensitive poly(acrylic acid-co-*N*-isopropyl acrylamide (NIPAM)) gel shell containing SPIONs that was stabilized with PEG. The hollow core could be loaded with drug and the particles could be magnetically guided to tumor cells before being internalized. Drug release is induced at acidic pHs (present in intracellular endosomes and lysosomes) and could be enhanced ~12-fold by AMF application [132]. The particles were cytotoxic against tumor cells via drug release and hyperthermia individually, with further enhanced efficacy in when they were used in combination. Another strategy utilized “smart” microgel nanocomposites consisting of gold nanoparticles encapsulated with a p(NIPAM-co-acrylic acid) hydrogel shell that could be internalized by specific cancer cells and release drug due to the lower pH of local intracellular environment [136].

There are several current nanocarrier systems in clinical trials designed to target cancer regions, much more than any other disease or region of the body. The fact that there are much more nanoparticles for chemotherapeutic delivery than any other treatment speaks to the prevalence and threat of cancer to global healthcare and the importance of finding better therapies to combat it. These clinical examples of nanomedicines that target cancers are neatly summarized in an excellent review by Xie et al. [88]. To be fair, most of these nanocarriers are liposomes, which can be functionalized with similar moieties to polymeric nanoparticles, but are cheaper, easier to manufacture, and simpler to get approved by regulatory bodies. They are also less stable and prone to bursting upon injection, a significant issue that polymeric nanomedicines are not as liable to do [108]. Liposomes have been PEGylated to avoid their rapid clearance by the MPS and prolong their circulation time [6, 94], including Caelyx, which has been clinically approved to treat metastatic breast and ovarian cancers as well as doxorubicin but with lesser side effects [137]. A polymeric micelle called Genexol-PM has been approved to deliver paclitaxel, a chemotherapeutic, to treat breast cancer [138]. Polymer-drug conjugates have also been approved to treat leukemia and hepatocellular carcinoma, with asparaginase functionalized with PEG [139] and neocarzinostatin functionalized with poly(styrene-co-maleic acid) [140] respectively, to improve their circulation half-lives. Advanced to preclinical trials are underway for several other drug-loaded polymeric systems, including PLA microgels with a PEG coating, micelles, dendrimers, and polymer-drug conjugates [88].

These delivery systems in preclinical trials and already in the clinic represent significant strides for targeting with nanoparticles in the right direction. However these materials are nowhere close to the “magic bullet” that this field is pursuing. The

development of nanocarriers that can effectively target solid tumors represents the major bottleneck in the advancement of cancer therapeutics and any gains that have been made thus far in their targeting efficiency have been modest [88]. This is because tumors are highly diverse and malleable entities that are extremely hard to predict, with the variations in tumor type and conditions from patient to patient, so it may be impossible to develop a particle to treat a given cancer type or even to predict what a given particle will do and how effective it will be. In fact, even the way that cancers are classified may be not be correct [141], which could inhibit the development of clinical treatment methods. Incremental improvements in targeted delivery will ultimately lead to substantially improved health outcomes, but the large focus on drug delivery using targeting nanoparticles in this field at present may be not be the best route for the field as a whole. As opposed to attempting to do everything at once (nanoparticles are still relatively new, after all), an intensification of simpler, macroscale cancer treatment systems might present as a more logical first step towards using controlled release systems and getting polymeric release systems approved for clinical use in the short term.

3.4 Alternative Cancer Therapies

Macroscale cancer therapies offer extended therapies over nanoparticles as they can be implanted/injected adjacent to solid tumors, can be loaded with more drug, and are not cleared nearly as rapidly. As noted in the section on brain delivery, biodegradable poly(carboxyphenoxypropane-co-sebacic acid) wafers that are implanted after a tumor is removed and can release its payload as it degrades over 3 weeks in this localized treatment regime have been in clinical use for years [57, 58]. Similar implantable systems composed of biodegradable polymers have been explored and clinically utilized post-surgery to help ensure that the cancerous tissues are fully removed, deliver drug locally to decrease the impact of side-effects, and aid in the infiltration of healthy tissues [142].

Similarly, macroscale hydrogel-based controlled release systems can improve chemotherapy by delivering the chemotherapeutic directly to the tumor locally, decreasing the degree of exposure of healthy tissues to the drug to avoid side effects, increasing the half-life of the chemotherapeutic, prolonging the duration of action, and protecting the activity of the drug of interest [121]. Hydrogels have been explored for treating cancers with traditional chemotherapeutics, and combinations of therapeutics, as well as for the delivery to siRNA to improve clinical outcomes [121]. Prefabricated hydrogels made from “bottom-up” processes can be implanted post-surgery or placed adjacent to tumorous regions to treat cancers. A clinical example of this is the biodegradable VANTAS hydrogel that is implanted to deliver controlled, sustained release of histrelin acetate to treat prostate cancer [143]. A significant drawback of “bottom-up” hydrogels is that they have to be synthesized outside of the body and subsequently must be surgically implanted, which is inconvenient for the patient and requires a significant amount of time from medical professionals.

Hydrogels capable of controlled release that can make use in situ gelation via the physical or chemical cross-linking of presynthesized polymer chains, using thermogelation or the use of various biorthogonal (click) reactions, would be much more convenient for all parties involved in cancer treatment [78, 144, 145]. As a result, injectable hydrogels that can be administered to the body without invasive surgery are being explored extensively in drug delivery research. For example, a hydrogel comprised of dendrimers that thermoaggregate to form a gel after injection in the body to locally deliver Dox and the radioisotope [131]. It was shown to exhibit reduced side effects and improved tumor growth suppression and survival outcomes in murine breast cancer models with this combination therapy [146]. This is an example of the combination or concurrent therapies involving multiple chemotherapeutics that have been used for years to combat the heterogeneity and diversity of tumors, as well as the ability of cancer cells to develop resistance to drugs, to achieve better patient outcomes [147].

Numerous strategies involving the delivery of a chemotherapeutic drug along with radiotherapy and gene delivery are now being explored, within both nanomedicines and macroscale hydrogel systems. For example, an in situ forming hydrogel composed of Pluronic F27 (PEO₉₉-PPO₆₇-PEO₉₉) was able to show significant breast tumor suppression via the localized delivery of both paclitaxel, a common chemotherapeutic, and lapatinib, a HER2 kinase inhibitor, in an example of multiple chemotherapeutic combination therapy [148]. Chemotherapeutics have also been combined with microRNA in an implanted hydrogel scaffold for combined therapy (cisplatin was the chemotherapeutic in this case) to show efficacy in shrinking the tumor and prevent its metastasis for a specific form of breast cancer [149]. These studies are examples of the clear benefits of treating tumors with a combination of strategies to eliminate as much of the tumor as possible.

The same can be said for combining chemotherapy with hyperthermia treatments [124, 126, 127]. Magnetic hyperthermia was discussed in the nanoparticle section, but it is often difficult to accumulate sufficient quantities of magnetic nanoparticles at the desired site to make the treatment effective [121]. Magnetic hydrogels with a known concentration of magnetic nanoparticles (often SPIONs) can be placed or injected into specific locations to obtain improved control over hyperthermia treatments. Hydrogel-based materials can have other embedded nanoparticles to create nanocomposite materials capable of facilitating hyperthermia as well, including gold nanoparticles/nanoshells, graphene oxide, and carbon nanotubes, which generate heat in response to near-IR irradiation [150]. Gold nanoparticles are generally used more often than carbon nanotubes, due to their lesser toxicity, but neither can be efficiently cleared from the body, unlike SPIONs [150]. “Smart” nanocomposite hydrogels capable of externally-controlled release can be designed if the hydrogel is made of thermosensitive polymers or if other thermosensitive components are imbedded in the hydrogel along with the inorganic nanoparticles. A good example of a “smart” nanocomposite hydrogels with the potential for concurrent chemotherapy/hyperthermia is a thermosensitive injectable and PNIPAM-based hydrogel with SPION cross-links was able to heat in response to an AMF and release a burst of the model drug as the hydrogel heated and deswelled/compressed [151].

Another thermosensitive PNIPAM-based hydrogel nanocomposite containing gold nanoshells that can generate heat in response to near-IR irradiation was shown to release both Dox and DNA concurrently, and were shown to have an enhanced burst release when near-IR was applied and induced deswelling of the hydrogel (albeit only for a single cycle) [152]. These systems, particularly if they are also injectable and biodegradable, are very promising as they could be capable of achieving remotely-controlled, precise periodic delivery of therapeutics, also termed chronopharmaceutical drug delivery, which would not only be useful for cancer, but many other ailments as well [153].

Nanocomposites capable of chronopharmaceutical drug delivery that could deliver externally-mediated bursts of release over multiple cycles would represent a significant step towards improved “on-demand” cancer therapy [153, 154]. In fact, periodic bursts of chemotherapeutics have shown advantages over the sustained release strategies [1]. The study that determined this was an interesting injectable and self-healing alginate hydrogel that was able to have its calcium cross-links temporarily disrupted by an external ultrasound source before rapidly self-healing. Ultrasound applications were applied daily to delivered daily burst doses of mitoxantrone to effectively shrink xenograft breast cancer tumors [1]. Another nanocomposite system with chronopharmaceutical capability was an injectable hydrogel with embedded SPIONs, thermosensitive microgels, and a model drug [2, 155]. This system could be heated by short AMF applications, shrinking the thermosensitive microgels to enhance the release of drug from the system, and this could be achieved for multiple cycles for at least 5 days [2]. The field as a whole is edging closer and closer towards injectable and degradable systems capable of improved chronopharmaceutical delivery over longer time frames that could benefit a wide range of therapies.

Responsive systems that respond to remote stimuli still have several challenges ahead of them. Chiefly among these is that better chronopharmaceutical control is required for nearly all systems before they can become clinically available, particularly for any of the injectable and biodegradable systems. Even if these advanced “smart” systems were currently capable of well-defined spatiotemporal drug delivery, the trigger mechanisms for nearly all stimuli-responsive materials would have to undergo numerous and complex enhancements and optimizations to scale these actuators up from benchtop to clinical scales.

Another promising new avenue of cancer research is immunotherapy. Immunotherapy can successfully utilize the immune system to detect and treat cancers, highlighted by recent clinical trials involving checkpoint blockade antibodies [156–158]. Cancer vaccines are intended to initiate immune reactivity against existing cancerous tissues through activating antigen presenting cells (APCs) to provoke T lymphocyte cells to specifically lyse tumor cells [147]. Porous polymeric biomaterials (made from gelatin, PLGA, and alginate hydrogels) can improve the efficiency of these immunotherapies by controlling the environment that immune cells come across antigens, cancerous cells, and stimulatory signals [147]. For example, biomaterials can be used to control the rate at which antigens are exposed to APCs, as a short, low-dose of antigen may lead to the failure of a T cell response, and an overexposure to the antigen may lead to T cell exhaustion [147].

A biomaterial vaccine system made from a PLGA hydrogel was shown to be capable of the sustained release of granulocyte macrophage-colony stimulating factors (GM-CSFs) to promote APC accumulation in the scaffold [159, 160]. Within this scaffold, nanoparticles of CpG oligonucleotides are presented to the APCs, which become activated and then migrate to lymph nodes to initiate an anti-cancer immune response. This response was sufficient to show complete the regression of melanoma tumors in 47% of the mice studied [161]. This system is currently undergoing clinical trials, and implantable scaffolds such as this are entirely modular, allowing for a wide range of immunostimulants to be incorporated in their networks [147]. Adjuvants can also be incorporated to further promote immune responses, such as aluminum salts, silica nanoparticles, or cage-like nanoparticles called ISCOMATRIX [147, 162]. There are also several examples nanoscale systems designed to target lymph nodes or APC receptors, based on polystyrene (with optimized sizes of 40 nm), pluronic, and PEGylated nanoparticles [147]. A significant portion of the macroscale hydrogel work has originated from David Mooney's lab, which recently developed porous, injectable, sponge-like cryogel that release GM-CSFs and CpG oligonucleotides to recruit APC to promote specific antitumor immune responses [163]. Overall, using polymeric release systems to mediate the delivery of cancer vaccines at controlled rates presents as a promising emerging methodology to treat cancers from within the patient's own body.

In summary, developing effective methods to treat the dynamic tumor microenvironment has proven challenging. Polymeric controlled release systems have made great advances in cancer therapy, to the point where several advanced controlled release systems have reached the clinic. These systems include both targeting nanomedicines and macroscale biodegradable polymers and hydrogels. Research towards more effective treatments involves the delivery of traditional chemotherapeutic drugs, hyperthermia treatments, gene delivery, immunotherapy, and combinations thereof. There are positive and negative qualities to each strategy and there is no obvious single path to pursue. A single method or strategy to cancer or even a specific subtype of cancer may be unrealistic, as the treatment strategy (along with its regulatory approval process) would likely have to be as malleable as cancers are known to be. Thus, a combination of these strategies is likely the best route, so ensuring that there are minimal side effects for any given strategy/treatment will be important. This is the direction that current cancer research is striving towards. As a result, the successive small improvements in technology that are currently taking place will likely lead to achieving minimizing side effects during treatment while attaining consistently better outcomes in cancer therapy.

4 Current Understanding/Trends and Future Prospective

The general theme underlying much of drug delivery research thus far is that while there are extensive amounts of research taking place, few of these systems are in clinical trials or have reached the market. This is due to the fact that the bulk of the research is currently focused on the development of nanomedicines that are

attempting to be “silver bullets” that solve all of the issues associated with conventional delivery all at once. This is despite the fact that much of the nanomedicines with targeting potential do not reach their intended site of action, with, at best, only ~5% of the best nanomedicines reaching their target [93, 118]. Thus far, nanomedicines have only achieved marginal gains over much of the simple, conventional drug delivery, which has stunted their commercialization potential. Indeed, in terms of nanoparticles, mainly cancer-related treatments are clinically approved or are undergoing clinical trials due to the toxicity of chemotherapeutics and the subsequent benefits of even minor improvement in targeting effectiveness [164, 165].

Achieving effective targeting will continue to be difficult to achieve, due to the heterogeneity of the target tissues, especially between different individuals, and the limited accessibility of many of the biological targets [118]. For example, cancer nanomedicines mostly still rely on the EPR effect, which is unlikely to be clinically relevant, as this is highly dependent on the specific tumor and individual [93]. The rise of personalized medicine might shed light on how to detect some of these differences to predict whether or not specific therapeutic strategies should be effective for specific individuals. In forthcoming decades, personalized medicine could be coupled with more effective targeting therapeutics to achieve better outcomes to a wide variety of therapies.

As the small but consistent improvements in the efficiency of these delivery polymer-based delivery strategies continue, increasing numbers of improved delivery systems will ultimately be introduced into the clinic to improve the healthcare of millions of people. Nanotechnology could revolutionize medicine, and, as indicated by the rapidly increasing number of innovations in the field and the substantial increase in nanotechnology-related patents, one thing is clear: it is here to stay.

That does not mean that the degree to which the drug delivery field as a whole is focusing on targeting systems cannot be questioned. While targeting potential will certainly improve much further as polymer technology and our understanding of the underlying biology advance, the current emphasis on achieving better control over drug release using nanotechnology may be neglecting alternative macroscale delivery strategies that have a good degree of potential. Such technologies are easier to be characterized by regulatory agencies and could allow for novel, improved therapies to help people all over the world in the next few years rather than decades. Indeed, several of the more revolutionary breakthroughs in recent years regarding controlled delivery are from macroscale system, namely the implantable MicroCHIPS device that has unparalleled remote chronopharmaceutical control to treat osteoporosis [166] and the injectable hydrogel scaffolds for immunotherapy [163]. While nanomedicines have a bright future in the long term, the extent of the current shift away from the development of macroscale therapeutic devices may inhibit the commercialization of implantable or injectable polymer-based delivery systems that could improve the healthcare system in the short term (and provide as a platform for “smart” delivery strategies before more beneficial nanoscale examples arise).

There are, however, several scientific and regulatory challenges that must be solved before much of this research leads to tangible commercial products. There are significant challenges regarding the cost of commercializing these systems and the

regulatory concerns associated with new developments. For example, the cost of developing novel hydrogel controlled release systems is estimated as \$50 million to \$800 million USD, providing significant barriers to commercialization [167]. The systems discussed in this and the previous chapter involve drug release systems have drug contained within a polymeric systems and are thus considered combination products by the regulatory agencies, which slows the regulatory process to 7–10 years [167]. In comparison, scaffolds without containing drug typically take 1–5 years to successfully advance through the regulatory process. This longer timeframe can limit commercial viability with the finite timeframe for patent protection [167]. There is also a balance that must be met between complex “smart” drug releasing systems that can improve therapy and simple systems that can more easily traverse the FDA process.

Nanomedicines are generally trickier to achieve FDA approval from, as assessing their safety is much more difficult. Most nanoparticles will end up in the lungs (particularly if they are large, >150 nm), liver, kidney, and spleen [168]. Safety concerns regarding the accumulation of materials in these organs are paramount, and new methods of safely studying and analyzing the cumulative effects of nanoparticles over time must be developed. This is why the development of new innovations in materials and polymer systems that are biodegradable and can be efficiently cleared from the body is of such importance. Furthermore, the toxicological effects of functionalizing nanoparticles with specific targeting ligands must be further studied. An important step towards realizing this will be the development of standardized nanotoxicity assessments, along with innovations in tagging nanocarriers and observing their biodispersity over time, that will result in improved knowledge of what properties and characteristics of nanoparticles cause toxicity and lead to safer, more effective nanomedicines in the future [169]. A nanotoxicological classification system (NCS) is currently being proposed in order to establish such a standardized methodology for evaluating the safety of nanomedicines [170].

There are several other barriers that currently impede the process of getting a controlled drug delivery system from the benchtop to the clinic. One major issue is that there are often poor relations between 2D *in vitro* models and *in vivo* animal studies, and incompatibilities between the animal models used in *in vivo* studies and the humans that the drug systems are being developed for. These incompatibilities have led to thousands of drug delivery systems failing as they go from *in vitro* to *in vivo* studies or failing in preclinical and clinical studies as technologies that were shown to be effective in animal models are ineffective or cause hazardous side effects in humans. This unfortunately may be the case of several of the studies showing success in mouse studies discussed in this chapter. The inverse is likely true too, as several systems that may have been effective in humans and shown real commercial promise may have been phased out earlier on when they exhibited insufficient efficacies in 2D cell culture or in animal models.

Tissue engineering that focuses on the development of 3D models to test drugs and polymeric drug releasing systems on are a potential solution to this issue. Hydrogels can be used to engineer small scale 3D *in vitro* systems or can be incorporated into emerging organ-on-a-chip technologies to better mimic conditions within the human

body. This, along with improvements in tissue engineering of larger scale organoids (often using hydrogels with specific functionalities to mirror human soft tissues), could result in improved relations between preclinical and clinical studies [121]. These systems could ultimately replace the use of 2D *in vitro* and animal *in vivo* work in the future. If they are effective enough at mimicking human tissues, they may ultimately be incorporated into and accelerate the regulatory process for new drugs and drug delivery systems, and could be used to test how specific individuals react to specific drugs or drug delivery systems [171].

There are several other emerging technologies that could significantly impact and alter the direction of drug delivery research are on the horizon. Clustered regularly interspaced short palindromic repeats (CRISPR)-Cas9 is a new disruptive gene editing technology that is capable of site-specific modifications of DNA using guide RNAs that recognizes the specific DNA target sequences in a surprisingly simple process [172]. As a result, laboratories worldwide are utilizing this technology throughout biology, but it will be crucial for many of these applications to develop methods to safely and efficiently deliver Cas9 and its guide RNA via novel nanoscale polymeric drug delivery systems. These early systems would likely attempt to target specific cells by having certain surface functionalities to deliver their payload within the cell.

The cells in your body constantly regulate the nutrients that they take in and the waste products they excrete. Specialty cells can also regulate important proteins, hormones, and growth factors in your body. This is how glucose levels are maintained in the body to sustain normoglycemia. In this case, functioning beta islet cells optimized to monitor glucose levels and deliver the appropriate amount of insulin to regulate bodily glucose concentrations. Cellular therapies utilize regulatory cells like this to deliver appropriate levels of hormones and other materials to the body. However, it is difficult to maintain healthy allogeneic or xenogeneic cells without activating the immune system, which limits the duration of cellular therapies [173]. As such, much research centers on prolonging the lifetime and efficacy of these cellular therapies. The most successful example of this may be a system where beta islet cells that produce and deliver insulin where encased in 1.5-mm triazole-thiomorpholine dioxide-functionalized alginate hydrogel spheres [173]. The size and functionality of the hydrogel spheres were carefully selected via combinatorial library of materials as they were found to elicit minimal foreign body responses over long time frames (>6 months) [174, 175]. The resulting hydrogel spheres were able to keep the beta cells active and able to maintain normoglycemia in non-human primates for an unprecedented 6 months, an extraordinary result [173]. This is a perfect example of how effective cellular therapies can be in delivering drugs when the integration of polymers and cells is designed correctly.

There are also several theories to counter the effects of aging that are currently being explored. Senescent cells are cells that no longer grow and remain viable [176]. These cells are thought to be a significant proponent of aging (and multiple other chronic diseases) [176], as they build up over time, and a study that cleared just 30% of senescent cells showed significant improvements in age related phenotypes in mice as a result [177]. These cells are believed to be dependent on antiapoptotic

pathways to persist in the body and are susceptible to be cleared by several drugs and siRNAs known as synolytic agents [176]. “Smart” polymeric drug delivery devices that are capable of delivering intermittent doses, potentially by periodic or chronopharmaceutical delivery, of synolytic agents thus could have the potential to treat the effects of aging and other chronic diseases [176].

There are also new mechanisms for targeting nanomedicines being developed. For example, self-propelled nanocarriers are in the proof-of-concept stage, making use of chemical reactions to aid the targeting of a nanomedicine to its desired target [178]. This is a small step towards nanorobots that circulate in the blood stream and search out diseases, what some people envision as the ultimate “silver bullet.”

Overall, the field of drug delivery still has a wide range of challenges that must be overcome to translate some of the research involving polymeric systems into commercial real-world products. Drug delivery is at the intersection of several other complementary disciplines, including polymer chemistry, biology, nanotechnology, medicine, toxicology, and more. It requires knowledge of each of these broad fields in order to successfully design and produce novel drug carriers for specific purposes. This is also still a young, cutting-edge field, and yet we may just be on the cusp of many of these release systems reaching the market sooner rather than later.

The landscape of the field of drug delivery is constantly shifting and will change significantly in the coming decades, with the recent disruptive technologies and ideas spread within this field, including CRISPR technology, antiaging techniques, the prospect of individualized medicine, organ-on-a-chip technologies, and many more, as well as the introduction of new technologies that there is no way of anticipating. The field is continuing to transition into improved solutions, there are significant challenges up ahead. Issues associated with the regulatory system, quality control, reproducibility, and toxicity are will be particularly important if clinical drug delivery is to transition further towards nanoscale materials and systems [168]. However, these obstacles will be overcome, and, until then, the field of drug delivery using polymer systems will continue to expand and become immensely beneficial to health and well-being of people all over the world.

References

1. N. Huebsch, C.J. Kearney, X. Zhao, J. Kim, C.A. Cezar, Z. Suo, D.J. Mooney, Ultrasound-triggered disruption and self-healing of reversibly cross-linked hydrogels for drug delivery and enhanced chemotherapy. *Proc. Natl. Acad. Sci. U. S. A.* **111**, 9762–9767 (2014)
2. D. Maitland, S.B. Campbell, J. Chen, T. Hoare, Controlling the resolution and duration of pulsatile release from injectable magnetic “plum pudding” nanocomposite hydrogels. *RSC Adv.* **6**, 15770–15781 (2016)
3. S.V. Sastry, J.R. Nyshadham, J.A. Fix, Recent technological advances in oral drug delivery – a review. *Pharm. Sci. Technol. Today* **3**, 138–145 (2000)
4. L.M. Ensign, R. Cone, J. Hanes, Oral drug delivery with polymeric nanoparticles: the gastrointestinal mucus barriers. *Adv. Drug Deliv. Rev.* **64**, 557–570 (2012)
5. E.M. Pridgen, F. Alexis, O.C. Farokhzad, Polymeric nanoparticle technologies for oral drug delivery challenges of oral delivery. *Clin. Gastroenterol. Hepatol.* **12**, 1605–1610 (2014)
6. R. Langer, Drug delivery and targeting. *Nature* **392**, 5–10 (1998)

7. K. Sonaje, K. Lin, S. Wey, C. Lin, T. Yeh, H. Nguyen, C. Hsu, T. Yen, J. Juang, H. Sung, Biodistribution, pharmacodynamics and pharmacokinetics of insulin analogues in a rat model: oral delivery using pH-responsive nanoparticles vs. subcutaneous injection. *Biomaterials* **31**, 6849–6858 (2010)
8. Q. Xu, L.M. Ensign, N.J. Boylan, A. Schon, X. Gong, J.-C. Yang, N.W. Lamb, S. Cai, T. Yu, E. Freire, J. Hanes, Impact of surface polyethylene glycol (PEG) density on biodegradable nanoparticle transport in mucus ex vivo and distribution in vivo. *ACS Nano* **9**, 9217–9227 (2015)
9. K.Y. Win, S. Feng, Effects of particle size and surface coating on cellular uptake of polymeric nanoparticles for oral delivery of anticancer drugs. *Biomaterials* **26**, 2713–2722 (2005)
10. E. Cochran, C. Musso, P. Gorden, The use of U-500 in patients with extreme insulin resistance. *Diabetes Care* **28**, 1240–1244 (2005)
11. M. Chen, K. Sonaje, K. Chen, H. Sung, A review of the prospects for polymeric nanoparticle platforms in oral insulin delivery. *Biomaterials* **32**, 9826–9838 (2011)
12. L.T. Kuhn, *Biomaterials*, in *Introduction to Biomedical Engineering*, 4th edn., ed. by J. Enderle, S. Blanchard, J. Bronzino (Elsevier Academic, Burlington, 2005)
13. N.A. Peppas, P. Bures, W. Leobandung, H. Ichikawa, Hydrogels in pharmaceutical formulations. *Eur. J. Pharm. Biopharm.* **50**, 27–46 (2000)
14. Y. Kim, J. Park, M.R. Prausnitz, Microneedles for drug and vaccine delivery. *Adv. Drug Deliv. Rev.* **64**, 1547–1568 (2012)
15. M.R. Prausnitz, R. Langer, Transdermal drug delivery. *Nat. Biotechnol.* **26**, 1261–1268 (2008)
16. N.R. Mathias, M.A. Hussain, Non-invasive systemic drug delivery: developability considerations for alternate routes of administration. *J. Pharm. Sci.* **99**, 1–20 (2010)
17. J.J. Norman, J.M. Arya, M.A. McClain, P.M. Frew, M.I. Meltzer, M.R. Prausnitz, Microneedle patches: usability and acceptability for self-vaccination against influenza. *Vaccine* **32**, 1856–1862 (2014)
18. E.M. Saurer, R.M. Flessner, S.P. Sullivan, M.R. Prausnitz, D.M. Lynn, Layer-by-layer assembly of DNA- and protein-containing films on microneedles for drug delivery to the skin. *Biomacromolecules* **11**, 3136–3143 (2010)
19. B.P.C. Demuth, X. Su, R.E. Samuel, P.T. Hammond, D.J. Irvine, Nano-layered microneedles for transcutaneous delivery of polymer nanoparticles and plasmid DNA. *Adv. Mater.* **22**, 4851–4856 (2010)
20. M. Kim, B. Jung, J. Park, Hydrogel swelling as a trigger to release biodegradable polymer microneedles in skin. *Biomaterials* **33**, 668–678 (2012)
21. G. Wiedermann, Patient compliance in the use of Vivotif Berna vaccine, typhoid vaccine, live oral Ty21a. *J. Travel Med.* **5**, 1–2 (1998)
22. J.S. Boateng, K.H. Matthews, H.N.E. Stevens, G.M. Eccleston, Wound healing dressings and drug delivery systems: a review. *J. Pharm. Sci.* **97**, 2892–2923 (2008)
23. H. Ueno, T. Mori, T. Fujinaga, Topical formulations and wound healing applications of chitosan. *Adv. Drug Deliv. Rev.* **52**, 105–115 (2001)
24. Y. Sawadal, M. Ara, T. Yotsuyanagi, K. Sonet, Treatment of dermal depth burn wounds with an antimicrobial agent-releasing silicone gel sheet. *Burns* **16**, 347–352 (1990)
25. A.C. Lee, H. Leem, J. Lee, K. Chan, Reversal of silver sulfadiazine-impaired wound healing by epidermal growth factor. *Biomaterials* **26**, 4670–4676 (2005)
26. S. Park, J. Koo, H. Suh, Evaluation of antibiotic-loaded collagen-hyaluronic acid matrix as a skin substitute. *Biomaterials* **25**, 3689–3698 (2004)
27. H. Storrie, D.J. Mooney, Sustained delivery of plasmid DNA from polymeric scaffolds for tissue engineering. *Adv. Drug Deliv. Rev.* **58**, 500–514 (2006)
28. M.M. Bailey, C.J. Berkland, Nanoparticle formulations in pulmonary drug delivery. *Med. Res. Rev.* **29**, 196–212 (2008)
29. J.S. Patil, S. Sarasija, Pulmonary drug delivery strategies: a concise, systematic review. *Lung India* **29**, 44–49 (2012)

30. D.A. Edwards, J. Hanes, G. Caponetti, J. Hrkach, A. Ben-Jebria, M. Lou Eskew, J. Mintzes, D. Deaver, N. Lotan, R. Langer, Large porous particles for pulmonary drug delivery. *Science* **276**, 1868–1871 (1997)
31. E. Rytting, J. Nguyen, X. Wang, T. Kissel, Biodegradable polymeric nanocarriers for pulmonary drug delivery. *Expert Opin. Drug Deliv.* **5**, 629–639 (2008)
32. M. Beck-Broichsitter, O.M. Merkel, T. Kissel, Controlled pulmonary drug and gene delivery using polymeric nano-carriers. *J. Control. Release* **161**, 214–224 (2012)
33. F. Ungaro, I. Angelo, A. Miro, M.I. La Rotonda, F. Quaglia, Engineered PLGA nano- and micro-carriers for pulmonary delivery: challenges and promises. *J. Pharm. Pharmacol.* **64**, 1217–1235 (2012)
34. M. Paranjpe, C.C. Müller-Goymann, Nanoparticle-mediated pulmonary drug delivery: a review. *Int. J. Mol. Sci.* **15**, 5852–5873 (2014)
35. J.S. Patton, C.S. Fishburn, J.G. Weers, The lungs as a portal of entry for systemic drug delivery. *Proc. Am. Thorac. Soc.* **1**, 338–344 (2004)
36. J.C. Sung, D.J. Padilla, L. Garcia-Contreras, J.L. Verberkmoes, D. Durbin, C.A. Peloquin, K.J. Elbert, A.J. Hickey, D.A. Edwards, Formulation and pharmacokinetics of self-assembled rifampicin nanoparticle systems for pulmonary delivery. *Pharm. Res.* **26**, 1847–1855 (2009)
37. M. Dutt, G.K. Khuller, Chemotherapy of *Mycobacterium tuberculosis* infections in mice with a combination of isoniazid and rifampicin entrapped in poly(DL-lactide-co-glycolide) microparticles. *J. Antimicrob. Chemother.* **47**, 829–835 (2001)
38. M. Dutt, G.K. Khuller, Sustained release of isoniazid from a single injectable dose of poly(DL-lactide-co-glycolide) microparticles as a therapeutic approach towards tuberculosis. *Int. J. Antimicrob. Agents* **17**, 115–122 (2001)
39. I.M. El-Sherbiny, S. McGill, H.D.C. Smyth, Swellable microparticles as carriers for sustained pulmonary drug delivery. *J. Pharm. Sci.* **99**, 2343–2356 (2010)
40. E. Kleemann, M. Neu, N. Jekel, L. Fink, T. Schmehl, T. Gessler, W. Seeger, T. Kissel, Nano-carriers for DNA delivery to the lung based upon a TAT-derived peptide covalently coupled to PEG-PEI. *J. Control. Release* **109**, 299–316 (2005)
41. J. Nguyen, T.W.J. Steele, O. Merkel, R. Reul, T. Kissel, Fast degrading polyesters as siRNA nano-carriers for pulmonary gene therapy. *J. Control. Release* **132**, 243–251 (2008)
42. W. Zhang, H. Yang, X. Kong, S. Mohapatra, H.S. Juan-Vergara, G. Hellermann, S. Behera, R. Singam, R.F. Lockey, S.S. Mohapatra, Inhibition of respiratory syncytial virus infection with intranasal siRNA nanoparticles targeting the viral NS1 gene. *Nat. Med.* **11**, 56–62 (2005)
43. X. Kong, W. Zhang, R.F. Lockey, A. Auais, G. Piedimonte, S.S. Mohapatra, Respiratory syncytial virus infection in Fischer 344 rats is attenuated by short interfering RNA against the RSV-NS1 gene. *Genet. Vaccines Ther.* **5**, 1–8 (2007)
44. H. Yamamoto, Y. Kuno, S. Sugimoto, H. Takeuchi, Y. Kawashima, Surface-modified PLGA nanosphere with chitosan improved pulmonary delivery of calcitonin by mucoadhesion and opening of the intercellular tight junctions. *J. Control. Release* **102**, 373–381 (2005)
45. K.K. Gill, S. Nazzal, A. Kaddoumi, Paclitaxel loaded PEG5000–DSPE micelles as pulmonary delivery platform: formulation characterization, tissue distribution, plasma pharmacokinetics, and toxicological evaluation. *Eur. J. Pharm. Biopharm.* **79**, 276–284 (2011)
46. S. Wohlfart, S. Gelperina, J. Kreuter, Transport of drugs across the blood – brain barrier by nanoparticles. *J. Control. Release* **161**, 264–273 (2012)
47. P.R. Lockman, R.J. Mumper, M.A. Khan, D.D. Allen, Nanoparticle technology for drug delivery across the blood-brain barrier. *Drug Dev. Ind. Pharm.* **28**, 1–13 (2002)
48. M. Elsbahy, K.L. Wooley, Design of polymeric nanoparticles for biomedical delivery applications. *Chem. Soc. Rev.* **41**, 2545–2561 (2012)
49. H.-L. Liu, M.-Y. Hua, P.-Y. Chen, P.-C. Chu, C.-H. Pan, H.-W. Yang, C.-Y. Huang, J.-J. Wang, T.-C. Yen, K.-C. Wei, Blood-brain barrier disruption with focused ultrasound enhances delivery of chemotherapeutic drugs for glioblastoma treatment. *Radiology* **255**, 415–425 (2010)

50. J. Nicolas, S. Mura, D. Brambilla, N. Mackiewicz, P. Couvreur, Design, functionalization strategies and biomedical applications of targeted biodegradable/biocompatible polymer-based nanocarriers for drug delivery. *Chem. Soc. Rev.* **42**, 1147–1235 (2013)
51. Z. Pang, L. Feng, R. Hua, J. Chen, H. Gao, S. Pan, X. Jiang, P. Zhang, Lactoferrin-conjugated biodegradable polymersomes holding doxorubicin and tetrandrine for chemotherapy of glioma rats. *Mol. Pharm.* **7**, 1995–2005 (2010)
52. Z. Pang, H. Gao, Y. Yu, L. Guo, J. Chen, S. Pan, J. Ren, Z. Wen, X. Jiang, Enhanced intracellular delivery and chemotherapy for glioma rats by transferrin-conjugated biodegradable polymersomes loaded with doxorubicin. *Bioconjug. Chem.* **22**, 1171–1180 (2011)
53. H. Gao, J. Qian, S. Cao, Z. Yang, Z. Pang, S. Pan, L. Fan, Z. Xi, X. Jiang, Precise glioma targeting of and penetration by aptamer and peptide dual-functioned nanoparticles. *Biomaterials* **33**, 5115–5123 (2012)
54. U. Bickel, T. Yoshikawa, W.M. Pardridge, Delivery of peptides and proteins through the blood–brain barrier. *Adv. Drug Deliv. Rev.* **46**, 247–279 (2001)
55. L. Illum, Nasal drug delivery – possibilities, problems and solutions. *J. Control. Release* **87**, 187–198 (2003)
56. J. Piazza, T. Hoare, L. Molinaro, K. Terpstra, J. Bhandari, P.R. Selvaganapathy, B. Gupta, R.K. Mishra, Haloperidol-loaded intranasally administered lectin functionalized poly(ethylene glycol)–block-poly (D,L)-lactic-co-glycolic acid (PEG-PLGA) nanoparticles for the treatment of schizophrenia. *Eur. J. Pharm. Biopharm.* **87**, 30–39 (2014)
57. F.J. Attenello, D. Mukherjee, G. Dato, M.J. McGirt, E. Bohan, J.D. Weingart, A. Olivi, A. Quinones-Hinojosa, H. Brem, Use of Gliadel (BCNU) wafer in the surgical treatment of malignant glioma: a 10-year institutional experience. *Ann. Surg. Oncol.* **15**, 2887–2893 (2008)
58. H. Brem, S. Piantadosi, P.C. Burger, M. Walker, R. Selker, N.A. Vick, K. Black, M. Sisti, S. Brem, G. Mohr, P. Muller, R. Morawetz, S.C. Schold, Placebo-controlled trial of safety and efficacy of intraoperative controlled delivery by biodegradable polymers of chemotherapy for recurrent gliomas. *Lancet* **345**, 1008–1012 (1995)
59. S. Kunwar, S. Chang, M. Westphal, M. Vogelbaum, J. Sampson, G. Barnett, M. Shaffrey, Z. Ram, J. Piepmeyer, M. Prados, D. Croteau, C. Pedain, P. Leland, S.R. Husain, B.H. Joshi, R.K. Puri, Phase III randomized trial of CED of IL13-PE38QQR vs Gliadel wafers for recurrent glioblastoma. *Neuro Oncol.* **12**, 871–881 (2010)
60. G.Y. Kim, B.M. Tyler, M.M. Tupper, J.M. Karp, R.S. Langer, H. Brem, M.J. Cima, Resorbable polymer microchips releasing BCNU inhibit tumor growth in the rat 9L flank model. *J. Control. Release* **123**, 172–178 (2007)
61. U.B. Kompella, A.C. Amrite, R. Pacha, S.A. Durazo, Nanomedicines for back of the eye drug delivery, gene delivery, and imaging. *Prog. Retin. Eye Res.* **36**, 172–198 (2013)
62. M.E. Myles, D.M. Neumann, J.M. Hill, Recent progress in ocular drug delivery for posterior segment disease: emphasis on transscleral iontophoresis. *Adv. Drug Deliv. Rev.* **57**, 2063–2079 (2005)
63. M.N. Yasin, D. Svirskis, A. Seyfoddin, I.D. Rupenthal, Implants for drug delivery to the posterior segment of the eye: a focus on stimuli-responsive and tunable release systems. *J. Control. Release* **196**, 208–221 (2014)
64. Y. Chun, B. Chiang, X. Wu, M.R. Prausnitz, Ocular delivery of macromolecules. *J. Control. Release* **190**, 172–181 (2014)
65. E. Lavik, M.H. Kuehn, Y.H. Kwon, Novel drug delivery systems for glaucoma. *Eye* **25**, 578–586 (2011)
66. N. Kuno, S. Fujii, Recent advances in ocular drug delivery systems. *Polymers* **3**, 193–221 (2011)
67. N. Nagai, H. Kaji, H. Onami, Y. Ishikawa, M. Nishizawa, A polymeric device for controlled transscleral multi-drug delivery to the posterior segment of the eye. *Acta Biomater.* **10**, 680–687 (2014)
68. M. Allansmith, A. De Ramus, D. Maurice, The dynamics of IgG in the cornea. *Invest. Ophthalmol. Vis. Sci.* **18**, 947–955 (1979)

69. H. Sheardown, Critical role for drug delivery in the development of new ophthalmic treatments. *Future Med. Chem.* **4**, 2123–2125 (2012)
70. S.D. Fitzpatrick, M.A. Jafar Mazumder, F. Lasowski, L.E. Fitzpatrick, H. Sheardown, PNIPAAm-grafted-collagen as an injectable, in situ gelling, bioactive cell delivery scaffold. *Biomacromolecules* **11**, 2261–2267 (2010)
71. V. Delplace, S. Payne, M. Shoichet, Delivery strategies for treatment of age-related ocular diseases: from a biological understanding to biomaterial solutions. *J. Control. Release* **219**, 652–668 (2015)
72. T.R. Thrimawithana, S. Young, C.R. Bunt, C. Green, R.G. Alany, Drug delivery to the posterior segment of the eye. *Drug Discov. Today* **16**, 270–277 (2011)
73. F.M. Veronese, A. Mero, The impact of PEGylation on biological therapies. *BioDrugs* **22**, 315–329 (2008)
74. J. Jiang, J.S. Moore, H.F. Edelhauser, M.R. Prausnitz, Intrasceral drug delivery to the eye using hollow microneedles. *Pharm. Res.* **26**, 399–403 (2009)
75. S.R. Patel, A.S. Lin, H.F. Edelhauser, M.R. Prausnitz, Suprachoroidal drug delivery to the back of the eye using hollow microneedles. *Pharm. Res.* **28**, 166–176 (2011)
76. A.L. Gomes dos Santos, A. Bochot, A. Doyle, N. Tzapis, J. Siepmann, F. Siepmann, J. Schmalzer, M. Besnard, F. Behar-Cohen, E. Fattal, Sustained release of nanosized complexes of polyethylenimine and anti-TGF- β 2 oligonucleotide improves the outcome of glaucoma surgery. *J. Control. Release* **112**, 369–381 (2006)
77. T. Hoare, S.B. Campbell, W.-I. Wu, J. Yang, P.R. Selvaganapathy, A microinjection device for delivering in situ-gelling hydrogels for posterior segment drug delivery. *Invest. Ophthalmol. Vis. Sci.* **55**, 478 (2014)
78. M. Patenaude, N.M.B. Smeets, T. Hoare, Designing injectable, covalently cross-linked hydrogels for biomedical applications. *Macromol. Rapid Commun.* **35**(6), 1–20 (2014)
79. G. Zhu, Y. Zhang, K. Wang, X. Zhao, H. Lian, H. Wang, J. Wu, Y. Hu, H. Guo, G. Zhu, Y. Zhang, K. Wang, X. Zhao, H. Lian, G. Zhu, Y. Zhang, K. Wang, X. Zhao, H. Lian, W. Wang, H. Wang, Visualized intravesical floating hydrogel encapsulating vaporized perfluoropentane for controlled drug release. *Drug Deliv.* **23**, 2820–2826 (2016)
80. D. Zhang, P. Sun, P. Li, A. Xue, X. Zhang, H. Zhang, X. Jin, A magnetic chitosan hydrogel for sustained and prolonged delivery of Bacillus Calmette-Guérin in the treatment of bladder cancer. *Biomaterials* **34**, 10258–10266 (2013)
81. Y.L. Traore, Y. Chen, A. Bernier, A. Ho, Impact of hydroxychloroquine-loaded polyurethane intravaginal rings on Lactobacilli. *Antimicrob. Agents Chemother.* **59**, 7680–7686 (2015)
82. E.A. Ho, Intravaginal rings as a novel platform for mucosal vaccination. *Mol. Pharm. Org. Process Res.* **1**, 1–2 (2013)
83. S. Kim, Y. Chen, E.A. Ho, S. Liu, Reversibly pH-responsive polyurethane membranes for on-demand intravaginal drug delivery. *Acta Biomater.* **47**, 100–112 (2017)
84. S. Yang, Y. Chen, R. Ahmadie, E.A. Ho, Advancements in the field of intravaginal siRNA delivery. *J. Control. Release* **167**, 29–39 (2013)
85. W.C. Carlyle, J.B. McClain, A.R. Tzafiriri, L. Bailey, G. Brett, P.M. Markham, J.R.L. Stanley, E.R. Edelman, Enhanced drug delivery capabilities from stents coated with absorbable polymer and crystalline drug. *J. Control. Release* **162**, 561–567 (2015)
86. L. Lei, S. Guo, W. Chen, H. Rong, F. Lu, Stents as a platform for drug delivery. *Expert Opin. Drug Deliv.* **8**, 813–831 (2011)
87. T. Keler, V. Ramakrishna, M. Fanger, Mannose receptor-targeted vaccines. *Expert Opin. Biol. Ther.* **4**, 1953–1962 (2004)
88. T. Sun, Y.S. Zhang, B. Pang, D.C. Hyun, M. Yang, Y. Xia, Engineered nanoparticles for drug delivery in cancer therapy. *Angew. Chem. Int. Ed.* **53**, 12320–12364 (2014)
89. D. Hanahan, R.A. Weinberg, The hallmarks of cancer. *Cell* **100**, 57–70 (2000)
90. D. Peer, J.M. Karp, S. Hong, O.C. Farokhzad, R. Margalit, R. Langer, Nanocarriers as an emerging platform for cancer therapy. *Nat. Nanotechnol.* **2**, 751–760 (2007)

91. R. Tong, D.S. Kohane, New strategies in cancer nanomedicine. *Annu. Rev. Pharmacol. Toxicol.* **56**, 41–57 (2016)
92. T.M. Allen, P.R. Cullis, Drug delivery systems: entering the mainstream. *Science* **303**, 1818–1822 (2003)
93. Y.H. Bae, K. Park, Targeted drug delivery to tumors: myths, reality and possibility. *J. Control. Release* **153**, 198–205 (2012)
94. A.A. Gabizon, Stealth liposomes and tumor targeting: one step further in the quest for the magic bullet. *Clin. Cancer Res.* **7**, 223–225 (2001)
95. A.K. Iyer, G. Khaled, J. Fang, H. Maeda, Exploiting the enhanced permeability and retention effect for tumor targeting. *Drug Discov. Today* **11**, 812–818 (2006)
96. G. Bergers, L.E. Benjamin, Tumorigenesis and the angiogenic switch. *Nat. Rev. Cancer* **3**, 401–410 (2003)
97. B. Haley, E. Frenkel, Nanoparticles for drug delivery in cancer treatment. *Urol. Oncol.* **26**, 57–64 (2008)
98. Y. Matsumura, H. Maeda, A new concept for macromolecular therapeutics in cancer chemotherapy: mechanism of tumorotropic accumulation of proteins and the antitumor agent smancs. *Cancer Res.* **46**, 6387–6392 (1986)
99. M.J. Alonso, Nanomedicines for overcoming biological barriers. *Biomed. Pharmacother.* **58**, 168–172 (2004)
100. R.K. Jain, T. Stylianopoulos, Delivering nanomedicine to solid tumors. *Nat. Rev. Clin. Oncol.* **7**, 653–664 (2010)
101. P. Decuzzi, S. Lee, B. Bhushan, M. Ferrari, A theoretical model for the margination of particles within blood vessels. *Ann. Biomed. Eng.* **33**, 179–190 (2005)
102. P. Decuzzi, R. Pasqualini, W. Arap, M. Ferrari, Intravascular delivery of particulate systems: does geometry really matter? *Pharm. Res.* **26**, 235–243 (2009)
103. V.P. Torchilin, Recent advances with liposomes as pharmaceutical carriers. *Nat. Rev. Drug Discov.* **4**, 145–160 (2005)
104. H.M. Warenius, G. Galfre, N.M. Bleehen, C. Milstein, Attempted targeting of a monoclonal antibody in a human tumour xenograft system. *Eur. J. Cancer Clin. Oncol.* **17**, 1009–1015 (1981)
105. D.E.L. De Menezes, L.M. Pilarski, T.M. Allen, In vitro and in vivo targeting of immunoliposomal doxorubicin to human B-cell lymphoma. *Cancer Res.* **58**, 3320–3331 (2000)
106. J.W. Park, K. Hong, D.B. Kirpotin, G. Colbern, R. Shalaby, J. Baselga, Y. Shao, U.B. Nielsen, J.D. Marks, D. Moore, D. Papahadjopoulos, C.C. Benz, Anti-HER2 immunoliposomes: enhanced efficacy attributable to targeted delivery. *Clin. Cancer Res.* **8**, 1172–1181 (2002)
107. J. Majoros, B.G. Orr, J.R. Baker, S. Hong, P.R. Leroueil, M.M.B. Holl, The binding avidity of a nanoparticle-based multivalent targeted drug delivery platform. *Chem. Biol.* **14**, 107–115 (2007)
108. D. Peer, P. Zhu, C.V. Carmen, J. Lieberman, M. Shimaoka, Selective gene silencing in activated leukocytes by targeting siRNAs to the integrin lymphocyte function-associated antigen-1. *Proc. Natl. Acad. Sci. U. S. A.* **104**, 4095–4100 (2007)
109. O.C. Farokhzad, J. Cheng, B.A. Tepy, I. Sherifi, S. Jon, P. Kantoff, J.P. Richie, R. Langer, Targeted nanoparticle-aptamer bioconjugates for cancer chemotherapy in vivo. *Proc. Natl. Acad. Sci. U. S. A.* **103**, 6315–6320 (2006)
110. Y.N. Dou, J. Zheng, W.D. Foltz, R. Weersink, N. Chaudary, D.A. Jaffray, C. Allen, Heat-activated thermosensitive liposomal cisplatin (HTLC) results in effective growth delay of cervical carcinoma in mice. *J. Control. Release* **178**, 69–78 (2014)
111. S. Heilmann, S. Kuchler, C. Wischke, A. Lendlein, C. Stein, M. Schäfer-Korting, A thermosensitive morphine-containing hydrogel for the treatment of large-scale skin wounds. *Int. J. Pharm.* **444**, 96–102 (2013)
112. R. Pelton, Temperature-sensitive aqueous microgels. *Adv. Colloid Interface Sci.* **85**, 1–33 (2000)

113. C. Ju, R. Mo, J. Xue, L. Zhang, Z. Zhao, L. Xue, Q. Ping, C. Zhang, Sequential intra-intercellular nanoparticle delivery system for deep tumor penetration. *Angew. Chem. Int. Ed.* **53**, 6253–6258 (2014)
114. C.L. Lay, J.N. Kumar, C.K. Liu, X. Lu, Y. Liu, A rocket-like encapsulation and delivery system with two-stage booster layers: pH-responsive poly(methacrylic acid)/poly(ethylene glycol) complex-coated hollow silica vesicles. *Macromol. Rapid Commun.* **34**, 1563–1568 (2013)
115. X. Yao, L. Chen, X. Chen, C. He, J. Zhang, X. Chen, Metallo-supramolecular nanogels for intracellular pH-responsive drug release. *Macromol. Rapid Commun.* **35**, 1697–1705 (2014)
116. T. Hoare, R. Pelton, Charge-switching, amphoteric glucose-responsive microgels with physiological swelling activity. *Biomacromolecules* **9**, 733–740 (2008)
117. A. Matsumoto, K. Yamamoto, R. Yoshida, K. Kataoka, T. Aoyagi, Y. Miyahara, A totally synthetic glucose responsive gel operating in physiological aqueous conditions. *Chem. Commun.* **46**, 2203–2205 (2010)
118. S. Mura, J. Nicolas, P. Couvreur, Stimuli-responsive nanocarriers for drug delivery. *Nat. Mater.* **12**, 991–1003 (2013)
119. S. Merino, C. Martin, K. Kostarelos, M. Prato, E. Vazquez, Nanocomposite hydrogels: 3D polymer-nanoparticle synergies for on-demand drug delivery. *ACS Nano* **9**, 4686–4697 (2015)
120. S. Laurent, D. Forge, M. Port, A. Roch, C. Robic, L. Vander Elst, R.N. Muller, Magnetic iron oxide nanoparticles: synthesis, stabilization, vectorization, physicochemical characterizations, and biological applications. *Chem. Rev.* **108**, 2064–2110 (2008)
121. M. Sepantafar, R. Maheronnaghsh, H. Mohammadi, F. Radmanesh, M.M. Hasani-Sadrabadi, M. Ebrahimi, Engineered hydrogels in cancer therapy and diagnosis. *Trends Biotechnol.* **35**, 1074–1087 (2017)
122. T. Tagami, W.D. Foltz, M.J. Ernsting, C.M. Lee, I.F. Tannock, J.P. May, S. Li, MRI monitoring of intratumoral drug delivery and prediction of the therapeutic effect with a multifunctional thermosensitive liposome. *Biomaterials* **32**, 6570–6578 (2011)
123. S. Lee, H. Park, J. Choi, Y.N. Park, C. Yun, H. Yoo, Multifunctional nanoparticles for targeted chemophotothermal treatment of cancer cells. *Angew. Chem. Int. Ed.* **50**, 7581–7586 (2011)
124. P. Wust, B. Hildebrandt, G. Sreenivasa, B. Rau, J. Gellermann, H. Riess, R. Felix, P.M. Schlag, Review. Hyperthermia in combined treatment of cancer. *Lancet Oncol.* **3**, 487–497 (2002)
125. I. Hilger, W.A. Kaiser, Iron oxide-based nanostructures for MRI and magnetic hyperthermia. *Nanomedicine* **7**, 1443–1459 (2012)
126. P. Pradhan, J. Giri, F. Rieken, C. Koch, O. Mykhalyyk, M. Döblinger, R. Banerjee, D. Bahadur, C. Plank, Targeted temperature sensitive magnetic liposomes for thermochemotherapy. *J. Control. Release* **142**, 108–121 (2010)
127. B. Thiesen, A. Jordan, Clinical applications of magnetic nanoparticles for hyperthermia. *Int. J. Hyperthermia* **24**, 467–474 (2008)
128. J. Gautier, E. Allard-Vannier, E. Munnier, M. Soucé, I. Chourpa, Recent advances in theranostic nanocarriers of doxorubicin based on iron oxide and gold nanoparticles. *J. Control. Release* **169**, 48–61 (2013)
129. C.S. Brazel, Magnetothermally-responsive nanomaterials: combining magnetic nanostructures and thermally-sensitive polymers for triggered drug release. *Pharm. Res.* **26**, 644–656 (2009)
130. S. Hu, S. Chen, X. Gao, Multifunctional nanocapsules for simultaneous encapsulation of hydrophilic and hydrophobic compounds and on-demand release. *ACS Nano* **6**, 2558–2565 (2012)
131. M. Mahmoudi, S. Sant, B. Wang, S. Laurent, T. Sen, Superparamagnetic iron oxide nanoparticles (SPIONs): development, surface modification and applications in chemotherapy. *Adv. Drug Deliv. Rev.* **63**, 24–46 (2011)
132. W.-H. Chiang, V.T. Ho, H.-H. Chen, W.-C. Huang, Y.-F. Huang, S.-C. Lin, C.-S. Chern, H.-C. Chiu, Superparamagnetic hollow hybrid nanogels as a potential guidable vehicle system of stimuli-mediated MR imaging and multiple cancer therapeutics. *Langmuir* **29**, 6434–6443 (2013)

133. Z. Deng, Z. Zhen, X. Hu, S. Wu, Z. Xu, P.K. Chu, Hollow chitosan-silica nanospheres as pH-sensitive targeted delivery carriers in breast cancer therapy. *Biomaterials* **32**, 4976–4986 (2011)
134. K. Hyun, J. Kim, S. Mun, H. Shin, M. Sang, S. Park, H. Lee, R. Park, I. Kim, K. Kim, I. Chan, S. Young, D. Sung, Tumoral acidic pH-responsive MPEG-poly(β -amino ester) polymeric micelles for cancer targeting therapy. *J. Control. Release* **144**, 259–266 (2010)
135. G. Hui Gao, M. Jung Park, Y. Li, G. Ho Im, J. Kim, H. Nyun Kim, J. Won Lee, P. Jeon, O. Young Bang, J. Hee Lee, D. Sung Lee, The use of pH-sensitive positively charged polymeric micelles for protein delivery. *Biomaterials* **33**, 9157–9164 (2012)
136. W. Wu, T. Zhou, A. Berliner, P. Banerjee, S. Zhou, Smart core-shell hybrid nanogels with Ag nanoparticle core for cancer cell imaging and gel shell for pH-regulated drug delivery. *Chem. Mater.* **22**, 1966–1976 (2010)
137. M.E.R. O'Brien, N. Wigler, M. Inbar, R. Rosso, E. Grischke, A. Santoro, R. Catane, D.G. Kieback, P. Tomczak, S.P. Ackland, F. Orlandi, L. Mellars, L. Alland, C. Tendler, Reduced cardiotoxicity and comparable efficacy in a phase III trial of pegylated liposomal doxorubicin HCl (CAELYX™/Doxil) versus conventional doxorubicin for first-line treatment of metastatic breast cancer. *Ann. Oncol.* **15**, 440–449 (2004)
138. K.S. Lee, H.C. Chung, S.A. Im, Y.H. Park, C.S. Kim, S.-B. Kim, S.Y. Rha, M.Y. Lee, J. Ro, Multicenter phase II trial of Genexol-PM, a Cremophor-free, polymeric micelle formulation of paclitaxel, in patients with metastatic breast cancer. *Breast Cancer Res. Treat.* **108**, 241–250 (2008)
139. P.A. Dinndorf, J. Gootenberg, M.H. Cohen, P. Keegan, R. Pazdur, FDA drug approval summary: pegaspargase (oncaspar) for the first-line treatment of children with acute lymphoblastic leukemia (ALL). *Oncologist* **12**, 991–998 (2007)
140. T. Okusaka, S. Okada, H. Ueno, M. Ikeda, R. Iwata, H. Furukawa, K. Takayasu, N. Moriyama, T. Sato, K. Sato, Transcatheter arterial embolization with zinstatin stimalamer for hepatocellular carcinoma. *Oncology* **62**, 228–233 (2002)
141. Q. Song, S.D. Merajver, J.Z. Li, Cancer classification in the genomic era: five contemporary problems. *Hum. Genomics* **9**, 1–8 (2015)
142. L.K. Fung, W.M. Saltzman, Polymeric implants for cancer chemotherapy. *Adv. Drug Deliv. Rev.* **26**, 209–230 (1997)
143. P.N. Schlegel, Efficacy and safety of histrelin subdermal implant in patients with advanced prostate cancer. *J. Urol.* **175**, 1353–1358 (2006)
144. D.J. Overstreet, D. Dutta, S.E. Stabenfeldt, B.L. Vernon, Injectable hydrogels. *J. Polym. Sci. B Polym. Phys.* **50**, 881–903 (2012)
145. Y. Li, J. Rodrigues, H. Tomás, Injectable and biodegradable hydrogels: gelation, biodegradation and biomedical applications. *Chem. Soc. Rev.* **41**, 2193–2221 (2012)
146. P. Huang, Y. Zhang, W. Wang, J. Zhou, Y. Sun, J. Liu, D. Kong, J. Liu, A. Dong, Co-delivery of doxorubicin and 131 I by thermosensitive micellar-hydrogel for enhanced in situ synergetic chemoradiotherapy. *J. Control. Release* **220**, 456–464 (2015)
147. L. Gu, D.J. Mooney, Biomaterials and emerging anticancer therapeutics: engineering the microenvironment. *Nat. Rev. Cancer* **16**, 56–66 (2016)
148. H. Hu, Z. Lin, B. He, W. Dai, X. Wang, J. Wang, X. Zhang, H. Zhang, Q. Zhang, A novel localized co-delivery system with lapatinib microparticles and paclitaxel nanoparticles in a peritumorally injectable in situ hydrogel. *J. Control. Release* **220**, 189–200 (2015)
149. D. Weissglas-Volkov, N. Oliva, E. Friedman, N. Artzi, A. Gilam, N. Shomron, Local micro-RNA delivery targets Palladin and prevents metastatic breast cancer. *Nat. Commun.* **7**, 12868 (2016)
150. S.B. Campbell, T. Hoare, Externally addressable hydrogel nanocomposites for biomedical applications. *Curr. Opin. Chem. Eng.* **4**, 1–10 (2014)
151. S.B. Campbell, M. Patenaude, T. Hoare, Injectable superparamagnets: highly elastic and degradable poly(*N*-isopropylacrylamide)-superparamagnetic iron oxide nanoparticle (SPION) composite hydrogels. *Biomacromolecules* **14**, 644–653 (2013)

152. L.E. Strong, S.N. Dahotre, J.L. West, Hydrogel-nanoparticle composites for optically modulated cancer therapeutic delivery. *J. Control. Release* **178**, 63–68 (2014)
153. B.C. Youan, Chronopharmaceutical drug delivery systems: hurdles, hype or hope? *Adv. Drug Deliv. Rev.* **62**, 898–903 (2010)
154. R. Tong, H.D. Hemmati, R. Langer, D.S. Kohane, Photoswitchable nanoparticles for triggered tissue penetration and drug delivery. *J. Am. Chem. Soc.* **134**, 8848–8855 (2012)
155. S. Campbell, D. Maitland, T. Hoare, Enhanced pulsatile drug release from injectable magnetic hydrogels with embedded thermosensitive microgels. *ACS Macro Lett.* **4**, 312–316 (2015)
156. P.W. Kantoff, C.S. Higano, N.D. Shore, E.R. Berger, E.J. Small, D.F. Penson, C.H. Redfern, A.C. Ferrari, R. Dreicer, R.B. Sims, Y. Xu, D. Ph, M.W. Frohlich, P.F. Schellhammer, Sipuleucel-T immunotherapy for castration-resistant prostate cancer. *N. Engl. J. Med.* **363**, 411–422 (2012)
157. O. Hamid, C. Robert, A. Daud, F.S. Hodi, W.-J. Hwu, R. Kefford, J.D. Wolchok, P. Hersey, R.W. Joseph, J.S. Weber, R. Dronca, T.C. Gangadhar, A. Patnaik, H. Zarour, A.M. Joshua, K. Gergich, J. Ellassais-Schaap, A. Algazi, C. Mateus, P. Boasberg, P.C. Tumeh, B. Chmielowski, S.W. Ebbinghaus, X.N. Li, S.P. Kang, A. Ribas, Safety and tumor responses with lambrolizumab (anti-PD-1) in melanoma. *N. Engl. J. Med.* **369**, 134–144 (2013)
158. M.A. Postow, J. Chesney, A.C. Pavlick, C. Robert, K. Grossmann, D. McDermott, G.P. Linette, N. Meyer, J.K. Giguere, D. Minor, A.K. Salama, M. Taylor, P.A. Ott, L.M. Rollin, C. Horak, P. Gagnier, J.D. Wolchok, F.S. Hodi, Nivolumab and Ipilimumab versus Ipilimumab in untreated melanoma. *N. Engl. J. Med.* **372**, 2006–2017 (2015)
159. O.A. Ali, N. Huebsch, L. Cao, G. Dranoff, D.J. Mooney, Infection-mimicking materials to program dendritic cells in situ. *Nat. Mater.* **8**, 151–158 (2009)
160. S.T. Koshy, D.J. Mooney, Biomaterials for enhancing anti-cancer immunity. *Curr. Opin. Biotechnol.* **40**, 1–8 (2016)
161. O.A. Ali, D. Emerich, G. Dranoff, D.J. Mooney, In situ regulation of DC subsets and T cells mediates tumor regression in mice. *Sci. Transl. Med.* **1**, 1–10 (2009)
162. P. Duedwell, U. Kisser, K. Heckelsmiller, S. Hoves, P. Stoitzner, S. Koernig, A.B. Morelli, B.E. Clausen, M. Dauer, A. Eigler, D. Anz, C. Bourquin, E. Maraskovsky, S. Endres, M. Schnurr, ISCOMATRIX adjuvant combines immune activation with antigen delivery to dendritic cells in vivo leading to effective cross-priming of CD8+ T cells. *J. Immunol.* **187**, 55–63 (2015)
163. S.A. Bencherif, R.W. Sands, O.A. Ali, W.A. Li, S.A. Lewin, T.M. Braschler, T. Shih, C.S. Verbeke, D. Bhatta, G. Dranoff, D.J. Mooney, Injectable cryogel-based whole-cell cancer vaccines. *Nat. Commun.* **6**, 1–13 (2015)
164. A.Z. Wang, R. Langer, O.C. Farokhzad, Nanoparticle delivery of cancer drugs. *Annu. Rev. Med.* **63**, 185–198 (2012)
165. M.E. Davis, J.E. Zuckerman, C.H.J. Choi, D. Seligson, A. Tolcher, C.A. Alabi, Y. Yen, J.D. Heidel, A. Ribas, Evidence of RNAi in humans from systemically administered siRNA via targeted nanoparticles. *Nature* **464**, 1067–1070 (2010)
166. R. Farra, N.F. Sheppard Jr., L. McCabe, R.M. Neer, J.M. Anderson, J.T. Santini Jr., M.J. Cima, R. Langer, First-in-human testing of a wirelessly controlled drug delivery microchip. *Sci. Transl. Med.* **4**, 122ra121 (2012)
167. J. Li, D.J. Mooney, Designing hydrogels for controlled drug delivery. *Nat. Rev. Mater.* **1**, 1–18 (2016)
168. E. Blanco, H. Shen, M. Ferrari, Principles of nanoparticle design for overcoming biological barriers to drug delivery. *Nat. Biotechnol.* **33**, 941–951 (2015)
169. G. Oberdorster, Safety assessment for nanotechnology and nanomedicine: concepts of nanotoxicology. *J. Intern. Med.* **267**, 89–105 (2009)
170. C.M. Keck, R.H. Müller, Nanotoxicological classification system (NCS) – a guide for the risk-benefit assessment of nanoparticulate drug delivery systems. *Eur. J. Pharm. Biopharm.* **84**, 445–448 (2013)

171. D. Huh, D.C. Leslie, D. Benjamin, J.P. Fraser, S. Jurek, A. Geraldine, K.S. Thorneloe, M. Allen, D.E. Ingber, A. Human Disease, Model of drug toxicity – induced pulmonary edema in a lung-on-a-chip microdevice. *Sci. Transl. Med.* **4**, 1–8 (2012)
172. J.A. Doudna, E. Charpentier, The new frontier of genome engineering with CRISPR-Cas9. *Science* **346**, 1258096-1–1258096-9 (2014)
173. A.J. Vegas, O. Veiseh, M. Gürtler, J.R. Millman, F.W. Pagliuca, A.R. Bader, J.C. Doloff, J. Li, M. Chen, K. Olejnik, H.H. Tam, S. Jhunjhunwala, E. Langan, S. Aresta-DaSilva, S. Gandham, J.J. McGarrigle, M.A. Bochenek, J. Hollister-Lock, J. Oberholzer, D.L. Greiner, G.C. Weir, D.A. Melton, R. Langer, D.G. Anderson, Long-term glyceimic control using polymer-encapsulated human stem cell-derived beta cells in immune-competent mice. *Nat. Med.* **22**, 306–311 (2016)
174. O. Veiseh, J.C. Dolo, M. Ma, A.J. Vegas, H.H. Tam, A.R. Bader, J. Li, E. Langan, J. Wycko, W.S. Loo, S. Jhunjhunwala, A. Chiu, S. Siebert, K. Tang, J. Hollister-Lock, S. Aresta-Dasilva, M. Bochenek, J. Mendoza-Elias, Y. Wang, M. Qi, D.M. Lavin, M. Chen, N. Dholakia, R. Thakrar, I. Lacik, G.C. Weir, J. Oberholzer, D.L. Greiner, R. Langer, Size- and shape-dependent foreign body immune response to materials implanted in rodents and non-human primates. *Nat. Mater.* **14**, 643–652 (2015)
175. A.J. Vegas, O. Veiseh, J.C. Doloff, M. Ma, H.H. Tam, K. Bratlie, J. Li, A.R. Bader, E. Langan, K. Olejnik, P. Fenton, J.W. Kang, J. Hollister-Locke, M.A. Bochenek, A. Chiu, S. Siebert, K. Tang, S. Jhunjhunwala, S. Aresta-DaSilva, N. Dholakia, R. Thakrar, T. Vietti, M. Chen, J. Cohen, K. Siniakowicz, M. Qi, J. McGarrigle, A.C. Graham, S. Lyle, D.M. Harlan, D.L. Greiner, J. Oberholzer, G.C. Weir, R. Langer, Combinatorial hydrogel library enables identification of materials that mitigate the foreign body response in primates. *Nat. Biotechnol.* **34**, 345–352 (2016)
176. Y. Zhu, T. Tchkonina, T. Pirtskhalava, A.C. Gower, H. Ding, N. Giorgadze, A.K. Palmer, Y. Ikeno, G.B. Hubbard, S.P.O. Hara, N.F. Larusso, D. Jordan, C.M. Roos, G.C. Verzosa, K. Nathan, J.D. Wren, J.N. Farr, M.B. Stout, S.J. McGowan, A.U. Gurkar, J. Zhao, A. Dorronsoro, Y.Y. Ling, S. Amira, D.C. Navarro, T. Sano, D. Paul, L.J. Niedermhofer, J.L. Kirkland, The Achilles’ heel of senescent cells: from transcriptome to senolytic drugs. *Aging Cell* **14**, 644–658 (2015)
177. D.J. Baker, T. Wijshake, T. Tchkonina, N.K. Lebrasseur, B.G. Childs, B. Van De Sluis, J.L. Kirkland, J.M. Van Deursen, Clearance of p16Ink4a-positive senescent cells delays ageing-associated disorders. *Nature* **479**, 232–236 (2011)
178. D. Patra, S. Sengupta, W. Duan, H. Zhang, R. Pavlick, A. Sen, Intelligent, self-powered, drug delivery systems. *Nanoscale* **5**, 1273–1283 (2013)



Organic-Inorganic Hybrid Materials and Their Applications

28

Rizwana Mobin, Tauseef Ahmad Rangreez, Hamida Tun Nisa Chisti, Inamuddin, and Mashallah Rezakazemi

Contents

1	Introduction	1136
1.1	Synthesis of Organic-Inorganic Hybrids	1137
1.2	Classification of Organic-Inorganic Hybrid Materials	1142
1.3	Applications of Organic-Inorganic Composites	1143
2	Conclusion	1150
	References	1150

Abstract

The organic-inorganic composites in addition to providing new alternate materials represent a class that exhibit novel, astonishing features, and their properties can be tailored to suit a particular application. These are developed by combinations of two or more materials that differ in form or composition on a macroscale. The matrix and the filler are two indispensable components of a composite. In this chapter, synthetic routes, viz., sol-gel, blending, and emulsion polymerization,

R. Mobin

Government College for Women, Srinagar, India

e-mail: rizwanambn013@gmail.com

T. A. Rangreez (✉) · H. T. N. Chisti

National Institute of Technology, Srinagar, India

e-mail: tauseefjh@gmail.com; hamida@nitsri.net

Inamuddin

Advanced Functional Materials Laboratory, Department of Applied Chemistry, Faculty of Engineering and Technology, Aligarh Muslim University, Aligarh, India

e-mail: editorinamuddin@gmail.com

M. Rezakazemi

Faculty of Chemical and Materials Engineering, Shahrood University of Technology, Shahrood, Iran

e-mail: mashallah.rezakazemi@gmail.com

classification, and application of organic-inorganic composites as ion-selective membrane electrodes has been discussed. The ion-selective electrodes provide simple, reliable, low cost, on-spot methods for the detection of heavy metal ions. The field of hybrid materials is vast open and promising and newer possibilities to improve their application are to be explored.

Keywords

Composite · Sol-gel synthesis · Selectivity · Ion-selective membrane electrode

1 Introduction

Since ages, nature has provided various materials that exhibit astonishing properties and features (radiolarian and diatoms). It appears that nature has its own way of combining/mixing materials at nanoscale, resulting in the formation of “smart materials” that have characteristics which are a blend of the combining components [1]. One of the greatest advantages of integration of components at this level is miniaturization (maximum elementary functions) along with hybridization between combining organic-inorganic components [2]. Bamboo, bone, wood, feathers, etc are some examples of naturally occurring composites. Bamboo is cellulose reinforced by silica, bone is an organic-inorganic composite of protein (collagen) and minerals (calcium apatite), while as wood is a composite of cellulose fiber in a matrix of lignin.

Man has long tried to replicate what nature has bestowed him with. It has always had a quest for such materials which possess several distinct features simultaneously. The mission to combine the properties of composite organic and inorganic components seems to be too old as it dates back when Mesopotamians used a straw to strengthen mud bricks, Egyptians used plywood with resistance to thermal expansion and swelling. It is, however, important to note that these hybrid organic-inorganic materials do not represent a simple mixture of components; rather these have organic-inorganic components intimately mixed [3, 4]. In brief, the hybrids are either homogeneous or heterogeneous systems. The homogeneous system is composed of monomers and the miscible organic and inorganic component while as the heterogeneous system has one component with dimensions from a few angstroms to nanometers. It is also to be kept in mind that the properties of hybrids are not just summed total of properties of individual components but the interface also plays a major role [2]. On the basis of the nature of the interface, the hybrids have been broadly grouped into two types. The organic and inorganic components are embedded and only weak bonds (hydrogen, Van der Waals or ionic bonds) give the cohesion to the whole structure in class I while in class II hybrids strong chemical bonds (covalent or ionic-covalent bonds) are present between the two phases.

The composite materials or composites may be considered to consist of two or more constituent materials with different physical or chemical properties that are designed in a manner which allows the components to remain separate and distinct at macroscopic level [5]. The composites are electrically conducting when the organic

conducting polymers are incorporated into the inorganic precipitates of polyvalent metal acid salts. These materials have attained great significance owing to their mechanical, chemical, and electrochemical properties. During the past decade, researchers have shown great interest in the development of electrically conducting organic-inorganic composite materials that exhibit higher conductivity at high and subambient temperature. The composites can be expected to exhibit a wide range of applications such as electronic, electrochromic, photoelectrochemical, ion-exchange, photochromic, and electrodes, if the organic portion is composed of intrinsically conducting polymers such as polyaniline, polypyrrole, poly(3,4-ethylene dioxythiophene), and polystyrene sulfonate (PEDOT: PSS) [6].

1.1 Synthesis of Organic-Inorganic Hybrids

Hybrid organic-inorganic materials played important role in the development of numbers of advanced nanomaterials. These hybrid materials are not only used as an alternative for the synthesis of new material for academic and research purpose but also open new and innovative ways in developing a variety of smart materials with promising applications used in the various field such as electronics, medicine, biology, environment, optics, mechanics, etc. For the synthesis of organic-inorganic hybrid materials, variety of methods have been developed. The commonly used methods include sol-gel method, blending, and emulsion polymerization especially the miniemulsion method is effective and promising in the preparation of polymer-based hybrid materials.

1.1.1 Sol-Gel Method

For over two decades, the sol-gel method has been used for the synthesis of polymer-based hybrid materials, and this method is still a promising method in developing advanced hybrid materials enabling the configurational and structural control simultaneously because of newly developed sol-gel methods [7]. In this method, organic polymers combine with inorganic solid materials at the nanoscale, form hybrid materials with properties similar to both the materials used and also exhibiting some new properties. These hybrid materials extensively used in biological, mechanical, catalytic, optical, and other applications [8].

How Does the Sol-Gel Method Work?

In the sol-gel method, metal alkoxides are used which undergo hydrolysis reaction followed by a condensation reaction (Fig. 1). These two stepwise reactions produce inorganic networks. The organic molecules incorporate within the inorganic networks produced by the sol-gel method which generally include alumina, silica, titania, vanadia, etc. is practicable when mild reaction condition is employed [9–11]. By this sol-gel method, number of hybrid materials has been developed. Due to easy availability, the well-known chemistry of silica and high stability of Si-O bond, silica-based hybrids are extensively used.

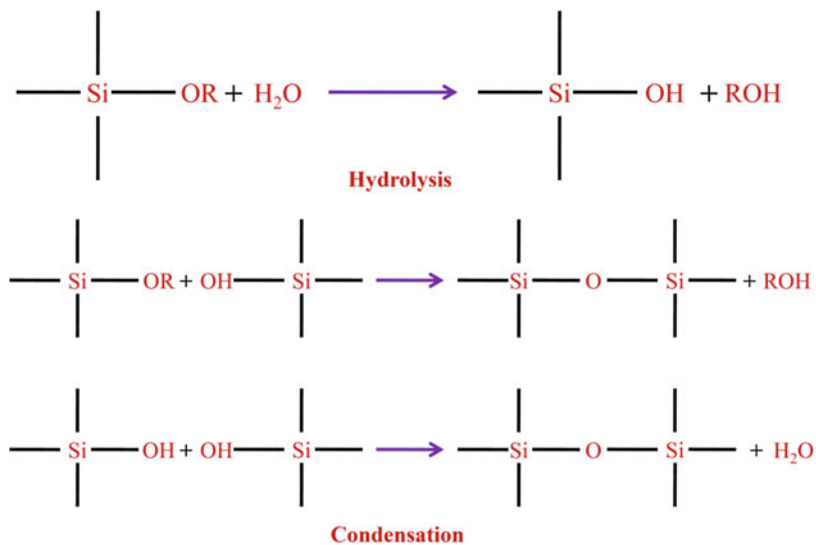


Fig. 1 Steps involved in sol-gel synthesis

The principal requirement for the sol-gel method to produce materials of high homogeneity and transparency is the proper dispersion of organic part into the inorganic matrix. The high reactivity of metal oxide other than silica causes aggregation and nonhomogeneity in the sol-gel method. The interaction between organic and inorganic material in sol-gel methods may be chemical or physical, depending upon its interaction polymer-based hybrid materials are classified into two categories.

1. Class I: It includes the hybrid materials in which physical interaction takes place between organic and inorganic molecules.
2. Class II: It includes the hybrid materials in which chemical interaction takes place between organic and inorganic molecules.

In Situ Hybrid Formation Via Sol-Gel Methods

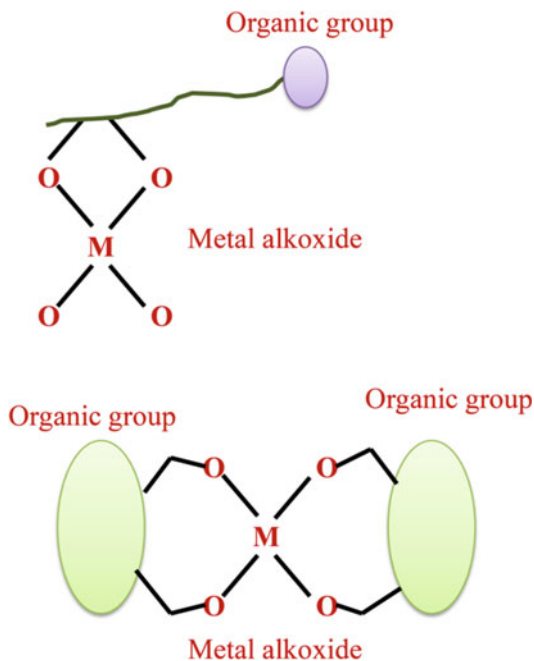
In-situ hybrid materials prepared via the sol-gel method can be divided into three types:

- (i) Water catalyzed sol-gel method
- (ii) Nonhydrolytic sol-gel method
- (iii) The interpenetrating polymer network approach

Water Catalyzed Sol-Gel Method

In this method, monomeric unit combines with organic and metal alkoxide group, which simultaneously forms an inorganic network and polymer chain in the presence of a solvent (water). Depending on the type of organic group used, different methods

Fig. 2 In-situ preparation of polymer-metal oxide hybrid materials by H₂O-catalysed sol-gel polymerization



have been used for the formation of in-situ hybrid materials which include a ring opening process, the free radical process [8]. Figure 2 shows the general scheme for the water catalyzed sol-gel method.

Nonhydrolytic Sol-Gel Method

In the nonhydrolytic sol-gel method, the reaction takes place in the absence of a solvent. The first report in this regard appeared in 2001, which shows that the sol-gel methods (polymerization of an organic monomer in bulk takes place simultaneously with the formation of the inorganic network), are carried out in the absence of solvent or water as a catalyst [12]. In this method, ligand exchange takes place in the presence of metal halide or an organic molecule with oxygen donor moiety such as alcohol, ether.

The silica-dimethylsiloxane hybrid material has been produced by nonhydrolytic sol-gel (NHSG) method, in which NHSG synthesis occurs simultaneously along silica ring-opening polymerization of hexamethylcyclotrisiloxane in the presence of FeCl₃ as a catalyst [13]. General reaction scheme for the nonhydrolytic sol-gel method has been shown in Fig. 3.

The Interpenetrating Polymer Network

This process involves the simultaneous cross-linking process of organic and inorganic groups, which results in the formation of the interpenetrated organic-inorganic hybrid network. Figure 4 shows the general scheme of an interpenetrating network. Example of interpenetrating polymer network is thermo-reversible interpenetrating

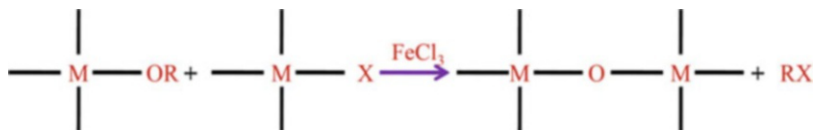


Fig. 3 General reaction involved in NHSG method

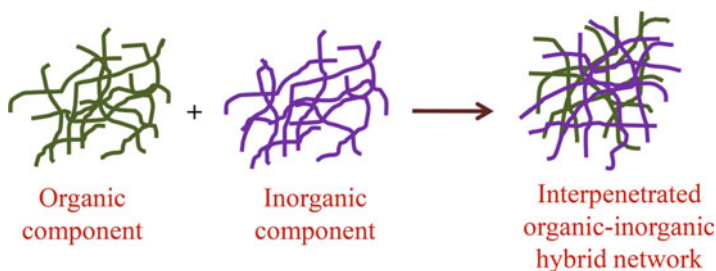


Fig. 4 Representation of interpenetrated organic-inorganic composites

polymer network hybrids, prepared by an acid catalyzed sol-gel method in which reaction of tetramethoxysilane takes place to produce silica network, as this hybrid consists of the organic polymer chain and silica gel. This reaction took place via Diels-Alder reaction, to produce an organic network in the presence of polyoxazoline polymers with maleimide and furan groups [14]. Bipyridyl which consists of polystyrene and poly(ethylene oxide) is another example where a network is formed in the presence of ruthenium salt.

1.1.2 Blending Method

There are three types of blending methods used in the synthesis of hybrid materials.

- (i) Solution blending
- (ii) Melt blending
- (iii) Powder blending

Solution Blending

Solution blending method is one of the simplest methods for the synthesis of organic-inorganic hybrid materials. This method first involves the preparation of organic solution by dissolving the organic material in a suitable solvent and then the inorganic material is introduced. Dispersion is carried out by ultrasonication or by stirring. The resulting hybrid material can be easily processed to generate in the solid state by solvent evaporation. This method is very simple and cost-effective but one drawback is the aggregation of hybrid materials due to the agglomeration properties of inorganic materials, which causes the inferior physical, chemical, and mechanical properties of the hybrid material. To overcome this problem, good intermixing of

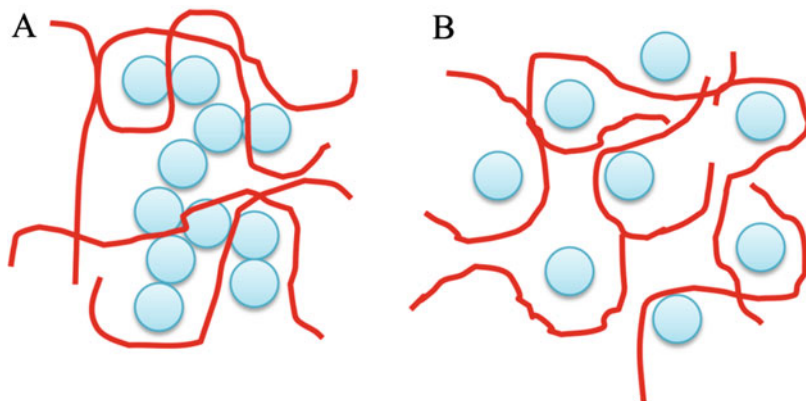


Fig. 5 Organic-inorganic composites: (a) agglomeration (b) dispersion

organic and inorganic materials has been done so that the inorganic material is properly dispersed in organic component (Fig. 5).

Melt Blending

Melt blending is similar to solution blending; the only difference is that in the case of melt blending, organic solvent is not used, which makes this method more environmental friendly as compared to solution blending. In this method, organic material is present in a melt state when the inorganic component is mixed. Polymer-based hybrid materials are generally prepared by this method. In polymer-based hybrid materials, polymers are combined with a variety of inorganic materials such as silica, nanoclays, alumina, etc. [15–18].

Powder Blending

In the powder blending method, solid state powder is used in the synthesis of organic-inorganic hybrid materials. This method is more advantageous as it does not require any solvent (solvent blending) or heating to melt the organic substances (melt blending). Organic materials with poor solubility in the organic solvent or high melting materials cannot be processed with inorganic materials by solution and melt blending methods; therefore, for such materials, powder blending is used. In the powder blending method, high energy ball milling is used for the synthesis of hybrid materials [19]. In case of high energy ball milling, organic and inorganic materials have been mixed by a series of energy transfer. Agglomerates of inorganic materials breakdown into smaller particles which results in homogeneous mixing of the inorganic group into an organic matrix. The hybrid material formed by this method exhibits the properties of the individual component as well as new properties depending on the interaction of inorganic and organic matrix.

Some examples of hybrid materials prepared by these methods are polymers combined with silica [20, 21], barium titanate [22, 23], titanium oxide [24], nickel ferrite nanopowder [25], etc.

1.1.3 Emulsion Polymerization

The process of emulsion polymerization is mainly used by industries to develop adhesives, modifiers, paints, etc. The in-situ polymerization in the presence of preformed inorganic particles which usually act as “seeds” and stabilizers results in the development of composite colloids. The polymer latexes which are developed by conventional emulsion polymerization can also be used for further growth of inorganic domains either within or on the surface of these particles. Polymer silica composites have been mostly developed by this method [26].

1.2 Classification of Organic-Inorganic Hybrid Materials

Hybrid materials are prepared by dispersing inorganic materials into the organic matrix by various methods as described above. There are two types of interaction between organic and inorganic materials. Depending upon these interactions, hybrid materials are classified into two categories (Fig. 6).

1. Class I
2. Class II

Class I In this type of hybrid materials, the interaction between organic and inorganic material is only physical interaction which includes hydrogen bonding, π - π interaction (aromatic interaction), etc. In class I type hybrid material, both the organic and inorganic material consists of some specific functional group which develops physical interaction between these two materials. Polyamides, polycarbonates, polyurethanes, biopolymers possess H-bond functionality are widely used in the synthesis of class I type hybrid materials [27–30]. Physical interaction and homogenous mixture of organic and inorganic material forms occur only when both the compounds have some specific functional groups if such groups are not present then, in hybrid material incomplete homogeneity occurs which result in phase separation between organic and inorganic materials. For example, silicate

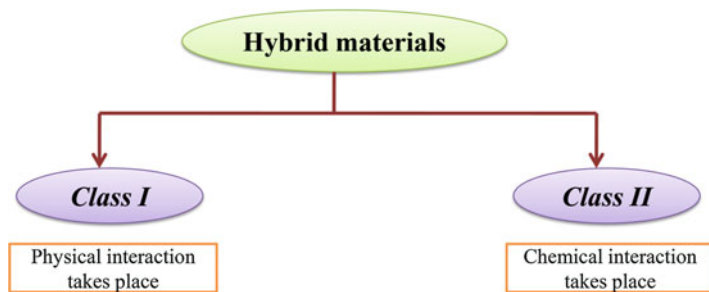


Fig. 6 Classification of hybrid materials on the basis of the interaction between organic and inorganic components

(inorganic matrix) contain aromatic moiety easily generate the homogenous mixture with an organic matrix which contains an aromatic group [31].

Class II In this type of hybrid materials, chemical bonding occurs between two different phases. Different methods have been used for this purpose. Miscibility between two different phases or the homogenous mixture of noncompatible organic and inorganic materials can be obtained by adding compatibilizers. Compatibilizers are macromolecules exhibiting good miscibility properties with both the organic and inorganic parts which are incompatible with each other. For example, class II type of hybrid material can be prepared by alkoxy silane ($-\text{Si}(\text{OR})_3$)-functionalized organic compound and telechelic (with two identical reactive group) organic compounds with functional moieties by co-condensation reaction [32–37].

1.3 Applications of Organic-Inorganic Composites

The commercial application of composites dates back to 1950. The organic-inorganic composites represent materials with unusual properties often modified in order to optimize their performance for a specific use. The use of composites has gained momentum in the last 50 years as new analytical/spectroscopic techniques and tools have become available which have led to the better understanding of structure/properties relationship in these composites. The hybrid/composites have revolutionized the field of biotechnology as biosensors and bioreactors. Active biospecies have been immobilized on or in solid substrates to protect these from denaturation [38]. The most widely used enzyme in sol-gel matrices is the glucose oxidase (GOD) which catalyzes the oxidation of glucose by molecular oxygen and finds application for diagnostic purpose (diabetes) and food industry. These hybrids find wide application in paint industry leading to the development of all-weather resistant coatings. In recent past, the hybrids have been used as barrier system/protective coatings in solar cells, optics, electronics, and food packaging. In the field of dentistry, organic-inorganic hybrids are used in fillings because it gives the same color and texture to the tooth of a patient by adding different fillers [39]. These can be used to change the shape, size, and color of the tooth and easily stick with tooth and hence less tooth has to be removed.

Besides this, the organic-inorganic hybrids find a wide variety of application particularly in the field of water processing, clinical diagnostics, safety, industrial hygiene, process controls, quality controls, human comfort, critical care, emissions monitoring, automotive, safety alarms, and more recently as ion-selective membrane electrodes. The widespread application of hybrids as sensors in these fields has economic, aesthetic, and social utility [40]. The ion-selective membrane electrodes represent an important and widely used class of potentiometric sensors. The applications of organic-inorganic composites are so vast that it is beyond the scope of this chapter, to sum up these all, thus the focus will be laid on only a few applications of organic-inorganic composites.

1.3.1 Water Softening

The hard water contains sparingly soluble magnesium (Mg^{2+}) and calcium (Ca^{2+}) ions. The hardness is considered undesirable even leading to kidney stones due to higher quantities of calcium ions and it influences the processing of water [41]. The most commonly used technique for softening of water includes precipitation of Mg^{2+} and Ca^{2+} (ions) in the form of their carbonates. In chemical precipitation, bicarbonates and alkaline chemicals are added which cause the formation of $MgCO_3$ and $CaCO_3$ precipitates. The boiling of hard water is considered as a physical method but the process consumes too much energy and is costly. Also being partially soluble (carbonates) causes hindrance in the complete removal of these ions from the drinking water [42].

The cation and anion exchangers can be used to selectively remove cations (Mg^{2+} and Ca^{2+}) and anions (sulfate and dissolved organic matter (DOM)). The electrodiagnosis, electrodeionization (EDI), and capacitive deionization (CDI) are better techniques in water softening.

In comparison to calcium, magnesium is abundant in seawater and constitutes about 83% of total hardness (TH) of seawater. Magnesium is necessary for several life processes and is essential for normal cardiac electrophysiology, lipid metabolism, and proper enzyme functions. Its deficiency causes hypomagnesemia and cardiovascular diseases [43]. Mg^{2+} ions can be supplemented in the drinking water in chloride/sulfate form but the process is not feasible cost-wise. Therefore, a new approach of selective desalination of seawater to enrich for Mg^{2+} in the drinking water has been adopted as an alternate method. A combination of ion exchange and filtration-based approaches are used. Tang et al. [44] used a combination of ion exchange and nanofiltration (NF) (filtration of water through a nanometer pore size membrane), to selectively separate Mg^{2+} and SO_4^{2-} from seawater. Cation exchanger was used initially to remove salts and then NF to obtain $MgSO_4$ rich concentrate solution. Similarly, Enterazi et al. [45] showed that a combination of ultrasound and ion exchange increased the efficiency of removal of Mg^{2+} and Ca^{2+} .

1.3.2 Enzyme Immobilization Agents

The immobilization by ionic/electrostatic interactions is an adsorption approach that works on the same principle as ion exchange chromatography [46]. The charged groups present on the protein surface interact with oppositely charged ions on the ion exchange resin. The pH plays a significant role in the loading of proteins (operational pH). If the operational pH is higher than the isoelectric point of the protein, it exhibits a net negative charge and interacts with positively charged exchange media. On the other hand, if the operational pH is lower than the isoelectric point of protein; it shows a positive net charge and therefore interacts with negative exchange agents [47]. Hence, it is possible to use cationic and anionic media for enzyme separation and immobilization based on their net surface charge. Ion exchange is one of the oldest approaches for enzymatic immobilization and is simple, fast, and cost-effective. However, the enzyme immobilization by ion exchange is a multistep process, wherein the enzyme is attached to the carrier only if the number of charge interactions is high enough to compensate for the medium's

ionic strength [48]. Since the adsorption involves weak interactions, therefore, the effects of immobilization on enzyme conformational structure tend to be less drastic, promoting high catalytic activities [49, 50]. However, the possible solution to increase the adsorption strength is the use of polymer-coated carriers. Polymers tend to increase the load bearing capacity using a flexible and adaptable bed for the enzyme. This allows adsorption of the larger part of the protein surface, increasing the contact surface [51]. Several instances using ion exchange resins as immobilization carriers in the food industry have already been reported [49]. These carriers are inexpensive, abundant, mechanically strong, chemically stable, nontoxic, non-polluting, and easily regenerated after use [52].

1.3.3 Decolourization

The traditional sugar processing is a broad area that can benefit from technologies based on ion-exchangers as most of the coloring matter present in sugar liquors show an anionic character and can be removed by ion-exchange resins. These processes have been an important part of sugar processes since the 1980s and significantly improve the profitability of the sugar processing; however, they are still not a standard in sugar production facilities [53]. Till recently, the ion-exchangers have been used either as processing aids (decalcification) in sugar-recovering technologies and in decolorizing of sugar solutions.

1.3.4 Ion-Selective Membrane Electrode

The International Union of Pure and Applied Chemistry (IUPAC) described [54] an ion-selective membrane electrode (ISME) as: an electrochemical sensor, based on thin films or selective membranes as recognition elements, and is an electrochemical half-cell equivalent to other half-cells of the zeroth (inert metal in a redox electrolyte), 1st, 2nd, and 3rd kinds. These devices are distinct from systems that involve redox reactions (electrodes of zeroth, 1st, 2nd, and 3rd kinds), although they often contain a 2nd kind electrode as the “inner” or “internal” reference electrode. The potential difference response has, as its principal component, the Gibbs energy change associated with permselective mass transfer (by ion-exchange, solvent extraction or some other mechanism) across a phase boundary. The ISME has to be used in conjunction with a reference electrode (i.e., “outer” or “external” reference electrode) in order to form a complete electrochemical cell. The measured potential differences (ISME versus outer reference electrode potentials) are linearly dependent on the logarithm of the activity of a given ion in solution.

The foundation of work on the ion-selective membrane was laid by Oswald (1890) with the discovery that for an electrolyte a membrane can be impermeable [55]. The membrane potential at the boundary is a result of the difference in concentration at the membrane. Latter Donan confirmed the same in 1911 [56]. The basic work related to ISME is still considered that of Michaelis and Fujita [57].

The use of ion-exchange membranes for industrial use got impetus from the work of Juda and MC Rae [58] and Winger et al. [59] who developed stable, highly selective ion-exchange membranes exhibiting low resistance. The ion-selective membrane electrode selectively determines the activity of a particular ionic species. The main

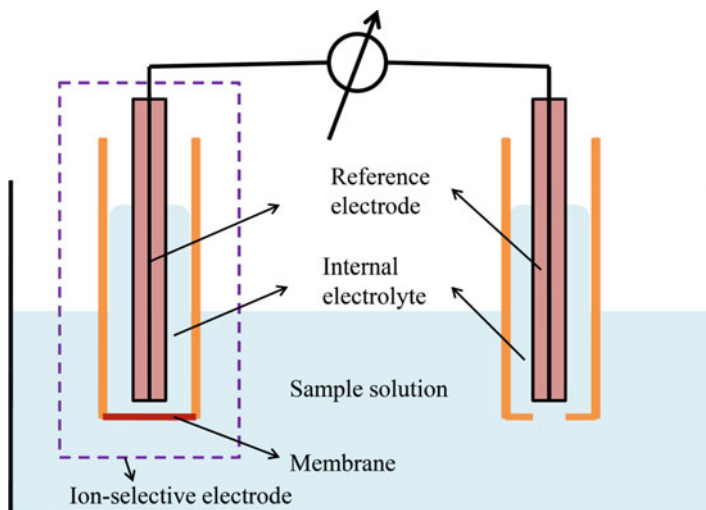


Fig. 7 Schematic representation of the ion-selective membrane electrode cell

constituent of these electrodes is membrane composed of permselective ion-conducting materials separating the sample from the inside of the electrode (Fig. 7).

The surrounding environment determines the potential of the working electrode while the reference electrode potential is kept constant by a solution containing the ion of interest at a constant activity. The potential difference (cell potential) is related to the concentration of the dissolved ion as the potential of reference electrode remains constant. The development of an ion-selective membrane electrode specific to a given ion is very typical and different strategies to produce a specific electrode, selective to particular species depend primarily on the nature and composition of the membrane material. Hence the research in this area is wide open and has applications to an almost unlimited number of analytes; with the preparation of particular analyte selective membrane electrode based on dopant and ionophore matrix of the membrane being the only limitation. These find potential application in several diverse fields of food, drug, biological, waste material treatment, and environmental monitoring owing to their better selectivity, low electrical resistance, improved thermal and mechanical properties. The ion-selective membrane electrodes offer low cost, nondestructive, robust, portable, higher sensitive, and selective procedure for the determination of heavy toxic metal ions. The harmful/hazardous effects of heavy toxic metals have necessitated the rapid, on-spot, selective determination of these ions in portable and groundwater. The ion-selective electrodes can be used for the detection of both the cationic and anionic ions.

Physicochemical Properties of Ion-Selective Membrane Electrodes

Several parameters, viz., electrode response or membrane potential, detection limit, response time, working pH range, selectivity, and interference, are to be evaluated to study the characteristics of the membrane electrode.

Electrode Response or Membrane Potential

The potential determination is one of the main characteristics involved in the working of ion-selective membrane electrode. Since the potential of an individual electrode cannot be determined, it is required to measure emf of the half-cell of an electrochemical cell. The two half-cells are separated by the ion-selective membrane with their respective reference electrodes. A membrane potential (emf) is developed across the membrane separating the two solutions 1 and 2 with both having the same ions. This potential developed across the membrane is given by the Eq. (1)

$$E_m = \frac{RT}{Z_A F} \left[\ln \frac{[a_A]_1}{[a_A]_2} - (Z_y - Z_A) \int_1^2 t_y d \ln a_{\pm} \right] \quad (1)$$

where A = counter ion, Y = co-ion, Z = charge on ions, t_y = transference number of co-ions in the membrane phase, $[a_A]_1$ and $[a_A]_2$ = activities of the counter ions in the solution 1 and 2, a_{\pm} = mean ionic activity of the electrolyte.

Detection Limit

The working concentration range of an ISME is evaluated from the analyte concentration range within which it follows Nernstian equation. It is also defined as the activity range of an ion between the upper and lower detection limits of an ion-selective membrane electrode. The ISMEs exhibit a point where the electrode response starts to deviate from the theoretical value and the ISME loses its specificity towards the primary ion. The presence of various interfering ions in the form of impurities also plays a significant role in governing the detection limit of ISME. The extrapolation of the linear part of the calibration curve of ISME gives the limit of detection of the membrane electrode (Fig. 8).

Response Time

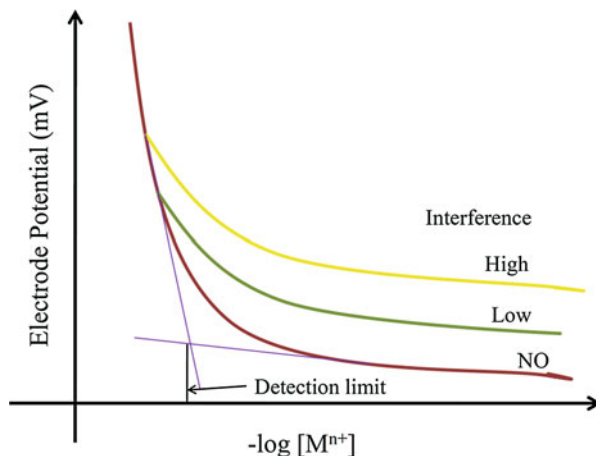
According to the IUPAC recommendations, the time which elapses between the instant when an ion-selective membrane electrode and a reference electrode (ISME cell) are brought into contact with a sample solution (or at which the activity of the ion of interest in a solution is changed) and the first instant at which the emf/time slope ($\frac{\Delta E}{\Delta t}$) becomes equal to a limiting value selected on the basis of the experimental conditions and/or requirements concerning the accuracy (e.g., 0.6 mV/min.) is defined as response time.

It has also been described as the time necessary to attain an equilibrium value (steady potential) within ± 1 mV after a tenfold increase or decrease in the concentration of the test solution.

Selectivity Coefficients

The selectivity coefficient is one of the important factors of ion-selective membrane electrodes, which determines the potential applicability of an electrode. The ISME yield a potential that is primarily due to the ion of interest usually called the primary

Fig. 8 Ion-selective membrane electrode calibration curve



ion while other interfering ions are called secondary ions. However, the ISME cannot be exclusively specific to a single ion. The actual response of a binary mixture of primary (A) and secondary (B) ions is given by *Nikoloskii-Eisenman* Eq. (2) [60]. A detailed theory of the processes at the interference of these membranes, which generate the potential, is available elsewhere [61–63].

$$E = E_0 + \frac{2.303 RT}{Z_A F} \log \left[a_A + \sum K_A^{pot} (a_A)^{\frac{Z_A}{Z_B}} \right] \quad (2)$$

The lower the value of $K_{A,B}^{pot}$, the more selective is the electrode. For ideally selective electrodes, the $K_{A,B}^{pot}$ would be zero. Thus, the selectivity coefficient plays a great role while determining the selectivity of a particular ion-selective membrane electrode. Figure 8 shows the effect on selectivity of ISME due to the presence of the various interfering ions. As such the inconsistent nature of the selectivity coefficient is not considered a desirable trait of ISME [64–66]. Two main methods, separate solution method and mixed solution method, are generally used for determining the selectivity coefficient of ISME [67].

Life Time

The period of time during which the slope and detection limit of an ISME do not undergo any significant change represents its lifetime. Several factors which include the deterioration of the plasticizer, polymer, and the electroactive material are the main reasons for the deviation in the response of the membrane electrode. Thus, the period during which the electrode response remains reasonably constant represents the lifetime of ISME.

Effect of pH

These ISMEs work only within a specific pH range, and thus it is essential to find out the effect of pH on the electrode response. In order to determine the working pH

Table 1 Some important heavy metal ion-selective composite ion-exchangers

S. No.	Composite material	Application	Ref.
1	Polypyrrole Th(IV) phosphate	Pb(II) selective	[72]
2	Poly- <i>o</i> -toluidine Ce(IV) phosphate	Cd(II) selective	[73]
3	Polyaniline Sn(IV) phosphate	Pb(II) selective	[74]
4	Poly(methylmethacrylate) Zr(IV) phosphate	Pb(II) selective	[75]
5	Polyacrylamide Th(IV) phosphate	Pb(II) selective	[76]
6	Acrylamide aluminum tungstate	Pb(II) selective	[77]
7	Poly- <i>o</i> -anisidine Sn(IV) arsenophosphate	Pb(II) selective	[78]
8	Acrylonitrile Sn(IV) tungstate	Pb(II) selective	[79]
9	Polyacrylamide apatite	Pb(II) selective	[80]
10	Macrocyclic diamide sulfur	Cd(II) selective	[81]
11	B ₂ O ₃ /TiO ₂ nanocomposite	Cd(II) selective	[82]
12	Ethylenediamine tetra acetic acid Sn(IV) iodate	Pb(II) selective	[83]
13	Acrylamide Zr(IV) arsenate	Pb(II) selective	[84]
14	Acrylamide stannic silicomolybdate	Pb(II) selective	[85]
15	Poly(methylmethacrylate) Ce(IV) molybdate	Pb(II) selective	[86]
16	Polyaniline Ce(IV) molybdate	Cd(II) selective	[87]
17	Poly- <i>o</i> -methoxyaniline Zr(IV) molybdate	Cd(II) selective	[88]
18	Poly- <i>o</i> -toluidine stannic molybdate	Pb(II) selective	[89]
19	Poly- <i>o</i> -anisidine Sn(IV) phosphate	Cd(II) selective	[90]
20	Polyaniline Sn(IV) molybdate	Pb(II) selective	[91]
21	Polyaniline zirconium titanium phosphate	Hg(II) selective	[92]
22	Nylon-6,6 Sn(IV) phosphate	Hg(II) selective	[93]
23	Poly- <i>o</i> -toluidine Zr(IV) phosphate	Hg(II) selective	[94]
24	Poly- <i>o</i> -toluidine Th(IV) phosphate	Hg(II) selective	[95]
25	Polyaniline Sn(IV) phosphate	Hg(II) selective	[96]
26	Poly- <i>o</i> -anisidine Sn(IV) phosphate	Sb(II) selective	[97]
27	Cellulose acetate-Zr(IV) molybdophosphate	Cr(III) selective	[98]
28	Polyaniline-Sn(IV)tungstophosphate	Pb(II) selective	[99]
29	Polyaniline Sn(IV) silicomolybdate	Pb(II) selective	[100]
30	Polyaniline Zr(IV) arsenate	Pb(II) selective	[101]
31	Poly- <i>o</i> -toluidine Zr(IV) tungstate	Pb(II) selective	[102]
32	Polyaniline Ti(IV) arsenate	Pb(II) selective	[103]
33	Polyaniline Ti(IV) phosphate	Pb(II) selective	[104]
34	Polyaniline Sn(IV) tungstoarsenate	Cd(II) selective	[105]
35	Polyaniline Sn(IV) silicate	Cd(II) selective	[106]
36	Poly- <i>o</i> -toluidine Sn(IV) tungstate	Pb(II) selective	[107]
37	Polyaniline Sn(IV) tungstomolybdate	Pb(II) selective	[108]
38	Polyaniline Ti(IV) arsenophosphate	Cd(II) selective	[109]
39	Polyaniline Sn(IV) silicophosphate	Pb(II) selective	[110]
40	Poly(3,4-ethylenedioxythiophene)-poly(styrenesulfonate) Zr(IV) phosphate	Cd(II) selective	[111]
41	Polyaniline tungstophosphate	Pb(II) selective	[112]

(continued)

Table 1 (continued)

S. No.	Composite material	Application	Ref.
42	Carboxymethyl cellulose Sn(IV) phosphate	Pb(II) selective	[113]
43	Polyaniline Zr(IV) sulfosalicylate	Pb(II) selective	[114]
44	Poly(3,4-ethylenedioxythiophene)-poly(styrenesulfonate) Zr(IV) monothiophosphate	Pb(II) selective	[115]
45	Cellulose acetate Zr(IV) molybdophosphate	Cd(II) & Pb(II) selective	[116]
46	Single-walled carbon nanotubes Ce(IV) phosphate	Cd(II) selective	[117]

range of the ion-selective membrane electrode, different solutions of varying pH with constant ion concentration are prepared and the electrode potential is recorded at each pH. The electrode potential is plotted against pH value and the pH over which the potential of ion-selective membrane electrode remains constant is taken as the working pH range of the electrode.

Thus these ion-selective membrane electrodes have several attractive features as a simple instrument, high sensitivity and selectivity, low cost, and fast response [68–71].

Table 1 represents various composites that are specifically selective for various heavy metal ions.

2 Conclusion

The organic-inorganic composites have already made in-roads in various industries. The advance research in the field is moving at a very fast rate owing to usefulness in various sciences, physical, chemical, material, biological, etc. The composites provide both integration and miniaturization, thus opening the vast field for their application. The simple methods of development of these composites provide ample opportunities to alter, modify, and club various distinguishing characteristics in a single entity. The composites as ion-selective membrane electrodes provide fast, on-spot, reliable, cost-effective means for the detection, determination, and removal of various heavy metal ions.

Acknowledgments Tauseef Ahmad Rangreez is thankful to SERB, New Delhi for grant under SERB N-PDF (File No. PDF/2017/001724).

References

1. C. Sanchez, H. Arribart, M.M.G. Guille, Biomimetism and bioinspiration as tools for the design of innovative materials and systems. *Nature Mater.* **4**, 277–288 (2005)
2. C. Sanchez, B. Julian, P. Belleville, M. Popall, Applications of hybrid organic-inorganic nanocomposites. *J. Mater. Chem.* **15**, 3559–3592 (2005)
3. D. Avnir, D. Levy, R. Reisfeld, The nature of the silica cage as reflected by spectral changes and enhanced photostability of trapped Rhodamine 6G. *J. Phys. Chem.* **88**, 5956–5959 (1984)

4. C.J. Brinker, G.W. Scherrer, *Sol-Gel Science, The Physics and Chemistry of Sol-Gel Processing* (Academic, San Diego, 1990)
5. A.M. El-Kanarh, B. El-Gannal, A.A. El-Sayid, Preparation and evaluation of cerium (IV) tungstate powder as inorganic exchanger in sorption of cobalt and europium ions from aqueous solutions. *J. Hazard. Mater.* **141**, 719–728 (2007)
6. G. Albewrti, U. Costantino, F. Digregorio, E. Torracca, Crystalline insoluble salts of polyvalent metals and polybasic acids-VIII: synthesis and ion-exchange properties of cerium (IV) arsenate. *J. Inorg. Nucl. Chem.* **31**, 3195 (1969)
7. S. Pandey, S.B. Mishra, Sol-gel derived organic-inorganic hybrid materials: Synthesis, characterizations and applications. *J Sol-Gel Sci. Technol.* **59**, 73–94 (2011)
8. T. Ogoshi, Y. Chujo, Organic-inorganic polymer hybrids prepared by the sol-gel method. *Compos. Interfaces* **11**, 539–566 (2005)
9. Y. Chujo, T. Saegusa, Organic polymer hybrids with silica-gel formed by means of the sol-gel method. *Adv. Polym. Sci.* **100**, 11–29 (1992)
10. J.E. Mark, Ceramic-reinforced polymers and polymer-modified ceramics. *Polym. Eng. Sci.* **36**, 2905–2920 (1996)
11. H. Zou, S. Wu, J. Shen, Polymer/silica nanocomposites: Preparation, characterization, properties, and applications. *Chem. Rev.* **108**, 3893–3957 (2008)
12. J.N. Hay, H.M. Raval, Synthesis of organic-inorganic hybrids via the non-hydrolytic sol-gel process. *Chem. Mater.* **13**, 3396–3403 (2001)
13. D. Apperley, J.N. Hay, H.M. Raval, Silica-dimethylsiloxane hybrids non-hydrolytic sol-gel synthesis and characterization by NMR spectroscopy. *Chem. Mater.* **14**, 983–988 (2002)
14. Y. Imai, H. Itoh, K. Naka, Thermally reversible IPN organic-inorganic polymer hybrids utilizing the Diels-Alder reaction. *Macromolecules* **33**, 4343–4346 (2000)
15. S.M. Lai, J.R. Chen, J.L. Han, Preparation and properties of melt-blended polylactic acid/polyethylene glycol-modified silica nanocomposites. *J. Appl. Polym. Sci.* **130**, 496–503 (2013)
16. C.S. Reddy, C.K. Das, HLDPE/organic functionalized SiO₂ nanocomposites with improved thermal stability and mechanical properties. *Compos. Interfaces* **11**, 687–699 (2005)
17. G.C. Psarras, S. Siengchin, P.K. Karahaliou, Dielectric relaxation phenomena and dynamics in polyoxymethylene/polyurethane/alumina hybrid nanocomposites. *Polym. Int.* **60**, 1715–1721 (2011)
18. M.T. Albdiry, B.F. Yousif, H. Ku, A critical review on the manufacturing processes in relation to the properties of nanoclay/polymer composites. *J. Compos. Mater.* **47**, 1093–1115 (2013)
19. P.D. Castrillo, D. Olmos, D.R. Amador, Real dispersion of isolated fumed silica nanoparticles in highly filled PMMA prepared by high energy ball milling. *J. Colloid Interface Sci.* **308**, 318–324 (2007)
20. D. Olmos, E. Rodriguez-Gutierrez, J. Gonzalez-Benito, Polymer structure and morphology of low density polyethylene filled with silica nanoparticles. *Polym. Compos.* **33**, 2009–2021 (2012)
21. R. Pantaleon, J. Gonzalez-Benito, Structure and thermostability of PMMA in PMMA/silica nanocomposites: Effect of high-energy ball milling and the amount of the nanofiller. *Polym. Compos.* **31**, 1585–1592 (2010)
22. D. Olmos, G. Gonzalez-Gaitano, A.L. Kholkin, Flexible PVDF-BaTiO₃ nanocomposites as potential materials for pressure sensors. *Ferroelectrics* **447**, 9–18 (2013)
23. R. Serra-Gomez, G. Gonzalez-Gaitano, J. Gonzalez-Benito, Composites based on EVA and barium titanate submicrometric particles: Preparation by high-energy ball milling and characterization. *Polym. Compos.* **33**, 1549–1556 (2012)
24. G. Ouyang, K. Wang, X.Y. Chen, TiO₂ nanoparticles modified polydimethylsiloxane with fast response time and increased dielectric constant. *J. Micromech. Microeng.* **22**, 074002 (2012)
25. B. Azhdar, B. Stenberg, L. Kari, Polymer-nanofiller prepared and high velocity cold by high-energy ball milling compaction. *Polym. Compos.* **29**, 252–261 (2008)
26. E.B. Lami, M. Lansalot, Organic/inorganic composite latexes: the marriage of emulsion polymerization and inorganic chemistry. *Adv. Polym. Sci.* **233**, 53–123 (2010)

27. M.I. Sarwar, S. Zulfiqar, Z. Ahmad, Investigating the property profile of polyamide-alumina nanocomposite materials. *Scr. Mater.* **60**, 988–991 (2009)
28. P. Zhang, Z. Weng, J. Guo, Solution-dispersible, colloidal, conjugated porous polymer networks with entrapped palladium nanocrystals for heterogeneous catalysis of the Suzuki-Miyaura coupling reaction. *Chem. Mater.* **23**, 5243–5249 (2011)
29. K. Lioni, B. Toury, C. Boissiere, Hybrid silica coatings on polycarbonate: Enhanced properties. *J. Sol-Gel Sci. Technol.* **65**, 52–60 (2013)
30. T. Coradin, J. Allouche, M. Boissiere, Sol-gel biopolymer/silica nanocomposites in biotechnology. *Curr. Nanosci.* **2**, 219–230 (2006)
31. R. Tamaki, K. Samura, Y. Chujo, Synthesis of polystyrene and silica gel polymer hybrids via pi-pi interactions. *Chem. Commun.* **10**, 1131–1132 (1998)
32. S.Q. Huang, D.Q. Fan, Y.Q. Lei, Alkoxysilane-functionalized acrylic copolymer latexes. I. Particle size, morphology, and film-forming properties. *J. Appl. Polym. Sci.* **94**, 954–960 (2004)
33. H. Sardon, L. Irusta, M.J. Fernandez-Berridi, Synthesis of room temperature self-curable waterborne hybrid polyurethanes functionalized with (3-aminopropyl)triethoxysilane (APTES). *Polymer* **51**, 5051–5057 (2010)
34. J.J. McDowell, N.S. Zacharia, D. Puzzo, Electroactuation of alkoxysilane-functionalized polyferrocenylsilane microfibers. *J. Am. Chem. Soc.* **132**, 3236–3237 (2010)
35. B. Julián, C. Gervais, M.N. Rager, Solid-State 17O NMR characterization of PDMS–MxOy (M = Ge(IV), Ti(IV), Zr(IV), Nb(V), and Ta(V)) organic–inorganic nanocomposites. *Chem. Mater.* **16**, 521–529 (2004)
36. J.M. Uilk, A.E. Mera, R.B. Fox, Hydrosilation-cured poly(dimethylsiloxane) networks: intrinsic contact angles via dynamic contact angle analysis. *Macromolecules* **36**, 3689–3694 (2003)
37. Y. Chujo, E. Ihara, S. Kure, Synthesis of triethoxysilyl-terminated polyoxazolines and their cohydrolysis polymerisation with tetraethoxysilane. *Macromolecules* **26**, 5681–5686 (1993)
38. J. Livage, T. Coradin, C. Roux, in *Functional Hybrid Materials*, ed. by P. Gomez Romero, C. Sanchez (Wiley VCH, Weinheim, 2004), ch. 7
39. H. Wolter, W. Storch, A new silane precursor with reduced polymerization shrinkage. *J. Sol-Gel Sci. Technol.* **2**, 93 (1994)
40. C.C. Liu, Electrochemical sensors, in *The Biomedical Engineering Handbook*, 2nd edn, ed. by J.D. Bronzino (CRC Press, LLC, Boca Raton, 2000)
41. V. Bellizzi, L. DeNicola, R. Minutolo, D. Russo, B. Cianciaruso, M. Andreucci, G. Conte, V. Andreucci, Effects of water hardness on urinary risk factors for kidney stones in patients with idiopathic nephrolithiasis. *Nephron* **81**, 66–70 (1999)
42. E. Yildiz, A. Nuhoglu, B. Keskinler, G. Akay, B. Farizoglu, Water softening in a cross-flow membrane reactor. *Desalination* **159**, 139–152 (2003)
43. L.C. Del Gobbo, F. Imamura, J.H. Wu, M.C. de Oliveira Otto, S.E. Chiuve, D. Mozaffarian, Circulating and dietary magnesium and risk of cardiovascular disease: a systematic review and meta-analysis of prospective studies. *Am. J. Clin. Nutr.* **98**, 160–173 (2013)
44. S.C. Tang, L. Birnhack, Y. Cohen, O. Lahav, Selective separation of divalent ions from seawater using an integrated ion-exchange/nanofiltration approach. *Chem. Eng. Process-Process Intensification* **126**, 8 (2018)
45. M.H. Entezari, M. Tahmasbi, Water softening by combination of ultrasound and ion exchange. *Ultrason. Sonochem.* **16**, 356–360 (2009)
46. R.R. Ribeiro, M. Vitolo, Anion exchange resin as support for invertase immobilization. *J. Basic Appl. Pharm. Sci.* **26**, 175–179 (2005)
47. A. Williams, V. Frasca, in *Ion-Exchange Chromatography*, ed. by J.E. Coligan (Wiley, Weinheim, 2001)
48. X.D. Tong, X.Y. Dong, Y. Sun, Lysozyme adsorption and purification by expanded bed chromatography with a small-sized dense adsorbent. *Biochem. Eng. J.* **12**, 117–124 (2002)

49. K. Gupta, A.K. Jana, S. Kumar, M. Maiti, Immobilization of α -amylase and amyloglucosidase onto ion-exchange resin beads and hydrolysis of natural starch at high concentration. *Bioprocess Biosyst. Eng.* **36**, 1715–1724 (2013)
50. L.D.S. Marquez, B.V. Cabral, F.F. Freita, V.L. Cardoso, E.J. Ribeiro, Optimization of invertase immobilization by adsorption in ionic exchange resin for sucrose hydrolysis. *J. Mol. Catal. B Enzym.* **51**, 86–92 (2008)
51. M. Fuentes, B.C.C. Pessela, J.V. Maquiese, C. Ortiz, R.L. Segura, J.M. Palomo, O. Abian, R. Torres, C. Mateo, R. Fernández-Lafuente, J.M. Guisán, Reversible and strong immobilization of proteins by ionic exchange on supports coated with sulfate-dextran. *Biotechnol. Prog.* **20**, 1134–1139 (2004)
52. C.Z. Guidini, J. Fischer, L.N.S. Santana, V.L. Cardoso, E.J. Ribeiro, Immobilization of *Aspergillus oryzae* β -galactosidase in ion exchange resins by combined ionic-binding method and cross-linking. *Biochem. Eng. J.* **52**, 137–143 (2010)
53. M. Asadi, *Ion Exchange Resin, Beet-Sugar Handbook* (Wiley, Hoboken, 2007), pp. 483–488
54. R.P. Buck, E. Lindner, Recommendations for nomenclature of ion-selective electrodes. *Pure Appl. Chem.* **66**, 2527–2536 (1994)
55. W. Ostwald, Elektrische Eigenschaften Halbdurchlässiger Scheidewände. *J. Phys. Chem.* **6**, 71–82 (1890)
56. L. Michaelis, A. Fujita, Permselectivity of biological membranes. *Biochem. Z.* **148**, 28–37 (1925)
57. W. Juda, W.A. McRae, Coherent ion-exchange gels and membranes. *J. Am. Chem. Soc.* **72**, 1044–1044 (1950)
58. A.G. Winger, G.W. Bodamer, R. Kunin, Some electrochemical properties of new synthetic ion exchange membranes. *J. Electrochem. Soc.* **100**, 178–184 (1953)
59. B.P. Nikoloskii, *Acta Physiochim. URSS* **7**, 597 (1937)
60. R.P. Buck, Electroanalytical chemistry of membranes. *Crit. Rev. Anal. Chem.* **5**, 323–420 (1976)
61. D. Amman, W. Morf, P. Anker, P. Meier, E. Pret, W. Simon, Neutral carrier based ion-selective electrodes. *Ion Sel. Electrode Rev.* **5**, 3–92 (1983)
62. A.K. Covington, Ion-selective electrodes. *Crit. Rev. Anal. Chem.* **3**, 355–406 (1973)
63. M.F. Wilson, E. Haikala, P. Kivalo, An evaluation of some sodium ion-selective glass electrodes in aqueous solution: part I. Electrode calibration characteristics and selectivity with respect to hydrogen ions. *Anal. Chim. Acta* **74**, 395 (1975)
64. A. Hulanicki, A. Lewenstam, Model for treatment of selectivity coefficients for solid-state ion-selective electrodes. *Anal. Chem.* **53**, 1401–1405 (1981)
65. D.J. Clarke, D.B. Kell, J.G. Morris, A. Burns, The role of ion-selective electrodes in microbial process control. *Ion Sel. Electrode Rev.* **4**, 75–131 (1982)
66. Y. Umezawa (ed.), *Handbook of Ion Selective Electrodes: Selectivity Coefficients* (CRC Press, Boca Raton, 1990)
67. D.W.O. Connell, C. Birkinshaw, T.F.O. Dwyer, Heavy metal adsorbents prepared from the modification of cellulose: a review. *Bioresour. Technol.* **99**, 6709–6724 (2008)
68. K.S. Low, C.K. Lee, Cadmium uptake by the Moss, *Calymperesdelessertii*, *Besch. Bioresour. Technol.* **38**, 1–6 (1991)
69. K. Mulder, N. Hagens, B. Fisher, Burning water: a comparative analysis of the energy return on water invested. *Ambio* **39**, 30–39 (2010)
70. G.M. Naja, B. Volesky, Treatment of metal-bearing effluents: removal and recovery, in *Handbook on Heavy Metals in the Environment*, ed. by L.K. Wang, J.P. Chen, Y.T. Hung, N.K. Shammam (Taylor and Francis, Boca Raton, 2009), pp. 247–291
71. A.A. Khan, Inamuddin, M.M. Alam, Preparation, characterization and analytical applications of a new and novel electrically conducting fibrous type polymericinorganic composite material: polypyrrole Th(IV) phosphate used as a cationexchanger and Pb(II) ion-selective membrane electrode. *Mater. Res. Bull.* **40**, 289–305 (2005)

72. A.A. Khan, T. Akhtar, Synthesis, characterization and analytical application of nano-composite cation-exchange material, poly-*o*-toluidine Ce(IV) phosphate: its application in making Cd(II) ion selective membrane electrode. *Solid State Sci.* **13**, 559–568 (2011)
73. A.A. Khan, Inamuddin, Preparation, physico-chemical characterization, analytical applications and electrical conductivity measurement studies of an ‘organic–inorganic’ composite cation-exchanger: polyanilineSn(IV) phosphate. *React. Funct. Polym.* **66**, 1649–1663 (2006)
74. W.A. Siddiqui, S.A. Khan, Inamuddin, Synthesis, characterization and ionexchange properties of a new and novel ‘organic–inorganic’ hybrid cation-exchanger: poly(methyl methacrylate) Zr(IV) phosphate. *Colloid Surf. Physicochem. Eng. Aspect.* **295**, 193–199 (2007)
75. M. Islam, R. Patel, Polyacrylamide thorium (IV) phosphate as an important lead selective fibrous ion exchanger: synthesis, characterization and removal study. *J. Hazard. Mater.* **156**, 509–520 (2008)
76. S.A. Nabi, A.S. Ganai, A.H. Shalla, New organic-inorganic type acrylamide aluminum-tungstate: preparation, characterization and analytical applications as a cation exchange material. *Sep. Sci. Technol.* **43**, 3695–3711 (2008)
77. A.A. Khan, U. Habiba, A. Khan, Synthesis and characterization of organicinorganic nano-composite poly-*o*-anisidinesn(IV) arsenophosphate: its analytical applications as Pb(II) ion-selective membrane electrode. *Int. J. Anal. Chem.* **659215**, 10 (2009)
78. S.A. Nabi, M. Naushad, R. Bushra, Synthesis and characterization of a new organic–inorganic Pb²⁺ selective composite cation exchanger acrylonitrile stannic(IV) tungstate and its analytical applications. *Chem. Eng. J.* **152**, 80–87 (2009)
79. U. Ulusoy, R. Akkaya, Adsorptive features of polyacrylamide-apatite composite for Pb²⁺, UO₂²⁺ and Th⁴⁺. *J. Hazard. Mater.* **163**, 9–108 (2009)
80. M. Shamsipur, A.S. Dezaki, M. Akhond, H. Sharghi, Z. Pazirae, K. Alizadeh, Novel PVC-membrane potentiometric sensors based on a recently synthesized sulfur-containing macrocyclicdiamide for Cd²⁺ ion. Application to flow-injection potentiometry. *J. Hazard. Mater.* **172**, 566–573 (2009)
81. O.M. Kalfa, O. Yalcinkaya, A.R. Turker, Synthesis of nano B₂O₃/TiO₂ composite material and its application to preconcentration and separation of cadmium. *J. Hazard. Mater.* **166**, 455–461 (2009)
82. S.A. Nabi, A.H. Shalla, EDTA-stannic (IV) iodate: preparation, characterization and its analytical applications for metal content determination in real and synthetic samples. *J. Porous Mater.* **16**, 587–597 (2009)
83. S.A. Nabi, A.H. Shalla, Synthesis, characterization and analytical application of hybrid; Acrylamide zirconium (IV) arsenate a cation exchanger, effect of dielectric constant on distribution coefficient of metal ions. *J. Hazard. Mater.* **163**, 657–664
84. A.M. Khan, S.A. Ganai, S.A. Nabi, Synthesis of a crystalline organic-inorganic composite exchanger, acrylamide stannic silicomolybdate: binary and quantitative separation of metal ions. *Colloid Surf. Physicochem. Eng. Aspect.* **337**, 141–145 (2009)
85. Z. Alam, Inamuddin, S.A. Nabi, Synthesis and characterization of a thermally stable strongly acidic Cd(II) ion selective composite cation-exchanger: polyanilineCe(IV) molybdate. *Desalination* **250**, 515–522 (2010)
86. Inamuddin, Y.A. Ismail, Synthesis and characterization of electrically conducting poly-*o*-methoxyanilineZr(IV) molybdate Cd(II) selective composite cationexchanger. *Desalination* **250**, 523–529 (2010)
87. S.A. Nabi, R. Bushra, M. Naushad, A.M. Khan, Synthesis, characterization and analytical applications of a new composite cation exchange material poly-*o*-toluidine stannic molybdate for the separation of toxic metal ions. *Chem. Eng. J.* **165**, 529–536 (2010)
88. A.A. Khan, A. Khan, Ion-exchange studies on poly-*o*-anisidine Sn(IV) phosphate nano composite and its application as Cd(II) ion-selective membrane electrode. *Cent. Eur. J. Chem.* **8**, 396–408 (2010)
89. Z.A. Al Othman, M. Naushad, A. Nilchi, Development, characterization and ion exchange thermodynamics for a new crystalline composite cation exchange material: application for the

- removal of Pb^{2+} ion from a standard sample (rompin hematite). *J. Inorg. Organomet. Polymer Mater.* **21**, 547–559 (2011)
90. A.A. Khan, L. Paquiza, Characterization and ion-exchange behavior of thermally stable nano-composite polyaniline zirconium titanium phosphate: its analytical application in separation of toxic metals. *Desalination* **265**, 242–254 (2011)
 91. A.A. Khan, T. Akhtar, Synthesis, synthesis, characterization and ion-exchange properties of a fibrous type 'polymeric-inorganic' composite cation-exchanger Nylon-6,6 Sn(IV) phosphate: its application in making Hg(II) selective membrane electrode. *Electrochim. Acta* **54**, 3320–3329 (2009)
 92. A.A. Khan, A. Khan, Inamuddin, Preparation and characterization of a new organic-inorganic nano-composite poly-*o*-toluidine Th(IV) phosphate: its analytical applications as cation-exchanger and in making ion-selective electrode. *Talanta* **72**, 699–710 (2007)
 93. A.A. Khan, Inamuddin, Preparation, physico-chemical characterization, analytical applications and electrical conductivity measurement studies of an 'organic-inorganic' composite cation-exchanger: polyaniline Sn(IV) phosphate. *React. Funct. Polym.* **66**, 1649–1663 (2006)
 94. A.A. Khan, A. Khan, Synthesis, characterization and electrical conductivity measurement studies of poly-*o*-anisidine Sn(IV) phosphate [POASn(IV)P] nano-composite cation-exchange material. *Mater. Sci. Eng. B* **158**, 92–97 (2009)
 95. S.A. Nabi, M. Naushad, Synthesis, characterization and analytical applications of a new composite cation exchanger cellulose acetate-Zr(IV) molybdophosphate. *Colloids Surf. A Physicochem. Eng. Aspects* **316**, 217–225 (2008)
 96. S.A. Nabi, A. Akhtar, M.D.A. Khan, M.A. Khan, Synthesis, characterization and electrical conductivity of polyaniline-Sn(IV)tungstophosphate hybrid cation exchanger: analytical application for removal of heavy metal ions from wastewater. *Desalination* **340**, 73–83 (2014)
 97. S.A. Nabi, S.A. Ganai, A.M. Khan, Synthesis, characterization and ion exchange behavior of polyaniline stannic silicomolybdate, an organic-inorganic composite material: quantitative separation of Pb^{2+} ions from industrial effluents. *J. Inorg. Organomet. Polym.* **21**, 25–35 (2011)
 98. S.A. Nabi, R. Bushra, M. Shahadat, Removal of toxic metal ions by using composite cation-exchange material. *J. Appl. Polymer Sci.* **125**, 3438–3446 (2012)
 99. M. Shahadat, S.A. Nabi, R. Bushra, A.S. Raeissi, K. Umar, M.O. Ansari, Synthesis, characterization, photolytic degradation, electrical conductivity and applications of a nanocomposite adsorbent for the treatment of pollutants. *RSC Adv.* **2**, 7207–7220 (2012)
 100. A.A. Khan, U. Baig, Electrically conductive membrane of polyanilinetitanium (IV) phosphate cation exchange nanocomposite: applicable for detection of Pb(II) using its ion-selective electrode. *J. Ind. Eng. Chem.* **18**, 1937–1944 (2012)
 101. M.M. Alam, Z.A. Alothman, M. Naushad, Analytical and environmental applications of polyaniline Sn(IV) tungstoarsenate and polypyrrrolepolyantimonic acid composite cation-exchangers. *J. Ind. Eng. Chem.* **19**, 1973–1980 (2013)
 102. M. Naushad, Z.A. AL-Othman, M. Islam, Adsorption of cadmium ion using a new composite cation-exchanger polyaniline Sn(IV) silicate: kinetics, thermodynamic and isotherm studies. *Int. J. Environ. Sci. Technol.* **10**, 567–578 (2013)
 103. A.A. Khan, S. Shaheen, Synthesis and characterization of a novel hybrid nano composite cation exchanger poly-*o*-toluidine Sn(IV) tungstate: its analytical applications as ion-selective electrode. *Solid State Sci.* **16**, 158–167 (2013)
 104. R. Bushra, M. Naushad, R. Adnan, M.N.M. Ibrahim, M. Rafatullah, Polyaniline supported nanocomposite cation exchanger: synthesis, characterization and applications for the efficient removal of Pb^{2+} ion from aqueous medium. *J. Ind. Eng. Chem.* (2014). <https://doi.org/10.1016/j.jiec.2014.05.022>
 105. R. Bushra, M. Shahadat, A. Ahmad, S.A. Nabi, K. Umar, M. Oves, A.S. Raeissi, M. Muneer, Synthesis, characterization, antimicrobial activity and applications of polyaniline Ti (IV) arsenophosphate adsorbent for the analysis of organic and inorganic pollutants. *J. Hazard. Mater.* **264**, 481–489 (2014)

106. M.A. Khan, A. Ahmad, K. Umar, S.A. Nabi, Synthesis, characterization, and biological applications of nanocomposites for the removal of heavy metals and dyes. *Ind. Eng. Chem. Res.* **54**, 76–82 (2015)
107. A. Khan, A.M. Asiri, M.A. Rub, N. Azum, A.A.P. Khan, S.B. Khan, M.M. Rahman, I. Khan, Synthesis, characterization of silver nanoparticle embedded polyaniline tungstophosphate-nanocomposite cation exchanger and its application for heavy metal selective membrane. *Compos. B Eng.* **45**, 1486–1492 (2013)
108. Inamuddin, M. Naushad, T.A. Rangreez, Z.A. Al-Othman, Ion-selective potentiometric determination of Pb(II) ions using PVC-based carboxymethyl cellulose Sn(IV) phosphate composite membrane electrode. *Desalin. Water Treat.* **56**, 806–813 (2015)
109. M. Shahadat, R. Bushra, Synthesis, characterization and significant applications of PANI-Zr(IV) sulphasalicylate nanocomposite. *Adv. Nanotechnol.* **6**, 181–206 (2015)
110. T.A. Rangreez, Inamuddin, M. Naushad, H. Ali, Synthesis and characterisation of poly(3,4-ethylenedioxythiophene)-poly(styrenesulfonate) (PEDOT:PSS) Zr(IV) monothiophosphate composite cation exchanger: analytical application in the selective separation of lead metal ions. *Int. J. Environ. Anal. Chem.* **95**, 556–568 (2015)
111. T.A. Khan, Inamuddin, M. Naushad, Heavy metal ion-exchange kinetic studies over cellulose acetate Zr(IV) molybdophosphate composite cation-exchanger. *Desalin. Water Treat.* **53**, 1675–1682 (2015)
112. Inamuddin, T.A. Rangreez, A. Khan, Synthesis of single-walled carbon nanotubes cerium (IV) phosphate composite cation exchanger: ion exchange studies and its application as ion-selective membrane electrode for determination of Cd(II) ions. *Polymer Compos.* (2015). <https://doi.org/10.1002/pc.23664>
113. F.G. Donan, The theory of membrane equilibrium in presence of a non-dialyzable electrolyte. *Z. Elektrochem.* **17**, 572–581 (1911)
114. R. Bushra, M. Shahadat, M.A. Khan, R. Inamuddin, M. Adnan, Rafatullah, Optimization of polyaniline supported Ti(IV) arsenophosphate composite cation exchanger based ion-selective membrane electrode for the determination of lead. *Ind. Eng. Chem. Res.* **53**, 19387–19391 (2014)
115. A.A. Khan, T. Akhtar, Preparation, physico-chemical characterization and electrical conductivity measurement studies of an organic–inorganic nanocomposite cation-exchanger: poly-*o*-toluidine Zr(IV) phosphate. *Electrochim. Acta* **53**, 5540–5548 (2008)
116. R. Bushra, M. Shahadat, A.S. Raeissi, S.A. Nabi, Development of nano-composite adsorbent for removal of heavy metals from industrial effluent and synthetic mixtures; its conducting behavior. *Desalination* **289**, 1–11 (2012)
117. A. Mohammad, Inamuddin, S. Hussain, Poly(3,4-ethylenedioxythiophene): polystyrene sulfonate (PEDOT:PSS) Zr(IV) phosphate composite cation exchanger: sol-gel synthesis and physicochemical characterization. *Ionics* **21**, 1063–1071 (2014)